



**FAA CENTER OF EXCELLENCE FOR  
ALTERNATIVE JET FUELS & ENVIRONMENT**

**Annual Technical Report**

**2020**

**For the period**

October 1, 2019 – September 30, 2020

Boston University  
Georgia Institute of Technology  
Massachusetts Institute of Technology  
Missouri University of Science and Technology  
Oregon State University  
Pennsylvania State University  
Purdue University  
Stanford University  
University of Dayton  
University of Hawaii  
University of Illinois  
University of North Carolina  
University of Pennsylvania  
University of Tennessee  
University of Washington  
Washington State University



FAA CENTER OF EXCELLENCE FOR ALTERNATIVE JET FUELS & ENVIRONMENT



This work was funded by the US Federal Aviation Administration (FAA) Office of Environment and Energy as a part of ASCENT Project AJFE under FAA Award Number 13-C. Any opinions, findings, and conclusions or recommendations expressed in this material are those of the authors and do not necessarily reflect the views of the FAA or other ASCENT Sponsors.





## Table of Contents

Overview Michael Wolcott and R. John Hansman, Center Directors	1
Project 001(A)   Alternative Jet Fuel Supply Chain Analysis Lead Investigators: Michael Wolcott, Christina Sanders, Manuel Garcia-Perez, Xiao Zhang, Ji Yun Lee	6
Project 001(B)   Alternative Jet Fuel Supply Chain Analysis Lead Investigator: Scott Q. Turn	22
Project 001(C)   Alternative Jet Fuel Supply Chain Analysis Lead Investigator: Farzad Taheripour	39
Project 001(D)   Alternative Jet Fuel Supply Chain Analysis Lead Investigator: Saurabh Bansal	46
Project 001(E)   Alternative Jet Fuel Supply Chain Analysis Lead Investigators: Burton C. English, Timothy Rials	52
Project 001(F)   Alternative Jet Fuel Supply Chain Analysis Lead Investigators: Steven R. H. Barrett, Raymond L. Speth, Florian Allroggen	71
Project 002   Ambient Conditions Corrections for Non-Volatile PM Emissions Measurements Lead Investigator: Phil Whitefield	93
Project 003   Cardiovascular Disease and Aircraft Noise Exposure Lead Investigator: Junenette Peters	97
Project 009   Geospatially Driven Noise Estimation Module Lead Investigators: Dimitri N. Mavris, Holger Pfaender	108
Project 010   Aircraft Technology Modeling and Assessment Lead Investigators: Dimitri N. Mavris, William Crossley, Jimmy Tai, Daniel A. DeLaurentis	115
Project 017   Pilot Study on Aircraft Noise and Sleep Disturbance Lead Investigator: Mathias Basner	235
Project 018   Health Impacts Quantification for Aviation Air Quality Tools Lead Investigator: Kevin J. Lane, Jonathan Levy	332
Project 019   Development of Aviation Air Quality Tools for Airport-Specific Impact Assessment: Air Quality Modeling Lead Investigator: Saravanan Arunachalam	354
Project 020   Development of NAS wide and Global Rapid Aviation Air Quality Lead Investigator: Steven R. H. Barrett	382



Project 021   Improving Climate Policy Analysis Tools Lead Investigators: Steven R.H. Barrett, Florian Allroggen	385
Project 022   Evaluation of FAA Climate Tools Lead Investigator: Donald Wuebbles	388
Project 023   Analytical Approach for Quantifying Noise from Advanced Operational Procedures Lead Investigator: R. John Hansman	394
Project 025   National Jet Fuels Combustion Program – Area #1: Chemical Kinetics Combustion Experiments Lead Investigator: Ronald K. Hanson	399
Project 027   National Jet Fuels Combustion Program – Area #3: Advanced Combustion Tests Lead Investigator: Tim Lieuwen	407
Project 029(A)   National Jet Fuels Combustion Program – Area #5: Atomization Tests and Models Lead Investigator: Robert P. Lucht	423
Project 031(A)   Alternative Jet Fuels Test and Evaluation Lead Investigator: Steven Zabarnick	437
Project 033   Alternative Fuels Test Database Library Lead Investigator: Tonghun Lee	446
Project 034   National Jet Fuels Combustion Program – Area #7: Overall Program Integration and Analysis Lead Investigator: Joshua S. Heyne	455
Project 036   Parametric Uncertainty Assessment for AEDT2b Lead Investigators: Dimitri N. Mavris, Yongchang Li	467
Project 037   CLEEN II Technology Modeling and Assessment Lead Investigator: Dimitri N. Mavris	471
Project 038   Rotorcraft Noise Abatement Procedures Development Lead Investigator: Kenneth Brentner	477
Project 039   Naphthalene Removal Assessment Lead Investigator: Steven R. H. Barrett	487
Project 040   Quantifying Uncertainties in Predicting Aircraft Noise in Real-world Situations Lead Investigators: Victor W. Sparrow, Kai-Ming Li	500
Project 041   Identification of Noise Acceptance Onset for Noise Certification Standards of Supersonic Airplanes Lead Investigator: Victor W. Sparrow	534
Project 043   Noise Power Distance Re-Evaluation Lead Investigator: Dimitri N. Mavris	543



Project 044   Aircraft Noise Abatement Procedure Modeling and Validation Lead Investigators: R. John Hansman, Jacqueline Thomas	570
Project 045   Takeoff/Climb Analysis to Support AEDT APM Development Lead Investigators: Dimitri N. Mavris, Michelle R. Kirby	576
Project 046   Surface Analysis to Support AEDT APM Development Lead Investigator: Hamsa Balakrishnan	590
Project 047   Clean Sheet Supersonic Aircraft Engine Design and Performance Lead Investigator: Steven R. H. Barrett	599
Project 048   Analysis to Support the Development of an Engine nvPM Emissions Standards Lead Investigator: Steven R. H. Barrett	615
Project 049   Urban Air Mobility Noise Reduction Modeling Lead Investigator: Kenneth Brentner	629
Project 050   Over-Wing Engine Placement Evaluation Lead Investigators: Dimitri N. Mavris, Chung Lee	643
Project 051   Combustion Concepts for Next-Generation Aircraft Engines Lead Investigator: Steven R. H. Barrett	664
Project 052   Comparative Assessment of Electrification Strategies for Aviation Lead Investigators: Steven R. H. Barrett, Florian Allroggen, Raymond Speth	668
Project 053   Validation of Low Exposure Noise Modeling by Open Source Data Management and Visualization Systems Integrated with AEDT Lead Investigator: Juan J. Alonso	681
Project 054   AEDT Evaluation and Development Support Lead Investigators: Dimitri N. Mavris, Michelle Kirby	691
Project 055   Noise Generation and Propagation from Advanced Combustors Lead Investigator: Tim Lieuwen	749
Project 056   Turbine Cooling through Additive Manufacturing Lead Investigator: Karen A. Thole	772
Project 057   Support for Supersonic Aircraft En-route Noise Efforts in ICAO CAEP Lead Investigator: Victor W. Sparrow	781
Project 058   Improving Policy Analysis Tools to Evaluate Higher-Altitude Aircraft Operations Lead Investigators: Steven R. H. Barrett, Sebastian D. Eastham	789
Project 059(A/E)   Jet Noise Modeling to Support Low Noise Supersonic Aircraft Technology Development Lead Investigators: Dimitri N. Mavris, Philip J. Morris, Jimmy Tai	798



Project 059(B)   Jet Noise Modeling and Measurements to Support Reduced LTO Noise of Supersonic Aircraft Technology Development Lead Investigator: Krishan Ahuja	804
Project 059(C)   Modeling Supersonic Jet Noise Reduction with Global Resolvent Modes Lead Investigator: Daniel J. Bodony	820
Project 059(D)   Physics-Based Analyses and Modeling for Supersonic Aircraft Exhaust Noise Lead Investigator: Sanjiva K. Lele	826
Project 060   Analytical Methods for Expanding the AEDT Aircraft Fleet Database Lead Investigators: Dimitri N. Mavris, Yongchang Li	832
Project 061   Noise Certification Streamlining Lead Investigators: Dimitri N. Mavris, Jimmy Tai	851
Project 062   Noise Model Validation for AEDT Lead Investigators: Dimitri N. Mavris, Victor W. Sparrow	869
Project 063   Parametric Noise Modeling for Boundary Layer Ingesting Propulsors Lead Investigators: Dimitri N. Mavris, Jonathan Gladin	891
Project 064   Alternative Design Configurations to Meet Future Demand Lead Investigators: Dimitri N. Mavris, Michelle R. Kirby	907
Project 065(A)   Fuel Testing Approaches for Rapid Jet Fuel Prescreening Lead Investigator: Joshua Heyne	918
Project 065(B)   Fuel Testing Approaches for Rapid Jet Fuel Prescreening Lead Investigator: Tonghun Lee	929
Project 066   Evaluation of High Thermal Stability Fuels Lead Investigator: Joshua Heyne	937
Project 067   Impact of Fuel Heating on Combustion and Emissions Lead Investigator: Robert P. Lucht	944
Project 068   Combustor Wall Cooling with Dirt Mitigation Lead Investigator: Karen A. Thole	951
Project 069   Transitioning a Research nvPM Mass Calibration Procedure to Operations Lead Investigator: Philip Whitefield	960
Project 070   Reduction of nvPM Emissions from Aero-Engine Fuel Injectors Lead Investigator: Wenting Sun	964
Project 071   Predictive Simulation of nvPM Emissions in Aircraft Combustors Lead Investigator: Suresh Menon	970



Project 072   Aircraft Noise Exposure and Market Outcomes in the United States Lead Investigators: R. John Hansman, Christopher R. Knittel, Steven R.H. Barrett, Jing Li, Florian Allroggen	976
Project 073   Fuel Composition Impact on Combustor Durability Lead Investigator: Steven Zabarnick	979
Project 074   Low Emissions Pre-Mixed Combustion Technology for Supersonic Civil Transport Lead Investigator: Adam Steinberg	983
Project 075   Improved Engine Fan Broadband Noise Prediction Capabilities Lead Investigator: Sheryl Grace	996
Project 076   Improved Open Rotor Noise Prediction Capabilities Lead Investigators: Dimitri N. Mavris, Jimmy Tai	999
Project 077   Measurements to Support Noise Certification for UAS/UAM Vehicles and Identify Noise Reduction Lead Investigator: Eric Greenwood	1003
Publications Index	1023
Funding Tables	1035



## Overview

This report covers the period October 1, 2019 through September 30, 2020. The Center was established by the authority of FAA solicitation 13-C-AJFE-Solicitation. During that time the ASCENT team launched a new website, which can be viewed at [ascent.aero](http://ascent.aero). The next meeting will be held virtually April 27-29, 2021.

Over the last year, the ASCENT team has made great strides in research, outreach, and education. The team's success includes the following:

- **60 active research projects.**

The projects are divided into five main categories: tools, operations, noise, emissions, and alternative fuels, with cross-cutting research in aircraft technology innovation and supersonics. See the project category descriptions for more detail on each category and a summary of the projects. Funding for these projects comes from the FAA in partnership with Transport Canada.

- **125 publications, reports, and presentations by the ASCENT team.**

Each project report includes a list of publications, reports, and presentations. A comprehensive list of the publications, reports, and presentations for all projects is available in the publications index on page 546.

- **186 students participated in aviation research with the ASCENT team.**

Each project report includes the names and roles of the graduate and undergraduate students in the investigator's research. Students are selected by the investigators to participate in this research.

- **57 industry partners involved in ASCENT.**

ASCENT's industry partners play an important role in the Center. The members of the ASCENT Advisory Board provide insight into the view of stakeholders, provide advice on the activities and priorities of the Center's co-directors, and ensure research will have practical application. The committee does not influence FAA policy. Industry partners also play a direct role in some of the research projects, providing matching funds, resources and expertise to the project investigators.

## Leadership

Dr. Michael Wolcott  
Center Director and Technical Lead for Alternative Jet Fuels Research  
Washington State University  
(509) 335-6392  
[wolcott@wsu.edu](mailto:wolcott@wsu.edu)

Dr. R. John Hansman  
Center Co-Director and Technical Lead for Environmental Research  
Massachusetts Institute of Technology  
(617) 253-2271  
[rjhans@mit.edu](mailto:rjhans@mit.edu)

Dr. John Holladay  
Federal Research Laboratories and Agency Liaison  
[john.holladay@pnnl.gov](mailto:john.holladay@pnnl.gov)

Dr. James Hileman  
Chief Scientific and Technical Advisor for Environment and Energy  
Office of Environment and Energy  
Federal Aviation Administration  
[james.hileman@faa.gov](mailto:james.hileman@faa.gov)





## Research Topics

Research projects within ASCENT are divided into five categories: alternative fuels, emissions, noise, operations, tools, aircraft technology innovation and supersonics.

### Alternative Fuels

The development of alternative jet fuels (AJFs) -- or sustainable aviation fuels (SAF) -- is of great interest to an array of aviation stakeholders, including aircraft and engine manufacturers and airlines. Alternative fuels that are produced from bio-based materials provide sustainable jet fuel alternatives that not only help alleviate environmental impacts from aviation emissions but can also create jobs in rural areas and lessen our reliance on foreign petroleum supplies.

Effective research and development, co-funded by the federal government and industry, enables SAF development by reducing the costs of producing renewable fuel. ASCENT research provides the scientific expertise and data to evaluate the environmental benefits associated with these sustainable fuels. ASCENT's collaborative R&D activities focuses on evaluating promising sustainable aviation fuel pathways to ensure environmental and social benefits, reduce technical uncertainties, inform aviation emission policies, and promote private sector investment in production.

Projects include:

- 001A-F - Alternative Jet Fuel Supply Chain Analysis
- 025 - National Jet Fuels Combustion Program – Area #1: Chemical Kinetics Combustion Experiments
- 026 - (COMPLETE) - National Jet Fuels Combustion Program – Area #2: Chemical Kinetics Model Development and Evaluation
- 027 - National Jet Fuels Combustion Program – Area #3: Advanced Combustion Tests
- 028 - National Jet Fuels Combustion Program – Area #4: Combustion Model Development and Evaluation
- 029 - National Jet Fuels Combustion Program – Area #5: Atomization Tests and Models
- 030 - National Jet Fuels Combustion Program – Area #6: Referee Swirl-Stabilized Combustor Evaluation/Support
- 031 - Alternative Jet Fuels Test and Evaluation
- 032 - (COMPLETE) - Worldwide LCA of GHG Emissions from Petroleum Jet
- 033 - Alternative Fuels Test Database Library
- 034 - National Jet Fuels Combustion Program – Area #7: Overall Program Integration and Analysis
- 052 - Comparative Assessment of Electrification Strategies for Aviation
- 065 - Fuel Testing Approaches for Rapid Jet Fuel Prescreening
- 066 - Evaluation of High Thermal Stability Fuels
- 067 - Impact of Fuel Heating on Combustion and Emissions
- 073 - Combustor Durability with Alternative Fuel Use

### Emissions

The demand for passenger and cargo air transportation has grown rapidly over the last several decades. According to the International Air Transport Association (IATA), in 2016 there were 3.8 billion air travelers, a number it predicts will rise to 7.2 billion passengers by 2035—a near doubling of current levels. This staggering growth is accompanied by airport expansions and increases in emissions from aircraft, ground services equipment, and vehicle traffic on and near airports. The increases in these activity-based emissions impact the air quality around airports, cumulatively contribute to global climate change, and can negatively affect human health.

ASCENT researchers are analyzing data and improving predictive models to understand the effects of aircraft and ground vehicle emissions, create and refine emission-based analytical techniques at both airport-specific and global scales, and assess how policy changes affect emissions and its impacts.

Projects include:

- 002 - Ambient Conditions Corrections for Non-Volatile PM Emissions Measurements
- 013 - (COMPLETE) - Micro-Physical Modeling & Analysis of ACCESS 2 Aviation Exhaust Observations
- 014 - (COMPLETE) - Analysis to Support the Development of an Aircraft CO<sub>2</sub> Standard
- 018 - Community Measurement of Aviation Emission Contribution of Ambient Air Quality
- 019 - Development of Improved Aviation Emissions Dispersion Capabilities for AEDT
- 020 - (COMPLETE) - Development of NAS wide and Global Rapid Aviation Air Quality



- 021 - (COMPLETE) - Improving Climate Policy Analysis Tools
- 022 - Evaluation of FAA Climate Tools
- 024 - (COMPLETE) - Emissions Data Analysis for CLEEN, ACCESS, and Other Recent Tests
- 039 - Naphthalene Removal Assessment
- 047 - Clean Sheet Supersonic Aircraft Engine Design and Performance
- 048 - Analysis to Support the Development of an Engine nvPM Emissions Standard
- 051 - Combustion Concepts for Next-Generation Aircraft Engines
- 052 - Comparative Assessment of Electrification Strategies for Aviation
- 058 - Improving Policy Analysis Tools to Evaluate Higher-Altitude Aircraft Operations
- 064 - Alternative Design Configurations to Meet Future Demand
- 067 - (NEW) - Impact of Fuel Heating on Combustion and Emissions
- 068 - (NEW) - Combustor Wall Cooling Concepts for Dirt Mitigation
- 069 - Transitioning a Research nvPM Mass Calibration Procedure to Operations
- 070 - (NEW) - Reduction of nvPM emissions via innovation in aero-engine fuel injector design
- 071 - Predictive Simulation of nvPM Emissions in Aircraft Combustors
- 074 - (NEW) - Low Emissions Pre-Mixed Combustion Technology for Supersonic Civil Transport

### **Noise**

ASCENT researchers work to understand all aspects of the aircraft operations that contribute to aviation's noise impact. They are working on understanding how aircraft and rotorcraft performance and operation affect noise generation and how they could be modified for mitigation measures. Research is also under way to look how noise propagates from the source to the ground and how it affects human health, wellbeing, and quality of life. This research will improve the modeling tools used to estimate the noise impacts from aviation operations and provide data to inform policy development as well as public engagement and education.

Projects include:

- 003 - Cardiovascular Disease and Aircraft Noise Exposure
- 004 - (COMPLETE) - Estimate of Noise Level Reduction
- 005 - (COMPLETE) - Noise Emission and Propagation Modeling
- 007 - (COMPLETE) - Civil, Supersonic Over Flight, Sonic Boom (Noise) Standards Development
- 008 - (COMPLETE) - Noise Outreach
- 009 - Geospatially Driven Noise Estimation Module
- 017 - (COMPLETE) - Pilot Study on Aircraft Noise and Sleep Disturbance
- 038 - Rotorcraft Noise Abatement Procedures Development
- 040 - Quantifying Uncertainties in Predicting Aircraft Noise in Real-world Situations
- 041 - Identification of Noise Acceptance Onset for Noise Certification Standards of Supersonic Airplane
- 042 - Acoustical Mode of Mach Cut-off
- 043 - Noise Power Distance Re-Evaluation
- 044 - Aircraft Noise Abatement Procedure Modeling and Validation
- 049 - Urban Air Mobility Noise Reduction Modeling
- 050 - (NEW) - Over-Wing Engine Placement Evaluation
- 053 - Validation of Low Exposure Noise Modeling by Open Source Data Management and Visualization Systems Integrated with AEDT
- 055 - Noise Generation and Propagation from Advanced Combustors
- 057 - Support for Supersonic Aircraft En-route Noise Efforts in ICAO CAEP
- 059A-E - Modeling and Measurements of Supersonic Civil Transport Jet Noise
- 061 - Noise Certification Streamlining
- 062 - Noise Model Validation for AEDT
- 063 - Parametric Noise Modeling for Boundary Layer Ingesting Propulsors
- 072 - (NEW) - Aircraft noise exposure and market outcomes in the US
- 075 - (NEW) - Improved Engine Fan Broadband Noise Prediction Capabilities
- 076 - (NEW) - Improved Open Rotor Noise Prediction Capabilities

### **Operations**

Aviation operations result in fuel burn, emissions, and noise impacts. The nature and scale of these effects depends on a number of related factors, including:



- Aircraft flight paths and profiles,
- Schedule and frequency of operations, and
- Aircraft fleet mix.

ASCENT research focuses on identifying and accelerating the implementation of operational concepts that will reduce aviation environmental impacts and/or improve energy efficiency while maintaining the efficiency of the National Airspace System. The research spans multiple phases of flights and targets all environmental impact areas.

Projects include:

- 006 - (COMPLETE) - Rotorcraft Noise Abatement Operating Conditions Modeling
- 015 - (COMPLETE) - Cruise Altitude and Speed Optimization
- 016 - (COMPLETE) - Airport Surface Movement Optimization
- 023 - Analytical Approach for Quantifying Noise from Advanced Operational Procedures
- 038 - Rotorcraft Noise Abatement Procedures Development
- 044 - Aircraft Noise Abatement Procedure Modeling and Validation
- 053 - Validation of Low Exposure Noise Modeling by Open Source Data Management and Visualization Systems Integrated with AEDT
- 077 - (NEW) - Measurements to Support Noise Certification for UAS/UAM Vehicles and Identify Noise Reduction Opportunities

## Tools

The aviation system operation involves complex interactions between many different components when aircraft are on the ground, taking off, in the air, and when landing. Aviation system operations also require the understanding of how to optimize aviation activities, which is best done by implementing advanced modeling tools.

The Federal Aviation Administration's suite of modeling tools have been developed to characterize and quantify the interdependences of aviation-related noise and emissions, impacts on human health and welfare, and the costs and market impacts to industry and consumers under varying policies, technologies, operations and market scenarios.

The ASCENT researchers are further developing and expanding the capabilities of these modeling tools in a variety of ways, from improving the way basic physical properties are represented and effectively modeled to how new technologies will enter the aircraft fleet and identifying the benefits of such technologies.

Projects include:

- 009 - Geospatially Driven Noise Estimation Module
- 010 - Aircraft Technology Modeling and Assessment
- 011 - (COMPLETE) - Rapid Fleet-wide Environmental Assessment Capability
- 012 - (COMPLETE) - Aircraft Design and Performance Assessment Tool Enhancement
- 035 - (COMPLETE) - Airline Flight Data Examination to Improve flight Performance Modeling
- 036 - (COMPLETE) - Parametric Uncertainty Assessment for AEDT2b
- 037 - CLEEN II Technology Modeling and Assessment
- 040 - (COMPLETE) - Quantifying Uncertainties in Predicting Aircraft Noise in Real-world Situations
- 043 - Noise Power Distance Re-Evaluation (NPD+C) to Include Airframe Noise in AEDT
- 045 - Takeoff/Climb Analysis to Support AEDT APM Development
- 046 - Surface Analysis to Support AEDT APM Development
- 049 - Urban Air Mobility Noise Reduction Modeling
- 053 - Validation of Low Exposure Noise Modeling by Open Source Data Management and Visualization Systems Integrated with AEDT
- 054 - AEDT Evaluation and Development Support
- 058 - Improving Policy Analysis Tools to Evaluate Higher-Altitude Aircraft Operations
- 060 - Analytical Methods for Expanding the AEDT Aircraft Fleet Database
- 062 - (NEW) - Noise Model Validation for AEDT
- 064 - (NEW) - Alternative Design Configurations to meet Future Demand



## **Aircraft Technology Innovation**

The evolution of airframes and engines has resulted in modern designs that significantly reduce aviation fuel use, emissions and noise on a per-flight basis. ASCENT researchers conduct the analyses, modeling and testing required to demonstrate the viability of innovative airframe, engine and flight management technologies that reduce noise, emissions, and fuel burn. Future innovations will drive further improvements and the ASCENT research helps accelerate technology development.

### Projects include:

- 010- Aircraft Technology Modeling and Assessment
- 037 - CLEEN II System Level Assessment
- 047 - Clean Sheet Supersonic Aircraft Engine Design and Performance
- 050 - Over-Wing Engine Placement Evaluation
- 051 - Combustion Concepts for Next-Generation Aircraft Engines
- 052 - Comparative Assessment of Electrification Strategies for Aviation
- 055 - Noise Generation and Propagation from Advanced Combustors
- 056 - Turbine Cooling through Additive Manufacturing
- 059 - Modeling and Measurements of Supersonic Civil Transport Jet Noise
- 063 - Parametric Noise Modeling for Boundary Layer Ingesting Propulsors
- 064 - Alternative Design Configurations to Meet Future Demand
- 066 - Evaluation of High Thermal Stability Fuels
- 067 - (NEW) - Impact of Fuel Heating on Combustion and Emissions
- 068 - Combustor Wall Cooling with Dirt Mitigation
- 070 - (NEW) - Reduction of nvPM emissions via innovation in aero-engine fuel injector design
- 071 - (NEW) - Predictive Simulation of Soot Emission in Aircraft combustors
- 074 - (NEW) - Low Emissions Pre-Mixed Combustion Technology for Supersonic Civil Transport
- 075 - (NEW) - Improved Engine Fan Broadband Noise Prediction Capabilities
- 076 - (NEW) - Improved Open Rotor Noise Prediction Capabilities
- 077 - Measurements to Support Noise Certification for UAS/UAM Vehicles and Identify Noise Reduction Opportunities

## **Supersonics**

ASCENT supersonics research supports implementation of new technologies by advancing the understanding of the perception of sonic boom noise over a range of sonic boom levels, assessing Mach cut-off levels that will allow supersonic flight over land and furthering development of supersonic aircraft noise certification standards.

### Projects include:

- 007 - (COMPLETE) - Civil, Supersonic Over Flight, Sonic Boom (Noise) Standards Development
- 010- Aircraft Technology Modeling and Assessment
- 022 - Evaluation of FAA Climate Tools
- 041 - Identification of Noise Acceptance Onset for Noise Certification Standards of Supersonic Airplanes
- 042 - Acoustical Model of Mach Cut-off
- 047 - Clean Sheet Supersonic Aircraft Engine Design and Performance
- 057 - (NEW) - Support for Supersonic Aircraft Noise Efforts in ICAO CAEP
- 058 - (NEW) - Improving Policy Analysis Tools to Evaluate Aircraft Operations in the Stratosphere
- 059 - (NEW) - Jet Noise Modeling to Support Low Noise Supersonic Aircraft Technology Development
- 074 - (NEW) - Low Emissions Pre-Mixed Combustion Technology for Supersonic Civil Transport



# Project 001(A) Alternative Jet Fuel Supply Chain Analysis

## Washington State University

### Project Lead Investigator

Michael P. Wolcott  
Regents Professor  
Department of Civil & Environmental Engineering  
Washington State University  
PO Box 642910  
Pullman, WA 99164-2910  
509-335-6392  
wolcott@wsu.edu

### University Participants

#### Washington State University (WSU)

- PIs: Michael P. Wolcott, Regents Professor; Christina Sanders, Acting Director, DGSS; Manuel Garcia-Perez, Professor; Xiao Zhang, Associate Professor; and Ji Yun Lee, Assistant Professor
- FAA Award Number: 13-C-AJFE-WaSU-016
- Period of Performance: August 1, 2019 to September 30, 2020
- Tasks:
  1. WSU 1. Design cases. (Garcia-Perez, Zhang)
  2. WSU 2. Evaluate the most promising biorefinery concepts for alternative jet fuel (AJF) production. (Garcia-Perez, Zhang)
  3. WSU 3. Supplement and maintain the current inventory of biorefinery infrastructures that are useful for the production of AJF, as identified in the conversion design cases. (Wolcott)
  4. WSU 4. Perform a community social asset assessment. (Gaffney)
  5. WSU 5. Refine and deploy facility siting tools to determine regional demand and to identify potential conversion sites to be used in regional analyses. (Wolcott)
  6. WSU 6. Perform a refinery-to-wing stakeholder assessment. (Gaffney)
  7. WSU 7. Conduct a supply chain analysis. (Wolcott, Garcia-Perez)
  8. WSU 8. Provide analytical support for regional Commercial Aviation Alternative Fuels Initiative (CAAFI) and USDA jet fuel projects. (Wolcott)

### Project Funding Level

\$510,918 FAA funding and \$510,918 matching funds. State-committed graduate school contributions for four PhD students. Faculty time for Michael Wolcott, Manuel Garcia-Perez, and Xiao Zhang contributes to the cost share.

### Investigation Team

- Michael Wolcott, WSU, Project Director/PI
- Christina Sanders, WSU, Co-Project Director/Co-PI
- Season Hoard, WSU, Co-Project Director/Co-PI
- Manuel Garcia-Perez, WSU, Co-Project Director/Co-PI
- Xiao Zhang, WSU, Co-Project Director/Co-PI
- Ji Yun Lee, WSU, Co-Project Director/Co-PI
- Michael Gaffney, WSU, Faculty
- Kristin Brandt, WSU, Staff Engineer
- Dane Camenzind, WSU, Staff Engineer
- Lina Pilar Martinez Valencia, WSU, Graduate Student



- Tanzil Abid Hossain, WSU, Graduate Student
- Anamaria Paiva, WSU, Graduate Student
- Daniel Mueller, WSU, Graduate Student
- Kelly Nguyen, WSU, Graduate Student
- Jie Zhao, WSU, Graduate Student
- Fangjiao Ma, WSU, Graduate Student

## Collaborating Researchers

- Burton English, University of Tennessee
- Greg Latta, University of Idaho
- Kristin C. Lewis, Volpe National Transportation Systems Center

## Project Overview

As part of an effort to realize an “aviation system in which air traffic will move safely, swiftly, efficiently, and seamlessly around the globe,” the FAA has set a series of goals and supporting outcomes, strategies, and performance metrics (Hileman et al., 2013). The goal entitled “Sustaining our Future” outlines a number of strategies that are collectively aimed at reducing the environmental and energy impacts of the aviation system. To achieve this goal, the FAA set an aspirational goal for the aviation industry to utilize one billion gallons of AJF by the year 2018. This goal was created from an economic, emission, and overall feasibility perspective (Richard, 2010; Staples et al., 2014).

Current approaches to supply chain analysis for AJF optimize the feedstock-to-refinery and refinery-to-wing transportation logistics (Bond et al., 2014). One of the greatest barriers to large-scale AJF production is the high capital of greenfield facilities, which translates to risk in the investment community (Huber et al., 2007). The cost of cellulosic ethanol plants ranges from \$10 to \$13 per gallon capacity (Hileman and Stratton, 2014); moreover, the additional processing steps required to convert the intermediate to a drop-in AJF could increase this cost to over \$25 per gallon capacity (Hileman, 2014).

Motivated by the realities of converting these initial commercialization efforts into second-generation AJF, researchers have considered alternate conversion scenarios, including the transitioning of existing facilities (Brown, 2013). Currently, Gevo is employing retrofit strategies for corn ethanol plants to produce isobutanol, a potential intermediate for the alcohol-to-jet (ATJ) process of producing iso-paraffinic kerosene (Pearlson, 2011; Pearlson et al., 2013). Research on approaches for achieving the aspirational FAA goal of AJF consumption has relied upon “switching” scenarios, in which the existing and planned capacity are used to produce drop-in fuel (Malina, 2012). These approaches require the identification of existing industrial assets that can be targeted for future AJF production. Thus, siting becomes not only an exercise for optimizing feedstock transportation, but a necessary task for aligning this critical factor with the existing infrastructure, markets within regions, and the appropriate social capital for developing this new industry (Henrich et al., 2007; Seber et al., 2014).

Thus far, all published AJF supply chain analyses have been limited to stand-alone jet fuel production technologies that do not generate bio-products. Hence, the potential techno-economic and environmental benefits of using existing industrial infrastructure and the production of coproducts with respect to the development of jet fuel production scenarios must be considered in future studies.

Design cases of stand-alone AJF production facilities will be used in supply chain evaluations. Social asset modeling is not well developed, and efforts are likely hampered by difficulties in quantifying social assets when compared to improved environmental performance or reductions in AJF costs, which may be better observed by optimizing economic and environmental constraints. However, the community characteristics of a potential site must be considered when determining preferred locations for a new biorefinery. Community resistance or enthusiasm for the AJF industry can strongly influence the success or failure of a facility (Martinkus et al., 2014; Rijkhoff et al., 2017). Thus, community social asset modeling efforts conducted within this project, such as those based on the Community Asset and Attribute Model (CAAM), will inform disciplinary applications and advances. Clearly, social factors can have a significant effect—positive or negative—on project adoption and implementation, particularly in high technology or energy-related projects (Lewis et al., 2012; Martinkus et al., 2012; Mueller et al., 2020). The consideration of social factors in site selection and implementation decisions can maximize positive social support and minimize opposition and social negatives, which can significantly promote the success of a project. In this regard, the CAAM originally piloted in the Northwest Advanced Renewables Alliance (NARA) project was designed to provide a quantitative rating of select social factors at the county level (Martinkus et al., 2014).



Focusing on regional supply chains, this research aims to identify the key barriers that must be overcome to produce one billion gallons of AJF. We will address this overall goal by developing tools to support the AJF supply chain assessment performed at the Volpe Center. Our effort will provide facility siting analyses that assess conversion design cases combined with regional supply chain assets and social capacity assessments for communities to act collectively toward development goals. Finally, a refinery-to-wing stakeholder assessment will support modeling and accounting of AJF distribution for downstream fuel logistics.

## References

- Bond, J.Q., Upadhye, A.A., Olcay, H., Tompsett, G.A., Jae, J., Xing, R., Alonso, D.M., Wang, D., Zhang, T., Kumar, R., Foster, A., Sen, S.M., Maravalias, C.T., 13, R., Barret, S.R., Lobo, R., Wayman, C.E., Dumesic, J.A., & Huber, G.W. (2014). Production of renewable jet fuel range alkanes and commodity chemicals from integrated catalytic processing of biomass. *Energy Environ. Sci.*, 7:1500.
- Brown, N. (2013). FAA Alternative Jet Fuel Activities. Overview. Presented to: CLEEN Consortium, November 20, 2013.
- Henrich, E. (2007). The status of FZK concept of biomass gasification. 2<sup>nd</sup> European Summer School on Renewable Motor Fuels. Warsaw, Poland 29-31, August 2007.
- Hileman, J.I., De la Rosa-Blanco, E., Bonnefoy, P.A., & Carter, N.A. (2013). The carbon dioxide challenge facing aviation. *Progress in Aerospace Sciences.* 63:84-95.
- Hileman, J. I., & Stratton, R. W. (2014). "Alternative jet fuel feasibility." *Transport Policy*, 34:52-62.
- Hileman, J. (2013). Overview of FAA alternative jet fuel activities. Presentation to the Biomass R&D Technical Advisory Committee, Washington DC, August 14, 2013.
- Huber, G.W. & Corma, A. (2007). Synergies between bio- and oil refineries for the production of fuels from biomass. *Angewandte Chemie.* 46(38):7184-7201.
- Lewis, K., Mitra, S., Xu, S., Tripp, L., Lau, M., Epstein, A., Fleming, G., & Roof, C. (2012). Alternative jet fuel scenario analysis report. No. DOT/FAA/AEE/2011-05. (<http://ntl.bts.gov/lib/46000/46500/46597/DOT-VNTSC-FAA-12-01.pdf>) (Retrieved on 2014-07)
- Malina, R. (2012). HEFA and F-T jet fuel cost analyses. Laboratory for Aviation and the Environment. MIT, Nov 27, 2012.
- Martinkus, N., Kulkarni, A., Lovrich, N., Smith, P., Shi, W., Pierce, J., & Brown, S. (2012). An Innovative Approach to Identify Regional Bioenergy Infrastructure Sites. Proceedings of the 55th International Convention of Society of Wood Science and Technology, Beijing, China.
- Martinkus, N., Shi, W., Lovrich, N., Pierce, J., Smith, P., & Wolcott, M. (2014). Integrating biogeophysical and social assets into biomass-to-alternative jet fuel supply chain siting decisions. *Biomass and Bioenergy*, 66:410-418.
- Mueller, D., Hoard, S., Roemer, K., Sanders, C., & Rijkhoff, S. (2020). Quantifying the Community Capitals Framework: Strategic Application of the Community Assets and Attributes Model. Community Development.
- Pearlson, M.N. (2011). A techno-economic and environmental assessment of hydroprocessed renewable distillate fuels. MSc Thesis in Technology and Policy, MIT.
- Pearlson, M., Wollersheim, C., & Hileman, J. (2013). A techno-economic review of hydroprocessed renewable esters and fatty acids for jet fuel production. *Biofuels, Bioproducts and Biorefining*, 7(1):89-96.
- Rijkhoff, S., Hoard, S., Gaffney, M., Smith, P., & Wolcott, M. (2017). Communities Ready for Takeoff: Integrating Social Assets for Biofuel Site-Selection Modeling. *Politics and Life Sciences*, 36; 14-26.
- Richard, T.L. (2010). Challenges in scaling up alternative jet fuels infrastructure. *Science*, 329:793.
- Seber, G., Malina, R., Pearlson, M.N., Olcay, H., Hileman, J.I., & Barret, S.R.H. (2014). Environmental and economic assessment of producing hydroprocessed jet and diesel fuel from waste oil and tallow. *Biomass and Bioenergy*, 67:108-118.
- Staples, M.D., Malina, R., Olcay, H., Pearlson, M.N., Hileman, J.I., Boies, A., & Barrett, S.R.H. (2014). Lifecycle greenhouse gas footprint and minimum selling price of renewable diesel and jet fuel from fermentation and advanced fermentation technologies. *Energy & Environmental Science*, 7:1545.

## Task 1 - Design Cases

Washington State University

### Objectives

In previous years, our team has worked towards completing the reviews and final reports of design cases for six stand-alone AJF technologies (Table 1) and four relevant industries (sugarcane, pulp and paper, corn ethanol, and petroleum refineries). The status of each stand-alone AJF techno-economic analysis (TEA) and report are shown in Table 1. The results from pyrolysis



and ATJ pathways have been published in the peer-reviewed journals referenced, while the work conducted from October 1, 2019 to September 30, 2020 has focused on the following tasks:

1. Conduct a detailed analysis of a “catalytic hydrothermolysis pathway for jet fuel production.”
2. Conduct a detailed analysis of a new AJF pathway for hydrothermal liquefaction (HTL) processing.
3. Conduct TEA analyses on the integration of lignin coproduct technologies in the ATJ pathway to determine the potential for reducing fuel costs.
4. Develop a new case report, focusing on a technology review and an evaluation of lipid conversion processes (HEFA, CH, SBI, Forge, Tyton, decarboxylation; see Table 1) and new technologies for the production of alternative lipids (HTL and sugar-to-lipid).
5. Prepare manuscripts for publication.

**Table 1.** Evaluated Stand-alone AJF Technologies

	Literature review and design report date	Publications	TEA model
Pyrolysis	Literature review based on a design report, 138 pages (2017).	Energy & Fuels 33:4683, 2019; <i>Fuel Process Technology</i> 195:106140, 2019	Standardized TEA complete and available for use by university partners.
Alcohol-to-jet (ATJ)	Literature review based on a design report, 28 pages (2015).	ChemSusChem 11:3728, 2018	Standardized TEA complete and available for use by partners.
Synthetic kerosene and synthetic aromatic kerosene (SK-SKA)	Literature review based on a design report, 36 pages (2015).	A manuscript based on the case design report in preparation.	This is based on the Sasol process for which we have not found any significant development since 2016. There is a lack of adequate process information/data on SK-SKA production from renewable feedstock. Thus, we are not able to build a reliable TEA.
Direct sugar-to-hydrocarbon (DSHC)	Literature review based on a design report, 88 pages (2017).	Manuscript submitted and under review by Biomass and Bioenergy that includes DSHC.	Standardized TEA complete and available for use by partners.
Virent BioForming process	Literature review based on a design report, 46 pages (2015).	Manuscript submitted and under review by Biomass and Bioenergy that includes Virent.	Standardized TEA complete and available for use by partners.
Catalytic hydrothermolysis (CH)	Literature review based on a design report, 35 pages (2018).	Manuscript has been submitted for journal publication.	Standardized TEA complete.
Gasification Fischer Tropsch (GFT)	No literature review conducted.	Manuscript submitted and under review by Biomass and Bioenergy that includes GFT.	Standardized TEA complete and available for use by partners.
Microchannel gasification Fischer Tropsch (microGFT)	No exhaustive literature review was written. The capital costs found in the open literature for microchannel FT were not reliable.	The capital cost results were considered of poor reliability.	A standardized microGFT TEA was completed, however the cost information is considered unreliable.
Hydroprocessed esters and fatty acids (HEFA)	No written literature review conducted.	Manuscript submitted and under review by Biomass and Bioenergy that includes HEFA.	Standardized TEA complete and available for use by partners.



## **Research Approach**

### **Background**

We have conducted a detailed literature review and prepared design case reports on six AJF pathways, including pyrolysis, ATJ, synthetic kerosene and synthetic aromatic kerosene, direct sugar-to-hydrocarbon (DSHC), Virent BioForming, and catalytic hydrothermolysis (CH). We have also collected data from the literature to conduct TEA for these pathways. The results from these design cases are being applied in the development of supply chains and the identification of synergisms that may eventually lead to the construction of integrated AJF production systems that take advantage of the infrastructure in a given region. An analysis of the locations of existing infrastructure demonstrated that the United States can be divided into regions based on the dominant biomass. Thus, we believe that the generation of advanced biorefinery concepts focused on petroleum refineries, pulp and paper mills, sugarcane mills, and corn ethanol mills is a viable approach for evaluating the synergism among AJF pathways, existing infrastructure, and coproducts. We can then compare the biorefinery concepts developed for each technology to identify the most promising approach, which will then be used in supply chain analyses.

Stand-alone design case reports were generated by conducting reviews of relevant research in the academic literature and public information provided by commercial entities developing the corresponding technology. The published papers were subjected to an industrial expert review, and the reports provide details regarding the processes involved in each conversion pathway and outline the technology readiness and particular barriers to implementation. Publicly available information regarding the commercial processes and research literature will provide a foundation of information to be used in modeling efforts. Where detailed process engineering information is lacking, new models will be built to estimate the parameters needed to complete assessments such as techno-economic modeling and supply chain modeling. Aspen Plus is primarily used to generate process models and details, including mass balances, energy balances, energy requirements, and equipment size and cost. These results will also provide the basis for a comparative analysis between design cases, which will identify the key advantages and markets for each technology.

Each design case has the following components:

1. Feedstock requirements
2. Companies developing/commercializing the technology
3. Current location of units in the U.S. and worldwide
4. Block and flow diagram of the technology
5. Unit operations and process conditions (reactor type, separation unit type, catalysts, product yield, jet fuel yield)
6. Properties of the produced jet fuel
7. Identification of potential intermediates
8. Current and potential uses of wastes and effluents
9. Developed coproducts
10. Potential ways to co-process intermediates, wastes, and coproducts using existing infrastructure (petroleum refineries, pulp and paper mills, etc.)
11. Preliminary TEA
12. Technological challenges and gaps

We have submitted technical reports and supplementary Microsoft Excel files with mass and energy balances and TEAs for the pathways listed below. Furthermore, we have conducted a strategic analysis to identify the overall weaknesses of the technologies under study. All files are available on shared drives for the ASCENT Project 01 team members. Where indicated, the TEAs are still undergoing internal review.

- Pyrolysis-bio-oil hydro-treatment concept (hydro-treated depolymerized cellulosic jet): TEA is complete.
- ATJ: A manuscript with information regarding the mass and energy balances and the TEA has been published.
- Gasification Fischer Tropsch (GFT): Two design cases have been prepared for biomass gasification. The first case focuses on microreactors and the second design case is applicable to technology based on larger, standard reactors. Reviews on the TEAs for GFT and microGFT have been completed. However, the limited reliability of the microreactor capital costs hinders the value of the practical impact of our microreactor TEA study. The TEAs are available for use by partners.
- HEFA: A stochastic TEA was created in MATLAB and was confirmed to match the completed, deterministic TEA when assumptions and costs match. The deterministic TEA review is complete and it is now available for use.
- CH: TEA is complete.

We have submitted a manuscript to *Biomass and Bioenergy* comparing the economic and environmental performance of the AJF technologies discussed above and the overall weaknesses of the technologies studied. This manuscript presents a strategic analysis of the yield increases needed to achieve a minimum selling price (MSP) comparable to those of current commercial fuels. Over the last year, we also made progress in design cases for existing industries (corn ethanol, sugarcane mills) that could be used to reduce the production cost of AJFs. The analyses are complete.

Major progress has been made on the analysis of corn ethanol, sugarcane, and petroleum refinery infrastructure that could support jet fuel production. A paper on conversion of corn ethanol mills is under review by *Biomass and Bioenergy*. Two additional papers, using either sugarcane mills or petroleum refineries to reduce AJF production costs, are under internal review.

We have worked with the Pacific Northwest National Laboratory (PNNL) and completed a case design report on HTL for AJF conversion.

A summary report on several lipid conversion pathways, including SBI, Forge, Tyton, decarboxylation, and coprocessing, has been prepared. A manuscript entitled “Techno-economic analysis of the CH pathway for jet fuel production” has been reviewed by Agrisoma and the FAA, before submission for journal publication in September 2020.

### **Milestones**

An Excel file with TEAs for all AJF technologies has been completed and design cases for the corn ethanol and sugarcane industries are still being reviewed by the standardization team. A detailed analysis entitled “Catalytic hydrothermolysis pathway for jet fuel production” has been completed and a design case report entitled “Jet Fuel Design Case: Hydrothermal liquefaction case design report” has been completed. A summary report entitled “Lipid and Bio-processing Technologies: Process Intensification and Continuous Flow-Through Reaction (PICFTR), Lipid-to-Hydrocarbon (LTH), TYTON, Decarboxylation and Co-processing” has been produced and manuscripts have been prepared for publication.

### **Major Accomplishments**

A manuscript entitled “Comparison of Techno-economic and Environmental Performance of Alternative Jet Fuel Production Technologies” has been prepared and reviewed. Another manuscript entitled “Economic Analysis of Catalytic Hydrothermolysis Pathway for Jet Fuel Production” has been submitted for journal publication. “Hydrothermal liquefaction case design report” has been updated in preparation for FAA review. We intend to submit these manuscripts to the FAA for review within the next four months. We are working on the construction of a TEA for lignin extraction and utilization in a biorefinery process (National Renewable Energy Laboratory [NREL] biochemical conversion, <https://www.nrel.gov/docs/fy19osti/71949.pdf>).

A paper detailing the impact of coproducts on the financial viability of a forest-residual based ATJ process was published in *Biofuel, Bioproducts and Biorefining*. A companion paper that details the combined effect of siting and repurposing industrial facilities with multiple levels of capital cost avoidance on the economic viability of AJF is being written with submission for internal review expected in late 2020.

We have assisted the Committee on Aviation Environmental Protection (CAEP) through participation on the Fuel Task Group (FTG). ASCENT HEFA, ATJ, and GFT TEAs have been revised, streamlined, and generalized for use by both scientists and non-scientists from around the world. The TEAs can be modified to reflect local costs and feedstocks. The TEAs were used to develop a “Rules of Thumb” or heuristics approach to estimating capital requirements and relative fuels costs from these technologies. This output is compiled in both Word document and Excel spreadsheet formats. These documents illustrate the influence of key variables in AJF costs: yield, CAPEX, feedstock price, and conversion technology maturity.

Data generated from the design cases have been made available to ASCENT Project 01 partners to assist with supply chain analysis and techno-economic modeling by improving the conversion and cost figure database values. Evaluations of the effects of process variations on the chemical properties of the generated products are being used to provide insight into the challenges that will be faced when AJFs are blended into commercial jet fuel.



## **Publications**

### **Peer-reviewed journal publications**

Brandt, K.L., Wooley, R.J., Geleynse, S.C., Gao, J., Zhu, J., Cavalieri, R.P., Wolcott, M.P. (2020). Impact of co-product selection on techno-economic analyses of alternative jet fuel produced with forest harvest residuals. *BioFPR*, 14(4):764-775.

Geleynse, S., Jiang, Z., Brandt, K., Garcia-Perez, M., Wolcott, M., Zhang, X. (2020). Fuel Processing Technology 201:106338

Tanzil, A.H., X. Zhang, M. Wolcott and M. Garcia-Perez, Strategic Assessment of Sustainable Aviation Fuel Production Technologies: Yield Improvement and Cost Reduction Opportunities (submitted to *Biomass and Bioenergy*, 2020).

## **Outreach Efforts**

During the preparation of design case reports, we have closely interacted with industrial companies, including Gevo, LanzaTech, and Agrisoma. These companies have also helped us review reports and draft manuscripts. Our results have been presented to the FAA, the Washington State Academy of Science, and specialized conferences (TCS 2020). We have also made several presentations to graduate and undergraduate students.

Malina, R., Wolcott, M., Brandt, K. Update on TEA tool development. CAEP/12 Fuels Task Group, TPP subgroup. 20 May 2020.

## **Awards**

None

## **Student Involvement**

Several graduate students (Senthil Subramaniam, Sudha Eswaran, Kelly Nguyen, Tanzil Hossain, Anamaria Paiva, and Lina Martinez) and one undergraduate student (Kitana Kaiphanliam) participated in the creation, editing, and updating of the design cases for stand-alone AJF technologies, relevant existing infrastructure, and lignin coproducts.

## **Plans for Next Period**

We intend to submit 3-5 manuscripts for the lignin coproduct analyses and others based on the AJF analyses. The following are the proposed manuscripts to be completed this project year:

1. Methodology of quantifying the Impact of Repurposing Existing Manufacturing Facilities: Case Study using Pulp and Paper Facilities for SPORL Sustainable Aviation Fuel Facility.
2. Lipid and Bio-processing Technologies: Process Intensification and Continuous Flow-Through Reaction (PICFTR), Lipid-to-Hydrocarbon (LTH), TYTON, Decarboxylation and Co-processing.
3. Economic Analysis of Catalytic Hydrothermolysis Pathway for Jet Fuel Production.
4. The Potential of SK-SKA for Production of Sustainable Aviation Fuel.
5. The Opportunity for Lignin Co-products to Improve the Economics of Sustainable Aviation Fuel Production.

## **Task 2 – Evaluation of the Most Promising Biorefinery Concepts for AJF Production**

Washington State University

### **Objectives**

#### **Continuation from previous years**

During this upcoming year, we will complete our evaluation of biorefinery scenarios for AJF production using corn ethanol, sugarcane, pulp and paper mills, and petroleum refineries. Over the past year, we advanced our analyses for corn ethanol and pulp and paper mills, and in the coming year, we aim to complete our analyses for sugarcane and petroleum refineries.

We will conduct detailed TEA analyses on the integration of lignin coproduct technologies and the ATJ pathway to determine the potential for reducing fuel costs.

### **Research Approach**

#### **Background**

In this Task, we will utilize the design cases for existing infrastructure, AJF production technology, and identified coproducts to generate new biorefinery concepts for petroleum refineries, pulp and paper mills, sugarcane mills, and corn ethanol mills. The results from this effort will allow us to identify and select the most commercially feasible biorefinery concepts. Major

technical gaps/barriers toward the commercialization of each biorefinery concept will also be determined from the results of this study.

The integration of process technologies will be assessed using an approach similar to that for the stand-alone design cases. The integration concepts will be developed by pairing stand-alone cases with these concepts to evaluate the economic and environmental advantages of the integration approaches. Over this period, we have conducted detailed analyses of ATJ conversion and integration with pulp mill operations. We have also investigated the potential contribution of lignin coproducts to the overall process economy.

A dry grind corn ethanol mill (DGCEM) with a capacity of 80 million gallons of ethanol per year was studied in order to evaluate potential biorefinery scenarios for AJF production. Similarly, we used a sugarcane mill with a sugarcane processing capacity of 12,444 MTD that produces raw sugar, molasses, surplus bagasse, and surplus electricity. The petroleum refinery used as base case processes 120,000 barrels per day of crude oil. Five AJF technologies were studied: Virent's BioForming, ATJ, DSHC, fast pyrolysis, and GFT. A standardized methodology was adopted to compare DGCEM, sugarcane mill and petroleum refineries biorefinery concepts in a number of integration scenarios with six jet fuel production scenarios. For all of the cases we estimated the minimum fuel selling price and greenhouse gas emissions.

A manuscript on the integration of ATJ technologies in pulp mill infrastructure was published. Three new papers will be published with the results for corn ethanol mills, sugarcane mills, and petroleum refineries.

### **Major Accomplishments**

Building upon the ATJ pathway analyses, we have analyzed the integration of the ATJ process in a pulp mill infrastructure. A manuscript entitled "Pulp Mill Integration with Alcohol-to-Jet Conversion Technology" has been published in *Fuel Processing Technology*. Following the reviewer's input, a revised manuscript has been submitted. Economic models and life cycle assessments have been applied to select the most promising biorefinery concepts for corn ethanol, sugarcane, and pulp and paper, and petroleum refineries. The manuscript on corn ethanol was submitted to *Biomass and Bioenergy*. The other two papers (sugarcane and petroleum refineries) are under internal review.

### **Publications**

#### **Written reports under peer review**

- Brandt, K.L., Wooley, R.J., Geleynse, S.C., Gao, J., Zhu, J., Cavalieri, R.P., Wolcott, M.P. (2020). Impact of co-product selection on techno-economic analyses of alternative jet fuel produced with forest harvest residuals. *BioFPR*, 14(4):764-775
- Geleynse, S., Jiang, Z., Brandt, K., Garcia-Perez, M., Wolcott, M., Zhang, X. (2020). *Fuel Processing Technology* 201:106338
- Tanzil, A.H., Zhang, X., Wolcott, M., Garcia-Perez, M. Evaluation of Biorefinery Alternatives for the Production of Sustainable Aviation Fuels in a Dry Grind Corn Ethanol Mill (submitted to *Biomass and Bioenergy*)
- Tanzil, A.H., Zhang, X., Wolcott, M., Garcia-Perez, M. Evaluation of Biorefinery Alternatives for the Production of Sustainable Aviation Fuels in a Sugarcane Mill (internal review)
- Tanzil, A.H., Zhang, X., Wolcott, M., Garcia-Perez, M. Evaluation of Biorefinery Alternatives for the Production of Sustainable Aviation Fuels in a Petroleum Refinery (internal review)

### **Outreach Efforts**

Senthil Subramaniam, who has been supported by this project, has graduated with a PhD degree from WSU (December 2020).

Kelly Nguyen, who has been supported by this grant, has graduated with master's degree from WSU (May 2020).

Abid Tanzil has now submitted his PhD dissertation to defend during the fall 2020 semester.

### **Awards**

None

### **Student Involvement**

Graduate students (Senthil Subramaniam, Kelly Nguyen, Abid Tanzil Hossain, Lina Martinez Valencia, and Anamaria Paiva) have received training in this project. An undergraduate student (Kitana Kaiphanliam), funded under a National Science Foundation Research Experience for Undergraduates (NSF-REU) grant, assisted in building techno-economic models for coproduct production scenarios.

### **Plans for Next Period**

During the next period, Dr. Garcia-Perez's team will focus on publications.

## **Task 3 – Supplement and Maintain the Current Inventory of Biorefinery Infrastructures that are Useful for AJF Production, as Identified in the Conversion Design Cases**

Washington State University

### **Objective**

This Task requires periodic evaluation of the databases to add new or update the status of closed facilities in each category such that the geospatially specific assets are current.

### **Research Approach**

The use of existing infrastructure assets is a key component of retrofit approaches for advances in this industry. To differentiate between the relative value of different options, the specific assets must be valued with respect to their potential use within a conversion pathway. Regional databases of industrial assets that might be utilized by a developing AJF industry have been assessed on a national level. These baseline databases are compiled from a variety of sources, including industry associations, universities, and news outlets. These databases will be expanded, refined, and validated as the conversion design cases articulate additional needs for the regional analyses.

### **Milestones**

National databases have been compiled, geolocated, validated, and shared for biodiesel, corn ethanol, energy pellet, pulp and paper, and sugar mill production. We evaluate the databases as needed to add new or change the status of closed facilities in each category to ensure that the geospatially specific assets are current.

The geospatial infrastructure data was converted for use in the supply chain resiliency models. Tools were updated for transportation cost modeling, which will lead to future improvements.

### **Major Accomplishments**

National databases have been compiled, validated, and shared with the ASCENT Project 01 teams. All of the metadata are available for use in the regional analyses.

### **Publications**

None

### **Outreach Efforts**

N/A

### **Awards**

None

### **Student Involvement**

None

### **Plans for Next Period**

N/A

## **Task 4 – Continue Work on Social Asset Decision Tools Developed in Phase 1 for Plant Siting (CAAM), Including Additional Validation and Incorporation of Multi-decision-making Tools. Extend Applications to Another U.S. Region in Coordination with Other Team Members (Inland Northwest, Appalachian Region). Prepare for National Extension and Replication in Select Countries.**

Washington State University

### **Objective**

Update CAAM with available data and strategically apply to additional U.S. regions.

### **Research Approach**

Based on key measures of social, cultural, human, and political capitals, WSU finalized the CAAM for strategic application to communities to determine appropriate outreach to aid project development and implementation. The first tool with only three community assets—social, human and cultural—was initially applied to the NARA region in the Pacific Northwest, and a refined tool that added more complete measures of social, cultural, and human capital was deployed in two sub-regions of NARA. The model was updated in 2019 to include political capital and further refined through factor analysis to capture more parsimonious measures of each capital using factor analysis. The 2019 updated model was strategically applied to case studies of biorefineries in the Pacific Northwest and Montana to provide community engagement recommendations in order to increase the likelihood of project success. The case study analysis was used to validate the strategic application model which has been published online in *Community Development*. Additional efforts to apply the final CAAM in the BANR region and the Inland Northwest are ongoing.

### **Milestones**

The CAAM dataset and codebook is available and was shared with FAA ASCENT colleagues in Tennessee. CAAM benchmark measures have been developed for the additional two regions of BANR and the Inland Northwest.

### **Major Accomplishments**

A strategic application model has been created using completed CAAM measures and supplementary data to provide engagement recommendations for improving the likelihood of success when making initial contacts with communities. A manuscript which explains the development of the new CAAM and applies the model to case studies in the Pacific Northwest and Montana has been published online in *Community Development*. The manuscript will be available in an upcoming issue of *Community Development* in 2020. Two additional manuscripts for BANR on an application of the CAAM in Colorado and Wyoming are still underway.

### **Publications**

#### **Written report under peer review**

Mueller, D., Hoard, S., Roemer, K., Rijkhoff, S., Sanders, C. (2020). Quantifying the Community Capitals Framework: Strategic Application of the Community Assets and Attributes Model. *Community Development*. DOI: 10.1080/15575330.2020.1801785

### **Outreach Efforts**

None

### **Awards**

None

### **Student Involvement**

None

### **Plans for Next Period**

Update model with new data (where available); complete application to BANR and Inland Northwest regions.

# Task 5 – Refine and Deploy Facility Siting Tools to Determine Regional Demand and Potential Conversion Sites to be Used in Regional Analyses

Washington State University

### Objective

Develop tools to site potential conversion facilities. There are two primary needs: a generalized tool to site initial locations that meet the needs of a specific conversion facility type and a second tool to select optimal conversion facility sites from the initial set of locations.

### Research Approach

The geospatial siting pre-selection tool (GSP) began development in early 2019. It is a Python-based script that automates ArcGIS to produce points that represent locations that suit the needs of a conversion facility. The GSP uses a combination of buffer and cost datasets. Buffer datasets ensure that a candidate is sited within proximity to necessary infrastructure such as roads, rail, and natural gas pipelines. The set of candidates generated using only buffers would be very large, thus cost datasets are added to distinguish candidates from each other. Cost datasets represent geospatially variable costs including electricity, natural gas, and transportation. An additional script has been developed to model the input transportation costs for the GSP by taking a feedstock point dataset and using that to develop an equation relating feedstock density to the average cost to supply a set amount of feedstock to that location. In early 2020, a graphic user interface was added to the GSP to make it more user-friendly.

The Many Step Transshipment Solver (MASTRS) is another Python-based script that models large supply chains across multiple levels by building and solving mixed integer linear programming problems. The model starts with feedstock spread across many locations and then models the distribution and conversion of feedstock into biofuels and other co-products through multiple levels of intermediate facilities that may include temporary storage, pre-treatment, and fuel production before sending the new products to their destinations. Intermediate facilities may include existing facilities or new candidate facilities that are generated by the GSP. Output from MASTRS shows the flow of materials throughout the supply chain and the most cost-efficient capacities and locations of new facilities.

The modeling combination of GSP and MASTRS scripts has been implemented on several regional supply chains. MASTRS was first implemented with Pacific Northwest oilseed-to-jet-fuel supply chain in 2018. Since 2019, GSP and MASTRS scripts have been used together for two supply chain models both for the production of jet fuel from forest residuals and lumber production byproducts in the Pacific Northwest. The first uses single-stage conversion at integrated biorefineries and the second is a multi-stage model with distributed pre-processing facilities.

### Milestones

GSP and MASTRS have undergone continuous progress to become much more practical tools. Along with expansion of tool capabilities, significant improvements have been made to tool accessibility for new potential users.

### Major Accomplishments

None

### Publications

None

### Outreach Efforts

None

### Awards

None

### Student Involvement

None

### **Plans for Next Period**

Begin process to publish papers that define GSP and MASTRS. Continue implementation of GSP and MASTRS in regional supply chain analyses, particularly in completing the BANR supply chain analysis.

## **Task 6 – Refinery-to-Wing Stakeholder**

Washington State University

(The report is provided in Award No. 13-C-AJFE-PSU-002)

### **Objectives**

We will extend the stakeholder assessment to a limited sample of informed stakeholders in the remaining sections of the country to provide insight into market and industry dynamics, with the aim of optimizing successful outcomes.

### **Research Approach**

In 2019, the team collected primary data via surveys to better understand the awareness, opinions, and perspectives of key aviation fuel supply chain stakeholders regarding the potential impacts and key factors for an economically viable biojet fuel production industry in the United States. These aviation fuel supply chain stakeholders include airport management, fixed-base operators (FBOs), aviation fuel handlers, relevant airlines, and CAAFI personnel. Data were collected to assess the opinions, awareness, and perceptions of aviation fuel supply chain stakeholders regarding factors impacting the adoption and diffusion of AJF. A national survey of aviation management and FBOs was distributed to several hundred stakeholders across the United States and was completed in the summer of 2019.

### **Milestones**

Data has been assessed for potential manuscripts due to low response rates and potential publications identified.

### **Major Accomplishments**

None

### **Publications**

None

### **Outreach Efforts**

N/A

### **Awards**

None

### **Student Involvement**

None

### **Plans for Next Period**

Complete updated publication based on national results.

## **Task 7 – Supply Chain Analysis**

Washington State University-Volpe

### **Objective(s)**

WSU and the Volpe Center have each developed modeling tools that apply trans-shipment optimization to model the geospatial layout of developing supply chains. A comparison of these tools would be useful to identify the strengths and weaknesses of each.

We have developed a framework for assessing the resilience of a sustainable aviation fuel (SAF) supply chain subjected to multiple uncertain hazards and conditions and have modified the Freight and Fuel Transportation Optimization Tool (FTOT) for its extensive utilization in a continuous re-optimization process. The team has applied the proposed resilience assessment framework to a forest residue-based SAF supply chain in the Pacific Northwest region to demonstrate its feasibility.

## **Research Approach**

Focusing on the use of woody-biomass-to-jet-fuel conversion via fast pyrolysis and the upgrading of a supply chain centered in the Northern Rockies, a series of comparison studies was conducted using optimization tools from the Volpe Center and WSU. Each modeling approach was required to determine sites for new pyrolysis depots and upgrading refineries. Forest production data were provided by the LURA model from the University of Idaho. Pyrolysis depot locations were selected by candidate generation tools included in each approach and existing petroleum refineries were used as candidates for upgrading refineries. Cities, ports, and airport hubs throughout the U.S. West Coast and Rocky Mountain regions were used as markets for road transportation fuel, bunker fuel, and jet fuel.

## **Resilience**

A supply chain can be exposed to multiple unpredictable events and conditions over the medium- to long-term horizon. These events and conditions include natural (e.g., earthquakes, hurricanes, floods, wildfires, and tsunamis) and manmade hazards (e.g., terrorist attacks, cyberattacks, and industrial accidents), climate change, technology development, evolving customer preferences, dynamic changes in government regulation and political circumstances, etc., which may have negative or positive impacts on supply chain performance. Although supply chain resilience assessments should address the combined effects of multiple negative and positive events and conditions that may occur over the planning horizon, most existing studies have focused on negative consequences induced by a single type of natural hazard, which often leads to the under- or over-estimation of potential risks. Moreover, previous studies have assessed supply chain resilience in a more qualitative manner, utilizing either conceptual or empirical analysis. To address these deficiencies in the existing literature, the proposed framework quantitatively assesses the effect of both negative and positive events and conditions on the performance of a supply chain and supports resilience-enhancing strategies that minimize negative impacts while capitalizing on opportunities. Furthermore, in contrast to conventional resilience assessments, which focus on a single type of hazard and provide a snapshot of the resilience index immediately following a hazardous event, the proposed resilience assessment considers the medium- to long-term performance of a supply chain, thereby providing the resilience index as a function of time over the planning horizon. In this way, the time-dependent performance-based supply chain resilience index enables the quantification of multiple components of resilience.

In the previous period of performance (October 2018 to September 2019), we developed a multi-component resilience assessment framework for a supply chain system subjected to multiple uncertain hazards and conditions. During this period (Oct 2019 – Sep 2020), our task consists of two parts: (a) the modification and utilization of FTOT, and (b) the application of the resilience assessment framework to a forest-residue-based SAF supply chain system in the Pacific Northwest (PNW) region. We have investigated the utilization of FTOT in solving re-routing problems following a major disruption and computing time-dependent supply chain system performance. First, we have studied FTOT Python package and scenarios thoroughly to identify the implicit assumptions and methodologies adopted in FTOT. Then, we have communicated with the Volpe FTOT team during the period from March 2020 to August 2020 through bi-weekly meetings and FTOT GitHub to incorporate the risk and resilience assessment process into the current FTOT framework. We have made major modifications in FTOT, including (a) a separate Python package that simulates multiple risk factors, (b) the modification of main objective function and constraints, and (c) a new iterative structure embedded in the existing codes to enable the continuous evaluation of system performance over the planning horizon.

In order to facilitate the Volpe team's understanding of the incorporation of risk and resilience assessment into the current FTOT framework, we have utilized a simple supply chain system. Specifically, the quick scenario 2 from the FTOT package, was used for the purpose of communication. Subsequently, the newly added modules and modified FTOT codes have been validated with this example. After the initial validation was completed, we have utilized a more realistic forest-residue-based SAF supply chain system distributed over the PNW region to find any challenges that may arise from the application of the modified and/or newly added modules to a larger-scale supply chain system and demonstrate the feasibility and practicability of the proposed framework. We have identified multiple risk factors that may potentially affect the supply chain system. Among them, seismic hazards may induce the greatest negative impact on the system performance, as some parts of the system are located in high seismic hazard zones. While seismic risk assessment of civil infrastructure and regional transportation system has been well investigated in the past decades, their concern has focused on a city- or county-scale

risk assessment. However, the supply chain system is distributed over a much larger geographical region, including three states (WA, ID, and OR), and a new approach has been developed to generate a finite set of stochastic seismic events for the study region which can appropriately represent all possible events. An importance sampling technique has been employed to sample large-magnitude seismic events while improving computational efficiency. In the next quarter, all the risk factors will be combined to assess their effects on supply chain system performance and resilience to complete the case study.

### **Milestones**

The team has developed risk and resilience modules that are compatible with the FTOT to incorporate the resilience assessment framework into the current FTOT package.

The proposed assessment framework has been illustrated with a forest-residue-based SAF supply chain system distributed over the PNW region to demonstrate its feasibility and practicability.

### **Major Accomplishments**

The WSU MASTRS and Volpe FTOT were compared for siting analyses in the BANR region. Similar and differing modeling assumptions were identified and the appropriate model for a given objective was determined.

The team has developed a theoretical framework for multi-component resilience assessment. The Python-based risk and resilience modules and the supporting document have been shared with the Volpe FTOT team. A manuscript describing the resilience assessment framework and its illustration with a forest-residue-based SAF supply chain system has been prepared and will be submitted to *Transportation Research Part E: Logistics and Transportation Review*. A conference abstract on this topic (but with a case study of transportation system) has been accepted, and we have been invited to submit a full paper to the 13<sup>th</sup> International Conference on Structural Safety & Reliability.

We have performed a preliminary study on wildfire risk assessment of a supply chain system to investigate the potential effects of wildfire on a forest-residue-based SAF supply chain system.

### **Publications**

None

### **Outreach Efforts**

N/A

### **Awards**

None

### **Student Involvement**

Dane Camenzind, MS Environmental Engineering, Washington State University – graduated in September 2019 and is currently employed by WSU as an operations research engineer.

Jie Zhao, PhD candidate, Civil Engineering, Washington State University

### **Plans for Next Period**

We will utilize regional supply chain tools to assess forest residuals for SAF using pyrolysis methods, as described in Task 8 below.

The team will submit a manuscript on a multi-component resilience assessment framework for a supply chain system in January 2021 and another manuscript on wildfire risk assessment of a forest residual-based SAF supply chain system in December 2020. During the upcoming year, we will extend this study to determine the most resilient supply chain layout among alternatives and support cost-effective resilience-enhancing activities. Moreover, we will also investigate various negative effects of wildfires on supply chain performance, including forced closedown of several facilities, delayed delivery schedule due to health risk, closure of essential transit routes due to landslides, rock falls, etc.

In the following year, the research team will incorporate the proposed resilience assessment framework into FTOT to (a) assess the integrated effects of multiple types of hazards/conditions on long-term supply chain performance and (b) quantify

the overall resilience of a supply chain system under a wide range of plausible future scenarios. In order to make FTOT compatible with the proposed resilience assessment framework, several modifications of the FTOT Python file package are required. For example, the framework has an iterative structure to measure supply chain performance at each time step which generates a set of future scenarios. This structure is necessary to capture the dynamic nature of supply chain performance over a planning horizon under diverse scenarios, and thus, should be included in FTOT. Moreover, FTOT needs to be modified to incorporate the restoration costs and processes following a hazard event to quantify the restorative capacity of a supply chain, which is one of the three resilience components. In addition to the modifications to FTOT simulation structure and procedure, minor modifications to variables and constraints in FTOT will be required. While the unmet-demand ratio (UDR) in FTOT can take on either 0 or a positive value, the resilience assessment framework considers the positive effect of risk factors on supply chain performance and allows the redundancy of the system. Accordingly, the lower bound of UDR should be changed from 0 to negative infinity. Furthermore, additional Python files need to be developed for generating the realizations of each type of risk factor and integrating the factors in supply chain analysis. In order to maintain the consistency between the proposed framework and FTOT, this work will be actively collaborated with the Volpe Center. The incorporation of resilience assessment into FTOT will provide supply chain managers and stakeholders with information on (a) the key risk factors that should be mitigated to enhance supply chain resilience and (b) which supply chain design is the most resilient one among alternative designs in the future. Such information can be further used to determine cost-effective resilience-enhancing solutions.

## Task 8 – Analytical Support for Regional CAAFI and USDA Jet Fuel Project

Washington State University

### Objectives

We will develop a readiness level tool to assess the status of regional SAF production projects and will use supply chain and stand-alone design cases to support the USDA BANR project in TEA and supply chain analysis. This regional CAP project focuses on the use of softwood forest salvage feedstock for fuels via a catalyzed pyrolysis conversion pathway.

We will assess the regional feedstock, conversion pathways, and the fuel minimum selling price (MSP) for SAF manufactured in the Northwest U.S. The focus of this work, requested by the Port of Seattle, is to determine if the Seattle-Tacoma International Airport can attain the 10% SAF goal using SAF manufactured in the region from regional feedstock.

### Research Approach

We will develop readiness level tools for regional projects to assess the status of developing fuel projects and to identify critical missing components. This tool will be similar in form to the CAAFI Feedstock and Fuel Readiness Levels and will be used to assist CAAFI in understanding the stage of development for projects of interest and to assess critical gaps. In addition, we will assist the regional USDA BANR team in deploying TEA and supply chain analysis for their project. This effort will be focused on the use of softwood forest salvage feedstock in a thermochemical conversion process to produce fuels and coproducts.

The facility siting tools discussed in Task 5, GSP and MASTRS, have been implemented on the BANR supply chain and Port of Seattle project. The most recent model runs included feedstock and markets in a 11-state region that includes the West Coast and intermountain regions. Feedstocks include forest residue from logging operations and mill residues from lumber production. A future expansion will also include beetle-killed timber. The model run results generated by MASTRS will help determine the relationship between facility location, fuel MSP, and conversion facility revenue.

The Port of Seattle project required a detailed feedstock survey for forest residuals, municipal solid waste (MSW), and lipids. Forest residuals were quantified using the LURA model for OR, WA, ID, and MT. Regional landfills were identified, located, scales determined, and remaining lifetime assessed to determine the most viable biorefinery location. The composition of MSW in the region was determined, as was a method and the related costs to sort the material to match the SAF conversion pathway. Lipids were separated into two major categories: waste fats, oils, and greases (FOGs) and vegetable oil. Each feedstock was quantified and then paired with a compatible SAF conversion pathway to determine SAF MSP using ASCENT-developed TEAs.



## **Milestones**

We are progressing on the use of supply chain and stand-alone design cases to support the USDA BANR project in TEA and supply chain analysis. Additionally, we have supported the BANR team in creating TEAs for the technologies under consideration.

The Port of Seattle analysis and report have been completed, submitted, and presented.

## **Major Accomplishments**

We have collaborated with the USDA BANR project and attended their annual meeting to coordinate analysis. We currently await their completion of dead wood estimates to complete the supply chain analysis. Moreover, analyses with previous forest residue data have been successfully modeled.

The Port of Seattle feedstock and SAF assessment was completed, presented to the Port of Seattle, and released to the public.

## **Publications**

### **Public Reports**

Potential Northwest Regional Feedstock and Production of Sustainable Aviation Fuel: 2019 Report from the Port of Seattle and Washington State University. Prepared February 2020. [https://www.portseattle.org/sites/default/files/2020-08/PofSeattleWSU2019updated\\_appendix.pdf](https://www.portseattle.org/sites/default/files/2020-08/PofSeattleWSU2019updated_appendix.pdf)

## **Outreach Efforts**

Wolcott, M., Holladay, J. Supply chains for sustainable aviation fuels: Why, What, Who? CleanTech Alliance Breakfast. 11 December 2019. Seattle, WA.

Wolcott, M., Brandt, K., Camenzind, D. Potential Northwest Regional Feedstock and Production of Sustainable Aviation Fuel. Energy and Sustainability Committee - WSU Briefing. 12 February 2020. Seattle, WA.

Wolcott, M., Brandt, K., Camenzind, D., Meyn, S. Potential Northwest Regional Feedstock and Production of Sustainable Aviation Fuel: Port of Seattle. ASCENT Spring Meeting. 31 March 2020.

Wolcott, M.P., K. Brandt, and D. Camenzind. Potential Northwest Regional Feedstock and Production of Sustainable Aviation Fuel: Port of Seattle. Washington State Aviation Biofuels Work Group. Virtual Meeting held on June 3, 2020.

Wolcott, M. Potential Northwest Regional Feedstock and Production of Sustainable Aviation Fuel: Port of Seattle. Washington Clean Fuel Forum: 2021 Industry and Policy Forecast. 22 October 2020.

## **Awards**

None

## **Student Involvement**

Dane Camenzind, MS Environmental Engineering, Washington State University, graduated in September 2019 and is currently employed by WSU as an operations research engineer.

Lina Martinez, PhD candidate, Biosystems Engineering, Washington State University

## **Plans for Next Period**

Analysis of the BANR region is underway and will be completed in 2021.

The Port of Seattle report will be adapted for peer-reviewed publication.



# Project 001(B) Alternative Jet Fuel Supply Chain Analysis

## University of Hawaii

### Project Lead Investigator

Scott Q. Turn  
Researcher  
Hawaii Natural Energy Institute  
University of Hawaii  
1680 East-West Rd., POST 109; Honolulu, HI 96822  
(808)-956-2346  
sturn@hawaii.edu

## University Participants

### University of Hawaii

- PI: Scott Q. Turn, Researcher
- FAA Award Number: 13-C-AJFE-UH, Amendment 005
- Period of Performance: October 1, 2015 to August 4, 2021
- Task):
  1. Informing regional supply chains.
  2. Identification of supply chain barriers in the Hawaiian Islands.

### University of Hawaii

- PI: Scott Q. Turn, Researcher
- FAA Award Number: 13-C-AJFE-UH, Amendment 007
- Period of Performance: October 1, 2016 to August 4, 2021
- Tasks:
  1. Informing regional supply chains.
  2. Support of Indonesian alternative jet fuel supply initiatives.

### University of Hawaii

- PI: Scott Q. Turn, Researcher
- FAA Award Number: 13-C-AJFE-UH, Amendment 008
- Period of Performance: August 1, 2017 to August 4, 2021
- Tasks:
  1. National lipid supply availability analysis.
  2. Hawaii regional project.

### University of Hawaii

- PI: Scott Q. Turn, Researcher
- FAA Award Number: 13-C-AJFE-UH, Amendment 011
- Period of Performance: May 31, 2019 to August 4, 2021
- Task:
  1. Hawaii regional project.

### University of Hawaii

- PI: Scott Q. Turn, Researcher
- FAA Award Number: 13-C-AJFE-UH, Amendment 013
- Period of Performance: June 5, 2020 to August 4, 2021
- Task:
  1. Hawaii regional project.



## Project Funding Level

Under **FAA Award Number 13-C-AJFE-UH, Amendment 005**, the Alternative Jet Fuel Supply Chain Analysis-Tropical Region Analysis project received \$75,000 in funding from the FAA and cost share funding of \$75,000 from the State of Hawaii.

Under **FAA Award Number 13-C-AJFE-UH, Amendment 007**, the Alternative Jet Fuel Supply Chain Analysis-Tropical Region Analysis project received \$100,000 in funding from the FAA and cost share funding of \$75,000 from the State of Hawaii and \$25,000 of in-kind cost match in the form of salary support for Scott Turn from the University of Hawaii.

Under **FAA Award Number 13-C-AJFE-UH, Amendment 008**, the Alternative Jet Fuel Supply Chain Analysis-Tropical Region Analysis project received \$125,000 in funding from the FAA and cost share funding of \$125,000 from the State of Hawaii.

Under **FAA Award Number 13-C-AJFE-UH, Amendment 011**, the Alternative Jet Fuel Supply Chain Analysis-Tropical Region Analysis project received \$200,000 in funding from the FAA and cost share funding of \$200,000 from the State of Hawaii.

Under **FAA Award Number 13-C-AJFE-UH, Amendment 013**, the Alternative Jet Fuel Supply Chain Analysis-Tropical Region Analysis project received \$200,000 in funding from the FAA and cost share funding of \$200,000 from the State of Hawaii.

## Investigation Team

### Lead

Scott Turn, University of Hawaii, PI

### Other Lead Personnel

Tim Rials, Professor, and Burt English, Professor (University of Tennessee Co-PIs)

Manuel Garcia-Perez, Professor (Washington State University (WSU) Co-PI)

Kristin Lewis, Principal technical advisor (Volpe National Transportation Systems Center PI)

Michael Wolcott, Professor (WSU PI)

Lara Fowler, Professor (The Pennsylvania State University, PI)

### UH Investigation Team

Under **FAA Award Number 13-C-AJFE-UH, Amendment 005**, Task 1 and Task 2 include

Dr. Scott Turn, researcher, Hawaii Natural Energy Institute, University of Hawaii (UH)

Dr. Trevor Morgan, assistant researcher, Hawaii Natural Energy Institute, UH

Dr. Richard Ogoshi, assistant researcher, Department of Tropical Plant and Soil Sciences, UH

Dr. Adel H. Youkhana, junior researcher, Department of Tropical Plant and Soil Sciences, UH

Under **FAA Award Number 13-C-AJFE-UH, Amendment 007**, Task 1 and Task 2 include

Dr. Scott Turn, researcher, Hawaii Natural Energy Institute, UH

Dr. Trevor Morgan, assistant researcher, Hawaii Natural Energy Institute, UH

Dr. Richard Ogoshi, assistant researcher, Department of Tropical Plant and Soil Sciences, UH

Dr. Adel H. Youkhana, junior researcher, Department of Tropical Plant and Soil Sciences, UH

Dr. Curtis Daehler, professor, Department of Botany, UH

Ms. Sharon Chan, junior researcher, Hawaii Natural Energy Institute, UH

Mr. Gabriel Allen, undergraduate student, Biochemistry Department, UH

Under **FAA Award Number 13-C-AJFE-UH, Amendment 008**, Task 1 and Task 2 include

Dr. Scott Turn, researcher, Hawaii Natural Energy Institute, UH

Dr. Trevor Morgan, assistant researcher, Hawaii Natural Energy Institute, UH

Dr. Jinxia Fu, assistant researcher, Hawaii Natural Energy Institute, UH

Dr. Quang Vu Bach, postdoctoral fellow, Hawaii Natural Energy Institute, UH

Ms. Sabrina Summers, undergraduate student, Bioengineering Department, UH

Ms. Sarah Weber, undergraduate student, Molecular Biosciences and Biotechnology, UH

Mr. Taha Elwir, undergraduate student, Chemistry Department, UH

Under **FAA Award Number 13-C-AJFE-UH, Amendment 011**, Task 1 includes

Dr. Scott Turn, researcher, Hawaii Natural Energy Institute, UH



Dr. Quang Vu Bach, postdoctoral fellow, Hawaii Natural Energy Institute, UH

Under **FAA Award Number 13-C-AJFE-UH, Amendment 013**, Task 1 includes

Dr. Scott Turn, researcher, Hawaii Natural Energy Institute, UH

Ms. Sharon Chan, Hawaii Natural Energy Institute, UH

## Project Overview

Under **FAA Award Number 13-C-AJFE-UH, Amendment 005**, the research effort has two objectives. The first objective is to develop information on regional supply chains for use in creating scenarios of future alternative jet fuel (AJF) production in tropical regions. Outputs from this project may be used as inputs to regional supply chain analyses being developed by the FAA and Volpe Center. The second objective is to identify the key barriers in regional supply chains that must be overcome to produce significant quantities of AJF in the Hawaiian Islands and similar tropical regions.

The **FAA Award Number 13-C-AJFE-UH, Amendment 005** project goals are to:

- Review and summarize
  - the available literature on biomass feedstocks for the tropics,
  - the available literature on pretreatment and conversion technologies for tropical biomass feedstocks, and
  - the available literature on geographic information systems (GIS) datasets available for assessment of AJF production systems in the tropics.
- Identify AJF supply chain barriers in the Hawaiian Islands.

Under **FAA Award Number 13-C-AJFE-UH, Amendment 007**, the research effort has two objectives. The first objective is to develop information on regional supply chains for use in creating scenarios of future AJF production in tropical regions. Outputs from this project may be used as inputs to regional supply chain analyses being developed by the FAA and Volpe Center. Included in this objective is the development of fundamental property data for tropical biomass resources to support supply chain analysis. The second objective is to support the memorandum of understanding between the FAA and Indonesian Directorate General of Civil Aviation (DGCA) to promote development and use of sustainable, alternative aviation fuels.

The **FAA Award Number 13-C-AJFE-UH, Amendment 007** project goals are to:

- Support the Volpe Center and Commercial Aviation Alternative Fuels Initiative (CAAFI) Farm to Fly 2.0 supply chain analysis.
- Use GIS-based estimates of fiber crop production potential to develop preliminary technical production estimates of jet fuel in Hawaii.
- Develop fundamental property data for tropical biomass resources.
- Transmit data and analysis results to other ASCENT Project 1 researchers to support improvement of existing tools and best practices.
- Support Indonesian AJF supply initiatives.

Under **FAA Award Number 13-C-AJFE-UH, Amendment 008**, the research effort has two objectives. The first objective is to support a national lipid supply availability analysis that will inform industry development and guide policy. The second objective is to conduct a targeted supply chain analysis for AJF production facility based on the Hawaii regional project.

The **FAA Award Number 13-C-AJFE-UH, Amendment 008** project goals are to:

- Support ASCENT partners conducting the national lipid supply availability analysis by contributing information on tropical oilseed availability.
- Evaluate supply chains for targeted waste streams and purpose-grown crops in Hawaii to a location in the principal industrial park on the island of Oahu.

Under **FAA Award Number 13-C-AJFE-UH, Amendment 011**, the main objective of the research effort is to conduct bench-scale testing of tropical feedstocks for use in targeted supply chain analysis for AJF production facility based on the Hawaii regional project initiated under Amendment 008.



The FAA Award Number 13-C-AJFE-UH, Amendment 011 project goals are to:

- Survey bench-scale systems available for relevant sustainable aviation fuel (SAF) conversion technology options.
- Down select from the available bench-scale systems to no more than two systems capable of conducting feedstock testing and quantify product yields and contaminant concentrations.
- Conduct bench-scale feedstock tests and quantify product yields and quality and contaminant concentrations.

The FAA Award Number 13-C-AJFE-UH, Amendment 013 project goals are to:

- Conduct tropical oil to AJF supply chain analysis.
- Develop management strategies for elements present in construction and demolition waste that impact use in thermochemical conversion based AJF production pathways

## Task 0.1 – Informing Regional Supply Chains

University of Hawaii

### Objectives

This Task included two activities: (1) a review of the archival literature on existing tropical crops and potential new crops that could provide feedstocks for AJF production, and (2) a review of relevant pretreatment and conversion technology options and experience with feedstocks identified in (1).

### Research Approach

Activity 1: The archival literature will be reviewed to construct an updated database of relevant citations for tropical crops; new potential energy crops will be identified and added to the database. Available information on agronomic practices, crop rotations, and harvest techniques will be included. The database will be shared with and serve as a resource for the ASCENT Project 1 team and Volpe Center analyses of regional supply chains.

Activity 2: A database of relevant pretreatment and conversion technology options and experience with potential tropical feedstock materials will be assembled from the archival literature and from existing Project 1 team shared resources. Of particular interest are inventories of material and energy flows associated with the pretreatment and conversion unit operations fundamental to the design of sustainable systems and the underlying analysis. Pairings of pretreatment and conversion technology options provide the starting point for evaluation of tropical biorefineries that can be integrated into ASCENT Project 1 team and Volpe Center activities.

### Milestones

Task 1, Activity 1: Identify target list of databases to search for relevant literature.

Task 1, Activity 1: Interim report summarizing progress on literature search.

Task 1, Activity 2: Identify target list of databases to search for relevant literature.

Task 1, Activity 2: Interim report summarizing progress on literature search.

### Major Accomplishments

This work is completed. A report was produced for each of the two activities, and the two reports were combined to form a manuscript published in the journal *Energy & Fuels*.

### Publications

#### **Peer-reviewed journal publication**

Morgan, T.M., Youkhana, A., Ogoshi, R., Turn, S., & Garcia-Perez, M. (2019). Review of biomass resources and conversion technologies for alternative jet fuel production in Hawai'i and tropical regions. *Energy & Fuels*, 2699-2762.

### Outreach Efforts

On February 21, 2018, the PI participated in a ThinkTech Hawaii broadcast focused on AJFs with collaborators from WSU and CAAFI (<https://www.youtube.com/watch?v=Ci4oWITPRKQ&feature=youtu.be>).

### **Awards**

None

### **Student Involvement**

None

### **Plans for Next Period**

N/A

## **Task 0.2 – Identification of Supply Chain Barriers in the Hawaiian Islands**

University of Hawaii

### **Objective**

Identify the key barriers in regional supply chains that must be overcome to produce significant quantities of AJF in the Hawaiian Islands and similar tropical regions.

### **Research Approach**

UH developed the Hawaii Bioenergy Master Plan for the State of Hawaii (<https://www.hnei.hawaii.edu/sites/www.hnei.hawaii.edu/files/Hawaii%20Bioenergy%20Master%20Plan.pdf>), which was completed in 2009. In that plan, UH was tasked with determining whether Hawaii had the capability to produce 20% of land transportation fuels and 20% of electricity from bio-based resources. To this end, the plan included assessments of (1) land and water resources that could support biomass feedstock production, (2) potential biomass resources and their availabilities, (3) technology requirements, (4) infrastructure requirements to support logistics, (5) economic impacts, (6) environmental impacts, (7) availability of human capital, (8) permitting requirements, and (9) limitations to developing complete value chains for biomass-based energy systems. In keeping with the stakeholder-driven development of the Hawaii Bioenergy Master Plan, barriers to development of regional supply chains for ASCENT will be identified by interacting with key stakeholder groups. Green Initiative for Fuels Transition Pacific (GIFTPAC) meetings are held quarterly and attended by biofuel development interests in Hawaii, including representatives of large landowners, producers of first-generation biofuels, petroleum refiners, electric utilities, the State Energy Office, U.S. Pacific Command, biofuel entrepreneurs, county government officials, and UH. Additional stakeholders are invited as necessary to fill information and value chain gaps. These meetings are excellent opportunities to receive stakeholder input, identify barriers to supply chain development, and organize data collection efforts that span supply chain participants.

### **Milestones**

Task 2: Introduce activities at next regularly scheduled GIFTPAC meeting after contract executed.

Task 2: Prepare interim report outlining two tropical supply chain scenarios developed in consultation with Project 1 team and with input from GIFTPAC participants.

### **Major Accomplishments**

This Task is completed. A stakeholder meeting was held and documented in a report submitted to the FAA. The stakeholders identified barriers to AJF production in Hawaii and ranked the barriers in order of importance as indicated below:

- Economic constraints (e.g., high costs of entry for production factors such as land) throughout the whole production chain.
- Issues associated with access to capital, including high initial risks and uncertain return on investment.
- Insufficient government support in the form of incentives and favorable policies to encourage long-term private investment.
- Cost, availability, and competition for water.
- AJF production technologies (emerging but have not yet demonstrated full commercial viability).
- Insufficient or inadequate infrastructure (e.g., harbors, roads, fuel distribution infrastructure, irrigation systems) to support the whole production chain.

Several of the barriers are held in common with other locations in the continental U.S. but those related to water and infrastructure are unique characteristics of an island state.

## Publications

N/A

## Outreach Efforts

This activity engaged stakeholders to identify barriers to AJF production in Hawaii. Preparation included reviewing stakeholder lists from previous activities. Facilitators appropriate to the stakeholder group were retained. The stakeholder meeting included a presentation about the scope and goals of the larger ASCENT program and other aspects of the UH ASCENT project.

## Awards

None

## Student Involvement

None

## Plans for Next Period

This Task is complete, but stakeholder outreach activities will continue under other tasks outlined below.

## **Task 0.3 – Informing Regional Supply Chains**

University of Hawaii

### Objectives

Building on FY16 activities, additional supporting analysis will be conducted for proposed supply chains in Hawaii, including:

- 0.3.1 Support Volpe Center and CAAFI Farm to Fly 2.0 supply chain analysis.
- 0.3.2 Use GIS-based estimates of fiber crop production potential to develop preliminary technical production estimates of jet fuel in Hawaii.
- 0.3.3 Develop fundamental property data for tropical biomass resources.
- 0.3.4 Transmit data and analysis results to support improvement of existing tools (e.g., POLYSYS; <https://bioenergykdf.net/content/polysys>).

### Research Approach

Activity 0.3.2 has been conducted using GIS data to identify areas suitable for purpose-grown crop production of feedstocks for AJF production in Hawaii. The approach has been to use GIS layers for land capability class (LCC), slope, and zoning as preliminary screens for suitability. Lands are classified by the Natural Resources Conservation Service (NRCS) with ratings from 1 to 6. LCCs from 1 to 3 are generally suitable for agricultural production; LCC of 4 can be productive with proper management; and LCCs of 5 or 6 can support less intensive production and could be suitable for forestry. The slopes of terrains affect aspects of production, including mechanization and erodibility. An elevation GIS layer was used to derive a slope layer. Zoning layers were acquired from state and county GIS offices. Only agricultural zoning was deemed suitable for this analysis.

The EcoCrop model was used to develop yield models for the crops selected in Task 0.1 based on the annual rainfall and mean minimum monthly temperature data. EcoCrop includes model parameters on sugarcane, bana grass, five species of eucalyptus, gliricidia, leucaena, pongamia, jatropha, and sorghum. The parameters for sugarcane have been used to provide a base case assessment for comparison with historical sugarcane acreage and yield. Using sensitivity analysis, the model can be tuned to account for the differences between parameters developed from global sugar production and a century of production experience in Hawaii that was refined through plant breeding to adapt sugarcane varieties to a wide variety of agro-ecosystems. Analysis has purposely avoided land use conflict with food production by limiting suitability to areas capable of sustaining AFJ feedstocks under rain fed conditions. Areas suitable for AJF production that do not conflict with current agricultural land use (i.e., fallow land) have also been identified.

Pongamia (*Millettia pinnata*) was the initial focus of Activity 0.3.3. Pongamia is an oilseed-bearing, leguminous tree that has production potential in Hawaii and Florida. The tree produces pods containing oil-bearing seeds. Pods, oilseed cake,

and oil were evaluated from a number of trees growing on the island of Oahu. Fundamental measurements of chemical composition will be conducted and reported. Torrefaction of pods as a coproduct to oil production has been conducted. Investigation of pretreatment methods to improve pod feedstock properties for thermochemical conversion applications are currently underway.

### **Milestones**

- Identify target opportunities to augment POLYSYS, Alternative Fuel Transportation Optimization Tool (AFTOT; <https://trid.trb.org/view/1376122>), and conversion modules.
- Review previously developed GIS information layers for tropical fiber crops and identify updating requirements.
- Conduct preliminary estimates of AJF technical potential in Hawaii based on previously developed GIS information layers.

### **Major Accomplishments**

The GIS-based analysis of AJF production potential is ongoing. The assessment of potential lands meeting requirements for LCC, slope, and land-use zoning is complete. The EcoCrop model is being implemented to predict yield as a function of minimum mean monthly temperature and annual rainfall. This will allow prescription of potential AJF feedstock crops on land areas capable of supporting their production under both rain-fed and irrigated conditions. This analysis will provide information necessary in determining cropping patterns and assessing transport costs to processing facility locations. The EcoCrop model's prediction of sugarcane potential was determined and the results were compared with historic sugarcane acreage, both rain-fed and irrigated. EcoCrop's upper and lower values for temperature and rainfall that support optimal sugarcane production were varied to calibrate the prediction against historic acreage. The difference between the EcoCrop values and those representative of Hawaii conditions can be attributed to improvements due to plant breeding and unique combinations of environmental conditions. An example of the latter is the relatively young volcanic soils present in high-rainfall areas on the island of Hawaii that allow for high drainage rates and accommodate sugar production.

Calibration of the EcoCrop model using historic sugarcane planted acreages was completed in 2018. This effort used a confusion matrix approach to validation (resulting in a kappa value >0.4) and demonstrated that mean annual temperature was a better indicator of environmental capability than the minimum mean monthly temperature recommended by the EcoCrop developers. This effort highlights the need to adapt models to local conditions. Model predictions for suitable cropping are being compared with current land uses to provide another indicator of agreement.

The GIS analysis of SAF feedstock production potential has been completed to include statewide working maps for each of the species summarized in a draft report currently undergoing internal review. This report will serve as the basis for a publication targeted for the upcoming, ASCENT-organized, special issue of *Frontiers in Energy Research*.

Dr. Curtis Daehler (University of Hawaii, Department of Botany) completed a report assessing the invasiveness of pongamia. Retrospective analyses show that predictive weed risk assessment systems correctly identify many major pest plants, but such predictions are not 100% accurate. The purpose of this study was to make field observations of pongamia planted around Oahu to look for direct evidence that pongamia is escaping from plantings and becoming an invasive weed. Seven field sites were visited in varying environments across Oahu. Although some pongamia seedlings were found in the vicinity of some pongamia plantings, particularly in wetter, partly shaded environments, almost all observed seedlings were restricted to areas directly beneath the canopy of mother trees. This finding suggests a lack of effective seed dispersal away from pongamia plantings. Based on its current behavior in the field, pongamia is not invasive or established outside of cultivation on Oahu. Because of its limited seed dispersal and low rates of seedling establishment beyond the canopy, the risk of pongamia becoming invasive can be mitigated through monitoring and targeted control of any rare escapes in the vicinity of plantings. Seeds and seed pods are water dispersed, so future risks of pongamia escape and unwanted spread would be minimized by avoiding planting at sites near flowing water, near areas exposed to tides, or on or near steep slopes. Vegetative spread by root suckers was not observed around plantings on Oahu but, based on reports from elsewhere, monitoring for vegetative spread around plantations is recommended; unwanted vegetative spread might become a concern in the future that could be addressed with localized mechanical or chemical control.

Pods, oilseed cake, and oil were evaluated from a number of trees growing on the island of Oahu. TerViva, a company pursuing pongamia commercialization, has provided material from orchards on Oahu. Fundamental measurements of chemical composition were made for seeds, pods, extracted oil, and post-extraction seed material. Measured values included C, H, N, and S elemental composition; energy content; volatile matter, fixed carbon and ash content; and trace element

composition. Oils were characterized for peroxide value, iodine value, fatty acid profile, free fatty acid content, flash point, density, viscosity, and phase transition temperatures. Chemical composition and fuel properties of the oilseed cake and the pod material have been characterized. A manuscript summarizing the results of this effort was submitted to the journal *Industrial Crops and Products*.

Coproduct evaluation of pongamia pods feedstock for thermochemical conversion has been conducted. Evaluation included both untreated pods and those pretreated by a torrefaction process to improve their properties. Torrefaction produces a material that has better grindability, reduced oxygen content, improved storage stability, and reduced microbial availability. The effects of process conditions on feedstock properties relevant to thermochemical conversion technologies, proximate and ultimate composition, heating value, and Hardgrove grindability index (HGI), were measured. The chemical structure, reactivity, and changes in elemental composition of the torrefied materials were also investigated. A manuscript summarizing the results of this effort was submitted to the journal *Fuel*.

## **Publications**

### **Written report**

Chan, S., Ogoshi, R. & Turn, S. Feedstocks for sustainable jet fuel production: An assessment of land suitability in Hawaii. Draft report. 82 pp.

### **Peer reviewed publication**

Fu, F., Summers, S., Morgan, T.J., Turn, S.Q., & Kusch, W. 2020. Fuel properties of *Milletia pinnata* seeds and pods grown in Hawaii. *Industrial Crops and Products*. In review.

Fu, J., Summers, S., Turn, S.Q., & Kusch, W. 2020. Upgraded pongamia pod via torrefaction for the production of bioenergy. *Fuel*. In review.

## **Outreach Efforts**

Outreach in this Task has focused on interactions with TerViva, a startup company that has identified pongamia germplasm production and marketing as the central focus of their business plan.

A poster entitled "Feedstocks for Sustainable Jet Fuel Production: An Assessment of Land Suitability in Hawaii" was presented at the European Biomass Conference and Exhibition held virtually July 6–9, 2020.

"Upgraded *Milletia Pinnata* Pod via Torrefaction for the Production of Bioenergy in Hawaii" was orally presented at the 2020 Thermal & Catalytic Sciences Virtual Symposium.

Information from this Task was included in the, "Regional Supply Chain Analysis for Alternative Jet Fuel Production in the Tropics," presentation at the Hawaii Aviation and Climate Action Summit, December 3, 2019, at the Hawaii State Capitol.

## **Awards**

The poster entitled, "Feedstocks for Sustainable Jet Fuel Production: An Assessment of Land Suitability in Hawaii" presented at the European Biomass Conference and Exhibition held virtually July 6-9, 2020, received the Best Visual Presentation Award.

## **Student Involvement**

Three undergraduate students are involved in the project, with primary responsibility for processing and analyzing samples of biomass materials selected for evaluation as potential AJF feedstocks. The pongamia torrefaction work was the focus of an Undergraduate Research Opportunity Program project for Sabrina Summers, a bioengineering and chemistry double major. The results of her work were presented at the fall 2019 American Chemical Society meeting in San Diego, California.

## **Plans for Next Period**

The report summarizing the analysis of the GIS analysis of SAF feedstock production potential will be completed and submitted as a manuscript for the upcoming, ASCENT-organized, special issue of *Frontiers in Energy Research*.

Statewide working maps for each of the feedstock species will be used as the basis for ongoing discussions with targeted stakeholder groups including landowners and NRCS staff. Funding for planting and evaluating the more promising feedstock plants on UH experiment station land will be pursued in collaboration with stakeholders, e.g., TerViva.

The current manuscript submitted to *Industrial Crops and Products* summarizing fuel properties of pongamia seed, pod, and oilseeds will be finalized and published.

The current manuscript submitted to *Fuel* summarizing torrefaction pretreatment of pongamia pods will be finalized and published.

Analysis of coproduct development based on pongamia oilseeds and husks will be continued.

## Task 0.4 – Support of Indonesian Alternative Jet Fuel Supply Initiatives

University of Hawaii

### Objective

This Task supports the memorandum of understanding between the FAA and the Indonesian DGCA to promote development and use of sustainable, alternative aviation fuels. Under the coordination of the FAA, efforts to establish points of contact and coordinate with Indonesian counterparts are ongoing.

### Research Approach

This Task will support the memorandum of understanding between the FAA and Indonesian DGCA to promote development and use of sustainable, alternative aviation fuels. This will begin with working with the FAA to establish points of contact to coordinate efforts with Indonesian counterparts. The Indonesian Aviation Biofuels and Renewable Energy Task Force (ABRETF) membership includes Universitas Indonesia, Institut Teknologi Bandung, and Universitas Padjadjaran. A prioritized list of tasks will be developed in consultation with Indonesian counterparts and data required to inform sustainability and supply analyses and potential sources of information will be identified. This could include data collection on Indonesian jet fuel use and resources for AJF production, airport locations, and annual and monthly jet fuel consumption patterns. Characterization of sustainable biomass resources with potential for use in producing AJF supplies could include developing preliminary GIS mapping information of their locations and distributions and preliminary estimates of their technical potentials.

### Milestones

- Identify points of contact at Indonesian universities participating in ABRETF.
- Identify research needs and develop project plan.
- Develop data on potential project.

### Major Accomplishments

The PI traveled to Jakarta in the first week of August 2017 and met with the following individuals:

- Cesar Velarde Catolffi-Salvoni (International Civil Aviation Organization)
- Dr. Wendy Aritenang (International Civil Aviation Organization)
- Dr. Ridwan Rachmat (head of Research Collaboration, Indonesian Agency for Agricultural Research and Development)
- Sylvia Ayu Bethari (head of Aviation Fuel Physical & Chemical Laboratory, Research and Development Centre for Oil and Gas Technology)
- Dr. Ina Winarni (Forest Product Research and Development Center, Ministry of Environment and Forestry)
- Dr. SD Sumbogo Murti (Center of Technology Energy Resources and Chemical Industry, Agency for the Assessment and Application of Technology)

The activities of the tropical supply chain analysis effort were presented to the group, followed by a general discussion. The conclusion from this introductory meeting was that the Indonesian counterparts would seek agreement on how to move forward with future cooperation.

The PI traveled to Jakarta and met with Dr. Wendy Aritenang of the International Civilian Aviation Organization Jakarta office. The same trip included meetings with renewable energy researchers at Universitas Indonesia. Following the meeting, Dr.

Aritenang suggested points of contact for future engagement: Frisda Panjaitan from the Palm Oil Research Institute and three researchers from the Bandung Institute of Technology: Tatang Soerawidjaja, Tirto Prakoso Brodjonegoro, and Imam Reksowardojo.

A source of funds external to ASCENT has been identified to hold a post-pandemic workshop on alternative jet fuel production in Indonesia. Scott Turn requested and received encouragement from FAA ASCENT program management. FAA will provide guidance on personnel, participation, and workshop content when planning begins in earnest.

### **Publications**

N/A

### **Outreach Efforts**

Outreach efforts by the PI are described in the Major Accomplishments section above.

### **Awards**

None

### **Student Involvement**

None

### **Plans for Next Period**

The PI will continue to develop the cooperative research agenda between UH and Indonesian universities through continued dialog with FAA, the International Civil Aviation Organization, and the Indonesian DGCA. Travel to Southeast Asia for other projects is anticipated in 2021 and meetings with the researchers at Indonesian institutions (delayed by pandemic in 2020) suggested by Dr. Aritenang will be pursued. Planning for a workshop on AJF will move forward as the situation returns to normal.

## **Task 2.2 – National Lipid Supply Availability Analysis**

University of Hawaii

### **Objective**

Activities under this Task will support ASCENT partners working on a national lipid supply availability analysis by sharing data on tropical oilseed availability developed under previous years' activities.

### **Research Approach**

Activities under this Task will support ASCENT partners working on a national lipid supply availability analysis by sharing data on tropical oilseed availability developed under previous years' activities. This support will include estimates of pongamia production capability in the state, in addition to assessments of waste cooking oil and tallow.

### **Milestones**

Milestones will coincide with the schedule of the lead institution (WSU) for the national lipid supply analysis.

### **Major Accomplishments**

Additional seeds and pods were collected from the pongamia tree on the UH campus, Foster Botanical Garden, and the Ke'ehi Lagoon Beach Park. Large quantities (tens of kilograms) of material were acquired from TerViva's plantings on Oahu's north shore for use in oil evaluation. Two oilseed presses were acquired and safety documents were developed. Pods, oilseed cake, and oil were evaluated from a number of trees growing on the island of Oahu. Fundamental measurements of chemical composition were made for seeds, pods, extracted oil, and post-extraction seed material. Measured values included C, H, N, and S elemental composition; energy content; volatile matter, fixed carbon, and ash contents; and trace element composition. Oils were characterized for peroxide value, iodine value, fatty acid profile, free fatty acid content, flash point, density, viscosity, and phase transition temperatures. Development of coproducts from the pods and oilseed cake will be explored.

The assessment of areas in Hawaii with agricultural zoning that are suitable for rainfed production of pongamia have been identified. Conflicts with current agricultural land use have been identified.

Waste oil resources in Hawaii are estimated to be on the order of two to three million gallons per year based on defacto population and are directed to biodiesel production.

### **Publications**

N/A

### **Outreach Efforts**

Data were presented at the April 2019 ASCENT review meeting in Atlanta, Georgia.

### **Awards**

None

### **Student Involvement**

Three undergraduate students—Sabrina Summers, Sarah Weber, and Taha Elwir—are involved in the project, with primary responsibility for processing and analyzing samples of biomass materials selected for evaluation as potential AJF feedstocks.

### **Plans for Next Period**

Characteristics and suitable production areas for additional oilseed crops in Hawaii will be assessed as needed. Information will be provided to the lead institution (WSU).

## **Task 3.2 – Hawaii Regional Project**

University of Hawaii

### **Objectives**

A supply chain based on fiber feedstocks transported to a conversion facility located at Campbell Industrial Park (CIP) on Oahu will be evaluated (Figure 1). CIP is the current site of two oil refineries. Construction and demolition (C&D) wood waste from the PVT Land Company's landfill could be the primary source of feedstock. Other sources will be evaluated from elsewhere on Oahu and from outer islands, including municipal solid waste (MSW) stream from outer islands and mining of current stocks of waste-in-place. Waste streams and purpose-grown crops form the basis for a hub-and-spoke supply system with the hub located on Oahu. Pipelines for jet fuel transport are in place from CIP to Daniel K. Inouye International Airport and adjacent Joint Base Pearl Harbor/Hickam. Other coproduct off-takers for alternative diesel fuel include Hawaiian Electric Co. and several military bases, including Schofield Barracks (~50 MW alternative fuel-capable power plant under development) and Kaneohe Marine Corp Base. Hawaii Gas (a local gas utility) is also seeking alternative sources of methane if methane or feedstock suitable for methane production is available as a coproduct. Hawaii Gas currently off-takes feedstock (naphtha) from refinery.



## Possible Locations of Value Chain Participants



### PVT Land Company



Figure 1. Possible locations of value chain participants for fiber-based alternative jet fuel production facility located at Campbell Industrial Park, Oahu.

### Research Approach

**Task 3.2.G1. Analysis of feedstock-conversion pathway efficiency, product slate (including coproducts), maturation**  
 Building on activities from previous years, additional supporting analysis will be conducted for proposed supply chains in Hawaii, as follows:

- 3.2.G1.1 Assess feedstock suitability for conversion processes (e.g., characterization, conversion efficiencies, contaminants). [UH and WSU (Manuel Garcia-Perez)]
- 3.2.G1.2 Acquire data on feedstock size reduction, particle size of materials, bulk densities. [UH, WSU (Manuel Garcia-Perez)]
- 3.2.G1.3 Evaluate coproducts at every step of the supply chain. [ASCENT Project 1 team]

### Task 3.2.G2. Scoping of techno-economic analysis (TEA) issues

This Task will determine the current TEA status of targeted AJF production technologies that use fiber feedstocks as production inputs. [UH, WSU (Manuel Garcia-Perez), Purdue University (Wally Tyner)]

### Task 3.2.G3. Screening-level greenhouse gas (GHG) life-cycle assessment (LCA)

This Task will conduct screening-level GHG LCA on the proposed target supply chains and AJF conversion technologies.



Subtasks:

- 3.2.G3.1 Assess Massachusetts Institute of Technology (MIT) waste-based GHG LCA tools in context of Hawaii application. [MIT (Mark Staples)]
- 3.2.G3.2 Assess requirements to link previously completed eucalyptus energy and GHG analysis to the edge of the plantation with available GHG LCA information for conversion technology options. [MIT (Mark Staples), UH]
- 3.2.G3.3 Identify and fill information/data gaps.

**Task 3.2.G4. Identification of supply chain participants/partners**

Subtasks:

- 3.2.G4.1 Define C&D landfill case.
- 3.2.G4.2 Identify eucalyptus in existing plantations: landowners, leaseholder/feedstock producer, harvesting contractor, trucking, etc. [UH]
- 3.2.G4.3 Define other feedstock systems as identified. [ASCENT Project 01 Team]

**Task 3.2.G5. Develop appropriate stakeholder engagement plan**

Subtasks:

- 3.2.G5.1 Review stakeholder engagement methods and plans from past work to establish baseline methods. [UH, WSU (Season Hoard)]
- 3.2.G5.2 Identify and update engagement strategies based on updated Community Social Asset Modeling (CSAM) /Outreach support tool. [UH, WSU (Season Hoard)]

**Task 3.2.G6. Identify and engage stakeholders**

Subtasks:

- 3.2.G6.1 Identify stakeholders along the value chain and create database based on value chain location. [UH]
- 3.2.G6.2 Conduct stakeholder meeting using instruments developed in Task 3.2.G5. [UH, WSU (Season Hoard)]
- 3.2.G6.3 Analyze stakeholder response and feedback to process. [UH, WSU (Season Hoard)]

**Task 3.2.G7. Acquire transportation network and other regional data needed for Freight and Fuel Transportation Optimization Tool (FTOT) and other modeling efforts**

Subtasks:

- 3.2.G7.1 Acquire necessary data to evaluate harbor capacities and current usage. [UH, Volpe (Kristin Lewis), WSU (Mike Wolcott)]
- 3.2.G7.2 Acquire data on interisland transport practices. [UH, Volpe (Kristin Lewis), WSU (Mike Wolcott)]

**Task 3.2.G8. Evaluate infrastructure availability**

Subtasks:

- 3.2.G8.1 Evaluate interisland shipping options and applicable regulation. [UH, Volpe (Kristin Lewis), WSU (Mike Wolcott)]
- 3.2.G8.2 Evaluate transport or conveyance options from conversion location to end user and applicable regulation. [UH, Volpe (Kristin Lewis), WSU (Mike Wolcott)]

**Task 3.2.G9. Evaluate feedstock availability**

Subtasks:

- 3.2.G9.1 Refine/ground truth prior evaluations of options for purpose-grown feedstock supply. [UH]
- 3.2.G9.2 Conduct projections of C&D waste supply moving forward and mining of waste-in-place on Oahu, MSW, and mining of waste-in-place on other islands. [UH]

**Task 3.2.G10. Develop regional proposal**

This Task will use the information collected in Tasks 3.2.G1 through 3.2.G9 to develop a regional project proposal.

**Milestone**

One milestone is associated with each of the subtask activities identified in the Research Approach section above.

**Major Accomplishments**

Characteristics of the feedstock generated at the landfill have been determined and summarized in a draft publication.

Elemental compositions of the feedstock materials have been used as the basis for equilibrium analysis of gasification systems using oxygen, steam, and steam-oxygen mixtures.

Material flows relevant to the screening level GHG analysis of construction and demolition waste as SAF feedstock have been assembled. Preliminary discussions on GHG analysis of C&D-based SAF systems with landfill operators have been initiated.

Solid waste management plans from all counties in Hawaii have been used to provide a broader picture of the waste stream composition, diversion and recycling practices, and planned uses.

### **Publications**

Bach, Q.V., Fu, J., & Turn, S.Q. Fuel Characterization of Construction and Demolition Wastes as Feedstock for Thermochemical Gasification, draft manuscript to be submitted to *Waste Management*.

### **Outreach Efforts**

Results of the fuel sampling, fuel analyses, and gasification equilibrium analyses were presented at the October 2019 Thermochemical Biomass 2019 conference, in Chicago, Illinois.

Information from this task was included in the talk, “Regional Supply Chain Analysis for Alternative Jet Fuel Production in the Tropics,” was presented at the Hawaii Aviation and Climate Action Summit, December 3, 2019, at the Hawaii State Capitol.

Data acquired under this task were presented to the management of PVT Land Company and their consultants from Simonpietri Enterprises and T.R. Miles Technical Consultants Inc.

“Construction and Demolition Waste as an Alternative Energy Source: Fuel Characterization and Ash Fusion Properties” was presented as a poster at the 2020 Thermal & Catalytic Sciences Virtual Symposium.

As suggested by FAA Management, UH worked with the Servicios y Estudios para la Navegación Aérea y la Seguridad Aeronáutica (SENASA) to identify a counterpart university in the Canary Islands, Spain. Universidad de la Laguna (ULL) was selected and a memorandum of understanding was signed between the UH and ULL. A non-disclosure agreement was subsequently signed between SENASA, ULL, UH, and the Spanish company Abengoa Energía, S.A.

Discussion with the Dr. Kristin Lewis and Volpe Center staff on the addition of Hawaii transportation infrastructure to the *Freight and Fuel Transportation Optimization Tool* was initiated and deferred until a clearer definition of the system emerges.

### **Awards**

None

### **Student Involvement**

Three undergraduate students—Sabrina Summers, Sarah Weber, and Taha Elwir—have been involved in sample preparation and in operating the laboratory analytical equipment used for sample analysis.

### **Plans for Next Period**

Manuscripts covering the feedstock characteristics and prediction of gasification product streams including contaminant concentrations will be submitted.

Work on the greenhouse gas analysis of construction and demolition waste use for AJF production will be extended from the landfill to a point of use (to be determined) and interfaced to the system TEAs described by WSU.

Outreach to interested industries will be continued.

## Task 4 – Hawaii Regional Project

University of Hawaii

### **Objective**

This Task builds upon the results from the previous years' work under the Hawaii regional project. The focus is the data and analysis necessary to plan a project that uses C&D waste as feedstock for SAF production. Using previous years' C&D feedstock characterization data and thermochemical equilibrium analysis, the Task 4 objective is to conduct bench-scale gasification tests and quantify the product gas yield and composition and contaminant concentrations. These results will be compared with equilibrium prediction used to identify contaminants that must be addressed prior to end use and provide the basis for contaminant control system design.

### **Research Approach**

Using samples of construction and demolition wastes characterized in the earlier Tasks, bench-scale gasification tests will be conducted to measure product yields, identify contaminants, and investigate element partitioning between product phases.

Information gained from the tests will be used to identify opportunities to improve TEA, identify coproducts, inform supply chain participants and stakeholders, and identify needed infrastructure improvements.

### **Milestones**

- Identify and evaluate capabilities of experimental bench-scale facilities to gasifier tests.
- Specify system performance parameters to be measured.
- Specify techniques to sample and analyze contaminants.
- Select and engage experimental bench-scale facility for testing.
- Prepare and ship feedstock from Hawaii to experimental test facility.
- Conduct tests, reduce data, and prepare summary report of results.

### **Major Accomplishments**

Preliminary listings of bench-scale facilities have been assembled and discussions for accessing them have begun.

Operational measurements to be conducted as part of bench-scale tests have been summarized to drive test plan developments and evaluate capabilities of bench-scale units.

### **Publications**

N/A

### **Outreach Efforts**

N/A

### **Awards**

None

### **Student Involvement**

None

### **Plans for Next Period**

During the next period, activities identified in the Research Approach section above will continue. The primary focus will be to conclude the planning phase and conduct the bench-scale gasification tests. The sequence of milestones identified above provide a roadmap of necessary subtasks.

## Task 5 – Hawaii Regional Project

University of Hawaii

### Objective

Task 5 includes two subtasks:

Subtask 5.1: Tropical oil to AJF supply chain analysis.

Subtask 5.2: Contaminants in gasification of construction and demolition wastes.

The goal of subtask 5.1 is to develop a model for tropical oil supply chains for alternative jet fuel and associated coproducts. Hawaii will be used as the initial focus, but the modeling tools will be developed for wider use in island settings.

The goal of subtask 5.2 is to develop management strategies for elements present in C&D waste that impact its use as a feedstock for thermochemical conversion.

### Research Approach

Subtask 5.1: Prior ASCENT EcoCrop GIS modeling activities identified growing locations for pongamia, kamani, croton, and jatropha, based on suitable environmental conditions, geography, and zoning. Where unavailable, primary data were also developed for chemical and physical characteristics of these tropical oils and their coproducts (pods/shell, oil seed cake, etc.). The project will use these earlier results as the basis for developing supply chain models for alternative jet fuel production. Model results will identify feedstock production areas, and locations and scales of primary processing sites for shell and pod separation, oil extraction from seeds, and oil conversion to AJF. Potential sources of hydrogen from oil seed coproducts, other renewable resources, and fossil sources will be analyzed and included in the model. Options for points of production, AJF production technologies (ARA, SBI, or Forge, etc.), transportation strategies, and blend ratios at airports (or for specific end users, i.e., military) across Hawaii will affect model outcomes and will be evaluated. Options for coproducts such as animal feeds and higher valued materials will be evaluated and incorporated into the model decision making. Criteria used to drive the model solution might include minimizing AJF production costs while meeting a minimum total production benchmark or minimum blending rate for annual State jet fuel consumption. Other criteria such as system resiliency to extreme weather events and climate change, provision of environmental services, and stakeholder acceptability will also be of importance and will be used to evaluate model solutions.

Subtask 5.2: Thermochemical gasification of biorenewable resources is the initial conversion process for two entry points to alternative jet fuel production; (1) synthesis gas used in direct production of Fischer-Tropsch (FT) liquids and/or (2) green/renewable hydrogen used in biorefineries for hydrotreating lipids or in existing petroleum refining activities for the production of hybrid jet fuel. Urban wood waste from C&D activities provides a reliable source of biorenewable material and requires a tipping fee for disposal, characteristics that enhance feedstock attractiveness. Negative aspects of C&D feedstock are its physical and chemical inhomogeneity. In the latter case, inorganic elements present in the feedstock can negatively impact the gasification process (e.g., corrosion of or accumulation on reactor working surfaces, bed material agglomeration, catalyst deactivation, pollutant emissions, etc.). Using data generated from previous ASCENT Project 01 tasks, this project will assess methods for managing contaminants in C&D feedstocks. This project will be based around gasification systems proposed for production of syngas-FT liquids and green hydrogen. Technology options for contaminant removal or conversion to benign forms will be assessed at each step in the conversion process, i.e., presorting at the waste generation site, sorting/diversion at the C&D waste intake facility, removal by physical/chemical/other methods prior to gasification, in situ reactor control methods, and gas clean up. Technology options from existing process industries and from the scientific literature will be considered. Lab-scale testing of removal techniques will be conducted to provide preliminary assessment of selected, promising technology options. Integrated gasification process options and contaminant control options will be evaluated as complete systems to guide system design and allow system comparisons. Risks associated with the technology options will also be assessed to guide implementation and risk mitigation of the system as a whole. Impacts of processing scale (e.g., Mg waste/day) on selection of technology options will also be assessed.

### Milestone

Subtask 5.1: Establish model framework for oil seed based AJF supply chain in an island setting using Hawaii scenario.

Subtask 5.2: Complete review of options to manage contaminants along the supply chain. Conduct bench scale tests to confirm the efficacy of options



### **Major Accomplishments**

Funding for this Task was received recently and the Task is in the planning stage.

### **Publications**

N/A

### **Outreach Efforts**

N/A

### **Awards**

None

### **Student Involvement**

None

### **Plans for Next Period**

Subtask 5.1: GIS data for oilseed crop production areas and petroleum jet fuel use data at Hawaii airports will be used as the starting points for building AJF model scenarios.

Subtask 5.2: A review of options to manage contaminants along the supply chain will be conducted. Results of the review and contaminant measurements from the bench scale gasification tests in Task 4 will be used to target bench-scale contaminant control tests.



# Project 001(C) Alternative Jet Fuel Supply Chain Analysis

## Purdue University

### Project Lead Investigator

Farzad Taheripour  
Research Associate Professor  
Department of Agricultural Economics  
Purdue University  
403 West State Street  
West Lafayette, IN 47907-2056  
765-494-4612  
tfarzad@purdue.edu

### University Participants

#### Purdue University

- Farzad Taheripour, Research Associate Professor
- FAA Award Number: 13-C-AJFE-PU, Amendments 25, 29, 34, 36
- Period of Performance: October 1, 2019 to September 30, 2020
- Tasks:
  1. Lead: Taheripour; supported by Chepeliev and Stevenson—Develop stochastic techno-economic models for relevant pathways and identify key stochastic variables to be modeled for assessing risk in conversion pathways. This work will lead to our capability to compare pathways, their expected economic cost plus the inherent uncertainty in each pathway.
  2. Lead: Taheripour; supported by Sajedinia, Aguiar, and Malina (Hasselt University) —Life cycle analysis (LCA) of alternative jet fuel pathways in coordination with the International Civil Aviation Organization’s Committee on Environmental Protection Fuels Task Group (ICAO-CAEP-FTG). Work with the CAEP/FTG life cycle assessment group on issues such as system boundaries, induced land use change (ILUC), LCA methodology, and pathway greenhouse gas (GHG) emissions assessment.
  3. Lead: Taheripour; supported by Sajedinia, Aguiar, and Chepeliev—Develop estimates of land use change (LUC) associated emissions for alternative jet fuels for the ICAO-CAEP-FTG. This task is closely related to Task 2,
  4. Lead: Taheripour—Provide support for the other ASCENT universities on alternative jet fuel policy analysis.

### Project Funding Level

- Amendment 3: \$250,000
- Amendment 6: \$110,000
- Amendment 10: \$230,000
- Amendment 15: \$373,750
- Amendment 19: \$400,000
- Amendment 29: \$400,000
- Amendment 36: \$523,000

Current cost sharing for this project year was from Alex Menotti from Neste US, Inc.

### Investigation Team

- Farzad Taheripour (PI): Research Associate Professor
- EhsanReza Sajedinia (PhD student Purdue University): stochastic techno-economic analysis and Global Trade Analysis Project (GTAP) ILUC analysis.
- Xin Zhao (former PhD student, Purdue University): stochastic techno-economic analysis and GTAP ILUC analysis. (Zhao graduated and left Purdue but still voluntarily contributes to the project)



- Jeremiah Stevens (MS student, Purdue University): stochastic techno-economic analysis. (Stevens graduated in December 2019, continued to work for the project as a consultant until August 2020, and still voluntarily contributes to project.)
- Maksym Chepeliev (PhD, Research Associate, GTAP Center): collaborates part time with the project.
- Angel H. Aguiar (PhD, Research Associate, GTAP Center): collaborates part time with the project.

## Project Overview

This project has five main components: First is advancement of stochastic techno-economic analysis (TEA) for aviation biofuel pathways. Second is life cycle and production potential analysis of alternative jet fuel pathways in coordination with ICAO CAEP-FTG. The third component also involves working with FTG, specifically on estimation of land use change (LUC) associated emissions for alternative jet fuels. The fourth is to provide support for the policy sub-group in FTG by providing policy guidelines to facilitate expansions in using sustainable aviation fuels. This task includes bridging existing TEA for alternative jet fuels with partial and general equilibrium economic models to develop alternative scenarios for alternative jet fuels in the fuels mix used by the industry. The fifth task supported “Farm to Fly 2.0” (F2F2). F2F2 was a collaboration of government and industry to enable commercially viable, sustainable alternative jet fuel supply chains in the U. S. at state and regional levels to support the goal of one billion gallons of alternative jet fuel production capacity and use by 2019. Purdue University provided necessary analytical support for this effort.

## Task 1 – Develop Stochastic Techno-economic Models for Relevant Pathways and Identify Key Stochastic Variables for Assessing Risk in Conversion Pathways

Purdue University

### Objective

Develop stochastic techno-economic models for relevant pathways and identify key stochastic variables to be modeled for assessing risk in conversion pathways. This work will lead to our capability to compare pathways, their expected economic cost, plus the inherent uncertainty in each pathway.

### Research Approach

For each fuel pathway being evaluated, we develop a stochastic model that covers the entire pathway so that it can be used for both techno-economic and life cycle analysis. Over this period, we continued to work on alcohol-to-jet (ATJ) and the catalytic hydrothermolysis (CH) processes. We have also developed some harmonized TEA.

### Milestone(s)

We developed a new a stochastic TEA for a plant designed to use the CH technology to produce renewable diesel fuel, renewable jet fuel, and renewable naphtha from pennycress seed oil produced in Iowa and Indiana. In addition to the standard stochastic practices, this TEA considers uncertainty in biofuel policies and highlights the existing policies that can be altered to support production of alternative jet fuels. This research shows that with proper policies in place, producing alternative jet fuels could be commercially viable in the near future. This research has been fully and successfully conducted. We will continue to publish results of these case studies.

### Major Accomplishments

- An Excel-based framework has been developed to conduct stochastic TEA in combination with @Risk program.
- An archive from the exiting TEAs has been created and summarized in an Excel file for future uses.

### Publications

The following paper has been developed and presented:

Stevens J. and Taheripour F. (2020) “A stochastic techno-economic analysis of aviation biofuel production from pennycress seed oil,” Selected paper *presented at the 2020 Agricultural & Applied Economics Association Annual Meeting, Virtual Meeting August 10-1, 2020.*

### **Outreach Efforts**

None

### **Awards**

None

### **Student Involvement**

Jeremiah Stevens, MS student, Purdue University

### **Plans for Next Period**

We will work on the publication of the result of the TEA of producing alternative jet fuels from pennycress.

## **Task 2 – Life Cycle Analysis of Alternative Jet Fuel Pathways in Coordination with ICAO-AFTF-FTG**

Purdue University

### **Objective(s)**

- Provide required data and analysis to support the low LUC risk practices adopted in CAEP.
- Provide required data and analysis to support the core LCA group with respect to ILUC for co-processing of esters and fatty acids in petroleum refineries and other tasks as needed.

### **Research Approach**

There are many varied assignments and pieces under this Task. We follow standard approaches to support FTG subgroups including core LCA, Technology Production Policy (TPP), Emission Reductions Accounting (ERA), and Sustainability subgroups. We use the GTAP-BIO model, collected data, and provided proper analyses to accomplish this Task.

Taheripour is co-chair of the FTG induced land use change (ILUC) group.

Taheripour collaborates with the LCA, TPP, ERA, and Sustainability subgroups of ICAO-CAEP-FTG.

### **Milestones**

Taheripour participated in the following FTG meetings: FTG3 in Dubai and virtual FTG4 and FTG5. Taheripour has been involved in many of the tasks and document preparation activities for the meetings. He responded to other subgroups requests for help and collaboration. He leads the efforts on ILUC modeling and the ILUC-related tasks associated with other subgroups. We developed a framework to examine regional ILUC and rank countries according to their LUC determinants. We collected data on LUC determinants and developed some primary analysis.

### **Major Accomplishments**

- We developed a template to collect information from the existing TEAs. Using this template and in collaboration with ASCENT projects, we collected and reviewed the existing TEA on alternative jet fuels and summarized and synthesized their findings, advantages, and limitations. The results of this work helped us to bridge the TEA approach with a modeling framework that aims to develop a supply schedule for alternative jet fuels. The results of this effort have been used by the FTG-TPP subgroup to help the ICAO-CAEP-FTG group to identify future research on supply of sustainable aviation fuels (SAFs), see CEAP/12-FTG/03-WP/10.
- We also developed two harmonized TEAs for: hydroprocessed esters and fatty acids (HEFA) from vegetable oils and ATJ from grain-based ethanol. These TEAs have been developed in collaboration with ASCENT projects.
- A dataset including historical observations on crop yields has been developed to support TPP subgroup projections. This dataset covers yield trends for maize, wheat, soybean, rapeseed, oil palm crop, sugar beet, and sugarcane for two time slices of 1961–2028 and 2000–2018. These crops are the main feedstocks for biofuel production. Data provided by the Food and Agricultural Organization (FAO) data have been used to determine yields for the 10 largest producers of each crop.



## **Publications**

Taheripour, F., & Tyner, W. E. (2020). US biofuel production and policy: implications for land use changes in Malaysia and Indonesia. *Biotechnology for Biofuels*, 13(11), 17.

## **Outreach Efforts**

- Taheripour attended the CRC meeting and made a presentation on regional land use change values. The meeting was in Argonne National Laboratory, Lemont, IL, October 15–17, 2019.
- Taheripour attended the ASCENT Advisory Group Meeting and made a presentation on limiting deforestation from palm oil in Malaysia and Indonesia. The meeting was in Washington DC., October 22–23, 2019.
- Taheripour attended the virtual ASCENT Advisory Group Meetings in March 2020 and September 2020 and presented the following posters entitled:
  - Alternative Jet Fuel Supply Chain Analysis - CORSIA Fuels Support,
  - Land Use in Computable General Equilibrium models - CORSIA Support.

## **Awards**

None

## **Student Involvement**

EhsanReza Sajedinia, PhD student Purdue University  
Jeremiah Stevens, MS student, Purdue University

## **Plans for Next Period**

We will continue to support FTG subgroups.

# **Task 3 – Develop Estimates of Land Use Change Associated Emissions for Alternative Jet Fuels for the ICAO Fuels Task Group**

Purdue University

## **Objective(s)**

- Computation of induced land use change emissions of alternative jet fuels for use in Carbon Offsetting and Reduction Scheme for International Aviation (CORSIA).
- Improvements in GTAP-BIO model and its database and making proper modification in the Agro-ecological Zone Emission Factor (AEZ-EF) emissions model.
- Define and implement a method to determine regional ILUC values and rank countries according to their LUC determinants.

## **Research Approach**

We modify, update, and use the GTAP-BIO model to produce estimates of ILUC for FTG. We also collaborate with the International Institute for Applied Systems Analysis (IIASA) and Hugo Valin to evaluate the outcomes of GTAP-BIO and GLOBIOM models. We collect data and develop new approaches to assess issues related to ILUC emissions due to production of alternative jet fuels.

## **Milestones**

We added several new pathways to the GTAP-BIO model. We examined new regional ILUC values. We developed primary analyses to rank countries according to their land use change determinants and determine global ILUC values.

## **Major Accomplishments**

Most of the accomplishments under this Task are in the form of work progress of ICAO-CAEP-FTG. Some of the working papers and information papers we have produced over this period are listed in this section and in the overall publication list at the end of this report. In addition, an Excel-based model has been developed to estimate direct land use change (DLUC) emissions values.



## **Publications**

There have been several working papers and information papers produced for the AFTF/FTG work. In what follows, we only presented the working and information papers presented at FTG meetings:

- CAEP/12-FTG/03-WP/07: “Progress on Modelling of ILUC values for CORSIA LCA”, Abu Dhabi, United Arab Emirates, February 2020.
- CAEP/12-FTG/03-WP/08: “Progress of ILUC Subgroup on Low LUC Risk Practices”, Abu Dhabi, United Arab Emirates, February 2020.
- CAEP/12-FTG/03-WP/11: “Guidance document for calculation and submission of LCA data for new pathways”, Abu Dhabi, United Arab Emirates, February 2020.
- CAEP/12-FTG/03-IP/04: “Possible methodologies to derive regional ILUC values based on current modelling”, Abu Dhabi, United Arab Emirates, February 2020.
- CAEP/12-FTG/03-IP/05: “Land Use Change Emission Accounting in GLOBIOM and GTAP-BIO”, Abu Dhabi, United Arab Emirates, February 2020.
- CAEP/12-FTG/03-IP/08: “Method proposed for DLUC values”, Abu Dhabi, United Arab Emirates, February 2020.
- CAEP/12-FTG/04-WP/07: “Guidance on Direct Land Use change calculation for Sustainability Criterion 2.2”, Virtual, June 2020.
- CAEP/12-FTG/04-WP/08: “Expanding Regional ILUC Values Coverage Based On Model Simulations”, Virtual, June 2020.
- CAEP/12-FTG/04-IP/09: “Progress on ILUC values for additional SAF pathways”, Virtual, June 2020.
- CAEP/12-FTG/04-IP/10: “Low LUC risk practices: scoping for case studies analysis”, Virtual, June 2020.
- CAEP/12-FTG/05-WP/05: “Updated ILUC values for carinata oil HEFA”, Virtual, July 2020.
- CAEP/12-FTG/05-WP/06: “Updated ILUC values for ETJ perennial grass pathways”, Virtual, July 2020.
- CAEP/12-FTG/05-WP/07: “DLUC safeguard for unused land approach in LMP”, Virtual, July 2020.
- CAEP/12-FTG/05-WP/08: “Revised guidance on Direct Land Use Change calculation”, Virtual, July 2020.
- CAEP/12-FTG/05-IP/05: “Overview of ILUC modelling assumptions applied across pathways”, Virtual, July 2020.

In addition to the above reports we have the following papers in press or already published:

- Zhao X. Taheripour F., Malina R. Tyner W. (2020) “Aviation biofuels: A viable and sustainable option to curb aviation emissions,” Selected paper *presented at the 2020 Agricultural & Applied Economics Association Annual Meeting, Virtual Meeting August 10-1, 2020.*
- Taheripour F. Zhao X., Horridge M. Farrokhi F. Tyner W (2020: In press) “Modeling Land Use in Computable General Equilibrium Models: Preserving Physical Area of Land” (In press), *Journal of Global Economic Analyses.*

## **Outreach Efforts**

Taheripour attended several meetings to present the research outcomes on ILUC values, including:

- National Biodiesel Conference & Expo, Tampa, Florida, January 2020.
- GTAP 23<sup>rd</sup> Annual Conference on Global Economic Analysis, Virtual meeting, June 2020.
- AAEA Annual Meeting, Virtual, August 2020.
- EPA Brownbag seminar, September 10, 2020.

## **Awards**

- Farzad Taheripour, Award for Quality of Communication, The Agricultural and Applied Economic Association, 2020,
- Farzad Taheripour, Award for Outstanding Publication in the journal of *Environmental and Resource Economics* published in 2019, The European Association of Environmental and Resource Economics, 2020

## **Student Involvement**

EhsanReza Sajedinia, PhD student Purdue University

## **Plans for Next Period**

- We will continue working with ICAO on ILUC emission estimates including the following highlights:
- The current model uses a database which represent the world economy in 2011. We plan to update to this data base to 2014. This is a major task and requires new development.
- We will work to develop regional ILUC values.
- We are in the process of developing a method to rank countries according to their LUC determinant factors.



- We are now working on DLUC values.

## Task 4 – Provide Support for the other ASCENT Universities on Alternative Jet Fuels Policy Analysis

Purdue University

### **Objective**

To provide support for the other ASCENT universities on alternative jet fuels policy analysis.

### **Research Approach**

See Task 1

### **Milestone(s)**

See Task 1

### **Major Accomplishments**

See Task 1

### **Publications**

None

### **Outreach Efforts**

None

### **Awards**

None

### **Student Involvement**

Jeremiah Stevens, MS student, Purdue University

### **Plans for Next Period**

We will continue to collaborate with ASCENT as needed.

## Task 5 – Provide Support for the Farm-to-Fly Initiative as Needed

Purdue University

### **Objectives**

To provide support for the Farm-to-Fly (F2F2) initiative as needed.

### **Research Approach**

This activity is a general support for other initiatives. Our main role is to consult with other projects and activities and provide assistance as needed.

### **Milestones**

There has been little activity under this Task in this reporting period.

### **Major Accomplishments**

None



**Publications**

None

**Outreach Efforts**

None

**Awards**

None

**Student Involvement**

None

**Plans for Next Period**

Support for this effort has concluded.



# Project 001(D) Alternative Jet Fuel Supply Chain Analysis

## The Pennsylvania State University

### Project Lead Investigator

Saurabh Bansal  
Associate Professor of Supply Chain Management  
Department of Supply Chain and Information Systems  
The Pennsylvania State University  
405 Business  
University Park, PA 16802  
814-863-3727  
sub32@psu.edu

### University Participants

#### The Pennsylvania State University (Penn State)

- PI: Saurabh Bansal, Associate Professor of Supply Chain Management.
- PI: Lara Fowler, Senior Lecturer, Penn State Law School; Assistant Director, Penn State Institutes of Energy and the Environment
- PI: Ekrem Korkut, Penn State Law School

#### The Washington State University (WSU)

- Kristin Brandt, Staff Engineer

#### University of Tennessee

- Tim Rials, Associate Dean Ag Research
- Burt English, Professor of Agricultural and Resource Economics

### Project Funding Level

FAA Funding: \$200,000  
Matching, Penn State: \$200,000  
Total Funding: \$400,000

### Investigation Team

Task 1.3.1 (Lead: Bansal; supported by Brandt and English): risk-reward profit sharing modeling for first facilities.

Task 1.3.2 (Lead: Bansal; supported by Brandt and English): additional quantification of risk and uncertainties in supply chains (foundational part of Task above).

Task 1.3.3 (Lead: Bansal; supported by Brandt and English): supply chain risk analysis tools for farmer adoption.

Task 1.4.1 (Lead: Fowler; supported by Korkut): national survey of current and proposed state and federal programs that monetize ecosystem services.

Task 1.4.3 (Lead: Fowler; supported by Korkut): support in stakeholder engagement efforts.

### Project Overview

The project focuses on developing a qualitative and quantitative understanding of factors that can help the establishment of biofuel supply chains aimed at supplying alternative jet fuels. Efforts are being made to establish these supply chains. However, many of these efforts are challenged because of a lack of clarity regarding the incentives that stakeholders would require to engage in these supply chains and devote their resources to invest in the facilities required for these supply chains. To this end, the project has two goals:

1. Develop proforma cash flows that represent the financial status of various participants in biofuel supply chains for

- alternative jet fuels to inform a transparent risk-sharing tool, and
2. Understand the policy landscape that exists in various parts of the U.S. to encourage these supply chains and identify further policy initiatives that may be needed.

## Task 1.3.1 – Risk-Reward Profit Sharing Modeling for First Facilities

The Pennsylvania State University

### **Objective**

Develop a transparent risk-sharing tool to provide all partners with an understanding of the cash flows and risks faced by all supply chain partners.

### **Research Approach**

We first collected a large number of risk-sharing tools that have been proposed in the supply chain literature. Subsequently, we narrowed the list down to 9–12 mechanisms. We created an Excel-based framework in which the cash flows of all supply chain partners are modeled by using the numbers from the techno-economic analyses developed by WSU. This framework incorporates the risk sharing mechanisms.

### **Milestone**

We developed the Excel models for four realistic configurations by using data from techno-economic analysis models from WSU.

### **Major Accomplishments**

We developed an Excel-based framework showing the cash flows of four key stakeholders of alternative jet fuel supply chains: farmers, preprocessors, refineries, and airlines. The framework shows various risk-sharing contracts that each of the stakeholders can extend to others, as well as the financial burden or opportunity associated with these mechanisms. The framework also shows the government’s financial burden of supporting these mechanisms. The framework is developed for four levels of refinery capacities. Overall, this framework can be used as a decision support tool by various stakeholders to determine whether to engage in alternative jet biofuel supply chains and negotiate with each other.

### **Publications**

We anticipate publishing a paper based on combined work from the last year and the coming year.

### **Outreach Efforts**

The tool has been presented and discussed at three ASCENT advisory committee meetings.

### **Awards**

None

### **Student Involvement**

None

### **Plans for Next Period**

We were planning on running laboratory studies with graduate students. However, the behavioral research lab was closed at Penn State due to the COVID-19 situation. We will run these studies when students are back to campus. We would be able to run these studies only when students are able to interact with each other in a simulated negotiation environment. We will provide the tool and a training in use of the tool to project sponsor.

## Task 1.3.2 – Additional Quantification of Risk and Uncertainties in Supply Chains (Foundational Part of Task Above)

The Pennsylvania State University

### **Objective**

Develop methods to rely on expert judgments to quantify uncertainties associated with biofuel supply chains.

### **Research Approach**

We developed a new econometric approach to quantify probability distributions of uncertain quantities such as yield or demand when a panel of experts provides judgments regarding the most-likely values. This approach exploits the well-known theory of generalized least squares in statistics for the context in which historical data are available to calibrate expert judgments or when these data are not available.

### **Milestones**

We have described the method in two manuscripts. In the first manuscript, [\*Using Subjective Probability Distributions to Support Supply Chain Decisions for Innovative Agribusiness Products\*](#), we develop a two-stage procedure to calibrate expert judgments for the distribution of biofuel uncertainties, such as the uncertain yield of new varieties of oil seeds, demand, or selling price. In the first step of the procedure, we calibrate the expert judgments by using historical data. Specifically, we use prior judgments provided by experts and compare them with actual realizations (such as predicted yield versus actual yield) to determine the frequency with which each expert over- or underestimated the uncertainty, e.g., Expert 1 underestimated the yield 60% of the time, but Expert 2 underestimated the yield 90% of the time. In the second manuscript, [\*Optimal Aggregation of Individual Judgmental Forecasts to Support Decision Making in a R&D Program\*](#), we use this information to determine the optimal way to aggregate the experts' judgments to determine the mean and standard deviation of the probability distributions. In the second manuscript, we develop a new optimization protocol to determine the optimal acreage for growing specific crops, by taking into account the estimated mean and standard deviation as well as incorporating the variability in these estimates.

### **Major Accomplishments**

Theoretical development and a numerical study have demonstrated the promise of this approach.

### **Publications**

One paper has been accepted. The second paper is finished.

### **Outreach Efforts**

N/A

### **Awards**

None

### **Student Involvement**

None

### **Plans for Next Period**

The second paper has been submitted for review. It will be sent out for a publication during this period.

## Task 1.3.3 – Supply Chain Risk Analysis Tools for Farmer Adoption

The Pennsylvania State University

### **Objectives**

Understand farmers' risk preferences over a long duration and how these preferences affect their decisions to grow crops that can support alternative jet fuel supply chains

### **Research Approach**

We surveyed farmers to understand their risk preferences over extended durations. Specifically, we showed them sample yield ranges over extended periods and asked them to estimate the lowest equivalent guaranteed yield that they would be willing to accept given the uncertain yields. We used these responses for statistical analyses.

### **Milestones**

We have completed the survey and finished a manuscript based on the survey.

### **Major Accomplishments**

We compiled data from 43 farmers in central Pennsylvania regarding their preferences given the uncertain yields from their land. The results quantify the loss of value that farmers attribute to an uncertain yield. The reported results are for both 1-year and 10-year horizons. For the 10-year horizon, we also report results with an initial yield buildup, as is the case with most biofuel crops. The key takeaways from this study are that: (a) farmers' valuation of a new crop decreases acutely as the uncertainty in yield increases, and (b) the initial build-up period of low yields can be a large deterrent to farmers' adopting new crops for the purpose of supporting biofuels.

### **Publications**

The paper was finished and was provided to the sponsor.

### **Outreach Efforts**

N/A

### **Awards**

None

### **Student Involvement**

None

### **Plans for Next Period**

The results in the first version of the paper revealed something interesting: when faced with uncertain yields, say from  $x$  to  $y$ , farmers were willing to swap their output for a consistent output at levels that were lower than  $x$ . This finding was surprising at first. However, the research team has recently found prior research in economics documenting similar behavior. We would like to collect more data during the year to bolster the manuscript, pending a resolution to the COVID-19 situation.

## **Task 1.4.1 – National Survey of Current and Proposed State and Federal Programs that Monetize Ecosystem Services**

The Pennsylvania State University

### **Objective**

Conduct a survey and summarize current and proposed state and federal programs to monetize ecosystem services.

### **Research Approach**

This Task builds on and continues the work done under ASCENT Project 01, Task 8.1, which focused on the biomass and water quality benefits to the Chesapeake Bay watershed. Under this Task, we examined the biofuel law and policy landscape of the Pacific Northwest and Southeast regions, as well as the state of Hawaii. We also researched federal biofuel law and policy. We have had a change in personnel working on this project. Lara Fowler remains the lead; however, Gaby Gilbeau left the project in August 2018, and Ekrem Korkut joined the project during the fall of 2018.

### **Milestones**

We have captured this research in three region-specific white papers describing the biofuel law and policy incentives, and the ecosystem service drivers for the subregions. In addition, we added another U.S.-level white paper to the list of tasks.

- Project 01A, Tasks 3.1, the Pacific Northwest.



- Project 01B, Task 3.2, Hawaii.
- Project 01E, the Southeast.

Copies of these documents are available online:

- Western U.S. policy paper (with a focus on Washington State): <https://psu.box.com/s/l9ektkr8lk10qjqu93l4jmm9djmmhf>
- Southeast policy paper (with a focus on Tennessee): <https://psu.box.com/s/iyeowdfo0447t4ya8dl5md2zu5un48u6>
- Hawaii policy paper: <https://psu.box.com/s/92a7tl19tpphg69t4ff12t9d4rdshgq1>
- **Federal level white paper:** <https://psu.app.box.com/file/629416796137?s=5r15l1xg8yeg1nnms1nfjx023p3wzkfu>
- **Poster:** <https://psu.box.com/s/20ugtneqsmu8ufjrjahos87hp47dk2zm>

### **Major Accomplishments**

We have captured this research in three regional white papers describing the biofuel law and policy incentives. In addition, we have researched and finished drafting a document summarizing aviation and biofuel at the national level in the U. S. As part of this, we have examined how legal and policy drivers from other parts of the world are affecting U.S. incentives.

### **Publications**

The white papers have been sent to ASCENT leads for review and comment (including Nate Brown and Michael Wolcott); comments on the federal white paper have been addressed and incorporated.

We are working on turning these papers into publications for the *Frontiers in Energy* special edition. In addition, we have circulated the white papers to ASCENT team members for their background and information.

### **Outreach Efforts**

Lara Fowler and Ekrem Korkut created and shared a poster for the September 29, 2020 annual meeting. This poster is linked above and addresses the federal, state, regional and international aspects of aviation biofuel law and policy.

### **Awards**

None

### **Student Involvement**

Ekrem Korkut continues to be a full-time student at the Penn State School of International Affairs. He has continued to work on the ASCENT project as a part-time research assistant while conducting his studies.

### **Plans for Next Period**

As noted above, we are turning the existing white papers into published papers (at least one policy related piece for the *Frontiers in Energy* special issue) and planning on an additional review at the state/regional level. In addition, we are working with other ASCENT team members on law and policy research questions they have identified, including how landfill regulations shape opportunities in Hawaii and other related topics.

## **Task 1.4.3 – Help Support Stakeholder Engagement Efforts**

The Pennsylvania State University

### **Objective**

Facilitate dialogue among producers, industry, government, and other affected stakeholders.

### **Research Approach**

Our work under this objective focused on stakeholder engagement and facilitation of effective dialogue to help bridge the gaps among producers, industry, government, and other affected stakeholders. This role supports other team members' needs.



### **Milestone**

These efforts supported the stakeholder engagement efforts led by other teams, including but not limited to the regional partners identified in ASCENT Project 01, Tasks 3.1, 3.2, and 3.3.

### **Major Accomplishments**

This set of tasks has been more limited, with no major accomplishments to date. We have continued to participate in discussions and calls related to potential stakeholder engagement needs.

### **Publications**

N/A

### **Outreach Efforts**

N/A

### **Awards**

None

### **Student Involvement**

None

### **Plans for Next Period**

Future work under this objective will include presenting to the project partners on facilitation skills and tactics. Additional support for regional projects will be offered as needed for facilitation and stakeholder engagement sessions as the regional projects move to the deployment stage.



## Project 001(E) Alternative Jet Fuel Supply Chain Analysis

### University of Tennessee

#### Project Lead Investigator

Timothy Rials  
Professor and Director  
Center for Renewable Carbon  
University of Tennessee  
2506 Jacob Dr. Knoxville, TN 37996  
865-946-1130  
trials@utk.edu

#### University Participants

##### University of Tennessee

- PI: Burton English, Professor
- FAA Award Number: 13-C-AJFE-UTenn, Amendments 09, 11, 13
- Period of Performance: August 1, 2019 to August 10, 2021
- Tasks:
  1. Assess and inventory regional forest and agricultural biomass feedstock options.
  2. Develop national lipid analysis.
  3. Lay the groundwork for lipid and/or biomass in Tennessee (TN) and Southeastern U.S.
  4. Biorefinery infrastructure and siting (supporting role).

#### Project Funding Level

Total six-year funding/This year funding

Total Estimated Project Funding: \$1,075,000/\$500,000

Total Federal and Non-Federal Funds: \$2,150,000/\$1,000,000

The University of Tennessee, Institute of Agriculture provided faculty salary in support of the project.

#### Investigation Team

- Tim Rials – Project Director(s)/Principal Investigator (PD/PI)
- Burton English – Co-Principal Investigator (Co-PD/PI)
- Lixia He – Other Professional
- Kim Jensen – Faculty
- Jim Larson – Faculty
- Carlos Trejo-Pech – Faculty
- Ed Yu – Faculty
- David Hughes – Faculty
- Jada Thompson – Faculty
- Bijay Sharma – Post Doc
- K. Alan Robertson – Graduate Student
- McKenzie Thomas – Masters Graduate Student
- Luis Vizcaya – Masters Graduate Student
- Patwary, A. Latif – Masters Student
- Mackenzie Gill – Masters Student
- Ty Wolaver – Masters Student



## Project Overview

The University of Tennessee (UT) will lead the Feedstock Production (Task 1) component of the project. This component targets the need to assess and inventory regional forest and agricultural biomass feedstock options and delineate the sustainability impacts associated with various feedstock choices, including land use effects. UT will lead the national lipid supply availability analysis employing POLYSYS to develop information on the potential impacts and feasibility of using lipids to supply aviation fuel. The team at UT will facilitate regional deployment/production of jet fuel by laying the groundwork and developing a regional proposal for deployment. Additionally, UT will support activities in Task 3 with information and insights on feedstocks, along with potential regional demand centers for aviation fuels and coproducts, along with information on current supply chain infrastructure, as required.

Major goals include:

1. Develop a rotation-based oil seed crop scenario and evaluate potential with POLYSYS.
2. Develop database on infrastructure and needs for the Southeast U.S.
3. Organize and convene workshop on the alternative jet fuel supply chain for Appalachia stakeholders (completed).
4. Initiate aviation fuel supply chain studies in the Southeast using pine and oilseeds.
5. Continue with sustainability work for both goals 1 and 4.

A journal manuscript will be prepared based on the biochar survey data in this project. McKenzie Thomas will complete her M.S. thesis using this data.

## Task 1– Assess and Inventory Regional Forest and Agricultural Biomass Feedstock Options

University of Tennessee

### Objectives

As the markets for lignocellulosic biomass (LCB) feedstock (i.e., grasses, short-rotation woody crops, and agricultural residues) are currently not well-established, it is important to evaluate the feasibility of supplying those LCB feedstocks. The opportunity cost of converting the current agricultural lands to LCB feedstocks production will be estimated. In addition, the production, harvest, storage, and transportation cost of the feedstocks are included in the assessment. A variety of potential crop and biomass sources will be considered in the feedstock path, including:

**Oilseed crops:** Potentials include mustard/crambe (*Sinapsis alba/Crambe abyssinicia*); pennycress (*Thlaspi arvense*); rapeseed/canola (*Brassica napus/B. campestris*); safflower (*Carthamus tinctorius*); sunflower (*Helianthus spp.*); soybean (*Glycine max*); camelina (*Camelina sativa*); carinata.

**Perennial grasses:** switchgrass (*Panicum virgatum*); miscanthus (*Miscanthus sinensis*); energy cane (*Saccharum complex*).

**Short-rotation woody crops:** poplar (*Populus species*); willow (*Salix species*); loblolly pine (*Pinus taeda*); sweetgum (*Liquidambar styraciflua*); sycamore (*Plantanus occidentalis*).

**Agricultural residue:** wheat straw; corn stover.

**Forest residue:** logging and processing residue.

POLYSYS will be used to estimate and assess the supply and availability of these feedstock options at regional and national levels. This U.S. agricultural sector model forecasts changes in commodity prices and net farm income over time.

County level estimates of all-live total woody biomass, as well as average annual growth, removals, and mortality will be obtained from the Forest Inventory and Analysis Database (FIADB). Mill residue data will be obtained from the U.S. Forest Service's Forest Inventory and Analysis (FIA) Timber Product Output (TPO) data. The ForSEAM model will be used to estimate and predict logging residues. ForSEAM uses U.S. Forest Service FIA data to project timber supply based on the U.S. Global Forest Product Model module of the Global Forest Product Model (USFPM/GFPM) demand projections. Specific tasks related

to this objective are outlined below. These supply curves will be placed in both ForSEAM and POLYSYS and estimates into the future will be made.

**Task 1 Goals** (support/continue ongoing work from previous year)

- Complete the economic viability analysis on switchgrass, short rotation woody crops, crop residues, forest residues, and cover crops.
- Assist risk-reward profit sharing modeling by providing information from past work on cellulosic supply chains to PSU.
- Assist the Pennsylvania State University (Penn State) in a national survey of current and proposed programs that incentivize ecosystem services.
- Finish environmental impact analysis for the aforementioned crops looking at soil, water, greenhouse gas emissions and sequestration, and direct land use change.

**Research Approach**

1. Completed developing a consistent set of budgets for pennycress, camelina, and carinata as cover crops.
2. Yields for camelina, carinata, and pennycress have been estimated. Camelina and carinata were estimated using the Environmental Policy Integrated Climate (EPIC) model and pennycress from secondary source information.
3. Initiated a risk analysis for the three cover crops.
4. Developing two articles on carinata and switchgrass.
5. Taking information from a project titled *Next Generation Logistics Systems for Delivering Optimal Biomass Feedstocks to Biorefining Industries in the Southeastern US* (LEAF) funded by the Bioenergy Technologies Office (BETO) on pine and switchgrass blend examine the potential in the Southeast. Completed 100% pine scenario and initiated the 75% pine, 50% pine, and 25% pine scenarios (Figures 1 and 2). We found the average transportation cost, average feedstock cost, the distance feedstock had to travel, and the location of potential biorefineries of the 2000/million (M) dry short tons (t) and 2500 Mt/day capacities. The results are displayed in Table 1.

**Table 1.** Average transportation cost, average feedstock cost, the distance feedstock had to travel, and the location of potential biorefineries of the 2000/Mt and 2500 Mt/day capacities

2000 Mt/day Biorefinery				
Location Indicator	Tons	Average Feedstock Cost	Average Transportation Cost (\$/t)	Average Distance (ton-mile)
24746	723,456	\$52.19	\$21.19	68
39134	723,538	\$52.39	\$21.39	69
56464	724,124	\$55.82	\$24.82	80
110865	721,866	\$58.30	\$27.30	88
44009	722,242	\$58.75	\$27.75	90
2500 Mt/day Biorefinery				
Location Indicator	Tons	Average Feedstock Cost	Average Transportation Cost (\$/t)	Average Distance (ton-mile)
39134	902,214	\$56.16	\$25.16	81
24746	901,099	\$57.10	\$26.10	84
51468	904,468	\$59.44	\$28.44	92
110865	899,182	\$63.08	\$32.08	103

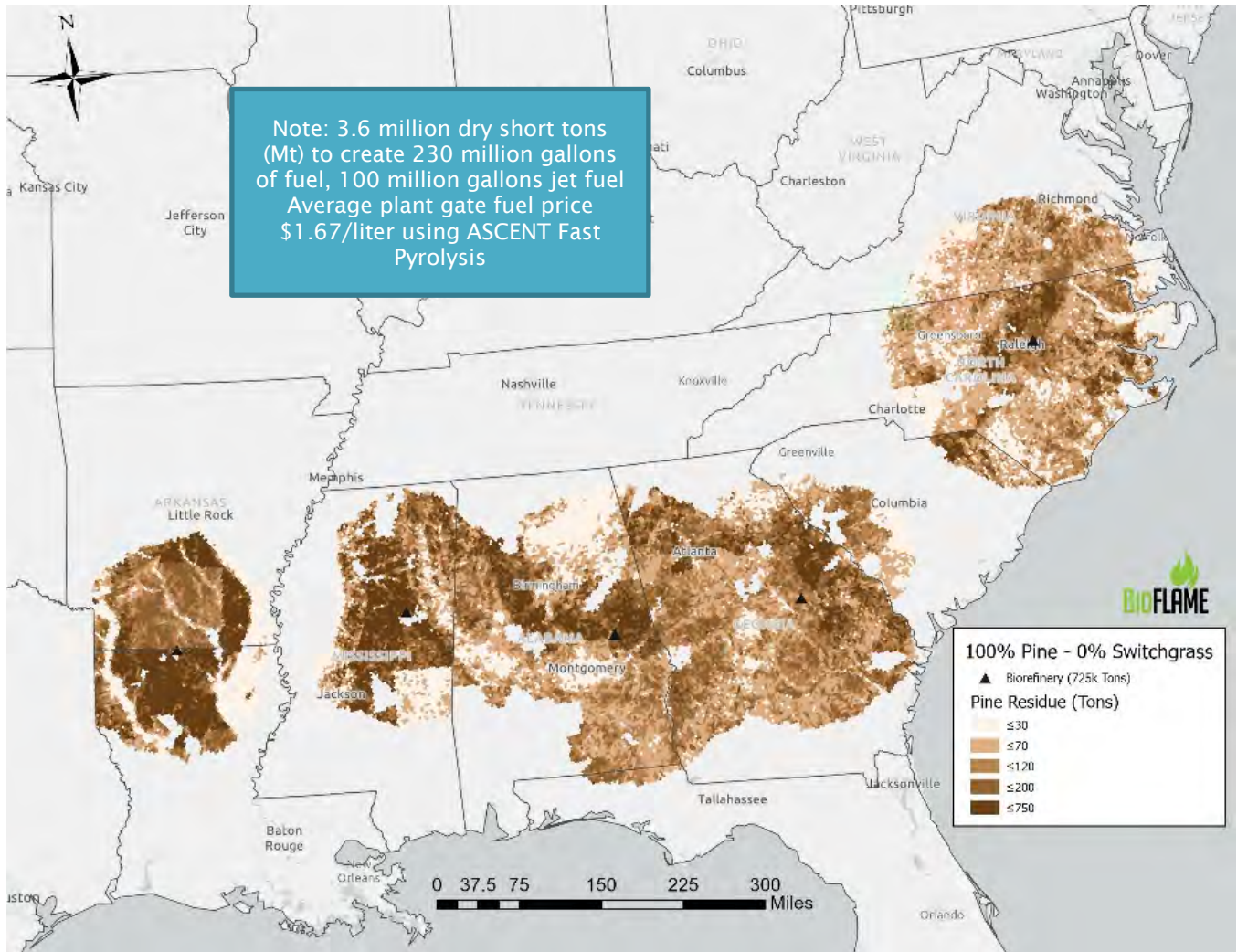
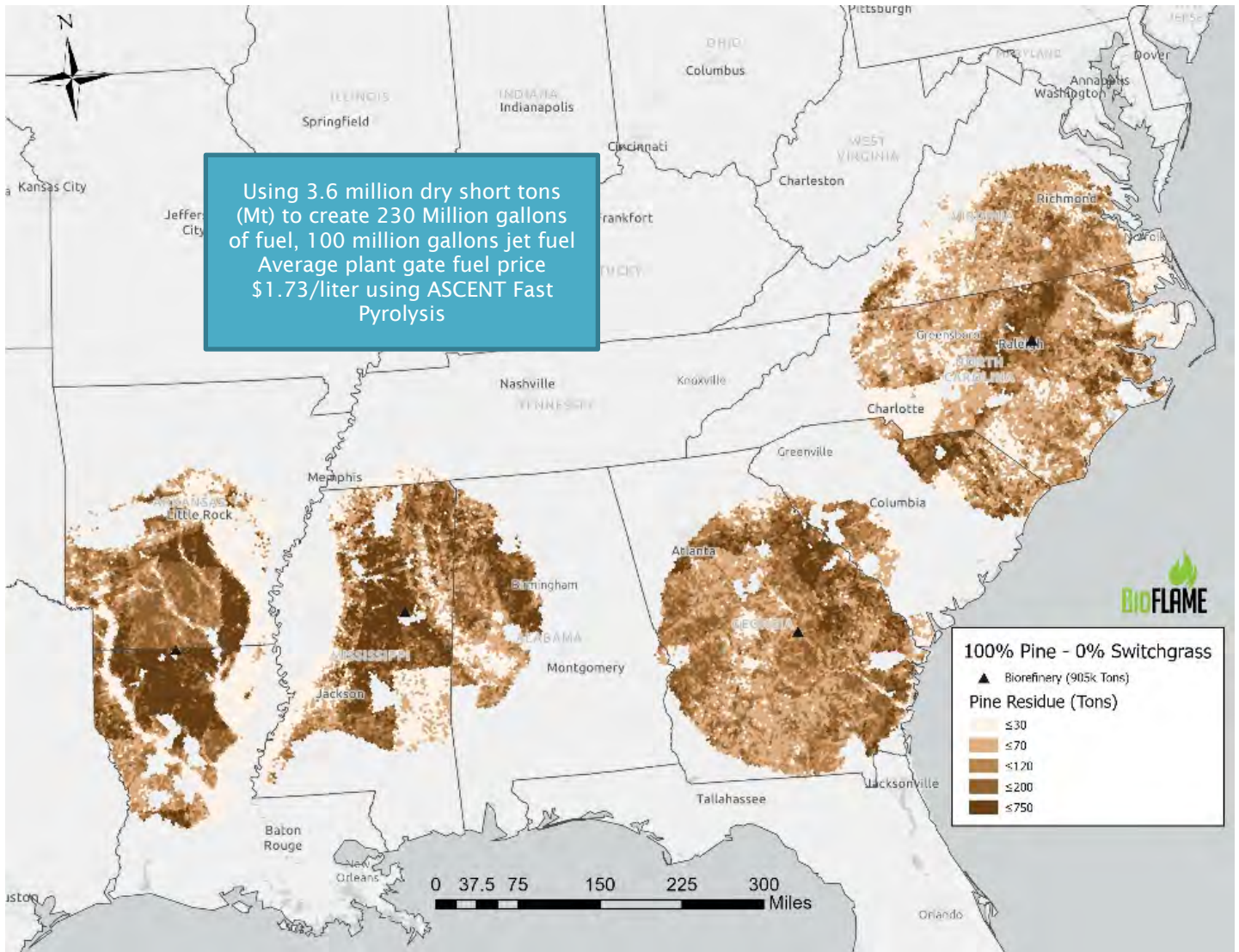


Figure 1. Projected biorefinery locations and their feedstock draw area; 2000 dry Mt/day.



**Figure 2.** Projected biorefinery locations and their feedstock draw area; 2500 dry Mt/day.

With a 50% pine and 50% switchgrass blend, the region has the capability of using 4.7 million dry short tons of forest residues to produce 225 to 258 million gallons of sustainable aviation fuel (SAF) with the average price ranging from \$1.74 to \$1.78 per liter for the two different plant sizes.

6. Developed new forest layer for the nation. Focus is the cellulosic pathway potential of the southeast and in Appalachia area specifically. Forest residues for the United States have been re-estimated and quantities have been evaluated.

Two scenarios were used. The initial analysis uses the Department of Energy's 2016 Billion-Ton Report assumptions, with medium demand for traditional forest products and a sustainable, 50-million-ton demand for forest residues. The model ForSEAM was rerun from 2015 to 2040 with the bioenergy demand for forest residues initiated in 2020 and continued to 2040. The model met this level of forest demand indicating that U.S. forests can produce the 50 million tons of forest residues sustainably. The second scenario assumed that harvest could extend beyond the limit of one mile from the road used by the 2016 Billion-Ton Report. With this assumption, it was found that the nation's forests can provide 75 million tons

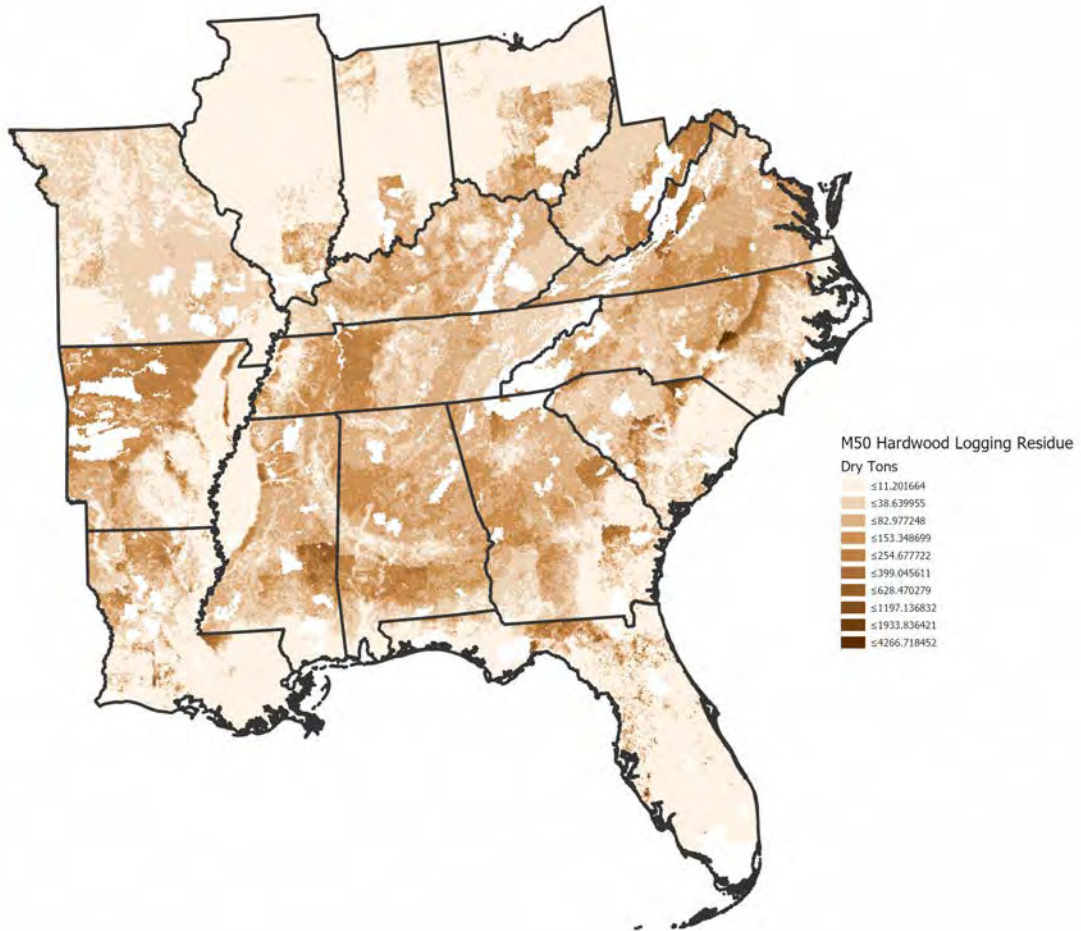


of forest residues for energy production over the same 20-year period (Table 2). The cost varies between \$20 to \$70 per ton delivered in chipped form with logging residues on the low end and pulpwood on the higher end. Locations of the hardwoods are shown in Figure 3, panels 1 and 2.

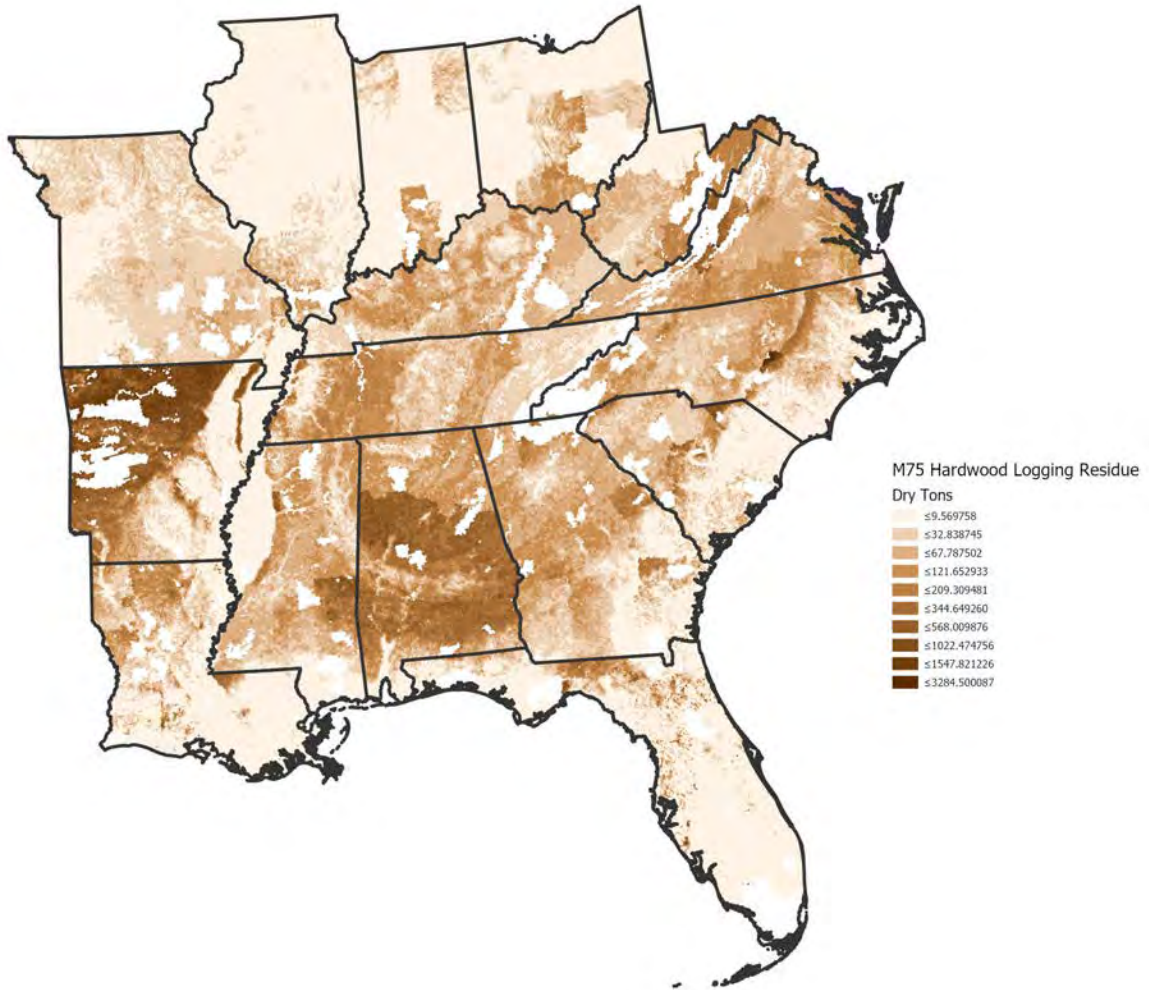
**Table 2.** Annual average hardwood and softwood timber available for energy feedstock, U.S.

	Hardwood		
	Upland and Lowland Hardwoods	Mixed Stands <sup>a</sup>	Total
	Dry tons		
Logging Residues	8,272,586	1,585,603	9,858,189
Whole Trees (pulp)	24,841,533	446,370	25,287,903
Whole Trees (Pre-pulp)	3,928,157	31,480	3,959,636
	37,042,275	2,063,453	39,105,729
	Softwoods		
	Natural and Planted Softwood	Mixed Stands	Total
Logging Residues	3,736,821	2,335,513	6,072,335
Whole Trees (pulp)	22,585,690	743,951	23,329,641
Whole Trees (Pre-pulp)	1,538,978	52,466	1,591,444
	27,861,490	3,131,930	30,993,420

<sup>a</sup> Stands identified as mixed are assumed to have 37.5% hardwood and the remainder softwood.



Panel 1. Hardwood forest residues, 50 million dry ton scenario with one mile from road limitation



Panel 2. Hardwood forest residues, 75 million dry ton scenario with three miles from road limitation

**Figure 3.** Hardwood logging residue potential in the Southeast under the 2016 Billion-Ton Report medium demand and sustainability assumptions relaxing the one mile to the road restriction.

### Milestones

- Generated data incorporated into the ASCENT Project 001 database for hardwood and softwood forest residues in the Southeast for two different sustainability scenarios.
- Developed a pine pathway for the Southeast. Examined its potential using ASCENT cellulosic pathway.
- Delivered pennycress and crush facility spreadsheet to Penn State for use in risk-reward profit sharing modeling.
- Developed economic multipliers for Fischer-Tropsch Synthetic Paraffinic Kerosene (FT-SPK); Feedstock - Conversion temp. - 1200~1600 deg. C; Product - jet and naphtha; Microsoft Excel model of economic analysis; and Alcohol to Jet Synthetic Paraffinic Kerosene (ATJ-SPK); Feedstock - yeast biocatalyst converts purified sugar to ethanol, followed by oligomerization and hydrogenation; Product - jet fuel.

### **Major Accomplishments**

A new logging residue spatial layer for hardwoods and softwoods was completed. This spatial layer contains forest residues from logging and thinning activities, along with sustainability criteria used in the 2016 Billion-Ton Report as well as relaxing the one mile to the road limitation to three miles.

### **Publications**

None

### **Outreach Efforts**

The University of Tennessee, Institute of Agriculture (UTIA) and the Commercial Aviation Alternative Fuels Initiative (CAAFI) are partnering to identify sites with optimal woody biomass and essential supply chain infrastructure because these factors present challenges for processors with limited resources to conduct site assessments with enough detail needed to attract investment capital. The initial attempt will highlight the availability of woody biomass in the region, and thereby extend its potential utilization.

### **Awards**

None

### **Student Involvement**

Alan Robertson graduated and was employed by Pilot. He worked on oilseeds and switchgrass quality.

Luis Vizcaya is working on a forest harvesting model and biorefinery siting given forest residue availability. Vizcaya was also included in the project to analyze the optimal harvest pattern of forestry residues that will be the derived supply for biorefineries.

Latif Patwary is examining potential environmental benefits.

### **Plans for Next Period**

- Complete blend study.
- Develop forest harvest model
- Complete several manuscripts.
- Continue work on forest sector.
- Develop a stochastic analysis focusing on pennycress, carinata, and camelina feasibility in the Southeast.
- Continue to work on Memphis International Airport region analysis using camelina and pennycress as feedstocks.
- Work on feedstock sustainability issues.
- Develop stakeholders for the Central Appalachia region.

## **Task 2 – Develop National Lipid Analysis**

University of Tennessee

### **Objectives**

The UT team will complete the national lipid supply availability analysis employing POLYSYS to develop information on the potential impacts and feasibility of using lipids to supply aviation fuel.

### **Research Approach**

POLYSYS will be used to estimate and assess the supply and availability of lipid feedstock options at regional and national levels. This U.S. agricultural sector model forecasts changes in commodity prices and net farm income over time. Analysis requires consistency amongst the crops. Budgets have been reevaluated for pennycress, camelina, and carinata for consistent



assumptions where possible. Yields have been compared to literature sources and cover crop estimates appear to be consistent. See yield maps (Figures 4-6) below.

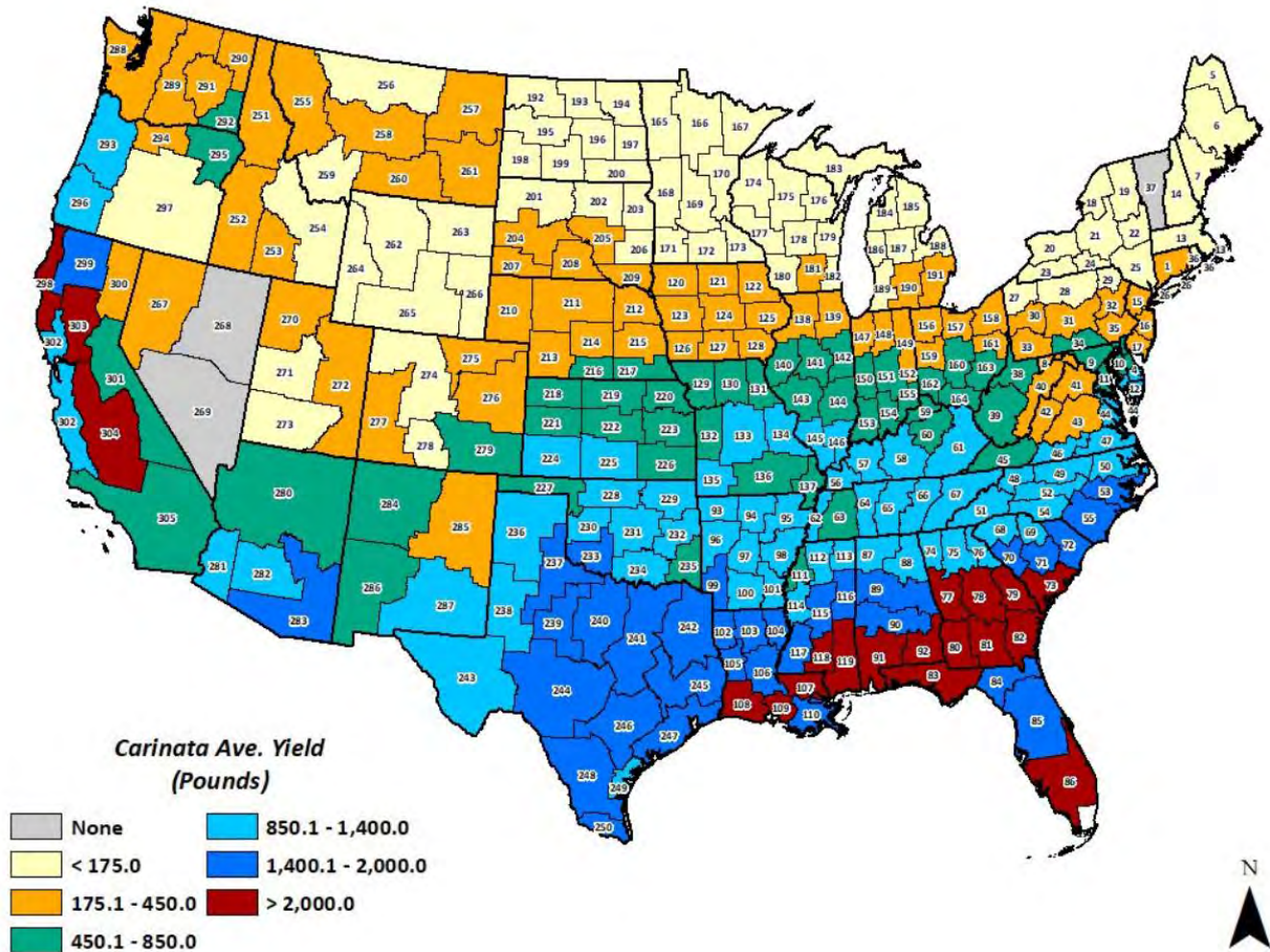


Figure 4. Yield map for carinata.

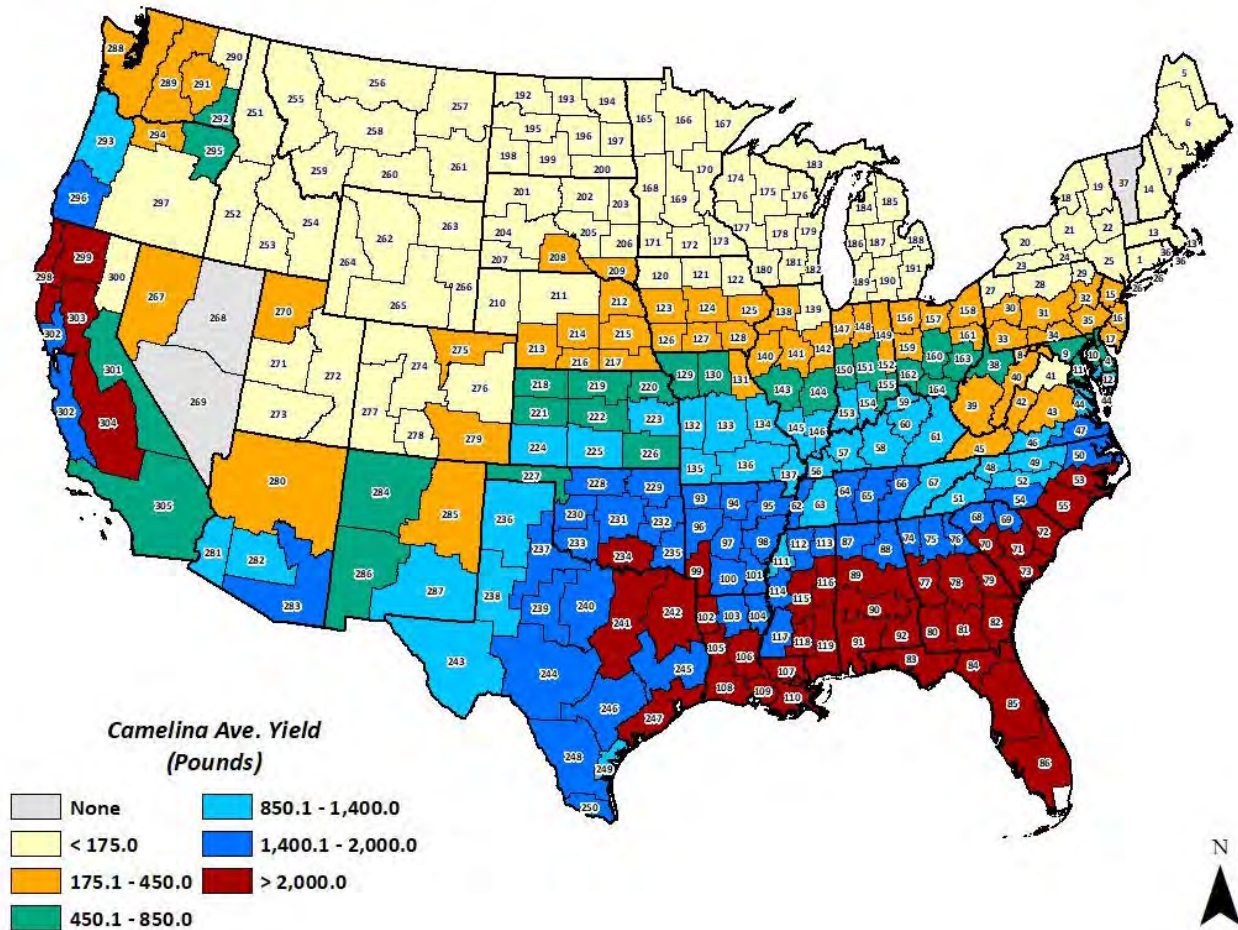


Figure 5. Yield map for camelina.

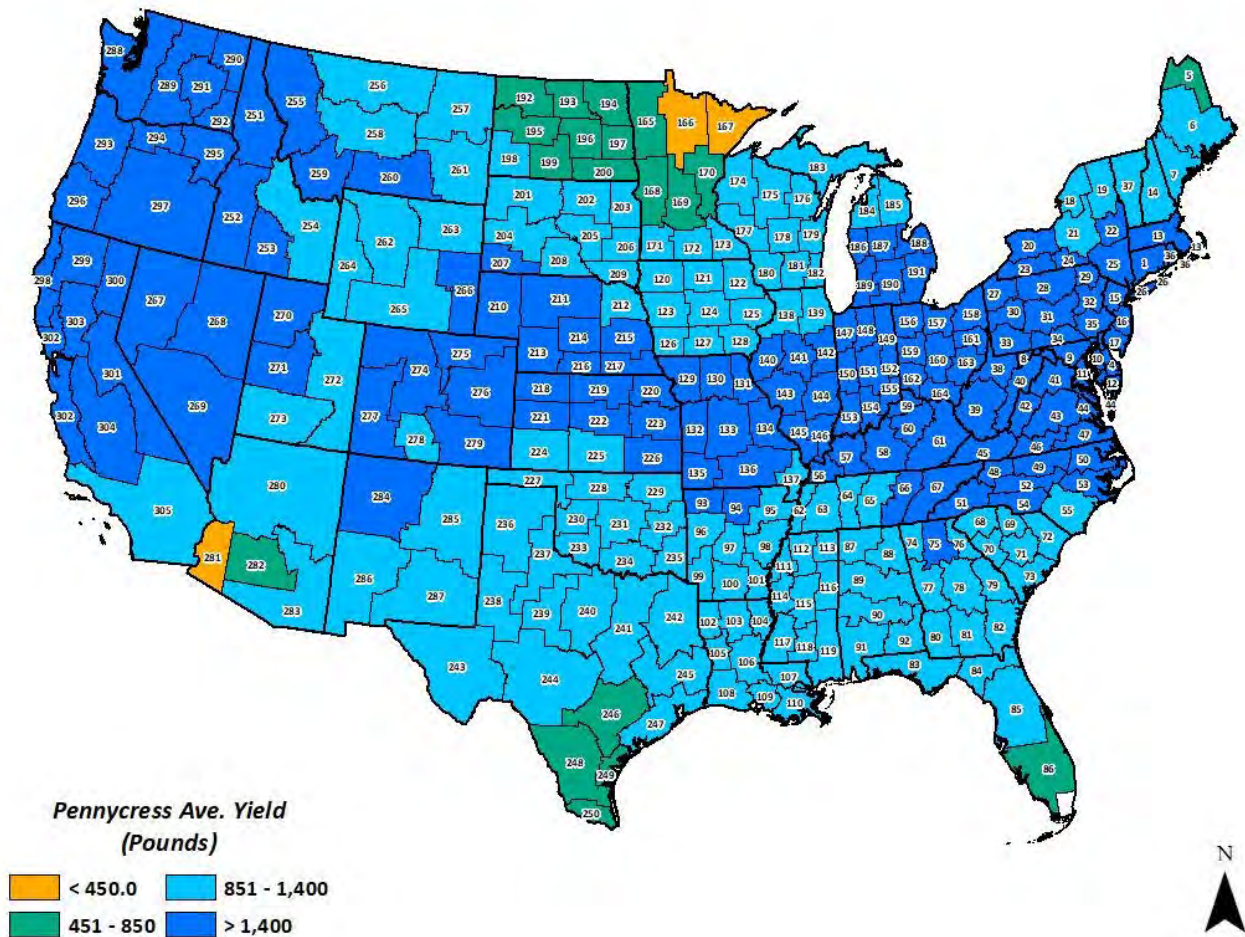


Figure 6. Yield map for pennycress.

### Milestones

This Task is behind schedule because COVID-19 has limited access to POLYSYS. The situation will improve in the next quarter. The analysis will be completed and written up for the ASCENT-organized, special issue of *Frontiers in Energy Research*, featuring the work ASCENT Project 001 has completed up to this point. The issue will include articles that provide an introduction and overview, covering sustainability as a key value proposition for SAF, feedstocks and economic sustainability, techno-economic analysis of conversion pathways, supply chain development and de-risking, environmental performance including greenhouse gas life cycle analysis (LCA) and local air quality/ emissions benefits, recent advances in indirect land use change (ILUC) modeling, ecosystem services provided by SAF pathways, SAF and social sustainability, and policy effects on deployment and sustainability performance, including future scenario analyses of the potential for deployment, targets and policies, and fuel testing/analysis and properties. The planned article, written about this project, will address both feedstock and economic sustainability of oilseed cover crops.

### Major Accomplishments

- Crops are consistent and ready to be placed into POLYSYS. Last year the POLYSYS modeling was completed to accommodate additional cover crops.
- Completed the carinata spreadsheet, incorporating risk into the analysis. The spreadsheet is under review.



- Compared the assumptions between the three oilseed crops and attempted to develop spreadsheets that contain similar price data and other assumptions.

### **Publications**

Choi, Yejun; Lambert, Dayton M.; Jensen, Kimberly L.; Clark, Christopher D.; English, Burton C.; Thomas, McKenzie. 2020. "Rank-Ordered Analysis of Consumer Preferences for the Attributes of a Value-Added Biofuel Co-Product" *Sustainability* 12, no. 6: 2363.

Trejo-Pech, C., J. A. Larson, B. C. English, and T. E. Yu. 2019. Cost and Profitability Analysis of a Prospective Pennycress to Sustainable Aviation Fuel Supply Chain in Southern USA. *Energies*, 12, no. 16: 3055.

A carinata article is in draft form.

### **Outreach Efforts**

None

### **Awards**

None

### **Student Involvement**

Alan Robertson

### **Plans for Next Period**

Complete national oilseed analysis.

## **Task 3 – Lay the Groundwork for Lipid and/or Biomass in TN and Southeastern U.S.**

University of Tennessee

### **Objectives**

The team at UT will facilitate regional deployment/production of renewable jet fuel by completing the groundwork phase of the regional oilseed feedstock to biofuel pathway and developing a proposal for regional deployment in the Southeastern U.S. and in Central Appalachia leading to the development of SAF regional deployment plans..

### **Research Approach**

- Same as Task 1 but focused on small areas such as the Central Appalachia, Memphis, and Nashville regions.
- Softwood analysis is focused on the Southeast and findings are displayed in Task 1 above.
- Developed seed trial for oilseed cover crops using funding from UT seed money. The findings will be incorporated in this report for the first year under subproject 2.

### **Central Appalachia—first year of a multi-year project**

This project was initiated about the time when COVID-19 hit. The project was rearranged to reflect laboratory closures and travel restrictions. The research approach was modified somewhat to reflect these changes. The hardwood forest residue layer was developed for BioFLAME and Freight and Fuel Transportation Optimization Tool (FTOT) (Figures 7 and 8).

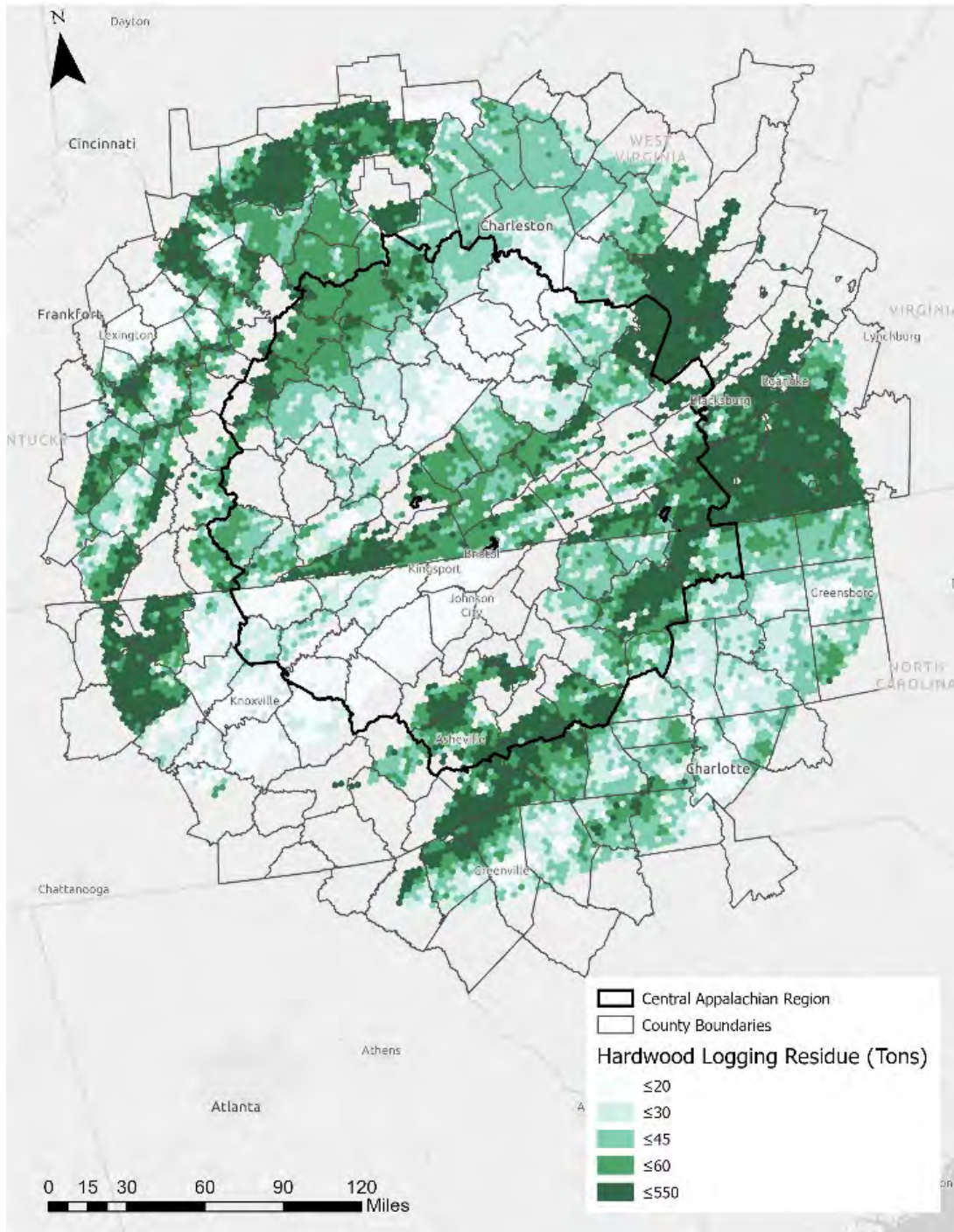
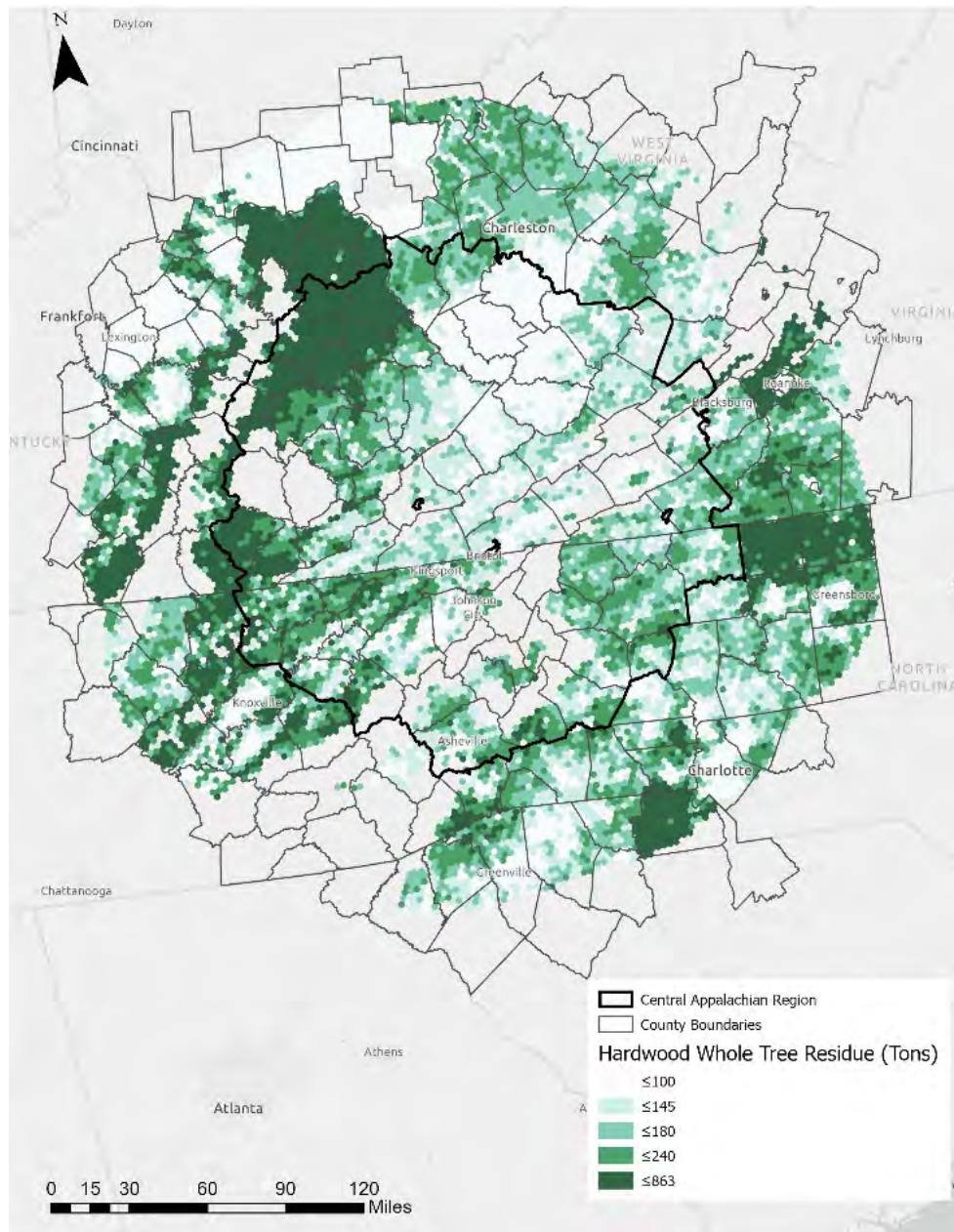
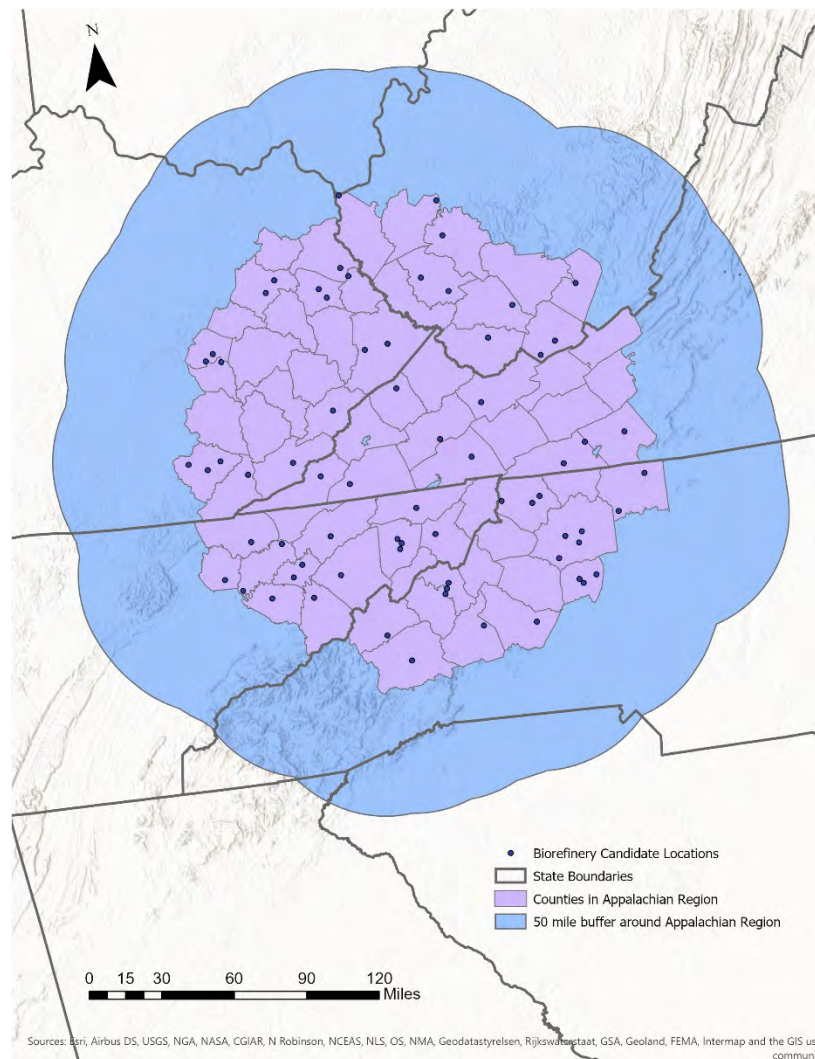


Figure 7. Estimated privately owned hardwood forest residues



**Figure 8.** Estimated whole tree, privately owned forest residue from thinning and pulpwood material.

In addition, the potential locations of a biorefinery were developed and located within the region (Figure 9). Existing sawmills were identified in the region. Contract was established with the Center for Natural Capital, and the development of stakeholder advisory board and stakeholder group has been initiated. The initial brainstorming meeting is scheduled for mid-November.



**Figure 9.** Industrial park within the Central Appalachian study region or in West Virginia at towns of a pre-specified size.

### Survey of producers

A total of 206 farmers in AL, AR, IL, KY, MO, MS, and TN responded to a survey conducted using Qualtrics and the Farm Journal contact online service.

### Survey of consumers

A survey of consumers and their use of biochar as a soil amendment was conducted. The pre-test and survey were administered online through Qualtrics, an online hosting service. A total of 771 Tennesseans responded.

### Milestones

The Nashville modeling work using cover crop oilseeds is completed. The next step will be to develop a regional deployment plan once risk and uncertainty are evaluated.

The Memphis modeling work is completed, but analysis has not begun. Analysis will be initiated during the second quarter of 2021.

**Major Accomplishments**

**Survey of producers results**

Of the survey respondents, 55% stated they would plant a cover crop (pennycress), 38% said no but they supported SAF, and 7% said no and they do not support SAF. Of the 55% of respondents who answered yes to growing pennycress, 50% of them would need to earn at least \$0.10 per pound. The farmers' concerns about growing an oilseed crop as a cover were ranked in order of concern on a 1 to 5 scale, with 5 being extremely concerned. The results are shown in Figure 10.

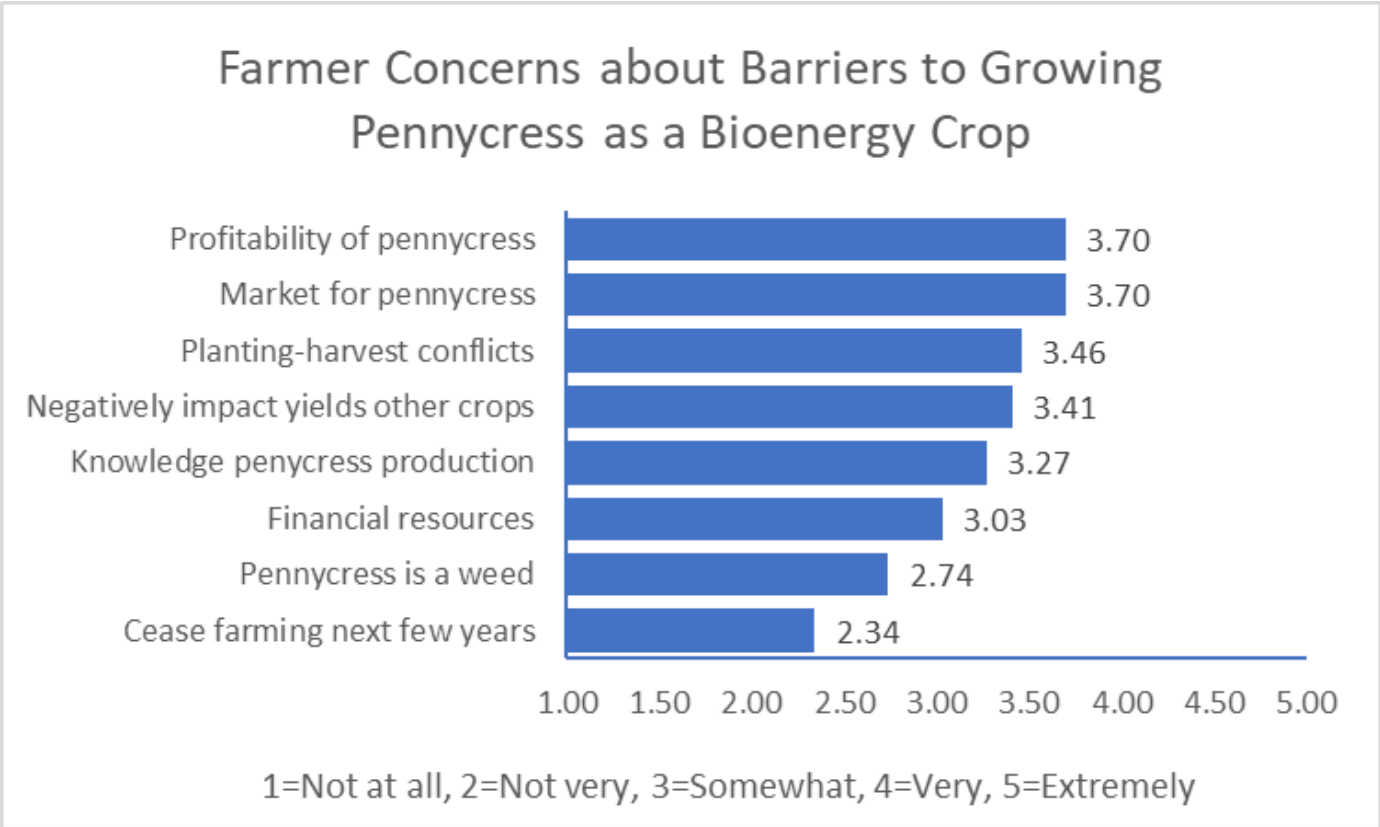


**Figure 10.** Farmer concerns about barriers to growing pennycress as a bioenergy crop.

**Survey of consumers**

The participants of the consumer biochar survey were asked to choose between two potting mix products: a conventional eight-quart bag of potting mix priced at \$4.99, and an eight-quart potting mix bag with 25% biochar priced at either \$4.99, \$6.49, \$7.99, \$9.49, or \$10.99. The estimate of willingness to pay (WTP) for a 25% biochar potting mix was \$8.52, a significant premium over the potting mix with no biochar at \$4.99. Overall, 54.42% of the respondents were willing to pay the price offered for the 25% biochar potting mix. Other factors and influences on WTP included greater percent of income spent on gardening supplies, greater potting mix purchases, likely purchase at garden centers, importance of product being a biofuel co-product, and greater concerns about climate change.

**Task 4 – Biorefinery Infrastructure and Siting (Supporting Role)**

University of Tennessee

**Objective**

Provide feedstock support to other members of ASCENT as requested.



## **Research Approach**

The research approach to Task 4 is to provide necessary input through research efforts using feedstock tools developed prior to or as a part of this project. The approach will differ as questions surface from other universities. This year, we provided input to Penn State on the cost of feedstock production, and to FTOT asking for information on feedstock availability in the Central Appalachian region. Discussions were also held about the potential of assisting Scott Q. Turn at the University of Hawaii with an economic analysis of Hawaii feedstock and conversion efforts.

## **Milestone(s)**

1. Delivered potential hardwood feedstock layer to FTOT.
2. Delivered crushing facility and pennycress budget information to Penn State for risk analysis project

## **Major Accomplishments**

See Tasks 1 and 3 above.

## **Publications**

Sharma, B. P., T. E. Yu, B. C. English, C. Boyer, and J. A. Larson. 2019. Stochastic Optimization of Cellulosic Biofuel Supply Chain under Feedstock Yield Uncertainty. *Energy Procedia*, 158: 1009-1014.

Trejo-Pech, C., J. A. Larson, B. C. English, and T. E. Yu. 2019. Cost and Profitability Analysis of a Prospective Pennycress to Sustainable Aviation Fuel Supply Chain in Southern USA. *Energies*, 12, no. 16: 3055.

Choi, Y., D. Lambert, K. L. Jensen, C. D. Clark, B. C. English, and M. Thomas, 2020. Rank-Ordered Analysis of Consumer Preferences for the Attributes of a Value-Added Biofuel Co-Product, *Sustainability*, 12, 2363.

Gill, MacKenzie, K. L. Jensen, D. M. Lambert, S. Upendram, B. C. English, N. Labbé, S. Jackson, and R. J. Menard, 2020. Consumer Preferences for Eco-Friendly Attributes in Disposable Dinnerware, *Resources, Conservation and Recycling*, Volume 161, October 2020, 104965.

Yu, T. E., B. C. English, J. Zhong, J. A. Larson, J. S. Fu, L. H. Lambert, and B. S. Wilson, 2020. High-resolution Multi-objective Optimization of Sustainable Supply Chains for a Large Scale Lignocellulosic Biofuel Industry, *Pursuing Sustainability: OR/MS Applications in Sustainable Design, Manufacturing, Logistics, & Resources*, C. Chen, V. Jayaraman, and Y. Chen, ed., Springer International Series in Operations Research and Management Science.

Lewis, K.C., E. K. News, S. Peterson, M. N. Pearlson, E. A. Lawless, K. Brandt, D. Camenzind, M. P. Wolcott, B. C. English, G. S. Latta, A. Malwitz, J. I. Hileman, N. L. Brown, and Z. Haq., 2019. U.S. Alternative Jet Fuel Deployment Scenario Analyses Identifying Key Drivers and Geospatial Patterns for the First Billion Gallons, *BioFPR*, Society of Chemical Industry and John Wiley & Sons, Ltd, December, 13, pp 471-485.

Markel, E, B. C. English, C. M. Hellwinckel, and R. J. Menard., 2019. Potential for Pennycress to Support a Renewable Jet Fuel Industry, *Ecology, Pollution and Environmental Science*, *SciEnvironm* 1:121.

Choi, Y., D.M. Lambert, K.L. Jensen, C.D. Clark, B.C. English, and M. Thomas. 2020. "Rank-Ordered Analysis of Consumer Preferences for the Attributes of a Value-Added Biofuel Co-Product. *Sustainability*, 12, 2363; doi:10.3390/su12062363.

Thomas, M., K.L. Jensen. C. Clark., B. English, D. Lambert, and F. Walker. 2019. "Tennessee Home Gardener Preferences for Environmental Attributes in Gardening Supplies: A Multiple Indicators Multiple Causation Analysis." *2019 SNA Research Conference* 63: 87-93 (refereed proceedings).

Sharma, B.P, T. E. Yu, B. C. English, C. Boyer, and J. A. Larson, Impact of Government Subsidies on a Cellulosic Biofuel Sector with Diverse Risk Preferences toward Feedstock Uncertainty, *Energy Policy*, in press.

Thomas, M.\*, K.L. Jensen, M. Velandia, C. Clark, B. English, D. Lambert, and F.Walker. 2020. "Outdoor Home Gardener Preferences for Environmental Attributes in Gardening Supplies and Use of Ecofriendly Gardening Practices." *HortTech*. Accepted, in press.



Thomas, M.\*, K. L. Jensen, C. D. Clark, D. M. Lambert, B. C. English, and F. R. Walker. 2020. "Consumer Preferences for Potting Mix with Biochar." *Journal of Cleaner Production*, in review.

Gill, Mackenzie (August 2020). Consumer Preferences for Environmentally Friendly Disposable Dinnerware Alternatives, University of Tennessee M.S. Thesis.

Patwary, A. Latif (May 2020). "Efficiency Studies of the U.S. Transportation Sector", University of Tennessee M.S. Thesis.

Robertson, A. (May 2020). "Biomass Potential in Sustainable Aviation Fuel Development: Switchgrass Production Optimization and Carinata Oilseed Enterprise Viability Analysis", University of Tennessee M.S. Thesis.

Thomas, M. (May 2019). "An Analysis of Consumer Preferences for Gardening Products with Environmentally Friendly Attributes." University of Tennessee M.S. Thesis.

### **Outreach Efforts**

Trejo-Pech, C., J. A. Larson, B. C. English, and T. E. Yu., 2019. Return and Risk Profile of a Potential Pennycress Processing Facility for the Aviation Industry, Southern Agricultural Economics Association Annual Meeting. Birmingham, AL, February 2-5.

Larson, J. A., C. Trejo-Pech, B. C. English, and T. E. Yu. 2019. Farm-level Risk Management Potential of Pennycress as a Bioenergy Cover Crop in a Corn-Soybean Rotation. Southern Agricultural Economics Association Annual Meeting. Birmingham, AL, February 2-5.

Thomas, L., K.L. Jensen, C. Clark, D. Lambert, B. English, and F. Walker. 2019. Consumers' Willingness to Pay for Potting Mix with Biochar. Selected Paper. Southern Agricultural Association Meetings, Birmingham, AL. February 2 - 5.

Choi, Y., D. Lambert, K.L. Jensen, C. Clark, B. English, and M. Thomas. 2019. "Estimating Consumer Preferences for Biochar Using Best and Worst Scaling." Selected Paper. 2019 Western Agricultural Association Meetings, Coeur D'Alene, ID. June 30-July 2.

Thomas, M., K.L. Jensen, C. Clark., B. English, D. Lambert, and F. Walker. 2019. "Tennessee Home Gardener Preferences for Environmental Attributes in Gardening Supplies: A Multiple Indicators Multiple Causation Analysis." Presentation at 2019 SNA Research Conference, Baltimore, MD, Jan. 7-8.

### **Awards**

None

### **Student Involvement**

McKenzie Thomas – Masters Graduate Student – Survey work

Luis Vizcaya – Masters Graduate Student – Modelling forest residues

Patwary, A. Latif – Masters Graduate Student – Sustainability and GHG emissions

Mackenzie Gill – Masters Graduate Student – Survey work

Ty Wolaver – Masters Graduate Student – Co-product evaluation

### **Plans for Next Period (Year)**

- Complete oilseed national analysis
- Complete farm survey analysis
- Continue to react to ASCENT Project 001 needs
- Complete Nashville deployment plan
- Respond to UT-CAAFI analysis needs
- Complete website to place simulation analysis
- Complete FTOT-BioFLAME comparison findings.
- Continue to add social capital into supply chain framework.
- Enhance economic indicator analysis.



# Project 001(F) Alternative Jet Fuel Supply Chain Analysis

## Massachusetts Institute of Technology

### Project Lead Investigator

PI: Steven R. H. Barrett  
Professor of Aeronautics and Astronautics  
Director, Laboratory for Aviation and the Environment  
Massachusetts Institute of Technology  
77 Massachusetts Ave, Building 33-322, Cambridge, MA 02139  
+1 (617) 253-2727  
sbarrett@mit.edu

Co-PI: Dr. Raymond L. Speth  
Principal Research Scientist  
Laboratory for Aviation and the Environment  
Massachusetts Institute of Technology  
77 Massachusetts Ave, Building 33-322, Cambridge, MA 02139  
+1 (617) 253-1516  
speth@mit.edu

Co-PI: Dr. Florian Allroggen  
Research Scientist  
Laboratory for Aviation and the Environment  
Massachusetts Institute of Technology  
77 Massachusetts Ave, Building 33-115A, Cambridge, MA 02139  
+1 (617) 715-4472  
fallrogg@mit.edu

## University Participants

### Massachusetts Institute of Technology (MIT)

- PI: Professor Steven R. H. Barrett
- FAA Award Number: 13-C-AJFE-MIT, Amendment Nos. 003, 012, 016, 028, 033, 040, 048, 055, 058, and 067
- Period of Performance: August 1, 2014 to August 10, 2021
- Tasks (those listed here are for the reporting period October 1, 2019 to September 31, 2020):
  1. Support U.S. participation in the International Civil Aviation Organization (ICAO) Committee on Aviation Environmental Protection (CAEP) to enable appropriate crediting of the use of sustainable aviation fuels (SAF) under the Carbon Offsetting and Reduction Scheme for International Aviation (CORSIA), especially as it relates to assessments for low-carbon aviation fuels (LCAF).
  2. Support U.S. participation in ICAO CAEP by carrying out core life cycle analysis (CLCA) to establish default values for use under CORSIA, especially for SAF produced from co-processing of biogenic feedstocks with fossil feedstocks.
  3. *Omitted; Task led by Hasselt University Team.*
  4. Develop methods for probabilistic life-cycle analyses of SAF.
  5. Support knowledge-sharing and co-ordination across all ASCENT Project 01 universities' work on SAF supply-chain analyses.

### Hasselt University (through subaward from MIT)

- PI: Robert Malina
- Period of Performance: September 1, 2016 to January 31, 2021
- Tasks (those listed here are for the reporting period October 1, 2019 to September 31, 2020):



1. Support U.S. participation in ICAO CAEP to enable appropriate crediting of the use of SAF under CORSIA especially as it relates to feedstock classification and pathway definitions.
2. Support U.S. participation in ICAO CAEP by carrying out CLCA to establish default values for use under CORSIA, especially for SAF produced using the ethanol-to-jet (ETJ) conversion technology.
3. Contribute to the development of the fuel production assessment for CORSIA-eligible fuels out to the year 2035/
4. *Omitted; Task led by MIT.*
5. *Omitted; Task led by MIT.*

## Project Funding Level

FAA provided \$3,135,000 in funding and matching funds of \$3,135,000 have been contributed by: approximately \$497,000 from MIT, plus third-party in-kind contributions of \$809,000 from Byogy Renewables, Inc., \$1,038,000 from Oliver Wyman Group, and \$791,000 from NuFuels LLC.

## Investigation Team

Principal Investigator:

Principal Investigator (Hasselt Subaward):

Co-Principal Investigator:

Postdoctoral Associates:

Research Specialist:

Graduate Research Assistants:

Prof. Steven Barrett (MIT) (all MIT tasks)

Prof. Robert Malina (Hasselt University) (all Hasselt University tasks)

Dr. Florian Allroggen (MIT) (all MIT tasks)

Dr. Raymond Speth (MIT) (Task 4)

Hakan Olcay (Hasselt University) (all Hasselt University tasks)

Gonca Seber (Hasselt University) (all Hasselt University tasks)

Katrijn Gijbels (Hasselt University) (all Hasselt University tasks)

Matthew Pearlson (MIT) (Tasks 1 and 4)

Tae Joong Park (MIT) (Task 2)

Walter Kelso (MIT) (Tasks 1 and 4)

## Project Overview

The overall objectives of ASCENT Project 01 (A01) are to (i) derive information on regional supply chains to explore scenarios for future sustainable aviation fuel (SAF) production, and (ii) identify supply chain-related obstacles to commercial-scale production in the near term, and larger-scale adoption in the longer term.

For the assessment year (AY) 2019/20, the MIT/Hasselt University team contributed to these goals by: (1) providing leadership in the context of the International Civil Aviation Organization Committee for Aviation Environmental Protection (ICAO CAEP) core life cycle analysis (CLCA) task group of the Fuels Task Group (FTG), which is mandated to calculate lifecycle greenhouse gas (GHG) emissions associated with SAF use under the Carbon Offsetting and Reduction Scheme for International Aviation (CORSIA); (2) carry out CLCA analyses to enable the inclusion of additional SAF pathways under CORSIA; (3) contribute to the methodological development and analysis of SAF availability out to 2035 in the context of the Technology, Production & Policy (TPP) task group of FTG; (4) develop probabilistic estimates of life cycle GHG emissions for a number of SAF pathways; and (5) provide support for coordination of the A01 team.

## Task 1 – Co-lead and Support U.S. Participation in ICAO-CAEP to Enable Appropriate Crediting of the Use of SAF Under CORSIA

Massachusetts Institute of Technology

Hasselt University

### Objectives

The overall objective of this task is to provide support to the FAA in their engagement with the ICAO CAEP FTG (during CAEP/12). The specific focus of the work during this reporting period was to (1) refine feedstock classifications; and (2) support the discussion leading toward the development of a CLCA method for LCAF.

## **Research Approach**

In order to achieve the goals outlined above, the team continued to co-lead the Core LCA Task Group of FTG. Prof. Malina acted as a co-lead. This role ensures that Prof. Malina can act as a focal point of CLCA research, so that the specific research tasks can be guided efficiently and effectively. The following research has been conducted in support of the leadership role:

### **Feedstock classifications**

During CAEP/11, the Alternative Fuels Task Force (AFTF) established a process for defining feedstocks as either primary, residues, wastes, or by-products. An initial list of feedstocks in each of these categories was agreed upon. However, it was recognized that the list is incomplete. Under the leadership of the co-lead of the core LCA group, Professor Malina, FTG continuously updates this list during CAEP/12.

### **Pathway definitions**

Under the leadership of the core LCA task lead, Professor Malina, a review of assumptions made in the development of default core LCA values has been conducted. This review aimed to understand if Sustainable Certification Schemes (SCS) require additional guidance on the applicability of a certain default value. The results of this assessment will be discussed at the FTG/6 meeting (AY20–21).

It was found that the publicly available ICAO document "CORSIA SUPPORTING DOCUMENT CORSIA Eligible Fuels – Life Cycle Assessment Methodology" already contains definitions within the sections for the different CORSIA-eligible fuels. For example, these sections contain definitions of the feedstocks for which default core LCA values have been calculated (a definition of used cooking oil, corn oil, palm fatty acid distillate (PFAD), etc.). These sections can be used as a concise source of reference and guidance by the SCS. Based on an analysis of how much the assumptions incorporated into the default pathway influence LCA calculations, several additional clarifications have been recommended to ensure that default values are applied appropriately to a SAF pathway. Recommendations included facility type definitions for the ethanol-to-jet (ETJ) pathway, definitions of open and closed pond palm hydroprocessed esters and fatty acids (HEFA) pathways and updated definitions of agricultural residue pathways, specifically with regard to additional nutrient replacement requirements on the primary crop.

### **Assessment of LCAF**

In preparation of the FTG/04 Meeting, MIT outlined potential technologies and practices to produce LCAF and quantified potential cost and GHG emission impacts. The work was conducted in collaboration with Argonne National Laboratory (ANL). MIT evaluated renewable electricity use at the crude oil field, while ANL evaluated renewable hydrogen use at the refinery, and carbon capture and sequestration (CCS) at the refinery.

More specifically, MIT analyzed the costs and potential reduction of lifecycle impacts associated with electrification of oil field operations and on-site production of electricity from renewable sources. The Uthmaniyah oil field (1.6 million barrels of crude daily output from 472 producing wells) located in Eastern Saudi Arabia was chosen for the case study. The LCA results are presented in terms of the amount of GHG emissions for each megajoule (MJ) of oil produced ( $\text{gCO}_2\text{e/MJ}$ ). The techno-economic analysis (TEA) results are presented in terms of change in minimum selling price per barrel of crude oil produced when LCAF technologies are implemented. GHG abatement costs are derived from the TEA and LCA results.

#### ***Electricity demand at oil field***

MIT analyzed the potential for electrification and on-site production of renewable electricity (i.e., solar electricity) to meet electricity demand at the Uthmaniyah oil field. The electricity requirements and emissions at the field were computed using the Oil Production Greenhouse gas Emissions Estimator (OPGEE) model. OPGEE is a peer-reviewed, publicly available, and editable LCA tool for the measurement of GHG emissions from the production, processing and transport of crude petroleum. Specifically, OPGEE v2.0b and inputs for the Uthmaniyah field from Masnadi et al., (2018) were used.

In the baseline scenario, in which no additional processes at the field are electrified, 463 MWh of electricity are used daily in the field, mainly for water treatment, pumps, and air coolers for gas processing. When the downhole pumps are powered by 600 hp electric motors instead of natural gas (NG) engines, the daily electricity required at the field increases to 4.931 GWh.

#### ***Power generation and storage system sizing***

The assumed power generation system is composed of a photovoltaic (PV) array consisting of monocrystalline solar modules. Complete specifications for the PV system follow Almarshoud (2016). Global Horizontal Irradiance (GHI) and temperature

data are available in 5-minute intervals from the Solar Village in Saudi Arabia for the year 2002 (NREL, n.d.). The PV system is sized such that it produces enough electric energy during the daytime to meet instantaneous electricity demand from the oil field and charge an energy storage system (i.e., a battery system) which covers the night-time electricity demand of the field. The system is sized under four assumptions for back-up power. Under the worst-case sizing assumption, electricity production meets daily electricity demand in the oil field on all days using the year-2002 irradiance data. Under the 1st percentile case, the PV array is sized to meet electricity demand on 99% of the days (361 days). On the remaining days of the year, electricity is imported from the grid. The 5th and 10th percentile case are defined accordingly.

The electricity storage system is sized to store the electric energy to sustain night-time operations of the oil field and is composed of lithium-ion batteries. Based on the specifications of the battery system and the night-time electricity requirements at the field, the required minimum battery storage capacity is found to be 3.6 GWh.

**Costs of PV and battery system**

Discounted cash flow analysis is used to determine the increase in jet fuel selling price associated with electrification of oil well operations (i.e., downhole pumps) and production of renewable electricity at the well. The analysis is run over a 20-year period which reflects the assumed lifetime of the PV system. All costs are adjusted to year-2020 USD and are allocated to products by output volume.

Capital cost, construction labor cost, land cost and operation cost for the PV and inverter system are taken from Apostoleris et al., (2018). A Weighted Average Cost of Capital (WACC) of 7.5% is assumed, in line with the current WACC of large petrochemical companies. Utility scale lithium-ion battery storage capital, installation labor, and structural balance of system costs are taken from Fu et al., (2018), fixed and operating costs are from Mongrid (2019), and future capital cost reductions are from Cole and Frazier (2019). Labor costs are reduced by 50% relative to U.S. benchmarks due to lower labor costs in Saudi Arabia (Apostoleris et al., 2018).

Lifetimes and costs for electric motors and gas-powered engines are taken from Frazier (2014). Additionally, excess natural gas, which was previously used for combustion, and excess generated electricity is exported from the field at market value.

**Minimum selling price impacts**

Table 1 shows the increase in selling price per barrel of crude oil input for the four PV sizing scenarios, both with and without the additional revenue streams from selling excess natural gas and electricity.

**Table 1. MSP impacts for PV array sizing assumptions (\$/bbl of crude oil)**

PV Sizing Assumption	MSP Impact [USD per barrel of crude oil]	MSP revenue adjustments *		Net-cost-based MSP impact [USD per barrel of crude oil]
		Natural Gas Sales [USD per barrel of crude oil]	Electricity Sales [USD per barrel of crude oil]	
Worst Case	1.13	0.03	0.50	0.60
1 <sup>st</sup> Percentile	0.53	0.03	0.15	0.35
5 <sup>th</sup> Percentile	0.36	0.03	0.05	0.28
10 <sup>th</sup> Percentile	0.32	0.03	0.02	0.27

\* Note that the cost estimate disregards potential investments required for connecting the oil field to the grid

**Life cycle GHG analysis of renewable electricity at the oil field**

Well-to-refinery emissions at the oil field are modeled with OPGEE v.2.0b using the implemented assumptions for the Uthmaniyah oil field. Table 2 shows the break-down of well-to-refinery emissions for the baseline case, and the worst-case PV sizing scenario. In the renewable electricity scenario, combustion emissions are reduced due to the elimination of the natural gas engines, and offsite emissions are reduced because electricity is produced from renewable sources.



**Table 2.** Breakdown of Well-to-Refinery Emissions

GHG Emissions Source	Baseline (gCO <sub>2</sub> e/MJ)	Renewable Electricity (gCO <sub>2</sub> e/MJ)
Combustion	0.58	0.29
Venting and Flaring	2.41	2.40
Land Use	1.14	1.14
Transport	1.27	1.26
Small Source	0.50	0.50
Offsite Emissions	0.25	0.21
<b>Total</b>	<b>6.16</b>	<b>5.80</b>

Additionally, the sensitivity of the lifecycle emissions reductions to the PV sizing assumption are calculated because smaller PV systems will require additional back-up power with non-zero emissions index. As shown in Table 3, this impact was found to be small.

**Table 3.** Potential well-to-refinery carbon intensity (CI) reduction for PV array sizing assumptions

PV Sizing Assumption	Average Daily CI (gCO <sub>2</sub> e/MJ)
Worst Case	5.80
1 <sup>st</sup> Percentile	5.80
5 <sup>th</sup> Percentile	5.80
10 <sup>th</sup> Percentile	5.81
<b>CI Reduction from Baseline</b>	<b>0.35-0.36</b>

**Abatement costs**

The results from the cost and emissions analysis are combined to derive the abatement cost of one unit of CO<sub>2</sub>-equivalent emissions. The results are shown in Table 4. Additionally, Table 4 shows the impact of natural gas and electricity exports on the cost of avoided CO<sub>2</sub> in the renewable electricity scenario.

**Table 4.** Costs of avoided CO<sub>2</sub> for PV array sizing assumptions (\$/tonne CO<sub>2</sub> avoided)

PV Sizing Assumption	CO <sub>2</sub> e abatement costs, <i>no additional energy export revenue</i> (in USD per tCO <sub>2</sub> e)	CO <sub>2</sub> e abatement costs, <i>net impact after energy export revenue</i> (in USD per tCO <sub>2</sub> e)
Worst Case	547	290
1 <sup>st</sup> Percentile	258	171
5 <sup>th</sup> Percentile	176	138
10 <sup>th</sup> Percentile	159	132

**Summary of results**

Table 5 provides a summary of the MIT results from above, as well as the results for the other LCAF technologies assessed by ANL.

**Table 5. Summary of case study results**

LCAF Technologies	Reductions in CI [gCO <sub>2</sub> e/MJ]	Changes in cost [\$/gal]	Abatement cost [\$/tCO <sub>2</sub> e]
Renewable energy use at oil field [Uthmaniyah oil field]	0.35 - 0.36	0.006 - 0.013 <sup>a</sup>	132 - 290
Carbon capture in the refinery	3.86	0.09	171
Hydrogen from renewable sources in the refinery	0.54	0.014	190

<sup>a</sup> Calculated as net change in minimum selling price for jet fuel after additional revenue streams from additional sales of natural gas and electricity.

### **Milestones**

The work described above has been documented in numerous Working Papers and Information Papers submitted to the FTG. This includes FTG/02 (Montreal, September 2019), FTG/03 (Abu Dhabi, February 2020), FTG/04 (Virtual, June 2020), and FTG/05 (Virtual, July 2020). Team members from Hasselt University and MIT participated in and contributed to all meetings.

### **Major Accomplishments**

The MIT and Hasselt University team accomplished the following under this task:

1. As co-lead of the FTG-CLCA Task Group, Prof. Malina drafted CLCA progress reports to all FTG meetings during the current reporting period and co-lead several Task Group meetings.
2. The team submitted Information Paper (IP08) to FTG/04, which summarized the findings of the analysis on LCAF. The LCAF abatement cost analysis will allow assessments of economic viability and will facilitate comparisons between LCAF and biofuels.
3. The team contributed to the FTG report to SG2020/2, outlining the progress made within the core LCA and TPP tasks.

### **Publications**

- CAEP/12-FTG04-IP08. Potential LCAF Technologies and Practices. June 2020.
- CAEP/12-FTG/02-WP/06. Summary of the work of CLCA-TG since FTG/01. September 2019.
- CAEP/12-FTG/03-WP/04. Summary of the work of CLCA-TG since FTG/02. February 2020.
- CAEP/12-FTG/04-WP/05. Summary of the progress of the Core LCA Subgroup since FTG/03. June 2020.
- CAEP/12-FTG/05-WP/02. Summary of the progress of the Core LCA Subgroup since FTG/04. July 2020.

### **Outreach Efforts**

Progress on these tasks was communicated during weekly briefing calls with the FAA and other U.S. delegation members to FTG, as well as during numerous FTG teleconferences between meetings.

### **Awards**

None.

### **Student Involvement**

During the reporting period, the MIT graduate student involved in this task was Walter Kelso.

### **Plans for Next Period**

In the coming year, the MIT ASCENT Project 1 team will continue its work in FTG. Default core LCA values will be calculated and proposed for additional pathways. Prof. Robert Malina will continue to lead the core LCA Task Group. Work on pathway definitions and LCAF are currently expected to be the focus of attention. The work of the core LCA Task Group during CAEP/12 will be summarized in a series of working and information papers presented to FTG.

### **References**

- Almarshoud, A. (2016). Performance of solar resources in Saudi Arabia. *Renewable and Sustainable Energy Reviews*, 66, 694-701



- Apostoleris, H., Sgouridis, S., Stefancich, M., & Chiesa, M. (2018). Evaluating the factors that led to low-priced solar electricity projects in the Middle East. *Nature Energy* 3, 1109-1114.
- Cole, W. & Frazier, A. (2019). Cost Projections for Utility-Scale Battery Storage. *NREL Technical Report* NREL/TP-6A20-73222.
- Fraizer, R. (2014). Comparative Energy Costs for Irrigation Pumping. Retrieved from <http://pods.dasnr.okstate.edu/docushare/dsweb/Get/Document-2979/BAE-1204web.pdf>
- Fu, R., Remo, T., & Margolis, R. (2018). 2018 U.S. Utility-Scale Photovoltaics-Plus-Energy Storage. Retrieved from <https://www.nrel.gov/docs/fy19osti/71714.pdf>
- Masnadi, M. S., El-Houjeiri, H. M., Schunack, D., Li, Y., Englander, J. G., Badahdah, A., ... & Brandt, A. R. (2018). Global carbon intensity of crude oil production. *Science* 361(6405), 851-853.
- Mongrid, K. (2019). Energy Storage Technology and Cost Characterization Report. Retrieved from [https://www.energy.gov/sites/prod/files/2019/07/f65/Storage Cost and Performance Characterization Report\\_Final.pdf](https://www.energy.gov/sites/prod/files/2019/07/f65/Storage_Cost_and_Performance_Characterization_Report_Final.pdf)
- NREL (n.d.): NASA Remote Sensing Validation Data: Saudi Arabia. (n.d.). Retrieved from <https://www.nrel.gov/grid/solar-resource/saudi-arabia.html>

## Task 2 – Support U.S. Participation in ICAO CAEP by Carrying out CLCA to Establish Default Values for Use Under CORSIA

Massachusetts Institute of Technology  
Hasselt University

### Objective

During AY 2019/20, the team carried out attributional CLCA to establish or validate default values for use under CORSIA. During the CAEP/11 cycle, the MIT ASCENT Project 1 team took leadership in applying the agreed-upon CLCA method to establish default CLCA values for 26 unique pathways. However, the list of 26 pathways is not exhaustive, and further CLCA analysis is required to enable inclusion of SAF technologies that are nearing commercialization. During the current reporting period, the team supported the calculation of default CLCA values for fuels which are produced from co-processing of biogenic feedstocks and fossil feedstocks in conventional refineries. In addition, the team contributed towards the verification of a set of eight ethanol-to-jet production pathways.

### Research Approach

#### Co-processing

Co-processed fuels are produced by upgrading biogenic feedstocks to jet fuel alongside petroleum feedstock in existing refineries. In their current specification (ASTM D1655-20, A.1.2.2 (ASTM International, 2020)), ASTM allows co-processed jet fuels to be produced by co-processing mono-, di-, triglycerides, free fatty acids, and fatty acid esters as biogenic feedstocks at up to 5% inputs by volume through either hydrocracking or hydrotreating and fractionation. For our initial analyses, we limited the scope of pathways under investigation to hydroprocessing via hydrotreater or hydrocracker, dependent upon the biogenic feedstocks and petroleum derived distillates used. A simplified refinery configuration example using middle distillates and a hydrotreater is shown in Figure 1.

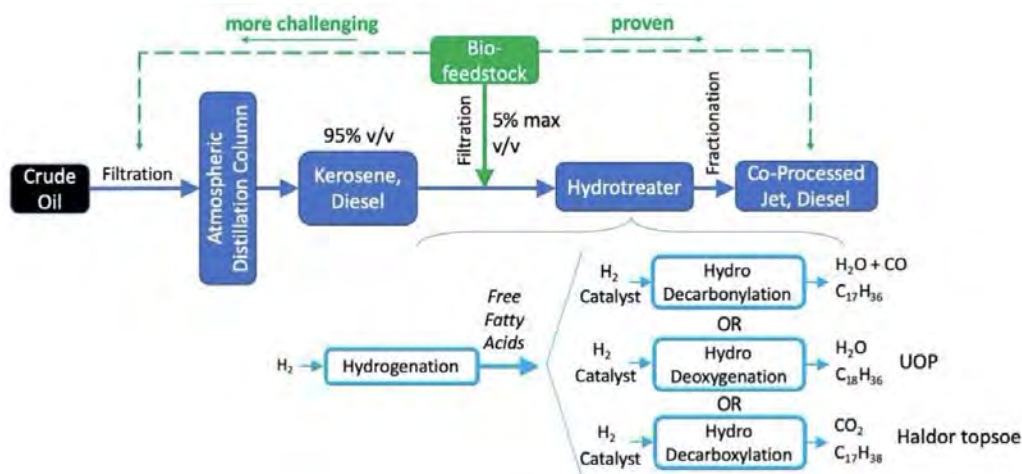


**Figure 1.** Illustration of co-processing of HEFA bio-feedstock with middle distillates.

The initial list of feedstocks (Table 6) follows the HEFA SAF feedstocks for which CLCA values have been published (ICAO, 2019). Co-processing is not limited to these feedstocks and the analysis can be expanded to include other feedstocks.

**Table 6.** List of HEFA feedstocks to be considered for co-processing

Feedstock	Type	Details
Used cooking oil (UCO)	Waste	Cooked vegetable oil
Tallow	By-product	Fats from cattle slaughtering
Palm fatty acid distillate		Stripped from crude palm oil during refined palm oil production
Corn oil	Main	Extracted from distillers dry grains/solubles
Oil crops		Soybean, canola/rapeseed, camelina
Palm oil		Closed (w/methane capture) or open pond (w/o methane capture)
Brassica Carinata		Primary summer crop in US/Canada

*Conceptual questions for calculating the lifecycle emissions of jet fuel produced from co-processing*

LCA analysis of co-processed fuels was found to require addressing the following four conceptual questions:

1. **Process yield/bio-yield calculations:** The goal of the yield analysis is to determine both the total output fuel volume and biogenic fuel volume which results from the addition of biogenic feedstock into the refinery. The potential approaches for the analysis include: a mass balance approach that accounts for process efficiencies; an energy balance which assumes the input feedstock fractions to apply to the outputs; and carbon dating.
2. **GHG emissions savings:** A potential approach for analyzing the lifecycle emissions of co-processed fuels is to analyze the incremental changes of GHG emissions as compared to a refinery configuration without co-processing of biogenic feedstocks. GHG emissions savings are then calculated as the sum of the changes in GHG output associated with inputs such as natural gas, hydrogen, or electricity, with by-products or waste streams, and with the emissions of petroleum-derived fuels. We note that the CORSIA CLCA method assumes combustion emissions of the biogenic fuel portion to be zero (ICAO, 2019).
3. **Eligible SAF volume:** In the regulatory framework, the regulator needs to determine which portions of fuel are considered as the eligible SAF volume. The conceptual options include the (estimated) biogenic portion of the fuel output or the total fuel output (including both the petroleum-derived and biogenic fractions).
4. **GHG allocation:** Since refineries produce multiple products, GHG emissions need to be allocated to the different products. This step can be completed through (1) proportional attribution following mass or energy of the output fuel portion; (2) carbon dating to directly measure biogenic content in the output fuel; or (3) free attribution which allocates the carbon saving to any chosen portion of the output fuel.

Fuels produced through co-processing are considered in existing regulatory frameworks including the California Low Carbon Fuel Standard (LCFS). For yield calculations under the LCFS, fuel producers can apply carbon dating, a total or carbon mass balance-based method, and an input biogenic energy content method (CARB, 2017A; CARB, 2017B). For computing CI, a default value approach is used which relies on average refining emissions of conventional fuel production, output energy content allocation, or hybrid marginal allocation by calculating the energy use difference between baseline and co-processing production. Other methods not outlined by CARB may also be allowed but are subject to approval (California LCFS, 17 CCR §95491 (d) (C)). CARB requires both the biogenic and total output fuel CIs to be reported (California LCFS, 17 CCR §95488.4). Other regulatory frameworks that include co-processed fuels include the International Sustainability & Carbon Certification System (ISCC) which suggests using an energy balance and/or carbon dating approach for yield analyses (ISCC, 2016).

During the reporting period, MIT conducted an analysis of the sensitivity of CLCA values to the different conceptual choices outlined above. The analyses are illustrative in nature and do not provide guidance on the expected lifecycle values for co-processed fuels. The work was conducted on the basis of two publications: Bezergianni et al., (2014), which showed laboratory experimental results of co-processing heavy atmospheric gas oil (HAGO) with UCO at 4.8% v/v, and Garrain et al., (2014), which showed refinery experimental results of co-processing diesel distillate with soybean oil at 9.6% v/v. We assumed that the soybean/diesel case would still provide valuable insight despite exceeding the ASTM limit of 5% v/v biogenic input feedstock. Both studies present data for producing co-processed renewable diesel, and we assumed no additional resource use for upgrading to jet fuel.

The HAGO/UCO case resulted in a lifecycle impact of 7.8 gCO<sub>2</sub>e/MJ for the 0.039 kg biogenic portion and 84.8 gCO<sub>2</sub>e/MJ for the 0.788kg entire jet fuel output. This result confirms that the definition of the eligible fuel will have significant impacts on the availability and lifecycle impact associated with the eligible fuel. We note that only one output fuel is reported in Bezergianni et al., thus only this single set of values is presented. A summary of the results for the soybean/diesel case is shown in Table 7. The results confirm the high sensitivities to the different conceptual choices outlined above.

**Table 7.** LCA sensitivities and associated eligible fuel volumes for the diesel/soybean case, jet only

GHG allocation approach	Eligible fuel	Eligible fuel mass (kg)	Lifecycle emissions (gCO <sub>2</sub> e/MJ)
Energy-based	All co-processed jet fuel	42,735	86.7
Energy-based	Biogenic diesel portion only	3,519	60.5
Total-mass-based	All co-processed jet fuel	42,735	86.6
Total-mass-based	Biogenic diesel portion only	3,519	60.3
Carbon-mass-based	All co-processed jet fuel	42,735	88.1
Carbon-mass-based	Biogenic diesel portion only	3,519	72.0
Free attribution to Jet	All co-processed jet fuel	42,735	86.4
Free attribution to Jet	Biogenic diesel portion only	3,519	57.8

*Two approaches for computing the lifecycle impacts of co-processed fuels*

We outlined two approaches to perform the default CLCA value calculations:

- **Bottom-up approach:** This method calculates CIs from detailed process data for each well-to-wake process step. The approach is similar to the approaches for SAF pathways described in ICAO (2019). An example process diagram for the biogenic portion of a fuel produced from co-processing tallow is shown in Figure 2. During the reporting period, MIT supported ANL in setting up a linear programming study to help obtain the data for a bottom-up assessment from refinery modeling.

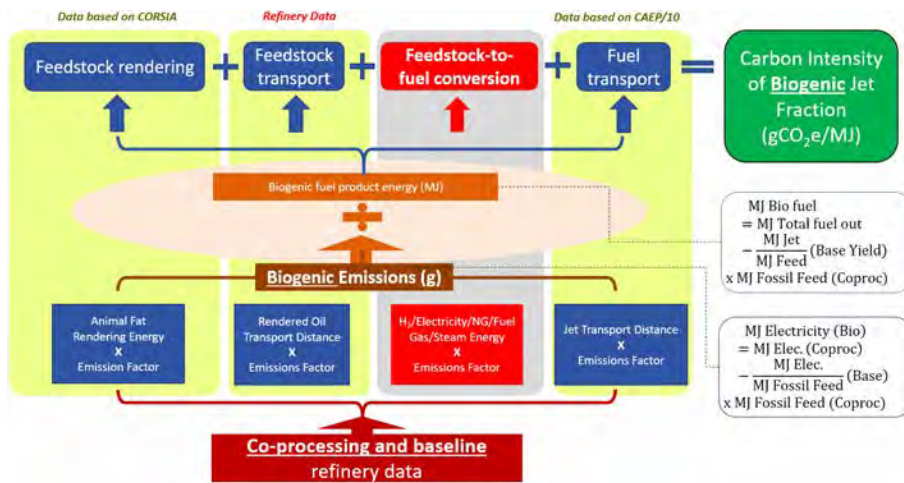


Figure 2. Bottom-up approach outline for calculating carbon intensity of biogenic jet fraction.

- Top-down approach:** This method relies on (published) CI data for certain process steps, which are adjusted to reflect the specific conditions of the production process under investigation. As such, it does not derive CIs from detailed process data (e.g., GHG emissions associated with heavy duty truck transport of fuel). For example, existing data from existing SAF assessments could be combined with data from an approved application to the Californian LCFS for producing co-processed renewable diesel using tallow at BP Cherry Point, WA (CARB, 2019). The resulting calculation method is outlined in Figure 3. Due to a lack of published data, this method was determined to be viable for validating results from a detailed bottom-up analysis only.

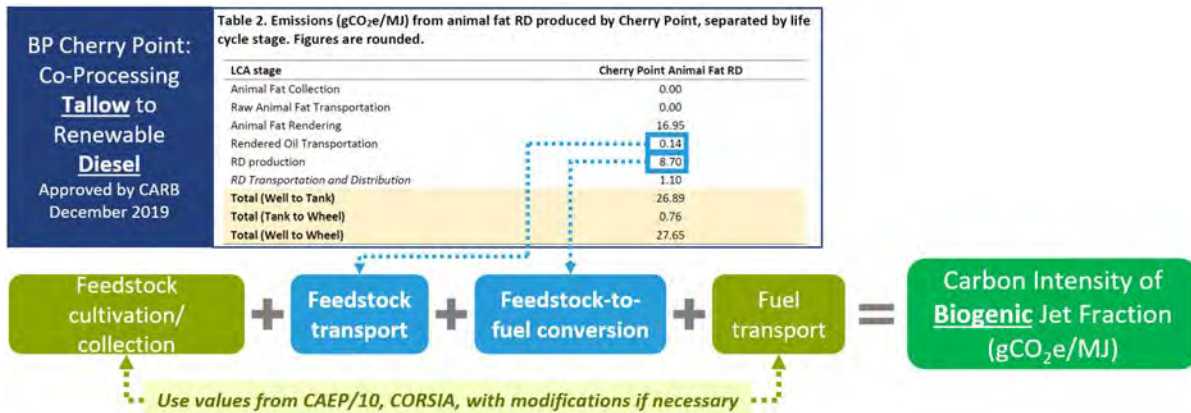


Figure 3. BP Cherry Point tallow co-hydrotreating report data and top-down approach outline.

### CLCA Validation and verification

The Hasselt University (UHasselt) team served as the verifier for a set of eight new core LCA pathways based on (EtJ) conversion technologies. Separate default core LCA values were calculated for four types of feedstocks and two distinct conversion technologies (integrated EtJ and stand-alone EtJ process).

Core LCA values for EtJ pathways from agricultural residues, forest residues, miscanthus, and switchgrass were modelled and the resulting default CLCA values were proposed at FTG/4 initially. Because the heat integration assumption in ethanol and jet fuel production changes the CLCA values significantly, two sets of default CLCA values for the standalone (without heat integration) and integrated (with heat integration) pathway were proposed. The CLCA TG used the same inputs and outputs of the EtJ process for calculating the approved default CLCA values of the approved corn grain EtJ pathway.

Since FTG/3, the core LCA modelling groups, including Hasselt University, reviewed the standalone EtJ process through an extensive literature review and collected a life-cycle inventory of the EtJ process from various research papers. With the literature review, detailed analyses, and discussion among the modeling group and industry, the CLCA modeling group has included the dataset provided by LanzaTech and two more life-cycle inventories. The modelers used the average datasets for the standalone pathways within the Greenhouse Gases, Regulated Emissions, and Energy Use in Technologies (GREET) model. The calculations have been verified by Hasselt University and approved by the modelling team from the three institutions. Table 8 shows the approved default core LCA values for the four standalone EtJ pathways.

**Table 8.** Default CLCA values for FTG approval for the standalone EtJ pathways

Technology	Feedstock	Data source	Model	Feedstock collection	Feedstock transportation	Jet fuel production	Jet fuel transportation	Total emissions	Proposed default CLCA values
Standalone	Agricultural residues	Consensus model	GREET	3.5	3.1	32.7	0.4	39.7	<b>39.7</b>
	Forest residues	Consensus model	GREET	1.8	2.4	35.5	0.4	40.0	<b>40.0</b>
	Miscanthus	Consensus model	GREET	8.8	1.4	32.7	0.4	43.3	<b>43.3</b>
	Switchgrass	Consensus model	GREET	9.6	1.2	32.7	0.4	43.9	<b>43.9</b>

In order to guarantee consistency in the final results, the CLCA values of the four EtJ pathways with the integrated design were recalculated, using the appropriate parts of the agreed-upon life-cycle inventories for the standalone design pathways. ANL was the modeler of this pathway, with UHasselt serving as verifying institution. Table 9 shows the approved default core LCA values for the integrated EtJ pathways.

**Table 9.** Default CLCA values for FTG approval for the integrated EtJ pathways

Conversion Design	Feedstock	Data source	Model	Feedstock collection	Feedstock transportation	Jet fuel production	Jet fuel transportation	Total emissions	Proposed default CLCA values
Integrated	Agricultural residues	Consensus model	GREET	3.6	3.2	17.4	0.4	24.6	<b>24.6</b>
	Forest residues	Consensus model	GREET	1.8	2.4	20.3	0.4	24.9	<b>24.9</b>
	Miscanthus	Consensus model	GREET	9.0	1.4	17.4	0.4	28.3	<b>28.3</b>
	Switchgrass	Consensus model	GREET	9.8	1.2	17.4	0.4	28.9	<b>28.9</b>

**Milestone**

The work described above has been documented in numerous Working Papers and Information Papers submitted to the FTG. This includes paper for FTG/02 (Montreal, September 2019), FTG/03 (Abu Dhabi, February 2020), FTG/04 (Virtual, June 2020), and FTG/05 (Virtual, July 2020). Team members from Hasselt University and MIT participated in and contributed to all meetings. In addition, progress on the co-processing analysis was presented at the Spring ASCENT meeting (Virtual, March 2020).

**Major Accomplishments**

The MIT and Hasselt University team accomplished the following under this task:

1. The team submitted and presented working paper WP/06 to FTG/02.
2. The team submitted and presented information paper IP/07 and working paper WP/04 to FTG/03, which summarize approaches and challenges for CLCA analyses of co-processed fuels.



3. The team submitted and presented information paper IP/07 and working paper (WP/05) to FTG/04, which proposed the bottom-up and top-down approach for calculating CLCA values for co-processed fuels.
4. The team submitted and presented working paper WP/02 to FTG/05, which reported progress towards working with fuels industry experts towards obtaining data and better understanding of methods.
5. The team presented "Updates on Lifecycle Analysis: Methods for Analyzing Co-processing and for Systematically Capturing Uncertainty" at the Spring ASCENT meeting.

## **Publications**

### **Written reports**

CAEP/12-FTG/02-WP/06. Summary of the work of CLCA-TG since FTG/01. September 2019.

CAEP/12-FTG/03-IP/07. Summary of the work of CLCA-TG on co-processing since FTG/02. February 2020.

CAEP/12-FTG/03-WP/04. Summary of the work of CLCA-TG since FTG/02. February 2020.

CAEP/12-FTG/04-IP/07. Summary of progress since FTG/03 on calculating LCA values for fuels produced through co-processing of biogenic feedstock with petroleum feedstock. June 2020.

CAEP/12-FTG/04-WP/05. Summary of the progress of the Core LCA Subgroup since FTG/03. June 2020.

CAEP/12-FTG/05-WP/02. Summary of the progress of the Core LCA Subgroup since FTG/04. July 2020.

### **Presentations**

Project 1 ASCENT Spring Meeting. "Updates on Lifecycle Analysis: Methods for Analyzing Co-processing and for Systematically Capturing Uncertainty," March 2020.

## **Outreach Efforts**

Progress on these tasks was communicated during weekly briefing calls with the FAA and other U.S. delegation members to FTG, as well as during numerous FTG teleconferences between meetings. Furthermore, the team collaborated extensively with experts from the fuels industry for obtaining reliable data to model LCA values for co-processed fuels. In addition, MIT presented its work under Project 1 to ASCENT at the bi-annual meeting in Spring 2020 (virtual meeting, March 31–April 1) in the form of a presentation.

## **Awards**

None

## **Student Involvement**

TJ Park, Master's degree student at MIT, performed most of the analysis on co-processing.

## **Plans for Next Period**

The team will continue to carry out attributional CLCA to establish default values for use under CORSIA. More specifically, the team expects to support efforts to determine CLCA values for co-processed fuels and for novel fuel pathways (e.g., catalytic thermolysis), as well as establishing additional default core LCA values for pathways such as jatropha HEFA, for example.

## **References**

ASTM International. *D1655-20 Standard Specification for Aviation Turbine Fuels*. West Conshohocken, PA; ASTM International, 2020. doi: <https://doi.org/10.1520/D1655-20>

CARB, 2017A. Co-processing of biogenic feedstocks in petroleum refineries. Draft Staff Discussion Paper. Retrieved from [https://ww3.arb.ca.gov/fuels/lcfs/lcfs\\_meetings/020717\\_staffdiscussionpaper.pdf](https://ww3.arb.ca.gov/fuels/lcfs/lcfs_meetings/020717_staffdiscussionpaper.pdf).

CARB, 2017B. Co-processing of low-carbon feedstocks in petroleum refineries. Draft Discussion Paper. Retrieved from [https://ww3.arb.ca.gov/fuels/lcfs/lcfs\\_meetings/053017draft\\_discussion\\_paper\\_coprocessing.pdf](https://ww3.arb.ca.gov/fuels/lcfs/lcfs_meetings/053017draft_discussion_paper_coprocessing.pdf).

CARB, 2019. GREET modelling technical support document. California LCFS Tier 2 fuel pathway application: Renewable diesel produced from co-processed animal fat at the BP Products North America Inc Cherry Point Refinery using natural gas, steam, and electricity as process energy. Retrieved [ww3.arb.ca.gov/fuels/lcfs/fuelpathways/comments/tier2/b0018\\_report.pdf](https://ww3.arb.ca.gov/fuels/lcfs/fuelpathways/comments/tier2/b0018_report.pdf).

ICAO, 2019. CORSIA supporting document, CORSIA Eligible Fuels – Life Cycle Assessment Methodology. Retrieved from [https://www.icao.int/environmental-protection/CORSIA/Documents/CORSIA%20Supporting%20Document\\_CORSIA%20Eligible%20Fuels\\_LCA%20Methodology.pdf](https://www.icao.int/environmental-protection/CORSIA/Documents/CORSIA%20Supporting%20Document_CORSIA%20Eligible%20Fuels_LCA%20Methodology.pdf).

ISCC, 2016. Guidance for the Certification of Co-Processing, International Sustainability & Carbon Certification (2016). Retrieved from [https://www.iscc-system.org/wp-content/uploads/2017/02/ISCC-Guidance-Document-203-01\\_Co-processing-requirements.pdf](https://www.iscc-system.org/wp-content/uploads/2017/02/ISCC-Guidance-Document-203-01_Co-processing-requirements.pdf)

## Task 3 – Contribute to the Development of the Fuel Production Assessment for CORSIA-eligible Fuels out to the Year 2035

Hasselt University

### **Objective**

The UHasselt team aimed to contribute to the development of the fuel production assessment for CORSIA-eligible fuels out to the year 2035. The results of this scenario exercise will then be extrapolated to 2050 and fed into the CAEP Modelling and Databases Group (MDG) process. During the reporting period, this work was accelerated and re-scoped to inform efforts under ICAO's Long-Term Aspiration Goals (LTAG) Task. The research will be completed jointly with researchers from Washington State University and Purdue University.

### **Research Approach**

The work for this task focused on two items:

1. The development of a set of techno-economic models for representative SAF pathways that can be used to estimate capital costs and financial public support needs in the 2035 fuel production scenarios and during the ramp-up; and
2. A comprehensive update of the short-term production database, which will be used to develop an intermediate waypoint (year 2025) for the short-term production scenarios.

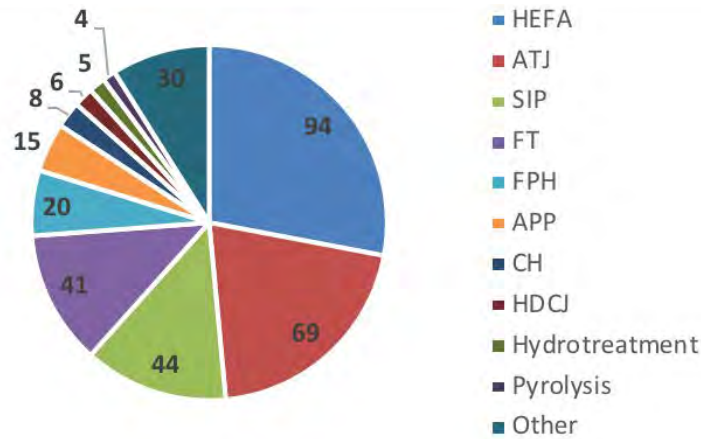
### **Techno-economic models for scenario development**

UHasselt and Purdue University conducted a review of the archival literature and SAF-specific research projects. A total of 56 distinct studies were identified that contained 336 different cases. A case refers to one or more combinations of different parameters for which a (MSP) or net present value (NPV) is estimated in a reference paper. These parameters differ by case and may include process types, feedstocks, co-products, plant sizes, financial assumptions, plant location, etc.

A database was built that captures assumptions and parameter estimates as presented in the studies reviewed. Assumptions and parameters include but are not limited to: feedstock (type and amount), fuel production process, location of plant, location of feedstock sourcing, plant capacity, co-products, discount rate, reference year, plant life, equity/loan fraction, inflation rate, depreciation rate, loan interest rate, base year, internal rate of return.

Not all parameters have yet been filled in for the 336 cases. However, based on initial assessment, assumptions differ significantly across the studies. The 336 cases were compared based on the reference year (year that fuel production is assumed to start), feedstock considered, and the fuel production pathways considered.

Five pathways account for almost 80% of all cases (Figure 4). In particular, the HEFA process is the one most frequently reported pathway (94 cases), followed by alcohol-to-jet (ATJ) (69 cases), synthesized iso-paraffins from hydroprocessed fermented sugars (SIP) (44 cases), Fischer-Tropsch processing (FT) (42 cases), and fast pyrolysis and hydroprocessing (FPH) (20 cases).



Note: Numbers on the chart represent the number of corresponding conversion pathways reported in the constructed dataset. The following abbreviations are used on the figure: Hydroprocessed esters and fatty acid (HEFA), Alcohol-to-jet (ATJ), Synthesized iso-paraffins (SIP), Fischer-Tropsch (FT), Fast pyrolysis and hydroprocessing (FPH), Aqueous-phase processing (APP), Catalytic hydrothermolysis (CH), Hydrotreated depolymerized cellulosic jet fuel (HDCJ).

Figure 4. Pathways considered in TEA studies (frequency)

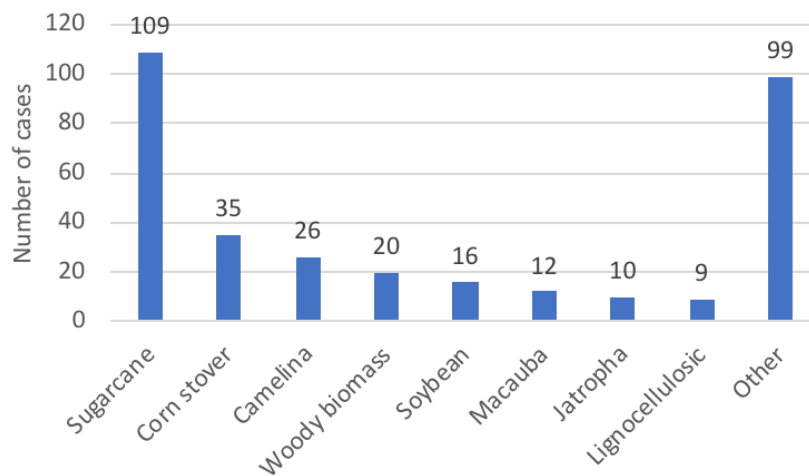
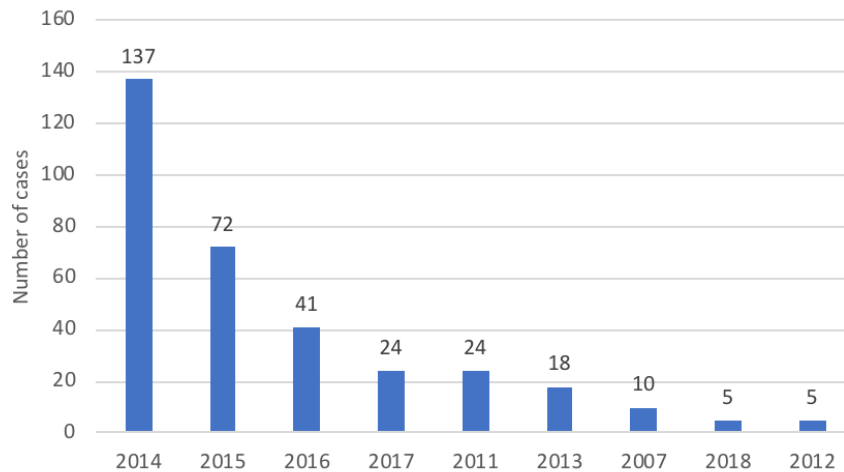


Figure 5. Feedstocks considered in TEA studies (frequency)

Over 30% of the analyzed cases use sugarcane as an input feedstock, followed by corn stover (10% of all cases) and camelina (8%) (Figure 5). The set of the feedstock inputs is highly diversified, representing over 50 varieties. Note that the high number of sugarcane cases is driven by several sugarcane studies assessing multiple cases.

The reported studies rely on different reference years, spanning from 2007 to 2018 (Figure 6). There are 13 cases with non-identified reference year. To make these cases comparable within our dataset, we assumed that the reference year is three years prior to the publication year.



**Figure 6,** Reference years of TEA studies considered.

Based on the comprehensive literature review, a set of spreadsheet models has been developed for three ASTM-approved fuel pathways: HEFA, FT, and ATJ. Feedstocks considered include vegetable and waste oils, municipal solid waste, forest and agricultural residues, and bulk ethanol and isobutanol. A subset of the models is available to FTG experts in the ICAO portal. The models estimate the financial viability for a specific fuel pathway. They account for capital expenses, operating expenses and revenue streams from co-products in order to estimate the minimum selling price of the fuel pathway under a set of user-determined financial assumptions. The current model parameters reflect the state of the knowledge from the archival literature.

The models also have the capability to quantify the impact of a set of policies (e.g., loan guarantee, capital grant, feedstock subsidy, fuel production) on the financial viability of different fuel pathways. The policy impact calculated by the model builds upon the results of a previous AFTF analysis conducted by MIT, Purdue University, and UHasselt as documented in CAEP/11-AFTF/07-IP/14. The models, in their current form, represent U.S. production characteristics. However, production characteristics in other world regions will be different from the U.S., and the U.S. results from the tool are not representative of other parts of the world. Table 10 contains a list of parameters that can be assumed to be dependent on the location of the CORSIA eligible fuel (CEF) production.

Each Excel file, which was developed under the leadership of the Washington State University team, is a combination of multiple feedstocks and conversion pathways and includes both capital and operating costs. Inside battery limit (ISBL) equipment costs were determined from literature, Aspen modeling, and quotations. The ISBL equipment costs were increased using ratio factors to cover all other capital costs.

**Table 10.** Proposal for location-specific parameters in the techno-economic models

OPERATING EXPENSES	CAPITAL EXPENSES	FINANCIAL ASSUMPTIONS	
feedstock - purchase and transport	construction	corporate tax rate	property insurance
utility prices, e.g. electricity, natural gas, hydrogen	installation	inflation	local taxes
consumables	land value	depreciation schedule	equity
labor wages and burden	region factor for purchases	discount rate	loan interest rate
<b>REVENUE</b>			loan term (yrs)
Distillate co-product prices			

The outputs of the analysis are minimum selling price (MSP) values for the applicable fuel. In addition, capital costs, operating costs and fuel volumes are calculated. The capital costs are presented as equipment costs, equipment cost totals by manufacturing area, total direct costs (TDC), fixed capital investment (FCI), and total capital investment (TCI). Operational costs are reported as single line items, manufacturing area totals, variable and fixed costs. The details allow users to focus on costs that are most relevant for a given process and feedstock combination for each region, country, or specific location. All fuel distillate values are linearly related to jet fuel MSP using relationships developed by historical fuel cost data available from the U.S. Energy Information Administration. World-region relationships can be added as an option if FTG decides to pursue this option and if the necessary data is obtained.

Users can input a variety of information to tune the analysis to a specific world region, facility scale, and yield. Economic parameters (discount rate, inflation, percent equity, depreciation schedule, etc.), cost parameters (electricity, natural gas, hydrogen, etc.), technical data/assumptions (feedstock, yield, distillate split, etc.) and policy impact (output subsidies, feedstock subsidy, capital grant, etc.) can be altered.

### Short-term production database

The short-term production projections database has been updated and revised for the current timeframe (2020–2025). Furthermore, it has been reorganized for ease of management and scenario filtering. It includes six sheets: Announcements & Projections; Codes, ASTM Spec, Facility Type; Conversions & Jet Fuel Ratios; Maturity Definitions; Scenario Definitions; and Updates. The “Announcements and Projections” sheet is organized alphabetically by company, with a single row for each known facility. The database currently includes 131 companies/ventures and 247 facilities. Drop-down menus are used in columns C (Code), L (ASTM specification), and P (Facility Type) to ensure consistency of entries. The “Code” in column C helps to track whether the company has indicated specific plans to produce jet fuel (code 1, green), has indicated jet as a possible product (2, blue), has a process that is compatible with producing jet fuel but no announced intent (3, purple), has a process that provides an intermediate for jet fuel (4, peach), if the company is defunct (5, grey), etc. Total fuel production is entered in original units in column U and then harmonized to kilotonnes/year (kt/y) in column V. If a specific jet fuel production quantity has been announced for the facility, it is included in column W. Alternatively, default product slate values for low and high SAF production are calculated in columns Y and Z, respectively, utilizing the default product slates found on the “Conversions & Jet Fuel Ratios” sheet. Defunct companies are kept on the list to avoid re-researching the same companies later (but these will be excluded from scenario analyses). The goal is to have all projections referenced with a link or other public information in column N. Currently, placeholder columns for low, medium, and high production scenarios are in columns AA to AY. These will be populated during the CAEP/12 cycle based on decisions regarding maturity and scenario definitions (see 2.7 and 2.8 below).

The “Codes, ASTM Spec, Facility Type” sheet provides the definitions for three of the drop-down columns in the Announcements & Projections sheet. The “Conversions & Jet Fuel Ratios” sheet provides conversion factors for various units of production (e.g., millions of gallons or liters per year, cubic meters, etc.) into kt/y, and provides default low and high jet fuel product slates for various processes to populate the low/high jet fuel entries in the Announcements & Projections sheet. It is planned to align the jet fuel conversion factors and product slate ratios between the techno-economic analyses for the various processes and the short-term database assumptions.

The “Maturity Definitions” sheet provides criteria for assessing company maturity as an element that will be used to determine inclusion in future production scenarios. The CAEP/10 analysis used the technology maturity (i.e., a fuel being qualified under ASTM, under evaluation, or not yet in process) and company maturity (experience producing fuel, financial backing, etc.) as criteria for inclusion in various production scenarios. Draft CAEP/12 criteria for assessing maturity are included; however, these maturity criteria have not yet been discussed/developed by the TPP subgroup and are provided solely as an example to aid FTG in understanding how maturity criteria will be developed during the CAEP/12 cycle. Further development of maturity definitions and their application to producers is planned by the TPP sub-group.

The “Scenario Definitions” sheet provides a set of potential rules for inclusion of companies and extent of commercial deployment success that take into account the industry-wide challenges of bringing company plans to fruition. An initial table of scenario definitions is included; however, these scenario definitions have not yet been discussed/developed by the TPP subgroup and are solely provided as an example to aid FTG in understanding how scenarios will be developed during the CAEP/12 cycle. Further development is planned.

The “Updates” sheet provides space for proposed modifications to the Announcements & Projections sheet. The use of the Updates sheet allows TPP to vet changes before they are made and track changes over time. It also ensures that all entries made into the Announcements & Projections sheet can be made consistently using the revised format.

### **Milestone**

The work described above has been documented in several Working Papers submitted to the FTG. This includes papers submitted to FTG/02 (Montreal, September 2019), FTG/03 (Abu Dhabi, February 2020), and FTG/04 (Virtual, June 2020). Team members from Hasselt University and MIT participated in and contributed to all meetings.

### **Major Accomplishments**

- The team presented the comprehensive literature review at the FTG/3 meeting.
- The team presented and led a discussion on the spreadsheet TEA models at the FTG/4 meeting.
- A subset of the spreadsheet TEA models is available for FTG-internal use at the ICAO portal.

### **Publications**

#### **Written reports**

CAEP/12-FTG/02-WP/09: Potential Methodology for the Fuel Production Evaluation Task

CAEP/12-FTG/03-WP/10: Summary of the progress on inventory of techno-economic analyses on sustainable aviation fuel

CAEP12/FTG04/WP03: Update on fuel production assessment and TEA

CAEP12/FTG04/IP05 TPP Short Term Projections Database

### **Awards**

None

### **Student Involvement**

None

### **Plans for Next Period**

The team will draft year-2035 fuel production scenarios based on using a market diffusion approach on the production ramp-up contained within the short-term production database and will bring forward scenario results at the Spring 2020 FTG meeting. The team will also provide guidance for MDG and LTAG TG on 2050 production scenarios.

## **Task 4 – Develop Methods for Probabilistic Life-cycle Analyses and Probabilistic Techno-economic Analyses of SAF**

Massachusetts Institute of Technology

### **Objective**

Previous studies have shown that there is significant variability and uncertainty in the life cycle emissions of renewable drop-in fuels (e.g., Sills et al., 2012, Fortier 2014). Variability has been addressed by calculating local sensitivities and by generating a deterministic range of estimates including maximum, minimum, and most likely values (e.g., Staples et al. 2014, Stratton et al., 2011, Seber et al. 2014, Galligan 2018, Rosen 2017). Uncertainty has been quantified for selected pathways (Suresh et al., 2018), however a probabilistic quantification of uncertainty across a number of AJF pathways has not been carried out.

Similarly, MIT previously conducted stochastic TEA studies for a wide set of feedstock-to-fuel pathways to convert biomass or industrial and household wastes into alternative aviation fuel in the U. S. The resulting literature (e.g., Bann et al., 2017; Yao et al., 2017; Suresh et al., 2018; Pearlson et al., 2013, Seber et al., 2014; Bond et al., 2014; Staples et al., 2014) shows that alternative aviation fuels will remain more expensive to produce than conventional jet fuel in the short- to medium-term, but also highlights the range of potential cost outcomes.

These existing TEA and LCA studies have evaluated nationwide uncertainty but did not intend to capture or disentangle this this nationwide uncertainty from regional variability in key inputs. The latter variability manifests itself in factors such as yield, utility prices, and emissions factors, and capital area cost factors. Under this task, we develop a high-resolution

stochastic TEA and LCA model to disentangle the impacts of regional variability and nationwide uncertainty in key input parameters on costs and lifecycle impacts. The results of a combined probabilistic LCA would help researchers, policymakers, technology developers, and investors to evaluate the risks and likely emissions outcomes of AJF production and use in a systematic way. In addition, disentangling variability from uncertainty would guide decisionmakers in choosing the most efficient implementation strategies.

## **Research Approach**

### **High Resolution Feedstock Availability**

MIT has previously investigated the production potential of SAF in 2050 in the U. S. across scenarios assuming different economic, climate, and land use assumptions (Galligan 2018). This high-resolution feedstock availability model coupled with regional stochastic LCA and TEA modeling enables the proposed work.

County level crop availability is determined using 2035 land use projections and future crop yield assumptions. Land use patterns in the U.S. in 2035 are modeled with a spatial resolution of 250 meters by the U.S. Geological Survey FORE-SCE project under Intergovernmental Panel on Climate Change (IPCC) Special Report Emissions Scenarios (SRES) A1B, A2, B1, and B2 (Sohl et al., 2014). Land use changes for crop cultivation is considered on the following land classifications: mechanically disturbed lands, barren, grassland, shrubland, herbaceous and woody wetland, and hay and pasture land. For all crops except switchgrass and miscanthus, historical U.S. Department of Agriculture (USDA) county level yield data is extrapolated to 2035 and capped by the agro-climatically attainable yield from the Global Agro-Ecological Zone (GAEZ) version 3.0 model (Fischer, 2012). County level switchgrass and miscanthus yields in 2035 are drawn from the baseline scenario in the 2016 Billion Ton Report (Langholtz, Stokes, and Eaton, 2016).

Crop residue availability is determined using present day crop-specific land cover data, 2035 cropland area, residue quantity per unit crop yield, and sustainable residue removal rates. Crop-specific land cover data is used to determine the distribution of crops on cropland in each county in 2035 and is assumed equal to the crop distribution in 2019 (USDA National Agricultural Statistics Service Cropland Data Layer, 2019). The residue quantity per unit crop yield is available for each crop from Lal (2005), and county level sustainable crop residue removal rates are available from Muth et al., (2013).

Forest residue availability is taken from 2035 county level results from the baseline scenario in the 2016 Billion Ton Report.

Waste products evaluated include animal fats, waste grease, and municipal solid waste (MSW). Waste grease production is available on a per capita basis from Wiltsee (1998), while animal fat production on a per capita basis is calculated using 2017 USDA census data, 2017 USDA animal slaughter data and animal byproduct fractions (USDA, 2018). Municipal solid waste availability is calculated on a per capita basis in 2035 with data from Hoornweg (2012), and 2017 discard fractions from the U.S. Environmental Protection Agency (EPA, 2019). County level population projections in 2035 are available from Hauer (2019) for the five Shared Socioeconomic Pathways (SSP). The SSP data is mapped to the SRES scenarios according to Riahi et al., (2017) for consistency with the USGS FORE-SCE land use models.

### **Stochastic Life Cycle Assessment**

The stochastic LCA model builds off deterministic LCA models which quantify GHG emissions along the AJF supply chain from feedstock cultivation and collection to transportation and combustion. Key stochastic inputs for each step in the LCA model are shown in Table 11.

**Table 11. Stochastic LCA inputs**

Life Cycle Step	Stochastic Inputs
Feedstock cultivation	<ul style="list-style-type: none"> <li>■ Crop yield</li> <li>■ Soil nutrient requirements</li> </ul>
Feedstock harvesting, collection, and recovery	<ul style="list-style-type: none"> <li>■ Cultivation energy</li> <li>■ Electricity emissions factor</li> </ul>
Feedstock transportation	<ul style="list-style-type: none"> <li>■ Transportation distance</li> <li>■ Transportation fuel emissions factor</li> </ul>
Feedstock pre-processing and fuel conversion	<ul style="list-style-type: none"> <li>■ Energy utility requirements</li> <li>■ Feedstock-to-fuel conversion efficiency</li> <li>■ Utility emissions factors</li> </ul>
Fuel transportation	<ul style="list-style-type: none"> <li>■ Transportation distance</li> <li>■ Transportation fuel emissions factor</li> </ul>

The LCA method uses energy allocation for allocating emissions among energy products along the conversion process. The calculated LCA values include emissions generated during ongoing operational activities and emissions embedded in all utilities used. Preliminary stochastic LCA results for the corn grain iso-butanol ATJ pathway in the year 2018 are shown in Figure 7 for a sample of ten U.S. states, along with preliminary stochastic LCA results when U.S.-wide uncertainty is evaluated. The results assume that all life cycle steps occur within the same U.S. state.

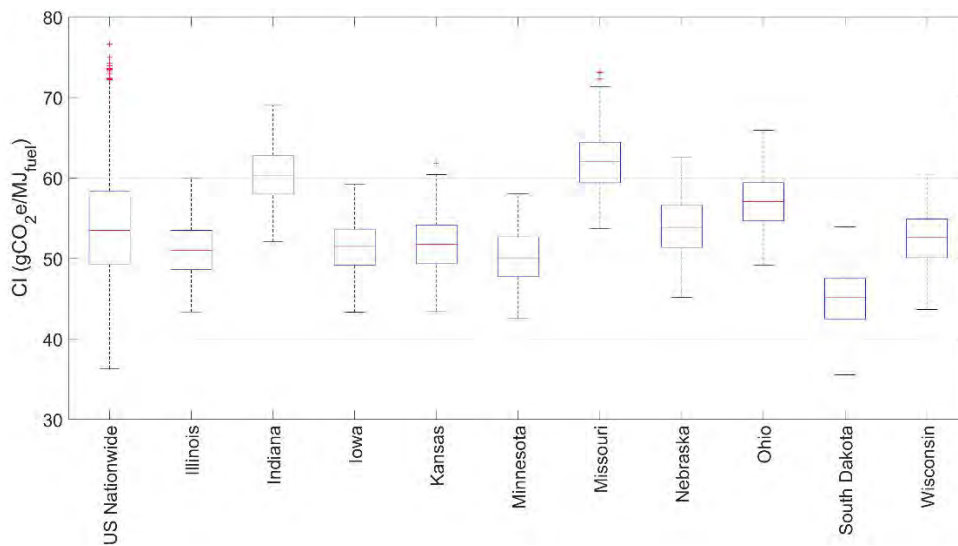


**Figure 7. Preliminary regional stochastic LCA for corn grain iso-butanol ATJ.**

Preliminary results indicate that regional stochastic LCA modeling can reduce life cycle emissions uncertainty for the ATJ pathway by capturing regional variability in key inputs. Further development of the stochastic LCA modeling is ongoing for all feedstocks and pathways.

**Stochastic Techno-Economic Analysis**

The stochastic TEA model and stochastic LCA model use harmonized inputs where appropriate, including feedstock yield, chemical and utility requirements, and transportation distance and method. Key stochastic inputs for each step in the TEA model are shown in Table 12.



**Table 12. Stochastic TEA inputs**

Life Cycle Step	Stochastic Inputs
Feedstock cultivation	<ul style="list-style-type: none"> <li>▪ Crop yield</li> <li>▪ Soil nutrient requirements</li> <li>▪ Fertilizer and chemical costs</li> </ul>
Feedstock harvesting, collection, and recovery	<ul style="list-style-type: none"> <li>▪ Cultivation energy</li> <li>▪ Utility and labor costs</li> </ul>
Feedstock transportation	<ul style="list-style-type: none"> <li>▪ Transportation distance</li> <li>▪ Transportation fuel costs</li> </ul>
Feedstock pre-processing and fuel conversion	<ul style="list-style-type: none"> <li>▪ Energy utility requirements</li> <li>▪ Feedstock-to-fuel conversion efficiency</li> <li>▪ Utility and chemical emissions costs</li> <li>▪ Refinery capital costs</li> <li>▪ Non-fuel product prices</li> </ul>
Fuel transportation	<ul style="list-style-type: none"> <li>▪ Transportation distance</li> <li>▪ Transportation fuel costs</li> </ul>

**Milestone**

The team briefed FAA on progress during the ASCENT meetings in Spring and Fall 2020.

**Major Accomplishments**

MIT has developed the framework for harmonized regional stochastic LCA and TEA models. Further development of the TEA and LCA models and integration with regional feedstock availability will occur in the next period.

**Publications**

N/A

**Outreach Efforts**

MIT presented the work under this task at the biannual meeting in Spring 2020 (virtual meeting, March 31–April 1) in the form of a presentation. During the ASCENT Fall 2020 meeting (virtual meeting, September 29–30), MIT provided an update through a poster presentation.

**Awards**

None

**Student Involvement**

The MIT graduate students involved in this task was Walter Kelso.

**Plans for Next Period**

MIT will further develop methods for probabilistic life-cycle analyses and probabilistic techno-economic analyses. More specifically, the MIT team will disentangle uncertainty from stochasticity by using a higher-resolution LCA model. This high-resolution approach will provide insights in the regional variability of lifecycle emissions for different SAF pathways in the U.S. and the associated risks by area. This data will further be combined with a regionalized stochastic TEA model (Bann et al., 2017) and previous work on U.S.-specific assessments of long-term SAF availability (Galligan 2018) to obtain a holistic assessment of U.S.-sourced SAF availability in 2035. The results will guide researchers, policymakers, technology developers, and investors in prioritizing geographic areas of SAF development and in better understanding the risks and uncertainties associated with specific choices.

**References**

Bann, S. J., Malina, R., Staples, M. D., Suresh, P., Pearlson, M., Tyner, W. E., . . . Barrett, S. (2017). The costs of production of alternative jet fuel: A harmonized stochastic assessment. *Bioresource Technology*, 227, 179-187. doi:10.1016/j.biortech.2016.12.032



- Bond, J. Q., Upadhye, A. A., Olcay, H., Tompsett, G. A., Jae, J., Xing, R., . . . Huber, G. W. (2014). Production of renewable jet fuel range alkanes and commodity chemicals from integrated catalytic processing of biomass. *Energy Environ. Sci.*, 7(4), 1500-1523. doi:10.1039/c3ee43846e
- Fischer, G. (2012). *Global Agro-ecological Zones (GAEZ v3.0) Model Documentation* [PDF]. IIASA, Laxenburg, Austria and FAO, Rome, Italy.
- Fortier, M. P., Roberts, G. W., Stagg-Williams, S. M., & Sturm, B. S. (2014). Life cycle assessment of bio-jet fuel from hydrothermal liquefaction of microalgae. *Applied Energy*, 122, 73-82. doi:10.1016/j.apenergy.2014.01.077
- Galligan, T. (2018). *Carbon dioxide emissions reduction potential of aviation biofuels in the US* (Unpublished master's thesis). Massachusetts Institute of Technology.
- Hauer, M. E. (2019). Population projections for U.S. counties by age, sex, and race controlled to shared socioeconomic pathway. *Scientific Data*, 6(1). doi:10.1038/sdata.2019.5
- Hoorweg, D., & Bhada-Tata, P. (2012). What a Waste : A Global Review of Solid Waste Management. 281.
- Lal, R. (2005). World crop residues production and implications of its use as a biofuel. *Environment International*, 31(4), 575-584. doi:10.1016/j.envint.2004.09.005
- Langholtz, M. H., Stokes, B. J., & Eaton, L. M. (2016). 2016 Billion-Ton Report: Advancing Domestic Resources for a Thriving Bioeconomy. doi:10.2172/1271651
- Muth, D., Bryden, K., & Nelson, R. (2013). Sustainable agricultural residue removal for bioenergy: A spatially comprehensive US national assessment. *Applied Energy*, 102, 403-417. doi:10.1016/j.apenergy.2012.07.028
- Pearlson, M., Wollersheim, C., & Hileman, J. (2013). A techno-economic review of hydroprocessed renewable esters and fatty acids for jet fuel production. *Biofuels, Bioproducts and Biorefining*, 7(1), 89-96. doi:10.1002/bbb.1378
- Riahi, K., Vuuren, D. P., Kriegler, E., Edmonds, J., O'Neill, B. C., Fujimori, S., . . . Tavoni, M. (2017). The Shared Socioeconomic Pathways and their energy, land use, and greenhouse gas emissions implications: An overview. *Global Environmental Change*, 42, 153-168. doi:10.1016/j.gloenvcha.2016.05.009
- Rosen, C. (2017). *Scenario based lifecycle analysis of greenhouse gas emissions from petroleum-derived transportation fuels in 2050*. Master's thesis. Massachusetts Institute of Technology.
- Seber, G., Malina, R., Pearlson, M. N., Olcay, H., Hileman, J. I., & Barrett, S. R. (2014). Environmental and economic assessment of producing hydroprocessed jet and diesel fuel from waste oils and tallow. *Biomass and Bioenergy*, 67, 108-118. doi:10.1016/j.biombioe.2014.04.024
- Sills, D. L., Paramita, V., Franke, M. J., Johnson, M. C., Akabas, T. M., Greene, C. H., & Tester, J. W. (2012). Quantitative Uncertainty Analysis of Life Cycle Assessment for Algal Biofuel Production. *Environmental Science & Technology*, 47(2), 687-694. doi:10.1021/es3029236
- Sohl, T. L., Sayler, K. L., Bouchard, M. A., Reker, R. R., Friesz, A. M., Bennett, S. L., . . . Hofwegen, T. V. (2014). Spatially explicit modeling of 1992-2100 land cover and forest stand age for the conterminous United States. *Ecological Applications*, 24(5), 1015-1036. doi:10.1890/13-1245.1
- Staples, M. D., Malina, R., Olcay, H., Pearlson, M. N., Hileman, J. I., Boies, A., & Barrett, S. R. (2014). Lifecycle greenhouse gas footprint and minimum selling price of renewable diesel and jet fuel from fermentation and advanced fermentation production technologies. *Energy Environ. Sci.*, 7(5), 1545-1554. doi:10.1039/c3ee43655a
- Stratton, R. W., Wong, H. M., & Hileman, J. I. (2011). Quantifying Variability in Life Cycle Greenhouse Gas Inventories of Alternative Middle Distillate Transportation Fuels. *Environmental Science & Technology*, 45(10), 4637-4644. doi:10.1021/es102597f
- Suresh, P., Malina, R., Staples, M. D., Lizin, S., Olcay, H., Blazy, D., . . . Barrett, S. R. (2018). Life Cycle Greenhouse Gas Emissions and Costs of Production of Diesel and Jet Fuel from Municipal Solid Waste. *Environmental Science & Technology*, 52(21), 12055-12065. doi:10.1021/acs.est.7b04277
- USDA National Agricultural Statistics Service Cropland Data Layer. (2019). Published crop-specific data layer [Online]. Available at <https://nassgeodata.gmu.edu/CropScape/>. USDA-NASS, Washington, DC.
- US Department of Agriculture. (2018). *Livestock Slaughter 2017 Summary*.
- US Environmental Protection Agency. (2019). *Advancing Sustainable Materials Management: 2017 Fact Sheet* [PDF]. Washington, DC.
- Wiltsee, G. (1999). Urban Waste Grease Resource Assessment. doi:10.2172/9782
- Yao, G., Staples, M. D., Malina, R., & Tyner, W. E. (2017). Stochastic techno-economic analysis of alcohol-to-jet fuel production. *Biotechnology for Biofuels*, 10(1). doi:10.1186/s13068-017-0702-7

# Task 5 – Support Coordination of All A01 Universities’ Work on SAF Supply-chain Analyses

Massachusetts Institute of Technology

### **Objective**

The objective of this task is to provide support for coordination of all ASCENT Project 1 (A01) Universities’ work on SAF supply-chain analysis. The sharing of methods and results decreases the replication of A01 Universities’ work on similar topics.

### **Research Approach**

The MIT A01 team performed several functions to accomplish this task.

- Participated in the bi-weekly A01 coordination teleconferences, which were used as a venue to discuss progress on various grant tasks and learn about the activities of other ASCENT universities. The team also presented current research on co-processing to the A01 universities.
- Contributed to efforts for developing a special journal issue on SAF based on the research conducted under A01.

### **Milestone**

The MIT ASCENT A01 team presented current research to other ASCENT universities.

### **Major Accomplishments**

The major accomplishments associated with this task include participation in bi-weekly A01 coordination teleconferences; presentation of current research to other ASCENT universities; and contribution to the development of a journal special issue.

### **Publications**

N/A

### **Outreach Efforts**

See above.

### **Awards**

None

### **Student Involvement**

N/A

### **Plans for Next Period**

Continued engagement in bi-weekly teleconferences and other events to disseminate MIT’s A01 work. In particular, the MIT team expects to contribute to a collection of articles on SAF development.



## Project 002 Ambient Conditions Corrections for Non-volatile PM Emissions Measurements

Missouri University of Science and Technology, Aerodyne Research Inc., and Honeywell

### Project Lead Investigator

Philip D. Whitefield  
 Chancellor's Professor of Chemistry  
 Missouri University of Science and Technology  
 400 W 11<sup>th</sup> Street, Rolla, MO 65409  
 573-341-4420  
 pwhite@mst.edu

### University Participants

#### Missouri University of Science and Technology

- PI: Philip D. Whitefield, Chancellor's Professor of Chemistry
- FAA Award Number: 13-C-AJFE-MST Amendments: 002, 003, 005, 008, 010, and 012
- Period of Performance: September 18, 2014, to February 28, 2021
- Tasks:
  - Task 1. Engine-to-engine variability at Honeywell (completed and reported in the ASCENT 2018-19 annual report).
  - Task 2. Ground-based non-volatile particulate matter (nvPM) emissions from an IAE V2527-A5 engine burning four different fuel types (completed and reported in the 2018-19 annual report).
  - Task 3. Re-examination of engine-to-engine particulate matter (PM) emissions' variability using an Aerospace Recommended Practice (ARP) reference sampling and measurement system (being executed).

### Project Funding Level

PROJECT	FUNDING	MATCHING	SOURCE
13-C-AJFE-MST-002	\$1,288,836.34	\$1,288,836.34	EMPA LETTER
	\$284,613.66	\$284,613.66	TRANSPORT CANADA
13-C-AJFE-MST-003	\$500,000.00	\$500,000.00	EMPA LETTER
13-C-AJFE-MST 005	\$500,000.00	\$500,000.00	EMPA LETTER
13-C-AJFE-MST-008	\$579,234.00	\$579,234.00	EMPA LETTER
13-C-AJFE-MST-010	\$725,500.00	\$725,500.00	EMPA LETTER
13-C-AJFE-MST-012	\$1,217,221.00	\$1,217,221.00	EMPA LETTER

### Investigation Team

- Professor Philip Whitefield, Missouri University of Science and Technology
- Steven Achterberg, research technician, Missouri University of Science and Technology
- Max Trueblood, research technician, Missouri University of Science and Technology
- Dr. Richard Miake-Lye, subcontractor, Aerodyne Research Inc.
- Rudy Dubebout, subcontractor, Honeywell Aerospace
- Paul Yankowich, subcontractor, Honeywell Aerospace



## Project Overview

The International Civil Aviation Organization (ICAO) has published the revised ICAO Annex 16 Vol. II specifying a standardized sampling system for the measurement of non-volatile particulate matter (nvPM) from aircraft engines for use in certification. The Missouri University of Science and Technology (MS&T) owns and operates the ICAO Annex 16 Vol. II compliant North American mobile reference system (NARS) to measure nvPM emissions from the exhaust of aircraft engines. The work under this project exploits the use of the NARS to address issues associated with ambient condition corrections, engine-to-engine variability, and fuel formulation sensitivity. Under ASCENT Project 2, work has been performed on three major Tasks:

### Task 1

Testing has taken place at Honeywell as part of a series of measurements to acquire certification-like data on a set of engines identified by ICAO Committee on Aviation Environmental Protection (CAEP) Working Group 3 (Emissions Technical) Particulate Matter Task Group (CAEP/WG3/PMTG) to be representative of the commercial fleet for entry into the nvPM values database. The engine-to-engine variability of nvPM emissions data from a sample of a large number of engines is required in order to assess the characteristic variability of these engines, which is critical in establishing a regulatory limit for nvPM number- and mass-based emissions. The measurement activity in this Task has been undertaken by Honeywell personnel under subcontract to MS&T. Technical oversight was provided by the MS&T team. This Task was completed in 2019 and reported upon in the 2018–19 annual report.

### Task 2

The NARS and its ancillary equipment have been used to characterize ground-based nvPM emissions from an IAE V2527-A5 engine burning four different fuel types. This work was conducted as part of the NASA/DLR Multidisciplinary Airborne Experiment (ND-MAX) campaign. This Task was completed in 2019 and the results of this study have been described in the 2018–19 annual report. In 2019–20 the data has been uploaded to NASA-DLR database for the ECLIF/ND-MAX and discussions leading to a publication are currently underway.

### Task 3

The NARS and its ancillary equipment are being prepared to quantify the impact of changing conditions on nvPM emissions from a combustor rig and to develop methods for the use of inventory modeling. This Task has been the primary focus of Project 2 in the period October 2019 through September 2020. The preparation has included the recalibration of the mass instruments (LII and MSS+) and the number (APC) and the size instrument (DMS500). The NARS has been operated in its entirety using a minicast as a surrogate source to ensure its continued operability during the pandemic waiting period.

## Task 1 – Engine-to-Engine Variability at Honeywell

Missouri University of Science and Technology

Completed and reported in 2018–19 annual report.

## Task 2 – Ground-Based non-volatile Particulate Matter (nvPM) Emissions from an IAE V2527-A5 Engine Burning Four Different Fuel Types

Missouri University of Science and Technology

In 2019–20, the data was uploaded to NASA-DLR database for the ECLIF/ND-MAX and discussions leading to a publication are currently underway.



## Task 3 – Re-Examination of Engine-to-Engine Particulate Matter (PM) Emissions Variability Using an Aerospace Recommended Practice (ARP) Reference Sampling and Measurement System

Missouri University of Science and Technology

This Task has been the primary focus of Project 2 in the period October 2019 through September 2020.

### Objectives

Changing inlet conditions affect nvPM emissions from aircraft engines. A combustor rig test provides the most flexibility to quantify the impact of changing conditions on nvPM emissions and to develop methods for use in inventory modeling. The MS&T/Aerodyne team will work with Honeywell to conduct combustor rig tests, collect nvPM mass and number emissions data, and analyze data to determine nvPM ambient corrections.

### Research Approach

- Define and assemble a standardized nvPM measurement system that will include the same mass measurement system that was used to sample nvPM from 25 Honeywell HTF7350 production engines in 2017.
- Design and fabricate nvPM emissions rakes and combustor rig adaptive hardware required to enable nvPM and gaseous emissions data to be acquired from Honeywell's existing HTF7000 Combustor Test Rig.
- Perform four combustor rig tests with Jet A and three alternative fuels.
- Vary combustor test conditions (derived from engine cycle performance analysis, covering a range of engine ambient inlet conditions on the ground and at altitude) and measure nvPM emissions.
- Analyze data to inform performance-based nvPM emissions modeling for all altitudes.

### Milestone

The funding for the Honeywell and Aerodyne sub awards is in place and work is underway to prepare for testing at Honeywell's combustor rig facilities in Phoenix, AZ.

### Major Accomplishments

- Honeywell and the MS&T/Aerodyne team have assembled two standardized nvPM emissions measurement systems. Key components are in the process of being recalibrated.
- Honeywell has completed design and fabrication of rakes and adaptive rig hardware required to enable nvPM emissions measurements in the HTF7000 Combustor Test Rig.
- Honeywell has completed the initial set up of the sampling system and performed the shakedown test.
- Honeywell found some hardware interferences in the shakedown tests and these have been corrected.
- Honeywell has conducted a second shakedown test and the sampling system was deemed ready for testing.
- It was anticipated that testing would start in March 2020, however, the onset and continuation of the COVID-19 pandemic throughout the remainder of this reporting period has thwarted all attempts to initiate the testing phase of this Task. This is mainly due to the fact that the initial testing phase required the MS&T team (i.e., MS&T and Aerodyne) to deploy instrumentation and personnel from Missouri and Massachusetts, respectively.
- The Honeywell team, MS&T team, and the FAA have conducted bi-weekly planning teleconferences, but these have largely focused on potential alternative deployment strategies should things improve with travel restrictions driven by the pandemic.
- During the pandemic delay, the calibrations required for the Honeywell and NARS nvPM measurement systems expired. These instruments are currently undergoing recalibration with the hope that the testing can be resumed in early 2021.

### Publications

N/A

### Outreach Efforts

Presentations on the project plan to date have been made at:

- ASCENT virtual advisory board meetings held in April and September 2020.



- AEC Roadmap virtual meeting held in May 2020.

### **Awards**

None

### **Student Involvement**

Three undergraduate research assistants (Christian Hurst, Nicholas Altese, and Susan Donaldson) were employed in pre-test activities, including individual component testing and calibration and data reduction and interpretation. None of these students have graduated.

### **Plans for Next Period**

- Re-install and shakedown of nvPM combustor rig measurement system with rig in test cell.
- Conduct initial rig test with Jet A (Phase I).
- Conduct rig test with three sustainable aviation fuel blends (Phase II).



# Project 003 Cardiovascular Disease and Aircraft Noise Exposure

## Boston University

### Project Lead Investigator

Junenette L. Peters  
Assistant Professor  
Department of Environmental Health  
Boston University School of Public Health  
715 Albany St., T4W  
Boston, MA 02118  
617-358-2552  
petersj@bu.edu

## University Participants

### Boston University (BU)

- Pls: Prof. Jonathan Levy (University PI), Prof. Junenette Peters (Project PI)
- FAA Award Number: 13-C-AJFE-BU-016
- Period of Performance: October 1, 2019 to September 30, 2020

### Massachusetts Institute of Technology (MIT)

- Sub-PI and Co-I: Prof. R. John Hansman, Dr. Florian Allroggen

#### Tasks (Performance Period)

*Related to 2018 FAA Reauthorization, Section 189, Tasks 1-3*

1. Generate final results for analyses of hypertension and aircraft noise exposure.
2. Generate preliminary results of supporting analyses.
  - a. Trends of aircraft noise exposure.
  - b. Sociodemographic patterning of aircraft noise exposure.
3. Assess suitability of existing cohort data on sleep quality and develop a noise-sleep analysis plan.
4. Develop an analysis plan for cardiovascular disease (CVD) and aircraft noise exposure and generate descriptive statistics.

*Related to 2018 FAA Reauthorization, Section 189, Task 4*

5. Develop a model for measuring change in business activities attributable to aircraft noise exposure prototyping a model city.

## Project Funding Level

Total funding (three-year funding): \$1,729,286

Matching: \$1,729,286

Source of matching funds: Nonfederal donors to the Nurses' Health Study (NHS), Health Professional Follow-up Study (HPFS), and Women's Health Initiative (WHI) cohorts.

## Investigation Team

### Junenette Peters, PI, Boston University

Dr. Peters is responsible for directing all aspects of the proposed study, including study coordination, design and analysis plans, and co-investigator meetings.

**Jonathan Levy, Boston University**

Dr. Levy will participate in noise exposure assessment and provide expertise in the area of predictive modeling and air pollution.

**Francine Laden, Jaime Hart, and Susan Redline, Harvard Medical School/Brigham and Women's Hospital**

Dr. Laden is our NHS and HPFS sponsor for this ancillary study. Dr. Hart will assign aircraft noise exposures to the geocoded address history coordinates of each cohort member. Dr. Laden and Dr. Hart will also assist in documenting data from the NHS and HPFS based on their previous experience in air pollution and chronic disease outcome research in these cohorts and in appropriate analyses of hypertension and cardiovascular outcomes. Dr. Redline will lead efforts related to noise and sleep disturbance in the NHS and WHI.

**John Hansman and Florian Allroggen, Massachusetts Institute of Technology**

Dr. Hansman will participate in the economic impact assessment and will provide expertise on analytical approaches for quantifying noise. Dr. Allroggen will perform an economic impact assessment based on his expertise in analyzing the societal costs and benefits of aviation.

## Project Overview

Exposure to aircraft noise is considered the most significant perceived environmental impact of aviation in communities surrounding airports (Wolfe et al., 2014). Exposure to aircraft noise has been associated with physiological responses and psychological reactions (Bluhm & Eriksson, 2011; Hatfield et al., 2001), including sleep disturbances, sleep-disordered breathing, nervousness, and annoyance (Hatfield et al., 2001; Rosenlund et al., 2001). Recent literature, primarily from European studies, provides evidence of a relationship between aircraft noise and self-reported hypertension (Rosenlund et al., 2001), increased blood pressure (Evrard et al., 2017; Haralabidis et al., 2008; Haralabidis et al., 2011; Jarup et al., 2008; Matsui et al., 2004), antihypertensive medication use (Bluhm & Eriksson, 2011; Floud et al., 2011; Franssen et al., 2004; Greiser et al., 2007), and incidence of hypertension (Dimakopoulou et al., 2017; Eriksson et al., 2010). However, the extent to which aircraft noise exposure increases the risk of adverse health outcomes is not well understood. Impacts related to annoyance have been empirically studied using the stated preference approach (Bristow et al., 2015) and the revealed preference approach, which often relies on analyses of house prices (Almer et al., 2017; Kopsch, 2016; Wadud, 2013). Although the impacts of aircraft noise on individuals are well understood, little evidence has been presented on the impact of aircraft noise exposure on companies located beneath flight paths. Section 189 of the 2018 FAA Authorization has called for a study on the potential health and economic impacts attributable to aircraft overflight noise.

The goal of this ongoing project is to examine the potential health impacts attributable to noise exposure resulting from aircraft flights, and this project will leverage ongoing work within ASCENT to respond to Section 189. This study aims to assess the potential association between aircraft noise exposure and outcomes such as sleep disturbance and elevated blood pressure. The study will leverage existing collaborations with well-recognized and respected studies that have followed over 250,000 participants through the course of their lives to understand factors that affect health. These studies include the NHS and HPFS. Furthermore, this work is aligned with an ongoing National Institutes of Health (NIH)-funded effort to examine these associations in the WHI. The research team will leverage aircraft noise data for 90 U.S. airports from 1995–2015, as generated using the Aviation Environmental Design Tool (AEDT); these data will then be linked to demographic, lifestyle, and health data for the participants of long-term health studies. These studies provide considerable geographic coverage of the United States, including all the geographic areas specified in Section 189.

This work will also respond to the aspect of Section 189 calling for the study of economic harm or benefits for businesses located underneath regular flight paths. The study will involve a first-of-its-kind empirical assessment of the economic impacts on businesses located beneath flight paths at selected U.S. airports. Such impacts are expected to be driven by (a) potential positive economic impacts related to the airport and its connectivity and (b) environmental impacts such as noise, which may reduce the revenue and productivity of businesses beneath flight paths. The team will evaluate whether such impacts can be empirically identified while considering economic outcome metrics such as the gross domestic product (GDP), employment, and revenue.

The overall aims for the three-year project are as follows:

- Perform Tasks 1–3 [Sec. 189. (b)(1–3)]: Potential health impacts attributable to aircraft overflight noise.
  - Investigate the relationship between aircraft noise exposure and the incidence of hypertension in the NHS and HPFS, accounting for other individual- and area-level risk factors.



- Investigate the relationship between aircraft noise exposure and the incidence of cardiovascular disease (CVD) in the NHS and HPFS cohorts and determine whether sufficient data exist to prove a causal relationship.
- Determine whether a relationship exists between annual average aircraft noise exposure and general sleep length and quality in the NHS and the Growing Up Today Study (GUTS) and report whether sufficient data exist to prove a causal relationship.
- Evaluate the potential relationship between residing under a flight path and measures of disturbed sleep in the WHI WHISPER sub-study.
- Perform Task 4 [Sec. 189. (b)(5)]: Potential economic impacts attributable to aircraft overflight noise.
  - Model noise exposure before and after the introduction of area navigation (RNAV) procedures on the basis of FAA flight trajectory data.
  - Combine noise data with yearly county-level data from the Bureau of Economic Analysis (BEA) (e.g., GDP, employment) and with city-level statistics for the years 2007, 2012, and 2017 from the Economic Census (e.g., revenue, employment).
  - Compare economic outcomes using state-of-the-art econometric approaches while controlling for regional and national economic trends.
  - Evaluate whether the spatial resolution of the available data can significantly impact the study results.

## Task 1 – Generate Final Results for Analyses of Aircraft Noise and Hypertension

Boston University

### Objective

To generate final results of analyses of aircraft noise (day-night average sound level (DNL)) and hypertension.

### Research Approach

We will intersect modeled noise exposure surfaces for 1995, 2000, 2005, 2010, and 2015 with geocoded addresses of the participants over the follow-up period. We will select a large set of *a priori* variables to be examined as confounders and/or effect modifiers and will use time-varying Cox proportional hazards models to estimate hypertension or CVD risks associated with time-varying aircraft noise exposure, while adjusting for both fixed and time-varying covariates. We will also perform a sensitivity analysis to address potential biases.

### Milestones

Generate results from analyses of aircraft noise (DNL and Leq Night) and hypertension (January 2020).  
Present at the University of California, Davis Aviation Noise and Emissions Symposium (March 2020).

### Major Accomplishments

- Determined the person-time of people free of hypertension at baseline (1995).
- Incorporated updated NHS and NHS II data relevant to this analysis.
- In response to comments, reevaluated the process for selecting variables (potential confounders) to include in the analysis from the variables: age, alcohol use (g/day), body mass index (BMI), calendar year, comorbidities (diabetes, hearing loss, and hypercholesterolemia), smoking status, diet (dietary approaches to stop hypertension [DASH] score), hearing problems, family history of hypertension, individual-level socioeconomic status (SES) variables (educational attainment, marital status, and partner's educational attainment), medication use (current statin and non-narcotic analgesic drug use), menopausal status, physical activity (metabolic equivalent hours per week), and race, as well as region, latitude, area-level SES variables (census-tract median income and house value), and air pollution (PM<sub>2.5</sub> and PM<sub>2.5-10</sub>). Initially chose potential confounders *a priori* through literature review, then ran bivariable models adjusting for each potential confounder separately examining model Akaike information criterion (AIC; a mathematical method for evaluating model fit), then built multivariable models by adding one variable in at a time and comparing AICs.
- Using updated NHS and NHS II data and final variable selection, reran time-varying Cox proportional hazards models to estimate hypertension risks associated with time-varying aircraft noise exposure, while adjusting for both fixed and time-varying covariates. Analysis performed with the DNL noise metric.



- Performed analysis for each cohort separately (Tables 1 and 2 for NHS and NHS II, respectively).
- Performed meta-analysis to combine the results found for each cohort, NHS and NHS II.
- Performed the following sensitivity analyses (assessing the sensitivity of each primary analysis to underlying issues).
  - Restricted participants to those living close to one of the 90 modeled airports ( $\geq 45$  dB) to address potential exposure errors, for example, to exclude those living near an airport that is not included in the 90 airports and to minimize the impact of potential differences in populations living close to airports versus those living farther away.
  - Analyzed the potential effect of noise abatement programs for DNLs higher than 65 dB to address possible exposure errors related to noise abatement programs among those with noise exposure above the FAA threshold ( $> 65$  dB).
  - Adjusted for air pollution and area-level SES, which is available for only a portion of the time period.
- Presented on "Long-term aircraft noise exposure and the risk of hypertension in national US studies" at the University of California, Davis Aviation Noise and Emissions Symposium in San Diego, CA on March 2, 2020.

**Table 1.** Hazard ratios (95% confidence intervals (Cis)) for hypertension associated with aircraft noise in the NHS, comparing results for  $\geq 55$  dB with those for  $< 55$  dB

Model for DNL Beta Estimate	Ratio	LCL	UCL	p-value
Age and calendar-year adjusted	1.08	0.97	1.21	0.17
Multivariable*	1.05	0.94	1.17	0.42

\*Multivariable model: Adjusted for age, calendar year, race, menopause status, family history of hypertension, and comorbidities (diabetes, hypercholesterolemia), body mass index (BMI), physical activity, alcohol use, DASH (dietary approaches to stop hypertension), medication use (current statin and NSAID use), spouse's education attainment, neighborhood level socioeconomic status (SES), and region of residence

**Table 2.** Hazard ratios (95% confidence intervals (Cis)) for hypertension associated with aircraft noise in the NHS II, comparing results for  $\geq 55$  dB with those for  $< 55$  dB

Model for DNL Beta Estimate	Ratio	LCL	UCL	p-value
Age and calendar-year adjusted	1.11	0.99	1.24	0.08
Multivariable*	1.08	0.97	1.21	0.17

\*Multivariable model: Adjusted for age, calendar year, race, menopause status, family history of hypertension, and comorbidities (diabetes, hypercholesterolemia), BMI, physical activity, alcohol use, DASH, medication use (current statin and NSAID use), spouse's education attainment, neighborhood level SES, and region of residence

The results suggest an increased risk for incident hypertension associated with higher aircraft noise exposure in both NHS and NHS II (Tables 1 and 2). In the multivariable models of the meta-analysis across both cohorts, when compared to participants exposed to aircraft noise at levels below 55 dB, those exposed to 55 dB and above had an estimated risk of hypertension (probability of an incident of hypertension) of 1.06 times. The 95% confidence, which gives a range of estimates between which we are confident that the true value lies, was 0.98 to 1.15. The hazard ratios were relatively stable across the sensitivity analyses.

## Task 2 – Generate Preliminary Results from Supporting Analyses: (a) Trends in Aircraft Noise Exposure and (b) Sociodemographic Patterning of Aircraft Noise Exposure

Boston University

### Objective

To understand changes in exposure that will facilitate our interpretation of time-varying exposure measures in noise-health analyses and to understand sociodemographic patterning of noise exposure that may confound or modify potential associations of noise and health.



### Research Approach

For (a, Noise Trend), we will overlay noise contours for 2000, 2005, 2010, and 2015 and census block data from the U.S. Census Bureau and American Community Surveys for 2000, 2010, and 2015 in a geographic information system to estimate population changes within noise levels. We will utilize linear fixed-effects models to estimate changes in the sizes of exposure areas based on U.S. census regions/divisions with DNL values  $\geq 65$  dB or  $\geq 55$  dB. For (b, Sociodemographic Patterning), we will describe the characteristics of populations exposed to aviation noise by race/ethnicity and income/education using the U.S. Census Bureau and American Community Survey for 2010 and will perform univariate and multivariable hierarchical analyses.

### Milestone

Perform supporting analyses characterizing aircraft noise trends and sociodemographic patterns of exposure to aviation noise - N/A.

### Major Accomplishments

- Overlaid noise contours for 2000, 2005, 2010, and 2015 and census block data from the U.S. Census Bureau and American Community Surveys for 2000, 2010, and 2015
- Determined the exposure area and number of people exposed to aircraft noise using data over time (2000–2015); preliminary results are presented in Figure 1.
- Determined social patterning of aircraft noise exposure by race/ethnicity and income/education for 2010 using univariate and multivariable analysis; preliminary results are presented in Figure 2 (univariable) for % black and Table 3 (multivariable; mixed effects) for airports with at least 100 census block groups.
- Investigated other statistical approaches for determining social patterning that account for multiple variables and clustering around airports and reduce potential bias. Investigated other regression methods for analyzing clustered data, such as Bayesian approaches and separating between and within cluster (airport) effects.

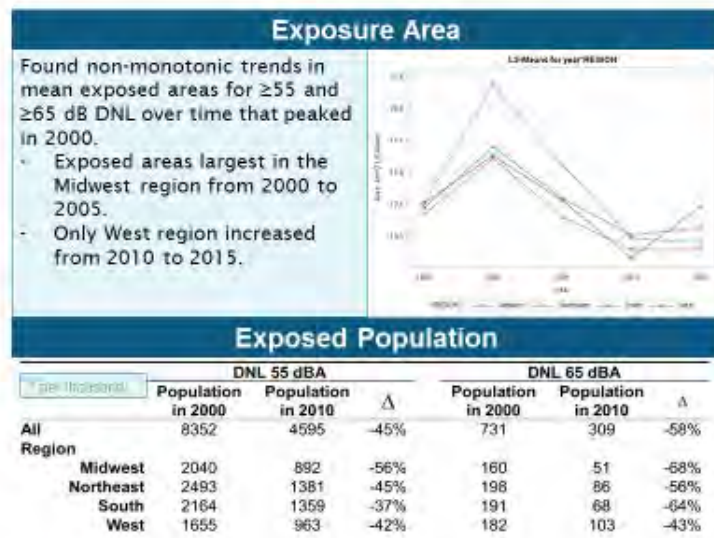
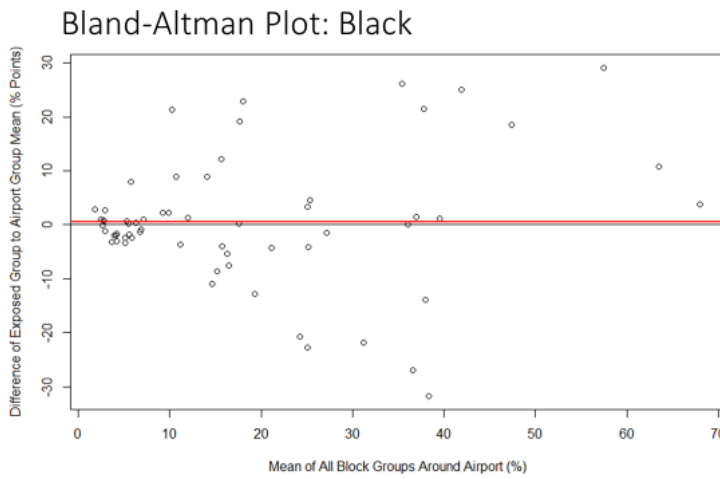


Figure 1. Preliminary results for noise trends based on exposure area (top) and number of people exposed (bottom).



**For example**, point at approx. (68, 4) would be interpreted as an airport where the mean block group percentage around the airport is a population that is 68% black, but if looking at just the block groups in the exposed group, the mean block group percentage is 4 percentage points higher (i.e., mean is population that is 72% black).

**Plot Interpretation:**

(true for all following figures)

- Each point represents a single airport (n=61).
- X-axis represents the mean of all block groups included in the analysis around an airport (both exposed and unexposed groups).
- Y-axis represents the mean difference of the exposed block groups from the entire airport group mean (the x-axis value for that airport).
- Points along the black line at y=0 would be interpreted as there is no difference between block groups exposed vs. the entire airport group for that airport.
- Red line is the mean difference for all airports.

4

**Figure 2.** Preliminary results for sociodemographic patterning in aircraft noise exposure showing univariate analysis by airport of differences from mean of % black in census blocks within DNL 55 dB contours; using airport surrounded by at least 100 census blocks within the buffer zone.

**Table 3.** Preliminary results for sociodemographic patterning in aircraft noise exposure showing mixed-effect multivariable analysis providing odds ratio that represent percent increase (or decrease) in odds of living within DNL 55 dB noise contour per percent increase in a block group’s specific population characteristic

Variable	Odds Ratio	95% Confidence Interval	
		2.5%	97.5%
(Intercept)	0.032	0.024	0.042
BlkGrp_PCT_Black	0.997	0.995	0.999
BlkGrp_PCT_Asian	1.003	1.000	1.007
BlkGrp_PCT_Hispanic	1.003	1.001	1.006
BlkGrp_PCT_Other	1.001	0.992	1.009
PCT_edu0to8	1.013	1.008	1.019
PCT_edu9toC	1.015	1.012	1.018
PCT_LT25k	0.996	0.992	0.999
PCT_25100k	1.002	0.998	1.005

Variables in block groups: Blk\_grp\_PCT\_Black = percent black; Blk\_grp\_PCT\_Asian = percent Asian; Blk\_grp\_PCT\_Hispanic = percent Hispanic; Blk\_grp\_PCT\_Other = percent other race; Blk\_grp\_PCT\_white = percent white (reference); PCT\_edu0to8 = percent with 0 to 8<sup>th</sup> grade education; PCT\_edu9toC = percent with 9<sup>th</sup> grade to college education; PCT\_C= = percent college and > education (reference); PCT\_LT25k = percent with income <25K; PCT\_25100k = percent with income 25-100K; PCT\_GT100k = percent with income >100K (reference).

## Task 3 – Assess Suitability of Data on Sleep Quality and Develop a Noise-Sleep Analysis Plan

Boston University

### **Objective**

To identify sleep measures that may be used to evaluate potential associations between noise and sleep outcomes.

### **Research Approach**

We will review the available measures of sleep quality for the NHS to determine their timing and frequency and their relationship to the timing of the noise exposure data. We will also determine which measures, if any, are relevant to the average exposure measures. If suitable measures are found, we will develop an analysis plan to be presented to the NHS and HPFS committees.

### **Milestones**

Assess potential analysis approaches and suitability of sleep quality data from the NHS (January 2020).  
Preliminary results of analysis of annual aircraft noise and sleep quality (NHS) (September 2020).

### **Major Accomplishments**

- Identified sleep measures in NHS and HPFS that could be used to evaluate potential association between noise and sleep outcomes.
- Developed analysis plan for noise and sleep research effort. Submitted and presented the analysis plan to NHS and HPFS oversight committees. Analysis plan was approved.
- Boston University School of Public Health Postdoc replaced Brigham and Women's Hospital Research Fellow who accepted an international faculty position.

## Task 4 – Develop an Analysis Plan for Cardiovascular Disease and Aircraft Noise and Generate Descriptive Statistics

Boston University

### **Objective**

To generate an analysis plan for studying the potential relationship between CVD and aircraft noise.

### **Research Approach**

We will develop an analysis plan for studying CVD and aircraft noise and gain approval from the NHS and HPFS oversight committees. We will design the statistical analysis and select a large set of *a priori* variables to be examined as confounders and/or effect modifiers. We will compile appropriate data sets and run descriptive statistics.

### **Milestone**

Generate preliminary results of analysis of aircraft noise and CVD (October 2020).

### **Major Accomplishments**

- Developed an analysis plan for evaluating the potential relationship between CVD and noise. Submitted and presented the analysis plan to NHS and HPFS oversight committees. Analysis plan was approved.
- Determined definition of CVD to be used and inclusion and exclusion criteria.
- Determined the person-time of people free of CVD at baseline (1995).
- Determined the number of people exposed (Table 4).

**Table 4.** Number of CVD cases, including number of exposed cases in different exposure groups.

	NHS	NHS II
<b>Total CVD cases</b>	7,818	1,667
<b>Unexposed cases</b>	7,284	1,549
<b>Exposed cases</b>	534	118
<i>At 45-54 dB(A)</i>	456	101
<i>At 55-64 dB(A)</i>	74	17
<i>At ≥65 dB(A)</i>	3	0

## Task 5 – Develop a Model for Measuring Change in Business Activities Attributable to Aircraft Noise Exposure Prototyping a Model City

Massachusetts Institute of Technology

### Objective

To develop a model for measuring changes in business activities attributable to aircraft noise exposure and begin data analysis to assess potential impacts on business dynamics, controlling for confounding, prototyping one or two cities.

### Research Approach

We will create a set of methods to analyze the potential economic impact of noise exposure. The methods will center on the difference-in-difference approach. In an effort to enable causal inference, this approach will focus on differences between levels of business activity before and after exogenous noise exposure changes. In addition, the approach implicitly controls for outside factors that have remained constant from start year to end year.

We will apply our approach to Boston Logan International Airport as an initial case study. This will allow us to refine choices surrounding the economic sectors selected for study and modeling choices such as the spatial resolution of gridding process.

Analyses will include, but are not limited to:

- stratification by economic sector (e.g. retail),
- stratification by geographic concentration at the community-level,
- starting with sufficiently low noise, due to perceptual effects,
- threshold-setting to detect the effects of crossing certain critical noise levels,
- identification of comparable regions (e.g., urban-to-urban, rural-to-rural).

### Milestone

Briefing on airport sample, experimental setting and noise contour data for economic analysis (April 2020).

### Major Accomplishments

- Completed a review of the validity and internal consistency of high-resolution business data that is used to determine changes in economic outcomes. Business data was cleaned and reorganized.
- Identified necessary noise data required for comparing between and within cities and determined the timeline for obtaining that data.
- In our preliminary case studies for Boston Logan (BOS), no significant relationship between noise exposure and business dynamics has yet been found (see Figures 3 and 4).

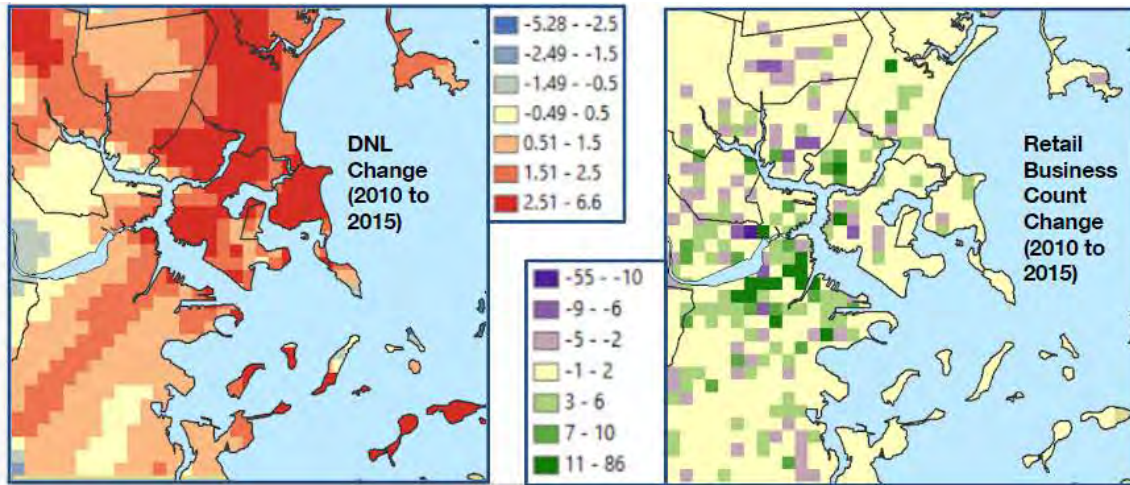


**Figure 3.** Change to DNL in dB from 2010 to 2015, centered on BOS, gridded at 500 m resolution (left). Change in number of retail business in each cell from 2010 to 2015 (right).

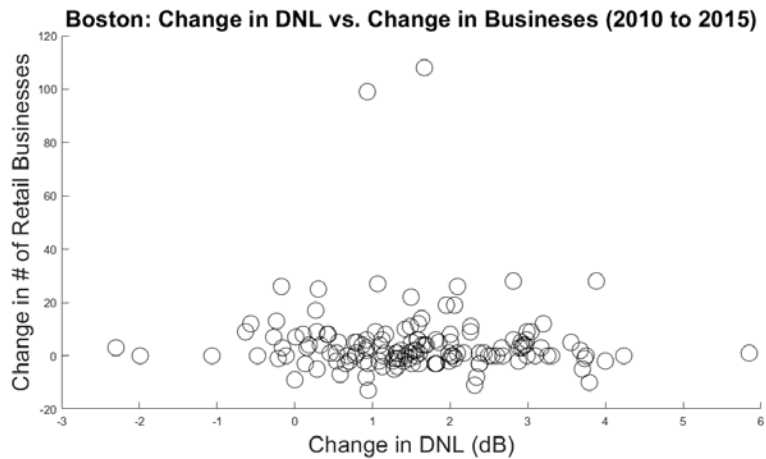


**Figure 4.** Scatterplot of business dynamics against noise change. Each point represents a cell in the Boston area shown in Figure 3. Cells with business decline are not overrepresented among cells with high-magnitude noise increases.

**Publications**

N/A

**Outreach Efforts**

Presented on current progress orally during the ASCENT Spring Meeting (March 31-April 1, 2020) and as a poster during the ASCENT Fall Meeting (September 29-30, 2020).

Presented on "Long-term aircraft noise exposure and the risk of hypertension in national US studies" at the University of California, Davis Aviation Noise and Emissions Symposium in San Diego on March 2, 2020.

**Awards**

None



## **Student Involvement**

The dissertation of Chloe Kim (doctoral graduate, BU) includes the development and implementation of statistical analyses on the noise and hypertension risk. Chloe Kim graduated in the fall of 2019 and is currently working for the Environmental Science, Policy, and Research Institute.

The dissertation of Daniel Nguyen (doctoral candidate, BU) includes a characterization of the temporal trends in aviation noise surrounding U.S. airports.

The research rotation of Stephanie Grady (doctoral student, BU) includes the development and running of statistical analyses on noise and cardiovascular event risk.

Carson Bullock (master's student, MIT) is conducting economic impact analysis.

## **Plans for Next Period**

(October 1, 2020 to September 30, 2021)

*Related to 2018 FAA Reauthorization, Section 189, Tasks 1-3*

- Assign noise exposure estimates to participants for Leq Day and Leq Night metrics.
- Complete models estimating the risk of hypertension associated with aircraft noise exposure and finalize a manuscript for publication in a peer-reviewed journal.
  - Update current draft of the manuscript.
  - Submit manuscript for Channing (Harvard/Brigham and Women's Hospital) and FAA review and to a professional journal.
- Perform analyses to estimate the risk of CVD events associated with aircraft noise exposure.
- Perform analyses to evaluate the relationship between noise and sleep.
- Develop abstracts for presentations at professional conferences and give presentation at ASCENT meetings.

*Related to 2018 FAA Reauthorization, Section 189, Task 4*

- Finalize methods to analyze the impacts of noise exposure on economic activity.
- Apply methods to other airports across the U.S. in order to analyze heterogeneities in potential business responses.
- Compare potential noise impacts to potential economic benefits of airport proximity, using results from the economic literature.

## **References**

- Allroggen F. & Malina, R. (2014). Do the regional growth effects of air transport differ among airports? *Journal of Air Transport Management*. 37:1-4.
- Brueckner, J.K. (2003). Airline traffic and urban economic development. *Urban Studies*. 40(8):1455-1469.
- Campante, F. & Yanagizawa-Drott, D. (2018). Long-range growth: Economic development in the global network of air links. *Quarterly Journal of Economics*. 133(3):1395-1458.
- Lakshmanan, T.R. (2011). The broader economic consequences of transport infrastructure investments. *Journal of Transport Geography*. 19(1):1-12.

## **Project Overview References**

- Almer, C., Boes, S., & Nuesch, S. (2017). Adjustments in the housing market after an environmental shock: Evidence from a large-scale change in aircraft noise exposure. *Oxford Economic Papers*. 69(4):918-938.
- Bluhm, G. & Eriksson, C. (2011). Cardiovascular effects of environmental noise: Research in Sweden. *Noise and Health*. 13(52):212-216.
- Bristow, A.L., Wardman, M., & Chintakayala, V.P.K. (2015). International meta-analysis of stated preference studies of transportation noise nuisance. *Transportation*. 42(1):71-100.
- Dimakopoulou, K., Koutentakis, K., Papageorgiou, I., Kasdagli, M.I., Haralabidis, A.S., Sourtzi, P., Samoli, E., Houthuijs, D., Swart, W., Hansell, A.L., & Katsouyanni K. (2017). Is aircraft noise exposure associated with cardiovascular disease and hypertension? Results from a cohort study in Athens, Greece. *Occupational and Environmental Medicine*. 74(11):830-837.
- Eriksson, C., Bluhm, G., Hilding, A., Ostenson, C.G., & Pershagen, G. (2010). Aircraft noise and incidence of hypertension--gender specific effects. *Environmental Research*. 110(8):764-772.



- Evrard, A.S., Lefevre, M., Champelovier, P., Lambert, J., & Laumon, B. (2017). Does aircraft noise exposure increase the risk of hypertension in the population living near airports in France? *Occupational and Environmental Medicine*. 74(2):123-129.
- Floud, S., Vigna-Taglianti, F., Hansell, A., Blangiardo, M., Houthuijs, D., Breugelmans, O., Cadum, E., Babisch, W., Selander, J., Pershagen, G., Antoniotti, M.C., Pisani, S., Dimakopoulou, K., Haralabidis, A.S., Velonakis, V., Jarup, L.; HYENA Study Team. (2011). Medication use in relation to noise from aircraft and road traffic in six European countries: Results of the HYENA study. *Occupational and Environmental Medicine*. 68(7):518-524.
- Franssen, E.A., van Wiechen, C.M., Nagelkerke, N.J., & Leuret, E. (2004). Aircraft noise around a large international airport and its impact on general health and medication use. *Occupational and Environmental Medicine*. 61(5):405-413.
- Greiser, E., Janhsen, K., & Greiser, C. (2007). Air traffic noise increases prescriptions of cardiovascular drugs in the vicinity of a major airport. *Epidemiology*. 18(5):S33-S33.
- Haralabidis, A.S., Dimakopoulou, K., Vigna-Taglianti, F., Giampaolo, M., Borgini, A., Dudley, M.L., Pershagen, G., Bluhm, G., Houthuijs, D., Babisch, W., Velonakis, M., Katsouyanni, K., Jarup, L.; HYENA Consortium. (2008). Acute effects of night-time noise exposure on blood pressure in populations living near airports. *European Heart Journal*. 29(5):658-664.
- Haralabidis, A.S., Dimakopoulou, K., Velonaki, V., Barbaglia, G., Mussin, M., Giampaolo, M., Selander, J., Pershagen, G., Dudley, M.L., Babisch, W., Swart, W., Katsouyanni, K., Jarup, L.; HYENA Consortium. (2011). Can exposure to noise affect the 24 h blood pressure profile? Results from the HYENA study. *Journal of Epidemiology and Community Health*. 65(6):535-541.
- Hatfield, J., Job, R., Carter, N.L., Peploe, P., Taylor, R., & Morrell, S. (2001). The influence of psychological factors on self-reported physiological effects of noise. *Noise and Health*. 3(10):1-13.
- Jarup, L., Babisch, W., Houthuijs, D., Pershagen, G., Katsouyanni, K., Cadum, E., Dudley, M.L., Savigny, P., Seiffert, I., Swart, W., Breugelmans, O., Bluhm, G., Selander, J., Haralabidis, A., Dimakopoulou, K., Sourtzi, P., Velonakis, M., Vigna-Taglianti, F.; HYENA Study Team. (2008). Hypertension and exposure to noise near airports: The HYENA study. *Environmental Health Perspectives*. 116(3):329-333.
- Kopsch, F. (2016). The cost of aircraft noise - does it differ from road noise? A meta-analysis. *Journal of Air Transport Management*. 57:138-142.
- Matsui, T., Uehara, T., Miyakita, T., Hiramatsu, K., Yasutaka, O., & Yamamoto, T. (2004). The Okinawa study: Effects of chronic aircraft noise on blood pressure and some other physiological indices. *Journal of Sound and Vibration*. 277:469-470.
- Rosenlund, M., Berglund, N., Pershagen, G., Jarup, L., & Bluhm, G. (2001). Increased prevalence of hypertension in a population exposed to aircraft noise. *Occupational and Environmental Medicine*. 58(12):769-773.
- Wolfe, P.J., Yim, S.H.L., Lee, G., Ashok, A., Barrett, S.R.H., & Waitz, I.A. (2014). Near-airport distribution of the environmental costs of aviation. *Transport Policy*. 34:102-108.



## Project 009 Geospatially Drive Noise Estimation Module

### Georgia Institute of Technology

#### Project Lead Investigator

Principal Investigator:

Professor Dimitri N. Mavris

Director, Aerospace Systems Design Laboratory

School of Aerospace Engineering

Georgia Institute of Technology

Phone: (404) 894-1557

Fax: (404) 894-6596

Email: dimitri.mavris@ae.gatech.edu

Co-Principal Investigator:

Dr. Holger Pfaender

Aerospace Systems Design Laboratory

School of Aerospace Engineering

Georgia Institute of Technology

Phone: (404) 385-2779

Fax: (404) 894-6596

Email: holger.pfaender@ae.gatech.edu

#### University Participants

##### Georgia Institute of Technology

- PIs: Dr. Dimitri Mavris, Dr. Holger Pfaender
- FAA Award Number: 13-C-AJFE-GIT-059
- Period of Performance: June 5, 2020 to June 4, 2021
- Tasks:
  1. Literature Review and GIS Software Evaluation.
  2. Investigation of Emerging Computational Technologies.
  3. Collaboration with UAS Computation Module Development Team.
  4. Noise Computation Engine Integration.

#### Project Funding Level

This project is funded at the following levels: Georgia Institute of Technology (\$250,000). The Georgia Institute of Technology has agreed to a total of \$250,000 in matching funds. This total includes salaries for the project director, research engineers, and graduate research assistants and for computing, financial, and administrative support, including meeting arrangements. The institute has also agreed to provide tuition remission for students whose tuition is paid via state funds.

#### Investigation Team

##### Georgia Institute of Technology

- PI: Dimitri Mavris
- Co-Investigator: Holger Pfaender
- Graduate Students: Aroua Gharbi, Cem Yumuk, Anthony Markowitz

#### Project Overview

The goal of this task is to develop a novel geospatially driven noise estimation module to support computation of noise resulting from the operation of Unmanned Aircraft Systems (UAS) and other upcoming vehicle concepts. The development

of the module will leverage emerging computational technologies in order to achieve fast and efficient modeling of a potentially large number of vehicles and operations. The module will be designed to be integrated as a component module or plug-in to other applications relying on a Geographic Information System (GIS) interface. The noise estimation approach will be based on the concept of precomputed noise grid tiles addition. The module’s design phase will identify what emerging open-source geospatial and data processing technologies would be best suited to serve as the module’s computational infrastructure and assess if they can provide innovative, maintainable, and affordable solutions.

## Task 1 – Literature Review and GIS Software Evaluation

Georgia Institute of Technology

### Objectives

Develop a novel geospatially driven noise estimation module to support computation of noise resulting from the operation of UAS and other upcoming vehicle concepts.

### Research Approach

This Task aims to identify the leading GIS software. This review focused on open-source options. For an adequate evaluation of the options, six criteria were set forth:

1. Data import: Ability to read shape files format of input geometrical data as well as rasterized (gridded) data.
2. Data storage: Capability to store geospatial data in either shape/vector formats or rasterized data.
3. Geometric calculations: Conversion to and from Cartesian coordinate system and other Earth model coordinates and ability to compute polygon areas and lengths as well as unions and substructions.
4. Geospatial calculations: Ability to perform calculations on given vector or raster data and draw contour plots.
5. Display: Ability to print raw or processed geospatial data as various map displays.
6. Map data: Capability to display results with relation to landmasses, political boundaries such as states and counties, as well as roads and buildings.

### QGIS

QGIS is a user-friendly open-source GIS written in C++. It runs on Linux, Unix, Mac OSX, Windows, and Android and supports numerous vectors, raster, and database formats and functionalities. Apart from built-in functionalities, QGIS allows users to install and create their own plugins. New applications can also be created in QGIS through C++ and Python languages.

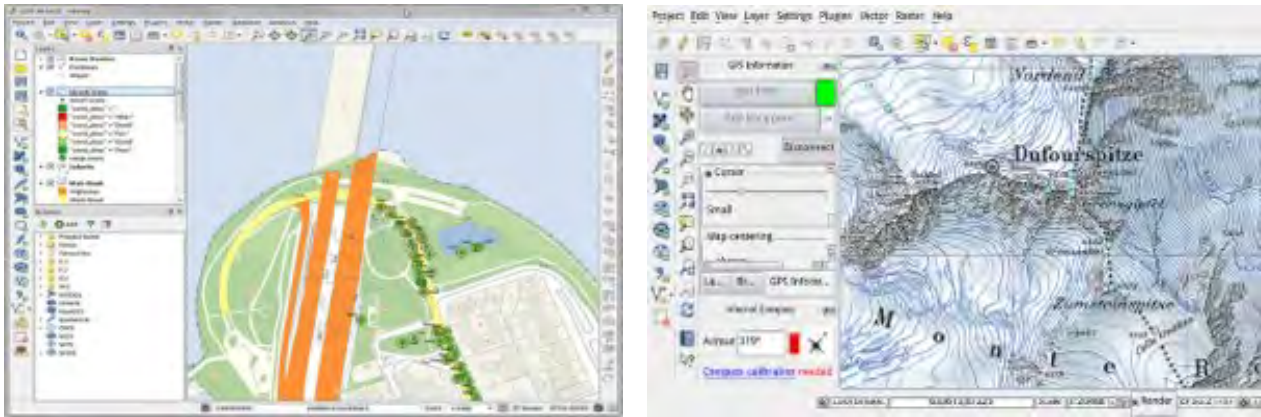


Figure 1. Screenshot of QGIS.

### Evaluation Criteria

1. Data import: Imports shape and raster files.
2. Data storage: Stores geospatial data in vector and raster formats.
3. Geometric calculations: Supports Cartesian (x, y), polar (length, angle), projected (x-north, y-east); calculates length or area of geometry features; and provides overlay, union and difference between areas.



4. Geospatial calculations: Creates vector contour map from an elevation raster; and carries out raster to vector conversion.
5. Display: Web mapping is available with QGIS2Web.
6. Map data: Displays geospatial data such as countries, states, and counties as well as roads.

### Open JUMP

OpenJUMP is a Java-based open-source GIS. It works on Windows, Linux, and Mac platforms having Java 1.7 or later. Reading and writing vector formats, displaying geospatial data, and execution of geometric calculations are some of OpenJUMP's features. Additional plugins for more capabilities are also available.

#### Evaluation Criteria

1. Data import: Imports shape and raster files.
2. Data storage: Stores geospatial data in vector and raster formats.
3. Geometric calculations: Supports Coordinate Reference System (CRS), (Cartesian (x, y, z), geographic (longitude, latitude, height) and projected (x-north, y-east)); provides CRS transformation library called PROJ; calculates length or area of geometry features; provides overlay, union and subtraction.
4. Geospatial calculations: Provides conversion between desired file formats (raster to vector conversion); does NOT feature contour plot.
5. Display: Does NOT provide web application.
6. Map data: Display geospatial data such as countries, states, and counties as well as roads.

### SAGA (System for Automated Geoscientific Analyses)

SAGA is an open-source cross-platform GIS software written in C++. It can be run on Windows, Linux, FreeBSD, and Mac (OS X). SAGA provides multiple libraries for GIS calculations: digital terrain analysis, image segmentation, fire spreading analysis and simulation, etc. In addition to these libraries, SAGA allows the scripting of custom models through the Command Line Interface and the Python interface.

#### Evaluation Criteria

1. Data import: Imports shape and raster files.
2. Data storage: Stores geospatial data in vector and raster formats.
3. Geometric calculations: Supports Geographic Coordinate System (latitude, longitude) and Universal Transverse Mercator (UTM).
4. Geospatial calculations: Performs raster to vector conversions and can create contour lines.
5. Display: Displays data with histogram and scatter plot; provides web mapping service.
6. Map data: Enables visualization of spatial data into cartographic maps. It can also import maps from Web Map Service (WMS) and Open Street Map.

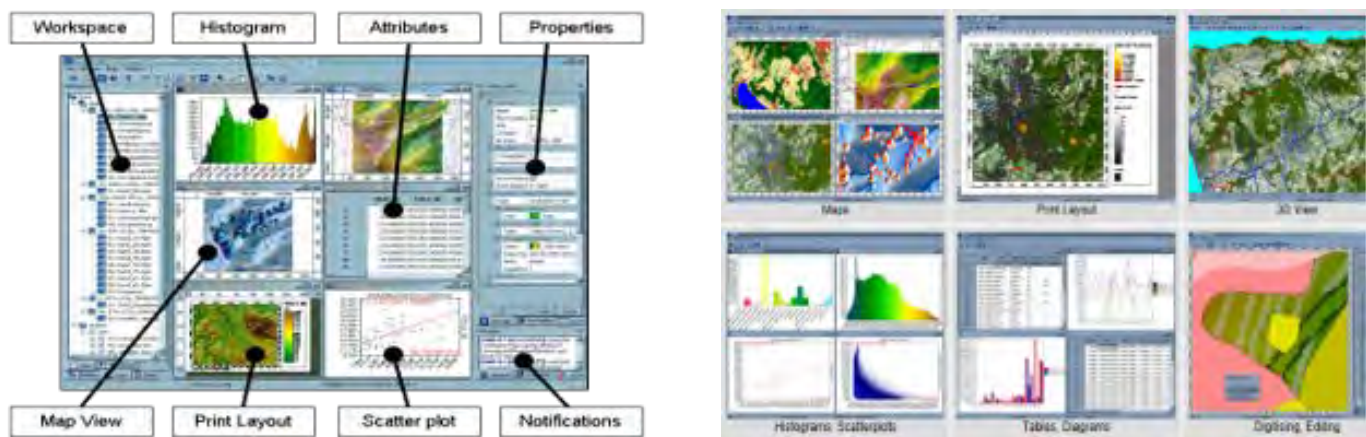


Figure 2. Screenshot of SAGA.



## Deck.gl

Deck.gl is a WebGL visualization framework for large data sets. It allows the users to map data (JSON objects, csv) into a stack of layers. These layers can be imported directly from a catalogue or built by the user.

### Evaluation Criteria

1. Data import: Reads only csv files.
2. Data storage: Doesn't store geospatial data into vector or shape files.
3. Geometric calculations: Supports Geographic Coordinate System (latitude, longitude) using Web Mercator.
4. Geospatial calculations: Doesn't convert raster data to vector data. Can create contour lines for a given threshold and cell size.
5. Display: Offers an architecture for packaging advanced WebGL based visualizations; enables users to quickly get impressive visual results with limited effort.
6. Map data: Displays geospatial data with relation to roads and buildings easily.

## GRASS GIS

GRASS stands for Geographic Resources Analysis Support System. It is an open-source Java-based software for vector and raster geospatial data management, geoprocessing, spatial modelling, and visualization. It has compatibilities with QGIS, meaning that QGIS can run some features of GRASS GIS as a plugin. Already developed addons along with capability to develop own addons are available.

### Evaluation Criteria

1. Data import: Imports vector and raster files.
2. Data storage: Stores geospatial data in vector and raster formats.
3. Geometric calculations: Supports Coordinate Reference System (CRS), (Cartesian (x, y, z) and geographic (longitude, latitude, height)); provides CRS transformation library called PROJ; calculates length or area of geometry features; provides overlay, union, and subtraction.
4. Geospatial calculations: Provides conversion between desired file formats (raster to vector conversion); creates contour lines.
5. Display: Provides web mapping service.
6. Map data: Displays geospatial data such as countries and states by using Inkspace.

## GeoPandas

GeoPandas is an open-source project developed in Python to provide a useful library for working with geospatial data. It is able to run on distributions of Linux and Windows. It primarily uses the Python packages pandas (as a base for its data storage), shapely (to manipulate the shapes stored in the advanced database), Fiona (for file access), and Descartes and matplotlib (for plotting the visuals of the data). It is most adept at displaying discrete sections of data in a geospatial visualization. It is limited in its ability to display graphics outside of the Python environment and does not support conversion to the desired raster/vector formats.

### Evaluation Criteria

1. Data import: Read almost any vector-based spatial data format.
2. Data storage: Store geospatial data in vector and raster formats.
3. Geometric calculations: Supports Coordinate Reference System (CRS); cannot calculate length or area of geometry features; has overlay functions, such as intersections between two or more areas, union (merges the areas of one layer to one single area), difference (A-B areas), and polygons.
4. Geospatial calculations: No conversion to any desired file formats (no raster to vector formats); does not provide contour plot function.
5. Map data: Uses various map projection using CartoPy, Python library.
6. Display: Does not provide web application; good representation in 3D colorspace using matplotlib.



Figure 3. GeoPandas can overlay processed geospatial data over existing maps.

### WorldWind

WorldWind is an open-source virtual 3D globe visualization API developed by NASA in partnership with the European Space Agency. It is written in both Java (for desktop and Android devices) and JavaScript (for web applications). After being suspended from development in 2019, it was refunded in August of 2020. It can import a variety of input files with geospatial data, stores the data in both raster and vector formats, does sufficient geometric and geospatial calculations, and produces good visualizations with comprehensive map data.

### Evaluation Criteria

1. Data import: Import shapefile, KML, VPF, GML, GeoJSON, GeoRSS, GPX, NMEA, etc.
2. Data storage: Store geospatial data in vector and raster formats.
3. Geometric calculations: Support Geographic Coordinate System (latitude, longitude), Universal Transverse Mercator (UTM), and MGRS; draw and measure distance and area across the terrain.
4. Geospatial calculations: Display contour lines on surface terrain at a specified elevation.
5. Map data: Visual representation of scalar values, like noise, over a grid of geographic positions; visualize the results on web and Android platform.
6. Display: Display geospatial data divided into country, states, and city.

### Overall Evaluation

	Intuitive GUI	Compatibility	Statistical Analyses	Data Import	Data Storage	Geometric Calculations	Geospatial Calculations	Map Data	Display	Total
QGIS	3	5	3	5	5	5	5	5	4	40
Open JUMP										
SAGA	3	3	4	5	5	4	5	5	4	38
Deck.gl	4	3	1	1	1	3	3	5	5	26
Kepler.gl										
GRASS										
gvSIG										
MapWindow										
GeoPandas		3		5	5	4	1	2	2	19
WorldWind		5		5	5	4	4	5	5	28

GIS applications can be broadly classified in two categories, desktop and web-based applications.



WebGIS applications use web technologies to display and communicate geospatial information to an end user. There are five common elements in every webGIS application:

1. A web application
  - The interface used by the client. It has tools to visualize, analyze, and interact with geographic information. It can be run on a web browser or a GPS-enabled device.
2. Digital basemaps
  - The geographical context for the application. E.g., transportation, topography, imagery, etc.
3. Operational layers
  - The layer to display the results of an operation. E.g., observations, sensor feeds, query results, analytic results, etc.
4. Tasks and tools in the webGIS application
  - Tools to perform operations beyond mapping.
5. Geodatabase(s)
  - Container of geo data. It can be geodatabase(s), shape files, tabular databases, CAD files, etc.

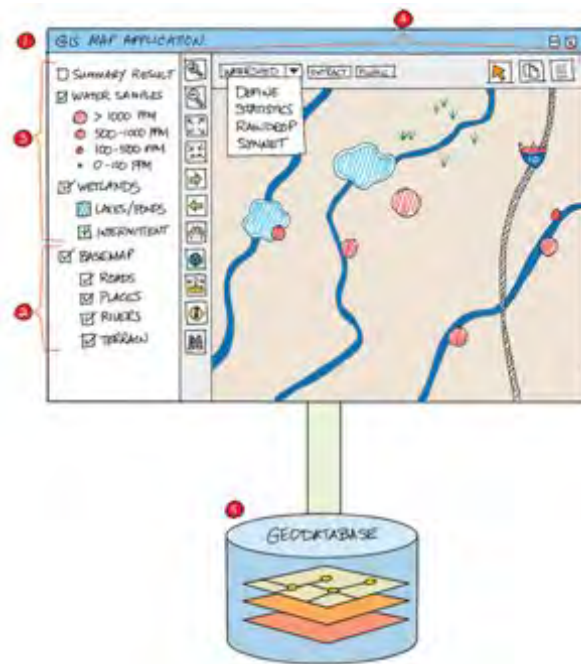


Figure 4. A sketch of a webGIS application.

WebGIS applications come with multiple advantages as well as limitations. These are provided in the non-exhaustive list in table below:

Advantages of WebGIS	Drawbacks of WebGIS
<ul style="list-style-type: none"> <li>• Provide a broader reach for the customers compared to a traditional desktop application</li> <li>• Better cross-platform capability with the different web browsers that can be used</li> <li>• Easy to use for customers with different levels of GIS expertise</li> <li>• Extendable to cloud services hence allowing manipulation and use of big GIS data</li> <li>• Lower cost to entry. Most of the libraries and tools are open source with good community support</li> <li>• Allows real-time analysis</li> </ul>	<ul style="list-style-type: none"> <li>• Harder to build. The developers need to have a good knowledge of multiple scripting languages to build the app (Python, JavaScript, html, etc.)</li> <li>• Security of the data might be dependent on a third party</li> <li>• The application might need to be hosted outside of the organization</li> </ul>

The team has also started a dialogue with the Aviation Environmental Design Tool (AEDT) development team as to which GIS functionality will be required in order to be able to integrate the UAS noise engine into AEDT in the future.

## Task 2 – Investigation of Emerging Computational Technologies

The Ascent 9 team has started to develop an initial testing plan to investigate the emerging computational technologies with a sample test problem in various GIS and computational environments.

## Task 3 – Collaboration with UAS Computation Module Development Team

The ASCENT Project 9 team started an initial dialogue with the UAS Computation Module Development team at Mississippi State University to explore way that both teams can effectively collaborate and exchange data and ideas.

## Task 4 – Noise Computation Engine Integration

This task has not been started yet.

### Milestone

The team presented an initial overview of candidate GIS systems to FAA and members of the AEDT development team.

### Major Accomplishments

None yet.

### Publications

None

### Outreach Efforts

Initial outreach and coordination with the ASSURE Center of Excellence team and their work at Mississippi State University.

### Awards

None

### Student Involvement

The Georgia Institute of Technology student team consists of three graduate research assistants (GRA). At the beginning of the project, all seven GRAs engaged in the GIS background research. The team is now being divided into tackling the different aspects and implementation of the noise engine and the novel computational technology testing.

### Plans for Next Period

This project is still in the middle of the Year 1 work plan. Therefore, the plan for the reporting period is to finish the current work plan and test the emerging computational technologies on a defined sample problem. After further collaboration with the team at Mississippi State University, the noise computation engine will be integrated into a user interface as planned.



# Project 010 Aircraft Technology Modeling and Assessment

**Georgia Institute of Technology and Purdue University**

## Project Lead Investigators

Dimitri Mavris (PI)  
Regents Professor  
School of Aerospace Engineering  
Georgia Institute of Technology  
Mail Stop 0150  
Atlanta, GA 30332-0150  
Phone: 404-894-1557  
E-mail: dimitri.mavrisatae.gatech.edu

William Crossley (PI)  
Professor  
School of Aeronautics and Astronautics  
Purdue University  
701 W. Stadium Ave  
West Lafayette, IN 47907-2045  
Phone: 765-496-2872  
E-mail: crossleyatpurdue.edu

Jimmy Tai (Co-PI)  
Senior Research Engineer  
School of Aerospace Engineering  
Georgia Institute of Technology  
Mail Stop 0150  
Atlanta, GA 30332-0150  
Phone: 404-894-0197  
E-mail: jimmy.taiatae.gatech.edu

Daniel DeLaurentis (Co-PI)  
Professor  
School of Aeronautics and Astronautics  
Purdue University  
701 W. Stadium Ave  
West Lafayette, IN 47907-2045  
Phone: 765-494-0694  
E-mail: ddelaureatpurdue.edu

## University Participants

### Georgia Institute of Technology

- PIs: Dr. Dimitri Mavris (PI), Dr. Jimmy Tai (Co-PI)
- FAA Award Numbers: 13-C-AJFE-GIT-006, -012, -022, -031, -041
- Period of Performance: September 1, 2019 to August 31, 2020
- Tasks: 16



### Purdue University

- PIs: Dr. William A. Crossley (PI), Dr. Daniel DeLaurentis (Co-PI)
- FAA Award Numbers: 13-C-AJFE-PU-004, -008, -013, -018, -026, -032, -035
- Period of Performance: September 1, 2019 to August 31, 2020
- Tasks: 1, 2, 4, 5

## Project Funding Level

The project is funded at the following levels: Georgia Institute of Technology (\$1,200,000); Purdue University (\$222,116). Cost share details are below:

The Georgia Institute of Technology has agreed to a total of \$1,200,000 in matching funds. This total includes salaries for the project director, research engineers, and graduate research assistants, as well as computing, financial, and administrative support, including meeting arrangements. The institute has also agreed to provide tuition remission for the students, paid for by state funds. During the period of performance, in-kind cost share is also obtained for cost share.

Purdue University provides matching support through salary support of the faculty PIs and through salary support and tuition and fee waivers for one of the graduate research assistants working on this project.

## Investigation Team

### Georgia Institute of Technology

- PI: Dimitri Mavris
- Co-Investigator: Jimmy Tai (Task 4)
- Fleet Modeling Technical Leads: Holger Pfaender, Michelle Kirby, and Mohammed Hassan (Tasks 1, 2, and 5)
- Graduate Students: Thomas Dussauge, Thayna Da Silva Oliveira, Nadir Ougazzaden, Taylor Fazzini, Rick Hong, Nikhil Iyengar, Barbara Sampaio, Kevyn Tran, Edan Baltman, Kaleb Cornick, Brennan Stewart, Ezgi Balkas, Nadir Ougazzaden, David Shalat, Joao De Azevedo, Eddie Li, Colby Weit, Jiajie Wen

### Purdue University

- PI: William Crossley (Tasks 1,2, 4, and 5)
- Co-Investigator: Daniel DeLaurentis (Tasks 1, 2, 4, and 5)
- Graduate Students: Samarth Jain, Suzanne Swaine, Kolawole Ogunsina, Hsun Chao

## Project Overview

Georgia Institute of Technology (Georgia Tech) and Purdue have partnered to investigate the future demand for supersonic air travel and the environmental impact of supersonic transports (SSTs). In the context of this research, environmental impacts include direct CO<sub>2</sub> emissions and fuel consumption. The research is conducted as a collaborative effort to leverage capabilities and knowledge available from the multiple entities that make up the ASCENT university partners and advisory committee. The primary objective of this research project is to support the Federal Aviation Administration (FAA) in modeling and assessing the potential future evolution of the next-generation supersonic aircraft fleet. Research under this project consists of five integrated focus areas: (a) establishing fleet assumptions and performing demand assessment; (b) performing preliminary SST environmental impact prediction; (c) testing the ability of the current Aviation Environmental Design Tool (AEDT) to analyze existing supersonic models; (d) performing vehicle and fleet assessments of potential future supersonic aircraft; and (e) modeling SSTs by using a modeling and simulation environment named Framework for Advanced Supersonic Transport (FASST).

In order to better understand the potential demand for supersonic air travel, the team developed a parametric airline operating cost model in order to be able to explore the sensitivities of key vehicle, operational, and cost parameters on the required yield an airline would have to target for ticket prices on such a potential new supersonic aircraft. The current model, however, assumes fixed parameters for key vehicle metrics—which can be changed—but do not include sensitivities to key vehicle design choices such as vehicle size, design cruise Mach number, and maximum range. This task will examine the implications of the physical and technical dependencies on the airline operational cost. Through the vehicle performance sensitivities such as passenger capacity and design cruise Mach number, it will be possible to determine the combined “sweet spot” that would be the most profitable vehicle to operate for an airline. In order to accomplish this, the existing vehicle models created in the prior year will be utilized and supplemented by additional vehicles proposed in Task 4. These vehicles



together will serve as the foundation to create credible sensitivities with regards to parameters such as vehicle size and design cruise Mach number. These sensitivities will then be embedded into the airline operating cost estimation model and utilized to explore the combined vehicle and airline operational space in order to identify the most economically feasible type of supersonic vehicle.

In an independent but complementary approach to consider demand and routes for supersonic aircraft, the Purdue team developed a ticket pricing model for possible future supersonic aircraft that relies upon current as-offered fares for business class and above, for routes that could have passenger demand for supersonic aircraft. Via an approach considering the size of the potential demand at fares business class and above on a city-pair route, the distance of that city-pair route, an adjustment to allow for the shortest trip time by increasing the overwater distance of the route, and the range capability of a simplistically modeled medium SST (55-passenger capacity) to fly that route, the Purdue team identified 205 potential routes that could see supersonic aircraft service in a network of routes with at least one end in the United States. Of these 205 potential routes, 193 are direct routes, and 12 are routes that would require fuel stops but would still save travel time over a subsonic nonstop flight on the same route. By providing these potential routes to the Fleet-Level Environmental Evaluation Tool (FLEET) simulation, the allocation problem in FLEET then determines how many supersonic aircraft would operate on these routes, giving a prediction of which routes would see supersonic aircraft use and the number of supersonic flights operated on those routes at dates in the future.

One of the accomplishments of the project during the performance period is the development of two FASST models. Two supersonic vehicles, a medium and large SST, have been modeled in FASST. The large SST is designed to carry 100 passengers for 5,000 nmi cruising at Mach 1.8. The medium SST is designed to carry 55 passengers for 4,500 nmi cruising at Mach 2.2. The propulsion system for both the medium and large SST models are of a clean sheet design.

Georgia Tech and Purdue exercised their respective fleet analysis tools—the Global and Regional Environmental Analysis Tool (GREAT) and FLEET—and produced estimates of the fleet-level impact of a potential fleet of supersonic aircraft operating in the future. The SSTs required for these fleet-level analyses are provided by the vehicle modeling tasks with FASST, a derivative framework from Environmental Design Space (EDS). The outcome of this study provides a glimpse into the future potential state of supersonic air travel by using physics-based models of supersonic vehicle performance. Future work should build on current estimates to conduct more detailed analyses of vehicle and fleet performance.



## Table of Acronyms and Symbols

$\alpha$	$T/T_{sl}$ , installed full-throttle thrust lapse
A4A	Airlines for America
$A_c$	Inlet capture area
ADP	Aerodynamic design point
AEDT	Aviation Environmental Design Tool
ANP	Aircraft noise performance
$A_0$	Reference inlet area
AoA	Angle of attack
APU	Auxiliary power unit
$\beta$	Multiplier used to capture impacts of both fuel burn and utilization on airline costs
BADA	Base of Aircraft Data
BFFM	Boeing Fuel Flow Method
BPR	Bypass ratio
BTS	Bureau of Transportation Statistics
CAEP	Committee on Aviation Environmental Protection
$C_{all-other}$	All other costs
CART3D	NASA Inviscid Computational Fluid Dynamics Program
CAS	Calibrated airspeed
$C_{D0}$	Profile drag
$C_{DR}$	Additional drag caused by flaps, ground friction, etc.
$C_{fixed}$	Fixed proportions of airline operating cost
$C_{fuel}$	Fuel cost of airline operating cost
CG	Center of gravity
$C_L$	Lift coefficient
CLEEN	Continuous lower energy, emissions, and noise
CMPGEN	NASA Program for Compressor Map Generation
$CO_2$	Carbon dioxide
$d$	Distance between center of inoperative engine and aircraft longitudinal axis
$\delta_{amb}$	Ratio of total pressure
$\Delta t$	Total segment flight time
$\Delta T$	Change in temperature from standard atmospheric temperature
$\Delta X$	Distance between CG of vehicle and aerodynamic center of tail
$\Delta z_e$	Total change in segment energy height
D	Drag
DNL	Day-night level
DoE	Design of Experiment
EDS	Environmental Design Space
EEDB	Engine Emissions Databank
$eff_{REF}$	Reference fuel efficiency metric
EI	Emissions index
EINO <sub>x</sub>	NO <sub>x</sub> emissions index
EIS	Entry into service
EPNdB	Effective perceived noise in decibels
$\phi$	Cooling effectiveness
FAA	Federal Aviation Administration
FAR	Fuel to air ratio
FASST	Framework for Advanced Supersonic Transport
$FB_A$	Fuel penalty to accelerate
$FB_{D\&L}$	Fuel penalty to descend from cruising altitude and land
$FB_{REF}$	Reference subsonic fuel burn
$FB_{SST}$	Supersonic fuel burn
$FB_{T\&C}$	Fuel penalty to takeoff and climb to cruising altitude
FF	Fuel flow
FLEET	Fleet-Level Environmental Evaluation Tool



FLOPS	Flight Optimization System
FPR	Fan pressure ratio
$\gamma$	Acquisition multiplier used to scale the proportion of ownership costs
$\gamma_{\text{airline}}$	Average yield per unit distance for a commercial subsonic airline
GC	Great circle
GRA	Graduate research assistant
GREAT	Global and Regional Environmental Analysis Tool
HPC	High-pressure compressor
HPCPR	High-pressure-compressor pressure ratio
HPT	High-pressure turbine
ICAO	International Civil Aviation Organization
IDEA	Interactive Dynamic Environmental Analysis
IGV	Inlet guide vanes
ISA	International standard atmosphere
$K_1$	Coefficients of parabolic lift-drag polar
$K_2$	Coefficients of parabolic lift-drag polar
KEI	Key environmental indicators
JFK	John F. Kennedy International Airport code
LAX	Los Angeles International Airport code
L/D	Lift-to-drag ratio
LE	Leading edge
LPC	Low-pressure compressor
LPCPR	Low-pressure-compressor pressure ratio
LPP MRA	Lean Pre-mixed Pre-vaporized Multi Radial Axial
LPT	Low-pressure turbine
LSA	Large single aisle
LTA	Large twin aisle
LTO	Landing and takeoff
M	Mach number
$Mach_{\text{sub}}$	Subsonic cruise Mach number
$Mach_{\text{super}}$	Supersonic cruise Mach number
MDP	Multi-design point
MFTF	Mixed flow turbofan
MTOM	Maximum takeoff mass
MTOW	Maximum takeoff weight
$n$	Load factor or number of flight segments
$n_a$	Number of accelerations
NASA	National Aeronautics and Space Administration
$n_f$	Number of fuel stops
NO <sub>x</sub>	Nitrogen oxide
NPD	Noise power distance
NPR	Nozzle pressure ratio
NPSS	Numerical Propulsion System Simulation
OGV	Outlet guide vanes
OpenVSP	Open Vehicle Sketch Pad
OPR	Overall pressure ratio
PACI	Passenger Airline Cost Index
$PAX_{\text{REF}}$	Reference subsonic number of passengers
$PAX_{\text{SST}}$	Number of passengers of the supersonic aircraft
PCBOOM	NASA PC Software for Predicting Sonic Boom on the Ground
PDEW	Passengers daily each way
PI	Principal investigator
PIPSI	Performance of Installed Propulsion System Interactive
PLdB	Sound pressure level in dB
$P_s$	Weight specific excess power
$q$	Dynamic pressure
Pt3	Combustor inlet total pressure
$\rho$	Air density
R	Rolling resistance force



$R_{C,max}$	Maximum cruise range for supersonic vehicles
RJ	Regional jet
RQL	Rich Burn, Quick Quench, Lean Burn
S	Wing area
SAR	Specific air range
$SAR_{sub}$	Specific air range for subsonic aircraft
$SAR_{super}$	Specific air range for supersonic aircraft
$S_C$	Cruise range
SA	Single aisle (includes both SSA and LSA classes)
SEL	Single event level
SFTF	Separate flow turbofan
SLS	Sea level static
SP	Switching percentage
SSA	Small single aisle
SST	Supersonic transport
STA	Small twin aisle
$S_{tail}$	Tail area
$\theta_{amb}$	Ratio of total temperature
T	Thrust
T3	Compressor exit temperature
T41	Turbine rotor entrance temperature
$t_{cool}$	Cooled temperature
$t_{C,sub}$	Cruise time for subsonic vehicle
$t_{C,sup}$	Cruise time for supersonic vehicle
$t_{D\&L}$	Time to descent from cruising altitude and land
TE	Trailing edge
$t_{gas}$	Gas temperature
TO	Takeoff
$t_{metal}$	Metal temperature
TOC	Top of climb
$t_{REF}$	Flight times for reference subsonic aircraft
$t_{re-fuel}$	Time delay (90 minutes) for fuel stops
TSFC	Thrust specific fuel consumption
$T_{SL}$	Thrust at sea level
$t_{SST}$	Flight time for supersonic aircraft
Tt3	Combustor inlet total temperature
$t_{T\&C}$	Time to takeoff and climb to cruising altitude
$t_{total,sub}$	Total subsonic flight time
$t_{total,sup}$	Total supersonic flight time
$U_{REF}$	Utilization for subsonic aircraft used as reference
$U_{SST}$	Utilization for supersonic aircraft
V	Velocity
$V_C$	Cruise speed
$V_{C,sub}$	Subsonic cruise speed
$V_{C,sup}$	Supersonic cruise speed
$V_{SR1}$	Reference stall speed
VLA	Very large aircraft
VT	Vertical tail
VTTs	Value of travel time savings
WATE	Weight approximation for turbine engines
$W_E$	Empty weight
$W_f$	Fuel weight
$W_f$	Weight of aircraft at the end of a mission segment
$W_i$	Weight of aircraft at the beginning of a mission segment
$W_p$	Payload weight
$W_{TO}$	Takeoff weight
x	Percentage of flight over water



## Project Introduction

Georgia Tech and Purdue partnered to investigate the effects of supersonic aircraft on future environmental impacts of aviation. Impacts assessed at the fleet level include direct CO<sub>2</sub> emissions and fuel consumption. The research is conducted as a collaborative effort to leverage capabilities and knowledge available from the multiple entities that make up the ASCENT university partners and advisory committee.

The primary objective of this research project is to support the FAA in modeling and assessing the potential future evolution of the next-generation supersonic aircraft fleet. Research under this project Task 1 focuses on development of fleet demand drivers for supersonic transport. This Task will explore and estimate the potential demand for supersonic travel. In Task 3, Georgia Tech will continue to support the development of supersonic aircraft analysis capabilities into AEDT and identify modeling issues and work with the AEDT development team to identify required modifications. Task 2 will perform a fleet impact assessment using the scenarios and vehicle performance metrics developed in Tasks 1. Task 4 will develop detailed supersonic aircraft model for 100-passenger class and support Committee on Aviation Environmental Protection (CAEP) supersonic exploratory study, and Task 5 is will develop capability to generate Base of Aircraft Data 4 (BADA4) coefficients in order to provide additional BADA4 vehicles for AEDT.

Because of extensive experience in assessing the FAA Continuous Lower Energy, Emissions, and Noise project (CLEEN I), Georgia Tech is selected as the lead for all four objectives described above. Purdue supported the objectives shown in Table 1, which lists the high-level division of responsibilities.

**Table 1.** University Contributions for Year 3.

Objectives		Georgia Tech	Purdue
1	Fleet Assumptions and Demand Assessment	Expand airline cost model: Capture vehicle performance sensitivities (passenger capacity, cruise Mach number); Evaluate which size vehicle the most likely to be able to close the business case.	Airline fleet composition and network; Passenger choice for supersonic/subsonic demand; Effect of supersonic aircraft on subsonic aircraft operations and pricing.
2	Fleet Analysis	Develop assumptions for supersonic scenarios relative to 12 previously developed subsonic focused fleet scenarios; Perform fleet analysis with the gradual introduction of SST vehicles into the fleet.	Develop assumptions for supersonic scenarios relative to 12 previously developed subsonic focused fleet scenarios; Perform fleet-level assessments, including additional SST vehicle types; Develop FLEET-like tool for supersonic business jet operations; Simple SST sizing to support FLEET development and studies.
3	AEDT Vehicle Definition	Develop methods to model supersonic flights in AEDT.	n/a
4	Support CAEP Efforts	FASST vehicle modeling: Develop additional SST class for 100 passengers; Develop AEDT coefficient generation algorithm for BADA3 supersonic coefficient (redirected to BADA4); Perform trade studies to support CAEP Exploratory Study.	Provide representative supersonic demand scenarios; Develop and assess airport noise model to account for supersonic aircraft.
5	BADA4 Coefficient Generation	Develop, implement, and test BADA4 coefficient generation algorithms; Identify gaps and needs for BADA4 coefficient generation for SST.	n/a
6	Coordination	Coordinate with entities involved in CAEP Supersonic Exploratory Study; Coordinate with clean-sheet supersonic engine design project.	Coordinate with entities involved in CAEP MDG/FESG, particularly the SST demand task group; Maintain ability to incorporate SST vehicle models that use the engine design from ASCENT Project 47 and/or NASA-developed SST models.

Georgia Tech led the process of developing a supersonic routing tool that was used to create the basic information about potential time savings and the additional cost. This information was then used to develop a demand forecast for commercial supersonic travel. This work is performed under Objective 1, and the outcome was used to support Objective 2. Under Objective 2, Georgia Tech also produced results for multiple scenarios to assess the fleet-level impacts of supersonic vehicles.

Purdue applied their FLEET tool under Objective 2, using a subset of the fleet assumptions defined in Objective 1 and preliminary vehicle impact estimates from Objective 4. This activity demonstrated the capabilities of FLEET for assessment of fleet-level environmental impacts as a result of new aircraft technologies and distinct operational scenarios.

Georgia Tech developed additional aircraft concepts in FASST under Objective 4. This was done in consideration of supporting a trade study that will help potentially support the CAEP Exploratory Study. For Objectives 3 and 5, Georgia Tech explored the requirements for modeling supersonic vehicles in AEDT, and under Objective 5 developed an approach to generate BADA4 coefficients. After discussion with the sponsor, it was decided that rather than attempting to model supersonic aircraft in BADA3 under Objective 3 to instead utilize the capabilities developed under Objective 5.

Under Objective 6, Georgia Tech supported coordination and meetings with the member entities of CAEP Modeling and Databases Group (MDG)/ Forecasting and Economic Analysis Support Group (FESG) as well as NASA and ASCENT Project 47. This involved a series of weekly meetings, ad-hoc groups, and in-person meetings, as well as virtual versions of those meetings that could no longer be held in person.

## Milestones

Georgia Tech had four milestones for this year of performance:

1. Fleet assumptions and demand analysis.
2. Fleet analysis and demand results.
3. FASST SST descriptions and characteristics in PowerPoint format.

For Purdue, the proposal covering this year of performance listed three milestones:

1. Complete modeling of the chosen contractor's technologies.
2. Update fleet assessment.
3. Support CAEP efforts.

The Purdue team is using its in-house simplistic "back of the envelope" representation of the ASCENT Project 10 (A10) notional medium SST aircraft to characterize the potential supersonic routes based on a number of filters. The team identified 258 potential "supersonic-eligible" routes, including 241 nonstop routes and 17 routes with fuel stops.

The Purdue team has also incorporated the detailed A10 notional medium SST aircraft flown on the detailed supersonic routing path (both provided by Georgia Tech) in FLEET and performed fleet-level assessments for the single Current Trends Best Guess (CTBG) scenario. The FLEET allocation results indicate routes where supersonic aircraft might be used and the number of operations, along with changes in the utilization of the subsonic aircraft in the fleet.

## Major Accomplishments

The following are the major tasks completed under A10 during the period of performance:

### Fleet-Level Assumptions and Demand Assessment (Task 1)

Georgia Tech team has developed a parametric airline operating cost model in order to be able to explore the sensitivities of key vehicle, operational, and cost parameters on the required yield an airline would have to target for ticket prices for a potential new supersonic aircraft. As a starting point, the team established a baseline airline cost structure representative of subsonic operations using A4A airline operating costs.

The Purdue team updated FLEET's passenger demand and route network using historical Bureau of Transportation Statistics (BTS) data for years from 2005 through 2018, and model-based predictions for years 2019 and beyond. The team used the previously developed "back of the envelope" representation of the A10 notional medium SST aircraft to identify "supersonic-eligible" routes, including both nonstop routes and routes with one fuel stop. The team also incorporated the detailed A10 notional medium SST aircraft from Georgia Tech into FLEET along with the detailed supersonic routing path (also from Georgia Tech).

### **Fleet Analysis (Task 2)**

One of the major accomplishments during the period of performance for this Task is the capability to identify routes that are suitable for SST operations. This demand route algorithm also evaluates the penalties associated with the restriction of supersonic overland flight, and it becomes a crucial enabler for commercial supersonic demand assessment.

Purdue conducted fleet-level assessments for the updated route network in FLEET using the detailed A10 notional medium SST aircraft (flown on detailed supersonic routing path). The outputs included number of operations and number of passengers served by supersonic aircraft on routes profitable supersonic-eligible routes, and similar details about subsonic aircraft on both supersonic and subsonic routes.

### **AEDT Supersonic Modeling (Task 3)**

The original intent of Task 3 is to develop methods for AEDT to model supersonic transports. At the writing of the proposal, AEDT utilizes BADA3 for vehicle modeling; therefore, the proposal has been focused on BADA3 approaches. Since then and at the writing of this report, AEDT is transitioning to BADA4 for new vehicle representation in AEDT; therefore, rendering the proposed tasks obsolete. Based on conversation with FAA technical monitors at the Spring 2019 ASCENT Advisory Board meeting, Georgia Tech is directed to focus on BADA4 coefficient generation for supersonic transport, which is described in Task 5.

### **Support of CAEP Supersonic Exploratory Study (Task 4)**

Although EDS is developed for subsonic vehicles, its structure is still relevant and useful to adapt for the design of supersonic vehicles. One of the major accomplishments during the previous period of performance is the development of the supersonic version of EDS called FASST. Several major accomplishments are completed during the period of performance using FASST. The first accomplishment is the development of a closed vehicle for the Georgia Tech (GT) Medium SST (designated as version 11.4) which carries 55 passengers with a range of 4,500 nmi cruising at Mach 2.2. The second accomplishment is the development of a preliminary model of a large SST carrying 100 passengers with a range of 5,000 nmi cruising at Mach 1.8. The final accomplishment is the generation of preliminary results of the design Mach trade study for three classes of SSTs.

The Purdue team provided fleet-level assessments in the form of a data packet and a report for the broader CAEP studies of future supersonic aircraft operations, which included the resulting “pseudo-schedule” for where the FLEET aggregate airline operates supersonic aircraft.

### **AEDT BADA4 Coefficient Generator (Task 5)**

The Georgia Tech team developed an approach on conducting regression analysis for the BADA4 formulation and implemented the approach for both subsonic and supersonic aircraft. With the current functional form of BADA4, the accuracy of the regression models is deemed insufficient. As a result, the team has proposed possible alternative functional forms, which are more representative of the underlying physics. The implementation of the proposed approach is a continuing discussion with the FAA.

### **Coordination with Other ASCENT Projects (Task 6)**

The Georgia Tech team attended in-person or, once travel became restricted, eleven CAEP-related meetings of Working Group 1 (Noise), Working Group 3 (Emissions), and the MDG/FESG meetings. This included up to six telecons per week depending on schedule and needs. The Georgia Tech team authored and presented eight papers to these meetings and contributed additional presentations and technical data in support of the CAEP supersonic exploratory study and related progress reports. The Georgia Tech modeling team has been in communications with Massachusetts Institute of Technology (MIT) researchers working on ASCENT Project 47 in regard to results of a medium-sized SST.

The Purdue team has maintained its ability to incorporate any “type” of supersonic aircraft in the FLEET tool without many modifications to the tool itself.

## **Task 1 – Fleet-Level Assumption Setting and Demand Assessment**

Georgia Institute of Technology and Purdue University

### **Objectives**

In order to better understand the potential demand for supersonic air travel, the Georgia Tech team developed a parametric airline operating cost model in order to be able to explore the sensitivities of key vehicle, operational, and cost parameters

on the required yield an airline would have to target for ticket prices on such a potential new supersonic aircraft. The current model, however, assumes fixed parameters for key vehicle metrics—which can be changed—but do not include sensitivities to key vehicle design choices such as vehicle size, design cruise Mach number, and maximum range. This Task will examine the implications of the physical and technical dependencies on the airline operational cost. Through the vehicle performance sensitivities such as passenger capacity and design cruise Mach number, it will be possible to determine the combined “sweet spot” that would be the most profitable vehicle to operate for an airline. In order to accomplish this, the existing vehicle models created in the prior year will be utilized and supplemented by additional vehicles proposed in Task 4. These vehicles together will serve as the foundation to create credible sensitivities with regards to parameters such as vehicle size and design cruise Mach number. These sensitivities will then be embedded into the airline operating cost estimation model and utilized to explore the combined vehicle and airline operational space in order to identify the most economically feasible type of supersonic vehicle.

**Research Approach (Georgia Tech)**  
**Potential Airline Market for Supersonic Travel**

After analyzing the potential demand from a passenger perspective, the Georgia Tech team has investigated the market for supersonic travel from an airline perspective. A4A data for airline operating costs are used to establish a baseline airline cost structure representative of subsonic operations. Specifically, Passenger Airline Cost Index (PACI) data for the fourth quarter of 2016 are used to establish the structure shown in Figure 1. As can be seen, “labor” and “fuel” costs account for approximately 50% of all airline operating costs. Other major contributors include “aircraft rents and ownership” and “professional services.” This baseline structure is assumed to be representative for a currently operational reference subsonic aircraft with certain specifications. To estimate a similar cost structure representative of operating costs for a concept supersonic aircraft, the specifications of the latter needed to be estimated relative to those of the reference aircraft. Engineering judgement is used, along with some feedback input based on the results of Task 2, to define the specifications of the concept supersonic vehicle. With these specifications, and by normalizing the cost structure by flight hour, the baseline airline structure could be adjusted to reflect the differences in various component costs (e.g., fuel and maintenance).

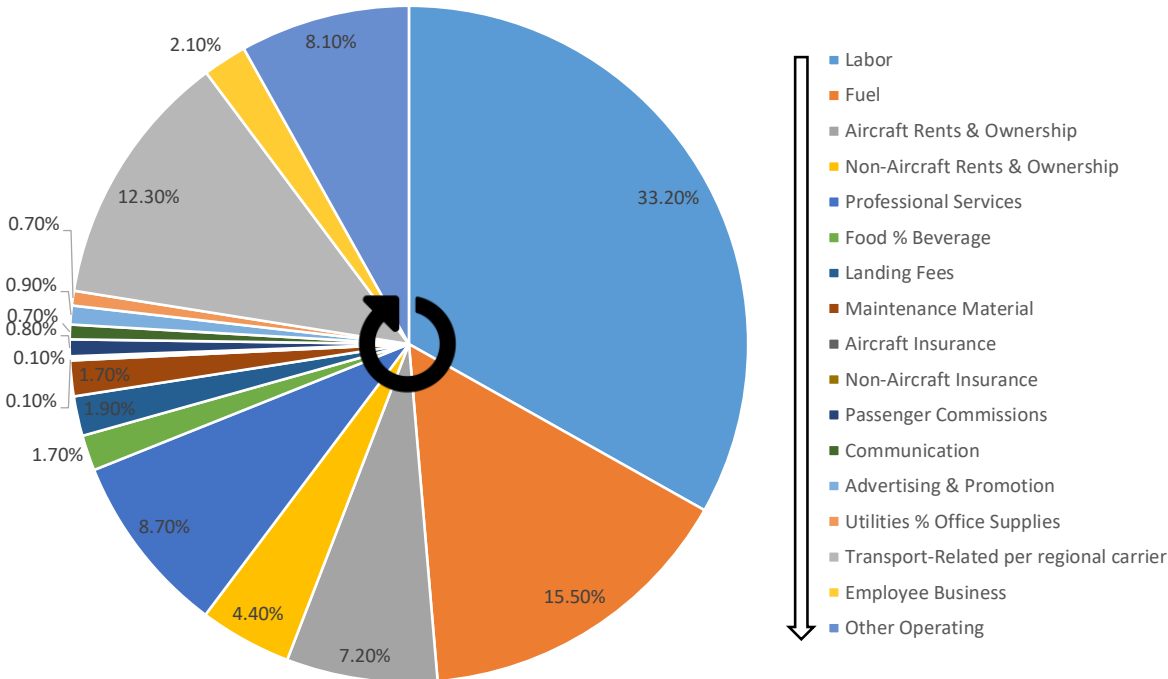


Figure 1. Commercial Airline Cost Index.

An important parameter that is estimated with this procedure is the required yield per seat mile (i.e., the average fare per seat mile). If airline profit margins are assumed to remain the same as those for subsonic operations, yield directly correlates with operating costs. The operating cost is estimated for different utilization and fuel consumption scaling values. The

complete analysis for the various size and speed combinations has been delayed pending finalization of the vehicle trades in Task 4.

### Demand Assessment

Another objective of this Task is to develop an all-encompassing framework to assess demand for commercial supersonic air travel, while simultaneously accounting for flight routing that abides by current regulations. There is presently no established method to adequately predict SST demand. Often such demand is accounted for by assuming a fixed proportion of premium passengers (i.e., business and first-class travelers) would switch from subsonic to supersonic flights across all routes. This approach, however, does not account for the effects of time savings and fare changes that are route specific. A more accurate approach would therefore quantify demand on a route-by-route basis according to the time saved during the supersonic flight translated to an extra amount of fare paid.

Demand forecasting for commercial supersonic flight is achieved by considering current forecasts for commercial subsonic flight. The approach relies on calculating a "switching percentage" of premium passengers who would switch to supersonic flights if enough value, in terms of time savings, would be provided. Induced demand could also exist, which is defined as the additional demand that could occur purely due to the availability of supersonic service that would otherwise not exist. However, induced demand is difficult to quantify and it is unclear if this would constitute a significant amount of additional demand. As a result, the impact of induced demand is neglected. Figure 2 summarizes the overall approach implemented.

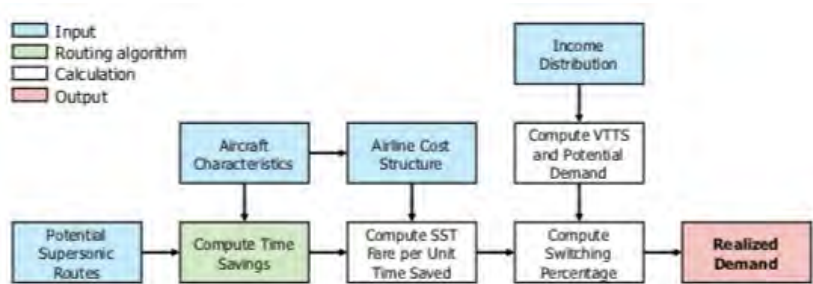


Figure 2. Overall Approach for Demand Forecasting.

### Potential Supersonic Routes

To assess the future market of supersonic transport, current subsonic routes with potential for supersonic operations need to be identified first. Such routes have to exceed a certain minimum distance to guarantee value in time savings. They also need to be of high demand to guarantee a high switching percentage of premium passengers. Generally, any long-distance route with high demand would be considered a potential supersonic route.

This study relied on the FAA Global Inventory of 2015 to establish information regarding commercial service routes around the world, including the total number of operations and total number of seats (FAA, 2015). This inventory is combined with another one retrieved from the AEDT, which contains data for over 35,000 airports around the world, including location (in terms of latitude and longitude) and runway length (FAA, 2020). Together, both inventories provide the necessary information to filter routes based on distance and seating capacity (or demand).

While distances between airports remain fixed, seating capacity could grow or shrink based on future passenger demand growth. For instance, a route with low demand in 2015 could still be considered a potential supersonic route if growth rates for that route are such that it exceeds a certain seating capacity for a future year. Therefore, the identification of potential supersonic routes could not only rely on current and/or historical operations but also had to account for future growth. To that effect, aviation traffic forecasts are utilized to estimate demand growth rates in different regions of the world.

The inventories along with the aviation traffic forecasts provide a complete picture of future aviation growth. Applying a conservative assumption for the number of premium passengers per flight provides an initial estimate for supersonic demand in terms of premium Passengers Daily Each Way (PDEW). Finally, by enforcing the minimum requirements for distance and capacity on each route, the Georgia Tech researchers have identified an initial set of potential supersonic routes.



### Supersonic Fare

Once the potential supersonic routes are identified, they need to be analyzed in order to determine the switching percentage of premium passengers. To do so, it is necessary to compare the extra cost to passengers from flying supersonic with the value gained from time savings. While the latter is a direct outcome of the routing algorithm (discussed later), the former needed to be determined. For each route, the subsonic fare is estimated using economic assumptions for yield and cost index of current commercial airlines. The extra costs of flying supersonic ( $\Delta\text{Fare}$ ) are then computed by scaling the airline yield and costs to account for changes in fuel consumption and aircraft utilization. This process is detailed as follows.

Reference subsonic fuel burn per passenger ( $\text{FB}_{\text{REF}}/\text{PAX}_{\text{REF}}$ ) values for every route are first computed using the great circle distance between the departure and arrival airports and a fuel efficiency metric. The latter is a user input that averages gate-to-gate (i.e., accounts for all phases of flight: taxi, takeoff, climb, cruise, descent, and landing) fuel burn for a subsonic aircraft. An appropriate estimate for such value could be found in the literature based on historical performance specific to certain aircraft types or averaged for an overall fleet. The metric is usually defined in terms of passenger distance per fuel quantity (e.g., (pax·nmi)/ton). Accordingly,  $\text{FB}_{\text{REF}}/\text{PAX}_{\text{REF}}$  is calculated as:

$$\frac{\text{FB}_{\text{REF}}}{\text{PAX}_{\text{REF}}} = \text{distance}_{\text{GC}}/\text{eff}_{\text{REF}} \quad (1)$$

where the subscript GC denotes great circle distance, and  $\text{eff}_{\text{REF}}$  is the reference fuel efficiency metric. Alternatively, supersonic fuel burn for every route is calculated based on the results of the routing algorithm. Outputs of the algorithm include the cruise distances covered in subsonic and supersonic regimes, the number of accelerations  $n_a$ , and the number of fuel stops  $n_f$  (if any). This information is used along with the aircraft characteristics to establish supersonic fuel burn:

$$\text{FB}_{\text{SST}} = \frac{\text{distance}_{\text{sub}}}{\text{SAR}_{\text{sub}}} + \frac{\text{distance}_{\text{super}}}{\text{SAR}_{\text{super}}} + n_a \cdot \text{FB}_A + (n_f + 1) \cdot (\text{FB}_{\text{T\&C}} + \text{FB}_{\text{D\&L}}) \quad (2)$$

where  $[\text{FB}_A; \text{FB}_{\text{T\&C}}; \text{FB}_{\text{D\&L}}]$  are the fuel penalties to accelerate, takeoff and climb to cruising altitude, and descend from cruising altitude and land, respectively.

Another important parameter affected by supersonic operations is aircraft utilization, which is typically measured in terms of block hours per day or per year. Higher aircraft utilization allows for fixed airline costs to be spread over more block hours, effectively decreasing those costs on a per mile or per passenger basis. For supersonic aircraft, it is expected that utilization would be less than that of subsonic aircraft, thus increasing costs to airlines.

The impacts of both fuel burn and utilization on airline costs are captured through the definition of a multiplier  $\beta$ :

$$\beta = [1 - C_{\text{fuel}} - C_{\text{fixed}}] + \frac{\text{FB}_{\text{SST}} \text{PAX}_{\text{REF}}}{\text{FB}_{\text{REF}} \text{PAX}_{\text{SST}}} \cdot C_{\text{fuel}} + \frac{U_{\text{REF}}}{U_{\text{SST}}} \cdot C_{\text{fixed}} \quad (3)$$

where  $[C_{\text{fuel}}; C_{\text{fixed}}]$  are the fuel and fixed proportions of airline operating costs,  $\text{PAX}_{\text{SST}}$  is the number of passengers of the supersonic aircraft, and  $[U_{\text{REF}}; U_{\text{SST}}]$  are the utilization values for the subsonic and supersonic aircraft. Moreover, within the fixed cost proportion of airline operating costs are ownership costs, which are directly affected by the cost of acquisition of a supersonic aircraft. To account for that,  $C_{\text{fixed}}$  is further broken down into an ownership cost proportion and an "all-other" one:

$$C_{\text{fixed}} = \gamma \cdot C_{\text{ownership}} + C_{\text{all-other}} \quad (4)$$

where  $\gamma$  is an acquisition multiplier used to scale the proportion of ownership costs. Finally,  $\Delta\text{Fare}$  is calculated using an average yield per unit distance for a commercial subsonic airline ( $\gamma_{\text{airline}}$ ):

$$\Delta\text{Fare} = (\beta - 1) \cdot \text{distance}_{\text{GC}} \cdot \gamma_{\text{airline}} \quad (5)$$

### Switching Percentage

Once  $\Delta\text{Fare}$  is computed for every potential supersonic route, the switching percentage is determined by comparing the  $\Delta\text{Fare}$  per unit time saved to the Value of Travel Time Savings (VTTS) of the passengers. Essentially, if the cost per hour saved

is lower than a passenger’s hourly income, it is assumed that such a passenger would find value in switching to a supersonic flight. Time savings along a given route are calculated using results from the routing algorithm (see Task 2 section):

$$\text{time savings} = t_{REF} - t_{SST} \tag{6}$$

$$t_{REF} = t_{R\&C} + t_{D\&L} + \text{distance}_{GC} / \text{speed}_{REF} \tag{7}$$

$$t_{SST} = t_{R\&C} + t_{D\&L} + \text{distance}_{sub} / \text{speed}_{sub} + \text{distance}_{super} / \text{speed}_{super} + n_f \cdot t_{re-fuel} \tag{8}$$

where  $[t_{REF}; t_{SST}]$  are the flight times for the reference subsonic and SST vehicles,  $[t_{R\&C}; t_{D\&L}]$  are the takeoff and landing times, and  $t_{re-fuel}$  is the 90-minute delay assumed for fuel stops. The switching percentage (SP) along a given route is thus defined as follows:

$$SP = 100 \times \frac{\text{no. passengers with VTTS} > \Delta\text{Fare per hour saved}}{\text{no. of passengers}} \tag{9}$$

Evaluating the equation above requires information regarding the income distribution among passengers of every potential supersonic route. This information is impossible to determine precisely. However, it could be approximated based on the income distribution of a certain country or region (e.g., the income distribution of the departure country, or the arrival country, or the region in which both airports lie, etc.). Such data is available in the literature. Accordingly, the switching percentage is approximated as:

$$SP \approx 100 \times \frac{\text{no. of individuals in a population with VTTS} > \Delta\text{Fare per hour saved}}{\text{no. of individuals in a population who could afford to travel at least once}} \tag{10}$$

While the numerator of the equation above correctly accounts for individuals who would find value in flying supersonic, it does not account for the frequency of their trips along the route. This is important because the number of weekly/monthly/yearly trips made by an individual tends to increase with income. Such relationship between trips per capita and income per capita is also readily available in the literature. By accounting for this effect, the final form of switching percentage utilized in this study is as follows:

$$SP \approx 100 \times \frac{\text{no. of trips made by individuals in a population with VTTS} > \Delta\text{Fare per hour saved}}{\text{no. of individuals in a population who could afford to travel at least once}} \tag{11}$$

Using data available for the income distributions of passengers and their trip frequencies, the equation above is evaluated for every potential supersonic route to compute demand. However, a distinction has to be made between passengers traveling for leisure versus business when applying these distributions since they may differ based on the nature of travel.

Once SP is evaluated for a given route, supersonic demand in terms of PDEW is calculated as:

$$\text{PDEW} = SP \cdot \frac{\text{daily available seats}}{\text{load factor}} \tag{12}$$

where the daily available seats on a specific route are those determined using the aviation traffic forecasts and the load factor is a user input. The number of daily flights along the route is derived based on PDEW:

$$\text{daily flights} = \frac{\text{PDEW}}{\text{PAX}_{SST}} \tag{13}$$

Finally, the number of aircraft required to satisfy the yearly demand is computed using yearly aircraft utilization:

$$\text{no. of aircraft} = \frac{\text{daily flights} \cdot t_{SST}}{U_{SST}/365} \tag{14}$$

Aviation Traffic Growth Rates

In order to identify the initial set of potential supersonic routes, an air traffic forecast is needed to estimate growth rates in different regions of the world. In this study, those growth rates are derived from the 2019 Boeing Commercial Market Outlook

(CMO) (Boeing, 2019). The Boeing CMO divides the world into 12 different regions and includes the forecasted traffic growth between them, as shown in Table 2. Those different growth rates are applied to the baseline network of operations derived from the FAA inventories in order to project the operational network for a given future year. Each airport in the baseline network is mapped to one of the Boeing regions, and growth along the different network routes is determined depending on the regions in which the origin and destination airports lay.

**Table 2. 2019 Boeing Commercial Market Outlook and Forecasted Traffic Growth.**

Africa – Africa	6.6%	Europe – Southeast Asia	2.8%
Africa – Europe	4.1%	Middle East – Middle East	4.7%
Africa – Middle East	7.3%	Middle East – North America	4.7%
Central America – Central America	3.0%	Middle East – Oceania	4.2%
Central America – Europe	3.9%	Middle East – Russia and Central Asia	4.9%
Central America – North America	5.1%	Middle East – South Asia	6.4%
Central America – South America	5.9%	Middle East – Southeast Asia	4.8%
China – China	6.2%	North America – North America	3.1%
China – Europe	5.2%	North America – Northeast Asia	1.2%
China – Middle East	9.4%	North America – Oceania	3.3%
China – North America	4.9%	North America – South America	5.4%
China – Northeast Asia	4.2%	Northeast Asia – Northeast Asia	1.1%
China – Oceania	4.7%	Northeast Asia – Southeast Asia	4.1%
China – Southeast Asia	6.1%	Oceania – Oceania	3.7%
Europe – Europe	3.6%	Oceania – Southeast Asia	3.6%
Europe – Middle East	4.3%	Russia and Central Asia – Russia and Central Asia	3.1%
Europe – North America	2.9%	South America – South America	6.7%
Europe – Northeast Asia	1.6%	South Asia – South Asia	7.7%
Europe – Russia and Central Asia	2.7%	Southeast Asia – South Asia	8.6%
Europe – South America	4.5%	Southeast Asia – Southeast Asia	7.1%
Europe – South Asia	4.7%	Rest of the World	5.1%
Overall annual growth		4.6%	

Once traffic growth is applied, potential supersonic routes for a given future year are identified through filtration based on distance and seating capacity. An example of such a filtration process is shown in Figure 3. Essentially, routes with PDEW less than the SST vehicle seating capacity are considered to be of low demand and are disregarded. Long distance (>1,500 nmi) routes above that limit are considered to be potential supersonic routes. Those routes are identified for the years 2025, 2035, 2045, and 2050. Even though the Boeing CMO only extends to 2038, growth rates are extrapolated to 2050 to gauge the full potential of the commercial supersonic market. Supersonic vehicles are currently not in production; if they are to be introduced within the next decade (i.e., by 2030–2035), the introduction will be slow at first. Full market saturation will probably occur within 10–15 years after entry into service following historical trends for subsonic aircraft. The year 2050 is assumed to be an appropriate reference point for a comprehensive assessment of demand for supersonic air travel. Extrapolation beyond 2050 would increase uncertainty and diminish the reliability of results.

Aircraft and Airline Characteristics

Parameters required for demand forecasting and flight routing are listed in Table 3. Those parameters can be divided into three primary groups. The first group describes the commercial SST vehicle and includes: seating capacity, load factor,  $Mach_{sub}$ ,  $Mach_{super}$ ,  $SAR_{sub}$ ,  $SAR_{super}$ ,  $FB_A$ ,  $FB_{T\&C}$ , and  $FB_{D\&L}$ . The second group describes the reference subsonic vehicle and includes  $Mach_{REF}$  and  $eff_{REF}$ . The final group describes the airline economics and includes  $U_{REF}$ ,  $U_{SST}$ ,  $C_{fuel}$ ,  $C_{ownership}$ ,  $C_{all-other}$ ,  $\gamma$ , and  $\gamma_{airline}$ .

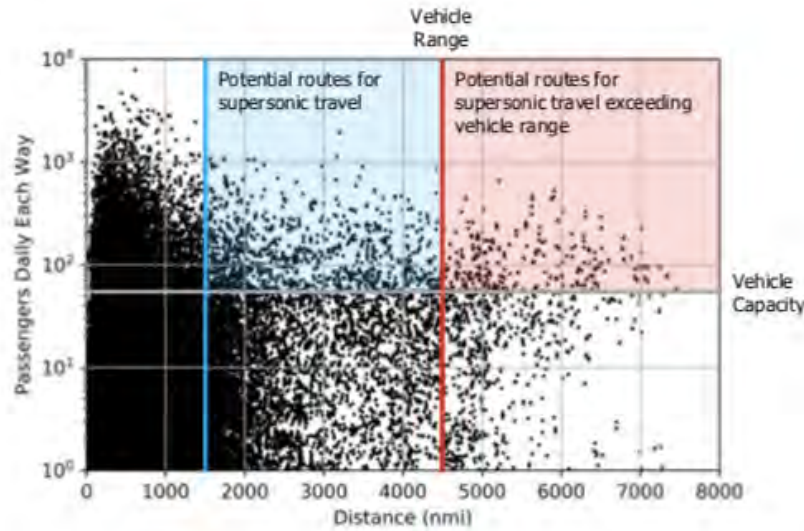


Figure 3. Filtration Process to Identify Potential Supersonic Routes.

Table 3. Parameters Required for Demand Forecasting and Flight Routing.

Parameter	Value	Parameter	Value
Seating capacity	55	Mach <sub>REF</sub>	0.80
Load factor	0.80	eff <sub>REF</sub> (pax·nmi/t)	24,911
Range (nmi)	4,500	U <sub>REF</sub> (h/year)	4,500
Mach <sub>sub</sub>	0.95	U <sub>SST</sub> (h/year)	1,000
Mach <sub>super</sub>	2.20	C <sub>fuel</sub>	0.155
SAR <sub>sub</sub> (nmi/t)	61.5	C <sub>ownership</sub>	0.072
SAR <sub>super</sub> (nmi/t)	75.1	C <sub>all-other</sub>	0.300
FB <sub>A</sub> (t)	3.3	γ	3
FB <sub>T&amp;C</sub> (t)	4.0	γ <sub>airline</sub> (\$/pax/nmi)	0.1483
FB <sub>D&amp;L</sub> (t)	2.0		

Values for the first group of parameters are either based on advertised values for the Boom Overture concept (e.g., seating capacity and Mach<sub>super</sub>) or are estimated using historical performance data of the Concorde while accounting for technological improvements. Passenger load factor is set to 0.80 based on projected trends for subsonic international operations (FAA, 2018), while Mach<sub>sub</sub> is set to 0.95, similar to the Concorde. Specific air range (SAR) values are a function of the instantaneous weight of the aircraft and its cruising altitude. According to the technical manual of the Concorde, ranges for SAR<sub>sub</sub> and SAR<sub>super</sub> in nautical miles per ton of fuel are found to be approximately 33–48 and 47–68, respectively (Air France, 2003). Averaged SAR values for the SST vehicle are derived from those of the Concorde by accounting for performance improvements in both the subsonic and supersonic regimes. Fuel penalty [FB<sub>A</sub>; FB<sub>T&C</sub>; FB<sub>D&L</sub>] values are based on conservative estimates for fuel burn during the respective flight phases. An SST conceptual design tool developed by the Georgia Tech researchers and calibrated using Concorde data is utilized to derive those estimates (Hassan, Pfaender and Mavris, 2020).

Moreover, values for the second group of parameters are based on typical subsonic operations. Cruising Mach number, M<sub>REF</sub>, is set to 0.80. Gate-to-gate fuel efficiency eff<sub>REF</sub> is based on two recent studies by the International Council on Clean Transportation (ICCT). One study analyzed the fuel efficiency of 20 major airlines along transatlantic routes in 2017 and found the industry average to be 34 pax·km/L (Graver and Rutherford, 2018). The other study analyzed the fuel efficiency of 10 major airlines along the U.S. to/from South America routes in 2018 and found the industry average to be 37 pax·km/L (Zheng and Rutherford, 2019). The latter value is the one used to derive the value shown in Table 3 assuming jet-A fuel density to be 0.802 kg/L.

Finally, values for the third group of parameters are either based on assumptions regarding future supersonic operations (e.g., U<sub>SST</sub> and γ), or derived from historical cost data for airlines. An appropriate estimate of utilization for a current subsonic

aircraft would be 4,500 hours per year. Given the smaller market size of supersonic air travel, utilization for the SST vehicle is assumed to be 1,000 hours per year. The acquisition cost of an SST vehicle is also assumed to be three times that of a subsonic vehicle of similar size (e.g., Boeing 737-800). As for the airline cost proportions [ $C_{fuel}$ ,  $C_{ownership}$ ,  $C_{all-other}$ ], they are determined based on data retrieved from Airlines for America Passenger Airline Cost Index (A4A PACI) derived from airline data submissions to the U.S. Department of Transportation (Airlines for America, 2017). Last, the average yield value for a commercial subsonic airline is derived from yield values for international operations reported in the FAA aerospace forecast (FAA, 2018).

Trips per Capita and Income Distributions

In order to compute switching percentage (SP), trips per capita and income distribution data are needed. First, the relationship between trips per capita and income per capita is established using socioeconomic data from the International Air Transport Association (IATA). IATA relates the average frequency of air travel in terms of trips per capita to the living standards measured in GDP per capita (IATA, 2019). To convert from GDP per capita to income per capita, a factor of 0.9 is applied. The resulting relationship is plotted in Figure 4. Since the IATA data only extends to an hourly income of \$40, extrapolation is required to account for premium passengers with much higher incomes. Extrapolation is linear based on the last two data points (rather than all data points) to avoid over estimation. Moreover, the maximum number of trips per year is capped at 20 assuming that passengers with a higher trip frequency would shift to the business jet market. The final relationship between trips per capita and income per capita is as follows:

$$\text{yearly trips per capita} = \begin{cases} 0.0959 \cdot VTTS - 0.0603 & \text{if } VTTS \leq \$40/h \\ 0.0330 \cdot VTTS + 2.4324 & \text{if } \$40/h < VTTS \leq \$530/h \\ 20 & \text{if } VTTS \geq \$530/h \end{cases} \tag{15}$$

where value of travel time savings (VTTS) is assumed equivalent to the hourly income per capita and \$530/h is the value at which the extrapolated line crosses 20 trips per year.

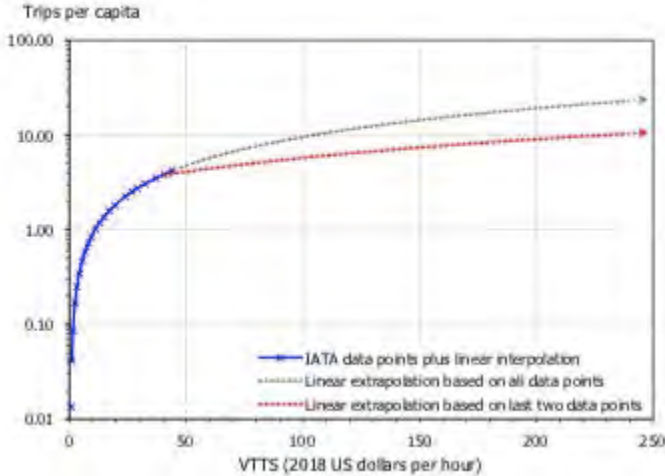


**Figure 4.** Relationship between Average Frequency of Air Travel to Value of Travel Time Savings.

After establishing the relationship between trips per capita and VTTS, income distributions need to be defined. Ideally, a separate income distribution would be utilized for each supersonic route depending on the origin/destination countries or regions. However, this is very difficult to implement due to the lack of complete and/or high-quality income data for many countries around the world. This study relies on income data from the World Inequality Database (WID), which not only includes the data, but also rates its quality (WID, 2019). Even though data for countries like the U.S. are available and their quality is rated very highly, data for many other countries in the WID are either incomplete or unreliable.

Income distributions for countries with complete data are examined. It is observed that the distributions across different countries have a similar shape, as shown in Figure 5. Furthermore, when only accounting for the "traveling" adults of the

population (i.e., adults whose income allowed for at least one trip per year— quantified using Figure 5), the high-end fraction of the distributions almost overlapped. Effectively, for higher income values, most income distributions exhibit similar behavior. This is an important observation since the high-end fraction of the distribution is the one of concern for SP calculations. VTTs values of premium passengers who would switch to supersonic travel will be towards the high-end of the income distribution.

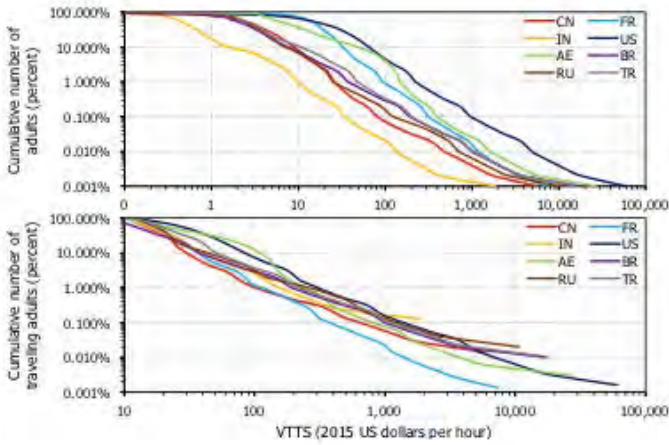


Figure 5. Income Distributions for Countries with Complete Data.

Based on this observation and due to the lack of complete income data for many countries, the Georgia Tech researchers have decided to utilize only one representative distribution for all SP calculations. The U.S. income distribution of 2014 is selected due to its completeness and high-quality rating. Additionally, differentiation between leisure and business travel is achieved by considering the type of income and the share of travel. For leisure travel, post-tax income data is used, and a 0.596 share is assumed according to historical trends from the U.S. Bureau of Transportation Statistics (BTS) (BTS, 1995). Alternatively, for business travel, pre-tax income is used, and a 0.404 share is assumed. The resulting cumulative number of U.S. adults as a function of hourly income is shown in Figure 6. Finally, the numerator of Eq. (11), and hence SP, is evaluated by combining the cumulative number of adults with the corresponding number of yearly trips based on income (Figure 6).

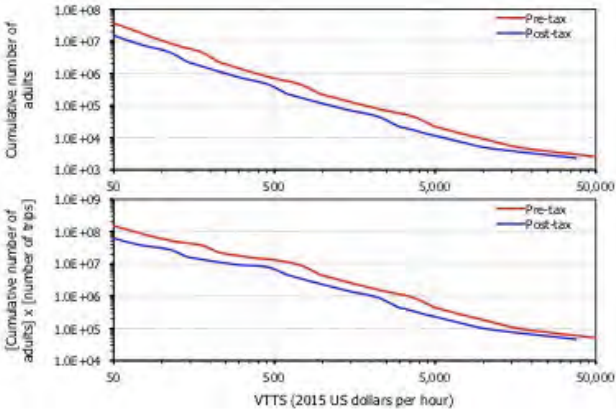


Figure 6. Cumulative Number of U.S. Adults as a Function of Hourly Income.

**Results**

The initial set of potential supersonic routes derived from combining the FAA inventories with the Boeing CMO nominal growth rates consists of 2,045 one-way origin-destination pairs. The flight routing algorithm is utilized to determine the time savings across these routes. To that effect, the Partnership for an Advanced Computing Environment (PACE) at Georgia Tech is leveraged to access a cluster of Intel Xeon Gold 6226 processor nodes. One core is utilized per route. The resulting



cumulative distribution function of computational run time is shown in Figure 7. As illustrated in the figure, half of the routes took less than 10 minutes to run (each), while 90% took no more than three hours. Outcomes of the routing algorithm are then used to calculate SP, the cumulative distribution function of which is shown in Figure 8. A third of the routes had SP values greater than 7%, while nearly 60% had SP values of at least 5%. Figure 7 and Figure 8 provide an overview of the computational efficiency of the routing algorithm and the sizable market capture of supersonic air travel along many candidate routes.

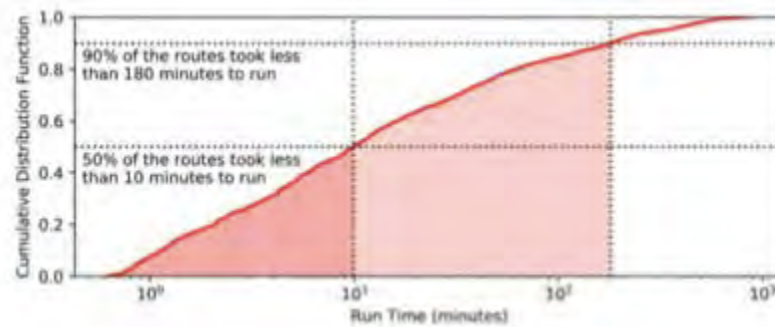


**Figure 7.** Cumulative Distribution Function of Computational Run Time.

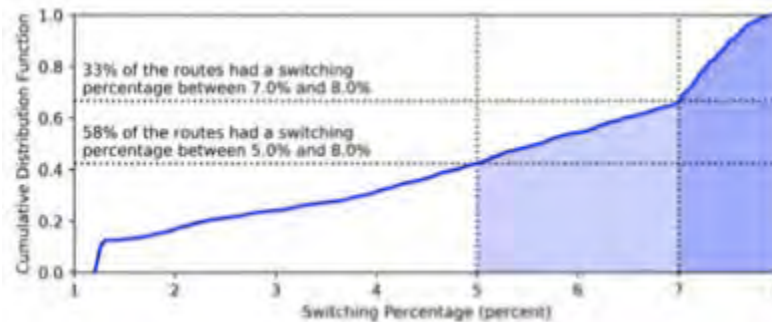


**Figure 8.** Cumulative Distribution Function of Computed Switching Percentage.

After routing the initial set of one-way origin-destination pairs, outcomes are collected and processed in order to calculate SP and assess future demand. Based on the flight routing outcomes and the SP calculations, this initial set is then filtered so that only viable routes are used for demand forecasting. For a route to be deemed viable, it has to meet the following criteria:

1. time savings relative to the reference subsonic aircraft are more than 20%.
2. time savings relative to the reference subsonic aircraft are more than two hours.
3. number of accelerations are less than four if no fuel stop is needed.
4. number of accelerations are less than six if fuel stops are needed.
5. number of flights per day in 2050 are at least one.
6.  $\Delta$ Fare per hour saved is less than \$1,000.

Out of the initial set of 2,045 routes, 1,084 (53%) met the above-mentioned criteria. This filtered set of routes is used to forecast demand for commercial supersonic air travel. The top 10 two-way origin-destination routes in 2050, ranked by PDEW, are summarized in Table 4. Besides the very top Dubai–Hong Kong route, which is hugely driven by the Middle East–China annual traffic growth rate of 9.4% (Table 2), routes on the top 10 list are generally characterized by a balanced combination of high time savings, low distance penalties, high SP, and high traffic growth rates between the origin and destination regions. Moreover, it is not surprising that the majority of the cities on the list are coastal cities. Those coast-to-coast city pairs give the routing algorithm direct access to open water and an opportunity to fly the SST vehicle at its supersonic speed for the majority of the flight in order to maximize time savings.



**Table 4.** Top 10 Two-way Origin-Destination Routes in 2050 Ranked by PDEW.

Route	Distance (nmi)		Time Savings		SP	PDEW	Daily Flights	Regions
	GC	Penalty	Hours	Percent				
Dubai (OMDB) – Hong Kong (VHHH)	3,201	1,239	3.3	43%	5%	3,927	90	Middle East – China
Shanghai (ZSPD) – Singapore (WSSS)	2,048	91	2.7	53%	7%	2,992	68	China – Southeast Asia
Mumbai (VABB) – Singapore (WSSS)	2,117	19	2.2	42%	6%	2,583	58	South Asia – Southeast Asia
New York (KJFK) – London (EGLL)	2,999	140	3.9	55%	8%	2,069	47	North America – Europe
Hong Kong (VHHH) – Jakarta (WIII)	1,751	50	2.2	52%	7%	2,064	46	China – Southeast Asia
New Delhi (VIDP) – Singapore (WSSS)	2,242	42	2.1	38%	6%	1,990	46	South Asia – Southeast Asia
Dubai (OMDB) – Johannesburg (FAOR)	3,450	479	4.1	49%	7%	1,874	42	Middle East – Africa
Beijing (ZBAA) – Singapore (WSSS)	2,416	309	3.2	46%	7%	1,854	42	China – Southeast Asia
Colombo (VCBI) – Dubai (OMDB)	1,774	42	2.3	51%	7%	1,769	40	South Asia – Middle East
Bangkok (VTBS) – Dubai (OMDB)	2,650	551	3.0	46%	7%	1,743	40	Southeast Asia – Middle East

A more holistic view of demand in 2050 is provided in Figure 9 and Figure 10. These figures illustrate the connectivity of the different regions of the world in terms of daily passengers (Figure 9) and distances flown (Figure 10). Southeast Asia is the region with the highest number of daily passengers due to its access to both the Indian and Pacific Oceans (i.e., over water connections with the Middle East (Indian), South Asia (Indian), China (Pacific), and Northeast Asia (Pacific)). Alternatively, the biggest connectivity between two regions in terms of passengers and flown distances is the one between North America and Europe over the Atlantic Ocean.

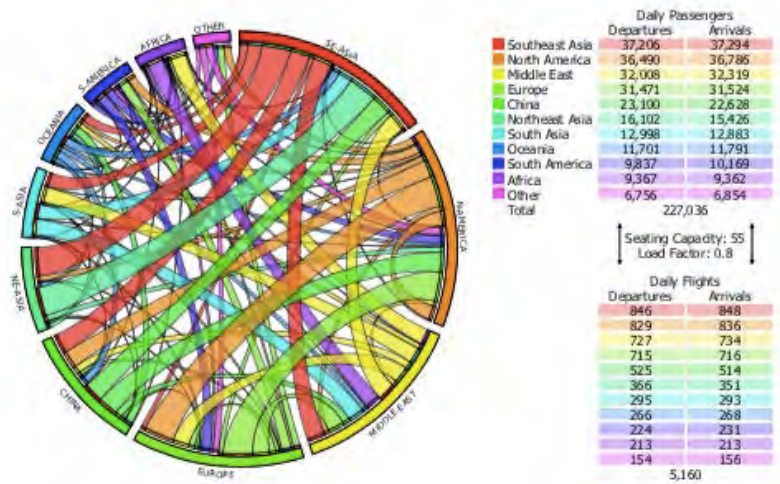


**Figure 9.** Holistic View of 2050 Demand for Supersonic Travel in Terms of Daily Passengers.

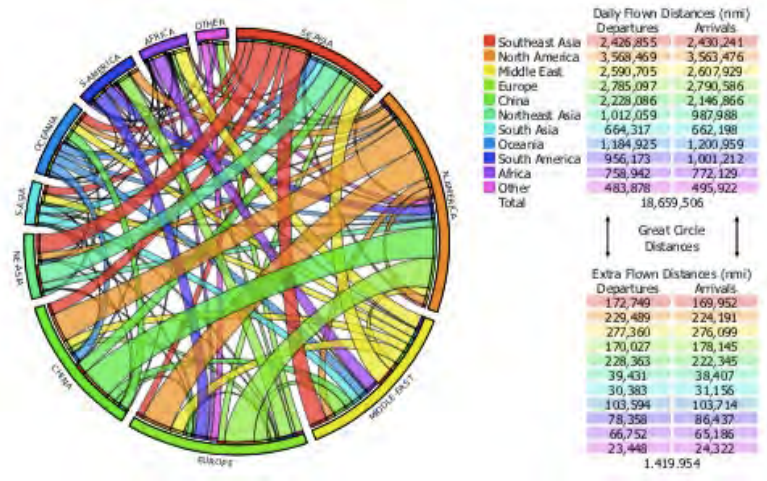


**Figure 10.** Holistic View of 2050 Demand for Supersonic Travel in Terms of Daily Flown Distances.

Consequently, both regions rank first and second, respectively, in terms of daily flown distances. The connectivity between North America and China is similarly high but only in terms of flown distances because of cross-Pacific routes. Furthermore, the Middle East ranks third in terms of both passengers and distances flown due to its central location that helps it connect different regions of the world over the Mediterranean Sea and the Indian Ocean.

To satisfy passenger demand in 2050 using SST vehicles with a seating capacity of 55, passenger load factor of 0.8, and utilization  $U_{SST}$  of 1,000 hours per year, the number of SST vehicles required is 8,081, as calculated using Eq. (14). To put this number in context, it is compared to the Boeing CMO projection for the worldwide subsonic fleet. The CMO reports that the 2018 fleet count, not including freighter aircraft, is 23,860 and projects it to grow at an annual rate of 3.4%. Thus, the subsonic fleet count by 2050 is expected to be 69,555. At 8,081 vehicles in 2050, the SST fleet size would be 11.6% of that of the subsonic fleet (or 10.4% of that of the overall fleet).

## Research Approach (Purdue)

### FLEET's Passenger Demand and Route Network

FLEET predictions for routes and passenger demand build upon reported data from the BTS (Airline Origin and Destination Survey—DB1B). The FLEET simulations presented in this paper use 2005 as the starting year for all simulations, because most stated aviation emissions goals use 2005 as the reference year. FLEET uses historical BTS data for years from 2005 through 2018, then uses model-based predictions for years 2019 and beyond. This causes FLEET to have a dynamic route network that follows how U.S. flag carrier airlines updated their route networks as reported in the BTS data until 2018, followed by a static route network from 2018 and beyond. In 2018 (and all the subsequent years), there are 1,974 routes in the FLEET network that connect a subset of Worldwide Logistics Management Institute Network Queuing Model (WWLMINET) 257 airports<sup>1</sup>. All these routes are either U.S.-domestic routes or international routes with direct flights originating or ending at a U.S. airport.

### Extracting and Processing Data from BTS Datasets

The BTS demand data employed in this work is the T-100 Segment Data (all carriers). The T-100 segment demand data comes in either monthly or yearly entries, with all data from both domestic and international carriers, passengers, and cargo services (scheduled and unscheduled), all types of carriers (regional, major, small certified, etc.), and all types of aircraft configuration. This raw data contains information irrelevant to FLEET and therefore needs to be filtered before using it to generate the route network in FLEET. For this work, the authors use yearly data for years from 2005 to 2018, but the filtering approach is applicable to monthly data also.

<sup>1</sup> The "World-Wide LMI Network (WWLMINET) 257" airports as reported by Logistics Management Institute are those "worldwide" airports that have the most operations.

**Filtering the Data**

The authors use the filters numbered 0 to 11 in Table 5 to trim the raw data from BTS to relevant data that can be used as an input for further processing in FLEET. After these filters are applied to the raw data in the order listed in Table 5, the final demand data contains information about the number of passengers per year on directional routes by all domestic carriers combined. For instance, after filtering, the demand data for the JFK-LHR route has a single entry that represents the yearly number of passengers carried by all U.S.-flag carrier airlines combined.

**Processing the Data**

The filtered data is input into FLEET and additional filters for aircraft performance and airport characteristics are applied to the data. The yearly data is then transformed to daily demand (dividing the yearly demand by 365 and then ceiling the result for integer number of passengers) applicable to both directions of a route (bi-directional routes) by choosing the larger demand of the two directions to represent the demand for each direction. For instance, if JFK-LHR has a daily demand of 10,000 passengers and LHR-JFK has a daily demand of 10,500 passengers, then the daily demand in FLEET for the JFK-LHR route will be 10,500 passengers. Routes with daily demand greater than or equal to 10 passengers constitute the route network in FLEET for that year. This step is included in Table 5 as filter number 12.

**Table 5.** List of Filters for Extracting and Processing BTS T-100 Segment Data (All Carriers) Using Year 2005 as an Example.

ID	Step	Purpose	Data
0	Initial BTS data for 2005 T-100 Segment (all carriers)		Monthly records on directional routes by both different international and domestic carriers; More than one record/month possible  <i>Example: American Airlines (AA) has two entries for JFK-LAX route in Jan, one entry in Feb, four entries in Mar, etc.</i>
1	All origin- and destination-airports are in the WWLMINET 257 airport network	Keep entries for routes with origin or destination in the U.S. only	Same as above
2	Filter out cargo carrier group	Keep entries for scheduled passengers service (this can include flights by regional, commuter, small certified carriers)	Same as above
3	Filter out freight configuration and seaplane configuration aircraft		Same as above
4	Filter out all cargo scheduled service, unscheduled passenger service		Same as above
5	Filter out all routes by international carriers	Keep entries for flights by U.S.-flag carrier airlines only	Monthly records on directional routes by different domestic carriers; More than one record/month possible
6	Filter for non-zero passengers and seats	Keep entries with non-zero demand only	Same as above
7	Filter for non-zero distance	Keep entries for "real" flights	Same as above
8	Aggregate to get monthly performance		Monthly records on directional routes by different domestic carriers; Only one record/month  <i>Example: AA has one entry for JFK-LAX route in Jan, Feb, Mar, etc.</i>
9	Group by directional routes to combine demand of all airlines on each route together	Assume one large "aggregate" U.S.-based airline, no competition considered	Monthly records on directional routes by one large "aggregate" airline representing all domestic carriers  <i>Example: JFK-LAX route has 12 entries, one for each month, and the demand shown is sum of all airlines' demand</i>

10	Aggregate to get yearly performance	Aggregate monthly data into yearly data	Yearly records on directional routes by one large "aggregate" airline representing all domestic carriers  <i>Example: One entry for JFK-LAX route for year 2005</i>
11	Filter for routes with regular departures performed	Keep only entries for routes with regular operations (at least 1 flight/week or 52 flights/year performed on directional routes)  <i>Example: JFK-LAX has 105 flights performed in 2005 → kept JFK-IND has 50 flights performed in 2005 → out</i>	Same as above
12	Turn each subset into a 257x257 matrix	Prepare for input to FLEET	Same as above, in matrix form
13	Process in FLEET	Filter for minimum passengers per day, minimum runway length, etc. Turn yearly demand to daily demand	Daily demand on bi-directional routes by one large "aggregate" airline representing all domestic carriers

### Updated Route Network

FLEET's route network updates every year from 2005 to 2018 using the corresponding year's BTS T-100 Segment data (yearly). This causes FLEET's route network to have 1,965 routes in the year 2005 and 1,974 routes in the year 2018. FLEET's route network stays static beyond 2018, hence, there are 1,974 routes in FLEET from years 2018 to 2050. Earlier, FLEET had a static route network with 1,940 routes from years 2005 to 2050. The updated route network allows FLEET to include some current "popular" trans-Pacific and trans-Atlantic routes, like SJC-HND, that were missing from FLEET's previous route network, and to remove some outdated routes, like ATL-LGW, from its route network.

### Characterizing Supersonic Passenger Demand

To estimate the supersonic passenger demand, the Purdue team began using the discussion on Boom Supersonic's website about passengers paying same fares for supersonic flights as today's business class (Boom Supersonic). Using this concept is not intended to endorse this position; instead, it provides a convenient and publicly presented starting point for characterizing potential supersonic aircraft passenger demand. The work presented in this report assumes that the potential supersonic passengers are the current passengers who pay "business class or above" fares. In FLEET, the travel demand is split such that supersonic (business class or above) demand is a fixed percentage (5%) of the total travel demand on each route and the remaining demand is passengers only willing to pay subsonic fares. As a starting point to estimate the number of potential paying passengers in business class or above, the Purdue team considered typical aircraft currently flying transoceanic routes. Those aircraft have enough seats in business and above cabins that are roughly 10% of the total seat capacity, albeit with fairly significant variation. From this, the team assumes that 50% of the daily business class or above passengers in the historical data (or 5% of the total demand) are willing to pay the supersonic fare, and this 5% of total passenger demand on a route becomes the supersonic passenger demand on that route. This is a coarse approximation that half of the passengers flying in the business class or above cabin are paying the higher fare, while the other half are using upgrades or similar promotions rather than paying the full fare. A direct comparison with BTS database is not possible for our 5% supersonic demand assumption, because the DB1B Coupon database (Airline Origin and Destination Survey—DB1B) sample consists of ticket prices paid only for domestic routes. However, an indirect comparison indicates that for all domestic routes in the DB1B for 2016, 4.82% of the reported tickets were business class or above; focusing on U.S. domestic flights between 2350 nmi and 4500 nmi, 6.89% of the reported tickets were business class or above. This supports that the 5% assumption is not unrealistic. This approach will be replaced by a passenger-choice model to estimate the supersonic passenger demand in the future.

### Identifying Potential Supersonic Routes

This report considers potential airport pairs that are connected with both nonstop (direct) flights and flights with a fuel stop (indirect) as potential supersonic routes. The Purdue team identified potential supersonic routes from FLEET's latest route network of 1974 routes using a set of route filters based on the performance characteristics of a "placeholder" supersonic aircraft. Details about the placeholder supersonic aircraft are provided in the following sub-section. The potential supersonic routes are filtered based on the placeholder supersonic aircraft's maximum design range (differentiating between routes that require a fuel stop and those that do not require one), the aircraft's maximum range capability for different percentages of supersonic and subsonic flight segments, and the block time savings incurred when flying supersonic aircraft compared to subsonic aircraft. To calculate the minimum time flight path for a supersonic route, the team employs a very simple

supersonic route path adjustment strategy that gives the block time, percentage of flight path over water, updated departure heading for the route, and minimum time route distance as outputs.

“Placeholder” supersonic aircraft model

To identify potential supersonic routes, this work used a placeholder 55-seat supersonic aircraft with a maximum design range of 4,500 nmi using a relatively simplistic approach to identify the potential supersonic routes from the overall route network in FLEET. The supersonic aircraft modeled here makes no attempt at sonic boom reduction, so that it flies over water at a supersonic cruising speed of Mach 2.2 and flies overland at a subsonic cruising speed of Mach 0.95. The simplistic sizing and performance analysis for this placeholder aircraft model uses the Breguet range equation to calculate the fuel burn and block time for routes of different lengths and different values of percentage of overwater flight. The simplistic supersonic aircraft modeling uses the following abstractions:

- The overland segment is assumed to be equally split at each end of the overwater segment. For example, for a mission of 3000 nmi with 75% of flight over water, the overland portion of the flight is split into 375 nmi segments at the beginning and at the end of the 2250 nmi overwater segment, so that the total over-land flight segment for the mission is 750 nmi. In reality, the overland segment is airport pair- and route-dependent (e.g., for one airport pair, the origin might be close to the ocean, and the destination further inland; the return flight on this pair would have the opposite), so a higher resolution representation of the routes will lead to different fuel burn characteristics for each direction on each route.
- There is no range credit for the climb and acceleration segments from 35,000 ft @ Mach = 0.95 to 55,000 ft @ Mach = 2.2 for the supersonic aircraft. There is a simple estimate for fuel burn for these accelerations.
- There is no range credit for the descent and deceleration from supersonic to subsonic speeds. Also, no fuel burn is considered for this descent segment.

Using the team's engineering judgement, the lift-to-drag ratio (L/D ratio) for sizing the placeholder supersonic aircraft changes for supersonic (Mach = 2.2) and subsonic (Mach = 0.95) flight regime, varying from a value of 8.0 @ Mach = 2.2 to a value of 13.0 @ Mach = 0.95. These are meant to be a bit better than the Concorde to reflect improved aerodynamic design. The fuel burn estimates also vary for the two flight regimes. Again, guided by information about the Concorde, the specific fuel consumption (SFC) value of the notional 55-passenger supersonic aircraft is 1.0338 (1/hr) @ Mach = 2.2. The subsonic flight regime's fuel burn is estimated using a product of the supersonic flight regime's SFC value and Concorde's subsonic flight to supersonic flight SFC ratio, leading to an SFC value of 1.2025 (1/hr) @ Mach = 0.95.

The simple sizing and performance assessment allow estimation of supersonic aircraft maximum range as a function of route overwater percentage. Figure 11 shows the supersonic aircraft maximum range capability as a function of the percentage of flight over water. The supersonic aircraft has an all-supersonic (100% overwater flight) range capability of 4,500 nmi. The range capability reduces with an increase in percentage of overwater flight because the supersonic aircraft has to fly further at subsonic speeds, which is less efficient in the placeholder model of the supersonic aircraft, leading to an increased fuel burn and a reduced aircraft range. The supersonic aircraft modeled here shows a maximum range of 2790.5 nmi when flying completely over land.

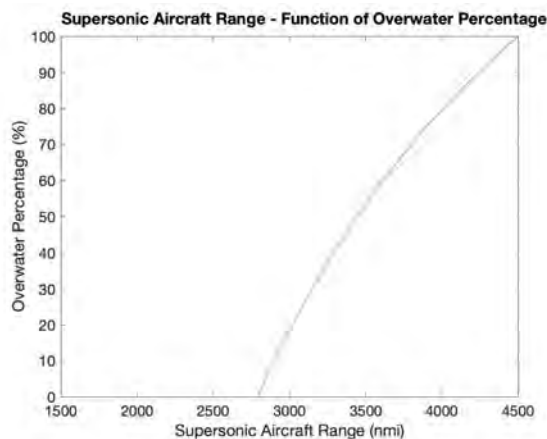


**Figure 11.** Supersonic Aircraft Maximum Range Capability as a Function of the Percentage of Overwater Flight.

### Simplistic supersonic route path adjustment

The percentage of overwater flight calculations form the second component used in determining the route-specific range capability of supersonic aircraft (shown in Figure 11). The method presented here identifies route adjustments that lead to minimum flight time for a particular route (using supersonic speeds over water and subsonic speeds over land). Because the current work considers that the supersonic aircraft can operate over Mach 1.0 only while flying over water, the desire to minimize flight time through route adjustments corresponds to finding route path deviations from its great circle path to allow the aircraft to operate at supersonic speeds for the longest overwater route segment possible. The percentage of flight over water calculations with re-routing technique have the following characteristics:

- These calculations consider the longest route portion over water without any land portions. The great circle distance is based on the longitudes and latitudes of airports on a spherical Earth model.
- In case small islands lie under the flight path (in the great circle path or during path re-routing), the algorithm checks if the sum of path length before and after the island is greater than 40% of the total flight path. If yes, then the small island is ignored, because of the assumption that an aircraft can avoid the island by flying around it.
- The re-routing technique finds 14 alternate flight path deviations above and below the great circle path. For generating the alternate flight path, the coordinates of the mid-point of the great circle path are determined, followed by incrementing (or decrementing) the mid-point latitude by 1° for each alternate flight path, ultimately changing the departure heading of the aircraft. The 14 alternate routes generated in this study correspond to incremental deviations in departure heading to a maximum of +7° and -7° from the great circle path. This is very simplistic for computational efficiency but does recognize that the supersonic aircraft might fly a longer distance so that the overwater portion of the flight minimizes block time. Higher resolution flight paths would likely be adopted in actual operations, but the optimal path determination problem was deemed too computationally expensive for the route characterization part of the study.
- Among the great circle path and all the alternate flight paths generated for a route, the minimum time flight path is selected for supersonic aircraft operation. The flight time is determined using different flight speeds for overwater and overland flight operation. The minimum time flight path from the 15 options is selected. The flight time for every route is calculated using a supersonic flight speed of Mach 2.2 (at 55,000 ft) for the longest segment over water and subsonic flight speed of Mach 0.95 (at 35,000 ft) for remaining segments. These simplistic calculations are performed using the following equation:

$$t_{flight} = \frac{P_{overwater}}{100 * vel_{sup}} + \frac{100 - P_{overwater}}{100 * vel_{sub}} \quad (16)$$

Here,  $t_{flight}$  denotes flight time,  $P_{overwater}$  is the percentage of flight over water,  $vel_{sup}$  is the aircraft's supersonic speed (Mach 2.2 at 55,000 ft), and  $vel_{sub}$  is the aircraft's subsonic speed (Mach 0.95 at 35,000 ft).

For example, considering the JFK-LHR route shown in Figure 12, the overwater calculation technique finds a minimum time flight path (denoted by red dotted line) with a deviation from the great circle flight path (denoted by solid red line). In this case, the minimum flight time path also has the longest segment over water amongst all the route path deviations generated by the technique. This simplistic routing provides the inputs for the filters used to identify potential airport pairs for supersonic aircraft service. The FLEET allocation problem to predict the routes on which supersonic aircraft will operate (and how many flights on those routes) uses the higher resolution flight path approach developed by our colleagues at Georgia Tech.

### Nonstop Supersonic-Eligible Routes

The following route filters are employed to identify the nonstop potential supersonic routes:

- Routes with minimum time route distance less than or equal to 4,500 nmi.
- Routes satisfying placeholder supersonic aircraft's range capability as a function of overwater flight percentage.
- Routes with block time savings of one hour or more when flying the placeholder supersonic aircraft on the simplistic supersonic routing. The authors believe that only routes that show potential time savings of more than 60 minutes will be to attract passengers given the cost difference; airlines would want to operate their supersonic aircraft on these routes only for maximizing their profit. A more rigorous passenger choice model might provide a better approach to this filter.

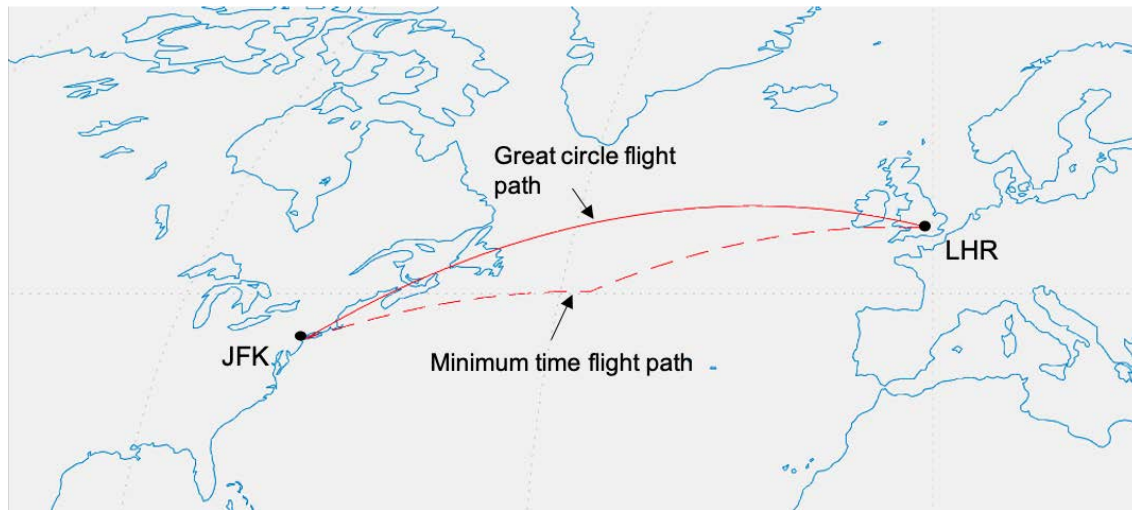


**Figure 12.** Supersonic Flight Path Re-routing Example for JFK–LHR Route to Find the Minimum Flight Time Route Path.

These filters lead to the identification of 241 nonstop potential supersonic routes in the FLEET network. Out of these 241 routes, using our fairly simple route path adjustment, 191 routes have greater than or equal to 75% of overwater flight segment, 35 routes have overwater flight segments between 50% and 75%, and the remaining 32 routes have overwater flight segments lesser than 50%.

#### Supersonic-eligible Routes with Fuel Stops

There are some intercontinental routes with sufficiently high passenger demand to suggest the potential for profitable supersonic operations that have ranges that exceed the un-refueled range of the supersonic aircraft. Even with the increase in distance flown and with the time required to land, refuel, and takeoff again, the total trip time savings suggests that a potential supersonic passenger demand would exist on routes with an intermediate fuel stop between the origin airport and the destination airport. For this work, only airports currently in the FLEET network are considered for potential fuel stops; there are two trans-Pacific potential fuel stop airports—Honolulu, Hawaii (HNL) and Anchorage, Alaska (ANC); and five trans-Atlantic potential fuel stop airports—Shannon, Ireland (SNN); Keflavik, Iceland (KEF); Oslo, Norway (OSL); Dublin, Ireland (DUB); and San Juan, Puerto Rico (SJU). The team recognizes that there exists a number of other potential fuel stop airports in the Pacific and the Atlantic; however, these airports do not have enough U.S. flag carrier service to appear in the BTS database and are not in the FLEET network. For routes with fuel stops, this work assumes that the fuel stops are just technical stops, hence, there is no boarding of any new passenger from the fuel stop airport into the flight or debarkation of any existing passenger from the flight. The fuel stop adds 60 minutes to the block time of the supersonic aircraft flying on the with-fuel-stop route (includes time for descent, landing, taxi, refueling, taxi, takeoff, and climb). The supersonic route path adjustment method for with-fuel stop routes optimizes the heading deviation for each "hop" of the flight, i.e., from origin to fuel stop (first hop) and then from fuel stop to destination (second hop), while also selecting the optimum fuel stop airport that minimizes the overall block time. Figure 13 shows the route adjustment approach for routes with fuel stops using the DFW–HNL–NRT route as an example. The following route filters are employed to identify the with-fuel stop potential supersonic routes:

- Routes with minimum time route distance less than or equal to 9,000 nmi. This work does not consider more than one fuel stop on a route.
- Routes satisfying placeholder supersonic aircraft's range capability as a function of overwater flight percentage. This step is implemented for each hop of the flight. The route heading deviation is also adjusted for each hop.
- Routes with block time savings of 1 hour or more when flying the placeholder supersonic aircraft on simplistic supersonic routing. This block time savings includes additional 60 minutes gained in block time due to the technical stop.

These filters lead to identification of 17 additional potential supersonic routes with a fuel stop in the FLEET network. All of the 17 potential routes with fuel stops indicate a block time savings of more than two hours over the nonstop subsonic flight.

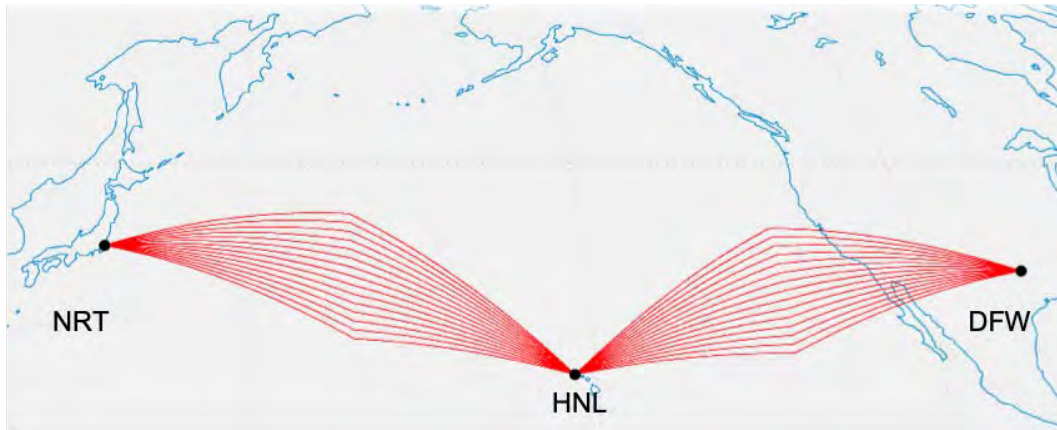


**Figure 13.** Supersonic Flight Path Re-routing Example for Routes with Fuel Stop using DFW-NRT Route with Fuel Stop at HNL.

Supersonic-eligible Route Network in FLEET

The supersonic-eligible route network in FLEET consists of a total of 258 potential supersonic routes, out of which 241 are nonstop routes and 17 are with-fuel stop routes. Figure 14 depicts the whole potential supersonic route network for FLEET on a world map. The route path for the 258 potential routes plotted in this figure are selected using the approach described in the preceding paragraphs. The routes without fuel stops are shown in gray and the routes with fuel stops are shown in red.

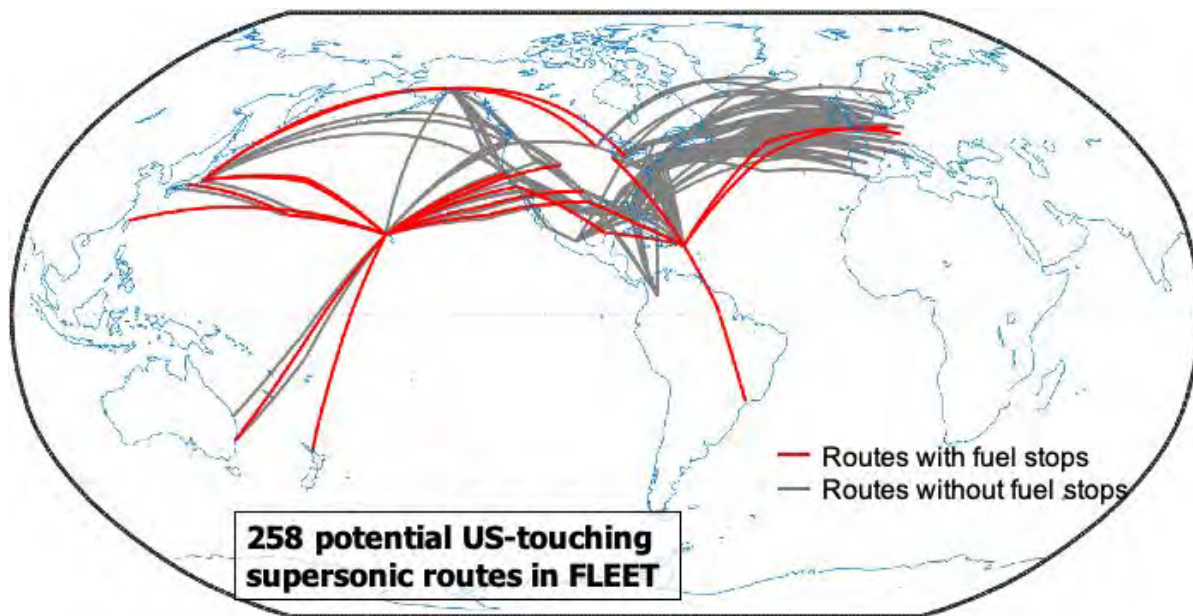


**Figure 14.** Supersonic-Eligible Route Network in FLEET (Airport Minimum Time Connections Shown Here; Not the Exact Route Path Flown).

The current allocation problem setup in FLEET uses the 258 potential supersonic routes as an input. FLEET chooses which routes to allocate to supersonic aircraft according to the route profitability, which is specific for each year of the simulation. As with all routes in FLEET, the aircraft will travel a roundtrip on the route, so the Amsterdam Schiphol (AMS)-JFK route also covers JFK-AMS flights. Table 6 provides information about a few of the routes for potential supersonic service.

**Table 6.** Details about Selected Potential Supersonic Routes in FLEET (Based on Simplistic Routing).

	Parameter	Airport A	Airport B	Great Circle Distance (nmi)	% Over-Water*	Min Time Distance* (nmi)	Block Time* (in hours)		Time Savings* (in hours)
							Subsonic	SST	
Nonstop routes	Max % overwater	HNL	SYD	4412.03	<b>99.79</b>	4425.70	9.14	3.52	5.62
	Min % overwater	MIA	SEA	2364.89	<b>18.75</b>	2414.53	4.90	3.87	1.03
	Max time savings	SFO	NRT	4442.35	99.47	4442.36	9.20	3.55	<b>5.65</b>
	Min time savings	DTW	MEX	1584.08	36.20	1588.23	3.28	2.27	<b>1.01</b>
Fuel stop routes	Max % overwater	SFO	AKL	5674.26	<b>99.42</b>	5910.17	11.75	5.72	6.03
	Max time savings	LAX	SYD	6512.48	99.22	6639.63	13.48	6.31	<b>7.17</b>

### FLEET Supersonic Simulation Requirements

#### Higher-resolution Supersonic Aircraft Model and Routing

As mentioned before, the Purdue team employed the placeholder supersonic aircraft model to only identify the supersonic-eligible route network in FLEET. The team used the 55-seat A10 notional medium supersonic aircraft model to run FLEET and conduct all the fleet-level analyses. The computational model of the 55-seat A10 notional medium SST aircraft implemented in this work was developed by our colleagues at Georgia Tech. This model provides mission performance characteristics—including fuel consumption and block time—for the supersonic aircraft to operate on routes in the FLEET network. Because the supersonic aircraft can only operate supersonically over water, the ground path of the flight to optimize a combination of fuel consumption and block time can deviate significantly from typical subsonic aircraft routes. For consistency in the project, this work uses flight path ground tracks also generated by the team at Georgia Tech.

The Purdue team considers two generations of supersonic aircraft with entry into service (EIS) dates of 2025 (generation 1) and 2038 (generation 2). The generation 2 supersonic aircraft show a 10% improvement in the fuel burn with no change in the aircraft noise or sonic boom characteristics.

The detailed supersonic routing developed by Georgia Tech works to identify the optimum supersonic route path by solving an optimization problem to minimize a weighted sum “cost to the goal” objective function. The goal here is to minimize a combination of the block time and the block fuel values for flying supersonic aircraft on a supersonic route. This approach essentially finds a supersonic route path that is a trade-off between the time optimal-only route and fuel optimal-only supersonic route path. A simplistic representation of this approach is shown in the equation below:

$$weightedsum_{objective} = \alpha * \left( \frac{BlockFuel}{BlockFuel_{min}} \right) + (1 - \alpha) * \left( \frac{BlockTime}{BlockTime_{min}} \right) \quad (17)$$

Here,  $BlockFuel_{min}$  and  $BlockTime_{min}$  is the minimum block fuel and block time value possible for a route, respectively. This work uses  $\alpha = 0.4$  as the recommended value for the weighted sum supersonic routing (based on various supersonic routing tests conducted by our partners at Georgia Tech).

The Purdue team uses NASA's Flight Optimization System (FLOPS) to “fly” the detailed notional 55-seat supersonic aircraft on the weighted sum routes (with an  $\alpha$  value of 0.4), conducting separate FLOPS runs for each direction of a supersonic route. The team observed different block fuel values (and in some cases, block time) when flying the detailed notional supersonic aircraft in different directions on a supersonic route.

#### Supersonic aircraft cost model

With no commercial supersonic aircraft currently in production/service, the Purdue team used some rational assumptions to model aspects of the supersonic aircraft cost. The assumptions used for supersonic aircraft cost modeling in FLEET are as follows:

- The 55-seat supersonic aircraft acquisition cost equals that of a very large commercial subsonic aircraft (a “class 6” aircraft in FLEET with 400+ seats) (Mavris et al., 2017).
- 100% of the supersonic aircraft acquisition cost is amortized over a 15-year period. This is reflected in the total operating cost of the supersonic aircraft.
- Fuel costs per gallon are the same for supersonic and subsonic aircraft.
- Crew costs for the 55-seat supersonic aircraft have a higher hourly rate, like those for a large subsonic aircraft, reflecting the “premier” status that the supersonic aircraft crews might have. The operating cost per flight also reflects the faster speed (shorter block hour flights) of the supersonic aircraft.
- Yearly maintenance costs used to inform aircraft retirement decisions follows the same Boeing maturity curve as the subsonic aircraft. This curve predicts maintenance cost as aircraft ages up to 40 years from EIS. Using this may be problematic given the operating conditions of the supersonic aircraft —particularly the in-flight heating and subsequent cooling and the cruise operating throttle settings of the engines—differ from subsonic aircraft.
- Aircraft age-based fuel economy follows Airbus trends that are also used for subsonic aircraft. This means an increased fuel consumption each year of service to reach 10% increase over original fuel consumption after 40 years from EIS.

Table 7 summarizes the multipliers used for developing the cost model for the simplistic A10 notional medium SST aircraft in FLEET.

**Table 7.** Cost Parameters used for Developing the Simplistic “Back-of-the-Envelope” Supersonic Aircraft Model in FLEET.

Cost Parameters of Simplistic Supersonic Aircraft	Multipliers/Modeling Characteristics
Crew Cost	Block time calculations and subsonic class 5 aircraft
Maintenance Hours	1.5 times that of subsonic class 5 aircraft
Insurance	Subsonic class 5 aircraft Insurance
Indirect Operating Cost	Subsonic class 5 aircraft
Acquisition Cost	Subsonic class 6 aircraft

Supersonic ticket price model

One of the first steps in determining ticket prices for supersonic flights is identifying the potential routes where the supersonic aircraft might operate and then use available pricing information about those routes. Considering that the Boom Overture concept (Boom Overture) is a possible first supersonic passenger-carrying entrant that does not make an attempt at low boom flight, the initial supersonic aircraft are most likely to operate on over-ocean routes, where they can fly supersonically over the water. This means that mostly international routes will be “supersonic eligible.” Following the discussion from Boom’s website that indicates their aircraft could operate with a ticket price similar to current business class tickets (Boom Supersonic), the Purdue team assumes that the supersonic ticket price would be similar to the current business class ticket prices. With data about historical ticket prices paid for international routes difficult to obtain, the team is dependent on the most recent (2018) offered business class or above ticket pricing data to model supersonic ticket prices for FLEET simulations. The business class or above offered ticket price data is procured through matrix.itasoftware.com (Matrix Airfare Search) as round-trip data for a subset of 26 supersonic-eligible trans-Atlantic origin-destination pairs (and destination-origin pairs) for February 9, 2018 and the median of the ticket price data for every route is selected as the current offered business class or above ticket fare.

Using the offered ticket fares for business class or above, this work builds a range-dependent delta-yield model, wherein delta-yield is the markup or profit per passenger-nautical mile (\$/pax-nmi). The model builds a simplistic linear fit for ticket delta-yield with respect to the range elasticity. This simplistic model attempts to account for the passenger’s willingness to pay more for increased time savings when flying longer distances in a supersonic aircraft. The supersonic ticket fare is hence equal to the sum of the supersonic aircraft operating cost per passenger and a margin term, expressed as the following equation:

$$Fare_{SST, route i} = (\Delta yield_{per nmi} * range_{route i}) + \frac{CostofSST_{route i}}{55 pax} \tag{18}$$

The operating cost of the aircraft (represented by the term *CostofSST*) includes the non-fuel direct operating cost (maintenance cost, crew cost, servicing cost, indirect operating cost, insurance cost, and amortized acquisition cost) and the fuel cost for operating the supersonic aircraft on a specific route.



### Supersonic Aircraft Production and Aircraft Available in FLEET

The Purdue team assumes that the supersonic aircraft production follows the trend of Boeing 787 deliveries over the last decade. The available Boeing 787 annual aircraft delivery data from first delivery until 2018 provides the absolute supersonic aircraft production numbers for eight years (2011–2018), followed by extrapolation of the lower-slope production rates for years beyond the eighth year of production. There are two reasons for selecting the Boeing 787 production curve as a baseline for the simplistic supersonic aircraft. First, the Boeing 787 is a recent high-technology introduction aircraft and given that the commercial supersonic aircraft are also expected to be high-technology (owing to the addition of supersonic cruising abilities in the commercial sector), this assumption does not seem unfair. Second, because the deliveries of the Boeing 787 began in 2011, this assumption provides a historical basis for predicting supersonic aircraft deliveries from their initial delivery. Then, to use this as a guide for supersonic aircraft availability in the FLEET simulations, the total production must be scaled to reflect the number of aircraft available to the airline model that reflects U.S. flag carrier airlines on a U.S.-touching route network. On the basis of the Boeing Market Outlook, the share of future aircraft deliveries to North America is approximately 40% of the total aircraft production. In Figure 15, the red dotted line depicts the Boeing 787 production/delivery curve (which provides a model of the total number of supersonic aircraft delivered worldwide), and the black solid line depicts the number of supersonic aircraft delivered to FLEET's airline each year.

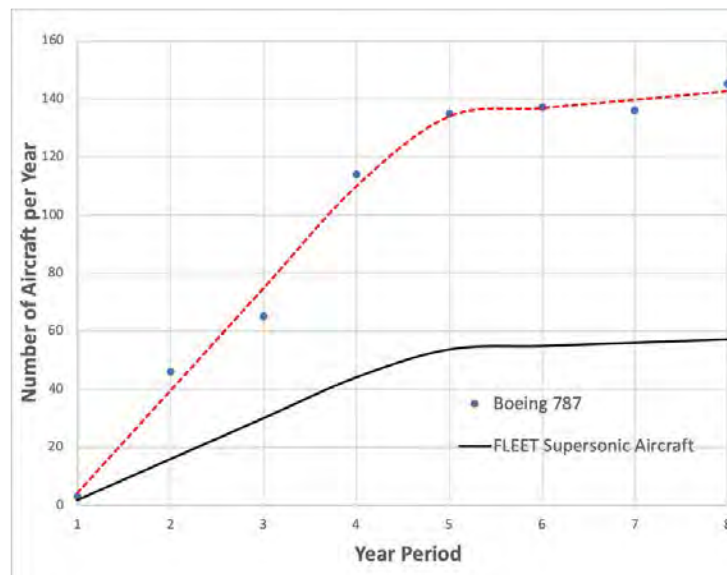


**Figure 15.** Supersonic Aircraft Production Curve in FLEET.

## Task 2 – Fleet Analysis

Georgia Institute of Technology and Purdue University

### Objective

Georgia Tech used the GREAT fleet prediction tool to perform an assessment of the impact of subsonic aircraft, and then with the help of FLOPS-based performance models, the team developed similar capability for supersonic aircraft using the scenarios from prior ASCENT Project 10 work and the key environmental indicators (KEIs) from vehicle models developed in Tasks 4 and 5. Georgia Tech has been working to define supersonic demand scenarios to estimate the fleet level impact of supersonic travel. Similarly, the Purdue team has been utilizing their FLEET tool to analyze this impact.

### Research Approach (Georgia Tech)

Retired SST vehicles struggle with environmental and economic challenges primarily due to the generation of sonic booms during flight. Sonic booms are generated when traveling at speeds greater than the speed of sound. These booms cause significantly higher disturbance and annoyance when reaching the ground relative to subsonic aircraft. This fact has resulted in the prohibition of overland supersonic operations for SST vehicles, which has severely reduced the number of permissible

routes and the overall utilization of these vehicles (Liebhardt, Gollnick and Lütjens, 2011; Liebhardt, 2019). Moreover, SST vehicles consume much more fuel compared to their subsonic counterparts along the same missions. The lower utilization coupled with the higher fuel consumption for SST vehicles increases operating costs for airlines significantly, which leads to very high-ticket prices that further shrinks the market for supersonic air travel (Henne, 2005; Liebhardt, Lütjens, Tracy and Haas, 2017).

New SST vehicles are expected to face the same environmental and economic challenges that previous SST vehicles faced. Whether technological advancements would sufficiently lower fuel consumption and whether smart flight routing would enable more routes to be flown remain unanswered questions. If those vehicles do make supersonic flight more affordable, the projected demand for such service also remains unknown.

Previous research has investigated different aspects of these questions. Liebhardt et al. (2011) assessed the global market for SST vehicles based on premium airline ticket sales and found that insufficient demand exists to support the production of large SST vehicles, but smaller vehicles, with a seating capacity of approximately 20, could represent a more realistic opportunity. However, limited focus was given to the impact of SST routing on the aircraft mission and on overall SST operations. The impact of prohibited overland operations on flight routes and mission performance was separately analyzed by Liebhardt, Linke, and Dahlmann (2014). It was shown that only small trade-offs, manifested by detours and subsonic overland segments, are required for high demand routes, emphasizing the opportunity for SST. Yet, routing was based on maximizing time savings without regards to fuel consumption. When exploring SST-specific routing, a need to evaluate time-versus fuel-optimal routes arose in order to examine the resulting implications on demand for those routes. Finally, the effect of the sonic boom carpet on SST routing was studied by Liebhardt (2019) to evaluate a pool of permissible supersonic routes. Correlations to demand were not investigated, however.

As a result, identifying routes that are suitable for SST operations and evaluating the penalties associated with the restriction of supersonic overland flight both become crucial enablers for assessing the demand for commercial supersonic.

### General SST Flight Rules

For an algorithm to route an aircraft over water/land, it has to know the location of water/land at any location on the globe, which can be done using a set of polygon-based data or gridded data. The toolset described here exclusively uses Natural Earth Data, which is a continuously updated public domain, free vector and raster map data set available online.

Since current regulations state that sonic booms shall not reach land, the analysis needs to consider where and how a sonic boom could reach land. In general, a sonic boom depends on multiple factors, some of which are specific to the aircraft (e.g., cruise Mach number and weight), atmospheric conditions (e.g., temperature gradients, wind speed/direction), and operational characteristics (e.g., cruising altitude, maneuvering effects from turning, or acceleration/deceleration). Until such time that detailed, aircraft-specific sonic boom characteristics become available from other tasks of the project, the current algorithm focuses on sensible generic rules that can be widely applied.

Using the Concorde as a reference, the Cross-track Projection Distance (CPD) is computed to be 20 nmi. The CPD is the side distance covered by the primary boom carpet on the ground. However, this value changes with turning (Air France, 2003). Currently, how CPD values would change for an aircraft with different characteristics is unknown. For this analysis, a generic value of 27 nmi is assumed, corresponding to a maximum routing angle of 45 deg and based on the specifics of the algorithm to be described later. This value is used to define a “buffer” distance around land masses by using the ocean polygon dataset and shrinking it by a fixed Cartesian distance of 27 nmi converted into geospatial angles.

Besides buffer distances, there are additional areas to be avoided for flight routing. These areas can include entire countries where overflight is not permissible due to a variety of reasons, as well as closed airspace areas that aircraft are not allowed to enter. These additional areas can be included as long as the areas are known and agreed upon, such as through country border vector data or Notice-To-Airmen (NOTAM) polygon shapes. In this analysis, no-fly-zones or restricted airspaces are not considered since it is deemed premature when trying to understand the routing options for supersonic aircraft. Furthermore, weather variability is also not considered in this analysis and instead, the International Standard Atmosphere (ISA) model with still air is utilized.

### Routing Algorithm

During the development of the routing algorithm, the Georgia Tech team quickly recognized that even for routes that the Concorde flew regularly, the great circle track falls over land in many places. It is possible, however, to slightly shift the

ground track away from land and the buffer zone and arrive at a track with a significantly higher fraction over water so that the aircraft can make use of its speed for a much larger portion of the flight. For example, two coastal cities on the same continent, where the great circle track falls entirely over land, can become an almost entirely over water flight by simply moving the ground track out to sea and then following the coastline with the buffer distance to the destination.

Raster-based algorithms can be utilized to determine such tracks for any given route. These algorithms make use of a discretized representation of a physical space by dividing it into small/equal boxes (i.e., a grid) in order to search for an optimum path. The simplest of these pathfinding algorithms is the Breadth First Search (BFS), which explores the grid equally in all directions to discover paths. Alternatively, Dijkstra’s algorithm associates movements between grid nodes with costs and as a result, seeks and prioritizes paths of lower costs.

Computational complexity for raster-based algorithms scales strongly with the size of the grid or grid resolution. BFS and Dijkstra’s algorithm can quickly become computationally prohibitive for a large grid or one with fine resolution. To tackle this issue, other raster-based algorithms have employed heuristics or heuristic cost functions to add search directionality (rather than exploring equally in all directions) and increase computational speed, while preserving accuracy. Examples include the A\* and Theta\* algorithms. The latter is the basis for the routing algorithm utilized in this research.

Definitions

As previously mentioned, raster-based algorithms operate on a discretized representation of the physical space. This technique leads to the definition of grid nodes, which lie in the middle of the boxes representing the search space. For algorithms to establish a grid path from any node to another in the search space, it is necessary to explore the neighboring nodes of the start node, and then the neighboring nodes of those neighboring nodes, and so on until the goal node is reached. If a ‘shortest’ path is to be established, a cost function is defined in order to inform the algorithm as to which paths are considered “shorter” and need to be prioritized. Algorithms, such as Dijkstra’s or A\*, typically follow a series of steps below to seek those shortest paths:

1. Identify neighboring nodes of the current node.
2. Evaluate cost function for all the neighboring nodes.
3. Select the neighboring node(s) with the lowest cost to explore next.
4. Repeat until the goal node is reached.

The performance of these algorithms is therefore directly affected by the definitions of neighboring nodes and the cost function. As shown in Figure 16, the simplest definition of neighbor nodes only allows for lateral and longitudinal movements in a two-dimensional space, essentially presenting the algorithm with four options to explore for every node. While this ensures that the step size is preserved in every iteration, it often results in non-smooth paths. This can be remedied by allowing diagonal (45 deg) movements, which doubles the number of options. For the routing algorithm utilized in this research, diagonal movements could ensure smooth paths between origins and destinations. Furthermore, the algorithm is set up to account for the two cruising regimes of supersonic aircraft (i.e., subsonic and supersonic) and therefore, 16 total options are available for every node (Figure 16).

As for the cost function  $f(n)$  evaluated for every neighbor node  $n$ , it is typically of the following form:

$$f(n) = g(n) + h(n) \tag{19}$$

where  $g(n)$  is the exact cost from the start node to the neighbor node, and  $h(n)$  is the heuristic estimated cost from the neighbor node to the goal node, as illustrated in Figure 16. For Dijkstra’s algorithm,  $h(n) = 0$  such that  $f(n)$  only relies on exact costs, which guarantees accuracy but compromises speed. Alternatively, other raster-based algorithms, such as the Greedy Best-First-Search, solely rely on heuristics such that  $g(n) = 0$ , which significantly increases speed but does not guarantee accuracy. A\* and Theta\* algorithms provide a good compromise between accuracy and speed by accounting for both exact costs and heuristics.

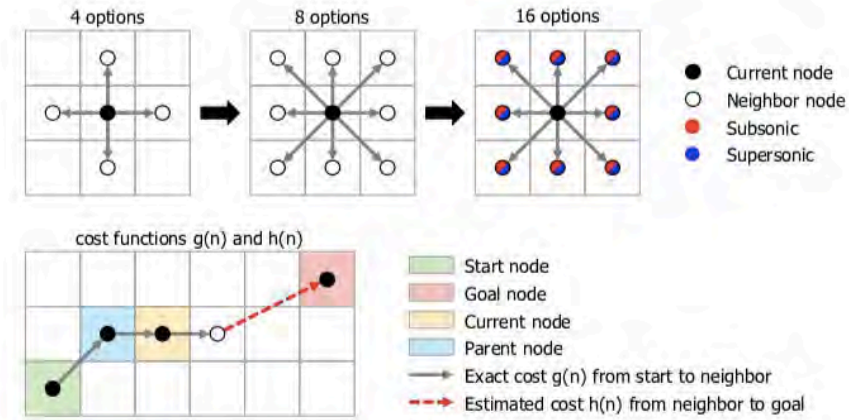


Figure 16. Definition of Neighboring Nodes and Search Options.

Cost Functions

To determine the optimum paths between origins and destinations, two primary metrics are considered: time and fuel. To minimize time, the most obvious choice would be to fly the aircraft at its supersonic speed along the great circle track. However, for many routes, this path would feature an excessive number of fuel-expensive accelerations since the aircraft would need to decelerate every time it flies over land. Alternatively, fuel-optimum paths might avoid accelerations altogether and fly the aircraft at its subsonic speed, which is not ideal since it would result in minimal time savings. Therefore, the cost functions need to account for both time and fuel simultaneously and not just a single metric. Actual airline operations utilize a cost index that captures the trade-off between time-based operating costs and fuel use. At this point, there is not enough information available to construct this type of trade-off for supersonic vehicles.

To that effect, the definitions of  $g(n)$  and  $h(n)$  included an artificial scaling parameter  $\alpha$  to trade between time and fuel. Values of alpha range from 0 to 1 such that a value of 0 represents a time-optimal choice, and a value of 1 represents a fuel-optimal choice, and any value in between represents a scaled blend:

$$g(n) = \alpha \cdot g_f(n) + (1 - \alpha) \cdot g_t(n) \tag{20}$$

$$h(n) = \alpha \cdot h_f(n) + (1 - \alpha) \cdot h_t(n) \tag{21}$$

where subscripts  $t$  and  $f$  denote time and fuel evaluations, respectively. Furthermore, the time and fuel absolute values need to be normalized by appropriate reference values in order to scale them to non-dimensional values close to unity in magnitude. The reference values represent idealized time  $f_{t,GC}$  and fuel  $f_{f,GC}$  to fly the great circle distance from origin to destination at supersonic speed such that the cost functions are of the following final form:

$$g(n) = \alpha \cdot [g_f(n)/f_{f,GC}] + (1 - \alpha) \cdot [g_t(n)/f_{t,GC}] \tag{22}$$

$$h(n) = \alpha \cdot [h_f(n)/f_{f,GC}] + (1 - \alpha) \cdot [h_t(n)/f_{t,GC}] \tag{23}$$

Time and fuel are calculated based on distance traveled and aircraft characteristics such as speed and specific air range (SAR). Time spent from one node to the other is simply the distance between the nodes divided by the speed of the aircraft. To calculate fuel, the distance is divided by SAR instead. The value of SAR is not a constant; however, it is a function of the instantaneous weight of the aircraft and its cruising altitude. For simplification, average SAR values are assumed for both the subsonic and supersonic regimes.

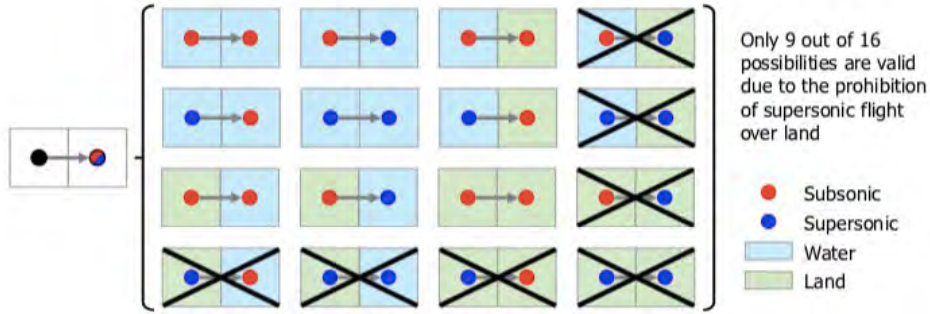


Figure 17. Possible Movements within the Search Grid.

The cost functions are formulated for all possible movements within the search grid. As shown in Figure 17, only nine possibilities are valid for any given movement from a current node to a neighboring one. Every possibility falls into one of four categories, where the aircraft will either accelerate, decelerate, or continue to cruise at either subsonic speed or supersonic speed. Thus, the cost functions  $g(n)$  and  $h(n)$  are formulated as follows:

$$g_f(n) = g_f(\text{Current}) + \hat{g}_f \quad (24)$$

$$\hat{g}_f = \begin{cases} \text{fuel penalty} & \text{if accelerate,} \\ \text{distance}/SAR_{sub} & \text{if decelerate,} \\ \text{distance}/SAR_{sub} & \text{if subsonic cruise,} \\ \text{distance}/SAR_{super} & \text{if supersonic cruise.} \end{cases} \quad (25)$$

$$h_f(n) = \text{distance to goal}/SAR_{super} \quad (26)$$

$$g_t(n) = g_t(\text{Current}) + \hat{g}_t \quad (27)$$

$$\hat{g}_t = \begin{cases} \text{distance}/\text{speed}_{super} & \text{if accelerate,} \\ \text{distance}/\text{speed}_{sub} & \text{if decelerate,} \\ \text{distance}/\text{speed}_{sub} & \text{if subsonic cruise,} \\ \text{distance}/\text{speed}_{super} & \text{if supersonic cruise.} \end{cases} \quad (28)$$

$$h_t(n) = \text{distance to goal}/\text{speed}_{super} \quad (29)$$

where  $h(n)$  is always evaluated based on the great circle distance from the neighbor node to the goal node, assuming a 100% supersonic flight. The latter ensures that  $h(n)$  is optimistic and monotonically decreasing (i.e., the estimated cost to the goal node is always equal or less than the best possible solution). It is worth noting that  $f_{f,GC}$  and  $f_{t,GC}$  of Eqns. (22) and (23) are equivalent to  $h_f(n)$  and  $h_t(n)$  evaluated for the start node.

### Path Optimality

As previously mentioned, the Theta\* algorithm (Daniel, Nash, Koeing and Felner, 2010) is the basis for the routing algorithm utilized in this research. While closely related to the A\* algorithm, Theta\* differs in that it performs a "line of sight" check after every iteration. This check determines whether a clear path from the parent node of the current node to the chosen neighbor node exists. If so, the current node is eliminated and the shortest path is adjusted. This procedure is illustrated in Figure 18.

Within the search grid, the Bresenham line of sight algorithm (Bresenham, 1965) is employed to identify grid nodes that intersect the line of sight. These intersection nodes are then checked for any constraint violation (e.g., the presence of obstacles). If no violations are present, the algorithm proceeds with eliminating the current node and constructing a new path that directly links the neighbor node with the parent node. This allows for smoother paths to be established, as shown in Figure 18. In this implementation, an obstacle is defined as the presence of land in a supersonic cruise segment. This means that if a purely supersonic parent-current-neighbor path is established and land is present along the parent-neighbor

path, the latter constitutes an obstacle and does not pass the line-of-sight check. In such a case, the current node would not be eliminated.

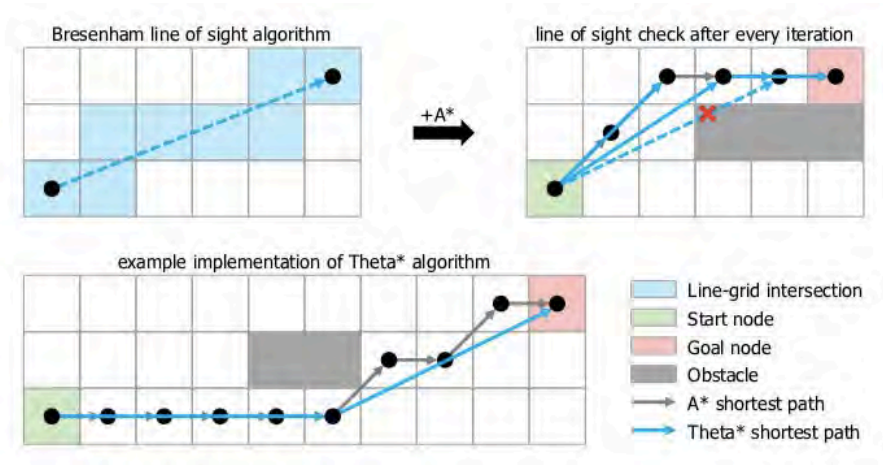


Figure 18. Search Algorithm.

Although the Theta\* algorithm resulted in paths smoother than the paths produced by the A\* algorithm, a few further refinements are still required to derive optimal paths. These refinements tackle two primary issues: first, situations where the algorithm would be presented with neighbor nodes of equal or numerically very close  $f(n)$  evaluations, and second, the fact that not all neighboring nodes are of equal step size since both lateral/longitudinal and diagonal nodes are considered.

If the cost function for all neighbors is equal or numerically very close, the algorithm is essentially presented with a tie. Typically, search functions for lowest value in a list will simply return the first encountered of all the tied values. The algorithm will therefore repeatedly return the same direction neighbor every time it is presented with a tie. Usually in a discretized space this is not an issue because the resulting path is still optimal; however, the solution mapped back to the physical space will be decidedly non-optimal. This issue is tackled by randomizing the list of tied neighbors each iteration. This approach guarantees that the algorithm returned different directions in the case of repeated ties.

The second issue stems from the fact that diagonal steps are significantly longer than the lateral/longitudinal steps, which leads the algorithm to prefer (or in some cases not to prefer) to take these steps since they get closer to the goal relatively faster. This issue is addressed by adding a cross-product term to the heuristic function, essentially adding a penalty for solutions that are away from the straight line connecting the start and goal nodes. This cross-product term therefore forces the routing algorithm to favor paths that are closer to the great circle track connecting the origin and destination, rather than those that follow the diagonal nodes.

Coordinate Systems

Proper functioning of the routing algorithm depends heavily on distance computations in a geospatial context. The most commonly used geospatial coordinate system is World Geodetic System (WGS) 84 (or European Petroleum Survey Group (EPSG) 4326), which defines latitude and longitude in degrees for a slightly elliptical spheroid with zero coordinates for Greenwich and the equator. This is originally developed for the GPS system and is widely used for many datasets. However, this coordinate system is not Cartesian and has extreme variations in unit coordinate sizes, especially between the poles and the equator, as well as discontinuities at the poles and the dateline.

It is therefore advisable to project this spherical coordinate system into a flat, near-2D Cartesian space. While many ways exist to accomplish this, some basic properties are desired: 1) the coordinates need to be continuous, 2) a straight line should approximate the shortest distance, and 3) a discretization should result in a mostly evenly sized grid.

Unfortunately, the most common and well-known projections such as Mercator or Web-Mercator (used in Google Maps, for example) do not provide these properties since they are cylindrical projections, as shown in Figure 19. Straight lines in these



projections represent constant heading but not shortest distance and there still is extreme distortion near the poles. Both of these issues are highlighted in FIGURE 20 for the New York (JFK) to Paris (CDG) route.

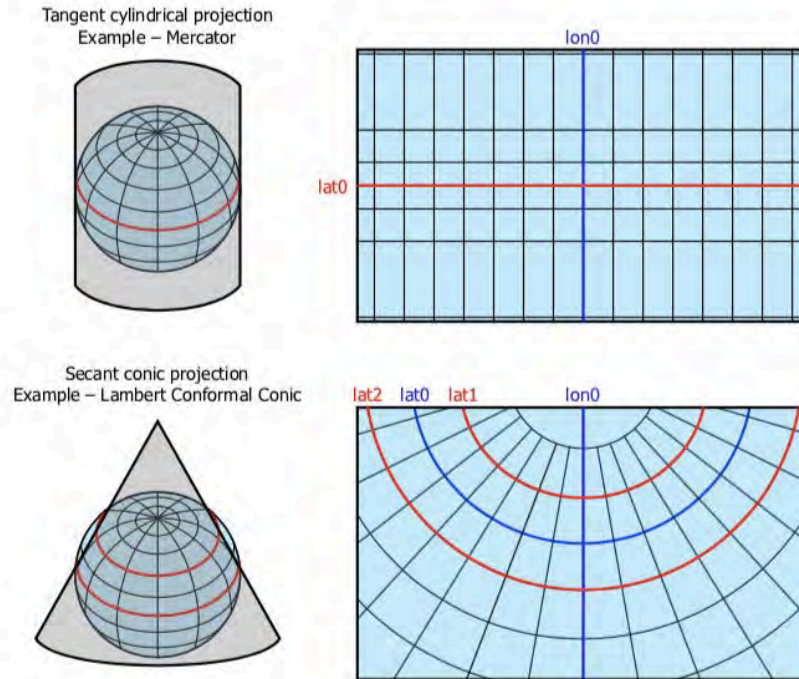


**Figure 19.** Typical Methods for Projecting Spherical Coordinate System into a Flat, Near-2D Cartesian Space.

However, there are projections that do fit the stated criteria. A commonly used aeronautical chart map projection is the Lambert Conformal Conic (LCC) projection (Figure 19), which has the advantage of preserving distances and at the same time has straight lines close to great circle routes (Figure 20). The disadvantages are that the areas are not preserved and that such a projection has to be customized to a specific area or region of the globe. These two disadvantages can be overcome by careful selection of the region at hand while avoiding or splitting antipodal routes into pieces. This process can be successfully automated.

The process of projection is shown in Figure 21. The implementation of customizing this for every route or origin-destination pair is accomplished as follows. Based on the locations of both airports, a buffer is added to define a box in which the route is likely to fall. From this box, three latitudes are defined: the maximum (lat1), the minimum (lat2), and a mid-point (lat0). These three values are then used to define the route specific LCC projection. It should be noted that libraries developed by the Open-Source Geospatial Foundation (OSGeo) are utilized to accomplish this. The PROJ library in particular is used to provide coordinate transformation and projection capabilities, whereas the GDAL/OGR library is used to provide translation capabilities for raster and vector geospatial data formats.

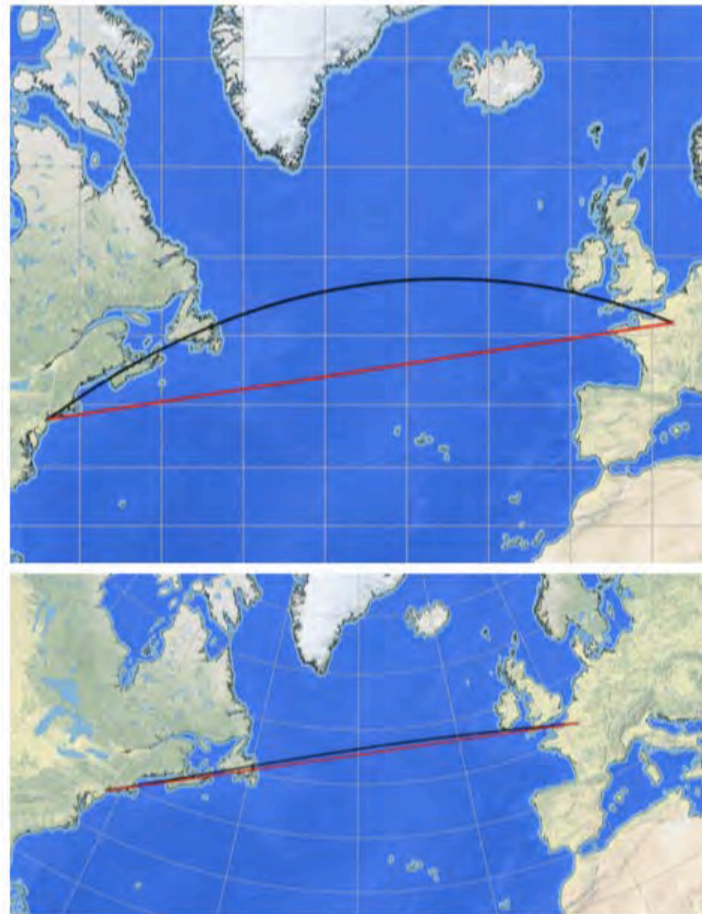


**Figure 20.** New York (JFK) to Paris (CDG) route.

It should also be noted that the actual grid size used can be dynamically adjusted up or down. The trade-off between computational speed and accuracy for a large sample of routes is investigated. In most cases, the resulting grid cells are just below 10 nmi in size but varied slightly depending on where on the globe the routes are, as well as the specific size of the area selected for the LCC projection. Automation of the projection procedure is the final element required for the routing algorithm (Algorithm 1) to be fully functional.

#### Fuel Stops

For routes exceeding the maximum supersonic range, it becomes necessary to select appropriate refuel stops. The fuel stops are selected based on the aircraft runway length requirement, and/or potential current commercial service, and the exclusion of conflict zone country airports. This selection is done while minimizing the great circle deviation for the refuel stop from the full great circle track of the entire route. The resulting pieces are routed separately and then added together while assuming a 90-minute delay for the time to descend, land, refuel, takeoff, climb, and resume cruise.




---

**Algorithm 1**

---

**Input:** aircraft characteristics; origin and destination WGS coordinates;  $\alpha$   
**Output:** optimal path from origin to destination

**procedure**

  load world map with buffer zones  
   $f_{f,GC} \leftarrow$  fuel to fly great circle distance from origin to destination 100% supersonic  
   $f_{t,GC} \leftarrow$  time to fly great circle distance from origin to destination 100% supersonic  
  **function** PROJECTLCC(origin and destination WGS coordinates) ▷ LCC projection  
   **return** search grid; start node; goal node  
  **end function**

**procedure** RUNTHETA STAR ▷ Theta\* algorithm

  OPEN, CLOSED  $\leftarrow$  {}, {}  
  add start node to OPEN  
   $g(\text{start}) \leftarrow 0$   
   $f(\text{start}) \leftarrow 1$   
  **while** OPEN **do**  
   current node  $\leftarrow$  node with minimum  $f$  in OPEN  
  **if** current node is goal node **then**  
    **break**  
  **else**  
   remove current node from OPEN and add it to CLOSED  
   determine neighbor nodes and randomize their order  
   **for all** neighbor nodes **do**  
     $\hat{g}_f, \hat{g}_t \leftarrow$  exact fuel and time from current node to neighbor node  
    $\hat{g} \leftarrow g(\text{current}) + \alpha \cdot [\hat{g}_f / f_{f,GC}] + (1 - \alpha) \cdot [\hat{g}_t / f_{t,GC}]$   
   **if** neighbor node is in CLOSED and  $\hat{g} \geq g(\text{neighbor})$  **then**  
    **skip**  
   **else if** neighbor node is not in CLOSED or  $\hat{g} < g(\text{neighbor})$  **then**  
     $h_f, h_t \leftarrow$  heuristic fuel and time from neighbor node to goal node  
    $h(\text{neighbor}) \leftarrow \alpha \cdot [h_f / f_{f,GC}] + (1 - \alpha) \cdot [h_t / f_{t,GC}]$   
   **if** line of sight to parent node is clear **then**  
     $\hat{g}_f, \hat{g}_t \leftarrow$  exact fuel and time from parent node to neighbor node  
    $g(\text{neighbor}) \leftarrow g(\text{parent}) + \alpha \cdot [\hat{g}_f / f_{f,GC}] + (1 - \alpha) \cdot [\hat{g}_t / f_{t,GC}]$   
   **else**  
    $g(\text{neighbor}) \leftarrow \hat{g}$   
   **end if**  
    $f(\text{neighbor}) \leftarrow g(\text{neighbor}) + h(\text{neighbor})$   
   **if** neighbor node is not in OPEN **then**  
    add neighbor node to OPEN  
   **end if**  
   **end if**  
   **end for**  
  **end if**  
  **end while**  
  construct reverse path from goal node to start node  
  **return** grid path from start node to goal node  
  **end procedure**

transform LCC grid path to WGS coordinates  
**return** optimal path from origin to destination  
**end procedure**

Figure 21. Pseudo-code for Automation of the Projection Procedure.

### Calculating $\alpha$ Value for Cost Functions

The artificial scaling parameter  $\alpha$  is introduced to trade between time-optimum and fuel-optimum paths for a given origin-destination route. Ideally, the appropriate  $\alpha$  value would be determined on a route-by-route basis by running the algorithm for a sweep of values ranging from 0 to 1, and then selecting the value that resulted in a path that maximized time savings at minimum fuel costs. However, running such a sweep for every potential supersonic route would increase computational run time significantly (e.g., if  $\alpha$  values of 0, 1, and all 0.1 increments in between would be examined, 10 additional runs would be required for every single route).

Instead, a subset of the potential supersonic routes is examined to determine a fixed  $\alpha$  value that could be used universally. One of the routes examined is the Hong Kong to Sydney route shown in Figure 22. For that route,  $\alpha = 0$  produces a time-optimal path with four accelerations, and  $\alpha = 1$  produces a fuel-optimal path along the great circle path with zero accelerations, and  $\alpha = 0.5$  produces a path that preserved the savings of the time-optimal path to a great extent but reduced the number of accelerations by two. For most routes examined, an  $\alpha$  value of 0.4 provides the best trade between time and fuel. This value is therefore used for all subsequent evaluations.

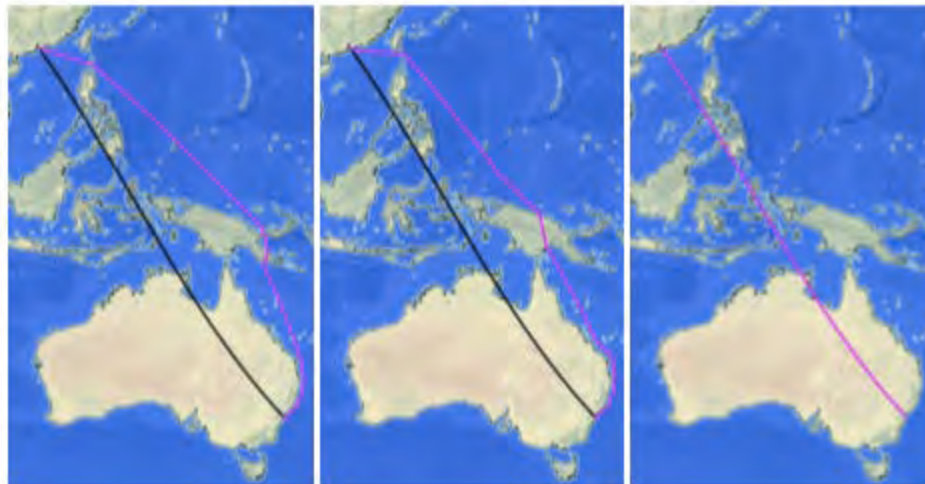


Figure 22. Hong Kong to Sydney Route.

### Flight Routing Results

Flight routing results for all origin-destination pairs are shown in Figure 23. Because the scaling parameter  $\alpha$  is set to 0.4, the performance of the algorithm for certain routes is predictable beforehand. For example, for routes whose great circle paths fall entirely over water (e.g., Honolulu, Hawaii to San Francisco, California), the algorithm did fly the SST vehicle at its supersonic speed for the entire route, as expected. For other routes whose great circle paths fall entirely over land and away from open water (e.g., Los Angeles, California to New York City, New York), the algorithm did fly the SST vehicle at its subsonic speed for the entire route, as expected. To gauge the performance of the routing algorithm, routes that are neither entirely over water nor entirely over land and away from open water need to be investigated. Two such examples are presented here.

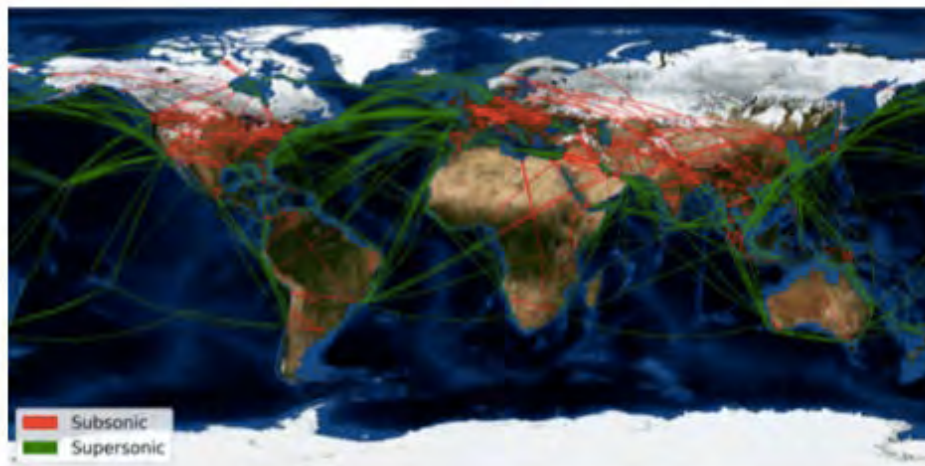


Figure 23. Flight Routing Results for All Origin-Destination Pairs.

The first route to examine is the Dubai to Singapore route shown in Figure 24. Although a big portion of the great circle path for this route lies over water, it cuts through the Indian peninsula. To fly the great circle path at its supersonic speed, the SST vehicle would have to slow down to its subsonic speed before it crosses the peninsula, and then re-accelerate to its supersonic speed once it clears it (i.e., two accelerations). In order to maximize time savings while minimizing fuel consumption, the algorithm instead routes the flight around the peninsula and flies the vehicle almost the entire time at its supersonic speed (i.e., only one acceleration). Such routing results in 52%-time savings at a minimal distance penalty of 7%,



while avoiding the fuel consumption penalty associated with a second acceleration. The algorithm efficiently weaves the flight around the coastlines and islands of India, Sri Lanka, and Indonesia to stay as close as possible to the great circle path.



**Figure 24.** Dubai to Singapore Route.

Another route that highlights the efficiency of the algorithm is the London to Dubai route shown in Figure 25. The great circle path for this route lies almost entirely over land (with the exception of a small portion over the Black Sea); hence, flying supersonically for the non-over land portion would yield minimal time savings. However, big bodies of water exist around the great circle path. The algorithm makes use of those bodies to route the flight along a two-acceleration path that enabled the SST vehicle to fly at its supersonic speed over the Adriatic Sea, the Mediterranean Sea, and the Persian Gulf. This flight route results in 33%-time savings at a distance penalty of just 9%. Once again, the algorithm efficiently threads the flight track around many coastlines and islands, especially over the Mediterranean, to stay as close as possible to the great circle path.



**Figure 25.** London to Dubai Route.

### Discussion: Demand Forecast and SST Flight Routes

The above-mentioned results show a promising market capture for future commercial supersonic air travel. However, it is important to realize that these results are derived based on a set of modeling inputs and assumptions, which if varied, could influence the results in different ways. The sensitivity of both flight routing and demand forecasting to various inputs and/or assumptions is discussed in this section.

Flight routing results derived in this study are influenced by a number of factors including: 1) the definition of a 27 nmi buffer distance around land masses, 2) the lack of consideration for weather patterns around the world, and 3) the SST aircraft characteristics embedded in the cost functions.

While the buffer distance value is set based on Concorde data, there is no guarantee that future supersonic flight rules would not consider a different value. If a much greater value is to be respected, a number of routes in this study would no longer be viable. For example, a much larger buffer zone for the London to Dubai route shown in Figure 25 could eliminate the possibility of supersonic flight over both the Adriatic Sea and the Persian Gulf, severely reducing the time savings for that route. The buffer distance value is therefore an important driver for routing results, especially for routes that utilize narrow bodies of water such as seas and gulfs.

Another factor that would impact flight routing is the consideration of weather patterns. It is assumed throughout this study that the great circle path between any city pair would be the choice for the subsonic reference vehicle and that the SST vehicle should adhere to it as much as possible to maximize time savings. In reality, weather plays a huge role in determining routes flown on a daily basis. Decisions are often made to deviate from great circle paths to avoid areas with intense head winds or make use of other areas with favorable tail winds. Wind patterns around the globe throughout the year have not been considered in this study, but they could influence routing results if they are included.

Moreover, SST aircraft characteristics that drive the cost functions have a strong and direct impact on the results of the routing algorithm. As previously discussed, SAR is a function of the instantaneous weight of the aircraft and its cruising altitude. All evaluations within the routing algorithm use averaged estimates for SAR in the subsonic and supersonic regimes. Similarly, the supersonic cruise speed of the aircraft is set to that of the Boom Overture concept. If this value would change, the cost evaluations and time savings along many routes would change as a result. Demand forecasting results in this study are driven by an alternative set of factors including: 1) the Boeing CMO air traffic growth rates, 2) the aircraft and airline characteristics, and 3) the implicit assumption that everyone who could afford to switch to supersonic travel would switch.

Air traffic growth rates are based on the 2019–2038 Boeing CMO. These rates were projected and published before the COVID-19 pandemic caused an abrupt and significant decline in air travel during 2020. It is assumed in this study that air travel would fully recover to pre-COVID levels and resume growth as projected. If growth rates would deviate from those of the CMO, the initial and filtered sets of potential routes—and consequently the overall demand for supersonic air travel—would be altered.

Similarly, aircraft and airline characteristics directly influence the  $\Delta$ Fare calculations for demand forecasting. The  $eff_{REF}$  value of 37 pax-km/L is based on an industry average reported in 2019. If instead a value corresponding to the state-of-the-art single aisle aircraft is utilized, the projected demand for supersonic travel would decrease, since the SST vehicle would be compared to a much more efficient reference in terms of fuel performance. Values of airline cost proportions and the assumed utilization for both the reference and SST vehicles would likewise impact demand calculations.

The switching percentage of premium passengers to supersonic air travel along the different routes is determined based on the implicit assumption that any passenger with a VTTS higher than the  $\Delta$ Fare per hour saved would switch. In reality, that may well not be the case for a variety of reasons. For example, passengers may choose not to switch to supersonic air travel even if they could afford it in order to avoid inconvenient departure and arrival times due to time zone variations. Effectively, demand forecasting results are based on an optimistic estimate of switching percentage, everything else being held the same.

## **Research Approach (Purdue)**

### **Incorporating Supersonic Aircraft in the FLEET Allocation Problem**

For the work presented here, the allocation of the airline's supersonic aircraft occurs before the allocation of the airline's subsonic aircraft. This approach allows for the characterization of a subset of total passenger demand as the passengers who would be willing to pay for the supersonic fare, and it currently assumes that the supersonic fare will be similar to the

as-offered fares for business class or above available in 2018. Because these passengers would be willing to pay more for the higher-speed and shorter-time trips, this subset of demand is identified on all of the potential supersonic routes, and an allocation problem determines how many supersonic aircraft roundtrips operate on which of the potential routes to maximize the profit from the supersonic aircraft in the airline's fleet. Then, for any routes that have potential supersonic demand but do not receive supersonic aircraft service, and for any routes that have supersonic aircraft service but do not have enough roundtrips to serve all the supersonic passenger demand, the unserved supersonic passenger demand is recombined with the subsonic passenger demand. The subsonic allocation problem then determines the number of roundtrips operated by each subsonic aircraft type on all of the routes in the network to serve the recombined passenger demand. Figure 26 depicts the subsonic and supersonic aircraft sequential allocation approach in a flowchart.

In the future, the team plans to implement a simultaneous allocation approach in which the airline would allocate the supersonic and subsonic aircraft at the same time (to satisfy both supersonic and subsonic flight demands). Such an approach could provide insights about passengers' travelling preferences via supersonic and subsonic aircraft while allowing for the enforcement of noise and/or airport capacity constraints in FLEET, if those are desired in the simulation. The simultaneous allocation approach will require some restructuring of the allocation problem (because of which the team chose to use the sequential allocation approach for the current work).

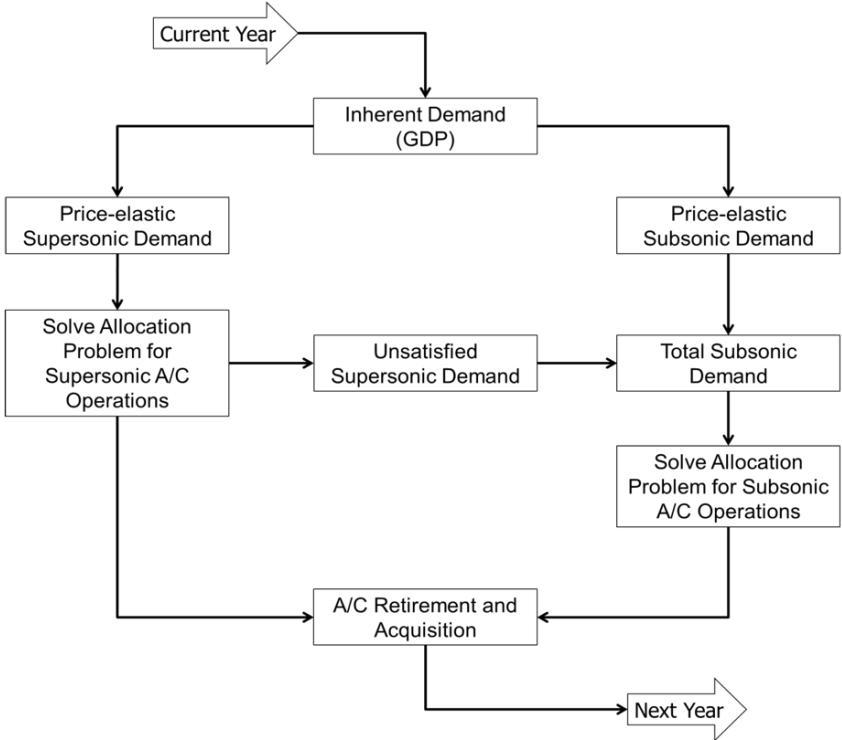


Figure 26. Sequential aircraft Allocation Approach in FLEET.

In each simulation year, FLEET predicts the inherent growth in airline passenger demand due to the economic growth described in the scenario and then includes the effects of price-demand elasticity to account for the influence of airline ticket price changes from the previous year on passenger demand. For instance, if a new aircraft is introduced that is far more fuel efficient than its predecessors, some of the cost savings associated with that fuel reduction leads to a lower ticket price. That would drive the passenger demand up, separately from the inherent economic demand driver. After the sequential allocation problems are complete, the model can make assessments on the need for more aircraft to meet future demand and the future profitability of retiring a currently operating aircraft in favor of a newer model in the following year.

**Preliminary FLEET Simulation Results**

The FLEET simulation is run from years 2005 to 2050 with the supersonic aircraft introduced in 2025 (generation 1) and

2038 (generation 2). In FLEET simulations, the aircraft are available to the airline to use one year after the EIS date (i.e., the aircraft was first available during the EIS year, but the representative day when that aircraft was part of regular service is the year following the EIS). Hence, the first-generation supersonic aircraft becomes available for allocation by the airline for a representative day in 2026. Similarly, the second-generation supersonic aircraft becomes available for allocation in 2039. The second-generation supersonic aircraft has the same block time on routes but consumes less fuel for the mission assuming incremental improvements in empty weight, aerodynamics, and propulsive efficiency.

The simulation results presented here are based on the higher-resolution A10 notional medium SST aircraft, detailed supersonic route path data, and the sequential aircraft allocation approach; i.e., supersonic aircraft allocation is performed before the subsonic aircraft allocation and, consequently, FLEET is accommodating the premium passengers first. The FLEET run presented here has no constraints on the number of airport operations. The current set of results demonstrate the ability of FLEET to indicate the routes where supersonic aircraft might be used and the number of daily operations on those supersonic routes. Further, the results demonstrate the possible changes in the subsonic fleet allocations due to the introduction of supersonic aircraft on select routes. This work considers only the previously developed CTBG scenario, utilizing the previously obtained subsonic-only CTBG results for comparing and analyzing the supersonic FLEET CTBG allocation and fleet fuel burn results.

The FLEET setup for the CTBG scenario is defined as follows:

- The network consists of 169 airports including U.S. domestic routes and international routes that have either their origin or destination in the U. S.
- The annual gross domestic product (GDP) grows at a constant value of 4.3% in Asia, 4.2% in Latin America, 2.4% in Europe, and 2.8% for airports in the U. S.
- The annual population growth rate is a constant value of 1.1% in Asia, 1.26% in Latin America, 0% in Europe, and 0.58% in the U. S.
- Jet fuel prices grow according to the Energy Information Administration (EIA) reference fuel price (Annual Energy Outlook 2011, 2011) case and are adjusted to meet the ASCENT survey fuel price, \$77.08/bbl, by 2050.
- Carbon emission prices grow linearly from \$0/MT in 2020 to \$21/MT by 2050.

The set of subsonic aircraft utilized in the CTBG scenario for the current work is listed in Table 8. The aircraft denoted “GT Gen1 DD” are the Generation 1 aircraft modeled by Georgia Tech with a “direct drive” engine. The Generation 2 aircraft are labeled “GT Gen2 DD.” These include aircraft belonging to the following classes: regional jet (RJ), single aisle (SA), small twin aisle (STA), large twin aisle (LTA), and very large aircraft (VLA). According to the amount and speed of technology incorporated into aircraft, in each of the scenarios, the new-in-class and best-in-class aircraft models will vary. Given the observation that new orders for 50-seat regional jet aircraft have diminished to zero, there are no small regional jet (SRJ) aircraft in the new- and future-in-class technology ages.

**Table 8.** Subsonic Aircraft Types used in Simulation.

Subsonic Aircraft Types in Study				
	Representative in Class	Best in Class	New in Class	Future in Class
Class 1 (SRJ)	Canadair RJ200/RJ440	Embraer ERJ145		
Class 2 (RJ)	Canadair RJ700	Canadair RJ900	GT Gen1 DD RJ (2020)	GT Gen2 DD RJ (2030)
Class 3 (SA)	Boeing 737-300	Boeing 737-700	GT Gen1 DD SA (2017)	GT Gen2 DD SA (2035)
Class 4 (STA)	Boeing 757-200	Boeing 737-800	GT Gen1 DD STA (2025)	GT Gen2 DD STA (2040)
Class 5 (LTA)	Boeing 767-300ER	Airbus A330-200	GT Gen1 DD LTA (2020)	GT Gen2 DD LTA (2030)
Class 6 (VLA)	Boeing 747-400	Boeing 777-200LR	GT Gen1 DD VLA (2025)	GT Gen2 DD VLA (2040)

Because FLEET models the behavior of a profit-seeking airline, the FLEET allocation problem decides which routes to operate the supersonic aircraft on while maximizing its profit over the whole network. This essentially allows FLEET to choose the routes for supersonic aircraft operation from the 258 supersonic-eligible routes presented in the previous section. If the 5% passenger demand on a route is too low for profitable supersonic operations, the result has no trips allocated to that routes. This ensures that FLEET airline does not forcefully operate supersonic aircraft on a set of user-defined routes. Rather, it has the freedom to operate supersonic aircraft on profitable routes only, mimicking the behavior of an actual profit-seeking airline.

With the current modeling, the 2050 fleet fuel burn with supersonic aircraft is 6.48% higher than the subsonic-only fuel burn. Figure 27 shows the normalized fuel burn for both supersonic and subsonic-only cases. The supersonic run refers to the case in which both supersonic and subsonic aircraft are available for allocation in an airline fleet, whereas the subsonic-only run refers to the case in which only subsonic aircraft are available for allocation in an airline fleet (no supersonic aircraft are introduced in this case). Figure 28 shows the normalized total daily passenger demand served for both supersonic and subsonic-only cases, which appears to be similar for most years. For year 2050, the demand served for the case with supersonic aircraft is actually greater than the subsonic aircraft-only case by 14,696 passengers per day. Figure 28 does not help the reader to identify this demand difference, but it still informs the reader about the total daily passenger demand trend for the two cases.

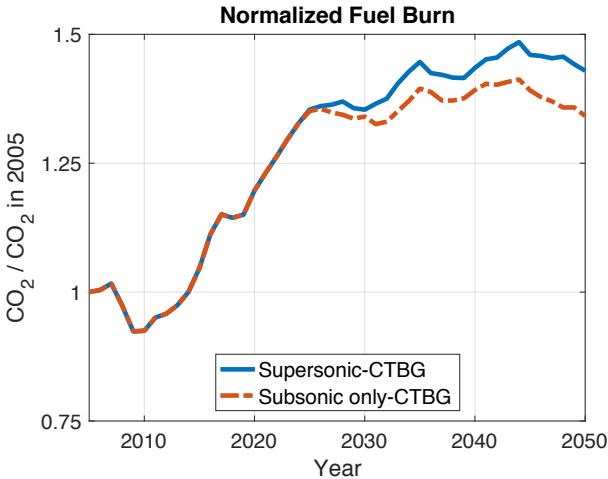


Figure 27. Normalized Fuel Burn from FLEET Simulation.

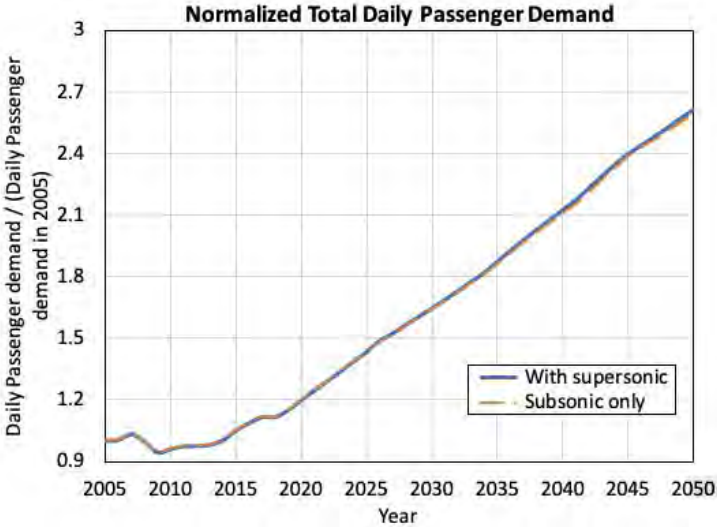


Figure 28. Normalized Total Daily Passenger Demand from FLEET Simulation.

The Purdue team noted that the introduction and allocation of the supersonic aircraft changes the use, retirement, and acquisition of the subsonic aircraft. That is, the airline modifies its subsonic fleet allocation to accommodate the new class of aircraft, i.e., supersonic aircraft, to maximize its overall profit. The change in the usage of the subsonic fleet can be seen by comparing the two charts in Figure 29 and Figure 30. In the first figure, the first six layers from the bottom in both charts

indicate the fuel burn from the six classes of subsonic aircraft in FLEET, and the topmost layer in the upper chart indicates fuel burn from the supersonic aircraft in FLEET. Analysis of the two charts reveals that the pattern of the six common color layers in the two charts changes after 2025, indicating a change in the fuel burn (and the allocation) of the subsonic fleet after the introduction of the supersonic aircraft.

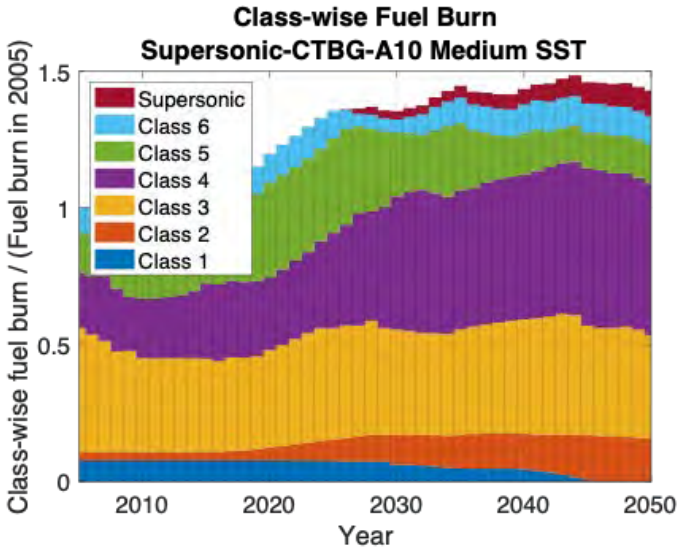


Figure 29. Class-Wise Fuel Burn Plots for Supersonic Case with A10 Notional Medium SST Aircraft.

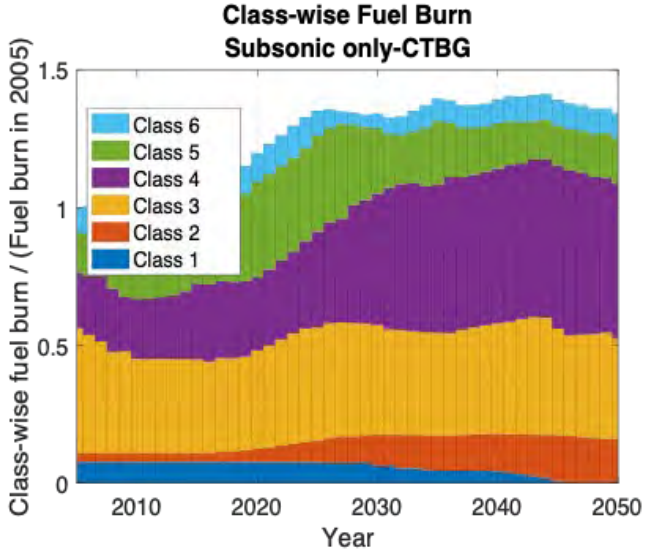


Figure 30. Class-Wise Fuel Burn Plots for Subsonic-Only Case.

The simulation results include details about the daily round-trip supersonic and subsonic aircraft allocations and the number of daily round-trip passengers carried on every route by each aircraft type each year. This data is used to generate different sets of output tables that provide yearly information about which routes the airline chose to operate their supersonic aircraft on and how did the airline change its subsonic aircraft allocation on those routes (and even on the non-supersonic-eligible routes in the FLEET network).

Table 9 depicts a partial output of FLEET aircraft allocations on supersonic-eligible and supersonic-ineligible routes for the year 2038. Here, we selected year 2038 as a year of interest because the second generation of supersonic aircraft becomes available to the airline next year in the simulation (i.e., only one “type” of supersonic aircraft available to simulation in 2038). The table contains aircraft allocation information for selected routes, including the distance flown (different for supersonic and subsonic aircraft), fuel stops (for supersonic routes with route length greater than 4,500 nmi), and the number of roundtrips conducted by each type (size) and class (generation) of aircraft in FLEET for a representative day. Considering Table 9, the daily aircraft allocation (roundtrips) columns for supersonic-eligible routes (JFK-LHR, LAX-HNL, and DFW-NRT) show that the introduction of supersonic aircraft influences the subsonic aircraft allocation. The rows labeled "supersonic" show the number of roundtrips operated on the route by each type of subsonic or supersonic aircraft. For all three routes in the table, there are small, but noticeable changes in the type and number of subsonic aircraft used when comparing the allocation when supersonic aircraft become available to the allocation when only subsonic aircraft are available. With the FLEET model introducing supersonic aircraft in 2025, there are 13 predicted years of demand evolution with supersonic aircraft present, so the passenger demand on each route varies between the supersonic and the subsonic-only scenarios. Additionally, when supersonic aircraft are available, they take some of the business class and above passenger demand away from the subsonic aircraft. A combination of these two factors shows that on some routes, the subsonic aircraft capacity has actually increased when supersonic aircraft are also available (JFK-LHR and LAX-HNL indicate this). The DFW-NRT route indicates a decrease in the number of subsonic seat capacity on the route decreases when supersonic aircraft are available.

**Table 9.** FLEET Aircraft Allocations on Selected Supersonic Routes in 2038.

Route Information		FLEET Allocation Information			Number of Daily Roundtrips for different A/C Size and Generation					
Airport A	Airport B	Allocation Model	Fuel Stop	Distance Flown (nmi)	Future-in-Class 3	Best-in-Class 4	New-in-Class 4	New-in-Class 5	Future-in-Class 5	Best-in-Class Supersonic
JFK	LHR	<i>Supersonic</i>		3150.63	0	0	8	2	0	2
		<i>Subsonic-only</i>		2991.45	0	1	9	1	0	
LAX	HNL	<i>Supersonic</i>		2225.47	1	0	22	0	0	4
		<i>Subsonic-only</i>		2217.99	0	1	22	1	0	
DFW	NRT	<i>Supersonic</i>	HNL	6619.53	0	0	6	0	0	1
		<i>Subsonic-only</i>		5573.40	0	0	5	0	1	

Considering Table 10, this specific example shows the subsonic aircraft allocation on a non-supersonic eligible route, EWR-LAS, for with supersonic and subsonic-only cases. As visible from this allocation chart, even though supersonic aircraft service is not available on this route, the subsonic aircraft allocation is different in the two cases.

**Table 10.** FLEET Aircraft Allocations on Selected Supersonic-Ineligible Route in 2038.

Route Information		FLEET Allocation Information		Number of Daily Roundtrips for different A/C Size and Generation				
Airport A	Airport B	Allocation Model	Distance Flown (nmi)	New-in-Class 3	Future-in-Class 3	Best-in-Class 4	New-in-Class 4	Best-in-Class Supersonic
EWR	LAS	<i>Supersonic</i>	1930.89	0	1	0	11	N/A
		<i>Subsonic-only</i>	1930.89	2	0	2	9	N/A

This output shows that, given FLEET’s current modeling techniques, the introduction of supersonic aircraft influences the subsonic aircraft allocation on both supersonic and non-supersonic routes. Hence, the Purdue team noted that the introduction and allocation of the supersonic aircraft changes the use, retirement, and acquisition of the subsonic aircraft. In other words, the airline modifies its subsonic fleet allocation to accommodate the new class of aircraft, i.e., supersonic aircraft, to maximize its profit over the whole route network. The FLEET airline serves a total of 57 routes with supersonic aircraft in the year 2038 and a total of 87 routes with supersonic aircraft in the year 2050; Figure 31 plots the number of routes served by supersonic aircraft in FLEET every year. Figure 32 shows the routes with supersonic service in the year 2038.

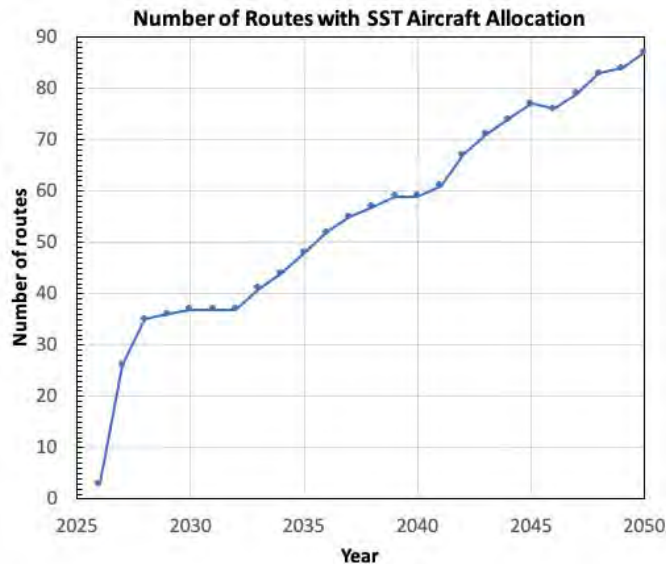


Figure 31. Number of Routes in FLEET that See Supersonic Aircraft Allocation from 2026 to 2050.

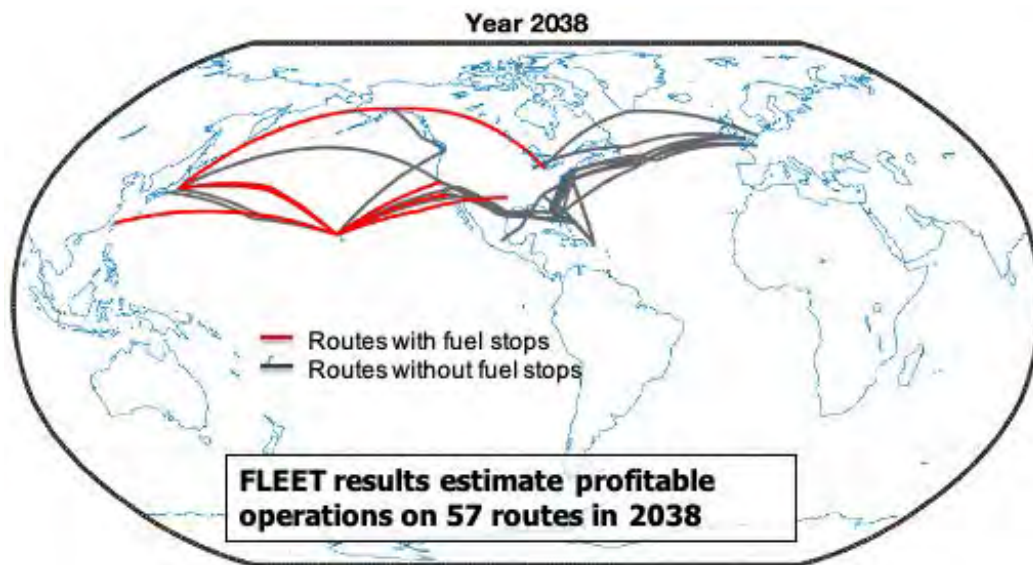


Figure 32. Routes with Supersonic Service in 2038 in FLEET.

**Support CAEP Efforts**

This task is for Purdue to support CAEP supersonic studies by providing potential future supersonic aircraft demand scenarios, including the resulting “pseudo-schedule” for where the FLEET aggregate airline operates supersonic aircraft.

Fleet-level Assessments

The Purdue team provided fleet-level assessments in the form of a data packet and a report to the MDG/FESG for the broader CAEP studies of future supersonic aircraft operations. The Purdue team documented our process for identifying potential supersonic routes and FLEET’s approach to predict both supersonic and subsonic passenger demand, while also providing the resulting pseudo-schedule for where the FLEET aggregate airline operates supersonic aircraft. For a given year, the pseudo-schedule provides information about nonstop routes and routes with fuel stops that see supersonic aircraft allocation

due to profitability in operation, number of daily allocated roundtrips for supersonic aircraft on these routes, and number of daily allocated roundtrips for subsonic aircraft on these routes. The pseudo-schedule also provides similar data for the number of daily roundtrip supersonic and subsonic passengers.

Because FLEET’s model-based predictions rely upon historically based information about U.S.-touching airline routes and passenger demand carried by U.S. flag-carrier airlines from BTS, the resulting pseudo-schedule only indicates the supersonic aircraft operations by U.S. flag carriers. To estimate the overall supersonic operations on a route with supersonic aircraft allocation for a given year in FLEET, the Purdue team implemented a multiplier-based approach to project the supersonic “all carriers” daily allocation numbers. The multipliers were generated using three different approaches: (1) number of passengers carried by U.S. domestic and international carriers on each route, (2) number of U.S. domestic and international carriers on each route, and (3) number of flights operated by U.S. domestic and international carriers on each route. These projections were based on 2013 BTS T-100 Segment data because year 2013 was the latest year that we used historical demand in FLEET (this was before FLEET’s route network was updated, as described under Task 1). The multipliers for each route were set as the ratio of number of passengers/carriers/flights by both U.S. domestic and international carriers and number of passengers/carriers/flights by U.S. domestic carriers only. The projected supersonic all carriers daily allocated roundtrip numbers using all three approaches were then included in the data packet along with the numbers from FLEET. Table 11 shows supersonic aircraft daily roundtrips along with the projected all carrier roundtrips for selected routes in 2038.

**Table 11. FLEET Aircraft Allocations on Selected Supersonic Routes in 2038 with “All Carriers” Projections for Supersonic Aircraft Allocation (Based on Runs before FLEET’s Route Network was Updated, as Described under Task 1).**

Airport A	Airport B	Fuel Stop	GT's Weighted Sum Route Distance (alpha = 0.4) [nmi]	Number of Daily Allocated Roundtrips for different A/C Size and Generation									
				Future in Class 3	Best in Class 4	New in Class 4	New in Class 5	Future in Class 5	New in Class 6	Supersonic - FLEET US Flag Carriers only	Supersonic - projected total number – all carriers Based on pax carried	Based on # of carriers	Based on # of flights
JFK	LHR	-	3150.63	0	0	12	0	0	1	2	7	6	6
LAX	HNL	-	2225.47	1	0	27	0	1	0	5	5	5	5
DFW	NRT	HNL	6619.53	0	0	1	3	0	1	1	1	1	1

For a given year, other important information provided by the data packet includes daily roundtrip fuel burn for routes that see supersonic aircraft allocation, average supersonic aircraft utilization (in terms of daily supersonic flight hours), fleet composition (i.e., number of supersonic and subsonic aircraft used), and total roundtrip demand on all potential supersonic routes (with split-up values for supersonic and subsonic demand).

The data packet also included the sensitivity of the fleet-level assessments to the fidelity of supersonic aircraft model and the supersonic routing scheme. The Purdue team ran multiple FLEET simulations using Purdue’s low-fidelity 55-seat placeholder supersonic aircraft (along with our simplistic supersonic route path adjustment strategy) and using Georgia Tech’s higher-fidelity 55-seat A10 notional medium SST aircraft (flown on detailed weighted sum supersonic route paths). The comparative assessments for these cases comprised a major portion of the data packet. For a given year, the comparison parameters included the number of routes (and city-pairs) that see supersonic aircraft allocations, number of daily supersonic roundtrips, number of supersonic passengers carried, airline fleet composition (both supersonic and subsonic aircraft), supersonic aircraft utilization, changes in subsonic aircraft allocation, and fleet-level fuel burn. The team noted that when the airline's supersonic aircraft are allocated before the airline's subsonic aircraft, the difference in fidelity of the supersonic aircraft does not impact the number of routes (and city-pairs) that see supersonic aircraft allocations, i.e., the city-pairs that see profitable supersonic aircraft operation remain the same for both the cases. However, the other parameters do change with changes in the supersonic aircraft model. Table 12 and Table 13 show the FLEET allocation results using Purdue’s low-fidelity models and Georgia Tech’s higher-fidelity models, respectively.

**Table 12.** FLEET Allocation Results using Purdue’s Low Fidelity “Placeholder” SST Aircraft Model and Simplistic Supersonic Route Path (Based on Runs Before FLEET’s Route Network was Updated, as Described under Task 1).

Route Information		FLEET Allocation Information			Number of Daily Roundtrips for different A/C Size and Generation using higher-fidelity models							
Airport A	Airport B	Allocation Model	Fuel Stop	Distance Flown (nmi)	New-in-Class 3	Future-in-Class 3	Best-in-Class 4	New-in-Class 4	New-in-Class 5	Future-in-Class 5	New-in-Class 6	Best-in-Class Supersonic
JFK	LHR	Supersonic		3150.63	0	0	0	12	0	0	1	2
		Subsonic-only		2991.45	0	0	0	12	0	0	1	
LAX	HNL	Supersonic		2225.47	0	1	0	27	0	1	0	5
		Subsonic-only		2217.99	0	0	0	28	2	0	0	
DFW	NRT	Supersonic	HNL	6619.53	0	0	0	1	4	0	3	2
		Subsonic-only		5573.40	0	0	0	0	1	6	0	

**Table 13.** FLEET Allocation Results using GT’s Higher-Fidelity A10 Notional Medium SST Aircraft Model and Detailed Weighted Sum Supersonic Route Path (Based on Runs before FLEET’s Route Network was Updated, as Described under Task 1).

Route Information		FLEET Allocation Information			Number of Daily Roundtrips for different A/C Size and Generation using lower-fidelity models							
Airport A	Airport B	Allocation Model	Fuel Stop	Distance Flown (nmi)	New-in-Class 3	Future-in-Class 3	Best-in-Class 4	New-in-Class 4	New-in-Class 5	Future-in-Class 5	New-in-Class 6	Best-in-Class Supersonic
JFK	LHR	Supersonic		3093.34	0	0	0	12	0	0	1	2
		Subsonic-only		2991.45	0	0	0	12	0	0	1	
LAX	HNL	Supersonic		2227.44	0	0	1	26	2	0	0	5
		Subsonic-only		2217.99	0	0	0	28	2	0	0	
DFW	NRT	Supersonic	HNL	6619.53	0	0	0	6	0	0	0	1
		Subsonic-only		5573.40	0	0	0	0	1	6	0	

The fleet-level data packet also provided insights on the changes in the usage, retirement, and acquisition of subsonic aircraft when supersonic aircraft are made available to the airline. This included details about subsonic aircraft allocation (and passengers carried) for all routes that see supersonic aircraft allocation (and some routes that are supersonic ineligible in FLEET’s network).

**Impact of COVID-19 on Passenger Demand and Fleet-level Assessments**

The CAEP meetings included some discussions about studying the impact of the COVID-19 pandemic on aviation travel demand and the related fleet level assessments. Because Purdue had the capability to perform such studies, the team used FLEET to assess the impact of the pandemic on future passenger demand and its fleet-level implications in a preliminary study.

We considered two different recovery scenarios: “2022 recovery” and “2022 recovery + GPD slowdown to 75% until 2030.” In the former scenario, we assume that passenger demand returns to 2019 levels (pre-COVID-19) by the year 2022 and continues its growth based on the inherent demand and GDP growth. In the latter, we assume that demand returns to 2019 levels in the year 2022 but demand grows at 75% of the inherent demand and GDP growth assumptions. For both scenarios, we also assume that there is a 50% reduction in passenger demand in 2020 and the recovery follows a V-shape. By using these demand projection scenarios as inputs to FLEET, we are able to estimate the impact that the changes in future demand can have on airline operations and emissions. Figure 33 presents these projected demand scenarios in terms of passengers (left) and trips (right) and makes clear the possible ~16% reduction in passenger demand and ~23% reduction in trips flown by 2050 for the worst of the two scenarios.

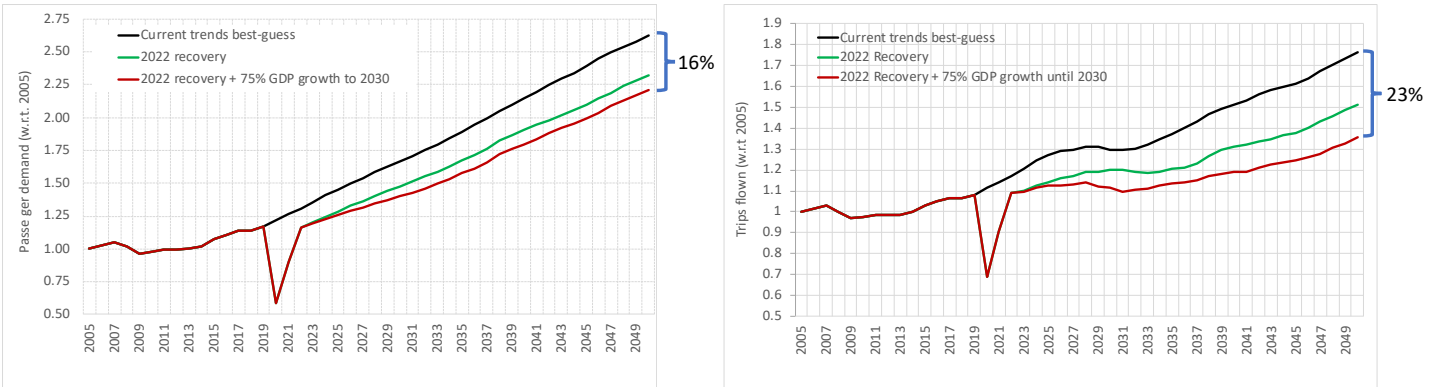


**Figure 33.** Passenger Demand Projection and Trips Flown for COVID-19 Recovery Scenarios.

This expected reduction in demand (both in terms of passengers and trips) has the obvious implication of reducing the number of aircraft in the fleet that are needed to satisfy all demand. In fact, when comparing the fleet size and fleet mix projections of the pre-COVID (Figure 34 left) and the two post-COVID scenarios (Figure 34 center and right), one can see the drop in fleet size of ~13% in the “2022 Recovery” and ~23% in the “2022 Recovery + GDP slowdown to 75% until 2030” scenarios.

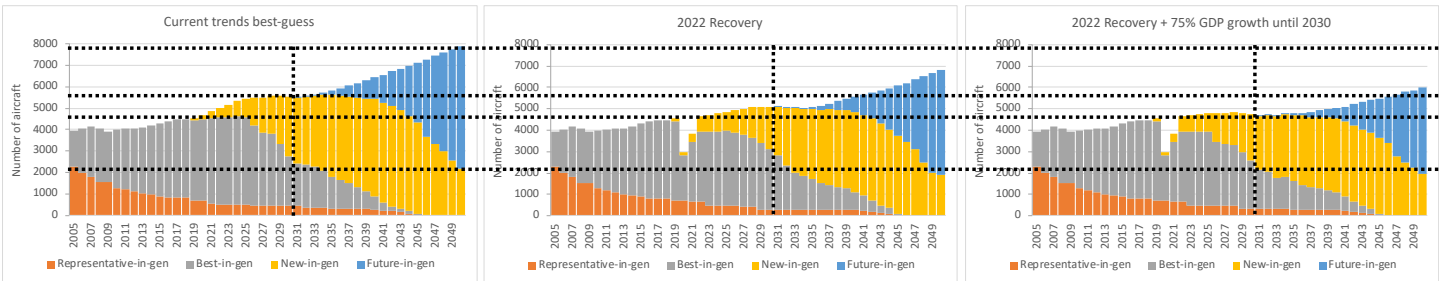


**Figure 34.** Fleet Mix Projections by Aircraft “Technology Age”.

Of note in these predicted fleet mixes is the reduction in the best-in-class and future-in-class fleet size. The former implies early retirement of these type of aircraft and the latter implies a delay in the acquisition and introduction of the new aircraft to the fleet. If such scenarios were to materialize, the delay and smaller fleet size of the more environmental-friendly future-in-class aircraft does not seem to negatively impact the projected emissions. As Figure 35 (right) shows, CO<sub>2</sub> emissions, for example, are still expected to see a decline due to the reduction in passenger demand and overall less flying activity.

This confirms results of prior analyses and explorations that show that changes in demand have the largest impact on emissions. While new aircraft technologies that improve fuel consumption and emissions do contribute to the reduction of overall emissions, the combined effect of an increasing air travel demand and the gradual phasing out of older generation aircraft and slow introduction of newer-technology aircraft results in a relatively slow reduction in overall emissions. The two scenarios considered here may not reflect the exact demand that the airline industry is likely to see in the future, but the trends make it clear that, as long as demand continues to increase, so will emissions, until the future generation of aircraft start to become a large proportion of the operational fleet.

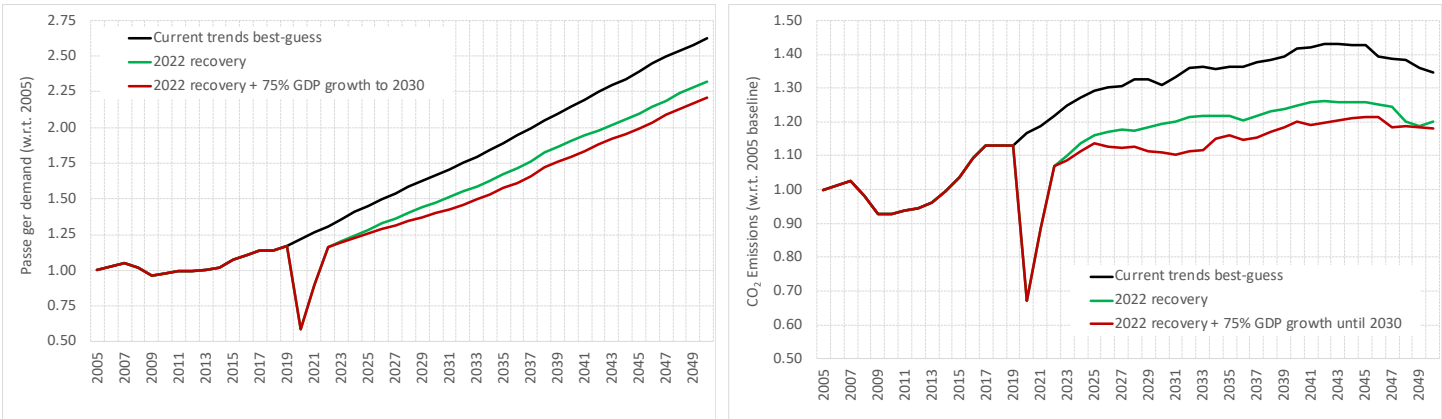


Figure 35. Passenger Demand Projection and Projected CO2 Emissions.

### Task 3 – AEDT Supersonic Modeling

Georgia Institute of Technology

The original intent of Task 3 is to develop methods for AEDT to model supersonic transports. At the writing of the proposal, AEDT utilizes BADA3 for vehicle modeling; therefore, the proposal has been focused on BADA3 approaches. Since then and at the writing of this report, AEDT is transitioning to BADA4 for new vehicle representation in AEDT; therefore, rendering the proposed tasks obsolete. Based on conversation with FAA technical monitors at the Spring 2019 ASCENT Advisory Board meeting, Georgia Tech is directed to focus on BADA4 coefficient generation for supersonic transport, which is described in Task 5.

### Task 4 – Support CAEP Supersonic Exploratory Study

Georgia Institute of Technology

**Objective**

The top-level objective of this Task is to model the supersonic vehicles needed to support FAA technology trade studies. Concurrently, the modeling team also support OEMs participating in the CAEP SST Exploratory study. During the period of performance, Georgia Tech emphasized the design for both medium SST (55 passengers) and large SST (100 passenger) classes and the design Mach study.

**Research Approach**

To model the vehicles, the Georgia Tech researchers utilized a well-established modeling environment for subsonic vehicles, the Environmental Design Space (EDS), as a starting point. The existing infrastructure of EDS is modified and developed into a modeling and simulation (M&S) environment for Supersonic Transports (SSTs) called the Framework for Advanced Supersonic Transports (FASST). The connectivity and flow of information between the various aspects of FASST are shown in Figure 36. The overall approach starts with defining the requirements and design mission and then proceeding to configuration exploration.

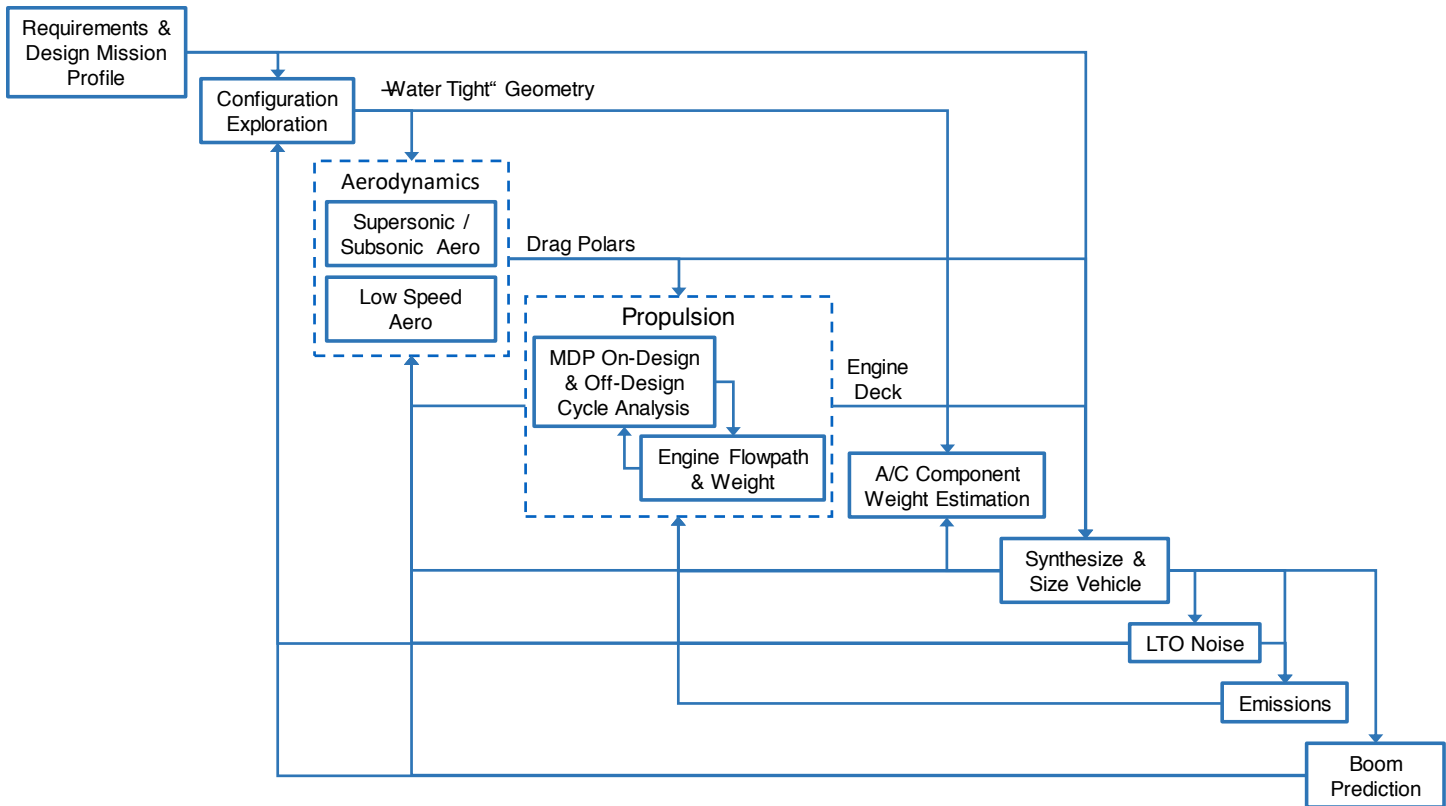


Figure 36. FASST Overall Architecture.

The configuration exploration step is partially done off-line from FASST, in a brainstorming exercise in which candidate configurations are developed with Engineering Sketch Pad (ESP) and OpenVSP (NASA’s open-source parametric geometry tool). These geometries are run through CART3D (NASA’s inviscid computational fluid dynamics tool) and CART3D’s viscous drag correction module to examine the wave and viscous drag characteristics. Based on these preliminary results, the research team selects a configuration class, and proceed to perform aerodynamic shaping to maximize the cruise lift to drag ratio (L/D). After the aerodynamic shaping is completed, a set of supersonic and subsonic drag polars is generated. The supersonic drag polars are generated in CART3D (with viscous module enabled) by sweeping vehicle’s angle of attack for multiple supersonic Mach numbers. The subsonic drag polars (i.e., Mach 0.3–0.8) are generated with the set of tools depicted in Figure 37. The subsonic aerodynamic module uses two empirically based aerodynamic codes from NASA to calculate lift and specific components of drag. OpenVSP’s Parasite Drag Tool, based on turbulent flat plate theory and form factor corrections, is used to compute parasite drag. Then, AERO2S (NASA’s low-fidelity subsonic induced drag estimation tool) is used to compute drag due to lift. AERO2S is based on linearized aerodynamics assumptions with empirical data corrections to estimate lift and drag. This set of aerodynamic tools are integrated into a Python module called AFASST (Aerodynamics for Framework for Advanced Supersonic Transports). AFASST computes the drag polar for a given Mach number, angle of attack, and aircraft geometry. The last element of the aerodynamic module for FASST is the landing and takeoff (LTO) drag polars which is also generated using AFASST. Once the vehicle geometry has been frozen, multi-element wing geometries are developed for LTO conditions. Flaps are created on the existing wing planform for different trailing edge deflections. A sensitive study of perturbing leading edge slats resulted in negligible effects on LTO aero; therefore, the combination of leading slats and trailing edge flaps is not considered. If time and resources permit, a couple of CFD Reynolds-Average Numerical Simulations (CFD-RANS) are performed to validate AFASST LTO results. The resulting LTO drag polars are input into FLOPS’ detailed takeoff and landing module to compute balance takeoff field length and landing field length.

The propulsion module for FASST, like EDS, utilizes the object-oriented code Numerical Propulsion System Simulation (NPSS). Cycle design is conducted using the Multi-Design Point (MDP) algorithm which allows requirements at both on-design and off-design conditions to be met simultaneously. The thrust sizing points are initially estimated until the aero shaping is

complete. The propulsion system analysis also includes a flowpath analysis to estimate the propulsion system weight including the inlet and nozzle. The flowpath and weight analysis is conducted using WATE++. The propulsion analysis is described in more detail in below.

Once the aero and propulsion models are matured, then the thrust sizing points and inlet capture area can be converged between aero and propulsion. Aero discipline provides vehicle coefficient of drag ( $C_D$ ) for the takeoff (deflected flap), top of climb, and cruise conditions to the propulsion disciplines to compute thrust sizing points. However, the drag estimates are based on assumed inlet capture area from the propulsion discipline. These parameters are iterated upon until they are converged between aero and propulsion disciplines.

After the thrust sizing points, capture area, and drag characteristics are converged, the next step is to select the best engine cycle for the vehicle. This step starts with generating an engine deck containing thrust and fuel flow at various Mach and altitude combinations and passed over to the mission analysis, which is performed using FLOPS. FLOPS internal aircraft component weight estimation (except for propulsion systems weight) is used for the mission sizing. A design of experiment (DoE) is constructed, varying key engine design parameters. The FASST environment is executed in accordance to the DoE and response (both metrics and constraints) are recorded to generate cycle selection surrogate models. With the help of JMP statistical software, the best engine cycle is selected based on minimum mission fuel burn and subject to constraints, such as bypass ratio and jet velocity for noise considerations. Future iterations of FASST will have noise metrics directly.

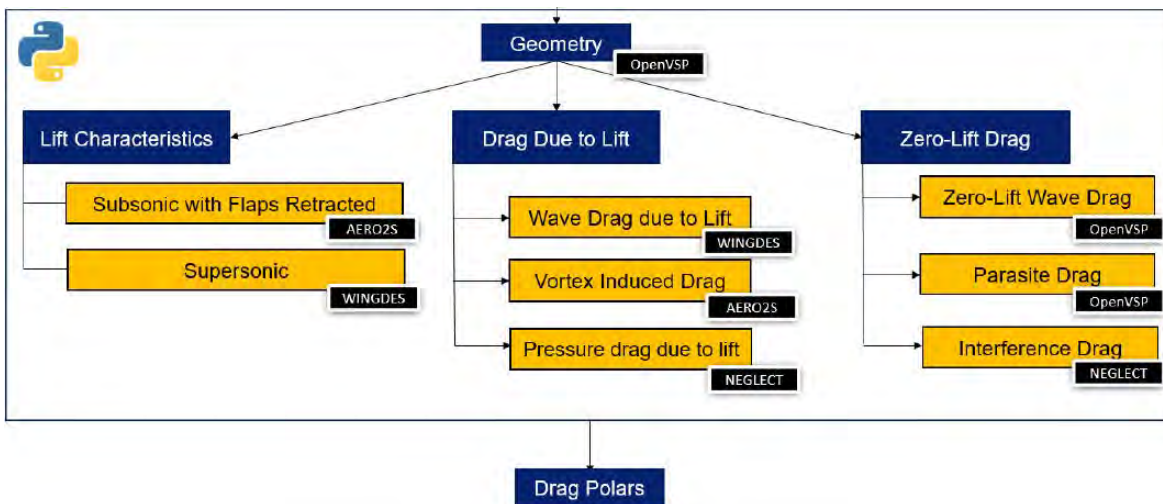


**Figure 37.** Subsonic Drag Polar Generation (Wave Drag Effects are Neglected in Subsonic Aerodynamics).

Another major difference between EDS and FASST is the iteration required between aerodynamic and propulsion modules during the vehicle synthesis and sizing process. For subsonic vehicles, as the aircraft drag increases or decreases during this process, the engine can be scaled by using mass flow, and the only drag impact is the engine profile and parasitic drag due to the engine nacelle being sized up and down. For supersonic vehicles, engine and airframe integration effects are much stronger and thus the size of the engine affects the entire vehicle drag and lift characteristics. In order to capture the change in vehicle drag due to engine size being scaled up and down, a surrogate of delta vehicle drag as function of capture area and flight condition is also generated after the propulsion and aero discipline has converged on the initial capture area. Note that this initial capture area is converged without flying the mission.

After the aerodynamics, propulsion, and mission analysis (i.e., synthesis and sizing) modules converge, the resulting vehicle and engine are then used to predict LTO noise, emissions, and boom levels. If any of the last three analysis results are unacceptable, the aircraft and engine design will need to be changed, and the entire convergence loop is repeated until all metrics are satisfied. Currently, FASST is not envisioned to incorporate an optimizer to find the optimal configuration. It is envisioned as a framework to perform design space exploration via design of experiments to determine whether there is a feasible space that satisfies fuel burn, emission, LTO noise, and potentially boom.

The subsequent section of the report describes the propulsion and airframe modeling performed during the period of performance, for both the GT Medium SST and GT Large SST, in more detail.

## GT Medium SST

The GT Medium SST vehicle is designed and sized to cruise at Mach 2.2, carrying 55 passengers at 4,500 nmi with no subsonic cruise mission segments.

### Propulsion System

#### Cycle Architecture Selection

Most modern subsonic aircraft use a high bypass ratio separate flow turbofan (SFTF). This type of engine allows for high overall efficiency by moving a greater amount of air for high propulsive efficiency while being able to maintain a high overall pressure ratio for high thermal efficiency. As a result of the higher mass flow rate, these engines have lower jet velocities for the same thrust, which is desirable from a noise perspective. However, moving more air comes at a cost of larger engine diameters and greater thrust lapse in altitude as density decreases. This is detrimental for supersonic aircraft, which have much higher drag and fly at much higher altitudes. In addition, supersonic engines have very long inlets and nozzles relative to subsonic engines and the lengths of these components are proportional to engine diameter and heavily influence the weight of the engine. To address all these challenges, a low bypass ratio mixed flow turbofan (MFTF) is chosen for this study. The MFTF is a simple modification of the SFTF accomplished by mixing the bypass and core flow before exiting through a single exhaust nozzle. The mixing of the two streams offers some efficiency gains and higher specific thrust, which reduces the thrust lapse problem (Hartmann, 1967; Pearson, 1962). Although more advanced architectures exist that may provide even greater benefits, the MFTF is chosen because of its simplicity relative to an adaptive or variable cycle architecture (Welge et al., 2010).

#### Cycle Modeling

A schematic is included in Figure 38, depicting the components in the engine model and their connectivity. This model inherited much of its structure from previous supersonic work done by Georgia Tech (Welge et al., 2010) with some changes. A different inlet map is used to parametrically model total pressure recovery as well as installation drag due to spillage, bypass, and bleed flow. The map is obtained from a library of maps in the PIPSI method (Kowalski & Atkins Jr., 1979) and models a 2D, four-ramp variable geometry inlet. Due to the age of the maps, a technology scalar is applied to the bleed flow. The fan and high-pressure compressor (HPC) maps are generated with the NASA tool CMPGEN within the FASST environment to avoid the need for map scaling. The turbine maps are notional maps that are scaled, because the FASST environment does not currently include a routine to parametrically generate turbine maps.

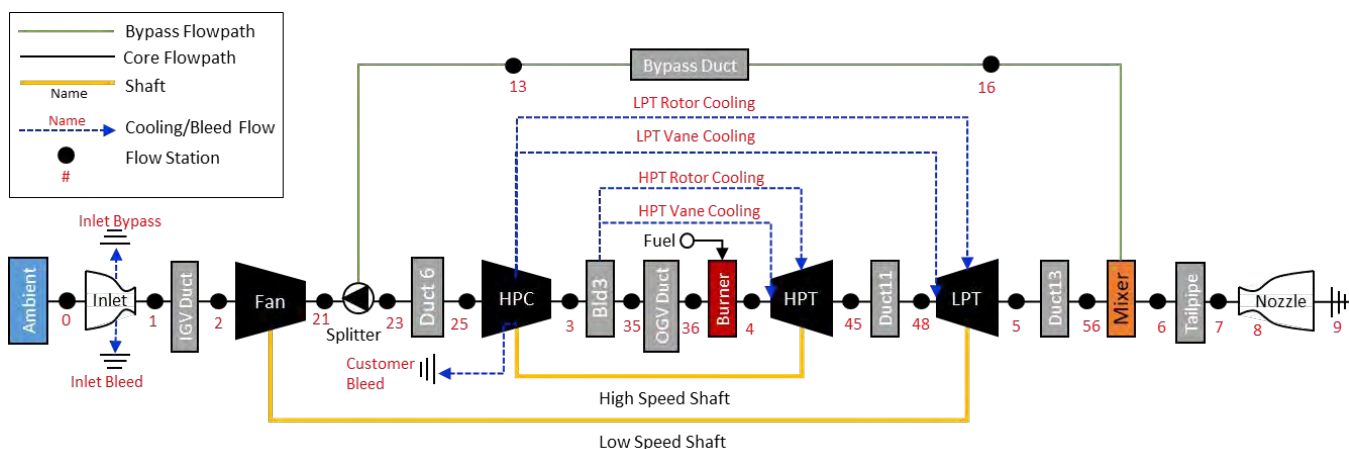


Figure 38. Engine schematic of clean sheet design for medium SST.

To obtain the design performance, dimensions, and number of stages of the turbomachinery, a simple preliminary estimation is conducted to determine such parameters as flow coefficient, work coefficient, RPM, tip-speed, efficiency, hub-tip ratio, and number of stages. This is important in order to trade-off the efficiency, size and weight of these components. Turbine cooling flows are determined from NASA developed Coolt model, which computes the required cooling flow as a function

of metal temperature and the cooling effectiveness parameter  $\phi = (T_{gas} - T_{metal}) / (T_{gas} - T_{cool})$ . A mixer gain term is used (0% for unmixed and 100% for perfectly mixed) to model how well the two streams mixed before expanding through the nozzle. This mixer gain essentially accounts for the loss of thrust due to imperfect mixing. The nozzle chosen is an axisymmetric plug nozzle and is modeled with a gross thrust coefficient curves as a function of the nozzle pressure ratio and expansion ratio from the PIPSI library (Kowalski & Atkins Jr., 1979). For preliminary estimates, 100 HP is extracted from the high-speed shaft and 1.5 lbm/s of air is extracted from the HPC for customer usage.

Cycle Design Methodology

Classical thermodynamic cycle analysis sizes the engine (i.e., determines the airflow requirement to meet a certain requirement, such as thrust) for a single flight condition, such as takeoff. However, the engine must operate over a wide range of conditions, and thus, the engine set at the design flight condition may not meet requirements under other flight conditions. This classical method called “single design point” requires an iterative procedure whereby the design is updated and then reevaluated under other flight conditions. MDP is a technique developed by the Aerospace Systems Design Laboratory (ASDL) to size an engine to simultaneously ensure that requirements are met at multiple flight conditions (Schutte, 2009). This is enabled by the object-oriented structure of NPSS, which allows for copies of the design engine to be simulated at the same time as the design case. A system of equations can then be set up such that the independent design variables may be set by a numerical solver to meet specified targets for different flight conditions.

As mentioned above, MDP allows for requirements under multiple flight conditions to be met simultaneously. To that end, several flight conditions of interest are determined, along with relevant requirements for each of them. The flight conditions chosen are listed in Table 14. The Aerodynamic Design Point (ADP) is the sizing point of the engine and a reference point for defining the turbomachinery component performance. It is selected in this study to be a transonic acceleration point at which having enough thrust to get through without afterburners or the need to dive is critical. The top of climb (TOC) point is typically a critical point at which adequate thrust for a required rate of climb must be ensured. Additionally, this point is part of the supersonic cruise segment, and thus efficiency is of critical concern. The takeoff point ensures enough thrust at aircraft rotation. The takeoff point is critical to ensure there is enough thrust at rotation and for one engine inoperative (OEI). The sea level static (SLS) point is a typical point of interest for certification. The cooling flow sizing point sizes the turbine cooling flows for the condition of max gas temperature and max cooling flow temperature.

The NPSS solver is then used to determine a set of independent parameters (fuel flow, airflow, bypass ratio (BPR), etc.) that would meet specified target values of certain dependent parameters. Some of these dependent parameters are design targets and others are to ensure conservation of mass, momentum, and energy. For example, the fuel flow is varied to produce a target value for turbine rotor inlet temperature (T41). The target T41 is determined from a user input throttle ratio (ratio between max T41 and T41 at SLS). The max T41 is set to 3300 °R to be a slight improvement of the technology level of the High-Speed Civil Transport (HSCT) [Pratt & Whitney and General Electric, 2005]. The value of MDP is that it allows changing an independent design variable at one condition to target a desired value of another metric at a different flight condition. For example, the ADP BPR is set to target an extraction ratio at TOC. Extraction ratios are set near 1.0 to avoid excessive mixing losses. The ADP airflow is set to meet a TOC thrust requirement subject to constraints on thrust requirements at other points. The thrust requirements are scaled as the vehicle is run through mission analysis. The inlet capture area is sized to ensure the inlet and engine are perfectly matched at TOC.

**Table 14.** Cycle design points for a medium SST engine.

Flight Condition	Mach	Altitude	$\Delta T$
ADP	1.2	39,000	0
TOC	2.2	60,000	0
Cooling Flow Sizing	Set for max Tt3 or Mach 2.2 whichever is lower	55,000	0
Takeoff	0.25	0	27
SLS	0	0	0

Off-design Power Management

This section describes how the engine is operated in off-design through the entire flight envelope. Full power at any flight condition is determined by running the fuel control to target a turbine rotor entrance temperature set as the product of max turbine rotor entrance temperature and the ratio of the dimensionless temperature  $\theta_{t2} = T_{t2} / (518.67 \text{ }^\circ\text{R})$  and throttle ratio.



This is constrained, however, by SLS thrust as a maximum value and by maximum temperature limits on the compressor discharge ( $T_{t3max} = 1790^\circ R$ ) and turbine rotor entrance ( $T_{t41} = 3300^\circ R$ ). In addition, the nozzle throat is variable and set to hold an R-line of 2.0. R-lines are arbitrary lines drawn through the map such that values of flow, pressure ratio, and efficiency are tabulated at the points where speed lines and R lines intersect. This enables creating tabulated maps for use in numerical simulations like NPSS. R-lines should be roughly parallel to the stall line or the nominal operating line. By convention, R-line = 1 corresponds to the nominal stall line, and R-line = 2 corresponds to the nominal operating line (approximately), which is typically just below the peak efficiency line. Therefore, holding an R-line = 2 approximates holding a desired stall margin or operating line. The use of a plug nozzle allows for full expansion of the flow through the nozzle at any flight condition without the use of variable geometry mechanisms. At part power, the fuel flow control is set based on a power code schedule defining the percent of the thrust desired relative to the full power thrust at any flight condition. The nozzle controls at part power are the same as the full power case.

#### Flowpath and Weight Model

The flowpath and weight model for the engine is developed with WATE++ and is inherited from previous supersonic study in which Georgia Tech is involved (Welge et al., 2010). The model is modified for a 2D supersonic inlet, an axisymmetric plug nozzle, and changes to some turbomachinery parameters based on a preliminary analysis method that is developed for this study. The inlet model is modified to be based on the geometry determined from a preliminary inlet design code called IPAC (Barnhart, 1997), and the inlet weight is modeled using the regressions from PIPSI (Kowalski & Atkins Jr., 1979). The nozzle model is modified for an axisymmetric plug nozzle by extending the internal plug outside the nozzle with a 15-degree half-angle and setting the external convergent flap to match the plug half-angle. A custom module for calculating the weights of variable geometry actuators is also developed. A preliminary analysis code based on constant-meanline assumptions is developed to estimate the number of stages of turbomachinery required along with parameters such as hub-tip ratio, area, radii, and blade speeds. This preliminary turbomachinery code is run in conjunction with cycle analysis to set the component efficiency and the geometric parameters, and the results are then passed to the WATE++ input to ensure consistency in the geometry used to compute both final component efficiency and component weight.

#### Propulsion Systems Modeling Results

The engine cycle presented is as of the writing of this report (i.e., August 2020). Table 15 shows the efficiencies, pressure losses, bleeds, and modeling assumptions used in the model at each of the design points for the MDP analysis of the current design. Table 16 shows the cycle parameters and performance metrics at each of the design points of the current design. The choice of cycle is conducted in the context of the vehicle by minimizing vehicle fuel burn as opposed to Thrust specific fuel consumption (TSFC), which is an engine-level metric. This approach considers the tradeoff of TSFC, weight, and drag due to engine size. The minimization of mission fuel burn is constrained by limits on inlet capture area (max  $3000 \text{ in}^2$ ) to prevent excessive vehicle drag and a jet velocity below 1,650 ft/s at takeoff as a surrogate for noise. The details of the mission fuel burn and vehicle gross weight are in the mission analysis section. A DoE is created to simulate different combinations of cycle design variables, and FASST is executed accordingly and relevant responses (both metrics and constraints) are recorded. The resulting responses are used to generate surrogate models for various metrics and constraints of interest (e.g., fuel burn, inlet capture area, TSFC, jet velocity, weight, etc.). These surrogates are used to conduct the cycle selection via the desirability function within the JMP software, which is essentially an optimization exercise utilizing the surrogate models generated. Figure 39 shows an example of a profiler for the response of mission fuel burn as a function of cycle design variables. The curves in each window are the partial derivative of the response with respect to the x-value of that window and at the current values of all other x-values. The selected x-value settings represent the results of the surrogate optimization exercise, and they are run through FASST a final time to verify the predictions of the surrogate models.

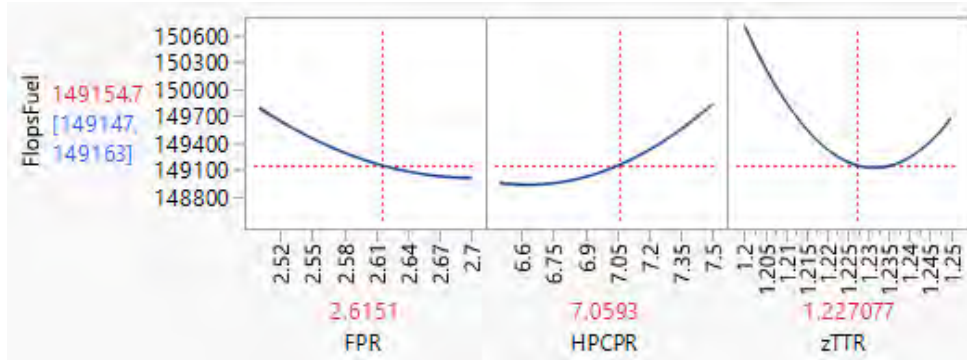


Figure 39. Example [not final results] of JMP Profiler for Fuel Burn as a function of cycle variables.

Table 15. Cycle modeling assumptions for a medium SST engine.

Component	ADP	TOC	TO	SLS (Uninstalled)
Inlet Recovery	99.26%	90.17%	96.0%	100.0%
Fan Adiabatic Efficiency	89.85%	91.26%	92.33%	92.75%
HPC Adiabatic Efficiency	88.61%	88.75%	89.17%	89.5%
HPT Adiabatic Efficiency	91.36%	91.47%	92.1%	92.15%
LPT Adiabatic Efficiency	91.06%	90.7%	91.45%	91.42%
Nozzle Gross Thrust Coefficient	98.8%	97.22%	98.8%	98.8%
Imperfect Mixing Coefficient	99.06%	99.06%	99.21%	99.29%
Nozzle Discharge Coefficient	96.4%	96.3%	96.1%	96.5%
Shaft Horsepower Extraction	100	100	100	0
Customer Bleed, lbm/s	1.5	1.5	1.5	0
IGV Duct Pressure Loss	0.00% (currently no IGV)			
Duct 6 Pressure Loss	2.50%			
OGV Duct	0.0% (bookkept in burner)			
Fuel LHV, BTU/lbm				18,580
Fuel Temperature, °R				518.67
Burner Efficiency				99.70%
Burner Pressure Drop				4.00%
Duct 11 Pressure Loss				2.00%
Duct 13 Pressure Loss				3.00%
Tailpipe Pressure Loss				2.00%
Bypass Duct Pressure Loss				4.00%



Table 16. Cycle variables and performance metrics.

	ADP	TOC	TO	SLS (Uninstalled)
<b>Mach</b>	1.2	2.2	0.25	0
<b>Altitude [kft]</b>	39	60	0	0
<b><math>\Delta T + ISA</math> [R]</b>	0	0	27	0
<b>FPR</b>	2.61	2.06	2.28	2.13
<b>%Nc Fan</b>	100.0%	90.5%	94.6%	91.7%
<b>N1 [RPM]</b>	6598	7372	6545	6146
<b>Wc2 [lbm/s]</b>	570	489	507	508
<b>HPCPR</b>	6.72	5.98	6.34	6.12
<b>N2 [RPM]</b>	11220	12990	11360	10800
<b>OPR</b>	17.1	12.0	14.1	12.7
<b>BPR</b>	0.967	1.21	1.11	1.18
<b>Extraction Ratio</b>	0.99	1.05	1.03	1.05
<b>Throttle Ratio</b>	1.234			
<b>Turbine Cooling Flow [%W<sub>25</sub>]</b>	27%			
<b>T4 [R]</b>	2779	3523	2749	2468
<b>T41 [R]</b>	2590	3300	2565	2305
<b>T3 [R]</b>	1212	1615	1245	1134
<b>NPR</b>	5.83	17.88	2.10	1.93
<b>Vjet [ft/s]</b>	2395	3275	1646	1468
<b>Installed Net thrust [lbf]</b>	9323	8895	21696	23005
<b>Installed TSFC [lbm/(hr × lbf)]</b>	0.968	1.22	0.72	0.554

Figure 40 and Figure 41 show a notional flow path and weight breakdown for the current engine design, respectively.

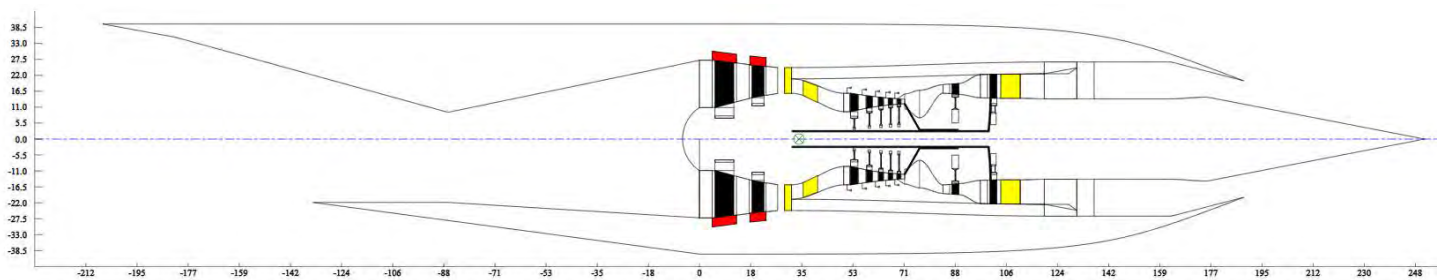


Figure 40. Flowpath of Medium SST Engine.



ENGINE COMPONENT WEIGHT LISTING			
	weight	length	
WATEa.WATE_Fan	1228.1	31.86	
WATEa.WATE_Splitter	0.0	0.00	
WATEa.WATE_Duct6	269.3	18.04	
WATEa.WATE_HPC	776.8	21.08	
WATEa.WATE_Bld3	43.6	5.17	
WATEa.WATE_Burner	374.9	8.10	
WATEa.WATE_HPT	841.7	5.39	
WATEa.WATE_Duct11	34.9	7.57	
WATEa.WATE_LPT	1500.3	13.74	
WATEa.WATE_Duct13	27.3	8.33	
WATEa.WATE_Duct15	36.0	87.43	
WATEa.WATE_Mixer	34.7	11.25	
WATEa.WATE_Tailpipe	21.8	6.00	
WATEa.WATE_Core_Nozz	1597.5	39.15	
WATEa.WATE_LP_Shaft	216.0	71.04	
WATEa.WATE_HP_Shaft	80.6	18.67	
WATEa.WATE_Inlet	2154.9	255.81	

PROPULSION SYSTEM WEIGHT SUMMARY			
bare engine weight	7083.6 lbs	engine length	188.2 in.
accessories weight	750.0 lbs	inlet length	255.8 in.
engine mount weight	167.6 lbs	engine pod length	444.0 in.
total engine weight	8001.2 lbs	engine pod C.G.	34.4 in.
inlet & nacelle weight	2154.9 lbs	engine max diameter	54.4 in.
engine pod weight	10232.3 lbs	nacelle max diameter	64.4 in.

Figure 41. Weight Summary of Medium SST Engine.

## Emissions Modeling

### Nitrogen Oxides

One of the important issues in the development of any aircraft is environmental acceptability (NASA CPC Vol2, 2005). This is true even more so for SSTs which consume more fuel than their subsonic counterparts. This section discusses the various methods found in the literature for modeling LTO and in-flight cruise emissions indices as represented by various combustor configurations. Each method is evaluated in the context of the GT Medium SST engine cycle and with respect to the CAEP limits.

To predict the Medium SST NO<sub>x</sub> emissions, NASA CFM56 P3T3, BFFMv2 (Dubois & Paynter, 2006), NASA HSCT P3T3 (Niedzwiecki, Richard W., 1992), and GE LPP MRA (lean pre-mixed/pre-vaporized multistage radial/axial) (S.Greenfield, P.Heberling, G.Moertle, 2005) combustor correlations are explored. Each of the models are evaluated for LTO Dp/F00 for the Medium SST engine cycle and compared with existing engines from the ICAO databank and plotted against overall pressure ratio (OPR). Along with CAEP limits. For consistency with the existing engines, all of which are for subsonic aircraft, subsonic rules for LTO Dp/F00 are used. A table is created to compare EI NO<sub>x</sub> at max power takeoff and max power top-of-climb predicted by each of the methods. Finally, the emissions indices, predicted by each method, are evaluated throughout the flight envelope as additional comparison.

The first method evaluated is a NASA CFM56 P3T3 correlation that is developed by NASA Glenn Research Center and based on the CFM56 combustor. This correlation development is done using the combustor inlet total pressure (Pt3), inlet temperature (Tt3), and the fuel-to-air ratio (FAR) at both the reference test condition and the operational condition being modeled. This correlation is called the “updated P3T3” model since 87 data points, collected from GE/Peebles test facility,

are used to cross-correlate these emission indices with Pt3 and Tt3 from NASA CFM56-7B engine cycle model. The resulting model assumed an  $Pt3^{0.4}$  dependency and a polynomial fit in Tt3 to calculate  $EINO_x = f(Pt3, Tt3)$ .

Another method to predict LTO NOx for supersonic engines is the Boeing Fuel Flow Method, version 2 (BFFMv2). This method was introduced by Boeing Company and presented to the ICAO CAEP WG3 Certification Subgroup on March 6, 1995 (SAE AIR, Procedure for the Calculation of Aircraft Emissions, 2009-07). An updated version of this method has been published as a technical paper by Dubois in 2006. The basic approach of the BFFMv2 is to generate a correlation between EI and fuel flow (FF). Dubois's method also contained an update for supersonic engines to adjust the model for higher Mach numbers. The process for the BFFMv2 is as follows:

1. Formulate correlation of log (FF) versus log ( $EINO_x$ ) from LTO EIs.
2. Compute  $\delta_{amb}, \theta_{amb}$  (used values from NPSS ambient element).
3. Compute the reference fuel flow at altitude using the cycle model (max power setting at a given Mach number/altitude).
4. Compute the reference fuel flow by using  $FF_{ref} = \frac{FF}{\delta} \theta^{3.8} e^{0.2M^2}$ .
5. Interpolate/extrapolate the correlation in item 1 using  $\log(FF_{ref})$  to obtain  $EINO_{x_{ref}}$ .
6. Humidity correction.
7.  $EINO_x$  computed from the following equation  $EINO_x = EINO_{x_{ref}} e^H \left(\frac{\delta^{1.02}}{\theta^{3.3}}\right)^y$ .

Using the BFFMv2 at Mach numbers above 1.6 showed large error relative to the P3T3 method discussed above. In the original BFFMv2, the term  $e^{0.2M^2}$  substituted in place of the term  $(1 + 0.2M^2)$ , which is from the theory of compressible flow. Figure 42 shows a comparison of these two Mach number correction terms. It can be seen that at low Mach numbers they coincide, but at high Mach numbers they diverge. At Mach 2.2, the fuel flow is being overestimated by 25% due to the use of the term  $e^{0.2M^2}$  instead of  $(1 + 0.2M^2)$ . In addition to the Mach number correction, a fuel flow correction factor ( $k$ ), is added to the BFFMv2 equation  $\frac{FAR}{\theta_1} = k \left(\frac{T_3}{\theta_1}\right)$ . This correction factor acts as an additional free parameter to better fit the data. When implementing the correct Mach number correction and fuel flow correction factor, the error of the BFFMv2 relative to the P3T3 method reduces from 25% to 8%.

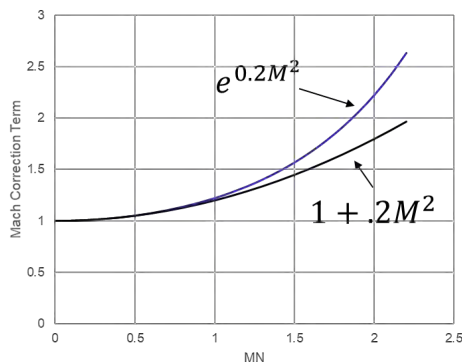


Figure 42. Mach Number Correction Term versus Mach Number.

The P3T3 correlation developed from the CFM56 is deemed inappropriate for the GT Medium SST because the engine is a clean-sheet design versus a refan using the core of the CFM56 engine. The BFFMv2, even after the corrections presented above, still has a level of error higher than acceptable and is a general methodology that neglects the specifics of a given combustor configuration. Given these shortcomings of both the CFM56 based P3T3 correlation and the BFFMv2, two additional advanced combustor configurations that have been previously proposed for supersonics are examined. The two combustor configurations are the Rich Burn, Quick Quench, Lean Burn (RQL) combustor and the LPP MRA combustor. For the RQL configuration, shown in Figure 43, the initial section of this combustor is a rich-front to obtain and stabilize the flame structure. Since the rich-front is low in oxygen, combustion is incomplete and only about 50% of the total energy release occurs here. This incomplete combustion results in the formation of CO without any NOx. After the rich-front, air is rapidly added into what is called the quench-section to enable the reactions to complete to CO<sub>2</sub>. After the quench-section is the lean-zone where liner cooling air is added and the remaining energy release occurs. The excess air in lean combustion zone



results in a reduction of NO<sub>x</sub> emissions (NASA CPC Vol2, 2005). The initially evaluated correlation comes from the NASA HSCT study (Niedzwiecki, Richard W., 1992) and is presented below:

$$EINO_x = 23.8 \left(\frac{P_3}{432.7}\right)^{0.4} \exp\left[-\frac{(T_3 - 1027.6)}{349.9} + 0.014\right]$$

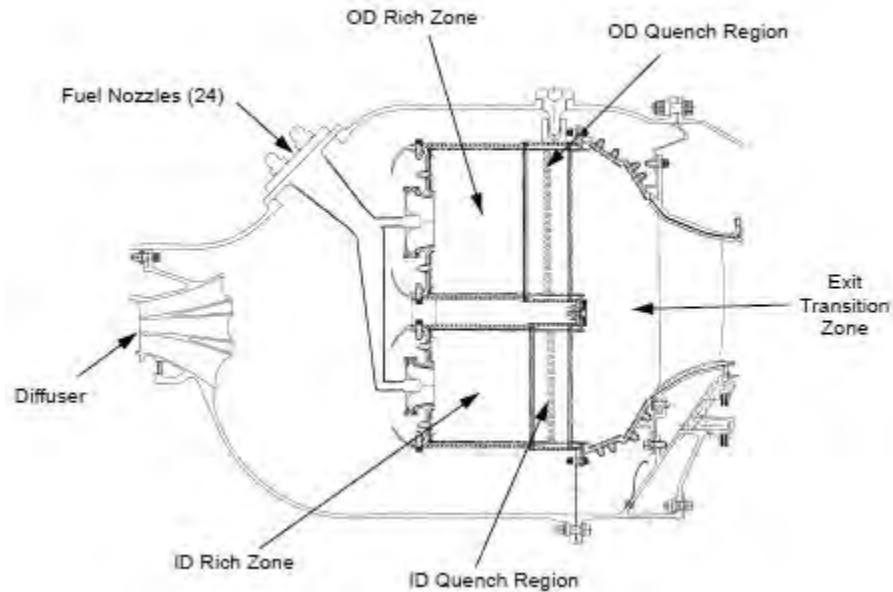


**Figure 43.** Rich/Quench/Lean HSCT Combustor (NASA CPC Vol2, 2005).

The LPP MRA combustor concept (S. Greenfield, P. Heberling, G. Moertle, 2005), shown inworks by rapidly atomizing and uniformly mixing the fuel in the air prior to the combustion zone. This is done by injecting the fuel near a venturi throat, where the high-swirl and high velocity air rapidly atomize the fuel. The lean fuel/air mixture, well-atomized and uniformly mixed, will reduce the NO<sub>x</sub> levels (NASA CPC Vol2, 2005). The LPP MRA configuration is one of the lean combustion architectures introduced that has a more mechanically durable dome structure (NASA CPC Vol2, 2005). To predict the NO<sub>x</sub> emissions of this advanced configuration, GE Aviation developed the following correlations using 120 test data points:

- 1)  $SP_{NO_x} = \frac{P_3^{0.4}}{432.7} \exp\left[\frac{T_3 - 460 - 1027.6}{349.9} + \frac{6.29}{53.2}\right]$ ;  $P_3$  in psia,  $T_3$  in Rankine
- 2)  $EI_{gasl} = \tau \exp\left[-72.28 + 2.8\sqrt{T_4} - \frac{T_4}{38.2}\right]$ ;  $\tau$  in msec,  $T_4$  in Kelvin
- 3)  $NO_{x,corrected} = 0.824159 + 4.166818(EI_{gasl})(SP_{NO_x})$
- 4)  $NO_x(EI) = 0.7136 [NO_{x,corrected}]^{0.8449}$

Figure 45 shows the LTO dP/F00, calculated by subsonic rules, for each of the correlations when applied to the GT Medium SST engine cycle. For context, the CAEP limits and values for other engines from the CAEP database are also plotted on the same graph. Table 17, Table 18, and Table 19 present the EINO<sub>x</sub> results for the GT Medium SST cycle using the NASA HSCT P3T3 correlation.

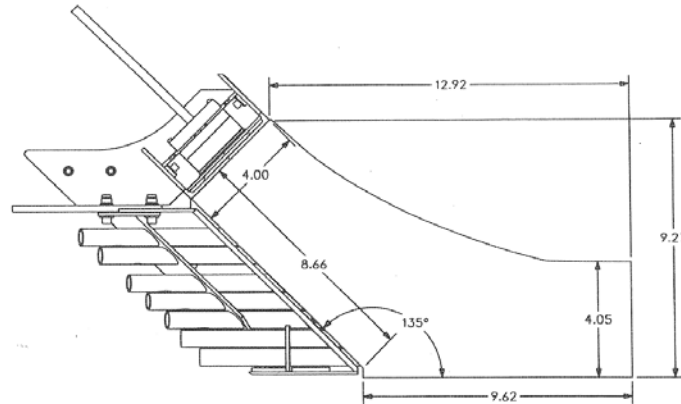


Figure 44. LPP MRA 2D Section View (S. Greenfield, P. Heberling, G. Moertle, 2005).

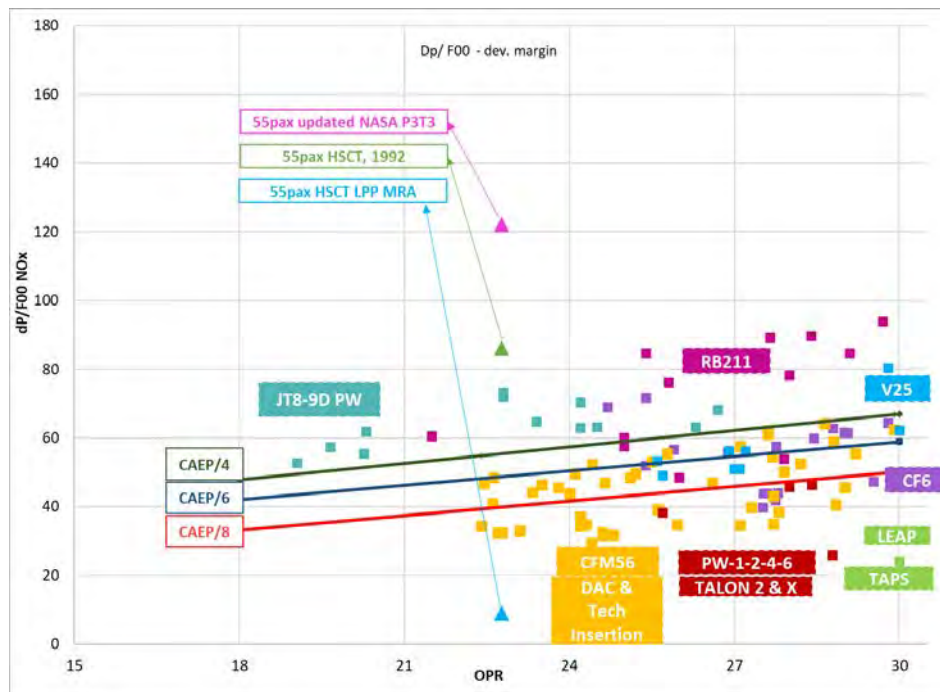


Figure 45. Plot of LTO Dp/F00 Using NASA CFM56 P3T3, NASA HSCT 1992 and GE Based HSCT LPP MRA Correlations.

Table 17. GT Medium SST LTO EINO<sub>x</sub> (Subsonic Rules).

Mode	Time	Thrust % (max)	Thrust (lbf)	OPR	P <sub>13</sub> (psi)	T <sub>13</sub> (°R)	Fuel Flow (lbm/sec)	EINO <sub>x</sub> (g/kg)
Takeoff	0.7	100	23005	12.7	186.7	1134	3.51	6.34
Climb Out	2.2	85	19554	11.2	163.9	1091	2.91	5.31
Approach	4	30	6902	5.7	83.2	896	1.07	2.32
Idle	26	7	1610	3.1	46.2	762	0.51	1.25


**Table 18.** GT Medium SST LTO EINO<sub>x</sub> (Supersonic Rules).

Mode	Time	Thrust % (max)	Thrust (lbF)	OPR	P <sub>13</sub> (psi)	T <sub>13</sub> (°R)	Fuel Flow (lbm/sec)	EINO <sub>x</sub> (g/kg)
Takeoff	1.2	100	23005	12.7	186.7	1134	3.51	6.34
Climb Out	2.0	85	19554	11.2	163.9	1091	2.91	5.31
Approach	2.3	30	6902	5.7	83.2	896	1.07	2.32
Descent	1.2	15	3451	4.1	59.9	818	0.69	1.63
Idle	26	5.8	1334	3.0	44.0	753	0.49	1.20

**Table 19.** GT Medium SST LTO NO<sub>x</sub> Dp/Foo.

Rule	Dp/Foo Calculated, [g/kN]	Corrected for engine tested	Corrected for dev. margin	Dp [g]	CAEP 8 Limit
Subsonic	15.81	17.39	20.16	463826	25.76
Supersonic	14.95	16.44	19.06	438447	25.76

#### Nonvolatile Particulate Matter (nvPM)

The cruise nvPM emissions for the NASA STCA are computed using the methodology described in CAEP11-WG3-PMTG09-IP06, “nvPM Cruise Modeling Methodology.” Two modifications are made to the CAEP methodology. The first modification takes the parameters P<sub>3</sub>, T<sub>3</sub>, and FAR directly from the NASA cycle model run at the required flight conditions, rather than using the CAEP estimation procedure. The data is provided by NASA Glenn Research Center. The second modification is based upon recommendations by members of CAEP WG3 to change the Döpelheuer-Lecht equation by replacing the combustor primary zone equivalence ratio  $\phi$  with the combustor FAR, resulting in the following equation:

$$EI = EI_{ref} \left( \frac{FAR}{FAR_{ref}} \right)^{2.5} \left( \frac{P3}{P3_{ref}} \right)^{1.35} \frac{\exp(-20000/T_{fl})}{\exp(-20000/T_{fl,ref})}$$

where the flame temperature is calculated by:

$$T_{fl}[K] = 2281[P3^{0.009375} + 0.000178P3^{0.055}(T3 - 298)]$$

with T<sub>3</sub> in Kelvin and P<sub>3</sub> in Pascals.

In addition, the sea level reference emissions data is taken from CAEP10-WG3-PMTG4-WP09, “GE0E1 nvPM Emissions Data Description.” This document reports test results for a CFM56-7B26/3 engine. Data is presented both with and without liner loss corrections, so the analysis is carried out for both cases. Finally, the sea level reference values of P<sub>t3</sub>, T<sub>t3</sub>, and FAR are taken from Georgia Tech’s EDS model of the CFM56-7B27/3 engine, an up-rated version of the test engine. The EDS model is run at the approximate test conditions of 1,400 ft elevation and ISA + 10C day. The results of the analysis are presented in Table 20 below. At this point in time, the correct methodology of predicting nvPM emissions are still under discussion with the CAEP community.

**Table 20.** nvPM mass EI, mg/kg fuel.

Condition	With Line Loss Correction	Without Line Loss Correction
Start of cruise (43774 ft / 1.4)	25.90	17.80
End of cruise (50916 ft / 1.4)	15.52	10.64
Sea level static, 100% thrust	42.84	27.81
Sea level static, 85% thrust	25.32	15.66
Sea level static, 30% thrust	1.62	1.62
Sea level static, 7% thrust	1.54	1.54

**Airframe Modeling**

This section details the process of modeling the airframe including using the viscous drag correction from CART3D, the area ruling, and aero shaping of the vehicle.

Viscous Drag Prediction

The previous aerodynamic analysis of all aircraft developed in this project was done using inviscid CFD, which neglects viscous drag but has lower analysis time compared to CFD (i.e., RANS) that considers all types of drag. At first, it is assumed that the viscous portion of the drag could be neglected in the context of supersonic cruise, but a single point RANS solution is obtained for the GT Medium SST, and it shows that the viscous portion of drag is 23.5% of total drag at Mach = 2.2 and angle of attack (AoA) of 2 degrees. This result invalidates the assumption previously made and the need for a viscous drag calculation is recognized. Predicting viscous drag using RANS-based CFD software is very computationally expensive. RANS solutions may take days to be evaluated, and the Euler equations often used neglect that portion of drag. For this reason, the viscous drag for the Medium SST is estimated using the CART3D viscous correction module. This software add-on uses the Euler solution provided by CART3D’s inviscid solver with an interactive boundary-layer approach to estimate viscous drag (Aftomis et al. 2006), greatly decreasing CFD evaluation time compared to RANS. This methodology uses loops around the geometry to specify boundary layer stations (BLcuts) and boundary layer axis (BLaxis), which can be specified in any of the x, y, z Cartesian directions.

An initial attempt uses the viscous correction in CART3D simply applying the BLcuts and BLaxis to the exiting geometry, but there are many errors related to both the software use in the Georgia Tech computers and how the geometry is specified. The CART3D viscous drag add-on is originally created to run on computers with different software and operating system versions; therefore, additional assistance for the NASA developers (with much appreciation) is needed. The first geometry files generated by the Georgia Tech team used the airframe as one body and used several BLcuts in all directions to cover said body. This procedure generated many errors because BLcuts are not supposed to intersect each other. The developers of CART3D at NASA suggested that the geometry had to be created by components with different IDs, which enables the creation of BLcuts and BLaxis that do not interfere with each other and still cover the entire geometry. Therefore, in order to properly obtain the viscous drag for the Medium SST, the geometry definition in ESP had to change significantly. Each component of the vehicle (i.e., engines) is assigned a component ID to identify it, and an in-house code is developed to transform the new ESP geometry file into the triangulated files used by CART3D. Other adjustments are also made to other input files for CART3D. Once the new files are obtained and the viscous drag module from CART3D is executed, a comparison between the viscous correction results and the RANS solution for the Medium SST at Mach = 2.2 and AoA of 2 degrees is made. The results of both CART3D and RANS CFD are shown in Table 21. Table 22 shows the percent difference of the results at the same Mach number and angle of attack. As it can be seen, the deviation of CD and CL is less than 10%, which shows that the CART3D viscous module has an acceptable agreement to higher fidelity CFD.

**Table 21.** Comparison between Cart3D viscous drag correction and RANS for Mach = 2.2 and AoA = 2 deg.

	CART3D Results			RANS CFD Results		
	Inviscid	Viscous	Total	Inviscid	Viscous	Total
<b>CD</b>	0.0187	0.006083	0.02479	0.0197	0.006061	0.02579
<b>CL</b>	0.1813	-0.000292	0.18103	0.1986	-0.000310	0.19833

**Table 22.** Percent difference in the results from Cart3D and RANS for the medium SST for Mach = 2.2 and AoA = 2 deg.

	% Difference in results		
	Inviscid	Viscous	Total
<b>CD</b>	5.21	-0.37	3.90
<b>CL</b>	8.72	5.81	8.73

Another comparison is performed by trying to match CL between the CART3D simulation and the RANS CFD solution. The CART3D simulation with viscous correction is executed at Mach = 2.2 and AoA of 2.375 degrees, and the RANS CFD solutions are obtained at Mach = 2.2 and AoA of 2.0 degrees. The results for both simulations are shown in Table 23. Table 24 shows

the percent difference of the results at the same CL and Mach number. Using this comparison approach, CART3D predicts 5.1% more total drag than RANS CFD at the same CL conditions. Given the small change in results for both comparisons made and a great reduction in computational expenses given by the viscous drag correction, the CART3D viscous module is used to predict viscous drag at all other flight conditions and for all other aircraft analyzed in the project.

**Table 23.** Comparison between Cart3D Viscous Drag Correction and RANS CFD matching CL. Cart3D calculations obtained at Mach = 2.2 and AoA = 2.375 deg. RANS solutions obtained at Mach = 2.2 and AoA = 2.0 deg.

	CART3D Results			RANS		
	Inviscid	Viscous	Total	Inviscid	Viscous	Total
<b>CD</b>	0.02103	0.0060813	0.02711	0.01973	0.006061	0.025791
<b>CL</b>	0.1986	-0.00033156	0.19829	0.19864	-0.000310	0.198334

**Table 24.** Percent difference in the results from Cart3D and RANS for the medium SST. Cart3D calculations obtained at Mach = 2.2 and AoA = 2.375 deg. RANS solutions obtained at Mach = 2.2 and AoA = 2.0 deg.

	% Difference in results		
	Inviscid	Viscous	Total
<b>CD</b>	-6.57	-0.33	5.11
<b>CL</b>	0.01	-6.95	0.02

Implementation of CART3D viscous module into the drag polar generation process results in a lower overall L/D at cruising and peak L/D occurs at a higher coefficient of lift. Figure 46 shows the comparison between a purely inviscid drag polar and one which has CART3D viscous correction implemented for 60,000 ft. Viscosity introduces dependency of L/D to altitude. Higher altitudes will have more prominent viscous effects and cruise Reynolds number will decrease due to decreasing density, resulting in a decreased L/D. Table 25 expresses the relationship between altitude and peak cruise L/D. Currently, the Medium SST is projected to cruise at 62,000 ft resulting in a peak cruise L/D of approximately 7.1 occurring at a CL of 0.169. For comparison, an aircraft operating in purely inviscid conditions would have a cruise L/D of approximately 9.7 occurring at a CL of 0.112. Therefore, there is a significant difference in the performance and ideal operating conditions of the airframe in inviscid flow compared to viscous flow and indicating that airframes designed in a inviscid environment may not necessarily be ideal in a viscous environment. Moving forward studies on airframes will be conducted in a viscous environment from the start.

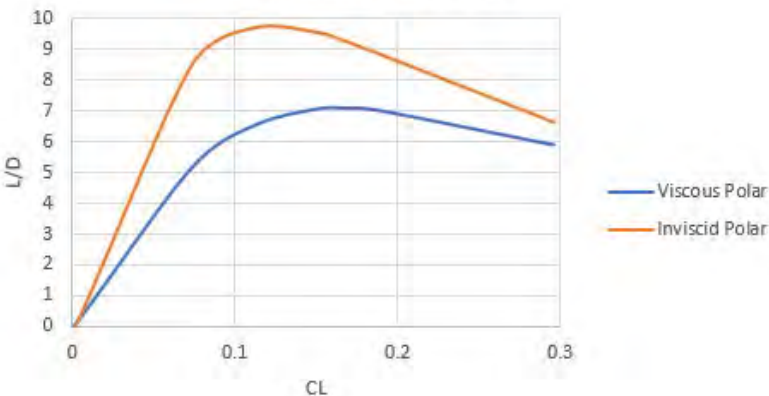


**Figure 46.** Inviscid/Viscous Lift over Drag Performance Comparison.

**Table 25.** Peak Lift to Drag Dependence on Altitude.

Altitude	Peak Operating L/D @ Mach 2.2
50000	7.23
55000	7.18
60000	7.12
65000	7.06
70000	7.00

**Area Ruling**

With a cruise Mach of 2.2, the Medium SST must minimize wave drag to increase efficiency. One way to decrease wave drag is to area rule an aircraft. Area ruling involves reducing area jumps along the length of the fuselage of the aircraft. To minimize these area jumps, the wing and engines are strategically placed along the length of the aircraft. The nose is very sharp leading to the body, the wing is moved forward, and as the wing ends, the rear engine and vertical tail prevent the area distribution from drastically changing. An area ruling plot corresponding to the configurations shown in Figure 50 is shown in Figure 47. In this figure, the smooth blue line represents an ideal Sears-Haack body, a shape demonstrated to minimize wave drag for supersonic flight, and the black line shows the total area distribution of the aircraft at the cruise Mach number. The other colored lines represent the area contributions of the separate aircraft components, such as the wing, fuselage, and engines. To minimize wave drag, the total area distribution should follow the Sears-Haack body curve as closely as possible. The plot on the left shows the area ruling of the initial configuration and the plot on the right shows the current area ruling. Two major configuration updates that adversely affected the area ruling are the expansion of the underside of the fuselage to allow for landing gear storage (see Figure 48) and the integration of the nacelles into the wings. These changes result in a configuration with worse area ruling compared to the initial configuration that did not address these concerns. Future design processes will include nacelles in the initial planform selection process. This inclusion should lead to the selection of a planform which better reduces the nacelles adverse area ruling impact.

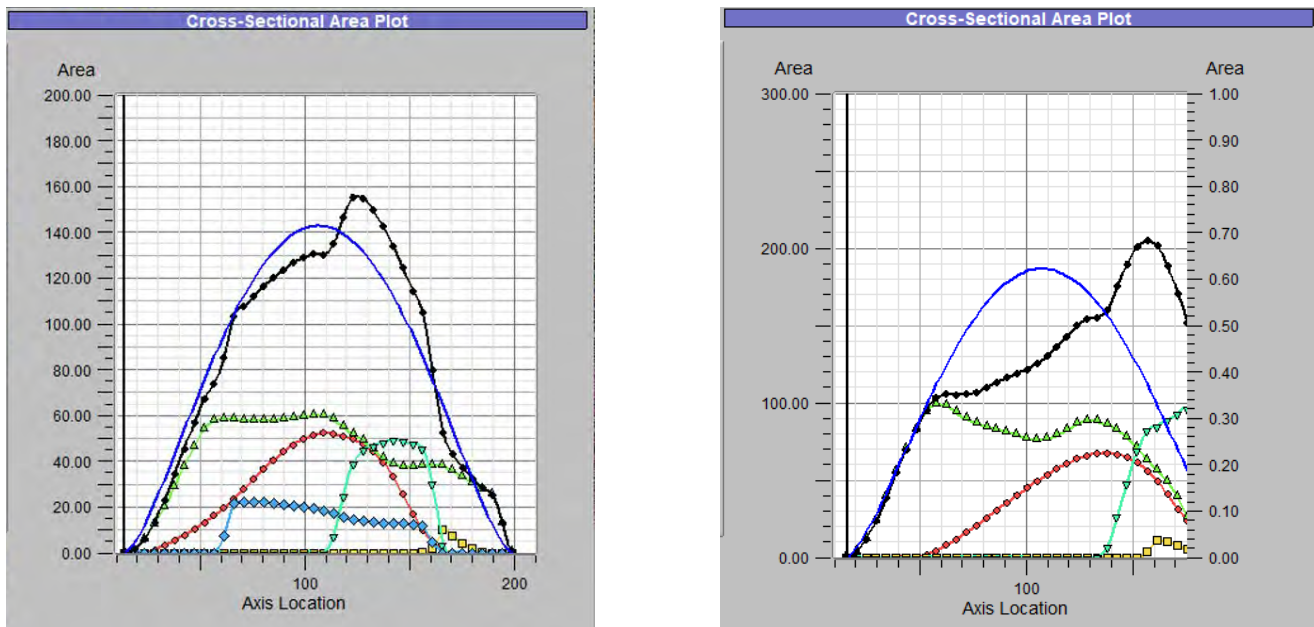


**Figure 47.** Area Ruling Distribution Plot Before (left) and After (right) Landing Gear Storage and Nacelle Integration.



**Figure 48.** Configuration before (left) and after (right) landing gear storage considerations.

#### Aero Shaping

In the supersonic flight regime, small geometric aspects of a configuration can have major effects on cruise efficiency (i.e., L/D). By visualizing the pressure distribution across the body of the aircraft, the aero team identifies areas of very high or low pressure, and these areas are smoothed or modified to prevent the pressure buildup. The major areas investigated are the sweep of the outboard section of the wing, the area ruling of the aft region of the fuselage, and nacelle integration. Figure 49 shows flow visualization of the initial aero shaping of the Medium SST. Flow visualization revealed a large high-pressure region on the leading edge of the outboard section of the wing. This high-pressure region can be reduced by increasing the sweep of the wings. Additionally, the addition of the nacelles to the aircraft negatively impacted the area ruling of the aircraft, necessitating a reduction in fuselage area behind the passenger cabin in reducing the impact caused by the integration of the nacelles. Finally, minimization of interactions between the nacelle and the rest of the configuration will be discussed extensively in the next section. Figure 50 shows the flow visualization over the Medium SST after the aero shaping has been improved, revealing that the flow distribution on the wings had been smoothed out and thus resulting in improved aerodynamic performance.

#### **Airframe-Engine Integration**

A major modeling challenge is integrating the engine into the ESP model for aerodynamic analysis. Due to the fact that the primary purpose of airframe shaping is to define the outer mold line of the aircraft and due to engine cycle constantly evolving during this process, only unpowered flow-through nacelles are modeled in the aerodynamic analysis. Even with this simplification, modeling the engine installation effects parametrically remained a difficult task. Initial attempts to integrate the engines into the wings result in very adverse interactions between the engines and the leading edge of the wing. Manual improvements to the engine placements result in a much cleaner engine integration and an improved L/D, as can be seen in the reduction in leading edge pressure in Figure 51. Unfortunately, manually improving the placement of the engines is a time-consuming process and not feasible in design space explorations, which is why engine location design relations are developed to parametrically place the engines. This approach will be discussed in more detailed in the Large SST section where it is first implemented.

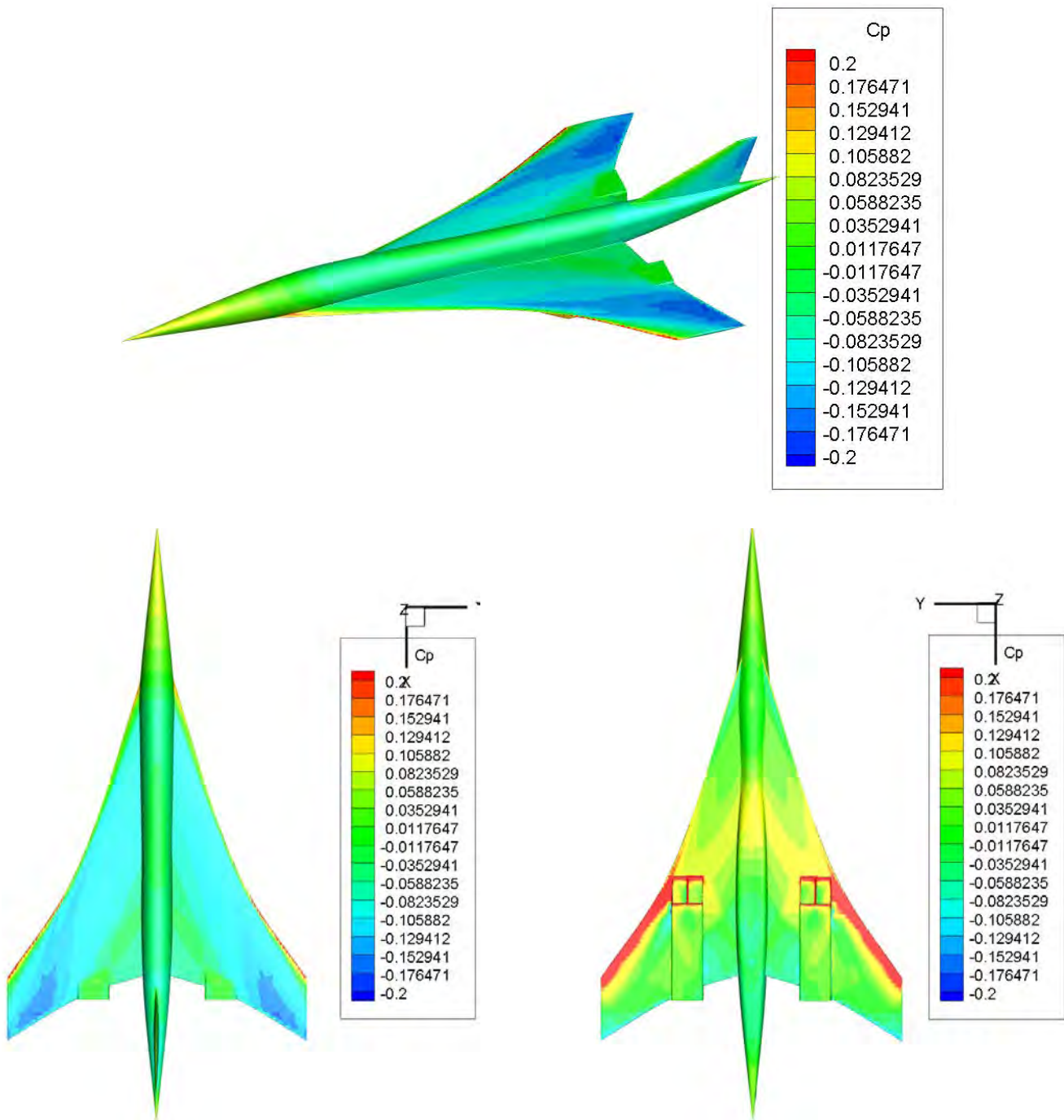


Figure 49. Initial Medium SST Aero Shaping.

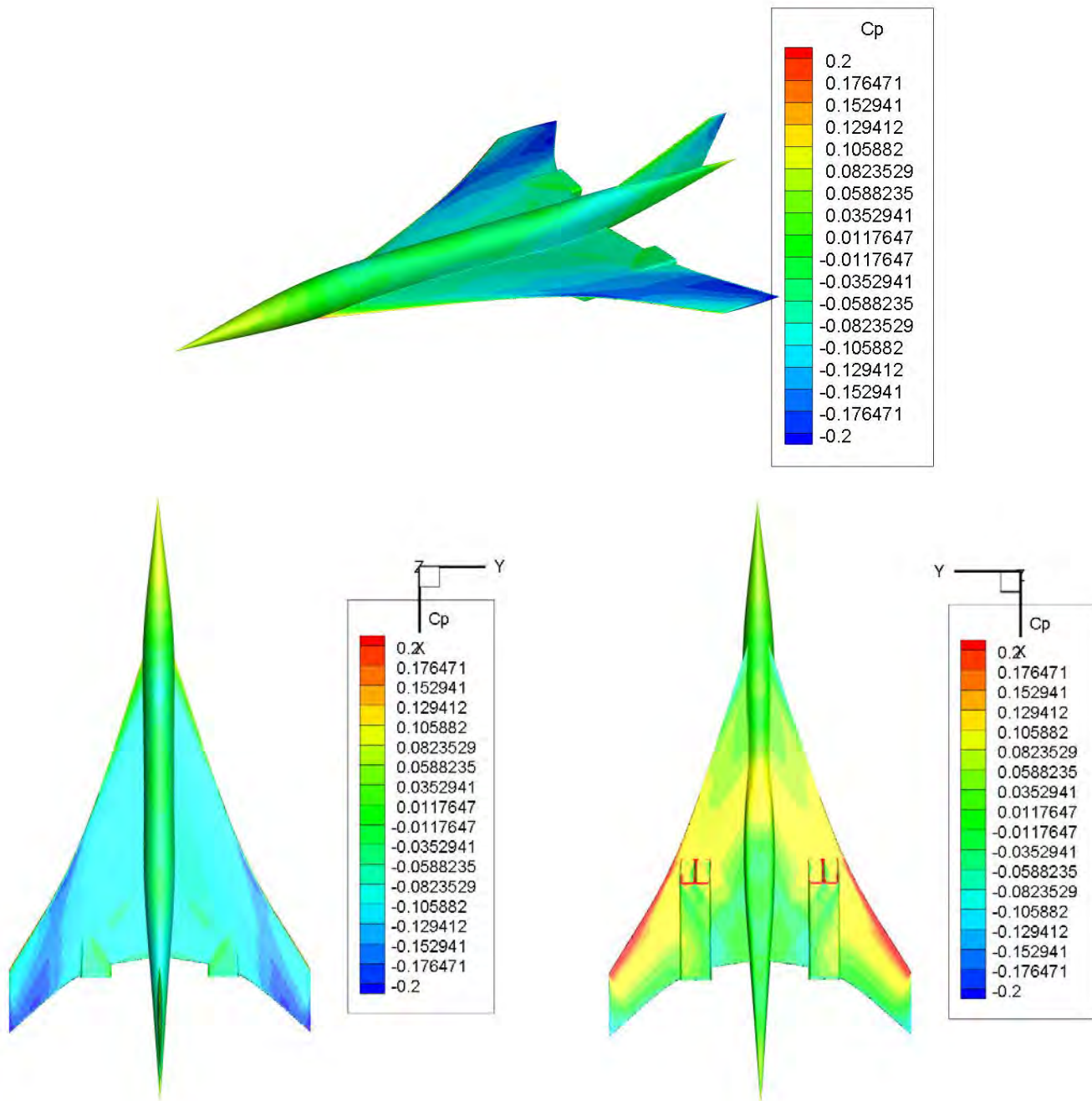


Figure 50. Improved Medium SST Aero shaping.

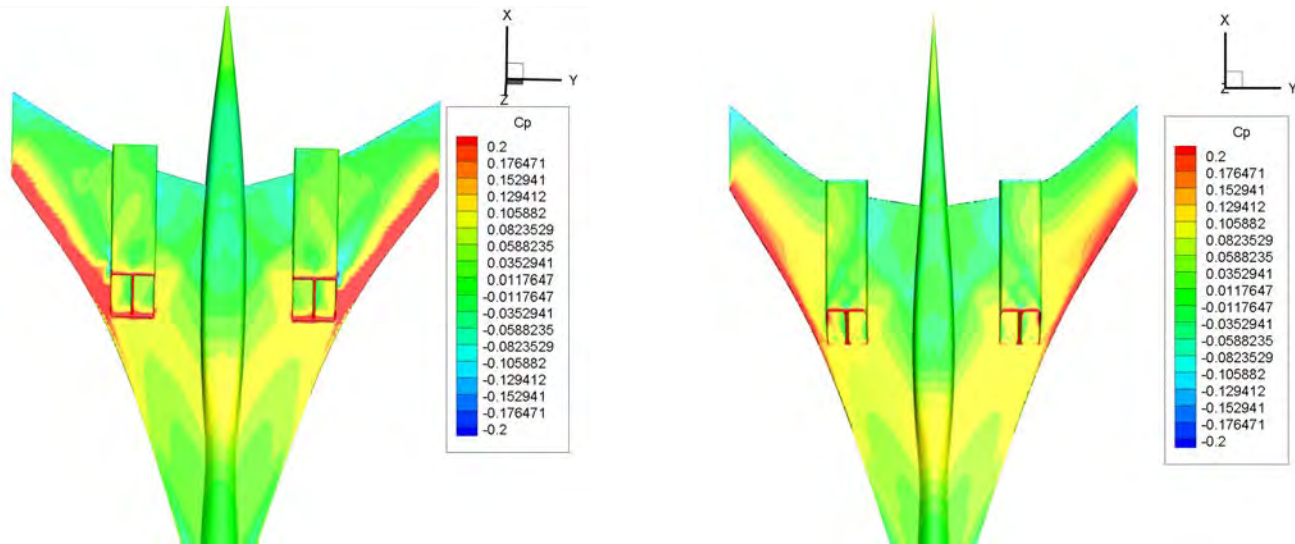


Figure 51. Comparisons between the initial engine integration and Improved engine integration.

**Landing and Takeoff Drag Polar Prediction**

This section describes the process to generate the low-fidelity LTO drag polar. The tools used for LTO polar generation are AERO2S and OpenVSP parasite drag tool. Parasite drag module in OpenVSP is used to calculate the parasitic drag (which is not included in AERO2S), while AERO2S is used for lift and drag due to lift generation. Figure 52 is the overview workflow of this process. If not specifically mentioned, the flight conditions for LTO drag polar analysis are Mach 0.25, 0 ft altitude, and with AoAs ranging from -2 degrees to 16 degrees.

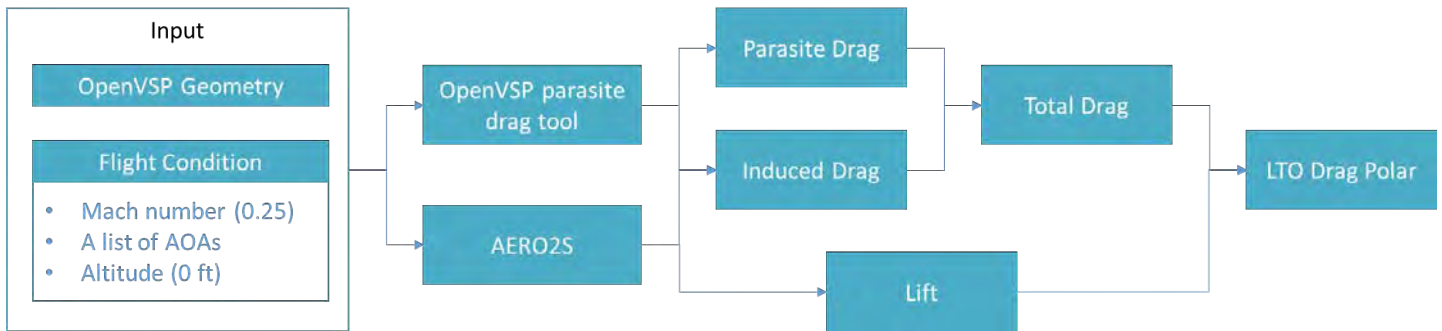


Figure 52. workflow for lto drag polar generation.

For each OpenVSP geometry, multiple flap deflection settings are applied for LTO drag polar comparison. In this study, the TE flap deflections ranges from 0 degree to 30 degree with a step size of 5 degree. Figure 53 shows the spanwise location and length of the TE flaps in AERO2S. Note that the LE slats are not activated in this study due to the aforementioned leading-edge slat sensitivity study. Figure 54 shows the LTO drag polar for the GT Medium SST with multiple TE flap settings.

**Mission Analysis**

This section presents the preliminarily results of the GT Medium SST closed vehicle design, designated as version 11.4 or v1 1.4 for short. The preliminary results shown in this section are the result of executing the processes/iterations described in the previous sections.



**Design point**

For synthesis and sizing of an aircraft, both the thrust-to-weight ratio (T/W) and the wing loading (W/S) are major design parameters that are generally determined by performing a constraint analysis. For the current supersonic study, the T/W and W/S are chosen to meet balanced field length under 10,000 ft and an approach speed below 165 kts.

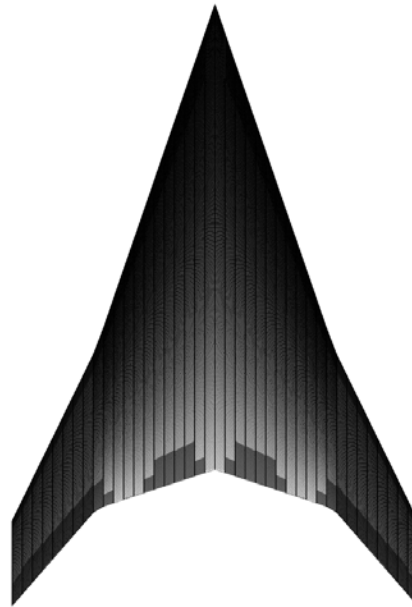


**Figure 53. GT Medium SST TE Flap Locations.**

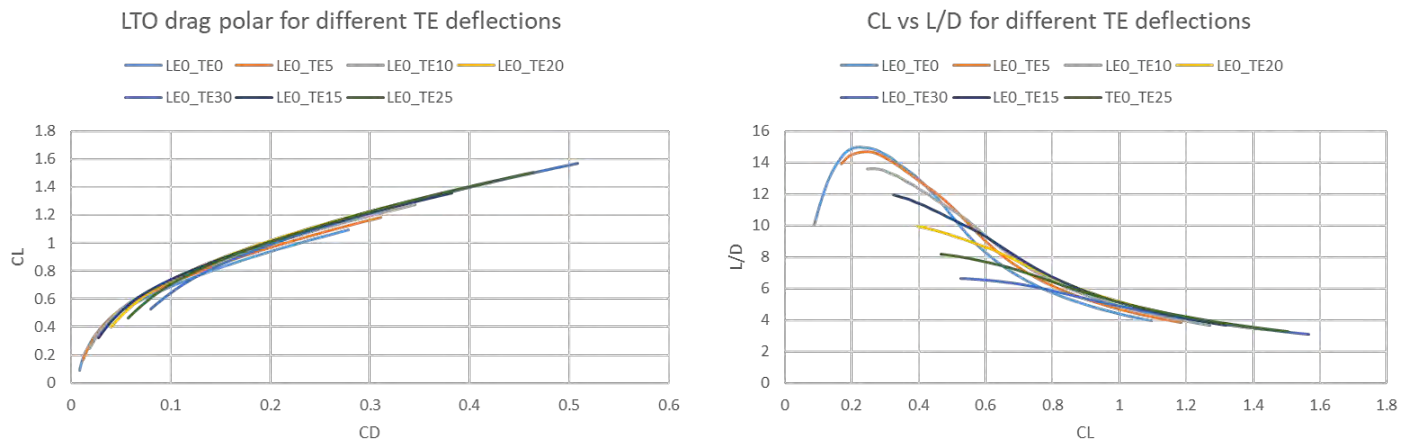


**Figure 54. LTO Drag Polar for GT Medium SST.**

**Mission Profile**

The vehicle is sized for a mission with a total range (excluding reserve mission) of 4,500 nmi. The chosen mission profile is as follows:

- Takeoff: Mach = 0 - 0.30 at altitude of 0 ft.
- Subsonic climb: M = 0.30 - 0.95; altitude changing from 0 ft to 25,000 ft.
- Supersonic climb: M = 0.95 - 2.20; altitude changing from 25,000 ft to 58,000 ft.
- Cruise climb: constant cruise M = 2.2; altitude changing from 58,000 ft to 66,000 ft.



- Descent: deceleration from  $M = 2.2 - 0.30$ ; altitude decreasing from 66,000 ft to 0 ft.

The reserve mission is defined as follows:

- Reserve fuel available: equal to 10% of total fuel used in main mission.
- Total hold time: 15 min.
- Climb: from 0 to 35,000 ft, with Mach increasing up to 0.80.
- Cruise: 35,000 ft at  $M = 0.80$ .

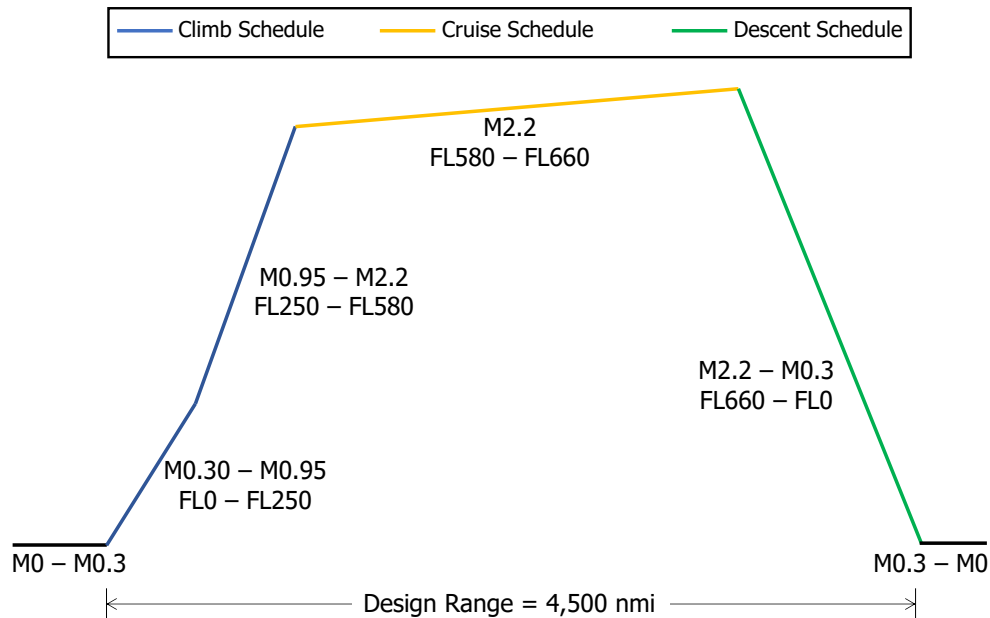


Figure 55. Mission Profile for Medium SST.

### Vehicle Sizing

The vehicle sizing loop is performed with NASA’s FLight Optimization System (FLOPS). The vehicle is defined by using the aerodynamic and propulsion information defined in this report along with the mission profile discussed above. The preliminary vehicle characteristics results are shown in Table 26 and Table 27. *Again, these results are preliminary at the writing of this annual report.*

Table 26. Key metrics for medium SST (preliminary).

Key Metric	Value
Takeoff Gross Weight, lbs	367,000
Design Cruise Mach	2.2
Wing Reference Area (ft <sup>2</sup> )	3,863
Design Range (nmi)	4,500
Beginning of Cruise L/D	7.13



**Table 27.** Weight breakdown of medium SST (preliminary).

Component	Weight (lbs)	% Empty Weight (lbs)	Component (Cont'd)	Weight (lbs)	% Empty Weight (lbs)
Wing	44,765	29.11	Control Surfaces	3,191	2.07
Horizontal Tail	0	0.00	Auxiliary Power	727	0.47
Vertical Tail	902	0.59	Instruments	1,030	0.67
Fuselage	24,411	15.87	Hydraulics	2,268	1.47
Landing Gear	11,100	7.22	Electricals	2,899	1.88
Nacelle (bookkept with engine)	0	0.00	Avionics	1,407	0.92
<b>Structures Total</b>	<b>81,178</b>	<b>52.78</b>	Air Conditions	3,794	2.47
Engines	54,080	35.16	Anti-icing	260	0.17
Propulsion Miscellaneous	271	0.18	<b>Systems and Equipment Total</b>	<b>15,576</b>	<b>10.13</b>
Fuel System: Tanks and Plumbing	2,697	1.75	<b>Weight Empty</b>	<b>153,801</b>	<b>100.00</b>
<b>Propulsion Total</b>	<b>57,048</b>	<b>37.09</b>			

### GT Large SST

The GT Large SST is sized to cruise at Mach 1.8 carrying 100 passengers, at 4,500 nmi with no subsonic mission segments.

#### Propulsion System

##### Architecture Selection

A MFTF engine architecture is also chosen for this class of supersonic transport for the same reasons as aforementioned for the GT Medium SST.

##### Cycle Modeling

The propulsion model used for this aircraft is the same as the GT Medium SST. The differences in engine design are being driven by the different design Mach number and number of passengers. The inlet map used is again based on a configuration from the library of maps in the PIPSI database (Kowalski & Atkins Jr., 1979). It models a 2D, 4-shock, variable ramp, external compression inlet which is optimized for Mach 2.0. The different design Mach number (1.8 versus 2.0) will require a different selection of cycle variable and the larger number of passengers will result in larger thrust requirements.

##### Cycle Design Methodology

The GT Large SST uses the same MDP points as the GT Medium SST except that the TOC Mach number is 1.8 and the altitude is 55 kft, whereas the Medium SST is designed for a TOC at Mach 2.2 and an altitude of 60 kft. The cycle design points are summarized in Table 28. Initial thrust estimates are made based on the current vehicle drag polar for the Large SST, assumed vehicle weight, and specific excess power requirements. The vehicle maximum takeoff weight (MTOW) is assumed around 400,000 lbs, since this is about what the Concorde weighed. Another assumption made for determining the thrust required at TOC is that 15% of fuel is consumed so the vehicle weight would be 85% of MTOW. From these assumptions and the wing loading from the Concorde to estimate wing area, the required lift coefficient is computed. Using the drag coefficient at the required lift coefficient and a required 300 fpm of specific excess power, the TOC thrust is estimated. The thrust at other points of interest such as ADP, takeoff, and SLS are kept in the same proportions as the Medium SST. The computed thrust requirements are implemented as a target within the cycle design environment and FPR, HPCPR, and Throttle Ratio (i.e., design T41) are varied to evaluate the performance of different engine designs. Using the MDP methodology, a design space is studied and optimized to minimize TSFC.



**Table 28.** Cycle Design Points for Large SST Engine.

Flight Condition	Mach	Altitude	$\Delta T$
ADP	1.2	39,000	0
TOC	1.8	55,000	0
Cooling Flow Sizing	Set for max Tt3 or Mach 1.8, whichever is lower	55,000	0
Takeoff	0.25	0	27
SLS Uninstalled	0	0	0

Off-design Power Management

The off-design power management is the same for the GT Large SST as the GT Medium SST.

Flowpath and Weight Model

The flowpath model will be largely based on the one developed for the GT Medium SST. Appropriate modifications are being made for the inlet, turbomachinery, and nozzle. At the writing of this report, the flowpath / engine weight model is still under development.

Results

The engine cycle presented is as of August 2020. Table 29 shows the efficiencies, pressure losses, bleeds, and modeling assumptions used in the model at each of the design points for the MDP analysis of the current design. Table 30 shows the cycle parameters and performance metrics at each of the design points of the current design. At the time of the writing of this annual report, these propulsion results are still preliminary and have not been completely matched to aircraft performance.

**Table 29.** Cycle Modeling Assumptions for Large SST Engine.

Component	ADP	TOC	TO	SLS
Inlet Recovery	97.74%	92.72%	95.75%	100.0%
Fan Adiabatic Efficiency	90.69%	89.94%	93.30%	92.21%
HPC Adiabatic Efficiency	87.72%	87.35%	88.48%	88.30%
HPT Adiabatic Efficiency	90.77%	90.71%	91.53%	91.63%
LPT Adiabatic Efficiency	92.94%	92.77%	93.30%	93.52%
Nozzle Gross Thrust Coefficient	98.80%	97.91%	98.80%	98.80%
Imperfect Mixing Coefficient	98.98%	98.87%	99.11%	99.06%
Nozzle Discharge Coefficient	96.3%	96.3%	97.3%	96.1%
Shaft Horsepower Extraction	100	100	100	0
Customer Bleed, lbm/s	1.52	1.40	2.74	0
IGV Duct Pressure Loss	0.00% (currently no IGV)			
Duct 6 Pressure Loss	2.50%			
OGV Duct	0.0% (bookkept in burner)			
Fuel LHV, BTU/lbm	18,580			
Fuel Temperature, °R	518.67			
Burner Efficiency	99.70%			
Burner Pressure Drop	5.00%			
Duct 11 Pressure Loss	2.00%			
Duct 13 Pressure Loss	3.00%			
Tailpipe Pressure Loss	2.00%			
Bypass Duct Pressure Loss	4.00%			


**Table 30.** Cycle Variables and Performance Metrics.

	ADP	TOC	TO	SLS
Mach	1.2	1.8	0.3	0
Altitude [kft]	39	55	0	0
$\Delta T + ISA$ [R]	0	0	27	0
FPR	2.27	2.27	1.96	2.20
%Nc Fan	100.0%	100.0%	93.4%	98.5%
N1 [RPM]	4935	5591	4850	4940
Wc2 [lbm/s]	1018	1012	946	1012
HPCPR	7.93	7.91	7.31	7.81
N2 [RPM]	8948	10127	9035	9010
OPR	17.55	17.54	13.95	16.72
BPR	1.63	1.62	1.87	1.68
Extraction Ratio	1.00	1.00	1.04	1.01
Throttle Ratio	1.218			
Turbine Cooling [%W <sub>25</sub> ]	26%			
T4 [R]	2783	3492	2734	2736
T41 [R]	2624	3300	2581	2583
T3 [R]	1224	1543	1249	1236
NPR	4.96	11.20	1.83	2.04
Vjet [ft/s]	2142	2862	1392	1507
Installed Net thrust [lbf]	13124	14073	30000	47151
Installed TSFC [lbm/(hr × lbf)]	0.916	1.067	0.687	0.549

### Emissions Modeling

The emissions model for the GT Large SST is under development at the writing of this report.

### Airframe Modeling

This section details the process of modeling the airframe for a 100-passenger SST that cruises at Mach 1.8. The development of the cabin layout, area ruling, conceptual design process of the vehicle and initial configuration selection processes are described.

### Cabin Sizing

The passenger cabin is sized to conform to the FAA requirements of emergency exits and number of flight attendants for a 100-passenger vehicle. The seat width, seat pitch, and aisle width are assumed to be equal to the ones from the Medium SST, and its values are shown in Table 31. These values were defined during previous work in this project, and they are based on the seat width/pitch of first-class seats in long domestic flights (e.g., JFK to LAX, approximately 6.5 h).

**Table 31.** Seat pitch and width for Medium SST and Large SST cabins.

Class	Seat Pitch (in)	Seat Width (in)
First Class	32	21
VIP	45	24

The arm rests are chosen to be 3 in for the single seat in first class and the non-shared arm rest of the double seats in first class. The shared arm rest in first class and the arm rest in the VIP class are set to 3.5 in. The fuselage thickness is assumed to be 6 in, and the cabin cross-section is a circle with a 12.3-ft diameter. Three exits in each side of the fuselage and two steward's seats are added to fulfill the FAA requirements listed in 14 CFR 25.807 and 14 CFR 121.391. One type I exit and two type II exits are used. The type I exit has a width of 36 in in order to accommodate passenger boarding, and the type II exits width is 20 in. The final cabin layout also contains two lavatories and two galleys. The final cabin length is 111.6 ft. Figure 56, Figure 57 and Figure 58 show the first-class cross-section, the final cabin layout, and its dimensions, respectively.

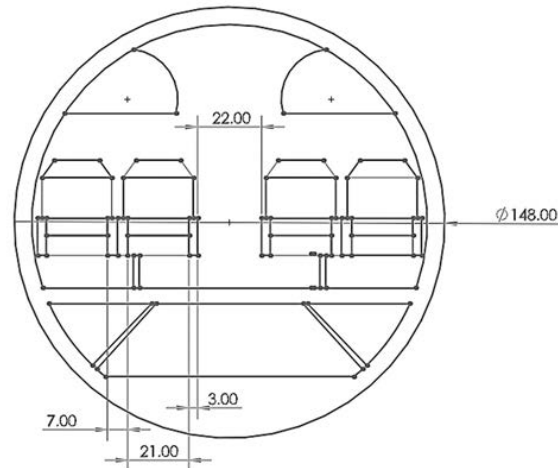


Figure 56. Cross-section of the First-Class cabin for the Large SST. All dimensions are in inches.

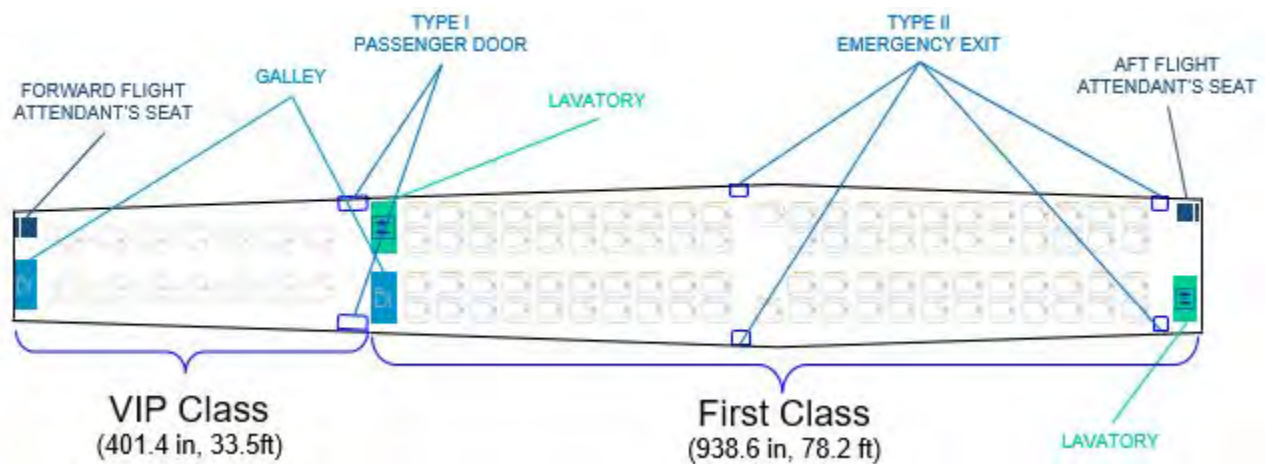


Figure 57. Cabin layout for the large sst.

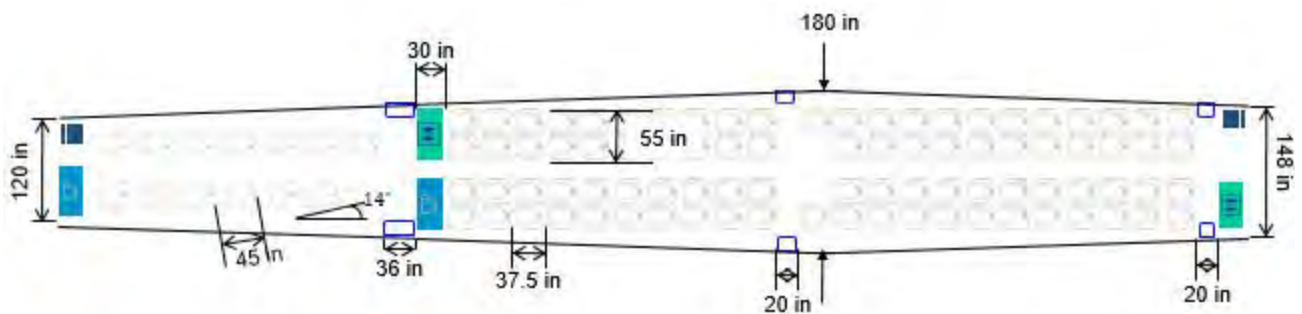


Figure 58. Cabin dimensions for the large sst.

Area Ruling

During the conceptual design, the minimization of wave drag governed the aerodynamic shaping of the aircraft. This drag contribution can be calculated by using slender body theory and supersonic area rule (Whitcomb, 1966). Area rule means that a smooth change in cross-sectional area of the vehicle going from the nose to the tail of the aircraft is desired. Some cross-sectional area distributions have been shown to minimize wave drag. In order to design a vehicle that minimizes drag, area rule is used to shape the fuselage of the vehicle along with the cabin size. For this reason, the fuselage of the Large SST did not maintain a constant width as seen in Figure 58.

Parametric Design Relations

The design of the GT Large SST used the knowledge learned on the design of the Medium SST; however, the change in passenger count and design Mach number are enough to require a new design for all parts of the vehicle. The fuselage is designed to fit the cabin layout developed, to be area ruled, and to have a total length of 254.2 ft (3050.3 in). The vertical tail, wing, and engine inlet capture areas are increased compared to the GT Medium SST. The vertical tail is assumed to double in area of that of the GT Medium SST; this assumption will be re-evaluated once the aerodynamics and propulsion designs iterate to ensure the vehicle can fly safely with one-engine-out condition. The wing area is increased compared to the 55-passenger vehicle. The aircraft is assumed to have four engines, each one with 4490 sq. in inlet capture area and length of 500 in. The baseline vehicle just described is shown in Figure 59, and it has an L/D of 6.76 at Mach 1.8, AoA = 2 degrees, and it has an L/D = 6.42 at Mach 1.8, AoA = 3 degrees.

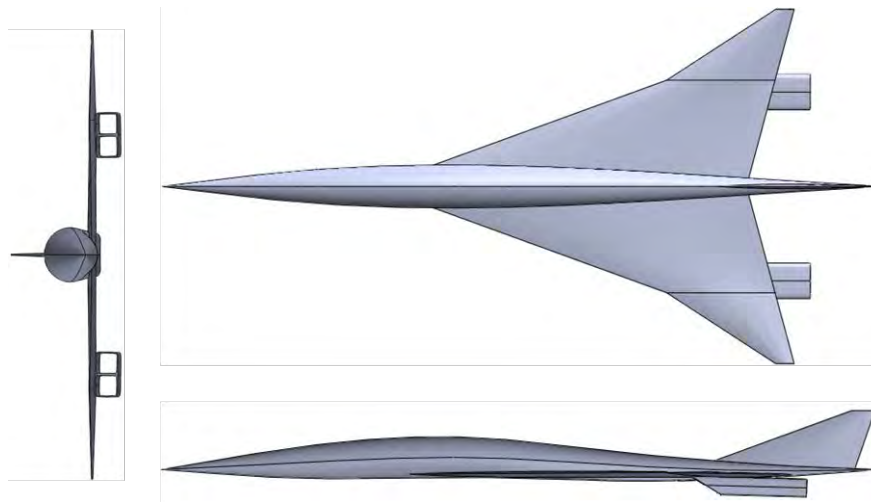


**Figure 59.** Baseline vehicle created for the GT Large SST configuration.

Given that the fuselage, vertical tail, and engines will be sized to conform to the vehicle passenger, thrust, and safety requirements, the only component that can be changed to improve L/D in the beginning of the conceptual design is the wing. In order to obtain a wing planform with higher L/D compared to the baseline, a DoE is performed to find wing geometries that perform better with respect to cruise L/D.

DoEs are a way of choosing variable combinations in the design space such that the points are within the ranges of variables set by the designer, and there are sampling points spanning the entire range of variables. The first DoE performed did not impose constraints on the points chosen. Engines are also not included in the initial set of experiments. The resulting configurations that are obtained as the optimum are unreasonable, such as the design shown in Figure 60.

In order to avoid looking at designs that are obviously infeasible, the next DoEs added constraints to the design parameters. Specifically, the following requirements are specified:

- Flow through nacelles must be included in the geometry model to account for engine-wing interference effects.
- Engine location must change as the planform design changes.
- Infeasible or invalid design combinations need to be avoided.
- Design space needs to be large enough to find sufficient improvement over the baseline.

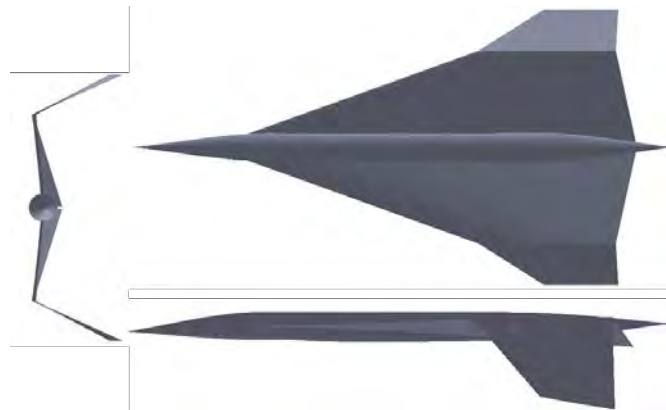


**Figure 60.** Optimum Design Obtained from DoE without Parametric Design Relations.

To satisfy the above requirements, the following procedural steps are established:

1. Define a baseline geometry seed from which subsequent designs can be generated.
2. Define the design variables and ranges.
3. Define engine location design relations.
4. Formulate constraints on the design space.

Step 1 requires the definition of a realistic design that is also geometrically valid (i.e., engines are not sticking through the wing). The baseline can be any design since the only purpose of this configuration is to provide reference values for use in the engine location design relations and the design space constraints. As such, the geometry shown in Figure 59 is defined as the baseline for step 1. Step 2 requires defining the design parameters that can be varied as part of the DoE. The vertical tail and fuselage geometries are frozen for this exercise and only the wing is considered as part of the design space. Table 32 shows the design variables and their ranges considered. The upper and lower bounds are set somewhat arbitrarily large to ensure a large enough design space, recognizing that the constraints developed in step 4 will help in filtering out unrealistic design combinations.

**Table 32.** design variable ranges for DoE created to optimize GT Large SST.

VARIABLE	Lower Bound	Upper Bound
Root Chord (in)	1000	1800
Mid Chord (in)	250	1000
Tip Chord (in)	50	250
Root Twist (deg)	-6	6
Mid Twist (deg)	-6	6
Tip Twist (deg)	-6	6
Root Thickness to Chord Ratio	1%	2%
Mid Thickness to Chord Ratio	2.5%	6.5%
Tip Thickness to Chord Ratio	2.5%	10%
Sweep of LE of Inboard Section (deg)	55	80
Sweep of LE of Outboard Section (deg)	35	80
Inboard Span (in)	450	650
Outboard Span (in)	100	400
Inboard Dihedral (deg)	-6	6
Outboard Dihedral (deg)	-6	6

The purpose of step 3 is to define a set of relations that automatically allow for the through flow nacelle geometry to move with the changes in the wing design. The idea is to prevent situations where the nacelles are not connected to the wing or stick through the wing geometry and produce invalid designs. While these situations can be manually corrected, doing so for hundreds of cases in a DoE is impractical. Lastly, step 4 aims to develop realistic constraints on the design space that

are a function of the chosen design variables. These constraints will filter out infeasible design combinations. Steps 3 and 4 are described in more detail below.

**Engine Location Design Relations (Step 3)**

To develop a set of robust and realistic relations, the following assumptions are made:

- The engine will always be on the inboard wing section → for structural considerations (avoid mounting engine on span location with thin airfoils) and directional stability purposes (engine out yawing moment).
- The airfoils on the wings are biconvex → allows for linear variation of thickness between cross sections and simplifies engine-wing z direction mate relationship.
- No droop on any airfoil either at LE or TE → prevents engine from accidentally sticking through the fore section of the wing due to a change in camber.
  - Note: Droop is added after the high-speed DoE study and parameters are varied manually to improve low speed performance.
- Engine length and cross section area are fixed (not part of design space). The relations made are tested for four engines with 4490 sq. in inlet capture area and length of 500 in.

Figure 61 shows the dependency between the engine location and wing design parameters. All these relations are accounted for as algebraic equations when generating the geometry for a given set of design parameters. The following relations are implemented:

- Changes in the x location of the engine due to changes in wing sweep and chord length to prevent the engine from sticking out in front of the wing leading edge or too far back behind the trailing edge.
- Changes in the y location of the engine to keep it within the inboard wing section as the wingspan changes.
- Changes in the z location due to changes in all design variables to keep the engine from sticking through the wing or from having a large clearance between the wing and nacelle upper surface.
- Changes in the engine pitch angle due to changes in wing twist or span.
- Changes in the engine roll angle due to changes in span or wing dihedral.

**Design Space Constraints (Step 4)**

The design space constraints are integrated as part of the DoE generation script, thereby allowing for the creation of DoEs where each sample satisfies the constraints and infeasible cases are filtered out during the generation stage. These constraints also leverage the algebraic equations developed as part of step 3 above. These constraints are listed below:

- Wing/engine cannot extend beyond fuselage TE.
- Engine inlet must be at least 10 in behind the mid chord LE to avoid engine sticking out ahead of the wing LE.
- Outboard span must be smaller than inboard (aeroelasticity constraint).
- Wing TE should be monotonic. This constraint is later replaced by the stricter straight TE requirement to allow for easier TE spar construction.
- Engine pitch should be within +/- 3 degrees from horizontal → to minimize loss in thrust.
- Wing root TE cannot travel more than 6 in in positive z direction and more than 2 in in the negative z direction relative to the reference z location of its LE → to avoid wing sticking out from above/below the fuselage.
- Outboard sweep must be smaller than inboard sweep → to avoid compromising low-speed performance.
- Wing thickness at the root should be greater than thickness at the mid, which should be greater than the tip thickness → structural constraint.

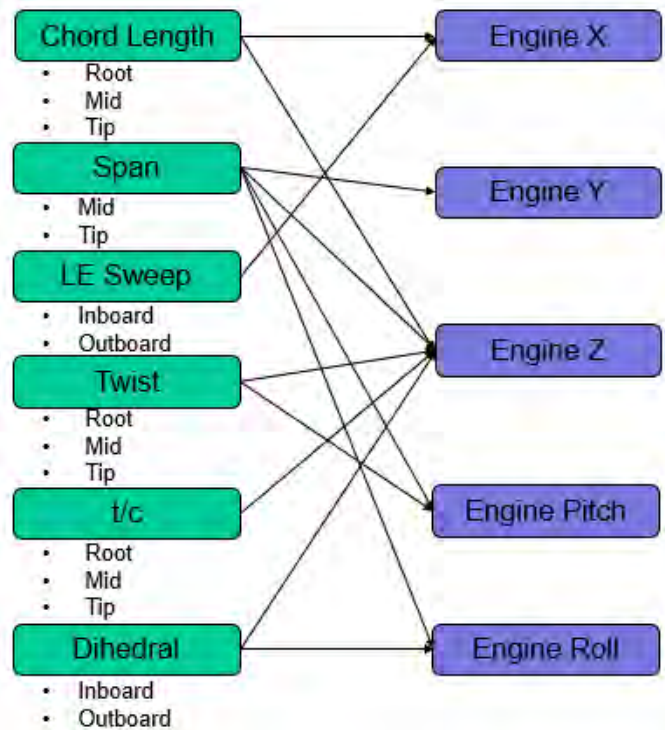


**Figure 61.** Dependency of engine location, pitch and roll angles on the design variables



- Minimum thickness at the mid chord is 18 in → to allow space for fuel pipes/cables to/from engine.
- Maximum height of either the mid or tip LE z location cannot be more than +/- 18 in from the root LE z location → stability/ground clearance/structural constraint.

After all the constraints mentioned above are implemented, a DoE with 250 cases is executed using CART3D with viscous correction. The designs with highest L/D are shown in Figure 62; however, these designs have structural issues, namely the wing box would not support the planforms created because there are drastic changes in the TE sweep between the inboard and outboard sections of the wing. The ribs in the wing box are usually not created to conform to such changes in the wing TE. The rightmost vehicle in Figure 62 is a good example of this issue.

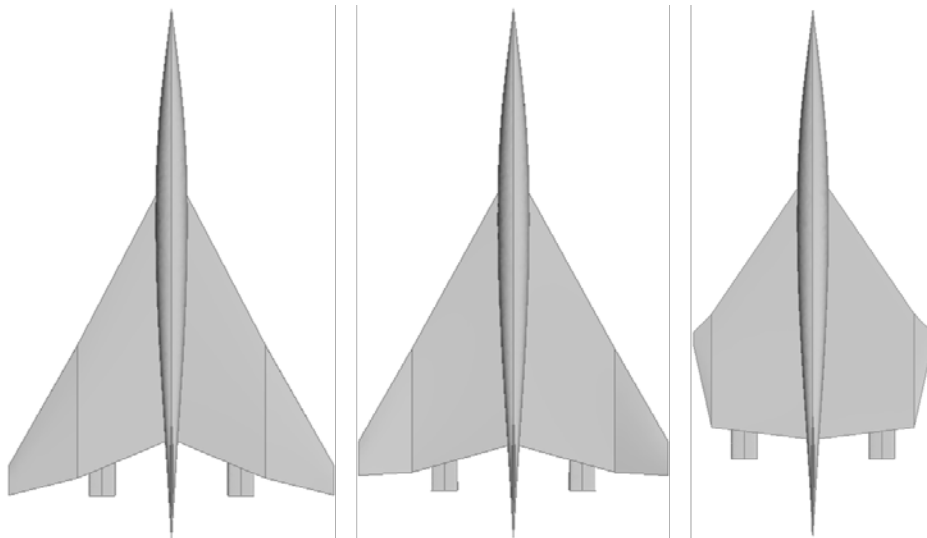


**Figure 62.** Best Designs from Constrained DoE without Enforcing Straight TE (Configurations with L/D Decreasing from Left to Right).

The odd planform shapes are avoided by imposing another constraint: a straight TE throughout the entire wingspan. This constraint changes the geometric design space by substituting mid and tip chord with TE sweep in the independent variable list. The addition of this design relation allows the generation of 250 valid and realistic geometries, but many resulting designs with high L/D have oversized wings due to long wingspans and tip chords. Long tip chords are not desired for structural considerations during supersonic cruise and large wing areas lead to high total drag, which would worsen the overall performance of the vehicle. For these reasons, planforms with wing areas greater than 1.55 times the Concorde wing area are filtered out. The configurations that resulted from this final DoE and that had reasonable wing areas are shown in Figure 63.

The main considerations used to choose the final planform are L/D, outboard sweep, and planform area. The wing planform chosen is the leftmost design in Figure 63. This planform has the highest L/D, which is important for vehicle performance; the smallest outboard sweep, which indicates best low-speed performance; and the second smallest wing area, showing it does not perform well simply for the having oversized wing and that the overall drag of the wing will be acceptable. It is observed that the wing area from this design could be decreased by shortening the root chord and the wingspan by 3.5%, improving the overall characteristics of the planform. The final design obtained after the scaling the wing parameters for the GT Large SST is shown in Figure 64.

The wing characteristics for the GT Large SST are shown in Table 33. Figure 65 and Figure 66 show the L/D versus AoA curve and the drag polar for this vehicle at Mach 1.8. The peak L/D is equal to 7.07, and it occurs at AoA of 3 degrees. The reference wing area is 5183.2 ft<sup>2</sup>. To improve the performance of this vehicle even further, an engine inlet capture area study will be performed to understand the change in drag caused by the change in inlet capture area. Droop will be added to the airfoil sections to improve L/D. An iteration between the high speed and low speed aerodynamics can affect the outboard characteristics of the chosen wing planform. Geometry updates will also arise as the engine cycle, engine capture area, and



length change are updated. Changes to the vertical tail and engine span-wise location will occur for the one-engine-out condition and landing gear sizing, which depends on the estimation of center of gravity obtained when the vehicle is sized in FLOPS.

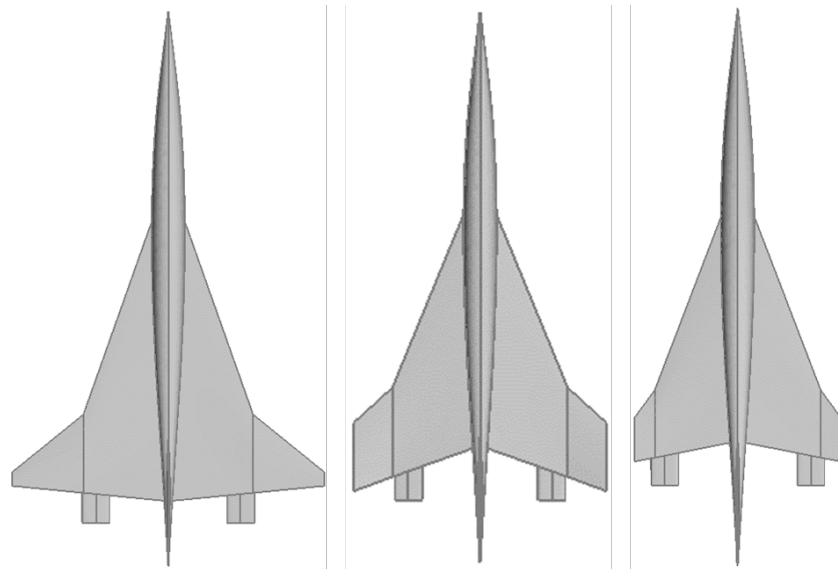


**Figure 63.** Best Designs from Constrained DoE Enforcing Straight TE and Wing Area (Configurations with L/D Decreasing from Left to Right).

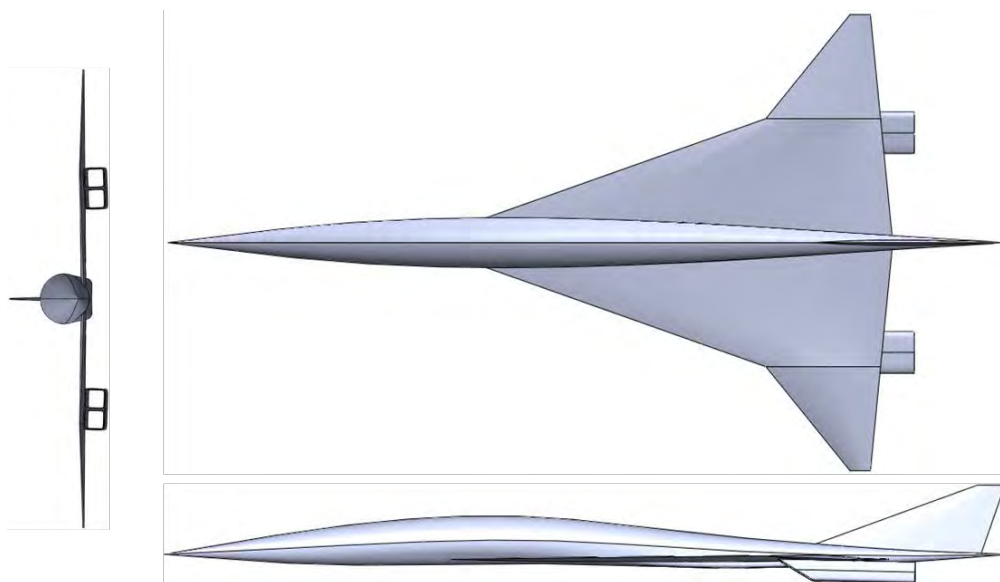


**Figure 64.** Final vehicle geometry with wing planform chosen for the GT Large SST.



**Table 33. Wing Geometry Definition for GT Large SST.**

VARIABLE	Baseline	GT Large SST
Root Chord (in)	1576.2	1734.3
Mid Chord (in)	460.4	417.2
Tip Chord (in)	78.8	75.3
Root Twist (deg)	0.00	-0.0846
Mid Twist (deg)	2.17	1.95
Tip Twist (deg)	2.01	-3.36
Root Thickness to Chord Ratio	1.77%	1.07%
Mid Thickness to Chord Ratio	4.50%	4.36%
Tip Thickness to Chord Ratio	8.00%	7.05%
Sweep of LE of Inboard Section (deg)	70.0	70.5
Sweep of LE of Outboard Section (deg)	57.0	39.0
Inboard Span (in)	450	450.9
Outboard Span (in)	300	378.1
Inboard Dihedral (deg)	0.892	1.84
Outboard Dihedral (deg)	-1.14	-2.15

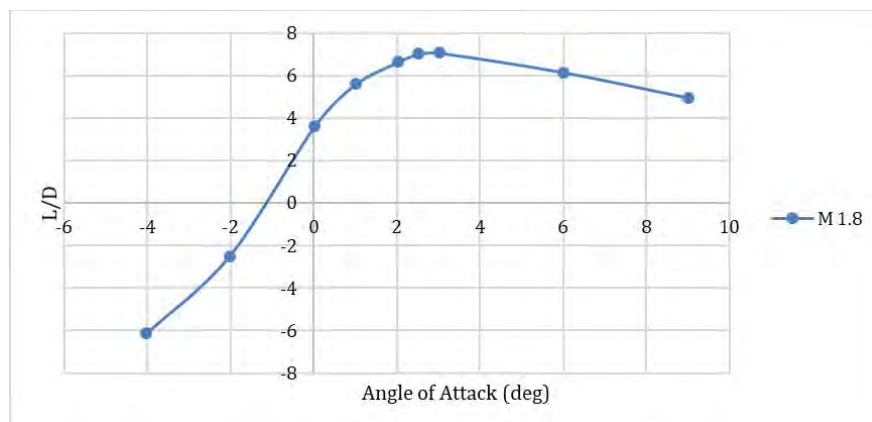


**Figure 65.** L/D versus Angle of Attack for GT Large SST at Mach 1.8. Peak L/D of 7.07 at 3 Degrees AoA.

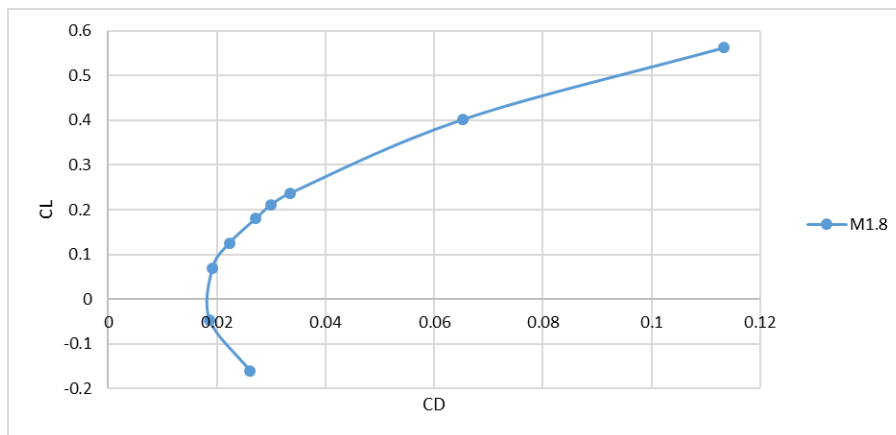


**Figure 66.** Drag Polar for GT Large SST at Mach 1.8.

**Landing and Takeoff Drag Polar Prediction**

The process for generating GT Large SST LTO drag polar is the same as that for the GT Medium SST. Same flight condition and workflow are used for GT Large SST. Figure 67 shows the spanwise locations and length of the TE flaps. Figure 68 shows the generated LTO drag polar of GT Large SST with different TE flap deflections.

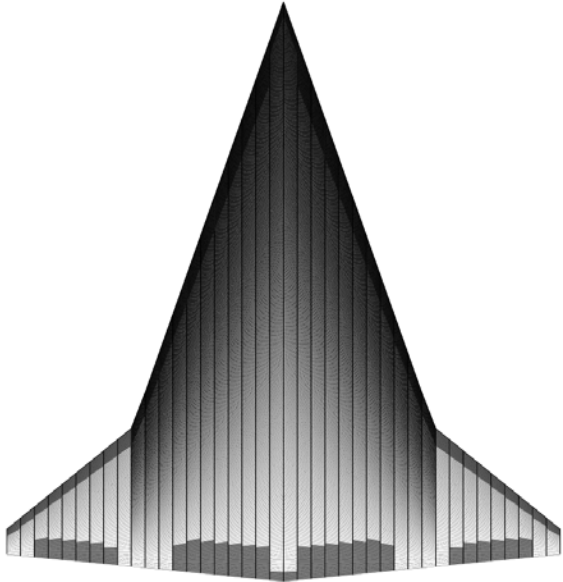


Figure 67. GT Large SST TE Flap Locations.

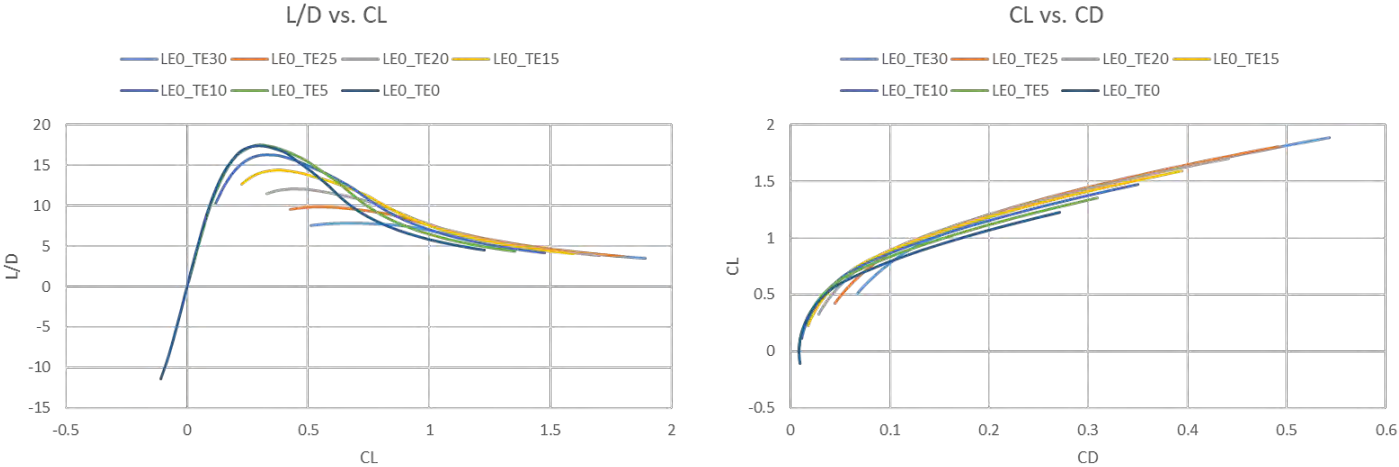


Figure 68. LTO Drag polar for GT Large SST.

**Design Mach Number Trade Study**

At the request of the FAA AEE office, additional technology trade studies are added to the work scope to examine design fuel burn, LTO NOx, and noise trends as a function of design Mach number for three classes of SST. As a result, six additional vehicles are expected to be modeled. The Mach number in red fonts in Table 34 lists these extra vehicle models.

**Table 34.** Design Mach Number Trade Study for Different Vehicle.

Notional SST	Baseline Design Mach Number	Possible Design Mach Number Range for Trades	Design Range (nm)	Design Payload (Number of Passengers)
NASA 55t STCA	1.4	1.4, 1.6, 1.8	4,000	8
GT Medium SST	2.2	1.8, 2.0, 2.2	4,500	55
GT Large SST	1.8	1.6, 1.8, 2.0	4,240	100

Considering the large computational time spent using inviscid CFD aero shaping as mentioned in the Aerodynamic Shaping section of the report, it is infeasible to apply the same workflow for the design of the six additional vehicles at different design Mach numbers. Therefore, a low-fidelity approach is proposed, and Figure 69 demonstrates the general workflow for the approach. For each baseline geometry (NASA 55t STCA, GT Medium SST, and GT Large SST), firstly, a set of uncalibrated drag polars generated from low-fidelity aero model and drag polars from high-fidelity CART3D CFD are used to create calibration functions to correct the low-fidelity drag polar to match the CFD data (details will be described later). Meanwhile, a design space is created by sweeping each baseline geometry design parameter. The design parameters used for the Mach number study are listed in Table 35. Design space sampling is done by using Latin Hypercube Sampling (LHS) to fill the design space. Design space constraints described for the GT Large SST are adjusted and applied here to filter out infeasible design and generate the design candidates for further study. Based on the design Mach number and its corresponding optimization criterion, calibrated drag polars for each design candidate are generated. The design criterion used in this study is a combination of both low-speed and high-speed performance. As shown below, the objective function for optimization is a weighted sum of 80% high-speed drag polar and 20% low-speed drag polar.

$$objective\ function = 0.8 * \left(\frac{L}{D}\right)_{high\ speed} + 0.2 * \left(\frac{L}{D}\right)_{low\ speed}$$

The high-speed drag polar is calculated at design Mach number to represent its cruise performance while the low-speed drag polar is calculated at Mach 0.25 to represent its low-speed performance. A weighted sum objective function can enforce the final optimum design to have good performance at both cruise and low speed. The configuration maximizing the objective function will be chosen as the optimum.

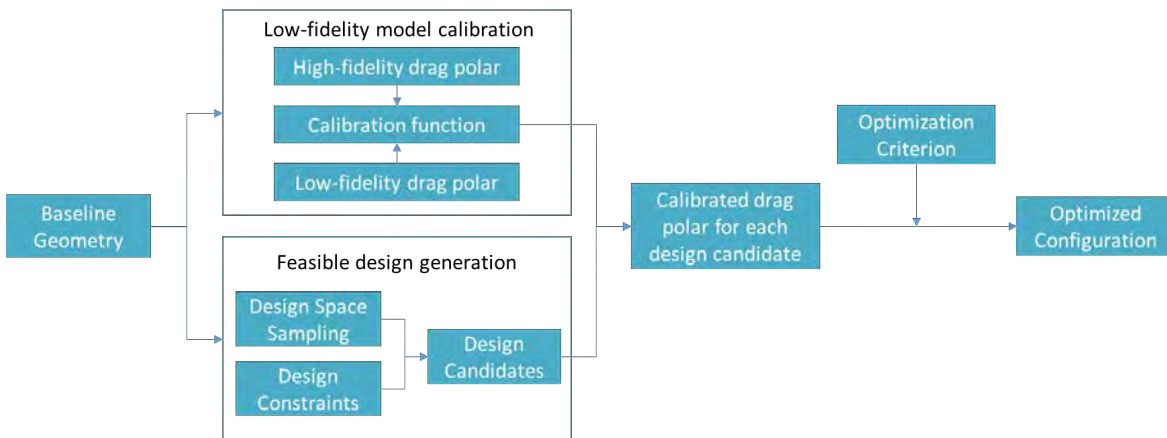


**Figure 69.** general workflow for low-fidelity design mach number trade study.

**Table 35.** Design parameters for optimization.

Design parameters	
Inboard sweep	Outboard dihedral
Outboard sweep	Inboard span
Inboard twist	Outboard span
Outboard twist	Mid chord
Inboard dihedral	

The baseline geometry is taken from vehicle design described in the former sections in this report. Figure 70 is a detailed description of calibration function calculation. Low-fidelity tools including AERO2S, WINDES, and OpenVSP are used to generate drag polars for all range of Mach numbers. Detailed function for each tool can be found in Figure 37. Calibration functions are calculated by fitting a non-linear model. Calibration only covers drag polar from Mach 0.88 to Mach 2.4. Low-speed drag polar and LTO drag polar have no calibration since there are no higher fidelity data to calibrate against.

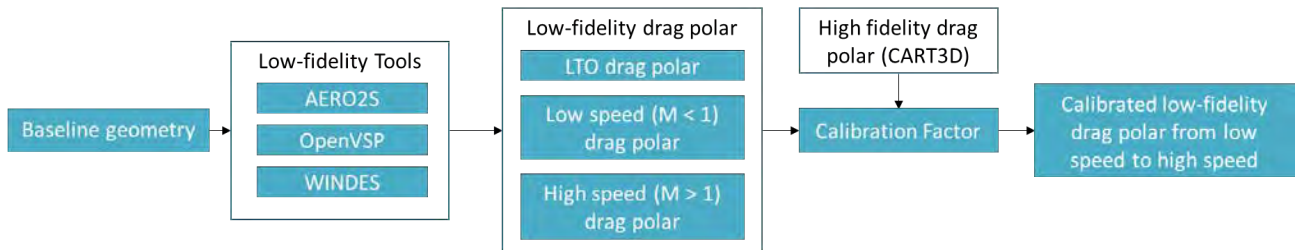


**Figure 70.** Detailed workflow for calibration factor generation.

The design candidates are selected by combining an LHS design space sampling and design constraint sampling. The number of survived design candidates vary from case to case as the design space is randomly filled. In this study, at least 100 cases for each design dimension are considered. Sections below are calibration and optimization results for each vehicle for its corresponding design Mach number.

**NASA 55t STCA**

The design Mach number study for the NASA 55t STCA is based on NASA-provided geometry definition and drag polar. Although NASA’s drag polar for STCA used similar low-fidelity tools as those depicted in Figure 37, differences are still observed which makes calibration a worthy exercise. Based on observations of the drag polar data and AFASST-generated data, a single calibration function is sufficient for calibrating supersonic drag polar. Low-speed drag polar (i.e., Mach < 1, excluding LTO drag polar) does not need calibration since their differences are negligible. Figure 71 depicts the calibration result for Mach 1.4 at 20,000 ft altitude.

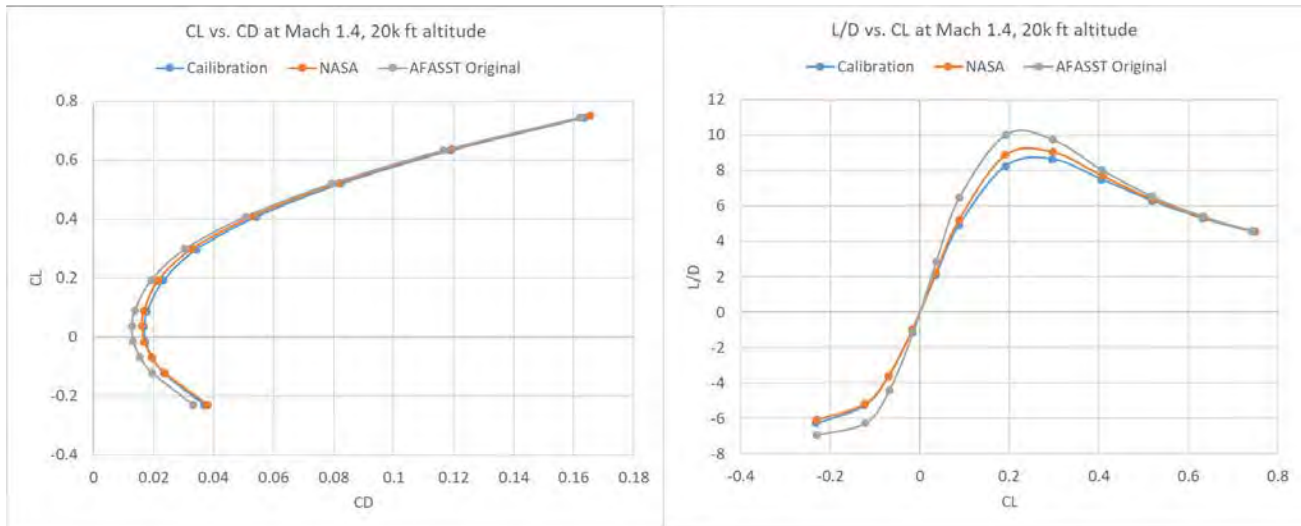


**Figure 71.** Calibration result for NASA 55t STCA.

As listed in Table 34, two additional business class configurations, one for Mach 1.6 and the other for Mach 1.8, are studied. However, since the exact optimization methodology is unknown, the original NASA 55t STCA designed for Mach 1.4 is also redesigned (using the same optimization philosophy) for consistency. Figure 72 shows the original NASA 55t STCA (subplot a), redesigned Mach 1.4 STCA (subplot b), Mach 1.6 design (subplot c), and Mach 1.8 design (subplot d).



Table 36 shows the resulting detailed design parameters for each configuration. Note that for the original NASA 55t STCA, the wing is divided into four sections; therefore, instead of having only two variables for inboard twist and outboard twist, four twist and dihedral angles are chosen as design parameters. Since there is only one kink location, sweep angles are kept as two design parameters—one inboard and one outboard. The optimization results show good consistency, meaning maximum L/D decreases as design Mach number increases as expected.

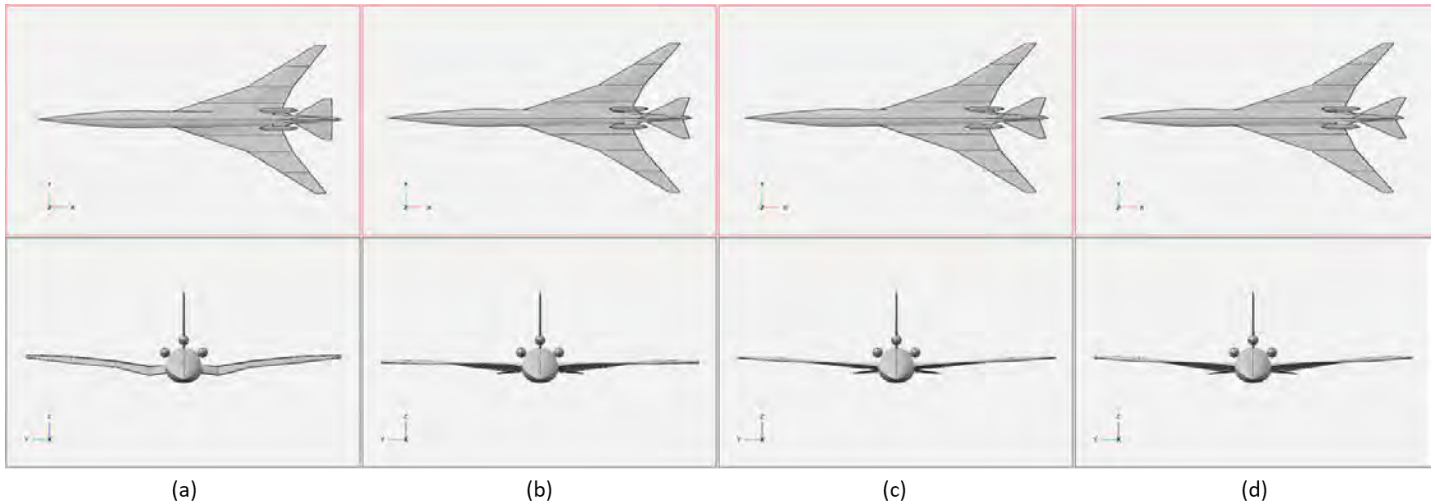


**Figure 72.** Geometry configurations for different design Mach number.

**Table 36.** Design Parameters for different re-design configurations.

Design Parameter	STCA@Mach 1.4	STCA@Mach 1.6	STCA@Mach 1.8
Inboard sweep	28	28	28
Outboard sweep	41	41	42
Section 1 twist	3	2	3
Section 2 twist	3	2	3
Section 3 twist	-3	-2	-3
Section 4 twist	-3	-2	-3
Section 1 dihedral	2	2	2
Section 2 dihedral	0	2	2
Section 3 dihedral	0	2	2
Section 4 dihedral	0	2	2
Horizontal tail sweep	65	65	67
Maximum L/D	9.37	9.03	8.36

### GT Medium SST

For GT Medium SST and GT Large SST, some of the assumptions used in the NASA 55t STCA optimization no longer hold. During the calibration process, contrary to single calibration function for the whole supersonic Mach number regime, calibration factors fitted for GT Medium SST and GT Large SST can only be used for one single Mach number. Moreover, for NASA 55t STCA optimization, calibration is not required for Mach < 1; for GT Medium SST and GT Large SST, drag polar with Mach number greater than 0.8 needs to be calibrated. One potential reason could be that for the NASA 55t STCA, the calibration is performed using two low-fidelity tools that share the same physics and similar logic. For the GT Medium SST and GT Large SST, calibration is based on high-fidelity CFD data (i.e., CART3D with viscous correction). The differences between the theories used in low-fidelity and high-fidelity tools make it difficult to have one single calibration function to cover the entire Mach range. Therefore, multiple sets of calibration factors have been developed and currently the model has

the capability to predict aerodynamic coefficients from Mach 0.88 to 2.4. Also, both GT Medium SST and GT Large SST have only two wing sections, i.e., inboard and outboard; therefore, the number of design parameters are reduced.

Figure 73 shows one single example for the calibration factor developed for GT Medium SST. Good approximation has been achieved through a linear calibration function. Note that poor calibration performance is observed at negative AoA, a region the mission analysis will not be exploring.

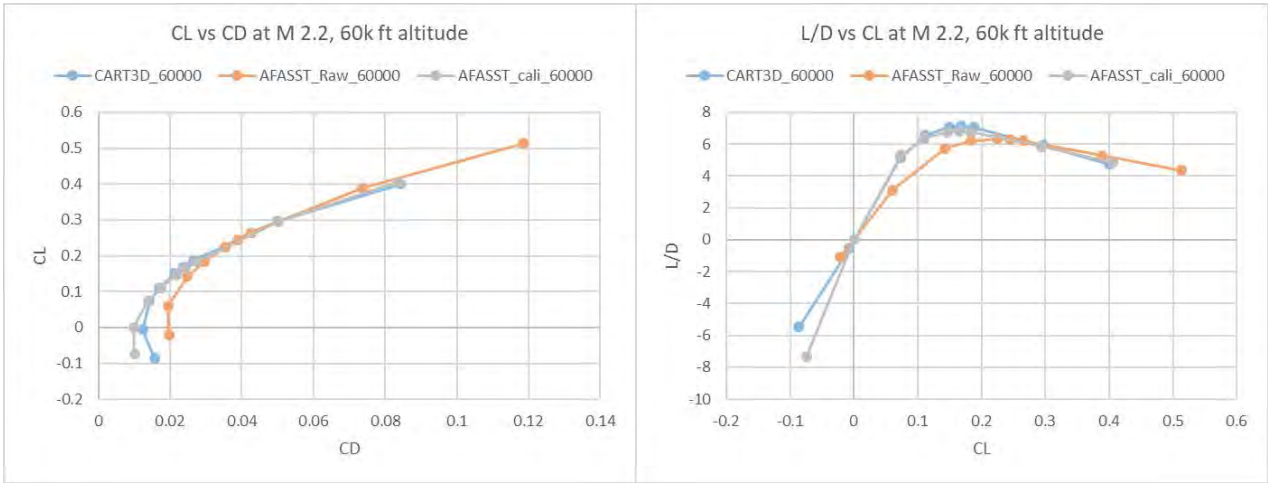


**Figure 73.** Calibration Results for GT Medium SST.

Figure 74 shows the optimization result for the GT Medium SST. Similar to the optimization process for the NASA 55t STCA, geometry optimization has been applied for both design point and the other two trade study design Mach numbers for consistency consideration. Four subplots in Figure 74 represents the original configuration at design point Mach 2.2 (subplot a), optimized configuration at design Mach number (subplot b), additional configurations for trade study design Mach number Mach 1.8 (subplot c) and Mach 2.0 (subplot d). Table 37 lists the values for the optimized design parameters for comparison. The optimization is done by manually sweeping design variables around the baseline value and seeking to improve the maximum L/D.

**Table 37.** Design Parameters for Different Re-design Medium SST Configurations.

Design Parameter	GT Medium SST Redesign@Mach 2.2	GT Medium SST Redesign@Mach 2.0	GT Medium SST Redesign@Mach 1.8
Inboard sweep	71	72	71
Outboard sweep	64	62	64
Inboard twist	3	4	4
Outboard twist	-3	-3	-3
Inboard dihedral	2	2	2
Outboard dihedral	-5	-5	-5
Maximum L/D	7.39	7.55	7.71

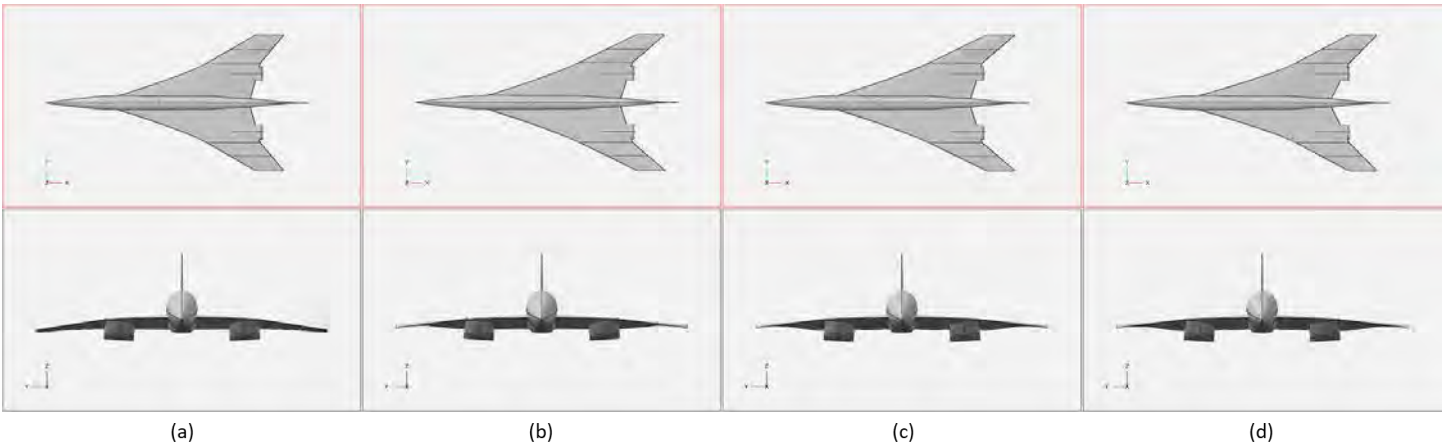


**Figure 74.** Geometry Configurations for Different Design Mach Numbers for Medium SST.

Meanwhile, LTO drag polar has been generated for the three redesign configurations. The process for generation is exactly the same as formerly described in an earlier section. Figure 75 shows LTO drag polars of different TE flap settings for each redesign configurations.

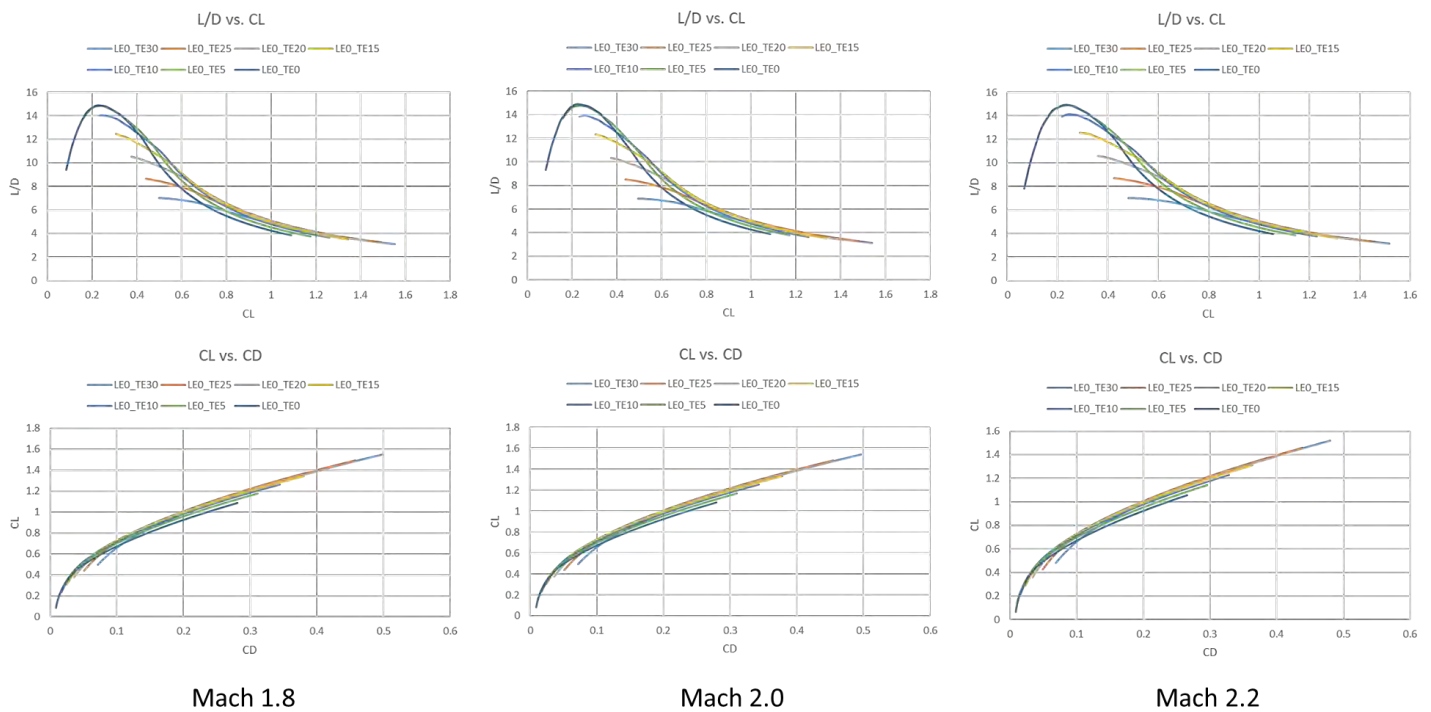


**Figure 75.** Comparison of LTO Drag Polar for Redesign Medium SST Configurations.

**GT Large SST**

Recalling that the calibration for the GT Large SST shares the same process as for the GT Medium SST, Figure 76 shows the calibration results for GT Large SST at Mach 1.8 and 55,000 ft altitude. Good approximation has been achieved at positive AoA.

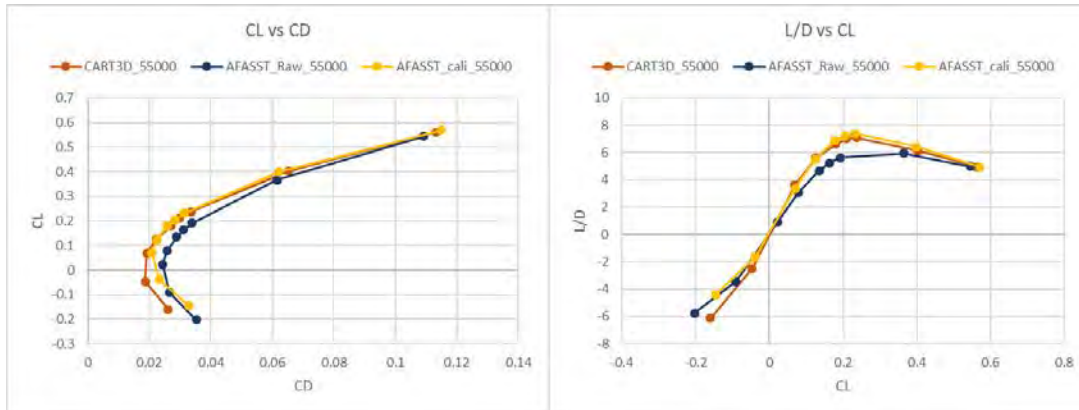


**Figure 76.** Calibration result for GT Large SST (Preliminary Results).

Similar optimization procedures as for the GT Medium SST are applied to the GT Large SST for design Mach numbers 1.6 and 2.0. Figure 77 depicts the optimization results. Subplots from left to right corresponds to original configuration design for Mach 1.8, optimized configuration for Mach 1.8, optimized configuration for Mach 1.6, and optimized configuration for Mach 2.0. Table 38 lists the detailed optimized design parameter values for these configurations for comparison. Similarly, LTO drag polars shown in Figure 78 have been generated for these three redesign configurations. The process for generation is exactly the same as described for the GT Medium SST. *Note that these results are very preliminary since the baseline design has not been frozen.*

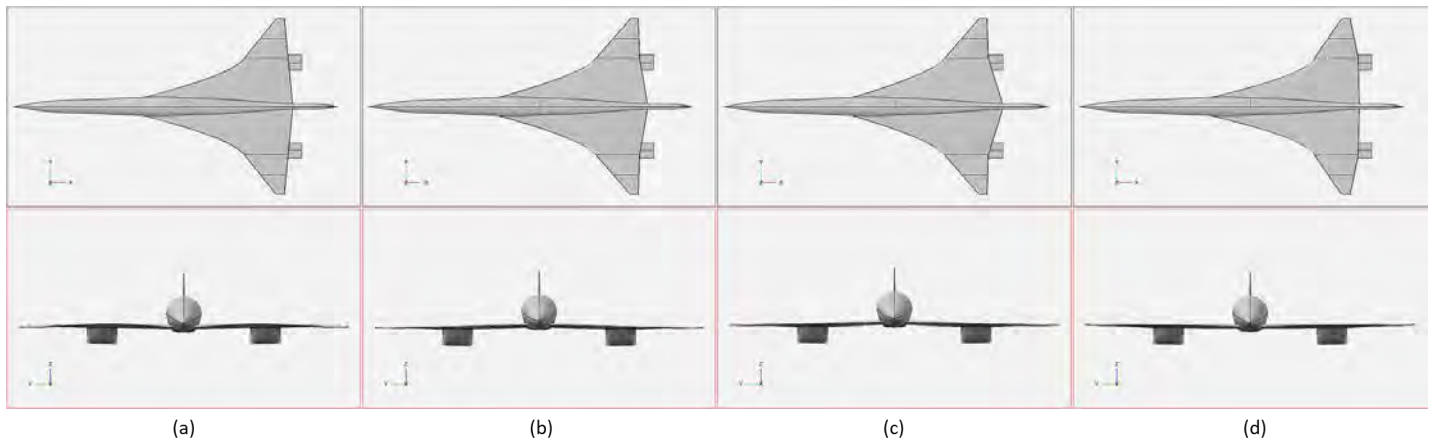


**Figure 77.** Preliminary Geometry Configurations for different Mach numbers (Preliminary Results).

**Table 38.** Design parameters for different preliminary re-design configurations (Preliminary Results).

Design Parameter	GT Large SST Redesign@Mach 1.8	GT Large SST Redesign@Mach 1.6	GT Large SST Redesign@Mach 2.0
Inboard sweep	70	69	71
Outboard sweep	41	41	35
Inboard twist	2	2	2
Outboard twist	-3	-3	-3
Inboard dihedral	-1	-1	1
Outboard dihedral	-1	-1	0
Maximum L/D	8.03	9.52	7.95

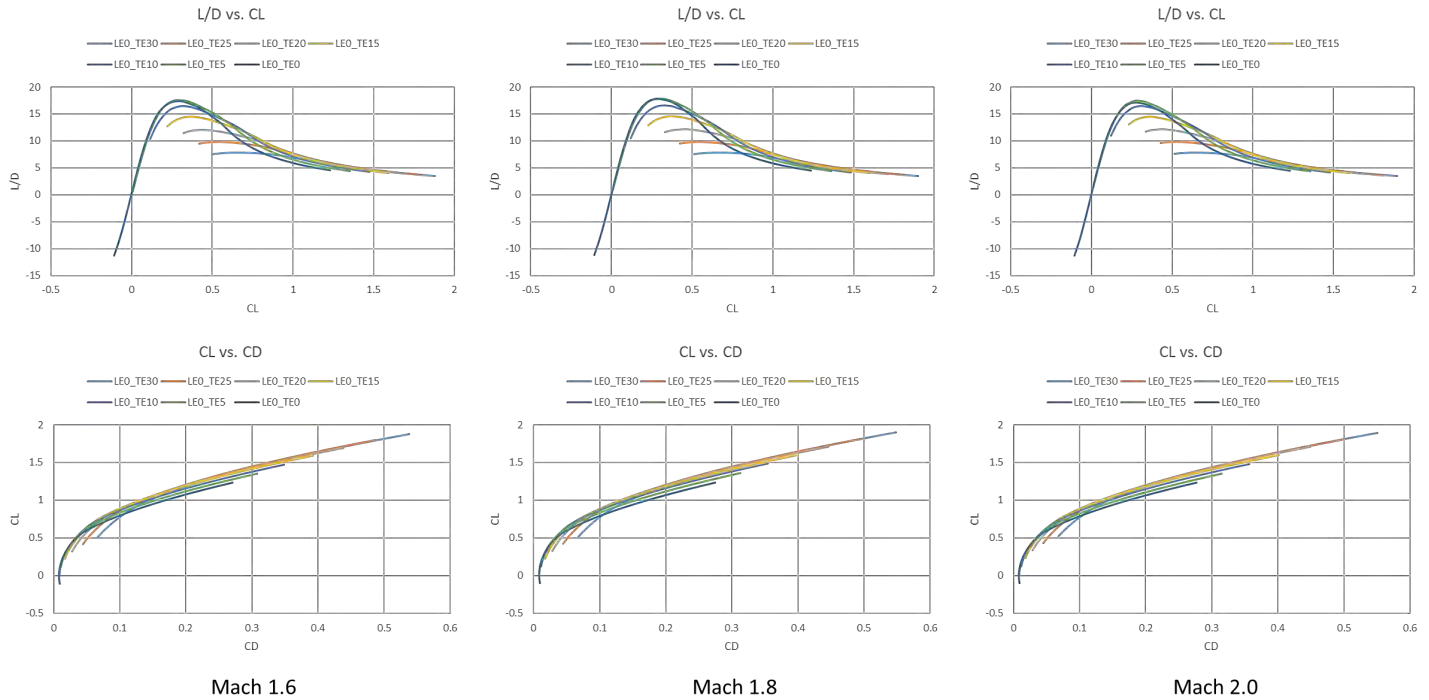


Figure 78: Comparison of LTO Drag Polar for Redesign Large SST Configurations (Preliminary Results).

## Task 5 – AEDT BADA4 Coefficient Generator

### Objective

This Task's objective is to investigate the representation of SST aircraft generated using EDS in AEDT. Aerodynamics and propulsion coefficients of the BADA4 method (which is adopted in AEDT for subsonic aircraft) are to be generated using data fitting techniques for SST aircraft. Recommendations are to be provided on whether the BADA4 method is sufficient to capture SST aircraft performance.

### Research Approach

The Georgia Tech team makes a distinction between the aerodynamics and propulsion coefficients of the BADA4 method due to the different BADA4 equation forms and the different underlying physics. These differences are assumed to necessitate the need for different regression techniques. Within aerodynamics, drag coefficients for clean and non-clean configurations are investigated. Alternatively, for propulsion, thrust and fuel flow coefficients for the idle and non-idle settings are investigated.

### Aerodynamic Coefficient Generation

The main BADA4 equations for aerodynamics are those for clean and non-clean drag coefficients as reported in the BADA4 user manual published by EUROCONTROL. For the clean configuration, the drag coefficient is represented in equations 3.2-3 to 3.2-6 of the manual, as shown in Figure 79.

For the non-clean configuration, the drag coefficient is represented in equation 3.2-8 of the manual, as shown in Figure 80.



$$C_D = \text{scalar} \cdot [C_0 + (C_2 \cdot C_L^2) + (C_6 \cdot C_L^6)] \quad (3.2-3)$$

With:

$$C_0 = d_1 + \frac{d_2}{(1-M^2)^2} + \frac{d_3}{(1-M^2)} + \frac{d_4}{(1-M^2)^3} + \frac{d_5}{(1-M^2)^5} \quad (3.2-4)$$

$$C_2 = d_6 + \frac{d_7}{(1-M^2)^2} + \frac{d_8}{(1-M^2)^3} + \frac{d_9}{(1-M^2)^4} + \frac{d_{10}}{(1-M^2)^5} \quad (3.2-5)$$

$$C_6 = d_{11} + \frac{d_{12}}{(1-M^2)^7} + \frac{d_{13}}{(1-M^2)^{15}} + \frac{d_{14}}{(1-M^2)^8} + \frac{d_{15}}{(1-M^2)^{17}} \quad (3.2-6)$$

Where:

- scalar is a scaling factor [-]
- $C_L$  is the lift coefficient [-]
- $M$  is the Mach number [-]
- $d_1$  to  $d_{15}$  are clean drag coefficients [-], from the DPM

Figure 79. BADA4 Equation for Clean Drag Coefficient.

$$C_D = d_{1,\delta_{HL},\delta_{LG}} + d_{2,\delta_{HL},\delta_{LG}} \cdot C_L + d_{3,\delta_{HL},\delta_{LG}} \cdot C_L^2 \quad (3.2-8)$$

Where:

- $C_L$  is the lift coefficient [-]
- $\delta_{HL}$  is the position of the high-lift devices [-], see section 3.2.1
- $\delta_{LG}$  is the position of the landing gear [-], see section 3.2.1
- $d_{1,\delta_{HL},\delta_{LG}}$  to  $d_{3,\delta_{HL},\delta_{LG}}$  are non-clean drag coefficients [-], from the AFCM

Figure 80. BADA4 Equation for Non-clean Drag Coefficient.

Data fitting for aerodynamics followed a general procedure:

1. Utilize drag datasets for representative *subsonic* aircraft first to analyze if fitting issues exist. Two vehicle classes are selected: the large single aisle (150pax) and the small twin aisle (210pax).
2. Experiment with a subset of aerodynamic data for the *SST* aircraft. If no generalized model results in a good fit for the original form of the BADA4 equations, derive alternate forms for the BADA4 equations.

By examining the BADA4 equation for clean drag, the Georgia Tech researchers immediately recognized that the current formulation is not suitable for the supersonic regime since the denominator values for multiple terms in the equation would result in complex numbers for Mach numbers greater than one. Different alternate formulations listed below are tested:

1. **Method 1.** Using the same formulation but considering only the real portion of complex numbers when Mach > 1. This method results in one set of coefficients for all flight regimes and cruising altitudes.
2. **Method 2.** Using a slightly different formulation by implementing an "IF" statement: If Mach > 1, the denominators of terms with a square root power would have their base changed to  $M^2-1$  instead of  $1-M^2$  (this applies to terms with coefficients  $d_2$ ,  $d_4$ ,  $d_7$ ,  $d_9$ ,  $d_{13}$ , and  $d_{15}$ ). This method also results in one set of coefficients for all flight regimes and cruising altitudes.
3. **Method 3.** Using a slightly different formulation by setting the coefficients of terms with denominators that include a square root power to zero (i.e.,  $d_2=d_4=d_7=d_9=d_{13}=d_{15}=0$ ). This method also results in one set of coefficients for all flight regimes and cruising altitudes.
4. **Method 4.** Using two different formulations for the two different flight regimes, subsonic and supersonic. For the subsonic regime, use the BADA4 formulation as-is with no changes. For the supersonic regime, set the bases of all terms with a denominator to  $M^2-1$  instead of  $1-M^2$  (this applies to terms with coefficients  $d_2$ ,  $d_3$ ,  $d_4$ ,  $d_5$ ,  $d_7$ ,  $d_8$ ,  $d_9$ ,  $d_{10}$ ,  $d_{12}$ ,  $d_{13}$ ,  $d_{14}$ , and  $d_{15}$ ). This method results in two sets of coefficients for each flight regime.



For all these methods, the scalar term of the BADA4 formulation (in equation 3.2-3) is not included in any of the fits since it is a constant term applied to all the coefficients. This decision is made in order to convert the optimization problem to a linear regression problem with a closed form solution.

Results for Methods 1, 2, and 3 are shown in Figure 81. These methods clearly do not result in good fits. By generating two sets of coefficients, however, Method 4 results in a much better fit, and these results are shown in Figure 82. Based on these results, Method 4 is chosen for all subsequent data fitting efforts. (Note: for subsonic aircraft, Method 4 is just the original BADA4 formulation.)

Given the results of Method 4, an attempt to reduce the number of coefficients utilized to achieve a good regression fit is examined. As shown in Figure 83, this attempt resulted in poorer fits (i.e., higher residuals) and therefore, all coefficients are considered in subsequent data fitting efforts.

### **Aerodynamic Data Fitting Results**

#### Clean Drag Data Fitting for Subsonic Aircraft

Drag datasets generated using FLOPS for the two EDS models, 150pax and the 210pax vehicles, are used for fitting. Values or drag coefficients are solved for using a regression model that minimized the root mean square error (RMSE) between the predicted BADA4 values and the actual EDS values. Results are shown in Figure 84 and Figure 85. The results show that a good generalized fit for all altitudes simultaneously could not be achieved.

#### Non-clean Drag Data Fitting for Subsonic Aircraft

Unlike clean drag, non-clean drag fits are of good accuracy, since a separate fit is required for each flap setting. As shown in Figure 86 and Figure 87, good accuracy polynomial fits are achieved for the drag polar data for multiple flap settings. (Note: for the 210pax vehicle, fitting is limited to the convex portion of the drag polar.)

#### Clean Drag Data Fitting for SST Aircraft

Drag datasets for the Georgia Tech 55pax Medium SST are used for fitting considering two flight regimes. Results are shown in Figure 88. Similar to the subsonic aircraft, no good generalized fit for all altitudes and Mach regimes could be achieved for the SST aircraft.

#### Non-clean Drag Data Fitting for SST Aircraft

Similar to the non-clean drag fits of the subsonic aircraft, good accuracy is achieved for the non-clean drag fits of the SST aircraft. Results are shown in Figure 89.

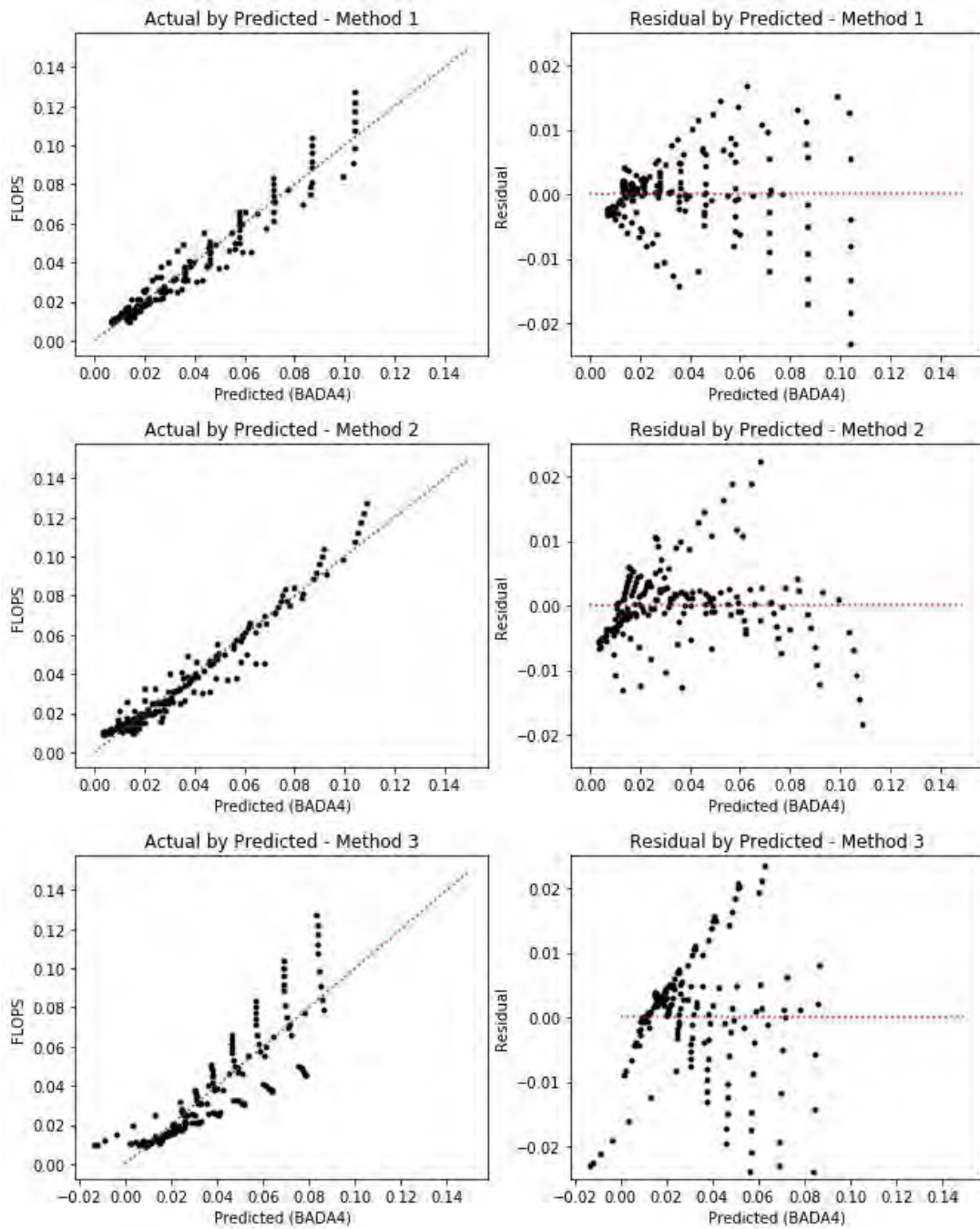


Figure 81. Actual versus Predicted and Residual vs. Predicted Plots for Methods 1, 2, and 3.

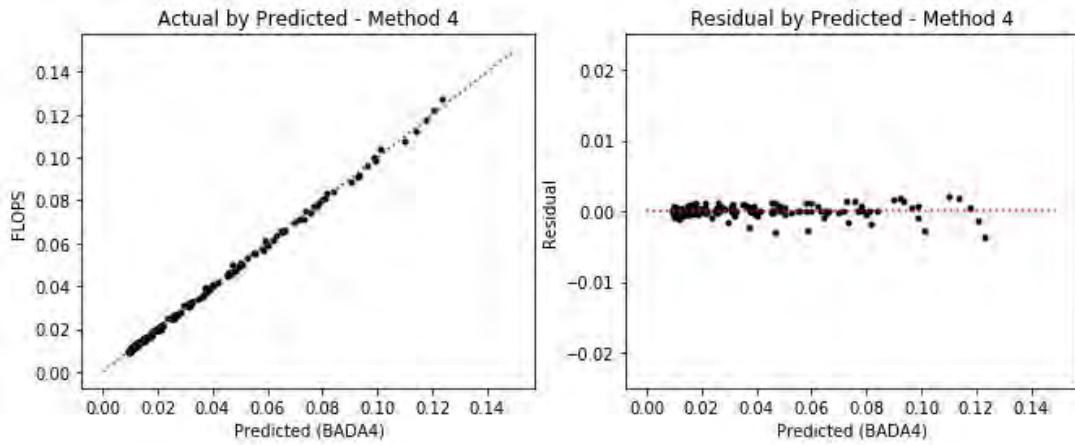


Figure 82. Actual versus Predicted and Residual vs. Predicted Plots for Method 4.

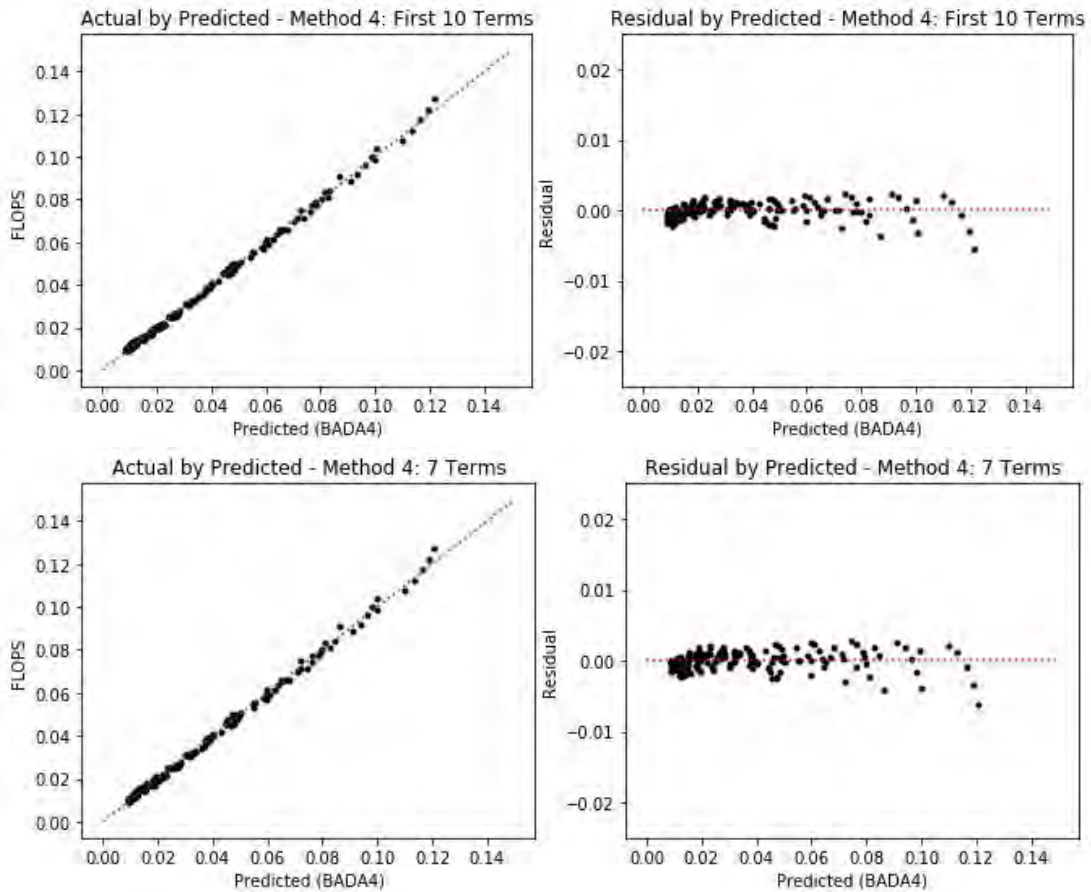


Figure 83. Actual versus Predicted and Residual versus Predicted Plots for Method 4 with Reduced Number of Coefficients.

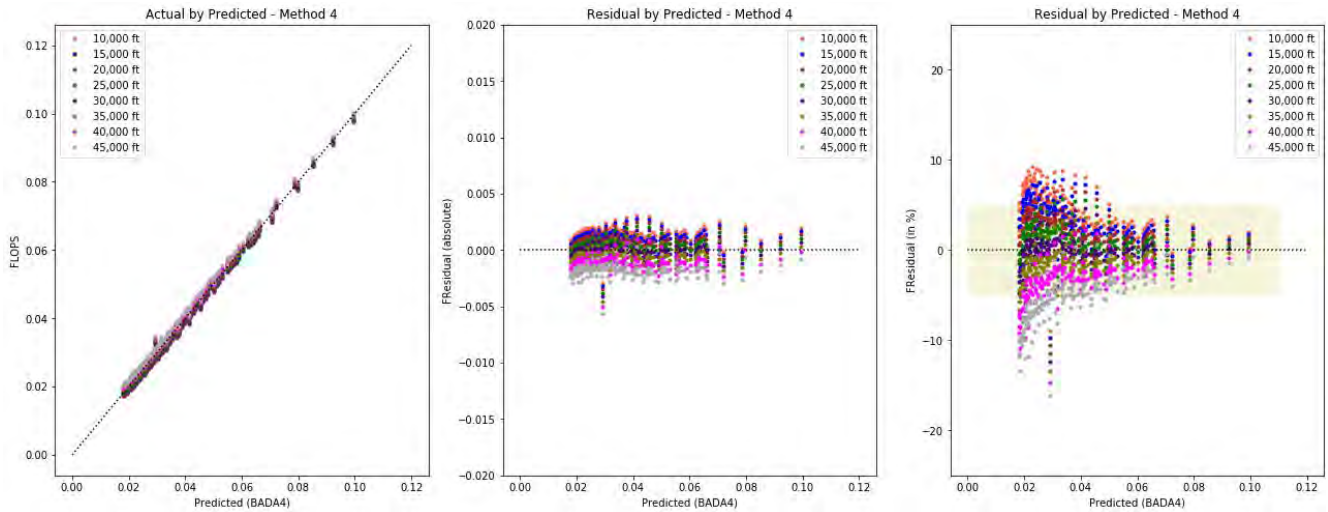


Figure 84. Clean Drag Data Fitting Results for the 150pax Vehicle.

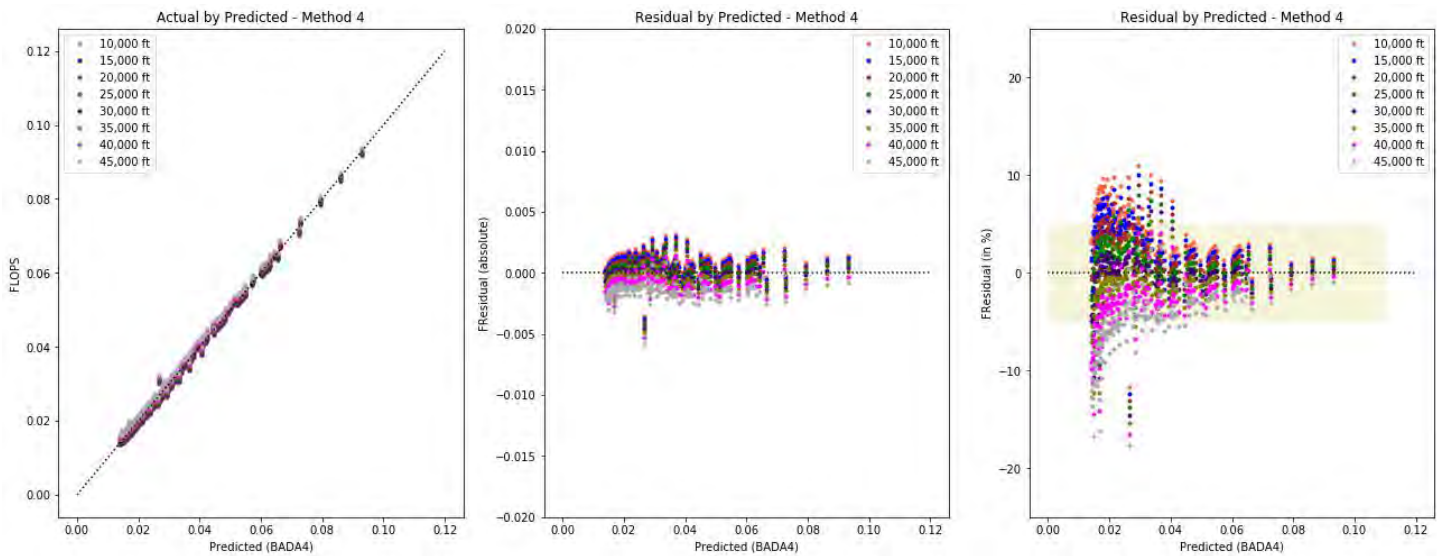
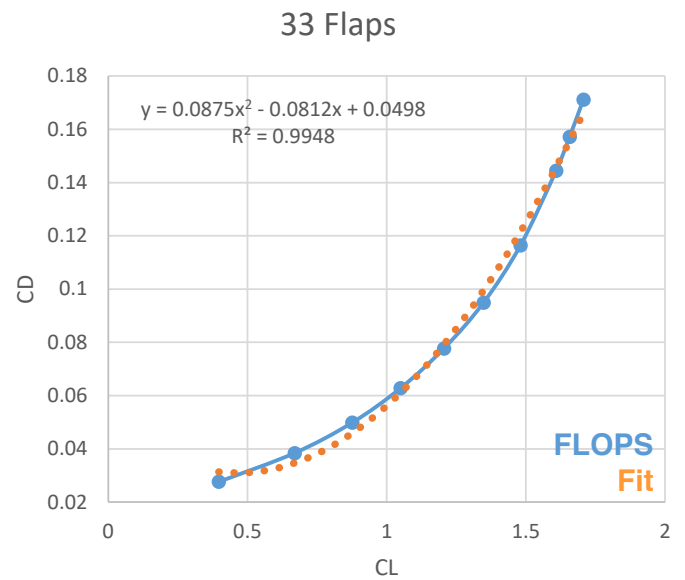
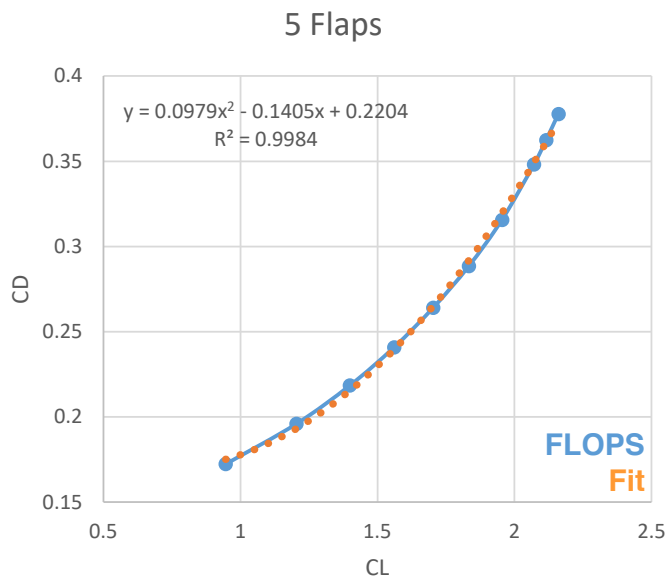
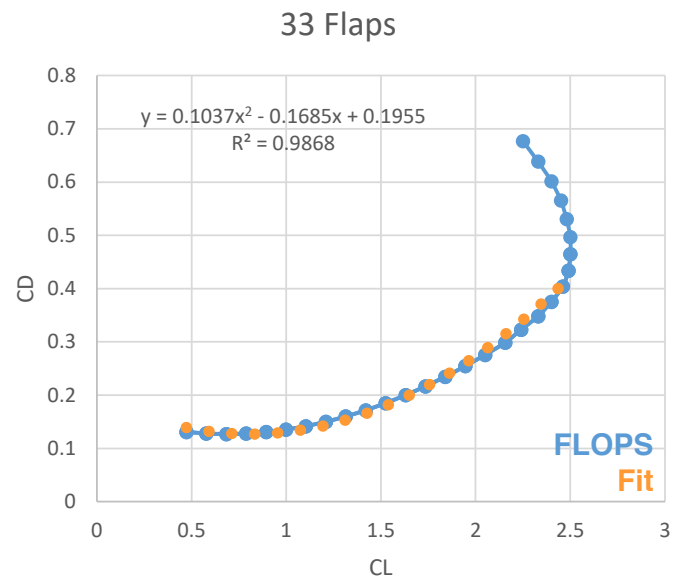
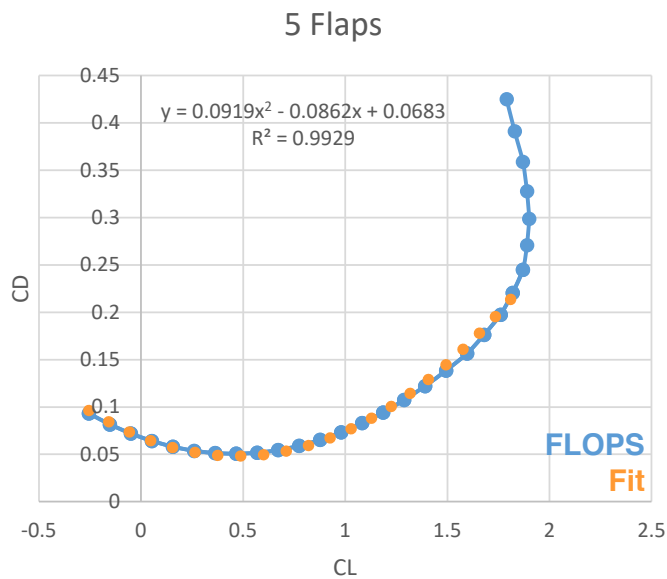


Figure 85. Clean Drag Data Fitting Results for the 210pax Vehicle.



**Figure 86.** Non-clean Drag Data Fitting Results for the 150pax Vehicle.



**Figure 87.** Non-clean Drag Data Fitting Results for the 210pax Vehicle.

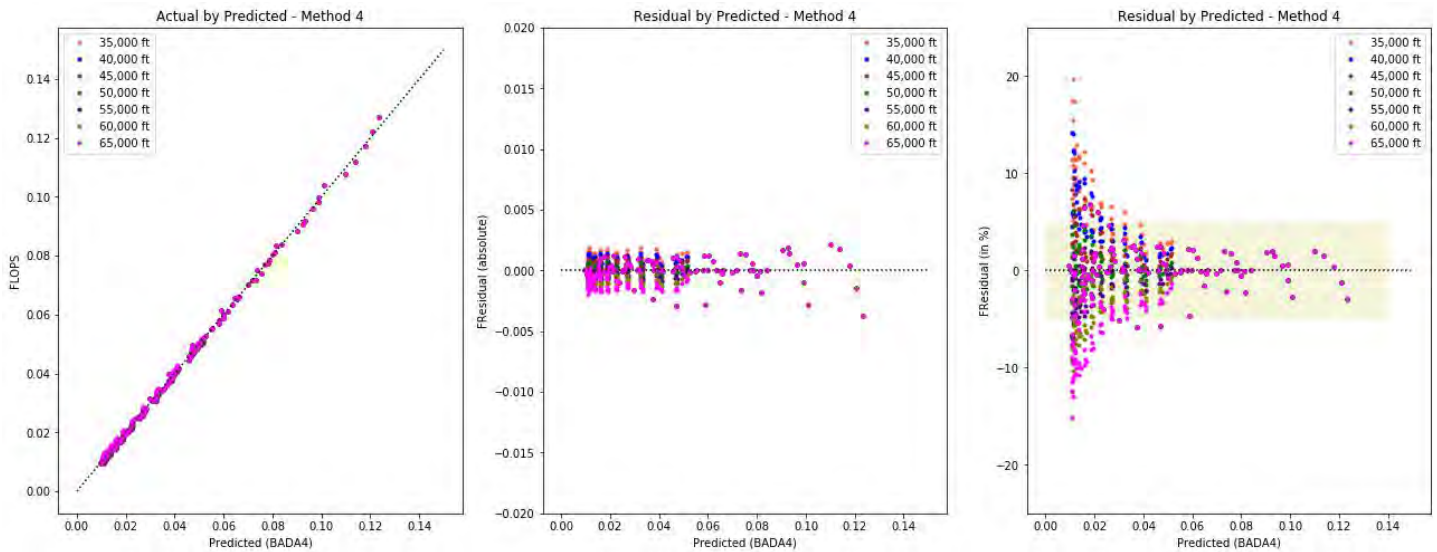


Figure 88. Clean Drag Data Fitting Results for the SST Aircraft.

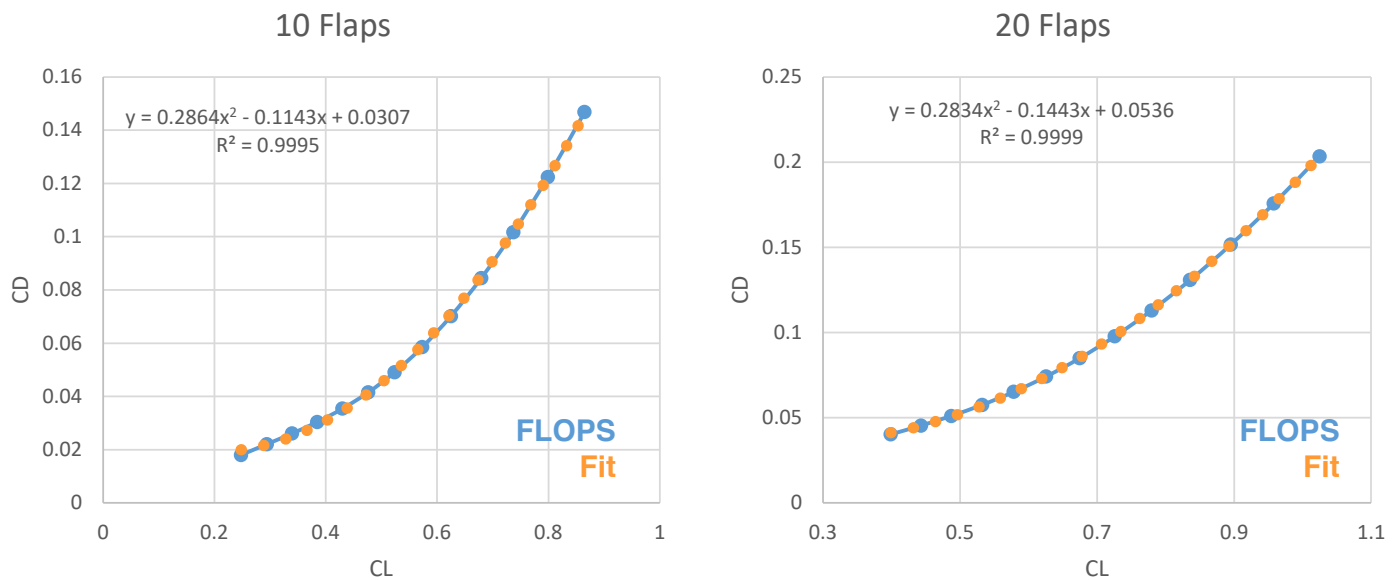


Figure 89. Non-clean Drag Data Fitting Results for the SST Aircraft.

### Aerodynamic Recommendations

Based on the aforementioned results, it is clear that the current BADA4 method and its alternate formulations fail to accurately fit the clean drag data at the different flying regimes and cruising altitudes for both the subsonic and supersonic aircraft. Alternatively, data fits for the non-clean drag data are very accurate since they follow the underlying physics of the problem and are localized to specific control surface and gear settings. An attempt to locally fit clean drag data in a similar manner is examined, and a second degree polynomial model seems to provide sufficiently accurate fits for specific altitude and cruise Mach combinations. Sample results for the supersonic aircraft are shown in Figure 90. Hence, within AEDT, it is recommended to have such fits for a representative set of combinations and to implement in an interpolation procedure for all other combinations.



## **Propulsion**

### BADA4 Propulsion Objective

The main purpose of this study is to develop a regression approach to obtain coefficients idle, non-idle thrust, and fuel consumption of the various engines with standard and non-standard day. The initial approach is to determine if the functional form of BADA4 could represent the subsonic fleet and then apply a similar methodology to a supersonic aircraft if possible. If BADA4 is not sufficient to model an SST, recommendations would be provided to the FAA on how to simulate the performance within AEDT.

### Summary of Proposed Methodology

To prepare a regression model, the original BADA4 equations are used as the starting point for modeling the Notional B737-800 CFM56-7B and notional B767-300 GT-CF6-80C2B5F thrust and fuel consumption. Engine decks of these aircraft are extracted from EDS (NPSS engine model). To solve for the relevant coefficients, Excel Solver GRG (Generalized Reduced Gradient) Nonlinear Solving function is used. At best, the GRG Solving method alone can find a locally optimal solution to a reasonably well-scaled, non-convex model. After extracting the engine decks, data is divided according to rating structure such as MTKF (Max takeoff) < Mach 0.4 and MCMB (Max Climb)  $\geq$  Mach 0.4. A solver tool is created by leveraging the Excel Solver GRG Nonlinear Solving function to fit various BADA4 ratings for subsonic fuel flow and thrust. Then, error is compared between fit and engine deck data.

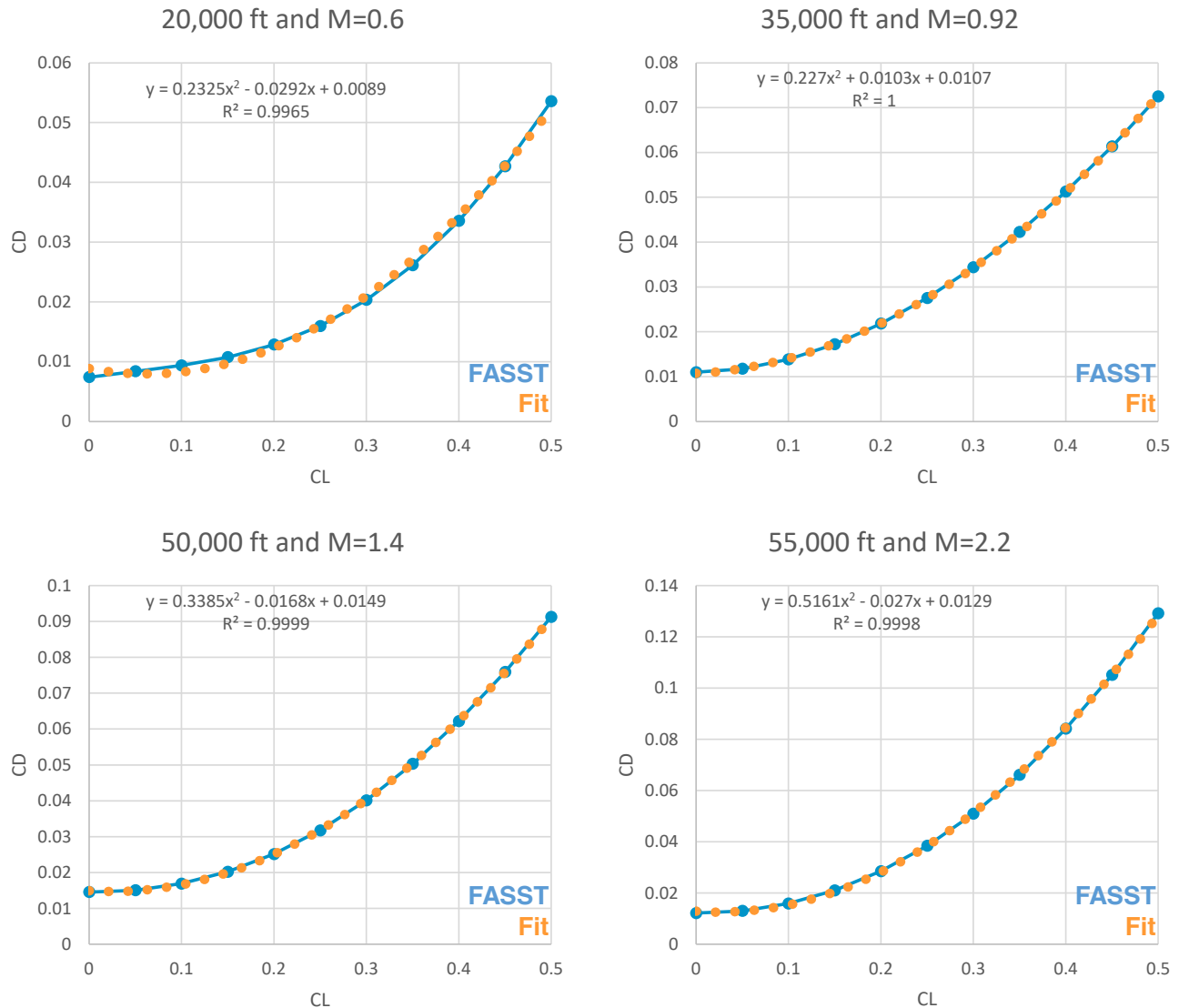


Figure 90. Polynomial Fits for Clean Drag Data for Individual Altitude and Cruise Mach Combinations.

Tool Introduction

To observe the model’s limitations, relative error and sum squares of the relative error are calculated, and Excel Solver function is used to minimize the error between fit and engine data. Detailed methodologies for each regression are summarized via flow chart diagrams, and an example is depicted in Figure 91.

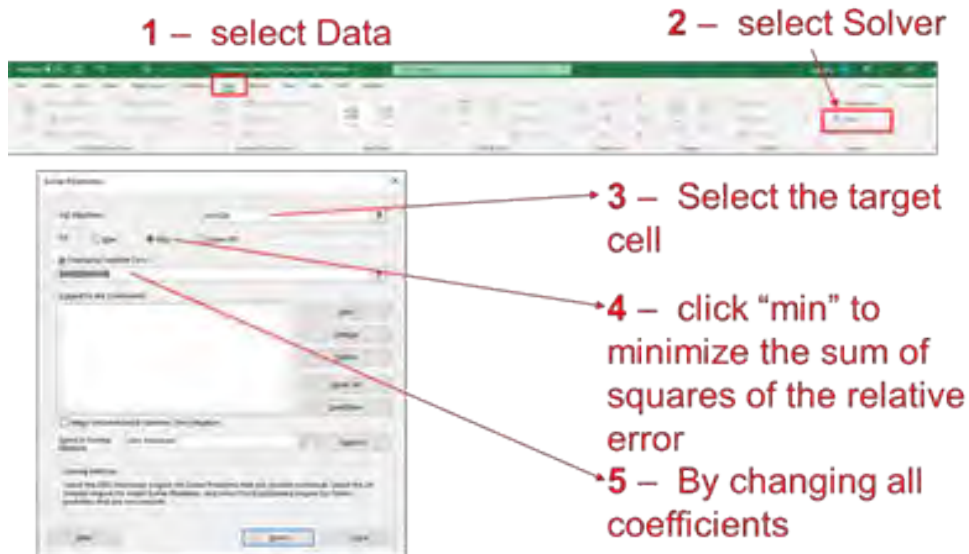


Figure 91. Excel Tool Introduction.

Process Flow for the Regressions

Within this section, engine thrust and fuel consumption models are studied. Models can be itemized as following:

- 1) Idle thrust
- 2) Non-idle thrust
- 3) Idle fuel consumption
- 4) Non-idle fuel consumption

Initially, the BADA4 equations are used without modifications to predict notional B737 and B747 aircraft engine thrust and fuel consumption. The BADA4 model provides three separate thrust models as part of the Propulsive Forces Model (PFM), depending on the type of engine:

- turbofan: TurboFan Model (TFM)
- turboprop: TurboProp Model (TPM)
- piston: Piston Engine Model (PEM)

Each model includes the contribution from all engines and provides the thrust as a function of airspeed, throttle setting, and atmospheric conditions. The general formulation of the thrust force,  $Th$  [N], is:

$$Th = \delta \cdot W_{ref} C_T f(n) = g(n) + h(n) \tag{30}$$

Where:

- $\delta$  is the pressure ratio [-]
- $m_{ref}$  is the reference mass [kg], from the PFM
- $W_{ref}$  is the weight force at  $m_{ref}$  [N]
- $C_T$  is the thrust coefficient [-]

Due to selected notional aircraft, the turbofan model will be leveraged for this study. A turbofan engine may be operated either by direct control of the throttle or through the use of predefined settings called ratings. The following ratings are modelled for turbofan engines: low idle thrust (LIDL), maximum climb thrust (MCMB), maximum cruise thrust (MCRZ) and maximum takeoff thrust (MTKF). The MCMB, MCRZ, and MTKF ratings have their own respective set of coefficients but share the same formulas, whereas the LIDL rating is modelled by different formulas, as detailed in the following subsections.

### Idle Rating Thrust

The idle rating model for the turbofan engine model directly provides the thrust coefficient  $C_T$  as a function of the Mach number and the atmospheric conditions. Mach, Altitude, and Thrust data are extracted from engine deck, which is an output of NPSS. Related data is selected by filtering the power code equal to 20 for idle rating. Weight assumption is made based on the selected notional aircraft. Then, thrust is calculated by using NPSS data output with Eq. (31). Twelve random equations are assigned to calculate  $C_T$ :

$$C_T = ti_1\delta^{-1} + ti_2 + ti_3 + ti_4\delta^2 + (ti_5\delta^{-1} + ti_6 + ti_7\delta + ti_8\delta^2)M + (ti_9\delta^{-1} + ti_{10} + ti_{11}\delta + ti_{12}\delta^2)M^2 \quad (31)$$

$C_T$  also can be calculated by Eq. (27) since  $\delta$ , weight, and thrust are known from the engine deck. Therefore, coefficients can be generated by using Excel Solver since the thrust coefficient is known. Coefficients ( $ti$ ) are iterated by the solver to minimize the sum of squares of the relative error between calculated and predicted  $C_T$ . This process is described in Figure 92.

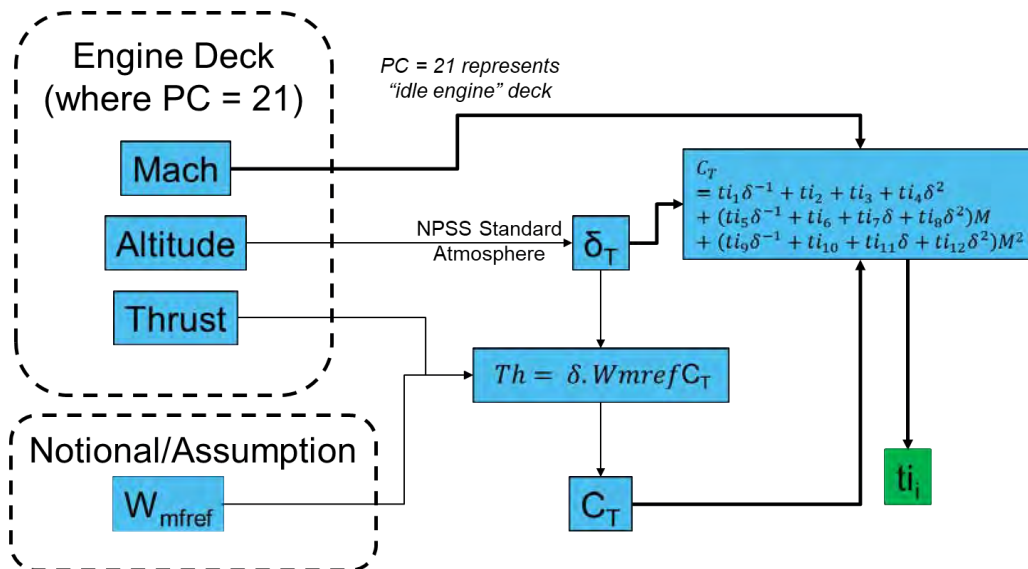


Figure 92. Idle Thrust Prediction Flow Chart.

Results using the original BADA4 equations are shown in Figure 93. The areas highlighted with black circles show that BADA4 equations result in +/- 6% error. The highest error is observed near the border between the MCMB/MTKF ratings.

To reduce the initial error, the engine deck and fits are split into low versus high Mach number, as shown in Figure 94. Splitting the fits at the Mach = 0.4 line does help the fits in that area. Furthermore, to reduce the error, total pressure is used in the  $C_T$  equation instead of static pressure. Results with total pressure are shown in Figure 95.

Using total pressure instead of static pressure does improve the high-altitude fits. A fourth order term is added to the BADA4 equations to obtain better results. Results are plotted for second order terms, fourth order terms, and total and static properties in Figure 96.

### Non-idle Thrust Ratings (MCMB, MCRZ, MTKF)

The generalized thrust form for the turbofan engine model provides  $C_T$  as a function of the Mach number  $M$  and the throttle parameter  $\delta_T$ .  $C_T$  is calculated as a fifth order polynomial of  $\delta_T$  with coefficients that are fifth order polynomials of  $M$ :

$$\delta_T = (C_{T,actual} - a_1 + a_2M + a_3M^2 + a_4M^3 + a_5M^4 + a_5M^5)/(a_7 + a_8M + a_9M^2 + a_{10}M^3 + a_{11}M^4 + a_{12}M^5) \quad (32)$$

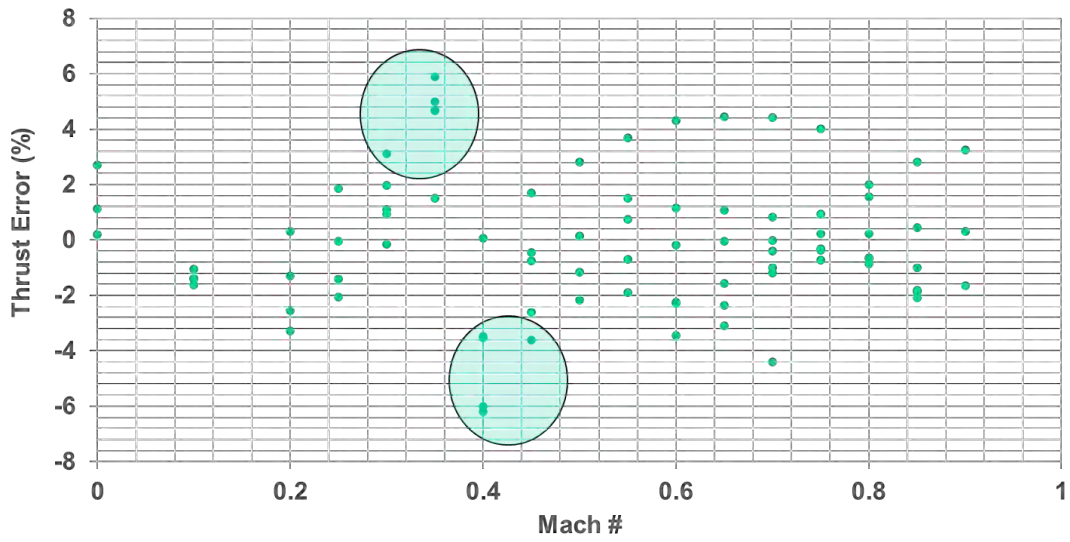


Figure 93. Results Using BADA4 Equations.

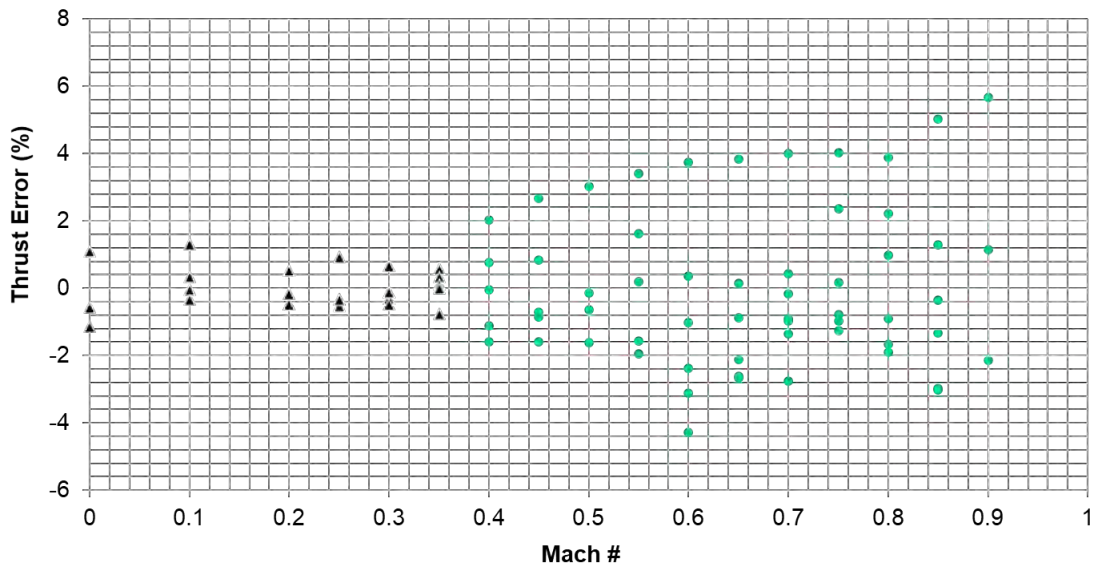


Figure 94. Splitting the Fits by Low versus High Mach.

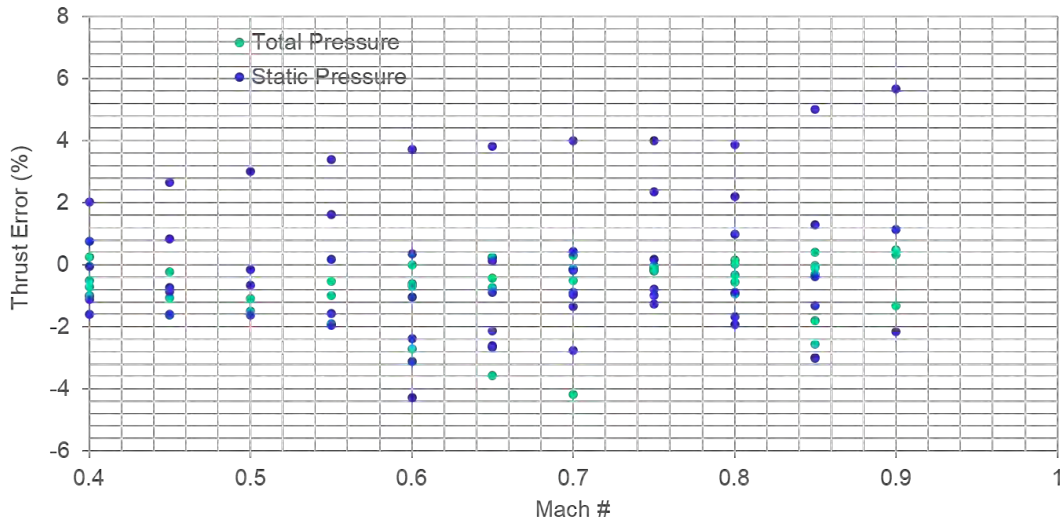


Figure 95: Total Pressure versus Static Pressure Comparison for Notional B737-800.

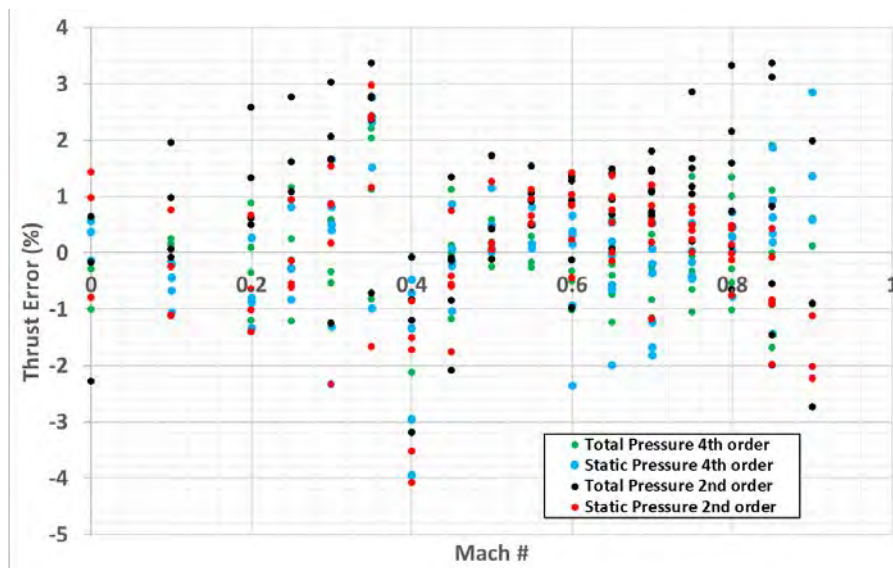


Figure 96. Notional B767 Idle Thrust Error (%).

As shown in Figure 97,  $PC = 50$  represents the maximum thrust. To apply the rating appropriately, two sets of coefficient fits are used for  $Mach < 0.4$  (MKTF) and  $Mach \geq 0.4$  (MCMB). To extract Mach, Altitude, Thrust, and temperature data, the NPSS output engine deck is leveraged. This model takes up to 12  $a_i$  coefficients to calculate  $C_T$ . The above equation shows the complete case containing all  $a_i$  coefficients. However, the number of coefficients is not fixed and depends on the quantity and quality of the reference data with which the coefficients are identified, together with the modeler preferences. According to the BADA4 manual, for many occasions this results in simpler expressions where some  $a_i$  coefficients are deactivated.

A rating model is provided to determine the throttle position and this rating model is made available for several different ratings, namely:

- maximum cruise (MCRZ)
- maximum climb (MCMB)
- maximum takeoff (MTKF)

Turbofan engines behave differently whether they are operated at a temperature deviation below or above a threshold temperature deviation called the kink point, which defines two operation areas:

- The flat-rated area
- The temperature-rated area

When the atmospheric conditions result in a temperature deviation inferior to the kink point, the turbofan operates in the flat-rated area, in which the engine behavior is limited by the internal pressure. When the temperature deviation exceeds the kink point, the amount of fuel being injected into the combustion chamber must be reduced to control the turbine entry temperature; the turbofan then operates in the temperature-rated area.

The two areas are thus inherently different and as such are modeled by two independent functions, each with its respective coefficients:

$$\delta_T = \begin{cases} \delta_{T,flat} & \text{when } \Delta T \leq \Delta T_{kink} \\ \delta_{T,temp} & \text{when } \Delta T > \Delta T_{kink} \end{cases} \quad (33)$$

Where:

- $\delta_T$  is the throttle parameter [-]
- $\delta_{T, flat}$  is the throttle parameter in the flat-rated area
- $\delta_{T, temp}$  is the throttle parameter in the temperature-rated area [-]
- $\Delta T_{kink}$  is the kink point [K], from the turbofan model

#### Flat-rated Area

The rating model for the turbofan engine in the flat-rated area provides the throttle parameter  $\delta_{T,flat}$  as a function of the Mach number and the atmospheric conditions:

$$\begin{aligned} \delta_{Tflat} = & b_1 + b_2M + b_3M^2 + b_4M^3 + b_5M^4 + b_6M^5 + (b_7 + b_8 + b_9M^2 + b_{10}M^3 + b_{11}M^4 + b_{12}M^5)\delta \\ & + (b_{13} + b_{14}M + b_{15}M^2 + b_{16}M^3 + b_{17}M^4 + b_{18}M^5)\delta^2 \\ & + (b_{19} + b_{20}M + b_{21}M^2 + b_{22}M^3 + b_{23}M^4 + b_{24}M^5)\delta^3 \\ & + (b_{25} + b_{26}M + b_{27}M^2 + b_{28}M^3 + b_{30}M^4 + b_{31}M^5)\delta^4 f(n) = g(n) + h(n) \end{aligned} \quad (34)$$

Where:

- $\delta$  is the pressure ratio [-]
- $M$  is the Mach number [-]
- $b_1$  to  $b_{31}$  are flat-rated area throttle coefficients [-], from the TFM

#### Temperature -rated area:

The rating model for the turbofan engine in the temperature-rated area provides the throttle parameter  $\delta_{T,temp}$  as a function of the Mach number and the atmospheric conditions:

$$\begin{aligned} \delta_{Ttemp} = & c_1 + c_2M + c_3M^2 + c_4M^3 + c_5M^4 + (c_7 + c_8 + c_9M^2 + c_{10}M^3 + c_{11}M^4)\theta \\ & + (c_{13} + c_{14}M + c_{15}M^2 + c_{16}M^3 + c_{17}M^4)\theta^2 + (c_{19} + c_{20}M + c_{21}M^2 + c_{22}M^3 + c_{23}M^4)\theta^3 \\ & + (c_{25} + c_{26}M + c_{27}M^2 + c_{28}M^3 + c_{30}M^4)\theta^4 \end{aligned} \quad (35)$$

Where:

- $M$  is the Mach number [-]
- $c_1$  to  $c_{30}$  are temperature-rated area throttle coefficients [-], from the TFM
- $\theta$  is the total temperature ratio
- Coefficients ( $a_i, b_i, c_i$ ) are iterated by solver to minimize the sum of squares of the relative error between calculated and predicted  $C_T$  and  $\delta_T$

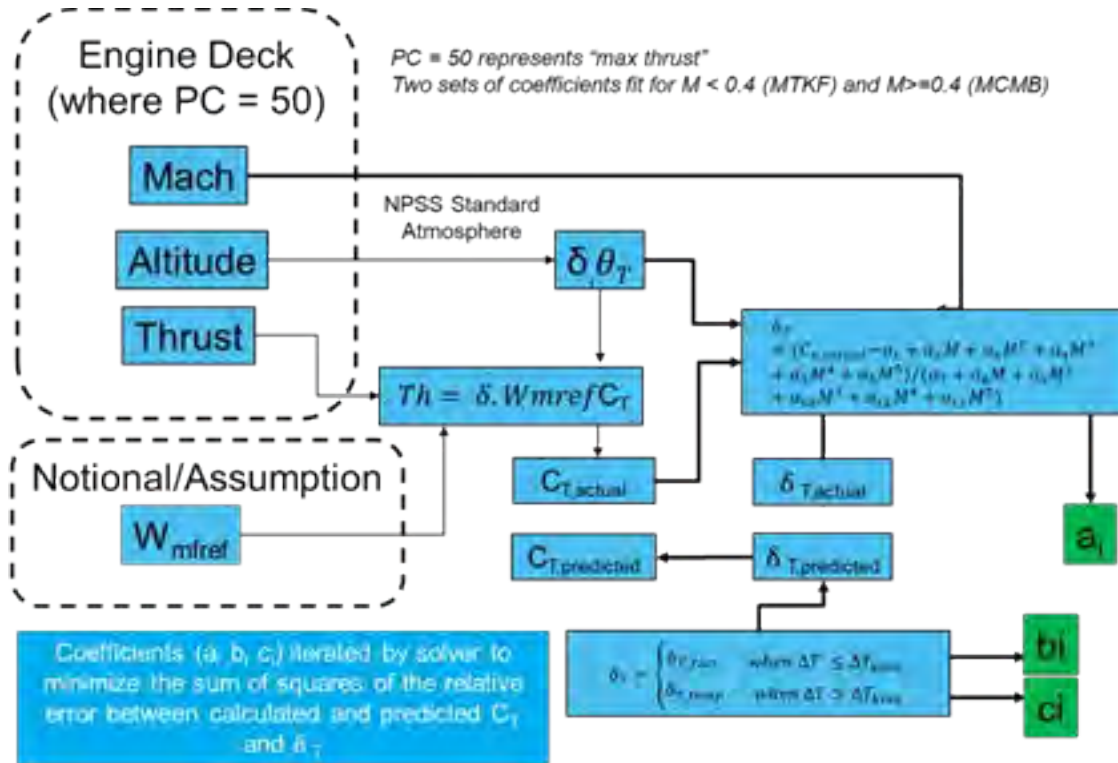


Figure 97. Non-Idle Thrust Flow Chart.

Basic BADA4 equations work relatively well (+/- 5%) except at a few outlier points. MTKF has lower error than MCMB, which can be observed from Figure 98.

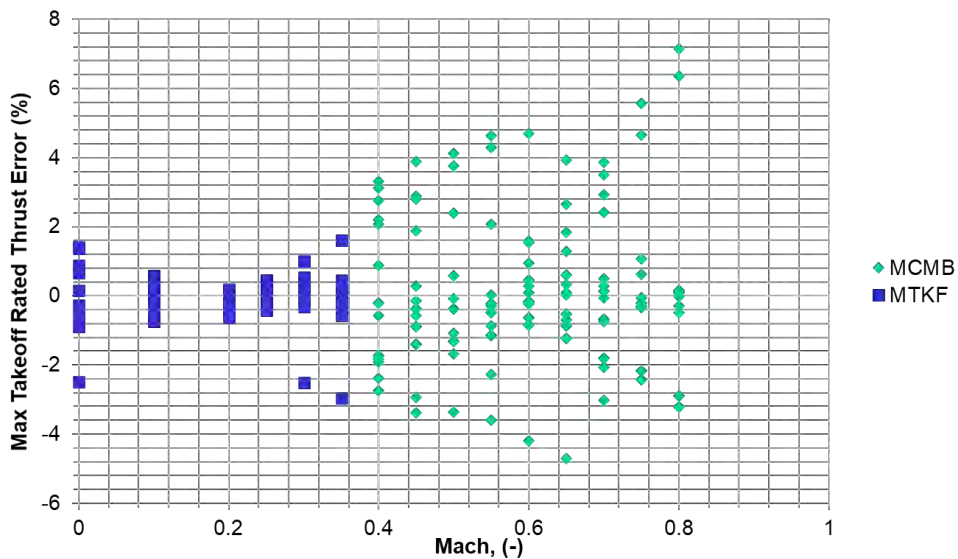


Figure 98. Non-Idle Thrust for Notional B737-800.

Similar results were replicated for the notional B767 engine deck as shown in Figure 99.

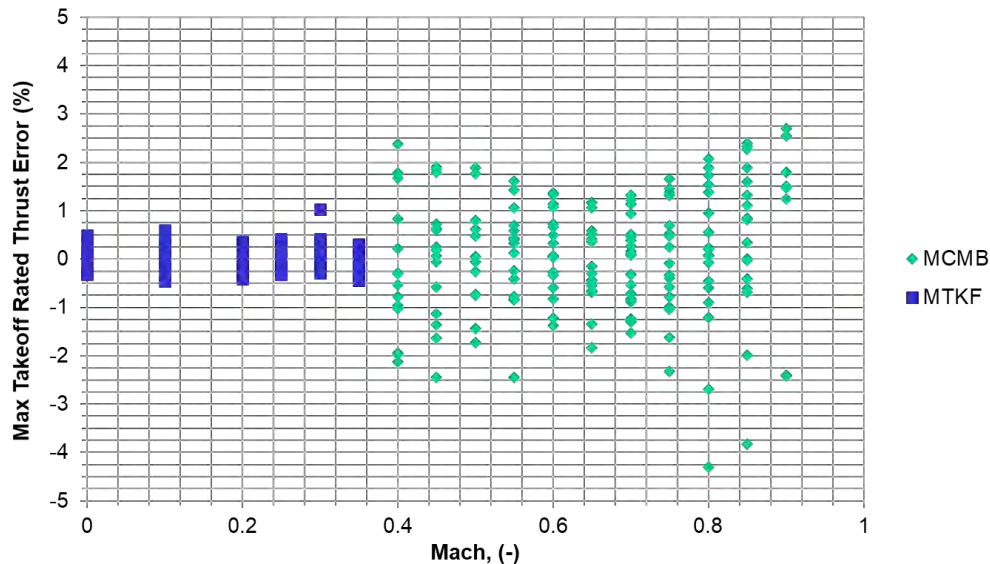


Figure 99. Non-Idle Thrust Results for Notional B767.

The approach described here only uses the first 12 terms of the regression model for the thrust as shown below:

$$C_T = -a_1 + a_2M + a_3M^2 + a_4M^3 + a_5M^4 + a_5M^5 + (a_7 + a_8M + a_9M^2 + a_{10}M^3 + a_{11}M^4 + a_{12}M^5)\delta_T + (a_{13} + a_{14}M + a_{15}M^2 + a_{16}M^3 + a_{17}M^4 + a_{18}M^5)\delta_T^2 + (a_{19} + a_{20}M + a_{21}M^2 + a_{22}M^3 + a_{23}M^4 + a_{24}M^5)\delta_T^3 + \dots$$

This may improve fits by a few percent, but Georgia Tech could not figure out an appropriate numerical scheme for performing the fits with higher order terms. We recommend attempting to use at least the quadratic term in the rating parameter in this equation to improve error if needed

#### Fuel Consumption

The purpose of this section is to explain turbofan fuel consumption model for both idle and non-idle ratings. Each model includes the contribution from all engines and provides the fuel consumption as a function of airspeed, throttle parameter, and atmospheric conditions. The general formulation of the fuel consumption, F [kg/s], is:

$$F = \begin{cases} TFA \cdot 60^{-1} & \text{during taxi (if TFA is defined)} \\ \delta \cdot \theta^{0.5} \cdot W_{ref} \cdot a_0 \cdot L_{hv}^{-1} \cdot C_F & \text{otherwise} \end{cases} \quad (36)$$

Where:

- TFA is the taxi fuel allowance [kg/min], from the PFM
- $\delta$  is the pressure ratio [-]
- $\theta$  is the temperature ratio [-]
- $m_{ref}$  is the reference mass [kg], from the PFM
- $W_{ref}$  is the weight force at  $m_{ref}$  [N],
- $a_0$  is the speed of sound at MSL in standard atmosphere [m/s],
- LHV is the fuel lower heating value [ $m_2/s_2$ ], from the PFM
- $C_f$  is the fuel coefficient [-].

This section provides the formulas to compute the fuel coefficient used, depending on the engine rating. The fuel coefficient  $C_f$  is determined by:



$$F = \begin{cases} C_{F,idle} & \text{when idle rating is used} \\ \max(C_{F,gen}, C_{F,idle}) & \text{when a non - idle rating or no rating is used} \end{cases} \quad (37)$$

Where:

$C_{F,idle}$  is the idle fuel coefficient [-],

$C_{F,gen}$  is the general fuel coefficient [-]

**Idle Rating**

The idle rating model for the turbofan engine model directly provides the idle fuel coefficient  $C_{F,idle}$  as a function of the Mach number and the atmospheric conditions:

$$C_{F,idle} = f_{i_1} + f_{i_2}\delta + f_{i_3}\delta^2 + (f_{i_4} + f_{i_5}\delta + f_{i_6}\delta^2) + (f_{i_{10}} + f_{i_{11}}\delta + f_{i_{12}}\delta^2)M^3 + (f_{i_{13}} + f_{i_{14}}\delta + f_{i_{15}}\delta^2)M^4 \quad (38)$$

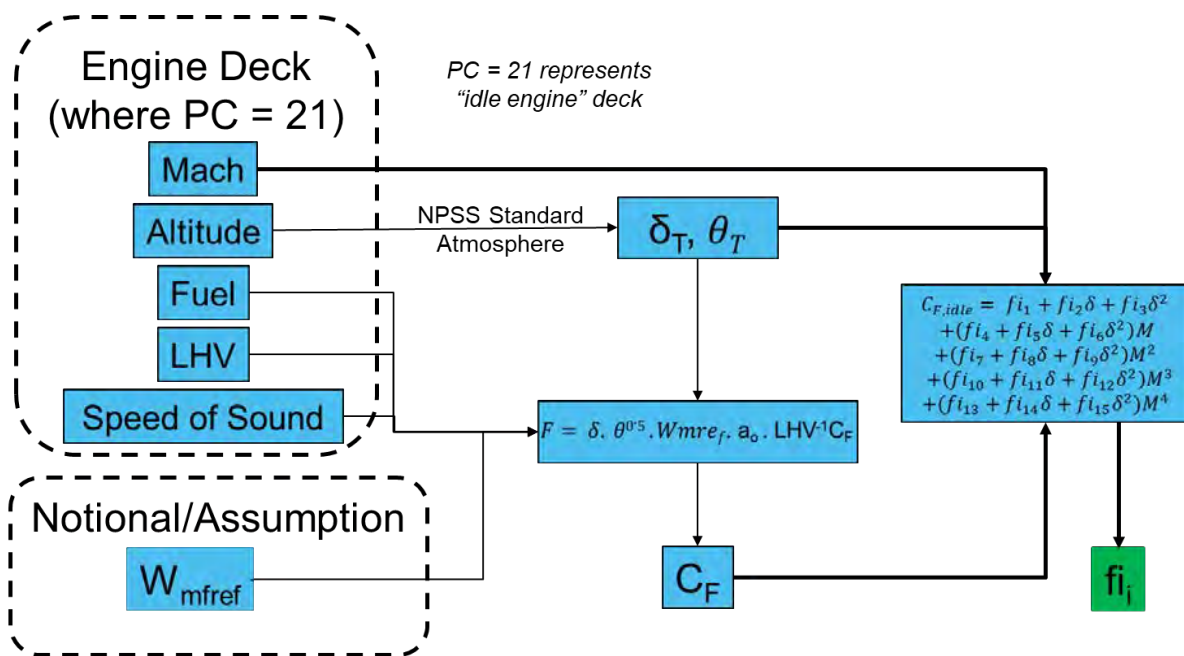
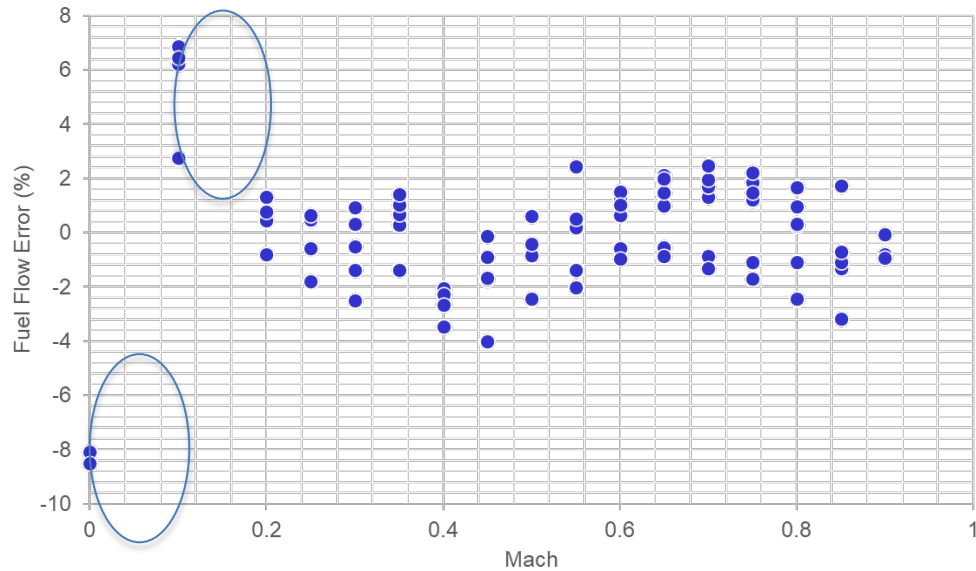


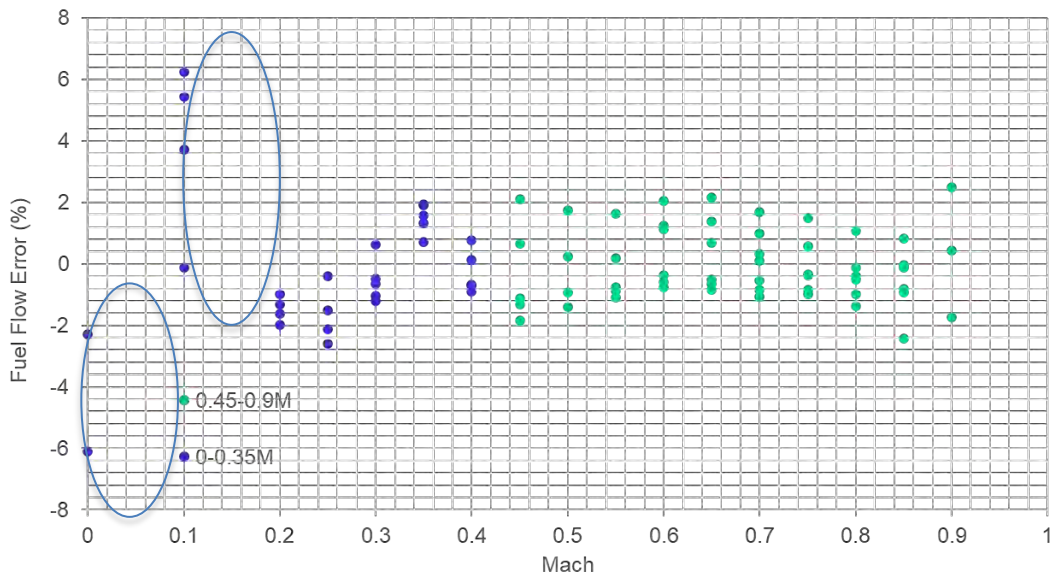
Figure 100. Idle Rating Fuel Consumption Model Generation Process Chart.

Figure 100 shows the process by which the coefficients are iterated by the solver to minimize the sum square of relative error between calculated and predicted  $C_F$ . Before recommending any new equation forms, BADA4 equations are used to observe error %, which is shown in Figure 101.



**Figure 101.** Idle Rating Fuel Consumption Error for Notional B737-800.

Basic BADA4 equations do work well except at very low Mach. Therefore, the Georgia Tech team decided to split the engine deck by rating for  $M = 0.4$  to see if this would help, shown in Figure 102.



**Figure 102.** Idle Rating Fuel Consumption Error for Notional B737-800 with Divided Engine Deck.

Splitting the data by Mach does not help to reduce the idle rating fuel consumption error for the notional B737-800.

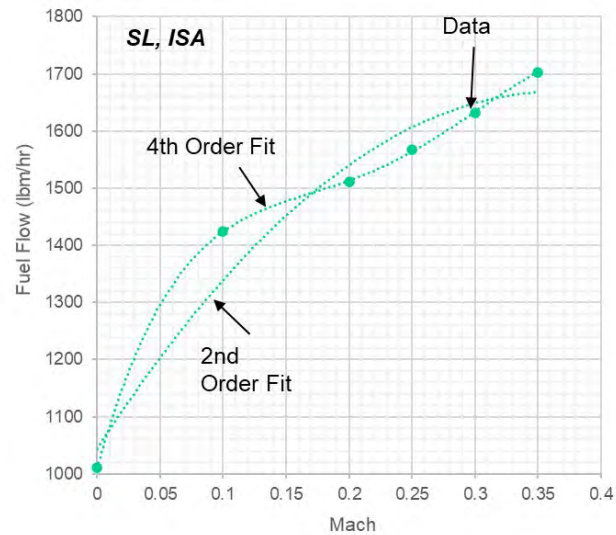


Figure 103. Fuel Flow versus Mach Trend Observation.

The following new idle fuel flow equation is recommended:

$$C_{F,Idle} = \frac{\left( \begin{aligned} &f_{i_1} + f_{i_2}\delta + f_{i_3}\delta^2 \\ &+ (f_{i_4} + f_{i_5}\delta + f_{i_6}\delta^2) \cdot M \\ &+ (f_{i_7} + f_{i_8}\delta + f_{i_9}\delta^2) \cdot M^2 \end{aligned} \right) \cdot \delta^{-1} \theta^{\frac{1}{2}}}{\begin{aligned} &+ (f_{i_{10}} + f_{i_{11}}\delta + f_{i_{12}}\delta^2) \cdot M^3 \\ &+ (f_{i_{13}} + f_{i_{14}}\delta + f_{i_{15}}\delta^2) \cdot M^4 \end{aligned}} \quad (39)$$

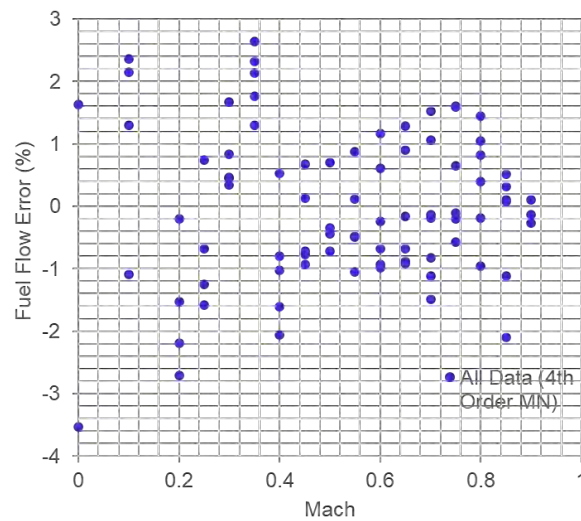


Figure 104. Error % with Recommended Equation for Notional B737-800.

Fourth order Mach fit helps at low speed because the data is a bit more non-linear in that regime, which can be seen in Figure 103 and Figure 104. The notional B767 exhibits the same trend as shown in Figure 105 and Figure 106.

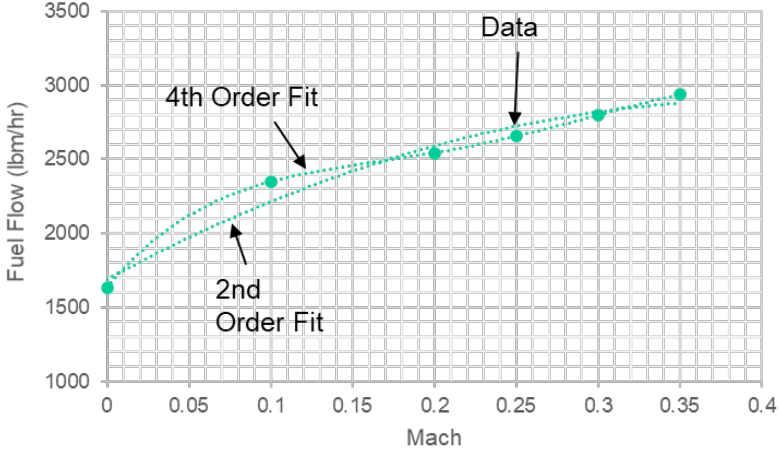


Figure 105. Fuel Flow Trend for Notional B767.

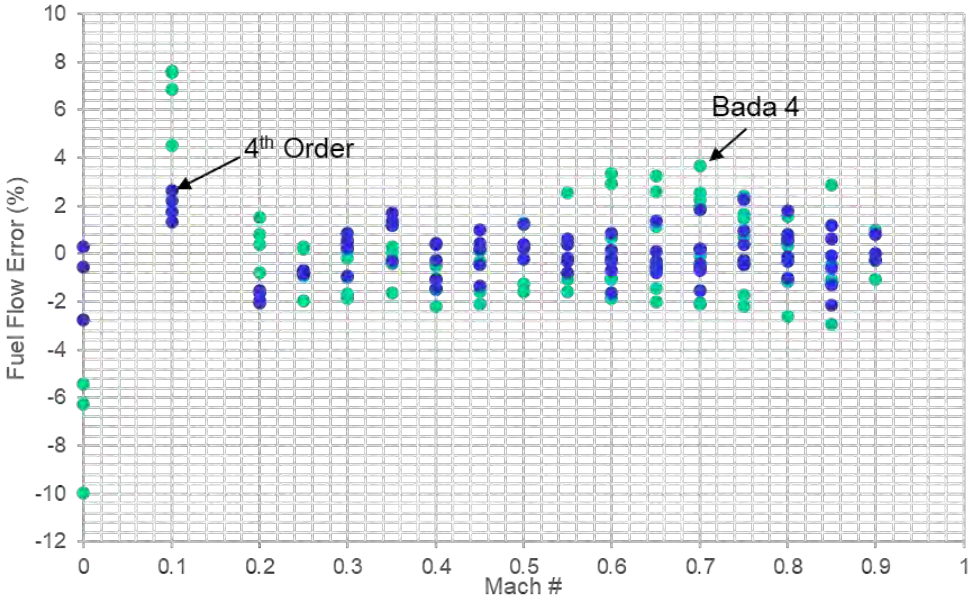


Figure 106. Results Comparison with fourth Order and BADA AS IS Equations for Notional B767.

**Non-idle Fuel Consumption**

The generalized fuel form for the turbofan engine model provides the general fuel coefficient  $C_{F,gen}$  as a function of the Mach number  $M$  and the thrust coefficient  $C_T$ .  $C_{F,gen}$  is calculated as a fourth order polynomial of  $M$  with coefficients that are fourth order polynomials of  $C_T$ . The team started to use the BADA4 equation as follows:

$$\begin{aligned}
 f_1 + f_2 C_T + f_3 C_T^2 + f_4 C_T^3 + f_5 C_T^4 + (f_6 + f_7 C_T + f_8 C_T^2 + f_9 C_T^3 + f_{10} C_T^4) M + (f_{11} + f_{12} C_T + f_{13} C_T^2 + f_{14} C_T^3 \\
 + f_{15} C_T^4) M^2 + (f_{16} + f_{17} C_T + f_{18} C_T^2 + f_{19} C_T^3 + f_{20} C_T^4) M^3 + (f_{21} + f_{22} C_T + f_{23} C_T^2 + f_{24} C_T^3 + f_{25} C_T^4) M^4
 \end{aligned}
 \tag{40}$$

To predict non-idle rating fuel consumption, the following process shown in Figure 107 is applied.

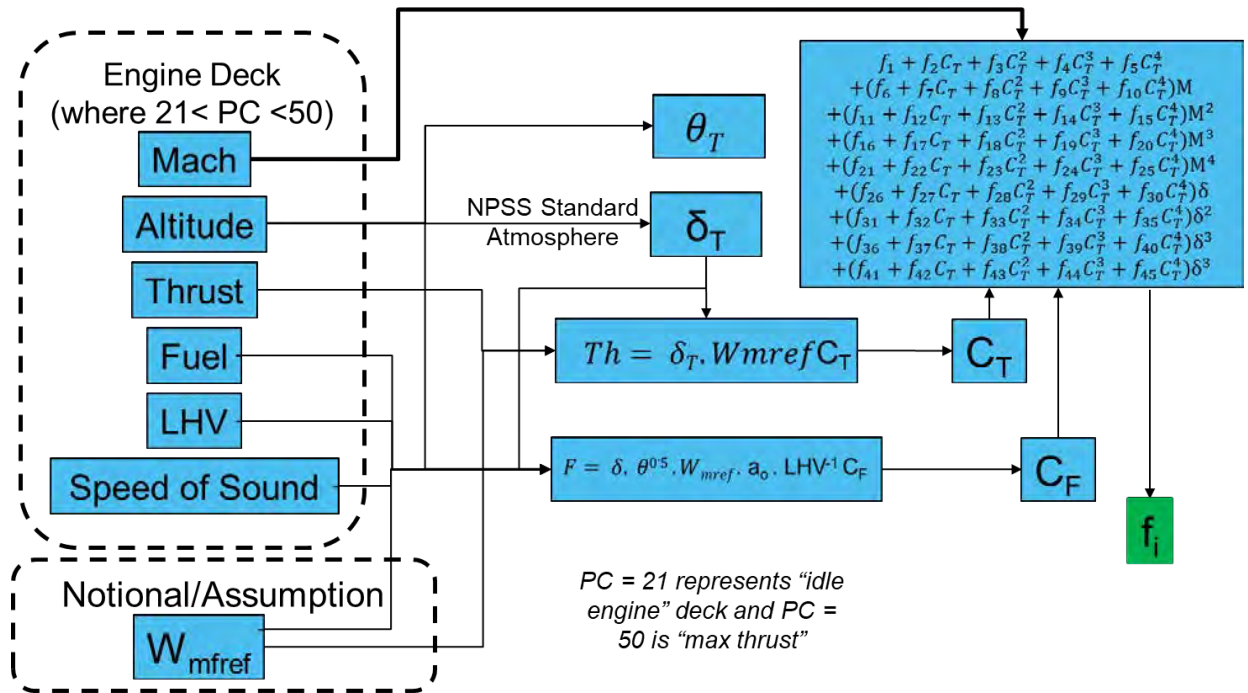


Figure 107. Non-idle Rating Fuel Consumption Model Generation Process Chart.

A new model is introduced with total properties to reduce the relative error % and coefficients iterated by the solver to minimize the sum of the squares of relative error between calculated and predicted  $C_F$ . Using total properties enhanced the current BADA4 model. However, the MCMB error rate % is still high ( $\pm 6\%$ ).

The following steps are applied to enhance the BADA4 original equation:

- 1) Started with original BADA4 equation.
- 2) Split the engine deck MCMB and MTKF (@Mach 0.4 per engine rating).
- 3) Total and static properties are compared with original BADA4 equation, which is shown in Figure 108.
- 4) Regarding the initial results of BADA4 model as is, the team decided to check the engine deck's source data.
- 5) Only to check the data and instead of using the BADA4 model, another model (artificial neural net) is randomly selected (see Figure 109).

The data does not necessarily preclude a good model, but the team observed issues with functional forms in BADA4. Given these initial results of the BADA4 model, the Georgia Tech team decided to try a new model as shown in Figure 110. Higher order terms with ambient conditions were added to enhance the current BADA4 model. The new fit works a good bit better, with the error range within  $\pm 1\%$  as shown in Figure 111. Figure 112 shows that the maximum climb rated fuel flow consumption of the notional B767 also has better results with the new model.

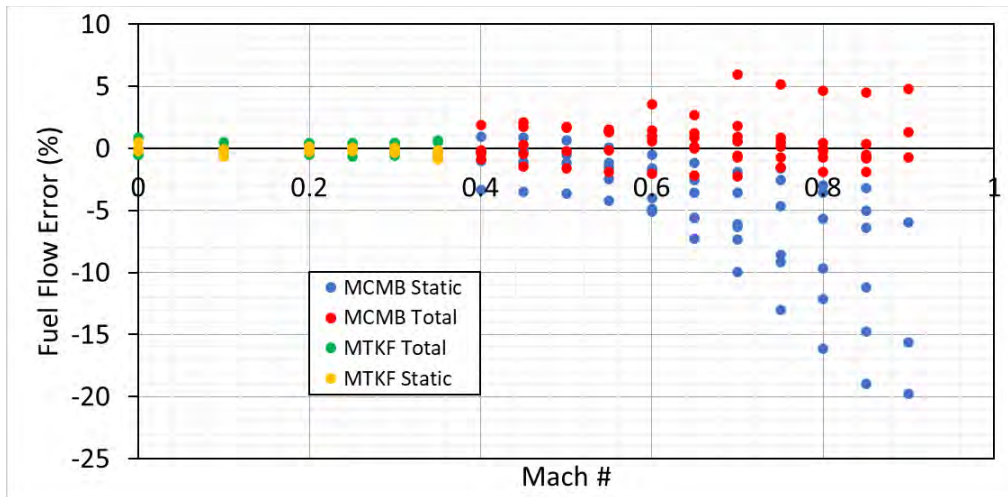


Figure 108: Non-Idle Fuel Consumption for Notional B737.

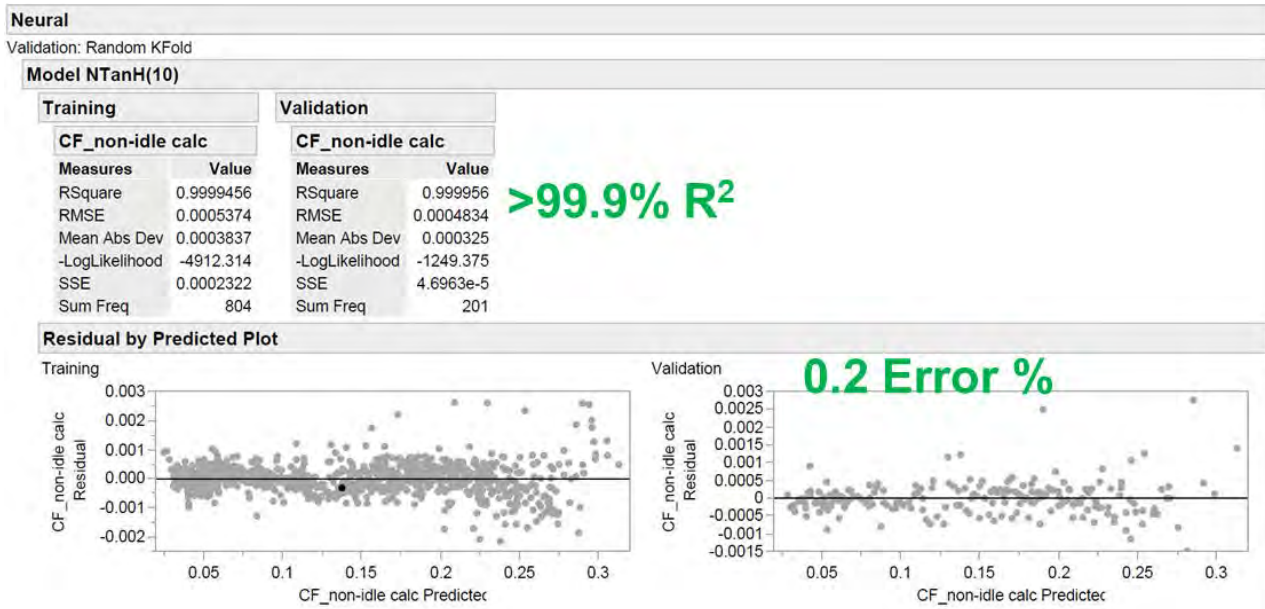


Figure 109. Engine Deck (Data Source) Evaluation with Artificial Neural Network Analysis.

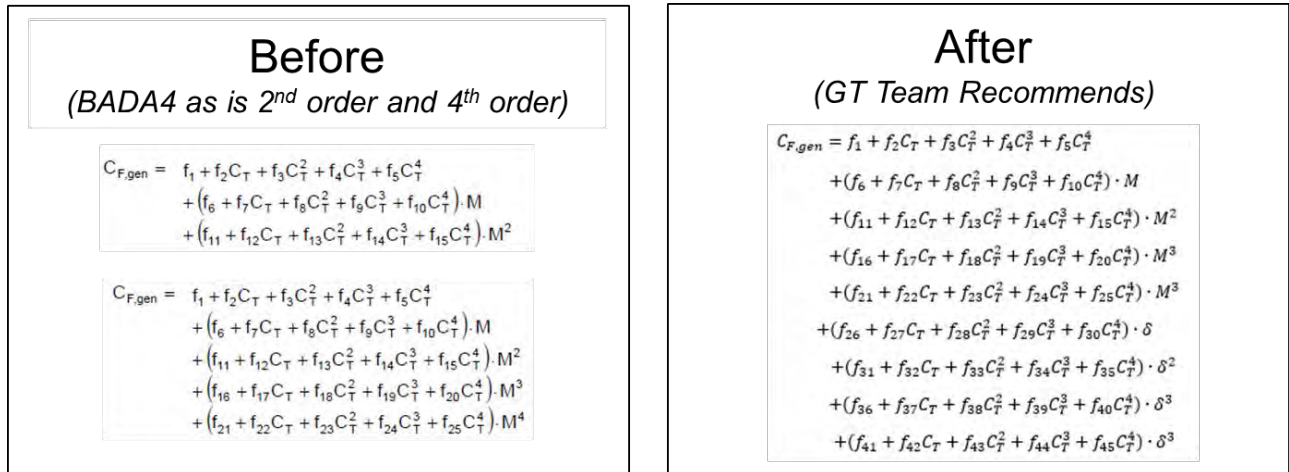


Figure 110: Recommended Equation and BADA4 As Is Comparison.

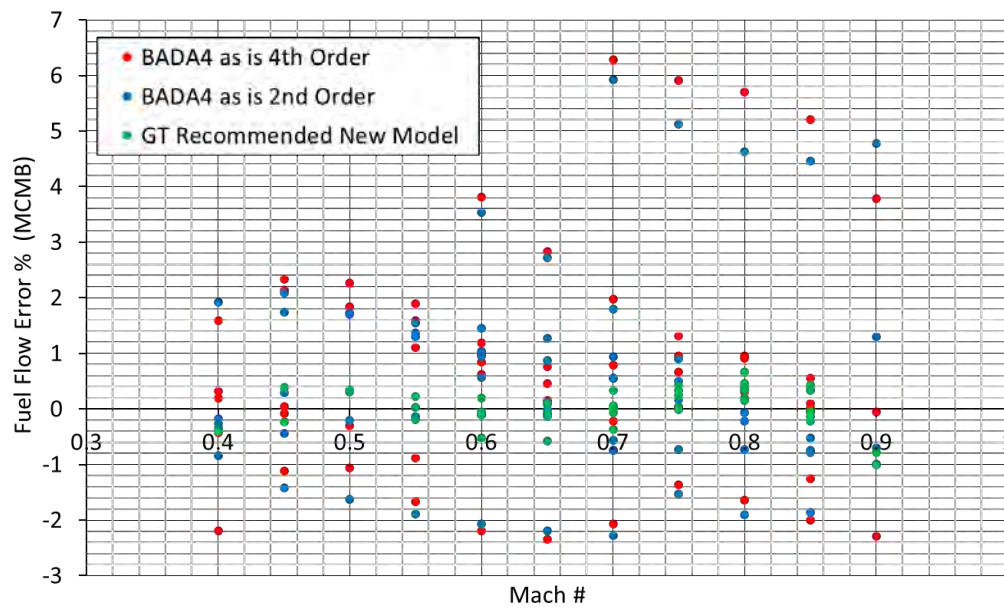


Figure 111. Notional B737 Results comparison for Three Different Equations.

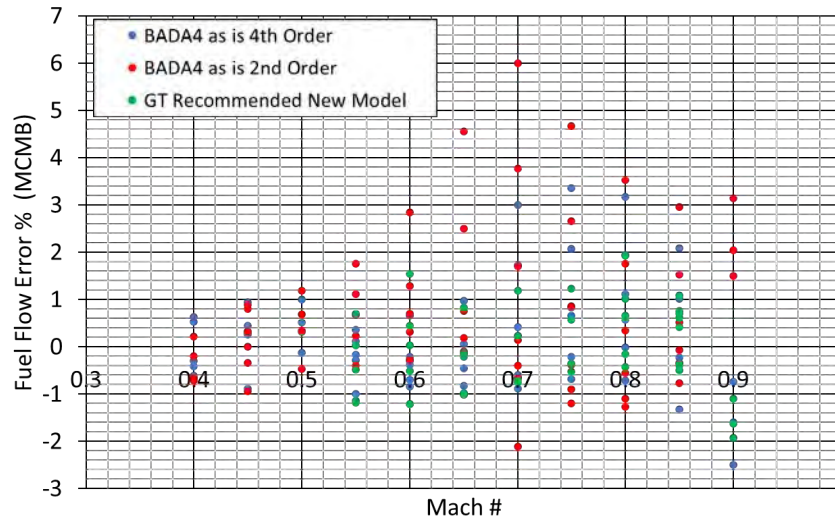


Figure 112. Notional B767 Results comparison for Three Different Equations.

Summary of the Propulsion Coefficient Generation Results:

Error comparison charts are created to determine the difference between BADA4 as is equations and recommended models to reduce the errors. In general, the functional form did not represent the actual behavior of thrust nor fuel flow for the two subsonic aircraft of interest. As a result, a set of modifications to each of the propulsion equations are recommended and provided in Table 39. For SST regressions, even larger errors are observed. As a result, new functional forms of the thrust and fuel flow equations will be developed in subsequent research.

Table 39. BADA4 Propulsion Regression Models' Results & Recommendations.

Regression Type	Aircraft	Error Before (BADA4 as is)	Recommendation	Error After (Recommendation)
Idle Thrust	Notional B737	+/- 6 %	To improve fits beyond base BADA 4, there is a need to split the fits by flight condition. Using total pressure instead of static also improved results at higher Machs.	+/- 2%
	Notional B767	+/- 4%		+/- 2%
Idle Fuel Consumption	Notional B737	+/- 2% (+/- 8% M<0.25)	Add 4th order Mach terms to BADA Equation to improve M < 0.25	+/- 3% (M<0.25)
	Notional B767	+/- 2% (+/- 9% M<0.25)		+/- 3% (M<0.25)
Non- Idle Thrust (MTKF)	Notional B737	+/- 2%	No change recommended. Approach seems suitable.	--
	Notional B767	+/- 0.5%		--
Non- Idle Thrust (MCMB)	Notional B737	+/- 6%	BADA approach is reasonable given that only linear ratings terms were used. Recommend utilizing higher order terms in the thrust equation.	--
	Notional B767	+/- 4%		--
Non-Idle Fuel Consumption (MTKF)	Notional B737	+/- 1%	No Change recommended but may want to update functional form to be consistent with MCMB if that approach is taken	--
	Notional B767	+/- 2%		--
Non-Idle Fuel Consumption (MCMB)	Notional B737	+/- 6%	Add 4 <sup>th</sup> order correlation with ambient pressure ratio $\delta$ or other alternative way of capturing altitude impact.	+/- 1%
	Notional B767	+/- 6%		+/- 2%

## Task 6 – Coordination

Georgia Institute of Technology and Purdue University

### Objective

This Task's objective is to maintain awareness and to coordinate among the different telecons in supporting the various elements supporting the CAEP supersonic exploratory study. It is envisioned that there could be a minimum of six different telecons occurring from week to week.

This Task will also coordinate with ASCENT Project 47 led by MIT on the clean-sheet supersonic engine design. The Georgia Tech/ASDL team will serve as the airframer providing requirements to the engine manufacturer. In this case, the MIT team will serve as the engine manufacturing. Georgia Tech/ASDL will generate requirements in terms of thrust and thrust specific fuel consumption (TSFC) at critical points in the mission. Since the application is a supersonic aircraft, engine maximum diameter and weight are also potential constraint requirements. In addition to providing design requirements and constraints, Georgia Tech/ASDL will also evaluate the performance of the engine on the aircraft and provide feedback to the MIT team.

This Task's objective is also to ensure that the Purdue team maintains the ability to incorporate other SST vehicle models in FLEET.

### Research Approach (Georgia Tech)

The team attended in person or, once travel became restricted, eleven CAEP related meetings of Working Group 1 (Noise), Working Group 3 (Emissions), and MDG/FESG meetings. This included up to six telecons per week depending on schedule and needs. The team authored and presented eight papers to these meetings and contributed additional presentations and technical data in support of the CAEP supersonic exploratory study and related progress reports.

The Georgia Tech modeling team has been in communications with the ASCENT Project 47 MIT researchers in regard to results of the Medium SST. At the time of this report, the ASCENT Project 47 researchers have provided an extensive list of requested information shown below, and the Georgia Tech modeling team is currently compiling the information for transmission using the GT Medium v1.1.4 closed vehicle.

- General aircraft properties
  - Number of engines
  - Wing Area
  - Wing inclination angle with the horizontal
  - Thrust inclination angle with the horizontal
  - Maximum take-off weight (MTOW)
- Overall mission analysis
  - Design mission design
  - Total fuel wing capacity
  - Drag polar for clean configuration
  - Detailed mission segment performance
- Airframe constraint on engine size
- Takeoff and landing trajectories
  - Low speed ( $M < 0.35$ ) aerodynamic properties of the full aircraft
- Noise footprint analysis
  - Airframe flap area
  - Horizontal tail area
  - Vertical tail area
  - Wing area
  - Flap span
  - Horizontal tail span
  - Vertical tail span
  - Wingspan
  - Tire diameter main landing gear
  - Tire diameter nose landing gear
  - Main landing gear strut length



- Nose landing gear strut length
- Number of wheels per main landing gear
- Number of wheels on nose landing gear
- Number of main landing gear
- Number of nose landing gear
- Number of slots for trailing edge flaps
- Flap setting [degrees deflected]
- Coordinates of the wing planform relative to the engine (i.e., top view of the aircraft)

### **Research Approach (Purdue)**

#### **Coordinate with CAEP MDG/FESG**

The Purdue team provided relevant data to the entities involved in CAEP MDG/FESG (particularly the demand task group) as outlined in the Purdue efforts under Task 4.

#### **Incorporating Supersonic Aircraft from Other Partners in FLEET**

The Purdue team used FLOPS to generate relevant aircraft coefficients for the 55-seat A10 notional medium supersonic aircraft developed by our colleagues at Georgia Tech in FLEET. The supersonic aircraft were essentially “flown” on the supersonic flight path ground tracks (also generated by the team at Georgia Tech) using FLOPS. To do so, the team wrote a wrapper code to “force” FLOPS to fly the supersonic aircraft on the supersonic flight path ground tracks. The wrapper code employed an optimizer with an objective function of minimizing the sum of the squares of the differences in the supersonic and subsonic distance flown by the supersonic aircraft on a given route in FLOPS and the flight path ground tracks data provided by Georgia Tech. There were some routes for which the supersonic aircraft ground tracks flown in FLOPS could not exactly match the required supersonic flight path ground tracks, but the difference in ground tracks were still not significant enough to project any major discrepancies in terms of the block fuel and the block time for those handful routes. This optimization-based approach to generate the aircraft performance coefficients required for implementation in FLEET enables the Purdue team to incorporate any “type” of supersonic aircraft in FLEET from any of our partners (provided that the supersonic aircraft models are provided to us in FLOPS).

### **Publications**

Jain, S., Ogunsina, K. E., Chao, H., Crossley, W. A., and DeLaurentis, D. A., Predicting Routes for, Number of Operations of, and Fleet-level Impacts of Future Commercial Supersonic Aircraft on Routes Touching the United States, 2020. <https://doi.org/10.2514/6.2020-2878>, URL <https://arc.aiaa.org/doi/abs/10.2514/6.2020-2878>.

Mohammed Hassan, Holger Pfaender and Dimitri Mavris, “Design Tools for Conceptual Analysis of Future Commercial Supersonic Aircraft”, AIAA Aviation 2020 Forum, AIAA 2020-2620, June 2020

#### **Submitted conference proceedings**

Jain, S., Mane, M., Crossley, W. A., & DeLaurentis, D. A. Investigating How Commercial Supersonic Aircraft Operations Might Impact Subsonic Operations and Total CO<sub>2</sub> Emissions. Abstract submitted to AIAA Aviation Forum for presentation in June 2021

Mane M., Jain, S., Crossley, W. A. Estimating Market Size for Supersonic Passenger Transport Aircraft. Abstract submitted to AIAA Aviation Forum for presentation in June 2021

### **Outreach Efforts**

Multiple interactions with government, industry, and academia have occurred during the course of the project.

ASCENT 10: Aircraft Technology Modeling and Assessment, poster presentation to ASCENT Spring Advisory Committee Meeting, Georgia Tech, Virtual, March 2020.

ASCENT 10: Aircraft Technology Modeling and Assessment, oral presentation to ASCENT Fall Advisory Committee Meeting, Georgia Tech, Virtual, September 2020.

### **Awards**

None

### **Student Involvement**

The Georgia Tech student team consists of seven graduate research assistants (GRA). At the beginning of the project, all seven GRAs engaged in determining supersonic configurations for both the business jet and medium SST, and then the team

was divided into geometry, aerodynamics, propulsion, weights, noise, mission analysis, and fleet assessment, with each student taking on multiple topics. GRA leads are identified for each topic. Ms. Barbara Sampaio and Mr. Brennan Stewart are the student leads for aerodynamics; Mr. Edan Baltman is the student lead for propulsion; Mr. Brennan Stewart is the student lead for geometry; Mr. Joao De Azevedo is the student lead for noise; Mr. Colby Weit is the student lead for mission analysis; and Mr. Nadir Ougazzaden is the student lead for fleet assessment.

The Purdue team included four graduate students over the one-year period, all of whom have been conducting tasks in support of the effort. Samarth Jain is a continuing PhD student at Purdue and worked on the effort for the entire period. Kolawole Ogunsina and Hsun Chao are PhD students; both of these students moved to other research projects during the period covered by this report; Mr. Chao still supports the ASCENT 10 effort in an advisory capability. Suzanne Swaine, a PhD student, joined the Purdue team in August of 2020.

## **Plans for Next Period**

### **Georgia Tech**

The Georgia Tech team investigated routes that would be capable of carrying enough demand to fill a 50- to 60-seat supersonic aircraft with significant time advantages. It was also demonstrated that an estimate of vehicle demand can be converted to equivalent passenger traffic in GREAT.

The next phase in fleet level analysis will focus on identifying and predicting significant drivers of commercial supersonic travel demand. Using scenarios from prior ASCENT Project 10 work, Georgia Tech will build on the prior work of identifying the key drivers of supersonic demand. Georgia Tech will work with Purdue to coordinate the final scenario assumptions. This information together with the vehicle performance and characteristics will be used to estimate the fleet level impact of supersonic travel.

In order to better understand the potential demand for supersonic air travel, the team developed a parametric airline operating cost model in order to be able to explore the sensitivities of key vehicle, operational, and cost parameters on the required yield an airline would have to target for ticket prices on such a potential new supersonic aircraft. This development was followed by an SST routing tool that allows the computation of actually possible potential time savings for any potential SST based on key performance characteristics. These combined models are then fed into a potential SST demand model that is based on passenger income distributions.

The team envisions improvements to all three models in various ways. The operating cost model will be improved by using improved vehicle characteristics and performance as they become available. The routing tool will be improved by including significant air space exclusions, as well as improving the selection of fuel stop airports for routes that exceed the vehicle range. Additional improvements include accommodating potential for Mach cutoff operations as well as including vehicle kinematics and secondary boom avoidance. The potential SST demand model will be improved by including a larger variety of and improved income distributions compared to the current simplified data being used.

Georgia Tech will then use the GREAT fleet prediction tool to perform an assessment of the impact of supersonic aircraft using the scenarios from prior ASCENT 10 work and use the supersonic demand scenarios to estimate the fleet level impact of supersonic travel. This includes emissions, such as water vapor and NO<sub>x</sub>, at cruise altitude and emissions around the airports. The results for each scenario will then be formatted to be compatible with the APMT input format. This will be coordinated with the APMT users and developers. Additionally, any updated vehicle models, new vehicle models, or new information that should become available will be used to re-examine the fleet level impacts of supersonic aircraft.

### **Purdue**

The Purdue team successfully demonstrated FLEET's capabilities for modeling and analyzing the introduction of commercial supersonic aircraft to an existing all-subsonic airline fleet model. This demonstration has shown that FLEET is capable of predicting the potential routes for profitable supersonic service, along with predicting the number of supersonic and subsonic aircraft operations, number of roundtrips, and the number of passengers carried on such routes. The Purdue team also successfully updated its route network to use a dynamic route network until 2018 that follows how U.S. flag carrier airlines updated their route networks as reported in the BTS data, followed by a static network from year 2019 and onwards.

The preliminary results from FLEET by using the placeholder supersonic aircraft model indicate an increase in the fleet-level total fuel burn for the subsonic-only fleet mix compared with a mix including supersonic aircraft along with subsonic aircraft. In the fleet-mix scheme in which supersonic aircraft become available, the future total fuel burn exceeds that predicted for

the subsonic-only fleet by an amount larger than would be expected for the number of supersonic aircraft operated by the airline. When the allocation approach first satisfies passenger demand for business class and above with supersonic aircraft and subsequently satisfies remaining demand with the subsonic fleet, the results indicate a different use, retirement, and acquisition of the subsonic fleet from that predicted in the subsonic-only fleet mix scheme. These changes lead to the increased fleet-level fuel burn trend observed in the preliminary results. These results are based on the detailed A10 notional medium SST aircraft.

Future work (elucidated in detail in the fourth-year proposal for the current supersonic effort) will include extending FLEET's airline network to a global network (moving away from the U.S.-flag-carrier-airlines-only route network currently implemented in FLEET). The team will also study the impact of increasing the load factor for subsonic aircraft in FLEET that operate on routes where supersonic aircraft also operate (to compensate for the shifting of subsonic business class and above passengers to supersonic aircraft based on supersonic demand).

The Purdue team plans to develop a passenger choice model that can replace the supersonic passenger demand assumption of 5% of the total passenger demand. The current idea for this model will combine both the value of travel time to help monetize time savings, which will be a major contributor, and a relationship between trip duration and volume per passenger to help address considerations of comfort, which will be a minor contributor.

The preliminary results presented in this report are based on the allocation approach, which satisfies travel demand first by using supersonic aircraft and next by using subsonic aircraft. In the near term, the Purdue team intends to replace this "supersonic-first" allocation approach with a "simultaneous" allocation approach wherein the supersonic and subsonic aircraft are allocated together on the basis of supersonic and subsonic passenger demand.

Future work will also include developing a FLEET-like tool for supersonic business jet operations and assessing the fleet-level advantage of having different types and sizes of supersonic aircraft, defined by certain operational specifications (e.g., Mach cutoff over land) and passenger capacity (e.g., 100-seat supersonic aircraft), available to the FLEET airline.

Table 40 shows the expected objectives and contributions developed among Georgia Tech, Purdue, and FAA. It shows the expected contributions by task and university. This table highlights the plans for the next research period for Georgia Tech. Full details on these plans can be found in the third-year proposal submitted earlier in the summer.

Table 41 shows the anticipated list of Milestones for the Georgia Tech portion.

Table 42 highlights the plans for the next research period for Purdue. Full details on these plans can be found in the second-year proposal submitted earlier in the summer.



**Table 40.** University Contributions for Year 4.

Objectives		Georgia Tech	Purdue
1	Fleet Analysis	<p>Improve airline cost model</p> <p>Improve SST routing tool</p> <p>Improve SST demand estimation</p> <p>Develop assumptions for supersonic scenarios relative to 12 previously developed subsonic focused fleet scenarios</p> <p>Perform fleet analysis with the gradual introduction of SST vehicles into the fleet including additional SST vehicle types</p>	<p>Extend FLEET airline network to global network, introduce passenger choice for supersonic / subsonic demand, and implement simultaneous allocation model</p> <p>Perform fleet-level assessments for supersonic scenarios relative to 12 previously developed subsonic focused fleet scenarios</p> <p>Perform fleet-level including additional SST vehicle types, simple sizing of “placeholder” SST aircraft to support FLEET studies, integrate detailed SST aircraft models from Georgia Tech in FLEET</p> <p>Develop FLEET-like tool for supersonic business jet operations</p>
2	AEDT Vehicle Definition	Develop methods to model supersonic flights in AEDT	N/A
3	Support CAEP Efforts	<p>FASST vehicle modeling: develop additional SST class for 100 passengers</p> <p>Develop AEDT coefficient generation algorithm for BADA3 supersonic coefficient</p> <p>Perform trade studies to support CAEP Exploratory Study</p>	<p>Provide representative supersonic demand scenarios</p> <p>Examine change in routes where supersonic aircraft might operate based upon different aircraft types and sizes</p> <p>Model impact of supersonic aircraft noise at airports and other emission metrics as requested</p>
5	BADA4 Coefficient Generation	<p>Develop, implement, and test BADA4 coefficient generation algorithms</p> <p>Identify gaps and needs for BADA4 coefficient generation for SST</p>	N/A
6	Coordination	<p>Coordinate with entities involved in CAEP Supersonic Exploratory Study</p> <p>Coordinate with clean-sheet supersonic engine design project</p>	<p>Coordinate with entities involved in CAEP MDG/FESG, particularly the SST demand task group</p> <p>Maintain ability to incorporate SST vehicle models that use the engine design from ASCENT Project 47 and/or NASA-developed SST models</p>

**Table 41.** List of anticipated milestones for the next research period (Georgia Tech).

Milestone	Planned Due Date
Fleet Assumptions and Demand Analysis Results	31 July 2021
Fleet Analysis Results	31 July 2021
Initial AEDT BADA4 SST Model Recommendations	31 December 2020
Refined AEDT BADA SST Model Recommendations	31 July 2021
75-Passenger SST Vehicle Definition (Data Pack)	28 February 2021
25-Passenger SST Vehicle Definition (Data Pack)	31 July 2021
Trade Study Results	31 July 2021



**Table 42.** List of anticipated milestones for the next research period (Purdue).

Milestone	Planned Due Date
<ul style="list-style-type: none"> <li>Extend the FLEET route network to include global routes</li> <li>Develop and test passenger choice model based on the “effective cost” metric</li> <li>Develop type 2 and type 3 “textbook” models for 55-seat, 10-seat, and 100-seat supersonic aircraft</li> </ul>	01/2021
<ul style="list-style-type: none"> <li>Provide updated supersonic demand scenario information based upon updated baseline year and network topology</li> <li>Integrate type 1, type 2, and type 3 supersonic aircraft models for different seat capacities in FLEET</li> <li>Employ aircraft representations from Georgia Tech teammates into FLEET and provide FLEET results with these models</li> </ul>	04/2021
<ul style="list-style-type: none"> <li>Implement simultaneous allocation model</li> <li>Identify airport / certification noise metrics for all aircraft—including supersonic—and implement airport noise area constraint approach in FLEET</li> </ul>	06/2021
<ul style="list-style-type: none"> <li>Develop a separate FLEET-like tool to assess business jet operations and their subsequent impacts on fleet allocation</li> </ul>	07/2021
<ul style="list-style-type: none"> <li>Coordinate with colleagues at Georgia Tech to provide a project report summarizing this fourth phase of work studying the introduction of supersonic aircraft</li> </ul>	08/2021

## References

- Aftomis, Michael J., Berger, Marsha J. and Alonso, Juan J. (2006) “Applications of a Cartesian Mesh Boundary-Layer Approach for Complex Configurations”. 44<sup>th</sup> AIAA Aerospace Sciences Meeting, Reno NV.
- Blake, M., Smith, J., Wright, K., Mediavilla, R., Kirby, M., Pfaender, H., Clark, J.P., Volovoi, V., Dorbian, C., Ashok, A. (2010). “Advanced Vehicle concepts and implications for NextGen.” NASA CR-2010-216397.
- Dubois, D. & Paynter, G.C. (2006), “Fuel flow method 2 for estimating aircraft emissions,” SAE Transactions Vol. 115, pp. 1-14, Section 1: Journal of Aerospace.
- The Concorde Flying Manual Volume II. (1976). British Airways Overseas Division with later amendments.
- Annual Energy Outlook 2011. (2011). U.S. Energy Information Administration.
- Bachman, J. (2016). “Supersonic is coming back. Will the airlines buy it?” Bloomberg.
- Barnhart, P. J. *IPAC - Inlet Performance Analysis Code*. 1997.
- Bogaisky, J. (2018). “GE reveals engine that could make Aerion’s ambitious supersonic business jet take flight.” Forbes.
- Crichton, D., de la Rosa Blanco, E., Law, T., & Hileman, J. (2007). “Design and operation for ultra-low noise take-off,” AIAA 45<sup>th</sup> Aerospace Sciences Meeting and Exhibit, January 8-11, 2007.
- de la Rosa Blanco, E., Hall, C., & Crichton, D. (2007). “Challenges in the silent aircraft engine design,” AIAA 45<sup>th</sup> Aerospace Sciences Meeting and Exhibit, January 8-11, 2007.
- Hartmann, A. (1967). “Theory and test of flow mixing for turbofan engines,” AIAA 3rd Propulsion Joint Specialist Conference, Vol. 5, No. 6, pp. 522-527. DOI:10.2514/3.43978.
- Kowalski, E.J. & Atkins Jr., R.A. (1979). “A computer code for estimating installed performance of aircraft gas turbine engines.” Advanced Airplane Branch Boeing Military Airplane Company, Vol. I - Final Report.
- Kuchar, A.P. (1989). “Variable convergent-divergent exhaust nozzle. General Electric Company Aircraft Engine Group”, AIAA Education Series, 1989, Chapter 5 of Aircraft Propulsion Systems Technology and Design.
- Li, W., Shields, E., & Le, D. (2008). “Interactive inverse design optimization of fuselage shape for low-boom supersonic concepts.” *Journal of Aircraft*, Vol. 45, No. 4, July-August 2008.
- Mattingly, J. (2002). *Aircraft engine design*, AIAA Education Series.
- Ozgen, S. (2017). AE 451 aeronautical engineering design I. Middle East Technical University.



- Pearson, H. (1962). "Mixing of exhaust bypass flow in bypass engine," *Journal of The Royal Aeronautical Society*, Vol. 66, No. 620, pp. 528-530.
- Pratt & Whitney, and General Electric Aircraft Engines. Critical Propulsion Components Volume 1: Summary, Introduction, and Propulsion Systems Studies. 2005.
- Raymer, D. (2004). *Aircraft design: A conceptual approach*. AIAA 1992.
- Rech, J. & Leyman, C.S. (1981). A case study by Aerospatiale and British aerospace on the Concorde. AIAA Professional Study Series.
- Scholz, E. (2017). Aircraft design – an open educational resource. Hamburg Open Online University.
- Schutte, J.S. (2009). "Simultaneous multi-design point approach to gas turbine on-design cycle analysis for aircraft engines," Ph.D. Thesis, Georgia Institute of Technology, May 2009.
- Thornock, R.L. & Brown, E.F. (1972). "An experimental study of compressible flow through convergent-conical nozzles, including a comparison with theoretical results," *Journal of Basic Engineering*, pp.926-930.
- Welge, H.R., Bonet, J., Magee, T., Chen, D., Hollowell, S. Kutzmann, A., Mortlock, A., Stengle, J., Nelson, C., Adamson, E., Baughcum, S., Britt, R., Miller, G., Tai, J. (2010). "N+2 supersonic concept development and systems integration," NASA-CR-2010-216842.
- Whitcomb, R.T. (1966). "Some consideration regarding the application of the supersonic area rule to the design of airplane fuselages," NACA Research Memorandum, National Advisory Committee for Aeronautics, Washington, July 1966.
- Young, J.B. & Wilcock, R.C. (2002). "Modeling the air-cooled gas turbine part 2-coolant flows and losses," *Journal of Turbomachinery*, 124(2): pp. 214-221.
- Air France, 2003. Manuel d'utilisation Concorde.
- Airlines for America, 2017. A4A Passenger Airline Cost Index (PACI).
- Boeing, 2019. Commercial market outlook 2019-2038.
- Bresenham, J.E., 1965. Algorithm for computer control of a digital plotter. *IBM Systems Journal* 4, 25-30.
- BTS, 1995. American Travel Survey (ATS) 1995. <https://www.transtats.bts.gov/>.
- Daniel, K., Nash, A., Koeing, S., Felner, A., 2010. Theta\*: Any-angle path planning on grids. *Journal of Artificial Intelligence Research* 39, 533-579.
- FAA, 2015. 2015 inventory as modeled in Aviation Environmental Design Tool (AEDT).
- FAA, 2018. FAA aerospace forecast – fiscal years 2018-2038.
- FAA, 2020. Aviation Environmental Design Tool (AEDT) version 3c – user manual.
- Graver, B., Rutherford, D., 2018. Transatlantic airline fuel efficiency ranking, 2017.
- Hassan, M., Pfaender, H., Mavris, D., 2020. Design tools for conceptual analysis of future commercial supersonic aircraft, in: AIAA Aviation 2020 Forum. doi:10.2514/6.2020-2620.
- Henne, P.A., 2005. Case for small supersonic civil aircraft. *Journal of Aircraft* 42, 765-774.
- IATA, 2019. IATA economics chart of the week: Air travel frequency flattens in developed markets, rises in emerging markets.
- Liebardt, B., 2019. Sonic boom carpet computation as a basis for supersonic flight routing, in: AIAA Aviation 2019 Forum, p. 3387.
- Liebardt, B., Gollnick, V., Lütjens, K., 2011. Estimation of the market potential for supersonic airliners via analysis of the global premium ticket market, in: 11th AIAA Aviation Technology, Integration, and Operations (ATIO) Conference, p. 6806.
- Liebardt, B., Linke, F., Dahlmann, K., 2014. Supersonic deviations: Assessment of sonic-boom-restricted flight routing. *Journal of Aircraft* 51, 1987-1996. doi:10.2514/1.C032591.
- Liebardt, B., Lütjens, K., Tracy, R., Haas, A., 2017. Exploring the prospect of small supersonic airliners – A case study based on the Aerion AS2 jet, in: 17th AIAA Aviation Technology, Integration, and Operations (ATIO) Conference, p. 3588.
- Sun, Y., Smith, H., 2017. Review and prospect of supersonic business jet design. *Progress in aerospace sciences* 90, 12-38.
- WID, 2019. World Inequality Database (WID). <https://wid.world/data/>.
- Zheng, X.S., Rutherford, D., 2019. U.S.-Latin America airline fuel efficiency ranking, 2017-2018.



# Project 017 Pilot Study on Aircraft Noise and Sleep Disturbance: Final Report

## University of Pennsylvania

### Project Lead Investigator

Mathias Basner, MD, PhD, MSc  
Associate Professor of Sleep and Chronobiology  
Department of Psychiatry  
University of Pennsylvania  
1019 Blockley Hall, 423 Guardian Dr.  
Philadelphia, PA 19104-6021  
215-573-5866  
basner@penncmedicine.upenn.edu

### University Participants

#### University of Pennsylvania

- PI(s): Mathias Basner, associate professor
- FAA Award Number: 13-C-AJE-UPENN-011
- Period of Performance: October 01, 2015 to September 30, 2018
- Task(s):
  - Pilot study on aircraft noise and sleep disturbance around Atlanta (ATL) airport

### Investigation Team

Mathias Basner, Associate Professor, University of Pennsylvania: P.I. and lead on all tasks

Michael Smith, Postdoctoral researcher, University of Pennsylvania: Data analysis on all tasks

Sarah Rocha, Research assistant, University of Pennsylvania: Data collection and technical and administrative support on all tasks

Maryam Witte, Research assistant, University of Pennsylvania: Data collection and technical and administrative support on all tasks

Katharine Casario, Research assistant, University of Pennsylvania: Technical and administrative support on all tasks

### Project Overview

The long-term goal of this line of research is to derive exposure–response relationships for aircraft noise-induced sleep disturbance that are representative of the exposed U.S. population. Studies will have to investigate samples around multiple airports; therefore, it will not be possible to use polysomnography [i.e., simultaneous recording of the electroencephalogram (EEG), electromyogram, and electrooculogram] to monitor sleep because this would require trained personnel at the measurement site in the evening and morning, which would be too costly. An alternative method of using



a single-channel electrocardiogram (ECG) and actigraphy to monitor sleep has been examined. This would allow investigation of a greater number of subject samples at lower cost because individuals can be taught how to apply the electrodes themselves. Also, in contrast to polysomnography, awakenings can be identified automatically. Awakenings are defined as brain activations (so-called EEG arousals) that last 15 s or longer. As part of previous research, we refined an algorithm for identifying EEG arousals (Basner et al., 2007) based on increases in heart rate to identify only those arousals  $\geq 15$  s in duration, which is the most agreed upon indicator of noise-induced sleep disturbance. High agreement was obtained between arousals scored visually from the EEG and those identified using the refined ECG-based algorithm. The method of using ECG and actigraphy to monitor sleep has been implemented in two pilot field studies to evaluate the quality of data that can be obtained for unattended physiological and noise measurements. Based on lessons learned, the study protocol is being refined to inform the design and cost of a potential multi-airport study on the effects of noise on sleep.

## Task 1 - Pilot Study on Aircraft Noise and Sleep Disturbance Around Atlanta Airport

### Objective(s)

Aircraft noise can disturb sleep and impair recuperation. Research is needed to develop exposure-response relationships that are representative of noise-exposed communities around multiple airports and that can be used to inform noise mitigation policy in the United States. To achieve this goal, we will conduct a field study around airports throughout the U.S. in which we will measure both aircraft noise exposure in the bedroom and physiologic response to this noise during sleep. In order for this National Sleep Study (NSS) to be feasible, which is anticipated to involve scores of airports and several hundred participants, an inexpensive yet sound study methodology is needed. In an earlier pilot study around Philadelphia International Airport (PHL) we demonstrated that electrocardiograph (ECG) electrodes and actigraphs measuring body movements could easily and non-invasively be applied to the torso by study participants themselves. This greatly reduces the methodological study cost compared to fully attended studies. In a second pilot study, which forms the basis of this report, the methodology of using ECG and actigraphy to monitor sleep was implemented around Atlanta Hartsfield-Jackson International Airport (ATL). The primary objective of this study was to continue improving study methodology, in particular evaluating the quality and quantity of data that could be obtained when recruiting participants by postal questionnaire, shipping them the physiological and noise measurement equipment, and the unattended setup of the equipment and recording of data by the participants themselves, in preparation for the larger-scale NSS. A secondary objective of the study was to compare objective and subjective measures of sleep and health between groups exposed to different levels of nocturnal aircraft noise.

### Research Approach

#### I. Summary

We mailed 4080 questionnaires containing items on sleep, health and noise disturbance to residences around ATL that were exposed to at least 35 dB  $L_{\text{Night}}$  aircraft noise. A number of different mailing strategies were adopted to maximize response rates. Prepaid cash incentives and sending follow-up reminder and survey waves were an effective method of improving response rates.

Completed questionnaires were received from 407 respondents, who were broadly representative of their geographical region. Among these respondents, calculated outdoor nighttime air traffic noise was significantly associated with self-reports of worse overall sleep quality, trouble falling asleep within 30 minutes, annoyance, and sleep disturbance. Residents in areas exposed to higher levels of aircraft noise coped by closing the windows at night.

From among the questionnaire respondents, 37 participants were initially recruited into the field study, with 34 participants completing five nights of unattended sleep measurements and 3 recruits dropping out before the study began. Data of sufficient quality and quantity to investigate the effects of aircraft noise on sleep were obtained, despite some data loss in the field study due to technical issues with the equipment and non-compliance among the participants. The technical issues were the main cause of data loss however, and non-compliance was low, with both physiologic and acoustic data collected by the participants in 87.6% of all study nights.



Concerning the primary objective of the study, evaluation of the feasibility of the study methodology, we demonstrated both the feasibility of recruiting field study participants by postal questionnaire in a larger, more nationally representative sample for future studies around multiple airports, and the feasibility of mailing equipment to participants to obtain unattended physiologic and acoustic measurement data.

Regarding the secondary objective of the study, investigating noise-induced effects on physiologic and self-reported sleep, a number of statistically significant outcomes were found, including associations between aircraft noise and physiologic and recalled awakenings. However, these findings are from a sample population of limited size, living close to a single airport. The findings of physiologic and self-reported effects of aircraft noise on sleep may not be representative of response among a demographically diverse national study population exposed to different patterns of nocturnal aircraft noise. A larger-scale study among such a population should be performed in the future, and the approach used in the present pilot study has been demonstrated to be feasible for this purpose.



## II. Glossary of terms

ATL	Hartsfield-Jackson Atlanta International Airport
A-Weighting	Frequency weighting filter applied to a sound measurement to mimic the frequency-dependence of human hearing
dB	Decibel, relative to the threshold of human hearing ( $2 \times 10^{-5}$ Pa)
dB(A)	A-weighted decibel
CI	Confidence interval
DLR	German Aerospace Center (Deutsches Zentrum für Luft- und Raumfahrt)
ECCG	Electrocardiogram
EEG	Electroencephalogram
EMG	Electromyogram
EOG	Electrooculogram
FAA	Federal Aviation Administration
FRA	Frankfurt Airport
H5	Zoom H5 Handy Recorder
ICBEN	International Commission on the Biological Effects of Noise
INM	Integrated Noise Model
$L_{Aeq,sleep}$	A-weighted equivalent continuous sound pressure level during an individual's sleep period time from sleep onset to sleep cessation
$L_{Aeq,t}$	A-weighted equivalent continuous sound pressure level over specified time period $t$
$L_{AF,max}$	Maximum A-weighted sound pressure with fast (0.125 s) time constant
$L_{AS,max}$	Maximum A-weighted sound pressure with slow (1 s) time constant
$L_{Night}$	Nighttime (23:00-07:00) A-weighted outdoor equivalent sound pressure level from aircraft
$L_{Night,cat}$	Nighttime (23:00-07:00) A-weighted outdoor equivalent sound pressure level from aircraft, categorized into 5 dB bins
NSS	National Sleep Study
PHL	Philadelphia International Airport
PSQI	Pittsburgh Sleep Quality Index
PSG	Polysomnography
SPL	Sound pressure level
SSS	Stanford Sleepiness Scale
UPenn	The University of Pennsylvania
XL2	NTi Audio XL2 Class 1 sound level meter



### III. Background and introduction

Humans spend approximately one third of their lives asleep, yet the core function or functions of sleep remains elusive. Some of the proposed functions of sleep include clearance of neural waste products that build up in the central nervous system during wakefulness, reducing cellular stress, synthesis of cellular components in preparation for the next period of wakefulness, consolidation of memories and restoration of cognitive performance [1-5]. Whatever the core function of sleep, it is critical for good physical and mental health, and chronic short sleep duration is associated with increased risk for obesity in both adults and children, diabetes, hypertension, cardiovascular disease and all-cause mortality [6-10]. Nocturnal traffic noise can impair physiologic and subjective sleep, by causing cortical awakenings and self-reported sleep disturbance [11]. With the most recent US sleep study dating back to 1996 [12], US research on the effects of aircraft noise on sleep, particularly compared to the efforts of some European countries, has lagged over the past 20 years. During the intervening time, US air traffic has changed significantly, with substantial increases in traffic volume over the past 30 years on one hand, and significant reductions in noise levels of single aircraft on the other. Due to inter-cultural differences and different operational procedures, results from studies performed outside the US may not translate directly to US domestic airports. Therefore, it is important that field studies be conducted in the US to acquire current data on sleep disturbance relative to varying degrees of noise exposure.

The long-term goal is to perform a National Sleep Study (NSS) throughout the U.S. to derive exposure-response relationships for aircraft noise-induced sleep disturbance that are representative for the exposed US population. Since airports differ in nocturnal traffic volume and pattern, it will be necessary to investigate several airports across the US that are representative for all US airports with relevant nocturnal air traffic to achieve this goal. The pilot study presented in the current report represents a preparatory step towards implementing the NSS. Prior to this point, we made significant progress during our work within the FAA Centers of Excellence PARTNER and ASCENT to achieve this long-term goal (Table 1).

Table 1. Overview of previous accomplishments made as part of the PARTNER COE.

Funding Period	Result
2010-11	Proposed an initial study design for a US field study on the effects of aircraft noise on sleep.
2011-12	Refined the ECG-based algorithm for the automatic detection of cortical arousals to better reflect EEG awakenings. This refinement was based on the 2011 NORAH <sup>1</sup> data.
2012-13	Validated the refined ECG-based algorithm with the 2012 NORAH data. Wrote a MatLAB™ software interface that facilitates the automatic identification of EEG awakenings based on a single channel ECG and body movements.
2013-14	Completed preparation for a field study examining the effects of aircraft noise on sleep around Philadelphia International Airport (PHL). GIS modeling of socio-demographic characteristics were completed to select the control area. Developed study materials including recruitment flyers and questionnaires. New hardware was purchased and coupled with software.
2014-15	Completed a pilot field study on the effects of aircraft noise on sleep around PHL and in a control area not exposed to aircraft noise.

**In 2010/2011**, we proposed an initial study design for the NSS [13]. Models relating noise characteristics of single aircraft events (e.g. maximum A-weighted sound pressure level,  $L_{AS,max}$ ) and physiological reactions (e.g. awakenings) will be the primary outcome of the NSS, which will have to investigate samples representative of exposed populations, and therefore sample more subjects than similar studies that have been conducted in the past. The gold standard for measuring sleep is polysomnography (PSG), which is the simultaneous measurement of the electroencephalogram (EEG), electrooculogram

<sup>1</sup> NORAH was a multi-disciplinary study on the effects of aircraft noise performed around FRA Frankfurt Airport (Frankfurt, Germany).



(EOG), and electromyogram (EMG). This method has been implemented in a few field studies on the effects of road, rail, or aircraft noise on sleep [14-17]. However, PSG is methodologically expensive to implement. Trained staff are needed at the measurement site in the evening and the morning to respectively apply and remove the electrodes. Trained sleep technologists are needed to visually score sleep stages, which has both high intra- and inter-rater variability [18, 19]. Finally, the methodology is somewhat invasive and may itself influence sleep, especially during the first night(s) [20]. For these reasons, it is not viable to implement PSG in studies of the planned scale; as of July 2019 the NSS is anticipated to involve 400 field study participants living around 77 airports within the U.S. Based on the 2010/2011 results of PARTNER Project 25B, it was proposed to use a combination of actigraphy (skeletal muscle movement) and electrocardiography (heart rate) instead of PSG, which will allow a cost-effective and methodologically sound investigation of large subject cohorts.

Awakenings are typically associated with arousals of the autonomic nervous system, which include increases in heart rate and blood pressure. In prior publications, we were able to show the potential of an automatic ECG-based algorithm to predict cortical arousals [21, 22]. During an earlier project, this algorithm was refined in order to only identify cortical arousals that are 15 seconds or longer in duration [23], which is the indicator of noise-induced sleep disturbance most commonly used [24].

**In 2011/2012**, the University of Pennsylvania (UPenn) and the German Aerospace Center (DLR) collaborated to develop common methodological approaches to be used both in the NSS and in a DLR field study (called NORAH) [25-27]. The first two waves of the NORAH study (summers of 2011 and 2012) used standard PSG to investigate 120 subjects living around Frankfurt Airport (FRA) for 3 consecutive nights. In the third wave, 187 volunteers (including 39 who participated in all 3 waves) were investigated with the less methodologically expensive ECG-based method for the detection of awakenings [28]. The advantage of replacing PSG with the less costly actigraphy and ECG-algorithm is that much larger and representative subject populations can be investigated at an acceptable cost. However, the validity of the ECG-based algorithm is crucial for the success of the NSS that will rely only on actigraphy and the ECG.

The ECG algorithm was originally programmed to detect cortical arousals (defined as activations lasting 3 s or longer) rather than EEG awakenings (defined as cortical activations lasting 15 seconds or longer). In terms of noise effects prediction and noise policy, EEG awakenings may be superior indicators of noise induced sleep disturbance than cortical arousals [29]. Noise policy and noise indices based on awakening probability are already in use at the airports in Leipzig/Halle, Zurich, and Frankfurt [30, 31]. A 2012 assessment of the effects of aircraft noise on sleep at Montreal airport was also based on awakening probability [32].

In the 2011-2012 period, the ECG algorithm was thus refined to better reflect EEG awakenings (i.e., it was the goal to detect cortical arousals 15 seconds or longer). However, with  $\kappa=0.733$ , the agreement fell short of an a priori set goal of  $\kappa=0.80$  which marks the beginning of "almost perfect" agreement [33].

**In 2012-2013**, the ECG algorithm was thus further refined. It now combines arousals that are scored based on the ECG and actigraphically-determined body movements, and it is able to estimate sleep onset and offset based on heart rate and movement activity alone. A comparison of kappa values based on the refined algorithm is shown in Figure 1.

The pre-defined threshold of  $\kappa=0.80$  was surpassed (0.86). As UPenn's algorithm outperformed DLR's algorithm, we moved forward with Penn's algorithm only. We developed a MatLAB™ software interface that allows an easy analysis of ECG and actigraphy data, and automatically outputs start and end times of automatically detected arousals.

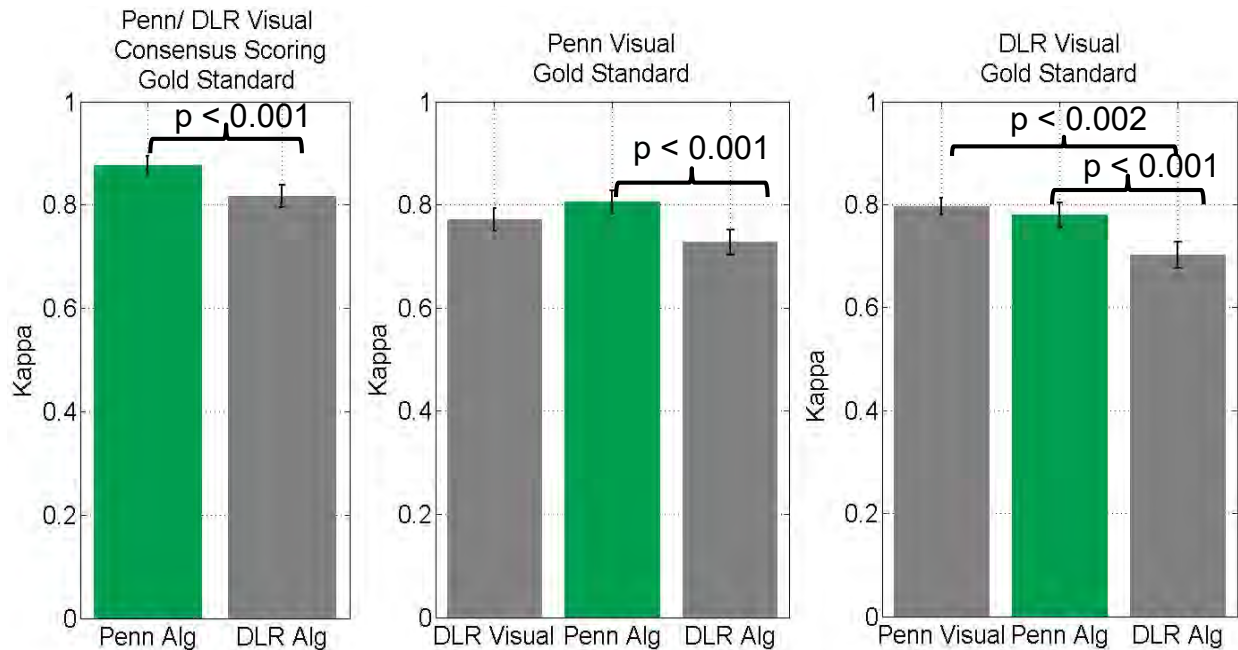


Figure 1. Chance corrected agreement (kappa) between visual (DLR, Penn) and automatic (DLR Alg, Penn Alg) arousal scorings is shown for a consensus arousal scoring (left graph), for Penn visual scoring being the gold standard (middle graph), and for DLR visual scoring being the gold standard (right graph). Kappa values indicated almost perfect (kappa>0.80) agreement between both algorithms and the consensus scoring. Penn's algorithm significantly outperformed DLR's algorithm in all three comparisons. Importantly, the agreement with the gold standard did not differ significantly between Penn's algorithm and both of the two visual scorings (p>0.05). Arousals had to last 15 s or longer to better reflect traditionally defined EEG awakenings [34].

**In 2013-2015**, we performed a pilot field study around Philadelphia International Airport (PHL) using the developed ECG and actigraphy methodology, with measurements performed unattended in order to assess the feasibility of such an approach in the NSS. In order to determine the airport for the study we examined flight operations for 4 months: from June 2012 to September 2012, for PHL. Cumulative nighttime metrics (LNight) and single event metrics (LAS,max) were predicted using the FAA's Integrated Noise Model (INM). Although the number of people exposed to high noise levels ( $\geq 55$  dB LNight) was found to be low around the airport, due to the airports close proximity to UPenn and the number of night events (on average 130 events between 11:00 PM and 7:00 AM), the decision was made to conduct this pilot study at PHL. To select a control region where dwellings were not exposed to aircraft noise, GIS modeling of data from the American Community Survey was performed on the census tract level. Eighty participants were recruited, 40 from a region with aircraft noise exposure near the airport and 40 from a control region in Philadelphia County. Control region participants were comparable to the exposed group of subjects in terms of sociodemographic characteristics and non-aircraft traffic exposure, but without relevant amounts of nighttime air traffic. Each participant completed three consecutive nights of ECG and actigraphy measurements with concomitant noise level measurements and sound recordings each night in their bedroom. Additionally, participants completed brief questionnaires subjectively assessing their sleep each morning. All objective and subjective measurements were performed unattended, with staff going to the participant's home only on the first and last day of the study to setup and collect the equipment, respectively. Overall, it was found that participants were able to follow the study protocol well. For 93.4% of the nights, there were no missing periods of ECG data due to participants not wearing the device or due to improper use of the device, electrodes, or cables. For 5.7% of the nights, partial ECG recordings were obtained and for only 0.9% of nights no valid ECG data was recorded. For 89.4% of the nights, full sound recordings were obtained. Data loss was due to either equipment problems or participants failing to turn on the sound recorder at night. All questionnaires for the study were completed. The surveys were web-based which allowed staff members to verify completion of the surveys in real time and contact participants if the study protocol was not being followed.



Single event awakening analysis based on random effect logistic regression was conducted to examine whether the indoor noise level of single aircraft events ( $L_{AS,max}$ ) was related to awakenings determined with the ECG and actigraphy. The coefficient for  $L_{AS,max}$  was positive and statistically significant (i.e., higher noise levels were associated with increased awakening probability). One limitation of the derived exposure-response relationship was the wide confidence interval due to the small sample size and the comparatively low number of events per subject in this pilot study. The results of the PHL study indicated that the protocol needed further refinement for a potential future multi-site US field study on the effects of aircraft noise on sleep. While the target enrollment was met, the response rate was low, which restricts generalizability of the findings.

**In 2015-2017**, we performed a follow-up pilot study, around Atlanta Hartsfield-Jackson International Airport (ATL), and completed data analysis in 2019. The method and results of this study are presented in this report. The primary objective of this current study was to evaluate the feasibility of the study methodology that could be implemented in the future NSS, in particular the quantity and quality of data that could be obtained when recruiting participants by postal questionnaire, shipping them the physiological and noise measurement equipment, and the setup of the equipment and recording of data by the participants themselves, completely unattended. A secondary objective of the study was to compare objective and subjective measures of sleep and health between groups exposed to different levels of nocturnal aircraft noise.



## IV. Study Methodology

### A. Overview

The study was designed to assess the feasibility of obtaining in-home aircraft noise measurements and physiologic measurements of awakening from sleep, without the need for trained staff on-site. Atlanta Hartsfield-Jackson International Airport (ATL) was one of several US airports with relevant nocturnal air traffic, and chosen by the FAA as the study site for this pilot study. Modelled nighttime noise exposure around ATL and census tract demographic data were used as the basis for selecting the field study target population (section IV.C). Participants for the study were recruited by postal questionnaires (section IV.D), with a number of different mailing strategies used in order to determine how to maximize response rates (sections IV.E and V.A ). Prospective study participants received one of three recruitment surveys of different length (section IV.D and Appendix 2). Field study eligibility (see section IV.E.2 for eligibility criteria) could be determined with the long and medium versions of the survey. Participants had to be re-contacted to determine eligibility for the short survey. Participants were then shipped equipment to measure aircraft noise and physiologic data during sleep (sections IV.B, IV.F), which they set up themselves in their own bedrooms. After recording five nights of data (Monday night/Tuesday morning through to Friday night/Saturday morning) and completing questionnaires each morning on subjective sleep (sections IV.F.3 and V.D), participants mailed the equipment back. Data were then downloaded and analyzed using a suite of software developed for the project in collaboration with investigators at DLR (section IV.G). Noise and ECG recordings were used to determine noise-induced event-related awakening probabilities (section V.E), with particular attention given to the efficacy of the methodology on providing usable data in the future NSS (section V.G).

The protocol of the pilot study was approved by the Institutional Review Board of the University of Pennsylvania (IRB #823726). Participants in the field study provided informed, written consent prior to taking part in the study. All private contact information for study participants was stored in a Redcap database, a secure web application designed to support data capture for research studies. Web-based community surveys were implemented through Redcap's secure system. Participant responses to paper copies of the community survey were entered separately by two staff members into Redcap's online survey database. Any discrepancy between the two data entries were resolved in consensus. For participants interested in participating in the in-home sleep study, eligibility was determined (see section IV.E.2 for eligibility criteria). Information on those participating in the in-home sleep study was stored in Redcap as well. Data were recorded on when participants were scheduled to complete measurements, which equipment was shipped to their home, when it was returned, and if there were equipment failures or damage to equipment.



## B. Equipment identification and testing

For the study to be feasible on a national scale, it was important to obtain high quality acoustic and physiologic data while keeping equipment costs low. A breakdown of the equipment used in the field study is given in section IV.B.1. Equipment was tested before buying multiple units to ensure it met the required data acquisition specifications (section IV.B.2).

### 1. Equipment selection and cost breakdown

Study equipment (see Appendix 1) was shipped directly to participants, who unpacked and set-up equipment unattended (i.e., without research staff on site). It was therefore necessary that the noise and sleep measurement equipment we used could be set up and operated easily, with the participants able to follow simple instructions to do so, even if they did not have technical knowledge. Just as importantly, in order for the study to be feasible on a large scale, it was necessary to select recording equipment that was both low-cost and accurate in its measurement.

The H5 Handy Recorder (Zoom Corp, Tokyo, Japan) with an Earthworks M23 measurement microphone (Earthworks Inc., Milford, NH) was selected for recording acoustic data in participants' bedrooms (see section IV.B.2 for equipment testing results). Prior to shipment, the H5 recorder and microphone were fastened to a tripod and a remote control was provided to subjects for their convenience.

The Faros 90 (Bittium Corp, formerly eMotion, Oulu, Finland) was chosen to measure heart rate and actigraphy data. We have previously demonstrated the ability of the Faros 90 devices to reliably capture ECG and actigraphy data for the scoring of noise-induced awakenings among field study participants at PHL and FRA airports [35].

A total of twenty sets of equipment were prepared for use in the field study. A breakdown of equipment cost for a set of study equipment is given in Appendix 1. A single set of equipment cost \$1261. In total, purchasing of study materials and testing of potential equipment designs cost \$28,381. These costs do not include those for personnel, storage, or expenses for shipping the study equipment to and from study participants.

### 2. Equipment testing

#### Noise recorder testing

Prior to purchasing all twenty Zoom H5 Handy Recorders and Earthworks M23 measurement microphones, two units were purchased and tested to ensure they met the manufacturer stated specifications, and that they were suitable for accurate measurement of aircraft noise levels.

To measure the noise floor of the H5 we used the following approach. A recording was initialized, the recorder was isolated from noise by placing a cap over the microphone, sealing the recorder in a box filled with foam, and then placing the sealed box in a cupboard in the quietest room available at our laboratory. The resulting noise floor of the equipment was 22 dB(A).

Measurements were made with the H5 and compared against measurements of the same sound signal made with two Class 1 sound level meters (XL2, NTi Audio). All systems were first calibrated using a 1 kHz calibration signal at 94 dB (Larson Davis CAL200). This calibration signal was stored for the H5 recorders. As in the actual field study, the sounds recorded with the H5 were stored as MP3 files (320 bit). The stored calibration signal was used to convert these MP3 files into A-weighted sound pressure levels (see section IV.G.1 for a description of the software that was developed for this conversion). One XL2 unit was owned by us, and is hereafter termed XL2-UPenn. The second XL2 was loaned to us by the manufacturer NTi, and is hereafter termed XL2-NTI. An audio file of airplane flyovers and train pass-bys was used as the acoustic test signal, since the H5 recorders were to be used for traffic noise measurements. Sound pressure level measurements made with the H5, XL2-UPenn and XL2-NTI are presented in Figure 2. The region around the highest measured level (173-177 s) is presented in higher sound level resolution in Figure 3 for clarity. The difference in level measured with H5 and XL2-NTI relative to the level measured with XL2-UPenn during traffic noise playback is given in Figure 4. As expected there was almost no difference between both XL2 units. The noise floor of the XL2 units was around 3 dB lower than the H5. During noise measurement, there was close agreement between the H5 and XL2-UPenn, agreeing to within approximately 1.5 dB. There were very short intervals with slightly higher deviation between 160-175s (Figure 4), but at these points there were also deviations between both XL2 units. These deviations could be due to slight spatial variation in the microphone positions during measurement.

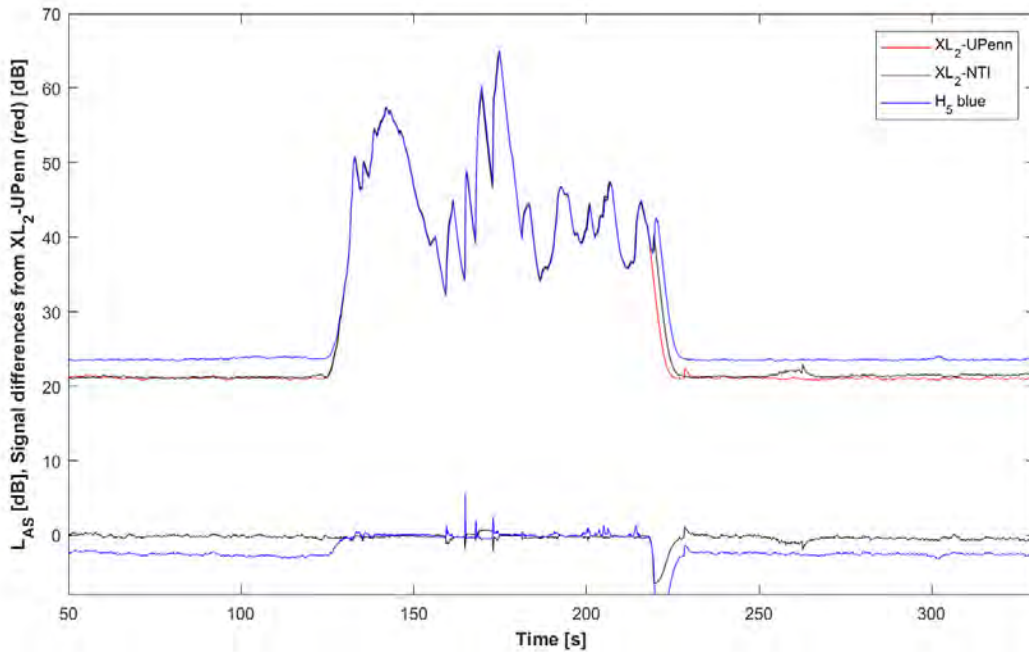


Figure 2. Measurement of traffic noise made with ZoomH5 (blue) and two XL2 sound level meters (black and blue). The upper lines represent the sound pressure level measurement (A-Weighted, slow time filter) made with each device. The lower lines represent the difference between the sound pressure level measured with H5 and XL2-NTI compared to measurements made with the XL2-UPenn. Note that the disparity between devices around 220-230 s is due to slight differences in noise cessation timing.

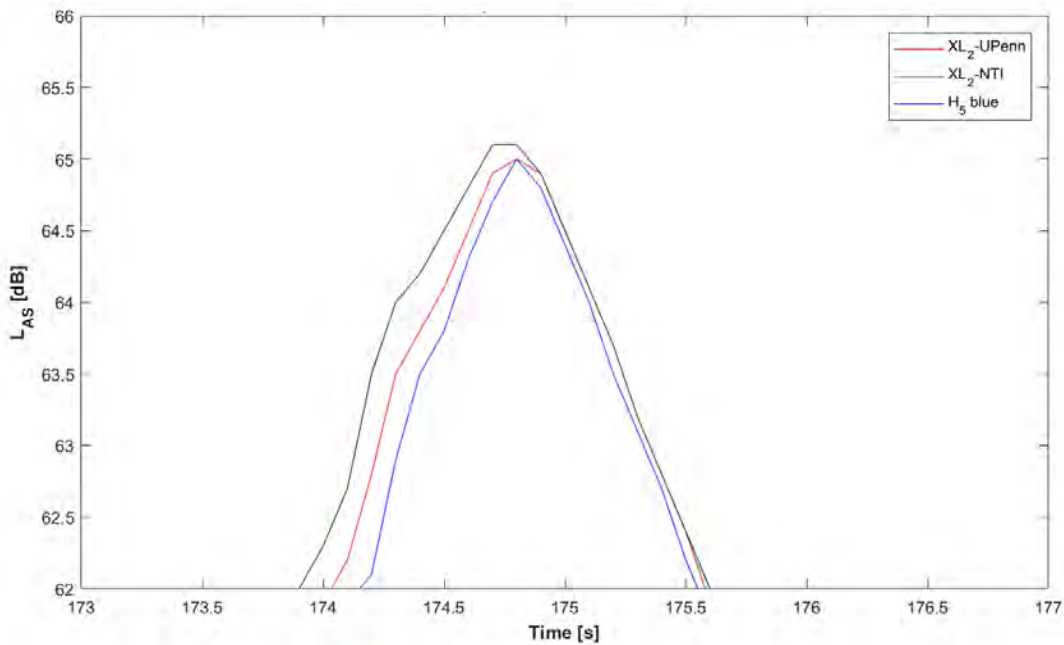


Figure 3. Measurement of traffic noise made with ZoomH5 (blue) and two XL2 sound level meters (black and blue) around the noise maximum.

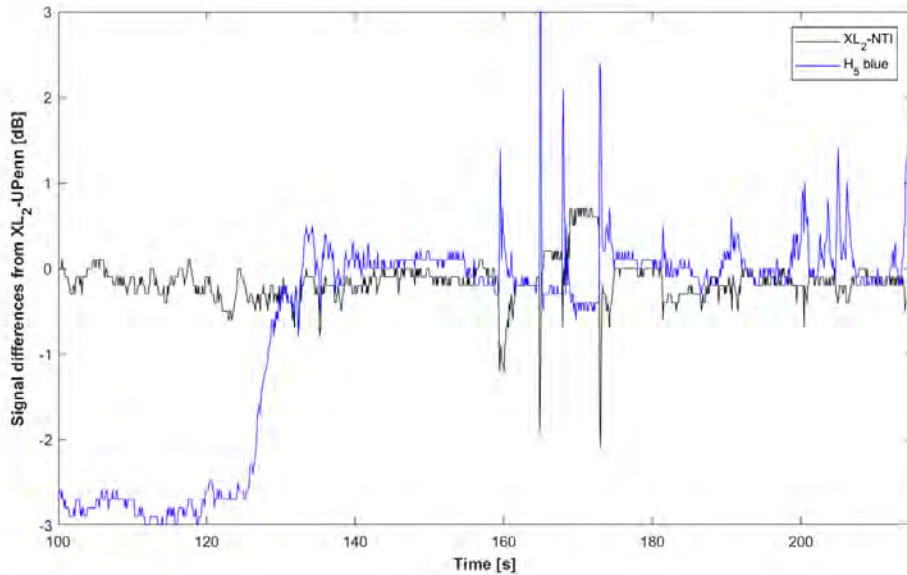


Figure 4. Difference in sound pressure level made with XL2-NTI (black) and H5 (blue) relative to measurement of the same noise signal made with XL2-UPenn.

We also compared the H5 unit used in the above measurements against a second H5 unit to examine inter-unit variability. The same procedure as above was used, and recordings were compared against those made with XL2-UPenn. The difference in level during the noise signal is given in Figure 5. Both H5 units generally agreed to within  $\pm 1$  dB, which is within the tolerance limits for Class 1 sound level meters [36].

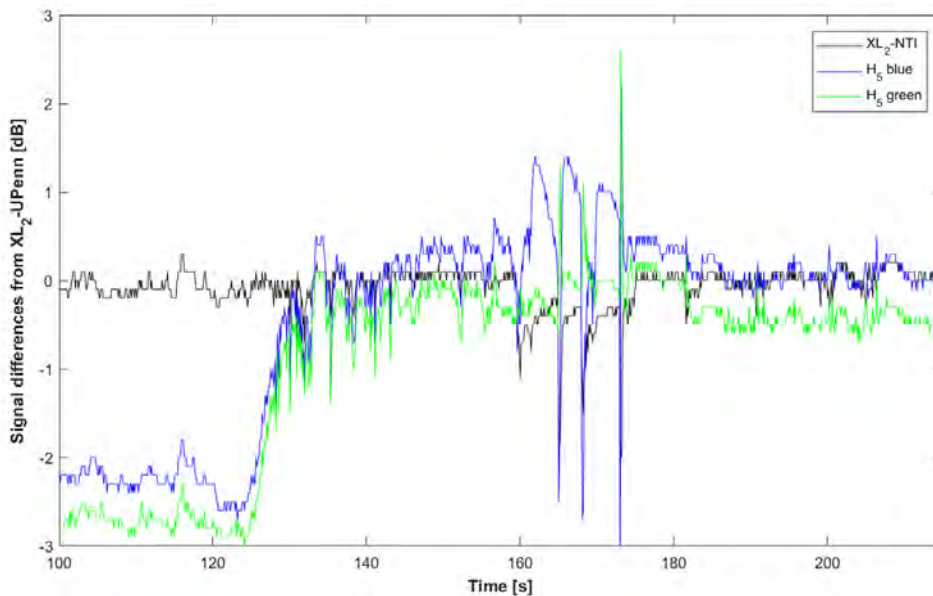


Figure 5. Difference in sound pressure level made with XL2-NTI (black), H5 (blue) and a second H5 (green) relative to measurement of the same noise signal made with XL2-UPenn. Measurements with H5 units generally agreed to within  $\pm 1$  dB.

In summary, Zoom H5 recorders using with Earthworks M23 microphones represent a cost-effective approach of performing accurate measurements of aircraft noise in a field study. All microphones were calibrated by the manufacturer.



### Faros and H5 time drift testing

For the event-related analysis, it is very important that acoustic and physiological events are recorded on a synchronized same timeline, so that an awakening in the physiologic data can be attributed to a concurrent aircraft event in the noise data. As we used two separate devices to record sounds (H5) and physiological data (Faros 90), we needed to ensure that there was minimal time drift between the devices, or alternatively develop a method allowing us to synchronize both data streams post-hoc. Prior to shipment to study participants, the internal clocks on the Faros 90 and H5 sound recorder were synchronized with the network time; however, study equipment was in the field for approximately 20 days, during which time was the potential for time drift in either or both devices. To investigate time drift between the devices, we performed a study in which movement detected in the physiological data and noise events detected in the acoustic data were matched. We tested all 20 Faros 90 devices (Figure 6-Figure 8) and four H5 recorders (Figure 9). We also tested an updated version of the Faros device, the Faros 180, for comparison (this device was not used in the ATL study, but may be used in future studies). The Faros devices and H5 recorders were initialized with the network time and then powered off. They were kept in a cool location for 1 week, simulating the time devices are in transit to participants. After 1 week, the Faros 90 and 180 were placed on a rotating table that rotated the devices at fixed intervals. The start of the rotation was indicated by a clicking sound which was recorded by the H5 sound recorders. We recorded differences in the event times, relative to the network master clock, between the acoustic and physiologic data throughout the 5 study days. These recordings were completed under a variety of test conditions to simulate common scenarios expected in the field. Recordings on the Faros devices were made in either a room-temperature environment (23 °C, Figure 6) or in a warm room (35 °C, Figure 7). In both the warm and cold room scenarios, the Faros devices recorded for 8 hours per day, simulating an anticipated 8 hour recording of sleep during the field study, and were turned off for the remaining 16 hours. Additionally, we also examined the time drift when the Faros devices were left running for the duration of the simulation (Figure 8), i.e. not turned off for the 16 hours each day, as subjects may forget to turn off the devices in the morning.

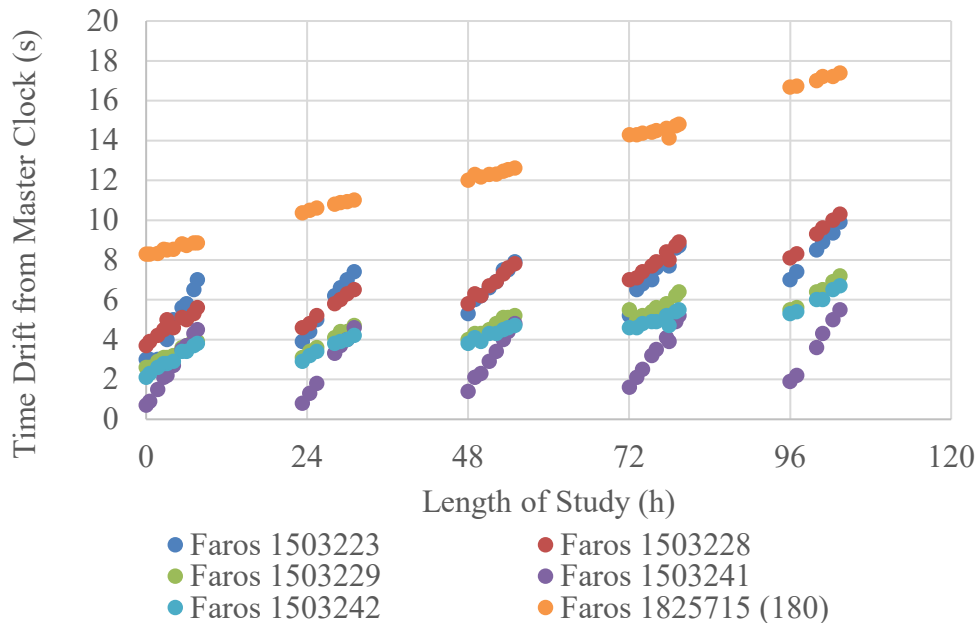


Figure 6. Time drift between master clock and five Faros 90 and one Faros 180 recorder internal clocks, recorded at room temperature (23 °C). Different colored points indicate different Faros units.

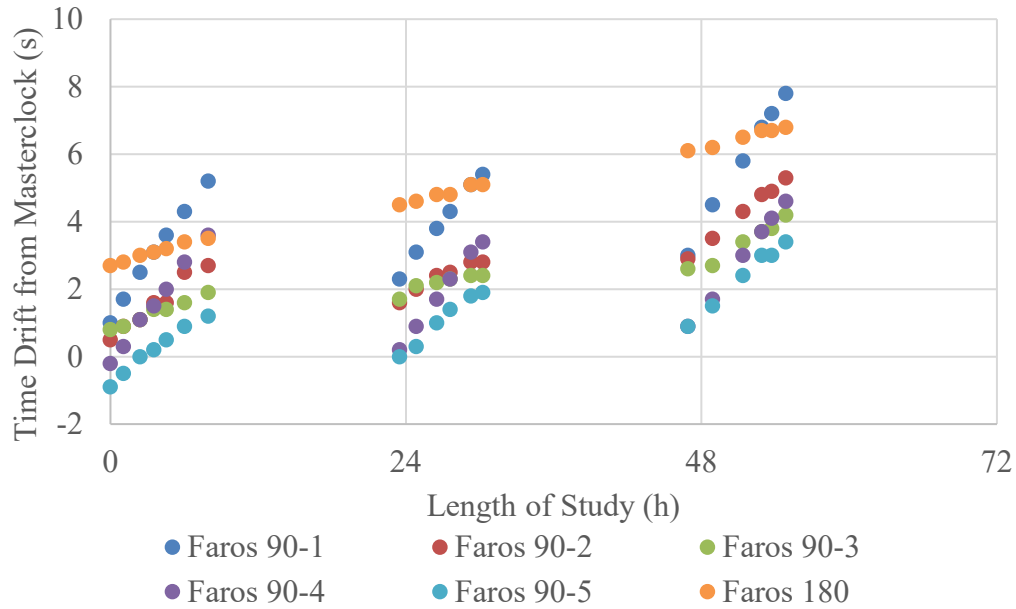


Figure 7. Time drift between master clock and five Faros 90 and one Faros 180 recorder internal clocks, recorded in a warm room (35 °C). Different colored points indicate different Faros units.

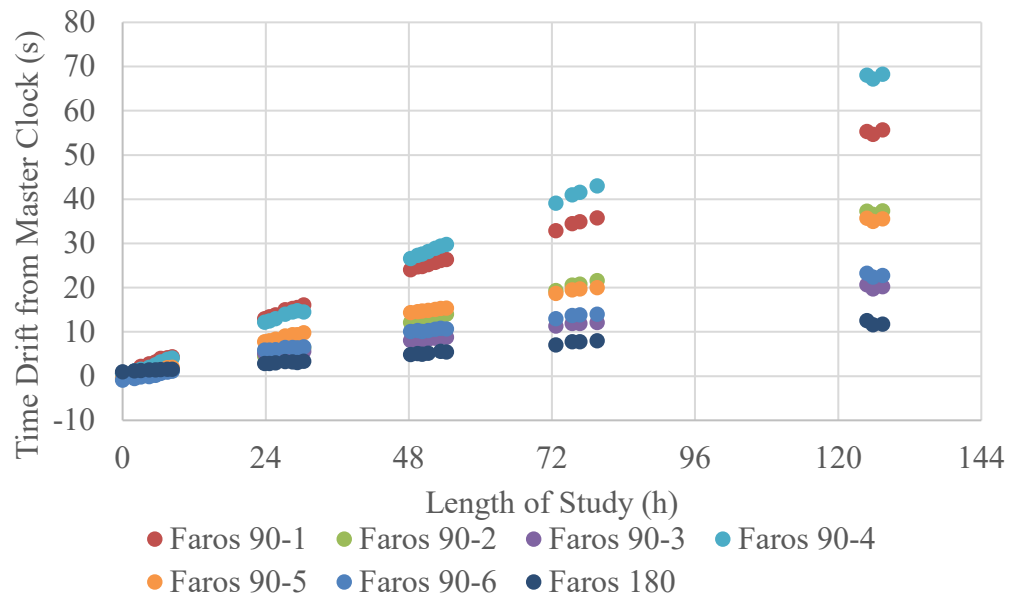


Figure 8. Time drift between the Faros devices and the master clock for the simulation in which the Faros are left running for the duration of the simulation, mimicking the scenario in which a participant forgets to turn off the Faros prior to charging. At the end of each day, the Faros were plugged into a charging port but continued running. It was found that the Faros 180 automatically turns off when plugged into a power source, and so this device did not run continuously during the simulation. At 96 hours of the simulation, technical staff were unavailable to run the simulation, and so the Faros were not rotated on the rotating table until hour 120 of the simulation.

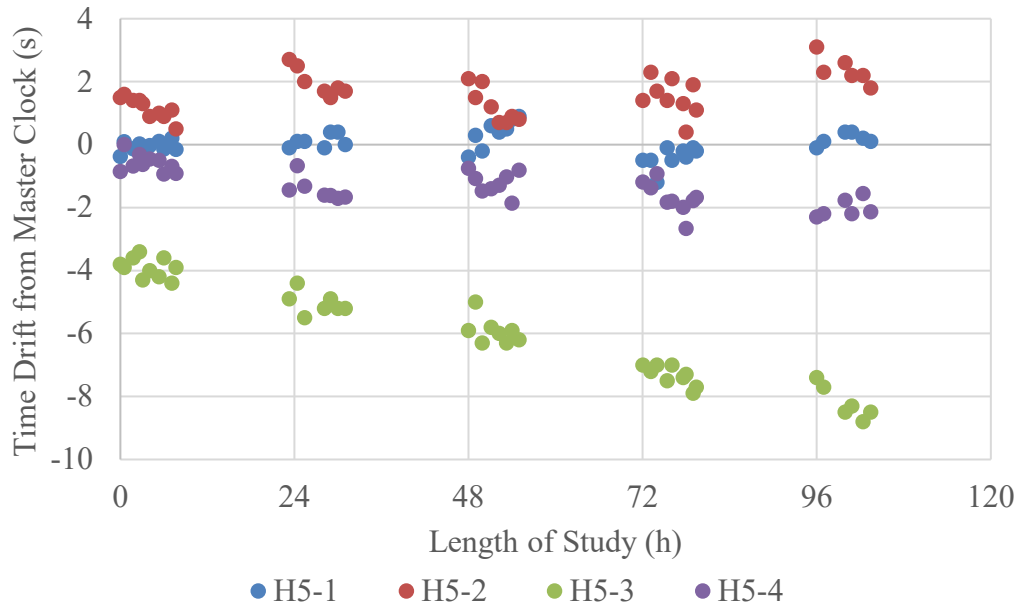


Figure 9. Time drift between master clock and H5 recorder internal clocks. Different colored points indicate different H5 units.

It was found that the Faros 90 clocks drifted approximately linearly within recording nights, both at room temperature and in a warm room, but did not appear to drift between nights when the devices were turned off. The Faros 180 clock also drifted linearly within recording nights, but continued drifting between nights when turned off. Out of the four H5 sound recorders that were tested, three drifted approximately  $\pm 2$  seconds from the master clock in a seemingly random pattern. A fourth H5 recorder drifted approximately 4 seconds from the master clock during the simulated transit week, and drifted a further 4 seconds during the five recording nights in a linear fashion. When switched on (and therefore recording) for extended periods of time, the Faros devices were found to continue to drift linearly for the duration of the simulation. Based on this evidence of time drift between the acoustic and physiologic data streams from our simulations, our DLR collaborator, Dr. Uwe Müller generated a time-synchronization software that matches body movements scored in the acoustic data with the body movements recorded in the physiological data (see section IV.G.3). Based on the simulation results above, a linear time drift across the measurement night was assumed for correction purposes.



### C. Selection of field study target sample region

The purpose of the field study was to investigate effects of aircraft noise on sleep. It was therefore necessary to stratify the sample population by nighttime aircraft noise exposure levels, so that recruitment from appropriate regions could be performed.

#### 1. Generating and validating noise contours around ATL airport

Noise exposure around ATL was modelled using the FAA’s Integrated Noise Model (INM) [37], implemented using the ArcGIS software (Esri, Redlands, CA).

Radar track data and flight plan data from the Performance Data Analysis and Reporting System (PDARS) [38] around ATL were provided by the FAA for the period of September 1<sup>st</sup> 2014 to August 31<sup>st</sup> 2015. Along with runway location and orientation, the PDARS data were used to model individual nighttime (23:00-07:00) aircraft noise events over 84 nights. These noise data were used to calculate outdoor nighttime A-weighted noise level ( $L_{Night,outdoor}$ ) contours around ATL. These modelled contours are presented as filled contours in Figure 10.

To validate the modelled contours, they were visually compared with yearly average  $L_{Night}$  contours from 2012 for 45, 50, 55 and 60 dB, which were also provided by the FAA. These are presented as lines in Figure 10. There was a good agreement between the FAA contours and our own modelled contours.

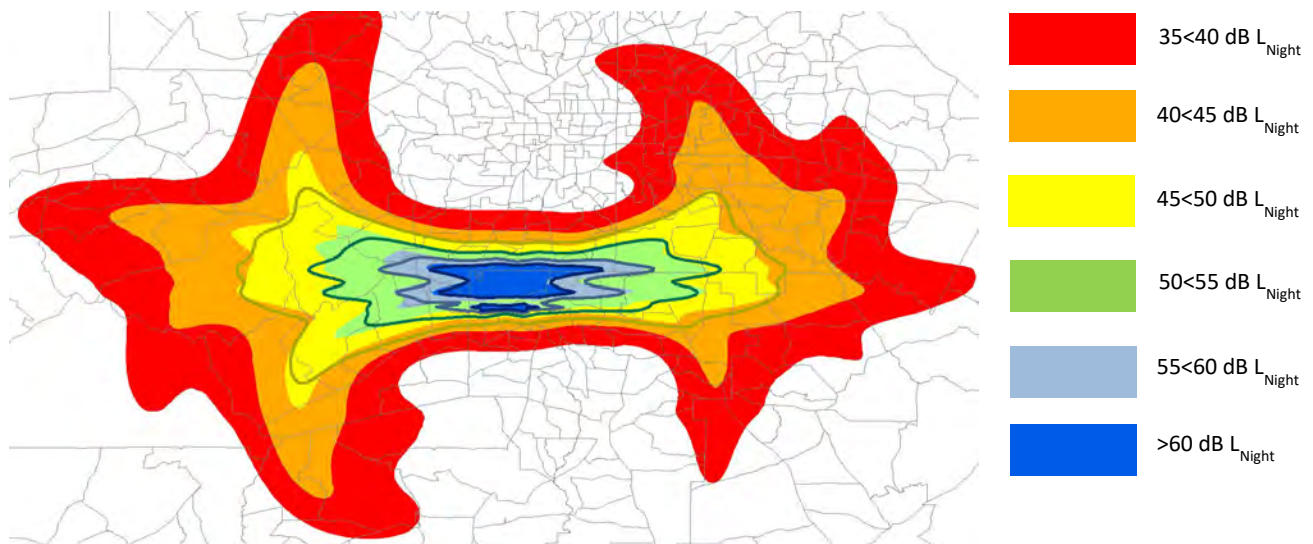


Figure 10.  $L_{Night}$  noise contours around ATL. Filled contours represent those calculated by UPenn. Line-only contours represent the 2012 average, provided by the FAA, and used only to validate the UPenn contours. Contours are overlaid on Atlanta census tract geographical boundaries.

Since  $L_{Night}$  was the primary exposure variable of interest, it was necessary to sample the study population from addresses with different noise exposure. We therefore stratified into five sampling regions: 35-39.9 dB, 40-44.9 dB, 45-49.9 dB, 50-54.9 dB and  $\geq 55$  dB. This stratification was performed based on the UPenn contours since the FAA contours had a lower limit of 45 dB  $L_{Night}$ , as compared to the UPenn contour lower limit of 35 dB  $L_{Night}$ .

#### 2. Population sampling procedure

Geographical shape information for the census tracts in and around Atlanta were extracted from TIGER/Line® Shapefiles (<https://www.census.gov/geo/maps-data/data/tiger-line.html>). These shapefiles are an extract of selected geographic and cartographic information from the U.S. Census Bureau's Master Address File / Topologically Integrated Geographic Encoding and Referencing (MAF/TIGER) Database (MTDB). Demographic data for these census tracts were extracted from



American FactFinder (<http://factfinder2.census.gov/>). For each census tract in each noise exposure category, the population weighted centroid was calculated using the extracted geographical and demographic information. The noise levels at each centroid were then calculated, before assigning the census tract into the 35, 40, 45, 50 or 55 dB  $L_{Night}$  category. The resulting assignment of each census tract is shown in Figure 11.

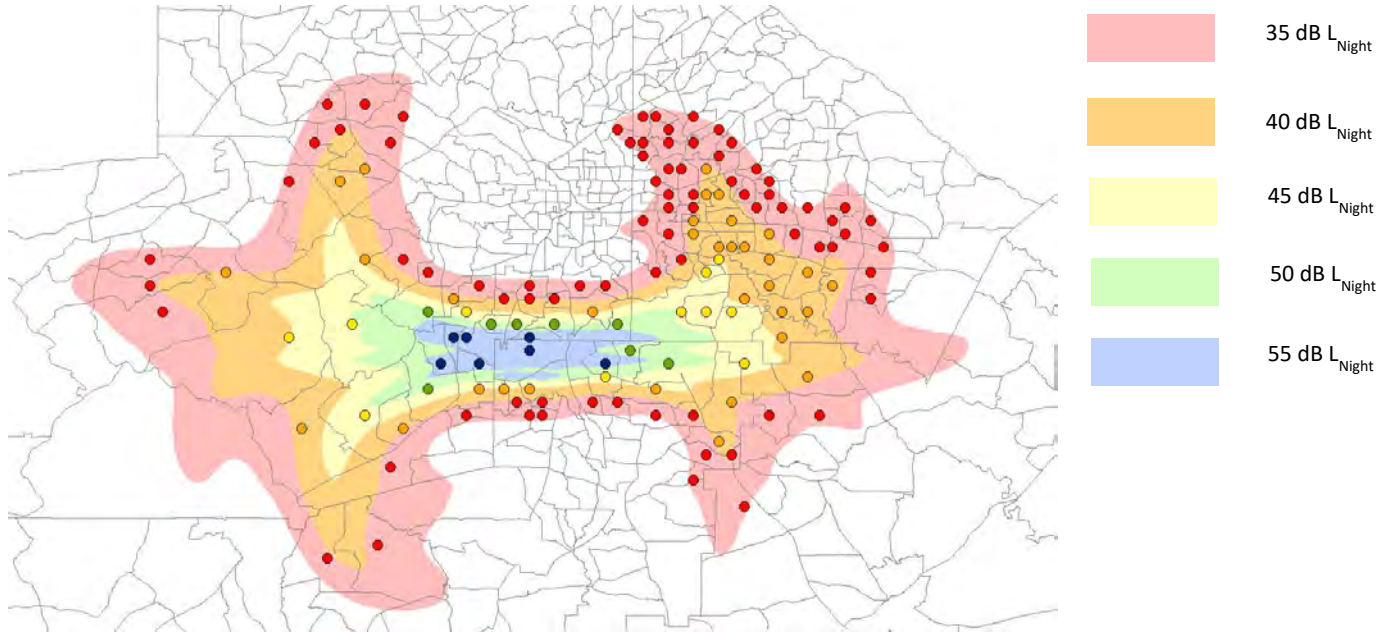


Figure 11. Population weighted centroid of each census tract, colored according to noise exposure category (noise contour) in which it is located.

In addition to classifying census tract by noise exposure, they were further sub-divided into their orientation relative to ATL airport, either west or east. The location of the population weighted centroid of each census tract relative to the airport coordinate (33.640444° N, 84.4269444° W) was used to assign whether the census tract was east or west of the airport. The number of census tracts in each noise exposure category is given in Table 2. Demographic data from the 2010-2014 American Community Survey 5-Year Estimates for the census tracts in each noise exposure category are given in Table 3.

Table 2. Number of census tracts in each noise category.

Noise category	n	West	East
≥55 dB	5	4	1
50-54.9 dB	8	4	4
45-49.9 dB	11	4	7
40-44.9 dB	34	10	24
35-39.9 dB	79	22	57
Total	137	44	93



Table 3. Demographic characteristics of census tracts within each noise category.

Noise category	Direction re: ATL	Houses (n)	% No College Education	% Black or African American	Mean income (\$)	Mean age (years)	Mean house price (\$)
≥55 dB	East	1949	59.5	55.1	33,624	29.4	60,300
≥55 dB	West	7305	50.8	90.7	26,737	29.4	105,975
50-54.9 dB	East	9464	59.7	59.6	31,126	30.7	78,950
50-54.9 dB	West	11,123	34.8	77.3	40,938	35.5	161,200
45-49.9 dB	East	14,489	46.3	83.6	46,964	35.4	102,971
45-49.9 dB	West	20,457	32.2	32.2	59,955	35.1	138,625
40-44.9 dB	East	53,391	41.9	77.4	50,249	38.4	126,300
40-44.9 dB	West	30,674	45.1	81.2	39,677	30	101,260
35-39.9 dB	East	118,182	35.7	52.7	50,684	35	182,782
35-39.9 dB	West	55,842	41.1	58.5	54,040	36.6	139,109

The 35-39.9 dB category was the control region for the study. The cost for obtaining addresses was \$50 for each census tract. To minimize cost we selected 16 census tracts from the 35-39.9 dB category (8 west and 8 east). These 16 control region census tracts were chosen so as to have a similar mean and variance of household income as in all 79 census tracts in the <40 dB category (Table 4).

Table 4. Demographic characteristics of 35-39.9 dB census tracts. Demographics of the census tracts selected as the control region are highlighted.

Direction re: ATL	Houses (n)	% No College Education	% Black or African American	Mean (M), range (R) and standard deviation (SD) income (\$)	Mean age (years)	Mean house price (\$)
East (n=57)	118,182	35.7	52.7	M: 50,684 R: 14,879-136,813 SD: 25,689	35.0	182,782
East, selected (n=8)	12,300	47.1	36.8	M: 50,376 R: 14,879-92,000 SD: 25,710	35.1	156,157
West (n=22)	55,842	41.1	58.5	M: 54,040 R: 24,129-103,333 SD: 19,177	36.6	139,109
West, selected (n=8)	22,302	38.4	60.2	M: 54,302 R: 37,446-83,969 SD: 19,191	35.7	148,450

Once the 74 census tracts from which we would sample was finalized, 10,000 residential addresses and inhabitant names within these tracts were purchased from MSG Marketing Group at a cost of \$1,325 (\$425 initial setup cost, \$50 for each of the 9 additional survey tracts, and \$450 for the 10,000 address-based sampling records). Each address was provided with its associated latitude and longitude.  $L_{Night}$  was then calculated for each individual address. Addresses were reclassified into the appropriate noise categories based on these  $L_{Night}$  noise levels and not based on the census tract population weighted centroid noise levels.



## D. Postal surveys

Postal questionnaires are an inexpensive and unobtrusive method of data sampling among large study populations, and so are widely used in epidemiological research. One of the challenges faced by public health research is the current trend for decreasing response rates to all survey modes [39], which leads to reduced effective sample sizes, and furthermore may bias the acquired data and subsequent conclusions [40]. To minimize threats to internal and external validity, the highest attainable response rate is therefore desirable. Researchers have adopted a number of methods to improve response rates, which include monetary and non-monetary incentives, changes in the length and appearance of questionnaires, different methods of returning completed questionnaires, pre-notification and different approaches to follow-up contact [41]. Reduced survey length, the use of incentives and follow-up contact for postal surveys can improve response rates, but these findings are not found universally across different studies [41, 42]. There is also a risk that incentives may introduce bias, by being more appealing to those with lower socioeconomic status [43]. Survey follow-up and incentivization also increases methodological expense, although this may be offset by the reduced need for further sampling from a study population to obtain an equivalent sample size.

Postal questionnaires can, in addition to furnishing researchers with valuable epidemiological data, serve as useful pre-screening instruments. Pre-screening questionnaires can determine a person's eligibility for, as well as their interest in, recruitment into later studies, although when relying on self-report there can be some risk for respondents to misrepresent themselves so that they can participate in the study [44]. Low response rates for questionnaires used for pre-screening may lead to non-representative sample populations in any subsequent studies, so it remains important to obtain the greatest achievable number of responses. For this pilot study, we therefore adopted a number of different survey strategies in order to determine how to maximize survey response and field study recruitment while minimizing cost.

### 1. Survey instruments

The primary purpose of the postal surveys was to recruit participants for the field study on the effects of nocturnal aircraft noise on sleep. Of primary importance therefore were questions regarding suitability as pertains to the study inclusion criteria (see section IV.E.2). The survey included a checkbox for respondents to indicate whether they were interested in participating in the field study, along with their contact details.

The secondary purpose of the surveys was comparison of eventual field study participants with non-participants. This allows for determining whether those who are eligible for the field study are representative of those who respond. This comparison can potentially inform weights to adjust for non-response bias.

Of tertiary importance in the questionnaires were items regarding the effects of noise on annoyance, sleep disturbance and health outcomes, to allow a cross-sectional analysis of community response to aircraft noise. The addition of these items increased the questionnaire length, which as a result could risk lowering response rates, while at the same time providing useful data on the effects of aircraft noise. We therefore used questionnaires of different lengths to investigate if longer questionnaires had a significant adverse effect on response rate.

Survey instructions indicated that only a single household member should fill out the survey (the person who most recently celebrated a birthday). Complete versions of the questionnaires are given in Appendix 2, and are only summarized here. Questionnaires differed in length and were characterized as short (11 questions), medium (26 questions) or long (57 questions). The long form of the survey asked respondents to provide basic demographic information, such as age, sex, race, income, marital status, education level, and employment status. Respondents were asked to rate their overall sleep quality on a 4-point Likert-type scale over the past month, which is an item taken directly from the Pittsburgh Sleep Quality Index (PSQI) [45]. They also indicated how often (on a 4-point scale from "not during the past month" to "three or more times per week") they experienced trouble falling asleep, waking up in the night or early morning, took medication for sleep, or had difficulty staying awake during the day, all of which are items from the PSQI. The survey asked about coping behaviors to environmental noise. Survey respondents were asked to estimate over the past month how often (on a 5-point Likert-type scale from "never" to "always") they "wear earplugs," "use alcohol," "use medication," "turn on the TV," "turn on music," "close windows," "use a sound machine," or "turn on a fan" because of noise when trying to sleep. Sensitivity to noise in the community was another variable examined, and respondents were asked to estimate on a 6-point ordinal scale their agreement with statements: "I am easily awakened by noise," "I get used to most noises without difficulty," "I find it hard to relax in noisy places," "I am good at concentrating no matter what is going on around me," "I get mad at people who make noise," and "I am sensitive to noise." All of the noise sensitivity questions and response scales were taken from the Weinstein Noise Sensitivity Scale [46]. Also, participants were asked to describe how much they were annoyed over the last 12 months (on a 5-point Likert-type scale with endpoints "not at all" and "extremely", per



recommendations by the International Commission on the Biological Effects of Noise (ICBEN) [47]) to “road traffic,” “trains,” “aircraft,” “industry/factory,” “construction,” “neighbors,” and “air conditioner” noise. They also indicated on the same ICBEN scale how often their sleep was disturbed by those noise sources over the past 12 months. Respondents estimated their general health on a 5-point Likert-type scale (poor to excellent) and indicated if they had ever been diagnosed with any of the following sleep disorders: sleep apnea, periodic limb movement syndrome, narcolepsy, insomnia, or restless leg syndrome. Participants also reported any diagnosis of hypertension, migraines, arrhythmia, heart disease, stomach ulcer, or diabetes, and indicated whether they had received treatment in the past month.

The short and medium questionnaires did not include the items on habitual sleep and wake times, frequency of sleep difficulties, expanded noise sensitivity, annoyance by traffic, industry and community noise, diagnosis and treatment for a number of the medical conditions, marital status, income, education level, employment status or residence sound proofing treatment. Furthermore, the short form questionnaire did not include items on sleep medication, sleep disorders, sleep-promoting coping strategies, hearing acuity, diagnosed hypertension and/or arrhythmia, shift work, residence duration, household children, height or weight.

The medium and long versions were sufficiently comprehensive to determine whether a respondent met the field study inclusion criteria, but the short version required us to contact the respondents via telephone for additional information. This telephone contact was only done if the respondent indicated that they were interested in participating in the study and as such gave permission to be contacted.



## E. Field study participant selection process and recruitment

### 1. Survey protocol

Between September 2016 and July 2017, we sent paper surveys along with a letter of introduction to 4080 randomly selected households around ATL. The introduction letter, provided in Appendix 3, briefly described the purpose of the survey, informed the recipient that participation was voluntary, assured the confidentiality of their responses, and provided contact information for the research group. Also provided was the survey eligibility criteria: 21 or more years of age and only one respondent per household, preferably the adult whose birthday was most recent. Respondents returned surveys by mail using an included pre-paid addressed envelope, or completed them online by following a URL or scanning a QR code.

The surveys indicated the financial compensation that would be awarded for participating in the field study (which varied between \$100, \$150 or \$200; see below), and included items on whether respondents would be interested in taking part in such a study.

Surveys were sent in batches of 240 in seventeen mailing rounds. An equal number of surveys were sent to each noise exposure category within each round (24 surveys to each of the 10 noise exposure categories). Mailing rounds differed in the incentive for completing the survey, the length of the survey, the number of follow-up (reminder) waves issued after the initial mailing, and the monetary incentive for participating in the field study if eligible (Table 5). The incentive for completing the survey was either \$2 cash included in the initial survey mailing wave, or an Amazon gift card of \$2, \$5 or \$10 value provided upon completion of the survey. The United States Postal Service could not always deliver the surveys to the listed address. We classed a survey as “non-deliverable” if at least one survey, from any wave within a round, was returned to sender. Such reasons for returning to sender included vacant address, unable to be forwarded, incorrect address or reasons unknown. The percentage of surveys that were deliverable within each mailing round are given in Table 5. On average, (87.6%) of the surveys were deliverable. If a completed survey was received for a recipient that had been classed as non-deliverable (n=9), we reclassified the survey as deliverable. A number of surveys were returned to the sender because the recipient was deceased (n=1), refused delivery of the survey (n=23) or returned a blank survey indicating they were not interested (n=5): these instances were classed as deliverable but as non-response.

Prior to the initial survey wave, a pre-survey notification postcard was sent out only in round 5. Following the initial survey wave within each round, there were 0, 2 or 3 follow-up waves sent if a completed survey had not yet been received from a specific household. The first follow-up, sent 7 days after the initial survey, consisted of a postcard encouraging the recipient to return and complete the original survey if they had not yet already done so. The second follow-up, sent 21 days after the initial survey, consisted of a reminder letter, a new paper copy of the survey and a new pre-paid envelope for returning the survey. The third follow up, sent 42 days after the initial survey consisted of a reminder letter, a further new paper copy of the survey and a further new pre-paid envelope for returning the survey.

Mailing rounds 1-2 were addressed to “Current Resident” and rounds 3-17 were personalized and addressed to a named individual or current resident, for example “A. N. Onymous or Current Resident”. Rounds 1-2 were mailed in envelopes measuring 24×10.5 cm, and rounds 3-17 were sent in 23×15.5 cm envelopes. In addition to a University of Pennsylvania logo on the envelope of all mailing rounds, rounds 1-2 indicated that “Perelman School of Medicine, University of Pennsylvania, Department of Psychiatry, Division of Sleep and Chronobiology” sent the mail, and rounds 3-17 indicated only “University of Pennsylvania” as the sender.



Table 5. Overview of each survey round.

Round	Incentive for completing the survey	Survey length	Number of follow-up waves	Incentive for participating in field study	Addressee	% deliverable
1	Gift card	Long	0	\$100	"Current Resident"	91.3
2	Gift card	Long	0	\$100	"Current Resident"	92.9
3	Gift card	Long	0	\$100	Personalized	91.7
4	Gift card	Long	0	\$100	Personalized	88.8
5	Gift card	Long	0†	\$100	Personalized	91.3
6	\$2 cash	Long	3	\$150	Personalized	88.3
7	\$2 cash	Long	3	\$150	Personalized	89.6
8	\$2 cash	Medium	3	\$150	Personalized	87.5
9	\$2 cash	Short	3	\$150	Personalized	86.3
10	\$2 cash	Long	3	\$200	Personalized	84.6
11	\$2 cash	Long	0	\$200	Personalized	91.3
12	\$2 cash	Long	3	\$200	Personalized	85.0
13	\$2 cash	Long	3	\$200	Personalized	86.3
14	\$2 cash	Long	2	\$200	Personalized	85.4
15	\$2 cash	Long	2	\$200	Personalized	84.2
16	\$2 cash	Long	2	\$200	Personalized	83.8
17	\$2 cash	Long	2	\$200	Personalized	82.1

† Included pre-survey notification postcard sent before the initial survey mailing



## 2. Recruitment into field study

Upon receiving completed surveys where respondents indicated they were interested in participating in the field study, responses were checked to see whether an individual was eligible for the field study. In the case of short survey respondents, follow-up contact via telephone was required to determine eligibility.

Exclusion criteria were as follows:

- Use of medication (either prescribed or “over-the counter”) to help with sleep three times or more per week, over the past month.
- Diagnosed by a health professional with any sleep disorder, including but not limited to the following: sleep apnea, narcolepsy, restless leg syndrome, period limb movement syndrome, insomnia.
- Diagnosed by a health professional with arrhythmia.
- Self-reported problems or difficulties with hearing.
- Overnight shift work, defined as working for at least 4 hours between 00:00 to 06:00.
- Under 21 years of age.
- Any children in the household under 5 years of age.
- Body mass index (BMI) of  $>35$  or  $<17$   $\text{kgm}^2$ , corresponding to classification as Obesity Class II (“severely obese”) and moderately underweight respectively [48].

Out of 407 completed surveys, 237 respondents (58.2%) were interested in participating in the field study. Among respondents interested in the field study, 79 respondents (19.4% of all completed surveys, 33.3% of those interested) met the eligibility criteria. Of those interested and eligible, 37 respondents (9.1% of completed surveys, 15.6% of those interested) were enrolled into the field study. Three participants dropped out before the study commencement. Demographic data of the 34 remaining participants who completed the study are given in Table 6. Further analysis on the effectiveness of the different survey protocols for eliciting questionnaire response, interest for participating in the field study, and eventual participation in the field study, are given in section V.A.



Table 6. Demographics of participants completing the field study.

Variable		Mean ( $\pm$ S.D.)	Range
Age, years (n=34)		50.2 ( $\pm$ 14.7)	21-81
BMI, kgm <sup>2</sup> (n=34)		27.0 ( $\pm$ 3.25)	21.8-33.5
Categorical variable	Level	Count (n)	% of responses
Sex (n=34)	Women	22	64.7
	Men	12	35.3
General health (n=34)	Poor	1	2.9
	Fair	2	5.9
	Good	8	23.5
	Very good	18	52.9
	Excellent	5	14.7
Race (n=34)	White	11*	32.4
	Black	19	55.9
	Other	3*	8.8
	Prefer not to answer	2	5.9
Marital status (n=23)	Single	11	47.8
	Married	6	26.1
	Widowed	1	4.3
	Separated	1	4.3
	Divorced	3	13.0
	Dom. Partner	1	4.3
Education (n=23)	< High school	0	0
	High school	9	40.9
	College or more	13	59.1
Job status (n=23)	Employed	15	65.2
	Unemployed	2	8.7
	Retired	6	26.1
Household income (n=23)	<\$25k	5	21.7
	\$25-50k	6	26.1
	\$50-75k	4	17.4
	\$75-100k	2	8.7
	\$100-150k	2	8.7
	>\$150k	2	8.7
	Prefer not to answer	2	8.7

\* One participant listed race as both White and Other and is counted for both categories.



## **F. Field study procedure**

### **1. Telephone recruitment**

Survey respondents who indicated that they would like to be contacted about participating in the in-home sleep study were contacted by telephone. These prospective participants were read a script detailing the study length, procedures and compensation. They were informed that the study was a 5 consecutive night, in-home, unattended sleep study, and that sounds inside the bedroom would be recorded at night using a sound recorder. Participants would wear a small device attached to two electrodes that would measure heart rate and body movement. In the morning, study participants complete a brief questionnaire concerning their sleep. The eligibility of prospective participants was verified. Those determined ineligible according to exclusion criteria were informed that they did not meet eligibility criteria for the in-home sleep study, and thanked for their time. Eligible participants were mailed an informed consent form for their review together with a pre-paid return envelope. Prospective participants who completed and signed a consent form were called and scheduled for participation in the in-home study.

### **2. Field study procedures**

#### **Unpacking Study Equipment**

Study equipment was shipped directly to participants by staff (Figure 12B). Participants received an instruction manual detailing step-by-step instructions for setting up the equipment and completing measurements. Included in the manual was a link for online-instructional videos on how to unpack and setup the equipment. Participants were called on the first and last day of the study to review procedures and answer questions. Participants were encouraged to call the 24 hour hotline to contact staff for questions regarding study procedures. Also included in the equipment package were five copies of morning surveys (Appendix 4), a photocopy of their signed consent form, return shipping instructions, and forms for payment. Participants were instructed to setup the sound recorder on the first evening (Monday), at any time prior to bedtime. For five consecutive nights (Monday to Friday), immediately before going to bed, they would put on and start the heart rate device, and begin the recording on the sound recorder. On each of the following mornings (Tuesday to Saturday), they would stop the sound recorder, stop and remove the heart rate device, and complete the morning survey. During the day after the final study morning (Saturday), the participants would then pack up and return the measurement equipment.

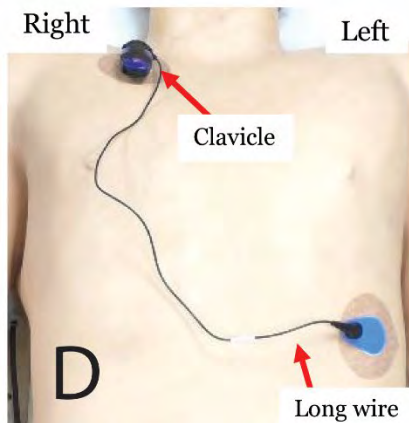


Figure 12. Field study measurement equipment.

- A: Set-up of H5 sound recorder.
- B: Study equipment as received by the participants.
- C: Faros 90 and associated accessories, as they are received by the subjects.
- D: Faros 90 actigraphy and heart rate monitor worn each night by participants.



### **Setting up the Sound Recorder:**

Participants were allowed to sleep at their normal times and wake up at their normal times each day. They were asked to turn off any noise producing items such as the TV, radio, or music during the night. However, in order to preserve a typical sleeping environment, participants were allowed to turn on fans, air conditioners and heaters for their comfort. Also, participants were allowed to sleep with their pets (such as dogs and cats) as they would have normally in their bedrooms. It was desired to have participants maintain as close to their normal sleep routine as possible. Participants were instructed to place the sound recorder near where they slept at night, preferably on a night stand near their head, and to keep the recorder plugged in during measurements (Figure 12A). An extension cord was provided in case it was required. A remote control was supplied for convenience in turning the recorder on/off. The recorder was to be turned on before getting into bed and turned off once awake in the morning.

### **Setting Up the Heart Rate Device:**

During the night, participant's sleep was monitored using one device (eMotion Faros 90) which measured both heart rate and body movements. The device was battery powered and attached with two electrodes to the chest of the subjects. The ECG was sampled at 1 kHz and the peak of each R-wave was detected and recorded. Movement was also measured using a 3-axis accelerometer at a sample rate of 10 Hz, 14 bit resolution, range set to 2 g. As movement was recorded with a high resolution, breathing patterns could be inferred from movements of the chest and it could be determined whether participants had chest movements that would be suggestive of sleep apnea during the night.

Along with the Faros 90 device, participants received a charger, electrodes, tape, alcohol wipes, and cortisone cream in case of skin irritation from the electrodes (Figure 12C). Participants were instructed to place one electrode just below the right clavicle, and another below the left breast (Figure 12D). The heart rate device snaps onto the electrode below the clavicle and the cable snaps onto the bottom electrode. The device is secured with Velcro and medical tape is supplied for extra security if needed. Participants were instructed to turn the device on when they get in bed, and turn it off when waking up. They were instructed to charge the device every morning after awakening.

## **3. Morning survey**

On each morning after measurements took place, participants were instructed to fill out a short questionnaire on the previous night's sleep. Surveys could be completed either online or on the provided hard copies (Appendix 4). The morning survey asked participants at what time they went to sleep, how long it took them to fall asleep, and how many times (if any) they woke up during the night. They were also asked about their quality of sleep, how refreshed or tired they felt in the morning, and whether they felt disturbed by environmental noise during the night. Online morning surveys were checked daily and participants contacted if survey comments mentioned difficulties or concerns with equipment.

To ensure accuracy of the data when coding the paper versions of the morning questionnaires, we adopted an approach to minimize human error. The responses indicated on the questionnaires were manually entered into RedCap by two or three different investigators using the same coding scheme. An automated algorithm was then implemented to check for any discrepancies between the entered data. If a discrepancy was identified, i.e. at least one of the investigators had entered a value that did not match exactly with the entries of the other investigators, the data point was cross-checked against the original questionnaire and the correct value entered.

## **4. Returning study equipment**

After completing five nights of measurements, participants were instructed to pack all equipment back into the shipping box. Photos of how the box should appear when properly packed were included for their assistance. Participants filled out their personal information on payment forms in order to receive compensation for participating in the study. Return shipping instructions indicated the FedEx phone number and shipping order number to schedule an at-home pick-up of study equipment. Subjects could also drop off the equipment at any location that accepts FedEx shipments.

## G. Data Analysis

### 1. SPL converter

The H5 recorder used in the in-home sleep study records noise in mp3 format. Acoustic data from the field study thus had to be converted from mp3 to sound pressure level (SPL) prior to analysis. A sound pressure level converter program was developed to calculate the correct A-weighted sound pressure levels with fast (0.125 s) and slow (1 s) time constants ( $L_{AF}$  and  $L_{AS}$  respectively), for a given mp3 file using an existing calibration file for each measurement. Calibration files (1 kHz at 94 dB) were recorded prior to shipment into the field study, and again upon return.

First, the  $L_{AS}$  and  $L_{AF}$  of the initial and final calibration files were calculated (Figure 13). If the deviation between the two calibration files was less than  $\pm 2$  dB, then the SPL for the measurement was calculated. In total, of the data of 9 subjects were excluded from the analysis due to large deviations in the pre- and post-calibration files. This deviation was due to shifting in the dials of the sound recorders, and was remedied for future subjects by securing the dials in a fixed position with adhesive prior to shipment.

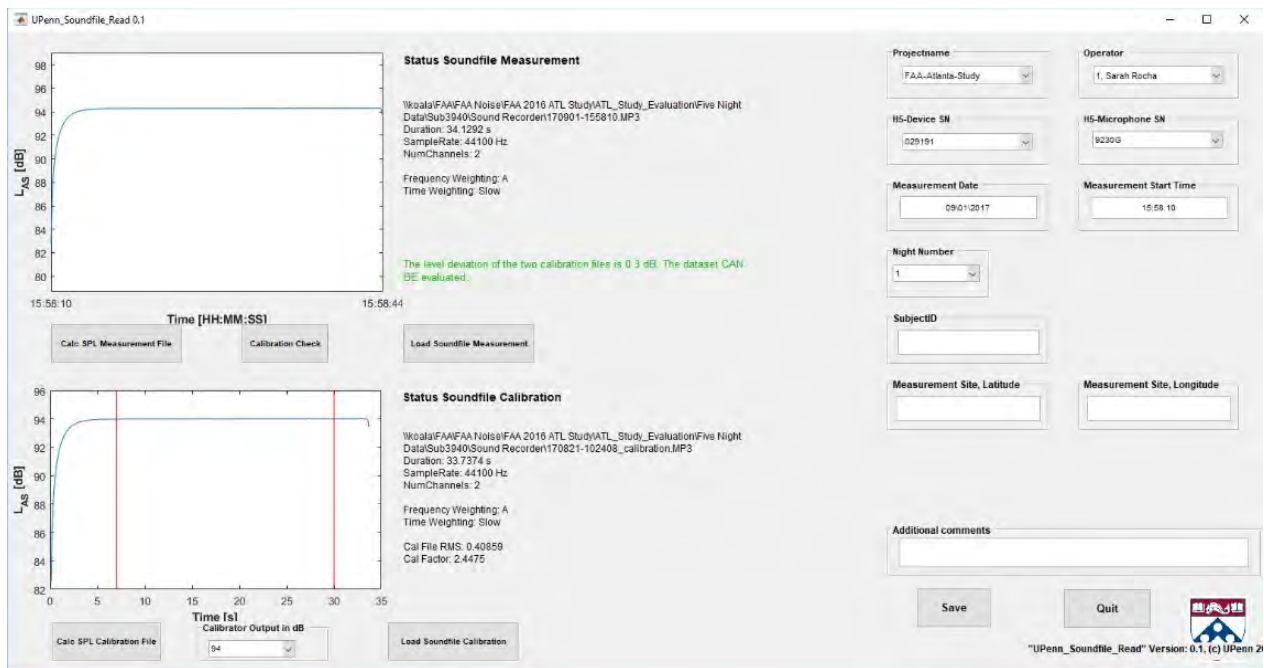


Figure 13. Sound Pressure Level Converter compares the initial and final calibration files for a given subject.

Next the program calculated the  $L_{AS}$  and  $L_{AF}$  of the measurement file using the calibration file and the calibrator output value. The converted sound pressure level could then be scored for aircraft noise in the acoustic scoring program, Akustikview (see section IV.G.2).

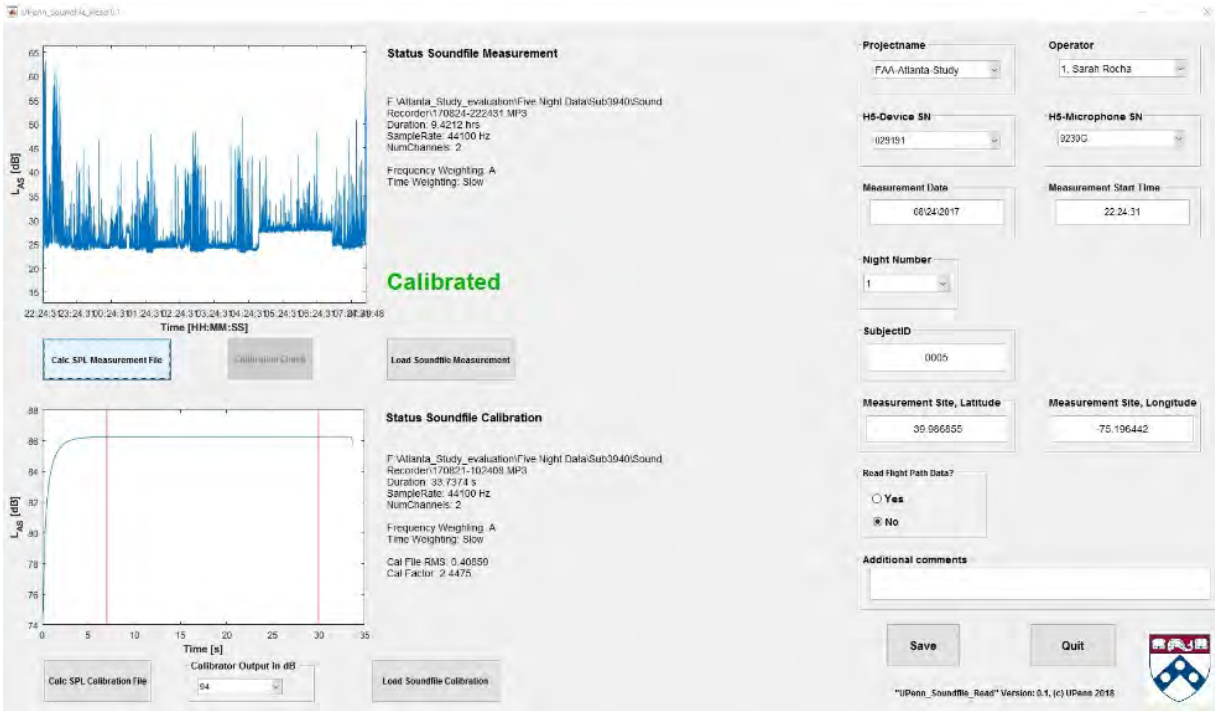


Figure 14.  $L_{AS}$  of a measurement file plotted using the Sound Pressure Level Converter program.



## 2. Akustikview

Research assistants listened to and scored acoustic data using the acoustic scoring software, Akustikview, which is a non-commercial software developed in-house by our collaborators at DLR. Staff members marked when they heard subjects get into and out of bed, aircraft noise, background noise, traffic sounds, and any other relevant noise events in the bedroom. These notations were used to determine periods of time where the subject was not sleeping or was affected by non-aircraft noise events. In case of other noise events during an aircraft noise event, the maximum SPL of the aircraft noise event had to be the highest noise level for the aircraft noise event to be scored as the primary noise event. Akustikview recorded the  $L_{ASmax}$  for aircraft noise events as well as a number of other acoustical whole night and event related acoustical indicators (e.g., the average sound level in the minute preceding the start of the noise events). Once staff had scored a full night of acoustic data, Akustikview generated a text file with information on nightly aircraft noise events, for later use in the statistical analysis. The background noise level is automatically selected and scored by Akustikview, but the selection can be manually overwritten. Akustikview also synchronized the timeline of the acoustic data with the physiological data timeline using input from a time adaptation software (see section IV.G.3). Scoring all acoustic events in a given night is cumbersome, can take 2 hours or more, and is likely not feasible for a larger National Sleep Study. For this study, we plan to integrate flight rack radar data into the Akustikview software, that, based on the minimal distance to the receiver site on the ground, suggests times of expected aircraft noise events that can then be listened to and scored, probably including the minute before the start of the aircraft noise event.

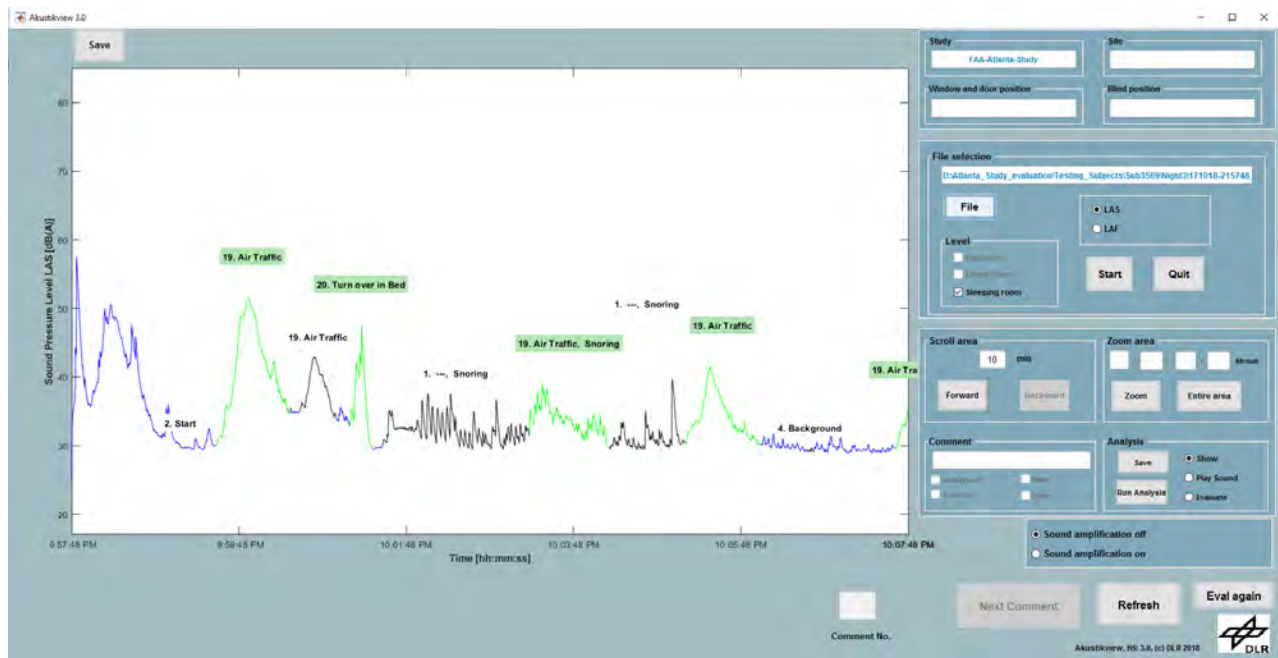


Figure 15. A ten-minute window of an acoustic file scored for aircraft noise and other sounds heard in the bedroom. Noise events are scored by staff and are displayed alternately in green and black. A caption appears above a noise event describing the type of noise heard by staff (e.g. air traffic). Unscored periods of the acoustic file appear in blue.

## 3. Time adapt

Physiological signals recorded with the Faros 90 heart rate devices and acoustical signals recorded with the H5 sound recorders were recorded on the individual devices. Although the devices were synchronized before they were shipped, it often took more than a week before data collection began. Therefore, over the course of the study, their internal clocks could potentially drift apart in time. A software called “Time Adapt” was developed by our collaborator at DLR to synchronize the timeline of the acoustic and physiological data (Figure 16). In this time adaptation software, body movements scored in the acoustic data were paired against movements detected in the physiological data. Time Adapt recorded the difference between movement events in the acoustic and physiological data. The differences were then plotted across the measurement night, as the time drift may increase throughout the night. Time Adapt fitted a linear

regression to the time drift data and outputted this information in a text file to be read by the acoustic scoring software, Akustikview (section IV.G.2).

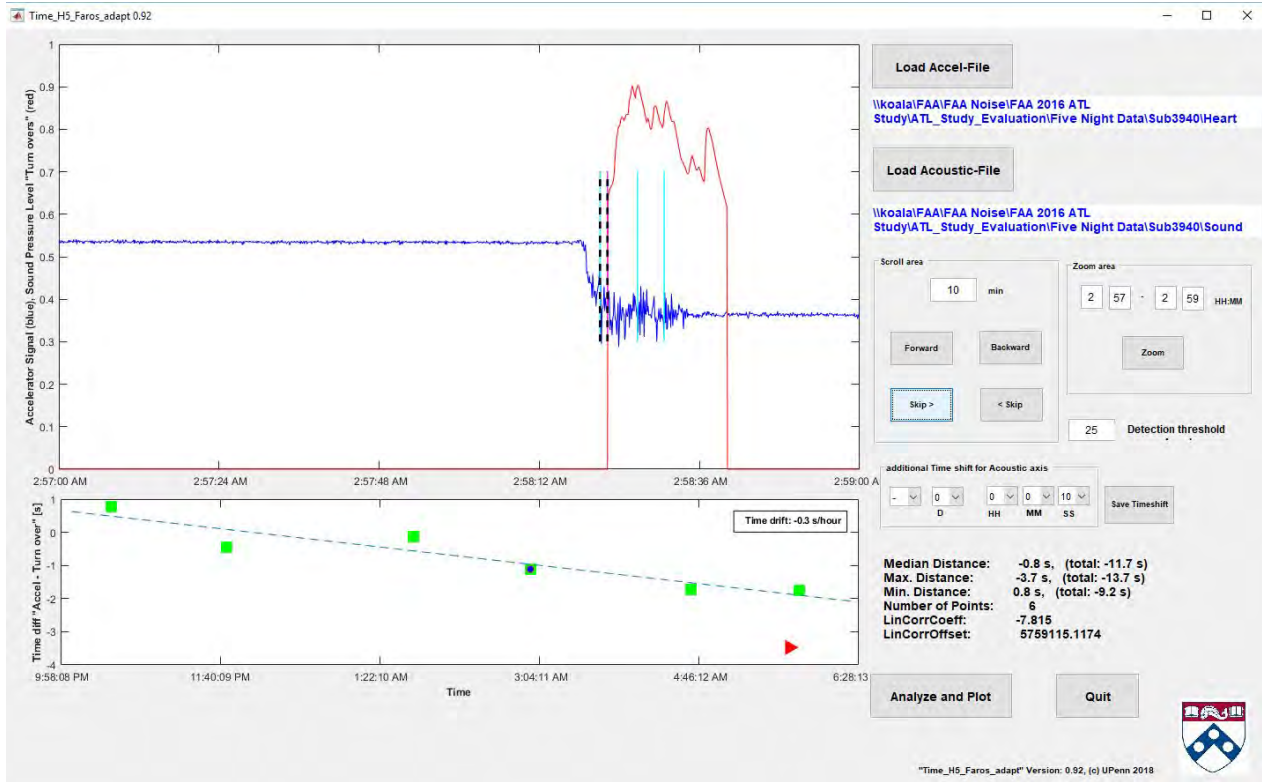


Figure 16. The Time Adapt program matches the start of major body movements with movements scored in the acoustic data. In the upper window, the accelerometer signal is plotted in blue for a given time window and marks the start of major body movements with pale blue lines. A body movement scored in the acoustic data is depicted in red. When the program pairs a body movement scored in both the physiologic and acoustic data, it adds a dashed line to the start of each event. In cases where there are multiple body movements in succession, staff can manually adjust which movement in the physiologic data is paired with the movement in the acoustic data by adding or subtracting time in the program. In the lower window, within-night time drift is shown (see section IV.B.2).



#### 4. Heart rate file splitter

If subjects forget to turn off the heart rate device when they woke up and took off the device, it was possible that movement and heart rate data from multiple days were stored in one large file. Before physiological data could be read by the arousal detection software, the large file had to be split in two or more separate files. A software was developed for this purpose, which detects body movement recorded in the Faros 90 above a minimum threshold. The program then marks these periods of movement, and a human scorer manually adjusted the boundaries to encompass the actual time spent in bed (see Figure 17). Once adjustments had been made, the program then generated separate new data files.

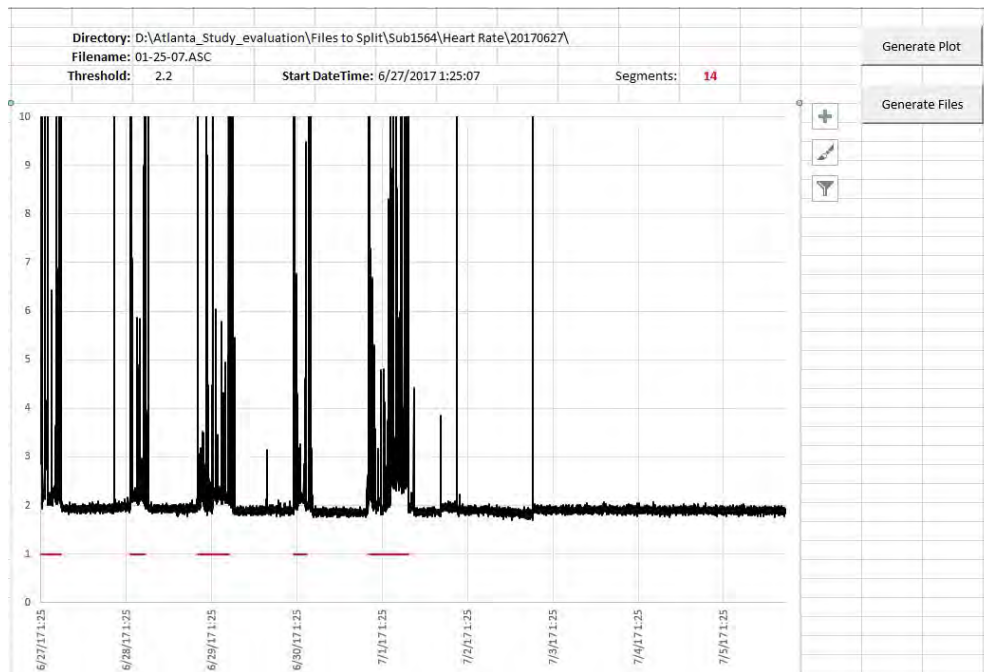


Figure 17. The Heart Rate Splitter program detects periods of body movement, indicated by red horizontal dashes, which can be exported into separate files.

### 5. Automatic identification of awakenings based on heart rate and actigraphy data

Awakenings during the night were identified automatically based on the heart rate and actigraphy data. The software (Figure 18) was based on the algorithm of Basner et al. [21] which identified EEG arousals ( $\geq 3$  seconds) based on heart rate alone. This algorithm was refined to identify EEG awakenings ( $>15$  seconds) using heart rate and actigraphy data, which is a more specific indicator of noise-induced sleep disturbance due to the lower frequency of occurrence on nights without noise exposure [49]. Awakenings are identified in the algorithm by using matrices of likelihood ratios which indicate whether the difference in the beat to beat heart rate to a 3 minute median heart rate or the amount of movement is associated with an awakening [50]. Awakenings were calculated for every subject night. After the calculations were completed, artefacts in the heart rate signals or missing data were visually identified, and these periods were removed from data analysis.

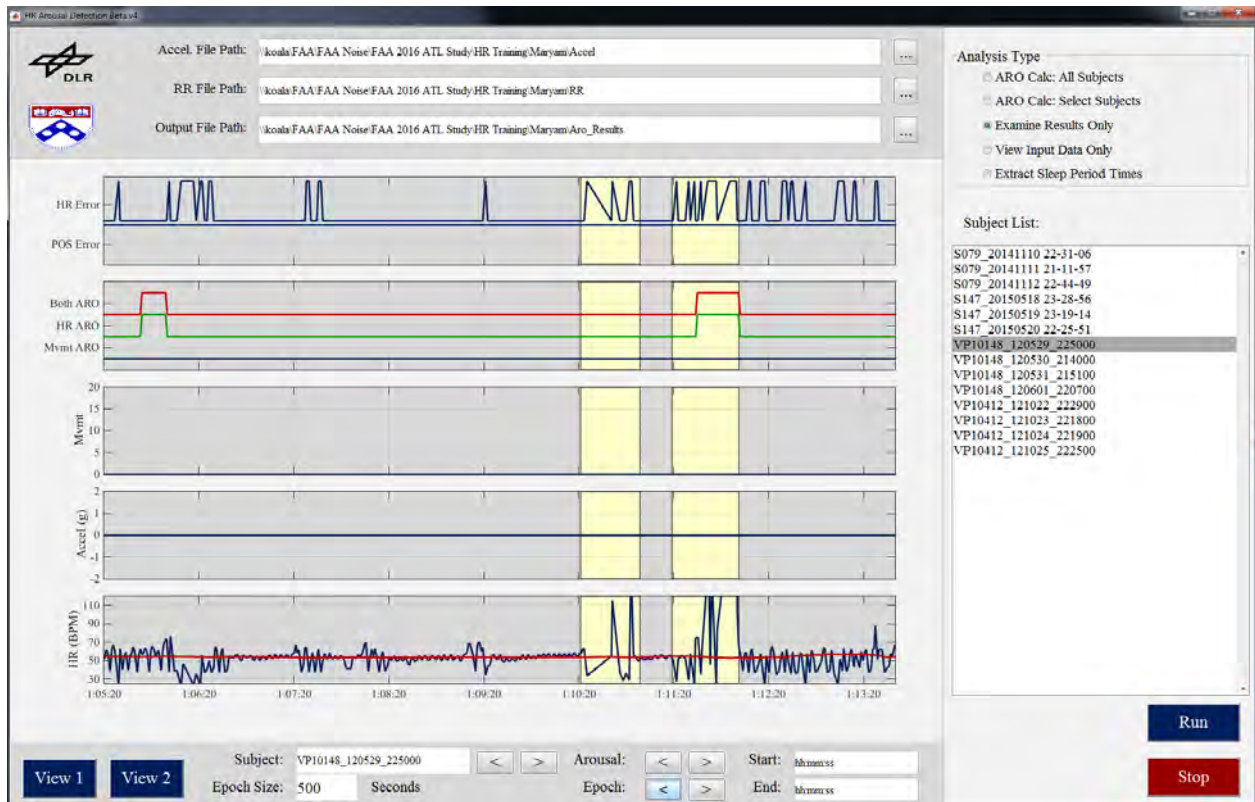


Figure 18. Physiological arousals were detected using the software’s algorithm. Artefacts in the data were highlighted by staff (yellow sections) and removed from the dataset.

## 6. Respiratory signal viewer

We tried to recruit only subjects without intrinsic sleep disorders (like sleep apnea, restless leg movements syndrome, or periodic limb movements in sleep) into the study. However, subjects are often not aware of these sleep disorders, and therefore some intrinsic sleep disorders may not be captured by the questions of the recruitment survey addressing these disorders. Obstructive sleep apnea is characterized by partial or complete obstructions of the upper airways during sleep, that lead to decreases in blood oxygenation levels that ultimately cause an arousal which re-opens the airway. In a sleep laboratory, several physiological signals are used to identify obstructive respiratory events (measurements of movements of movements of the rib cage and abdomen, airflow measurements at the mouth and nose, and blood oxygenation measurements with pulse oximetry). Most of these signals were not available in our study, but the FAROS device, which was attached to the rib cage, is very sensitive, and we thus developed a software that displayed movements of the rib cage along all three orthogonal axes (Figure 19). We inspected rib cage movement for all subject nights for signs of possible obstructive or central sleep apnea, which would be indicated by repeated periods of no activity during times of restricted respiration, followed by an abrupt increase in activity as respiration was resumed. In this case, participants would be notified with a recommendation to seek out their primary care physician for further diagnostic procedures, and the collected data would be excluded from data analysis. In this study, none of the participants demonstrated potential signs of sleep apnea, and thus no data were subsequently excluded from our analyses.

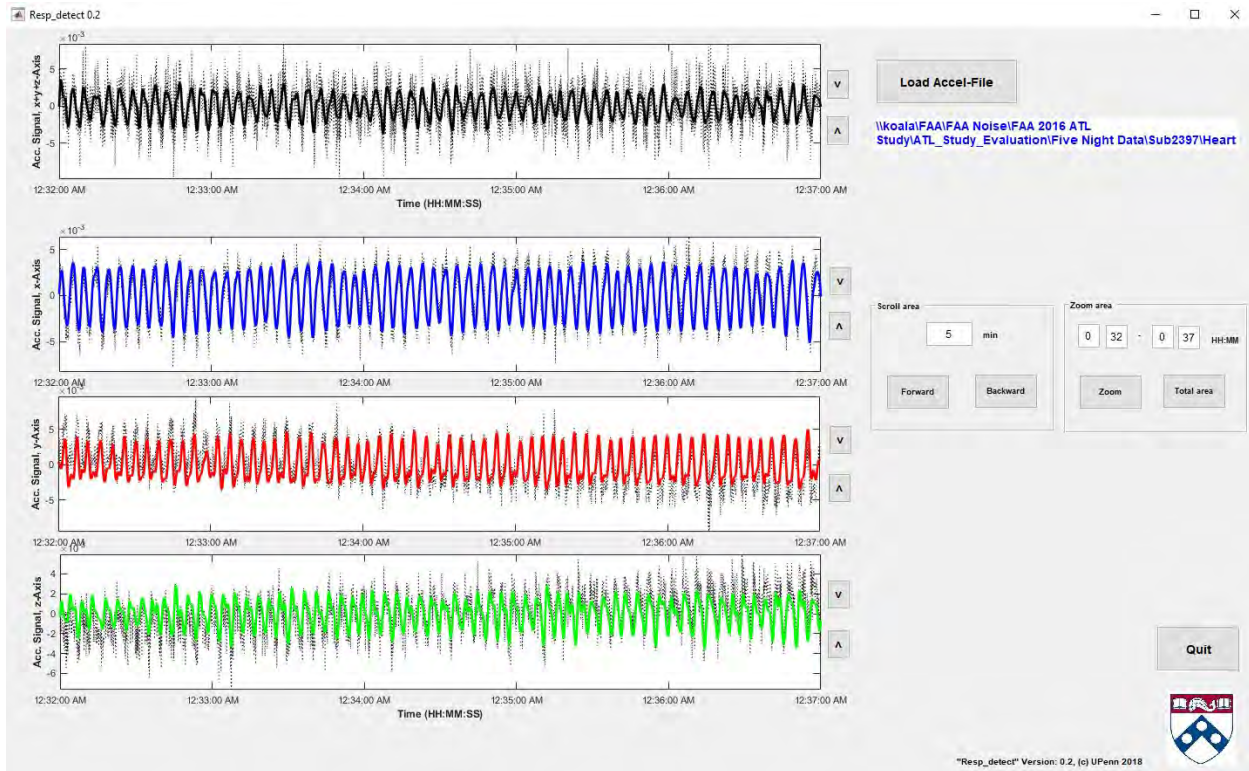


Figure 19. Respiratory signal of a healthy subject shown along the three axes and in a combined axis view.



## 7. Physiological analysis

The main outcome of interest of the event-related analysis is an exposure-response function between the maximum sound pressure level  $L_{AS,max}$  of an aircraft noise event and the probability of the exposed subject to wake up.

### Acoustic analysis – Aircraft event scoring

As described in detail earlier, sounds were continuously recorded in the bedroom of study participants with calibrated sound recorders. Sound levels were calculated based on these recordings. Trained research personnel listened to the sound recordings of each night and marked the beginning and the end of each aircraft noise event using Akustikview (see section IV.G.2). An aircraft noise event was only scored as such if it was the dominant noise source. For example, if a car drove by the house at the same time and generated a higher  $L_{AS,max}$  than the aircraft, the event was classified as road traffic noise (primary) and aircraft (secondary). Only aircraft noise events characterized as the dominant (primary) noise source contributed to data analysis. In addition to the maximum SPL of aircraft noise events, the average noise level  $L_{Aeq}$  in the minute prior to the start of the aircraft noise event was calculated as a proxy for the background noise level prior to the start of the aircraft noise event.

### Automatic identification of awakenings based on heard rate and actigraphy data

Awakenings during the night were identified automatically based on the heart rate and actigraphy data, using the procedure and software described in IV.G.5.

### Time drift correction

Time measured both by the sound recorders and by the Faros devices drifted in an approximately linear fashion relative to actual time determined by Network Time Protocol Internet servers. We wrote special software (see section IV.G.3 above) to correct for the time drift between acoustical and physiological data. We also added 5 seconds prior to the start of an aircraft noise event to the screening window to allow for minor inaccuracies in the time drift correction (see below).

### Single event awakening analysis

All aircraft events were included in the single event analysis regardless of whether another noise source occurred at the same time, such as an aircraft event occurring at the same time as a car pass-by, as long as the aircraft noise was the dominant noise source. In analyses performed for WHO based on data from DLR's STRAIN study, it was found that for aircraft noise, exposure-response relationships did not vary relevantly when including all events or only events that did not co-occur with noise events from other sources [50]. A 50-second time window extending from -5 seconds until +45 seconds relative to the start of each aircraft noise event was screened for an awakening. A noise event was excluded from analysis if an awakening started before the start of this screening window and extended into or even beyond it. Five seconds before the start of the aircraft noise event were added to the screening window to account for any inaccuracies in synchronizing acoustical and physiological measurement equipment (see 2.5.3). The 50-second duration of the screening window was derived empirically from data collected at four different airports (PHL, ATL, FRA, and CGN), which maximized slope estimates for the maximum sound pressure level.

## 8. Statistical analyses

### Survey protocol

We performed statistical analysis in IBM SPSS Statistics (version 25). We excluded surveys that were non-deliverable from all analyses with the exception of analysis of survey delivery rates. Binomial logistical regression models were constructed with completed survey (yes/no), interest in taking part in the field study (yes/no), or participation in the field study (yes/no) as the dependent variables. A number of regression models were constructed, including a combination of survey incentive (gift card/\$2 cash), survey length (short/medium/long), number of follow-up waves (0/2/3), noise exposure category (<40/40-45/45-50/50-55/>55 dB) and orientation to the runway (West/East) as nominal predictor variables. Furthermore, sex (woman/man) and age category (18-29/30-39/40-49/50-59/60-69/70+) data from completed surveys were used as predictor variables in a regression model for both interest and participation in the field study. For each model, we performed an overall omnibus test ( $\chi^2$  tests) relative to the intercept-only model, and  $\chi^2$  tests within each model to examine whether there were significant fixed effects for any of the independent variables. Respondents with missing data were excluded from analyses involving the missing variables. Age data were missing for 43 respondents (10.6%), sex

data were missing for 21 respondents (5.2%), and interest in the field study data were missing for 5 respondents (1.2%). The level of statistical significance was set at  $\alpha=0.05$ . Results are reported as odds ratios (OR) and 95% confidence intervals (CI).

We calculated the cost effectiveness of the different survey strategies based on the cost of envelopes (both for mailing the surveys to the study population and the enclosed pre-paid envelopes for returning the completed surveys), paper, color printing, survey incentive and postage. Color printing cost \$0.075 per page, with 3 pages for the short survey and 4 pages for the medium and long surveys. Mailing envelopes cost \$0.086 each, which also required printing in color. Pre-printed return envelopes cost \$0.093 each. We used the current cost of first class postage (\$0.50) rather than the cost when we mailed the surveys.

### Postal questionnaire results

Statistical analysis of the postal questionnaire data are described in detail in Rocha et al. 2019 [51] and are only summarized here. Only the long questionnaire versions were included in the analysis, corresponding to 3600 surveys across 15 mailing rounds. A logistic regression was performed using SAS (version 9.4, SAS Institute, Cary, NC). Each survey response variable was re-coded on a binomial scale. Responses in the top two categories (i.e. “very” & “extremely”) were coded as “1” and all responses below as “0”.  $L_{\text{night}}$  was analyzed as a continuous variable using the outdoor  $L_{\text{night}}$  estimate for each household.

We first analyzed each outcome separately in a crude, unadjusted model, with  $L_{\text{night}}$  only as an independent variable. We then analyzed each outcome in an adjusted multilevel regression model. We used directed acyclic graphs in DAGitty v2.3 to determine the minimal adjustment required to estimate the total effect of  $L_{\text{night}}$  on outcomes of interest [52]. Adjustment for age and income were minimally necessary, so we did not include occupational status or education in analysis models. In addition to  $L_{\text{night}}$  and income, we furthermore included sex, BMI, noise sensitivity and hearing problems as independent covariates in the adjusted model since we were interested in their influence on our outcomes. Fifteen missing values for age and 14 missing values for BMI were replaced with the mean age (53 years) and mean BMI (29 kg/m<sup>2</sup>). Where categorical covariate data (sex, income, hearing problems and/or noise sensitivity) were missing, we excluded the respondent from analysis.

Wald Chi-Squared tests were performed to determine the significance of the predictor variables, and statistical significance was set to  $\alpha=0.05$ . We did not correct for multiple testing in this exploratory analysis of pilot study data. Odds ratios with 95% confidence intervals and p-values are reported for both the crude and fully-adjusted models.

### Field study morning questionnaires

Data were analyzed in repeated measures multiple logistic regression assuming an independent working correlation matrix (SPSS Generalized Estimating Equation). For each outcome variable, four models were performed. Two crude models used either the equivalent indoor aircraft noise over the individualized sleep period from physiologically-determined sleep onset to sleep cessation ( $L_{\text{Aeq, sleep}}$ ) or the maximum aircraft noise level during the sleep period ( $L_{\text{AS, max}}$ ) as the primary independent predictor variable. Two adjusted models used the same noise exposures as the primary independent variables of interest but were further adjusted to account for the number of measured aircraft noise events during sleep (covariate), sex (dichotomous), age (covariate) and if the window was open or closed. There was only one single study night where the participant slept with fully open windows, therefore window closing was coded as a dichotomous variable as “fully closed” or “partially or completely open”.

Numerical outcome variables (sleep latency, number of awakenings, tiredness, difficulty sleeping, sleep restlessness and sleep quality) were analyzed as continuous outcomes. Categorical outcome variables (Stanford Sleepiness Scale [SSS, question 7] [53] and sleep disturbance by aircraft, road, rail and general noise) were analyzed as dichotomous outcomes, where a score of  $\geq 4$  on the 7-point Likert scale for SSS was classified as “sleepy”, and scores of  $\geq 4$  on the 5-point Likert scales for sleep disturbance were classified as “disturbed”.

### Event-related physiological data

Statistical analysis was performed using SAS (version 9.4, SAS Institute, Carey, NC). For the calculation of single event exposure-response relationships for the probability of an awakening, logistic mixed models with random subject intercept were calculated using Proc NL MIXED. The random intercept term accounts for the correlation of the repeated observations within each subject. In this case, the repeated observations are multiple reactions to aircraft noise events observed per subject. A p-value of 0.05 or less was considered statistically significant. We ran an unadjusted model with  $L_{\text{AS, max}}$  as the only predictor, as well as models adjusting for age (continuous), BMI (continuous), time from sleep onset (continuous), and sex (nominal; value of 1=male, 0=female).



## V. Results and discussion

### A. Survey protocol

#### 1. Delivery rates

Across all 17 mailing rounds, 3576 out of 4080 surveys (87.6%) were deliverable. A breakdown of the delivery rate, by survey round, is given in Table 5. When the survey was addressed only to “Current Resident”, the mean deliverable rate was 92.1% (95% CI: 89.3-94.2%). When the survey address was personalized, the mean deliverable rate was 87.1% (95% CI: 85.9-88.1%). Regression analysis showed that there were lower odds (OR=0.578, 95% CI: 0.409-0.817) of delivery to personalized individuals than “Current Resident” only ( $\chi^2(1, n=4080)=9.668, p=0.002$ ).

The delivery rate was lower for surveys sent to named individuals, perhaps due to the mail carrier not delivering if the name on the envelope did not match a name at the address despite the appended “or Current Resident”, but this was more than offset by higher response rates among those named addressees. This increased response rate when personalizing the surveys is generally in agreement with previous research. A meta-analysis of 14 trials including over 12,000 participants found that the inclusion of names on health survey letters increased the odds of response by one fifth [54]. A later study however found that addressing surveys to named individuals significantly increased the response rate to reminder letters, but the increased response rate to the initial survey waves was not significant, although in this study of 1000 participants the absence of significance could be due to insufficient power [55]. As well as personalization, the higher response rate could be in part due to the removal of “School of Medicine” and “Department of Psychiatry” from the envelope, since psychiatry as a medical profession continues to suffer from public stigma [56]. We would not anticipate the change in envelope size to influence response [57].

## 2. Response rate

Out of 3576 delivered surveys, 407 were completed, a response rate of 11.4%. The majority (n=309; 75.9%) were returned by mail, with a minority (n=98; 24.1%) completed online. There was a statistically significant effect of respondent age category on the response mode ( $\chi^2=54.9$ ,  $p<0.0001$ ), with younger respondents generally preferring to respond online and older respondents generally preferring to respond by mail (Figure 20).

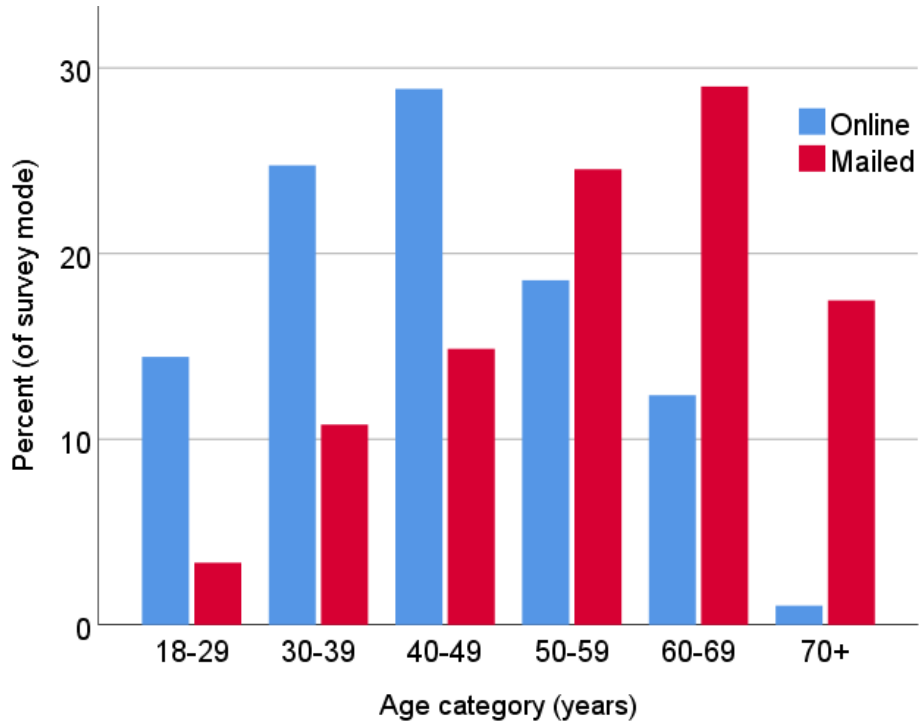


Figure 20. Effect of age of respondent on preferred response mode.

Among deliverable surveys within rounds 1-5, there was a 4.3% response rate when addressing the survey to a named individual in larger envelopes that indicated only “University of Pennsylvania” as the sender. The response rate was 1.4% when addressing the survey to only “Current resident” in smaller envelopes that indicated “Perelman School of Medicine” and “Department of Psychiatry, Division of Sleep and Chronobiology” as the sender. The higher response rate among personalized, larger envelope, “University of Pennsylvania” sender surveys was statistically significant (Wald  $\chi^2(1, n=1094)=6.772$ ,  $p=0.009$ , OR=3.261, 95% CI: 1.339-7.942).

A total response rate of 11.4% is lower than rates of 30-76% for postal surveys on aircraft noise annoyance in Europe and East Asia that were reported in a recent systematic review [58]. Our response rate is however in line with some more general attitudinal surveys [55, 59]. Possible reasons for non-response in our sample might include concerns about privacy and confidentiality despite assurances given in the introduction letter [60], illiteracy or language issues [61] or lack of interest in the survey topic or low community engagement [62]. In the United States, 37.6 million people speak Spanish at home [63], and including Spanish language surveys along with the English versions could improve response rates among this population without lowering response rates from non-Spanish speakers [64].

We received the majority of responses by mail, at a ratio of around 3:1 compared to online response. There is inconsistency among earlier studies regarding the influence of response mode, with some reporting higher response rates for paper surveys compared to online surveys e.g. [59, 65], and others finding an increased preference for completing questionnaires electronically e.g. [66]. We do not know whether those who completed our survey online would have returned it by post if the online option was not available, or vice versa for respondents who completed the survey by mail, and therefore cannot draw any conclusions regarding the optimal choice if only one survey mode were to be used in future



studies. Offering web and mail response modes concurrently, rather than sequentially, may have reduced the overall response rate [67], although evidence is mixed [68]. Hypothesized reasons for this effect include, firstly, increased complexity in the decision to respond by introducing the choice of response mode; secondly, respondents choosing to respond online but never actually doing so since it involves a break in the response process; and thirdly sample members attempting to respond by web but not completing the survey due to computer or internet connectivity issues [69]. Initial mail contact offering a web-based response, and withholding paper surveys until later mailing rounds, may increase response rates compared to a paper-only method, but without significantly improving respondent representativeness [70]. A higher response rate, while not necessarily indicating greater respondent representativeness or data quality [71-73], may at least reduce the risk of nonresponse bias [67]. The pilot study presented in the current paper is a preceding step towards a national study of the potential effects of aircraft noise on sleep, and this future study offers the opportunity to more rigorously address nonresponse bias. One approach that has been widely used is comparing respondent characteristics to known characteristics of the whole population of interest [74, 75], in this case residents exposed to a certain minimum level of aircraft noise, using demographic data at the census tract level from the decennial U. S. Census [76] and the American Community Survey [77].

The survey rounds were not issued concurrently, but the earlier rounds were sent in autumn, the middle rounds were sent in winter or spring and the final rounds were sent in early summer. We cannot totally exclude there are subsequent effects on response rate, perhaps because residents were not home at certain times of year, or that there are seasonal effects influencing the predisposition of an individual to complete the questionnaire [78].

### 3. Effect of protocol on survey completion

We performed a regression analysis including the only round with pre-notification (round 5) and the two rounds that were otherwise identical except for pre-notification (rounds 3 and 4). There were higher odds for survey response when issuing a pre-notification postcard (OR=1.759, 95% CI: 0.821-3.765), but the effect was not statistically significant (Wald  $\chi^2(1, n=652)=2.113, p=0.146$ ).

Results of the regression models for completing the surveys are presented in Table 7, and are graphically illustrated in Figure 21 in green. Regression model 1 (survey incentive, survey length, follow-up waves and field study incentive) indicated that a survey was more likely to be completed if including a \$2 cash incentive compared to a gift card of any value (OR=2.792), and if 3 follow-up waves were issued compared to no follow-ups (OR=2.121). Survey length and field study incentive had no significant effect on survey completion rate. The inclusion of noise exposure category as a predictor (model 2) revealed results similar to that of model 1, with higher response rates for the \$2 cash incentive (OR=2.798) and 3 follow-up waves (OR=2.120), but there was no effect of noise exposure or direction on survey completion rate.



Table 7. Results of the regression models for recipients completing the survey (including only deliverable surveys). All analyses excluded surveys that could not be delivered for any reason. OR=Odds Ratio. CI=Confidence Interval. Ref=Reference category. df=Degrees of Freedom. Statistically significant ( $p < 0.05$ ) results are indicated with bold typeface.

Model and test relative to intercept-only model	Variable	Fixed effects			Variable level	Completing survey		
		df	Wald $\chi^2$	p		p-value	OR	95% CI
Model 1 $\chi^2(6, n=3576)=158.793, p < 0.0001$	Survey incentive	1	11.599	<0.001	Gift card	Ref		
					\$2	<0.001	2.792	1.546-5.041
	Survey length	2	2.569	0.277	Short	Ref		
					Medium	0.752	0.927	0.579-1.484
					Long	0.139	0.730	0.482-1.107
	Follow-up waves	2	9.627	0.008	0	Ref		
					2	0.114	1.530	0.903-2.591
					3	0.005	2.121	1.250-3.597
	Field study incentive	1	0.150	0.699	150	Ref		
					200	0.699	0.936	0.671-1.306
Model 2 $\chi^2(11, n=3576)=162.574, p < 0.0001$	Survey incentive	1	11.643	<0.001	Gift card	Ref		
					\$2	<0.001	2.798	1.550-5.054
	Survey length	2	2.505	0.286	Short	Ref		
					Medium	0.759	0.929	0.580-1.488
					Long	0.144	0.733	0.483-1.112
	Follow-up waves	2	9.592	0.008	0	Ref		
					2	0.114	1.530	0.903-2.592
					3	0.005	2.120	1.249-3.596
	Field study incentive	1	0.170	0.680	150	Ref		
					200	0.680	0.932	0.668-1.301
	Noise exposure category	4	3.397	0.494	<40	Ref		
					40-45	0.562	0.907	0.651-1.263
					45-50	0.306	0.839	0.599-1.175
					50-55	0.671	1.073	0.776-1.484
					>55	0.594	1.093	0.787-1.519
Direction	1	1.073	0.300	West	Ref			
				East	0.538	0.936	0.758-1.156	

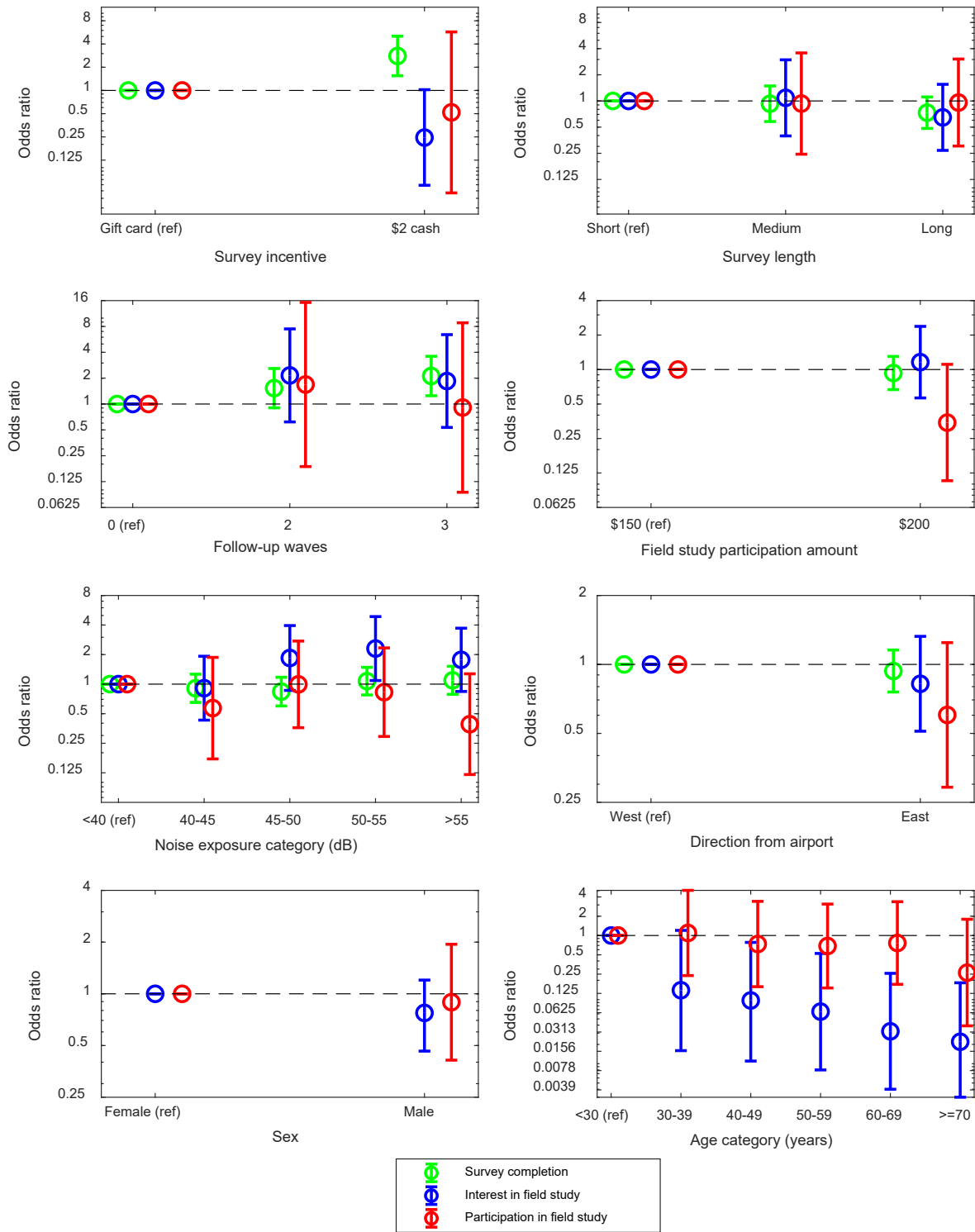


Figure 21. Odds ratios and 95% confidence intervals for the effect of different survey approaches and situational factors on receiving completed surveys (green), eliciting interest in the study (blue) and recruiting a participant into the study (red). The horizontal dashed line indicates the reference value OR=1.0.



Our findings on the effectiveness of different surveying strategies are in good agreement with the existing literature. For instance, a previous meta-analysis found that response to health research postal questionnaires could be improved by implementing repeat mailing strategies and, to a lesser degree, using shorter questionnaires [42]. In particular, the effectiveness of follow-ups on increasing response is rather well established in the existing literature [41, 79]. Similarly, we attained the highest response rate when using the most intensive follow-up strategy, but observed no significant increases in response when shortening the questionnaire length.

Only the mailing rounds with gift card incentives offered \$100 for field study participation, and only the rounds with cash incentives offered \$150 or \$200 for field study participation, which is a limitation of the study design. The almost three times higher odds in survey response when we used a cash incentive is most plausibly due to the \$2 cash outperforming the gift card as an incentive, rather than the difference in field study participation incentives. This is supported by the lack of observed differences in response rates between \$150 and \$200 field study incentives, the fact that monetary incentives have previously been found to outperform non-monetary incentives and that prepaid incentives outperform promised incentives [41, 80-83]. Furthermore, completion of the survey did not obligate field study participation, so we did not anticipate that field study compensation would influence survey response rates.

#### 4. Effect of protocol on interest in field study

Out of 407 completed surveys, 237 respondents (58.2%) were interested in participating in the field study. Regression models for interest, calculated only using data from completed surveys, are given in Table 8, and are graphically illustrated in blue in Figure 21. The crude model (model 1) was not significantly different from the intercept-only model. In the fully adjusted regression model 3, residents exposed to 50-55 dB  $L_{\text{Night}}$  were more interested in taking part than those exposed to <40 dB (OR=2.304). There was a significant effect of age, with a monotonic decrease in the odds of interest in the field study with increasing age. There was also a statistically borderline effect ( $p=0.054$ ) of survey incentive, whereby recipients of the \$2 cash incentive were less likely to be interested in the field study (OR=0.245). No effects of survey incentive, survey length, number of follow-up waves or the field study participation incentive were found.

Older people are, for multiple reasons, frequently more difficult to recruit into experimental studies [84]. Accordingly, younger people in our survey sample were more interested in taking part in the field study. When endeavoring to recruit evenly distributed age groups in studies, oversampling from the target population might be needed.



Table 8. Results of the regression models for respondent interest in participating in the field study (including only completed surveys). All analyses excluded surveys that could not be delivered for any reason. df=Degrees of Freedom. OR=Odds Ratio. CI=Confidence Interval. Ref=Reference category. Statistically significant ( $p < 0.05$ ) results are indicated with bold typeface. Results of borderline statistical significance ( $p = 0.05-0.1$ ) are indicated with italic typeface.

Model and test relative to intercept-only model	Variable	Fixed effects			Variable level	Interest in field study		
		df	Wald $\chi^2$	p		p-value	OR	95% CI
Model 1 $\chi^2(6, n=402)=6.885$ , $p=0.332$	Survey incentive	1	2.106	0.147	Gift card	Ref		
					\$2	0.147	0.417	0.128-1.359
	Survey length	2	2.628	0.269	Short	Ref		
					Medium	0.819	1.111	0.452-2.733
					Long	0.233	0.621	0.284-1.358
	Follow-up waves	2	1.735	0.420	0	Ref		
					2	0.366	1.595	0.581-4.384
					3	0.811	1.130	0.414-3.090
	Field study incentive	1	0.001	0.971	150	Ref		
					200	0.971	1.011	0.550-1.861
Model 2 $\chi^2(11, n=402)=20.832$ , $p=0.035$	Survey incentive	1	2.095	0.148	Gift card	Ref		
					\$2	0.148	0.408	0.121-1.373
	Survey length	2	2.854	0.240	Short	Ref		
					Medium	0.753	1.158	0.463-2.899
					Long	0.234	0.615	0.277-1.369
	Follow-up waves	2	1.564	0.457	0	Ref		
					2	0.422	1.529	0.543-4.310
					3	0.876	1.086	0.388-3.038
	Field study incentive	1	0.010	0.921	150	Ref		
					200	0.921	0.969	0.519-1.808
	Noise exposure category	4	<b>10.830</b>	<b>0.029</b>	<40	Ref		
				40-45	0.311	0.721	0.383-1.358	
				45-50	0.150	1.619	0.841-3.118	
				50-55	<i>0.072</i>	<i>1.775</i>	<i>0.949-3.318</i>	
				>55	0.171	1.558	0.826-2.940	
Direction	1	2.049	0.152	West	Ref			
				East	0.152	0.738	0.487-1.119	
Model 3 $\chi^2(17, n=359)=63.308$ , $p < 0.0001$	Survey incentive	1	3.719	<i>0.054</i>	Gift card	Ref		
					\$2	<i>0.054</i>	<i>0.245</i>	<i>0.059-1.023</i>
	Survey length	2	1.659	0.436	Short	Ref		
					Medium	0.873	1.086	0.396-2.973
					Long	0.330	0.647	0.270-1.553
	Follow-up waves	2	1.461	0.482	0	Ref		
					2	0.228	2.153	0.619-7.489
					3	0.332	1.851	0.534-6.421
	Field study incentive	1	0.164	0.685	150	Ref		
					200	0.685	1.160	0.565-2.381
	Noise exposure category	4	<i>8.904</i>	<i>0.064</i>	<40	Ref		
					40-45	0.803	0.909	0.430-1.924
					45-50	0.114	1.846	0.863-3.949
					50-55	<b>0.029</b>	<b>2.304</b>	<b>1.088-4.875</b>
					>55	0.132	1.768	0.842-3.713
	Direction	1	0.642	0.423	West	Ref		
					East	0.423	0.823	0.511-1.326
Sex	1	0.961	0.327	Female	Ref			
				Male	0.327	0.774	0.464-1.202	
Age category	5	<b>33.150</b>	<b>&lt;0.0001</b>	<30	Ref			
				30-39	<i>0.073</i>	<i>0.140</i>	<i>0.016-1.202</i>	
				40-49	<b>0.029</b>	<b>0.094</b>	<b>0.011-0.781</b>	
				50-59	<b>0.010</b>	<b>0.065</b>	<b>0.008-0.525</b>	
				60-69	<b>0.001</b>	<b>0.032</b>	<b>0.004-0.257</b>	
				≥70	<b>&lt;0.001</b>	<b>0.022</b>	<b>0.003-0.183</b>	



## 5. Effect of protocol on participation in field study

Among respondents interested in the field study, 79 respondents (19.4% of all completed surveys, 33.3% of those interested) met the eligibility criteria. Of those interested and eligible, 37 respondents (9.1% of completed surveys, 15.6% of those interested) were enrolled into the field study (see section V.G.2 for discussion of attrition at the different stages of recruitment). Regression models for participating in the field study, calculated only using data from completed surveys, are given in Table 9 and illustrated in red in Figure 21. In no models were any statistically significant effects of survey incentive, survey length, follow-up waves, field study incentive, age or sex found for the likelihood that respondents would participate in the field study.

The lack of significant difference in the odds of participation for different field study compensation amounts could suggest that the participants had more self-determined motivational traits [85], and/or that general interest in the research was a primary reason for taking part rather than financial interests alone. The hypothesis for personal interest is supported by the doubled odds of interest in the study for respondents exposed to 50-55 dB noise relative to the lowest noise category. Populations exposed to higher noise levels could be expected, through personal experience, to be more acutely aware of the issue of nocturnal aircraft noise, and therefore more willing to contribute to research on its effects. The odds in the highest exposure category (>55 dB) were not significantly higher than in the lowest category, which on one hand would not substantiate the idea for greater interest among those most affected, but could alternatively be explained by the most adversely affected people self-selecting themselves out of the area by moving to a quieter neighborhood.

Although rounds 1-5 offered \$100 for field study participation, these mailing rounds also exclusively included gift cards as survey incentives, and so we cannot draw conclusions regarding differences in participation rates between \$100 and \$150/\$200 amounts. Furthermore, the absence of significant findings could result from insufficient statistical power, since only 34 subjects eventually participated in the field study.

The highest probability of field study participation, achieved with the short survey - although not statistically significant - may reflect a modest advantage of using a reduced survey length. On the other hand, the short survey required additional telephone contact, which may be the cause of a potential higher participation likelihood, rather than the short survey *per se*.

The study design was not perfectly balanced, so we cannot conclude whether increasing the field study compensation from \$100 to \$150 or \$200 would have affected recruitment. To avoid possible confounding, an alternative study design, but with additional expense, could involve a 2×2×3×3 factorial design with the factors of pre-/post-completion incentive, \$2/gift card incentive, short/medium/long survey length and 0/2/3 follow-up waves.



Table 9. Results of the regression models for recipients participating in the field study (including only completed surveys). All analyses excluded surveys that could not be delivered for any reason. df=degrees of freedom. OR=Odds Ratio. CI=Confidence Interval. Ref=Reference category.

Model and test relative to intercept-only model	Variable	Fixed effects			Variable level	Field study participation		
		df	Wald $\chi^2$	p		p-value	OR	95% CI
Model 1 $\chi^2(6, n=407)=4.707,$ p=0.582	Survey incentive	1	0.174	0.677	Gift card	Ref		
					\$2	0.9677	0.608	0.059-6.305
	Survey length	2	0.058	0.809	Short	Ref		
					Medium	0.809	0.855	0.241-3.040
					Long	0.896	0.929	0.307-2.811
	Follow-up waves	2	0.805	0.669	0	Ref		
					2	0.698	1.528	0.179-13.022
					3	0.936	0.914	0.100-8.300
	Field study incentive	1	2.828	0.093	150	Ref		
					200	0.093	2.657	0.851-6.588
Model 2 $\chi^2(9, n=407)=10.502,$ p=0.486	Survey incentive	1	0.294	0.588	Gift card	Ref		
					\$2	0.588	0.521	0.049-5.505
	Survey length	2	0.065	0.968	Short	Ref		
					Medium	0.810	0.854	0.236-3.095
					Long	0.843	0.892	0.290-2.748
	Follow-up waves	2	1.012	0.603	0	Ref		
					2	0.628	1.703	0.197-14.691
					3	0.971	0.960	0.104-8.834
	Field study incentive	1	3.254	0.071	150	Ref		
					200	0.071	2.890	0.912-9.153
	Noise exposure category	4	3.662	0.454	<40	Ref		
					40-45	0.258	0.519	0.166-1.619
					45-50	0.906	1.061	0.399-2.818
					50-55	0.605	0.770	0.285-2.079
					>55	0.142	0.427	0.137-1.330
Direction	1	1.917	0.166	West	Ref			
				East	0.166	0.607	0.299-1.231	
Model 3 $\chi^2(17, n=364)=13.496,$ p=0.702	Survey incentive	1	0.286	0.593	Gift card	Ref		
					\$2	0.593	0.520	0.047-5.730
	Survey length	2	0.011	0.995	Short	Ref		
					Medium	0.919	0.933	0.244-3.569
					Long	0.944	0.959	0.303-3.036
	Follow-up waves	2	1.092	0.579	0	Ref		
					2	0.642	1.687	0.187-15.238
					3	0.935	0.910	0.094-8.817
	Field study incentive	1	3.190	0.074	150	Ref		
					200	0.074	2.904	0.901-9.354
	Noise exposure category	4	3.432	0.488	<40	Ref		
					40-45	0.354	0.570	0.173-1.873
					45-50	0.992	0.995	0.360-2.746
					50-55	0.722	0.828	0.293-2.340
					>55	0.119	0.391	0.120-1.274
	Direction	1	1.877	0.171	West	Ref		
					East	0.171	0.602	0.291-1.245
	Sex	1	0.081	0.776	Female	Ref		
					Male	0.776	0.894	0.411-1.942
Age category	5	3.223	0.666	<30	Ref			
				30-39	0.906	1.096	0.237-5.064	
				40-49	0.696	0.737	0.159-3.410	
				50-59	0.624	0.686	0.152-3.093	
				60-69	0.722	0.764	0.173-3.368	
				$\geq 70$	0.173	0.263	0.039-1.793	



## 6. Questionnaire completion and field study participation probabilities

Probabilities of completing the survey and participating in the field study were calculated using regression model 1. The probability of surveys being completed for each observed combination of survey incentive, survey length and follow-up waves are given in Table 10. The more follow-up waves were sent and the shorter the survey length, the more likely it was to receive a completed survey, with a response rate of 21.7% for survey rounds with 3 follow-up waves, a short survey and a \$2 cash incentive.

Table 10. Predicted probability and 95% confidence intervals (CI) of receiving a completed survey, stratified by number of follow-up waves, survey length and survey incentive. Data calculated excluding non-deliverable surveys.

Sample size (n)	Probability of completing survey and 95% CIs (%)	Follow-up waves	Survey length	Survey incentive
207	21.7 (16.6-27.9)	3	Short	\$2
210	20.5 (15.6-26.5)	3	Medium	\$2
1041	16.3 (14.2-18.7)	3	Long	\$2
805	12.0 (10.0-14.5)	2	Long	\$2
219	8.2 (5.2-12.7)	0	Long	\$2
1094	3.1 (2.2-4.3)	0	Long	Gift card
Total=3576				

Since the \$2 cash incentive was superior to gift cards for receiving completed surveys, and therefore likely a more representative sample, we restricted analysis of field study participation to rounds where only the cash incentive was used (rounds 6-17). The probability of respondents participating in the field study for each combination of survey length, follow-up waves and field study incentive, are given in Table 11. We calculated probabilities based on both the total number of surveys mailed and from among completed surveys only. Since the field study incentive of \$100 was offered only in rounds 1-5, probabilities are presented for incentive amounts of \$150 and \$200 only. The shorter the survey length, the more likely it was for a respondent to participate in the field study. Generally, participation was more likely with more follow-up waves and with the lower field study incentive, although there may be some confounding among these variables due to the unbalanced design.

Table 11. Predicted probability and 95% confidence intervals (CI) of a recipient participating in the field study, stratified by number of follow-up waves, survey length, and field study participation amount. Data calculated excluding non-deliverable surveys and gift card incentive rounds.

Sample size (n)*	Probability of participating in field study (% with 95% CIs)*	Probability of participating among survey respondents (% with 95% CIs)†	Follow-up waves	Survey length	Field study participation amount
207	2.9 (1.3-6.3)	13.3 (6.1-26.7)	3	Short	\$150
210	2.4 (1.0-5.6)	11.6 (4.9-25.1)	3	Medium	\$150
427	2.1 (1.1-4.0)	12.5 (6.6-22.3)	3	Long	\$150
805	1.0 (0.5-2.0)	8.2 (4.2-15.6)	2	Long	\$200
614	0.8 (0.3-1.9)	5.1 (2.1-11.7)	3	Long	\$200
219	0.5 (0.1-3.2)	5.6 (0.8-30.7)	0	Long	\$200
Total=2482					

\*Based on total number of surveys mailed (n=2482)

†Based only on completed surveys (n=407)



## B. Postal questionnaires

### 1. Delivery rates

Out of 3600 surveys mailed, 3159 surveys could be delivered. Of deliverable surveys, 319 were completed and returned, resulting in a response rate of 10.1%. Twenty one surveys with missing information for sex (n=21), income (n=9), noise sensitivity (n=7) and/or hearing problems (n=33) were excluded from analysis, resulting in an effective sample size of n=268 (8.5 %) of the surveyed population.

### 2. Respondent demographics

summarizes the demographics for respondents to the noise and sleep survey for whom there were no missing sex, income, noise sensitivity or hearing problem data. There were 57 participants in the 35<40 dB noise exposure category, 46 in the 40<45 dB category, 51 in the 45<50 dB category, 64 in the 50<55 dB category and 50 in the  $\geq 55$  dB category. Respondents ranged in age from 21 to 97 years, with a mean of 52.4 years (SD $\pm$ 15.2) and had a mean BMI of 29.3 kg/m<sup>2</sup> (SD $\pm$ 6.5). Sixty one percent of respondents were black, which is a similar proportion to the 62.5% mean proportion for the sampled sampling region. For highest level of completed education, 46.4% of respondents had no college education, which is slightly higher than the 40.0% of the population without college education in the sampling region. Among respondents who disclosed their income, 50.9% had a household income below \$50,000, with 31.3% of respondents and the median value lying in the \$25-50k category. This is in agreement with the mean household income for the sampled census tracts of \$49,100.

Table 12 summarizes the demographics for respondents to the noise and sleep survey for whom there were no missing sex, income, noise sensitivity or hearing problem data. There were 57 participants in the 35<40 dB noise exposure category, 46 in the 40<45 dB category, 51 in the 45<50 dB category, 64 in the 50<55 dB category and 50 in the  $\geq 55$  dB category. Respondents ranged in age from 21 to 97 years, with a mean of 52.4 years (SD $\pm$ 15.2) and had a mean BMI of 29.3 kg/m<sup>2</sup> (SD $\pm$ 6.5). Sixty one percent of respondents were black, which is a similar proportion to the 62.5% mean proportion for the sampled sampling region. For highest level of completed education, 46.4% of respondents had no college education, which is slightly higher than the 40.0% of the population without college education in the sampling region. Among respondents who disclosed their income, 50.9% had a household income below \$50,000, with 31.3% of respondents and the median value lying in the \$25-50k category. This is in agreement with the mean household income for the sampled census tracts of \$49,100.



Table 12. Demographic characteristics of survey respondents (N=268) for whom complete data were available for regression analysis. Respondents could provide multiple answers for Race.

Variable	Level	Percent
Sex (n=268)	Women	64.9
	Men	35.1
Race (n=268)	Black	61.2
	White	24.6
	Other	8.2
	Prefer not to answer	10.4
Marital Status (n=267)	Single	36.9
	Married or domestic partners	38.6
	Widowed	7.9
	Separated/divorced	16.5
Income (n=268)	<\$50,000	41.8
	\$50,000-\$100,000	27.2
	>\$100,000	13.1
	Prefer not to answer	17.9
Education (n=265)	<High School	4.2
	High School	42.3
	College or greater	53.6
Employment (n=265)	Working	53.6
	Unemployed	9.1
	Student	1.9
	Retired	30.9
	Homemaker	4.5
Hearing (n=268)	No problems	85.8
	Problems	14.2
Noise sensitivity (n=268)	Not sensitive	69.0
	Sensitive	31.0

### 3. Survey responses

#### Sleep disturbance by noise, annoyance by noise and sleep quality

Results of the unadjusted logistic regression models for annoyance, sleep disturbance and sleep quality are presented in Table 13. With increasing nocturnal aircraft noise exposure  $L_{night}$  there were significant increases in the following outcomes: sleep disturbance by aircraft noise; annoyance by aircraft noise; likelihood of rating overall sleep quality as “bad” or “fairly bad”; trouble falling asleep within 30 minutes at least once a week; trouble sleeping at night due to nocturnal awakenings or waking too early in the morning at least once a week; and trouble staying awake during the daytime at least once a week. Only use of sleep medications was not significantly associated with  $L_{night}$ . Nighttime aircraft noise was therefore associated with higher sleep disturbance and decreased subjective sleep quality.

Table 13. Odds ratios and 95% confidence intervals from unadjusted logistic regression models for sleep quality variables.

Covariate	Outcome measure						
	Sleep disturbance	Annoyance	Overall sleep quality	Trouble falling asleep	Trouble sleeping at night	Sleep medication	Trouble staying awake
$L_{night}$	1.15 [1.10-1.20]****	1.17 [1.11-1.22]****	1.05 [1.01-1.08]*	1.05 [1.02-1.09]**	1.04 [1.01-1.08]*	0.99 [0.95-1.04]	1.06 [1.01-1.11]*

P-values for odds ratios that are statistically significant are denoted with asterisks (\*<0.05; \*\*<0.01; \*\*\*\*<0.0001).



The odds ratios for the associations between  $L_{\text{night}}$  and sleep in the adjusted regression models (Table 14) closely match results from the unadjusted models, although trouble staying awake during the daytime is no longer significant. Furthermore, there were significant effects of noise sensitivity for all of the sleep outcomes, with noise sensitive individuals reporting higher disturbance, annoyance and trouble sleeping than non-sensitive individuals. Respondents with hearing problems were more likely to report trouble falling asleep and staying asleep. There were also effects of income bracket, with respondents in the highest annual income bracket (>\$100k) less annoyed and sleep disturbed by aircraft noise than respondents in the lowest income bracket (<\$50k).

Table 14. Odds ratios from logistic regression models for sleep quality variables, adjusted for age, BMI, sex, hearing problems, noise sensitivity and income.

Covariate	Level	Outcome measure						
		Sleep disturbance	Annoyance	Overall sleep quality	Trouble falling asleep	Trouble sleeping at night	Sleep medication	Trouble staying awake
$L_{\text{night}}$ [95% CI]	Continuous	1.15 [1.10-1.21]****	1.17 [1.11-1.23]****	1.04 [1.00-1.08]*	1.06 [1.02-1.10]**	1.04 [1.00-1.08]*	0.98 [0.94-1.03]	1.05 [1.00-1.11]
BMI	Continuous	0.95*	0.95*	1.00	0.99	1.00	1.04	1.00
Sex <sup>a</sup>	Male	1.05	1.13	0.99	1.23	0.59	0.66	0.58
Age	Continuous	1.00	1.00	0.99	0.99	0.99	0.99	0.99
Hearing problems <sup>b</sup>	Hearing problems	0.72	0.66	1.44	2.46*	2.51*	1.57	1.98
Noise sensitivity <sup>c</sup>	Noise sensitive	3.05***	3.10***	2.09**	2.74***	4.01****	2.10*	2.03*
Income <sup>d</sup>	\$50-100k	0.49	0.69	1.08	0.94	0.89	1.13	1.53
	>\$100k	0.21*	0.17*	0.72	0.63	0.72	1.70	0.83
	Prefer not to answer	0.67	0.85	0.82	0.61	0.56	1.88	0.62

Reference categories as follows: <sup>a</sup>Female; <sup>b</sup>No hearing problems; <sup>c</sup>Not noise sensitive; <sup>d</sup><\$50k; P-values for odds ratios that are statistically significant are denoted with asterisks (\*<0.05; \*\*<0.01; \*\*\*<0.001; \*\*\*\*<0.0001). CI: Confidence interval.

**Use of sleep aids in response to noise**

Results of the unadjusted logistic regression models for often or always using different sleep aids are presented in Table 15. With increasing nocturnal aircraft noise exposure  $L_{\text{night}}$ , respondents were significantly more likely to report using alcohol, television, music closing their windows in response to noise. Nighttime aircraft noise was therefore positively associated with increased prevalence of a number of coping behaviors.

Table 15. Odds ratios and 95% confidence intervals from unadjusted logistic regression models for always or often using sleep aids because of noise.

Covariate	Outcome							
	Earplugs	Alcohol	Medication	TV	Music	Close windows	Sound machine	Fan
$L_{\text{night}}$	1.04 [0.98-1.12]	1.11 [1.01-1.21]*	1.01 [0.97-1.06]	1.06 [1.02-1.10]**	1.08 [1.02-1.13]**	1.05 [1.01-1.08]**	0.97 [0.90-1.05]	1.02 [0.99-1.06]

P-values for odds ratios that are statistically significant are denoted with asterisks (\*<0.05; \*\*<0.01; \*\*\*<0.001).



The odds ratios and tests of significance for the associations between  $L_{night}$  and sleep aid use in the adjusted regression models (Table 16) closely match results from the unadjusted models. Furthermore, there were some significant effects of age, hearing problems and noise sensitivity. Older individuals were increasingly less likely to use music or fans as a sleep aid. Noise sensitive respondents and respondents with hearing problems were more than twice as likely to use either medication or television as a sleep aid. Noise sensitive individuals were also more likely to close their windows and use fans than non-sensitive individuals. Individuals with hearing problems were over 5 times as likely to use music as a sleep aid against noise compared to individuals without hearing problems.

Table 16. Odds ratios from logistic regression models for always or often using sleep aids because of noise, adjusted for age, BMI, sex, hearing problems, noise sensitivity and income.

Covariate	Level	Outcome							
		Earplugs	Alcohol	Medication	TV	Music	Close windows	Sound machine	Fan
$L_{night}$ [95% CI]	Continuous	1.04 [0.96-1.12]	1.10 [1.00-1.21]*	1.01 [0.96-1.06]	1.05 [1.01-1.10]*	1.07 [1.01-1.13]*	1.05 [1.01-1.09]**	0.99 [0.91-1.07]	1.01 [0.97-1.06]
BMI	Continuous	1.08*	0.99	1.03	1.02	1.04	0.96	0.95	1.03
Sex <sup>a</sup>	Male	0.90	1.12	0.85	0.82	0.84	1.16	0.97	0.77
Age	Continuous	1.00	0.97	1.00	0.98	0.94****	0.99	1.00	0.97**
Hearing problems <sup>b</sup>	Hearing problems	3.00	0.55	2.91*	5.14***	5.18***	1.05	1.14	2.07
Noise sensitivity <sup>c</sup>	Noise sensitive	2.42	2.29	2.29*	2.37*	1.08	1.71	0.96	2.04*
Income <sup>d</sup>	\$50-100k	2.46	1.23	0.89	1.42	1.35	0.98	1.59	0.80
	>\$100k	1.77	1.12	1.74	0.91	0.45	0.62	2.25	1.00
	Prefer not to answer	0.91	1.80	1.22	2.51	0.99	0.50	1.13	0.91

Reference categories as follows: <sup>a</sup>Female; <sup>b</sup>No hearing problems; <sup>c</sup>Not noise sensitive; <sup>d</sup><\$50k; P-values for odds ratios that are statistically significant are denoted with asterisks (\*<0.05; \*\*<0.01; \*\*\*<0.001; \*\*\*\*<0.0001). CI: Confidence interval.

## Health

Results of the unadjusted logistic regression models for self-reported general health and diagnosis of relevant health outcomes are presented in Table 17. With increasing nocturnal aircraft noise exposure  $L_{night}$ , respondents were significantly more likely to rate their health as worse, i.e. as fair or poor rather than good to excellent. This association was not statistically significant after adjusting for BMI, sex, age, hearing problems, noise sensitivity and income (Table 18). With increasing BMI, respondents were more likely to rate their health as worse and report a prior diagnosis of a sleep disorder, hypertension, and diabetes. With increasing age, respondents were more likely to report a prior diagnosis of a sleep disorder, hypertension, arrhythmia, heart disease and diabetes. There were no significant effects of sex or noise sensitivity on any of the measured health outcomes.



Table 17. Odds ratios and 95% confidence intervals from unadjusted logistic regression models for general health and diagnosis of different health outcomes.

Covariate	Outcome measure							
	General health†	Sleep disorder	Hypertension	Chronic headaches/Migraine	Arrythmia	Heart disease	Stomach ulcer	Diabetes
<i>L</i> <sub>night</sub>	1.06 [1.02-1.11]**	1.00 [0.96-1.04]	1.00 [0.97-1.04]	1.04 [0.98-1.11]	0.98 [0.92-1.04]	1.06 [0.97-1.15]	0.95 [0.86-1.05]	0.98 [0.93-1.03]

† Odds ratio of reporting health as poor or fair. P-values for odds ratios that are statistically significant are denoted with asterisks (\*<0.05; \*\*<0.01).

Table 18. Odds ratios from logistic regression models for general health and diagnosis of different health outcomes, adjusted for age, BMI, sex, hearing problems, noise sensitivity and income.

Covariate	Level	Outcome measure							
		General health†	Sleep disorder	Hypertension	Chronic headaches/Migraine	Arrythmia	Heart disease	Stomach ulcer	Diabetes
<i>L</i> <sub>night</sub> [95% CI]	Continuou s	1.04 [1.00-1.09]	0.99 [0.95-1.03]	1.00 [0.96-1.04]	1.03 [0.96-1.10]	0.99 [0.92-1.06]	1.08 [0.98-1.18]	0.95 [0.85-1.06]	0.96 [0.90-1.01]
BMI	Continuou s	1.08***	1.07**	1.13****	0.98	1.01	1.02	0.95	1.10***
Sex <sup>a</sup>	Male	1.33	0.85	1.04	0.51	1.14	1.86	0.52	0.82
Age	Continuou s	0.99	1.03*	1.10****	0.98	1.07**	1.06*	1.03	1.06***
Hearing problems <sup>b</sup>	Hearing problems	2.28*	2.03	1.25	1.24	2.12	2.27	0.67	0.85
Noise sensitivity <sup>c</sup>	Noise sensitive	1.28	1.61	0.87	1.36	1.65	1.02	0.35	1.31
Income <sup>d</sup>	\$50-100k	0.78	1.13	1.15	0.84	1.27	1.42	0.78	0.64
	>\$100k	0.22	2.03	1.98	0.36	0.94	1.03	1.47	1.30
	Prefer not to answer	1.30	1.60	1.10	0.60	0.73	0.57	-	3.09*

† Odds ratio of reporting health as poor or fair. Reference categories as follows: <sup>a</sup>Female; <sup>b</sup>No hearing problems; <sup>c</sup>Not noise sensitive; <sup>d</sup><\$50k; P-values for odds ratios that are statistically significant are denoted with asterisks (\*<0.05; \*\*<0.01; \*\*\*<0.001; \*\*\*\*<0.0001). CI: Confidence interval. Among respondents who chose not to report income, none reported stomach ulcers, so the odds ratio could not be determined.

#### 4. Subjective sleep quality, disturbance and coping strategies

From the 3600 long form versions of the postal surveys sent out, we found that residents living in regions with higher levels of nighttime aircraft noise were more likely to report poor overall sleep quality. They also reported greater difficulty falling asleep within 30 minutes and trouble sleeping at night due to waking in the middle of the night or too early in the morning. These findings are consistent with those of a recent World Health Organization (WHO) review on environmental noise and self-reported sleep outcomes [11]. While the WHO report found a statistically significant relationship between aircraft noise and disruptions to sleep only when noise was referred to in the question, in our study *L*<sub>night</sub> was associated with poorer self-reported sleep quality without a reference to noise. However, the title of our survey referenced noise, which may have influenced respondents when answering questions about their sleep. Furthermore, the choice of classification we used for coding the dichotomous variables of reporting difficulty sleeping, i.e. we coded a sleep difficulty



as present if it occurred once a week or more rather than the single highest response of three times a week or more, should moderate conclusions regarding associations between aircraft noise and subjective sleep. According to the American Psychiatric Association, a criterion for diagnosis of insomnia is that sleep difficulty occurs at least 3 times per week [86]. Few respondents reported that trouble with sleep occurred at least 3 times a week, precluding statistical analysis of this response category only, and further illustrating the need for the larger sample sizes that will be obtained in the nationwide study. Respondents were increasingly likely to report that they were very or extremely annoyed and sleep disturbed with increasing  $L_{\text{night}}$ , which are responses corresponding to the “highly annoyed” and “highly sleep disturbed” classifications used by the WHO in their estimations of the disease burden of environmental noise [87]. These level-dependent associations between aircraft noise and annoyance and sleep disturbance are consistent with what has been found previously in the literature [11, 88, 89]. Good quality sleep is important for many biological functions and overall health, and so public perception that aircraft noise is disrupting sleep is a relevant concern. However, questionnaires on self-reported sleep may not fully capture the magnitude of the effect of environmental noise on sleep. Nighttime awakenings due to noise often occur without conscious awareness, and so residents may not accurately estimate the degree to which noise affects their sleep. There is also some evidence that self-reported sleep may only be weakly associated with objective sleep measures of sleep [90]. Thus, future field studies on the physiological responses to nighttime aircraft noise are needed to elucidate the objective impact of aircraft noise on sleep.

Along with disrupting sleep, aircraft noise can be annoying to residents living near airports. It was found that residents living in regions with higher  $L_{\text{night}}$  levels were significantly more likely to report feeling highly annoyed by aircraft noise over the last twelve months. This finding is consistent with previous annoyance studies (e.g., [91-93]). A limitation of this finding is that we only examined the associations between  $L_{\text{night}}$  and annoyance to aircraft noise, and so we cannot exclude daytime noise exposure as the main source of annoyance. A high level of annoyance to aircraft noise is concerning not just because of its impact on mood, but also because of its potential to influence sleep. While we sleep, the brain continues to process and evaluate auditory stimuli, and so noise events that have emotional relevancy may induce a nighttime arousal with a higher probability compared to those that are less emotionally relevant [94]. Addressing annoyance to aircraft noise may thus be an important component in preventing aircraft noise-induced sleep disturbance. Because of the limited sample size and low response rate, annoyance levels found in this study should not be generalized to the studied, or other, airports. A much larger national survey across a more representative selection of 20 airports was recently conducted by the FAA and is expected to provide more precise exposure-response functions for daytime and nighttime aircraft noise annoyance [95].

Residents who were sensitive to noise were more likely to report annoyance and sleep disturbance by aircraft noise, as well as worse subjective sleep overall in all measures of sleep quality. This is in line with previous findings that noise sensitive individuals report worse sleep [96-98]. As a result of noise, sensitive respondents were also more likely to report using three of the eight measured sleep aids at least once a week, further supporting the idea they were more psychologically susceptible to, or more cognizant of, nocturnal noise. It is however unclear how sensitivity might influence the impact of noise on sleep biology, with several studies finding minimal or no physiologic effects of sensitivity [97, 99, 100], or even that their sleep was objectively better [101]. Regardless of whether or not physiologic effects of noise are moderated by an individual’s sensitivity, consistent findings, both here and previously, that they report worse subjective sleep and increased annoyance and disturbance remain relevant when considering the public health implications of nocturnal aircraft noise exposure.

Those exposed to high levels of aircraft noise during sleep may try to adapt to the noise using various sleeping aids, such as putting in earplugs or closing windows. We found that  $L_{\text{night}}$  was significantly associated with an increased likelihood to frequently close windows when trying to sleep and to use alcohol, television and/or music as sleep aids because of noise. These findings suggest that residents in communities with higher  $L_{\text{night}}$  are concerned with noise affecting their sleep, and they engage in coping behaviors to adapt to the noise at night. A limitation is that our survey questions on sleep aids referenced noise in general—rather than aircraft noise specifically. It may be possible that residents living in neighborhoods with higher  $L_{\text{night}}$  use sleep aids to block out other sources of nighttime noise as well. However, given that these residents were significantly annoyed and disturbed in their sleep by aircraft noise it is plausible that aircraft noise was the primary noise source that induced these coping behaviors.

In the long-term, exposure to high levels of aircraft noise may have adverse health consequences [102, 103]. It is thought that nighttime aircraft noise exposure increases the risk of cardiovascular disease [104] and is known to disturb sleep, which—when restricted on a chronic basis—is associated with increased risk of cancer, obesity, and diabetes [105]. However, we did not find an association between  $L_{\text{night}}$  and poorer self-reported general health after adjusting for individual-level covariates and sociodemographic factors. Nor did we find an association between  $L_{\text{night}}$  and diagnosis of heart disease,



hypertension or diabetes. However, we were underpowered to detect the small effect sizes expected for these health outcomes. However, the significant relationships between BMI and age with a number of the health outcomes are all positive, as would be expected for sleep disorders, hypertension, heart disease and diabetes, indicating that the questionnaire items may be suitable for capturing the prevalence of diagnosis among the sampled population.

## 5. Limitations

There are a number of limitations with results of the survey results, most notably that our sample size was small (268 surveys or 8.5% of the surveyed population). Our response rate was lower (10.1%) than the 46-76% response rates seen in other postal questionnaires on attitudes towards aircraft noise [58], and so survey responses may not accurately represent the attitudes and sleep patterns of the population around Atlanta airport. However, this survey was primarily aimed at recruitment for a field study, and its response rate may not be comparable to other attitudinal questionnaires). Additionally, we did not have information on noise exposure levels in the bedrooms of survey participants. Our survey study used estimated outdoor nighttime aircraft exposure levels based on flight traffic data; however, these estimates may not always reflect actual noise levels in the bedroom (see section V.F). If residents close their windows at night, noise levels can be diminished by up to 28 dB [106], and indeed in the field study we measured lower indoor levels among participants who slept with the windows closed compared to those who did not (see Figure 27 and Figure 28 in section V.F on Noise Expose Validation). Aircraft noise can also be masked by noise from air conditioning, television or white noise machines. Accurate bedroom noise levels can only be obtained with measurement, such as was performed for a small sample of survey respondents in the field study. Lastly, because of the exploratory design of this study, we decided not to correct for multiple testing, and therefore inferences drawn from these tests may not be reproducible [107]. Despite these limitations, evidence of adverse effects of aircraft noise warrants further investigation in larger subject cohorts.



### C. Non-participation analysis

It is important that participants in the field study are representative of the population from which they are recruited. We therefore compared demographic data for survey respondents who participated or did not participate in the field study. The percentages of participant and non-participant race, sex, age,  $L_{\text{Night}}$ , marital status, household income, education, employment, noise sensitivity, sleep disturbance by aircraft noise at home, general health and sleep quality over the past month are presented in Appendix 5.

A number of categories for certain items had low numbers of responses, and the total sample size ( $n=407$ ) was less than 1000. We therefore used Fisher's exact test of independence, rather than the more general  $\chi^2$  test, to test whether the proportion of responses for the demographic variables were different between participants and non-participants [108]. Exact p-values are reported in the figure captions. There were no statistically significant indications of differences between the participation groups for race, sex, age,  $L_{\text{Night}}$ , marital status, household income, education, employment, noise sensitivity or sleep disturbance by aircraft noise at home. There were statistically significant differences between the participation groups for self-reported general health ( $p=0.0004$ ) and sleep quality over the past month ( $p=0.023$ ).

The lack of differences between participation groups for the majority (10 of 12) of the variables suggests a good representativeness of the field study participants relative to the wider population. However, a greater proportion of non-participants rated their sleep quality and general health as worse than the field study participants. In other words, survey respondents with poorer health and/or sleep quality were less likely to enroll in the field study. Part of this may be explained by subjects not meeting eligibility criteria for inclusion into the study.

Fifty eight percent of respondents were black, which is a similar proportion to the 62.5% mean proportion for the sampled sampling region (calculated based on proportions and number of houses in each sampling region, see Table 3). The mean age of respondents was 53.0 years. Although this is greater than the mean age of 35.1 years for the sampled census tracts (calculated as  $(\sum (\text{houses per tract} \times \text{mean age per tract})) / \text{total number of houses in all tracts}$ ), see Table 3), this is an expected result since census data includes children, whereas our survey contact letters specified that respondents must be an adult (Appendix 3). For highest level of completed education, 48.6 % of respondents had no college education, which is slightly higher, although not greatly so, than the 40.0% of the population without college education in the sampling region (calculated based on proportions and number of houses in each sampling region, see Table 3). For annual household income, 42.6% of all responses were in the 25-50k category and below, and 61.6% of all responses were in the \$50-75k category. The median household income of respondents is therefore between \$50-75k. The mean for the sampled census tracts is \$49.0k (see Table 3 calculated based on proportions and number of houses in each tract). On one hand, if the median income was in the lower range of the \$50-75k category, there would be a good agreement between survey respondents and the general population in the sampling region. On the other hand, an income in the higher range of the category would suggest that respondents earned substantially more than their counterparts. In the absence of more precise income data, no firm conclusions can therefore be drawn in this regard.



#### D. Field study morning questionnaires

Six participants entered questionnaire data directly into RedCap using their own computer. Twenty eight participants completed paper versions of the same questionnaire (Appendix 4).

There were a total of 165 completed questionnaires from 33 field study participants (expected N=170). One participant did not complete the morning questionnaires during the field study.

Results of the crude models are presented in Table 19, with equivalent ( $L_{AEq, sleep}$ ) or maximum ( $L_{AS, max}$ ) noise level during the individualized sleep period as the independent variables. The number of self-reported awakenings and sleep disturbance by aircraft noise significantly increased with increasing  $L_{AS, max, sleep}$ . There were no statistically significant effects for any other outcomes in the crude models.

Table 19. Effect of equivalent nighttime aircraft noise ( $L_{AEq, sleep}$ ) or maximum aircraft noise ( $L_{AS, max}$ ) during sleep on questionnaire outcomes. Crude noise-only model. Parameter estimates are presented as regression coefficients ( $\beta$ ). Statistically significant ( $p < 0.05$ ) Type III effects are highlighted in bold typeface. df=degrees of freedom. CI=confidence interval. SSS=Stanford Sleepiness Scale.

Response	$L_{AEq, sleep}$		$L_{AS, max}$	
	p	$\beta$ (95% CI)	p	$\beta$ (95% CI)
Sleep latency (minutes)	0.448	-0.512 (-1.835; 0.811)	0.552	0.141 (-0.323; 0.604)
Awakenings (n)	0.075	0.031 (-0.003; 0.065)	<b>&lt;0.001</b>	<b>0.037 (0.019; 0.054)</b>
Tiredness (0-10)	0.571	0.046 (-0.113; 0.205)	0.058	0.069 (-0.002; 0.141)
Sleepiness (dichotomous SSS)	0.792	-0.019 (-0.157; 0.120)	0.438	-0.029 (-0.102; 0.044)
Difficulty falling asleep (0-10)	0.444	-0.049 (-0.173; 0.076)	0.495	0.030 (-0.055; 0.115)
Sleep restlessness (0-10)	0.229	-0.086 (-0.226; 0.054)	0.844	0.009 (-0.083; 0.101)
Sleep quality (0-10)	0.959	0.005 (-0.189; 0.199)	0.134	0.059 (-0.018; 0.135)
Disturbance by aircraft noise (dichotomous)	0.334	0.133 (-0.137; 0.403)	<b>0.003</b>	<b>0.106 (0.036; 0.175)</b>

Results of the adjusted models are presented in Table 20. There was quasi-complete separation of the data, whereby the dichotomous sleepiness variable separated the predictor variables to a certain degree, and therefore the regression model could not estimate the maximum likelihood ratio. Where complete or quasi-complete separation occurred, the problematic predictor variable were excluded from the model.

No statistically significant effects of  $L_{AEq, sleep}$  were found. With increasing  $L_{AS, max}$  there were significant increases in tiredness ( $\beta=0.005$ ,  $p=0.005$ ) and, as with the crude model, self-reported awakenings ( $\beta=0.051$ ,  $p < 0.001$ ). These findings provide some support to the hypothesis that nocturnal aircraft noise can have adverse effects on sleep. Physiologic awakening probability increased with the maximum noise level of a discrete aircraft noise event (see section V.E), and based on the questionnaire data the participants seem to recall at least some of these awakenings. Furthermore, recalled awakenings can have a moderate correlation with self-reported tiredness [109].

There was a significant effect of the number of airplane noise events on sleepiness in the  $L_{AEq, sleep}$  model, and tiredness in  $L_{AS, max}$  model, whereby participants reported lower sleepiness and lower tiredness with higher numbers of airplanes. On the one hand, this could indicate that individuals who are chronically exposed to a high number of aircraft noise events habituate to the exposure. There is evidence that physiologic habituation to single noise events occurs within nights, but not between-nights in the short-term, particularly for autonomic arousal [110]. However, in the long-term, there might be some level physiologic habituation to nocturnal noise, but this habituation does not seem to be total, i.e. at least some degree of response persists [111]. An alternative explanation for the finding of lower sleepiness and tiredness could be that individuals exposed to a high number of events over time have more impaired sleep than counterparts exposed to fewer events. Incongnizant of this decreasing objective sleep quality, they may downwardly adjust their criteria for what



they consider as good subjective sleep, i.e. they “get used” to this poorer sleep as the norm, such as seems to occur with aging [112]. Such a process would manifest superficially as a psychological habituation, with lower levels of sleepiness and tiredness than an individual may have reported previously even with adversely impacted sleep physiology. However, in the absence of more detailed data on the objective sleep of the participants in the current field study, both explanations of the lower tiredness and sleepiness following nights with a higher number of aircraft noise events remain speculative.

There was a significant effect of sex on tiredness in the  $L_{Aeq, sleep}$  model, whereby men were less tired than women. There was a similar effect in the  $L_{AS, max}$  model, but the result was of borderline statistical significance ( $p=0.052$ ). This result is in line with some earlier work finding that although women may have better objective sleep than men, they frequently report greater sleep disturbance [113], and are at increased risk for developing sleep disorders including insomnia and restless legs syndrome [114, 115].

There was a significant effect of age on sleep latency in the  $L_{Aeq, sleep}$  model. This increasing sleep latency with age is in line with typical age-related alterations in sleep [116].

There were significant effects of sleeping with open windows on sleep latency in the  $L_{Aeq, sleep}$  and  $L_{AS, max}$  models, and on awakenings in the  $L_{AS, max}$  model. With fully or partially open windows, sleep latency was shorter and there were fewer recalled awakenings. One possible explanation is that individuals who find it difficult to sleep, and therefore have longer sleep latencies and more awakenings, may be more likely to close their window to lower noise levels. Alternatively, open windows, while resulting in higher indoor noise levels, could lead to better air quality and temperature in the bedroom, which may *per se* help promote certain aspects of subjective sleep [117].

No statistically significant effects were found for any of the independent variables in either of the  $L_{Aeq, sleep}$  and  $L_{AS, max}$  models for difficulty falling asleep, sleep restlessness, sleep quality or disturbance by aircraft noise. The absence of an effect on disturbance by aircraft noise in particular is surprising, as self-reported sleep disturbance by a particular noise source has frequently been reported in the literature [11, 118]. However, as part of eligibility for the field study, participants did not regularly use sleep medication, did not suffer from sleep disorders, and were generally free from internal and external factors that could interfere with sleep, all of which indicates they were habitually good sleepers. Taken with the fact that they generally reported better sleep quality than postal survey respondents who did not participate in the field study (see section V.C), the current study population may represent a particularly resilient subgroup who do not feel their sleep is disturbed, or the size of any disturbance effect in this group was too small to be detected with our limited sample size.



Table 20. Effect of equivalent nighttime aircraft noise ( $L_{Aeq, sleep}$ ) or maximum nighttime aircraft noise ( $L_{AS, max}$ ) during sleep on questionnaire outcomes. Fully adjusted model. Parameter estimates are presented as regression coefficients ( $\beta$ ). Statistically significant ( $p < 0.05$ ) Type III effects are highlighted in bold typeface. \* Reference category=women. † Reference category=completely closed. ‡ Excluded from model due to quasi-complete separation. df=degrees of freedom. CI=confidence interval. SSS=Stanford Sleepiness Scale.

Response	Independent variable	$L_{Aeq, sleep}$		$L_{AS, max}$	
		p	$\beta$ (95% CI)	p	$\beta$ (95% CI)
Sleep latency (minutes)	Noise ( $L_{Aeq, sleep}/L_{ASmax}$ )	0.090	-0.947 (-2.041; 0.146)	0.482	-0.181 (-0.686; 0.324)
	Sex *	0.268	5.456 (-4.206; 15.117)	0.739	-0.086 (-0.595; 0.422)
	Number of planes	0.143	0.140 (-0.047; 0.327)	0.332	0.097 (-0.099; 0.293)
	Age	<b>0.013</b>	<b>0.443 (0.095; 0.790)</b>	<b>0.024</b>	<b>0.457 (0.061; 0.853)</b>
	Windows †	<b>0.012</b>	<b>-11.769 (-20.904; -2.635)</b>	<b>0.013</b>	<b>-13.392 (-24.012; -2.773)</b>
Awakenings (n)	Noise ( $L_{Aeq, sleep}/L_{ASmax}$ )	0.079	0.040 (-0.005; 0.085)	<b>&lt;0.001</b>	<b>0.051 (0.028; 0.074)</b>
	Sex (ref=women)	0.857	-0.039 (-0.468; 0.390)	0.467	0.161 (-0.272; 0.593)
	Number of planes	0.978	0.000 (-0.006; 0.006)	0.263	-0.004 (-0.011; 0.003)
	Age	0.074	0.014 (-0.001; 0.030)	0.067	0.011 (-0.001; 0.022)
	Windows †	0.063	-0.578 (-1.187; 0.031)	<b>0.016</b>	<b>-0.783 (-1.418; -0.148)</b>
Tiredness (0-10)	Noise ( $L_{Aeq, sleep}/L_{ASmax}$ )	0.322	0.092 (-0.090; 0.273)	<b>0.005</b>	<b>0.118 (0.036; 0.199)</b>
	Sex *	<b>0.008</b>	<b>-2.054 (-3.579; -0.530)</b>	0.052	-1.591 (-3.195; 0.014)
	Number of planes	0.070	-0.022 (-0.045; 0.002)	<b>0.001</b>	<b>-0.031 (-0.048; -0.013)</b>
	Age	0.275	0.026 (-0.021; 0.074)	0.471	0.018 (-0.031; 0.068)
	Windows †	0.373	-0.887 (-2.837; 1.063)	0.140	-1.365 (-3.177; 0.447)
Sleepiness (dichotomous SSS)	Noise ( $L_{Aeq, sleep}/L_{ASmax}$ )	0.558	0.046 (-0.108; 0.200)	0.832	0.012 (-0.097; 0.121)
	Sex *	0.131	-1.808 (-4.153; 0.537)	0.145	-1.805 (-4.233; 0.624)
	Number of planes	<b>0.026</b>	<b>-0.050 (-0.094; -0.006)</b>	0.072	-0.051 (-0.106; 0.005)
	Age	0.463	0.020 (-0.033; 0.073)	0.462	0.018 (-0.031; 0.067)
	Windows †‡		-		-
Difficulty falling asleep (0-10)	Noise ( $L_{Aeq, sleep}/L_{ASmax}$ )	0.472	-0.053 (-0.196; 0.091)	0.428	0.044 (-1.197; 0.154)
	Sex *	0.976	0.021 (-1.386; 1.429)	0.750	0.233 (-1.197; 1.663)
	Number of planes	0.874	-0.001 (-0.017; 0.015)	0.298	-0.010 (-0.028; 0.009)
	Age	0.056	0.045 (-0.001; 0.091)	0.050	0.043 (0.000; 0.085)
	Windows †	0.176	-1.045 (-2.559; 0.469)	0.083	-1.420 (-3.023; 0.183)
Sleep restlessness (0-10)	Noise ( $L_{Aeq, sleep}/L_{ASmax}$ )	0.375	-0.069 (-0.221; 0.083)	0.560	0.033 (-0.077; 0.143)
	Sex *	0.224	-0.835 (-2.181; 0.512)	0.323	-0.668 (-1.993; 0.657)
	Number of planes	0.293	-0.008 (-0.024; 0.007)	0.096	-0.016 (-0.036; 0.003)
	Age	0.115	0.032 (-0.008; 0.072)	0.105	0.031 (-0.006; 0.068)
	Windows †	0.094	-1.212 (-2.629; 0.205)	0.068	-1.559 (-3.231; 0.113)



Table 20. continued

Response	Independent variable	p	$L_{AEq,sleep}$	p	$L_{AS,max}$
			$\beta$ (95% CI)		$\beta$ (95% CI)
Sleep quality (0-10)	Noise ( $L_{AEq,sleep}/L_{AS,max}$ )	0.587	-0.063 (-0.292; 0.165)	0.122	0.058 (-0.016; 0.132)
	Sex *	0.507	-0.563 (-2.227; 1.101)	0.731	-0.290 (-1.943; 1.363)
	Number of planes	0.465	0.009 (-0.016; 0.034)	0.894	-0.001 (-0.023; 0.020)
	Age	0.188	-0.038 (-0.094; 0.018)	0.137	-0.040 (-0.093; 0.013)
	Windows †	0.127	1.640 (-0.465; 3.745)	0.275	1.157 (-0.921; 3.235)
Disturbance by aircraft noise (dichotomous)	Noise ( $L_{AEq,sleep}/L_{AS,max}$ )	0.433	0.060 (-0.089; 0.208)	0.183	0.092 (-0.043; 0.226)
	Sex *	0.668	-0.456 (-2.539; 1.627)	0.962	-0.053 (-2.235; 2.129)
	Number of planes	0.378	0.016 (-0.019; 0.051)	0.464	0.015 (-0.025; 0.055)
	Age	0.378	0.023 (-0.136; 0.183)	0.859	0.015 (-0.151; 0.181)
	Windows †	0.763	-0.285 (-2.137; 1.568)	0.263	-0.765 (-2.106; 0.575)

In summary, only minimal effects of aircraft noise were found on self-reported sleep outcomes. Maximum and average nighttime aircraft sound pressure levels have previously been found to predict event-related awakenings [11]. Accordingly, even with a small sample size by questionnaire study standards, we saw a statistically significant increase in the number self-reported awakenings with increasing  $L_{AS,max}$ , although the effect of  $L_{AEq,sleep}$  was of only borderline significance ( $p=0.079$ ), which could be due to insufficient statistical power resulting from the limited sample size.

There may have been some misinterpretation of the questionnaire response scales among the participants, as response scales were sometimes in different directions relative to one another. For instance, the three items of question 8 (ease of falling asleep, sleep restlessness and sleep quality) had a 0-10 response scale, with a value of 10 indicating the worst sleep on two scales (most difficult to sleep and most restless), but the best sleep quality. In one case, a participant rated themselves as very restless (10 out of 10) and having difficulty falling asleep (8 of 10), but with very good sleep quality (9 out of 10). It is unlikely, albeit not impossible, that this rating of sleep quality is accurate, but instead results from the inversion of the response scale. Rather than taking what would be an unethical and unscientific approach of trying to guess what we believed the respondent intended, we always used the actual responses. In future field studies it will be important to minimize the possibility of confusion or misinterpretation of any questionnaire items, improving data quality.



## E. Event-related analysis

This section describes the physiologic event-related response to aircraft noise events during sleep.

### 1. Study participants and data loss

Thirty-four subjects consented to participate in the study, and provided at least some data (a single subject consented but did not participate in the measurements nor returned the equipment). Of the 34 subjects, the acoustical calibration before the equipment was sent out and after it was returned differed by  $>2$  dBA and was considered invalid in 10 subjects. These differences were caused by an unprotected gain controller that, likely unwillingly, was moved by research staff or study participants after initial calibration (see Figure 22).



Figure 22. Sound recorder gain controller issues. The left pane shows two gain controllers behind a metal bar. As the protection of these controllers is minimal, the position of the controllers was changed in  $N=10$  study participants after initial calibration. A 3D-printed gain control stabilizer (middle pane) was used for all remaining measurements. In the final approach, which will be used in the future National Sleep Study (but was not implemented around ATL), the gain controller was fixed in one position with a hot glue gun before calibration (right pane).

Of the remaining 24 subjects, one subject contributed only one valid night of physiological data, and only a single aircraft noise event was recorded in this period. In another subject, not a single aircraft noise event was recorded during the measurement nights. These two participants were thus excluded from data analysis. Therefore, 22 subjects (8 male; mean  $\pm$  SD age  $50.0 \pm 14.0$  years; mean  $\pm$  SD BMI  $27.8 \pm 3.3$   $\text{kgm}^{-2}$ ) contributed to the final analysis. A total of 1,900 aircraft noise events were recorded in the bedroom. In 154 aircraft noise events (8.1%), no physiological data were available. Finally, in 79 aircraft noise events (4.2%), an awakening reaction started prior to the start of the aircraft noise event, and so were excluded. A total of 1,667 aircraft noise events (87.7% of 1,900) therefore contributed to the data analysis.

### 2. Aircraft noise levels

The distribution of indoor maximum noise levels for the 1,667 aircraft events within participant's homes that contributed to the data analysis is shown in Figure 23. The average  $L_{AS,max}$  of aircraft events was 40.1 dB (median 39.4 dB, range 28.9 dB-63.4 dB). A distribution of average noise levels in the minute preceding the start of each aircraft noise event is also shown in Figure 23 (average 30.9 dB, median 29.8 dB, range 22.4 dB-56.5 dB).

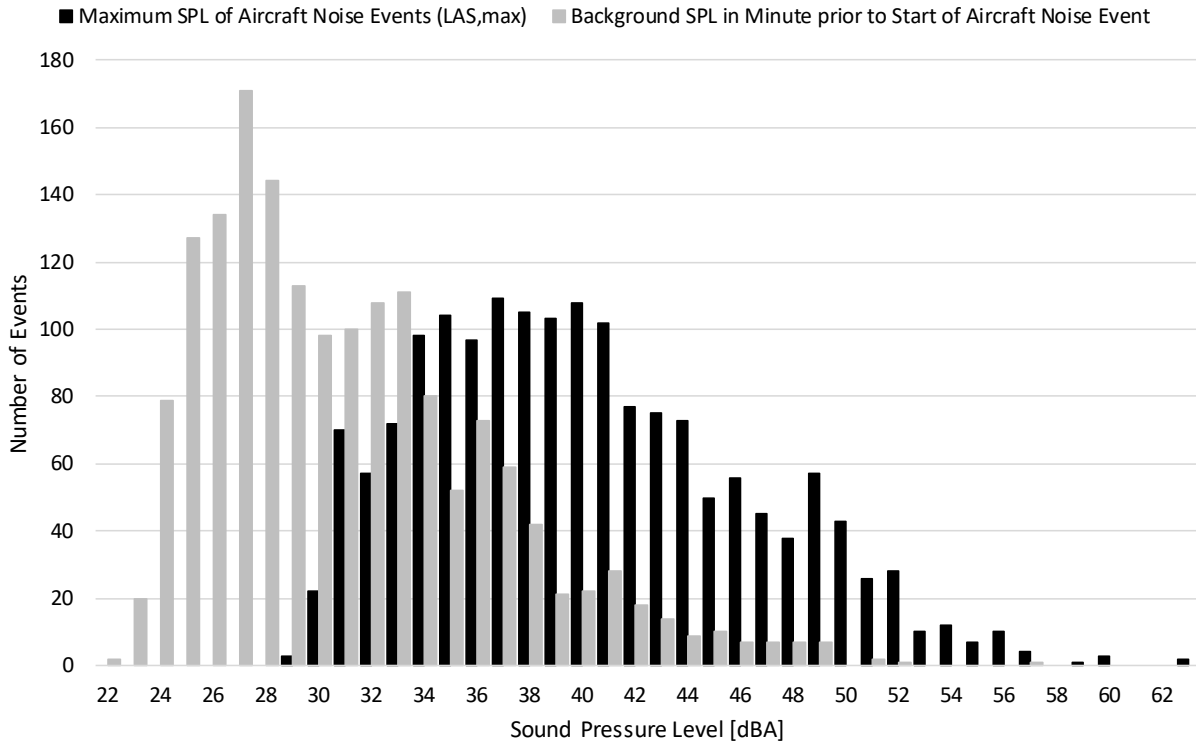


Figure 23. Indoor noise levels for participants near the airport. Black:  $L_{AS,max}$  of aircraft events; Gray:  $L_{AEq}$  one minute before the start of each aircraft event.

The number of events per night per subject who lived near the airport is shown in Figure 24. Out of the 22 participants that contributed to data analysis, the median number of aircraft noise events experienced across the 5 study nights was 43 (range 5-297).

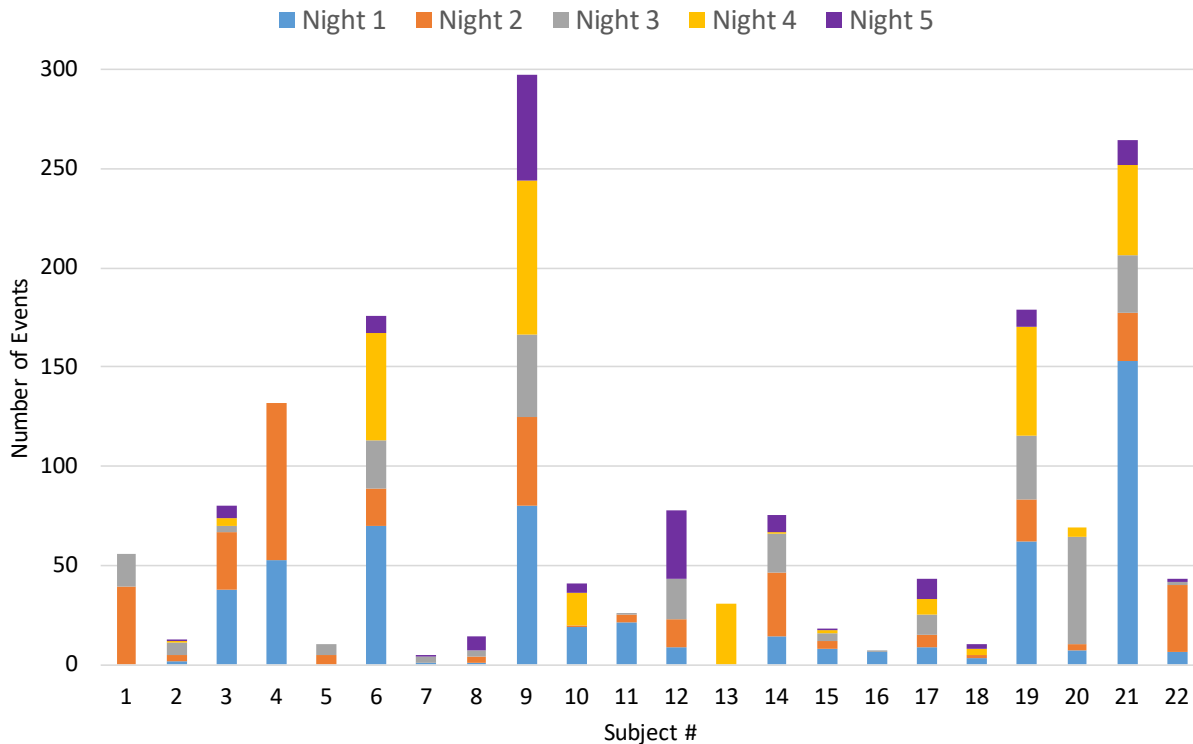


Figure 24. Number of aircraft noise events per subject near ATL airport for each of the 5 study nights. The colors indicate study nights.

### 3. Single event awakening analysis

Random intercept logistic regression models were calculated for the probability of awakening to an aircraft. Model 1 contained only the indoor maximum noise level, Model 2 was adjusted for age, sex, BMI, and time from sleep onset (Table 21). A total of 1,667 aircraft noise events contributed to the analysis. In both models the coefficient for  $L_{ASmax}$  was positive (i.e., awakening probability increased statistically significantly with increasing  $L_{ASmax}$ ) but not statistically significant, likely due to the low sample size and power of the study. In Model 2, adjustment had little influence on the estimate of the coefficient for  $L_{ASmax}$  (0.0288 in Model 1 vs. 0.0254 in Model 2, respectively). None of the investigated confounders (age, sex, BMI, and time from sleep onset) had a statistically significant influence on awakening probability.

Table 21. Random effect logistic regression models for the probability of awakening.

	Model 1			Model 2		
	Estimate	SE	p-value	Estimate	SE	p-value
$L_{ASmax}$ [dB]	0.0288	0.0148	0.0647	0.0254	0.0126	0.0572
Age [years]				-0.0054	0.0052	0.3159
Male				-0.1359	0.2910	0.6454
BMI				-0.0021	0.0304	0.9450
Time [min]				-0.0005	0.0005	0.3346

SE: Standard Error



The exposure-response relationship for additional awakenings due to aircraft events ( $P_{\text{noise}} - P_{\text{spontaneous}}$ ), based on unadjusted Model 1 above, is shown in Figure 25. To account for spontaneous awakenings in the exposure-response function [119], an estimate statement was used in NLMIXED to subtract awakening probability at 29 dB from the awakening probability at the maximum SPL of interest. The threshold of 29 dB was based on the median background noise level one minute prior to the start of the aircraft noise events in this study (29.8 dB). Due to the relatively low number of subjects and aircraft noise events per subject, the 95% confidence interval of the exposure-response function is relatively wide. As the p-value for the  $L_{AS,max}$  estimate was  $\geq 0.05$ , the 95% confidence intervals in Figure 25 includes 0% for higher noise levels (negative estimates were converted to 0%).

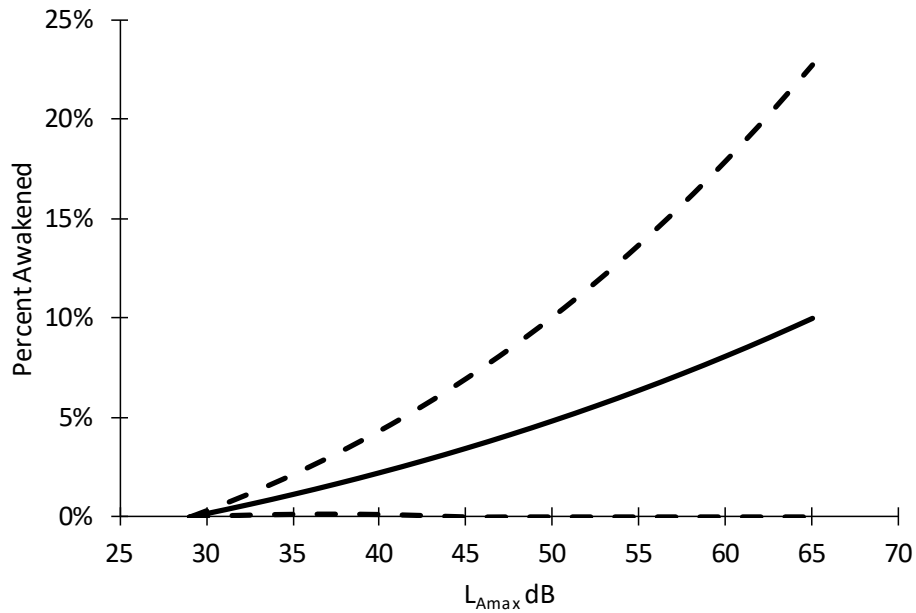


Figure 25. The unadjusted probability of an additional awakening induced by aircraft noise depending on indoor maximum SPL  $L_{Amax}$  (slow time weighting) for ATL International Airport. Dashed lines indicate 95% confidence intervals.



### F. Noise exposure validation

Selection of geographical areas from which to recruit field study participants and analysis of survey response data were both based on modelled outdoor, rather than measured indoor, aircraft noise data. Effects of noise on sleep depend on noise levels during sleep in the bedroom, and therefore are affected by the accuracy of the modelling and GIS coding, sound insulation (including window opening and closing), position of the bedroom in the dwelling (for instance facing towards or away from flight paths), and sleep times of the occupants (for instance if they sleep during low- or high- air traffic volume times). The modelled outdoor aircraft noise exposure  $L_{night}$  correlated significantly with  $L_{Aeq,sleep}$  ( $r=0.63$ ,  $p=0.001$ ) and  $L_{AS,max,sleep}$  ( $r=0.57$ ,  $p=0.004$ ), shown in Figure 26. There were lower measured aircraft noise levels in the bedroom when participants closed their windows (mean  $\pm$  SD level  $27.2 \pm 0.4$  dB  $L_{Aeq,sleep}$ ;  $44.8 \pm 0.9$  dB  $L_{AS,max,sleep}$ ) compared to when it was partially or completely open ( $30.2 \pm 1.2$  dB  $L_{Aeq,sleep}$ ;  $52.7 \pm 2.5$  dB  $L_{AS,max,sleep}$ ). These data stratified by window closing were averaged across all noise exposure categories, and we do not have outdoor noise measurements, so the difference between the window closed and partially/completely open groups does not reflect the noise reduction effect of closing a window. For instance, individuals with higher outdoor aircraft noise levels were more likely to close their windows [51], which may also be the case in this field study. Given the number of factors that can influence indoor noise levels compared to  $L_{night}$ , the correlation coefficient indicates a rather good capability of the noise modelling procedure to predict average aircraft noise levels in the bedroom during sleep.

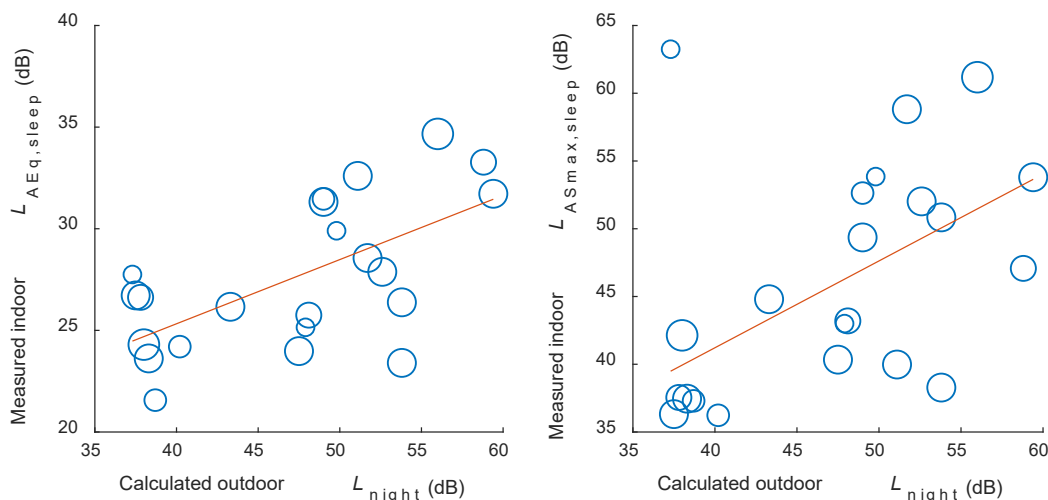


Figure 26. Scatter plot of between calculated outdoor  $L_{night}$  (abscissa) and mean measured indoor aircraft noise level during sleep for each participant (ordinate; left pane  $L_{Aeq,sleep}$ ; right pane  $L_{ASmax,sleep}$ ). The number of observations (nights) for each participant is indicated by the circle radius. The least squares regression line, calculated with weighted data, is shown in red.

Cross-sectional information on the influence of window closing/opening on indoor noise level can be determined by stratifying measured aircraft noise levels by the morning questionnaire item on window position. As anticipated, there were generally lower noise levels, both sleep period average (Figure 27) and maximum (Figure 28), when the window was closed compared to when it was partially or completely open. Note that these data were averaged across all noise exposure categories, and we do not have outdoor noise measurements, so the difference between the window closed and partially/completely open groups does not necessarily reflect the noise reduction effect of closing a window. For instance, as found in the postal surveys, individuals with higher outdoor aircraft noise levels were more likely to close their windows (see section V.B.3), which may also be the case in the field study.

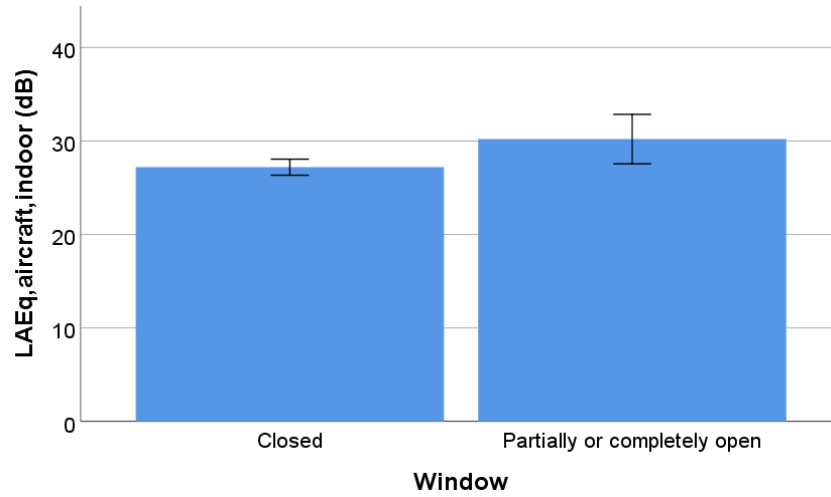


Figure 27. Mean  $L_{AEq}$  during sleep stratified by window position during the night. Error bars indicate 95% confidence intervals.

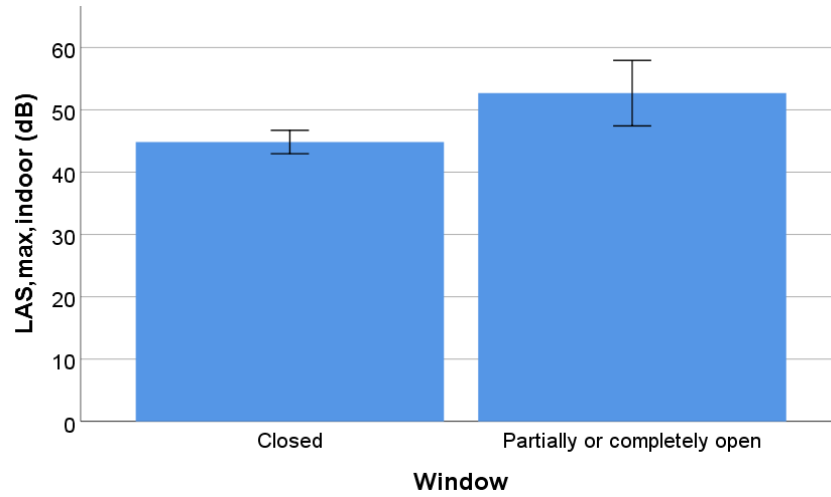


Figure 28. Mean  $L_{AS,max}$  during sleep stratified by window position during the night. Error bars indicate 95% confidence intervals.



**G. Feasibility assessment**

The following sections describe whether the approach adopted in the study presented in this report is feasible to implement on a larger scale in the National Sleep Study.

**1. Cost effectiveness of postal surveys for study recruitment**

In rounds 1-5, the gift card amount was randomized among respondents, so we used the mean cost of the possible \$2, \$5 and \$10 amounts (\$5.67) in the cost calculations. In rounds 6-17, 12.4% of initial survey waves were non-deliverable and returned to us with the \$2 cash incentive still included. For each individual survey that was delivered, an average of \$0.248 (i.e. 12.4% of \$2) was recouped from these non-deliverable initial waves, and accounted for in the cost calculations. The costs for each individual survey and follow-up wave mailed out, the total cost per individual and the resulting total cost to receive a single completed survey are presented in Table 22, stratified by the different survey sampling protocols. The number of surveys sent out to receive a single response are the reciprocals of the response probabilities in Table 10. These data do not account for any associated personnel costs.

Table 22. Survey sampling cost effectiveness, ordered from the most to least cost effective method to receive a single completed survey.

Sampling protocol			Surveys needed to receive 1 response (n)*	Surveys sent to recruit 1 participant (n)*#	Costs (\$)							
Follow-up waves (n)	Survey length	Survey incentive			Initial wave	Follow-up wave 1	Follow-up wave 2	Follow-up wave 3	Total per mailed individual	Per response received*	Total to receive 1 response †	Recruit 1 participant †#
3	Short	\$2	4.61	50.7	3.01	0.70	1.01	1.01	5.74	26.44	28.89	317.51
3	Medium	\$2	4.88	53.6	3.09	0.70	1.09	1.09	5.96	29.09	31.84	349.88
0	Long	\$2	12.20	134.1	3.09	-	-	-	3.09	37.65	39.54	434.48
3	Long	\$2	6.13	67.4	3.09	0.70	1.09	1.09	5.96	36.59	39.99	439.50
2	Long	\$2	8.33	91.5	3.09	0.70	1.09	-	4.88	40.64	44.01	483.66
0	Long	Gift card	32.26	354.5	1.09	-	-	-	1.09	40.83‡	46.81‡	503.38

\*Assumes 100% delivery rate

†Assumes 87.6% delivery rate and, if applicable, \$0.248 recouped from non-deliverable initial survey waves.

‡Includes a mean gift card cost of \$5.67

#Assumes 9.1% participation rate from completed surveys across all survey mailing rounds, independent of mailing protocol. Does not include cost for actual participation in the field study (\$150 or \$200).

The most cost effective approach was the short survey with a \$2 cash incentive and 3 follow-up waves, whereby on average 50.7 surveys were sent, with a total associated cost of \$317.51, to recruit one participant into the field study. A slightly higher number of medium length surveys were sent to recruit one participant (n=53.6), which when combined with the slightly higher cost of mailing each individual survey resulted in a total associated cost of \$349.88, to recruit one participant into the field study. The long surveys were the least cost effective approaches, due to the lower response rates.

The most inexpensive sampling protocol had the lowest response rate, with the consequence that it the least effective approach in terms of the financial cost to receive one completed survey. Conversely, the three sampling protocols with three follow-up waves were the most expensive, but when using the short and medium length survey were the most cost effective approaches owing to their increased response rates. The short survey was the most cost effective in terms of materials due to a slightly lower cost and a higher response rate. We required additional telephone contact with the short survey respondents to obtain further information regarding field study eligibility, but since personnel costs were not included, this approach may not truly be the most cost effective approach overall for field study recruitment.

Three follow-up waves approximately doubled the response rate compared to sending no follow-up. The additional cost of those follow-up waves (\$2.88 for long surveys) was comparable with the cost of mailing a new long survey to a new household with no follow-ups (\$3.09), hence both approaches could be anticipated to yield similar response rates at

similar costs. This is consistent with findings reported by Mayfield et al. [120]. It would be preferable to increase response rate from initial non-responders to minimize bias and increase the representativeness of the sample.

**2. Study attrition**

An overview of attrition of recruitment of study participants is given in Figure 29. Of 237 survey respondents interested in the field study, only 79 met the inclusion criteria. Of those 79 who were eligible, 64 were contacted and sent consent forms for review. The main reason for not sending consent forms was being unable to reach survey respondents by telephone, typically because they did not respond to voicemail messages left by the research team, who were therefore unable to confirm their interest and eligibility. Of the 64 respondents who were sent consent forms, 45 consented and signed and returned the forms. Of those 45 who consented, 37 were enrolled into the field study and sent the equipment. Of those who were enrolled, 3 dropped out before the start of their study period, resulting in a total of 34 participants who completed (or partially completed) the study.

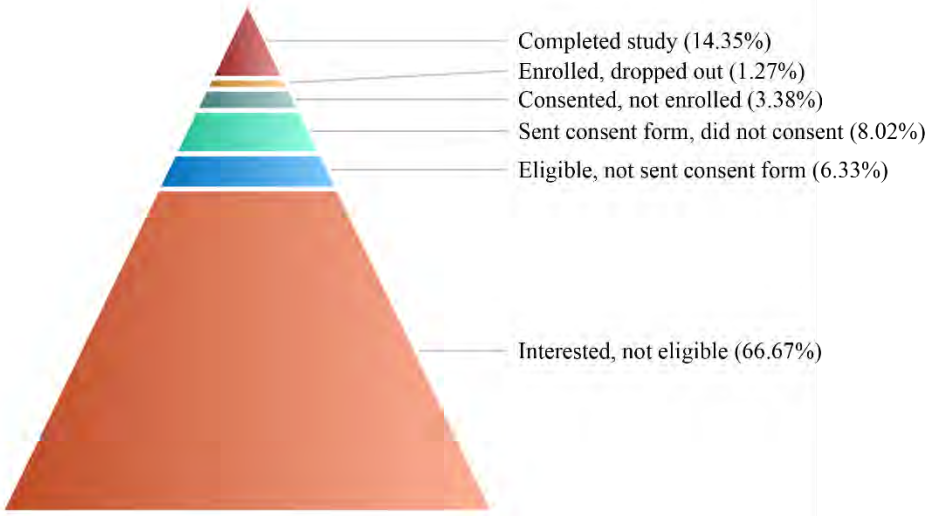


Figure 29. Graphical illustration of attrition at progressive stages of field study recruitment and implementation. Percentages are relative to the total number of survey respondents who indicated an interest in participating in the field study (n=237).

**3. Study compliance and data loss**

The purpose of this pilot study was to determine feasibility for a large-scale national field study. Thirty-four participants recorded acoustic and physiological data using equipment sent directly to their homes for 5 nights. In total, we received 160 nights of ECG data out of an anticipated 170 nights (94.1% successful data collection; Table 23). Participants also recorded 153 nights of acoustic data (90.0%), and completed 165 morning questionnaires (97.1%). Two participants accidentally began data collection a day ahead of schedule on the Sunday evening, but both agreed to record an extra night of physiological and acoustic data so that we had data from the same days of the week as other participants. These extra two days of data were included in both physiologic and morning questionnaire analysis. One participant found the Faros 90 device somewhat uncomfortable and collected only 3 nights of ECG data, but continued to collect acoustic data and complete the morning questionnaires. The most common reason for missing acoustic data was failure of the participants to initialize correctly the noise recorder. For one participant, only three nights of acoustic data were collected due to a technical error prior to sending them the equipment.

In order to perform analysis of study data, measurements of physiological and acoustic data must occur concurrently. Participants did not always record physiological and acoustic data in the same evenings. In total, we received 149 nights of overlapping acoustic and physiological data (87.6% data matching). For 9 subjects, acoustic data were excluded from the



analysis due to large discrepancies in the sound recorder calibration value prior to and after completing study measurements. During transit and while participants are handling equipment, the calibration dials of the sound recorder can shift. When this happens, it is no longer possible to convert the mp3 recording to sound pressure levels, which is necessary to determine the  $L_{AS,max}$  of aircraft noise events. After removing a total of 38 acoustic data files from the analysis due to calibration errors, our data collection rate was 65.3%. However, this problem was remedied for future subjects by securing the dials on the sound recorder in a fixed position with adhesive prior to shipment.

Table 23. A total of 170 overlapping nights of acoustic and ECG data were expected for 34 study participants. Amount of data collected and percent of usable data received is detailed below.

	ECG	Acoustic	Morning surveys	Matched ECG and acoustic data	Matched ECG and acoustic data included in analysis
Total Nights of Data Collected (n)	160	153	165	149	111
Proportion of anticipated data successfully collected (%)	94.1	90.0	97.1	87.6	65.3

#### 4. Equipment loss

One set of equipment was lost, whereby after enrollment in the study one participant did not complete study measurements and could not be reached after repeated attempts at contact via phone and mail. Equipment was returned undamaged and in a timely manner by all other study participants enrolled in the study.

#### 5. Summary

The study design is feasible to implement on a larger scale in the National Sleep Study. Thirty-four out of 37 enrolled participants recruited by postal surveys were able to receive and set-up study equipment, record measurements, and return equipment with minimal assistance from staff. In total, participants recorded 87.6% of requested data. Data loss as a result of calibration errors was remedied during the study and is not anticipated to be a continued problem in future studies.



## VI. Acknowledgement

This research was funded by the U.S. Federal Aviation Administration Office of Environment and Energy through ASCENT, the FAA Center of Excellence for Alternative Jet Fuels and the Environment, project 017 through FAA Award Number 13-C-AJFE-UPENN-004 under the supervision of Sean Doyle and Natalia Sizov. Any opinions, findings, conclusions or recommendations expressed in this material are those of the authors and do not necessarily reflect the views of the FAA.

We would like to thank Sarah McGuire for her invaluable contributions during the design and data gathering stage of this study. We would also like to thank Uwe Müller for spending 3 months at the University of Pennsylvania and for developing software critical for the success of the project. We would like to thank Emanuel Hermosillo and Jad Nasrini for assisting in the scoring of acoustic events. We are grateful to students working at the Unit for Experimental Psychiatry who assisted with survey mailings and data entry. Finally, we would like to thank colleagues from the German Aerospace Center (DLR) for their continued collaboration on projects on the effects of aircraft noise on sleep.

## Major Accomplishments

Prepaid cash incentives and sending follow-up reminder and survey waves were an effective method of improving response rates to postal questionnaires. Although no factors of the different sampling protocols improved the probability of a respondent participating in the field study *per se*, using a pre-issued cash incentive and sending more follow-up waves, and subsequently improving response rates and achieving higher numbers of people from which to recruit, may be an effective strategy for improving recruitment into field studies.

Among postal survey respondents, calculated outdoor nighttime air traffic noise was significantly associated with self-reports of worse overall sleep quality, trouble falling asleep within 30 minutes, annoyance, and sleep disturbance. Residents in areas exposed to higher levels of aircraft noise coped by closing the windows at night. After adjustment for sociodemographic factors, we did not find a significant effect of nocturnal aircraft noise exposure on any of the investigated self-reported health outcomes. The low sample size and response rate are limitations of this study warranting a replication of the findings in larger, representative subject cohorts.

Postal survey respondents were, based on available census data, representative of their geographical region. The respondents who eventually participated in the field study were in many, but not all, ways similar to survey respondents who either did not wish to or were not eligible to take part in the field study. Recruitment by postal questionnaire is therefore a feasible approach in obtaining a large, representative sample for future studies around multiple airports.

Two thirds of survey respondents who were interested in the field study did not meet the eligibility criteria. Among the interested and eligible respondents there was some attrition at each stage of the study enrollment process, with 34 individuals (43% of interested and eligible respondents) eventually completing the study. Based on lessons learned during this pilot study, a lower attrition rate could be expected in future studies.

Data of sufficient quality and quantity to investigate the effects of aircraft noise on sleep were obtained, despite some data loss in the field study due to technical issues with the equipment and non-compliance among the participants. The technical issues were the main cause of data loss, and a number of approaches to minimize data loss during the field study were identified. Non-compliance was low, with both physiologic and acoustic data collected by the participants in 87.6% of all study nights. The study therefore demonstrates the feasibility of mailing equipment to participants to obtain unattended physiologic and acoustic measurement data.

The current study was an investigation among a sample population of limited size, living close to a single airport. The findings of physiologic and self-reported effects of aircraft noise on sleep may not be representative of response among a demographically diverse national study population exposed to different patterns of nocturnal aircraft noise. A larger-scale study on the effects of aircraft noise on sleep around a representative sample of US airports is needed to provide up-to-date exposure-response functions. The approach used in the present pilot study has been demonstrated to be feasible for the purpose of this National Sleep Study.



## A. Recommendations for National Sleep Study

### 1. Methodological approaches demonstrated as feasible in the current ATL study

In the pilot study presented in this report, we demonstrated the feasibility of a number of key methodological approaches for the National Sleep Study. These include:

- Recruiting participants who are representative of their geographical area for a field study via postal questionnaires.
- Aside from field study eligibility, the postal surveys for recruitment are useful for collecting community response data in their own right.
- A recruitment strategy using a random sampling stratified by noise exposure strata ensured a broad range of measured noise level in the bedroom, allowing for a wide range of exposure in the physiologic exposure-response awakening curve.
- Using the measurement equipment deployed around ATL, to collect unattended noise and physiological data of sufficient quality over five consecutive nights.
- Collecting questionnaire data allowing for non-response analysis and non-participation analysis.
- Telephone contact on the first and last day of the field study, as well as offering 24-hour support should the participants require assistance, was effective at mitigating data loss.

### 2. Updates to methodology

Based on the findings of the pilot study presented in this report, we would make the following recommendations for changes in the study methodology when implementing the study on a national scale. The reasons for these recommendations can be found in the appropriate section of this report.

#### Questionnaires, including postal survey and field study morning survey

- Use a consistent number of levels in response scales; 5-point Likert.
- Ensure the direction of the response scales is consistent; leftmost is the most positive rating, rightmost is the most negative rating.
- Collect data allowing for non-response analysis and non-participation analysis.

#### Postal survey mailing strategy

- Send three follow-up waves: one reminder postcard after 7 days, a second paper copy of the survey after 28 days, and a third paper copy of the survey after 48 days.
- Include a \$2 pre-paid cash incentive with the initial mailing.
- Use a medium length survey; around 26 questions.
- Include all field study eligibility questions in the survey.
- Offer mail response mode only with initial mailing, and offer both mail and online response modes with follow-up mailings.
- Offer a \$150 incentive for volunteering for the field study.
- Omit "Department of Psychiatry" and "Unit for Experimental Psychiatry" from the recruitment survey envelope

#### Eligibility criteria for field study

- Change "children in the household under 5 years of age" to "Any individuals in the household requiring care during the night"

#### Field study

- Hot glue the gain control dials on the noise recorder firmly in place.
- Use the data analysis software developed in this project
- Consider time synchronicity issues between measurement devices, and correct deviations in the data streams accordingly



- Scoring all acoustic events in Akustikview in a given night is cumbersome, can take 2 hours or more, and is likely not feasible for the National Sleep Study . Efforts will be made to minimize manual effort in identifying aircraft noise events, which may include integrating flight rack radar data into the Akustikview software, or using scheduled flight operations data to identify periods in which to score acoustic events.



## **Publications**

### **Peer Reviewed Journal Publications**

- Basner, M., Witte, M., & McGuire, S. (2019). Aircraft noise effects on sleep – Results of a pilot study near Philadelphia International Airport. *International Journal of Environmental Research and Public Health*, 16(17): 3178.
- Rocha, S., Smith, M., Witte, M., & Basner, M. (2019). Survey results of a pilot sleep study near Atlanta International Airport. *International Journal of Environmental Research and Public Health*, 16(22): 432.
- Smith, M., Rocha, S., Witte, M., & Basner, M. (2020). On the feasibility of measuring physiologic and self-reported sleep disturbance by aircraft noise on a national scale: A pilot study around Atlanta airport. *Science of the Total Environment*, 718: 137368
- Smith, M., Witte, M., Rocha, S., & Basner, M. (2019). Effectiveness of incentives and follow-up on increasing survey response rates and participation in field studies. *BMC Medical Research Methodology*, 19: 230.

### **Published Conference Proceedings**

- Basner, M., Smith, M., Rocha, S., & Witte, M. (2019). Pilot field study on the effects of aircraft noise on sleep around Atlanta International Airport. Presentation and conference paper 23<sup>rd</sup> International Congress on Acoustics, Aachen, Germany.

## **Outreach Efforts**

### **Conference presentations**

- Basner, M., Smith, M., Rocha, S. and Witte, M. Pilot Field Study on the Effects of Aircraft Noise on Sleep Around Atlanta International Airport. Conference paper to be presented as an oral presentation at 23<sup>rd</sup> International Congress on Acoustics, 2019, Aachen, Germany
- Smith, M., Rocha, S., Witte, M. and Basner, M. Self-reported sleep disturbance by aircraft noise around Atlanta airport. Abstract only, presented as a poster at SLEEP 2019, San Antonio, TX

## **Awards**

None

## **Student Involvement**

None

## **Plans for Next Period**

This task is complete.

## **References**

1. Xie L, Kang H, Xu Q, Chen MJ, Liao Y, Thiyagarajan M, et al. Sleep drives metabolite clearance from the adult brain. *Science*. 2013;342(6156):373-7. doi: 10.1126/science.1241224. PubMed PMID: 24136970.
2. Naidoo N. Cellular stress/the unfolded protein response: relevance to sleep and sleep disorders. *Sleep Med Rev*. 2009;13(3):195-204. doi: 10.1016/j.smrv.2009.01.001. PubMed PMID: 19329340; PubMed Central PMCID: PMC2964262.
3. Mackiewicz M, Shockley KR, Romer MA, Galante RJ, Zimmerman JE, Naidoo N, et al. Macromolecule biosynthesis: a key function of sleep. *Physiol Genomics*. 2007;31(3):441-57. doi: 10.1152/physiolgenomics.00275.2006. PubMed PMID: 17698924.
4. Rasch B, Born J. About Sleep's Role in Memory. *Physiol Rev*. 2013;93(2):681-766. doi: 10.1152/physrev.00032.2012. PubMed PMID: WOS:000317599400006.



5. Banks S, Van Dongen HP, Maislin G, Dinges DF. Neurobehavioral dynamics following chronic sleep restriction: dose-response effects of one night for recovery. *Sleep*. 2010;33(8):1013-26. PubMed PMID: 20815182; PubMed Central PMCID: PMC2910531.
6. Cappuccio FP, Taggart FM, Kandala NB, Currie A, Peile E, Stranges S, et al. Meta-analysis of short sleep duration and obesity in children and adults. *Sleep*. 2008;31(5):619-26. PubMed PMID: 18517032; PubMed Central PMCID: PMC2398753.
7. Knutson KL, Spiegel K, Penev P, Van Cauter E. The metabolic consequences of sleep deprivation. *Sleep Med Rev*. 2007;11(3):163-78. doi: 10.1016/j.smrv.2007.01.002. PubMed PMID: 17442599; PubMed Central PMCID: PMC1991337.
8. Gottlieb DJ, Redline S, Nieto FJ, Baldwin CM, Newman AB, Resnick HE, et al. Association of usual sleep duration with hypertension: the Sleep Heart Health Study. *Sleep*. 2006;29(8):1009-14. PubMed PMID: 16944668.
9. Badran M, Yassin BA, Fox N, Laher I, Ayas N. Epidemiology of Sleep Disturbances and Cardiovascular Consequences. *Can J Cardiol*. 2015;31(7):873-9. doi: 10.1016/j.cjca.2015.03.011. PubMed PMID: 26037823.
10. Cappuccio FP, D'Elia L, Strazzullo P, Miller MA. Sleep duration and all-cause mortality: a systematic review and meta-analysis of prospective studies. *Sleep*. 2010;33(5):585-92. PubMed PMID: 20469800; PubMed Central PMCID: PMC2864873.
11. Basner M, McGuire S. WHO Environmental Noise Guidelines for the European Region: A Systematic Review on Environmental Noise and Effects on Sleep. *Int J Env Res Pub He*. 2018;15(3). doi: 10.3390/ijerph15030519.
12. Fidell S, Pearsons K, Tabachnick BG, Howe R. Effects on sleep disturbance of changes in aircraft noise near three airports. *Journal of the Acoustical Society of America*. 2000;107(5):2535-47. doi: Doi 10.1121/1.428641. PubMed PMID: WOS:000086967900025.
13. Basner M. Design for a US field study on the effects of aircraft noise on sleep. Cambridge, MA: Partnership for Air Transportation Noise and Emissions Reduction (PARTNER), 2012 PARTNER-COE-2012-003 Contract No.: PARTNER-COE-2012-003.
14. Aasvang GM, Overland B, Ursin R, Moum T. A field study of effects of road traffic and railway noise on polysomnographic sleep parameters. *J Acoust Soc Am*. 2011;129(6):3716-26. Epub 2011/06/21. doi: 10.1121/1.3583547. PubMed PMID: 21682396.
15. Basner M, Samel A, Isermann U. Aircraft noise effects on sleep: application of the results of a large polysomnographic field study. *J Acoust Soc Am*. 2006;119(5 Pt 1):2772-84. Epub 2006/05/20. PubMed PMID: 16708935.
16. Elmenhorst EM, Pennig S, Rolny V, Quehl J, Müller U, Maass H, et al. Examining nocturnal railway noise and aircraft noise in the field: sleep, psychomotor performance, and annoyance. *Sci Total Environ*. 2012;424:48-56. Epub 2012/03/27. doi: S0048-9697(12)00234-3 [pii] 10.1016/j.scitotenv.2012.02.024. PubMed PMID: 22444069.
17. Flindell IH, Bullmore AJ, Robertson KA, Wright NA, Turner C, Birch CL, et al. Aircraft Noise and Sleep, 1999 UK Trial Methodology Study. Southampton, UK: Institute of Sound and Vibration Research, University of Southampton, 2000.
18. Danker-Hopfe H, Anderer P, Zeitlhofer J, Boeck M, Dorn H, Gruber G, et al. Interrater reliability for sleep scoring according to the Rechtschaffen & Kales and the new AASM standard. *J Sleep Res*. 2009;18(1):74-84. Epub 2009/03/03. doi: 10.1111/j.1365-2869.2008.00700.x. PubMed PMID: 19250176.
19. Basner M, Griefahn B, Penzel T. Inter-rater agreement in sleep stage classification between centers with different backgrounds. *Somnologie*. 2008;12(1):75-84.
20. Agnew HW, Jr., Webb WB, Williams RL. The first night effect: an EEG study of sleep. *Psychophysiology*. 1966;2(3):263-6. Epub 1966/01/01. PubMed PMID: 5903579.
21. Basner M, Griefahn B, Muller U, Plath G, Samel A. An ECG-based algorithm for the automatic identification of autonomic activations associated with cortical arousal. *Sleep*. 2007;30(10):1349-61. Epub 2007/11/01. PubMed PMID: 17969469; PubMed Central PMCID: PMC2266280.
22. Basner M, Müller U, Elmenhorst EM, Kluge G, Griefahn B. Aircraft noise effects on sleep: a systematic comparison of EEG awakenings and automatically detected cardiac activations. *PhysiolMeas*. 2008;29(9):1089-103.
23. McGuire S, Müller U, Plath G, Basner M. Refinement and validation of an ECG based algorithm for detecting awakenings. 11th International Congress on Noise as a Public Health Problem (ICBEN); Nara, Japan 2014.
24. Basner M, Brink M, Elmenhorst EM. Critical appraisal of methods for the assessment of noise effects on sleep. *Noise & health*. 2012;14(61):321-9. doi: 10.4103/1463-1741.104902. PubMed PMID: WOS:000313350600011.
25. Schreckenber D, Eikmann T, Faulbaum F, Haufe C, Herr C, Klatte M, et al. NORAH – study on Noise Related Annoyance, Cognition and Health: a transportation noise effects monitoring program in Germany. ICBEN 2011; London, UK 2011.



26. Müller U, Elmenhorst EM, Mendolia F, Quehl J, Basner M, McGuire S, et al. A comparison of the effects of night time air traffic noise on sleep at Cologne/Bonn and Frankfurt Airport after the night flight ban. ICBEN; 18-22 June; Zürich 2017.
27. NORAH study: Publications [cited 2019 March 18th]. Available from: <https://www.norah-studie.de/en/alle.html>.
28. Müller U, Elmenhorst EM, Mendolia F, Quehl J, Basner M, McGuire S, et al. The NORAH-sleep study: Effects of the night flight ban at Frankfurt airport. *Internoise 2016*; August 21-24, ; Hamburg, Germany 2016.
29. Griefahn B, Bröde P, Marks A, Basner M. Autonomic arousals related to traffic noise during sleep. *Sleep*. 2008;31(4):569-77. Epub 2008/05/07. PubMed PMID: 18457245; PubMed Central PMCID: PMC2279756.
30. Basner M, Isermann U, Samel A. Aircraft noise effects on sleep: Application of the results of a large polysomnographic field study. *JAcoustSocAm*. 2006;119(5):2772-84.
31. Brink M, Schreckenber D, Thomann G, Basner M. Aircraft Noise Indexes for Effect Oriented Noise Assessment. *Acta Acustica United with Acustica*. 2010;96(6):1012-25. doi: Doi 10.3813/Aaa.918364. PubMed PMID: ISI:000285082200003.
32. Tetreault LF, Plante C, Perron S, Goudreau S, King N, Smargiassi A. Risk Assessment of Aircraft Noise on Sleep in Montreal. *Can J Public Health*. 2012;103(4):E293-E6. PubMed PMID: WOS:000208937500012.
33. Landis JR, Koch GG. The measurement of observer agreement for categorical data. *Biometrics*. 1977;33(1):159-74. Epub 1977/03/01. PubMed PMID: 843571.
34. Rechtschaffen A, Kales A. A manual of standardized terminology, techniques and scoring system for sleep stages of human subjects. Los Angeles: UCLA; 1968.
35. McGuire S, Witte M, Kallarackal A, Basner M. Pilot Study Examining the Effects of Aircraft Noise on Sleep in Communities near Philadelphia International Airport. *Sleep*. 2017;40:A60-A1. doi: DOI 10.1093/sleepj/zsx050.161. PubMed PMID: WOS:000433175000163.
36. International Electrotechnical Commission. IEC 61672-1 Electroacoustics - Sound level meters. 2013.
37. Federal Aviation Administration. Integrated Noise Model (INM) [cited 2019 November]. Available from: [https://www.faa.gov/about/office\\_org/headquarters\\_offices/apl/research/models/inm\\_model/](https://www.faa.gov/about/office_org/headquarters_offices/apl/research/models/inm_model/).
38. Federal Aviation Administration. Performance Data Analysis and Reporting System (PDARS) [cited 2019 November]. Available from: [https://www.faa.gov/about/office\\_org/headquarters\\_offices/ato/service\\_units/systemops/perf\\_analysis/perf\\_tools/](https://www.faa.gov/about/office_org/headquarters_offices/ato/service_units/systemops/perf_analysis/perf_tools/).
39. Czajka JL, Beyler A. Declining response rates in federal surveys: Trends and implications. Final report - Volume I. Mathematica Policy Research, 2016 June 15th. Report No.: 40146.D4C.
40. Armstrong JS, Overton TS. Estimating Nonresponse Bias in Mail Surveys. *J Marketing Res*. 1977;14(3):396-402. doi: Doi 10.2307/3150783. PubMed PMID: WOS:A1977DS66100020.
41. Edwards PJ, Roberts I, Clarke MJ, DiGiuseppi C, Wentz R, Kwan I, et al. Methods to increase response to postal and electronic questionnaires. *Cochrane Db Syst Rev*. 2009;(3). doi: ARTN MR000008  
10.1002/14651858.MR000008.pub4. PubMed PMID: WOS:000268037800036.
42. Nakash RA, Hutton JL, Jorstad-Stein EC, Gates S, Lamb SE. Maximising response to postal questionnaires--a systematic review of randomised trials in health research. *Bmc Med Res Methodol*. 2006;6:5. Epub 2006/03/01. doi: 10.1186/1471-2288-6-5. PubMed PMID: 16504090; PubMed Central PMCID: PMCPMC1421421.
43. Knoll M, Soller L, Ben-Shoshan M, Harrington D, Fragapane J, Joseph L, et al. The use of incentives in vulnerable populations for a telephone survey: a randomized controlled trial. *BMC Res Notes*. 2012;5:572. Epub 2012/10/23. doi: 10.1186/1756-0500-5-572. PubMed PMID: 23083313; PubMed Central PMCID: PMCPMC3503563.
44. Chandler JJ, Paolacci G. Lie for a Dime: When Most Prescreening Responses Are Honest but Most Study Participants Are Impostors. *Soc Psychol Pers Sci*. 2017;8(5):500-8. doi: 10.1177/1948550617698203. PubMed PMID: WOS:000408630200003.
45. Buysse DJ, Reynolds CF, 3rd, Monk TH, Berman SR, Kupfer DJ. The Pittsburgh Sleep Quality Index: a new instrument for psychiatric practice and research. *Psychiatry Res*. 1989;28(2):193-213. Epub 1989/05/01. doi: 0165-1781(89)90047-4 [pii]. PubMed PMID: 2748771.
46. Weinstein ND. Individual differences in reactions to noise: a longitudinal study in a college dormitory. *J Appl Psychol*. 1978;63(4):458-66. Epub 1978/08/01. PubMed PMID: 701213.
47. Fields JM, De Jong RG, Gjestland T, Flindell IH, Job RFS, Kurra S, et al. Standardized general-purpose noise reaction questions for community noise surveys: Research and a recommendation. *Journal of Sound and Vibration*. 2001;242(4):641-79. doi: DOI 10.1006/jsvi.2000.3384. PubMed PMID: WOS:000168482600006.
48. Barba C, Cavalli-Sforza T, Cutter J, Darnton-Hill I, Deurenberg P, Deurenberg-Yap M, et al. Appropriate body-mass index for Asian populations and its implications for policy and intervention strategies. *Lancet*. 2004;363(9403):157-63. PubMed PMID: WOS:000187939200021.



49. Basner M, Brink M, Elmenhorst EM. Critical appraisal of methods for the assessment of noise effects on sleep. *Noise Health*. 2012;14(61):321-9. Epub 2012/12/22. doi: 10.4103/1463-1741.104902. PubMed PMID: 23257586.
50. McGuire S, Müller U, Plath G, Basner M, editors. Refinement and validation of an ECG based algorithm for detecting awakenings. 11th International Congress on Noise as a Public Health Problem; 2014; Nara, Japan: International Commission of Biological Effects of Noise (ICBEN).
51. Rocha S, Smith MG, Witte M, Basner M. Survey Results of a Pilot Sleep Study Near Atlanta International Airport. *Int J Env Res Pub He*. 2019;16(22):4321. PubMed PMID: doi:10.3390/ijerph16224321.
52. Textor J, van der Zander B, Gilthorpe MS, Liskiewicz M, Ellison GTH. Robust causal inference using directed acyclic graphs: the R package 'dagitty'. *Int J Epidemiol*. 2016;45(6):1887-94. doi: 10.1093/ije/dyw341. PubMed PMID: WOS:000398261100024.
53. Hoddes E, Zarcone V, Smythe H, Phillips R, Dement WC. Quantification of sleepiness: a new approach. *Psychophysiology*. 1973;10(4):431-6. PubMed PMID: 4719486.
54. Scott P, Edwards P. Personally addressed hand-signed letters increase questionnaire response: a meta-analysis of randomised controlled trials. *Bmc Health Serv Res*. 2006;6. doi: Artn 111  
10.1186/1472-6963-6-111. PubMed PMID: WOS:000240734000001.
55. Sahlqvist S, Song Y, Bull F, Adams E, Preston J, Ogilvie D, et al. Effect of questionnaire length, personalisation and reminder type on response rate to a complex postal survey: randomised controlled trial. *Bmc Med Res Methodol*. 2011;11. doi: Artn 62  
10.1186/1471-2288-11-62. PubMed PMID: WOS:000291362600001.
56. Möller-Leimkühler AM, Möller H-J, Maier W, Gaebel W, Falkai P. EPA guidance on improving the image of psychiatry. *European Archives of Psychiatry and Clinical Neuroscience*. 2016;266(2):139-54. doi: 10.1007/s00406-016-0678-5.
57. Halpern SD, Ubel PA, Berlin JA, Asch DA. Randomized Trial of \$5 Versus \$10 Monetary Incentives, Envelope Size, and Candy to Increase Physician Response Rates to Mailed Questionnaires. *Medical Care*. 2002;40(9):834-9. PubMed PMID: 00005650-200209000-00012.
58. Guski R, Schreckenber D, Schuemer R. WHO Environmental Noise Guidelines for the European Region: A Systematic Review on Environmental Noise and Annoyance. *Int J Env Res Pub He*. 2017;14(12). doi: ARTN 1539  
10.3390/ijerph14121539. PubMed PMID: WOS:000423699400102.
59. Sinclair M, O'Toole J, Malawaraarachchi M, Leder K. Comparison of response rates and cost-effectiveness for a community-based survey: postal, internet and telephone modes with generic or personalised recruitment approaches. *Bmc Med Res Methodol*. 2012;12. doi: Artn 132  
10.1186/1471-2288-12-132. PubMed PMID: WOS:000311347600001.
60. Singer E, Van Hoewyk J, Neugebauer RJ. Attitudes and behavior - The impact of privacy and confidentiality concerns on participation in the 2000 Census. *Public Opin Quart*. 2003;67(3):368-84. doi: Doi 10.1086/377465. PubMed PMID: WOS:000186082100003.
61. Bowling A. Mode of questionnaire administration can have serious effects on data quality. *J Public Health-Uk*. 2005;27(3):281-91. doi: 10.1093/pubmed/fdi031. PubMed PMID: WOS:000231762400005.
62. Groves RM, Singer E, Corning A. Leverage-saliency theory of survey participation - Description and an illustration. *Public Opin Quart*. 2000;64(3):299-308. doi: Doi 10.1086/317990. PubMed PMID: WOS:000166024000004.
63. Ryan C. Language Use in the United States: 2011. U.S. Department of Commerce. Economics and Statistics Administration. U.S. Census Bureau., 2013 ACS-22 Contract No.: ACS-22.
64. Brick JM, Montaquila JM, Han DF, Williams D. Improving Response Rates for Spanish Speakers in Two-Phase Mail Surveys. *Public Opin Quart*. 2012;76(4):721-32. doi: 10.1093/poq/nfs050. PubMed PMID: WOS:000311670600005.
65. Guo YM, Kopec JA, Cibere J, Li LC, Goldsmith CH. Population Survey Features and Response Rates: A Randomized Experiment. *Am J Public Health*. 2016;106(8):1422-6. doi: 10.2105/Ajph.2016.303198. PubMed PMID: WOS:000384981200034.
66. Ryan JM, Corry JR, Attewell R, Smithson MJ. A comparison of an electronic version of the SF-36 General Health Questionnaire to the standard paper version. *Qual Life Res*. 2002;11(1):19-26. doi: Doi 10.1023/A:1014415709997. PubMed PMID: WOS:000175137200003.
67. Dillman DA, Smyth JD, Christian LM. Internet, phone, mail, and mixed-mode surveys : the tailored design method. 4th edition. ed. Hoboken: Wiley; 2014. xvii, 509 pages p.
68. Patrick ME, Couper MP, Laetz VB, Schulenberg JE, O'Malley PM, Johnston LD, et al. A Sequential Mixed-Mode Experiment in the U.S. National Monitoring the Future Study. *J Surv Stat Methodol*. 2018;6(1):72-97. doi: 10.1093/jssam/smx011. PubMed PMID: WOS:000433601600004.



69. Medway RL, Fulton J. When More Gets You Less: A Meta-Analysis of the Effect of Concurrent Web Options on Mail Survey Response Rates. *Public Opin Quart.* 2012;76(4):733-46. doi: 10.1093/poq/nfs047. PubMed PMID: WOS:000311670600006.
70. McMaster HS, LeardMann CA, Speigle S, Dillman DA, Tea MCFS. An experimental comparison of web-push vs. paper-only survey procedures for conducting an in-depth health survey of military spouses. *Bmc Med Res Methodol.* 2017;17. doi: ARTN 73  
10.1186/s12874-017-0337-1. PubMed PMID: WOS:000400239100001.
71. Groves RM, Peytcheva E. The impact of nonresponse rates on nonresponse bias - A meta-analysis. *Public Opin Quart.* 2008;72(2):167-89. doi: 10.1093/poq/nfn011. PubMed PMID: WOS:000256523900001.
72. American Association for Public Opinion Research. Response rates - An overview 2019 [cited 2019 November]. Available from: <https://www.aapor.org/Education-Resources/For-Researchers/Poll-Survey-FAQ/Response-Rates-An-Overview.aspx>.
73. Cook C, Heath F, Thompson RL. A meta-analysis of response rates in Web- or internet-based surveys. *Educ Psychol Meas.* 2000;60(6):821-36. doi: Doi 10.1177/00131640021970934. PubMed PMID: WOS:000165284000001.
74. Johnson TP, Wislar JS. Response Rates and Nonresponse Errors in Surveys. *Jama-J Am Med Assoc.* 2012;307(17):1805-6. doi: 10.1001/jama.2012.3532. PubMed PMID: WOS:000303386800018.
75. Halbesleben JRB, Whitman MV. Evaluating Survey Quality in Health Services Research: A Decision Framework for Assessing Nonresponse Bias. *Health Serv Res.* 2013;48(3):913-30. doi: 10.1111/1475-6773.12002. PubMed PMID: WOS:000318700900002.
76. United States Census Bureau. 2010 Decennial census of population and housing 2010 [cited 2019 July]. Available from: <https://www.census.gov/programs-surveys/decennial-census/decade.2010.html>.
77. United States Census Bureau. American Community Survey (ACS) 2019 [cited 2019 November]. Available from: <https://www.census.gov/programs-surveys/acs>.
78. Saleh A, Bista K. Examining Factors Impacting Online Survey Response Rates in Educational Research: Perceptions of graduate students. *J MultiDisciplinary Evaluation.* 2017;13(29):63-74.
79. Funkhouser E, Vellala K, Baltuck C, Cacciato R, Durand E, McEdward D, et al. Survey Methods to Optimize Response Rate in the National Dental Practice-Based Research Network. *Eval Health Prof.* 2017;40(3):332-58. doi: 10.1177/0163278715625738. PubMed PMID: WOS:000406071500003.
80. Church AH. Estimating the Effect of Incentives on Mail Survey Response Rates - a Metaanalysis. *Public Opin Quart.* 1993;57(1):62-79. doi: Doi 10.1086/269355. PubMed PMID: WOS:A1993KY41200004.
81. Edwards P, Roberts I, Clarke M, DiGiuseppi C, Pratap S, Wentz R, et al. Increasing response rates to postal questionnaires: systematic review. *British medical journal.* 2002;324(7347):1183-5. doi: DOI 10.1136/bmj.324.7347.1183. PubMed PMID: WOS:000175763200015.
82. Mercer A, Caporaso A, Cantor D, Townsend R. How Much Gets You How Much? Monetary Incentives and Response Rates in Household Surveys. *Public Opin Quart.* 2015;79(1):105-29. doi: 10.1093/poq/nfu059.
83. Han DF, Montaquila JM, Brick JM. An Evaluation of Incentive Experiments in a Two-Phase Address-Based Sample Mail Survey. *Surv Res Methods-Ger.* 2013;7(3):207-18. PubMed PMID: WOS:000328484700006.
84. Weil J, Mendoza AN, McGavin E. Recruiting older adults as participants in applied social research: Applying and evaluating approaches from clinical studies. *Educ Gerontol.* 2017;43(12):662-73. doi: 10.1080/03601277.2017.1386406. PubMed PMID: WOS:000418681700008.
85. Sharp EC, Pelletier LG, Levesque C. The Double-Edged Sword of Rewards for Participation in Psychology Experiments. *Can J Behav Sci.* 2006;38(3):269-77. doi: 10.1037/cjbs2006014. PubMed PMID: WOS:000207230700007.
86. American Psychiatric Association. DSM-5 Task Force. Diagnostic and statistical manual of mental disorders : DSM-5. 5th ed. Washington, D.C.: American Psychiatric Association; 2013. xlvii, 947 p. p.
87. Fritschi L, Brown AL, Kim R, Schwela DH, Kephelopoulos S. Burden of disease from environmental noise. Fritschi L, editor. Bonn: World Health Organization; 2011.
88. Miedema HME, Vos H. Associations Between Self-Reported Sleep Disturbance and Environmental Noise Based on Reanalyses of Pooled Data From 24 Studies. *Behavioral Sleep Medicine.* 2007;5(1):1-20. doi: 10.1080/15402000709336723.
89. Kim SJ, Lee KW, Park JB, Min KB, Kil HG, Lee C, et al. Exposure-Response Relationship Between Aircraft Noise and Sleep Quality: A Community-based Cross-sectional Study. *Osong Public Health and Research Perspectives.* 2014;5(2):108-14.
90. Jackowska M, Ronaldson A, Brown J, Steptoe A. Biological and psychological correlates of self-reported and objective sleep measures. *Journal of psychosomatic research.* 2016;84:52-5. doi: 10.1016/j.jpsychores.2016.03.017. PubMed PMID: WOS:000375237000008.



91. Miedema HM, Oudshoorn CG. Annoyance from transportation noise: relationships with exposure metrics DNL and DENL and their confidence intervals. *Environmental Health Perspectives*. 2001;109(4):409-16. PubMed PMID: PMC1240282.
92. Quehl J, Müller U, Mendolia F. Short-term annoyance from nocturnal aircraft noise exposure: results of the NORAH and STRAIN sleep studies. *International archives of occupational and environmental health*. 2017;90(8):765-78. doi: 10.1007/s00420-017-1238-7. PubMed PMID: WOS:000412896400005.
93. Babisch W, Houthuijs D, Pershagen G, Cadum E, Katsouyanni K, Velonakis M, et al. Annoyance due to aircraft noise has increased over the years-Results of the HYENA study. *Environ Int*. 2009;35(8):1169-76. doi: 10.1016/j.envint.2009.07.012. PubMed PMID: WOS:000271360900010.
94. Portas CM, Krakow K, Allen P, Josephs O, Armony JL, Frith CD. Auditory processing across the sleep-wake cycle: simultaneous EEG and fMRI monitoring in humans. *Neuron*. 2000;28(3):991-9. Epub 2001/02/13. doi: S0896-6273(00)00169-0 [pii]. PubMed PMID: 11163282.
95. Cointin R, Sizov N, Hileman JI. U.S. Civil Aircraft Noise Annoyance Survey Design. Hamburg2016.
96. Miedema HME, Vos H. Demographic and attitudinal factors that modify annoyance from transportation noise. *Journal of the Acoustical Society of America*. 1999;105(6):3336-44. doi: Doi 10.1121/1.424662. PubMed PMID: ISI:000080778100034.
97. Marks A, Griefahn B. Associations between noise sensitivity and sleep, subjectively evaluated sleep quality, annoyance, and performance after exposure to nocturnal traffic noise. *Noise Health*. 2007;9(34):1-7. Epub 2007/09/14. PubMed PMID: 17851221.
98. Park J, Chung S, Lee J, Sung JH, Cho SW, Sim CS. Noise sensitivity, rather than noise level, predicts the non-auditory effects of noise in community samples: a population-based survey. *Bmc Public Health*. 2017;17. doi: ARTN 315  
10.1186/s12889-017-4244-5. PubMed PMID: WOS:000400798400001.
99. Smith MG, Croy I, Ögren M, Hammar O, Lindberg E, Persson Waye K. Physiological effects of railway vibration and noise on sleep. *J Acoust Soc Am*. 2017;141(5):3262-9.
100. Di Nisi J, Muzet A, Ehrhart J, Libert JP. Comparison of cardiovascular responses to noise during waking and sleeping in humans. *Sleep*. 1990;13(2):108-20. Epub 1990/04/01. PubMed PMID: 2330471.
101. Smith MG, Ogren M, Ageborg Morsing J, Persson Waye K. Effects of ground-borne noise from railway tunnels on sleep: A polysomnographic study. *Build Environ*. 2019;149:288-96. doi: 10.1016/j.buildenv.2018.12.009. PubMed PMID: WOS:000457118300025.
102. Basner M, Babisch W, Davis A, Brink M, Clark C, Janssen S, et al. Auditory and non-auditory effects of noise on health. *Lancet*. 2014;383(9925):1325-32. doi: 10.1016/S0140-6736(13)61613-X. PubMed PMID: 24183105.
103. Basner M, Clark C, Hansell A, Hileman JI, Janssen S, Shepherd K, et al. Aviation Noise Impacts: State of the Science. *Noise & health*. 2017;19(87):41-50. doi: 10.4103/nah.NAH\_104\_16. PubMed PMID: WOS:000404119700001.
104. Babisch W. Cardiovascular effects of noise. *Noise Health*. 2011;13(52):201-4. doi: 10.4103/1463-1741.80148. PubMed PMID: WOS:000290490700001.
105. Watson NF, Badr MS, Belenky G, Bliwise DL, Buxton OM, Buysse D, et al. Joint Consensus Statement of the American Academy of Sleep Medicine and Sleep Research Society on the Recommended Amount of Sleep for a Healthy Adult: Methodology and Discussion. *Sleep*. 2015;38(8):1161-83. doi: PII sp-00367-15  
10.5665/sleep.4886. PubMed PMID: WOS:000358838100006.
106. Locher B, Piquerez A, Habermacher M, Ragetti M, Roosli M, Brink M, et al. Differences between Outdoor and Indoor Sound Levels for Open, Tilted, and Closed Windows. *Int J Env Res Pub He*. 2018;15(1). doi: ARTN 149  
10.3390/ijerph15010149. PubMed PMID: WOS:000424121200148.
107. Perneger TV. What's wrong with Bonferroni adjustments. *British medical journal*. 1998;316(7139):1236-8. doi: DOI 10.1136/bmj.316.7139.1236. PubMed PMID: WOS:000073224100034.
108. McDonald JH. *Handbook of Biological Statistics*. 3rd ed. Baltimore, Maryland: Sparky House Publishing; 2014.
109. Croy I, Smith MG, Gidlöf-Gunnarsson A, Persson Waye K. Optimal questions for sleep in epidemiological studies: Comparisons of subjective and objective measures in laboratory and field studies. *Behav Sleep Med*. 2017;15(6):466-82. doi: 10.1080/15402002.2016.1163700. PubMed PMID: 27159152.
110. Basner M, Müller U, Elmenhorst EM. Single and combined effects of air, road, and rail traffic noise on sleep and recuperation. *Sleep*. 2011;34(1):11-23. Epub 2011/01/05. PubMed PMID: 21203365; PubMed Central PMCID: PMC3001788.
111. Tassi P, Rohmer O, Schimchowitsch S, Eschenlauer A, Bonnefond A, Margiocchi F, et al. Living alongside railway tracks: Long-term effects of nocturnal noise on sleep and cardiovascular reactivity as a function of age. *Environ Int*. 2010;36(7):683-9. Epub 2010/06/24. doi: 10.1016/j.envint.2010.05.001



S0160-4120(10)00087-5 [pii]. PubMed PMID: 20569986.

112. Åkerstedt T, Schwarz J, Gruber G, Lindberg E, Theorell-Haglöw J. The relation between polysomnography and subjective sleep and its dependence on age - poor sleep may become good sleep. *J Sleep Res.* 2016;25(5):565-70. doi: 10.1111/jsr.12407. PubMed PMID: 27122391.

113. Vitiello MV, Larsen LH, Moe KE. Age-related sleep change: Gender and estrogen effects on the subjective-objective sleep quality relationships of healthy, noncomplaining older men and women. *Journal of psychosomatic research.* 2004;56(5):503-10. doi: 10.1016/S0022-3999(04)00023-6. PubMed PMID: 15172206.

114. Mong JA, Cusmano DM. Sex differences in sleep: impact of biological sex and sex steroids. *Philos Trans R Soc Lond B Biol Sci.* 2016;371(1688):20150110. doi: 10.1098/rstb.2015.0110. PubMed PMID: 26833831; PubMed Central PMCID: PMC4785896.

115. Mallampalli MP, Carter CL. Exploring sex and gender differences in sleep health: a Society for Women's Health Research Report. *J Womens Health (Larchmt).* 2014;23(7):553-62. doi: 10.1089/jwh.2014.4816. PubMed PMID: 24956068; PubMed Central PMCID: PMC4089020.

116. Ohayon MM, Carskadon MA, Guilleminault C, Vitiello MV. Meta-analysis of quantitative sleep parameters from childhood to old age in healthy individuals: developing normative sleep values across the human lifespan. *Sleep.* 2004;27(7):1255-73. PubMed PMID: 15586779.

117. Mishra AK, van Ruitenbeek AM, Loomans MGLC, Kort HSM. Window/door opening-mediated bedroom ventilation and its impact on sleep quality of healthy, young adults. *Indoor Air.* 2018;28(2):339-51. doi: 10.1111/ina.12435. PubMed PMID: WOS:000425083500013.

118. Miedema HM, Vos H. Associations between self-reported sleep disturbance and environmental noise based on reanalyses of pooled data from 24 studies. *Behav Sleep Med.* 2007;5(1):1-20. Epub 2007/02/23. doi: 10.1207/s15402010bsm0501\_1. PubMed PMID: 17313321.

119. Brink M, Basner M, Schierz C, Spreng M, Scheuch K, Bauer G, et al. Determining physiological reaction probabilities to noise events during sleep. *Somnologie.* 2009;13(4):236-43.

120. Mayfield A, Amaya A, Carris K. A matter of time: The value and optimal timing of follow-up questionnaire mailings in a multimode survey 68th Annual Conference of the American Association for Public Opinion Research May 16-19; Boston, MA. *Proceedings of the Survey Research Methods Section: American Statistical Association;* 2013.



## VII. Appendices

### Appendix 1. Field study equipment

Table 24. List of all field study equipment and associated quantities and costs

Equipment category	Item	Quantity per box	Cost per item(s) (\$)
Sound	Zoom H5 Handy Recorder	1	216.39
Sound	Earthworks M23 Measurement Microphone	1	376.92
Sound	SM Series XLR Microphone Cable	1	2.99
Sound	Remote Control for Zoom H5 Handy Recorder	1	18.71
Sound	Rechargeable AA NiMH Batteries	2	4.89
Sound	Foam Windscreens for 3/8" Diameter Microphones	1	2.23
Sound	Multi-Function Ball Head with Removable Bottom Shoe Mount	1	19.99
Sound	Hot Shoe Post Adapter	1	5.21
Sound	4" Cold Shoe Extension	1	14.21
Sound	Transcend 32 GB microSDHC	1	16.99
Sound	USB 2.0 Digital Camera Cable	1	2.44
Sound	USB Wall Plug	1	8.70
Sound	Reversible Thread Adapter (Steel)	1	3.71
Physiology	Faros 90 Sensor Kit (includes eMotion Faros 90 sensor, cable set, eMotion LAB software, docking station)	1	527.00
Physiology	VELCRO(R) Brand Dots	9	2.60
Physiology	Slim Micro USB Charger Cable	1	3.23
Physiology	Ambu BlueSensor VLC Electrodes	16	8.08
Shipping	Pick and Pack Foam Sheet	1	5.75
Shipping	Convolute Foam Set	1	2.39
Shipping	Soft Foam Charcoal Sheet 2" Thickness	1	2.87
Shipping	Soft Foam Charcoal 1" Thickness	1	1.81
Shipping	Corrugated Shipment Box	1	0.98
Shipping	Gusseted Polyester Bag	1	0.46
Shipping	Packing Tape Sheets	5	3.18
Medical	Alcohol Prep Pads Wipes	4	0.08
Medical	Durapore Medical Tape	1	0.55
Medical	Hydrocortisone 1% Anti-Itch Cream 1 Oz Tube	1	2.39
Miscellaneous	Ziploc(R) 1 Quart Storage Bags	5	0.36
Miscellaneous	Office Depot(R) Brand File Folder	1	0.46
Miscellaneous	Brother(R) Black-On-White Tape Labels	7	5.69
		<b>Total</b>	<b>1261.24</b>



**Appendix 2. Postal questionnaires**

**A. Short questionnaire**

**Q1.** During the **past month**, how would you rate your sleep quality overall?

<b>Very Good</b>	<b>Fairly Good</b>	<b>Fairly Bad</b>	<b>Very Bad</b>
▼	▼	▼	▼
<input type="checkbox"/>	<input type="checkbox"/>	<input type="checkbox"/>	<input type="checkbox"/>

**Q2.** In general, would you say your health is...?

<b>Poor</b>	<b>Fair</b>	<b>Good</b>	<b>Very Good</b>	<b>Excellent</b>
▼	▼	▼	▼	▼
<input type="checkbox"/>				

**Q3.** Rate how strongly you agree or disagree to the statement: I am sensitive to noise

<b>Strongly Disagree</b>						<b>Strongly Agree</b>
1	2	3	4	5	6	
▼	▼	▼	▼	▼	▼	▼
<input type="checkbox"/>						

**Q4.** Thinking about the **last 12 months** or so, when you were here at home, how much was your sleep disturbed by noise from the following sources?

	<b>Not at all</b>	<b>Slightly</b>	<b>Moderately</b>	<b>Very</b>	<b>Extremely</b>
	▼	▼	▼	▼	▼
<b>Q4a.</b> Road Traffic	<input type="checkbox"/>				
<b>Q4b.</b> Trains	<input type="checkbox"/>				
<b>Q4c.</b> Aircraft	<input type="checkbox"/>				
<b>Q4d.</b> Neighbors	<input type="checkbox"/>				

**Q6.** What race do you consider yourself to be? (mark all that apply)

<input type="checkbox"/> American Indian or Alaska Native	<input type="checkbox"/> Native Hawaiian or Other Pacific Islander
<input type="checkbox"/> Asian	<input type="checkbox"/> White
<input type="checkbox"/> Black or African American	<input type="checkbox"/> Other (please specify): _____
<input type="checkbox"/> Prefer Not to Answer	

<b>Q7. Gender:</b> <input type="checkbox"/> Male <input type="checkbox"/> Female	<b>Q8. Age:</b> _____(years)
--	------------------------------



**B. Medium questionnaire**

**Q1.** During the **past month**, how would you rate your sleep quality overall?

<b>Very Good</b>	<b>Fairly Good</b>	<b>Fairly Bad</b>	<b>Very Bad</b>
▼	▼	▼	▼
<input type="checkbox"/>	<input type="checkbox"/>	<input type="checkbox"/>	<input type="checkbox"/>

**Q2.** How often have you have taken medicine (prescribed or “over the counter”) to help you sleep in the **past month**?

<b>Not during the past month</b>	<b>Less than once a week</b>	<b>Once or twice a week</b>	<b>Three or more times a week</b>
▼	▼	▼	▼
<input type="checkbox"/>	<input type="checkbox"/>	<input type="checkbox"/>	<input type="checkbox"/>

**Q3.** How often in the **past month** have you done the following because of noise when trying to sleep at home?

	<b>Never</b>	<b>Rarely</b>	<b>Sometimes</b>	<b>Often</b>	<b>Always</b>
	<b>1</b>	<b>2</b>	<b>3</b>	<b>4</b>	<b>5</b>
	▼	▼	▼	▼	▼
<b>Q3a.</b> Wear earplugs or headphones	<input type="checkbox"/>				
<b>Q3b.</b> Turn on the TV	<input type="checkbox"/>				
<b>Q3c.</b> Turn on music	<input type="checkbox"/>				
<b>Q3d.</b> Close windows	<input type="checkbox"/>				
<b>Q3e.</b> Use a sound machine	<input type="checkbox"/>				
<b>Q3f.</b> Turn on a fan	<input type="checkbox"/>				

**Q4.** Rate how strongly you agree or disagree to the statement: I am sensitive to noise

<b>Strongly Disagree</b>					<b>Strongly Agree</b>
<b>1</b>	<b>2</b>	<b>3</b>	<b>4</b>	<b>5</b>	<b>6</b>
▼	▼	▼	▼	▼	▼
<input type="checkbox"/>					

**Q5.** Thinking about the **last 12 months** or so, when you were here at home, how much was your sleep disturbed by noise from the following sources?

	<b>Not at all</b>	<b>Slightly</b>	<b>Moderately</b>	<b>Very</b>	<b>Extremely</b>
	▼	▼	▼	▼	▼
<b>Q5a.</b> Road Traffic	<input type="checkbox"/>				
<b>Q5b.</b> Trains	<input type="checkbox"/>				
<b>Q5c.</b> Aircraft	<input type="checkbox"/>				
<b>Q5d.</b> Neighbors	<input type="checkbox"/>				



**Q6.** In general, would you say your health is...?

- |                          |                          |                          |                          |                          |
|--------------------------|--------------------------|--------------------------|--------------------------|--------------------------|
| <b>Poor</b>              | <b>Fair</b>              | <b>Good</b>              | <b>Very Good</b>         | <b>Excellent</b>         |
| ▼                        | ▼                        | ▼                        | ▼                        | ▼                        |
| <input type="checkbox"/> |

**Q7.** Have you ever been diagnosed by a health professional with any of the following sleep disorders?

- |  |                                     |  |
|--|-------------------------------------|--|
| <input type="checkbox"/> Sleep Apnea                     | <input type="checkbox"/> Narcolepsy | <input type="checkbox"/> Restless Leg Syndrome |
| <input type="checkbox"/> Periodic Limb Movement Syndrome | <input type="checkbox"/> Insomnia   | <input type="checkbox"/> None                  |
| <input type="checkbox"/> Other (please specify): _____   |                                     |  |

**Q8.** Do you have any problems or difficulties with your sense of hearing?

- Yes  No

**Q9.** Have you ever been diagnosed by a health professional with the following conditions (mark all that apply)?

- |   |   |                               |
|---|---|-------------------------------|
| <input type="checkbox"/> Hypertension/<br>High blood pressure | <input type="checkbox"/> Arrhythmia/<br>Irregular heartbeat | <input type="checkbox"/> None |
|---|---|-------------------------------|

**Q10.** If currently employed, does your job require overnight shift work?

(Overnight shift work refers to work for at least 4 hours between 12 a.m. midnight to 6 a.m. in the morning)

- Yes  No

**Q11.** How long have you lived at your current residence

- |                          |                          |                          |                           |
|--------------------------|--------------------------|--------------------------|---------------------------|
| <b>Less than 1 year</b>  | <b>1-5 years</b>         | <b>5-10 years</b>        | <b>More than 10 years</b> |
| ▼                        | ▼                        | ▼                        | ▼                         |
| <input type="checkbox"/> | <input type="checkbox"/> | <input type="checkbox"/> | <input type="checkbox"/>  |

**Q12.** Are there children in this household under the age of 5?

- Yes  No

**Q13.** Are you Hispanic or Latino?

- Yes  No  Prefer Not to Answer

**Q14.** What race do you consider yourself to be? (mark all that apply)

- |   |  |
|---|--|
| <input type="checkbox"/> American Indian or Alaska Native | <input type="checkbox"/> Native Hawaiian or Other Pacific Islander |
| <input type="checkbox"/> Asian                            | <input type="checkbox"/> White                                     |
| <input type="checkbox"/> Black or African American        | <input type="checkbox"/> Other (please specify): _____             |
| <input type="checkbox"/> Prefer Not to Answer             |  |



<b>Q15. Gender:</b> <input type="checkbox"/> Male <input type="checkbox"/> Female	<b>Q16. Age:</b> _____(years)
<b>Q17. What is your height?</b>	_____feet_____inches
<b>Q18. What is your weight?</b>	_____lbs



C. Long questionnaire

<b>Q1a.</b> During the <b>past month</b> , at what time have you usually gone to bed on weekdays or workdays?	_____ (HH:MM AM/PM)
<b>Q1b.</b> During the <b>past month</b> , at what time have you usually woken up on weekdays or workdays?	_____ (HH:MM AM/PM)
<b>Q1c.</b> During the <b>past month</b> , how much sleep did you usually get on weekdays or workdays?	_____ (Hours)

<b>Q2.</b> During the <b>past month</b> , how would you rate your sleep quality overall?			
<b>Very Good</b>	<b>Fairly Good</b>	<b>Fairly Bad</b>	<b>Very Bad</b>
▼	▼	▼	▼
<input type="checkbox"/>	<input type="checkbox"/>	<input type="checkbox"/>	<input type="checkbox"/>

<b>Q3.</b> For the following questions, select the response that best reflects how often the following occurred during the <b>past month</b> .				
	<b>Not during the past month</b>	<b>Less than once a week</b>	<b>Once or twice a week</b>	<b>Three or more times a week</b>
	▼	▼	▼	▼
<b>Q3a.</b> You had trouble sleeping because you cannot get to sleep within <b>30 minutes</b> ?	<input type="checkbox"/>	<input type="checkbox"/>	<input type="checkbox"/>	<input type="checkbox"/>
<b>Q3b.</b> You had trouble sleeping because you wake up in the middle of the night or early morning?	<input type="checkbox"/>	<input type="checkbox"/>	<input type="checkbox"/>	<input type="checkbox"/>
<b>Q3c.</b> You have taken medicine (prescribed or “over the counter”) to help you sleep?	<input type="checkbox"/>	<input type="checkbox"/>	<input type="checkbox"/>	<input type="checkbox"/>
<b>Q3d.</b> You had trouble staying awake while driving, eating meals, or engaging in social activity?	<input type="checkbox"/>	<input type="checkbox"/>	<input type="checkbox"/>	<input type="checkbox"/>

<b>Q4.</b> How often in the <b>past month</b> have you done the following because of noise when trying to sleep at home?					
	<b>Never</b>	<b>Rarely</b>	<b>Sometimes</b>	<b>Often</b>	<b>Always</b>
	1	2	3	4	5
	▼	▼	▼	▼	▼
<b>Q4a.</b> Wear earplugs or headphones	<input type="checkbox"/>				
<b>Q4b.</b> Use alcohol	<input type="checkbox"/>				
<b>Q4c.</b> Use medication	<input type="checkbox"/>				
<b>Q4d.</b> Turn on the TV	<input type="checkbox"/>				
<b>Q4e.</b> Turn on music	<input type="checkbox"/>				
<b>Q4f.</b> Close windows	<input type="checkbox"/>				
<b>Q4g.</b> Use a sound machine	<input type="checkbox"/>				
<b>Q4h.</b> Turn on a fan	<input type="checkbox"/>				



**Q5.** For the following statements respond how strongly you agree or disagree.

	Strongly Disagree 1 ▼	2 ▼	3 ▼	4 ▼	5 ▼	Strongly Agree 6 ▼
<b>Q5a.</b> I am easily awakened by noise	<input type="checkbox"/>	<input type="checkbox"/>	<input type="checkbox"/>	<input type="checkbox"/>	<input type="checkbox"/>	<input type="checkbox"/>
<b>Q5b.</b> I get used to most noises without much difficulty	<input type="checkbox"/>	<input type="checkbox"/>	<input type="checkbox"/>	<input type="checkbox"/>	<input type="checkbox"/>	<input type="checkbox"/>
<b>Q5c.</b> I find it hard to relax in a place that is noisy	<input type="checkbox"/>	<input type="checkbox"/>	<input type="checkbox"/>	<input type="checkbox"/>	<input type="checkbox"/>	<input type="checkbox"/>
<b>Q5d.</b> I am good at concentrating no matter what is going on around me	<input type="checkbox"/>	<input type="checkbox"/>	<input type="checkbox"/>	<input type="checkbox"/>	<input type="checkbox"/>	<input type="checkbox"/>
<b>Q5e.</b> I get mad at people who make noise that keeps me from falling asleep or getting work done	<input type="checkbox"/>	<input type="checkbox"/>	<input type="checkbox"/>	<input type="checkbox"/>	<input type="checkbox"/>	<input type="checkbox"/>
<b>Q5f.</b> I am sensitive to noise	<input type="checkbox"/>	<input type="checkbox"/>	<input type="checkbox"/>	<input type="checkbox"/>	<input type="checkbox"/>	<input type="checkbox"/>

**Q6.** Thinking about the last 12 months or so, when you were here at home, how much was your sleep disturbed by noise from the following sources?

	Not at all ▼	Slightly ▼	Moderately ▼	Very ▼	Extremely ▼
<b>Q6a.</b> Road Traffic	<input type="checkbox"/>				
<b>Q6b.</b> Trains	<input type="checkbox"/>				
<b>Q6c.</b> Aircraft	<input type="checkbox"/>				
<b>Q6d.</b> Industries/Factories	<input type="checkbox"/>				
<b>Q6e.</b> Construction	<input type="checkbox"/>				
<b>Q6f.</b> Neighbors	<input type="checkbox"/>				
<b>Q6g.</b> Air Conditioner	<input type="checkbox"/>				

**Q7.** Thinking about the last 12 months or so, when you are here at home, how much does noise from each of the following bother, disturb, or annoy you?

	Not at all ▼	Slightly ▼	Moderately ▼	Very ▼	Extremely ▼
<b>Q7a.</b> Road Traffic	<input type="checkbox"/>				
<b>Q7b.</b> Trains	<input type="checkbox"/>				
<b>Q7c.</b> Aircraft	<input type="checkbox"/>				
<b>Q7d.</b> Industries/Factories	<input type="checkbox"/>				
<b>Q7e.</b> Construction	<input type="checkbox"/>				
<b>Q7f.</b> Neighbors	<input type="checkbox"/>				
<b>Q7g.</b> Air Conditioner	<input type="checkbox"/>				

**Q8.** In general, would you say your health is...?

Poor ▼	Fair ▼	Good ▼	Very Good ▼	Excellent ▼
<input type="checkbox"/>				



**Q8. In general, would you say your health is...?**

<b>Poor</b>	<b>Fair</b>	<b>Good</b>	<b>Very Good</b>	<b>Excellent</b>
▼	▼	▼	▼	▼
<input type="checkbox"/>				

**Q9. Have you ever been diagnosed by a health professional with any of the following sleep disorders?**

<input type="checkbox"/> Sleep Apnea	<input type="checkbox"/> Narcolepsy	<input type="checkbox"/> Restless Leg Syndrome
<input type="checkbox"/> Periodic Limb Movement Syndrome	<input type="checkbox"/> Insomnia	<input type="checkbox"/> None
<input type="checkbox"/> Other (please specify): _____		

**Q10. Do you have any problems or difficulties with your sense of hearing?**     Yes     No

<b>Q11a. Have you ever been diagnosed by a health professional with the following conditions (mark all that apply)?</b>	<b>Q11b. If you have been diagnosed with a condition listed under Q11a, have you been treated for the condition in the <b>past month</b>?</b>
<input type="checkbox"/> Hypertension/High blood pressure	<input type="checkbox"/> Yes <input type="checkbox"/> No
<input type="checkbox"/> Chronic headaches/Migraines	<input type="checkbox"/> Yes <input type="checkbox"/> No
<input type="checkbox"/> Arrhythmia/Irregular heartbeat	<input type="checkbox"/> Yes <input type="checkbox"/> No
<input type="checkbox"/> Heart disease	<input type="checkbox"/> Yes <input type="checkbox"/> No
<input type="checkbox"/> Stomach ulcer	<input type="checkbox"/> Yes <input type="checkbox"/> No
<input type="checkbox"/> Diabetes	<input type="checkbox"/> Yes <input type="checkbox"/> No
<input type="checkbox"/> None of the above	

**Q12. What is your marital status?**

- Single
- Married
- Widowed
- Separated
- Divorced
- Domestic Partners

**Q13. What was your total household income last year?**

- < \$25,000
- \$25,000-\$50,000
- \$50,000-\$75,000
- \$75,000-\$100,000
- \$100,000-\$150,000
- >\$150,000
- Prefer Not to Answer

**Q14. What is the highest level of education you have completed?**

- Less than High School
- High School Graduate
- College Graduate or Higher

**Q15. What is your current employment status?**

- Working
- Unemployed
- Student
- Retired
- Homemaker

**Q16. If currently employed, does your job require overnight shift work?**  
 (Overnight shift work refers to work for at least 4 hours between 12 am midnight to 6 am in the morning)     Yes     No



**Q17.** Are you Hispanic or Latino?  Yes  No  Prefer Not to Answer

**Q18.** What race do you consider yourself to be? (mark all that apply)

- American Indian or Alaska Native  Native Hawaiian or Other Pacific Islander
- Asian  White
- Black or African American  Other (please specify): \_\_\_\_\_
- Prefer Not to Answer

**Q20.** How long have you lived at your current residence?

- Less than 1 year
- 1-5 years
- 5-10 years
- More than 10 years

**Q21.** Do you have an air conditioner in your bedroom?

- No Unit
- Central Air Conditioner
- Window Unit

**Q22.** How many people (including yourself) reside in this household? \_\_\_\_\_

**Q23.** How many children in this household are under the age of 5? \_\_\_\_\_

**Q24.** Gender:  Male  Female **Q25.** Age: \_\_\_\_\_(years)

**Q26.** What is your height? \_\_\_\_\_ feet \_\_\_\_\_ inches

**Q27.** What is your weight? \_\_\_\_\_ lbs



**Appendix 3. Initial contact letters**

Text highlighted in yellow indicates text that was changed based on recipient and mailing round.



# Community Noise Study

Sponsored by the Federal Aviation Administration



Forename Surname  
or Current Resident  
Street  
City, GA Zip code

Dear Forename Lastname or Current Resident,

Your household has been selected to take part in an important study on the effect of noise in your community on sleep which is sponsored by the Federal Aviation Administration. We encourage 1 adult in the household to complete the attached brief survey. The information you provide will be used to develop and revise nighttime noise policies.

Your participation is voluntary. However, your participation is essential to inform us about your neighborhood. Your answers will be treated as confidential. We have enclosed \$2.00 as a token of our appreciation for your participation.

In addition to the survey, we are conducting a 5 night in home study which includes measurements of heart rate and body movement and the indoor noise levels in the bedroom at night. Participants of this additional study will receive \$20/30/40.00 per night, for a total of \$100/150/200.00. For information on how to participate in this optional study please refer to the last page of the attached survey booklet.

If you have any questions about this study:

**Call:** 215-573-3815

**Email:** noise@mail.med.upenn.edu

**Visit:** [https://www.med.upenn.edu/uep/projects\\_pcns.html](https://www.med.upenn.edu/uep/projects_pcns.html)

Thank you in advance for your participation!

Sincerely,

*Basner*

Mathias Basner, MD, PhD

Associate Professor, University of Pennsylvania



## Community Noise and Sleep Study



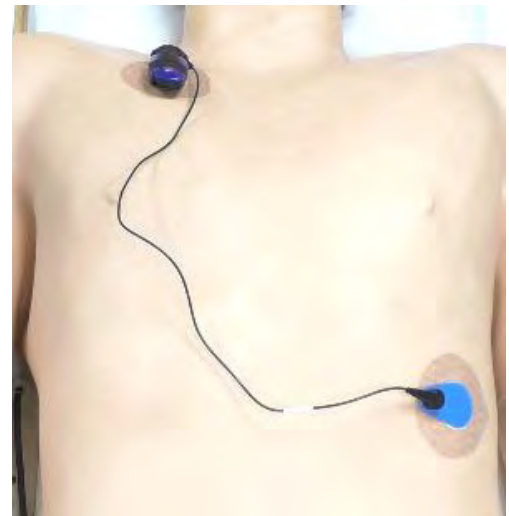
### Indoor Noise Measurements

Indoor sound recordings will be made during the sleep period. The microphone and sound recorder should be placed near the sleeping position on a dresser or nightstand. Participants will need to start/stop the sound recorder each night/morning.



### Heart Rate and Body Movement Measurements

During the night both heart rate and movement will be measured. The device used is battery operated. There are two electrodes for measuring heart rate there are two electrodes. One electrode will go just below the right clavicle; the other electrode will go on the left side of the chest below the pectoral muscle/breast. There is a button on the device for starting and stopping the measurements each night/morning.



**Appendix 4. Morning questionnaire**

---

**Morning Questionnaire**

---

**Instructions**

- Please mark all answers clearly
- If the question is multiple choice, mark your answer by placing an x in the box:
- If there are no response alternatives listed, write in your response in the provided space

---

1. **Current Date:** \_\_\_\_\_ **Current Time:** \_\_\_\_\_

2. **Last night did you sleep with the windows...**

- Closed
- Partially Open
- Completely Open

3. **At what time did you...**

go to bed and switch off the light last night? \_\_\_\_\_ (Hour: Minute)

wake up this morning? \_\_\_\_\_ (Hour: Minute)

get out of bed this morning? \_\_\_\_\_ (Hour: Minute)

4. **How long did it take you to fall asleep after you turned the lights off?**

\_\_\_\_\_ (minutes)

5. **Did you wake up during the night?**

- Yes
- No

If so, how many times? \_\_\_\_\_

What were the reasons, please describe: \_\_\_\_\_

\_\_\_\_\_

**6. How do you feel right now?**

awake, active, refreshed	<input type="checkbox"/>	tired, dull, sleepy										
	0	1	2	3	4	5	6	7	8	9	10	

**7. Please check the box next to the statement that best describes how sleepy you feel right now...**

- Feeling active, vital, alert, or wide awake
- Functioning at high levels, but not at peak; able to concentrate
- Awake, but relaxed; responsive but not fully alert
- Somewhat foggy, let down
- Foggy; losing interest in remaining awake; slowed down
- Sleepy, woozy, fighting sleep; prefer to lie down
- No longer fighting sleep, sleep onset soon; having dream-like thoughts

**8. Please evaluate last night's sleep:**

**Falling asleep was:**

<input type="checkbox"/>										
0: very easy	1	2	3	4	5	6	7	8	9	10: very difficult

**My sleep was:**

<input type="checkbox"/>										
0: very calm	1	2	3	4	5	6	7	8	9	10: very restless

**Overall Sleep Quality:**

<input type="checkbox"/>										
0: low	1	2	3	4	5	6	7	8	9	10: high



**9a. How bothered, disturbed, or annoyed do you feel by last night's Aircraft noise?**

- Not at all       Slightly       Moderately       Very       Extremely

**10. How bothered, disturbed, or annoyed do you feel by last night's Road Traffic noise?**

- Not at all       Slightly       Moderately       Very       Extremely

**11. How bothered, disturbed, or annoyed do you feel by last night's Train noise?**

- Not at all       Slightly       Moderately       Very       Extremely

**12. How bothered, disturbed, or annoyed do you feel by noise in general last night?**

- Not at all       Slightly       Moderately       Very       Extremely

**13. Other comments?**

.....

.....

.....



**Appendix 5. Non-participation figures**

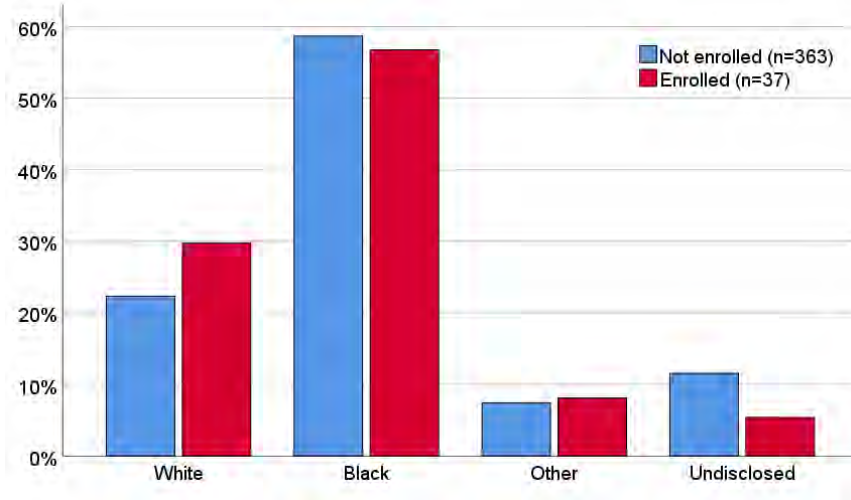


Figure 30. Race. Respondents indicating multiple ethnicities are classified as “Other”. p=0.557.

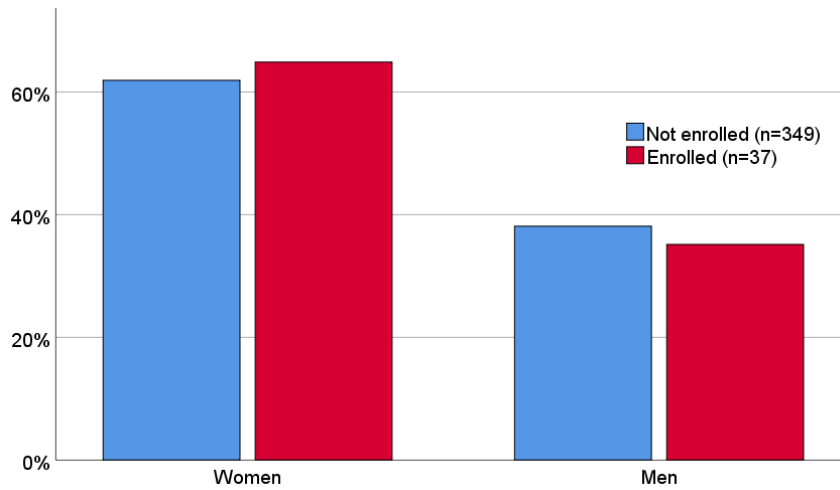


Figure 31. Sex. p=0.859.

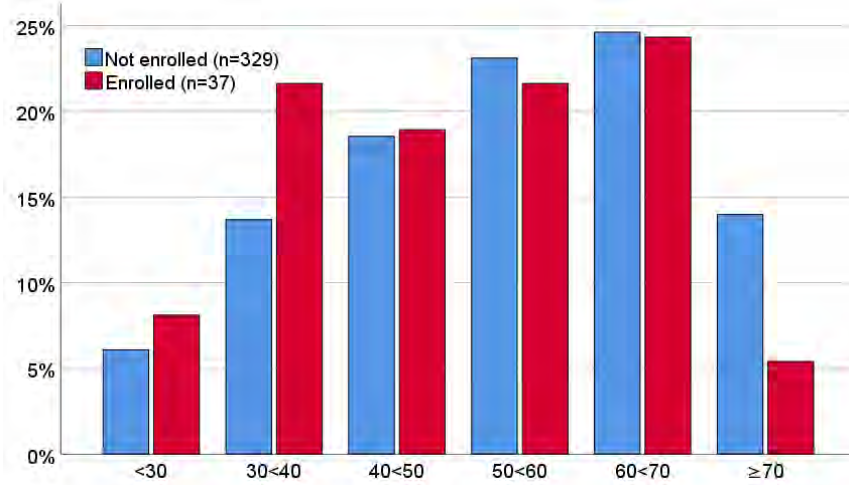


Figure 32. Categorical age. Excludes one non-participant respondent listing an age of 4 years.  $p=0.580$

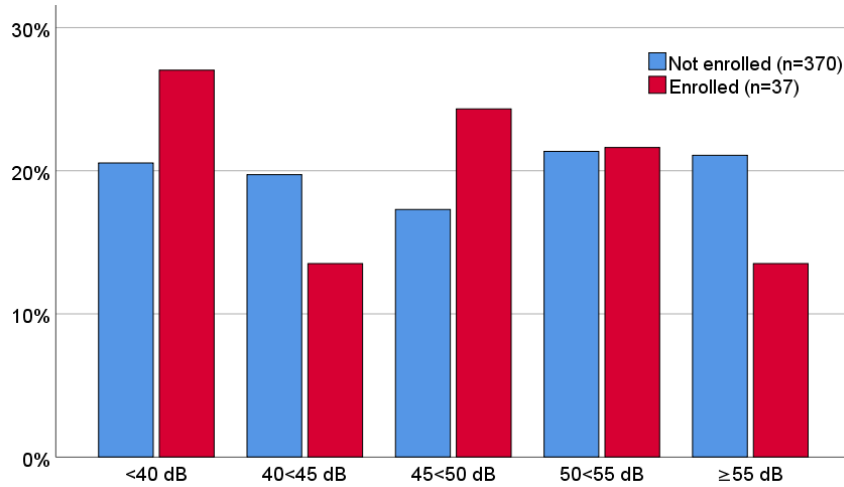


Figure 33. Categorical  $L_{Night}$ .  $p=0.527$ .

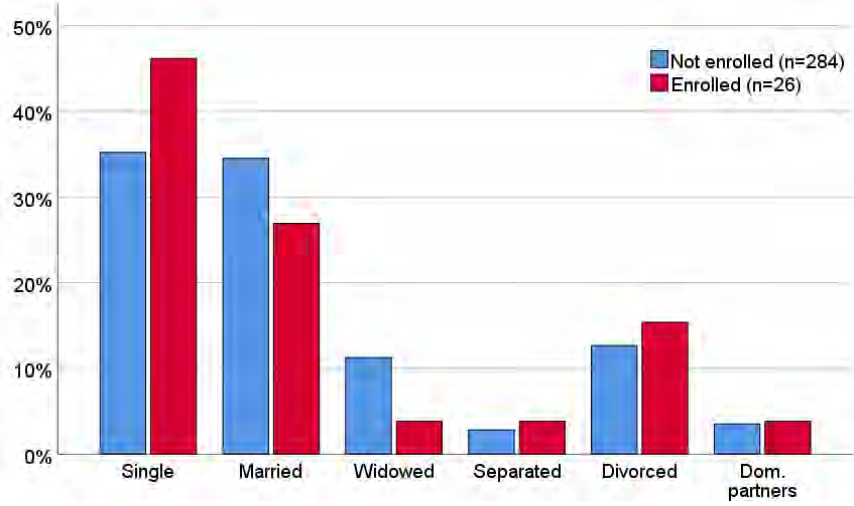


Figure 34. Marital status.  $p=0.649$ .

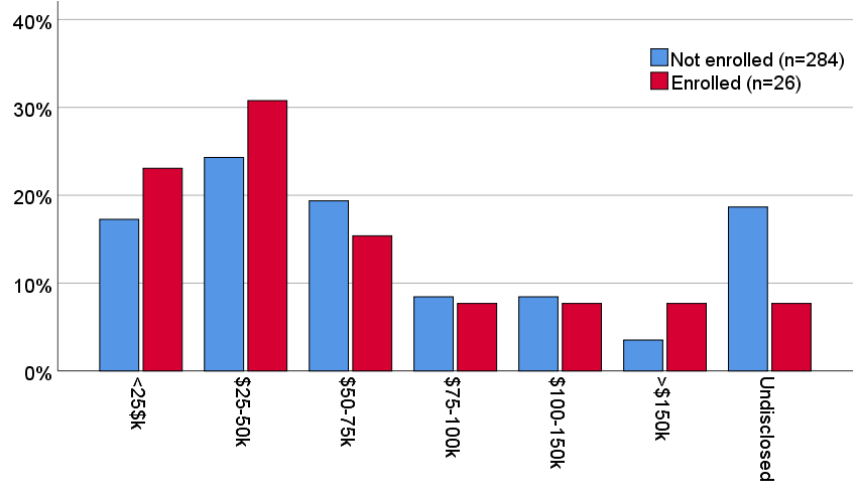


Figure 35. Annual household income.  $p=0.634$ .

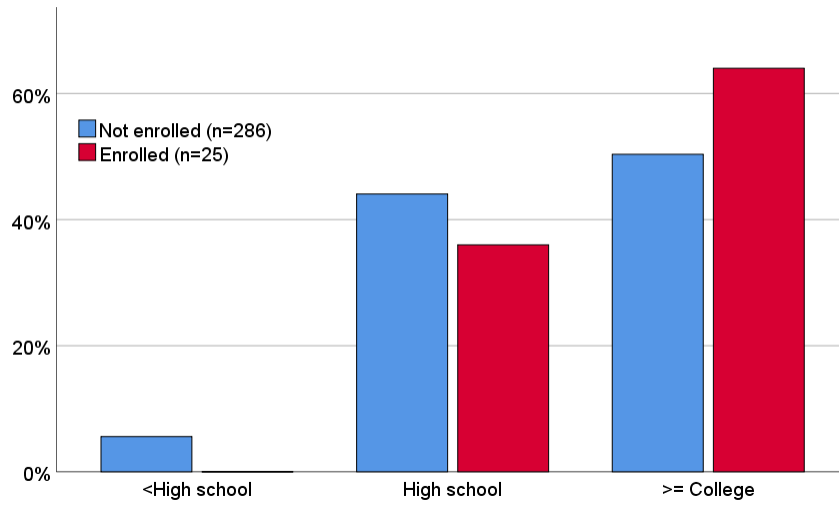


Figure 36. Highest education level completed.  $p=0.374$ .

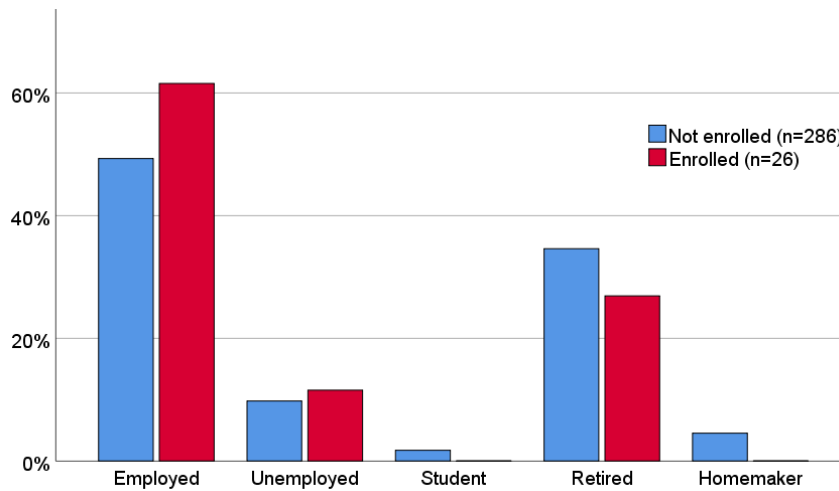


Figure 37. Employment status.  $p=0.733$ .

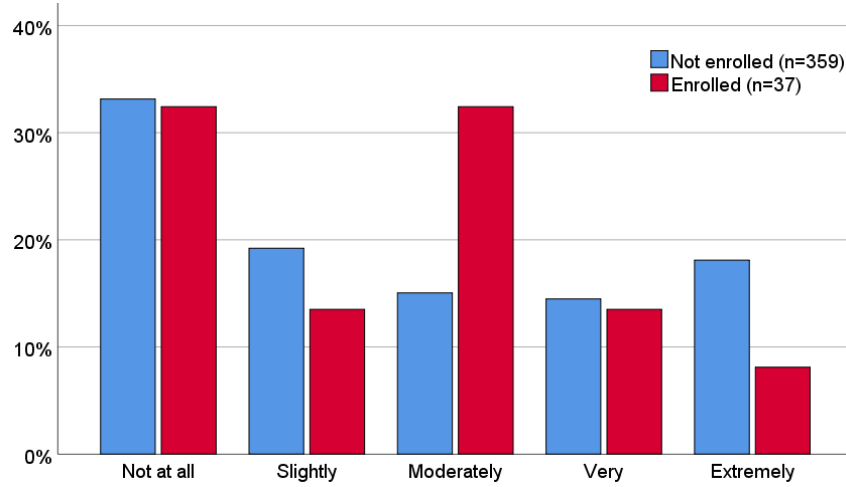


Figure 38. Sleep disturbance by aircraft noise over past 12 months.  $p=0.100$ .

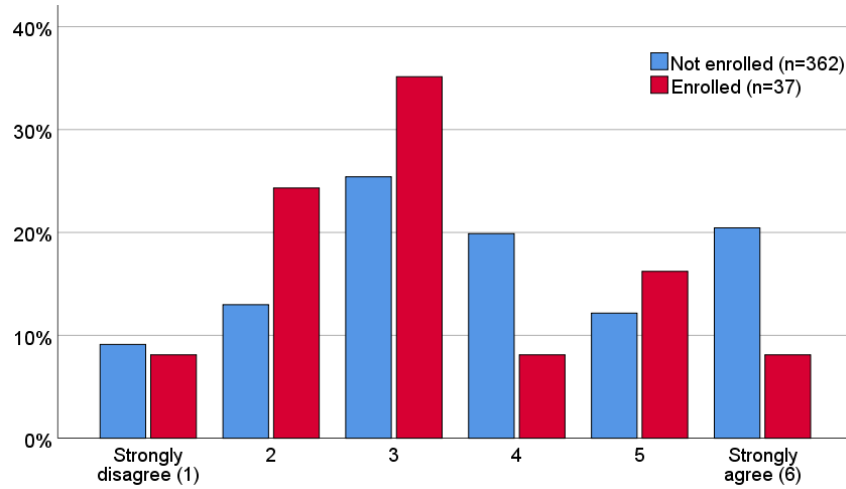


Figure 39. I am sensitive to noise.  $p=0.065$ .

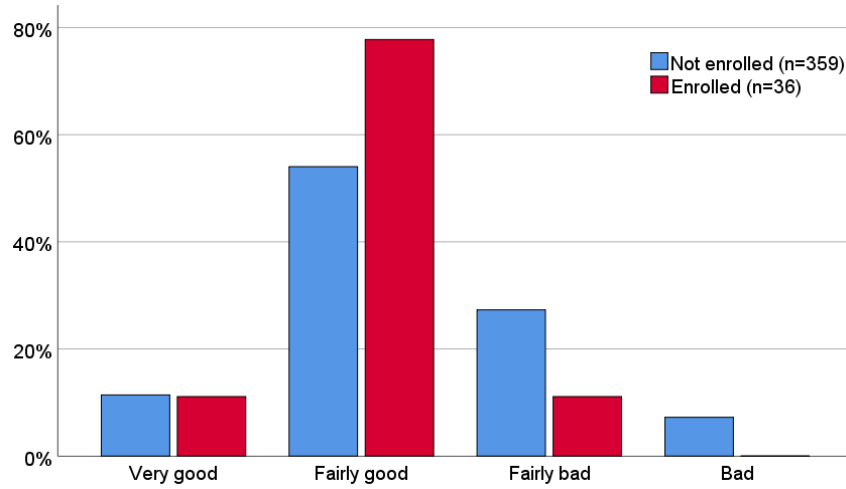


Figure 40. Overall sleep quality during past month.  $p=0.023$ .

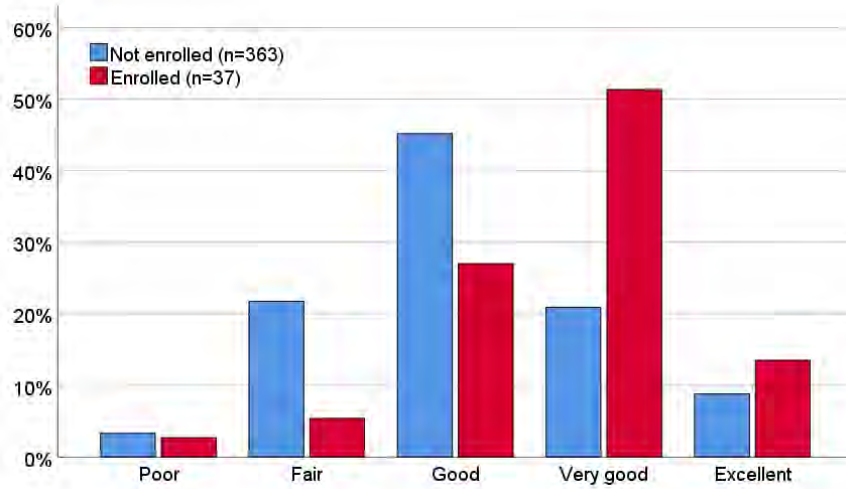


Figure 41. Self-rated general health.  $p=0.0004$ .



# Project 018 Community Measurements of Aviation Emissions Contribution to Ambient Air Quality

## Boston University School of Public Health

### Project Lead Investigator

Kevin J. Lane  
Assistant Professor  
Department of Environmental Health  
Boston University School of Public Health  
715 Albany St. T4W  
Boston, MA 02118  
617-414-8457  
klane@bu.edu

Jonathan I. Levy (through September 30, 2017)  
Interim Chair and Professor  
Department of Environmental Health  
Boston University School of Public Health (BUSPH)  
715 Albany St. T4W  
Boston, MA 02118  
617-358-2460  
jonlevy@bu.edu

### University Participants

#### Boston University School of Public Health

- PIs: Kevin J. Lane, Assistant Professor; and Jonathan I. Levy, Professor and Associate Chair
- FAA Award Number: 13-C-AJFE-BU, Amendment 7
- Period of Performance: March 1, 2020 to September 30, 2020
- Tasks:
  - Task 1: Continue long-term monitoring of air pollution at both new and existing stationary sites to assess temporal variation in aviation source contributions in greater Boston area communities.
  - Task 2: Incorporate particle size distribution at each of our monitoring sites to inform our understanding of inflight contributions to community ultrafine particles (UFP) relative to background sources.
  - Task 3: Conduct mobile monitoring in selected communities near Boston Logan International Airport to determine spatial and short-term temporal variation in aviation emissions contributions to concentrations at ground level.
  - Task 4: Compile from FAA essential flight activity covariates needed for regression modelling under ASCENT Project 18 and dispersion modelling under ASCENT Project 19 for a data-sharing platform that would allow for comparisons between atmospheric dispersion models implemented by collaborators on Project 19 and monitored pollutant concentrations and related regression models from Project 18.
  - Task 5: In Year 1, construct regression models using the 2017–2018 data and the flight activity data and covariates developed under Task 4 to determine the contributions of aviation sources to UFP and black carbon (BC) concentrations measured during our 2017–2018 monitoring campaign. In Year 2, analyze the combined mobile monitoring and stationary data collected under Tasks 1–3 for the 2020 sampling campaign for community-level contributions from aviation sources.



## Project Funding Level

FAA provided \$675,092 in funding. Matching funds provided by non-federal donor to the Women's Health Initiative (WHI) cohort studies, as cost share support to Boston University through ASCENT Project 3.

## Investigation Team

- ASCENT BUSPH Director and Project 18 Co-Investigator: Jonathan I. Levy, ScD (Professor of Environmental Health, Chair of the Department of Environmental Health, Boston University School of Public Health). Dr. Levy is the Boston University PI of ASCENT. He initiated ASCENT Project 18 and serves as the director of BUSPH ASCENT research.
- ASCENT Project 18 Principal Investigator: Kevin J. Lane, PhD (Assistant Professor of Environmental Health, Department of Environmental Health, Boston University School of Public Health). Dr. Lane joined the Project 18 team in July 2017. Dr. Lane has expertise in the assessment of UFP exposure, geographic information systems, statistical modeling of large datasets, and cardiovascular health outcomes associated with air pollution exposure. He has contributed to study design and data analysis strategies and, as of October 1, 2017, has taken over the primary responsibility for project execution; Dr. Lane also contributes to the manuscripts and reports produced.
- Tufts University Associate Professor Dr. John Durant, PhD. Dr. Durant oversees the Tufts Air Pollution Monitoring Laboratory (TAPL) team, leads development of the field study design and scientific manuscript preparation.
- Tufts University Research Professor Dr. Neelakshi Hudda, PhD. Dr. Hudda joined the Project 18 team in September 2020 and is managing the TAPL team and mobility data analysis, field study design and implementation, and scientific manuscript preparation.
- BUSPH Assistant Professor Dr. Prasad Patil. Dr. Patil is a machine learning and regression modeling expert that is assisting Dr. Lane with modeling of the 2017–2019 UFP data.
- Graduate Students: Sean Mueller is a doctoral student at Boston University School of Public Health.
- Undergraduate Students: Ida Weiss and Taylor Adams at Tufts University are working on the mobile monitoring platform and helping to clean the air pollution data and create map plots.

## Project Overview

The primary goal of this project was to conduct new air pollution monitoring beneath flight paths to and from Boston Logan International Airport (Logan Airport), using a protocol specifically designed to determine the magnitude and spatial distribution of UFP in the vicinity of arrival flight paths. Data were collected to assess whether aircraft emissions, particularly arrival emissions, significantly contribute to UFP concentrations at appreciable distances from the airport. Task 1–3 are an extension of the previous air pollution monitoring performed under ASCENT Project 18. Tasks 2 and 3 leverage the infrastructure developed for our field campaign and enable measurements that address a broader set of research questions than those evaluated in the previous monitoring year, with additional data collection for UFP size distributions and a new air pollutant (NO/NO<sub>2</sub>). These Tasks provide a strong foundation for Task 4 and 5, which increases the potential for future collaborative efforts with Project 19, in which we interpret and apply the collected measurements to inform ongoing dispersion modeling efforts at UNC and regression modeling at BUSPH.

We reestablished a new monitoring campaign to collect and analyze community air pollution measurements to determine the contributions of inflight arrival and departure aircraft to ground-based concentrations. Previous studies have not had the monitoring infrastructure and real-time flight activity data necessary to determine how much of the pollution measured is from aviation sources. We will use state of the art air pollution monitoring technology that can measure different air pollutants every 1–5 seconds. Stationary sites will be established at varying distances from flight paths for Logan Airport, with measurements collected across multiple seasons. We also will use a mobile monitoring system (electric vehicle) that has been outfitted with the same monitoring equipment to drive throughout these communities to better characterize geographic variation in air pollution. Statistical analyses will compare the stationary and mobile measurements with flight activity data from the U.S. Federal Aviation Administration and meteorology to determine aircraft contributions to the ground measurements. We will compare these source attribution estimates with comparable outputs from atmospheric dispersion models.

A summary of the current project methods and data collection is included below to describe the continued application of Project 18 data, including bivariate statistical analysis and multiple regression model development conducted under Task 5.



## Task 1 – Continue Long-term Monitoring of Air Pollution at Both New and Existing Stationary Sites to Assess Temporal Variation in Aviation Source Contributions in Greater Boston Area Communities

Boston University School of Public Health

### **Objectives**

Task 2 for the 2017–2018 funding cycle focused on designing and implementing an air pollution monitoring study that would allow us to determine contributions from arriving aircraft to ambient air pollution in a near-airport setting. The objective of this Task was to determine whether aircraft emissions, particularly in-flight arrival and departure emissions, can significantly contribute to ground-level UFP concentrations at appreciable distances from the airport.

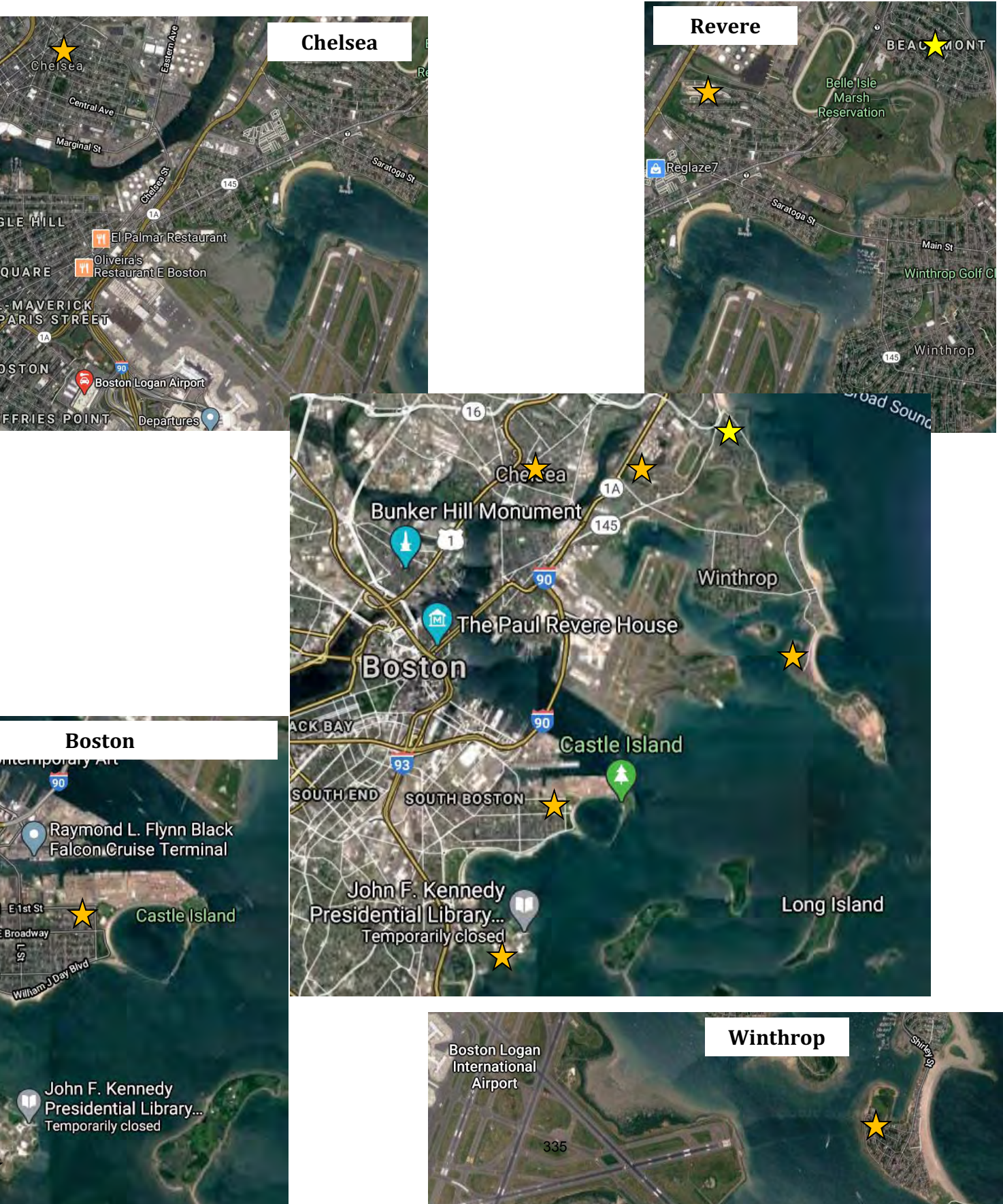
### **Research Approach**

An air pollution monitoring campaign was conducted at five sites located at varying distances from the airport and arrival/departure flight paths for Logan Airport (Figure 1). Sites were selected through a systematic process, considering varying distances from the airport and laterally from each flight path and excluding locations close to major roadways or other significant sources of combustion. These sites were specifically chosen to isolate the contributions of in-flight aircraft, which is important for the flight activity source attribution task. Particle number concentration (PNC, a proxy for UFP) monitoring instruments were established at each monitoring site in a preselected scheme to allow for multiple levels of comparison (e.g., sites beneath versus not beneath flight paths given prevailing winds, sites at varying distances from the airport, and sites at varying lateral distances beneath flight paths). The PNC was measured using TSI condensation particle counters (model 3783). In addition, BC was measured using AethLabs microaethalometers (model AE51), and meteorological data at each site were collected using Davis Vantage Pro2 weather stations.

**Field Monitoring:** Due to COVID-19 there was substantial difficulty with gaining access to monitoring locations and visits to potential new sites during the spring and summer. However, we have collected air pollution data since April on a total of 140 days from April–September (April = 15 days; May = 18 days; June = 22 days; July = 26 days; August = 29 days; September = 30 days). UFP data have come from two different long-term monitoring sites in Chelsea and South Boston allowing for comparison of PNC to be compared within our monitored communities this fall. Multiple new monitoring sites were visited during this month to identify locations for Revere and Winthrop that were greater than 200 m away from major roadways and intersections and would be near arrival and takeoffs on runways 22 and 9, respectively. Agreements have been made to sample at locations for the next 12–18 months with property owners. The maps in Figure 1 indicate where the stationary monitors will be configured during the rest of the 2020–2021 field monitoring campaign. We will have a monitor in the cities of Boston, Chelsea, Revere, and Winthrop (Figure 1).



Figure 1. Stationary sites for 2020-2021 monitoring campaign.





We also have reconfigured the long-term monitoring boxes to allow for year-round sampling of all our monitoring devices. At each site there will be UFP, NO/NO<sub>2</sub> and BC measured. Example of the box setup with climate control can be seen in Figure 2.

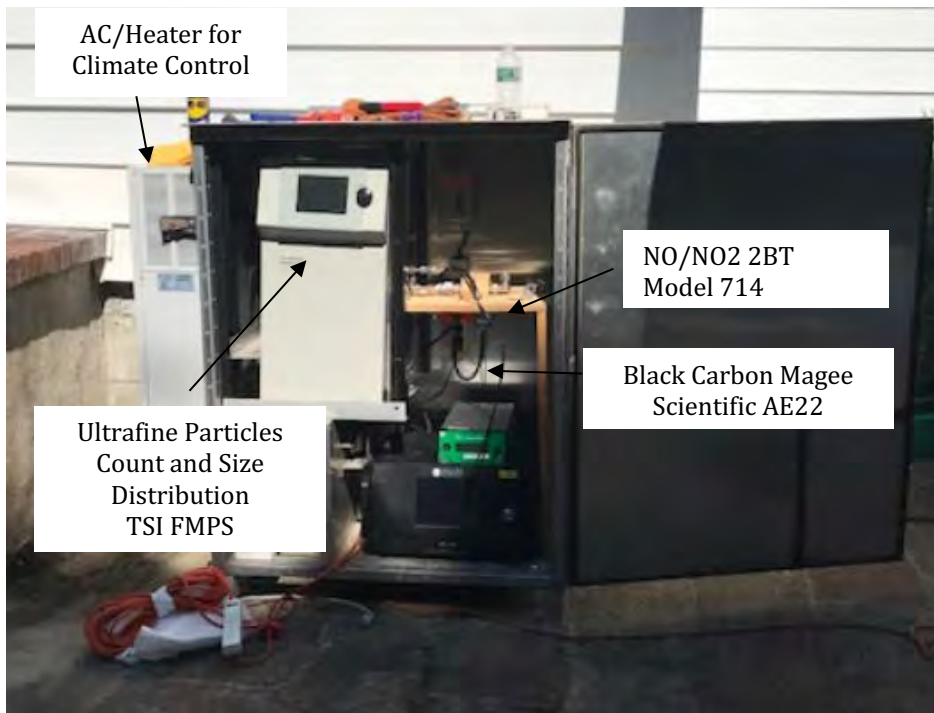


Figure 2. BUSPH long-term air pollution monitoring box for Winthrop, MA.

The monitoring site equipment configurations at other sites are as follows:

- **Chelsea**
  - UFP – measured using condensation particle counter (CPC)
  - BC – Micro-aethalometer
- **Revere**
  - UFP – measured using CPC
  - NO/NO<sub>2</sub> – 2BT Model 714
  - BC – Micro-aethalometer
- **Winthrop**
  - UFP – FMPS
  - NO/NO<sub>2</sub> – 2BT Model 714
  - BC – Magee AE33

### Milestones

We have relaunched our monitoring sites and have been sampling for the 2020–2021 funding cycle in multiple locations.

- Obtained permission to resample and/or sample new locations and developed a sampling schedule.
- Obtained new monitoring equipment and completed annual manufacturer cleaning and calibration of CPCs.
- Implemented air pollution monitoring protocols, including measurements of meteorological parameters.

### Major Accomplishments

Field tests were performed for comparison of CPCs for low and high air pollution exposure sampling scenarios. Comparisons between instruments were made using a recent factory calibrated instruments and all had an agreement with  $r \geq 0.97$ - $0.99$

and within device comparison of 0.96 (Figure 3). These tests will be conducted every six months or when a monitor requires factory recalibration.

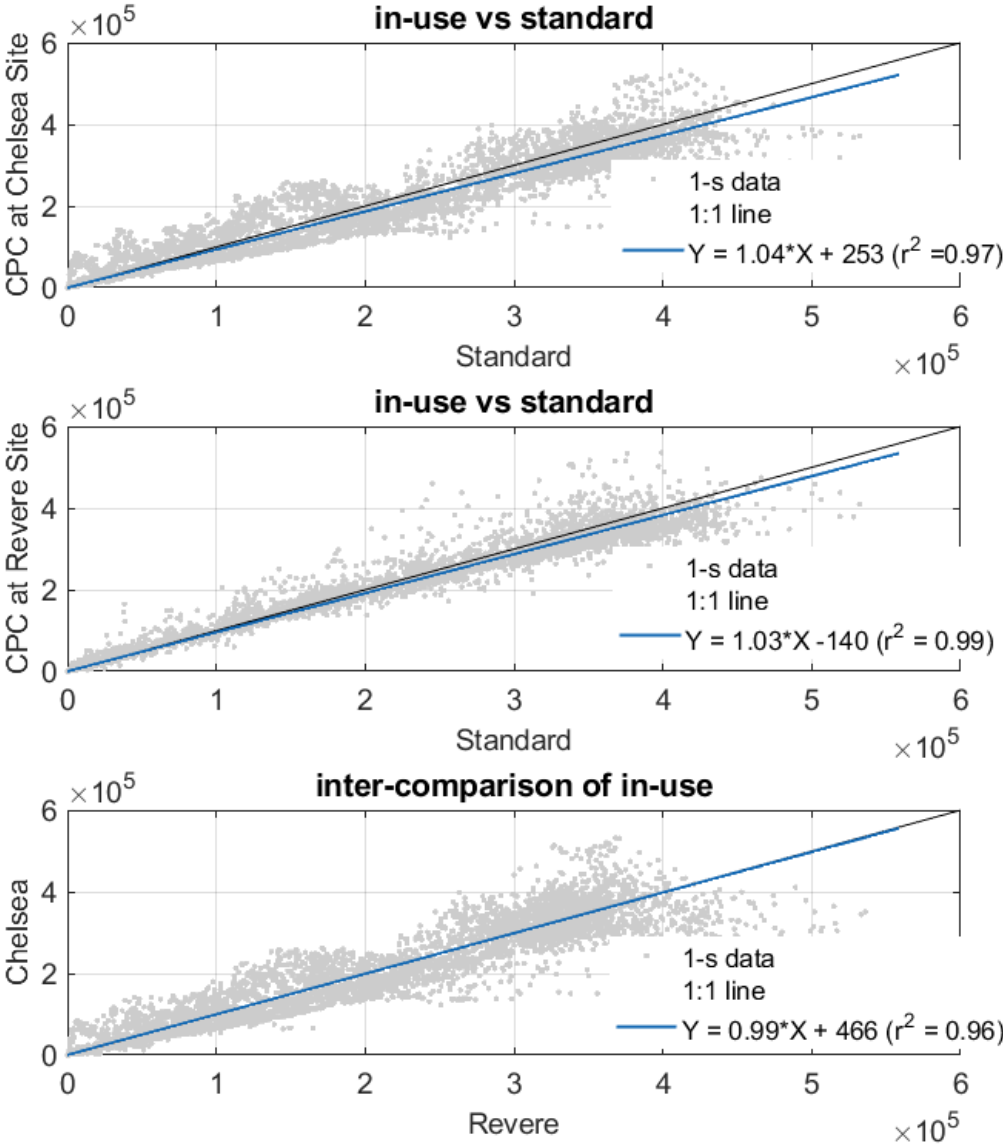
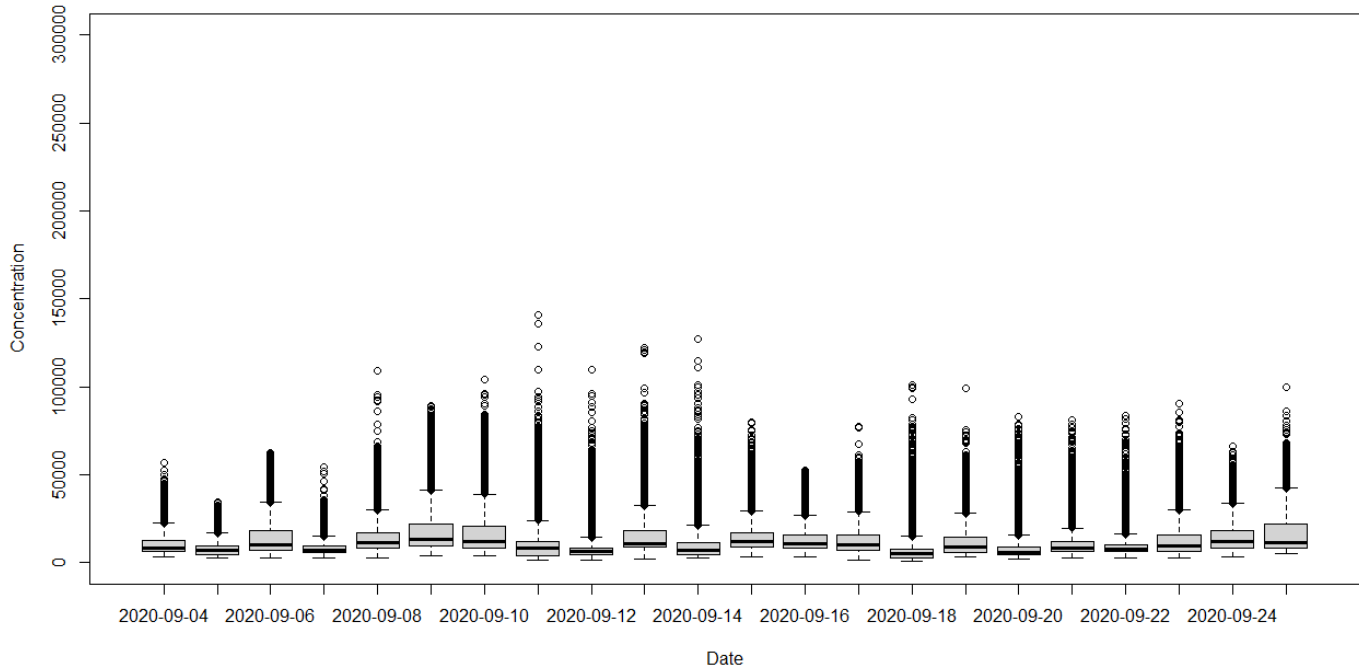


**Figure 3.** Side-by-side particle count comparisons between CPCs in the field to test for inter-monitor comparisons.

The CPC monitors have been recalibrated and will be rotated through every 5–6 months for retesting and factory calibration. Stationary monitors have been collecting data that is compiled and merged with meteorological data. Figure 4 provides a time-series plot for two of our monitoring locations as an example of the data being collected on UFP. We observed elevated levels at the Winthrop site compared to the Chelsea site, with significantly elevated peak exposures.



### Chelsea, MA



### Winthrop, MA

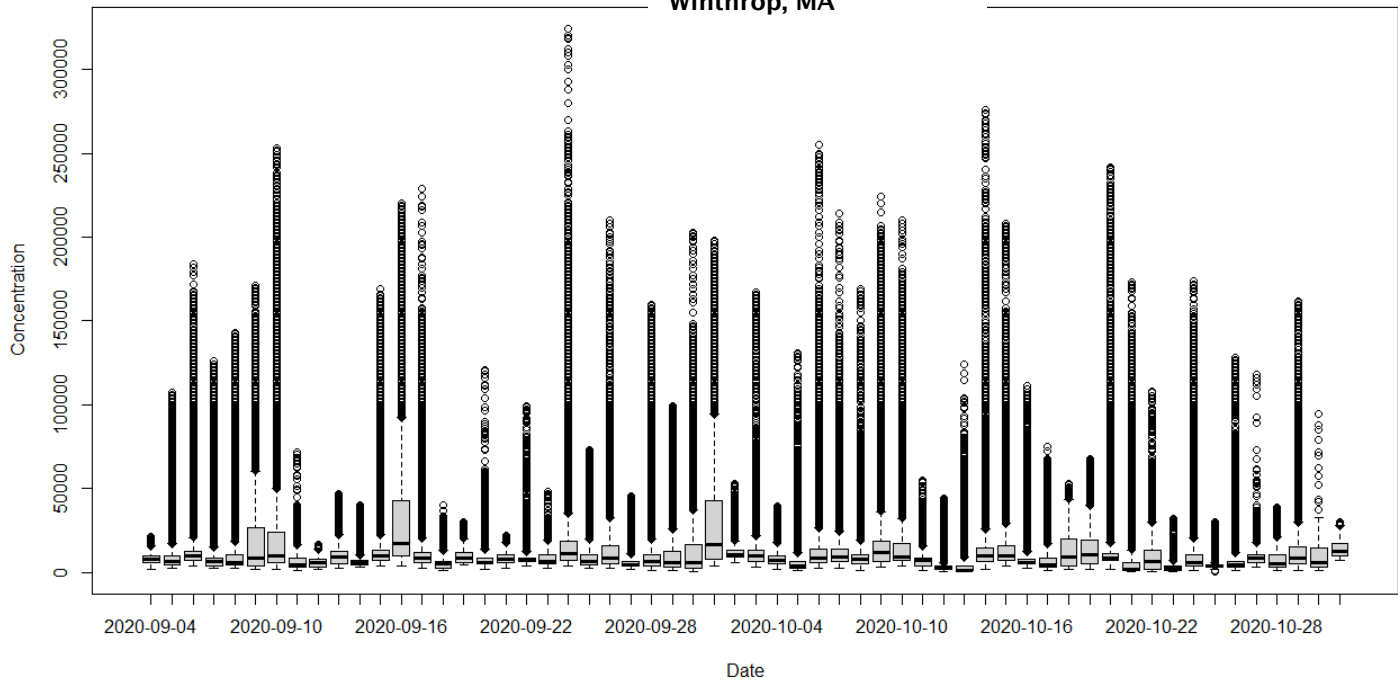


Figure 4. Example of PNC at stationary monitoring in boxplots by day since September for Chelsea and Winthrop sites.



## **Publications**

N/A

## **Outreach Efforts**

N/A

## **Awards**

None

## **Student Involvement**

Sean Mueller, a doctoral student on the study, has been analyzing the descriptive statistics of the stationary monitoring data. Ida Weiss, an undergraduate student at Tufts University, has been assisting with stationary site monitoring data collection.

## **Plans for Next Period**

Tasks proposed over the next study period (October 1, 2020 to September 30, 2021): We will continue monitoring at our stationary sites and evaluate the potential for future monitoring locations.

# **Task 2 – Incorporate Particle Size Distribution at Each of Our Monitoring Sites to Inform Our Understanding of Inflight Contributions to Community UFP Relative to Background Sources**

Boston University School of Public Health

## **Objective**

The objective of this Task is to incorporate particle size distribution into our UFP monitoring campaign using two TSI Fast Mobility Particle Sizers (FMPS). FMPS is routinely used to make accurate nanoparticle size measurements of particles to assess the shape of the particle size distribution, providing broad size range from 1 nm to 1,000 nm at a fine temporal scale (<10 second scans) that can bin categorize a wide concentration range up to  $10^7$  particles/cm<sup>3</sup>. The method is independent of the refractive index of the particle or fluid and has a high degree of absolute sizing accuracy and measurement repeatability.

Inclusion of two FMPS in our study design allows for the particle size distribution to be examined. Given literature showing differences in particle size distributions for aircraft versus motor vehicles, as well as for aircraft plumes at different points in time, this could further inform our understanding of inflight contributions to community UFP relative to background sources.

## **Research Approach**

There are two different particle size distribution monitors that we will be deploying in mobile and stationary monitoring platforms. We have two FMPS and the scanning mobility particle sizer (SMPS) that will be deployed. There will be one SMPS in the mobile electric vehicle (EV) platform, with the FMPS at our Winthrop site and the other FMPS rotated through our other monitoring locations. During this summer, we started our comparison of the FMPS and SMPS laboratory testing. The FMPS and SMPS particle number at different particle size channels were compared under 10 test runs with a correlation coefficient average of  $r = 0.97$  and differences in time coincident points that were below the instrument error for both monitors (< 800 particles/cm<sup>3</sup>). Below are two figures illustrating the laboratory tests. The SMPS can measure many more size channels than the FMPS but has a higher limit of detection (LOD) on the particle size it can detect at 10 nm than the FMPS, which can accurately measure down to 6 nm. We therefore only conducted the statistical analysis on the channels that were able to detect coincident size distribution values. Below in Figure 5, we present two examples of the test runs. As these are laboratory tests, the concentrations are much lower than ambient exposure conditions.

## **Milestones**

The core milestones for Task 2 included incorporating particle size distribution into our monitoring campaign and testing for comparability between UFP monitoring equipment and deploying into the field.

**Major Accomplishments**

We successfully integrated monitoring of particle size distribution into our 2020–2021 monitoring campaign.

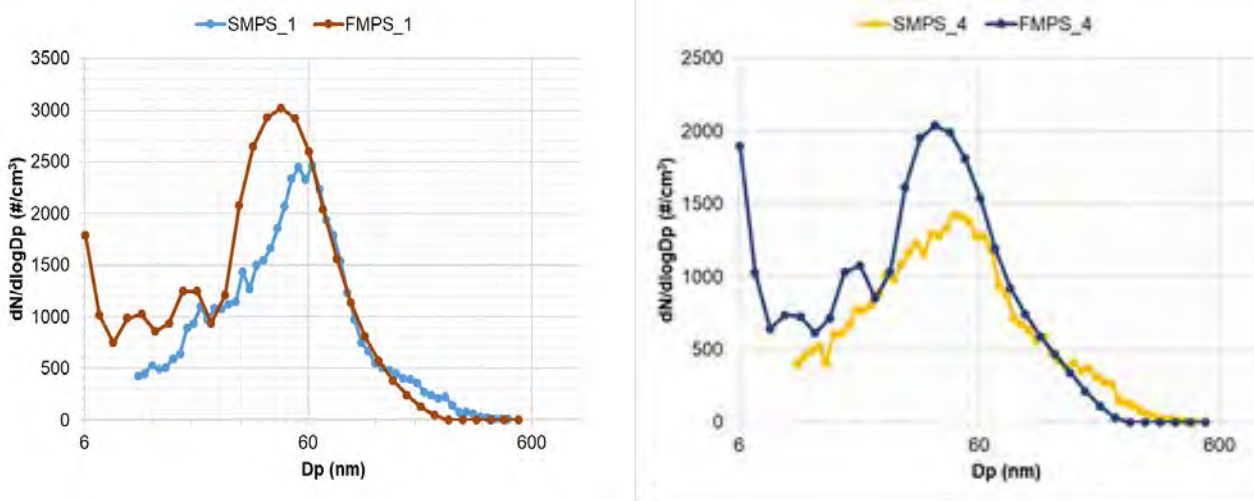


**Figure 5.** Example of two side-by-side particle size total comparisons between SMPS and FMPS in laboratory. Dots represent the particle size channels being measured between 6 nm and 600 nm.

We also conducted mobile monitoring test runs with the FMPS and a CPC in the Tufts EV. The chart below (Figure 6) shows the data from a test run conducted the first week of April.

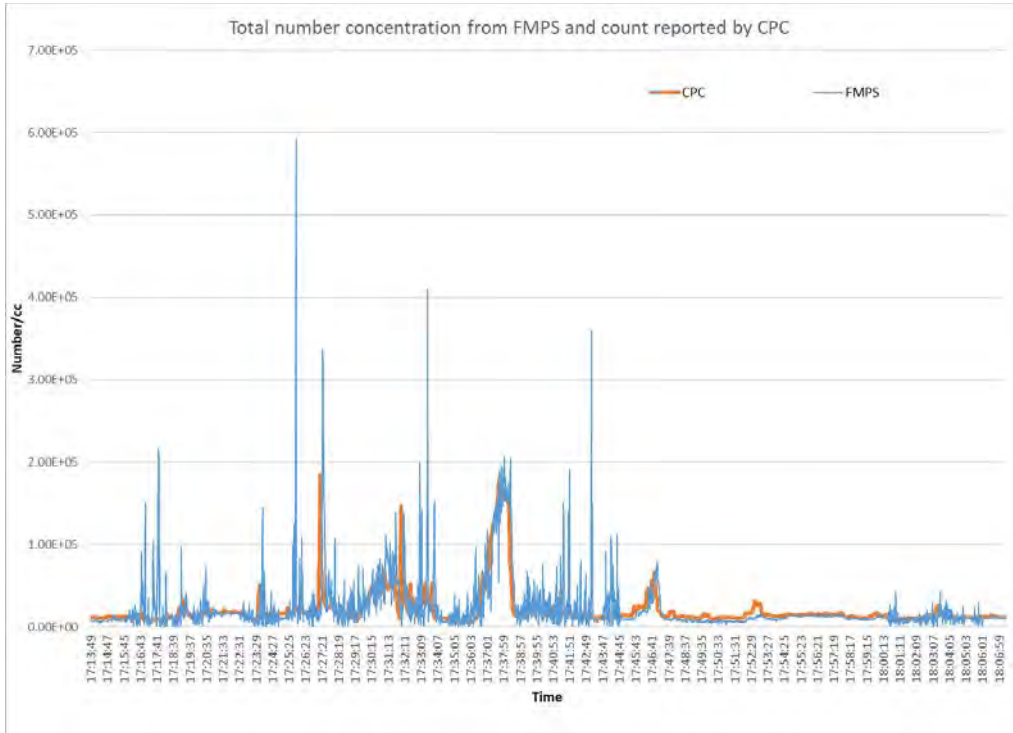


**Figure 6.** Mobile monitoring route CPC and FMPS total particle number concentration data collected on April 4, 2020.

From the test run, we were able to identify that the FMPS tracks well with the CPC, but measurements from the FMPS are impacted more from vibration, creating zero values that need to be cleaned. In the mobile and lab testing scenarios, both monitoring devices captured similar data.

### **Publications**

N/A

### **Outreach Efforts**

N/A

### **Awards**

None

### **Student Involvement**

Doctoral student Sean Mueller will analyze the particle distribution data as part of a source apportionment analysis.

### **Plans for Next Period**

Continue monitoring particle size distribution as part of the ongoing community monitoring campaign.

## **Task 3 – Conduct Mobile Monitoring in Selected Communities Near Logan Airport to Determine Spatial and Short-term Temporal Variation in Aviation Emissions Contributions to Concentrations at Ground Level**

Boston University School of Public Health

### **Objectives**

New to our scope of work in 2019–2021, we added high-resolution mobile monitoring to improve spatial characterization of UFP and other air pollutants in near-airport communities. Under the current project, we are collaborating with Dr. John Durant at Tufts University to deploy a mobile monitoring platform concurrent with our stationary monitoring under Tasks 1 and 2, which will allow us to efficiently monitor more spatially diverse communities near Logan Airport in less time, with a limited number of monitoring devices. Dr. Durant has the mobile monitoring infrastructure and expertise to allow us to collect these data in a reliable and robust manner, as described in more detail below. Real-time measurements of air pollutants will be made with the Tufts Air Pollution Monitoring Laboratory (TAPL), a mobile platform equipped with fast-response instruments for monitoring gas- and particle-phase pollutants.

### **Research Approach**

TAPL is a 2017 Chevrolet Bolt electric vehicle (Figure 7). The instruments are powered by six 12-volt marine deep cycle batteries, which are connected in parallel to a 2-kW inverter/charger (Xantrex 2000). The TAPL is driven slowly (~10 m/s) to allow measurement of local-scale (~20 m) changes in pollutant concentrations. Individual measurements are matched to location by 1-second-interval GPS readings. The TAPL monitoring setup can be outfitted to include a combination of air pollution monitoring equipment that includes a condensation particle counter (CPC; Model 3775, TSI; 4-2,000 nm), a particle size classifier (Scanning Mobility Particle Sizer (SMPS; Model 3080 electrostatic classifier and a Model 3085 Nano DMA, TSI; 6-200 nm)), a photoelectrical aerosol sensor to detect particle-bound polycyclic aromatic hydrocarbons (PAS, Model PAS2000, EcoChem Analytics, Inc.), an aethelometer to measure black carbon (BC) (Model AE-16, Magee Scientific), and a laser photometer (Dusttrak DRX Aerosol Monitor, 8533, TSI) to measure PM<sub>2.5</sub>. Nitric oxide (NO) and nitrogen oxides (NO<sub>x</sub>; sum of NO<sub>2</sub> and NO concentrations) are measured using a chemiluminescence analyzer (Model 42i, Thermo Scientific). The measurement frequency of the instrument's ranges from 1 second for the CPC to 135 seconds for a full scan (32 bins) with the SMPS.



Figure 7. TAPL exterior and interior pictures.

### TAPL Instruments

The monitoring instruments used in TAPL are listed in Table 1. Measurements were taken every 1 second to 1 minute depending on the instrument. All instruments were factory calibrated by the equipment manufacturers before the start of the campaign. Quality assurance measures performed before each monitoring run include a flow rate and zero-concentration check, and instrument clock resets to the National Institute of Standards and Time (NIST). Periodic side-by-side tests of the instruments area also performed as part of the quality assurance process to determine instrument-specific measurement differences prior to data analysis.

Table 1. Air pollution monitoring equipment in the TAPL used for this study.

Instrument	Parameter measured	Instrument Flow Rate (L min <sup>-1</sup> )	Response Time (s)	Detection Limit, Sensitivity
TSI portable CPC (Ethanol-based) model 3007	UFP count, 10 nm - 1 um	0.8	<9 sec for 95% response	10 nm, <0.01 particles/cm <sup>3</sup>
TSI EPC (water-based) model 3783	UFP count, 7 nm - 3 um	3	<3 sec for 95% response	7 nm, <0.01 particles/cm <sup>3</sup>
2B Technology Model 408	NO	1	8	Greater of 3 ppb or 3% of reading
Magee Scientific Aethalometer AE-33	BC	5	<60	Proportional to time-base and sample flow rate settings: approximately 0.03 µg/m <sup>3</sup> @ 1 min, 5 LPM.
Garmin GPSMAP 76CSx	GPS location	N/A	1	3 m

### Data Acquisition and Preliminary Checks

Data from the instruments are recorded in real-time on a laptop in the TAPL. After each monitoring day, the data files are screened and collated in a master database. Air pollution measurements are matched to location by 1-second-interval GPS readings. The database then goes through a quality assurance and quality check process where the data is screened for



errors flagged by instruments and quality criteria developed by the research team. Both the raw data and quality assured database are stored on a secure server.

**Monitoring Routes**

We have developed two monitoring routes that encompass the communities that are impacted by the most commonly used runways at Logan Airport: (1) a route to the north—the North Route—that includes all, or parts of the communities of Winthrop, Revere, Chelsea, East Boston, and Lynn located 1–4 miles from the airport, and (2) a route to the south—the South Route—that includes all or parts of the communities of South Boston, Dorchester, and Quincy located 1–6 miles from the airport. The routes are shown in Figures 8. The following criteria informed the route design:

- (1) Coverage in communities in proximity of the airport.
- (2) Coverage under main flight paths.
- (3) Spacing of transects underneath flight paths such that altogether they offer the ability to assess spatial gradients of air pollutants over a large area.
- (4) Ability to measure on multiple transects in an area within a relatively short period of time (1–2 hours) to capture both the spatial and temporal changes in aviation impacts within the study area.
- (5) Ability to cover the entire route within the period of window associated with peak and off-peak flight activity periods (3–4 hours).

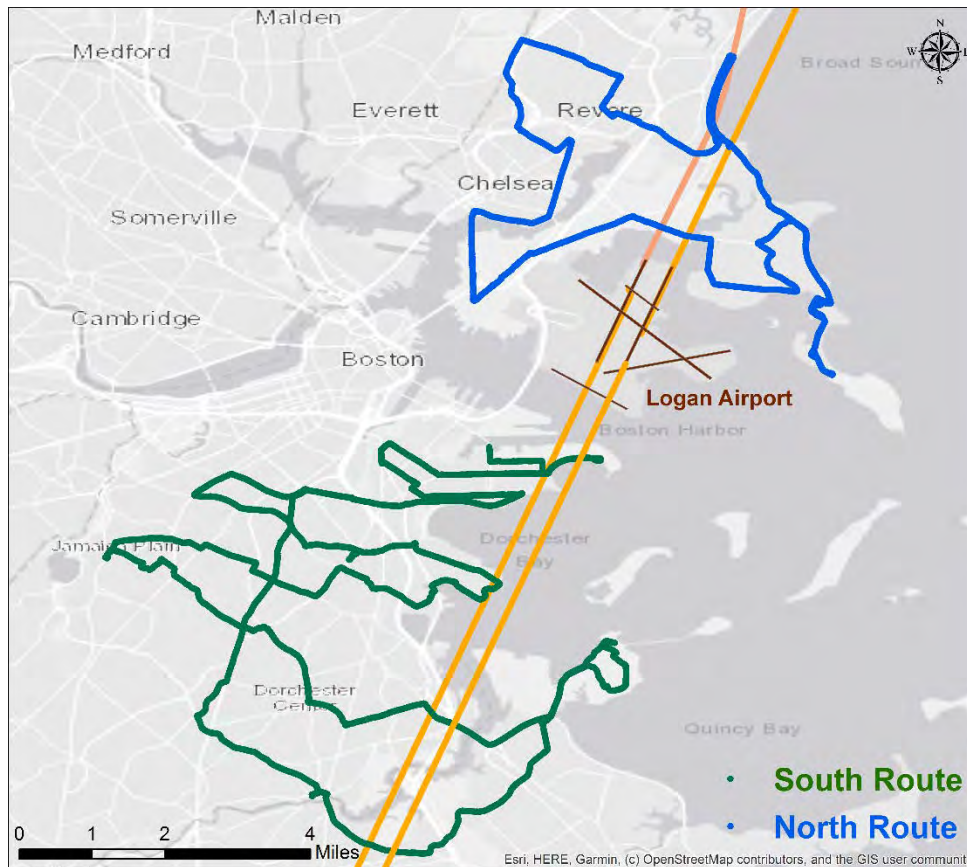


**Figure 8:** Map shows north and south monitoring routes, the airport, and typical flight trajectories for arrivals on runways 4R, 4L, 22R and 22L.

**Monitoring Schedule**

We are collecting measurements on these two routes under a variety of different meteorological and airport-activity conditions. We have adopted a purposeful, flexible monitoring approach rather than a rigid, repetitive schedule. The

advantage of this approach is that it allows us to capture a much wider range of meteorological and airport-activity conditions, and thereby more fully characterize the main factors that influence aviation-related pollutant concentrations in the two study areas. The following criteria are being used to guide the monitoring schedule:

1. Maximize coverage of the periods of the day associated with peak and off-peak flight activity.
2. Coverage of the periods of the day associated with predictable diurnal variations in air pollution due to changes in meteorological factors (e.g., temperature, mixing height, on-shore and off-shore winds).
3. Coverage of the seasonal wind patterns. We are aiming to reasonably mimic the natural distribution (2/3 westerly flow versus 1/3 easterly flow) that is prevalent in the research area. We are also scheduling the monitoring runs to cover different wind speed/direction combinations.
4. Coverage of various temperature regimes (e.g., seasonal, diurnal).
5. Coverage of various active runway configurations.

The record of monitoring to date is summarized in Tables 2 and 3.

**Table 2.** Monitoring dates for the North Route and meteorological conditions during monitoring hours.

Monitoring Date	Time	Temp (F)	Winds	Wind Speed (mph)
8/18/2020	1200-1500	82-84	W-WSW	9-14
8/22/2020	0700-1200	63-80	SW	7-10
8/31/2020	1500-1700	69	E	9-13
9/8/2020	1400-1800	72-78	SE-ESE	10-15
9/11/2020	0700-1200	54-66	N-NE	12-15
9/22/2020	1300-1700	62-65	N-NW	14-18
9/25/2020	1400-1800	64-68	E-ENE	13-14
10/2/2020	1300-1700	59-62	NNW-WNW	7-13
10/6/2020	1500-2000	62-66	S	10-13
10/15/2020	1300-1700	69-71	S-SSW	17-25
10/20/2020	1300-1600	57-59	S-SW	7-13
10/25/2020	0800-1100	43-46	N-NNW	9-12
11/1/2020	0700-1000	35-38	S-W	3-9
11/5/2020	0700-1000	48-51	SW-SSW	10-14

**Table 3.** Monitoring dates for the South Route and meteorological conditions during monitoring hours.

Monitoring Date	Time	Temp (F)	Winds	Wind Speed (mph)
8/27/2020	1300-1700	62-66	ENE-WSW	3-6
8/28/2020	0800-1200	55-61	NNW-WNW	5-7
8/31/2020	1400-1500	68	ESE	15
9/20/2020	1200-1500	58-60	NNE-ENE	14-16
10/4/2020	1700-2100	56-59	SE	8-12
10/20/2020	0600-0900	50-56	SE	3-9
10/23/2020	1500-1800	59-62	E	9-13

**Mobile Monitoring Protocol**

Mobile monitoring has continued with 2-3 routes per week being decided on the day-of between north or south routes based on weather, current flight activity patterns on arrival and takeoff for that day of sampling. Route selection is being designed to maximize variation in meteorology and landing and takeoff (LTO) activity over a community to inform regression modeling. The standard operating procedure for the mobile monitoring route (see Figure 2) preparation begins with (1) checking weather conditions as the wind direction and speed are used by Massport to identify the LTO runways; (2) check the real-time flight tracker to identify the flight paths and which communities are being flown over, (3) warmup of the monitoring

equipment and driving to the starting points of the routes; (4) drive routes and then download and QA/QC data. This standard operating procedure is depicted in Figure 9.

## Mobile Monitoring Setup & Processing

(1) Check weather and record wind, temperature, and other conditions

(2) Check Flight Tracker to predict where planes will be landing

FlightAware <https://flightaware.com/>  
 Weather data <https://forecast.weather.gov/MapClick.php?lat=42.38&lon=-71.09&lg=english&FcstType=digital>

Monitoring Date	Route	Time (24 hr)	Temp (F)	Winds	Wind Speed (m)	Sky Cover (%)	Precipitation (%)	Ending On (Runw)
8/10/2020	Winthrop		90-92	SW (5-7 mph)				
8/12/2020	Winthrop		90-84	W (6-9 mph)				
8/14/2020	Dorchester	13	81	NE		40		4's
8/14/2020	Dorchester	14	82	E		40		4's
8/14/2020	Dorchester	15	82	E		40		4's
8/14/2020	Dorchester	16	82	E		40		4's
8/14/2020	Dorchester	17	81	E		41		4's
08/18/2020	Winthrop	12	83	WSW		9		22
08/18/2020	Winthrop	13	82	W		14		22
08/18/2020	Winthrop	14	84	W		14		22
08/21/2020	Winthrop							



- (3) Start machinery and wait for warmup period (30 minutes)
- CPC 3007/3783 (UFP)
  - LI-840A (CO2 and H2O)
  - AE33 (Black Carbon)
  - Nitrogen dioxide

Commute time to routes:  
 South route: 40 mins round trip  
 North route: 40 mins round trip

South Route: 3 hrs/loop  
 North Route: 1.25 hrs/loop

(4) Post monitoring data processing in MapSource, Aerosol Instrument Manager, Excel, and ArcMap (1.5 hrs)

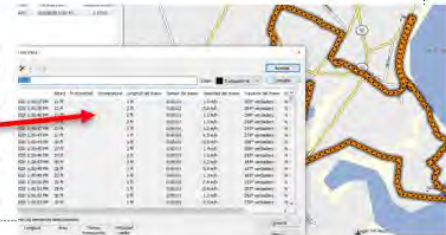


Figure 9. Standard operating procedure for mobile monitoring route preparation.

### Milestones

We have designed monitoring routes and protocol to integrate mobile monitoring for community measuring of aviation-related UFP. Data are being compiled and examined for wind rose plotting and to be included in regression modeling for UFP.

### Major Accomplishments

We have started to conduct preliminary analysis of the patterns of UFP under different wind conditions and flight activity. Here we provide examples of mobile monitoring data from upwind and downwind sampling runs to illustrate the PNC data being collected along the monitoring routes. Figure 10 includes a map showing spatial trend observed on the afternoon of October 23, 2020 during easterly flow on the South Route, with transects in South Boston and a time-series plot of the data collected that highlights elevated baseline concentration on two parallel streets.



**South Route Monitoring**  
**Oct 23, 2020**  
**1500-1800 hours**

**Winds: E at 9-13 miles/h**  
**Temp: 59-62 F**  
**Runways Active: 4L and 4R arrivals**

**(a) Total on-road PNC**

- 3059 - 4615
- 4616 - 7072
- 7073 - 8943
- 8944 - 10944
- 10945 - 13891
- 13892 - 17926
- 17927 - 26103
- 26104 - 235010

**(b) Total on-road PNC in S. Boston**

- 3336 - 15884
- 15885 - 32115
- 32116 - 125257
- 125258 - 235010

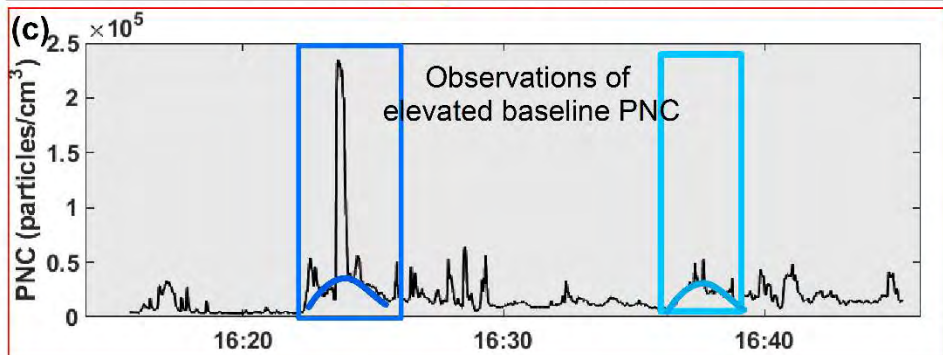
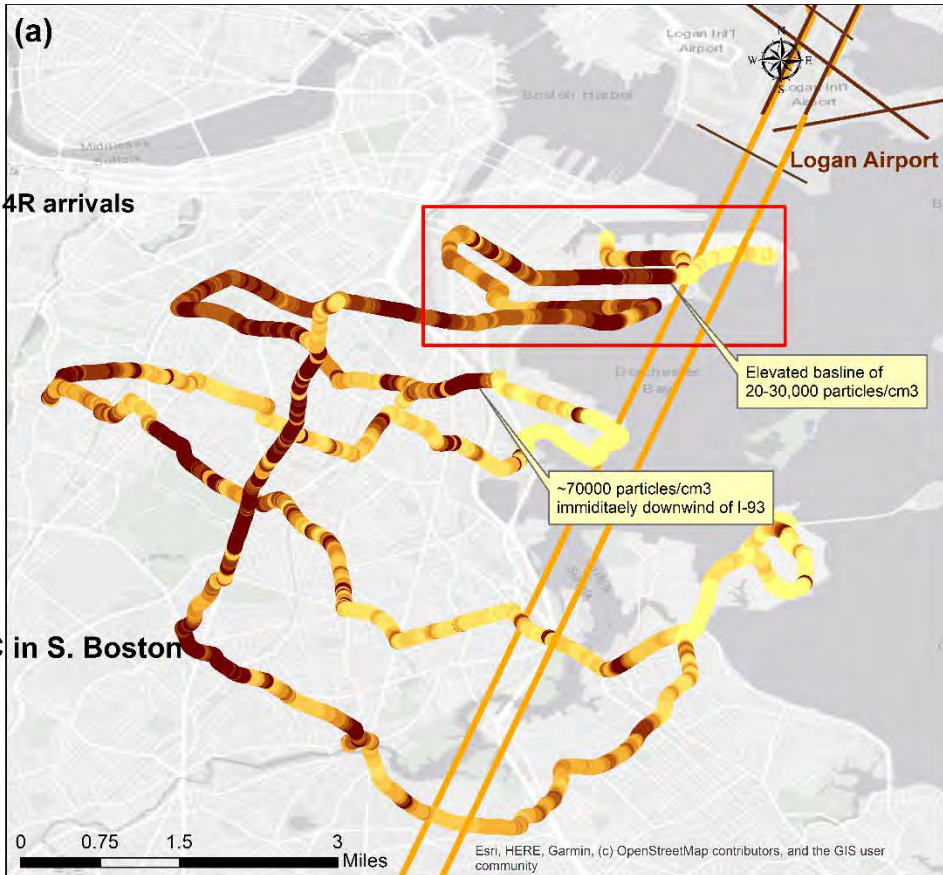


**Figure 10.** (a) Map showing spatial trend observed on the afternoon of October 23, 2020 during easterly flow on the South Route; (b) map showing the spatial trend on several transects in the South Boston area; and (c) time-series of PNC in South Boston area highlighting observations of elevated baseline concentration on two parallel streets.

**Publications**

N/A

**Outreach Efforts**

N/A

### Awards

None

### Student Involvement

Two undergraduate students at Tufts University (Ida Weiss and Taylor Adams) have been trained on the air pollution monitoring equipment and are driving the TAPL as part of their degrees in environmental engineering.

### Plans for Next Period

No new Tasks are currently planned over the next study period (October 1, 2019 to September 30, 2020).

## **Task 4 – Compile from FAA Essential Flight Activity Covariates Needed for Regression Modelling Under Project 18 and Dispersion Modelling Under Project 19 for a Data-Sharing Platform that Would Allow for Comparisons Between Atmospheric Dispersion Models Implemented by Collaborators on ASCENT Project 19 and Monitored Pollutant Concentrations and Related Regression Models from Project 18**

Boston University School of Public Health

### Objectives

We are currently analyzing the data from the 2017 stationary site monitoring campaign to provide insight regarding the ability of statistical analyses of real-time UFP concentration measurements to capture arrival aircraft source contributions to UFP, providing a roadmap for future investigations. Our analyses thus far indicate that we can explain significant variability in UFP across multiple monitoring sites, with statistically significant terms for aviation flight activity as well as meteorology and other site attributes. To our knowledge, this is the only study to date that has incorporated all of the attributes needed to determine the contribution of aviation activity to UFP concentrations in communities, including the collection of UFP concentrations at multiple sites concurrently, with sites selected specifically for the purpose of aircraft-source attribution, insight about detailed flight activity tracks, and application of statistical methods to separate the aviation signal from other sources of UFP.

### Research Approach

The monitoring data and regression model outputs can also directly inform UFP dispersion model development under ASCENT Project 19 directed by Dr. Sarav Arunachalam at the University of North Carolina at Chapel Hill. Under this Task, we plan to work directly with Project 19 and improve both dispersion and regression modelling approaches to quantify arrival and takeoff aircraft contributions to UFP concentrations in communities near Logan Airport. In collaboration with Project 19, we will develop a data sharing platform to provide UFP monitored data and coordinate collection of flight activity data to be used in both projects. The importance of having accurate and highly resolved flight activity data from the FAA (e.g. aircraft type, number of engines, engine type, latitude, longitude, elevation, tail number) is an essential step for both Projects 18 and 19 in the development of an UFP regression model and emissions inventory for dispersion modelling, respectively. We will use PDARS data and other related data as the foundation of the shared data inputs needed for both projects.

Using a shared data platform will allow us to 1) compare UFP monitoring data collected under Project 18 to SCICHEM and CMAQ dispersion model outputs developed under Project 19; 2) identify key predictors in both dispersion and regression modelling of UFP; 3) use the same flight activity data and covariates to develop a regression model (Project 18) and dispersion model (Project 19) of UFP; and 4) compare with the dispersion model outputs. Future modelling efforts will incorporate mobile monitoring data to enhance spatial-resolution of UFP prediction. Comparisons of both project models will guide future efforts towards development of a robust hybrid regression and dispersion model to predict fine scale concentrations of aviation-attributable UFP and other air pollutants.

### Milestones

Currently this Task is on hold and prepared to begin summer of 2021.

### **Major Accomplishments**

Currently this Task is on hold and prepared to begin summer of 2021.

### **Publications**

N/A

### **Outreach Efforts**

N/A

### **Awards**

None

### **Student Involvement**

N/A

### **Plans for Next Period**

Task proposed to begin summer of 2021.

## **Task 5 – In Year 1, Construct Regression Models Using the 2017–2018 Data and the Flight Activity Data and Covariates Developed under Task 4 to Determine the Contributions of Aviation Sources to UFP and BC Concentrations Measured During our 2017–2018 Monitoring Campaign. In Year 2, Analyze the Combined Mobile Monitoring and Stationary Data Collected Under Tasks 1-3 for the 2020 Sampling Campaign for Community-level Contributions from Aviation Sources**

Boston University School of Public Health

### **Objectives**

From 2017–2019, we conducted a monitoring campaign to inform an aviation source attribution analysis as an expansion of the Task 1 regression model development. Our instrumentation and protocol were similar to that of the 2017–2019 monitoring campaign, but with some key enhancements to improve insights regarding aviation source contributions.

### **Research Approach**

Utilizing the air pollution data collected during the 2017–2018 monitoring campaigns, we will build on the methods and insights developed as part of our ongoing analyses of stationary site monitoring data collected during our initial 2017 monitoring campaign. We will begin by analyzing concentrations as a function of wind conditions and flight activity to help inform the structure and form of the subsequent regression models. The contributions of aircraft to ambient UFP and BC concentrations will be preliminarily examined by comparing the measurements during periods of high versus low aviation activity and by considering concentration patterns as a function of meteorological conditions and other key predictors across sites and pollutants. In particular, we will examine concentrations across sites as a function of wind speed and direction under varying flight activity conditions, as our analyses to date have shown elevated UFP concentrations at sites close to arrival flight paths only when the sites are downwind from those flight paths. Results from these and other descriptive analyses will inform the regression model development process.

For the regression models, we are developing multivariable generalized linear models to examine the association between air pollutant concentrations and real-time flight activity, accounting for aircraft locations in space relative to the monitor including terms for wind speed/direction, temperature, mixing height, and other relevant meteorological covariates. Each study site will be modeled individually to look at the location-specific impact of aircraft arrivals and departures along with meteorological and other local environmental conditions, and then combined models will be explored. Because of some of the complex interactions among predictors (i.e., flight activity will be influenced by wind speed and direction, which will also

affect plume dispersion and resulting concentrations at individual monitors), we are exploring advanced statistical techniques for covariate selection, including random forest regression and other machine learning regression techniques. Preliminary findings from an application of machine learning techniques to our 2017 UFP measurements indicate that machine learning methods are able to explain more variability than generalized linear models or related techniques.

We anticipate completing all core regression models from 2017–2018 measurements within Year 1. In Year 2, we would focus on our 2020 monitoring data and develop analogous regression models. The primary distinction would be the inclusion of mobile monitoring data in the 2020 campaign, which would necessitate an analogous but slightly different statistical analysis approach given concurrent spatial and temporal variation in concentrations.

With each of these regression models, we will be able to estimate on a short-term and long-term basis the amount of the measured air pollution attributable to flight activity. In other words, by zeroing out the flight activity terms and determining the predicted concentrations, we will ascertain the portion of measured concentrations attributable to aircraft arrivals and departures. These predictions would subsequently be shared with Project 19, where investigators are developing comparable estimates of aviation-attributable concentrations near Logan Airport, and we would conduct analyses comparing the predictions from dispersion models and regression models.

We conducted a monitoring campaign in 2018 to inform ground contributions from in-flight aviation sources beneath multiple landing and takeoff runways at various distances from the airport and flight path. The instrumentation and protocol used were the same as the 2017 monitoring campaign, but with some key enhancements to improve insights regarding aviation source contributions to NO/NO<sub>2</sub>. The monitoring instruments included the TSI model 3783 water-based CPC for UFP, our primary measure of interest, which was used in the 2017 monitoring campaign. The 3783 model is intended for long-term deployment and can record 1-s average concentrations, which is a valuable time resolution for capturing short-term concentration spikes. Of note, because the model 3783 CPC is temperature-sensitive, we developed and deployed instrumentation in a temperature-conditioned space to protect against extreme heat and cold, allowing for long-term deployment.

In addition, the AethLabs model AE51 micro-aethalometer was used to measure BC. We also deployed the 2BT NO/NO<sub>x</sub> monitor, which gives high-fidelity outputs and can be used in future studies with simultaneous real-time measurements at numerous sites. This approach provides an additional pollutant for future comparisons with atmospheric dispersion model outputs, which can help isolate factors that influence predictions of particulate matter versus gas-phase pollutants. Local Davis Vantage Pro2 weather stations were used to capture real-time wind speed/direction and other meteorological parameters at each sampling site.

Similar to the 2017 campaign, obtaining flight activity data from the FAA for the sampling time periods is essential for future regression model development, which will include the location of each flight as well as basic aircraft characteristics, which can be linked using the Aviation Environmental Design Tool (AEDT) to determine aircraft-specific attributes that may be predictive of emissions and corresponding concentrations.

## **Milestones**

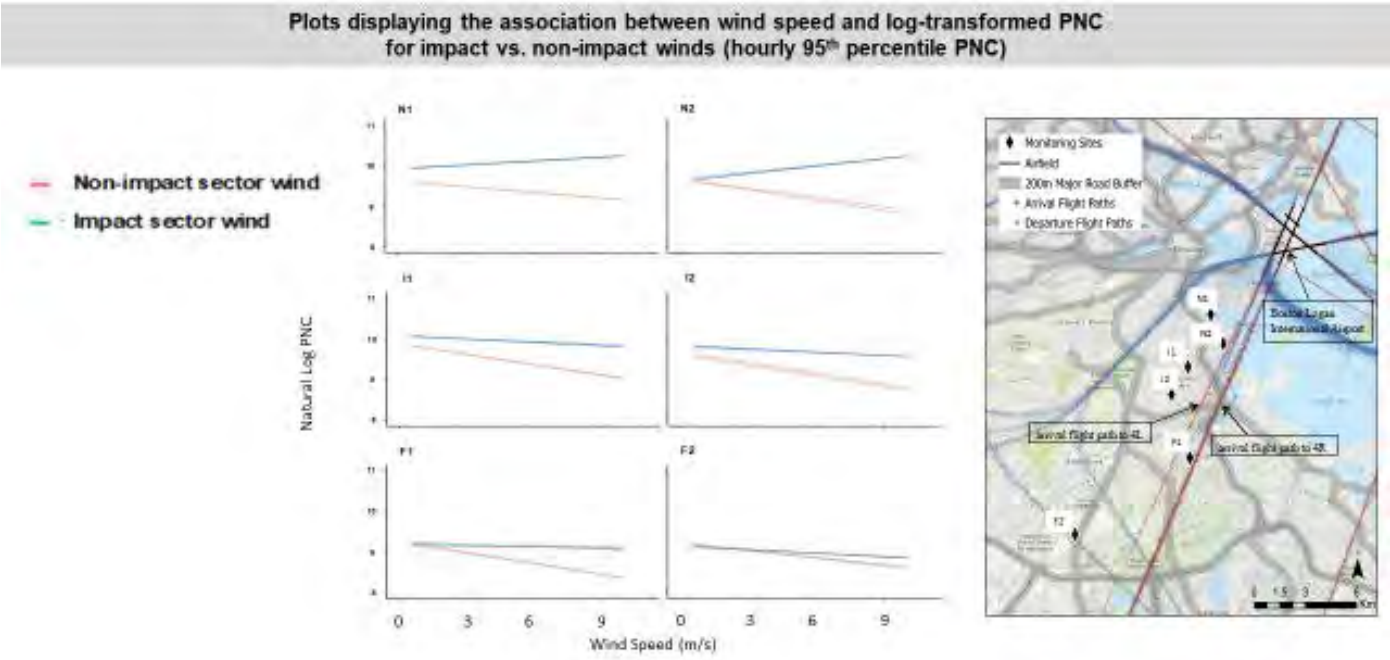
- Submitted 2017 descriptive data for publication in Environmental Science and Technology.
- Completed regression modeling analysis of aviation-related contribution to community level UFP and have presented at conferences.
- Drafted two additional manuscripts for submission on generalized regression modeling of aviation-related UFP and machine learning regression modeling of UFP

## **Major Accomplishments**

### **Aviation-related PNC modeling**

We have continued analyzing PNC regression models and developed new figures that have been shared at the Aviation Emissions Committee meeting in 2020 that illustrated modeled in-flight and ground contributions to community level PNC (Figure 11). Here we share the results from the ground-based airport operations contributions to community exposures at each monitoring site. In order to quantify aircraft contributions, we used the regression models to predict hourly 95th percentile PNC and present here the natural log PNC values under wind trajectories from the airport (impact sector wind). This was an effort to compare the different magnitudes of arrival aircraft impact across the sites while controlling for all

other aircraft activity as well as meteorological conditions. Several plots were generated using the coefficients from the regression models.



14

**Figure 11.** Estimated associations between airport wind speed for impact versus non-impact wind sectors (hourly 95<sup>th</sup> percentile PNC).

Plots in Figure 11 display the association between wind speed and log-transformed PNC for impact versus non-impact winds (hourly 95<sup>th</sup> percentile PNC). We see inverse association between wind speed and measured PNC under all conditions except at N1 and N2 under impact sector wind, confirming the positive association between wind speed and aircraft-PNC shown by other studies. Previous results from our regression models showed in-flight aircraft impact at all sites, so this may indicate different dispersion pattern of PNC coming from ground-based emissions which require being closer to the airport since farther-away sites did not have an impact.

As described above, the air pollution field monitoring campaign was conducted from November 2017 to September 2019 at sites located at varying distances from the airport under multiple arrival and takeoff flight paths into Logan Airport. We have started to analyze these data to inform regression model development under Task 5. Below are descriptive tables of the distribution of UFP at each monitoring site and by season.

**Table 4.** Particle number concentration (PNC) distribution at five monitoring sites

	<u>UMASS</u>	<u>Chelsea</u>	<u>East Boston</u>	<u>South Boston</u>	<u>Winthrop</u>
<b>Sample Size (days)</b>	264	250	167	123	43
<b>Location</b>	Ground Level	Roof 4th Floor	2nd Floor Window	Roof 5th Floor	Ground Level
<b>Other Samplers</b>	BC, meteorology, NO, NO2	BC, meteorology, NO, NO2	BC, NO, NO2	BC, meteorology, NO, NO2	BC, meteorology
<b>0.1st percentile</b>	169	863	172	471	521
<b>1st percentile</b>	379	1750	904	1160	676
<b>5th percentile</b>	975	3270	2020	2610	1400
<b>50th percentile</b>	7440	11900	10800	8260	8680
<b>95th percentile</b>	24500	43700	65000	36300	47000
<b>99th percentile</b>	47200	87800	124000	66300	70300
<b>99.9th percentile</b>	76900	152000	229000	100000	111000

The summary statistics presented in Table 4 cannot provide definitive insights regarding the aviation contributions to the measured PNC but are helpful for hypothesis generation and for informing future modeling efforts. For example, Chelsea and East Boston have the highest concentrations for the 95th and 99th percentiles of the distribution, which is expected because these sites are closest to the airport and are affected by planes at a lower elevation compared with farther locations such as UMASS. This trend suggests that there may be a more rapid decline in PNC with increasing distance from the airport compared with that observed in the 2017 sampling campaign, which focused on only a single arrival pathway. Consistent seasonal patterns were observed at three monitor sites with data from winter, spring, and summer.

**Table 5.** Seasonal particle number concentration (PNC) distribution at three monitoring sites

<b>Sample Size (days)</b>	<u>UMASS</u>			<u>Chelsea</u>			<u>East Boston</u>		
	80	79	93	64	75	105	20	85	54
<b>Season</b>	Winter	Spring	Summer	Winter	Spring	Summer	Winter	Spring	Summer
<b>0.1st percentile</b>	493	309	139	1460	1090	552	879	137	862
<b>1st percentile</b>	1040	496	262	2460	1660	1610	1260	564	1300
<b>5th percentile</b>	3250	1640	547	4350	3210	2950	3290	1810	2230
<b>50th percentile</b>	10100	5970	6390	14100	11200	11100	13800	10600	9920
<b>95th percentile</b>	28600	20200	22800	42200	42100	46000	60100	65400	66100
<b>99th percentile</b>	50500	44800	45300	79900	92200	90300	172000	127000	113000

The median PNC levels were consistently elevated during winter at all three sites, with greater variation at the 95th and 99th percentile. It should be noted that East Boston did not have the same number of sampling days over the winter season. As shown in Table 4, East Boston and Chelsea exhibit an elevated PNC at the median and 95th percentile compared with the UMASS sites across all seasons. Additionally, lower PNC levels were observed during the summer compared with the winter and spring across all three sites.

The impact of COVID-19 on flight activity has been well-documented, with commercial aircraft still substantially below pre-COVID-19 levels. PNC analysis for the 2020 data collection is being considered as flight activity at Logan Airport has continued to be less than 50% compared to 2019. The data in Table 6 and Figure 12 indicate that the flight activity has not stabilized, and we are continuing to collect monitoring data during an irregular time-period.

**Table 6.** Comparison of total flights at Logan Airport between 2019 and 2020 by month

<u>Month</u>	<u>2020</u>	<u>2019</u>	<u>% Difference</u>
August	15582	40075	-61.1
July	16140	38627	-58.2
June	10361	37483	-72.4
May	7455	37991	-80.4
April	7983	35952	-77.9
March	28682	34350	-16.5
February	31635	28975	9.2
January	33,001	30,330	8.8



**Figure 12.** Comparison of flight activity at Logan Airport between 2019 and 2020.

While there has been some increase during the monitoring campaign setup and testing period this summer, the flight activity data shows that we are collecting air pollution data in a period of substantial flight reduction. The pandemic has led to a natural experiment of lower flight activity that will allow us to collect data during airline industry’s recovery period over the next 12-18 months. This presents a novel opportunity for source apportionment analysis to examine the change in community exposure to air pollution as the number of flights steadily increases.

We have started collecting PNC data as part of preliminary test runs for mobile monitoring routes during the month of May and map to examine the mobile data. Data collected during the pandemic is being analyzed and compared with values collected during other time periods (Figure 13).

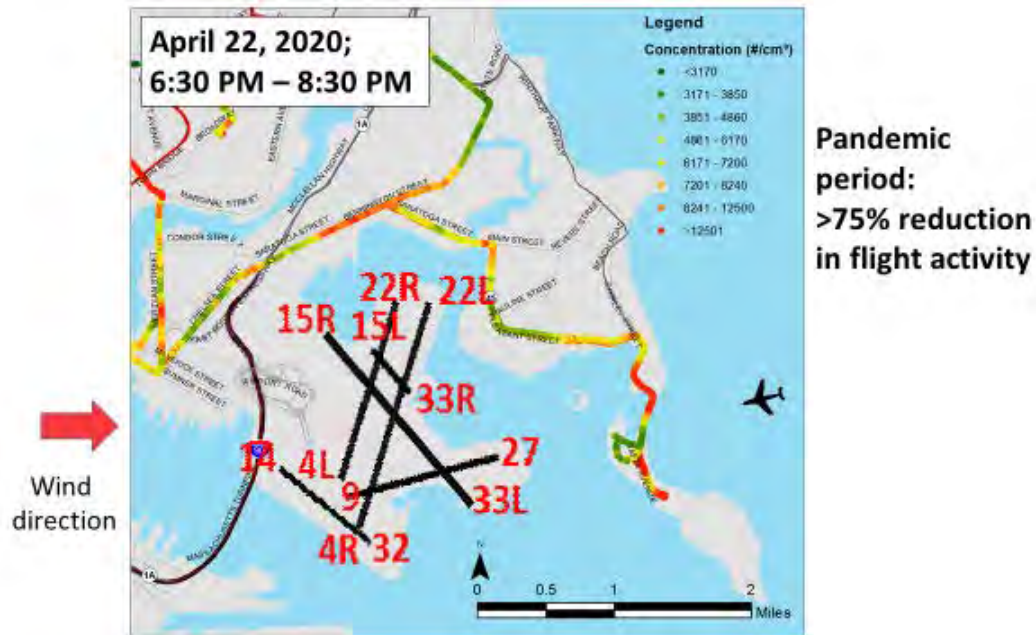


Figure 13. Maps of PNC in East Boston and Winthrop during the pandemic.

PNC concentrations during this time period are being compared to the data collected by the mobile monitoring vehicle for other studies previously conducted in the same area during 2018 and 2019.

**Publications**

N/A

**Outreach Efforts**

N/A

**Awards**

None

**Student Involvement**

Sean Mueller, a doctoral student at BUSPH, has been involved with field monitoring, data cleaning, and calculations of descriptive statistics.

**Plans for Next Period**

We are developing descriptive data plots of wind roses under various flight conditions to inform regression modeling and will continue this development. We anticipate completing all core regression models from 2017-2018 measurements within Year 1. In Year 2, we would focus on our 2020 monitoring data and develop analogous regression models. The primary distinction would be the inclusion of mobile monitoring data in the 2020 campaign, which would necessitate an analogous but slightly different statistical analysis approach given concurrent spatial and temporal variation in concentrations.

With each of these regression models, we will be able to estimate on a short-term and long-term basis the amount of the measured air pollution attributable to flight activity. In other words, by zeroing out the flight activity terms and determining the predicted concentrations, we will ascertain the portion of measured concentrations attributable to aircraft arrivals and departures. These predictions would subsequently be shared with Project 19, where investigators are developing comparable estimates of aviation-attributable concentrations near Logan Airport, and we would conduct analyses comparing the predictions from dispersion models and regression models.



# Project 019 Development of Aviation Air Quality Tools for Airshed-Specific Impact Assessment: Air Quality Modeling

## University of North Carolina at Chapel Hill

### Project Lead Investigator

Saravanan Arunachalam, Ph.D.  
Research Professor  
Institute for the Environment  
University of North Carolina at Chapel Hill  
100 Europa Drive, Suite 490  
Chapel Hill, NC 27517  
919-966-2126  
sarav@email.unc.edu

### University Participants

#### University of North Carolina at Chapel Hill (UNC)

- PI: Saravanan Arunachalam, Research Professor and Deputy Director
- FAA Award Number: 13-C-AJFE-UNC Amendments 1-12
- Period of Performance: September 10, 2019 to September 30, 2020
- Tasks: Development of a framework for a new dispersion model for aircraft sources.

### Project Funding Level

FAA provided \$350,064 in funding. Matching cost-share was provided by the Los Angeles World Airports (LAWA) and Environmental Defense Fund (EDF).

### Investigation Team

Prof. Saravanan Arunachalam (UNC) (Principal Investigator) [Tasks 1, 2, 3, 4]  
Dr. Chowdhury Moniruzzaman (UNC) (Co-Investigator) [Task 4]  
Dr. Gavendra Pandey (UNC) (Co-Investigator) [Task 4]  
Prof. Akula Venkatram (University of California, Riverside) (Consultant) [Task 4]

### Project Overview

Aviation is predicted to grow steadily in upcoming years;<sup>1</sup> thus, a variety of aviation environmental policies will be required to meet emission reduction goals in aviation-related air quality and health impacts. Tools are needed to rapidly assess the implications of alternative policies for an evolving population and atmosphere. In the context of the International Civil Aviation Organization (ICAO)'s Committee on Aviation Environmental Protection (CAEP), additional approaches are required to determine the implications of global aviation emissions.

The overall objective of this project is to develop a new aircraft-specific dispersion model and continue the development and implementation of tools, both domestically and internationally, to allow for an assessment of year-to-year changes in significant health outcomes. These tools must be acceptable to the FAA (in the context of Destination 2025) and/or other decision-makers. More importantly, this new model must have the capability to address the 1-hour form of the NO<sub>2</sub> National Ambient Air Quality Standard (NAAQS) in the U.S., as well as support National Environmental Policy Act (NEPA) and/or NAAQS analyses that may be needed by airports. The developed methods must also rapidly provide output in order to support a

---

<sup>1</sup> Boeing Commercial Airplane Market Analysis, 2010.



variety of “what if” analyses and other investigations. While the tools for use within and outside the U.S. need not be identical, a number of goals are desirable for both cases:

- Enable the assessment of premature mortality and morbidity risks due to aviation-attributable particulate matter (PM) having diameter up to 2.5- $\mu\text{m}$  (PM<sub>2.5</sub>), ozone, and other pollutants known to exert significant health impacts;
- Capture airport-specific health impacts at regional and local scales;
- Account for the impact of landing/takeoff (LTO) versus non-LTO emissions, including a separation of effects;
- Allow for an assessment of a wide range of aircraft emission scenarios, including differential growth rates and emission indices;
- Account for changes in non-aviation emissions;
- Allow for assessments of sensitivity to meteorology;
- Provide domestic and global results;
- Include quantified uncertainties and differences with respect to Environmental Protection Agency (EPA) practices, which are to be minimized when scientifically appropriate; and
- Be computationally efficient such that tools can be used in time-sensitive rapid turnaround contexts and for uncertainty quantification.

During this period of performance, The University of North Carolina at Chapel Hill's Institute for the Environment (UNC-IE) team was expected to perform research on multiple fronts, as described below. However, the FAA has requested that Tasks 1–3 be placed on hold because the collaborative ASCENT Project 18 at BU did not receive funding from the FAA during FY2019. Thus, our report is limited to our progress on Task 4.

1. Create Boston Logan International Airport emission inventories.
2. Create a WRF-SMOKE-CMAQ modeling application.
3. Perform a model–monitoring intercomparison at Boston Logan International Airport.
4. Develop a new dispersion model for aircraft sources.

## Task 4 – Develop a Framework for a New Dispersion Model for Aircraft Sources

University of North Carolina at Chapel Hill

### Objectives

The FAA's Aviation Environmental Design Tool (AEDT) is currently coupled with the U.S. EPA's AERMOD dispersion model for modeling aircraft sources and is the required regulatory model in the U.S. for modeling airport-level aircraft operations during landing and takeoff cycles.

Recent studies have shown several limitations in the use of AERMOD for modeling aircraft sources. The Airport Modeling Advisory Committee (AMAC) developed a series of recommendations in 2011 to improve modeling jet exhaust. Since then, Airport Cooperative Research Program (ACRP) project 02-08 developed a guidance for airport operators on conducting measurement and modeling for air quality at airports, published in ACRP Report 70 (Kim et al., 2012). This study conducted a measurement and modeling study at Washington Dulles International Airport (IAD). More recently, ACRP project 02-58 developed a final report ACRP Report 171 (Arunachalam et al., 2017a) for providing dispersion modeling guidance for airport operators for local air quality and health. This study applied four different dispersion models—AERMOD, CALPUFF, SCICHEM, and the U.K.'s ADMS-Airport—for the Los Angeles International Airport (LAX) and compared modeled predictions with high resolution measurements taken during the Los Angeles Air Quality Source Apportionment Study (AQSAS). All these reports identified several limitations with AERMOD and developed a series of recommendations for improving dispersion modeling of aircraft emissions for airport-level air quality.

UNC recently developed the C-AIRPORT dispersion model for application to LAX (Arunachalam et al., 2017c). Initially, C-AIRPORT was designed to be part of the C-TOOLS series of community-scale, web-based modeling systems. The objective of C-TOOLS was to create a web-based interface to model multiple source types for short-term or long-term pollutant concentration averages and perform various what-if scenarios that assess the changes in air quality at local scales due to changes in inputs. C-AIRPORT uses a line-source based approach to model aircraft sources, based upon the C-LINE modeling system (Barzyk et al., 2015), and preliminary evaluation of the algorithms against LAX AQSAS was conducted.



Under previous year's funding, UNC-IE developed a comprehensive plan or a modeling framework that addresses known limitations from the above Tasks and proposed a viable and most suitable approach for modeling pollutants from aircraft sources. The primary objective of this plan is to demonstrate that a robust, improved pollutant dispersion model for aircraft can be developed for U.S. regulatory compliance purposes. The proposed new model will disperse pollutants from aircraft sources in a more technically and scientifically advanced manner (when compared to current AERMOD capabilities), with the ultimate goal of becoming a potential U.S. regulatory compliance tool, based on ongoing discussions between FAA and EPA. This plan will include an itemized list of known limitations along with a corresponding proposed developmental approach with recommendations on how to address them.

As part of this Task, we proposed implementing the plan with specific focus on three broad areas, over a period of two years.

Our approach would be to ensure that the new model will be "robust" and based on the state-of-science on source and plume characterization and the associated algorithms.

a) Source Characterization

This area looks at alternate options beyond the current area source-based approach in the AERMOD model. Some approaches we explored include:

- Volume treatment in AERMOD.
- Puff-based treatment like in SCICHEM.
- Line-based treatment like in C-AIRPORT.
- Line-puff or Jet Sources like in ADMS-Airport.

b) Physical Processes

This area will look at all relevant processes for aircraft dispersion including treatment of plume rise, wing tip vortices, low wind speed conditions, etc. Some specific approaches include:

- Coupled plume rise—wake model for assessing the effects of wake vortices on plume rise, dispersion, and ground-level concentrations.
- An integral approach called the Fluid-mechanical Entrainment model (FEM), which has been evaluated against LIDAR observations from Heathrow Airport (see Arunachalam et al., 2017a).

c) Chemical Processes

This area will look at adequate treatment of chemical conversation relevant to LTO cycles, such as NO<sub>x</sub>-to-NO<sub>2</sub> (see Kinney et al., 2016), PM<sub>2.5</sub> (see Arunachalam et al., 2017a), etc. Some approaches include:

- AERMOD includes the Plume Volume Molar Ratio Method (PVMRM), the Ozone Limiting Method (OLM), and the Ambient Ratio Method (ARM). But these methods are designed primarily for emissions from tall stacks there is thus a need for algorithms specific to aircraft sources.
- OLM neglects photolysis of NO<sub>2</sub> during the daytime and is thus likely to overestimate NO<sub>2</sub> concentrations. Further, OLM does not account for gradual background O<sub>3</sub> entrainment into the plume and does not account for the NO/NO<sub>2</sub> ratio depending on engine power.
- Similarly, for PM<sub>2.5</sub>, we consider bringing in background estimates to account for secondary PM<sub>2.5</sub> or look at other reduced-form chemical schemes.
- In both cases, we will review newer approaches that decouples transport from the chemistry as described in Venkatram et al., 1998 and implemented in ADMS-Airport by Carruthers et al., and more recently in R-LINE as described in Valencia et al., 2017.

## **Research Approach**

In this research, we describe progress made on four fronts.

### **1. Diagnostic Evaluation of Observations from LAX AQSAS**

#### **1.1 Brief Description of LAX AQSAS**

LAX is situated within the South Coast Air Basin (Basin). LAX is close to residential neighborhoods to the north, south, and east. The impact of airport operations on air quality is a key public health concern for the population surrounding this or any airport. For illustration, the NO<sub>x</sub> and SO<sub>x</sub> concentration measurements from the Los Angeles Source Apportionment Study (LAX AQSAS III) conducted at LAX in 2012 have been utilized. The air quality monitoring during Phase III was done in two separate six-week field measurement campaigns: "winter monitoring season" from January 31, 2012 to March 13, 2012 and "summer monitoring season" from July 18, 2012 to August 28, 2012. Three types of monitoring sites (four "core," four

“satellite,” and nine “gradient”), with different combinations of continuous monitors and time-integrated (24-hour and 7-day) samples, were used to determine how the ambient concentrations of various chemical species of interest vary by location, time of day, day of the week, and season (Figure 1.1). There are two main airfield runways at LAX, namely the South Airfield and the North Airfield. The most extensive air quality measurements were obtained at the four core sites. These core sites were identified in the study as the “Community East (CE)” site, the “Community North (CN)” site, the “Community South (CS)” site, and the “Air Quality (AQ)” site. The core monitoring station CE was in Lennox approximately one mile east of the South Airfield Runways and approximately one-third mile east of the I-405 Freeway. The CN core monitoring station was in Westchester approximately one mile east of the North Airfield Runways. The CS core monitoring station was located at the former Imperial Avenue School in El Segundo, approximately 600 feet from the LAX southern boundary. The fourth core monitoring station, AQ, was located at the South Coast Air Quality Management District (SCAQMD) Hastings site, which was northwest of the airport in Playa del Rey (Figure 1.1) (Arunachalam et al., 2017, ACRP Report 179). In this study, we have used only the NO<sub>x</sub> and SO<sub>x</sub> concentration measurements from these four core sites, collected in February 2012.

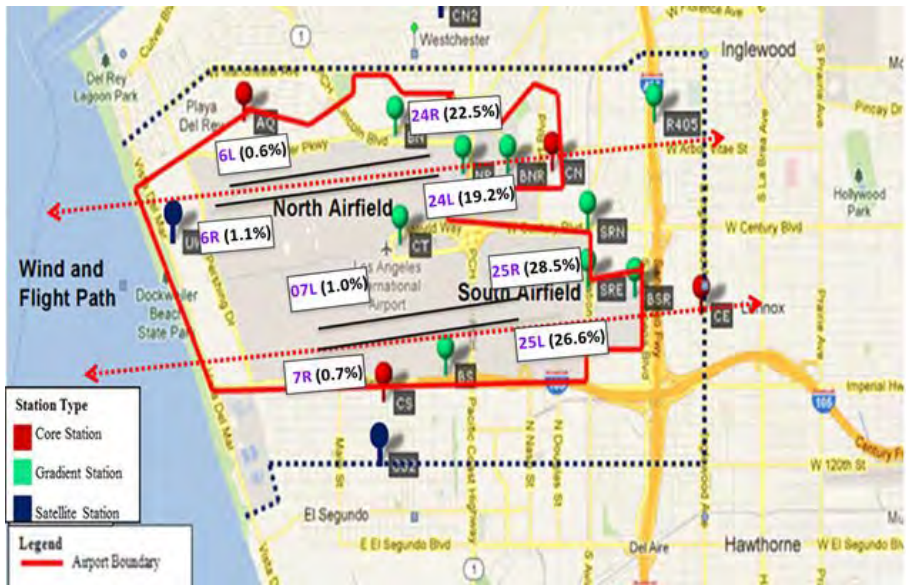


Figure 1.1. Location of core, gradient and satellite monitoring stations during LAX AQSAS Phase III (Arunachalam et al., 2017, ACRP Report 179).

During February 2012, morning winds were from the northeast until about 11:00 AM, resulting in greater contributions from non-airport emissions at the CE and CN sites, whereas in daytime and nighttime, the LAX airport was consistently downwind as winds were westerly during this time (Figure 1.2).

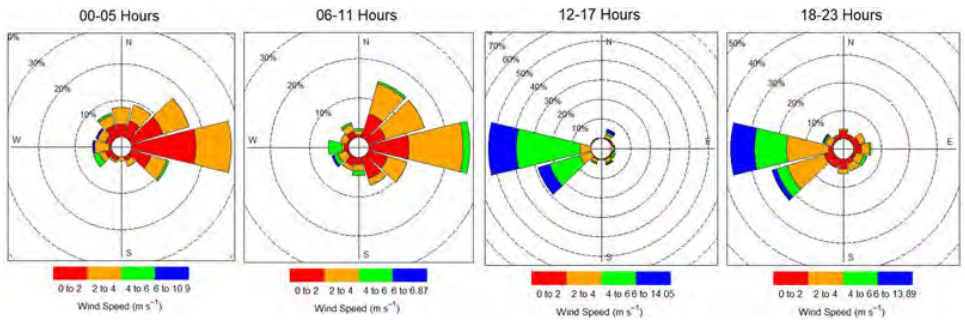
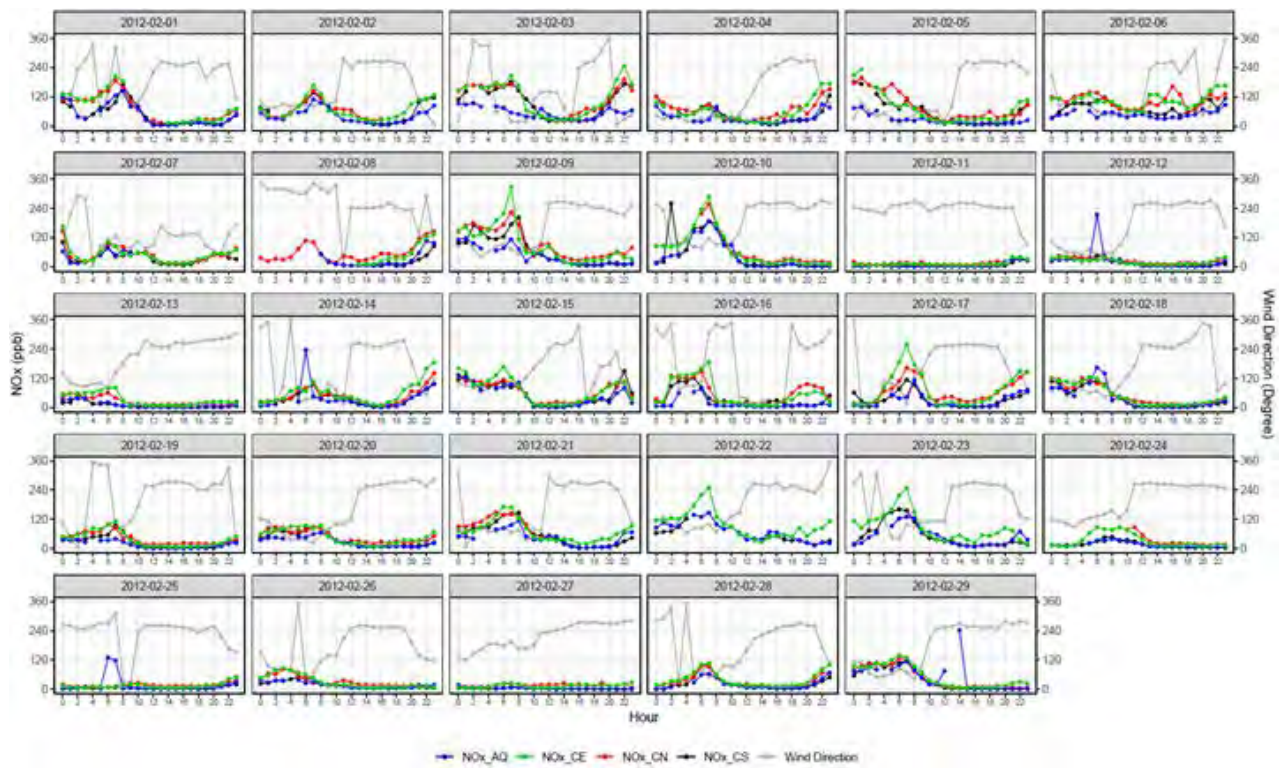


Figure 1.2. Wind rose plots for LAX during February 2012.



To understand the plume behavior at the LAX airport, we did an extensive observation analysis with the main species such as NO<sub>x</sub> and SO<sub>x</sub>. The hourly observed NO<sub>x</sub> concentrations are plotted on each day of February 2012 in the form of line plots at all four core sites (AQ, CN, CS, and CE) (Figure 1.3). The peak in NO<sub>x</sub> concentrations at the sites CE and CN, during the weekdays (Monday through Friday) can be attributed due to morning commute period (on-road vehicle emissions, mainly local traffic in the region north of the I-405 and east of the I-405 freeways (Figure 1.1) (Figure 1.3)). On the other hand, the significantly lower concentrations during the same time period on Sundays (February 5, 12, 19, and 26, 2012) provide additional confirmation of this source contribution. It appears that CN and CE sites were potentially impacted by airport NO<sub>x</sub> emissions from the late morning to evening during February 2012. The CE and CN sites were downwind of LAX during consistent westerly winds from about 11:00 AM to 10:00 PM. LAX was downwind of all the core sites during this time of the day except the CS site. The CS site was impacted during a relatively brief period from about 06:00 AM to 11:00 AM, whereas the morning data from the AQ site show little evidence of impact from airport NO<sub>x</sub> emissions (Figure 1.3). However, sources southeast of the study area include refineries and seaports, potentially impacted the observed concentrations at all four core sites, especially the CS and CN sites (Figure 1.1).



**Figure 1.3.** Daily Observed NO<sub>x</sub> concentrations and wind direction at all four core (AQ, CN, CS, and CE) sites during February 2012 at LAX.

In contrast to NO<sub>x</sub>, the SO<sub>x</sub> concentrations were low during the morning period at all sites except the CS site. SO<sub>x</sub> concentrations gradually increased throughout the day at both the CE and CN sites during February 2012. The relatively high SO<sub>x</sub> concentrations were occurring at the CN site especially because this site was next to the North Airfield, as well as downwind during most of the time of the day in February 2012. The highest SO<sub>x</sub> occurred on February 6 and 24, 2012 at the CN site (Figure 1.4). These results, coupled with the main source of SO<sub>x</sub>, indicate airport emissions were the main source of SO<sub>x</sub> at the CE and CN sites during February 2012.

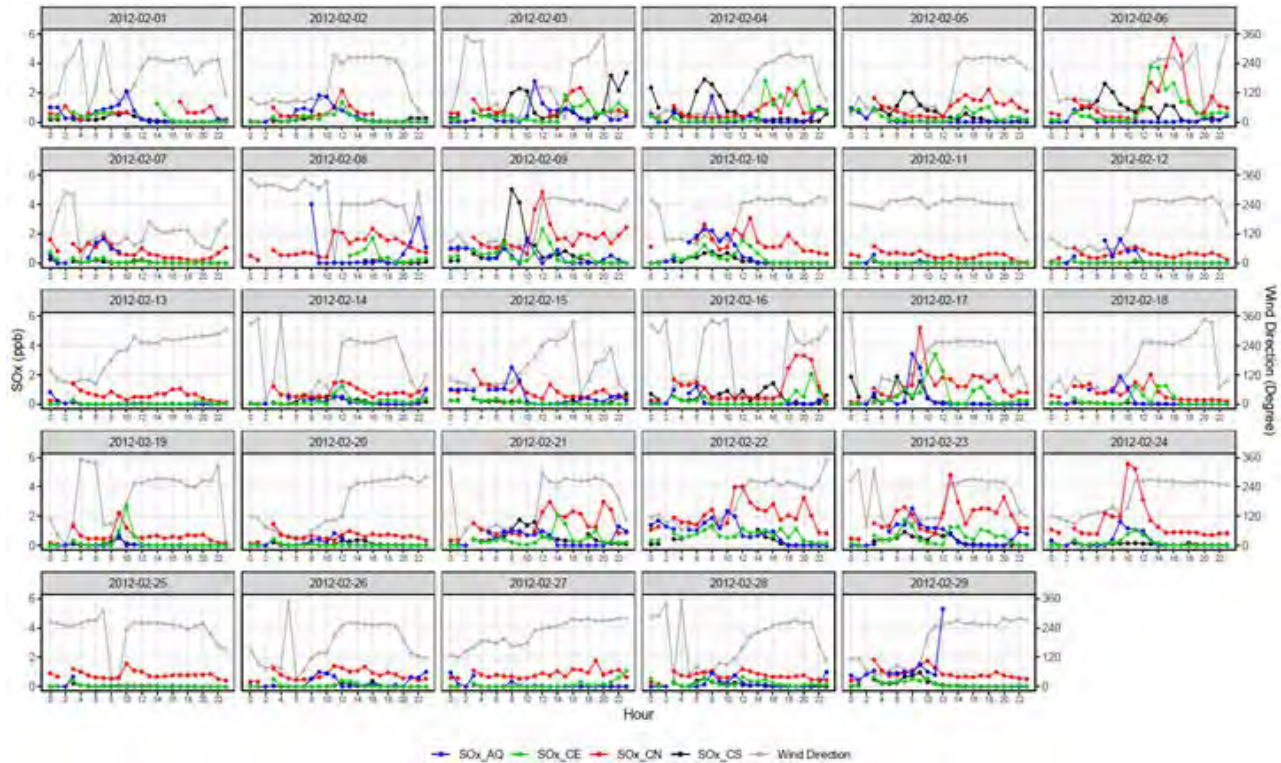


**Figure 1.4.** Daily observed SO<sub>x</sub> concentrations and wind direction at all four core (AQ, CN, CS, and CE) sites during February 2012 at LAX.

### 1.2 Plume behavior at Core Sites

Bivariate polar plots are useful in understanding the plume behavior for different pollutants (here NO<sub>x</sub> and SO<sub>x</sub>) and a potential signal from aircraft operations (Carslaw et al., 2006). From Figure 1.5a and b displaying all four core sites (AQ, CN, CS, and CE), we can see that the observed NO<sub>x</sub> and SO<sub>x</sub> concentrations vary with both the wind speed and wind direction. In Figure 1.5a, the highest observed NO<sub>x</sub> concentrations occur when the wind is blowing from the northeast at all four core sites. The highest NO<sub>x</sub> concentrations vary little with wind speed. On the other hand, at the AQ site, the highest SO<sub>x</sub> concentrations occur when the wind is blowing from the north with a speed of around 4 m/s (Figure 1.5b). At the CN site, the highest mean observed SO<sub>x</sub> concentrations occur when the wind is coming from the southwest direction and at high wind speed around 4–5 m/s (Figure 1.5b). The unusual behavior of concentrations is due to the aircraft related operations as the CN site, which is located downwind of LAX most of the time during the day and it is next to the North Airfield (Figure 1.1). The CS site is located south of the South Airfield and it is largely impacted by the winds passing over the tall buildings of Los Angeles city (Figure 1.1). The peak observed SO<sub>x</sub> concentration is from the northeast direction at high wind speed (Figure 1.5b). The site CE is largely impacted by its location next to major highways and it has less SO<sub>x</sub> concentrations but large NO<sub>x</sub> concentrations.

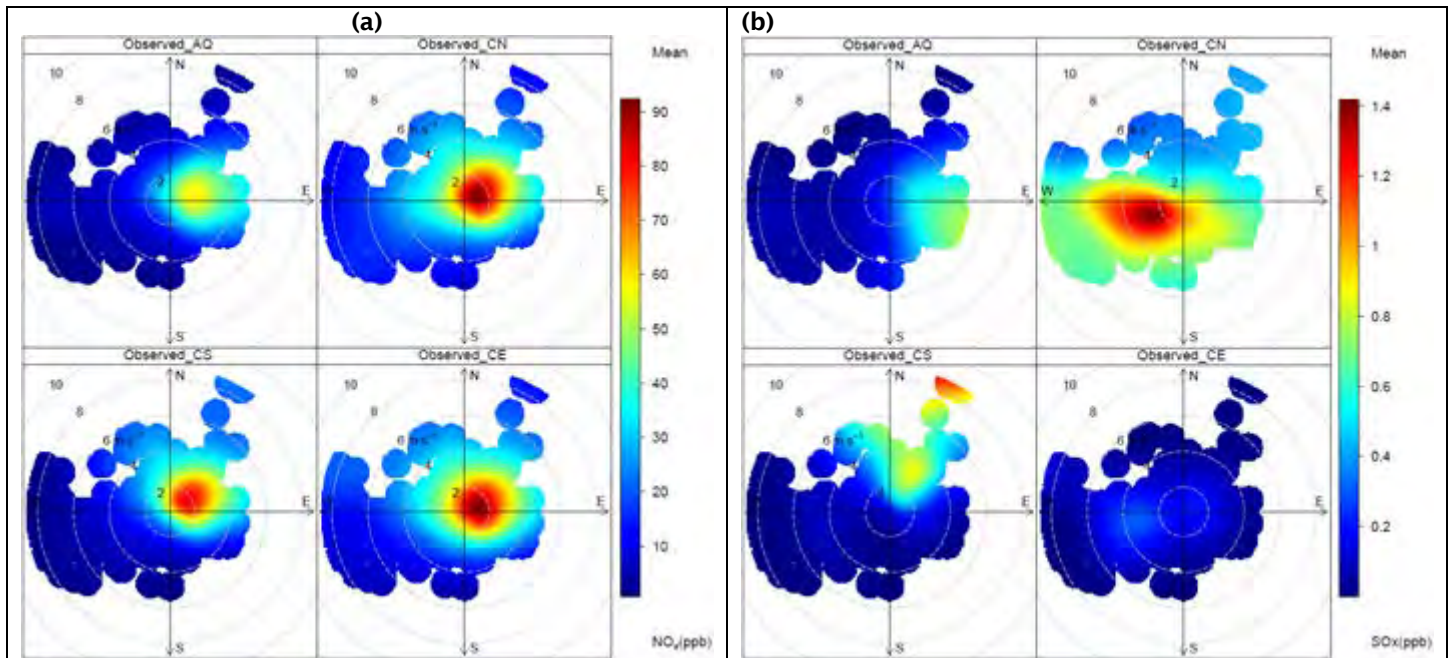


**Figure 1.5.** Bivariate polar plots of observed NO<sub>x</sub> and SO<sub>x</sub> concentrations at all four core (AQ, CN, CS, and CE) sites during February 2012 at LAX.

## 2. Emissions Processing of AEDT Emissions

AEDT-produced aircraft segmented data (termed hereafter as “AEDT-S” data) for both flight activity and emissions, provided by FAA to UNC-IE for LAX for February 2012, was used for the new Airport Dispersion Model (ADM) currently being developed at UNC-IE. The ADM needs the emission data of aircraft sources in the hourly emission rate in units of g/s for all the sources on the surface and in air. A Python-based emission processor code has been developed at UNC-IE which can postprocess the AEDT segment’s raw aircraft data to produce AMD-compatible hourly flight activity and emission rate data for any type of source characterization (area, line, volume, and point source). The AEDT-S data were compared with other emission processor data such as AEDT-area (AEDT-A) and EDMS-area (EDMS-A) (Arunachalam et al., 2017) for the AERMOD model.

### 2.1 Emissions Processing of AEDT-S Emissions

The AEDT-S file has time series flight segment data (each flight has about 45 segments), which has flight information including 3D location coordinates, aircraft and engine data, fuel burn, and emission data for 15 species. To produce the emission data in a desired format for the ADM, a Python-based emission processor has been developed at UNC-IE that can process the raw, high-temporal-resolution time series flight segment data and can produce the hourly emission rate (in g/s) and hourly flight activity (number of flights in an hour) for any desired source characterization.

#### 2.1.1. Source characterization

The surface sources for the ADM model have been characterized as line-thermal source (which is an area source) aligned with the 19 rectangles shown in Figure 2.1. Out of these 19 rectangles, four rectangles (red color in Figure 2.1) are for four runways, further divided into four more sources (two directions and two LTOs) for each runway rectangle, making a total number of 31 surface sources (15 non-runway sources and 4x4 = 16 runway sources), listed and described in Table A1 in Appendix A1.

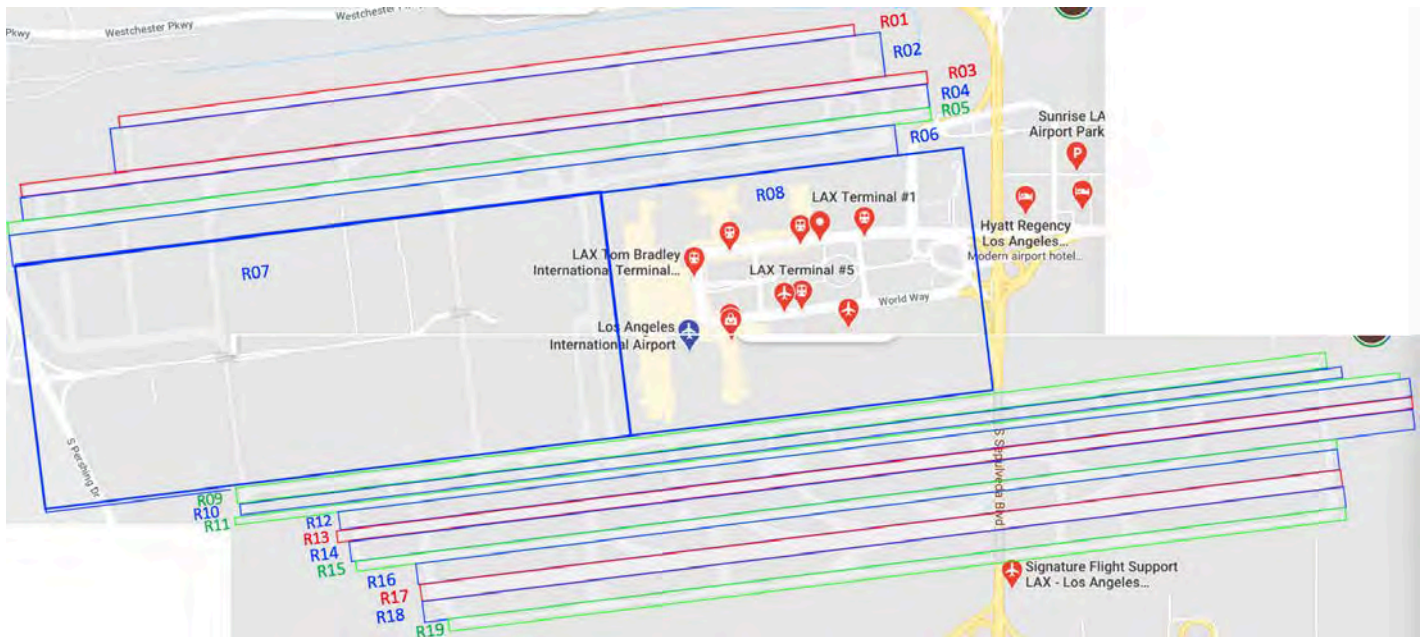


**Figure 2.1.** Airport runways, taxiways, terminal, and other areas have been divided into 19 horizontal rectangles (West to East) to extract emission data on surface sources. Four rectangles are for four runways (red rectangles), five rectangles are for the East-West taxiway (green rectangles), and 10 rectangles are for other areas such as ramps, taxiways, buildings, and grass (blue rectangles).

The source characterization in the ADM model (right column in Figure 2.2) is different than that of EDMS (left column in Figure 2.2) and AEDT (middle column in Figure 2.2) for the AERMOD model. The number of surface sources in ADM is lower than EDMS (Arunachalam et al., 2017) and AEDT, shown in Figure 2.2. The flight paths are not straight lines in the AEDT area and AEDT segment, unlike the EDMS area model shown in Figure 2.2. The hourly emission rate in the 31 surface area sources (listed in Table A1 in Appendix A) for 19 surface rectangles (shown in Figure 2.1) and in 144 air sources for nine air layers for each of the 16 flight paths (four runways x two directions x two LTOs) listed in Table A1 in Appendix A are determined using the AEDT segment's raw data.

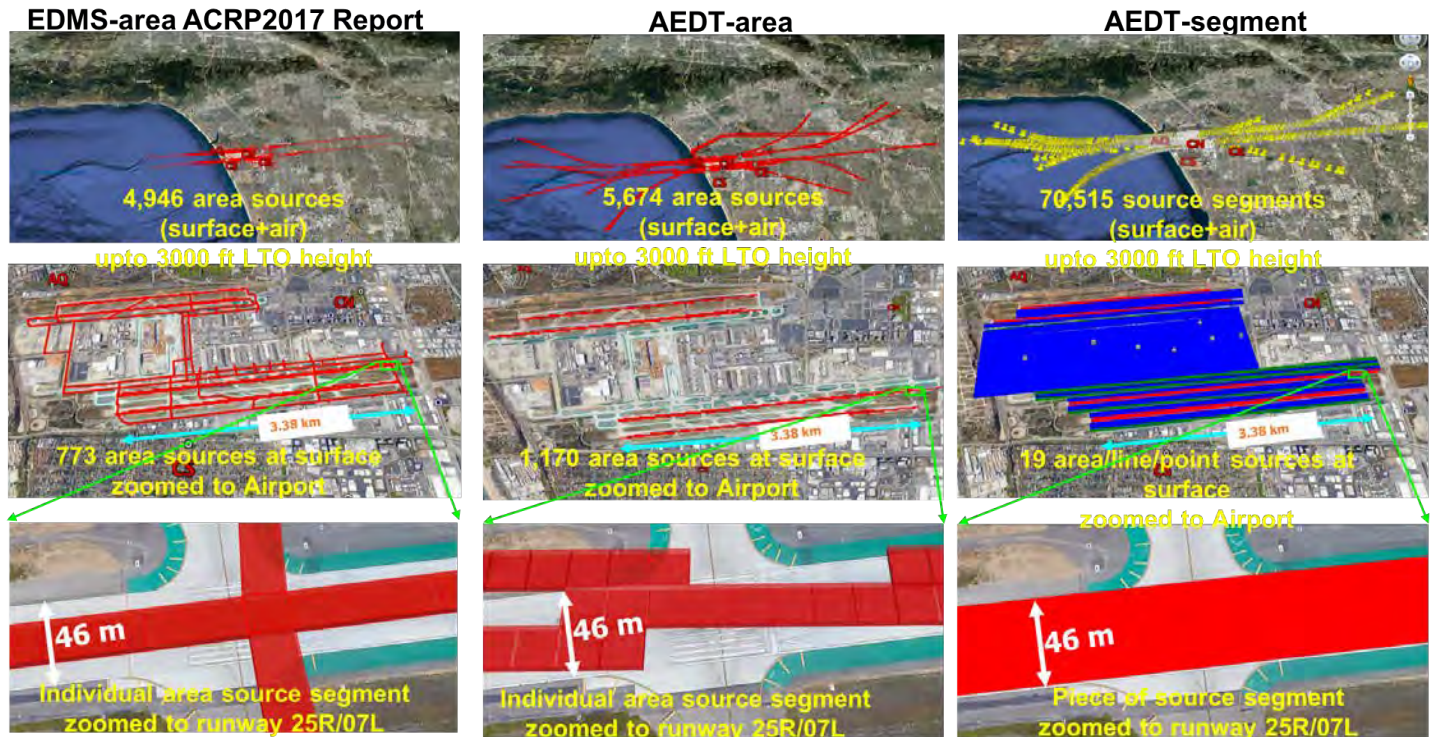


**Figure 2.2.** The source characterization in three emission processor models for aircraft sources. From left: EDMS-A, AEDT-A, and AEDT-S.

### 2.1.2. Preparation of Emissions Inputs for ADM

The AEDT segment flight and emission data were processed in three steps. In the first step, we extracted the data (making a smaller data set) by different categories. Then in the second step, the hourly flight number and emission rate for each of the sources are determined. In the third step, the non-aircraft source data (such as ground support equipment (GSE) and others) are determined by a correlation using a reference data (Arunachalam et al., 2013). The three steps are further described below.

#### Step 1:

1. Extract the data by a date.
2. Extract the data by the LTO cutoff height (3000 ft or 914 m).
3. Extract the data by eight AEDT LTO modes: 1) Taxi-out, 2) Takeoff ground, 3) Takeoff airborne, 4) Terminal climb, 5) Approach, 6) Landing ground roll, 7) Landing ground rolls with reverse thrust and 8) Taxi. The relative magnitudes of these eight LTO modes as a % of total emissions are shown in Figure A1 in Appendix A.
4. Extract surface data (having altitude up to 0 m) in 16 flight paths (four runways x two directions, two LTOs) for four runways and 15 non-runway rectangles using the user input latitude-longitude coordinates for each corner of the 19 rectangles shown in Fig. 2.1 and listed in Table A1 in Appendix A.
5. Extract air data for 144 air sources for nine air layers for each of the 16 flight paths (four runways x two directions x two LTOs) listed in Table A1 in Appendix A. The percentage of these nine air layers of the total emissions from LTO to 914 m are shown in Figure A2 in Appendix A. The latitude-longitude locations of the 144 air sources are shown in a Google Earth map in Figure A3 in Appendix A.

#### Step 2:

1. All the segmented emission data (emission amounts during a flight segment) are accumulated for each hour and then the hourly accumulated emissions are divided by 3,600 to estimate the hourly emission rate (g/s) for the above categories in Step 1. The number of flights are accumulated for each hour to get the hourly number of flights (#/hour) for the above categories in Step 1.



**Step 3:**

1. The AEDT segment data file does not have non-aircraft surface source emission data (such as GSE and others). The non-aircraft surface emission data are determined by a correlation using the AEDT-S's total aircraft emission data and the ratio of non-aircraft source categories to the total aircraft source from a reference report (Arunachalam et al., 2013). These emissions are then distributed among the 15 non-runway surface rectangles by an approximation.

2.1.3. Source Characterization by LTO Mode.

Table 1 below lists the actual source type for each mode during LTO activity at LAX.

**Table 1.** Source characterization of eight AEDT LTO modes in the ADM

No	LTO modes	Source characterization
1	Taxi Out	Area
2	Takeoff Ground Roll	Area, line thermal
3	Takeoff Airborne	Point
4	Terminal Climb	Point
5	Approach	Point
6	Landing Ground Roll	Area, line thermal
7	Landing Ground Roll with Reverse Thrust	Area, line thermal
8	Taxi In	Area

**2.2 Comparison of EDMS-A, AEDT-S, AEDT-A**

The post-processed emission and flight data have been evaluated by comparing the data with other reference data.

2.2.1 Evaluation of flight activity data

The hourly flight activity data from AEDT-S were compared with the Los Angeles World Airport's (LAWA's) actual flight data (LAWA, 2020) for February 6, 2012, shown in Figure 2.3 and Table A2 in Appendix A. The flight activity in AEDT-S for LAX's four runways have similar hourly flight activity to LAWA's actual data and the differences between the AEDT-S model and the LAWA actual data were from 1 to 6%, shown in Table A2 in Appendix A.

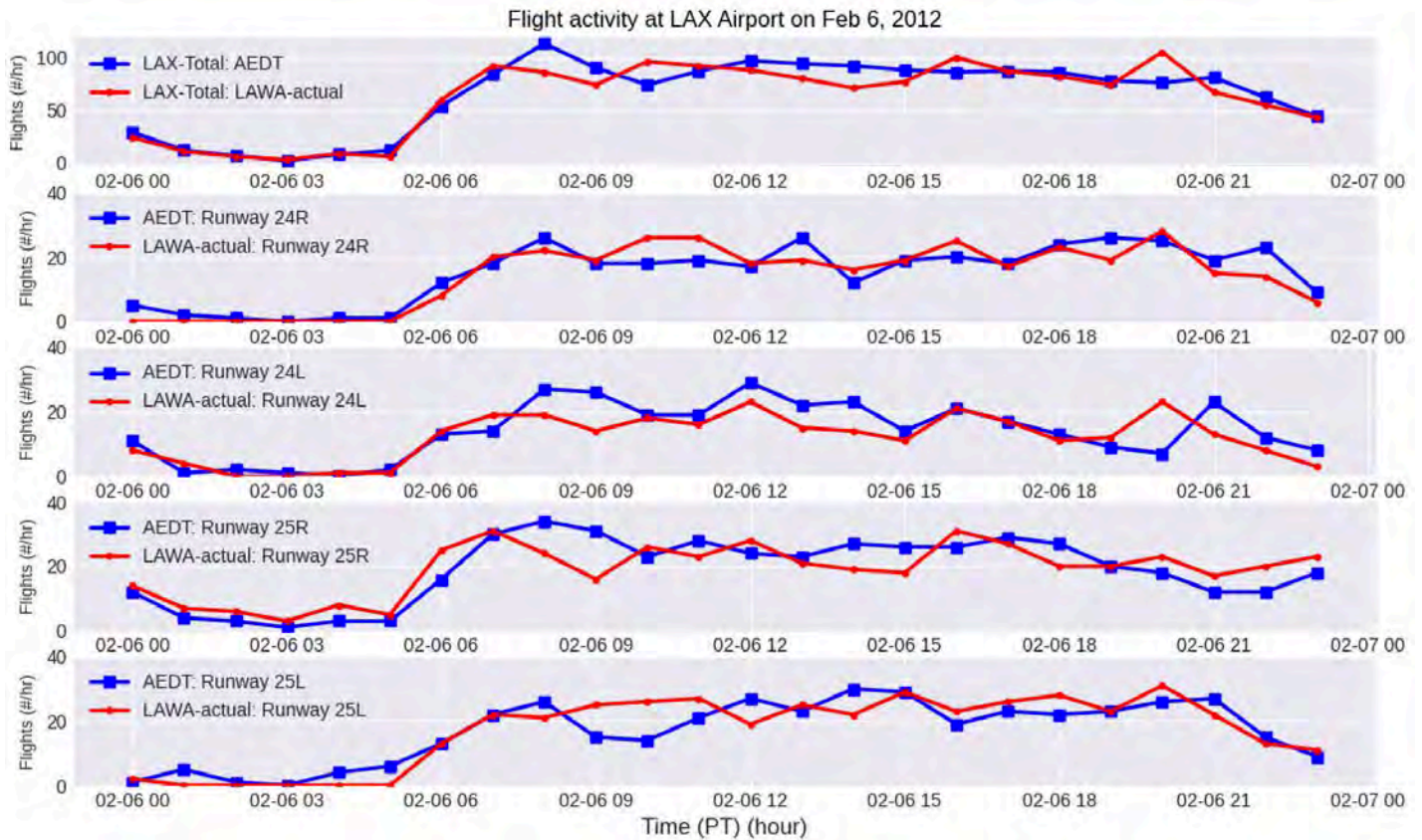
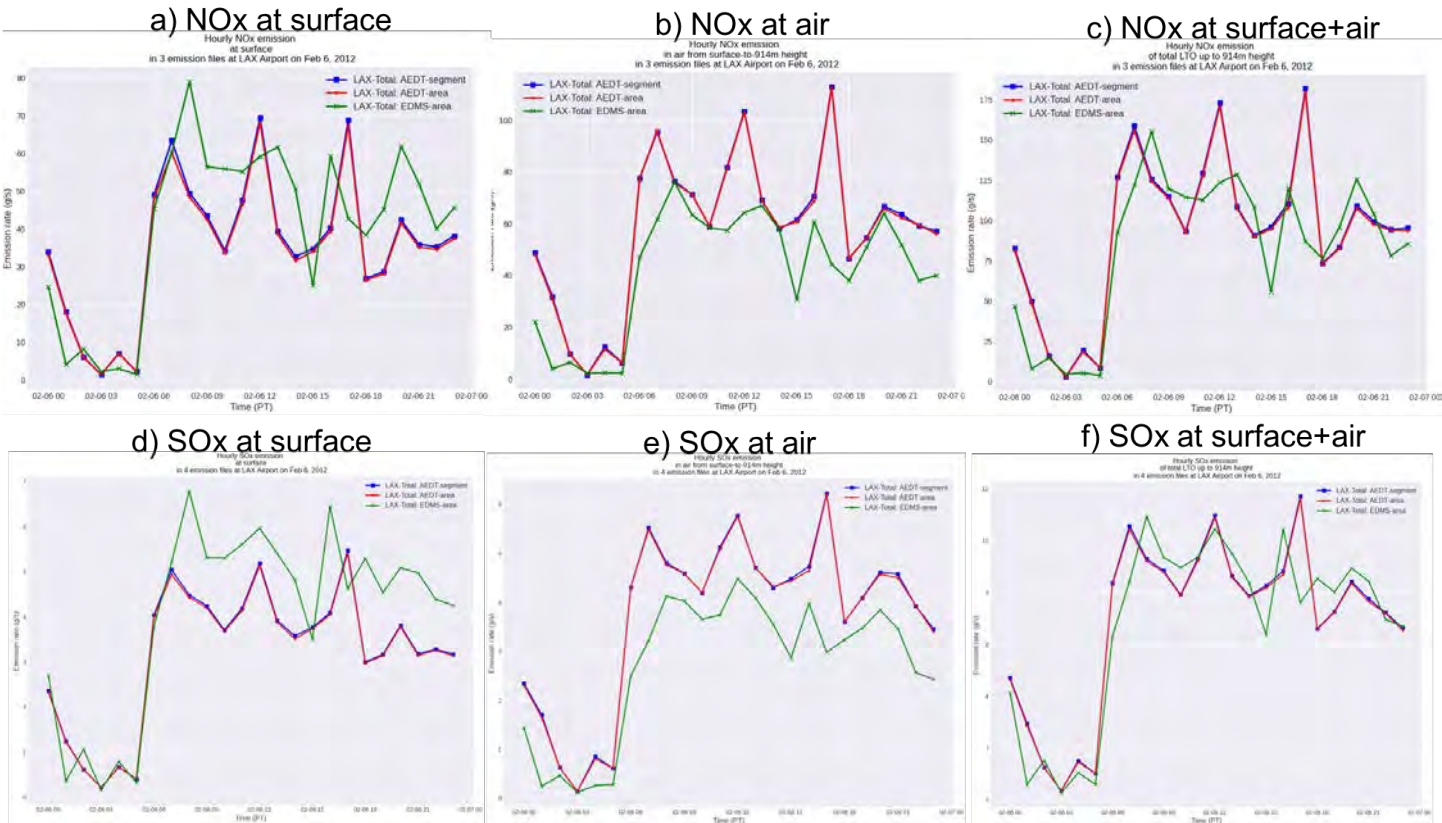


Figure 2.3. Hourly flight activity at LAX on February 6, 2012 by AEDT and LAW-actual for total LTO.

2.2.2 Evaluation of emission data of AEDT-S comparing with AEDT-A and EDMS-A data

The hourly NO<sub>x</sub> and SO<sub>x</sub> emission rate by AEDT-S emission processor was compared with the AEDT-A and EDMS-A (Arunachalam et al., 2017) emission processor models for Feb 6, 2012 at LAX, shown in Figure 2.4. The emission rate of both NO<sub>x</sub> (shown in Figure 2.4a, b, c) and SO<sub>x</sub> by AEDT-S and AEDT-A were exactly matched, indicating that the AEDT-S emission processor’s emission data are reasonable. The emission trends in AEDT-S and AEDT-A were consistent with the diurnal trend of EDMS-A both for NO<sub>x</sub> (shown in Figure 2.4a, b, c) and SO<sub>x</sub> (shown in Figure. 2.4 d, e, f). The EDMS-A NO<sub>x</sub> and SO<sub>x</sub> emissions were overpredicted at the surface (shown in Figure 2.4a and d, respectively) and underpredicted in air (shown in Figure 2.4b and e, respectively) when compared with AEDT-S and AEDT-A, likely due to differences in the altitude cutoff used in EDMS versus AEDT for the different configurations.



**Figure 2.4.** Hourly NOx and SOx emission rate at LAX on Feb 6, 2012 by AEDT-S (blue line), AEDT-A (red line), and EDMS-A (green line) for NOx (top row) a) LTO-surface, b) LTO-air from surface to 914 m (3000 ft) and c) LTO total-surface-&air 914m and for SOx (bottom row) d) LTO-surface, e) LTO-air from surface to 914 m (3000 ft) and f) LTO total-surface-&air 914m.

### 3. Alternate Treatment of Meteorological Inputs

#### 3.1 Methodology

When an airport is situated near a shoreline, where meteorological conditions significantly vary from spatial uniformity, an added complexity occurs during dispersion. In this condition, the airport region neither becomes unstable nor very stable due to the cold breeze from the ocean. The input preprocessor (AERMET) of AERMOD does not account for important features of the boundary layer that occurs on the shoreline, where many of the large U.S. airports are situated. In this study, we have modified the meteorological outputs from AERMET as discussed below to account for formation of the internal boundary layer, where stable air from the ocean flows onto the warmer land surface of the airport. Based on this, we have done a sensitivity analysis for the meteorological input parameters of the AERMOD and evaluated the AERMOD model by comparing model estimates of SOx with measurements made during February 2012 from the Los Angeles Source Apportionment Study (LAX AQSAS III) conducted at LAX. The measurements consisted of 1-hour averaged concentrations made at the four core sites, AQ, CN, CS, and CE, shown in Figure 1.1. For this analysis, we have taken the emissions from the EDMS emission inventory of LAX accounting for all the airport sources. The sensitivity analysis led to the following changes:

- To account for the shoreline effect at LAX, stable and convective conditions in the AERMET file are replaced by neutral conditions: the Monin-Obukhov length is set to 1000 m, and the friction velocity is computed using the neutral formulation,

$$u_* = kU_r / \ln(z_r / z_0)$$

where  $k$  is the von-Karman constant,  $U_r$  is the wind speed at  $Z_r$  (reference height), and  $Z_0$  is the roughness length.



- Roughness lengths ( $Z_0$ ) altered when the winds blew from the northeast quadrant, reflecting the flow passing over the tall buildings in Los Angeles' urban core.

### 3.2 Simulated Results

The performance of the AERMOD model is assessed at all the four core sites using 1) diurnal variation of concentrations averaged over the month, and 2) quantile-quantile (Q-Q) plots constructed with 1-hour averaged concentrations measured during the 29 days of February. In addition, model performance is also characterized using fractional bias (FB) of the robust highest concentrations (RHC) using the procedures described in Cox and Tikvart (1990). The U.S. EPA recommends this metric to measure performance of models that are used in regulatory applications. A negative/positive value of FB indicates an over/under prediction of the observed concentrations. We have calculated the factor of two (FAC2) to the observations..

#### 3.2.1 Diurnal variation of concentrations averaged over the month

The diurnal variation of concentrations averaged over the month at all four core sites (AQ, CN, CS, and CE) are exhibited in the form of diurnal line plots for both observed and AERMOD model predicted concentrations with interquartile range for original as well as modified meteorology (Figures 3.1 and 3.2).

At the AQ site, there are two observed peaks above 2 ppb, in the early morning and afternoon, that the model underestimates for both meteorological conditions (Figures 3.1 and 3.2). The model predictions have a large peak in late evening for both meteorological conditions. However, with the modified meteorology, the model predicted lowering concentrations in comparison to the original meteorology. There is little correspondence between the observed and modeled diurnal patterns for both meteorological conditions (Figures 3.1 and 3.2).

The modeled concentrations above 0.8 ppb are higher than the measured values at the CN site, and the model shows a large peak in the late evening with the original meteorology. After modifying the model inputs based on the neutral and roughness change, the model predictions are improved and closer to the observed diurnal behavior from 10 AM onward, whereas in the early morning, the model is still underestimating the observed diurnal concentrations. On the other hand, the correlation coefficient is improved from -0.30 to 0.38 (Figures 3.1 and 3.2).

The CS site is largely impacted by the emissions when the wind direction is from the northeast. We examined the possibility that the effective roughness seen by this site is governed by the flow over Los Angeles, where tall buildings can increase roughness. Therefore, we set the roughness length to 1.2 m when the wind is blowing from the northeast (Figure 1.2). The observed diurnal concentration has a single peak in morning, whereas the model has two large peaks (one in the morning and second in the late evening) with original meteorology (Figure 3.1). After applying the stability and roughness changes, the model predicted concentrations are closer to the observed diurnal concentrations, with the model able to slightly capture the morning observed peak, whereas the late evening peak is still missing. In addition, the correlation coefficient improves from 0.5 to 0.6 (Figures 3.1 and 3.2). We can say that the model predictions are getting close to observations after modifications in the meteorology at the CS site.

The model predictions are close to observations in the early morning to noon for both the original and modified meteorology. In the late evening, the model prediction has a large peak when run with original meteorology versus the modified meteorology (Figures 3.1 and 3.2). However, the model predictions are improved after modifications in meteorology.

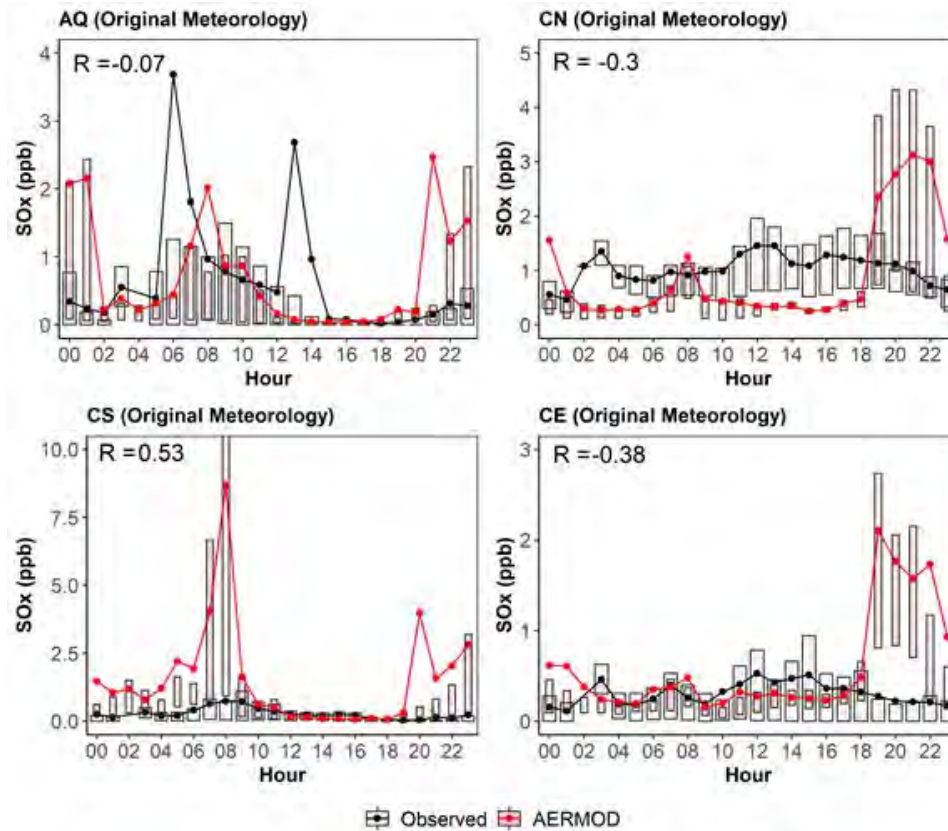


**Figure 3.1.** Diurnal variability in observed and modeled SOx concentrations with original meteorology at all four core sites (AQ, CN, CS, and CE). Bars represent interquartile ranges and lines represents mean of values.

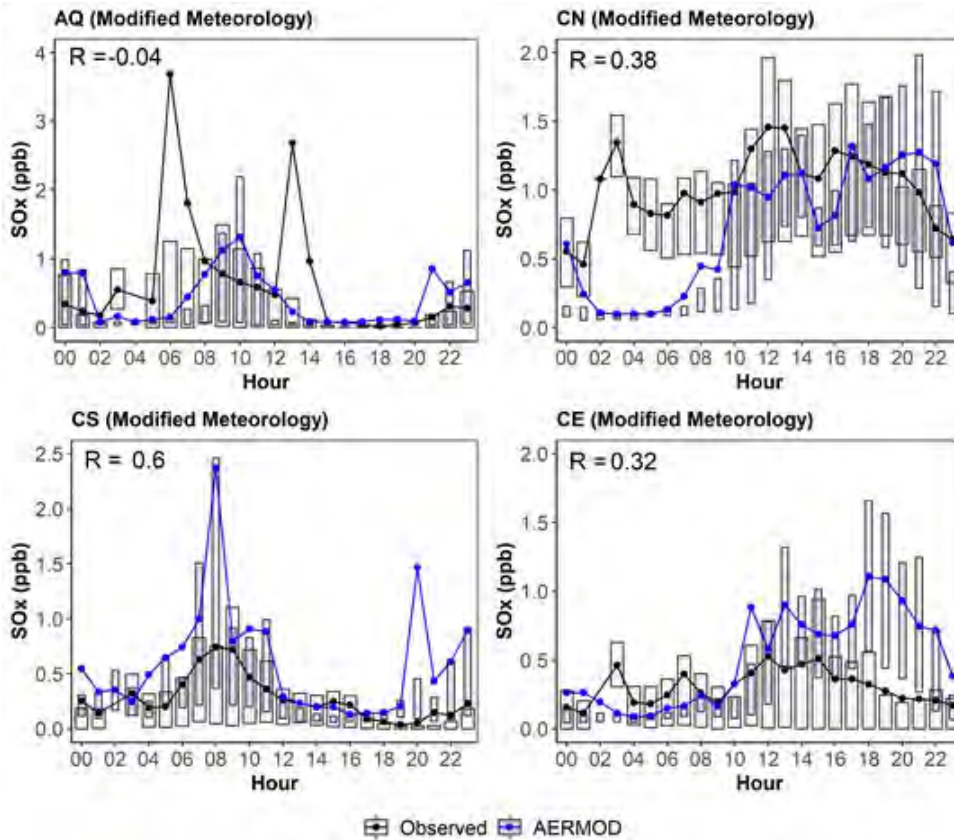


**Figure 3.2.** Diurnal variability in observed and modeled SO<sub>x</sub> concentrations with modified meteorology at all four core sites (AQ, CN, CS, and CE). Bars represent interquartile ranges and lines represents mean of values.

### 3.2.2 Quantile-Quantile (Q-Q) distribution analysis

It is important to examine/evaluate the performance of a model for high concentrations because the assessment of the model for high ground-level concentrations, in compliance with air quality, is necessary (Weil et al., 1992). In unpaired concentration distribution plots or Q-Q plots, first the predictions and observations are ranked from highest to lowest and then both ranked predictions and ranked observations are plotted (Venkatram, 1999). The dotted (-----) line represents that the predicted concentrations are one-to-one to the observations. The solid lines of half and double slope indicate under and over-predictions, respectively.

At the AQ site, the highest concentrations are overpredicted by the model with original meteorology, whereas the concentrations from the middle to lower range are within the factor of two lines. On the other hand, with the modified meteorology, the lower concentrations are becoming less accurate, whereas the highest concentrations are getting closer to one-to-one line, which is very important for air quality assessment. However, the FAC2 is decreasing from 35% to 28% with modified meteorology (Figure 3.3).

For the CN site, the model is overpredicting the higher concentrations and underpredicts the middle to lower concentrations with original meteorology. On the other hand, with modified meteorology, the model is predicting the higher concentrations very close to the one-to-one line whereas it slightly underpredicts the lower concentrations (Figure 3.3). In addition, the FAC2 is improved from 33% to 50% after modification of the input parameters. The prediction of FAC2 greater than 50% is good for air quality assessment (Chang and Hanna, 2004). The fractional bias is also decreased from -0.99 to -0.21 (Figure 3.3).

At the CS site, the model is highly overpredicting the concentrations with original meteorology, this leads to the negative FB. After applying the modifications in the input parameters, we can easily see that the improvements from the figure 3.3. The

overall concentration is getting close to the one-to-one line with modified meteorology (Figure 3.3). The FB is decreased from -1.62 to -1.07 whereas the FAC2 to the observations is improved substantially from 0 to 27% (Figure 3.3).

The CE site shows little change after the modifications to the input parameters. The higher concentrations are getting closer to the one-to-one line with modified meteorology. The FB is improved from -1.13 to -0.52 and FAC2 is almost the same (Figure 3.3).

Hence, overall, the higher concentrations are getting close to the one-to-one line after modifications in the input meteorological parameters. From all the above analysis, we can say that the meteorology matters a lot, and suggests the need to re-examine the meteorology that governs concentrations at AQ. Note that we obtain the best results when it is assumed that stable conditions govern the concentrations at this site. However, apart from this aspect, there are additional issues related to source characterization and treatment of physical and chemical processes that will be addressed as part of the ADM development.

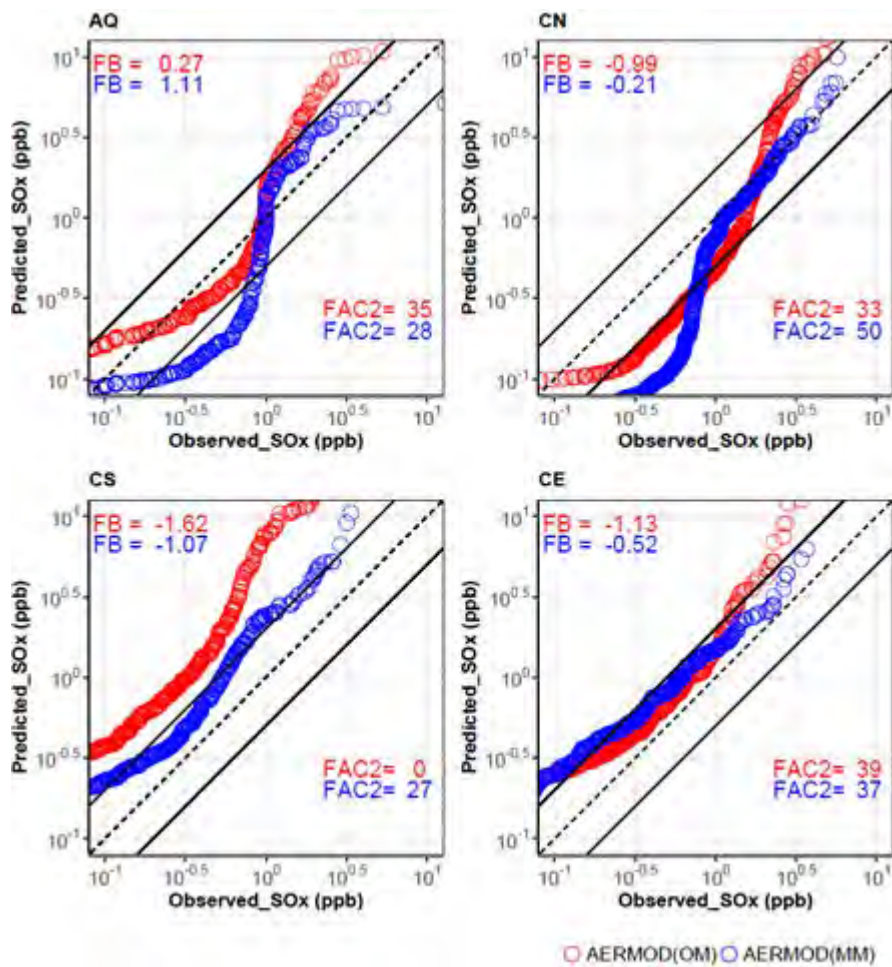


Figure 3.3. Quantile-quantile plots between observed and modeled SOx concentrations with original (red color) and modified meteorology (blue color) at all four core sites (AQ, CN, CS, and CE).

## 4. Development of Airport Dispersion Model (ADM)

### 4.1 Model Algorithm Development

We developed and tested code to treat dispersion of emissions from different types of sources at LAX. The sources include aircraft during takeoff roll, climb out, and taxiing. Emissions along the runway are modeled as line sources or area sources. Each runway is described with two lines along the length of the runway, spaced by the width of the runway. The line sources include meandering and plume rise of jet exhaust described using the line thermal model.

The runway can be treated as an area source with plume rise modeled with an initial plume spread. Emissions during taxiing are also treated using area sources. The treatment of area sources differs from that used in models such as AERMOD in that vertical dispersion is modeled using the solution of the mass conservation equation. As shown by Nieuwstadt and van Ulden (1978), this solution provides a more realistic description of observations than the commonly used Gaussian distribution. Emissions during climb out in the air are modeled using point sources along the path of the aircraft after takeoff. The path is specified as an inclined line starting at the end of the runway and ending at 914 m (3000 ft), which is considered to be the height at which an aircraft starts reducing power.

### 4.2 Evaluation against LAX AQSA

The main objective of this task is to develop a new airport dispersion model (ADM), that can address past issues involving aircraft dispersion modeling such as source characterization, unconventional plume behavior of the aircraft sources, and treatment of low wind and meander, etc. A new ADM is being developed that will address these issues. In the new ADM, we have characterized the aircraft sources as area sources (that are aligned, in a line, to each runway), airborne sources as point sources, and other aircraft-related sources as area sources. In this section, we discuss preliminary results of this ADM.

The preliminary results of predicted NO<sub>x</sub> and SO<sub>x</sub> concentrations (obtained from LAWA AQSA study for February 2012 only) are in the form of diurnal line plots and Q-Q distribution for both the original (OM) and modified meteorology (MM) at all four core sites (AQ, CN, CS, and CN). We have also characterized the source in two ways: not including the plume rise with line thermal source (ADM), and inclusion of a plume rise algorithm with the line thermal source (ADM\_PR). To simulate both models, we have utilized the emissions from AEDT-segment (ASA) calculations which are discussed in section 2 of this report. Here, in this study, we have modeled the aircraft sources only. In addition, model performance is also characterized using Fractional Bias (FB) of the robust highest concentrations (RHC) using the procedures described in Cox and Tikvart (1990). The USEPA recommends these metrics to measure performance of models that are used in regulatory applications.

#### 4.2.1 NO<sub>x</sub> concentration analysis

##### 4.2.1.1 Without plume rise algorithm (ADM)

The ADM predicted NO<sub>x</sub> diurnal concentrations with OM are slightly able to capture the morning peaks of observed diurnal concentrations, whereas after 9 AM to late evening, ADM underpredicts the observed concentrations at the AQ and CS sites. On the other hand, during this period at the CN and CS sites, ADM highly underpredicts the observed concentrations with original meteorology (Figure 4.1a).

In the Q-Q plots between ADM predicted and observed overall NO<sub>x</sub> concentrations, the ADM predicted concentrations are close to the one-to-one observed line, but ADM highly underpredicts the middle-to-lower range concentration at all four core sites. ADM predicts approximately 9%, 7%, 11%, and 1% concentrations within the FAC2 at the AQ, CN, CS, and CE sites, respectively, with original meteorology (Figure 4.1b).

With the modified meteorology, the ADM highly underpredicts the NO<sub>x</sub> concentrations most of the time as the values of FB are positive (Figure 4.1d). In capturing the diurnal behavior at all four core sites, ADM captures the observed diurnal pattern from noon to after noon at the CN site especially well (Figure 4.1c). In addition, and only at the AQ site, the ADM predicts 9% concentrations within a FAC2 with modified meteorology (Figure 4.1d).

##### 4.2.1.2 With plume rise algorithm (ADM\_PR)

The ADM\_PR-predicted NO<sub>x</sub> diurnal concentration highly underpredict the observed concentrations, most of the time during February 2012, with both the original and modified meteorology (Figure 4.1a and c). However, with both meteorology conditions, ADM\_PR is capturing the pattern of observed NO<sub>x</sub> concentrations (Figure 4.1a and c). In addition, the FAC2 is 1% by ADM\_PR at the CS site only with both meteorological conditions.



Hence, we have modeled only the NO<sub>x</sub> emissions related to aircraft sources. Still, we are not taking account of or modeling most of the NO<sub>x</sub> emissions of other airport sources as well as non-airport sources, which were contributing during that time and especially at the CE site. This site was highly impacted by the on-road sources because CE was located next to the major highways. We are assuming that after including the other on-airport and off-airport sources in plume rise model (ADM\_PR), we will be able to capture the diurnal patterns as well as the high concentrations, which is very important for air quality assessment especially at the CN and CS sites.

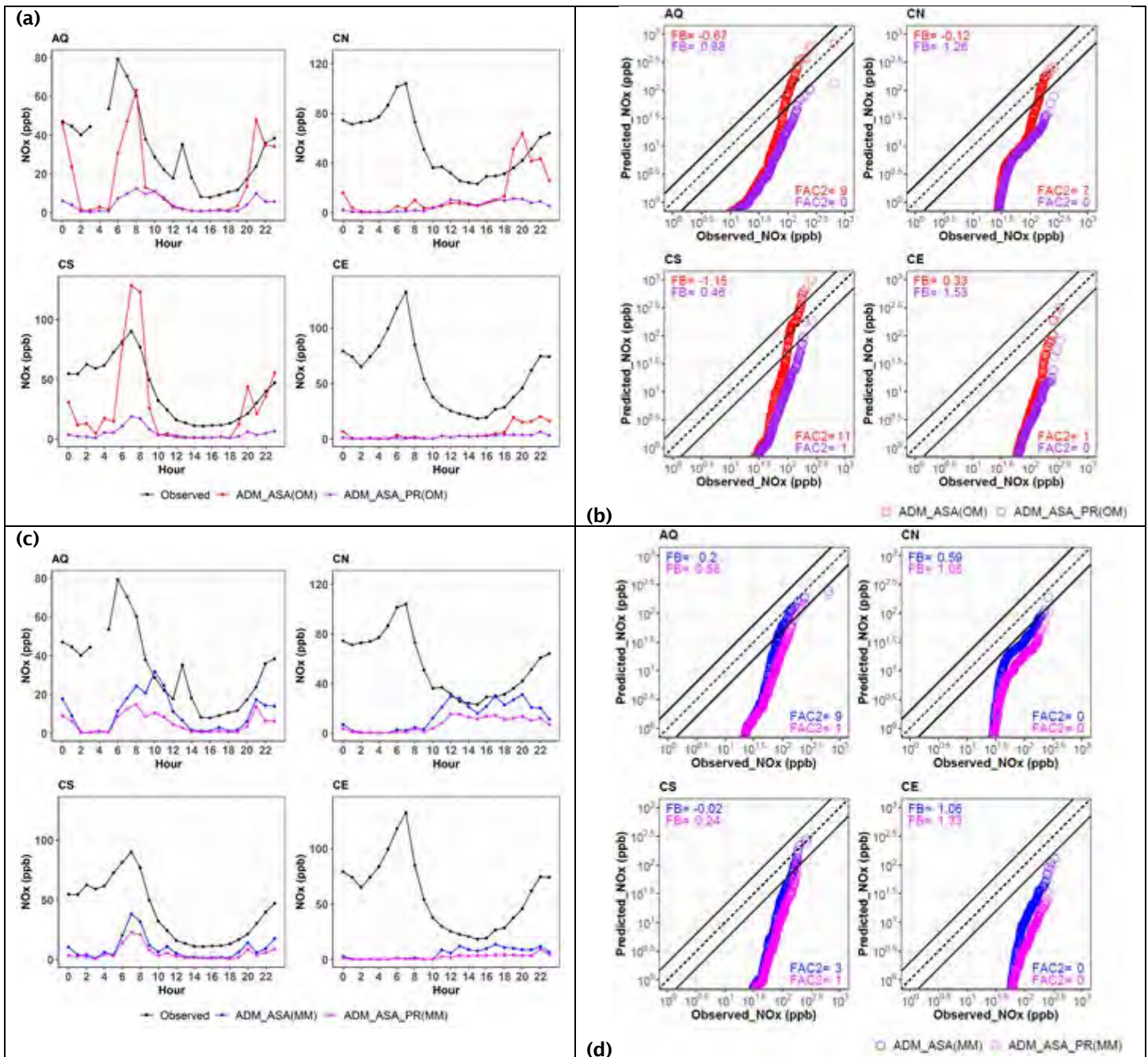


**Figure 4.1.** Diurnal variability (a and c) and Q-Q distribution (b and d) between observed (black) and modeled (ADM with and without plume rise) NOx concentrations with original (a and b) and modified meteorology (c and d) at all four core sites (AQ, CN, CS, and CE). The initialisms are as follows: ADM (Airport Dispersion Model); ASA (AEDT Segment Area); PR (With Plume Rise); OM (Original Meteorology); MM (Modified Meteorology).

#### 4.2.2 SO<sub>x</sub> concentration analysis

##### 4.2.2.1 Without plume rise algorithm (ADM)

With original meteorology, the ADM-predicted SO<sub>x</sub> diurnal concentrations are slightly able to capture the morning peak of diurnal observed concentrations at the AQ site whereas ADM is missing the second peak at the AQ. In addition, at all four core sites (AQ, CN, CS, and CE), the ADM is overpredicting the observed SO<sub>x</sub> concentrations in late evening. During late morning to afternoon, ADM is underpredicting the observed concentrations at all four core sites with original meteorology. At the CS site, ADM substantially overpredicts the morning peak with original meteorology (Figure 4.2a).

However, with the modified meteorology, the diurnal patterns of the observed concentrations distribution are captured well by ADM, especially at the CN site, from late morning to the evening. In contrast, ADM is substantially underpredicting the observed concentration between 0:00 hours to 10:00 hours at all core sites, except CS. At the CS site during this period, ADM highly overpredicts the morning observed peak, but the prediction is improved from original meteorology (Figure 4.2d).

In the Q-Q plots between ADM-predicted and observed overall SO<sub>x</sub> concentrations, the high concentrations are overpredicted by the ADM at all four core sites, whereas lower concentrations are underpredicted at the CN, CS, and CE sites with original meteorology (Figure 4.2b). ADM is predicting approximately 33%, 16%, 19%, and 19% concentrations within the FAC2 at the AQ, CN, CS, and CE sites, respectively, with original meteorology (Figure 4.1b).

On the other hand, with modified meteorology, the ADM-predicted high concentrations are close to the one-to-one line or within a factor of two lines at all four core sites. However, the middle-to-lower concentrations are still underpredicted by the ADM at all four core sites (Figure 4.2d). In addition, the values of FB are improved from -0.67, -1.61, and -0.81 to 0.29, -0.73, and 0.11 at the sites CN, CS, and CE, respectively, with original and modified meteorology. The values of FAC2 are improved from 33%, 16%, 19%, and 19% when using original meteorology to 44%, 44%, 40%, and 38% with the modified meteorology at the sites AQ, CN, CS, and CE, respectively (Figures 4.2(b and d)).

##### 4.2.2.2 With plume rise algorithm (ADM<sub>PR</sub>)

ADM<sub>PR</sub> either underpredicts or is close to the diurnal observed concentrations most of the time at all four core sites, whereas at the CS site, ADM<sub>PR</sub> predicted morning peak is very close to the observed peak as compare to ADM (without plume rise) with original meteorology (Figure 4.2a).

Therefore, with the modified meteorology, the ADM- and ADM<sub>PR</sub>-predicted diurnal concentrations are similar at the AQ and CS sites. At the other two sites, CN and CE, the ADM<sub>PR</sub>-predicted concentrations are close to the ADM for 0:00 hours to 10:00 hours, whereas after 10 AM, the ADM<sub>PR</sub> is slightly more underpredictive compared to ADM with modified meteorology (Figure 4.2c). However, there is a high peak with ADM<sub>PR</sub> with modified meteorology at 10 PM at the CE site (Figure 4.2c).

As shown in Figure 4.2b, the ADM<sub>PR</sub>-predicted high concentrations are getting close to the one-to-one line at the AQ and CS sites, whereas at the other two sites, ADM<sub>PR</sub> underpredicts more with the original meteorology. In addition, the FAC2 improves from 19% to 46% at the CS site with ADM<sub>PR</sub> (Figure 4.2b and d) with original meteorology.

On the other hand, with modified meteorology, ADM<sub>PR</sub> predicts the high concentrations closer to the one-to-one line of observation at the AQ and CS sites than ADM with modified meteorology. However, at the other two sites, ADM<sub>PR</sub> with modified meteorology more significantly underpredicts the high concentrations, whereas the lower concentrations are similar to ADM with modified meteorology (Figure 4.2d).

Hence, here, we have modeled only the SO<sub>x</sub> emissions related to aircraft sources. Still, we are not taking into account a substantial contribution of emissions coming from the south of the South Airfield, where a Chevron refinery is situated beyond CS, as well as some of the SO<sub>x</sub> on-airport and off-airport emissions. We expect that after including the contribution of these sources with plume rise model (ADM<sub>PR</sub>), we will be able to capture the diurnal patterns as well as the high and low concentrations adequately at all four core sites.

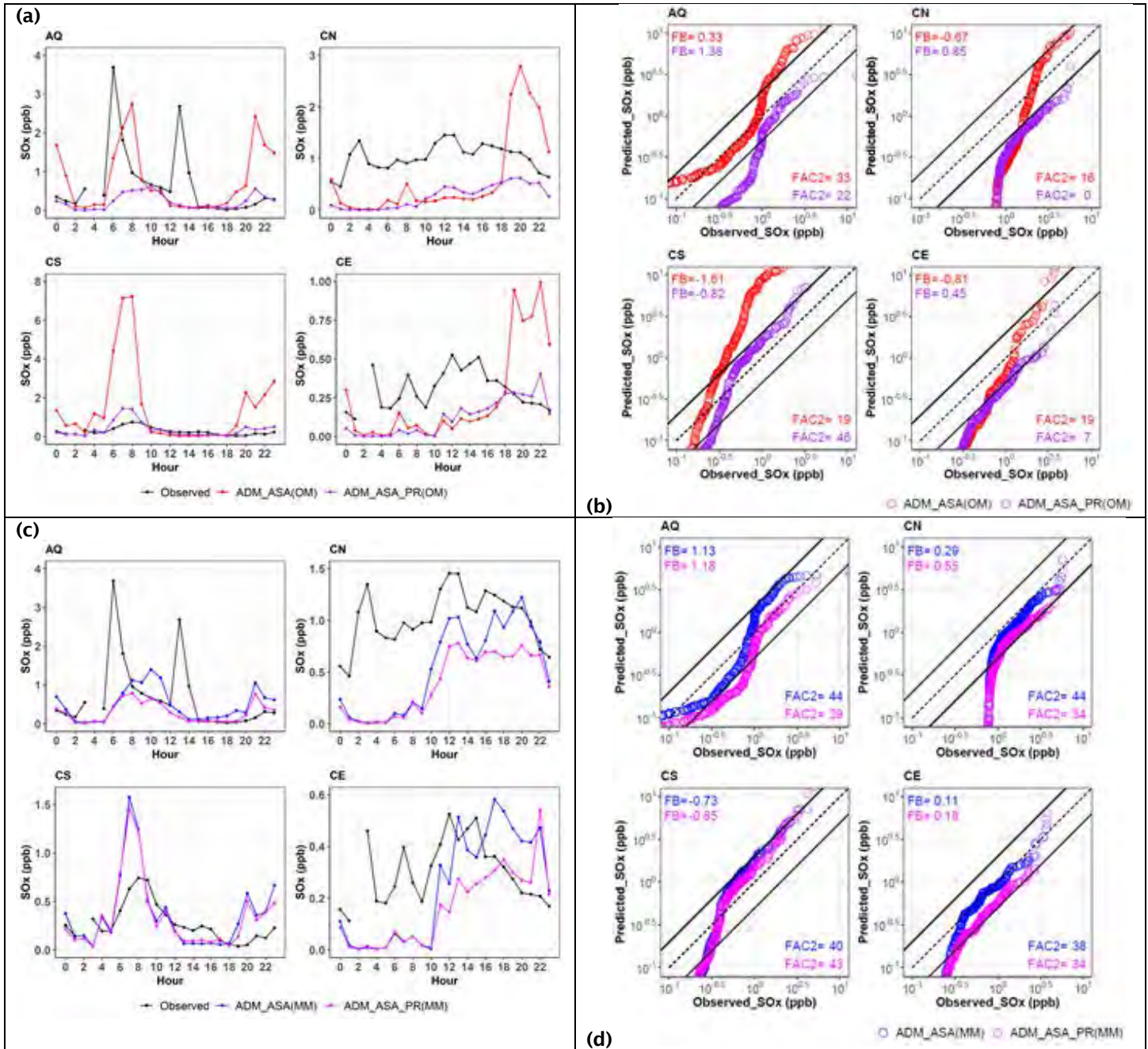


**Figure 4.2.** Diurnal variability (a and c) and Q-Q distribution (b and d) between observed and modeled (ADM with and without plume rise) SOx concentrations with original (a and b) and modified meteorology (c and d) at all four core sites (AQ, CN, CS, and CE). The initialisms are the same as those in Figure 4.1.

### Milestone

We submitted a draft of the modeling results and code to the FAA. A revised version with additional cleanup and additional treatment of physical and chemical processes will be submitted.



## Major Accomplishments

- Design document detailing features that will go into the new ADM.
- Initial conceptual approach for plume behavior at LAX using data from LAX AQSAS.
- Initial treatment of source characterization to treat aircraft sources during LTO cycles.
- Initial prototype of dispersion model to treat aircraft emissions at LAX and preliminary evaluation completed.

## Publications

N/A

## Outreach Efforts

Presentation at semi-annual ASCENT stakeholder meetings in the spring and fall of 2020, held virtually.  
Presentation and collaborative discussion during monthly meetings with the FAA and EPA.

## Awards

None

## Student Involvement

None

## Plans for Next Period

Finalize the ADM with all physical and chemical processes and complete evaluation.

## References

- Arunachalam, S., Blanchard, C., Henry, R., Tombach, I., 2013. LAX Air Quality and Source Apportionment Study Volume 1. Executive Summary. Los Angeles World Airports [Available at: <https://www.lawa.org/lawa-environment/lax/lax-air-quality-and-source-apportionment-study/final-report-and-materials> ]
- LAWA, 2020. LAWA Flight Data. Los Angeles World Airt. Flight Data, Obtained through Personal Communication.
- Arunachalam, S., A. Valencia, M. Woody, M. Snyder, J. Huang, J. Weil, P. Soucacos and S. Webb (2017). Dispersion Modeling Guidance for Airports Addressing Local Air Quality Concerns. Transportation Research Board Airport Cooperative Research Program (ACRP) Research Report 179, Washington, D.C. Available from: <http://nap.edu/24881>
- Arunachalam, S., Naess, B., Seppanen, C., Valencia, A., Brandmeyer, J.E., et al. (2019b). A new bottom-up emissions estimation approach for aircraft sources in support of air quality modelling for community-scale assessments around airports Akula Venkatram Jeffrey Weil Vlad Isakov and Timothy Barzyk. *Int. J. Environ. Pollut.* 65, 43-58. doi:10.1504/IJEP.2019.101832
- Carshaw, D. C., Beevers, S. D., Ropkins, K., Bell, M. C., 2006. Detecting and quantifying aircraft and other on-airport contributions to ambient nitrogen oxides in the vicinity of a large international airport. *Atmos. Environ.* 40, 5424-5434.
- Chang, J.C., Hanna, S.R., 2004. Air quality model performance. *Meteorol. Atmos. Phys.* 87, 167-196.
- Cox, W.M., Tikvart, J.A., 1990. A statistical procedure for determining the best performing air quality simulation model. *Atmos. Environ. Part A, Gen. Top.* 24, 2387-2395. [https://doi.org/10.1016/0960-1686\(90\)90331-G](https://doi.org/10.1016/0960-1686(90)90331-G)
- Nieuwstadt, F.T.M., van Ulden, A.P., 1978. A numerical study on the vertical dispersion of passive contaminants from a continuous source in the atmospheric surface layer. *Atmos. Environ.* 12, 2119-2124. [https://doi.org/10.1016/0004-6981\(78\)90166-X](https://doi.org/10.1016/0004-6981(78)90166-X)
- Valencia, A., S. Arunachalam, D. Heist, D. Carruthers, and A. Venkatram (2018). Development and Evaluation of the R-LINE Model Algorithms to Account for Chemical Transformation in the Near-road Environment, *Transp. Res. Part D: Transp. Environ.*, 59, 464 - 477.
- Venkatram, A., Du, S., Hariharan, R., Carter, W., Goldstein, R. (1998). The concept of species age in photochemical modeling. *Atmos. Environ.* 32. doi:10.1016/S1352-2310(98)00032-6
- Venkatram, A., 1999. Applying a framework for evaluating the performance of air quality models. In: Proceedings of the Sixth International Conference on Harmonisation within Atmospheric Dispersion Modeling for Regulatory Applications, Rouen, France, 11-14 October, 1999.
- Weil, J. C., Sykes, R. I., Venkatram, A., 1992. Evaluating air-quality models: review and outlook, *J. Applied Meteorol.* 31, 112-1145.



## Appendix A: Emission processing

Table A1. The list and the description of the surface and air sources for the ADM model.

No	Source name	Description of sources
	<b>Surface sources</b>	
1	ER01R06L_TG	Surface emission (g/s) for Take-Off Ground (TG) West-to-East (06L) direction
2	ER01R24R_TG	Surface emission (g/s) for Take-Off Ground (TG) East-to-West (24R) direction
3	ER01R06L_LG	Surface emission (g/s) for Landing Ground (LG) West-to-East (06L) direction
4	ER01R24R_LG	Surface emission (g/s) for Landing Ground (LG) East-to-West (24R) direction
5	ER02	Surface emission (g/s) in rectangles "R02"
6	ER03R06R_TG	Surface emission (g/s) for Take-Off Ground (TG) West-to-East (06R) direction
7	ER03R24L_TG	Surface emission (g/s) for Take-Off Ground (TG) East-to-West (24L) direction
8	ER03R06R_LG	Surface emission (g/s) for Landing Ground (LG) West-to-East (06R) direction
9	ER03R24L_LG	Surface emission (g/s) for Landing Ground (LG) East-to-West (24L) direction
10	ER04	Surface emission (g/s) in rectangles "R04"
11	ER05	Surface emission (g/s) in rectangles "R05"
12	ER06	Surface emission (g/s) in rectangles "R06"
13	ER07	Surface emission (g/s) in rectangles "R07"
14	ER08	Surface emission (g/s) in rectangles "R08"
15	ER09	Surface emission (g/s) in rectangles "R09"
16	ER10	Surface emission (g/s) in rectangles "R10"
17	ER11	Surface emission (g/s) in rectangles "R11"
18	ER12	Surface emission (g/s) in rectangles "R12"
19	ER13R07L_TG	Surface emission (g/s) for Take-Off Ground (TG) West-to-East (07L) direction
20	ER13R25R_TG	Surface emission (g/s) for Take-Off Ground (TG) East-to-West (25R) direction
21	ER13R07L_LG	Surface emission (g/s) for Landing Ground (LG) West-to-East (07L) direction
22	ER13R25R_LG	Surface emission (g/s) for Landing Ground (LG) East-to-West (25R) direction
23	ER14	Surface emission (g/s) in rectangles "R14"
24	ER15	Surface emission (g/s) in rectangles "R15"
25	ER16	Surface emission (g/s) in rectangles "R16"
26	ER17R07R_TG	Surface emission (g/s) for Take-Off Ground (TG) West-to-East (07R) direction
27	ER17R25L_TG	Surface emission (g/s) for Take-Off Ground (TG) East-to-West (25L) direction
28	ER17R07R_LG	Surface emission (g/s) for Landing Ground (LG) West-to-East (07R) direction
29	ER17R25L_LG	Surface emission (g/s) for Landing Ground (LG) East-to-West (25L) direction
30	ER18	Surface emission (g/s) in rectangles "R18"
31	ER19	Surface emission (g/s) in rectangles "R19"



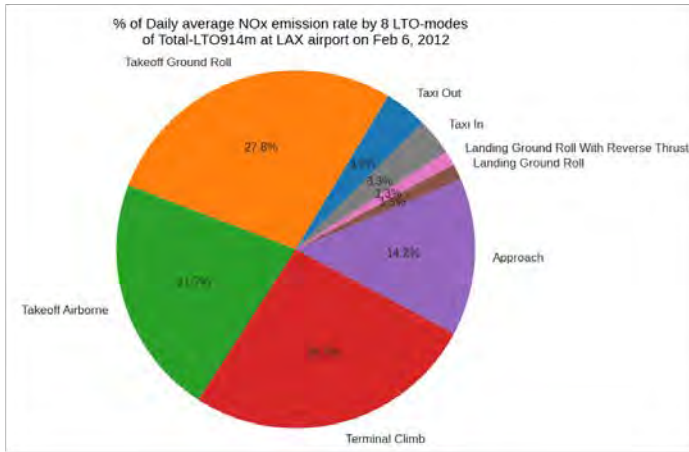
Air sources		
	<b>Air-layer 01</b>	<b>Air-source for air-layer 01</b>
32	ER01R06L_TA1	Air emission (g/s) for Take-Off (T) West-to-East (06L) direction in air layer 1 (altitudes 0 to 100 m)
33	ER01R24R_TA1	Air emission (g/s) for Take-Off (T) East-to-West (24R) direction in air layer 1 (altitudes 0 to 100 m)
34	ER01R06L_LA1	Air emission (g/s) for Landing (L) West-to-East (06L) direction in air layer 1 (altitudes 0 to 100 m)
35	ER01R24R_LA1	Air emission (g/s) for Landing (L) East-to-West (24R) direction in air layer 1 (altitudes 0 to 100 m)
36	ER03R06R_TA1	Air emission (g/s) for Take-Off (T) West-to-East (06R) direction in air layer 1 (altitudes 0 to 100 m)
37	ER03R24L_TA1	Air emission (g/s) for Take-Off (T) East-to-West (24L) direction in air layer 1 (altitudes 0 to 100 m)
38	ER03R06R_LA1	Air emission (g/s) for Landing (L) West-to-East (06R) direction in air layer 1 (altitudes 0 to 100 m)
39	ER03R24L_LA1	Air emission (g/s) for Landing (L) East-to-West (24L) direction in air layer 1 (altitudes 0 to 100 m)
40	ER13R07L_TA1	Air emission (g/s) for Take-Off (T) West-to-East (07L) direction in air layer 1 (altitudes 0 to 100 m)
41	ER13R25R_TA1	Air emission (g/s) for Take-Off (T) East-to-West (25R) direction in air layer 1 (altitudes 0 to 100 m)
42	ER13R07L_LA1	Air emission (g/s) for Landing (L) West-to-East (07L) direction in air layer 1 (altitudes 0 to 100 m)
43	ER13R25R_LA1	Air emission (g/s) for Landing (L) East-to-West (25R) direction in air layer 1 (altitudes 0 to 100 m)
44	ER17R07R_TA1	Air emission (g/s) for Take-Off (T) West-to-East (07R) direction in air layer 1 (altitudes 0 to 100 m)
45	ER17R25L_TA1	Air emission (g/s) for Take-Off (T) East-to-West (25L) direction in air layer 1 (altitudes 0 to 100 m)
46	ER17R07R_LA1	Air emission (g/s) for Landing (L) West-to-East (07R) direction in air layer 1 (altitudes 0 to 100 m)
47	ER17R25L_LA1	Air emission (g/s) for Landing (L) East-to-West (25L) direction in air layer 1 (altitudes 0 to 100 m)
	<b>Air-layer 02</b>	<b>Air-source for air-layer 02 ( from 100m to 200m)</b>
...	.....	.....
...	.....	.....
...	.....	.....



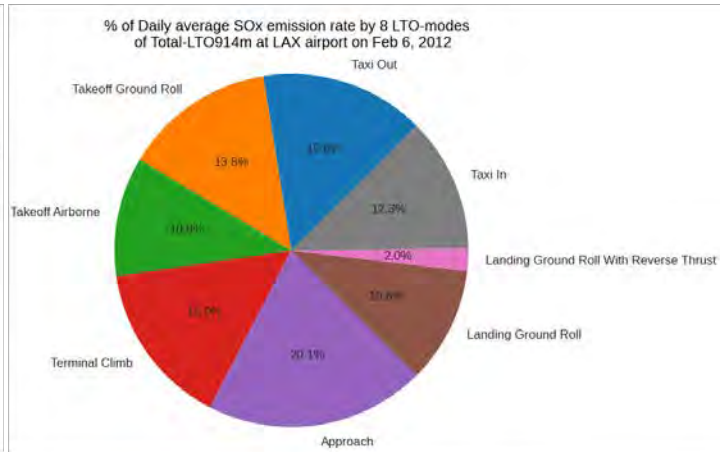
Air-layer 08		Air-source for air-layer 08 ( from 700m to 800m)
...	.....	.....
	<b>Air-layer 09</b>	<b>Air-source for air-layer 09</b>
<b>160</b>	ER01R06L_TA9	Air emission (g/s) for Take-Off (T) West-to-East (06L) direction in air layer 9 (altitudes from 800 to 914.4m)
<b>161</b>	ER01R24R_TA9	Air emission (g/s) for Take-Off (T) East-to-West (24R) direction in air layer 9 (altitudes from 800 to 914.4m)
<b>162</b>	ER01R06L_LA9	Air emission (g/s) for Landing (L) West-to-East (06L) direction in air layer 9 (altitudes from 800 to 914.4m)
<b>163</b>	ER01R24R_LA9	Air emission (g/s) for Landing (L) East-to-West (24R) direction in air layer 9 (altitudes from 800 to 914.4m)
<b>164</b>	ER03R06R_TA9	Air emission (g/s) for Take-Off (T) West-to-East (06R) direction in air layer 9 (altitudes from 800 to 914.4m)
<b>165</b>	ER03R24L_TA9	Air emission (g/s) for Take-Off (T) East-to-West (24L) direction in air layer 9 (altitudes from 800 to 914.4m)
<b>166</b>	ER03R06R_LA9	Air emission (g/s) for Landing (L) West-to-East (06R) direction in air layer 9 (altitudes from 800 to 914.4m)
<b>167</b>	ER03R24L_LA9	Air emission (g/s) for Landing (L) East-to-West (24L) direction in air layer 9 (altitudes from 800 to 914.4m)
<b>168</b>	ER13R07L_TA9	Air emission (g/s) for Take-Off (T) West-to-East (07L) direction in air layer 9 (altitudes from 800 to 914.4m)
<b>169</b>	ER13R25R_TA9	Air emission (g/s) for Take-Off (T) East-to-West (25R) direction in air layer 9 (altitudes from 800 to 914.4m)
<b>170</b>	ER13R07L_LA9	Air emission (g/s) for Landing (L) West-to-East (07L) direction in air layer 9 (altitudes from 800 to 914.4m)
<b>171</b>	ER13R25R_LA9	Air emission (g/s) for Landing (L) East-to-West (25R) direction in air layer 9 (altitudes from 800 to 914.4m)
<b>172</b>	ER17R07R_TA9	Air emission (g/s) for Take-Off (T) West-to-East (07R) direction in air layer 9 (altitudes from 800 to 914.4m)
<b>173</b>	ER17R25L_TA9	Air emission (g/s) for Take-Off (T) East-to-West (25L) direction in air layer 9 (altitudes from 800 to 914.4m)
<b>174</b>	ER17R07R_LA9	Air emission (g/s) for Landing (L) West-to-East (07R) direction in air layer 9 (altitudes from 800 to 914.4m)
<b>175</b>	ER17R25L_LA9	Air emission (g/s) for Landing (L) East-to-West (25L) direction in air layer 9 (altitudes from 800 to 914.4m)



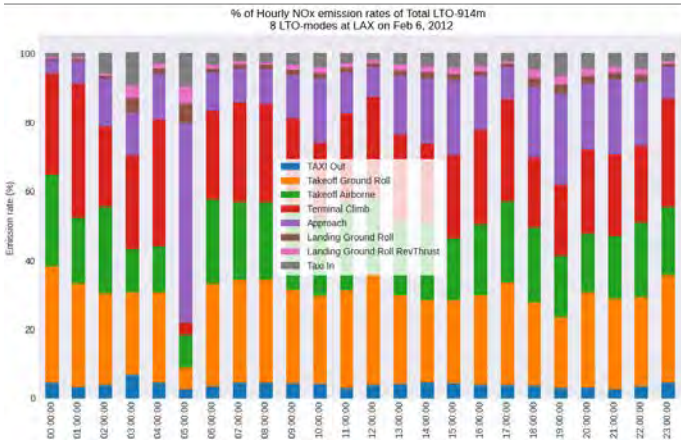
a) NOx : Daily %



b) SOx : Daily %



c) NOx : Hourly %



d) SOx : Hourly %

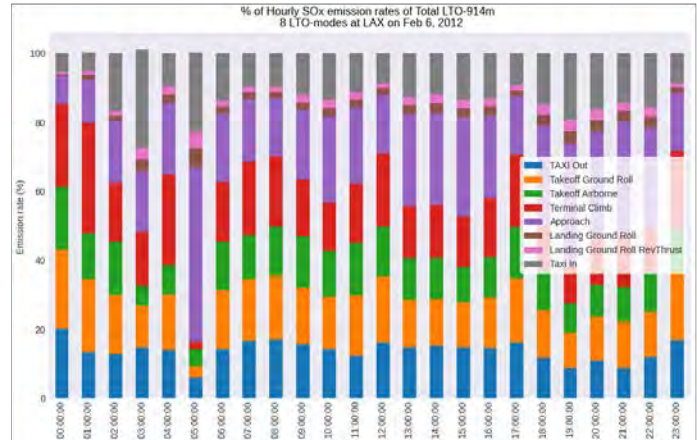
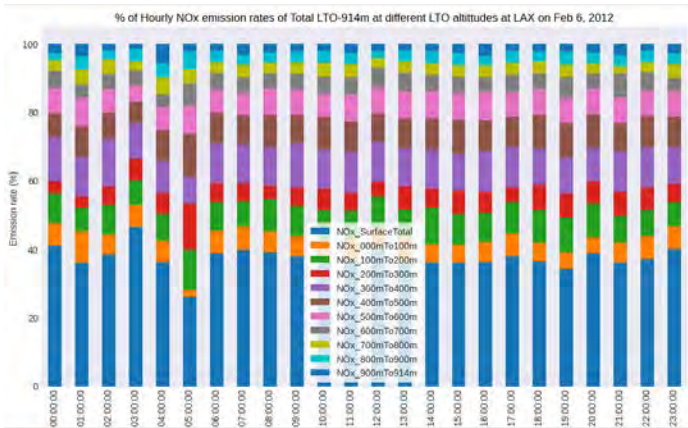
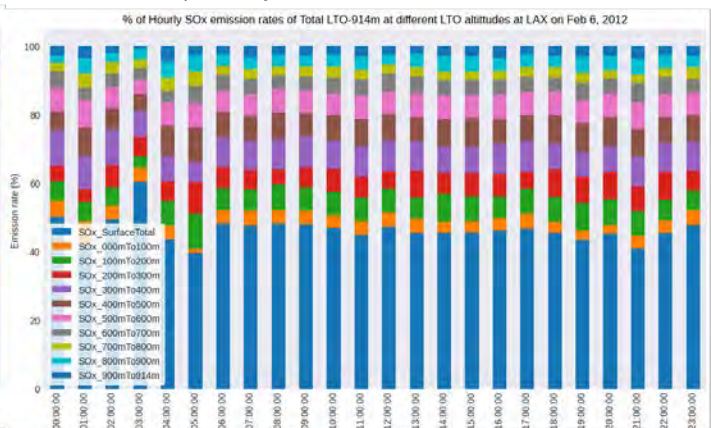


Figure A1. The % of hourly a) NOx and b) SOx of total-LTO-914m emission, the % of hourly c) NOx and d) SOx of total-LTO-914m emission in eight AEDT-LTO modes on February 6, 2012 at LAX in AEDT emission data.

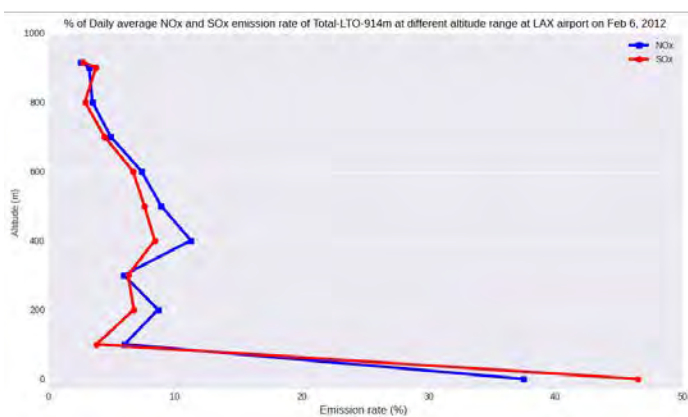
a) Hourly NOx % at different altitude



b) Hourly SOx % at different altitude



c) Daily NOx and SOx % at different altitude



d) Cumulative Daily NOx and SOx % at different altitude

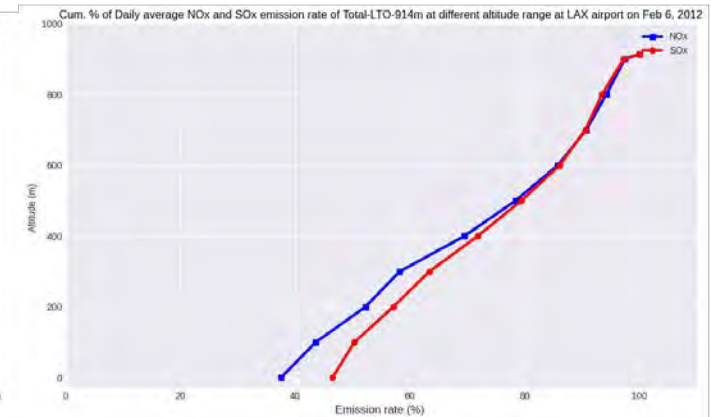


**Figure A2.** The % of hourly a) NOx and b) SOx of total-LTO-914m emission in different altitudes and % of daily emission of c) NOx and d) SOx of total-LTO-914m emission in different altitudes on February 6, 2012 at LAX in AEDT emission data.

**Table A2.** Daily total number of flights by AEDT-S and LAWA-actual (LAWA, 2020) and % change from LAWA-actual for flights at LAX on February 6, 2012.

	AEDT-S	LAWA-actual	% Change from LAWA-actual
Runway 24R/06L	359	340	5.59
Runway 24L/06R	333	295	16.84
Runway 25R/07L	450	455	-1.1
Runway 25L/07R	401	408	-1.72
LAX-total	1543	1488	3.7

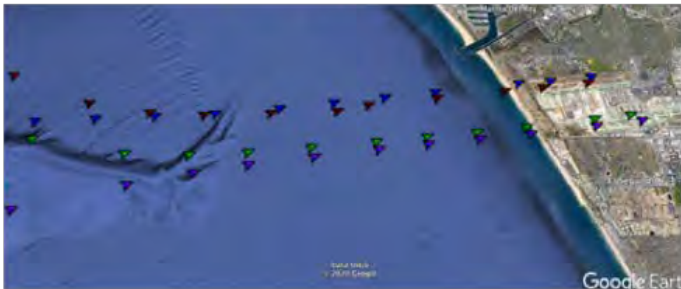


Average lat-lons in air at 9 altitudes (also 2 surface runway points given)

a) Landing: 24R (Blue), 24L (Red), 25R (Green), 25L (Purple)    b) Take-Off: 24R (Blue), 24L (Red), 25R (Green), 25L (Purple)



c) Landing: 06L (Blue), 06R (Red), 07L (Green), 07R (Purple)    d) Take-Off: 06L (Blue), 06R (Red), 07L (Green), 07R (Purple)



Sources in air: 9 Altitudes : 100m, 200m, 300m, 400m, 500m, 600m, 700m, 800m, 914m  
 Source at surface: 1<sup>st</sup> 2-points (for take-off) and last 2 points (for landing) at the runway

**Figure A3.** Latitude–longitude (lat-lons) pairs of each of the nine, air layer height for eight runways and two LTOs (produced based on aircraft location data for February 2012. (These latitude–longitude pairs are assumed to be fixed for all 29 days of February to be used in the model at any hour.)



# Project 020 Development of NAS-Wide and Global Rapid Aviation Air Quality Tools

## Massachusetts Institute of Technology

### Project Lead Investigator

Professor Steven R.H. Barrett  
Raymond L. Bisplinghoff Professor of Aeronautics and Astronautics  
Department of Aeronautics & Astronautics  
Massachusetts Institute of Technology  
77 Massachusetts Ave.  
Cambridge, MA 02139  
(617) 452-2550  
sbarrett@mit.edu

### University Participants

#### Massachusetts Institute of Technology (MIT)

- Pls: Steven R. H. Barrett
- FAA Award Number: 13-C-AJFE-MIT, Amendment Nos. 007, 018, 025, 032, and 041
- Period of Performance: August 19, 2014, to August 31, 2020 (via no-cost extension)
- Tasks for current period (September 1, 2019, to August 31, 2020)
  - No additional funding was provided for the project for this reporting period. All tasks were previously finalized, but outreach was conducted on the following Task:
    1. Provide surface air quality analysis and quantify the effects of aviation on surface air quality.

### Project Funding Level

\$800,000 FAA funding + \$50,000 Transport Canada funding = \$850,000 total sponsored funds, of which only the FAA-funded portion requires matching funds. Sources of match are that same \$50,000 Transport Canada funding (it constitutes both matching funds itself and sponsored funds that do not need to be matched), plus approximately \$215,000 from MIT, and third-party in-kind contributions of \$114,000 from Byogy Renewables Inc. and \$421,000 from Oliver Wyman Group.

### Investigation Team

- PI: Professor Steven Barrett, MIT (All tasks)
- Co-PI: Dr. Raymond L. Speth, MIT (All tasks)
- Co-investigator: Dr. Florian Allroggen, MIT (All tasks)
- Research scientist: Dr. Sebastian Eastham, MIT (All tasks)
- Postdoctoral associate: Dr. Irene Dedoussi, MIT (All tasks)
- Graduate student: Guillaume Chossière, MIT (All tasks)

### Project Overview

The aim of this project is to develop tools that enable the rapid assessment of the health impacts of aviation emissions. The focus of the project is aviation-attributable particulate matter  $\leq 2.5 \mu\text{m}$  ( $\text{PM}_{2.5}$ ) and ozone on the National Airspace System (NAS)-wide and global scales. These tools allow for rapid policy analysis and scenario comparison. The adjoint method on which these tools are based provides a computationally efficient way of calculating sensitivities of an objective function with respect to multiple model inputs. The project enhances existing tools in terms of the domains and impacts covered, and in terms of uncertainty quantification. The enhanced tools support the FAA in its strategic vision to reduce the health impacts of aviation emissions and allow for detailed and quantified policy analyses.

For the current reporting period, no additional funding was provided, and the project team finalized all tasks in previous years. During the current period, the team led some additional outreach efforts and finalized the documentation of the project and its results.

## Task 1 – Provide Surface Air Quality Analysis and Quantify the Effects of Aviation on Surface Air Quality

Massachusetts Institute of Technology

### **Objective**

The objective is to apply the tools developed under ASCENT Project 20 to quantify the surface air quality impacts of aviation. This Task was completed during the no-cost extension.

### **Research Approach**

This project provides a set of metrics which can be used directly to perform rapid policy assessment. Previous MIT research found that aviation emissions result in ~16,000 premature deaths annually due to impaired air quality (Eastham & Barrett, 2016; Yim et al., 2015). When aiming to reduce these impacts and those from climate change, decision makers often face trade-offs between different emission species or impacts in different times and locations. To inform rational decision-making, the sensitivity data computed for ASCENT Project 20 were applied to compute aviation’s marginal air quality impacts per tonne of species emitted, while accounting for the altitude and chemical composition of the emissions. Uncertainty in chemistry transport modeling was incorporated using scaling factors based on prior literature. Uncertainty in climate, health impact, and economic factors was also quantified.

### **Milestone**

The task has been completed and a paper published in the past and current reporting period (Grobler et al., 2019).

### **Major Accomplishments**

We found that air quality impacts accounted for 64% of combined climate and air quality impacts, based on fuel burn in 2015, and that the majority of these impacts were associated with cruise-level NO<sub>x</sub> emissions. A sensitivity study was conducted to find the contribution of each of the uncertain Monte Carlo input variables to the observed output variance. We found uncertainty in climate sensitivity and the DICE (Dynamic Integrated Climate-Economy model) damage function to be the largest drivers of total output uncertainty.

A detailed description of the research approach and results can be found in a paper which was published as a result of work under both ASCENT Projects 20 and 21 (Grobler et al., 2019).

### **Publications**

#### **Peer-reviewed journal publications:**

Grobler, C., Wolfe, P.J., Dasadhikari, K., Dedoussi, I.C., Allroggen, F., Speth, R.L., Eastham, S.D., Agarwal, A., Staples, M.D., Sabnis, J. & Barrett, S.R.H. (2019). Marginal climate and air quality costs of aviation emissions. *Environmental Research Letters*, 14 114031, <https://doi.org/10.1088/1748-9326/ab4942>

### **Outreach Efforts**

#### **Presentations:**

- A summary of the paper approach and results were presented to the FAA (November 2019).
- Presented at Aerospace Europe conference in Bordeaux in February 2020.
- Presented at the fall ASCENT meeting (September 2020) for winning Joseph Hartman best paper award

FAA funding was acknowledged in all presentations.

### **Student Involvement**

The outreach activities were completed by Carla Grobler (PhD student, MIT).



### **Plans for Next Period**

N/A

### **References**

- Eastham, S. D. & Barrett, S. R. H. (2016). Aviation-attributable ozone as a driver for changes in mortality related to air quality and skin cancer. *Atmospheric Environment*, doi:10.1016/j.atmosenv.2016.08.040.
- Grobler, C., Wolfe, P. J., Dasadhikari, K., Dedoussi, I. C., Allroggen, F., Speth, R. L., Eastham, S. D., Agarwal, A., Staples, Sabnis, J., & Barrett, S. R. H. (2019). Marginal climate and air quality costs of aviation emissions. *Environmental Research Letters*, 14 114031, <https://doi.org/10.1088/1748-9326/ab4942>.
- Yim, S. H. L., Lee, G. L., Lee, I. W., Allroggen, F., Ashok, A., Caiazzo, F., Eastham, S. D., Malina, R. & Barrett, S. R. H. (2015). Global, regional and local health impacts of civil aviation emissions. *Environmental Research Letters*, 10 034001.



## Project 021 Improving Climate Policy Analysis Tools

### Massachusetts Institute of Technology

#### Project Lead Investigator

PI: Steven R. H. Barrett  
Professor of Aeronautics and Astronautics  
Department of Aeronautics and Astronautics  
Massachusetts Institute of Technology  
77 Massachusetts Avenue, 33-316  
Cambridge, MA 02139  
+1 (617) 452-2727  
sbarrett@mit.edu

Co-PI: Dr. Florian Allroggen  
Research Scientist  
Department of Aeronautics and Astronautics  
Massachusetts Institute of Technology  
77 Massachusetts Avenue, 33-115A  
Cambridge, MA 02139  
+1 (617) 715-4472  
fallrogg@mit.edu

#### University Participants

##### Massachusetts Institute of Technology (MIT)

- PIs: Steven R. H. Barrett, Florian Allroggen (co-PI)
- FAA Award Number: 13-C-AJFE-MIT, Amendment Nos. 004, 017, 024, 037, and 042
- Period of Performance: August 1, 2014, to August 31, 2020 (via no-cost extension)
- Tasks for current period (September 1, 2019 to August 31, 2020)
  - No additional funding was provided for the project for this reporting period. All tasks were previously finalized, but outreach was conducted on the following Task:
    1. Derive and publish marginal climate costs per unit of aviation emissions for rapid assessments of emissions interventions

#### Project Funding Level

FAA provided \$600,000 in funding and \$600,000 in matching funds were contributed by: approximately \$162,000 from MIT, and third-party in-kind contributions of \$114,000 from Byogy Renewables, Inc. and \$324,000 from Oliver Wyman Group.

#### Investigation Team

- Prof. Steven R. H. Barrett, PI, MIT (All tasks)
- Dr. Florian Allroggen, co-PI, MIT (All tasks)
- Dr. Raymond Speth, co-investigator, MIT (All tasks)
- Dr. Sebastian Eastham, MIT (All tasks)
- Carla Grobler (PhD student), MIT (All tasks)

## Project Overview

The objective of ASCENT Project 21 is to facilitate continued development of climate policy analysis tools that will enable impact assessments for different policy scenarios at the global, zonal, and regional scales and will enable FAA to address its strategic vision on sustainable aviation growth. Following this overall objective, the particular objectives of ASCENT Project 21 are (1) to continue the development of a reduced-order climate model for policy analysis consistent with the latest scientific understanding; and (2) to support FAA analyses of national and global policies as they relate to long-term atmospheric and environmental impacts.

For the current reporting period, no additional funding was provided, and the project team finalized all tasks in previous years. During the current period, the team led additional outreach efforts and finalized the documentation of the project and its results.

## Task 1 – Derivation of Marginal Climate Costs Per Unit Aviation Emissions

Massachusetts Institute of Technology

### Objectives

Aviation emissions have been found to cause 5% of global anthropogenic radiative forcing (RF) and ~16,000 premature deaths annually due to impaired air quality (Eastham & Barrett, 2016; Lee et al., 2009; Yim et al., 2015). When aiming to reduce these impacts, decision makers often face trade-offs between different emission species or impacts in different times and locations. To inform rational decision-making, the objective of this Task is to compute aviation’s marginal climate and air quality impacts per tonne of species emitted during different flight stages and by emission location. This Task has been completed in collaboration with ASCENT Project 20.

### Research Approach

The research approach involves applying Aviation environmental Portfolio Management Tool - Impacts Climate (APMT-IC) to calculate costs for full flight emissions by running APMT-IC for an emissions pulse in 2015. Impacts per unit of precursor emissions are derived by normalizing each of the short-lived forcers by its respective precursor emissions.

Full flight results are computed using APMT-IC and landing and takeoff (LTO) and cruise impacts are obtained by modifying the LTO and cruise RF per unit of fuel burn. LTO RF results are based on the global warming potential values for ground emissions from the Intergovernmental Panel on Climate Change (IPCC) report (Myhre et al., 2013), whereas cruise radiative impacts are calculated as the difference between the Aviation Climate Change Research Initiative (ACCRI) (Brasseur et al., 2016) full flight radiative impacts and the LTO results. Climate results are derived for discount rates ranging from 2% to 7%.

A detailed description of the research approach can be found in the publication (see below).

### Milestones

Results were derived as described above. The journal paper was prepared and submitted to *Environmental Research Letters*, where it was reviewed, accepted, and published (Grobler et al., 2019).

### Major Accomplishments

Results were successfully derived using APMT-IC. Our results indicate that three components are responsible for 97% of climate and air quality damages per unit fuel burn, with individual contributions of NO<sub>x</sub> at 58%, CO<sub>2</sub> at 25%, and contrails at 14%. Air quality impacts account for 64% of total impacts. A sensitivity study was conducted to find the contribution of each of the uncertain Monte Carlo input variables to the observed output variance. We found uncertainty in the climate sensitivity and the Dynamic Integrated Climate-Economy model (DICE) damage function to be the largest drivers in the output uncertainty.

This work was submitted and published in *Environmental Research Letters*.



## **Publications**

### **Peer-reviewed journal publications:**

Grobler, C., Wolfe, P.J., Dasadhikari, K., Dedoussi, I.C., Allroggen, F., Speth, R.L., Eastham, S.D., Agarwal, A., Staples, M.D., Sabnis, J. & Barrett, S.R.H. (2019). Marginal climate and air quality costs of aviation emissions. *Environmental Research Letters*, 14 114031, <https://doi.org/10.1088/1748-9326/ab4942>

## **Outreach Efforts**

### **Presentations:**

- A summary of the paper approach and results were presented to the FAA (November 2019).
- Presented at Aerospace Europe conference in Bordeaux in February 2020.
- Presented at the Fall ASCENT Meeting (September 2020).

FAA funding was acknowledged in all presentations.

## **Student Involvement**

The outreach activities were completed by Carla Grobler (PhD student, MIT).

## **Awards**

Carla Grobler received the ASCENT Joseph Hartman best paper award.

## **Plans for Next Period**

There are no further research plans under this project. The project has ended.

## **References**

- Brasseur, G.P., Gupta, M., Anderson, B.E., Balasubramanian, S., Barrett, S., Duda, D., Fleming, G., Forster, P.M., Fuglestvedt, J., Gettelman, A. & Halthore, R.N. (2016). Impact of aviation on climate: FAA's aviation climate change research initiative (ACCRI) phase ii. *Bulletin of the American Meteorological Society*. 97(4), pp.561-583
- Eastham, S.D. & Barrett, S.R.H. (2016). Aviation-attributable ozone as a driver for changes in mortality related to air quality and skin cancer. *Atmospheric Environment*. 144 17-23
- Lee, D.S., Fahey, D.W., Forster, P.M., Newton, P.J., Wit, R.C.N., Lim, L.L., Owen, B., & Sausen, R. (2009). Aviation and global climate change in the 21st century. *Atmospheric Environment*, 43 3520-37, <http://dx.doi.org/10.1016/j.atmosenv.2009.04.024>
- Myhre, G., Shindell, D., Bréon, F., Collins, W., Fuglestvedt, J., Huang, J., Koch, D., Lamarque, J., Lee, D., Mendoza, B., Nakajima, T., Robock, A., Stephens, G., Takemura, T., & Zhang, H. (2013). Anthropogenic and natural radiative forcing. Contribution of Working Group I to the Fifth Assessment Report of the Intergovernmental Panel on Climate Change [Stocker, T.F., Qin, D., Plattner, G.K., Tignor, M., Allen, S.K., Boschung, J., Nauels, A., Xia, Y., Bex, V., & Midgley, P.M. (eds.). Cambridge, United Kingdom and New York, NY, USA: Cambridge University Press] [https://www.ipcc.ch/pdf/assessment-report/ar5/wg1/WG1AR5\\_Chapter08\\_FINAL.pdf](https://www.ipcc.ch/pdf/assessment-report/ar5/wg1/WG1AR5_Chapter08_FINAL.pdf).
- Yim, S.H.L., Lee, G.L., Lee, I.H., Allroggen, F., Ashok, A., Caiazzo, F., Eastham, S.D., Malina, R. & Barrett, S.R.H. (2015). Global, regional and local health impacts of civil aviation emissions. *Environmental Research Letters*, 10 034001



## Project 022 Evaluation of FAA Climate Tools: APMT

### University of Illinois at Urbana-Champaign

#### Project Lead Investigator

Dr. Donald Wuebbles  
Dept. of Atmospheric Sciences  
University of Illinois  
105 S. Gregory Street  
Urbana, IL 61801  
Tel: 217-244-1568  
Fax: 217-244-4393  
Email: wuebbles@illinois.edu

#### University Participants

##### University of Illinois at Urbana-Champaign

- PI: Dr. Donald Wuebbles
- Period of Performance: October 1, 2019 to September 30, 2020 (project started January 31, 2020)
- Tasks:
  1. Revisit High Speed Civil Transport and the potential effects on ozone and climate using the state-of-the-art Community Earth System Model (CESM) global chemistry-climate model.
  2. Conduct cruise altitude sensitivity study.

#### Project Funding Level

Support from the FAA over this time period was about \$70,000 with an additional \$70,000 in matching support, including about \$70,000 from the University of Illinois at Urbana-Champaign.

#### Investigation Team

Dr. Donald Wuebbles: project oversight.

Jun Zhang (graduate student): conduct studies and perform analyses using the CESM Whole Atmosphere Community Climate Model (WACCM), a 3D atmospheric climate-chemistry model.

### Task 1 – Revisiting HSCTs and Their Potential Effects on Ozone and Climate

University of Illinois at Urbana-Champaign

#### Objective(s)

This project has the primary objective of understanding how the understanding of atmospheric processes over the last few decades has affected analyses of the potential environmental effects on ozone and climate from assumed future fleets of supersonic aircraft. The aim here is to conduct a series of sensitivity global chemistry-climate modeling studies that revisit case studies run for High Speed Civil Transport (HSCT) emission scenarios for a mature fleet of aircraft. The emission scenarios analyzed in this study are developed from the NASA HSCT program from the late 1990s through the early 2000s and/or from the 1999 Intergovernmental Panel on Climate Change (IPCC) special assessment on aviation.

#### Research Approach

The study will use the Whole Atmosphere Community Climate Model (WACCM) of the Community Earth System Model (CESM), developed by the National Center for Atmospheric Research (NCAR). This model has 66 layers from the ground to the middle of the mesosphere and provides a comprehensive treatment of tropospheric and stratospheric chemical processes.



## Results and Discussions

The calculated total column ozone percentage change from the HSCT emission scenarios are shown in Table 1 for different nitrogen oxides (NO<sub>x</sub>) emission indexes and fleet sizes in a 2015 background atmosphere. The results from the earlier 1999 NASA Atmospheric Effects of Aviation Project (AEAP) and IPCC aviation assessments (Kawa et al, 1999; Penner et al., 1999) using 2D and 3D models from that time period are shown here for comparison. The calculated percentage change in total column ozone from this study with WACCM is shown in the last row. All total column ozone changes are shown here for each emission scenario relative to the subsonic-only background atmosphere.

The results are more similar to the earlier results from the 2D models than the early-stage 3D models. For the baseline scenario Case A, this study determines a change in percentage ozone of -0.21% and -0.13% for the Northern Hemisphere (NH) and Southern Hemisphere (SH), respectively. This change falls into the range of +0.2 to -0.4% in the NH and +0.05 to -0.8 in the SH calculated from previous models shown in Table 1. For Cases B and C, with increasing NO<sub>x</sub> Emissions Index (EINO<sub>x</sub>) to either 10g or 15g NO<sub>2</sub>/kg fuel, the WACCM derived ozone loss in the NH tends to be larger than that from most of the earlier models. Case D, for only NO<sub>x</sub> emissions with EINO<sub>x</sub>=15g NO<sub>2</sub>/kg fuel, was not considered in the earlier assessments.

For the water vapor (H<sub>2</sub>O)-only emissions scenario Case E, the WACCM results are lower than all of the earlier models in the NH. Doubling the fleet to 1000 HSCTs assumed to be in operation (Case F), the total column ozone percentage change calculated from WACCM is -0.45% and -0.27% in the NH and SH respectively, which is in the range of values calculated from previous models.

Figure 1 shows the sensitivity of ozone depletion in the NH as a function of NO<sub>x</sub> emission indices for a fleet of 500 supersonic aircraft calculated from WACCM and the comparison to earlier models. In general, WACCM derives a higher sensitivity in the NH between the levels of NO<sub>x</sub> emissions and the resulting ozone changes. As the EINO<sub>x</sub> goes from no NO<sub>x</sub> emission (the H<sub>2</sub>O-only perturbation case) to 5g/kg fuel, WACCM has a higher sensitivity in ozone depletion than all of the earlier models. Increasing the EINO<sub>x</sub> from 5 to 15 g/kg fuel also shows WACCM having a stronger sensitivity compared to most of the earlier models, with one exception, the THINAIR 2D model.

**Table 1.** Percentage changes (%) in total column ozone for the WACCM results relative to the earlier NASA AEAP and IPCC aviation assessment results taken from Kawa et al. (1999) and Penner et al. (1999). The first and second value is for the Northern Hemisphere (NH) and Southern Hemisphere (SH) average percent change in total column ozone, respectively.

Models	Case A EINO <sub>x</sub> = 5 with H <sub>2</sub> O	Case B EINO <sub>x</sub> = 10 with H <sub>2</sub> O	Case C EINO <sub>x</sub> = 15 with H <sub>2</sub> O	Case D EINO <sub>x</sub> = 15 without H <sub>2</sub> O	Case E EINO <sub>x</sub> = 0 H <sub>2</sub> O only	Case F EINO <sub>x</sub> = 5 with H <sub>2</sub> O Fleet 1000
AER 2D	-0.3, -0.1	-0.3, -0.1	-0.3, -0.05	-	-0.6, -0.3	-0.7, -0.3
GSFC 2D	-0.4, -0.8	-0.6, -0.7	-0.8, -0.7	-	-0.4, -0.8	-0.9, -1.4,
LLNL 2D	-0.2, -0.2	-0.3, -0.1	-0.4, -0.01	-	-0.3, -0.3	-0.5, -0.3
CSIRO 2D	-0.2, -0.1	-0.3, -0.2	-0.5, -0.3	-	-0.2, -0.07	-0.5, -0.2
UNIVAQ 2D	-0.002, +0.02	+0.2, +0.1	+0.4, +0.2	-	-0.4, -0.2	-0.06, +0.005
SUNY 2D	-0.2, -0.1	-0.2, -0.06	-	-	-0.2, -0.1	-0.3, -0.2
THINAIR 2D	-0.2, -0.2	-0.5, -0.3	-0.9, -0.5	-	-	-0.4, -0.3
GMI 3D	+0.2, +0.05	-	-	-	-	-
LaRC 3D	-0.05, -0.1	+0.07, -0.03	-	-	-	-
SLIMCAT 3D	-0.4, -0.6	-0.5, -0.7	-	-	-0.6, -0.7	-
<b>This study</b>	<b>-0.21, -0.13</b>	<b>-0.38, -0.11</b>	<b>-0.66, -0.14</b>	<b>-0.62, -0.003</b>	<b>-0.13, -0.16</b>	<b>-0.45, -0.27</b>

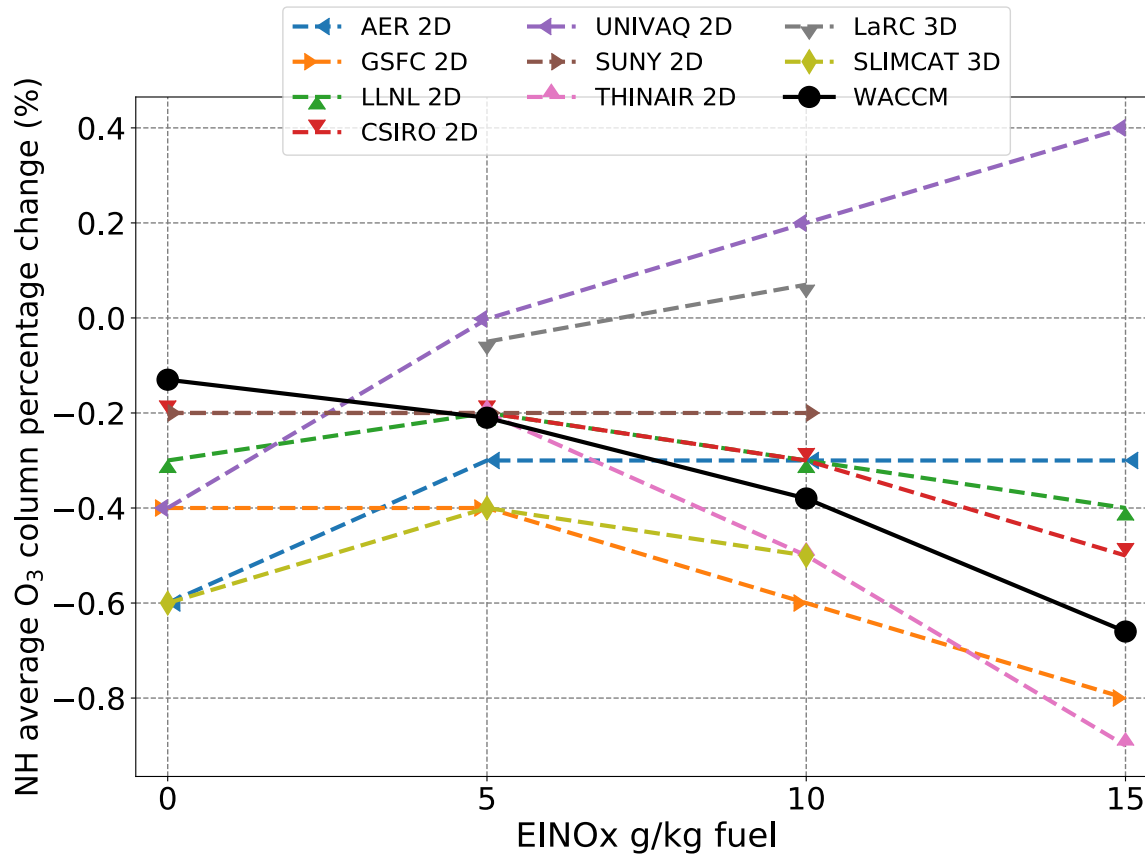


**Figure 1.** Northern Hemisphere (NH) total ozone column change (%) as a function of EINOx for a fleet size of 500 supersonic aircraft. Results from earlier models are shown in dashed lines while the WACCM results are shown in solid black line.

### Milestones

- Journal paper completed to examine effects of historical projected fleets of supersonic aircraft on stratospheric ozone and climate. Paper under review with the *Journal of Geophysical Research*. This paper provides a historical context for further studies of supersonic aircraft effects on ozone and climate.
- NO<sub>x</sub> and H<sub>2</sub>O emissions from fleets of HSCTs can potentially affect stratospheric ozone and climate.
- New analyses on ozone change from HSCTs are similar to results from the 1999 NASA and IPCC aviation assessments, although with a greater sensitivity to NO<sub>x</sub> emissions.
- Ozone effects from an HSCT fleet depends on the amount of NO<sub>x</sub> and H<sub>2</sub>O emissions and resulting chemical interactions through ozone destroying catalytic cycles.
- These studies provide important context for the studies of actual projected fleets that we will be examining next in our studies.

## Task 2 – Conducting Sensitivity Studies on Cruise Altitude

University of Illinois at Urbana-Champaign

### Objectives

This study is intended to show how the stratosphere responds to different cruise altitudes. The potential effects from hypothetical fleets of stratospheric-flying aircraft will be evaluated by conducting a series of sensitivity studies in a projected realistic 2050 background atmosphere.

### Research Approach

Here we use a state-of-the-art 3D chemistry-transport model to evaluate the sensitivity of the atmosphere, especially the stratosphere, to different cruise altitudes from a possible supersonic aircraft fleet. A parametric approach is applied in which the fleet fuel use, NO<sub>x</sub> emission index as well as the geographical distribution of the emissions are all treated constant while the emission altitude varies systematically at a 2 km cruise range. The cruise emissions are assumed to be uniformly distributed vertically over a 2 km band ranging from 13 to 23 km, with a total of eight emission scenarios.

### Results and Discussions

This study has evaluated the sensitivity of the potential environmental effects at different cruise altitudes of supersonic transport on atmospheric ozone and radiative forcing. A series of sensitivity studies of possible future cruise altitudes were conducted to evaluate the relative atmospheric response from NO<sub>x</sub> and H<sub>2</sub>O emissions for a fleet of supersonic aircraft assumed to fully operational by 2050. For these calculations, a fixed fleet fuel use and geographical distribution is assumed.

For a range of cruise altitudes from 13 to 23 km evaluated in this study, the resulting ozone impacts depending on the altitude and can be either positive or negative if examining the annual and global averaging total ozone column change (Figure 2). For emissions in the upper troposphere and lower stratosphere, such as the cases for cruise altitude between 13 and 17 km, total column ozone indicates a slight increase. At these altitudes, the ozone chemistry is affected by the coupling of HO<sub>x</sub>/NO<sub>x</sub>/ClO<sub>x</sub>/BrO<sub>x</sub> chemistry and the resulting ozone impact is less significant and much less dependent on the altitude of the aircraft emissions. At higher cruise altitudes from 17 to 23 km, where the ozone chemistry is dominated by NO<sub>x</sub> and the stratospheric lifetimes are longer, stratospheric ozone is reduced, primarily as a result of the NO<sub>x</sub>-O<sub>3</sub> catalytic cycles, and the magnitude of the ozone destruction increases with higher cruise altitude. The resulting changes in total column ozone at these altitudes is highly dependent on the cruise altitude. A cruise altitude from 16 to 18 km shows a minimal total column ozone change resulting from the offsetting effects of ozone production and reduction at different heights. The inflection point is at around 17 km, where the effect from supersonic emission on ozone transitions from ozone production to ozone depletion. The maximum total column ozone loss occurs in the NH high latitudes in the fall to winter season. With higher cruise altitudes, more ozone depletion is found in the SH as more emitted NO<sub>x</sub> and H<sub>2</sub>O are lifted upward and transported southward across the equator.

This study looked at a range of cruise altitudes that encompass the range of the concepts currently being discussed by the industry for supersonic business jets and smaller supersonic airliners. The sensitivity study is based on an assumed Mach-2.4, 300-passenger conceptual supersonic airliner and a projected network based on its 5000 nautical mile range that was developed in the 1990s. As a consequence, the fleet fuel use in these studies is likely larger than any of the much smaller business jets being considered. Likewise, their range, projected markets, utilization, and fleet sizes could be much different, which would result in changes to the geographical patterns of the emissions. If developers are successful at developing designs with low sonic boom, then the geographical distributions could also be quite different because of flights occurring over land. When viewed as impact scaled by fleet fuel use, this study provides insights on the potential impacts on ozone relative to cruise altitudes (Figure 2). As such, this study suggests that developing low NO<sub>x</sub> combustors could be important if large fleets of supersonic aircraft flying at the highest altitudes ever become viable. In future studies, the environmental effects of other design and operation parameters need to be evaluated thoroughly to facilitate technological development in order to make widespread supersonic travel more environmentally feasible.

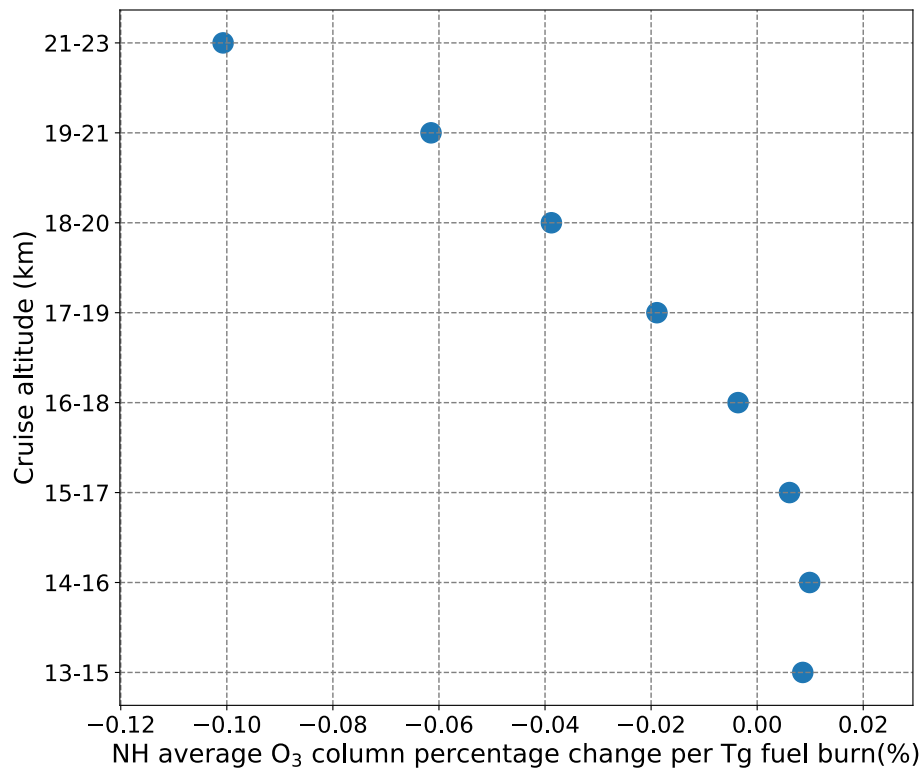


**Figure 2.** Northern Hemisphere total column ozone change (%) per Tg of fuel burn as a function of cruise altitudes.

### Milestones

- Journal paper completed and submitted to the *Journal of Geophysical Research* examining the sensitivity of fleets of supersonic aircraft on stratospheric ozone and climate. This study provides further context for future studies of the environmental effects from future fleets of supersonic aircraft.
- Stratospheric ozone response of supersonic aircraft emissions depends on cruise altitudes and the sensitivity of ozone to emissions was found to increase with altitudes.
- The calculated ozone impact is small for cruise altitudes below 17 km and the ozone depletion increase sharply as the cruise altitudes increase above 17 km.
- Low NOx combustors may be important to consider for fleets of potential future supersonic aircraft with cruise altitudes above 17 km.
- These studies provide important context for the studies of actual projected fleets that we will be examining next in our studies.

### Major Accomplishments

The model performs well and the results establish a new paradigm for studies of the impacts from fleets of supersonic aircraft, while also being consistent with earlier studies.

Completed the sensitivity studies. Submitted the journal paper.

### Publications

Zhang, J., Wuebbles, D. J., Kinnison, D. E., & Baughcum, S. L. Potential Impacts of Supersonic Aircraft Emissions on Ozone and Resulting Forcing on Climate. Volumes 1 and 2. Both papers are submitted to the *Journal of Geophysical Research*, September 2020.



### **Outreach Efforts**

ASCENT Advisory Committee Meeting, September 2020 (Presentation).

Bi-weekly meeting with project manager.

ICAO Impacts and Science Group (ISG) meetings (monthly) for Dr. Wuebbles.

### **Student Involvement**

Graduate Student Jun Zhang is responsible for the analyses and modeling studies within the project and leading the initial preparation of the project reports.

### **Plans for Next Period**

- Begin studies based on the emission inventories developed by ASCENT Project 10 to consider specific designs of supersonic transports (SSTs).
- Use the results from this study to inform the development of Aviation Portfolio Management Tool – Impacts Climate (APMT-IC) for supersonic impacts (ASCENT Project 58).

### **References:**

Kawa, S. R., Anderson, J. G., Baughcum, S. L., Brock, C. A., Brune, W. H., Cohen, R. C., ... & Waugh, D. (1999). Assessment of the effects of high-speed aircraft in the stratosphere: 1998. National Aeronautics and Space Administration report. NASA/TMM1999-209237.

Penner, J. E., Lister, D. H., Griggs, D. J., Dokken, D. J., & McFarland, M. (Eds). (1999). Aviation and the global atmosphere (pp. 1-373). Cambridge, UK: Cambridge University Press.



# Project 023 Analytical Approach for Quantifying Noise from Advanced Operational Procedures

## Massachusetts Institute of Technology

### Project Lead Investigator

R. John Hansman  
T. Wilson Professor of Aeronautics & Astronautics  
Department of Aeronautics & Astronautics  
Massachusetts Institute of Technology  
Room 33-303  
77 Massachusetts Ave  
Cambridge, MA 02139  
617-253-2271  
rjhans@mit.edu

### University Participants

#### Massachusetts Institute of Technology

- PI: R. John Hansman
- FAA Award Number: 13-C-AJFE-MIT, Amendment Nos. 008, 015, 022, 031, 046, and 051
- Period of Performance: October 1, 2019 to September 30, 2020
- Tasks:
  1. Evaluate the noise impacts of flight track concentration or dispersion associated with performance-based navigation (PBN) arrival and departure procedures.
  2. Identify the key constraints and opportunities for procedure design and implementation of noise-minimizing advanced operational procedures.
  3. Develop concepts for arrival and departure procedures that consider noise impacts in addition to operational feasibility constraints.
  4. Analyze location-specific approach and departure design procedures in partnership with affected industry stakeholders.

### Project Funding Level

FAA provided \$860,000 in funding and \$860,000 in matching funds were provided by the Massachusetts Institute of Technology (MIT) (approximately \$80,000) and from the Massachusetts Port Authority (Massport) (approximately \$780,000).

### Investigation Team

- Professor R. John Hansman (PI)
- Jacqueline Thomas (research scientist)
- Sandro Salgueiro (graduate student)
- Clement Li (graduate student)
- Madeleine Jansson (graduate student)
- Ara Mahseredjian (graduate student)
- Kevin Zimmer (graduate student)



## Project Overview

This project is evaluating the noise reduction potential from advanced operational procedures in the terminal (arrival and departure) phases of flight. The noise impact from these procedures is not well understood or modeled in current environmental analysis tools, presenting an opportunity for further research to facilitate air traffic management (ATM) system modernization. This project is leveraging a noise analysis framework developed at MIT under ASCENT Project 23 to evaluate a variety of sample procedures. In conjunction, the project is contributing to the memorandum of understanding between the FAA and Massport to identify, analyze, and recommend procedure modifications at Boston Logan International Airport (Boston Logan hereafter).

## Task 1 – Evaluate the Noise Impacts of Flight Track Concentration or Dispersion Associated with Performance-Based Navigation (PBN) Arrival and Departure Procedures

Massachusetts Institute of Technology

### Objectives

This Task evaluates the impact of flight track concentration arising from PBN procedure implementation and the potential noise mitigation impact of track dispersion. The effects of track concentration due to PBN procedure implementation have not been fully explored. Although the potential benefits of PBN for flight efficiency and predictability are well understood, the resulting environmental impact has caused increased community awareness and concern over the procedure design process. Current methods and noise metrics do not provide adequate information to inform policy decisions relating to noise concentration or dispersion due to PBN implementation.

In this Task, models were used to evaluate noise concentration scenarios using a variety of metrics and procedure design techniques. Noise data from Massport were used to support the simulation effort. The impact of track dispersion was compared with potential community noise reduction through noise-optimal required navigation performance procedure designs that avoid noise-sensitive areas and use background noise masking where possible.

### Research Approach

- Evaluate the impact of noise dispersion directly through modeling of a dispersed set of flight tracks in the Aviation Environmental Design Tool (AEDT).
- Analyze population exposure impact using multiple metrics, including day-night average sound level (DNL) and  $N_{above}$ .
- Validate which metrics best capture the impacts of noise concentration and dispersion.

### Major Accomplishments

- Reviewed previously proposed dispersion-based procedure concepts with stakeholders (FAA, controllers, airlines, communities) and identified key procedure design constraints.
- Developed new procedure alternatives for achieving dispersion of flight tracks on departure at Boston Logan based on early divergence of area navigation (RNAV) paths. The new design is believed to satisfy all previously identified stakeholder concerns.
- Conducted detailed design of the new proposed procedures using the FAA's standard procedure design tool, TARGETS, and sent them for evaluation by an FAA PBN design group.



## Task 2 – Identify the Key Constraints and Opportunities for Procedure Design and Implementation of Noise-Minimizing Advanced Operational Procedures

Massachusetts Institute of Technology

### Objectives

Arrival and departure procedure design is subject to physical, regulatory, and workload constraints. Procedures must be flyable by transport-category aircraft using normal, stabilized maneuvers and avionics. The procedures must comply with Terminal Instrument Procedures (TERPS) guidelines for obstacle clearance, climb gradients, and other limitations. The procedures must be chartable and work within the limitations of current flight management systems. Advanced operational procedures must also be compatible with airport and air traffic control operations, avoiding workload saturation for air traffic controllers and pilots.

This Task involved evaluating the key constraints affecting advanced operational procedures and opportunities to improve noise performance, identifying those that may affect design and implementation. This process involved collaboration with pilots, air traffic controllers (ATC), procedure designers, and community members. The Task also considered current research and evidence on physical, psychological, and social impacts of aircraft noise, as well as emerging issues such as community perceptions of equity and the effect of overflight frequency on noise perception.

### Research Approach

- Meet with key stakeholders in the implementation pathway to understand procedure development processes, timeline, and constraints.
- Research documentation on regulations and operational standards influencing new flight procedure development.
- Consult with stakeholders during candidate advanced operational procedure development to identify potential implementation obstacles.

### Major Accomplishments

- Met with airport operators, airline technical pilots, and air traffic controllers to discuss potential concepts for advanced operational procedures.
- Identified key constraints in procedure design related to criteria, air traffic control operational rules, and airspace.
- Implemented all previously proposed Boston Block 2 procedures in the FAA's standard procedure design tool, TARGETS, and verified that the new identified constraints are met. All proposed procedures for RWY 22L/R, 27, and 33L currently pass all criteria and flyability tests in TARGETS.

## Task 3 – Develop Concepts for Arrival and Departure Procedures that Consider Noise Impacts in Addition to Operational Feasibility Constraints

Massachusetts Institute of Technology

### Objectives

This Task applied the findings from Task 2 to identify a set of generic constraints and procedures for designing feasible and flyable advanced operational procedures to minimize noise perception as measured by traditional metrics (e.g., 65 dB DNL) and alternative metrics that address noise concentration concerns introduced by PBN procedures and emerging equity issues. Given an understanding of technology capabilities and operational constraints, in this Task we developed potential operational concepts and identified potential implementation pathways for both specific locations and generalizable operational concepts. Some of the approaches considered were:

- Lateral track management approaches (e.g., dispersion, parallel offsets, equivalent lateral spacing operations, multiple transition points, vectoring, high background noise tracks, and critical point avoidance tracks).
- Vertical/speed thrust approaches (e.g., thrust tailoring, steep approaches, and delayed deceleration approaches).

In addition, procedures were identified and categorized for the noise reduction effort at Boston Logan. These included Block 1 procedures, which were characterized by clear predicted noise benefits, limited operational/technical barriers, and a lack



of equity issues, and Block 2 procedures, which exhibited greater complexity due to potential operational and technical barriers, as well as equity issues (defined as noise redistribution between communities).

### **Research Approach**

- Use feedback from Task 2 to identify procedures with noise reduction potential.
- Model procedures using AEDT and the Aircraft Noise Prediction Program (ANOPP) for generic runways to evaluate noise impacts for candidate procedures on a single-event or integrated basis.
- Determine noise impacts based on multiple metrics that are location-agnostic (i.e., contour area) as well as location-specific (i.e., population exposure at specific runways).

### **Major Accomplishments**

- Identified key constraints for lateral, vertical, and speed profile redesign based on ATC operational guidelines and FAA procedure design criteria.
- Investigated a *thrust cutback* concept for departure procedures, in which aircraft momentarily reduce engine thrust by flying a procedural level segment on departure, therefore also reducing engine noise.
- Identified final candidate Block 2 procedures for noise reduction at Boston Logan. These include procedures that shift lateral tracks, procedures that increase total flight track dispersion, and procedures that allow for more optimal descent and deceleration on approach.

## **Task 4 – Analyze Location-Specific Approach and Departure Design Procedures in Partnership with Affected Industry Stakeholders**

Massachusetts Institute of Technology

### **Objectives**

Advanced operational procedures may be particularly applicable for specific airports based on local geography, population density, operational characteristics, fleet mix, and local support for procedure modernization (among other factors). Specific procedures are being evaluated at a series of representative airports around the United States. This Task involves collaboration with multiple airports and air carriers on potential opportunities at locations that would benefit from advanced PBN procedures.

For the Boston Logan noise reduction project, this Task also involves collaboration with the FAA 7100.41 PBN working group, which is the initial operation evaluation group for new procedure design concepts.

### **Research Approach**

- Coordinate with a specific airport operator to evaluate procedure design opportunities with noise reduction potential.
- Work closely and communicate with affected stakeholders throughout the procedure evaluation, design, and analysis process to ensure that key constraints and objectives are appropriate for the selected location on a procedure-by-procedure basis.

### **Major Accomplishments**

- Continued regular meetings and collaboration with Massport to finalize Block 2 procedure recommendations for Boston Logan.
- Conducted redesign of specific Block 2 procedures after initial feedback from stakeholder group that included FAA, controllers, and airlines.
- Presented revised detailed procedure design conducted in TARGETS to FAA PBN group and sent proposed procedure implementation for review.
- Performed detailed noise analysis for all Block 2 procedure concepts that addressed community concerns, including population impact estimation based on census data.

### **Publications**

- “Block 1 Procedure Recommendations for Logan Airport Community Noise Reduction,” 2017.  
Link: <http://hdl.handle.net/1721.1/114038>



- Thomas, J; Hansman, J. “Framework for Analyzing Aircraft Community Noise Impacts of Advanced Operational Flight Procedures,” *Journal of Aircraft*, Volume 6, Issue 4, 2019. <https://doi.org/10.2514/1.C035100>
- Thomas, J., Yu, A., Li, C., Toscano, P., and Hansman, R.J. “Advanced Operational Procedure Design Concepts for Noise Abatement” In *Thirteenth USA/Europe Air Traffic Management Research and Development Seminar*, Vienna, 2019.
- Yu, A., and Hansman, R.J. “Approach for Representing the Aircraft Noise Impacts of Concentrated Flight Tracks” *AIAA Aviation Forum 2019*, Dallas Texas, 2019.

### **Outreach Efforts**

- September 27, 2017: Poster to ASCENT Advisory Board.
- December 5, 2017: Call with Boeing to discuss procedure noise impact validity.
- March 16, 2018: Discussion with Minneapolis-St. Paul (MSP) Airport about metrics.
- April 4, 2018: Poster to ASCENT Advisory Board.
- May 7, 2018: Presentation to FAA 7100.41 PBN Working Group.
- June 24, 2018: Discussion with air traffic controllers about dispersion concepts.
- July 23, 2018: Briefing to FAA Joint University Program research update meeting.
- October 9, 2018: Poster to ASCENT Advisory Board.
- November 8, 2018: Presentation to Airline Industry Consortium.
- March 3, 2019: Presentation to the Aviation Noise and Emissions Symposium
- October 15, 2019: Presentation to the ASCENT Advisory Board.
- November 12, 2019: Presentation to Airline Industry Consortium.
- Numerous community meetings.
- Numerous briefings to politicians representing eastern Massachusetts (local, state, and federal).
- Briefing to FAA Management Advisory Council.
- In-person outreach and collaboration with Massport, operator of Boston Logan and ASCENT Advisory Board member.

### **Awards**

2018 Dept of Transportation/FAA COE Outstanding Student of the Year Award to Jacqueline Thomas.

### **Student Involvement**

Graduate students have been involved in all aspects of this research in terms of analysis, documentation, and presentation.

### **Plans for Next Period**

The next phase of this project will involve a detailed review with all key stakeholders of the latest procedure redesigns proposed for Boston Logan and conducted in TARGETS. Following procedure acceptance by FAA and airline stakeholders, a new round of community outreach will be conducted to communicate the noise impact of these new procedures, as well as to inform communities of potential tradeoffs among procedure options. Finally, MIT will produce a Block 2 report for Massport with the final proposals for Boston Logan that have been generated after multiple rounds of stakeholder feedback. The final procedure ideas are expected to also inform recommendations to airport operators, airlines, and the FAA to develop noise-mitigating advanced operational procedures at other locations in the National Airspace System.



# Project 025 Shock Tube Studies of the Kinetics of Jet Fuels

## Stanford University

### Project Lead Investigator

Ronald K. Hanson  
Woodard Professor  
Mechanical Engineering Department  
Stanford University  
452 Escondido Mall  
650-723-6850  
rkhanson@stanford.edu

### University Participants

#### Stanford University

- Pls: Prof. Ronald K. Hanson
- FAA Award Number: 13-C-AJFE-SU-027
- Period of Performance: October 1, 2019, to September 30, 2020
- Task:
  1. Area #1: Chemical kinetics combustion experiments.

### Project Funding Level

2019/2020: FAA provided \$110,000 in funding and Stanford University provided 1:1 in matching funds of \$110,000.  
2020: FAA provided \$300,000 in funding and Stanford University provided 1:1 in matching funds of \$300,000.

### Investigation Team

- Prof. Ronald K Hanson, principal investigator, research direction
- Dr. David F Davidson, senior research engineer, research management
- Yu Wang, graduate student, research assistant
- Nicolas Pinkowski, graduate student, research assistant
- Vivek Boddapati, graduate student, research assistant
- Alison Ferris, graduate student, research assistant

### Project Overview

The sixth year of this program has focused on developing strategies for the accurate prediction of jet fuel properties (chemical and physical) and the further development of a fundamental kinetics database to describe the combustion behavior of modern jet fuels. To achieve these two goals, research focused on two project areas: correlation of chemical, physical, and combustion fuel properties with infrared (IR) spectral features, and shock tube/laser absorption kinetics measurements to characterize JP8, JP5, and Jet-A pyrolysis. The results of the infrared (IR) spectral analysis work will be used to reveal the sensitivity of combustion properties to jet fuel composition, with the ultimate goal of developing a rapid pre-screening approach, requiring minimal fuel volume, to simplify the alternative jet fuel certification process. The shock tube/laser absorption results will be used as input constraints for the development and refinement of hybrid-chemistry (HyChem) models for jet fuel combustion.



## Task 1 – Chemical Kinetics Combustion Experiments

Stanford University

### Objectives

This work aims to develop fuel prescreening tools based on the IR absorption cross-section measurements of jet fuels and their constituent molecules. Specific fuel analysis objectives include developing effective strategies for correlating (1) functional group and molecular species composition and (2) chemical, physical, and combustion properties of jet fuels with their IR spectra.

A second area of research includes shock tube/laser absorption experiments to characterize JP8/JP5/Jet-A fuels and extend the fundamental kinetics database built over the past five years. One particular objective has been to conduct shock tube experiments to obtain species time-history measurements of alkane, alkene, and aromatic formation during pyrolysis under conditions comparable to those used to characterize previous FAA fuels.

This multi-year research program aims to culminate in the completion of American Institute of Aeronautics and Astronautics (AIAA) book chapters describing the research progress of the past six years, notably, advancements in our understanding of jet fuel chemical kinetics and fuel prescreening techniques.

Finally, it should be noted that species time-history measurements conducted in shock tubes provide valuable fundamental kinetics data for FAA fuels. These data are a critical input for Area #2, which seeks to develop a new hybrid and detailed kinetics model for jet fuels (HyChem). The data provided will also ensure that the combustion models developed in Area #4 (combustion model development and validation) to model the extinction and ignition processes controlling lean blowout, cold ignition, and high altitude relight are chemically accurate.

### Research Approach

An important goal of the current research is to investigate the possibility of characterizing jet fuel composition and combustion behavior based on the fuel's mid-IR absorption spectrum, measured using a Fourier transform IR (FTIR) spectrometer. As the shock tube/spectroscopic research has progressed under FAA support, a large database of kinetic and spectroscopic measurements for a variety of jet fuels and jet fuel components has been acquired. Using this database, we have developed correlations between the spectroscopic properties of neat jet fuel with fuel composition and with important combustion parameters such as derived cetane number (DCN), lean blowout, and C<sub>2</sub>H<sub>4</sub> pyrolysis yields. Presented here is an overview of the two research thrusts (IR fuel analysis and shock tube/laser absorption measurements), along with exemplary experimental results obtained over the past year.

#### **IR fuel analysis: methods and results**

An FTIR instrument (Nicolet 6700) and heated cell are used to measure the mid-IR spectra of gas-phase fuel samples. Analysis of gas-phase samples allows for the detection of sharper spectral features, even individual absorption transitions, which can in turn be tied directly to structural characteristics of fuel molecules. This work focuses on analysis of mid-IR absorption spectra, due to the strong sensitivity of the mid-IR region to hydrocarbon bonding. Initial investigations have focused primarily on the 3- $\mu\text{m}$  region, although future work aims to extend this range to 2–15  $\mu\text{m}$ . Advanced statistical methods, including cross-validated models with Lasso regularization, are used to interpret the mid-IR spectra.

In the previous year of this program, a strategy (Strategy 1) was developed for estimating physical and chemical properties of fuels directly from mid-IR spectra. In the current year of this program, three additional strategies (referred to as Strategy 2, 3, and 4) were developed for estimating molecular functional group fractions, global fuel properties, and molecular species constituents, respectively. The workflow of the three newest strategies is shown in Figure 1, and the methods and results for each will be described here.

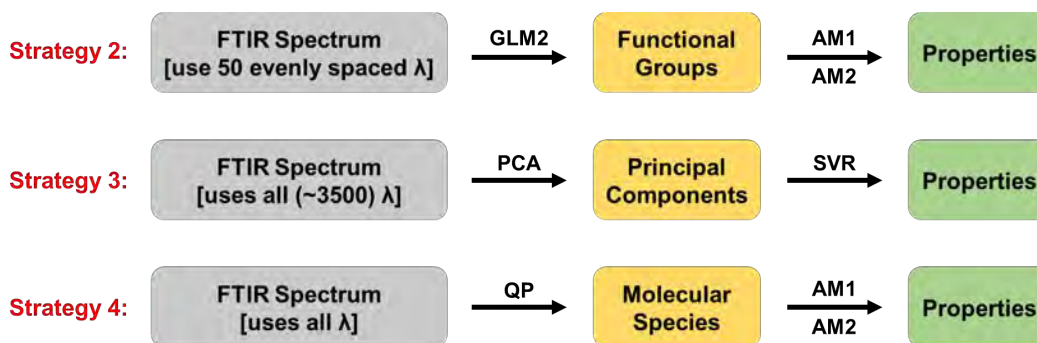


**Figure 1.** Flow chart of three new strategies developed to estimate physical and chemical properties of conventional jet fuels and sustainable aviation fuels from FTIR spectra. (GLM2 = Generalized Linear Model with Grouped-Lasso Regularization, AM1/AM2 = linear (1)/nonlinear (2) group additivity models, PCA = principal component analysis, SVR = support vector regression, QP = quadratic programming).

Strategy 2 was implemented and used to demonstrate the correlation between FTIR spectra from 3300–3500 nm and  $-\text{CH}_2$ ,  $-\text{CH}_3$ , and “other” functional groups; subsequent linear and nonlinear group additivity models were then used to estimate 14 physical and chemical properties for 69 hydrocarbon fuels. Optimization of a generalized linear model with grouped-Lasso regularization indicates that 10 wavelengths are necessary to accurately correlate measured absorption cross-sections with the number of  $-\text{CH}_2$  and  $-\text{CH}_3$  functional groups in each fuel. Figure 2 shows a comparison of known  $-\text{CH}_2$  and  $-\text{CH}_3$  functional group fractions, defined as the fraction of a fuel’s hydrogen atoms contained in each functional group type, to fitted functional group fractions. The two plots indicate that the linear model with grouped-Lasso regularization is generally a good fit to the data, but that smaller molecules (e.g., hexane, 2,2-dimethylbutane, etc.) may be fit better with alternative spectrum-functional group relations.

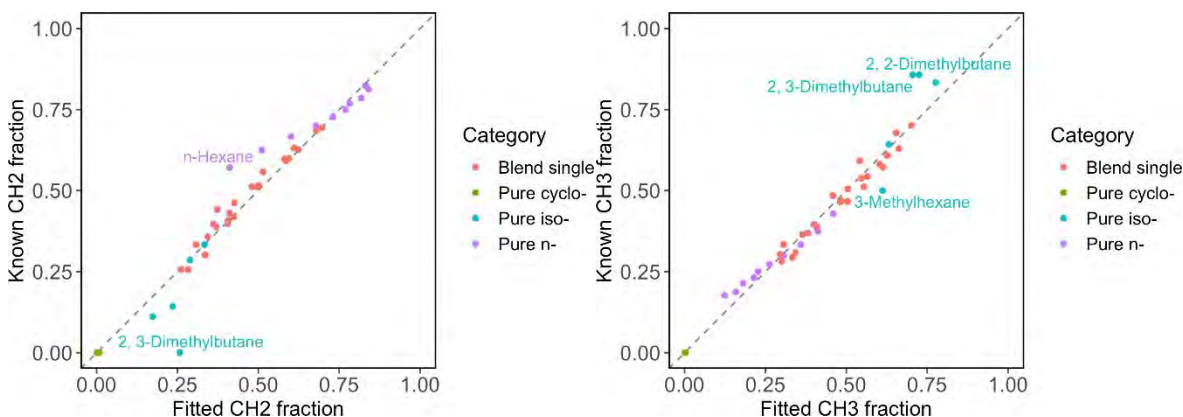


**Figure 2.** Known fraction of alkyl  $\text{CH}_2$  versus fitted fraction of alkyl  $\text{CH}_2$  (left) and known fraction of alkyl  $\text{CH}_3$  versus fitted fraction of alkyl  $\text{CH}_3$  (right). Dashed gray line denotes line of equivalence.

After estimating the functional group fractions of each fuel, the number of each functional group present in each average fuel molecule can be calculated by multiplying the fractions by the total number of hydrogen atoms per average molecule. With the number of each type of functional group in a given fuel known, group additivity models can be used to determine physical and chemical properties.

Strategy 3 uses principal component analysis (PCA) and support vector regression (SVR) to directly correlate mid-IR spectral features with physical and chemical fuel properties. PCA is a preprocessing step that transforms input data (FTIR spectra) into its principal components. These principal components are independent linear combinations of the input features, arranged in decreasing order of importance, thereby enabling significant dimensionality reduction without significant information loss. Use of PCA eliminates redundancies in the training data, reduces the chance of overfitting data, and extracts

data-driven latent features that would otherwise not be readily apparent. SVR maps this input data onto a high-dimensional feature space where it can be fit by an appropriate linear hyperplane. Optimal SVR model parameters are chosen by performing a grid search, using the minimum cross-validation error (RMSE) as the performance metric. Table 1 shows the prediction error for three fuel properties—molecular weight (MW), kinematic viscosity (KV) at -20 C, and DCN—as calculated using the Strategy 1 and Strategy 3 approaches. As seen in the tabulated results, Strategy 3 has a lower prediction error than Strategy 1 for all of the properties considered.

**Table 1.** Prediction errors for three properties (molecular weight, kinematic viscosity, derived cetane number), as calculated using Strategy 1 and Strategy 3.

Method	Prediction Error (RMSE %)		
	MW	KV (-20 C)	DCN
Strategy 1	3.45	9.62	6.51
Strategy 3	2.29	7.09	3.91

Strategy 4 was developed to infer the molecular species content of a fuel from its IR spectrum. This strategy uses a constrained least squares optimization approach to accurately identify the components of a blended fuel and predict their respective mole fractions. This information is then used to determine the C and H number, and consequently, the average molecular weight of the composite fuel. Although still in development, Strategy 4 has been tested on a real fuel (gasoline) and excellent agreement between the estimated and actual fuel composition was observed (see Figure 3).

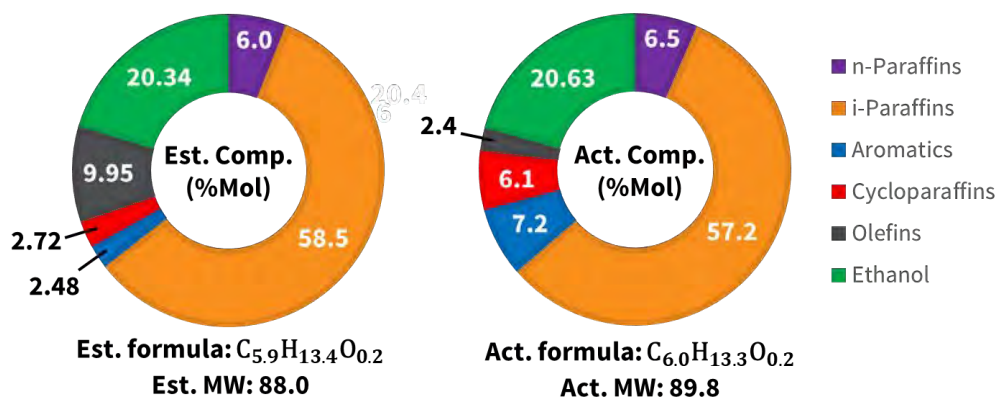


**Figure 3.** Comparison of estimated and actual compositional breakdown of a real fuel sample (gasoline). Estimates were obtained using Strategy 4.

Overall, the IR analysis results obtained using the three strategies developed over the past year show improved predictive performance relative to the initial spectral analysis strategy developed in the first year of this work (Strategy 1). In addition to being able to predict physical and chemical fuel properties, the newly developed analysis strategies also provide valuable insight into the functional groups and molecular species present in a fuel mixture.

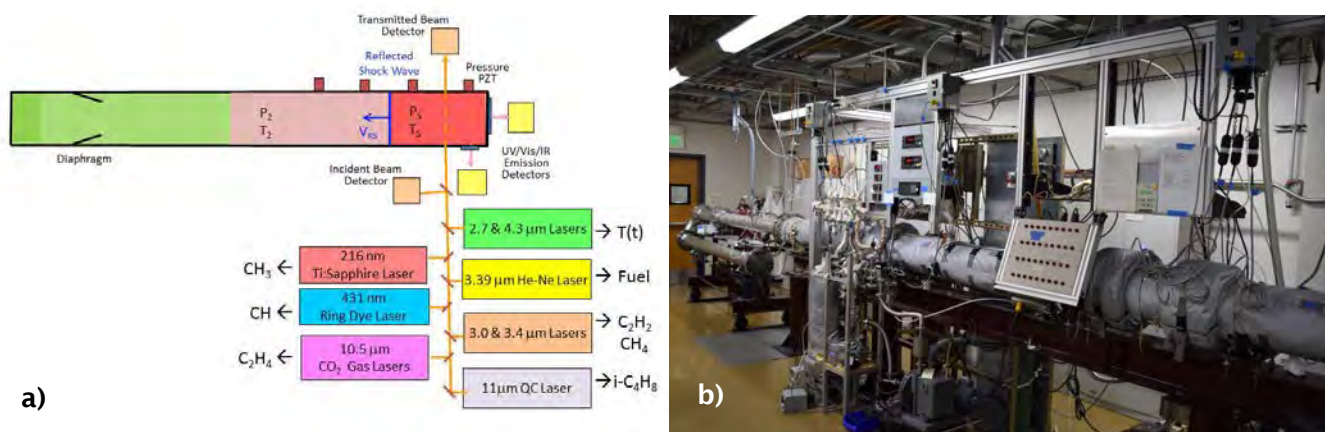
### Shock tube experiments: methods and results

The development, refinement, and validation of detailed reaction mechanisms describing the pyrolysis and oxidation of fuels require experimental data as targets for kinetics models. Experimentally, the best way to provide these targets at high temperatures and pressures is with shock tube/laser absorption experiments, conducted over a wide range of pressures, temperatures, and fuel and oxidizer compositions.

Reflected shock wave experiments provide a test environment that does not introduce additional fluid mechanics, turbulence, or heat transfer effects to the target phenomena. This allows isolation of the target phenomena (ignition time delays (IDTs) and species concentration time-histories) in a quiescent high-temperature, high-pressure environment that is very well characterized and hence amenable to modeling. In these experiments, temperatures from <500 to >3000 K, and pressures

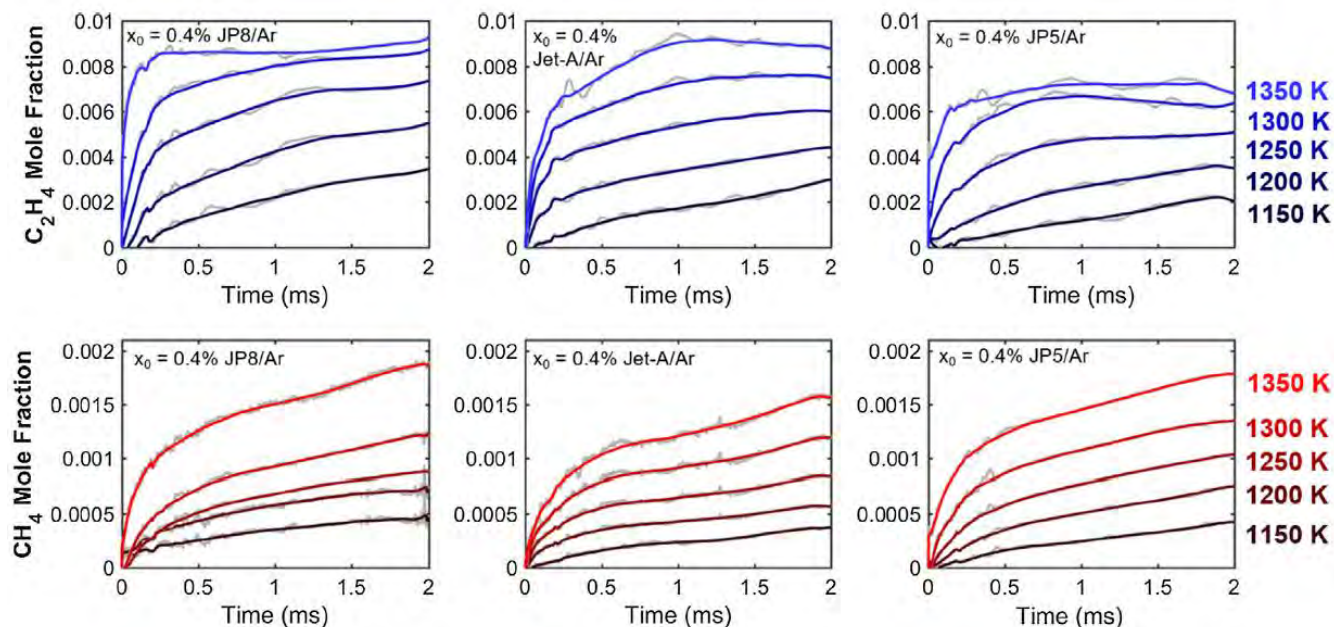
from sub-atmospheric (0.2 atm) to >500 atm can be achieved in different carrier gases, such as argon or air, with demonstrated test times up to and exceeding 50 ms at low temperatures.

The strength in the Stanford shock tube approach comes from the implementation of laser diagnostics that enable the simultaneous measurement of species time-histories. Using laser absorption diagnostics developed over the past 30 years, we are able to provide quantitative time-histories during fuel pyrolysis and oxidation of the fuel, including transient radicals (e.g., OH, CH<sub>3</sub>), stable intermediates (e.g., CH<sub>4</sub>, C<sub>2</sub>H<sub>4</sub>, isobutene, CH<sub>2</sub>O, and aromatics), combustion products (including CO, CO<sub>2</sub>, and H<sub>2</sub>O), and temperature (see Figure 4a). Furthermore, measurements of the pyrolysis and oxidation systems of real fuels, rather than of surrogates or solvent surrogates, provide a direct link to actual fuel behavior. To facilitate shock-tube studies of low-vapor pressure fuels like jet fuels, the shock tube facility must be heated, as is the case in the high-purity, large-diameter (14 cm internal diameter) shock tube facility used in this work (pictured in Figure 4b).



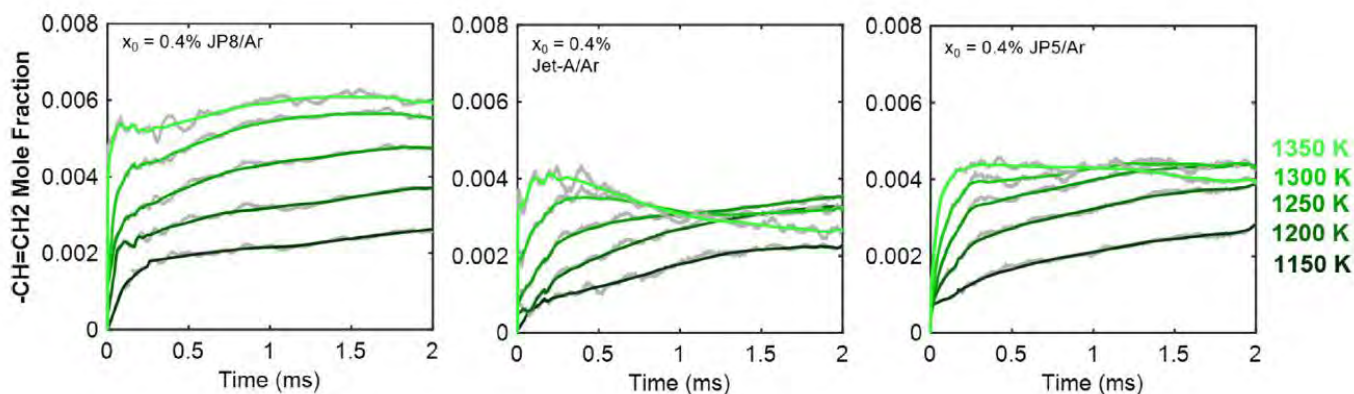
**Figure 4.** (a) Schematic of shock tube/laser absorption setup. Simultaneous measurement of multiple species time-histories and temperature with microsecond time resolution are enabled using this arrangement (only a partial list of accessible species is indicated); and (b) Stanford 14-cm-diameter, heated shock tube.

In our recent work, an absorbance model, connecting data spanning three years and eight laser wavelengths, was developed to enable the improved spectroscopic study of three jet fuels: JP8, Jet-A, and JP5. Specifically, methane (CH<sub>4</sub>), ethylene (C<sub>2</sub>H<sub>4</sub>), and lumped vinyl-group time-histories, in addition to aromatics (benzene and toluene) yields, were quantified using eight wavelengths over conditions 1040–1480 K, 1–3 atm. Figure 5 shows the C<sub>2</sub>H<sub>4</sub> and CH<sub>4</sub> species time-histories at five temperatures for each of the three fuels. Both C<sub>2</sub>H<sub>4</sub> and CH<sub>4</sub> time-histories are relatively consistent across each fuel, with JP8 showing stronger C<sub>2</sub>H<sub>4</sub> formation at earlier times at high temperatures, and higher CH<sub>4</sub> formation at the highest temperature.



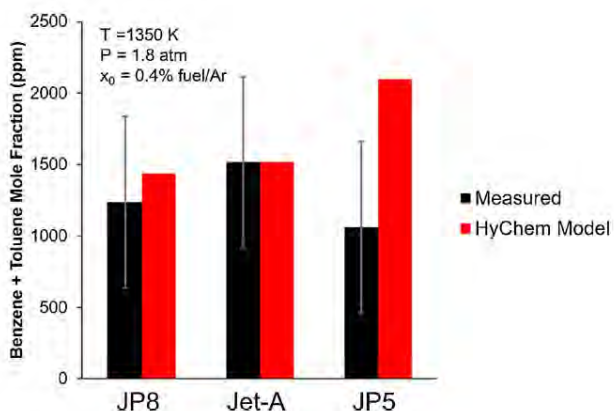
**Figure 5.** Mole fraction time-histories of ethylene (top row) and methane (bottom row) during pyrolysis of 0.4% JP8 (left), Jet-A (center), and JP5 (right) at 1.8 atm.

Figure 6 shows the mole fraction time-histories of vinyl groups during the pyrolysis of JP8, Jet-A, and JP5. The mole fractions shown correspond to the combined formation of propene (one vinyl group), 1-butene (one vinyl group), and twice 1,3-butadiene (two vinyl groups). Notably, the vinyl-group time-history for Jet-A begins to decay at high temperatures, while JP8's vinyl-group time-histories continue to grow. This is likely caused by a different blend of vinyl-group-containing species between the two fuels: the larger molecules 1-butene and 1,3-butadiene break down faster than propene, indicating their presence is more prevalent in the Jet-A pyrolysis system than the JP8 pyrolysis system.



**Figure 6.** Mole fraction time-histories of vinyl groups during the pyrolysis of JP8 (left), Jet-A (center), and JP5 (right) between 1150–1350 K.

Figure 7 shows aromatics (benzene and toluene) yields at 2 ms, 1350 K, and 1.8 atm for the three jet fuels. The JP8 and Jet-A results show close agreement with HyChem model predictions, while the JP5 measurements show lower aromatics yields than predicted by HyChem.



**Figure 7.** Inferred aromatics (benzene and toluene) mole fractions at 1350 K and 2 ms during the pyrolysis of JP8, Jet-A, and JP5 (black) compared with HyChem models (red).

Overall, this shock tube/laser absorption work has provided valuable new insights into the formation of jet fuel pyrolysis products methane, ethylene, propene, 1-butene, 1,3-butadiene, benzene, and toluene. Data were generally found to agree with existing HyChem model results and serve as independent validation of our understanding of jet fuel pyrolysis and oxidation chemistry.

### Milestones

Major milestones included regular reporting of experimental results and analysis at monthly meetings for both the Kinetics Working Group and the Steering Working Group, as well as reporting at FAA Quarterly and ASCENT annual meetings.

### Major Accomplishments

During the sixth year of this program, major advances were made in several areas:

- Measurements of methane ( $\text{CH}_4$ ), ethylene ( $\text{C}_2\text{H}_4$ ), and lumped vinyl-group time-histories, in addition to aromatics (benzene and toluene) yields, were acquired in pyrolysis experiments for three jet fuels (JP8, Jet-A, JP5) spanning 1040–1480 K, 1–3 atm.
- A strategy (Strategy 2) was developed for using IR spectra (3.3–3.6  $\mu\text{m}$ ) to estimate the number/fractional presence of  $\text{CH}_2$ ,  $\text{CH}_3$ , and “other” functional groups in a fuel, which in turn can be used to infer physical/combustion properties of the fuel.
- A strategy (Strategy 3) was developed to infer physical and combustion properties of fuels from their IR spectra (3.3–3.6  $\mu\text{m}$ ) via principal component analysis using complex, non-linear models.
- A strategy (Strategy 4) was developed to more accurately identify individual molecular species components and their mole fractions in blended fuels.
- A paper entitled “Spectroscopic inference of alkane, alkene, and aromatic formation during high-temperature JP8, JP5, and Jet-A pyrolysis” was published in the journal *Fuel* (Pinkowski et al., 2020). A paper entitled “A new strategy of characterizing hydrocarbon fuels using FTIR spectra and generalized linear model with grouped-Lasso regularization” was accepted for publication in the journal *Fuel* (Wang et al., 2020).
- Our contribution to the jet fuel prescreening section of the AIAA volume titled *Fuel Effects on Operability of Aircraft Gas Turbine Combustors* was completed.

### Publications

#### Peer-reviewed journal publications

N. Pinkowski, S. Cassady, D.F. Davidson, R.K. Hanson, “Spectroscopic inference of alkane, alkene, and aromatic formation during high-temperature JP8, JP5, and Jet-A pyrolysis,” *Fuel* 269 117420 (2020).

<https://doi.org/10.1016/j.fuel.2020.117420>

Y. Wang, W. Wei, R.K. Hanson, “A new strategy of characterizing hydrocarbon fuels using FTIR spectra and generalized linear model with grouped-Lasso regularization,” *Fuel*, accepted September 30, 2020.



### **Outreach Efforts**

Our IR fuel analysis work was presented via poster at the Fall ASCENT Virtual Meeting, September 29-30, 2020.

### **Awards**

Professor Hanson delivered the 100<sup>th</sup> Beacon lecture at Tsinghua University, China.

### **Student Involvement**

Graduate students are actively involved in the acquisition and analysis of all experimental data. Nicolas Pinkowski (current graduate student) performed the multi-wavelength speciation experiments. Yu Wang and Vivek Boddapati (current graduate students) performed the IR spectral analysis/fuel prescreening. Alison Ferris (current graduate student) has additionally contributed to the project through compilation of experimental results and report writing.

### **Plans for Next Period**

In the next period, we plan to:

- Expand the capability of the Stanford FTIR spectrometer to collect measurements over an expanded mid-IR spectral range (2–15  $\mu\text{m}$ )
- Compile a training dataset containing the full (2–15  $\mu\text{m}$ ) vapor-phase FTIR spectra of real fuels and neat hydrocarbons (specifically those larger than C<sub>8</sub> and relevant to jet fuels) using spectral databases and measurements at Stanford.
- Assess the improvement in predictive performance of Strategies 1–4 using the full spectral range compared to just the 3.4  $\mu\text{m}$  region.
- Apply these wide-spectrum IR analysis methods to prescreening and characterization of real, sustainable aviation fuel (SAF) candidates.
  - Acquire candidate SAF fuel samples and property data from National Jet Fuels Combustion Program (NJFCP) partners.
- Investigate further refinement in IR spectral analysis methods to enhance prediction accuracy and applicability to a wider range of jet fuels, particularly those derived from bio-derived feedstocks.



## Project 027 Advanced Combustion (Area #3)

**Georgia Institute of Technology**  
**Oregon State University**

### Project Lead Investigator

Tim Lieuwen  
Professor  
Aerospace Engineering  
Georgia Institute of Technology  
270 Ferst Drive, G3363 (M/C 0150)  
Atlanta, GA 30332-0150  
404-894-3041  
tim.lieuwen@ae.gatech.edu

### University Participants

#### Georgia Institute of Technology

- PIs:
  - Professor Tim Lieuwen
  - Professor Jerry Seitzman
  - Professor Wenting Sun
- FAA Award Number: 13-C-AJFE-GIT-008
- Period of Performance: 12/1/2014 to 3/31/2020
- Tasks:
  - Task 1 - Lean Blowout. This Task measures the lean blowout (LBO) characteristics of alternative jet fuels and compares them to the LBO characteristics of Jet A.
  - Task 2 - Ignition. This Task measures the ignition probabilities of alternative jet fuels and compares them to the ignition probabilities of Jet A.

#### Oregon State University

- P.I.(s): David Blunck
- FAA Award Number: 13-C-AJFE-OSU-02
- Period of Performance: 12/1/2014 to 3/31/2020
- Task:
  - Task 3 - Turbulent Flame Speed. This Task measures the turbulent flame speeds of alternative jet fuels and compares them to the turbulent flame speeds of Jet A.

### Project Funding Level

#### Georgia Institute of Technology (Georgia Tech)

FAA Funding: \$30,000

Cost Share: \$30,000 provided by Georgia Tech.

#### Oregon State University (OSU)

During the reporting period, the remaining funds were spent and an additional \$4,441 was provided by OSU to complete the project.

### Investigation Team

**Tim Lieuwen (Georgia Institute of Technology):** Principal Investigator. Professor Lieuwen is the PI overseeing all tasks, and is manager of Task 1- Lean Blowout.

**Jerry Seitzman (Georgia Institute of Technology):** Co-Principal Investigator. Professor Seitzman is the manager of Task 2- Ignition.

**David Blunck (Oregon State University):** Co-Principal Investigator. Professor Blunck is the manager of Task 3- Turbulent Flame Speed.

**Wenting Sun (Georgia Institute of Technology):** Co-Principal Investigator. Professor Sun is acting as an internal expert consultant on kinetic mechanisms.

**Tonghun Lee (University of Illinois Champaign):** Co-Principal Investigator. Professor Lee is the lead diagnostic expert.

**Benjamin Emerson (Georgia Institute of Technology):** Research Engineer. Dr. Emerson is responsible for designing and maintaining experimental facilities, as well as experimental operations and management and safety of graduate students. He is also acting as the administrative coordinator for all three Tasks.

**David Wu (Georgia Institute of Technology):** Research Engineer. Mr. Wu is responsible for designing and maintaining experimental facilities, as well as experimental operations and management and safety of graduate students.

**Glenda Duncan (Georgia Institute of Technology):** Administrative Staff. Mrs. Duncan provides administrative support.

**Tiwanna Williams (Georgia Institute of Technology):** Administrative Staff. Mrs. Williams provides administrative support.

**Seth Hutchins (Georgia Institute of Technology):** Lab Coordinator. Mr. Hutchins maintains the core lab facilities and provides technician services.

**Machine Shop Staff (Georgia Institute of Technology):** The Aerospace Engineering machine shop provides machining services for experimental facility maintenance/construction.

**Nick Rock (Georgia Institute of Technology):** Graduate Student. Mr. Rock is leading Task 1.

**Hanna Ek (Georgia Institute of Technology):** Graduate Student. Ms. Ek is the lead data analyst for Task 1.

**Sheng Wei (Georgia Institute of Technology):** Graduate Student. Mr. Wei currently leads Task 2.

**Jonathan Bonebrake (Oregon State University):** Graduate Student. Mr. Bonebrake was the lead grad student experimentalist on Task 3.

**Nathan Schorn (Oregon State University):** Graduate Student. Mr. Schorn recently started and has transitioned to leading the effort to operate the burner and collect and analyze data.

## Project Overview

The objective of this project was to provide advanced combustion testing of alternative jet fuels. We performed this advanced combustion testing to accomplish two goals. The first goal was to rank the lean blowout (LBO) boundaries, ignition probabilities, and turbulent flame speeds of alternative fuels relative to conventional Jet A. The second goal was to produce data that could support the modeling and simulation tasks of other teams. For this second goal, data were measured as needed and as requested by the other teams. These data typically consisted of velocity field measurements, high speed flame images, and test rig boundary conditions.

During this program we have tested twenty total fuel mixtures. Sixteen of these fuels have been pure (un-blended) fuels, known to the program as: A1, A2, A3, C1, C2, C3, C4, C5, S1, S2, S3, high TSI, C7, C8, C9, and n-dodecane. The A1, A2, and A3 fuels represent the range of conventional Jet A fuels. The other fuels have different physical and/or chemical properties. We have also tested three different sets of blends: A2/C1 blends, A2/C5 blends, a C1/n-heptane blend, and a C1/n-dodecane blend. These fuels have been tested under three different Tasks, which are summarized next and which are detailed in the rest of this report.

- (1) The first Task consisted of LBO measurements. The highest priority LBO measurement was fuel screening, where the blowout boundaries of various fuels were compared to the blowout boundary of Jet A. This Task also included measurements of the combustor velocity field, the spatio-temporal evolution of the flame position, and several thermodynamic rig boundary conditions. Thermodynamic boundary conditions included measurements such as air flow rates, surface temperatures, gas temperatures, and gas pressures.
- (2) The second Task consisted of forced ignition measurements. As with Task 1, the highest priority forced ignition measurement was fuel screening. In the case of this forced ignition Task, the fuel screening activity measured the ignition probabilities of various fuels and compared them to the ignition probability of Jet A. Ignition probability is a common measure of combustor ignitability. It was measured by sparking the igniter hundreds of times and measuring the fraction of spark events that successfully ignited the combustor. This Task included a modeling component which began to develop predictive capability for ignition probability. Such a predictive capability would take combustor conditions (pressure, temperature, and fuel-air ratio) in addition to key fuel properties (vaporization and chemical kinetic properties) as inputs and would produce an ignition probability as the output. To support this modeling effort,

Task 2 produced measurements of detailed ignition physics. These detailed measurements captured fuel spray images, ignition kernel images, and flame images.

- (3) The third Task consisted of turbulent flame speed measurements. Like the other two Tasks, the high priority measurement was fuel screening. For this Task, fuel screening compared the turbulent flame speeds of various fuels to the turbulent flame speed of Jet A. This Task additionally had a significant rig development aspect. The rig development added sub-atmospheric pressure capability.

This report covers the last 1.5 years of a 5.5-year program. This report is nearly identical to the year 5 report because funding was expended during year 5 and no further work was performed. The following sections provide a summary of the most important results from all five years and for each of the three Tasks. The first and third Tasks were funded during the fifth year, so new results are included relative to previous years' reports. The second Task was not funded during the fifth year, so its results are repeated from the year 4 report.

## Task 1 – Lean Blowout

Georgia Institute of Technology

### Objectives

The objective of this Task was to obtain two types of measurements in a combustor rig operating near LBO. The two types of measurements were fuel screening and detailed diagnostics. The objective of the fuel screening was to rank the blowout boundaries of each fuel relative to the blowout boundary of Jet A. The objective of the detailed diagnostics was to produce data that could support the modeling teams. These data would support the modeling teams by providing physical insight and by providing important simulation boundary conditions. To summarize, the objectives of this Task were to obtain fuel screening data and detailed diagnostic measurements.

### Research Approach

This Task was performed with a combustor rig, shown in Figure 3. The rig was a high-pressure, swirl-stabilized spray combustor with original equipment manufacturer (OEM)-relevant hardware. The combustor was configured similarly to the referee rig at the Air Force Research Lab. The difference between the Georgia Tech rig and the referee rig was their dome and liner cooling arrangements. The referee rig had a greater level of complexity of these components, providing a closer simulation of a real combustor. However, the reduced complexity of the Georgia Tech rig enabled a greater rate of data generation. The reduced complexity of the Georgia Tech rig also enabled laser-based diagnostics that were not possible in the referee rig.

The research approach consisted of four major activities. The first of these activities was to collaboratively select the test conditions. This activity was conducted through the LBO working group. Thus, test condition selection included input from the OEMs as well as other stakeholders such as the referee rig team and the modeling teams. Together, these teams selected one combustor pressure and three air preheat temperatures for LBO testing. These were designed to simulate idle and altitude conditions where LBO poses the greatest risk. The selected combustor pressure was 3 atmospheres and the selected air preheat temperatures were 300 K, 450 K, and 550 K.

The second activity was to acquire screening data. This was accomplished by outfitting the combustor test rig with an advanced fuel cart. The fuel cart had ten different fuel tanks, each of which could hold a different fuel. The cart could rapidly switch between these fuels, which enabled the LBO testing of ten different fuels in a single sitting. The testing of many fuels in one sitting was advantageous because it promoted repeatability by eliminating the potential for uncontrolled variations in test conditions between test days. Fuel screening was conducted by igniting the combustor and intentionally leaning it to the LBO limit. Conditions where the combustor blew out were recorded, and the process was repeated until the first fuel tank was empty. This repetition process typically produced 20–30 blowout points for a single fuel. This was then repeated for the fuels in the other nine tanks. Figure 1 shows the screening data that was measured during the third year of the project. Correlations between the cetane number and the blowout equivalence ratio at elevated temperatures first became evident from this third-year dataset. For example, Figure 1 shows greater correlation of the blowout equivalence ratio to cetane number at the two higher inlet temperatures (450 K and 550 K) versus the lower inlet temperature (300 K).

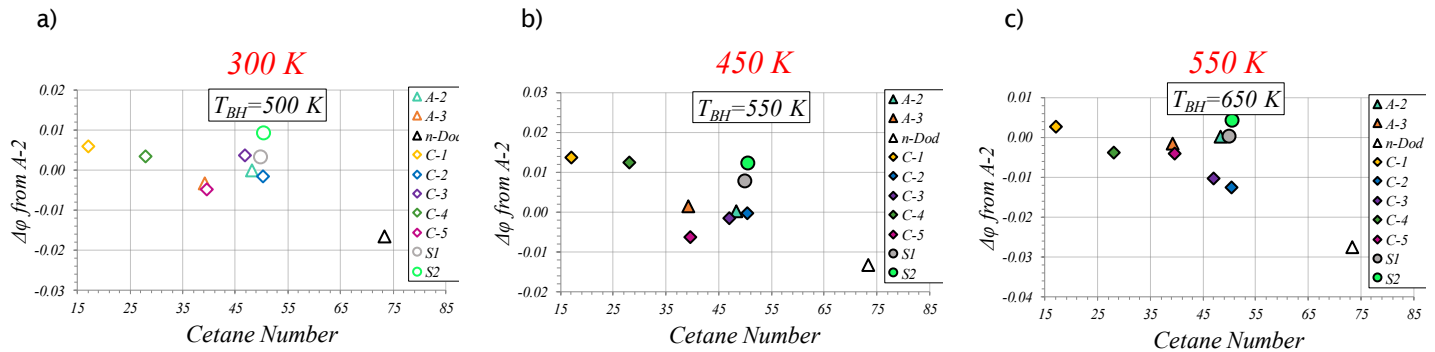


**Figure 1.** Sample of year 3 screening data at three different preheat temperatures and three different bulkhead temperatures, demonstrating the strong correlation of LBO with cetane number. The correlation coefficients between blowout equivalence ratio and the cetane number are -0.21 at 300 K, -0.79 at 450 K, and -0.76 at 550 K.

The third activity was detailed data acquisition. This activity produced data to support the modeling groups, and it also produced data to improve the program’s understanding of the physics of LBO. In support of the modeling groups, the LBO team performed detailed laser-based measurements. These measurements were delivered to the modeling groups to help them refine and validate their simulations. The measurements incorporated several different laser-based techniques that were synchronized together at 5,000 frames per second. These diagnostics included:

- Stereoscopic particle image velocimetry (s-PIV) to obtain planar measurements of the three-component velocity field.
- Planar laser-induced fluorescence of the OH molecule (OH PLIF) to obtain measurements of the flame position.
- Planar laser-induced fluorescence of the liquid fuel (fuel PLIF) to obtain measurements of the liquid fuel spray location.

The third activity also produced high speed chemiluminescence images. Figure 2 shows an example of one chemiluminescence image. These measurements were easier to perform and analyze than the laser-based diagnostics outlined above. Therefore, the advantage of the chemiluminescence imaging was that it was faster to implement. Because it was faster to implement, it was applied for more fuels and test conditions than the laser-based techniques. The chemiluminescence images helped reveal the qualitative burning characteristics near LBO. The chemiluminescence images also produced data to help the program determine the roles of ignition and extinction in the lean blowout process. Area 3 and Area 7 have both been analyzing these data to try to make such a determination. In addition to these optical measurements, the third activity also produced measurements of combustor boundary conditions. The measured boundary conditions included air flow rates, air and fuel temperatures, combustor pressure, and surface temperatures.

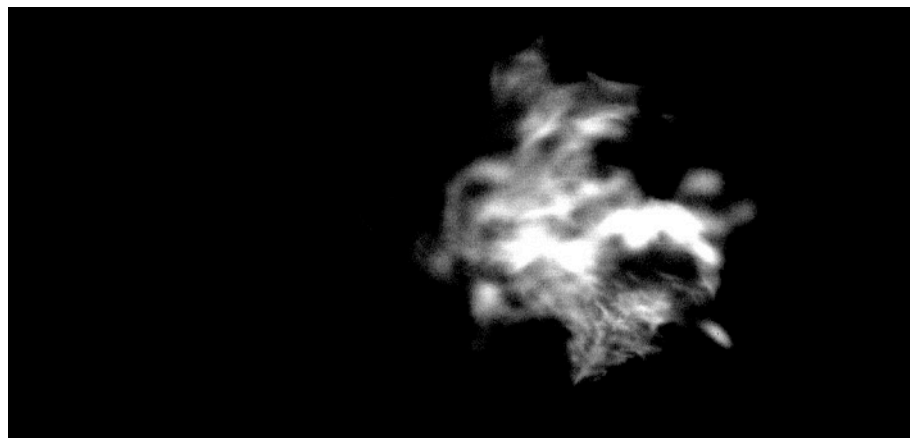


**Figure 2.** Sample flame chemiluminescence image from n-dodecane burning at 300 K air preheat temperature.

The fourth activity was data analysis. This activity was very important because it converted the raw measured data into useful data. In the case of screening data, analysis was performed on the combustor operational data to identify LBO events and their associated operating points. Analysis of screening data also included uncertainty analysis. The uncertainty analysis was necessary in order to determine the statistical significance of the results, and in some cases it motivated the LBO group to take additional data in order to tighten the uncertainty. In the case of detailed data, analysis was performed in two steps, pre-processing and post-processing. Pre-processing was applied to the velocity field measurements, and consisted of an intensive cross-correlation algorithm to convert raw images into velocity fields. This was extremely time-consuming and was the most difficult data analysis step. Post-processing was conducted to produce the time-averaged velocity field, to produce the root-mean square velocity field, and to extract key vortical flow features. These post-processed data were the deliverable to the modeling teams.

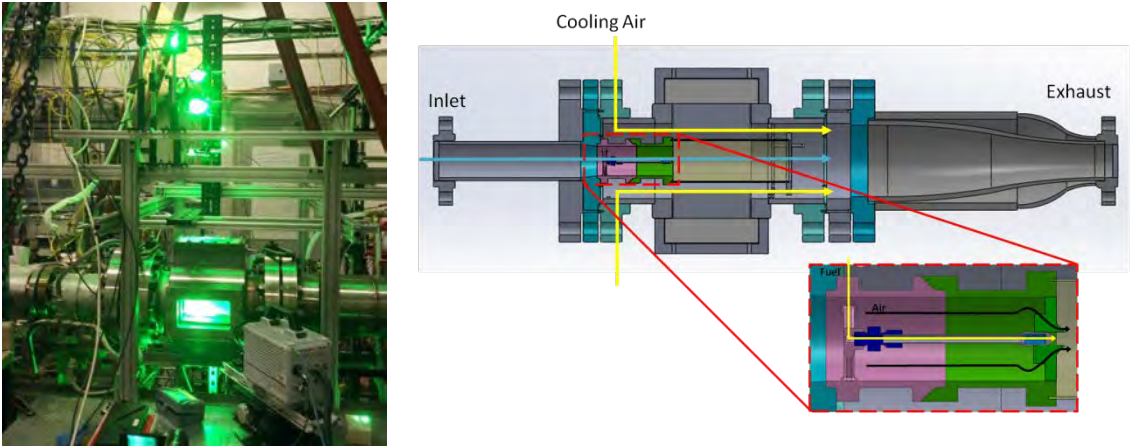


**Figure 3.** High shear swirl combustor, showing a) pressure vessel instrumented for high-speed stereo PIV and OH PLIF, and b) a cross section with generic swirler holder/injector for illustrative purposes.

**Fifth Year Results**

A supervised machine learning regression technique was conducted on the fuel screening data during the fifth year. The objective of this analysis was to determine cause-and-effect relationships between fuel properties and blowoff characteristics. These cause-and-effect relationships have been hard to identify with classical statistics because the fuel properties are strongly intercorrelated. These intercorrelations can be very misleading with classical statistics.

The regression procedure consisted of a Hierarchical Non-Negative Garrote with a two-step approach. This procedure has two steps. The first step is to identify important groups of variables or parameters. Examples of such groups would be “physical properties” and “chemical properties.” This step requires a physical understanding of the system. The second step involves a series of regressions of the data against the groups and the variables within the groups. The groupings used in this study are shown in Table 1.

**Table 1.** Hierarchical Non-Negative Garrote Groupings

Group 1	Group 2	Group 3	Group 4	Group 5	Group 6	Group 7
$T_{10}$	$v$ (mm <sup>2</sup> /s) 313 (K)	$T_{30}$	% iso-Paraffins	H/C	% Aromatics	DCN
MW	$\rho$ (kg/m <sup>3</sup> ) 288 K	$T_{90}$	$\sigma$ (mN/m) 300 K	LHV (MJ/kg)	Smoke Point (mm)	Ri

The regression model consists of tuning parameters. These parameters are determined from the cross-validation procedure. During cross-validation, a subset of the data (the training data set) and the regression is tested against the remaining data (the validation data set). This is repeated with different portions of the data serving as the training data set until all data have served as training data. The cross-validation procedure is illustrated in Figure 4.

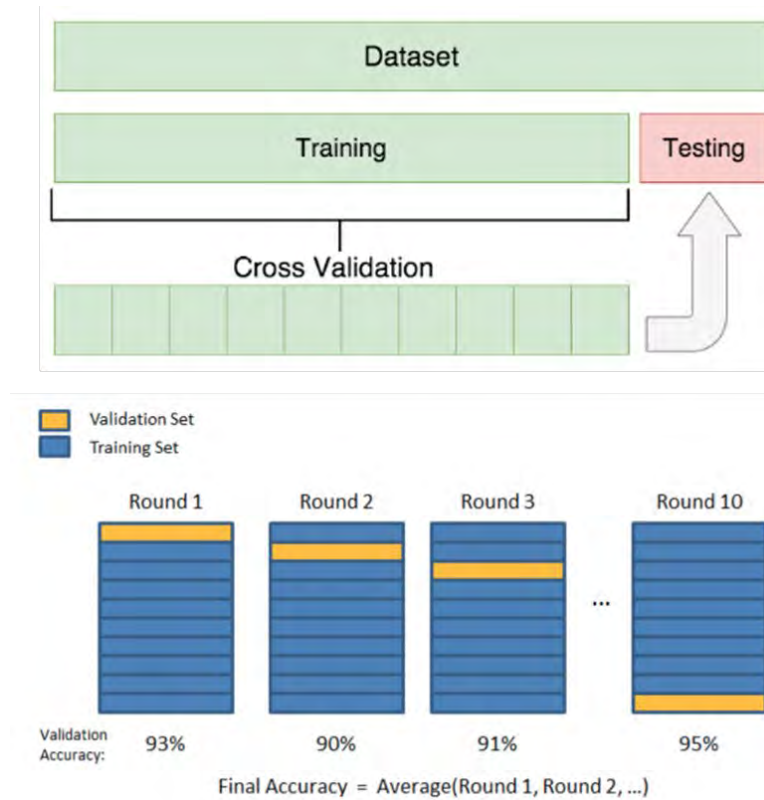


**Figure 4.** Illustration of the cross-validation procedure

The results of this analysis indicated that different parameters influenced blowout at different combustor inlet temperatures. These results are shown graphically in Figure 5, which shows the regression coefficients that relate LBO equivalence ratio to the fuel properties. At low combustor inlet temperatures, the 90% boiling point has the strongest influence on LBO characteristics (see the right-most blue bar in Figure 5). However, at higher combustor inlet temperatures, the Derived Cetane Number (DCN) has the strongest influence on LBO characteristics (see the left-most yellow and orange bars in Figure 5). This result strongly supports the hypothesis from the University of Dayton Research Institute (UDRI) that physical properties are important for LBO at low temperatures, and that autoignition properties are important for LBO at high temperatures. In addition, these results identify the individual parameters that are most important. Finally, we note that the regression model worked the best when we adjusted the DCN for the 20% most volatile fuel constituents. This is significant because it supports the preferential vaporization hypothesis that has been proposed by other teams.

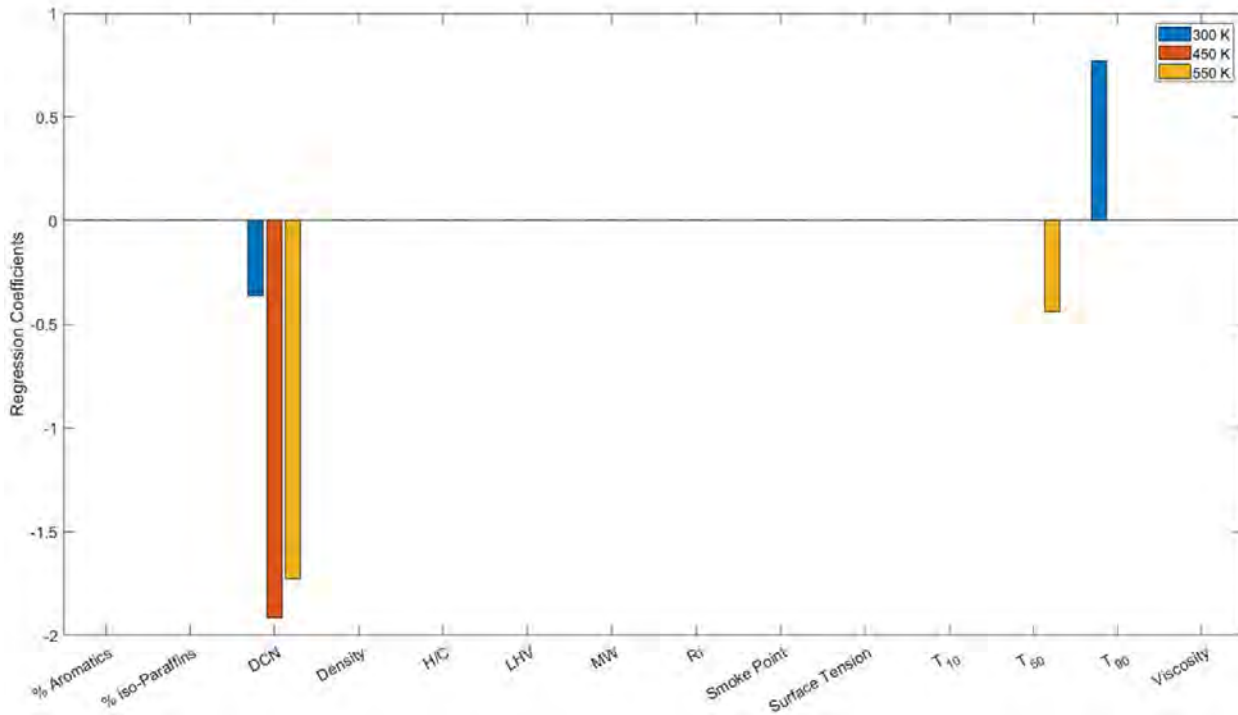


Figure 5. Results of the Hierarchical Non-Negative Garrote for three different combustor inlet temperatures.

### Milestones

1. Boundary condition measurements. This was completed during years 1 and 2.
2. Detailed diagnostic measurements. This was completed during years 1 and 2.
3. Screening data. This was completed during year 4.
4. Analysis. This was completed during year 5.

### Major Accomplishments

1. We have built a data analysis framework that explains the sensitivity of LBO to different fuel characteristics. This framework is robust against the intercorrelation of parameters. The results of the analysis support several hypotheses that have been presented by various National Jet Fuels Combustion Program (NJFCP) team members over the years.
2. We have supported the LBO chapter of the American Institute of Aeronautics and Astronautics (AIAA) book during year 5.

### Publications

Chterev, I., Rock, N., Ek, H., Emerson, B.L., Seitzman, J.M., Lieuwen, T.C., Noble, D.R., Mayhew, E. and Lee, T., 2017. Simultaneous High Speed (5 kHz) Fuel-PLIE, OH-PLIF and Stereo PIV Imaging of Pressurized Swirl-Stabilized Flames using Liquid Fuels. In 55th AIAA Aerospace Sciences Meeting (p. 0152).

Chterev, I., Rock, N., Ek, H., Emerson B., Seitzman J., Jiang, N., Roy, S., Lee, T., Gord, T., and Lieuwen, T. 2017. Simultaneous Imaging of Fuel, OH, and Three Component Velocity Fields in High Pressure, Liquid Fueled, Swirl Stabilized Flames at 5 kHz. *Combustion and Flame*. 186, pp. 150-165.

Chterev, I., Rock, N., Ek, H., Smith, T., Emerson, B., Noble, D.R., Mayhew, E., Lee, T., Jiang, N., Roy, S. and Seitzman, J.M., 2016, June. Reacting Pressurized Spray Combustor Dynamics: Part 2—High Speed Planar Measurements. In *ASME Turbo*



*Expo 2016: Turbomachinery Technical Conference and Exposition* (pp. V04AT04A020-V04AT04A020). American Society of Mechanical Engineers.

Ek H., Chterev I., Rock N., Emerson B., Seitzman J., Jiang N., Proscia W., Lieuwen T., Feature Extraction from Time Resolved Reacting Flow Data Sets, Proceedings of the ASME Turbo Expo, Paper #GT2018-77051, 2018.

Emerson, B., and Ozogul, H. 2018. Experimental Characterization of Liquid-gas Slip in High Pressure, Swirl Stabilized, Liquid-fueled Combustors, in Western States Section of the Combustion Institute – Spring 2018 Meeting.

Rock, N., Chterev, I., Emerson, B., Seitzman, J. and Lieuwen, T., 2017, June. Blowout Sensitivities in a Liquid Fueled Combustor: Fuel Composition and Preheat Temperature Effects. In ASME Turbo Expo 2017: Turbomachinery Technical Conference and Exposition (pp. V04AT04A022-V04AT04A022). American Society of Mechanical Engineers.

Rock, N., Chterev, I., Smith, T., Ek, H., Emerson, B., Noble, D., Seitzman, J. and Lieuwen, T., 2016, June. Reacting Pressurized Spray Combustor Dynamics: Part 1—Fuel Sensitivities and Blowoff Characterization. In *ASME Turbo Expo 2016: Turbomachinery Technical Conference and Exposition* (pp. V04AT04A021-V04AT04A021). American Society of Mechanical Engineers.

### **Outreach Efforts**

We provided research opportunities to undergraduate students and a high school student with this program. We had a graduate student present his work at the 2019 AIAA Scitech conference. We had a graduate student complete his Ph.D. on the work conducted under this program.

### **Awards**

Graduate student Nick Rock was awarded ASCENT student of the year in April 2017.

### **Student Involvement**

- Dr. Nick Rock has been actively involved in the LBO experimental effort for all years. Nick was the Ph.D. student responsible for operating the experimental facility. He led the screening measurements and operated the facility for the detailed diagnostic efforts, and has also performed the analysis of the screening data. Dr. Rock has now graduated with his Ph.D. and works for Spectral Energies in Dayton, OH.
- Hanna Ek was involved in the LBO effort as a data analyst. Hanna has been responsible for processing and analyzing the large volume of detailed data produced by the PIV, PLIF, and Mie scattering measurements.
- Dr. Ianko Chterev was also actively involved in the LBO experimental effort. His primary responsibility was the design of experimental procedures and support of detailed diagnostic measurements. Dr. Chterev has now graduated with his Ph.D. and works as a Postdoctoral Researcher for the German Aerospace Center (DLR) in Stuttgart, Germany.
- Dr. Eric Mayhew visited Georgia Tech from the University of Illinois at Urbana-Champaign. Dr. Mayhew helped lead the execution of the laser and optical diagnostics. Dr. Mayhew has graduated with his Ph.D. and works as a Postdoctoral Fellow at the U.S. Army Research Laboratory.

### **Plans for Next Period**

We have completely expended our budget during the fifth year. We plan to continue to author and present papers from this work, and we will continue to support the LBO chapter of the AIAA book that is being produced from this program.

## **Task 2 – Ignition**

Georgia Institute of Technology

### **Objectives**

There were four objectives for this year's ignition task. The first objective was to expand the database of room temperature ignition probability measurements. The second objective was to acquire and analyze ignition probabilities for chilled fuels. The third objective was to characterize the droplet size distribution in the liquid spray. The fourth objective was to couple liquid droplet heating and vaporization physics to the previously developed perfectly stirred reactor (PSR) model. This

enhanced model would simulate the spark kernel development process to show the relative effect of chemical reactions, dilution cooling, and droplet heating and vaporization on the ignition process.

## **Research Approach**

The first activity in the ignition task back in 2018 was to test ignition probabilities of liquid sprays for room temperature and chilled fuels. This began with modification of the test facility. The fuel delivery system was modified to provide liquid sprays rather than pre-vaporized fuels. The most important fuel system modifications were the installation of a solid core pressure atomizer (a fuel injector) near the entrance to the test section and the addition of a fuel chiller. Also, the splitter plate was removed from the test rig to provide a single pure air stream. The fuel injector location was selected to produce ignition probabilities in the range of 1–10%. The injector location was also fine-tuned to prevent fuel droplet impingement on the igniter. Scattering of a HeNe laser from the liquid droplets was used to monitor the fuel spray trajectory. The schematic of the fuel delivery system is shown in Figure 6.

Liquid fuel testing was conducted with a crossflow air velocity of 10 m/s and an equivalence ratio of  $\phi=0.55$ . The crossflow air temperature was 80 °F and its pressure was 1 atmosphere. For room temperature fuel sprays, ignition probabilities were measured for A2, A3, C1, C2, C3, C5, C7, C8, and C9. For chilled fuel, ignition probabilities were measured for A1, A2, A3, C1, C3, C4, C5, C7, and C8. Some fuels could not be chilled in this system as they would freeze. The ignition probabilities of each fuel relative to A2 are shown in Figure 7. For comparison, the figure also includes the results from earlier testing of pre-vaporized fuels. There are several noteworthy differences between the ignition probabilities of liquid versus pre-vaporized fuels. One of these noteworthy differences is a change in the ranking of ignition probabilities. For example, the ignition probabilities of A3, C2, and C3 are reduced relative to the other fuels when tested as liquid sprays. Another noteworthy difference is the range in probabilities is larger for chilled fuel sprays than for room temperature fuel sprays.

The differences in the ignition probabilities of liquid sprays versus pre-vaporized fuels provide some important insight. For example, the rate-limiting properties of pre-vaporized fuels should be the chemical properties. This is because the physical properties govern the vaporization process, which has been bypassed by pre-vaporization. However, the rate-limiting properties for liquid sprays may include physical properties in addition to chemical properties. Therefore, the differences in ignition probability demonstrate the important role of physical properties (such as viscosity, boiling points, etc.) for ignition of liquid fuel sprays. Special attention has been paid to properties that govern vaporization (recovery temperature, vapor pressure) and atomization (viscosity). The correlations to the viscosities and the 10% recovery temperatures for the fuel sprays are shown in Figure 8 and Figure 9.

The third activity in the ignition task was to measure the droplet distribution with a phased Doppler particle analyzer (PDPA) system. In aviation gas turbine combustors, jet fuels are injected as liquid sprays. These liquid sprays transition to gaseous fuel vapors before they burn. The droplet sizes can play an important role in the phase transition process by affecting the droplet heat transfer process. Therefore, PDPA measurement of droplet size and velocity distribution for an array of fuels was acquired. Normalized size distribution data for fuel C3 (high viscosity), A2 (middle viscosity), and C5 (low viscosity) at ~5 mm above the igniter center are presented in Figure 10. Significant differences in droplet size distributions were observed. The C3 fuel has more droplets at the larger size range (above 30  $\mu\text{m}$ ), and the C5 fuel only has a small percentage of droplets in that size range. The PDPA data can be used for more advanced computational fluid dynamics (CFD) simulation.

Lastly, a reduced order model was enhanced to study the physics of forced ignition in liquid fuel spray. The conceptual model construction is shown in Figure 11. An example case study simulates forced ignition in a spray of 5  $\mu\text{m}$  single size droplets uniformly distributed with an equivalence ratio of 1. The heat release, the dilution cooling, and the droplet heating and vaporization rates are shown in Figure 12. The initial results show that the energy required to heat and vaporize a droplet is 10 times smaller than the heat release rate and the dilution cooling. Therefore, droplet during ignition heating is not expected to substantially affect the ignition kernel's temperature. Thus, the time delay that is observed before chemical heat release occurs is likely due the heating of the droplets. If this time is too long, the kernel will be cooled significantly by dilution and ignition will not occur.

## **Fifth Year Results**

This Task was not funded during the fifth year. There is no new technical progress to report.

## **Milestones**

- Produced high-quality, repeatable ignition probability data for room temperature liquid fuel sprays.



- Produced high-quality, repeatable ignition probability data for chilled liquid fuel sprays.
- Acquired droplet size and velocity distribution data for several fuels.
- Enhanced a reduced order ignition model that includes droplet heating and vaporization processes.

### Major Accomplishments

- Fuel spray ignition probabilities correlate to properties that controls droplet sizes and vaporization.
- The acquired droplet distribution data is useful for CFD modelers.
- The reduced order ignition model shows the magnitude of the droplet cooling effect is small compared to those of the chemical heat release and the dilution cooling.

### Publications

Wei, S., Sforzo, B., and Seitzman, J., 2018, "Fuel Composition Effects on Forced Ignition of Liquid Fuel Sprays," *ASME Turbo Expo 2018: Turbomachinery Technical Conference and Exposition*, Oslo, Norway

### Outreach Efforts

Conference presentation at ASME Turbo Expo 2018, Oslo, Norway.

### Awards

None

### Student Involvement

- Sheng Wei was the lead student on all of the ignition task objectives.
- Daniel Cox was involved in data analysis.
- Sabrina Noor helped analyzed results for pre-vaporized ignition simulation.
- Vedant Mehta conducted a parametric study on droplet ignition.
- John Ryu helped with the multi-size droplet ignition study.

### Plans for Next Period

This Task will not continue into the next period.

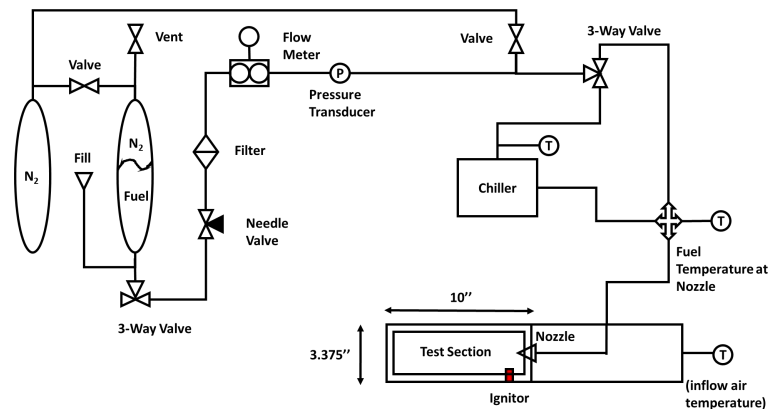
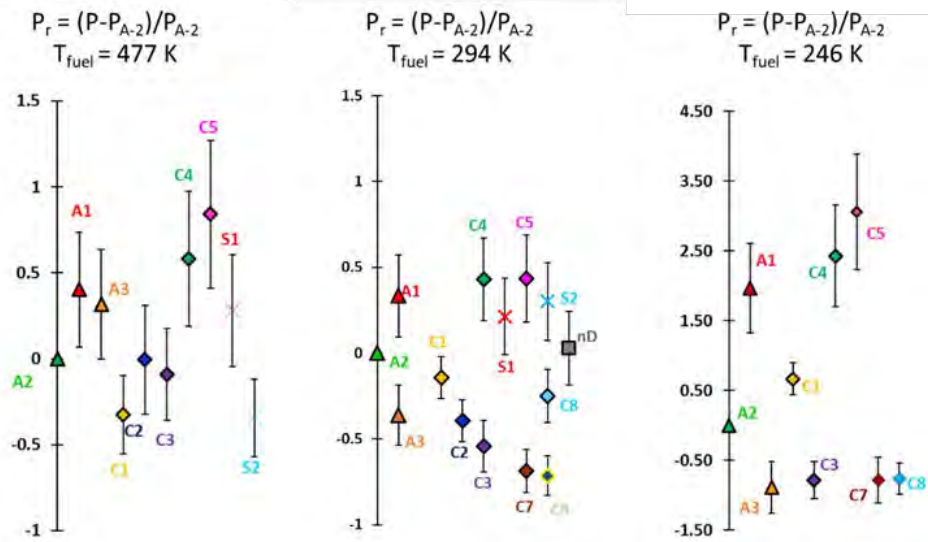
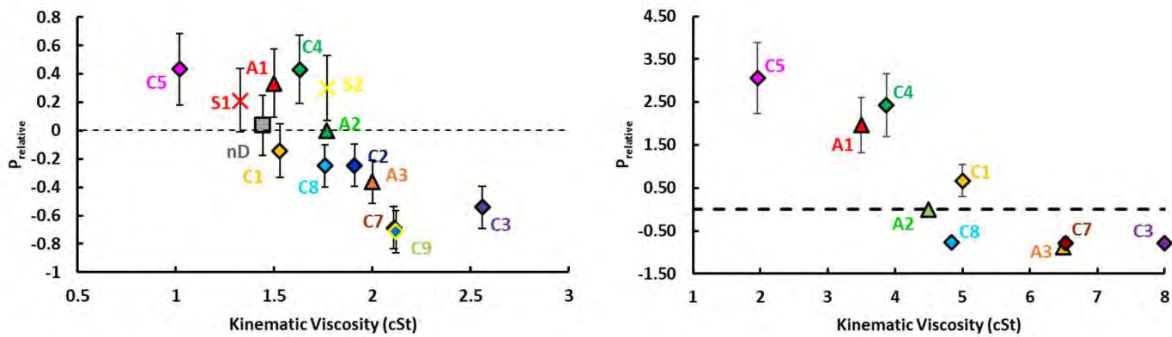


Figure 6. Schematic of the liquid fuel delivery system.



**Figure 7.** Ignition probability rankings, scaled with respect to A2 probability. Error bars show 68% uncertainty. Left: pre-vaporized fuel/air mixture. Middle: room temperature liquid fuel spray. Right: chilled liquid fuel spray.



**Figure 8.** Relative probabilities versus relative viscosity for room temperature fuel spray. Left: probability results for room temperature fuel spray. Right: probability results for chilled fuel sprays.

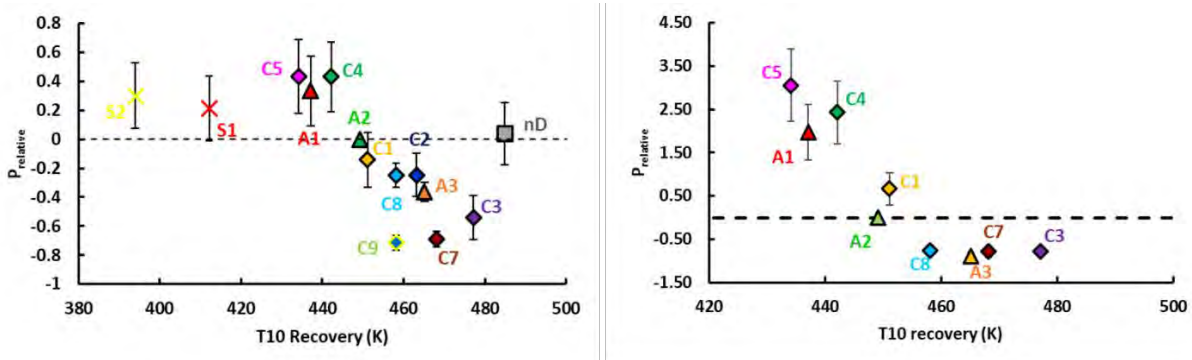


**Figure 9.** Relative probabilities versus 10% recovery temperature. Left: probability results for room temperature fuel spray. Right: probability results for chilled fuel sprays.

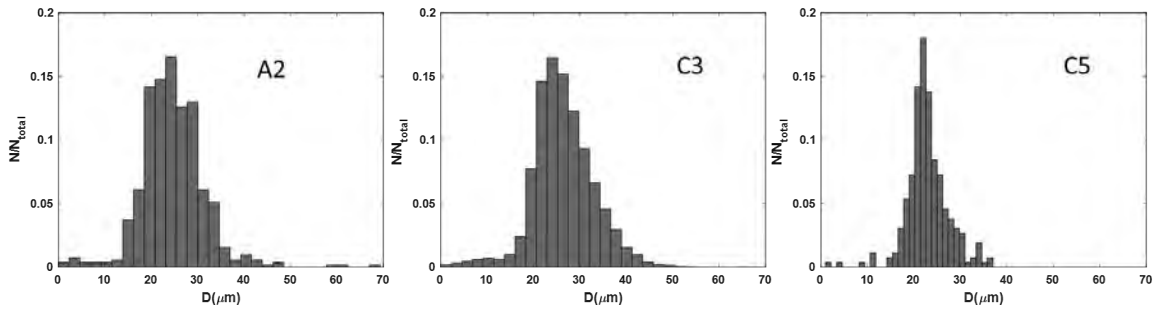


Figure 10. Normalized size distribution at 5 mm above the igniter center.

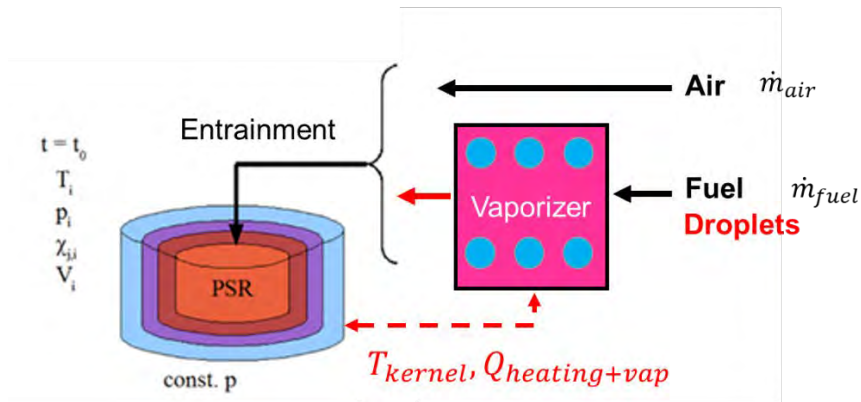


Figure 11. Conceptual model PSR modeling with droplet vaporization.

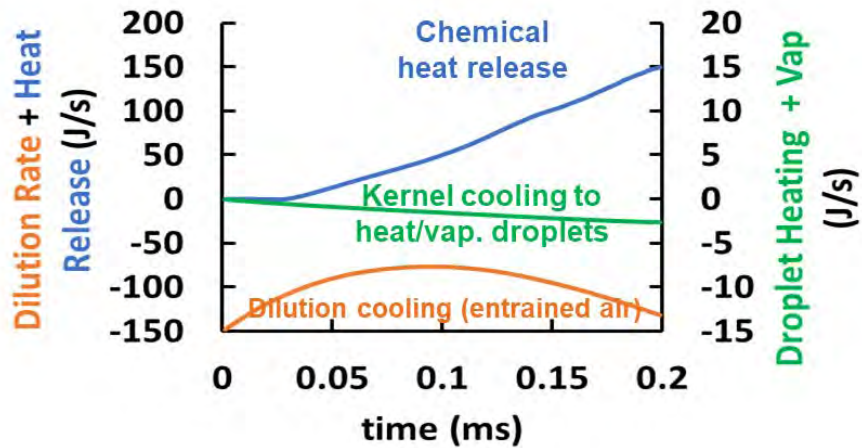


Figure 12. Chemical heat release, dilution cooling, and droplet heating/vaporization rates for a successful ignition of  $5 \mu\text{m}$  droplets at an equivalence ratio of 1.

## Task 3 – Turbulent Flame Speed

Oregon State University

### Objectives

This Task had three objectives. The first objective was to measure and identify the sensitivity of the turbulent flame speed to fuel composition. This objective spanned a range of jet fuels and test conditions (including atmospheric and sub-atmospheric pressures). The second objective was to build a database of turbulent flame speeds for pre-vaporized jet fuels. This year we initiated a collaboration with Suresh Menon (Georgia Tech) who is performing simulations of the turbulent flames anchored to the burner. The third objective was to measure the sensitivity of turbulent flames to local extinction.

### Research Approach

Testing was conducted using a laboratory test rig that produced turbulent flames. The rig featured a pre-vaporizer based on designs developed by the Air Force Research Laboratory, and a burner based on designs developed by Lieuwen and colleagues. The experimental arrangement consisted of fuel and air metering systems that delivered pre-vaporized jet fuel and air to the burner. Fuel was vaporized using a series of heaters, and elevated to a temperature near 200 °C (473 K). The air/fuel mixture flowed through an adjustable turbulence generator which produced turbulence intensities (TI) ranging from 10% to 20% of the bulk flow velocity. The TI is independent of bulk flow velocity. A premixed methane pilot flame was used for ignition and to stabilize the Bunsen burner flame.

Data was collected for three fuels (A2, C1, and C5). Test conditions included two pressures (1 and 0.7 atm), Reynolds numbers near 10,000, a range of equivalence ratios ( $0.75 \leq \phi \leq 1.0$ ), and turbulence intensities near 20%. The test data consisted of chemiluminescence imaging for all conditions and high-speed imaging for a subset of the tests. Chemiluminescence imaging was conducted using a 16-bit intensified charge-coupled device (ICCD) camera with a 1024 x 1024 pixel resolution and a 25 mm f/4.0 UV camera lens. For each flow condition (Re,  $\phi$ , and TI), data were typically collected over a 3-minute period at 2 Hz.

The most important accomplishment of this activity was sub-atmospheric pressure testing (i.e., objective one). Such measurements are relevant to relight conditions in engines at high altitudes. Figure 13 shows a photograph of the burner operating at sub-atmospheric conditions. Figure 14 (left panel) shows measured turbulent consumption speeds for C1, C5, and A2 at 1 and 0.7 atm. The right hand panel shows normalized turbulent consumption speeds. Note that the flame speeds increase as the pressure is reduced, and a fuel sensitivity is observed between C1, C5, and A2. This observation indicates that the relight characteristics between C1, C5, and A2 may be different when an aircraft is at altitude. More testing of practical systems are required to verify this postulate. It is noted that while the turbulent consumption speed increases with decreasing pressure, the mass consumption rate of the fuel decreases with decreases in pressure (Figure 15). The latter trend is consistent with the literature.

The second objective was partially addressed by initiating a collaboration with Suresh Menon (Georgia Tech). His team has simulated the cold-flow conditions through the burner and has plans to simulate the reacting flow. It is anticipated that this collaborate will serve as a baseline for evaluating the chemistry models created as part of the NJFCP program.

The third activity (i.e., objective three) was evaluating a methodology to detect the onset of local extinction events in the flame brush. Earlier in this program, a fuel sensitivity to the onset of instabilities of the flame was detected based on large changes in the apparent turbulent flame speed. However, using this technique to evaluate fuels was quite time-consuming and it was difficult to link the physics of flame speed measurements to local extinction. This year, efforts were made to develop a better method to more readily determine breaks in the flame front. High-speed images were collected of flames, and analysis tools were developed to quantify the turbulent statistics of emissions from the flames. Figure 16 provides a representative image of a turbulent statistic (i.e., integral length scale) that was evaluated to determine if it could be used as a metric of the onset of breaks in the flame front. Our current approach is to use the shape of the radial distribution of intensity as a marker of flame tip opening. Further testing is required to verify that this approach is valid.

### Fifth Year Results

This Task had very modest funding. The focus was on completing data collection and analysis, as well as writing up and distributing the results. The publications and pending publications resulting from this period or work are shown below. The student funded by this project (Nathan Schorn) completed and defended his thesis.



### Milestones

- Nathan Schorn successfully defended his M.S. thesis.
- Three publications were prepared. Two of these publications were from Nathan’s work while the third was from the research from a previous student (Aaron Fillo).
- The experimental arrangement was used to support research for two undergraduate honors theses. One project focused on identifying how preheating the fuel alters flame speeds. The other project has focused on measuring the fraction of radiative heat released by a Bunsen flame with and without dilution.

### Major Accomplishments (Cumulative)

- Turbulent flame speeds at atmospheric and sub-atmospheric conditions were measured. A fuel sensitivity is evident.
- Observation was made that flame extinction is sensitive to fuel composition. This can be important for the program’s LBO tasks, which aim to understand how ignition and extinction influence the LBO process.
- It was found that the surrogate fuel (S1) has similar flame speeds as Jet A.



Figure 13. Picture of flame operating in pressure vessel at sub-atmospheric conditions.

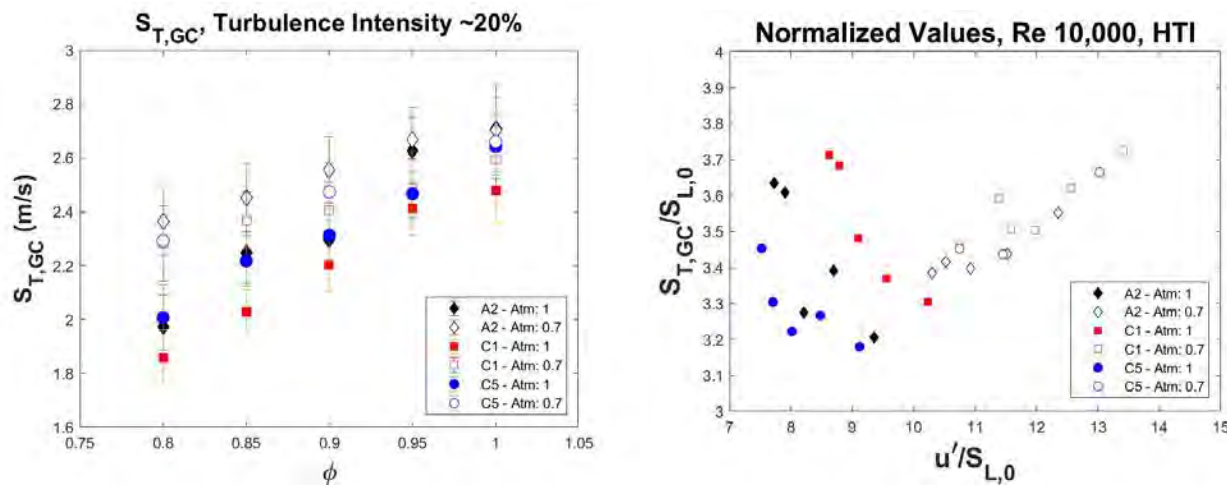


Figure 14. Turbulent consumption speeds (left panel) and normalized turbulent consumption speeds (right panel) for A2, C1, and C5 when tested at 1 and 0.7 atm.

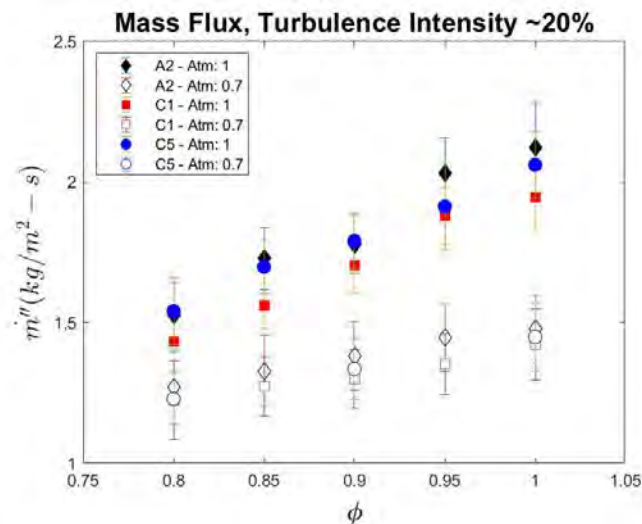


Figure 15. Mass consumption speeds of jet fuels for 1 and 0.7 atm.

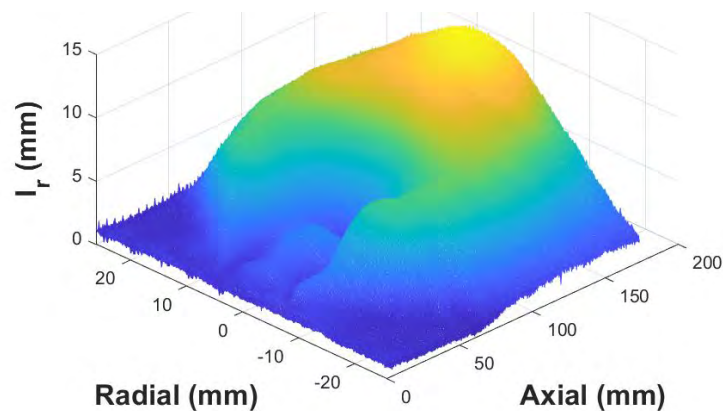


Figure 16. Radial integral length scale of visible light emissions from turbulent Bunsen burner flame burning A2 fuel. Such statistics have been considered as a marker of the onset of openings of the flame brush.

### **Publications (to date)**

N. Schorn, Z. Hoter, D. Blunck, "Turbulent Combustion Behavior of a Surrogate Jet Fuel," in preparation for submission to Fuels.

N. Schorn, J. Bonebrake, Z. Hoter, A. Fillo, D. Blunck, "Pressure Effects on the Turbulent Consumption Speed of Large Hydrocarbon Fuels," *AIAA Journal*, under review.

N. Schorn, J. Bonebrake, B. Pendergrass, A. Fillo, D. Blunck, "Turbulent Consumption Speed of Large Hydrocarbon Fuels at Sub-Atmospheric Conditions," *AIAA Science and Technology Forum and Exposition 2019*, San Diego, CA (2019).

Schorn, M, M.S., Thesis, "Turbulent Bunsen Burner Analysis," Oregon State University (2019).

N. Schorn, D. Blunck, "Flame Stability of Turbulent Premixed Jet Flames of Large Hydrocarbon Fuels," *Western States Section of the Combustion Institute Meeting*, Laramie, WY (2017).



A. Fillo, J. Bonebrake, D. Blunck, "Impact of Fuel Chemistry and Stretch Rate on the Global Consumption Speed of Large Hydrocarbon Fuel/Air Flames," *10<sup>th</sup> US Combustion Meeting*, College Park, ME (2017).

Fillo, Aaron, M.S., Thesis, "The Global Consumption Speeds of Premixed Large- Hydrocarbon Fuel/Air Turbulent Bunsen Flames," Oregon State University (2016).

### **Outreach Efforts**

None

### **Awards**

Fillo, Aaron, M.S., Thesis, "The Global Consumption Speeds of Premixed Large- Hydrocarbon Fuel/Air Turbulent Bunsen Flames," received a 2017 OSU Distinguished Master's Thesis Award.

### **Student Involvement (over the duration of the project)**

- Jonathan Bonebrake, a Ph.D. student, has helped to collect and analyze data. He also designed and built the sub-atmospheric pressure vessel and vacuum system.
- Aaron Fillo, a Ph.D. student, has worked tangentially on this project to analyze results and further investigate scientific phenomena.
- Nathan Schorn, a M.S. student, has collected and analyzed data.
- Multiple undergraduate students, including underrepresented students, have worked with the graduate students to operate the burner and collect data. This has provided a significant opportunity for the students to experience research.

### **Plans for Next Period**

The team from OSU will provide two remaining contributions. First, we will complete the publication process. One paper is currently under peer review, a second paper will be submitted by the end of December, and a third paper will be revised and resubmitted for peer review. Our second contribution will be to support the LBO book chapter as needed. Previously, the team provided content for the introduction to the LBO section. We will gladly help to revise the introduction or provide new content as requested.



## Project 029(A) National Jet Fuel Combustion Program – Area #5: Atomization Test and Models

### Purdue University

#### Project Lead Investigator

Robert P. Lucht  
Ralph and Bettye Bailey Distinguished Professor of Combustion  
School of Mechanical Engineering  
Purdue University  
West Lafayette, IN 47907-2088  
765-714-6020 (Cell)  
Lucht@purdue.edu

### University Participants

#### Purdue University

- PIs: Robert P. Lucht, Jay P. Gore, Paul E. Sojka, and Scott E. Meyer
- FAA Award Number: 13-C-AJFE-PU, Amendments: 27, 28, 30
- Period of Performance: October 1, 2019 to September 30, 2020
- Tasks:
  1. Obtain phase Doppler anemometry (PDA), Mie scattering, and fuel laser-induced fluorescence data in the variable ambient pressure spray (VAPS) test rig operated with the referee rig nozzle for numerous fuels under near-lean blowout (LBO) conditions and under cold fuel/cold air flow conditions approximating ground light-off (GLO) and high-altitude relight (HAR) conditions.
  2. Perform computational fluid dynamics (CFD) simulations of the referee rig under near-LBO and LBO conditions for different fuels.

### Project Funding Level

No additional funding was executed in the period of performance. A no-cost extension was awarded through December 19, 2020.

### Investigation Team

- PI Dr. Robert Lucht, Bailey Distinguished Professor of Mechanical Engineering, is responsible for overseeing the project at Purdue University. He is also responsible for mentoring one of the graduate students, coordinating activities with Stanford, working with all parties for appropriate results, and reporting results as required.
- Co-PI Dr. Jay P. Gore, Reilly Professor of Mechanical Engineering, works closely with the PI and oversees the work performed by one of the graduate students. He is also responsible for interacting with the CFD groups to suggest comparisons with experiments and with results of an adaptive grid solver.
- Co-PI Dr. Paul Sojka, Professor of Mechanical Engineering, is mentoring one of the graduate students and is responsible for supervising the spray measurements.
- Co-PI Scott Meyer, Managing Director of Maurice J. Zucrow Laboratories, is responsible for coordinating facility upgrades and for performing facility design reviews.
- Graduate Student (until December 2019) and Research Assistant Professor now, Hasti Veeraraghava Raju has conducted simulations with an adaptive grid solver and has performed comparisons with experimental results and results from the other CFD groups.
- Graduate student Daniel Shin is responsible for performing the PDA measurements and for modifying the VAPS test rig for operation under near-LBO and cold start conditions.



- Graduate student Neil Rodrigues contributes to the project by providing advice for the PDA measurements and technical editing.

## Project Overview

The objectives of this project, as stated in the Invitation for ASCENT COE Notice of Intent (COE-2014-29), are to “measure the spray characteristics of the nozzles used in the Referee Combustor used in Area 6 tests and to develop models for characterizing the atomization and vaporization of the reference fuels.” We are conducting experiments within the joint experimental and modeling effort. The experimental tasks are being performed at Purdue University, and the modeling tasks are being performed by Prof. Matthias Ihme’s group at Stanford University, Prof. Suresh Menon’s group at Georgia Tech, and Vaidya Sankaran’s group at United Technologies Research Center (UTRC). Nader Rizk is developing spray correlations based on the measurements.

Purdue University has highly capable test facilities for measuring spray characteristics over wide ranges of pressure, air temperature, and fuel temperature. The experimental diagnostics applied in this project include PDA and high-frame-rate shadowgraphy. The atomization and spray dynamics for multiple reference and candidate alternative fuels have been characterized for the referee rig nozzle operating under near-LBO conditions. In the future, measurements will be performed for these fuels under operating conditions characteristic of HAR. A new fuel, IH<sup>2</sup> (Shell CPK-0), has been added to the test matrix and is being investigated under LBO and cold start conditions.

## Task 1 – Measurement of Spray Characteristics under Near-Lean-Blowout and High Ambient Pressure Conditions

Purdue University

### Objectives

The objectives of this Task are to visualize and measure the characteristics, including drop size distributions and axial velocity components, of sprays generated by a nozzle in the Referee Combustor in the Area 6 tests. The resulting data are being applied by Nader Rizk to develop spray correlations and by Matthias Ihme (Stanford University), Suresh Menon (Georgia Tech), and Vaidya Sankaran (UTRC) to develop a sub-model for detailed computer simulations. The spray data are being shared with the FAA National Jet Fuel Combustion Program (FAA-NJFCP) team members for their interpretation and for the development of modeling, simulation, and engineering correlation-based tools.

An upgraded VAPS test rig at Purdue University is utilized to measure spray characteristics over a range of pressures, atomizing gas temperatures, and fuel temperatures. Our work has led to the identification of challenges associated with performing reliable and reproducible spray measurements while keeping the windows of the apparatus clean. PDA has emerged as the technique of choice for obtaining drop size distribution and axial velocity data for comparison with numerical simulations. The VAPS facility was upgraded to support experiments over the entire range of fuel/air temperatures and pressures of interest and to enable planar spray measurement. We have compared reacting and nonreacting spray data by collaborating with the University of Illinois Urbana Champaign (UIUC), University of Dayton Research Institute (UDRI), and Air Force Research Laboratory (AFRL) Area 6 team.

The experimental data have supported the continued development and evaluation of engineering spray correlations, including the dependence of the Sauter mean diameter, spray cone angle, and particle number density per unit volume on the fuel properties at the fuel and air temperatures of interest. The experimental data provide detailed statistical measurements for comparison with high-fidelity numerical simulations of mixing and combustion processes. The predicted spatial distribution of the liquid fuel and of the resulting vapor and breakdown components from the liquid fuels critically affects the ignition, flame stabilization, and pollutant formation processes.

The project objectives are summarized as follows:

1. Obtain PDA data across different planes in the VAPS test rig operating with the referee rig nozzle for numerous fuels under near-LBO conditions and under cold fuel/cold air flow conditions approximating GLO and HAR conditions.
2. Provide data to the research groups of Suresh Menon, Vaidya Sankaran, Matthias Ihme, and Jay P. Gore for simulations.



3. Conduct PDA measurements for selected operating conditions in the VAPS test rig to provide data for the spray correlation analysis of Nader Rizk.
4. Ensure data quality through repeated tests at Purdue and through comparisons with spray measurements at Pratt & Whitney, UDRI/AFRL, and UIUC.

### **Research Approach**

The Purdue University VAPS test rig facility is designed to measure spray characteristics over wide ranges of pressure, atomizing gas temperature, and fuel temperature. Liquid fuels can be supplied to the test rigs by multiple systems. A facility-integrated system draws fuel from one of two certified flame-shield fuel containments to test standard aviation fuels as well as alternative blends. A mobile fuel system, developed under the combustion rules and tools (CRATCAF) program and redeployed during the first year of the NJFCP program, is being utilized for further control of additional injector circuits and for supplying alternative fuel blends. Both systems were designed with two independently controlled and metered circuits to supply fuel to the pilot and main injector channels of the test injector. The mass flow rates of both fuel supplies are measured with Micro Motion Elite® Coriolis flow meters. A nitrogen sparge and blanket ullage system is used to reduce the dissolved oxygen content of the fuel, which is monitored by a sensor immediately upstream of the fuel control circuits. High-pressure gear pumps provide fuel at rates of up to 30 kg/hr, which is supplied to the control circuits at a regulated line pressure of 10 MPa. The mobile fuel system was built with two onboard heat exchangers, and a chilling unit controls the fuel temperature over a range of 193–263 K (-80 °C to -10 °C).

### **Milestones**

The milestones for the work performed in FY2020 are listed below:

#### **Quarter 1**

1. New window on the pressure vessel of the VAPS test rig was added to enable planar laser-induced fluorescence (PLIF), structured laser illumination planar imaging (SLIPI), and particle image velocimetry (PIV) measurements of the spray.
2. First shake down test was done in upgraded VAPS test rig with modified fuel supply system.
3. First PLIF measurement was performed using 266 nm excitation wavelength at 10 Hz.
4. The work accepted by the American Institute of Aeronautics and Astronautics (AIAA) *Journal of Propulsion and Power* was published in press.
5. Revised the spray book chapter.

#### **Quarter 2**

1. No experimental work had been done in this period due to nationwide shutdown by COVID-19.
2. A phenomenological three-step atomization model for the hybrid pressure-swirl air blast atomizer was developed to predict the drop size at LBO and cold start conditions.
3. Continued work on the book chapter revision.

#### **Quarter 3**

1. Simultaneous PLIF and Mie scattering measurements were performed high ambient pressure LBO conditions for A-2 and C-5 using 266 nm excitation wavelength at 10 Hz.
2. Cone angle estimation and liquid and vapor discrimination analysis were completed using previously obtained PLIF and Mie images.
3. The laser head for the PDA system at Purdue had failed, therefore an equivalent laser head was borrowed from UIUC and was successfully integrated with the PDA system at Purdue.
4. Continued revising the AIAA volume book chapter on sprays.

#### **Quarter 4**

1. The laser head from UIUC was integrated to PDA system and the laser alignment was re-done.
2. The drop size and drop velocity measurement was performed using PDA system at LBO and high ambient pressure conditions with 1, 2, 5, and 9.5 bar for A-2 and C-5.
3. Data processing is in progress.
4. Completed spray book chapter 5.

### **Major Accomplishments**

#### **Experimental contributions**

The work described in this section is a part of the Purdue contribution to a larger FAA-funded effort, the NJFCP. The major objective of the experimental work at Purdue was to measure spray properties (droplet size, droplet velocity, spray cone angle) for a variety of jet fuels and candidate jet fuels under a wide range of conditions, including LBO and GLO conditions.

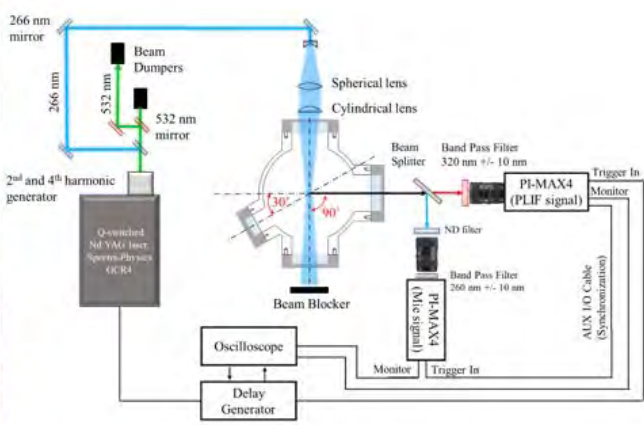
These measurements were successfully performed last year using a PDA, which provided single-point measurements of the spray. This year, two-dimensional (2D) planar imaging measurements were completed for A-2 and C-5 fuels for a more detailed investigation of the spray. Simultaneous PLIF and Mie imaging were performed in the upgraded VAPS test rig at high ambient pressure and LBO conditions. The PDA measurements were also performed at the same operating conditions as the PLIF and Mie scattering measurements. The remainder of this section presents the results of PLIF and Mie imaging and PDA measurements.

**Experimental systems**

The Purdue VAPS test rig comprises two major components: the airbox assembly and the pressure vessel. The airbox assembly is a length of pipe in which the hybrid air-blast pressure-swirl atomizer is mounted. The airbox is placed within the pressure vessel, which allows a pressurized atomizing gaseous flow through the airbox to be isolated from the vessel to create a pressure difference across the gas swirler. The pressure vessel is rated to withstand 4.14 MPa (600 psi) at 650 °C (1200 °F).

A new 127 mm window was added to the pressure vessel so that three 127 mm windows are oriented at a 90° angle each other and a 72.6 mm is oriented at a 60° angle from one of the 127 mm windows. With this new window system, Simultaneous PLIF and Mie imaging measurement was performed at LBO and high ambient pressure conditions (1, 2, 5, and 9.5 bar) for A-2 and C-5 fuels to provide a 2D representation of the spray. Figure 1 shows the image of simultaneous PLIF and Mie imaging measurement system in upgraded VAPS test rig. A 266 nm excitation wavelength laser beam was expanded into a 40 mm of sheet in height and illuminated a plane of the spray. Two synchronized intensified charge-coupled device (ICCD) cameras were used to obtain simultaneous PLIF and Mie images of the spray at 5 Hz with the laser power of approximately 70 mJ per pulse.

The laser head used for the PDA system at Purdue died due to old age. Another compatible laser head was borrowed from UIUC and was integrated to the existing PDA system at Purdue. Figure 2 shows the schematic diagram of the PDA system around upgraded VAPS test rig. The window modification on the pressure vessel allowed us to set the PDA transmitter and receiver probes at a 30° of scattering angle, which was suggested to get a strong signal from the forward scattering when the droplets passes through the probe volume.



(b)

(a)

**Figure 1.** (a) Photographs of simultaneous PLIF and Mie imaging measurement system in VAPS test rig. (b) Schematic diagram of simultaneous PLIF and Mie system around the VAPS rig.

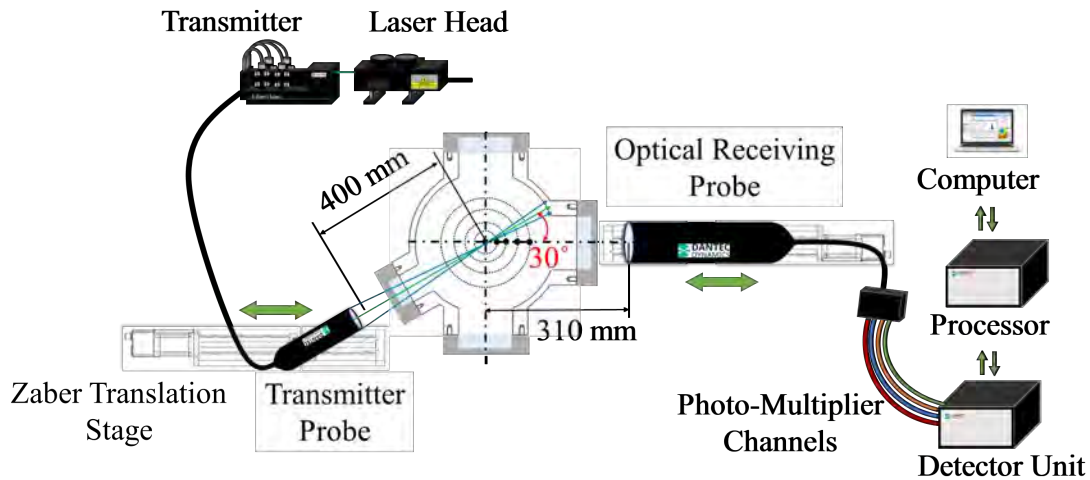


Figure 2. Schematic diagram of PDA system in upgraded VAPS rig.

#### Results from PLIF/Mie imaging and PDA measurements

Both PLIF/Mie and PDA measurements were performed at  $T_{fuel} = 328K$ ,  $T_{airbox} = 394K$ ,  $\Delta P/P = 3\%$ ,  $\Delta P_{pilot} = 1.72$  bar, and  $\dot{m}_{fuel} = 2.52$  g/s for A-2 and C-5 fuels. The operating condition with ambient pressure of 2 bar case is corresponding to the near-LBO conditions.

The drop size and drop velocity were measured using PDA measurement system at LBO and high ambient pressure conditions (1, 2, 3, 4, 5, and 9.5 bar) for A-2 and C-5 fuels. Some 20,000 samples were recorded within  $\pm 30$  mm from the center of the spray at increments of 5 mm. Figure 3 shows the comparison of  $D_{32}$  and axial velocity ( $U_z$ ) at different ambient pressure conditions. A decrease in  $D_{32}$  was observed with increases in ambient pressure. Higher ambient gas density with an increase in pressure caused the drag force on a droplet to increase. This resulted in smaller droplet diameter with increasing ambient pressure. The significant reduction in  $D_{32}$  was observed from 1 bar to 2 bar. However, minimal decrease in  $D_{32}$  was observed with further increase in ambient pressure beyond 5 bar. This indicated that the effect of ambient pressure on the drop size diminished with further increasing in ambient pressure. Similar trends were observed for both A-2 and C-5 fuels.

No significant variations were observed in axial velocity at different ambient pressures for most radial locations within the spray. However, at near the spray edge ( $r=30$ mm), the drop axial velocity decreased with ambient pressures as the droplet encountered higher drag force due to higher ambient pressure.

Figure 4 shows the instantaneous and averaged PLIF and Mie images at different ambient pressure conditions: 1, 2, 5, and 9.5 bar. The hollow-cone spray structure was observed from both PLIF and Mie images. At lower ambient pressure, it can be seen that the larger droplets were presented from both PLIF and Mie images. The cone angle estimation was done using a Sobel edge detection technique using averaged Mie images at different ambient pressure conditions. The ambient pressure had minimal effect on the spray cone angle as shown in Fig. 5. The LIF/Mie drop sizing analysis was also performed at different ambient pressures to predict  $D_{32}$  of the entire spray as shown in Fig 6. The drop size measurements by PDA at measurement plane of 12.7 and 25.4 mm were used to calibrate the LIF/Mie ratio with measured  $D_{32}$  values. The percentage difference between the predicted  $D_{32}$  and measured  $D_{32}$  were found to be within 17% for ambient pressure of the 1-bar case and 19% for ambient pressure of the 5-bar case.

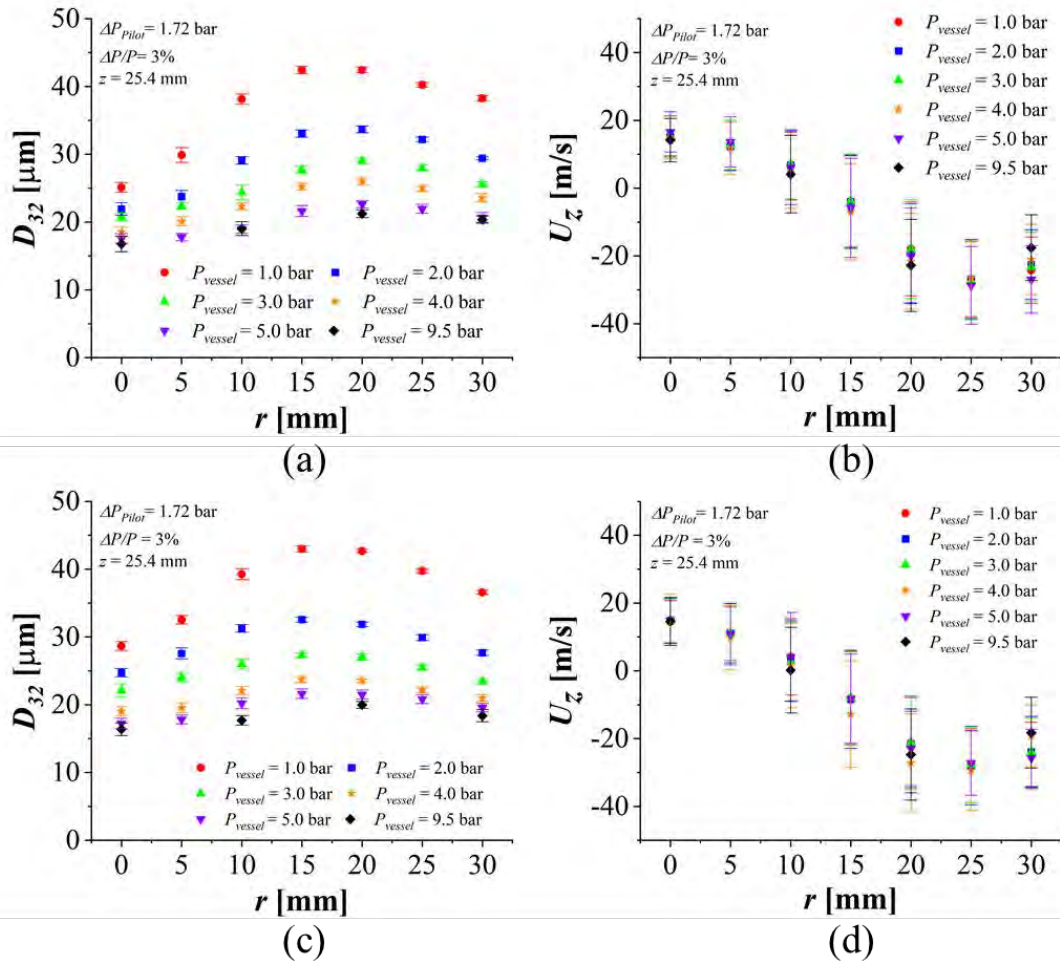
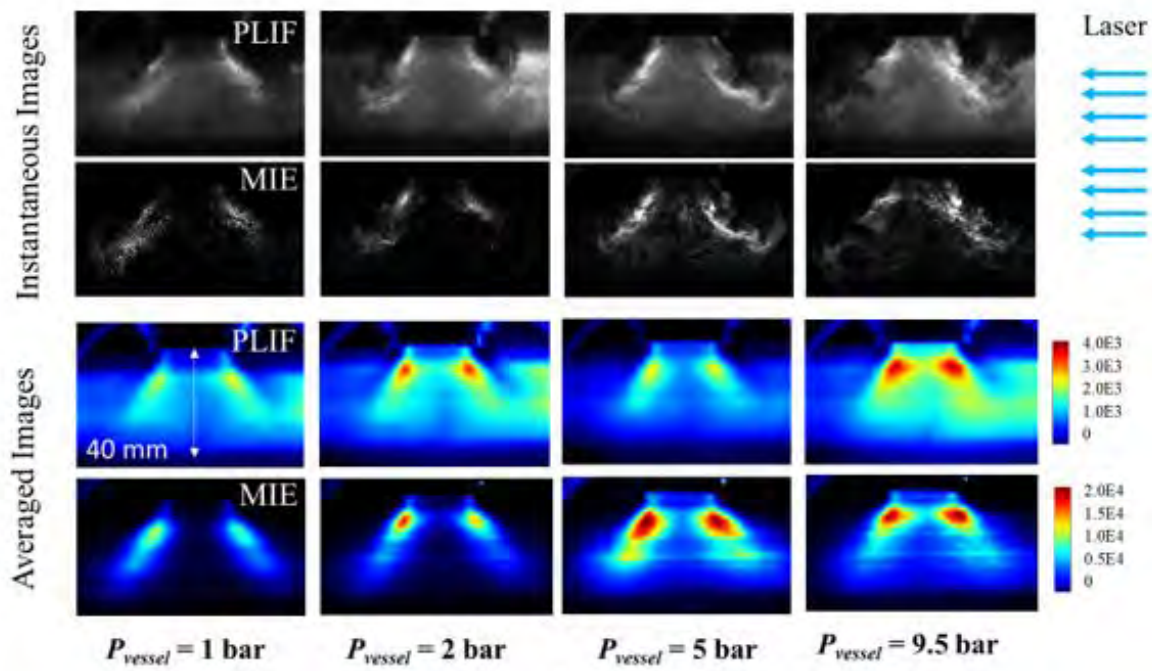
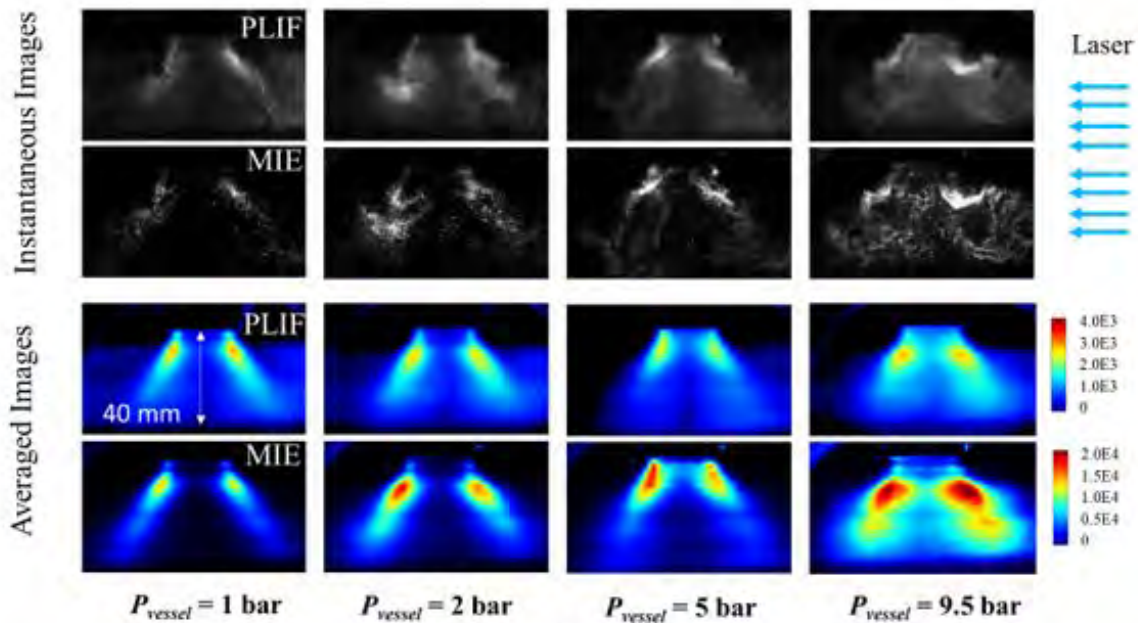


**Figure 3.** D32 and axial velocity at different ambient pressures of 1, 2, 3, 4, 5, and 9.5 bar,  $T_{fuel} = 328\text{K}$ , and  $T_{airbox} = 394\text{K}$  for A-2 and C-5 fuels. (a) D32 comparison for A-2 fuel. (b) Axial velocity comparison for A-2 fuel. (c) D32 comparison for C-5 fuel. (d) Axial velocity comparison for C-5 fuel.



(a)



(b)

**Figure 4.** Instantaneous and averaged images of PLIF and Mie measurements at ambient pressures of 1, 2, 5, and 9.5 bar. The 2-bar case is corresponding to the LBO condition. (a) A-2 fuel. (b) C-5 fuel.

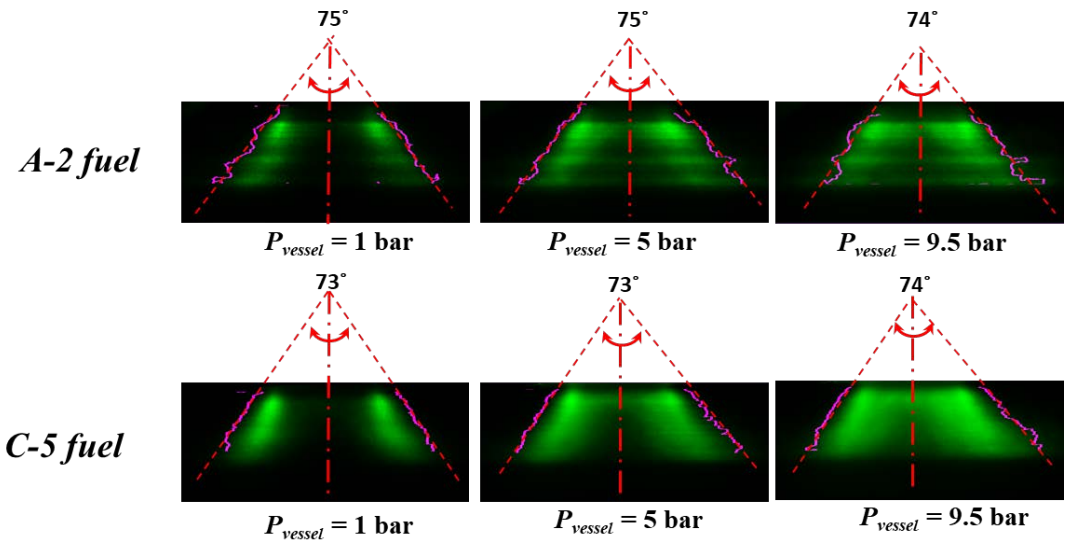


Figure 5. Cone angle comparison for A-2 and C-5 at different ambient pressures.

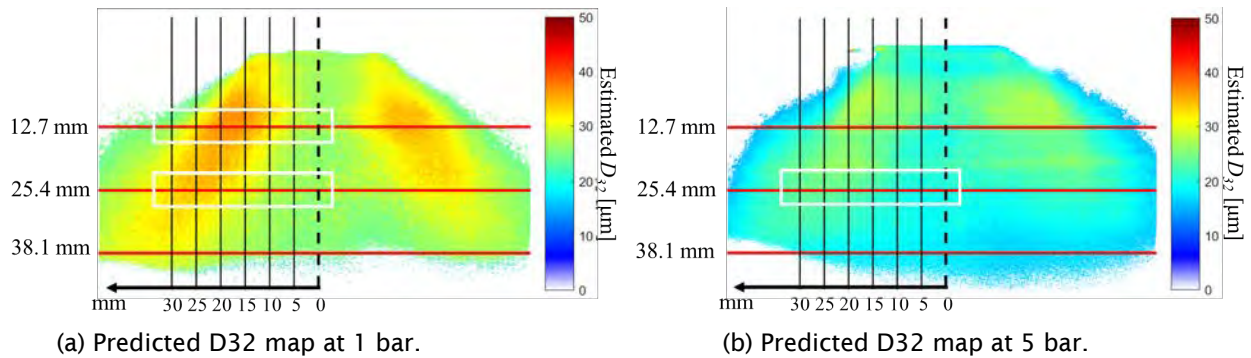


Figure 6. D32 map resulted from LIF/Mie ratio drop sizing.

## Task 2 – CFD Simulations of the Referee Rig Under Near-LBO and LBO Conditions

### Milestones

The milestones for the work performed in FY2020 are listed below:

#### Quarter 1

1. Updated the CFD model for domain sensitivity studies and performed non-reacting simulations.

#### Quarter 2

1. Updated the CFD model for domain sensitivity studies and performed non-reacting simulations.

#### Quarter 3

1. Analyzed the non-reacting large eddy simulations (LES) results to understand the impact of plenum size on the combustor flow field.
2. Contributed to the CFD modeling and simulations section of the AIAA volume book chapter on CFD.

#### Quarter 4

1. Completed the Purdue section on LBO modeling in the CFD book chapter.

## Major Accomplishments

### Domain sensitivity study

The reacting LES simulations reported in the previous year were performed with a reduced plenum size and excluded bypass air passages near the combustor exit. During 2019, we initiated efforts to model the actual size of the plenum in the rig hardware and included all bypass air passages near the combustor exit. The reduced and actual plenum domains are compared in Figure 7. A domain sensitivity study was performed under non-reacting conditions and LES simulations were completed during the 4<sup>th</sup> quarter of 2019. A detailed investigation of the results in the first quarter of 2020 revealed that we had failed to include a few effusion holes on the liners in the 2019 CFD model. We have now updated the CFD model to include all of the liner effusion holes. Revised non-reacting LES simulations have been completed in the first quarter of 2020 with the actual plenum size, all combustor passages, and the full rig inlet air flow rate of 391.4 g/s at the computational domain inlet.

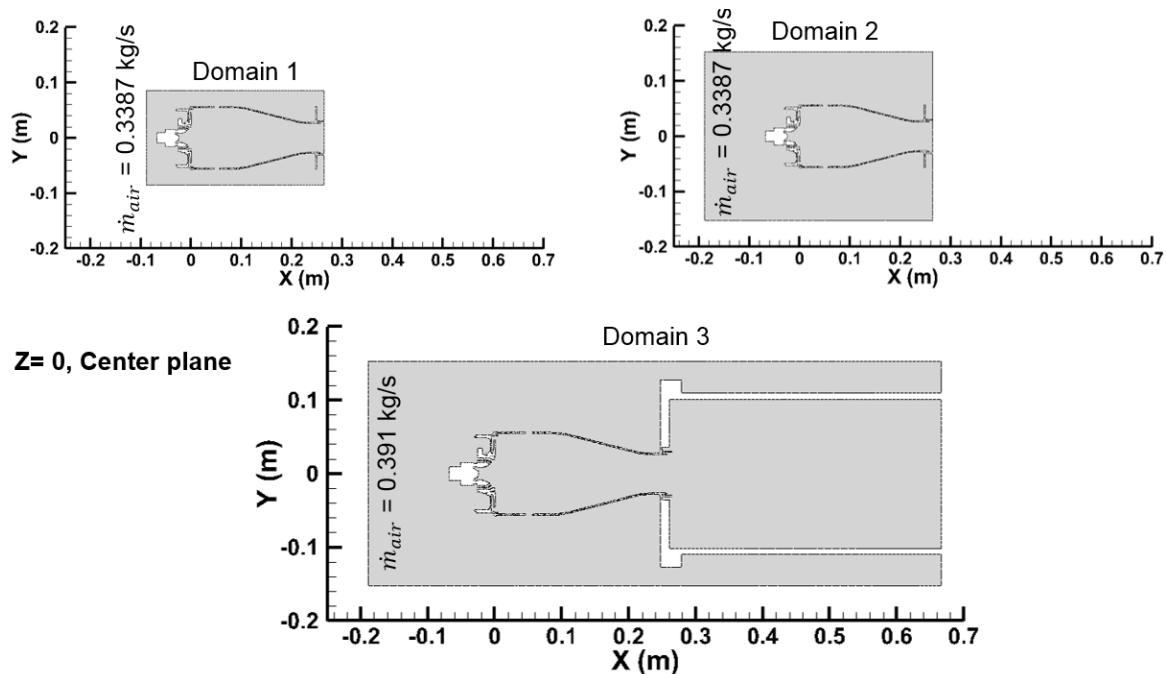


**Figure 7.** Comparison of computational domains at the Z=0 center plane for the three computational domains.

Combustor aft effusion holes are not included in domains 1 and 2. The flow-splits are compared in Table 1. The combustor aft effusion holes account for a total air flow rate of 52.9 g/s. This air flow rate is excluded in the CFD simulations for domains 1 and 2. An air mass flow rate of 338.5 g/s is specified at the inlet for the domain 1 and 2 CFD simulations. An air mass flow rate of 391.4 g/s is specified for domain 3 since it includes all the effusion holes, including those at the combustor aft end. In addition, the flow rates are increased by 4.9% and 2.5% for the first row of dilution holes and the second row of dilution holes, respectively, for domain 3. In order to maintain the total mass flow rate of air at 391.4 g/s, the swirler flow is decreased by 1.6%.



Table 1. Comparison of Flow Splits

	Exp (g/s)	Domain 1 Non-Reacting (g/s)	Domain 1 Reacting A2-0.096 (g/s)	Domain 2 Non-Reacting (g/s)	Domain 3 Non-Reacting (g/s)
Dilution Row 1	39.5	45.22	46.3	47.03	47.45
Dilution Row 2	45.4	50.01	52.4	50.57	51.27
Total swirler	60.7	75.37	72.9	73.12	74.17
Radial swirler	14.3	15.56	14.7	15.68	15.34
Axial int. swirler	18.9	25.18	23.8	23.92	24.93
Axial ext. swirler	24.6	32.37	31.9	31.3	31.64
Swirler cooling	2.9	2.25	2.3	2.22	2.24
Effusive plate	245.4	167.66	166.7	164.82	210
Total (sum)	391	338.26	338.3	335.54	382.89

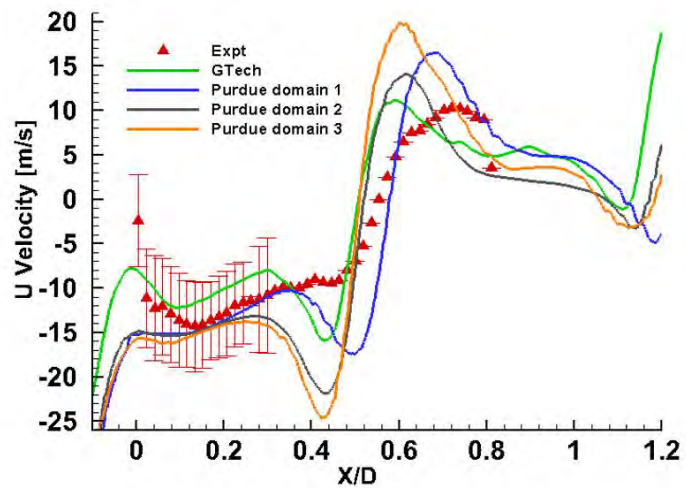
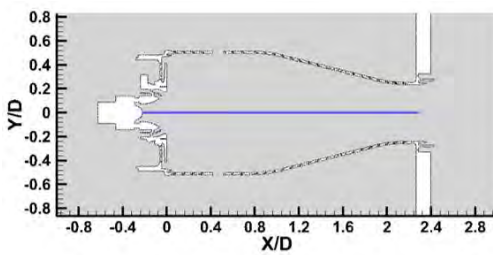
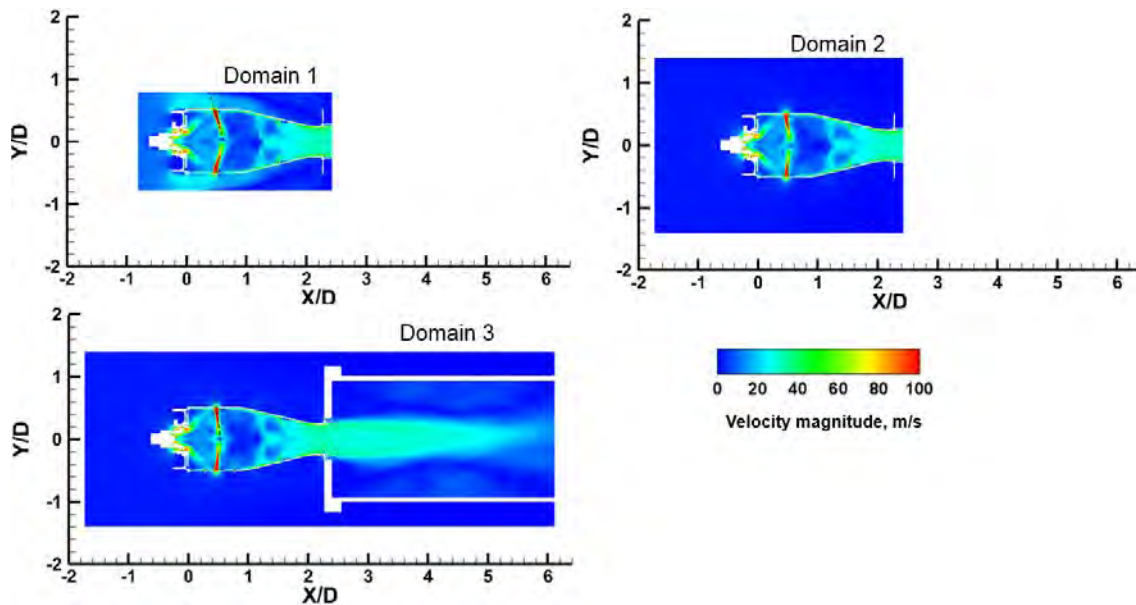


Figure 8. Comparison of the measurements of the mean axial velocity with results of the Georgia Tech (GTech) computations and the Convex-PU computations with three computational domains.



**Figure 9.** Comparison of velocity magnitude on the middle plain ( $Z=0$ ) of the combustor.

The measurements of mean axial velocity along the centerline of the combustor and the results of the Argonne National Laboratory-Purdue University (ANL-PU) computations using the three domains and the Georgia Tech computations are compared in Figure 8. The contour plots for the velocity magnitude on the middle plane of the combustor ( $Z=0$ ) are compared in Figure 9. For domain 1, the dilution jets in the first row enter the combustor with a higher velocity because of the smaller width of the annulus and therefore show an  $8^\circ$  greater angle. The results also show that the domain size does not have a significant effect on the flow patterns and velocity magnitudes in the critical primary flame stabilization zone. This zone is dominated by the swirling flow.

## Publications

### Peer-reviewed journal publications

- V. R. Hasti, R. P. Lucht, and J. P. Gore, "Large Eddy Simulation of Hydrogen Piloted  $\text{CH}_4$ /Air Premixed Combustion with  $\text{CO}_2$  Dilution," *Journal of the Energy Institute* **93**, 1099-1109 (2020). DOI: [10.1016/j.joei.2019.10.004](https://doi.org/10.1016/j.joei.2019.10.004)
- D. Shin, A. J. Bokhart, N. S. Rodrigues, P. E. Sojka, J. P. Gore, and R. P. Lucht, "An Experimental Investigation of Spray Characteristics of Alternative Aviation Fuels Using a Hybrid Pressure Swirl Airblast Atomizer at Lean Blowout Conditions," *Journal of Propulsion and Power* **36**, 323-334 (2020). DOI: [10.2514/1.B37712](https://doi.org/10.2514/1.B37712)

### Published conference proceedings

- Bokhart, J.A., Shin, D., Gejji, R., Buschhagen, T., Naik, S.V., Lucht, R.P., Gore, J.P., Sojka, P.E., & Meyer, S.E. (2017). Spray measurements at elevated pressures and temperatures using phase doppler anemometry. Presented at the 2017 AIAA SciTech Meeting, Grapevine, TX. Paper Number AIAA-2017-0828.
- Buschhagen, T., Zhang, R.Z., Naik, S.V., Slabaugh, C.D., Meyer, S.E., Gore, J.P., & Lucht, R.P. (2016). Effect of aviation fuel type and fuel injection conditions on non-reacting spray characteristics of hybrid air blast fuel injector. Presented at 2016 AIAA SciTech Meeting, San Diego, CA. Paper Number AIAA 2016-1154.
- Hasti, V.R., Liu, S., Kumar, G., & Gore, J.P. (2018). Comparison of premixed flamelet generated manifold model and thickened flame model for bluff body stabilized turbulent premixed flame. 2018 AIAA Aerospace Sciences Meeting, AIAA SciTech Forum, (AIAA 2018-0150)
- Hasti, V.R., Kundu, P., Kumar, G., Drennan, S.A., Som, S., & Gore, J.P. (2018). A numerical study of flame characteristics during lean blow-out in a gas turbine combustor. 2018 Joint Propulsion Conference, AIAA Propulsion and Energy Forum, (AIAA 2018-4955)



- Hasti, V.R., Kundu, P., Kumar, G., Drennan, S.A., Som, S., & Gore, J.P. (2018). Numerical simulation of flow distribution in a realistic gas turbine combustor. 2018 Joint Propulsion Conference, AIAA Propulsion and Energy Forum, (AIAA 2018-4956)
- Hasti, V.R., Kundu, P., Kumar, G., Drennan, S.A., Som, S., Won, S.H., Dryer, F.L., & Gore, J.P. (2018). Lean blow-out (LBO) computations in a gas turbine combustor. 2018 Joint Propulsion Conference, AIAA Propulsion and Energy Forum, (AIAA 2018-4958)
- May, P.C., Nik, M.B., Carbajal, S.E., Naik, S., Gore, J.P., Lucht, R.P., & Ihme, M. (2016). Large-eddy simulations of fuel injection and atomization of a hybrid air-blast atomizer. Presented at the 2016 AIAA SciTech Meeting, San Diego, CA. Paper Number AIAA 2016-1393.
- Shin, D., Bokhart, J.A., Rodrigues, N.S., Lucht, R.P., Gore, J.P., Sojka, P.E., & Meyer, S.E. (2018). Spray characteristics at lean blowout and cold start conditions using phase doppler anemometry. Presented at the 2018 AIAA SciTech Meeting, Kissimmee, Florida.
- Shin, D., Bokhart, J.A., Rodrigues, N.S., Naik, S.V., Lucht, R.P., Gore, J.P., Sojka, P.E., & Meyer, S.E. (2018). Spray characteristics of a hybrid airblast pressure-swirl atomizer at cold start conditions using phase doppler anemometry. Presented at ICLASS 2018 14<sup>th</sup> Triennial International Conference on Liquid Atomization and Spray Systems, Chicago, Illinois.
- Shin, D., Bokhart, J.A., Rodrigues, N.S., Sojka, P., Gore, J.P., & Lucht, R.P. (2019). Experimental study of spray characteristics at cold start and elevated ambient pressure using hybrid airblast pressure-swirl atomizer. Presented at 2019 AIAA SciTech Meeting, San Diego, CA. Paper Number AIAA 2019-1737.

## Outreach Efforts

N/A

## Awards

- Veeraraghava Raju Hasti received the Outstanding Research Award from the College of Engineering, Purdue University, May 2020.
- Veeraraghava Raju Hasti served as the subject matter expert and global judge for the NASA Space Apps COVID-19 Challenge Competition, May 2020.
- Veeraraghava Raju Hasti received the 2019 Gordon C. Oates Air Breathing Propulsion Graduate Award from the AIAA Foundation. The AIAA Foundation presents this award to a graduate student performing excellent research in air and space science.
- Veeraraghava Raju Hasti received the Computational Interdisciplinary Graduate Program's Bilisland Dissertation Fellowship from Purdue University in 2019.
- Veeraraghava Raju Hasti received the Outstanding Graduate Student Mentor award from Purdue University in May 2019.
- Veeraraghava Raju Hasti received the Outstanding Service award from the College of Engineering, Purdue University in May 2019.
- Veeraraghava Raju Hasti won 1<sup>st</sup> prize (best poster) under the 100 Years Category in the Sustainable Economy and Planet Poster Competition for PhD Students, Ideas Festival, 150 Years Celebrations at Purdue University for his poster presentation entitled "Quantum Computers on Artificial Intelligence: Automatic and Adaptive Solutions," given February 6, 2019.
- Veeraraghava Raju Hasti delivered an invited talk entitled "Computational methodology for biofuel performance assessment" at the Spring CIGP Symposium, Purdue University, April 17, 2019.
- Veeraraghava Raju Hasti and Jay P. Gore delivered a keynote speech entitled "Computational Study of Fuel Effects on Lean Blow-Out in a Realistic Gas Turbine Combustor" at the Modeling and Simulation of Turbulent Mixing and Reaction: For Power, Energy and Flight, April 12-13, 2019.
- Veeraraghava Raju Hasti was elected as Chair for the Membership Committee of the Gas Turbine Engines Technical Committee (GTE TC), AIAA, August 2019.
- Veeraraghava Raju Hasti delivered an invited talk entitled "Computational Methodology for Biofuel Performance Prediction" at the Academic Research Colloquium, University of Dayton, September 10-12, 2019.
- Veeraraghava Raju Hasti successfully defended his PhD dissertation on October 30, 2019.
- Veeraraghava Raju Hasti served as a Global Ambassador following selection by the Purdue Graduate School for interactions with prospective international students on November 8, 2019.



- Veeraraghava Raju Hasti represented Purdue University at the Big Ten Grad Expo on September 22, 2019, following selection by the Office of Interdisciplinary Graduate Programs and Computational Interdisciplinary Graduate Programs. Hasti also served on a Panel at the Big Ten Grad Expo on September 22, 2019.
- Veeraraghava Raju Hasti was invited by the College of Engineering to serve on the Graduate Students Panel on May 21, 2019 to interact with global undergraduate summer interns through the Purdue Undergraduate Research Experience (PURE).
- Veeraraghava Raju Hasti delivered a presentation on computational research opportunities in combustion and energy at the Mechanical Engineering Visitation Program for prospective graduate students on February 14, 2019 at Purdue University.
- Jay P. Gore delivered an invited talk entitled “Radiation Heat Transfer in High Pressure Gas Turbine Combustors” at the United Technologies Research Center (UTRC) Workshop on Combustor-Turbine Wall Heat Transfer Modeling and Prediction, East Hartford, CT, March 11, 2019.
- Jay P. Gore delivered an invited talk entitled “Radiation and Soot Measurements in High Pressure Gas Turbine Combustors” at the United Technologies Research Center (UTRC) Follow-up Meeting for Combustor-Turbine Wall Heat Transfer at the ASME IGTI Conference, Phoenix, AZ, June 16, 2019.

### **Student Involvement**

PhD student Daniel Shin is primarily responsible for performing PDA measurements under LBO and HAR/GLO conditions and for upgrading the VAPS test rig in a new test cell. PhD student Neil Rodrigues and postdoctoral research associate Rohan Gejji assist with the project when their expertise is required. PhD student Veeraraghava Raju Hasti is primarily responsible for developing and performing the LES simulations. Veeraraghava Raju Hasti has graduated and is currently a Research Assistant Professor in the School of Mechanical Engineering at Purdue.

### **Plans for Next Period**

The proposed deliverables and tasks for FY2021 are listed below.

#### **Year-5 deliverables**

The year-5 deliverables for Area 5, Project 29A is focused on spray experiments and the deliverables are as follows:

1. Continue revisions and complete the spray section in the AIAA book chapter.
2. Continue interactions with the three CFD groups (Ihme, Vaidya, and Menon).
3. Prepare a journal paper for the measurements at high ambient pressure conditions.
4. Graduate student Daniel Shin will complete his thesis and defend for his Ph.D.

### **References**

- Bokhart, A., Shin, D., Gejji, R.M., Sojka, P., Gore, J.P., Lucht, R. P., Naik, S. V., and Buschhagen, T. (2017). Spray measurements at elevated pressures and temperatures using phase doppler anemometry. 55th AIAA Aerospace Sciences Meeting. American Institute of Aeronautics and Astronautics.
- Bokhart, A., Shin, D., Rodrigues, N.S., Sojka, P., Gore, J.P., & Lucht, R.P. (2018). Spray characteristics of a hybrid airblast pressure-swirl atomizer at near lean blowout conditions using phase doppler anemometry. American Institute of Aeronautics and Astronautics.
- Convergent Science, Inc. (2017). CONVERGE CFD, Version 2.4., Madison, WI
- El-Asrag, H.A., Braun, M., & Masri, A.R. (2016). Large eddy simulations of partially premixed ethanol dilute spray flames using the flamelet generated manifold model. Combustion Theory and Modelling Vol. 20, No. 4, pp. 567-591. doi: 10.1080/13647830.2016.1159732
- Elasrag, H. & Li, S. (2018). Investigation of extinction and reignition events using the flamelet generated manifold model. ASME Turbo Expo 2018: Turbomachinery Technical Conference and Exposition. Vol. Volume 4A: Combustion, Fuels, and Emissions.
- Giusti, A. & Mastorakos, E. (2017). Detailed chemistry LES/CMC simulation of a swirling ethanol spray flame approaching blow-off. Proceedings of the Combustion Institute Vol. 36, No. 2, pp. 2625-2632. <https://doi.org/10.1016/j.proci.2016.06.035>
- Hasti, V.R., Kundu, P., Kumar, G., Drennan, S.A., Som, S., & Gore, J.P. (2018). A numerical study of flame characteristics during lean blow-out in a gas turbine combustor. 2018 Joint Propulsion Conference, No. AIAA 2018-4955. doi:10.2514/6.2018-4955



- Hasti, V.R., Kundu, P., Kumar, G., Drennan, S.A., Som, S., & Gore, J.P. (2018). Numerical simulation of flow distribution in a realistic gas turbine combustor. 2018 Joint Propulsion Conference, No. AIAA 2018-4956. doi: doi:10.2514/6.2018-4956
- Hasti, V.R., Kundu, P., Kumar, G., Drennan, S.A., Som, S., Won, S.H., Dryer, F.L., & Gore, J.P. (2018). Lean blow-out (LBO) computations in a gas turbine combustor. 2018 Joint Propulsion Conference, No. AIAA 2018-4958. doi:10.2514/6.2018-4958
- Ihme, M., Cha, C.M., & Pitsch, H. (2005). Prediction of local extinction and re-ignition effects in non-premixed turbulent combustion using a flamelet/progress variable approach. *Proceedings of the Combustion Institute* Vol. 30, No. 1, pp. 793-800. doi: <https://doi.org/10.1016/j.proci.2004.08.260>
- Ihme, M. & Pitsch, H. (2008). Prediction of extinction and reignition in nonpremixed turbulent flames using a flamelet/progress variable model: 1. A priori study and presumed PDF closure. *Combustion and Flame* Vol. 155, No. 1, pp. 70-89. doi: <https://doi.org/10.1016/j.combustflame.2008.04.001>
- Ma, P.C., Wu, H., Labahn, J.W., Jaravel, T., & Ihme, M. (2019). Analysis of transient blow-out dynamics in a swirl-stabilized combustor using large-eddy simulations. *Proceedings of the Combustion Institute* Vol. 37, No. 4, pp. 5073-5082. doi: <https://doi.org/10.1016/j.proci.2018.06.066>
- Mayhew, E., Mitsingas, C.M., McGann, B., Hendershott, T., Stouffer, S., Wrzesinski, P., Caswell, A.W., & Lee, T. (2017). Spray characteristics and flame structure of jet a and alternative jet fuels. 55th AIAA Aerospace Sciences Meeting. doi: 10.2514/6.2017-0148
- Pomraning, E. & Rutland, C.J. (2002). Dynamic one-equation nonviscosity large-eddy simulation model. *AIAA Journal* Vol. 40, No. 4, pp. 689-701. doi: 10.2514/2.1701
- van Oijen, J.A., Donini, A., Bastiaans, R.J.M., ten Thijsse Boonkamp, J.H.M., & de Goey, L.P.H. (2016). State-of-the-art in premixed combustion modeling using flamelet generated manifolds. *Progress in Energy and Combustion Science* Vol. 57, pp. 30-74. doi: 10.1016/j.pecs.2016.07.001

# Project 31 Alternative Jet Fuel Test and Evaluation

## University of Dayton Research Institute

### Project Lead Investigator

Steven Zabarnick, PhD  
 Division Head  
 Fuels and Combustion Division  
 University of Dayton Research Institute  
 300 College Park  
 Dayton, OH 45469-0043  
 937-255-3549  
 Steven.Zabarnick@udri.udayton.edu

### University Participants

#### University of Dayton Research Institute

- PIs: Steven Zabarnick, Division Head
- FAA Award Number: 13-C-AJFE-UD
- Overall Period of Performance: April 8, 2015 to August 10, 2021
- Tasks:
  - Period of Performance: April 8, 2015 to March 14, 2016 – Amendment No. 006
    1. Evaluate the performance of candidate alternative fuels via the ASTM D4054 approval process.
  - Period of Performance: August 13, 2015 to August 31, 2016 – Amendment No. 007
    2. Evaluate the performance of candidate alternative fuels via the ASTM D4054 approval process.
  - Period of Performance: August 5, 2016 to August 31, 2017 – Amendment No. 012
    3. Manage the evaluation and testing of candidate alternative fuels.
  - Period of Performance: July 31, 2017 to August 31, 2019 – Amendment No. 016
    4. Manage the evaluation and testing of candidate alternative fuels.
  - Period of Performance: August 30, 2018 to August 31, 2019 – Amendment No. 021
    5. Manage the evaluation and testing of candidate alternative fuels.
  - Period of Performance: Extended period of performance end from September 10, 2019 to September 9, 2020 – Amendment No. 023
  - Period of Performance: February 5, 2020 to February 4, 2021 – Amendment No. 25
    6. Manage the evaluation and testing of candidate alternative fuels.
  - Period of Performance: Extended period of performance end from September 9, 2019 to September 9, 2021 – Amendment No. 028.
  - Period of Performance: August 11, 2020 to August 10, 2021 – Amendment No. 32
    7. Manage the evaluation and testing of candidate alternative fuels.

### Project Funding Level

Amendment No. 006	\$309,885
Amendment No. 007	\$ 99,739
Amendment No. 012	\$693,928
Amendment No. 016	\$999,512
Amendment No. 021	\$199,966
Amendment No. 025	\$1,926,434
Amendment No. 032	\$1,049,700
<b>Total</b>	<b>\$5,279,164</b>



In-kind cost sharing has been obtained from:

Organization	Amount	Year
LanzaTech	\$ 55,801	2015
LanzaTech	\$ 381,451	2016
UDRI	\$ 43,672	2016
Neste	\$ 327,000	2017
Boeing	\$2,365,338	2017
Shell	\$ 280,000	2019
IHI	\$1,150,328	2019
Shell	\$ 325,000	2020
<b>Total</b>	<b>\$4,928,590</b>	

## Investigation Team

- Steven Zabarnick, PI, New candidate fuel qualification and certification.
- Richard Striebich, Researcher, Fuel chemical analysis and composition.
- Linda Shafer, Researcher, Fuel chemical analysis and composition.
- John Graham, Researcher, Fuel seal swell and material compatibility.
- Zachary West, Researcher, Fuel property evaluation.
- Rhonda Cook, Technician, Fuel property testing.
- Sam Tanner, Technician, Fuel sampling and shipping.
- Carlie Anderson, Researcher, Fuel chemical analysis.
- Tak Yamada, Researcher, Fuel chemical analysis.

## Project Overview

Alternative jet fuels offer the potential benefits of reduced global environmental impacts, increased national energy security, and stabilized fuel costs for the aviation industry. The FAA is committed to the advancement of “drop-in” alternative fuels. The successful adoption of alternative fuels requires approval for use by the aviation community, followed by large-scale production of a fuel that is cost-competitive and that meets the safety standards of conventional jet fuel. Alternative jet fuels must undergo rigorous testing to become qualified for use and be incorporated into ASTM International specifications.

Cost-effective, coordinated performance testing capability (in accordance with ASTM D4054) is needed to support the evaluation of promising alternative jet fuels. The objective of this project is to provide the necessary capability to support fuel testing and evaluation of novel alternative jet fuels.

The proposed program should provide the following capabilities:

- Identify alternative jet fuels, including blends with conventional jet fuel, with the potential to be economically viable and to support FAA’s NextGen environmental goals for testing.
- Perform engine, component, rig, or laboratory tests or any combination thereof to evaluate the performance of alternative jet fuels in accordance with ASTM International standard practice D4054.
- Identify and conduct unique testing, beyond that defined in ASTM International standard practice D4054, to support the evaluation of alternative jet fuels for inclusion in ASTM International jet fuel specifications.
- Obtain baseline and alternative jet fuel data to assess any effects of an alternative jet fuel on aircraft performance, maintenance requirements, and reliability.
- Coordinate efforts with activities sponsored by the Department of Defense and/or other government parties that may be supporting relevant work.
- Report relevant performance data for the alternative fuels tested, including quantified effects of the alternative fuel on aircraft and/or engine performance and on air quality emissions relative to conventional jet fuel. Reported data will be shared with the FAA National Jet Fuel Combustion Program, the broader community (e.g., ASTM International), and the ASCENT COE Program 33 “Alternative Fuels Test Database Library.”



## Tasks 1 and 2 – Evaluate the Performance of Candidate Alternative Fuels via the ASTM D4054 Approval Process and Manage the Evaluation and Testing of Candidate Alternative Fuels

University of Dayton Research Institute

### Objective

Cost-effective, coordinated performance testing capability (in accordance with ASTM D4054) is needed to support the evaluation of promising alternative jet fuels. The objective of this project is to provide the capability necessary to support either a) the evaluation of to-be-determined alternative fuel(s) selected in coordination with the FAA or b) a fuel test and evaluation project with a specific alternative fuel(s) in mind.

### Research Approach

The intent of this program is to provide the capability needed to perform specification and fit-for-purpose evaluations of candidate alternative fuels, with the aim of providing a pathway forward through the ASTM D4054 approval process. The University of Dayton Research Institute (UDRI) team is capable of performing a large number of these evaluations, and we are prepared to work with other organizations, such as Southwest Research Institute (SwRI) and engine original equipment manufacturers (OEMs), with unique test capabilities, as needed. These assessments include additional engine, auxiliary power unit (APU), component, and rig evaluations. The UDRI testing capabilities include efforts at the laboratories of the Fuels Branch of the Air Force Research Laboratory (AFRL) and at our campus laboratory facilities.

The following lists provide examples of the evaluations that can be provided by UDRI:

#### **Tier 1**

1. Thermal stability (quartz crystal microbalance)
2. Freeze point (ASTM D5972)
3. Distillation (ASTM D86)
4. Hydrocarbon range (ASTM D6379 & D2425)
5. Heat of combustion (ASTM D4809)
6. Density, API gravity (ASTM D4052)
7. Flash point (ASTM D93)
8. Aromatics (ASTM D1319)

#### **Tier 2**

1. Color, saybolt (ASTM D156 or D6045)
2. Total acid number (ASTM D3242)
3. Aromatics (ASTM D1319 and D6379)
4. Sulfur (ASTM D2622)
5. Sulfur mercaptan (ASTM D3227)
6. Distillation temperature (ASTM D86)
7. Flash point (ASTM D56, D93, or D3828)
8. Density (ASTM D1298 or D4052)
9. Freezing point (ASTM D2386, D5972, D7153, or D7154)
10. Viscosity at -20°C (ASTM D445)
11. Net heat of combustion (ASTM D4809)
12. Hydrogen content (ASTM D3343 or D3701)
13. Smoke point (ASTM D1322)
14. Naphthalenes (ASTM D1840)
15. Calculated cetane index (ASTM D976 or D4737)
16. Copper strip corrosion (ASTM D130)
17. Existent gum (ASTM D381)
18. Particulate matter (ASTM D2276 or D5452)
19. Filtration time (MIL-DTL-83133F Appendix B)
20. Water reaction interface rating (ASTM D1094)
21. Electrical conductivity (ASTM D624)



## 22. Thermal oxidation stability (ASTM D3241)

### Extended physical and chemical characterization

1. Lubricity evaluation: BOCLE test (ASTM D5001).
2. Evaluation of low-temperature properties: scanning Brookfield viscosity.
3. Detection, quantification, and/or identification of polar species: as necessary.
4. Detection, quantification, and/or identification of dissolved metals: as necessary.
5. Initial material compatibility evaluation: optical dilatometry and partition coefficient measurements to determine the fuel-effected swell and fuel solvency in three O-ring materials (nitrile, fluorosilicone, and fluorocarbon) and up to two additional fuel system materials.
6. Experimental thermal stability evaluation: quartz crystal microbalance to measure thermal deposit tendencies and oxidation profiles at elevated temperatures.
7. Evaluation of viscosity versus temperature: ASTM D445 to determine the fuel viscosity at 40°C and -40°C to assess the viscosity variation with temperature.

In addition to the above physical and chemical fuel evaluation capabilities, UDRI has extensive experience in the evaluation of microbial growth in petroleum-derived and alternative fuels. These evaluations include standard lab culturing and colony counting methods and advanced techniques such as quantitative polymerase chain reaction (QPCR) and metagenomic sequencing. These methods enable quantitative measurements of microbial growth rates in candidate alternative fuels for comparison with petroleum fuels.

UDRI also has extensive experience in the evaluation of elastomer degradation upon exposure to candidate alternative fuels. Various methods are used to evaluate seal swell and O-ring fixture leakage, including optical dilatometry, sealing pressure measurements, fuel partitioning into the elastomer, and the use of a pressurized temperature-controlled O-ring test device.

Moreover, UDRI can perform fuel-material compatibility testing using the D4054 procedures for fuel soak testing, postexposure nonmetallic and metallic material testing, and surface and microstructural evaluation. The 68 “short-list” materials and the 255 materials on the complete list can be tested.

### Milestones

The schedule for this project is dependent upon the receipt of alternative fuel candidates for testing. As candidate fuels are received, a testing schedule will be established via coordination with the FAA and collaborators. Our existing relationships with these organizations will help expedite this process.

### Major Accomplishments

#### **Shell IH<sup>2</sup> testing**

Discussions with Shell on their IH<sup>2</sup> fuel and process (hydropyrolysis and hydrotreating of woody biomass, municipal solid waste (MSW), and agriculture residue) began in 2017 and proceeded through 2018. In January 2019, samples of their CPK-0 (zero aromatics) fuel were received by the Clearinghouse for testing. Testing proceeded at UDRI and SwRI through the spring of 2019, with a draft research report produced in the summer. In October 2019, initial warm lean blowout (LBO) testing of the CPK-0 fuel blends was performed in the referee combustor. We await the production of larger quantities of IH<sup>2</sup> fuel for additional cold LBO and ignition studies in the referee rig. In addition, a Phase 1 research report was presented to the OEM committee in the June 2020, with the anticipation of OEM APU and engine combustor sector testing in 2021. The unusually high cycloparaffin content (>95%) of this fuel will dictate the need for additional Tier 3 testing, with the extent of testing potentially being limited by the fuel’s excellent performance in the referee rig. We anticipate that OEM feedback from the Phase 1 research report will be available to the fuel producer in early November 2020.

#### **IHI Bb-Oil SPK testing**

Discussions with IHI of Japan on their Bb-oil fuel and process (algae cultivation with hydrocarbon and oil extraction) began in 2018, with initial fuel samples received in January 2019. Testing proceeded during the winter and spring of 2019, with a resulting Fast Track research report being submitted for OEM review in June 2019. This fuel consists of approximately 40% cycloparaffins and thus has a higher density than that specified in the Fast Track guidelines. The OEM review was completed in August 2019, and we completed additional testing on another production sample to address OEM questions during the year. The ASTM ballot was approved in March 2020 for the creation of D7566-20 Annex 7 with the fuel now referred to as HC-HEFA SPK (hydroprocessed hydrocarbons, esters, and fatty acids).



### **Fischer-Tropsch coprocessing**

Fulcrum Bioenergy is interested in adding Fischer-Tropsch (FT) coprocessing to the D1655 fuel specification to permit small quantities (<10%) of FT waxes to be used as feed to petroleum refinery hydrocracking reactors. This change would allow the use of FT waxes produced from the gasification of MSWs in petroleum refinery operations, enabling jet fuel to be produced without operation modifications. To support this effort, this project received vacuum gas oil (VGO)-produced jet fuel and fuel produced from a co-feed of VGO and FT wax product. We assessed the D1655 Table 1 properties, JFTOT thermal stability, trace metals, GCxGC hydrocarbon type, GCxGC polars, lubricity additive responses, and conductivity additive responses. A research report was produced and FT coprocessing was balloted in an ASTM October 2019 ballot. The FT coprocessing ballot was approved in March 2020 with subsequent publication of D1655-20 which includes this process in paragraphs A1.2.2.2 of Annex A1.2 "Acceptable Fuels from Non-Conventional Sources."

### **Publications**

#### **Written reports**

ASTM Ballot. (2019). Modification of ASTM D1655: Co-processing of Fischer-Tropsch feedstocks with petroleum hydrocarbons for jet production using hydrotreating and hydrocracking.

D4054 Fast Track Research Report. (2019). Evaluation of synthesized paraffinic kerosene from algal oil extracted from *botryococcus braunii* (ihi bb-spk).

ASTM D1655-20, Standard Specification for Aviation Turbine Fuels.

### **Outreach Efforts**

Presentations on Project 31 activities were given at the March/April 2020 and September 2020 ASCENT virtual meetings. Meetings were held with the OEM team, FAA, fuel producers, and others at numerous virtual (generally two per month) FAA/OEM meetings.

### **Awards**

None

### **Student Involvement**

None

### **Plans for Next Period**

We are awaiting the receipt of larger quantities of the Shell IH<sup>2</sup> fuel for further evaluation, including cold LBO testing, ignition testing, APU cold start and ignition evaluation, and engine OEM sector evaluation. We expect the Shell IH<sup>2</sup> Phase 1 research report OEM feedback to be returned to the fuel producer in November 2020. We will likely be performing additional testing of the Shell IH<sup>2</sup> fuel as a result of this feedback. We will continue discussions with new fuel producers and expect new candidates to enter the process in the coming months, such as fuels from Global Bioenergies, OMV, Revo, CSIR-IIP.

## **Tasks 3 and 4 – Manage the Evaluation and Testing of Candidate Alternative Fuels**

University of Dayton Research Institute

### **Objective**

The objective of this work is to manage the evaluation and testing of candidate alternative jet fuels in accordance with ASTM International standard practice D4054 (see Figure 1).

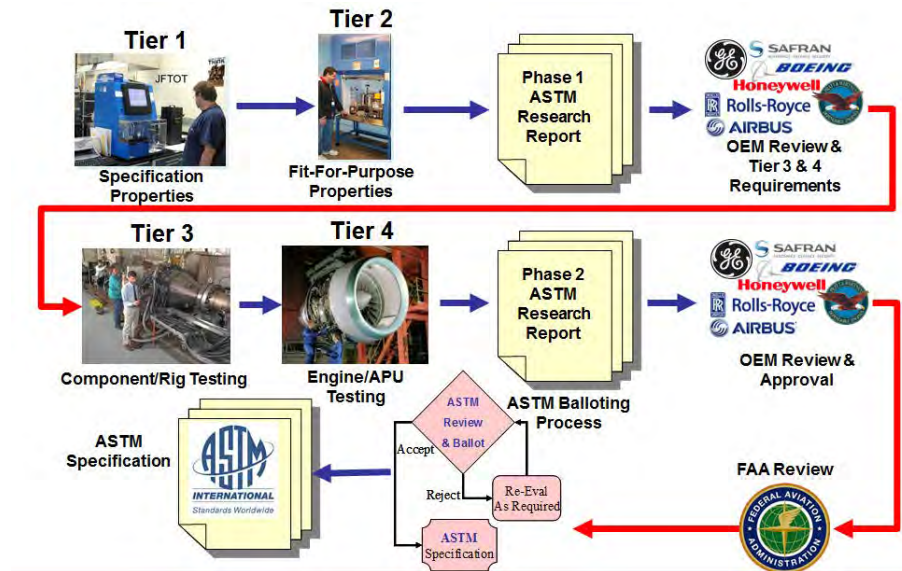


Figure 1. ASTM D4054 qualification process.

### Research Approach

UDRI will subcontract with other research organizations, test laboratories, and/or OEMs to conduct the following tasks in support of the evaluation and ASTM specification development for alternative jet fuels. The purpose of this project is to manage and coordinate the D4054 evaluation process illustrated in Figure 2 in order to facilitate the transition of alternative fuels to commercial use.

#### Subtask 1: General support

- Develop and make available a D4054 process guide that describes logistical procedures for the handling of test fuels, documentation requirements, test report issuance and delivery, and contact information. This guide is intended to provide clear instructions to candidate fuel producers for entering the ASTM D4054 process.

#### Subtask 2: Phase 1 support

- Coordinate the handling of Phase 1 candidate test fuel samples for Tier 1 and 2 testing.
- Review process descriptions provided by the fuel producer to determine acceptability for incorporation into the Phase 1 research report.
- Review test data from Tier 1 and 2 testing to determine acceptability for incorporation into the Phase 1 research report.
- Issue and deliver a Phase 1 research report to OEMs.
- In conjunction with the fuel producer, review and respond to comments regarding the Phase 1 research report, as submitted by the OEMs.
- Conduct additional Tier 1 or 2 testing in response to OEM comments as required.
- Review and consolidate OEM requirements for D4054 Tier 3 and 4 testing, as submitted by the OEMs.
- Deliver consolidated D4054 Tier 3 and 4 testing requirements to the fuel producer.

#### Subtask 3: Phase 2 support

- Coordinate the funding and scheduling of D4054 Tier 3 and 4 testing with OEMs and other test facilities.
- Coordinate the handling of Phase 2 candidate test fuel samples for Tier 3 and 4 testing.
- Review test data from Tier 3 and 4 testing to determine acceptability for incorporation into the Phase 2 research report.
- Issue and deliver the Phase 2 research report to OEMs.
- In conjunction with the fuel producer, review and respond to comments submitted by OEMs regarding the Phase 2 research report.



- Conduct additional Tier 3 or 4 testing in response to OEM comments as required.
- Issue and deliver Phase 2 research report addendums reporting the additional Tier 3 or 4 test results as required.

**Subtask 4: OEM review meetings**

- Schedule periodic OEM meetings to review the testing status and the research report evaluations.
- Identify suitable meeting venues and support equipment.
- Develop agendas and coordinate with attendees for participation in these meetings.
- Record meeting minutes, including agreements, commitments, and other action items
- Issue and distribute meeting minutes to all attendees

**Subtask 5: Single-laboratory GCxGC method documentation**

- Document UDRI GCxGC methodology for hydrocarbon type analysis
- Develop reference materials for the creation of GCxGC hydrocarbon type templates
- Measure single-laboratory precision of the GCxGC methods

**Subtask 6: Multi-laboratory GCxGC method documentation**

- Validate the precision of GCxGC methods over multiple laboratories
- Identify alternative GCxGC methods, including column selection and order, and modulation techniques
- Perform a correlation study to determine the agreement among laboratories, methods, and hardware choices

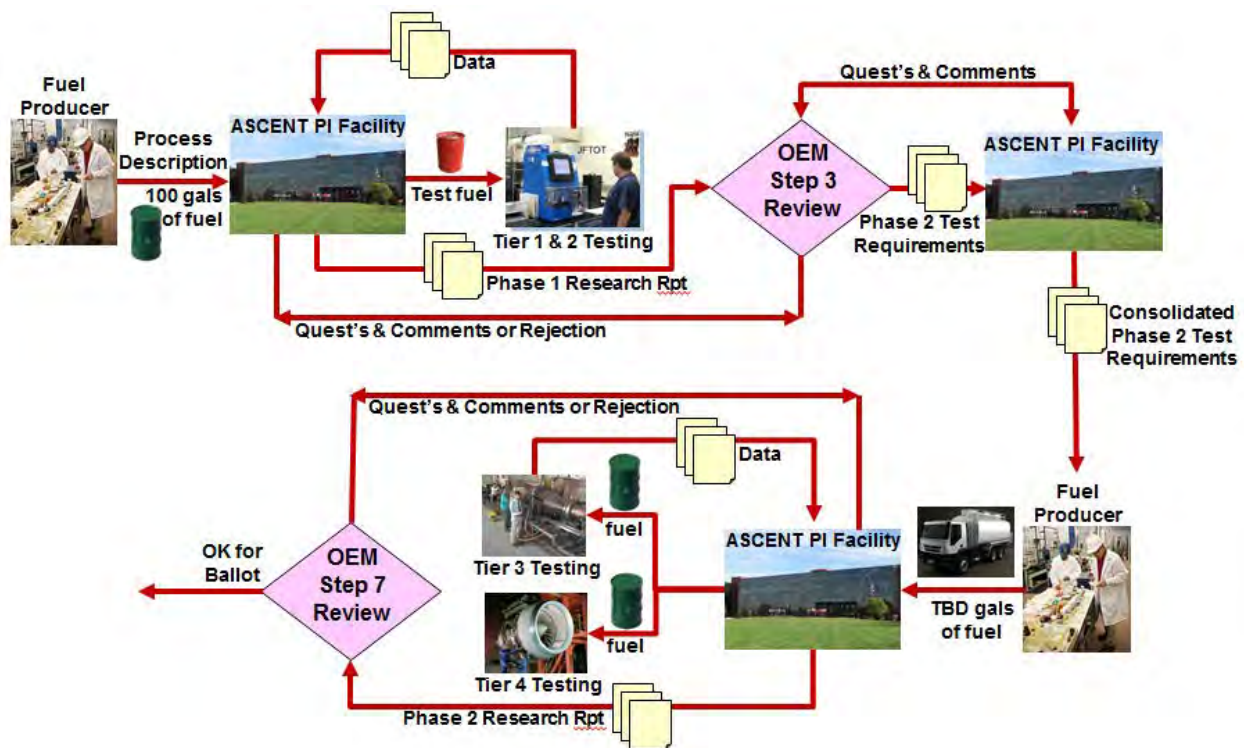
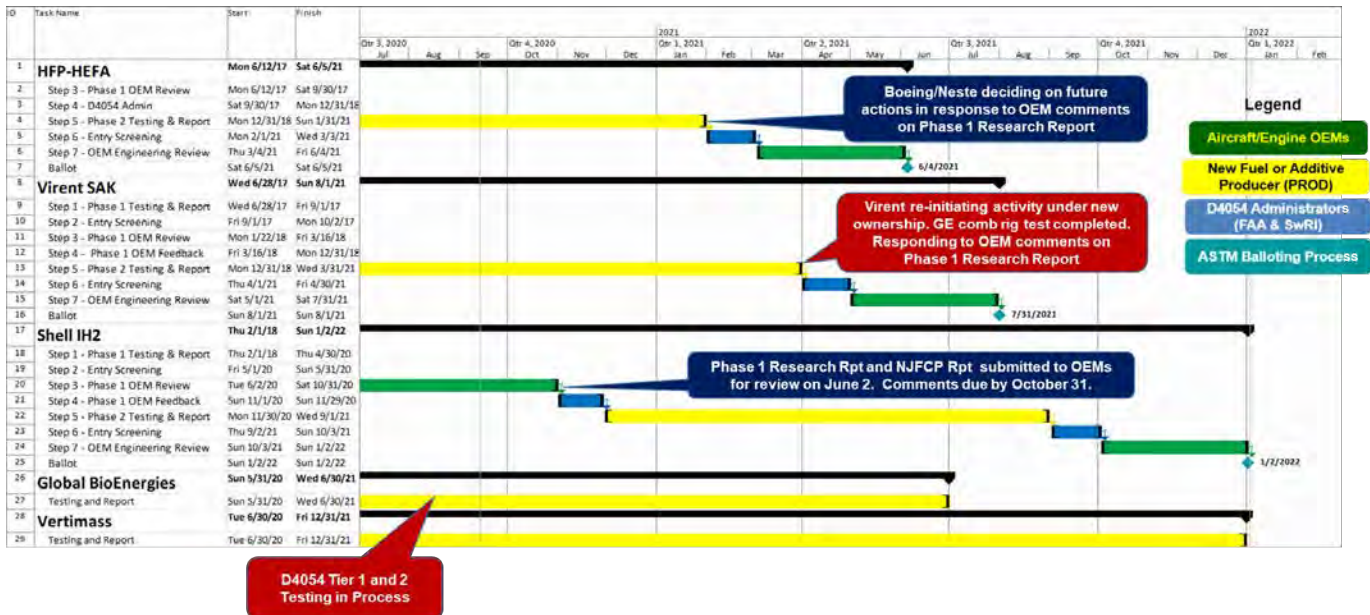


Figure 2. D4054 evaluation process.

**Milestone(s)**

The schedule for this project is dependent upon the receipt of alternative fuel candidates for testing. As candidate fuels are received, a testing schedule will be established via coordination with the FAA and collaborators. Our existing relationships with these organizations will help expedite this process. Figure 3 shows a Gantt chart schedule for the testing and approval of candidate fuels that are currently under evaluation or that will soon enter the evaluation process.

## D4054 Clearinghouse Forecasted Fuel Evaluation Schedule



September 14, 2020

Figure 3. Schedule for fuel evaluations.

### Major Accomplishments

#### Fast Track annex development

A D7566 Generic Annex concept was originally presented to the OEM committee, in which a set of highly stringent property requirements would be used to create a D7566 annex without the feedstock or process being defined. This annex would enable the rapid approval of a wide variety of fuels that closely resemble already approved fuels with regard to composition and physical properties. However, the OEM committee was concerned about the lack of an OEM review for each fuel approved through this process. Thus, the Generic Annex pathway was abandoned in the spring/summer of 2018. In response to OEM concerns, a Fast Track Annex to D4054 was proposed in the winter of 2018/19, which included a list of stringent properties and chemical composition requirements. This Fast Track Annex would require an identification of the feedstock and processing, along with a required OEM review of the research report results. The goal would be an allowed 10% blend limit with a much more rapid approval pathway. Fast Track approval would result in the creation of a D7566 annex for each approved fuel. Ultimately, the Fast Track Annex was balloted in the spring of 2019 and approved in April 2019. To date, one candidate fuel has been approved via the Fast Track process, the IHI HC-HEFA D7566 Annex 7 fuel.

#### GCxGC method documentation

Two GCxGC method reports were completed and made available to the fuel community (UDRI Method FC-M-101 Flow Modulation GCxGC for Hydrocarbon Type Analysis of Conventional and Alternative Aviation Fuels; UDRI Method FC-M-102 Identification and Quantitation of Polar Species in Conventional and Alternative Aviation Fuels Using SPE-GCxGC). The first report documents the UDRI/AFRL hydrocarbon type analysis method based on flow modulation GCxGC and “normal phase” column order (nonpolar followed by polar columns). The second report documents the UDRI/AFRL polar analysis, which uses a solid-phase extraction pre-separation technique to separate and concentrate trace polar species. After pre-separation, the fuel polars are analyzed by GCxGC separation. These reports are being made available to any parties that express interest. These documents are now included in the ASTM D4054 Fast Track Annex A4 (ASTM D4054 Annex A4. Fast Track OEM Qualification and Approval Process for New Aviation Turbine Fuels). These methods provide the fuel community with new tools to enable accurate fuel composition analysis and improved techniques for evaluating and qualifying new candidate alternative fuels.



### **GCxGC precision – intra- and interlab comparisons**

To investigate the precision of GCxGC hydrocarbon type analyses, we assessed a single fuel over a number of years using a single instrument (intralab comparison). We also compared two different GCxGC systems, i.e., flow modulation with a nonpolar initial column and a polar secondary column versus thermal modulation with a polar initial column and a nonpolar secondary column. We also compared measurements between two labs (UDRI/AFRL versus NASA Glenn) for a number of fuels using the same instrument type and column configuration.

### **OEM committee coordination**

The ongoing effort of ASTM OEM committee coordination continued during this period. This effort involves coordinating the engine and airframer OEM meetings, which have occurred in concert with the biannual ASTM D02 sessions and at the annual UK MoD AFC meeting in London. SwRI continues to receive funding to aid in coordinating the OEM meetings and in communicating with the OEMs for discussions and research report reviews of new candidate alternative jet fuels. In addition, a Gantt schedule is updated monthly; this schedule shows a queue of candidate fuels and the completed and expected schedule as these fuels move through the ASTM D4054 process of testing, review, balloting, and approval. A recent version of this schedule is shown in Figure 3. In support of the ongoing OEM committee coordination, subcontracts were extended to our ASCENT grant end date of February 4, 2021 with Boeing, GE Aviation, Honeywell, Rolls Royce, Pratt & Whitney, and SwRI. As the current end date was recently extended to August 10, 2021, we are in the process of extending these subcontracts to reflect the new end date.

### **Publications**

#### **Written reports**

UDRI Method FC-M-101. Flow modulation GCxGC for hydrocarbon type analysis of conventional and alternative aviation fuels. UDR-TR-2018-40.

UDRI Method FC-M-102. Identification and quantification of polar species in conventional and alternative aviation fuel using SPE-GCxGC. UDR-TR-2018-41.

Evaluation of Integrated Hydrolysis and Hydroconversion (IH<sup>2</sup>) Cycloparaffinic Kerosene (CPK-0), D4054 Phase 1 Research Report, May 2020.

Evaluation of Synthesized Paraffinic Kerosene from Algal Oil Extracted from *Botryococcus braunii* (IHI Bb-SPK), Fast Track Research Report, 2019.

### **Outreach Efforts**

Presentations on Project 31 activities were given at the March/April 2020 and September 2020 ASCENT virtual meetings. Meetings were held with the OEM team, FAA, fuel producers, and others at numerous virtual (generally two per month) FAA/OEM meetings. We continue to have biweekly teleconferences with Shell on their IH<sup>2</sup> fuel candidate. We have had meetings with a number of candidate fuel producers, including Global Bioenergies, OMV, CSIR-IIP, and Revo.

### **Awards**

None

### **Student Involvement**

### **Plans for Next Period**

We plan to continue coordination of the OEM committee reviews. We held an OEM committee meeting at the December 2019 ASTM D02 meeting in Denver and will hold virtual OEM committee meetings until the coronavirus situation is resolved to allow business travel.



## Project 033 Alternative Fuels Test Database Library (Year VI)

### University of Illinois Urbana-Champaign

#### Project Lead Investigator

Tonghun Lee  
Professor  
Mechanical Science & Engineering  
University of Illinois at Urbana-Champaign  
1206 W. Green St.  
Urbana, IL 61801  
517-290-8005  
tonghun@illinois.edu

#### University Participants

##### University of Illinois at Urbana-Champaign

- PI: Tonghun Lee, Professor
- FAA Award Number: 13-C-AJFE-UI-026
- Period of Performance: October 1, 2019 to September 30, 2020
- Tasks:
  1. Generation II Online Database Update and JETSCREEN Connection.
  2. Machine Learning-Based Online Analysis,

#### Project Funding Level

FAA funding Level: \$130,000

Cost Share: Software license support from Reaction Design (ANSYS)

#### Investigation Team

- Tonghun Lee (Professor, University of Illinois at Urbana-Champaign): Overall research supervision.
- Isabel Anderson (Graduate Student, University of Illinois at Urbana-Champaign): Database development and Machine Learning-Based Analysis.

#### Project Overview

This study seeks to develop a comprehensive and foundational database of current and emerging alternative jet fuels by integrating relevant pre-existing jet fuel data into a common archive that can support scientific research, enhance operational safety, and provide guidelines for the design and certification of new jet fuels. In previous years of this project, efforts were focused on the integration and analysis of pre-existing jet fuel data from various government agencies and individual research groups. Recently, we have converted all of the compiled data to a new nonstructured query language (NoSQL) format using a JavaScript object notation (JSON) schema, thus allowing the data to be analyzed in a flexible manner using various programming languages. To this end, we have launched the second generation of our online database, which utilizes the new nonrelational database structure. This version is equipped with interactive analysis functions for users and flexible methods for plotting and downloading data. In the previous year, we have extended this effort to incorporate advanced machine learning algorithms in the analysis process. Additionally, we have worked on integrating our database with the database assembled by the European JETSCREEN program, potentially leading to a global database structure in the future. We hope that the database will one day not only serve as a comprehensive and centralized knowledge base utilized by the jet fuel research community, but will also serve as a resource that can enhance global operation efficiency and safety. Future efforts will include not only expansion of the international framework with JETSCREEN, but also efforts to potentially include

real-time data being used at the airports. With the prolific diversification of new alternative jet fuels expected in the near future, the ability to track critical fuel properties and test data from both research and operation perspectives will be highly valuable for the future of commercial aviation.

## Task 1– Generation II Online Database Update and JETSCREEN Connection

University of Illinois Urbana-Champaign

### Objectives

The main objective of this Task is to upgrade/debug the generation II online National Alternative Jet Fuels Test Database functions and link the database to the European JETSCREEN program. The generation II database is designed using a new architecture that allows for flexible analysis and scaling based on a NoSQL data format. This format can accommodate various data types and that can be easily accessed by any common programming language, and basic analysis functions have been built right into the web interface. Following the launch of the generation II web interface, significant effort has been made in the past year to upgrade the functionalities and address bugs based on user feedback. We have also converted much of the data to a comma-separated values (CSV) format to enable machine learning-based analysis in the future, of which more will be discussed in Task 2. The specific goals in Task 1 are as follows:

- Test and improve functionality of the generation II online web interface and database structure.
- Convert dataset from nonrelational JSON (Schema) format to CSV for machine learning-based analysis.
- Link database with the European JETSCREEN program with automatic file sharing.
- Link database with real-time airport fuels data (delayed due to COVID-19, efforts restarted as of September 2020).

### Research Approach

#### Generation II Database Debugging and Upgrade

A beta version of the generation II database was launched online in the summer of 2019. The web interface of the generation II database is shown in Figure 1. All of the functionality of the previous database is maintained, and the security login features have been migrated from the previous version. The generation II web interface, much like generation I, is a HTML-oriented program that is built on a layer of metadata which supports search functions for the users. The tree structure that was applied to organize the data folders in the first database was also retained in this version, allowing the user to access the data in a similar manner. The main difference is that there is an additional inner core which houses the JSON files, and it is here where the test data resides. Currently, the database has grown to house over 25,000 separate fuel records.

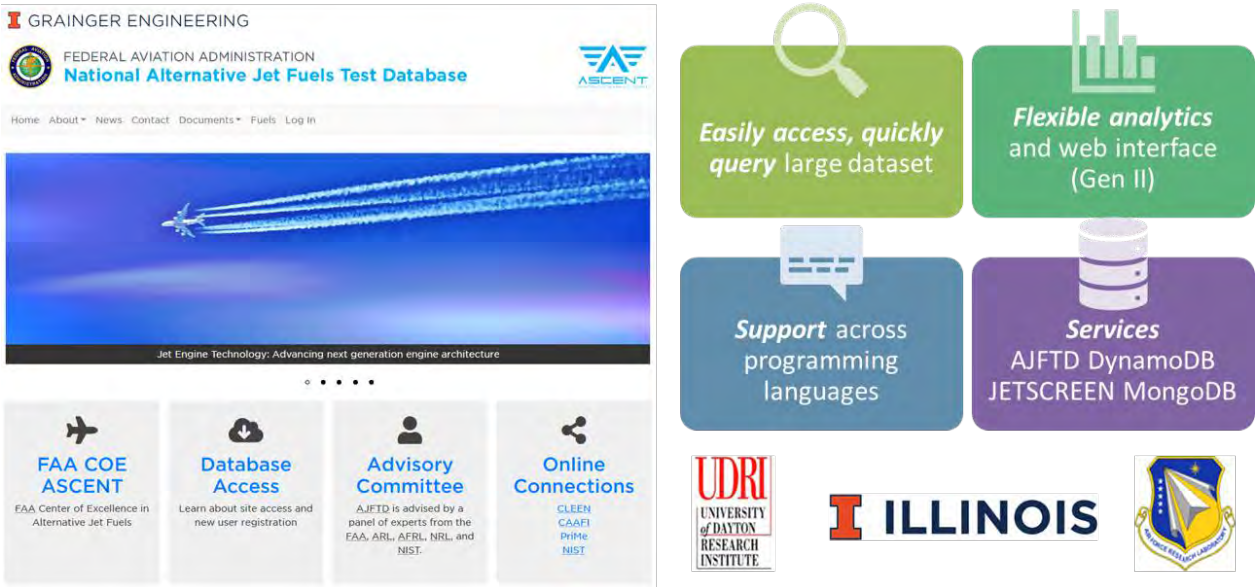
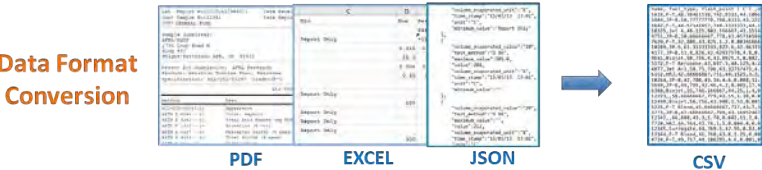


Figure 1. Generation II National Alternative Jet Fuels Test Database web interface. (altjetfuels.illinois.edu)

The catalogue of data currently available in the database is primarily assembled from four separate sources. The fuels with POSF (Air Force Research Laboratory (AFRL) fuel database code) number designations were added from the internal database maintained by the AFRL at the Wright Patterson Air Force Base. The second dataset was obtained from the PQIS reports of the Naval Air Systems Command (NAVAIR) and corresponds to a compilation of fuel data geared primarily towards government use. The third set was provided by Metron Aviation, who compiled fuel properties from samples collected at airports through a previous ASCENT project. The dataset resulting from this study proved valuable by providing a landscape of fuels currently used in commercial aviation and will guide our future efforts focused on capturing this type of data in real time. The final dataset was obtained from the National Jet Fuel Combustion Program (NJFCP) within ASCENT.

-  **Search function** optimized to include multiple categories for specific searches (POSF, JETSCREEN, airport, fuel ID, etc.)
-  **Export & Compare features** updated for JETSCREEN fuels
-  **Display** of keys and values updated (security)
-  **GCxGC** specific section being added
-  **Daily & hourly syncs** with AWS S3 buckets



**Figure 2.** Modifications to the Generation-II Database and conversion of data to CSV for machine learning.

Following the launch of the generation II database (summer 2019), significant effort was required to fix bugs and upgrade various aspects of the database. Some of the key changes to the database are listed in Figure 2 and summarized below.

- During the integration of the database with JETSCREEN, we modified the labeling structure to ensure that files were coded as JETSCREEN data and separately searchable. Similar to how the Metron data is labeled according to the airport the data was retrieved from, JETSCREEN was added as a separate search label also. This search filter can be integrated with additional search filters to allow users to view tests for a specific fuel type from the JETSCREEN group if so desired. The search page was also updated to include options to search by POSF number and GCxGC data. Searching by POSF number allows the user to find not only the specific POSF fuel they are looking for, but also any fuels that include it in a blend. Searching “GCxGC” in this search bar also returns any files that contain “GCxGC” in the fuel description. The user can also combine this search with a “Search by Fuel Type” or “Search by Airport” to narrow the results. This function is still being optimized based on user experience.
- After the search page was updated to include JETSCREEN files, the Export and Compare features required updates as well. Although we had worked with JETSCREEN extensively to create a standard JSON format, the files generated from the two camps had minor differences which caused the current code on the database to fail at times. Slight differences between the JETSCREEN files themselves were also causing errors not only for comparing the data with FAA files, but also with other JETSCREEN files. The Export and Compare features were updated to work around these issues and to support the comparing of all test files on the database.
- The display of data on the database was also changed to allow for more privacy and security. Authors of the files (which included student names) were removed from the JETSCREEN display. The sharing function, which was put in place to share selected FAA data with JETSCREEN via Amazon Web Services (AWS), was set to display for admin accounts only. These

shared FAA files sync with the AWS S3 bucket every hour. The JETSCREEN bucket on AWS is checked each day for new files, which are then downloaded to the website (more detail will be provided in Figure 3).

- Effort was made to convert the JSON format on the database to a CSV format for select files so that we could utilize machine learning-based analysis, which will be addressed further in Task 2. The actual files that are being stored will utilize the NoSQL JSON format, which is more conducive to maintaining a flexible database. However, certain parts of the data that are to be analyzed using machine learning will need to be converted to CSV format for which multiple Python based machine learning scripts are available. In the future, there may need to be a process to automate this conversion in real-time for when it is needed.

**Integration of Database with JETSCREEN**

During the past year, we have made significant progress in integrating our database with the European JETSCREEN program. The JETSCREEN program was initiated to provide fuel producers, air framers, and aero-engine and fuel system original equipment manufacturers (OEMs) with knowledge-based screening tools for fuels and also have a similar database that could be linked with ours. We first started discussing a potential merger with the JETSCREEN database in 2018, after which we started methodically synchronizing the data structure so that a merger could be possible. After much beta testing, the two databases were first linked in Spring of 2020, and the data sharing process is shown in Figure 3.

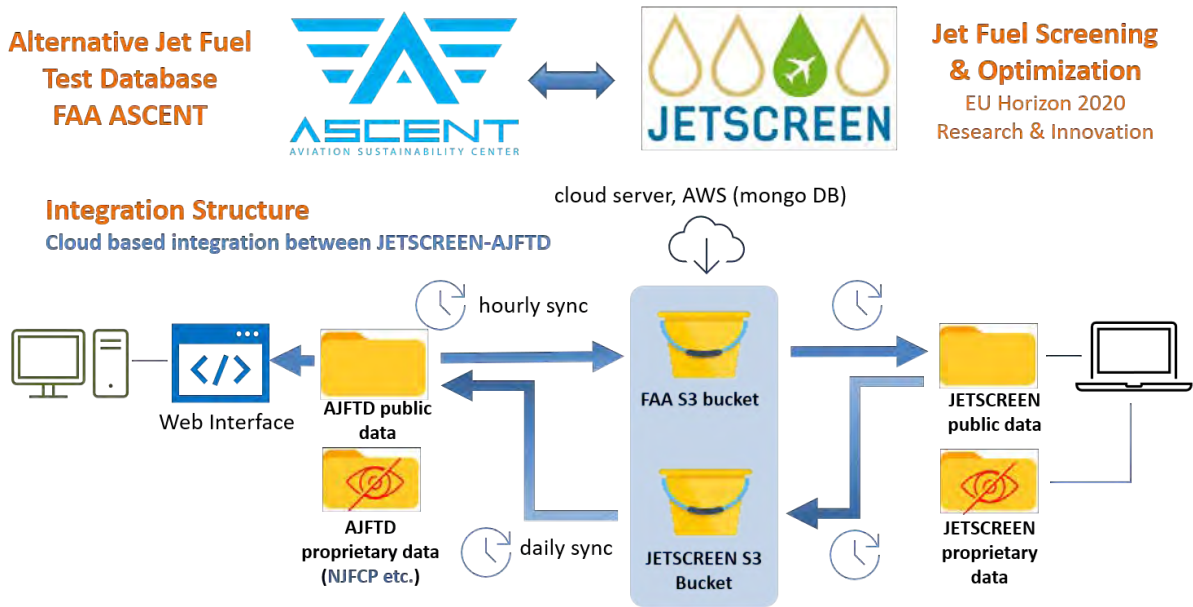


**Figure 3.** Database integration schematic with JETSCREEN.

As shown, the JETSCREEN and FAA databases are joined by a common cloud storage. AWS was selected as the server to store the shared data, mainly due to their affiliation with the University of Illinois. S3 buckets (Amazon database structure) were created for both FAA and JETSCREEN to share their JSON files. Each can pull files from the other’s folder, but read and write access is only granted for the owners of the bucket. The FAA data is shared to its S3 bucket via altjetfuels.illinois.edu. All public FAA data on the website will have an option to be shared with JETSCREEN, which can be toggled by administrators. The website syncs hourly with the bucket to upload newly shared data. No proprietary data is shared to the FAA S3 bucket. Any files uploaded to the FAA bucket can be viewed and downloaded by JETSCREEN. For downloading new JETSCREEN data to the website, a script runs daily to check JETSCREEN’s S3 bucket for newly shared data. Any new files are then downloaded to our local database and can be consumed by the users. We note that the actual interface of the database will be left to each entity to decide. For us, we have adopted an open web interface, whereas JETSCREEN has a proprietary software with no direct web access currently.

We feel that this is a monumental first step in linking many other fuel databases across the globe in the future. From this joint effort between FAA and JETSCREEN, we hope to establish a foundation which can help to both monitor and evaluate fuels used around the international airspace in the future. As new fuels are integrated into the global supply chain, a means to keep track of their properties will become critical. Such an interconnected database will ensure that we are able to provide both the information needed for research and certification of new fuels, but also to uphold quality standards and demonstrated the feasibility of sustainable aviation fuels (SAFs) in our future. The database integration impacts are outlined in Figure 4.



Figure 4. Database integration impacts.

**Milestones**

**3 months**

- Initiation of debugging and optimization of data structure in the generation II database.
- Collaboration with JETSCREEN to standardize the data format for a potential merger in the near future.

**6 months**

- Completion of most debugging in the generation II database and further improvements to online analysis tools.
- Writing of scripts for integration of database with JETSCREEN on cloud server and selection of provider (Amazon).
- Conversion of data from NoSQL to additional CSV format.

**9 months**

- Launch of the joint cloud server with JETSCREEN and turning on of data sharing scripts.
- Continued discussions with JETSCREEN to optimize data sharing protocols and set security protocols.

**12 months**

- Preliminary tests with JETSCREEN for optimization of file sharing and identification of problems.
- Modification of Compare, Export, and other functions to accommodate integration of JETSCREEN data.

**Major Accomplishments**

**Launching of the Integrated Database with JETSCREEN**

We have finally merged our FAA database with the JETSCREEN database at <https://altjetfuels.illinois.edu/>. The database is linked with JETSCREEN through a cloud archive (AWS) where FAA and JETSCREEN data are kept in separate secure online folders. Data is automatically shared and downloaded to the local servers for both us and JETSCREEN several times each day through the execution of customized scripts. On our side, new JETSCREEN data will be pulled into our local database each

day and available for processing through our regular analysis tools. This new database structure can be a foundation for a global database in the future, contributing to the development and certification of new fuels in the global aviation pipeline as well as monitoring fuel quality and safety concerns.

#### **Modifications to the Generation II Online Database and Conversion of Data to CSV**

Upon launching of the generation II database and migrating more than 25,000 fuel records in a NoSQL JSON format, the web interface and analysis tools have been rigorously tested and debugged. These improvements will continue in the future as new data are added and new analysis techniques are developed. In anticipation of using machine learning-based analysis in the future, parts of the database have been converted to a CSV format so that Python-based machine learning scripts could be utilized. Significant upgrades to the search functions have been carried out so that users can search for specific fuel type and other cross-referenced properties directly online.

#### **Publications**

N/A

#### **Outreach Efforts**

Database made accessible through <https://altjetfuels.illinois.edu/>

#### **Awards**

N/A

#### **Student Involvement**

This project was primarily conducted by one graduate student (Isabel Anderson).

#### **Plans for Next Period**

In the next period, we intend to optimize the integration with JETSCREEN as well as develop common online analysis tools based on "big data" analysis. New discussions regarding management of proprietary data will need to take place with JETSCREEN. Most importantly, we will need to engage with airports in the U.S. to capture real-time fuel data and determine the feasibility of integrating it into our current database.

## **Task 2 – Machine Learning-Based Analysis**

University of Illinois Urbana-Champaign

#### **Objectives**

The main objective of this Task was to develop advanced analysis methods based on machine learning algorithms for analysis of the data in the alternative jet fuel database. The effort is inspired by the notion that the intricate relations between properties of fuels and their chemical signatures are critical, but maybe beyond the complexity that can be addressed with routine, classical, regression-based analysis. The effort is ever more important when new analysis techniques such as GCxGC can provide large amounts of data that are difficult to process using simple analytical algorithms. Machine learning can provide the means for the most advanced analysis to be applied to our current data and will prove to be even more powerful as the size of the data grows in the future. This effort was also established through a series of discussions with the JETSCREEN team and both programs will devote considerable effort to this cause. The major goals of this Task are as follows:

- Identify best machine learning-based approach for the jet fuel data.
- Identify the best data format for implementation of machine learning algorithms.
- Carry out binary regression analysis of key jet fuel properties.
- Conduct prediction analysis of jet fuel properties based on classical machine learning.
- Conduct prediction analysis of jet fuel properties based on neural network (deep learning) machine learning.

#### **Research Approach**

##### **Classical Regression-Based Analysis**

The need to utilize basic regression analysis came from joint collaborative work with JETSCREEN during a phase when we were trying to synchronize the data scripts to merge the two databases. A key insight was that many properties of the fuels are correlated and having a strong understanding of such correlations would help reduce the number of testing procedures

for certification. Naturally, our interests extend to understanding if this type of correlation extends to alternative fuel sources with different chemical makeups. On the JETSCREEN side, a separate effort was also initiated in looking into the correlation between different fuel properties; the results were presented at the International Association for Stability, Handling and Use of Liquid Fuels (IASH) meeting in 2019.

On our side, we approached this in two steps. The first was to carry out an extensive binary correlation to understand the relationship between all the major properties that we had access to. The second step was to utilize the correlation information to test out classical regression-based machine learning algorithms to see if we could predict certain properties based on other properties through a training algorithm. The two approaches are shown in Figure 5.

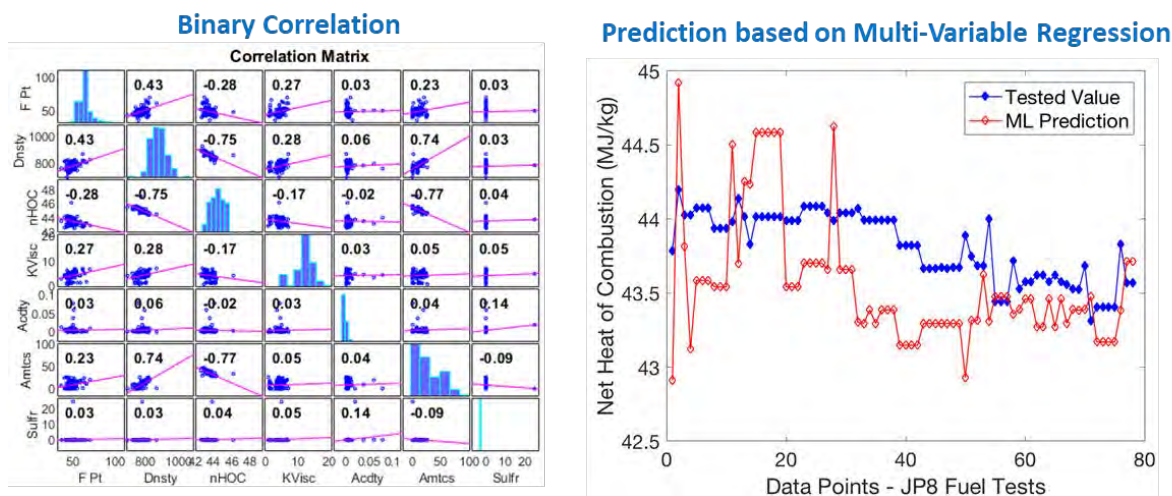


Figure 5. Classical regression-based machine learning.

In order to extract the relationships between the jet fuel properties, the Pearson Coefficients for several properties were investigated using MATLAB's Corrplot tool. The binary correlation matrix in Figure 5 shows the Pearson Coefficients for binary relationships between flash point, density, net heat of combustion, kinematic viscosity, acidity, aromatics, and sulfur content. After correlations were confirmed, the data was transferred to Microsoft's ML.Net program to make predictions. ML.Net is a machine learning platform developed by Microsoft to integrate multiple machine learning algorithms and find the best performing model for the input data. This reduces the computation time for testing various algorithms by hand and provides the user with the reassurance of knowing they are using one of the best models for their data from the extensive Microsoft archive. Our database provides the extensive training set to ensure accurate models are created.

After specifying which properties to predict, ML.net was given a training set containing approximately 9,000 fuel tests to find the highest performing regression model for each predicted property. ML.net tests about 30 varying algorithms for each property and returns the top one. Figure 5 shows the results from prediction net heat of combustion for JP8 fuel type using Fast Tree Regression. This test set had a nominal error percentage of ~1.8%. Fast Tree Regression is a multiple additive regression tree gradient boosting algorithm. It goes through multiple regression trees and calculates the error for each step and corrects for in the next step. This algorithm was found by ML.NET to be the top performing model for this data.

### Deep Learning (Neural Network)-based Data Analysis

While it is recognized that estimating various properties of fuels will be helpful for investigating alternative jet fuels and even for drop-in fuels, the problem itself is complex. Traditionally, a mathematical description of the physical relationships was used to predict properties. This process requires a study of the underlying physicochemical characteristics and the use of classical correlations to determine the outcome. Jet fuels, however, are highly complex mixtures with thousands of hydrocarbon species as opposed to single-component fuels. This complexity obscures the direct implementation of simplified laws, and simple correlations are difficult to find. Over the years, tremendous effort has been made to correlate and estimate various properties based on knowledge of other properties which were generally measured. The work here strives to push this effort to the next level where nonlinear and complex relations can be more accurately modeled. The

proposed methods in this section are based on predictor selection and multivariate linear regressions through an artificial neural network. In so doing, we will strive to build a foundation to enhance the accuracy of the predictions to within 1~2 % for the most well correlated properties.

To improve the accuracy and performance of an artificial neural network and regression analysis, we have employed deep learning methodologies that can be used to learn complex prediction models between input and output variables by utilizing multi-layer neural networks with multiple hidden layers. A benefit of deep learning is that features of the data are connected mathematically and statistically, which enables the representation of intricate nonlinear functions. The correlation used in deep learning has proven to be a reliable property model for nonlinear prediction, even though it is typically shown as a black box.

The prototype of our deep learning-based machine learning approach is shown in Figure. 6. Similar to classical regression process learning in Figure 5, one of the properties among flash point, density, net heat of combustion, kinematic viscosity, acidity, aromatics, and sulfur content have been labeled as output and the other properties are labeled as input. Values are normalized with mean 0 and standard deviation 1 to prevent distortion due to differences in the range of values. A PyTorch (Facebook machine learning code library)-based, fully connected deep learning network was built and trained with 138 fuels' datasets by dividing 100 batches over 7000 epochs of iteration. To ensure nonlinearity in the correlation and prevent vanishing gradient problems for training, LeakyReLU was selected as the activation function. In order to improve calculation without overfitting, four different sets of hidden layer compositions were tested.

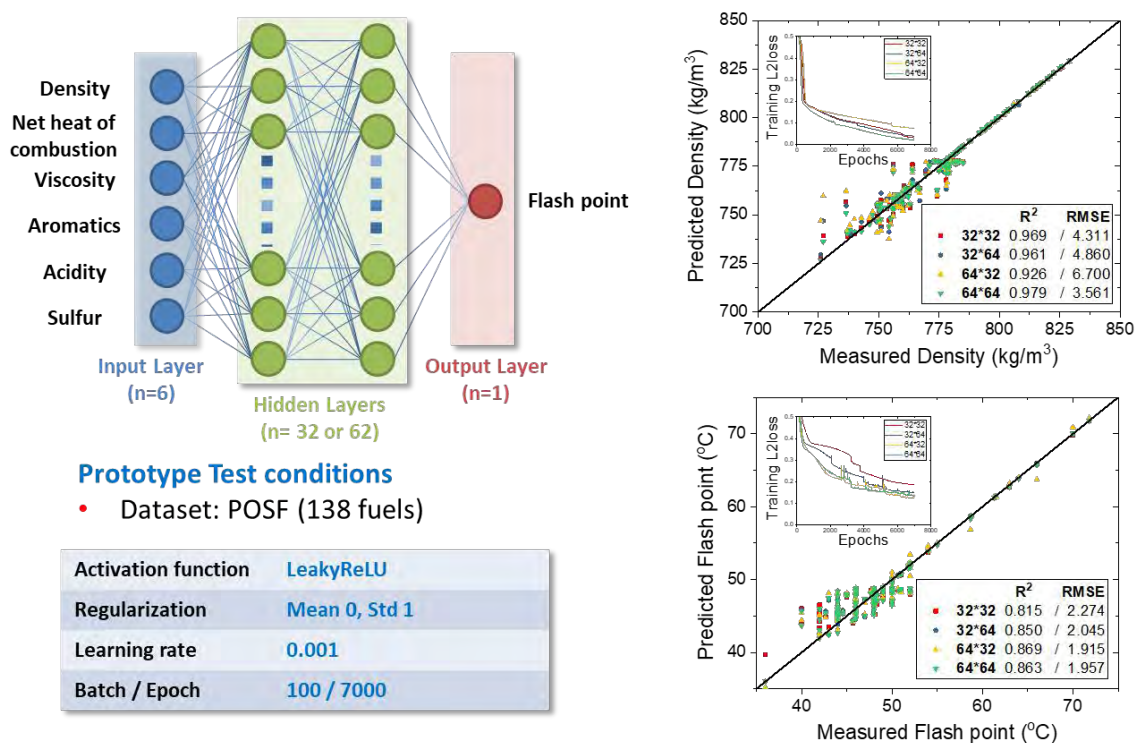


**Figure 6.** Neural network-based machine learning.

The right side of Figure 6 shows the results of the predictions of density and flashpoint by using other properties. The prototype predicted well, even under low numbers of test sets. In the future, it will be meaningful if this method can be tested under well-organized big data samples. Based on our preliminary studies, we have identified several aspects of the prediction method which could be improved. First, the correlation/prediction results should be explanatory and transparent. The black box model in deep learning, due to its multilayer nonlinear structure, is often criticized for being non-transparent and its predictions untraceable by the user. We feel that we should find underlying comprehensive physical laws to give

insights for guiding the machine learning algorithms. Second, we have to pay attention to prevent overfitting or underfitting to the training dataset. Wrongly trained models will give prediction errors under different sets of data. Generally, deep learning is more suitable for learning from large datasets and could potentially be more difficult to train with small datasets or datasets with skewed characteristics. We should systematically explore this limitation and present guidelines for training datasets in the future.

## **Milestones**

### **3 months**

- Discussion with JETSCREEN on machine learning focus and direction.
- Formalization of machine learning implementation plan (binary correlation, prediction, neural network, etc.).

### **6 months**

- Setting up scripts and algorithms for implementation of machine learning.
- Organization of target data from the database for implementation of machine learning.
- Conversion of data from NoSQL to additional CSV format.

### **9 months**

- Binary correlation analysis using Corrplot (MATLAB).
- Prediction of properties using ML.NET and classical regression machine learning routines.

### **12 months**

- Coding and preliminary implementation of neural network (deep learning) algorithms.

## **Major Accomplishments**

We have started the preliminary implementation of using advanced machine learning algorithms for analysis of data in our database. We have adopted an approach that starts from classical machine learning algorithms based on regression-based analysis with optimization of the specific mathematical routines being used. We then transitioned to more advanced neural network (deep learning)-based analysis where multiple layers of learning nodes should provide superior flexibility in terms of nonlinear computations for property predictions. The comparison between the two methods should allow us to gauge how proficient the implementation of machine learning will turn out to be when we increase the data size. We are coordinating these efforts with our collaborators in the JETSCREEN program and will work on joint publications in the near future.

## **Publications**

N/A

## **Outreach Efforts**

Database made accessible through <https://altjetfuels.illinois.edu/>

## **Awards**

N/A

## **Student Involvement**

This project was primarily conducted by two graduate students (Isabel Anderson and Keunsoo Kim).

## **Plans for Next Period**

We will expand our machine learning capabilities and provide tangible performance metrics for various datasets in the database. In particular, we are strongly interested in whether machine learning can discern differences in alternative fuel blends and provide predictions that work across an entire range of conventional fuels and SAFs. This will require a focused and extensive analysis of the data in the next period of the program.



# Project 034 National Jet Fuels Combustion Program – Area #7: Overall Program Integration and Analysis

## University of Dayton

### Project Lead Investigator

Joshua Heyne  
Associate Professor  
Mechanical Engineering  
University of Dayton  
300 College Park  
Dayton, OH 45458  
937 229-5319  
Jheyne1@udayton.edu

### University Participants

#### University of Dayton

- PI: Joshua Heyne
- FAA Award Number: 13-C-AJFE-UD (Amendment Nos. 9, 10, 13, 17, 18, and 24)
- Period of Performance: October 1, 2019 to September 30, 2020
- Tasks:
  1. Overall National Jet Fuels Combustion Program (NJFCP) integration and coordination.
  2. Investigation of chemical and physical effects on lean blowout (LBO).

### Project Funding Level

Amendment No. 9: \$134,999 (September 18, 2015, to February 28, 2017)

Amendment No. 10: \$249,330 (July 7, 2016, to December 31, 2017)

Amendment No. 13: \$386,035 (August 30, 2016, to December 31, 2017)

Amendment No. 17: \$192,997 (August 3, 2017, to September 30, 2018)

Amendment No. 18: \$374,978 (December 7, 2017, to December 31, 2018)

Amendment No. 24: \$374,978 (February 5, 2020, to February 4, 2022)

### Investigation Team

- Joshua Heyne (University of Dayton) is the project lead investigator for coordinating all NJFCP teams (both ASCENT and non-ASCENT efforts).
- Jen Colborn (University of Dayton) is a graduate research student assistant aiding in the testing of fuels on the Referee Combustor rig.
- Katherine Opacich (University of Dayton) is a graduate research assistant working to document NJFCP activities and analyze ignition data across NJFCP teams.
- Zhibin Yang (University of Dayton) is a graduate student research assistant working to develop jet fuel blend optimizer (JudO).

### Project Overview

The NJFCP is composed of more than two dozen member institutions contributing information and data, including expert advice from gas turbine original equipment manufacturers (OEMs), federal agencies, other ASCENT universities, and corroborating experiments at the German Aerospace Center (DLR Germany), National Research Council Canada, and other international partners. The project is tasked to coordinate and integrate research among these diverse program stakeholders and academic PIs; cross-analyze results from other NJFCP areas; collect data for modeling and fuel comparison purposes in

a well-stirred reactor; conduct large eddy simulations of sprays for the Area 3 high-shear rig; procure additional swirler geometries for the NJFCP areas and allied partners while developing an interface of NJFCP modeling capabilities with OEM requirements. Work under this program consists of, but is not limited to:

- conducting meetings with member institutions to facilitate the consistency of testing and modeling,
- coordinating timely completion of program milestones,
- documenting results and procedures,
- creating documents critical for program process (e.g., fuel down selection criteria),
- soliciting and incorporate program feedback from OEMs,
- reporting and presenting on behalf of the NJFCP at meetings and technical conferences,
- integrating state-of-the-art combustion and spray models into user-defined-functions (UDFs), and
- advising the program steering committee.

## Task 1 – Integration and Coordination of NJFCP Teams

University of Dayton

### Objective

The objective of this Task is to integrate and coordinate all ASCENT and non-ASCENT team efforts by facilitating meetings, summarizing results, presenting results external to the NJFCP, communicating regularly with the steering committee, and other related activities.

### Research Approach

The NJFCP is integrated and coordinated by two main techniques: (1) the structural combining of various teams into six topic areas, and (2) routine meetings and discussion both internal and external to individual topic areas. The topic areas are distinguished by the dominant physics associated with them (topics I and IV), the culmination of all relevant combustion physics (topics II, III, and V), and wrapping all work into a singular OEM graphical user interface package (topic VI). These six topic areas are as follows:

- Topic I. Chemical kinetics: Foundational to any combustion model is a chemical kinetic model and the validation data anchoring modeling predictions.
- Topic II. LBO: This topic covers data, screening, and validation under relevant conditions to statistically and theoretically anticipate fuel property effects on this figure of merit (FOM).
- Topic III. Ignition: Similar to the LBO topic, the focus here is experimental screening and validation data for statistical and theoretical predictions.
- Topic IV. Sprays: Historically, the dominant effect of fuel FOM behavior has been the spray character of the fuel relative to others. Experimentalists in this topic area focus on measuring effects of fuel property on spray behavior. Analogous to topic I, spray behavior is not an FOM like topics II and III, although it is critical to bound the physical property effects on combustion behavior relative to other processes (i.e., chemical kinetics).
- Topic V. Computational fluid dynamics (CFD) modeling. Complementary to the empirical topics II, III, and IV, the CFD modeling topic focuses on the theoretical prediction of measured data and facilitates the development of theoretical modeling approaches.
- Topic VI. UDF development: Once the theoretical modeling approaches matured in topic V are validated, UDFs are developed for OEM evaluation of fuel performance in proprietary rigs.

These topic area teams meet and coordinate regularly. The coordination meetings have been reduced in the current reporting period.

### Milestones

NJFCP AIAA Book.

Developed Tier Alpha prescreening tool for novel sustainable aviation fuel (SAF) prescreening.

### Major Accomplishments

- Book editing and coordination.



- Developing and publishing a Commercial Aviation Alternative Fuels Initiative (CAAFI) R&D prescreening document to provide guidance to novel companies and producers in the refinement and development of fuels to facilitate reduced testing in later stages.

## **Publications**

### **Peer-reviewed journal publications**

Colborn JG, Heyne JS, Stouffer SD, Hendershott TH, Corporan E. Chemical and physical effects on lean blowout in a swirl-stabilized single-cup combustor. Proc Combust Inst 2020. doi:10.1016/j.proci.2020.06.119.

### **Published conference proceedings**

None

## **Outreach Efforts**

### **Invited talks**

Heyne, J. (2020). Prescreening of sustainable aviation fuels. ACS Fall 2020 National Meeting & Exposition, San Francisco, CA

### **Conference presentations**

Yang Z, Heyne J, Ave P, States U. A GCxGC Tier Alpha and Combustor Figure-of-Merit Approach on Sustainable Aviation Fuels Prescreening 2018:1-6. Eastern States Section of the Combustion Institute. University of South Carolina

## **Awards**

None

## **Student Involvement**

Katherine Opacich, graduate research assistant, October 2019 to September 2020. Katherine is working on writing an ignition book chapter.

Jen Colborn, graduate research assistant, October 2019 to September 2020. Jen is working on writing an LBO book chapter.

Zhibin (Harrison) Yang, Ph.D. student, October 2019 to September 2020. Harrison is working on developing Tier Alpha prescreening tool.

## **Plans for Next Period**

Finalize the AIAA book editing.

## **Task 2 – Investigation of Chemical and Physical Effects on LBO**

University of Dayton

### **Objective**

The objective of this Task is to investigate chemical and physical effects on LBO in a swirl-stabilized single-cup combustor.

### **Research Approach**

#### **Introduction**

The lower stability limit of gas turbine engines, or lean blowout (LBO), is an important limit phenomenon for safety, the approval of novel sustainable aviation fuels, and identifying transitions between competing physics [1]. LBO is a complex process that can be impacted by engine design, operating conditions, or any number of fuel properties.

Combustor configuration strongly influences LBO limits. Recirculation zones, air velocity, and combustor dome pressure drop ( $\Delta P$ ) are all influenced by the combustor, nozzle, and swirler design. These different features can impact fuel spray and mixing quality. Nozzle atomization technique and cone angle have been found to influence the equivalence ratio at LBO ( $\varphi_{LBO}$ ) [2,3]. The presence of a swirler, as well as the number of vanes, swirl angle, and swirl direction impact the spray quality which will influence  $\varphi_{LBO}$  [4-8].

Fuel properties have also been found to impact  $\phi_{LBO}$  strongly. Lefebvre found that varying fuel atomization and evaporation properties strongly influenced  $\phi_{LBO}$  in a variety of engine geometries [9]. Physical properties have been shown to strongly impact LBO due to their influence on atomization [9–12]. Fuel property variance can be found within petroleum-derived fuels, impacting LBO limits regardless of engine configuration [9,13].

Changes in operating conditions can also heavily influence  $\phi_{LBO}$ . Variances in combustor pressure (P) and  $\Delta P$  can lead to differences in air velocity, which can affect fuel atomization. Fuel and air temperatures highly influence evaporation as well as droplet breakup, since the physical properties that control fuel atomization are highly temperature dependent [3]. Increased temperatures cause less required energy from the combustion process to vaporize the fuel, leading to an improved LBO limit.

Aircraft engines must operate over a wide range of pressures and temperatures where LBO performance is important. Combustor conditions vary throughout flight, which can influence LBO limits. Fuels must be able to perform acceptably under these varying conditions. Lefebvre described  $\phi_{LBO}$  with Eq. 1, where combustor design parameters, thermo-fluid effects, and fuel-dependent properties demonstrate the multi-property dependency of LBO [9].

$$\phi_{LBO} = \underbrace{\left[ \frac{f_{pz}}{v_{pz}^{(1+x)}} \right]}_{\text{Geometry}} \underbrace{\left[ \frac{\dot{m}_A^{(1+x)}}{p_3^{(1+nx)} \exp(x T_3/b)} \right]}_{\text{Thermofluids}} \underbrace{\left[ \frac{D_0^2}{\lambda_{eff} LHV} \right]}_{\text{Fuel Effects}} \quad (1)$$

Burger, Plee, and Mellor have extended the work of Lefebvre, evaluating LBO by considering the effects of chemical kinetics, operating conditions, and combustor geometry [14–16]. Through a combination of relevant fuel parameters and combustor geometries, the chemical, evaporative, and mixing timescales can represent autoignition and extinction, fuel volatility, and combustor properties, respectively, as shown in Eq. 2. Peiffer utilized this method to compare the variance of  $\phi_{LBO}$  in experimental rigs with varying geometries and operating conditions to explain the relative importance of fuel properties [17]. Dependence on physical properties was noted in rigs without swirlers, which hinders atomization [18].

$$\phi_{LBO} \sim \left( \frac{1}{\tau_{chem}} + \frac{1}{\tau_{evap}} + \frac{1}{\tau_{mix}} \right)^{-1} \quad (2)$$

Recent LBO investigations have also shown high sensitivity to fuel properties [19,20]. A swirl-stabilized, single-cup combustor showed strong correlation to derived cetane number (DCN) at relatively high temperature and increased pressure conditions ( $T_{air} = 394K$ ,  $T_{fuel} = 322K$ ,  $P = 207kPa$ ,  $\Delta P/P = 3\%$ ) [19]. In contrast, Peiffer demonstrated that at relatively low temperatures and pressures physical properties, such as distillation temperatures and density were important for describing  $\phi_{LBO}$  in an auxiliary power unit (APU) [17,18]. The difference in physical and chemical property dependence between different operating conditions implies competition between spray characteristics and autoignition stabilization.

While the extreme operational conditions detailed above demonstrated a difference in property importance, the transition between the physical and chemical regime has not been thoroughly investigated. This study seeks to investigate a transition from LBO performance physical property dependence (spray characteristics) to chemical property dependence (autoignition characteristics) with varying  $\Delta P/P$  as well as air and fuel temperatures.

### Test article

A swirl-stabilized single-cup combustor designed with turbine engine OEM input to simulate key characteristics of actual turbine engine combustors was used for LBO limit investigation (Figure 1). Referred to as the “Referee Combustor”, it features effusion cooling and dilution holes as well as an injector and swirler that allow for the reproduction of important turbine engine combustor features [21]. The combustor is housed in a pressure vessel surrounded with fused silica windows to allow for optical access. The reduced combustor scale allows for ignition and LBO experiments with reduced fuel quantities for both elevated and cold fuel and air temperatures. Fuel impact assessments on these performance metrics in this combustor have shown similar trends to actual engines [19,21,22].

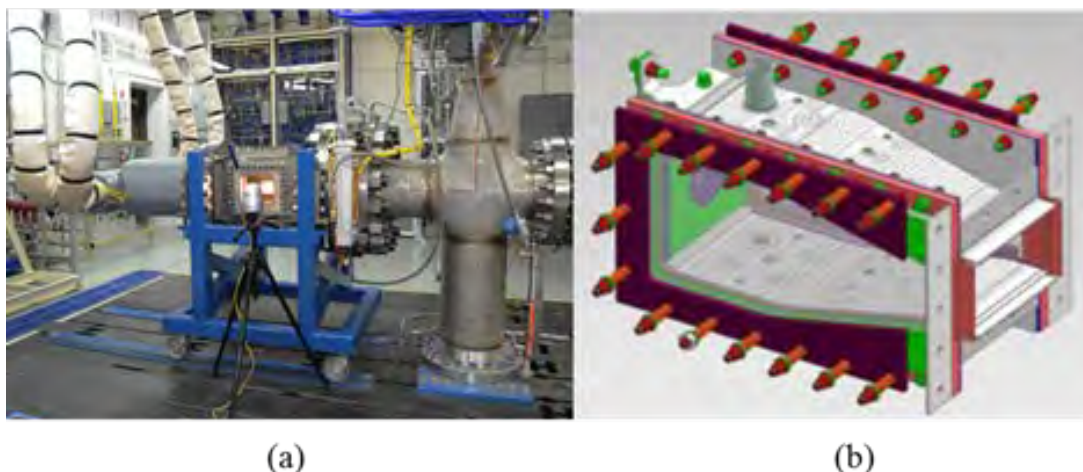


**Figure 1.** (a) Referee Combustor rig at the Air Force Research Laboratory (AFRL). (b) Swirl-stabilized (Referee) Combustor design.

Air mass flow to the combustor is metered using two Coriolis meters and pressure was regulated upstream of the control valves. Approximately 15% of the total air flow passes through the swirler, 22% through the dilution holes, and the other 63% through the effusion holes. The volume between the combustor dome and first stage dilution holes is 617 cm<sup>3</sup>. Pressure transducers along the combustor wall measured  $\Delta P$  at 15 Hz and a high-frequency response transducer at 150 kHz detected any pressure oscillations via semi-infinite tube technique. K-type thermocouples positioned on the outside of the combustor as well as the pressure vessel and surrounding supports allow for temperature monitoring to prevent structural damage. When required, fuel is heated using a heat exchanger with water supplied by a process fluid heater to deliver fuel at the nozzle at the desired fuel temperature. The fuel mass flow is measured using Coriolis meters upstream of the heat exchanger, before the nozzle. The fuel and air temperature were typically maintained within  $\pm 1.5K$  of the desired value. Two syringe pumps allow for fine control of the fuel flow.

Combustor LBO is very sensitive to fluctuations in the test conditions such as flow rate, pressure, temperature, and  $\Delta P$ . Due to an emphasis on repeatability, control of these parameters was imperative. Proportional-Integral-Derivative (PID) loops were used extensively for fine control of various parameters. Pressure drop across the control valves was enough to choke the valves, keeping the mass flow supplied to the combustor independent of any downstream pressure fluctuations. In order to prevent fuel contamination from the previous test fuel, it was paramount to properly purge the fuel lines. Prior to each test, a fuel sample was collected near the fuel nozzle and tested for fuel purity via chemical analysis (GC-FID).

### Experimental procedures

LBO tests were conducted by establishing pressure, air temperature, air mass flow, and  $\Delta P$ . Fuel flow was then introduced and ignited. Adjustments were then made to the fuel temperature and flow rate until the desired condition was reached. After steady conditions were established within the combustor, the LBO test was initiated by slowly decreasing the fuel flow rate via syringe pumps at a rate of 0.25 mL/min every two seconds. For each condition, the LBO test was initiated from the same fuel mass flow rate, approximately 10% above the LBO limit. A slow ramp rate was important for achieving an unbiased LBO. Too fast a ramp rate may lead to a lower  $\phi_{LBO}$  due to higher wall temperatures. Previous experiments determined that this rate allowed for a repeatable, smooth ramp, wall temperatures to adjust during experimentation, and maximized the number of experiments performed [19]. The LBO limit was determined by a rapid drop in the photodiode signal, which was directed at the primary combustion region. A sufficient number of LBO tests, usually between ten and fifteen, were conducted to ensure that agreement in values was achieved before moving to a different condition. Statistics were updated with each LBO test, and when the 95% confidence interval for the mean  $\phi_{LBO}$  dropped below 0.75%, agreement was considered to be reached. This estimated  $\phi_{LBO}$  was usually within a percent of the actual  $\phi_{LBO}$  determined from more thorough post-test analysis of the 15 Hz photodiode signal. Experiments were performed at the conditions included in Table 1.

**Table 1. Test Conditions Evaluated**

P	T <sub>air</sub> = T <sub>fuel</sub> [K]	ΔP/P [%]
107kPa	338	2,3,3.5,4,5,6
	305,322,338,355	3.5

**Fuels**

Four fuels were tested to study physical or chemical property influence (Table 2) on combustor LBO performance. The fuels were selected due to their wide range of physical and chemical properties. For reference, these were designated either A or C type fuels within the NJFCP [13]. A-type fuels are conventional petroleum fuels commercially available and C-type fuels are research fuels meant to highlight potential sensitivity to varying fuel properties.

**Table 2. Fuels Evaluated and Corresponding Selected Physical and Chemical Properties Including 20 and 90% Recovered Temperatures (T<sub>20</sub> and T<sub>90</sub>, respectively, Molecular Weight (MW), and Lower Heating Value (LHV)**

Property	ASTM Standard	A-2 Jet A	C-1 Alcohol-to-Jet	C-3 64% JP-5, 36% Farnesane	C-7 75% RP-2, 23% JP-5, 2% Decalin
DCN	D6890	48.3	17.1	47	42.6
Kinematic Viscosity, ν (253K, mm <sup>2</sup> /s)	D445	4.5	4.9	8.3	6.53
Surface Tension, σ (295K, dynes/cm)	D1331	24.8	23.4	26.1	26.1
Density, ρ (288K, kg/m <sup>3</sup> )	D4052	0.803	0.76	0.808	0.817
T <sub>20</sub> (K)	D2887	447	445	478	464
T <sub>90</sub> (K)	D2887	533	513	528	534
MW	n/a	159	178	180	170
LHV (MJ/kg)	D4809	43.06	43.8	42.39	43.3

A-2, a nominal Jet A with average properties, was selected as a baseline fuel. C-1 is an alcohol-to-jet, which features a very low DCN to test for chemical property dependence. To study physical property effects, C-3 was selected due to its high viscosity (ν). C-7 is a high cycloparaffin fuel (~62% cycloparaffins) with a high surface tension. Figure 2 displays the relative values of several physical and chemical properties for the tested fuels.

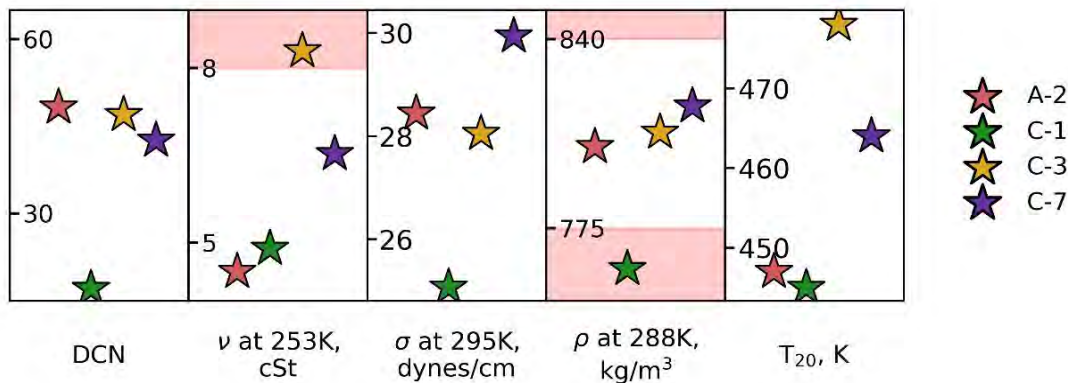


**Figure 2** Physical and chemical properties of tested fuels. Red regions denote current specification limits.

### Results and discussion

Combustor LBO performance is based on the  $\phi_{LBO}$  as in previous studies [9,19,23]. The lower the  $\phi_{LBO}$ , the less fuel is required to maintain the flame, indicating better LBO performance. Figure 3 shows  $\phi_{LBO}$  response with varying  $\Delta P/P$  and constant air and fuel temperature.

Increasing  $\Delta P/P$  resulted in a non-monotonic  $\phi_{LBO}$  ranking response across all fuels except C-3 were seen to collapse at 3.5%  $\Delta P/P$ , at which point  $\phi_{LBO}$  began to increase with increasing  $\Delta P/P$ . As observed, the LBO limits for C-3 consistently decreased with increasing  $\Delta P/P$ . Unfortunately, LBO tests for C-3 were not conducted at 6%  $\Delta P/P$  due to heavy soot formation on the combustor liner and windows. At 2%  $\Delta P/P$ , C-1 had the lowest (i.e., best) stability limit ( $\phi_{LBO}$ ) among fuels tested. In contrast, at  $\Delta P/P=5$  and 6% C-1 was observed to have the highest (i.e., worst) stability limit. The data for A-2 and C-7 diverge above 3.5%  $\Delta P/P$ , below which they had almost identical performance.

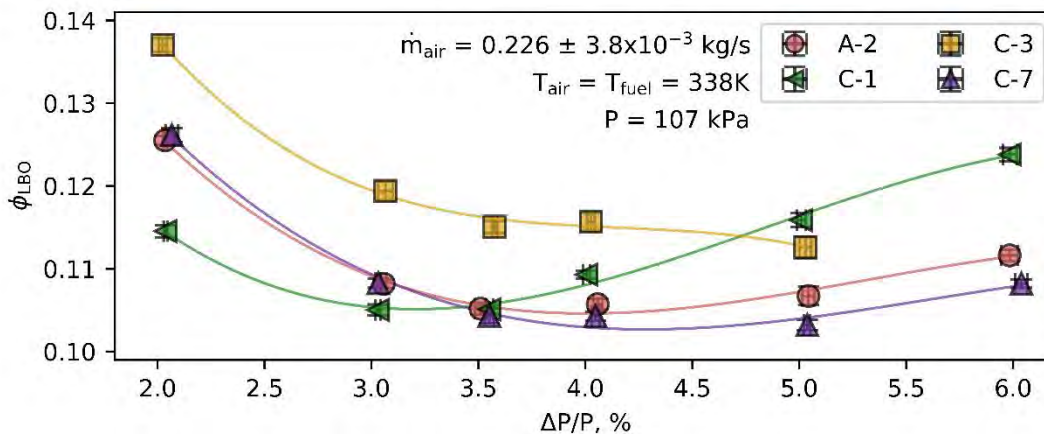


**Figure 3.** LBO limits ( $\phi_{LBO}$ ) as a function of combustor  $\Delta P/P$ . Error bars denote the 95% confidence interval for  $\phi_{LBO}$  and two standard deviations for  $\Delta P/P$ .

At 2%  $\Delta P/P$ , the LBO performance ordering of the fuels corresponded to physical property impacts. C-1, which possesses the lowest  $\phi_{LBO}$ , had beneficial physical properties (lower surface tension, viscosity, and density) relative to other fuels, thus, promoting fuel atomization. Conversely, C-3 had less favorable physical properties (e.g., very high viscosity) which were detrimental to fuel atomization resulting in higher  $\phi_{LBO}$ . The physical properties of A-2 and C-7 between the more extreme C-1 and C-3, resulting in  $\phi_{LBO}$  between the two fuels. Low combustor  $\Delta P/P$  consequently led to poor fuel atomization due to decreased aerodynamic forces acting upon the fuel droplets. With low aerodynamic forces, physical properties highly influenced fuel atomization and droplet size.

When considering the high  $\Delta P/P$  cases of 5% and 6%, fuel performance changed dramatically compared to the 2% condition. At  $\Delta P/P=5\%$ , C-3 had a lower  $\phi_{LBO}$  than C-1, which cannot be accounted for when only considering physical properties. C-1 had more favorable physical properties than C-3, which would result in better LBO performance if only physical properties were affecting LBO limits. It is clear that some other property or properties impacted fuel LBO performance at higher  $\Delta P/P$ . In previous higher temperature and pressure studies ( $T_{air} = 394K$ ,  $T_{fuel} = 322K$ ,  $P = 207kPa$ ,  $\Delta P/P = 3\%$ ), DCN was identified as the dominant property for LBO performance due to its strong inverse correlation to  $\phi_{LBO}$  [19,24,25]. The lower DCN of C-1 could account for its higher  $\phi_{LBO}$  relative to C-3, indicating that chemical properties were beginning to impact  $\phi_{LBO}$ . Once  $\Delta P/P$  was high enough to minimize physical property impact, chemical properties began to dominate the lean stability limit. At 3.5%  $\Delta P/P$ , A-2, C-1, and C-7 all demonstrate the beginning of a transition from physical property to chemical property dependence due to the collapse of their LBO limits at 3.5%  $\Delta P/P$  and the increase in LBO limit above 3.5%  $\Delta P/P$ . However, since C-3 did not attain a lower  $\phi_{LBO}$  than C-1 at  $\Delta P/P$  less than 5%, physical properties still had an influence between these two conditions. These trends indicated a transition regime rather than a single point, wherein fuels with very poor atomization characteristics shift the minima (improved LBO) to higher  $\Delta P/P$ .

Random forest regression analysis was leveraged in similar techniques as those used by Peiffer [17]. Random forest analysis is a machine learning technique that utilizes random sampling and replacement, or bagging, to evaluate how different



variables (e.g., fuel properties) impact a particular result (e.g., fuel performance). Around twenty data points are required for a normal pattern to appear [26]. For this analysis, a minimum of thirty data points were considered at each condition. By using bagging techniques, random forests can evaluate and predict importance values for given properties without bias and with lower error than other statistical techniques with small sample sizes [27,28]. Each parameter in the selected regression was evaluated against  $\phi_{LBO}$ . Linear regression analyses to correlate LBO performance to fuel properties were attempted, but no correlations could be discerned because of the non-monotonic trends. Since only four fuels and relatively small data sets (between 30–40 data points per condition) were used, a more robust statistical analysis method was required.

Weber number ( $We$ ), defined in Eq. 3, was selected to evaluate physical property and operating condition effects on the fuel spray. Weber number is a dimensionless spray parameter which considers the disruptive aerodynamic forces ( $\rho v^2$ ) and the fuel binding forces ( $\sigma/l$ ). It is the ratio between fluid inertial and surface tension forces. By considering the competition between breakup inhibiting and promoting forces, fuel spray quality can be evaluated [3].

$$We = \frac{\rho v^2 l}{\sigma} \quad (3)$$

For the present study, the fuel velocity ( $v$ ) was unknown so the pressure drop across the nozzle ( $\Delta P_{noz}$ ) was used, due to  $\Delta P_{noz}$  scaling with  $v^2$ . Since the same fuel nozzle was used for all experiments, the characteristic length ( $l$ ) was equivalent for all fuels tested, which allowed for approximation of Weber number ( $We_{apr}$ ) as shown in Eq. 4. Density ( $\rho$ ) and surface tension ( $\sigma$ ) were calculated based on the fuel temperature at each point. Random forest analysis was also performed using all three properties considered in  $We_{apr}$ , as well as substituting each property individually for  $We_{apr}$ , and it was found that the inclusion of only  $We_{apr}$  resulted in higher adjusted  $R^2$  ( $R_{adj}^2$ ) values.

$$We_{apr} = \frac{\rho(T)\Delta P_{noz}}{\sigma(T)} \quad (4)$$

The Ohnesorge number ( $Oh$ ) was additionally considered to evaluate physical property effects on LBO performance. As shown in Eq. 5, the Ohnesorge number only considers physical properties and was able to be fully evaluated [3].

$$Oh = \frac{\mu(T)}{[\rho(T)\sigma(T)D]^{0.5}} \quad (5)$$

When  $\Delta P/P$  was set at 2%,  $We_{apr}$ , as well as viscosity, were shown to be the most influential parameters to  $\phi_{LBO}$  (Figure 4a). At the low  $\Delta P/P$  conditions, atomization was strongly controlled by physical properties such as viscosity and those included in  $We_{apr}$ . These physical properties affected fuel atomization, which in turn impacted  $\phi_{LBO}$ . For the range of  $\Delta P/P$ ,  $\Delta P_{noz}$  was found to be between 48 and 200 kPa. Lefebvre [3] calls out 100 kPa being the minimum  $\Delta P_{noz}$  required to produce a cone-shaped spray in pressure-swirl nozzles like the one used in this study. This value was not reached for most fuels with  $\Delta P/P$  below 3.5%, because the fuel mass flow was low enough that the spray was most likely tulip or onion-shaped rather than a conical sheet, meaning physical properties strongly influenced the LBO limit. Interestingly, DCN was also observed to have measurable impact at 2%  $\Delta P/P$ . However, it is not near the collective impact that  $We_{apr}$  and  $\mu$  have at low  $\Delta P/P$ , allowing low  $\Delta P/P$  to be considered physical property-dominated.

At higher  $\Delta P/P$ , fuel chemical property influence is observed (Figure 4a) where DCN is the most important property, followed by molecular weight (MW) and  $We_{apr}$ . The improved atomization at higher  $\Delta P/P$  caused physical properties to have a lesser impact on fuel performance once the 100kPa  $\Delta P_{noz}$  atomization threshold was surpassed. With comparable atomization characteristics between the fuels, regardless of physical properties, fuel chemical properties evidently impact the LBO limit.

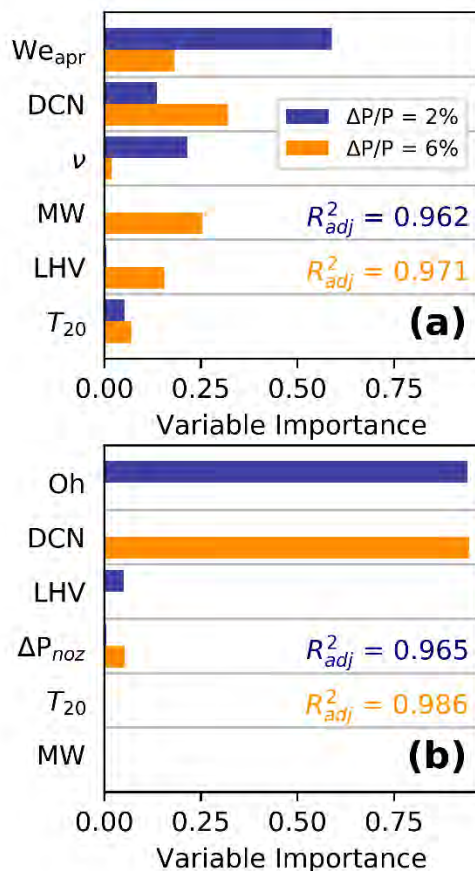


**Figure 4.** (a) The random forest regression including approximated Weber Number for  $\Delta P/P$  of 2% and 6%, and (b) random forest results for  $\Delta P/P$  of 2% and 6% for Ohnesorge number. The Ohnesorge regression results show higher adjusted  $R^2$  values than the approximated Weber number.

As shown in Figure 4, the Ohnesorge number clearly illustrates the transition from physical to chemical property dependency with increasing  $\Delta P/P$ . In Fig. 4b, at 2%  $\Delta P/P$ , the Ohnesorge number, which considers only physical properties, is observed to be the most important parameter. Because of the low  $\Delta P/P$ , atomization will be poor, allowing physical properties to dominate LBO performance. In contrast, at 6%  $\Delta P/P$ , the Ohnesorge has no impact on LBO due to improved atomization, thus, transition to a DCN dominated effect.

Fuel and air temperature was varied at constant  $\Delta P/P=3.5\%$  to examine potential physical-to-chemical transitions via temperature impacts (Figure 5). The fuel performance variance over the temperature range reported here was modest compared to previous studies [27]. Experimental limitations at this configuration required temperatures below 360K. To first order,  $\varphi_{LBO}$  decreased with increasing temperatures, as all break-up and vaporization rates increased at higher temperatures. While most of the fuels were closely grouped, C-3 did not overlap with any of the other fuels, most likely due to its higher viscosity and relatively high distillation temperatures. Together, these properties would account for poorer atomization and vaporization, which led to worse LBO performance for C-3. The  $\varphi_{LBO}$  for C-1 was unaffected by increases in temperature from 34 -355K, which suggests a transition to chemical property transition. Conversely, fuels A-2 and C-7 continued to have a decreased  $\varphi_{LBO}$  at similar conditions. The effect of fuel I and air temperature on the C-3  $\varphi_{LBO}$  was more pronounced than for the other fuels as evident by its steeper slope.

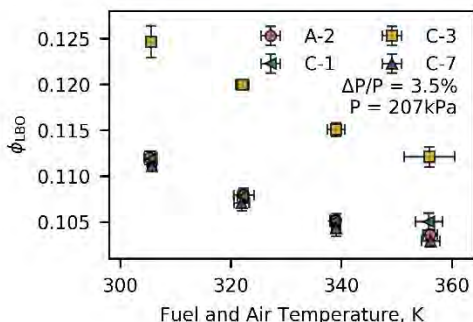


Figure 5. Impact of varying fuel and air temperature on equivalence ratio.

### Conclusion

LBO experiments were conducted in a single-cup swirl-stabilized combustor (Referee Combustor) to study the impacts of fuel chemical and physical properties under varying pressure drops across the dome and at varying fuel and air temperatures. The Referee Combustor was designed with turbine engine OEMs input to simulate key characteristics of actual turbine engine combustors. LBO has previously been found to correlate with chemical properties (i.e. DCN) at relatively high air and fuel temperatures and pressures, while at low fuel and air temperatures and pressures LBO correlates most strongly with physical properties such as viscosity.

Results showed that LBO performance ( $\phi_{LBO}$ ) responded non-monotonically to fuel properties and to combustor  $\Delta P/P$ , and the relative performance of the fuels was found to change with varying  $\Delta P/P$ . At lower combustor  $\Delta P/P$ , LBO dependence on physical properties due to poorer fuel atomization was demonstrated. At higher  $\Delta P/P$  the trends appear to shift to LBO performance being impacted by chemical properties (i.e., DCN). The changeover from physical to chemical property dependence was found to be a range rather than a single temperature or  $\Delta P/P$  point. Random forest regression analysis using dimensionless parameters demonstrated that an approximate Weber Number and Ohnesorge number were the most influential parameters at low  $\Delta P/P$ , while DCN was the most impactful property at high  $\Delta P/P$ .

### Milestones

Chemical and physical effects on LBO at various temperature was determined.

### Major Accomplishments

Reported the LBO results at various temperature for various fuels.

### Publications

#### Peer-reviewed journal publications

Colborn JG, Heyne JS, Stouffer SD, Hendershott TH, Corporan E. Chemical and physical effects on lean blowout in a swirl-stabilized single-cup combustor. Proc Combust Inst 2020. doi:10.1016/j.proci.2020.06.119. (Article in press)

### Outreach Efforts

None

### Awards

None

### Student Involvement

Jen Colborn, graduate research assistant, leads this effort.

### Plans for Next Period

Finalize the publication in progress and for Jen Colborn to finish her M.S.



## References

- [1] M. Colket, J. Heyne, M. Rumizen, et al., Overview of the National Jet Fuels Combustion Program, *AIAA Journal* 55 (4) (2016) 1087-1104.
- [2] N. Papanikolaou, I. Wierzba, Effect of Burner Geometry on the Blowout Limits of Jet Diffusion Flames in a Co-Flowing Oxidizing Stream. *J. Energy Resour. Technol.* 118 (2) (1996) 134-139.
- [3] A.H. Lefebvre, D.R. Ballal, *Gas Turbine Combustion: Alternative Fuels and Emissions*, CRC Press Taylor & Francis Group, Boca Raton, Fl., U.S.A., 2010, p. 221-240.
- [4] M.D. Durbin, D.R. Ballal, Studies of Lean Blowout in a Step Swirl Combustor. *J. Eng. for Gas Turbines Power* 118 (1) (1994) 1-8.
- [5] C. Liu, F. Liu, J. Yang, et al., Experimental Investigation of Spray and Combustion Performances of a Fuel-Staged Low Emission Combustor: Effects of Main Swirl Angle, *J. Eng. Gas Turbines Power* 139 (12) (2017) 1-10.
- [6] J.F. Bourgouin, J. Moeck, D. Durox, et al., Sensitivity of swirling flows to small changes in the swirler geometry. *Comptes Rendus - Mec* 341 (1) (2013) 211-219.
- [7] A. Ateshkadi, V.G. McDonell, G.S. Samuelsen, Lean blowout model for a spray-fired swirl-stabilized combustor, *Proc. Combust. Inst.* 28 (2007) 1281-1288.
- [8] A. Ateshkadi, V.G. McDonell VG, G.S. Samuelsen, Effect of mixer geometry on fuel spray distribution, emissions and stability, *American Institute of Aeronautics and Astronautics*, 1998.
- [9] A.H. Lefebvre. Fuel Effects on Gas Turbine Combustion, Report No. AFWAL-TR-83-2004, Air Force Wright Aeronautical Laboratories, 1983.
- [10] J.W. Blust, D.R. Ballal, G.J. Sturgess, Fuel Effects on Lean Blowout and Emissions from a Well-Stirred Reactor, *J. Propuls. Power* 15 (2) 1999 216-223.
- [11] Q. Zhang, D.R. Noble, A. Meyers, K. Xu, T. Lieuwen, Characterization of Fuel Composition Effects in H<sub>2</sub>/CO/CH<sub>4</sub>, *Turbo Expo* (2) (2005) 657-668.
- [12] L. Esclapez, P.C. Ma, E. Mayhew, et al., Fuel effects on lean blow-out in a realistic gas turbine combustor. *Combust. Flame* 181 (2017) 82-99.
- [13] J.T. Edwards, Reference Jet Fuels for Combustion Testing, *American Institute of Aeronautics and Astronautics*, 2017.
- [14] V. Burger. The Influence of Fuel Properties on Threshold Combustion in Aviation Gas Turbine Engines, PhD thesis, University of Cape Town, Cape Town, South Africa, 2017.
- [15] S.L. Plee, A.M. Mellor, Characteristic Time Correlation for Lean Blowoff of Bluff-Body-Stabilized Flames, *Combust. Flame* 35 (1979) 61-80.
- [16] A.M. Mellor. Semi-Emperical Correlations for Gas Turbine Emissions, Ignition, and Flame Stabilization, *Prog. Energy Combust. Sci.* 6 (4) (1980) 347-538.
- [17] E.E. Peiffer, J.S. Heyne, M. Colket, Sustainable Aviation Fuels Approval Streamlining: Auxiliary Power Unit Lean Blowout Testing, *AIAA J* 57 (11) (2019) 1-9.
- [18] E.E. Peiffer, J.S. Heyne. Characteristic Timescales for Lean Blowout of Alternative Jet Fuels in Four Combustor Rigs, *AIAA Prop. Eng. Forum*, 2018.
- [19] S.D. Stouffer, T.H. Hendershott, J.R. Monfort, et al., Lean Blowout and Ignition Characteristics of Conventional and Surrogate Fuels Measured in a Swirl Stabilized Combustor, *American Institute of Aeronautics and Astronautics*, 2017.
- [20] A.J. Bokhart, D. Shin, N.S. Rodrigues, et al., Spray Characteristics of a Hybrid Airblast Pressure-Swirl Atomizer at Near Lean Blowout Conditions using Phase Doppler Anemometry, *American Institute of Aeronautics and Astronautics*, 2018.
- [21] T.H. Hendershott, S.D. Stouffer, J.R. Monfort, et al., Ignition of Convectional and Alternative Fuels at Low Temperatures in a Single-Cup Swirl-Stabilized Combustor, *American Institute of Aeronautics and Astronautics*, 2018.
- [22] E. Corporan, R. Casselberry, M. Wagner, et al., Fuel Effects on the Lean Operational Limits of a T63 Turboshift Engine, *American Institute of Aeronautics and Astronautics*, 2019.
- [23] X.F. Wang, A.H. Lefebvre, Influence of Fuel Temperature on Atomization Performance of Pressure-Swirl Atomizers, *J. Propuls. Power* 4 (3) (1988) 222-227.
- [24] J.S. Heyne, N. Glenn, J.T. Edwards, et al., Year 2 of the National Jet Fuels Combustion Program: Moving Towards a Streamlined Alternative Jet Fuels Qualification and Certification Process, *American Institute of Aeronautics and Astronautics*, 2017.
- [25] J.S. Heyne, E.E. Peiffer, M. Colket, et al., Year 3 of the National Jet Fuels Combustion Program: Practical and Scientific Impacts, *American Institute of Aeronautics and Astronautics*, 2018.
- [26] K. Seefeld and E. Liner, *Statistics Using R with Biological Examples*, University of New Hampshire (2007), Chap. 13.
- [26] T. Hastie, R. Tibshirani, J. Friedman, *The Elements of Statistical Learning, Data Mining, Inference, and Prediction*, Stanford, California: 2008, p. 587-603.



- [27] J.G. Colborn, J.S. Heyne, T.H. Hendershott, et al., Fuel and Operating Condition Effects on Lean Blowout in a Swirl-Stabilized Single-Cup Combustor, American Institute of Aeronautics and Astronautics, 2020.
- [28] G. Biau and E. Scornet, "A Random Forest Guided Tour," TEST 25 (2016) 197-227.



# Project 036 Parametric Uncertainty Assessment for the Aviation Environmental Design Tool (AEDT)

## Georgia Institute of Technology

### Project Lead Investigator

Principal Investigator:

Professor Dimitri N. Mavris

Director, Aerospace Systems Design Laboratory

School of Aerospace Engineering

Georgia Institute of Technology

Phone: (404) 894-1557

Fax: (404) 894-6596

Email: [dimitri.mavris@ae.gatech.edu](mailto:dimitri.mavris@ae.gatech.edu)

Co-Principal Investigator:

Dr. Yongchang Li

Chief, Aviation Environmental Policy Branch

Aerospace Systems Design Laboratory

School of Aerospace Engineering

Georgia Institute of Technology

Phone: (404) 385-2776

Fax: (404) 894-6596

Email: [yongchang.li@ae.gatech.edu](mailto:yongchang.li@ae.gatech.edu)

### University Participants

#### Georgia Institute of Technology (GT)

- FAA Award Number: 13-C-AJFE-GIT, Amendments 19, 29, 30, 40, and 49
- Period of Performance: October 1, 2019 to September 30, 2020
- Task: AEDT uncertainty quantification (UQ) reports development.

### Project Funding Level

The current funding for this project is based on amendments 30, 40, and 49 for a total of \$300,000 from May 31, 2019 to May 30, 2020. The Georgia Institute of Technology has agreed to a total of \$300,000 in matching funds.

### Investigation Team

- Prof. Dimitri Mavris (PI), Georgia Institute of Technology, oversees the entire project.
- Dr. Yongchang Li (Co-PI, project lead), Georgia Institute of Technology, leads the research team in performing capability demonstrations and tests and in validating various functionalities of different AEDT versions.
- Dr. Michelle Kirby (Co-PI), Georgia Institute of Technology, oversees the entire project and supports all of the research activities.
- Bogdan Dorca (graduate student), Georgia Institute of Technology, conducts AEDT capability demonstration, feature evaluation, and system testing.
- Zhenyu Gao (graduate student), Georgia Institute of Technology, conducts parametric uncertainty quantification analyses for the BADA4 model, created the AEDT study, and performed a sensitivity analysis for this study.
- Santusht Sairam (graduate student), Georgia Institute of Technology, conducts AEDT capability demonstration, feature evaluation, and system testing.
- Dr. Holger Pfaender (research staff) provides consultation and support.

## Project Overview

The FAA's Office of Environment and Energy (AEE) has developed a comprehensive suite of software tools that allow for a thorough assessment of the environmental effects of aviation, particularly for assessments of interdependencies among aviation-related noise, emissions, performance, and cost. As the heart of this tool suite, the high-fidelity Aviation Environmental Design Tool (AEDT) is a software system that models aircraft performance in space and time to estimate fuel consumption, emissions, noise, and air quality impacts. This software has been developed by the FAA AEE for public release as the next-generation FAA environmental consequence tool. AEDT enables evaluations of interdependencies among aircraft-related fuel consumption, emissions, and noise. AEDT 2 was released in four phases. The first version, AEDT 2a, was released in March 2012 (US FAA, AEDT 2a Uncertainty Quantification Report, 2014; US FAA, AEDT 2a SP2 UQ Supplemental Report, 2014) and the second version, AEDT 2b, was released in May 2015 (US FAA, AEDT 2b UQ Report, 2016). The third and fourth versions, AEDT 2c and AEDT 2d, respectively, were released in September 2016 and September 2017. A new version, AEDT 3b, was released in September 2019 with major updates, including the inclusion of the Base of Aircraft Data family 4 (BADA4) performance model for fuel consumption, emissions, and noise and the implementation of reduced thrust and alternative weight profiles for departure operations.

The uncertainty quantification (UQ) applied in this project comprehensively assesses the accuracy, functionality, and capabilities of AEDT during the development process. The major purposes of this effort are as follows:

- Contribute to the external understanding of AEDT.
- Demonstrate and evaluate AEDT's capability and fidelity (ability to represent reality).
- Help AEDT users to understand the sensitivities of output responses to variations in input parameters/assumptions.
- Identify gaps in functionality.
- Identify high-priority areas for further research and development.

The UQ consists of verification and validation, capability demonstrations, and parametric uncertainty/sensitivity analysis.

## Task 1 – AEDT UQ Reports Development

Georgia Institute of Technology

### Objectives

In order to provide the best possible environmental impacts modeling capabilities in AEDT, the FAA/AEE continues to develop AEDT, improving existing modeling methods and data and adding new functionalities. The AEDT development team has been exercising an agile development process, where minor updates are released in new Sprint versions every three weeks, and major updates and/or new functionalities are incorporated as new versions of AEDT. The FAA/AEE seeks an independent effort in system testing to evaluate the accuracy, functionality, and capabilities of AEDT and support the future development process. Thus, the objective of this effort is to provide FAA with high-quality UQ analysis of AEDT and its future releases to evaluate AEDT's capability, while identifying gaps in the tool's functionality and areas for further development.

GT has been conducting UQ on AEDT's releases since 2015 and recently completed UQ analysis on the BADA4 model, reduced thrust profiles, and other new features for AEDT 3b. All the work was concluded in 2019 and GT has been focusing on developing AEDT reports including AEDT 3b UQ report and the ASCENT Project 36 final report. Project 36 was officially closed out on May 30, 2020 and the work that has been performed under the project was transitioned to ASCENT Project 54.

### Research Approach

GT developed the final report summarizing the work that has been accomplished before ASCENT Project 36 was officially closed out. In addition, the AEDT 3b UQ report was also created to document the UQ effort on AEDT 3b to inform and educate the user regarding the methodologies used in AEDT 3b, as well as the thorough verification and validation (V&V), capability demonstration, and parametric uncertainty/sensitivity analysis of AEDT using the BADA4 aircraft performance model. The report consists of four analyses which were designed as the V&V of the newly implemented capabilities in AEDT 3b. Within the analyses, all of the relevant functionality specific to a given algorithm was evaluated to determine if it functioned as intended. In addition, test cases were designed to conduct further analysis to ensure the functionality was implemented properly.



- **Analysis 1—Reduced Thrust Profile V&V Analysis:** A V&V analysis of AEDT 3b’s new feature to model aircraft performance and environmental impact using alternative weight and reduced thrust profiles. A comprehensive study was conducted to analyze the performance, fuel burn, emissions, and noise impacts of these new modified profiles. The analysis showed that the results produced by the alternative weight and reduced thrust profiles were reasonable and as expected.
- **Analysis 2—BADA4 V&V Analyses:** A comparison of BADA4 model and Aircraft Noise and Performance (ANP) model at aircraft and fleet level. Three levels of analysis at flight segment, single flight, and fleet level were conducted to ensure that the BADA4 algorithm and associated data are properly implemented into AEDT 3b. Further V&V analyses were done by comparing the results produced by BADA4 and ANP at the fleet level. Analysis results implied that BADA4 provides more accurate and unified results in aircraft performance modeling.
- **Analysis 3—AEDT 3c Features V&V Analyses:** This analysis consists of two comprehensive studies: (1) The ANP performance comparison between AEDT 3b and AEDT 3c to investigate the effects of new speed limit, and (2) BADA4 versus ANP comparison within AEDT 3c. It was identified that the speed limit change generally increases fuel burn and NOx emissions, which is expected. The results of the AEDT 3c verification and validation analyses display reasonable general trends of the new AEDT implementations.
- **Analysis 4—Parametric UQ on BADA4:** This parametric uncertainty/sensitivity analysis on BADA4 strives to quantify and identify how the algorithms and methodologies of BADA4 performance model respond to variations in inputs. Major contributors that have big effects on the outputs were identified. These analyses serve to inform the user as to the expected variation of BADA4 performance resulting from the variation of input parameters, as well as future data collection and tool development.

An inventory of UQ analysis was also compiled to summarize the UQ analysis that has been conducted for AEDT 3b. In addition, the bugs and issues found during the UQ analysis were listed, and the status of each bug were discussed as well.

**Milestones**

Milestone	Due Date	Estimated Completion Date	Actual Completion Date	Status
A36 Kickoff Meeting	5/3/2016	5/3/2016	5/3/2016	Completed
Quarterly Report (Aug)	7/31/2016	7/31/2016	7/31/2016	Completed
ASCENT Meeting	9/27-28/2016	9/27-28/2016	9/27-28/2016	Completed
Quarterly Report (Nov)	10/31/2016	10/31/2016	10/31/2016	Completed
Annual Report	1/18/2017	1/18/2017	1/13/2017	Completed
Quarterly Report (Jan)	1/31/2017	1/31/2017	1/27/2017	Completed
Quarterly Report (Mar)	3/31/2017	3/31/2017	3/31/2017	Completed
ASCENT Meeting	4/18/2017	4/18/2017	4/18/2017	Completed
Quarterly Report (Jun)	6/30/2017	6/30/2017	6/30/2017	Completed
ASCENT Meeting	9/26/2017	9/26/2017	9/26/2017	Completed
Quarterly Report (Oct)	10/30/2017	10/30/2017	10/30/2017	Completed
Annual Report	11/30/2017	11/30/2017	11/30/2017	Completed
Quarterly Report (Jan)	1/31/2018	1/31/2018	1/31/2018	Completed
Quarterly Report (Mar)	3/31/2018	3/31/2018	3/31/2018	Completed
ASCENT Meeting	4/3-4/2018	4/3-4/2018	4/3-4/2018	Completed
Quarterly Report (Jun)	6/30/2018	6/30/2018	6/30/2018	Completed
ASCENT Meeting	10/9-10/2018	10/9-10/2018	10/9-10/2018	Completed
Quarterly Report (Oct)	10/30/2018	10/30/2018	10/30/2018	Completed
Annual Report	11/30/2018	11/30/2018	11/30/2018	Completed
Quarterly Report (Jan)	1/31/2019	1/31/2019	1/31/2019	Completed
ASCENT Meeting	4/18-19/2019	4/18-19/2019	4/18-19/2019	Completed
Quarterly Report (Apr)	4/30/2019	4/30/2019	4/30/2019	Completed
Quarterly Report (Jul)	7/31/2019	7/31/2019	7/31/2019	Completed
ASCENT Meeting	10/22-23/2019	10/22-23/2019	10/22-23/2019	Completed
Quarterly Report (Oct)	10/31/2019	10/31/2019	10/31/2019	Completed
Annual Report	11/30/2019	11/30/2019	11/30/2019	Completed
Quarterly Report (Dec)	12/31/2019	12/31/2019	12/31/2019	Completed
Quarterly Report (Mar)	3/31/2020	3/31/2020	3/31/2020	Completed

ASCENT Meeting	3/31-4/1/2020	3/31-4/1/2020	3/31-4/1/2020	Completed
Quarterly Report (Jun)	6/30/2020	6/30/2020	6/30/2020	Completed
Final Report	8/31/2020	8/31/2020	8/31/2020	Completed
Annual Report	11/30/2020	11/30/2020	11/30/2020	Completed

**Major Accomplishments**

As of May 2020, all new AEDT Sprint releases, including Sprints 124-138, have been tested. Fifteen AEDT Sprints have been tested, focusing on new features and added capabilities. Some of the new features/capabilities were minor updates to the GUI, bug fixes, or data updates. Major updates included modified weight and reduced thrust profile, BADA4 performance model, and user-defined profile editor. To understand the background of new AEDT features, all relevant documents were reviewed, including software requirement documents, database design documents, AEDT Sprint release notes, updated technical manuals, user manuals, and research papers/reports. Basic tests of all new AEDT versions were completed to confirm their functionality, and issues were reported to the FAA and the development team via biweekly ASCENT project teleconferences and weekly AEDT development-lead calls. Identified issues and follow-up actions taken by the developers were documented and shared through the Team Foundation Server (TFS) online system. The TFS also allows for reporting of any potential areas of improvements in AEDT algorithms and user friendliness.

Finally, two reports were developed including a final project report and AEDT 3b UQ report which documented the UQ efforts on AEDT 3b. Though the project officially ended on May 30, 2020, the work that has been conducted under this project will be continued under ASCENT Project 54.

**Publications**

**Written reports**

ASCENT quarterly reports (Jan. 2019; Apr. 2019; Jul. 2019, Oct. 2019)  
 ASCENT annual report (Nov. 2018)

**Peer-reviewed journal publications**

Gao, Z., Behere, A., Li, Y., Lim, D., Kirby, M., & Mavris, D.M. Quantitative assessment of the new departure profiles with improved weight and thrust modeling. Approved for publication, Journal of Aircraft.

**Outreach Efforts**

N/A

**Awards**

None

**Student Involvement**

Bogdan Dorca is a third year PhD student at Georgia Institute of Technology. Mr. Dorca conducted AEDT capability demonstration, feature evaluation and system testing. Mr. Dorca is being trained on related tools such as INM, AEDT Tester, AEDT 2e, and AEDT 3b.

Zhenyu Gao is a fourth year PhD student at Georgia Institute of Technology. Mr. Gao conducted parametric uncertainty quantification analyses for the BADA4 model, created the AEDT study, and performed a sensitivity analysis for this study. Mr. Gao is being trained on related tools such as INM, AEDT Tester, AEDT 2e, and AEDT 3b.

Santusht Sairam is a second year Master student at Georgia Institute of Technology. Mr. Sairam conducted AEDT capability demonstration, feature evaluation and system testing. Mr. Sairam is being trained on related tools such as INM, AEDT Tester, AEDT 2e, and AEDT 3b.

**Plans for Next Period**

This project officially closed out on May 30, 2020; however, some of the tasks performed by GT will be continued under the new ASCENT Project 54. GT will perform the system testing, validation, and verification tasks for the new versions of AEDT 3d and beyond to identify any issues that should be addressed by the development team.



## Project 037 CLEEN II System Level Assessment

### Georgia Institute of Technology

#### Project Lead Investigator

Dimitri Mavris (PI)  
Regents Professor  
School of Aerospace Engineering  
Georgia Institute of Technology  
Mail Stop 0150  
Atlanta, GA 30332-0150  
Phone: 404-894-1557  
Email: dimitri.mavris@ae.gatech.edu

#### University Participants

##### Georgia Institute of Technology

PIs: Dr. Dimitri Mavris (PI), Dr. Jimmy Tai (Co-PI)  
FAA Award Number: 13-C-AJFE-GIT-055  
Period of Performance: August 31, 2019 to August 31, 2020

#### Project Funding Level

FAA funding was distributed at the levels of \$240,000. The Georgia Institute of Technology has agreed to a total of \$240,000 in matching funds. This total includes salaries for the project director, research engineers, and computing, financial and administrative support, including meeting arrangements. The institute has also agreed to provide tuition remission for any students paid for by state funds.

#### Investigation Team

Georgia Institute of Technology  
Principal Investigator: Dimitri Mavris  
Co-Investigators: Jimmy Tai  
Fleet Modeling Technical Lead: Holger Pfaender  
Supporting Engineers: Greg Busch, Joshua Brooks

#### Project Overview

The objective of this research project is to support the FAA by independently modeling and assessing the technologies that will be developed under the Continuous Lower Energy, Emissions, and Noise Phase II (CLEEN II) program. This will involve direct coordination and data sharing with companies developing technologies under CLEEN II, in order to accurately model the environmental benefits of these technologies at the vehicle and fleet levels.

The Georgia Institute of Technology (GT) was previously selected to perform all of the system level assessments for the original CLEEN Phase I (CLEEN I) program under PARTNER Project 36 and ASCENT Project 10. As a result, GT is in a unique position from both a technical and programmatic standpoint to continue the system level assessments for CLEEN II. From a technical perspective, GT has significantly enhanced the Environmental Design Space (EDS) over the last five years to incorporate advanced, adaptive, and operational technologies targeting fuel burn, noise, and emissions. EDS was successfully applied to all CLEEN I contractor technologies including: GE open rotor, TAPS II combustor, FMS-Engine and FMS-Airframe; Pratt & Whitney geared fan; Boeing adaptive trailing edge and CMC nozzle; Honeywell hot section cooling and materials; and Rolls-Royce turbine cooling technologies. GT also gained significant experience in communicating system-level modeling requirements to industry engineers and translating the impacts to fleet-level fuel burn, noise, and emissions assessments.

This broad technical knowledge base covering both detailed aircraft and engine design and high-level benefits assessments puts GT in a unique position to assess CLEEN II technologies.

As the ultimate goal of this work is to conduct fleet-level assessments for aircraft representative of future "in-service" systems, GT will need to create system-level EDS models using a combination of both CLEEN II and other public domain N+1 and N+2 technologies. The outcomes of the technology and fleet assumptions-setting workshops conducted under ASCENT Project 10 will be heavily leveraged for this effort. Non-CLEEN II technologies for consideration along with potential future fleet scenarios will help to bound the impact of CLEEN II on future fleet fuel burn, emissions, and noise.

Since the FAA will also be performing a portion of the EDS technology modeling work, EDS training has been provided to the FAA in 2016 under ASCENT Project 10. The training has provided the requisite skill set required to use EDS.

In the prior year of this project, GT began modeling activities with Collins, GE, Honeywell, and Pratt & Whitney. This modeling process included validation of underlying EDS models, information and data exchange necessary to model the individual technologies, and related EDS modeling activities. In addition, GT has assisted the FAA with in-house modeling of GE combustion technologies. This process has increased the FAA's use of FAA personnel for EDS system level assessment modeling.

This year's work will focus on moving toward the end of the project by completing vehicle- and fleet-level assessments for CLEEN II. This includes final technology modeling details for each CLEEN II industry contractor generation of vehicle-level assessments of fuel burn, emissions, and noise compared to current best-in-class along with fleet-level estimates of fuel burn, emissions, and noise, including community noise impact estimates at multiple relevant airports. Quantifying this impact will provide understanding on the number of increased operations per day that CLEEN II technologies enable without worsening noise exposure to the surrounding community. While airports in the U.S. are not generally noise-constrained, there are European airports that do have limited capacity to meet noise constraints. Understanding the impact of technologies on the future U.S. fleet is critical to quantifying the interaction between economic growth (i.e., increased flight operations at a given airport) and community noise impacts.

GT has completed most of the technology modeling to date. Remaining items include updating technology models using the most recent data from contractors and conducting a final fleet assessment. The table in the next section shows the current status of technology modeling. Where work remains, a brief description is provided after the table.

**Major Accomplishments**

- The modeling for GE MESTANG is complete.
- The modeling for GE Flight Management System is complete.
- The modeling for Collins Slim Nacelle is complete.
- The modeling for Honeywell Blade Outer Air Seal is complete, awaiting contractor review.
- The modeling for Pratt & Whitney Compressor and Turbine Aero-Efficiency Technologies is complete, awaiting contractor review.
- Preliminary fuel burn assessment completed.
- The data exchange and assumptions were defined for Honeywell Compact Combustor.
- Ongoing effort to model Collins zoned liner technology.
- Ongoing effort to model GE LPR Advanced Acoustic technology.

Contractor	Technology / Model Impact Area	Initial Modeling Discussions Held with Contractor?	Modeling Underway	Percentage Complete	Might Require Update?
Aurora (Techs listed are sub-parts of Double Bubble Fuselage)	D8 configuration	✓	✓	100%	No
Boeing	Structurally Efficient Wing	✓	✓	100%	No
	Compact Nacelle	✓	✓	100%	No



Contractor	Technology / Model Impact Area	Initial Modeling Discussions Held with Contractor?	Modeling Underway	Percentage Complete	Might Require Update?
Delta/MDS/America's Phenix	Leading Edge Protective Fan Blade Coating	✓	✓	100%	No
GE	TAPS III Low NOx Combustor	✓	✓	100%	No
	More Electric Systems and Technologies for Aircraft in the Next Generation (MESTANG)	✓	✓	100%	Yes
	Flight Management System (FMS)	✓	✓	100%	Yes
	Low Pressure Ratio Advanced Acoustic	✓		15%	Yes
Honeywell	Compact Combustor	✓	✓	75%	Yes
	Turbine Blade Outer Air Seal	✓	✓	80%	No
Pratt & Whitney	Compressor and Turbine Aero-Efficiency Technologies	✓	✓	80%	Yes
Collins/Rohr/UTAS	Slim Nacelle	✓	✓	100%	Yes
	Noise Liner Technologies	✓	✓	75%	Yes
Rolls-Royce	Advanced Rich Quench Lean Low NOx Combustor	✓		25%	Yes

**Remaining Modeling Work**

- GE Low Pressure Ratio Advanced Acoustic
  - Waiting on information from GE.
  - Modeling not yet started. Modeling approach formulated.
- Honeywell Compact Combustor
  - Received preliminary combustor correlation estimates from Honeywell.
  - When Honeywell completes high pressure testing at NASA facility, correlations will be updated and model finalized. This only requires minor modeling changes.
- Honeywell Turbine Blade Outer Air Seal
  - Have received modeling impacts from Honeywell. Have modeled similar technology for CLEEN I from Honeywell. Will implement and confirm at same time as Compact Combustor validation.
- Pratt & Whitney Compressor and Turbine Aero-Efficiency Technologies
  - Have held several working meetings with Pratt & Whitney. Modeling approach agreed upon. Modeling data required has been provided by Pratt & Whitney. GT needs to run sensitivity studies and verify trends with Pratt & Whitney.
- Collins Noise Liner Technologies
  - GT has developed a new modeling approach based on feedback from Collins and is currently in the process of implementing this approach.
- Rolls-Royce Advanced RQL Low NOx Combustor
  - When Rolls-Royce completes testing, the same modeling approach as Honeywell will be used, but with empirical NOx model specific to Rolls-Royce.

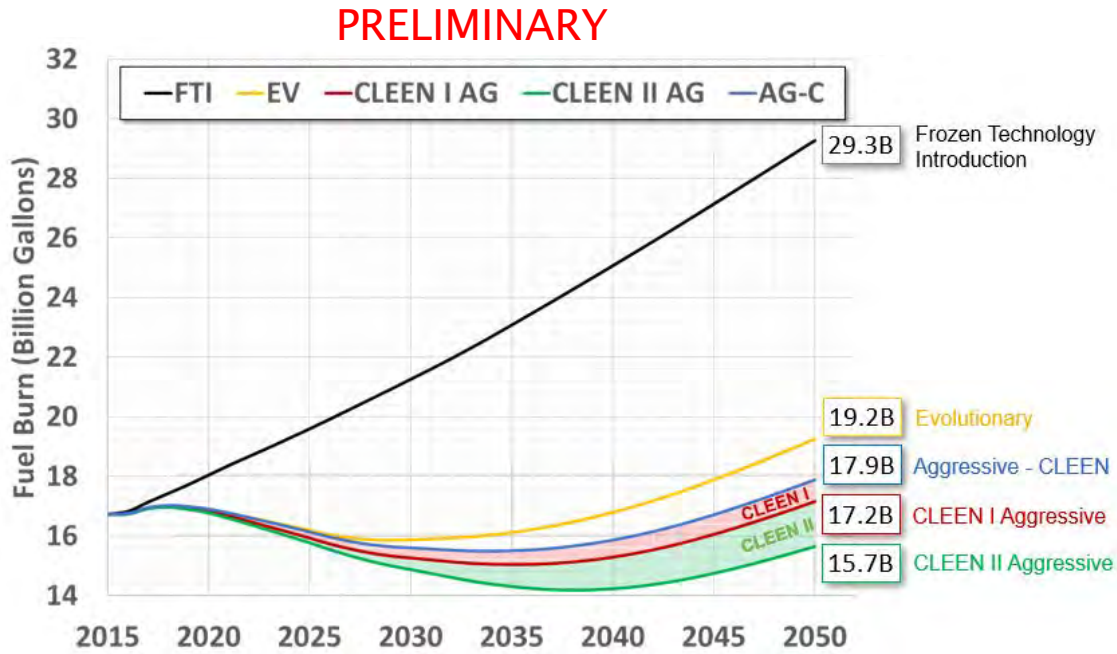


Preliminary Fuel Burn Assessment

GT and FAA have completed a preliminary fleet-level fuel burn assessment. This does not include the entire set of CLEEN II technologies. The following technologies are included in this assessment:

- All relevant CLEEN I Technologies
- Aurora Double Bubble (fuselage weight reduction)
- Boeing SEW
- Boeing Compact Nacelle
- Delta/MDS/America's Phenix Leading Edge Protective Coating
- GE MESTANG
- Honeywell Turbine Blade Outer Air Seal
- Pratt & Whitney Compressor and Turbine Aero-Efficiency Technologies
- Collins Slim Nacelle

Figure 1 below depicts the estimated fuel burn (in billions of gallons) under the technology introduction scenarios considered by GT. These results are estimated for the fleet of U. S. domestic and internationally departing aircraft. The red and green shaded areas represent the estimated fuel burn savings enabled by the CLEEN Phase I and Phase II programs, respectively.



**\*Not all technologies are modeled/included at this time.\***

Figure 1. Preliminary fuel burn assessment.



**PRELIMINARY**

**CLEEN Fuel Savings relative to Evolutionary Scenario**



**\*Not all technologies are modeled/included at this time.\***

**Figure 2.** Preliminary fuel burn assessment: savings relative to evolutionary scenario.

Figure 2 has been provided to display fuel savings (%) relative to the evolutionary scenario.

According to the analysis performed above, the technologies matured in the first five-year phase of CLEEN will reduce U.S. fleet-wide fuel burn by 2 percent by 2030 and 3.7 percent by 2050 relative to the evolutionary scenario, providing a cumulative savings of 13.2 billion gallons of jet fuel. The CO<sub>2</sub> savings are the equivalent of taking 1.11 million cars off of the road from 2020 to 2050.

This preliminary analysis projects the technologies matured in the CLEEN Phase II program to reduce fuel consumption 2.5 percent by 2030 and 7.9 percent by 2050 relative to the evolutionary scenario, bringing the contribution of CLEEN Phase I and II to 11.6 percent fuel burn reduction in the fleet by 2050.

Cumulatively, CLEEN Phase I and II are estimated to save 36.4 billion gallons of fuel by 2050, worth approximately 72.8 billion dollars in savings for airlines, and resulting in a reduction in CO<sub>2</sub> emissions of approximately 424 million metric tons. These CO<sub>2</sub> reductions are equivalent to removing 3.05 million cars from the road from 2020 to 2050.

Assessment of CLEEN Phase II's other benefit areas are ongoing. Quantification of the program's fleet-level noise benefits is expected to be complete in 2022.

**Publications**

None

**Outreach Efforts**

CLEEN Consortium

**Awards**

None



**Student Involvement**

None currently, anticipated in 2021.

**Plans for Next Period**

Future work will focus on completing technology modeling and updating fleet analysis assessments with remaining technologies. The next period will also include the transition of efforts toward the incoming CLEEN III initiative (e.g., NDAs).

This work will also support attendance at CLEEN consortium meetings and contractor preliminary and detailed design reviews to identify any updates required to technology models developed in prior years.

**References**

None



# Project 038 Rotorcraft Noise Abatement Procedure Development

The Pennsylvania State University, Continuum Dynamics, Inc.

## Project Lead Investigator

Kenneth S. Brentner  
Professor of Aerospace Engineering  
Department of Aerospace Engineering  
The Pennsylvania State University  
233 Hammond Building  
University Park, PA  
(814) 865-6433  
ksbrentner@psu.edu

## University Participants

### The Pennsylvania State University (Penn State)

- PI: Kenneth S. Brentner, Professor of Aerospace Engineering
- FAA Award Number: 13-C\_AJFE-PSU-038, Amendment No. 53
- Period of Performance: February 5, 2020 to February 4, 2021
- Tasks (during this period):
  14. Continue evaluating flight test data to determine the effectiveness of noise abatement procedures
  15. Evaluate and refine noise abatement procedure development strategy
  16. Demonstrate the potential of refined noise abatement procedures
  17. Continue effort to develop noise abatement flight procedures for various helicopter classes

## Project Funding Level

FAA provided \$150,000 in funding. In-kind matching funds of \$150,000 were provided by Continuum Dynamics, Inc. and Penn State provided \$30,617 in faculty academic year cost sharing.

## Investigation Team

- Kenneth S. Brentner, PI, The Pennsylvania State University; acoustic prediction lead on all Tasks.
- Joseph F. Horn, Co-PI, The Pennsylvania State University; flight simulation lead supporting all Tasks.
- Daniel A. Wachspress, Co-PI, Continuum Dynamics, Inc.; responsible for rotor loads, wake integration, and Comprehensive Hierarchical Aeromechanics Rotorcraft Model (CHARM) coupling.
- Damaris R. Zachos, Graduate Research Assistant, The Pennsylvania State University; primarily responsible for establishing new aircraft models, developing simulations for new helicopter types, performing acoustic predictions, and developing flight abatement procedures; involved in all Tasks.

## Project Overview

Rotorcraft noise consists of several components, including rotor noise, engine noise, gearbox and transmission noise, etc. Rotor noise is typically the dominant component of rotorcraft noise to which the community is exposed upon takeoff and landing and along the flight path of the helicopter. Rotor noise consists of multiple noise sources, including thickness noise and loading noise (typically combined as rotational noise), blade-vortex-interaction (BVI) noise, high-speed-impulsive (HSI) noise, and broadband noise. Each noise source has its own unique directivity pattern around the helicopter. Furthermore, aerodynamic interactions among rotors, interactions between the airframe wake and a rotor, and unsteady time-dependent loading generated during maneuvers typically result in significant increases in loading noise. The combination of all potential rotor noise sources makes the prediction of rotorcraft noise highly complex, even though not all noise sources are present

at any given time in the flight (e.g., BVI noise usually occurs during the descent, and HSI noise only occurs during high-speed forward flight).

In ASCENT Project 6, “Rotorcraft Noise Abatement Operating Conditions Modeling,” the project team coupled a MATLAB-based flight simulation code with CHARM and PSU-WOPWOP to perform rotorcraft noise prediction. This noise prediction system was used to develop noise abatement procedures through computational and analytical modeling. Although this noise prediction system cannot predict engine noise or HSI noise, it was thoroughly validated via a comparison between predicted noise levels for a Bell 430 aircraft and flight test data (Ref. 19) for several observer positions and operating conditions.

In previous work for ASCENT Project 38, representative helicopters were recommended for noise abatement procedure development. These helicopters were selected to enable a determination of whether noise abatement procedures could be developed for various categories of helicopters, (i.e., 2-blade light, 4-blade light, 2-blade medium, etc.) or whether aircraft-specific design considerations would be required. Aircraft models were established for the following aircraft: Bell 430, Sikorsky S-76C+ and S-76D, Bell 407 and 206L, Airbus EC130 and AS350, and Robinson R66 and R44. Predictions were made before the 2017 FAA/NASA noise abatement flight test to provide guidance for the flight test. After the flight test, a comparison of  $L_A$  time histories and sound exposure level (SEL) contour plots revealed a problem in the broadband noise prediction, which was subsequently corrected. Initial validation comparisons demonstrated that the simulations were within a few dBA of the flight test data; however, some discrepancies in the simulations (simplifications) remained, requiring a detailed examination.

The objective of this continuing project is to utilize computational and analytical modeling to develop noise abatement procedures for various helicopters in different phases of flight. The extension of this project also includes predictions aiming to analyze various flight procedures to determine their effectiveness in noise reduction. Comparisons of predictions and flight test data provide further validation of the noise prediction system and allow a deeper understanding of the impact of noise abatement procedures on noise directivity and amplitude. Emphasis is given to more complicated flight procedures (turns with deceleration or descending turns) and validation of the noise prediction system for these complex procedures. The predictions help to explain the details of the noise generated in various procedures, which will aid in the design of refined noise abatement flight procedures. New flight test data from NASA became available in August 2020. This data included new aircraft data for a Bell 205, Leonardo AW139, Sikorsky S76D, and a Eurocopter MH-65. These aircraft are of a heavier class than the aircraft tested in 2017 and may have different acoustic characteristics, not present in lighter class helicopters. The extension of this project aims to evaluate the noise sources of these larger aircraft and determine if noise abatement procedures defined by aircraft size are appropriate. If new flight procedures are necessary, this project aims to assist FAA/NASA in developing these procedures following a similar approach used for the 2017 flight test aircraft.

## Task 14 – Determine the Effectiveness of Noise Abatement Procedures by Class of Helicopter Using the 2017 and 2019 Flight Test Data

The Pennsylvania State University

### Objective

In this Task (Task 8.1 in the 2019 proposal), helicopter models representing the aircraft in the 2019 FAA/NASA flight test will be developed from publicly available sources. Several of the noise abatement procedures flown during the flight test will be simulated with the noise prediction system. Using both the noise predictions and measured data, the noise abatement procedures will be analyzed. The effectiveness of the procedures for the heavier helicopters in the 2019 flight test will be compared to that for the lighter helicopters in the 2017 test.

### Research Approach

The noise prediction system developed in ASCENT Projects 6 and 38 will be used and updated as necessary. The PSU-WOPWOP code will be used for noise prediction and will be coupled with a PSUHeloSim flight simulator and CHARM to form a rotorcraft noise prediction system. The flight test data will be examined, and the measured and predicted results will be compared to help explain any significant details of the noise measurements. This evaluation can also identify the primary and secondary noise sources involved in each flight procedure and can clarify how the noise abatement was achieved (which can lead to generalized procedures for other helicopter categories, weights, etc.). After validation of the prediction system with 2019 flight test aircraft, comparison between similar aircraft of the 2017 flight test and the 2019 flight test will be developed.

Identical maneuver cases will be developed for comparable aircraft and various noise metrics will be evaluated for signs of significant differences in noise sources between the heavier and the lighter designs. The results of this study will provide guidance on the importance of aircraft weight in the development of noise abatement procedures and determine if separate procedures are necessary for aircraft in different weight classes.

**Milestones**

The milestones for this Task include (a) validation of predictions for aircraft flow in the 2019 flight test and (b) comparison of noise metrics between the two predictions. This Task will examine various predicted noise sources and will investigate which sources are important in the flight test data (for several different microphones). Dissimilarities between comparable aircraft with differences in weight will be used to determine the use of noise abatement procedures to reduce noise.

**Major Accomplishments**

A significant number of the parameters required to model the Bell 205 and S-76D have been collected. These parameters include blade, airframe, and aerodynamic properties for each helicopter. Engineering judgment has been used to populate some of the parameters for these aircraft. Validation with other experts is underway, which will improve the flight simulation solutions. Careful documentation of the sources used for the input parameters has been maintained to ensure validation and repeatability of the predictions.

The late release of the 2019 flight test data in August of 2020 delayed significant progress on this Task to date, but data is now available at Penn State and validation of the predictions against measured data will begin soon. As a new student, Damaris R. Zachos needed to learn the prediction system. She was able to generate identical flight maneuver predictions as her predecessor for the Bell 206 and Bell 407 for multiple flight test cases (Figure 1 and Figure 2). NASA corrected the acoustic pressure in the flight test to remove ground reflections; hence, the predictions were free-field predictions. Atmospheric absorption was accounted for in the predictions. Some new flight test cases from the 2017 flight tests, previously unassessed, were also evaluated. The capability to output MaxdBA contours was added to PSU-WOPWOP during this period, and the predicted MaxdBA contour plots for the Bell 206 and Bell 407 were generated.

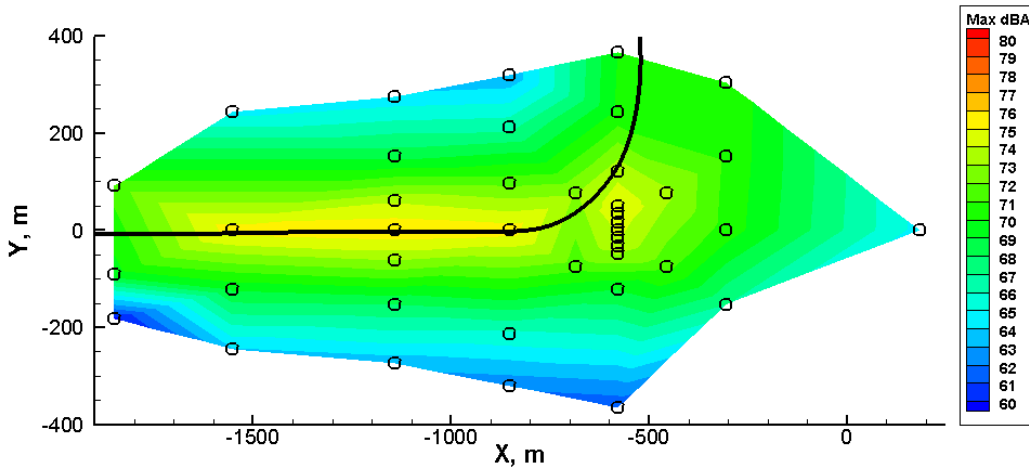


Figure 1. Predicted MaxdBA contours for Bell 407, Run 283122.

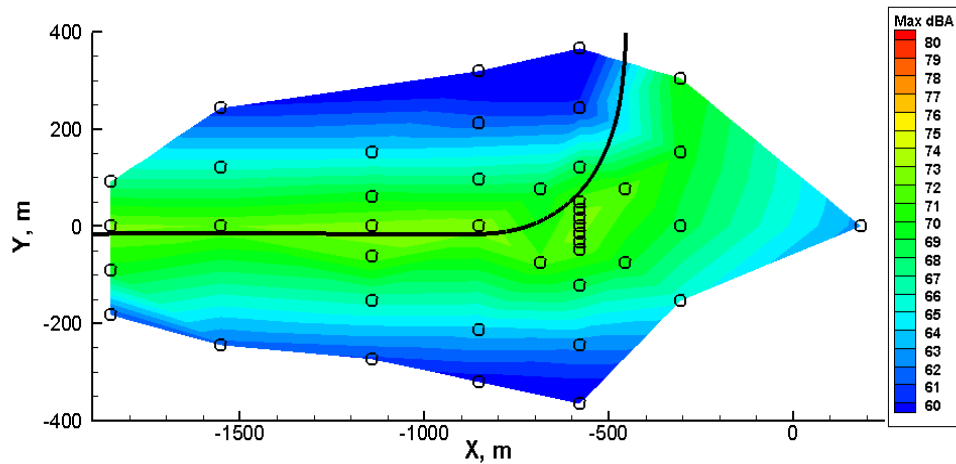


Figure 2. Predicted MaxdBA contours for Bell 206, Run 278208.

### Publications

N/A

### Outreach Efforts

N/A

### Awards

None

### Student Involvement

Damaris R. Zachos, a graduate assistant currently working toward her master's degree at Penn State, gathered the data for the Bell 205 (2019 flight test), modified PSU-WOPWOP to generate MaxdBA contours, and simulated Bell 206 and Bell 407 cases, including MaxdBA contours.

### Plans for Next Period

During the next period, helicopter models representing the remaining aircraft in the 2019 FAA/NASA flight test will be developed from publicly available sources. Several of the noise abatement procedures executed during the flight test will be simulated with the noise prediction system. Based on both the noise predictions and measured data, the noise abatement procedures will be analyzed. The effectiveness of these procedures for the heavier helicopters in the 2019 FAA/NASA flight test will be compared to that for the lighter helicopters in the FAA/NASA 2017 test, which will indicate the need and feasibility of developing noise abatement procedures based on the helicopter size, type, and weight.



## Task 15 – Assist in Data Analysis of 2019 FAA/NASA Acoustic Flight Test Data

The Pennsylvania State University

### Objective

The goal of this Task (Task 8.2 in the 2019 proposal) is to provide continued assistance in the evaluation of the 2017 and 2019 FAA/NASA flight test data and the assessment of the effectiveness of various noise abatement procedures. This will involve evaluation of the flight test data and examination and comparison of measured and predicted results to help explain any significant unexpected differences in the noise measurements. This evaluation can also identify which noise sources are the primary and secondary noise sources involved in a flight procedure and provide understanding about how the noise abatement was achieved (which can lead to generalizing the procedure to other helicopter categories, weights, etc.).

### Research Approach

Flight test data for the 2017 and 2019 FAA/NASA flight tests signal processing methods will be evaluated. Comparison between PSU-WOPWOP and NASA signal processing will indicate if there are any differences between the predictions and measured data not caused by modeling discrepancies. NASA TM-2019-220264 contains data published on the 2017 flight tests, including MaxdBA contours and hemispheres for various flight maneuvers. This Task relies on the ability to recreate these same plots using the predictions from PSU-WOPWOP to determine any modeling differences, which may indicate inaccuracy in the helicopter model or noise prediction sources. During the review of the signal processing methods, recommendations regarding different signal processing methods may be made. Examination of the processed acoustic signal at each stage of processing may indicate if a certain noise source is being attenuated or reduced via signal processing. If a particular noise source is both significant and distorted by processing, then the knowledge learned should lead to improved data analysis techniques.

### Milestones

The milestones for this Task are (a) determination of the signal processing methods used on the 2017 and 2019 NASA flight test data, (b) replication of identical cases in PSU-WOPWOP, (c) comparison of the results to ensure similarity in the signal processing, and (d) potential recommendation of new signal processing methods for 2019 flight test data.

### Major Accomplishments

The ability to output MaxdBA contours was not present in PSU-WOPWOP at the start of 2020. It has since been added and select 2017 flight test cases have been replicated to compare results published in NASA TM-2019-220264. Additionally, the ability to incorporate a moving average into the signal processing chain was added to PSU-WOPWOP. Insight from Kyle Pascioni (NASA Langley) provided detailed information about the signal processing methodology used to generate the MaxdBA contours published in the NASA TM, and the data processing methodology that will be published for the FAA/NASA 2019 flight test data. The NASA process used includes de-Dopplerization, which is not currently included in PSU-WOPWOP. Other signal processing methods, such as overlap and windowing, are available in both the prediction and the published results. PSU-WOPWOP also can account for atmospheric absorption and reflection from a ground plane. Figure 3 shows some preliminary results that highlight the differences in flight test data processed by PSU-WOPWOP (top) and the NASA post-processing used in NASA TM-2019-220264 (bottom).

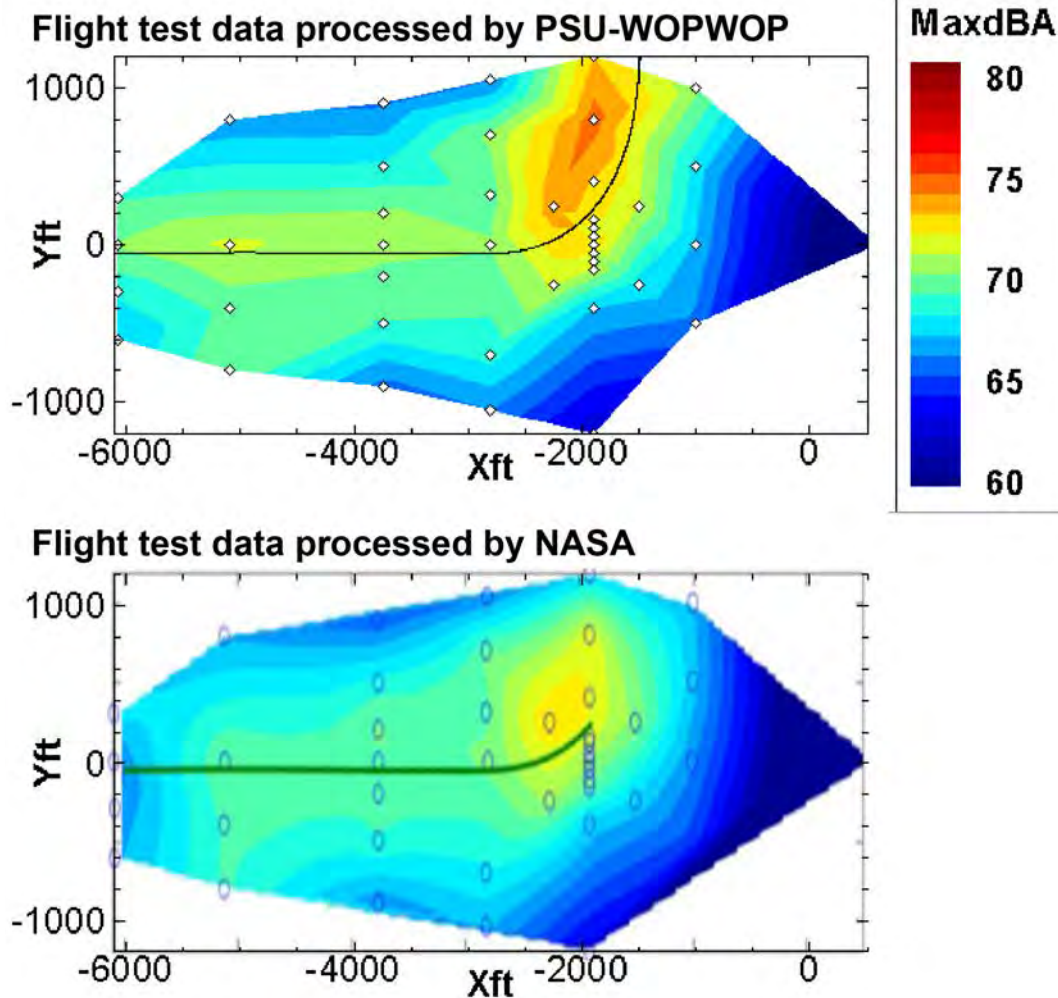


**Figure 3.** Comparison of MaxdBA contours for flight test data processed with PSU-WOPWOP (top) and NASA’s processing in NASA TM-2019-220264 (bottom) for Bell 206 Run, 278208.

**Publications**

N/A

**Outreach Efforts**

N/A

**Awards**

None

**Student Involvement**

Damaris R. Zachos, a graduate assistant currently working toward her master’s degree at Penn State, post-processed the flight test data for this Task, added the capability to output MaxdBA contours to PSU-WOPWOP, implemented moving averaging into PSU-WOPWOP, and worked with NASA to determine the signal processing methods they used.

### **Plans for Next Period**

Evaluation of the significance of de-Dopplerization used to generate MaxdBA contours will be conducted via a comparison of predictions with and without moving observers (observers moving with the vehicle do not have Doppler shift). New plots comparing the NASA TM and PSU-WOPWOP results will be generated to ensure identical results between the two signal processing methods. Assessment of the signal processing used for these plots and the hemispheres published in NASA TM-2019-220264 will be conducted for assistance in validating transient maneuvers. Evaluation of each independent noise source and an assessment of the impact of the signal processing methods for each noise source will be performed to determine if any important information is neglected using the current NASA processing method.

## **Task 16 – Assessment of Noise Prediction System and Provide Potential Improvements for Broadband Noise, Engine Noise, and Improved Interface with FAA Noise Codes**

The Pennsylvania State University

### **Objective**

In this Task (Task 8.3 in the 2019 proposal), predictions of noise abatement procedures executed in the flight test will be simulated and compared to the optimal procedures developed under the new strategy. The process will be thoroughly documented and will provide the basis for future low-noise operational guideline development. Both linear flight profiles and turns will be considered, along with more complex procedures. These demonstrations will consider flight conditions both with and without BVI noise.

### **Research Approach**

Predictions for various aircraft from 2017 and 2019 FAA/NASA flight tests will be generated using the PSUHeloSim/CHARM/PSU-WOPWOP prediction system. These results will have been validated as a result of Task 14's milestones. New flight paths will then be predicted via the same prediction system, but with a noise-optimized command input generator. Various noise metrics for these predictions will be evaluated to determine the effectiveness of these maneuvers on reduced noise generation. To assist the FAA in evaluating helicopter noise, the capability to process prediction data from PSU-WOPWOP will be streamlined for use with Advanced Acoustic Model (AAM) software.

### **Milestones**

The milestones for this Task are (a) completion of the validation of the prediction system from Task 14, (b) evaluation of the prediction of individual noise sources, and (c) add the capability to PSU-WOPWOP to output noise files for AAM.

### **Major Accomplishments**

Significant modifications to the internal data structures in PSU-WOPWOP have been performed to enable the additional data processing capabilities required in Task 15 and other data output. As a direct result of the internal improvements to PSU-WOPWOP, the ability to output moving averaged data was possible (see Figure 4). **Figure 1** This code revision applied changes to the signal processing hierarchy used in PSU-WOPWOP that enable addition of new post-processing methods to PSU-WOPWOP and simplify the process of writing out the data PSU-WOPWOP already computes but does not output. By evaluating flight test signals through a moving average filter, information about the presence of non-tonal noise, such as broadband noise, can be determined to better validate the prediction results. Additionally, this architecture change allows the user to evaluate the prediction results with multiple signal processing methods during one case, instead of a single processing method per run. This will significantly improve the speed at which new flight test cases can be evaluated for noise abatement flight procedures. The architecture change also lays the groundwork necessary to output files for use with AAM. Discussions with Juliet Page and Chris Cutler at the Department of Transportation's Volpe National Transportation Systems Center provided Penn State with the some of the information necessary to output files for AAM. Work is underway to update the flapping motion of the blade surface files required for noise predictions. This will improve the thickness noise predictions for all aircraft.

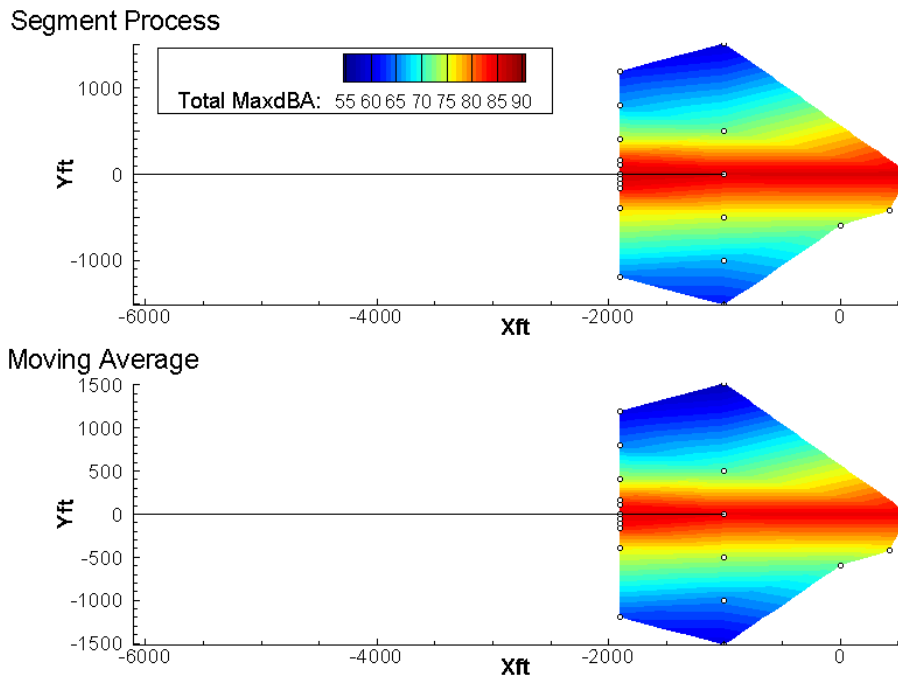


**Figure 4.** Comparison of results for small aircraft (Bell 206) on a level flight trajectory with legacy processing method (top) and moving average implementation (bottom). Note the decrease along the flight path line.

**Publications**

N/A

**Outreach Efforts**

N/A

**Awards**

None

**Student Involvement**

Damaris R. Zachos, a graduate assistant currently working toward her master’s degree at Penn State, made the code architecture changes to PSU-WOPWOP and added the capability for moving average post-processing. She also initiated communication with Volpe on the needs for AAM output file generation.

**Plans for Next Period**

Changes to PSU-WOPWOP are still needed to output the files needed for AAM. Once completed, the documentation on how to use PSU-WOPWOP with that capability will be generated. Regarding prediction improvements, a scaling factor may need to be added to the Pegg broadband noise model to account for inaccuracies in that method during a maneuver. Thickness noise predictions will also be improved upon the completion of the blade flapping motion integration in PSUHeloSim.

## Task 17 – Continue Effort to Develop Noise Abatement Flight Procedures for Various Helicopter Classes

The Pennsylvania State University

### **Objective**

This Task (Task 8.4 in the 2019 proposal) will continue the development of noise abatement procedures. The noise abatement procedures demonstrated in the FAA/NASA acoustic flight test will be simulated and compared to the best procedures that can be developed with the new strategy. The strategy for developing noise abatement procedures will be evaluated/demonstrated for various helicopter classes (light to medium weights). The process will be thoroughly documented and provide the basis for future low noise operational guideline development.

### **Research Approach**

Following the validation of noise predictions with the 2019 FAA/NASA flight test data (Task 14), the prediction system will have been authenticated for multiple maneuvers. Using both predicted and experimental data, a flight path optimizer tool will be created to develop flight paths with the lowest noise. Optimal flight paths will be tested in the noise prediction system to verify the noise is minimized. Predictions from these generated flight paths will yield new insight about noise abatement procedures for different class size aircraft. Evaluation of the noise results from these optimized flight paths will be compared against flight path recommendations from the Fly Neighborly guide to update the guidance as needed.

### **Milestones**

The milestones for this Task are (a) creation of a noise-optimized flight trajectory generator, (b) evaluation of the noise metrics for fully simulated flight test cases, and (c) the recommendation of noise abatement flight maneuvers for aircraft.

### **Major Accomplishments**

A flight path generation code which follows user input waypoints was created in August 2020. This code adapted the strict trajectory following command input design used for validation runs into a more lenient waypoint following code that more readily utilized the helicopter dynamics modeled in PSUHeloSim. This code set the groundwork for the noise-optimized trajectory generator which will be used to determine optimal noise abatement maneuvers. Preliminary work, which will incorporate the ability to turn in this command generation code, was also started.

Revisions to the MATLAB-based simulation code, PSUHeloSim, have been made to improve the helicopter simulation utilized in the predictions. These changes removed erroneous trim conditions which may have flown the simulated aircraft in an unrealistic manner. The combination of the waypoint following method described above and these changes improved the pilot control outputs. The significance of the pilot inputs in noise generation could be evaluated during this Task with these results. The improvements also enhanced the accuracy of the helicopters modeled. The improvement caused by allowing the simulated model to fly according to its dynamics instead of the trajectory following method, indicate that improvements to the simulated trajectory may be inherent in the noise-optimizer tool design.

### **Publications**

N/A

### **Outreach Efforts**

N/A

### **Awards**

None

### **Student Involvement**

Damaris R. Zachos, a graduate assistant currently working toward her master's degree at Penn State, created the preliminary trajectory following command program and worked with Professor Horn on improvements to the PSUHeloSim code to better predict the command outputs.



### **Plans for Next Period**

Further development of the waypoint trajectory generator will be needed to perform more complicated maneuvers and to add the capability to optimize the flight path based on noise results. An in-depth analysis of the changes in noise sources during each point in a maneuver is also required to determine which sound sources may be causing the high noise levels. This information should be included in an optimizer tool for determining low noise flight maneuvers. Evaluation of the effects of pilot commands on the noise generated may also be assessed.



## Project 039 Naphthalene Removal Assessment

### Massachusetts Institute of Technology

#### Project Lead Investigator

Prof. Steven R. H. Barrett  
Leonardo Associate Professor of Aeronautics and Astronautics  
Department of Aeronautics and Astronautics  
Massachusetts Institute of Technology  
77 Massachusetts Avenue – Bldg. 33-316  
Cambridge, MA 02139  
(617)-452-2550  
sbarrett@mit.edu

#### University Participants

##### Massachusetts Institute of Technology

- PIs: Prof. Steven R. H. Barrett and Dr. Raymond Speth (Co-PI)
- FAA Award Number: 13-C-AJFE-MIT, Amendment Nos. 026, 034, 043, and 053
- Period of Performance: July 8, 2016 to February 28, 2021 (with the exception of funding and cost share information, this report covers the period from October 1, 2019 to September 30, 2020)
- Tasks:
  1. Evaluate changes in emissions resulting from removal of naphthalene.
  2. Conduct integrated cost-benefit analysis of impacts of naphthalene removal in the United States.

#### Project Funding Level

The funding comprises \$840,000 in FAA funding and \$840,000 in matching funds. Sources of match are approximately \$233,000 from the Massachusetts Institute of Technology (MIT), plus third-party in-kind contributions of \$361,000 from Oliver Wyman Group and \$246,000 from Byogin Renewables, Inc.

#### Investigation Team

- Prof. Steven Barrett (MIT) serves as PI for ASCENT Project 39 as head of the Laboratory for Aviation and the Environment. Prof. Barrett both coordinates internal research efforts and maintains communication among investigators in the various MIT research teams mentioned below.
- Dr. Raymond Speth (MIT) serves as co-PI for ASCENT Project 39. Dr. Speth directly advises students performing research in the Laboratory for Aviation and the Environment, with a focus on assessment of naphthalene removal refinery options; climate and air quality modeling; and fuel alteration life-cycle analysis. Dr. Speth also coordinates communication with FAA counterparts.
- Prof. William Green (MIT) serves as a co-investigator for ASCENT Project 39, as head of the Green Research Group. Prof. Green advises students on work in the Green Research Group focused on computer-aided chemical kinetic modeling of polycyclic aromatic hydrocarbon (PAH) formation.
- Mr. Randall Field (MIT) is the Executive Director of the MIT Energy Initiative and a co-investigator ASCENT Project 39. Drawing upon his experiences as a business consulting director at Aspen Technology Inc., Mr. Field provides mentorship to student researchers in the selection and assessment of naphthalene removal refining options and process engineering at large.
- Mr. Drew Weibel (MIT) was a graduate student researcher in the Laboratory for Aviation and the Environment. Mr. Weibel was responsible for conducting selection and assessment of naphthalene removal refining options; calculation of refinery process requirements and fuel composition effects from selected processes; estimation of capital and operating costs of naphthalene removal processes; air quality and climate modeling; and integrated cost-benefit analysis.



- Mr. Lukas Brink (MIT) is a graduate student researcher in the Laboratory for Aviation and the Environment. Mr. Brink is responsible for the development of a combustor model quantifying the effect of naphthalene removal on soot emissions, the modeling of air quality and climate impacts, and integrated cost-benefit analysis.

## Project Overview

Aircraft emissions impact the environment by perturbing the climate and reducing air quality, thus leading to adverse health impacts including an increased risk of premature mortality. As a result, understanding how different fuel components can influence pollutant emissions, as well as the resulting impacts and damage to human health and the environment, is important in guiding future research aims and policy. Recent emissions measurements have shown that removal of naphthalenes can dramatically decrease emissions of particulate matter (Brem et al., 2015; Moore et al., 2015). The objective of this research is to determine the benefits, costs, and feasibility of removing naphthalenes from jet fuel, with regard to the refiner, the public, air quality, and the environment. Specific goals of this research include:

- Assessment and selection of candidate refining processes for the removal of naphthalenes from conventional jet fuel, including details of required technology, steady-state public cost, and changing life-cycle emissions impacts at the refinery.
- Development of a chemical kinetics model to better understand the link between fuel aromatic composition and the resulting particulate matter (PM) emissions due to jet fuel combustion.
- Assessment of the climate and air quality impacts associated with naphthalene reduction and/or removal from jet fuel.
- Development of a life-cycle analysis of the relative costs of removing naphthalene from jet fuel and the associated benefits due to avoided premature mortalities and climate damage for a range of possible scenarios.

## References

- Brem, B.T., Durdina, L., Siegerist, F., Beyerle, P., Bruderer, K., Rindlisbacher, T., Rocci-Denis, S., Andac, M.G., Zelina, J., Penanhoat, O., & Wang, J. (2015). Effects of fuel aromatic content on nonvolatile particulate emissions of an in-production aircraft gas turbine. *Environmental Science and Technology* 49 13149-57
- Moore, R.H., Shook, M., Beyersdorf, A., Corr, C., Herndon, S., Knighton, W.B., Miake-Lye, R., Thornhill, K.L., Winstead, E.L., Yu, Z., Ziemba, L.D. & Anderson, B.E. (2015). Influence of jet fuel composition on aircraft engine emissions: A synthesis of aerosol emissions data from the NASA APEX, AAFEX, and ACCESS missions. *Energy Fuels* 29 2591-600

## Task 1 - Evaluate Changes in Emissions Resulting from Removal of Naphthalene

Massachusetts Institute of Technology

### Objective

Changes to jet fuel composition, such as those achieved by removal of naphthalene using available refining technologies, affect the chemical kinetics of the combustion process in gas turbine engines, which in turn affects the resulting emissions. To enable evaluation of the sensitivity of soot emissions to fuel composition, this Task develops a combustor model that includes the detailed chemical kinetic pathways for formation of polycyclic aromatic hydrocarbon (PAH) species from different fuel components and the conversion of these PAH species to soot particles or non-volatile particulate matter (nvPM) emissions. The model also provides the ability to predict changes to CO and NO<sub>x</sub> emissions resulting from changes to fuel composition.

### Research Approach

The aircraft engine emissions model developed here has three main components: a soot model, an engine model, and a combustor model. The combustor model consists of a reactor network coupled with a gas-phase kinetic mechanism, which is modeled using Cantera (Goodwin et al., 2018). A soot model is added to the reactor network and the interactions between the gas phase and the solid soot phase are modeled in detail. The altitude- and thrust-specific input conditions for the combustor are generated with the engine model. The model is called Pycaso (Python Cantera Soot). The model is used to predict emissions for a CFM56-7B/3 engine because it is one of the most prevalent engines in the commercial fleet, and measurement data for soot emissions from this engine have been published.



### Soot model

Due to the uncertainty in soot modeling in gas turbine combustors, a two-equation model is used, which captures all the major soot formation and depletion processes while minimizing complexity. In a two-equation model, the soot number density ( $N$ ) and mass density ( $M$ ) are modeled using two equations, which represent the change in soot  $N$  and  $M$  in response to four soot formation and depletion steps. The standard two-equation model assumes that oxidation solely affects  $M$  and does not directly destroy soot particles. However, experiments have shown that oxidation can destroy particles and can thus reduce  $N$  (Garo et al., 1988; Lindstedt, 1994). Therefore, an additional term is included in the number density equation to capture the effect of particle destruction through oxidation. It is assumed that for every change in soot mass equivalent to the average soot particle mass, a variable fraction of a particle is destroyed as well. The resulting equations for  $N$  and  $M$  are

$$\frac{dN}{dt} = C_{\text{nuc}} \left( \frac{dN}{dt} \right)_{\text{nuc}} + C_{\text{coag}} \left( \frac{dN}{dt} \right)_{\text{coag}} + C_{\text{ox},N} \frac{N}{M} C_{\text{ox}} \left( \frac{dM}{dt} \right)_{\text{ox}}, \quad (1)$$

and

$$\frac{dM}{dt} = C_{\text{nuc}} \left( \frac{dM}{dt} \right)_{\text{nuc}} + C_{\text{sg}} \left( \frac{dM}{dt} \right)_{\text{sg}} + C_{\text{ox}} \left( \frac{dM}{dt} \right)_{\text{ox}}. \quad (2)$$

During nucleation, the inception of soot particles happens through collisions of precursor species (Blanquart & Pitsch, 2009). These precursor species are considered to primarily consist of heavy PAH molecules (Dobbins et al., 1998; Schuetz & Frenklach, 2002). When two PAH molecules collide and stick together, they form a PAH dimer, which again increases in size through collisions with other PAH species and dimers. This growth through collisions allows for transitioning from the gas phase to the solid phase and results in the first solid incipient soot particle (Martini, 2008). PAH-PAH collision rates are considered for nucleation in the model, while PAH-soot collisions are modeled as surface growth. The nucleation rate resulting from collisions of PAH species  $i$  and  $j$  is based on the collision frequency  $\beta_{i,j}$  and is given by

$$\left( \frac{dN}{dt} \right)_{\text{nuc},ij} = \frac{\gamma_i + \gamma_j}{2} \varepsilon \sqrt{\frac{8\pi k_B T}{\mu_{i,j}}} N_A^2 (r_i + r_j)^2 [\text{PAH}_i] [\text{PAH}_j], \quad (3)$$

where  $\varepsilon = 2.2$  is the Van der Waals enhancement factor,  $k_B$  is the Boltzmann constant,  $N_A$  is Avogadro's constant,  $r_i$  and  $r_j$  are the radii of PAH species  $i$  and  $j$ ,  $\mu_{i,j}$  is the reduced mass of PAH species  $i$  and  $j$ , and  $[\text{PAH}_i]$  is the concentration of PAH species  $i$  (An et al., 2016; Atkins et al., 2018; Blanquart & Pitsch, 2009). The sticking coefficient  $\gamma < 1$  is computed using the assumption that it scales with PAH mass to the fourth power (Blanquart & Pitsch, 2009). The PAH species are chosen such that no direct pathways from species in the fuel surrogates to soot mass through nucleation exist, as these pathways might result in an overestimation of sensitivities to fuel composition. The total nucleation rate is calculated by taking the sum over all the PAH species in the gas-phase mechanism.

Nucleation is followed by surface growth and coagulation. During surface growth, the soot particles grow in size and mass due to the adsorption of gas phase molecules, mainly acetylene (Omidvarborna et al., 2015). Growth rates are found to be much higher than nucleation rates and most of the soot mass is thought to form during this step in the process (Martini, 2008). Here, two types of surface growth mechanisms are implemented. The first assumes surface growth solely by acetylene, whereas the second also includes surface growth through condensation of PAH species on the soot surface. In order to include surface growth through the adsorption of PAH species, the surface growth source term is expanded with an additional term. This term is based on the collision frequency of soot particles with PAH species  $i$  and is given by

$$\left( \frac{dM}{dt} \right)_{\text{sg,PAH}} = \sum_{i=1}^L n_{C,i} W_C \frac{\gamma_i + \gamma_{\text{soot}}}{2} \varepsilon \sqrt{\frac{8\pi k_B T}{\mu_{\text{soot},i}}} \left( r_i + \frac{d_p}{2} \right)^2 [\text{PAH}_i] N. \quad (4)$$

Since this term is similar to the nucleation term, it is scaled with  $C_{\text{nuc}}$  instead of  $C_{\text{sg}}$ .

During coagulation, soot particles grow further in size through particle-particle collisions (Blanquart & Pitsch, 2009; Omidvarborna et al., 2015). The total number of soot particles decreases during coagulation whereas the total mass across all particles stays constant. The implemented coagulation mechanism is based on the collision of two spherical particles with a collision rate as defined by Puri et al. (1993). The resulting source term for the number density equation is given by



$$\left(\frac{dN}{dt}\right)_{\text{coag}} = -K_{\text{coag}} \sqrt{\frac{24R_u T}{\rho_{\text{soot}} N_A}} \sqrt{d_p} N^2, \quad (5)$$

where  $\rho_{\text{soot}}$  is assumed to be equal to 2000 kg/m<sup>3</sup> and  $K_{\text{coag}}$  is a constant ranging between 1 and 9 in the literature (Brookes & Moss, 1999; Wen et al., 2003).

In contrast to the previous three steps, soot is destroyed during oxidation. Oxidation significantly reduces the amount of soot and measurements suggest that most of the soot formed at the start of the combustion process is oxidized before reaching the combustor exit (Toone, 1968). Carbon and hydrogen atoms are removed from the soot agglomerates by reactions with primarily diatomic oxygen (O<sub>2</sub>), hydroxyl radicals (OH), and atomic oxygen (O) (Louloudi, 2003; Neoh et al., 1981). Their respective contributions to the oxidation source term (Guo et al., 2016; Martini, 2008; Schiener & Lindstedt, 2018) are given by

$$\left(\frac{dM}{dt}\right)_{\text{ox},\text{O}_2} = -745.88\eta_{\text{O}_2} W_C \sqrt{T} \exp\left(-\frac{19,680}{T}\right) [\text{O}_2] A_s, \quad (6)$$

and

$$\left(\frac{dM}{dt}\right)_{\text{ox},\text{OH}} = -\eta_{\text{OH}} W_C \sqrt{T} [\text{OH}] A_s, \quad (7)$$

and

$$\left(\frac{dM}{dt}\right)_{\text{ox},\text{O}} = -1.82\eta_{\text{O}} W_C \sqrt{T} [\text{O}] A_s, \quad (8)$$

where the collision efficiencies for O<sub>2</sub> and O ( $\eta_{\text{O}_2}$  and  $\eta_{\text{O}}$ ) are assumed to be unity (Mueller et al., 2009; Wen et al., 2003). For oxidation through OH, collision efficiency values ranging from 0.01 to 0.65 have been proposed (Fenimore & Jones, 1967; Ghiassi et al., 2017; Guo et al., 2016; Haudiquert et al., 1997; Neoh et al., 1981; Puri et al., 1994; Richter et al., 2005; Schiener & Lindstedt, 2018). We use a value of 0.13, determined by Neoh et al. (1981), as baseline value in this model.

### Engine model

The combustor inlet temperature ( $T_3$ ) and pressure ( $P_3$ ), as well as the mass flows of fuel ( $\dot{m}_{\text{fuel}}$ ) and air ( $\dot{m}_{\text{air}}$ ) entering the combustor are computed using a detailed engine model of the CFM56-7B engine. The engine model is developed using the Numerical Propulsion System Software (NPSS) and matches fuel flows, thrust levels, and pressure ratios from the International Civil Aviation Organization (ICAO) engine Emissions Databank (EDB) within 5%. The temperature of the gas-phase mixture entering the combustor is corrected for vaporization of the fuel by adjusting the specific enthalpy of the gas-fuel mixture as follows:

$$h_{\text{mix}} = \frac{1}{\dot{m}_{\text{air}}} [\dot{m}_{\text{air}} h_{\text{air},P_3,T_3} + \dot{m}_{\text{fuel}} h_{\text{fuel},P_3,T_3} - \dot{m}_{\text{fuel}} (L + \Delta h)], \quad (9)$$

where  $L$  represents the enthalpy of vaporization at standard conditions ( $T = 298.15$  K and  $P = 101,325$  Pa),  $h$  is the specific enthalpy, and  $\Delta h$  is the change in specific enthalpy going from standard conditions to  $T_3$  and  $P_3$ .  $\dot{m}_{\text{fuel}}$  and  $\dot{m}_{\text{air}}$  are the mass flow rates of fuel and air, respectively.

### Combustor model

The combustor model developed for this project represents a rich-burn quick-mix lean-burn (RQL) combustor. Figure 1 shows a schematic overview of the model. The model is divided into two parts called the primary zone and the secondary zone. In the primary zone, air and fuel are mixed at a certain equivalence ratio. Then, the quenching happens at the start of the secondary zone through to the addition of secondary air in the slow and fast mixing zones. In the second part of the secondary zone, dilution air is added to represent the lean burn zone. As NO<sub>x</sub>, CO, and soot reactions are found to be quenched at the end of the secondary zone, the turbine is not modeled. The gas phase chemistry inside the combustor model is modeled using a kinetic mechanism which determines the structure of the flame and specifies the species profile

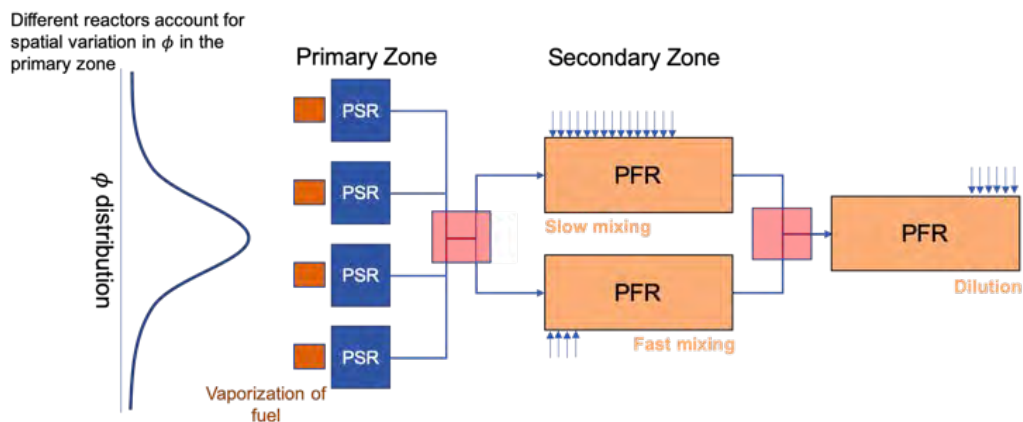


**Figure 1.** Schematic overview of the combustor model. Multiple well-stirred reactors (WSR) are used in the primary zone. The secondary zone uses a combination of plug flow reactors (PFR) to simulate different mixing times. The arrows represent secondary and dilution air entering the combustor.

(Appel et al., 2000). A high temperature kinetic mechanism for transportation fuels is coupled with a  $\text{NO}_x$  mechanism, resulting in a chemical mechanism consisting of 218 species and 7047 reactions (Ranzi et al., 2012, 2014, 2015).

The combustor model can be used to represent different (RQL) combustors. In order to represent a specific combustor design, combustor model parameters are calibrated using emissions data from the EDB for an engine containing that specific combustor. Since the combustor model can be considered a "black box" function and obtaining a (numerical) gradient is computationally expensive, gradient-free optimization is used to calibrate the model parameters. More specifically, the Divided RECTangles (DIRECT) method is applied (Finkel, 2003; Hicken et al., 2012; Jones, 2009).

## Milestones

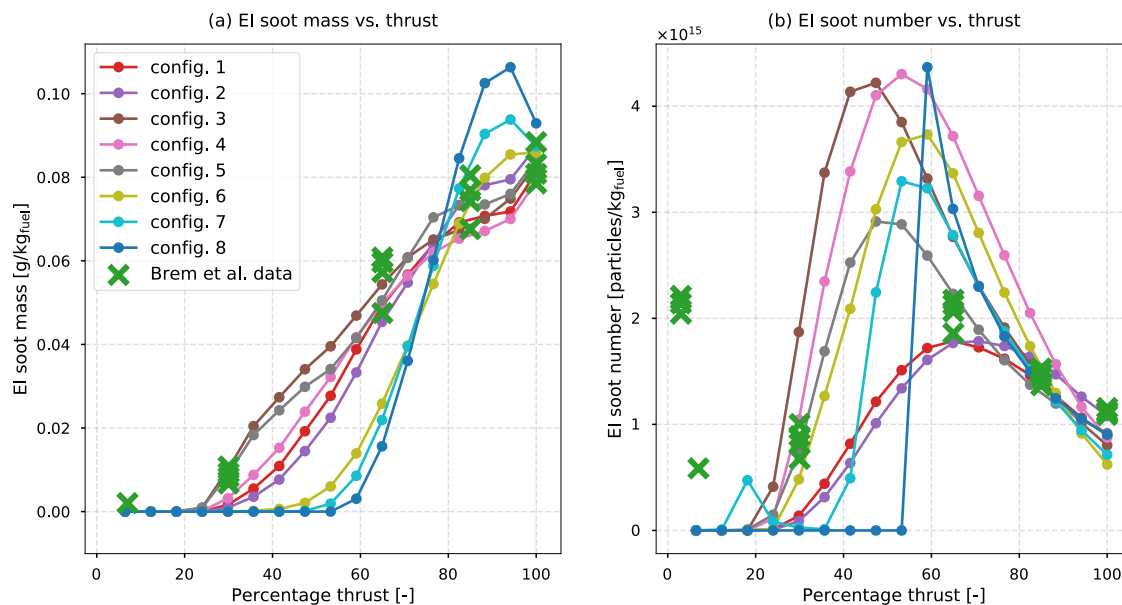
The combined combustor, soot, and engine model described above were implemented, and used to explore the impact of different jet fuel compositions on  $\text{NO}_x$ , CO, and soot emissions.

## Major Accomplishments

### Model validation

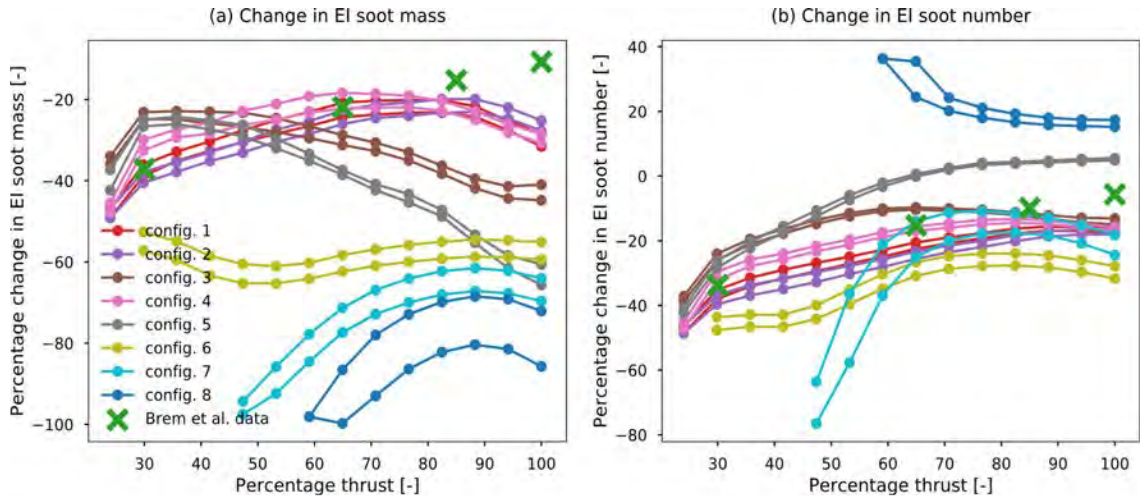
Eight different soot model configurations (C1–C8) were developed. Each configuration consists of a different set of reaction rate coefficients and/or soot mechanisms. These eight configurations are selected in order to capture a range of soot mechanisms in literature and to quantify the impact and behavior of each step of the soot formation process. The performance of the configurations against measurements for both emission index (EI) mass and number is summarized in Figure 2. Starting with EI soot mass, two clusters of configurations are visible. Configurations 1–5 capture the trends in the validation data for thrust levels  $\geq 30\%$ . On the other hand, configurations 6–8 capture the trend in the data for thrust settings larger than approximately 75% but underpredict soot mass emissions thrust settings lower than 75%. For soot number EI, the models all capture the trend in the validation data of decreasing number EI with increasing thrust between approximately 60% and 100% thrust. Configurations 4, 5, and 6 also capture the 30% thrust point, whereas configurations 1, 2, 7, and 8 underpredict soot number at this thrust setting, while configuration 3 overpredicts it.

We find that primary zone soot mass formation peaks at  $\varphi \approx 2.3$ , where the EI soot is approximately seven times higher than at  $\varphi \approx 3.0$  and  $\varphi \approx 2.0$ . On the other hand, soot number increases with equivalence ratio and peak EI soot number values are observed in the richest reactors. This difference is explained by the PAH concentration being the limiting factor for nucleation (soot number), whereas temperature and  $\text{C}_2\text{H}_2$  concentration are the limiting factors for soot mass (surface growth).



**Figure 2.** Comparison of EI soot (a) mass and (b) number with validation data (surrogate 4).

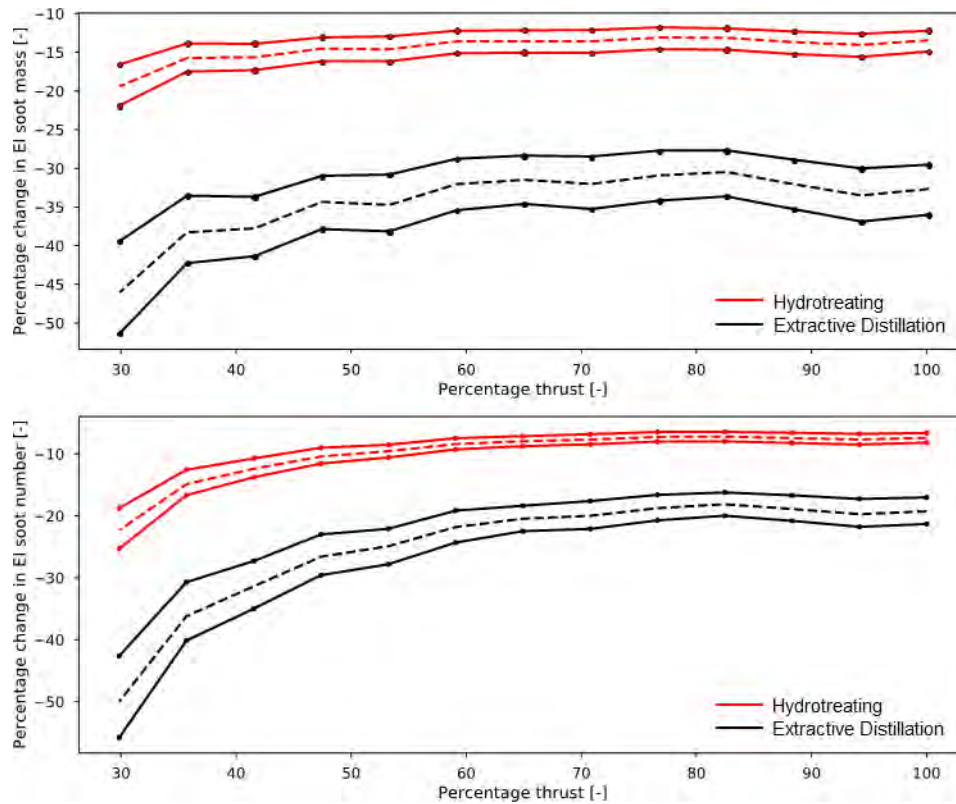
In order to validate the model's capability to predict changes in soot emissions in response to changing fuel compositions, we simulate a subset of the experiments conducted by Brem et al. (2015) where soot emissions are measured for two fuel blends with different naphthalene and aromatic content. The soot predictions of each of the model configurations for two versions of each of the five surrogates are evaluated. The total aromatics % v/v, naphthalene % v/v, and hydrogen content of these two fuels match the values used in experiments by Brem et al. (2015). The resulting changes in EI soot mass and number are shown in Figure 3. We see that the three configurations using the hydrogen abstraction acetylene addition (HACA) mechanisms show large discrepancies for both soot mass and number. The five other configurations can be grouped based on their values for  $C_{coag}$  and  $C_{ox,N}$ . The three configurations (1, 2, and 4) with relatively low coagulation factors ( $<30$ ) and relatively large  $C_{ox,N}$  values ( $> 0.65$ ) match the soot mass data from Brem et al. (2015) within 5 percentage points (p.p.) at 30% and 65% thrust, 8 p.p. at 85% thrust, and 18 p.p. at 100% thrust, and within 15 p.p. of the soot number data for all thrust conditions. When increasing the coagulation factor and decreasing  $C_{ox,N}$  (configurations 3 and 5), these differences grow to a maximum of 51 p.p. at 100% thrust for configuration 5. A possible explanation for the relatively large discrepancies at high thrust for the configuration using high coagulation factors is that these configurations rely on a large  $N$  in the primary zone (PZ) to increase the average particle size (and thus the  $M/A_s$  ratio). When reducing the naphthalene content of the fuel, less nucleation occurs and the soot number density decreases. This again reduces coagulation and increases  $M/A_s$ , which leads to more oxidation in the secondary zone. On the other hand, configurations relying on  $C_{ox,N}$  to reduce  $N$  are not affected as much by a decreasing  $N$ . Due to their superior performance compared on the validation data, configurations 1, 2, and 4 are selected to assess the sensitivity of soot to naphthalene removal and biofuels in the subsequent analysis of fuel composition effects.



**Figure 3.** Comparison of model predictions with experimental data by Brem et al. (2015). Percentage change in EI soot (a) mass and (b) number for all eight configurations.

### *Effects of fuel composition*

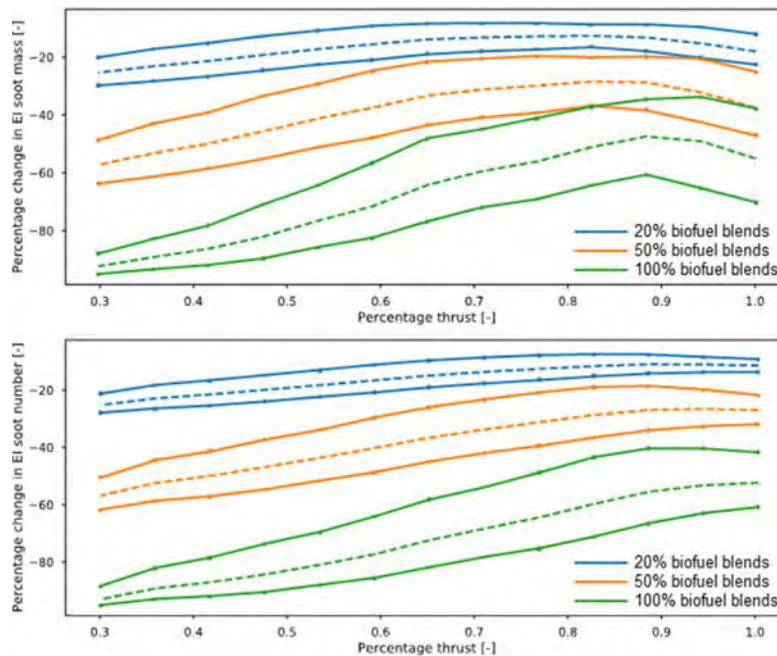
Figure 4 shows the computed ranges of soot mass and number emissions reductions associated with the naphthalene removal through extractive distillation and hydrotreating. These ranges represent both variations in the three soot model configurations as well as the five baseline fuel compositions. The mean reductions in EI mass are approximately 20 p.p. higher for extractive distillation than for hydrotreating. For EI soot number, the differences between the means of the two methods range from 12 p.p. at 100% thrust to 28 p.p. at 30% thrust. These differences are explained by tetralin, the product of hydrotreating naphthalene, still being an aromatic species and having a relatively short pathway to becoming a PAH species during combustion. Reductions in mass are predicted to be larger than reductions in number (for >35% thrust), which is consistent with the literature (Brem et al., 2015; Speth et al., 2015).



**Figure 4.** Ranges of predicted effects of naphthalene removal from jet fuel by hydrotreating (red) and extractive distillation (black) on EI soot (a) mass and (b) number emissions indices. The dashed lines represent the means of the prediction ranges, which capture variations in three different soot configurations and five different surrogates.

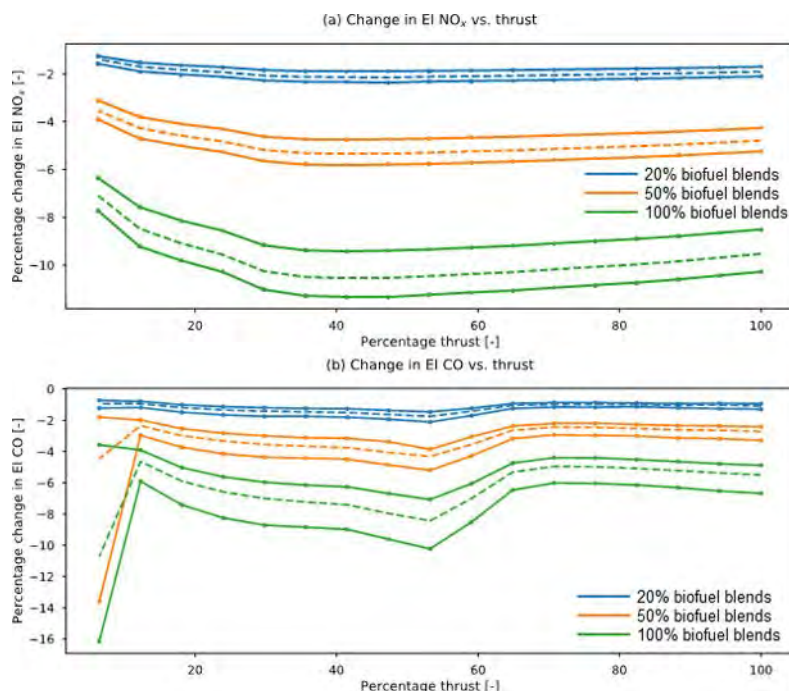
Furthermore, especially for number emissions, reductions increase with decreasing thrust. This effect is also observed in experiments in the literature (Brem et al., 2015; Corporan et al., 2007; Naegeli & Moses, 2015; Speth et al., 2015). We find that the increasing change in soot emissions with decreasing thrust is explained by two main factors. The first one is that sensitivity to fuel composition increases with decreasing PZ equivalence ratio. The changes in EI soot mass and number due to naphthalene removal are found to be approximately 1.5 and 2–3 times higher at  $\varphi=2.2$  compared to  $\varphi=3.0$ , respectively. The lower the thrust setting, the lower the primary zone equivalence ratio(s), and thus the higher the sensitivity to fuel composition. The second factor is that for a given  $\varphi$ , the reductions in both soot mass and number increase with decreasing thrust. This is explained by the temperature difference between the thrust conditions. Higher temperatures at higher thrust settings make the reactor more resilient to changes in naphthalene concentrations.

Figure 5 shows the predicted effects of using 20%, 50%, and 100% biofuel blends on soot emissions. As expected, mean reductions increase with increasing the biofuel fraction and decreasing thrust. The predicted reductions for soot mass range from 17%, 37%, and 55% at 100% thrust to 25%, 56%, and 92% at 30% thrust. For soot number, mean reductions at 100% thrust are 11%, 26%, and 51% compared to reductions of 24%, 56%, and 92% at 30% thrust.



**Figure 5.** Effects of using 20% (blue), 50% (orange) and 100% (green) biofuel blends on EI soot (a) mass and (b) number. The dashed lines represent the means of the prediction ranges, which capture variations in three different soot mechanisms and five different surrogates.

The effect of using 20%, 50%, and 100% biofuel blends on  $\text{NO}_x$  and CO emissions is shown in Figure 6. The model predicts mean reductions in  $\text{NO}_x$  emissions of 2%, 5%, and 10% and reductions in CO emissions of 1%, 2%, and 5% for the three blends, respectively. The sharp drop in CO at the lowest thrust setting is a consequence of the finite number of reactors in the model and the corresponding CO values are therefore not considered. This sharp drop in CO occurs because the leanest reactor blows out for the standard surrogate and does not for the 50% and 100% biofuel blends. This leads to an increase in secondary zone (SZ) mixing temperature and thus CO depletion.



**Figure 6.** Effects of using 20% (blue), 50% (orange) and 100% (green) biofuel blends on (a) NO<sub>x</sub> and (b) CO emissions. The dashed lines represent the means of the prediction ranges, which capture variations in five different surrogates.

## Publications

N/A

## Outreach Efforts

The results of this work were presented at the Aviation Emissions Characterization (AEC) Roadmap annual meeting held in May 2020.

## Awards

None.

## Student Involvement

This task was conducted primarily by Lukas Brink, working directly with Prof. Steven Barrett and Dr. Raymond Speth. Mr. Brink graduated with a Master of Science in 2020.

## Plans for Next Period

Task is complete. A journal paper based on this work is being prepared for submission.

## References

- An, Y., Li, X., Teng, S., Wang, K., Pei, Y., Qin, J., & Zhao, H. (2016). Development of a soot particle model with PAHs as precursors through simulations and experiments. *Fuel*, 179, 246–257. <https://doi.org/10.1016/j.fuel.2016.03.100>
- Appel, J., Bockhorn, H., & Frenklach, M. (2000). Kinetic modeling of soot formation with detailed chemistry and physics: Laminar premixed flames of C<sub>2</sub> hydrocarbons. *Combustion and Flame*, 121(1–2), 122–136.
- Atkins, P. W., De Paula, J., & Keeler, J. (2018). *Atkins' physical chemistry*. Oxford University Press.
- Blanquart, G., & Pitsch, H. (2009). A joint volume-surface-hydrogen multi-variate model for soot formation. *Combustion Generated Gine Carbonaceous Particles*, 437–463.
- Brookes, S. J., & Moss, J. B. (1999). Predictions of soot and thermal radiation properties in confined turbulent jet diffusion flames. *Combustion and Flame*, 116(4), 486–503. [https://doi.org/10.1016/S0010-2180\(98\)00056-X](https://doi.org/10.1016/S0010-2180(98)00056-X)



- Corporan, E., DeWitt, M. J., Belovich, V., Pawlik, R., Lynch, A. C., Gord, J. R., & Meyer, T. R. (2007). Emissions Characteristics of a Turbine Engine and Research Combustor Burning a Fischer-Tropsch Jet Fuel. *Energy & Fuels*, 21(5), 2615–2626. <https://doi.org/10.1021/ef070015j>
- Dobbins, R. A., Fletcher, R. A., & Chang, H.-C. (1998). The evolution of soot precursor particles in a diffusion flame. *Combustion and Flame*, 115(3), 285–298. [https://doi.org/10.1016/S0010-2180\(98\)00010-8](https://doi.org/10.1016/S0010-2180(98)00010-8)
- Fenimore, C. P., & Jones, G. W. (1967). Oxidation of soot by hydroxyl radicals. *The Journal of Physical Chemistry*, 71(3), 593–597. <https://doi.org/10.1021/j100862a021>
- Finkel, D. (2003). *DIRECT optimization algorithm user guide*. North Carolina State University. Center for Research in Scientific Computation.
- Garo, A., Lahaye, J., & Prado, G. (1988). Mechanisms of formation and destruction of soot particles in a laminar methane-air diffusion flame. *Symposium (International) on Combustion*, 21(1), 1023–1031. [https://doi.org/10.1016/S0082-0784\(88\)80333-3](https://doi.org/10.1016/S0082-0784(88)80333-3)
- Ghiassi, H., Lignell, D., & Lighty, J. S. (2017). Soot Oxidation by OH: Theory Development, Model, and Experimental Validation. *Energy & Fuels*, 31(3), 2236–2245. <https://doi.org/10.1021/acs.energyfuels.6b02193>
- Goodwin, D. G., Speth, R. L., Moffat, H. K., & Weber, B. W. (2018). *Cantera: An object-oriented software toolkit for chemical kinetics, thermodynamics, and transport processes*. Version 2.4.0. <https://www.cantera.org>.
- Guo, H., Anderson, P. M., & Sunderland, P. B. (2016). Optimized rate expressions for soot oxidation by OH and O<sub>2</sub>. *Fuel*, 172, 248–252. <https://doi.org/10.1016/j.fuel.2016.01.030>
- Haudiquert, M., Cessou, A., Stepowski, D., & Coppalle, A. (1997). OH and soot concentration measurements in a high-temperature laminar diffusion flame. *Combustion and Flame*, 111(4), 338–349. [https://doi.org/10.1016/S0010-2180\(97\)00003-5](https://doi.org/10.1016/S0010-2180(97)00003-5)
- Hicken, J., Alonso, J., & Farhat, C. (2012). *Introduction to multidisciplinary design optimization: Chapter 6: Gradient-free optimization*. Stanford University.
- Jones, D. R. (2009). Direct global optimization algorithm. *Encyclopedia of Optimization*, 1(1), 431–440.
- Lindstedt, P. R. (1994). Simplified Soot Nucleation and Surface Growth Steps for Non-Premixed Flames. In H. Bockhorn (Ed.), *Soot Formation in Combustion: Mechanisms and Models* (pp. 417–441). Springer. [https://doi.org/10.1007/978-3-642-85167-4\\_24](https://doi.org/10.1007/978-3-642-85167-4_24)
- Louloudi, S. (2003). *Transported probability density function: Modelling of turbulent jet flames*. Imperial College London (University of London).
- Martini, B. (2008). *Development and assessment of a soot emissions model for aircraft gas turbine engines* [Thesis, Massachusetts Institute of Technology]. <https://dspace.mit.edu/handle/1721.1/45256>
- Mueller, M. E., Blanquart, G., & Pitsch, H. (2009). Hybrid Method of Moments for modeling soot formation and growth. *Combustion and Flame*, 156(6), 1143–1155. <https://doi.org/10.1016/j.combustflame.2009.01.025>
- Naegeli, D. W., & Moses, C. A. (2015, April 17). *Effect of Fuel Molecular Structure on Soot Formation in Gas Turbine Engines*. ASME 1980 International Gas Turbine Conference and Products Show. <https://doi.org/10.1115/80-GT-62>
- Neoh, K. G., Howard, J. B., & Sarofim, A. F. (1981). Soot Oxidation in Flames. In D. C. Siegla & G. W. Smith (Eds.), *Particulate Carbon: Formation During Combustion* (pp. 261–282). Springer US. [https://doi.org/10.1007/978-1-4757-6137-5\\_9](https://doi.org/10.1007/978-1-4757-6137-5_9)
- Omidvarborna, H., Kumar, A., & Kim, D.-S. (2015). Recent studies on soot modeling for diesel combustion. *Renewable and Sustainable Energy Reviews*, 48, 635–647. <https://doi.org/10.1016/j.rser.2015.04.019>
- Puri, R., Richardson, T. F., Santoro, R. J., & Dobbins, R. A. (1993). Aerosol dynamic processes of soot aggregates in a laminar ethene diffusion flame. *Combustion and Flame*, 92(3), 320–333.
- Puri, R., Santoro, R. J., & Smyth, K. C. (1994). *Oxidation of Soot and Carbon Monoxide in Hydrocarbon Diffusion Flames*. 97, 125–144.
- Ranzi, E., Cavallotti, C., Cuoci, A., Frassoldati, A., Pelucchi, M., & Faravelli, T. (2015). New reaction classes in the kinetic modeling of low temperature oxidation of n-alkanes. *Combustion and Flame*, 162(5), 1679–1691. <https://doi.org/10.1016/j.combustflame.2014.11.030>
- Ranzi, E., Frassoldati, A., Grana, R., Cuoci, A., Faravelli, T., Kelley, A. P., & Law, C. K. (2012). Hierarchical and comparative kinetic modeling of laminar flame speeds of hydrocarbon and oxygenated fuels. *Progress in Energy and Combustion Science*, 38(4), 468–501. <https://doi.org/10.1016/j.pecs.2012.03.004>
- Ranzi, E., Frassoldati, A., Stagni, A., Pelucchi, M., Cuoci, A., & Faravelli, T. (2014). Reduced Kinetic Schemes of Complex Reaction Systems: Fossil and Biomass-Derived Transportation Fuels. *International Journal of Chemical Kinetics*, 46(9), 512–542. <https://doi.org/10.1002/kin.20867>
- Richter, H., Granata, S., Green, W. H., & Howard, J. B. (2005). Detailed modeling of PAH and soot formation in a laminar premixed benzene/oxygen/argon low-pressure flame. *Proceedings of the Combustion Institute*, 30(1), 1397–1405. <https://doi.org/10.1016/j.proci.2004.08.088>



- Schiener, M. A., & Lindstedt, R. P. (2018). Joint-scalar transported PDF modelling of soot in a turbulent non-premixed natural gas flame. *Combustion Theory and Modelling*, 22(6), 1134–1175. <https://doi.org/10.1080/13647830.2018.1472391>
- Schuetz, C. A., & Frenklach, M. (2002). Nucleation of soot: Molecular dynamics simulations of pyrene dimerization. *Proceedings of the Combustion Institute*, 29(2), 2307–2314. [https://doi.org/10.1016/S1540-7489\(02\)80281-4](https://doi.org/10.1016/S1540-7489(02)80281-4)
- Speth, R. L., Rojo, C., Malina, R., & Barrett, S. R. H. (2015). Black carbon emissions reductions from combustion of alternative jet fuels. *Atmospheric Environment*, 105, 37–42. <https://doi.org/10.1016/j.atmosenv.2015.01.040>
- Toone, B. (1968). A Review of Aero Engine Smoke Emission. In I. E. Smith (Ed.), *Combustion in Advanced Gas Turbine Systems* (pp. 271–296). Pergamon. <https://doi.org/10.1016/B978-0-08-013275-4.50019-2>
- Wen, Z., Yun, S., Thomson, M. J., & Lightstone, M. F. (2003). Modeling soot formation in turbulent kerosene/air jet diffusion flames. *Combustion and Flame*, 135(3), 323–340. [https://doi.org/10.1016/S0010-2180\(03\)00179-2](https://doi.org/10.1016/S0010-2180(03)00179-2)
- Wen, Z., Yun, S., Thomson, M. J., & Lightstone, M. F. (2003). Modeling soot formation in turbulent kerosene/air jet diffusion flames. *Combustion and Flame*, 135(3), 323–340. [https://doi.org/10.1016/S0010-2180\(03\)00179-2](https://doi.org/10.1016/S0010-2180(03)00179-2)

## Task 2 – Conduct Integrated Cost-Benefit Analysis of Impacts of Naphthalene Removal in the United States

Massachusetts Institute of Technology

### Objective

The objective of this Task is to produce an integrated cost-benefit analysis of naphthalene removal in the United States, accounting for the additional refining cost as well as the air quality and climate impacts.

### Research Approach

The overall cost-benefit assessment of naphthalene removal includes fuel production costs, air quality benefits, and climate impacts from fuel production and fuel consumption. Fuel production costs were evaluated in tasks that were completed in previous project years. Air quality benefits and non-contrail climate impacts were calculated per unit reduction in nvPM mass and number emissions, based on the results of Grobler et al. (2019). These impacts are then scaled using the emissions reductions determined in the results of Task 1. Contrail impacts are estimated based on contrail modeling studies which investigated the effect of reductions in the soot number EI (Caiazza et al., 2017; Bier & Burkhardt, 2019). Finally, all effects are placed on a common monetized basis to compare different naphthalene removal scenarios. We consider uncertainties in the assessment of each component and use these uncertainties to compute the likelihood of a net benefit for different scenarios.

### Milestone

The work completed for this Task was presented at the Aviation Emissions Characterization (AEC) Roadmap annual meeting in May 2020.

### Major Accomplishments

The processing costs, air quality benefits, and climate impacts of naphthalene removal are converted to a common basis of cents per liter, as presented in Table 1. The benefits of widespread naphthalene removal are outweighed by the costs of processing the fuel and the CO<sub>2</sub> emissions associated with that processing.

**Table 1.** Costs (positive) and benefits (negative) of naphthalene removal.

	Component	Hydrotreatment (¢/liter)		Extractive Distillation (¢/liter)	
		Median	95% CI	Median	95% CI
<b>Processing</b>	Refinery	2.4	2.0 - 2.7	1.7	1.5 - 2.0
<b>Air quality</b>	nvPM	-0.004	0 - -0.01	-0.009	0 - -0.03
	Fuel sulfur	-0.51	-0.28 - -0.73	0	
<b>Climate</b>	nvPM	-0.02	0 - -0.04	-0.04	-0.01 - -0.09
	Fuel sulfur	1.06	0.15 - 2.85	0	
	Contrails	-0.16	-0.04 - -0.44	-0.38	-0.09 - -1.0
	Refinery CO <sub>2</sub>	0.46	0.08 - 1.19	0.48	0.08 - 1.27
<b>Total</b>		<b>3.2</b>	<b>2.2 - 4.7</b>	<b>1.8</b>	<b>1.0 - 2.5</b>

For hydrotreatment, the climate impacts of the refinery CO<sub>2</sub> emissions exceed the expected air quality and climate benefits associated with the reduction in soot emissions. Furthermore, the net present value (NPV) of the climate warming associated with sulfur removal is greater than the NPV of the reduced air-quality-related damages. For extractive distillation, the median air quality and climate benefits are approximately equal to the societal cost of the refinery CO<sub>2</sub> emissions. In addition to these environmental costs, the costs associated with processing jet fuel in the refinery must also be considered. These results suggest that, in the absence of a strong contrail effect, naphthalene removal on a nationwide basis is unlikely to be cost beneficial using either extractive distillation or hydrotreatment. However, it may be possible that naphthalene removal could be beneficial under certain circumstances, e.g., if applied to fuels used at individual airports with particular air quality concerns, or if used at times in locations where the formation of net warming contrails is most likely.

### Publications

N/A

### Outreach Efforts

The results of this work were presented at the Aviation Emissions Characterization (AEC) Roadmap annual meeting held in May 2020.

### Awards

None

### Student Involvement

This task was conducted primarily by Drew Weibel, working directly with Prof. Steven Barrett and Dr. Raymond Speth. Mr. Weibel graduated with a Master of Science in 2018.

### Plans for Next Period

Task is complete.

### References

- Bier, A., & Burkhardt, U. (2019). Variability in Contrail Ice Nucleation and Its Dependence on Soot Number Emissions. *Journal of Geophysical Research: Atmospheres*, 124(6), 3384–3400. <https://doi.org/10.1029/2018JD029155>
- Caiazzo, F., Agarwal, A., Speth, R. L., & Barrett, S. R. H. (2017). Impact of biofuels on contrail warming. *Environmental Research Letters*, 12(11), 114013. <https://doi.org/10.1088/1748-9326/aa893b>
- Grobler, C., Wolfe, P. J., Dasadhikari, K., Dedoussi, I. C., Allroggen, F., Speth, R. L., Eastham, S. D., Agarwal, A., Staples, M. D., Sabnis, J., & Barrett, S. R. H. (2019). Marginal climate and air quality costs of aviation emissions. *Environmental Research Letters*, 14(11), 114031. <https://doi.org/10.1088/1748-9326/ab4942>



# Project 040 Quantifying Uncertainties in Predicting Aircraft Noise in Real-world Scenarios

## The Pennsylvania State University Purdue University

### Project Lead Investigator

Victor W. Sparrow  
Director and United Technologies Corporation Professor of Acoustics  
Graduate Program in Acoustics  
The Pennsylvania State University  
201 Applied Science Bldg.  
University Park, PA 16802  
+1 (814) 865-6364  
vws1@psu.edu

### University Participants

#### The Pennsylvania State University (Penn State)

- PI: Victor W. Sparrow, United Technologies Corporation Professor of Acoustics
- Co-PI: Philip J. Morris, Boeing/A.D. Welliver Professor of Aerospace Engineering
- FAA Award Number: 13-C-AJFE-PSU, Amendment 49
- Period of Performance: May 31, 2019 through April 30, 2021.
- Tasks:
  1. Assess uncertainty in aircraft noise events, examining the background noise levels and noise levels from en-route aircraft (BANOERAC) and similar datasets.
  2. Assess uncertainty in realistic noise source models in the (Aircraft Noise Prediction Program) ANOPP.

#### Purdue University

- PI: Kai Ming Li, Professor of Mechanical Engineering
- FAA Award Number: 13-C-AJFE-PU, Amendment 31
- Period of Performance: May 31, 2019 through December 31, 2020.
- Task:
  3. Validate the noise model capabilities of the Aviation Environmental Design Tool (AEDT) by comparing numerical results with field data and quantify uncertainties of both model prediction and measurement in trying to predict aircraft noise (or pattern of change) in the real world.

### Project Funding Level

FAA funding to Penn State in 2019–2020 is \$170,000. FAA funding to Purdue in 2019–2020 is \$85,000.

Airbus has committed in-kind cost share for both Penn State and Purdue regarding the SILENCE-R data set, and this in-kind cost share is currently in-process, awaiting a non-disclosure agreement. The point of contact for this cost sharing is Pierre Lempereur, pierre.lempereur@airbus.com.

### Investigation Team

#### The Pennsylvania State University

Victor W. Sparrow (PI)  
Philip J. Morris (Co-PI)  
Graduate Research Assistant Harshal P. Patankar



## Purdue University

Kai Ming Li (PI)  
Graduate Research Assistant Yiming Wang  
Graduate Research Assistant Jianxiong Feng

## Special Acknowledgments

### European Union Aviation Safety Agency

Illimar Bilas, Section Manager  
Willem Franken

### Anotec Engineering, S.L.

Nico van Oosten

The BANOERAC data has been provided to Penn State and Purdue by the European Union Aviation Safety Agency (EASA) via a special licensing agreement, with the assistance of Anotec Engineering, S.L. This in-kind data contribution is greatly appreciated.

## Project Overview

The ASCENT R&D portfolio is designed to assist the FAA in meeting the overarching environmental performance goal for the Next Generation Air Transportation System (NextGen) in order to attain environmental protection that allows sustained aviation growth. This project is part of the aviation modeling and analysis work in the ASCENT R&D portfolio that has the goal of improving the accuracy of the FAA's environmental modeling tools. Specifically, this project is providing data and methods to improve the aircraft weight and takeoff thrust modeling capabilities within the FAA Aviation Environmental Design Tool (AEDT). Atmospheric conditions and ground properties have significant impacts on accurate predictions of aircraft noise. It is well known that the accuracy of these inputs is critical for the predictions. The research performed by Penn State and Purdue through FAA ASCENT Center research grants has informed FAA regarding the limitations of existing noise tools and helped advance the state-of-the-art in aircraft noise modeling. Appropriate models were enhanced and developed to account for the effects of meteorological conditions, atmospheric absorption, and the Doppler effect due to source motions on the propagation of aircraft noise. The purpose of this project is to understand and quantify uncertainty in the prediction of noise propagation of aircraft.

ASCENT Project 40 is developing numerical methods that could later be used in FAA tools for predicting aircraft noise. The current research addresses an improved approach to extend the uncertainty quantification methods of Wilson et al. (2014) and other algorithms. Realistic aircraft trajectories and meteorology in the atmosphere are being used to predict aircraft flyover noise levels. The results will be compared with field data already acquired in Discover-AQ Acoustics, the Vancouver Airport Authority, BANOERAC, and SILENCE(R) databases. In addition, the uncertainties on geometric locations of source and receivers, the effective surface impedance and the ground topography, and the source motion have been incorporated in this year of effort.

If successful, the outcomes of ASCENT Project 40 will lead to the development of improved methodologies that could be later used to improve the FAA tools for predicting aircraft noise in the presence of real-world weather. By having faster predictions and predictions verified with field data, the project will help to improve confidence when making decisions regarding aircraft noise. Examples of these decision include choosing the sites for new runways and implementing new landing approach and takeoff patterns over populated areas. The project team has identified the key drivers for quantifying uncertainties in predicting aircraft noise. To assess these uncertainties, an integrated approach will be used to understand uncertainties in (a) the aircraft state and resulting noise levels and directivity (source), (b) the atmospheric and meteorological conditions (propagation), and (c) the ground impedance and terrain model (receiver). This integrated approach will include all predominant uncertainties between the source and receiver. One of the main motivations of the current project is to guide these recent advancements for reaching a sufficient Research Readiness Level (RRL) that leads to a possible implementation in AEDT in the future.

This research will enhance the accuracy of AEDT through improved aircraft noise propagation modeling. This improvement is needed to support the evaluation and development of aircraft flight routes and procedures that could reduce community noise. These improvements will also facilitate the implementation of NextGen through improved characterization of the efficiency benefits it would deliver. If this research is not performed, then the accuracy of the noise prediction tool may not be representative of real-world operations affecting studies used by airport authorities.



In 2020, the Project 40 team continued the collaborative initiative with National Aviation University of Ukraine and close cooperation with the Georgia Tech team working on ASCENT Project 43.

## Task 1 – Assess the Propagation Uncertainty in Aircraft Noise Events, Examining the BANOERAC and Similar Data Sets

The Pennsylvania State University

### Research Approach

#### Overview of the BANOERAC data

Background noise level and noise levels from en-route aircraft (BANOERAC) was a project initiated by EASA in 2009 (contracted to ANOTEC Consulting, S.L.) [1]. The project had two main goals, the first of which was to prepare maps for Europe showing background noise levels. The calculation method relied on the population density to come up with background noise levels (based on work done earlier by SINTEF). The measurements of the background noise and the en-route aircraft noise were conducted in Spain (see Figure 1). The first part of the BANOERAC study focused on correcting the SINTEF model for the cases of extremely low population density areas by taking background noise measurements. (This correction will not be the focus of the analysis presented here.) The second goal of the study involved the measurements of en-route aircraft noise. These measurements were conducted from February 2009 to July 2009 (to cover both the winter and the summer season). The data collection was spread across twenty days over the six-month period.

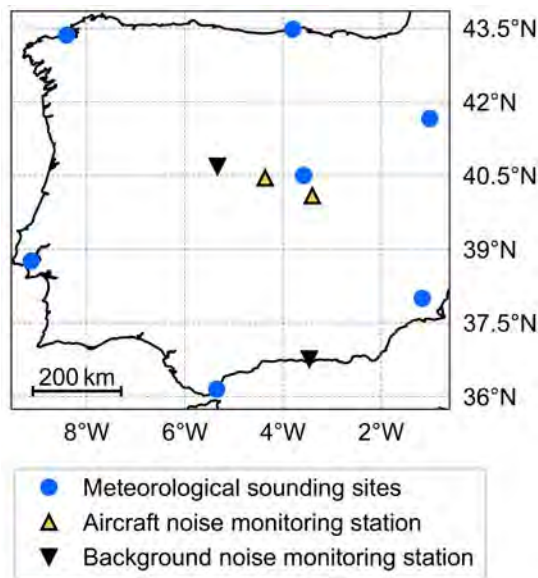


Figure 1. Map of Spain showing locations of measurement sites.

The measured data includes time histories of aircraft tracking data and noise measurement data (third-octave levels), obtained from two microphones, with one microphone placed at 1.2 m height above the ground, and the second microphone inverted and placed on a flat plate on the ground. The locations of the noise monitors can be seen in Figure 1 (shown by upward pointing yellow triangles). Meteorological data from a ground meteorological station (time synchronized with the noise monitors) and seven far-away sounding stations (seven Spanish airports shown by blue circles in Figure 1) are also provided.

#### Choosing noise events for analysis

As described in the last year’s (2019) ASCENT annual report, the raw data from the BANOERAC dataset has been parsed and visualized to identify aircraft noise events that might be useful for validating the existing noise modeling capabilities. After carefully skimming through the events, the events that seemed to have the least amount of non-aircraft noise have been chosen for further investigation. Out of those events, three events (a descent event, a cruise event, and a climb event)

Involving Boeing 737-800 aircraft are analyzed and discussed in this report. To get an idea about the aircraft altitudes, slant distances, and the maximum overall sound pressure levels (OASPL) involved in these events, a brief summary is shown in Table 1.

**Table 1.** Brief Summary of the Noise Events Selected for Analysis

	Event ID 30609	Event ID 120301	Event ID 30214
<b>Event type</b>	Descent	Cruise	Climb
<b>Aircraft altitude (min. value to max. value)</b>	4.6 km to 5.9 km	11.2 km	6.4 km to 8 km
<b>Maximum OASPL (50 Hz to 5000 Hz) for the ground microphone</b>	58 dB	54 dB	60 dB
<b>Slant distance (min. value to max. value)</b>	4.6 km to 18 km	11 km to 21 km	7.2 km to 28.6 km

**The data associated with the selected events**

The data available for each of the three selected events are shown in Figures 2–5 (the descent event), Figures 6–9 (the cruise event), and Figures 10–13 (the climb event), respectively. Since the figures corresponding to each event are laid out identically, only Figures 2–5 (the descent event) are explained in detail in the following subsection.

**Detailed explanation of the data visualization for the descent event**

The event shown in Figures 2–5 involves a descending Boeing 737-800 aircraft. Figure 2 shows the aircraft track (with timestamps) along with the location of the noise monitor (the yellow upward-pointing triangle). Figure 3 shows the time history of the aircraft altitude (solid black line on the left-hand side Y-axis) as well as the slant distance (dashed blue line on the right-hand side Y-axis). Figure 4 shows the time history of the aircraft ground speed (solid black line on the left-hand side Y-axis) and the time history of the aircraft heading (dashed blue line on the right-hand side Y-axis). As can be seen from Figure 4, the aircraft ground speed is dropping from 650 km/h to about 600 km/h during the event (a slow descent). The heading angle time-history shown in Figure 4 can be corroborated with the aircraft track shown in Figure 2. The time-history of third-octave sound press levels (SPLs) is shown in Figure 5 using a colormap (dark blue to yellow) along with the OASPL in red color (right-hand side Y-axis). The upper part of Figure 5 shows the data from the microphone on the ground and the lower part of the figure shows the data from the microphone placed at 1.2 m height above the ground. The aircraft is approaching the noise monitor until about 65 seconds, as can be seen from Figure 2 (aircraft track), and this gets reflected in the time-history of the slant distance (dashed blue line reaching its minimum value) in Figure 3. After that point in time, the aircraft continues to go away from the noise monitor. The direct effect of this kind of a trajectory is evident in the noise monitor data where the OASPL is seen to be increasing for the first part of the event and then it starts dropping off as the aircraft flies away from the noise monitor.

The descent event (Event ID 30609):

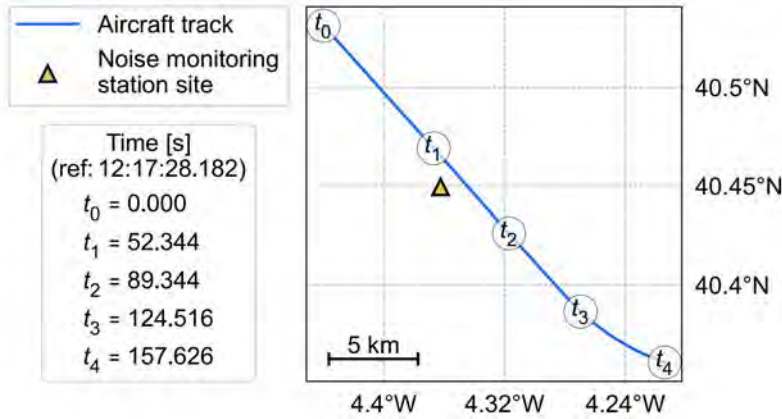


Figure 2. Time history of the aircraft trajectory (descent event).

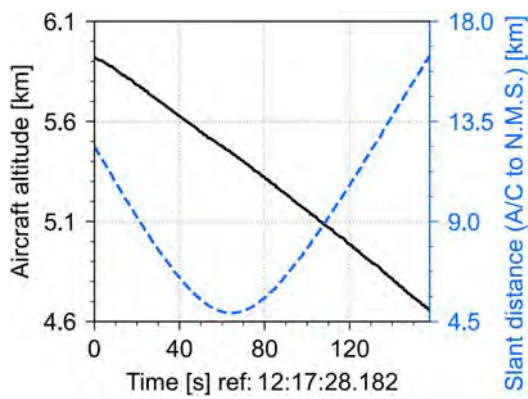


Figure 3. Time history of the aircraft altitude and the slant distance between the aircraft and the noise monitor station (descent event).

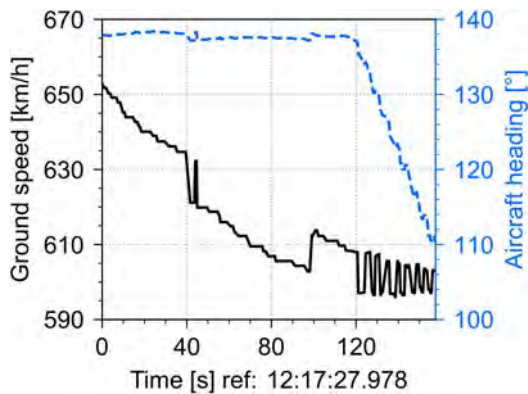


Figure 4. Time history of the aircraft ground speed and heading angle (descent event).

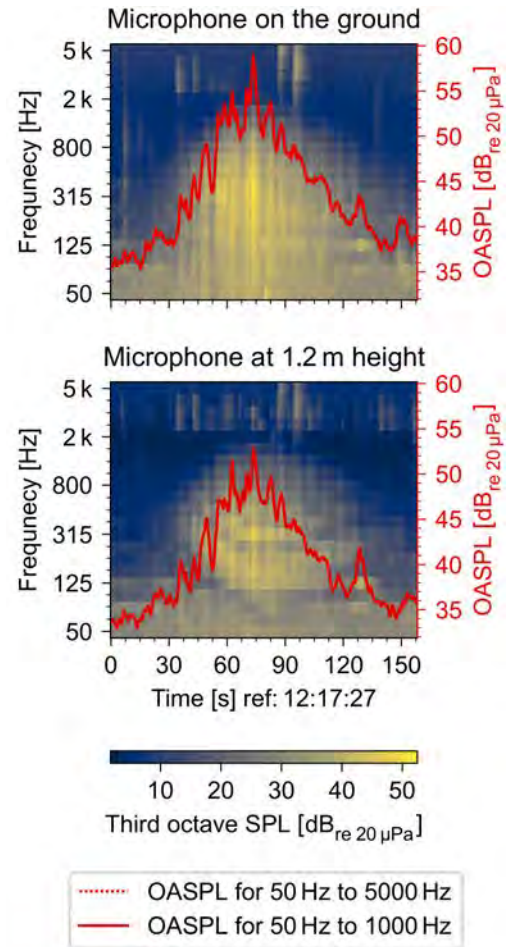


Figure 5. Time history of third-octave SPLs and OASPL for microphone on the ground and microphone at 1.2 m height (descent event).

The cruise event (Event ID 120301):

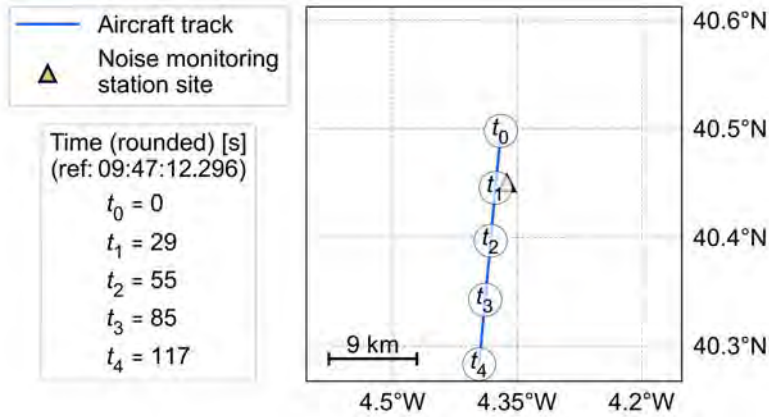


Figure 6. Time history of the aircraft trajectory (cruise event).

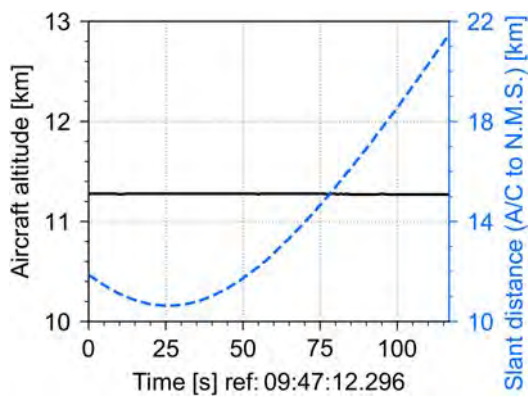


Figure 7. Time history of the aircraft altitude and the slant distance between the aircraft and the noise monitor (cruise event).

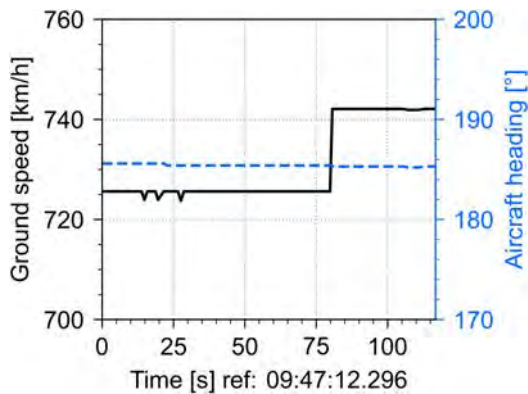


Figure 8. Time history of the aircraft ground speed and heading angle (cruise event).

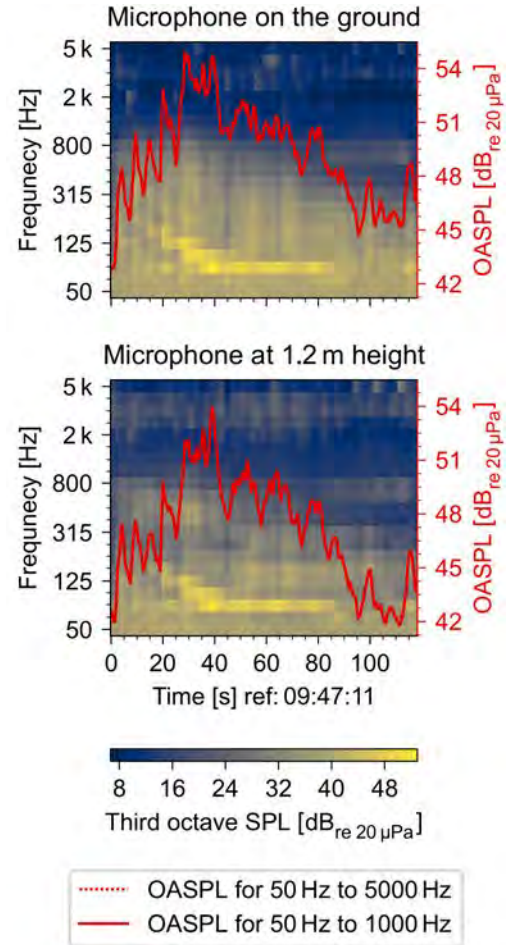


Figure 9. Time history of third-octave SPLs and OASPL for microphone on the ground and microphone at 1.2 m height (cruise event).

The climb event (Event ID 30214):

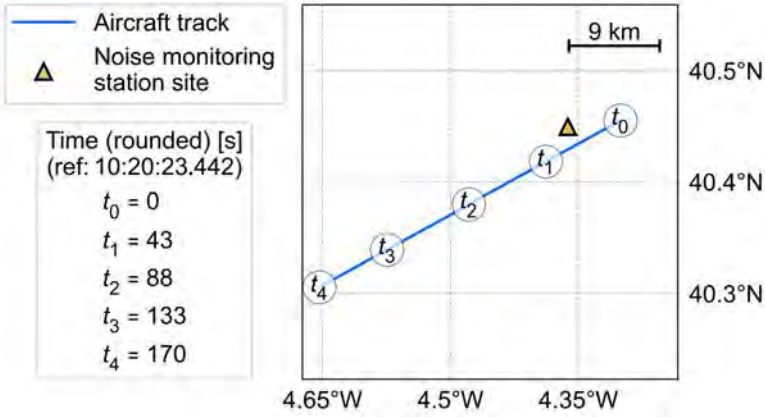


Figure 10. Time history of the aircraft trajectory (climb event).

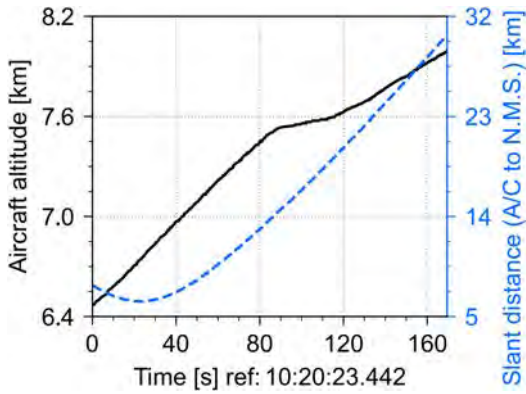


Figure 11. Time history of the aircraft altitude and the slant distance between the aircraft and the noise monitor (climb event).

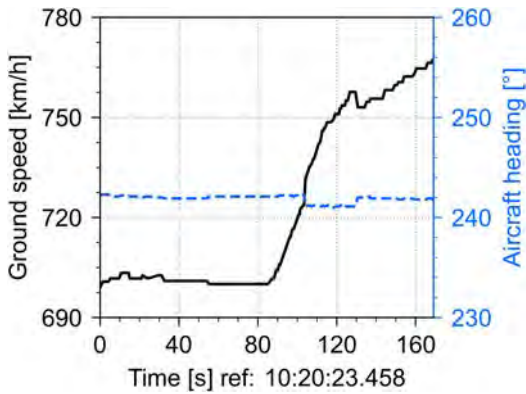


Figure 12. Time history of the aircraft ground speed and heading angle (climb event).

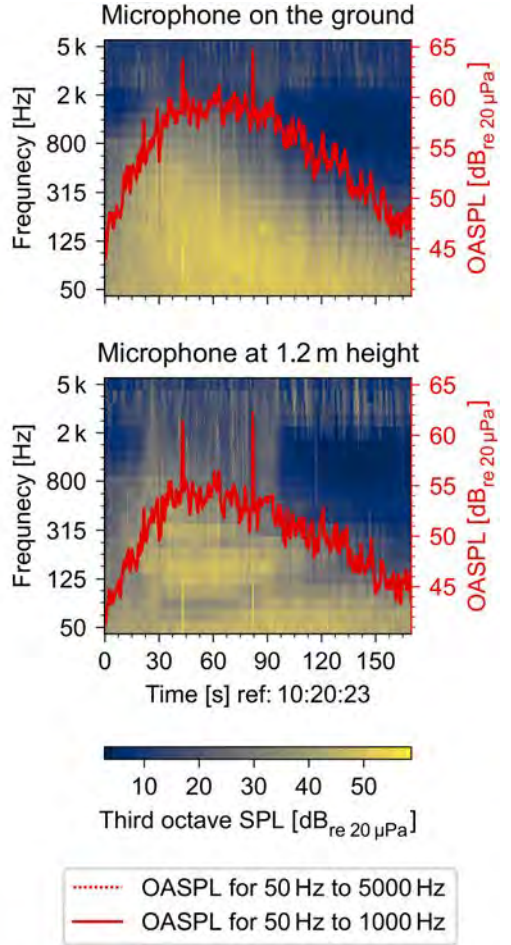


Figure 13. Time history of third-octave SPLs and OASPL for microphone on the ground and microphone at 1.2 m height (climb event).

### Modeling the acoustic propagation

The Penn State team developed an in-house acoustic ray-tracing code that takes into account wind (vector), sound speed profile, and ground reflections. The in-house code assumes a vertically stratified atmosphere (i.e., the temperature and the wind profiles are specified as functions of the vertical coordinate). The code has been validated using a benchmark problem.

The atmospheric absorption is modeled using ISO 9613-1 and uses SAE-ARP-5534 to correctly calculate the losses when dealing with the third-octave band data. To take into account the inhomogeneity in the humidity and the temperature profile (since both affect the absorption), the atmospheric absorption is successively calculated every 10 m in distance from the source to the receiver.

### Limitations of the available meteorological data

The BANOERAC data provides two types of meteorological data. The first kind of data are from a ground meteorological system. The data from the ground meteorological system (placed on a 1.8 m high mast at the noise measurement site) consist of temperature, relative humidity, wind speed, wind direction, and atmospheric pressure. Although the data are synchronized in time with the noise measurement data, the data only provide information at one physical location (i.e., not along a vertical profile).

The second kind of data are from meteorological sounding stations (seven Spanish airports shown by blue circles in Figure 1). The data from the seven meteorological sounding stations do provide vertical profiles of the meteorological variable but the data are available every 12 hours (and not in sync with the noise events). In addition, the sounding stations are far away from the noise measurement sites. For the noise events under consideration, the closest meteorological sounding station (Madrid airport) is about 66 km away from the noise monitor; hence, the sounding data might not be the best choice for use in the acoustic propagation calculations.

### Obtaining the meteorological conditions necessary to analyze the events

The Penn State team considered alternative sources (such as ERA5 [8], CFSv2 [9], and HRRR [10]) for obtaining meteorological conditions relevant to the noise events under consideration. Because of the geographical location of the BANOERAC test sites (the country of Spain in the European continent), the meteorological data source with the best possible resolution (both spatial and temporal) seems to be the ERA5 reanalysis product. It is hosted by the European Centre for Medium-Range Weather Forecasts (ECMWF). The horizontal grid of the ERA5 product has a 0.25° resolution in both latitude and longitude (which corresponds to about 15 km–20 km for Spain). The temporal resolution of the product is one hour, and the vertical grid consists of 37 pressure levels from 1000 hPa to 1 hPa.

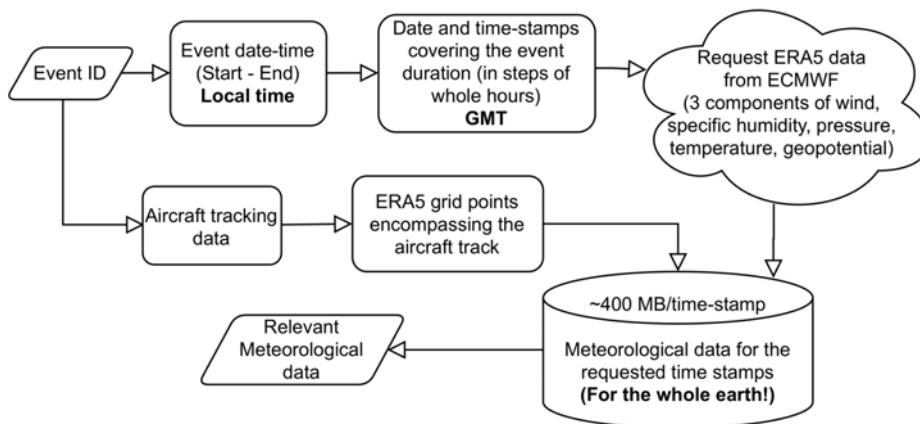


Figure 14. Procedure to extract the relevant meteorological data from the ERA5 reanalysis product.

The ERA5 data can be downloaded for a specific timestamp but it needs to be downloaded for the whole Earth and then sliced spatially to obtain the data close to the aircraft track. Figure 14 shows a flowchart summarizing the process followed to obtain the meteorological data from the ERA5 reanalysis product. As an example, Figure 15 shows the aircraft track for the descent event along with the four closest grid points from the horizontal grid of the ERA5 reanalysis product.

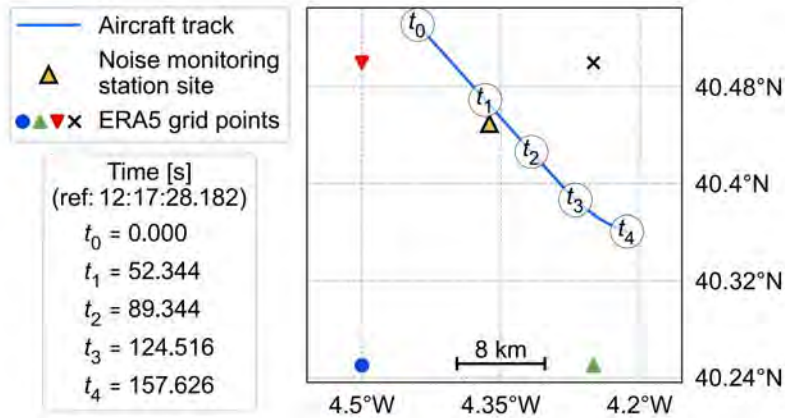


Figure 15. Time history of the aircraft track (for the descent event, Event ID 30609) and the selected ERA5 grid points (shown using four different colors and markers) for obtaining meteorological data.

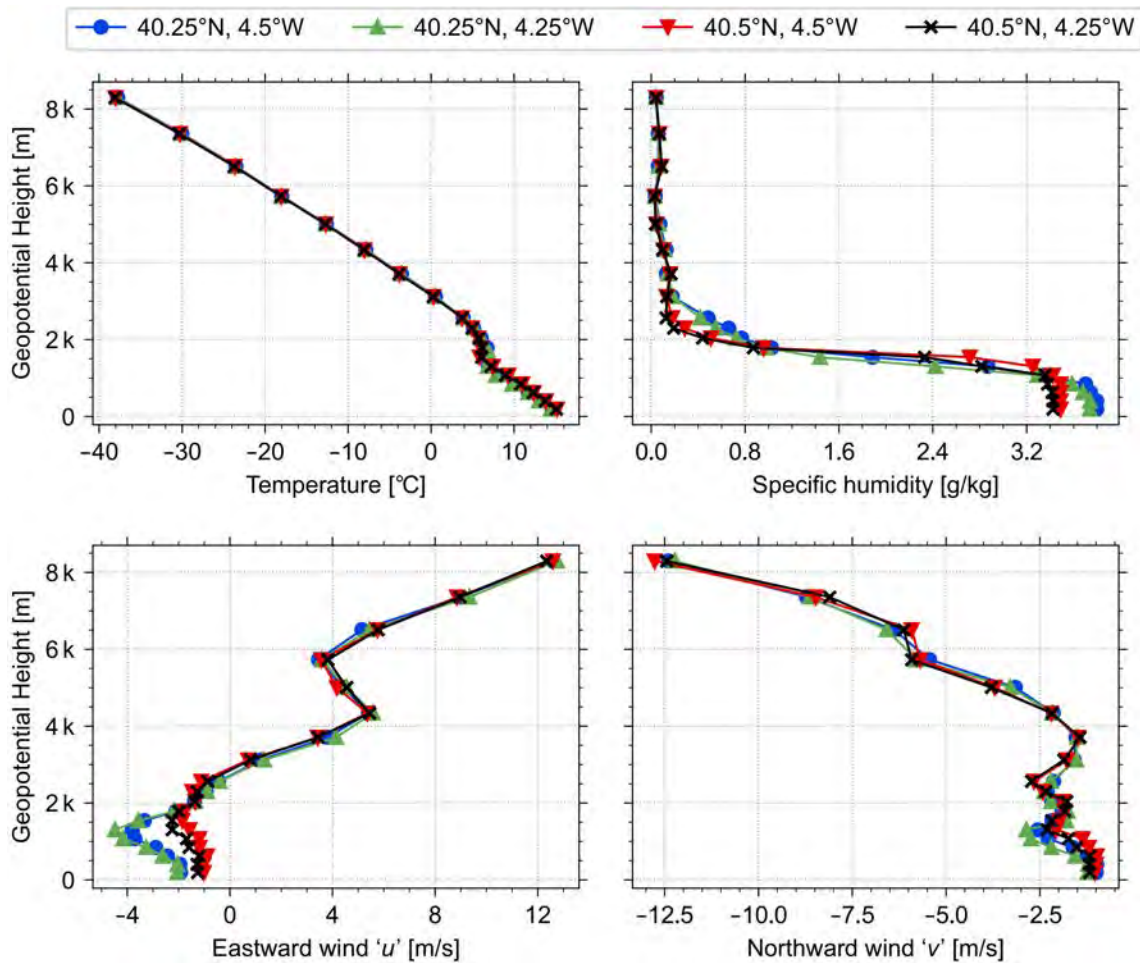
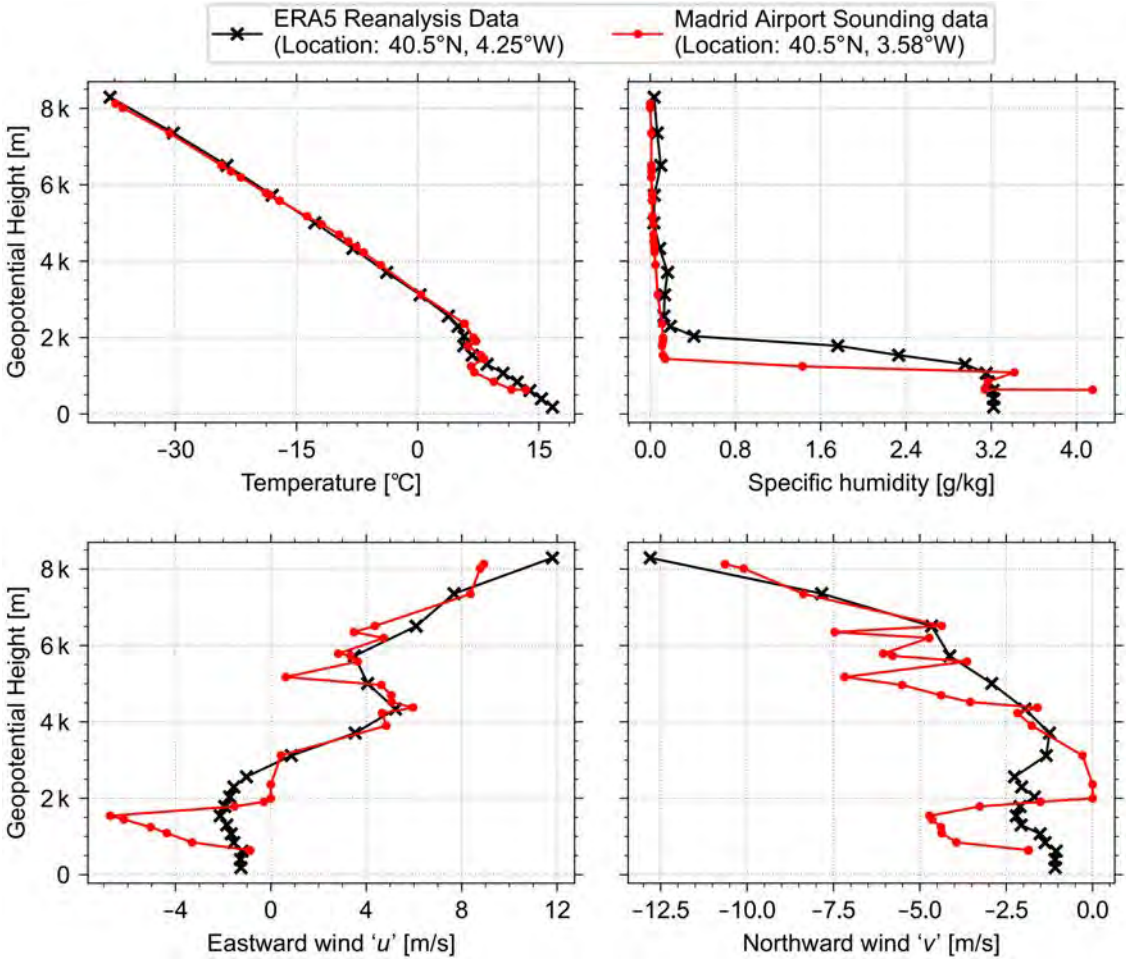


Figure 16. Meteorological data obtained from ERA5 for the four grid points surrounding the aircraft track shown in Figure 15. The data are obtained for 12:00 local time (17 minutes before the noise event, Event ID 30609).

Figure 16 shows the meteorological data (temperature, specific humidity, two components of the horizontal wind) for the four closest grid points that surround the aircraft track under consideration. It is important to note that because the ERA5 reanalysis product has a temporal resolution of one hour, the data obtained are for 12:00 local time (17 minutes before the descent event). It can be observed in Figure 16 that the meteorological profiles from the four grid points (shown using the four symbols and colors) do not differ from each other significantly. This is consistent with the expectation that meteorological conditions will not vary drastically within the span of 15–20 km (this is the distance between the adjacent grid points shown in Figure 15). Hence, the profiles from the grid point closest to the aircraft track (shown using a black 'x' marker in Figures 15 and 16) are utilized for the propagation calculations. Note that this grid point is about 8 km away from the noise monitor.

**Validating the meteorological data obtained from the ERA5 reanalysis product**

As a sanity check, the selected meteorological data from the ERA5 reanalysis product is compared with the meteorological sounding data from the Madrid airport (about 66 km away from the noise monitor) in Figure 17.



**Figure 17.** Comparison of the ERA5 reanalysis data (for the descent event, Event ID 30609) with the data from the Madrid airport sounding data.

As can be seen from Figure 17, the temperature profile obtained from the ERA5 reanalysis product (black line with 'x' markers) is similar to the temperature profile obtained from the Madrid airport sounding data (red line with small dots) except for the geopotential heights less than 2 km. There is a considerable difference between the specific humidity profiles obtained using the two sources, especially for the geopotential heights less than 2 km. Even though the wind speed profiles

follow a similar trend, there is quite a bit of difference between the two profiles (ERA5 data and the Madrid airport sounding data). These differences are expected since the sounding station is about 66 km away from the noise monitor, whereas the ERA5 grid point is only about 8 km away from the noise monitor. It is important to note that profiles from both the sources are obtained for 12:00 (local time), which is 17 minutes before the noise event. It is a mere coincidence that the noise event time is close to one of two 12-hourly timestamps for which the meteorological sounding data from the Madrid airport is available. In general, the 12-hour resolution of the sounding data is a severe limitation since not all the noise events will be this close to the 12-hourly timestamp.

Next, the data obtained from the ERA5 reanalysis product is compared with the data from the Ground Meteorological System (provided with the BANOERAC data). Before making the comparison, it is important to note that the vertical coordinate shown in Figures 16 and 17 is the geopotential height (which is not the same as the altitude). The vertical coordinate has been transformed correctly before making the comparison with the data from the Ground Meteorological System (placed directly next to the noise monitor at a 1.8-m height). The Ground Meteorological System data consist of the temperature, the relative humidity, and the wind speed at a single location. The instantaneous wind speed and direction close to the ground are expected to be highly sensitive to the exact time and the exact location; hence, only the temperature and the relative humidity values measured by the ground meteorological system are compared with the data obtained from the ERA5 reanalysis product. The comparison between the two is shown in Table 2. The temperature from the ERA5 grid point is off by about 4 °C and the relative humidity is off by about 3%. This discrepancy is reasonable because the grid point for the ERA5 reanalysis data is about 8 km away from the Ground Meteorological System and the reanalysis data is from 17 minutes before the event.

**Table 2.** Comparing the Ground Meteorological Station Data with the Data from the ERA5 Reanalysis Product

	Data from the Ground Meteorological System (in sync with the noise event)	Data from the closest ERA5 grid point (8 km away from the noise monitor, 17 minutes before the event)
Temperature	16.1 °C	12.3 °C
Relative Humidity	39.8%	36.08%

**Aircraft source levels and directivity**

Preliminary noise propagation predictions (shown in last year’s annual report) have shown the importance of using a realistic noise source directivity when estimating the ground-based measurements. To provide such a noise source description, the NASA Aircraft Noise Prediction Program 2 (ANOPP2) is being used. The details of obtaining the noise source description are explained in a separate Task (Task 2) in this report. The noise directivity data obtained from ANOPP2 is visually represented in Figure 19, which shows the source levels as a function of the azimuthal angle and the polar angle. The schematic in Figure 18 explains the way the polar angle and the azimuthal angle is defined. This information is used along with the in-house ray-tracing code to predict the aircraft noise levels near the ground.

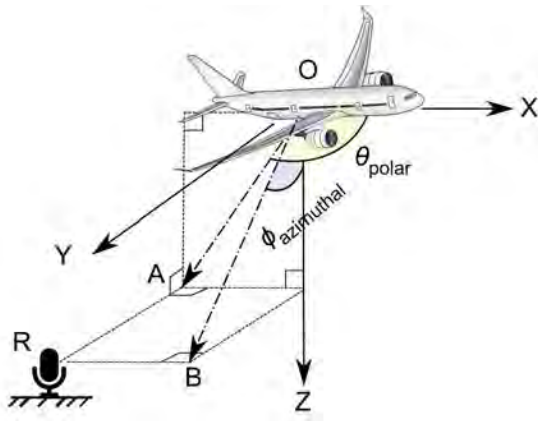


**Figure 18.** A schematic showing the polar and the azimuthal angle used in describing the aircraft directivity.

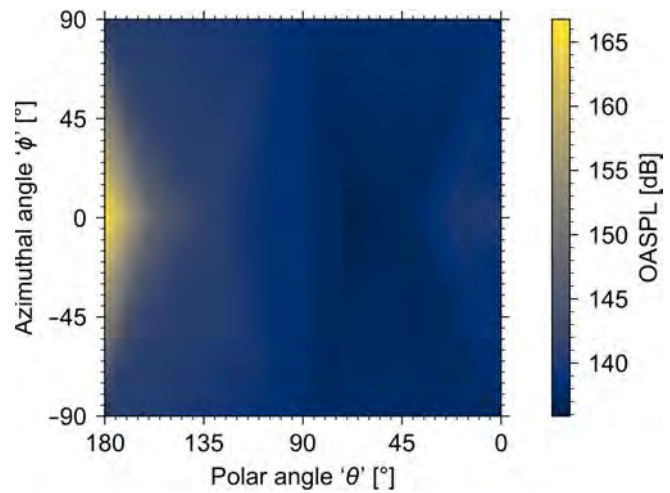


**Figure 19.** Aircraft directivity (for the descent event, Event ID 30609) as a function of the azimuthal angle and the polar angle. Note that the values shown are OASPLs calculated at 1 m away from the aircraft.

**Initial results assuming a stationary source (for the descent event, Event ID 30609)**

As a first pass, the in-house ray-tracing code (explained earlier in this report) is used to simulate the noise event assuming a stationary source (only the location of the source is updated to get the time history of noise received on the ground). The aircraft source level and directivity information appropriate for this event are used along with the meteorological data obtained from the ERA5 reanalysis product. The results of the simulations are shown in Figure 20 along with the measured OASPL data from the ground microphone (black line). The OASPL time history obtained using the 3D version of the code (blue line with filled circles as markers) and 2D version of the code (cyan colored line with upward-pointing triangles) are shown in Figure 20. The ray-tracing results seem to agree well with the measured data for the first part of the event but for the later part of the event, the ray-tracing results are off by about 15 dB. The mismatch between the ray-tracing results and the measured data could be because of not including the moving source effects. This is investigated in the following subsection of this report.

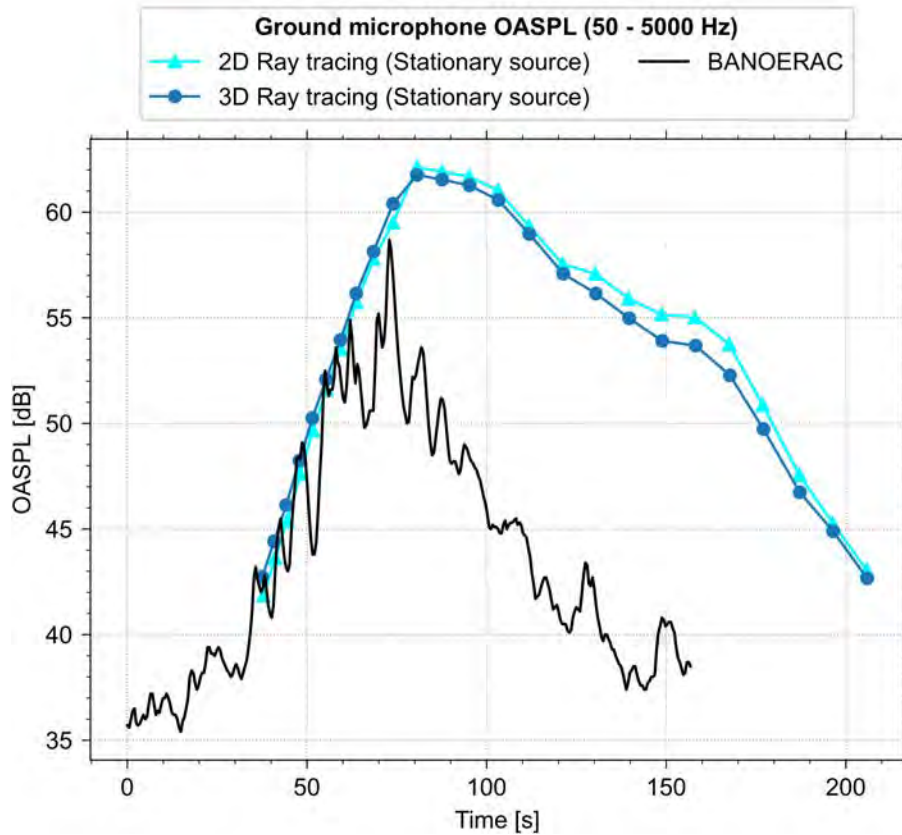


**Figure 20.** Time histories of the 2D and the 3D ray-tracing results (stationary source) with the measured data from the ground microphone (for the descent event, Event ID 30609).

The 2D version of the ray-tracing code only performs calculations in the vertical plane that includes the source and the receiver (i.e., the component of wind perpendicular to this plane is ignored). The 2D version of the ray-tracing code does take into account the wind profile, the temperature profile, and the humidity profile. The 3D version of the ray-tracing code additionally takes into account the component of the wind perpendicular to the vertical plane that includes the source and the receiver. As can be seen from Figure 20, the difference between the results obtained using the 3D ray-tracing and the 2D ray-tracing code is negligible (about 1.5 dB at maximum). Since the 3D ray-tracing is computationally expensive to run and does not seem to have a significant impact, it is not used for analyzing the other two events (the cruise event and the climb event).

#### Effect of a moving source

For a moving source, the effect of convection on the received sound pressure level depends on the Mach number ( $M$ ) and the emission angle (as shown in the schematic in Figure 21). This effect can be calculated using Equation (40.1) where  $n = 1$  for a monopole or a dipole source and  $n = 2$  for a quadrupole source [3]. In general, aircraft noise could be represented using multipole expansion (i.e., as a combination of a monopole, a dipole, a quadrupole, and higher-order sources). For the analysis shown in this report, the aircraft is assumed to be represented by a monopole source for the sake of calculating the convective amplification (this is consistent with the ANOPP2 [4] model).

$$\text{Convective amplification} = -20(n + 1) \log(1 - M \cos \theta_{\text{emission}}) \quad (40.1)$$

The Mach number needs to be calculated using the airspeed of the aircraft, but the available data are only for the groundspeed; hence, the airspeed is calculated using the wind speed from the ERA5 reanalysis data. Figure 22 shows the

time history of emission angle (on the left-hand side Y-axis in black) and the corresponding convective amplification (shown on the right-hand side Y-axis in red). The evolution of the emission angle shown in Figure 22 can be corroborated with the aircraft trajectory shown in Figure 2. Until about 65 seconds, the aircraft is approaching the noise monitor which causes the noise to be amplified, and thereafter the moving source results in the noise getting attenuated as the aircraft goes away from the noise monitor.

The effect of a moving source on the frequency content of the noise can be described using the Doppler effect as shown in Equation 40.2.

$$(\text{Apparent frequency})/(\text{Actual frequency}) = (1 - M \cos \theta_{\text{emission}})^{-1} \tag{40.2}$$

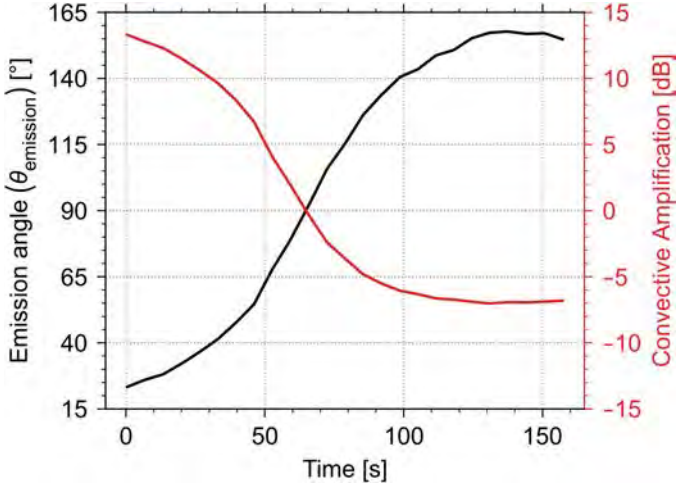
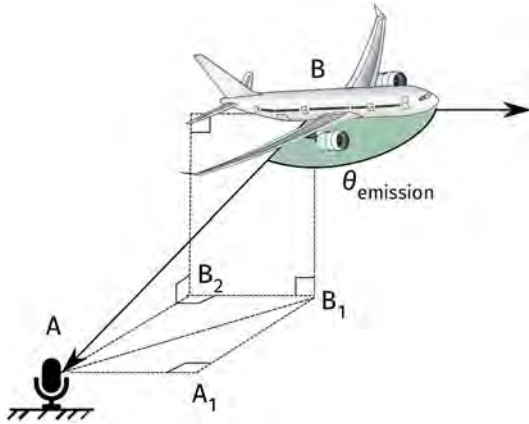


**Figure 21.** A schematic showing the emission angle and its relation to the aircraft and the receiver location.

**Figure 22.** Time history of the emission angle and the convective amplification (for the descent event, Event ID 30609).

**Results including the effects of a moving source**

The results obtained after including the effect of a moving source are shown in Figure 23 along with the results obtained assuming a stationary source (blue line with filled circles). The orange line (with downward point triangles) shows the results obtained after only applying the amplitude correction to account for a moving source. As expected, the OASPL is amplified when the source (the aircraft) is approaching the observer (noise monitor). The blue line (stationary source) and the orange line (amplitude correction) intersect at about the 80-seconds mark, implying that there is no contribution from the convective amplification at that point of time. At a first glance, this might seem contradictory to what is observed in Figure 22 (i.e., the convective amplification is zero at about 65 seconds). This apparent discrepancy is due to the fact that it takes a finite amount of time for sound to reach the noise monitor (in this case about 15 seconds). The sound that starts off from the aircraft at about 65 seconds (emission angle 90°, see Figure 22) reaches the observer at about 80 seconds (see the point of intersection of the blue and the orange line in Figure 23). This explanation can be further corroborated with the data from Figure 3, where the dashed blue line shows a slant distance of about 5 km at 65 seconds. The 15-second delay is because of the time required for the sound from the aircraft to travel about 5 km to reach the observer.

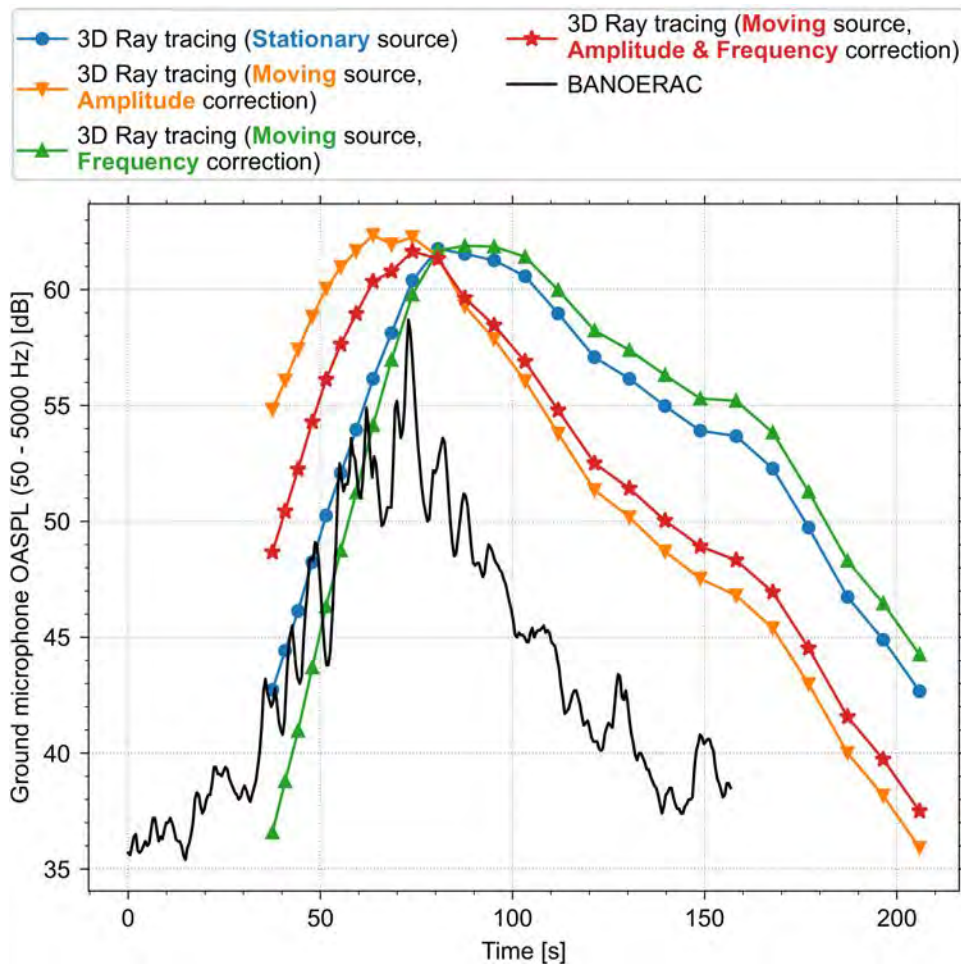


**Figure 23.** Results obtained assuming a stationary source and with the moving source effects included (for the descent event, Event ID 30609).

The effect of frequency correction (i.e., Doppler effect to account for a moving source) is shown with a green line (and upward pointing triangles) in Figure 23. As the aircraft approaches the observer, the frequency spectrum gets shifted towards higher frequencies, thereby increasing the atmospheric attenuation. This results in lower OASPL compared to the results obtained assuming a stationary source (blue line with filled circles) for the first 80 seconds as seen in Figure 23. For the latter part of the event, as the aircraft goes away from the observer, the apparent frequency spectrum gets shifted towards lower frequencies, thereby amplifying the OASPL (compared to the stationary source case).

The overall effect of a moving source (including both the amplitude and the frequency correction) is shown using the red line with asterisks in Figure 23. The trend in these results resembles the trend seen in the OASPL measured on the ground (shown using the solid black line). Even though there is a qualitative agreement between the simulation results and the measured data, quantitatively there is still an offset of about 5-8 dB (overprediction). All the results shown in the remaining portion of this report include the moving source effects (i.e. both the frequency correction and amplitude correction).

**Assessing the effect of inhomogeneity in the meteorological conditions on propagation calculations (for the descent event, Event ID 30609)**

One of the focus areas of project is to look at how meteorological conditions affect noise propagation; hence, a number of numerical experiments are conducted to investigate the role of inhomogeneity of meteorological variables such as temperature and relative humidity. Figure 24 shows the results of all the numerical experiments conducted for the descent



event. The results obtained using the inhomogeneous meteorological conditions (temperature, specific humidity, and two components of wind) from the ERA5 reanalysis product are shown using the red color and asterisk symbols. These include the effect of wind on the acoustic propagation and represent the best possible prediction with the available data. Next, the effect of assuming homogeneity in meteorological variables is discussed.

1. **Effect of wind on acoustic propagation:** The results obtained without including the wind are shown in a cyan color line with squares as the markers (these results do include the effects of inhomogeneity in temperature and humidity). As can be seen from the difference between the red line (with the wind) and the cyan line (no wind), the effect of including wind in the propagation calculations seems to be negligible when comparing the OASPL results for the microphone on the ground.

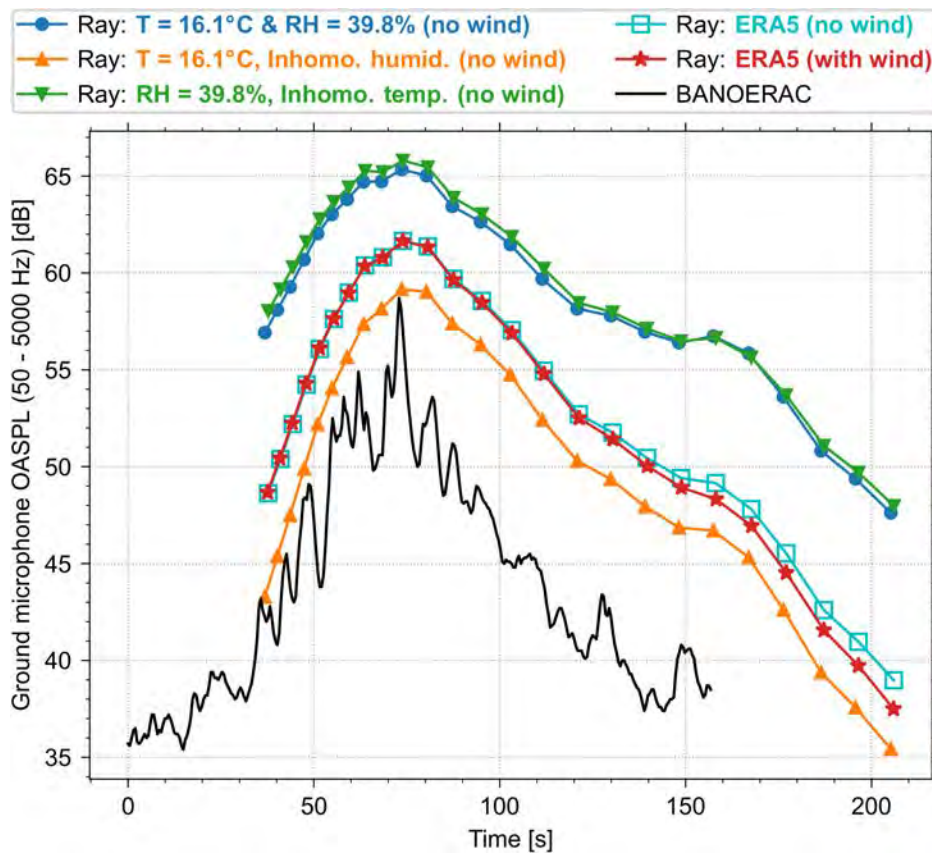


**Figure 24.** Comparing the ray-tracing results obtained assuming various levels of inhomogeneity in meteorological conditions (for the aircraft descent event, Event ID 30609).

2. **Effect of assuming a homogenous atmosphere:** The aircraft noise modeling tools typically assume meteorological conditions to be homogenous. The temperature and the relative humidity values that are used in predicting aircraft noise are typically measured on the ground and assumed to be constant throughout the propagation path. The results of a numerical experiment assuming homogenous meteorological conditions for the descent event are shown in the blue color in Figure 24 (with filled circles as markers). The constant values of temperature and relative humidity are taken from the measurements done on the ground during the noise events (as reported in the BANOERAC data). In assuming complete homogeneity of the atmosphere, the wind is assumed to be absent. Compared to the red line (which is the best possible prediction with all the inhomogeneity included), the results obtained using homogenous conditions are off by as high as 10 dB (with respect to the prediction based on the inhomogeneous atmosphere).
3. **Effect of assuming a homogenous relative humidity profile:** If the inhomogeneity in temperature profile is



considered while keeping the relative humidity profile homogenous, the results (green color line with downward-pointing triangles in Figure 24) do not differ significantly from the results obtained using a completely homogenous atmosphere.

4. **Effect of assuming a homogenous temperature profile:** If the inhomogeneity in relative humidity profile is taken into account while keeping the temperature profile homogenous, the results (orange color line with upward-pointing triangles in Figure 24) differ by as high as 15 dB from the results obtained using a completely homogenous atmosphere. This implies that the inhomogeneity in the relative humidity profile seems to be a significant factor in correctly predicting aircraft noise propagation. It is a mere coincidence that the results which include only the inhomogeneity in humidity profile (orange line with upward-pointing triangles) are closer to the measured data (black line) than the fully inhomogenous case (red line with asterisks). In general, ignoring the inhomogeneity in either temperature or the humidity profile can result in large errors in predicting aircraft noise.

#### **Assessing the effect of inhomogeneity in the meteorological conditions on propagation calculations (for the cruise event, Event ID 120301):**

The detailed analysis shown in the previous sections is repeated for the aircraft cruise event (shown in Figures 6–9) involving Boeing 737-800 aircraft. The meteorological data are obtained from the ERA5 reanalysis product for the hour closest to the event. The source level/directivity appropriate for this event is used (see Task 2) along with the ray-tracing results. The key challenge faced in analyzing this event can be appreciated by looking at the results shown in Figure 25. The red line shows the ray-tracing results which include the effect of inhomogeneities in the temperature, the humidity, and the wind. The first available data point in the ray-tracing results is at about 37 seconds. This is due to the finite amount of time required by the noise from the aircraft to travel about 12 km (see the dashed blue line showing the slant distance in Figure 7). It is important to note that even though the noise monitor data and the aircraft tracking data are time-synchronized, the aircraft noise emitted at an instance in time shows up on the noise monitor at a later time thereby not allowing any prediction for the initial part of the event. To overcome this limitation, the aircraft track is extrapolated as shown in Figure 26. Extrapolating the aircraft track is a reasonable assumption since the aircraft is in the cruise phase of the flight and seems to maintain the heading angle throughout the event.

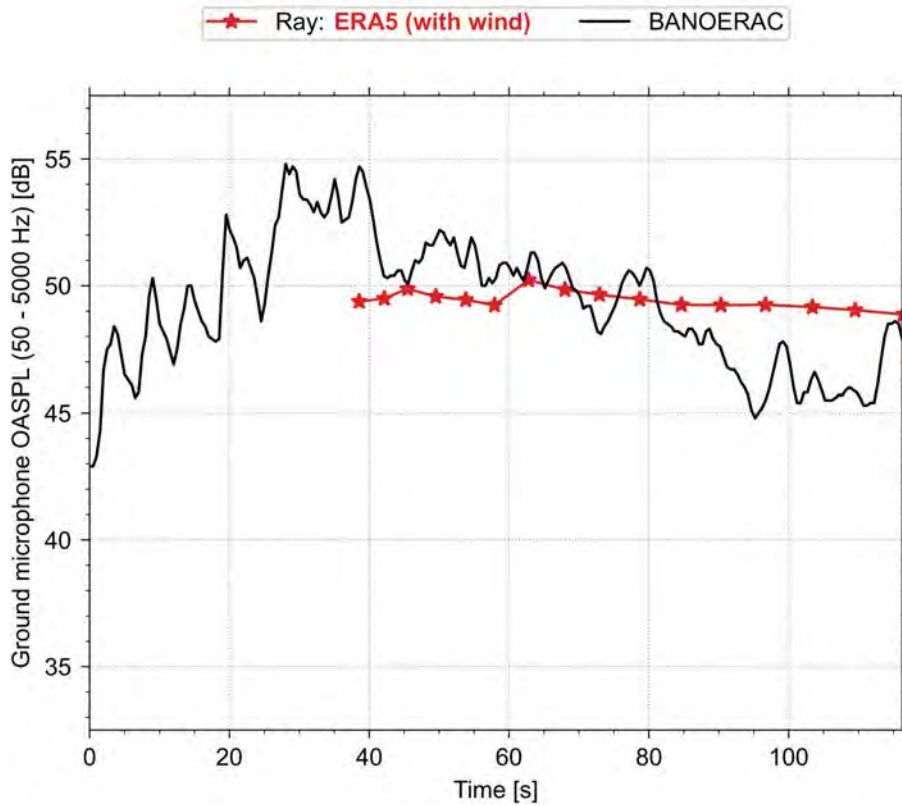


Figure 25. Comparing the ray-tracing results obtained assuming various levels of inhomogeneity in meteorological conditions (cruise event, Event ID 120301).

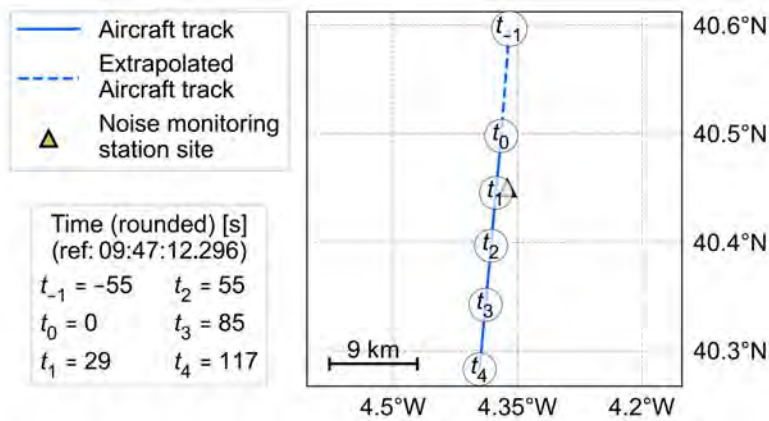
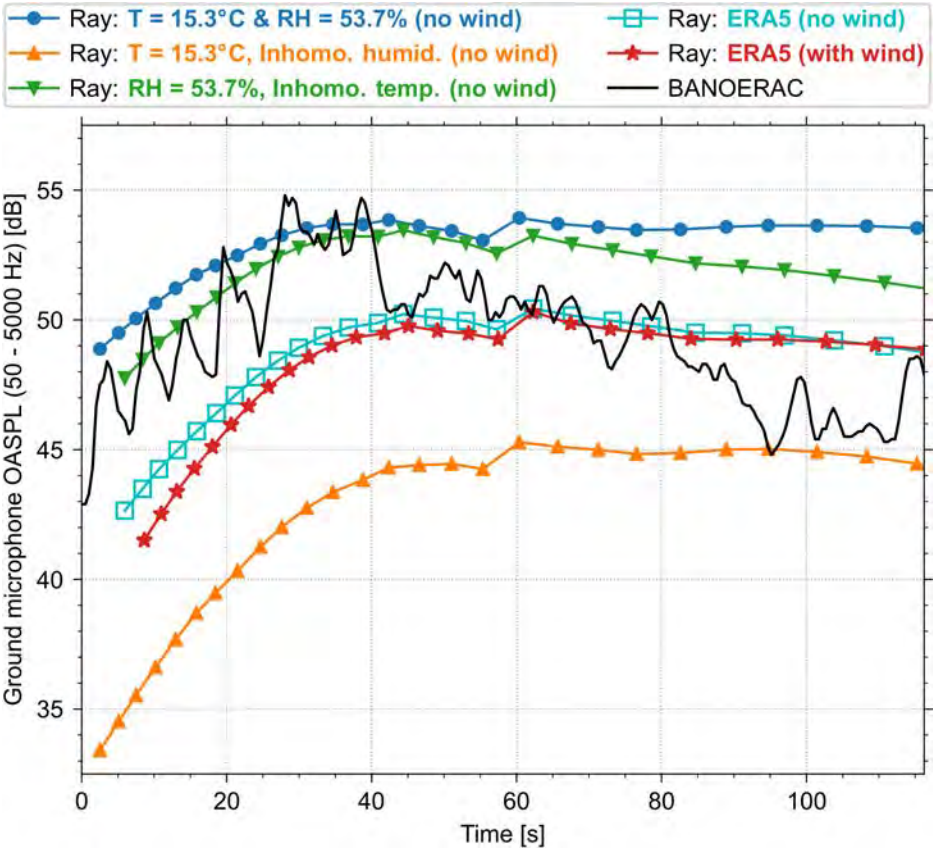


Figure 26. Time history of the aircraft trajectory (cruise event, Event ID 120301) with the added extrapolated aircraft track (compare with Figure 6).

The ray-tracing results obtained assuming the extrapolated aircraft track are shown in Figure 27. As observed in the previous case (the descent event), the wind seems to have a negligible effect on the propagation calculations for OASPL received on

the ground microphone (the red line with asterisk markers versus the cyan line with square markers). The best possible prediction (red line) which includes all the inhomogeneities in the meteorological profiles is still off by about 5-7 dB from the measured data (black line). Consistent with the observations in Figure 24, assuming a homogenous atmosphere results in errors in predictions as high as 9 dB (the blue line with filled circles as markers versus the red line with asterisks as markers). Assuming the inhomogeneity in humidity profile alone seems to have a more significant impact on the predicted levels than assuming the inhomogeneity in the temperature profile alone. Contrary to what is observed in the case of the descent event (Figure 24), only assuming the inhomogeneity in the humidity profile has worsened the prediction (orange line in Figure 27).



**Figure 27.** Comparing the ray-tracing results obtained assuming various levels of inhomogeneity in meteorological conditions (for the cruise event, Event ID 120301).

**Assessing the effect of inhomogeneity in the meteorological conditions on propagation calculations (for the climb event, Event ID 30214)**

The detailed analysis shown in the previous sections is repeated for the aircraft climb event (shown in Figures 10–13) involving Boeing 737-800 aircraft. The meteorological data is obtained from the ERA5 reanalysis product (for the hour closest to the event) and the appropriate source-level/directivity information (see Task 2) for this event is used to obtain the ray-tracing results shown in Figure 29. Similar to the cruise event, the aircraft track shown in Figure 10 is extrapolated (see Figure 28). As seen before, assuming a homogenous atmosphere results in a prediction which is off by about 9 dB from the prediction obtained assuming an inhomogeneous atmosphere. Assuming a homogenous atmosphere results in predictions that agree well with the measured data for the latter part of the event (a coincidence), but not for the first part (until about 40 seconds in Figure 29). As seen before, the inhomogeneity in the humidity profile seems to have a significant effect on the predicted levels.

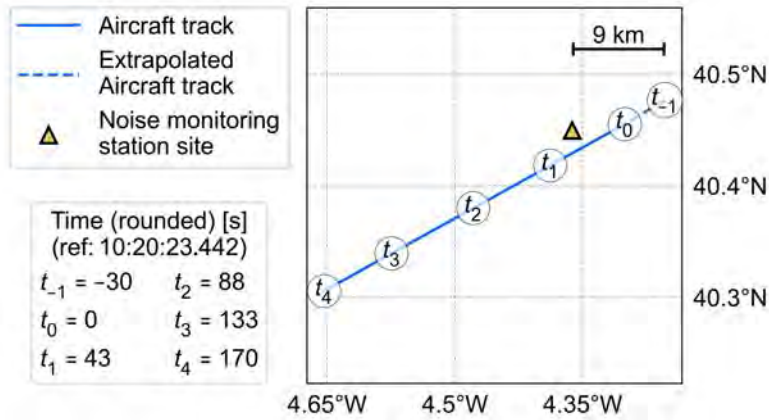


Figure 28. Time history of the aircraft trajectory (the climb event, Event ID 30214) with the added extrapolated aircraft track (compare with Figure 10).

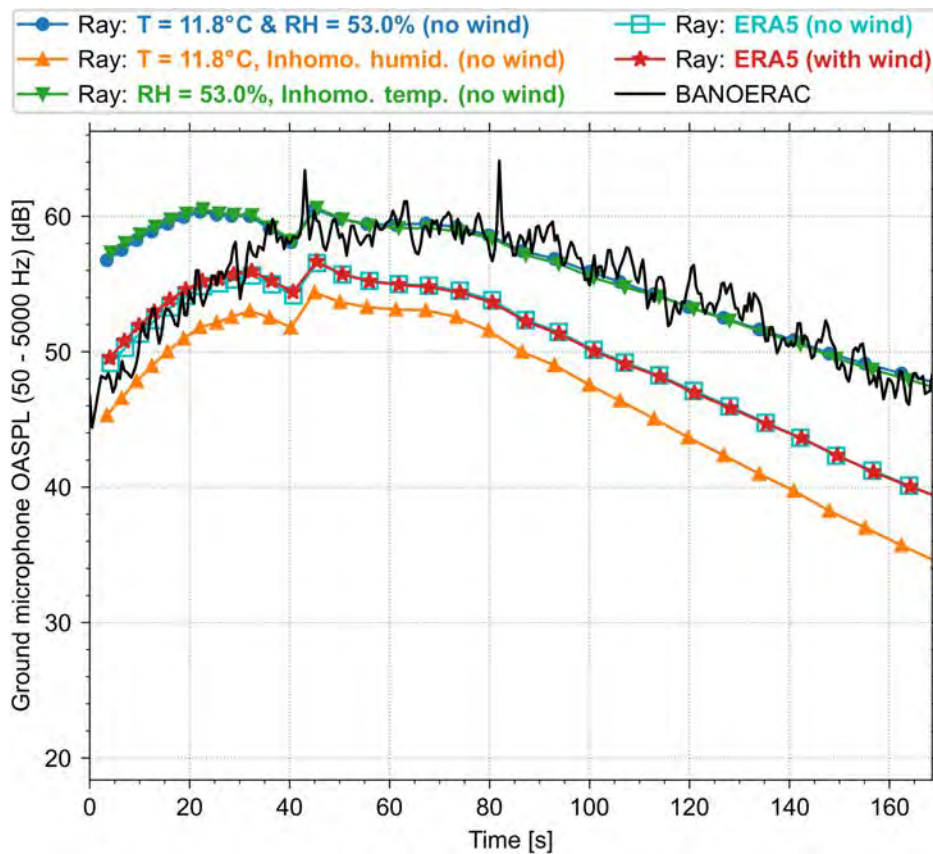


Figure 29. Comparing the ray-tracing results obtained assuming various levels of inhomogeneity in meteorological conditions (the climb event, Event ID 30214).



### **Conclusions based on the analysis of the three events (descent, cruise, climb)**

1. Knowing the accurate aircraft source levels and directivity is important to achieve a quantitative agreement between predictions and measurements (see Task 2).
2. Including the inhomogeneity in meteorological variables is shown to be an important factor in accurately predicting the aircraft noise. Even with the meteorological data from a location 8 km away from the noise monitor, a good qualitative (trends) agreement is achieved between the predictions and the measurements for the microphone on the ground.
3. Inhomogeneity in the humidity profile seems to have a significant effect on propagation calculations (more significant than the inhomogeneity in the temperature profile).
4. The effect of wind on the OASPL predictions seems to be negligible for the microphone on the ground.

### **Milestones**

A descent event, a cruise event, and a climb event from the BANOERAC data involving a Boeing 737-800 aircraft have been analyzed. To achieve this, appropriate meteorological data have been extracted using the ERA5 meteorological product. The acoustic propagation has been modeled using an in-house ray-tracing code and an atmospheric absorption routine that can handle inhomogeneities in the temperature, the humidity, and the wind profile. A number of numerical experiments have been successfully conducted to assess the effect of meteorological inhomogeneities on acoustic propagation.

### **Major Accomplishments**

For accurate aircraft noise predictions, the importance of including the inhomogeneity in the meteorological conditions has been demonstrated with the help of real-world meteorological data and real-world aircraft noise data. The importance of correctly modeling the noise source and directivity (see Task 2) along with the effects of high-speed source motion (convective amplification, Doppler effect) have been demonstrated. A qualitative agreement has been achieved between the predicted aircraft noise and measured aircraft noise.

### **Publications**

None

### **Outreach Efforts**

None

### **Awards**

None

### **Student Involvement**

Graduate Research Assistant Harshal P. Patankar has been the primary person working on this Task.

### **Plans for Next Period**

1. Penn State plans to analyze the noise events from the BANOERAC data to look at the differences between the ground microphone and the microphone at 1.2 m height (measured data versus predictions). The predictions for the third-octave band levels have not been looked at carefully yet and could give more insight into the uncertainties in propagation path.
2. Penn State had previously shown that the overall approach of Wilson et al. (2014) [5] is adaptable for the aircraft noise prediction problem [6, 7]. This approach will be extended with the help of a 2D ray-tracing model to comment on the uncertainty in predictions caused by the lack of/insufficient meteorological conditions.

### **References**

1. BANOERAC Project final report, Document ID PA074-5-0, ANOTEC Consulting S.L. (2009).
2. Delivery of flight trajectory data of BANOERAC project (Document Number: PAT001-1, ANOTEC Consulting S.L.)
3. Ruijgrok, G.J., *Elements of aviation acoustics*, Delft Univ. Press, 1994.
4. ANOPP documentation, NASA.
5. Wilson, D. Keith, *et al.*, "Description and quantification of uncertainty in outdoor sound propagation calculations." *The Journal of the Acoustical Society of America* 136(3) 1013-1028 (2014).



6. Patankar, Harshal and V. Sparrow, "Quantifying the effect of uncertainty in meteorological conditions on aircraft noise propagation," Proc. of Internoise 2018, Chicago, IL (2018).
7. Patankar, Harshal and V. Sparrow, "Effect of uncertainty in meteorological conditions on aircraft noise levels," J. Acoust. Soc. Am. **145**(3, Pt. 2) 1885 (2019).
8. Copernicus Climate Change Service (C3S) (2017): ERA5: Fifth generation of ECMWF atmospheric reanalyses of the global climate . Copernicus Climate Change Service Climate Data Store (CDS), Accessed in February/March 2020. <https://cds.climate.copernicus.eu/cdsapp#!/home>
9. Saha, S., et al. 2011, updated daily. NCEP Climate Forecast System Version 2 (CFSv2) 6-hourly Products. Research Data Archive at the National Center for Atmospheric Research, Computational and Information Systems Laboratory. <https://doi.org/10.5065/D61C1TXF>.
10. Horel, J., and B. Blaylock. "Archive of the High-Resolution Rapid Refresh model." University of Utah: Salt Lake City, UT, USA (2015).

## Task 2 – Assess Uncertainty in Realistic Noise Source Models in ANOPP

Pennsylvania State University

### Objectives

Firstly, three events from the BANOERAC dataset were chosen for noise prediction with ANOPP. All events chosen were for Boeing 737-800 aircraft. The event flightpaths correspond to a climb event, a cruise event, and a descent event. ANOPP input decks were generated for each event and noise was predicted for the BANOERAC ground monitor location.

Secondly, source spheres of 1 m radius around the aircraft were developed. The acoustic predictions from ANOPP included OASPL and 1/3 octave SPL for each event. These were necessary to employ ray-tracing techniques through a realistic atmosphere.

### Part 1: ANOPP Input Deck Creation

#### Research Approach

A sample input deck for a Boeing 737-800 aircraft was provided by Chris Perullo from the Georgia Institute of Technology. The sample input deck had all geometry parameters for a Boeing 737-800, including a set of engine state tables for various altitudes. The input decks were adapted to each BANOERAC case by developing flight path geometry modules for each event and substituting them in the sample input deck. In addition, the engine state tables for the appropriate altitude were substituted. Finally, the atmosphere module was modified from a standard atmosphere to the local atmosphere at the time of the event by substituting the ERA5 atmospheric data in the input deck.

#### BANOERAC Event ID 30609 (Descent)

Flightpath:

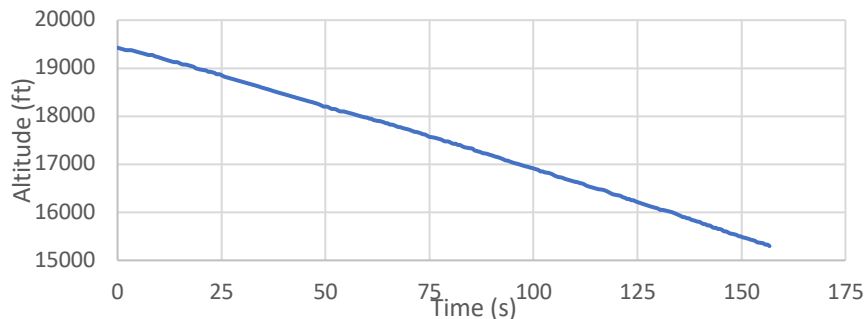


**Figure 30.** Time history of the aircraft altitude (descent event). The aircraft travels 33.5 km horizontally over the event duration.

Ground monitor noise prediction:

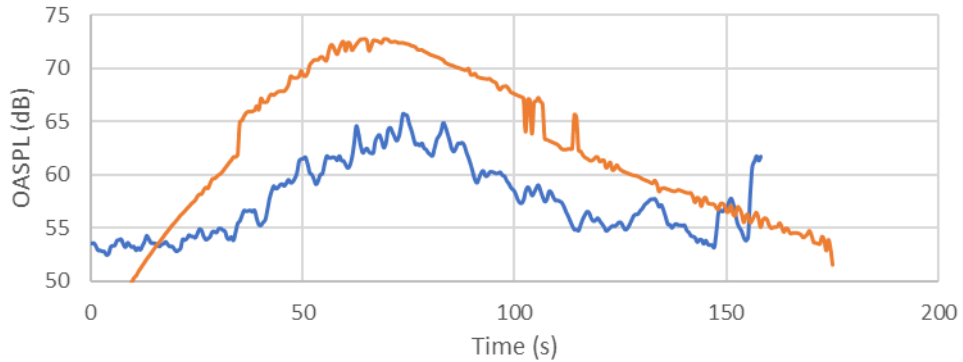


**Figure 31.** OASPL time histories for the ground microphone (descent event); ANOPP (orange), BANORAC (blue).

**BANOERAC Event ID 120301 (Cruise)**

Flightpath:

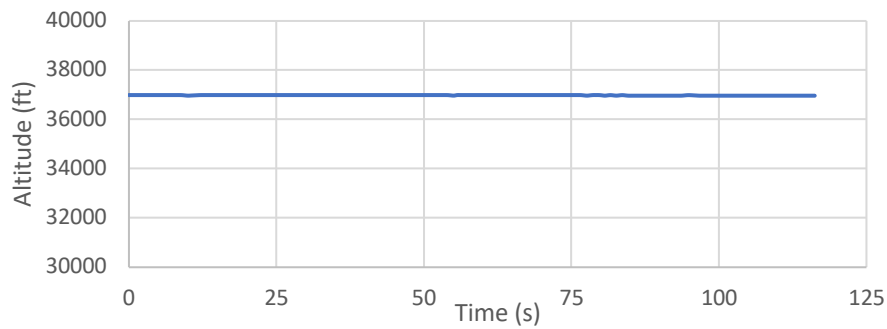


**Figure 32.** Time history of the aircraft altitude (cruise event). The aircraft travels 23.9 km horizontally over the event duration.

Ground monitor noise prediction:

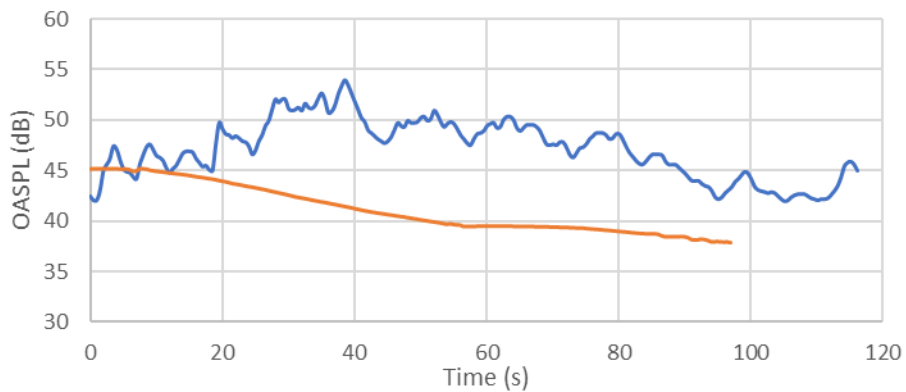


**Figure 33.** OASPL time histories for the ground microphone (cruise event); ANOPP (orange), BANORAC (blue).

**BANOERAC Event ID 30214 (Climb)**

Flightpath:

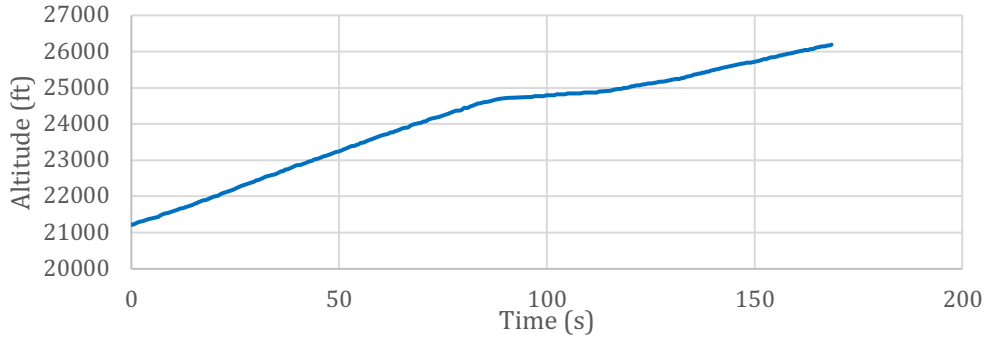


**Figure 34.** Time history of the aircraft altitude (climb event). The aircraft travels 34.0 km horizontally over the event duration.

Ground monitor noise prediction:

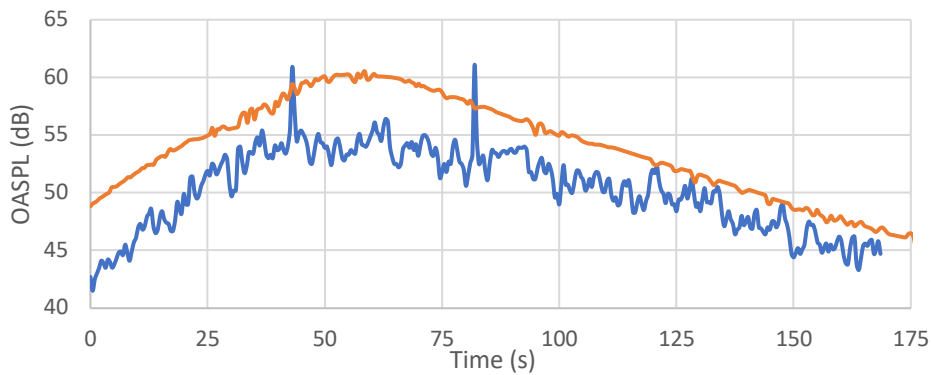


**Figure 35.** OASPL time histories for the ground microphone (climb event); ANOPP (orange), BANORAC (blue).

1/3 Octave band SPL:

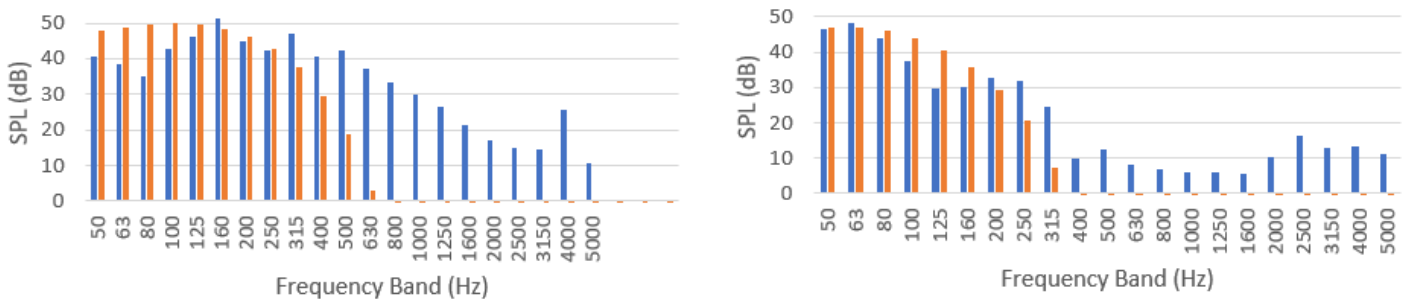


**Figure 36.** 1/3 octave SPL comparison between ANOPP (orange) and BANOERAC (blue).

Figure 36 shows a comparison of the ANOPP predictions for 1/3-octave spectra at two observer times. The predicted levels are confined to the lowest frequency bands as expected, since the propagation distance from the aircraft to the observer is very large. The levels at the higher frequencies are likely due to ambient noise unrelated to the aircraft.



## Part 2: Noise Source Spheres

### Research Approach

For each event, a source sphere was generated at the flight event time when the aircraft was closest to the ground monitor. These contours were generated with 58 observers. Both OASPL and 1/3 octave band SPL were extracted from the output. The noise sources in ANOPP, including core and bypass jet noise, fan noise, and airframe noise were considered separately to better understand the directivity and magnitudes of the summed source spheres.

### Summed Source Sphere: BANOERAC Event ID 30609 (Descent)

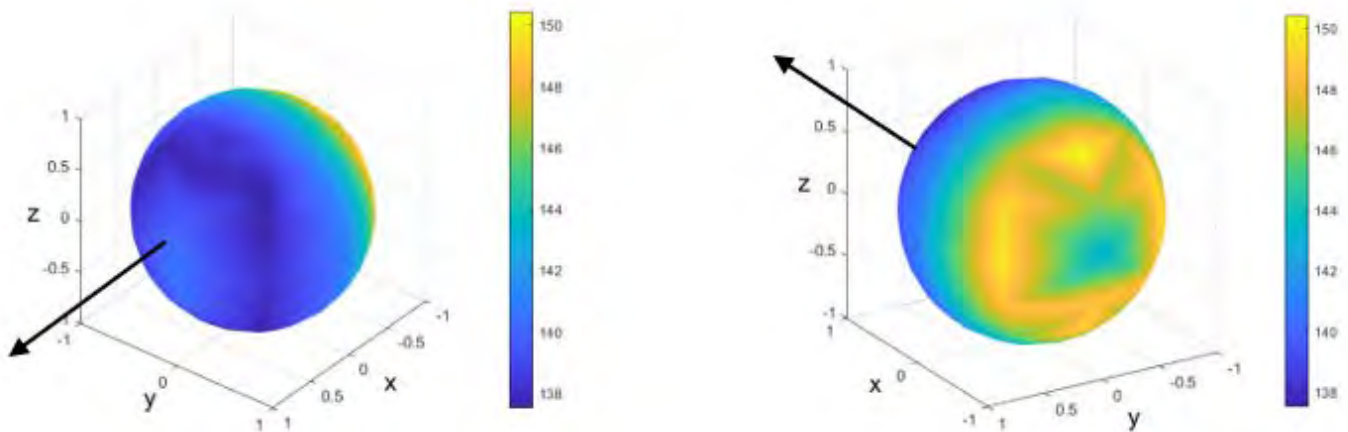


Figure 37. OASPL source sphere from front (left) and rear (right) of aircraft. Arrows indicate direction of flight.

### Component Source Spheres: BANOERAC Event ID 30214 (Climb)

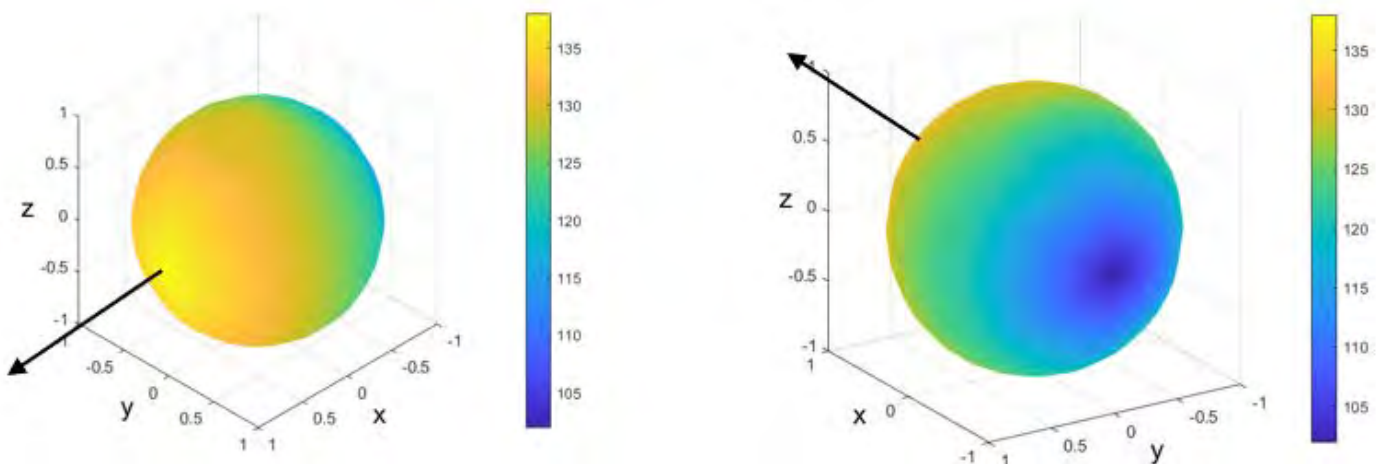


Figure 38. Airframe noise OASPL sphere from front (left) and rear (right) of aircraft. Arrows indicate direction of flight.

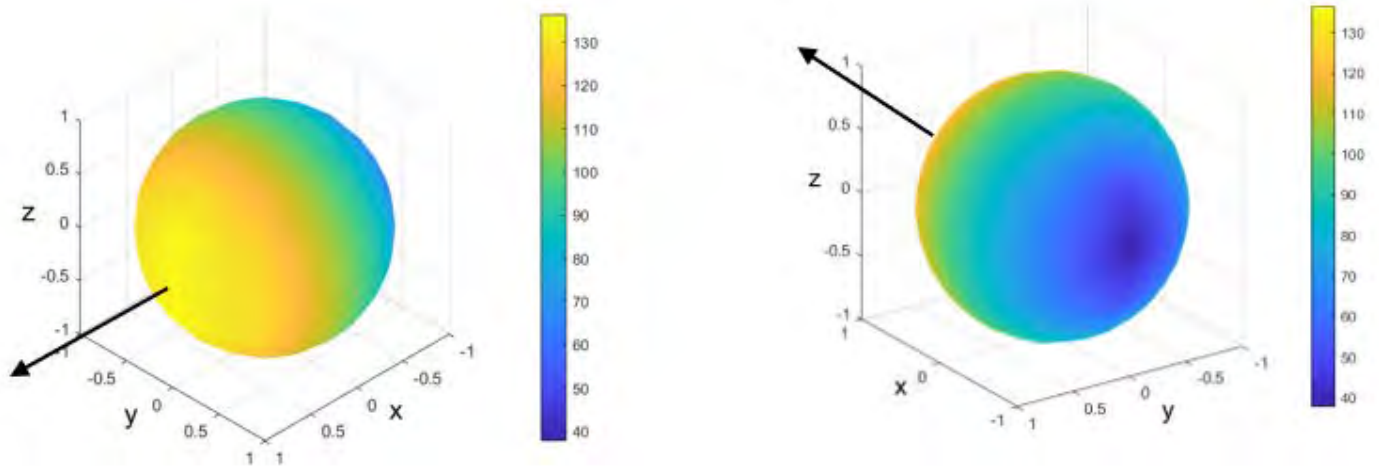


Figure 39. Fan noise OASPL sphere from front (left) and rear (right) of aircraft. Arrows indicate direction of flight.

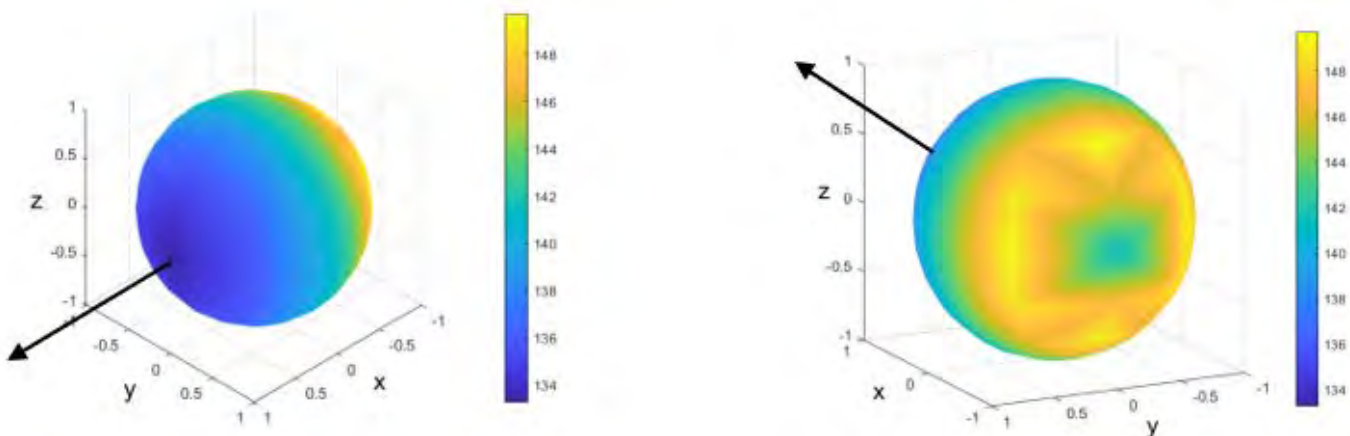


Figure 40. Core and bypass jet noise OASPL sphere from front (left) and rear (right) of aircraft. Arrows indicate direction of flight.

**Milestones**

Not applicable.

**Major Accomplishments**

Extraction and analysis of the flightpaths was a prerequisite to developing geometry modules for ANOPP input decks. The flightpath allowed for the generation of aircraft body Euler angles, ground speeds, and Mach number needed by ANOPP. The climb and descent rates were used to tabulate slat and flap deflections over the duration of the events. These input decks were used to give preliminary information about the propagation to the ground observer through a simple atmosphere with no ray-tracing algorithms.

In addition, the information on the OASPL and 1/3-octave levels were provided to Task 1 of the project for propagation calculations through a realistic atmosphere using two- and three-dimensional ray-tracing algorithms.

**Publications**

None

### **Outreach Efforts**

None

### **Awards**

None

### **Student Involvement**

Stephen Willoughby also has strongly contributed to this Task, initially as an undergraduate student and as a graduate research assistant during Fall 2020.

### **Plans for Next Period**

Penn State will continue to provide noise source spheres for selected BANOERAC cases. In addition, contributions to the source spheres from different aircraft noise sources will be evaluated to further assess their correctness and quality.

## **Task 3 – Validate the Noise Model Capabilities of AEDT by Comparing Numerical Results with Field Data and Quantify Uncertainties of Both Model Prediction and Measurement in Trying to Predict Aircraft Noise (or pattern of change) in Real World**

Purdue University

### **Objectives**

1. Analyze DISCOVER-AQ dataset.
2. Quantify the influence of various effects such as the Doppler effect and the ground effect on the propagation of en-route aircraft noise.

### **Background**

In 2013, NASA conducted a series of flight tests in Houston, Texas for the Deriving Information on Surface Conditions from Column and Vertically Resolved Observation to Air Quality (DISCOVER-AQ) campaign to support their research efforts for air quality studies. As part of this campaign, the FAA and the Department of Transportation's Volpe National Transportation Systems Center were involved with making acoustic measurements at various locations around the Houston metropolitan areas. The precise locations of the test aircraft were collected during the period of the acoustic measurements. The high-quality dataset also included meteorological data measured with a weather balloon and other monitoring equipment on the aircraft. The details of acoustic measurements and information on the dataset were reported in Boeker et al. [11].

In the previous study, the Purdue team summarized the influence of the Doppler effect on the propagation of aircraft noise. Additionally, the Purdue team identified two datasets with high signal-to-noise ratios after reviewing all the noise data recorded in the overall DISCOVER-AQ dataset, containing spiral down data and level flight data. These two datasets were used over the past year in the analysis of propagation effects.

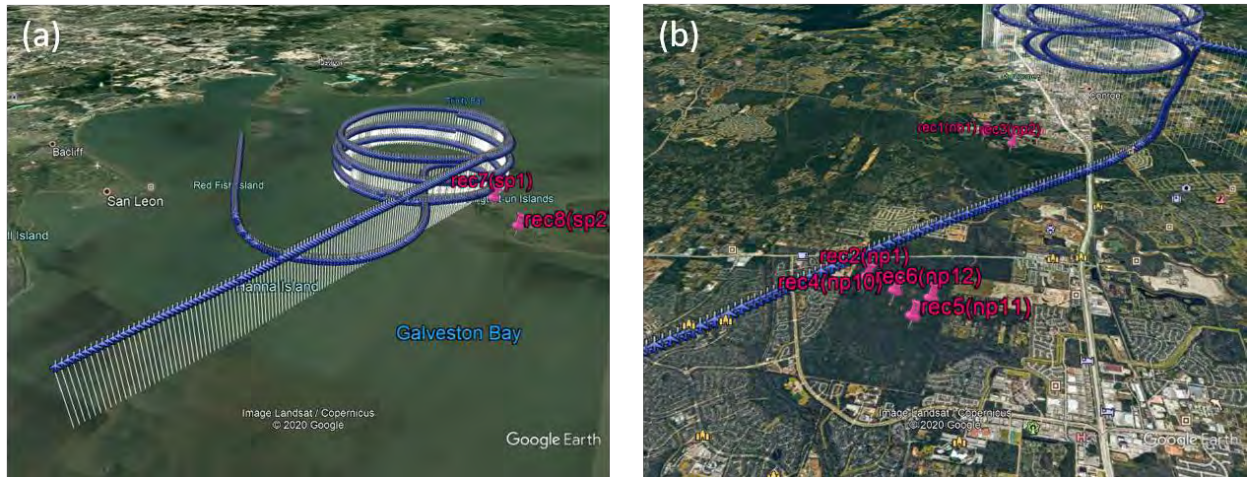


**Figure 41.** (a) Aircraft path in the spiral down dataset. (b) Aircraft path in the level flight dataset.

The typical aircraft path in spiral down events and level flight events are illustrated in Figure 41a and 41b, respectively. The spiral down dataset was recorded around Conroe, Texas when the aircraft was descending in a counterclockwise spiral pattern. The level flight data was recorded near Trinity Bay in the Houston area when aircraft were flying in a nearly straight path before entering a spiral up course.

Per a detailed consultation at the onset of the current project year, it was agreed that the Purdue team will continue to analyze the noise data obtainable from the DISCOVER-AQ dataset. More details of the study will be discussed in the following sections.

### Research Approach

To analyze the propagation effects, the aircraft path is split into a number of sub-sections in the first step. The spiral down loops and the level flight section are illustrated in Figure 42a and 42b, respectively. For spiral down events, the loops of the flight path are separated into two to four sub-sections. Each of the spiral loops is labeled as Loop 1 to Loop 4 in Figure 42a. A nearly straight section of 60 seconds is used for every event of the level flight data. The lengths of each sub-section in both spiral down events and level flight events are sufficiently long so that the truncation errors have minimum influences on the total measured sound exposure levels (SELs).

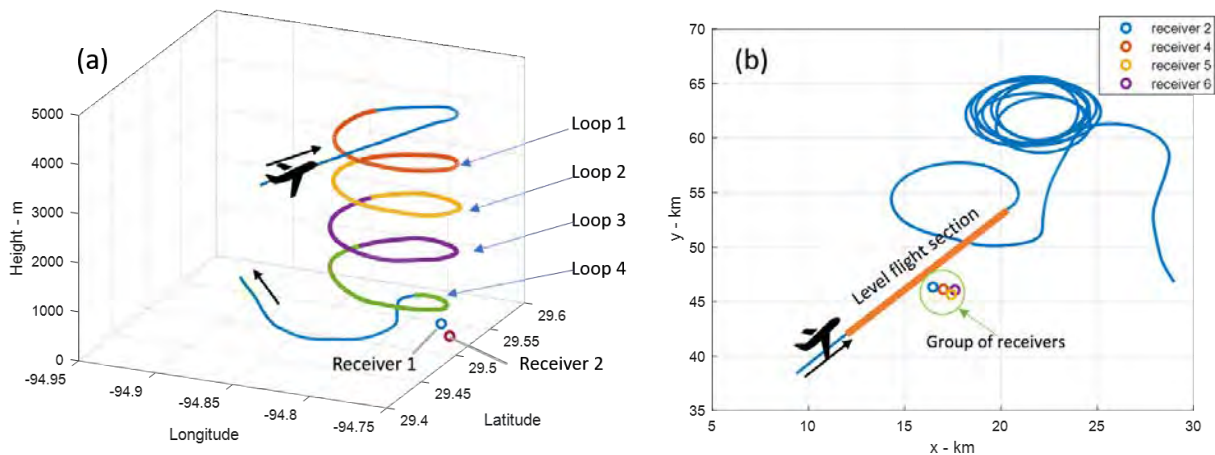


**Figure 42.** The geometry of (a) the spiral down loops and (b) the level flight section.

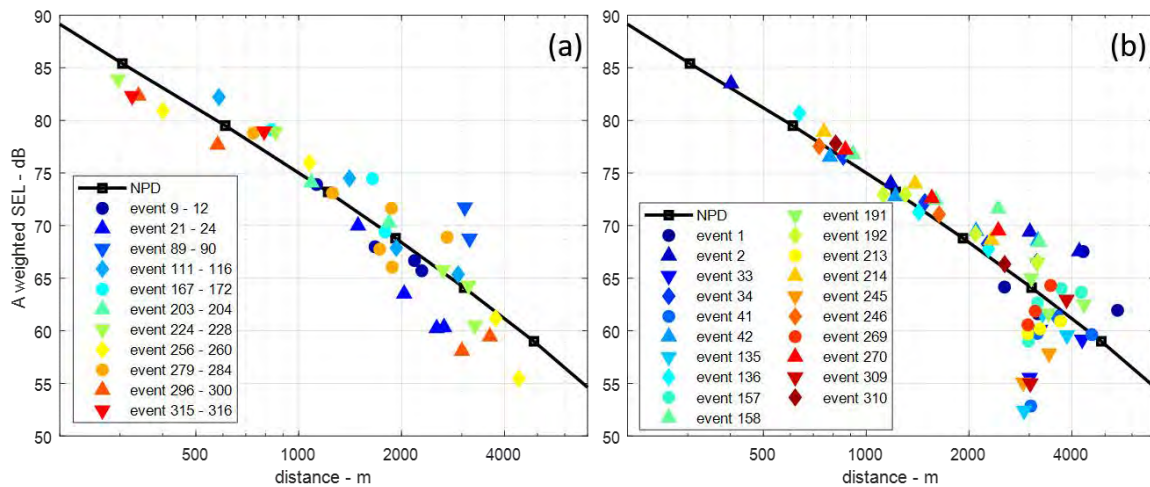


**Figure 43.** SEL measurement of (a) spiral down loops and (b) level flight versus NPD curve of P3C Orion at 20% power setting.

The measurement results in both datasets are first adjusted to the standard condition according to SAE-AIR-1845 [12] and compared with noise-power-distance (NPD) curve stored in the AEDT database for the P3C Orion aircraft. In both Figure 43a and 43b, the rate of change of the SEL against distance has good agreement to that of NPD predictions at short ranges. However, the disagreement becomes more apparent when the distance between the source and receiver is greater than 2000 m. The variance in the measured SEL is also larger when the distance between source and receiver is larger than 2000 m.

In our prior study, it was noted that the acoustic power emitted by the aircraft cannot be predicted accurately because of the complexity of the aeroacoustics problem and the available information on the power setting, source directivity, etc. of the test aircraft. It is necessary to use the method of subtraction in order to minimize any possible uncertainties caused by the variation in the acoustic power of the test aircraft during the flight tests. In essence, the method of subtraction is based on the subtraction of two simultaneously measured noise levels. By using this method, the dependency on the knowledge of the source acoustic power can be minimized. In other words, the SEL is not predicted directly at any single receiver location but the differences in SELs between two receiver locations are used instead. The method of subtraction is based on the analysis described as follows. Suppose the SEL at the  $i^{\text{th}}$  receiver is denoted by  $SEL(i)$ . It can be linked with attenuation due to the propagation effect by

$$SEL(i) = SEL_{source} - Att_{propagation}(i),$$

where,  $Att_{propagation}(i)$  is the attenuation at the  $i^{\text{th}}$  receiver due to a sum of all of the propagation effects during the transmission of noise from the test aircraft to the  $i^{\text{th}}$  receiver. For the same flight path and same test aircraft, the difference between the received SELs at two different receiver locations can be expressed as

$$\Delta SEL(i,j) = Att_{propagation}(i) - Att_{propagation}(j),$$

where  $\Delta SEL(i,j)$  is the difference of SEL levels between the  $i^{\text{th}}$  and the  $j^{\text{th}}$  receivers. It can be observed that  $\Delta SEL$  represents the pure propagation effect since the acoustic power of the source at the two receivers is assumed to be identical, which can be canceled out in the subtraction of the respective SELs.

Two slightly different strategies are used for spiral down events and level flight events. For the spiral down events, the flight path is divided into a number of different loops (usually four loops). Two receivers are available in the spiral down events. For each loop, an overall SEL can be calculated based on the measurements at each of the two receiver locations. Then subtraction is made between the two measured SELs to yield  $\Delta SEL$  for a particular pair of receivers. In fact, four  $\Delta SEL$  can be calculated and used for propagation analysis in the present dataset at Trinity Bay, Texas. There is only one level flight path

in each flight event in Conroe, Texas. However, more receivers are usually available in this dataset series. Typically, there are four receivers recording the noise levels of these fly-over events. Consequently, six  $\Delta SEL$  events can be calculated if four receivers are available (choose any two from a total of four receivers).

Using  $\Delta SEL$  in favor of SEL, the measured results can be compared with various prediction models described in Y. Wang and K.M. Li [13]. The prediction models have incorporated the divergence effect, air absorption factor, ground effect, and Doppler effect in the analysis. To facilitate the presentation of the comparison results, the difference between the measured and predicted  $\Delta SEL$  is used where

$$Error = \Delta SEL_{model} - \Delta SEL_{measurement},$$

and error (or absolute error) is plotted against the altitude (height) of the test aircraft in Figures 44 to 46.

**Spiral down data analysis**

The error in the AEDT model and theoretical model is first compared in Figure 44 for the spiral down events. The error for the calculated  $\Delta SEL$  is plotted against the height of each loop. It can be observed that the theoretical model has smaller error most of the time. The error of the AEDT model is good at lower heights but it is particularly worse in the height range between 1000 m and 2500 m.

The influences of different absorption models are compared and presented in Figure 45. Blue crosses represent the model that uses the atmospheric parameters (temperature, pressure, and relative humidity) at the mean aircraft height within a layer. Red crosses represent the model that uses a layered absorption model, which evaluates absorption in each 250 m layer separately. Figure 45 suggests that these two different models have less than 0.5 dB differences for all data points. Hence, it may be concluded that the use of a layer absorption model does not improve the accuracy for the simple model in which the mean aircraft height is used to represent the layer of 250 m thick.

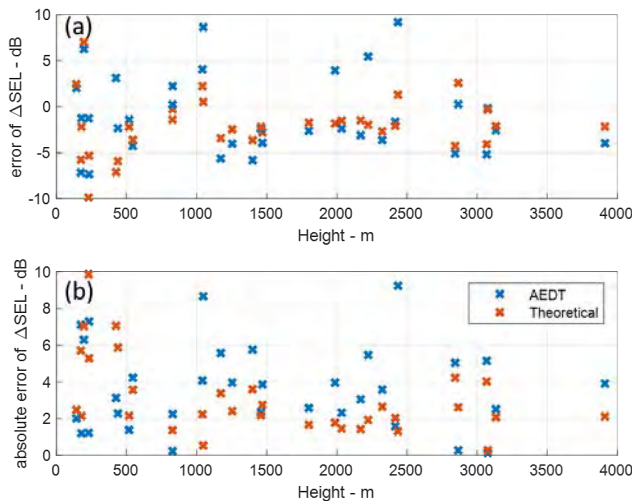


**Figure 44.** Comparison of the AEDT model’s error and the theoretical model’s error. (a) Error. (b) Absolute error.

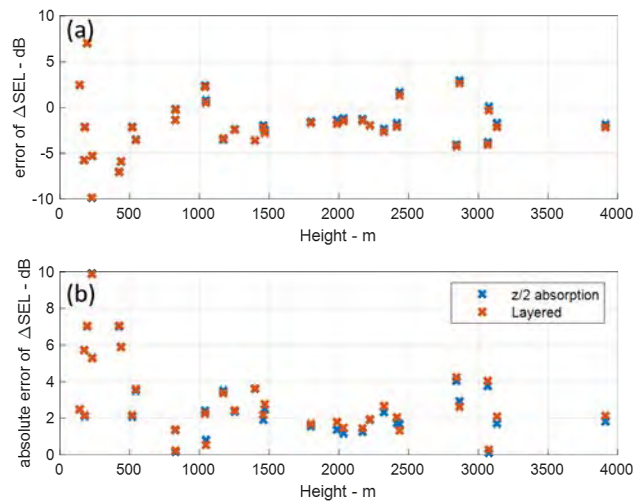


**Figure 45.** Comparison of the theoretical model's error with two different absorption models.

The influence of the Doppler effect is removed in the next comparison. The results are shown in Figures 46a and 46b with all other propagation effects (except the Doppler effect) kept in the model. Next, the influence of the ground effect is removed. The results are displayed in Figure 46c and 46d, with all other effects kept in this set of comparisons. The errors in these two groups of data have similar behaviors. The error in the theoretical model increases when either the Doppler effect or the ground effect is removed, especially at lower heights; at a high elevation, the influences of both the Doppler effect and the ground effect are negligible. The Doppler effect and the ground effect have the same impact on the propagation of aircraft noise in a comparable way as the spiral down events.

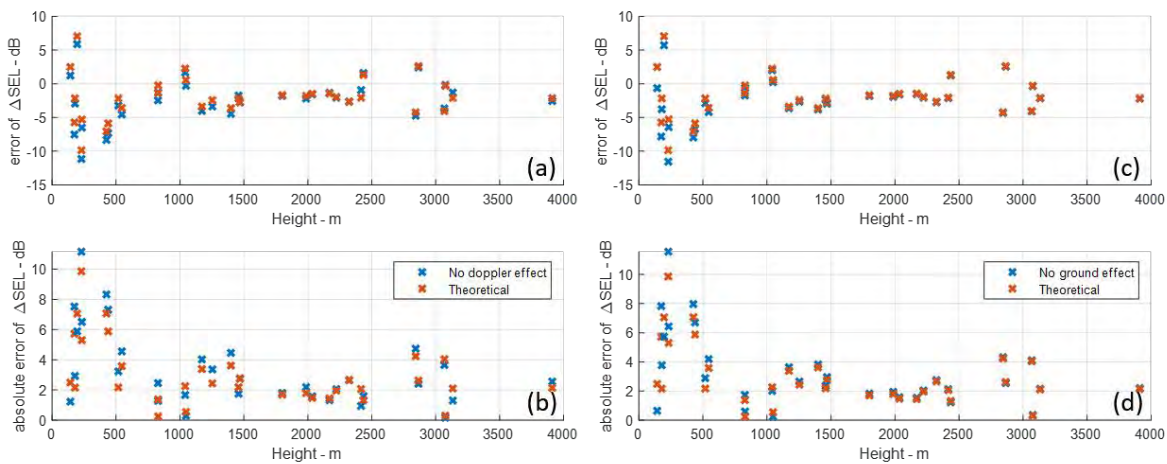


**Figure 46.** Comparison of the complete theoretical model's error and theoretical models without the Doppler effect (a,b) and without the ground effect (c,d).

The average errors of several models discussed above are then calculated and collected in Table 3. It can be observed that the AEDT has the largest error among all the models used in the present analysis. Removing the Doppler effect increases the error of the theoretical model by 0.3 dB. Removing the ground effect increases the error by 0.26 dB. Removing both the ground and Doppler effects increases the error by 0.66 dB. It should be noted that the Doppler effect changes the frequency of the received noise, which as a result changes the ground effect since the ground effect is frequency-dependent. Table 3 summarizes the difference of error in  $\Delta\text{SEL}$  for various models.



**Table 3. Average Error for Different Models**

	Error of $\Delta$ SEL [dB]
Theoretical	3.02
AEDT	3.69
No Doppler	3.32
No ground	3.28
No Doppler and no ground	3.68

**Level flight analysis**

Data regarding level flight events are analyzed in the same approach. However, they can be represented in a different way due to the wide range of available sideline distances in level flight events. Additionally, a simple propagation model of a divergence effect is used as reference where the attenuation can be expressed as  $20\log(1/d)$ , where  $d$  (meters) is the distance between source and receiver.

The error of AEDT is plotted in Figure 47a against  $d_1$  and  $d_2$ .  $\Delta$ SEL( $i, j$ ) is decided by two receivers,  $i$  and  $j$ . The  $d_1$  indicates the distance between the source to the closer receiver among the  $i^{\text{th}}$  and  $j^{\text{th}}$  receivers, and  $d_2$  indicates the distance between the source to the further receiver. In Figure 47b, the error of a simple divergence model is plotted as a reference. It can be observed that AEDT and the simple divergence model are both good at short distances. The error of both models increases as  $d_2$  increases; however, the error of the simple divergence law increases much quicker because of the lack of air absorption and other propagation effects. Comparing 47a with 47c, one can see that the error of the theoretical model is very similar to that predicted by AEDT. However, the predictions according to the theoretical model are marginally better than those predicted by AEDT at far ranges.

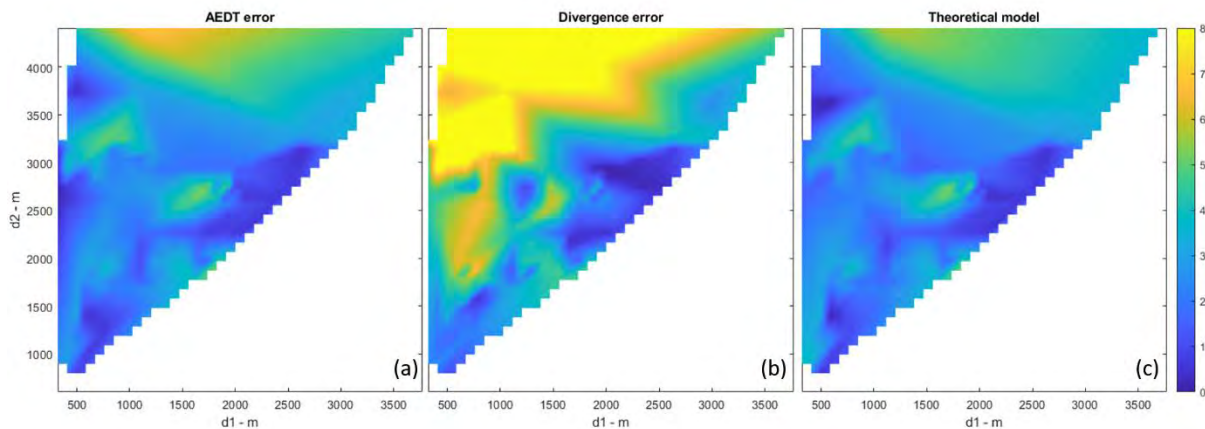


**Figure 47.** Error of (a) AEDT versus error of (b) a simple divergence law and (c) the theoretical model.

Next, the Doppler effect and the ground effect are removed from the theoretical model separately in Figure 48b and 48c. Comparing with the theoretical model, one can see the Doppler effect and the ground effect influence the total error in a very similar way. This is comparable with the results that have been discussed earlier for the spiral down events.

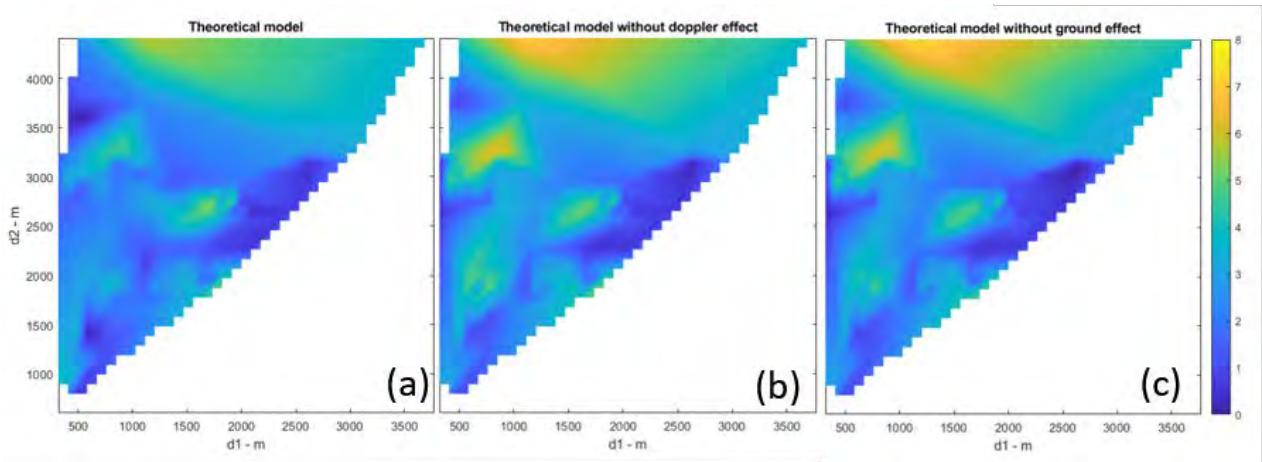


Figure 48. Error of theoretical models (b) without the Doppler effect and (c) without the ground effect.

### Conclusions

To analyze the influence of the Doppler effect and the ground effect, we analyzed the two datasets with high signal-to-noise ratios concerning spiral down events and level flight events. Through the use of the subtraction method, the influence of source power is removed, and the influence of various propagation effects can be analyzed via comparing  $\Delta SEL$  calculated with different propagation models. The comparison results have suggested that both the Doppler effect and the ground effect are crucial to the total attenuation during propagation. Both effects influence error of propagation in a very similar way for both spiral down and level flight events. Removing the Doppler effect and the ground effect increases the error of the propagation model in the region with small elevation angles (i.e., low source height cases in spiral down events and long sideline distance cases in level flight events). The Doppler effect is only subtly included in the NPD data in AEDT. When the speed of the aircraft is changed, there is no explicit mechanism to adjust the changes of the propagation effect caused by the Doppler effect directly. Similarly, AEDT assumes a uniform ground property (i.e., that the ground is hard), which is independent of ground properties and sound source spectra. Based on available theoretical propagation models, there is room for improvement for AEDT in modeling the two effects more accurately.

### Milestones

Yiming Wang has completed his PhD thesis entitled “Propagation of en route aircraft noise.” He has progressed to serve as a Postdoctoral Research Assistant.

### Major Accomplishments

Most of the Tasks and objectives have been completed; see earlier reports for the details of the Accomplishments. The project is due for completion by December 31, 2020.

### Outreach Efforts

None

### Awards

Yiming Wang has been awarded the INCE Best Graduate Student Award, 2018.

### Student Involvement

Jianxiong Feng has been involved partially on this project.

### Plans for Next Period

In the next few months, we plan to complete a final report for submission. We also plan to prepare a technical paper on the relevant topic for submission to a refereed journal for publication and possibly for a conference presentation of the findings.



## References

- [11] E. Boeker, J. Cumper, A. Rapoza, C. Cutler, N. Schulz, J. Rosenbaum, R. Samiljan, C. Roof, K. Shepherd, J. Klos, H. He, B. Harper, P. Nwokeji "DISCOVER-AQ Acoustics: Measurement and Data Report." U.S. Department of Transportation, 2015.
- [12] SAE, AIR1845. "Procedure for the Calculation of Airplane Noise in the Vicinity of Airports." (1986)
- [13] Y. Wang, and K.M. Li, 2018, December. Uncertainties due to Doppler's Shift on Aircraft Noise Prediction. In INTER-NOISE and NOISE-CON Congress and Conference Proceedings (Vol. 258, No. 5, pp. 2657-2669). Institute of Noise Control Engineering.



# Project 041 Identification of Noise Acceptance Onset for Noise Certification Standards of Supersonic Airplanes

## The Pennsylvania State University

### Project Lead Investigator

Victor W. Sparrow  
Director and United Technologies Corporation Professor of Acoustics  
Graduate Program in Acoustics  
The Pennsylvania State University  
201 Applied Science Bldg.  
University Park, PA 16802  
+1 (814) 865-6364  
vws1@psu.edu

### University Participants

#### The Pennsylvania State University (Penn State)

- PI: Vic Sparrow, United Technologies Corporation Professor and Director, Graduate Program in Acoustics
- FAA Award Number: 13-C-AJFE-PSU Amendment Nos. 45 and 60
- Period of Performance: March 29, 2019 to February 28, 2021
- Tasks:
  1. Obtaining confidence in signatures, assessing metrics sensitivity, and adjusting for reference day conditions.
  2. Assessing secondary sonic boom propagation.

#### Queensborough Community College, City University of New York

- Co-Investigator: Kimberly A. Riegel, subrecipient to The Pennsylvania State University (Penn State)

### Project Funding Level

This project supports the identification of noise acceptance onset for noise certification standards of supersonic airplanes through research conducted on multiple tasks at Penn State. The FAA funding to Penn State in 2019–2021 is \$390,000. Matching funds are expected to meet cost share on both Tasks. Boom Supersonic has pledged \$300,000 and Gulfstream has pledged \$100,000.

### Investigation Team

For 2019–2021, the investigation team includes:

- Victor W. Sparrow, PI (Tasks 1 and 2), The Pennsylvania State University
- Joshua Kapcsos, graduate research assistant (Task 1), The Pennsylvania State University
- Juliet Page, coinvestigator, subrecipient to Penn State, Volpe National Transportation Systems Center
- Kimberly A. Riegel, coinvestigator (Task 2), subrecipient to Penn State, Queensborough Community College, City University of New York
- Michael Rybalko, Joe Salamone, et al., Boom Supersonic [industrial partner]
- Brian Cook and Charles Etter, Gulfstream [industrial partner]

### Project Overview

FAA participation continues in International Civil Aviation Organization, Committee on Aviation Environmental Protection (ICAO CAEP) efforts to formulate a new civil supersonic aircraft sonic boom (noise) certification standard. This research investigates elements related to the potential approval of supersonic flight over land for low-boom aircraft. The efforts include investigating certification standards, assessing community noise impact, and developing methods to assess the

public acceptability of low-boom signatures. The proposed research will support NASA in the collaborative planning and execution of human response studies that gather the data to correlate human annoyance with low-level sonic boom noise. As the research progresses, this may involve the support of testing, data acquisition and analyses, field demonstrations, laboratory experiments, or theoretical studies; for example, see Maglieri et al. (2014).

## Task 1 – Obtaining Confidence in Signatures, Assessing Metrics Sensitivity, and Adjusting for Reference Day Conditions

The Pennsylvania State University

This task has transitioned into the new ASCENT Project 57. Please see the 2020 report for ASCENT Project 57, *Support for supersonic aircraft en-route noise efforts in ICAO CAEP*, which describes developments on this Task.

## Task 2 – Assessing Secondary Sonic Boom Propagation

The Pennsylvania State University  
Queensborough Community College, City University of New York

### Research Approach

#### **Background**

As both conventional “N-wave” (normal) boom and low-boom supersonic aircraft are getting closer to implementation, it is important to assess all aspects of the sonic boom noise that reaches the ground. This includes the need to more completely understand secondary sonic booms, when/why they occur, and the resulting signatures.

Most of the research done in the United States was completed in 1980 to understand the regular occurrence of secondary sonic booms observed along the New England coastline as a result of Concorde flights approaching New York. There are two main types of secondary sonic booms: Type I is the ground boom resulting from shock waves emanating off the top of the aircraft that refract downward for certain atmospheric conditions, and Type II is the boom that bounces off of the ground or water surface and is bent in the atmosphere to come back down to the ground a second time. In order to better predict the conditions that result in these secondary sonic booms, the variance in the atmospheric conditions, type of aircraft, and trajectory should be examined.

In the recent work for Project 41 in 2019, the original work of Rickley and Pierce [2] was recreated using the PCBoom [1] modeling software. The sound ray arrival locations, resulting from the PCBoom simulations, showed very good agreement with the original Rickley and Pierce arrival locations.

With the confidence that PCBoom is appropriately predicting the ray trajectories for secondary sonic booms, the work for this year was focused on predicting the arrival locations for a variety of atmospheric conditions and locations in the United states. The Climate Forecast System (CFS) v2 [3] was used to obtain weather conditions for different times and locations.

#### **East Coast Concorde Results**

In order to better understand the way that secondary booms behave for different seasons, the arrival locations were modeled covering several years for all twelve months with an average weather profile for each month. This allowed us to look for trends in the arrival of secondary sonic booms throughout the year to better understand when they would most likely be heard. In this simulation, the same trajectory for a New York City arrival of a Concorde was used. In addition, the Concorde pressure information built into PCBoom was used as the aircraft, as if Concorde were flying today. Meteorological data for the years 2012, 2014, 2016, and 2018 were obtained using the CFS v2 database. The profiles for February, a typical winter month, are shown for all four years in Figure 1. The profiles for July, a typical summer month, are shown for all four years in Figure 2. In these figures, the biggest difference between the summer and winter months is the high-altitude wind directions. Using these atmospheric profiles, the ray arrival locations for these years for February and July are shown in Figure 3 and Figure 4, respectively. It is clear from Figures 3 and 4 that in the winter months there are no secondary sonic boom arrivals, but in the summer months there are strong arrivals of both Type 1 and Type 2 secondary sonic booms. This is consistent across all four years that were simulated. Hence, one can conclude that these secondary sonic booms would be expected to occur every summer on an annual basis, if Concorde were still flying. The noise mitigation method used in the

late 1970s was to push the deceleration of Concorde from supersonic to subsonic out further from the coastline, and that method would still be expected to work today.

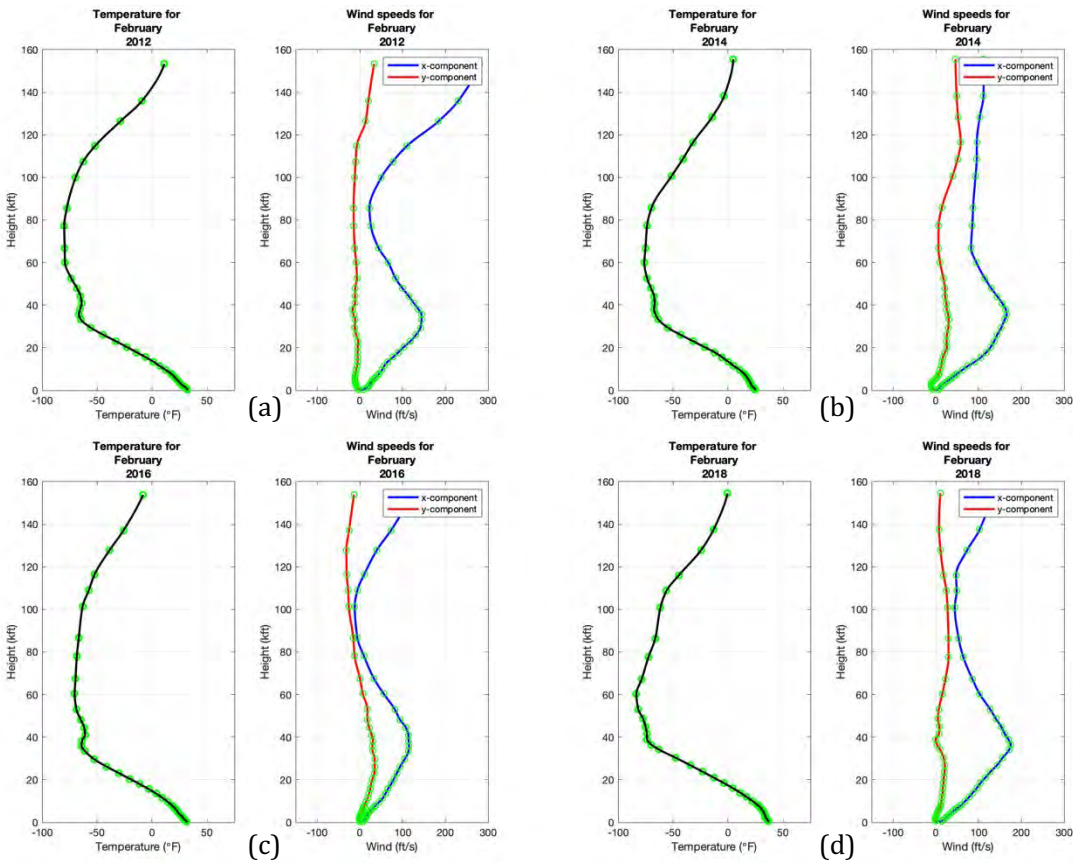


**Figure 1.** The monthly average temperature and wind speed profiles for February on the East Coast for (a) 2012, (b) 2014, (c) 2016, and (d) 2018.

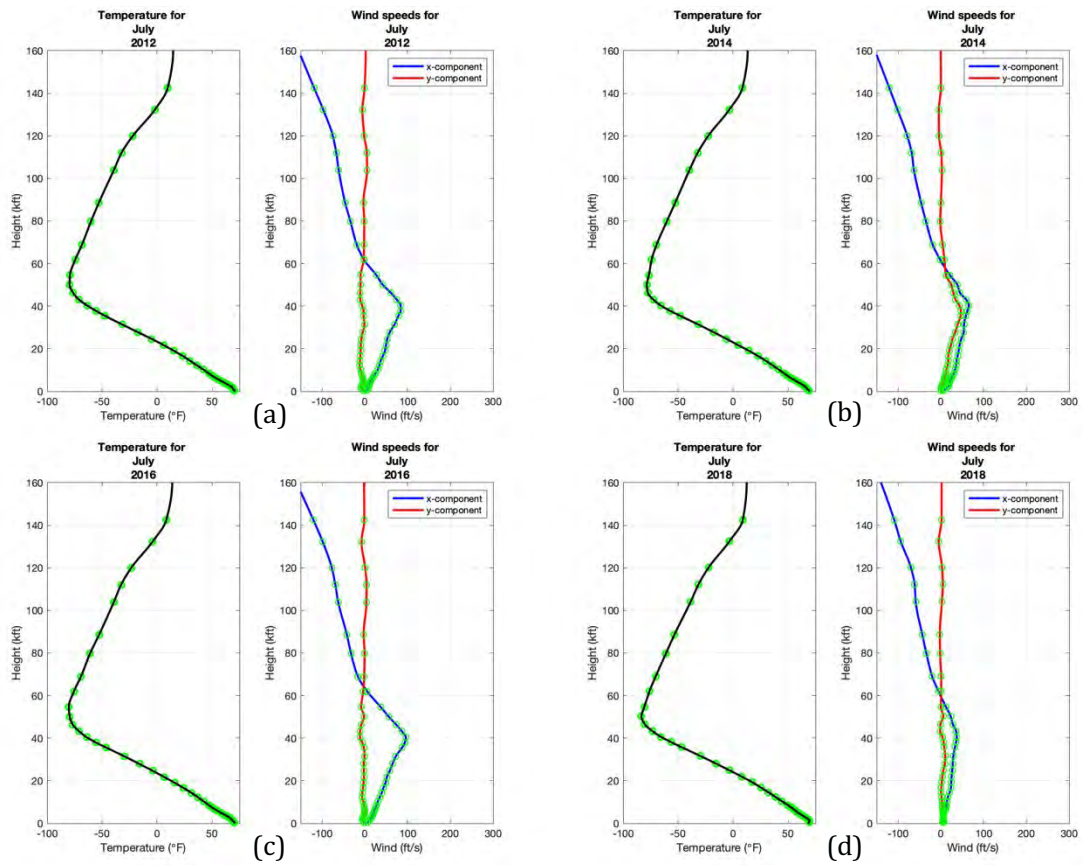


**Figure 2.** The monthly average temperature and wind speed profiles for July on the East Coast for (a) 2012, (b) 2014, (c) 2016, and (d) 2018.

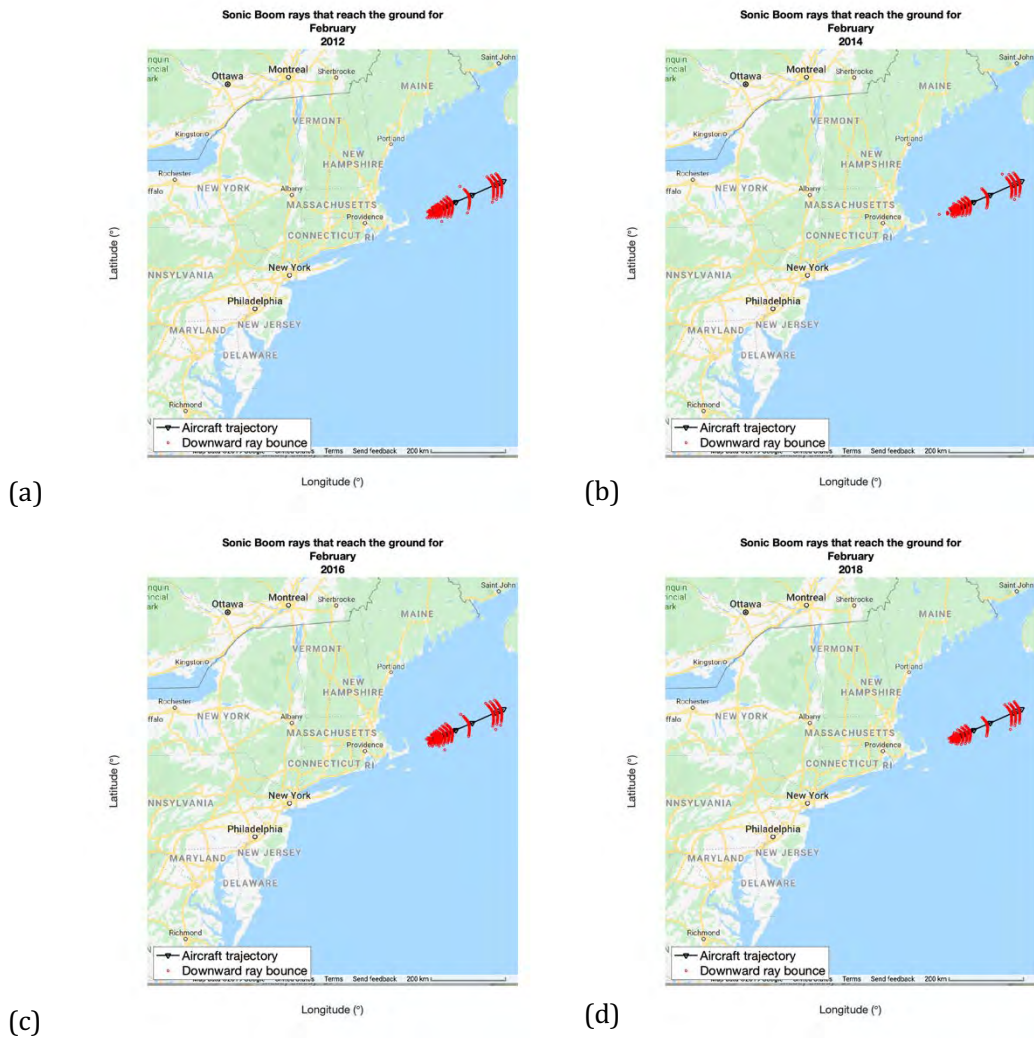


**Figure 3.** Ray arrival locations for a hypothetical Concorde aircraft approaching New York City for February in the years (a) 2012, (b) 2014, (c) 2016, and (d) 2018.

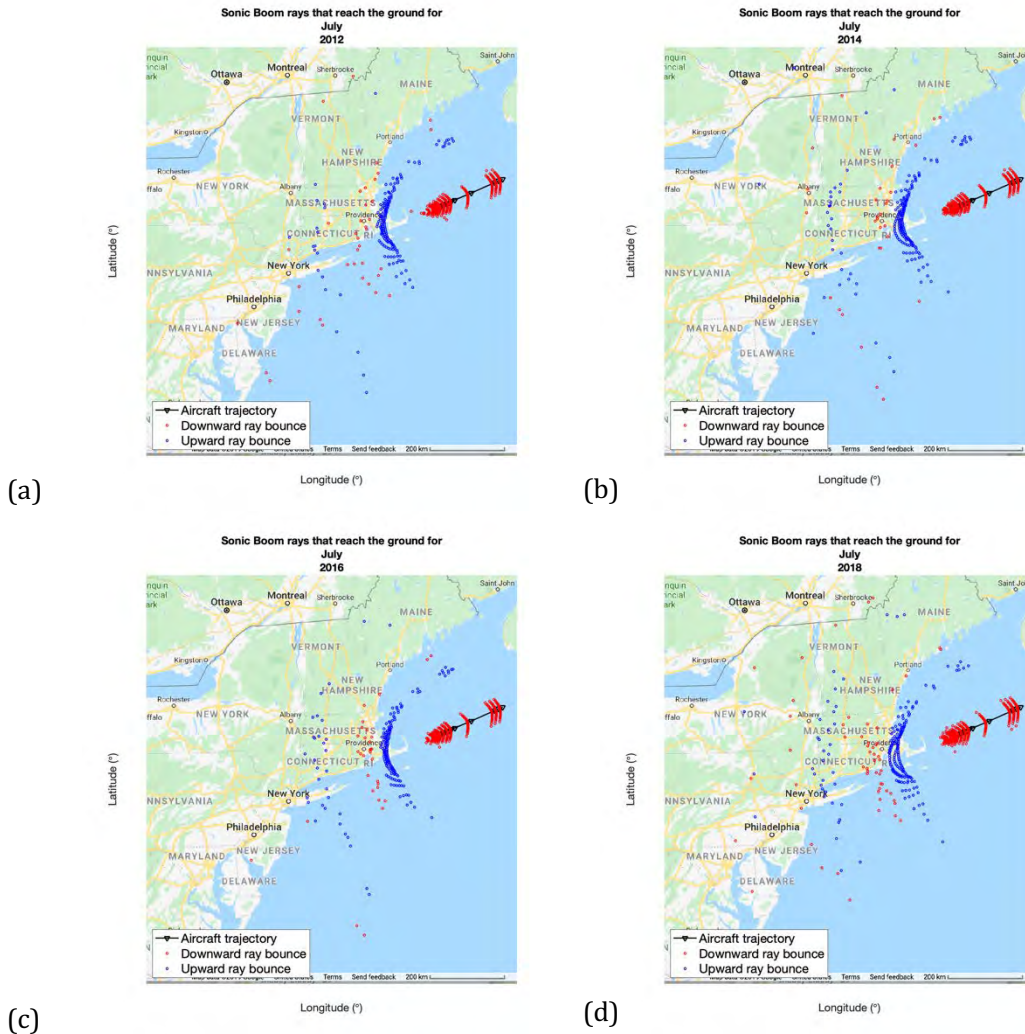


**Figure 4.** Ray arrival locations for a hypothetical Concorde aircraft approaching New York City for July in the years (a) 2012, (b) 2014, (c) 2016, and (d) 2018.

**West Coast Concorde Results**

The arrival locations of secondary sonic booms of a trajectory from a hypothetical Concorde approaching Los Angeles International Airport (LAX) from the south were modeled with PCBoom. Weather data for the West Coast was obtained from the CFS v2 for a location off the coast of LAX. This was used as the atmospheric conditions for PCBoom. Figure 5 shows the monthly average temperature and wind directions for February and July of 2018 for the West Coast. It should be noted that the wind directions are consistent with the East Coast in that during the summer months, there is a significant change in the wind between February and July where the winds come from the west during the winter and from the east during the summer. The trajectory as an approach to LAX was created using a similar speed profile (deceleration and waypoints) as for the East Coast study. The trajectory is shown in ray arrival plots in Figure 6. The consequence of the change in wind direction on the West Coast is that secondary booms impact the land during the winter months. While there are still secondary sonic booms that reach the Earth’s surface, they are all impacting the ocean, far from the land, during the summer months. One notices the trend that the secondary sonic booms would more likely impact the West Coast during the winter months, while the impacts would more likely be in the summer months for the East Coast.

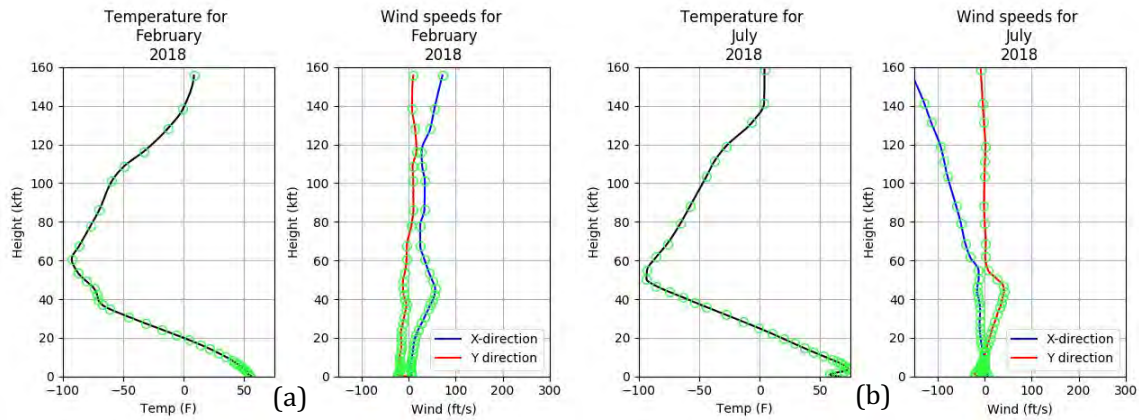


Figure 5. The monthly average temperature and wind speed profiles for (a) February and (b) July on the West Coast in 2018.

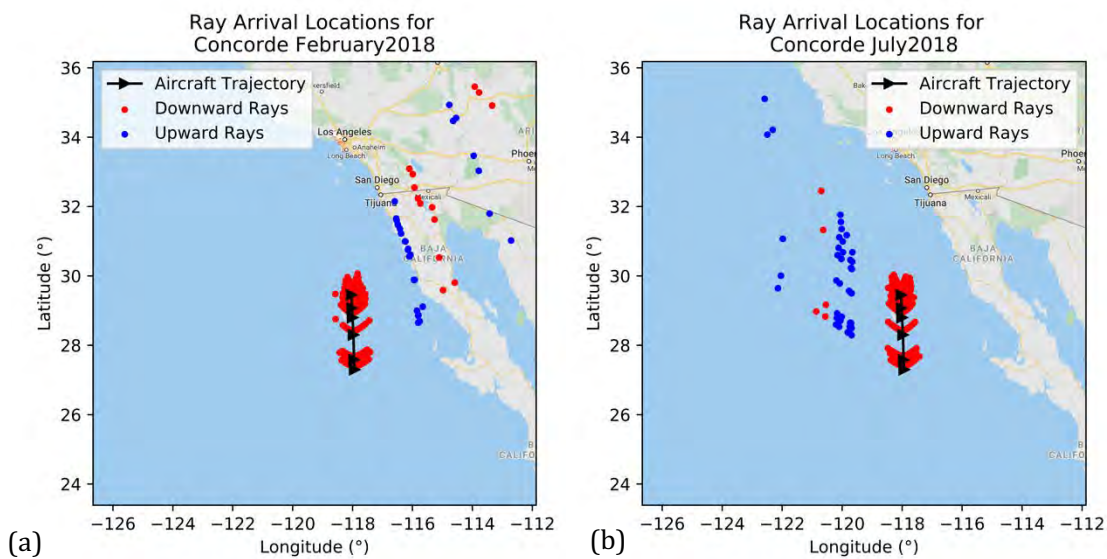


Figure 6. Ray arrival locations for a hypothetical Concorde aircraft approaching LAX for (a) February and (b) July in 2018.

### Boom Supersonics Cylinder Data

Looking at an aircraft other than Concorde, Boom Supersonics provided computational fluid dynamics (CFD) data for their XB-1 demonstrator aircraft to the team at Penn State and Queensborough. These data were adapted to create cylinder input data for PCBoom. The ray arrival locations were successfully run with the cylinder option on PCBoom. The ray arrival locations are shown in Figure 7 for the same trajectory and atmospheric conditions provided in the original Rickley and Pierce report. The ray arrival locations are similar to the arrival locations for the Concorde for the same conditions.



Ray Arrival Locations for  
XB1 July 1980

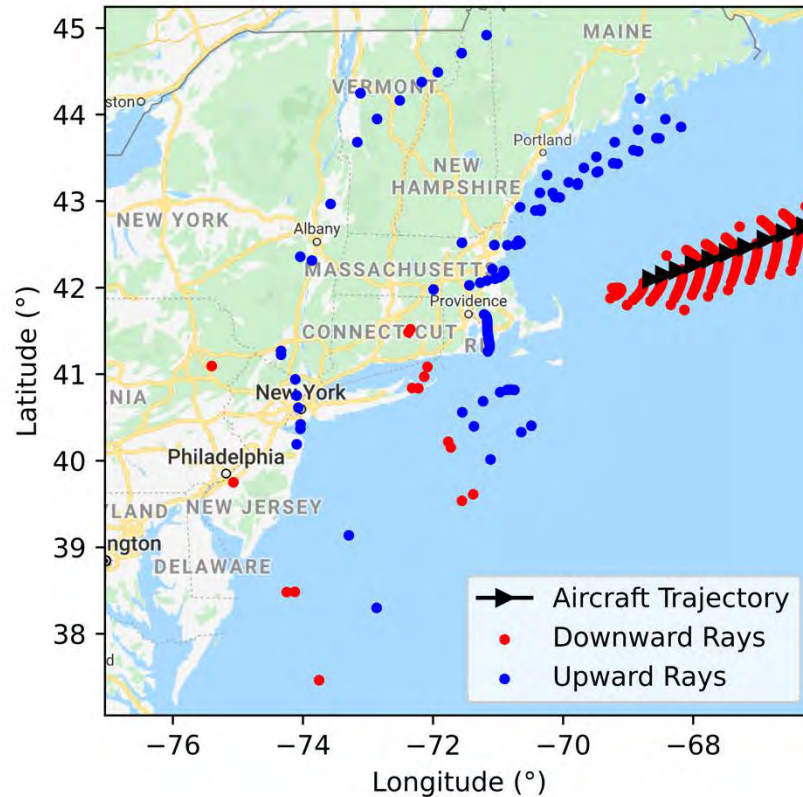


**Figure 7.** Predicted ray arrival locations for the XB-1 demonstrator aircraft approaching New York City, flying the original trajectory flown by Concorde, as documented in the Rickley and Pierce report.

**Comprehensive Literature Review**

In addition to the simulation subtasks, the project team also constructed a comprehensive literature review of known references related to the subject of secondary sonic boom. A summary paper, including 50 references, was presented at the December 2020 online meeting held by the European Acoustics Association. The original meeting was to take place in Lyon, France in April 2020, but it was delayed due to the Covid-19 pandemic and became the e-Forum Acusticum. The authors greatly appreciate the suggestions of colleagues acknowledged in the paper who provided feedback on initial drafts of the literature review to maximize the inclusion of all available references.

**Milestone**

The team successfully used Boom Supersonic CFD data, a requirement for in-kind cost sharing for Project 41.

**Major Accomplishments**

The team successfully demonstrated that secondary sonic booms are possible annually on both the United States' East and West Coasts and has shown that another aircraft produces ray arrival locations on the East Coast, similar to Concorde, if the same flight trajectory is flown. Furthermore, a comprehensive literature review on secondary sonic booms has been constructed and presented.

**Publications**

V. Sparrow and K. Riegel, "2020 literature review of secondary sonic boom," Written paper in Proc. 2020 e-Forum Acusticum (European Acoustics Association, Dec. 2020). This paper will be open-access, available online in 2021.



### **Outreach Efforts**

None

### **Awards**

None

### **Student Involvement**

None for Task 2.

### **Plans for Next Period**

The project team will investigate the pressure signatures at the ground for various aircraft to determine the pressure signatures on the ground. Changes to the current propagation models used in PCBoom for secondary sonic booms will need to be updated in order to accomplish this next step.

### **References**

- [1] Plotkin, K., Page, J., and Haering, E. (2007). Extension of PCBoom to over-the-top booms, ellipsoidal earth, and full 3-D ray tracing. AIAA 2007-3677, 13th AIAA/CEAS Aeroacoustics Conference
- [2] Rickley, E. and Pierce, A. (1980). Detection and assessment of secondary sonic booms in New England. FAA-AEE-80-22, accessible as ADA088160
- [3] Saha, S., et al. (2014). The NCEP Climate Forecast System Version 2. J. Climate, Vol. 27, 2185-2208, accessible as DOI: 10.1175/JCLI-D-12-00823.1



## Project 043 Noise-Power-Distance Re-Evaluation

### Georgia Institute of Technology

#### Project Lead Investigator

Dimitri Mavris (PI)  
Regents Professor  
School of Aerospace Engineering  
Georgia Institute of Technology  
Mail Stop 0150  
Atlanta, GA 30332-0150  
Phone: 404-894-1557  
Email: dimitri.mavris@ae.gatech.edu

#### University Participants

##### Georgia Institute of Technology

- PIs: Dr. Dimitri Mavris (PI), Mr. Christopher Perullo (Co-PI), Dr. Michelle Kirby (Co-PI)
- FAA Award Number: 13-C-AJFE-GIT-048
- Period of Performance: June 28, 2016 to February 4, 2022
- Tasks:
  1. Year 3 Task 1: Investigate the impact of frequency content on standard noise-power-distance (NPD) curves through a sensitivity study of weather effects in the Aviation Environmental Design Tool (AEDT).
  2. Year 3 Task 2: Investigate the impact of frequency content on NPD + configuration (NPD+C) data by utilizing NASA's Aircraft Noise Prediction Program (ANOPP) tool.
  3. Year 3 Task 3: Perform a validation with noise data in AEDT.
  4. Year 4 Task 1: Development and Testing of NPD+C Correction Function.
- Other Work Supporting Tasks: Development of AEDT Tester.

#### Project Funding Level

This project is funded at the following levels: Georgia Institute of Technology (\$200,000). \$200,000 in matching funds is based on in-kind contributions from a major airline. This total includes salaries for the project director, research engineers, and graduate research assistants and for computing, financial, and administrative support, including meeting arrangements. The institute has also agreed to provide tuition remission for students whose tuition is paid via state funds.

#### Investigation Team

- Dimitri Mavris, Principal Investigator, Georgia Institute of Technology
- Michelle Kirby, Co-Investigator, Georgia Institute of Technology
- Tejas Puranik, Research Faculty, Georgia Institute of Technology
- Yongchang Li, Research Faculty, Georgia Institute of Technology
- Mohammed Hassan, Research Faculty, Georgia Institute of Technology
- Christopher Perullo, Research Faculty, Georgia Institute of Technology
- Ameya Behere, graduate student, Georgia Institute of Technology
- Sarah Malak, graduate student, Georgia Institute of Technology
- Shilpa Ravoory, graduate student, Georgia Institute of Technology
- Wenxin Zhang, graduate student, Georgia Institute of Technology
- Alex Ostrow, graduate student, Georgia Institute of Technology
- Max Geissbuhler, graduate student, Georgia Institute of Technology



## Project Overview

The standard technique for evaluating fleet noise is to estimate flight procedure source noise using noise-power-distance (NPD) curves. Noise calculations within the Aviation Environmental Design Tool (AEDT) rely on NPD curves provided by aircraft manufacturers. This dataset reflects representative aircraft categories at set power levels and aircraft configurations. Noise levels are obtained as a function of slant distance via spherical spreading through a standard atmosphere, and other correction factors are applied to obtain the desired sound field metrics at the location of the receiver. The current NPD model does not consider the aircraft configuration (e.g., flap settings) or alternative flight procedures being implemented. These factors are important, as the noise characteristics of an aircraft depend on thrust, aircraft speed, and airframe configuration, among other contributing factors such as ambient conditions. The outcome of this research is an approach based on the suggested NPD + configuration (NPD+C) format, which will enable more accurate noise predictions due to its inclusion of aircraft configuration and speed changes.

This project is currently in its fourth year and finished up the third-year effort in the last calendar year. During the third year, this work focused on two main topics. First, prior work was extended to examine the impact of NPD spectral (frequency) content on noise contours. This first focus was divided into two aspects: 1) the manner in which the spectral data are used within AEDT while all other parameters are held constant, and 2) the manner in which the noise contours change when utilizing spectral data generated from the Environmental Design Space (EDS) in a fashion similar to that of the NPD+C approach. Second, the NPD+C approach will be validated using available aircraft operation and airport noise monitoring data. A brief description of the prior work is provided for reference.

## Year 3 Task 1– Investigate the Impact of Frequency Content on Standard NPD Curves

Georgia Institute of Technology

This task was completed in the previous year. Please refer to the 2019 Annual Report for this project for details.

## Year 3 Task 2 – Investigate the Impact of Frequency Content on NPD+C Data

Georgia Institute of Technology

### Objective(s)

This Task extends the work which was completed under Year 3 Task 1. Test cases from Year 3 Task 1 are re-executed using NPD+C data with spectral content to include configuration information (flight speed, flap setting, and gear setting). The AEDT sensitivity study will be repeated, and the results will be compared to those obtained using the standard NPD approach. Changes to the noise grid and contours will be analyzed to determine whether the increased complexity due to the inclusion of configuration-dependent spectral data is outweighed by the increased fidelity of community noise predictions for typical weather at the airport.

### Research Approach

The overall research approach can be summarized in the following steps:

1. Selection of aircraft and their ANOPP simulations to obtain NPD+C data.
2. Selection of airport and weather conditions for simulations.
3. Simulations in AEDT to obtain noise metrics for each combination of spectral condition and weather condition for all selected aircraft.
4. Comparison of noise grids and conclusions.

The first step involved in this Task was the selection of aircraft for consideration. While a large number of aircraft are available in AEDT, only a handful of them have been matched to calibrated models for ANOPP; therefore, the following aircraft were selected for this study: CRJ900ER, 737-700, 737-800, 767-300ER, and 777-200ER. Modeling efforts began with the 737-700, followed by the 767-300ER. The results from these two aircraft were sufficient to provide conclusions for this Task; hence, the other aircraft were not modeled.

Once the aircraft were selected, different configuration and speed settings were identified from the aircraft’s default STANDARD Arrival profile in AEDT. These settings were then used in ANOPP to obtain the spectral variation and NPD tables for both aircraft. The spectral datasets obtained for the 737-700 representing the one-third octave band spectrum are shown in Figure 1. The subplot on the left shows the raw spectral data visualized as the spectral correction in dB against frequency in Hz for each configuration and speed setting. The subplot on the right shows the difference of each ANOPP dataset to the AEDT baseline. The labels for the plots refer to the configuration and speed setting. For example, 133\_D\_F39 refers to a condition of 133 kts airspeed, landing gear extended or “down”, and flaps deployed to 39°. Such a condition would be present in the final approach of the aircraft, immediately preceding the touchdown.

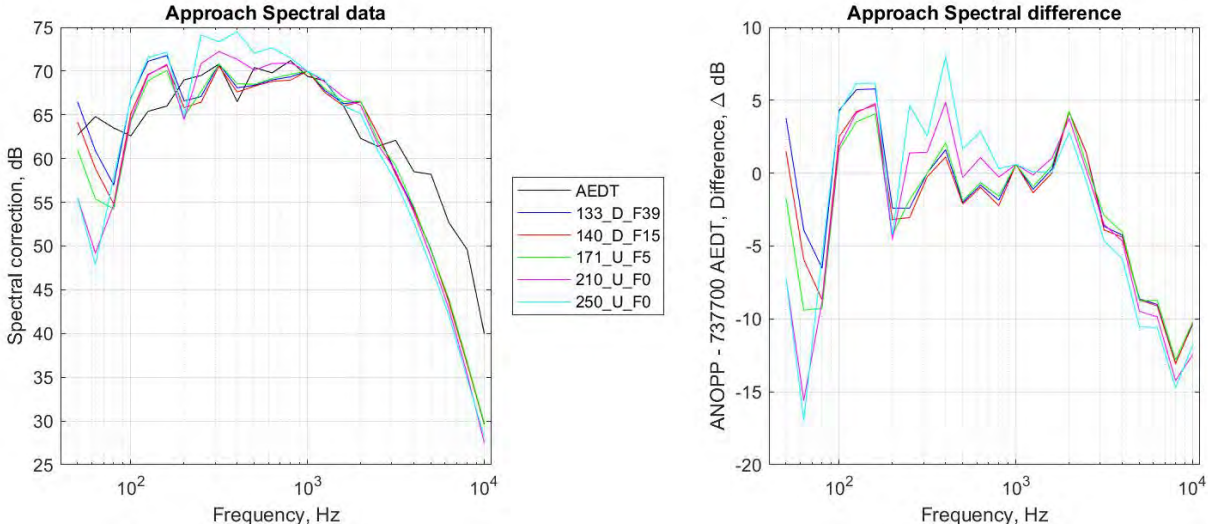


Figure 1. Comparison of spectral data obtained from ANOPP to AEDT baseline for 737-700.

The next step is to setup an AEDT study with the selected airport and the weather conditions. For this Task, Hartsfield-Jackson Atlanta International Airport (KATL) was selected along with 13 weather conditions as shown in Table 1. These weather conditions were selected based on historical weather trends. Additional information for the selection of these conditions is available in the 2019 Annual Report under Task 1.

Table 1. Weather conditions modeled at KATL airport

WEATHER CASE	JOB NUMBER	TEMPERATURE	SEA-LEVEL PRESSURE	STATION PRESSURE	DEW POINT, °F	RELATIVE HUMIDITY, %	WIND SPEED, kts
BASELINE	1	62	1018.02	980.61	50.86	67.65	7.03
TEMP	2	40	1018.02	980.61	30	67.65	7.03
	3	100	1018.02	980.61	87	67.65	7.03
HUMIDITY	4	62	1018.02	980.61	-40.03	1	7.03
	5	62	1018.02	980.61	20.44	20	7.03
	6	62	1018.02	980.61	37.4	40	7.03
	7	62	1018.02	980.61	47.96	60	7.03
	8	62	1018.02	980.61	55.76	80	7.03
	9	62	1018.02	980.61	62	100	7.03
WIND	10	62	1018.02	980.61	50.86	67.65	0
	11	62	1018.02	980.61	50.86	67.65	30
PRESSURE	12	62	985.56	950	50.86	67.65	7.03
	13	62	1141.17	1100	50.86	67.65	7.03

Using these weather definitions, one study in AEDT was created per configuration and speed setting. Each of these studies flew the identical operation for the selected aircraft, namely a fixed-point arrival profile on a straight ground track. If the selected aircraft contained procedural profile definitions, they were converted to fixed-point profiles with the help of performance reports. This step is important because it removes the effect of weather condition on the aircraft trajectory and performance characteristics, while retaining the effect of weather on the noise propagation and spectral correction. For each weather condition, four noise metrics were evaluated on an adequately sized sensor grid surrounding the airport. These four noise metrics were chosen because they represent a mix of both “maximum-level” type metrics and “time-integrated” metrics and are listed below.

1. Sound Exposure Level (SEL/S).
2. Maximum Perceived Noise Level with Tonal corrections (PNLTM/P).
3. Effective Perceived Noise Level (EPNL/E).
4. Maximum A-Weighted Sound Pressure Level (LMAX/L).

Thus, a total of  $6 \times 13 \times 4 = 312$  noise results were obtained. Each noise result consists of a 2D grid of sensors which record the dB level of the noise metric being modeled. Each noise grid was sized as  $251 \times 41 = 10,291$  points spaced 0.1 nmi in both directions. In order to effectively analyze such a large set of results, box plots were created to assess the sensitivities of the noise metrics to the spectral data at the various noise conditions.

One such result is shown in Figure 2. This figure makes use of box and whisker plots to condense a large amount of data from the noise reports into useful information. A boxplot is interpreted as follows;

1. The central point in each box denotes the median.
2. The top and bottom edges of the box indicate the 75<sup>th</sup> and 25<sup>th</sup> percentiles.
3. Each whisker extends to 2.7 times the standard deviation of the dataset.
4. All data points outside the whiskers are outliers and are showed as red crosses.

The values being plotted in this figure are the differences in noise dB values over an entire grid; therefore, each box plot represents 10,291 sensors at which this difference was calculated. The noise metric represented by each box plot is labeled on the x-axis as L, P, E, or S. Each collective group of four boxplots represents one weather condition.

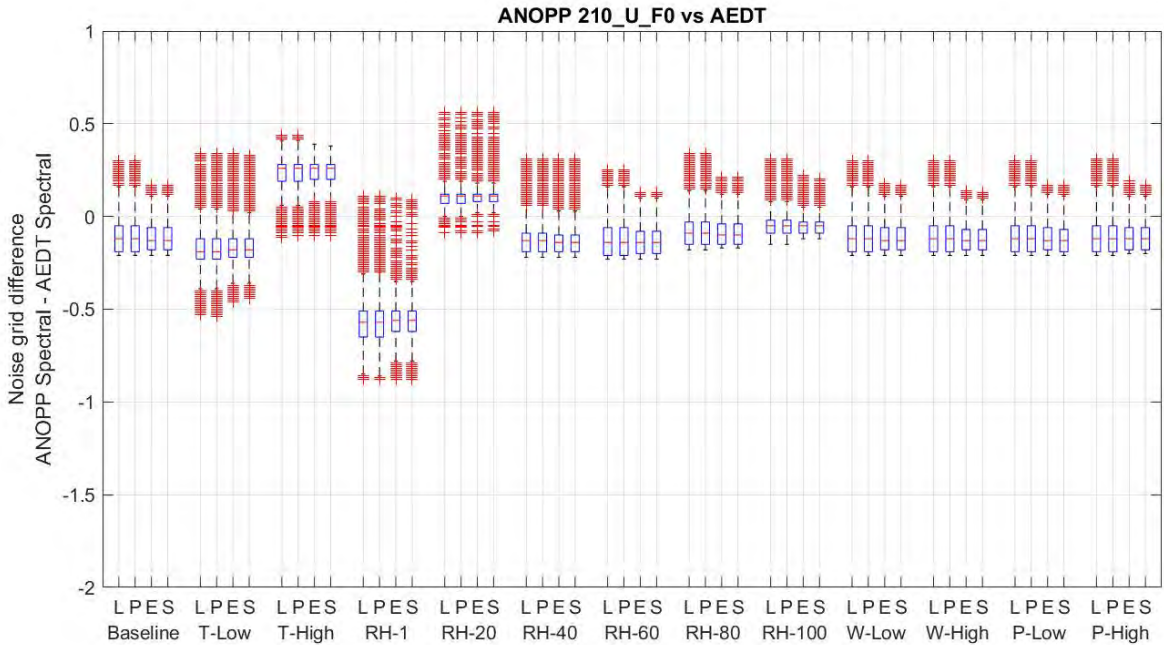


**Figure 2.** Comparison of noise grids obtained from ANOPP spectral data versus AEDT spectral data, for various weather conditions.

Based on the figure, it is observed that the differences in the noise metrics are very small across all noise metrics and weather conditions for the spectral condition of 210 kts, gear retracted, and flaps at 0°. Similar results were obtained for the other spectral conditions as well for both aircraft. Across all such plots, the RH-1 case was a consistent outlier. This represents a weather condition of 1% relative humidity. In order to further investigate these results, contour plots were made for all four noise metrics at this condition. This collection of contour plots is shown in Figure 3.

For each noise metric, contours are created at various appropriate dB levels. The solid lines represent results from ANOPP spectral, whereas the dashed lines represent results for AEDT spectral. In addition to the contour comparison, the difference in noise levels at each point in the grid is also shown as a heatmap. This visualization aids in the identification of exact regions where the noise level from ANOPP spectral is higher or lower than the AEDT spectral. It is observed that dB differences across the entire grid are limited to  $\pm 1$  dB, with most regions of the grid well below  $\pm 0.5$  dB. Additionally, it is also observed that for all four noise metrics, the contours from ANOPP and AEDT spectral are mostly concurrent with each other. Hence, it was observed that the introduction of spectral data from ANOPP did not appreciably change noise grids and contours.

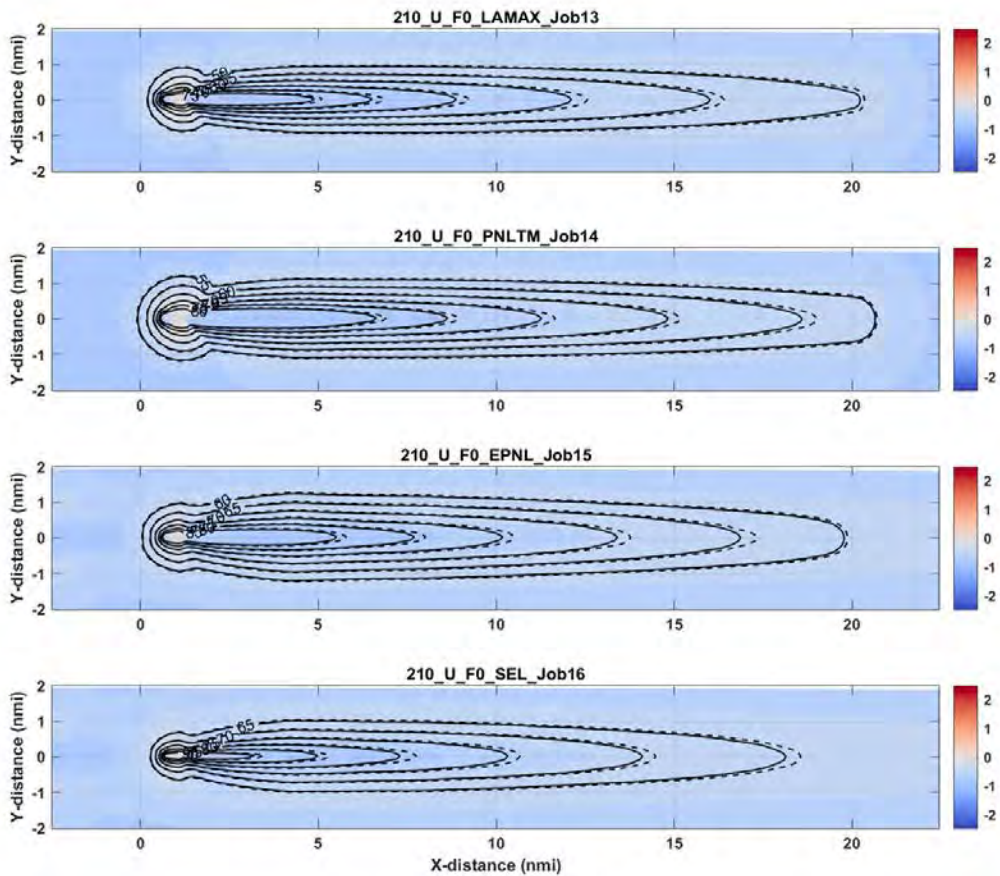


**Figure 3.** Noise contours comparing ANOPP and AEDT spectral datasets at the 1% relative humidity weather condition.

This observation was consistently present across all 312 noise results; therefore, it was concluded that the inclusion of additional spectral data from ANOPP did not appreciably change noise results when compared to the results for the baseline spectral data in AEDT. The increased complexity due to the inclusion of configuration-dependent spectral data was deemed to not have been outweighed by the increased fidelity of community noise predictions for typical weather at the airport; therefore, implementation of this configuration-dependent spectral data is not recommended.

**Milestone**

The objective of this Task was completed.

**Major Accomplishments**

It was found that configuration-dependent spectral data does not appreciably change noise results when compared to the use of baseline AEDT spectral data. As such, no further research is needed for this theme.

**Plans for Next Period**

This Task is now complete.

**Year 3 Task 3 – Validation of AEDT with Noise Data**

Georgia Institute of Technology

**Objectives**

The main objective of this Task was to validate AEDT noise calculations using data obtained from the real-world operations of a commercial airline and noise monitoring data from a partner airport. A secondary objective of this task which served as an enabler for the main objective was modeling real-world airline data (such as radar or flight operations quality assurance (FOQA)) in AEDT using fixed-point profiles in an automated manner.

**Research Approach**

The overall research approach for this Task is outlined in Figure 4. The process starts with a mapping of airline FOQA data to the noise monitoring data obtained from San Francisco International Airport (SFO) airport. Once this mapping is available, FOQA operations are then modeled in AEDT as fixed-point profiles, flown on user-defined ground tracks. Noise metrics for these operations are then obtained from AEDT at sensor locations which are mapped to the noise monitoring program data at SFO. Finally, the obtained noise metrics can be compared at these noise sensor locations to assess the validity of AEDT models.

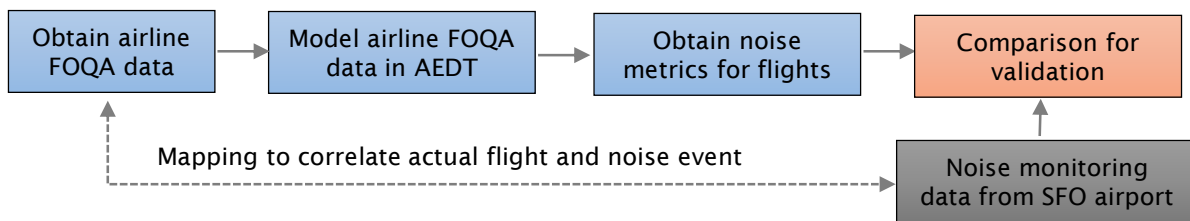


Figure 4. Outline of AEDT noise validation Task.

The real-world validation data sources for this task are FOQA and the SFO noise monitoring program. The FOQA data contains detailed tabulated information obtained from aircraft flight recorders. For each flight, about 600 parameters are available, recorded once per second. Some of the parameters important for this task are height above takeoff/touchdown, airspeeds and groundspeed, geo-location (latitude, longitude), configuration (flaps, slats, landing gear, spoilers), gross weight, and thrust levels. The availability of thrust and weight data is especially important as both are required for the creation of fixed-point profiles in AEDT.

There are several potential sources of difference between AEDT and real-world observations of noise metrics. The use of fixed-point profiles in conjunction with custom ground tracks eliminates the difference associated with aircraft position. Another source of difference is the NPD lookup table which models the noise produced by the aircraft at different speeds and configurations. This was addressed in this task with the use of mode-based NPD lookups in AEDT. Mode-based NPD modeling instructs AEDT to make use of specific NPD sets, instead of a typical lookup based on the aircraft thrust. This allows the user to define multiple NPD sets and associate them with each segment of a fixed-point profile, thereby increasing accuracy of the computed noise metrics. These multiple NPD sets are obtained from ANOPP for each aircraft type under consideration.

In order to effectively perform this Task, many processes had to be automated. This was done primarily through SQL scripts which work on the AEDT backend databases to create studies much faster than through the graphical user interface (GUI).

Additional programming scripts were written to create fixed-point profiles and user defined ground tracks from FOQA datasets.

A dashboard was created in Tableau in order to visualize the large number of flights that were available for modeling, A sample screen from the dashboard, depicting noise sensor locations, flight trajectories, and ground tracks, is shown in Figure 5. This effort was shifted to ASCENT Project 62 in 2020.

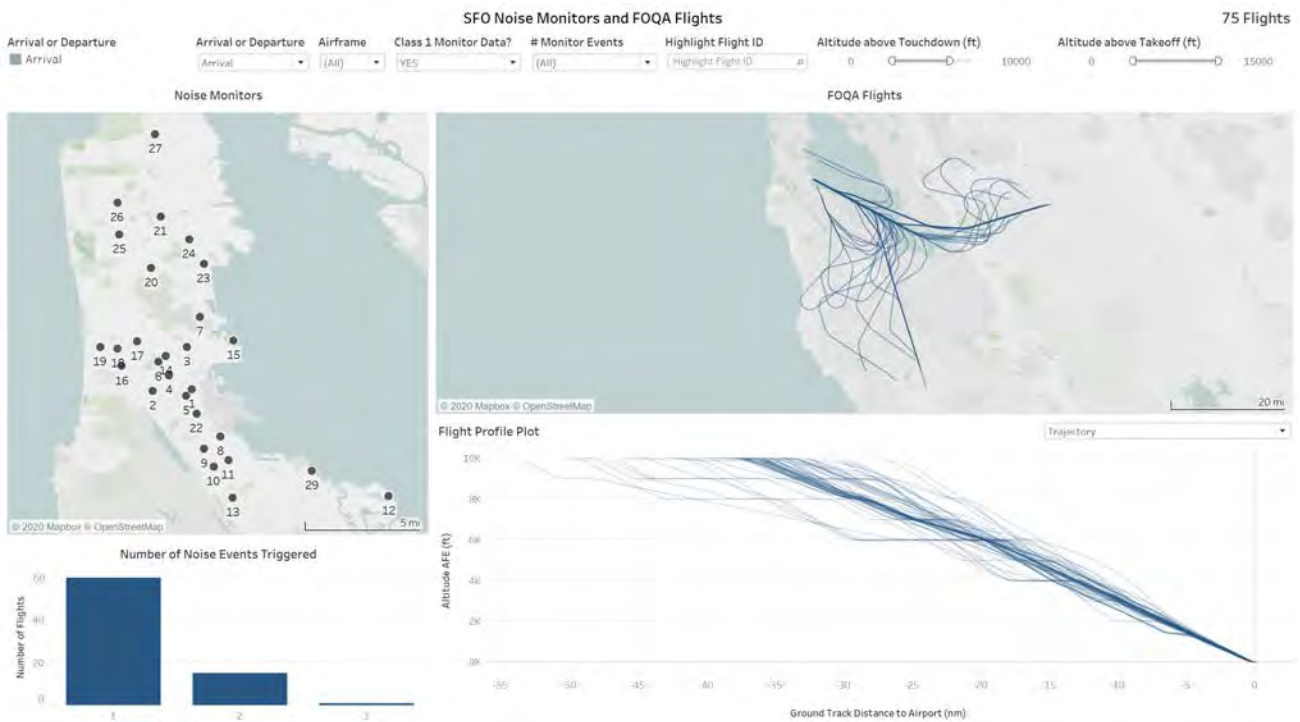


Figure 5. Dashboard created for flight visualization.

### Milestone

A process for the validation of noise models based on the component trajectories, weather, ground track, and NPD data was created and implemented for an initial set of flights.

### Major Accomplishments

A dashboard was created to visualize noise modeling validation efforts at SFO.

### Plans for Next Period

This Task has been migrated to ASCENT Project 62.

## Year 4 Task 1 – NPD+C Correction Function

Georgia Institute of Technology

### Objectives

The objective of this Task is to create a correction function which will serve to correct an aircraft class' baseline NPD to match a given flight configuration, incorporating flight speed, flap deflection angle, and gear setting.

## Research Approach

### Overview

Fitting the NPD correction function involved four primary steps. The first was the aircraft class definition, in which the bypass ratios, overall pressure ratios, and rated thrusts were collected for a given aircraft class. Next, these values were used to create a series of engine variants for the aircraft class and were evaluated using the Environmental Design Space (EDS) software to generate engine state tables for use in ANOPP. Following this, ANOPP was used to produce a series of configuration and engine-specific NPDs. The final step of this process was to fit a model to this data, so that the difference between a given configuration and a baseline condition could be predicted. This process is shown in the left column of Figure 6.

### Class Definition

The first phase of the correction function modeling process involved defining the scope of the model; specifically, selecting the aircraft and corresponding engines from AEDT for which the model would be based on. A baseline engine was also selected to match the baseline aircraft represented in the ANOPP model. Once this list had been compiled, the engine bypass ratio (BPR), overall pressure ratio (OPR), and sea-level static (SLS) thrust values were collected from AEDT. With this information, the minimum, maximum, and mean values for each parameter could be found, and a full factorial design of experiments (DoE) could be created. This DoE would consist of 27 cases (three BPR values \* three OPR values \* three thrust values). A 28<sup>th</sup> case would also be added to account for the baseline engine settings.

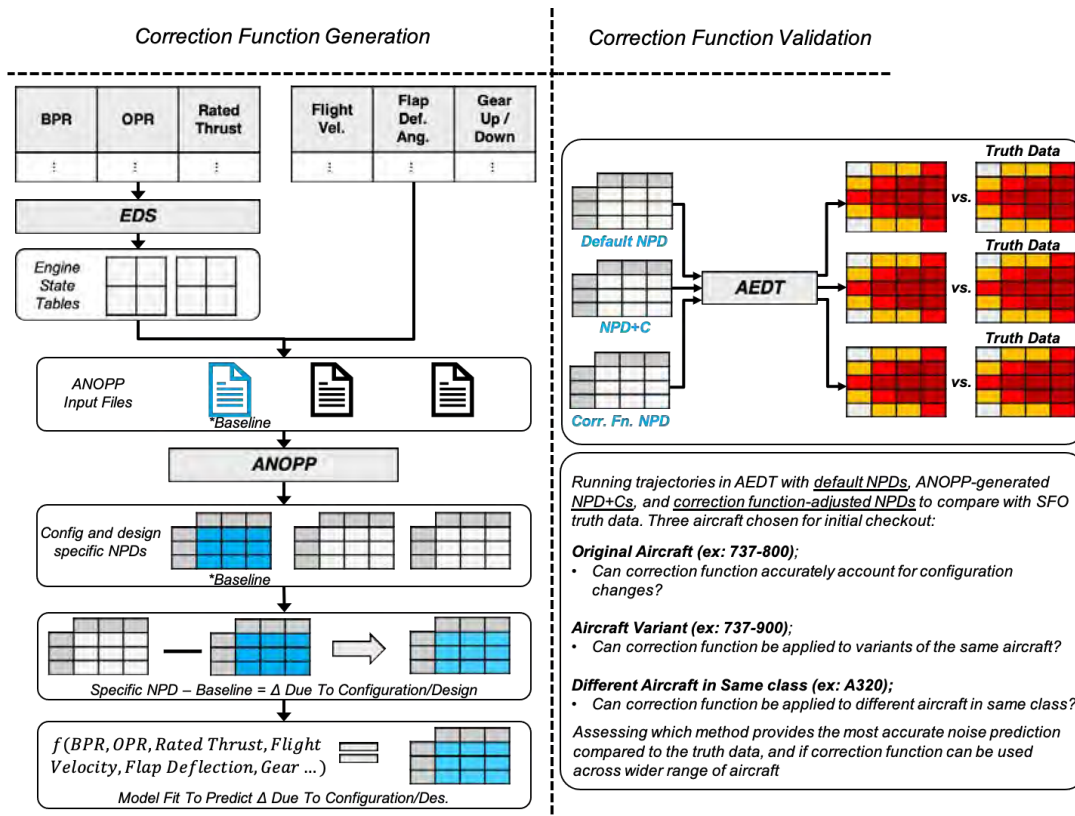


Figure 6. Correction function process.

### Environmental Design Space (EDS) Simulations

The next phase of the correction function modeling process involved creating the engine variants to model in EDS. This was done by modifying the baseline EDS engine input of the same class by adjusting the values of the SLS thrust, takeoff thrust, top-of-climb thrust, fan pressure ratio, low-pressure compressor pressure ratio, and high-pressure compressor pressure ratio. Once the values were modified, to match the engine settings from the DoE, the simulation was initiated, and the

resulting outputs were compiled. These results were then post-processed to extract the specific engine and thrust information needed for use in ANOPP.

**ANOPP Simulations**

Next, the post-processed EDS data was used to modify aircraft input files for use in ANOPP to generate NPD curves. This consisted of running a given aircraft model with each engine variant at several different flap, speed, and gear settings to generate a full sweep of the configurations that the model would be applied to. Once the ANOPP simulation was completed, the outputs were compiled and transferred to the statistical software package JMP.

**Model Fit**

The final phase of the correction function modeling process involved creating models within JMP. For a given aircraft class, two models were fit—one with gear down, and one with gear up. The model was fit to the difference between configuration-specific NPDs and the baseline NPD (both coming from the set of ANOPP cases) at the thrust settings corresponding to approach. With this prediction formula, a default NPD could be adjusted to represent different flap, gear, and speed configurations.

**150pax Model Fit**

When determining the simulation cases to use in creating the correction function, it was found that both the engine parameters and approach NPD for the 100pax model (represented in ANOPP as a 737-700) were close to those of the 150pax model (represented in ANOPP as a 737-800). As such, it was decided to fit a model for both classes simultaneously. Engine variants for the Boeing 737-700/800/900 and the Airbus A318/319/320 were obtained from the equipment database in AEDT, and the minimum and maximum values were found. This domain is shown in Figure 7.

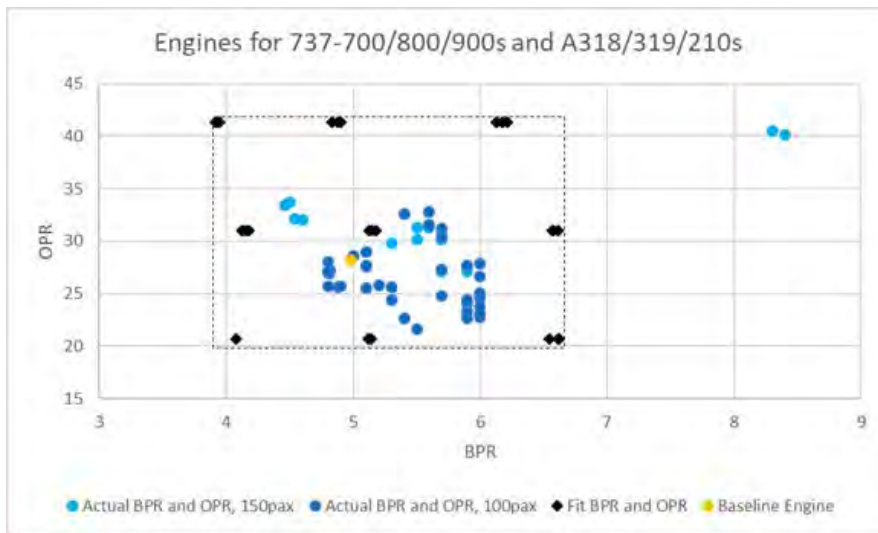


**Figure 7.** 150pax correction function domain.

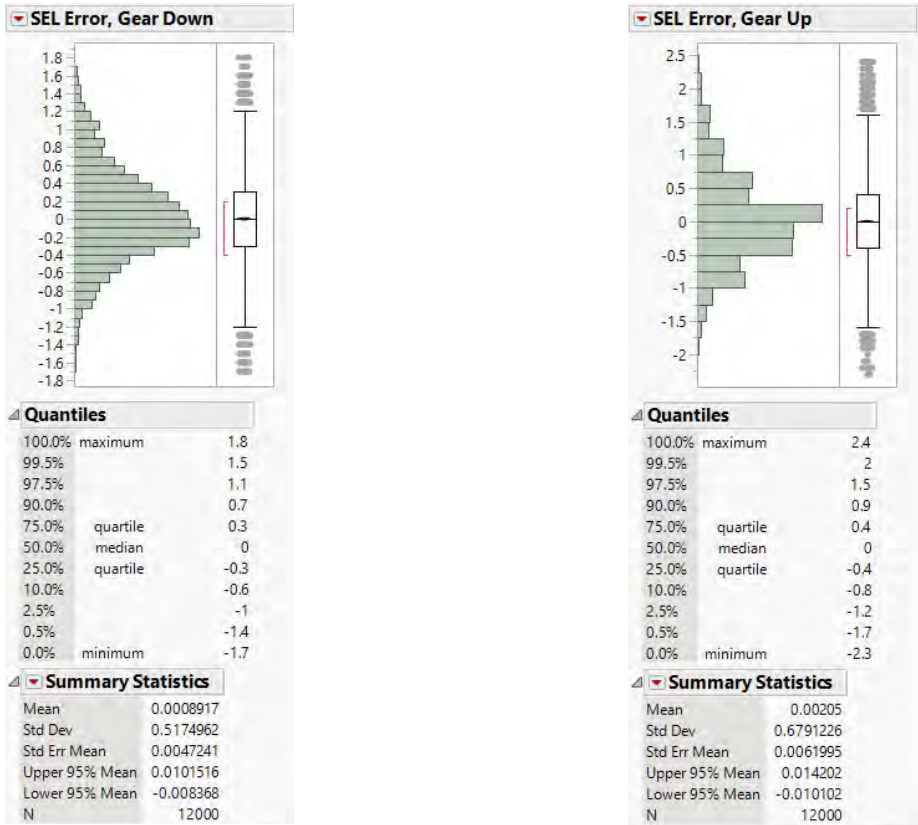
Figure 7 shows that the correction function for the 150pax class would be usable for bypass ratios ranging from slightly less than 4 to 6.75, and overall pressure ratios ranging from 20 to 42. To capture all of the relevant rated thrust values, the model was fit using SLS thrust values ranging between 25,350 lbs and 28,400 lbs.

Next, the engines representing the minimum, mean, and maximum OPR, BPR, and rated thrust values were simulated using EDS, and the results postprocessed for use in ANOPP simulations. ANOPP was used to generate the baseline NPD for this aircraft (at a setting of 160 kts, 15° flaps, and gear down) and configuration specific NPDs, with simulations completed at speeds of 130 kts, 160 kts, 190 kts, and 210 kts, flap settings at deflections of 0°, 15°, and 40°, and gear set at both up and down.

The resulting NPDs from the ANOPP cases were post-processed and imported into JMP. Using this tool, two models were fit for approach thrust settings—one with gear up and another with gear down. The models were fit on the difference between the configuration-specific NPDs and the baseline NPD as a function of BPR, OPR, SLS thrust, flap deflection angle, gear setting, aircraft speed, thrust fraction, and distance. Following the creation of the two models, they were tested by comparing the predicted configuration-specific NPDs from the correction function with the original configuration-specific NPDs from ANOPP. The SEL error distributions for this comparison for the gear-down configuration are shown in Figure 8a, and for the gear-up configuration in Figure 8b.

Figure 8 shows that for the gear-down configurations, the error between the baseline NPD corrected for a given configuration and the original configuration-specific NPDs from ANOPP was within the bounds of -1.7 dB and 1.8 dB, with 95% of the cases resulting in an SEL error within -1 dB and 1.1 dB. The model was slightly less accurate for the gear-up configurations, but the SEL error was still within -2.3 dB and 2.4 dB, with 95% of the cases resulting in an SEL error within -1.2 dB and 1.5 dB.

Figure 9 shows the baseline NPD for the 737-800 aircraft. As a demonstration of how the function works, Figure 10 shows the correction function being used to predict the difference between the baseline NPD and the NPD for a flight configuration of 187 kts, flap deflection angle of 1°, and gear-down. Figure 11 is the sum of Figures 9 and 10, reflecting the corrected NPD for the 737-800 in the aforementioned flight configuration.



(a). Gear-down configuration (b). Gear-up configuration

Figure 8. SEL error distributions for the gear-down model (left) and gear-up model (right).

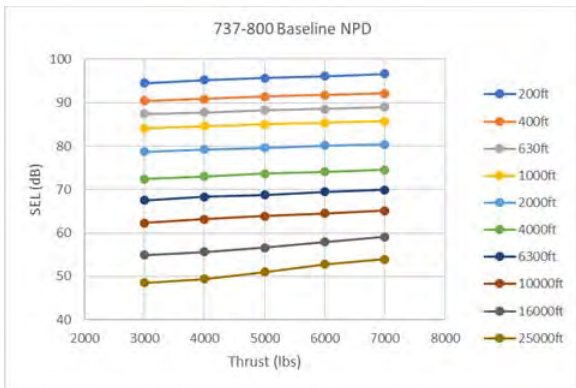


Figure 9. Baseline NPD.

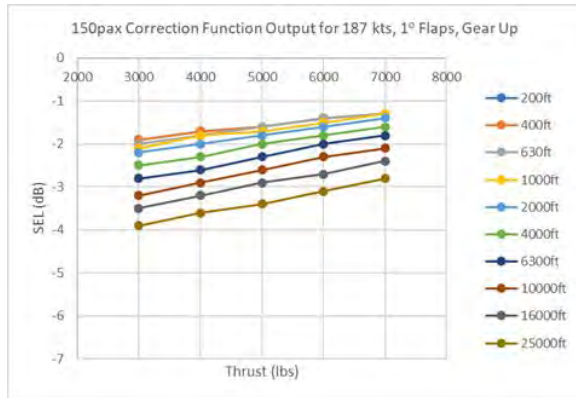


Figure 10. Correction function results for 187 kt, 1° FDA, gear-down configuration.

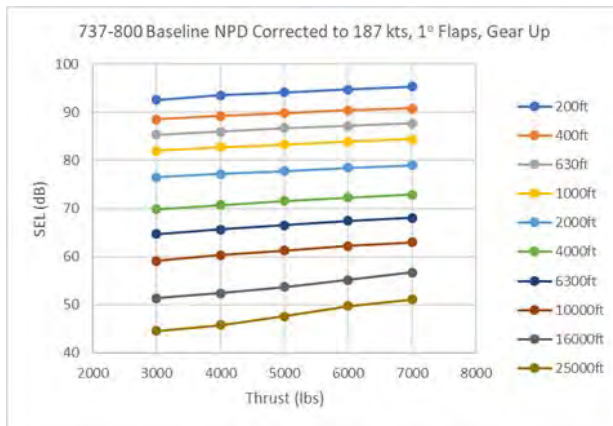


Figure 11. Corrected NPD.

Figures 9–11 illustrate that the correction function model is not creating a new NPD for a given flight configuration; rather, it is predicting the change from the baseline NPD for a given configuration. For each thrust and distance value in the NPD, the correction function predicts the change in SEL from the baseline NPD as a result of the flight configuration. Once the corrected NPD was generated, a series of tests were performed to assess the results.

**150pax Model Test**

To test the correction function, new ANOPP NPDs were generated for a range of aircraft configurations and compared with the AEDT default NPD with the correction function applied to account for the same configurations. First, the standard approach profiles were collected from AEDT for the baseline aircraft, as shown in Table 2. Although it was understood that the Flap IDs might not correspond to exact flap deflection angles, for the purpose of this Task they were assumed to match.

**Table 2. 737-800 Approach Profile From AEDT**

Flap ID	Thrust Level	Altitude AFE (ft)	Calibrated Airspeed (kt)
A_00	Unknown Thrust	6000	248.93
A_00	Idle Approach	3000	249.5
A_01	Idle Approach	3000	187.18
A_05	Idle Approach	3000	174.66
A_15	Unknown Thrust	3000	151.41
A_30	Unknown Thrust	2817	139.11

The approach configurations were then used to create configuration-specific NPDs using the correction function applied to the AEDT default NPD for this aircraft class. ANOPP was also used to generate NPDs for each configuration in the profile so that the corrected AEDT NPD could be compared against the configuration-specific NPD created with ANOPP; thus, the correction function results could be compared against the ANOPP results to determine the accuracy of the correction function. A series of figures comparing the data were created for each configuration in the profile, as well as tables containing the error between the ANOPP and the corrected baseline NPD. For the sake of brevity, only two of the six cases will be described in this report; however, the procedure for all configurations was the same.

The first configuration consisted of gear up, flap deflection of 1°, and a velocity of 187 kts. The error between ANOPP and correction function data was calculated as the difference between the solid and dashed lines shown in Figures 12a and 12b where they overlapped. Table 3 shows the calculated error at each distance.

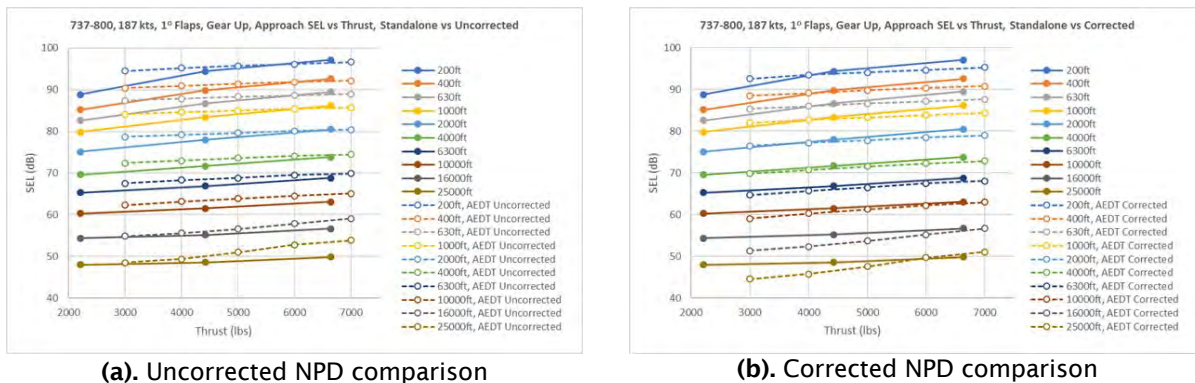


**Figure 12.** Correction function and ANOPP comparison for 187 kt, 1° FDA, gear-up configuration.

**Table 3.** Correction Function Error versus ANOPP for 187 kt, 1° FDA, Gear-Up Configuration

Distance	Uncorrected Error	Corrected Error
200 ft	1.02	-0.57
400 ft	1.17	-0.42
630 ft	1.09	-0.53
1000 ft	1.08	-0.61
2000 ft	1.12	-0.70
4000 ft	1.36	-0.71
6300 ft	0.43	-0.90
10000 ft	1.86	-0.78
16000 ft	1.02	-1.95
25000 ft	1.94	-1.45

As Table 3 shows, the correction function improved the absolute error between the AEDT NPD and the configuration-specific ANOPP NPD for all but two of the distance values. Moreover, there were only two distance values with SEL errors greater than one dB in magnitude. Figure 12 shows this graphically, where the solid lines indicate the ANOPP data and the dashed lines indicate the uncorrected (Figure 12a) and corrected AEDT default NPD (Figure 12b).

This process was repeated for a second case, involving a flight configuration of gear down, flap deflection angle of 30°, and velocity of 139 kts. As before, the uncorrected and corrected NPDs were compared against the ANOPP data in Figure 13, and the error between the ANOPP and uncorrected and corrected NPDs are shown in Table 4.

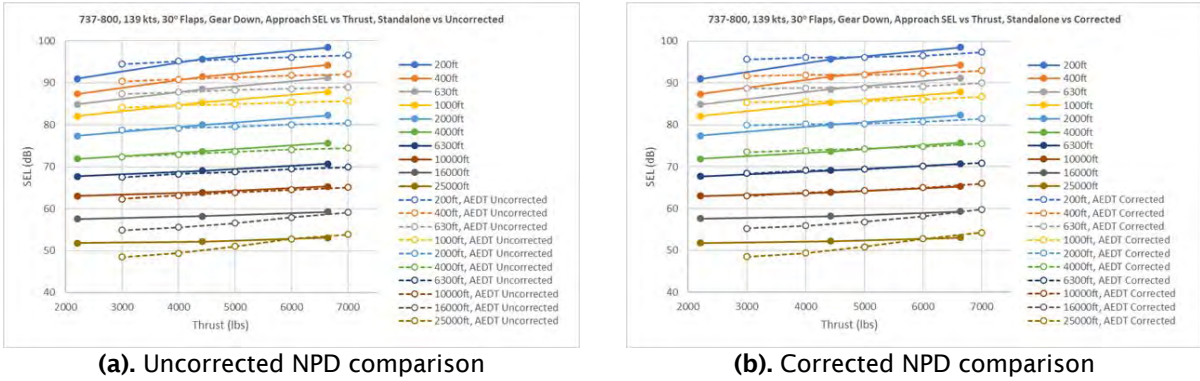


Figure 13. Correction function and ANOPP comparison for 139 kt, 30° FDA, gear-down configuration.

Table 4. Correction Function Error versus ANOPP for 139 kt, 30° FDA, Gear-Down Configuration

Distance	Uncorrected Error	Corrected Error
200 ft	-0.42	0.27
400 ft	-0.58	0.21
630 ft	-0.73	0.1
1000 ft	-0.80	0.08
2000 ft	-0.84	0.03
4000 ft	-0.64	0.19
6300 ft	-0.69	0.05
10000 ft	-0.51	0.05
16000 ft	-1.86	-1.55
25000 ft	-1.54	-1.54

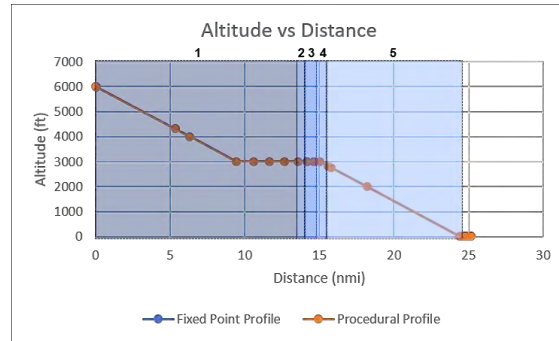
As Table 4 shows, the correction function reduced the difference between the AEDT NPD and ANOPP data for all but one of the distances and resulted in only two SEL errors greater than 0.3 dB. This reduction of error is made more apparent in Figure 13, where the overlap between the NPD and ANOPP data increases upon application of the correction function.

Next, a fixed-point profile was derived from the standard procedural profile for the 737-800 in AEDT. This profile is shown in Figure 14a. Figures 14b-14d compare the altitude, speed, and noise thrust against distance for the fixed-point and procedural profiles. As these figures show, both profiles are nearly identical such that only one is visible in each plot. The correction function was applied to the AEDT default NPD to create configuration-specific NPDs for all of the states in the profile, and the profile was simulated in AEDT using both the default and configuration-specific NPDs. Figure 15 shows the difference in the noise contours between the default and configuration-specific NPDs.

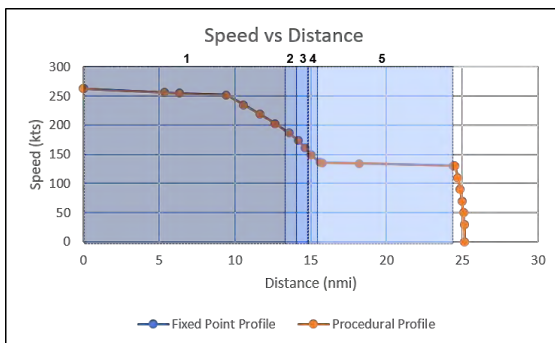


NPD	Speed	Flap Setting	Gear Setting
1	201 kts	0	Up
2	187 kts	1	Up
3	174 kts	5	Up
4	151 kts	15	Up
5	139 kts	30	Down

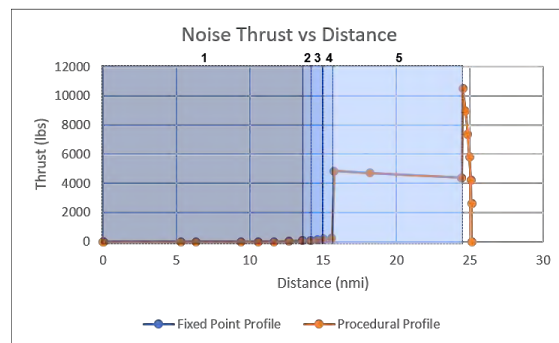
(a). Standard approach profile



(b). Altitude comparison



(c). Speed comparison



(d). Noise thrust comparison

Figure 14. Comparison of fixed-point and procedural profiles.

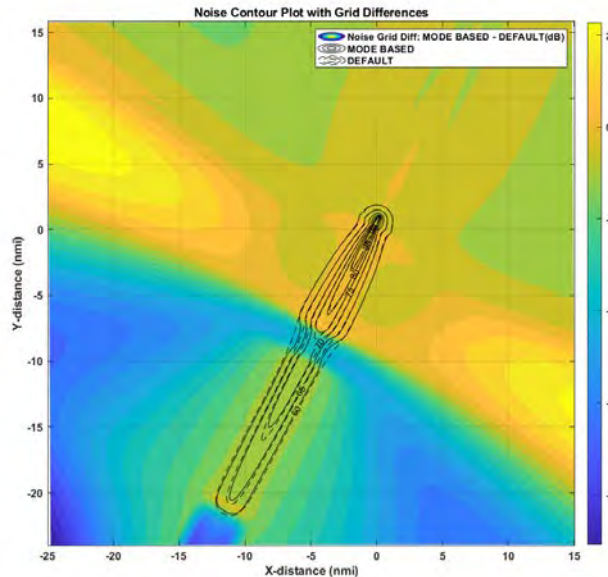


Figure 15. Comparison of uncorrected and corrected noise contours.

As Figure 15 shows, the largest difference between corrected and uncorrected NPDs occurs in segments/configurations 1-4, which is also seen in Figure 16. As the approach profile in Figure 14a shows, segments 1-4 reflect different flap settings with the gear retracted, while segment 5 reflects a 30° flap deflection and gear-down configuration. The contour plot reveals that the difference between the corrected and uncorrected noise contours is relatively small for the gear-down segment (shown in yellow and light green), while the difference is larger for the gear-up cases as shown via the dark blue levels in the contour plot.

The areas for several SEL values were calculated for both the uncorrected and corrected NPD simulation in AEDT, as shown in Table 5. This table shows that for SEL values below 75 dB, the predicted contour areas for the corrected NPD simulations were smaller than for the uncorrected NPD simulations. For SEL values at or above 75 dB, the predicted contour areas for the corrected NPD simulations were greater than for the uncorrected simulations.

**Table 5. Contour Area Changes by SEL**

Level (dB)	Contour Area (Default) (nm <sup>2</sup> )	Contour Area (Mode based) (nm <sup>2</sup> )	Δ (nm <sup>2</sup> )
60	76.63	72.12	-4.51
65	48.02	44.62	-3.40
70	24.56	22.51	-2.05
75	10.00	10.10	+0.10
80	4.21	4.56	+0.35
85	1.21	1.33	+0.12
90	0.34	0.37	+0.03

Finally, the predicted difference between the SEL values for the uncorrected and corrected NPD AEDT simulations was calculated directly underneath the flight path, as shown in Figure 16. This figure shows that for the entire simulation, the predicted SEL difference never exceeded 3 dB in magnitude. It also highlights that the difference was at its greatest between 12 and 15 nmi along the flight path, corresponding to flight segments 2-4.

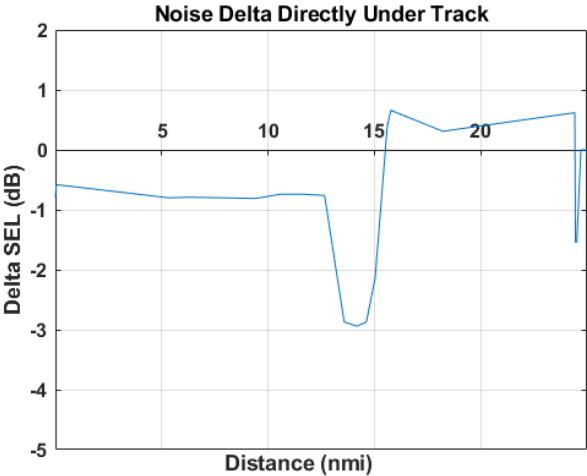
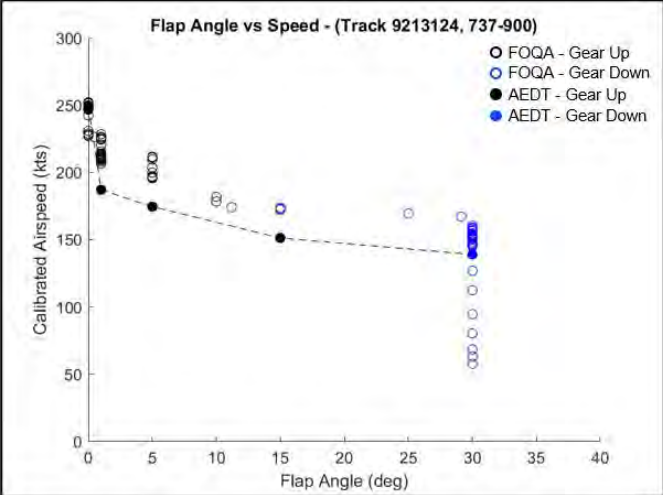


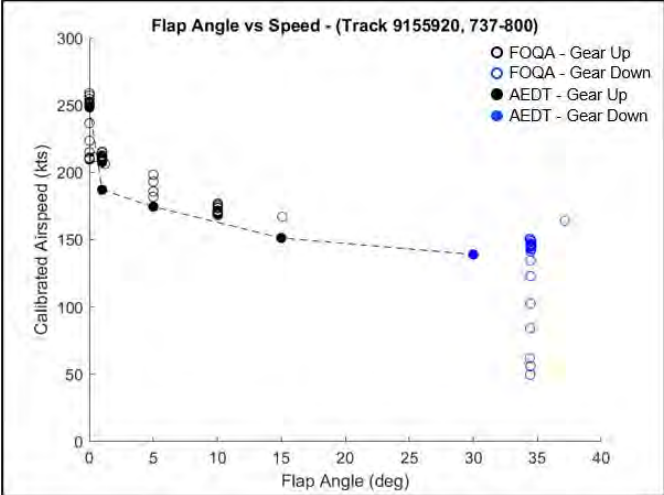
**Figure 16.** Plot of correction function values underneath track.

After developing the correction function for this aircraft class and testing it using a standard approach profile, it was then tested using FOQA data. Two representative tracks were selected from the FOQA dataset, consisting of approaches into SFO by a 737-800, a 737-900, and the corresponding matched noise monitor data. The objective of this was to see if the correction function improved the prediction in AEDT and was tested using the same method previously described—deriving a fixed-point profile from the track, correcting the default AEDT NPD for the configurations represented in the profile, and running the analysis using the mode-based NPD method to substitute configuration-specific NPDs.

First, the configurations represented in the FOQA tracks were plotted against the standard approach profile defined for these aircraft. This is shown below in Figures 17a-b, and indicates that although the true flight profile is similar to the standard profile as defined in AEDT, the configuration changes (in terms of flap and gear deployment) occur at higher speeds. Additionally, Figures 17c and 17d below show the tracks themselves modeled in AEDT.



(a)



(b)



(c)



(d)

**Figure 17.** FOQA tracks and configurations.

For each of these tracks, configuration-specific NPDs were generated using the correction function for the FOQA and Standard profiles and the tracks were simulated with the corresponding noise monitor site modeled. A total of four test cases were run for each profile. The first two cases used the Standard approach profile, tested with both default NPDs and corrected

NPDs accounting for the configurations in the Standard approach profile. The second two cases used the FOQA profile, tested with both default NPDs and corrected NPDs accounting for the configurations in the FOQA approach profile. Tables 6 and 7 below contain the results from each of the test cases.

**Table 6.** Results for Track 9213124.

	SEL
Measured Value, Noise Monitor (Site 12)	76.0 dB
Standard Profile, Default NPD	72.15 dB
Standard Profile, Corrected NPDs	72.63 dB
FOQA Profile, Default NPD	70.92 dB
FOQA Profile, Corrected NPDs	72.79 dB

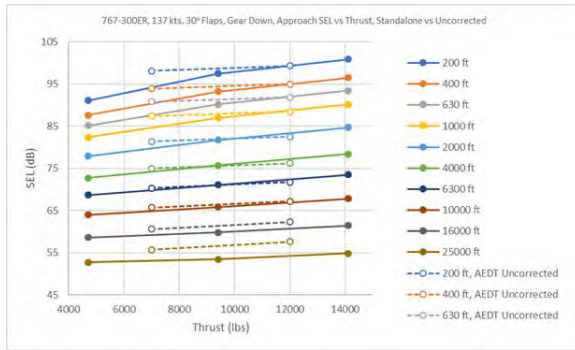
**Table 7.** Results for Track 9155920.

	SEL
Measured Value, Noise Monitor (Site 12)	81.6 dB
Standard Profile, Default NPD	81.44 dB
Standard Profile, Corrected NPDs	81.81 dB
FOQA Profile, Default NPD	80.25 dB
FOQA Profile, Corrected NPDs	81.37 dB

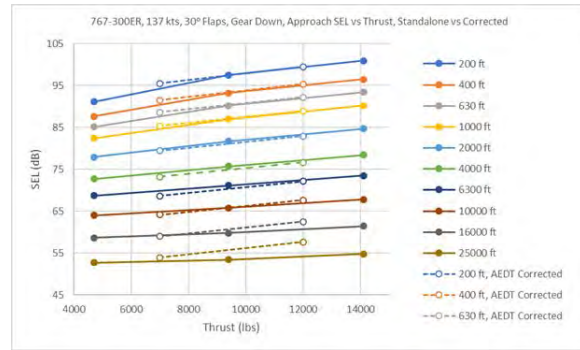
From these initial test cases, it can be seen that with the exception of the Standard profile for Track 9155920, the corrected NPDs improved the prediction at the noise monitor site. Additionally, the most pronounced change was observed between the FOQA profiles using the default and corrected NPDs. As a final check, the closest state to the noise monitor site was identified in order to see what was contributing the most at the nearest point. For the first instance (Track 9213124), the closest configuration in the FOQA profile was 154.25 knots, 30° flaps, and gear down. For the second instance (Track 9155920), the closest configuration in the FOQA profile was 167.25 knots, 15° flaps, and gear down. Given that the correction function predicts the difference from a baseline configuration of 160 knots, 15° flaps, and gear down, it makes sense that the changes observed were small for both tracks.

**210pax Model Test**

Once the model was completed and tested for the 150pax aircraft class, the entire process was repeated for the 210pax aircraft class using the 767-300ER as the baseline aircraft. Again, a correction function was developed using EDS, ANOPP, and JMP, and applied to the baseline NPD to test its accuracy. Figure 18 plots the default AEDT NPD for this aircraft against ANOPP for the same state, and Figure 18b plots the corrected AEDT NPD against the ANOPP results. These figures show that for each distance except for 2000, 4000, and 6300 ft, the correction function decreases the error between the NPD and the ANOPP prediction for the given configuration. The error between the uncorrected and corrected NPDs and the ANOPP results is shown in Table 8.



(a). Uncorrected NPD comparison



(b). Corrected NPD comparison

Figure 18. Correction function and ANOPP data comparison for 137 kt, 30° flap deflection, gear-down configuration.

Table 8. Correction Function Error versus ANOPP for 137 kt, 30° Flap Deflection, Gear-Down Configuration

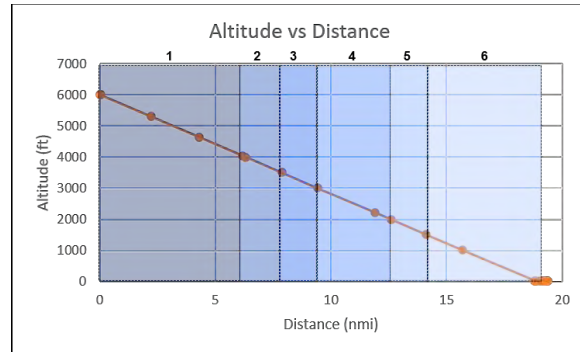
Distance	Uncorrected Error	Corrected Error
200 ft	1.51	0.31
400 ft	1.48	0.43
630 ft	1.33	0.38
1000 ft	1.06	0.21
2000 ft	0.29	-0.50
4000 ft	-0.11	-0.81
6300 ft	-0.14	-0.79
10000 ft	0.58	-0.01
16000 ft	1.56	0.86
25000 ft	3.13	2.23

Next, a fixed-point profile was derived using the Standard approach profile in AEDT for the 767-300ER aircraft class, and the uncorrected and corrected NPDs were tested in AEDT. Figure 19 shows the fixed-point profile used for testing the 210pax model.

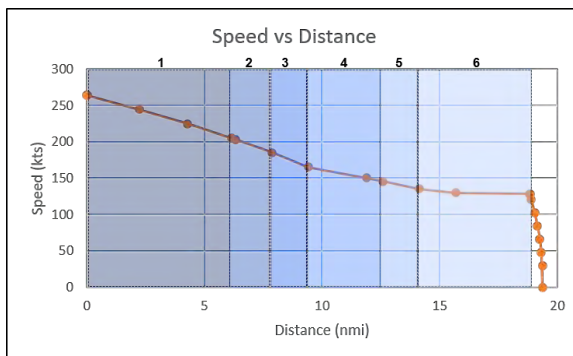


NPD	Speed	Flap Setting	Gear Setting
1	220 kts	0	Up
2	204 kts	0	Up
3	185 kts	0	Up
4	167 kts	5	Up
5	141 kts	25	Up
6	137 kts	30	Down

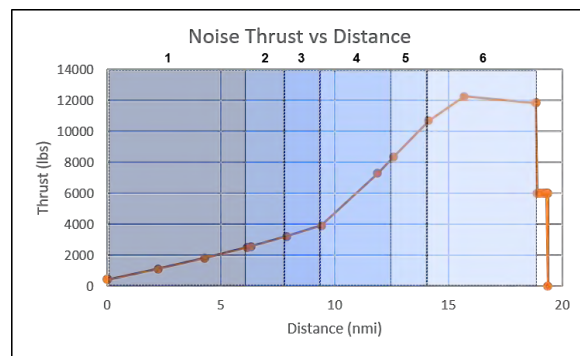
(a). ANOPP profile



(b). Altitude comparison



(c). Speed comparison



(d). Noise thrust comparison

Figure 19. Fixed-point profile used for testing.

As the profile shows, six different states made up the flight profile. Three configurations contained zero flap deflection at various speeds, one consisted of a flap deflection angle of 5° at a speed of 167 kts, another consisted of a flap deflection angle of 25° at a flight speed of 141 kts, and the final configuration consisted of a flap deflection angle of 30° and gear-down configuration.

With the profile identified, the default and corrected NPDs were used to simulate the approach and generate noise contours and grids for comparison. Figure 20 plots the difference between the uncorrected and corrected NPD simulation from AEDT.

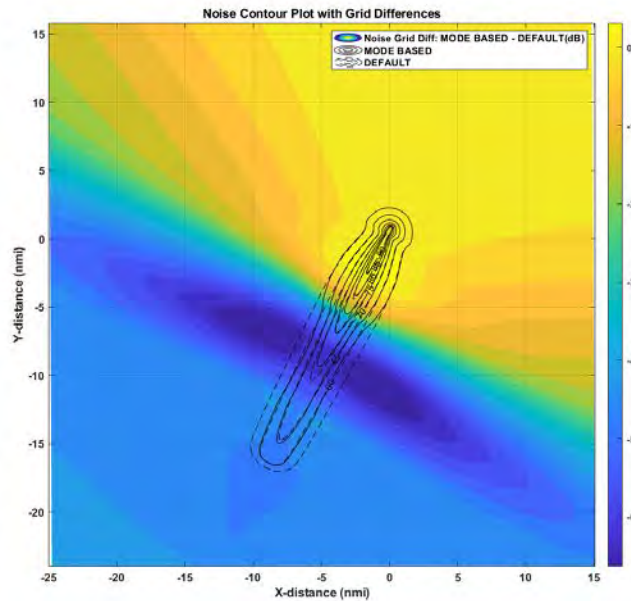


**Figure 20.** Noise contour plot of difference between uncorrected and corrected NPD.

As the contour plot shows, the largest difference between the uncorrected and corrected NPDs was located at the clean configuration states along the profile. As the flap deflection angle increased and the gear deployed, the difference in the uncorrected and corrected NPD decreased as shown by the lighter yellow contours near the origin of the contour plot. Once again, the contour areas were calculated for various SEL values, as shown in Table 9.

**Table 9.** Comparison of SEL Contour Areas

Level (dB)	Contour Area (Default) (nm <sup>2</sup> )	Contour Area (Mode based) (nm <sup>2</sup> )	Δ (nm <sup>2</sup> )
60	85.30	65.62	-19.68
65	54.44	37.23	-17.21
70	29.91	18.06	-11.85
75	14.25	9.79	-4.46
80	6.31	5.39	-0.92
85	2.60	2.60	0.0
90	0.92	0.99	+0.07

This table shows that for SEL values at or below 80 dB, using the corrected NPDs resulted in decreased contour areas, while for SEL values above 80 dB the contour areas were slightly increased. For SEL values of 60, 65, and 70 dB, the decrease in contour area between the uncorrected and corrected NPDs was significant, ranging in magnitude from 11.85 to 19.68 nm<sup>2</sup>. For SEL values of 85 and 90 dB, the change in contour area was less than 0.1 nm<sup>2</sup>. Figure 21 was also created from the AEDT simulation results to show how the correction function resulted in different SEL values across the fixed-point profile.

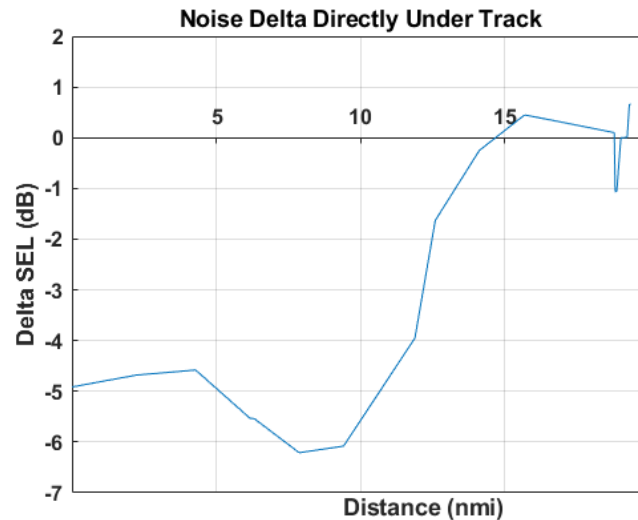


**Figure 21.** Difference in SEL values directly under flight path.

This plot shows that the greatest difference in SEL values underneath the flight path occurred between 7 and 10 nmi along the flight path. As Figure 19 shows, this corresponds to flight segments 2–4. This is sensible, given that the greatest difference in SEL values from the uncorrected and corrected AEDT simulations occurred when the aircraft was in a clean configuration at the slowest of the modeled speeds for that state, which the aircraft was in for segments 2 and 3.

Although the next step would be to test using FOQA tracks and associated noise measurements, at the time of this report the team did not have any matched tracks and noise data for aircraft in the 210-pax class. As such, although interim tests could be performed using aircraft outside of this class, additional data should be available soon and the corresponding evaluations will be able to be performed then.

**Milestone**

Develop correction functions across vehicle classes.

**Major Accomplishments**

Developed correction functions across vehicle classes and compared to real-world noise monitoring data.

**Plans for Next Period**

With the 150pax and 210pax class models complete, new models will be created for the 50pax and 300pax classes, following the same approach as described previously. Once the models are completed, they will be compared against “truth data” in the form of real-world noise observations for aircraft of the same class.

**Other Work Supporting Tasks (AEDT Tester Development)**

Georgia Institute of Technology

**Objective(s)**

Georgia Tech has developed a wrapper (AEDT Tester) around the AEDT source code that allows for the automation of reading aircraft definition and flight procedures input files with less user interaction and higher efficiency. AEDT Tester was initially developed to work with AEDT 2e. The first objective of this task is to synchronize AEDT Tester with the latest AEDT release – AEDT 3c.

Modifications were made to AEDT source code to incorporate NPD + Configuration (NPD+C), which accounts for varying aircraft speed and configuration parameters such as flap/gear/speed to achieve more accurate noise evaluation; however, the code was lost. The second objective of this task is to re-implement NPD+C.

## Research Approach

### AEDT Tester Synchronization

Figure 22 shows the general workflow of AEDT Tester. In order to synchronize AEDT Tester with the latest AEDT release - AEDT 3c. The team has rebuilt AEDT Tester by modifying its code to accommodate the new AEDT's interface.

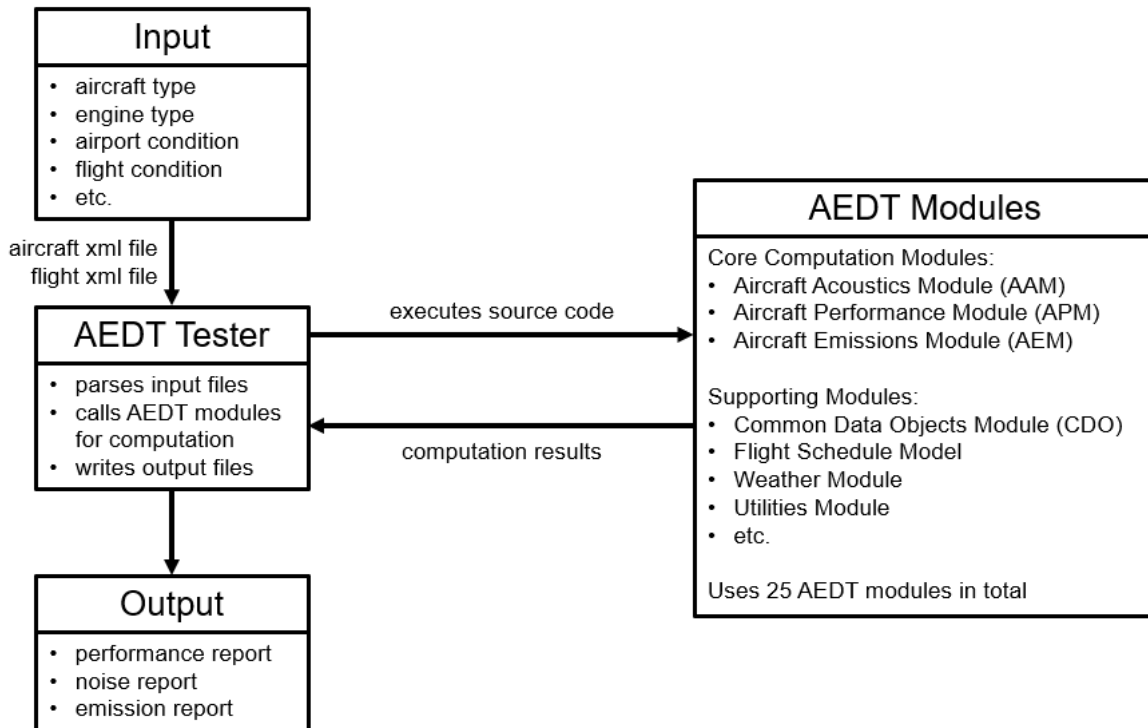


Figure 22. Workflow of AEDT Tester.

The new AEDT Tester achieved all expected functionalities, including parsing input aircraft and flight files, calling AEDT modules for computation, and writing output files. The team then performed a quantitative validation by running an identical case in AEDT Tester and AEDT 3c and comparing the results. The aircraft used was B737-800, the reference airport was SFO, and comparisons were done for both departure and arrival operations. Theoretically, the computational results of AEDT Tester, including performance, noise, and emission, should exactly match the results from AEDT 3c. The results showed that discrepancies, although not large, do exist between the two program's results. The team is investigating the reasons that have caused the differences.

### NPD+C Implementation

The Georgia Tech team has made modifications to both AEDT Tester and AEDT source code to incorporate NPD+C in noise computation. The modifications required an involvement within AEDT Tester itself and 3 main AEDT code modules which are: Aircraft Acoustics Module (AAM), the Aircraft Performance Module (APM) and the Common Data Objects (CDO) module. Here we provide a conceptual description to summarize the modifications in code. Detailed modifications are specified in Table 10.

**AEDT Tester:** The modifications in AEDT Tester focused on parsing the expanded input aircraft .xml file, which included a superset of NPDs. First, the input schema .xsd file was modified to accommodate multiple NPDs in the input file. Then, the code segments, such as `NpdCurveLongRecord_NPDC()` and `GetNoisePowerDistanceCurves_NPDC()`, for parsing the input .xml



file and constructing NPD+C curves were altered to read the multiple noise power distance curves and create NPD+C curves within the program. Functions for output purposes were updated to include flap and gear information for each flight segment.

CDO: The modifications in the CDO module were parallel to the changes in AEDT Tester's. Two new classes, `NpdDataAircraft_NPDC` and `NpdCurveLongRecord_NPDC`, were made to create new containers to store the information of the expanded NPDs, namely flap id, gear setting, and speeding setting. `TrajectorySegment` class was also adjusted to include flap id in flight segments.

APM: Much code was altered in the APM module to allow for the passing of aircraft configuration information obtained from the input .xml file all the way to flight segment containers, which were used for noise computation.

AAM: The majority of modifications in this task occurred in the AAM module for implementing the new noise interpolation method that works with NPD supersets. `NpdData.cs` class was modified to store the NPD superset in high dimensional matrices. `MainContainer.cs` was the key class that went through the heaviest modifications as it is where the noise interpolation takes place. `NoiseInterpolation_NPDC()` was altered to perform the 4-d interpolation, which took advantage of the original 2-d interpolation logic that AEDT originally had. The new noise interpolation did not make any internal changes to the existing one, but rather used the 2-d interpolation's results as the input for the high dimensional interpolation. To facilitate the new interpolation logic, a couple of other functions and interfaces were updated in `MainContainer.cs`

**Table 10. NPD+C Implementation Specifics.**

AEDT SOLUTION MODIFICATIONS FOR NPD+C IMPLEMENTATION						
Project	Class / File	Method / Class	Line(s)	Description	Related Mods	
AAM (Aircraft Acoustic Module)	CDOAAMInterface.cs	CopyCDONoiseParameterstoNPDObj()	1839-1841	Assign values for the aircraft configuration labels in NpdDataAircraft object		
			1947-1962	Assign number of different curves in NpdInfo	NpdData.cs	
		FindNPDIndices()	2420-2440	Find the first occurrence of departure curve in the npd curve list		
		CopyCDOTrajectorySegmenttoFlightPathSegment()	1555-1564	Pass flap_id and height from trajecotry segment to flight path segment airplane		
	FlightPathSegment.cs	FlightPathSegmentAirplane : FlightPathSegmentBase	171-174, 210-217	Include flap_id in the class		
	MainContainer.cs	SegmentContainer		4011-4012	Include gear setting in SegmentContainer class to be used for noise interpolation	
				3961-3965	Flap-related member variables in Segment Container class for interpolation	
				272-273	While initialization, pass flap_id from FlightPathSegmentAirplane to SegmentContainer and set the actual flap value	
				275-282	Initialize gear setting for segment container based on aircraft height	
				3985-3986, 274	Add height as a member variable and pass height when convert flight path segment into segment container	
			ParseFlapId()	381-394	Utility function to parse flap_id into float value	
			AircraftNoiseCurveStorage()	474-858	Fill values from npd curves into the noise matrix	
			Exposure()	1838-1842	Call new interpolation function to do noise computation	
			NoiseInterpolation_NPDC()	2799-2862	New interpolation algorithm based on AEDT original algorithm to do 4-d interpolation	
			FindFlapSpeedGearIndices()	3160-3195	Function to look for the two labels that box the desired flap/speed/gear values of the data point	
			NoiseInterpolation_ThrDist()	2864-3159	Modified AEDT's original algorithm's interface to perform interpolation on thrust and distance with NPD+C curves	
		NpdData.cs		NpdInfo	12-107	Include numbers of thrust, flap, speed, and gear settings into the NpdInfo class
			NpdDataAircraft : NpdBase	218-271	Include aircraft configuration settings into the class	
			NOISE_MATRIX_TYPE	379	Change the noise matrix dimension for it to be able to contain configuration data	

			399-409	Initialize the size of the noise matrix	
AEDTTester	AircraftXmlReader.cs	AircraftXmlReader	50	Modified AEDT's reader schema to incorporate the new vehicle XML input containing the information of the superset of NPDs.	EDS2AEDTFLEET_dummy.xsd
		GetNoiseParameters()	1887	Calling new method GetNoisePowerDistanceCurves_NPDC() to get NPD+C curves from xml elements.	
		NpdCurveLongRecord_NPDC()	2297-2416	Reading from xml element to construct the NPD+C records, which will later be used to create NPD+C curves	NpdCurveLongRecord_NPDC.cs
		GetNoisePowerDistanceCurves_NPDC()	2054-2120	Calls NpdCurveLongRecord_NPDC() funtion to create NPD+C curves.	NpdDataAircraft_NPDC.cs
		GetEngineEmissions()	664-685	Allow null values for some emission related data in the input	
		GetNoiseParameters()	1881-1918	Parsing the input data with "EDS_aircraft" format	
		GetNoisePowerDistanceCurves_NPDC_EDS()	2181-2185	Parse aircraft configuration data	
	ResultCSVWriter.cs	SavePerformanceAndEmission()	840-1131	Include flap and gear information	
		SavePerformanceAndNoise()	1194-1349	Include flap and gear information	
(APM) Aircraft Performance Module	FlightPath.cs	add_alt_interval_points_terminal()	433	Pass flap_id when interpolating new path points	
	AirplaneProfile.cs	AssignContextToStep()	365-367	Pass flap_id when going from profile steps to the original path points	
	TerminalOp.cs	CreateAirplaneTerminalFlightPathSegments()	432-433	Pass on flap_id when to flight path segment	FlightPathSegment.cs
	FlightPathSegment.cs	FlightPathSegmentAirplane	All	Add flap_id and height as member variables to the class	
	EventModeler.cs	PopulateCDOPerformanceEventResultFromFlightPath()	1002	Pass gear to trajectory segment	
			1091	Pass gear to the last trajectory segment	
			985	Pass flap_id to trajectory segment	TrajectorySegment.cs
1076			Pass flap_id to the last trajectory segment		
(CDO) Common Data Objects	NpdDataAircraft_NPDC.cs	NpdDataAircraft_NPDC	All	A sibling class of the original NpdDataAircraft class in AEDT, extra fields to include flap, gear, and speed settings so it becomes a superset of the original class	
	NpdCurveLongRecord_NPDC.cs	NpdCurveLongRecord_NPDC	All	A sibling class of the original NpdCurveLongRecord class in AEDT, extra fields to include flap, gear, and speed settings	
	TrajectorySegment.cs	TrajectorySegment	50-145, 448-453	Include flap_id in the class fields and created a new constructor	
	ITrajectorySegment.cs	ITrajectorySegment	120-124	Include flap_id in the interface	

The validation was done with respect to the NPD+C implementation. A test case was performed using B737-800 for an arrival flight at San Diego International Airport (SAN) and an NPD+C superset consisting of 12 identical baseline NPD curves was used as NPD+C noise curves. Since in this case the NPD+C algorithm essentially used the same baseline curve as the NPD algorithm, the algorithms had to produce identical noise results. Figure 23 shows the comparison of noise contours of the experiment, and a good match between the two result sets can be observed. The validation test has succeeded.

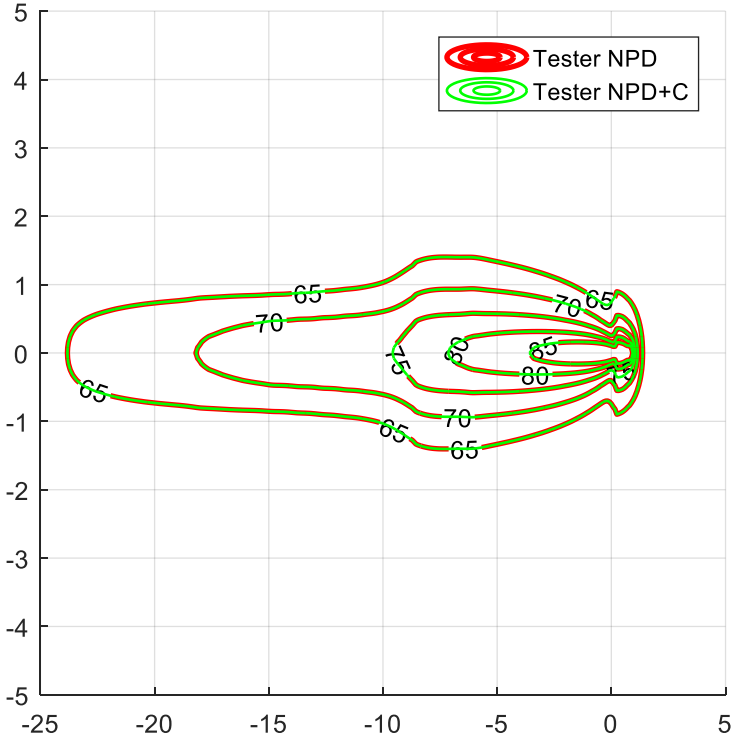


Figure 23. Noise contour comparison of NPD and NPD+C algorithms.

**Milestone**

N/A

**Major Accomplishments**

Recompiled the AEDT Tester.

**Plans for Next Period**

Continue debugging in the AEDT Tester to investigate the causes of the discrepancies between AEDT 3c and the AEDT Tester’s results, including performance, noise, and emissions.

Utilize AEDT Tester to perform experiments on FOQA flights with NPD and NPD+C and compare the noise results obtained by the two approaches against truth data to determine the effectiveness of incorporating NPD+C for noise evaluation.

**Publications**

N/A

**Outreach Efforts**

N/A



## **Awards**

N/A

## **References**

AEDT. (2016). Aircraft Environmental Design Tool, version 2.c. FAA, Washington, DC

ANOPP. (1998). Aircraft noise prediction program, version 1.0. NASA, Langley, VA. Ref. LAR-16809-GS

Aratani, L. (August 9, 2018) D.C. residents suffer major setback in fight over plane noise from National Airport. The Washington Post

Federal Aviation Administration (FAA). (Retrieved December 2019) Aircraft noise issues. United States Department of Transportation

John A. Volpe National Transportation Systems. (2008). Integrated Noise Model (INM) version 7.0 technical manual. FAA-AEE-08-01

Page, J.A., Hobbs, C.M., Plotkin, K.J., Stusnick, E., & Shepherd, K.P. (2000). Validation of aircraft noise prediction models at low levels of exposure. NASA technical report number: CR-2000-210112.

Plotkin, K.J., Page, J.A., Gurovich, Y., & Hobbs, C.M. (2013). Detailed weather and terrain analysis for aircraft noise modeling (No. Wyle Report 13-01). John A. Volpe National Transportation Systems Center (US)

Raymer, D.P. (2006). Aircraft design: A conceptual approach. 4<sup>th</sup> ed., AIAA Education Series, Reston, Virginia, pp. 197

U.S. DOT Volpe Center. (2017). Aviation Environmental Design Tool (AEDT) technical manual, version 2d. FAA, ATAC Corp, CSSI, Inc, Metron Aviation DOT-VNTSC-FAA-17-16

U.S. FAA. (2016). Aviation Environmental Design Tool (AEDT) technical manual version 2c. DOT-VNTSC-FAA-16-11



# Project 044 Aircraft Noise Abatement Procedure Modeling and Validation

## Massachusetts Institute of Technology

### Project Lead Investigator

R. John Hansman  
T. Wilson Professor of Aeronautics & Astronautics  
Department of Aeronautics & Astronautics  
Massachusetts Institute of Technology  
Room 33-303  
77 Massachusetts Ave  
Cambridge, MA 02139  
617-253-2271  
rjhans@mit.edu

### University Participants

#### Massachusetts Institute of Technology (MIT)

- PI: R. John Hansman
- FAA Award Number: 13-C-AJFE-MIT, Amendment Nos. 050, 057, and 073
- Period of Performance: Sept. 1, 2018 to Aug. 31, 2021
- Tasks: [to be added by project team]

#### University of California - Irvine (sub-award from MIT)

- PI: Jacqueline Thomas
- Award Number: MIT Subaward Purchase Order No. TBD
- Period of Performance: Sept. 1, 2020 to Aug. 31, 2021
- Tasks:
  1. Evaluate General Approaches to Aircraft Noise Validation
  2. Develop Validation Approach Options
  3. Develop Flight Test Plans
  4. Initial Experimental Runs on Targets of Opportunity
  5. Evaluate Experimental Results and Implications for Aircraft Noise Prediction Program (ANOPP) and Aviation Environmental Design Tool (AEDT) and Low-Noise Procedures

### Project Funding Level

FAA provided \$720,000 in funding. A total of \$720,000 in matching funds were provided by approximately \$125,000 from MIT and \$595,000 from Massachusetts Port Authority.

### Investigation Team

- Prof R. John Hansman (PI)
- Jacqueline Thomas (PI)
- Clement Li (graduate student)
- Sandro Salgueiro (graduate student)
- Madeleine Jansson (graduate student)
- Ara Mahseredjian (graduate student)



## Project Overview

This project will utilize empirical noise data to develop data-based/learned noise models and validate and improve existing noise models. Field measurements of aircraft noise on approach and departure have historically shown significant variation (on the order of 10 dB) which have traditionally been attributed to factors such as varied power settings, aircraft configuration differences, and propagation effects. Recent analysis under this and other ASCENT projects have attempted to account for these factors but are constrained by limited detailed flight data. This project will explore approaches to combine emerging sources of flight data from flight data recorders and other sources such as ADS-B with current and emerging networks of ground noise monitors to validate or improve aircraft noise models and to also validate proposed noise abatement procedures. The rise of data mining and machine learning techniques has enabled significant insight and modeling capabilities based on the use of large datasets and without requiring full a priori knowledge of all the relevant physics. The development of advanced data mining approaches applied to noise modeling is expected to provide insight into aircraft noise prediction for refining or validating noise models and developing strategies for noise mitigation, either through new aircraft technologies or operational changes. Furthermore, improved noise modeling capabilities would enable more informed decision-making for stakeholders when considering options and consequences of operational or technological changes, facilitating the minimization of noise impacts on communities. As noise is becoming an increasingly large factor in operational decisions around airports in the National Airspace System (NAS), an accurate understanding of noise impacts is necessary to minimize unnecessary disruptions or inefficiencies to NAS operations.

## Task 1 – Evaluate General Approaches to Aircraft Noise Validation

Massachusetts Institute of Technology

### Objectives

This goal of this Task is to evaluate the different options for validation of the ANOPP source component models and to confirm noise reductions from proposed low-noise procedures. Approaches to experimental design will be considered, which may include dedicated engineering flight trials that involve parametric sweeps of velocity and aircraft configuration at various power conditions. This process would involve collaborating with airline operators, who would need to be willing to fly trials of procedures, and air traffic control (ATC), who would have to approve the procedures. A ground measurement system would need to be in place under the departure tracks.

Potential monitoring approaches will also be considered, including distributed microphone arrays or single microphone installations, as well as potential phased-array microphone configurations. In addition, alternative flight data sources will be obtained either through airline sources or through available surveillance data. Sources of noise data from existing and emerging noise monitoring systems will be identified. Boston Logan International Airport (BOS) has agreed to provide data and additional airports will be approached to participate in the effort. Emerging open source and community noise monitoring systems such as those being developed under ASCENT Project 53 will also be investigated. Opportunities for collaboration will be explored with a focus on providing correlated flight data and noise datasets.

This Task will use a systems approach and will explore options with potential collaborators on experimental opportunities to validate research concepts.

### Research Approach

- Evaluate the different options for validation of the ANOPP source component models as well as confirmation of any noise reductions from proposed procedures.
- Identify potential existing data sources for noise validation.
- Collaborate with industry and operators to determine who would be willing to fly procedures.
- Evaluate potential challenges associated with flight testing and taking measurements.

### Major Accomplishments

- Flight radar and noise monitor data collected at Boston Logan International Airport and Seattle-Tacoma International Airport (SEA) was identified as a data source that can be used for noise model validation.
- Data from flight demonstrations conducted by Boeing was examined to validate flight procedure modeling methods and the feasibility of the flight procedure.

- Sources of weather data as a function of altitude were identified to make atmospheric absorption corrections for noise modeling validation.

## Task 2 – Develop Validation Approach Options

Massachusetts Institute of Technology

### Objectives

On the basis of the results of Task 1 and initial discussions with potential collaborators (measurement experts, model developers, manufacturers, operators, and test locations), one or more validation options will be identified. Targets of opportunity will be explored in which noise measurements may supplement other planned flight trials. For each option, the potential advantages and disadvantages will be identified, and preliminary flight test plans will be developed in coordination with the identified collaborators and in consultation with subject matter experts such as NASA. Potential advantages include the willingness of operators or collaborators to participate and provide test resources including aircraft and measurement systems. Other factors include measurement system resolution and discrimination of noise sources. Timing and location may also be considered. On the basis of this analysis, recommendations for next steps will be made.

### Research Approach

- Explore targets of opportunity for noise measurements or flight testing.
- Identify sources of data that can be used for validation from industry or other entities.

### Major Accomplishments

- Worked with a research team at Stanford University to identify noise monitor data of high-lift devices that could be used to validate noise of flight procedures with significant airframe noise contributors.
- Target of opportunity to fly a low-noise approach procedure in Boeing ecoDemonstrator tests were identified.
- Flight radar and noise monitor data collected at Boston Logan International Airport were identified as useful for evaluating noise of low-noise procedures like the delayed deceleration approaches when atmospheric absorption as a function of historical weather is properly taken into account.

## Task 3 – Develop Flight Test Plans

Massachusetts Institute of Technology

### Objectives

For the recommended validation options identified in Task 2, detailed flight test plans will be developed. Flight test plans for dedicated engineering flights would involve detailed planning of the speed, configuration, and thrust of each trial. Test plans for flight trails in collaboration with airline operators would focus more heavily on documenting the flown profiles to analyze the associated data measurements. Opportunity exists in both of these types of trials to validate not only the expected effects of aircraft speed versus noise in the analysis models, but also the expected noise impacts of procedures including delayed deceleration approaches, steeper approaches, and continuous approaches.

### Research Approach

- Develop flight test plans for validation of low-noise procedures.
- Collaborate with airline operators and industry to determine appropriate data collection for trial flight tests.

### Major Accomplishments

- Assisted in flight plan design for the delayed deceleration approach procedure and how to communicate the approach to pilots.
- Developed assessment methods to examine which attributes of the procedure contribute to which noise impacts.
- Developed assessment methods to model the noise impacts of flight profiles from radar data for comparison with noise data.



## Task 4 – Initial Experimental Runs on Targets of Opportunity

Massachusetts Institute of Technology

### Objective

If targets of opportunity are identified in Task 2 that would occur within the period of performance of this proposed research, initial experimental runs would be conducted after consultation with AEE and other relevant parties.

### Research Approach

- Document procedure recommendations so that flight trials are possible.
- Meet with airline technical pilots and representatives from aircraft manufacturers to discuss operational constraints and test opportunities.
- Develop test plans and protocols for potential flight trials.
- Develop test plans and protocols for potential noise measurement campaigns.
  - Specific flight test locations.
  - Operational field measurements.

### Major Accomplishments

- The delayed deceleration approach concept was identified as a noise abatement flight procedure as a candidate for flight test demonstration.
- A delayed deceleration approach combined with steeper approach were assessed for feasibility and noise reduction impacts by the MIT team and the Boeing team.
- Weekly meetings and discussions with industry were held to determine the feasibility of flying delayed deceleration approaches and steeper approaches.
- A delayed deceleration approach procedure was flight tested for operational demonstration.
- Flight data collected from operational demonstration was used to model procedure noise impacts.

## Task 5 – Evaluate Experimental Results and Implications for ANOPP and AEDT and Low-Noise Procedures

Massachusetts Institute of Technology

### Objectives

Contingent on data availability from Task 4 or other data identified as part of the experimental approach and discussions with collaborators, this Task in coordination with NASA will:

- Evaluate the ANOPP correlations relative to experimental results.
- Identify discrepancies that need to be corrected.
- Determine whether the results and data are sufficient to improve discrepancies or whether continued validation and testing are required.

The implications for AEDT from the data will be evaluated. The results of the flight tests, data exploration, and ASCENT Project 44 may create opportunities to continue to improve the noise-power-distance and configuration curves in AEDT. Validating the noise component modules in ANOPP would also allow for potential component corrections within the noise models of AEDT. The implications for AEDT will allow future research teams to continue to develop the AEDT noise models upon the results of the data analysis and flight tests from this project.

Implications for the development of low-noise procedures will also be evaluated. Validation and improvement of the noise models ANOPP and AEDT will allow for higher-fidelity development of low-noise procedures. Validation of procedures such as delayed deceleration approaches will also create opportunity for the development of further low-noise procedures.

### Research Approach

- Evaluate implications for modeling low-noise procedures with ANOPP and AEDT.
- Evaluate implications for the development of low-noise procedures.



## **Milestone**

The delayed deceleration approach was flown as an operational flight demonstration on the Boeing ecoDemonstrator at Atlantic City International Airport in November of 2019. Evaluation of the data from the Boeing ecoDemonstrator test and noise monitor data from Boston Logan International Airport were used to evaluate the modeling of low-noise procedures.

## **Major Accomplishments**

- Noise analysis was performed on ecoDemonstrator flight tests to show the impacts of different decisions made for actual flight test implementation, such as when and where the delayed deceleration would occur.
- Noise results were compared with data gathered at Boston Logan International Airport to predict flap deflection schedules for low-noise procedure modeling.

## **Publications**

- Jensen, L. & Hansman, R.J. (2018) Data-driven flight procedure simulation and noise analysis in a large-scale air MIT
- Jensen, L., O'Neill, G., Thomas, J., Yu, A., & Hansman, R.J. (2018). Block 1 procedure recommendations for Logan Airport community noise reduction. MIT ICAT Report
- Jensen, L., Thomas, J., Brooks, C., Brenner, M., & Hansman, R.J. (2017). Analytical approach for quantifying noise from advanced operational procedures. European Air Traffic Management Research and Development Seminar
- Reynolds, T., Sandberg, M., Thomas, J., & Hansman, R.J. (2016). Delayed deceleration approach noise assessment. 16th AIAA Aviation Technology, Integration, and Operations Conference.
- Thomas, J. & Hansman, R.J. (2020). Evaluation of the impact of transport jet aircraft approach and departure speed on community noise. MIT ICAT Report
- Thomas, J. & Hansman, R.J. (2020). Modeling and assessment of delayed deceleration approaches for community noise reduction. AIAA Aviation
- Thomas, J. & Hansman, R.J. (2019). Framework for analyzing aircraft community noise impacts of advanced operational flight procedures. *Journal of Aircraft*, Volume 6, Issue 4. <https://doi.org/10.2514/1.C035100>
- Thomas, J. & Hansman, R.J. (2017). Modeling performance and noise of advanced operational procedures for current and future aircraft. MIT International Center for Air Transportation
- Thomas, J., Jensen, L., Brooks, C., Brenner, M., & Hansman, R.J. (2017). Investigation of aircraft approach and departure velocity profiles on community noise. AIAA Aviation Forum, p. 1-12
- Thomas, J., Yu, A., Li, C., Toscano, P., & Hansman, R.J. (2019). Advanced operational procedure design concepts for noise abatement. In Thirteenth USA/Europe Air Traffic Management Research and Development Seminar, Vienna.
- Thomas, J., Yu, A., Li, C., Maddens Toscano, P., & Hansman, R.J. (2019). Advanced operational procedure design concepts for noise abatement. USA/Europe ATM R&D Seminar
- Yu, A. & Hansman, R.J. (2019). Aircraft noise modeling of dispersed flight tracks and metrics for assessing impacts. MIT ICAT Report
- Yu, A. & Hansman, R.J. (2019). Approach for representing the aircraft noise impacts of concentrated flight tracks. AIAA Aviation Forum 2019, Dallas, Texas. <https://doi.org/10.2514/6.2019-3186>

## **Outreach Efforts**

- September 30, 2020: Presentation to the ASCENT Advisory Board.
- October 15, 2019: Presentation to the ASCENT Advisory Board.
- November 8, 2019: Presentation to NASA.
- November 12, 2019: Presentation to Airline Industry Consortium.
- Weekly meetings with industry.
- Biweekly teleconferences and meetings with FAA Technical Monitors.
- In-person outreach and collaboration with Massport, operator of Boston Logan International Airport and ASCENT Advisory Board member.

## **Awards**

2018 Department of Transportation/FAA COE Outstanding Student of the Year Award to Jacqueline Thomas.

## **Student Involvement**

Graduate students have been involved in all aspects of this research in terms of analysis, documentation, and presentation.



### **Plans for Next Period**

The next phase of this project will include noise modeling validation of approach procedures using radar flights and noise measurements for several aircraft types, such as Boeing 737-800, Airbus A320, and Embraer E190. Noise monitor readings from Seattle-Tacoma International Airport have also been identified as a source for additional validation and will be included. The implications of the validation, including how data can be used to inform flight profile assumptions when assessing operational flights, as well as potential benefits and operational implications from advanced flight procedures such as the delayed deceleration approach will also be examined.



# Project 045 Takeoff/Climb Analysis to Support AEDT Aircraft Performance Model (APM) Development

## Georgia Institute of Technology

### Project Lead Investigator

Professor Dimitri N. Mavris

Director

Aerospace Systems Design Laboratory

School of Aerospace Engineering

Georgia Institute of Technology

Phone: (404) 894-1557

Fax: (404) 894-6596

Email: dimitri.mavris@ae.gatech.edu

Dr. Michelle R. Kirby, Co-PI

Chief, Civil Aviation Research Division

Aerospace Systems Design Laboratory

School of Aerospace Engineering

Georgia Institute of Technology

Phone: (404) 385-2780

Fax: (404) 894-6596

Email: michelle.kirby@ae.gatech.edu

### University Participants

#### Georgia Institute of Technology (GT)

- Pls: Prof. Dimitri Mavris, Dr. Michelle R. Kirby (Co-PI)
- FAA Award Number: 13-C-AJFE-GIT, Amendment 020, 035, 43, and 46
- Period of Performance: August 15, 2016 to March 28, 2019
- Tasks:
  - Task 1: Noise abatement departure profiles (NADP) library investigation.
  - Task 2: Arrival profile modeling.
  - Task 3: Integrated impact assessment of inaccuracies from thrust, weight, procedures, and noise-power-distance (NPD) curves.

### Project Funding Level

FAA provided \$175,000 in funding. Georgia Tech is providing \$175,000 in matching funds. Cost share details are as follows: GT has agreed to a total of \$175,000 in matching funds. This total includes salaries for the project director; research engineers; graduate research assistants; and computing, financial, and administrative support, including meeting arrangements. The institute has also agreed to provide tuition remission for the students, paid for by state funds.

### Investigation Team

- Prof. Dimitri Mavris, Principal Investigator, Georgia Institute of Technology
- Dr. Michelle Kirby, Co-Investigator, Georgia Institute of Technology
- Dr. Yongchang Li, Research Faculty, Georgia Institute of Technology
- Dr. Tejas Puranik, Research Faculty, Georgia Institute of Technology
- Dr. Don Lim, Research Faculty, Georgia Institute of Technology
- Ameya Behere, Graduate Student, Georgia Institute of Technology



- Zhenyu Gao, Graduate Student, Georgia Institute of Technology (Task 2)
- Yee Chan Jin, Graduate Student, Georgia Institute of Technology (Task 1)
- Dylan Monteiro, Graduate Student, Georgia Institute of Technology (Task 3)
- Ana Gabrielian, Graduate Student, Georgia Institute of Technology (Task 2)
- Loren Isakson, Graduate Student, Georgia Institute of Technology (Task 1)

## Project Overview

Accurate modeling of aircraft performance is a key factor in estimating aircraft noise, emissions, and fuel burn. Within the Aviation Environmental Design Tool (AEDT), many assumptions are made for aircraft performance modeling with respect to aircraft weight and departure procedure, coupled with aircraft departure typically being modeled by assuming that full rated takeoff power/thrust is used. As operations around airports continue to evolve, there is a need to examine those assumptions and to improve the modeling accuracy with flight data. In recent years, flight data are increasingly being used to enhance models and bring model estimation even closer to reality. Research is needed to build on prior work with a view to develop a robust set of recommendations for improved estimation processes for takeoff weight, reduced thrust takeoffs, and departure profiles within AEDT.

## Task 1 – NADP Library Investigation

Georgia Institute of Technology

### Objective

Previous research efforts under Project 45 led to the development of the NADP Library, a set of noise abatement departure profiles (NADPs) that are defined as procedural profiles in AEDT. The library is generic and can be applied to any aircraft or airport. Each such profile is based on the combination of three parameters: thrust cutback, initial acceleration, and final acceleration. The NADP Library contains 19 base profiles which can expand based on alternate weight and reduced thrust variants. The objective of this task is to recommend a subset of these 19 profiles for implementation in AEDT.

### Research Approach

There are six NADP-1 profiles and 13 NADP-2 profiles defined in the library. Even more modeling options are possible when the possibilities of alternate weight and reduced thrust are considered. Including such a high number of profiles as modeling options in future versions of AEDT is undesirable. Therefore, a grouping of profiles within NADP Library is required so that a subset of these 19 profiles can be selected. A single profile within each group can then be chosen to represent all other profiles within the group. The overall process is summarized by Figure 1.

The 2019 ASCENT Annual Report describes in detail the process created for the downsizing and the computation of similarity metrics between different profiles. Similarity metrics are calculated using performance, fuel burn, emissions, and noise reports for each profile at various stage lengths. Similarity metrics are a pair-wise measure of how “close” two profiles are in their environmental impact. All similarity metrics were normalized to be on the same relative scale.

Once noise metrics have been obtained, they are used as inputs to the clustering algorithm which groups similar profiles together. Three clustering algorithms are implemented using the “sklearn.cluster” Python library: K-means, Hierarchical, and DBSCAN. Table 1 shows the results obtained from two of these algorithms on the alternate weight version of the NADP-2 part of the NADP Library. The table entries represent the cluster label, i.e., all profiles labeled as 1 in a column belong to cluster 1. Note that different metrics and different algorithms result in different cluster assignments. Therefore, a consensus clustering algorithm was utilized to obtain final cluster assignments.

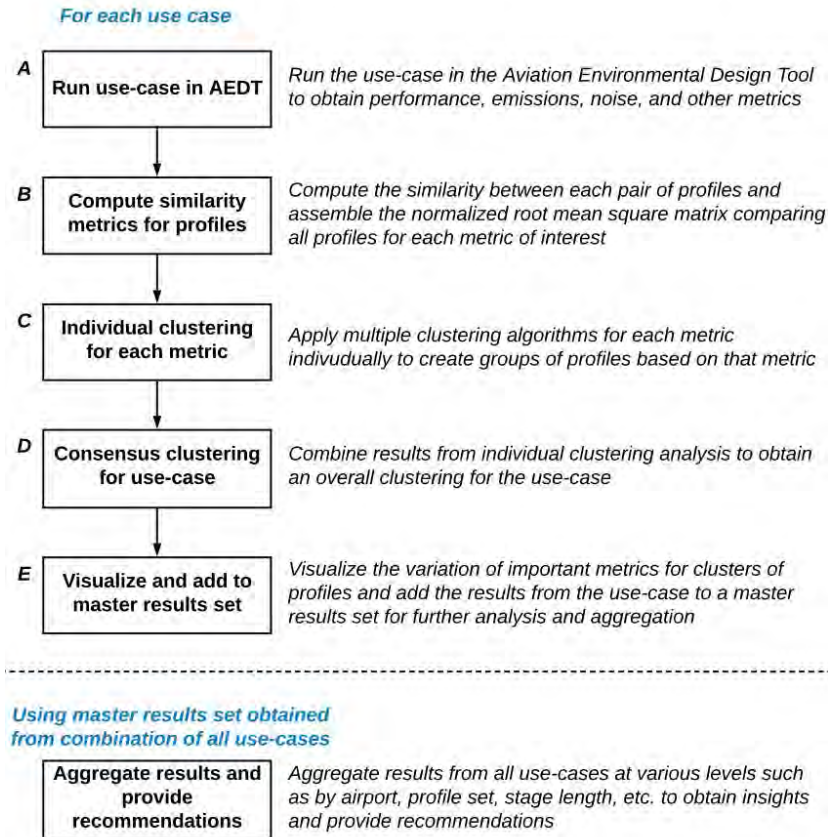


Figure 1. Overall clustering process for NADP Library.

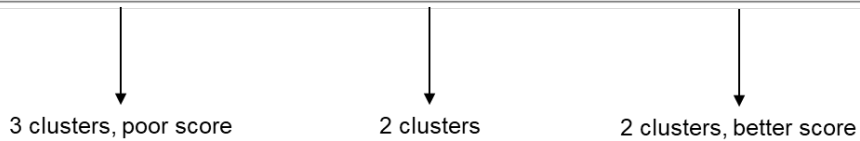
Table 1. Sample results from clustering algorithms

	Algorithm 1: K Means			Algorithm 2: DBSCAN		
	Noise SEL	Nox	Fuel Burn	Noise SEL	Nox	Fuel Burn
NADP2_1_AW-3	2	2	1	2	2	2
NADP2_2_AW-3	2	1	2	2	1	1
NADP2_3_AW-3	2	1	2	2	1	1
NADP2_4_AW-3	2	2	1	2	2	2
NADP2_5_AW-3	2	2	1	2	2	2
NADP2_6_AW-3	2	2	1	2	2	2
NADP2_7_AW-3	1	1	2	1	1	1
NADP2_8_AW-3	1	2	1	1	2	2
NADP2_9_AW-3	1	2	1	1	2	2
NADP2_12_AW-3	1	2	1	1	2	2
NADP2_11_AW-3	1	1	2	1	1	1
NADP2_12_AW-3	1	2	1	1	2	2
NADP2_13_AW-3	1	1	2	1	1	1

The “goodness” of clusters is evaluated using a silhouette score. This score is used to judge the efficacy of a clustering algorithm on the given set of similarity metrics. When the number of desired clusters is not fixed, this score can also help determine the optimal number of clusters. A comparison of silhouette scores is shown in Table 2.

**Table 2.** Comparison of silhouette scores for NADP-1 profiles flown by Airbus A320 at Hartsfield–Jackson Atlanta International Airport

	K-Means Algorithm				DBSCAN Algorithm			
	SEL	Emissions NO <sub>x</sub>	Fuel Burn	LA <sub>max</sub>	SEL	Emissions NO <sub>x</sub>	Fuel Burn	LA <sub>max</sub>
NADP1_1-1	0	1	0	0	1	0	0	0
NADP1_2-1	1	1	0	0	0	0	0	0
NADP1_3-1	1	0	1	0	0	1	1	0
NADP1_4-1	1	1	0	0	0	0	0	0
NADP1_6-1	1	0	1	0	0	1	1	0
NADP1_7-1	2	0	1	1	1	1	1	1
Silhouette Score	0.28	0.79	0.79	0.42	0.27	0.79	0.79	0.42



The final step for recommendation is to compare the clustered profiles with real-world flight operation data. For this task, flight operations quality assurance (FOQA) data was used as the validation data. FOQA data was grouped in accordance with the AEDT simulation results based on aircraft type and airport. Flight trajectories in each such group were condensed into a “median” FOQA profile. This median profile was then modeled in AEDT and compared to the modeled NADP profiles to identify the NADP profile which best represented the FOQA data.

In conclusion, the NADP-1\_1 and NADP-2\_11 profiles were found to consistently represent real world operations across a variety of aircraft types and airports. Hence, these profiles were recommended for implementation in AEDT.

**Milestone**

The objective of this task was to provide recommendations for the implementation of NADPs in AEDT, which has been accomplished.

**Major Accomplishments**

- Developed clustering process to perform down-selection of the NADP Library,
- Provided recommendations for additional departure profile options in AEDT to better represent real-world operations.

**Publications**

Ameya Behere, Loren Isakson, Tejas G. Puranik, Yongchang Li, Michelle Kirby, and Dimitri Mavris, Aircraft Landing and Takeoff Operations Clustering for Efficient Environmental Impact Assessment. AIAA AVIATION 2020 FORUM. June 2020, <https://doi.org/10.2514/6.2020-2583>

**Outreach Efforts**

Bi-weekly calls with the FAA, Volpe, and ATAC. Bi-annual ASCENT meetings.

**Awards**

None

**Student Involvement**

Ameya Behere and Loren Isakson, Graduate Research Assistants, Georgia Institute of Technology

**Plans for Next Period**

This Task is now complete.

## Task 2 – NextGen Arrival Profile Modeling

Georgia Institute of Technology

### Objective

Previous research has extensively investigated the difference between departure procedures in AEDT and the actual departure procedures observed by using data types such as radar data, FOQA data, and airline and airport documentation, thus resulting in a library of departure procedures. Under Task 2, a similar study will take place for arrival procedures. The use of FOQA data from one airline will be utilized to assess the accuracy of AEDT arrival procedures for 14 airframes. The FOQA data will be used to find different arrival characteristics such as level off altitude, velocity, gear setting, and flap setting. These different characteristics will then be compared to what is currently prescribed in AEDT. If a significant difference is found, new arrival profiles will be proposed. In essence, this will result in arrival procedures in AEDT that better capture existing operations as observed in data gathered via aircraft flight logs.

### Research Approach

Methods to model advanced NextGen profiles in AEDT were developed through recent research conducted for Airport Cooperative Research Program (ACRP) 02-55. The final deliverables for ACRP 02-55 included a report and technical guidance for selecting appropriate aircraft approach and departure profiles, which are available to the public. The GT team has conducted a thorough review of the work conducted in ACRP 02-55 and has created an actionable plan to incorporate the findings.

The ACRP 02-55 objective was to capture and represent arrival procedures used in the real world. This was done by creating additional standard or default procedures that are not currently within AEDT. The researchers working on this study had access to Performance Data Analysis and Reporting System (PDARS) data for more than 274,000 arrival procedures. The data was taken from 30 airports throughout the United States for 68 different aircraft types. From this, the flights were grouped according to the level off length, level off altitude and aircraft class. An example of this grouping would be “A-LJ-1-3000-40to49-5to14.” This signifies an approach operation for a large jet with a stage length of 1, which has a level off at 3,000 ft, for a distance between 40 and 49 nmi, ending with 5 to 14 nmi from the airport. The flights were then modeled to fly out of one airport, Hartsfield-Jackson Atlanta International Airport (KATL), to make the trajectories comparable. Level off “bins” for flights were created every 1,000 ft.

An averaged trajectory for these grouped flights was then created and compared to their analogous baseline trajectories, which were STANDARD AEDT approach procedures found in AEDT2a. The method used to average the flights was not explicitly defined within the airport. A trajectory score was computed for the average trajectories of the different groups with the following formula:

$$TrajScore = \frac{\sum_{i=1}^N |H_{avg,i} - H_{BL,i}|}{N}$$

where  $H_{avg}$  is the altitude from the averaged trajectory and  $H_{BL}$  is the altitude of the baseline from AEDT. These were then normalized to the number of samples taken. Samples were taken for every nautical mile in ground track distance. After the grouping process and the calculation of trajectory scores, the worst six profiles for six aircraft classes were chosen to create AEDT procedures by using AEDT’s altitude controls functionality. Then 36 approach profiles were generated for six different aircraft classes.

This document was helpful in providing a method to group different flight trajectories. The GT team will create their own algorithm for averaging a particular group of flights according to characteristics that will be discussed later. The averaging and grouping findings will then be compared to the findings in the ACRP 02-55 document to assess whether there is a correlation between the two.

A similar study will be conducted by the GT team with a new set of airline data acquired from one airline. FOQA data from more than 16,000 flights and 14 airframes will be used to assemble visualizations next to existing standard profiles in AEDT. This data includes information regarding aircraft altitude, ground track distance, thrust, velocity, gear position, flap position, etc. The aircraft state information available may bring to light more details that PDARS data is incapable of revealing. Popular arrival settings for each of the previously described parameters will be heavily inspected to find common departure modes. The following aircraft are in the dataset with operations at 71 airports across North and Central America.

- Boeing 717-200



- Boeing 737-700, 800, 900
- Boeing 757-200, 300
- Boeing 777-200LR, 200ER
- McDonnell Douglas 90
- Airbus 319-100, 320-200, 321-200
- Airbus 330-200, 300

A systematic parsing of the data is conducted because it includes the entire flight trajectory from taxi and takeoff to landing and taxi again. For the purposes of this task, the GT team will be investigating only the altitude from 6,000 ft until touchdown because this is the same altitude range that AEDT uses in its definition of approach. In addition, arrival profiles are categorized as a continuous descent approach (CDA) or a level off approach. A subroutine in Python is utilized to categorize trajectories based on distinguishable factors in each trajectory. A level off is detected for a particular flight segment when one of the two following criteria are met: either a calculated glide slope of less than  $0.6^\circ$  is found while performing a rolling average over two time steps ahead and behind the current altitude sample point, or the altitude up to three time steps ahead is within 30 ft of the current altitude. The second criterion sufficiently catches level offs with turbulent perturbations that exceed glide slope tolerance. On the other hand, the first criterion captures rare cases where the descent gradient is extremely shallow for a noticeable period and is more accurately categorized as a level-off. One time-step equates to about 0.1-0.3 nmi and decrease with a reduction in speed which progresses during the descent. There are still occasional “gray line” cases when detecting level offs at low altitudes, but that has been minimized through tuning of tolerances. An example would be a brief level off segment while an aircraft is getting established on vertical guidance provided by an instrument landing system. This brief level off detection is ignored when categorizing. Lastly, any level off detected below 1000 ft or above 5200 ft above ground level (AGL) is immediately discarded. Below 1000 ft, mostly noise is detected. Above 5200 ft, level offs are considered a part of the route, not the approach. These techniques overall proved useful and robust for the vast majority of arrival trajectories; however, the next logical step would make use of classification to categorize level offs versus CDAs.

Preprocessed data is then entered into visualization software. This software allows users to easily manipulate the data to see trends; an example is shown in Figure 2. An overview is provided on entire FOQA datasets at all airports for all airframes. Below, the size of the circle represents the number of data points at each airport, varying between approximately 5 and 2500. The color gradient represents the proportion of flights that are determined to be level offs at that respective airport, with nonlevel offs automatically categorized as CDAs. Immediately, it is noticeable that level offs are less common in the southwest portion of the United States. On the east coast, the opposite is true and most likely can be attributed to traffic congestion up and down the coast. Currently, standard profile runs for KATL, Denver International Airport (KDEN), and San Francisco International Airport (KSFO) are in the database so comparisons can be made along those lines. These airports, in addition to McCarran International Airport (KLAS), John F. Kennedy International Airport (KJFK), and Salt Lake City International Airport (KSLC), appear to be the most prominent in the United States in terms of operations according to the figure.

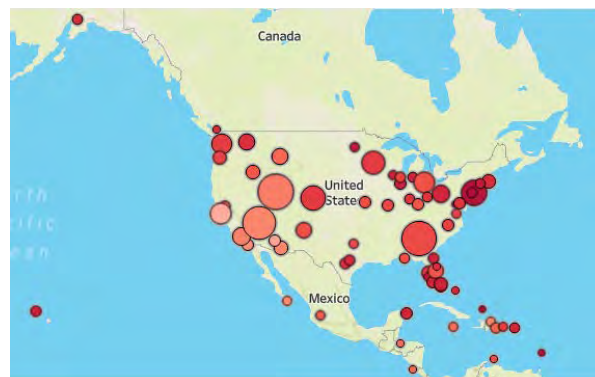


**Figure 2.** Percentage level offs detected at each airport in FOQA dataset.

The following process can be employed at any airport using the constructed dashboard. Selecting KATL for examination in Figure 3 alongside the default AEDT profiles, for the aircraft mentioned above, it is observed that AEDT profiles are either a CDA or a level off at 3000 ft AGL, with slight variation in level off segment distance. Fairly large discrepancies are immediately apparent between modeled AEDT profiles and FOQA data with respect to thrust. Thrust is underpredicted at distances greater than 10 nmi from touchdown. This difference is evident with all aircraft. The same can be said regarding airspeed. Airspeed changes in real aircraft appear to less abrupt between 15 and five nmi from touchdown.

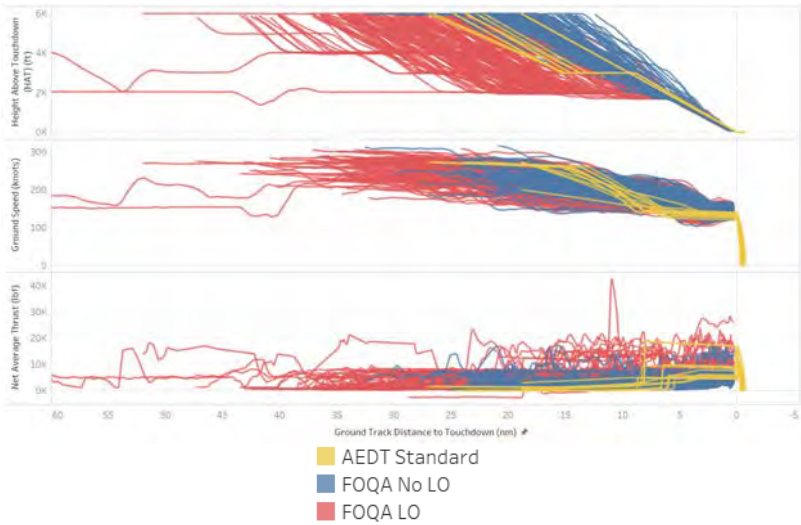


Figure 3. AEDT standard profiles next to FOQA data at KATL.

As shown in Figure 4(a), it is recommended that a CDA and level off profile be available for every type of aircraft. There is a relatively consistent proportion of level offs regardless of aircraft type at KATL. Level off proportions are less dependent on aircraft type and are airport-specific due to airspace, traffic, and obstacles. This assumption can be made after viewing the same breakdown performed at KJFK in Figure 4(b), which proves to consist almost entirely of level offs. However, on the whole, there are a significant number of airports with trends similar to KATL as shown by the final aircraft breakdown across all 71 airports in Figure 5.

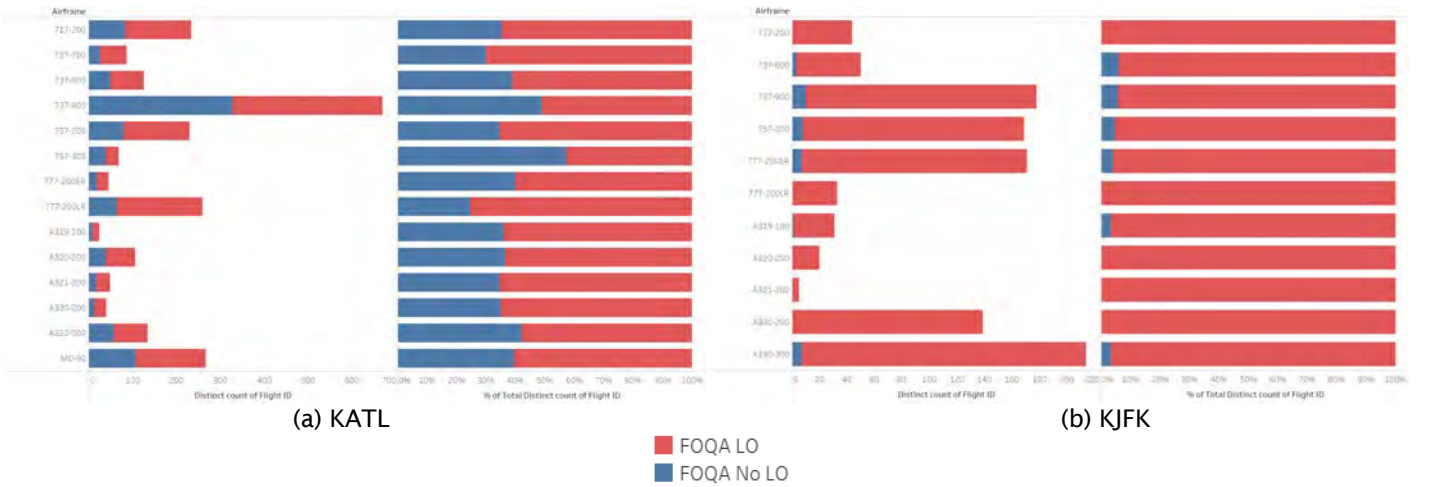


Figure 4. Level off percentage breakdown by aircraft at specific airports.

Distinct count of flight ID is simply the number of unique flights counted in each respective category, with red and blue representing level offs and CDAs, respectively. This color scheme is consistent throughout the report in accordance with the legend in Figure 3. On the right-hand side of each image, the relative proportion or percentage is shown of the counting performed on the left-hand side. Clearly, the number of wide body arrivals, currently solely modeled in AEDT using level offs, is significantly less. However, CDAs are still seen 20% to 30% of the time.



Figure 5. Level off percentage breakdown by aircraft including all 71 airports in the database.

In summary, it is recommended that all aircraft with a single arrival profile in AEDT have both a CDA and level off defined. Addressing discrepancies in thrust and speed may be prioritized as needed. However, noise prediction quality may degrade beyond 10 nmi. Effects of thrust underprediction and speed overprediction do act in opposition of each other. These effects, although possibly negligible, together may mask the issue at long distances and high altitudes.

The next portion of this section seeks to recommended altitudes and distances for level off arrival profiles in AEDT. There are a number of ways this can be done with varying fidelity. The best solution would be to examine every airport individually, but that is impractical, especially with a handful of airports dominating the dataset. Therefore, prominent airports will be selected. These airports, generally located near metropolitan areas, will also capture where the greatest concern is regarding noise. A recommendation made with respect to these airports will likely sufficiently reflect more remote regions in the vicinity, sometimes in the same airspace. The following airports are selected for this subset for their prominence in Figure 2 and for the reasons put forth in this paragraph.

- KATL
- KDEN
- KSFO
- KJFK
- KLAS
- KSLC

In Figure 6, a detailed visual analysis is conducted on the airport subset including trajectory, level off altitude, thrust setting, airspeed, and level off distance. Once popular altitudes are determined, additional filters will be applied to pinpoint distance. At this point, level off distance is somewhat nonsensical because it counts distances at all level off altitudes. Note that a miniscule proportion of level offs occur below 2000 ft height above touchdown (HAT); however, they are not interpreted as a traditional level off profile but rather a temporary level off assigned to intercept vertical guidance. In decreasing popularity,

altitudes of approximately 2000 ft, 3000 ft, 4000 ft, and 5000 ft appear. The peak level off altitude at 5000 ft primarily belongs to approaches at KSLC and does not entirely represent a national trend. The noise between dominant altitudes is largely due to KDEN, which seems to have consistent separation of 1000 ft between popular level off altitudes. However, these altitudes are also consistently 200-300 ft lower on average. Hence, premature peaks are shown before 2000 ft, 3000 ft, 4000 ft, and 5000 ft.

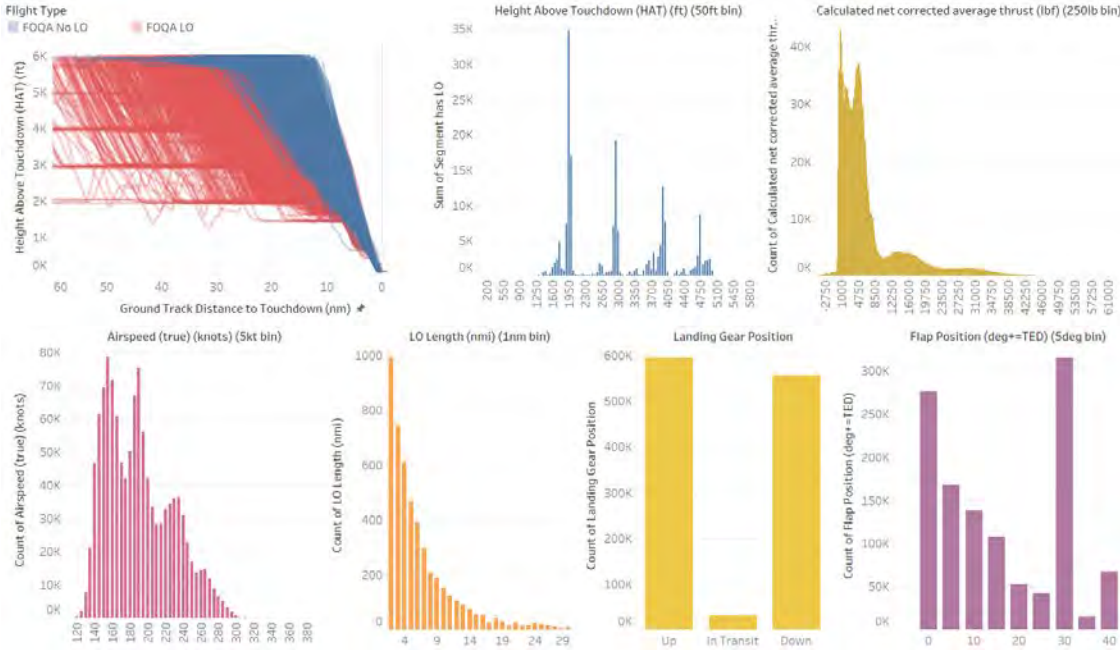


Figure 6. Level off analysis of airport subset.

On average, it can be shown that this trend holds for all other airports in the database. In Figure 7, the total count of level off altitudes is shown. A case can be made to discard 5000 ft as a level off to model due to the inconsistency. This altitude also appears to be associated with a select few airports such as KSLC. Altitudes of 2000 ft, 3000 ft, and 4000 ft remain in order of popularity. To address any uncertainty, level offs at 2000 ft do appear legitimate according to Figure 8 trajectories. The airport subset assumption holds quite well.

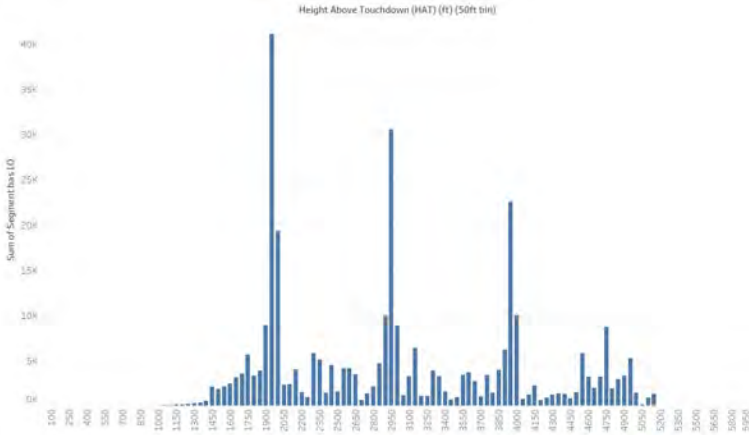
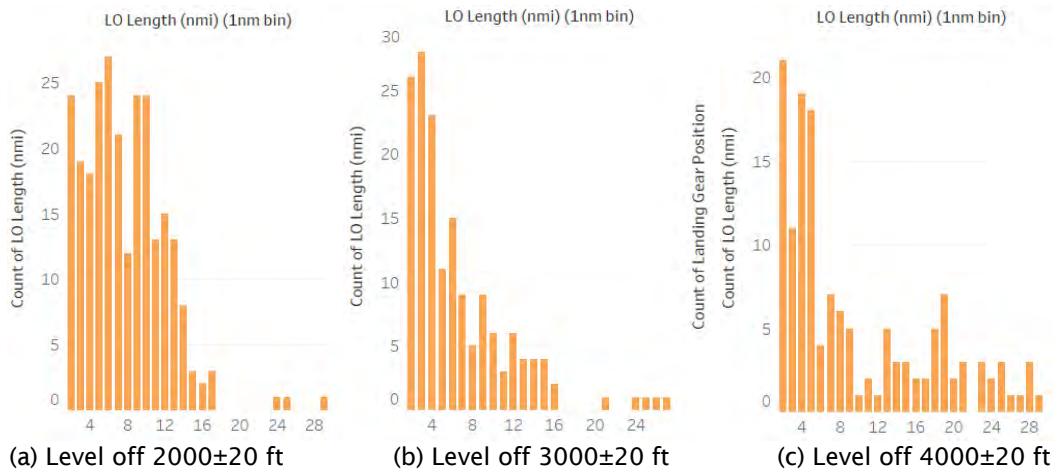


Figure 7. Level off altitude count for all aircraft at all 71 airports in the database.

Therefore, this technique is extended to level off distance. Thus, not only is better clarity observed when looking at the subset with respect to level off distance, but it validates previous and future analyses conducted at these airports. Level off distance is especially noisy when viewing all airports at the same time, masking any observable trend. The airport subset is selected and all datapoints outside of a centered 20 ft interval of the selected level off altitude are filtered out. Below in Figure 8, level off distances are examined. Stringent filtering is required to observe any trend beyond the previously observed simplistic trend of the shortest distance being most common in Figure 6.



**Figure 8.** Level off distance examined at each level off altitude.

Outliers in the figure above could be holding patterns or other anomalies. Still, no clear trend is observable, so level off distance recommendations remain inconclusive according to Figure 8. It is recommended that the manufacturer-supplied level off distance be utilized. Level offs modeled for the aircraft above in AEDT currently are around six nmi. This is actually a nice median in the figure above. If any adjustment is to be made, it would be to shorten the level off distance.

Final recommendations for level off altitude are summarized in Table 3. Note that existing profiles have either a CDA or a level off at 3000 ft. Profiles that already exist are marked with an “X”, whereas profiles that would be inserted are numbered in order of significance with “1” as the highest priority. Much of the older aircraft already have CDAs, while the newer aircraft have level offs at 3000 ft. All Airbus aircraft have only level offs defined when about 40% of approaches actually use CDAs. That is one of the more significant discrepancies.

With these recommendations in order, future work would involve incorporating threaded track data from radar to confirm these findings. Further analysis can be done on level off distance if required.



**Table 3.** Aircraft AEDT profile recommendations.

Aircraft	CDA	LO 2000	LO 3000	LO 4000
B717-200	X	1	2	3
B737-700	X	1	2	3
B737-800	1	2	X	3
B737-900	1	2	X	3
B757-200	X	1	2	3
B757-300	1	2	X	3
B777-200ER	1	2	X	3
B777-200LR	1	2	X	3
MD-90	X	1	2	3
A319-100	1	2	X	3
A320-200	1	2	X	3
A321-200	1	2	X	3
A330-200	1	2	X	3
A330-300	1	2	X	3

**Milestone**

The objective of this Task is to provide insight as to how accurately the current AEDT approach profile represents the performance of real-world flight trajectories, and if the AEDT approach profiles are not accurate, to propose new profiles for use.

**Major Accomplishments**

- Obtained real-world FOQA performance data from airline partner for 14 airframes,
- Created a parsing algorithm which observes only the approach phase of flight.
- Created an algorithm which detects a level segment during the approach phase,
- Used this algorithm to create a detailed statistical analysis of the FOQA data in order to observe common approach procedural patterns

**Publications**

None

**Outreach Efforts**

Bi-weekly calls with the FAA, Volpe, and ATAC. Bi-annual ASCENT meetings.

**Awards**

None

**Student Involvement**

Ana Gabrielian and Loren Isakson, Graduate Research Assistants, Georgia Institute of Technology

**Plans for Next Period**

- This Task is being continued in ASCENT 54

# Task 3 – Integrated Impact Assessment of Inaccuracies from Thrust, Weight, Procedures, and NPD Curves

Georgia Institute of Technology

### Objective

Assess the total impact of proposed improvement in accuracy in modeling assumptions from thrust, weight, procedures, and NPD curves in AEDT versus real-world settings. The final comparisons will be among standard baseline AEDT modeling assumptions, improved AEDT modeling assumptions (based on real-world data), and actual real-world noise contours.

### Research Approach

The overall research approach is presented in Figure 9. The focus of this Task was the departure phase of flight. Detailed information about the processing of FOQA data, the determination of departure modes, and the creation of new NPDs and fixed-point profiles can be found in the 2019 ASCENT 45 Annual Report.

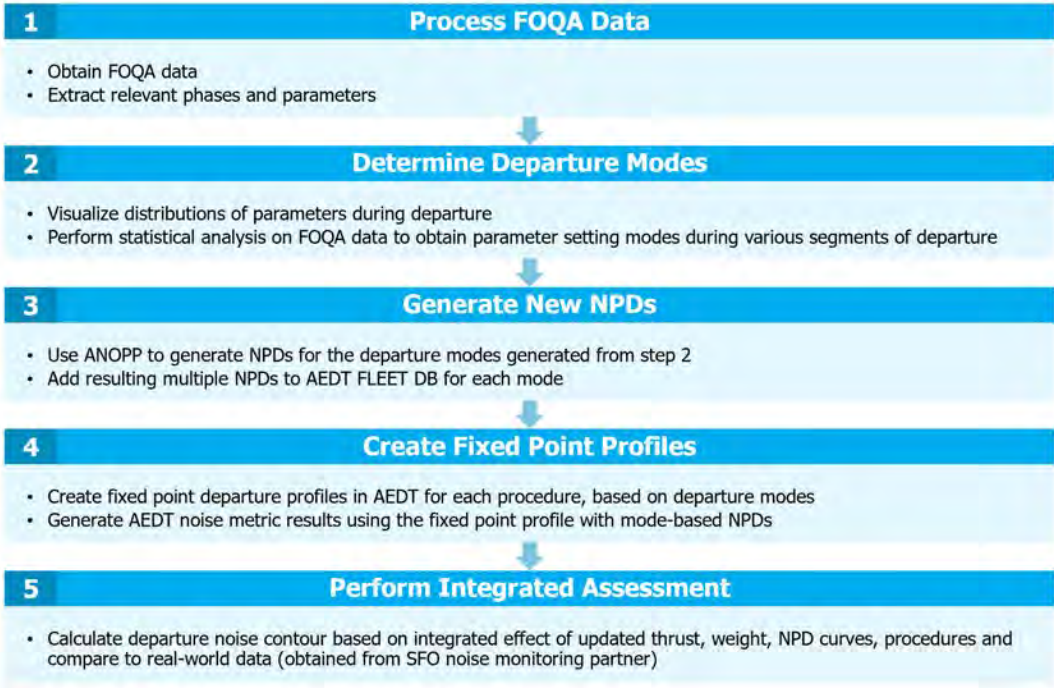
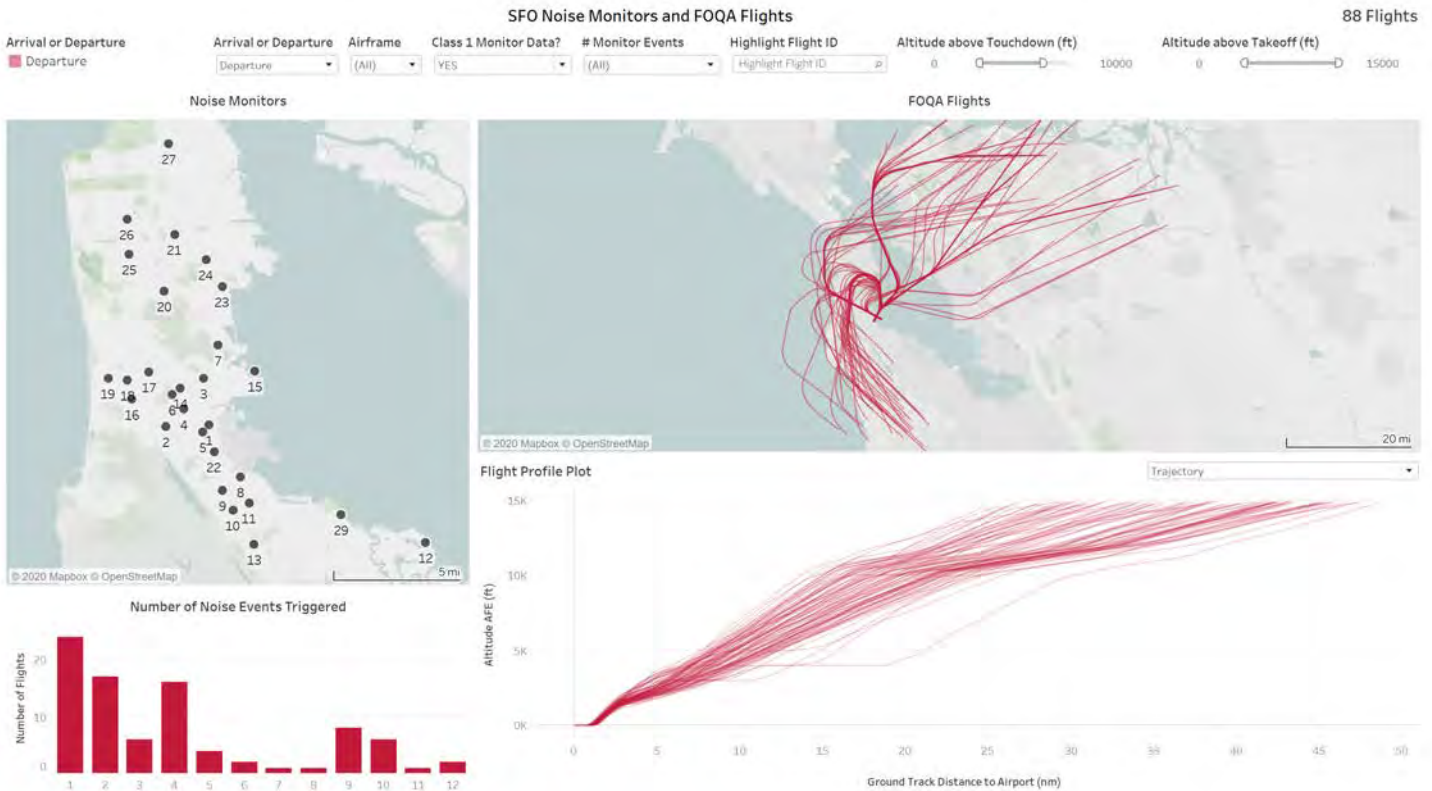


Figure 9. Task 3 research approach.

In order to visualize the results from the integrated impact assessment, a dashboard was created in Tableau. A sample view of the input side of the dashboard is shown in Figure 10. A breakdown of all 88 flights shown in this sample view is described in Table 4. The dashboard is useful in visualizing both the vertical profile and the ground track of the aircraft, in addition to the noise sensor locations. Many filters are available to isolate different flights based on airframe type, noise monitors triggered by the flight, etc. Each of the 88 flights shown in the sample view represents a real-world FOQA flight which has been modeled in AEDT and has linked noise validation data from the KSFO noise monitoring program.



**Figure 10.** Sample view of input section of dashboard.

**Table 4.** Number of flights by aircraft type for input dashboard

FOQA Aircraft	AEDT Aircraft	# Flights
737-800	737-800	21
737-900ER	737-800	59
757-200	757-300	3
757-300	757-300	4
A320-200	A320-211	1

Additional progress on this task is covered in the ASCENT Project 62 “Noise Model Validation for AEDT” 2020 Annual Report.

**Milestones**

None

**Major Accomplishments**

- Created visualization dashboards and statistical analysis codes to visualize validation flights and their associated noise data,



### **Publications**

None

### **Outreach Efforts**

Bi-weekly calls with the FAA, Volpe, and ATAC. Bi-annual ASCENT meetings.

### **Awards**

N/A

### **Student Involvement**

Dylan Monteiro, Graduate Research Assistant, Georgia Institute of Technology

### **Plans for Next Period**

Further efforts on this task are covered under ASCENT Project 62 "Noise Model Validation for AEDT".



# Project 046 Surface Analysis to Support AEDT Aircraft Performance Model (APM) Development

## Massachusetts Institute of Technology and Massachusetts Institute of Technology Lincoln Laboratory

### Project Lead Investigator

Hamsa Balakrishnan  
William E. Leonhard (1940) Professor  
Aeronautics and Astronautics  
Massachusetts Institute of Technology  
77 Massachusetts Ave., 33-207  
Cambridge, MA 02139  
617-253-6101  
hamsa@mit.edu

### University Participants

#### Massachusetts Institute of Technology (MIT) and MIT Lincoln Laboratory

- PI: Hamsa Balakrishnan
- FAA Award Number: 13-C-AJFE-MIT, Amendment Nos. 021, 035, 044, 047, 063, and 068
- Period of Performance: July 7, 2016 to August 10, 2021
- Tasks:
  1. Undertake more detailed studies to extend Aviation Environmental Design Tool (AEDT) capabilities to model surface noise and emissions impacts.
  2. Identify representative application scenarios and estimate the impact of improved surface movement modeling capability.
  3. Develop implementation plan to transition appropriate surface modeling enhancements into the operational AEDT product.

### Project Funding Level

FAA provided \$625,000 in funding and \$625,000 matching funds are from MIT.

### Investigation Team

- Prof. Hamsa Balakrishnan, co-PI (MIT)
- Dr. Tom Reynolds, co-PI (MIT Lincoln Laboratory)
- Sandeep Badrinath (graduate student)
- Emily Joback (MIT Lincoln Laboratory staff)

### Project Overview

The objective of this research project is to identify and evaluate methods for improving taxi performance modeling in the Aviation Environmental Design Tool (AEDT) in order to better reflect actual operations. This objective is being met through the analysis of relevant data sources, including surface surveillance (Airport Surface Detection Equipment, ASDE-X), Aviation System Performance Metrics (ASPM) taxi time, Flight Data Recorder (FDR), and air quality monitor datasets. Prior phases of the ASCENT Project 46 have identified first order enhancements to the AEDT Aircraft Performance Model (APM) for surface operations. Specific improvement areas include enhanced baseline taxi fuel flow models; improved taxi times at different airports; and estimation of pre-taxi engine and auxiliary power unit (APU) fuel burn. These enhancements were described in the 2019 annual report. This phase of the work has extended and refined fuel burn modeling in these areas, as well as

undertaking initial studies to explore whether improved surface emissions models can leverage these enhanced fuel models. In particular, the research team has undertaken a detailed assessment of surface operations and associated air quality impacts at Los Angeles International Airport (LAX) due to extensive data availability at that location. The next focus is on expanding the LAX findings to more airports and exploring the impacts of findings on the current implementation of the Delay, Sequence, and Queuing Model (DSQM). We will make recommendations on AEDT improvements from all these analyses.

## Task Progress and Plans

This report summarizes the latest accomplishments in each of the ASCENT46 task areas.

### Task 1 – Undertake More Detailed Studies to Extend AEDT Capabilities to Model Surface Noise and Emissions Impacts

Massachusetts Institute of Technology

In prior phases of the work, relevant literature sources and other modeling approaches were identified and reviewed with respect to surface noise and emissions modeling (e.g., ACRP 02-27, (Martin et al., 1996), ACRP 02-45, (Kyprianidis et al., 2015), and P3-T3 emissions models (Doppelheuer & Lecht, 1998)). Based on these activities, a roadmap has been developed of how researchers will use the enhanced surface fuel flow models to benefit noise and emissions modeling in AEDT. The work on this Task to date has focused on leveraging the enhanced surface fuel burn models to determine taxi emissions on the airport surface for any given airport operating condition (fleet mix, demand profile, etc.) and meteorological conditions using the approach presented in Figure 1. It comprises two elements: a statistical model of emissions dispersion patterns built on the enhanced surface fuel burn models from prior phases of the work, and a model of the queuing areas on the airport surface.

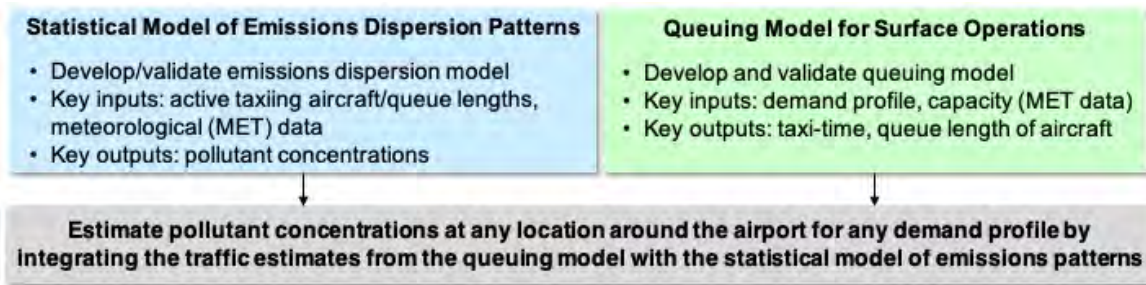


Figure 1. Enhanced air quality modeling approach.

Implementation of these models has been demonstrated initially for LAX due to the availability of detailed airport Performance Data Analysis and Reporting System (PDARS) surface surveillance and associated high resolution air quality monitor measurements over a six-week period from February 1 to March 16, 2012. Over this period, the airport was operating in west-flow configuration (i.e., taking off and landing to the west) for over 90% of the time, and hence was the focus for the analysis. Air pollutant measurements for CO, NO, NO<sub>2</sub>, NO<sub>x</sub>, PM<sub>2.5</sub>, and ultra-fine particulate (UFP) were available from four air quality monitor locations termed Community North, East, and South (CN, CE, and CS respectively) and AQ to the north located 500-5,000 ft from the airport boundary as illustrated in Figure 2. Because of their location in the urban environment in communities around LAX, these monitors measured both airport and non-airport pollutant sources, and this needed to be carefully considered in the analysis.

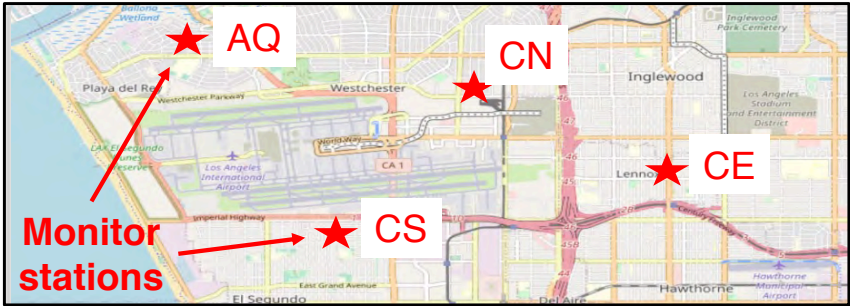


Figure 2. LAX air quality monitor locations.

Each monitor recorded measurements of CO, NO, NO<sub>x</sub>, SO<sub>2</sub>, PM<sub>2.5</sub>, and UFP concentrations every minute. The median measurements over the six-week measurement period for some of these species as a function of local time are presented in Figure 3. It is seen that variations in the species are influenced greatly by diurnal photochemical reactions which makes their dynamics as a function of airport traffic very hard to discern.

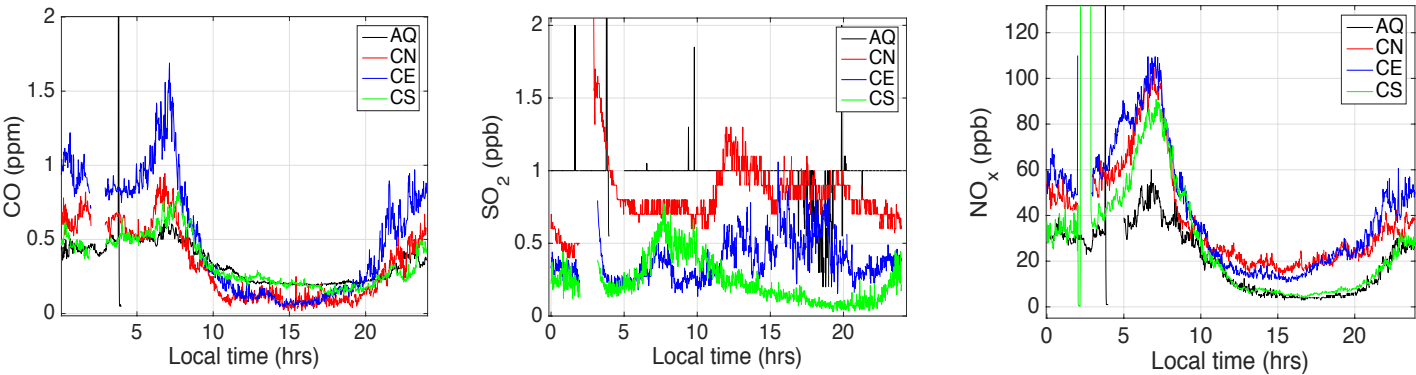


Figure 3. Sample air quality monitor median measurements of CO, SO<sub>2</sub>, and NO<sub>x</sub> species as a function of local time over the six-week test period.

Therefore, there was a need to consider other pollutants in order to identify good correlations with airport activity. UFPs are aerosols with an aerodynamic diameter of 0.1 μm (100 nm) or less. There is a growing concern in the public health community about the contribution of UFPs to human health. Despite their modest mass and size, they dominate in terms of the number of particles in the ambient air. Figure 4 presents a plot of median 100 nm UFP measurements from a representative monitor (the CE site, in this example) relative to aircraft movements as a function of local time. These UFP concentrations are seen to be a very good signature for airport traffic: PM particle diameter depends on the thrust setting of the engine which helps isolate taxi emissions from other phases of flight, and particle diameter from aircraft emissions is much lower than vehicular emissions or other sources.

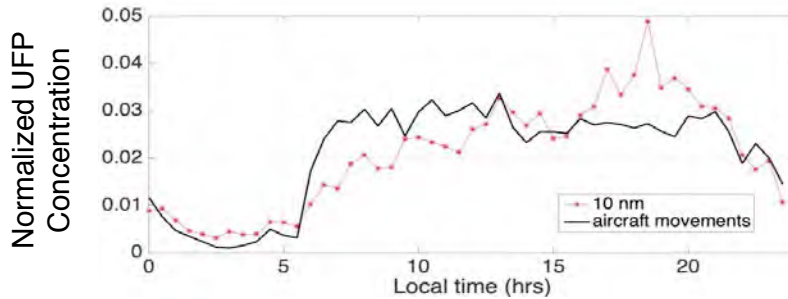


Figure 4. 100 nm UFP and aircraft movement correlation.

Given this strong UFP correlation to aircraft traffic on the airport surface, we built a preliminary statistical model of emissions dispersion patterns that estimates the UFP concentration (i.e., what the monitor observes) as a function of the aircraft traffic on the surface and meteorological conditions (winds, temperature, and solar irradiance). We developed two classes of models: a temporal one that only focuses on each monitor location (and does not try to generalize to all locations on the surface), and another spatial model that tries to infer the spatial impacts as well (which is a much harder problem, especially given we had data from only four monitor locations, and there are a lot of effects at play). Time-delays are found to be important, since the advection of the pollutants is not instantaneous. We investigated both linear regression and Gaussian Process Regression (GPR) models (which are non-parametric, can capture nonlinear effects, and estimate the probability distribution of the dependent variable).

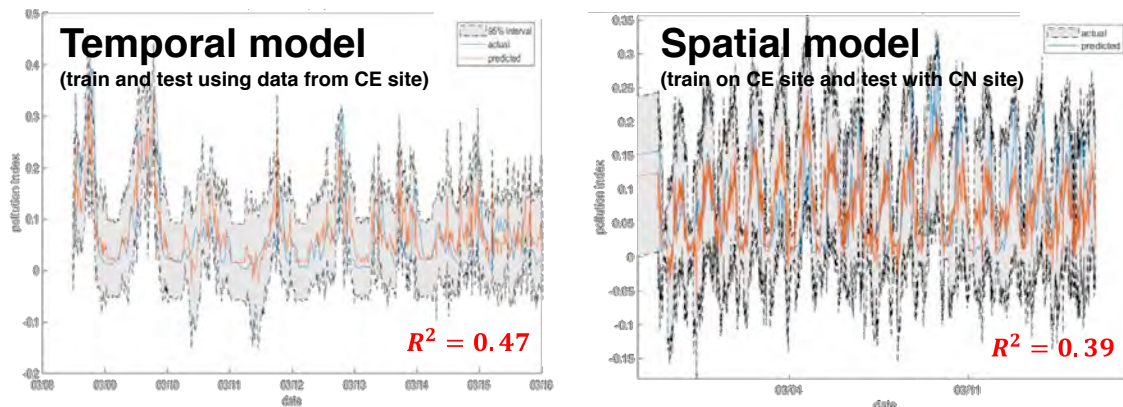


Figure 5. Preliminary emissions model based on GPR (left) temporal and (right) spatial models.

Figure 5 shows sample results from the temporal and spatial GPR models. The blue lines are the mean predicted values, the grey regions are the 95% confidence intervals, and the red lines are the observed values of a weighted UFP concentration. As expected, the temporal model performs better than the spatial model, as shown by the respective  $R^2$  scores. We also find that the performance of the spatial model varies by monitor (location), with better performance at the downwind sites (which makes sense since the pollutants are being transported and dispersed towards them).

The second element of Figure 1 is the development of a model of airport surface queuing locations. For LAX, PDARS and FAA Aviation System Performance Metrics (ASPM) data was available for the same six-week period as the air quality monitor data. This was used to identify the taxi time distributions for departures from the airport, as shown in Figure 6 for the case of taxi-out time.

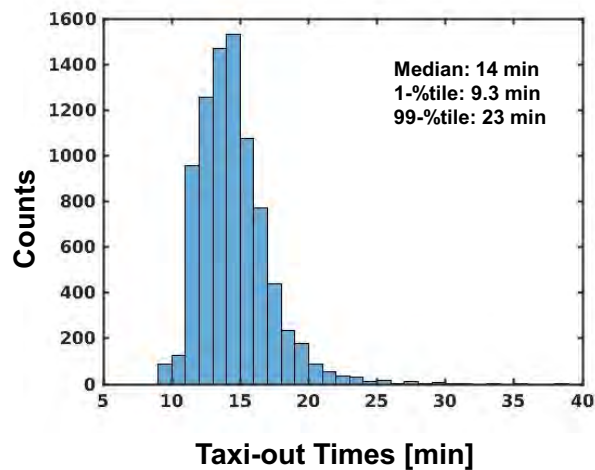


Figure 6. LAX taxi-out time distribution for a 6-week test period.

The time periods making up the 99th percentile taxi-out times were taken to be representative of periods when the airport was most congested. These were then used to identify heat maps of queueing locations on the airport surface, as shown in Figure 7. The hypothesized causes of the observed queueing locations are also presented, which fall into general “queue building block” categories of:

- departure runway queues
- terminal/spot queues
- runway crossing queues
- other areas (e.g., remote/corporate pad queues)

These results are now being used to develop queueing models for the various parts of the LAX airport surface. A particular finding in our initial analysis relates to the need to calibrate the unimpeded taxi times of aircraft, rather than relying on the ASPM calculated values, while building the queueing models. We use the ASPM records of gate and runway times to infer various parameters of the queueing model, such as the service times of different runway queues, as well as the unimpeded taxi times. By estimating the time spent idling in different queues (corresponding to hotspots on the surface), we can estimate the emissions that occur at different locations on the airport surface.

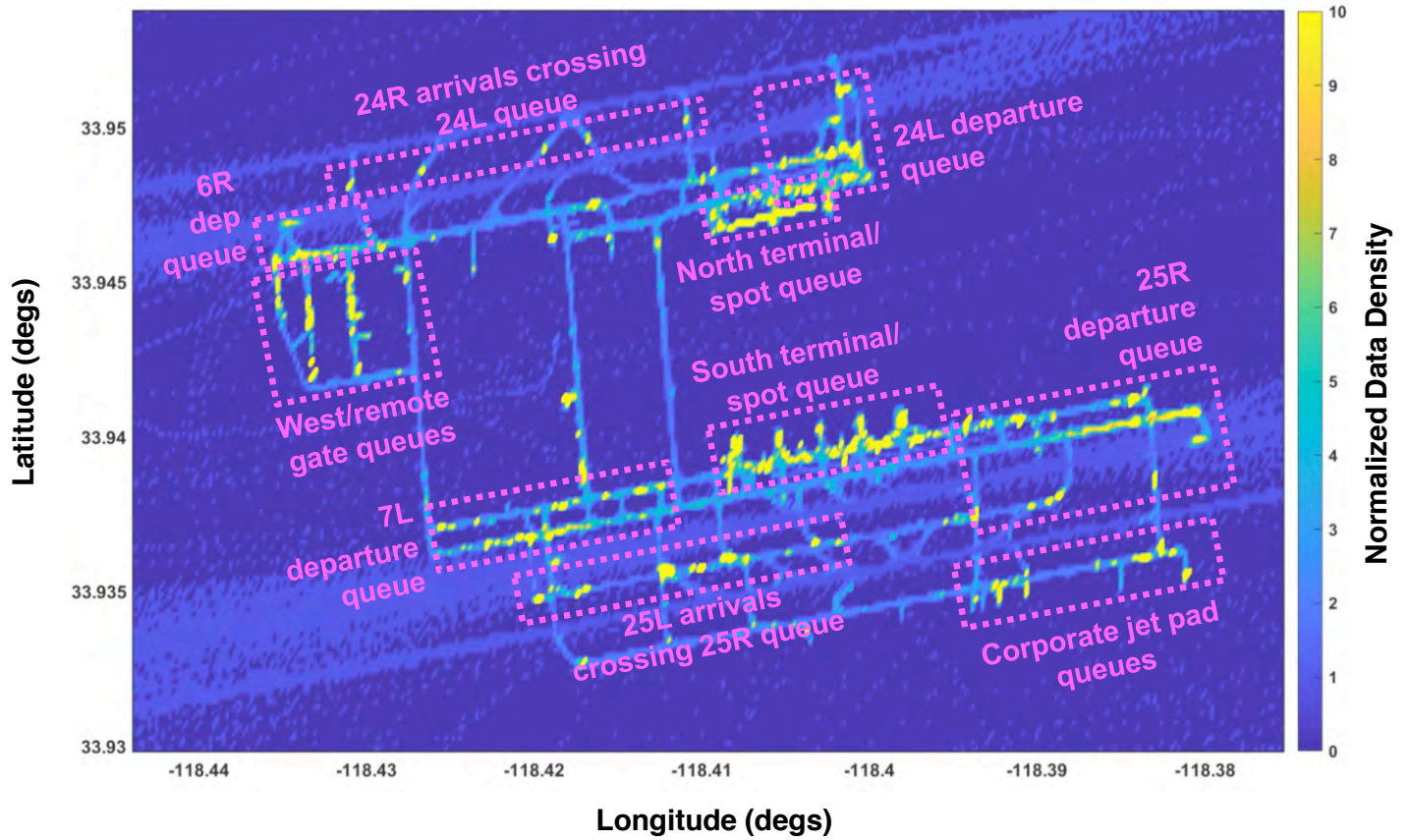


Figure 7. LAX queuing location heat map and hypothesized causes.

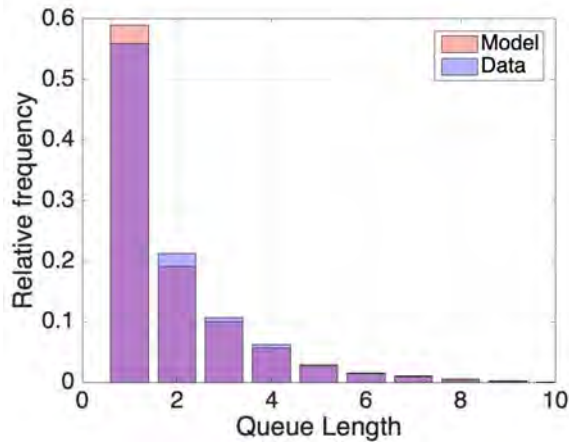


Figure 8. LAX queuing model preliminary results, showing a comparison of modeled and observed runway queue length frequency distributions. The purple regions correspond to an overlap of the model estimates and observed values, while light red regions correspond to the model estimates exceeding the observed values, and the blue regions correspond to the observed values exceeding the model estimates.

Figure 8 shows a comparison of the queuing model-predicted runway queue lengths and the observed values for an independent training set. The mean error is 0.02 aircraft and the mean absolute error is 0.64 aircraft. Next, we propose to validate the queuing model by comparing the queue lengths with those estimated from ASDE-X data (i.e., the heat map in Figure 7).

## Task 2 – Identify Representative Application Scenarios and Estimate the Impact of Improved Surface Movement Modeling Capability

Massachusetts Institute of Technology

Plans for this Task moving forward include:

- Improve the performance of emissions model by:
  - Exploring other input features
  - Different machine learning methods
- Develop and validate queuing model for LAX
  - Model will be developed using larger quantities of historical ASDE-X and ASPM operational data
  - Capable of estimating surface traffic based on demand, capacity (meteorological data)
- Integrate the queuing model with the statistical model of emissions dispersion patterns to evaluate the performance of the resulting emissions estimate
- Explore generalizing results to other airports
  - Develop lookup table of queue building blocks for a set of different classes of airports and runway configurations
  - Leverage prior ASCENT-funded efforts to inform this task (e.g., CLT, DFW, PHL, BOS, and LGA airports)
- Evaluate implications for AEDT/DSQM

Priorities for extensions will be established through continued engagement with FAA sponsors, AEDT developers, and other appropriate stakeholders.

## Task 3 – Develop Implementation Plan to Transition Appropriate Surface Modeling Enhancements into the Operational AEDT Product

Massachusetts Institute of Technology

The research team conducts regular analysis status and results review with FAA sponsors and AEDT developers. This will continue moving forward, with the intent to identify an implementation plan and schedule to transition specific surface modeling enhancements into appropriate versions of the operational AEDT product given their developmental maturity and programmatic priorities.

### Milestones

Task 1 has been the primary focus in CY2020. Tasks 2 and 3 will be the focus of the next three months of the current period of performance. In particular, based on discussions with FAA sponsors and AEDT developers, we plan to develop a lookup table that identifies the components of queuing network models for different types of airports.

### Publications

N/A

### Outreach Efforts

N/A

### Awards

None

## **Student Involvement**

MIT students have been involved in this research. Sandeep Badrinath is currently a PhD candidate in Aeronautics and Astronautics at MIT. We also had an undergraduate student, James Abel, involved in this project over the summer.

## **Plans for Next Period**

The ongoing phase of work involves enhancing AEDT's surface performance modeling to augment its dispersion modeling capabilities for airport air quality analysis, using a statistical model of emissions dispersion patterns. In particular, the research team will assess the current implementation of the DSQM and associated issues, will make recommendations on improvements, and if appropriate, develop a new/improved surface queuing model that would address these issues. The next extension to this work focuses on maturing the surface fuel, noise, and emissions models to a point they are suitable for implementation in the operational AEDT. Implementation pathways into the operational AEDT product will then be created for the surface fuel, noise, and emissions modeling enhancements. This will be conducted in close collaboration with the AEDT developers and key stakeholders and will focus on AEDT capabilities matched to the needs of different user classes. Sensitivity studies will also be conducted as needed. Specific planned tasking is described below.

### **Task 1: Undertake more detailed studies to extend AEDT capabilities to model surface noise and emissions impacts**

In the prior phase of the work, relevant literature sources and other modeling approaches have been identified and reviewed with respect to surface noise and emissions modeling (e.g., ACRP reports, P3-T3 emissions models, etc.). Based on these activities, a roadmap has been developed of how the researchers will use the enhanced surface fuel flow models to benefit noise and emissions modeling in AEDT. The current proposal is to map engine power settings for different taxi phases (stops, idle taxi, and accelerations) to noise and emissions effects. By considering the accuracy of resulting noise and emissions effects as a function of location on the airport surface, we can start to understand the potential utility of these proposed enhancements. We are initially using the case of A320 FDR data to illustrate how we can analyze taxi speed profiles to identify acceleration events on the airport surface. These in turn can be used to determine correlations between acceleration events and fuel flow and thrust spikes from the relevant parameters in the FDR data. In this Task, similar correlations will be found for other aircraft types contained in our FDR data archive which can then be used for airports where we do not have FDR data but do have ASDE-X data, from which we can identify acceleration events as a function of time and location. The resulting fuel flow and thrust profiles will be used as inputs to appropriate noise and emissions analyses for those airports. Sensitivity studies will also be conducted as appropriate.

The main subtasks will be:

1. **Enhance noise modeling** by incorporating location-specific thrust levels during taxi (e.g., ramp area, taxiways, runway queues).
2. **Evaluate and refine baseline emissions indices** by considering modeling techniques that are based on analysis of FDR data, as has been considered for cruise emissions (e.g., DLR or P3-T3 methods). We will also consider ranges provided by different methods, and the discrepancies with the International Civil Aviation Organization (ICAO) Emissions Databank values. We have begun to analyze the A4A fuel burn data for this purpose and will continue to do so.
3. **Initial investigation and assessment of APU emissions** by considering prior Airport Cooperative Research Program (ACRP) studies (e.g., ACRP 02-25 and ACRP 02-03a). We will also look into the possibility and value of obtaining FDR data that includes APU parameters.

### **Task 2: Identify representative application scenarios and estimate the impact of improved surface movement modeling capability**

The main subtasks undertaken will be:

1. Identify a few practical scenarios that represent environmental analysis of typical airport settings.
2. Use AEDT baseline modeling and user defined inputs to predict noise, emission, and fuel burn for the scenarios identified.
3. Compare the predictions and evaluate the impact of the improved surface movement modeling capabilities from the ongoing phase.
4. Compare with field measurement data if such data are available.

Priorities for extensions will be established through continued engagement with FAA sponsors, AEDT developers, and appropriate other stakeholders.



### Task 3: Develop implementation plan to transition appropriate surface modeling enhancements into the operational AEDT product

The research team conducts regular analysis status and results review with FAA sponsors and AEDT developers. This will continue in the current tasking with the intent of identifying an implementation plan and schedule to transition specific surface modeling enhancements into appropriate versions of the operational AEDT product given their developmental maturity and programmatic priorities. Further engagement with AEDT developers in prior phases of the work identified the need for functionality tailored to different user classes, ranging from:

1. **Basic users** wanting the ability to select “pre-canned” options representative of typical operating conditions, e.g., based on ASPM-derived empirical distributions. We can also analyze the impact of infrastructure development (for example, runway construction) that can change the airport capacity and traffic flows on the surface and have a subsequent effect on fuel burn, noise, and emissions.
2. **Intermediate users** wanting the ability to modify behaviors based on appropriate modeled parameters, e.g., available in the existing AEDT delay and sequence model.
3. **Advanced users** wanting complete control over all aspects of aircraft and airport dynamics, e.g., based on ASDE-X data.

### References

- ACRP 02-25. (2012). Handbook for evaluating emissions and costs of APUs and alternative systems. Transportation Research Board
- ACRP 02-27. (2009). Enhanced modeling of aircraft taxiway noise, volume 1: Scoping. Transportation Research Board
- ACRP 02-27. (2013). Enhanced modeling of aircraft taxiway noise, volume 2: Aircraft taxi noise database and development process. Transportation Research Board
- ACRP 02-45. (2016). Methodology to improve EDMS/AEDT quantification of aircraft taxi/idle emissions. Transportation Research Board
- S. Badrinath, M. Li and H. Balakrishnan. “An Integrated Surface-Airspace Model of Airport Departures,” AIAA Journal of Guidance, Control, and Dynamics, Vol. 42, No. 5, pp. 1049-1063, 2018.
- S. Badrinath, H. Balakrishnan, E. Joback and T.G. Reynolds. “Impact of Uncertainty on the Control of Airport Surface Operations,” *Transportation Science*, Vol. 54, No. 4, 2020, <https://doi.org/10.1287/trsc.2019.0957>.
- S. Badrinath, J. Ma, H. Balakrishnan and D. Delahaye. “A Comparative Analysis of Departure Metering at Paris (CDG) and Charlotte (CLT) Airports,” USA/Europe Air Traffic Management R&D Seminar, June 2019.
- Chati, Y.S., and Balakrishnan, H., “Analysis of Aircraft Fuel Burn and Emissions in the Landing and Takeoff Cycle using Operational Data,” Intl. Conf. on Research in Air Transportation, Istanbul, 2014.
- E. Clemons, T.G. Reynolds, S. Badrinath, Y. Chati and H. Balakrishnan, “Enhancing Aircraft Fuel Burn Modeling on the Airport Surface”, AIAA Aviation Conference, Atlanta, June 2018.
- Doppelheuer, A. & Lecht, M. (1998). Influence of engine performance on emission characteristics. RTO AVT Symposium on Gas Turbine Engine Combustion, Emissions and Alternative Fuels, Lisbon.
- DOT-VNTSC-FAA-16-11, “Aviation Environmental Design Tool – Technical manual, Version 2b”, U.S Department of Transportation (FAA), 2016.
- International Civil Aviation Organization (ICAO). (2014). Aircraft Engine Emissions Databank. Online database
- H. Khadilkar and H. Balakrishnan, “Estimation of Aircraft Taxi Fuel Consumption using Flight Data Recorder Archives”, Transportation Research Part D: Transport and the Environment, 17(7), 2012.
- Martin, R.L., Oncina, C.A., & Zeeben, J.P. (1996). A simplified method for estimating aircraft engine emissions. Appendix C of Scheduled Civil Aircraft Emission Inventories for 1992: Database Development and Analysis.
- I. Simaiakis and H. Balakrishnan. “A Queuing Model of the Airport Departure Process,” *Transportation Science*, 50(1), pp. 94-109, February 2016.



# Project 47 Clean-Sheet Supersonic Aircraft Engine Design and Performance

## Massachusetts Institute of Technology

### Project Lead Investigator

Prof. Steven R. H. Barrett  
Professor of Aeronautics and Astronautics  
Department of Aeronautics and Astronautics  
Massachusetts Institute of Technology  
77 Massachusetts Avenue – Building 33-322  
(617)-452 2550  
sbarrett@mit.edu

### University Participants

#### Massachusetts Institute of Technology

- PI: Prof. Steven R. H. Barrett
- FAA Award Number: 13-C-AJFE-MIT, Amendment Nos. 052, 059, and 074
- Period of Performance: March 29, 2019 to August 10, 2021 (with the exception of funding and cost share information, this report covers the period from October 1, 2019 to September 30, 2020)
- Tasks:
  1. Identify mission profiles and operating requirements for propulsion systems.
  2. Develop an engine cycle model for a supersonic aircraft propulsion system.
  3. Assess environmental footprint of an engine for a supersonic transport aircraft.
  4. Assess the effect of variable noise reduction systems on landing and takeoff (LTO) emissions of supersonic aircraft.

### Project Funding Level

FAA provided \$1,050,000 in funding and \$1,050,000 in matching funds were provided by the following sources: approximately \$239,000 from the Massachusetts Institute of Technology (MIT) and third-party in-kind contributions of \$177,000 from Byogy Renewables, Inc., and \$634,000 from NuFuels LLC.

### Investigation Team

- Prof. Steven Barrett (MIT) serves as PI for ASCENT Project 47 as head for the Laboratory for Aviation and the Environment. Prof. Barrett coordinates internal research efforts and maintains communication between investigators in the various MIT research teams.
- Dr. Raymond Speth (MIT) serves as co-investigator for Project 47. Dr. Speth directly advises student research in the Laboratory for Aviation and the Environment focused on assessment of fuel and propulsion system technologies targeting reduction of aviation's environmental impacts. Dr. Speth also coordinates communication with FAA counterparts.
- Dr. Jayant Sabnis (MIT) serves as co-investigator for Project 47. Dr. Sabnis co-advises student research in the Laboratory for Aviation and the Environment. His research interests include turbomachinery, propulsion systems, gas turbine engines, and propulsion system-airframe integration.
- Dr. Choon Tan (MIT) serves as co-investigator for Project 47. Dr. Tan directly advises student research in the Gas Turbine Laboratory focused on unsteady and three-dimensional flow in turbomachinery and propulsive devices, aerodynamic instabilities in aircraft gas turbine engines, and propulsion systems.
- Mr. Prashanth Prakash is a PhD student in the Laboratory for Aviation and the Environment. Mr. Prakash is responsible for developing engine models in the Numerical Propulsion System Simulation (NPSS) tool, for developing the combustor reactor network model, and for analyzing the sensitivity of engine emissions to design parameters.



- Mr. Laurens Voet is a PhD student in the Gas Turbine Laboratory. Mr. Voet is responsible for determining propulsion system requirements for supersonic aircraft designs, for relating the noise footprint to the relevant engine parameters, for estimating the effective perceived noise level (EPNL) for given aircraft trajectories, and for proposing clean-sheet engine design solutions to reduce its noise footprint.

## Project Overview

A number of new civil supersonic aircraft designs are currently being pursued by industry in different Mach regimes and for different size classes (e.g., supersonic business jets at low-supersonic Mach numbers and airliners at high-supersonic Mach numbers). Compared with those for subsonic aircraft, engines for supersonic aircraft present unique challenges in terms of their fuel consumption, noise, and emissions impacts because of their unique operating conditions. The propulsion systems currently proposed by the industry are developed around the core (high-pressure compressor, combustor, and high-pressure turbine) of existing subsonic engines, with modifications to the low-pressure spool (fan and low-pressure turbine).

ASCENT Project 47 aims to evaluate the design space of clean-sheet engines designed specifically for use on civil supersonic aircraft, and to determine the resulting environmental performance of such engines. Unlike previous commercial supersonic engines, which were adapted from military aircraft, or planned propulsion systems derived from current commercial engines, a clean-sheet engine takes advantage of recent advances in propulsion system technology to significantly improve performance and reduce emissions and noise footprints. This project will quantify these benefits for a range of engine designs relevant to currently proposed civil supersonic aircraft.

Specific goals of this research include:

- Development of a framework for quantifying the noise and emissions footprints of propulsion systems used on civil supersonic aircraft.
- Assessment of the difference in environmental footprint between a derived engine and a clean-sheet engine for a civil supersonic aircraft.
- Assessment of variable noise reduction systems used during noise certification of Supersonic Level 1 (SSL1) type aircraft and their effect on landing and take-off (LTO) emissions.
- Development of a roadmap for technology development, focusing on reducing the environmental footprint associated with engines for civil supersonic aircraft.

A summary of accomplishments to date include the following:

- A survey of supersonic transport concepts and existing designs was carried out, and the Stanford University Aerospace Vehicle Environment (SUAVE) was selected to analyze mission profiles and derive propulsion system requirements.
- Multiple engine models were developed in the NPSS tool. The baseline engine chosen for the derivative engine analysis was the CFM56-5B engine.
- The engine cycle model was used to evaluate the sensitivities of performance measures to design variables, technology assumptions, and propulsion system requirements.
- A reactor network framework was developed to estimate  $\text{NO}_x$  emissions. The model was calibrated to the International Civil Aviation Organization (ICAO) data for the CFM56-5B3 engine.
- A framework was set up to estimate the noise footprint sound pressure level (SPL), tone-corrected perceived noise level (PNLT) and effective perceived noise level (EPNL) of the engine given the relevant engine parameters using a semi-empirical model.
- Preliminary estimates have been made of the difference of pollutant emissions of engines for supersonic transport aircraft flying trajectories with and without variable noise reduction systems (VNRS).

## Task 1 – Identify Mission Profiles and Operating Requirements for Propulsion Systems

Massachusetts Institute of Technology

### Objectives

The first objective of this task is to identify representative mission profiles of commercial supersonic transport aircraft (i.e., characterize stages of the mission by defining parameters such as climb rates and accelerations). A second objective is to

use these mission profiles and representative aircraft parameters (e.g., wing area, drag and lift polars) of civil supersonic aircraft operating in different Mach regimes to derive propulsion system requirements for supersonic aircraft.

**Research Approach**

The mission profile of the NASA Supersonic Technology Concept Aeroplane (STCA) is used to get propulsion system requirements (Berton, 2019). The four critical sizing points of the NASA STCA, as illustrated in Table 1, are used in a multiple-design-point (MDP) model in the engine design process.

**Table 1.** Propulsion system requirements (per engine) for STCA. The top-of-climb conditions are chosen as the aerodynamic design point for any component that is purpose-designed for the application.

	Sea level static (SLS)	Takeoff (TO)	Top-of-climb (TOC)	End-of-cruise (EOC)
Altitude [kft]	0	0	41	51
Mach [-]	0	0.25	1.4	1.4
Thrust [lbf]	16,617	14,140	5,500	3,300

Mission requirements for other aircraft designs will be obtained through collaborations with ASCENT Project 10.

**Publications**

N/A

**Outreach Efforts**

None

**Awards**

None

**Student Involvement**

N/A

**Plans for Next Period**

Define the propulsion system requirements for different missions of supersonic transport aircraft (expected completion: April 2021)

**References**

Berton, J. & Geiselhart, K. (2019). NASA 55-tonne Supersonic Transport Concept Aeroplane (STCA) release package. NASA GRC/NASA LaRC.

**Task 2 – Develop an Engine Cycle Model for a Supersonic Aircraft Propulsion System**

Massachusetts Institute of Technology

**Objectives**

The objectives of this Task were to: 1) develop an engine cycle deck to analyze derivative and clean-sheet propulsion systems for commercial supersonic aircraft, 2) assess the sensitivities of engine performance metrics to constraints and propulsion system requirements to analyze the impact of design requirements and technology constraints on the engine performance, and 3) evaluate the design space constraints imposed by a constraint donor engine core on the environmental footprint.

**Research Approach**

The NPSS software (Claus, 1991) was chosen to develop the engine cycle decks for clean-sheet and derivative engines because it is an industry standard tool, which facilitates future collaboration with other users of the tool.



### Donor engine model

To develop the derivative engine, a baseline engine is first chosen and modeled. The CFM56-5B engine was chosen for this Task because it was the initial donor engine for the proposed GE Affinity engine. The engine architecture of the donor engine is illustrated in the bottom half of Figure 1. The baseline engine was modeled using published data from Jane's Aero Engines and data published in the Emissions Databank (EDB) by the European Union Aviation Safety Agency (EASA). The thrust versus fuel flow characteristic of the engine model is compared with data from the EDB of six CFM56 variants. The root mean square (RMS) error between the engine model results and the EDB data is 1.3%.

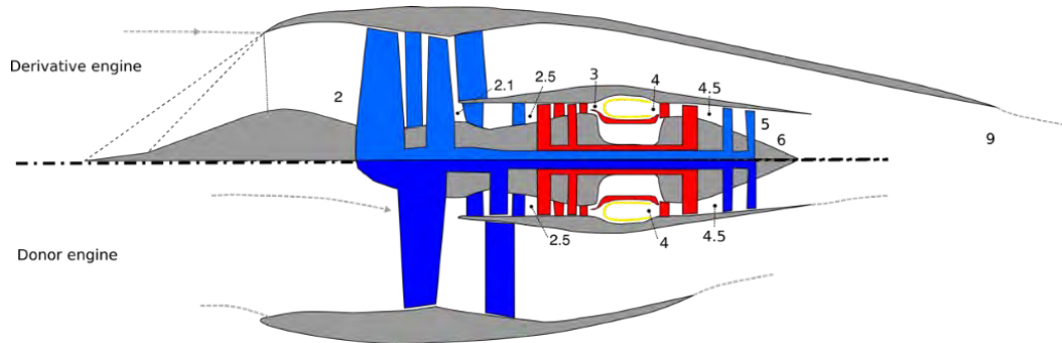


**Figure 1.** Engine architecture schematic. Lower half shows the subsonic donor engine. The high spool (red) core is used in the derivative engine along with modifications to the inlet, fan, and nozzle as shown on the top half.

### Derivative engine model

The thrust requirements of the derivative engine are given in Table 1. As shown in the engine architecture diagram in Figure 1, the derivative engine for supersonic application uses the high-pressure core of the donor subsonic engine. The low-pressure spool consists of a two-stage fan and a low-pressure turbine (LPT). An external compression supersonic inlet with two oblique shock stages is mounted upstream of the fan, with a pressure recovery modeled using standard oblique shock equations. A fully mixed, variable area nozzle is added downstream of the LPT. The engine is designed such that the nozzle is at the cusp of choke at takeoff conditions to avoid shock-cell noise. Polytropic efficiencies of the turbomachinery components are set to values representative of the CFM56-5B3 technology level. The map scalars of the turbomachinery components in the engine cycle model, the flow areas, and the cooling bleed flow fractions of the CFM56 donor engine core are applied as fixed constants to the derivative engine model.

### Clean-sheet engine model

The clean-sheet engine is also designed to meet the propulsion system requirements outlined in Table 1. The engine architecture for the clean-sheet design is the same as the derivative design. However, all the components for the clean-sheet engine, along with the high-pressure core, are purpose-designed. To have a fair comparison between the derivative and clean-sheet engine, the polytropic efficiencies of the turbomachinery are set to the CFM56 values to model the same technology level.

### Engine performance sensitivities

Sensitivities of engine performance metrics to constraints and propulsion system requirements are calculated for both the clean-sheet and derivative engine to analyze the impact of design requirements and technology constraints on the engine performance. A design vector,  $x$ , containing propulsion system requirements (net thrust,  $F_n$ , turbine inlet temperature,  $T_{t4}$ , flight parameter,  $\theta_{01}$ ) and design variables (mixer pressure ratio,  $Mix_{PR}$ , fan pressure ratio,  $\pi_{fan}$ , HPC pressure ratio,  $\pi_{hpc}$ ), and an objective vector,  $u$ , containing environmental response and performance metrics (specific fuel consumption, SFC,  $NO_x$  emission index,  $EINO_x$ , bypass ratio, BPR) are defined as:



$$\vec{x} = \begin{bmatrix} F_n \\ T_{I4} \\ \theta_0 \\ \text{Mix}_{PR} \\ \pi_{FPR} \\ \pi_{HPC} \end{bmatrix} \quad \begin{array}{c} \text{Requirements/} \\ \text{constraints} \\ \\ \text{Design Variables} \\ \\ \text{Response/ performance} \\ \text{metrics} \end{array} \quad \vec{u} = \begin{bmatrix} F_n \\ T_{I4} \\ \theta_0 \\ \text{Mix}_{PR} \\ \pi_{FPR} \\ \pi_{HPC} \\ \text{SFC} \\ \text{EINO}_x \\ \text{BPR} \\ \vdots \end{bmatrix} \quad (1)$$

The sensitivities of the objective vector with respect to the design vector

$$\frac{dU}{dx} = \begin{bmatrix} I_{n \times n} \\ \frac{\partial(SFC)}{\partial(F_n)} & \frac{\partial(SFC)}{\partial(T_{I4})} & \frac{\partial(SFC)}{\partial(\theta_0)} & \frac{\partial(SFC)}{\partial(FPR)} & \dots \\ \frac{\partial(EINO_x)}{\partial(F_n)} & \frac{\partial(EINO_x)}{\partial(T_{I4})} & \frac{\partial(EINO_x)}{\partial(\theta_0)} & \frac{\partial(EINO_x)}{\partial(FPR)} & \dots \\ \vdots & \vdots & \vdots & \vdots & \vdots \end{bmatrix} \quad (2)$$

are calculated using a 5-point finite difference stencil applied across the engine cycle model. The sensitivities of the engine model are also used in conjunction with the noise and emission model to assess sensitivities of the environmental footprint with respect to engine design parameters.

### Derivative engine design space constraints

A first-principle approach is used to evaluate design space constraints imposed by the donor core on the environmental footprint of the derivative engine. The engine cycle deck described above is used to calculate the engine performance in terms of SFC, emissions index, and noise of both the derivative and clean-sheet engine. Engine gaseous NO<sub>x</sub> emissions are quantified using the P<sub>3</sub>-T<sub>3</sub> method (DuBois and Paynter, 2006). The emissions index of NO<sub>x</sub> is assumed to be proportional to P<sub>t3</sub><sup>0.4</sup> and a polynomial fit in T<sub>t3</sub>, constructed based on engine emission data from the ICAO emission data bank, leading to the correlation

$$\frac{EI(NO_x)}{P_{t3}^{0.4}} = 6.26 \cdot 10^{-8} T_{t3}^3 - 0.00117 T_{t3}^2 + 0.0074 T_{t3} - 15.04 \quad (3)$$

The engine jet mixing noise is quantified using the SAE ARP876 jet noise power level method. The jet noise power, Π<sub>jet</sub>, is non-dimensionalized using the ambient density, ρ<sub>0</sub>, the ambient speed of sound, c<sub>0</sub>, and the jet area, A<sub>jet</sub>. The density exponent, ω, accounts for the effect of density on noise in heated jets. The power deviation factor, P, accounts for the variation of the classical 8-th power law by Lighthill.

$$\Pi_{jet}^* = \frac{\Pi_{jet}}{\rho_0 c_0^3 A_{jet}} = (6.67 \cdot 10^{-5}) \cdot P \cdot \left(\frac{\rho_{jet}}{\rho_0}\right)^\omega \cdot \left(\frac{V_{jet}}{c_0}\right)^8 \quad (4)$$

$$PWL_{jet} = 10 \log_{10} \Pi_{jet}^* - \frac{\Pi_{ref}}{\rho_0 c_0^3 A_{jet}} \quad (5)$$

### Milestones

Multiple engine models were developed in NPSS. The donor engine for the supersonic derivative core is chosen to be the CFM56-5B engine. The derivative engine model was used to evaluate the impact of design space constraints on the performance of the engine relative to the clean-sheet model.

## Major Accomplishments

### Engine performance sensitivities

Sensitivities of engine performance metrics with respect to design parameters are illustrated in Figure 2 for both the clean-sheet and derivative engine. In both cases we find that increasing the fan-pressure ratio (FPR) results in an increase in SFC. This is due to the increase in jet velocity and the corresponding reduction in the propulsive efficiency. Similarly, increasing the FPR also results in an increase in the compressor exit temperature and therefore results in an increase in the emissions index of  $\text{NO}_x$ . Increasing the turbine inlet temperature ( $T_{t4}$ ) results in an improvement in the thermal efficiency. However, it only results in a decrease in thrust-specific fuel consumption (TSFC) for the clean-sheet engine. This is due to the operation of the derivative core being a function of the turbine inlet temperature.

The derivative engine's high-pressure compressor (HPC) pressure ratio decreases as turbine inlet temperature are increased. This reduction in HPC pressure ratio as  $T_{t4}$  is increased results in a net increase in TSFC unlike the clean-sheet engine. Similarly, the HPC pressure ratio decreases as the FPR of the derivative engine is increased. The sensitivity of the TSFC of the derivative engine to the FPR is approximately twice as much as the clean-sheet engine due to the decreased thermal efficiency from the lower HPC pressure ratio and the decrease in propulsive efficiency from the increased FPR.

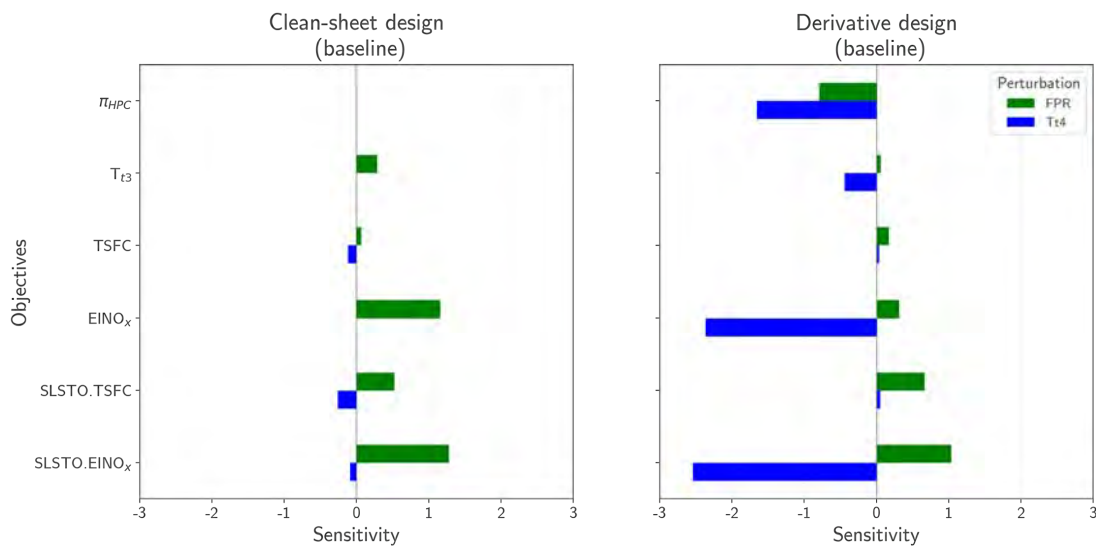


**Figure 2.** Sensitivities of engine performance parameters (HPC pressure ratio,  $\pi_{hpc}$ , compressor discharge temperature,  $T_{t3}$ , specific fuel consumption,  $TSFC$ , and  $\text{NO}_x$  emission index,  $EINO_x$ , at both design and sea-level static takeoff conditions) to engine design parameters (fan pressure ratio, FPR, and turbine inlet temperature,  $T_{t4}$ ) for the clean-sheet (left) and derivative (right) engine.

### Derivative engine design space constraints

Because the core of the derivative engine is sized by the donor-engine (CFM56) cycle, the pressure ratio of the high-pressure compressor of the derivative engine is not an independent design variable (in contrast to a clean-sheet engine where the HPC pressure ratio is a design variable that can be optimized). The design space of the derivative engine is illustrated in Figure 3. The core of the derivative engine also has cooling flows for the high-pressure turbine sized by the donor engine cycle. Therefore, there are regions of the design space where insufficient cooling flow can result in turbine metal blade temperatures exceeding the set limits. Therefore, the constraints from the donor core limit the feasible design space that can be used for the derivative engine.

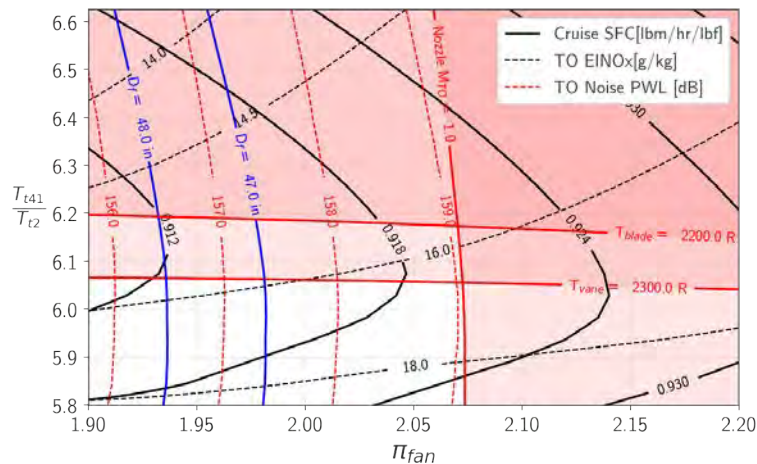


**Figure 3.** Design space of the derivative engine: turbine inlet temperature over compressor inlet temperature ratio,  $T_{t41}/T_{t2}$ , vs. fan pressure ratio,  $\pi_{fan}$ , at the engine aerodynamic design point. The performance contours are plotted at different engine operating points; cruise for specific fuel consumption (SFC) and takeoff for noise power level, PWL, and NOx emission index,  $EINO_x$ . Unshaded region represents the feasible design space of the derivative engine. The resulting fan diameter,  $D_f$ , for different designs in the design space is indicated.

### Publications

None

### Outreach Efforts

Mr. Prashanth Prakash and Mr. Laurens Voet gave a presentation titled "Clean-sheet supersonic engine design and performance" at the virtual ASCENT meeting on September 30, 2020.

### Awards

None

### Student Involvement

This task was conducted primarily by Prashanth Prakash, a graduate research assistant working under the supervision of Dr. Jayant Sabnis, Dr. Raymond Speth, and Dr. Choon Tan.

### Plans for Next Period

Various degrees of derivative engine models are to be developed, ranging from an "off-the-shelf" repurposing of an entire engine to using only the core of an existing engine (expected completion: May 2021).

A clean-sheet approach that ranges from redesigning a core with existing technology (e.g., metallurgy, cooling technology) to using new technology (e.g., advanced materials) and adaptive cycles to meet contrasting requirements at supersonic cruise and sea-level takeoff (expected completion: December 2021).

### References

Claus, Russell W., et al. "Numerical propulsion system simulation." *Computing Systems in Engineering* 2.4 (1991): 357-364.  
 D. DuBois and G. C. Paynter, "Fuel Flow Method 2 for estimating aircraft emissions," SAE Technical Paper, 2006.

# Task 3 – Assess Environmental Footprint of an Engine for a Supersonic Transport Aircraft

Massachusetts Institute of Technology

## Objective

The objective of this Task is to develop models to assess the environmental footprint of a supersonic transport aircraft. Models for both the noise footprint and the emissions footprint will be developed.

## Research Approach

The flow chart in Figure 4 illustrates the approach to model the environmental footprint of engines for supersonic transport.

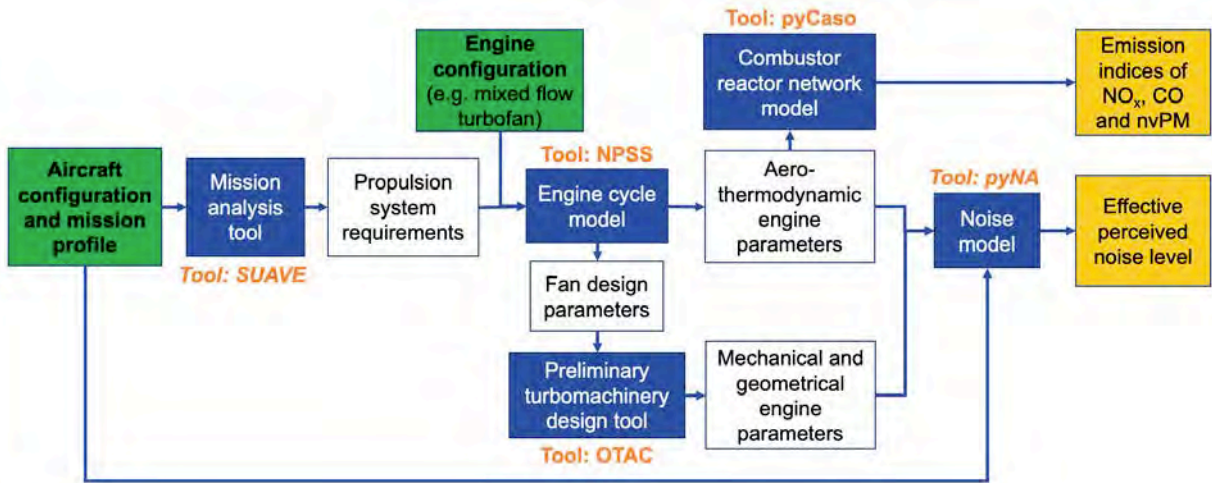


**Figure 4.** Overview of the framework to model environmental footprint of engines for supersonic transport (SST). The mission analysis is performed using the Stanford University Aerospace Vehicle Environment (SUAVE), the engine cycle model is made in the Numerical Propulsion System Simulation (NPSS) tool, the combustor reactor network model (pyCaso), and the noise model (pyNA) are used to calculate emission indices and effective perceived noise levels of the engines.

## Emissions modeling

A chemical reactor network combustor model (pyCaso) was developed to assess the emissions of the engines for supersonic transport. The combustor model represents CFM56-TechInsertion rich-quench-lean (RQL) combustor technology. The combustor model is illustrated in Figure 5. A series of perfectly stirred reactors in parallel, representing the primary zone of the combustor, are coupled to a secondary zone plug flow reactor. Similar to the engine model, the emission characteristics of the combustor model are validated against publicly available data from the EDB.

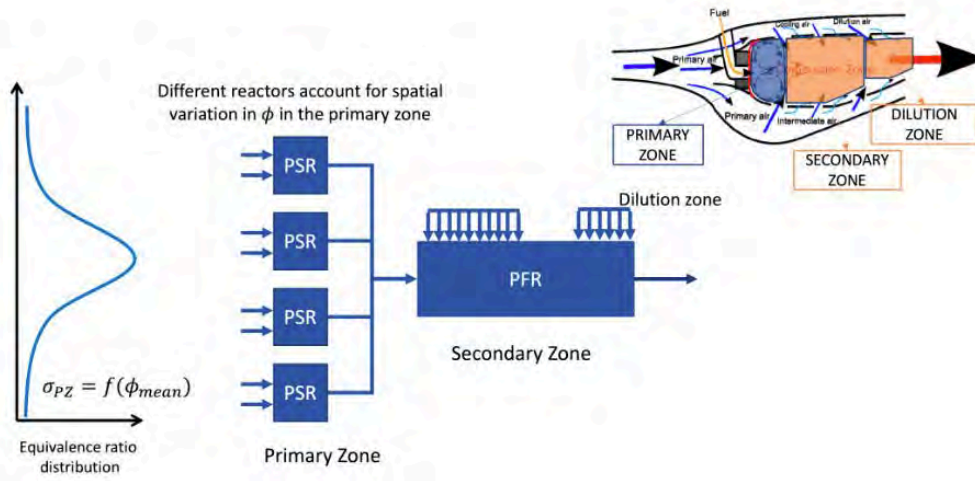


**Figure 5.** Chemical reactor network combustor model: a series of perfectly stirred reactors (PSR) in parallel, representing the primary zone, combined in parallel with a secondary zone plug flow reactor (PFR). The series of perfectly PRF represents a gaussian distribution, with standard deviation,  $\sigma_{PZ}$  being a function of the mean equivalence ratio,  $\phi_{mean}$ .

**Noise footprint modeling**

A python Noise Assessment (*pyNA*) model was developed to estimate the engine noise footprint as well as assess the sensitivities of the noise footprint with respect to relevant engine variables. The steps involved in estimating the effective perceived noise level (EPNL), given engine cycle and fan parameters, are shown in Figure 6.

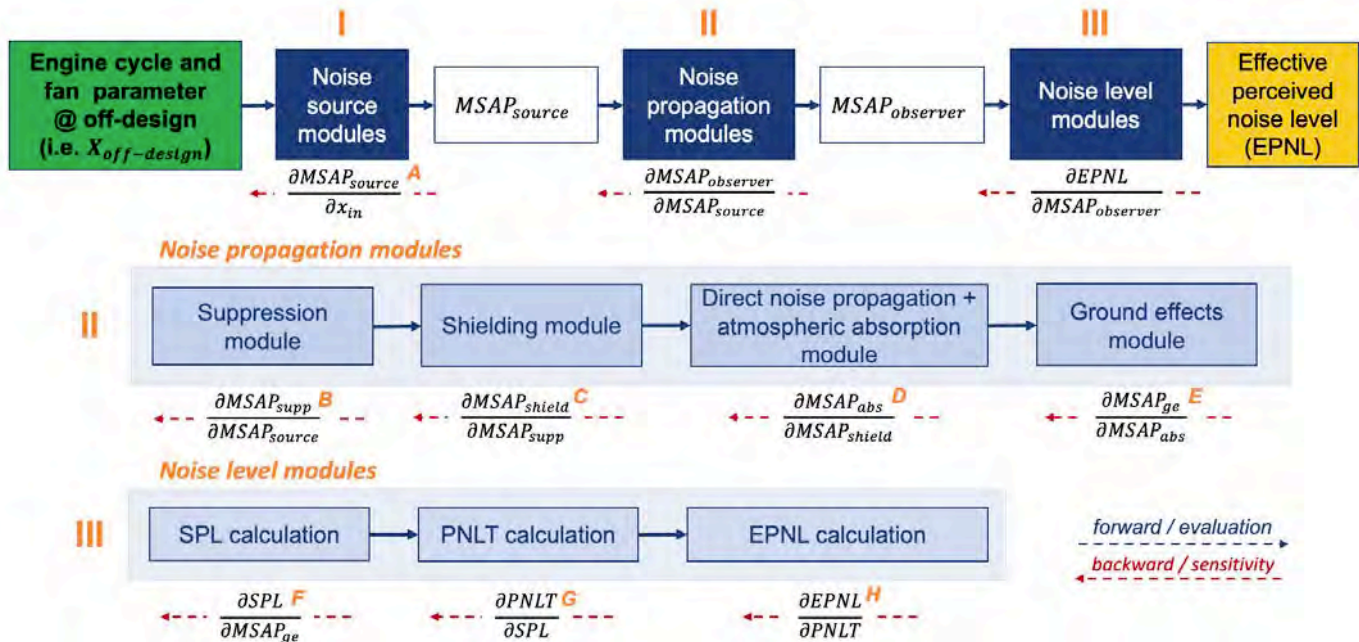


**Figure 6.** Flow chart of the python Noise Assessment (*pyNA*) model showing the different modules required to estimate the EPNL from engine cycle and fan parameters.

The different noise modules in *pyNA*, as shown in Figure 6, are developed using the methods from literature listed in Table 2, based on the Aircraft Noise Prediction Program (ANOPP) theoretical manual (Zorunski, 1981).



**Table 2.** Methods for the noise source, propagation, and levels modules.

Module	Method from literature
<b>Noise source modules</b> <ul style="list-style-type: none"> <li>Jet mixing noise</li> <li>Jet shock-cell noise</li> <li>Combustor noise</li> <li>Fan broadband and tones (inlet and discharge)</li> <li>Airframe noise</li> </ul>	Single-stream, shock-free jet mixing noise (SAE ARP876, 2012) Circular jet shock cell noise (SAE ARP876, 2012) Emmerling method FAA-RD-74-125 (Emmerling et al., 1976) Heidmann method NASA TM X-71763 (Heidmann, 1975) <ul style="list-style-type: none"> <li>with GEAE revision NASA CR-195480 for BB (Kontos et al., 1996)</li> <li>with AlliedSignal revision for RS tones (Hough et al., 1996)</li> <li>with fan treatment NASA CR-202309 (Kontos et al., 1996)</li> </ul> Fink method FAA RD-77-29 (Fink, 1977) with HSR calibration NASA CR-2004-213014 (Golub et al., 2004)
<b>Noise propagation modules</b> <ul style="list-style-type: none"> <li>Spherical spreading/ characteristic impedance</li> <li>Atmospheric absorption</li> <li>Ground reflection and attenuation</li> <li>Wing shielding module</li> </ul>	$R^2$ law and characteristic impedance ratio  Exponential decay from source based on absorption coefficient Chien-Soroka method (Chien et al., 1975) Maekawa method (copied shielding factors from STCA) (Maekawa, 1968)
<b>Certification Noise Levels modules</b> <ul style="list-style-type: none"> <li>Perceived noise level, tone corrected (PNLT)</li> <li>Effective perceived noise level (EPNL)</li> </ul>	ICAO Annex 16 Volume I: Aircraft noise App. 2-13 (ICAO, 2008)  ICAO Annex 16 Volume I: Aircraft noise App. 2-13 (ICAO, 2008)

The *pyNA* noise model is developed to have two different operating modes:

- **A forward, evaluation mode:** using engine off-design variables at takeoff/approach to calculate the certification EPNL (blue arrows in Figure 6). The noise source modules as well as the noise during the takeoff trajectory are verified with the NASA STCA noise assessment (Berton, 2019). The takeoff trajectory of the NASA STCA, including the noise source verification point are shown in Figure 7.
- **A backward, sensitivity mode:** calculating derivatives of the noise footprint with respect to engine off-design variables at takeoff/approach (red arrows in Figure 6). The partial derivatives of each module in Figure 6 are calculated using a pyTorch autograd implementation. The pyTorch derivative implementation is verified using a finite-difference scheme or analytical derivatives.

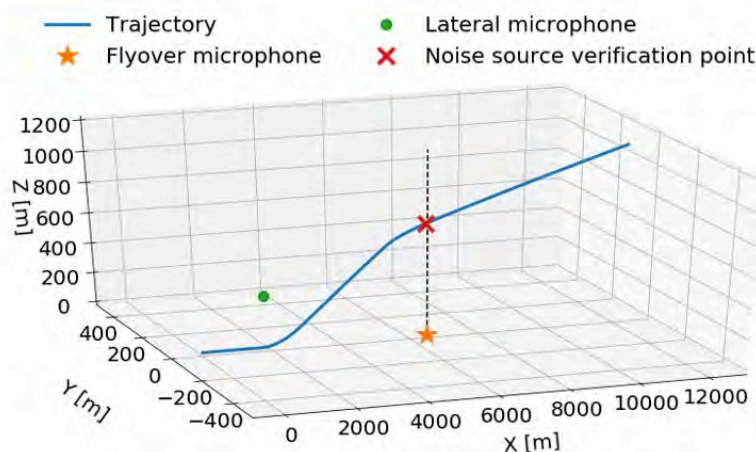


**Figure 7.** Standard takeoff trajectory of the 55-tonne STCA including lateral and flyover microphone positions. The noise source verification point is indicated with a red X.



## Milestones

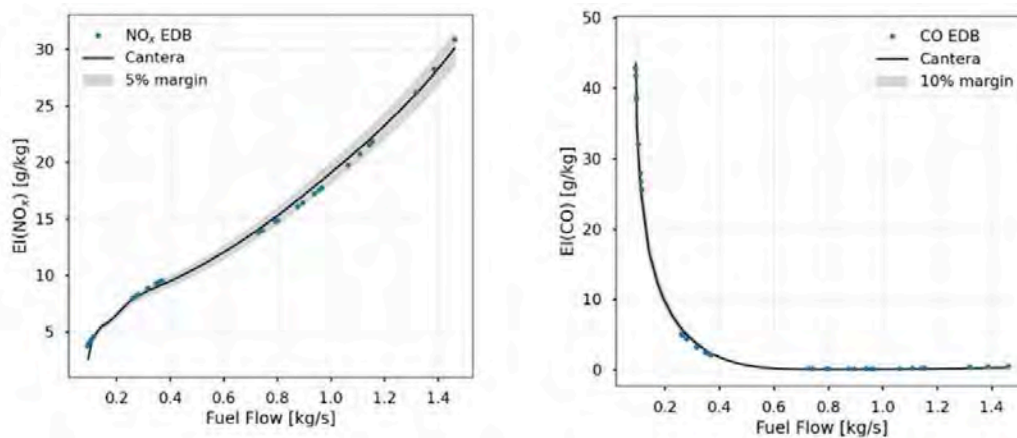
A chemical reactor network-based combustor model was developed, and NO<sub>x</sub> and CO emissions were calibrated to the EDB data using combustor inlet values obtained from the NPSS model of the CFM56-5B engine.

A model estimating the static noise database from relevant engine parameters, the static-to-flight noise projection, and the certification noise levels was set up.

## Major Accomplishments

### Emissions model

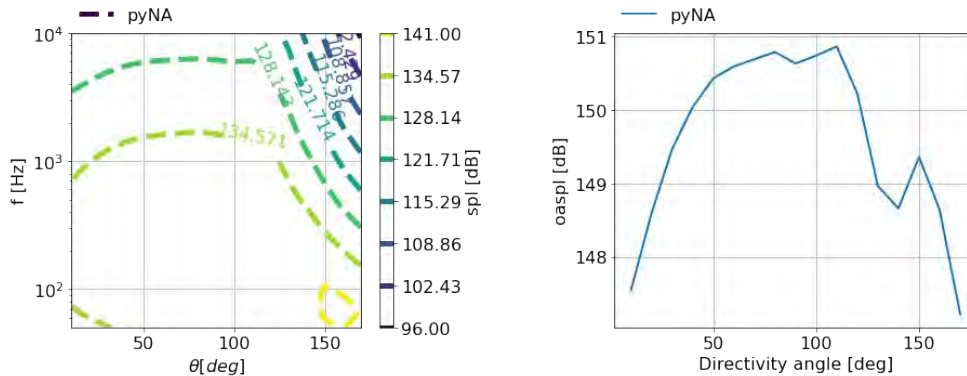
A framework was developed to estimate the NO<sub>x</sub> and CO emissions indices of the donor engine, given the relevant engine parameters using a reactor network model. A comparison of the model developed and the EDB data is shown in Figure 8. The derivative and clean-sheet engine analyzed in the work described here assumes that the combustor technology used is similar to that of the donor engine and therefore the calibrated parameters are assumed to hold for the clean-sheet engine as well. A soot model to estimate the non-volatile particulate matter (nvPM) concentrations is currently being integrated into the combustor model.



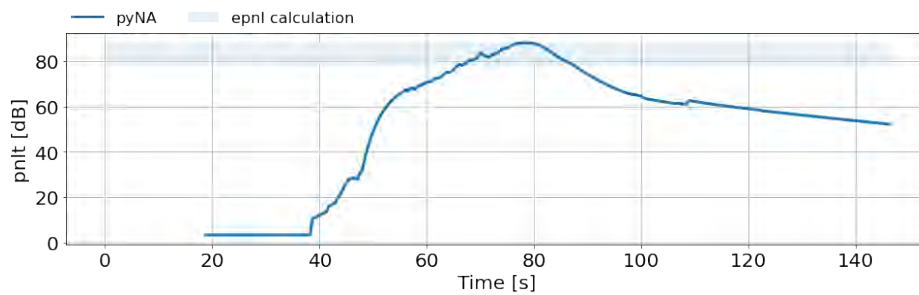
**Figure 8.** Comparison of NO<sub>x</sub> emission indices (left) and CO emission indices (right) of the combustor model and ICAO data from the EDB.

### Noise model (pyNA)

A framework was set up to estimate the noise footprint (SPL, PNLT, and EPNL) of the engine given the relevant engine parameters using a semi-empirical model. As an example, the jet mixing noise source SPL and the overall sound pressure level (OASPL) distribution are shown in Figure 9. The tone-corrected perceived noise level (PNLT) for jet mixing noise source, measured at the flyover microphone, is shown in Figure 10.



**Figure 9.** Jet mixing source SPL spectral and directivity distribution (left) and overall sound pressure level (OASPL) directivity distribution (right) at the noise source verification point.



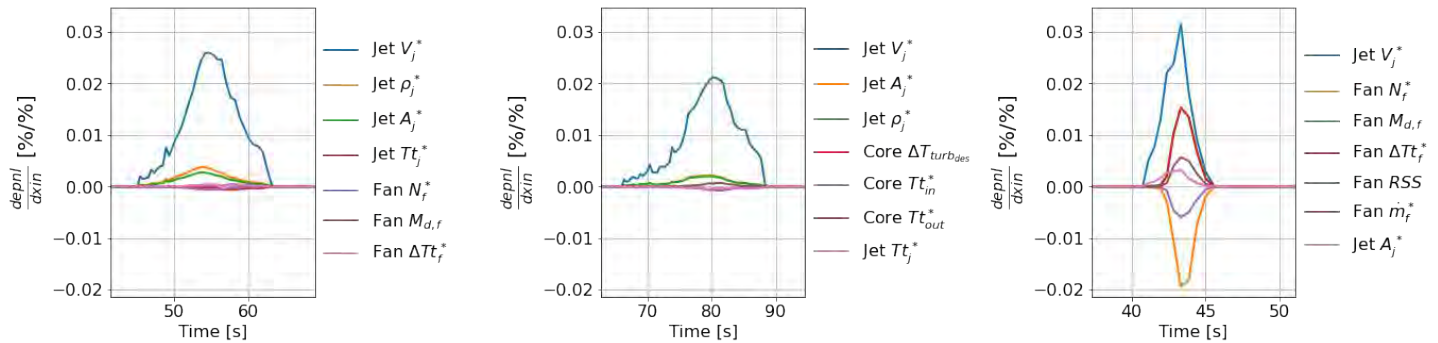
**Figure 10.** Jet mixing tone-corrected PNLt at the flyover microphone for the NASA STCA Standard take-off trajectory.

Table 3 shows the effective perceived noise level of the pyNA noise assessment for the NASA STCA aircraft for the lateral, flyover, and approach microphones. The EPNL are verified with the NASA STCA noise assessment. The individual EPNL have a maximum error  $\Delta EPNL_{max} < 5\%$ ; the total noise levels have an error  $\Delta EPNL < 0.5\%$  (Berton, 2019).

**Table 3.** pyNA results for the effective perceived noise levels for the lateral, flyover and approach microphone for the Standard take-off trajectory of the NASA STCA.

	Lateral [EPNdB]	Flyover [EPNdB]	Approach [EPNdB]
Fan inlet *	50.2	35.5	72.3
Fan exit *	77.1	71.7	91.0
Combustor	77.2	73.5	79.9
Jet mixing	94.8	88.0	90.5
<b>Total</b>	<b>95.2</b>	<b>88.7</b>	<b>95.9</b>

The pyNA backward sensitivity mode is used to calculate sensitivities of EPNL with respect to off-design parameters. The sensitivity results can be seen in Figure 11. The x-axis of the sensitivity plots is limited to the region in which PNLt contributes to the EPNL calculation (i.e., region 10dB below  $PNLT_{max}$ ).



**Figure 11.** Sensitivities of the EPNL at the lateral, flyover and approach microphone with respect to engine off-design variables ( $x_{in}$ ).

### Publications

None

### Outreach Efforts

Mr. Prashanth Prakash and Mr. Laurens Voet gave a presentation titled “Clean-sheet supersonic engine design and performance” at the at the virtual ASCENT meeting on September 30, 2020.

### Awards

None

### Student Involvement

This Task was conducted primarily by Prashanth Prakash and Laurens Voet, graduate research assistants working under the supervision of Dr. Jayant Sabnis, Dr. Raymond Speth, and Dr. Choon Tan.

### Plans for Next Period

- Extend the combustor model to include representation of staged combustors, and incorporate soot modeling capabilities to enable estimation of nvPM emissions (expected completion: May 2021)
- Enhance the noise model to calculate sensitivities between relevant engine parameters and the resulting noise footprint (expected completion: March 2021)
- Begin development of a preliminary turbomachinery design tool to determine noise-relevant geometrical engine parameters for an engine configuration (expected completion: August 2021)

### References

- W. E. Zorumski, Aircraft Noise Prediction Program Theoretical Manual Part 1-2, Technical report, NASA, 1982.
- Society of Automotive Engineers, ARP-876: Gas Turbine Jet Exhaust Noise Prediction, SAE, 1994.
- J. Emmerling, S. Kazin, R. Matta, Core engine noise program. Volume III. Prediction methods – Supplement I: Extension of prediction methods, Technical report, General Electric Co Cincinnati OH Aircraft Engine Business Group, 1976.
- M. F. Heidmann, Interim prediction method for fan and compressor source noise (NASA-TM-x71763), 1995.
- K. B. Kontos, B. Janardan, P. Gliebe, Improved NASA-ANOPP noise prediction computer code for advanced subsonic propulsion systems. Volume 1: ANOPP evaluation and fan noise model improvement (NASA CR-195480), 1996.
- K. B. Kontos, R. E. Kraft, P. R. Gliebe, Improved NASA-ANOPP noise prediction computer code for advanced subsonic propulsion systems. Volume 2: Fan suppression model development (NASA-CR- 202309), 1996.
- J. W. Hough, D. S. Weir, Aircraft noise prediction program (ANOPP) fan noise prediction for small engines (NASA-CR-198300), 1996.
- M. R. Fink, Airframe noise prediction method, Technical report, United Technologies Research Center East Hartford, CT, 1977.
- Golub, Robert, John W. Rawls Jr, and Jessie C. Yeager. High Speed Research Noise Prediction Code (HSRNOISE) User's and Theoretical Manual, 2004.

C. Chien, W. Soroka, Sound propagation along an impedance plane, *Journal of Sound and Vibration* 43 (1) (1975) 9–20  
 Z. Maekawa, Noise reduction by screens, *Applied Acoustics* 1 (3) (1968) 157–173.  
 ICAO, Annex 16 environmental protection. Volume I: Aircraft engine emissions (eight edition), 2017.  
 Berton, J. & Geiselhart, K. (2019). NASA 55-tonne Supersonic Transport Concept Aeroplane (STCA) release package. NASA GRC/NASA LaRC.

## Task 4 – Assess the Effect of Variable Noise Reduction Systems on LTO Emissions for Engines for Supersonic Transport Aircraft

Massachusetts Institute of Technology

### Objective

The objective of this Task is to assess the effects of variable noise reduction systems (VNRS) on the takeoff and climb emissions for supersonic transport engines. The objective of this task is to determine whether the current LTO cycle is relevant for supersonic transport engines and if not, characterize what such a relevant LTO cycle would look like.

### Research Approach

The approach to address the above-mentioned research objectives is shown in Figure 12. We start from a supersonic level 1-type aircraft (NASA STCA), and an engine model for that aircraft (a CFM56-based derivative). These are input in a takeoff trajectory model that is coupled to a noise model. Minimizing the noise footprint using a variable noise reduction system gives us a programmed lapse rate (PLR), characterized by a power setting schedule as a function of time,  $PS(t)$ . This power setting schedule is put into a combustor model to estimate takeoff emissions (i.e., Method 1 in Figure 12). These emissions are compared to a baseline trajectory, using a simple power setting schedule, without VNRS being applied (i.e., Method 2 in Figure 12). We are interested in comparing the takeoff emissions of both these methods.

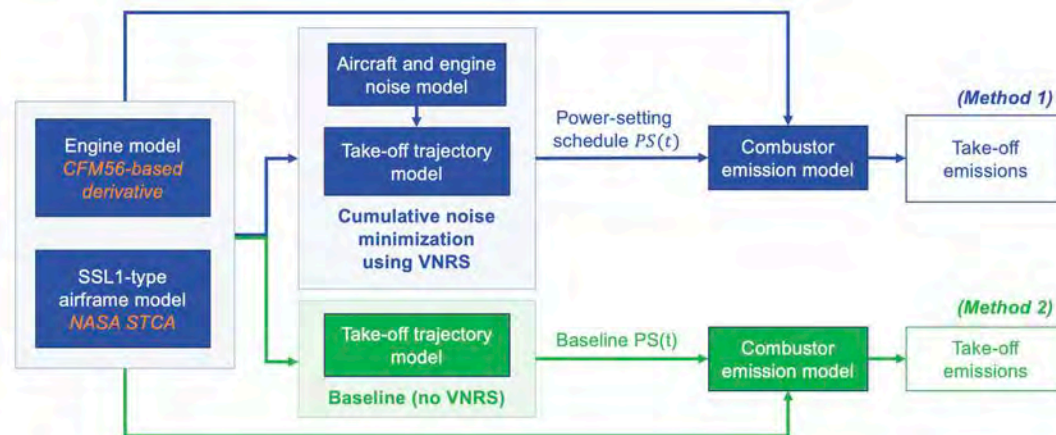


Figure 12. Flow chart of the approach to estimate the effect of VNRS on takeoff emissions of engines for supersonic transport.

### Milestone

A first estimate has been made of the difference of pollutant emissions of engines for supersonic transport aircraft flying trajectories with and without VNRS.

### Major Accomplishments

The takeoff and climb emissions of the NASA STCA "Standard" (having pilot-initiated cutback only) and "Advanced" (having a programmed lapse rate on top of a pilot-initiated cutback) takeoff trajectory are compared in Figure 13 (Berton, 2019). The instantaneous emission indices for  $NO_x$  and CO are calculated using a  $T_3-P_3$  method. It can be seen in these graphs, that applying a PLR affects both  $NO_x$  and CO emission indices.

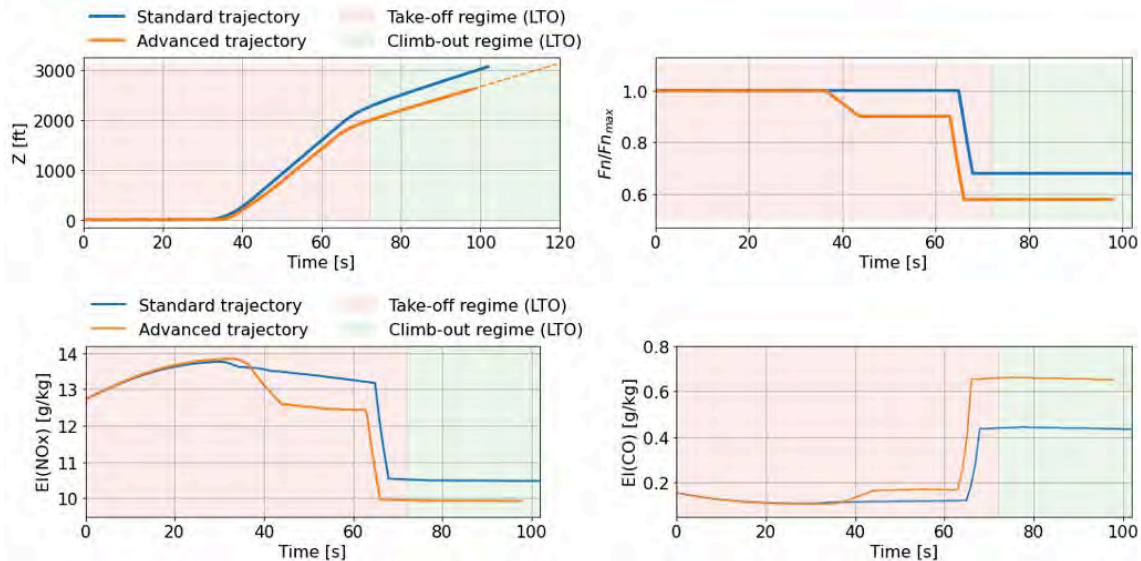


**Figure 13.** Comparison of NASA STCA Standard and Advanced takeoff trajectory (top left) and power setting (top right). The instantaneous emission indices during flight are compared for both NO<sub>x</sub> (bottom left) and CO (bottom right).

To quantify the overall difference in emissions, the total mass of pollutants emitted during the entire takeoff and climb regime of the current LTO cycle are calculated, thereby extrapolating the climb regime to 192 seconds, as shown in Table 4. A difference of 11% for NO<sub>x</sub> and 30% for CO is observed between the Standard and Advanced NASA STCA trajectory, mainly caused by applying the variable noise reduction system, the PLR.

**Table 4.** Comparison of NO<sub>x</sub> and CO emissions mass for takeoff and climb-out regime of the conventional LTO cycle for the Standard and Advanced NASA STCA takeoff trajectory.

Regime	Std. trajectory $m_{NO_x}$ [g]	Adv. trajectory $m_{NO_x}$ [g]	Std. trajectory $m_{CO}$ [g]	Adv. trajectory $m_{CO}$ [g]
Take-off	877	817	9	11
Climb-out	767	638	32	42
Total	1644	1455	41	53
$\Delta_{std-adv.}$	-11.5 %		+29.3 %	

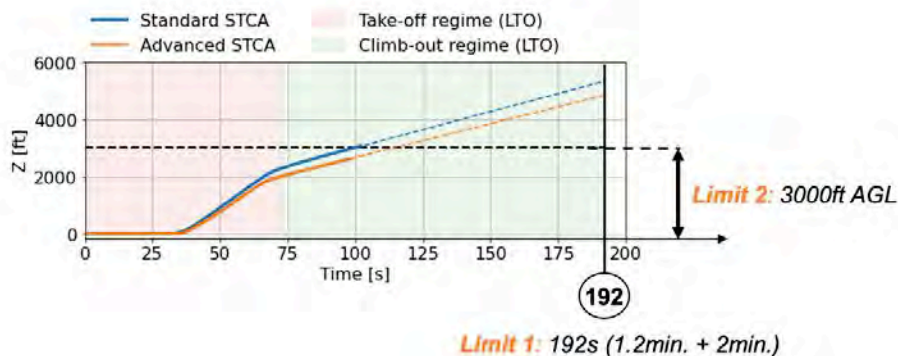


**Figure 14.** Comparison of NASA STCA Standard and Advanced takeoff trajectory (top left) and power setting schedule (top right). The instantaneous emission indices during flight are compared for both NO<sub>x</sub> (bottom left) and CO (bottom right).



The objective of the current emission standards is to limit pollutant emissions below 3000 ft above ground level (AGL). Looking at both the NASA Standard and Advanced takeoff trajectory, it can be seen that applying PLR changes the time at which the aircraft reaches this altitude, and this time might very well vary from aircraft to aircraft as each aircraft will have its own purposely designed VNRS. Therefore, instead of looking at the limit of 192 seconds for the climb phase, the mass of pollutant emissions is integrated until the time at which the aircraft reaches 3000 ft AGL, as shown in Table 5. The difference between the Standard and Advanced trajectory approximately doubles for CO and decreases to almost 0% for NO<sub>x</sub>.

**Table 5.** Comparison of NO<sub>x</sub> and CO emissions mass for take-off and climb-out regime of the conventional LTO cycle for the Standard and Advanced NASA STCA takeoff trajectory.

Limit	Trajectory	m <sub>NOx</sub> [g]	Δ	m <sub>CO</sub> [g]	Δ
192 seconds	Standard	1644	-11.5 %	41	+29.3 %
	Advanced	1455		53	
3000 ft AGL	Standard	1053	-0.6 %	16	+56.3 %
	Advanced	1046		25	

**Publications**

N/A

**Outreach Efforts**

Mr. Laurens Voet presented an information paper titled “Investigation of the effects of VNRS on LTO emissions of engines for supersonic transport aircraft” at the CAEP/12-WG3/5-ESTG meeting on November 3, 2020.

**Awards**

None

**Student Involvement**

This Task was conducted primarily by Laurens Voet, a graduate research assistant working under the supervision of Dr. Jayant Sabnis, Dr. Raymond Speth, and Dr. Choon Tan.

**Plans for Next Period**

- Applying this analysis to a wider range of aircraft designs in terms of number of engines, cruise Mach numbers, and maximum tak-off weight (MTOW).
- Applying this analysis to engines with different emissions characteristics to understand whether the emissions LTO cycle is relevant, even if it may not be precisely representative.

**References**

J. J. Berton, K. Geiselhart (2019). NASA 55-tonne Supersonic Transport Concept Aeroplane (STCA) release package. NASA GRC/NASA LaRC.



# Project 048 Analysis to Support the Development of an Engine nvPM Emissions Standard

## Massachusetts Institute of Technology

### Project Lead Investigator

Steven Barrett  
Associate Professor  
Department of Aeronautics & Astronautics  
Massachusetts Institute of Technology  
77 Massachusetts Ave  
Building 33-316  
Cambridge, MA 02139  
617-452-2550  
sbarrett@mit.edu

### University Participants

#### Massachusetts Institute of Technology

- PI: Prof. Steven Barrett
- Co-PI: Dr. Raymond Speth
- FAA Award Number: 13-C-AJFE-MIT, Amendment Nos. 027, 036, 045, 054, 065, and 069
- Period of Performance: July 8, 2016 to August 10, 2021 (reporting here with the exception of funding level and cost share only for the period October 1, 2019 to September 30, 2020)
- Tasks:
  1. Developing a no-change criterion for engine remeasurement.
  2. Comparing approaches to estimate non-volatile particulate matter (nvPM) particle number emissions.
  3. Extending the nvPM fuel correction method for blended fuels.

### Project Funding Level

FAA provided \$750,000 in funding. A total of \$750,000 of matching funds are contributed by approximately \$196,000 from the Massachusetts Institute of Technology (MIT), and third-party in-kind contributions of \$87,000 from University College London, \$158,000 from Oliver Wyman Group, \$156,000 from Byogy Renewables, Inc., and \$153,000 from NuFuels LLC.

### Investigation Team

- Prof. Steven Barrett (MIT) serves as PI for ASCENT Project 48 as head of the Laboratory for Aviation and the Environment. Prof. Barrett coordinates internal research efforts and maintains communication between investigators in the various MIT research teams.
- Dr. Raymond Speth (MIT) serves as co-PI for Project 48. Dr. Speth directly advises student research in the Laboratory for Aviation and the Environment focused on assessment of fuel and propulsion system technologies targeting reduction of aviation's environmental impacts. Dr. Speth also coordinates communication with FAA counterparts.
- Dr. Jayant Sabnis (MIT) serves as co-investigator for Project 48. Dr. Sabnis co-advises student research in the Laboratory for Aviation and the Environment. His research interests include turbomachinery, propulsion systems, gas turbine engines, and propulsion system-airframe integration.
- Akshat Agarwal (MIT) is a graduate student in the Laboratory for Aviation and the Environment. He is responsible for conducting the cost-benefit analysis of the nvPM emissions standard and developing methods for estimating nvPM emissions based on smoke number measurements.



## Project Overview

The FAA’s Office of Environment and Energy (FAA-AEE) is working with the international community to implement an international aircraft engine nvPM standard for engines of rated thrust greater than 26.7 kN. The proposed nvPM standard will influence the development of future engine technologies, resulting in reduction of nvPM emissions from aircraft engines, and thus lead to improved human health and climate impacts of aviation. During the Committee on Aviation Environmental Protection (CAEP)/11 cycle, the FAA, alongside other national aviation authorities, developed an nvPM emissions standard for the mass and particle number emitted by aircraft engines. During the current cycle (CAEP/12), the FAA needs support to provide a technical basis for the implementation of the nvPM emissions standards.

The objective of this project is to provide support for FAA decision-making related to the implementation of the nvPM certification standard. The first task focuses on developing a method to define the conditions in which an engine needs to re-certified for emissions after small changes are made to it—so-called no-change criteria. Second, we aided the CAEP and FAA decision-making process for choosing the best method to estimate particle number emissions to include in the airports air quality manual (Doc 9889). Finally, we extended the nvPM certification fuel correction approach for use with blended biofuels, so that the CAEP modeling and database group (MDG) is able to quantify reductions in emissions for using blended fuels.

## Task 1 – Developing a No-change Criterion for Engine Remeasurement

Massachusetts Institute of Technology

### Objective

The objective of this task was to identify when an engine, after small changes are made to it, needs its emissions remeasured.

### Research Approach

The landing and takeoff (LTO) nvPM mass and number standards were developed and agreed upon during CAEP/11. This process identified the total emissions per unit rated thrust that an engine can emit during the LTO procedure as the quantity to be evaluated. For gaseous emissions and the CAEP/10 maximum mass concentration standard, allowances are made for small changes to the engine design that do not require emissions re-certification. In this task, we developed no-change criteria for the CAEP/11 LTO nvPM mass and number standards by basing it on the uncertainty of the nvPM mass and number measurement system. If an engine’s nvPM mass or number metric value ( $D_p/F_{00}$ ) is estimated to change by more than the combined uncertainty of the underlying measurements, then an engine should be re-tested. This is because there is statistical certainty that the emissions of an engine have changed.

In order to quantify the uncertainty of a metric value, we first introduce the approach to estimate it. It is calculated as

$$MV = \frac{D_p}{F_{00}} = \frac{\sum_{i=1}^4 EI_i \dot{m}_{f,i}}{F_{00}}$$

where  $D_p$  is the total LTO emissions,  $F_{00}$  is the engine rated thrust,  $EI_i$  is the emissions index at International Civil Aviation Organization (ICAO) mode of operation  $i$ , and  $\dot{m}_f$  is the fuel flow rate. To calculate each  $EI_i$ , we use

$$EI_m \left[ \frac{\text{mg}}{\text{kg}_f} \right] = \frac{22.4 \times 10^{-3} \text{nvPM}_m k_t k_f}{\left( [CO_2]_{dil} + \frac{1}{DF_1} ([CO] - [CO_2]_b + [HC]) \right) (M_C + \alpha M_H)}$$

where  $\text{nvPM}_m$  is the mass concentration,  $k_t$  is the thermophoretic correction,  $k_f$  is the fuel correction,  $[X]$  is the diluted mass concentration of species  $X$ ,  $DF_1$  is dilution factor 1,  $M_C = 12.0$  g/mol,  $M_H = 1.0$  g/mol and  $\alpha$  is the ratio of moles of hydrogen to moles of carbon in the fuel. The subscripts b and dil represent the background and post-dilution concentrations of a species. The derivation of this equation can be found in AIR6241 (2013). A similar form of the equation is used for number emissions.

To calculate the uncertainty in the metric value, we must combine the uncertainties of each emissions index measurement together. For this task, we assume that  $\dot{m}_{f,i}$  and  $F_{00}$  have negligible uncertainty. The uncertainty in each value required for estimating the emissions index is defined by the SAE E31 team and the key values are included in Table 1.

**Table 1.** Uncertainty of each component of the nvPM mass and number measurement system. (Reproduced from CAEP/11-WG3-PMTG/10-WP/12)

	Mass	Number
Instrument $\left(\frac{u(\text{nvPM}_m)}{\text{nvPM}_m}\right)$	30 $\mu\text{g}/\text{m}^3 + 13\%$	$6 \times 10^4 / \text{cm}^3 + 7\%$
Dilution factor 1 $\left(\frac{u(\text{DF}_1)}{\text{DF}_1}\right)$	4%	4%
CO <sub>2</sub> concentrations $\left(\frac{u([\text{CO}_2]_{\text{dil}})}{[\text{CO}_2]_{\text{dil}}}, \left(\frac{u([\text{CO}_2]_{\text{b}})}{[\text{CO}_2]_{\text{b}}}\right)\right)$	4%	4%
Dilution factor 2 $\left(\frac{u(\text{DF}_2)}{\text{DF}_2}\right)$		10%
Thermophoretic losses $\left(\frac{u(k_t)}{k_t}\right)$	2%	2%
Fuel correction $\left(\frac{u(k_f)}{k_f}\right)$	8%	10%

We assume that all uncertain components follow a Gaussian distribution and are statistically independent. This allows us to combine uncertainties in quadrature. To calculate the relative uncertainties of each emissions index,  $u_{r,c}(\text{EI})$ , quadrature is performed as

$$u_{r,c}(\text{EI}) = \frac{1}{\text{EI}} \sqrt{\left(\frac{\partial \text{EI}}{\partial \text{nvPM}_m} u_r(\text{nvPM})\right)^2 + \left(\frac{\partial \text{EI}}{\partial k_t} u_r(k_t)\right)^2 + \left(\frac{\partial \text{EI}}{\partial k_f} u_r(k_f)\right)^2 + \left(\frac{\partial \text{EI}}{\partial [\text{CO}_2]_{\text{dil}}} u_r([\text{CO}_2]_{\text{dil}})\right)^2 + \left(\frac{\partial \text{EI}}{\partial \text{DF}_1} u_r(\text{DF}_1)\right)^2 + \left(\frac{\partial \text{EI}}{\partial [\text{CO}_2]_{\text{b}}} u_r([\text{CO}_2]_{\text{b}})\right)^2}$$

where  $u_r(X)$  is the relative uncertainty of component  $X$  as defined in Table 1. Finally, to get the uncertainty in the metric value, we again use quadrature, assuming that the uncertainty at each mode of operation is independent and follows a Gaussian distribution.

To identify potential options for the no-change criteria, we estimate the uncertainty of emissions indices and metric values for engines with reported data. Emissions are converted to concentrations by estimating the volumetric flow rate through the engine. The approach for this is described in detail in Agarwal et al. (2019). We can then propagate uncertainties using the previous set of equations. This is conducted for all engines with reported data.

Figure 1 and Figure 2 show the relative uncertainty in nvPM mass and number metric value ( $D_p/F_{00}$ ). The uncertainty in the metric value increases as the metric value decreases. This is caused by the limit of detection, which adds an absolute uncertainty of 30  $\mu\text{g}/\text{m}^3$  for mass and  $6 \times 10^4$  particles/ $\text{cm}^3$ . This trend can be modeled using an inverse proportional function as shown in each figure. The scatter in this relationship is caused by the differing contribution of each mode of operation to the overall  $D_p$  value. The relationships show that the uncertainty tends towards 9.6% for mass and 6.0% for number.

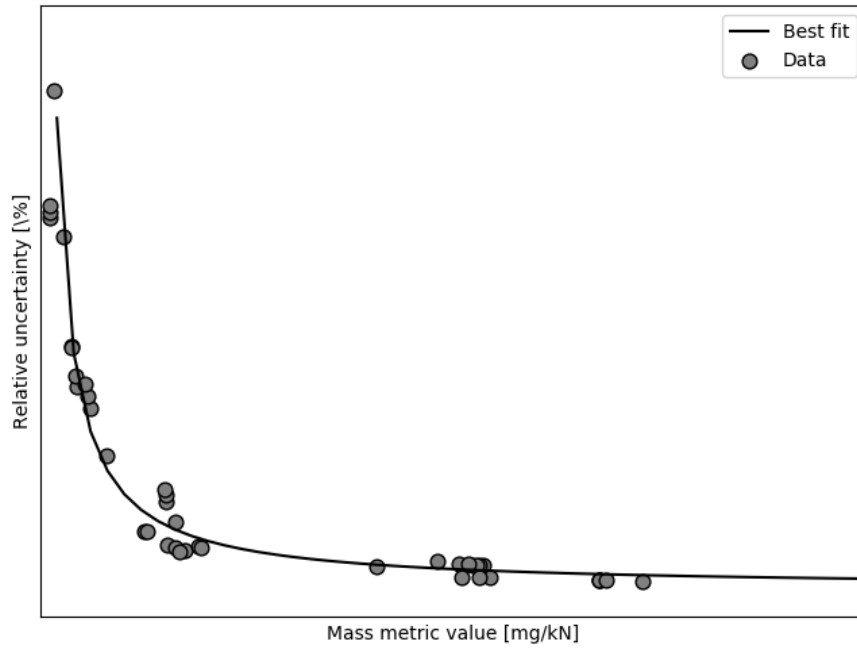


**Figure 1.** Relative uncertainty in mass metric value.

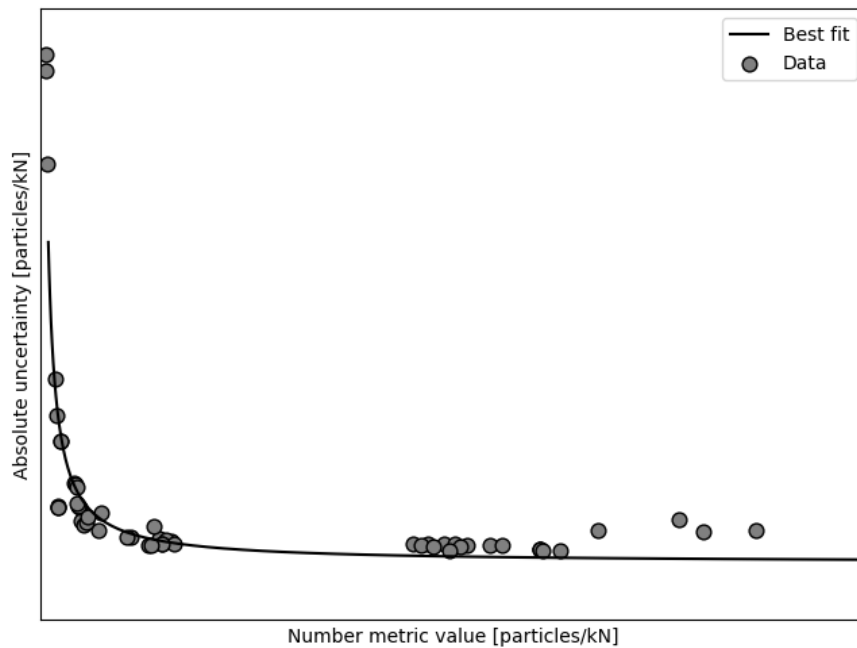


**Figure 2.** Relative uncertainty in number metric value.

Using the best fit lines, we can define a no-change criterion as a piecewise, continuous function. Below a threshold metric value, we use the absolute uncertainty to determine the no-change criteria. Above this threshold, we use the relative uncertainty. To define the values of the absolute and relative uncertainties in each region, we use the best-fit relationships



found in Figure 1 and Figure 2. First, we select the threshold metric value and identify the relative uncertainty according to the best fit relationships. This also defines the absolute uncertainty, which is calculated by multiplying the relative uncertainty with the metric value. This is used to determine the no-change criteria below the threshold metric value.

Three sample no-change criteria are shown in Figure 3 and Figure 4. This approach allows the no-change criteria to balance the increase in uncertainty at low emissions as well as the approximately constant uncertainty at higher emissions. It also accounts for the scatter in the relative uncertainty that is especially prevalent when the emissions are below approximately 200 mg/kN for mass and  $2 \times 10^{15}$  particles/kN for number. orange case. Mass (lower green case) and number (central orange case) provide sufficient balance between low and high emissions.

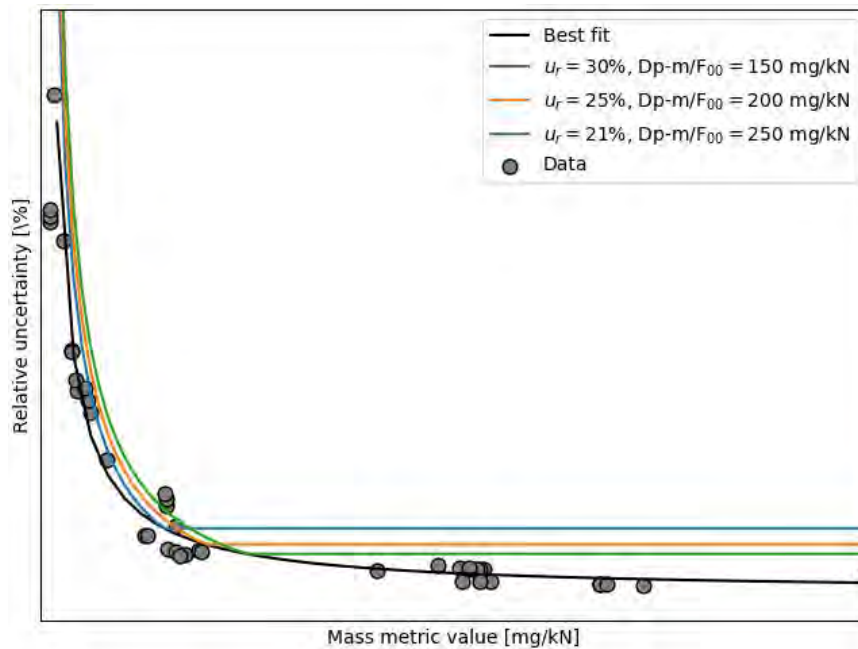


**Figure 3.** As in Figure 1 , but including three options for the mass no-change criterion.

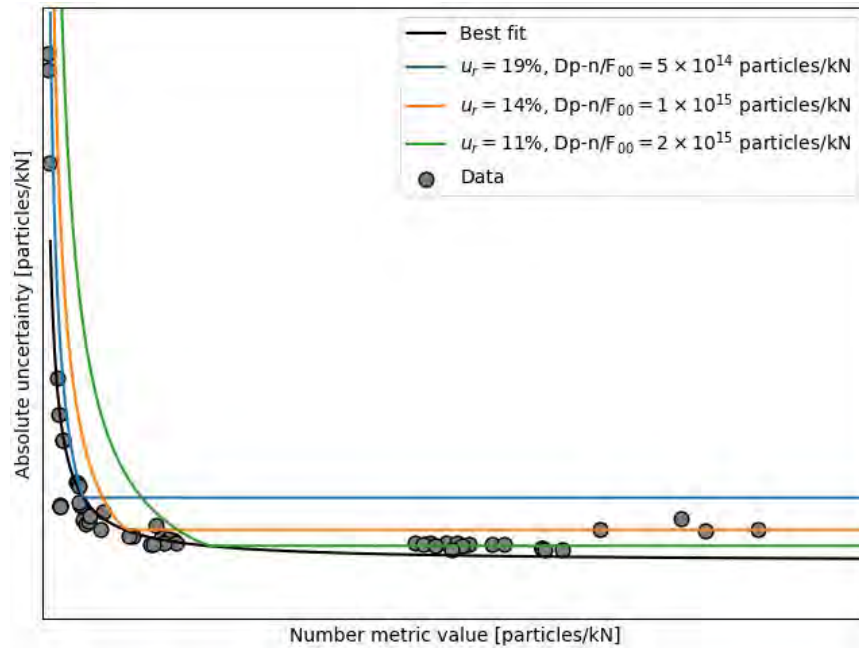


Figure 4. As in Figure 2, but including three options for the number no-change criterion.

### Milestone

The complete analysis was presented to the FAA and in a Working Paper for CAEP/12-WG3-ECTG/5.

### Major Accomplishments

This work has been presented to CAEP/12-WG3-ECTG/5.

### Publications

N/A

### Outreach Efforts

Our results have been communicated to the FAA and CAEP-WG3 in a detailed report and presentation.

### Awards

None

### Student Involvement

Graduate student Akshat Agarwal conducted the analyses and presented the work.

### Plans for Next Period

Feedback was received during the CAEP/12-WG3/5 meeting and we aim to refine the method and present updated results at the next meeting.

### References

- AIR6241. 2013. "Procedure for the Continuous Sampling and Measurement of Non-Volatile Particle Emissions from Aircraft Turbine Engines - SAE Aerospace Information Report 6241 (AIR6241)."
- Agarwal, Akshat, Raymond L. Speth, Thibaud M. Fritz, S. Daniel Jacob, Theo Rindlisbacher, Ralph Iovinelli, Bethan Owen, Richard C. Miake-Lye, Jayant S. Sabnis, and Steven R. H. Barrett. 2019. "SCOPE11 Method for Estimating Aircraft

Black Carbon Mass and Particle Number Emissions.” *Environmental Science & Technology* 53 (3): 1364–73.  
<https://doi.org/10.1021/acs.est.8b04060>.

## Task 2 – Comparing Approaches to Estimate nvPM Particle Number Emissions

Massachusetts Institute of Technology

### Objective

This Task aimed to compare three approaches to estimate nvPM particle number emissions developed during CAEP/11, as well as two additional approaches recently published in the literature (Zhang et al. 2019; Teoh et al. 2019).

### Research Approach

The Emissions Characterizations Task Group (ECTG) in WG3 has been trying to identify the best approach to estimate particle number emissions given information of nvPM mass emissions. This approach will be implemented in the ICAO airport air quality manual (Doc 9889) and be used by airports to quantify nvPM emissions. The goal of the approach is thus high accuracy without being overly complicated so as to be difficult for airports to implement. Three approaches have been developed by WG3 including:

- SCOPE11 approach (Agarwal et al. 2019).
- Fixed geometric mean diameter (GMD)-20 using 20 nm at idle, 20 nm at approach, 40 nm at climb-out, and 40 nm at takeoff.
- Fixed GMD-25, which is the same as Fixed GMD-20 but uses 25 nm at approach.

In addition, two approaches have been published in the literature that use the fractal aggregates approach to convert from mass to number emissions. These include:

- Zhang et al. (2019)
- Teoh et al. (2019)

We have implemented all five approaches and aim to capture the performance of all methods on estimating particle number emissions indices and the Dp number (mass of any pollutant emitted, expressed in grams) for the LTO cycle for all engines in the nvPM values database (VDB).

The results for estimating the number emissions index are shown in Figure 5, which shows the measured versus estimated emissions index using all five methods. The approach developed by Zhang et al. (2019) shows the highest error and bias, overpredicting the emissions index. The bias is highest for taxi emissions at  $9.8 \times 10^{17}$  particles/kg and the results show that there is an emissions-dependent offset with the parity line. The SCOPE11 (top left) and Teoh et al. (2019) (top right) approaches show similar results that are offset from each other. This is because the SCOPE11 mass and GMD approaches are used as input to the Teoh mass-to-number conversion. The bias of the SCOPE11 results is a factor of 1.3–21 lower than that for Teoh et al. Finally, the fixed GMD approach shown in the bottom right shows the highest variance in the results, however, these results seem to have low bias. This is expected since the GMD is a strong function of the engine and emissions level, thus it is difficult to identify optimum values fixed for each mode of operation.

Figure 6 shows the measured versus estimated Dp number emissions using all five methods, as well as the performance metrics on the right side of the figure. These results show that the fixed GMD approaches have the lowest root mean square error (RMSE), which can be up to 20% lower than that for the SCOPE11 method. The results do still show higher spread of the data when compared to the SCOPE11 method. This is evidenced in the bias of the results, which is a factor of 37.5 lower in SCOPE11 than the next-best, fixed-20 approach. For fleet estimates as required by Doc 9889, the bias is considered the best metric to assess performance.

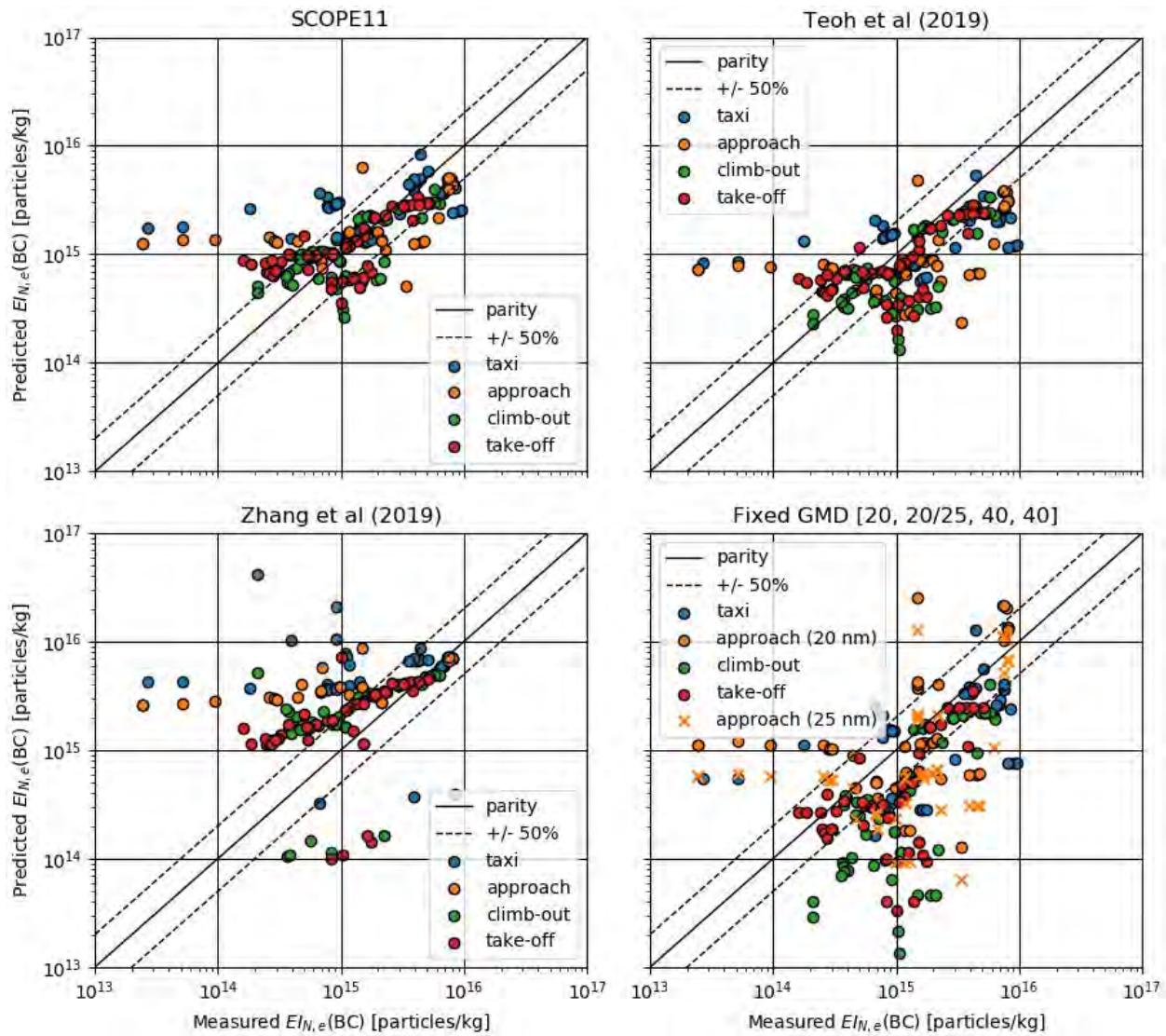
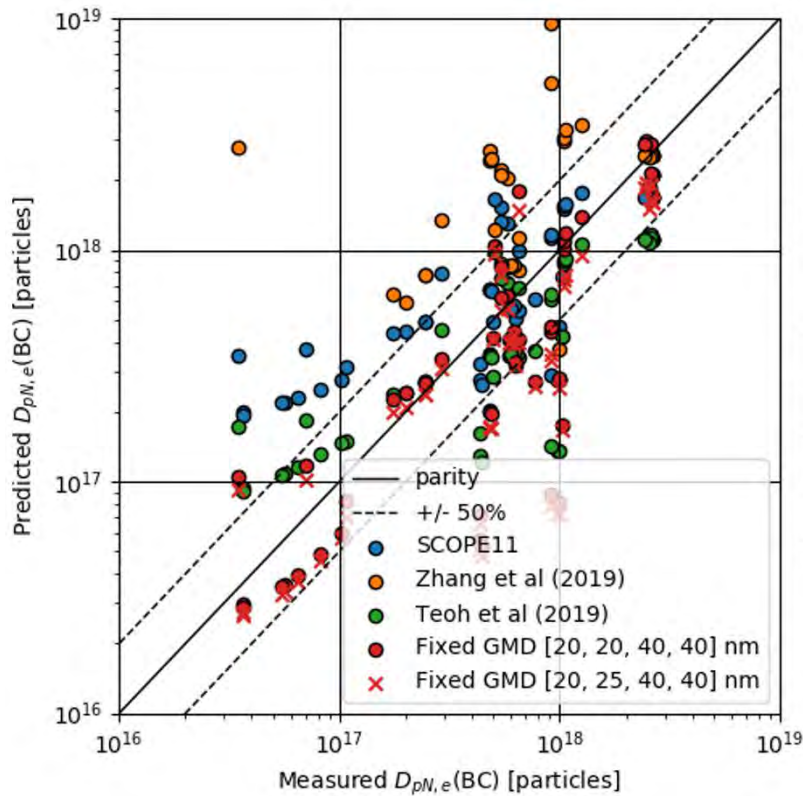


**Figure 5.** Measured versus predicted number emissions index for SCOPE11 (top left), Teoh et al. (2019) (top right), Zhang et al. (2019) (bottom left), and both fixed GMD approaches (bottom right). To distinguish between 20 nm and 25 nm for the fixed GMD at approach, orange circles or crosses have been used respectively.



	RMSE [#] $\times 10^{17}$	R <sup>2</sup>	Bias [#] $\times 10^{17}$
SCOPE11	5.1	0.78	-0.04
Zhang	59.0	-0.10	+20.2
Teoh	6.4	0.82	-3.4
Fix – 20	4.1	0.89	-1.5
Fix – 25	5.0	0.88	-3.0

**Figure 6.** Measured versus predicted  $D_p$  number emissions for the LTO cycle across each method. The key performance metrics are shown on the right side.

**Milestone**

The results were presented at the CAEP/12-WG3/5 meeting.

**Major Accomplishments**

The fixed-20 approach was accepted for use in Doc 9889.

**Publications**

N/A

**Outreach Efforts**

Our results were regularly communicated to the FAA and ICAO-CAEP in a detailed presentation.

**Awards**

None

**Student Involvement**

Graduate student Akshat Agarwal was responsible for completing the analysis.

**Plans for Next Period**

N/A



## References

- Agarwal, Akshat, Raymond L. Speth, Thibaud M. Fritz, S. Daniel Jacob, Theo Rindlisbacher, Ralph Iovinelli, Bethan Owen, Richard C. Miake-Lye, Jayant S. Sabnis, and Steven R. H. Barrett. 2019. "SCOPE11 Method for Estimating Aircraft Black Carbon Mass and Particle Number Emissions." *Environmental Science & Technology* 53 (3): 1364-73. <https://doi.org/10.1021/acs.est.8b04060>.
- Teoh, Roger, Marc E. J. Stettler, Arnab Majumdar, Ulrich Schumann, Brian Graves, and Adam M. Boies. 2019. "A Methodology to Relate Black Carbon Particle Number and Mass Emissions." *Journal of Aerosol Science* 132 (June): 44-59. <https://doi.org/10.1016/j.jaerosci.2019.03.006>.
- Zhang, Xiaole, Xi Chen, and Jing Wang. 2019. "A Number-Based Inventory of Size-Resolved Black Carbon Particle Emissions by Global Civil Aviation." *Nature Communications* 10 (1): 1-11. <https://doi.org/10.1038/s41467-019-08491-9>.

## Task 3 – Extending the nvPM Fuel Correction Method for Blended Fuels

Massachusetts Institute of Technology

### Objective

This Task aimed to identify the accuracy of the nvPM fuel correction method for blended fuels and compare the method to other formulations.

### Research Approach

Current fuel standards allow aircraft engines to use conventional fuels that are blended with biofuels up to 50% by volume. Biofuels tend to have higher hydrogen content than conventional jet fuels, so blended fuels also tend to have higher hydrogen content than conventional jet fuels. Increasing the hydrogen content of a fuel is expected to decrease nvPM emissions (Moore et al. 2017; Speth et al. 2015). In order to assess the reduction in emissions, the MDG requested WG3 to provide an approach to estimate the decrease in emissions associated with using blended fuels. In this Task, we first assessed the accuracy of using the current certification fuel correction approach developed during CAEP/11. In addition, we developed a different formulation that assumes a quadratic relationship between the change in emissions and the hydrogen content.

To test the performance and fit coefficients of all models, we combined several engine measurement datasets that comprise six different engines for mass emissions and two additional engines for number emission (Bulzan et al. 2010; Beyersdorf et al. 2014; Timko et al. 2011; 2010; Corporan et al. 2013; 2011; Cain et al. 2013; Corporan et al. 2010; Brem et al. 2015). In addition, we include auxiliary power unit (APU) emissions data provided by Prem Lobo, NRC Canada (private communication). Two forms of fits were tested on these datasets. The first follows an exponential trend in hydrogen content (H) and thrust setting ( $F/F_{00}$ ) as

$$\hat{E} = \exp((k_1 + k_2 F/F_{00})(H_0 - H))$$

where  $\hat{E}$  is the relative change in emissions,  $H_0 = 13.8\%$  is the reference fuel hydrogen content, and  $k_1$  and  $k_2$  are coefficients to be fitted. The second form assumes a quadratic relationship in the hydrogen content as

$$\hat{E} = (1 - \bar{H})[(k_1 + k_2 \bar{F})\bar{H} + 1]$$

where  $\bar{H} = \frac{H-H_0}{H_\infty-H_0}$  and  $H_\infty$ ,  $k_1$  and  $k_2$  are coefficients to be fitted. Both forms are fitted to the entire dataset and the coefficients are shown in Table 2 below. This table also includes the coefficients used for the certification fuel corrections approach.



**Table 2.** Fitted coefficient values for all models tested

	Certification		Exponential re-fitted		Quadratic	
	Mass	Number	Mass	Number	Mass	Number
$k_1$	1.12	1.05	1.33	1.11	-1.25	-1.30
$k_2$	-0.95	-0.99	-0.79	-0.69	1.54	1.98
$H_\infty$					15.92	15.93

The performance of the certification, the exponential re-fitted, and the quadratic approach are shown in Figure 6, Figure 7, and Figure 8. The certification approach exhibits low error for relative mass and number emissions above 1.0. This is expected since the model was fitted to this set of CFM56-7 data. Below this range, the performance degrades, and the approach tends to find a bias of -0.10 for mass and -0.09 for number. After re-fitting the coefficients in the certification approach for all the available data (Figure 7), the overall performance improves with the mean absolute error reducing by 20% for mass and 12.5% for number, and the mean error reducing by a factor of 3.2 and 6.0, respectively, for mass and number. The main region where the approach improves for biofuel prediction is for relative emissions below 1.0, which shows lower variance away from the parity line. Above relative emissions of 1.0, the approach does not perform as well as the certification approach and there is high bias in the results. Finally, the results of the quadratic approach are shown in Figure 8. This shows the lowest bias by a factor of 1.9 for mass and factor of 12.5 for number compared with the re-fitted exponential approach. This approach balances the performance at all relative emissions levels (above and below 1.0) better than the exponential form.

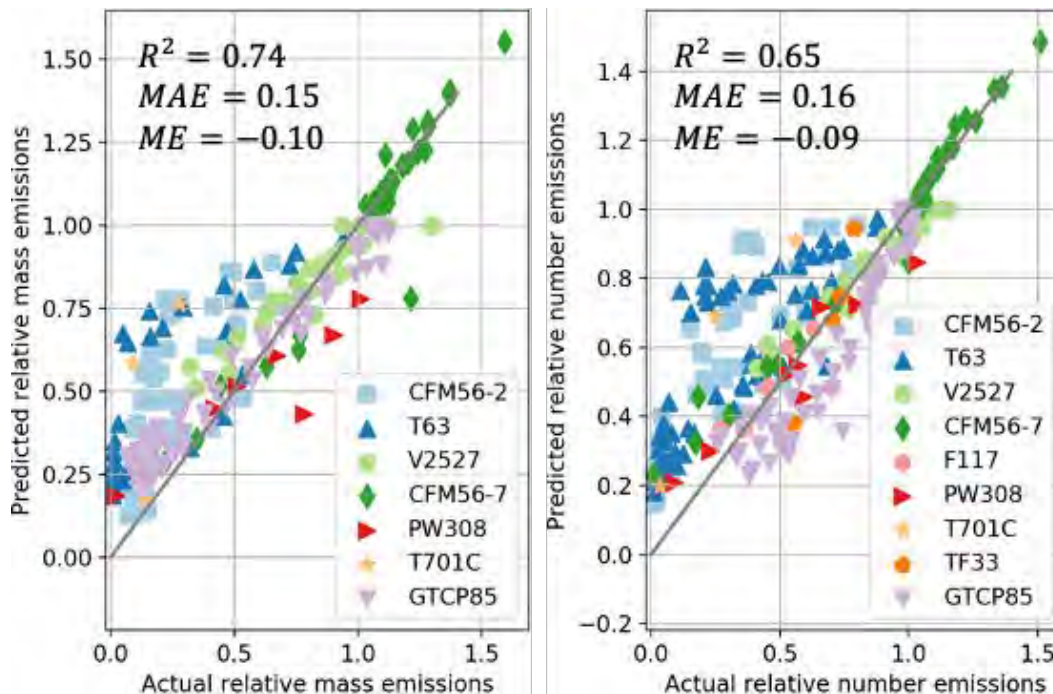


**Figure 7.** Actual/measured versus predicted relative mass emissions (left) and number emissions (right) using the certification fuel approach.

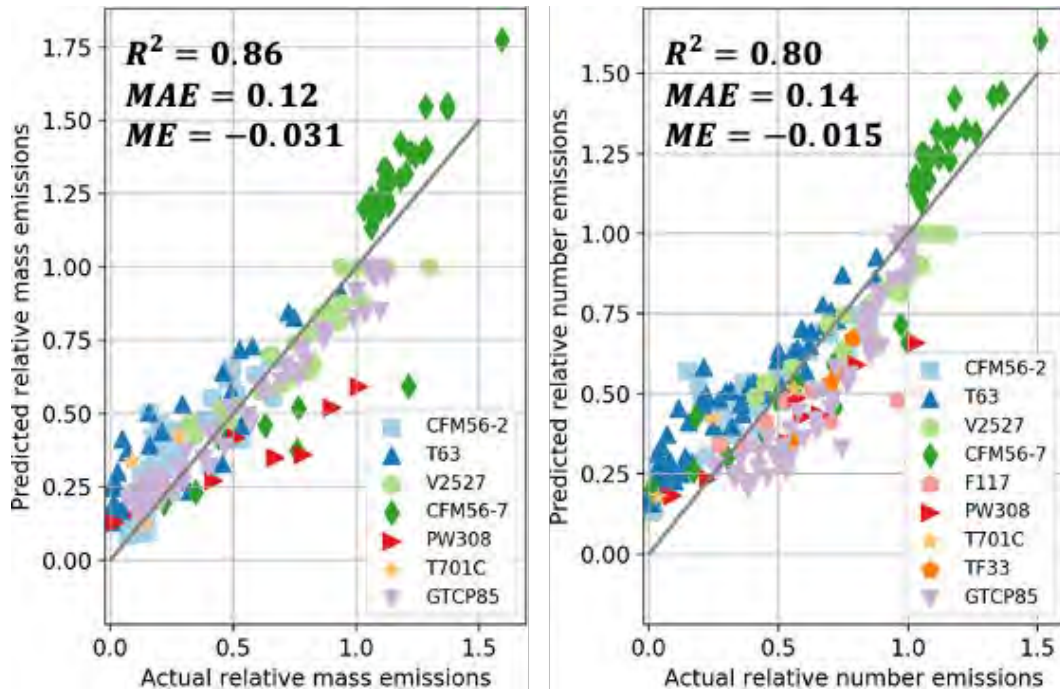


Figure 8. Actual/measured versus predicted relative mass emissions (left) and number emissions (right) using the exponential re-fitted approach.

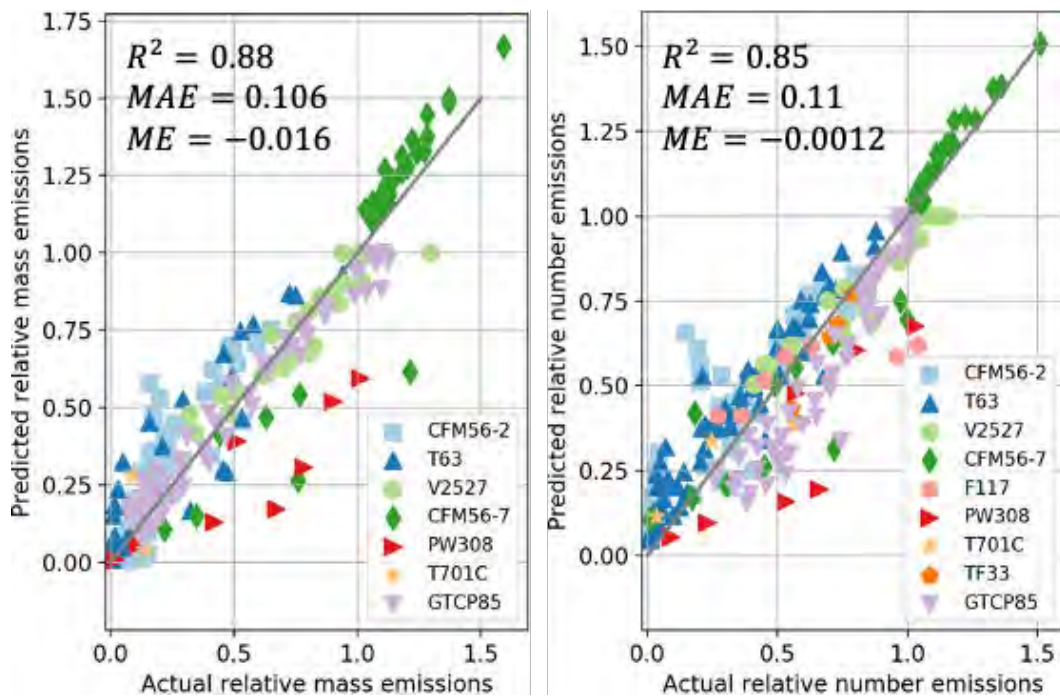


Figure 9. Actual/measured versus predicted relative mass emissions (left) and number emissions (right) using the quadratic approach.



### **Milestone**

The results of this analysis were presented to FAA project managers and to members of the ECTG group under WG3 at the 5<sup>th</sup> meeting of CAEP/12-WG3.

### **Major Accomplishments**

None

### **Publications**

None

### **Outreach Efforts**

Our results have been communicated to the FAA and ICAO-CAEP in a detailed report and presentation.

### **Awards**

None

### **Student Involvement**

Graduate student Akshat Agarwal conducted the analysis.

### **Plans for Next Period**

This work will be updated based on feedback with MDG and ECTG to complete the analysis by the next WG3 meeting.

### **References**

- Agarwal, Akshat, Raymond L. Speth, Thibaud M. Fritz, S. Daniel Jacob, Theo Rindlisbacher, Ralph Iovinelli, Bethan Owen, Richard C. Miake-Lye, Jayant S. Sabnis, and Steven R. H. Barrett. 2019. "SCOPE11 Method for Estimating Aircraft Black Carbon Mass and Particle Number Emissions." *Environmental Science & Technology* 53 (3): 1364-73. <https://doi.org/10.1021/acs.est.8b04060>.
- AIR6241. 2013. "Procedure for the Continuous Sampling and Measurement of Non-Volatile Particle Emissions from Aircraft Turbine Engines - SAE Aerospace Information Report 6241 (AIR6241)."
- Beyersdorf, A. J., M. T. Timko, L. D. Ziemba, D. Bulzan, E. Corporan, S. C. Herndon, R. Howard, et al. 2014. "Reductions in Aircraft Particulate Emissions Due to the Use of Fischer-Tropsch Fuels." *Atmospheric Chemistry and Physics* 14 (1): 11-23. <https://doi.org/10.5194/acp-14-11-2014>.
- Brem, Benjamin T., Lukas Durdina, Frithjof Siegerist, Peter Beyerle, Kevin Bruderer, Theo Rindlisbacher, Sara Rocci-Denis, et al. 2015. "Effects of Fuel Aromatic Content on Nonvolatile Particulate Emissions of an In-Production Aircraft Gas Turbine." *Environmental Science and Technology*, October. <https://doi.org/10.1021/acs.est.5b04167>.
- Bulzan, Dan, Bruce Anderson, Changlie Wey, Robert Howard, Edward Winstead, Andreas Beyersdorf, Edwin Corporan, et al. 2010. "Gaseous and Particulate Emissions Results of the NASA Alternative Aviation Fuel Experiment (AAFEX)," October, 1195-1207. <https://doi.org/10.1115/GT2010-23524>.
- Cain, Jeremy, Matthew J. DeWitt, David Blunck, Edwin Corporan, Richard Striebich, David Anneken, Christopher Klingshirn, W. M. Roquemore, and Randy Vander Wal. 2013. "Characterization of Gaseous and Particulate Emissions From a Turbohaft Engine Burning Conventional, Alternative, and Surrogate Fuels." *Energy & Fuels* 27 (4): 2290-2302. <https://doi.org/10.1021/ef400009c>.
- Corporan, Edwin, Matthew J. DeWitt, Christopher D. Klingshirn, David Anneken, Linda Shafer, and Richard Striebich. 2013. "Comparisons of Emissions Characteristics of Several Turbine Engines Burning Fischer-Tropsch and Hydroprocessed Esters and Fatty Acids Alternative Jet Fuels." In , 425-36. American Society of Mechanical Engineers Digital Collection. <https://doi.org/10.1115/GT2012-68656>.
- Corporan, Edwin, Matthew J. DeWitt, Christopher D. Klingshirn, Richard Striebich, and Meng-Dawn Cheng. 2010. "Emissions Characteristics of Military Helicopter Engines with JP-8 and Fischer-Tropsch Fuels." *Journal of Propulsion and Power* 26 (2): 317-24. <https://doi.org/10.2514/1.43928>.
- Corporan, Edwin, Tim Edwards, Linda Shafer, Matthew J. DeWitt, Christopher Klingshirn, Steven Zabarnick, Zachary West, Richard Striebich, John Graham, and Jim Klein. 2011. "Chemical, Thermal Stability, Seal Swell, and Emissions Studies of Alternative Jet Fuels." *Energy & Fuels* 25 (3): 955-66. <https://doi.org/10.1021/ef101520v>.



- Moore, Richard H., Kenneth L. Thornhill, Bernadett Weinzierl, Daniel Sauer, Eugenio D'Ascoli, Jin Kim, Michael Lichtenstern, et al. 2017. "Biofuel Blending Reduces Particle Emissions from Aircraft Engines at Cruise Conditions." *Nature* 543 (7645): 411–15. <https://doi.org/10.1038/nature21420>.
- Speth, Raymond L., Carolina Rojo, Robert Malina, and Steven R. H. Barrett. 2015. "Black Carbon Emissions Reductions from Combustion of Alternative Jet Fuels." *Atmospheric Environment* 105 (Supplement C): 37–42. <https://doi.org/10.1016/j.atmosenv.2015.01.040>.
- Teoh, Roger, Marc E. J. Stettler, Arnab Majumdar, Ulrich Schumann, Brian Graves, and Adam M. Boies. 2019. "A Methodology to Relate Black Carbon Particle Number and Mass Emissions." *Journal of Aerosol Science* 132 (June): 44–59. <https://doi.org/10.1016/j.jaerosci.2019.03.006>.
- Timko, M. T., Scott C. Herndon, Elena de la Rosa Blanco, Ezra C. Wood, Zhenhong Yu, Richard C. Miake-Lye, W. Berk Knighton, Linda Shafer, Matthew J. DeWitt, and Edwin Corporan. 2011. "Combustion Products of Petroleum Jet Fuel, a Fischer–Tropsch Synthetic Fuel, and a Biomass Fatty Acid Methyl Ester Fuel for a Gas Turbine Engine." *Combustion Science and Technology* 183 (10): 1039–68. <https://doi.org/10.1080/00102202.2011.581717>.
- Timko, M. T., Z. Yu, T. B. Onasch, H.-W. Wong, R. C. Miake-Lye, A. J. Beyersdorf, B. E. Anderson, et al. 2010. "Particulate Emissions of Gas Turbine Engine Combustion of a Fischer–Tropsch Synthetic Fuel." *Energy & Fuels* 24 (11): 5883–96. <https://doi.org/10.1021/ef100727t>.
- Zhang, Xiaole, Xi Chen, and Jing Wang. 2019. "A Number-Based Inventory of Size-Resolved Black Carbon Particle Emissions by Global Civil Aviation." *Nature Communications* 10 (1): 1–11. <https://doi.org/10.1038/s41467-019-08491-9>.



# Project 049 Urban Air Mobility Noise Reduction Modeling

The Pennsylvania State University, Continuum Dynamics, Inc.

## Project Lead Investigator

Kenneth S. Brentner  
Professor of Aerospace Engineering  
Department of Aerospace Engineering  
The Pennsylvania State University  
233 Hammond Building  
University Park, PA  
(814) 865-6433  
ksbrentner@psu.edu

## University Participants

### The Pennsylvania State University

- PI: Kenneth S. Brentner, Professor of Aerospace Engineering
- FAA Award Number: 13-C-AJFE-PSU-049, Amendment No. 52
- Period of Performance: February 5, 2020 to February 4, 2021
- Tasks:
  1. Update the flight simulation component of the noise prediction system for urban air mobility (UAM)/ electric vertical takeoff and landing (eVTOL) aircraft.
  2. Update the coupling of the new flight simulation software with Comprehensive Hierarchical Aeromechanics Rotorcraft Model (CHARM) and PSU-WOPWOP noise prediction software.
  3. Evaluate broadband noise models appropriate for UAM/eVTOL aircraft.
  4. Develop and test trim strategies for notional UAM/eVTOL vehicles.
  5. Evaluate the computational algorithm to ensure it is efficient enough for many rotors and noise generating bodies.

## Project Funding Level

FAA provided \$280,000 in funding. The Pennsylvania State University (PSU): \$147,454 faculty academic year cost sharing; \$102,000 equipment cost sharing.

## Investigation Team

- Kenneth S. Brentner, PI, The Pennsylvania State University; acoustic prediction lead on all tasks.
- Eric Greenwood, Co-PI, The Pennsylvania State University; acoustics prediction/analysis supporting acoustic tasks.
- Joseph F. Horn, Co-PI, The Pennsylvania State University; flight simulation lead supporting flight simulation tasks.
- Daniel A. Wachspress, Co-PI, Continuum Dynamics, Inc.; responsible for rotor loads, wake integration, and CHARM coupling.
- Ze Feng (Ted) Gan, Graduate Research Assistant, The Pennsylvania State University; primarily responsible for developing PSU-WOPWOP noise prediction software and performing acoustic predictions (Tasks 2, 3, 5).
- Bhaskar Mukherjee, Graduate Research Assistant, The Pennsylvania State University; primarily responsible for software coupling, establishing new aircraft models, developing simulations for new aircraft types, performing acoustic predictions, and developing flight abatement procedures (Tasks 1, 2, 4).

## Project Overview

A wide variety of unconventional configurations for UAM and eVTOL aircraft, with many electrically driven propellers and lifting rotors, have been proposed and are currently under development by companies worldwide. These novel configurations make up a new category of aircraft that will need to be certified and especially for acceptable noise levels, given their urban

operations. Furthermore, the noise of UAM and eVTOL vehicles is expected to be one of the determining factors for community and passenger acceptance. Therefore, first principles noise predictions of these aircraft will be important for providing information that is independent from manufacturers for the FAA, and before manufacturer flight test or certification noise data is available.

In ASCENT Project 38, the helicopter noise prediction system initially developed in ASCENT Project 6 was successful in accurately predicting the noise of 6 helicopters (usually within 1-3 sound exposure level (SEL) dBA), when comparing the predictions to flight test results from a FAA/NASA rotorcraft noise abatement flight test that was carried out in August and October of 2017. Sound exposure level contours from the flight test were compared with predictions for several flight procedures. This noise prediction system developed in Project 38 consisted of the PSUHeloSim flight dynamics simulation code coupled to the Comprehensive Hierarchical Aeromechanics Rotorcraft Model (CHARM) aeromechanics modeling software and the PSU-WOPWOP noise prediction code. This coupling with the flight simulation code was demonstrated to be important for noise predictions, which improved noticeably when the simulation was modified to track the time dependent aircraft position, velocity, and attitude flown in the individual run, rather than the nominal flight path.

To build upon the success of ASCENT Project 38, an analogous approach of coupling a flight simulation code with CHARM and PSU-WOPWOP is taken in this ASCENT Project 49. In this project, the PSUHeloSim flight simulation component of the noise prediction system used in Project 38 is replaced with DEPSim, a flight simulation code designed for many electrically driven rotors and the unique control strategies to fly such vehicles effectively. Coupling of DEPSim with CHARM was done in work outside of ASCENT, but the DEPSim-CHARM coupling with PSU-WOPWOP will be performed in this project.

The goal of this project is to develop a noise prediction system with the initial capability to analyze the noise from UAM and eVTOL vehicles with unique configurations under any flight conditions. This will enable the FAA, manufacturers, and related entities to investigate how this new class of vehicles—and their noise—might be integrated into the national airspace. Emphasis is placed on modeling the unique features of UAM and eVTOL configurations not commonly seen in conventional rotorcraft, such as variable rotation speed rotors and complex unsteady aerodynamic interactions between the many rotors and airframe. UAM vehicles will likely have lower tip speeds to achieve acceptable noise levels, so broadband noise is expected to become the dominant rotor noise source; accordingly, fast, accurate modeling of rotor broadband noise is a goal of this project. Another goal of this project is to use the noise prediction system developed in this project to provide guidance on how to fly these vehicles in a quiet manner through flight operations. Since the analysis and computations are based on fundamental physics, noise abatement procedures for novel new vehicles can be developed.

(Note: This is the first year of Project 49, which was authorized in February 2020. This report reflects approximately 7 months of effort).

## Task 1 – Update the Flight Simulation Component of the Noise Prediction System for UAM/eVTOL Aircraft

The Pennsylvania State University

### Objectives

This task will leverage the new flight simulator DEPSim to replace the PSUHeloSim component of the noise prediction system developed in ASCENT Projects 6 and 38. The DEPSim flight simulator will need to be tested for a variety of notional UAM and eVTOL configurations with distributed electric propulsion. For expediency, nominal configurations proposed by NASA will be used as example cases (Ref. 1.1). The trim envelope will be explored for these configurations in order to evaluate potential strategies for tailoring acoustics of these aircraft (as further explored in Task 4 below).

### Research Approach

Analogous to the PSUHeloSim system, the DEPSim flight simulator has been coupled with the CHARM Rotor Module (Ref. 1.2). This enables the flight simulator to capture necessary interactional effects between several moving components reasonably. Using DEPSim, a variety of control schemes will be explored to study the trim envelope. Based on experience from noise abatement strategies developed in ASCENT Project 38, control schemes with potential for noise reduction will be studied further. The impact of variable revolution per minute (RPM) and variable collective pitch control schemes is expected



to be an important factor. Realtime flight unsteadiness, such as gust (Ref 1.3), will also be included to study its impact on noise.

**Milestones**

The milestones for this task include 1) selecting a generic eVTOL configuration for preliminary study, 2) implementing a control scheme of choice (variable RPM, variable collective, variable RPM + collective), 3) studying trim envelope, and 4) studying the impact of control scheme choice on noise.

**Major Accomplishments**

A generic eVTOL configuration (Figure 1) previously developed (Ref. 1.2) was chosen for expediency. This configuration has four lift rotors and one cruise propeller along with a wing and other control surfaces included in the aerodynamic modeling.

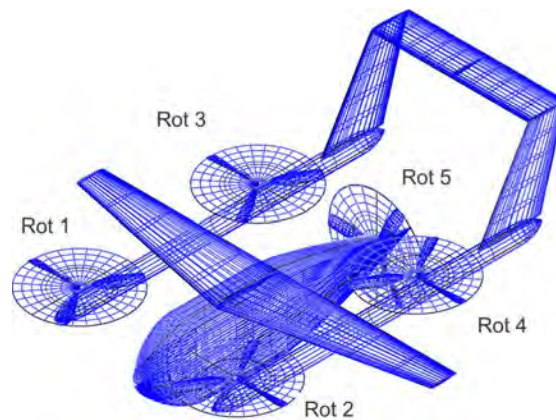


**Figure 1.** Generic eVTOL configuration for preliminary study.

The generic configuration shown in Figure 1 was simulated through the following maneuvers: hover, double doublet, and cruise (see Figure 2). The variable RPM fixed collective pitch control scheme was selected to trim the rotors for the entirety of this flight simulation.

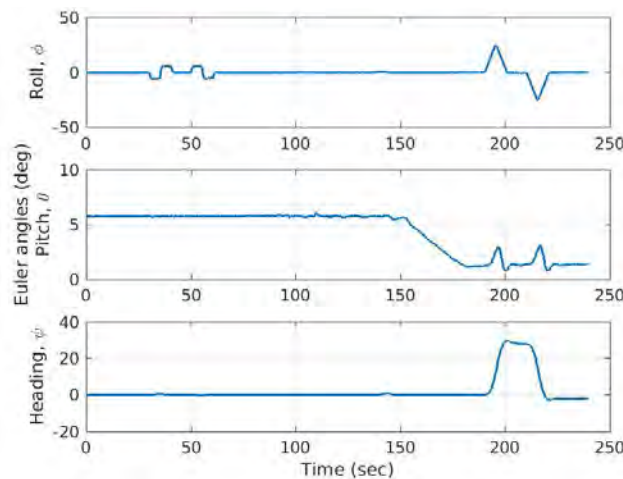


**Figure 2.** Aircraft Euler angles for entire flight trajectory.



Based on the maneuver commands, the variation in rotor angular velocity was studied (see Figure 3). The lifting rotors transition to zero angular velocity as the aircraft transitions to cruise and the wing provides the lift. The double doublet maneuver seems to have caused steep spikes in rotor RPM. A closer examination of Rotor 1 RPM reveals these spikes in greater detail (see Figure 4). These sudden spikes in rotor RPM are expected to have a strong impact on noise and will be an important focus in future work.

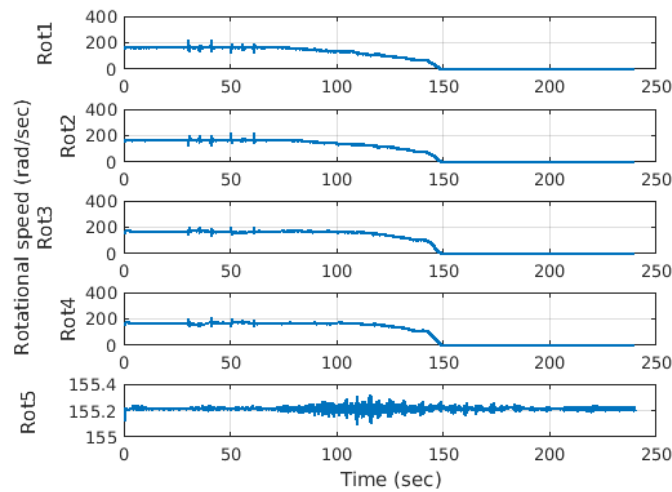


Figure 3. Rotor RPM response with respect to time.

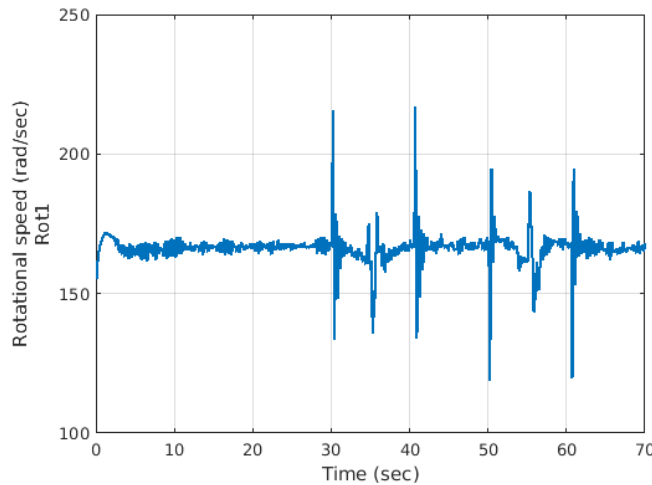


Figure 4. Rotor 1 RPM response during the double doublet maneuver.

**Publications**

**Published conference proceedings**

B. Mukherjee, Z. F. T. Gan, J.-P. Theron, M. Botre, K. S. Brentner, E. Greenwood, and J. F. Horn, “A New Distributed Electric Propulsion Aircraft Simulation Tool for Coupled Flight Dynamics, Free Wake, and Acoustic Predictions,” Vertical Flight Society 77th Annual Forum & Technology Display, May 11-13, 2021, *abstract submitted and under review.*

## **Outreach Efforts**

N/A

## **Awards**

None

## **Student Involvement**

Bhaskar Mukherjee, a graduate assistant just finishing his master's degree at PSU, has worked towards gaining proficiency in using DEPSim and CHARM Rotor Module.

## **Plans for Next Period**

The generic eVTOL vehicle in Fig. 1.1 will be studied for other flight operations. One to two more eVTOL vehicles (likely generic configurations developed by NASA) will be modeled in the coupled DEPSim/CHARM system. These aircraft models will be available for Task 2, which will include coupling of the current DEPSim/CHARM system with PSU-WOPWOP. The experience gained in this Task will support the activities of the other Tasks.

## **References**

- [1.1] Johnson, W., Silva, C., and Solis, E., "Concept Vehicles for VTOL Air Taxi Operations," AHS Technical Conference on Aeromechanics Design for Transformative Vertical Lift, San Francisco, CA, Jan. 16-19, 2018.
- [1.2] Theron, J.-P., Horn, J. F., and Wachspress, D., "An Integrated Simulation Tool for e-VTOL Aeromechanics and Flight Control Analysis," 2020 VFS Aeromechanics for Advanced Vertical Flight Technical Meeting, San Jose, CA, Jan. 2020
- [1.3] Theron, J.-P., Horn, J. F., Wachspress, D., and Enciu, J., "Nonlinear Dynamic Inversion Control for Urban Air Mobility Aircraft with Distributed Electric Propulsion," Vertical Flight Society 76th Annual Forum & Technology Display, Virginia Beach, VA, Oct. 2020.

## **Task 2 – Update the Coupling of the New Flight Simulation Software with CHARM and PSU-WOPWOP**

The Pennsylvania State University

### **Objective**

The objective of this task is to couple the DEPSim flight simulation system with PSU-WOPWOP and enable noise prediction. Emphasis will be on new changes to be made to the DEPSim flight simulation system and PSU-WOPWOP in order to enable computation of noise from rotors operating with variable angular velocity (variable RPM). This will enable the noise prediction of arbitrary eVTOL configurations and different trim strategies. The general approach used for PSUHelosim will be used in this Task, but will be modified as appropriate for DEP vehicles (i.e., variable RPM, many rotors, etc.)

### **Research Approach**

The DEPSim system is to be coupled with PSU-WOPWOP for enabling noise predictions. A schematic of the system is shown in Figure 5. The starting point for the coupling code was based of the work done for ASCENT Projects 6 and 38. The code needs modification in order to transfer time-varying rotor angular velocities to PSU-WOPWOP. High resolution blade loads are essential for noise prediction; therefore, the coupling with DEPSim and CHARM rotor module will require the azimuthal refinement of the wake and blade loads, known as reconstruction, to be passed to PSU-WOPWOP. CDI will extend the current reconstruction process to time-varying angular velocities. The new DEPSim/PSU-WOPWOP coupling will also need to extend what was previously done in PSUHelosim/CHARM/PSU-WOPWOP coupling. These changes are critical for noise prediction of UAM and eVTOL aircraft.

### **Milestones**

Milestones achieved for this task are 1) transferring aperiodic aircraft position, velocities, rotor angular velocities, aerodynamic blade loading, and geometry to PSU-WOPWOP; 2) generating input for broadband noise models (needed for Task 3); 3) updating PSU-WOPWOP to accept input data with arbitrary timestep spacing, regardless of whether the rotor has constant or variable RPM.

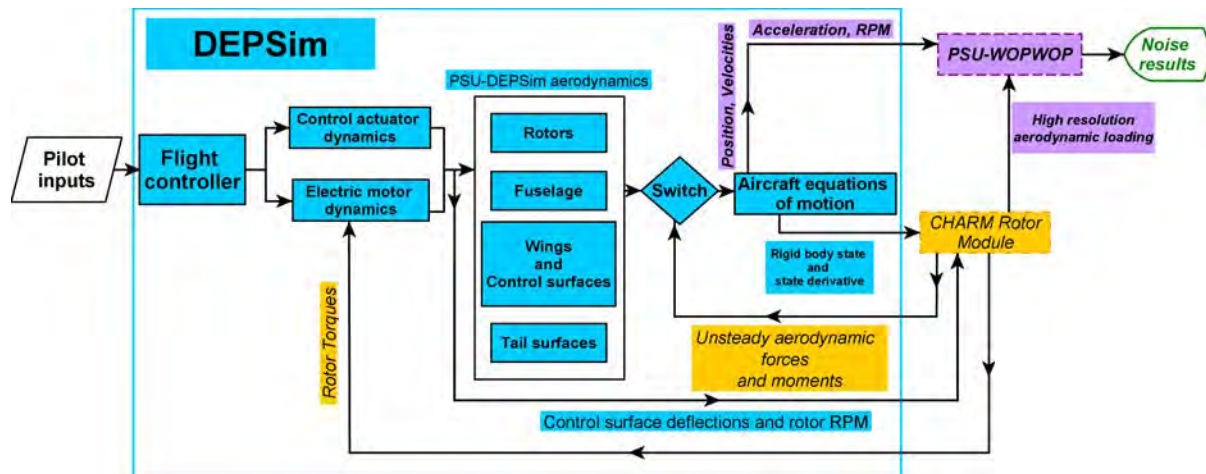


Figure 5. DEPSim system coupling schematic with CHARM rotor module and PSU-WOPWOP.

## Major Accomplishments

The code from ASCENT Projects 6 and 38 used in PSUHelosim for transferring the temporal aircraft, rotor, and blade loading data from CHARM rotor module to PSU-WOPWOP was used as a starting point for the development of a new interface for DEPSim. This code transfers data from CHARM and DEPSim using shared memory blocks. Work is ongoing in transferring the following data in aperiodic format:

1. Aircraft position, velocity
2. Position and orientation of rotors and other aircraft components
3. Rotor angular velocity

Previously, PSU-WOPWOP was able to calculate the noise for variable RPM rotors, but only if the input data was provided at discrete timesteps with constant time interval spacing. PSU-WOPWOP was updated to accept input data with arbitrary time spacing. To validate these changes to PSU-WOPWOP, the loading noise of a single rotating blade section with linearly-increasing RPM was calculated using two kinds of input data files: 1) with constant timestep spacing (and thus variable azimuthal spacing), and 2) with constant azimuthal spacing (and thus variable timestep spacing). Loading was approximated using blade element theory. The results from the two kinds of input data files coincide (see Figure 6), thus validating PSU-WOPWOP's capability in predicting the noise of rotors with arbitrary variable rotation speed, with input data from arbitrary timesteps.

## Publications

### Published conference proceedings

B. Mukherjee, Z. F. T. Gan, J.-P. Theron, M. Botre, K. S. Brentner, E. Greenwood, and J. F. Horn, "A New Distributed Electric Propulsion Aircraft Simulation Tool for Coupled Flight Dynamics, Free Wake, and Acoustic Predictions," Vertical Flight Society 77th Annual Forum & Technology Display, May 11-13, 2021, *abstract submitted and under review*.

## Outreach Efforts

N/A

## Awards

None

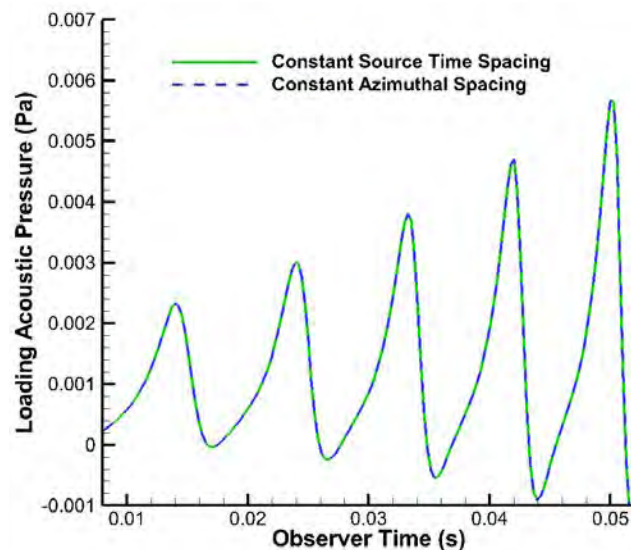


Figure 6. PSU-WOPWOP predictions for rotor with linearly increasing RPM.

### Student Involvement

Bhaskar Mukherjee, a graduate assistant just finishing his master’s degree at PSU, is working on the coupling of DEPSIm-CHARM and PSU-WOPWOP for this Task.

Ze Feng (Ted) Gan, a graduate assistant currently working towards his master’s degree at PSU, performed the modifications to PSU-WOPWOP to enable variable RPM rotors with nonuniform time step size for this Task.

### Plans for Next Period

Once the aircraft state data, such as velocities, position, and rotor trim data are transferred successfully, the focus will be on getting rotor geometry and high-resolution aerodynamic data to PSU-WOPWOP. When the coupling is complete, the system will be tested by simulating helicopters from the flight test data captured for ASCENT Project 6 and 38 and eVTOL vehicles modeled in Task 1.

## Task 3 – Evaluate Broadband Noise Models Appropriate for UAM/eVTOL Aircraft

The Pennsylvania State University

### Objective

The objective of this task is to predict the broadband noise of arbitrary UAM and eVTOL aircraft configurations. Broadband noise arises due to stochastic aerodynamic loading, usually due to turbulence. Broadband noise is expected to be important for UAM and eVTOL aircraft due to their complex configurations causing unsteady, turbulent aerodynamic interactions (e.g., between rotors, other rotors, and the airframe), and their low rotor tip speeds that reduce deterministic thickness and loading noise levels.

### Research Approach

To balance computational costs and physics-capturing fidelity, the semi-empirical physics-based Brooks, Pope, and Marcolini (BPM) model was chosen to model the rotor broadband noise (Ref. 3.1). The BPM model for airfoil self-noise is implemented within PSU-WOPWOP via an incoherent summation of the noise sound pressure level (SPL) spectrum generated at discrete airfoil sections along each blade span under a quasi-steady assumption. This implementation of the BPM model in PSU-WOPWOP was validated with other codes and experimental data.

Existing literature typically integrates the broadband noise spectrum for a time segment on the order of a rotor period; previously this was also done in PSU-WOPWOP. However, this may average out significant temporal/azimuthal variations in broadband noise that occur over one rotor period. For example, the rotor blade sections of helicopters and UAM aircraft may experience significant variations in unsteady aerodynamic loading, due to edgewise flight or interactional aerodynamics. Therefore, PSU-WOPWOP was updated to calculate the SPL spectrum as a function of time.

This approach is justified by rotor broadband noise frequencies being approximately 10 to 50 times higher than the blade passage frequency. This approach assumes that the time scale of the turbulence generating the self-noise is much smaller than the rotor period, such that only a short (compared to the rotor period) acoustic pressure time history is required to construct a representative broadband noise spectrum.

### **Milestones**

The milestones reached for this task include (1) validation of the implementation of the BPM model in PSU-WOPWOP, and (2) adding the capability to predict the time variation of broadband noise using the implementation of the BPM model in PSU-WOPWOP.

### **Major Accomplishments**

Two major activities were undertaken in this Task. The first activity was to validate the BPM model implementation in PSU-WOPWOP. Although the BPM model was available in PSU-WOPWOP, it had not been fully validated or widely used; thus, the first activity was to validate the model implementation. The second activity was to investigate the time varying nature of broadband noise in a way that has not been done previously. This is necessary before considering the broadband noise of time varying angular rotation rate of rotors. Both activities are described in more detail in the following.

#### **Validation of the BPM Model Implemented in PSU-WOPWOP**

To validate the implementation of the BPM model in PSU-WOPWOP, PSU-WOPWOP noise predictions were compared with experimental data of the higher-harmonic control aeroacoustic rotor test (HART) rotor (40% scale model BO-105 helicopter main rotor) in the DNW wind tunnel, and corresponding predictions made using the NASA ROTONET code (Ref. 3.2). The input data files required by PSU-WOPWOP were generated using CHARM, which solves for the rotor inflow.

Good agreement (within ~3-5 dB above 1000 Hz, where broadband noise dominates in the absence of rotor blade passage frequency harmonics) was obtained when comparing the PSU-WOPWOP predictions made using the BPM model with the experimental data and the ROTONET predictions (see Figure 7, from Ref. 3.2). The empirical Pegg model was found to be highly inaccurate (>20 dB over-prediction) compared to the experimental data. This inaccuracy was found to persist independently of the observer location (distance and directivity). The precise reasons for the observed discrepancies are difficult to determine, as the Pegg model combines numerous physical sources that are difficult to isolate and is heavily calibrated using experimental helicopter rotor data. The primary conclusion is that purely empirical models suitable for helicopters are probably not suitable for UAM aircraft. Accordingly, physics-based models, such as the BPM model, are needed. In Figure 8, a comparison of the BPM model implementation in PSU-WOPWOP (left) and the NASA BARC and ASNFIM codes (right, Ref. 3.3) is made. The PSU-WOPWOP predicts each of the self-noise components very close to the ASNFIM results (which is a newer implementation of the Brooks, Pope and Marcolini model, Ref. 3.1). The trailing-edge bluntness noise seems to be somewhat different, but more research is needed to determine the reason for this discrepancy.

The work summarized above provides validation of the BPM model implementation in PSU-WOPWOP. This accomplishment in Task 3 impacts the rest of the project by increasing confidence in the accuracy of broadband noise predictions to be made later in this project (Project 49).

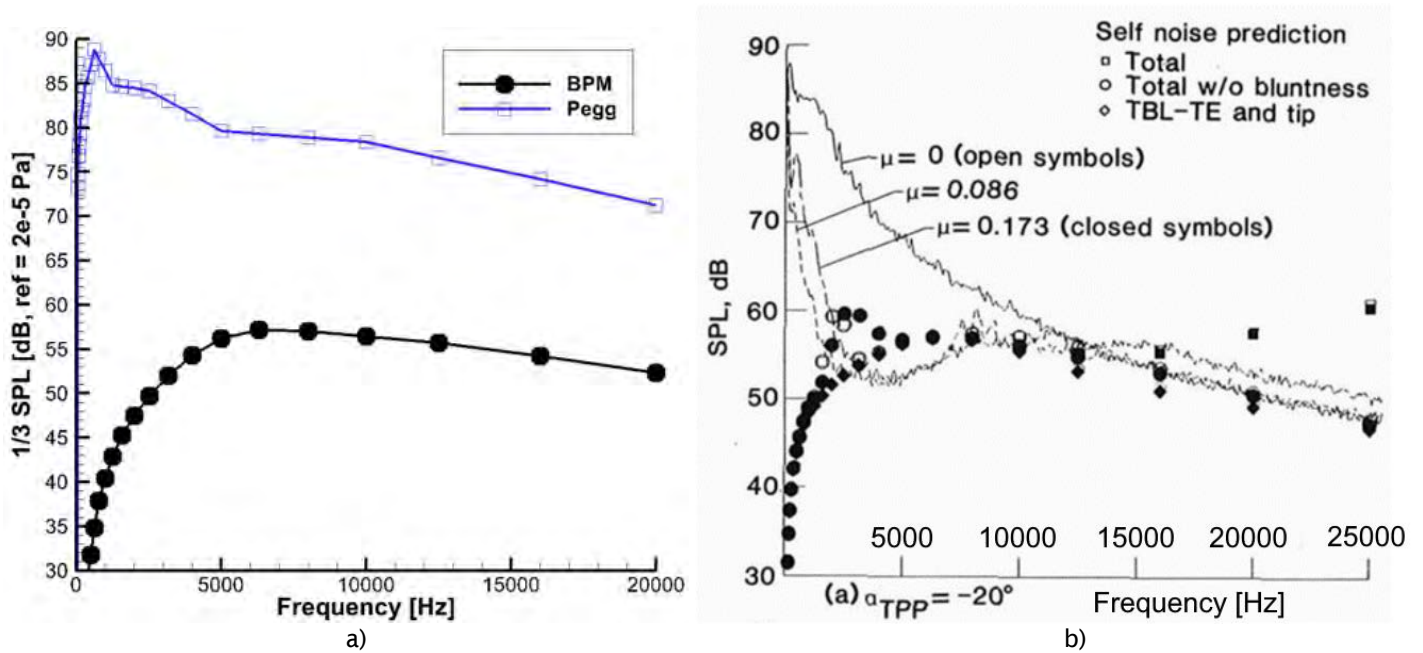


Figure 7. Broadband noise SPL spectrum for HART rotor case, advance ratio  $\mu = 0.173$ . a) PSU-WOPWOP prediction. b) Experimental data (lines) and ROTONET code predictions (symbols) (Ref. 3.2).

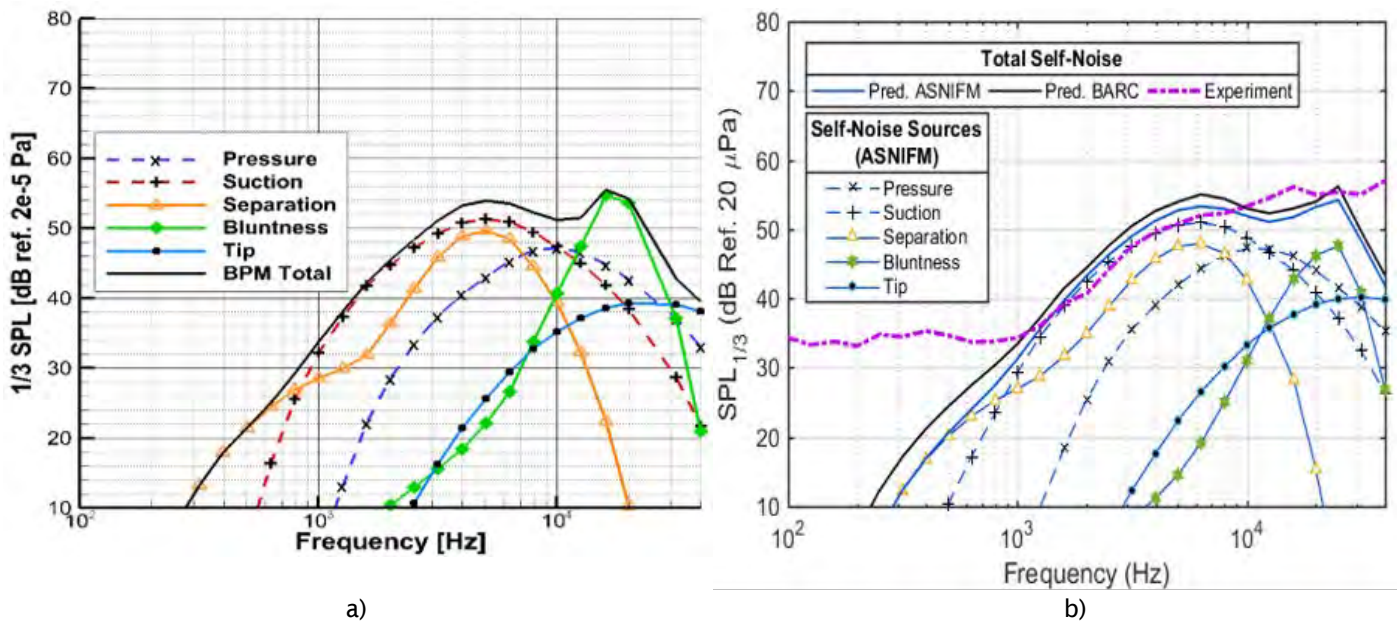
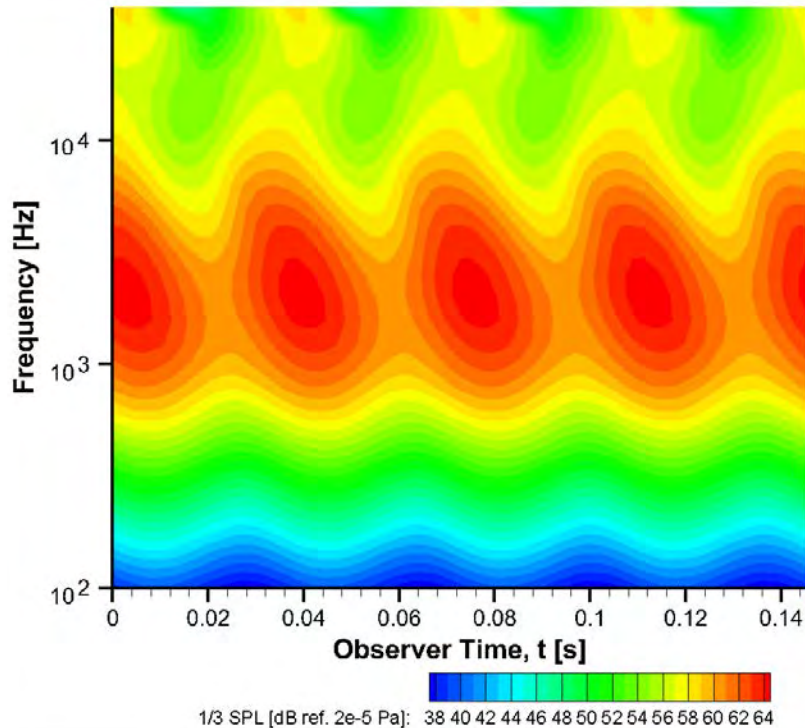


Figure 8. SPL spectrum from BPM model for ideally twisted rotor. a) PSU-WOPWOP prediction. b) BARC prediction (Ref. 3.3).

### Time Variation of Rotor Broadband Noise

Examples of time-varying broadband noise results are shown below for a Bell 407 helicopter main rotor (four blades,  $R = 5.34$  m) in steady level 80 knots forward flight (advance ratio  $\mu = 0.18$ , advancing tip Mach number  $M_{AT} = 0.8$ ). These sample plots demonstrate the new capabilities added to PSU-WOPWOP to analyze the time variation of broadband noise.

A spectrogram for a single observer (see Figure 9) demonstrates the time variation in the broadband noise SPL spectrum over a rotor period. At frequencies near 1 to 3 kHz, where SPL and human hearing sensitivity is highest, amplitude modulations of up to 4 dB peak-to-peak amplitude are observed. This demonstrates that averaging the SPL spectrum over a rotor period may average out important variations in the broadband noise.



**Figure 9.** Spectrogram for observer located at  $-45^\circ$  elevation relative to hub plane,  $180^\circ$  azimuth, and distance  $11R$  from hub.

Spectrograms can be extended to show the acoustic spectrum generated by each blade segment as a function of observer time. Such diagrams will be referred to as “spatial spectrograms”, which show the contribution from each blade segment for an observer time at a single observer location. Figure 10 shows the SPL spectrum from each radial segment for four observer time “snapshots”. These four observer times correspond to an approximately 1/4 revolution of the blade. Figure 10 shows that noise frequency and amplitude generally increase for radial stations approaching the blade tip.

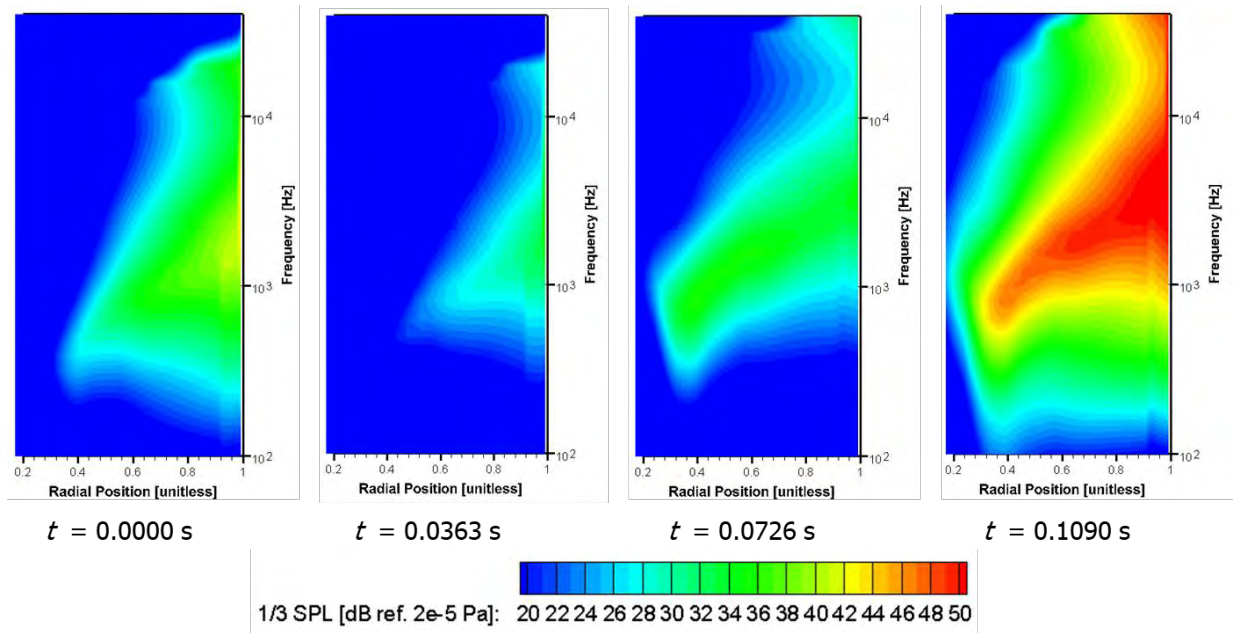


**Figure 10:** Observer time snapshots of spatial spectrogram of one rotor blade, for the same observer as Figure 9.

The time variation of the broadband noise directivity can be quantified using overall sound pressure level (OASPL). The noise levels (OASPL) are generally highest on the advancing side of the rotor due to convective amplification (see Figure 11). The broadband OASPL varies not only around the azimuth, but there is approximately a 3 dB OASPL difference between a single observer time ( $t = 0$  sec) and the observer time average, again for an observer on the advancing side and to the front of the rotor.

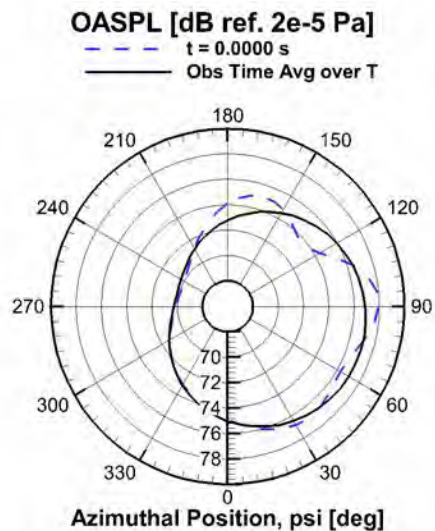


**Figure 11.** Broadband noise directivity in azimuthal plane, for observers located  $45^\circ$  below the tip-path-plane of the rotor, at a distance of  $11R$  from hub.

The impact of this work on the rest of the project consists of the development of new tools for calculating, visualizing, and analyzing time-varying broadband noise. This unique viewpoint may lead to better understanding of the physics of broadband noise, and improved prediction methodologies and metrics.

## **Publications**

### **Published conference proceedings**

Z. F. T. Gan, K. S. Brentner, and E. Greenwood, "Time Variation of Rotor Broadband Noise," Vertical Flight Society 8th Annual Electric VTOL Symposium, Jan. 26-28, 2021, *accepted for presentation*.

## **Outreach Efforts**

N/A

## **Awards**

None

## **Student Involvement**

Ze Feng (Ted) Gan, a graduate assistant currently working towards his master's degree at PSU, performed the modifications to PSU-WOPWOP, and the generation and analysis of the results for this Task.

## **Plans for Next Period**

Validation of the BPM model implemented in PSU-WOPWOP will continue, with diverse cases comprising a variety of flight conditions.

Future work will consist of parametric studies of the time-varying broadband noise spectrum. Parameters to vary include: number of blades and rotors, tip Mach number, advance ratio, and observer position (distance and directivity). These parametric studies will help determine conditions for which time variation of the broadband noise spectrum is important, which will in turn help determine how to incorporate knowledge of this spectrum time variation into UAM vehicle analysis and design. Both helicopter and UAM aircraft cases will be studied, including a Bell 407 helicopter in steady 6° descent, and a notional generic eVTOL aircraft. The relative contributions of the noise source mechanisms of the BPM model at different blade positions will be studied using spatial spectrograms. The correlation between deterministic and broadband loading noise will also be investigated. Some correlation is expected, as broadband noise is physically a type of loading noise, but at higher frequencies. This correlation will be investigated using the time-variation of contour plots and/or iso-surfaces of noise levels (e.g., acoustic pressure, OASPL). This work would help develop a deeper understanding of the underlying physics, enabling improved noise prediction. The impact of time varying rotor rotation rate on broadband noise will also be considered. The prediction of broadband noise for time-varying rotor rotation rate may require further noise prediction system implementation changes.

## **References**

- [3.1] T. F. Brooks, D. S. Pope, and M. A. Marcolini, "Airfoil self-noise and prediction," Tech. Rep. 1218, National Aeronautics and Space Administration, 1989.
- [3.2] T. F. Brooks, M. A. Marcolini, and D. S. Pope, "Main rotor broadband noise study in the DNW," Journal of the American Helicopter Society, vol. 34, no. 2, pp. 3-12, 1989.
- [3.3] N. A. Pettingill and N. S. Zawodny, "Ideally Twisted Rotor Testing and Predictions," presented at NASA Acoustics Technical Working Group, 2020.

## **Task 4 – Develop and Test Trim Strategies for Notional UAM/eVTOL Vehicles**

The Pennsylvania State University

### **Objectives**

UAM/eVTOL vehicles have significant control redundancy inherent in their design. This includes not only multiple propellers and rotors, but also lifting surfaces, such as wings and tail surfaces. As a result, the trim of the vehicle is not unique; hence, some strategies to determine an "optimal" trim will be required. In this Task, alternative trim approaches will be developed

and demonstrated. Baseline performance oriented trim strategies will be compared with trim for maximum noise reduction. These trim strategies and their use in anticipated flight operations will be evaluated in the PSU flight simulation facility to test feasibility for practical UAM operations.

### **Research Approach**

The development of trim strategies requires a thorough understanding of the correlation of interactional aerodynamics and fundamental acoustic mechanisms. Traditionally constant RPM rotors have discrete frequency peaks often corresponding to multiples of their blade passage frequency. Variable RPM rotors, however, are expected to introduce additional discrete frequencies whose characteristics will potentially be impacted by how the RPM will vary with time. The importance of parameters such as angular acceleration will need to be studied further in the context of acoustics.

### **Milestones**

This task has not yet been started, as correlating trim strategies with noise requires completing Task 2 first. The first milestone will be to demonstrate satisfactory trim with multiple trim approaches, and then to compare the acoustic field for each of the equivalent (in the sense of satisfying trim) trims. This will provide an example of how noise can be improved with a proper trim strategy for eVTOL aircraft. The next milestone will be to determine which aspects of the higher noise level trims are most important. A final milestone will be to develop new acoustically optimal trim strategies to reduce the noise. The new trim approach will be demonstrated/validated in the noise prediction system.

### **Major Accomplishments**

None

### **Publications**

None

### **Outreach Efforts**

N/A

### **Awards**

None

### **Student Involvement**

Bhaskar Mukherjee, a graduate assistant just finishing his master's degree at PSU, will perform this Task.

### **Plans for Next Period**

This Task will be initiated after the completion of Task 2, using the planned research approach.

## **Task 5 – Evaluate the Computational Algorithm to Ensure it is Efficient Enough for Many Rotors and Noise Generating Bodies**

The Pennsylvania State University

### **Objective**

The objective of this Task is to ensure that the computational algorithms used in the noise prediction software PSU-WOPWOP remain efficient for UAM aircraft, which generally have many rotors and noise-generating airframe components with significant aerodynamic interactions. This objective serves the more general goal of developing noise prediction that is fast but is also accurate in capturing the key underlying physics that generate the noise.

### **Research Approach**

The research approach taken will be to first use a code profiler to identify which parts of the computational algorithm serve as bottlenecks for noise prediction of UAM and eVTOL aircraft. These computational bottlenecks will be the focus of efforts to make the code more efficient, including techniques to make the code parallel. The eVTOL aircraft design attributes will



also be considered as part of the study on the computational algorithm, with the goal of using appropriate knowledge of the number of noise-producing components (rotors, wings, etc.), as part of the algorithm design of the noise predictions system in order to reduce computational bottlenecks.

### **Milestones**

This task has not yet been started because Task 2 must be completed first. The milestones for this task will be to 1) investigate where any bottlenecks show up in the noise predictions system, both for configurations with low number of rotors and eVTOL configurations with up to 10 rotors, and other noise generating surfaces; 2) review the configuration components and assess whether the computational algorithms can be improved by taking the aircraft configuration into account, especially in developing parallel processing strategies.

### **Major Accomplishments**

None

### **Publications**

None

### **Outreach Efforts**

None

### **Awards**

None

### **Student Involvement**

Ze Feng (Ted) Gan, a graduate assistant currently working towards his master's degree at PSU, will perform this Task.

### **Plans for Next Period**

This task will be initiated after the completion of Task 2, using the planned research approach.



# Project 050 Over-Wing Engine Placement Evaluation

## Georgia Institute of Technology

### Project Lead Investigator

Principal Investigator:

Professor Dimitri N. Mavris

Director, Aerospace Systems Design Laboratory

School of Aerospace Engineering

Georgia Institute of Technology

Phone: (404) 894-1557

Fax: (404) 894-6596

Email: dimitri.mavris@ae.gatech.edu

Co-Principal Investigator:

Dr. Chung Lee

Research Engineer

Aerospace Systems Design Laboratory

School of Aerospace Engineering

Georgia Institute of Technology

Phone: (404) 894-0197

Fax: (404) 894-6596

Email: chung.h.leei@ae.gatech.edu

## University Participants

### Georgia Institute of Technology

- PI: Dr. Dimitri Mavris, Co-PI Dr. Chung Lee
- FAA Award Number: 13-C-AJFE-GIT-057
- Period of Performance: February 5, 2020 to February 4, 2022
- Tasks relevant for this period:
  1. Formulate multidisciplinary analysis and optimization (MDAO) problem.
  2. Create tools to generate parametric geometry.
  3. Automate parametric mesh generation and computational fluid dynamics (CFD) solver on supercomputing cluster.
  4. Create and calibrate single aisle aircraft mission model.
  5. Develop high bypass turbofan propulsion cycle model.
  6. Create noise models.
  7. "Wrap" codes for multidisciplinary analysis.
  8. Perform screening or dimensionality reduction.
  9. Demonstrate MDAO or adaptive sampling scheme on reduced order or "placeholder" functions.

## Project Funding Level

Georgia Institute of Technology (Georgia Tech) was funded at \$590,000 for a two-year project. Georgia Techy has agreed to a total of \$590,000 in matching funds. This total includes salaries for the project director, research engineers, and graduate research assistants, as well as computing, financial, and administrative support, including meeting arrangements. The institute has also agreed to provide tuition remission for the students, paid for by state funds.

## Investigation Team

Georgia Institute of Technology

PI: Dimitri Mavris



Co-Investigator: Chung Lee

Propulsion and systems lead: Jonathan Gladin

Aerodynamics and CAD geometry: Srujal Patel

Graduate Students: Salah Tarazi, Kenneth Decker, Stephanie Zhu, Christopher Eggert, Christian Perron, Jai Ahuja

## Project Overview

The over-wing nacelle (OWN) aircraft concept has promising environmental benefits due to shielding of engine noise by the wings and the potential to reduce landing gear height and therefore gear noise. However, the engine placement may result in penalties in fuel burn due to aerodynamic interactions between the wing and propulsor if not optimized. The proposed work will develop a multidisciplinary analysis and optimization (MDAO) method for OWN aircraft. This task would build on past efforts by including noise shielding effects and analyzing multiple flight conditions to minimize fuel burn. One major challenge is the computational expense of analyses such as computational fluid dynamics (CFD). The proposed approach would rely on MDAO or efficient adaptive sampling techniques to use high fidelity analyses where they are most needed for system analysis.

The optimization of an OWN aircraft configuration over a mission with noise constraints will enable accurate tradeoffs between noise benefits and fuel burn. As a secondary benefit, the MDAO method will demonstrate efficient sampling methods for coupled, computationally intensive simulations in system analysis. These methods are useful to the FAA because many current applications require high fidelity simulations to accurately assess physics phenomena such as noise and emissions. Both the OWN results and the MDAO techniques will enable more physics-informed decisions about the environment.

2020 work focused on preliminary tasks to prepare a software tool chain and workflow for optimization. 2021 will focus on the execution of a full-scale MDAO process using supercomputing resources.

Major goals for this year thus focused on development:

- Creation of a baseline aircraft and engine deck for mission analysis.
- CFD studies for a fixed/non-parametric aircraft to estimate computational cost and requirements.
- Demonstration of MDAO or sampling methodologies using reduced order or “placeholder” analysis functions.

### *Notations and Abbreviations*

$\alpha$ : angle of attack

$C_D$ : drag coefficient

$C_L$ : lift coefficient

CFD: computational fluid dynamics

CRM: NASA Common Research Model

$\eta_{pr}$ : inlet pressure recovery

MDAO: multidisciplinary design analysis and optimization

OWN: over-wing nacelle

$p_{s_2}$ : static pressure at inlet

$p_{t_8}$ : total pressure at core nozzle exit

$p_{t_{18}}$ : total pressure at bypass nozzle exit

$T_{t_8}$ : total temperature at core nozzle exit

$T_{t_{18}}$ : total temperature at bypass nozzle exit

UWN: under-wing nacelle

## Task 1 – Formulate MDAO Problem

Georgia Institute of Technology

### Objectives

The overall goal is to state a MDAO problem to assess a single aisle OWN transport aircraft. The MDAO process will use CFD, noise analysis codes such as the Aircraft NOise Prediction Program (ANOPP), as well as weights, engine cycle, and mission analysis. The formulation will evolve during the project in light of physics results. However, for the performance period, a working MDAO problem statement was adopted:

- **Minimize:** fuel burn.



- **Subject to:** design variables including aircraft range, takeoff field length, and detailed side constraints such as wing/tail ground strike and tip-over requirements.
- **With respect to:** design variables including engine nacelle position (focusing on forward placement), nacelle and wing geometry, engine cycle and operating condition.
- **Given:** baseline single-aisle aircraft model and mission profile.
- **Returning:** fuel burn, noise

In discussion with FAA technical advisors, more emphasis is placed on aerodynamic performance optimization rather than noise, which is necessarily of lower fidelity. Accordingly, the single objective function of fuel burn is being minimized, though noise is evaluated as a response with respect to design variables. It is anticipated that the MDAO problem will undergo several iterations as information accumulates, so noise may be later treated as a constraint or secondary objective.

Given this general MDAO problem, this year’s performance on this Task focused on providing more detailed definition to the aero-propulsion aspect of the MDAO formulation.

### Research Approach

The most computationally expensive physics discipline is aerodynamics and it is closely coupled with propulsion cycle analysis. Therefore, the 2020 effort focused on the most important aero-propulsion aspects of MDAO, which drive the overall architecture of the problem. Noise and detailed side constraints mentioned above are important, as they allow solutions to capture realistically important physics trade-offs, such as the noise reduction, due to shorter landing gears enabled by over-wing engines. However, those constraints will be added in a full-scale MDAO effort of 2021. The 2020 developmental effort focuses on the following subset of the MDAO:

#### Preliminary aero-propulsion subset of MDAO problem:

<b>Minimize:</b>	fuel burn
<b>With respect to:</b>	geometry, angle of attack $\alpha$ , engine mass flow
<b>Given:</b>	fixed engine cycle design and throttle assumptions
<b>Subject to:</b>	continuity (mass flow balance between inlet and outlet)
	momentum balance (e.g. lift = weight, thrust = drag in steady level flight)
	Interdisciplinary consistency:
	Inlet pressure recovery $p_{t2,CFD} = p_{t2,cycle\ analysis}$
	Core nozzle total pressure $p_{t8,CFD} = p_{t8,cycle\ analysis}$
	Core nozzle total temperature $T_{t8,CFD} = T_{t8,cycle\ analysis}$
	Bypass nozzle total pressure $p_{t18,CFD} = p_{t18,cycle\ analysis}$
	Bypass nozzle total temperature $T_{t18,CFD} = T_{t18,cycle\ analysis}$
<b>Returning:</b>	fuel burn

Table 1 shows the aerodynamics, propulsion, and mission analyses in qualitative terms.

Table 1. Qualitative list of disciplinary analysis inputs and outputs

	Aerodynamics	Propulsion	Mission
Inputs	wing geometry	engine geometry	drag polar
	nacelle geometry	mass flow target	engine deck
	mass flow target	pressure recovery	
	$\rho_{t8}$		
	$T_{t8}$		
	$\rho_{t18}$		
Outputs	pressure recovery	$\rho_{t8}$	weights
	net force	$T_{t8}$	fuel burn
	drag polar	$\rho_{t18}$	
		$T_{t18}$	
		engine deck	

**On-Going Development of Design Structure Matrix**

This Task is also developing a design structure matrix (DSM) and maintaining a database of raw geometry variable descriptions that are to be included in the final MDAO implementation. Without emphasizing particular details, Figure 1 shows a snapshot in time of the DSM and variable descriptions. Note that geometry parameterization (Task 2), variable reduction/screening (Task 8), and actual MDAO trials will influence the final DSM and list of variables.

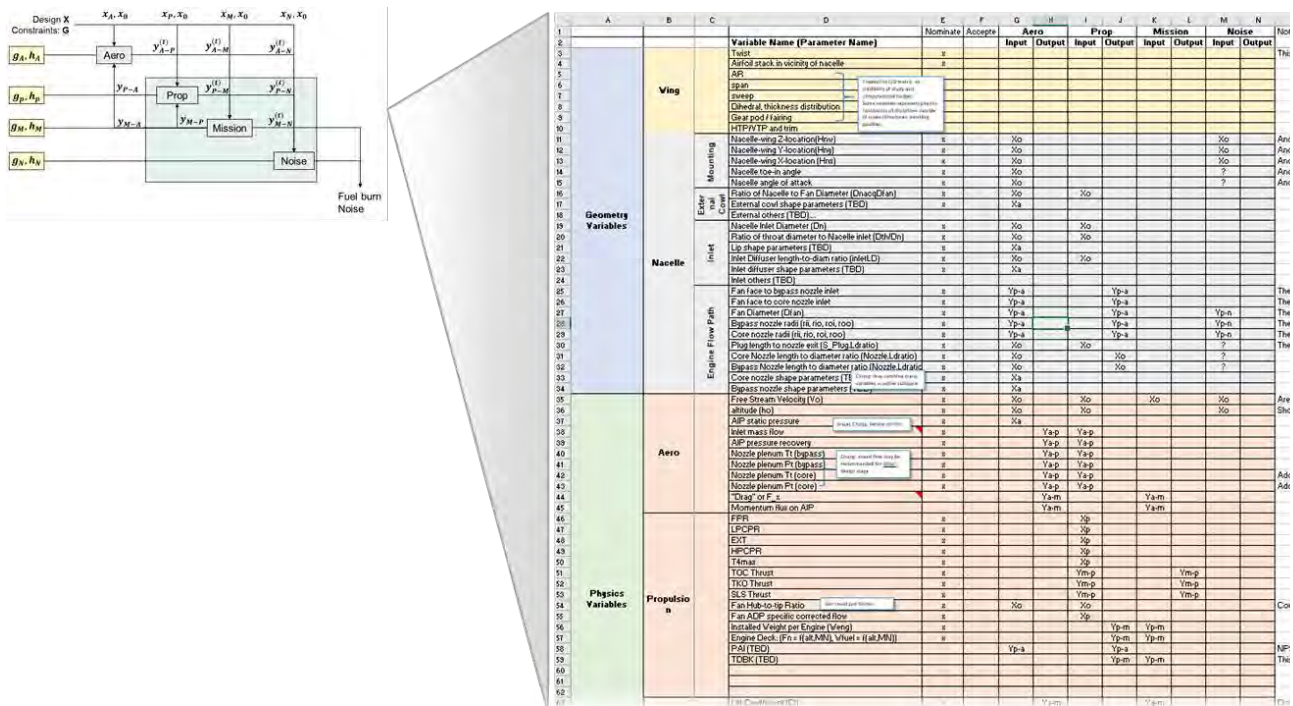


Figure 1. Example snapshot of DSM and variable database under development.

### **Scope of Design Variables**

The parameterization of geometric design variables is covered in the next Task, but the MDAO formulation effort provided bounds for the scope of optimization. In consultation with FAA technical advisors, the NASA Common Research Model (CRM) was chosen as a baseline geometry (Vassberg et al., 2008). Many parts of the aircraft geometry were deemed to be out of scope for the present research. Other than scaling from 300 to 150-passenger size, the fuselage is fixed. The justification for these decisions is an emphasis on credibility and reproducibility in the main research goal: a comparison between under-wing and over-wing nacelle configurations. In actual practice, an aircraft outer mold line (OML) geometry may involve thousands of detailed design variables, many more physics disciplines, flight scenarios, and constraints. For example, one consequence of simply scaling the fuselage shape is that the cockpit windows are much smaller. It is unlikely that pilot visibility requirements simply scale linearly with a fuselage length scale. Yet, this simple scaling of the CRM geometry is easily understood and replicable by the wider aeronautics research and industry communities. It avoids arbitrary detailed design decision by the researchers.

Because of this concern with credible and replicable comparison, several other parts of the aircraft geometry are not included in the MDAO study. The empennage requires flight mechanics and detailed mass estimation (e.g., trimming the horizontal tail plane requires knowledge of the center of gravity). Therefore, it is not included in high fidelity simulation, although mission analysis will include a friction drag penalty for empennage areas based on conceptual-level tail sizing rules. The landing gear pod region is not modified. The wing airfoils design space is constrained to a relatively small domain such that the structural thickness is not radically altered. The wing planform is also fixed.

The current approach is to not design a pylon joining the wing and nacelle, even though it undoubtedly plays an important role in interference drag for an OWN. Because the present effort includes no structural or thermal analysis, the pylon geometry would involve many potentially unrealistic guesses. To give decision-makers a fair assessment of potential benefits of OWN installation, we argue that a comparison of OWN and UWN should be made with no pylons or with thin placeholder/default pylons based on similar geometry rules for the two cases.

Finally, one of the most important variable scoping decisions is to limit the study to forward placement of nacelles. This decision was made in discussion with FAA and was driven by interest in the noise shielding effect from the wing.

### **Milestones**

Milestones for this task are not until 2021, but the MDAO formulation is under continuous development until high-fidelity optimization is executed.

### **Major Accomplishments**

A baseline aircraft design was successfully created based on reduction of the NASA Common Research Model (CRM). Aircraft wing and nacelle design variables were parameterized and implemented in Engineering Sketch Pad scripts. This directly supported Task 3 (parametric mesh generation and CFD solver on a supercomputing cluster), Task 7 (“wrapping” codes for multidisciplinary design analysis and optimization), and Task 8 (screening and reduction of design variables). The geometry generation also allowed preparatory activities for CFD such as initial mesh sensitivity studies.

### **Publications**

None

### **Outreach Efforts**

None

### **Awards**

None

### **Student Involvement**

Kenneth Decker and Bilal Mufti are continuing PhD students who contributed by testing different MDAO formulations on reduced order or inviscid test cases.



## Plans for Next Period

The next performance period will focus on the implementation of a specific MDAO architecture rather than a MDAO formulation. Whereas a formulation specifies the problem being solved (e.g., “Minimize fuel burn with respect to ....”), an architecture specifies the structure of information passing between the disciplinary analyses that comprise the MDAO. Examples that are currently being explored are the multidisciplinary feasible (MDF) architecture and various multi-level architectures such as collaborative optimization (CO) (Martins and Lambe, 2013).

## References

- Vassberg, J., Dehaan, M., Rivers, M., and Wahls, R., “Development of a Common Research Model for Applied CFD Validation Studies,” 26<sup>th</sup> AIAA Applied Aerodynamics Conference, AIAA Paper 2008-6919, 2008.
- Martins, Joaquim R. R. A. and Lambe, Andrew B., “Multidisciplinary Design Optimization: A Survey of Architectures,” AIAA Journal, 2013 51:9, 2049-2075.

## Task 2 – Parametric Geometry Generation

Georgia Institute of Technology

### Objective(s)

The solution of the MDAO problem involves reduction of physics disciplines to functions such as  $f(\mathbf{X})$  where  $\mathbf{X}$  is an array of design variables. An important and time-consuming preparatory step is to select candidate design parameters and create scripts through a CAD or CAD-like software to generate a water-tight geometry suitable for mesh generation. In the performance period, this parametric geometry effort focused on the outer mold line (OML) geometries of the fuselage, wing, and nacelles.

### Research Approach

The selection of a baseline aircraft mainly relied on two criteria: 1) applicability of the geometry to our current study of a single-aisle commercial airliner, and 2) existing wind-tunnel/CFD data for such geometry in open domain. By these two criteria, the NASA CRM (Vassberg et al., 2008) was deemed as the most appropriate geometry available in the open domain. Since the CRM geometry was derived from for a twin-aisle 300-passenger Boeing 777 design, it was determined that for the OWN problem, the baseline vehicle shall be a scaled-down version to match the overall dimensions of an Airbus A320 Neo, which is a 150-passenger single-aisle aircraft.

In order to generate the fully parametric CAD model, the section data for CRM fuselage, wing, horizontal tail, etc. were extracted from the original STEP file. Then the data was post-processed using Python-based scripts to make it import-ready for CAD model generation, which required the CST parametrization (explained in the next paragraph) and data re-organization for generating closed profile sketches. Figure 2 shows the sections extracted from the STEP file.

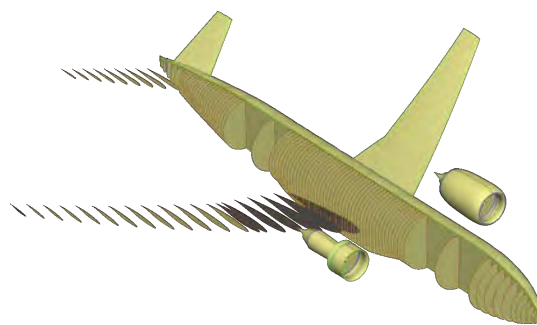


Figure 2. Cross sections extracted from NASA CRM model for parametric model creation.

### Implementation in Engineering Sketch Pad (ESP)

Two parametric geometry modeling tools were evaluated for this study: OpenVSP and Engineering Sketch Pad (ESP). ESP was chosen mainly due to two advantages over OpenVSP: a) ESP’s ability to design complex shapes and apply additional features

to those shapes such as blending/fillets that are crucial in aerodynamic optimization studies based on CFD, and b) OpenVSP initially did not interface to an adjoint feature in the inviscid CFD tool CART3D, which was the major drawback for its use in this study.

The ESP tool allows for a script-based bottom-up modeling approach to build the complex CAD models using constructive solid geometry concepts (Haimes et al., 2013). The tool generates complex geometries using feature-trees and parameters commonly used in CAD software and allows creation of both wire-bodies and sheet-bodies. The tool’s backend runs on LINUX, OSX, and Windows. The user interface is browser-based and is compatible on Firefox, Chrome, and Safari browsers. In the following subsections we will discuss how various OWN baseline aircraft components were modeled in ESP.

**Wing Design**

The wing was modeled using airfoil sections extracted from the original CRM wing geometry and then lofting the sketches through those sections, as shown in Figure 3. The airfoil geometry was specified using ESP’s built-in Kulfan function which uses the CST parametrization method (Kulfan, 2008).

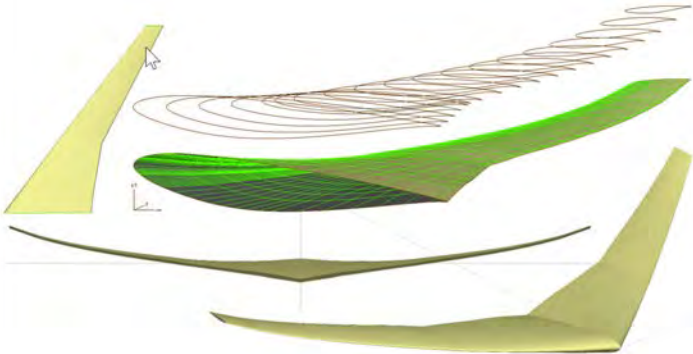


Figure 3. Example ESP output for wing.

The CST method allows for defining the airfoil shape using a simple analytic and well-behaved "shape function" that describes the geometry. The shape function provides the ability to directly control key geometry parameters that affect the airfoil drag, such as leading-edge radius, trailing edge boat-tail angle, and closure to a specified aft thickness. The shape function is mathematically represented by simple Bernstein polynomials, the coefficients of which become the parameters for controlling the airfoil shape. Therefore, the CST method requires relatively few variables to represent a large enough design space to contain optimum aerodynamic shapes for a variety of design conditions and constraints. Initially, the wing was parameterized with twist and four CST coefficients each for the top and bottom of airfoils at 21 spanwise stations. However, it was found that this parameterization allowed for physically unreasonable designs such as the exaggerated view in Figure 4.

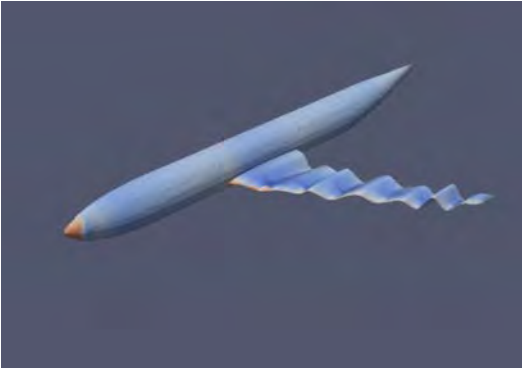


Figure 4. Example: parameterization of a physically unreasonable case in the design domain.

In particular, this parameterization did not account for spatial correlation or dependence of design variables. For example, the twist in one spanwise station is highly correlated to its adjacent, neighboring stations. Therefore, the twist and airfoil CST coefficients were modified such that each parameter type across 21 stations is governed by a spline with control points. In later Tasks such as design variable screening and reduction (Task 8), this spline parameterization was found to be much more efficient in terms of the fraction of feasible designs produced in sample domains.

**Engine/Nacelle Design**

The engine geometry was derived from approximating the overall dimensions of Pratt & Whitney PW1000G engines, which are part of the high-bypass geared turbofan engine family commonly seen on today’s aircraft, for example the Airbus A220, Mitsubishi SpaceJet, Embraer’s second-generation E-Jets, and as an option on the Irkut MC-21 and Airbus A320neo.

For CFD solver stability reasons, the engine bypass and core flows were implemented with plenums in CFD. The powered engine boundary conditions were implemented on surface patches in the plenums and the flow was allowed to expand through channels. These channels are non-physical (i.e., not a realistic representation of actual engines) but are used to represent the exhaust flow. The main reason for this strategy is numerical stability and robustness of the CFD solver setup across a wide range of nacelle designs and boundary conditions.

Particular geometry requirements arose because of this CFD strategy. The propulsion cycle analysis predicts properties such as mass flows that are linked to exit areas of bypass and core streams using 1D governing physics equations. However, it is difficult to define a corresponding area in 3D or 2D axisymmetric CFD. The geometry was parameterized using Bézier curves such that there is a constriction near the exit from bypass and core channels. This constriction was created such that the flow would choke (Mach = 1) close to the exit planes of the channels. This allows the estimation of an exit area that corresponds to the nozzle exit area in propulsion cycle analysis.

These geometry modeling decisions are not without drawbacks. In particular, there are difficulties in defining design domains *a priori* that produce physically reasonable designs. For example, if the tail cone angle is high, then the outer wall of the bypass channel (under the surface of the outer nacelle “airfoil”) must be deflected inward to avoid large regions of separated flow. Yet, this requires accompanying changes near the trailing edge of the outer airfoil for geometric compatibility. This can cause failed geometries or at least highly unfavorable aerodynamic designs. The nacelle parameterization was thus a compromise between robustness of CFD, ease of propulsion-aerodynamics integration, and the desire to yield feasible/reasonable geometries for much of the design space. Figure 5 shows the finished engine geometry ready for CFD simulation.

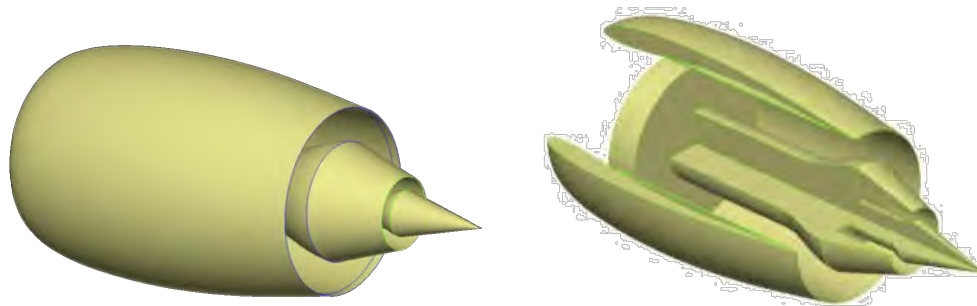


**Figure 5.** Fully parametric OWN engine geometry generated in ESP.

**Fuselage/Horizontal Tail Design**

A process similar to the previously described Wing Design was used to model the horizontal tail and fuselage of the aircraft, i.e., by generating sketches from extracted section data and then lofting those sketches together generate the respective surfaces. As described earlier, the OWN aircraft geometry is a scaled-down version of the original CRM geometry. Figure 6 depicts the complete CRM aircraft before and after the scale-down process for comparison.

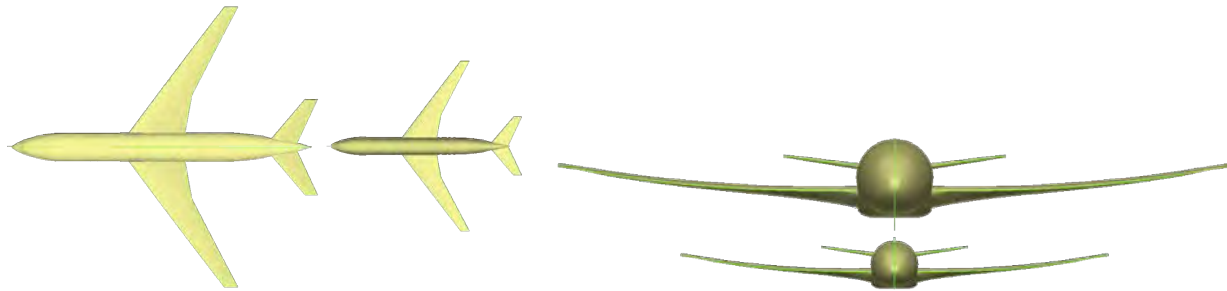


**Figure 6.** Side-by-side comparison of the original NASA CRM aircraft and scaled-down version of the OWN baseline aircraft (modeled in ESP), top view (left) and front view (right), with Fuselage scale factor 60.2%, wing scale factor 60.9%, and horizontal tail scale factor 62.25% (scaled with respect to longest dimension).

### **Milestone**

The entire aircraft including the engine geometry was parametrically modeled and is ready for CFD simulations.

### **Major Accomplishments**

A baseline aircraft design was successfully created based on reduction of the NASA CRM. Aircraft wing and nacelle design variables were parameterized and implemented in ESP scripts. This directly supported Task 3 (parametric mesh generation and CFD solver on a supercomputing cluster), Task 7 (“wrapping” codes for multidisciplinary design analysis and optimization), and Task 8 (screening and reduction of design variables). The geometry generation also allowed preparatory activities for CFD such as initial mesh sensitivity studies.

### **Publications**

None

### **Outreach Efforts**

None

### **Awards**

None

### **Student Involvement**

Salah Tarazi (continuing PhD student) played a major role in adapting the NASA CRM and implementing the baseline vehicle geometry in ESP.

Stephanie Zhu (continuing PhD student) was involved in wing parameterization in ESP and its linkage to CFD software.

### **References**

- Vassberg, J., Dehaan, M., Rivers, M., and Wahls, R., “Development of a Common Research Model for Applied CFD Validation Studies,” 26th AIAA Applied Aerodynamics Conference, AIAA Paper 2008-6919, 2008.
- Kulfan, Brenda M. “Universal parametric geometry representation method.” *Journal of aircraft* 45.1 (2008): 142-158.
- Haimes, Robert, and John Dannenhoffer. “The engineering sketch pad: A solid-modeling, feature-based, web-enabled system for building parametric geometry.” 21st AIAA Computational Fluid Dynamics Conference. 2013.
- Tejero, Fernando, et al. “Multi-objective optimisation of short nacelles for high bypass ratio engines.” *Aerospace Science and Technology* 91 (2019): 410-421.

### **Plans for Next Period**

In order to generate a more robust engine geometry, an extension of the CST parametrization approach (Tejero et al., 2019) will be explored. If this approach is successful, nacelle surfaces defined by Bézier curves will be replaced by the new parametric equations defined in the reference paper.

## Task 3 – Automation of Parametric Mesh Generation and CFD

Georgia Institute of Technology

### Objective

In order to solve an MDAO problem, the workflow between geometry generation to CFD solution and post-processing must be reduced to a robust function call. CFD meshing in particular is difficult to automate as a “fire-and-forget” process without human inspection or intervention. Yet, a high degree of automation is needed to allow modern design techniques such as active subspace, adaptive sampling, and multi-fidelity methods described in later tasks. This detailed development work may be of less interest to the stakeholder or decision-maker, but it is identified as a separate Task because it accounts for a large share of actual effort and calendar time.

### Research Approach

As with other Tasks, this is Task is currently under development until the first walk-through of an MDAO in 2021. In the example below, an off-line design of experiments (DoE), or sample specification, is used as a placeholder for an MDAO driver or optimizer.

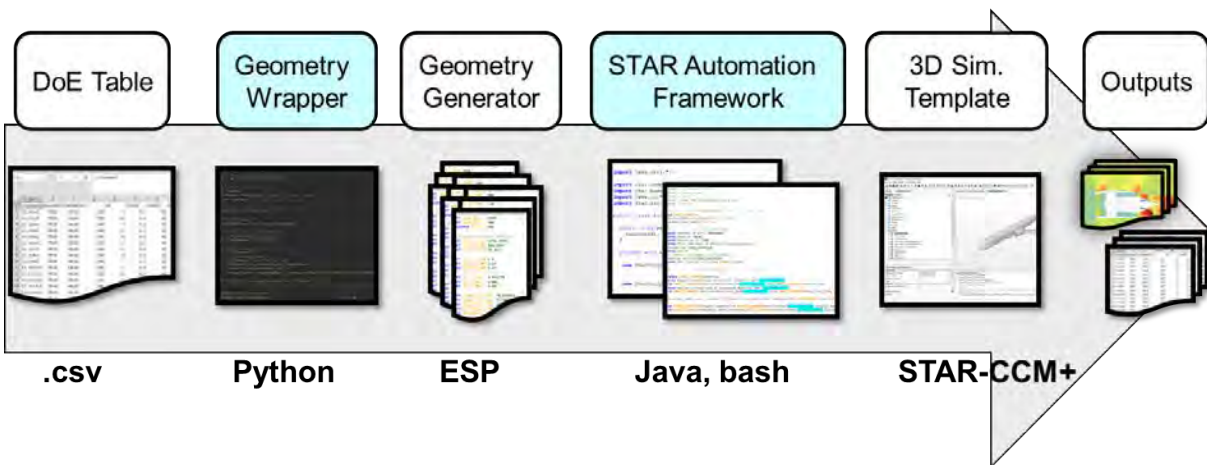


Figure 7. Automated work-flow for example design activity (design of experiments, or DoE).

### Risk Mitigation Strategies

Current development focuses on “wrapping” the Siemens STAR-CCM+ CFD suite. There have been delays in the performance period in legal arrangements to allow use of the tool on supercomputing resources supported by NASA. Therefore, two other CFD mesh and solver tool-chains have been linked to the parametric geometry generation as mitigation options. CREATE Capstone unstructured mesh generator and NASA’s Chimera Grid Tools were also “wrapped” with Python scripts and linked to ESP geometry for reduced cases in a pattern similar to Figure 7 above. These efforts leveraged ongoing academic efforts at Georgia Tech.

### Milestone

Related to this Task, initial grid sensitivity studies on the entire wing-body-nacelle geometry were conducted to fulfill a September 2020 milestone.

### Major Accomplishments

Initial automation of 2D axisymmetric CFD nacelles contributes to development of screening/variable reduction methods and MDAO techniques in later tasks.

### Publications

None



### **Outreach Efforts**

None

### **Awards**

None

### **Student Involvement**

Salah Tarazi (continuing PhD student) played a major role in adapting the NASA CRM and implementing the baseline vehicle geometry in ESP.

Stephanie Zhu (continuing PhD student) was involved in wing parameterization in ESP and its linkage to CFD software.

### **Plans for Next Period**

CFD automation and scripting shall be completed and tested with the full configuration on the NASA Advanced Supercomputing (NAS) facility.

## **Task 4 – Creation and Calibration of Single Aisle Aircraft Mission Model**

Georgia Institute of Technology

### **Objectives**

The study focuses on the impact of OWN installation on a specific aircraft class. An aircraft mission model is needed for a 150 passenger (“pax”) single-aisle aircraft. This mission model uses the propulsion cycle analysis and aerodynamic drag polars from CFD to yield fuel burn and other responses for a typical mission. The model is also used for comparison of OWN and UWN configurations.

### **Research Approach**

The mission analysis uses FLOPS (flight optimization system), which is a NASA code. The model discretizes a mission into segments and enforces conservation laws essentially for a point-mass representation of the aircraft. Even though the conservation laws are applied on a point mass, the aircraft has attributes such as drag and engine performance data from internal models and external data tables that are based on physics/geometry inputs such as wing area, aspect ratio, etc. Georgia Tech actually combines FLOPS along with the Numerical Propulsion System Simulation (NPSS) engine cycle analysis code and other tools in a multidisciplinary suite called the Environmental Design Space (EDS) (Kirby, 2008).

The detailed geometry used for CFD is substantially based on the NASA CRM in Task 2. For example, the baseline airfoil stack is adopted from the CRM. However, conceptual-level sizing parameters were adopted from the Airbus 320neo because this aircraft model has been used previously in FAA-sponsored mission analyses. Figure 8 below describes the development of the aircraft model.

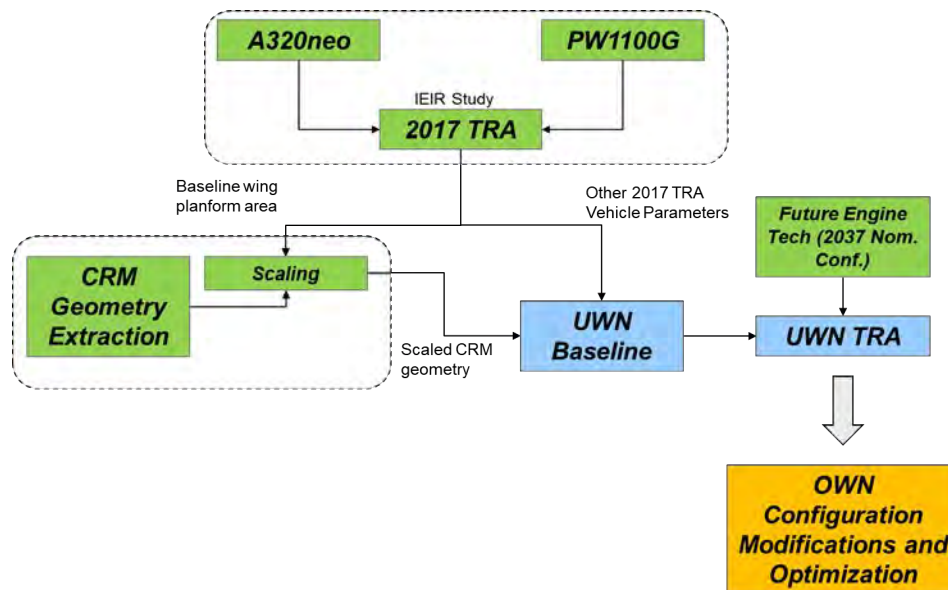


Figure 8. Development of 150-pax single-aisle aircraft model.

### Milestones

FLOPS aircraft baseline model and engine deck completed.

### Major Accomplishments

Baseline aircraft and engine model allow the propagation of aero-propulsion analysis to mission fuel burn and other system-level responses.

### Publications

None

### Outreach Efforts

None

### Awards

None

### Student Involvement

Andrew Burrell is a continuing graduate student.

### Plans for Next Period

The aircraft model is mainly complete, but detailed adjustments will be made as needed to the evolving aircraft design in the next period of performance.

### References

- Kirby, M.R. and Mavis, D.N., "The Environmental Design Space," 26th International Congress of the Aeronautical Sciences, Anchorage, AK, ICAS-2008-4.7.3, 2008.



## Task 5 – High Bypass Turbofan Propulsion Cycle Model

Georgia Institute of Technology

### **Objectives**

A cycle analysis is required to solve a coupling problem between aerodynamics (CFD) and mission analysis to compute thrust, fuel burn, and other key quantities. In particular, an engine model is created in the NPSS code to represent an appropriate technology level.

### **Research Approach**

The baseline engine was chosen to represent a future technology level (2027/2037) in consultation with FAA technical advisors. This was based on publicly available data for the PW1100G engine. The nominal bypass ratio is approximately 18. The large bypass is assumed because one of the main potential benefits of the OVN configuration is to enable larger diameter engines with their accompanying propulsive efficiency advantages.

This cycle information is linked to CAD and aerodynamic analysis through key geometry boundary conditions at different parts of the mission. For example, NPSS and its accompanying weight model WATE provides fan height as well as exit areas for core and bypass streams (at station 8 and 18) to the geometry generator. The cycle analysis also provides mass flow targets at the inlet as well as total pressure and temperature information at CFD core and bypass nozzle plenums.

### **Milestone**

Baseline engine deck (accompanying aircraft mission model) completed.

### **Major Accomplishments**

None

### **Publications**

None

### **Outreach Efforts**

None

### **Awards**

None

### **Student Involvement**

Andrew Burrell is a continuing graduate student.

### **Plans for Next Period**

An approach is being developed for landing gear sizing and constraint analysis for the 2037 engine, as the engine may be too large for reference/comparison UWN installations. The cycle shall be adjusted with respect to revised landing gear constraints. In addition, CFD analysis will likely reveal additional constraints and detailed modifications, especially due to nacelle shape.

## Task 6 – Noise Models

Georgia Institute of Technology

### Objective

One of the main benefits of the OWN configuration is noise shielding from the wing. Despite the importance of modeling noise, high fidelity physics modeling is out of scope for this present project due to the complexity and computational cost of analysis. Rather than a direct objective function in optimization, a lower-order analysis is used to model noise as a constraint (or simply tracked as a response) while optimization emphasizes aero-propulsion responses.

### Research Approach

Acoustics are modeled using a lower fidelity mode of ANOPP software. The code is used to model engine noise as a single source. Because of the relatively coarse spatial representation of noise, it is assumed that the dependence of noise responses with respect to nacelle geometry placement are crude at best. In other words, because the acoustical effect of the engine is concentrated at a point source, the ANOPP code in this lower fidelity mode cannot be used to capture the noise impact of moving the nacelle possibly within a tolerance of feet.

Nonetheless, keeping the above caveats in mind, initial configuration studies addressed the following questions:

- Does aft engine noise dominate the conversation moving forward?
- How much benefit does shielding provide for the forward mounted configuration?

A preliminary study was conducted by decomposing forward-radiated versus aft-radiated engine noise. The engine was simply moved above and below the wing by +/- 1.38 nacelle diameters for a baseline engine geometry. Comparisons were made for different technology assumptions (2017, 2027, 2037) for sideline and cutback noise. An example result is shown in Figure 9. It should be noted that these are preliminary results only, and results will change as geometry is optimized in the overall MDAO process.

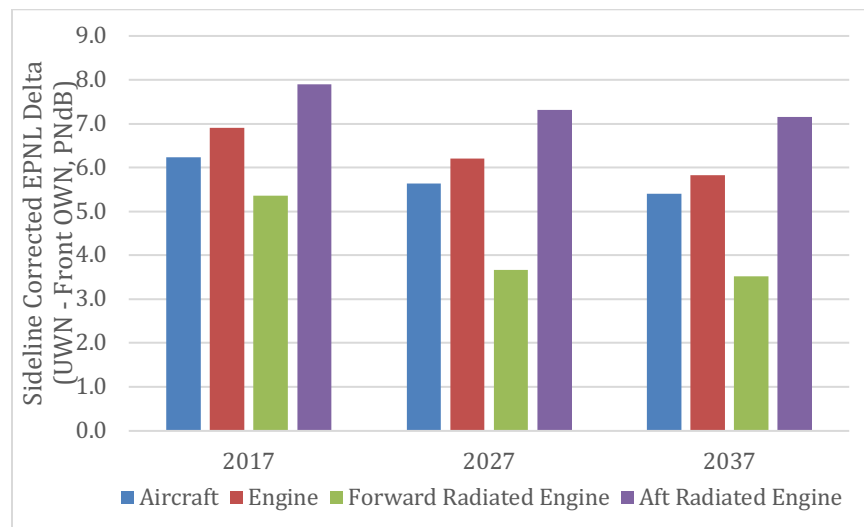


**Figure 9.** Sideline noise comparison of UWN and front-mounted OWN configurations under different technology assumptions. This example result is preliminary and before optimization.

### Milestones

None. This task contributes to an overall MDAO process for which a manual walk-through will be demonstrated in early 2021.



### **Major Accomplishments**

None

### **Publications**

None

### **Outreach Efforts**

None

### **Awards**

None

### **Student Involvement**

Andrew Burrell is a continuing PhD student who performed the ANOPP noise comparisons.

### **Plans for Next Period**

Noise models will be continually adjusted to reflect design changes in the high fidelity MDAO in the next period.

## **Task 7 – "Wrapping" of Codes for Multidisciplinary Analysis**

Georgia Institute of Technology

### **Objectives**

The multiple disciplinary codes such as CFD, engine cycle, mission, and noise analysis are scripted such that an MDAO driver script can direct function calls. This is essentially the preparation of interfaces to allow the codes to be connected to modern MDAO methods described in other Tasks.

As with other geometry and automation tasks, this present Task is also development work that is possibly of less direct interest to the stakeholder other than accounting for project schedule and workforce. There is considerable overlap with the automated meshing for CFD, which is emphasized separately (Task 3) due to its particular importance.

### **Research Approach**

In the period of performance, this wrapping of disciplinary codes focused on aerodynamics (also see Task 3), propulsion, and mission analysis. Interfaces are being prepared to allow each disciplinary analysis to be called from Python in a high-performance computing (HPC) environment. The use of Linux-based HPC initially posed a challenge because the propulsion, mission, and noise codes (NPSS, FLOPS, and ANOPP) have mainly been used in Windows. For this and related reasons, surrogate models (multivariable regressions) of these tools will be used rather than directly linking with Linux-based CFD.

Several regression options were investigated, including neural networks, linear regression, ridge regression, and lasso regression. For a full-scale optimization, larger DoE sample sizes will be used.

Full automation has been achieved for propulsion-aerodynamics integration (PAI) using STAR-CCM+ CFD on an axisymmetric nacelle case. Figure 10 below shows three columns, each with randomly generated nacelle designs. CFD is coupled with a NPSS polynomial surrogate model, and the plots show the evolution of responses as the two codes reach consistent flow properties.

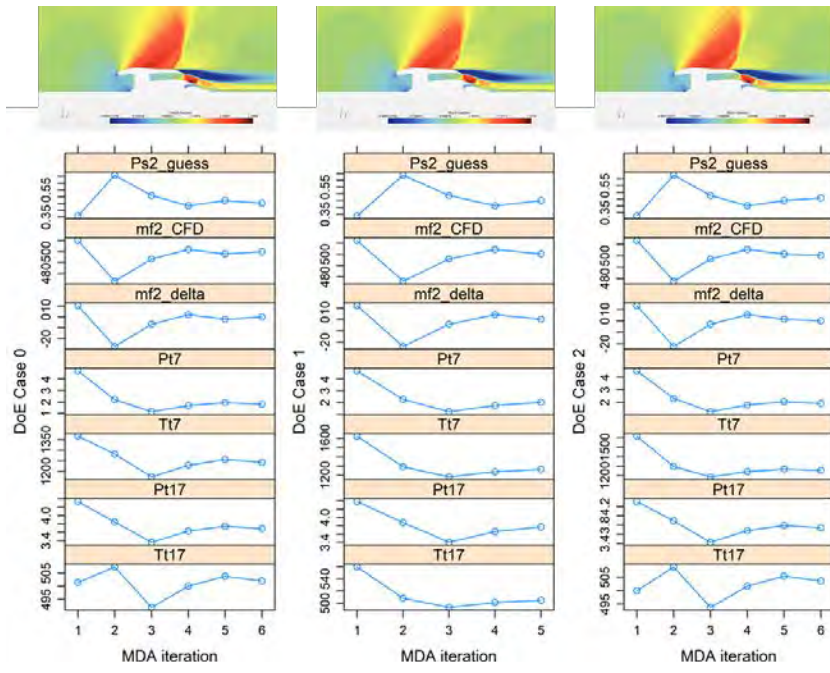


Figure 10. Automated CFD and propulsion analyses are shown in axisymmetric nacelle cases. The work is to be extended to the entire wing-body-nacelle configuration.

**Milestones**

None

**Major Accomplishments**

Preliminary methods for MDF method using a 2D nacelle inform later decision on MDAO architectures for the full wing-body-nacelle MDAO.

**Publications**

None

**Outreach Efforts**

None

**Awards**

None

**Student Involvement**

Bilal Mufti focused on Reynolds Averaged Navier-Stokes (RANS) CFD interfaces and propulsion surrogates. Stephanie Zhu and Kenneth Decker developed scripts to wrap inviscid CFD analysis. All are continuing graduate students pursuing PhDs.

**Plans for Next Period**

Surrogate models for mission and noise analysis shall be created. Interfaces to a Python MDAO driver shall be demonstrated.

# Task 8 – Screening and Dimensionality Reduction

Georgia Institute of Technology

## Objective

Realistic assessment of the OWN configuration depends on the degree of optimization. The degree of optimization depends on the dimensions or number of design variables. However, the computational cost of optimization can increase sharply with the number of design variables due to the “curse of dimensionality.” Therefore, the number of design dimensions must be minimized by finding the most important contributors to key metrics.

## Research Approach

The main approach to dimensionality reduction is the active subspace method (Constantine reference). Related variants of this method have been previously demonstrated for OWN at Georgia Tech. The method uses gradients of responses with respect to design variables to essentially rotate the design space such that new, hybrid design variables are aligned in directions where sensitivities have most variability.

The method requires the evaluation of gradients at a sample of design points. An eigen-decomposition problem is solved to yield new design variables that linear combinations of the former design variables. The new design variables are rank-ordered by their relative impact on a key metric such as lift-to-drag ratio for the aerodynamics discipline. In favorable cases, a small number of new, “active” design variables capture most of the effect of a much larger original set of design variables.

## Active Subspace Implementation with Adjoint Inviscid CFD

A key step in the active subspace method is to evaluate design gradients. For many simple analyses, this could be accomplished through finite differences. In other words, at each sample design point  $\underline{X}$ , the geometry would be perturbed by  $\Delta X_i$  for each design variable  $i$  and evaluated by a function (e.g., CFD). This is in turn used to estimate the gradient at the reference point. However, this finite differencing can become computationally expensive if there are many design variables. Many sample points  $\underline{X}$  are needed, and many perturbations are needed around each point.

Adjoint CFD is a type of analysis that modifies the original CFD governing equations to yield not just output functions like lift or drag but also their gradients with respect to design variables (Jameson 1988). This requires a relatively modest computational cost increase over the cost of a simple function evaluation of  $f(\underline{X})$ . The adjoint feature in the CART3D inviscid CFD code was used in this task (Aftosmis et al., 2011), as shown in Figure 11.

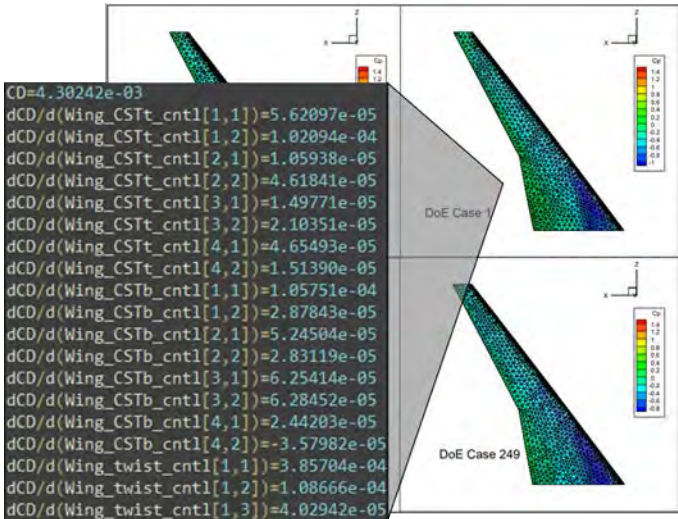


Figure 11. Adjoint inviscid CFD (CART3D) yields gradients for drag and other responses for a wing example.

A key hypothesis is that an active subspace for the OWN configuration learned from inviscid CFD is applicable to a viscous CFD design problem because there are enough similarities in the flow physics such that the relative impact of variables’



contributions to an objective may also be similar. This of course may not always be the case. In a design domain, if the principal physics phenomena that affect performance are inherently viscous (e.g., flow separation at the top of the wing near a nacelle), then the inviscid active subspace may not yield a major computational saving. However, the design variables under consideration include wing twist and airfoil variables that affect thickness, etc. These variables affect both lift distribution (associated with vortex induced drag that can be captured at low fidelity without viscosity) as well as wave drag (which also can be modeled to some degree without viscosity). This physical reasoning has justified taking the risk of using an inviscid CFD code to find an active subspace for a viscous/RANS CFD design task. Without performing two separate MDAO efforts in a controlled experiment, it is difficult to estimate beforehand the computational efficiency due to this active subspace implementation. The technique is therefore justified based on the above reasoning and may be tested with small-scale experiments.

**Preliminary Results**

Initial trials were performed using the OWN wing-body-nacelle configuration with relatively coarse grids in CART3D. A sample size of 48 was evaluated. The gradients for lift, drag, mass flow, and net thrust were calculated for a design domain around a CRM-based baseline geometry. Gradients were calculated for 28 design variables, including airfoil CST variables, wing twist, nacelle shape variables, flight conditions, and an engine boundary condition (fan face velocity). In Figure 12, the normalized eigenvalue corresponds to relative impact on response functions. The new, active subspace variables are ordered by their relative impacts. It can be seen that a small number of variables capture most of the effect of the original design variables.

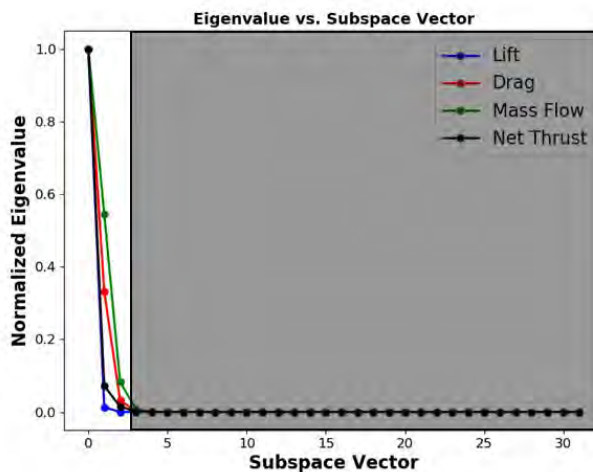


**Figure 12.** The first three or four new, “active” design variables (subspace vectors) have high eigenvalues which measure their relative contribution to variability in lift, drag, mass flow, and net thrust. It should be noted that this test was performed with a relatively coarse grid and with a small number of design variables.

**Milestones**

None

**Major Accomplishments**

Active subspace scripts written and demonstrated for wing-body-nacelle using a small sample of coarse-grid, inviscid CFD. A larger scale active subspace analysis will be used to finalize the reduced design space for full-scale MDAO.

**Publications**

None

**Outreach Efforts**

None

## Awards

None

## Student Involvement

Kenneth Decker performed the majority of the work for this task. Stephanie Zhu also contributed. They are continuing PhD students.

## Plans for Next Period

Currently, grid refinement studies are being conducted to more accurately estimate gradients. A future, larger scale DoE will be conducted to finalize the active subspace variables.

## References

- Jameson, Antony. "Aerodynamic design via control theory." *Journal of scientific computing* 3.3 (1988): 233-260.
- Aftosmis, Michael, Marian Nemec, and Susan Cliff. "Adjoint-based low-boom design with Cart3D." 29th AIAA Applied Aerodynamics Conference. 2011.

## **Task 9 – Demonstration of MDAO or Sampling Methods on Reduced Order or Placeholder Functions**

Georgia Institute of Technology

### Objective

The credibility of OWN assessment depends on the degree of design optimization. With limited computational resources, there is a strong need to use efficient, modern MDAO techniques. This Task focused on testing and down-selecting promising candidate methods from recent MDAO literature. The methods are first tested on reduced-order examples before committing large computer resources for final optimization.

### Research Approach

In addition to the active subspace method discussed in Task 8, this Task investigated two additional techniques in combination: Bayesian adaptive sampling and multi-fidelity methods.

#### **Bayesian Adaptive Sampling**

This class of methods relies on a type of surrogate model that yields probabilistic metrics of interpolation uncertainty for regions of the design space that have not yet been evaluated. The most famous of these methods relies on kriging or Gaussian process (GP) models (Jones, Schonlau, Welch, 1998). Different probabilistic criteria such as expected improvement are used to select the next design point for evaluation. This essentially behaves similarly to an optimizer, though if it is not run to convergence, it can be treated as an adaptive or sequential sampler that concentrates points near the optimum.

Bayesian adaptive sampling techniques are well-suited for batch analyses in HPC. Parallel or batch sampling techniques were tested on canonical algebraic test functions to sample multiple design points at a time. This is beneficial because multiple CFD or MDAO cases can be queued in a supercomputer job scheduler rather than running single design cases at a time.

#### **Multi-fidelity Methods**

Another potentially beneficial design technique combines two or more disciplinary analyses of different fidelity level and computational cost. The two codes are used in concert, with the cheaper low-fidelity code assisting in the estimation of a high-fidelity function across a design space. In the present research, we focused on inviscid and viscous CFD. A particular multi-fidelity method called hierarchical kriging was tested with the CRM-based wing parameterization discussed earlier (Han and Görtz, 2012).

#### **Initial Findings**

The two methods were combined and multi-fidelity adaptive sampling was tested on a wing example with three variables and coarse grids. NASA's FUN3D code was used in viscous/RANS mode for high-fidelity and in inviscid/Euler mode for low fidelity. For this coarse test case, the cost ratio was roughly 8:1. Results in Figure 13 show that both codes are used in combination to concentrate analyses in regions of favorable lift-to-drag ratio.

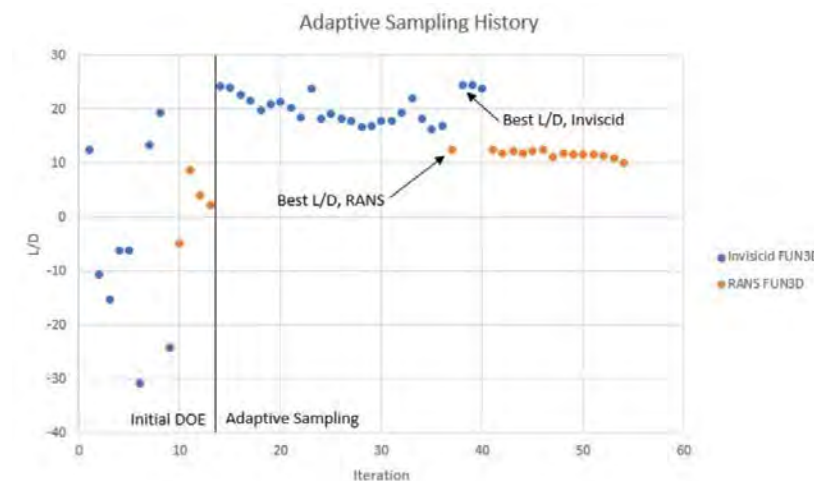


**Figure 13.** Multi-fidelity adaptive sampling concentrates low- and high-fidelity CFD analyses in regions of favorable lift-to-drag ratio.

Adaptive sampling balances between exploiting knowledge of favorable regions versus exploring regions that have not yet been sampled. In the example above, both low- and high-fidelity codes concentrate on designs with relatively high lift-to-drag ratio (L/D). Yet, after finding a favorable result (the current best result labeled in the figure), the algorithm continues exploring in other parts of the design space due to the remaining uncertainty. This explains why the L/D does not monotonically increase. This small-scale example will be expanded to the entire wing-body-nacelle using finer CFD meshes.

### **Milestone**

MDAO techniques were tested on reduced order/placeholder functions.

### **Major Accomplishments**

None

### **Publications**

None

### **Outreach Efforts**

None

### **Awards**

None

### **Student Involvement**

Christopher Eggert contributed to this task; he is graduating with a master's degree in December 2020 and will begin work at the NASA Langley Research Center.

### **Plans for Next Period**

The Bayesian adaptive sampling method will be implemented for full wing-body-nacelle CFD. A major challenge then is to adapt single-discipline (aerodynamics) adaptive sampling to a multidisciplinary problem. Currently, probabilistic design criteria are used to guide CFD analyses in isolation. In the future, a goal is to use the Bayesian approach to guide not only favorable design points but also efficient coupling between disciplines such as aerodynamics and propulsion.



## References

- Jones, D.R., Schonlau, M. & Welch, W.J. “Efficient Global Optimization of Expensive Black-Box Functions,” *Journal of Global Optimization*, Volume 13, 1998, pp. 455–492. <https://doi.org/10.1023/A:1008306431147>
- Han, Z.-H., and Görtz, S. “Hierarchical Kriging Model for Variable-Fidelity Surrogate Modeling.” *AIAA Journal*, Vol. 50, No. 9, 2012, pp. 1885–1896. <https://doi.org/10.2514/1.J051354>.



# Project 051 Combustion Concepts for Next-Generation Aircraft Engines

## Massachusetts Institute of Technology

### Project Lead Investigator

Steven R. H. Barrett  
Professor of Aeronautics and Astronautics  
Director, Laboratory for Aviation and the Environment  
Massachusetts Institute of Technology  
77 Massachusetts Ave, Building 33-322, Cambridge, MA 02139  
+1 (617) 253-2727  
sbarrett@mit.edu

### University Participants

#### Massachusetts Institute of Technology

- PI: Professor Steven R. H. Barrett
- FAA award number: 13-C-AJFE-MIT, Amendment nos. 061 and 071
- Period of Performance: February 5, 2020 to August 10, 2021 (reporting here with the exception of funding level and cost share only for the period February 5, 2020 to September 30, 2020)
- Task:
  1. Evaluate Water Injection to Extend Operating Envelope and Reduce Emissions

### Project Funding Level

FAA provided \$600,000 in funding. Matching fund sources are approximately \$140,000 from MIT, plus third-party in-kind contributions of \$460,000 from NuFuels LLC.

### Investigation Team

- Prof. Steven Barrett (MIT) serves as PI for ASCENT Project 51 as head of the Laboratory for Aviation and the Environment. Prof. Barrett coordinates internal research efforts and maintains communication between investigators in the various MIT research teams.
- Dr. Raymond Speth (MIT) serves as co-PI for ASCENT Project 51. Dr. Speth directly advises student research in the Laboratory for Aviation and the Environment focused on assessment of fuel and propulsion system technologies targeting reduction of aviation's environmental impacts. Dr. Speth also coordinates communication with FAA counterparts.
- Dr. Jayant Sabnis (MIT) serves as co-investigator for ASCENT Project 51. Dr. Sabnis co-advises student research in the Laboratory for Aviation and the Environment. His research interests include turbomachinery, propulsion systems, gas turbine engines, and propulsion system-airframe integration.
- Jad Elmourad is a graduate student in the Laboratory for Aviation and the Environment. He is primarily responsible for evaluating the impacts of emissions reduction technologies on fuel consumption and investigating the integration of advanced combustion technologies into the aircraft system.
- Syed Shayan Zahid is a graduate student in the Laboratory for Aviation and the Environment. He is primarily responsible for extending engine and emissions models to incorporate advanced combustion concepts.

### Project Overview

The purpose of this project is to identify design concepts for aircraft engine combustors which could decrease the combustor emissions for future aircraft engines that incorporate higher pressures and temperatures. The need to increase the thermal efficiency of the gas generator in aircraft engines has required designers to increase the overall pressure ratio ( $P_{03}/P_{02}$ ) as

well as the temperature ratio ( $T_{04}/T_{02}$ ). A higher pressure ratio increases the overall temperature in the combustor, thereby accelerating  $\text{NO}_x$  production. Increased combustor exit temperature results in higher cooling air requirements for the engine cycle, thus reducing the air available for  $\text{NO}_x$  reduction within the combustor. Hence, higher thermal efficiency engine cycles frequently result in higher  $\text{NO}_x$  production. The current state-of-the-art requires trade-off between engine fuel consumption and  $\text{NO}_x$ . In this project, we plan to develop numerical models for engine design concepts with promising new technologies. We will determine and compare performance characteristics associated with these technologies and will leverage detailed combustion chemistry models to understand how changes to fuel composition affect engine performance and emissions characteristics.

The design of combustors for aircraft engines is governed by the simultaneous need to ensure operability at low-power conditions (i.e., preventing combustion instabilities, blowout, etc.) and enabling operation at high power without excessive  $\text{NO}_x$  or soot emissions. For aircraft engines, the flight conditions and thrust setting of the engine fully determine the inlet conditions of the combustor, i.e., the temperature, pressure, and fuel flow rates, with very little adjustment to increase stability or decrease emissions being available. However, the introduction of additives into the engine at specific locations would provide secondary inputs that could be used to extend stability limits or reduce emissions.

When fuel flow rate is the only engine control parameter, the consequent variations in equivalence ratio result in wide variability in the combustion characteristics, e.g., flammability limits and flame speeds that must be accommodated across thrust settings ranging from idle to takeoff. Previous work has shown that the addition of a high-reactivity additive while holding the equivalence ratio constant can extend the lean blowout limit in a gas turbine-like combustor (Speth and Ghoniem, 2009). By changing the fuel composition to counteract the effect of the equivalence ratio, the combustor would not have to operate over as wide a range of conditions, allowing for more opportunities to optimize the combustor to control emissions at its design point. Furthermore, variations in fuel composition have been shown to decrease soot emissions from aircraft engines (Moore et al., 2015; Speth et al., 2015), suggesting that the use of a fuel additive could be effective at reducing emissions during specific operating regimes.

Although water injection is not used in any current commercial aircraft engines, it was used in several engines as a means of augmenting thrust at takeoff, such as the J-57 engines used on the B-52 and the JT9D engines used on the 747-200 (Daggett, 2004). The use of water injection at takeoff provided increased thrust without increasing the turbine inlet temperature. The temperature reduction, and therefore density increase, from the evaporation of the injected water allows the engine to handle a larger mass flow rate of air, which results in greater thrust. In modern engines with higher compression ratios, water injection into the compressor may also serve to alleviate limitations due to compressor exit temperature. Water injection has also been evaluated for its ability to reduce takeoff  $\text{NO}_x$  emissions (Daggett, 2004). While older engines that used water injection were known to have higher soot production, controlling soot emissions was not a design goal of these engines, and this does not imply that a modern engine design employing water injection could not meet limits on nonvolatile particulate matter emissions.

The work proposed here builds on work done in other ASCENT projects. Work under ASCENT Project 39 has resulted in a combustor model that can be used to predict soot emissions from conventional combustor designs and uses detailed chemical kinetic models to allow evaluation of the effects of different fuel compositions on emissions. Work done under ASCENT Project 47 has extended this model to include predictions of  $\text{NO}_x$  formation, as well as coupling the model to an engine cycle model, creating a consistent framework for modeling both ground and cruise emissions.

## Task 1 – Evaluate Water Injection to Extend Operating Envelope and Reduce Emissions

Massachusetts Institute of Technology

### Objectives

Water injection can be used to control temperatures in the engine, which may expand the design space and allow decreases in mission fuel burn and emissions. For this task, we will evaluate the impacts of water injection (1) at the compressor inlet, (2) into the diffuser (upstream of the combustor) and (3) into the combustor dilution zone. For each option, we will evaluate the effect of water injection on the engine cycle and determine engine designs which are optimized for the impacts of water injection, i.e., considering allowable limits on compressor discharge temperature and turbine inlet temperature. We expect that water injection can reduce peak temperatures and therefore  $\text{NO}_x$  formation. Tradeoffs with soot formation will also be

evaluated. Options to enable operation without the use of water injection will also be considered in order to address potential safety concerns. In the past, water injection was primarily used for thrust augmentation purposes when emissions were not thoroughly evaluated as part of the aircraft design process. For this reason, the existing literature on the effect of water injection on tailpipe emissions is sparse, justifying the need to conduct analyses on its feasibility.

## **Research Approach**

The research targets three sections for analysis: a thermodynamic cycle analysis, a chemical emissions analysis, and a weight analysis.

### **Preliminary Thermodynamic Cycle Analysis**

Water injection at different points in the Brayton cycle has varying effects on engine performance, depending on the state of the water being injected. There are, in general, two potentially competing effects affecting engine performance when using water injection as an emission-reduction approach. Injecting water into the thermodynamic cycle could lower the thermal efficiency due to its cooling effect on the flame temperature. At the same time, it has the potential to increase the engine thrust obtained. A preliminary thermodynamic cycle analysis was performed to assess the dominant effect of water injection at different points in the cycle to determine how much the performance parameters such as the thermodynamic states at various cycle locations, thrust, burner exit temperature, and the overall thrust-specific fuel consumption (TSFC) were affected as a result of this approach.

PyCycle, an open-source code for thermodynamic cycle analysis, was chosen as a tool for this preliminary analysis due to the added flexibility of making modifications to the source code in order to simulate water injection. Currently, other engine performance evaluation tools such as NPSS, do not include the flexibility to easily change the source code. Initially, manual calculations were performed as part of a zero-order analysis to observe the overall effects of water injection on engine performance using specified engine design variables as inputs. The PyCycle results will be compared to the performance trends obtained as a result of the zero-order approach.

### **Preliminary Chemical Analysis**

ASCENT Project 47 yielded an emissions model (Pycaso) based on Cantera to predict the  $\text{NO}_x$  and soot formation inside a CFM56-7B engine by using a reactor network to simulate the combustor. We aim to expand this model to add the capability to vary the engine design and configuration in order to simulate new emission-reduction technologies for a wider range of engines and observe the overall effect on emissions. In general,  $\text{NO}_x$  formation depends on complex reaction mechanisms that depend on the local temperatures and composition inside various zones of a combustor. In order to evaluate the effect of novel engine technologies on the amount of  $\text{NO}_x$  and other emissions, Cantera will be used to estimate the emissions index (EI) of  $\text{NO}_x$  inside the combustor. This chemical analysis will use the engine performance results obtained from the thermodynamic cycle analysis as inputs, such as the TSFC, burner inlet temperature, etc. The estimated emissions would help compare the benefits and disadvantages associated with water injection as a function of injection location and state of water being injected.

### **Preliminary Weight Analysis**

Water injection can reduce  $\text{NO}_x$  formation inside the combustor by lowering the combustor temperatures. This leads to a lower emission index for  $\text{NO}_x$ , where the emission index represents the amount of  $\text{NO}_x$  emitted per amount of fuel consumed. However, this does not necessarily imply that the total amount of  $\text{NO}_x$  emitted per mission decreases because the amount of fuel consumed could increase for a mission using water injection. The use of water injection could add significant weight to the aircraft in terms of the weight of the water and the associated system such as pumps, tanks, etc., and this extra weight would require additional fuel burn (assuming the other aircraft parameters such as the lift-to-drag ratio remain unchanged). Therefore, when considering the benefit of using water injection to reduce  $\text{NO}_x$  emissions, it is important to account for the penalty coming from the additional weight and the additional fuel burn associated with carrying the water injection system. A preliminary weight analysis was performed to assess whether this penalty would be significant and limiting to the use of water injection.

The results of the weight analysis depend on several factors including the weight of the water injection system, the mission range, the effect of water injection on the TSFC, the desired  $\text{NO}_x$  reduction, and the associated water flow rate. Therefore, a complete weight analysis would require input from a thermodynamic cycle analysis, specifically the relationship between the water flow rate and the TSFC, as well as input from a chemical analysis, specifically the relationship between the water flow rate and the  $\text{NO}_x$  formation.



## **Milestones**

A literature review was conducted to evaluate the known effects of water injection on aircraft performance and emissions, and the appropriate tools for evaluating the change in performance and emissions as a result of water injection were identified.

## **Major Accomplishments**

### **Literature review**

A survey of the existing literature on water injection techniques was conducted and the relevant information was used to conduct zero-order preliminary analyses on emission reduction as a result of water injection. The preliminary chemical emissions analysis will aim to verify the validity of the emission reductions proposed in the literature as a function of the amount of water injected at different cycle locations.

### **Preliminary analysis**

Tools were identified to conduct preliminary analyses on the thermodynamic cycle and the resulting emissions. PyCycle was selected to simulate water injection and compare the feasibility of injecting water at different locations in the cycle to determine the optimum approach. This will help confine and focus the scope of this project before making modifications to the existing Pycaso model.

## **Publications**

N/A

## **Outreach Efforts**

N/A

## **Awards**

None

## **Student Involvement**

This task was conducted primarily by Jad Elmourad and Syed Shayan Zahid, graduate research assistants working under the supervision of Dr. Jayant Sabnis and Dr. Raymond Speth.

## **Plans for Next Period**

After conducting the preliminary analyses, the best approach to water injection will be identified. This approach will add to the modeling capabilities of Pycaso in order to simulate water injection for different aircraft engine designs. The results will enable us to compare water injection with other emission-reduction technologies.

## **References**

Daggett, D.L.H. (2004). Water Misting and Injection of Commercial Aircraft Engines to Reduce Airport NO<sub>x</sub> (NASA/CR—2004-212957).

Moore, R.H., Shook, M., Beyersdorf, A., Corr, C., Herndon, S., Knighton, W.B., Miake-Lye, R., Thornhill, K.L., Winstead, E.L., Yu, Z., et al. (2015). Influence of Jet Fuel Composition on Aircraft Engine Emissions: A Synthesis of Aerosol Emissions Data from the NASA APEX, AAFEX, and ACCESS Missions. *Energy Fuels* 29, 2591–2600.

Speth, R.L., and Ghoniem, A.F. (2009). Using a strained flame model to collapse dynamic mode data in a swirl-stabilized syngas combustor. *Proceedings of the Combustion Institute* 32, 2993–3000.

Speth, R.L., Rojo, C., Malina, R., and Barrett, S.R.H. (2015). Black carbon emissions reductions from combustion of alternative jet fuels. *Atmospheric Environment* 105, 37–42.



# Project 052 Comparative Assessment of Electrification Strategies for Aviation

## Massachusetts Institute of Technology

### Project Lead Investigator

PI: Steven R. H. Barrett  
Professor of Aeronautics and Astronautics  
Director, Laboratory for Aviation and the Environment  
Massachusetts Institute of Technology  
77 Massachusetts Ave, Building 33-322, Cambridge, MA 02139  
+1 (617) 253-2727  
sbarrett@mit.edu

Co-PI: Dr. Florian Allroggen  
Research Scientist  
Department of Aeronautics and Astronautics  
Laboratory for Aviation and the Environment  
Massachusetts Institute of Technology  
77 Massachusetts Ave, Building 33-115A, Cambridge, MA 02139  
+1 (617) 715-4472  
fallrogg@mit.edu

Co-PI: Dr. Raymond Speth  
Principal Research Scientist  
Laboratory for Aviation and the Environment  
Department of Aeronautics and Astronautics  
Massachusetts Institute of Technology  
77 Massachusetts Ave, Building 33-322, Cambridge, MA 02139  
speth@mit.edu

## University Participants

### Massachusetts Institute of Technology

- PI: Professor Steven R. H. Barrett; co-PIs: Dr. Florian Allroggen, Dr. Raymond Speth
- FAA award number: 13-C-AJFE-MIT, amendment nos. 062 and 072
- Period of Performance: February 5, 2020 to August 10, 2021
- Tasks for the reporting period February 5, 2020 to September 31, 2020:
  1. Develop a suite of roadmaps for aircraft electrification.
  2. Develop a system-level engineering model of power conversion processes, aircraft energy requirements, and component production processes.
  3. Develop a model for analyzing the economics of electrification strategies.
  4. Comparative validation runs [to be started in the following reporting period – not covered in the current report].
  5. Analyze the system-level costs and benefits of the electrification strategies [to be started in following reporting periods – not covered in the current report].

## Project Funding Level

FAA provided \$600,000 in funding. Matching funds sources are approximately \$140,000 from the Massachusetts Institute of Technology (MIT) and third-party in-kind contributions of \$460,000 from NuFuels LLC.

## Investigation Team

Principal Investigator:	Prof. Steven Barrett (MIT) (all MIT tasks)
Co-Principal Investigators:	Dr. Florian Allroggen (MIT) (all MIT tasks) Dr. Raymond Speth (MIT) (Tasks 1, 2, and 4)
Co-Investigator:	Dr. Sebastian Eastham (MIT, Tasks 5)
Postdoctoral Associate:	Haofeng Xu (MIT, Tasks 2, 3, and 4)
Graduate Research Assistant:	Nicolas Gomez-Vega (MIT, Tasks 1, 2, and 4)

## Project Overview

The long-term goal of this project is to quantify the costs, emissions, and resulting environmental impacts (i.e., climate and air quality impacts) of different electrification approaches for commercial aviation. The electrification pathways considered range from battery-electric (or “all-electric”) aircraft to electrofuel-powered and liquid hydrogen-powered aircraft (both hydrogen fuel cell and hydrogen combustion) where electrofuels and hydrogen are produced using renewable electricity. As such, the project will help identify the best approach for using one unit of electric energy to power aviation.

In the project, we analyze the costs, emissions, and atmospheric impacts associated with each electrification strategy. We develop both a system-level engineering and system-level economic model which cover electricity generation, fuel production, transport and storage, aircraft energy requirements, and aircraft operations. The models analyze different electrification pathways using what can be described as a “power station-to-wake” approach. The models quantify differences in costs and emissions associated with each electrification approach as compared to a set of baseline aircraft powered by conventional petroleum-derived fuels or drop-in biofuels. The outputs from these models will be used in a cost-benefit model which provides insights into the costs associated with each technology—both investment and infrastructure as well as operating cost—and compares them with the lifecycle climate and air quality abatement potential. The results are differentiated by mission characteristics. When comparing electrification scenarios with the conventional petroleum-derived baseline, we take into account different electricity production scenarios (e.g., different fossil fuels and renewables). We expect the results to provide insights into the relative competitiveness of using electricity as a power source for aviation.

## Task 1 – Develop a Suite of Roadmaps for Aircraft Electrification

Massachusetts Institute of Technology

### Objectives

Under this Task, we develop a suite of roadmaps for aircraft electrification. Furthermore, we intend to discuss the mission characteristics which appear to be most suitable for each technology. Through these roadmaps, we aim to provide a high-level summary of conceptual opportunities and challenges as well as critical technologies for all electrification strategies. The results will inform the choice of pathways for detailed analysis.

In addition, this task includes defining future baseline scenarios for conventional aircraft powered by petroleum-derived fuels or drop-in sustainable aviation fuels (SAFs) considered under the International Civil Aviation Organization’s Carbon Offsetting and Reduction Scheme for International Aviation (CORSA). These baseline definitions will establish consistent comparisons for electric aircraft.

### Research Approach

Figure 1 shows the technology pathways for aircraft electrification as well as the baseline pathways. The electrification pathways under consideration in this study are all-electric (battery-electric) aircraft, drop-in electrofuels for conventional aircraft, and hydrogen aircraft. Turbo- and hybrid-electric aircraft which use an electrified power train in combination with other energy carriers are potentially considered in a later stage of the project.

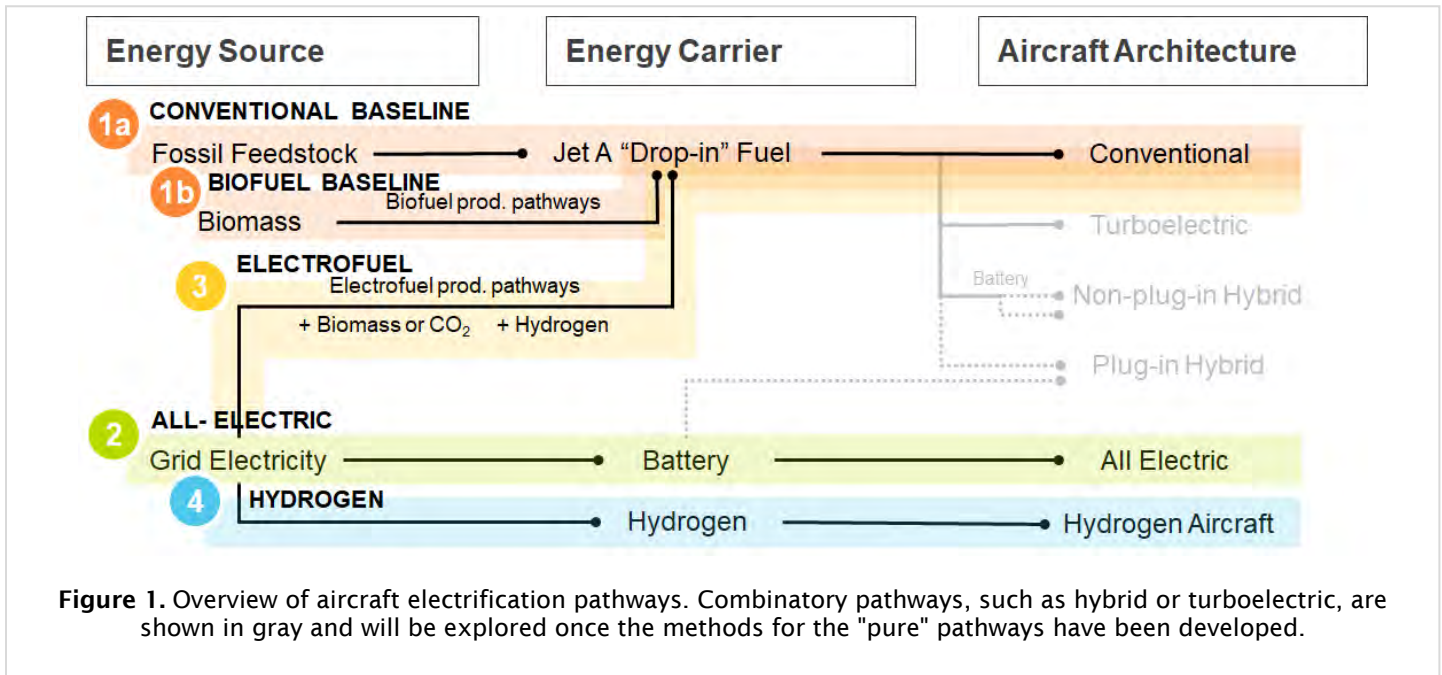


**Figure 1.** Overview of aircraft electrification pathways. Combinatory pathways, such as hybrid or turboelectric, are shown in gray and will be explored once the methods for the "pure" pathways have been developed.

### Conventional and SAF baseline

To establish a conventional and SAF baseline, fuel use and emissions impacts of aircraft powered by conventional jet fuel and SAF are needed. In their efforts to model all-electric aircraft, Gnad et al. (2019) use the aircraft design and optimization tool TASOPT (Drela, 2016) to establish reference conventional aircraft for missions similar to the missions proposed for all-electric aircraft. This approach allows them to conduct consistent comparisons between all-electric aircraft and their baseline aircraft. Lifecycle impacts of different fuels can be modeled using established and vetted results obtained in the CORSIA process (ICAO, 2019), while atmospheric impacts of aircraft emissions can be modeled to first order using results from Grobler et al. (2019).

### All-electric aircraft

An all-electric aircraft (AEA) is powered by batteries and uses an all-electric powertrain. As a result, AEA offer several advantages over traditional jet engine-propelled aircraft:

- **Reduced environmental impact:** AEA do not have direct emissions. Considering life-cycle impacts of power generation, Schäfer et al. (2018) estimate that a 150 passenger (PAX) AEA with a range of 400 nmi would produce 91 g of CO<sub>2</sub> per revenue passenger-kilometer (RPK), when the aircraft is powered by electricity drawn from an electric grid resembling the year-2015 U.S. grid. These emissions are 20% higher than those of conventional aircraft. However, once non-CO<sub>2</sub> impacts are taken into account (e.g., contrails), AEA would have a 30% lower impact than conventional aircraft (Schäfer, et al., 2018). The impacts of the proposed AEA could further be reduced by charging batteries with electric energy from renewable sources.
- **Reduced air quality impact:** AEA eliminate all emissions during takeoff, cruise, and landing. These are estimated to result in ~16,000 premature mortalities when accounting for all aviation (Yim, et al., 2015).
- **Reduced noise:** Schäfer et al. (2018) estimate a 36% reduction in the noise contour area compared to the best-performing conventional aircraft.

Current studies on AEA highlight limitations in the feasibility of AEA designs. Most importantly, Gnad et al. (2019) quantified the dependency of AEA on battery energy density: with a 400 Wh/kg battery, the only viable 180-seater aircraft design had a range of 200 nmi; this range could be improved to 1600 nmi with a 2000 Wh/kg battery. Current Li-ion technology has a theoretical maximum energy density of 387 Wh/kg; however, other battery architectures are theorized to provide significantly higher energy densities. For example, Bruce et al. (2011) show that the maximum energy density of Li-S is 2567 Wh/kg, and that of Li-O<sub>2</sub> is 3505 Wh/kg.



## Electrofuels

Electrofuels are liquid or gaseous synthetic fuels produced through converting syngas derived from electricity to a hydrocarbon fuel, often using Fischer-Tropsch (FT) synthesis. Syngas production requires a carbon source and a hydrogen source. In electrofuel pathways, the hydrogen is generally produced from renewable sources (i.e., electrolysis). The carbon may come from two sources: from biomass, resulting in a power and biomass-to liquid (PBtL) pathway; or from direct air capture, resulting in a power-to-liquid (PtL) pathway. For this project, we focus on liquid drop-in electrofuels which can be used onboard conventional aircraft.

Isaacs (2019) performed an environmental analysis of PBtL and PtL pathways for use in transportation. The study found that if electricity is obtained from renewable sources and carbon is captured from the air, PtL pathways have the potential to be near carbon neutral (Isaacs, 2019; Fasihi, Bogdanov, & Breyer, 2016), whereas PBtL pathways would reach approximately zero emissions, depending on the lifecycle impacts associated with obtaining carbon from biogenic sources. Generally, the lifecycle emissions of both PBtL and PtL pathways vary with grid emissions: with the current average grid emissions of the U.S., the lifecycle GHG emissions from PtL and PBtL fuels are between 1.5–3.5 times greater than conventional petroleum-derived fuel. The lifecycle impacts of PBtL pathways are less dependent on grid emissions due to lower electricity requirements as compared to the PtL pathway.

The economics of electrofuel production pathways have been studied by König et al. (2015), Herz et al. (2018), Blanco et al. (2018) and Isaacs (2019), among others. They concluded that electrofuels currently have a higher minimum selling price than conventional fuels: a PtL pathway with electrolysis and reverse water-gas shift (RWGS) drawing wind power would result in production costs of 3.0–5.2 \$/L depending on the electricity price and the electrolyzer cost (König, Freiberg, Dietrich, & Wörner, 2015). This is one order of magnitude higher than the selling price of conventional fuels. The underlying electricity price plays a key role in these costs—the minimum selling price has been found to vary approximately linearly with electricity price (Herz, Reichelt, & Jahn, 2018; Isaacs, 2019). However, these costs are projected to decrease significantly (Drünert et al., 2020).

## Hydrogen

Using hydrogen as an energy carrier onboard aircraft offers the potential to completely eliminate CO<sub>2</sub> emissions from fuel combustion. There are two main ways in which hydrogen can be used to produce thrust:

- **Combustion:** hydrogen replaces jet fuel in a jet engine. Challenges include the combustor design and flame stability (Khandelwal, Karakurt, Sekaran, Sethi, & Singh, 2013). Since combustion at high temperatures is still necessary, NO<sub>x</sub> is still likely to be emitted, resulting in surface air quality degradation.
- **Fuel cell:** Hydrogen can be used to produce electricity in an electrochemical fuel cell, which releases water and heat. The generated electricity then powers an electric motor attached to a fan or a propeller. Since this architecture relies on an electric powertrain, it offers opportunities for distributed propulsion and boundary layer ingestion. Potential drawbacks include low power density (resulting in high mass), excess residual heat, and relatively low demonstrated power output (Renouard-Vallet, et al., 2010).

If hydrogen is produced using renewable electricity, the lifecycle impacts of fuel production are small (e.g., production through electrolysis with renewable wind electricity: <11 g CO<sub>2</sub>e/MJ (Valente et al., 2017)). In contrast, if hydrogen is produced through steam-methane reforming (SMR), the lifecycle impacts of >100 g CO<sub>2</sub>e/MJ are larger than the impacts of conventional fuels at around 90 g CO<sub>2</sub>e/MJ.

Since hydrogen is a non-drop-in fuel, its introduction requires novel aircraft to be developed. In general, hydrogen storage onboard aircraft is associated with opportunities and challenges for aircraft design.

- First, since hydrogen has a lower heating value (LHV) of 120 MJ/kg—approximately 3 times higher than that of Jet-A—it is associated with lower fuel weight, which can result in payload advantages.
- Second, because jet fuel has four times the energy content per unit volume than liquid hydrogen, a hydrogen aircraft will require higher fuel storage volume than its conventional counterpart. In general, hydrogen can be stored onboard as a high-pressure gas or as a cryogenic liquid. For high-pressure gaseous storage, Colozza (2002) estimated that a high-pressure system at 62 MPa could store hydrogen with a density of 20 kg/m<sup>3</sup>. However, these high-pressure storage systems only offer storage mass fraction of approximately 5% due to the high mass of the pressure vessel (Colozza & Kohout, 2002). Liquid hydrogen can be stored at lower pressure and has a density of

71 kg/m<sup>3</sup> (Verstraete D. , 2013; Khandelwal, Karakurt, Sekaran, Sethi, & Singh, 2013; Brewer, 1982). However, it needs to be stored in spherical or cylindrical tanks to minimize the heat flux into the tank (Mital, et al., 2006).

### **Milestone**

The MIT team presented a first overview of the literature review and the resulting electrification roadmaps to the FAA project manager in September 2020.

### **Major Accomplishments**

MIT is producing an exhaustive overview of the current understanding of different electrification strategies as presented in the literature.

### **Publications**

None

### **Outreach Efforts**

The team summarized the preliminary findings outlined above in an overview presentation for the ASCENT Fall Meeting in September 2020.

### **Awards**

None

### **Student Involvement**

During the reporting period, the MIT graduate student involved in this task was Nicolas Gomez Vega.

### **Plans for Next Period**

The team is aiming to present an exhaustive overview of electrification roadmaps and rank their attainability based on an initial technical and economic assessment using data and results from the literature.

## **Task 2 – Develop a System-level Engineering Model of Power Conversion Processes, Aircraft Energy Requirements, and Component Production Processes**

Massachusetts Institute of Technology

### **Objectives**

The goal of this task is to develop an aircraft technology, production, and operation model (from here referred to as the “aircraft model”), which will enable comparisons of the technology pathways outlined above. This system-level engineering model aims to capture the most significant energy conversion processes, emissions, and costs.

In order to support the overall lifecycle cost-benefit assessment, the aircraft model considers both the operating and the production stages of “electrified” aircraft (see Task 1). Specifically, for a given aircraft type and mission combination, the model calculates the energy needed onboard the aircraft (either in the form of drop-in jet fuel, liquid hydrogen, or electric battery), the emissions resulting from onboard energy conversion and propulsion processes, and the operating costs of the mission. In addition to these outputs, the model estimates the emissions and costs associated with aircraft production, including the most significant component production processes (e.g., battery production for battery electric aircraft).

### **Research Approach**

#### **Aircraft Types**

ASCENT Project 52 aims to assess electrification options across the entire global civil aviation market. Therefore, in addition to modeling different technology options, the aircraft model applies these technologies to different types of aircraft with differing passenger capacities and to aircraft operating on routes with differing flight distance. Balancing the ability to cover

a broad spectrum of aircraft—and corresponding large portion of the relevant market (i.e., generalizability)—against the ability to model aircraft components and systems in high detail (i.e., fidelity) poses a significant challenge to model development. For this project, we divide the market into six “route classes” defined by route length. For each route class, we then model an aircraft (for each viable technology pathway). Figure 2 summarizes the class definitions and shows the route class breakdown for an example airport, Paris Charles de Gaulle (CDG).

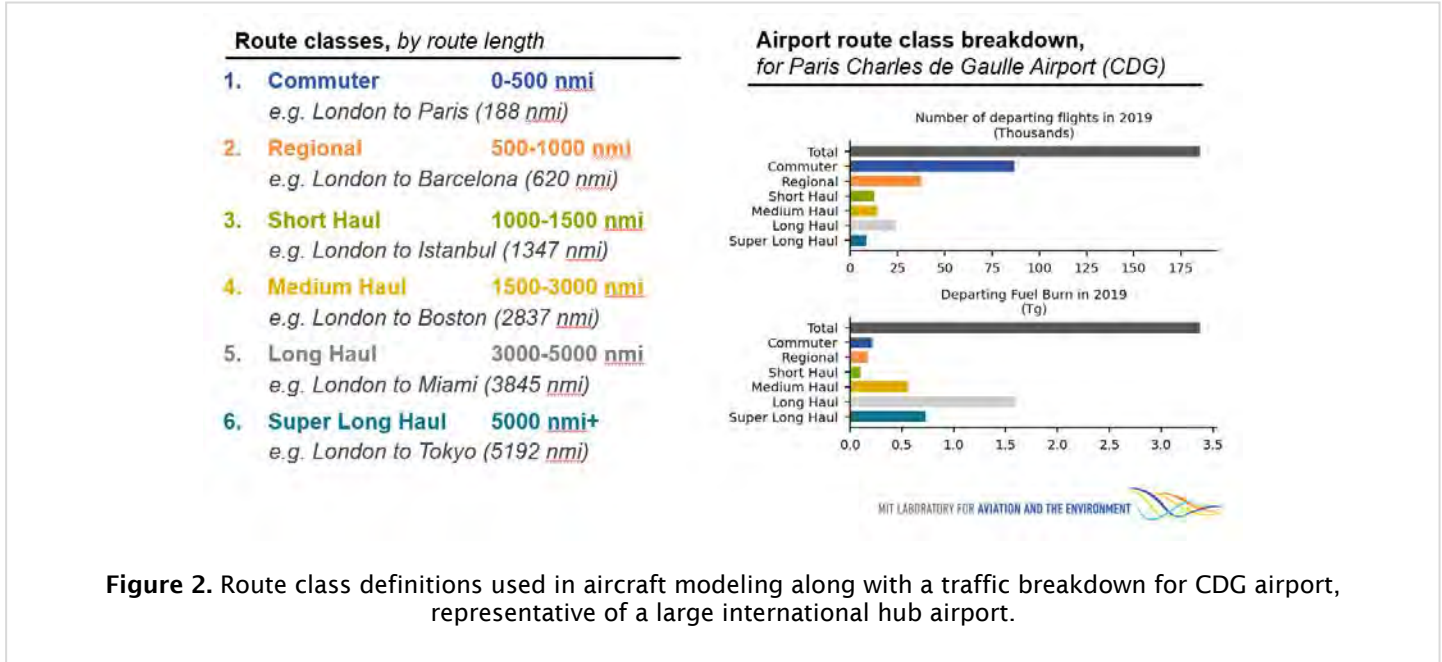
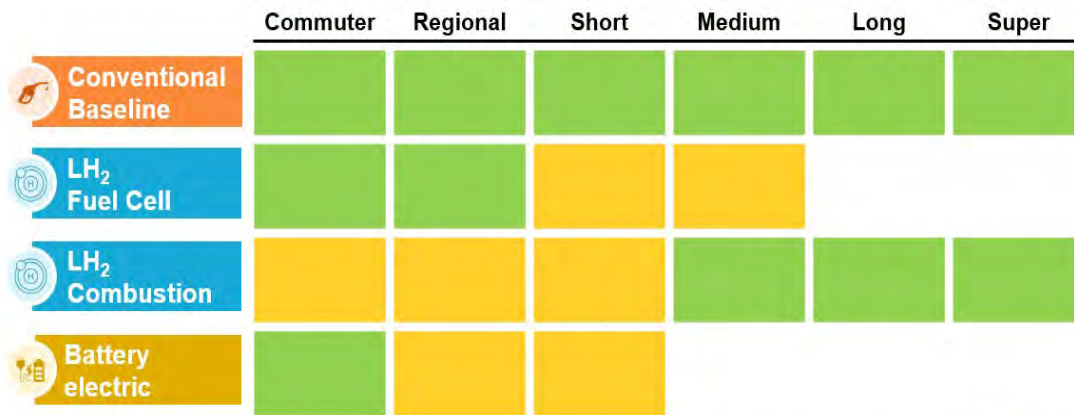


Figure 2. Route class definitions used in aircraft modeling along with a traffic breakdown for CDG airport, representative of a large international hub airport.

**Aircraft Technologies**

For each route class, our preliminary analysis considers four aircraft architectures described in Figure 1: 1) a conventional baseline, 2) a liquid hydrogen fuel cell aircraft, 3) a liquid hydrogen combustion aircraft, and 4) a battery electric aircraft.

While the baseline technology of Jet-A combustion aircraft currently covers all of the civil aviation market across all route classes, not all of the electrification pathways are technologically feasible for all route classes. In particular, the literature suggests that specific energy of batteries and the specific power of hydrogen fuel cells limit the feasibility of those technologies for use in longer range missions. Similarly, the added weight of onboard cryogenic hydrogen storage for smaller liquid hydrogen combustion aircraft are likely to make them less competitive. Figure 3 shows the route classes for which each technology is considered to be viable in our preliminary analysis in green, with areas of uncertainty in yellow (Gnadt, Speth, Sabnis, & Barrett, 2019; Verstraete D. , 2013; Brelje & Martins, 2019). This uncertainty stems from the exact performance capabilities of the various technology pathways and is currently driven by inconsistencies of assumptions and methods across different studies. This study will address these uncertainties in a consistent framework.



**Figure 3.** Aircraft technologies under consideration. Not all technologies are viable for all route classes. Green shows route classes for which a technology is currently viable and potentially competitive; yellow shows route classes where the viability of a technology is currently considered to be uncertain.

The aircraft modeling will build on prior work by the project team. The team has used the Transport Aircraft System OPTimization (TASOPT) tool (Drela, 2016) to establish baseline performance of conventional jet fuel aircraft and also developed a complementary electric version of TASOPT, TASOPTe, which adapted TASOPT for optimizing an all-electric tube-and-wing aircraft design based on first principles. The TASOPT tool was originally developed to analyze MIT’s D8 “double bubble” aircraft (Drela, 2011). TASOPT will be further extended to include hydrogen combustion and fuel cell technologies.

**Power Conversion and Energy Requirements**

The power conversion modeling will leverage the existing literature on power systems and their aircraft integration; they cover energy carrier storage and fueling systems, significant steps of power conversion, and propulsion. A range of current and feasible conversion efficiencies is considered. We aim to set up the model at a fidelity level which allows us to modularize the conversion chain. As a result, new technologies for aircraft electrification can be added to the assessment framework.

Our first version of the power conversion model for hydrogen aircraft is similar to that of jet fuel combustion, with the expectation that turbofan engines based on those existing today would be used (with modifications to the combustion chamber), although significant changes to the fuel system to incorporate cryogenic storage and distribution of liquid hydrogen and hence changes to overall aircraft configuration are likely necessary (Verstraete, Hendrick, Pilidis, & Ramsden, 2010).

The power conversion models for the battery electric and hydrogen fuel cell pathways share similar downstream electric transmission and propulsion architectures, which will be electric and likely distributed. Some components are already modeled in TASOPTe (Gnadt, Speth, Sabnis, & Barrett, 2019) and further work will draw on existing literature which addresses electric power systems (Chen, Wang, & Chen, 2018; Sarlioglu & Morris, 2015; Cao, Mecrow, Atkinson, Bennett, & Atkinson, 2012). The upstream battery and hydrogen fuel cells energy systems for these two pathways are significantly different and the model will include detailed considerations of battery performance and energy density (Bills, Sripad, Fredericks, Singh, & Viswanathan, 2020) for the former, as well as cryogenic hydrogen storage and fuel cell performance (Colozza & Kohout, 2002; Mital, et al., 2006; Verstraete D. , 2015) for the latter.

**Operating Emissions and Costs**

Direct emissions can be estimated from the aircraft fuel requirements, while upstream emissions will be calculated using the upstream system model developed as part of Task 3; the energy requirements calculated by the aircraft model here will be used as an input to the system model. Similarly, some direct operating costs can be estimated using the aircraft model, while costs of fuel will be a function of the upstream processes. The economic model will leverage prior work by the project team to derive the economics of aircraft electrification (Schäfer, et al., 2018).



### **Production Emissions and Costs**

To estimate the full lifecycle costs of electrification, it is necessary to account for potential changes in the production processes due to the adoption of certain electrification technologies. For example, the production emissions and cost of batteries are significantly different from the energy storage devices in other pathways; for this part of the analysis, we will leverage prior work in the literature (Kim, et al., 2016). In order to account for changes in individual components such as batteries, we will perform a bottom-up component-wise or aircraft-system-wise summation, again focusing on those aircraft systems which are sensitive to changes in energy carrier (e.g., the fuel system, the energy conversion system, and the propulsion system).

### **Milestone**

An initial outline of the modeling structure has been completed (see above).

### **Major Accomplishments**

An initial outline of the modeling structure has been compiled which will inform future research and will ensure consistent comparisons between the different pathways under consideration. In addition, the team has compiled an initial model of estimating energy and fuel demand under different electrification strategies.

### **Publications**

None

### **Outreach Efforts**

The team summarized the preliminary model structure above in an overview presentation for the ASCENT Fall Meeting in September 2020. In addition, the team prepared a presentation to ICAO's Long-term Aspiration Goal (LTAG) Task Group, to be held in October 2020.

### **Awards**

None

### **Student Involvement**

During the reporting period, the MIT graduate student involved in this task was Nicolas Gomez Vega.

### **Plans for Next Period**

Over the coming year, the team will expand the existing capabilities of TASOPT and TASOPTe, which are currently limited to A320-class aircraft that operate in medium-haul routes. The goal is to include models of aircraft of the other route classes which will have longer and shorter ranges.

In addition to the assessment of operating emissions, which will be a direct result of the aircraft performance, we will review the existing literature to provide estimates of cost for the different aircraft designs: that is, direct operating costs as well as production cost for the different aircraft technologies and components.

## **Task 3 – Develop a Model for Analyzing the Economics and Emissions of Electrification Strategies**

Massachusetts Institute of Technology

### **Objective(s)**

The team aims to develop a model that analyses the economics and emissions of each electrification strategy at the system level (the “system model”). The goal of this task is to develop a system-level analysis capability for modeling the possible electrification *pathways* (e.g., battery electric, hydrogen fuel cell, etc.) and their deployment in various aircraft electrification *scenarios* (e.g., replacing regional flights below 1000 nmi at a specific airport).

The system model focuses on the processes which occur upstream of the fueling and operation of the aircraft itself, but also incorporates the aircraft model developed in Task 2 in order to quantify the demands of the aircraft operations on the

upstream systems (both in terms of the amount of fuel or energy needed, but also the infrastructure required to fulfil this need in real-time). These upstream processes are significant for the overall environmental impact and for cost.

The system model aims to capture the most significant upstream fuel and power conversion processes in each pathway, including electricity generation, process inputs and outputs of materials and energy, process efficiency, cost (both investment and operating cost), and greenhouse gas emissions. When coupled with global flight data and models for onboard aircraft energy and costs (from Task 2), the overall system model assesses complete electrification scenarios for competing technological pathways to provide insight into their relative strengths and challenges and a quantitative comparison of their costs and potential benefits.

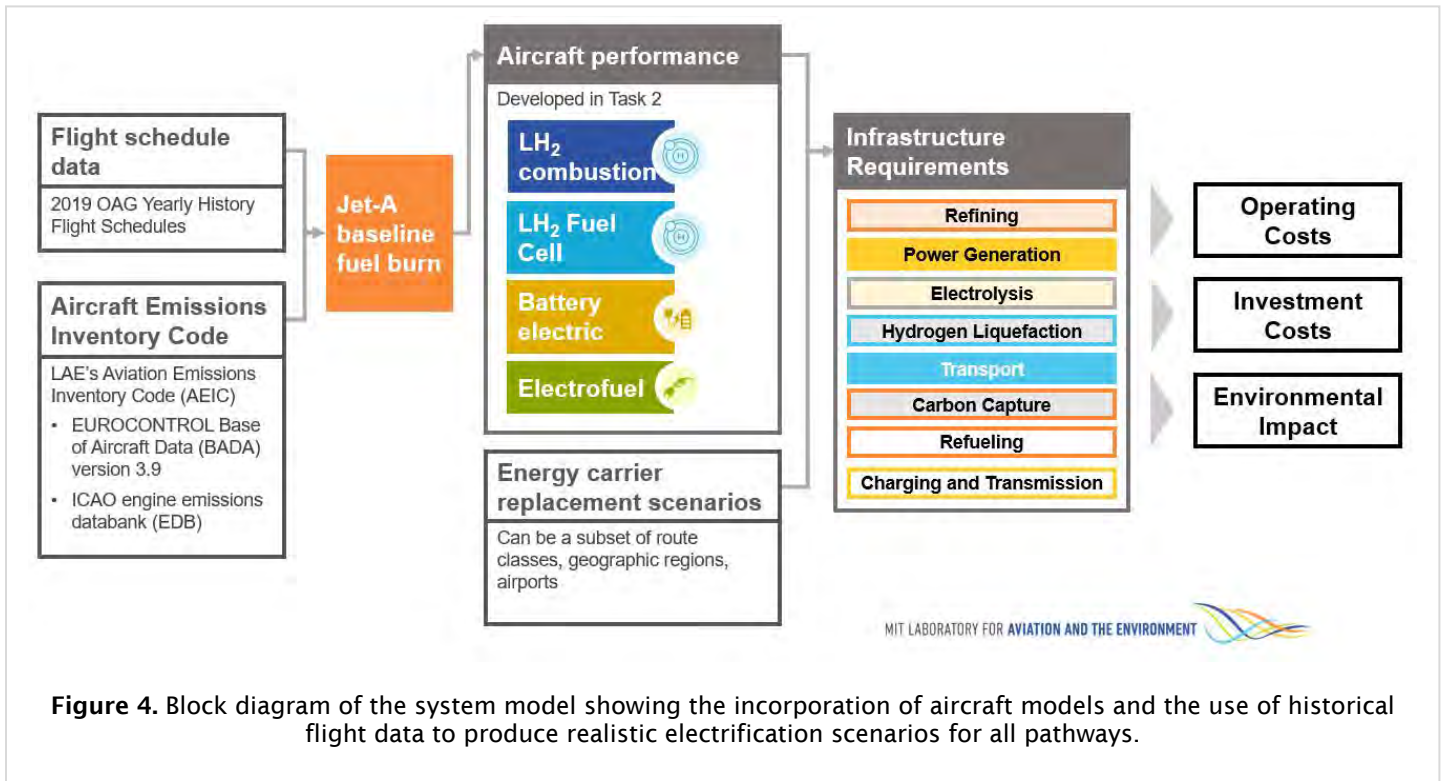
### **Research Approach**

Figure 4 provides an overview of the system model and its relation to the aircraft performance model described under Task 2. The aircraft models are used to produce realistic energy carrier replacement scenarios based on historical flight data, where subsets of the global market can be replaced. The tool can analyze the costs, environmental impacts, and infrastructure at the airport level and at the granularity of different route classes; this creates a scenario simulation tool, which not only allows us to compare different electrification strategies, but also enables us to analyze various combinations of electrification strategies applied to different geographic locations and markets. This approach is reflective of the diverse and multi-faceted approach to electrification which could be pursued by the aviation industry.

### **Baseline and Replacement Scenario Definition**

Since the objective of the project is to assess electrification pathways in policy-relevant scenarios, the first step of the system model is to establish a baseline scenario of “business as usual” for the aviation industry. The approach uses flight schedule data from the 2019 OAG database combined with a model for aircraft fuel burn to estimate the overall Jet-A fuel burn (and hence energy) requirements for each airport in the baseline case in the year 2019. Due to the nature of the flight schedule database, only scheduled passenger flights are accounted for in the study. The flights are divided into six route classes according to the distance flown as defined in Task 2. For any airport in the world, a time-resolved profile of energy demand (for departing flights) is generated for each route class.

The replacement scenarios that can be assessed in the model assume that traffic in a particular route class at particular airports is being replaced with a particular technology. The model is constructed in such a way that any combination of route class replacement with any combination of technologies at any combination of airports can be analyzed at a conceptual level. Results will be initially presented for scenario replacements at a single airport to understand the relative dynamics of the competing technologies. More complex country-wide, continent-wide, or global replacement scenarios representing progressive technology replacement will be developed to understand the overall system effects.



**Figure 4.** Block diagram of the system model showing the incorporation of aircraft models and the use of historical flight data to produce realistic electrification scenarios for all pathways.

### Infrastructure and Energy System Modeling

The infrastructure and energy system model is developed following the techno-economic approach, whereby the model incorporates operational and production costs within the overall system boundary. To estimate operational costs, the tool builds on the system-level engineering approach to derive the required process steps and understand each step's technical requirements and efficiencies. It then captures all relevant operational cost differences (as compared to the baseline specification developed under Task 1) for each technology pathway. The model will also estimate the initial investment required.

A key upstream infrastructure and energy system component is electric power generation, which will be required for all electrification pathways. The model includes solar, wind, and nuclear power generation. Geographically resolved estimates for cost, area requirement, and generation profiles will be made for each generation method.

The other major system considerations are fuel production, transport, and storage. Because there are multiple combinations possible for offsite and onsite production, which result in different requirements for transport and storage, the system model will use a modular building block approach to enable assessment and comparison of all relevant combinations of production, transport, and storage.

### Operating and Investment Costs

The modeling will be implemented using a discounted cash flow approach, which will enable consistent system-level comparisons between electrification pathways. Estimates for cost will be derived from the literature, drawing on previous work by the project team on the technoeconomic viability of electrofuels (Isaacs, 2019).

### Milestones

An initial outline of the system modeling structure has been completed (see above). The baseline scenario fuel burn and energy demand has been established, and initial simple replacement scenarios (i.e., at a single airport) have been defined.

## **Major Accomplishments**

An initial outline of the system modeling structure has been compiled which will inform future research and will ensure consistent comparisons between the different pathways under consideration.

In addition, the team has compiled an initial model for estimating energy and fuel demand under different electrification strategies. This model uses a simplified approach to aircraft modeling (which will be replaced by the more detailed model developed in Task 2) and incorporates a subset of the system processes which will eventually be included. Those already implemented are solar power generation, hydrogen production by electrolysis, hydrogen liquefaction, electrofuel production through co-electrolysis, and battery charging. Preliminary results from this model are presented to ICAO's Long-term Aspirational Goal task group.

## **Publications**

None

## **Outreach Efforts**

The MIT team prepared a presentation to ICAO's Long-term Aspirational Goal task group meeting, held in October 2020.

## **Awards**

None

## **Student Involvement**

None

## **Plans for Next Period**

The next step is to incorporate more of the modular process building blocks into the system model. These building blocks include wind power generation, nuclear power generation, and hydrogen transport and storage. At the same time, the operational and investment cost estimates for these processes will be refined, and first estimates of the emissions resulting from these processes made.

The scenario definitions will be extended to include regional and global replacement scenarios. An "optimization" capability, i.e., the ability to determine the most cost effective or most environmentally optimal electrification scenario, is a long-term aspiration of this Task.

## **References**

- Baroutaji, A., Wilberforce, T., Ramadan, M., & Olabi, A. G. (2019, 5). Comprehensive investigation on hydrogen and fuel cell technology in the aviation and aerospace sectors. *Renewable and Sustainable Energy Reviews*, 106, 31-40. doi:10.1016/j.rser.2019.02.022
- Barrett, S. R., Britter, R. E., & Waitz, I. A. (2010, 10). Global Mortality Attributable to Aircraft Cruise Emissions. *Environmental Science & Technology*, 44, 7736-7742. doi:10.1021/es101325r
- Bills, A., Sripad, S., Fredericks, W. L., Singh, M., & Viswanathan, V. (2020, 2). Performance Metrics Required of Next-Generation Batteries to Electrify Commercial Aircraft. *ACS Energy Letters*, 5, 663-668. doi:10.1021/acscenergylett.9b02574
- Blanco, H., Nijs, W., Ruf, J., & Faaij, A. (2018, 12). Potential for hydrogen and Power-to-Liquid in a low-carbon EU energy system using cost optimization. *Applied Energy*, 232, 617-639. doi:10.1016/j.apenergy.2018.09.216
- Brelje, B. J., & Martins, J. R. (2019, 1). Electric, hybrid, and turboelectric fixed-wing aircraft: A review of concepts, models, and design approaches. *Progress in Aerospace Sciences*, 104, 1-19. doi:10.1016/j.paerosci.2018.06.004
- Brewer, G. D. (1982). The prospects for liquid hydrogen fueled aircraft. *International Journal of Hydrogen Energy*, 7, 21-41. doi:10.1016/0360-3199(82)90205-1
- Bruce, P. G., Freunberger, S. A., Hardwick, L. J., & Tarascon, J.-M. (2011, 12). Li-O<sub>2</sub> and Li-S batteries with high energy storage. *Nature Materials*, 11, 19-29. doi:10.1038/nmat3191
- Brynnolf, S., Taljegard, M., Grahn, M., & Hansson, J. (2018, 1). Electrofuels for the transport sector: A review of production costs. *Renewable and Sustainable Energy Reviews*, 81, 1887-1905. doi:10.1016/j.rser.2017.05.288



- Cao, W., Mecrow, B. C., Atkinson, G. J., Bennett, J. W., & Atkinson, D. J. (2012, 9). Overview of Electric Motor Technologies Used for More Electric Aircraft (MEA). *IEEE Transactions on Industrial Electronics*, 59, 3523-3531. doi:10.1109/tie.2011.2165453
- Chen, J., Wang, C., & Chen, J. (2018, 6). Investigation on the Selection of Electric Power System Architecture for Future More Electric Aircraft. *IEEE Transactions on Transportation Electrification*, 4, 563-576. doi:10.1109/tte.2018.2792332
- CleanSky. (2020, 5). *Hydrogen-powered aviation*. Tech. rep., McKinsey and Company.
- Colozza, A. J., & Kohout, L. (2002). *Hydrogen storage for aircraft applications overview*. Tech. rep., NASA.
- Drela, M. (2016). *TASOPT 2.16 Transport Aircraft System OPTimization*. Tech. rep., Massachusetts Institute of Technology.
- Drünert, S., Neuling, U., Zitscher, T. & Kaltschmitt, M. (2020). Power-to-Liquid fuels for aviation - Processes, resources and supply potential under German conditions. *Applied Energy* 277, 115578.
- Fasihi, M., Bogdanov, D., & Breyer, C. (2016, 11). Techno-Economic Assessment of Power-to-Liquids (PtL) Fuels Production and Global Trading Based on Hybrid PV-Wind Power Plants. *Energy Procedia*, 99, 243-268. doi:10.1016/j.egypro.2016.10.115
- Glenk, G., & Reichelstein, S. (2019, 2). Economics of converting renewable power to hydrogen. *Nature Energy*, 4, 216-222. doi:10.1038/s41560-019-0326-1
- Gnadt, A. R., Speth, R. L., Sabnis, J. S., & Barrett, S. R. (2019, 2). Technical and environmental assessment of all-electric 180-passenger commercial aircraft. *Progress in Aerospace Sciences*, 105, 1-30. doi:10.1016/j.paerosci.2018.11.002
- Grobler, C., Wolfe, P. J., Dasadhikari, K., Dedoussi, I. C., Allroggen, F., Speth, R. L., . . . Barrett, S. R. (2019, 11). Marginal climate and air quality costs of aviation emissions. *Environmental Research Letters*, 14, 114031. doi:10.1088/1748-9326/ab4942
- Hall, D. K., Greitzer, E. M., Dowdle, A. P., Gonzalez, J. J., Hoburg, W. W., Lang, J. H., . . . Courtin, C. (2019, 12). *Feasibility of Electrified Propulsion for Ultra-Efficient Commercial Aircraft Final Report*. Tech. rep., NASA Glenn Research Center, Cleveland, OH, United States.
- Herz, G., Reichelt, E., & Jahn, M. (2018, 4). Techno-economic analysis of a co-electrolysis-based synthesis process for the production of hydrocarbons. *Applied Energy*, 215, 309-320. doi:10.1016/j.apenergy.2018.02.007
- ICAO (2019). *CORSIA eligible fuels - Lifecycle assessment methodology*. Montreal.
- Isaacs, S. A. (2019). *Environmental and Economic Characteristics of Electrofuel Production Pathways*. Master's thesis, Massachusetts Institute of Technology.
- Khandelwal, B., Karakurt, A., Sekaran, P. R., Sethi, V., & Singh, R. (2013, 7). Hydrogen powered aircraft : The future of air transport. *Progress in Aerospace Sciences*, 60, 45-59. doi:10.1016/j.paerosci.2012.12.002
- Kim, H. C., Wallington, T. J., Arsenault, R., Bae, C., Ahn, S., & Lee, J. (2016, 6). Cradle-to-Gate Emissions from a Commercial Electric Vehicle Li-Ion Battery: A Comparative Analysis. *Environmental Science & Technology*, 50, 7715-7722. doi:10.1021/acs.est.6b00830
- König, D. H., Freiberg, M., Dietrich, R.-U., & Wörner, A. (2015, 11). Techno-economic study of the storage of fluctuating renewable energy in liquid hydrocarbons. *Fuel*, 159, 289-297. doi:10.1016/j.fuel.2015.06.085
- Mital, S. K., Gyekenyesi, J. Z., Arnold, S. M., Sullivan, R. M., Manderscheid, J. M., & Murthy, P. L. (2006). *Review of Current State of the Art and Key Design Issues With Potential Solutions for Liquid Hydrogen Cryogenic Storage Tank Structures for Aircraft Applications*. Tech. rep., NASA.
- Nojumi, H., Dincer, I., & Naterer, G. (2009, 2). Greenhouse gas emissions assessment of hydrogen and kerosene-fueled aircraft propulsion. *International Journal of Hydrogen Energy*, 34, 1363-1369. doi:10.1016/j.ijhydene.2008.11.017
- Renouard-Vallet, G., Saballus, M., Schmithals, G., Schirmer, J., Kallo, J., & Friedrich, K. A. (2010). Improving the environmental impact of civil aircraft by fuel cell technology: concepts and technological progress. *Energy & Environmental Science*, 3, 1458. doi:10.1039/b925930a
- Sarlioglu, B., & Morris, C. T. (2015, 6). More Electric Aircraft: Review, Challenges, and Opportunities for Commercial Transport Aircraft. *IEEE Transactions on Transportation Electrification*, 1, 54-64. doi:10.1109/tte.2015.2426499
- Schäfer, A. W., Barrett, S. R., Doyme, K., Dray, L. M., Gnadt, A. R., Self, R., . . . Torija, A. J. (2018, 12). Technological, economic and environmental prospects of all-electric aircraft. *Nature Energy*, 4, 160-166. doi:10.1038/s41560-018-0294-x
- Smith, J. R., & Mastorakos, E. (2019, 8). An assessment of the uncertainty involved in predictions of energy consumption and carbon emissions from future fully-electrified aircraft. *AIAA Propulsion and Energy 2019 Forum*. American Institute of Aeronautics and Astronautics. doi:10.2514/6.2019-4493
- Valente, A., Iribarren, D. & Dufour, J. (2017). Hamronized life-cycle global warming impact of renewable hydrogen. *Journal of Cleaner Production* 149, 762-772.



- Verstraete, D. (2013, 11). Long range transport aircraft using hydrogen fuel. *International Journal of Hydrogen Energy*, 38, 14824-14831. doi:10.1016/j.ijhydene.2013.09.021
- Verstraete, D. (2015, 6). On the energy efficiency of hydrogen-fuelled transport aircraft. *International Journal of Hydrogen Energy*, 40, 7388-7394. doi:10.1016/j.ijhydene.2015.04.055
- Verstraete, D., Hendrick, P., Pilidis, P., & Ramsden, K. (2010, 10). Hydrogen fuel tanks for subsonic transport aircraft. *International Journal of Hydrogen Energy*, 35, 11085-11098. doi:10.1016/j.ijhydene.2010.06.060
- Yim, S. H., Lee, G. L., Lee, I. H., Allroggen, F., Ashok, A., Caiazzo, F., . . . Barrett, S. R. (2015, 2). Global, regional and local health impacts of civil aviation emissions. *Environmental Research Letters*, 10, 034001. doi:10.1088/1748-9326/10/3/034001



# Project 053 – Validation of Low Exposure Noise Modeling by Open-Source Data Management and Visualization Systems Integrated with AEDT

## Stanford University

### Project Lead Investigator

Juan J. Alonso  
Vance D. and Arlene C. Coffman Professor  
Department of Aeronautics & Astronautics  
Stanford University  
Stanford, CA 94305  
Phone: (650) 723-9954  
E-mail: [jjalonso@stanford.edu](mailto:jjalonso@stanford.edu)

## University Participants

### Stanford University

- PI: Prof. Juan J. Alonso
- FAA Award Number: 13-C-AJFE-SU-022
- Period of Performance: February 5, 2020 to February 4, 2021
- Tasks:
  1. Aviation Environmental Design Tool (AEDT) integration with Metroplex Overflight Noise Analysis (MONA) software
  2. Validation and verification of AEDT noise predictions in 55–65 db Day-Night Average Sound Level (DNL) areas.
  3. Software architecture infrastructure suggestions for AEDT.

## Project Funding Level

Year 1 of ASCENT Project 53 has been allocated FAA funds in the amount of \$169,903. Cost sharing in excess of this amount has been identified from various sources. Mr. Thomas Rindfleisch and Mr. Donald Jackson are contributing all of their time, uncompensated, to the project. In addition, contractor costs for the development of the MONA project website, the cost of undergraduate student support and summer interns, and some equipment purchases (and installation costs) are also being used to generate cost share for this project. During the first nine months of this project, a total of more than \$640,000 of cost share has already been accounted for.

## Investigation Team

The investigation team is made up of the faculty, graduate and undergraduate students, and collaborators listed below with their respective areas of expertise / areas of contribution:

1. Juan J. Alonso (PI, Stanford Aeronautics & Astronautics): overall responsibility for the project and its technical and administrative elements.
2. Nick Bowman (Graduate Student, Stanford Computer Science): MONA project cloud infrastructure, cloud-based execution of AEDT analyses, Apache Kafka-based data collection.
3. Brynne Hurst (Graduate Student, Stanford Computer Science): flight trajectory database analysis and synthesis.
4. Donald Jackson (Collaborator, independent consultant): overall MONA project infrastructure (servers, databases, hardware / software monitoring), GIS, web-based visualization deployment, technical guidance.
5. Priscilla Lui (Co-term Student, Stanford Computer Science): real-time Sound-Level Monitoring (SLM) software, metrics, Raspberry Pi connectivity.



6. Vikas Munukutla (Graduate Student, Stanford Computer Science): automation of AEDT analyses via generation/query of input/output databases on the cloud.
7. Chetanya Rastogi (Graduate Student, Stanford Computer Science): overall database infrastructure improvements, noise monitoring / filtering software.
8. Thomas Rindfleisch (Collaborator, Stanford University Emeritus): noise monitoring and filtering, aircraft trajectory collection / processing, visualization.
9. Aditeya Shukla (Undergraduate Student, Stanford Aeronautics & Astronautics): artificial intelligence/machine learning (AI/ML) classification of aircraft trajectories, real-time Sound-Level Monitoring (SLM) software
10. Kadin Hendricks (Undergraduate Student, Aeronautics & Astronautics): AEDT input/output database structure.

## Project Overview

The MONA project (Metroplex Overflight Noise Analysis) was started to provide real-time and objective data, analyses, and reports to key stakeholders and policy makers to mitigate the noise impacts of the deployment of new NextGen procedures. This system (a) collects and archives air traffic data using a network of antennae and receivers, (b) analyzes noise impacts using a variety of metrics, (c) visualizes resulting large-scale datasets, and (d) uses a network of sound-level monitors to enhance the quality of noise predictions. The focus of this ASCENT project is to improve upon the noise predictions of MONA through tighter integration with the FAA's Aviation Environmental Design Tool (AEDT). In particular, our work is focused on the following three tasks: (1) integrate and automate AEDT's noise analysis capabilities, (2) validate and verify (V&V) AEDT's noise predictions in 55-65 db Day-Night Average Sound Level (DNL) areas, and (3) propose software engineering/architectural choices for future AEDT development to enhance usability in multiple workflows including API formulation, visualization interfaces, resilient data acquisition and storage, and cloud computing.

The expected benefits of this project mirror the tasks mentioned above, including (a) ability to automate complex noise analyses in metroplexes so they are available in near-real time after the preceding 24-hr period, (b) a better understanding of the accuracy of AEDT's current noise models in low noise (55-65 db DNL) areas and the reasons for the discrepancies (if any) in existing predictions, and (c) guidance to software developers on flexible architectures and APIs for AEDT so that the tool is more versatile and generally applicable. AEDT predictions are built around the policy context of an average annual day. All the V&V results produced and shared by the MONA team will be focused on a cumulative daily basis for which flight track data is directly collected.

## Background and Previous Accomplishments

The MONA project (Metroplex Overflight Noise Analysis) started approximately 2.5 years ago with the main objective of providing real-time and objective data, analyses, and reports to key stakeholders and policy makers to help in mitigating the noise impacts of the deployment of new NextGen procedures. Since then, we have put together a preliminary open-source system that (a) collects, archives, and makes available air traffic data using a series of networked antennae and receivers 24/7, (b) analyzes noise impacts using a variety of metrics (based on both a MONA-developed noise prediction tool and, albeit manually, the noise predictions tools within AEDT), (c) visualizes resulting large-scale datasets in a simple, user-friendly fashion using both a bespoke website and Uber's kepler.gl and deck.gl large-scale data visualization toolboxes, and (d) is beginning to use a small network of low-cost sound-level monitors scattered across the Bay Area to enhance noise predictions so they describe exactly the actual noise levels experienced.

The longer-term objectives of the MONA project are to (a) ensure the validation and verification of all noise predictions provided (by AEDT or other tools) in both areas near the airport and in other areas further away from the airport, typically 55-65 db DNL, (b) achieve full automation of complex noise analyses in metroplexes in the United States, including AEDT-based noise predictions, (c) make all results web-accessible for in-depth interpretations of historical and proposed changes, (d) eventually study potential alternative traffic patterns in complex metroplexes to mitigate aviation environmental impacts, and (e) export the proven/validated MONA technology to other metroplexes via open-source software/hardware.

When ASCENT Project 53 started (Feb 2020), the MONA software had achieved several significant objectives which positioned the team to achieve the work described in the project proposal. MONA has:

1. Deployed a network of ADS-B / MLAT antennae and had completed initial versions of the software necessary to merge the data streams from all of these antennae including de-duplication of sightings, identification of aircraft



- equipment and routes flown, physical interpolation of data missing from the joint observations, and archiving (in appropriate json-based formats) of the information collected for successive analysis.
2. Begun the process of integration with FAA's AEDT (v2d, at the time) software that enables manual prediction of noise footprints at arbitrary receptor locations. Initial efforts to incorporate NASA's Aircraft Noise Prediction Program (ANOPP2) tools predictions had also been pursued and put aside until full AEDT integration is completed.
  3. Begun to incorporate measurements from networked sound-level monitors into the system and to develop preliminary versions of non-aircraft-noise filtering techniques (of the raw noise data) based on digital filtering, aircraft position information, and automated identification of background noise levels. Significant further efforts to improve the filtering techniques by using measurements and correlations from multiple sound-level monitors are also planned.
  4. Over the previous year, interfaced the above-described MONA preliminary software modules with the kepler.gl open-source visualization framework, developed by Uber, to be able to visualize and animate aircraft positions and paths, noise predictions, various routes and procedures, etc., to better communicate the results of our work (see Figure 1). A preliminary version of the MONA website, which helps visualize and makes accessible the same information but for a less experienced user, had also been started (see Figure 2 for an image from an early prototype).

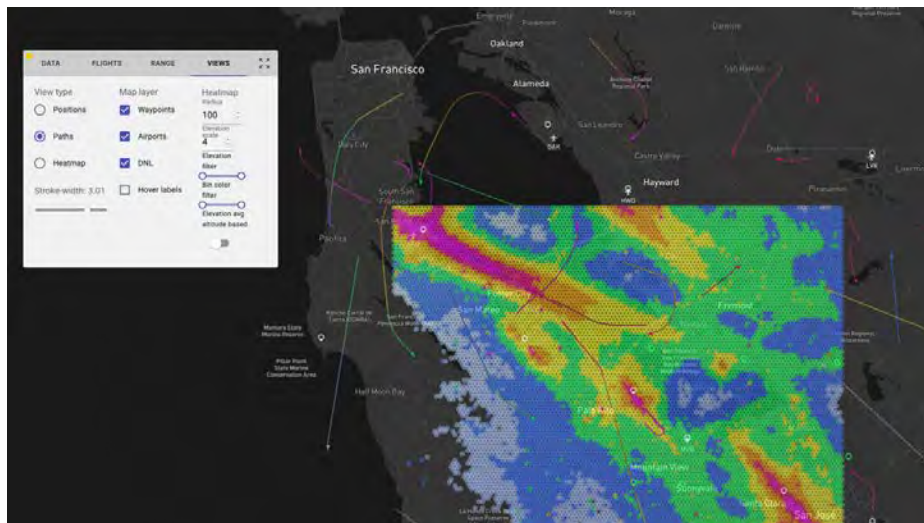


**Figure 1.** MONA visualization (using kepler.gl and deck.gl) of traffic patterns in the Bay Area.



Figure 2. Current MONA web-access prototype for real-time aircraft location and 24-hr DNL contours.

## Task 1 – AEDT Integration with MONA software

Stanford University

Given that the vision of MONA is to make 24/7 aircraft noise information available through a simple visualization interface, predictions of aircraft noise are a fundamental component of the entire effort. We eventually intend to validate these noise predictions with data collected from strategically located SLMs whose raw sound data has been appropriately filtered to eliminate non-aircraft noise sources. This Task, however, focuses on the necessary integration steps to make AEDT noise analyses available through the MONA interface. This Task will be complete when noise analyses in an entire metroplex (the Bay Area in our initial test case) for an entire 24-hr period can be performed, visualized, analyzed, and archived without user intervention. The automation of the entire workflow requires the implementation and automation of a number of key steps:

1. Starting from a set of MONA-acquired and pre-processed flight paths and associated aircraft equipment for the previous 24-hr period, the necessary AEDT inputs are generated in an SQL study database that can be later consumed by AEDT. The input database must contain the actual location of the aircraft as a function of time, the specific aircraft equipment, and other auxiliary parameters needed for the analysis.
2. The setup of a noise analysis in AEDT, including all the necessary metric descriptions, receptor locations, annualizations, and additional input data must be automatically generated and included in the input study database as permitted by AEDT v3.
3. Automated execution of arbitrary analyses can then be pursued so that AEDT can be run through a batch process without user intervention. For this batch process, we have developed a cloud-based solution that automatically fires up a cloud instance, sets up the necessary communication structures, runs the AEDT study, and returns the study results to the computer executing the study.
4. A module for the extraction of the computed metrics and their spatial distributions, for arbitrary metric computations, is being developed. The interaction with the output of AEDT analyses is intended to happen directly through the SQL output study database that contains and stores all the necessary information.

During the period covered by this report, we have completed a preliminary version of all four subtasks (some of which are described in more detail below) and are continuing the process of both automating every step, scaling our capabilities to handle larger and larger studies, and using automated AEDT analyses to support Task 2. In the process, we have created our own cloud-based AEDT execution environment (which we have named *raedt*, for *remote* AEDT) that works on Google Cloud Platform instances of arbitrary size (number of processors, memory, etc.)

## **Subtask Name: Remote and Automatable AEDT Execution in the Cloud**

### **Objective**

The main problem being addressed in this subtask is that AEDT can only run on the Windows operating system, which often requires the acquisition of specialized, standalone hardware in order to be able to run AEDT studies. In addition, studies can only be constructed via a graphical user interface (GUI), which is not easily automatable or executable in a scriptable, programmatic manner, making it difficult to efficiently run a large breadth and variety of surveys. The objective in this subtask is to move AEDT execution to the cloud by taking advantage of Windows Instances running on the Google Cloud Platform that are pre-configured with AEDT and all supporting software. Our goal was to create a system in which these instances can be remotely accessed from any platform/operating system in a programmatic manner. This would allow members of the team to write scripts to programmatically create and run AEDT studies in a scalable manner (discussed in a later subtask). To accomplish this goal, we proposed and developed a system that is based on templated creation of Windows-based virtual machines in the cloud and is controlled by a custom command-line software package uniquely tailored to carry out the necessary tasks and administrative actions necessary to run remote AEDT studies.

### **Research Approach**

There were three main components of our approach to achieve the goals set forward in this Task. First, we had to select a suitable cloud platform on which to build our cloud AEDT infrastructure. Of the three main cloud providers (Google Cloud Platform (GCP), Amazon Web Services, and Microsoft Azure), we found that GCP offered the best combination of cost effectiveness, well-documented command-line and language-specific APIs, and performance flexibility. We note, however, that the same capability can be replicated in any of the three major cloud providers with the necessary customization changes. Next, we had to manually construct a disk image (based on Windows Server) that would act as the template from which all AEDT-capable virtual machines (VMs) would be instantiated from. At the moment, this process involves manual installation of the necessary software packages on a Windows Server 2017 machine (including SQL Server), but we envision that this process can be automated in future versions of the project. Finally, we focused on developing a command-line software package implemented in a mix of Python and shell scripts that leveraged Google's GCP APIs to give users the ability to carry out important remote tasks in a programmatic manner. The outcome has been the possibility to create AEDT instances, open two-way communication channels between the computer / program running the analysis and the cloud instance executing it, run the AEDT analysis, and retrieve the results of the study. This software is currently being deployed and tested and will be available as open-source software to anyone who wants to benefit from its automation capabilities.

### **Milestones**

- Set up GCP infrastructure, with Windows Server "base install image" containing all necessary software, standardizing the environment for all team members.
- Defined library of command line tools (named `raedt`) to enable creation, control, and destruction of AEDT VMs in an easily scriptable format.
- Enabled seamless SSH connection, remote port tunneling for SQL Server access, connection via RDP for necessary GUI-based actions, and remote SSH command execution to support automated AEDT tools.

Overall, we have achieved cost-effective execution of AEDT studies (on the order of \$0.05-\$0.10 per hour for minimum required hardware specifications) and have set ourselves up in Project 53 for the scalable execution of much larger studies, repeatedly as needed, while allowing ourselves to tailor the cloud instance hardware resources that are needed for each individual study. This capability has been integrated with the capabilities described in the next subtask to automate our AEDT analyses, as we had suggested in our original proposal.

## **Subtask Name: Automatable AEDT Study Creation/Execution and Results Extraction**

### **Objective(s)**

One of the main goals of MONA / Ascent 53 (see Task 2) is to compare MONA SLM sensor output against AEDT predictions to see how similar the two measurements are and to gain a more nuanced understanding of the accuracy of AEDT predictions in 55-65 dB DNL areas. However, to run AEDT studies, one has to manually enter every flight using the AEDT GUI, and given that there are many thousands of flights per day in the San Francisco International Airport (SFO) region, this task is difficult to do through the GUI. This task would be both feasible and routine if, instead, the studies are automatically generated and executed by a script that can access the flights for the day. Moreover, if this script can run completely on the cloud using

the infrastructure described in the “Remote and Automatable AEDT Execution in the Cloud” subtask, then anyone on any laptop or remote server can run AEDT studies programmatically on their machine regardless of whether their machine is a Windows machine and independently of the resources needed (computer memory, number of processors, etc.) to carry out the AEDT analysis in reasonable time. The purpose of this subtask is to reverse-engineer the logic of AEDT study creation, execution, and results extraction as it would happen in the AEDT GUI to skip the overhead that comes with using the GUI for large, multi-flight studies, using a Windows VM and our internal command line tool `raedt` for cost-effective execution, ease of access, and flexibility.

## Research Approach

There are three main steps to this subtask. We first run an AEDT “create-study” script that creates a copy of the empty study database and populates the copy according to the various flights, airports, and desired noise metrics in the study. This step is the largest and most significant aspect of the subtask and involves researching the smallest details of every necessary value needed to be inserted into flight-related tables, airport-related tables, and metric-related tables. It also involves investigating how to replicate the simplest possible study—the empty study—in order to maintain all views, stored procedures, etc. for the new study. Next, the “remotely execute the study” step on the VM, which populates the results-related tables in the study’s database, is completed. This step simply issues a command called `RunStudy.exe` over SSH to the VM so that the VM can run the study on the AEDT databases that were just populated by the create-study script. Lastly, we run an “extract results” script which extracts the noise metric results produced after executing the study and stores the result in JSON files on the user’s machine. This step involves setting the right permissions in AEDT configuration files so that XML extraction is possible, running a SQL query to extract the XML results from the `EVENT_RESULTS` table of the study, and then converting the XML to JSON using Python libraries.

## Milestones

- Connected to the flights `postgres` databases and AEDT SQL Server databases.
- Created a backup of the empty study database and used the diff between an ASIF-generated study and empty study to fill in the appropriate flight, airport, and metric tables for a one-flight, multi-receptor study in which the flight is landing at SFO.
- Extracted results after running the one-flight study, converted the XML result to JSON, and saved the JSON file.
- Used Windows VM cloud execution to create an automation flow for AEDT studies which consists of starting the VM, starting SSH tunnel to VM, running create study script, running `RunStudy.exe` remotely on the VM using SSH, and running results extraction script.

## Task 2 – Validation and Verification of AEDT Noise Predictions in 55-65 db DNL Areas

Stanford University

The noise prediction modules inside of AEDT, based on noise power distance (NPD) relationships and certification data, were developed and calibrated mainly for areas of objectionable noise close to the airports (> 65 db DNL), at a constant velocity (160 knots), and for a particular aircraft high-lift system configuration. Even including efforts such as those in ASCENT Project 43 (which re-evaluated the noise power distance curves using ANOPP analyses and the ability to change the aircraft configuration during arrival/departure procedures), there is some evidence that the accuracy of AEDT’s predictions in areas of lower noise (between 55–65 db DNL) is lacking and must be improved. For these reasons, in this Task we proposed to undertake a thorough evaluation of the accuracy of AEDT’s predictions when measured against microphone readings from a small network of SLMs that the MONA project has acquired, tested, and sited. In order to accomplish the objectives of this Task, we will pursue the following steps:

1. Data acquisition and archiving for noise measurements at 3–4 locations. We will begin with the acquisition of the raw noise data (`Leq`, `Lmin`, `Lmax`) at a small number of locations. Even though we have already been collecting this data at one particular location, as part of this effort we will re-evaluate the most useful locations for the existing SLMs, place the SLMs at the desired locations, and begin collecting and archiving data for both the validation study and future use. Data will be collected 24/7, with particular attention paid to events that fall under the noise-level category that is the focus of this Task.
2. As a pre-processing step to the V&V portion of this work, we will focus our activities on the continued development of a series of non-aircraft noise removal algorithms that combine filtering techniques, automatic identification of



multiple aircraft peaks, automatic detection of background and peak noise levels, and real-time information regarding the position, velocity, and heading of the aircraft so we can maintain high levels of accuracy. In order to further improve the quality of our aircraft-only noise data, we also intend to use the noise measured at multiple, non-collocated but nearby SLMs and use the correlations between these measurements and aircraft locations to filter out false positives.

3. A validation campaign will then be pursued covering variations of the most important variables that can be observed in the 55–65 db DNL areas of the Bay Area metroplex: aircraft mass/weight, aircraft type, aircraft altitude at the time of the noise event, aircraft slant distance, and aircraft speed. No attempt to correct predictions for atmospheric conditions will be made, although we expect to pursue validation efforts over a number of different days and conditions that will span the range of the typically observed weather conditions.
4. The results of the validation study will be carefully documented in an archival publication. If possible, discrepancies between the measured noise levels and the AEDT predictions will be attributed to the main source causing the discrepancy.

Finally, all the data used for validation purposes will be processed at both the aggregate level and the level of individual flight predictions so that data-driven methods for the improvement of the NPD curves used in AEDT (or those produced in ASCENT Project 43) can be pursued in the future. For example, if all of the recorded overflights of a particular aircraft type, which have variability in mass, atmospheric conditions, high-lift system configuration, etc. have a corresponding time history of the recorded sound pressure level at an observer location, a learning algorithm could be devised to correct the AEDT predictions as functions of altitude, airspeed, and distance to the observer. Such a data-driven methodology can lead to significantly improved predictions in AEDT.

### **Subtask Name: Validation & Verification of AEDT predictions in 55–65 db DNL areas**

#### **Objectives**

The main objective of this Task is to evaluate the accuracy of AEDT noise predictions by directly comparing them with the metrics obtained from processing the raw data collected by the network of MONA SLMs. Another important aspect of this Task is to develop a well-documented library that abstracts the noise filtering and noise metric calculation aspects and can be open-sourced to assist future developments in this area.

#### **Research Approach**

The raw SLM data at multiple locations is currently captured and stored in a centralized database with associated timestamps which can be retrieved by running respective SQL queries. These data come from calibrated networked Convergence Instruments equipment that we have installed at various locations around the Bay Area and that have been tested with co-located sound measurement equipment loaned by SFO and found to agree with that equipment to within 0.1 dB. Such tests that we conducted lend credibility to the quality of the sound data recorded from our SLMs. The retrieved data is then processed through the noise filtering pipeline which was developed and implemented to remove any non-aircraft noise by following a multi-step process that identifying a noise matches the sound peaks with a corresponding flight and provides a summary statistic about the noise levels. The main steps of this process include:

- Retrieval of raw noise recording (including non-aircraft noise sources) from the MONA database.
- Calculation of a background noise profile to establish the (time-varying) identified background noise level.
- Development of a threshold profile, above the background level, below which all noise events are filtered.
- Signal processing of remaining signal to identify peak-like structures that might correspond to an aircraft event.
- Matching each potential *peaklet* to times and points of closest approach from ADS-B database. *Peaklets* whose time is within a specified time of a Time of Closest Approach (TCA) are retained and associated with a particular flight event. Peaks that do not have a corresponding potential aircraft are also filtered.

The result is a filtered signal that is guaranteed to correspond to a conservative estimate of the actual aircraft noise as the possibility exists that some aircraft noise events (such as some sensitive flights, etc) are recorded but not identified in our flight database collected simultaneously. Figure 3 below is an example of the interactive plots produced with this now fully automated process. This process can also be run during any subset of the day (a subset of the recorded data) to prepare actual recordings of flight events at multiple locations for comparisons with AEDT predictions. For example, flight recordings during the early hours of the day (between 1–4 AM) tend to have very low levels of background noise and, therefore, are prime candidates for the comparisons with AEDT predictions. We have now been collecting sound recordings at multiple locations for about a year and are beginning to prepare a database of test cases that will serve as the basis for our evaluation.

A Python client has also been developed to interact with the DB and provides APIs to process and perform required operations, including post-processing and plotting. For developing the Python client, the best software engineering practices were employed and provide configurable API access.

### Milestones

- Defined and documented APIs for communicating with the centralized database by abstracting the SQL queries.
- Verified the pipeline for obtaining TCAs and measuring associated peaks using the SLM data from the database.
- Restructured original noise-filtering code and modularized it for future reusability.
- Provided an end-to-end integration for running the noise filtering pipeline directly on the database data.
- Begun to create a database of flights that will be used for the comparisons with the automated AEDT analyses described in an earlier subtask.

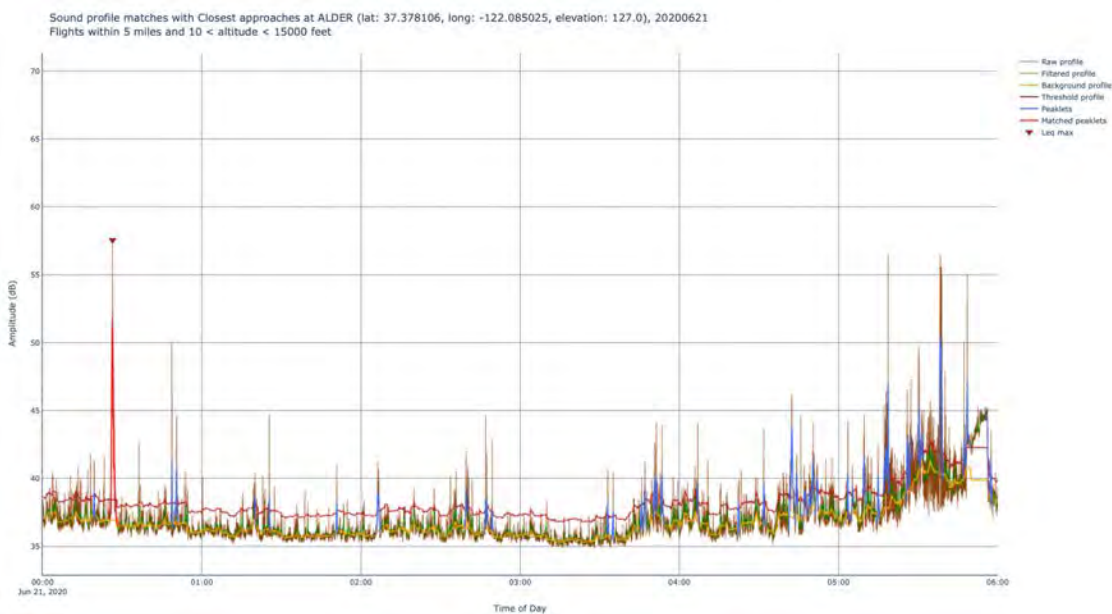


**Figure 3.** Graphical depiction of multi-step process used to filter non-aircraft data from SLM raw recordings. Example from 6-hour interval on June 21, 2020.

### Subtask Name: Real-time SLM Sound Recording and Metric Calculation

#### Objective

There are interesting real-time applications (versus post-processing data every 24 hours or every other reasonable time period) we would like to achieve with our noise data. However, before completion of this Task, those applications were impossible because ingesting the noise data involved waiting 6–24 hours for a file to be published to the cloud by the manufacturers of the SLM. Another downside was that this file contained already-computed metrics that were computed onboard the SLM, so we could not access the raw data which might prove useful for future analysis. Thus, this research task aimed to bypass the cloud file by using a Raspberry Pi to directly process the audio recorded by the SLM in real-time and send it to our database. The final vision is to integrate this SLM code and the ADSB-collector code onto a Raspberry Pi, to create an all-in-one MONA unit.

#### Research Approach

In terms of learning to compute the metrics ourselves, we consulted Dr. Bruno Paillard, the senior designer at the company that sold us the SLMs. With his guidance, we were able to replicate results for Leq, Lmax, and Lmin to near-perfect accuracy.

As for the goal of real-time, we leveraged past experiences implementing real-time applications on microprocessors to architect the final design of the software running on the Raspberry Pi.

### **Milestones**

- Designed and implemented an automated Python library that records audio from aSLM, computes metrics, and sends it to a server / database.
- Successfully wrote an algorithm to compute Lmin, Lmax and L<sub>Eq</sub> on streaming audio and verified it with 99.99% accuracy.
- Added a resilient way to store computed metrics in case of a network failure and implemented exponential back off for sending attempts.
- Made the script configurable (custom log intervals, custom frame rates, audio formats, etc.).
- Used multiprocessing and multithreading to leverage the Raspberry Pi's quadcore and improve throughput.
- Supported raw collection of audio samples (saving chunks of audio for later use).

## **Task 3 – Software Architecture Infrastructure Suggestions for Future AEDT Development**

Stanford University

The MONA project is working on a software infrastructure to setup hardware, collect data from various types of sensors, archive/store those data without interruptions in a fail-safe manner, and process the data (and store the results in appropriate databases) for future use that will be distributed in an open-source manner. Such use of multiple functional modules has resulted in the need to carefully think about the overall software architecture of the project, the standards used for the representation and communication of the data, the kinds of databases that can be used, the existing visualization standards that must be interfaced with, and the potential for cloud computing infrastructure to shorten the time to deployment of the MONA software in different metroplexes beyond the Bay Area.

### **Research Approach**

The FAA Office of Environment and Energy (AEE) has expressed interest in leveraging the ASCENT 53 experience (in software development-related aspects) and the expertise of professional software developers from Silicon Valley in the MONA team to provide suggestions / guidance to be used in deriving requirements for future AEDT development.

As part of this Task, our team is creating an architecture document that shows the organization of data, storage, processing, cloud-based analysis and automation, etc., so that future versions of AEDT can be more easily integrated into complex analysis workflows that we cannot do easily today. The integrity (and redundancy / resilience) of the data acquisition process is also of paramount importance to the success of environmental data collection and analysis efforts, and ASCENT 53 is using the latest tried-and-true distributed data collection approaches (which we will describe in a future report) and that have implications for interaction with AEDT. Our team has been pioneering visual representation approaches for the display of both the raw data and the processed data that could be more easily integrated with AEDT. All of these experiences from the ASCENT 53 team efforts, together with feedback from briefings (to Silicon Valley software developers and Stanford computer science faculty) that will provide additional suggestions regarding the typical workflows expected in AEDT v5, will be archived and provided as the output of this Task. Finally, we will create a report that will contain recommendations regarding (a) expected requirements for AEDT v5, (b) best software development practices / interfaces that might be followed, (c) organization of the overall code base, (d) APIs for external execution of AEDT's modules, and (e) suggestions for database and datafile formats and visualization interfaces. This Task is necessarily the last one for the first year of ASCENT 53 as it relies on the various experiences in Tasks 1 and 2 that are informing the outcome.

The output of these efforts will be communicated periodically with ASCENT's program managers, who will be invited to participate in the brainstorming sessions and in our internal deliberations.

### **Milestones**

- Completed architecture of MONA system (database data storage, multi-server / multi-computer communication, cloud instances of AEDT, two-way communication with cloud instances, software module architecture, postGIS



system, U.S. Census data incorporation, Apache Kafka / Zookeeper server for resilient/redundant data acquisition, and visualization infrastructure).

- Identified major elements that interact with AEDT to better understand potential changes to the AEDT structure and the availability of APIs that would be helpful.

### **Major Accomplishments**

- Created a completely new infrastructure for ASCENT 53 / MONA that can scale to the types of data collection and analysis expected of a complex metroplex such as that of the Bay Area.
- Developed a working version of the non-aircraft noise filtering process to compare sound recordings with AEDT predictions.
- Created a cloud-based automated approach to run AEDT studies so that they can be automated in the Bay Area metroplex.
- Collected necessary data to generate a database of individual flight data that will be used in our AEDT V&V study.
- Rewrote large portions of the software infrastructure to (a) make it more readily available via open-source, and (b) to provide input to Task 3, suggestions for AEDT improvements for better integration into MONA-like automated analyses and comparisons.

### **Publications**

None thus far. An initial publication detailing the infrastructure and early results of the MONA system is planned for later this year.

### **Outreach Efforts**

As part of our efforts to produce data of high quality that can be used for decision making, we have engaged with the Palo Alto City Council, with various citizen groups in the Bay Area, and like-minded individuals that may lend their help to the development of the ASCENT 53 / MONA infrastructure. Although we have been asked to participate in technical discussions in the existing local noise roundtables, these interactions have yet to take place and will be limited to discussions of technical elements of relevance to the community.

### **Awards**

None

### **Student Involvement**

A number of undergraduate and graduate students are / have been part of our team during this past nine months since the project started. Their names and areas of responsibility are listed at the beginning of this document. None of the students have yet graduated, although three of them will at the end (or before the end) of this academic year.

### **Plans for Next Period**

We intend to complete all three Tasks in our Statement of Work as planned. In addition to the completion of all milestones, the release of appropriate parts of the ASCENT 53 / MONA project and the demonstration of various capabilities through participation in aircraft noise related meetings / conferences is also envisioned.



# Project 054 AEDT Evaluation and Development Support

## Georgia Institute of Technology

### Project Lead Investigator

Principal Investigator:

Professor Dimitri N. Mavris

Director, Aerospace Systems Design Laboratory

School of Aerospace Engineering

Georgia Institute of Technology

Phone: (404) 894-1557

Fax: (404) 894-6596

Email: dimitri.mavris@ae.gatech.edu

Co-Principal Investigator:

Dr. Michelle Kirby

Chief, Civil Aviation Division

Aerospace Systems Design Laboratory

School of Aerospace Engineering

Georgia Institute of Technology

Phone: (404) 385-2780

Fax: (404) 894-6596

Email: michelle.kirby@ae.gatech.edu

### University Participants

#### Georgia Institute of Technology

- Pls: Dr. Dimitri Mavris, Dr. Michelle Kirby
- FAA Award Number: 13-C-AJFE-GIT-054
- Period of Performance: February 5, 2020 to February 4, 2021
- Tasks:
  1. Improved Departure Modeling (divided into four areas: High Altitude Airport Study; Refinement of Thrust and Weight Assumptions; Estimation of Thrust Using ANP Equations; and Comparison of NADP Profiles to Real-world Operations.
  2. Arrival Profile Modeling.
  3. Full Flight Modeling.
  4. System Testing and Evaluation of AEDT.

### Project Funding Level

The project is funded at the following levels: GT (\$700,000). In terms of cost-share details, GT has agreed to a total of \$700,000 in matching funds. This total includes salaries for the project director, research engineers, and graduate research assistants, as well as computing, financial, and administrative support, including meeting arrangements. GT has also agreed to provide tuition remission for the students, paid for by state funds.

### Investigation Team

**Prof. Dimitri Mavris**, Principal Investigator, Georgia Institute of Technology

**Dr. Michelle Kirby**, Co-Investigator, Georgia Institute of Technology

**Dr. Yongchang Li**, Research Faculty, Georgia Institute of Technology

**Dr. Tejas Puranik**, Research Faculty, Georgia Institute of Technology

**Dr. Mohammed Hassan**, Research Faculty, Georgia Institute of Technology

**Dr. Holger Pfaender**, Research Faculty, Georgia Institute of Technology





**Mr. David Anvid**, Research Faculty, Georgia Institute of Technology  
**Ameya Behere**, Graduate Student, Georgia Institute of Technology  
**Eleni Sotiropoulos-Georgiopoulos**, Graduate Student, Georgia Institute of Technology  
**Ayaka Miyamoto**, Graduate Student, Georgia Institute of Technology  
**Rukmini Roy**, Graduate Student, Georgia Institute of Technology  
**Jirat Bhanpato**, Graduate Student, Georgia Institute of Technology  
**Hyungu Choi**, Graduate Student, Georgia Institute of Technology  
**Bogdan Dorca**, Graduate Student, Georgia Institute of Technology  
**Zhenyu Gao**, Graduate Student, Georgia Institute of Technology  
**Santusht Sairam**, Graduate Student, Georgia Institute of Technology

## Project Overview

This project is providing data and methods to continue to improve the aircraft weight, takeoff thrust, and departure and arrival procedure modeling capabilities within the FAA’s Aviation Environmental Design Tool (AEDT). Some of the modeling assumptions in AEDT are considered overly conservative and could be improved using industry and airport flight operational data. This funding would continue to support the implementation of these methods and data into AEDT4. To facilitate this, the Georgia Tech team will utilize real-world data flight and noise monitoring data to improve departure, full flight, and arrival modeling. In addition, this research will provide the FAA Environment and Energy office with evaluations and assessments of AEDT’s future service pack releases.

## Task 1 – Improved Departure Modeling: High Altitude Airport Study

Georgia Institute of Technology

### Objectives

The conclusion of ASCENT Project 45 provided recommendations for noise abatement departure procedures (NADP) to be modeled in future versions of AEDT. While these procedures had been validated by comparison to real-world data at U.S. airports, it was not evident whether the recommended procedures would adequately represent operations at high altitude edge case airports. Project 54 aims to validate the recommended NADP profiles at very high-altitude airports

### Research Approach

#### Introduction

Very high-altitude airports present an edge case in terms of aircraft performance due to low ambient atmospheric temperatures, densities, and pressures. Such airports often require special considerations for operations such as limitations on max takeoff weight, use of modified flap, and reduced thrust settings. Hence, it is not evident whether the newly recommended NADP profiles would correctly represent real-world operations out of such airports. This task aims to verify whether the recommendations hold true, and what steps (if any) need to be taken to address any potential shortcomings.

#### Methodology

The validation dataset for this Task is Flight Operations Quality Assurance (FOQA) obtained from Georgia Tech’s airline partner. Subsequent considerations of airport and aircraft selection was based on the availability of associated data in the FOQA dataset. Based on an analysis of the metadata of all FOQA flights, the following high-altitude airports were selected for modeling in this Task:

**Table 1.** High altitude airports considered in this work

Airport Code	Location	Elevation, Mean Sea Level (MSL)
UIO/SEQM	Quito, Ecuador	7830 ft
MEX/MMMX	Mexico City, Mexico	7316 ft
JNB/JAOR	Johannesburg, South Africa	5558 ft
DEN/KDEN	Denver, Colorado	5433 ft

In this report, results are presented for 737-700 aircraft operations at MMMX airport. FOQA data contains information about the aircraft’s trajectory, thrust, weight, and numerous other characteristics. This information was compared against performance reports obtained from AEDT. AEDT simulations were set up to fly two NADP profile sets, NADP1\_1 and NADP2\_11. Each profile set contained the baseline profile definition along with alternate weight and reduced thrust versions. Detailed descriptions on the profile definitions are available in the 2019 ASCENT 45 Annual Report. Additionally, the default STANDARD profile set in AEDT was also modeled to serve as the baseline.

**Results and Discussion**

This section shows some of the preliminary results obtained in this research area. Figure 1, Figure 2, and Figure 3 show the comparison of trajectories, ground speed, and net corrected thrust, respectively, from AEDT profiles against the FOQA. These comparisons provide a visual comparison and a first assessment of the efficacy of NADP profiles at representing high altitude airport departure operations. Note that all FOQA flights are shown as solid lines in black color in all three figures.

The trajectory plot shows that the reduced thrust versions of profiles are a better representation of real-world flights than full thrust flights. Full thrust profile trajectories tend to be higher than the FOQA trajectories, due to the use of higher thrust levels. In the groundspeed plot, a wide variation is observed in the FOQA flights. The speed at liftoff for AEDT profiles tends to be lower, and the terminal speed at 10,000 ft above field elevation (AFE\_ altitude tends to be higher. A possible reason for this is the implication of wind speed in the calculation of groundspeed. AEDT assumes a constant headwind applied for all departure operations, whereas FOQA flights reflect actual wind conditions on the day of the flight, which leads to higher variability. In future analyses, true or calibrated airspeed will be used instead, which should eliminate this source of difference. Finally, the net corrected thrust comparisons also show better agreement with the reduced thrust profile versions at lower altitudes. Real-world thrust tends to be higher than AEDT in the latter half of the departure operation.

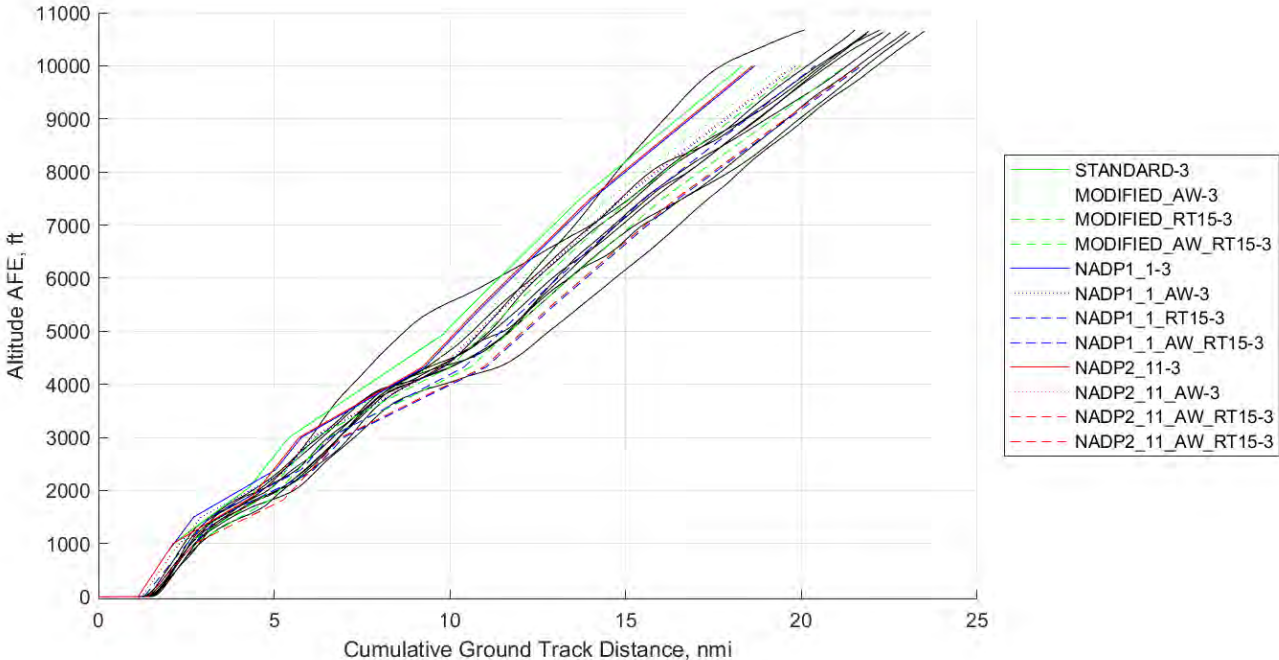


**Figure 1.** Flight trajectories from AEDT profile sets compared with FOQA flight data.

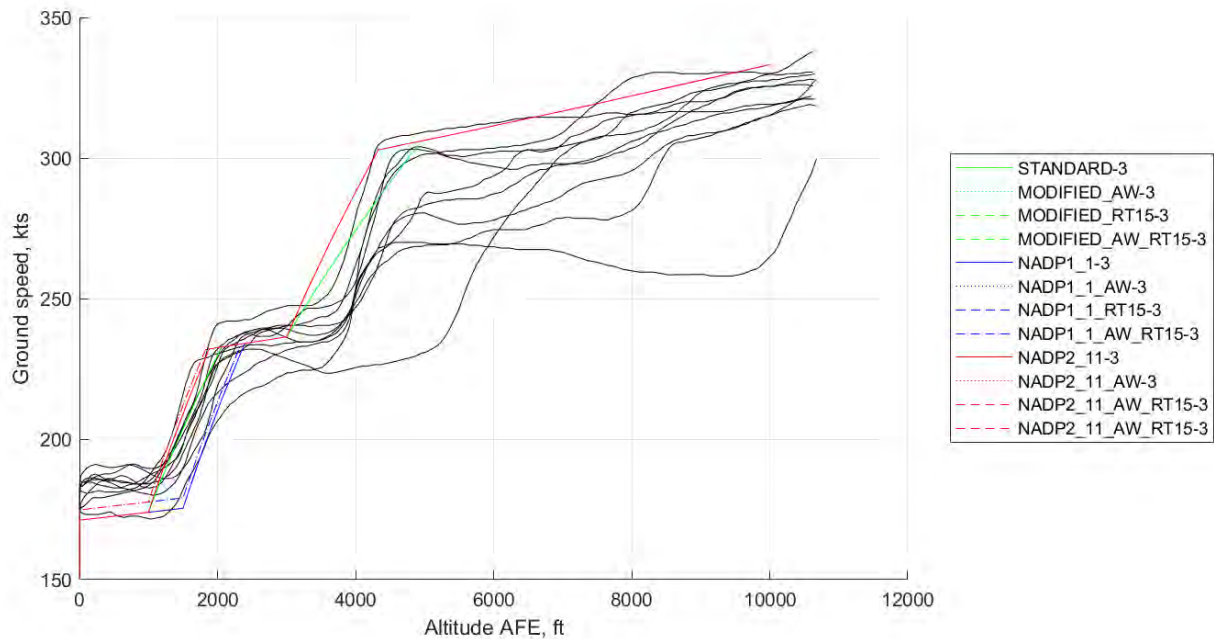


Figure 2. Groundspeed variation from AEDT profile sets compared with FOQA flight data.

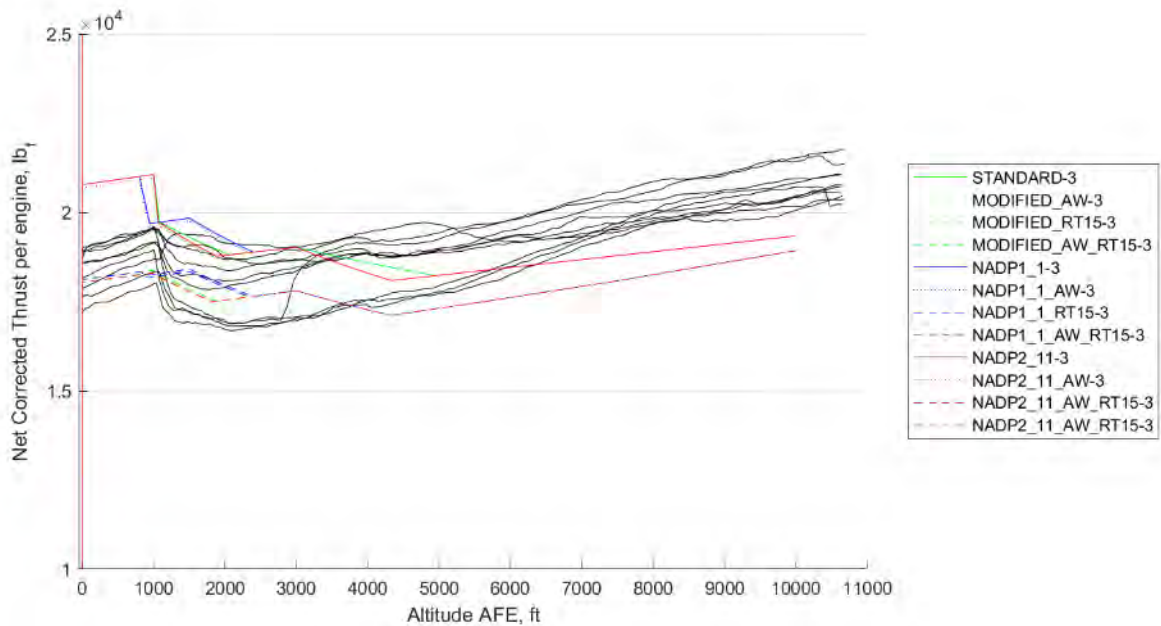


Figure 3. Thrust variation from AEDT profile sets compared with FOQA flight data.

Overall, initial comparative analysis shows that the reduced thrust variants of AEDT profile sets seem to reasonably represent real-world operations at high altitude airports. Additional analyses at other airports and with other aircraft types will be conducted.



## Task 1 – Improved Departure Modeling: Refinement of Thrust and Weight Assumptions

Georgia Institute of Technology

### **Objectives**

The objective of this Task is to use the new FOQA data to analyze previous takeoff thrust and weight assumptions and compare the results to previous years' weight model and thrust reduction models.

### **Research Approach**

#### ***Weight Assumptions***

#### **Introduction**

In this step, various linear, multilinear, and quadratic regression models have been used to determine relations between aircraft takeoff weights and Great Circle Distance (GCD), airport elevation, and runway length for each airframe of the FOQA data.

#### **Methodology**

First, it was necessary to clean and gather the takeoff weight, takeoff runway length, runway elevation, and GCD for each flight. According to the results from the ASCENT Project 35 team, it has been decided to neglect the presence of “tankered fuel”. Additionally, all flights with a GCD lower than 50 nmi were not considered since they correspond to repositioning or test flights. Finally, recording errors such as null or blank values were removed.

For each airframe, the following regression models were applied first to all data and later to the data averaged for each city-pair:

- $TOW=A0 \cdot GCD$
- $TOW=A1 \cdot GCD+A2 \cdot RXYlength+A3 \cdot RWYelev+A4$
- $TOW=A5 \cdot GCD^2+A6 \cdot GCD+A7$

#### **Results and Discussion**

Some of the plots obtained are presented in Figure 4. It is impossible to plot the results of multilinear regressions in 2D so only linear (in black) and quadratic (in red) regressions were plotted. On the non-averaged data, clusters of points can be observed. They correspond to data for the same city-pair, since those clusters are not present on the averaged plots.

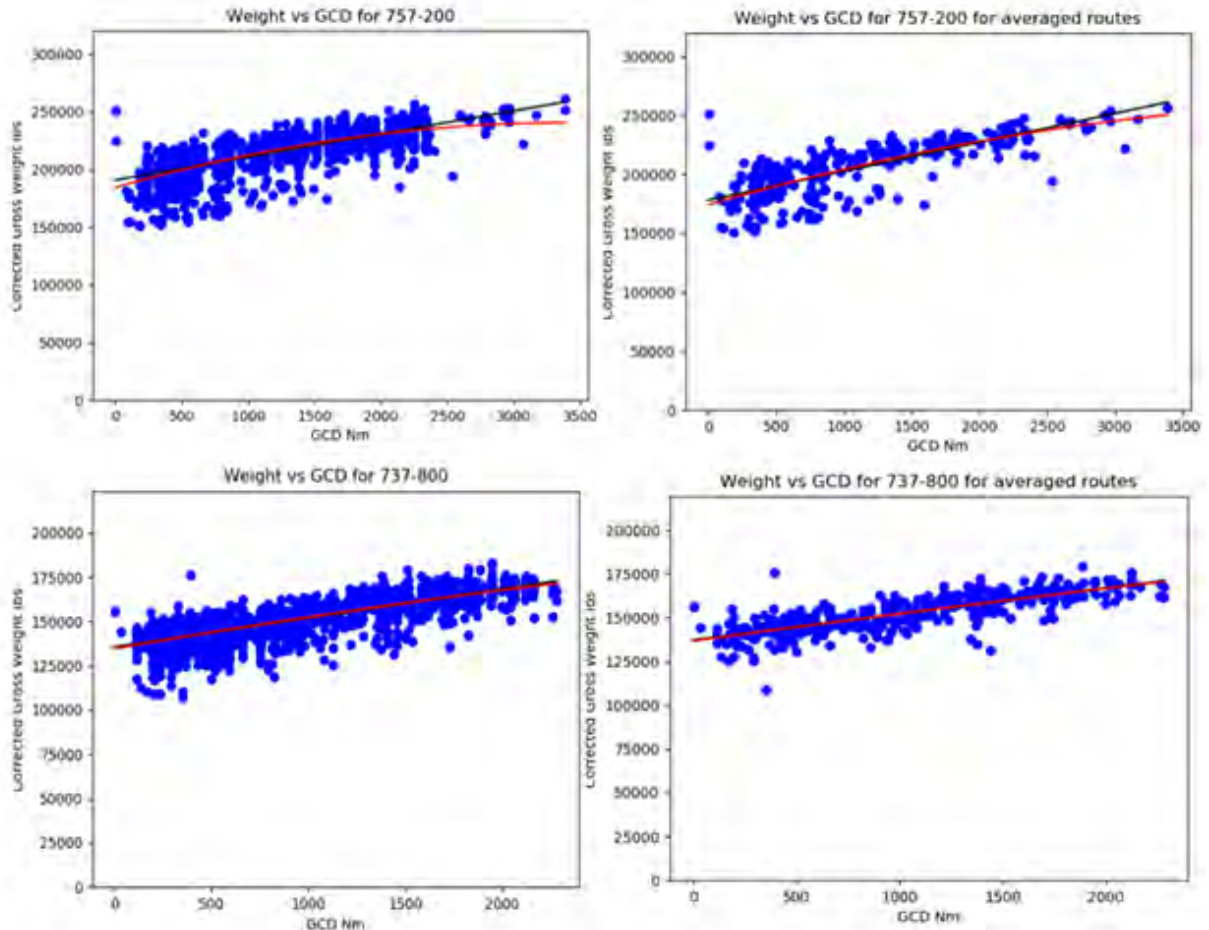


Figure 4. Weight versus GCD for 757-200 and 737-800.

The  $R^2$  and regression coefficients for each airframe and model are presented in the following table. The model that provides the best  $R^2$  for each airframe is highlighted in green. For those airframes that present low  $R^2$  values, two causes have been identified. First, some airframes have a small set of data points especially once averaged by city-pair. In addition, for short-range flights, there is more variability in the flight path since the departure and arrival procedures account for a larger share of the flight duration. The GCD does not take this variability into account.



Table 2. Regression results for all airframes

Airframe	Number of data points	Averaged by city-pair ?	Model	R <sup>2</sup>	Reg. Coeff. Weight	Reg. Coeff. elevation	Reg. Coeff. length	Reg. Coeff. quadratic Weight	Intercept
717-200	1992	No	Linear	0.300	12.289				98828.255
	1992	No	Quadratic	0.302	16.959			-0.004	97827.283
	304	Yes	Linear	0.320	11.088				99084.854
	304	Yes	Quadratic	0.355	26.178			-0.013	95738.690
	1992	No	Multi-	0.303	12.440	0.169	0.052		98027.002
	304	Yes	Multi-	0.321	11.061	-0.128	0.084		98367.382
737-700	114	No	Linear	0.502	10.685				123545.482
	114	No	Quadratic	0.507	15.221			-0.003	122361.263
	36	Yes	Linear	0.582	11.718				122579.044
	36	Yes	Quadratic	0.589	17.727			-0.004	120919.474
	114	No	Multi-	0.513	11.683	-0.394	0.098		122601.269
	36	Yes	Multi-	0.605	12.247	-0.295	0.500		117732.292
737-800	1926	No	Linear	0.617	16.373				135604.861
	1926	No	Quadratic	0.618	18.993			-0.001	134652.489
	389	Yes	Linear	0.627	14.864				137201.305
	389	Yes	Quadratic	0.627	16.027			-0.001	136742.694
	1926	No	Multi-	0.617	16.332	-0.017	0.162		133917.782
	389	Yes	Multi-	0.629	14.701	-0.317	0.189		135679.033
737-900	4844	No	Linear	0.624	16.807				143685.984
	4844	No	Quadratic	0.631	25.170			-0.004	140155.187
	388	Yes	Linear	0.647	15.365				143919.400
	388	Yes	Quadratic	0.647	16.234			0.000	143583.782
	4844	No	Multi-	0.629	16.316	-0.695	0.290		141795.918
	388	Yes	Multi-	0.658	15.058	-0.972	0.100		144072.997
757-200	1917	No	Linear	0.551	20.026				190667.481
	1917	No	Quadratic	0.565	32.645			-0.005	184338.703
	279	Yes	Linear	0.594	24.507				178122.597
	279	Yes	Quadratic	0.600	33.219			-0.003	174091.182
	1917	No	Multi-	0.556	20.087	0.868	0.503		184783.691
	279	Yes	Multi-	0.606	24.229	0.338	1.503		162850.011
757-300	478	No	Linear	0.496	21.857				208133.502
	478	No	Quadratic	0.513	40.764			-0.007	196485.663
	65	Yes	Linear	0.743	22.041				205428.409
	65	Yes	Quadratic	0.754	33.167			-0.004	199346.141
	478	No	Multi-	0.523	22.644	4.016	-0.524		209435.976
	65	Yes	Multi-	0.759	22.782	2.674	-0.644		209642.511
777-200LR	414	No	Linear	0.946	36.796				447798.275
	414	No	Quadratic	0.947	45.895			-0.001	435869.424
	47	Yes	Linear	0.831	41.091				431553.113
	47	Yes	Quadratic	0.835	52.819			-0.002	419400.774
	414	No	Multi-	0.947	38.713	-1.133	-2.231		470286.019
	47	Yes	Multi-	0.833	42.183	-2.223	-1.422		447037.943



Airframe	Number of data Points	Averaged by city-pair ?	Model	R <sup>2</sup>	Reg. Coeff. Weight	Reg. Coeff. elevation	Reg. Coeff. length	Reg. Coeff. quadratic Weight	Intercept
777-200ER	466	No	Linear	0.821	39.582				408355.484
	466	No	Quadratic	0.823	47.728			-0.001	396925.470
	56	Yes	Linear	0.798	42.299				399177.803
	56	Yes	Quadratic	0.806	59.856			-0.003	381719.896
	466	No	Multi-Linear	0.824	36.967	-14.003	1.453		404666.877
	56	Yes	Multi-Linear	0.798	42.138	-0.821	0.101		398848.892
A319-100	737	No	Linear	0.453	14.016				126774.658
	737	No	Quadratic	0.465	22.795			-0.005	123897.936
	234	Yes	Linear	0.486	13.214				127165.200
	234	Yes	Quadratic	0.507	22.902			-0.006	124012.509
	737	No	Multi-Linear	0.458	13.574	-0.324	0.067		126872.635
	234	Yes	Multi-Linear	0.489	13.124	0.047	0.227		124873.896
A320-200	957	No	Linear	0.476	18.216				133517.487
	957	No	Quadratic	0.482	26.469			-0.005	130459.344
	257	Yes	Linear	0.543	17.657				133157.523
	257	Yes	Quadratic	0.544	20.887			-0.002	132082.854
	957	No	Multi-Linear	0.488	17.509	-0.826	0.281		132111.273
	257	Yes	Multi-Linear	0.576	16.966	-1.398	0.496		130056.908
A321-200	325	No	Linear	0.584	17.724				157855.198
	325	No	Quadratic	0.584	17.002			0.000	158128.635
	92	Yes	Linear	0.600	16.376				158043.767
	92	Yes	Quadratic	0.604	9.394			0.004	160688.378
	325	No	Multi-Linear	0.584	17.666	-0.194	0.033		157747.549
	92	Yes	Multi-Linear	0.611	16.004	-0.846	0.471		154241.818
A330-200	491	No	Linear	0.794	31.086				341722.638
	491	No	Quadratic	0.812	49.715			-0.003	313121.055
	50	Yes	Linear	0.773	33.933				332352.394
	50	Yes	Quadratic	0.781	46.419			-0.002	320536.934
	491	No	Multi-Linear	0.796	30.539	-1.227	1.563		324727.594
	50	Yes	Multi-Linear	0.794	33.226	6.560	5.220		269574.853
A330-300	825	No	Linear	0.730	33.263				365027.300
	825	No	Quadratic	0.736	47.597			-0.003	349744.170
	98	Yes	Linear	0.641	34.518				353201.106
	98	Yes	Quadratic	0.642	28.616			0.001	357686.442
	825	No	Multi-Linear	0.733	32.734	0.386	1.818		345171.378
	98	Yes	Multi-Linear	0.662	32.314	-3.856	6.163		289707.955
MD-90	1860	No	Linear	0.466	20.927				132849.562
	1860	No	Quadratic	0.468	26.751			-0.004	131076.817
	227	Yes	Linear	0.518	19.644				133280.083
	227	Yes	Quadratic	0.518	22.243			-0.002	132593.858
	1860	No	Multi-Linear	0.479	21.240	-1.181	0.573		128177.782
	227	Yes	Multi-Linear	0.542	20.001	-1.239	0.569		128638.373



**Table 3.** Comparison with ASCENT 35 results for B757-200 and B737-800

Airframe			Number of flights	R <sup>2</sup>	Reg. Coeff. Weight	Reg. Coeff. elevation	Reg. Coeff. length	Intercept
757-200	Ascent 035 Report	All flights	45343	0.662				
		Average per city-pair	376	0.828	19.188	0	0.364	175571.496
	FOQA Data	All flights	1917	0.556	20.087	0.868	0.503	184783.691
		Average per city-pair	279	0.606	24.229	0.338	1.503	162850.011
Difference (average by city-pair model)				0.222	-5.041	-0.338	-1.139	12721.485
% Difference (average by city-pair model)				-36.6%	20.8%	100.0%	75.8%	-7.8%
737-800	Ascent 035 Report	All flights	33933	0.569				
		Average per city-pair	467	0.812	14.88	-0.094	0.625	128007.473
	FOQA Data	All flights	1926	0.617	16.332	-0.017	0.162	133917.782
		Average per city-pair	389	0.629	14.701	-0.317	0.189	135679.033
Difference (average by city-pair model)				0.183	0.179	0.223	0.436	-7671.56
% Difference (average by city-pair model)				-29.1%	-1.2%	70.3%	-230.7%	5.7%

Compared to previous years’ results, the FOQA data provides a significantly lower number of data points. The order of magnitude for each regression coefficient stay the same.

**Thrust assumptions**

**Introduction**

In this step, takeoff thrust data were used to determine reduced thrust distribution for each airframe.

**Methodology**

First, the data were cleaned by removing data recording errors, missing elements, and flight with a GCD lower than 20 nmi since they correspond to maintenance or repositioning flights. To limit computation time, it has been decided to only consider thrust values during takeoff roll when the speed of the aircraft is between 80 kts and 110 kts. The maximum calculated net corrected average thrust value, which is the thrust corrected for pressure difference, in this segment has been used. For each airframe, a histogram of takeoff thrusts has been plotted. The goal is then to obtain the reduced thrust percentage by dividing each thrust value by the maximum takeoff thrust of each airframe. However, this requires some tuning that has not been accomplished yet.

**Results and Discussion**

Histograms appear in the following Figures 5 and 6. It is important to check the total number of flights for each airframe before looking at thrust histograms. City-pairs and date and time can also create visible patterns on the thrust distributions.

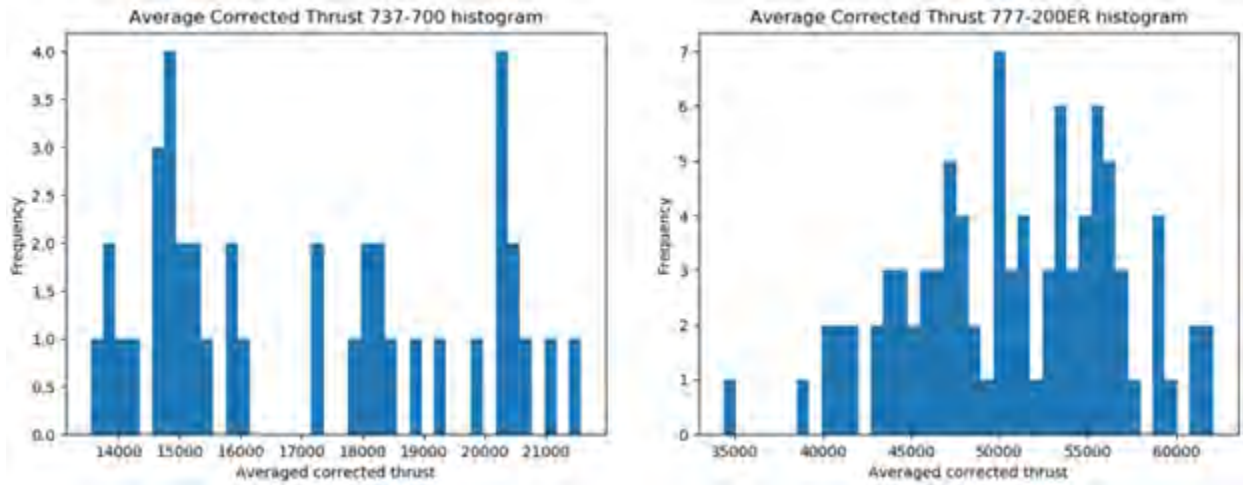


Figure 5. Thrust distributions for B737-700 and B777-200ER.

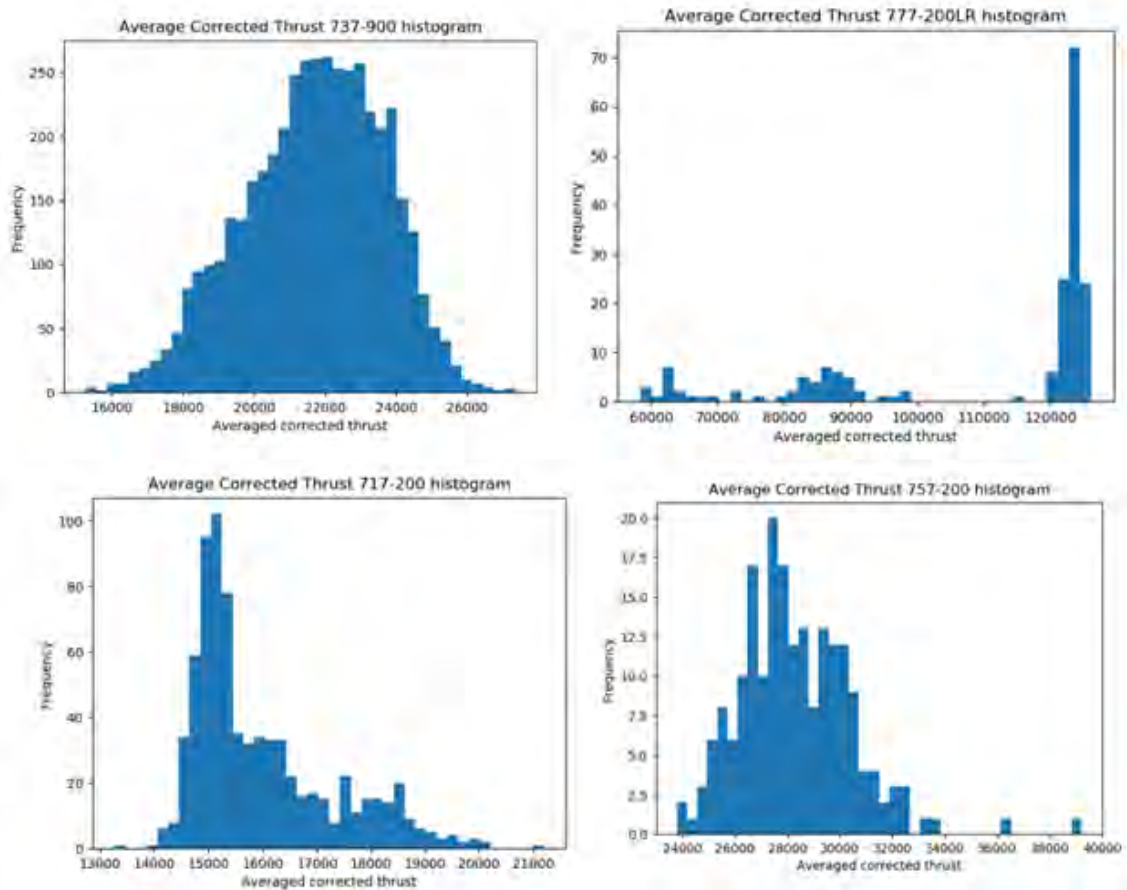
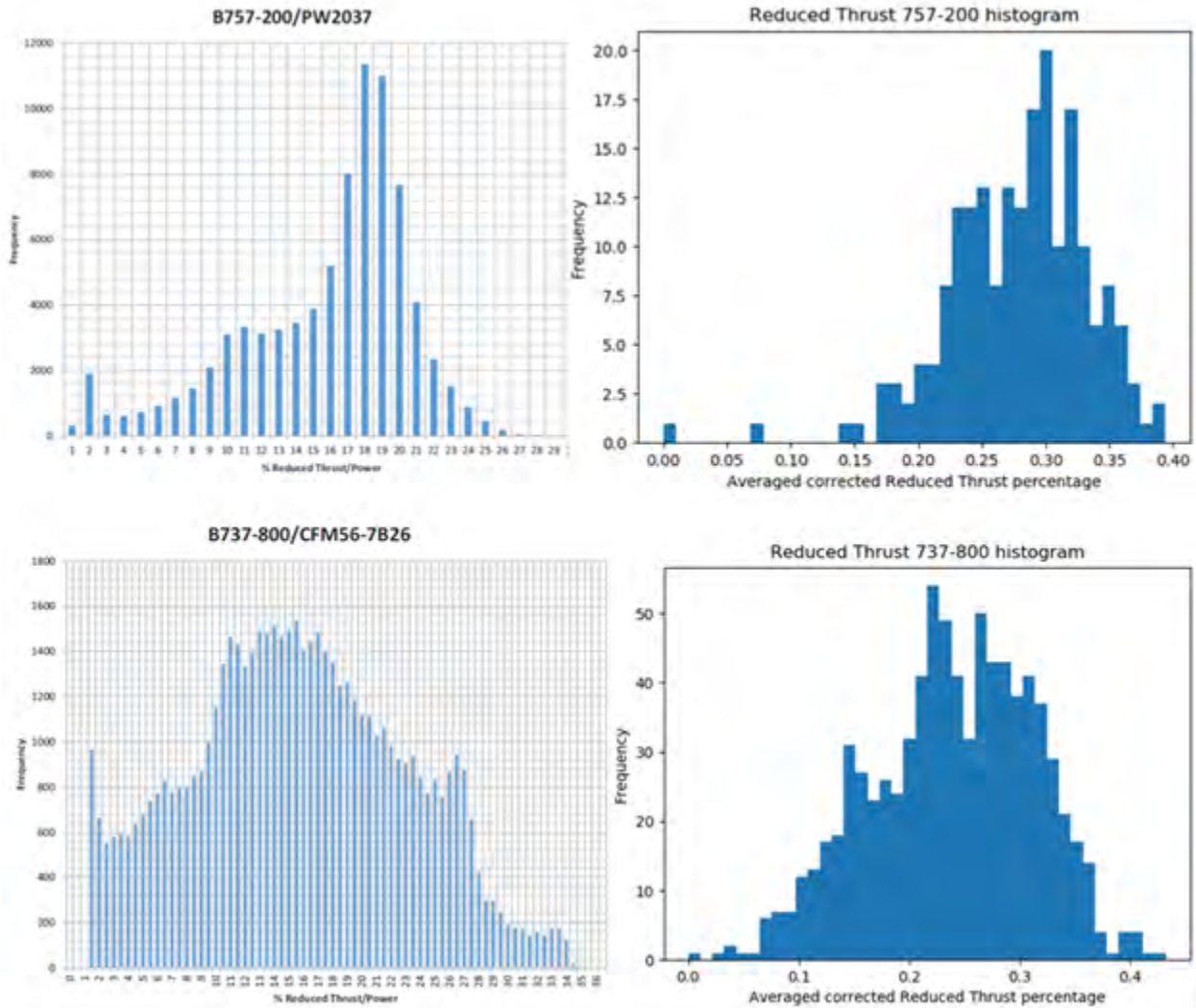


Figure 6. Thrust distributions for B737-900, B777-200LR, B717-200 and B757-200.



For the 777-200LR, we can observe a thrust distribution that is coherent with a long-range aircraft. Indeed, these aircraft almost always takeoff with the maximum fuel possible, which means maximum weight and thus maximum thrust. In the case of the 717-200, we observe the opposite trend. Since this aircraft is used for short-range flights, the maximum quantity of fuel is not required, therefore the maximum thrust at takeoff is not necessary. The 757-200 is another interesting case to study. Indeed, it is overpowered since it uses derated 767 engines. As a result, it always takes off at a reduced thrust. It also provides a comparison with previous years' results since this airframe was studied by ASCENT Project 35 in 2016, shown in Figure 7.



**Figure 7.** Comparison between ASCENT 35 and FOQA data thrust reduction results.

A comparison with previous year's results validates the shape of our thrust reduction distribution. Therefore, despite the small number of FOQA data points available, the observations are still consistent.

# Task 1 – Improved Departure Modeling: Estimation of Thrust Using ANP Equations

Georgia Institute of Technology

### Objectives

This research aims to develop regressions from FOQA data to obtain coefficients sets for the aircraft noise and performance (ANP) thrust equation. With these sets of coefficients, thrust can be estimated for flights based on radar/ADS-B tracking sources. This effort is directed at enabling estimation of thrust for threaded track or radar flights for which detailed information might not be available to model a fixed-point profile in AEDT.

### Research Approach

#### Introduction

The ANP thrust equations are used by AEDT as part of its performance model. The equation assumes that the net corrected thrust depends on a constant term, a linear dependency on airspeed and temperature, and a quadratic dependency on altitude. The equation is:

$$\frac{F_n}{\delta} = E + Fv + G_A h + G_B h^2 + HT$$

Where

$\frac{F_n}{\delta}$  is the net corrected thrust per engine (lbf)

$v$  is the equivalent/calibrated airspeed (kt)

$h$  is the pressure altitude MSL (ft)

$T$  is the temperature at the aircraft (°C)

$E, F, G_A, G_B, H$  are regression coefficients that depend on power state and temperature state

Typically, the regression coefficients are available in a database and can be used to compute the thrust value at various points in the aircraft trajectory. Here, thrust data is available in the FOQA data, and hence the regression coefficients can be estimated using a simple linear regression technique.

#### Methodology

The overall methodology for this task follows these steps:

1. Group FOQA data by aircraft type.
2. Isolate departure and arrival sections of each flight. Note that ANP performance models are only applicable in the terminal area (below 10,000 ft altitude), therefore the regression should only be applied to the dataset which conforms to these limits.
3. Identify power mode of the aircraft using normalized thrust lever angle (NTLA) variable in the FOQA data.
4. Perform linear regression on the data grouped by power mode to obtain the set of regression coefficients.
5. Use coefficients for thrust prediction.

### Results and Discussion

Some preliminary results have been obtained for step 3 of the methodology. Identification of the power mode of the aircraft requires grouping data by the NTLA variable. At present, AEDT contains six power modes for departure for most jet aircraft. These are outlined in Table 4.

**Table 4.** Description of ANP Thrust Codes and corresponding ranges in FOQA

ANP Thrust Code	Description	Range for NTLA
T	Full takeoff thrust	97.5% and above
F	5% reduced takeoff thrust	92.5% to 97.5%
X	10% reduced takeoff thrust	87.5% to 92.5%
Z	15% reduced takeoff thrust	82.5% to 87.5%
C	Full climb thrust	82.5% and below
D	10% reduced climb thrust	Not considered

One final data processing step is to remove the transient periods where the thrust is not stabilized. This was done by performing an analysis on the NTLA values, using finite differences to calculate derivatives. The time derivative was calculated using three finite difference formulas, the forward, central, and backward difference, respectively.

$$\frac{NTLA_{i+1} - NTLA_i}{t_{i+1} - t_i}, \frac{NTLA_{i+1} - NTLA_{i-1}}{t_{i+1} - t_{i-1}}, \frac{NTLA_i - NTLA_{i-1}}{t_i - t_{i-1}}$$

By applying a suitable threshold to these computed derivatives, unsteady regions of thrust can be identified and eliminated. Figure 8 shows the outcome of this process and its effect on the sampled trajectory altitude and airspeed. Once transient thrust data is removed, the remaining dataset can easily be grouped based on the ranges specified in Table 4.

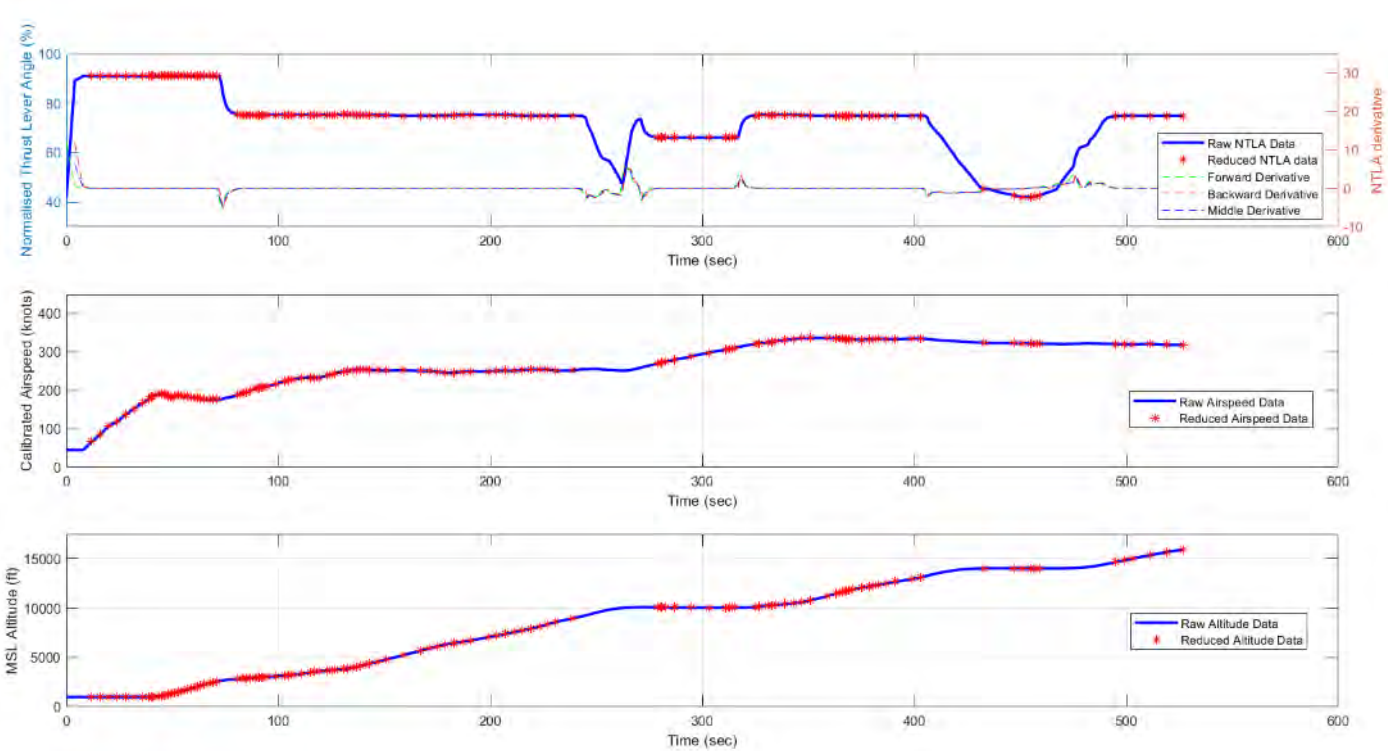


**Figure 8.** Filtering of FOQA data with finite difference time derivatives of NTLA.

This work is currently in progress and the next steps focus on the computation of the thrust coefficients using regression models.

# Task 1 – Improved Departure Modeling: Comparison of NADP Profiles to Real-world Operations

Georgia Institute of Technology

### Objective

Prior research in ASCENT Project 45 provided recommendations for NADPs to be modeled in future versions of AEDT. Comparisons were made between NADP profiles within the NADP library to determine the differences between each profile. As a result, the six NADP-1 and thirteen NADP-2 profiles were reduced to two profiles that are most representative of the variability among each group of NADPs. This task aims to investigate similarity between the recommended NADPs and real-world departure operations.

### Research Approach

Previous research efforts made in ASCENT Project 45 computed comparisons between the six NADP-1 and thirteen NADP-2 profiles defined in the NADP library. These profiles were modeled in AEDT for the B737-800, A320-211, and A330-301 at stage lengths 1, 3, and 5. NADP-1 profile 1 and NADP-2 profile 11 were found to be most representative, based on their ability to capture variability across all NADP profiles within their respective groups. However, comparisons between the two recommended NADP profiles and real-world operations are needed to ensure that the recommended NADP profiles are representative of real-world operations. For the purposes of this task, comparisons are made for the three airframes with NADP profiles already modeled in AEDT only. Table 5 outlines the 18 combinations of NADP settings to be used for comparison.

Table 5. NADP profiles to be compared.

NADP Type	Profile Number	Stage Length	Airframe
NADP-1	1	1, 3, 5	B737-800, A320-211, A330-301
NADP-2	11		

To accomplish this task, the trajectories to be compared are processed to align data points and remove anomalous flights. Next, the trajectories are grouped by airframe and stage length to enable comparisons between similar operating procedures across the two datasets. Comparison metrics are then computed between real and NADP trajectories for each grouping, enabling their similarities to be investigated. Figure 9 provides an overview of this approach.

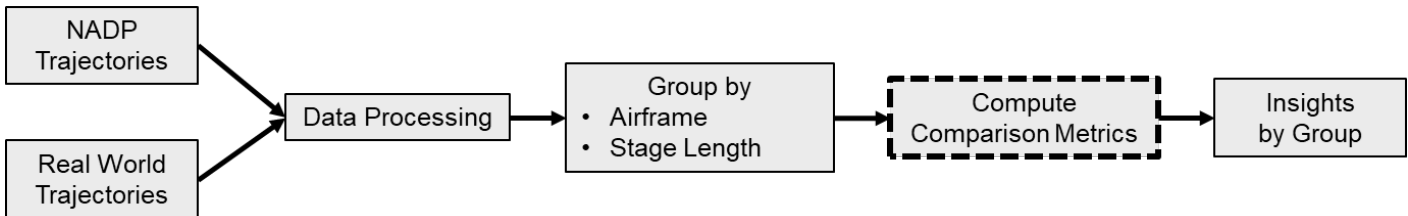


Figure 9. Summary of overall approach.

### Real-world Dataset

The real-world data to be utilized was obtained from publicly available OpenSky ADS-B data, which contains radar-tracked aircraft trajectories. For the purposes of this task, an OpenSky ADS-B dataset with one full year of departure operations from all airlines operating the B737-800, A320-211, and A330-301 at SFO for the year 2019 was selected for comparison. This real-world dataset contains a total of 8,517 flights operated by 23 airlines.

Performance-based parameters such as altitude and ground speed are readily available in this dataset. Due to the nature of radar-track data, important performance metrics which define operating conditions such as thrust and weight for each flight are missing. Flight great-circle distance computed from origin-destination pair was identified as a proxy for weight. Each flight within this dataset contains trajectory information sampled up to 25 nautical miles of cumulative ground track distance.

To accurately make comparisons, different operating conditions must be grouped and analyzed separately. The grouping parameters identified are airframe and flight great-circle distance. Because AEDT estimates weights by bins of stage lengths, flight distance was converted into stage lengths as defined by Table 6. The distribution of stage lengths by airframe is illustrated in Figure 10. Notably, only the B737-800 contains flights operated at stage length 5 and the A330 contains much smaller number of flights operated at only stage lengths 4, 6, and 7. By grouping the trajectories, direct comparisons to NADP profiles modeled for different airframes at varying stage lengths can be made. In future iterations, differences in operating procedures between airlines can also be investigated by further grouping the dataset by operator.

**Table 6.** Stage length bin definition

Stage Length	Flight Great-Circle Distance [nmi]
1	0-500
2	500-1,000
3	1000-1,500
4	1500-2500
5	2500-3500
6	3500-4500
7	4500-5500
8	5500-6500
9	6500-11,000
M	Maximum range at maximum takeoff weight

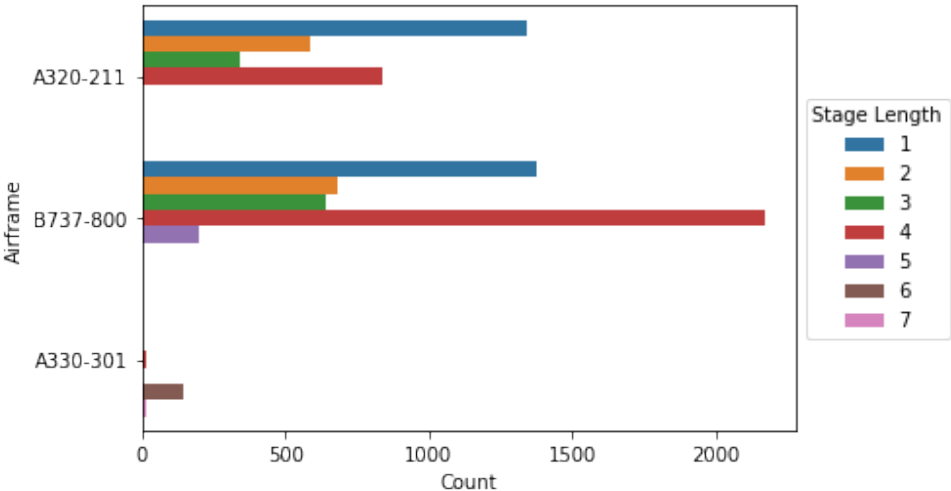


**Figure 10.** Number of flights by airframe and stage length in the real-world dataset.

**Data Processing**

The real-world dataset must be preprocessed to remove anomalous flights and adjusted such that pairwise comparison can be made against NADPs. Anomalous trajectories can be identified by examining the final altitude and the takeoff distance based on expected behaviors. Specifically, flights that do not cross 10,000 ft above ground level (AGL) at cumulative ground track distance of 25 nmi or have takeoff ground-roll segment greater than the maximum runway length of two nmi at SFO are removed from the comparison. Using this procedure, 2.88% of the flights are identified as anomalous, as shown in Figure 11.

Additionally, several flights contain marginally negative altitude data points during ground roll which can safely be shifted to 0 ft AGL. The remaining variation in the ground-roll segment can then be used to capture the effect of weight on takeoff distance. Finally, real-world trajectories exhibit climb acceleration beyond 10,000 ft AGL which is not modeled in the NADP profiles as illustrated in Figure 12. To avoid making comparisons beyond the departure segment, the trajectory of each flight is capped at 10,000 ft.

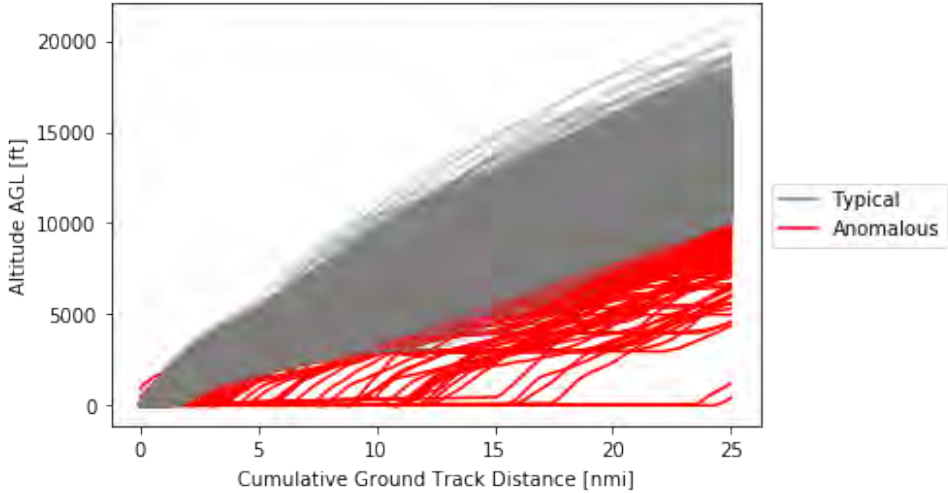


Figure 11. Real-world flights classified as anomalous and removed from comparison.

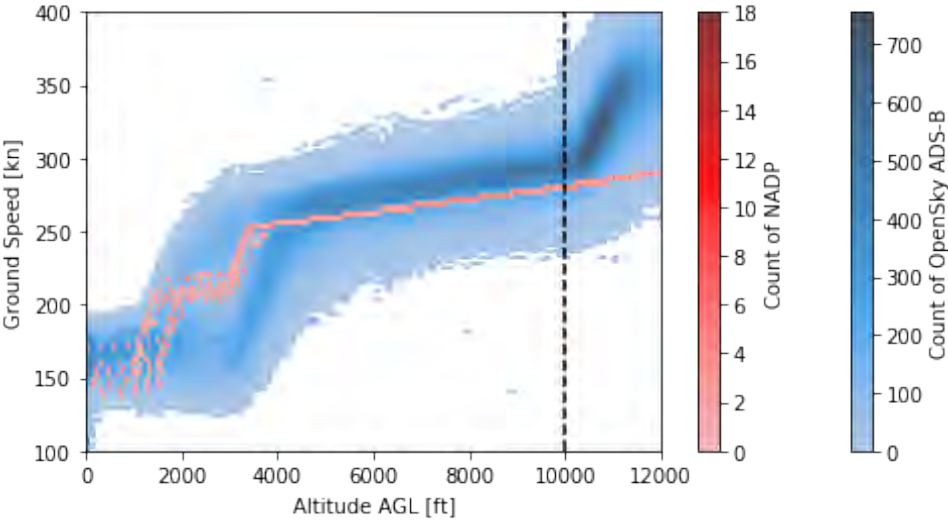
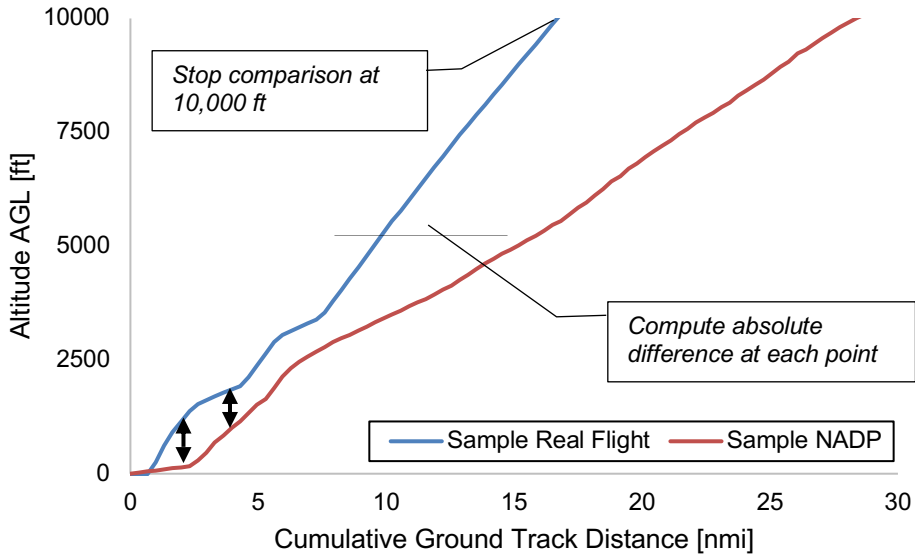


Figure 12. Distribution of ground speed as a function of altitude above ground level (AGL).

**Comparison Metrics**

In this task, altitude and ground speed profiles are utilized to compute comparison metrics as these parameters are already available across both the real-world and NADP datasets. In future iterations of this task, noise- and emissions-based metrics can be utilized as additional metrics once the real-world profiles have been sufficiently reduced to a feasible number of representative operating procedures and modeled in AEDT. This may be accomplished using clustering algorithms on existing metrics.

To facilitate computation of profile differences, profiles from both datasets are resampled using linear interpolation to align each point at a fixed cumulative ground track distance increment of 0.33 nmi. This enables computation of pairwise absolute differences at each data point along the profiles. Figure 13 visualizes this comparison process and Figure 14 provides examples for B737-800 comparison.



**Figure 13.** Trajectory comparison method visualization.

Because comparison is capped at 10,000 ft AGL, the number of data points per profiles being compared varies depending on the vertical speed. A flight that is rapidly climbing will reach 10,000 ft AGL at a shorter cumulative ground track distance and hence contain a smaller number of data points. For the current datasets, this yields a median of 49 data points per comparison.

To mitigate this, a root-mean-squared (RMS) based methodology is employed as an overall measure of discrepancy between any two profiles being compared, where  $x$  represents the comparison metric of interest and  $n$  is the minimum number of data points between either profile.

$$x_{rms} = \sqrt{\frac{\sum_{i=0}^n (x_{Real,i} - x_{NADP,i})^2}{n}}$$

The resulting RMS values indicate how separated the profiles are from each other on average, with higher values implying larger separation. Two matrices of altitude and speed RMS difference between real profiles and NADPs are then generated for each airframe. Then, the resulting RMS matrices are joined with meta data from the real-world trajectories to aggregate comparisons by stage length and by airline.

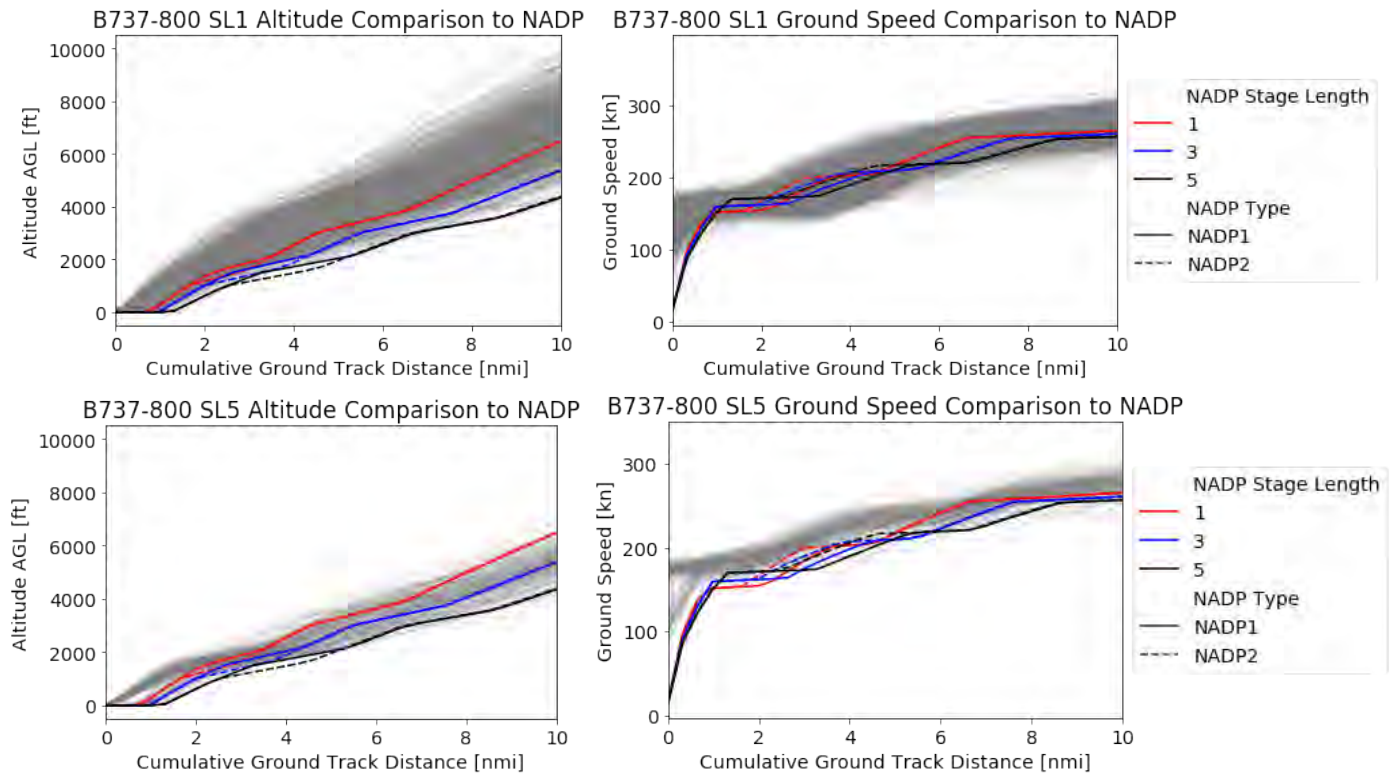
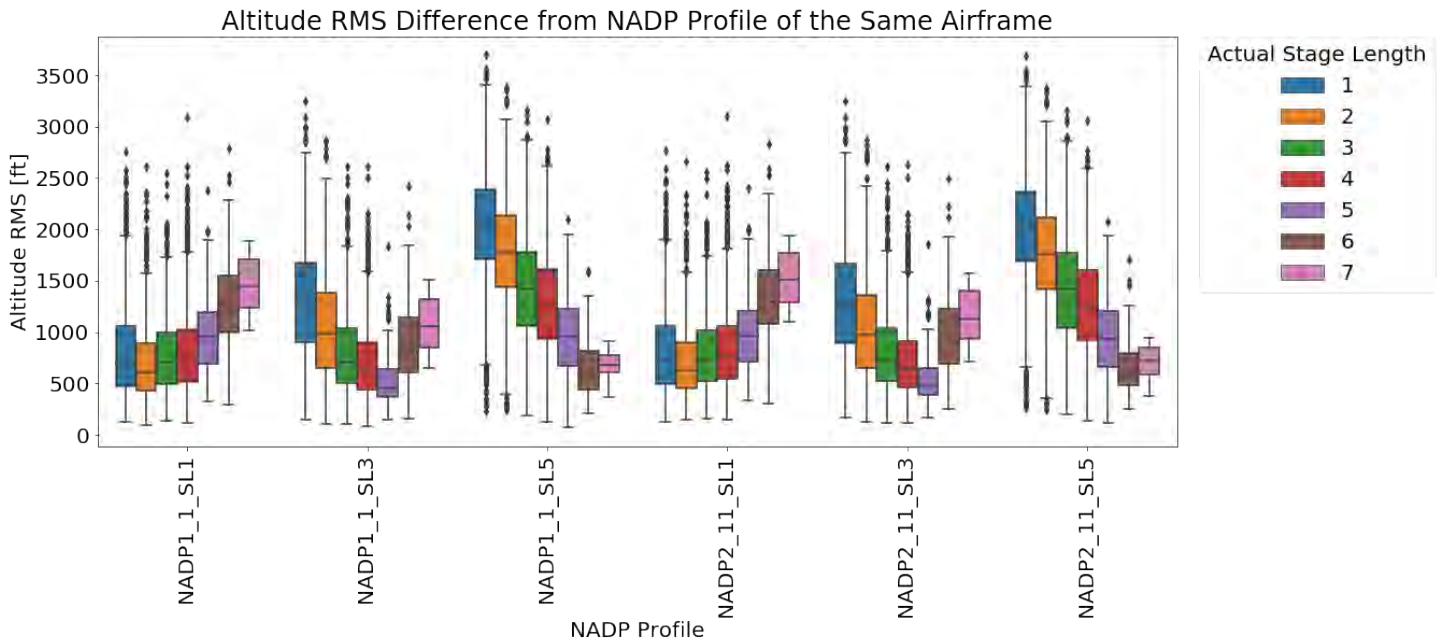


Figure 14. Sample comparison between NADP and real B737-800 flights

### Results and Discussion

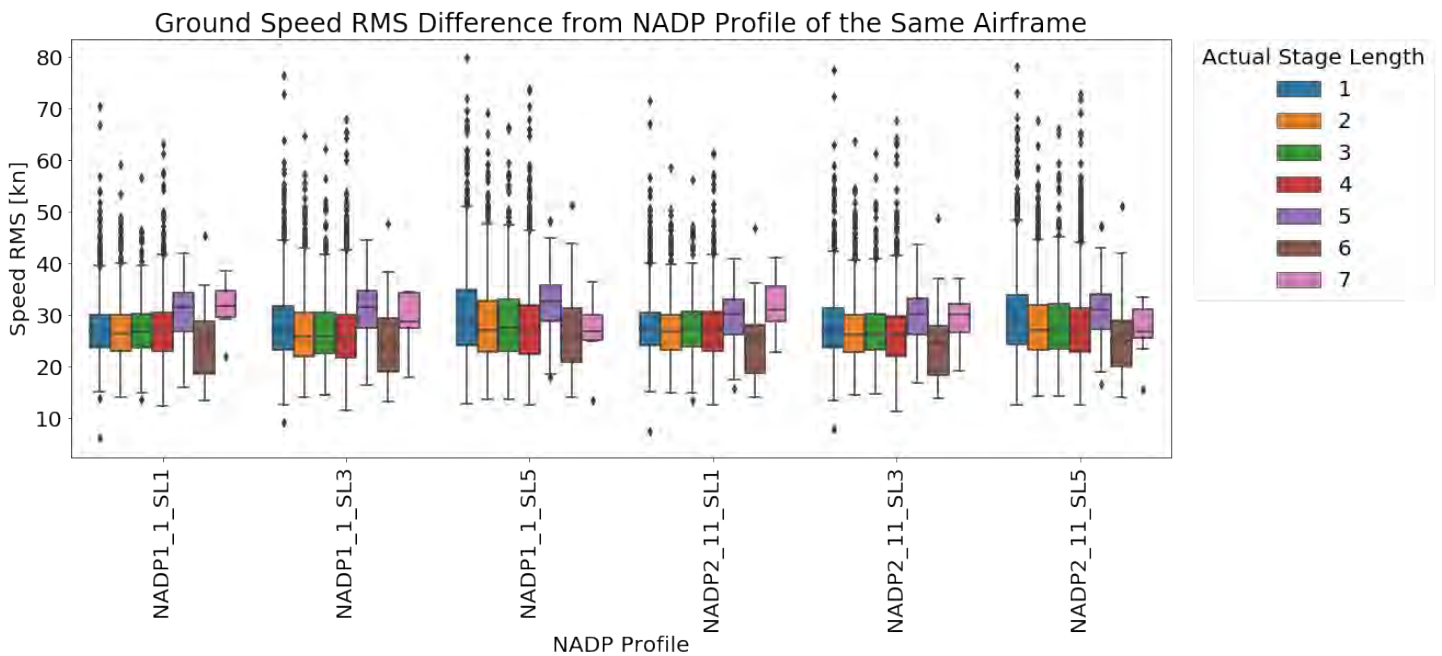
The resulting RMS differences between each real flight and each NADP profile are aggregated by comparison grouping. The grouped results are then visualized using boxplots. Figure 15 and Figure 16 illustrates the aggregated results where each box represents a distribution of RMS for all airframes (compared to NADP modeled using the same airframe) at a given stage length. Results separated by airframe are presented in Table 7 and Table 8. Such visualization enables the median and the interquartile range (IQR) of RMS distributions by group to be compared. The points plotted outside of the boxplot whiskers indicate outliers. Any RMS below  $Q1 - 1.5IQR$  or above  $Q3 + 1.5IQR$  are classified as outliers.

Figure 15 illustrates that varying NADP stage length noticeably influences altitude RMS. This makes intuitive sense since higher stage lengths imply higher weight and hence affect the altitude profile. When NADP is modeled at stage length 1, the resulting RMS distributions indicate that the profile is most similar to real flights flown at stage length 2 as indicated by the medians. At NADP stage lengths 3 and 5, real flights flown at stage length 5 and become the most similar, respectively. In all three NADP stage length cases, the distributions of RMS show an increasing shift when compared to other real flight stage lengths with increasing stage length difference. This trend is reflected across both NADP-1 profile 1 and NADP-2 profile 11. This result implies that NADP altitude profiles are generally more similar to real profiles flown at higher stage lengths. However, this does not imply that NADP altitude profiles are lower or higher than real profiles since RMS computation involves squaring the differences.



**Figure 15.** Altitude RMS difference from NADP profiles computed per airframe and grouped by stage length.

Figure 16 illustrates that varying NADP stage length result in marginal variation in ground speed RMS. This indicates that the results found for altitude RMS can be attributed to mostly differences in vertical speed utilized at different stage lengths. Furthermore, real flights flown at stage lengths 1-4 appear to be equally similar to NADP in all cases while stage lengths 5-7 deviate from this trend. This could be due to the lack of real flight data flown at stage lengths 5-7. Stage length 5 only contains flights flown by one airline using the B737-800 and stage lengths 6-7 only contain flights flown by A330-301, which has a much smaller number of flight records as shown in Figure 10.



**Figure 16.** Ground speed RMS difference from NADP profiles computed per airframe and grouped by stage length.



Table 7. Summary of median RMS differences for NADP-1 profile 1

NADP Profile	Actual Stage Length	Median Altitude RMS [ft]			Median Ground Speed RMS [kn]		
		A320-211	B737-800	A330-301	A320-211	B737-800	A330-301
NADP1_1_SL1	1	673.11	738.71		26.97	26.54	
	2	650.4	567.08		26.88	26.03	
	3	737.63	687.56		27.98	26.25	
	4	836.3	710.79	726.74	27.69	26.22	27.73
	5		955.25			31.5	
	6			1221.04			24.84
	7			1447.89			31.64
NADP1_1_SL3	1	1197.28	1368.38		27.19	26.58	
	2	972.85	998.47		25.96	25.7	
	3	701.52	713.78		26.16	25.86	
	4	659.08	612.47	1137.23	25.94	25.67	26.66
	5		464.28			31.43	
	6			830.45			24.23
	7			1060.67			28.82
NADP1_1_SL5	1	2011.37	2102.08		29.57	28.27	
	2	1794.11	1780.05		27.76	26.76	
	3	1448.09	1416.11		27.63	27.29	
	4	1220.7	1277.74	1910.05	26.58	26.73	26.71
	5		949.27			32.51	
	6			589.94			25.76
	7			687.11			26.87



**Table 8.** Summary of median RMS differences for NADP-2 profile 11

NADP Profile	Actual Stage Length	Median Altitude RMS [ft]			Median Ground Speed RMS [kn]		
		A320-211	B737-800	A330-301	A320-211	B737-800	A330-301
NADP2_11_SL1	1	695.28	745.53		27.6	26.88	
	2	685.32	578.21		27.77	26.12	
	3	780.55	706.21		28.91	26.39	
	4	896	728.52	747.36	28.52	26.01	29.65
	5		966.67			30.26	
	6			1298.96			25.04
	7			1511.74			31.04
NADP2_11_SL3	1	1164.64	1363		27.48	26.78	
	2	961.15	1000.38		26.56	25.82	
	3	725.97	722.39		27.65	25.78	
	4	694.28	627.93	1066.71	26.94	25.5	28.7
	5		482.17			30.16	
	6			917.22			24.67
	7			1130.19			30.06
NADP2_11_SL5	1	1975.8	2091.61		28.58	28.1	
	2	1763	1766.61		27.28	26.73	
	3	1423.33	1405.8		27.91	26.83	
	4	1188.94	1265.61	1836.9	26.74	26.7	27.46
	5		929.36			31.08	
	6			590.7			24.95
	7			728.38			26.85

# Task 2 – Arrival Profile Modeling

Georgia Institute of Technology

## Objective

The objective of Task 2 was to find and develop arrival procedures for AEDT that better capture existing operations as observed in airlines' flight data. The 2020-2021 objective specifically has been to determine what additional arrival profiles must be included in the AEDT models to represent real-life arrival profiles based on 2019 flight operations of multiple airlines. Previous research in this area has shown that a systemic statistical method must be developed to define the continuous descent approach and level-off for all aircrafts. In particular, the level-off trends remained unclear from the previous year's work. Hence it was recommended to incorporate threaded track data to confirm these findings and explore these uncertainties further.

## Introduction

AEDT currently models arrival profiles using specified fixed-point trajectories or manufacture-provided procedures. Task 2 compares data from real flights to the models in AEDT to make recommendations on how to improve AEDT models such that they capture real flight operations.

## Research Approach

To accomplish the objective outlined above, the goal was to examine prior years' research and arrival profile recommendations; study prior algorithms for level-off detection, level-off length calculation, and other parameters; conduct similar efforts with arrival profiles from other data sources available (threaded track, ADS-B); develop a modified algorithm for applying to threaded track/ADSB data; use statistical analysis to confirm the original recommendations and refine as needed; group airports into similar arrival procedure behaviours using machine learning or data analysis techniques based on threaded track data; obtain diversity of operational conditions, statistical trends, etc for clusters of data; and finally demonstrate implementation in AEDT.

Hence, the researchers for this task first enumerated and documented a summary of the recommendations for arrival modelling from the previous year, with a focus on understanding: What was done previously? How was it done? What needs improving? And most importantly, how can it be improved upon? In documenting the previous year's recommendations, the researchers were able to scope the level-off altitudes that were high priority in determining level-off trends as seen in Table 9 below:

**Table 9.** Summary of existing recommendations for AEDT arrival modeling

Aircraft	CDA	LO 2000	LO 3000	LO 4000
B717-200	X	1	2	3
B737-700	X	1	2	3
B737-800	1	2	X	3
B737-900	1	2	X	3
B757-200	X	1	2	3
B757-300	1	2	X	3
B777-200ER	1	2	X	3
B777-200LR	1	2	X	3
MD-90	X	1	2	3
A319-100	1	2	X	3
A320-200	1	2	X	3
A321-200	1	2	X	3
A330-200	1	2	X	3
A330-300	1	2	X	3

Here, X corresponds to "Already in AEDT", 1 is high priority, 2 is medium priority, and 3 is low priority.



From this, the task breakdown as prescribed was:

1. Expand one-airline analysis from previous year to new multi-airline flight data.
  - a. Identify popular altitudes and tolerances.
  - b. Define continuous descent approach and level-off based on aircraft.
  - c. Identify operational differences based on airline.
2. Continue analysis of level-off length histogram.
  - a. Evaluate the current assumption that manufacturer supplied level-off distance value is the best option for AEDT setting.
  - b. Conduct detailed analysis on airport subsets to look for level-off distance trends.
3. Edit/improve existing Python code for level-off detection and grouping to enable analysis of 2019 data.
  - a. Define statistics-based analysis methods

### **Methodology**

Despite having the intention of using threaded track data for this effort, a subset of 2019 OpenSky ADS-B data was used due to delays in receiving the threaded track dataset. The OpenSky dataset includes data from 415 flights operated by 32 airframes and 44 airlines which arrived at San Francisco International Airport (SFO). Statistical trends of approach profiles were identified in the OpenSky data and compared to existing arrival models in AEDT to locate gaps or inaccuracies in AEDT. The aircraft types observed in this dataset are:

'A21N' 'A319' 'A320' 'A321' 'A332' 'A343' 'A346' 'A359' 'A35K' 'A388' 'B38M' 'B39M' 'B737' 'B738' 'B739' 'B744' 'B748' 'B752' 'B753' 'B763' 'B764' 'B772' 'B77W' 'B788' 'B789' 'CL30' 'CRJ2' 'CRJ7' 'CRJ9' 'E75L' 'E75S' 'GLEX'

The dataset is in the form of a .csv table and is analyzed using Python. The code is built such that it may be implemented to larger datasets such as the threaded track data as they become available. The code differentiates between separate flights using the threaded track primary key associated to the flight. For each flight, potential level-offs are identified by finding consecutive data points which fall within some vertical speed tolerance. These flat portions of flights are compared against some ground track distance tolerance to determine if these points represent a level-off. All potential level-offs identified within 1500 feet above touchdown and within 5 miles of touchdown are disregarded as they fall in the category of final approach. Thus, the task in refining level-off detection for analysis is determining the appropriate vertical speed tolerance and ground track distance tolerance.

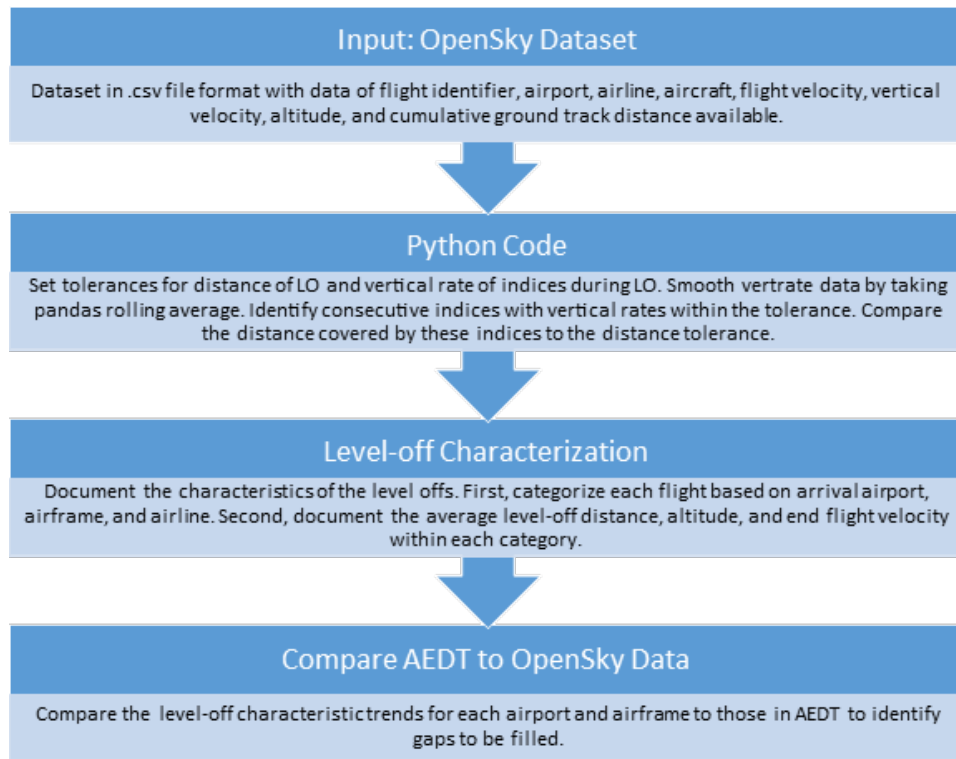


Figure 17. Flowchart of Task 2.

A systemic, statistical method for the determination of these key tolerances is being worked on. This was begun by conducting a design of experiments and writing a design of experiments (DoE) code in Python. The following DoE was created where the distance speed tolerances were one and two nmi corresponding to 0 and 1, respectively, and vertical speed tolerance levels of 200 to 500 ft/min corresponding to 0-3, respectively, as seen in Table 10:

Table 10. Level-off tolerance testing design of experiments

Experiment	Distance Tolerance (nmi)	Vertical Speed Tolerance (ft/min)
1	0	0
2	1	0
3	0	1
4	1	1
5	0	2
6	1	2
7	0	3
8	1	3

Using this to guide the cases or experiments that were run with various settings on the code, it was found that larger vertical speed tolerances did not affect the level-off detection and instead shorter level-off distances were not being detected by the code even if they seemed to be visually present in certain plots. This is best exemplified with the following plot in Figure 18. Examining distance tolerances was deemed high priority as seen with the level-off detected at 6000 ft by the code, and the potential level-off visually detected at 3000 ft which remains undetected by the Python code.

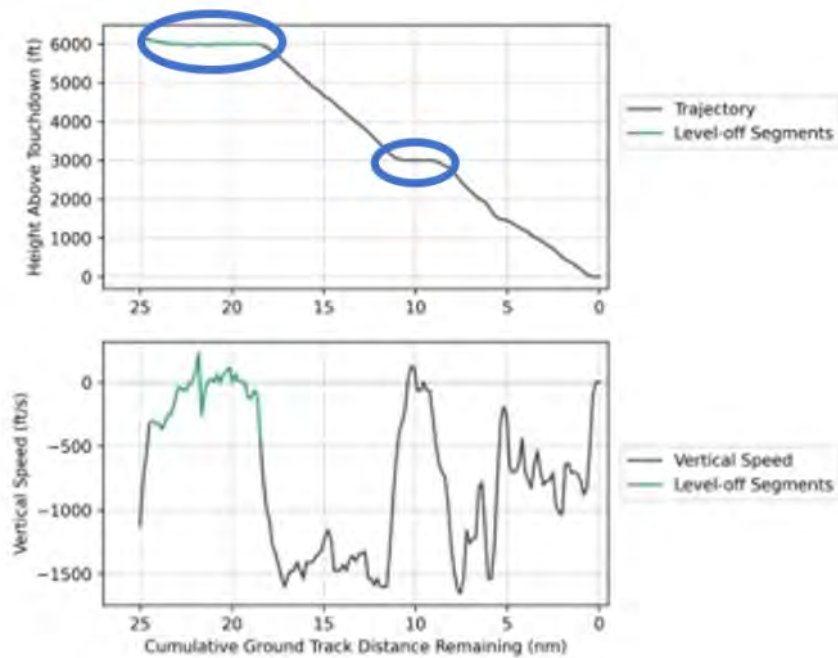


**Figure 18.** Distance tolerance two nmi, vertical speed tolerance 500 ft/min, Flight 110.

Hence lowering the level-off distance tolerances below two nmi would be required to help capture more flights with vertical speed tolerances in an appropriate range. A small sample set of code was run to understand the distribution of "shorter" level-offs across 10 flights, 50 flights, and soon the whole dataset to further examine these ambiguous level-offs.

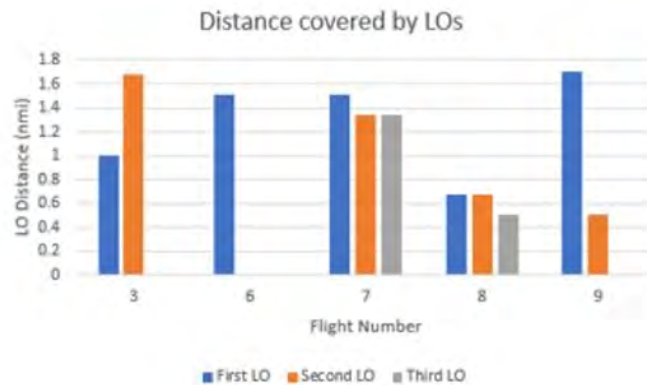


**Figure 19.** Level-off distances for first 10 flights.

When examining the first 10 flights, the researchers noted the clustering of level-off distances in the range 0.3–1 nmi and 1–2 nmi. Hence these groupings were used when examining the dataset of the first 50 flights and taking the two clusters of level-off distances and finding the mean, median, and mode between these two ranges. The findings for the two clusterings are captured in the tables below:

**Table 11.** Central tendencies for level-off distances for first 50 flights (0.3- 1 nmi)

Mean (0.3-1)	0.751324
<b>Median (0.3-1)</b>	<b>0.503356</b>
Mode (0.3-1)	0.671141

**Table 12.** Central tendencies for level-off distances for first 50 flights (1-2 nmi)

Mean (1-2)	1.339576
<b>Median (1-2)</b>	<b>1.342282</b>
Mode (1-2)	1.677853

However, when analysing the whole dataset, the airframes need to be accounted for and compared to AEDT. Hence the profile points were extracted from AEDT for each airframe, altitude, and distance with the intention of modifying the Python code such that it would have the ability to categorize level-offs by airframe and central tendencies.

Hence, in parallel with the statistical analysis of level-off tolerance determination, developments were made in the Python code to document and calculate characteristics of the level-offs such that they may be analyzed based on arrival airport, aircraft, and airline. In addition, the horizontal flight speed reached at the end of the level-off and the altitude at which the level-off occurs is documented. The three categorizations between airport, aircraft, and airline are made in anticipation of differences in arrival behavior for differences in each category. Upon grouping the flights by its category, the level-off characteristics of those flights are analyzed to identify prominent level-off altitudes, distances, and flight speeds. These level-off characteristic trends are then compared to the airframe-specific arrival models in AEDT.

**Results and Discussion**

Currently available results include a design of experiments approach to explore level-off distance tolerances and a baseline Python code to identify level-offs and plot these results.

The Python code is currently under development and has yet to yield notable results. Thus, next steps include the completion of the code such that level-off characterization can be performed for the entire dataset. The output of the code will include a calculation of the mean, median, and mode of the characteristics for each category. These statistical characteristics will be used in addition to a graphing of these metrics to identify significant trends that may be used to generalize the arrival profile for use in AEDT.

However, it should be noted that the OpenSky dataset which is currently being used only includes arrivals at SFO. Characterization of arrival profiles at multiple airports will be an important step in yielding results which can be translated into comparison with, and implementation into, AEDT’s arrival modelling.

**Task 3 – Full Flight Modeling**

Georgia Institute of Technology

**Objectives**

The objective of this Task is to improve the full flight modeling within AEDT. At present, to conduct a full flight in AEDT, a sensor path must be defined for each aircraft type and each origin-destination city-pair and is based on utilizing radar track data, which is being replaced with the new threaded track approach developed by The MITRE Corporation. Even with the threaded track data, this can be a daunting task for the user to set up an AEDT study. This task investigates the accuracy of the threaded track data compared to a truth model, FOQA, data, where all states of the aircraft flight are known, including thrust, weight, and fuel flow. Statistical analysis will be performed to determine how accurate the threaded tracks are and provide guidance to the FAA on improvement areas.

**Research Approach**

This Task's initial focus is to investigate the accuracy of thread track data and analyze the average behavior of FOQA flight data. Thus, the research approach will be described in two parts.

**Investigate the accuracy of the thread track data compare to FOQA data**

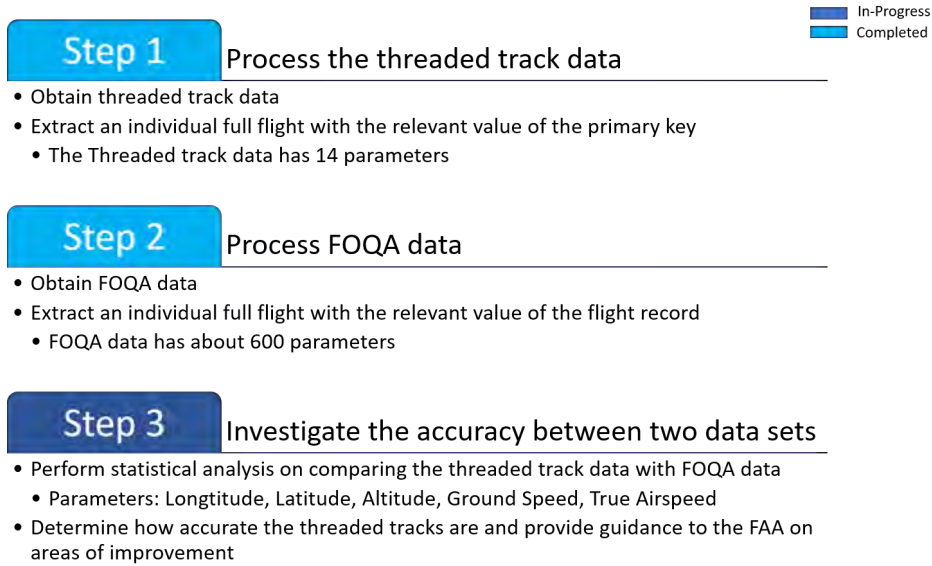


**Figure 20.** Research approach for investigating the accuracy of the threaded track data.

This section aims to study how accurate the threaded track data is compared to the true model FOQA data. The threaded track data has only 14 parameters and low-fidelity data compared with FOQA data. MITRE's new threaded track approach is used for establishing a sensor path to conduct the full flight modeling in AEDT. Therefore, it is necessary to analyze how accurate the threaded track data is because the full flight modeling performance in AEDT varies. Therefore, it is also necessary to analyze how accurate the threaded track data is because the full flight modeling performance in AEDT depends on the data's accuracy. The research method is represented in Figure 20. Step 3 of the method is currently in progress and is dependent on receiving the threaded track data.

**Study the average behavior within FOQA data**

This section's main objective is to analyze the average behavior of FOQA data and compare it to what AEDT has for full flight modeling. FOQA data includes about 21,000 flights from 14 different airframes. The first step is to find out if a specific flight pattern exists within each city pair. Instead of analyzing about 1001 city-pairs in the FOQA data, the top five city pairs were selected and investigated based on the highest flight operations. Scripts have been created to automate data extraction from the raw FOQA file so that only flight data corresponding to the relevant city pair can be extracted. Next, a trajectory was generated using each city pair's extracted data to analyze a specific pattern through the density-based spatial clustering of applications with noise (DBSCAN) algorithm. DBSCAN is a popular data clustering algorithm in machine learning and groups together points that are close to each other based on distance measurement. Two parameters of the DBSCAN algorithm are required to adjust the optimal clustering results. The first parameter is eps, which is the maximum distance between two samples for one to be considered in the other's neighborhood. The second one, min\_samples, is the number of points in a neighborhood considered a core point. Longitude and latitude were used for creating the trajectory and clustering. The detailed procedure is shown in Figure 21.

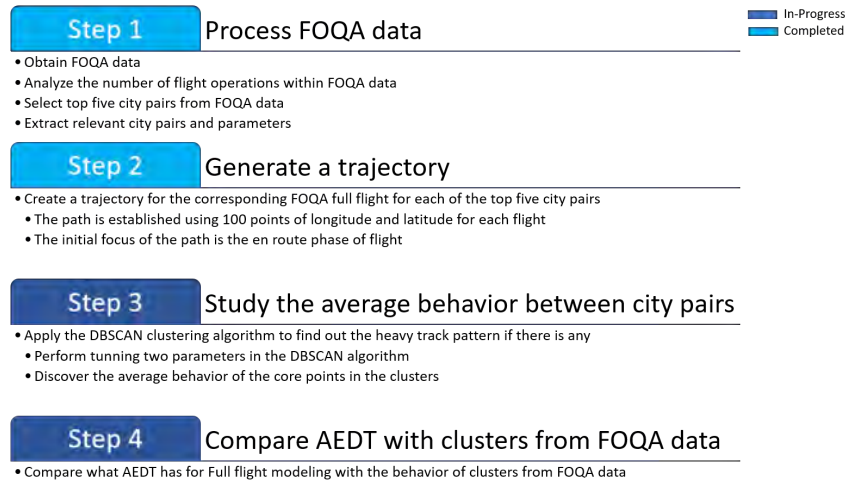


**Figure 21.** Research approach for analyzing the average behavior of FOQA data

**Results and Discussion**

This section presents preliminary results for investigating the average behavior for top city pairs. The results of the top five city pairs using Python scripts are presented in Table 13. The city pair from ATL to LAS has the highest number of flight operations with 417 flights, while the city pair from SEA to LAS has the lowest number of flight operations with 315 flights in the top five city pairs data. The city pair from SLC to LAS has the shortest length in terms of the great-circle distance.

**Table 13.** Top five city pairs from FOQA data

Origin	Destination	# of flights	Origin	Destination	# of flights	Total # of flight	GC distance (nm)
ATL	LAS	417	LAS	ATL	30	447	1514.488
MSP	LAS	378	LAS	MSP	24	402	1127.305
ATL	SLC	330	SLC	ATL	32	362	1378.838
SLC	LAS	255	LAS	SLC	104	359	319.622
SEA	LAS	315	LAS	SEA	18	333	753.300

\*\* ATL: Hartsfield-Jackson Atlanta International Airport  
MSP: Minneapolis-Saint Paul International Airport  
SLC: Salt Lake City International Airport  
LAS: McCarran International Airport  
SEA: Seattle-Tacoma International Airport

Figure 22 represents the clustering results with the DBSCAN algorithm performed to city pairs from ATL to LAS. Even though the total number of flight operations for city pairs from ATL to LAS is the same for both plots, the DBSCAN algorithm shows different results depending on the parameters' values. The first plot on the left shows results with five eps and three min\_samples, and the second plot on the right shows results with four eps and 15 min\_samples. The number of outliers for the first plot is 39, which is less than the second plot. However, the second plot shows a better clustering result displaying a good illustration of the meaningful track trajectory. The contents of parameters and outliers are given in Table 14.

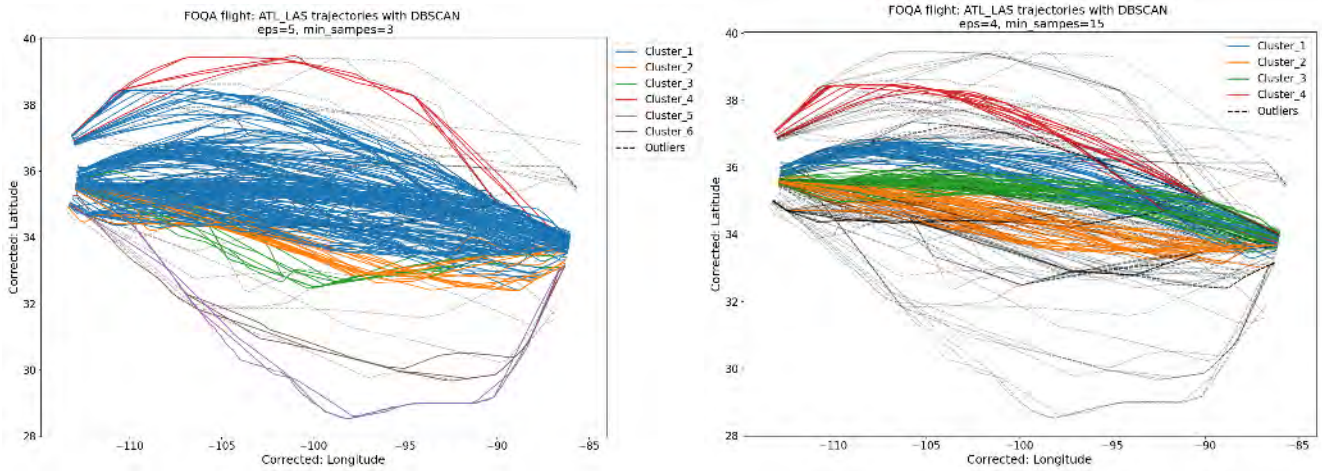


Figure 22. Clustering results of ATL to LAS trajectories with DBSCAN.

Table 14. Parameters and outliers in DBSCAN algorithm

City Pair	eps	Min_samples	Number of clusters	Number of outliers
ATL to LAS	5	3	6	39
ATL to LAS	4	15	4	164

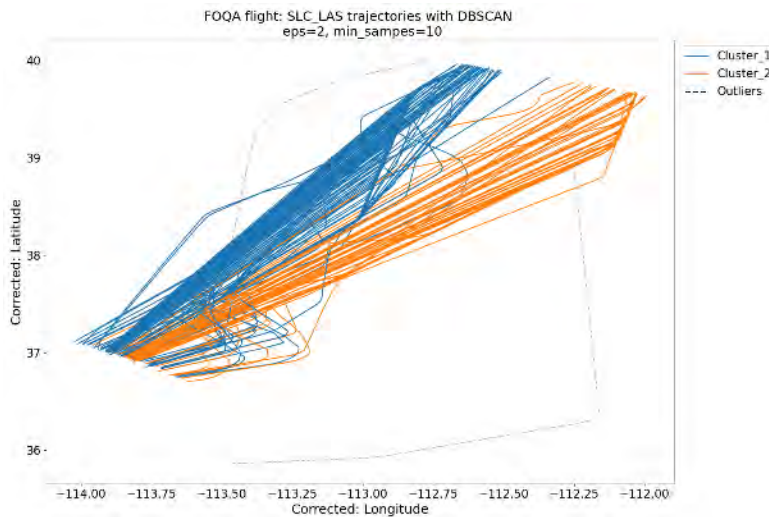


Figure 23. Clustering results of SLC to LAS trajectories with DBSCAN.

The clustering results of city pairs from LAS to SLC is illustrated in Figure 23. Most of the full flight trajectory from LAS to SLC is shown in two distinct patterns. Compared to the clustering results of city pairs from LAS to ATL, two patterns were well established. There are only two outliers and only 0.7% of the total flight. The city pair's clustering results from SLC to LAS are well detected compared to the city pair from ATL to LAS because the flight distance is relatively short. Moreover, there is less uncertainty, such as weather and traffic congestion.

## Task 4 – System Testing and Evaluation of AEDT

Georgia Institute of Technology

### Objective

To provide the best possible environmental impacts modeling capabilities in AEDT, the FAA AEE continues to develop AEDT by improving existing modeling methods and data and adding new functionalities. The AEDT development team has been exercising an agile development process, where minor updates are released in new Sprint versions every three weeks, and major updates and/or new functionalities are incorporated as new versions of AEDT. The FAA AEE seeks an independent effort in system testing to evaluate the accuracy, functionality, and capabilities of AEDT and support the future development process. Thus, the objective of this Task is to provide FAA with high-quality systematic testing and evaluation of AEDT 3 and its future releases to evaluate AEDT’s capability and identify gaps in the tools’ functionality and areas for further development.

### Research Approach

Under this area, the GT research team has been coordinating with FAA on the upcoming AEDT features and conducting necessary testing and evaluation efforts of the newly incorporated capability. For each of the AEDT releases, depending on the type of updates, we identify the key features and functionalities to first conduct capability demonstration to make sure the implemented features are working properly. Then we define the scope and test cases of the system testing and evaluation effort based on the key changes to the AEDT version from the previous releases. Due to the dynamic nature of the AEDT development process, we remain flexible in the choice of the testing and evaluation approach and the work scope. We always use the best available methods and data to ensure accuracy and functionalities of future AEDT versions. When it is applied, uncertainty quantification analysis is conducted to understand the sensitivities of output response to variation in input variables and quantify major contributors to output uncertainties.

### TGO/CIR Profile Development

This task focuses on updating the method of creating touch-and-go (TGO) and circuit (CIR) profiles from approach and departure procedures and using the updated method to develop TGO/CIR profiles for all 146 ANP fixed wing civil aircraft with procedure profiles. These newly developed TGO/CIR profiles are to be migrated into the FLEET database. The following goals are to be achieved:

1. Evaluate existing TGO and CIR profiles in the FLEET database to see how they are constructed.
2. Determine if the associated arrival/departure STANDARD stage 1 procedural profiles contain steps that are missing from the existing TGO and CIR profiles.
3. Create a method (program or script) to generate TGO and CIR profiles which utilize all available steps appropriately.
4. Develop TGO and CIR profiles for all civil aircraft with procedural arrival and departure profiles.

A sample C# code used for generating the original profiles was initially provided for this task. This code works by copying the procedure steps from the DEP/ARR (departure/arrival) profiles and re-arranging them in order to create TGO/CIR profiles compliant with the integrated noise model (INM) manual rules.

For a circuit profile, the code first copies the following procedure steps from the **DEPARTURE STAGE LENGTH 1** (steps shown in *italic* text were missing from the initial version of the code and were newly added as part of this feature):

1. TakeoffAirplaneProcedureStep
2. ClimbAirplaneProcedureStep
3. AccelerateAirplaneProcedureStep
4. *PercentAccelerateAirplaneProcedureStep*

This is done until an altitude of 1500 ft is reached for non-piston type large aircraft and 900 ft for piston type small aircraft. The code then creates Level steps and Fit-To-Track Distance steps at either 1500 ft or 900 ft altitude for a distance of 500 ft.

Finally, from the **ARRIVAL** procedure, at 900/1500 ft and downwards, the code copies (steps shown in *italic* text were missing from the initial version of the code and were newly added as part of this feature):



1. DescendAirplaneProcedureStep
2. *IdleThrustDescendAirplaneProcedureStep*
3. *DeceleratingThrustDescendAirplaneProcedureStep*
4. *IdleThrustLevelAirplaneProcedureStep*
5. *DeceleratingThrustLevelAirplaneProcedureStep*
6. LevelAirplaneProcedureStep
7. LandAirplaneProcedureStep
8. LandingDecelerateAirplaneProcedureStep

For a TGO profile, the code first creates a Level step at either 1500 ft or 900 ft altitude (depending on aircraft size and engine type) for a distance of 500 ft. It then copies the following procedure steps from the **ARRIVAL** procedure (steps shown in italic text were missing from the initial version of the code and were newly added as part of this feature):

1. DescendAirplaneProcedureStep
2. *IdleThrustDescendAirplaneProcedureStep*
3. *DeceleratingThrustDescendAirplaneProcedureStep*
4. *IdleThrustLevelAirplaneProcedureStep*
5. *DeceleratingThrustLevelAirplaneProcedureStep*
6. LevelAirplaneProcedureStep
7. LandAirplaneProcedureStep

From **DEPARTURE STAGE LENGTH 1**, the code then copies (steps shown in *italic* text were missing from the initial version of the code and were newly added as part of this feature):

1. TakeoffAirplaneProcedureStep
2. ClimbAirplaneProcedureStep
3. AccelerateAirplaneProcedureStep
4. *PercentAccelerateAirplaneProcedureStep*

As it can be seen in the earlier section, many new procedure steps that did not exist in the previous INM version of the code had to be defined inside the code. New arrival steps were inserted inside the code (*IdleThrustDescendAirplaneProcedureStep*, *DeceleratingThrustDescendAirplaneProcedureStep*, *IdleThrustLevelAirplaneProcedureStep*, *DeceleratingThrustLevelAirplaneProcedureStep*) that did not exist in the INM version of the code. Similarly, new departure steps were inserted inside the code (*PercentAccelerateAirplaneProcedureStep*) that did not exist in the INM code version.

Similar rules for the missing arrival steps were made based on the ones currently implemented for “DescendAirplaneProcedureStep”. Additionally, similar rules for the missing departure steps were created for the existing “AccelerateAirplaneProcedureStep”.

Besides the newly added step types, multiple problems were identified during the initial testing of the profiles that were being generated by the original INM code. New rules had to be added (code changes) in order to deal with the problems summarized below:

- **Problem 1:** Missing “DESCEND” steps that lead to invalid profiles that fail to run.
  - Solution: If there are no “Descend” steps, add one between the “Level” and “Land” steps.
- **Problem 2:** Missing “ACCELERATE” steps that lead to invalid profiles with 0 ft/min calibrated airspeed during the levelling step.
  - Solution: If there are no “ACCELERATE” steps, add one between the “Climb” and “Level” steps at 900/1500 ft.
- **Problem 3:** Non-zero/Too large climb rates that lead to the aircraft overclimbing.
  - Solution: Always climb to 1500 ft and add one acceleration step with 0 ft/min climb rate (ignore departure step order).

To deal with Problem 1, the code has been modified by first checking the entire aircraft TGO/CIR profile after it has been generated. If there are no “Descend” steps, one would be added between the “Level” and “Land” steps at 900/1500 ft with 3/5 degrees climb angle and same flap id/calibrated airspeed as the level step from earlier (complies with INM manual).

To deal with Problem 2, the code has been modified by first checking the entire aircraft TGO/CIR profile after it has been generated. If there are no “ACCELERATE” steps, one would be added between the “Climb” and “Level” steps at 900/1500 ft with the same calibrated airspeed as the first accelerate step in the departure profile and a 0 ft/min climb rate (complies with INM manual).

To deal with Problem 3, the code has been changed in order to do the following. Any aircraft now always climbs to 1500 ft and then one acceleration step with 0 ft/min climb rate (ignore departure step order) is added. This ensures that the aircraft will not overclimb.

Finally, it has been discovered that, for a few aircraft, there are multiple acceleration steps before the 1500 feet threshold that do not lead to the aircraft overclimbing. The only way to fix this is to do it manually via SQL scripts; it cannot be done via the code, hence not all the TGO/CIR profiles generated via the code are correct. Furthermore, minor issues such as incorrect flap IDs and missing thrust levels have been fixed. The original code also did not have any output files before, so this was a newly added feature. These are necessary for importing the new TGO/CIR profiles inside the FLEET database and for testing/validation purposes.

After running the code and making the necessary manual modifications using SQL scripts, a total of 146 aircraft have received new TGO/CIR profiles. The ALLPROFILES code was used to generate a study with operations for all the TGO/CIR profiles available. These have been validated by comparing the performance, noise, and emission results to the old TGO/CIR profiles (if available) and by checking that they are all compliant to the INM technical manual rules.

Performance, emissions, and noise reports were generated for each individual TGO/CIR aircraft operation from the ALLPROFILES study. In order to give a short summary of how the validation procedure was conducted, Table 15 shows how the new and the old TGO/CIR profiles compare in terms of altitude, thrust, and speed. Aircraft profiles are categorized into three classes. If the differences in thrust, altitude, and speed are very small, aircraft profiles are placed in Class 1. Small differences are the usual case because the old TGO/CIR profiles have not been updated while the departure/arrival profiles have. If there are noticeable differences in at most two metrics, aircraft are placed in Class 2. Finally, if there are differences in three or more metrics, the aircraft are placed in Class 3.

Similar validation exercises were conducted for emissions and noise results. In most cases, if an aircraft belongs to a certain class in the performance analysis, it will most likely belong to the same class in the emissions/noise analysis hence they are correlated. The new TGO/CIR profiles are correct in all cases, however, since they have been manually checked and modified to comply with the rules stated in the INM manual.

Table 15. TGO/CIR new profile validation – performance analysis

Aircraft	TGO Altitude	TGO Thru	TGO Speed	CIR Altitude	CIR Thru	CIR Speed	TGO Altitude	TGO Thru	TGO Speed	CIR Altitude	CIR Thru	CIR Speed	Number of Outlets	CLASS
757RR	1.2588	6.4518	23.7764	1.6705	6.1069	23.6409	1	1	1	1	1	1	6	3
GASEPV	7.7663	18.8621	28.6158	3.0623	17.7901	28.7757	1	1	1	1	1	1	6	3
7478	2.8058	6.4451	0.61077	2.8098	5.9656	1.9477	1	1	1	1	1	1	6	3
7878R	3.1345	4.4027	2.4121	3.0163	3.6005	2.1409	1	1	1	1	1	1	6	3
757PW	1.4162	3.8269	23.3915	1.876	3.9109	23.2478	1	1	1	1	1	1	6	3
CNA208	0.76438	13.5054	10.1363	0.76505	13.4839	10.1313	1	1	1	1	1	1	6	3
737300	0.35585	18.6295	11.0537	1.3005	12.6422	10.9606	0	1	1	1	1	1	5	3
GASEPF	3.865	1.4302	1.8325	3.0907	2.7288	1.8013	1	0	1	1	1	1	5	3
737400	0.17499	8.6473	10.5778	0.31587	8.6443	10.7225	0	1	1	0	1	1	4	3
7773ER	1.4004	1.2003	9.9733	1.4014	1.6407	10.8757	1	0	1	1	0	1	4	3
A7D	0.53831	26.532	36.5818	0.54065	25.0798	36.3189	0	1	1	0	1	1	4	3
BEC58P	7.8548	2.0912	1.8095	3.0837	2.6292	1.3411	1	0	1	1	0	1	4	3
CNA441	0.15572	18.3239	14.2388	0.15548	18.0642	14.1991	0	1	1	0	1	1	4	3
COMSEF	4.1603	1.58	2.4458	3.0871	2.4255	2.0209	1	0	1	1	0	1	4	3
DO228	0.26025	14.6117	17.2204	0.26292	14.5334	17.2079	0	1	1	0	1	1	4	3
DO328	0.10922	25.0217	7.7012	0.11378	24.6641	7.6842	0	1	1	0	1	1	4	3
F4C	0.42517	8.4394	13.6394	0.3308	8.1031	13.5413	0	1	1	0	1	1	4	3
PA42	0.3981	8.4198	23.1615	0.40376	8.2643	23.1064	0	1	1	0	1	1	4	3
EMB170	16.3683	1.9768	0.49652	16.8534	3.6723	0.65458	1	0	1	1	1	1	4	3
EMB175	16.6533	1.9787	0.50487	17.1477	3.7079	0.65679	1	0	0	1	1	1	4	3
CONCRD	1.4136	1.1503	0.52184	1.1318	1.1155	0.56848	1	0	0	1	0	1	3	3
GLIB	0.61549	28.9136	0.41479	0.61563	28.4992	0.41351	0	1	0	1	0	0	3	3
737700	1.2638	4.9429	0.48432	0.003227	0.89591	0.18952	1	1	0	0	0	0	2	2
747400	0.14553	1.052	0.82844	0.13867	1.0054	0.81918	0	0	1	0	0	1	2	2
CNA182	0.42672	24.3567	0.27829	0.42773	24.3432	0.27767	0	1	0	0	1	0	2	2
EMB190	8.0991	1.3891	0.26882	8.2999	2.4714	0.28696	1	0	0	1	0	0	2	2
EMB195	7.8999	1.3287	0.2575	7.7819	2.3565	0.26537	1	0	0	1	0	0	2	2
GII	0.46618	22.1061	0.26734	0.46644	21.799	0.26649	0	1	0	0	1	0	2	2
GIV	0.25405	32.0278	0.11198	0.25372	31.7593	0.11157	0	1	0	0	1	0	2	2
GV	0.42477	32.3935	0.25677	0.42508	31.8307	0.25616	0	1	0	0	1	0	2	2
MU3001	0.31299	10.2873	0.26152	0.23728	10.1786	0.29214	0	1	0	0	1	0	2	2
717200	0.033272	17.7628	0.32346	0.014823	0.31536	0.024225	0	1	0	0	0	0	1	2
737500	0.039278	1.0246	9.3699	0.019643	0.15805	0.034347	0	0	1	0	0	0	1	2
CNA172	0.60949	1.2432	0.38697	0.60877	1.2356	0.38603	0	0	0	1	0	0	1	2
DC3	0.1038	0.55899	0.50377	0.11346	0.55041	0.53487	0	0	0	0	0	1	1	2
1900D	0.093424	0.35253	0.039165	0.0049712	0.020242	0.046016	0	0	0	0	0	0	0	1
707320	0.0067908	0.0024614	0.00064674	0.0063304	0.0014562	0.00095019	0	0	0	0	0	0	0	1
707QN	0.0067908	0.0024614	0.00064674	0.0063304	0.0014562	0.00095019	0	0	0	0	0	0	0	1
720B	0.050674	0.26129	0.031031	0.0052844	0.0021059	0.030858	0	0	0	0	0	0	0	1
727100	0.013473	0.001616	0.036057	0.01374	0.0024865	0.035835	0	0	0	0	0	0	0	1
727D15	0.0029818	0.0030262	0.01748	0.0032144	0.0025467	0.017376	0	0	0	0	0	0	0	1
727D17	0.0072623	0.0047558	0.022315	0.0068498	0.0058001	0.022251	0	0	0	0	0	0	0	1
727EM1	0.013473	0.001616	0.036057	0.01374	0.0024865	0.035835	0	0	0	0	0	0	0	1
727EM2	0.0029818	0.0030262	0.01748	0.0032144	0.0025467	0.017376	0	0	0	0	0	0	0	1

The validation analysis was conducted for each of 146 aircraft individually by comparing the performance, emissions, and noise results between existing and updated TGO/CIR, and then grouped to the three classes based on the comparison differences. An example of a Class 1 aircraft (1900D) is shown below. There are no noticeable discrepancies to be found here.

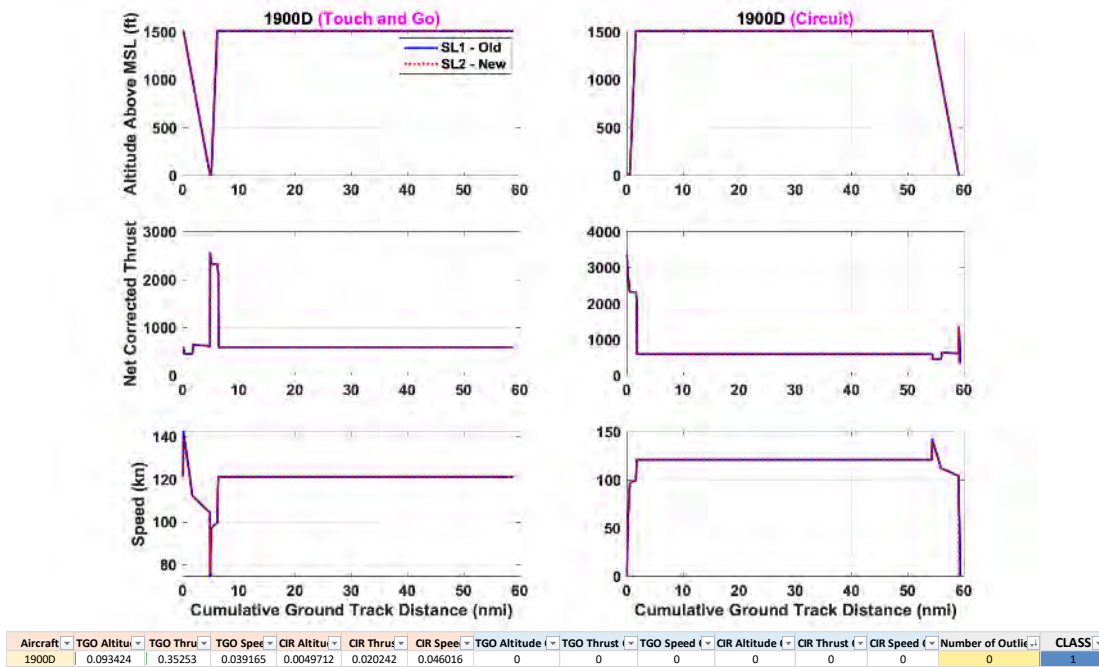


Figure 24. Class 1 aircraft—performance analysis.

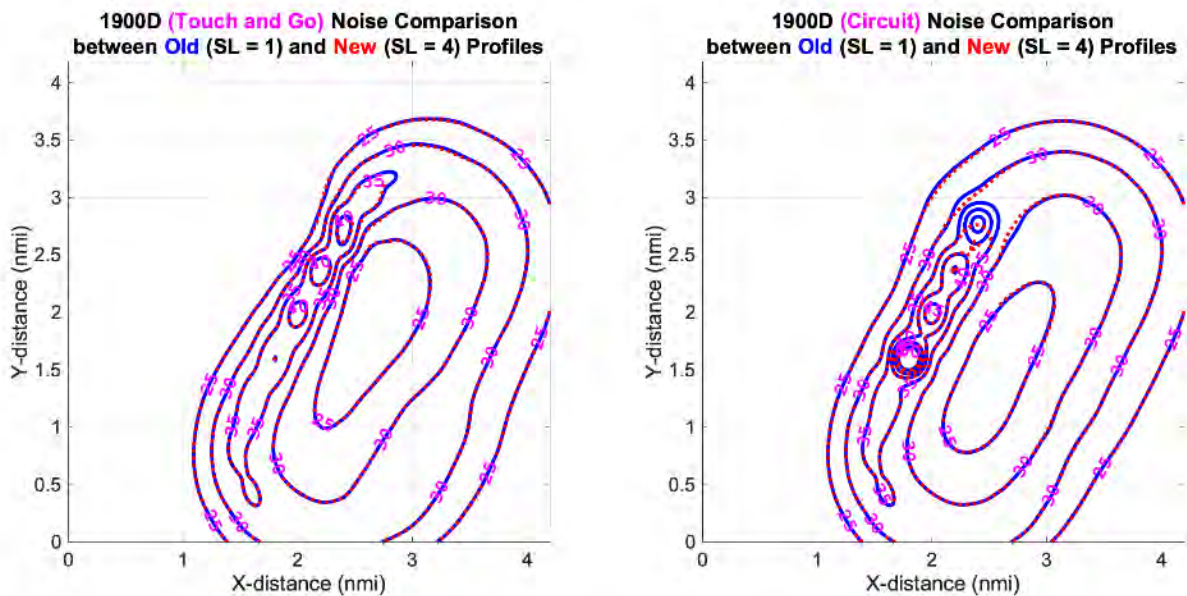


Figure 25. Class 1 aircraft—noise analysis.

An example of a Class 2 aircraft (EMB190) is shown below. As it can be seen, there are only two discrepancies here, namely the altitude for both the TGO and CIR profiles. This is due to the EMB190 overclimbing for the old TGO/CIR profiles. Discrepancies in terms of noise are thus present and expected because of the performance differences.

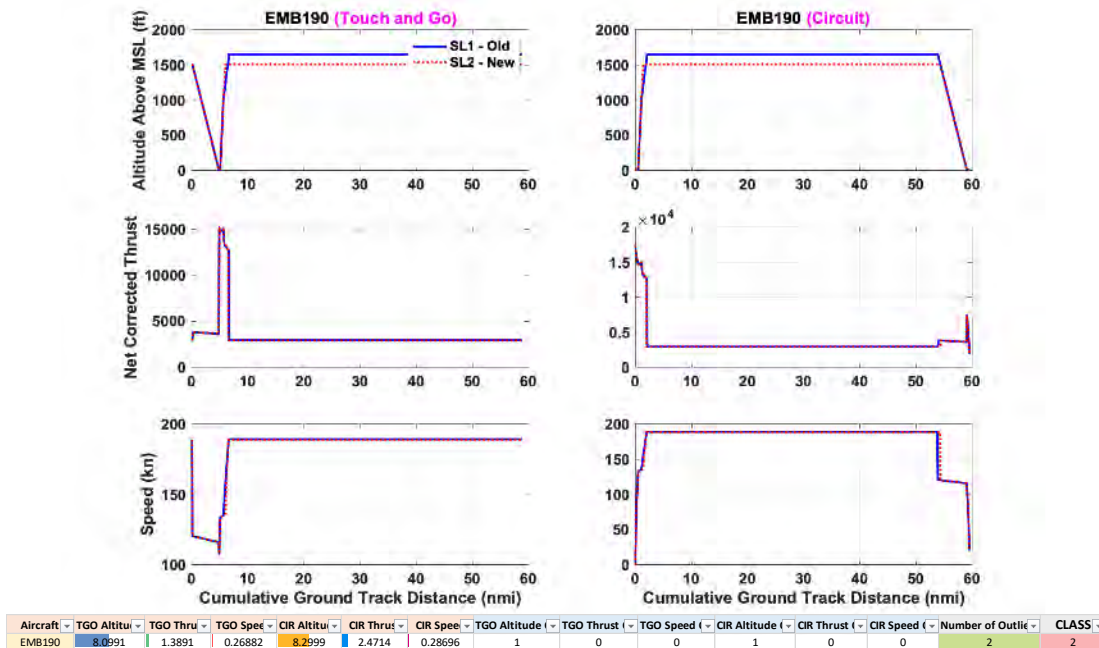


Figure 26. Class 2 aircraft—performance analysis.

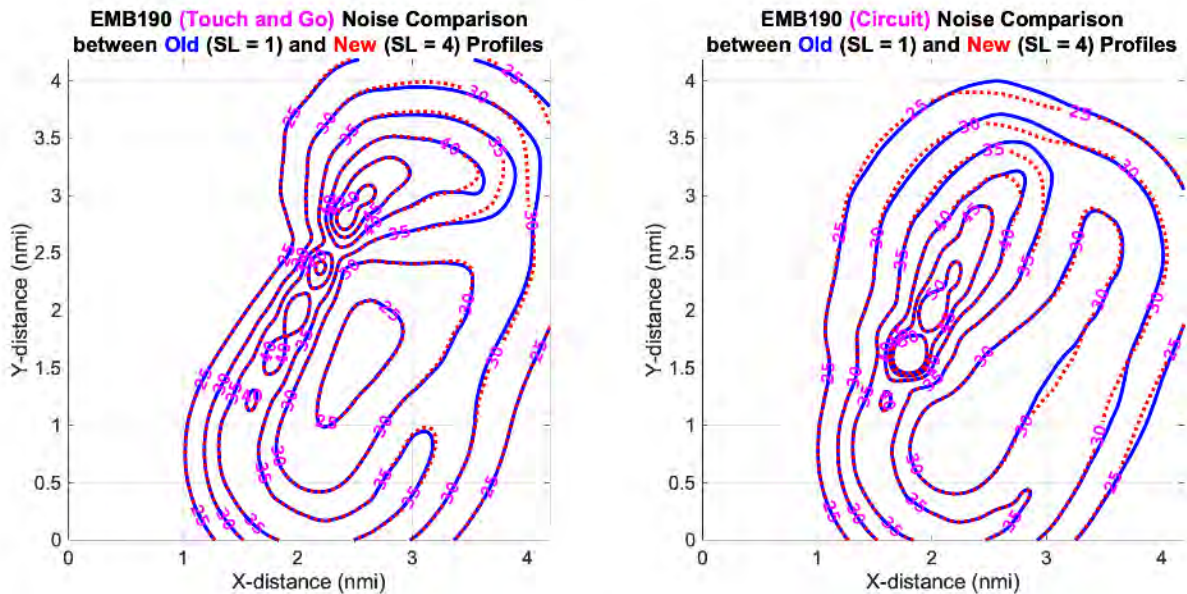


Figure 27. Class 2 aircraft—noise analysis.

An example of a Class 3 aircraft (757RR) is shown below. As can be seen, there are a total of four discrepancies, namely the thrust and speed for both the TGO and CIR profiles. This is mainly due to the old TGO/CIR profiles not having the updated

parameter values corresponding to the current version of the approach/departure profiles. Discrepancies in terms of noise are thus present and expected because of the performance differences.

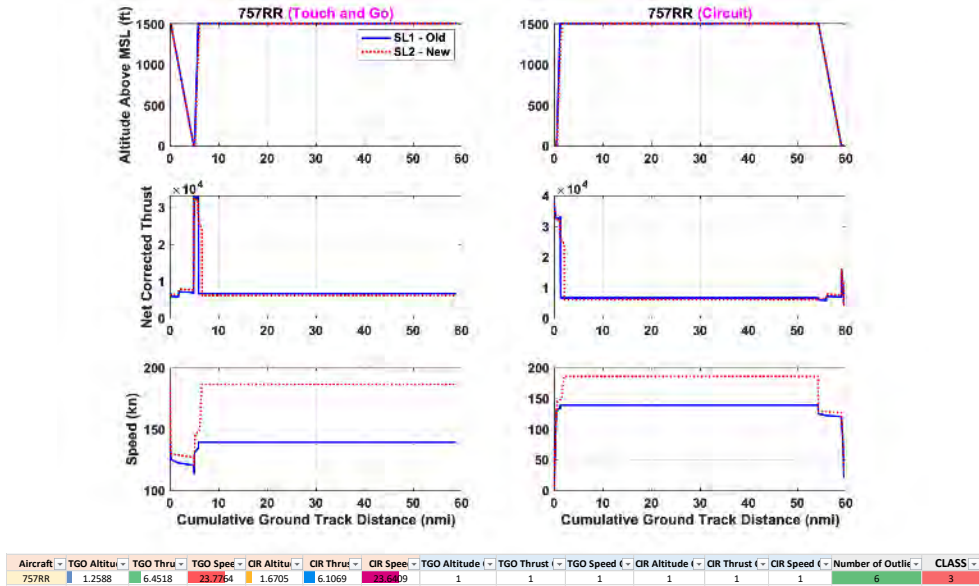


Figure 28. Class 3 aircraft—performance analysis.

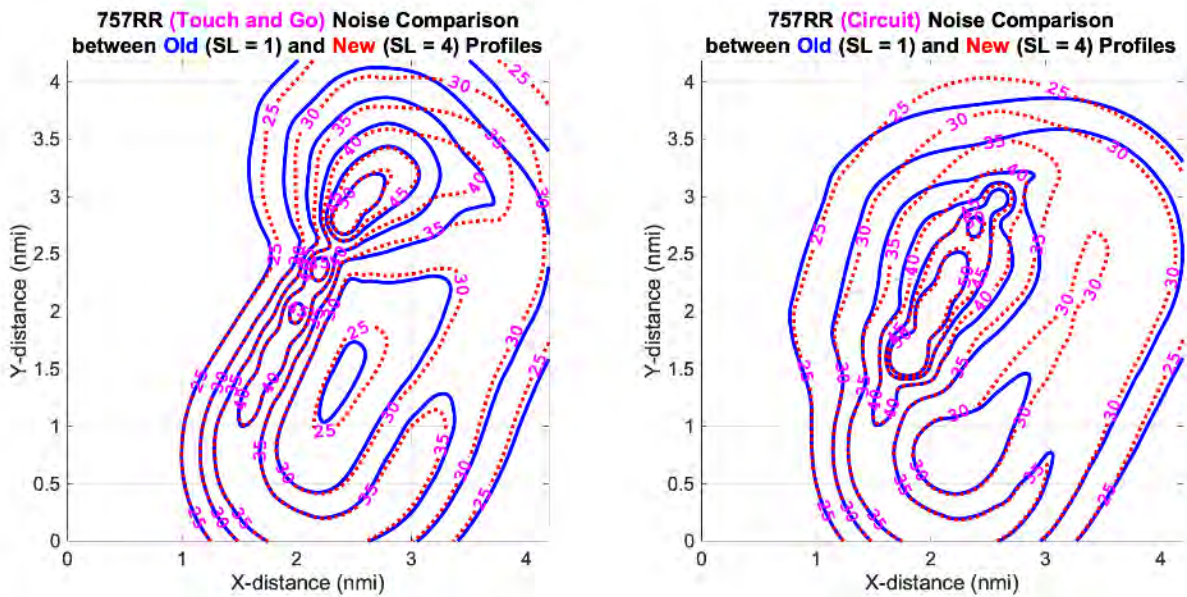


Figure 29. Class 3 aircraft—noise analysis.

Finally, it can be concluded that the noise class categorization is highly correlated with the performance class categorization, as it can be seen in the confusion matrix below in Table 16 which shows how many aircraft belong to which

performance/noise class combination. Many aircraft that are in Class 1 of the performance result (good agreement) and in Class 2 of the noise result (minor differences) have modified or new profiles as the final profile.

**Table 16.** TGO/CIR profiles performance/noise confusion matrix

Performance\Noise Classes	Noise = 1	Noise = 2	Noise = 3
Performance = 1	95	17	1
Performance = 2	6	5	2
Performance = 3	5	8	9

**Investigation on EUROCONTROL recommended ANP implementations**

**Investigation of BADA4 arrival fuel consumption inconsistencies**

The inconsistency identified is that for some aircraft type, such as the A300-622 shown in Figure 30, there is a reduction in the BADA4 fuel consumption levels near five nmi from the touchdown (the grey curve on the left plot), which does not correlate with the thrust variation (the grey curve on the right plot, which indicates thrust is increasing in that region).

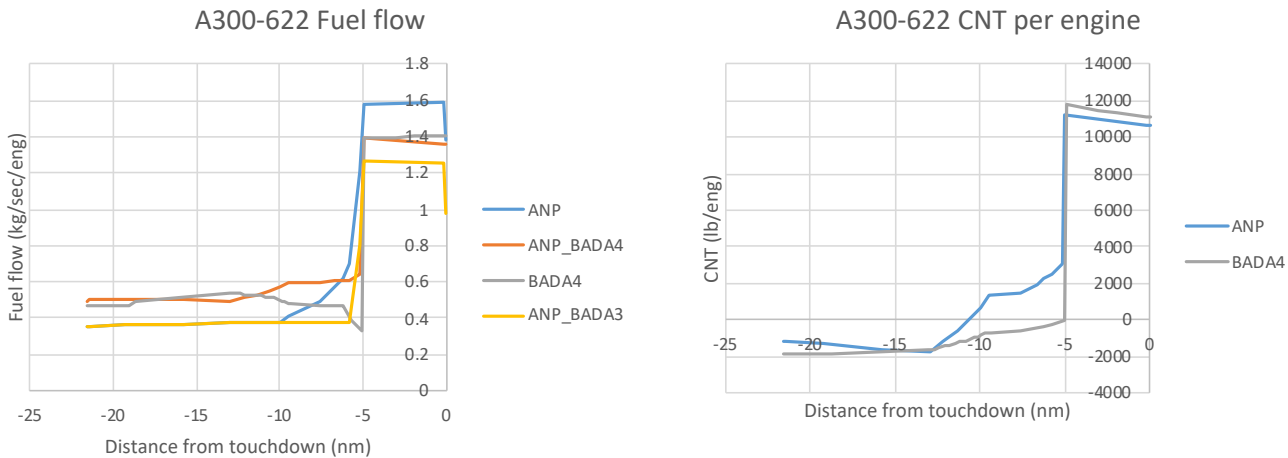


**Figure 30.** Example of arrival fuel consumption inconsistency.

Investigation of this problem starts from the STANDARD procedural approach profile of A300-622, which is shown below in Figure 31. It can be seen from Figure 31 that before touchdown, the landing approach procedure consists of two major sections: steps 1–6 belong to the idle descent section, while steps 7–8 belong to the non-idle section. After a matching processing between AEDT performance report and the approach profile, it can be identified that the BADA4 fuel consumption reduction region in the left plot of Figure 30 exactly matches the step 6 in the approach profile. As shown in Figure 32, the start and end of the reduction region correspond exactly to the two altitudes at the beginning and end of step 6. This leads to a crucial conclusion that the fuel consumption reduction region belongs to idle descent.

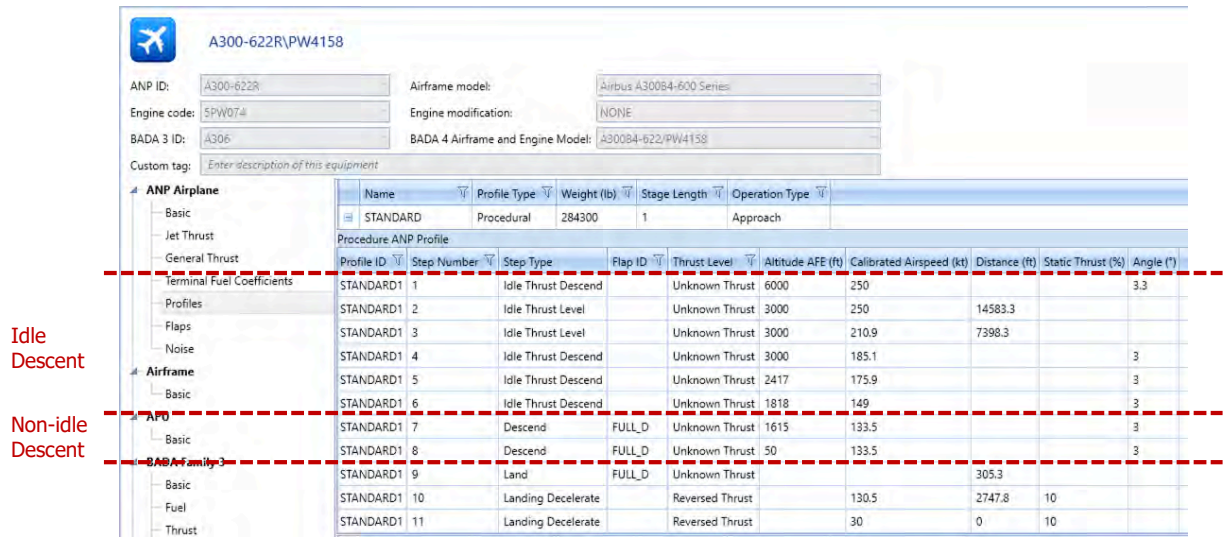


Figure 31. A300-622 STANDARD approach profile.

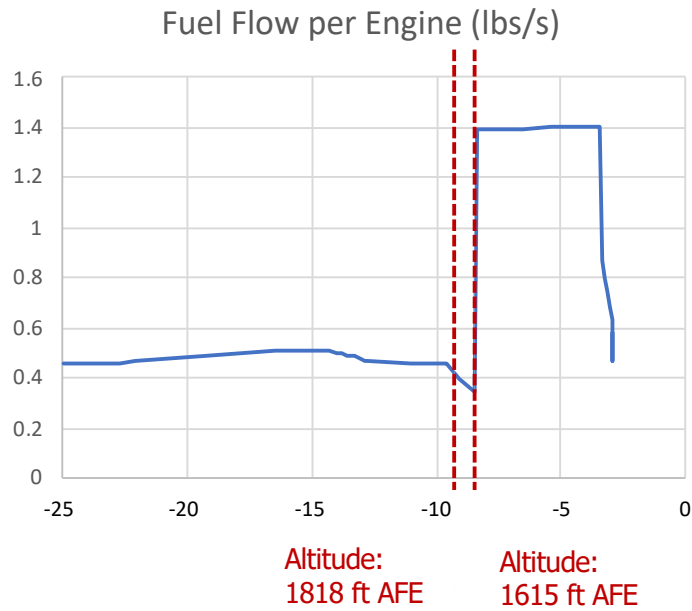


Figure 32. BADA4 fuel consumption for A300-622.

In the BADA4 fuel consumption equations, idle descent and non-idle descent are governed by two completely different equations.

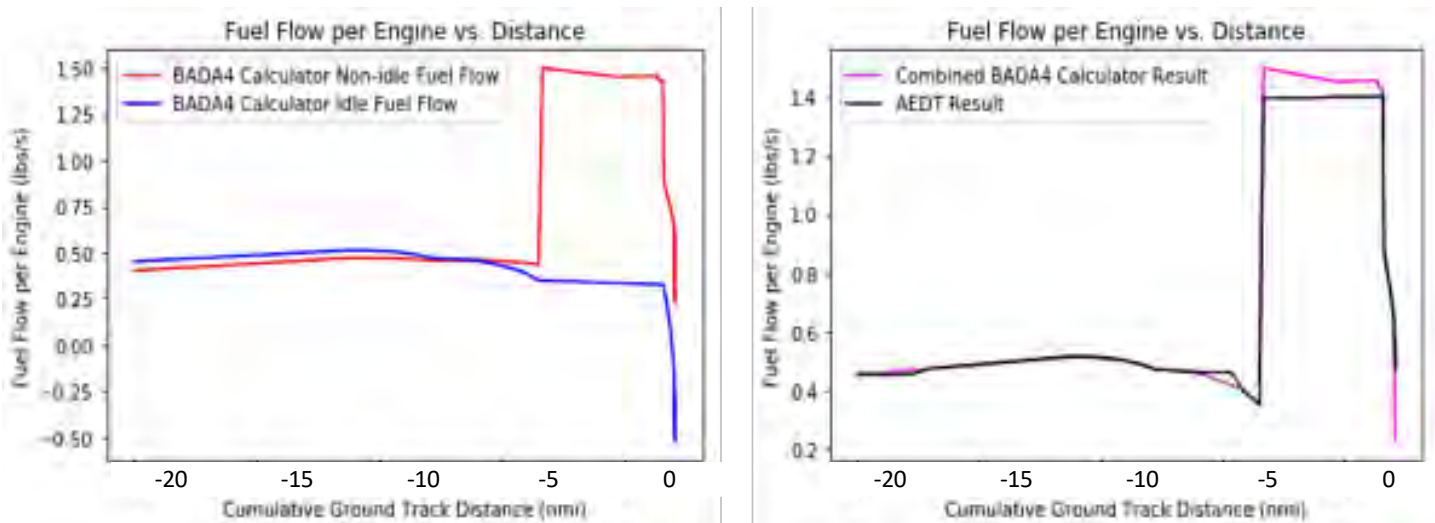


Figure 33. BADA4 calculator simulation results and comparisons.

After identifying the cutoff line between idle and non-idle fuel consumption regions, a simulation code called “BADA4 calculator” is utilized to further verify the result. In the BADA4 calculator, the same BADA4 performance equations and coefficients are used to simulate an aircraft’s performance for departure or approach operations. By implementing the BADA4 equations, it serves as a way to conduct model validation and verification for AEDT’s result. Figure 33 shows the simulation results from the BADA4 calculator for A300-622 STANDARD approach and a comparison to AEDT. The left plot of Figure 33 contains both idle fuel flow and non-idle fuel flow results from BADA4 calculator throughout the entire approach process. The magenta curve in the right plot of Figure 33 combines the idle fuel flow and non-idle fuel flow results such that it matches the approach profile in Figure 31. In this combined BADA4 calculator result, the idle fuel flow result is used before the around five nmi location on the x-axis; the non-idle fuel flow result is used after this point. It can be observed that right before the transition point, since idle fuel calculation is used, the reduction in fuel consumption in fact matches the BADA4 fuel flow calculation correctly. In the right plot of Figure 33, fuel consumption result from the AEDT performance report is also plotted as a comparison. There is a very good agreement between AEDT and BADA4 calculation. Therefore, the conclusion from this investigation is that the reduction in the BADA4 fuel consumption correctly reflects the real BADA4 fuel flow relationships.

A follow-up investigation here is that, in Figure 30, why does the ANP\_BADA4 fuel flow result not have such a reduction since it also used BADA4 idle fuel flow methods? For this question, we also use the BADA4 calculator to gain insights on the possible causes. The ANP\_BADA4 fuel flow result consists of ANP thrust and BADA4 fuel flow calculation, that is, the BADA4 fuel consumption coefficient uses the ANP thrust coefficient  $C_T$  in the calculation. Note that only the BADA4 non-idle fuel consumption coefficient is affected by  $C_T$ . The left plot of Figure 34 shows the non-idle and idle fuel flow variations during the arrival operation of A300-622, with a dashed line indicating the transition between idle and non-idle phases in the arrival profile. A possible reason here is that, in the ANP\_BADA4 result, transition from idle fuel flow to non-idle fuel flow happened earlier than the time point in the approach profile. The right part of Figure 34 shows two different combined idle and non-idle fuel flow results from BADA4 calculator, and one corresponds to the normal transition and the other corresponds to early transition. A reduction in the fuel flow is observed when the transition happens at the correct place near 5 nautical miles before touchdown. On the other hand, if the transition happens earlier or no transition from idle to non-idle happens during the arrival operation (only non-idle fuel flow), there is no such reduction. It is worth mentioning that the ANP\_BADA4 fuel flow result in Figure 30 has a very similar shape to the non-idle fuel flow curve in Figure 34.

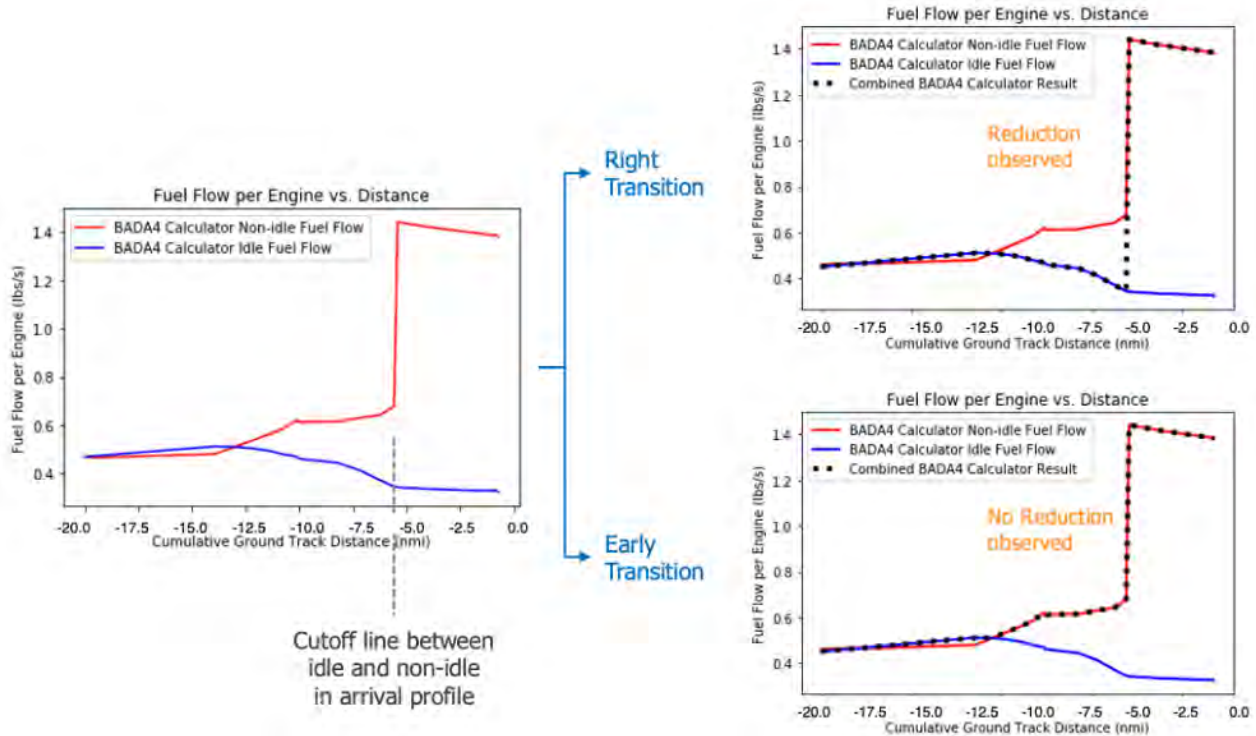
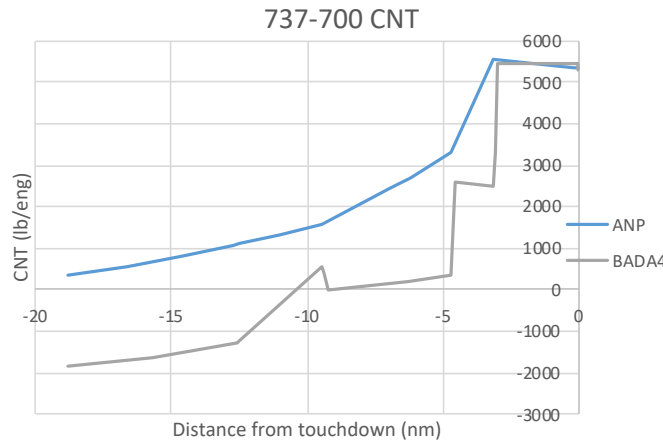


Figure 34. BADA4 calculator simulations for ANP\_BADA4 result.

**Investigation of arrival thrust bump near flap transition**

It was found that for some aircraft such as the 737-700, the BADA4 idle thrust model shows a small, unexpected bump in the transition near 10 nmi from touchdown. In Figure 35, the grey curve is the BADA4 idle thrust variation during 737-700 approach operation. The thrust bump near 10 nmi was deemed as a possible anomaly in the simulation process. After conducting AEDT tests on many other aircraft, it was identified that this phenomenon happens not only with the 737-700, but also with a few other aircraft. An initial inspection into the arrival profile shows that the unexpected bump normally happens near a flap transition region for some aircraft. However, a deeper investigation into the thrust calculation process is required to further uncover the possible reasons behind this phenomenon.



**Figure 35.** Unexpected bump of idle thrust in the flap transition region.

In BADA4, arrival thrust is calculated by the total energy model (TEM), given by

$$(T - D) \cdot V_{TAS} = mg_0 \frac{dh}{dt} + mV_{TAS} \frac{dV_{TAS}}{dt}$$

where  $T$  is thrust,  $D$  is drag, and  $V_{TAS}$  is the true airspeed. The right-hand side of the TEM equation has two components, namely the rates of change for potential energy and kinetic energy, respectively. In TEM, thrust is determined jointly by multiple factors, such as airspeed, rate of climb, acceleration, mass, and drag. Drag is a main influencer in the calculation of thrust, yet any other factor can contribute to the unexpected bump. In the following process, we use BADA4 calculator and AEDT intermediate performance outputs to investigate the problem.

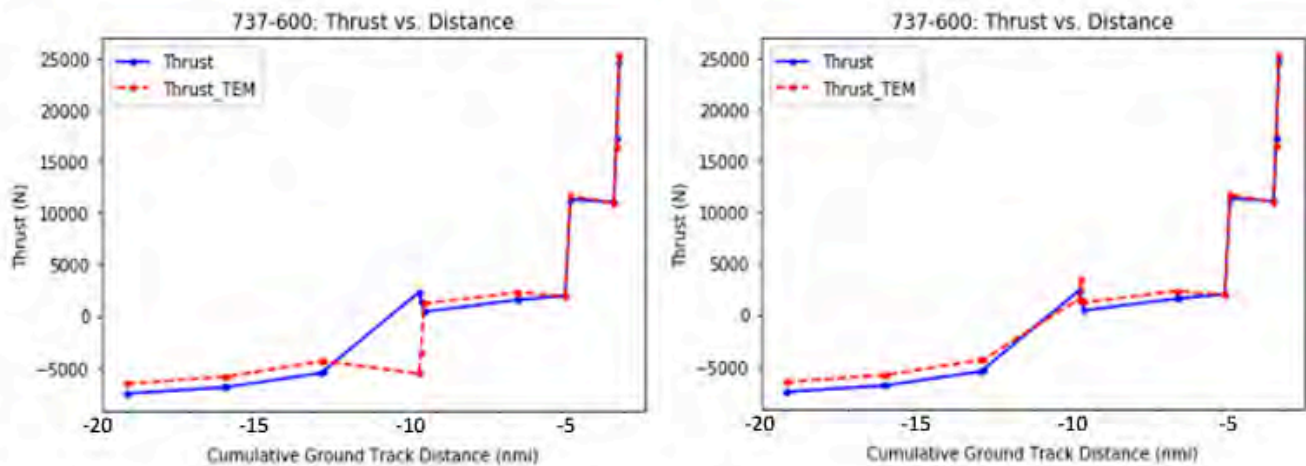


**Figure 36.** Arrival thrust comparison between AEDT and BADA4 calculator, with (left) and without (right) full TEM.

The left plot of Figure 36 shows a thrust comparison between AEDT and the BADA4 calculator for 737-600 arrival operation. The blue curve is from AEDT performance report; the red curve is the result calculated by the BADA4 calculator on the same operation with the full TEM implemented. One can observe from the left plot of Figure 36 that when the complete version of TEM is implemented, there is a disagreement between AEDT and the BADA4 calculator, especially in the "controversial region" around 10 nmi. Starting from the point around -13 nmi, the thrust result from the BADA4 calculator first decreases, then climbs sharply right before -10 nmi. In contrast, the AEDT result starts to climb right after -13 nmi and has a reduction in

the controversial region. A first assumption here is that the difference is caused by AEDT’s incomplete implementation of TEM. With this assumption, an action was taken on the BADA4 calculator simulation, in which the items in TEM are omitted one by one to see their influences in thrust calculation. The right plot of Figure 36 shows the BADA4 calculator result when the entire change in kinetic energy term in the TEM is omitted. Although slight differences still exist between the BADA4 calculator and AEDT, the trend is much closer compared to the full implementation of TEM in the BADA4 calculator.

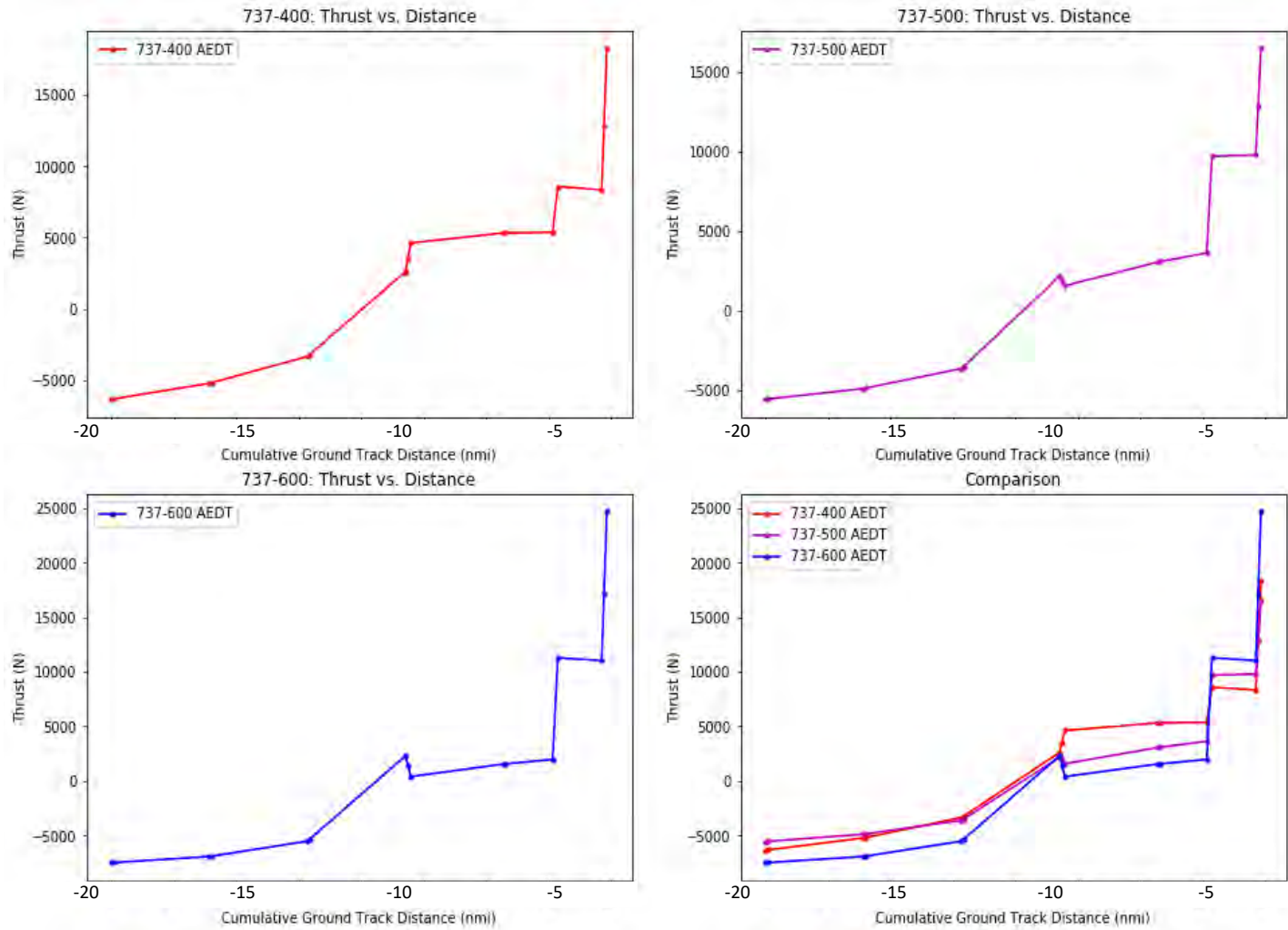


**Figure 37.** BADA4 thrust comparison between the 737 family.

After confirming that AEDT does not miss the kinetic energy term when calculating BADA4 idle thrust, a detailed comparison within the same aircraft family is utilized to further explore the role of the kinetic energy term and other factors in the unexpected bump. Figure 37 shows the BADA4 idle thrust comparison between three aircraft within the 737 family: 737-400, 747-500, and 737-600. The lower right plot of Figure 37 includes a direct comparison between the three aircraft. An interesting fact here is that, in the controversial region right before -10 nmi, three aircraft that have similar approach profiles show different characteristics. Compared to the 737-600, which has an obvious unexpected bump, the bump in the 737-500 becomes milder, as the reduction after the peak is smaller in magnitude. 737-400, however, does not have the bump at all as the idle thrust only increases in the controversial region. The three different patterns within the same aircraft family is worthy of a closer look into the intermediate results for these three aircraft.

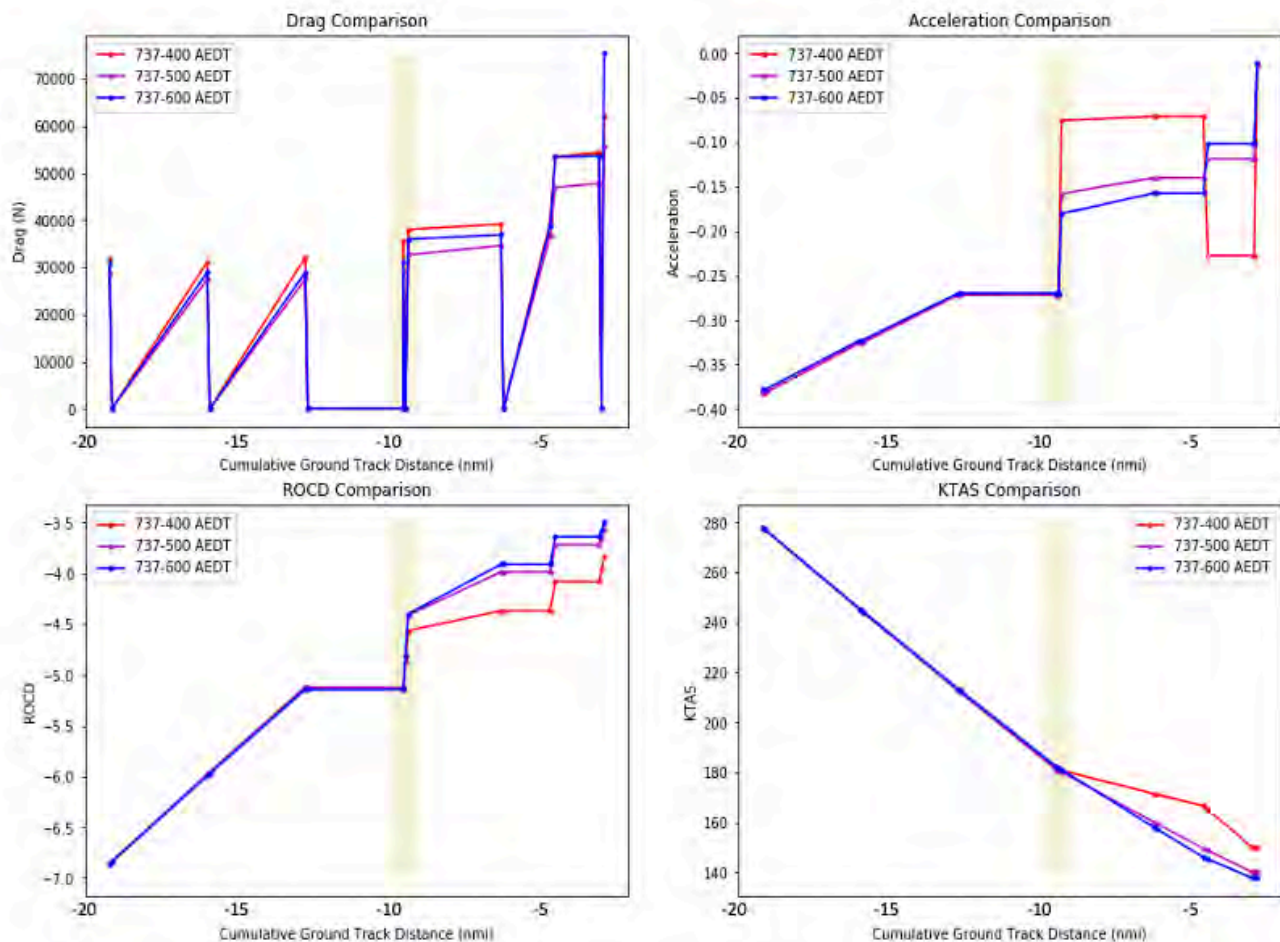


Figure 38. TEM components comparison between the 737 family.

Figure 38 shows the variations of four intermediate outputs for 737-400, 737-500, and 737-600: drag, acceleration, rate of climb (ROCD), and true airspeed (KTAS), which are all key terms in the TEM. In addition, the controversial region is also marked as a shaded region. It is observed that in the controversial region, all four intermediate outputs change trend to some extent. Among the four intermediate outputs, it is observed that acceleration is the most significant driving factor behind the thrust difference within the same 737 family. 737-400 has the smallest acceleration in absolute value, which leads to the only increasing thrust case among the three aircraft. On the other hand, 737-500 and 737-600 transit to more negative accelerations in the controversial region. In TEM, they result in a thrust reduction after the transition and cause a thrust bump. In conclusion, in the BADA4 idle thrust model, the unexpected thrust bump in the transition near 10 nmi from touchdown is mainly affected by the acceleration level of the aircraft.

### Profile editor testing

System testing and evaluation of AEDT's user-defined profile editor feature is conducted with the intent to verify both the functionality of graphical user interface (GUI) elements and the validity of performance results. Initial analysis consists of tests examining AEDT's response to conventional and unorthodox usage of the profile editor GUI shown in Figure 39, whereby parameters within both copies of existing profiles and newly generated alternatives are varied in an attempt to evaluate the feature. Existing arrival and departure profiles face alterations to weight, flap ID, airspeed, thrust and angle parameters across a range of values—both practical and infeasible—to discern AEDT's response to GUI alterations. Additional profiles are created with random step type combinations to confirm AEDT's capacity to reject and/or display warnings when

detecting irreconcilable profile components. This battery of tests demonstrates the full functionality of the profile editor GUI and reveals only a single bug (where modifications to thrust level under the BADA-4 tab result in program crashes) which has been reported and resolved.

Demonstrating GUI functionality facilitates the next round of testing, focused on ensuring the presence of accurate performance disparities across different profiles. Delayed deceleration approach (DDA) ([http://atmseminar.org/seminarContent/seminar12/papers/12th\\_ATM\\_RD\\_Seminar\\_paper\\_119.pdf](http://atmseminar.org/seminarContent/seminar12/papers/12th_ATM_RD_Seminar_paper_119.pdf)) is chosen as the candidate for comparison based on its ease of implementation within the profile editor, its clearly discernible differences across performance, noise, and emissions during real-word tests, and its potential for implementation across a number of U.S. airports.

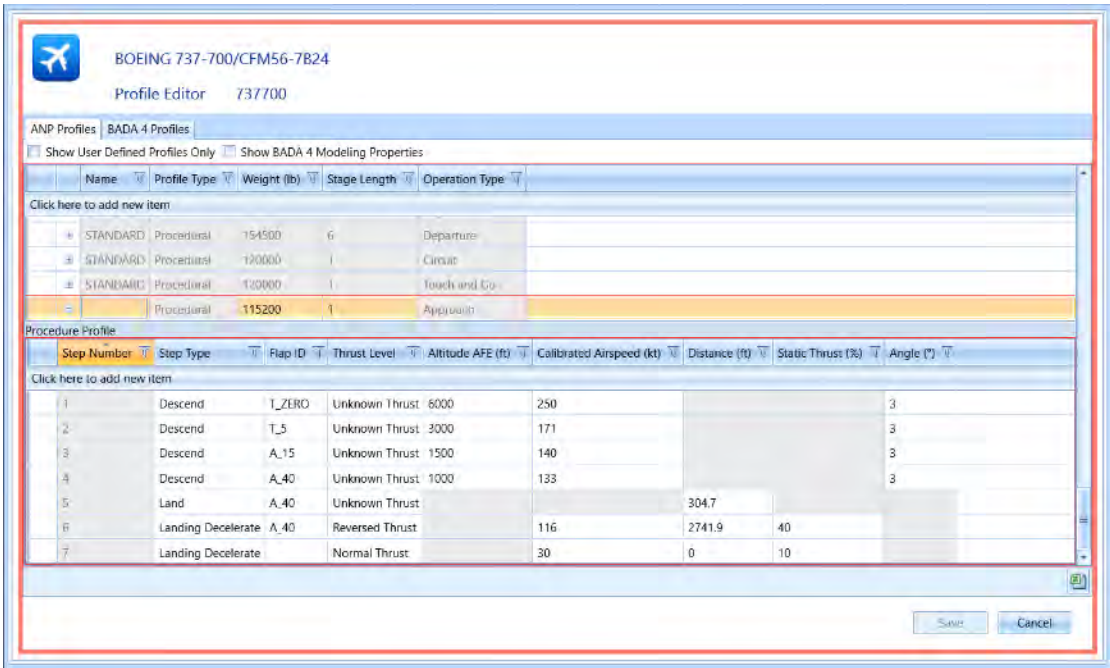


Figure 39. User-defined profile editor GUI.

Implementation of the DDA profile is preceded by the definition of a standard arrival procedure for comparison, shown in Table 17. Whereas the standard profile is quick to lower speed and deploy flaps, DDA profiles maintain their initial airspeed and delay flap deployment to reduce drag and engine power requirements. This results in a matching trajectory between both approaches and a linearly shifted (i.e. delayed) groundspeed profile in the latter case. Research thus far reveals varying degrees of correlation between speed and flap deployment on fuel savings and noise reductions across different aircraft but generally prioritizes the role of the latter in the B777 and A320 lines. The A320-211 is chosen as the test aircraft based on its prevalence in the industry alongside the KATL airport owing to its potential savings from DDA utilization.



**Table 17.** A320-211 standard arrival procedure

Step Number	Step Type	Flap ID	Thrust Level	Altitude—AFE (ft)	Airspeed (kts)	Distance (ft)	Static Thrust (%)	Angle (°)
1	Idle Thrust Descend	A_00	Idle Thrust	6000	248.93			3
2	Idle Thrust Level	A_00	Idle Approach	3000	249.5	5437		
3	Idle Thrust Level	A_01	Idle Approach	3000	187.18	3671		
4	Idle Thrust Level	A_05	Idle Approach	3000	174.66	5209		
5	Level	A_15	Unknown Thrust	3000	151.41	25000		
6	Descend	A_30	Unknown Thrust	3000	139.11			3
7	Land	A_30	Idle Approach			393.8		
8	Landing Decelerate		Reversed Thrust		139	3837.5	40	
9	Landing Decelerate		Normal Thrust		30	0	10	

Step 5 (highlighted in red) is absent in AEDT’s default arrival profile for the A320 and manually added to create a flexible level step simulating the effects of traditional and delayed approach. The same profile feature is recast as Step 2 in Table 18, which models extended time at higher altitudes to mimic a delayed approach.

**Table 18.** A320-211 DDA procedure

Step Number	Step Type	Flap ID	Thrust Level	Altitude—AFE (ft)	Airspeed (kts)	Distance (ft)	Static Thrust (%)	Angle (°)
1	Idle Thrust Descend	A_00	Idle Thrust	6000	248.93			3
2	Level	A_00	Idle Approach	3000	249.5	25000		
3	Idle Thrust Level	A_00	Idle Approach	3000	249.5	5437		
4	Idle Thrust Level	A_01	Idle Approach	3000	187.18	3671		
5	Idle Thrust Level	A_05	Idle Approach	3000	174.66	5209		
6	Descend	A_30	Unknown Thrust	2817	139.11			3
7	Land	A_30	Idle Approach			393.8		
8	Landing Decelerate		Reversed Thrust		139	3837.5	40	
9	Landing Decelerate		Normal Thrust		30	0	10	

Figure 40 examines the noise contours of the standard and DDA A320 profiles and reveals a noticeable reduction in noise across all decibel (dB) ranges. The 5–10% difference in contour area present across all noise levels conforms to values demonstrated in literature and confirms the accuracy of the profile editor with regards to its impact on noise calculations.

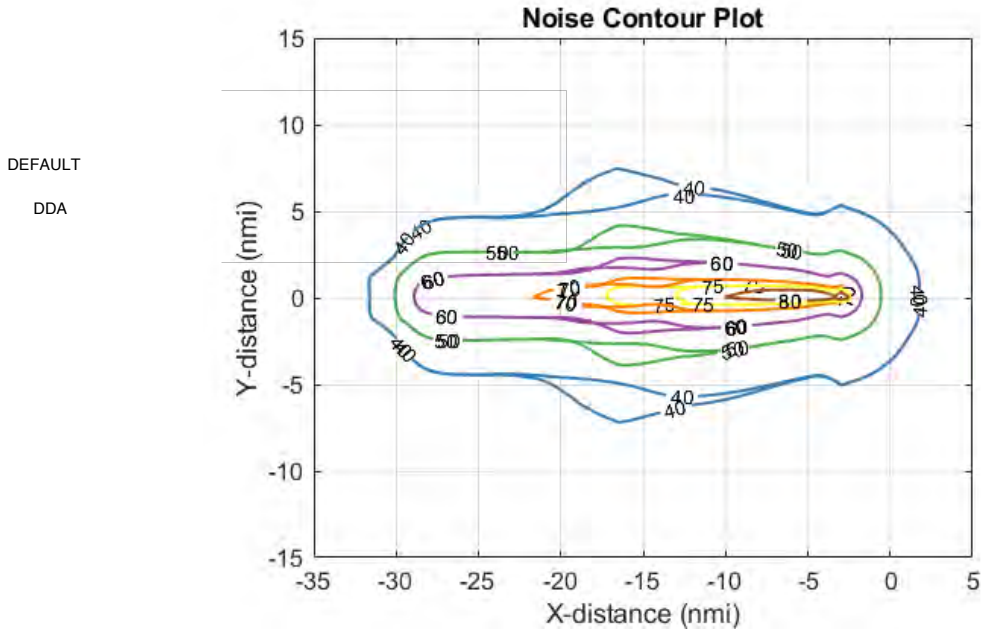


Figure 40. Noise contours for default and DDA profiles.

Figure 41 shows the general performance characteristics of default approach and DDA and reveals an identical trajectory and different ground speeds. These observations are once again validated by the literature, which aims to maintain a consistent trajectory and shift speed alterations to produce the noise reductions shown above.

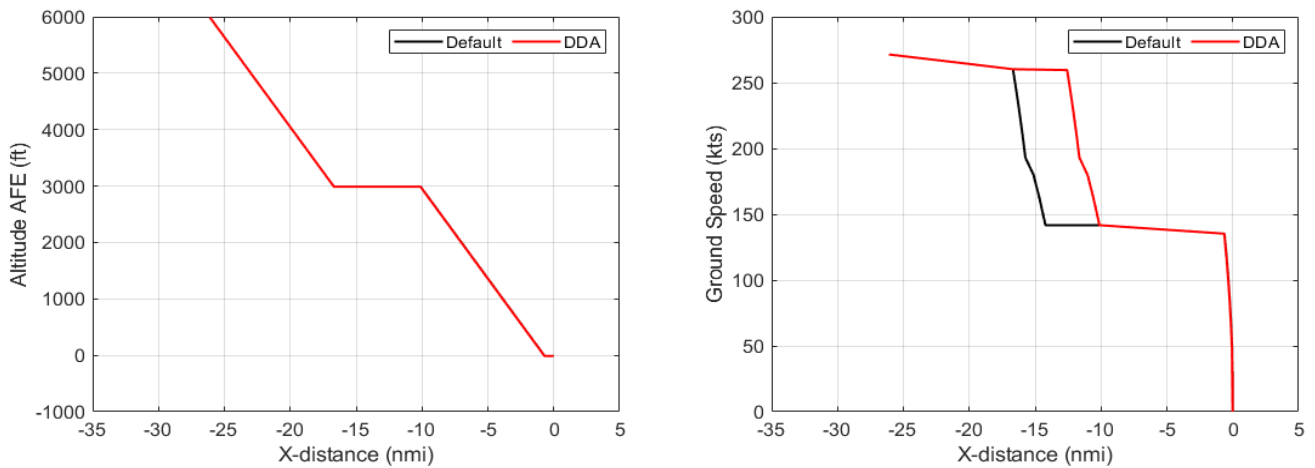
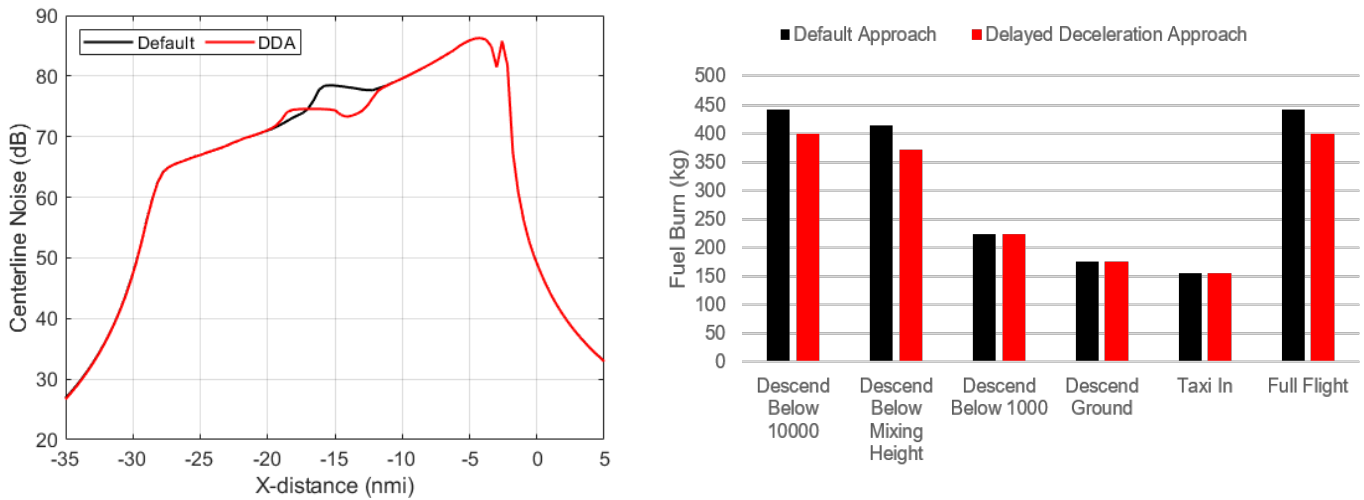


Figure 41. Default and DDA trajectory and speed.

Finally, Figure 42 displays centerline noise and compares fuel burn across each phase of arrival between both profiles. The graphs fall in line with earlier results, reiterate the overall reduction in noise, and confirm the reduction in DDA emissions.



**Figure 40.** Default and DDA centerline noise and emissions.

The successful generation of a DDA profile in accordance with the literature validates the functionality of the profile editor with respect to the modeling of conventional profiles and moderate deviations from standard procedures. The final set of tests models large departures from standard profiles and incorporates impractical or infeasible profile elements to determine AEDT’s response to unexpected inputs and potential fringe cases. The 737-800 and A320-211 aircraft are used to model variations in weight, step sequence, ground speed, and flap orientation across departures and arrivals at KATL.

Figure 43 and Figure 44 show the impact of weight variation on the 737-800’s arrival and departure performance respectively. Attempts to input negative or zero weight values during profile creation cause errors as expected; however, AEDT is robust in handling all positive weight values and generates accurate performance results across a wide range of weights. Values between 50,000–1,000,000 lbs are input to examine AEDT’s response and none cause errors despite their infeasibility.

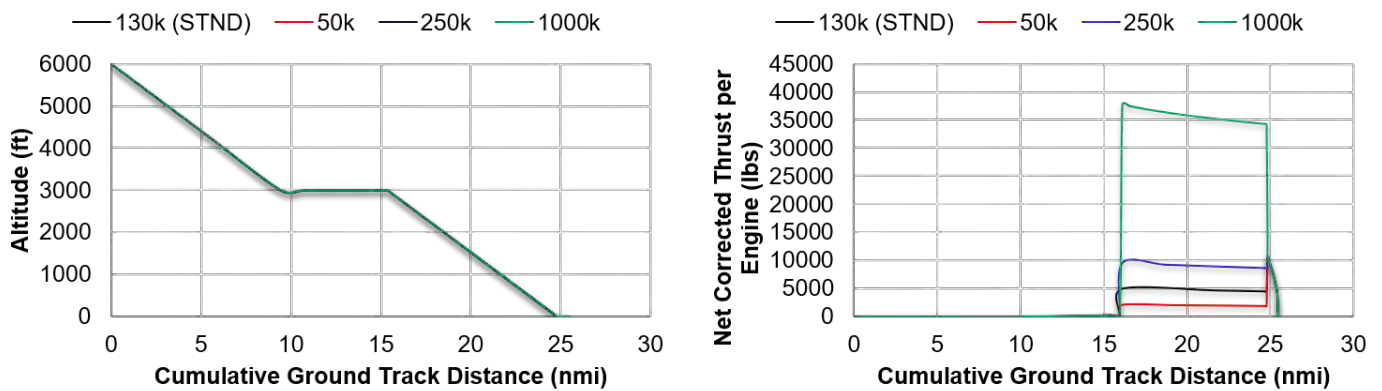


**Figure 41.** Comparing B737-800 arrival weights.

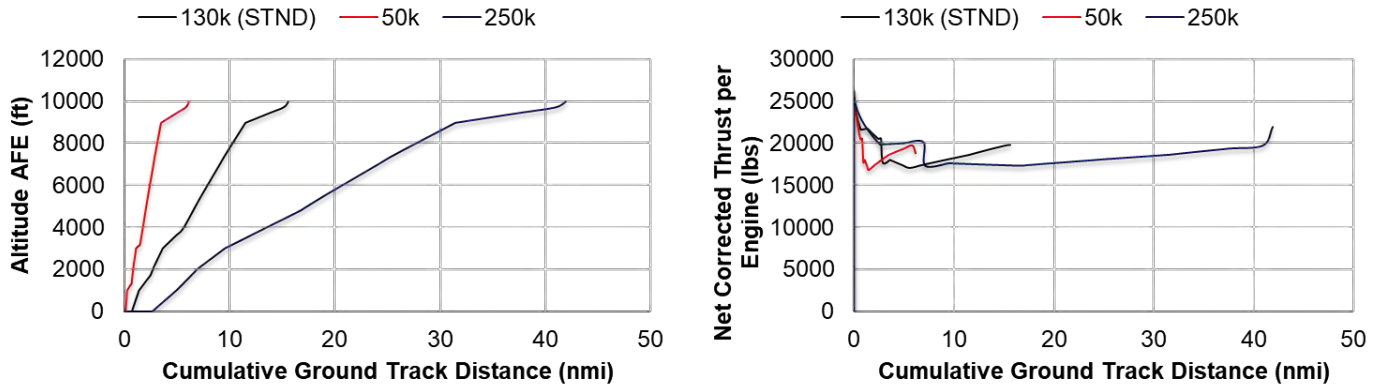


Figure 42. Comparing B737-800 departure weights.

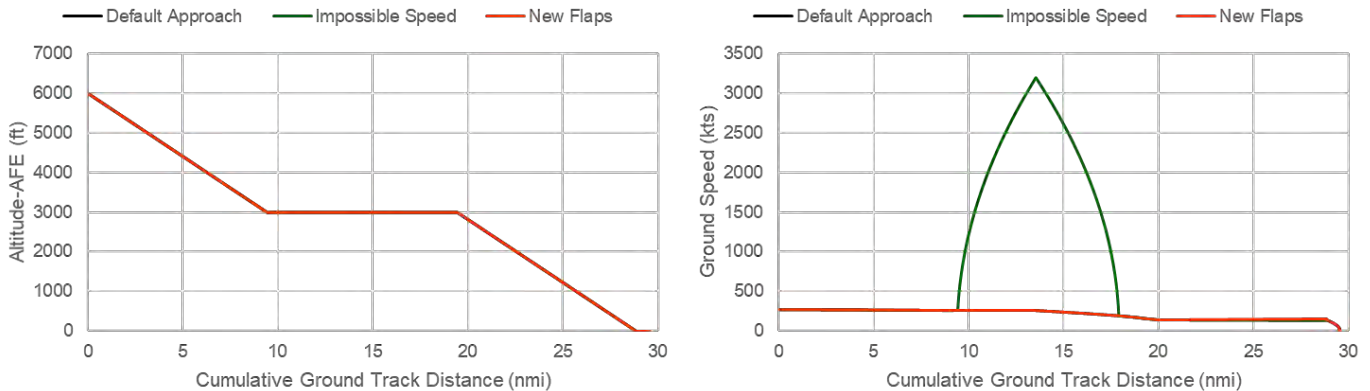
Alterations in weight are followed by modifications to arrival and departure steps to introduce new elements. The standard arrival profile is changed to begin with landing steps (as opposed to the default idle-step descent) and departure is modified to exhibit decreases in altitude and begin with climb and acceleration steps (rather than the default takeoff steps). All of these changes yield errors upon attempting to run the created profiles, with the log files indicating that ANP procedures can only begin with level flight, descent, takeoff ground roll, or cruise climb and cannot experience altitude decreases during climb and increases during descent.

Table 19 and Figure 45 compare the standard A320-211 departure profile to its modified counterparts, where flap settings and ground speeds are modified beyond conventional boundaries. AEDT demonstrates robustness in both cases, managing to capture the slight differences owing to flap variation and model a reasonable interpretation of performance owing to a climb speed of 3000 kts without any errors.

The range of tests examining AEDT’s response to variations in weight, step types, flap settings, and ground speeds indicates the profile editor’s capacity to handle both theoretical and physical impossibilities. Inputting exceedingly high speeds and flap settings continue to generate fairly accurate results and attempts at altering fundamental parameters such as departure or arrival sequencing and using negative weight causes errors with clear explanations in the log file.

Table 19. Comparing A320-211 departure flap and ground speed settings

Step Number	Step Type	Flap ID	Thrust Level	Altitude—AFE (ft)	Airspeed (kts)	Climb Rate (ft/min)
1	Takeoff	1+F	Max Takeoff		0	
2	Climb	1+F	Max Takeoff	1000		
3	Accelerate	1+F	Max Takeoff		186.2	1150.5
4	Accelerate	1	Max Takeoff		208.1	1300.7
5	Climb	ZERO	Max Climb	3000		
6	Accelerate	ZERO/1+F	Max Climb		3000/250	1230.7
7	Climb	ZERO/1+F	Max Climb	5500		
8	Climb	ZERO	Max Climb	7500		
9	Climb	ZERO	Max Climb	10000		



**Figure 43.** Comparing A320-211 departure flap and ground speed settings.

Considered in conjunction, the profile editor tests demonstrate GUI functionality and is capable of producing expected results for performance and noise metrics.

### Emissions Dispersion Computational Efficiencies

#### Background

Previous investigations have shown that emissions metrics in AEDT are more computationally expensive to run relative to other metrics. Georgia Tech was tasked to investigate whether this feature persisted and whether previous recommendations were still valid.

#### Approach

Two-step process:

1. Run study cases on a local machine  
STUDY\_DULLES was used to test if the feature persisted for one emissions dispersion and one emissions metric. Run times were documented and the study was backed up to a server.
2. Run the study on a different machine that enables Visual Studio profiling tools  
The study was retrieved from the server and rerun on a different machine with Visual Studio 2017 installed. Visual Studio profiling tools were used to investigate performance issues pertaining to the study. Visual Studio diagnostic capabilities analyzed memory and CPU usage, among others.

#### Results

This analysis was done using the performance profiling tools in Visual Studio 2017 running the main ribbon GUI in debug mode from within Visual Studio on a workstation machine with a six core (12 threads) Xeon CPU with 48Gb of memory, and a 1 Tb NVme system drive.

1. Emissions dispersion metric  
Figures 49 to Figure 51 show snapshots of the memory and CPU status timeline when running the emissions dispersion metric. The snapshots show memory usage and CPU performance while loading the study, processing operations, results extraction and generation, and finally results retrieval.
2. Emissions metric  
Figures 52 to Figure 57 show snapshots of the memory and CPU status timeline when running the emissions metric. The snapshots show memory usage and CPU performance while loading the study, processing operations, results extraction and generation, and finally results retrieval.

Moreover, Figures 58 to Figure 61 show further investigation into event processing threads, which were carefully isolated to identify opportunities for computational run time reductions.

Name	29% CPU	41% Memory	1% Disk	0% Network	3% GPU
> SQL Server Windows NT - 64 Bit	0.2%	7,435.3 MB	0 MB/s	0 Mbps	0%
> Microsoft Visual Studio 2017 (32 bit) (15)	13.5%	6,337.5 MB	0.4 MB/s	0 Mbps	6.9%
> AEDT (5)	2.5%	4,342.8 MB	0 MB/s	0 Mbps	0%

Figure 44. Task manager – Visual Studio CPU load.

Managed Memory (AEDT.exe)      Compare to: Select baseline      Search type names

Object Type	Count	Size (Bytes)	Inclusive Size (Bytes)
ResourceDictionary	792	171,808	96,137,792
ResourceDictionaryCollection	317	20,288	43,680,760
List<ResourceDictionary>	318	28,640	43,632,616
SystemResources+ResourceDictionaries	13	2,264	39,421,456
Hashtable	2,146	7,236,976	36,259,200
FAA.AEE.AEDT.GUI.View.Ribbon.App	1	232	36,158,928
FAA.AEE.AEDT.GUI.View.Ribbon.Windows.MainWindow	1	3,536	34,519,064
FAA.AEE.AEDT.DataAccessModule.Cache.AirportCacheSingleton	1	240	26,072,656
FAA.AEE.AEDT.GUI.View.Ribbon.Model.Study.Metrics.OperationsGroupNode	4	976	25,736,448
Lazy<FAA.AEE.AEDT.GUI.View.Ribbon.ViewModel.Workspaces.OperationGr...	1	40	25,736,400
Lazy+Boxed<FAA.AEE.AEDT.GUI.View.Ribbon.ViewModel.Workspaces.Oper...	1	24	25,736,296
FAA.AEE.AEDT.GUI.View.Ribbon.ViewModel.Workspaces.OperationGroupW...	1	168	25,736,272
Telerik.Windows.Data.RadObservableCollection<FAA.AEE.AEDT.GUI.View.Ri...	1	104	25,735,144
List<FAA.AEE.AEDT.GUI.View.Ribbon.Model.Study.Metrics.OperationsGrou...	1	96	25,735,016
Telerik.Windows.Data.RadObservableCollection<FAA.AEE.AEDT.CommonD...	4	416	25,734,000
List<FAA.AEE.AEDT.CommonDataObjects.Study.Metrics.IOperation>	4	262,384	25,733,488
FAA.AEE.AEDT.CommonDataObjects.Study.Movement	25,748	25,423,280	25,423,280
Baml2006Reader	327	44,472	18,725,264
List<Object>	30,691	4,707,800	17,356,848

Figure 45. Memory usage after loading study before run.

Managed Memory (AEDT.exe)      Compare to: Select baseline      Search type names

Object Type	Count	Size (Bytes)	Inclusive Size (Bytes)
ArrayList	65,058	4,355,888	386,455,304
log4net.Core.LogImpl	68	4,352	379,426,048
log4net.Repository.Hierarchy.DefaultLoggerFactory+LoggerImpl	68	7,960	379,424,576
log4net.Repository.Hierarchy.RootLogger	1	112	379,405,800
log4net.Util.AppenderAttachedImpl	1	72	379,405,664
FAA.AEE.AEDT.Utilities.MemoryAppenderWithEvents	1	160	379,402,680
log4net.Core.LoggingEvent	60,935	21,961,384	378,878,088
log4net.Core.LocationInfo	60,935	44,592,352	337,001,160
log4net.Core.StackFrameItem	958,974	201,449,896	292,408,936
log4net.Core.MethodItem	958,974	146,283,848	126,150,504
ResourceDictionary	792	159,952	55,682,008
FAA.AEE.AEDT.CommonDataObjects.Results.EmissionsEventResult	720	86,400	55,282,880
List<FAA.AEE.AEDT.CommonDataObjects.Results.EmissionsEventResult>	1	8,064	55,271,416
Hashtable	184,920	31,767,680	35,083,776
FAA.AEE.AEDT.CommonDataObjects.Movements.Event	720	214,376	29,648,528
FAA.AEE.AEDT.CommonDataObjects.Fleet.Aircraft.Airplane	699	201,352	27,920,784
FAA.AEE.AEDT.CommonDataObjects.Fleet.AircraftClass.AircraftClass	699	117,432	25,614,344
ResourceDictionaryCollection	317	20,288	25,509,832

Figure 46. Memory snapshot while processing operations.

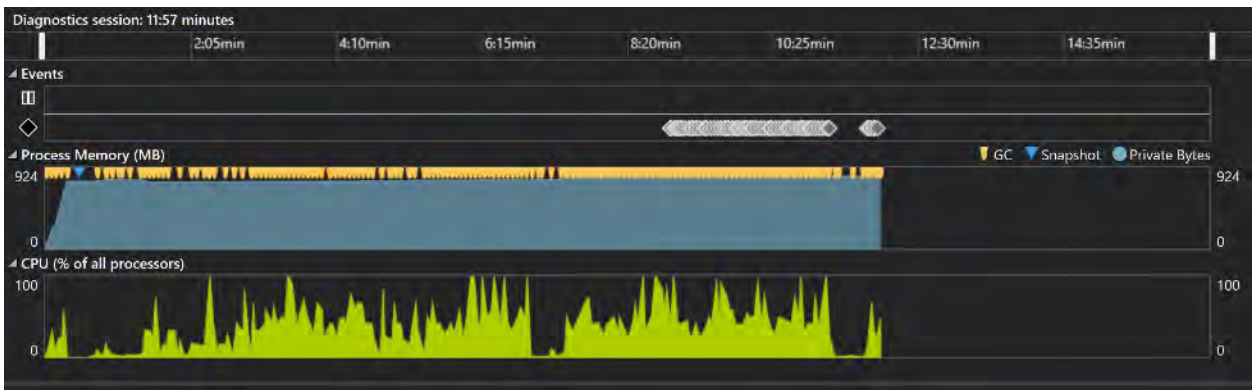


Figure 47. Processing operations.

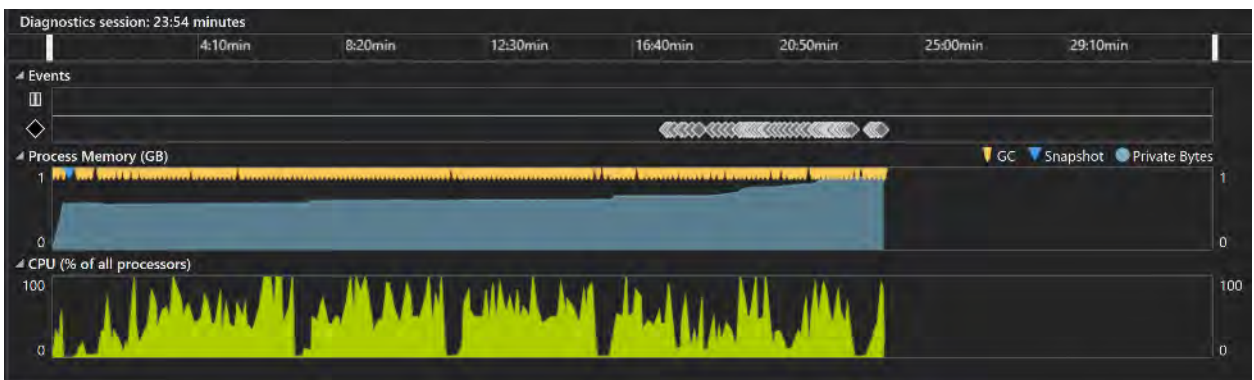


Figure 48. Start of result extraction after completing results generation, showing increase in memory use.

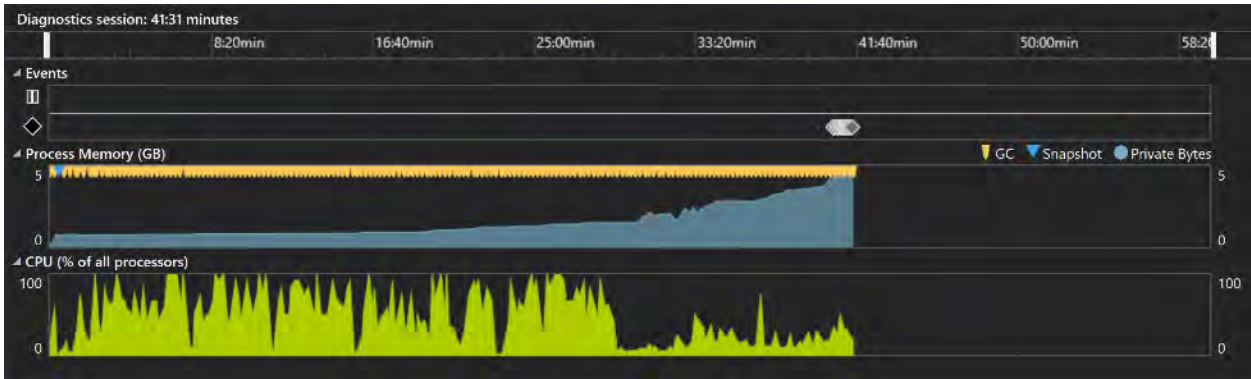


Figure 49. Retrieving event results.

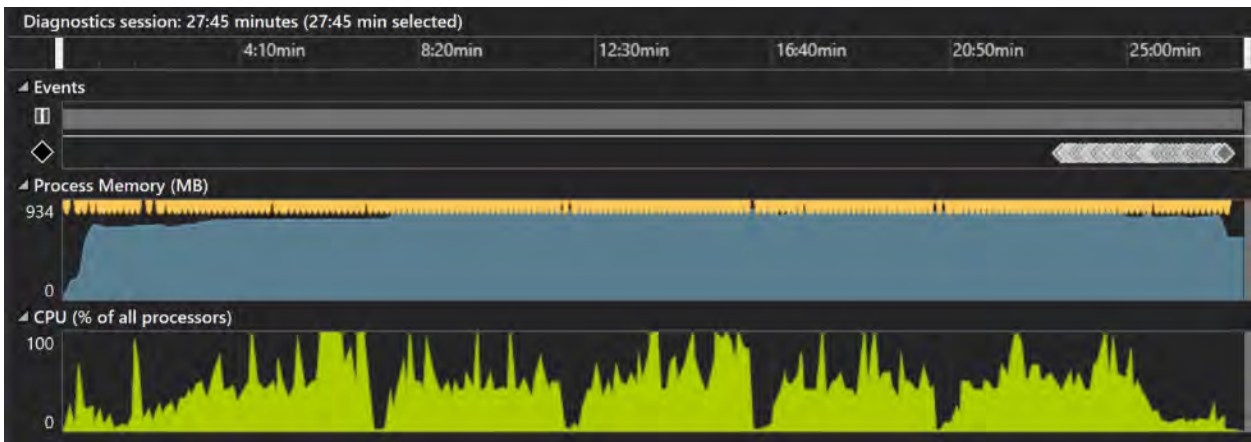


Figure 50. Overall snapshot of performance profiling.



Figure 51. Application start and loading STUDY\_DULLES (highlighted in yellow).

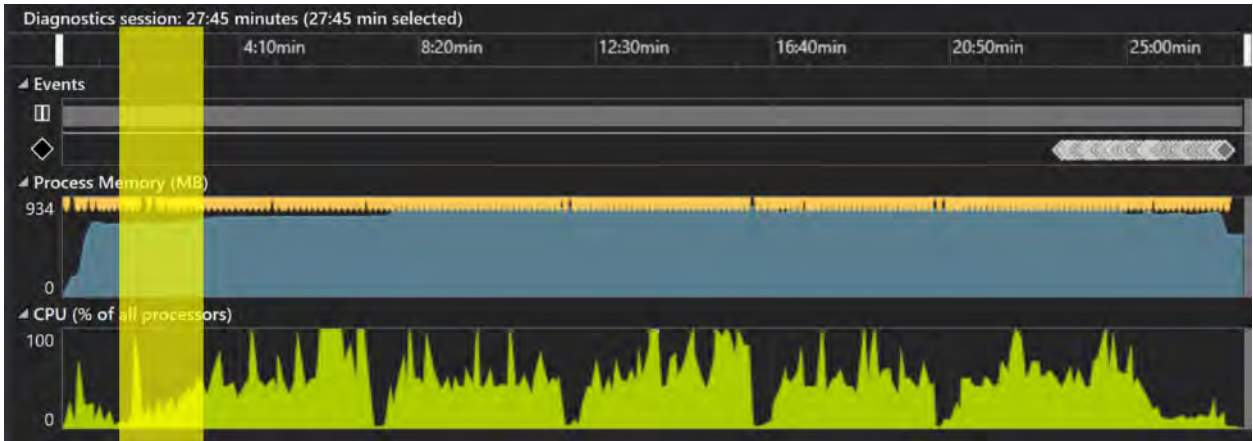


Figure 52. Run metric results and initial warmup (highlighted in yellow).

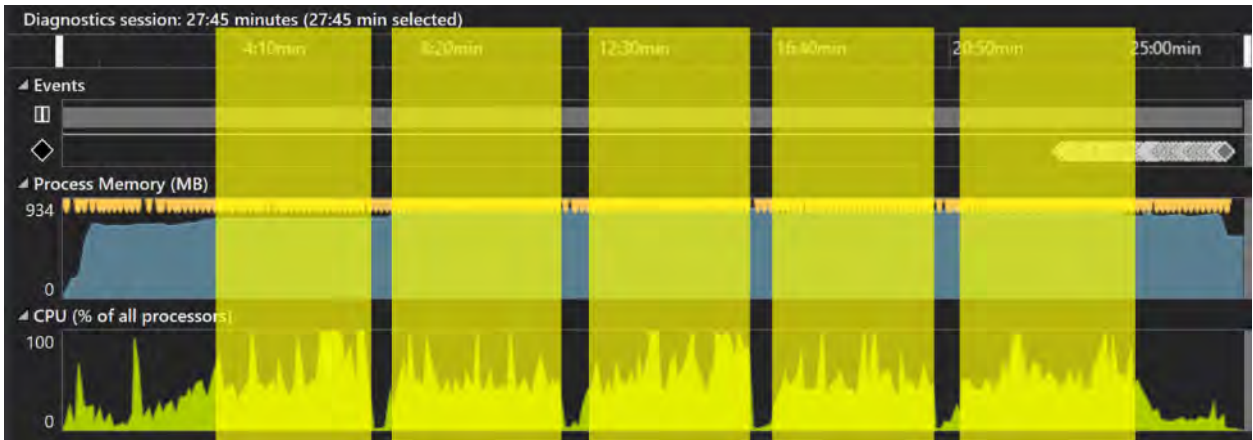


Figure 53. Processing operations (highlighted in yellow), appears to be a reasonable CPU load for hyper-threading.

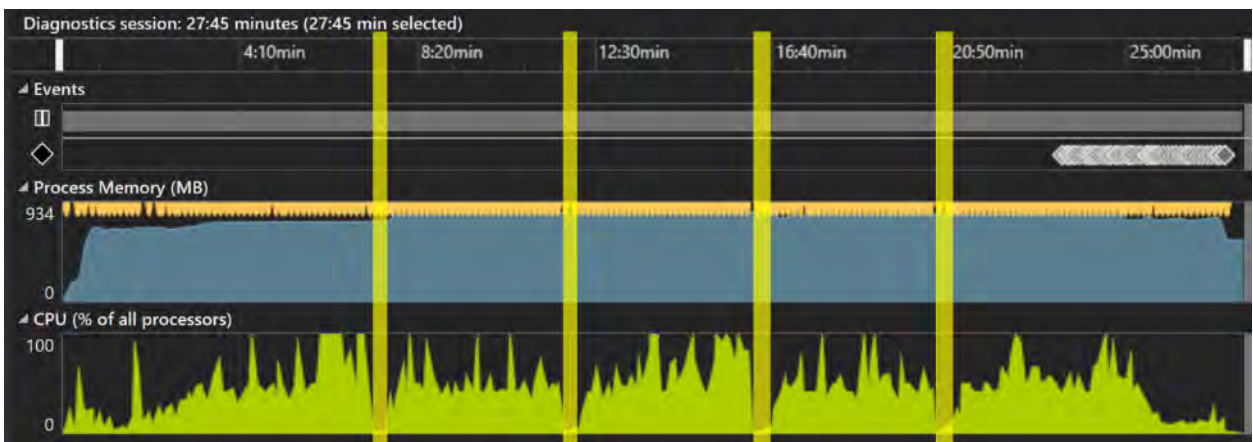


Figure 54. ~20 second pauses (highlighted in yellow). Unclear why this happens given no obvious memory or SQL delay.

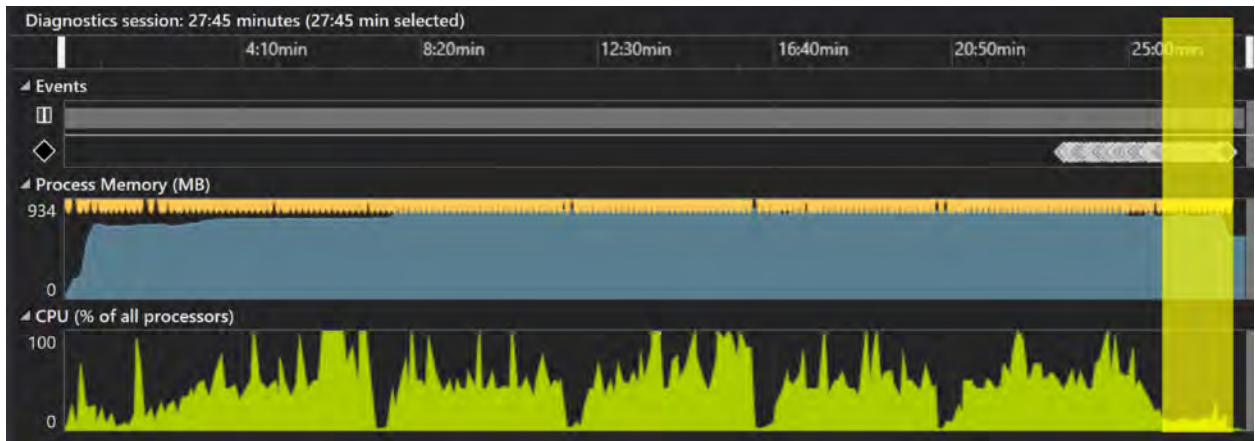


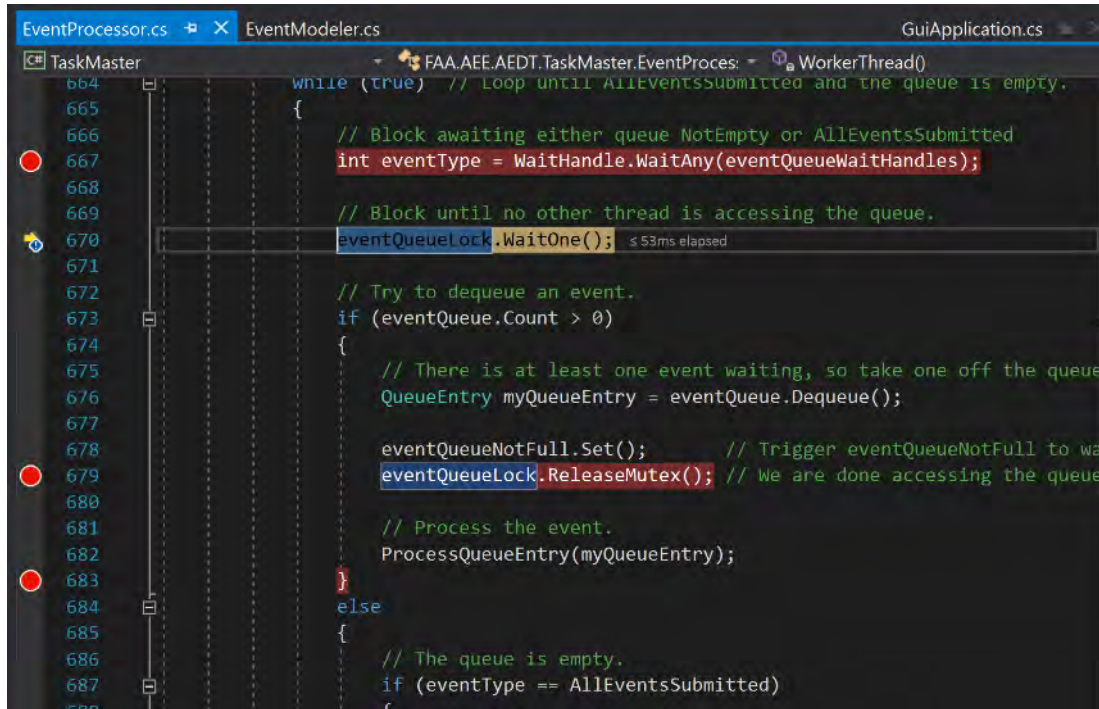
Figure 55. Reloading study and airport data and waiting for user input (highlighted in yellow).

```

EventProcessor.cs  EventModeler.cs  GuiApplication.cs
TaskMaster
664 while (true) // Loop until AllEventsSubmitted and the queue is empty.
665 {
666     // Block awaiting either queue NotEmpty or AllEventsSubmitted
667     int eventType = WaitHandle.WaitAny(eventQueueWaitHandles);
668
669     // Block until no other thread is accessing the queue.
670     eventQueueLock.WaitOne();
671
672     // Try to dequeue an event.
673     if (eventQueue.Count > 0)
674     {
675         // There is at least one event waiting, so take one off the queue
676         QueueEntry myQueueEntry = eventQueue.Dequeue();
677
678         eventQueueNotFull.Set(); // Trigger eventQueueNotFull to wa
679         eventQueueLock.ReleaseMutex(); // We are done accessing the queue
680
681         // Process the event.
682         ProcessQueueEntry(myQueueEntry); ≤ 59ms elapsed
683     }
684     else
685     {
686         // The queue is empty.
687         if (eventType == AllEventsSubmitted)
688         {

```

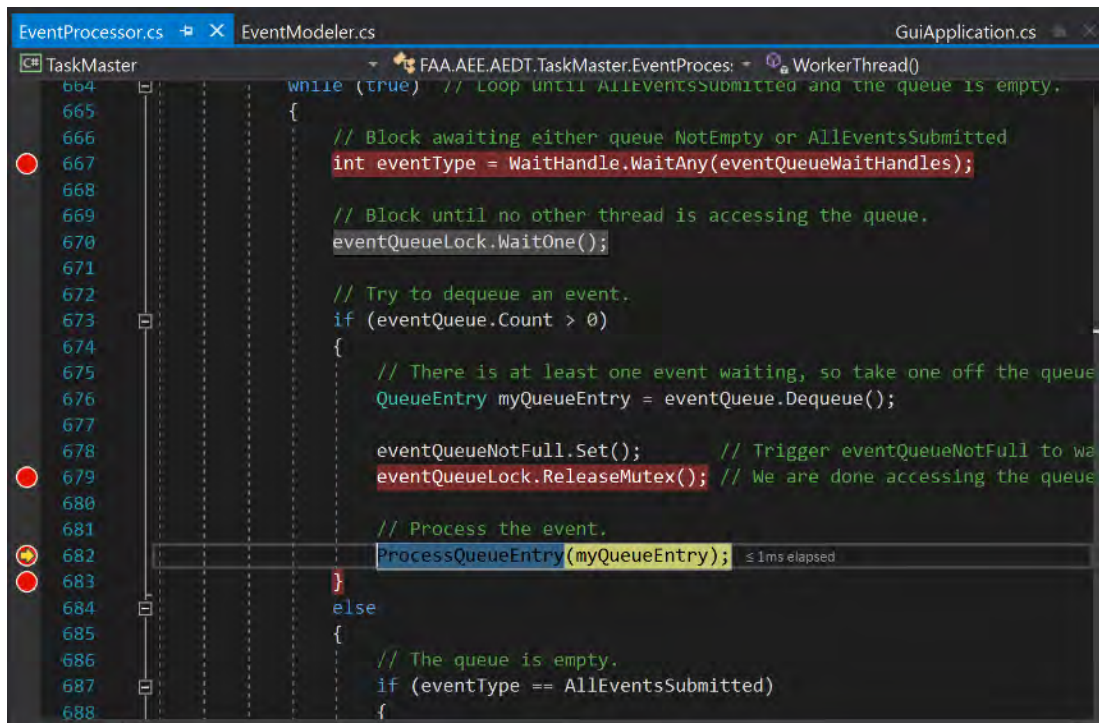
Figure 56. Event processing code for a single thread.

```

EventProcessor.cs | EventModeler.cs | GuiApplication.cs
TaskMaster
664 while (true) // Loop until AllEventsSubmitted and the queue is empty.
665 {
666 // Block awaiting either queue NotEmpty or AllEventsSubmitted
667 int eventType = WaitHandle.WaitAny(eventQueueWaitHandles);
668 // Block until no other thread is accessing the queue.
669 eventQueueLock.WaitOne(); ≤ 53ms elapsed
670 // Try to dequeue an event.
671 if (eventQueue.Count > 0)
672 {
673 // There is at least one event waiting, so take one off the queue
674 QueueEntry myQueueEntry = eventQueue.Dequeue();
675 eventQueueNotFull.Set(); // Trigger eventQueueNotFull to wa
676 eventQueueLock.ReleaseMutex(); // We are done accessing the queue
677 // Process the event.
678 ProcessQueueEntry(myQueueEntry);
679 }
680 else
681 {
682 // The queue is empty.
683 if (eventType == AllEventsSubmitted)
684 {
685 }
686 }
687 }
688 }
    
```

Figure 57. Time spent to block in line 667 was 53ms.



```

EventProcessor.cs | EventModeler.cs | GuiApplication.cs
TaskMaster
664 while (true) // Loop until AllEventsSubmitted and the queue is empty.
665 {
666 // Block awaiting either queue NotEmpty or AllEventsSubmitted
667 int eventType = WaitHandle.WaitAny(eventQueueWaitHandles);
668 // Block until no other thread is accessing the queue.
669 eventQueueLock.WaitOne();
670 // Try to dequeue an event.
671 if (eventQueue.Count > 0)
672 {
673 // There is at least one event waiting, so take one off the queue
674 QueueEntry myQueueEntry = eventQueue.Dequeue();
675 eventQueueNotFull.Set(); // Trigger eventQueueNotFull to wa
676 eventQueueLock.ReleaseMutex(); // We are done accessing the queue
677 // Process the event.
678 ProcessQueueEntry(myQueueEntry); ≤ 1ms elapsed
679 }
680 else
681 {
682 // The queue is empty.
683 if (eventType == AllEventsSubmitted)
684 {
685 }
686 }
687 }
688 }
    
```

Figure 58. Time spent to get to ProcessQueueEntry from block was <1 ms.



```

664 while (true) // Loop until AllEventsSubmitted and the queue is empty.
665 {
666     // Block awaiting either queue NotEmpty or AllEventsSubmitted
667     int eventType = WaitHandle.WaitAny(eventQueueWaitHandles);
668
669     // Block until no other thread is accessing the queue.
670     eventQueueLock.WaitOne();
671
672     // Try to dequeue an event.
673     if (eventQueue.Count > 0)
674     {
675         // There is at least one event waiting, so take one off the queue
676         QueueEntry myQueueEntry = eventQueue.Dequeue();
677
678         eventQueueNotFull.Set(); // Trigger eventQueueNotFull to wa
679         eventQueueLock.ReleaseMutex(); // We are done accessing the queue
680
681         // Process the event.
682         ProcessQueueEntry(myQueueEntry);
683         // <= 8ms elapsed
684     }
685     else
686     {
687         // The queue is empty.
688         if (eventType == AllEventsSubmitted)
        {

```

Figure 59. Time spent in ProcessQueueEntry was <8ms.

**Recommendations**

1. Emissions Dispersion

Attempts have been made to check if query can be improved using the SQL database tuning advisor. As shown in Figure 62, the estimated performance improvement was about 9%, which is less than a millisecond. This shows that only small improvements could be gained. The bigger issue was the 3-4 milliseconds for connection resets, shown in Figure 63, and the resulting lag from doing so repeatedly.

Database Name	Object Name	Recommendation	Target of Recommendation	Details	Partition Scheme	Size (KB)	Definition
STUDY_DULLES	[dbo].[AIR_OPERATION]	create	_jta_stat_457768688_1_2				[AIR_OP_ID].[AIRCRAFT_ID]
STUDY_DULLES	[dbo].[INPUT_TRAJECTORY_PART]	create	_jta_index_INPUT_TRAJECTORY_PART_11_...			11784	[INPUT_TRAJECTORY_ID].[INP_INPUT_TRAJECTORY_PART_ID]
STUDY_DULLES	[dbo].[RSLT_EVENTS]	create	_jta_stat_486292792_1_14_8_17_6				[RSLT_EVENT_ID].[AIR_OP_ID].[INPUT_TRAJECTORY_ID].[RU...
STUDY_DULLES	[dbo].[RSLT_EVENTS]	create	_jta_stat_486292792_1_17				[RSLT_EVENT_ID].[IRUNUP_ID]
STUDY_DULLES	[dbo].[RSLT_EVENTS]	create	_jta_stat_486292792_1_6				[RSLT_EVENT_ID].[ARRIVAL_AIRPORT_LAYOUT_ID]
STUDY_DULLES	[dbo].[RSLT_EVENTS]	create	_jta_stat_486292792_1_8_17_6_5_14				[RSLT_EVENT_ID].[INPUT_TRAJECTORY_ID].[IRUNUP_ID].[IAR...
STUDY_DULLES	[dbo].[RSLT_EVENTS]	create	_jta_stat_486292792_6_5_1_8				[ARRIVAL_AIRPORT_LAYOUT_ID].[DEPARTURE_AIRPORT_LAY...
STUDY_DULLES	[dbo].[RSLT_EVENTS]	create	_jta_stat_486292792_8_17_6_5_14				[INPUT_TRAJECTORY_ID].[IRUNUP_ID].[ARRIVAL_AIRPORT_L...

Figure 60. SQL database tuning advisor showing an estimated improvement of 9%.

TextData	ApplicationName	NTUserName	LoginName	CPU	Reads	Writes	Duration	ClientProcessID	SPID	StartTime	EndTime
exec sp_reset_connection	..Net SqlCl1e...	ae-hp52	AD\ae...	0	0	0	0	0	27664	65 2020-05-27 13:27:09.037	2020-05-27 13:27:09.037
exec sp_executesql N'SELECT [to].[RS...	..Net SqlCl1e...	ae-hp52	AD\ae...	0	18	0	0	0	27664	65 2020-05-27 13:27:09.037	2020-05-27 13:27:09.037
exec sp_executesql N'SELECT [to].[SU...	..Net SqlCl1e...	ae-hp52	AD\ae...	0	0	0	0	0	27664	65 2020-05-27 13:27:09.040	2020-05-27 13:27:09.040
exec sp_reset_connection	..Net SqlCl1e...	ae-hp52	AD\ae...	0	0	0	0	0	27664	65 2020-05-27 13:27:09.040	2020-05-27 13:27:09.040
exec sp_executesql N'SELECT [to].[RS...	..Net SqlCl1e...	ae-hp52	AD\ae...	0	18	0	0	0	27664	65 2020-05-27 13:27:09.040	2020-05-27 13:27:09.040
exec sp_executesql N'SELECT [to].[SU...	..Net SqlCl1e...	ae-hp52	AD\ae...	0	0	0	0	0	27664	65 2020-05-27 13:27:09.043	2020-05-27 13:27:09.043
exec sp_reset_connection	..Net SqlCl1e...	ae-hp52	AD\ae...	0	0	0	0	0	27664	65 2020-05-27 13:27:09.047	2020-05-27 13:27:09.047
exec sp_executesql N'SELECT [to].[RS...	..Net SqlCl1e...	ae-hp52	AD\ae...	0	18	0	0	0	27664	65 2020-05-27 13:27:09.047	2020-05-27 13:27:09.047
exec sp_executesql N'SELECT [to].[SU...	..Net SqlCl1e...	ae-hp52	AD\ae...	0	0	0	0	0	27664	65 2020-05-27 13:27:09.047	2020-05-27 13:27:09.047
exec sp_reset_connection	..Net SqlCl1e...	ae-hp52	AD\ae...	0	0	0	0	0	27664	65 2020-05-27 13:27:09.050	2020-05-27 13:27:09.050
exec sp_executesql N'SELECT [to].[RS...	..Net SqlCl1e...	ae-hp52	AD\ae...	0	18	0	0	0	27664	65 2020-05-27 13:27:09.050	2020-05-27 13:27:09.050
exec sp_executesql N'SELECT [to].[SU...	..Net SqlCl1e...	ae-hp52	AD\ae...	0	0	0	0	0	27664	65 2020-05-27 13:27:09.050	2020-05-27 13:27:09.050
exec sp_reset_connection	..Net SqlCl1e...	ae-hp52	AD\ae...	0	0	0	0	0	27664	65 2020-05-27 13:27:09.050	2020-05-27 13:27:09.050
exec sp_executesql N'SELECT [to].[RS...	..Net SqlCl1e...	ae-hp52	AD\ae...	0	18	0	0	0	27664	65 2020-05-27 13:27:09.050	2020-05-27 13:27:09.050
exec sp_executesql N'SELECT [to].[SU...	..Net SqlCl1e...	ae-hp52	AD\ae...	0	0	0	0	0	27664	65 2020-05-27 13:27:09.050	2020-05-27 13:27:09.050
exec sp_reset_connection	..Net SqlCl1e...	ae-hp52	AD\ae...	0	0	0	0	0	27664	65 2020-05-27 13:27:09.053	2020-05-27 13:27:09.053
exec sp_executesql N'SELECT [to].[RS...	..Net SqlCl1e...	ae-hp52	AD\ae...	0	18	0	0	0	27664	65 2020-05-27 13:27:09.053	2020-05-27 13:27:09.053
exec sp_executesql N'SELECT [to].[SU...	..Net SqlCl1e...	ae-hp52	AD\ae...	0	0	0	0	0	27664	65 2020-05-27 13:27:09.053	2020-05-27 13:27:09.053
exec sp_reset_connection	..Net SqlCl1e...	ae-hp52	AD\ae...	0	0	0	0	0	27664	65 2020-05-27 13:27:09.053	2020-05-27 13:27:09.053
exec sp_executesql N'SELECT [to].[RS...	..Net SqlCl1e...	ae-hp52	AD\ae...	0	18	0	0	0	27664	65 2020-05-27 13:27:09.053	2020-05-27 13:27:09.053
exec sp_executesql N'SELECT [to].[SU...	..Net SqlCl1e...	ae-hp52	AD\ae...	0	0	0	0	0	27664	65 2020-05-27 13:27:09.057	2020-05-27 13:27:09.057
exec sp_reset_connection	..Net SqlCl1e...	ae-hp52	AD\ae...	0	0	0	0	0	27664	65 2020-05-27 13:27:09.057	2020-05-27 13:27:09.057
exec sp_executesql N'SELECT [to].[RS...	..Net SqlCl1e...	ae-hp52	AD\ae...	0	18	0	0	0	27664	65 2020-05-27 13:27:09.057	2020-05-27 13:27:09.057

Figure 61. Connection resets.

Based on the previous documentation, it is not anticipated that any database tuning would result in much improvement. Additionally, the log shows that each of the queries gets run against the same ID what seems to be six or seven times (it is unclear why this is different). The issue needs to be looked into since it seems unnecessary to pull identical queries and results repeatedly this many times.

2. Emissions

Overall, memory usage for the application was limited to ~1Gb and a maximum of ~4-5Gb for the SQL server. CPU usage for the application made a relatively good use of the cores and no large usage was observed for the SQL server. As for the Disk/IO, no obvious impact or memory swap appears to be required, and there appears to be no obvious easy improvements.

A deep dive into event processing queues supports the recommendation to either increase queue length in order to reduce synchronization time, or alternatively rethink the way the queuing and synchronization interact. It should be possible to achieve ~5x speed up.

Milestones

- N/A

Major Accomplishments

High Altitude Airport Study

- Identification of test cases to assess validity of NADP profiles at high altitude airports.

Refinement of Thrust and Weight Assumptions

- Regressions (weight versus GCD) and multilinear regressions (weight vs CGD, airport elevation, and runway length) for each airframe for FOQA data.
- Comparison with previous years' weight model results.
- Plotting and interpretation of the thrust distribution for each airframe conditioning of FOQA data to perform regressions for ANP thrust coefficients.

Comparison of NADP Profiles to Real-world Operations

- Implemented data cleaning process to extract and group real-world flight trajectories for comparison.
- Computed overall altitude and ground speed differences between the two recommended NADP profiles and 1-year departures data from SFO for B737-800, A320-211, and A330-301.

Arrival Profile Modeling

- Produced a baseline Python script to identify level-offs based on a vertical speed tolerance and distance tolerance.
- Developed a systemic statistical method to evaluate the effect of different vertical speed and distance tolerances using a design of experiments.
- Identified key characteristics of arrival profiles and level-offs and began the addition of these capabilities to the baseline Python script.



#### Full Flight Modeling

- Generated a baseline Python script to compare the accuracy of the thread track data with the true model, which is FOQA data.
- Developed a Python script to identify top city pairs from FOQA data and apply the DBSCAN clustering algorithm to find specific trajectory patterns if there is any.

#### System Testing and Evaluation of AEDT

- Creation of a tool capable of automatically generating TGO/CIR profiles for aircraft with procedural profiles in AEDT and validation of these newly created TGO/CIR profiles.
- Conducted in-depth investigations on several AEDT new features on ANP/BADA4 fuel consumption and thrust modeling.
- Performed evaluation and validation on profile editor.
- Investigated the computational efficiency associated with emissions and emissions dispersion modeling and made recommendations to improve the efficiency.

#### Publications

- Behere, A., Bhanpato, J., Puranik, T.G., Li, Y., Kirby, M., Mavris D.N., “Data-driven Approach to Environmental Impact Assessment of Real-World Operations”, in AIAA SciTech Forum 2021

#### Outreach Efforts

Bi-weekly calls with the FAA, Volpe, and ATAC. Bi-annual ASCENT meetings. Attended AIAA Aviation conference to present conference paper publication.

#### Awards

None

#### Student Involvement

Ameya Behere, Eleni Sotiropoulos-Georgiopoulos, Ayaka Miyamoto, Rukmini Roy, Jirat Bhanpato, Hyungu Choi, Bogdan Dorca, Zhenyu Gao, Santusht Sairam, Graduate Research Assistants, Georgia Institute of Technology

#### Plans for Next Period

The primary focus for the next period will be:

- Evaluation of test cases for high altitude airport study.
- Comparison of NADP profiles to real-world operations: Expand comparison to other airports and implement comparison by airline to identify differences in operating procedures.
- For the refinement of thrust assumptions, comparisons with weights per stage length in the AEDT tool.
- Linear regression analysis of FOQA data to obtain ANP thrust coefficients.
- For arrival profile modeling, complete the existing development of the Python script with flight characterization capabilities such that this code may be used to identify arrival profile trends which can then be compared to existing AEDT arrival models.
- For full flight modeling, continue investigating the accuracy of the treaded track data with FOQA data and finding the average behavior for the top city pairs.
- Continue system testing and evaluation.



# Project 055 Noise Generation and Propagation from Advanced Combustors

**Georgia Institute of Technology (GT)**  
**Raytheon Technologies Research Center (RTRC)**

## Project Lead Investigator

Timothy Lieuwen  
Professor  
Aerospace Engineering  
Georgia Institute of Technology  
270 Ferst Drive, G3363 (M/C 0150)  
Atlanta, GA 30332-0150  
Phone: 404-894-3041  
E-mail: tim.lieuwen@aerospace.gatech.edu

## University Participants

### Georgia Institute of Technology

- Pls:
  - Timothy Lieuwen, Professor
  - Suresh Menon, Professor
  - Adam Steinberg, Professor
  - Vishal Acharya, Senior Research Engineer
  - Benjamin Emerson, Senior Research Engineer
  - David Wu, Research Engineer
  - Samuel Grauer, Post-Doctoral Researcher
- FAA Award Number: 13-C-AJFE-GIT-058
- Period of Performance: February 5, 2020 to February 4, 2021
- Tasks:
  1. **Facility Development at GT:** This task addresses the design of experiments that will be performed at GT. The task involves coordination between the teams for developing and defining the aerodynamic design of a Rich-Quench-Lean, quick quench, lean burn (RQL) combustor to study. The task is led by Professor Lieuwen, Professor Steinberg, and Dr. Emerson.
  2. **Simulations of GT experiment:** This task consists of the simulation of the GT experiment focusing on the pre-combustion flow dynamics, flame dynamics, and post-combustion dynamics of pressure and entropy disturbances. This task is led by Prof. Menon.
  3. **Reduced Order Modeling:** This task consists of creating a reduced order modeling framework for the unsteady response of the flame as well as the generation of entropy disturbances due to unsteady heat release. This task is led by Dr. Acharya and Prof. Lieuwen.

### Raytheon Technologies Research Corporation

- Pls:
  - Jeffrey Mendoza, Technical Fellow Acoustics
  - Duane McCormick, Principal Research Engineer
  - Julian Winkler, Staff Research Engineer
  - Peter Cocks, Project Leader, P&W Program Office
  - Lance Smith, Principal Research Engineer
- FAA Award Number: 13-C-AJFE-GIT-058 (sub-award through GT)
- Period of Performance: February 5, 2020 to February 4, 2021



- Tasks:
  4. **Facility Development at RTRC:** This task addresses the design of experiments that will be performed at RTRC. The task involves coordination between the teams for developing and defining the aerodynamic design of an RQL combustor to study. This task is led by Jeffrey Mendoza, Lance Smith, and Duane McCormick.
  5. **Spray Modeling:** This task consists of performing direct numerical simulation (DNS) of the air blast atomizer in the high shear swirler used for both the GT and RTRC experiment. The main goal of this task is to provide inputs for spray modeling used in the GT simulation task. This task is led by Jeff Mendoza and Xiaoyi Li.
  6. **Swirler Impedance Modeling:** This task focuses on modeling the acoustic impedance of the high shear swirler in order to provide boundary conditions for the GT simulations as well as for the direct noise modeling task. This task is led by Jeffrey Mendoza and Duane McCormick.
  7. **Post-Combustion Modeling:** This task consists of both a post-processing and simulation effort. First, data mining the post-combustion simulation data from the simulation of the GT experiment is used to understand the dynamics of entropy fluctuations and their transport. Next, simulations are used to model the propagation of noise in the post-combustion architecture of the engine. The simulations are split across the different sections: nozzle, turbine, and far-field. This task is led by Jeffrey Mendoza and Julian Winkler.

## Project Funding Level

**FAA funding:** \$1,500,000 split equally between Georgia Institute of Technology and sub-awardee Raytheon Technologies Research Corporation.

**Cost-share:** \$1,500,000 total, split equally between Georgia Institute of Technology and Raytheon Technologies Research Corporation.

**Total funding:** \$3,000,000.

## Investigation Team

**Tim Lieuwen (Georgia Institute of Technology):** Principal Investigator. Professor Lieuwen is the lead PI overseeing all tasks. Specifically, he leads the GT experiments and design in Task 1 and 2 along with Professor Steinberg. In addition, he also co-leads the modeling tasks in Task 1 for pre-combustion, flame response, and post-combustion along with Dr. Acharya.

**Adam Steinberg (Georgia Institute of Technology):** Co-Principal Investigator. Professor Steinberg manages the design of experiment diagnostics and the measurements.

**Suresh Menon (Georgia Institute of Technology):** Co-Principal Investigator. Professor Menon is the manager of the simulation tasks for simulations of the GT experiment.

**Vishal Acharya (Georgia Institute of Technology):** Co-Principal Investigator. Dr. Acharya co-manages all modeling tasks for the pre-combustion, combustion, and post-combustion physics along with Professor Lieuwen. In addition, as administrative coordinator, he is responsible for the general project management such as project deliverables and group meetings along with interfacing with the FAA project manager.

**Benjamin Emerson (Georgia Institute of Technology):** Co-Principal Investigator. Dr. Emerson is responsible for designing and maintaining experimental facilities, as well as experimental operations and management and safety of graduate students.

**David Wu (Georgia Institute of Technology):** Co-Principal Investigator. Mr. Wu is responsible for designing and maintaining experimental facilities, as well as experimental operations and management and safety of graduate students.

**Samuel Grauer (Georgia Institute of Technology):** Co-Principal Investigator. Dr. Grauer is a post-doctoral researcher and reports to Professor Steinberg. He is responsible for designing the post-combustion diagnostic capabilities in the GT experiment.

**Orlando Ugarte-Almeyda (Georgia Institute of Technology):** Post-Doctoral Researcher. Dr. Ugarte-Almeyda reports to Professor Menon and works on the simulation of the GT experiment.

**Lane Dillon (Georgia Institute of Technology):** Graduate Student. Mr. Dillon works on the design of the experiment at GT.

**Parth Patki (Georgia Institute of Technology):** Graduate Student. Mr. Patki works on the hydrodynamics modeling sub-task (pre-combustion disturbances).

**Tony John (Georgia Institute of Technology):** Graduate Student. Mr. John works on the entropy modeling sub-task (post-combustion disturbances).

**Jeffrey Mendoza (Raytheon Technologies Research Center):** Co-Principal Investigator. Dr. Mendoza is the team leader for the RTRC team and oversees their contributions to the project. He leads the sub-tasks related to modeling, measurements, and simulation for post-combustion disturbances, nozzle interactions, turbine interactions, and far-field sound propagation.

**Lance Smith (Raytheon Technologies Research Center):** Co-Principal Investigator. He is responsible for the design and measurements of the RTRC experiment. He works closely with the GT team to ensure similarities between both experiment setups.

**Duane McCormick (Raytheon Technologies Research Center):** Co-Principal Investigator. He is responsible for the design and measurements from the RTRC experiment as well as finite element calculations that are part of the design process.

**Jordan Snyder (Raytheon Technologies Research Center):** He is responsible for design, measurements, and data processing using tunable diode laser absorption spectroscopy (TDLAS) and chemiluminescence in the RTRC combustor rig.

**Julian Winkler (Raytheon Technologies Research Center):** Co-Principal Investigator. He is responsible for the simulation tasks at RTRC and focuses on the post-combustion disturbances, nozzle interactions, turbine interactions, and far-field sound propagation.

**Jin Lee (Raytheon Technologies Research Center):** He is responsible for the entropy wave transport modeling which models the transfer function for the entropy disturbances at the flame leading to pressure disturbances generated at the nozzle.

**Xiaoyi Li (Raytheon Technologies Research Center):** He is responsible for the pre-combustion DNS simulations of the spray dynamics. This task generates the spray information required for input to the GT simulation task led by Professor Menon.

**Kenji Homma (Raytheon Technologies Research Center):** He is responsible for the far-field sound propagation simulations.

**Aaron Reimann (Raytheon Technologies Research Center):** He is responsible for reduced order modeling and high-fidelity modeling of the propagation of direct and indirect noise sources through the turbine nozzle and supports the far-field sound propagation simulations.

## Project Overview

The objective of this project is to develop and validate physics-based design tools that are able to predict noise production mechanisms, the relative significance of the noise production mechanisms, and ultimately reduce the noise output from future engines. The motivation for this project stems from the recent advances and future advances in aircraft engine technology. High-bypass engine technology has significantly reduced the traditionally dominant engine noise sources; namely, fan and jet exhaust noise. The noise generated in the combustor has become a dominant source of engine noise for future advanced aircraft designs. In addition, as combustors evolve to increase efficiency and reduce pollutant emissions, methods of predicting and mitigating combustion noise have severely lagged; legacy methods are insufficient for predicting noise from next-generation combustors. This motivates the objective of this project which is a critical need to develop physics-based design tools. The resultant understanding of noise generation and propagation, along with the validated noise prediction tools, will enable more rapid and cost-effective design of low noise engines for future aircraft.

The project objectives will be achieved through a program of cooperative experiments, high-fidelity simulations, and physics-based reduced order modeling. The physical processes involved are tightly coupled and directly determine the project tasks as shown in Figure 1.

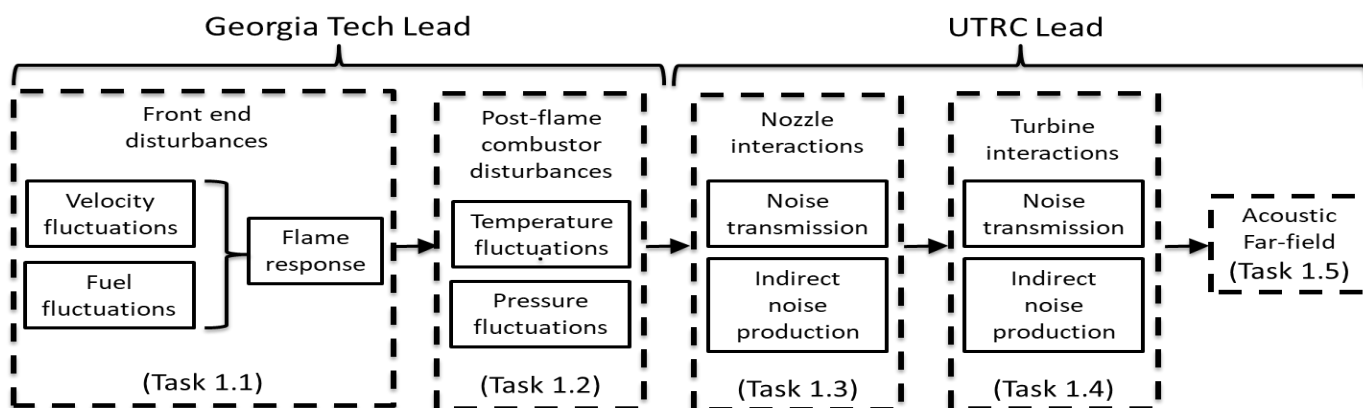


**Figure 1.** Physical processes and project tasks for noise generation.

The physics of noise generation begin with the source disturbances upstream of the combustion zone that involve unsteady dynamics in the flow and incoming fuel (spray). This is followed by the response of the combustion zone (flame) to these upstream disturbances. The fluctuations in the unsteady heat release, lead to both the generation of pressure fluctuations

as well as entropy fluctuations. These fluctuations propagate further downstream in the combustor and interact with the nozzle and turbine and eventually lead to far-field sound generation. With the complex interplay of unsteady physics in the different parts of the engine, developing reduced order models is a challenge.

An important goal of this project is to generate high-quality reference data from both measurements and validated high-fidelity simulations. This includes measurements of the flow, spray, and flame unsteadiness in the head-end of the combustor. Followed by this, the secondary combustion zone is characterized. The generation of entropy and pressure disturbances are then characterized through measurements of the temperature fluctuations and pressure fluctuations. This is followed by measurements of the reflection and transmission of noise through the turbine and nozzle section and finally measurement of sound in the far-field. The measurements are accompanied by large eddy simulations (LES) and finite element simulations that are validated against the measurements. Collectively, this data is generated across a range of operating parameters and serves as the source database for the modeling task.

The main goal of this project is the development of a robust design tool that can predict noise at operating points where prior measurements/data are unavailable. To achieve this goal, there are two major tasks involved. First, reduced order models and frameworks must be developed for different aspects of the engine architecture: flow/spray models, flame response models, entropy generation models, entropy propagation models, nozzle interaction models, turbine interaction models, and far-field noise generation models. The reduced order modeling for each of these involves simplifications and assumptions that are validated against the source database. This validation study and iterative improvement of model predictions serves as the second task to achieve this goal.

In this report, we summarize the effort by both teams from February 2020 (start of project) until September 2020. The effort primarily includes the development of the facilities at GT and RTRC. In addition, frameworks for the reduced order modeling and simulations have been setup and are being executed using available data and publications for validation.

## Task 1 – Facility Development at GT

Georgia Institute of Technology

### Objective

The objective of this task is to design an RQL combustor that closely mirrors the design by RTRC in order to measure different physics in the combustor architecture alone. The goal of the design is to allow for a multitude of optical diagnostics and other diagnostics capabilities that collectively measure the unsteady flow, spray, flame, temperature, and pressure fluctuations. The GT experiment will focus on the lower operating conditions to facilitate detailed optical measurements.

### Research Approach

The goal of this task at GT is to leverage an existing combustor test rig facility that was developed in partnership with Pratt & Whitney (PW). This task modified the facility to utilize the existing plumbing, instrumentation, data acquisition systems, pressure vessel, and structural steel. With these modifications, the new experiment setup resulted in: (a) a generalized hardware whose measurements can be shared in the public domain, (b) optical access and instrumentation access to measure flow, spray, flame, pressure, and temperature dynamics, and (c) replication of the general physics and operational characteristics of a modern RQL combustor. The modifications resulted in a new liner, fuel/air injection system, and exhaust system.

Aircraft engines use swirling inflow to aid both spray atomization as well as flame stabilization. In the project, we have used a swirler from an earlier FAA program in the current rig. This swirler is a high shear dual radial swirler as shown in Figure 2(a) and 2(b). The air blast atomizer is mounted in the center-body and is as shown in Figure 2(c). The air blast sprays are distributed evenly around the circular center-body. The collective flow path and spray are shown in Figure 2(d).

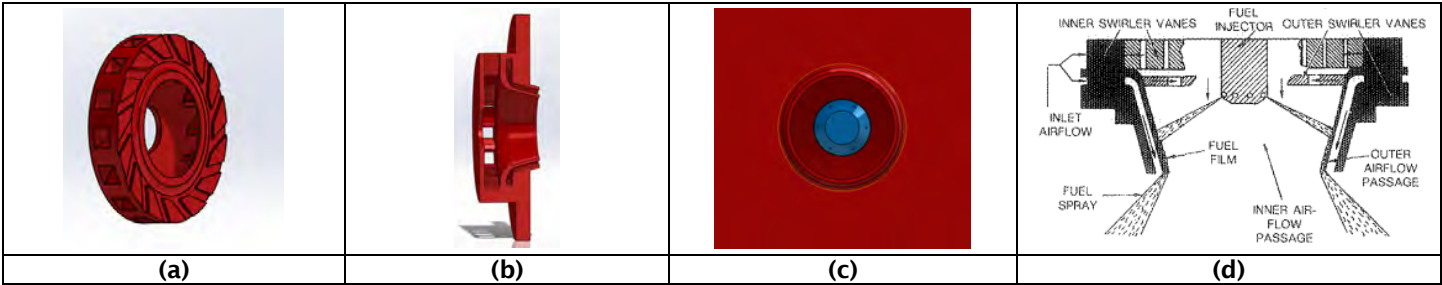


**Figure 2.** Inflow swirler showing: (a) one of the radial swirling inflow vanes, (b) side-view of the swirler cut-out without the center-body atomizer, (c) top view of center-body air blast atomizer (blue), and (d) side view of swirler showing swirler vanes, fuel injector, and spray.

The finalized liner design is as shown in Figure 3(a). It consists of five windows: two in the front and back, one in the bottom, and two in the top on either side of the quench hole section. Collectively, these optical access windows allow for highly detailed measurement of the flow, spray, and flame heat release. There are three quench holes in the top and two in the bottom. The quench holes are designed to have a “stepped” design as shown in Figure 3(b). The flow coming into the quench hole comes in the transverse direction as shown in Figure 4(a). The stepped design takes advantage of the recirculation flow created as shown in Figure 4(b). This creates a “turbulator” effect that induces components to the flow other than just the transverse component. This design is also adopted since it most closely represents the engine design and the rig designed/used by RTRC.



**Figure 3.** Combustor section showing: (a) liner with windows and frames, (b) “stepped” quench hole design.

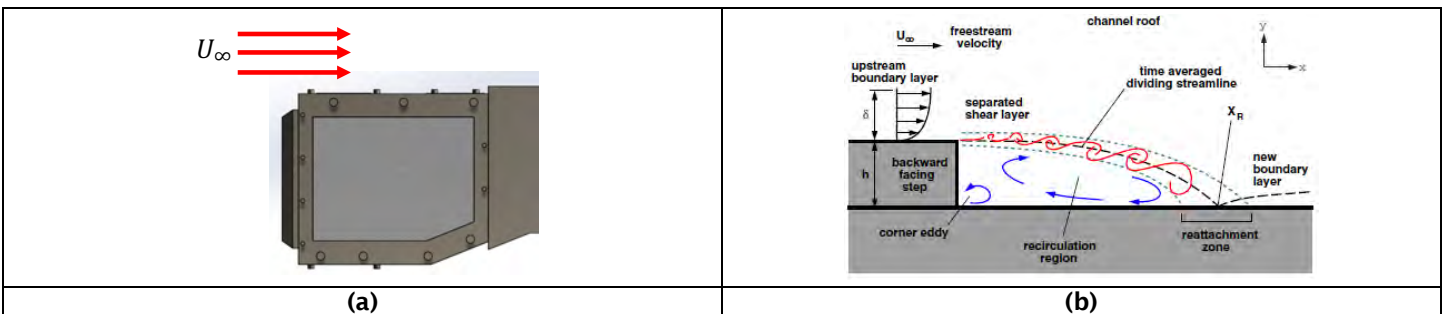


**Figure 4.** Physics of “stepped” quench hole design showing: (a) transverse flow over the liner coming to the quench, and (b) flow physics at a backward facing step.

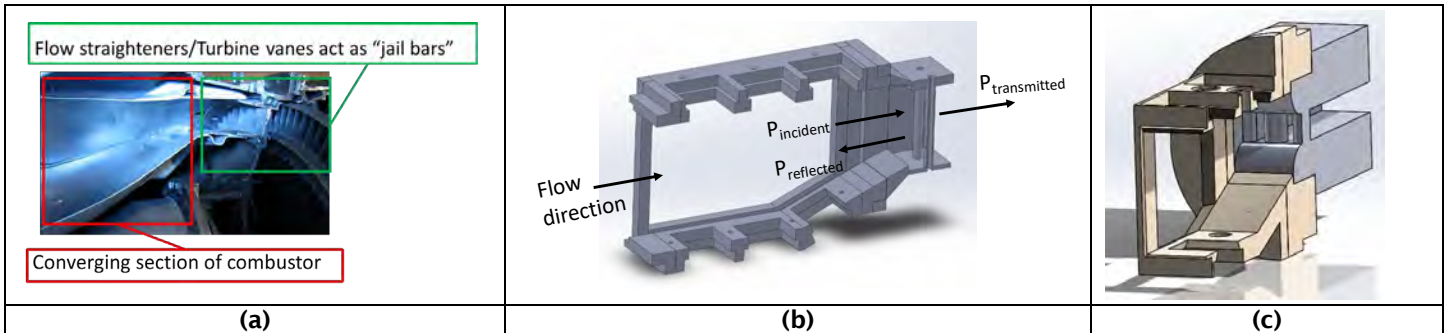


**Figure 5.** (a) Cross-section from a real engine showing converging section and array of turbine vanes, (b) cross-section from GT design showing converging section followed by, (c) “jail bars” to mimic turbine vanes.

The post-combustion zone architecture of the combustor is designed to closely resemble that seen in the real engine. As seen in Figure 5(a), the real engine architecture involves a converging section post-combustion that leads to the blade/vane array in the turbine section. This is replicated in the GT design. The repeating array of turbine blades is replicated through a jail bar type design. These designs in the GT rig are shown in Figure 5(b) and 5(c).

Finally, an important diagnostic feature of this rig is the measurement of post-combustion disturbances such as temperature and pressure fluctuations. Multiple pressure taps are installed, and the available pressure probes can be mounted at any of the taps and varied across different experiment runs. For temperature fluctuations, the TDLAS method is used. For this purpose, a TDLAS ring geometry is installed in the convergent section between the combustion zone and the jail bar exhaust as shown in Figure 6(a). In this ring, multiple lasers and absorption probes will be installed (see Figure 6(b)). Collectively, these measurement probes and lasers will allow for a detailed measurement of the temperature field that can then be used to understand the fluctuations in entropy that are a source of indirect noise.

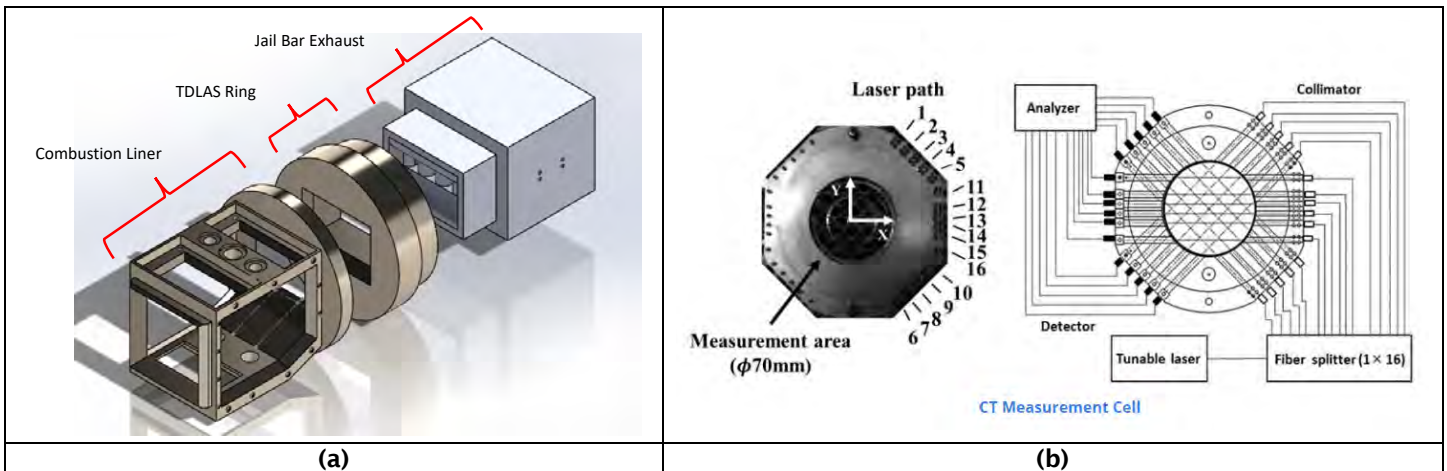


**Figure 6.** (a) Exploded view showing combustion liner, TDLAS, and jail bar exhaust system in the GT rig, (b) TDLAS probe array in the ring.

**Milestones**

- o GT experiment configuration finalized.
- o Operating conditions for the experiments have been finalized.

**Major Accomplishments**

The experiment rig has been designed to include a swirler relevant to aircraft engine operation and matching the experiment setup used by RTRC. The combustor section is designed as a RQL type borrowing from an existing lab-scale configuration.



In order to mimic the combustor exhaust to capture the effect of the turbine stage, jail bars were used to create periodic blockages that were each choked. The resultant configuration is suitable for detailed measurements of combustion noise. The range of operating conditions have been finalized. This has a major impact on this program as the second year shall focus on obtaining detailed measurements of unsteady flow, spray, flame, pressure, and temperature fluctuations. Collectively, these datasets will serve as validation data for the simulation as well as the reduced order model.

**Publications**

None

**Outreach Efforts**

None

**Awards**

None

**Student Involvement**

Lane Dillon is the graduate student taking the lead in the design of the GT experiment.

**Plans for Next Period**

In the second year of this project, the finalized GT rig design will be machined and installed in the pressure vessel as shown in Figure 7. The first step is to shakedown the experiment followed by which initial measurements will be taken across the board, covering flow, spray, flame, pressure, and temperature dynamics. The initial array of operating conditions and the corresponding measurements will serve as validation data for high-fidelity simulations. In addition to this, the measurements from the GT experiment campaign will be compared against those from the RTRC experiment campaign at similar operating conditions.

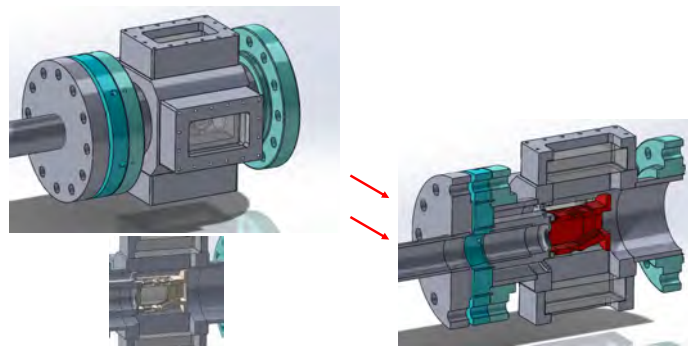


Figure 7. Placement of combustion liner inside the pressure vessel at the GT combustion lab.

**Task 2 – Simulations of GT Experiment**

Georgia Institute of Technology

**Objectives**

The objective of this task in the first year is to setup the facility geometry and flow conditions to begin the LES studies. The initial LES will involve cold-flow simulations without the swirler with appropriate boundary conditions. The spray modeling will take inputs from the RTRC Spray DNS task and a key objective of this task is to appropriately communicate the DNS data to the LES solver at GT.

**Research Approach**

The GT simulation effort uses the well-established compressible LES solver LESLIE to simulate the combustor configuration from the inflow swirler and spray to the choked downstream nozzle. The solver is well-suited to capture the required acoustic-vortex-heat release interactions. It is noted that the full combustor assembly has to be incorporated in order to produce

realistic acoustic disturbances and its coupling with the boundary conditions. The nozzle is needed to allow for the acoustic reflection/transmission by the throat and also to determine what disturbances are transmitted to the turbine and beyond. By modeling the entire combustor geometry, we can naturally couple the inflow with the spray and downstream choked throat's acoustic boundary. However, in this reporting period, the effort focused on a reduced geometry that incorporates a swirling inflow without the swirler but considers the jail bar exhaust as shown in Figure 8.

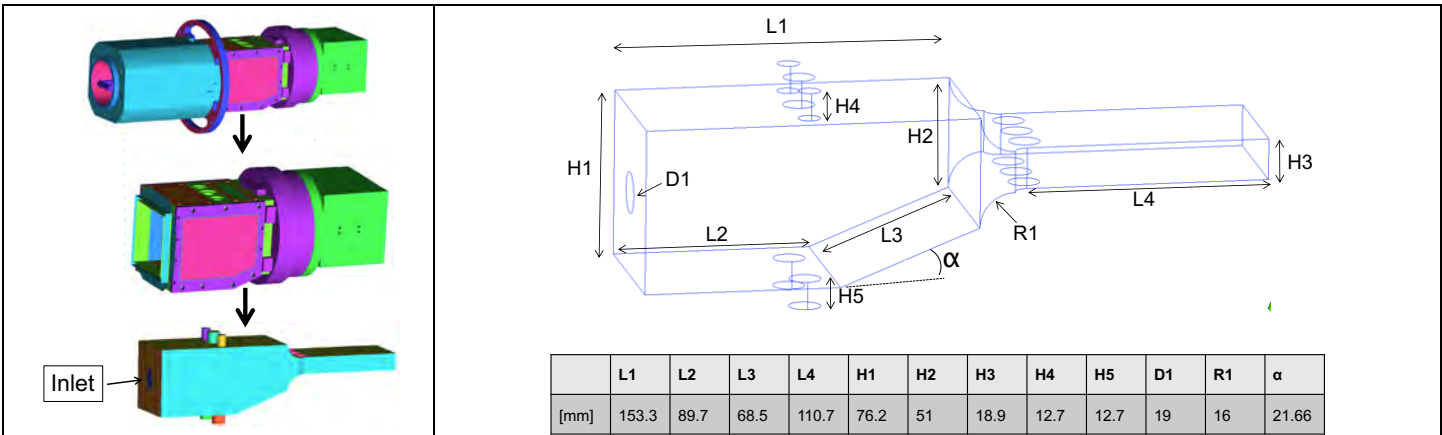


**Figure 8.** Initial computational domain used for the GT experiment simulation. Left: reduction from experiment CAD model to computational CAD model. Right: dimensions of computational domain.

The initial meshing effort on this geometry resulted in a hex-only grid with 5.6 million cells and 709 blocks. The cell sizes vary between 0.25 to 0.65 mm and are calculated depending on the flow velocity and length scales of the domain. The initial cold flow simulations are performed for an inflow with air incoming at 100 m/s, 300K, and a swirl number of 1. The dilution holes are set to inflow air at 10 m/s, 300K. Since the code is compressible, a subsonic non-reflective outlet boundary condition is used. An example snapshot from this simulation is shown in Figure 9. The simulation effort is on-going and further statistical analysis will be done at the different probe points (L1-L6) shown.

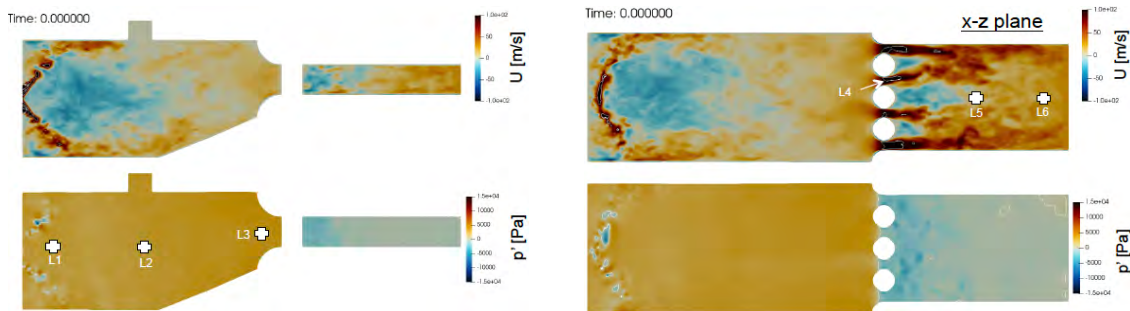


**Figure 9.** Snapshots of the velocity (top) and pressure fluctuations (bottom) in a cut-plane passing vertically through the center of the swirler (left) and in a cut-plane passing horizontally through the center of the exhaust section (right).

**Milestone**

Initial LES of cold flow in the computational domain of the GT experiment.

**Major Accomplishments**

The finalized GT experiment was reduced to an equivalent computational domain. This domain excludes the swirler and was meshed for an initial cold flow LES. The cold flow results are being analyzed for their statistics to understand the noise content and dominant features. In addition to this, the spray DNS by RTRC is generating data that is then being converted to an appropriate input form that can be read by the GT LESLIE code in order to perform both cold flow spray simulations as well as reacting flow simulations.



## **Publications**

None

## **Outreach Efforts**

None

## **Awards**

None

## **Student Involvement**

None

## **Plans for Next Period**

In the second year, the simulation efforts will focus on including an accurate representation of the swirling inflow along with a swirler impedance boundary condition measured by RTRC. In addition to this, the swirler geometry shall also be included as an option for future simulations, although will be considered secondary due to its computationally expensive nature. The spray modeling needed for reacting flow simulations will come from the spray DNS provided by RTRC. The cold flow and reacting flow simulations shall also be validated against measurements from the GT experiment. Finally, additional post-processing tools will be developed in order to generate the required information from the simulation for the RTRC post-combustion post-processing task geared towards entropy wave transport modeling.

## **Task 3 – Reduced Order Modeling**

Georgia Institute of Technology

### **Objectives**

The overarching objective of this task is to create quick-action, reduced order models that can accurately predict different aspects of the noise generation mechanism that then collectively feed into a design tool for noise prediction. The specific objective of the GT reduced order modeling task focuses on the head-end physics in the architecture, namely flow and spray dynamics, flame dynamics, and generation of entropy disturbances by the flame. The spray/flow dynamics feed into the flame dynamics that cause direct combustion noise. The flame dynamics also result in entropy disturbances which then lead to indirect combustion noise at the nozzle. The flame response modeling and the model for the generation of entropy disturbances are provided as inputs to the post-combustion models that will be developed by RTRC. Depending on the prediction results from the RTRC models, these “head-end” models will be iteratively refined.

### **Research Approach**

In this reporting period, the reduced order modeling activities at GT focused on developing the flame response framework in order to model the unsteady heat release disturbances. The generated unsteady heat release disturbances then lead to entropy disturbances at the flame.

#### **Flame Response Modeling**

The flame response modeling for a spray flame requires the extension of prior gaseous diffusion flame models to include the effect of spray droplets. The configuration used for this framework is as shown in Figure 10 with fuel droplets injected in a center duct and air injected in the outer ducts. The fuel flows in the inner duct  $0 < r < R_f$  and the air/oxidizer flows in the outer ducts  $R_f < r < R$ . The fuel exits the duct and enters the combustion zone as a mix of fuel gas and a spray of liquid fuel droplets, which after evaporation and diffusive mixing result in the spray diffusion flame being modeled.

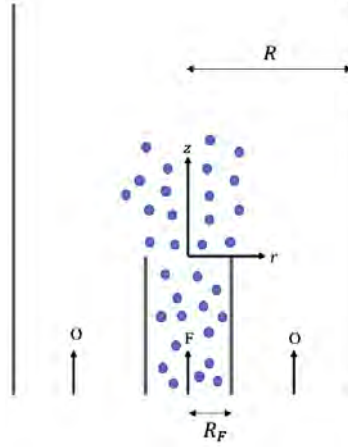


**Figure 10.** Schematic of the ducted spray flame configuration. Fuel droplets are injected in the center duct (shown in blue) and oxidizer gas is injected in the outer ducts.

In this work, the atomization physics for the liquid state is not considered. We assume the fuel to be injected as droplets far upstream that are then convected downstream in the fuel duct. These droplets are assumed to follow the gas flow in the combustion zone. A sectional approach is used to model the spray physics. In this approach, the continuous droplet-number distribution is divided into distinct size sections from which averaged sectional conservation equations are obtained. This simplifies the representation of an otherwise infinite size distribution of droplets. Note that while the droplets discretely exist, the sectional approach provides for a continuum representation of the droplets through their number density, which results in a continuum-based partial differential equations (PDE) for the droplet mass fraction. Under these assumptions, a governing equation for the droplet mass fraction can be derived. Following the Schvab-Zeldovich formulation, the gaseous phase is converted to a single gaseous mixture fraction ( $Z$ ), and along similar lines, the droplet phase is converted to a droplet mixture fraction ( $Z_d$ ). These mixture fractions are one-way coupled through vaporization of the droplet generating fuel gas. In non-dimensional form, the governing equations become:

$$\frac{\partial Z_d}{\partial t} + u_z \frac{\partial Z_d}{\partial z} + u_r \frac{\partial Z_d}{\partial r} = \frac{1}{Pe_d} \left[ \frac{\partial^2 Z_d}{\partial r^2} + \frac{\partial^2 Z_d}{\partial z^2} \right] - \Gamma_V Z_d \quad (1)$$

$$\frac{\partial Z}{\partial t} + u_z \frac{\partial Z}{\partial z} + u_r \frac{\partial Z}{\partial r} = \frac{1}{Pe_g} \left[ \frac{\partial^2 Z}{\partial r^2} + \frac{\partial^2 Z}{\partial z^2} \right] + \Gamma_V Z \quad (2)$$

Here,  $Pe_d = u_0 R / \mathcal{D}_d$  is the droplet Peclet number and  $Pe_g = u_0 R / \mathcal{D}_g$  is the gaseous Peclet number. The Peclet number is the ratio of the diffusion timescale to the axial convection timescale. A large Peclet number denotes diffusion dominant transport. The Damkohler number for vaporization is denoted by  $\Gamma_V$  and denotes the ratio of the axial convection timescale to the vaporization timescale. Large values of this parameter indicate that droplets tend to evaporate completely to fuel gas before they are transported sufficiently downstream. Notice that this parameter controls the one-way coupling from the droplet phase to gaseous phase and thus introduces the effect of the spray parameters on the gaseous mixture fraction and hence the local unsteady heat release. This local unsteady heat release is important for both the direct combustion noise modeling as well as for generation of entropy disturbances. The generation of noise by both mechanisms is a RTRC task and thus requires key inputs from this modeling task.

### Generation of Entropy Disturbances

The governing equation for entropy dynamics is given by:

$$\rho T \frac{Ds}{Dt} = -\nabla \cdot \vec{q} + \underline{\tau} : (\nabla \vec{u}) - \rho \sum_{i=1}^N \mathcal{D}_i \nabla Y_i \cdot \vec{F}_i - \sum_{i=1}^N \frac{\mu_i}{MW_i} [\dot{w}_i + \nabla \cdot (\rho \mathcal{D}_i \nabla Y_i)] \quad (3)$$

As seen from this equation, entropy generation can be attributed to molecular transport (diffusion and conduction) and chemical reactions (4<sup>th</sup> term). At the flame, molecular transport processes are negligible when compared to the chemical term. Retaining only the chemical term and expanding the chemical potential results in:

$$\rho T \frac{Ds}{Dt} = - \sum_{i=1}^N \tilde{\mu}_i \dot{w}_i = \dot{q} - \sum_{i=1}^N \dot{w}_i \int_{T_0}^T c_{p,i} dT + \sum_{i=1}^N T s_i \dot{w}_i \quad (4)$$

Here,  $\dot{q}$  is the chemical heat release term. Several prior research efforts on entropy dynamics during combustion have assumed that only the heat release term contributes to the generation of entropy disturbances at the flame and that the other terms are negligible, without evidence. A first focus of this task has been to investigate the relative contributions of the heat release term when compared to the full chemical term. To test the dominance of heat release rate over the remaining terms, a 1-D Cantera simulation was conducted for methane-air combustion. In the simulation, the ratio of the magnitude of the heat release rate to the sum of heat release rate and remaining terms was computed. The mathematical equivalent of this ratio,  $\alpha$ , is defined below. It can be noted that if  $\alpha$  is in close proximity to unity,  $\dot{q}$  can be considered the dominant term and the remaining terms can be neglected.

$$\alpha = \dot{q} / - \sum_{i=1}^N \tilde{\mu}_i \dot{w}_i \quad (5)$$

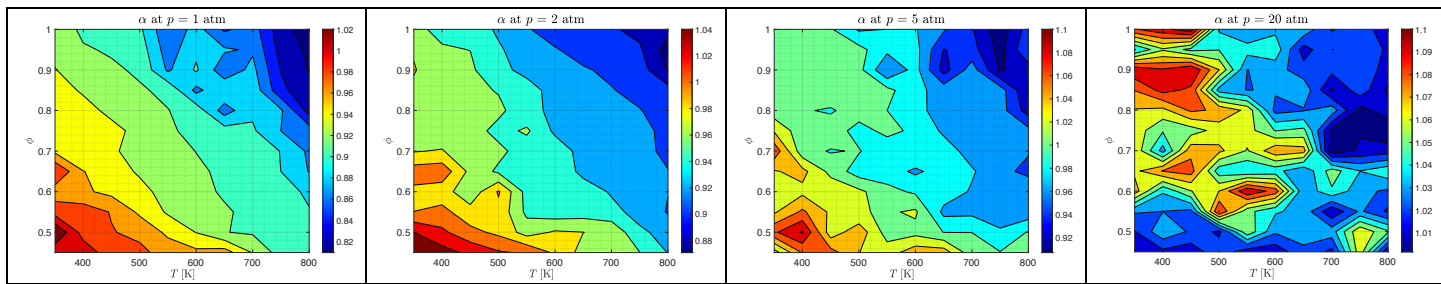


**Figure 11.** Variation in  $\alpha$  for methane-air combustion simulation for a range of equivalence ratio and pre-heating temperatures at different fixed pressures.

Figure 11 shows the variation of  $\alpha$  at different operating pressures, for a range of preheating ( $T$  ranging between 350K and 800K) and equivalence ratios ( $\phi$  ranging between 0.45 and 1). At lower pressures, the ratio is furthest from 1 and can go as low as 0.82, indicating that the assumption breaks down. In contrast, at the highest pressure, the ratio indicates that the heat release captures 90% of the source term. This indicates that the entropy dynamics at the flame can more or less be determined by the equation:

$$\rho T \frac{Ds}{Dt} = \dot{q} \quad (6)$$

Decomposing the entropy into its base state (subscript 0) and fluctuating component (subscript 1), the governing equation for the dynamics of the entropy fluctuations is given by:

$$\frac{Ds_1}{Dt} = \frac{\dot{q}_1}{\rho_0 T_0} \quad (7)$$

The unsteady heat release rate disturbance term is the source of the entropy disturbance generation at the flame. Although not shown here, a second term is present but can be shown to be negligible for multi-dimensional low Mach number flows. For a 2D flame in an axial only mean flow, the solution is given by:

$$s_1(x, y, t) = \frac{1}{\rho_0 T_0 u_0} \int_{-\infty}^x \dot{q}_1 \left( \eta, y, t - \frac{x - \eta}{u_0} \right) d\eta \quad (8)$$

The flame response modeling work then feeds the heat release model for the above equation. The resultant entropy fluctuations generated by the above model are then provided as inputs to the RTRC entropy wave modeling sub-task.

### **Milestones**

- Initial framework for the response of a spray flame.
- Initial framework for the generation of entropy disturbances by unsteady heat release.

### **Major Accomplishments**

The response of a premixed flame and gaseous diffusion flame to imposed disturbances has been significantly addressed in the literature. However, the framework developed in this task is the first step towards the response of a spray flame to imposed disturbances. Specifically, the formulation brings in the parameters of the spray and explicitly shows how they affect the diffusion flame and hence the overall heat release.

Prior research on entropy dynamics has assumed that the heat release was the only dominant source for the generation of entropy disturbances at the flame. However, this assumption was never validated. The chemical kinetics analysis showed that the heat release term covers between 80–100% of the source term, thus validating the assumption that the heat release is the sole contributor to the generation of entropy disturbances at the flame. In addition, the model for the generation of entropy disturbances shows how heat release disturbances are converted to entropy disturbances at the flame.

### **Publications**

Accepted submission to the 2021 AIAA SciTech virtual conference for the Flame Response Modeling task.

### **Outreach Efforts**

None

### **Awards**

None

### **Student Involvement**

- Graduate student Parth Patki has been involved in understanding the entropy budget of the entropy dynamics equation to determine the dominant source terms for entropy disturbances.
- Graduate student Tony John has been involved in modeling the generation of entropy disturbances due to a heat release source term.

### **Plans for Next Period**

In the next year, the reduced order modeling task will expand to include hydrodynamics stability analysis to model the pre-combustion flow disturbances. The velocity model generated from this analysis feeds directly into the flame response model. In addition to this, the spray measurements and spray DNS will be used to generate model parameters for the spray droplets used in the flame response model. In addition to this, the flame response model will be further improved to relax assumptions made in the current model. Furthermore, the results from the models will be validated against the new measurement and simulation data and iteratively improved.

The model for the entropy generation at the flame will be used with the validated flame response model to generate the source entropy disturbances which are then plugged into the entropy wave transport sub-task by RTRC. The predictions from RTRC's model at the nozzle will be validated against measurements of the temperature fluctuations. This will then iteratively feedback to improvements in both the GT entropy source model and the RTRC entropy wave transport model.



## Task 4 – Facility Development at RTRC

Raytheon Technologies Research Center

### Objective

The objective of this task is to design an RQL combustor that closely mirrors the design by GT, with the specific goal being to focus on the higher operating points not possible for the GT rig. Collectively, the GT and RTRC rig capabilities will encompass a broad range of operating conditions thus resulting in a robust data set to train the design tools.

### Research Approach

The approach to designing the RTRC rig largely mirrors the effort at GT through close discussions and iterations of the design process. The key features of the finalized RTRC rig are discussed here.

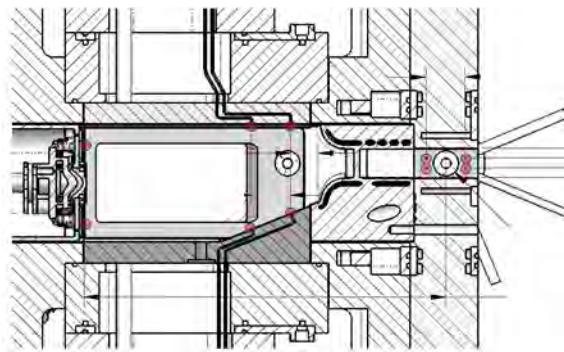


**Figure 12.** Cut-away of the RTRC experiment showing side view with the inflow in the left, combustion zone, convergent section, followed by bell mouth feature before jail bars. Pressure tap locations shown in red.

Figure 12 shows the cut-section of the RTRC experiment. The high shear swirler is inserted in the left. The optical access windows are present only on one side (unlike the GT rig where it is present on all sides). This RTRC liner design is incorporated into the GT rig discussed earlier with more optical windows being added for the GT experiment. The proposed pressure probe locations to measure pressure fluctuations is as shown in red. The intention of the pairs of probe locations upstream and downstream of the jail bars are for decomposing the acoustics into downstream and upstream propagating waves. This wave decomposition may help quantify the indirect noise magnitude.

### Milestones

- RTRC experiment configuration finalized.
- Operating conditions for the experiments have been finalized.

### Major Accomplishments

The experiment rig has been designed to include a swirler relevant to aircraft engine operation and has been designed in coordination with GT. The GT rig mirrors that of the RTRC rig except for the diagnostic capabilities. The combustor section is designed as a RQL type borrowing from an existing lab-scale configuration. In order to mimic the combustor exhaust to capture the effect of the turbine stage, jail bars were used to create periodic blockages that were each choked. The resultant configuration is suitable for detailed measurements of combustion noise. The RTRC rig shall focus on the higher end of the operating condition space.

### Publications

None

### Outreach Efforts

None



## Awards

None

## Student Involvement

None

## Plans for Next Period

In the second year of this project, the finalized RTRC rig design will be used to take initial measurements of the combustion heat release (deduced from chemiluminescence measurements), pressure fluctuations at various points, and temperature fluctuations. In conjunction with the GT experiment, the data will be used for validating GT simulations performed at higher conditions.

## **Task 5 – Spray Modeling**

Raytheon Technologies Research Center

### Objectives

The objective of this task is to perform direct numerical simulations (DNS) of the proposed high shear air blast atomizing swirler in order to capture the detailed atomization process and obtain the statistics of the spray. The output from these simulations will feed into the spray modeling settings used for the GT simulations.

### Research Approach

Accurate prediction of liquid fuel atomization is crucial for LES combustor noise prediction. RTRC has leveraged its internal DNS capability for spray atomization to predict droplet statistics near the injector exit. Over the last decade, RTRC has developed and extensively validated a state-of-the-art DNS capability in the form of the HiMIST code, which stands for High-fidelity Multiphase Injection Simulation Tool. This code has been applied to a wide variety of problems ranging from impinging jet atomization to liquid jet atomization in crossflow, as well as the first-ever full aero-engine swirling-flow injector atomization at ambient and high temperature-pressure conditions. Achieving these results involves some of the most advanced numerical methods, including the coupled level set and volume of fluid (CLSVOF) method for interface transport, the ghost fluid sharp-interface approach, adaptive mesh refinement (AMR), and the embedded boundary approach for flexible solid geometry handling. Realistic thermodynamic and transport properties are obtained using the National Institute of Standards and Technology's (NIST) Reference Fluid Thermodynamic and Transport Properties Database (REFPROP) in combination with established empirical correlations. The code is also massively parallelized in high performance computing (HPC) systems and can scale up to 10,000 cores.

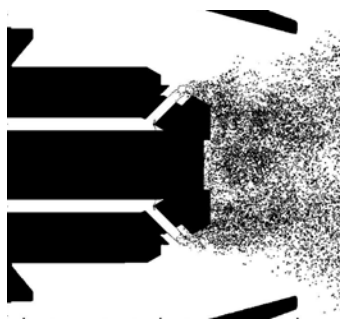


**Figure 13.** Snapshot of droplets and atomization from baseline production simulation. Spray is seen to remain in the core with minimal wall filming.

In this reporting period, a baseline condition was identified. This baseline production run used a 100-130 million grid on 1500-2000 HPC cores. The simulation completed roughly 2-3 flow through times and the flow-field reached a stationary state. A large region of Eulerian mesh refinement was applied in the startup simulation to ensure stability. The refinement region was manually adjusted to ensure both a stable and efficient production run. The computational cost was further reduced using grid coarsening with Lagrangian droplet transformation. These baseline conditions showed that a majority of

the droplets remained in the core of the inner swirling flow (see Figure 13), indicating that the filming process could be neglected when considering spray models for a larger combustor LES in the GT simulation task.

### **Milestones**

Established a baseline simulation to generate spray information from HiMIST.

### **Major Accomplishments**

The HiMIST code has been used for an initial baseline simulation case in order to interface its results with the GT simulation code (LESLIE).

### **Publications**

None

### **Outreach Efforts**

None

### **Awards**

None

### **Student Involvement**

None

### **Plans for Next Period**

In the next year, the efforts will focus on validating the simulations for conditions relevant to the GT rig. This will be done using the spray measurements from the GT experiment. In addition to this, the GT LESLIE code's spray input parameters/input file format will be used for post-processing the results from HiMIST in order to directly generate spray modeling input files for the GT simulation.

## **Task 6 – Swirler Impedance Modeling**

Raytheon Technologies Research Center

### **Objectives**

The major objective of this study is to characterize the acoustic impedance of the chosen high shear swirler at a range of operating conditions. This is achieved through a combination of impedance tube measurements and finite element simulations. The measurements and simulations collectively result in a validated data set of the swirler acoustic impedance. This data helps reduce the GT simulation cost by eliminating the swirler geometry from the computational domain and instead replacing it with the impedance and swirling inflow boundary condition. Additionally, the impedance is needed for the numerical Green's function approach used to characterize the direct combustion noise from unsteady heat release.

### **Research Approach**

The swirler geometry of the high shear swirler involves several small passages of air flow that along with the grid requirements can result in computationally expensive simulations. An alternative to modeling the effect of the swirler is to use an acoustic impedance boundary condition along with a swirling inflow. In addition, the numerical Green's function approach that is part of RTRC's direct combustion noise sub-task would require the heat release modeling from GT's sub-task and the swirler impedance for noise computations. The RTRC flowing impedance tube is a well-trodden and validated approach at RTRC to characterize the acoustic impedance of several geometries. The acoustic damping of the swirler pressure drop is modeled by locally linearizing flow resistance. An important drawback of these methods is that the effect of the fuel jets/spray is not captured.

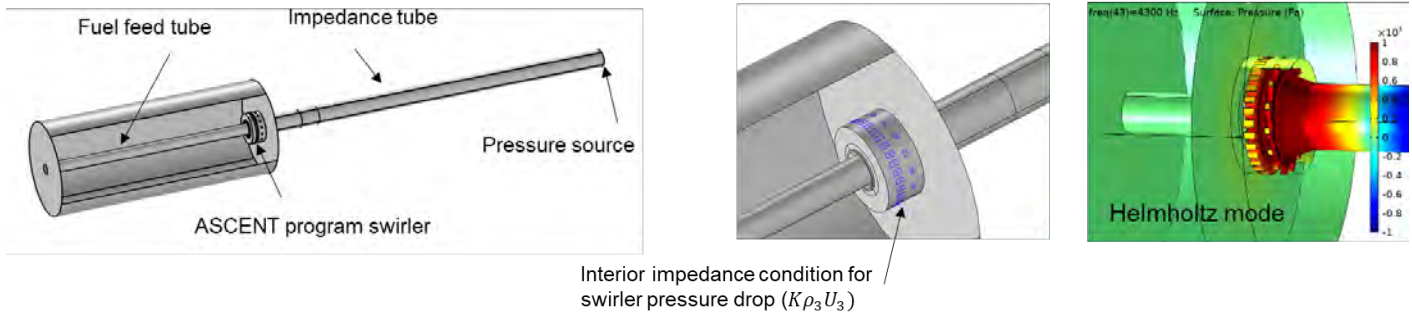


**Figure 14.** Geometry used for COMSOL simulations with boundary conditions to characterize swirler impedance and example mode visualization. Flow is from bottom left to top right.

In this reporting period, finite element calculations in COMSOL are used for modeling the swirler impedance as shown in Figure 14. The COMSOL simulations were performed at GT approach conditions of 118 psia, 752F. The swirler impedance is calculated just downstream of the swirler at the entrance to the impedance tube. In addition to the above geometry, the GT inlet, consisting of a perforated plate upstream of the swirler, is used.

### **Milestone**

Established a COMSOL simulation and post-processing framework to numerically characterize swirler impedance.

### **Major Accomplishments**

The high shear swirler has been used in a numerical impedance tube in COMSOL and its complex impedance was obtained for both the RTRC impedance tube plenum case as well as the GT combustion rig inlet case (includes perforated plate upstream of swirler). Once validated, the COMSOL finite element framework will continue to serve as a quick use tool to generate swirler impedance values at new operating conditions where impedance tube measurements are not available. This is helpful for reducing the computational cost of the corresponding GT simulations where this swirler boundary condition is required.

### **Publications**

None

### **Outreach Efforts**

None

### **Awards**

None

### **Student Involvement**

None

### **Plans for Next Period**

Validate the finite element results using the impedance tube when hardware is available.

## Task 7 – Post-Combustion Modeling

Raytheon Technologies Research Center

### Objectives

The goal of this task is to develop transfer functions from the combustion zone to the nozzle, nozzle to turbine, and turbine to far-field. This involves modeling the physics for:

- Entropy wave transport post-combustion, since unsteady heat release rate disturbances at the flame generates entropy disturbances that are then transported through the post-combustion zone.
- Direct noise modeling using a numerical Green’s function approach with the heat release model.
- Nozzle interactions for dynamics of pressure disturbances through the nozzle. Specifically, the effect of the jail bar configuration used in both GT and RTRC rigs is investigated.
- Turbine interactions for dynamics of pressure disturbances through the turbine.
- Far-field sound propagation.

### Research Approach

The post-combustion zone physics involves the effects of the combustion unsteady heat release rate disturbances and the post-combustion geometry on the eventual noise generation outside the engine. This involves:

- The direct generation of combustion noise due to the heat release and the interaction of these pressure disturbances with the rest of the engine geometry which and lead to far-field noise.
- The entropy disturbances generated by the flame interacting with geometric changes at the nozzle and causing pressure disturbances that then interact with the rest of the engine geometry and lead to far-field noise.

### Entropy Wave Transport Modeling

This task focuses on how the entropy disturbances at the upstream flame are transported through the combustor to the nozzle. The modeling in this task is performed through data mining from a simulation that generates and transports the entropy disturbances as shown in Figure 15. First, the rich combustion zone in the head-end labeled “A” generates entropy disturbances through unsteady heat release rate disturbances as the source. These disturbances are also manifested as temperature fluctuations. These disturbances are convected and diffused through the downstream region and also undergo turbulent dispersion. At the secondary lean combustion zone “B”, further disturbances are generated and collectively these disturbances are then transported downstream to the nozzle. At the nozzle, these disturbances are converted back into pressure disturbances depending on their magnitude at the nozzle. Thus, the important goal of this task is to measure the magnitude of the entropy disturbances at the nozzle and hence understand the importance of this indirect sound generation mechanism.

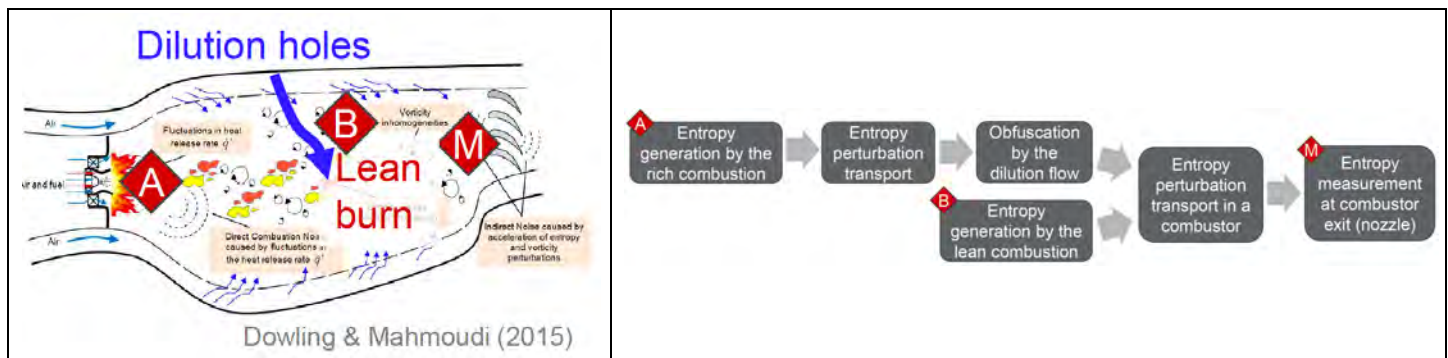


**Figure 15.** Mechanism of entropy wave generation and transport in combustor. Left: aeroengine combustor showing different regions with generation and transport. Right: flow chart for modeling and understanding entropy wave transport through simulation.

In order to accurately quantify the changes in magnitude of the entropy disturbances, the propagation of entropy disturbance is simulated with additional entropy fluctuations in the upstream controlled by user input. In this simulation, a fluctuation in temperature is introduced at “A” and then its magnitude is calculated at “M”. Additionally, the effect of the lean burn at the dilution holes is evaluated by introducing a temperature fluctuation at “B” and calculating the magnitude at “M”. In both

cases, a transfer function is evaluated between “A” and “M” and between “B” and “M”. The imposed disturbances in temperature are at an amplitude of 5% of the mean and the frequencies are varied. The analysis workflow is presented in Figure 16.

The results from the initial simulations showed that the transfer function between “A” and “M” is very small. The advection of the flow from “A” is much weaker than the turbulent diffusion by the lateral flow from “B”. The transfer function between “B” and “M” is greater. However, note that canonical RQL combustors can have different results. An important limitation from the current analysis is that the simulation time is shorter. Furthermore, additional probe locations must be used to continually track the changes in amplitude between the sources (“A” or “B”) and “M”.

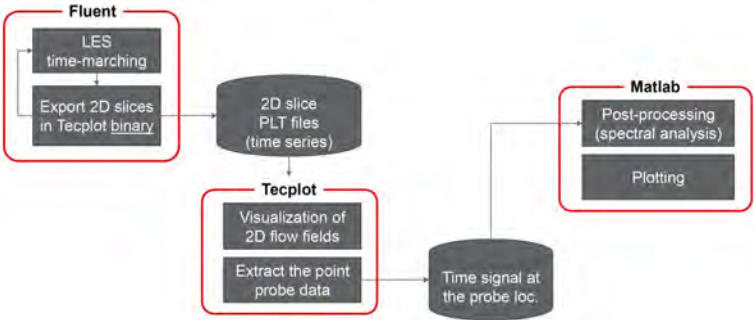


**Figure 16.** Analysis workflow from using Ansys Fluent for simulation to Tecplot for post-processing and visualization to Matlab for final transfer function calculation.

**Direct Noise Modeling**

The direct noise modeling is performed using a numerical Green’s function approach that uses an appropriate Green’s function in conjunction with either a measured or simulated/modeling unsteady heat release rate disturbance field, in order to calculate the pressure disturbance at a particular location in the combustor. While this was not performed in the current reporting period, a prior workflow established by RTRC under a NASA program has been reviewed and will be leveraged for this work.

**Nozzle Interactions Modeling**

The goal of this task is to use high-fidelity simulations to support the rig design of the jail bar configuration used by both GT and RTRC. This will help screen the jail bar nozzle design concept for potentially undesirable aerodynamics and acoustic behavior. The results also help with down selecting the final jail bar configuration and for placement of pressure sensors in the rigs. The jail bar configuration explored is as shown earlier in Figure 12(a). The equivalent computational domain is as shown in Figure 17 with a downstream extension to allow for numerical dampening of outgoing waves. A Lattice-Boltzmann compressible transonic scale-resolving flow simulation was performed. The grid consists of a total of 5 million voxels and the grid resolution used 40 points per diameter of the jail bar in the region of the jail bar as shown in Figure 17.

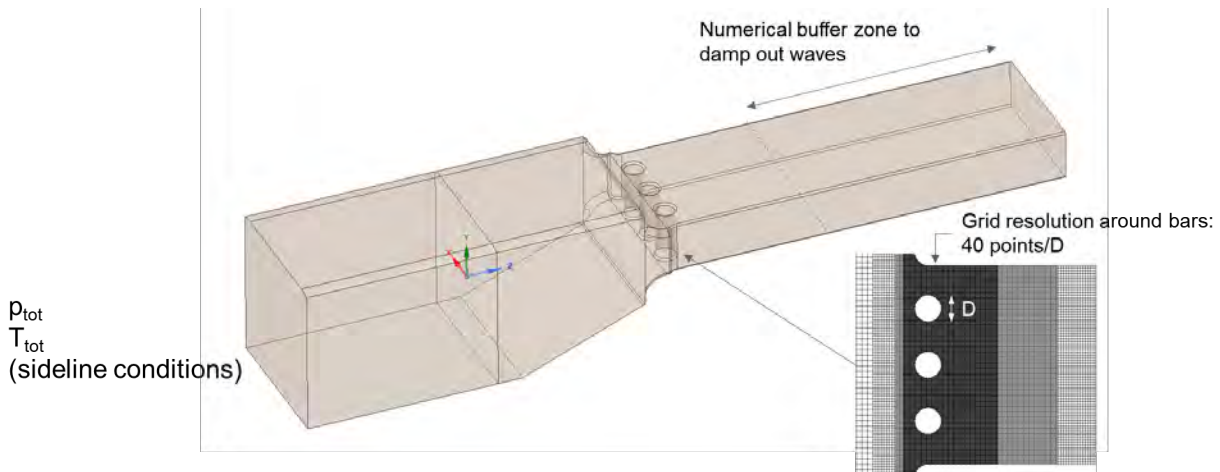


**Figure 17.** Computational domain and jail bar grid details for the Lattice-Boltzmann methods (LBM) simulations of the nozzle interactions.

The simulations were performed for different back pressure ratios ( $p_{s,outlet}/p_{s,inlet}$ ) in order to assess the reflection and transmission of sound through the jail bars. A snapshot of the results from the different back pressure cases is shown in Figure 18. For the choked case (which corresponds to the highest back-pressure ratio), the presence of the vortex shedding affects shock formation, leading to oscillations in the shock location. A dynamic coupling between cylinder wake vortex shedding and shock oscillation was observed that leads to the flow going in and out of choke. This flow condition may therefore be called “nominally” choked. As the ratio is decreased, shock oscillation is strongly reduced and an asymmetric shock pattern between bars is observed. For the lowest ratio, the shocks are stable and so are the wakes behind the cylinders.

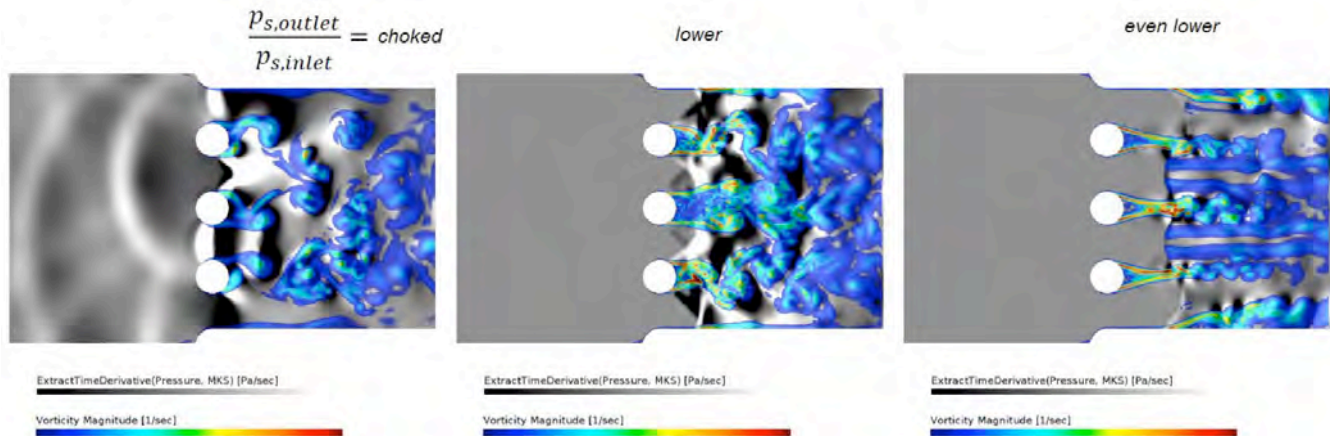


**Figure 18.** Snapshot of pressure field (grayscale) and vorticity (colors) for the three different cases simulated starting with a choked case until a lower back-pressure ratio.

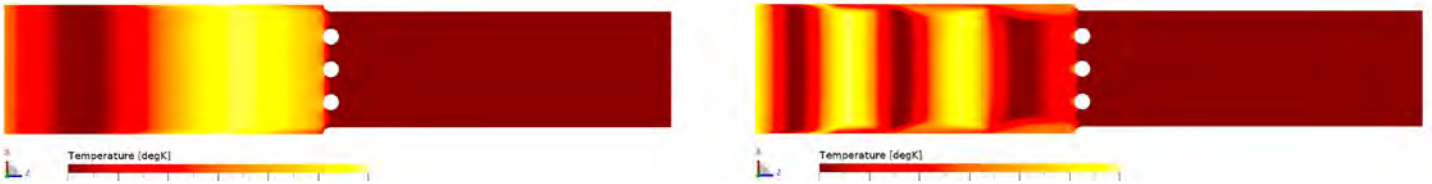


**Figure 19.** Snapshot of temperature field for two different frequencies. Left: lower frequency. Right: higher frequency.

In addition to the above analysis, the effect of indirect noise due to the jail bars was also investigated. For this analysis, a similar strategy as the entropy wave transport task was adopted. The inlet was forced with temperature fluctuations that are of a convective nature. This was analyzed for two different frequencies as shown in Figure 19. The higher frequency case shows multiple waves due to the shorter wavelength. As the temperature fluctuations pass through the area change introduced by both the bell mouth and jail bars, this acceleration leads to sound generation that is both transmitted and reflected. Using an upstream and downstream probe, the pressure signal was analyzed, and it was seen that in the region downstream of the jail bars there was broadband increase in noise levels, partially due to the complex flow field resulting from the cylinder wake flow and the shock-induced flow separation near the combustor rig walls. Additionally, at the forcing frequency, the noise level was seen to be slightly higher in the downstream region, due to the noise generation from the acceleration of the temperature disturbance passing through the flow contraction.

### Turbine Interaction Modeling

This task focuses on simulations of a high-pressure public domain turbine rig (Polytechnic University of Milan and the German Aerospace Center (DLR) to understand both direct and indirect noise propagation through a representative high-pressure turbine stage. The first set of simulations focused on ideal wave propagation through the turbine where there are no loss mechanisms to understand reflection and transmission of sound. For this study, the domain and mesh are as shown in Figure 20(a). The wave equation is solved using FEM Actran. This simulation provides a reference solution which can be used to verify the LBM setup and prediction results and to cross-compare with the experimental data. Plane wave acoustic duct modes are injected at the inlet of the domain and get either reflected or transmitted upon reaching the turbine stage. Both reflected and transmitted waves pass freely through the inlet and outlet of the domain via non-reflecting boundary conditions. Simulations were performed for the stator only and for the stator-rotor configuration. The transmitted (T) and reflected (R) sound power coefficients are shown in Figure 20(b). For the present turbine geometry, the stator alone provides increasing wave reflection with frequency. The combination of stator and rotor creates a dip near 900 Hz where almost no sound is reflected back. The cross-over frequency where reflection and transmission are on par is around 1200 Hz.

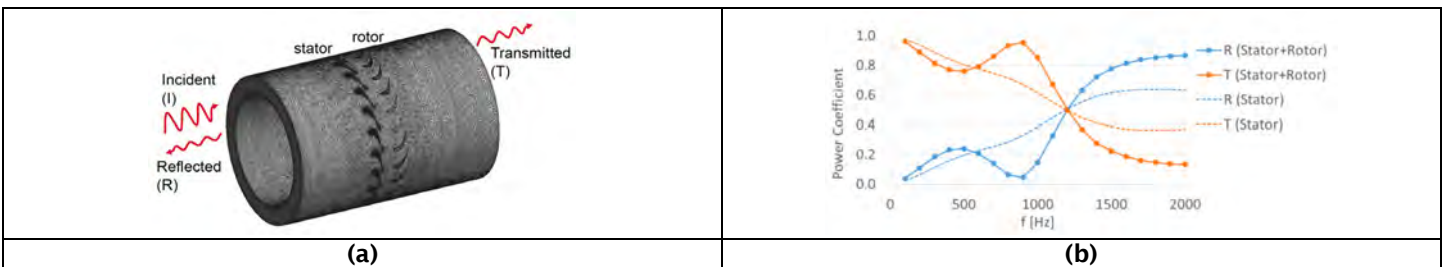


**Figure 20.** (a) Ideal wave simulation mesh. (b) Predicted sound power coefficients as a function of frequency.

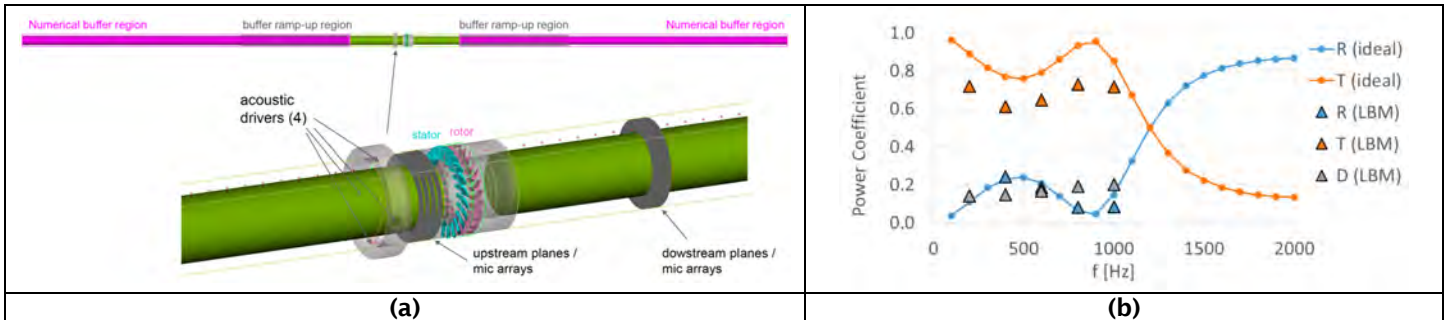


**Figure 21.** (a) Domain used for real wave simulations showing extended buffer regions to control wave damping. (b) Comparison of power coefficients between real and ideal wave simulations.

The next simulation focused on the real wave propagation through the turbine and used the setup shown in Figure 21(a). The simulations were performed using LBM in PowerFLOW. The comparison between the ideal wave and real wave simulations is shown in Figure 21(b). There is a close agreement for the reflection coefficients (R). The trend for the transmission (T) is the same, but some of the sound power is lost due to dissipation (D). The pumping of acoustic waves through the blade rows introduces viscous losses on the airfoil surfaces, with particularly high values at the nozzle guide vane throat (i.e., the minimum open area provided by the stator row). Upon scattering at the sharp vane and blade trailing edges and the rotor blade tip gap, vorticity waves are produced that add to the sound damping effect as shown in Figure 22 for the 1000 Hz case.

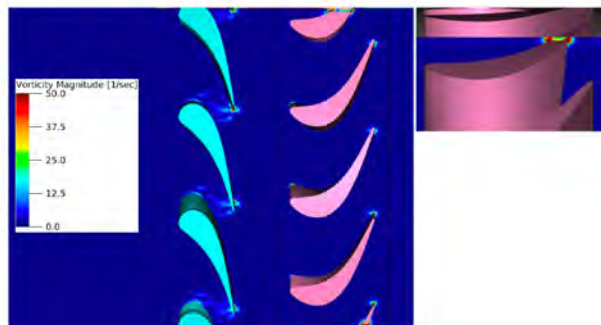


**Figure 22.** Induced vorticity generation in the LBM simulations of the acoustically forced stationary turbine (no flow). The forcing frequency is 1000 Hz.

The final simulation focused on the acoustic forcing for a high-subsonic flow operating condition for which the rotor speed is set to 7000 rpm. Horseshoe vortices are produced around the stator blade row, and the very large eddy simulation turbulence model quickly switches to scale-resolving mode downstream in the wake mixing region of the stator. The wave propagation behavior with acoustic forcing by the virtual duct speakers in presence of this unsteady high-subsonic flow is shown in Figure 23. As shown in Figure 23(a), the wave reflection behavior seems to be less sensitive to frequency compared to the no-flow case, with a reflection coefficient between 0.2 and 0.4. The transmitted noise is also much lower compared to the no-flow case, leaving larger values for the unaccounted term D, which is partly due to increased dissipation as the acoustic waves pass through the accelerated flow. The experimental data from DLR is plotted in Figure 23(b). The experimentally obtained reflection coefficient hovers around a similar value as in the LBM simulations and also shows little sensitivity to frequency. The transmission coefficient is also very low for all frequencies. Combined with the rather low reflection coefficient, this also leaves large values for the unaccounted part D, and the role of cut-off modes, mode scattering, and physical dissipation needs to be looked at in more detail to understand the different behavior.

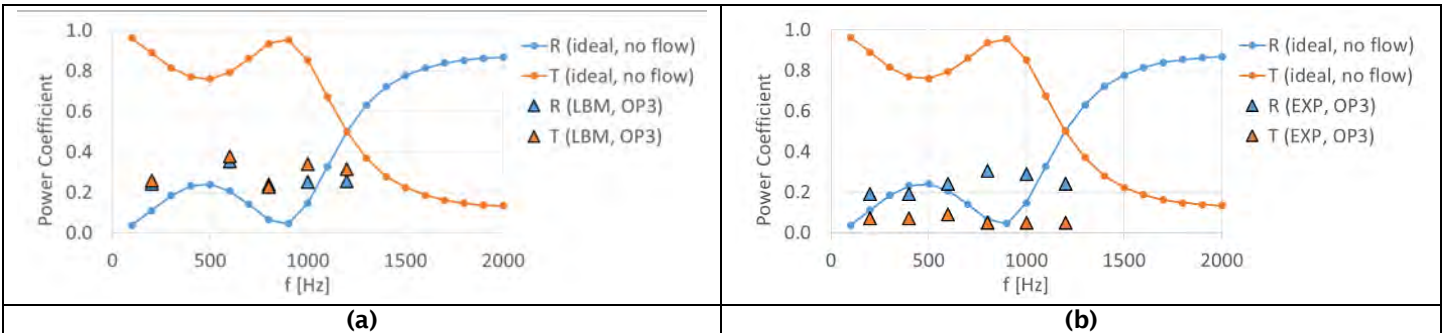


**Figure 23.** Comparison between (a) LBM with flow and ideal without flow, (b) experimental data with flow and ideal without flow.

**Far-field Noise Modeling**

This task uses the acoustic mode identified at the turbine exit as input and simulates the different physics involved in far-field noise propagation. This includes refraction due to sheared flow and temperature gradients before sound is perceived in the far-field.

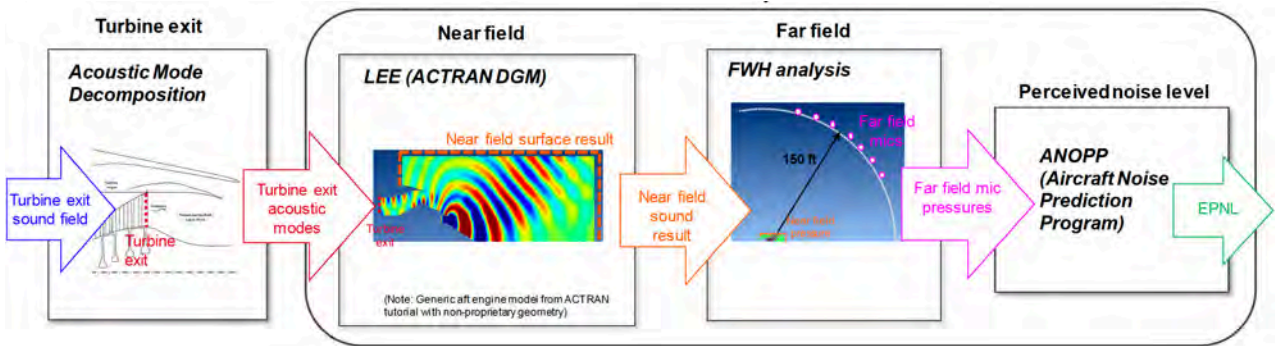


**Figure 24.** Simulation approach for turbine exit to far field pressure and perceived noise level.

The simulation approach used is as shown in Figure 24. First, the acoustic modes from the turbine exit are injected into the near-field simulation which uses a linearized Euler equation (LEE) approach in Actran DGM. From the near-field simulation output, the input to the far-field analysis is provided and calculated using the Ffowcs-Williams-Hawking equations. The far-field is set at 150 ft and from these far field mics, the pressure is used to measure the effective perceived noise level (EPNL) using the Aircraft Noise Prediction Program (ANOPP).

**Milestones**

- Entropy wave transport: Established a workflow from simulation to data processing to transfer function calculation.
- Nozzle interactions: Established an LBM simulation framework to simulate noise generation due to jail bars.
- Turbine interactions: Established a validated workflow to explore reflection/transmission of sound through a stator-rotor stage.
- Far-field sound generation: Established a multi-framework simulation workflow to go from turbine data to far-field noise.

**Major Accomplishments**

For the entropy wave transport modeling effort, a robust workflow has been established that performs the simulations in Fluent, post-processes the data in Tecplot, followed by which the final transfer functions are calculated using Matlab. This workflow can be used when simulation data specific to the GT rig is made available.

For the nozzle interaction task, the Lattice-Boltzmann simulation framework was used for the jail bar design to understand the effect of this geometry on noise propagation. An important result from this study was the identification of the back-pressure ratio at which there is a steady shock at the jail bars. This is important since it identifies operating conditions at which reflection from the nozzle section is minimized. It has important impacts on the transmitted noise through the nozzle which eventually affects the noise through the turbine and in the far-field.

For the turbine interaction task, a public domain turbine model with experiment data was simulated in the LBM framework and the resulted matched well with the measurements. This validates the simulation method that will be used to create a reduced order model for reflection/transmission of sound through the turbine stage.

For the far-field noise modeling task, a multi-framework simulation workflow was established and was successfully used with test data. When a validated turbine model is available, it can directly be used in this workflow to generate far-field sound data. Along with measurements, this will enable the creation of the final piece in the design tool which is to predict the perceived noise level in the far-field.

### **Publications**

Extended abstract submitted to AIAA Aviation 2021 Conference for work in the Turbine Interaction Modeling task.

### **Outreach Efforts**

None

### **Awards**

None

### **Student Involvement**

None

### **Plans for Next Period**

For the entropy wave modeling task, the main effort next year will be establishing a workflow pipeline that can take the raw simulation data from the GT LESLIE code and convert that to a form for post-processing in the exiting workflow. A new workflow will need to be established to analyze the LES data and generate transfer functions. In addition, a reduced order model for the transport physics will be developed, which will take the heat release model as input to generate source disturbances and then a transfer function for the disturbances at the nozzle.

For the nozzle interactions task, the main effort next year will be to perform simulations on the finalized rig with accurate inflow and exit boundary conditions and generate data that can then be used to create a reduced order model for the transmission and reflection of pressure waves before and after the nozzle.

For the turbine interaction task, there are several efforts that will be addressed in the coming year. In particular, the role of the downstream struts in the experiments in mode scattering and contribution to the “lost” sound power, captured by the D contribution will be studied numerically. More details and insight into the sound dissipation mechanisms will be explored. The analysis will be expanded towards transonic flow conditions, for which initial computations have already been performed. In addition, to address the indirect noise generation (entropy conversion to acoustics) at the turbine stage, entropy wave injection near the stator leading edge will be studied with the objective to perform validations with the available published experimental data. The injection ports and forcing are well-defined and the implementation into the current simulation setup is straightforward. The indirect noise source may be an important mechanism of future combustors and we expect to capture salient trends and observations with this initial study.

For the far-field noise propagation task, further simulations in the multi-simulation framework will be performed to build a database of core noise directivity as a function of frequency and source modes from turbine exhaust at multiple flight conditions. The results will be reduced into far field transfer functions mapping core source modes to far field pressures, which will be used for predicting total far field pressures once specific source modes are determined from upstream core propagation simulations.



# Project 056 Turbine Cooling through Additive Manufacturing

## The Pennsylvania State University

### Project Lead Investigator

Karen A. Thole  
 Distinguished Professor  
 Department of Mechanical Engineering  
 The Pennsylvania State University  
 136 Reber Building  
 University Park, PA 16802-4400  
 Phone: (814) 865-2519  
 E-mail: kat18@psu.edu

### University Participants

#### The Pennsylvania State University

- Pls: Dr. Karen Thole, Dr. Stephen Lynch
- FAA Award Number: 13-C-AJFE-PSU-054
- Period of Performance: February 5, 2020 to February 4, 2021
- Tasks:
  1. Manufacture and test existing FAA CLEEN (Continuous Lower Energy, Emissions, and Noise) II blade designs.
  2. Design new double-wall cooling technologies.
  3. Manufacture and test new double-wall cooling designs for linear cascade (2021–22).
  4. Manufacture and test optimal double-wall cooling designs for the Steady Thermal Aero Research Turbine (START) Lab turbine (2022–2023).

### Project Funding Level

The FAA has provided \$800,000 of funding to date with \$400,000 available to The Pennsylvania State University (Penn State) START. The other \$400,000 is processing through Penn State’s financial system and will be available soon to the team. In-kind cost share of \$1,500,000 has been provided to Penn State from Pratt & Whitney to cover the entire program.

### Investigation Team

Name	Affiliation	Role	Tasks Responsible For
Distinguished Professor Karen A. Thole	Penn State	PI	Management, reporting, oversight of all technical tasks
Associate Professor Stephen Lynch	Penn State	Co-PI	Management, reporting, oversight of Tasks 1–3
Assistant Research Professor Reid Berdanier	Penn State	Staff Scientist	Task 1, 4
Associate Research Professor Michael Barringer	Penn State	Staff Scientist	Task 1, 4
Scott Fishbone	Penn State	Project Manager	Task 1, 4
Jeremiah Bunch	Penn State	Laboratory Technician	Task 1, 4
Justin Wolff	Penn State	Graduate student	Tasks 1–4



## Project Overview

Gains in cooling performance of cooled turbine airfoils have a direct impact on the efficiency and durability (lifetime) of turbine engines and therefore are the subject of much development. Today, many cooling designs for turbine airfoils use complex micro-channels placed within the wall of the airfoil to extract heat, which is otherwise known as double-wall cooling. The geometric complexities (and thus effectiveness) of the micro-channels, however, are limited by the current design space available using conventional investment casting and core tooling methods to manufacture relatively small intricate internal cooling features. This project will investigate potential thermal performance and aerodynamic efficiency improvements made possible by exploring the expanded cooling design space opportunities by directly fabricating complex cooling geometries using three-dimensional laser powder bed fusion (L-PBF), a common type of metal-based additive manufacturing (AM) method. L-PBF AM has begun to see many uses in the gas turbine industry, particularly because of the new design space enabled by this new fabrication method. However, the ability to manufacture high-efficiency intricate complex double-wall cooling airfoils design concepts is unknown. This research would generate some of the first thermal performance data at engine-relevant conditions comparing traditional cast airfoils to advanced L-PBF AM manufactured airfoils. Understanding the potential of new innovative geometric heat transfer cooling design features coupled with unique airfoil cooling configurations will serve as an important guide to future investments in advanced manufacturing and cooling design technologies.

## Task 1 – Manufacture and Test Existing FAA CLEEN II Blade Designs

The Pennsylvania State University

### Objectives

The objective of this task is to measure the as-manufactured shape of FAA CLEEN II turbine blade airfoils using x-ray computed tomography and use that information to fabricate additively manufactured (AM) copies for direct comparison in the rotating turbine facility at Penn State. The outcomes of this effort will be: 1) to provide a direct back-to-back comparison of cast versus additively manufactured airfoils; 2) learn the unknown challenges with creating double-wall designs via AM and how to translate them to cast parts for commercialization; and 3) work through the design, fabrication, and testing of additive blades that will spin at engine-relevant conditions.

### Research Approach

#### Training

The initial portion of the project involved familiarizing the graduate student on the project with software such as Avizo (for computerized tomography (CT) scan analysis) and StarCCM (for cooling feature design). CT scan analysis training was performed with existing data on a previously published public microchannel coupon [1], which would be similar to the technology being deployed in this project. The training included the generation of a surface from raw CT data in Avizo, exporting said surface to SolidWorks (CAD program) to measure the CT surface and remodel it as a solid body, and comparing the solid body and CT surface via a nominal-actual comparison in Avizo.

Figure 1 shows the segmentation editor in Avizo, which was used to select the raw CT data that was rendered into a 3D surface. The CT surface was then exported into SolidWorks; its dimensions were analyzed and measured, and the solid body in Figure 2 was modeled.

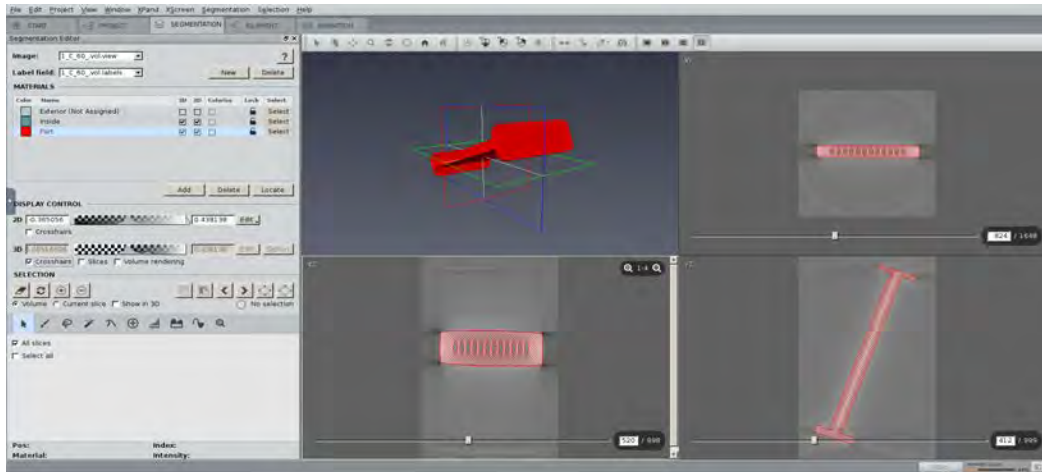


**Figure 1.** Segmentation editor views for the 1\_C\_60 public coupon.

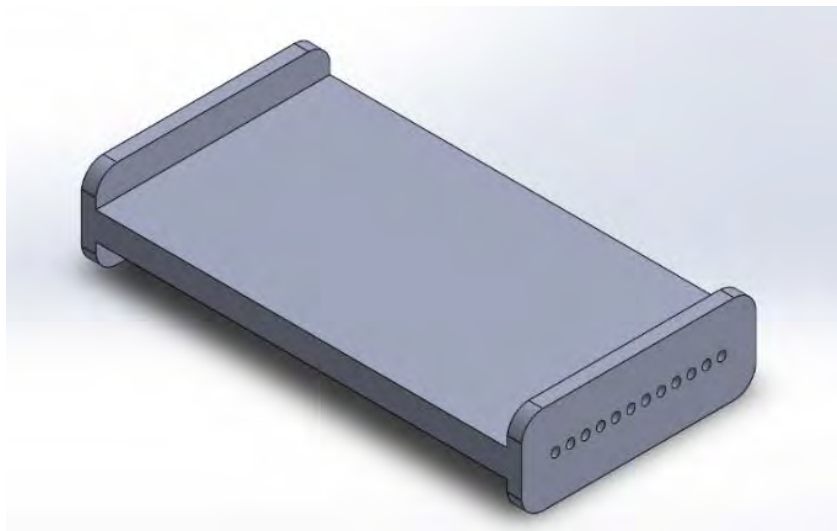


**Figure 2.** Solid body of the 1\_C\_60 public microchannel coupon in SolidWorks.

The nominal-actual comparison process is shown through Figures 3-5. The first step to a nominal-actual comparison starts with the registration or alignment of the two surfaces to be compared. Avizo has two ways of registering surfaces; one way is to attach an align surfaces operation to both surfaces and another is to add landmark pairs between the two surfaces. The align surfaces operation is used for an automatic registration of two surfaces, where Avizo utilizes its built-in computing code to align the centers, principal axes, and surfaces of the two bodies. Landmark pairs on the other hand are pairs of points that the user specifies to register the surfaces to one another. The landmark registration was used for the nominal-actual comparisons for the FAA CLEEN II blades but for the 1\_C\_60 public coupon, the align surfaces operation was used.

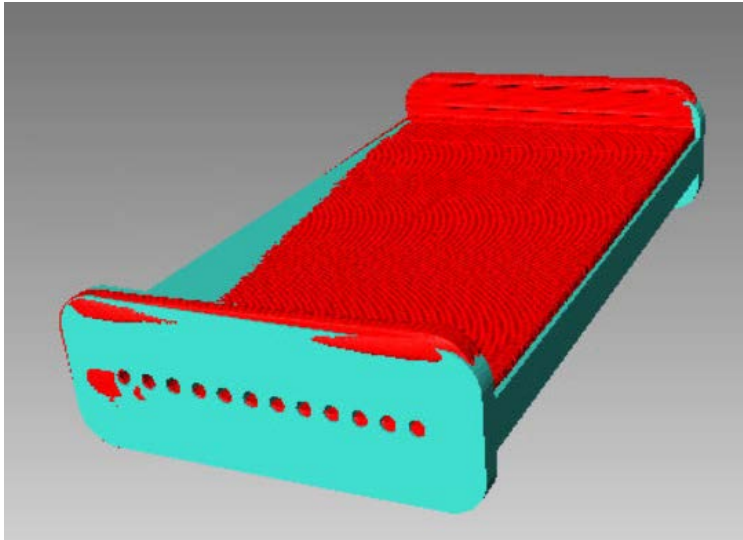


**Figure 3.** Registration/alignment of the 1\_C\_60 public coupon's CT surface and solid body model.

After registration, or alignment, of the surfaces, Figure 4 shows the steps used in Avizo to produce the image in Figure 5, and also shows the histogram produced from the surface distance calculations. The surface distance computation is the key step in completing the nominal-actual comparison; it is defined as the distance from the vertex of one surface to the closest point on another surface. Figure 5 shows the surface distance computation values mapped onto the 1\_C\_60 public coupon, where the colormap legend expresses the surface distance values in mm.

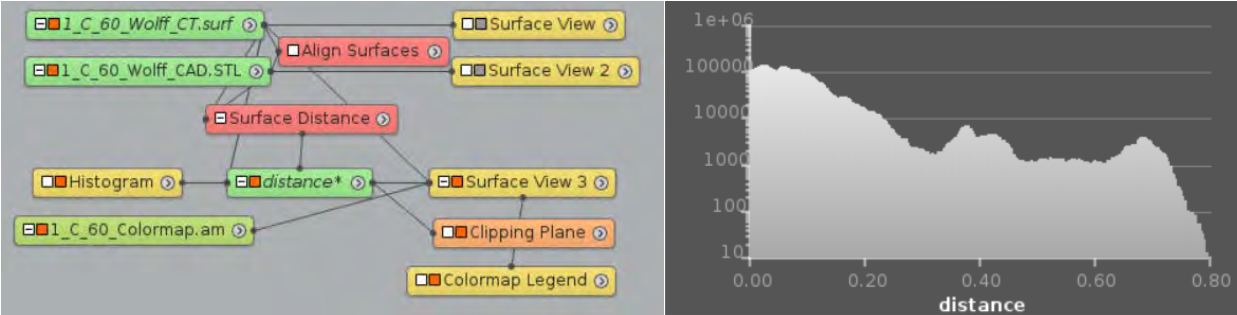


**Figure 4.** Steps performed in Avizo for a nominal-actual comparison, and the computed histogram of surface distance.

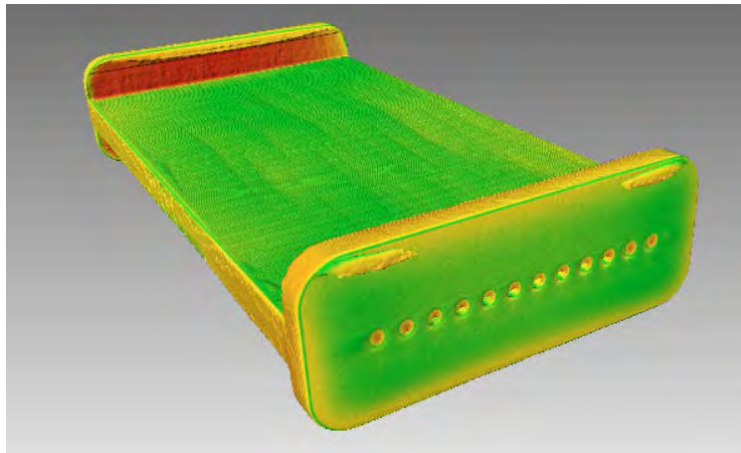


**Figure 5.** Nominal-actual comparison surface view with associated colormap legend.

After each of the steps explained above are completed, a nominal-actual comparison has been performed. Key information can be collected from the histogram of the surface distance calculations such as mean surface distance, range, and standard deviation. The same nominal-actual comparison process has been conducted on the FAA CLEEN II blades to determine which blades are appropriate to additively manufacture.

#### **Measurement of FAA CLEEN II Blades**

Substantial progress has been made in comparing the six desired FAA CLEEN II blades in order to decide which blade to fabricate using additive manufacturing techniques. Two different types of CT scans were obtained for each of six blades; one set of scans from a Pratt & Whitney vendor, and another set using on-campus facilities in the Center for Quantitative Imaging (CQI). The scan settings were changed for the two types, enabling either better determination of the solid wall boundary, or high resolution of small-scale cooling features. The learning from both types of scans will be compared, and scan settings have been documented for future use as the project progresses.

Several comparison techniques were employed for the blades: nominal-actual comparisons (CAD versus CT and CT versus CT) in Avizo, the overlap of blade cross-sectional slices, and plotting the overall cooling effectiveness (calculated from the infrared (IR) data). The CAD design intent was provided by Pratt & Whitney.

The process of nominal-actual comparisons in Avizo involves creating surfaces from raw CT data, registering the two surfaces that are to be compared, and computing a histogram that includes information such as mean surface distance, range, and standard deviation. The registration step was performed by aligning each surface based on points placed along the fir-tree (the airfoil root geometry). After the surfaces were aligned, the surface distance, which is the distance from the vertex of one surface to the closest point on another surface, was calculated. Then, the histogram was computed using the surface distance results to obtain the following: the mean surface distance (the average distance between the two triangulated surface), the range, and the standard deviation.

The nominal-actual comparisons that were calculated first involved comparison of the design intent of the blade (CAD model) compared to the six scanned airfoils. From this analysis, one airfoil (designated BA06) had an average surface deviation from CAD that was in the middle of the range among the six blades. Then, that airfoil was used as the “actual” in the nominal-actual comparisons to other airfoils. The surface distance determination from the nominal-actual comparison were mapped onto the blade surface to produce a qualitative image indicating distortion, whereas the quantitative results were summarized in a table.

Additional qualitative images that proved useful in the comparison of the blades were constructed as well. To qualitatively understand the variations between the CAD model and the CT surfaces, and between CT blade surface BA06 and the rest of the CT surfaces, cross-sectional slice images were compared at 10%, 50%, and 90% of blade height. The height is defined as the distance from just above the blade platform, to the tip of the blade.



Lastly, previously obtained infrared data on the blade surfaces from recent tests in the START turbine facility was post-processed to produce overall cooling effectiveness. This data has been reduced and is being compared to the CT data to understand any correlations between blade geometry deviation and overall cooling effectiveness.

The above data package is being discussed with Pratt & Whitney in order to make a final determination of the airfoils for which structural analysis will be performed and design drawings generated.

### **Mechanical Analysis and Manufacturing**

Pratt & Whitney was engaged as a subcontractor on the Task 1 effort, in order to provide mechanical analysis, generation of manufacturing drawings for the additively manufactured airfoils, and assistance with securing an additive manufacturing vendor. The subcontract was established on 9/28/2020, and a kickoff meeting was held on 10/2/2020. Pratt & Whitney engineers have started to perform some structural analyses of the existing FAA CLEEN II airfoil at the conditions of the START turbine rig and will update their models once a representative CT scan is selected. Pratt & Whitney has also helped to engage additive manufacturing vendors and the process of setting up non-disclosure agreements (NDAs) is underway.

### **References**

- [1] Wildgoose, A., Thole, K. A., Sanders, P. A., and Wang, L., 2020, "Impact of Additive Manufacturing on Internal Cooling Channels with Varying Diameters and Build Directions," *Proceedings of ASME Turbo Expo*, London, UK.

## **Task 2 – Design New Double-Wall Cooling Technologies**

The Pennsylvania State University

### **Objective(s)**

The objective of this task is to develop novel double-wall cooling designs that feature microchannel concepts being explored in literature and which are possible to achieve via AM. The designs will be generated with advice from Pratt & Whitney so that the concepts can be translated to the FAA CLEEN II airfoil later in this project, as well as leveraged for commercialization. The designs will be packaged into cascade test articles that will be measured in the high-speed linear cascade at Penn State using infrared thermography in Year 2 of the project. Best designs will be identified for re-integration into the FAA CLEEN II airfoil shape and run in the START turbine to confirm operational benefit.

### **Research Approach**

#### **Training**

StarCCM training was performed by the graduate student, as it will be used for design work later in this task. A tutorial for StarCCM was performed using a NASA C3X public first vane. A mesh was created, and boundary and initial conditions were set, to run a 2D analysis. Figures 6–8 show the mesh, Mach number, and temperature results.

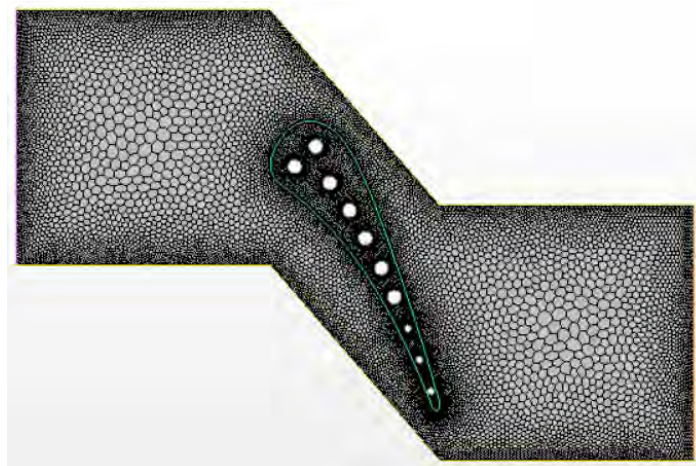


**Figure 6.** Mesh generated in StarCCM for the NASA C3X first vane.

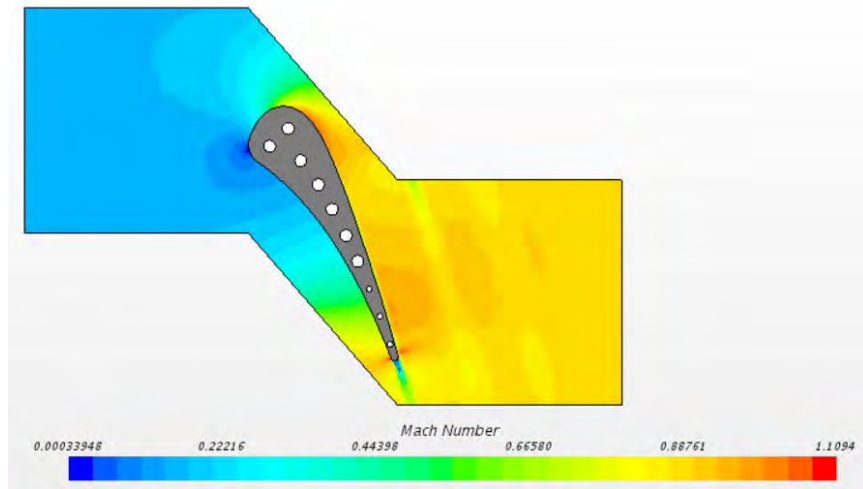


**Figure 7.** The predicted Mach number profile of the NASA C3X vane.

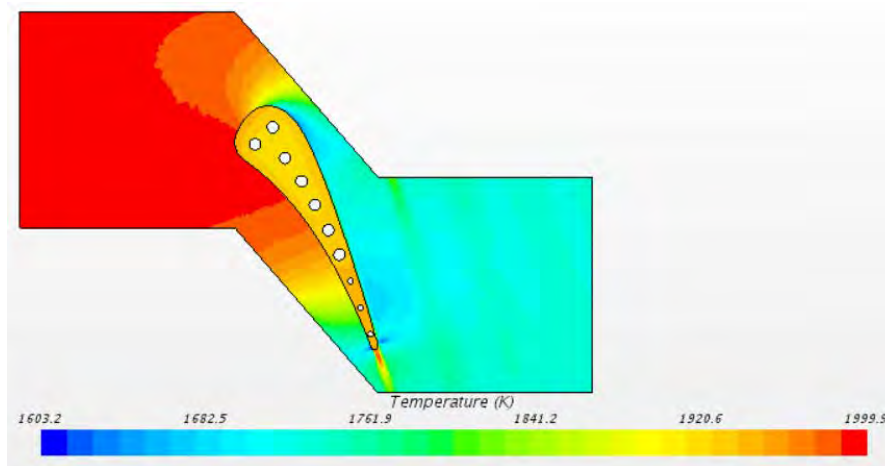


**Figure 8.** The predicted temperature profile of the NASA C3X vane.

An additively manufactured microchannel cooling design in [2] was also modeled in StarCCM to learn about internal cooling feature modeling. The triangle pin fin design from that study was modeled in SolidWorks and set up in StarCCM for a 2D analysis. More work on understanding the accuracy of the modeling is pending.

### **Milestones**

Milestone	Due Date	Estimated Date of Completion	Actual Completion Date	Status
Workplan	3/4/20	3/4/20	3/5/20	Completed
COE Meeting 1	4/1/20	4/1/20		Cancelled
COE Meeting 2	10/1/20	10/1/20	10/28-10/29/20	Completed
Annual Report	2/4/21	2/4/21		
Project Closeout	2/4/21	2/4/21		



## **Major Accomplishments**

The major activities are: 1) execution of the Pratt & Whitney subaward and a kickoff meeting to start design work; 2) completion of CT scans of existing FAA CLEEN II airfoils; 3) identification of the critical criteria (geometric match to design intent, cooling flow behavior relative to design intent, variation relative to other airfoils, etc.) to determine most appropriate airfoil design to additively manufacture. All of these activities will help us to execute Task 1, and the learning from these tasks will be leveraged throughout the rest of the project.

## **Publications**

Nothing to report yet.

## **Outreach Efforts**

Presented research findings to Pratt & Whitney (cost share partner) at bi-annual Center of Excellence review meeting on 11/30/2020.

## **Awards**

Nothing to report yet.

## **Student Involvement**

Justin Wolff (currently a first year Masters student) has been responsible for analyzing CT scan data of the FAA CLEEN II blades and compiling a review package to be discussed with Pratt & Whitney. Justin has learned the analysis tools and his next role will be designing novel double-wall cooling strategies that will be implemented by him into high-speed linear cascade hardware.

## **Plans for Next Period**

The most appropriate airfoil to model as an AM fabricated part will be decided in the near term and the design will be relayed to Pratt & Whitney. Structural analysis of the airfoil will be conducted to ensure that the airfoil will be safe to operate in the Penn State rig, and the design finalized. Once the design is complete, an AM vendor will be selected and a purchase order will be issued. The necessary post-processing steps will also be identified (blade machining operations, inspections, flow characterization, instrumentation, etc.) prior to installation in the rig.

The airfoils will be tested in the START turbine in the 2<sup>nd</sup> quarter of 2021 using the IR thermography capability recently developed, and the results will be compared to the original FAA CLEEN II cast airfoils.

The preliminary and detailed design of novel microchannel designs will begin shortly. The designs will use an appropriate airfoil geometry decided in conjunction with Pratt and Whitney, and the initial database for microchannel designs will be taken from public literature or patents. Test articles will be fabricated for the linear cascade at Penn State toward the middle of Year 2 and tested by the end of Year 2.

The current project plan is indicated below in the Gantt chart. Due to some delays attributed to COVID and shutdown of the facility in mid 2020, the design and fabrication of the AM blades for Task 1 is delayed and would be expected to be completed in 2021 Q1.



**Table 1. Project Schedule**

Calendar Year	2020				2021				2022				2023
Project Year	Year 1				Year 2				Year 3				
	Q2	Q3	Q4	Q1	Q2	Q3	Q4	Q1	Q2	Q3	Q4	Q1	
<b>Task 1:</b> Manufacture and test existing FAA CLEEN II blade designs	█	█	█	█									
1.1: Quote and purchase AM blades	█												
1.2: Fabricate AM blades		█											
1.3: Machining and heat treatment			█										
1.4: Installation, shakedown, and testing of blades in START Rig			█	█									
<b>Task 2:</b> Design new double-wall cooling technologies	█	█	█	█	█								
2.1: Evaluation of existing IP and concepts	█												
2.2: Conceptual designs		█											
2.3: Preliminary and detailed designs			█	█	█								
<b>Task 3:</b> Manufacture and test new double-wall cooling designs for linear cascade					█	█	█	█					
3.1: Purchase and fabricate AM airfoils					█								
3.2: Inspect and compare to design intent						█							
3.3: Instrumentation and flow checks							█						
3.4: Data collection at design conditions								█					
<b>Task 4:</b> Manufacture and test optimal double-wall cooling designs for START turbine									█	█	█	█	
4.1: Design blades for START turbine									█				
4.2: Quote and purchase AM blades										█			
4.3: Fabricate AM blades											█		
4.4: Machining and heat treatment												█	
4.5: Installation, shakedown, and testing of blades in START Rig												█	



## Project 057 Support for Supersonic Aircraft En-route Noise Efforts in ICAO CAEP

### The Pennsylvania State University

#### Project Lead Investigator

Victor W. Sparrow  
Director and United Technologies Corporation Professor of Acoustics  
Graduate Program in Acoustics  
The Pennsylvania State University  
201 Applied Science Bldg.  
University Park, PA 16802  
+1 (814) 865-6364  
vws1@psu.edu

#### University Participants

##### The Pennsylvania State University

- PI: Vic Sparrow, United Technologies Corporation Professor and Director, Graduate Program in Acoustics
- FAA Award Number: 13-C-AJFE-PSU Amendment 55
- Period of Performance: February 5, 2020 to August 4, 2021
- Tasks:
  1. Obtaining confidence in signatures, assessing metrics sensitivity, and adjusting for reference day conditions.
  2. Assessing secondary sonic boom propagation.

#### Project Funding Level

This project focuses on multiple Tasks at The Pennsylvania State University (Penn State) and its subcontractor Queensborough Community College. The FAA funding to Penn State in 2020–2021 is \$200,000. Matching funds are expected to meet cost share on both Tasks. Boom Supersonic has pledged \$100,000 and Gulfstream has pledged \$100,000.

#### Investigation Team

- Victor W. Sparrow, PI (Task 1 and 2), The Pennsylvania State University
- Joshua Kapcsos, graduate research assistant (Task 1), The Pennsylvania State University
- Kimberly A. Riegel, coinvestigator (Task 2), subrecipient to Penn State, Queensborough Community College, City University of New York
- Michael Rybalko, Joe Salamone, et al., Boom Supersonic [industrial partner]
- Brian Cook, Charles Etter, Gulfstream [industrial partner]

#### Project Overview

We are on the verge of a true revolution in passenger aircraft development. Companies such as Boom Supersonic, AERION, Gulfstream Aerospace Corporation, Lockheed Martin, and others are reaching the point where they can build, and deliver to users', aircraft capable of flying supersonically in an environmentally responsible way. This will allow for decreased air transportation travel times, to the great benefit of everyone.

To introduce new supersonic aircraft, these vehicles must be certified as being quiet enough so as to not highly annoy the public. Preparing for such a certification process has been ongoing for several years in the FAA Office of Environment and Energy (AEE). Working with its international partners in the International Civil Aviation Organizations (ICAO)'s Committee for Aviation Environmental Protection (CAEP), FAA has been laying the groundwork for certification standards. The FAA efforts

have been supported by both universities and other government agencies. Specifically, Penn State has supported FAA/AEE through Projects 8 and 24 in the PARTNER Center of Excellence (<http://partner.mit.edu/>) and in Projects 7, 41, and 42 more recently in the ASCENT Center of Excellence (<https://ascent.aero/>). Summaries of these research efforts can be found on the websites provided. Thus far, a group of six candidate metrics for sonic boom certification have been agreed upon in CAEP's Working Group 1 (Noise) Supersonic Task Group (SSTG). Several schemes for certification have been generated. A few schemes have been eliminated from further consideration, and others are currently being evaluated for possible implementation. Procedures have been proposed for acquiring and processing ground measurement of the sonic boom signatures, but all is still under discussion. The extent to which atmospheric conditions will affect the measurements and the requirements and role of numerical simulations of sonic booms propagating from the aircraft to the ground are being considered. One particularly tricky part is the influence of the atmosphere creating distortions in the sonic boom signatures, due to atmospheric turbulence, and the subsequent effects on the metric values. These are just a few of the gaps that need to be filled.

All of these topics are being worked, step by step, in FAA and in Working Group 1's SSTG. Recent efforts in ASCENT Project 041 are to support FAA with technical expertise with the development of the certification procedures, as well as to gain an initial understanding of secondary sonic booms. Secondary sonic booms, also known as over-the-top sonic booms, are the sound energy which travels upward at heights above the aircraft cruise altitude and land at distant locations. Secondary sonic booms are the reason that Concorde was requested to transition from supersonic to subsonic speeds at substantial distances before entering the continental United States. ASCENT Project 041 will be ending in 2020 (or soon thereafter) and ASCENT Project 57 has just begun, but there is still a lot more to do as an effort lasting over several more years will be required to move forward on certification standards for supersonic aircraft.

In 2020 and beyond, continued support for supersonic aircraft noise efforts will be necessary for FAA and its international partners to fill technical solution gaps and continue making progress toward certification procedures. Although other universities and industry will continue their focus on aircraft design and landing and takeoff (LTO) studies, it is essential to continue working on the sonic boom issues as these remain the greatest barrier for environmentally responsible supersonic aircraft. This new ASCENT Project will support the ongoing activities in ICAO CAEP and their Working Group 1 (Noise) with a focus on establishing supersonic aircraft en-route procedures and metrics for noise certification standards, and to support the interface with the ICAO Air Navigation Commission to address related noise issues.

In the 2020-2023 project period, the emphasis will be on continuing the support for supersonic aircraft en-route procedures. This includes the utilization of an agreed-upon reference day atmosphere, the establishment of techniques for incorporating measurement data and simulations into a draft certification procedure, and the consideration of off-design flight speed sonic booms, such as focus booms and acceleration booms. Support will also be provided for a more complete analysis of NASA's SonicBAT dataset and efforts on a methodology to remove the effects of atmospheric turbulence on measured sonic boom waveforms to support certification. The 2020-2023 research will also need to consolidate and process the results of research in 2019-2020 on the topic of secondary sonic booms that is a potential noise issue for initial supersonic airplanes. This material will be of particular interest to ICAO's Air Navigation Commission, since it could affect the operation of supersonic aircraft in the near-term. The project investigator, Dr. V. Sparrow, will also be available to assist the FAA in providing expert knowledge and scientific understanding on sonic booms, as requested, and to support the other CAEP committees, such as the Impacts and Science Group on their aircraft noise impacts activities.

## Task 1 – Obtaining Confidence in Signatures, Assessing Metrics Sensitivity, and Adjusting for Reference Day Conditions

The Pennsylvania State University

### Objectives

ASCENT Project 57 is a transition from Project 41: *Identification of Noise Acceptance Onset for Noise Certification Standards of Supersonic Airplanes*; as national aviation authorities move forward to develop noise certification standards for low-boom supersonic airplanes, several research gaps exist in the areas of signature fidelity, metrics, metrics sensitivity to real-world atmospheric effects, adjustments for reference-conditions, etc. The objective of this Task is to support the FAA in the development of technical standards for civil supersonic aircraft under ICAO CAEP. This effort provides FAA with technical noise expertise regarding the development of noise certification standards for future civil supersonic passenger aircraft, primarily in the area of en-route noise (sonic boom) minimization and/or abatement.

Task 1 in ASCENT Project 57 focuses on research initiatives needed to move toward the development of a low-boom supersonic en-route noise certification standard. An objective was to simulate the effects of turbulence within various planetary boundary layer heights above the ground. Additionally, Penn State was motivated to compare the results and evaluate agreement with data produced by organizations that use different turbulence tools.

## **Research Approach**

### **Background**

The Japan Aerospace Exploration Agency (JAXA) recently utilized the SPnoiseSB tool to simulate the effects of turbulence on NASA's concept aircraft C609 shaped sonic boom through various planetary boundary layer heights. During simulation, JAXA used the atmospheric conditions of the SonicBAT (Sonic Booms in Atmospheric Turbulence) project's Flight 5 that occurred on July 14, 2016 at the Armstrong Flight Research Center (AFRC). Simulated boundary layer heights included 268.2, 411.4, and 1026.7 meters. It is important to consider various boundary layers because these heights are determined by the point at which warm air begins to experience negative buoyancy, which depends on rapid increase in temperature and water vapor content. As one of the goals of Task 1 is to determine agreement with the results of other organizations that use different turbulence tools, Penn State was motivated to run similar simulations in order to compare to those of JAXA. NASA provided Penn State with sound metric analyses on JAXA data, and JAXA supplied additional databases.

### **Turbulence Modeling**

The computational tool that Penn State used above the planetary boundary layer was the PCBoom 6.7.1.1 sonic boom propagation software. PCBoom was developed by kbrWyle and is maintained in part by NASA, and version 6.7.1.1 was supplied to Penn State in August of 2019. Penn State matched the SonicBAT flight conditions used for the PCBoom portion above the boundary layer to those used by JAXA. The shaped sonic boom was propagated in PCBoom from a cruise altitude of 50,000 ft to the top of the planetary boundary layer. The signature outputs of PCBoom were quite smooth in each case, since the enhanced BURGERS algorithm was utilized, incorporating the effects of molecular relaxation absorption. The PCBoom output signatures at the top of the planetary boundary layer was then fed as input into the turbulence tool. Because different tools were used both above and below the planetary boundary layer and because the chosen turbulence tool does not take a ground reflection factor into account, the ground reflection factor was turned off in the PCBoom portion and instead applied during post-processing.

Penn State used the 2-dimensional version of KZKFourier as the turbulence tool to propagate the sonic boom through the planetary boundary layer to the ground. The KZKFourier code was developed by post-doctoral scholar Trevor Stout as a component of his 2018 Ph.D. dissertation, and the code uses an augmented nonlinear Khokhlov-Zabolotskaya-Kuznetsov (KZK) propagation equation that includes nonlinearity, diffraction, and absorption in directional sound beams. KZKFourier was designed to implement the Ostashev and Wilson (O&W) model throughout the turbulent boundary layer, which considers temperature and wind fluctuations corresponding to scalar and vector turbulence, respectively. The latter includes wind shear and buoyancy effects. The O&W model varies turbulence by defining length scale and root mean square (RMS) magnitude as a function of height, gradually changing which parts of the logarithmically spaced wavenumber spectrum are accentuated as the boom approaches the ground. The code features two Von Karman spectra equations, one for the energy spectra of the temperature (scalar) fluctuations and one for the wind (vector) fluctuations, and turbulent fields are produced by the Random Fourier Modes method. A binary switch to turn off the O&W model is included in the KZKFourier code; this switch instead prescribes a single length scale and RMS magnitude at all heights. The code does not include profiles for humidity and other ambient quantities.

### **Parameters**

Because KZKFourier does not include profiles for ambient atmospheric quantities, the relative humidity, temperature, and ambient pressure for the turbulence portion were extracted from the lowest altitude in the SonicBAT Flight 5 PCBoom atmospheric file provided by NASA. Penn State utilized these files in order to match the atmospheric parameters used by JAXA. The ray angle was determined by the angle of incidence of the output of the PCBoom portion and was held constant throughout the turbulence portion. KZKFourier generates atmospheres using random seeds, which were used for turbulence conditions 1 to 10. The amount and spacing of virtual microphones were set to correspond to JAXA parameters as well. KZKFourier output 100 ground pressure waveforms along the virtual microphone array to be plotted per JAXA's turbulence condition, but the output files are finer and had been prescribed as 4097 virtual microphones in each array.

### **Single Length Scale and RMS Magnitude without Temperature Fluctuations**

In order to match JAXA conditions, the temperature fluctuation was initially not considered and the O&W model was turned off with the KZKFourier binary switch, prescribing a single length scale and RMS magnitude at all heights, as the tool used



by JAXA did not take these factors into consideration. Penn State plotted 100 ground pressure waveforms for each of the three planetary boundary heights for turbulence condition 1, which are given below in Fig. 1. The plots for the latter nine turbulence conditions are visually similar and are therefore not shown. Because the O&W model was turned off and temperature fluctuation was not considered, the variability is not easily seen. The first plot features a magnified section to more clearly observe the small variation between ground pressure waveforms.

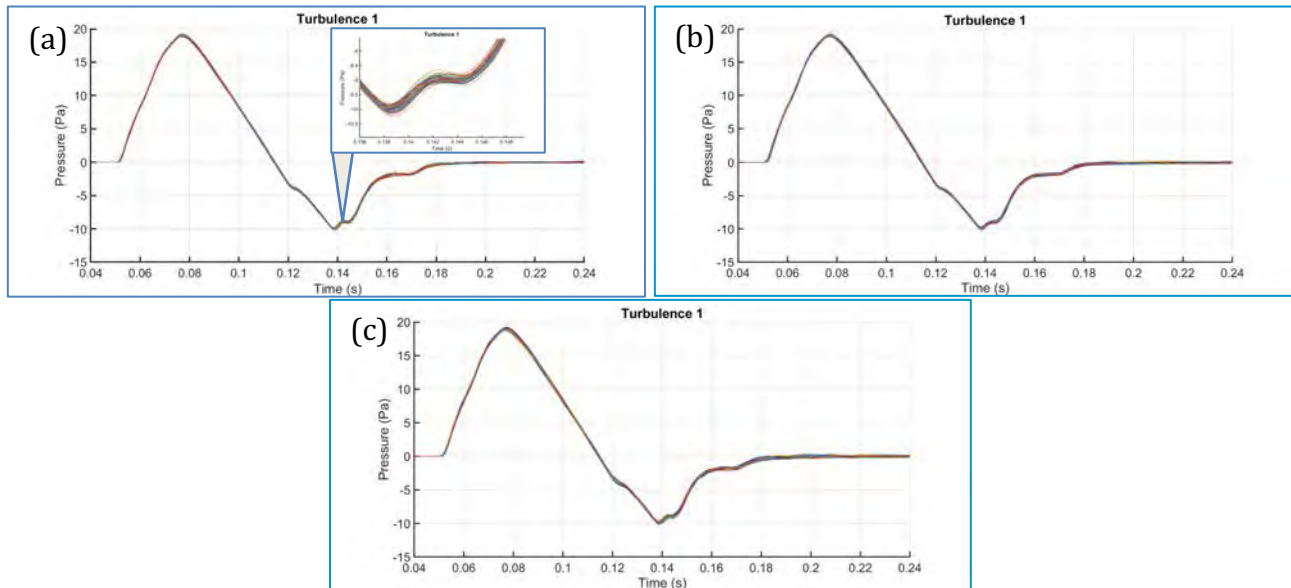


**Figure 1.** Plots of 100 ground pressure waveforms in Pa for turbulence condition 1 after propagation through boundary layer heights of 268.224 m (a), 411.38 m (b), and 1026.7 m (c) with single length scale and RMS magnitude.

In addition to plotting ground pressure waveforms, NASA ran analyses on the JAXA sound metric database. Penn State ran similar analyses, a portion of which are given below in Tables 1 and 2 that list the Steven’s Mark VII Perceived Level (PL) and Indoor Sonic Boom Annoyance Predictor (ISBAP) sound metrics, respectively. Sound exposure level (SEL) metrics A through E were also calculated and meet the ANSI/ASA S1.42 standard. The tables feature the mean, standard deviation, minimum, median, and maximum values of the applied sound metric of the 100 ground pressure waveforms for each of the 10 turbulence conditions and zero turbulence condition; condition 0 corresponds to no turbulence. It should be noted that KZKFourier does not include amplitude changes to account for geometrical spreading, which can reduce boom pressure amplitude by about 2% at AFRC. As such, the below PL output was corrected to account for geometric spreading by subtracting the difference between PCBoom and KZKFourier ground level realizations under zero turbulence.



**Table 1.** List of PLdB per turbulence analysis calculated via KZKFourier simulations with single length scale and RMS magnitude. Results have been corrected to account for geometric spreading.

Turb.	268.224 m BL					411.38 m BL					1026.7 m BL				
	Mean	SD	Min	Med.	Max	Mean	SD	Min	Med.	Max	Mean	SD	Min	Med.	Max
0	67.02	-	67.02	67.02	67.02	67.02	-	67.02	67.02	67.02	67.02	-	67.02	67.02	67.02
1	66.84	0.61	65.39	66.87	68.54	66.77	0.65	65.32	66.73	68.36	66.58	0.65	64.7	66.64	67.88
2	66.85	0.58	65.42	66.83	68.30	66.76	0.85	64.76	66.79	68.43	66.63	0.81	64.42	66.52	68.55
3	66.89	0.50	65.61	66.91	68.12	66.81	0.53	65.44	66.85	68.19	66.63	0.52	65.43	66.58	67.92
4	66.80	0.81	64.44	66.69	68.75	66.73	0.89	64.23	66.8	68.72	66.52	1.16	64.03	66.56	69.41
5	66.84	0.65	64.72	66.87	68.60	66.82	0.63	65.26	66.83	68.63	66.61	0.74	65.02	66.59	68.59
6	66.79	0.75	65.10	66.77	68.48	66.74	0.82	64.61	66.63	68.44	66.63	0.80	65.24	66.52	68.93
7	66.82	0.60	65.11	66.87	68.56	66.84	0.56	65.46	66.90	68.06	66.57	0.56	65.1	66.61	67.67
8	66.86	0.64	65.43	66.84	68.53	66.75	0.70	64.68	66.80	68.35	66.58	0.83	64.44	66.59	68.97
9	66.83	0.61	65.07	66.85	68.41	66.77	0.67	65.18	66.86	68.22	66.61	0.72	65.21	66.61	68.17
10	66.82	0.72	64.75	66.85	68.49	66.76	0.83	64.79	66.77	68.70	66.54	0.89	64.10	66.49	69.18

The ISBAP sound metric analysis is provided below in Table 2. Note that these ISBAP results were not corrected to account for geometric spreading.

**Table 2.** List of ISBAP per turbulence analysis calculated via KZKFourier simulations with single length scale and RMS magnitude. Geometric spreading is not considered.

Turb.	268.224 m BL					411.38 m BL					1026.7 m BL				
	Mean	SD	Min	Med.	Max	Mean	SD	Min	Med.	Max	Mean	SD	Min	Med.	Max
0	82.80	-	82.80	82.80	82.80	82.75	-	82.75	82.75	82.75	82.45	-	82.45	82.45	82.45
1	82.64	0.37	81.71	82.65	82.57	82.56	0.38	81.65	82.56	83.48	82.10	0.40	80.96	82.12	82.86
2	82.66	0.35	81.74	82.66	83.47	82.56	0.49	81.26	82.58	83.51	82.15	0.48	80.97	82.09	83.44
3	82.68	0.30	81.86	82.68	83.38	82.59	0.31	81.86	82.59	83.35	82.14	0.31	81.52	82.11	82.86
4	82.63	0.49	81.15	82.56	83.91	82.53	0.52	81.04	82.56	83.75	82.08	0.70	80.53	82.07	83.84
5	82.65	0.40	81.33	82.67	83.68	82.59	0.38	81.66	82.64	83.66	82.14	0.44	81.08	82.16	83.21
6	82.62	0.44	81.67	82.62	83.64	82.54	0.48	81.34	82.53	83.50	82.16	0.51	81.26	82.09	83.53
7	82.62	0.35	81.58	82.63	83.59	82.59	0.32	81.74	82.61	83.30	82.11	0.33	81.25	82.15	82.78
8	82.66	0.39	81.79	82.65	83.69	82.55	0.42	81.39	82.57	83.45	82.10	0.49	80.73	82.08	83.52
9	82.64	0.37	81.46	82.64	83.62	82.56	0.38	81.50	82.61	83.42	82.13	0.45	81.23	82.13	83.23
10	82.64	0.43	81.35	82.63	83.63	82.55	0.49	81.42	82.56	83.79	82.09	0.53	80.66	82.09	83.89

The above results were compared to the NASA analysis of JAXA results, and it was concluded that the Penn State data agreed closely with JAXA regarding means, but the standard deviations were higher than those of JAXA due to tool differences. The standard deviations of the Penn State results were all well within one standard deviation, and unincluded histograms and normal probability plots showed the turbulence conditions were approximately normally distributed for PL and ISBAP. The mean sound metric value decreased with increased boundary layer height, and the standard deviations increased with increased boundary layer height, both of which are intuitive because propagation over a longer distance results in more exposure to turbulence and its formulated randomness.



### Varied Turbulence as Function of Height with Temperature Fluctuations

As previously noted, the O&W model can be turned on or off using a binary switch in KZKFourier in order to vary turbulence as a function of height, in which higher wavenumbers become more important near the ground. Temperature fluctuations can also be prescribed in the KZKFourier code. Because there was good agreement between KZKFourier simulations and field measurement data for metric variability for N-waves during the SonicBAT project, Penn State performed a similar analysis with the shaped signature of the C609 concept aircraft, diverging from the previous JAXA scheme by turning on the O&W model and prescribing temperature fluctuations. Friction velocity, mixed-layer velocity scale, and surface layer temperature scale values required for the O&W model execution in KZKFourier match the parameters used for 2D and filter validation simulations as listed in the Stout thesis and SonicBAT contractor report. Again, flight conditions for the PCBoom portion above the boundary layer were the same used by JAXA and Penn State in previous runs.

Plots of 100 ground pressure waveforms for each of the three planetary boundary heights for turbulence condition 1 are given below in Fig. 2. The variability produced by the O&W model are very visible in comparison to the previous runs in which a single length scale was used. The plots for the latter nine turbulence conditions are visually similar to the below provided plots and are therefore not shown.

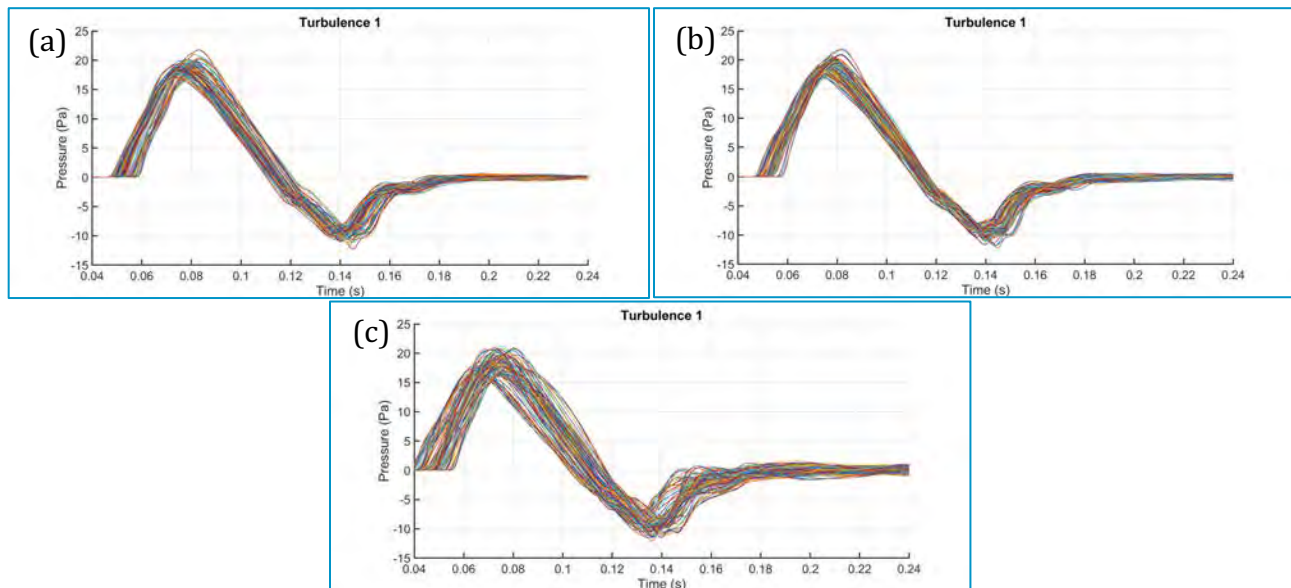


**Figure 2.** Plots of 100 ground pressure waveforms in Pa for turbulence condition 1 after propagation through boundary layer heights of 268.224 m (a), 411.38 m (b), and 1026.7 m (c) with O&W model and temperature fluctuations.

In addition to plotting ground pressure waveforms, Penn State again ran sound metric analyses, a portion of which are given below in Tables 3 and 4 in lists of the PL and ISBAP sound metrics, respectively. SEL metrics A through E were also calculated and meet the ANSI/ASA S1.42 standard. Neither of the below tables were modified to account for geometric spreading. The tables feature the mean, standard deviation, minimum, median, and maximum values of the applied sound metric of all 4097 ground pressure waveforms of the fine microphone array for each of the 10 turbulence conditions and zero turbulence condition.



**Table 3.** List of PLdB per turbulence analysis calculated via KZKFourier simulations with the O&W model and temperature fluctuations. Geometric spreading is not considered.

Turb.	268.224 m BL					411.38 m BL					1026.7 m BL				
	Mean	SD	Min	Med.	Max	Mean	SD	Min	Med.	Max	Mean	SD	Min	Med.	Max
0	67.81	-	67.81	67.81	67.81	67.76	-	67.76	67.76	67.76	68.14	-	68.14	68.14	68.14
1	67.27	1.76	63.05	67.33	71.99	67.11	1.97	62.01	67.00	72.89	66.65	2.59	58.01	66.72	75.69
2	67.39	1.52	64.10	67.35	71.53	67.19	1.88	62.32	67.11	71.90	66.70	2.60	60.50	66.87	74.00
3	67.26	1.87	62.98	67.25	72.97	67.03	2.16	62.37	66.74	73.36	66.41	2.88	60.31	65.93	75.00
4	67.28	1.83	63.21	67.38	73.57	66.86	2.47	61.38	66.63	75.02	66.35	3.09	59.93	65.94	74.02
5	67.31	1.80	62.70	67.44	71.44	67.26	2.26	60.42	67.64	72.87	66.33	3.21	58.86	66.62	73.78
6	67.27	1.88	61.78	67.19	72.16	66.89	2.60	60.62	66.90	73.23	66.03	3.62	56.26	65.87	76.77
7	67.33	1.66	63.26	67.34	72.53	67.01	2.22	62.34	67.02	73.46	66.36	3.09	58.66	66.40	73.77
8	67.37	1.55	63.01	67.42	70.77	67.20	1.77	63.62	67.13	72.32	66.86	2.17	62.55	66.85	72.60
9	67.21	1.95	62.00	67.09	72.70	66.71	2.76	59.86	66.37	73.19	66.20	3.44	57.10	66.08	75.40
10	67.24	1.91	62.56	67.18	72.51	67.03	2.21	61.51	67.08	73.46	66.69	2.71	57.63	66.78	74.50

**Table 4.** List of ISBAP per turbulence analysis calculated via KZKFourier simulations with the O&W model and temperature fluctuations. Geometric spreading is not considered.

Turb.	268.224 m BL					411.38 m BL					1026.7 m BL				
	Mean	SD	Min	Med.	Max	Mean	SD	Min	Med.	Max	Mean	SD	Min	Med.	Max
0	82.82	-	82.82	82.82	82.82	82.77	-	82.77	82.77	82.77	82.89	-	82.89	82.89	82.89
1	82.40	1.24	79.62	82.35	86.11	82.26	1.37	78.86	82.16	86.65	81.79	1.94	76.20	81.84	88.55
2	82.47	1.10	80.26	82.35	85.65	82.32	1.29	79.05	82.16	85.32	80.85	3.62	69.95	81.84	86.99
3	82.41	1.27	79.45	82.42	86.19	82.23	1.45	78.74	82.18	86.58	81.60	2.14	77.26	81.26	87.74
4	82.42	1.30	79.52	82.49	86.96	82.10	1.81	78.08	81.96	88.16	81.61	2.22	77.75	81.27	87.16
5	82.43	1.30	79.15	82.51	85.70	81.89	1.91	76.90	82.11	85.54	81.48	2.55	75.03	81.72	87.08
6	82.42	1.31	78.66	82.37	85.86	82.13	1.91	77.54	82.18	86.65	81.27	2.83	73.81	81.40	89.90
7	82.45	1.11	79.80	82.46	86.22	82.22	1.50	78.84	82.28	86.81	81.58	2.34	76.14	81.60	86.98
8	82.47	1.01	79.47	82.50	84.82	82.33	1.23	79.37	82.26	86.08	81.91	1.62	78.20	81.84	85.92
9	82.38	1.31	78.91	82.32	85.81	82.02	1.91	77.20	81.95	86.12	81.43	2.68	74.27	81.34	88.41
10	82.39	1.28	79.01	82.40	85.90	82.21	1.59	77.89	82.33	86.71	81.76	2.17	75.13	81.94	87.73

The standard deviations of the above tables were much higher than those of the previous runs as temperature fluctuations were considered and the O&W model was switched on in KZKFourier; the O&W model prescribed more turbulence that resulted in more variation. Similar to the previous runs, the standard deviations increased with increase in planetary boundary layer height, while mean sound metric decreased with increase in planetary boundary layer height.

**Milestone**

The impact of atmospheric turbulence on various planetary boundary layer heights was assessed in two different turbulence modeling schemes.

### **Major Accomplishments**

ASCENT Project 57 Task 1 has determined that sonic boom metrics are affected differently given the signature variability introduced by atmospheric turbulence, which may prove useful in sonic boom certification of supersonic aircraft.

### **Publications**

None

### **Outreach Efforts**

A summary of the procedure and findings of Task 1 were presented in the form of a virtual poster during the 2020 Fall Workshop of the Penn State Center for Acoustics and Vibration.

### **Awards**

None

### **Student Involvement**

Joshua Kapcsos was the Penn State graduate research assistant who worked on ASCENT Project 57 during the 2019-2020 academic year. In addition to the above research, he has been undertaking direct numerical comparisons of the fluctuation and spectral equations of different turbulence tools.

### **Plans for Next Period**

Additional simulations and corresponding recommendations regarding the potential sonic boom metrics for inclusion in a certification procedure will be conducted. Because sonic boom metrics are affected differently given the signature variability introduced by atmospheric turbulence, turbulent sonic boom propagation prediction software/code certification will be continued. Differences between turbulence models should be further evaluated for future agreement. The effects of temperature, wind, and humidity profiles on certification schemes will also be further studied. Task 1 of Project 57 will continue examining sonic boom propagation through turbulence for possible application to supersonic aircraft certification.

### **References**

<sup>1</sup>T. Stout, "Simulation of N-Wave and Shaped Supersonic Signature Turbulent Variations," Pennsylvania State University, Ph.D. Dissertation, December 2018.

<sup>2</sup>V. Ostashev, D. Wilson, *Acoustics in Moving Inhomogeneous Media* (2nd ed.), CRC Press, Boca Raton, FL, 2015.

<sup>3</sup>K. Bradley, *et al.*, "Sonic Booms in Atmospheric Turbulence (SonicBAT): The Influence of Turbulence on Shaped Sonic Booms" (NASA/CR-2020-220509), National Aeronautics and Space Administration, Armstrong Flight Research Center, Edwards, CA, 2020.

## **Task 2 – Assessing Secondary Sonic Boom Propagation**

The Pennsylvania State University  
Queensborough Community College / City University of New York

Information regarding this Task appears in the 2020 report for ASCENT Project 041: *Identification of Noise Acceptance Onset for Noise Certification Standards of Supersonic Airplanes*. In future years, information on this Task will appear in the annual report on Project 57.



# Project 058 Improving Policy Analysis Tools to Evaluate Higher-Altitude Aircraft Operations

## Massachusetts Institute of Technology

### Project Lead Investigator

PI: Steven R. H. Barrett  
Professor of Aeronautics and Astronautics  
Director, Laboratory for Aviation and the Environment  
Massachusetts Institute of Technology  
77 Massachusetts Ave, Building 33-322, Cambridge, MA 02139  
(617) 452-2550  
sbarrett@mit.edu

Co-PI: Dr. Sebastian D. Eastham  
Research Scientist  
Laboratory for Aviation and the Environment  
Massachusetts Institute of Technology  
77 Massachusetts Ave, Building 33-322, Cambridge, MA 02139  
seastham@mit.edu

### University Participants

#### Massachusetts Institute of Technology

- PI: Steven R. H. Barrett
- FAA Award Number: 13-C-AJFE-MIT, Amendment No. 064
- Period of Performance: Feb. 5, 2020 to Feb. 4, 2022
- Reporting Period: Feb. 5, 2020 to Sep. 30, 2020
- Tasks (Note: Tasks not covered during this reporting period are listed as "*pending*" and are discussed further only in the context of tasks for the coming period of performance):
  1. Develop a set of emissions scenarios for high-altitude aviation.
  2. Extend and validate the Massachusetts Institute of Technology's (MIT) existing atmospheric simulation capabilities.
  3. Simulate atmospheric impacts of high-altitude emissions using updated capabilities [*pending*].
  4. Conversion of estimated impacts into sensitivities [*pending*].
  5. Develop and update operational tools capable of quantifying environmental impacts of aviation.

### Project Funding Level

\$500,000 funding from FAA and \$500,000 matching funds. Sources of match are approximately \$109,000 from MIT, plus third-party in-kind contributions of \$391,000 from NuFuels LLC.

### Investigation Team

Principal Investigator: Prof. Steven Barrett (MIT) (all Tasks)  
Co-Principal Investigator: Dr. Sebastian Eastham (MIT) (all Tasks)  
Graduate Research Assistants: Inés Sanz-Morère (MIT) (Tasks 1-3, Task 5)  
Joonhee Kim (MIT) (Task 3- 5)



## Project Overview

Companies are proposing, developing, and testing aircraft operating at higher altitudes, such as commercial supersonic aircraft and high-altitude, long-endurance (HALE) unmanned aerial vehicles. These aircraft offer the potential to become enablers for new use cases and business models in the aviation sector. However, the combustion emissions of these vehicles will have atmospheric impacts which differ from conventional subsonic aviation due to the higher altitudes of emission. Emissions at higher altitudes are associated with a different chemical environment, longer emission lifetimes, and greater distances over which the emissions will be transported. In this project, we propose to quantify the environmental consequences of such high-altitude aviation emissions. For this purpose, we will perform high-fidelity atmospheric simulations by further developing and applying the GEOS-Chem UCX tropospheric-stratospheric chemistry-transport model and its adjoint. The results will be leveraged to: (1) evaluate the climate (radiative forcing) effects of high-altitude aircraft emissions; and (2) to estimate the sensitivity of the global ozone column and surface air quality to these emissions. As a result, the climate, air quality, and ozone impacts for a small number of different proposed supersonic aircraft designs and performance characteristics will be quantified and a rapid assessment approach for assessing the impacts of supersonic aircraft will be presented.

## Task 1 – Develop a Set of Emissions Scenarios for High-Altitude Aviation

Massachusetts Institute of Technology

### Objective

The overall objective of this task is to develop emissions inputs which cover scenarios relevant to near-future aviation, extending impact estimation to cover a range of altitudes exceeding those of current commercial airline activities. The specific focus of the work during this period was to develop physics-based parameterization which could be used to generate emissions maps resulting from a given supersonic aviation scenario.

### Research Approach

In order to achieve the goals outlined above, a mathematical model is necessary which can produce an estimate of emissions of key chemical species (nitrogen oxides ( $\text{NO}_x$ ), sulfur oxides ( $\text{SO}_x$ ), water vapor, soot, etc.) resulting from a single flight. This requires a physics-based approach. During the reporting period, the team has developed a prototype iterative model which can estimate the distribution of emissions along a supersonic aircraft flight path. This will support estimation of impacts resulting from aircraft design data provided from ASCENT Project 10, in addition to enabling perturbation analysis for plausible design and mission deviations. This prototype also incorporates engine modeling data developed under ASCENT Project 47.

### Milestones

- This Task was initiated during this project year. Bi-weekly project discussions with the FAA are now underway.
- The first prototype of this model has been completed and is now undergoing refinement and testing using representative aircraft designs.
- Regular meetings between members of the ASCENT Project 58 and ASCENT Project 47 teams have been established.

### Major Accomplishments

- The first prototype of a model to estimate fuel burn and emissions for a given mission under realistic constraints has been completed.

### Publications

None

### Outreach Efforts

Progress on all tasks was communicated during bi-weekly briefing calls with the FAA.

### Awards

None

### **Student Involvement**

During the reporting period of AY 2019/20, the MIT graduate student involved in this task was Inés Sanz-Morère.

### **Plans for Next Period**

In the coming year, the MIT ASCENT Project 58 team will complete the prototype code described above, including integration of engine model information from ASCENT Project 47 and adaptation to incorporate the supersonic fleet results from ASCENT Project 10, as processed by the Volpe Forecasting and Economics Support Group. This is expected to result in a set of emissions maps for representative supersonic aircraft designs, covering a range of possible scenarios.

### **References**

N/A

## **Task 2 – Extend and Validate MIT’s Existing Atmospheric Simulation Capabilities**

Massachusetts Institute of Technology

### **Objective**

The objective of Task 2 is to extend and validate MIT’s existing atmospheric simulation capabilities, with the specific goal of ensuring that they can accurately represent impacts on critical metrics of air quality and climate. During AY 2019/20, the team conceptualized and implemented an approach to estimate stratospherically adjusted radiative forcing using the GEOS-Chem UCX chemistry transport model.

### **Research Approach**

The team is using the GEOS-Chem UCX tropospheric-stratospheric global chemistry-transport model as the central tool to quantify climate, air quality, and ozone impacts resulting from high-altitude aviation. It is therefore necessary to evaluate the capabilities of this model for these purposes and to extend those capabilities where necessary. Two major subtasks have been identified: Task 2a, increasing the resolution of the model to capture localized impacts at a global resolution of 2°x2.5° or equivalent; and Task 2b, implementation of a technique to estimate stratospherically adjusted radiative forcing (RF), rather than instantaneous RF. Work in the AY 2019/2020 period has been on Task 2b.

As implemented in GEOS-Chem by Heald et al. (2014), the standard radiative transfer code in GEOS-Chem (RRTMG) calculates only the instantaneous RF and not the stratospherically adjusted RF which has been recommended for calculations of climate-relevant forcing (Maycock et al, 2011; IPCC 2007). Stratospheric adjustment has been shown to change the net RF attributable to changes in stratospheric water vapor by around 50%, and may therefore be important to accurate calculation of the impacts of high-altitude aviation (Solomon et al 2010).

We have now implemented a scheme in GEOS-Chem which can calculate the stratospheric adjustment using the Fixed Dynamical Heating approximation (Fels, 1980). For this purpose, we use a time-marching method. We assume a quasi-steady state such that, in a given baseline scenario, stratospheric heating is in equilibrium. Following Maycock et al (2011), this can be expressed as

$$\frac{dT}{dt} = Q_{\text{DYN}} + (Q_{\text{LW}}(T, \chi) + Q_{\text{SW}}(\chi)) = 0$$

where  $Q_{\text{LW}}$ ,  $Q_{\text{SW}}$ , and  $Q_{\text{DYN}}$  are the longwave radiative, shortwave radiative, and dynamical heating rates, respectively, each with units of  $\text{K day}^{-1}$ . Here we assume that dynamical heating is fixed, that shortwave heating changes as a function of species concentrations  $\chi$  only, and that longwave heating changes as a function of both species concentration and temperature,  $T$ .

In each of the non-baseline scenarios, the species concentrations will change from those in the baseline scenario, but the temperatures remain the same. This means that the net heating rate can become non-zero such that

$$\frac{dT}{dt} = Q'_{\text{DYN}} + (Q'_{\text{LW}}(T, \chi') + Q'_{\text{SW}}(\chi')) \neq 0$$

resulting in a change in temperature over time. Under the fixed dynamical heating assumption, we assume that the dynamical heating is the same with and without the perturbation such that  $Q'_{DYN} = Q_{DYN}$ . We can then estimate the temperature tendency as

$$\frac{dT}{dt} = -(Q_{LW}(T, \chi) + Q_{SW}(\chi)) + (Q'_{LW}(T, \chi') + Q'_{SW}(\chi'))$$

using the longwave and shortwave heating rates from the baseline simulation.

In each perturbation simulation, we calculate the temperature tendency and then integrate forwards in time using the Runge-Kutta 4<sup>th</sup> order method with a time step of 12 hours. Only stratospheric grid cells are considered. For each calculation we allow only  $T$  to vary, and therefore only  $Q'_{LW}$  needs to be recalculated. The integration is performed independently for each model column to find the net temperature adjustment  $\Delta T$  in each grid cell. Integration is stopped once the maximum temperature tendency anywhere in the stratospheric column is less than 1 mK per day, or if the integration time exceeds 150 simulation days.

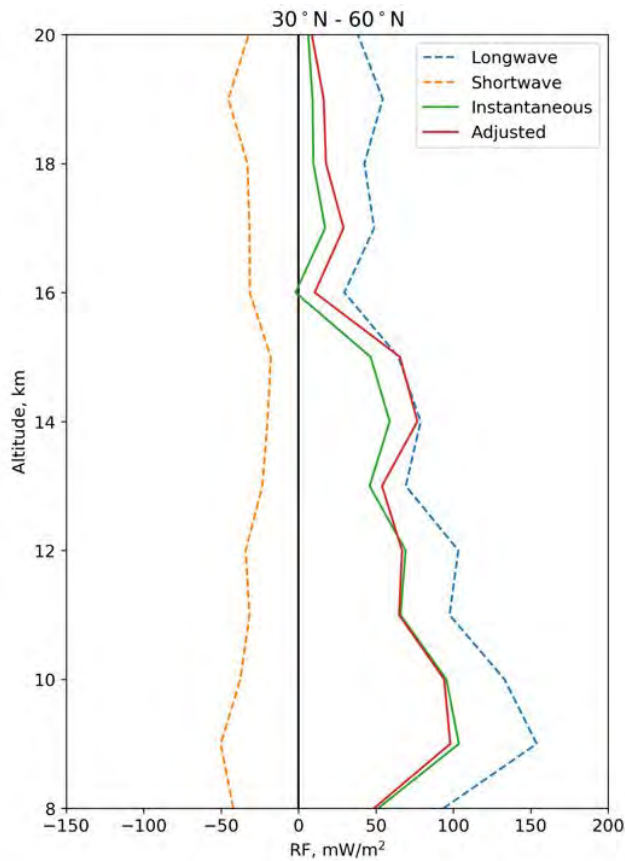


**Figure 1.** A comparison of the instantaneous RF components (dash), the instantaneous net RF (solid, green), and the stratospherically adjusted net RF (red) for a hypothetical contrail layer forming at a range of different altitudes.

The temperature adjustment is calculated using radiative transfer calculations including all constituents. The RF due to each constituent in a single simulation is then calculated by repeating the longwave and shortwave radiative transfer calculations with that constituent excluded. For these “excluded-constituent” calculations, the temperature adjustment is not recalculated; instead, the same temperature adjustment as was calculated for the “all-constituent” calculation is used.

Using this model, an initial assessment of the impacts of stratospheric water vapor emissions as a function of altitude has been carried out, comparing to the results from Solomon et al. (2010). We find that our results agree qualitatively with those shown in the reference paper. We also calculated the expected radiative impacts of a hypothetical contrail layer, with and without the adjustment (Figure 1).

These calculations demonstrate the importance of including stratospheric adjustment in RF calculations of higher-altitude aviation and will be used to perform all subsequent GEOS-Chem based RF calculations for ASCENT Project 58.

### **Milestones**

- Work has begun on familiarization of the graduate student team with the core modeling tool GEOS-Chem.
- A strategy to estimate stratospherically adjusted RF was identified, implemented, and tested.

### **Major Accomplishments**

- Stratospherically adjusted radiative forcing has been successfully implemented into the GEOS-Chem model.

### **Publications**

None

### **Outreach Efforts**

Progress on all tasks was communicated during bi-weekly briefing calls with the FAA.

### **Awards**

None

### **Student Involvement**

During the reporting period of AY 2019/20, the MIT graduate student involved in this task was Inés Sanz-Morère.

### **Plans for Next Period**

The team will feed the new RF scheme back to the GEOS-Chem community to maximize the impact of ASCENT Project 58's work. It will also perform an evaluation of the effect of stratospheric adjustment on aviation-attributable RF, verifying its results against literature estimates. Finally, the team will begin work on Task 2a, developing and validating a high-resolution version of the GEOS-Chem UCX model.

### **References**

- Fels, S. B., Mahlman, J. D., Schwarzkopf, M. D. and Sinclair, R. W.: Stratospheric Sensitivity to Perturbations in Ozone and Carbon Dioxide: Radiative and Dynamical Response, *J. Atmos. Sci.*, 37(10), 2265–2297, 1980.
- Heald, C. L., Ridley, D. a., Kroll, J. H., Barrett, S. R. H., Cady-Pereira, K. E., Alvarado, M. J. and Holmes, C. D.: Contrasting the direct radiative effect and direct radiative forcing of aerosols, *Atmos. Chem. Phys.*, 14(11), 5513–5527, 2014.
- IPCC: Contribution of Working Group I to the Fourth Assessment Report of the Intergovernmental Panel on Climate Change. Cambridge University Press, 2007.
- Maycock, a. C., Shine, K. P. and Joshi, M. M.: The temperature response to stratospheric water vapour changes, *Quart. J. Roy. Meteor. Soc.*, 137(657), 1070–1082, 2011.
- Solomon, S., Rosenlof, K. H., Portmann, R. W., Daniel, J. S., Davis, S. M., Sanford, T. J. and Plattner, G.-K.: Contributions of stratospheric water vapor to decadal changes in the rate of global warming, *Science*, 327(5970), 1219–1223, 2010.

## **Task 3 – Simulate Atmospheric Impacts of High-altitude Emissions Using Updated Capabilities**

Massachusetts Institute of Technology

### **Objective**

The objective of this task is to estimate the atmospheric response to each of the scenarios described in Task 1. This is a future task of the project and will begin in the coming project year.

### **Research Approach**

Specific outcomes to be investigated for each scenario are changes to the global ozone column; changes to the global average and northern hemispheric ozone layer; effects on polar ozone depletion; changes in surface air quality, including ozone and fine particulate matter (PM<sub>2.5</sub>); changes in UV-B radiation reaching the surface; and total induced radiative forcing. This will extend to limited-scale health impact evaluation, quantifying the human and economic impact of changes in surface air quality and exposure to UV-B. These outcomes will be estimated by performing simulations with the GEOS-Chem UCX model at the enhanced global resolution of 2°×2.5°. The outcomes will be calculated for each emissions scenario and in each case including different assumptions regarding cruise altitude, Mach number, engine NO<sub>x</sub> emissions index, and fuel sulfur content.

### **Milestones**

This task is planned for a later stage in the project and has not yet begun.

### **Major Accomplishments**

This task is planned for a later stage in the project and has not yet begun.

### **Publications**

None

### **Outreach Efforts**

This task is planned for a later stage in the project and has not yet begun.

### **Awards**

None

### **Student Involvement**

N/A

### **Plans for Next Period**

During the next project period, the project team will perform a baseline evaluation of subsonic aviation using the updated GEOS-Chem model to enable calibration of the future results to be used with the Aviation environmental Portfolio Management Tool - Impacts Climate (APMT-IC). It will also identify (and initiate) an experimental design which enables sensitivities of climate, air quality, and ozone to be evaluated using GEOS-Chem simulations.

### **References**

N/A

## **Task 4 – Conversion of Estimated Impacts into Sensitivities**

Massachusetts Institute of Technology

### **Objective**

The objective of this task is to convert the impacts calculated under Task 3 for each scenario into sensitivities of environmental impacts with regards to key parameters. This will then support the operationalization of these results in Task 5. This is a future task of the project and will begin in the coming project year.

### **Research Approach**

Sensitivities of each outcome will be calculated with respect to variables such as cruise altitude, Mach number, engine NO<sub>x</sub> emissions index, and fuel sulfur content. In addition, we will determine uncertainty distributions for each sensitivity. Due to the lack of recent literature on impacts from high-altitude aviation, there is not yet a scientific consensus from which uncertainties can be derived. The methods applied for past APMT-IC calculations are subsequently not applicable. Instead, impacts calculated from GEOS-Chem for high altitude scenarios will be compared to prior NASA studies to establish the appropriate shape and bounds for each outcome sensitivity.

### **Milestones**

This task is planned for a later stage in the project and has not yet begun.

### **Major Accomplishments**

This task is planned for a later stage in the project and has not yet begun.

### **Publications**

None

### **Outreach Efforts**

This task is planned for a later stage in the project and has not yet begun.

### **Awards**

None

### **Student Involvement**

N/A

### **Plans for Next Period**

During the next project period, the project team will survey the literature to establish the appropriate shape and bounds for the target set of outcome sensitivities. This will enable rapid adoption of the results generated by Task 3 into the APMT model, pending developments in Task 5.

### **References**

N/A

## **Task 5 – Develop and Update Operational Tools Capable of Quantifying Environmental Impacts of Aviation**

Massachusetts Institute of Technology

### **Objective**

This task aims to operationalize the results of Tasks 1–4. The eventual outcome will be a re-engineered version of APMT for climate and air quality impacts, calibrated based on updated sensitivity data and upgraded to provide monetized impacts which take into account the possibility of different cruise altitudes (among other characteristics).

### **Research Approach**

This task aims to produce a more broadly capable operational tool. The broad goal of incorporating new and updated sensitivity information must first be supported by an assessment of capabilities and requirements. This task is also expected to support updates of the tool to incorporate new information on impacts of existing aviation. During AY 2019/2020, this was accomplished through two subtasks.

First, an exercise was conducted to establish the extent of modifications required for APMT-IC and APMT-AQ (an air quality version) to account for higher-altitude aviation, including the effect of perturbations to the target altitude. Second, the existing version of APMT-IC was compared to the recent Lee et al. (2020) assessment of climate impacts of aviation. A summary of this comparison is shown in Figure 2.



## Radiative impact for emissions up to 2018

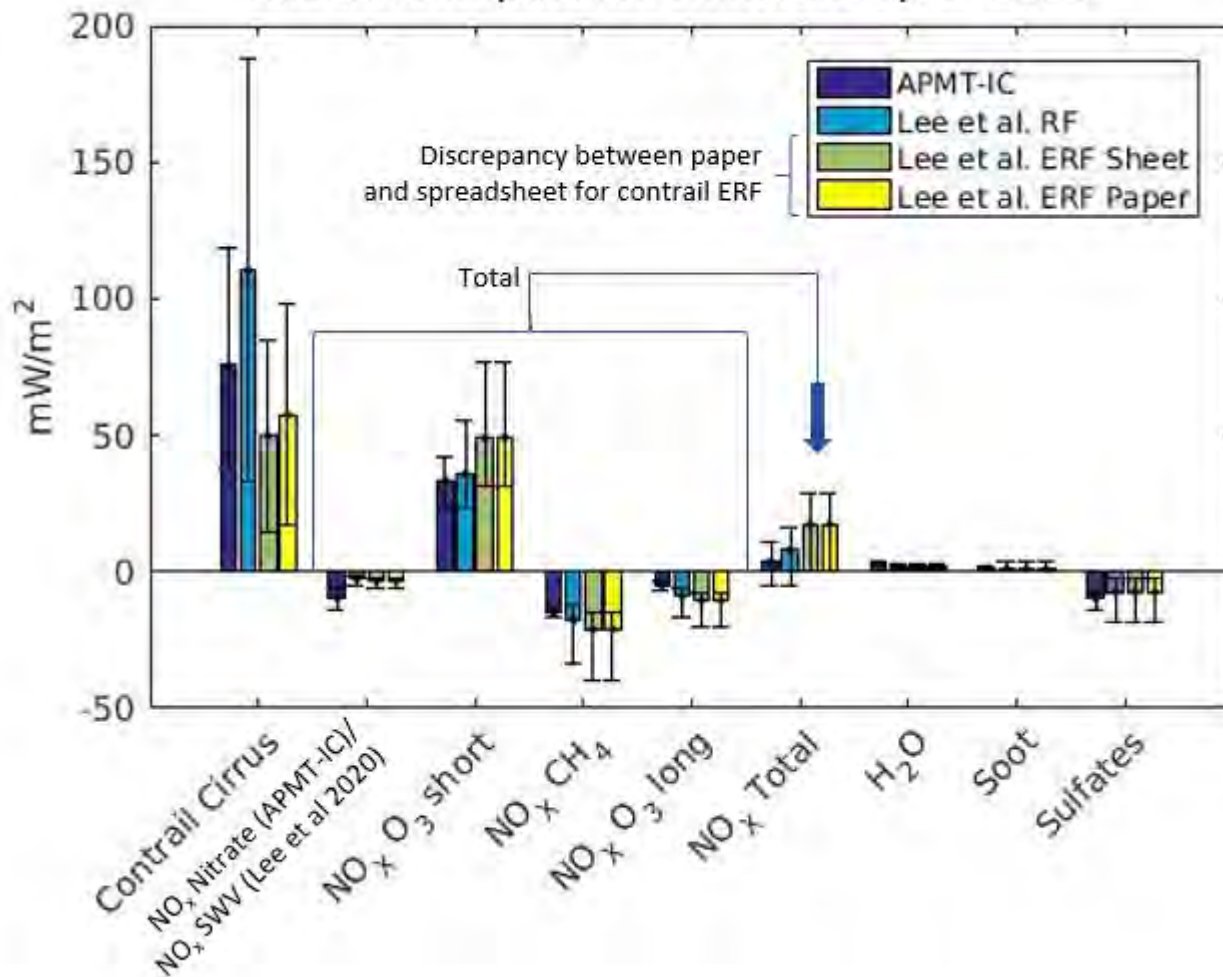


**Figure 2.** RF, in  $mW/m^2$ , estimated as a consequence of aviation to date using APMT-IC (dark blue) and compared to estimates from Lee et al. (2020). Results in light blue are for RF only and are most appropriate for comparison to APMT. Results in green and yellow show the “effective RF”, which includes tropospheric temperature adjustments. Two values are reported because the Lee et al. (2020) paper and supplementary information give conflicting results. The four  $NO_x$  components are summed to provide the “ $NO_x$  total” bar. SWV refers to stratospheric water vapor; SWV impacts were reported for Lee et al. (2020) but not for APMT, while nitrate formation due to  $NO_x$  is reported by APMT but not Lee et al. (2020). These are therefore provided together here for the sake of brevity.

Based on this comparison, a number of follow-up tasks—including separation of studies inside APMT-IC which estimate contrail RF from those which estimate contrail effective radiative forcing (ERF)—have been identified for future work.

### Milestones

- Work has begun on familiarizing both members of the student team with APMT, including both the climate and air quality assessment components.
- An initial assessment of the modifications required for APMT to incorporate higher-altitude aviation has been completed.



### **Major Accomplishments**

- A comparison of the Lee et al. (2020) results to those from APMT-IC has been completed.

### **Publications**

None

### **Outreach Efforts**

Progress on all tasks was communicated during bi-weekly briefing calls with the FAA.

### **Awards**

None

### **Student Involvement**

During the reporting period of AY 2019/20, the MIT graduate students involved in this task were Inés Sanz-Morère and Joonhee Kim.

### **Plans for Next Period**

The project team will incorporate updates to APMT-IC based on the comparison to Lee et al. (2020). The team also aims to generate a development plan to enable an upgraded version of APMT to quantify climate and air quality impacts for a range of higher-altitude aviation options.

### **References**

Lee, D. S., Fahey, D. W., Skowron, A., Allen, M. R., Burkhardt, U., Chen, Q., Doherty, S. J., Freeman, S., Forster, P. M., Fuglestvedt, J., Gettelman, A., De León, R. R., Lim, L. L., Lund, M. T., Millar, R. J., Owen, B., Penner, J. E., Pitari, G., Prather, M. J., Sausen, R. and Wilcox, L. J.: The contribution of global aviation to anthropogenic climate forcing for 2000 to 2018, *Atmos. Environ.*, 117834, 2020.



# Project 059A/E Jet Noise Modeling to Support Low Noise Supersonic Aircraft Technology Development

Georgia Institute of Technology and Pennsylvania State University

## Project Lead Investigators

Dimitri Mavris (PI)  
Regents Professor  
School of Aerospace Engineering  
Georgia Institute of Technology  
Mail Stop 0150  
Atlanta, GA 30332-0150  
Phone: 404-894-1557  
E-mail: dimitri.mavrisatae.gatech.edu

Philip Morris (PI)  
Professor  
Department of Aerospace Engineering  
Pennsylvania State University  
233C Hammond Building  
University Park, PA 16802  
Phone: 814-863-0157  
E-mail: pjm@psu.edu

Jimmy Tai (Co-PI)  
Senior Research Engineer  
School of Aerospace Engineering  
Georgia Institute of Technology  
Mail Stop 0150  
Atlanta, GA 30332-0150  
Phone: 404-894-0197  
E-mail: jimmy.taiatae.gatech.edu

## University Participants

### Georgia Institute of Technology

- PI: Dr. Dimitri Mavris (PI), Dr. Jimmy Tai (Co-PI)
- FAA Award Number: 13-C-AJFE-GIT-070
- Period of Performance: July 5, 2020 – December 31, 2020
- Task(s): 1,2,4,5

### Pennsylvania State University

- PI: Dr. Philip Morris (PI)
- FAA Award Number: 13-C-AJFE-GIT-070
- Period of Performance: July 5, 2020 – December 31, 2020
- Task(s): 1,3-5

## Project Funding Level

FAA provided \$200,000 in funding. Matching funds are provided by the Georgia Institute of Technology (\$100,000) and Pennsylvania State University (\$100,000). Cost share details are below:

The Georgia Institute of Technology has agreed to a total of \$100,000 in matching funds. This total includes salaries for the project director, research engineers, and graduate research assistants, as well as computing, financial, and administrative support, including meeting arrangements. The institute has also agreed to provide tuition remission for the students, paid for by state funds. During the period of performance, in-kind cost share is also obtained for cost share.

Pennsylvania State University provides matching support through salary support of the faculty PI, as well as computing and administrative support.

## Investigation Team

### Georgia Institute of Technology

- PI: Dimitri Mavris
- Co-Investigator: Jimmy Tai (Task(s) 1,2,4,5)
- Supporting Engineers: Greg Busch, Joshua Brooks
- Students: Edan Baltman, James Kenny, Madeline Bowne, Noah Chartier, Leon Chen, Jeremy Decroix

### Pennsylvania State University

- Principal Investigator: Dr. Phillip Morris (Task(s) 1,3-5)
- Graduate Students: Dana Mikkelsen, Stephen Willoughby

## Project Overview

During the reporting period, the Project 59A/E team focused on the assembly of 1) zeroth-order methods for predicting supersonic inlet performance, 2) introduction of an engine cycle modeling strategy, and 3) calculation of engine cycle boundary conditions. The last two tasks are closely tied to concurrent work in ASCENT Project 10. Preliminary steady simulations will be performed for the proposed nozzle geometries which involve grid generation and use of the STARCCM+ Computational Fluid Dynamics (CFD) solver. The operating conditions for the initial experimental geometry will be the result of discussions with other Project 59 performers.

If successful, the ASCENT Project 59 research will support development of methods to predict the noise generated and radiated by civil supersonic aircraft engines. The tools developed will enable airframe and engine manufacturers to assess the noise impacts of engine design changes and to determine if particular designs will meet current or anticipated noise certification requirements.

It should be noted that after discussions with FAA, the overall direction of this project was changed. The original purpose of Project 59A/E was to develop and assess computational tools to simulate the flow and noise of civil supersonic aircraft engines and to identify novel methods for noise reduction. The impact of the noise reduction methods on the overall engine performance also would be assessed. The predictions would include consideration of the engine inlet, the engine cycle, mixers and ejectors, and the unsteady jet exhaust. Accurate prediction of the engine exhaust flow would enable the noise it generates to be computed. Predictions were to be assessed by comparisons with available experimental measurements. In future years, the assessment of jet noise reduction technologies, as originally proposed, will be re-considered as part of this project.

## Project Introduction

The primary objective of this research project is to develop and assess computational tools to simulate the flow and noise of civil supersonic aircraft engines. In Task 1, the Georgia Institute of Technology (Georgia Tech) and the Pennsylvania State University (Penn State) will coordinate to select an initial jet nozzle geometry. In Task 2, Georgia Tech will analyze the engine cycle developed by ASCENT Project 10 for best operating conditions for take-off and landing to minimize certification noise levels [1, 2]. The resulting mixer and nozzle conditions will advise the researchers of ASCENT Project 59 on relevant test conditions. The test conditions for the initial geometry will also provide boundary conditions for Task 3 which will perform an internal and external flow simulation aimed at uncovering noise source information. Task4 will develop a process for

converting high fidelity simulation results into jet noise sources, and Task 5 will produce a final report detailing this research effort.

### Milestones

The anticipated major milestones and planned due dates are listed in the table below:

Task No.	Milestone	University	Planned Due Date
Task 1	Selection of initial geometry in coordination with other Project 59 Investigators	PSU & GIT	12/15/2020
Task 2.1	Assembly of zero-order methods to predict inlet performance	GIT	05/31/2021
Task 2.2	Determination of boundary conditions from “Vision SST Engine Cycle”	GIT	02/05/2021
Task 3.1	Completion of grid generation for internal flow calculations	PSU	03/05/2021
Task 3.2	Initial RANS Simulation of internal flow.	PSU	05/01/2021
Task 3.3	Preliminary grid generation for jet exhaust flow	PSU	04/01/2021
Task 4	Script construction for generation of ANOPP custom jet noise source	PSU & GIT	05/31/2021
Task 5	Submission of interim project report	PSU & GIT	05/31/2021

### Major Accomplishments

The ASCENT 59A/E team has received the geometry from the ASCENT 59 team and is currently gridding the geometry.

## Task 1 – Select Jet Nozzle Geometry

Georgia Institute of Technology and Pennsylvania State University

### Objective(s)

In order to unify and maximize the impact of work across relevant ASCENT projects, Georgia Tech and Penn State will coordinate efforts to select an initial jet nozzle geometry. Working with Dr. Krishnan Ahuja, the experimental data from this standard geometry (gathered in other ASCENT Project 59 research) will be used to inform the work of ASCENT project 59A/E.

### Research Approach

The research team will work together to identify promising geometries for use across the ASCENT projects. The selected geometry must be relevant to the project goals while also achievable regarding experimental measurement, computational analysis, and other supporting tasks. Specific evaluation criteria may include jet velocity reduction and thrust loss.

## Task 2 – Translate Installed Cycle Performance Requirements into Boundary Conditions

Georgia Institute of Technology

### Objectives

Task 2 aims to leverage engine cycle modeling capabilities to determine installed thrust for an engine of interest that is appropriate for civil supersonic transport. The thermodynamic properties across this mixed flow turbofan engine, with the install thrust value, are used to characterize the mixer exit, nozzle entrance, and nozzle exit operating conditions during take-off. Because the initial testing and high-fidelity simulations are not currently representative of a mixed flow turbofan, these operating conditions (i.e. total pressure, total temperature, mass flow, geometry, etc.) will advise the testing team on relevant testing conditions.



## **Research Approach**

### **Task 2.1: Determine Installed Thrust**

In order to ensure minimum thrust is lost, due to implementing potential jet noise reduction technology, the installed thrust requirement needs to be determined because it is directly proportional to jet velocity. One of the main contributors to installed thrust is inlet performance which is highly dependent on how the engine is integrated with the vehicle. This task will also investigate zero-order methods to predict inlet performance for different inlet configurations.

### **Task 2.2: Generate Boundary Conditions**

Georgia Tech will analyze the engine cycle developed by ASCENT Project 10 for best operating conditions for take-off and landing to minimize certification noise levels. The resulting mixer and nozzle conditions, i.e. total temperature, total pressure, and mass flow rate, will advise the researchers of ASCENT Project 59 on relevant test conditions. Test conditions for the initial geometry will also provide boundary conditions for the high-fidelity simulations to be performed in Task 3. The inlet investigation will represent an insurance plan on any thrust loss due to any mixer or nozzle design to minimize noise.

## **Task 3 – High Fidelity Simulation of Jet Noise Reduction Technology**

Pennsylvania State University

### **Objectives**

The objective of this task is to develop methodologies to accurately simulate the noise generated by jet nozzles of the type likely to be used on civil supersonic aircraft. A commercial computational fluid dynamics application, STARCCM+, will be used to perform both steady and unsteady flow simulations. The unsteady simulations will be coupled with an acoustic analogy solution to predict the radiated noise.

### **Research Approach**

Internal and external flows will be simulated in order to provide noise source information for Task 4.

Following discussions with FAA, it was decided to focus on a relatively simple geometry consisting of a dual stream jet followed by a mixing duct and a nozzle. The selected geometry is shown in Figure 1. The stages of the simulations follow those in the original work plan.

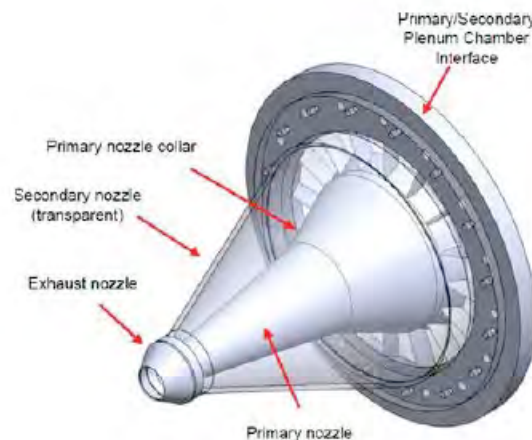


**Figure 1.** Schematic of proposed model geometry

### **Task 3.1: Grid generation for internal flow simulations**

The selected geometry was only made available close to the end of the calendar year, therefore an existing dual-flow nozzle geometry was used to train the new students in the use of STARCCM+ for grid generation and simulations., This geometry

was previously studied experimentally [3]. A grid was only generated for the inner nozzle. Figure 2 shows a grid for the inner nozzle. The nozzle includes a centerbody that can be seen in the grid.

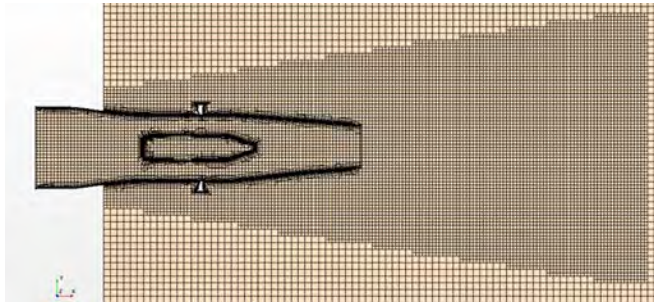


Figure 2. Grid generated for the inner nozzle

It is planned to use Reynolds-averaged Navier-Stokes (RANS) simulations for the internal flow. These simulations will provide boundary conditions at the nozzle exit. STARCCM+ will continue to be used to generate both the internal and external grid. The grid generator uses an extruder to generate the grid in the near wall regions and fills external regions with an unstructured mesh.

**Task 3.2: Perform RANS simulations for the internal flow**

RANS simulations will be performed using STARCCM+. Important outputs will be the degree of mixedness at the exit, which is expected to be an important factor in determining the radiated noise. The flow predictions will be assessed by comparison with available experimental data. The comparisons will be for both subsonic and supersonic nozzles and will include both flow and noise measurements.

**Task 3.3 Grid generation for Large Eddy Simulations of the jet exhaust flow**

The simulation of the jet exhaust flow will be performed using Large Eddy Simulation (LES). A key element in obtaining accurate and efficient simulations is the structure of the computational grid. The grid will be generated based on previous experience of the PI and his co-workers for supersonic nozzles. The simulations, once completed, will provide the unsteady flow properties in the exhaust and in the jet near-field. It is proposed to use the permeable surface Ffowcs Williams – Hawkings (FWH) acoustic analogy solution [4, 5] to determine the amplitude, spectral content, and directivity of the radiated noise, assuming noise radiating into a uniform stationary medium. The commercial CFD solver, STARCCM+ will be used for both the internal and external flow and noise simulations.

**Task 4 – Source Integration and Propagation**

Georgia Institute of Technology and Pennsylvania State University

**Objective(s)**

The knowledge acquired through the simulations performed in Task 3 must be translated into functional noise sources for use onboard aircraft analyses. These noise sources will allow for the assessment of observer perceived noise and the ability to assess the specific impacts of each of the promising noise technologies. The goal is to perform these analyses in terms of both certification noise levels and noise contours.

**Research Approach**

The combined research team will develop a process for converting high fidelity simulations (i.e. computational aeroacoustics, CAA) results into jet noise sources using the Aircraft Noise Prediction Program (ANOPP2) custom noise source feature. Once the process is developed and verified, the research team will be able to input CAA-simulated jet noise sources and propagate the noise to the observer using the ANOPP2 propagation module to assess the perceived noise levels. The latter step will require the research team to establish a baseline case with no active technology to assess the level of jet noise reduction. Furthermore, the combined research team will coordinate with ASCENT Project 10 (A10) to integrate the jet noise source results from the proposed research with other noise sources captured by the A10 team in order to examine the impact of the jet noise reduction technology in terms of both certification noise levels and noise contours.

**Publications**

None

**Outreach Efforts**

ASCENT Advisory Board Meeting

**Awards**

None

**Student Involvement**

The Georgia Tech student team consists of five graduate research assistants (GRA). Over the past performance period, all five GRAs engaged in formulating the approach being pursued for the inlet modeling activity. The team is divided into supersonic inlet aerodynamic and thermodynamic performance and mechanical and structural analysis, with each student taking on multiple topics. GRA leads are identified for each topic. Mr. James Kenny is the student lead for aerodynamic and thermodynamic performance and Mr. Jeremy Decroix is the student lead for mechanical and structural analysis.

For the first year, the Penn State team consists of two graduate research assistants. Ms. Dana Mikkelsen is the lead on the CFD simulations. Mr. Stephen Willoughby will assist with CAD work as well as the grid generation.

**Plans for Next Period**

**Georgia Tech**

The Georgia Tech team plans to complete the tasks listed in Table 1 with GT designation. Having completed Task 1, the team may use the selected nozzle geometry to assist in determining the relevant boundary conditions, based on the “Vision SST Engine Cycle”. Work will continue to completion in parallel on the assembly of a zero-order inlet design and analysis environment.

**Penn State**

The Penn State team plans to complete the tasks listed in Table 1 with PSU designation. Now that the geometry has been selected, Penn State researchers can continue with refining the grid generation and internal flow simulations. The jet exhaust flow will also be gridded and simulated using RANS. Unsteady simulations are planned for the second project year.

Table 1 shows the anticipated list of Milestones for the next research period:

**Table 1.** List of anticipated milestones for the next research period.

Milestone	Owner	Planned Due Date
Zero-order methods to predict inlet performance	GIT	05/31/2021
Determination of boundary conditions from “Vision SST Engine Cycle”	GIT	02/05/2021
Grid generation for internal flow calculations completed	PSU	03/05/2021
Initial RANS internal flow simulations completed	PSU	05/01/2021
Preliminary grid generated for jet exhaust flow	PSU	04/01/2021
Script for generation of ANOPP custom jet noise source	PSU & GIT	05/31/2021
Annual report will be submitted	PSU & GIT	05/31/2021

**References**

[1] Mavris, D., Tai, J., Kirby, M., Roth, B., “Systems Analyses of Pneumatic Technology for High Speed Civil Transport Aircraft,” NASA Funded Grant NAG-1-2015, NASA document ID: 19990105723.

[2] Welge, H., Bonet, J., Nelson, C., Tai, J., “N+2 Supersonic Concept Development and Systems Integration,” NASA/CR-2010-216842.

[3] Auhl, R. R., Willoughby, S. P., McLaughlin, D. K. and Morris, P. J., “Acoustic Measurements of Co-annular Jets at High Subsonic-Low Supersonic Jet Velocities,” AIAA Paper 2020-0264, 2020.

[4] Ffowcs Williams, J. and Hawkings, D. L., “Sound generation by turbulence and surfaces in arbitrary motion,” *Phil. Trans. Roy. Soc. A*, **264**(1151) 1969, 321–342.

[5] Farassat, F. and Succi, G. P., “The prediction of helicopter rotor discrete frequency noise,” *Vertica*, **7**(4), 1983, 497–507.



# Project 059B Jet Noise Modeling and Measurements to Support Reduced LTO Noise of Supersonic Aircraft Technology Development

## Georgia Institute of Technology/Gulfstream

### Project Lead Investigator

Krishan K. Ahuja  
Regents Professor  
School of Aerospace Engineering  
Georgia Institute of Technology  
Atlanta, GA 30342  
404-290-9873  
Krish.Ahuja@ae.gatech.edu

### University Participants

#### Georgia Institute of Technology (Georgia Tech)

- PI: Krishan K. Ahuja, Regents Professor
- FAA Award Number: 13-C-AJFE-GIT-060
- Period of Performance: June 5, 2020 to June 4, 2021
- Tasks:
  - Task 1: Form an Advisory Panel
  - Task 2: Identify a Baseline Nozzle Requirements and Design Tests
  - Task 3: Design and Fabricate a Baseline Nozzle
  - Task 4: Test Setup and Experimental Data Acquisition
  - Task 5: Data Dissemination
  - Task 6: Assess Readiness of Design Tools for a simple Baseline Nozzle Configuration
  - Task 7: Proposal for a Follow-on Effort for Years 2 and 3
  - Task 8: Reporting and Data Dissemination

### Project Funding Level

\$250,000 from FAA; \$250,000 cost share from Gulfstream.

### Investigation Team

- Dr. Krishan Ahuja, PI, Georgia Tech
- Dr. Dimitri Mavris (Co-PI) and Jimmy Tai (Co-PI), Georgia Tech
- Dr. Aharon Karon, Co-Investigator and Lead Experimentalist, Georgia Tech Research Institute (GTRI)
- Dr. Robert Funk, Experimentalist, GTRI
- David Ramsey, Graduate Research Assistant and Experimentalist, Georgia Tech

### Project Overview

The overall goal of this project is to perform cost-effective supersonic transport (SST) jet noise research/technology experiments to enable low-, medium-, and high-fidelity jet noise prediction methods. The specific objective is to design the experiments in collaboration with industry, NASA, DOD, FAA and Modelers funded by FAA to help develop improved jet noise prediction methods that have reduced uncertainty such that industry can design quieter supersonic jet engines with higher confidence of the noise that will be generated. Working with Gulfstream as Georgia Tech's industry partner on this project,

a representative baseline nozzle design will be selected for experiments at Georgia Tech. The data acquired will consist of farfield noise, high-speed flow visualization, source location, and detailed mean and unsteady flow measurements.

The experimental data acquired by Georgia Tech will be provided to key stakeholders and other computational teams funded by FAA to validate their computational simulations to confirm that jet noise predictions using semi-empirical and computational modeling approaches can be used reliably for jet noise evaluation.

## Task Objectives, Research Approach, and Accomplishments

This project is new and has the following eight Tasks. The Task titles are self-descriptive and reflect the Task objectives. A short objective statement, research approach, and a summary of the accomplishments to date for each Task is provided below under each Task description.

### Task 1 – Form an Advisory Panel

Georgia Institute of Technology

The objective of this task is to receive regular feedback from Industry and NASA subject matter experts (SMEs) in supersonic jet noise.

Dr. Liu, the FAA Project Manager for ASCENT 59, has already formed an advisory panel consisting of representatives of FAA, DOD, NASA, Aerion, GE, and Gulfstream and a kick-off meeting has already been held. Their feedback was used in the design of the test nozzle described below.

### Task 2 – Identify Baseline Nozzle Requirements and Design Tests

Georgia Institute of Technology

The objective of this Task is to define the nozzle requirements and design the experiments.

The baseline nozzle and tests were based on a paper engine design created by the Georgia Tech Aerospace Systems Design Lab (ASDL) guided by ASCENT Project 10 on engine cycle selection for GT Medium SST (55 passenger class). The GT nozzle model to be tested under this project will not have a plug. For the purpose of calculating the area of the outer (secondary flow) duct, the annular areas of the paper engine will be used to calculate the area of the secondary flow duct in the model nozzle facility. The GTRI model is a 0.045 scale of the paper engine. The mixing length/exhaust nozzle exit diameter (L/D) will be: 0.7, 1, 2, and 3.

As described below, tests have been designed with variations in nozzle design and/or operating parameters in order to explore the accuracy of semi-empirical and computational tools for predicting jet noise. Methodologies, the test matrix, and nozzle designs are detailed in Appendix A.

### Task 3 – Design and Fabricate a Baseline Nozzle

Georgia Institute of Technology

The objective of this Task is to design and fabricate a baseline nozzle that meets the requirements defined in Task 2 above and is also suitable for the tests needed to meet the objectives of the overall program.

Design has been completed and is shown in Figure 1. The model consists of the following parts: the primary nozzle with the collar to avoid any anomalous flow effects due to any geometrical protrusions/recesses, the secondary nozzle, mixer ducts, and the exhaust nozzle. There are three mixer ducts being fabricated to allow for different mixing length-to-nozzle-exit diameter ratios (L/D). The test model utilizes the coannular flow capabilities of the GTRI jet facilities. The primary and secondary flow streams converge into the mixer-duct and exhaust nozzle combination. The mixer-duct and exhaust nozzle combinations allow for L/Ds of 0.7 (exhaust nozzle mounted directly to the secondary nozzle), 1, 2, and 3. The jet stream is ultimately formed by the exhaust nozzle, which is a converging nozzle with geometry based on the converging section of the converging-diverging nozzle from the ASDL engine design.

The primary nozzle is ready to be used. The outer nozzle is being fabricated by Gulfstream. The COVID-19 situation has slowed down the availability of machinists.

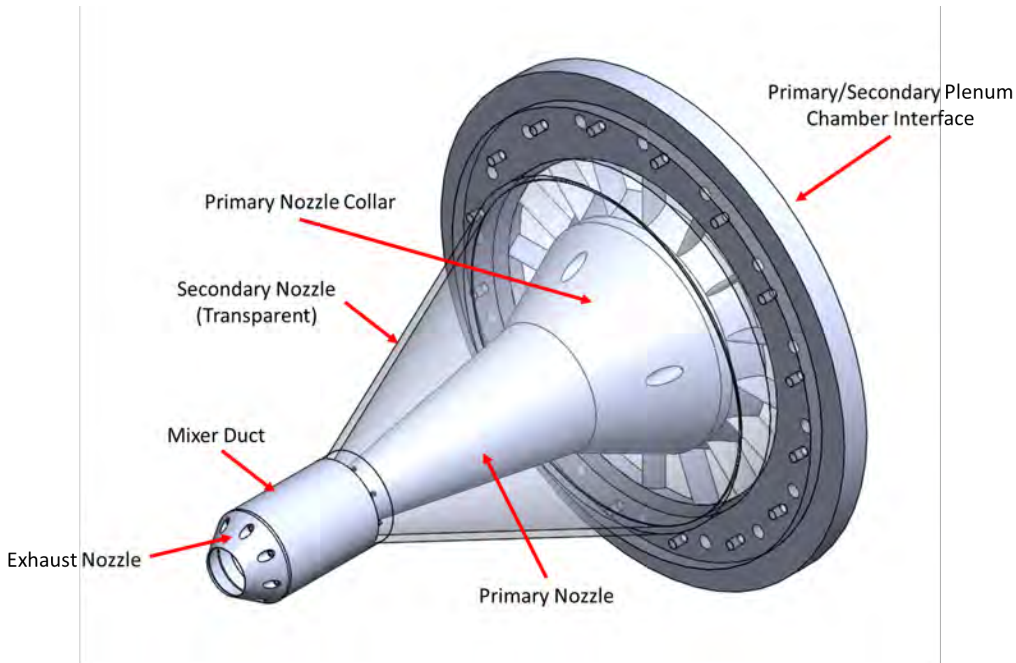


Figure 1. Experimental model design.

## Task 4 – Test Setup and Experimental Data Acquisition

Georgia Institute of Technology

The objective of this Task is to get ready to conduct the tests and acquire and analyze the data.

Test setup has been initiated; experiments are being planned. Acoustic and flow measurements will be acquired for the experimental model for a range of primary and secondary total pressures for both cold and heated flows. The acoustic measurements will be acquired in the GTRI Anechoic Static Jet-Facility, which is anechoic above 250 Hz. A photographic view of the chamber appears in Appendix A. A detailed description of the facility can be seen in Burrin et al. [1], Burrin and Tanna [2], and Ahuja [3]. In addition to recording the acoustic pressure time histories, the acoustic measurements will be processed into loss-less power spectra. This will follow the procedure found in Karon [4]. The flow measurements will be acquired in the GTRI Flow Diagnostic Facility, which is a non-anechoic jet-facility that can produce jet flow identical to those in the GTRI Anechoic Static Jet-Facility. This facility is instrumented with high-speed flow visualization, beamforming, and particle image velocimetry (PIV) capabilities. All of the acoustic and flow measurements will be analyzed by the Georgia Tech team and will be compared to the simulation results as validation for those simulations.

## Task 5 – Data Dissemination

Georgia Institute of Technology

The objective of this Task is stay in touch with the modelers being funded by FAA under Project 59 and provide them the nozzle design and both the acoustic and flow data from the current project.

The modelers were all informed of our preliminary design during the first Advisory Panel discussion. We have now provided the finalized design to the modelers. The data will be provided as it becomes available.

## Task 6 – Assess Readiness of Design Tools for a simple Baseline Nozzle Configuration

Georgia Institute of Technology

Whereas Task 5 just provides the data to the modelers, the objective of this Task is to interact with the modelers in terms of verification of their codes with the measurements made under this project at Georgia Tech. Partners Gulfstream and ASDL will also be comparing their low-fidelity codes with our data.

## Task 7 – Proposal for a Follow-on Effort for Years 2 and 3

Georgia Institute of Technology

Proposals for follow-on efforts will be prepared under this Task.

This Task has not been initiated yet.

## Task 8 – Reporting and Data Dissemination

Georgia Institute of Technology

This being a new project, so far only the first quarterly report has been submitted.

### Milestones

The experimental model design was completed and approved by the FAA. The primary nozzle is ready to be tested. The outer nozzle is now being fabricated.

### Major Accomplishments

The experimental model design was completed and approved by the FAA. This model design was passed along to the machine shops for fabrication and the simulation teams for use in their predictions. The microphones have been setup to start acquiring the data.

### Publications

N/A

### Outreach Efforts

N/A

### Awards

None

### Student Involvement

David Ramsey assisted with the design of the experimental model and put together the documents that were sent to the machine shop. He will continue to be the graduate research assistant on this project.

### Plans for Next Period

Acquire jet noise data for the primary nozzle alone. In parallel, complete the fabrication of the outer nozzle duct sections and start acquiring the data.

### References

[1] Burrin, R. H., Dean, P. D., and Tanna, H. K. "A New Anechoic Facility for Supersonic Hot Jet Noise Research at Lockheed-Georgia," *The Journal of the Acoustical Society of America* Vol. 55, No. 2, 1974, p. 400.



- [2] Burrin, R., and Tanna, H. "The Lockheed - Georgia coannular jet research facility," *The Journal of the Acoustical Society of America* Vol. 65, No. S1, 2005, pp. S44-S44.
- [3] Ahuja, K. "Designing clean jet-noise facilities and making accurate jet-noise measurements," *International Journal of Aeroacoustics* Vol. 2, No. 3, 2003, pp. 371-412.
- [4] Karon, A. Z., "Potential factors responsible for discrepancies in jet noise measurements of different studies," Ph.D. Dissertation, Daniel Guggenheim School of Aerospace Engineering, Georgia Institute of Technology, Atlanta, GA, 2016.

## Appendix A: Details of the Nozzle design



FAA CENTER OF EXCELLENCE FOR ALTERNATIVE JET FUELS & ENVIRONMENT

## Appendix A Project 59

Lead investigators: Krishan Ahuja (PI), Dimitri Mavris (Co-PI) and Jimmy Tai (Co-PI)  
Georgia Institute of Technology

Lead Experimentalists: Aharon Karon and Robert Funk, GTRI  
Industry Collaborator: Brian Cook (Gulfstream)

Project manager: Sandy Liu, FAA



## Introduction

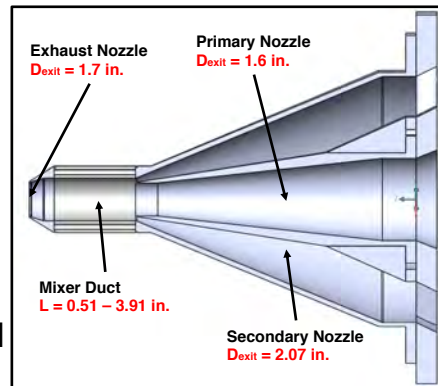


- Supersonic transports need small-sized engines to minimize drag when cruising at supersonic speeds.
- This requires higher jet exhaust velocities during landing and take-off (LTO), which will increase the noise at these conditions.
- The goal of this project is to improve jet noise prediction methods for supersonic transports at LTO conditions.
- This is to be done by acquiring high-quality acoustic data and the relevant flow data and providing that to separately-funded computational teams for validation using low, medium, and high fidelity codes.



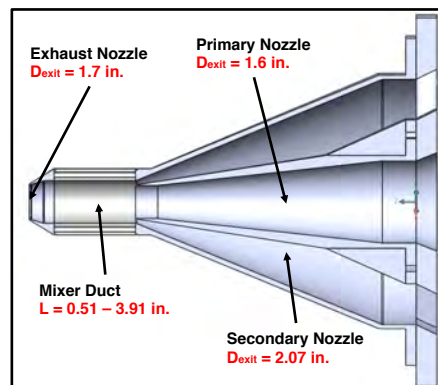
## Methodology

- The Georgia Tech team will collaborate with FAA-funded CFD teams from Stanford, Penn State and University of Illinois as well as Gulfstream.
- A common model-scale nozzle will be used by both the experimental and the computational teams.
- This model will initially be a simpler geometry to gain confidence in the noise prediction of the codes.
- In year 1, the mixer will be a straight duct as shown here.



## Methodology

- Measured noise and related flow data by the Georgia Tech team will be used by the computational teams to validate the noise prediction codes
- The final exhaust model will be a conical nozzle
- The scaled dimensions are based on an engine cycle design from the Georgia Tech Aerospace Systems Design Laboratory (GT ASDL). This is still to be finalized.
- A selected mixer nozzle (design TBD) will be added to the primary stream in years 2 and 3





## Data to Acquire



- Acoustic data will be acquired in GTRI's anechoic chamber

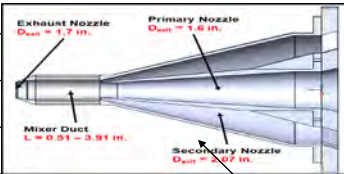


The following measurements will be made using model-scale nozzles

- Farfield noise
- Primary and secondary mass flow rates
- Primary and secondary total temperatures and pressures
- Ambient humidity and temperature
- Mean and turbulence velocities at the nozzle exits via PIV

## Test Matrix



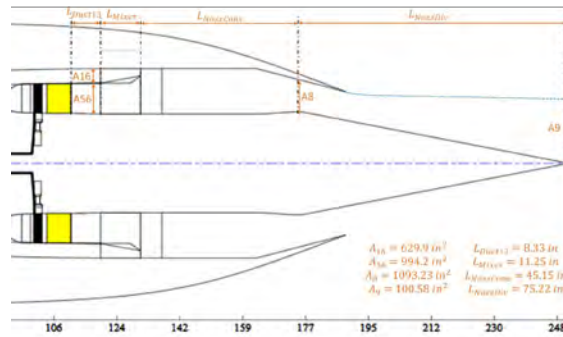
Configuration	M1	M2	Primary Temp	
	Primary Nozzle Alone	0.2 - 0.9	N/A	Unheated
	Primary Nozzle Alone	0.2 - 0.9	N/A	Heated
	Primary + Secondary	0.2 - 0.9	0.2 - 0.9	Unheated
	Primary + Secondary	0.2 - 0.9	0.2 - 0.9	Heated
Primary + Secondary + Exhaust Nozzle	0.2 - 0.9	0.2 - 0.9	Unheated	
Primary + Secondary + Exhaust Nozzle	0.2 - 0.9	0.2 - 0.9	Heated	
Primary + Secondary + Mixer Duct of Length L1 + Exhaust Nozzle	0.2 - 0.9	0.2 - 0.9	Unheated	
Primary + Secondary + Mixer Duct of Length L1 + Exhaust Nozzle	0.2 - 0.9	0.2 - 0.9	Heated	
Primary + Secondary + Mixer Duct of Length L2 + Exhaust Nozzle	0.2 - 0.9	0.2 - 0.9	Unheated	
Primary + Secondary + Mixer Duct of Length L2 + Exhaust Nozzle	0.2 - 0.9	0.2 - 0.9	Heated	
Primary + Secondary + Mixer Duct of Length L3 + Exhaust Nozzle	0.2 - 0.9	0.2 - 0.9	Unheated	
Primary + Secondary + Mixer Duct of Length L3 + Exhaust Nozzle	0.2 - 0.9	0.2 - 0.9	Heated	



## Test Model Reference



- The model used is based on the paper engine design by ASDL
- The GTRI model will not have a plug
  - Annular areas will become circular areas using area-equivalent diameters



- The GTRI Model of a 0.045 scale of the paper engine

## Notes on the Test Model Design



- The GTRI Model is a 0.045 scale of the paper engine
- The mixing length/exhaust nozzle exit diameter (L/D) will be: 0.7, 1, 2, and 3



## Complete Model

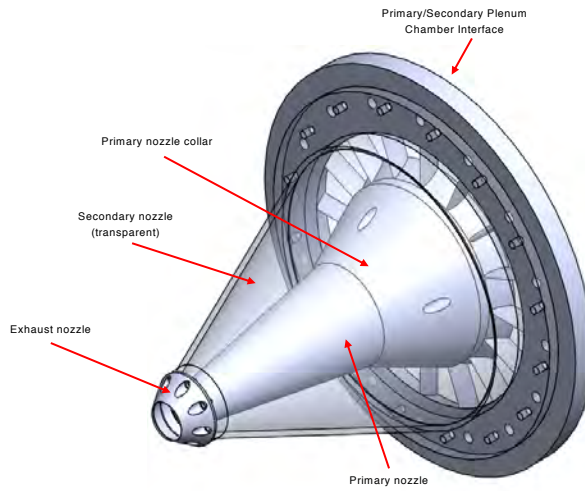


Figure 01. Isometric view of complete model with secondary nozzle shown as transparent

## Complete Model Exploded View

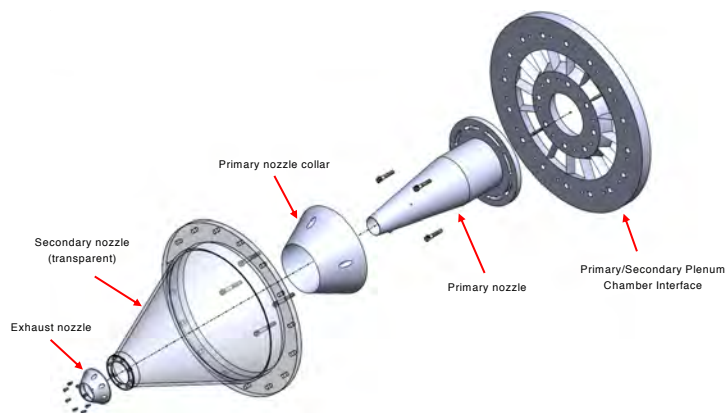
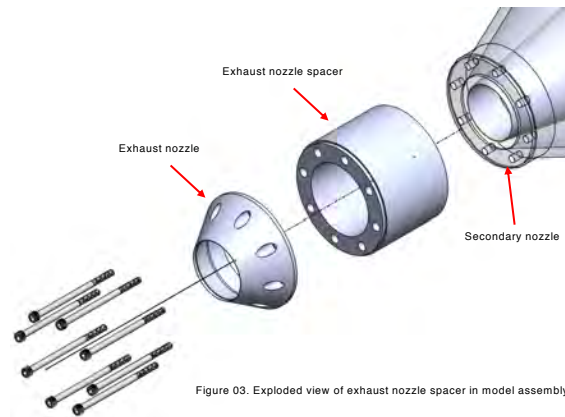


Figure 02. Isometric, exploded view of complete model with secondary nozzle shown as transparent



## Exhaust nozzle spacer length used to set L/D



## L/D convention shown with section view of exhaust nozzle



$$\frac{L_e}{D_e}$$

$L_e$ : Exhaust nozzle length after primary/secondary nozzle exit plane

$D_e$ : Exhaust nozzle exit diameter

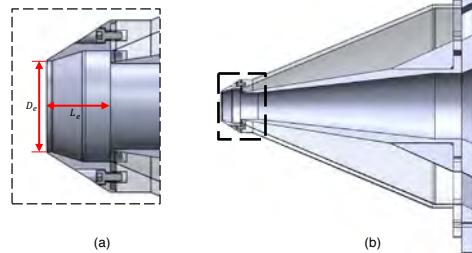


Figure 04. Section view of (a) exhaust nozzle with critical dimensions labeled and (b) region of view shown within context of model, both with secondary nozzle shown as transparent



### Exhaust nozzle spacers shown for each L/D value

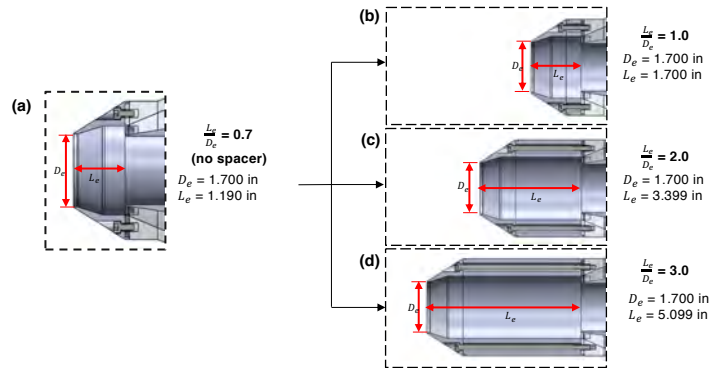


Figure 05. Section view of exhaust nozzle (a) with no spacer, (b) with L/D = 1.0 spacer, (c) with L/D = 2.0 spacer, and (d) with L/D = 3.0 spacer. Note that screws used for L/D = 2.0 and L/D = 3.0 must be cut to length.

### Complete Model for Hand-off to Simulation Engineers



No fasteners or fastener holes included. All fastener holes will be sealed with clay/plaster during experimentation.

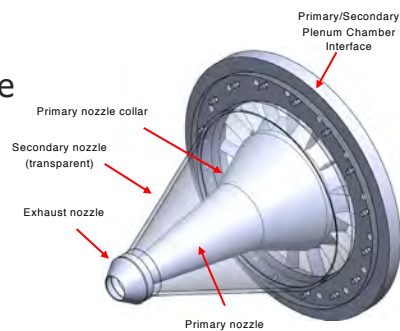


Figure 06. Isometric view of complete model as will be passed to simulation engineers with secondary nozzle shown as transparent



## Primary/Secondary Plenum Chamber Interface (Slide 1 of 2)

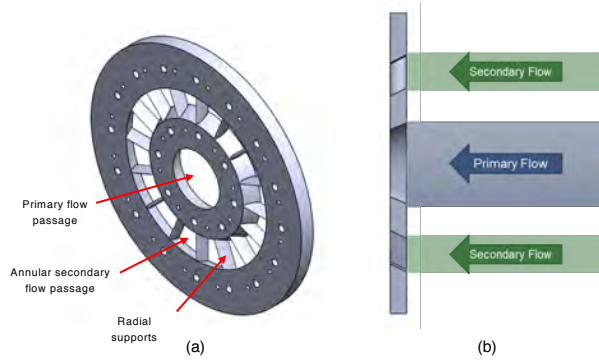


Figure 07. Primary/secondary plenum chamber interface (a) isometric view and (b) cross section view with primary and secondary flow shown

## Primary/Secondary Plenum Chamber Interface (Slide 2 of 2)

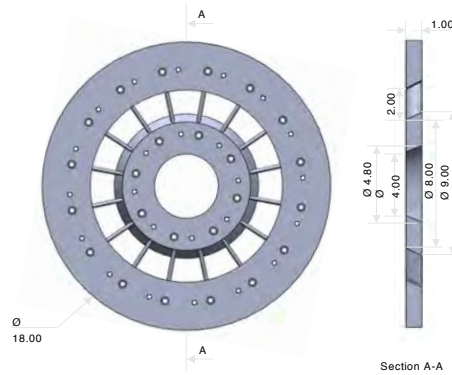


Figure 08. Primary/secondary plenum chamber interface dimensions (all dimensions are in inches)



## Primary Nozzle

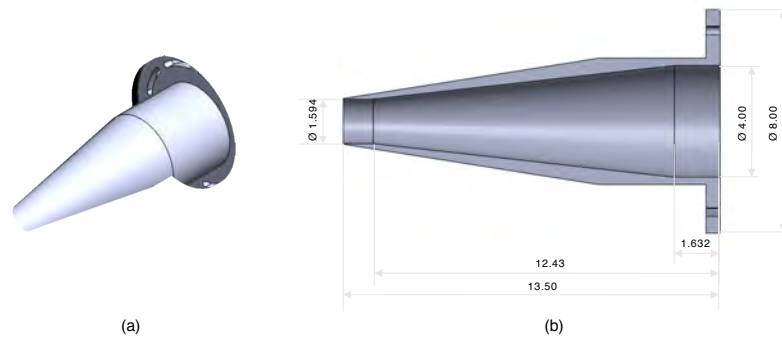


Figure 09. Primary nozzle (a) isometric view and (b) dimensioned cross section view (all dimensions are in inches)

## Primary Nozzle Collar



- This part is used to prevent a circulation zone from the backwards step in the secondary flow path

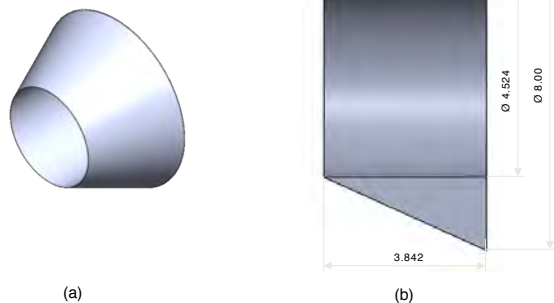


Figure 10. Primary nozzle collar (a) isometric view and (b) dimensioned cross section view (all dimensions are in inches)



## Secondary Nozzle

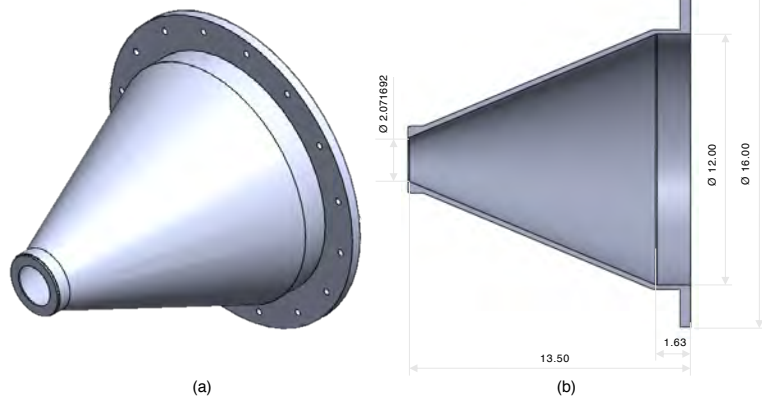


Figure 11. Secondary nozzle (a) isometric view and (b) dimensioned cross section view

## Exhaust Nozzle

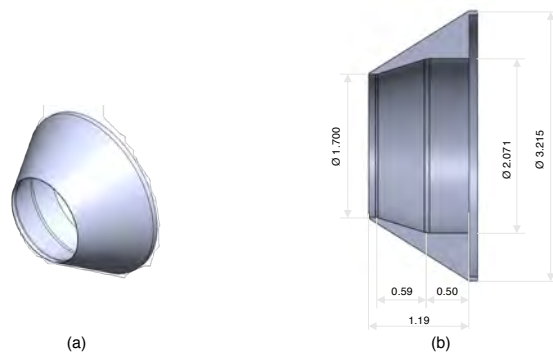


Figure 12. Exhaust nozzle (a) isometric view and (b) dimensioned cross section view (all dimensions are in inches)



## Exhaust Nozzle Spacer

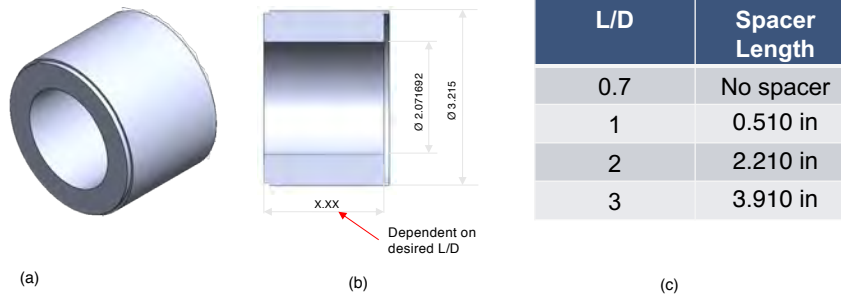


Figure 13. Exhaust nozzle (a) isometric view and (b) dimensioned cross section view (all dimensions are in inches) and (c) spacer length as a function of desired L/D



# Project 059C Modeling Supersonic Jet Noise Reduction with Global Resolvent Modes

## University of Illinois Urbana-Champaign

### Project Lead Investigator

Daniel J. Bodony  
Blue Waters Professor  
Department of Aerospace Engineering  
University of Illinois Urbana-Champaign  
306 C Talbot Labs  
104 S. Wright  
Urbana, IL 61801  
Phone: (217) 244-3844  
E-mail: bodony@illinois.edu

### University Participants

#### University of Illinois Urbana-Champaign (UIUC)

- Pls: Dr. Daniel J. Bodony, Dr. Tim Colonius
- FAA Award Number: 13-C-AJFE-UI-031
- Period of Performance: June 5, 2020 to June 4, 2021
- Tasks:
  1. Establish industry-relevant low bypass ratio (BPR) engine parameters and acoustic assessment workflow with cost-share partner.
  2. Automated Reynolds-averaged Navier–Stokes equations (RANS) predictions of jet exhaust.
  3. Resolvent mode computation—primary and sensitivity.
  4. Python resolvent mode interpolation tool.
  5. Python optimization tool for jet noise reduction (JNR)

### Project Funding Level

FAA provided \$199,956 in funding. Proposed cost match with GE Aviation (POC: Dr. Robert Babbitt) is no longer in force. Negotiations with Boom (POC: Dr. Joe Salamone) are in progress.

### Investigation Team

- Dr. Daniel Bodony, UIUC, PI
- Mr. Omar Gutierrez, UIUC, MS student
- Dr. Tim Colonius, California Institute of Technology (Caltech), Co-PI
- Mr. Ethan Pickering, Caltech, PhD student
- Mr. Liam Heidt, Caltech, PhD student

### Project Overview

This ASCENT project will leverage recent research in global resolvent mode-based descriptions of jet turbulence and associated noise to develop an efficient, physics-based tool for estimating the impact of jet noise reduction (JNR) strategies on the takeoff noise of civil supersonic transports. The software tool will quickly identify promising JNR technologies as well as more precisely evaluate the noise impact of parametric variation of a specific JNR approach. The tool will be compatible with the fleet-scale evaluation codes GREAT (Georgia Institute of Technology) and FLEET (Purdue University) developed in ASCENT Project 10 and integrated into the ASCENT Project 47 “clean sheet” evaluation tool targeting civil supersonic transport.

The proposed research will create a multi-fidelity JNR tool that can operate in two modes: one mode for specific engine estimates, and one mode for fleet-scale estimates:

1. *JNR evaluation for an engine* mode: Using the RANS-provided mean flow for a specific engine, the global resolvent description of wavepackets and their sensitivity to mean flow variations will be computed. The solutions will provide estimates of the low-frequency radiated noise while the sensitivity derivatives will estimate how the noise changes due to changes in the engine design, thus enabling JNR optimization.
2. *Fleet-level estimation* mode: The resolvent modes and their sensitivity derivatives for existing JNR strategies (e.g., chevrons, internal mixers) will be pre-computed for canonical jet exhaust profiles and flow conditions, compressed, and stored within an efficient data layout that can be quickly evaluated within FLEET, GREAT, and/or NASA's Aircraft Noise Prediction Program (ANOPP).

The original proposal outlined six tasks that were to be conducted. The project tasks have been modified in response to changes in the ASCENT Project 59 objectives as well as changes to our cost share partner. In particular, ASCENT Project 59 now includes a Georgia Tech Research Institute- (GTRI-) provided extensible dual stream, internally mixed nozzle that is to be studied computationally and whose noise is to be measured for validation. Further, our GE Aviation cost share partner has been removed due to personnel changes at GE Aviation coupled with pandemic financial impact.

## Task 1 – Establish Industry-Relevant Low-BPR Engine Parameters and Acoustic Assessment Workflow with Cost-share Partner

University of Illinois at Urbana-Champaign

### Objectives

Work with our cost share partner, identify the anticipated range of characteristics of the low-BPR engines being considered for business-class civil supersonic transport. These parameters include, but are not limited to diameter, BPR, mass flow rate, core and fan stream pressure ratios, core stream temperature ratio, thrust, nozzle configuration, plug designs, chevron designs, internal mixer designs, and afterburner design.

### Research Approach

Conduct face-to-face meetings and document exchanges to obtain industry-relevant low-BPR engine parameters and acoustic assessment workflows.

### Milestones

1. Find new cost share partner candidate.
2. Establish an NDA to initiate discussions.
3. Exchange low-BPR engine parameters and acoustic assessment workflow.

### Major Accomplishments

Milestone 1 has been completed with the help of Donald Scata (FAA). An initial discussion was held October 28, 2020, between UIUC (Bodony) and Boom Supersonics (Rachel Devine, Joe Salamone, Lourdes Maurice) to connect and establish the overall goals of the ASCENT 59 Project. Milestone 2 is in progress; UIUC is currently working with Boom (Devine) to agree to an NDA to initiate technical discussions with intent to formally agree on a cost-sharing arrangement.

### Publications

None

### Outreach Efforts

None

### Awards

None

### **Student Involvement**

None

### **Plans for Next Period**

Finalize NDA between UIUC and Boom and exchange JNR-relevant information, including low-BPR engine parameters and Boom-internal acoustic assessment workflows.

## **Task 2 – Automated RANS Predictions of Jet Exhaust**

University of Illinois at Urbana-Champaign

### **Objectives**

Develop and verify an automated toolchain for using RANS methods for predicting the jet exhaust plume from candidate near-sonic multi-stream jet nozzles.

### **Research Approach**

Achieving JNR will require changes to engine cycle and nozzle geometries. A Python-based software infrastructure that takes parametrically defined CAD-based descriptions of nozzle geometries, automatically generates meshes and boundary conditions for the nozzle internal flow path and the external nozzle plume, initiates an open-source RANS solver, and curates the data is to be developed.

### **Milestones**

1. Initial development of end-to-end Python infrastructure.
2. Verification of RANS solutions.

### **Major Accomplishments**

Milestone 1 has been completed using Python bindings for Gmsh, a 3D finite element mesh generator, to generate the mesh and boundary conditions for the SU2 open-source RANS solver. Challenges with the axisymmetric version of SU2 are being evaluated using a locally modified compressible OpenFOAM variant fitted with RANS models tuned for hot jet plumes. Milestone 2 is in progress and dependent on the outcome of the SU2-OpenFOAM selection.

### **Publications**

None

### **Outreach Efforts**

None

### **Awards**

Omar Gutierrez is a UIUC Grainger College of Engineering MERGE Fellowship recipient.

### **Student Involvement**

Omar Gutierrez is responsible for developing the entirety of the Python tool described previously.

### **Plans for Next Period**

Complete the SU2-OpenFOAM selection and complete Milestone 2. Review and revise, as necessary, the Python tool to integrate into the Python-based interpolator and optimizer of Task 3 and Task 4.



## Task 3 – Resolvent Mode Computation—Primary and Sensitivity

Caltech (lead) and University of Illinois at Urbana-Champaign

### Objectives

Develop and verify a resolvent mode computation tool suitable for evaluating the JNR potential of candidate near-sonic multi-stream jet nozzles.

### Research Approach

Achieving JNR will require changes to engine cycle and nozzle geometries. Estimation of the JNR potential of candidate cycles and geometries will use resolvent mode descriptions of the coherent, wavepacket-associated jet noise of the loudest sound sources. We term as “primary” the resolvent calculations that provide the input-gain-output modes of the resolvent operator  $(i\omega - A)^{-1}$  and as “sensitivity” the changes in those modes due to changes in the jet nozzle geometry and engine cycle. The resolvent operator requires knowledge of the linearized Navier-Stokes operator  $A$  generated for each nozzle and its exhaust plume and a global mode computational infrastructure. Sensitivity of the resolvent input-gain-output modes requires knowledge of the change in  $A$ , say  $\delta A$ , that result from changes in the nozzle design and/or engine cycle.

### Milestones

1. Primary resolvent mode computation capability.
2. Resolvent mode training data and fitting.
3. Resolvent mode sensitivity computation capability.

### Major Accomplishments

Milestone 1 has been completed and tested on single-stream sub- and supersonic jets. Milestone 2 is in progress for the low-BPR, near-sonic jets anticipated for the supersonic aircraft of interest to ASCENT Project 59.

### Publications

None

### Outreach Efforts

None

### Awards

None

### Student Involvement

Ethan Pickering is responsible for the primary resolvent mode computation and the preliminary training data and fitting tasks. Liam Heidt is a new student who is learning from Ethan and will assume leadership of the global mode computation and its data-driven alignment.

### Plans for Next Period

Complete Milestone 2 using to-be-acquired GTRI acoustic data and high-fidelity LES data from the Stanford University ASCENT Project 59 team. Initiate Milestone 3 by collaborating with UIUC on the sensitivity derivation and implementation.

## Task 4 – Python Resolvent Mode interpolation Tool

University of Illinois at Urbana-Champaign (lead) and Caltech

### Objectives

Develop and verify a Python-based interpolation tool computing resolvent input-gain-output modes at nozzle geometry and/or engine cycles for which RANS data are not available but are near to previously known input-gain-output modes from nearby nozzle geometries and/or engine cycles.



### **Research Approach**

Using gradient-enhanced interpolation methods, develop a response surface-based interpolation approach for estimating resolvent input-gain-output modes for estimating the radiated noise from an engine geometry / engine cycle for which previously computed RANS data, linearized operators, and resolvent data are not available.

### **Milestones**

1. Identify candidate interpolation methods and down select.
2. Develop Python tool to implement interpolation method.
3. Verify Python tool.

### **Major Accomplishments**

Work on this Task has not yet begun.

### **Publications**

None

### **Outreach Efforts**

None

### **Awards**

None

### **Student Involvement**

None

### **Plans for Next Period**

Begin Task 4.

## **Task 5 – Python Optimization Tool for JNR**

University of Illinois at Urbana-Champaign (lead) and Caltech

### **Objectives**

Develop and verify a Python-based optimization tool that searches the optimization space of engine geometry/cycle to identify design choices that improve JNR.

### **Research Approach**

Using gradient-informed optimization methods, develop an optimization approach for estimating JNR potential from a class of candidate engine geometries/cycles using resolvent mode predictions of the jet noise based on linearized operators described by RANS predictions of the jet exhaust plume.

### **Milestone(s)**

1. Identify candidate optimization methods and down select.
2. Develop Python tool to implement optimization method.
3. Verify Python tool.

### **Major Accomplishments**

Work on this Task has not yet begun.

### **Publications**

None



**Outreach Efforts**

None

**Awards**

None

**Student Involvement**

None

**Plans for Next Period**

Begin Task 5.



# Project 059D Physics-Based Analyses and Modeling for Supersonic Aircraft Exhaust Noise

## Stanford University

### Project Lead Investigator

Sanjiva K. Lele

Professor

Department of Aeronautics & Astronautics

Stanford University

Stanford, CA 94305

Phone: (650) 723-7721

E-mail: lele@stanford.edu

## University Participants

### Stanford University

- PIs: Dr. Sanjiva K. Lele, Dr. Juan J. Alonso
- FAA Award Number: 13-C-AJFE-SU-024
- Period of Performance: June 5, 2020 to September 30, 2020
- Tasks: (for three year effort)
  1. Develop and refine research plan in coordination with ASCENT Project 59 partners.
  2. Reynolds-averaged Navier-Stokes- (RANS)-based modeling, simulation, and validation of jet noise predictions for baseline configuration.
  3. Large eddy simulation- (LES)-based modeling, simulation, and validation of jet noise predictions for baseline configuration.
  4. RANS-based modeling, simulation, and validation of jet noise predictions with noise reduction concept.
  5. LES-based modeling, simulation, and validation of jet noise predictions with noise reduction concept.
  6. Improved LES-based modeling and jet noise predictions.
  7. Improved RANS-based jet noise source modeling and predictions.

## Project Funding Level

\$200,000 per year from FAA. In-kind matching from Stanford. Matching from industry is being arranged.

## Investigation Team

Dr. Sanjiva K. Lele (PI), Department of Aeronautics and Astronautics, Stanford University

Dr. Juan J. Alonso (PI), Department of Aeronautics and Astronautics, Stanford University

Gao Jun Wu, Ph.D. Student, Department of Aeronautics and Astronautics, Stanford University

Tejal Shanbhag, Ph.D. Student, Department of Aeronautics and Astronautics, Stanford University

Kristen Matsuno, Ph.D. Student, Department of Mechanical Engineering, Stanford University

## Project Overview

Improved methods for prediction and reduction of noise for civil supersonic aircraft would be highly valued by the research and technology (R&T) development community engaged in civil supersonic aircraft development. Besides the aircraft and engine companies, organizations such as NASA, FAA, and DoD R&T community would also benefit from the improved methods and tools. Ultimately, supersonic jet noise tools with predictive capabilities can be used to design better noise mitigation systems and to provide estimates of noise for certification studies.

The project involves coordinated development of both low- and high-fidelity approaches for jet noise predictions for civil supersonic aircraft being considered in ASCENT and involves the seven Tasks listed above.

## **Objectives**

In collaboration with ASCENT partners in Project 59, we plan to develop physics-based analyses for supersonic aircraft exhaust noise. The main goals of these analyses are to develop improved jet noise prediction methods and better understand the uncertainty associated with the noise predictions for a range of engine cycle parameters and operating conditions relevant for civil supersonic aircraft.

The Stanford team will develop a multi-fidelity analysis approach. High-fidelity simulations of the jet exhaust flow and noise will be developed for a carefully selected subset of configurations and operating points being tested by the Georgia Institute of Technology (Georgia Tech) team. In parallel, Reynolds-averaged Navier-Stokes (RANS) computations of a broader range of configurations and operating conditions relevant for civil supersonic aircraft will be carried out and used to develop improved jet noise source models and more accurate far-field noise propagation kernels. The noise source and noise propagation modeling will leverage high-fidelity simulation data and ongoing Georgia Tech experiments, as well as other noise and flow measurements available in the archival literature. Our goal is to understand the predictive quality of RANS-based noise prediction approaches with improved source- and/or propagation models so that designers can better capture tradeoffs typical in the development of full civil supersonic aircraft configurations.

## **Research Approach**

### **1) Project Planning**

The project began with a project planning exercise to define the range of operating conditions and possible nozzle configurations relevant for civil supersonic jet exhaust. These involved discussions with Project 59 partners and reaching out to external advisors at NASA and elsewhere in academia and industry. Based on this exercise, it was determined that the project should focus on axisymmetric dual-stream nozzles with internal mixer and with the possibility of internal and/or external nozzle plug. The operating conditions would include subsonic through low supersonic jet exhaust velocity and low-to-moderate bypass ratio (BPR). Research efforts were next focused on finding nozzle configurations and flow and noise measurement data in archival literature, which would be deemed relevant for civil supersonic aircraft and could be used in the development of noise prediction methods. Comprehensive exploration indicated that the bulk of jet noise data including studies of noise reduction concepts was in the regime of moderate-to-high BPR and thus not particularly relevant for civil supersonic aircraft. While this affirmed the need for the planned laboratory measurement campaign by Project 59 partner Georgia Tech, it also highlighted the need to use the most relevant data from the published literature to kickstart the modeling and simulation effort. Two specific datasets associated with jet noise tests at NASA Glenn were thus identified.

### ***Bridges and Wernet Internal Mixer***

In 2004, Bridges and Wernet (NASA Glenn) reported flow and noise measurements for internally mixed two-stream nozzles with variations in the mixer duct length and mixer geometry. The operating conditions involve transonic and low supersonic jet exhaust velocity and moderate BPR. This configuration, shown schematically in Figure 1, has also been used in previous RANS-based noise prediction studies by Rolls Royce and Purdue University, along with a more recent large eddy simulation (LES) study. We have been in touch with Rolls Royce and NASA regarding the nozzle geometry and the measurement data. It is hoped that the geometry and data will become available in the future. This configuration is of interest to us since it is unique in providing both jet flow measurements and far-field noise at conditions relevant to civil supersonic

### ***Recent Jet Noise Measurement at NASA Glenn***

As part of NASA's Commercial Supersonic Technology (CST) Project, under the Advanced Aero Vehicle Program (AAVP), Dr. James Bridges at NASA Glenn (personal communication, 2020) recently completed jet noise measurements on specially designed modular nozzle configurations (see Figure 2) at operating points selected to be relevant for commercial supersonic aircraft. He plans to make the nozzle geometry and measurement data available in the future. Included in NASA's plans are noise predictions using a variety of computational tools. We are interested in exploring a selected subset of NASA's test matrix in our Project 59 studies.

### **2) Progress in Jet Noise Modeling and Simulations**

#### ***Georgia Tech Dual Stream Nozzle***

The co-annular nozzle designed by Project 59 partner Georgia Tech is of special interest in our work. Figure 3 shows one of the four co-annular nozzles proposed for the first stage of the study, each with a different length of internal mixing region. For the geometry with the shortest mixing zone, a preliminary unstructured Voronoi mesh for LES is generated using the

grid generation tool developed by Cascade Technologies. The numerical domain spans from  $-20D_e$  to  $80D_e$  in axial direction ( $x$ ) and flares from  $20D_e$  to  $50D_e$  in the radial direction ( $r$ ), where  $D_e$  is the nozzle exit diameter and the origin is located at the geometric center of the nozzle exit. As suggested in the literature (Brès et al. 2018a, 2018b), near-wall mesh refinement is needed inside the nozzle in order to properly capture the development of the internal boundary layers. Near the internal walls of both primary and secondary nozzles starting from  $x = -3D_e$ , the target length scale is set to  $\Delta x = 0.005D_e$ , and then further reduced to  $\Delta x = 0.0025D_e$  between  $x = -1D_e$  and the nozzle exit. The current near-wall grid sizing is based on Bres et al. (2018a), in which LES for a conical nozzle of similar size were conducted at  $M_j = 0.9$ . Readjustment of the near-wall grid resolution will be applied once more information about the boundary layers is obtained from experiments and preliminary LES calculations. Immediately downstream the exit up to  $x = 1D_e$ , the grids near the liplines are set to  $\Delta x = 0.005D_e$  and then doubled in size between  $x = 1D_e$  and  $x = 2D_e$ . Further downstream, between  $x = 2D_e$  and  $x = 20D_e$ , the grids near the jet shear layers are set to be  $0.02D_e$ . Finally, the jet plume up to  $x = 40D_e$  is fully enclosed in a conical refinement zone with  $\Delta x = 0.04D_e$ . The rest of the domain is filled with successively coarser grids up to the boundaries. The resulting LES mesh contains around 64 million control volumes. Figure 4 (left) shows a schematic picture of the grid refinement near the nozzle surface and the jet shear layers in grayscale, with lighter color indicating a finer grid size. Figure 4 (right) shows a zoomed-in view of the Voronoi mesh near the nozzle exit, highlighting the fine isotropic grids placed near the nozzle wall and the exit shear layer.

By scaling the grids in the 64 million mesh by a factor of two, a coarse mesh containing around 15 million control volumes is generated. A preliminary test run using the coarse mesh is conducted at  $M = 0.9$  for the primary nozzle and  $M = 0.7$  for the secondary nozzle. This test run is done to further verify the numerical setup in preparation for the upcoming simulation plan. Figure 5 shows a contour plot of the instantaneous jet axial velocity near the nozzle exit, highlighting the interactions of the boundary layers inside the internal mixing region and the growth of the jet initial shear layers. Once the exact operating conditions of the nozzle are provided by the Georgia Tech experimental team, higher-fidelity simulations will be conducted on a finer mesh and validated with experimental data.

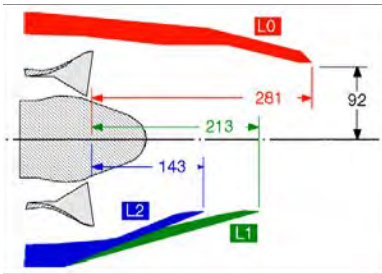


Figure 1. Internally mixed nozzle studied by Bridges and Wernet (AIAA 2004-2896).

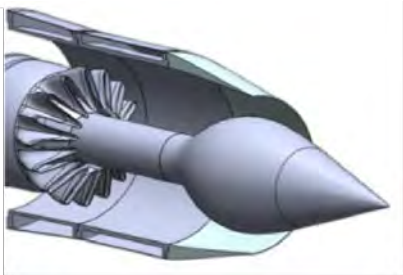


Figure 2. Dual stream internally mixed nozzle with external plug designed by Dr. Bridges at NASA.

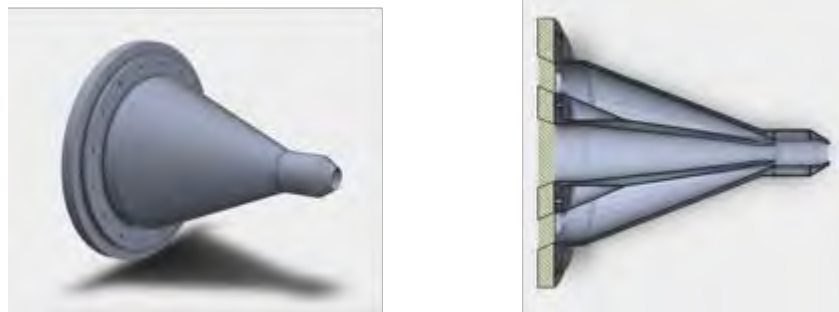


Figure 3. Coannular geometry provided by Georgia Tech team

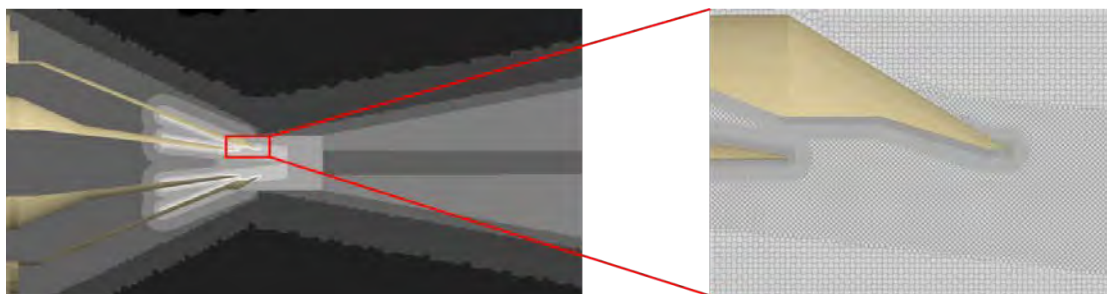


Figure 4. (Left) Preliminary LES mesh with refinement regions around the nozzle and the jet plume shear layers highlighted in grayscale; lighter color indicates finer grids. (Right) Zoomed-in view of the Voronoi mesh near the nozzle exit.

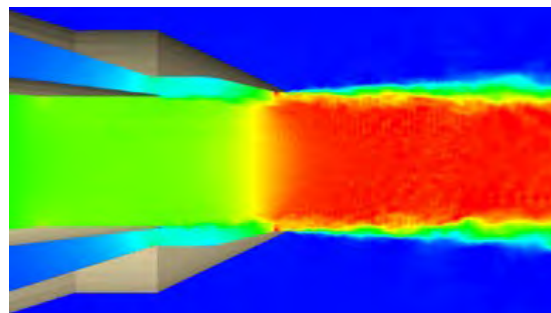


Figure 5. Instantaneous axial velocity from a test run using the Georgia Tech geometry on a coarse mesh.

### Jet Noise Propagation Modeling

A number of methods have been applied to predict jet noise from RANS (mean flow) calculations alone. Several of these build upon Lighthill's original acoustic analogy (Lighthill), where the Navier Stokes equations are rearranged into the form of an acoustic wave equation with a distribution of quadrupole source terms arising from local Reynolds stresses. Goldstein's generalized acoustic analogy (Goldstein) similarly rearranges the full flow equations, into a linear left-hand side representing the spatially developing mean flow and a non-linear right-hand side representing the acoustic sources. This framework allows for the effects of convection and refraction to be accounted for correctly and has been shown to be more robust to numerical errors in the jet mean flow than other commonly used acoustic analogy formulations (Samanta et al.).

In Generalized Acoustic Analogy (GAA), flow variables are decomposed into steady and fluctuating components using a Favre decomposition, resulting in a linearized form of the compressible flow governing equations with non-linear source terms

arising from Reynolds and shear stresses. Separate perturbation variables are defined for momentum and stagnation enthalpy.

The wave propagation problem is then solved efficiently in the frequency domain using an adjoint Green’s function method (Karabasov et al.). The Fourier transform of the adjoint Green’s function solution satisfies the adjoint PDE system to the linearized equations already obtained. Each adjoint variable corresponds to one of the base flow state variables—density, momentum, and temperature—and represents the sensitivity of this system to placing a point source at a given location in the domain. The adjoint equations are solved iteratively in a pseudo-time stepping scheme, controlling the step size in order to prevent inaccuracies arising from the shear layer instability. Our implementation of this adjoint solver has been tested on a time-averaged ensemble of unsteady jet realizations, taken from an SU2 (Molina) delayed detached-eddy simulation (DDES) calculation of a subsonic jet. This test case was previously studied in the framework of a European Union project Go4Hybrid (G4H) (Fuchs et al.), and the simulation results for this grid resolution have been validated against experimental data from Bridges and Wernet (Bridges and Wernet). Figure 6 shows an example calculation, the density sensitivity field obtained using the adjoint solver for the  $M = 0.9$  test jet, placing a point source underneath the jet.

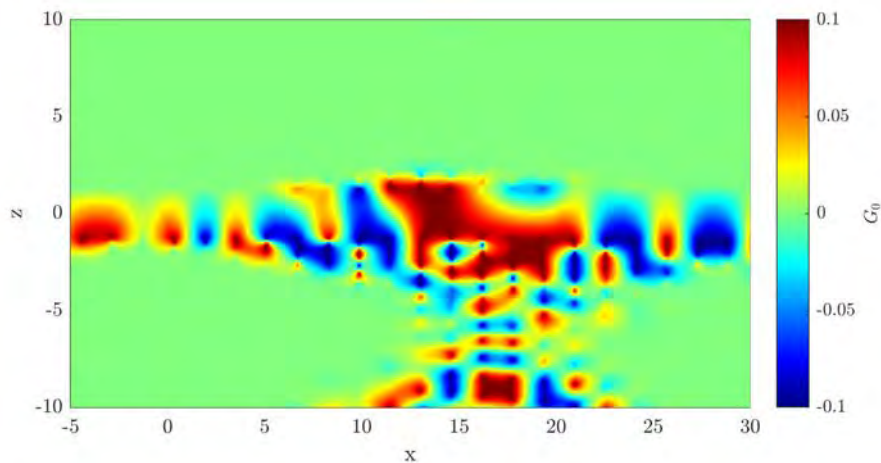


**Figure 6.** Adjoint density solution for point source placed in the x-z plane at  $y = -18$ .

The far-field acoustic pressure at a given observer location may then be calculated from a convolution integral over the domain volume of the adjoint fields with the non-linear sources obtained from the mean flow calculation. Calculating the power spectral density of the distant sound field in this way requires us to impose a model of the spatio-temporal cross-correlation of the source terms. This is assumed to take the form of a multivariate Gaussian, with the imposed length and time scales being assumed to scale with standard turbulent length and time scales according to universal non-dimensional constants (Karabasov et al.).

In addition to GAA, we have examined a number of other methods that could also be used to obtain far-field acoustic information from mean flow calculations alone. These include two lower order methods based on Lighthill’s equations (Morris and Farassat) and the linearized Euler equations (Tam and Auriault), as well as resolvent analysis (Schmidt et al.), whereby the operator representing the transfer function between the base flow’s forcing and response is decomposed to yield the most energetic acoustic modes present. These methods carry some advantages and drawbacks in comparison with GAA. The lower order methods carry the lowest computational cost while offering reasonable accuracy, and therefore appear to be well-suited for the purposes of design and optimization. However, this class of method requires significant tuning of empirical constants to provide the required accuracy. It is very difficult to attribute physical meaning to such parameters, and therefore difficult to come up with a universal tuning that would give sufficient predictive accuracy across the design space. Likewise, with resolvent analysis, the modes obtained are only indicative of the true energetic acoustic modes in the theoretical case of white noise forcing. In the true case, a model is required to account for non-forcing interactions within the flow. This model can range in complexity from simply including the eddy viscosity in the resolvent operator to more sophisticated solutions obtained from fitting to unsteady LES data. Work on each of these methods is ongoing.



## **Milestones**

None

## **Major Accomplishments**

To date, we have generated the preliminary grids for our RANS and LES studies. These preliminary grids serve as the starting point for quantifying the quality of our simulations. We expect the grid generation process to be an iterative process, especially as we receive more specifics on flow conditions from the experimental team.

We have also applied for and received some startup computer time on Extreme Science and Engineering Discovery Environment's (XSEDE) Stampede2 platform, on which we will begin running the preliminary simulations. This computer allocation and the anticipated preliminary runs will allow us to further refine our computational cost estimated in the future, larger allocation requests for production-sized runs.

## **Publications**

None

## **Outreach Efforts**

None

## **Awards**

None

## **Student Involvement**

Three graduate students are involved in this project. G. Wu has taken the lead on grid generation for the LES computations and computer time estimates for preliminary calculations. K. Matsuno has looked into previous literature relevant to this study and guided efforts to obtain more computer allocations. T. Shanbhag has led the modelling effort with the adjoint Green's function methods described in the previous sections and is in charge of running the RANS-level computations.

## **Plans for Next Period**

Research will be focused on Tasks 1-3, as listed above, for the following project year.

## **References**

- Brès, G. A., et al. "Importance of the nozzle-exit boundary-layer state in subsonic turbulent jets." *Journal of Fluid Mechanics*, vol 851, 2018a, pp. 83-124.
- Brès, G. A., et al. "Large-eddy simulations of co-annular turbulent jet using a Voronoi-based mesh generation framework." *AIAA/CEAS Aeroacoustics Conference*, 2018b.
- Bridges, J., and M. Wernet. "Establishing consensus turbulence statistics for hot subsonic jets." *AIAA/CEAS Aeroacoustics Conference*, 2010.
- Fuchs, M., et al. "Single-Stream Round Jet at  $M = 0.9$ ." *Go4Hybrid: Grey Area Mitigation for Hybrid RANS-LES Methods*, Springer International Publishing, 2018, pp. 125-137.
- Goldstein, M. E. "A generalized acoustic analogy." *Journal of Fluid Mechanics*, vol. 488, 2003, pp. 315-333.
- Karabasov, S. A., et al. "Jet Noise: Acoustic Analogy informed by Large Eddy Simulation." *AIAA Journal*, vol. 48, no. 7, 2010, pp. 1312-1325.
- Lighthill, M. J. "On Sound Generated Aerodynamically. I. General Theory." *Proceedings of the Royal Society of London. Series A. Mathematical and Physical Sciences*, vol. 211, no. 1107, 1952, pp. 564-587.
- Molina, E. "Detached Eddy Simulation in SU2 (PhD Thesis)."
- Morris, P. J., and F. Farassat. "Acoustic Analogy and Alternative Theories for Jet Noise Prediction." *AIAA Journal*, vol. 40, no. 4, 2002, pp. 671-680.
- Samanta, A., et al. "Robustness of Acoustic Analogies for Predicting Mixing-Layer Noise." *AIAA Journal*, vol. 44, no. 11, 2006, pp. 2780-2786.
- Schmidt, O. T., et al. "Spectral analysis of jet turbulence." *Journal of Fluid Mechanics*, vol. 855, 2011, pp. 953-982.
- Tam, C. K., and L. Auriault. "Jet Mixing Noise from Fine Scale Turbulence." *AIAA Journal*, vol. 37, no. 2, 1999, pp. 145-153.



# Project 060 Analytical Methods for Expanding the AEDT Aircraft Fleet Database

## Georgia Institute of Technology

### Project Lead Investigator

Principal Investigator:

Professor Dimitri N. Mavris

Director, Aerospace Systems Design Laboratory

School of Aerospace Engineering

Georgia Institute of Technology

Phone: (404) 894-1557

Fax: (404) 894-6596

Email: [dimitri.mavris@ae.gatech.edu](mailto:dimitri.mavris@ae.gatech.edu)

Co-Principal Investigator:

Dr. Yongchang Li

Senior Research Engineer

Aerospace Systems Design Laboratory

School of Aerospace Engineering

Georgia Institute of Technology

Phone: (404) 385-2776

Fax: (404) 894-6596

Email: [yongchang.li@ae.gatech.edu](mailto:yongchang.li@ae.gatech.edu)

### University Participants

#### Georgia Institute of Technology

- PIs: Dr. Dimitri Mavris, Dr. Yongchang Li
- FAA Award Number: 13-C-AJFE-GIT-065
- Period of Performance: June 5, 2020 to June 4, 2021
- Tasks:
  1. Identification and Review of Aircraft not in AEDT
  2. Analytical Method Development

### Project Funding Level

The current FAA funding for this project is \$150,000 from June 5, 2020 to June 4, 2021. The Georgia Institute of Technology has agreed to a total of \$150,000 in matching funds.

### Investigation Team

- Dr. Dimitri Mavris (PI), Georgia Institute of Technology, oversees the entire project.
- Dr. Yongchang Li (Co-PI), Georgia Institute of Technology, oversees the entire project and leads the research team in analyzing the AEDT ANP aircraft and developing the analytical methods to expand the FLEET database.
- Dr. Michelle R. Kirby (research staff), Georgia Institute of Technology, oversees the entire project and supports all of the research activities.
- Dr. Holger Pfaender (research staff), Georgia Institute of Technology, provides consultation and support.
- Zhenyu Gao (graduate student) and Ying Chen (undergraduate student), Georgia Institute of Technology, conduct the development of analytical methods derived from statistical learning methods and techniques.
- Bogdan Dorca (graduate student), Georgia Institute of Technology, performs literature study on databases for collecting performance, emissions and noise data for aircraft not modeled with ANP data.



- Chrysoula Pastra (graduate student) and Justin Coleman (undergraduate student), Georgia Institute of Technology, work on investigating and validating the ANP aircraft substitution method.
- Fabio Chiappina (undergraduate student), Georgia Institute of Technology, conducts the analysis to match ANP aircraft substitution with the equipment in AEDT FLEET DB.

## Project Overview

The Aviation Environmental Design Tool (AEDT) relies on the aircraft noise and performance (ANP) data provided by aircraft manufacturers to support the calculation of aircraft trajectories and noise at receptors using aircraft performance information and noise-power-distance (NPD) relationships for specific aircraft/engine combinations. In the ANP/BADA (Base of Aircraft Data) workflow, the ANP performance data is also used in the calculation of emissions inventories and air quality dispersion. However, not all aircraft in the fleet are represented in the ANP database. When ANP data is not available for a specific target engine/airframe combination, AEDT uses a substitute aircraft from the ANP database to model the target aircraft by closely matching certification noise characteristics and other performance parameters. A problematic issue, however, is that the best substitute based on noise criteria does not always match the best substitute for emissions criteria. In addition, substitute aircraft do not capture the environmental benefits of newer aircraft with noise and emissions reduction technologies, resulting in overly conservative noise and emissions estimates.

The goal of this research is to improve the accuracy of AEDT noise and emissions modeling of aircraft not currently in the ANP database. Georgia Tech will identify and review the aircraft not currently modeled in AEDT and collect information and necessary data to better understand the characteristics of the aircraft. Various statistical analysis methods will be utilized to classify the aircraft as different aircraft types in terms of size, age, technologies, and other engine/airframe parameters. Quantitative and qualitative analytical methods will be identified and evaluated for each aircraft type to develop the ANP and noise data for the aircraft. Validation data from real-world flight and physics-based modeling will be gathered to validate the methods. The Environmental Design Space (EDS) will be employed to generate NPD curves for the aircraft using physics-based modeling and simulation of new and existing aircraft designs and technologies which can support the method validation analysis. After the methods are validated, they will be applied to develop ANP and noise data for the aircraft. Finally, recommendations and guidelines will be developed for how to implement the developed data in AEDT to expand the AEDT FLEET database to include noise and performance data for the aircraft currently not in the ANP database.

## Task 1 – Identification and Review of Aircraft not in AEDT

Georgia Institute of Technology

### Objective

The objective of Task 1 is to identify the aircraft that are not currently modeled with ANP data in AEDT for noise and emissions modeling. In the FLEET database (DB), specific aircraft engine/airframe combinations are defined by a series of ANP and noise coefficients that are used with the BADA and SAE-AIR-1845 algorithms to conduct performance, emissions, and noise modeling. The FLEET DB contains representative aircraft of the entire fleet, with some modeled with ANP data and others represented by a substitution aircraft. This Task involves the identification of the aircraft that do not have ANP data and are represented by a substitution aircraft.

### Research Approach

The aircraft that are not currently modeled with ANP data are identified by reviewing the AEDT FLEET DB and conducting a literature survey. The identified aircraft of interest are further investigated to understand the gaps between them and the substitution aircraft in terms of performance, noise, and emissions. This involves reviewing the existing literature on these aircraft and acquiring the information and data necessary to better understand the engine/airframe characteristics of these aircraft. In addition, the ANP data in the FLEET DB are studied to summarize the key parameters for which the analytical methods will develop ANP data. The existing ANP aircraft substitution methods and the current substitution methods implemented in AEDT are also investigated to support the development of analytical methods.

### Task 1.1: Review the ANP Target-substitute Aircraft Pairs

The objective of this task is to review and identify target-substitute aircraft pairs. First the ANP aircraft substitution table was discovered from Eurocontrol's website [Eurocontrol, 2017] in the form of a spreadsheet through a literature study. This spreadsheet was provided for jet and heavy propeller-driven aircraft to help noise modelers map the aircraft from a given traffic sample to the types available in the ANP database. In the absence of a list directly indicating which aircraft in the AEDT

database are substitution aircraft, MATLAB functions were created to facilitate searching through the AEDT database and the acquired ANP aircraft substitutions spreadsheet. Once the AEDT aircraft substitutions list is acquired, these MATLAB functions can quickly match the target aircraft to the aircraft in the AEDT database and ANP substitutions spreadsheet and record the relevant data. Example calls to these MATLAB functions are provided below.

In order to sort out the target-substitution aircraft pairs, the first step is to identify the substitution aircraft in the ANP aircraft substitution spreadsheet and their associated data from AEDT FLEET DB. This was conducted by developing a MATLAB function which takes in an ANP ID as its only parameter and outputs all entries in the ANP substitutions spreadsheet and AEDT aircraft database with an ANP ID matching the input. The outputs are in the form of a cell array that can then easily be written to a spreadsheet for further analysis. For example, calling this function with the input "DHC8" yields the following output shown in Figure 1.

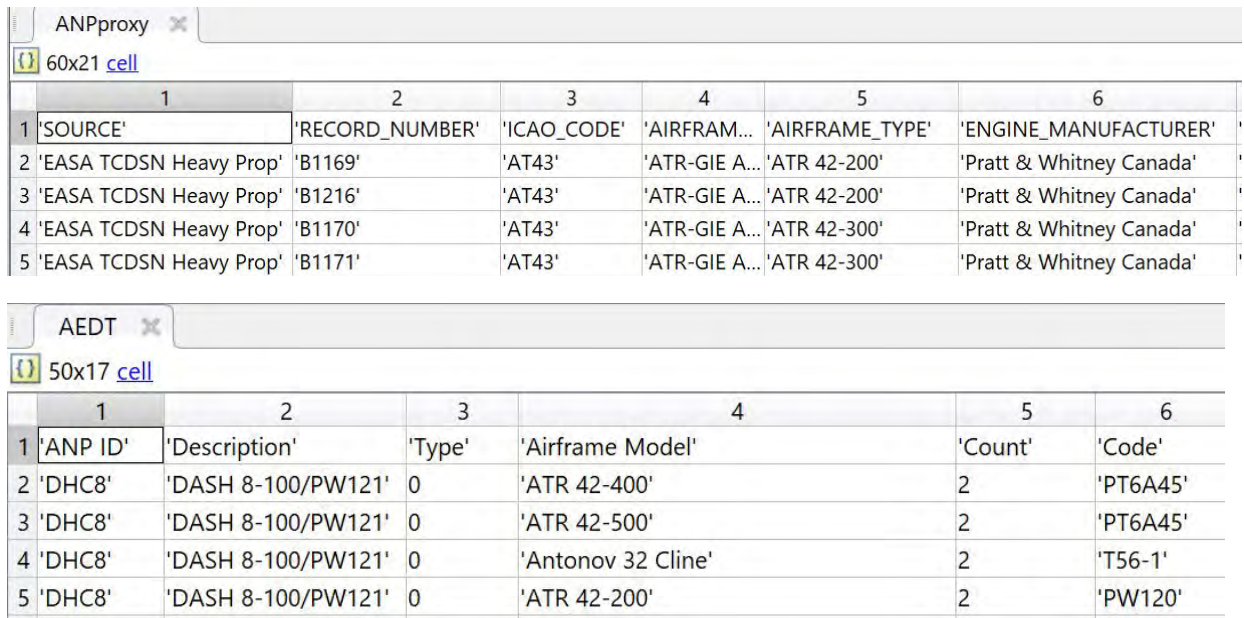


Figure 1. Queried data for ANP aircraft "DHC8."

The ANP proxy output shown above is a 60 x 21 cell array and contains many more columns of data than those shown, including maximum takeoff weight (MTOW), noise chapter, propeller type, and more. Similarly, the AEDT output is a 50 x 17 cell array that also contains various additional data.

Next, the target aircraft in the ANP aircraft substitution spreadsheet were studied. Each target aircraft is represented as a unique combination of airframe type and engine type. Another MATLAB function was developed which takes as its parameters an airframe type and engine type, outputting cell arrays with all data from the ANP substitutions spreadsheet with airframe type and engine type matching that of the input. It also outputs all entries in the AEDT database with an ANP ID matching that found in the ANP substitutions list. For example, calling this function with the inputs "BAe ATP" as airframe type and "PW126" as engine type yields the output shown in Figure 2.

ANP										
1	2	3	4	5	6	7	8	9	10	
1	'ICAO...	'AIRFRAME_MANU...	'AIRFRAME_TYPE'	'ENGINE_MANU...	'ENGINE_TYPE'	'ENGINE_NUM...	'MTOW_KG'	'MLW_KG'	'NOISE...	'ANP_PROXY'
2	'ATP'	'BAE Systems (Oper...	'BAe ATP'	'Pratt & Whitn...	'PW126'	2	22930	22250	4	'HS748A'
3	'ATP'	'BAE Systems (Oper...	'BAe ATP'	'Pratt & Whitn...	'PW126'	2	22930	22250	4	'HS748A'
4	'ATP'	'BAE Systems (Oper...	'BAe ATP'	'Pratt & Whitn...	'PW126'	2	22930	22250	5	'HS748A'
5	'ATP'	'BAE Systems (Oper...	'BAe ATP'	'Pratt & Whitn...	'PW126'	2	22930	22250	5	'HS748A'
6	'ATP'	'BAE Systems (Oper...	'BAe ATP'	'Pratt & Whitn...	'PW126'	2	23678	23133	4	'HS748A'
7	'ATP'	'BAE Systems (Oper...	'BAe ATP'	'Pratt & Whitn...	'PW126'	2	23678	23133	5	'HS748A'

AEDT							
1	2	3	4	5	6	7	
1	'ANP ID'	'Description'	'Type'	'Airframe Model'	'Count'	'Code'	'Model'
2	'HS748A'	'HS748/DART MK532-2'	0	'Saab 2000'	2	'4AL003'	'AE3007A'
3	'HS748A'	'HS748/DART MK532-2'	0	'Saab 2000'	2	'PW127A'	'PW127-A'

**Figure 2.** Queried data for ANP aircraft with "BAe ATP" airframe type and "PW126" engine type.

The function finds the ANP ID associated with the aircraft in the ANP output cell array—"HS748A" in this example—and searches the AEDT database for this ANP ID, outputting all rows with a matching ANP ID.

With a complete list of which aircraft in AEDT are substitution aircraft, these MATLAB functions will prove quite useful in easily accessing ANP and AEDT data for each of these aircraft.

In addition to these MATLAB functions, the basic ANP data for each of the 112 unique ANP proxy aircraft IDs in the ANP aircraft substitutions spreadsheet were queried from the AEDT FLEET database. Each of the aircraft obtained from these SQL queries was compared in airframe and engine model to all entries in the ANP aircraft substitutions list; if the SQL aircraft matched an ANP aircraft in both airframe model and engine model, then the matching entries from each spreadsheet were recorded; that is, the airframe and engine model combination was recorded exactly as it appeared both in the SQL database and in the ANP substitutions spreadsheet. An example of this procedure is shown below.

First, ANP data for all 112 unique ANP proxy aircraft were queried from SQL and stored in a spreadsheet. For each of the 2466 rows in the resulting spreadsheet, the listed airframe model and engine model combination were to be searched for within the ANP substitutions spreadsheet. For example, in Table 1 we consider a particular row in the spreadsheet comprised of SQL data:

**Table 1.** Queried data from AEDT FLEET database for an aircraft with equipment ID 128

EQUIP_ID	ANP_AIRPLANE_ID	AIRFRAME_ID	MODEL (AIRFRAME)	ENGINE_ID	MODEL (ENGINE)
128	737	4588	Boeing 737-200 Series	1263	JT8D-9 series

The ANP aircraft substitutions spreadsheet is thus searched for a match to "Boeing 737-200 Series" and "JT8D-9" series. Though no aircraft in the ANP spreadsheet has this exact string as its airframe type, "737-200" does exist within the ANP substitutions spreadsheet; this is considered an airframe match. Next, we locate aircraft in the ANP spreadsheet with "JT8D-9" as their engine type, and an engine match was found as well. Since there are aircraft in the ANP spreadsheet with both airframe type of "737-200" and engine type of "JT8D-9", this is considered a double match—a match of both airframe and engine simultaneously.

In Table 2, a different row in the SQL data spreadsheet is considered.

**Table 2.** Queried data from AEDT FLEET database for an aircraft with equipment ID 2360.

EQUIP_ID	ANP_AIRPLANE_ID	AIRFRAME_ID	MODEL (AIRFRAME)	ENGINE_ID	MODEL (ENGINE)
2360	7478	5224	Boeing 747-8F	1357	CF6-80C2B1F

Though the ANP spreadsheet does have aircraft with the airframe type "747-8F" and aircraft with the engine type "CF6-80C2B1F", there are no aircraft that match both criteria simultaneously. Thus, a match is recorded for airframe type and for engine type, but a double match is not recorded.

The task of matching aircraft in the SQL database to aircraft in the ANP aircraft substitutions list remains in progress, as this task requires more than two thousand comparisons and cannot be easily automated by a computer script due to the different formats in the two databases. Upon receiving a list indicating which AEDT aircraft are substitution aircraft, this same matching process can be applied to the substitution aircraft in AEDT, and the relevant data in the ANP aircraft substitutions spreadsheet can thus be easily obtained.

### Task 1.2: Aircraft Database Literature Study

The main objective of this task is to collect data from various publicly available databases for a wide range of aircraft. This information is helpful when determining which performance, emissions, and noise parameters will be used for the substitution algorithm.

With regards to performance, the following open-source databases have been identified:

- **AEDT ANP (FLEET + FLEET-FULL databases).** The most complete performance database available, the FLEET database contains multiple performance parameters for a wide variety of airframe/engine combinations. The FLEET-FULL database, while it is not publicly available, contains information for all the registered aircraft throughout the world. Minimum and maximum values for the same airframe/engine combinations are available for certain aircraft parameters (e.g., MTOW) depending on what aircraft equipment the airline is using onboard.
- **Aircraft Performance Database [Eurocontrol, 2020].** This database contains performance data for a wide variety of aircraft. It includes data regarding:
  - Aircraft geometry (e.g., wingspan, height, length).
  - Aircraft structure (e.g., tail configuration, wing position, engine type, landing gear configuration).
  - Aircraft performance parameters (e.g., MTOW, range).
  - Aircraft profile (e.g., takeoff, climb, approach, landing, and respective speeds, distances, rates of climb/rates of descent (ROC/ROD)).

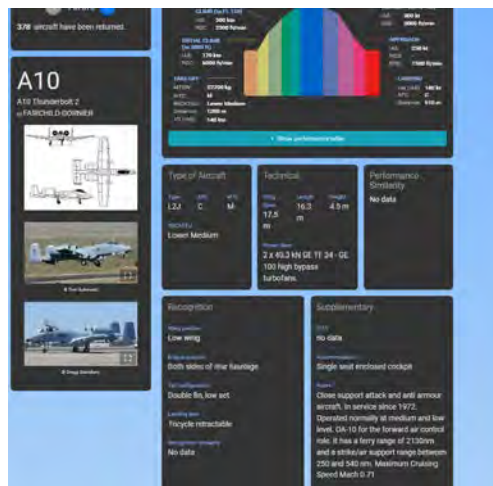


**Figure 3.** Aircraft performance database example.



- **RisingUp** [RingsUp Aviation, 2020]. This database contains performance data for a wide variety of general aviation aircraft (e.g., Cessna, Beechcraft). It includes information regarding:
  - Aircraft performance parameters (e.g., gross weight, empty weight, fuel capacity range).
  - Aircraft profile (e.g., takeoff, climb and landing and respective speeds, distances, ROCs/RODs, ceiling).

**AIRCRAFT PERFORMANCE DATA**  
[Home](#) > [Aircraft Specs](#) > [Manufacturers](#) > [Beechcraft Aircraft](#) > 56 TC Turbo Baron Performance Information

**Beechcraft 56 TC Turbo Baron - Performance Data**

<b>Horsepower:</b> 380	<b>Gross Weight:</b> 5990 lbs
<b>Top Speed:</b> 252 kts	<b>Empty Weight:</b> 3650 lbs
<b>Cruise Speed:</b> 247 kts	<b>Fuel Capacity:</b> 142 gal
<b>Stall Speed (dirty):</b> 73 kts	<b>Range:</b> 737 nm

<b>Takeoff</b>	<b>Landing</b>
<b>Ground Roll:</b> 1005 ft	<b>Ground Roll:</b> 1285 ft
<b>Over 50 ft obstacle:</b> 1420 ft	<b>Over 50 ft obstacle:</b> 2080 ft

<b>Rate Of Climb:</b> 2020 fpm	<b>Rate of Climb (One Engine):</b> 410 fpm
<b>Ceiling:</b> 32200 ft	<b>Ceiling (One Engine):</b> 18600 ft

**Related Specs:**

- [A56TC Turbo Baron](#)
- [E 55 Baron](#)
- [C55, D55 Baron](#)
- [B 55 Baron \(1978 & up\)](#)
- [B 55 \(SN up to 954\)](#)
- [A 55 Baron](#)
- [55 Baron](#)
- [B 55 \(SN 955 and up\)](#)

**Manufacturer:**

**Aircraft Model:**

[Search for aircraft meeting your performance criteria!](#)

**Navigation**

- [Manufacturer List](#)
- [Beechcraft Aircraft](#)
- [Advanced Search](#)
- [Specs Home](#)

Figure 4. RisingUp Aviation Database example

- **OpenSky** [The OpenSky Network, 2020]. This database provides limited information about a specific existing aircraft (e.g., an A320 that is currently operating). It includes information such as:
  - Engine type.
  - Aircraft owner, airline operator, number of years in service, etc.
  - Live tracking of aircraft including altitude, velocity, track, current location.

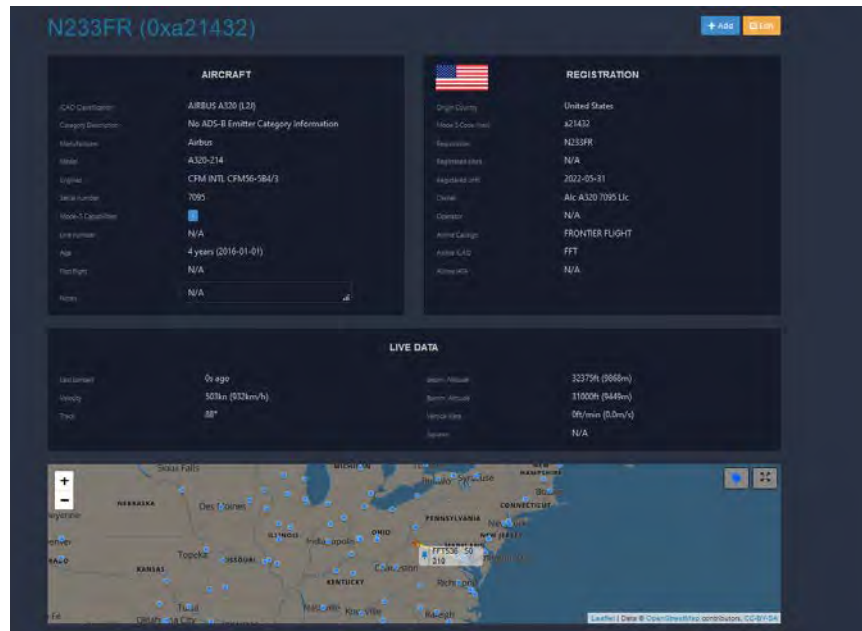


Figure 5. OpenSky Aircraft Database example

- **International Air Transport Association (IATA).** This source only provides a passenger data exchange database, which does not specifically relate to performance.

With regard to emissions, the following open-source databases have been identified:

- **ICAO Aircraft Engine Emissions Databank** [International Civil Aviation Organization (ICAO), 2020]. This Excel-based database covers turbojet and turbofan engines for which the emissions are regulated (27 kN or higher static thrust). It contains engine emissions for CO, NO<sub>x</sub>, and UHC as well as a few engine performance parameters like bypass ratio and thrust rated output.

With regards to noise, the following open-source databases have been identified:

- **EASA certification noise databases** [EASA, 2020]. A very large Excel database consisting of aircraft/engine types and effective perceived noise in decibels (EPNdB) and noise levels for lateral, flyover, and approach. It is a collection of four noise databases that address heavy propeller driven aeroplanes, jet aeroplanes, light propeller driven aeroplanes, and rotorcraft.
- **ICAO Noise Database (NoiseDB)** [ICAO, 2020]. Similar to the EASA certification noise database.

In order to see if these databases contain enough information, a case study involving the aircraft with ANP ID "737800" was performed and data were gathered for the 98 combinations of:

- Airframe (e.g., Boeing 737-800 Series, Boeing 737-800 with winglets, Boeing 737-900 Series, Boeing 737-900-ER, MC-21-300, etc.)
- Engine (e.g., CFM56-7B24, CFM56-7B27/2, LEAP-1B25, PW1130G-JM, etc.)

An Excel document was made containing various parameters of interest for all of the possible combinations. For this case study, the following ANP parameters which are necessary for substitution were identified:

- Engine related parameters (ENGINE\_CODE, ENGINE\_MOD\_CODE, ENGINE\_MOD\_DES, Number of Engines, Location of Engines, Type of Engine, Location of Engines, Engine Bypass ratio)
- Performance related parameters (INTRO\_YEAR, SIZE\_CODE, Maximum range, Max takeoff gross weight, Max landing gross weight, Static rated thrust or 100% thrust, in or out of production)
- Noise related parameters (EPNdB lateral/flyover/approach/cumulative levels, limits and margins)

**Table 3. B737-800 airframe/engine combinations**

EQUIP_ID	ANP ID	BADA3 ID	AIRFRAME	ENGINE	ENGINE	ENGINE	ENGINE	FLT_AIRFRAMES	FLT_AIRFRAMES	ENGINE
EQUIP_ID	ANP ID	BADA3 ID	AIRFRAME MODEL	ENGINE MODEL	ENGIN_CODE	ENGINE_MOD_CODE	ENGINE_MOD_DES	ENGINE_COUNT	ENGINE_LOCATION	BPR
EQUIP_ID	ANP ID	BADA3 ID	AIRFRAME MODEL	ENGINE MODEL	UID	ENGINE_MOD_CODE	ENGINE_MOD_DES	Number of Engines	Location of Engines	Engine Bypass ratio
210	737800B738		Boeing 737-800Series	CFM56-7B24		140 NONE	No engine modification.	2	W	5.2
211	737800B739		Boeing 737-900Series	CFM56-7B24		140 NONE	No engine modification.	2	W	5.2
	737800B738		Boeing 737-800withwinglets	CFM56-7B27/2		140 NONE	No engine modification.	2	W	5
	737800B739		Boeing 737-900-ER	CFM56-7B27E/B1		140 NONE	No engine modification.	2	W	5.1
	737800B738		MC-21-300	CFM56-5B2/3		140 NONE	No engine modification.	2	W	5.5
	737800B738		Boeing 737-800withwinglets	CFM56-7B24		140 NONE	No engine modification.	2	W	5.2
	737800B738		Boeing 737-800Series	CFM56-7B26/3		140 NONE	No engine modification.	2	W	5.1
	737800B738		Boeing 737-800Series	CFM56-7B26		140 NONE	No engine modification.	2	W	5.1
	737800B739		Boeing 737-900Series	CFM56-7B26/3		140 NONE	No engine modification.	2	W	5.1
	737800B739		Boeing 737-900Series	CFM56-7B26		140 NONE	No engine modification.	2	W	5.1
	737800B739		Boeing 737-900-ER	CFM56-7B26/3		140 NONE	No engine modification.	2	W	5.1

**Task 1.3: Summary of ANP Data in AEDT FLEET DB**

To understand the ANP data that need to be developed for the target aircraft, the ANP data in AEDT FLEET database were studied. A summary of ANP data was made to identify the locations and data structures of all ANP parameters. Going forward, this summary is expected to facilitate the identification of variables that play important roles in developing ANP data for the target aircraft as well as provide fast searches of relevant variables. A full list of summarized tables is given below:

- FLT\_AIRFRAMES
- FLT\_ANP\_AIRPLANES
- FLT\_ANP\_AIRPLANE\_NOISE\_GROUPS
- FLT\_ANP\_AIRPLANE\_NPD\_CURVES
- FLT\_ANP\_AIRPLANE\_PROCEDURES
- FLT\_ANP\_AIRPLANE\_PROCEDURES\_EXT
- FLT\_ANP\_AIRPLANE\_PROCEDURES\_MAP
- FLT\_ANP\_AIRPLANE\_PROFILE\_POINTS
- FLT\_ANP\_AIRPLANE\_PROFILE\_POINTS\_EXT
- FLT\_ANP\_AIRPLANE\_PROFILES
- FLT\_ANP\_AIRPLANE\_THRUST\_GENERAL
- FLT\_ANP\_AIRPLANE\_THRUST\_JET
- FLT\_ANP\_AIRPLANE\_THRUST\_PROP
- FLT\_ANP\_AIRPLANE\_THRUST\_TSFC\_COEFFICIENTS

The summary is made using an Excel sheet in a way that is easy to sort and filter information. Table 4 below shows a fraction of the complete ANP summary table, which only includes FLT\_AIRFRAMES. As a small part of the complete table, Table 4 gives an example of how data is sorted in the ANP summary. It contains six main columns plus a “Note” column. The function of each column is described below:

- **Table Name:** This column provides information regarding which table in the FLEET database a variable belongs to. This column can be used to look at a specific table in FLEET database.
- **Variable Name:** This column shows the variable name in the FLEET database, as well as links between tables.
- **Variable Description:** This column includes the descriptions of the variables. It can be used to find and locate similar variables across the entire FLEET database. For example, by searching the term “engine”, you will be able to find the location and information for variables such as “Number of engines”, “Location of engines”, “Type of engines”, “Engine bypass ratio”, etc. In addition, this column contains all the necessary information to locate crucial parameters that are mentioned in the aircraft grouping and substitution rules in Doc 29 (described in the next Task).
- **Discrete (Y/N):** Whether the variable is discrete or not. If the variable is discrete, it typically only contains a limited number of options. For example, for variable “Location of engines”, it has three discrete levels: Fuselage/Tail, Internal, and Wing. In contrast, a continuous variable usually spans across a numeric range. The variable “Maximum range” is an instance of a continuous variable.
- **Variable Possible Values:** Possible values of a variable. For each variable, it is in the form of either a range or a set that includes all discrete values.
- **Code Description (if applicable):** If the variable is discrete and its possible values are non-numeric, this column contains explanations of the abbreviation codes.



**Table 4.** Example of the ANP summary table

Table Name	Variable Name	Variable Description	Discrete (Y/N)	Variable Possible Values	Code Description (if applicable)
FLT_AIRFRAMES	MODEL	Detailed aircraft models	N	1136 models	
FLT_AIRFRAMES	ENGINE_COUNT	Number of Engines	Y	1, 2, 3, 4, 6, 8	
FLT_AIRFRAMES	ENGINE_LOCATION	Location of Engines	Y	I, W, F	F Fuselage/Tail I Internal W Wing C Civil
FLT_AIRFRAMES	DESIGNATION_CODE	Link to FLT_CAT_DESIGNATIONS table	Y	G, C, M	G General Aviation M Military
FLT_AIRFRAMES	EURO_GROUP_CODE	Link to FLT_CAT_EUROS_GROUPS table	Y	SS, PP, JB, H2, TP, LB, JR, JL, JS, H1, JM	H1 Helicopter Light H2 Helicopter Heavy JB Jet Business JL Jet Large JM Jet Medium JR Jet Regional JS Jet Small PP Propeller SS Supersonic TP Turboprop
FLT_AIRFRAMES	MAX_RANGE	Maximum range	N	513 possibilities within [11, 11000]	
FLT_AIRFRAMES	INTRO_YEAR	First year airframe was certified for flight operations	N	59 different years	
FLT_AIRFRAMES	USAGE_CODE	Link to FLT_CAT_USAGE table	Y	O, H, A, P, C, B	A Attack/Combat B Business C Cargo/Transport H Helicopter O Other P Passenger
FLT_AIRFRAMES	SIZE_CODE	Link to FLT_CAT_SIZES table	Y	T, H, S, L, M, V	H Heavy L Large M Medium S Small T Light V Very Light
FLT_AIRFRAMES	ENGINE_TYPE	Type of Engine	Y	J, T, P	E Electric J Jet P Piston R Rocket T Turboprop/Turboshaft

## Task 2 – Analytical Method Development

Georgia Institute of Technology

### Objective

The objective of this task is to formulate analytical methods that can be used to develop ANP data for the substituted aircraft in the AEDT FLEET database (DB). In this task, various statistical analysis techniques are investigated to analyze the distribution of the aircraft characteristics to distinguish different aircraft types. After the aircraft are classified into different aircraft types, the most appropriate analytical methods will be identified for each aircraft type to develop the ANP performance and NPD data by generating correction factors that can be applied to the substitution aircraft or new data for the aircraft. Multiple methods will be developed for different aircraft types that will span the current fleet depending on the data availability to develop the ANP performance data. This also requires an understanding of how to create correction factors or data suitable for integration into AEDT from higher fidelity noise and performance models. In addition, the substitution method implemented in AEDT is also to be examined and will be kept for use on some aircraft types if it is the most appropriate method. Georgia Tech will evaluate each method and identify the one most appropriate for the corresponding aircraft type.

## Research Approach

The existing aircraft substitution methods documented in Doc 29, a European Civil Aviation Conference (ECAC) report from 2016, are studied and validated. This will help with the development of analytical methods for the aircraft not modeled with ANP data in AEDT. Various statistical learning methods are investigated to understand the advantages and disadvantages of each method in order to select the most appropriate method for each aircraft type.

### Task 2.1: ANP Aircraft Substitution Method

The objective of this task is to study and validate the ANP substitution method from literary research. Doc 29 provided a comprehensive description of the substitution process which will be reviewed and studied in this section.

The ANP database contains noise and performance characteristics for various different airframe and engine combinations. In Doc 29, it is stated that when performing these combinations, it is often required that certain groupings of aircraft types with similar noise and performance characteristics be created and they are all represented by one aircraft category. There are three main reasons why this type of grouping would be necessary: 1) insufficient information, especially for forecast scenarios, 2) lack of separate data from different aircraft models or variants, and 3) a need to decrease modelling time and cost. Out of these three reasons, decreasing the time and cost is the most important due to the tedious nature and the magnitude of calculations that involves multiple aircraft variants operating at an airport. Furthermore, since the differences in noise performance are often relatively small, creating these groupings saves both time and money. Another reasoning behind the groupings is that very often the noise contours in airports are dominated by a few aircraft types, and therefore it is considered to be more efficient to emphasize the most significant noise-generating aircraft types rather than all.

The aircraft are initially grouped based on certain characteristics that are directly related to sound emission and the performance of the aircraft. These characteristics include the maximum takeoff mass (MTOM) of the aircraft, the type of engine, the number of engines, the bypass ratio, the installation of the engines, the type of operation, and lastly the ICAO noise certificate. The MTOM is a parameter that is widely used and is fairly simple, dividing existing aircraft into the three categories of light, medium, and heavy. The type of engine refers to the common engines that are usually paired with turbojet, turbofan, and turboprop aircraft and the number of engines in each configuration. When evaluating the bypass ratio, there is a distinction between the turbojet and turbofan aircraft due to the relation of the parameter-to-sound emissions. The distinction leads to a differentiation between turbojet and turbofan aircraft with low, medium, and high bypass ratios. The "installation of the engines" refers to fuselage-mounted engines or wing-mounted engines. This distinction is made due to the fact that studies have shown that lateral sound emission does depend on the installation of the engine. The "type of operation" is also a very important parameter used for aircraft grouping which might differ between departures and arrivals. The type of operation may also be extended with respect to takeoff procedures when considering more modern aircraft such as wide-bodied twins where reduced takeoff thrust is widely used. The final parameter that is considered, when the grouping is performed, is the ICAO certificate. This parameter is used for grouping if no other information is available, since for landing operations, the certified approach noise level can be a trusted way of recognizing the operational noise. When it comes to departures, unfortunately, the deep cut back method that is used is not representative of real-life operations. For the groupings to make sense, these parameters have to be used in a combinatorial manner, but the difficult part is selecting the correct combination for the grouping. A rule of thumb is that all possible combinations should be used so that a large group can be generated with many similar noise characteristics. Not compromising accuracy acoustic equivalency and noise significance, however, should also be considered. Acoustic equivalency is defined as the comparable noise produced by two aircraft and is expressed in terms of event level  $L_{Max}$  or  $L_E$  at multiple points on the ground or noise footprints. Acoustic equivalency depends on a variety of factors, such as operating procedures and aircraft mass, which means that all aircraft that are acoustically equivalent will not necessarily be grouped together, which is why an acoustic equivalency criterion is demanding in resource terms. Noise significance comes from the notion that the total noise at an airport is mostly driven by a small number of aircraft types. This is used so that the less noisy aircraft types can be grouped together in a simple way that can increase efficiency in potential noise studies.

Having defined the parameters used for grouping and the considerations for ensuring that accuracy and efficiency is not lost, a grouping approach can be set up by following three main steps. The first step consists of the introduction of a fundamental aircraft category scheme based on all of the combinations of parameters that can be used for grouping as mentioned above, such as MTOM, type of engine, number of engines, etc. The second step consists of identifying the different aircraft categories of low significance and grouping together based on a simple grouping scheme, such as engine type and takeoff mass. The third step combines the remaining groups depending on their acoustic equivalencies.



As mentioned earlier, one of the common reasons why a substitution is necessary is that the ANP database might be missing certain information about some possible airframe engine combinations. Therefore, since the information or model provided for this combination is not enough to model the required full set of operations at a specific airport, a substitution aircraft will be used instead in order to provide a noise model. This substitution aircraft will be similar to the ANP aircraft and is often referred to as a proxy aircraft. There are two options when using a proxy aircraft. One of the options is using the proxy aircraft as a one-to-one substitution, which means that it will be used, as is, without making any adjustments. The second option involves making adjustments to the NPD data or the number of movements of the proxy aircraft in the input operations. It is highly recommended that adjustments be made when a proxy is used so that the accuracy of the noise models is maintained. Two different types of adjustments are Method A and Method B. In Method A, a new entry is created in the ANP database and is defined as a duplicate of the proxy aircraft with the adjusted NPD data. The NPD data of the proxy are corrected by adding decibel adjustments, which are calculated using Equation (1) and (2). These equations are valid only for aircraft that have been certified under the ICAO Annex 16 Volume I Chapters 1, 3, 4, and 14, and different adjustments are made for arrival and departure as seen below.

$$\Delta_{dep} = \frac{FO_{LEVEL_{miss}} + LAT_{LEVEL_{miss}} - FO_{LEVEL_{proxy}} - LAT_{LEVEL_{proxy}}}{2} \quad (1)$$

$$\Delta_{arr} = APP_{LEVEL_{miss}} - APP_{LEVEL_{proxy}} \quad (2)$$

Equation (1) calculated the noise adjustment for departure and Equation (2) calculated for arrival. The subscript “miss” refers to the aircraft with the missing information, while the subscript “proxy” refers to the proxy aircraft.  $FO_{LEVEL}$  is defined as the flyover noise level,  $LAT_{LEVEL}$  is defined as the lateral noise level, and  $APP_{LEVEL}$  is the certified approach noise level. For the aircraft that are certified under Chapters 6 and 10, a different adjustment calculation is performed using the Equation (3).

$$\Delta_{certif} = CERTIF_{LEVEL_{miss}} - CERTIF_{LEVEL_{proxy}} \quad (3)$$

$CERTIF$  is defined as the overflight and takeoff levels in decibels for Chapter 6 and 10 aircraft, respectively. The adjustments that are made in Method A are reflected in all noise metrics, including the maximum sound level metrics such as  $L_{Amax}$ .

Method B takes a different approach. It adjusts the number of movements of the proxy aircraft in the input operation, which translates to one movement of the missing aircraft to  $N$  movements done by the proxy aircrafts. It may be easier to implement Method B than Method A, seeing that only the input operations need to be adjusted, but applied only to equivalent sound levels such as  $L_{Aeq}$ .

The variable  $N$  that is being calculated in this method is referred to as the movement adjustment factor and is derived by comparing the certified noise level of the aircraft with the missing information to the proxy aircraft. Just as with Method A, there are different equations that are being used to calculate the movement adjustment factor for aircraft that were certified in the ICAO ANNEX 16 Volume 1 Chapters 2, 3, 4, and 14 as well as Chapters 6 and 10. For the first set of chapters, the movement adjustment factor is calculated for both the departure and the arrival using Equations (4) and Equation (5).

$$N_{dep} = 10^{\frac{\Delta_{DEP}}{10}} \quad (4)$$

$$N_{ARR} = 10^{\frac{\Delta_{ARR}}{10}} \quad (5)$$

For the second set of Chapter -certified aircraft, the movement adjustment factor can be calculated from Equation (6).

$$N_{CERTIF} = 10^{\frac{\Delta_{CERTIF}}{10}} \quad (6)$$

It is important to note that the certified noise levels for the proxy aircraft can be located in the ANP database under the FLT\_NOISE\_CERTIFICATION Table. When there are no certified noise levels for the missing aircraft, then the users can decide

to apply a one-to-one substitution, as was mentioned earlier, where  $\Delta=0$  and  $N=1$ . Lastly, if the  $\Delta$  adjustments are large or if  $N$  deviates greatly from 1, then this is a good indication that the proxy selection is not appropriate.

In order to select the most appropriate proxy aircraft, certain criteria have to be compared and matched to the missing aircraft. Such criteria include engine category, number of engines, engine installation, MTOW, thrust-to-weight ratio (which is defined as the static thrust divided by MTOW), certified noise levels, airframe manufacturer, and engine manufacturer. Therefore, when initiating the proxy selection process, finding and comparing these characteristics is essential. If the MTOW or engine type of the missing aircraft is unknown, then the rule of thumb is that the variant with the largest MTOW should be used with the corresponding engine type and static thrust. The most ideal substitution would consist of the proxy and the missing aircraft having identical engine categories, number of engines, and engine installation, with MTOW, thrust-to-weight, and certified levels as close as possible. Unfortunately, it is not always trivial to find a proxy that satisfies all of the criteria, therefore a degree of relaxation of certain criteria might be necessary. In conclusion, when looking for the most appropriate proxy aircraft, the engine category and installation should be identical, while different variants such as engine and MTOW of the same aircraft type should be assigned to the same proxy unless the variants are present in the ANP database. Lastly, when the missing aircraft type is present in the ANP database but does not have the same engine, MTOW or another variant should be used as a proxy.

In order to validate this substitution process, the calculations for Method A were performed for four aircraft: the 737-700, 737-800, A320-211, and A330-343. For each aircraft, the process began by looking in the ANP substitutions spreadsheet for the first instance of the substituted aircraft. From there, the aircraft's FOLEVEL, LATLEVEL, and APPELVEL noise levels were recorded, along with the  $\Delta_{dep}$  and  $\Delta_{arr}$  values used in the ANP database, plus the ANP ID of the aircraft's proxy. Next, the proxy's ANP ID was used to find the specifications of the proxy aircraft in the FLT\_ANP\_AIRPLANES table. The three noise levels for this proxy were then found in the FLT\_NOISE\_CERTIFICATION table by finding the entry of the proxy aircraft type with a maximum takeoff mass matching that from the previous table. Lastly, these noise levels were used with those of the substituted aircraft to compute  $\Delta_{dep}$  and  $\Delta_{arr}$  which were compared to the values in the ANP database. In the case of the 737-800 and A320-211, both values were found to match, validating the substitution method. However, for the other two aircraft, only one of the values matched, with the other differing by a small amount. Repeating the calculations for other substituted aircraft with the same proxy found similar differences, suggesting that the problem is not with the substitution method but that one of the databases may be simply out of date. One additional complication was that there were several entries in the FLT\_NOISE\_CERTIFICATION table which matched both the proxy aircraft type and MTOW in each case. This suggests that more parameters from the proxy aircraft need to be considered when making this match to ensure the proper noise data is being used.

## Task 2.2: Review of Statistical Learning Methods

The objective of this task is to review the statistical learning methods that can be utilized to conduct analytical analysis for the tasks of this project. This section includes: (1) Review of the data analytics process; (2) Measuring data similarity and dissimilarity; (3) Data preprocessing; (4) Summary of common classification/regression and clustering algorithms.

### 2.2.1 The knowledge discovery from data (KDD) process

In the data mining literature, the KDD process contains seven main steps. The steps' names and roles are listed below [HPK, 2011]:

1. *Data cleaning*: To remove noise and inconsistent data.
2. *Data integration*: Where multiple data sources may be combined.
3. *Data selection*: Where data relevant to the analysis task are identified and chosen.
4. *Data transformation*: Where data are transformed and consolidated into forms appropriate for mining by performing summary or aggregation operations.
5. *Data mining*: An essential process where intelligent methods are applied to extract data patterns.
6. *Pattern evaluation*: To identify the truly interesting patterns representing knowledge based on interestingness measures.
7. *Knowledge presentation*: Where visualization and knowledge representation techniques are used to present mined knowledge to users.

Steps 1 through 4 are different forms of data preprocessing, where data are prepared for mining. *Data reduction* may also be performed to obtain a smaller representation of the original data without sacrificing its integrity. This multi-step process

is also representative of a typical machine learning project, where multiple steps—from collecting data to model delivery—are needed for the entire project cycle.

**2.2.2 Measuring Data Similarity and Dissimilarity**

Dissimilarities and similarities are assessed based on the attribute values describing the objects and often involve distance measures. Similarity and dissimilarity measures are related and referred to as measures of proximity. In this project, such measures can take important roles because of the need to quantitatively determine the closeness between, for example, two aircraft types or two engines. The challenging part is that an aircraft or an engine normally has multiple attributes that are different in type. Table 5 provides a summary of the four main attribute types: nominal attributes, binary attributes, numeric attributes, and ordinal attributes. The two right columns of Table 5 includes examples of such attributes in the FLEET database.

**Table 5.** Summary of the four main attribute types

Attribute Type	Description	ANP Example	Values
Nominal Attributes	A nominal attribute can take on two or more discrete states	ENGINE_LOCATION	F (Fuselage/Tail), I (Internal), W (Wing)
Binary Attributes	A binary attribute has only one of two states: 0 and 1	THR_RESTOR	N (No), Y (Yes)
Numeric Attributes	Has continuous state within certain range	MX_GW_TKO	Within [2200, 1254430]
Ordinal Attributes	The values of an ordinal attribute have a meaningful order or ranking about them	SIZE_CODE	H (Heavy), L (Large), M (Medium), S (Small), T (Light), V (Very Light)

Meanwhile, the crucial point here is that for different types of attributes, different similarity and dissimilarity measures must be used. Table 6 includes a summary of the corresponding metrics used in measure data dissimilarity for the four attributes in Table 5. The ratio of mismatches is used to measure nominal attributes, which are attributes with discrete and unordered states. Binary attributes can be either symmetric or asymmetric. Numerical attributes are the most common type in distance measuring. The Euclidean and Manhattan distances are commonly used in the literature, which are all special cases of the Minkowski distance (with *p* equal to 2 and 1, respectively). Chebyshev distance is another useful option that is also referred to as the supremum distance, and is the maximum difference in values between the two objects. Lastly, prior to calculating distance for ordinal attributes, data normalization is required to map the range of each attribute onto [0.0, 1.0].

Other than the individual measuring methods for the four types of attributes, an aircraft or engine typically has attributes of mixed types. Therefore, an approach is needed to combine the dissimilarity calculations from all four types into a single dissimilarity measure. The last row of Table 6 contains a brief introduction of how this can be done. When put into practice, the assignment of  $d_{ij}^{(f)}$  needs to be discussed on its type. Overall, the materials here can be utilized to quantitatively measure objects with attributes of mixed types.


**Table 6.** Metrics used to measure data similarity and dissimilarity

Type	Method of calculating dissimilarity
Nominal attributes	<u>The ratio of mismatches</u> : $d(i, j) = (p - m)/p$ ( $m$ is the number of matches and $p$ is the total number of attributes describing the objects).
Binary attributes	For <u>symmetric</u> binary attributes: $d(i, j)$ = summation of off-diagonal numbers / total number of attributes. The <u>asymmetric</u> binary dissimilarity therefore ignores the number of negative matches in the denominator of $d(i, j)$ .
Numeric attributes	1. Euclidean distance: $d(i, j) = \sqrt{(x_{i1} - x_{j1})^2 + (x_{i2} - x_{j2})^2 + \dots + (x_{ip} - x_{jp})^2}$ 2. Manhattan distance: $d(i, j) =  x_{i1} - x_{j1}  +  x_{i2} - x_{j2}  + \dots +  x_{ip} - x_{jp} $ 3. Minkowski distance: $d(i, j) = \left(  x_{i1} - x_{j1} ^p +  x_{i2} - x_{j2} ^p + \dots +  x_{ip} - x_{jp} ^p \right)^{1/p}$ 4. Chebyshev distance: $d(i, j) = \lim_{h \rightarrow \infty} \left( \sum_{f=1}^p  x_{if} - x_{jf} ^h \right)^{1/h}$
Ordinal attributes	Perform data normalization to map the range of each attribute onto [0.0, 1.0]: $z_{if} = (r_{if} - 1)/(M_f - 1)$ , and then use any dissimilarity method.
For attributes of mixed types	Process all attribute types together and combine the different attributes into a single dissimilarity matrix. Suppose that the data set contains $p$ attributes of mixed type, the dissimilarity $d(i, j)$ between objects $i$ and $j$ is defined as: $d(i, j) = \sum_{f=1}^p \delta_{ij}^{(f)} d_{ij}^{(f)} / \sum_{f=1}^p \delta_{ij}^{(f)}$

### 2.2.3 Data Preprocessing

Real-world data are highly susceptible to noise, incompleteness, and inconsistency due to their typically huge set sizes and their likely origin from multiple, heterogeneous sources. Data preprocessing is an important step in the knowledge discovery process because quality decisions must be based on quality data. Although numerous methods of data preprocessing have been developed, data preprocessing remains an active area of research. Major data preprocessing steps are listed below (and they are not mutually exclusive):

1. *Data cleaning*: “Clean” the data by filling in missing values, smoothing noisy data, identifying or removing outliers, and resolving inconsistencies.
2. *Data integration*: Merges data from multiple sources into a coherent data store. Additional data cleaning can be performed to detect and remove redundancies that may have resulted from data integration. An attribute may be redundant if it can be “derived” from another attribute or set of attributes.
3. *Data reduction*: Obtains a reduced representation of the dataset that is much smaller in volume, yet closely maintains the integrity of the original data and produces the same (or almost the same) analytical results. Data reduction strategies include the following two types:



- a. Dimensionality reduction: The process of reducing the number of random variables or attributes under consideration. Examples: include principal components analysis, attribute subset selection, attribute construction, and wavelet transform.
  - b. Numerosity reduction: The data are replaced by alternative, smaller representations. Examples include parametric models (regression, log-linear models, and nonparametric models), histograms, clusters, and sampling.
4. *Data transformation*: Can improve the accuracy and efficiency of algorithms involving distance measurements. An example is normalizing the data attempts to give all attributes an equal weight.
  5. *Data discretization*: Concept hierarchy generation, where raw data values for attributes are replaced by ranges or higher conceptual levels.

#### 2.2.4 Algorithms

This section provides a review of the common machine learning/data mining algorithms. The objective is to provide a list of candidate algorithms that can be chosen in this project and compare their characteristics.

Table 7 includes a summary of the common regression and classification algorithms [KJ, 2013]. We summarize these two types of algorithm in the same table for two reasons: (1) they are similar in that both belong to supervised learning methods, and (2) many algorithms can handle both regression and classification problems. Overall, the difference between regression and classification is that regression predicts continuous and numeric outputs, while classification predicts discrete outputs. Table 7 first classifies the algorithms into three categories: linear methods, nonlinear methods, and trees/rules-based methods. In the second column of Table 7, the collected candidate algorithms are listed. In the rest of the table, candidate algorithms are compared in eight different aspects:

1. Regression/Classification: What type of problem can the algorithm solve. “R”, “C”, and “R/C” stand for regression, classification, and both regression and classification, respectively.
2. Allows  $n < p$ : Whether or not the algorithm can be used when the number of observations  $n$  is less than the dimension of the predictors  $p$ .
3. Preprocessing: Which preprocessing methods must be used before applying the algorithm. “CS” stands for centering and scaling, “NZZP” stands for the removal of near-zero predictors, and “HCP” stands for the removal of highly correlated predictors.
4. Interpretability: To what extent is the model interpretable. “H” stands for high, “M” stands for medium, and “L” stands for low.
5. Feature Selection: Whether or not the algorithm can perform feature selection (also referred to as model selection). “H” stands for high, “M” stands for medium, and “L” stands for low.
6. No. of Tuning Parameters: How many tuning parameters the algorithm has.
7. Robustness to Predictor Noise: Whether or not the algorithm is robust to noise. “H” stands for high, “M” stands for medium, and “L” stands for low.
8. Comp. Time: The overall computational time required when running the algorithm. “H” stands for high, “M” stands for medium, and “L” stands for low.


**Table 7.** Summary of common regression/classification algorithms

Category	Method	Regression/ Classification	Allows $n < p$	Pre- processing	Inter- pretability	Feature Selection	No. of Tuning Parameters	Robustness to Predictor Noise	Comp. Time
Linear	Linear Regression	R	N	CS, NZP, HCP	H	L	0	L	L
	Partial Least Squares	R/C	Y	CS	H	M	1	L	L
	Ridge Regression	R/C	N	CS, NZP	H	L	1	L	L
	LASSO/ Elastic Net	R/C	Y	CS, NZP	H	H	1 to 2	L	L
	Logistic Regression	C	N	CS, NZP, HCP	H	L	0	L	L
	Linear Discriminant Analysis	C	N	NZP	M	L	0 to 2	L	L
	Nearest Shrunken Centroids	C	Y	NZP	M	H	1	L	L
Nonlinear	Neural Networks	R/C	Y	CS, NZP, HCP	L	L	2	L	H
	Support Vector Machines	R/C	Y	CS	L	L	1 to 3	L	H
	MARS/FDA	R/C	Y	-	M	H	1 to 2	M	M
	K-nearest Neighbors	R/C	Y	CS, NZP	L	L	1	M	L
	Nonlinear Discriminant Analysis	C	N	NZP	M	L	0 to 2	L	L
	Naïve Bayes	C	Y	NZP	L	L	0 to 1	M	M
Trees/Rules	Single Decision Trees	R/C	Y	-	M	H	1	H	L
	Rule-Based Models	R/C	Y	-	M	H	1 to 2	H	L
	Bagged Trees	R/C	Y	-	L	H	0	H	M
	Random Forest	R/C	Y	-	L	M	0 to 1	H	H
	Boosting	R/C	Y	-	L	H	3	H	H
	Cubist	R/C	Y	-	L	M	2	H	H
	C5.0	C	Y	-	M	H	0 to 3	H	H



Next, we provide a summary of the common clustering methods [HPK, 2011]. Clustering belongs to a category called unsupervised learning that is different from the regression and classification algorithms contained in Table 7. In unsupervised learning, the data are unlabeled, and there is no ground truth to evaluate the prediction accuracy. The difference between supervised and unsupervised learning leads to a different summary between them. Generally speaking, the discussion and comparison of clustering algorithms have more aspects to consider. Table 8 below provides a collection of clustering methods. In this table, candidate algorithms (listed in the second column) are classified into seven categories (listed in the first column). The first four categories—partition methods, hierarchical methods, density-based methods, and grid-based methods—indicate four different angles of conducting the clustering task. The last three categories—probabilistic modeled-based clustering, high-dimensional clustering, and clustering with constraints— belong to more advanced topics generated by higher level needs.

The third column of Table 8 summarizes the general characteristics of the seven categories listed in the first column. Through comparing the information in the third column to the contextual knowledge of the problem, one can better select candidate algorithms. (A comparison of other characteristics, such as the computational complexity of each algorithm is outside the scope of this table.) The clustering methods provided can be used together with other unsupervised learning steps, such as dimensional reduction.

**Table 8.** Summary of common clustering algorithms

Category	Method	General Characteristics
Partition Methods	K-means	Find mutually exclusive clusters of spherical shape. Distance-based. May use mean or medoid (etc.) to represent cluster center. Effective for small- to medium-size datasets. Heuristic methods: Global optimality is often computationally prohibitive.
	K-Medoids	
	CLARA	
	CLARANS	
Hierarchical Methods	DIANA	Clustering is a hierarchical decomposition (i.e., multiple levels). Cannot correct erroneous merges or splits. May incorporate other techniques like micro-clustering. Can be distance-based or density- and continuity-based.
	AGNES	
	Chameleon	
	BIRCH	
Density-based Methods	DBSCAN	Can find arbitrarily shaped clusters. Clusters are dense regions of objects in space that are surrounded by low-density regions. Each point must have a minimum number of points within its neighborhood. May filter out outliers.
	OPTICS	
	DENCLUE	
Grid-based Methods	STING	Use a multiresolution grid data structure. Fast processing typically independent of $n$ and dependent on grid size.
	CLIQUE	
Probabilistic Model-based Clustering	Fuzzy Clusters	Fuzzy or flexible cluster assignment. Each object is assigned a probability of belonging to a cluster. Each data point can belong to more than one cluster.
High-dimensional Clustering	CLIQUE	Conventional distance measures can be dominated by noise. Defined using a small set of attributes instead of the full data space. Methods include subspace clustering and dimensionality reduction.
	PROCLUS	
	PCA-based	
	Biclustering	
	MaPle	
Clustering with Constraints	COP-k-means	Can integrate background knowledge into cluster analysis. Constraints on instances, clusters, and similarity measurement.
	CVQE	



## Milestones

Milestone	Due Date	Estimated Date of Completion	Actual Completion Date	Status	Comments (Problems & Brief Resolution Plan)
Quarterly Report (Jun)	7/31/2020	7/31/2020	7/31/2020	Completed	
A60 Kickoff Meeting	8/13/2020	8/13/2020	8/13/2020	Completed	
ASCENT Meeting	9/29-30/2020	9/29-30/2020	9/29-30/2020	Completed	
Quarterly Report (Sep)	10/31/2020	10/31/2020	10/31/2020	Completed	
Annual Report	11/30/2020	11/30/2020	11/30/2020	In Progress	

## Major Accomplishments

The major accomplishments for this period performance include:

- Created MATLAB functions for searching through the AEDT aircraft database and ANP aircraft substitution list to match the target aircraft with the equipment in FLEET database.
- Matched aircraft from the AEDT FLEET database to aircraft in the ANP aircraft substitution list according to airframe model and engine model.
- Conducted literature study on databases for collecting performance, emissions, and noise data for target aircraft.
- Investigated the substitution method and how the groupings of the aircraft are performed.
- Validated the substitution method and identified gaps in the documentation and the data, since some substitution results could not be reproduced from the procedure described in Doc 29.
- Created a summary of the ANP database that asserts the data structure and location of all ANP parameters in a manner that is friendly to search and compare.
- Reviewed the knowledge discovery from data (KDD) process and common algorithms to conduct clustering and classification/regression tasks.

## Publications

### Written reports

ASCENT quarterly reports (Jun. 2020)

ASCENT quarterly report (Sep. 2020)

## Outreach Efforts

N/A

## Awards

None

## Student Involvement

Zhenyu Gao is a fourth year PhD student. Mr. Gao has conducted a literature review on the analytical methods to develop the analytical methods derived from statistical learning methods and techniques. Mr. Gao is being trained on related tools such as INM, AEDT Tester, AEDT 3b, and AEDT 3d.

Bogdan Dorca is a third year PhD student. Mr. Dorca has performed a literature study on databases for collecting performance, emissions and noise data for aircraft not modeled with ANP data. Mr. Dorca is being trained on related tools such as INM, AEDT Tester, AEDT 3b, and AEDT 3d.

Chrysoula Pastra is a first year PhD student. Ms. Pastra has investigated the ANP aircraft substitution method and conducted a validation exercise. Ms. Pastra is being trained on related tools such as INM, AEDT Tester, AEDT 3b, and AEDT 3d.

## Plans for Next Period

The ANP aircraft substitution dataset will be further investigated to continue matching the target aircraft in the spreadsheet with the equipment in AEDT FLEET database. Additional literature review will be conducted to collect data for the target aircraft in order to obtain performance, emissions, and noise data that can be used to develop ANP data for these aircraft.



The substitution methods implemented in AEDT will be studied to identify the capability gaps for potential improvement. Georgia Tech will coordinate with the AEDT development team to get a list of target-substitution aircraft to work on.

The problems associated with ANP data development will be defined. Based on the characteristics of the problem, the most appropriate statistical learning methods will be selected to formulate the analytical methods to develop ANP data for target aircraft.

## **References**

- EASA, <https://www.easa.europa.eu/domains/environment/easa-certification-noise-levels>, 2020 (accessed: Sept. 2020)
- ECAC.CEAC Doc 29, Report on Standard Method of Computing Noise Contours around Civil Airports, Volume 1: Applications Guide, As endorsed by DGCA/147 on 7 December 2016
- Eurocontrol, <https://contentzone.eurocontrol.int/aircraftperformance/default.aspx?>, 2020 (accessed: Sept. 2020)
- Eurocontrol, <https://www.aircraftnoisemodel.org/aircraft/substitutions>, 2017 (accessed: Sept. 2020)
- ICAO, <https://www.icao.int/environmental-protection/pages/modelling-and-databases.aspx>, (accessed: Sept. 2020)
- Jiawei Han, Jian Pei, and Micheline Kamber. *Data mining: concepts and techniques*. Elsevier, 2011.
- Max Kuhn, Kjell Johnson, et al. Applied predictive modeling, volume 26. Springer, 2013.
- NoisedB, <http://noisedb.stac.aviation-civile.gouv.fr/>, 2020 (accessed: Sept. 2020)
- RisingUp Aviation, <https://www.risingup.com/planespecs/> (accessed: Sept. 2020)
- The OpenSky Network, <https://opensky-network.org/aircraft-database>, 2020 (accessed: Sept. 2020)



## Project 061 Noise Certification Streamlining

### Georgia Institute of Technology

#### Project Lead Investigator

Principal Investigator:

Professor Dimitri N. Mavris

Director, Aerospace Systems Design Laboratory

School of Aerospace Engineering

Georgia Institute of Technology

Phone: (404) 894-1557

Fax: (404) 894-6596

Email: dimitri.mavris@ae.gatech.edu

Co-Principal Investigator:

Dr. Jimmy Tai

Division Chief, Propulsion & Energy

Aerospace Systems Design Laboratory

School of Aerospace Engineering

Georgia Institute of Technology

Phone: (404) 894-0197

Fax: (404) 894-6596

Email: jimmy.tai@ae.gatech.edu

#### University Participants

##### Georgia Institute of Technology

- Pls: Dr. Dimitri Mavris, Dr. Jimmy Tai
- FAA Award Number: 13-C-AJFE-GIT-066
- Period of Performance: June 5, 2020 to June 4, 2021
- Tasks:
  1. Task 1: Interview Industrial Partners on Current Noise Certification Process.
    - Task 1.1: FAA Noise Certification Regulation Review.
    - Task 1.2: Industrial Partner Interviews via Workshops.
  2. Task 2: Develop and Recommend a Streamlined Noise Certification Procedure for Existing Aircraft.
    - Task 2.1: Current Process Assessment.
    - Task 2.2: Streamlined Process Definition.
  3. Task 3: Develop a Flexible Noise Certification Procedure for New Aircraft.
    - Task 3.1: Flexibility Assessment of Streamlined Process.
  4. Task 4: Simulate Streamlined and Flexible Noise Certification Procedure.
    - Task 4.1: Identify Modeling Approach.
    - Task 4.2: Noise Certification Process Metric Definition.

#### Project Funding Level

The total amount of current funding from the FAA for ASCENT Project 61 is at \$250,000 for a 12-month period of performance.

#### Investigation Team

The ASCENT Project 61 Georgia Tech ASDL investigation team is shown in Figure 1. Prof. Dimitri Mavris is the PI of this project, joined by Dr. Jimmy Tai, Senior Research Engineer, and Dr. Evan Harrison, Research Engineer II, as the co-PIs. In support of the co-PIs, a team of four research faculty (two Research Engineers and two Postdoctoral Researchers) is leading efforts both at planning and technical development for the planned tasks. They are being joined by three graduate student

assistants, who are supporting the Project 61 as they work towards their M.Sc. and Ph.D. degrees. All team members are affiliated with the Aerospace Systems Design Laboratory (ASDL), under the School of Aerospace Engineering, Georgia Institute of Technology.

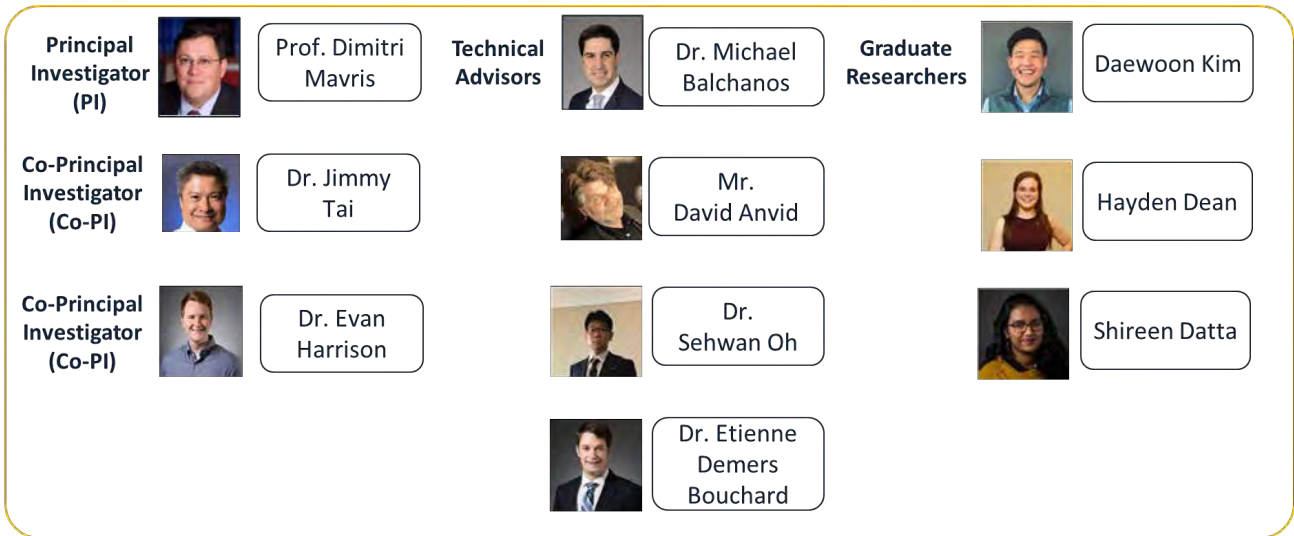


Figure 1. ASCENT Project 061 Georgia Tech ASDL Team.

From the team of technical advisors, the following roles and responsibilities have been defined:

- Dr. Michael Balchanos is a Research Engineer II, serving as the technical lead for Project 61. Aside from day-to-day coordination roles, he is responsible for planning a series of workshops with the industry partners and Subject Matter Experts (SMEs) on benchmarking efforts under Task 1 for current noise certification procedures. Moreover, he is looking into techniques for process modeling that could enable the certification modeling approach, as proposed under Task 4.
- Mr. David Anvid, Senior Research Engineer, is supporting Task 1 efforts in understanding of Parts 21 (on certification procedures) and 36 (on noise regulations) of Title 14 Part C. He joined ASDL on October 1 and his multi-year industry experience in noise certification has been invaluable for the team’s efforts to benchmark current certification procedures.
- Dr. Sehwan Oh, Postdoctoral Researcher, has been focusing on exploration of current certification regulations, understanding their structure (hierarchy, associations, etc.) linked to Task 1, and has been providing input on the application of discrete event and agent-based methods as part of the efforts planned for Task 4.
- Dr. Etienne Demers Bouchard, Postdoctoral Researcher, has been exploring process modeling methods from the literature, as well as formulating a canonical problem to assess feasibility and applicability of methods.

From the team of graduate student researchers, the following roles and responsibilities have been defined:

- Mr. Daewoon Kim, first year M.Sc. student who is leading the team’s MBSE efforts in representing the baseline certification process in SysML.
- Ms. Hayden Dean, first year M.Sc. student, who has been instrumental in capturing and understanding current regulations and certification procedures, as dictated by the Title 14 Subchapter C, Part 21 and Part 36, as well as Part 36 Advisory Circulars (AC), with particular focus on AC\_36-4D, and emphasis on the guidance instructions regarding the flight testing for noise certification.
- Ms. Shireen Datta, who has been supporting the efforts in documenting current procedures and exploring the exchange of regulations and processes with the planned noise certification process model.

### Project Overview

Noise certification process (with its inclusion of equivalent procedures) has served the aviation stakeholders (OEMs, regulators, operators, airports, et al.) well since the 1960s [1-3]. With new vehicles types and new technologies (including new entrants, digital technologies for airframe, propulsion, and measurements, etc.), it is necessary to critically examine the

existing certification processes. A key aspect of current certification practices is the equivalent procedures and supporting technology, which many OEMs utilize [4]. Equivalent procedures are anticipated both for existing as well as new standards to further accommodate for innovation down the road.

The project objective is to examine current noise certification procedures and identify opportunities to streamline the noise certification process while recommending process updates for building the needed flexibility to accommodate all air vehicle types. Project 61 seeks to propose quantifiable process improvements and facilitate the application of traditional systems engineering (SE) for complex systems, model-based systems engineering (MBSE), while leveraging these methods for the management of regulatory requirements. In order to perform the proposed research under this three-year effort, Georgia Tech has teamed with several industrial partners with extensive experience in noise certification. Each industrial partner represents different types of vehicles, such as large subsonic transports, propeller-driven small aircraft, and rotorcraft.

The ASCENT Project 61 team is seeking to accomplish the following goals:

- Identify opportunities for increased efficiency and flexibility in current noise certification process.
- Formulate and evaluate revised noise certification processes for current vehicles types and offer recommendations to the FAA (Part 36, AC 36-4D, etc.).
- Develop process modeling methods to enable quantitative assessment of noise certification.
- Facilitate the application of traditional SE processes for complex systems and MBSE, leveraging these methods for the management of regulatory requirements.

The timeline for completing the associated tasks in support of the above goals is shown in Table 1.

Table 1. ASCENT Project 61 Task Planning Timeline.

Task	Year 1												Year 2												Year 3											
	M1	M2	M3	M4	M5	M6	M7	M8	M9	M10	M11	M12	M13	M14	M15	M16	M17	M18	M19	M20	M21	M22	M23	M24	M25	M26	M27	M28	M29	M30	M31	M32	M33	M34	M35	M36
1 Interview Industrial Partners on Current Noise Certification Process	[Active]																																			
1.1 FAA Noise Certification Regulation Review	[Active]																																			
1.2 Industry Partner Interviews via Workshops	[Active]																																			
2 Develop a Streamlined Noise Cert. Procedure for Existing Aircraft	[Active]												[Active]																							
2.1 Current Process Assessment	[Active]												[Active]																							
2.2 Streamlined Process Definition	[Active]												[Active]																							
2.3 Streamlined Process Assessment and Revision	[Active]												[Active]																							
3 Develop a Flexible Noise Certification Procedure for New Aircraft	[Active]												[Active]												[Active]											
3.1 Flexibility Assessment of Streamlined Process	[Active]												[Active]												[Active]											
3.2 Flexible Process Definition	[Active]												[Active]												[Active]											
3.3 Flexible Process Assessment and Revision	[Active]												[Active]												[Active]											
4 Simulation Streamlined and Flexible Noise Certification Procedure	[Active]												[Active]												[Active]											
4.1 Identify Modeling Approach	[Active]												[Active]												[Active]											
4.2 Noise Certification Process Metric Definition	[Active]												[Active]												[Active]											
4.3 Model Calibration	[Active]												[Active]												[Active]											
4.4 Certification Process Simulation	[Active]												[Active]												[Active]											

## Task 1 – Interview Industrial Partners on Current Noise Certification Process

Georgia Institute of Technology

### Objectives

In support of the main research objective Project 61, Task 1 is examining current noise certification procedures (Task 1.1) and benchmarking against current industry practices in how these procedures are adopted and implemented (Task 1.2). In particular, subtasks are organized as follows (asterisk\* denotes Year 1 allocated efforts):

#### Task 1.1\*: FAA Noise Certification Regulation Review

- Perform a thorough review of FAA noise certification regulations for large subsonic jet and transport category airplanes, as well as rotorcraft types of vehicles (14 CFR, Chapter 1, Subchapter C, Part 36, Subparts B & H). With input from the FAA, an additional type that the Georgia Tech team will further explore is propeller-driven small airplanes and propeller-driven commuter category airplanes.
- Include recent certification regulations for new types of aircraft (e.g., advanced air mobility), in addition to conventional configurations.
- Document existing regulatory framework for aircraft noise certification, including both specified regulatory standards and accepted means of compliance.



### Task 1.2\*: Industrial Partner Interviews via Workshops

- Gather information through interviews and workshops on industry applied noise certification procedures, including equivalent procedures.
- Propose workshops and invite industry partners with subject matter expertise on airframe noise certification (large transport, small propeller aircraft, and rotorcraft).
- Facilitate dedicated workshop for each vehicle type and plan for follow-up events to iterate on feedback obtained, as well as to share lessons learned and the derived recommendations.
- Focus of workshop is to identify areas to streamline for each type of vehicle and potential solutions.
- Identify regulations that could be simplified and opportunities for improvements that would drive recommendations to the FAA.

## Research Approach

### Task 1.1

Starting with Task 1.1, the main effort pursued by the team was to review and understand the current certification process. Aside from the extensive literature review and the regulatory framework, the team produced a series of views to demonstrate the flow of procedures, the associations, and dependencies across regulatory items. One of the key outcomes of this exercise was to review the current procedures and identify opportunities for improvement.

Federal Aviation Administration rules are in the U.S. Code of Federal Regulations, Title 14 (14 CFR), Chapter 1. Aircraft Certification Procedures and Noise Standards are found in Subchapter C, Parts 21 and 36, respectively. Additional relevant sections of Subchapter C include:

- **Part 21 – Certification Procedures**
- Parts 23-31 – Airworthiness Standards for Aircraft
- Parts 33-35 – Airworthiness Standards for Aircraft Engines
- **Part 36 - Noise Standards**
- Part 39 – Airworthiness Directives
- Part 43 – Maintenance
- Part 45 – ID and Registration Marking
- Part 47 – Aircraft Registration
- Part 48 – Registration and Marking for Small Unmanned Aircraft
- Part 49 – Recording of Aircraft Titles and Security Documents

Benchmarking of current certification practices will be driven by Part 21, Part 36 [5], and Advisory Circular 36-4D (procedures and steps for noise certification) [6]. Please note that this list of requirements is derived from the FAA standards, guidance, and practices alone. The FAA works closely with the international community to ensure their standards align with International Civil Aviation Organization (ICAO) noise regulations and adapt with changing noise mitigation technologies [7]. ICAO noise regulations (Chapter 3) used FAA's FAR36 Stage 3 as a starting point. It is acknowledged that other national aviation authorities (NAAs), such as the European Union Aviation Safety Agency (EASA), have practices that may vary from FAA requirements.

The intent is to identify any potential gaps in the team's understanding of the noise certification procedures or detect any equivalent procedures and accepted means of compliance that should be noted. In Figure 2, an overview of the process is summarized and broken down into five Phases. This review covered the mapping of all detailed procedures contained in AC36-4D on the testing practices (the "how"), whereas Part 36 brings focus on the regulatory side (the "what") for compliance.

In the following subsections, the team's findings and high-level process views are included.



**Figure 2.** Overview of noise certification process as described in Parts 21 and 36 and AC36-4D.

**Phase 0: Checking Environmental Factors**

Under this Phase, the goal to measure and verify that weather and testing conditions are appropriate. These include checking the wind velocity and for abnormal meteorological conditions. Also, the terrain must be verified so that it meets the appropriate FAA specifications. In the case that a non-airport test site is sought, the test site criteria must be followed. Figure 3 provides a visual summary of what checks must be put in place before field setup occurs.

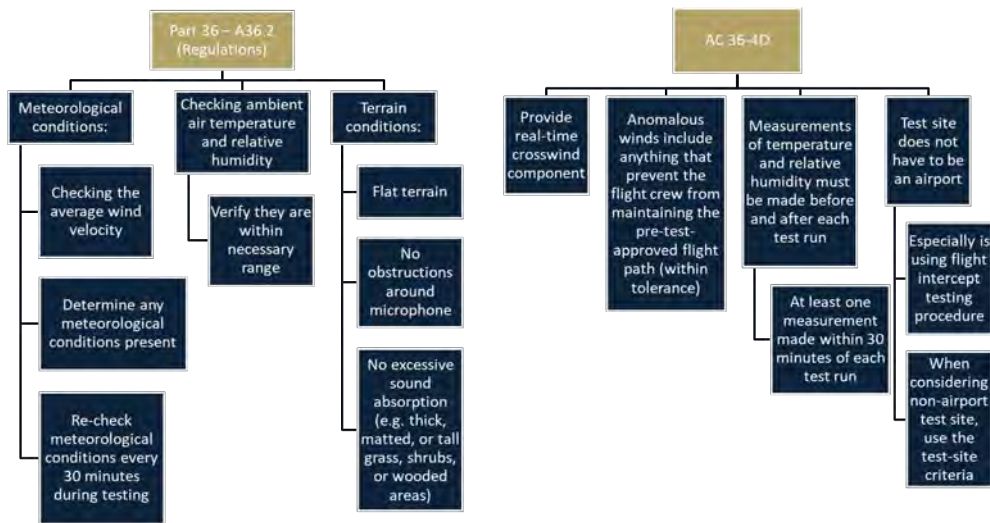


**Figure 3.** Phase 0: Checking environmental factors.

Based on Phase 0 benchmarking, the team prioritized the following inquiries to the industry partners, in support of Task 1.2:

- Is an airport used for testing, or is there another location that is typically used? If elsewhere, where are the certification procedures completed?
- How hard is it to get FAA approval to conduct the test at another location besides an airport?

- If an organization has multiple certification sites, how does testing differ amongst them (e.g., in the number of trials needed to successfully certify)?

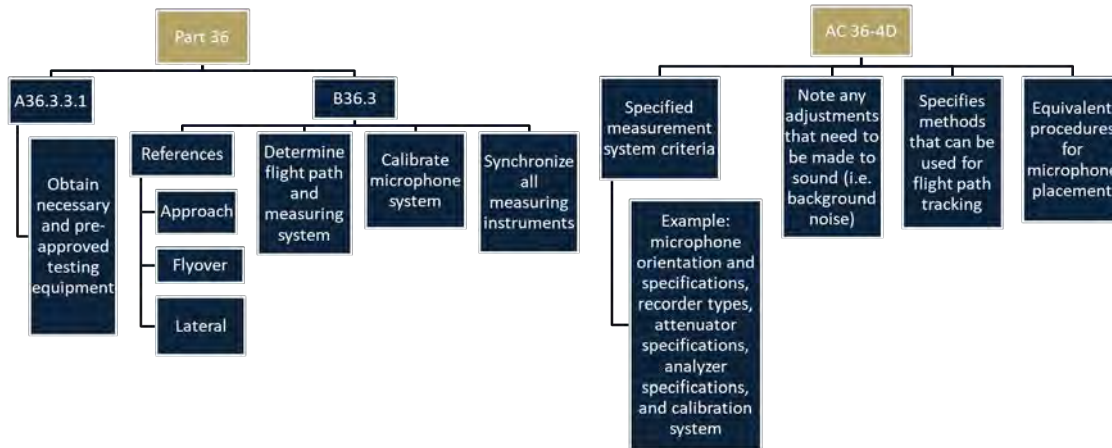


Figure 4. Phase 1: Field setup.

*Phase 1: Field Setup*

For Phase 1, the field setup procedures prioritize the selection and setup of equipment, calibration, and ensuring that equivalent procedures are fully defined. Figure 4 shows the complete steps of the setup procedure. Testing equipment must be preapproved. A lot of the hardware setup involves setting up approach, takeoff, and lateral microphones, which must be calibrated. There are two equivalent procedures that can be used for lateral microphone placement. Flyover and approach reference points remain the same. A flight tracking system must be determined, and all measuring instruments must be synchronized.

Based on Phase 1 benchmarking, the team has identified the following inquiries to industry partners:

- What equipment is used for certification?
- What equipment (if any) could be seen as an opportunity for upgrading or is potentially replaceable by a newer technology, but is required to use by the FAA?

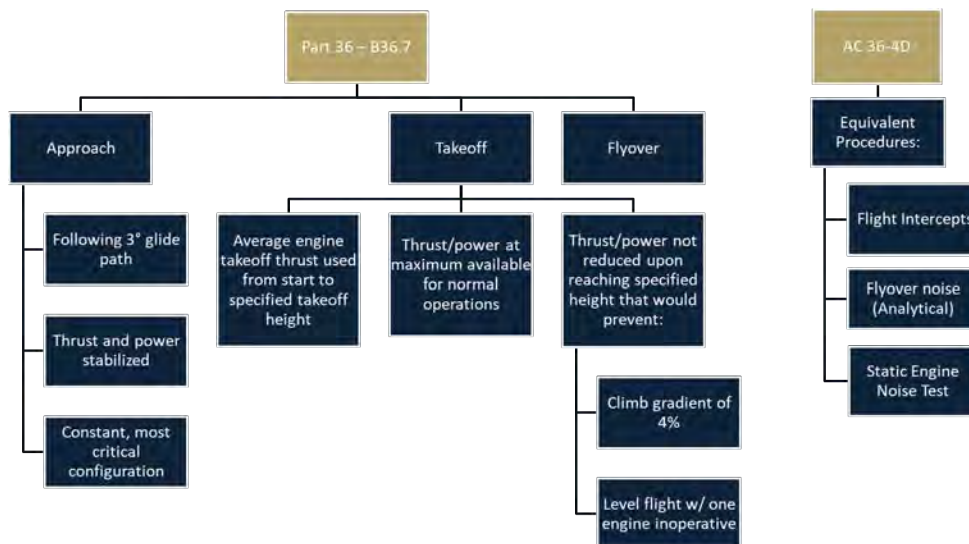


Figure 5. Phase 2: Testing.

**Phase 2: Testing**

Testing procedures, as listed in Part 36 and AC 36-4D, are outlined in Figure 5. The benchmarking exercise has also identified three equivalent testing procedures: flight intercepts, flyover noise, and static engine noise testing.

In lieu of full takeoff and/or landing profiles described in A36.9.2.1 and A36.9.2.2 of Part 36, *flight path intercepts* can be used. This procedure eliminates the need for actual takeoffs and landings. Moreover, it leads to significant cost and operational advantages at high gross weight, while it substantially reduces test time required and site selection issues. Following on these advantages, the shorter test time provides high probability of stable meteorological conditions, reduced wear, reduced fuel consumption, and adds to greater consistency of data generated.

*Flyover noise levels with thrust (power) reduction* may also be established without making measurements during takeoff with full thrust (power) followed by thrust (power) reduction. This is possible by merging tone-corrected perceived noise level (PNLT) versus time measurements obtained during constant power operations.

Last, *static engine noise tests and projections to flight noise levels (403.a.3)* are performed when are changes made to powerplant or similar powerplant installed. This process is also preferred after initial noise certification of "datum" airplane. It provides sufficient additional data or source noise characteristics, to allow for predictions about the effect of changes on the airplane certification noise levels.

In summary of Phase 2, commands that takeoff, flyover, and approach flight tests for noise certification still must be completed. Three types of equivalent procedures are recommended. When applicable, static engine noise tests are used, and flyover noise certification can be completed analytically.

As part of the team’s assessment for this Phase, the following inquiries were addressed to our industry partners:

- How often are equivalent procedures used instead of procedures specified in appendix A/B?
- How many test(s) (e.g., approach, takeoff, and flyover) are usually conducted for noise certification?

**Phase 3: Analysis**

Phase 3 involves the analysis for determining the effective perceived noise level (EPNL). This Phase involved the following steps, also outlined in detail in Figure 6:

- Find Perceived Noise Level (PNL(k))
- Correct for Spectral Irregularities
- Determine Duration Correction
- Determine EPNL

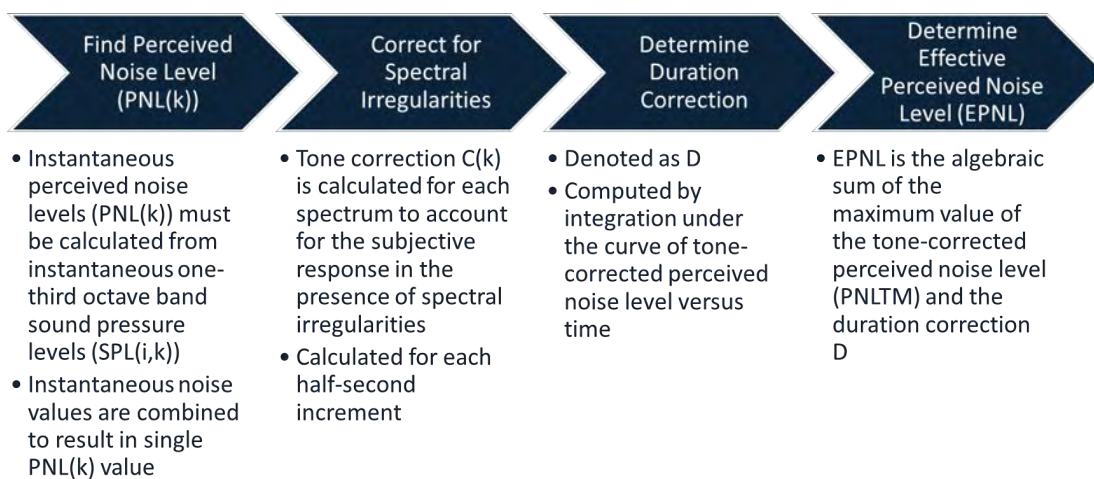


**Figure 6.** Phase 3: Analysis steps for calculating EPNL.

EPNdb (effective perceived noise in decibels) is a measure of human annoyance to aircraft noise which has special spectral characteristics and persistence of sounds. The EPNL (effective perceived noise level, measured in EPNdB) consists of instantaneous PNL corrected for spectral irregularities (tone correction factor) and for duration.

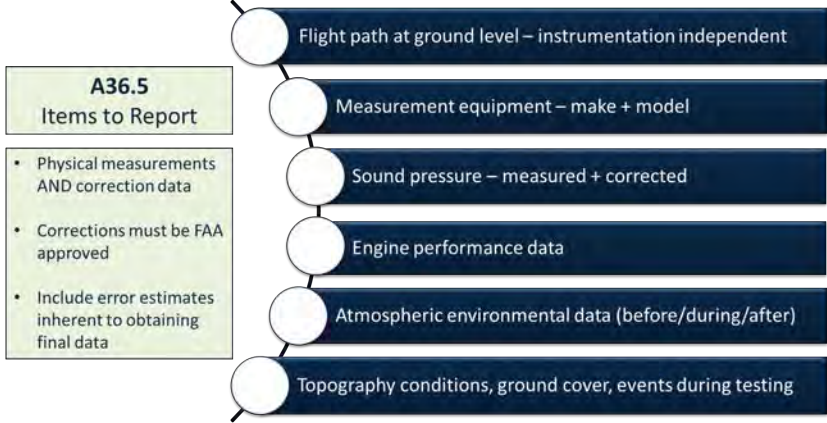


Figure 7. Phase 4: Reporting.

*Phase 4: Reporting*

In this phase, the goal is to ensure that the correct types of data, that need to be recorded during analysis, are selected and meet given FAA requirements, e.g., inclusion of error estimates. It also determines what material needs to be reported for FAA inspection and approval, ranging from test data and adjustments to noise recordings and instrument calibrations. The reporting requirements based on current regulations are summarized in Figure 7.

**Task 1.2**

To support Task 1.2, where SME input and feedback from industry practitioners is being solicited, the team has identified (through their work in Task 1.1) process items where certain efficiencies and synergies would be applied, as well as where more clarity for their understanding is needed. Accordingly, workshops are being planned with the objective of leveraging industry insight into practical aspects of noise certification requirements. The generic process, gathered from official FAA documentation and presented under Task 1.1 deliverables, has indicated where additional insight into ancillary or non-regulatory processes is needed.

The overarching goal of these workshops is to identify common practices, checkpoints, and milestones across industry partners, while soliciting feedback on steps in the process with high time and cost commitments. Moreover, the workshops will provide input on the identification of opportunities for potential process streamlining, such as steps or requirements that are out of sync with current technology and provide a forum for discussing potential solutions to the identified issues.

The first workshop was planned by the Georgia Tech team and was held virtually on November 5, 2020. Discussion centered on certification practices for large transport and business jet categories for aircraft, as applied by the team’s industry partners (representing airframers such as Boeing, Gulfstream, and Rolls-Royce). The Georgia Tech team produced discussion topics and questionnaires that were distributed prior to meeting. A high-level overview of the questions discussed is as follows:

- What is the current guidance provided by the FAA for noise certification?
- How does a company interact with the FAA to ensure that requirements for noise are satisfied and that the vehicle is compliant?
- How does the company perform the testing, internal processes, etc.?
- Can you identify regulations that should be revised or updated to reflect capabilities of modern configurations? Are there any opportunities for improvement?
- Are existing certification procedures and methods sufficient to meet future configurations?
- Certification amendments due to type design changes—if a vehicle needs to be recertified after making design changes, does your organization’s approach change from the first round of certification?



## Milestones

Since the project's start, the following milestones have been achieved (also shown in Table 2):

- Project work plan (July 5, 2020).
- Project Kickoff meeting (August 24, 2020).
- Participation in Fall 2020 ASCENT Advisory Committee Meeting (September 30, 2020).
- Workshop 1 on transport category aircraft (November 5, 2020).

**Table 2.** ASCENT Project 61 Milestone Status

Milestone	Due Date	Estimated Date of Completion	Actual Completion Date	Status
Workplan	7/5/20	7/5/20	7/5/20	Completed
Kick-off Meeting	8/30/20	8/30/20	08/24/20	Completed
COE Meeting 1	10/1/20	10/1/20	09/30/20	Completed
COE Meeting 2	4/1/21	4/1/21		
Annual Report	6/5/21	6/5/21		
Project Closeout	6/5/21	6/5/21		

## Major Accomplishments

The primary focus of the team's effort (for the research performance reporting period ending September 30, 2020) has been the completion of Task 1.1, as well as the planning for the series of workshops with industry partners (Boeing, Gulfstream, Rolls-Royce, Bell, GE, Pratt & Whitney) to support efforts under Task 1.2 for identification of noise certification practices as applied today, as well as opportunities for certification process streamlining.

With regard to Task 1.1, the following accomplishments are reported:

- Completed the literature review on current noise certification practices, as dictated by the Title 14 Part C, Part 21 on certification procedures and Part 36 on noise regulations. Moreover, the team incorporated the review of Part 36 Advisory Circulars (AC), with particular focus on AC\_36-4D, and emphasis on the instruction regarding the flight testing for certification.
- Summary and visual representation of the regulations and their respective relationships/associations, both in flow chart as well as SysML views.
- Identification of certain gaps in understanding of certification process, which have been documented and enabled the production of a topic questionnaire to further support the facilitation of workshops with industry partners, as planned for Task 1.2.

Task 1.1 accomplishments have formed the basis for supporting Task 1.2 (benchmarking current certification procedures) as well as activities under Task 2.1 (representation of current certification process in MBSE, in preparation of evaluation and assessment of current practices) and Task 4 (process modeling to leverage on evaluating current certification processes).

With regard to Task 1.2, the following accomplishments are reported:

- Workshop 1 for large transport category held virtually and completed on November 5.
- Collected feedback and input from industry partners during the workshop. Team is currently compiling and analyzing the responses.
- Questionnaire for the workshop has been compiled with input from Task 1.1's literature review and benchmarking activities. Additional responses by our industry partners are underway to be considered and will inform our modeling efforts under Tasks 2, 3, and 4.

## Publications

*Peer-reviewed journal publications*

- None



#### *Published conference proceedings*

- Mavris, D.N., Tai, J., Harrison, E., and Balchanos, M. (presenter), “ASCENT Project 61 – Noise Certification Streamlining”, presentation at the Fall 2020 ASCENT Advisory Committee Meeting, September 29 – 30, 2020.

#### *Written reports*

- September 2020 ASCENT Quarterly Report, ASCENT Project 61, “Noise Certification Streamlining”, Award number 13-C-AJFE-GIT-066, submitted October 30<sup>th</sup>, 2020.

### **Outreach Efforts**

- Virtual ASCENT Conference, ASCENT Project 61, “Noise Certification Streamlining”, Audio-recorded oral presentations, submitted at the Fall 2020 ASCENT Advisory Committee Meeting, September 29 – 30, 2020.
- Planned and help Workshop 1 with industry partners (Boeing, Gulfstream, Rolls-Royce, and the FAA) on transport category aircraft.

### **Awards**

None

### **Student Involvement**

- All three participating graduate students have supported Task 1 activities by performing literature and background search, reviewing current regulations and FAA instructed certification procedures (Parts 21, 36, and AC 36-4d). Special credit is extended to Ms. Hayden Dean and Ms. Shireen Datta for leading the process exploration and documentation efforts.
- All students contributed to producing the certification process views and compiling the questionnaire for supporting discussions and feedback solicitation as part of hosting Workshop 1.

### **Plans for Next Period**

- Coordinate on a follow-up meeting on Workshop 1 on large transport category aircraft with industry partners.
- Complete planned Workshop 2 on rotorcraft category aircraft.
- Leverage input from Workshop 1 and inform/update our current process views, as well as our MBSE baseline model.
- Identify process performance indicators and metrics, with input from workshop questionnaire responses.

## **Task 2 – Develop a Streamlined Noise Certification Procedure for Existing Aircraft**

Georgia Institute of Technology

### **Objectives**

Task 2 is focusing on the development of a more streamlined noise certification procedure, leveraging the benchmarking of current procedures as identified in Task 1, and developing a more streamlined and flexible noise certification process. Activities under this Task are performed in a coordinated effort with ICAO and NASA (asterisk\* denotes Year 1 allocated efforts):

#### **Task 2.1\*: Current Process Assessment**

- Identify which aspects of the present process, if any, would benefit from regulatory streamlining.

#### **Task 2.2\*: Streamlined Process Definition**

- Incorporate feedback from industry partners with identified areas of improvement over the present process to formulate a new certification process.
- Focus on areas which yield improvements in the cost and efficiency of the noise certification process.

#### **Task 2.3: Streamlined Process Assessment and Revision**

- Solicit feedback on the new process from the FAA and industry partners.
- Perform revision of suggested process, which incorporates key aspects of the collected feedback in order to build consensus between the research partners.

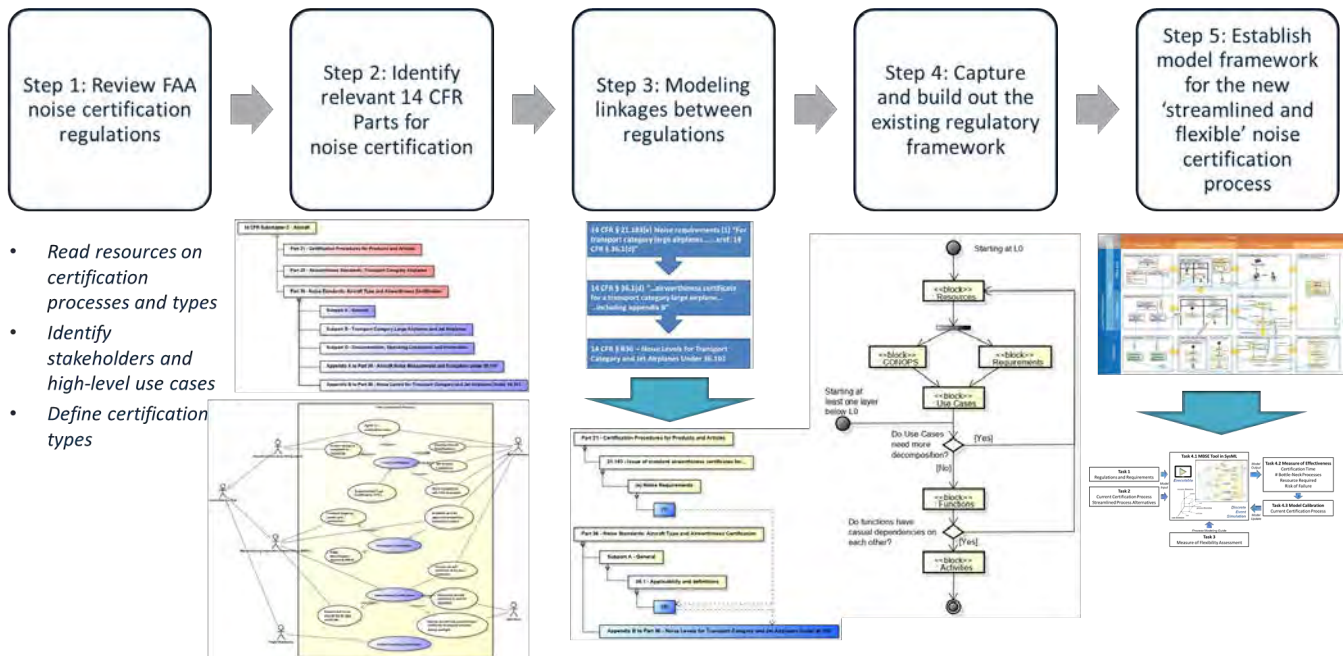


Figure 8. Proposed approach to serve as roadmap towards a model-based framework for exploring current and streamlined noise certification.

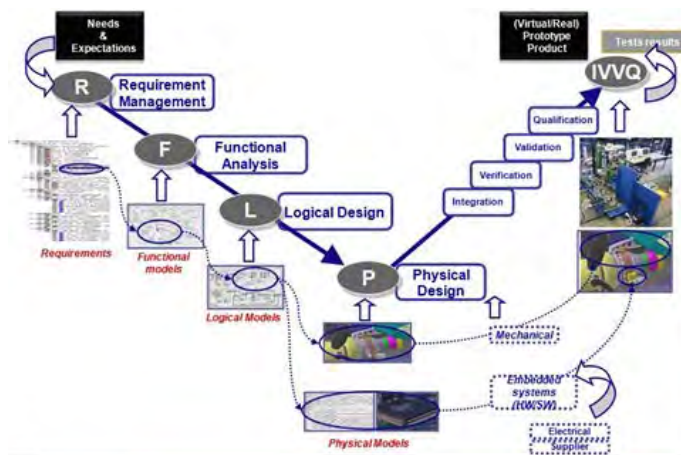
## Research Approach

### Task 2.1

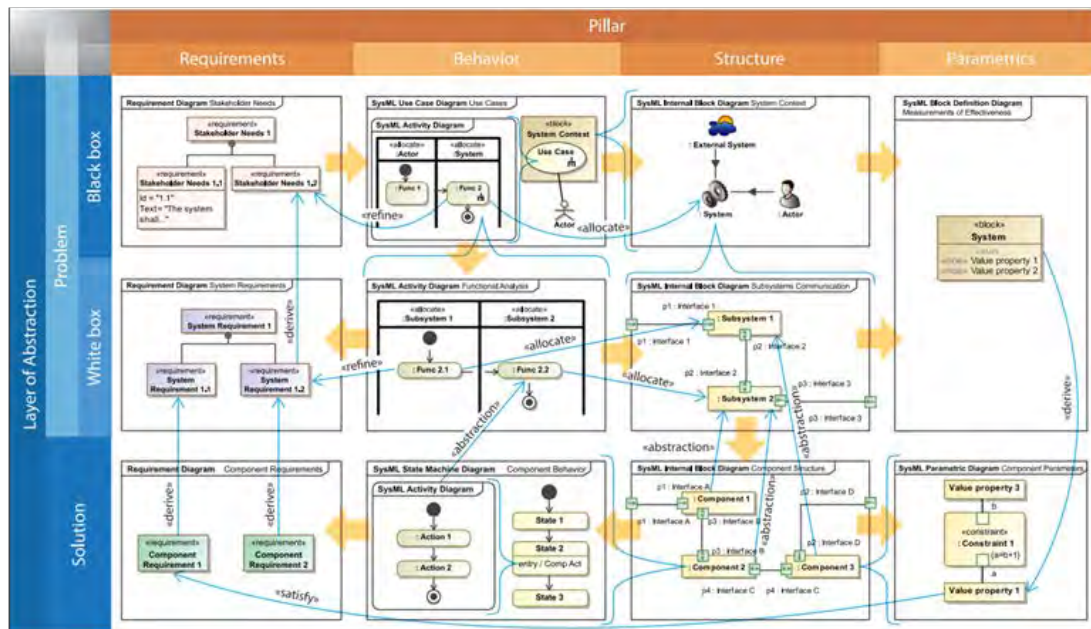
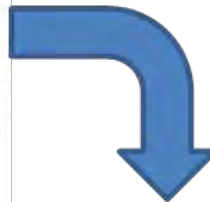
In order to assess current noise certification practices, a MBSE approach has been proposed. Work that is completed under Task 1, both benchmarking of current practices, as well as input from the workshop will be compiled and used to inform a process model formulated in SySML language and implemented in MagicDraw and Cameo Toolkit software tools. The views produced under Task 1 are being imported and represented in SySML towards the completion of an executable process architecture, from which certain assessments would be made possible.

MBSE allows for linking regulations and requirements to certification steps as well as representing links and associations between regulations. It is broad in scope over multiple modeling domains from SoS-level to component-level. It improves communication among stakeholders, management of complexity, and precision of operational use cases. It also addresses common issues that arise during certification audits, e.g., requirement traceability, configuration management, document control, and change impact analysis. Process assessments will then be possible in this framework, developed as the key capability for exploring and evaluating process alternatives (e.g., versions with reduced complexity, additional equivalent procedures, performing steps with newer technologies and equipment, etc.). The steps towards the development of this platform are showcased in Figure 8.

The development of an MBSE model for noise certification is one of the main targeted contributions of this research and a key advancement in state-of-the-art practices. Typically, MBSE methods are used to represent a vehicle's lifecycle and enable the use of data and information as an integrated system engineering approach. As the product is usually an executable vehicle architecture, in the case of Project 61 the product is a process architecture, within which flexibility levels will be added and tested. The roadmap for creating an MBSE system architecture is not unique; several approaches are introduced in the literature, but a commonly preferred option is the requirements-functional-logical-parametric (RFLP) approach, which maps to the traditional systems engineering "Vee" approach. Implementation of RFLP for a given application is also not unique, but the MagicGrid approach (see Figure 9 below) is one of the fastest emerging paradigms. This same approach will be adopted from a system to a process modeling use case and guide the team's noise certification modeling process development. A "mosaic" of all views in the team's current model is shown in Figure 10.



The RFLP approach, sourced by: "Aviles et al. - 2019 - Platform to Support Boeing's Digital Thread"



Aleksandraviene, A. "MagicGrid Book of Knowledge. Kansas, 2018. NoMagic.

Figure 9. The RFLP approach as the basis for the modeling approach for MBSE noise certification process modeling.

A custom model development process was created to capture the functional architecture of the noise certification process, as shown in Figure 11. The "blue" activities within the process are the aspects of the system modeling that are captured within the MBSE environment. As shown in the development flow, regulations and information about the certification process are captured as requirements and functional blocks within the model. A digital thread is created between the regulation, requirement, and function to build a verification thread. The form in the certification process that displays a function is also threaded by an <<allocation>> relationship to build a full digital thread from certification standard to the form which verifies the standard. From this point, parametric blocks are used to build an interface from the logical blocks to external analysis software to import detailed design data. An example of this import is importing the metric "time spent on test" from the test results into the activity of the model. Once all parameters are captured, they are integrated into the model as physical realizations of the logical blocks. An example of this realization is a specific test such as "Runway Noise Test Trial 2 Date 12/30/24" being realized as the physical element of a logical activity called "Runway Noise Test." Finally, the complete thread is verified within the model of tracing the specific requirement from a certification standard to the actual test which verifies the system worthiness of the specific standard.

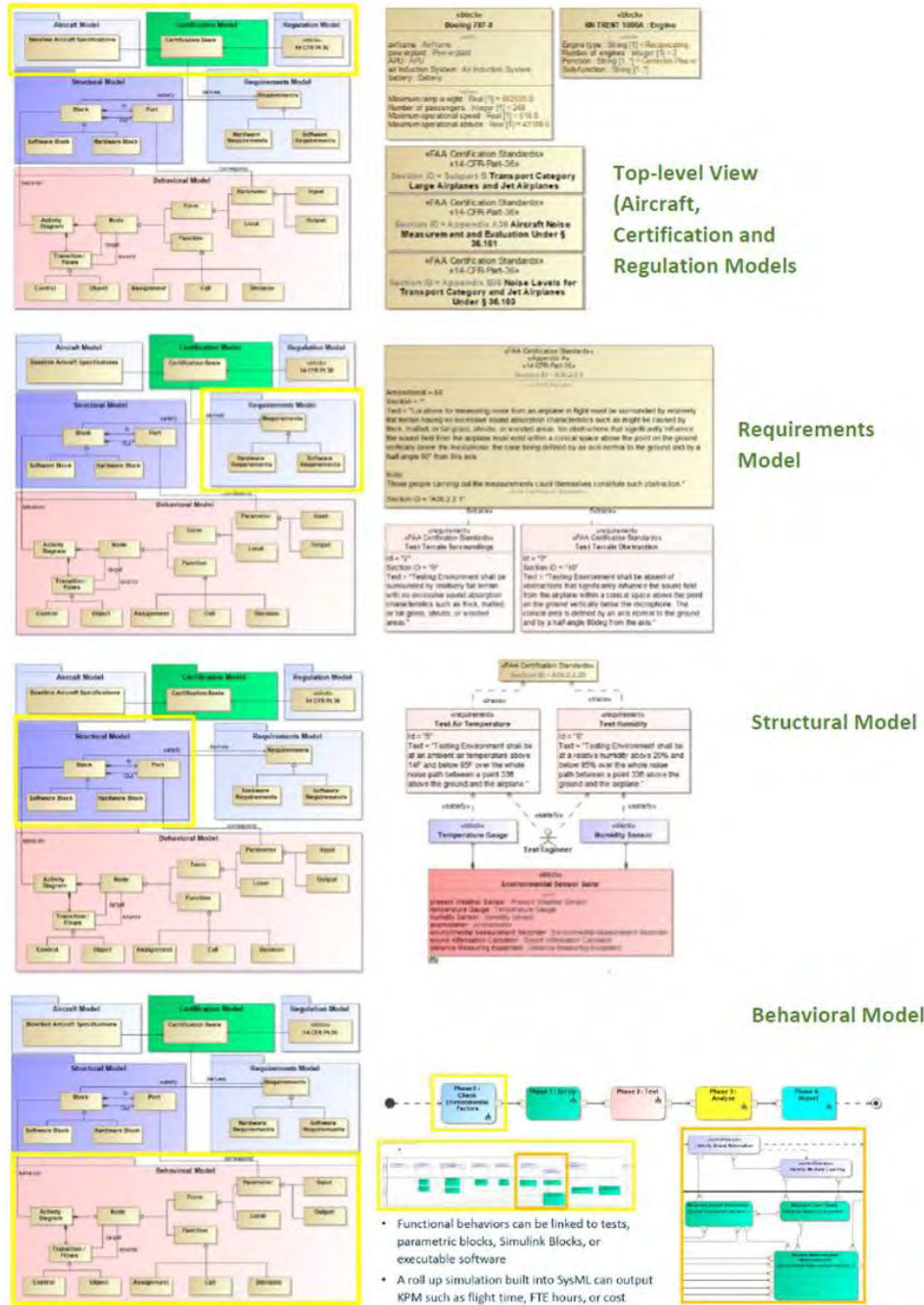


Figure 10. Current noise certification process model in development, leveraging the RFLP approach.

The same development process in Figure 11 will be used to capture both the Current Process Model and Streamlined Process Model. The Current Process Model captures within MBSE the currently practiced certification process of noise certification. The Streamlined Process Model will capture the streamlined version of the noise certification process our team will be proposing in Task 2.2. The two models will be used to assess the improvements given by the streamlined process. As shown

in Figure 12, the two models will share the same set of requirements and functions. This is built under the assumptions that both processes are operating under the same noise certification standard and must display the same functionality from the aircraft under testing through its certification process. However, the differences are captured as the logical blocks and activities performed by the blocks may change. As an example, the streamline process may suggest an alternative testing procedure (different activity) and an alternative testing equipment (different block). The parametrics captured within these blocks must still remain comparable (although not identical) so the improvement in the process can be measured.

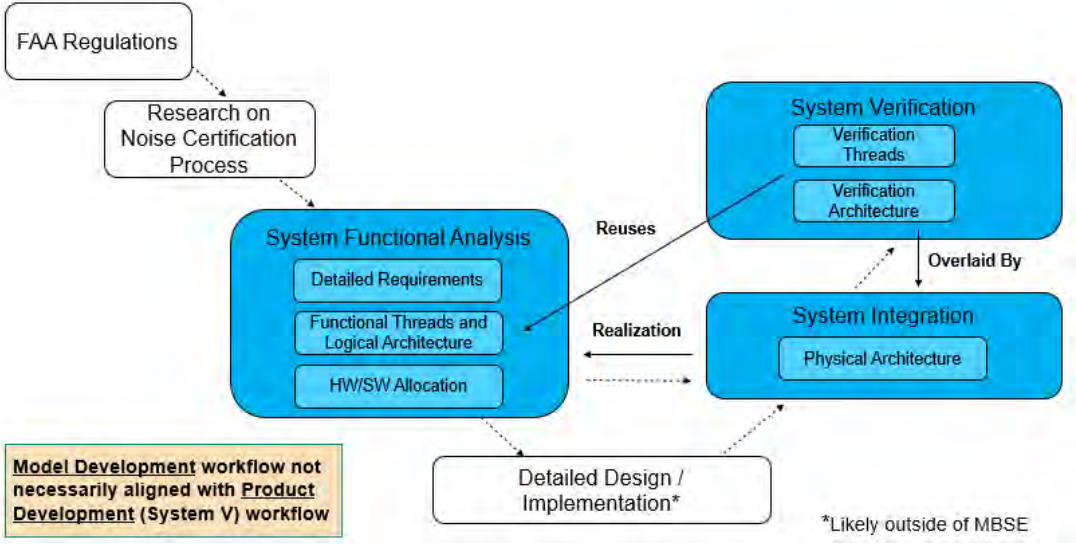


Figure 11. Architecture and model development process

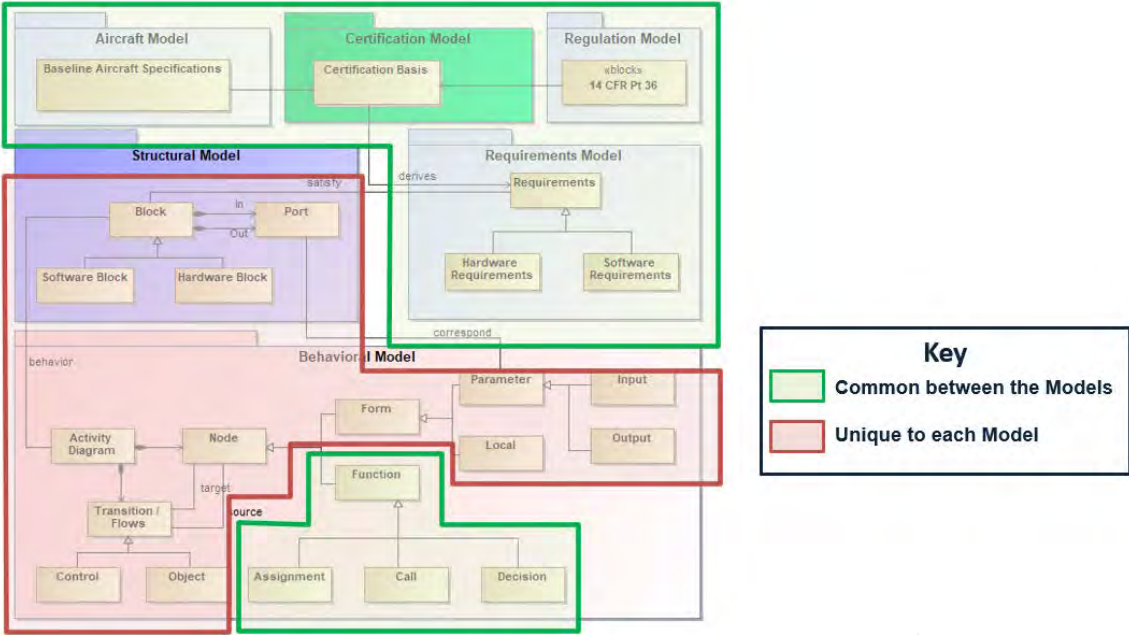


Figure 12. The meta-model distinction between Current Process Model and Streamlined Process Model



### **Task 2.2**

Feedback from the planned workshops will be used to inform the development of process alternatives where streamlining is the main improvement criterion. This task is currently underway and pending as additional workshops are planned ahead.

### **Task 2.3**

As in Task 2.2, this task is currently underway and pending as additional workshops are planned ahead, along with the team's further definition of metrics and evaluation criteria for the assessment and comparison of the baseline process to a streamlined alternative.

### **Milestones**

Please refer to Milestones listed under Task 1.

### **Major Accomplishments**

- Team became familiar with MBSE methods (e.g., SysML tutorials, RFLP approach, etc.).
- Team training in SysML software (MagicDraw) and setup/application for noise certification process modeling.
- A first complete version of the MBSE noise certification process model has been implemented in SysML and is being updated based on feedback from workshops.

These accomplishments, with the first baseline MBSE process model being central, are key in allowing the team to document and capture feedback from workshops in order to develop an executable platform allowing for experimentation and testing around process alternatives for a streamlined noise certification procedure.

### **Publications**

#### *Peer-reviewed journal publications*

- See list under Task1.

#### *Published conference proceedings*

- See list under Task1.

#### *Written reports*

- See list under Task1.

### **Outreach Efforts**

- See list under Task1.

### **Awards**

None

### **Student Involvement**

For the MBSE modeling of current noise certification processes, the leadership and contributions of Mr. Daewoon Kim have been instrumental.

### **Plans for Next Period**

- Finalize baseline model for current certification practices, incorporating feedback obtained by the workshops.
  - This model would primarily consist of documented regulations and certification procedures (both regulatory and equivalent procedures) all compiled in SysML views.
- Based on feedback from Workshop 1 and the FAA, flight test certification is what the Georgia Tech team will be working toward as part of the proof-of-concept exercise. One or two areas of improvement will suffice as examples of how the assessment would be applied.
- Based on current process models, perform a complete assessment of today's practices, and identify inefficiencies and complexities that could bottleneck the process and unnecessarily use resources (e.g., duplicate testing, time-intensive procedures, etc.). Of primary focus will be the flight-testing phase of the certification process.
- Formulate a simple certification problem (e.g., based on the flight-testing part of the process) per vehicle type and use it as a pilot for comparing and selecting the appropriate method.

# Task 3 – Develop a Flexible Noise Certification Procedure for New Aircraft

Georgia Institute of Technology

## Objectives

In support of the main research objective for this project, the focus of Task 3 is to define what a more flexible certification process would look like and what the evaluation criteria are for determining that the procedure is more streamlined than the baseline. Task 3 will build upon the capabilities of the integrated MBSE platform and leverage contributions from all other tasks. The breakdown of tasks under Task 3 is as follows (asterisk\* denotes Year 1 allocated efforts):

### Task 3.1\*: Flexibility Assessment of Streamlined Process

- Evaluate the flexibility of the streamlined noise certification process with respect to its use for new category air vehicles.

### Task 3.2: Flexible Process Definition

- Define and recommend improvements to the streamlined noise certification process to accommodate for a flexible noise certification process, with respect to vehicle type.

### Task 3.3: Flexible Process Assessment and Revision

- Solicit feedback on the new process from the FAA and industry partners.
- Perform revision of suggested process, which incorporates key aspects of the collected feedback in order to build consensus between the research partners.

## Research Approach

As a first iteration of the proposed concept for evaluating a flexible certification process, a first spiral has been formulated and is presented in Figure 13 below. Contributions, information, and capabilities from Tasks 1 and 2 are serving as inputs to the integrated MBSE platform, which will not only help formulate the alternatives, but also act as an enabler for simulating the performance of all process alternatives. Metrics also developed under Task 3 will allow for measuring process flexibility and other relevant figures of merit as part of comparing alternatives to the baseline.

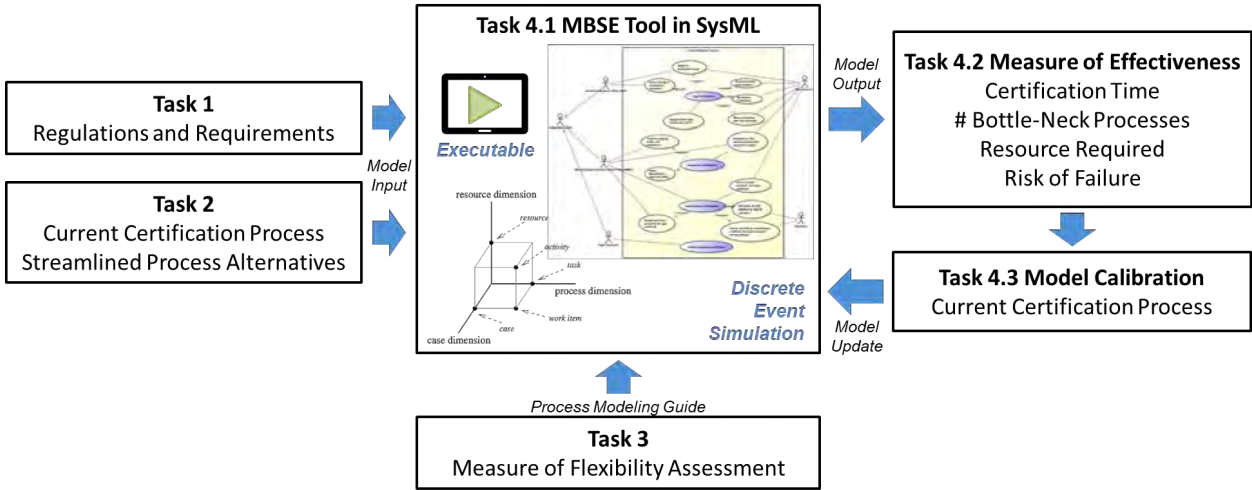


Figure 13. Integrated modeling and assessment framework for flexibility evaluation of certification procedures.

## Milestones

Please refer to Milestones listed under Task 1.

## Major Accomplishments

- Initial concept formulation of process and metrics development underway to support flexibility assessment.

- Showcase how the products and contributions of other tasks are coming together towards an integrated process exploration and assessment environment.

**Publications**

Peer-reviewed journal publications

- See list under Task1.

Published conference proceedings

- See list under Task1.

Written reports

- See list under Task1.

**Outreach Efforts**

- See list under Task1.

**Awards**

None

**Student Involvement**

No major contributions from the student team at this time.

**Plans for Next Period**

- Identify opportunities for noise certification process streamlining and propose alternatives.
- Develop and define metrics for assessment of process flexibility.
- Implement assessment and decision support capabilities in an integrated MBSE environment.

**Task 4 – Simulate Streamlined and Flexible Noise Certification Procedure**

Georgia Institute of Technology

**Objectives**

The mission behind Task 4 is to explore and identify suitable process modeling approaches for the purpose of simulating the noise certification procedure to serve as a benchmark against current practices and leverage this capability as part of the identification of more flexible process alternatives. The breakdown of tasks under Task 4 is as follows (asterisk\* denotes Year 1 allocated efforts):

**Task 4.1\*: Identify Modeling Approach**

- Potential methods: discrete event simulation (DES), agent-based modeling (ABM), or system dynamics (SD) simulation.

**Task 4.2\*: Noise Certification Process Metric Definition**

- Identify a set of metrics to allow for quantitative comparison of the current and proposed noise certification processes.

**Task 4.3: Model Calibration**

- Identify a benchmark for noise certification procedure simulation.
- Perform calibration of the noise certification procedure simulation.

**Task 4.4: Certification Process Simulation**

- Execute simulations of current and proposed noise certification procedures.

**Milestones**

Please refer to Milestones listed under Task 1.



## **Major Accomplishments**

- Literature review on process modeling methods (DES, ABM, and SD methods) for enabling simulation and assessment of noise certification process, as planned by Task 4.
- Team has been exploring the potential and applicability of the following methods: DES, ABM, or SD simulation.
- These techniques are evaluated on the basis of how well they could capture and simulate actual industry-applied procedures and their ability to interface with the process modeling in SysML under the MBSE-enabled proposed approach for this project.

## **Publications**

### *Peer-reviewed journal publications*

- See list under Task1.

### *Published conference proceedings*

- See list under Task1.

### *Written reports*

- See list under Task1.

## **Outreach Efforts**

- See list under Task1.

## **Awards**

None

## **Student Involvement**

Contributions by Mr. Daewoon Kim and Ms. Shireen Datta are acknowledged for supporting deliverables under Task 4.1.

## **Plans for Next Period**

- Based on current process models, define metrics for evaluation of today's certification practices. Next is identifying inefficiencies and complexities that could affect the process with bottlenecks and the unnecessary use of resources (e.g., duplicate testing, time-intensive procedures, etc.). Of primary focus will be the flight-testing part of the process.
- Compare process simulation methods (DES, ABM, SD) and explore their applicability for simulating noise certification.
- Formulate a simple certification problem per vehicle type and use it as a pilot for comparing and selecting the appropriate method.

## **References**

- [1] Metzger, F., & Foley, W. (1970). STOL Aircraft Noise Certification: A Rational Approach. SAE Transactions, 79, 1021-1031.
- [2] Federal Aviation Regulation, Part 21, Certification Procedures for Products and Parts; Part 36, Noise Standards: Aircraft Type Certification. December 1969.
- [3] J. B. Ollerhead, "Subjective Evaluation of General Aviation Aircraft Noise." FAA Technical Report NO-68-35, April 1968.
- [4] Senzig, D.A. and Marsan, M., 2018. UAS Noise Certification.
- [5] FAA 14 CFR Part 36 - NOISE STANDARDS: AIRCRAFT TYPE AND AIRWORTHINESS CERTIFICATION.
- [6] FAA Advisory Circular 36-4D - Noise Standards: Aircraft Type and Airworthiness Certification, date Issued October 12, 2017.
- [7] FAA, *Details on FAA Noise Levels, Stages, and Phaseouts* Available: [https://www.faa.gov/about/office\\_org/headquarters\\_offices/apl/noise\\_emissions/airport\\_aircraft\\_noise\\_issues/levels/](https://www.faa.gov/about/office_org/headquarters_offices/apl/noise_emissions/airport_aircraft_noise_issues/levels/).
- [8] Aleksandraviciene, A. "MagicGrid Book of Knowledge. Kansas, 2018. NoMagic.



## Project 062 Noise Model Validation for AEDT

### Georgia Institute of Technology The Pennsylvania State University

#### Project Lead Investigator

Principal Investigator:  
Professor Dimitri N. Mavris  
Director, Aerospace Systems Design Laboratory  
School of Aerospace Engineering  
Georgia Institute of Technology  
Phone: (404) 894-1557  
Fax: (404) 894-6596  
Email: dimitri.mavris@ae.gatech.edu

Principal Investigator:  
Dr. Victor W. Sparrow  
Director and United Technologies Corporation Professor of Acoustics  
Graduate Program in Acoustics  
The Pennsylvania State University  
201 Applied Science Bldg.  
University Park, PA 16802  
Phone: (814) 865-6364  
Email: vws1@psu.edu

#### University Participants

##### Georgia Institute of Technology

- PIs: Dr. Dimitri Mavris, Dr. Michelle Kirby
- FAA Award Number: 13-C-AJFE-GIT-061
- Period of Performance: June 5, 2020 to June 4, 2021

##### The Pennsylvania State University

- PI: Dr. Victor Sparrow
- FAA Award Number: 13-C-AJFE-PSU-059
- Period of Performance: June 5, 2020 to June 4, 2021

#### Project Funding Level

The project is funded by the FAA at the following levels: Georgia Institute of Technology (GT) \$235,000, The Pennsylvania State University (PSU) \$115,000. Cost-share details are below:

GT has agreed to a total of \$235,000 in matching funds. This total includes salaries for the project director; research engineers; graduate research assistants; and computing, financial, and administrative support, including meeting arrangements. The institute has also agreed to provide tuition remission for the students, paid for by state funds.

PSU's industrial partner, Spire Global (spire.com), is providing cost-share funds at a level of \$115,000 in the form of meteorological data and research support. The point of contact for this cost share is Mr. Cromarty +1 (650) 300-9997, [william.cromarty@spire.com](mailto:william.cromarty@spire.com).



## Investigation Team

Prof. Dimitri Mavris, Principal Investigator, Georgia Institute of Technology  
Dr. Michelle Kirby, Co-Investigator, Georgia Institute of Technology  
Dr. Tejas Puranik, Research Faculty, Georgia Institute of Technology  
Mr. Greg Busch, Research Faculty, Georgia Institute of Technology  
Ana Gabrielian, Graduate Student, Georgia Institute of Technology  
Emily Lembcke, Graduate Student, Georgia Institute of Technology  
Vinh Bui, Graduate Student, Georgia Institute of Technology

Prof. Victor Sparrow, Principal Investigator, The Pennsylvania State University  
Harshal Patankar, Graduate Student, The Pennsylvania State University

## Project Overview

This project focus is to assess the accuracy of the Aviation Environmental Design Tool (AEDT) in estimating noise in both the vicinity of airports as well as farther afield. The foundation of AEDT noise modeling is based on the Integrated Noise Modeling (INM) tool, which has undergone a number of validation and verification efforts in the past, specifically at the Denver International Airport (DIA) and has shown continually improving agreement of modeling with measurement data. During the development of AEDT, multiple algorithm updates have occurred, and this project seeks to quantify the new noise modeling capabilities based on comparison to field measurement data from DIA and other airport monitoring systems. The research team will develop a detailed model validation plan, review the plan with the FAA for concurrence, execute said plan, and provide recommendations for future AEDT development. The research, once completed, is expected to provide a noise model validation benchmark that can be used not only to respond to questions on AEDT noise prediction accuracy, but also to allow the tool development team to prioritize further development of modeling features and enhancements. The research team will also collaborate with PSU on the assessment of the noise propagation assumptions and the use of higher fidelity weather data.

## Task 1 – Literature Review

Georgia Institute of Technology

### Objective

The main goal of this task is to understand previous verification and validation studies done using AEDT. In order to better understand the functionalities that AEDT offers, a literature review had to be conducted. From previous verification and validation studies utilizing INM and AEDT, the evolution of AEDT's functionalities over time will guide this project.

### Research Approach

In 1997, a study conducted at DIA resulted in extremely thorough and useful data in terms of verification and validation studies. This data, as mentioned previously, has been used for multiple different INM studies, and these studies include: NASA /CR-2000-210112, NASA /CR-2006-214511, and Wyle Report 13-01.

The study conducted by Page et al. in 2000 with the 1997 DIA data focused on how different power prediction methods would impact INM's noise prediction calculations [1]. These methods included calculating thrust as a function of velocity (SAE AIR-1845), calculating thrust as a function of  $N_1$  and EPR (SAE AIR-1845), calculating thrust using J. P. Clarke's Mach equations, calculating thrust based on aircraft manufacturers'  $F_n/\delta$  charts, and finally, calculating thrust as a function of velocity (SAE AIR-1845) with the coefficients adjusted based on DIA's altitude. From this, it was determined that the implementation of the manufacturers'  $F_n/\delta$  information resulted in the most accurate noise predictions. As a result, INM's noise-power-distance (NPD) curves were updated using the correlating manufacturers' data.

Another verification and validation study was performed with the same DIA data in 2006 by Forsyth and Follet with a focus on higher altitude operations, thrust level, and flap and gear configurations [2]. At this point in time, INM offered full thrust as the only thrust option, so there was an interest in further updating INM's database with respect to thrust as well as flap and gear configurations. However, due to DIA being a high-altitude airport, aircraft had limited ability in utilizing reduced thrust operations, so the difference in noise contours between full thrust and 10% reduced thrust was minimal. It was also determined that the consideration of flap and gear configurations when calculating noise had little effect as well. In order to

properly include the effect on noise calculation that a high-altitude airport like DIA has, spectral classes were created in order to correct the NPD data with respect to the atmospheric absorption characteristics detailed in SAE AIR-1845.

A third and final study conducted using the 1997 DIA data was undertaken by Plotkin et al. in 2013 [3]. To incorporate weather and ground effects, a simulation was performed in the Advanced Acoustic Model (AAM), as INM lacked those capabilities at this time. By introducing weather data, it was determined that, while atmospheric layering had little impact on noise prediction calculations for receptors underneath the flight paths, atmospheric absorption characteristics were incredibly important to accurate noise predictions. In addition, terrain-processing algorithms from AAM and Noise Model Simulation (NMSim) were repackaged for future implementation within the FAA’s tools.

In May 2015, the FAA introduced AEDT, which was replacing not only INM but the Emissions and Dispersion Modeling System (EDMS) for emission and performance calculations as well [4]. In the figure below, the architectures of INM and EDMS are compared with that of AEDT. As a result, AEDT offers more functionality than the legacy models, but further improvement to the accuracy of noise predictions is still possible. Technical papers ACRP 02-52 and ACRP 02-79 highlight some of these possible improvements as well as the future of AEDT and its functionalities.

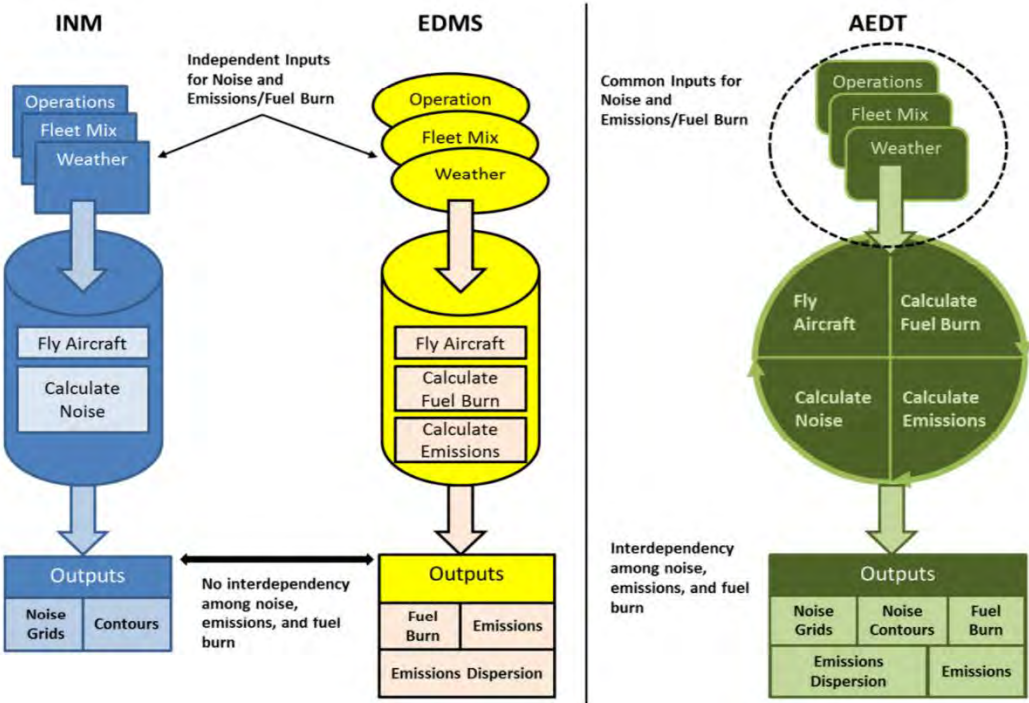


Figure 1. INM and EDMS architectures versus AEDT architecture. [5]

After the introduction of AEDT, the FAA’s verification and validation studies shifted to using AEDT instead of INM, as well as investigating the future functionalities of the model. Hobbs et al. explored the possibility of including the effects of terrain within AEDT’s noise propagation calculations [6]. At this point in time, AEDT only allowed for the use of soft surfaces, and thus, some accuracy in noise prediction was lost. To include these considerations into AEDT, terrain algorithms from AAM were considered. These algorithms are based in straight-ray theory which was originally developed for optics but has since been adapted for acoustics. An example of basic straight-ray theory geometry is below in Figure 2.

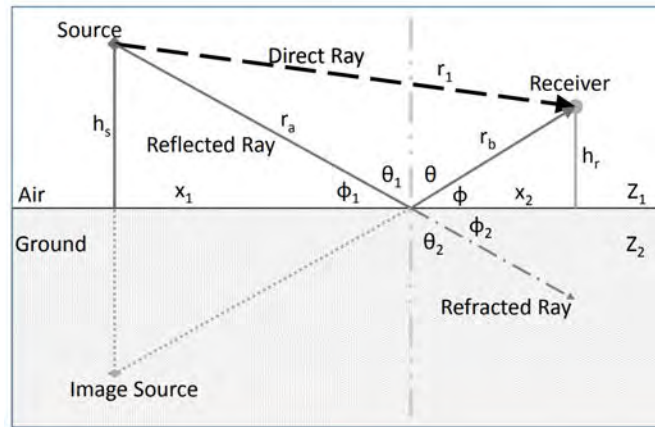


Figure 2. Basic straight-ray theory geometry. [6]

When the type of surface being analyzed changes, this creates a ground discontinuity. An example of geometry with multiple discontinuities is shown in Figure 3. To account for these discontinuities, the Fresnel ellipse method is used. By creating an ellipsoid between a given noise source, the point of impedance, and the correspond receiver, the different flow resistivities for different types of terrain can be weighted with respect to the amount of area a given terrain covers. With these weighted values, an overall average flow resistivity value for the area within the ellipsoid can be calculated. Figure 4 shows an example of a Fresnel ellipse in the context of partial obstruction.

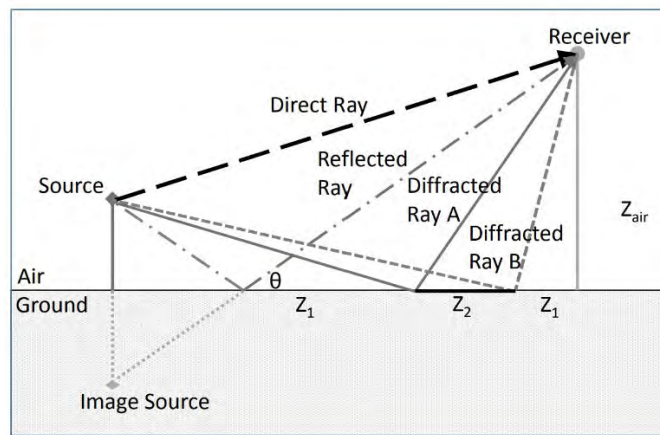
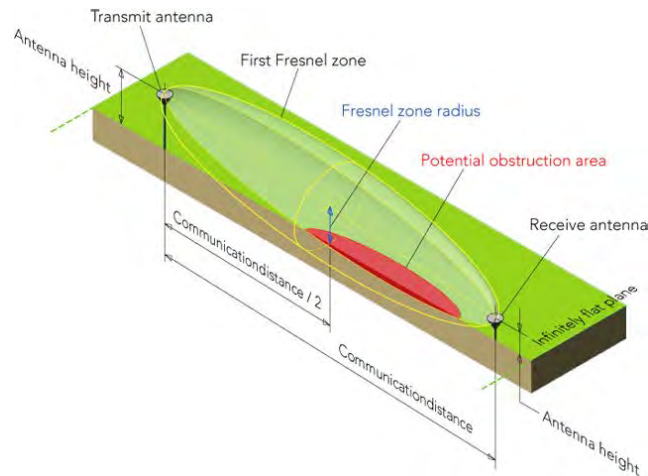
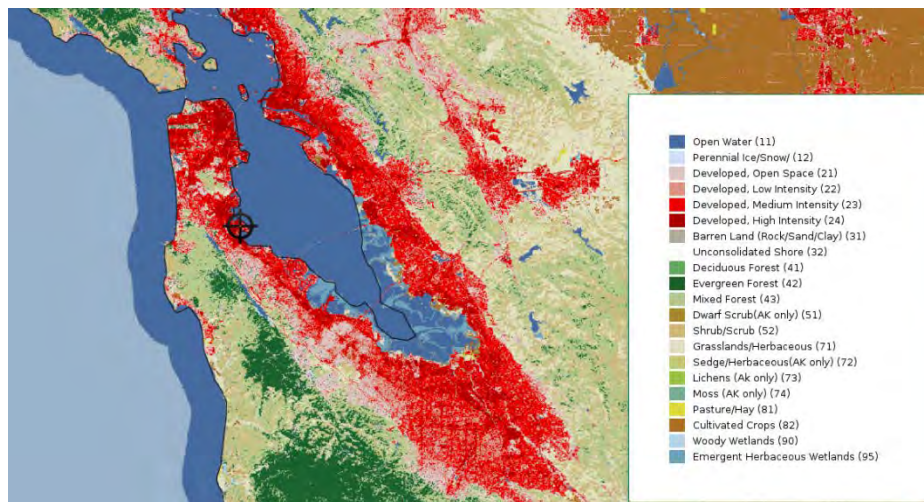


Figure 3. Straight-ray theory geometry with multiple ground discontinuities. [6]



**Figure 4.** Fresnel zone with partial obstruction. [7]

To obtain the flow resistivity values necessary to calculate an overall average value, a database was required, which was found in the Multi-Resolution Land Characteristics (MRLC) Consortium’s National Land Cover Database (NLCD). The most recent edition of the NLCD was published in 2019 and offers land cover information from the years of 2001, 2003, 2006, 2008, 2011, 2013, and 2016 for free use [8]. The data offered has 30 m resolution, which means that each pixel represents a 30 m by 30 m area, and it classifies terrain into 16 different categories. This information was then input into BASEOPS, which includes AAM and NoiseMap, to assign flow resistivity values to each of the categories. A visual example of the data offered by the NLCD is shown in Figure 5 for the San Francisco International Airport (SFO) and the surrounding area, where the crosshair represents SFO.



**Figure 5.** Land cover surrounding the San Francisco International Airport. [9]

Within INM and AEDT, the user must define the length of the flight segment, and this can be segmented into smaller lengths in order to calculate the flow resistivity for each segment that is needed for including ground and terrain effects in the noise propagation calculations. While investigating these segments, it was determined that decreasing segment length leads to an increase in accuracy but only to a point. As the segments of the flight track get smaller and smaller, more are required to model the same total length, which introduces bias to the overall calculation. Figure 5 represents the INM’s standard sound exposure level (SEL) calculations, where a single flight segment of a length of 10,000 ft is examined with a B737-300 aircraft at an altitude of 250 ft traveling at 250 knots and producing 19,000 lbs of thrust. It was also assumed that the ground

around the airport was uniform, flat, and soft, in addition to the airport being at sea level with a temperature of 59°F and a relative humidity of 70%.

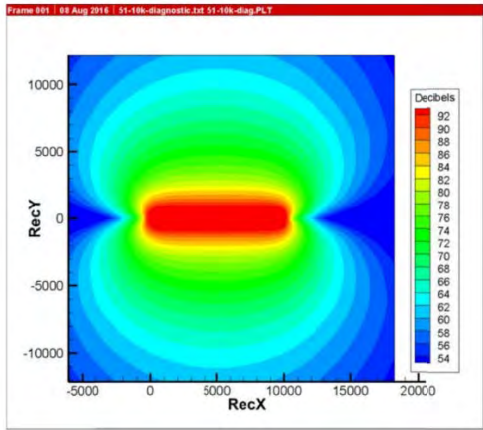


Figure 6. Baseline SEL results (dBA). [6]

Figure 7 represents the effect that varying the segment length has on SEL calculations within INM. Here, the same total flight segment (10,000 ft) is broken into multiple different length segments that were 5,000 ft, 1,000 ft, 500 ft, 200 ft, 100 ft, and 20 ft. As can be seen in Figure 6, most of this error occurs at either end of the segment and increases as the segment lengths decrease in size and increase in number. To help correct this bias, lateral attenuation from three points on each segment was applied at both ends of the segment and the point of closest approach. After applying attenuation, it was determined that segment lengths of up to 2,000 ft in length were the most accurate with an appropriate level of uncertainty.

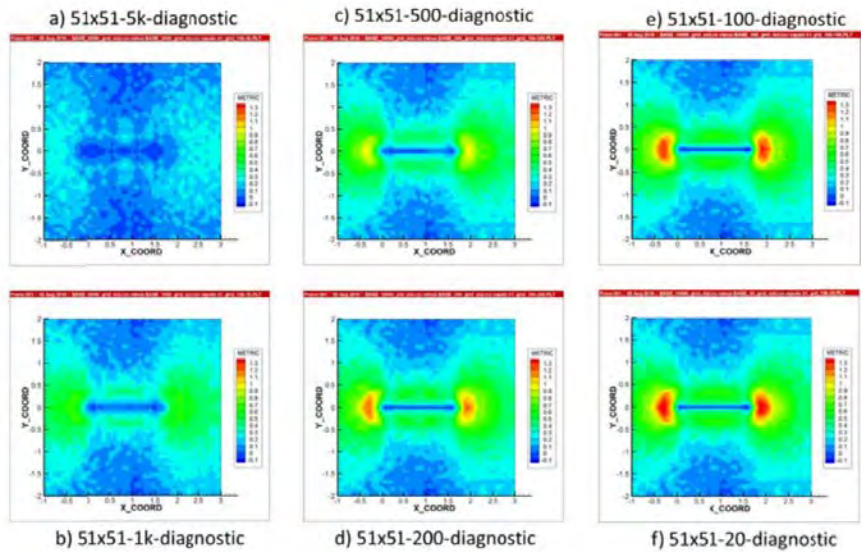


Figure 7. Difference between baseline SEL results and varying segment length SEL results (dBA). [6]

Overall, the introduction of variable ground impedance into the noise propagation calculations resulted in attenuation values that were within 1 dB of the actual measured values when validated using data from the Portland International Airport (PDX), SFO, and the Oakland International Airport (OAK). As a result of ACRP 02-52, it was recommended that the AAM algorithms used to apply this information about the terrain be implemented within AEDT’s workflow and that this process should be relatively simple; however, this functionality is not expected until AEDT’s 2022 release.

More recently, ACRP 02-79 investigated the possibility of including the effects of manmade structures and terrain on noise propagation calculations and how AEDT’s accuracy would be impacted [10]. Three different models were explored as to their accuracy with respect to two sets of aircraft data and two sets of highway data, and these models were the US Department of Transportation’s Traffic Noise Model (TNM) 3.0, SoundPLAN 7.4 (which implements the ISO 9613-2), and the National Cooperative Highway Research Program (NCHRP) Barrier Reflections Screening Tool. As a result, it was determined that TNM 3.0 and SoundPLAN 7.4 would be investigated further with respect to AEDT.

To calculate the effects that manmade structures have on noise propagation, the barrier effects models require information regarding buildings in the area being analyzed. For TNM, both terrain and building information was found using Google Earth and then used to specify building rows and barriers (such as building facades) in TNM. SoundPLAN 7.4, however, used terrain data from the United States Geological Survey’s (USGS) National Map. The building footprint data was sourced from lidar data and the heights from Google Earth.

To validate the results found by using TNM 3.0 and SoundPLAN 7.4, data from the Los Angeles International Airport (LAX) and the Long Beach Airport (LGB) were used. As a method of comparison, gain/loss factors  $GL_{BM}$  were calculated by comparing the noise results with and without buildings used in the models. Figure 8 details the averages and standard deviations for each model, as categorized as an arrival or departure operation and whether shielding or reflection effects were stronger.

Op Type	TNM Sorting	Measured-AEDT		Offset TNM		Offset ISO 9613-2		Offset NCHRP Pt.		Offset NCHRP Line	
		Ave	St Dev	Ave	St Dev	Ave	St Dev	Ave	St Dev	Ave	St Dev
Arrivals	Shielding	-0.9	3.5	-0.3	3.7	-1.8	5.3				
	Reflection	0.3	2.3	0.5	2.4	-0.9	3.2	1.9	2.6	2.2	2.4
Departures	Shielding	-5.8	4.6	2.0	5.0	2.1	5.2				
	Reflection	0.6	3.3	0.6	3.1	-0.6	3.1	0.5	3.4	0.7	3.3

Figure 8. Resulting statistics from LAX and LGB data analysis with grouping. [10]

Considering Figure 8, TNM shows  $GL_{BM}$  values that are consistent with and have the same variability as AEDT. As a result, it was recommended that TNM 3.0 be repackaged into an entirely new module for AEDT which increases the complexity of its implementation. Like the terrain algorithms discussed previously, structural effects will not be included in AEDT’s noise propagation workflow until its 2022 release.

**Conclusion**

The literature review presented here has provided a summary of recent and past efforts in noise model validation and verification and will be used by the team.

**Task 2 – Data Analysis and Dashboard Development**

Georgia Institute of Technology

**Objectives**

The goal for this research area is to have a comparison between noise modeling options in AEDT against real world noise monitoring data. This task aims to help with visualizing the differences between AEDT procedures, and their accuracy compared to the real-world data collected from noise receptors at SFO airport. The objective of this area is, therefore, to build a dashboard environment that can support the decision-making for assessing the sensitivities and to inform future modeling improvement in AEDT. Integrating from the main objective, this Task requires (1) collecting data from all different AEDT runs, (2) choosing the appropriate plots, filters, and highlights to best represent the noise data, flight trajectories, and flight performance, and (3) building a Tableau workbook that is readily available and consists all the components needed to best represent the data and benefit the study goals of ASCENT Project 062.

**Research Approach**

This research area consists of three steps that are presented in the flowchart below.

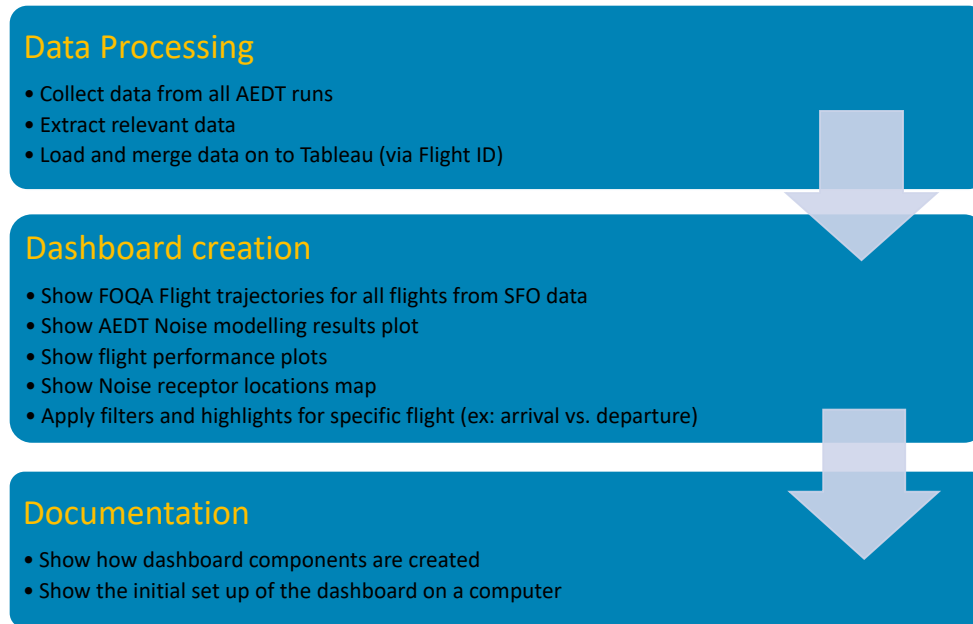


**Figure 9.** Research approach flowchart for data analysis and dashboard development.

In the following sub-sections, a detailed explanation for each step will be provided. The work is concluded with the demonstration of the dashboard design and discussions on the key learning points and milestones archived in this study.

### Data Processing

The objective of this step was to obtain the relevant data that can be used to show the difference between AEDT data and real-world aircraft noise data from SFO airport. A team effort was the key contribution to the success of this task. Data generated by AEDT modeling came from many different runs for an individual flight. The goal was to run as many flights as possible, then combine them into a library of flight and noise result data to be used in the data visualization process.

The process started with generating data from AEDT software for different flights with different profile groups in AEDT. Once all the runs finished, the results are saved in a list of text files. Since the study is only interested in specific numbers from the modeling results, a Python script was used to extract the data and save it into a new data file. The values that were needed for this study focused on the AEDT numerical noise values of SEL, maximum A-weighted sound pressure level (LAMAX), the AEDT result test matrix, and AEDT results in performance. In addition to the data generated from AEDT, this task required real-world data from the SFO airport; fortunately, this data was provided to the study by the SFO noise monitoring office and available to be used. In this data set, the information includes the Flight ID, the noise level for both SEL and LAMAX, the flight trajectory, airframe, and operation types. The study was also provided with the data of the SFO data frames for both arrival and departure flights. These data frames provide the information on the aircraft altitude before touchdown and after takeoff (ft), the thrust level (lbs), true airspeed (knots), corrected gross weight (lbs), and the distance, to touchdown or after takeoff, away from the airport (NM). The information on the noise receptor locations was also provided for this study. This is very beneficial for this study since it will help the team to correlate the locations of the noise receptors to the type of surface that the aircraft is flying over and how that affects the outcome of the noise data for that flight.

In total, the data processing task resulted in seven separate data files that are used for the purpose of building the dashboard. Once this step is concluded, these files are loaded onto Tableau to build an interactive dashboard environment.

### Dashboard Creation

A dashboard is necessary for the purpose of visualizing the study outcome and makes it easier to assess the effectiveness of AEDT. The use of the dashboard will allow the team to assess the differences in noise data from different AEDT procedures.

The dashboard will also allow users to see the exact flight correspond to that noise data on a live map. The dashboard will have multiple filters and highlight features that allow users to choose specific data, specific flight, specific trajectory, or data point of interest, then show the users what is the exact flight ID of that flight and the trajectory that it flies.

The first step of building the dashboard is to load all the data processed and collected, mentioned in the previous section, into the Tableau environment. Tableau software is capable of filtering data automatically and merging all the data needed for this study. The way that we can get the data we want by matching the data from our AEDT results to the data provided by SFO airport by way of matching Flight ID. Additionally, we can merge data between different AEDT result files by a similar process, but with “Case Combined ID” in this case. Once all the data files are merged using Tableau, the software is also used to build data visualization. The dashboard consisted of three main components. They are (1) a section showing the trajectory, speed, thrust, and weight of the flight for each flight, referred to as the performance section, (2) a section showing the satellite map of SFO airport with the noise monitor locations and the FOQA flights trajectory, and (3) a section showing the comparison of different AEDT procedure results with SFO real-world noise data via scatter plots. These components were combined on one big dashboard environment where they were all interconnected; other filters and highlights features were also applied. The dashboard will allow users to interact with the data and look at flight-specific data through built-in filters. Some of the main features include highlighting individual flights, arrival or departure, trajectory relative to the airport, the real-world noise data, the noise receptors that the flight triggered, and the AEDT noise results. Users can also highlight specific AEDT procedures to see the difference between that procedure noise results versus the real-world noise data. The noise data can be seen for all flights, individual flight, or by specific noise receptor as well. This step resulted in the creation of a working dashboard in which the layout can be seen in Figure 10 below. The three main sections mentioned above are also highlighted in this Figure.

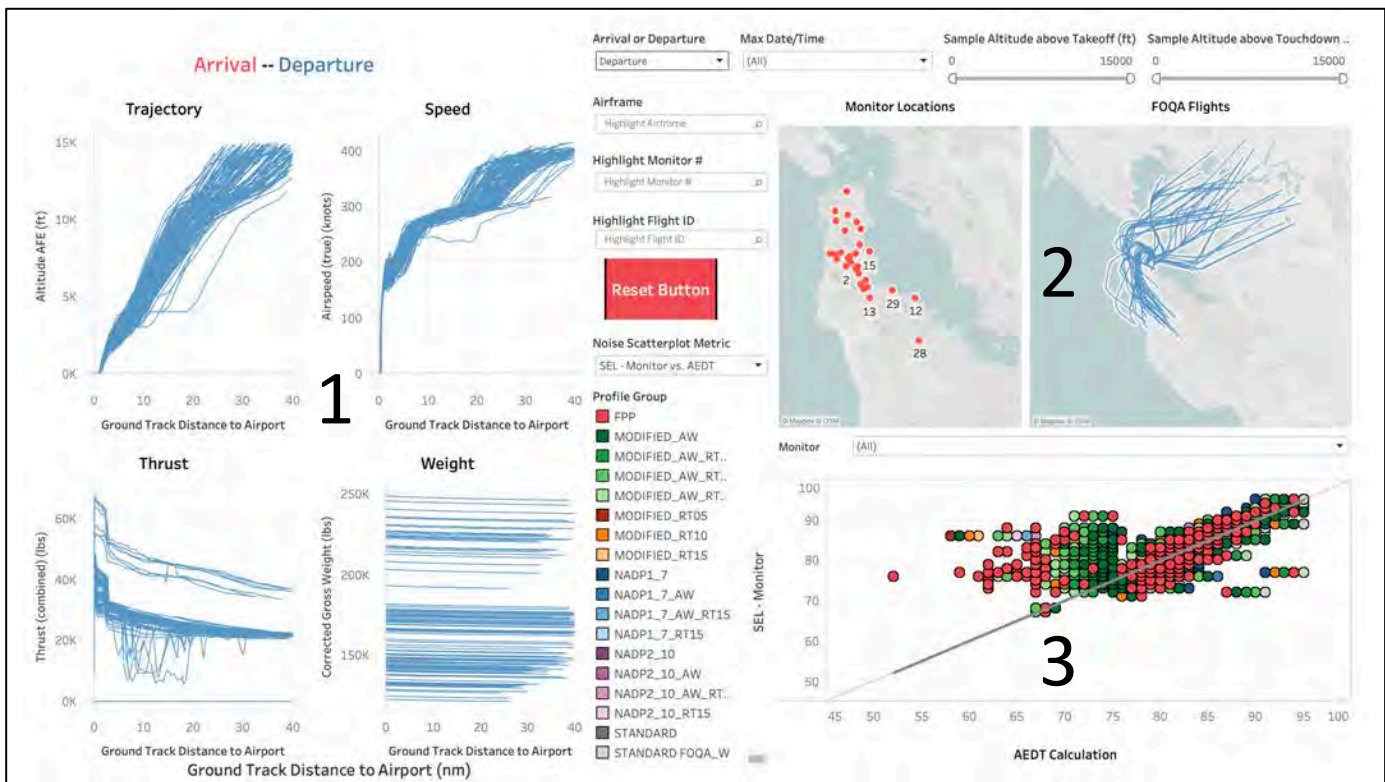


Figure 10. SFO noise study dashboard layout for departure.

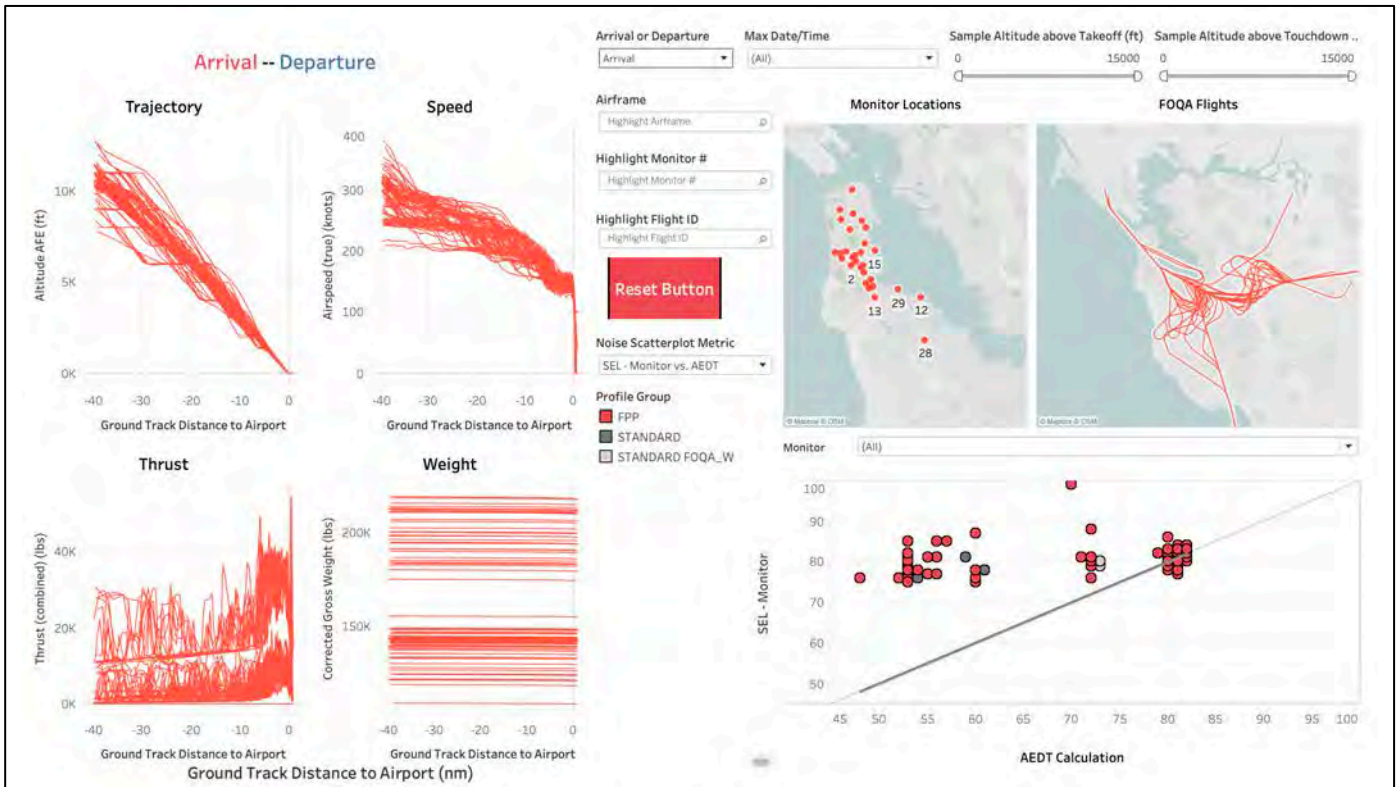


Figure 11. SFO noise study dashboard layout for arrival.

On the layout of this dashboard, there are a few additional features. There are filters for the date of the flight and airframe. The reset button on the layout will be used when the users are done with using the dashboard and want to return the dashboard back to its initial stage. There are also sliders for the altitude after takeoff or before touchdown to help users with knowing the exact location of the aircraft at the given altitude. The dashboard is usually split into just arrival or departure. On the dashboard this can be easily changed to either arrival or departure through a filter. An example of a departure and arrival layout can be found in Figures 10 and 11 above.

Figure 12 shows the filter for a specific flight, what noise monitor that flight triggered, and the noise data for that monitor generated by different AEDT procedure. Figure 13 then shows how the dashboard allows a user to choose a specific noise monitor and provide the user with the geographic location of that monitor and the noise data of that exact monitor. This feature was made to help users see the location of the noise monitor relative to the flight trajectory. In addition to these two figures, Figure 14 is provided with the purpose of showing how a specific AEDT feature can be highlighted and shown on the scatter plot. The noise value can be shown by hovering the cursor over any data point on the scatter plot. This highlight is beneficial since it can tell users how accurate this specific procedure is when comparing to the real-world noise data.

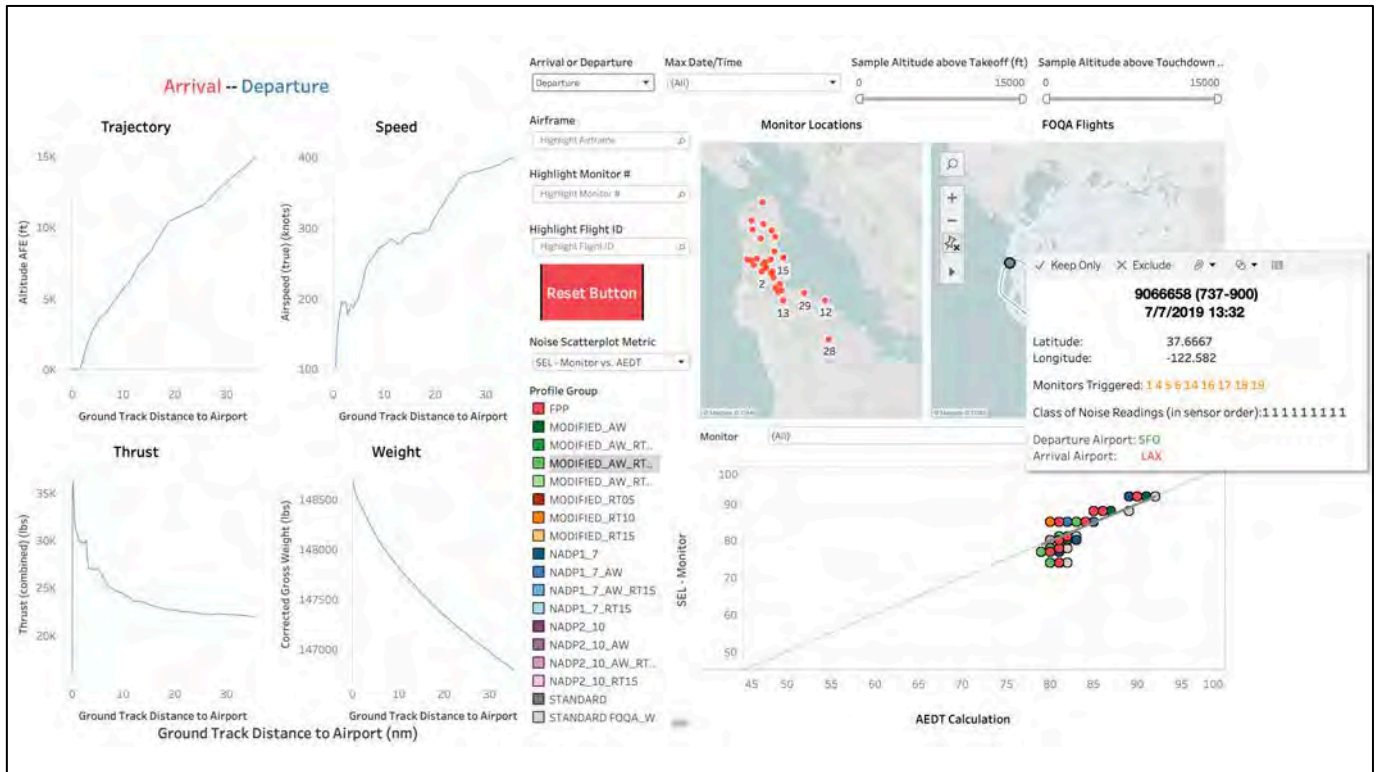


Figure 12. Flight specific filter.

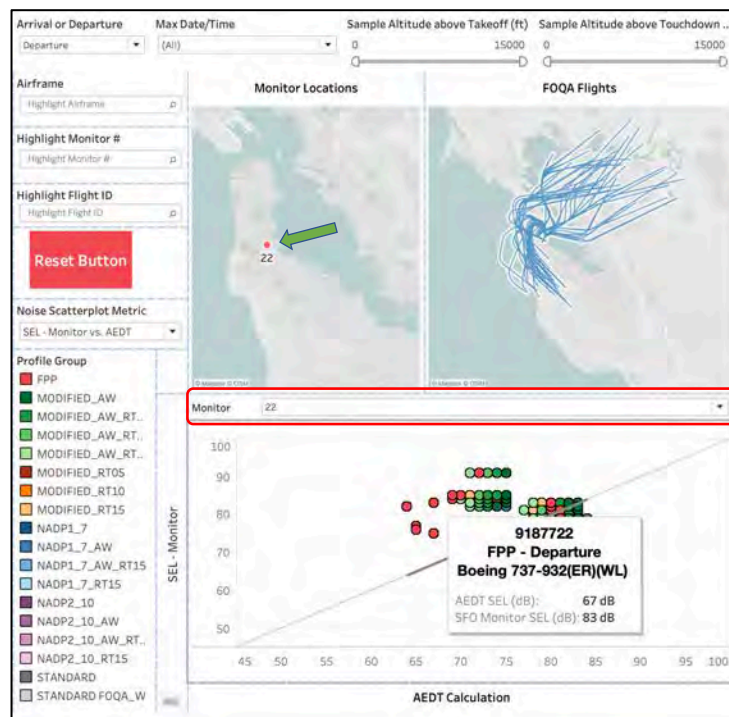


Figure 13. Noise monitor filter.

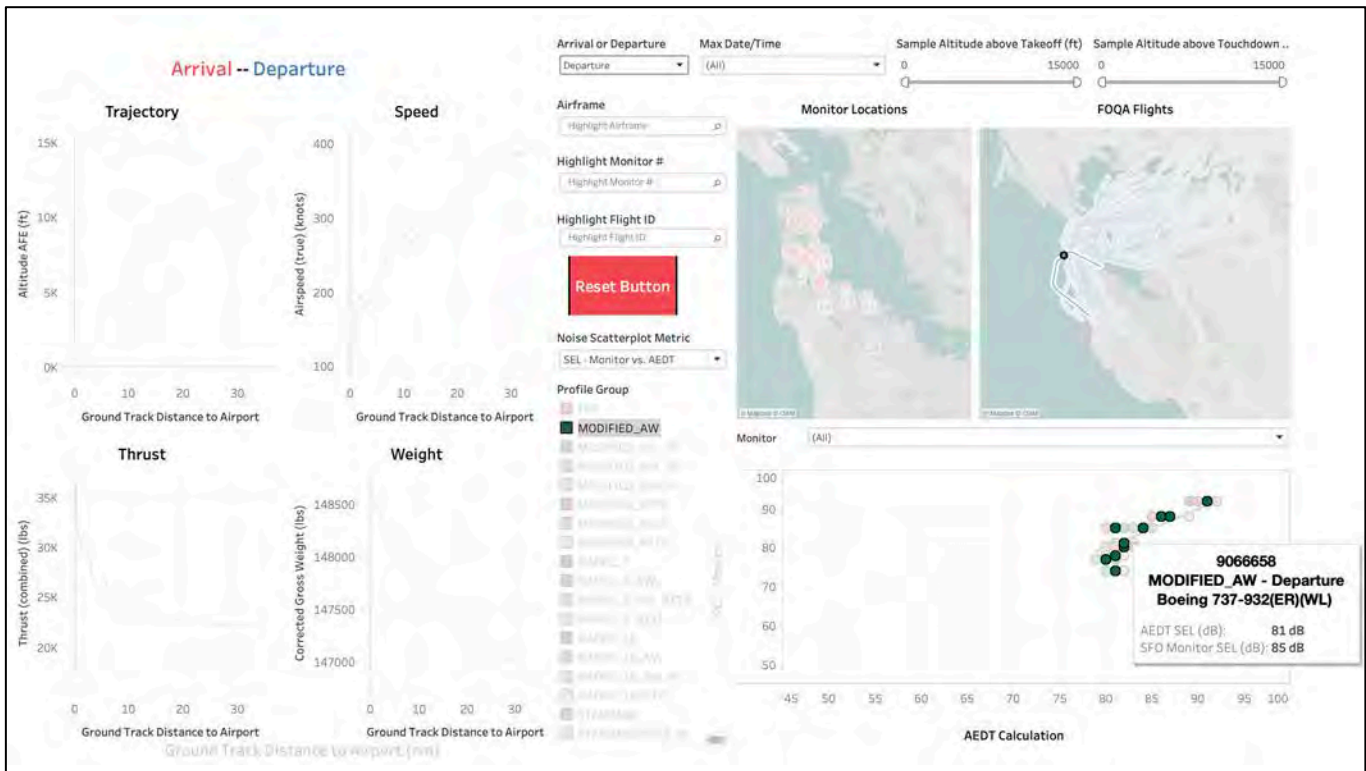


Figure 14. AEDT procedure highlight.

The creation of the dashboard for this study made it easier for the team and other users to observe the results visually. The framework used to build this dashboard can also be used for future dashboard versions as the study continues to different airports around the country. The current version of the dashboard is working and using the data from Project 045 output. Once the data is fully generated for Project 062, the next version of the dashboard will show the data from ASCENT Project 062. The team is also working on sharing this knowledge with undergraduate researchers to get them involved with future versions of the dashboard, while also hoping to spark the interest of these students in aircraft noise data studies. The dashboard will not be possible without the availability of the data generated from AEDT. This research area on data analysis and dashboard creation, therefore, depends heavily on the work that was done in the next research area on noise modeling with AEDT. The planning and execution of the noise model validation plan is crucial in ensuring that the data shown on the dashboard is accurate and provides value added to the goal of ASCENT Project 062.

### Task 3 – Model Validation Plan Development and Execution

Georgia Institute of Technology

#### Objective

The objective of this area is to create a plan to gather data from AEDT in a way that can be compared to real-world data (in the form of noise monitor data). Given a cursory observation of the options available for modeling within AEDT, the different ways to model a specific flight can be done in many ways which will be discussed in detail below. The model validation plan will take these options into account and prioritize them in order of most likely to make a large contribution to noise prediction. It is important to keep in mind during this plan to adhere closely to how an AEDT user would model an aircraft flight in order to make the data comparable to how AEDT is used on a day-to-day basis. The execution of the model validation plan will be done in a way that enables automation, yielding results that can be visualized easily and to provide recommendations on modeling techniques for future versions of AEDT.

## Research Approach

### Introduction

The research team has access to noise monitor data and Flight Operational Quality Assurance (FOQA) data for flights from SFO. FOQA data is high-resolution data that is recorded onboard an aircraft during the actual flight and is very reliable. The amount of noise recorded from a particular flight has been matched with the FOQA flight to match the aircraft configuration and state to the noise recorded from that operation.

### Methodology

The methodology for this research area is shown in Figure 15.

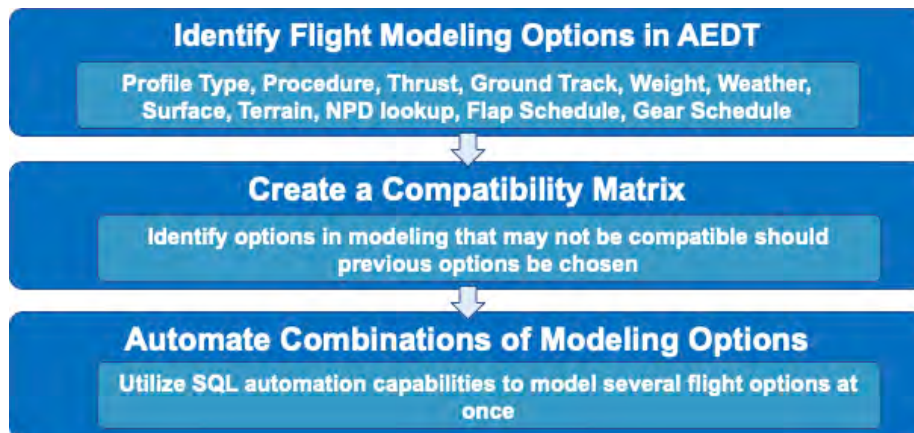


Figure 15. Methodology for Task 3.

### Flight Modeling Options

When modeling a flight in AEDT, there are multiple options for almost any settings chosen during a flight. When a user starts a new study, the first step is to choose a given airport that the flight will be taking off from. During this project, this option has been narrowed to SFO given that the noise comparison data obtained is from this airport only. For this methodology, the aircraft chosen has also been narrowed to the Boeing 737-800, although the same considerations for other aircraft would need to be taken. The end results of this project will also be shown for other aircraft as the noise monitor and FOQA data contain information for flights with other airframes.

The thrust options within AEDT can be seen in the pre-defined procedures in the FLEET database labelled MODIFIED\_RT05", "MODIFIED\_RT10", "MODIFIED\_RT15", and "STANDARD". These procedures are the same except for the additional designation of a change in thrust between them. The STANDARD procedure contains thrust values for 100% thrust upon takeoff. The other three procedures use 5% reduced thrust (RT), 10% reduced thrust, and 15% reduced thrust. Thrust settings upon takeoff and cutback were investigated in ASCENT Project 045 which concluded that other thrust options should be included in AEDT because operators usually use 15% reduced thrust in real-world operation. It has also been shown that this decrease in takeoff and cutback thrust results in a 30 % decrease in area of the 80 dB SEL contour for a single aisle aircraft. These thrust options can be changed by using these different procedures; however, they can also be changed by defining procedures themselves and using identifiers for 5%, 10%, and 15% reduced thrust. These reduced thrusts and other information are shown in Figure 16 from Project 045. The final thrust option that is available is the actual thrust from the flight given in the FOQA data.

PROF_ID1	Weight	Takeoff Thrust Level	Climb Thrust Level	RoC/ES	Takeoff Thrust	Climb Thrust
STANDARD	Standard Weight	0% Reduction	0% Reduction	RoC	T	C
MODIFIED_RT05	Standard Weight	5% Reduction	0% Reduction	ES	F (new)	C
MODIFIED_RT10	Standard Weight	10% Reduction	10% Reduction	ES	X (new)	D (new)
MODIFIED_RT15	Standard Weight	15% Reduction	10% Reduction	ES	Z (new)	D (new)
MODIFIED_AW	Alternative Weight	0% Reduction	0% Reduction	ES	T	C
MODIFIED_AW_RT05	Alternative Weight	5% Reduction	0% Reduction	ES	F (new)	C
MODIFIED_AW_RT10	Alternative Weight	10% Reduction	10% Reduction	ES	X (new)	D (new)
MODIFIED_AW_RT15	Alternative Weight	15% Reduction	10% Reduction	ES	Z (new)	D (new)

Figure 16. Identifiers in AEDT (T, C, F, X, D, and Z) to change thrust definitions within profile definitions.

The procedural options are the “STANDARD”, Noise Abatement Departure Procedure 1 (NADP1), Noise Abatement Departure Procedure 2 (NADP2), and the FOQA procedure. The NADPs are procedures that have been developed in order to abate noise near the airport and farther away from the airport by having shallower or steeper trajectories, changes in thrust settings, and locations for cutback.

The options for the ground track, or the latitude and longitude points on the ground of the aircraft during its flight, are the Straight in or Straight out Ground Track (depending on departure or arrival) or the FOQA ground track. The weight options available for modeling are the standard stage lengths which are derived from the distance between departure and arrival airports. There is also the MODIFIED\_AW (modified alternate weight) procedure which has a different weight from the stage length weights. These modifications have been made because of most airlines flying with larger payload fractions than the assumption within AEDT (payload fraction = 0.65). ASCENT Project 045 found that airlines usually fly with a payload fraction upwards of 0.80. Finally, the last weight option that can be used is the weight of the actual aircraft given in the FOQA data.

AEDT has multiple options for ingesting weather data and using it in its calculations. One of the major differences between AEDT and INM is that AEDT has the capability to use high-fidelity weather data which can come in multiple formats. If available, this will be provided by the PSU partners in this project from Spire Global.

In its default settings, AEDT uses average airport weather data acquired from the Airport Weather Database maintained by the National Oceanic and Atmospheric Administration (NOAA). These data in the airport database are included based on yearly averages. Other options for average weather data specific to an airport can be modified for each flight given the weather experienced by the aircraft during the flight which is available in the FOQA data and also through the Automated Surface Observing System (ASOS).

The surface options within AEDT have been developed mainly for rotor and propeller aircraft. There is a hard surface and a soft surface option. These will be considered in a one-off model test to observe any changes in the noise prediction for jet engine aircraft; however, it is predicted that the differences will be negligible. The flap and gear schedule for modeling in AEDT has two options: the schedules that are provided with each of the procedures, or the flap schedule defined in the FOQA data.

Finally, the method used to calculate the noise, the NPD curves, has two options as well: The default NPD curves defined already in the vehicle definition XML files, or a mode-based NPD lookup designated as NPD+c. All the options and settings can be seen in Figure 17.

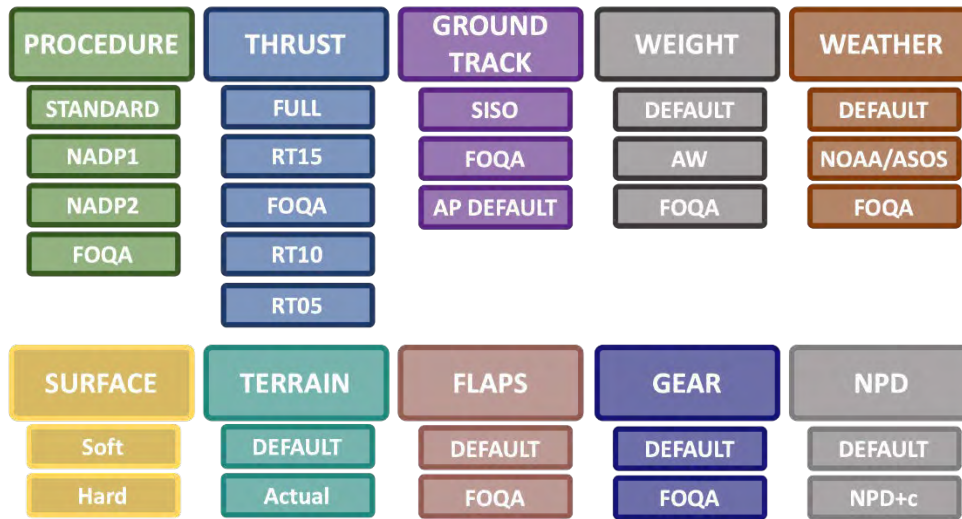


Figure 17. Modeling options.

**Compatibility Matrix**

If one were to create a combination of all these different settings, the outcome would be 17,280 different ways to model one FOQA flight in AEDT. These flights fall into two major modeling categories: fixed point and procedural. Taking the approach of modeling these flights, in a way that an AEDT user actually would, allows further narrowing of the combinations of flights to model. Flights with full FOQA data (speed, altitude, and thrust) will be modeled using the fixed-point profile method within AEDT; however, modeling flights using the full thrust or STANDARD procedure calls for modeling with a procedural method. If the fixed-point profile method were to be used when desiring results using, for example, the STANDARD procedure, one would have to model the STANDARD procedure, extract the performance results, and then plug those results back into a fixed-point profile for uploading to the FLEET database within AEDT, and finally, the running of another simulation. Given that an AEDT user would not perform this process, the researchers have decided to remove this option. An image of the compatibility matrix is shown in Figure 18. Given the choice of procedural modeling, then the amount of combinations is 1296. If fixed-point modeling is chosen, then the number of combinations is 108 for a total of 1404 combinations, which is 15,876 combinations smaller than 17,280.

								Combinations
Ground Track	AEDT	1 Airport Default	1 FOQA	1				3
Profile Type	Procedural	1 Fixed Point	0					1
Procedure	STANDARD	1 NADP1	1 NADP2	1 FOQA	0			3
Thrust	Full	1 RT15	1 FOQA	0 RT05	1 RT10	1		4
Weight	AEDT	1 AW	1 FOQA	1				3
Weather	AEDT	1 ASOS/NOAA	1 FOQA	1				3
Surface	Soft	1						1
Terrain	None	1						1
Flaps	AEDT	1 FOQA	1					2
Gear	AEDT	1 FOQA	1					2
NPD	AEDT	1						1
								1296

Figure 18. Compatibility matrix for departure procedural modeling.



								Combinations
Ground Track	AEDT	1 Airport Default	1 FOQA	1				3
Profile Type	Procedural	0 Fixed Point	1					1
Procedure	STANDARD	0 NADP1	0 NADP2	0 FOQA	1			1
Thrust	Full	0 RT15	0 FOQA	1 RT05	0 RT10	0		1
Weight	AEDT	1 AW	1 FOQA	1				3
Weather	AEDT	1 ASOS/NOAA	1 FOQA	1				3
Surface	Soft	1						1
Terrain	None	1						1
Flaps	AEDT	1 FOQA	1					2
Gear	AEDT	1 FOQA	1					2
NPD	AEDT	1						1
								108

Figure 19. Compatibility matrix for departure point profile modeling.

**Arrival**

The compatibility matrix for arriving flights is less complicated because it has fewer options. Of the procedures specified in AEDT, arrival only has the STANDARD defined. The thrust can only be one type of thrust as well since the reduction in thrust is only applied to takeoff and cutback. An option to note that differs between the arrival and the departure matrices is that the option of NPD+c is available in arrival modeling.

								Combinations
Ground Track	AEDT	1 Airport Default	1 FOQA	1				3
Profile Type	Procedural	1 Fixed Point	0					1
Procedure	STANDARD	1 FOQA	0					1
Thrust	Full	1 FOQA	0					1
Weight	AEDT	1 FOQA	1					2
Weather	AEDT	1 ASOS/NOAA	1 FOQA	1				3
Surface	Soft	1						1
Terrain	None	1						1
Flaps	AEDT	1 FOQA	1					2
Gear	AEDT	1 FOQA	1					2
NPD	AEDT	1 NPD+c	1					2
								144

Figure 20. Compatibility matrix for arrival procedural profile modeling.



						Combinations
Ground Track	AEDT	1 Airport Default	1 FOQA	1		3
Profile Type	Procedural	0 Fixed Point	1			1
Procedure	STANDARD	0 FOQA	1			1
Thrust	Full	0 FOQA	1			1
Weight	AEDT	1 FOQA	1			2
Weather	AEDT	1 ASOS/NOAA	1 FOQA	1		3
Surface	Soft	1				1
Terrain	None	1				1
Flaps	AEDT	1 FOQA	1			2
Gear	AEDT	1 FOQA	1			2
NPD	AEDT	1 NPD+c	1			2
						144

Figure 21. Compatibility matrix for arrival point profile modeling.

**Modeling Automation**

Given this large number of modeling combinations, an automated process will be needed to generate the data and output this data in such a way that is useful for comparison to the noise monitor data. This is achieved through SQL automation scripts that can execute the modeling of a flight using available FOQA data and various modeling assumptions. This capability has been leveraged from past ASCENT projects at GT.

**Extraction of Weather Parameters**

Another primary focus of the ASCENT 062 project was to analyze the weather-specific information available within the FOQA flight data. These datasets included over 1200 individual flights, which either took off or landed from SFO airport. Each of these flights included hundreds of measured values regarding aircraft positions and speeds as well as environmental factors at different points in the flight. These flights were sorted in a MATLAB script in order to manage this amount of information and were then pared down to analyze only weather-specific parameters for both the landing and takeoff of each flight, specifically ambient/dynamic/total air pressure, air density, air temperature, dewpoint, and wind direction and speed. Additionally, information regarding both the landing and takeoff airport was kept, as well as the flight date, such that the weather data could be analyzed within various subsets of time and location. This weather information is now organized in a spreadsheet with a pivot table, containing average values of the weather parameters that can be altered to include or omit values within certain dates. This organized data can be used to compare with the current weather assumptions within AEDT to determine how accurate of an approximation the software is operating off of currently and determine any improvements that can be made to reflect more accurately the reality of these flights.

Furthermore, as the FOQA weather data begins to be employed for analysis on individual flights, this spreadsheet and table allows specific flight information to be pulled, following the necessary format and content of parameters for AEDT:

Field	Description	Units
ID	A unique integer identifier for the weather case	
APT	The airport code for this weather case	
TEMPERATURE	Temperature	deg F
SLP_PR	Sea-level pressure	Millibars
ST_PR	Station ambient pressure	Millibars
DEW_P	Dew point	deg F
REL_HUM	Relative humidity	%
WND_SPD	Wind speed	Knots

Figure 22. Weather parameters available in the data.

Readily available within the FOQA data is ID (here represented as flight ID), airport code, temperature, station ambient pressure, dew point, and wind speed. Since SFO is located 14 ft above sea level, currently the operating assumption is that the takeoff or landing elevation (depending on which correlates to SFO) provides a close enough approximation to sea level to fulfill this parameter. Finally, relative humidity is a function of temperature and dew point. After running an analysis to ensure temperature and dew point have an appropriate relationship—temperature never exceeds the value of dew point for any of the datasets—the value of relative humidity can also be calculated; therefore, the FOQA data provides a complete set of the necessary parameters for AEDT, and these values are now readily available for any given FOQA flight, extractable from a complete spreadsheet using a simple MATLAB script.

Following the extraction of weather parameters, the modeling options highlighted earlier will be pursued, respecting the constraints imposed by the compatibility matrices. The results obtained from the automated modeling runs will then be used to update data in the developed dashboard.

## Task 4 – High Fidelity Meteorological Data

The Pennsylvania State University

### Objective

One of the challenges in validating aircraft noise models is knowing the state of the atmosphere during field tests. In collaboration with the industrial partner Spire Global [www.spire.com], PSU plans to provide the relevant high-fidelity meteorological data to support the AEDT noise model validation work being conducted by GT.

### Research Approach

Spire Global has launched a fleet of low Earth orbit satellites that will provide virtual soundings of the atmosphere worldwide. As additional satellites are being launched presently, the new meteorological data eventually will have a spatial resolution of 1 km by 1 km parallel to the ground, and a vertical resolution of 500 m, for every hour of the day. In short, the GPS signals sent out by other satellites are refracted (bent) by the atmosphere, and the Spire satellites analyze the data to provide virtual soundings. This could provide a very useful resource giving high-quality meteorological data for aviation studies.

For the noise model validation work, the project team is looking at the flight data and the noise monitor data for SFO. The PSU team learned from the GT team that the data is available from January 2018 to August 2019. The PSU team then requested Spire Global to provide a sample of the high-resolution meteorological data for the period of interest. During the interaction with Spire Global, it was learned that their meteorological data had an improvement in quality/resolution around August 2019. To assess if the low-resolution data before August 2019 was good enough for use in Project 062, Spire Global shared the data for three dates (July 30, 2019; August 30, 2019; and September 1, 2020). After receiving the sample data from Spire Global, it was established that they did have the high-resolution data beginning at least as early as July 30, 2019. Out of the variety of the data bundles provided by Spire Global, the "Aviation" and the "Upper-air" data bundles are found to be useful for Project 062 work. Both data bundles provide the temperature, the relative humidity, and the two components of horizontal wind (eastward and northward). Other variables provided by the bundles are not of interest for Project 062 (e.g., potential for aircraft icing). Table 1 summarizes the resolution of the data provided by the two bundles.

**Table 1.** Resolution of the Spire Global meteorological data.

Spire Global Data Bundle	Horizontal Resolution	Vertical Coordinate/Resolution	Temporal Resolution
Upper-air bundle	0.125° in latitude and longitude [11-14 km (near KSFO)]	Data available at 19 isobaric levels (non-uniformly spaced geopotential heights)	1 hour
Aviation bundle	0.125° in latitude and longitude [11-14 km (near KSFO)]	Data available at 36 specific altitudes above the mean sea level [from 3048 m to 13716 m (every ~305 m)]	1 hour

As a first step, the PSU team has written a Python script to read and extract the meteorological variables of interest from the sample files provided by Spire Global. To demonstrate the ability to read and extract the data, four grid points close to the KSFO airport were chosen from the horizontal grid contained in the Spire Global data. The locations of the four selected grid points and the location of the KSFO airport is shown in Figure 23.

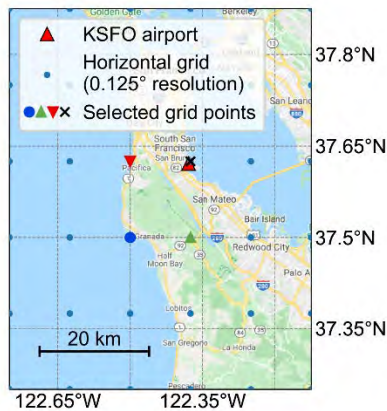


**Figure 23.** A map showing the location of KSFO airport and the four selected grid points from the rectangular grid.

Figure 24 and Figure 25 show the four meteorological variables of interest from the "Upper-air" and the "Aviation" bundle, respectively. The data shown in Figure 24 and Figure 25 is for July 30, 2019 00:00 UTC. Note that the vertical coordinate for the data from the "Upper-air" bundle is Geopotential height (Figure 24). This is different from the vertical coordinate for the data from the "Aviation" bundle, i.e., altitude above mean sea level (Figure 25). The four different markers and colors used in Figure 24 and Figure 25, correspond to the four grid points (shown in Figure 23) from the rectangular grid of the meteorological data. The four grid points are 11-14 km away from each other so, as would be expected, there is not a lot of variation in the meteorological variables obtained at these grid points (see Figures 24 and 25). This exercise has demonstrated that the PSU team can read the data from Spire Global and is able to extract the meteorological variables of interest for the locations and times of interest (constrained only by the resolution of the data). PSU will continue to work with GT and the other team members to move forward in carefully considering this and similar data in Project 062's AEDT validation efforts.

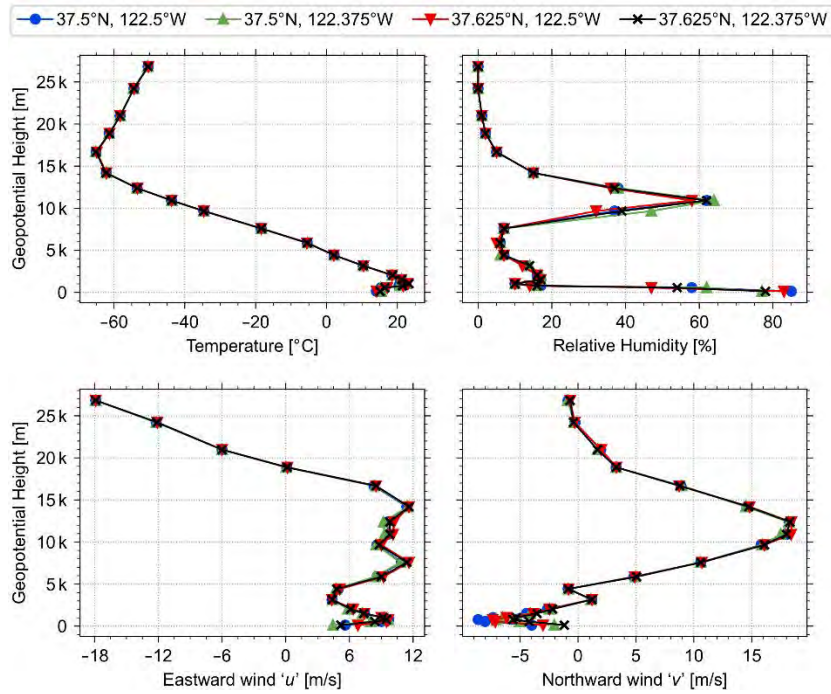


Figure 24. Data from the "Upper-air" bundle for July 30, 2019, 00:00 UTC. The symbols for the four locations are given in the legend above. (Data courtesy Spire Global)

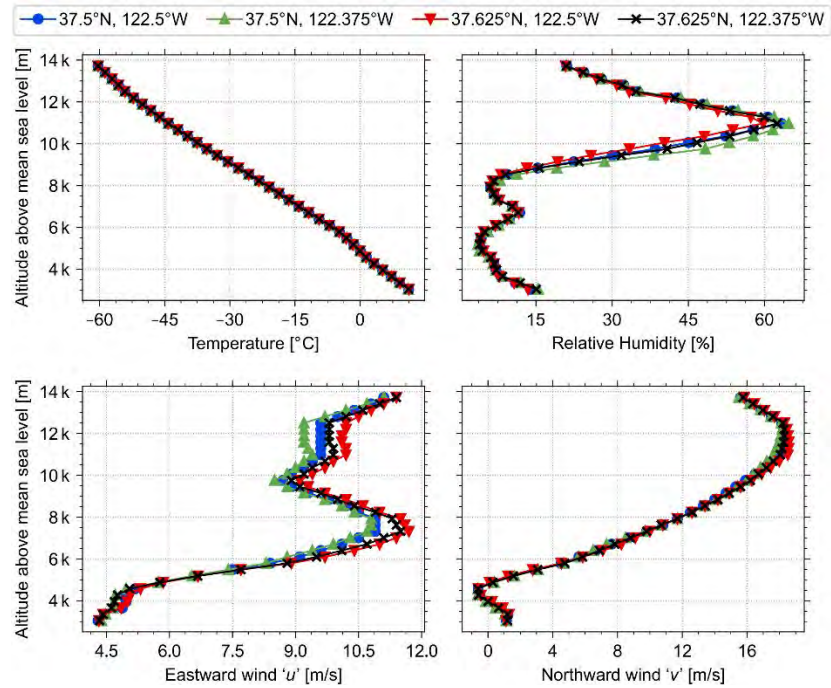


Figure 25. Data from the "Aviation" bundle for July 30, 2019, 00:00 UTC. The symbols for the four locations are given in the legend above. (Data courtesy Spire Global)



## **Milestones**

N/A

## **Major Accomplishments**

(Note that the Project started in July 2020.)

### Literature Review

- Completed literature review in November 2020.
- Compiled databases for future ASCENT projects.
- Created a literature review repository.
- Created a literature review summary.

### Data Analysis

- Completed a fully functional dashboard, ready to be loaded with new data from Project 062.
- Full documentation on the creation of the dashboard workbook.
- Transferred knowledge to undergrad researcher.
- Uploading new AEDT data, once enough cases are run, on the next updated version of the dashboard.

### Model Validation

- Identified all possible model validation combinations.
- Set up a preliminary model validation plan including a compatibility matrix to identify compatible combinations.
- Identified variations in weather conditions within the available data.

### PSU Accomplishments

- Conducted analysis on preliminary data available from Spire Global to assess its usefulness for project.
- Identified the resolution of the available data to communicate with team for use in validation tasks.

## **Publications**

N/A

## **Outreach Efforts**

Bi-weekly calls with the FAA, Volpe, and ATAC. Bi-annual ASCENT meetings.

## **Awards**

None

## **Student Involvement**

Ana Gabrielian, Emily Lembcke, Vinh Bui – Graduate Research Assistant, Georgia Institute of Technology

Harshal Patankar – Graduate Research Assistant, The Pennsylvania State University

## **Plans for Next Period**

The primary focus for the next period will be:

- Continue running AEDT cases and gathering the resulting data for different case combinations for a multitude of selected flights.
- Organize the results into the built dashboard to allow trade studies to be conducted for both arrival and departure procedures.
- Assess sensitivity of AEDT modeling outputs to variations in weather introduced via the modeling options identified this year.
- PSU plans to continue working closely with GT to identify aircraft noise events of interest for validating the publicly available version of AEDT. Once the aircraft noise events are identified, PSU in collaboration with Spire Global will provide high-fidelity meteorological data to be used in the validation study. For this, the aircraft trajectories and locations of the noise monitors provided by the GT team will be used to extract the relevant meteorological data

## **References**

[1] Page, J., Hobbs, C., Plotkin, K., Stusnick, E., and Shepherd, K., *Validation of Aircraft Noise Prediction Models at Low Levels of Exposure*, NASA /CR-2000-210112, April 2000.



- [2] Forsyth, D. and Follet, J., *Improved Airport Noise Modeling for High Altitudes and Flexible Flight Operations*, NASA /CR-2006-214511, October 2006.
- [3] Plotkin, K., Page, J., Gurovich, Y., and Hobbs, C., *Detailed Weather and Terrain Analysis for Aircraft Noise Modeling*, Wyle Report 13-01, April 2013
- [4] FAA, "Integrated Noise Model (INM)", Federal Aviation Administration, 2019. [Online]. Available: [https://www.faa.gov/about/office\\_org/headquarters\\_offices/apl/research/models/inm\\_model/](https://www.faa.gov/about/office_org/headquarters_offices/apl/research/models/inm_model/).
- [5] FAA, "AEDT & Legacy Tools Comparison", June 2016 [Online]. Available: [https://aedt.faa.gov/Documents/Comparison\\_AEDT\\_Legacy\\_Summary.pdf](https://aedt.faa.gov/Documents/Comparison_AEDT_Legacy_Summary.pdf).
- [6] Hobbs, C., Gurovich, Y., Boeker, E., Hasting, A., Rapoza, A., Page, J. and Volpe, J. *Improving AEDT Noise Modeling of Mixed Ground Surfaces*, ACRP 02-52, 2017.
- [7] Circuit Design, Inc., Fresnel zone. 2020 [Online]. Available: [https://www.cdt21.com/technical\\_tools/fresnel-zone/](https://www.cdt21.com/technical_tools/fresnel-zone/).
- [8] MRLC Consortium, "Land Cover Data", *Multi-Resolution Land Characteristics (MRLC) Consortium*, 2020. [Online]. Available: <https://www.mrlc.gov/data?f%5B0%5D=category%3ALand%20Cover>.
- [9] MRLC Consortium, "MRLC Viewer", *Multi-Resolution Land Characteristics (MRLC) Consortium*, 2020. [Online]. Available: <https://www.mrlc.gov/viewer/>.
- [10] Downing, J., Calton, M., Page, J., and Rochat, J. *Improving AEDT Modeling for Aircraft Noise Reflection and Diffraction from Terrain and Manmade Structures*, ACRP 02-79, 2019.



# Project 063 Parametric Noise Modeling for Boundary Layer Ingesting Propulsors

## Georgia Institute of Technology

### Project Lead Investigator

Principal Investigator:

Professor Dimitri N. Mavris

Director, Aerospace Systems Design Laboratory

School of Aerospace Engineering

Georgia Institute of Technology

Phone: (404) 894-1557

Fax: (404) 894-6596

Email: dimitri.mavris@ae.gatech.edu

Co-Principal Investigator:

Dr. Jonathan Gladin

Chief, Propulsion and Energy Division

Aerospace Systems Design Laboratory

School of Aerospace Engineering

Georgia Institute of Technology

Phone: (404) 894-5788

Fax: (404) 894-6596

Email: jgladin3@gatech.edu

### University Participants

#### Georgia Institute of Technology

- PIs: Dr. Dimitri N. Mavris, Dr. Jonathan Gladin
- FAA Award Number: 13-C-AJFE-GIT-064
- Period of Performance: June 5, 2020 to June 4, 2021
- Tasks:
  - Task 1 – Literature Review and Problem Parameterization
  - Task 2 – Develop Parametric Noise Model
  - Task 3 – Model Validation Exercises
  - Task 4 – Tool Documentation

### Project Funding Level

The project funding amount is \$300,000 from the FAA and a cost share match from Georgia Tech of \$300,000.

### Investigation Team

Dr. Jonathan Gladin – Research Engineer II – CO-PI, Overall task lead (Tasks 1 and 4)

Dr. Miguel Walter – Research Engineer II – Technical Aero-acoustics lead, Task 2 and Task 3 lead

Mr. Greg Busch – Research Engineer II – Noise analysis lead

Mr. Ross Weidman – Graduate Research Assistant – CAD and Geometry

Mr. José Zavala – Graduate Research Assistant – CFD Analysis



## Project Overview

Boundary layer ingestion (BLI) is a popular area of research by many entities in aerospace due to the potential for large fuel burn savings. However, the noise implications of this technology are not fully known at this time. The purpose of this project is to identify, develop, and validate a parametric fan noise module for a generic BLI propulsor based on the specifics of a given configuration and design. Parameters influencing the model will include aerodynamic distortion parameters along with others that may affect the noise of the propulsor. The module developed will be based on lower order methods but will seek to validate such methods against higher fidelity approaches and any publicly available experimental data sets. The goal is to quantify turbulence ingestion, mean flow distortion, and shielding in a generic enough way that multiple classes can be captured. Georgia Tech also expects that this module could be integrated into the NASA Aircraft Noise Prediction Program (ANOPP) in a future effort, especially if additional funding for supplementary experimentation or numerical solutions are provided within a future phase.

A recent study by Clark et al. attempted to demonstrate the impact on noise from the inlet distortion-fan interaction for the NASA D8 (ND8) concept and found it to be as much as a 15 EPNdB penalty on cumulative noise. While the study by Clark et al. is interesting in that it represents a first-cut approach for quantifying a BLI impact due to distortion based on experiment, there are several factors that may call such approaches into question. The first is the validity of the open rotor experiment for predicting the sound pressure level (SPL) impact for tonal noise impact on an embedded turbofan engine. The second is due to the fact that there are many ways to achieve BLI and the interaction may vary significantly depending on the kind and quantity of the distortion ingested, and for varying fan applications such as ducted electric fans, propellers, or turbofan engines. Georgia Tech therefore proposes to close the gap identified from this literature by developing a parametric fan noise module for a generic BLI propulsor based on the specifics of the BLI configuration and propulsor design. Parameters influencing the model would include distortion intensity, character (i.e., radial versus circumferential), frequency, multiple-per-rev, fan design parameters, location on the airplane, embedded versus flush mounted, and potentially other relevant physical parameters. The module will attempt to quantify the impact of BLI on turbulent ingestion and mean flow distortion noise based on lower-order methods but would seek to validate such methods against higher-fidelity approaches and any publicly available experimental data sets, such as those used in the above paper or others. The module will also seek to model the effects of ducted versus unducted shielding of BLI noise sources so as to quantify the validity of using “equivalent” experiment data sources for BLI approximations. A validation exercise will be conducted whereby the lower-order methods are tested against higher-fidelity analyses and compared against empirical approaches.

## Task 1 – Literature Review and Problem Parameterization

Georgia Institute of Technology

### Objectives

The objective of this task is to research existing approaches for the quantification of noise sources related to BLI fans and to determine an appropriate modeling approach for the parametric modules. The approach should fit within the statement of work and numerical computational budget afforded to the project.

### Research Approach

The approach for this task is to scan the literature associated with BLI and with distortion-related noise generation for ducted fans. Each reference will be ranked by relevance and appropriateness and its direct applicability and usefulness will be determined.

### Literature Review Results

A literature review on BLI, noise generation and prediction, model validation, and other related topics was conducted. The topics and research goals covered within a subset of the review are shown in Table 1. Most of the researched literature involved BLI, noise prediction, experimental validation, and numerical modeling. One limitation was the difficulty in finding literature that dealt with turbofans instead of open rotor engines. The identified numerical models emphasized that having well-understood correlations between the upwash of different rotor blades and the turbulence space-time correlations are critical in accurate noise estimation. This is partly due to the widely used rapid distortion theory (RDT) not being as useful in cases of inhomogeneous flow distortion, in which case sampling this correlation function becomes essential as a substitute to RDT. There also may be situations in which using this correlation function as a sampling distribution considerably accelerates computational time.



Table 1. Literature review topics

Literature	Topic Covered: BLI	Topic Covered: Inlet Distortions	Research Goal: Noise Prediction	Research Goal: Performance Prediction	Validation Method: Experimental Validation	Validation Method: CFD Validation	Results: Numerical Model Created	Topics Covered: Turbofans	Topics Covered: Open Rotor
Modelling of a Boundary Layer Ingesting Propulsor	X			X			X	X	
Predicting the Inflow Distortion Tone Noise of the NASA Glenn Advanced Noise Control Fan with a Combined Quadrupole-Dipole Model		X	X		X		X	X	
Discretized Miller Approach to Assess Effects on Boundary Layer Ingestion Induced Distortion	X			X	X	X	X	X	
An Analytical Model for Predicting Rotor Broadband Noise Due to Turbulent Boundary Layer Ingestion	X		X		X		X		X
Noise Produced by Turbulent Flow into a Rotor		X	X				X		X
Noise from a Rotor Ingesting a Thick Boundary Layer and Relation to Measurements of Ingested Turbulence	X		X		X				X
Noise from a Rotor Ingesting a Planar Turbulent Boundary Layer	X		X		X				X
Rotor Inflow Noise Caused by a Boundary Layer: Inflow Measurements and Noise Predictions	X		X		X				X
Enhanced Fan Noise Modeling for Turbofan Engines			X		X		X	X	

**Problem Parameterization and Approach**

Based on the results of the literature review, an approach to parameterizing the problem was developed. In order to develop a noise module that accounts for the impact of BLI parametrically and across a range of different applications, it was decided to develop this module using a “delta” approach. This approach will utilize a baseline non-BLI fan noise prediction from NASA’s ANOPP tool and attempt to correct the noise based on a semi-empirical model that accounts for the impact of BLI on fan noise. In order to achieve this, the Georgia Tech team is proposing to use computational aeroacoustics (CAA) to capture the acoustic impact of BLI parametrically, starting with one BLI configuration / architecture. The chosen configuration is a BLI tail cone thruster, similar to NASA’s STARC-ABL concept. This will be accomplished by parameterizing the modeling approach according to Figure 1.

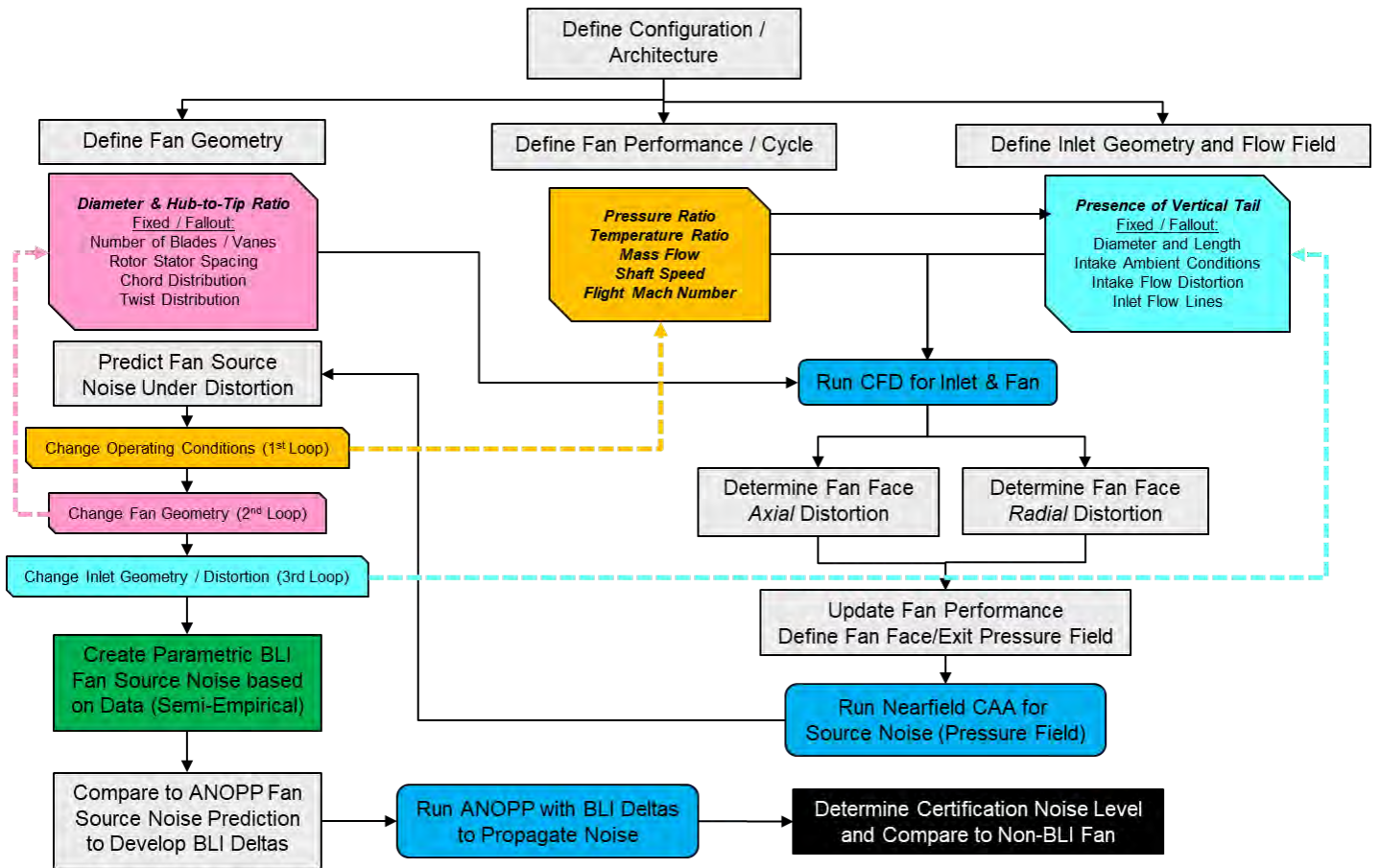


Figure 1. Proposed Modeling Approach to Create Parametric BLI Noise Module

To capture the sensitivity of the noise impact to a wide range of different BLI conditions, the acoustic impact of BLI will try to be captured at various fan geometries, operating conditions, and flow fields. To achieve the required number of runs needed to develop such a noise model, the scope of the varying parameters under each category was limited. The resulting proposed analysis cases needed to develop this initial parametric model are listed in Table 2. The analysis cases may change as the project progresses to accommodate computational resources and preliminary findings.



**Table 2.** Proposed analysis cases for modeling approach

Case Number	Operating Condition	Percent Power	Fan Diameter	Configuration
1	Takeoff	100%	Baseline	No Vertical Tail
2	Flyover / Cutback	65%	Baseline	No Vertical Tail
3	Approach	20%	Baseline	No Vertical Tail
4	Takeoff	100%	Baseline + 25%	No Vertical Tail
5	Flyover / Cutback	70%	Baseline + 25%	No Vertical Tail
6	Approach	35%	Baseline + 25%	No Vertical Tail
7	Takeoff	100%	Baseline - 25%	No Vertical Tail
8	Flyover / Cutback	70%	Baseline - 25%	No Vertical Tail
9	Approach	35%	Baseline - 25%	No Vertical Tail
10	Takeoff	100%	Baseline	With Vertical Tail
11	Flyover / Cutback	70%	Baseline	With Vertical Tail
12	Approach	35%	Baseline	With Vertical Tail
13	Takeoff	100%	Baseline + 25%	With Vertical Tail
14	Flyover / Cutback	70%	Baseline + 25%	With Vertical Tail
15	Approach	35%	Baseline + 25%	With Vertical Tail
16	Takeoff	100%	Baseline - 25%	With Vertical Tail
17	Flyover / Cutback	70%	Baseline - 25%	With Vertical Tail
18	Approach	35%	Baseline - 25%	With Vertical Tail

**Takeoff**  
Mach Number: 0.24  
Altitude: 1000 ft  
Angle of Attack: 8.5 deg

**Flyover / Cutback**  
Mach Number: 0.25  
Altitude: 2000 ft  
Angle of Attack: 4.5 deg

**Approach**  
Mach Number: 0.20  
Altitude: 400 ft  
Angle of Attack: 6.5 deg

**Milestone**

Task completed.

**Major Accomplishments**

The Task was completed and an approach for defining the methodology was conducted and finalized with FAA sponsor approval.

**Publications**

No publications during this reporting period.

**Outreach Efforts**

No forms of outreach were performed during this reporting period.

**Awards**

No awards received during this reporting period.

**Student Involvement**

Two graduate students, Ross Weidman and Jose Zevala, are involved with this work. Both are graduate research assistants in their first year at Georgia Tech.

**Plans for Next Period**

None. Task 1 has been completed.

**Task 2 – Develop Parametric Noise Model**

Georgia Institute of Technology

**Objective**

The objective of this task is to develop the parametric noise model, which will be the primary deliverable for the project. This module should be compatible with the ANOPP program.

**Research Approach**

After formulating the approach that was taken during the completion of Task 1, a more detailed Task schedule was defined and is shown in Table 3 below. The remaining Tasks 2, 3, and 4 and specific items relevant to each Task are broken down into a timeline through the end of the first year of the project. For Task 2, the baseline ANOPP, Fan, and computational fluid dynamics (CFD) models are the first items to have been worked and primarily accomplished during the current reporting period. Details on these items are shown below.

**Table 3.** Schedule for the implementation of Project 063's remaining Tasks (by month)

		S	O	N	D	J	F	M	A	M
Task 2	Baseline ANOPP Fan Model Development	█	█							
	Baseline Clean Fan Geometry w / SDT	█								
	Baseline Podded Fan CAA Cases		█	█	█					
	Baseline Distorted ANOPP Fan Model			█	█					
	Baseline STARC-ABL Geometry and Mesh		█	█	█					
	Parametric Perturbation Geometries and Mesh				█	█	█			
	Distorted CAA Cases					█	█	█		
Task 3	Reference ANOPP Fan Validation					█	█	█		
	Formulate Source Noise "Delta" Modules						█	█	█	
	Use Case Study, Single CAA Far Field Case								█	█
T4	Documentation of Theory, Setup, Results								█	█
	Documentation of Tool, Delta Modules, etc.								█	█

**Baseline Clean Fan Geometry with SDT Fan and Modifications Made**

The baseline configuration chosen for the current project is based on the STARC-ABL geometry and the NASA Source Diagnostic Test (SDT) fan. The former is chosen due to its BLI effect on the rear electric propulsor, while the latter is chosen because it is a benchmark geometry for acoustic fan studies. These two geometries are integrated, with SDT fan geometry replacing the original STARC-ABL propulsor geometry. Some modifications are needed in order to accomplish such integration.

The first modification concerns the NASA SDT fan. The SDT is a 1/5 scale model of a representative high bypass turbo fan, with three different vane variants, which differ from the type of outer guide vane (OGV). A baseline OGV that has 54 radial vanes to reduce the blade passing frequency (BPF) rotor-interaction tone, a low-count OGV which has 26 radial vanes to



reduce broadband noise, and a swept OGV which has 26 swept vanes with 30 degrees of sweep for reduced BPF noise. More information about the development of the SDT variants, can be found in the respective NASA program reports. The SDT provided by NASA for the current project is the first variant, and it is named SDT-A hereafter. SDT-A has a flat surface at the rear since it was developed to address fan noise only and thus it is not concerned with jet noise that would otherwise be generated from the rear part - core. In the current project, the chosen STARC-ABL utilizes an electric propulsor at the rear of the fuselage. Since the original STARC-ABL fan geometry is replaced with that of the SDT-A maintaining the concept of electric propulsor, then there is not core jet flow. Consequently, the SDT-A geometry is modified to have a plug shape at the rear so that it resembles the original STARC-ABL propulsor. The SDT-A geometry was modified in computer-aided design (CAD) to have a conical shape starting at the axial location of the trailing edge of the nacelle. A half-angle of the cone is  $20^\circ$  and the cone vertex is smoothed out with a small spherical cap. The resulting geometry is shown in Figure 2.

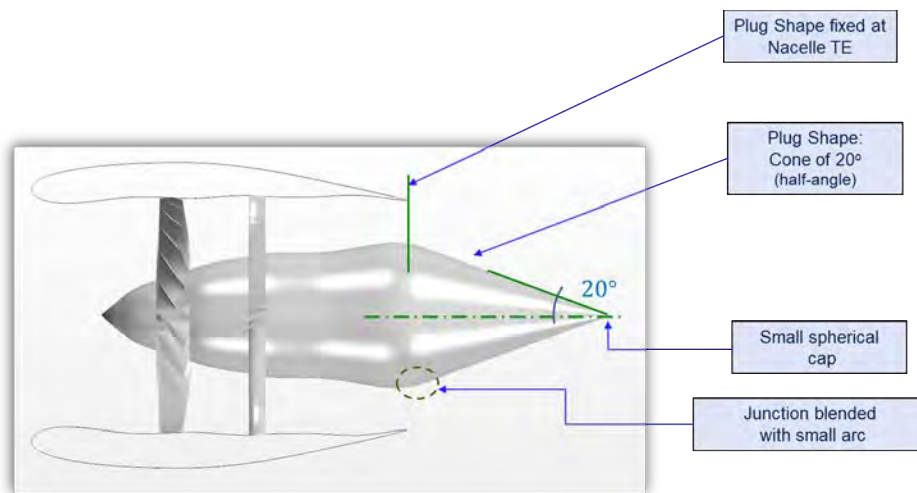


**Figure 2.** Modification to SDT-A geometry.

The second modification concerns changes at the STARC-ABL fuselage in order to integrate it with the modified SDT-A geometry. This integration uses two geometrical references in order to replace the original electric propulsor with that of the modified SDT-A. The first geometrical reference is the distance between the nose of the fuselage and the leading edge of the nacelle, which is maintained constant. The second geometrical reference, the axis of the original propulsor, is also maintained. These geometrical references are shown in Figure 3. Next, the modified SDT-A fan geometry is scaled up by a factor of 2.7272 so that it approximately meets the dimensions at the hub of the STARC-ABL propulsor. Then, the rear part of the fuselage is modified to allow a smooth transition with the scaled and modified SDT-A geometry. All of this is shown in Figure 4.

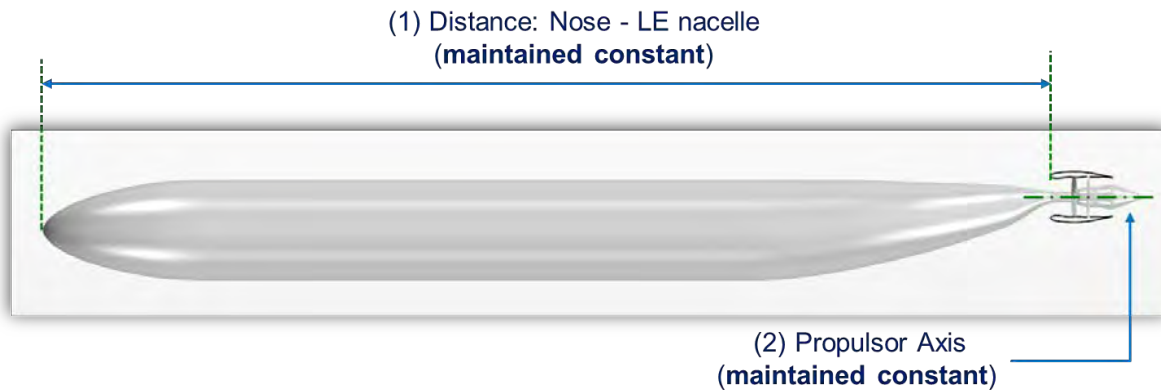


**Figure 3.** Geometry references for integration between the STARC-ABL and modified SDT-A.

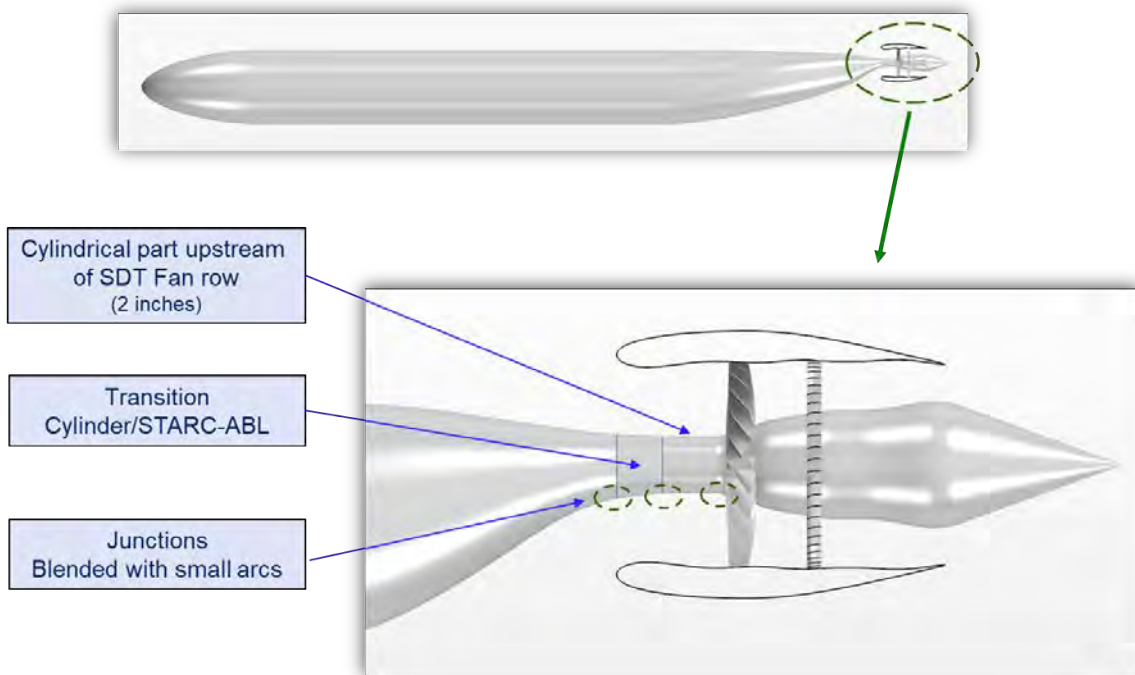


**Figure 4.** Modifications at the fuselage for integration.

#### Baseline Fan Performance Model for ANOPP

In order to create a baseline ANOPP noise model for the ducted SDT fan, it is necessary to model the performance of the fan over a range of flight conditions. To do that, a fan map was digitized from the reference material for the SDT fan and is shown below in Figure 5. The data points in the plots represent data digitized from the SDT test data, and the lines are the output of a computer code called CMPGEN, a NASA code that was used to approximately match the SDT fan map. This map is used to model the fan performance during off-design performance.

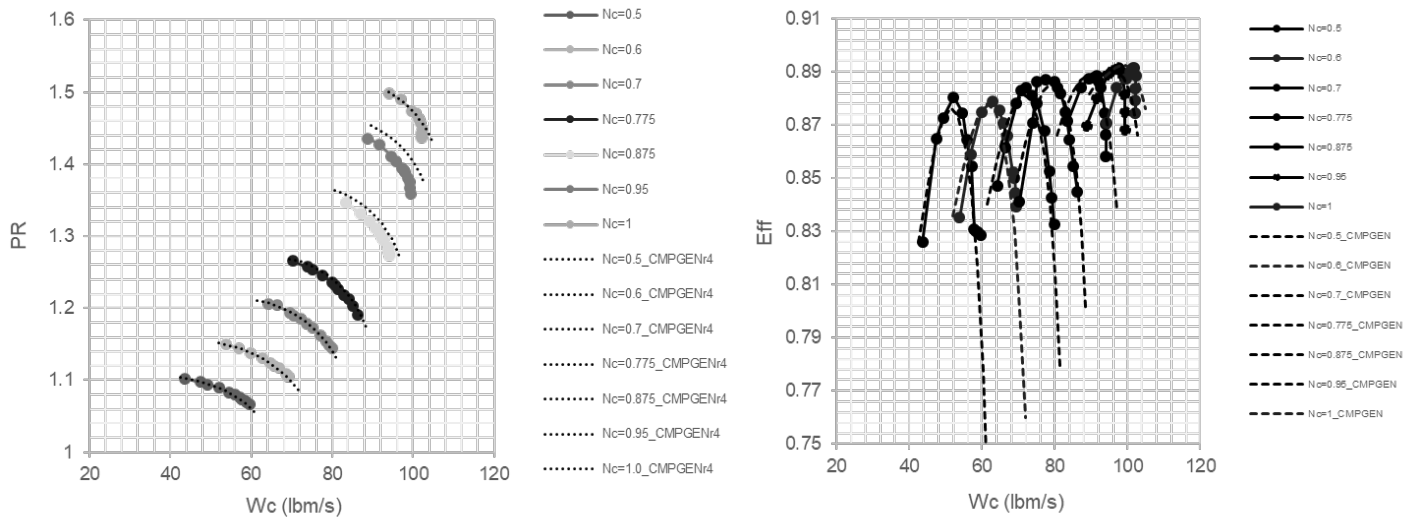


**Figure 5.** SDT fan map digitized from the SDT test data references and the lines representing the CMPGEN fan map performance that was matched to the SDT data set.

Next, the SDT fan needed to be scaled up to the size of the STARC-ABL geometry. The approach for doing this was to hold the fan shaft power constant at 3500 hp, which was taken from the STARC-ABL aircraft design. The criterion for scaling was to create a geometrically similar fan, but at the 3500 hp size. The scaling exercise results are shown below in Table 3. The scale factors for each of the main parameters of the fan are shown in the right column. The power of 3500 hp was used to determine the fan weight flow scale factor of 5.378. The square root of this number (2.31905) is therefore the geometric scale factor since the corrected flow is proportional to the area, which is in turn proportional to the radius of the fan squared. Therefore, the scale factor on the radii is 2.31905. The revolutions per minute (RPM) of the machine are also adjusted to keep the tip speed of the fan constant and maintain roughly constant aerodynamic performance. In this process, the stage pressure ratio and corrected specific flow are held constant. A numerical propulsion system simulation (NPSS) model of the ducted fan with these specifications and the fan map above was created. That model was then used to produce state tables to feed into the fan noise model.

**Table 4.** The parameters for the SDT and geometrically scaled SDT and the scale factors derived to scale the fan.

Parameter	SDT	Scaled SDT	Scale Factor
Tip Diameter	22 in.	51.0191 in.	2.31905
Hub Diameter	6.6 in. (Assuming 0.3 h/t ratio)	15.30573 in.	2.31905
Corrected Rotational Speed	12657 RPM	5457.83 RPM	1/2.31905
Corr. Tip Speed	1,215 ft/s	1,215 ft/s	1.0
Corrected Fan Weight Flow	100.5 lbm/sec	540.49	5.378 (2.31905 <sup>2</sup> )
Corrected Specific Flow	41.8 lbm/sec-ft <sup>2</sup>	41.8 lbm/sec-ft <sup>2</sup>	1.0
Stage Pressure Ratio	1.47	1.47	1.0

### Baseline Fan Noise Model

The development of the baseline fan noise model for the parametric model plus the fan performance and geometry were used to create an ANOPP noise model. This ANOPP model was used to predict the hard-wall forward and aft fan noise based on the Heidmann fan noise module within ANOPP. It was decided to forego modeling of acoustic liners for the development of the BLI noise module to fully capture the impact of BLI and remove acoustic liner assumptions. The baseline noise model was run for three representative conditions for noise certification: sideline, flyover, and approach. The baseline noise model will be used in conjunction with computational aeroacoustics results for the non-BLI baseline case to create a set of “baseline deltas” between ANOPP and CAA. These deltas will eventually serve as a calibration for the BLI noise module so the application of the module in ANOPP is captured correctly and will ensure that the magnitude of the BLI impacts on noise are

representative of BLI only, and do not include differences in the modeling methods. An outline of this process is shown in Figure 6.

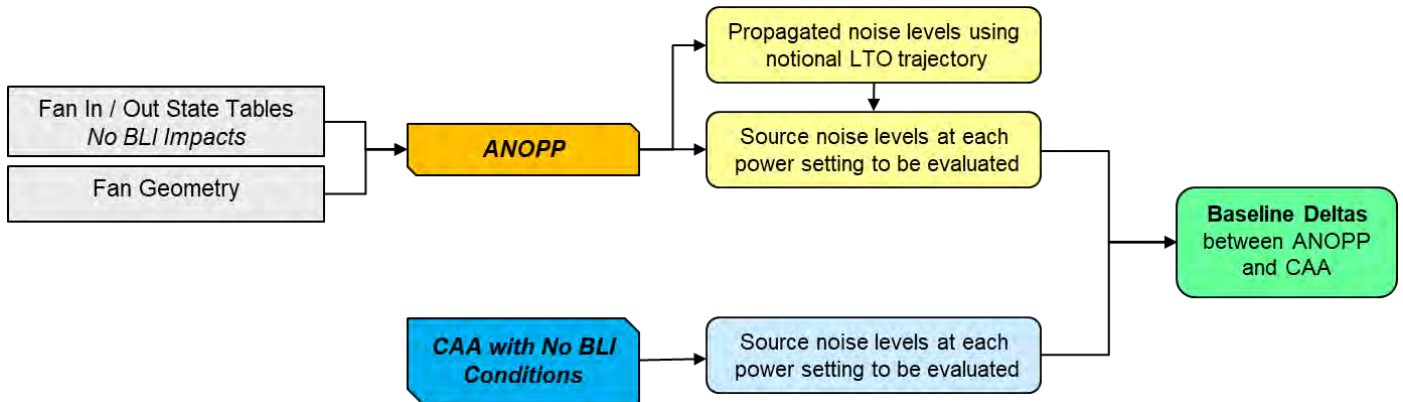


Figure 6. Modeling process to capture differences between ANOPP and CAA.

### Baseline Fan RANS CFD Cases

In order to ensure that the modification to the rear part of the SDT-A geometry does not introduce undesired flow features, axisymmetric CFD simulations are carried out. These simulations are carried with the scaled-up geometry of the modified geometry. The scale factor is 2.31905, which is the first scaling performed and it is lower than the final scale factor used for the integration with the STARC-ABL geometry. Simulations with the final scale factor will be provided in the next report.

The simulations consider that the flow is entirely axial at cruise condition with a flight Mach number of 0.8. Inlet and outlet boundaries are included slightly downstream of the vanes and slightly upstream of the rotor, respectively, in order to simulate the effect of the fan on the flow. These boundaries enforce thermodynamics conditions at the inlet and exit of the fan. The thermodynamic state at these boundaries is given by an engine NPSS model. At the inlet of the fan, outlet boundary conditions (BC) are enforced by prescribing static pressure and temperature so that they match the mass flow given by the NPSS model. At the exit of the fan inflow, boundary conditions are enforced by prescribing stagnation pressure and temperature. In an outer boundary far from the modified SDT-A fan, freestream conditions are imposed with a cruise flight Mach number of 0.8 and altitude of 35,000 ft.

Simulations are carried out with a Reynolds-averaged Navier-Stokes (RANS) solver provided by the commercial CFD solver, STAR-CCM+. Furthermore, the adopted turbulence model is  $k - \omega SST$ . The computational mesh consists of prismatic cells and polyhedral cells. The former are used at the surface walls of the nacelle and center body, while the latter are used everywhere else. The mesh ensures that  $y^+ \approx 1$  at all walls while the entire boundary layer is simulated with 25 prismatic cells. The computational set up and geometry are shown in Figure 7.

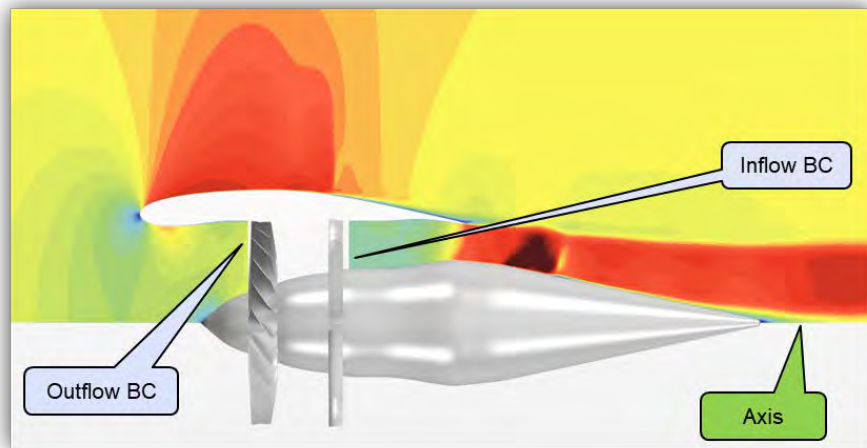


**Figure 7.** Axisymmetric CFD boundary conditions and geometry.

Flowfields of Mach number and magnitude of the density gradient are shown in Figure 8. It is observed that the resulting flow features of the modified SDT-A geometry are what would be typically expected for a turboprop at cruise conditions. Two relatively weak shock waves are observed at the nacelle, which is more evident in the gradient density flowfield. The flow exiting the fan undergoes expansion at the plug part, developing a relatively stronger shock wave. Immediately downstream of this shock, there is a very small separation of the flow; however, it reattaches at a very small distance downstream. All in all, no undesirable flow features such as strong separations and recirculations due to the plug shape geometry are observed.

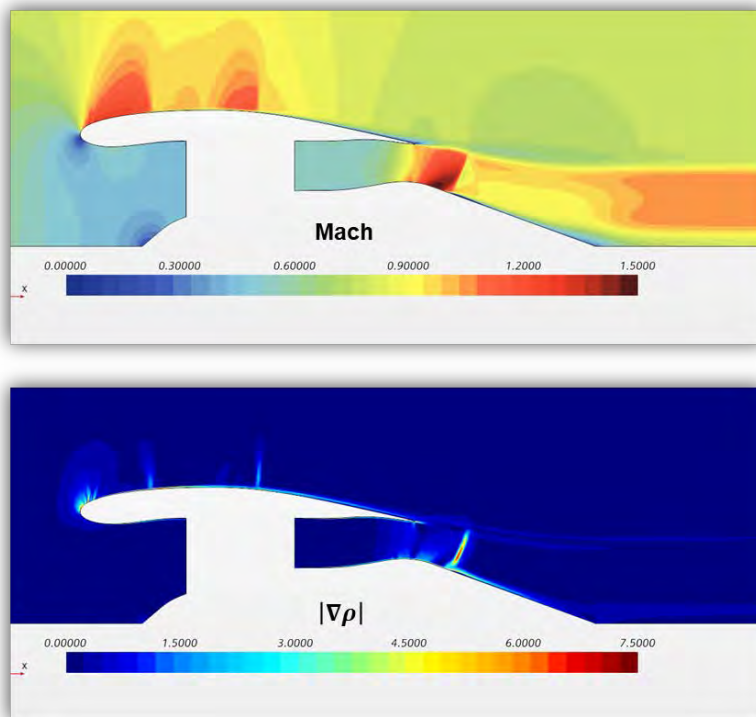


**Figure 8.** Flowfields of Mach and magnitude of density gradient



### **Milestones**

No major milestones yet reached in this task.

### **Major Accomplishments**

- SDT fan geometry and STARC-ABL aircraft geometry secured.
- Initial fan geometry run through RANS CFD codes.
- Geometry updated to baseline scaled model.
- Initial CAA meshes and test cases performed.

### **Publications**

No publications during this reporting period.

### **Outreach Efforts**

No forms of outreach yet performed during this reporting period.

### **Awards**

No awards received during this reporting period.

### **Student Involvement**

Two graduate students, Ross Weidman and Jose Zevala, are involved with this work. Both are graduate research assistants in their first year at Georgia Tech.

### **Plans for Next Period**

The plan for the next reporting period is to finish all of the items specified in the research approach under Task 3 and to fully finish the first phase of the Task before the end of the current period of performance.

## **Task 3 – Model Validation Exercises**

Georgia Institute of Technology

### **Objective**

The purpose of this task is to validate the creation of the parametric noise models with existing data or high-fidelity simulations.

### **Research Approach**

#### **Baseline Validation Approach**

To validate the baseline fan noise, the predicted fan noise from the ANOPP model will be compared to published acoustic results of the SDT fan and the differences will be documented. If there is a significant difference in the ANOPP prediction and published data, a correction function in the ANOPP model can be introduced to minimize these differences. In order to account for differences between the CAA results generated for the study and ANOPP, the proposed method is described in section 1.2, Figure 6. Further validation exercises may be needed depending on the results of the parametric model. The module will be used to generate both BLI and non-BLI noise results at various flight / operating conditions and compared to the CAA results at the corresponding conditions.

#### **High-Fidelity Computational Aero-Acoustics Modeling**

Since the objective is modeling the effect of BLI on noise, then the effect of distortion on noise must be addressed. BLI as well as other flow perturbations upstream of the fan lead to lack of uniformity in the axial flow ingested by the fan. This in turn causes variations of the blade loading in the azimuthal direction. Consequently, aeroacoustics performance is degraded.

In order to capture the effects of non-uniformities in the ingested flow, the aerodynamics analysis necessarily needs to be unsteady. In this study, the adopted analysis for performing CAA is a hybrid approach, consisting of unsteady CFD and integral method based on the Ffowcs Williams and Hawkings (FW-H) equations. The unsteady CFD simulates the aerodynamic

flowfield, which in turn provides noise sources. The FW-H approach is then used to propagate the noise sources to the farfield.

For the aforementioned CAA approach, unsteady Reynolds-averaged Navier-Stokes (uRANS), detached eddy simulations (DES,) and Lattice Boltzmann methods (LBM) are suitable approaches for unsteady aerodynamics. However, only the latter two can provide multi-scale noise sources that allow broadband noise assessment. In terms of computational cost, DES is the most computationally expensive, whereas uRANS and LBM have been reported to be more affordable. A summary of computational cost for similar applications is shown in Table 5. These costs suggest that uRANS and LBM have similar cost, which are between 60,000–66,000 CPU-hr, and thus they are considered for use in the current project.

**Table 5.** Computational cost for unsteady CFD in turbomachinery applications

Application	Purpose	Method	Cost (CPU-Hr)	Noise characteristics	Source	Remark
BLI Fan	Acoustics	LBM	62,000	Tonal & Broadband	Romani <i>et al.</i> , Aerospace Sci & Tech, 2020	Whole geometry
Turbo Fan	Acoustics	LBM	60,000	Tonal & Broadband	Casalino <i>et al.</i> , Vol 56, No 2, AIAA J. 2018	Whole geometry
Open-Rotor	Aerodynamics	uRANS	65,280	Tonal	Stuermer, AIAA paper 2008-5218 2008	Whole geometry
Turbo Fan	Acoustics	DES	1'080,000	Tonal & Broadband	Arroyo <i>et al.</i> , J. Sound and Vibration 2019	Sector (1/11) domain

The high-fidelity analysis workflow for the CAA approach considered in this study is shown in Figure 9. This process consists of the following:

- **Initialization:** This step refers to an initial solution for starting unsteady CFD simulations. For this purpose, a steady RANS simulation is performed and then used as an initial solution to uRANS.
- **Unsteady Aerodynamics:** This step refers to the unsteady CFD analysis. Initially, the unsteady CFD solver needs to be run long enough so that the initial solution is washed-out, i.e. convected down by the incoming flow from the geometry of interest. For the BLI turbo-fan application in this project, it is estimated that the time it takes for the rotor to undergo 2–5 revolutions is enough. After this initial step, unsteady CFD is executed along with the FW-H solver as described below.
- **CAA:** This step addresses the farfield aeroacoustics calculation using the FW-H model. Noise propagation is carried out from FW-H surfaces, where noise sources are captured, to FW-H receivers, where the acoustic pressure is recorded. It is pointed out that the FW-H solver is executed simultaneously with the unsteady CFD—after the initial solution is washed-out—and it is run long enough to collect acoustic pressure time histories. It is estimated that the run time for this step is about the time the fan rotor takes to undergo 10–12 revolutions.

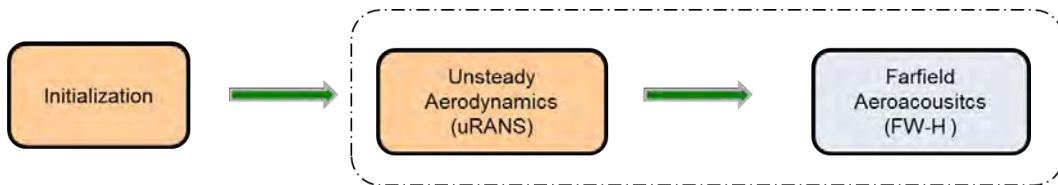


**Figure 9.** Workflow analysis chart.

In order to test the above workflow analysis, this process is applied to a simplified geometry based on the SDT-A turbofan. The main idea of this is to simplify the SDT geometry so that computational cost is reduced - reducing the total number of cells. As such, the geometry is simplified by removing the nacelle, vanes, and 20 blades from the SDT-A geometry. The



resulting geometry resembles a two-blade propeller. The computational domain is divided into two regions. The first region simulates the motion of the rotor and spinner by undergoing rigid body rotating motion with the same angular speed as that of the rotor. The second region is static and surrounds the inner regions and the rest of the geometry. The simplified geometry along with the inner region is shown in Figure 10.

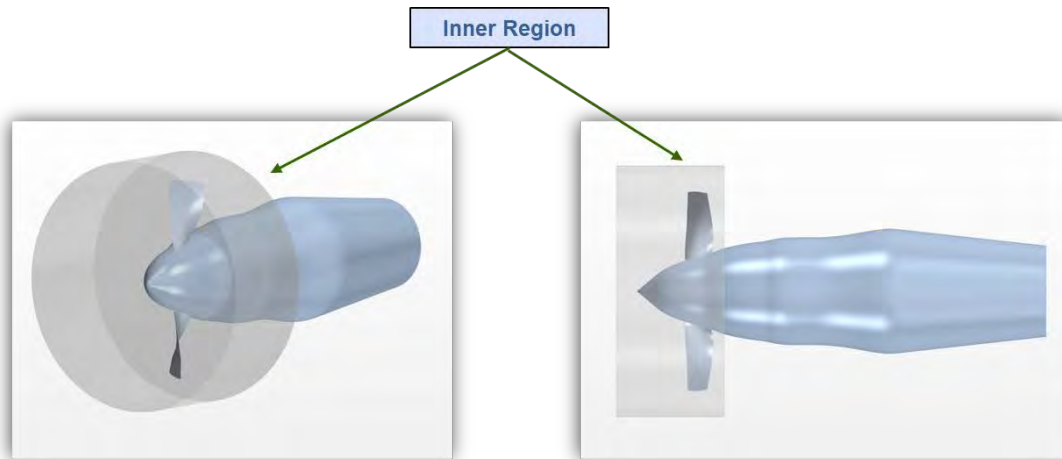


Figure 10. Simplified geometry

The CFD solver is uRANS with a  $k - \omega$  SST turbulence model, provided by STAR-CCM+. The assumed operating conditions for this test are free-stream Mach number of 0.25 and tip Mach number of 0.6, which lead to a rotational speed of 742 rad/s. The time step is  $10^{-5}$ , which approximately accounts for a half degree in the rotation of the fan rotor. The computational mesh has approximately 20 million cells and ensures  $y^+ \approx 1$  at all solid walls - blade and center body surface. Also, the mesh in the near field—between geometry and FW-H surface—is fine enough to resolve frequencies up to 6000 Hz.

The FW-H solver is executed with the same time step as the unsteady solver. The FW-H surface where the noise sources are captured is a permeable surface in the near field surrounding the simplified geometry. The receivers are located in a line parallel to the geometry axis and at a distance of five meters. All of this is shown in Figure 11.

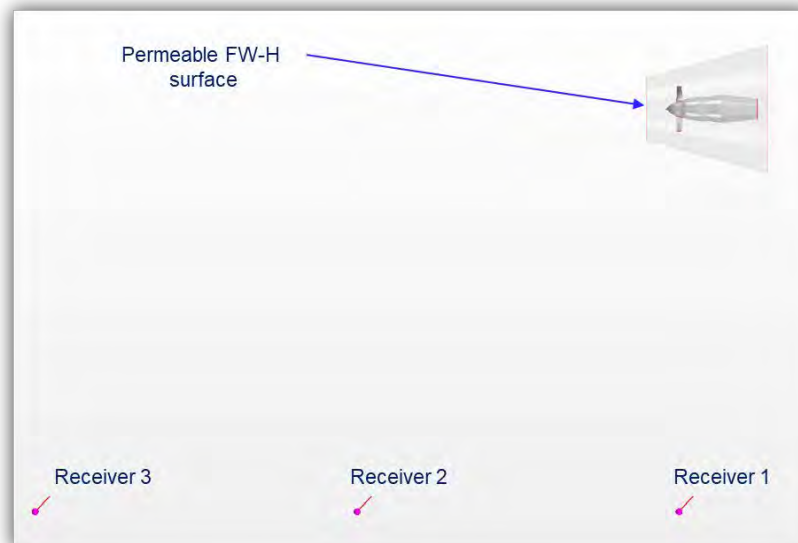


Figure 11. FW-H surfaces and receivers.



The acoustic pressure-time histories recorded in the receivers are shown in Figure 12. They have been recorded for approximately 1.5 revolutions of the simplified fan. Once run long enough, these pressure-time data can be used for assessing noise metrics such as spectrum and overall pressure sound level. It is noted that these pressure-time data will need to be recorded for a longer time—about 10 to 12 revolutions—in order to assess noise metrics. Nevertheless, the main purpose of this sample is to demonstrate the analysis workflow.

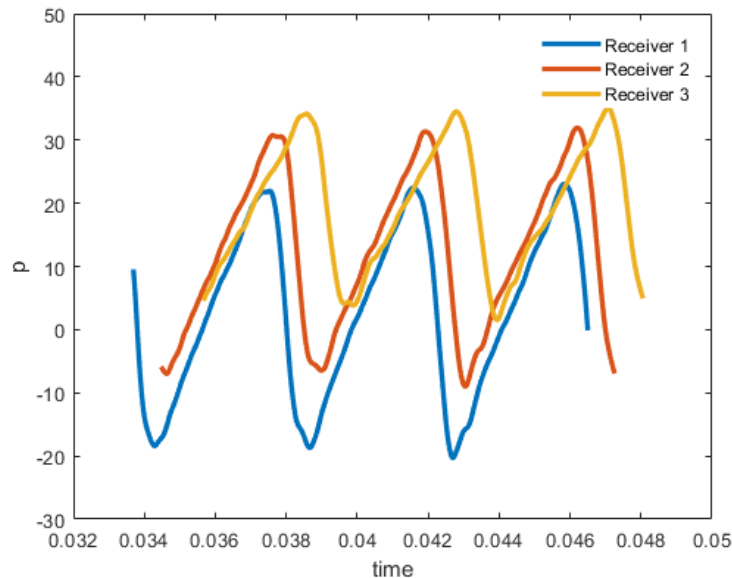


Figure 12. CAA results for the initial SDT fan test geometry.

### **Milestones**

No major milestones achieved.

### **Major Accomplishments**

Initial test cases for the SDT fan setup in CAA, including mesh, simulation, and unsteady CFD results.

### **Publications**

No publications during this reporting period.

### **Outreach Efforts**

No forms of outreach yet performed during this reporting period.

### **Awards**

No awards received during this reporting period.

### **Student Involvement**

Two graduate students, Ross Weidman and Jose Zevala, are involved with this work. Both are graduate research assistants in their first year at Georgia Tech.

### **Plans for Next Period**

The plan for the next reporting period is to finish all of the items specified in the research approach under Task 3 and to fully finish the first phase of the Task before the end of the current period of performance.



## Task 4 – Tool Documentation

Georgia Institute of Technology

### **Objective**

The purpose of this task is to create documentation of the parametric noise tool created.

### **Research Approach**

Georgia Tech will thoroughly document the tool and each of its modules including parameters involved, theoretical approach, algorithms utilized, output structure, and example use cases. This resulting theory manual will be in addition to the validation results which will be documented as a separate report.

### **Milestones**

None. This Task has not started yet.

### **Major Accomplishments**

None. This Task has not started yet.

### **Publications**

No publications during this reporting period.

### **Outreach Efforts**

No forms of outreach yet performed during this reporting period.

### **Awards**

No awards received during this reporting period.

### **Student Involvement**

Two graduate students, Ross Weidman and Jose Zevala, are involved with this work. Both are graduate research assistants in their first year at Georgia Tech.

### **Plans for Next Period**

The documentation for the modules will be completed during the next annual period of performance.



# Project 064 Alternative Design Configurations to Meet Future Demand

## Georgia Institute of Technology

### Project Lead Investigator

Principal Investigator:

Professor Dimitri N. Mavris

Director, Aerospace Systems Design Laboratory

School of Aerospace Engineering

Georgia Institute of Technology

Phone: (404) 894-1557

Fax: (404) 894-6596

Email: [dimitri.mavris@ae.gatech.edu](mailto:dimitri.mavris@ae.gatech.edu)

Co-Principal Investigator:

Dr. Michelle Kirby

Chief, Civil Aviation Division

Aerospace Systems Design Laboratory

School of Aerospace Engineering

Georgia Institute of Technology

Phone: (404) 385-2780

Fax: (404) 894-6596

Email: [michelle.kirby@ae.gatech.edu](mailto:michelle.kirby@ae.gatech.edu)

### University Participants

#### Georgia Institute of Technology

- PIs: Dr. Dimitri N. Mavris, Dr. Michelle Kirby
- FAA Award Number: 13-C-AJFE-GIT-062
- Period of Performance: June 5, 2020 to June 4, 2021
- Tasks:
  1. Support of LTAG-TG Meetings and Technical Ad-hoc Group Meetings
  2. Modeling & Simulation: Development of Turboprop Technology Reference Aircraft
  3. Modeling & Simulation: Assessment of 2050 Projections of Technology Reference Aircraft
  4. Modeling & Simulation: Assessment of 2050 Projections of Advanced Configurations

### Project Funding Level

FAA provided \$250,000 in funding and the Georgia Institute of Technology (Georgia Tech) has agreed to a total of \$250,000 in matching funds which includes salaries for the project director; research engineers; graduate research assistants; and computing, financial and administrative support, including meeting arrangements. The institute has also agreed to provide tuition remission for the students, paid for by state funds.

### Investigation Team

#### Faculty & Research Staff

Dr. Dimitri Mavris, Georgia Institute of Technology, Tasks 1-4

Dr. Michelle Kirby, Georgia Institute of Technology, Tasks 1-4

Mr. Greg Busch, Georgia Institute of Technology, Tasks 1-4

Dr. Jon Gladin, Georgia Institute of Technology, Tasks 2-4

Dr. Gokcin Cinar, Georgia Institute of Technology, Task 2



### Graduate Researchers

Melek Ozcan, Georgia Institute of Technology, Tasks 2-4

Luis Salas Nunez, Georgia Institute of Technology, Tasks 2-4

## Project Overview

The purpose of this ASCENT project is to support the Committee for Aviation Environmental Projection (CAEP) task group for a Long-Term Aspirational Goal (LTAG-TG), with a focus on aircraft technology modeling and analysis of fuel burn and CO<sub>2</sub> emissions. The LTAG-TG is working under the 12<sup>th</sup> CAEP cycle to develop scenarios that combine technology, fuels, and operations that represent a range of readiness and attainability for future air transportation. The work will be framed in the context of an analysis of achieving the current International Civil Aviation Organization (ICAO) aspirational goals. The future scenarios will be analyzed to understand the impacts on CO<sub>2</sub> emissions and relating this to current CO<sub>2</sub> levels. The costs associated with the scenarios and the economic impacts on aviation growth, noise, and air quality will be considered and the results will be placed within the context of the latest consensus scientific knowledge. Georgia Tech is supporting the modeling and simulation aspects of these analyses by leveraging the FAA's investment in Georgia Tech's Environmental Design Space (EDS) tool set, existing technology models, and previous work done in support of other CAEP efforts. The goals of Project 064 can be described at a high-level as follows:

- Supporting LTAG-TG and technical ad hoc group (Tahg) meetings.
- Development of a turboprop technology reference aircraft model.
- Execution and assessment of 2050 projections of all technology reference aircraft, all five classes of vehicles (turboprop, business jet, regional jet, narrow body, wide body).
- Execution and assessment of 2050 projection of advanced configuration aircraft; final list of concepts to be considered is still being discussed.

The completion of these tasks will inform the LTAG-TG as to the potential of aircraft technology to reduce fuel burn and CO<sub>2</sub> emissions under a variety of future scenarios.

## Task 1 – Support of LTAG-TG Meetings and Technical Ad-hoc Group Meetings

Georgia Institute of Technology

### Objective

The objective of Task 1 is to support LTAG-TG meetings and technical ad hoc group (Tahg) meetings within the LTAG Technology sub-group. The CAEP/12 LTAG-TG currently has four primary subgroups: Operations, Fuels, Technology, and Scenarios Development. The key interactions of the overall modeling process for the LTAG-TG are shown in Figure 1.

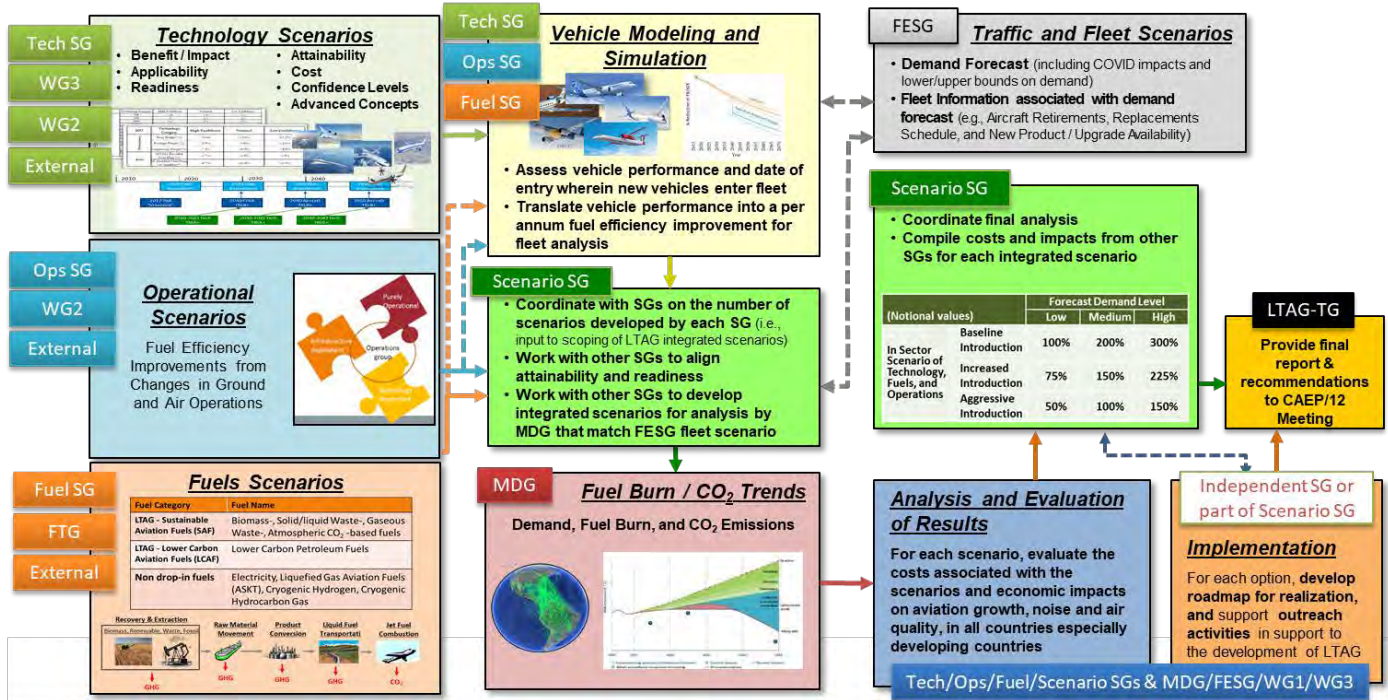


Figure 1. Key interactions for LTAG-TG modeling process.

Georgia Tech is primarily supporting the Technology subgroup, but is actively participating in the other subgroups to help facilitate coordination across the entire LTAG task group. The LTAG Technology subgroup (LTAG Tech SG) is divided into four Tahgs: Airframe, Propulsion, Vehicle Impact Assessment (VIA), and Advanced Concepts and Energy Sources (ACES). The VIA Tahg also contains a sub ad hoc group dedicated to Modeling & Simulation (M&S). Dr. Dimitri Mavris is a co-chair of the Technology subgroup, Dr. Michelle Kirby is a lead focal for the Airframe Tahg, and both Greg Busch and Dr. Dimitri Mavris are focals for the Modeling and Simulation group of the VIA Tahg. A breakdown of the LTAG Technology subgroup is shown in Figure 2.

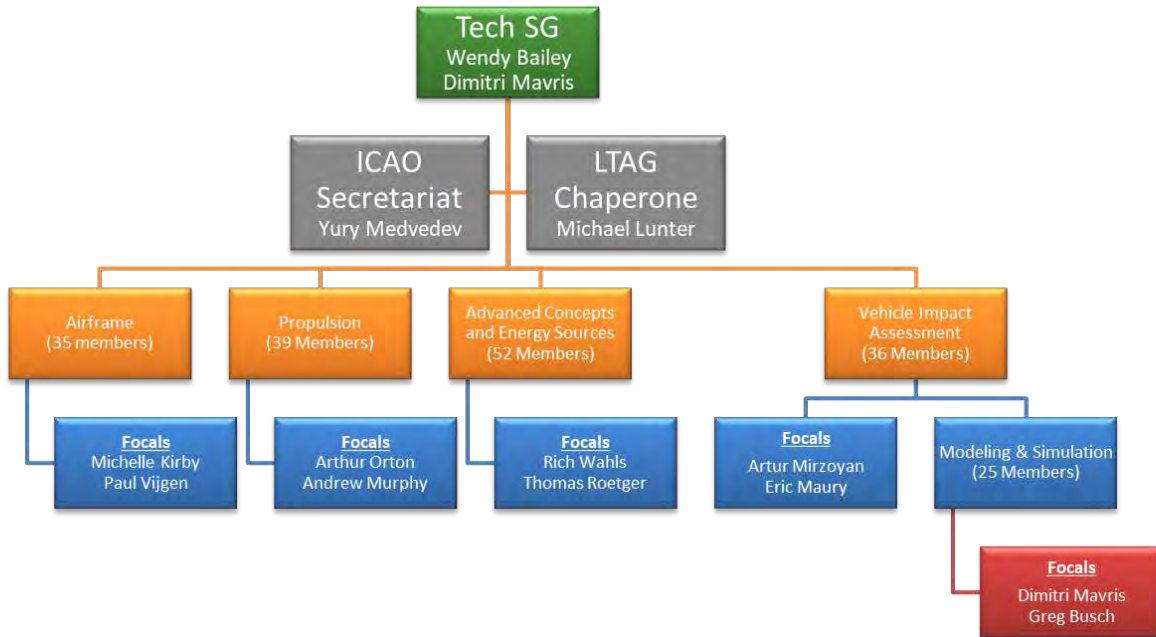


Figure 2. LTAG Technology subgroup structure.

**Research Approach**

Georgia Tech is supporting the task through hosting and attending various LTAG Tech SG calls, coordinating discussion between its members, and developing workplan proposals for the group. Georgia Tech has also taken on the responsibility for preparing presentations for these meetings, especially for the Tech SG and M&S meetings. There are a large number of LTAG related calls/meetings and many hours have been dedicated to supporting this task. The LTAG Tech SG call schedule continually changes based on the members’ availability, but the current schedule of LTAG calls is shown in Table 1. Other activity related to supporting this task are preparing presentations for plenary calls, writing status papers, information papers (IPs) and working papers (WPs), and presenting work summaries at CAEP/12 Steering Group meetings.

Table 1. Current LTAG Technology subgroup call schedule.

Group	Call time
Tech SG	Every other Wednesday, 9-11am
Joint Propulsion + Airframe Tahg	Every other Tuesday, 8-10am
ACES Tahg	Every Monday, 8:00-8:45am
Joint ACES Tahg + VIA Tahg	Every Monday, 8:45-9:15am
VIA Tahg	Every Monday, 9:15-10:00am
Tech SG Chairs + Focals	Every other Wednesday, 8-9am
Modeling & Simulation	Every other Wednesday 9-11am (Tech SG off weeks)

**Milestones**

- Developed workplan for ASCENT Project 064.



- Supported LTAG-TG at CAEP/12 steering group 2 (SG/2).

### **Major Accomplishments**

- Co-chairing the Tech SG and focals for the Airframe Tahg and M&S ad hoc group.
- Participation in all LTAG related meetings and calls.
- Participating in weekly Tech SG calls and ad hoc group meetings to develop technology impacts across five vehicle classes and preparing material for those calls.
- Refining the methodology, metrics, and process to assess the feasibility of a long-term aspirational goal
- Recurring calls with MDG on fleet level modeling and assumptions.
- Attended stocktaking event.
- Reviewed further submitted questionnaires.
- Wrote status papers for SG/2.

### **Publications**

None

### **Outreach Efforts**

None

### **Awards**

None

### **Student Involvement**

None

### **Plans for Next Period**

- Continue to support all LTAG-TG meetings and facilitate communication within LTAG.
- Prepare material to be presented and discussed during LTAG meetings.
- Host modeling and simulation meetings to inform members on the modeling objectives and progress.
- Attend and prepare content for LTAG Tech SG workshops 12/7/2020 and 12/14/2020.
- Support and prepare content for CAEP/12 Steering Group meeting 3 in Q2 2021.

## **Task 2 – Modeling & Simulation: Development of Turboprop Technology Reference Aircraft**

Georgia Institute of Technology

### **Objectives**

In order to support the modeling objectives of the LTAG-TG, representative vehicle models are developed and assessed at various timeframes to determine the potential impact of aircraft on the environment in the future. This information will then be used to help inform the LTAG leadership on potential long-term aspirational goals for aviation. The representative vehicle models are based on a current technology reference aircraft (TRA) and then infused with technology impacts in the 2030, 2040, and 2050 timeframes. LTAG-TG is also tasked with investigating advanced concepts for these timeframes and determining their performance characteristics. The current workplan for the LTAG M&S group is to use the TRA vehicles developed under the CAEP Independent Expert Integrated Review (IEIR). This included a TRA model for four different vehicle classes: business jets, regional jets, narrow body aircraft (single aisle), and wide body aircraft (twin aisle). It was requested by LTAG to develop an additional TRA for the turboprop vehicle class, as the electrification of this class of aircraft is likely to occur earlier than other vehicle classes. Georgia Tech is leading the effort to develop this turboprop TRA model to be used in the wider LTAG modeling effort.

### **Research Approach**

The Georgia Tech M&S team is working with industry experts to calibrate the turboprop TRA model. It was decided that the turboprop TRA would represent a notional De Havilland Canada Dash 8-400 aircraft.



Because a majority of the information required to create a TRA model is proprietary to the manufacturers, the TRAs are notional models-characteristics and performance are not required to match identically to the reference aircraft, but need to be close enough to be deemed “fit for purpose” to be used in the LTAG modeling effort. Georgia Tech has developed the turboprop TRA using EDS and currently in the process of getting it approved as fit for purpose. The TRA models are created using the modeling & simulation tool suite EDS by Georgia Tech/FAA/NASA and will go through the following process:

1. Collection of publicly available data on reference aircraft.
2. Review of data assembled with M&S ad hoc team and industry experts.
3. Develop EDS model comprising of a Flight Optimization System (FLOPS) vehicle model, Numerical Propulsion System Simulation (NPSS) engine model, and Aircraft Noise Prediction Program (ANOPP) noise model.
4. Calibrate EDS model to match performance characteristics.
5. Review calibrated weights, engine cycle, and performance with M&S ad hoc team.
6. If results are “fit for purpose” then modeling of TRA is complete. If not, then change modeling assumptions/inputs and return to step #4.

Georgia Tech has gone through multiple iterations of the turboprop TRA and has gotten valuable feedback from industry experts from De Haviland Canada, Pratt & Whitney Canada, and Dowty propellers. The current TRA model is very close to “fit for purpose,” and only requires some minor updates based on feedback from Dowty. The current performance metrics for the turboprop TRA are shown in Figure 3 and Figure 4. The current CO<sub>2</sub> metric value for the turboprop TRA stands at 0.517 kg/km. Georgia Tech is currently working on finalizing the TRA model and expects to accomplish this by the end of 2020.

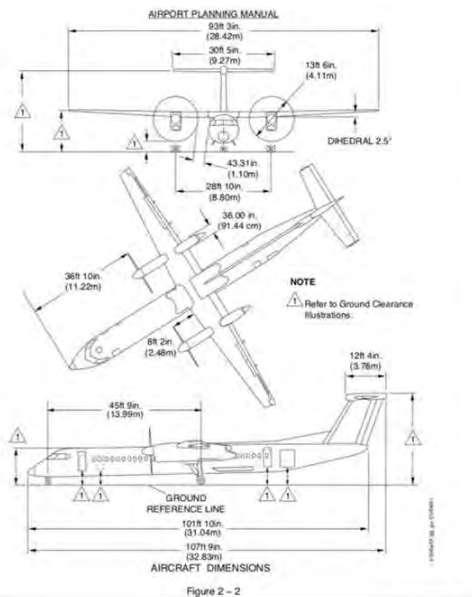


Image Ref: Bombardier, Q400 Airport Planning Manual  
Values obtained or measured from this reference.

Description	Value
Design Range	1,100 nmi
Design Payload	16,650 lbs / 7,552 kg
Design Cruise Mach No.	0.5 (Long Range Cruise)
Trip Fuel	7,459 lbs / 3,383 kg
Take-off Field Length	4,671 ft / 1,424 m
Approach Speed	117 kts / 60.2 mps
Max L/D (cruise)	16.2
CLmax Take-off	2.5
CLmax Landing	2.8
R1 Range	750 nmi
R1 Max Payload	18,696 lbs / 8,481 kg

Figure 3. Turboprop TRA current top-level metrics.

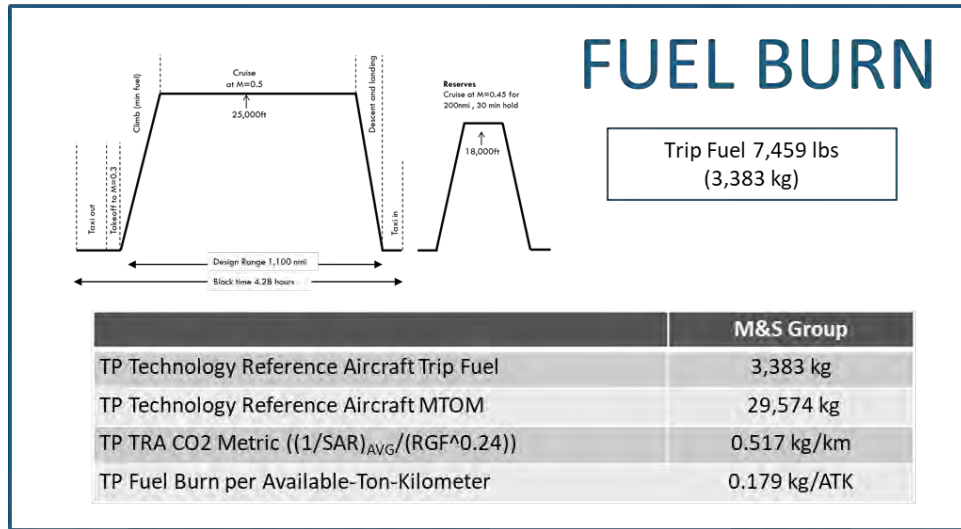


Figure 4. Turboprop (TP) TRA current fuel burn performance.

**Milestone**

Created a representative EDS model for the turboprop technology reference aircraft and iterated with industry experts to achieve “fit for purpose” status on fuel burn performance.

**Major Accomplishments**

- Gathered publicly available information on the De Haviland Canada Dash 8-400.
- Developed FLOPS vehicle model for turboprop TRA.
- Developed NPSS engine model for PW150A turboprop engine.
- Iterated with industry experts and are approaching finalized “fit for purpose” values.

**Publications**

None

**Outreach Efforts**

None

**Awards**

None

**Student Involvement**

Melek Ozcan, Graduate Research Assistant: Supporting modeling and simulation using EDS.

Luis Salas Nunez, Graduate Research Assistant: Supporting modeling and simulation using EDS.

**Plans for Next Period**

- Finalize turboprop TRA model by incorporating feed on propeller performance from Dowty.
- Model LTO noise of the turboprop TRA.
- Get approval from modeling and simulation ad hoc group to deem the turboprop TRA “fit for purpose.”

## Task 3 – Modeling & Simulation: Assessment of 2050 Projections of Technology Reference Aircraft

Georgia Institute of Technology

### Objectives

The objective of Task 3 is to perform assessments of future tube and wing (conventional) aircraft variants of the technology reference aircraft models. This task includes taking technology impacts for three different timeframes (2030, 2040, and 2050) and applying them to the five technology reference aircraft classes:

- Turboprop
- Business Jet
- Regional Jet
- Narrow body
- Wide Body

The technology impacts will be provided by the Propulsion and Airframe Tahgs within the LTAG technology subgroup and implemented onto the TRA models by the M&S group (led by Georgia Tech) of the VIA technical ad hoc groups. This task will initially be performed for the wide body vehicle class as the proposed “sample problem” to execute the entire LTAG modeling process. The objective of the sample problem is to go through the modeling methodology from front to back and include all the interactions and exchange of information between the various LTAG subgroups in an effort to establish a well-working methodology. This methodology will then be applied to the remaining four vehicle classes.

### Research Approach

The LTAG technology subgroup vehicle impact assessment process, shown in Figure 5, will be followed to accomplish the objectives of Task 3. This process includes all of the LTAG Tech SG technical ad hoc groups, with Georgia Tech primarily operating under the VIA Tahg. The Propulsion and Airframe Tahgs are currently in the process of down selecting technologies and determining the impacts to be provided to the VIA Tahg. These technology impacts will be provided at three different confidence levels: 80% confidence (high), 50% confidence (nominal), and 20% confidence (low). Once the technology impacts have been determined, they will be provided to Georgia Tech (as part of the VIA Tahg) and will be translated into modeling factors to be input in EDS for the modeling assessment. EDS will be used to model the future technology projection of all five vehicle classes at each timeframe and confidence level. For example, the wide body vehicle class assessments will result in fuel burn performance for nine different technology vehicles as follows:

- 2030 timeframe
  - High confidence technology wide body
  - Nominal confidence technology wide body
  - Low confidence technology wide body
- 2040 timeframe
  - High confidence technology wide body
  - Nominal confidence technology wide body
  - Low confidence technology wide body
- 2050 timeframe
  - High confidence technology wide body
  - Nominal confidence technology wide body
  - Low confidence technology wide body

The predicted noise levels for these aircraft models will also be assessed and tracked to ensure the technology packages on the future variants do not result in a significant increase in LTO noise. These assessments will be repeated for the other vehicle classes resulting in a total of 50 vehicle models being developed by Georgia Tech for Task 3: 45 technology aircraft (5 classes X 9 technology variants) and five 2017 technology reference aircraft. Once the performance metrics of the aircraft are determined, the fuel burn per available-ton-kilometer (ATK) relative to the 2017 TRA vehicles will be provided to the CAEP MDG group for fleet assessment. A notional table is shown in Table 2. MDG will use the fuel burn metrics to assess the impact of the technology vehicles on the fleet fuel burn projected out to the year 2070. The fleet results will be returned to the LTAG TG and the outcomes, along with economic impacts, will be utilized by LTAG to conduct a final analysis. LTAG will provide CO<sub>2</sub> emissions impacts, economic impacts, and technology roadmaps for each of the integrated scenarios to be brought forward to CAEP leadership.

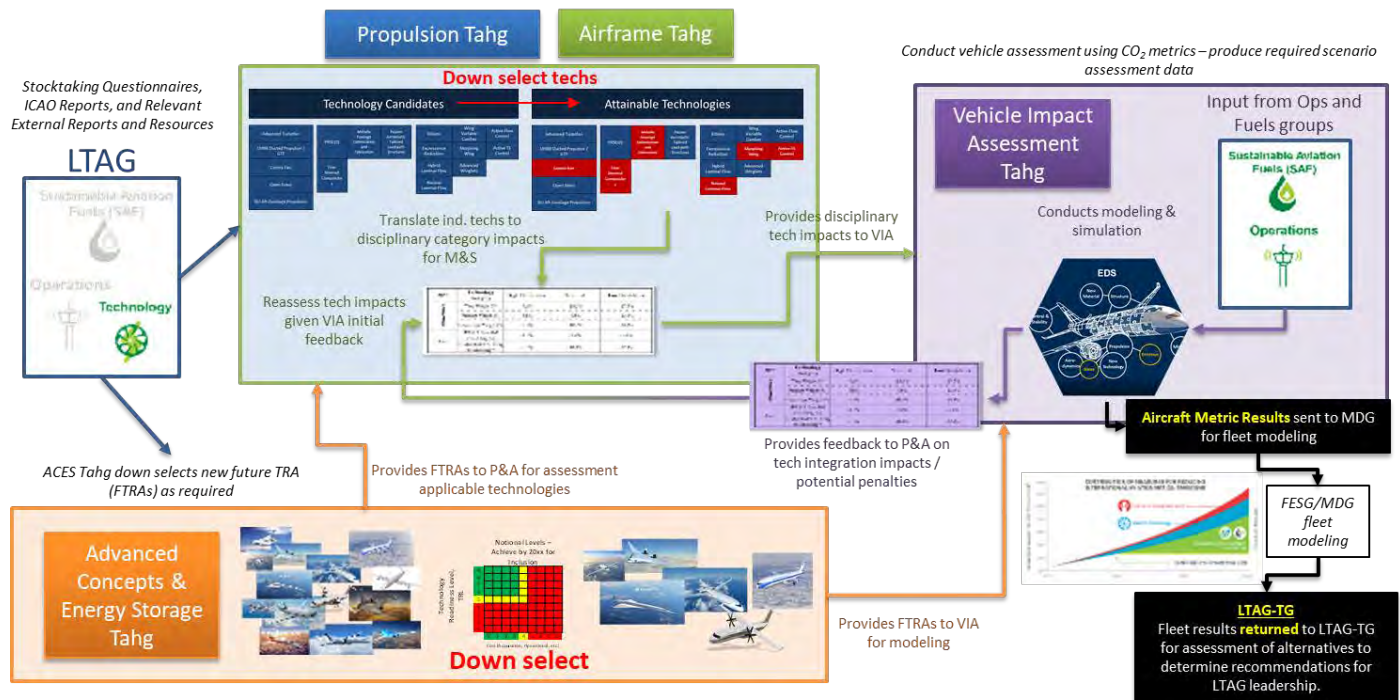


Figure 5. LTAG Tech SG assessment process.

Table 2. Notional table of fuel burn results to be provided to MDG.

Fuel Burn Per Annum Improvement rel. 2017 TRA (% Fuel Burn / ATK)					
Vehicle Class	Confidence Level	Timeframe			
		2017-2030	2030-2040	2040-2050	2050+
Turboprop	Low	0.67%	1.25%	0.96%	1.17%
	Nominal	0.72%	1.30%	1.01%	1.22%
	High	1.42%	2.00%	1.71%	1.92%
Business Jet	Low	0.37%	0.95%	0.66%	0.87%
	Nominal	0.42%	1.00%	0.71%	0.92%
	High	1.12%	1.70%	1.41%	1.62%
Regional Jet	Low	0.72%	1.24%	0.98%	0.95%
	Nominal	0.77%	1.29%	1.03%	1.00%
	High	1.47%	1.99%	1.73%	1.70%
Single Aisle	Low	1.21%	1.33%	1.17%	1.28%
	Nominal	1.26%	1.18%	1.22%	1.33%
	High	1.96%	1.88%	1.92%	2.03%
Twin Aisle	Low	0.99%	1.47%	1.23%	1.25%
	Nominal	1.04%	1.52%	1.28%	1.30%
	High	1.74%	2.22%	1.98%	2.00%
Adv. Concept A	Low	N/A	2.07%	2.05%	2.45%
	Nominal	N/A	2.12%	2.10%	2.50%
	High	N/A	2.82%	2.80%	3.20%
Adv. Concept B	Low	N/A	N/A	3.17%	4.15%
	Nominal	N/A	N/A	3.22%	4.20%
	High	N/A	N/A	3.92%	4.90%



### **Milestones**

- Established vehicle impact assessment methodology for LTAG Tech SG.
- Established timeline for LTAG modeling and simulation deliverables.
- Proposed wide body sample problem to use as a test case for modeling methodology.

### **Major Accomplishments**

- Verified performance of 2017 TRA models for business jet, regional jet, narrow body, and wide body classes (working on turboprop vehicle class as described in Task 2)
- Established required technology impact input to be delivered from Propulsion and Airframe Tahqs.

### **Publications**

None

### **Outreach Efforts**

None

### **Awards**

None

### **Student Involvement**

Melek Ozcan, Graduate Research Assistant: Supporting modeling and simulation using EDS.

Luis Salas Nunez, Graduate Research Assistant: Supporting modeling and simulation using EDS.

### **Plans for Next Period**

- Receive technology impacts for all five vehicle classes and translate impacts to modeling factors for use within EDS.
- Participate in LTAG Tech SG workshops to answer final outstanding questions regarding LTAG modeling process and establish required exchanges of information between the LTAG technology, fuels, and operations subgroups.
- Execute the modeling and simulation for the wide body sample problem.
- Complete modeling assessment for all vehicle classes/timeframes/confidence levels.
- Provide results to LTAG Tech SG and CAEP MDG for fleet assessment.
- Documentation of modeling and simulation process and methodology.

## **Task 4 – Modeling & Simulation: Assessment of 2050 Projections of Advanced Configurations**

Georgia Institute of Technology

### **Objectives**

The objective of Task 4 is to perform assessments of future advanced (unconventional) aircraft variants of the technology reference aircraft models. Task 4 is similar to Task 3 but applied to advanced aircraft configurations. These advanced configurations can include advanced airframe architectures, propulsion architectures and unconventional fuel systems. This task also includes taking technology impacts for three different timeframes (2030, 2040, and 2050) and applying them to the five technology reference aircraft classes:

- Turboprop
- Business Jet
- Regional Jet
- Narrow body
- Wide Body

The particular advanced configurations selected for use in the LTAG study will be done by the ACES Tahq, and has currently not been finalized. Georgia Tech is working with the focals of the ACES Tahq to help determine the advanced concepts to be used and provide potential options for modeling the impacts of these aircraft in the future timeframes of interest.



## **Research Approach**

The research approach for this task is still being finalized but will most likely follow the same process described in Task 3 and shown in Figure 5. The results of the task are similar to those in Task 3; the fuel burn performance metrics for the advanced concept aircraft are to be assessed for the 2030, 2040, and 2050 timeframes and provided to MDG for including in the fleet analysis. The approach for determining the performance of the advanced concepts is still under consideration. Georgia Tech has proposed that some of the advanced concept vehicles could be modeled and assessed through EDS, in a comparable way to the conventional tube and wing aircraft. Georgia Tech has also proposed that for the advanced concept variants that do not currently have a representative EDS model, the fuel burn performance could be determined through referencing studies and publications available in the public domain. Given the short time remaining to complete the entirety of the LTAG analysis, this could prove to be a prudent option for some or all of the advanced concepts that will be proposed by the ACES Tahg. It has been determined that the blended wing body (BWB) will be used as the advanced concept for the wide body sample problem. Georgia Tech is in the process of gathering information on the available models available for modeling and/or assessment.

## **Milestone**

- Helped guide the selection of an advanced concept for the wide body sample problem, a blended wing body variant.

## **Major Accomplishments**

- Helped establish a down selection process of the advanced concepts for the ACES Tahg.
- Provided information on available advanced concept models currently in Georgia Tech's EDS suite of aircraft models.

## **Publications**

None

## **Outreach Efforts**

None

## **Awards**

None

## **Student Involvement**

Melek Ozcan, Graduate Research Assistant: Supporting modeling and simulation using EDS.

Luis Salas Nunez, Graduate Research Assistant: Supporting modeling and simulation using EDS.

## **Plans for Next Period**

- Assist ACES Tahg in the down selection process for advanced concepts for all vehicle classes.
- Finalize the methodology to be used for assessing the fuel burn / emissions impact of advanced concepts.
- Perform the vehicle impact assessment for the blended wing body as part of the wide body sample problem.
- Perform the vehicle impact assessment for all other advanced concepts in all five vehicle classes, either through using EDS models or information from publicly available studies.



# Project 065(A) Fuel Testing Approaches for Rapid Jet Fuel Prescreening

## University of Dayton

### Project Lead Investigator

Joshua Heyne  
Associate Professor  
Mechanical Engineering  
University of Dayton  
300 College Park  
Dayton, OH 45458  
937 229-5319  
Jheyne1@udayton.edu

### University Participants

#### University of Dayton

- PI: Joshua Heyne
- FAA Award Number: 13-C-AJFE-UD, Amendments 26 and 31
- Period of Performance: June 5, 2020 to August 10, 2021
- Tasks:
  1. Prescreening of sustainable aviation fuels (SAF).
  2. Develop novel testing methods for the evaluation of SAF candidates.

### Project Funding Level

Amendment No. 026: \$159,998 (June 5, 2020, to June 4, 2021)  
Amendment No. 031: \$250,000 (June 5, 2020, to June 4, 2021)

Cost share is from the University of Dayton, VUV Analytics, and DLR Germany.

### Investigation Team

- Joshua Heyne (University of Dayton) is the Project Lead Investigator for coordinating all team member (both ASCENT and non-ASCENT efforts), communicating prescreening results with SAF producers.
- Linda Shafer (University of Dayton Research Institute) is a senior research engineer responsible for two-dimensional gas chromatography (GCxGC) measurement of SAFs.
- Zhibin (Harrison) Yang (University of Dayton) is a Ph.D. student conducting Tier Alpha prediction and Tier Beta measurement.
- Shane Kosir (University of Dayton) is a graduate student research assistant working on hydrocarbon properties prediction.
- Allison Coburn (University of Dayton) is an undergraduate student research assistant working on freeze point blending rule.

### Project Overview

This project will focus on further developing Tier Alpha and Beta test methods which can help minimize the fuel volume needed for testing and improve a fuels potential for meeting ASTM approval criteria. Tier Alpha refers to low-volume analytical testing approaches (i.e., GCxGC, nuclear magnetic resonance (NMR), and IR analytical testing). Tier Beta tests focus on testing the physical and chemical properties rather than predicting those key properties from GCxGC methods.

## Task 1 – Prescreening of Sustainable Aviation Fuels

University of Dayton

### Objective

A tiered prescreening process for new alternative jet fuels using low fuel volumes that will improve the potential for meeting ASTM approval criteria. This work lowers the technology readiness level (TRL) at which meaningful information can be provided to fuel producers, while simultaneously strengthening their readiness for the approval process.

### Research Approach

#### 1. Introduction

The aviation industry is facing mounting pressure to address current and growing anthropogenic emissions [1]. In response to the growing threat, the International Civil Aviation Organization (ICAO) has instituted emission reduction targets through the Carbon Offsetting and Reduction Scheme for International Aviation (CORSIA) [2]. Sustainable aviation fuels (SAFs) are identified as the only medium-term solution to the growing relative impact of aviation emissions on the environment. Recent life-cycle analysis (LCA) has shown that SAFs can reduce well-to-wake greenhouse gas (GHG) emissions by 60% to 104% relative to petroleum-based jet fuel [3]. To date, seven alternative fuels have been approved through the industry's standard approval and evaluation process (ASTM D4054 [4], D7566 [5]). The evaluation of alternative fuels through this process requires that novel fuels be compliant with safety, engine operability, compatibility, and minimal performance metrics. Safety, in the context of jet fuel, refers to the ability of a fuel to maintain acceptable properties under extreme conditions, such as maintaining a liquid state with acceptable viscosity under cold conditions, having a flash point above a determined limit, and others. A proposed prescreening test sequence requires that candidate fuels maintain these properties at a 50% blend ratio with Jet A.

Engine operability, in this context, refers to the ability of a fuel to ignite and hold a flame under potentially extreme conditions associated with the operating envelopes of main engines and auxiliary power units. Any novel fuel must exhibit acceptable performance within the same operating envelope as conventional jet fuels. Novel fuels that illustrate deleterious operability metrics pose a threat to safety and aircraft operations. Combustor and engine operability tests under ASTM D4054 (Tiers 3 and 4) involve significantly higher fuel volumes and capital expenditures than the fuel property tests of D4054, Tiers 1 and 2. Moreover, many of these operability tests have been the focus of the National Jet Fuels Combustion Program (NJFCP), which has measured the operability performance of multiple novel fuels with fundamental experiments and testing in more than a dozen combustor rigs. The results of these tests, hundreds of observations, nearly 20 different fuels, and numerous rigs are detailed in several publications [6–10].

The overarching results of the NJFCP work implies that nearly all observed combustor operability variance is captured by the physical and chemical properties, which in turn are controlled by the chemical composition of a fuel. Explicitly, deleterious operability behavior can be captured by bounding properties of a jet fuel within the typical experience of conventional fuels. The most important properties for combustor operability are viscosity at  $-20^{\circ}\text{C}$  and  $-40^{\circ}\text{C}$ , density, derived cetane number (DCN), distillation curve, flash point, and surface tension. DCN and surface tension have not historically needed independent specification requirements because they were constrained by other property limits of petroleum fuels. Recently, DCN has been shown to have a direct effect on lean blowout (LBO) performance in swirl-stabilized combustion [11,12]. Sensitivity to surface tension has also been identified [9], but its values may be constrained sufficiently by a fuel's density.

Compatibility and fungibility refer to the ability of a fuel to coexist, without deleterious effects, in existing hardware and infrastructure. Novel fuels, for example, must maintain the swelling character of O-rings and be non-corrosive. Furthermore, they cannot have deleterious effects for stakeholders responsible for parts of the existing fuel transport and delivery systems. The performance of jet fuels requires a minimum heat of combustion (HOC) and aromatic content within a range. Historically, novel fuels have not encountered issues with these two properties, but prescreening could cover these performance metrics if they did exist. SAFs that exhibit high HOC and density values also have the potential to be high-performance jet fuels (HPFs), which can confer benefits to end-users via increased aircraft payload, increased aircraft range, or reduced fuel volume required for a flight [13,14]. The use of gas chromatography (GC) to estimate specification tests properties for conventional jet fuel has been explored by Striebich et al. [15]. Striebich et al. were able to predict the distillation curve, freezing point, flash point, and sulfur content with a correlation for *n*-alkanes in conventional jet fuel. However, with the diverse profile of SAFs, they may deviate from this correlation or they might not contain *n*-alkanes. Here, a Tier Alpha testing procedure was developed to predict the above-mentioned important properties for combustor operability with only one mL of the candidate



fuel. This tool is intended to precede Tier 1 testing and provide fuel producers with information about the potential of a candidate fuel to pass subsequent tiered testing.

## 2. Material and methods

### 2.1 Material

A total of six SAFs were screened in this work, with their relevant information displayed in Table 1. The fuels encompassed three of the seven currently approved SAF conversion pathways [5]. All the fuels had high concentrations of *iso*-alkanes with smaller amounts of *n*- and cycloalkanes. Because of the high *iso*-alkane concentration of these fuels, it is expected that O-ring swelling, density, and DCN will represent the key limiting operability properties that necessitate blending with Jet A [16]. Properties for these SAFs were measured to validate Tier Alpha predictions, with testing methods and reproducibility errors detailed in the Supplementary Material.

**Table 1.** Information for SAFs screened in this work. Composition is in terms of *n*-alkanes, *iso*-alkanes, cycloalkanes, aromatics, and alkenes respectively.

Fuel	POSF	Average Formula	ASTM D7566 Annex	Composition, vol% ( <i>n/iso/cyclo/aro/alkene</i> )
Syntroleum FT-SPK	5018	C <sub>11.8</sub> H <sub>25.6</sub>	A1	24.2/75.2/0.6/<0.1/ND
Dynamic Fuels HEFA-SPK	7272	C <sub>12.4</sub> H <sub>26.7</sub>	A2	9.7/88.4/1.9/<0.1/ND
Sasol FT-SPK	7629	C <sub>10.8</sub> H <sub>23.4</sub>	A1	0.3/92.4/4.8/0.5/2.0
UOP HEFA-SPK	10301	C <sub>12.0</sub> H <sub>25.9</sub>	A2	10.2/86.2/3.5/0.1/ND
Gevo ATJ	11498	C <sub>12.6</sub> H <sub>27.2</sub>	A5	0/99.6/0.1/<0.1/0.3
Lanzatech ETJ	12756	C <sub>11.7</sub> H <sub>25.4</sub>	A5	0.8/96.5/2.6/<0.1/ND

### 2.2 Methods

The methodology for this study involved five components: (1) development of a hydrocarbon property database, (2) prediction of properties not available in the literature, (3) two-dimensional gas chromatography (GCxGC) measurements for SAFs, (4) random sampling using the hydrocarbon database and GCxGC data, and (5) SAF bulk property predictions using blending rules. These components are depicted relative to one another in Figure 1 and described in detail in the subsequent sections.

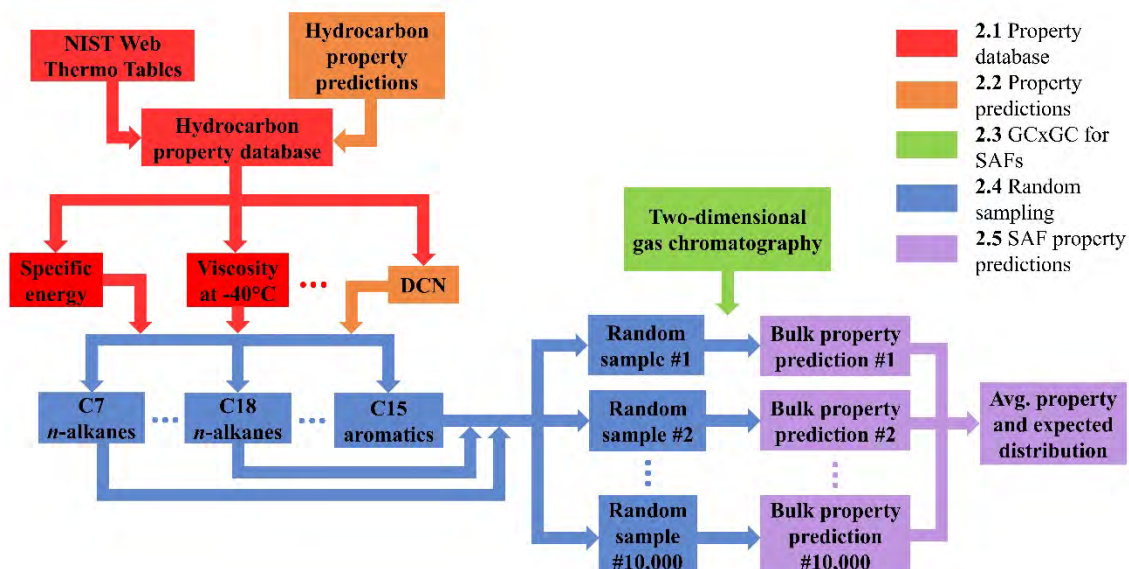
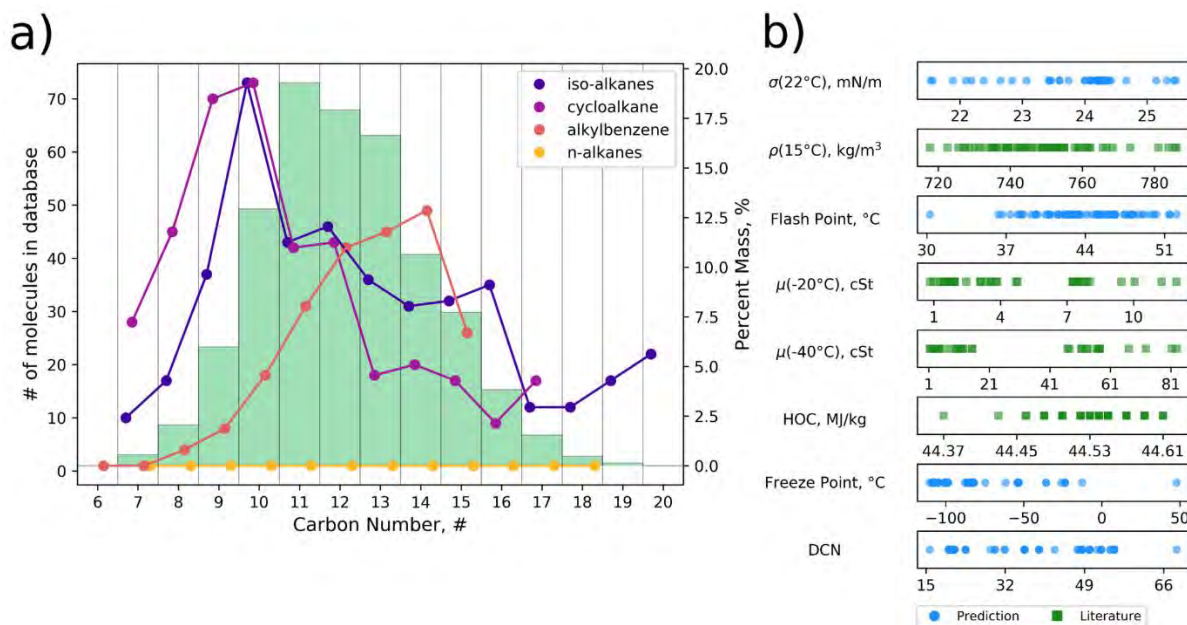


Figure 1. Flow chart of the methodology used for this study.

### 2.2.1 Hydrocarbon property database

Hydrocarbon property data used for this study consisted of 1,226 unique hydrocarbon compounds from nine molecular groups (i.e., *n*-alkanes, *iso*-alkanes, monocycloalkanes, dicycloalkanes, tricycloalkanes, alkylbenzenes, diaromatics, cycloaromatics, and dienes) ranging from C7 to C20. All the molecules were taken from the National Institute of Standards and Technology (NIST) Web Thermo Tables [17]. Each molecule had both temperature-dependent and temperature-independent properties. Surface tension at 22°C, density at 15°C, kinematic viscosity at -20°C, and kinematic viscosity at -40°C were temperature-dependent properties used in this study. Temperature-independent properties were boiling point, flash point, and HOC. Figure 2a shows the four most common molecular groups contained in SAFs that are in the hydrocarbon database plotted against a green histogram representing the composition of Jet A. The hydrocarbon database follows a quasi-normal distribution, indicating that it is a reasonable approximation of the composition and properties of Jet A. Because Jet A has a balanced distribution of all the major molecular groups, this means that the hydrocarbon database is representative of most fuels that can be expected for screening. Figure 2b illustrates property variance for 73 molecules that classify as C10 *iso*-alkanes. Blue circles are properties that were predicted for this work, and green squares represent properties taken from the literature. The large span for these properties indicates that the fidelity of predictions will be limited without further quantifying isomeric variance.



**Figure 2.** a) A frequency plot of the four most common molecular groups in the hydrocarbon database -*iso*-alkanes, cycloalkanes, alkylbenzenes, and *n*-alkanes- with green bars representing the composition by mass of Jet A and circles representing the number of molecules for each carbon number in the hydrocarbon database. b) A scatter plot of properties for 73 molecules that classify as C10 *iso*-alkanes. Green squares represent literature values and blue circles represent properties predicted in this paper.

### 2.2.2 Hydrocarbon property predictions

Properties not available on NIST were predicted with various methods. Flash point values for all molecules were predicted using Hshieh's work [18] on the relationship between boiling point and flash point. Hshieh developed a linear correlation of closed-cup flash points with normal boiling points with R-squared value of 0.966.

DCN values for molecules in the hydrocarbon database were predicted using a deep learning neural network trained using H<sub>2</sub>O Flow [19], with a five K-fold cross-validated mean absolute error (MAE) of 4.6 and an autocorrelation (R-squared) value of 0.94. 63 DCN observations for saturated hydrocarbons without heteroatoms were taken from the literature [20]. Only observations with DCN tested via ASTM D613 [21] and ASTM D6890 [22] were used for uniformity. Structural descriptors were generated from canonical smiles using the open-source cheminformatics software RDKit [23]. An overview of the training data can be seen in the Supplementary Material. H<sub>2</sub>O's automated machine learning (AutoML) feature was used to optimize weights and biases, with the final parameters displayed in the Supplementary Material. Feature importances from the neural network were subsequently used to screen observations from the hydrocarbon database with a threshold of 90% of the cumulative feature importance, similar to previous efforts in the literature [24]. This resulted in the removal of 161 molecules from the hydrocarbon database that did not fall within the range of structural variance encompassed by the training data.

A similar approach was taken to predict freezing point and surface tension for molecules in the hydrocarbon property database. 287 freezing point observations were taken from the literature [25] and used to train a neural network. A cross-validated MAE of 24.5°C and an R-squared value of 0.82 was achieved. The large MAE and modest R-squared value can be attributed to the fact that freezing point is widely regarded as a difficult property to predict because it is influenced by both crystal packing and neat molecule properties [26]. The surface tension model was trained using 260 observations from the literature [25]. The result was a cross-validated MAE of 0.83 mN/m and an R-squared value of 0.98. The low error achieved for surface tension is because it scales closely with density, which was used as a training feature.



### 2.2.3 Two-dimensional gas chromatography

GCxGC was used in this study to determine the hydrocarbon group-type composition of the SAFs using minimal volumes (i.e. one mL per SAF) [15]. The GCxGC analysis relies on the fact that hydrocarbon groups elute in certain regions of the GCxGC chromatogram based on both their volatility and polarity. All the compounds within a region have the same molecular formula and are identified and quantified as a group. Individual compounds are not identified except in the case of single-compound regions (e.g. n-alkanes, naphthalene). For instance, GCxGC results for Sasol SPK (POSF 7629) indicate that this fuel contains 31% C11 *iso*-alkanes, but 43 compounds can meet this classification. 2,2,3,4,5-pentamethylhexane and 3-ethylnonane are both C11 *iso*-alkanes; however, they have drastically different physical and chemical properties.

### 2.2.4 Random sampling of database properties

In the absence of any further information regarding the specific isomers contained within an eluted fraction (carbon number and molecular group), the best guess estimated properties corresponded to utilizing the hydrocarbon property database and GCxGC data to concurrently generate random samples of a given candidate fuel. From the respective GCxGC data, the corresponding weight or volume percent of the various hydrocarbon species can be identified for each molecular group and carbon number. Each relevant hydrocarbon grouping (via carbon number and molecular group) is paired with a random hydrocarbon with the same criteria in the hydrocarbon property database. This randomization of species primarily affected *iso*-alkanes and cycloalkanes as there are various isomerization and substitution patterns that affect their properties. Each of the randomly sampled species properties was extracted from the hydrocarbon property database and used for the bulk fuel property predictions. This randomization process occurred 10,000 times, creating 10,000 random candidate fuels to investigate variance and establish confidence in the given predictions. See Section 3 for discussion on random sampling convergence.

### 2.2.5 SAF property predictions

After random sampling of the molecules, appropriate blending rules were used to predict the properties of the bulk fuel being screened. For the average molecular weight, DCN, density, kinematic viscosity, and distillation curve, blending rules were taken from the work of Bell et al. [27]. Freezing point, flash point, and HOC blending rules were taken from the work of Flora et al. [28]. The surface tension blending rule used was the Macleod-Sugden correlation [29]. After 10,000 rounds of random sampling followed by bulk properties predictions, the average of each property was taken. The determined average of each property represented the most likely value for each property, and standard deviation was calculated to establish the confidence intervals.

## 3. Calculation

Random sampling, also known as Monte Carlo sampling, is used in this paper to predict the operability and safety properties of SAFs. Numerous examples of Monte Carlo sampling exist in the fuel literature, including for particulate matter segregation [30], combustion simulation [31], and separation modeling [32]. An important consideration for Monte Carlo sampling is to ensure that the samples have converged. In this study, convergence refers to the stability of the random sampling in terms of both the predicted average values and confidence intervals. If a property is converged, its fidelity can be considered as good as computationally possible without improving the accuracy of the hydrocarbon database or the capabilities of the GCxGC measurement.

As previously stated, 10,000 random samples were taken for each property considered in this study. Figure 3a depicts the running average property values plotted against the number of random samples and Figure 3b depicts the 95% confidence intervals plotted against the number of random samples. It can be seen that all properties have converged before reaching 10,000 random samples, justifying this threshold. The sporadic nature of the average values and the confidence intervals at low numbers of random samples can be attributed to the higher influence of outliers when the total number of samples is small. After about 2,000 random samples, density had few variations in its average value, indicating that the variance in each molecular group/carbon number bin was small. Properties like freezing point and DCN maintained larger variations in their average values, meaning that variance in each molecular group/carbon number bin was larger. This variation represents an inherent limitation for this approach unless molecules in SAFs can be identified with more exactness to inform the random sampling beyond molecular groups and carbon numbers.

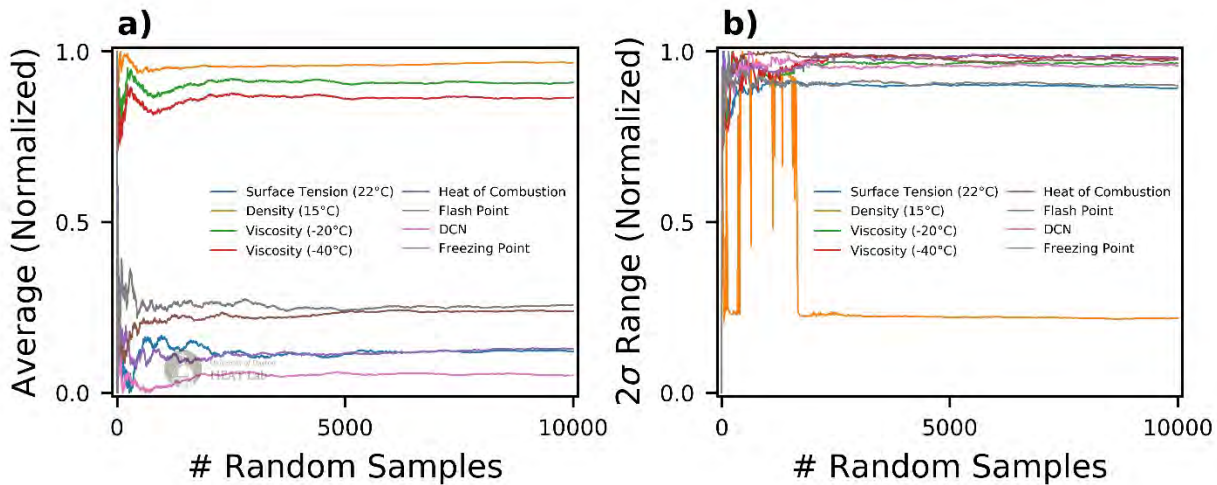


**Figure 3.** a) Average values and b) (95%) confidence intervals plotted against the number of random samples. Straight lines indicate that the predicted values have converged.

#### 4. Results and discussion

The measured properties for the six SAFs listed in Table 1 (black solid markers) and the Tier Alpha property predictions (colored open markers) of each SAF are plotted in Figure 4, with green shaded regions representing the conventional jet fuel range and red shaded regions representing violations of the specification limits. One sigma (solid colored lines) and two sigma (dashed colored lines) are plotted to show the confidence intervals of property predictions. Due to the known high uncertainty of the HOC and DCN measurements, the ASTM reproducibility (black solid line) is also reported for these properties. Relevant symbols include: surface tension ( $\sigma$ ), density ( $\rho$ ), and kinematic viscosity ( $\nu$ ).

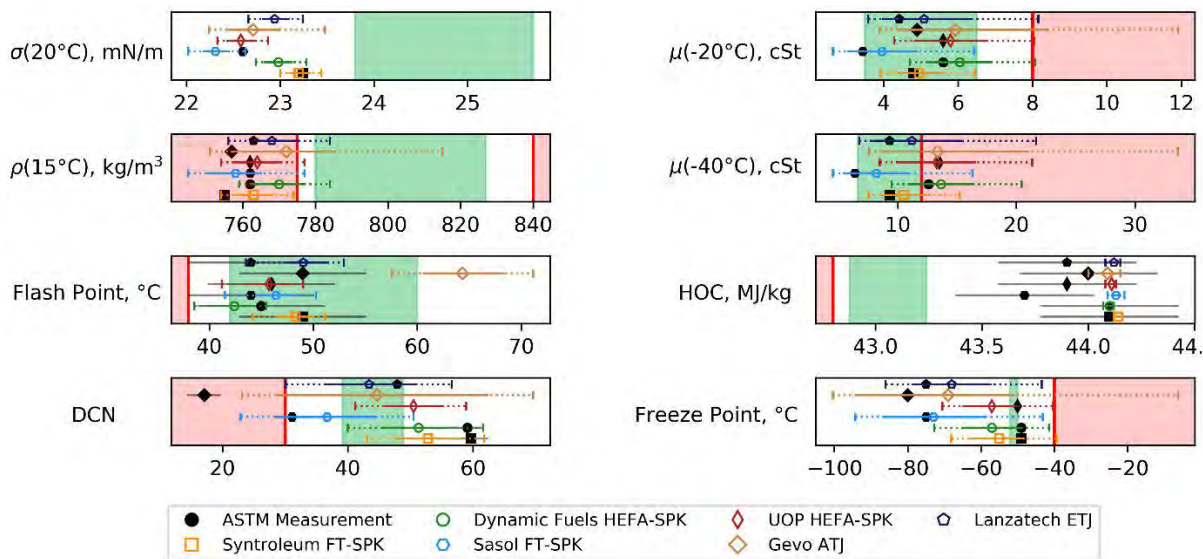


**Figure 4.** Tier Alpha property predictions and experimental measurements for SAFs. The open markers represent Tier Alpha predictions and solid markers are property measurements. The solid and dashed non-black lines represent one sigma and two sigma for the Tier Alpha predictions. The reproducibility of the ASTM measurements for HOC and DCN are reported as solid black lines.

The measured surface tension values for FT-SPK-Syntroleum and FT-SPK-Sasol are within the one sigma and two sigma range respectfully. There are only two surface tension measurements because surface tension has only recently been discovered as a key property to determine FOM. As Figure 4 shows, surface tension has a tight confidence range, which is because the majority of surface tension values for neat molecules have a positive linear correlation with density.

All SAF density measurements fall within the two sigma range and five are within the one sigma range. Dynamic Fuel HEFA SPK (POSF 7272) falls outside the one sigma range, largely because the range is very tight due to the low variance of density within the molecular group/carbon number bins.

Flash point had confidence intervals with medium magnitudes relative to the other properties. All flash point predictions except Gevo ATJ are within the two sigma range. Gevo ATJ likely fell outside the two sigma range because it contains 98% C12 *iso*-alkanes. Because of the specificity of C12 *iso*-alkanes, it is likely that they were not properly represented by the normal distribution generated during random sampling.

DCN and freezing point have some of the largest confidence intervals of any property. This is in part due to the uncertainty for neat molecule predictions, and also the result of factors influencing DCN and freezing point beyond molecular group and carbon number. Four out of five DCN measurements are within the two sigma range. Again, the outlier is Gevo ATJ, which could be due to the high concentration of a single carbon number molecule. All six measured freezing points are within the two sigma range and four of them are in the one sigma range. Dynamic Fuel HEFA SPK and UOP HEFA SPK fell slightly outside the one sigma range.

Viscosity experienced larger one sigma and two sigma ranges than the previously described properties because it is influenced by factors such as intermolecular attraction and bond rigidity in addition to molecule size. All viscosity measurements were inside the one sigma ranges.

There are only two measurements of HOC that fell outside the two sigma range. HOC also has the smallest confidence range of all the properties. There are four ways to test HOC (i.e., ASTM D1405, D3338, D4529, and D4909), and each one has different reported reproducibility errors. Because the HOC is directly linked to the hydrogen/carbon (H/C) ratio, and therefore easily predicted, it is preferred to use Tier Alpha rather than the ASTM methods to reduce uncertainty associated with the reproducibility errors.

The large uncertainty of Tier Alpha predictions came from property variance within a given molecular group and carbon number as shown in Figure 2b. Because the GCxGC data considered in this work only indicate molecular group and carbon number, the property variance associated with isomeric variance was propagated through to the final prediction. For instance, 2,2,3,3-tetramethylpentane and 2,2,3,4-tetramethylpentane are both classified as C9 *iso*-alkanes. However, the literature freezing points for these two molecules are -9.9°C and -121.1°C respectively [25]. That is a 111.2 °C difference from a single branch variance. Another example of significant property variance caused by a relatively small stereochemical difference is the experimentally determined DCN for *trans*-decalin and *cis*-decalin at 32.0 and 41.6 respectively [33]. With the vast range of properties for each carbon number and molecular group, it is inevitable to have a large uncertainty unless more information is provided by the fuel producer or the fidelity of the analytical technique is improved.

Figure 5 is a panel plot intended to show fuel producers SAF composition, Tier Alpha property predictions, and distillation properties. The left plot in Figure 5 shows GCxGC results for the SAF, with the green shaded region and the green line representing the carbon distribution and average carbon number for an average Jet A (POSF 10325). The carbon distribution of the SAF for various molecular groups is displayed on top of the green shaded region, and the vertical magenta line is the average carbon number of the sample. The middle plot in Figure 5 shows the Tier Alpha predictions (blue markers) with green shaded regions representing the conventional jet fuel range and red shaded regions representing violations of the specification limits. One sigma (solid blue lines) and two sigma (dashed blue lines) are plotted in these figures to show the confidence intervals of property predictions. The right plot in Figure 5 shows the distillation curve plotted to show the ASTM D2887 results as determined from the GCxGC data. The green shaded region is the conventional jet fuel range and the red shaded region is outside the ASTM D1655 specification limit.

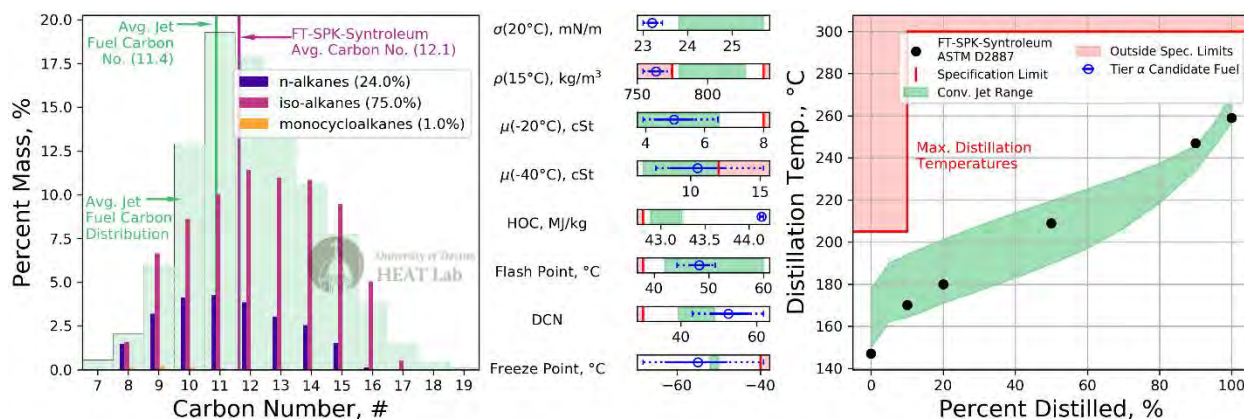


Figure 5. Panel plot for FT-SPK-Syntroleum (POSF 5018).

It is desirable for the fuel producer to match the general trend with the average conventional jet fuel on the left hand side of Figure 5 to reduce the risk of falling outside property specification limits. The risk of deleterious effects increases as the average carbon number of the SAF moves away from the average carbon number of Jet A. As the average carbon number of the SAF moves to the right, the SAF is expected to have higher density, surface tension, viscosity, flash point, and distillation curve. Having a high flash point is beneficial, but it could also push the viscosity outside the specification limit. Conversely, as the SAF becomes lighter, it is expected to have a lower density, surface tension, viscosity, flash point, and distillation curve.

#### 4. Conclusion

A Tier Alpha prescreening tool has been developed and validated to screen candidate alternative fuels at the earliest stage and to give the fuel producer early feedback regarding what is likely to occur during later tiered testing. Tier Alpha is capable of predicting eight properties that are the most important for combustor operability variance during Tier 3 and Tier 4 testing. Tier Alpha prescreening can be used as a proof of concept, as GCxGC requires less than one mL to run. In this way, the fuel producer only has to produce a small amount of fuel to test the concept instead of the 10 gallons required for Tier 1 testing [34]. If the producer has more available volume (i.e., ~150 mL), Tier Beta testing can be done at the University of Dayton to experimentally determine the properties that are important for combustor operability. As more volume is available, more tiered testing becomes possible and the uncertainty of the candidate fuels goes down. However, the required volume increases significantly relative to the uncertainty decrease as a candidate fuel passes through each technology tollgate as aligned with each tier of testing.

As previously stated, the GCxGC data considered in this work does not distinguish between molecules for each carbon number and molecular group. Instead, the GCxGC results show the fraction of each carbon number in each molecular group. Within each specific molecular group and carbon number, numerous isomers exist. Therefore, Tier Alpha does not predict the absolute value of each property, but rather it provides a range of possible values and the most likely value. If additional information is given by the fuel producer (i.e., molecules or functional groups that are expected to be in the SAF), then the confidence range can be significantly reduced. To date, Tier Alpha testing has been performed on 22 SAF samples from numerous national labs and industrial companies. The knowledge gained from Tier Alpha has helped fuel producers to adjust feedstock processing and conversion methods to achieve improved SAFs.

Tier alpha represents a work in progress, with significant reductions in the confidence intervals still possible. Future work should focus on the resolution of GCxGC or other analytical techniques to determine the composition of SAFs with greater fidelity. Neat molecule predictions for DCN and freezing point should be improved and the freezing point blending rule should be experimentally validated to narrow the confidence range of DCN and freezing point predictions. Filling gaps in the hydrocarbon database per Figure 2a would facilitate more accurate Tier Alpha predictions. Screened SAFs can also be optimized using the Jet Fuel Blend Optimizer (JudO) [35] to determine potential HPF blends that can provide performance benefits for aircraft and help eclipse the cost-benefit threshold of SAFs.



## References

- [1] Neumann B, Vafeidis AT, Zimmermann J, Nicholls RJ. Future Coastal Population Growth and Exposure to Sea-Level Rise and Coastal Flooding - A Global Assessment. *PLoS One* 2015;10:e0118571. doi:10.1371/journal.pone.0118571.
- [2] Chao H, Buyung D, Delaurentis D, Stechel EB. Carbon off setting and reduction scheme with sustainable aviation fuel options : Fleet-level carbon emissions impacts for U . S . airlines. *Transp Res Part D* 2020;75:42–56. doi:10.1016/j.trd.2019.08.015.
- [3] de Jong S, Antonissen K, Hoefnagels R, Lonza L, Wang M, Faaij A, et al. Life-cycle analysis of greenhouse gas emissions from renewable jet fuel production. *Biotechnol Biofuels* 2017;10:64. doi:10.1186/s13068-017-0739-7.
- [4] ASTM. Standard Specification for Aviation Turbine Fuel Containing Synthesized Hydrocarbons. *Annu B ASTM Stand* 2017:1–16. doi:10.1520/D1655-10.2.
- [5] ASTM D7566: Standard Specification for Aviation Turbine Fuel Containing Synthesized Hydrocarbons. West Conshohocken: 2020. doi:10.1520/D1655-10.2.
- [6] Heyne JS, Colket MB, Gupta M, Jardines A, Moder JP, Edwards JT, et al. Year 2 of the National Jet Fuels Combustion Program: Towards a Streamlined Alternative Jet Fuels Certification Process 2017:1–14. doi:10.2514/6.2017-0145.
- [7] Heyne JS, Peiffer E, Colket MB, Jardines A, Shaw C, Moder JP, et al. Year 3 of the National Jet Fuels Combustion Program: Practical and Scientific Impacts of Alternative Jet Fuel Research 2018. doi:10.2514/6.2018-1667.
- [8] Colket M, Heyne J, Rumizen M, Gupta M, Edwards T, Roquemore WM, et al. Overview of the National Jet Fuels Combustion Program. *AIAA J* 2017;55:1087–104. doi:10.2514/1.J055361.
- [9] Opacich KC, Heyne JS, Peiffer E, Stouffer SD. Analyzing the Relative Impact of Spray and Volatile Fuel Properties on Gas Turbine Combustor Ignition in Multiple Rig Geometries. *AIAA Sci Technol Forum* 2019:1–10. doi:10.2514/6.2019-1434.
- [10] Yang Z, Stachler R, Heyne JS. Orthogonal reference surrogate fuels for operability testing. *Energies* 2020;13:1–13. doi:10.3390/en13081948.
- [11] Heyne JS, Opacich KC, Peiffer EE, Colket M. The Effect of Chemical and Physical Fuel Properties on the Approval and Evaluation of Alternative Jet Fuels, 2019, p. 1–10.
- [12] Peiffer EE, Heyne JS, Colket M. Sustainable Aviation Fuels Approval Streamlining : Auxiliary Power Unit Lean Blowout Testing n.d.:1–9. doi:10.2514/1.J058348.
- [13] Kosir S, Behnke L, Heyne J, Stachler R, Flora G, Zabarnick S, et al. Improvement in Jet Aircraft Operation with the Use of High-Performance Drop-in Fuels. *AIAA SciTech Forum*, San Diego: AIAA SciTech; 2019.
- [14] Kosir S, Heyne J, Kirby M. High-Performance Jet Fuel Optimization and Aircraft Performance Analysis Considering O-ring Volume Swell 2018:1–6.
- [15] Striebich RC, Motsinger MA, Rauch ME, Zabarnick S, Dewitt M. Estimation of select specification tests for aviation turbine fuels using fast gas chromatography (GC). *Energy and Fuels* 2005;19:2445–54. doi:10.1021/ef050136o.
- [16] Flora G, Kosir S, Behnke L, Stachler R, Heyne J, Zabarnick S, et al. Properties Calculator and Optimization for Drop-in Alternative Jet Fuel Blends. *AIAA SciTech Forum*, San Diego: 2019.
- [17] Kroenlein K, Muzny CD, Kazakov AF, Diky V, Chirico RD, Magee JW, et al. NIST Standard Reference 203: TRC Web Thermo Tables (WTT) Version 2-2012-1 Professional. *Natl Inst Stand Technol* n.d.
- [18] Hshieh FY. Note: Correlation of closed-cup flash points with normal boiling points for silicone and general organic compounds. *Fire Mater* 1997;21:277–82. doi:10.1002/(SICI)1099-1018(199711/12)21:6<277::AID-FAM617>3.0.CO;2-3.
- [19] Using Flow - H2O's Web UI. *H2OAi* 2019.
- [20] Yanowitz J, Ratcliff MA, McCormick RL, Taylor JD, Murphy MJ. *Compendium of Experimental Cetane Numbers*. Golden: 2017.
- [21] ASTM D613: Standard Test Method for Cetane Number of Diesel Fuel Oil. West Conshohocken: 2000.
- [22] ASTM D6890: Standard Test Method for Determination of Ignition Delay and Derived Cetane Number (DCN) of Diesel Fuel Oils by Combustion in a Constant Volume Chamber. West Conshohocken: 2018.
- [23] Landrum G. *Getting Started with the RDKit in Python* 2016.
- [24] Kosir S, Heyne J, Graham J. A Machine Learning Framework for Drop-in Volume Swell Characteristics of Sustainable Aviation Fuel. *Fuel* 2020;274:1–7. doi:10.1016/j.fuel.2020.117832.
- [25] DIPPR 801 Database. *Am Inst Chem Eng* n.d.
- [26] Karthikeyan M, Glen RC, Bender A. General Melting Point Prediction Based on a Diverse Compound Data Set and Artificial Neural Networks 2005:581–90. doi:10.1021/ci0500132.
- [27] Bell D, Heyne JS, Won SH, Dryer F, Haas FM, Dooley S. On the Development of General Surrogate Composition Calculations for Chemical and Physical Properties. *55th AIAA Aerosp Sci Meet* 2017:1–5. doi:10.2514/6.2017-0609.
- [28] Flora G, Kosir S, Heyne J, Zabarnick S, Grupta M. Properties Calculator and Optimization for Drop-in Alternative Jet



- Fuel Blends. Aiaa 2018:1-14. doi:10.2514/6.2019-2368.
- [29] Poling B, Prausnitz J, O'Connell J. The Properties of Gases and Gas Mixtures. 2000. doi:10.1036/0070116822.
- [30] Rosato A, Prinz F, Swendsen R, Standburg KJ. Monte Carlo Simulation of Particulate Matter Segregation 1986;49:59-69.
- [31] Jovanović R, Marek E, Maletić S, Cvetinović D, Marković Z. Lattice Monte Carlo simulation of single coal char particle combustion under oxy-fuel conditions. Fuel 2015;151:172-81. doi:10.1016/j.fuel.2015.02.104.
- [32] Lei G, Liu C, Li Q, Xu X. Graphyne nanostructure as a potential adsorbent for separation of H<sub>2</sub>S / CH<sub>4</sub> mixture : Combining grand canonical Monte Carlo simulations with ideal adsorbed solution theory. Fuel 2016;182:210-9. doi:10.1016/j.fuel.2016.05.113.
- [33] Heyne JS, Boehman AL, Kirby S. Autoignition studies of trans- and cis-decalin in an ignition quality tester (IQT) and the development of a high thermal stability unifuel/single battlefield fuel. Energy and Fuels 2009;23:5879-85. doi:10.1021/ef900715m.
- [34] ASTM. ASTM D4054 – 20a Standard Practice for Evaluation of New Aviation Turbine Fuels and Fuel Additives 2020:1-45. doi:10.1520/D4054-20A.responsibility.
- [35] Kosir S, Stachler R, Heyne J, Hauck F. High-Performance Jet Fuel Optimization and Uncertainty Analysis. Fuel 2020.

### **Milestones**

- Tier Alpha performed 12 times.
- Tier Beta performed 15 times.
- Maximum blending ratio determined for three SAFs.

### **Major Accomplishments**

Reporting key combustor operability properties prediction for 12 SAFs, key combustor operability properties measurement of 15 SAFs, and maximum blending ratio for 3 SAFs.

### **Publications**

#### **Peer-reviewed Publications**

Yang, Z., Kosir, S., Stachler, R., Heyne, J., Shafer, L., and Anderson, C., "A GCxGC Tier Alpha Combustor Operability Prescreening Method for Sustainable Aviation Fuel," pp. 1-18. Fuel. (In review)

### **Outreach Efforts**

#### **Conference presentation**

ACS Fall 2020 National Meeting & Exposition in San Francisco, CA.

### **Awards**

None

### **Student Involvement**

Zhibin (Harrison) Yang, Ph.D. student, leads this effort.

### **Plans for Next Period**

Finalize the publication in progress, improve Tier Alpha prediction accuracy, and reduce volume required for Tier Beta measurement.



# Project 065(B) Fuel Testing Approaches for Rapid Jet Fuel Prescreening

## University of Illinois Urbana-Champaign

### Project Lead Investigator

Tonghun Lee  
Professor  
Mechanical Science & Engineering  
University of Illinois at Urbana-Champaign  
1206 W. Green St.  
Urbana, IL 61801  
517-290-8005  
tonghun@illinois.edu

### University Participants

#### University of Illinois at Urbana-Champaign

- PIs: Tonghun Lee, Professor
- FAA Award Number: 13-C-AJFE-UI-030
- Period of Performance: June 5, 2020 to June 4, 2021
- Tasks:
  1. General characterization of the M1 combustor.
  2. Measurements for comparison with referee combustor (NJFCP).

### Project Funding Level

FAA funding level: \$150,000

Cost share: 100% match provided by software license support from Converge, Inc.

### Investigation Team

- Tonghun Lee, Professor, University of Illinois at Urbana-Champaign (UIUC): Overall research supervision.
- Eric Wood, Jeongan Choi (Graduate Students, UIUC): Experimental efforts characterizing the M1 combustor including laser and optical diagnostics.

### Project Overview

This study (Prescreening 65b) will aim to introduce a new compact test rig (M1 combustor), developed with OEM support within the National Jet Fuel Combustion Program (NJFCP), which can screen fundamental combustor behavior with much reduced fuel volume (~gallons) prior to Tier 3 and 4 tests in the ASTM D4054 evaluation. In the NJFCP, the referee rig at the Air Force Research Laboratory (AFRL) was utilized as a foundational test rig for this goal. The M1 may have the potential to carry out these tasks at reduced fuel volumes (~gallons versus ~hundreds of gallons) in a simplified and open architecture that can be readily shared and operated at different locations at a fraction of the cost. Both Army Research Laboratory (ARL) and Argonne National Laboratory (ANL) will be partners in the effort to fully characterize the M1 facility. If successful, it would allow both fuel providers and OEMs to conduct basic combustor tests using identical testing architecture and the same test conditions at multiple test locations. Through the NJFCP program, the referee rig at AFRL has shown the ability for a combustor rig to produce results that can lead to reduced uncertainty in Tier 3 and 4 ASTM testing. The M1 combustor may potentially provide similar capabilities with less fuel consumption, and ease of access compared to the referee rig, which is housed in a secure government facility (AFRL). Tests in smaller test rigs can provide a platform for each supplier to independently test their new fuels and make predictions without resorting to the use of one single combustor facility. Over

time as test data is massed, the potential for test rigs such as the M1 to predict actual Tier 3 and 4 performance will increase and may even reduce the burden of relying on capital intensive ASTM rig and engine tests.

**Background of M1 Combustor**

During the FAA-funded NJFCP program in 2016, the Referee Rig combustor at AFRL was being used to determine the sensitivity of combustor performance parameters such as lean blow-out (LBO) and ignition on the chemical composition of novel fuels. The results from this investigation were instrumental in establishing a relationship between fuel chemistry and its impact on combustor performance. Professor Tonghun Lee’s research group carried out a significant portion of the laser and optical diagnostics in the referee rig as part of the NJFCP, including quantitative phase doppler particle analyzer (PDPA) measurements during full combustoring conditions which will be leveraged here.

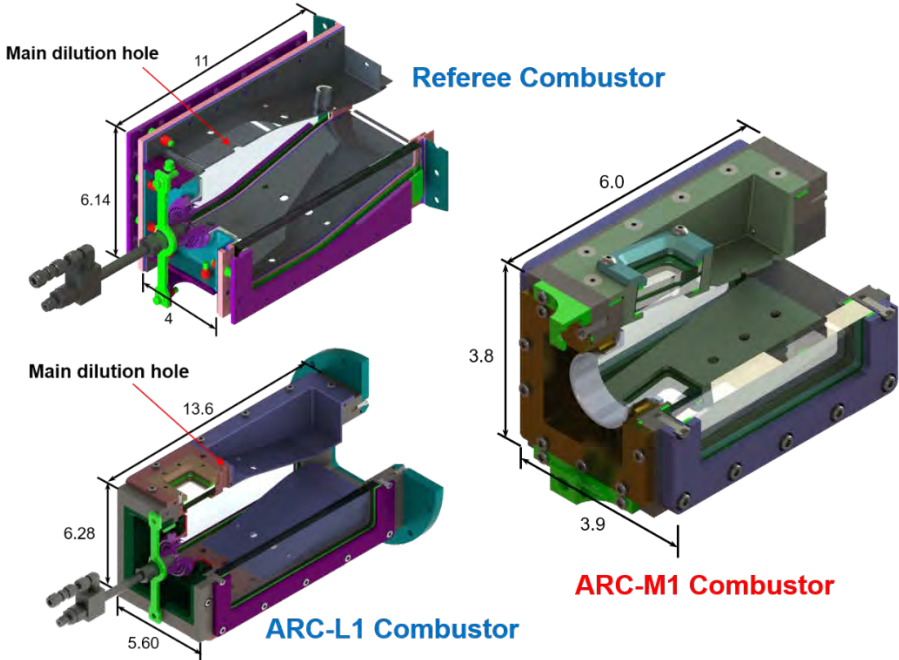


**Figure 1.** The referee combustor at AFRL, the ARC L1 combustor, and the M1 combustor.

Simultaneously, ARL was working with the NJFCP researchers to compliment the referee combustor work by carrying out high altitude relight tests at the ARL Aberdeen Proving Grounds, where a new altitude test chamber had just been commissioned. During the planning phase, ARL decided to build two new combustors for this purpose to address a couple of shortcomings of the referee combustor, namely optical access and flow split uncertainty. The first combustor would have the exact same dimensions as the referee combustor but with enhanced optical access and a less complicated liner for air cooling. Lack of vertical optical access had made velocity field measurements in the referee combustor virtually impossible, and the complicated liner had made accurate prediction of air flux into the combustor difficult. This new combustor would be code named ARC-L1 (Army Research Combustor-L1). Additionally, an effort was made to build a smaller combustor for more flexible testing with less fuel and air requirements. This smaller version would be code named the ARC-M1 and is the main architecture that is proposed in this study. Both combustors were designed through a subcommittee composed of NJFCP researchers and OEM representatives. The construction of both combustors was originally carried out in the research group of the PI (Tonghun Lee) at UIUC.

The referee combustor, L1, and M1 are shown in Figure 1. Continuing the heritage, ARL will be a key partner in the analysis of this combustor in terms of both numerical simulation efforts as well as x-ray imaging of spray break-up to be carried out at the Advanced Photon Source of ANL. In addition to the laser and optical measurements available at UIUC, the goal is to characterize the operating characteristics of the M1 in an unprecedented way so that it can be widely adopted in the academic/industrial community as a test platform for new fuel blends.



## Task 1 – General Characterization of the M1 Combustor

University of Illinois at Urbana-Champaign

### Objectives

The goal of this task is to perform a series of tests and diagnostics on the M1 combustor in order to quantify its operating characteristics in a manner which can allow it to be useful as a standard test platform for novel alternative fuels and for investigation of specific phenomena necessary for development of future combustion systems. This process includes developing the M1 combustion infrastructure to ensure repeatable and well-characterized operating conditions. The goal of the investigation is to characterize the M1 using x-ray diagnostics, laser and optical diagnostic techniques, as well as testing at LBO and high-altitude conditions to evaluate extremes of the operational envelope. This will allow the development of well-characterized numerical simulations for further study of complex combusting phenomena. Such information can be helpful for others who may choose to utilize the M1 architecture for future studies. The specific objectives in Task 1 are as follows:

- Setup and shakedown of the M1 combustor for testing.
- Selection of standard configuration and range of operating conditions.
- X-ray based spray imaging (ANL) and high-altitude testing at ARL.
- Laser and optical diagnostics in the laboratory at UIUC.

### Research Approach

The ARC-M1 combustor is a single-swirl cup gas turbine combustor that has been designed to allow application of an array of diagnostic techniques. The combustor has full optical access on four sides to allow application of many different types of laser and optical diagnostic techniques. In addition to the combustor itself, the infrastructure surrounding it has been built up to allow careful control of combustor operating parameters including inlet air system, combustor pressure, and fuel injection flow rate. This infrastructure includes mass flow controllers on the air and fuel inlets and a high-temperature control valve on the combustor outlet. The inlet air preheat temperature is also carefully controlled with independent temperature and power controllers on the main and dilution airflow. Figure 2 shows an image of the combustor installed for laser diagnostics measurements at UIUC and an image of A-2 fuel (conventional Jet-A) burning in the M1 combustor, showing the swirl-stabilized shape of the flame through a side window.

It is critical for a standard combustor to be carefully characterized at standard operating conditions and Table 1 shows the range of operating conditions at which the M1 combustor is designed to operate. These span a wide range of air flow rates and fuel flow rates, allowing investigation of many varying combusting conditions. The M1 has the capability of operating at higher pressures, but we are limiting it to three bars in the preliminary characterization, which can be easily accommodated in the future at separate locations.

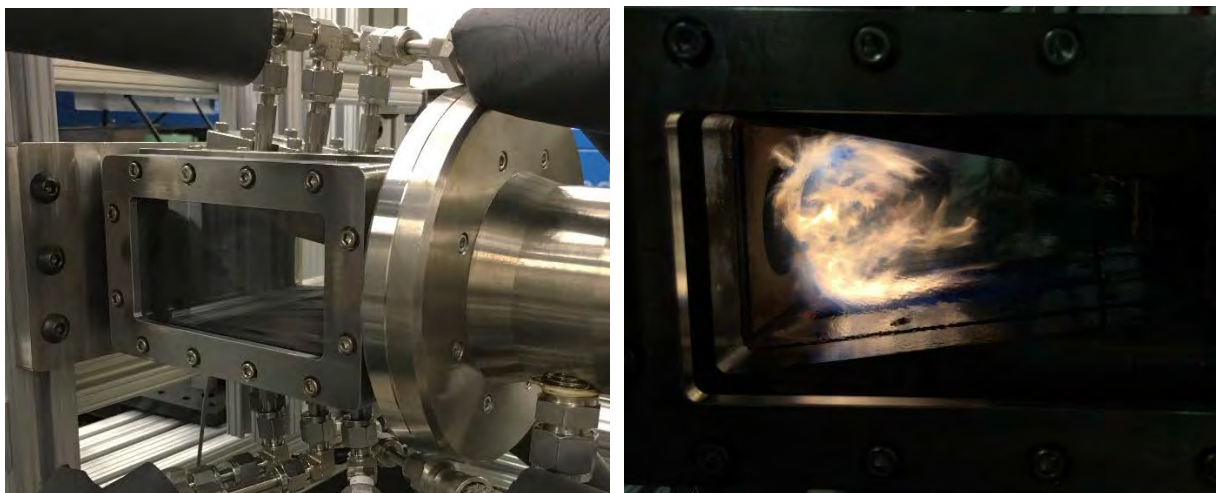


Figure 2. The ARC-M1 combustor installed at UIUC (left); the M1 combustor operating with A-2 jet fuel (right)



**Table 1: M1 Combustor Operating Conditions**

Input Variable	Conditions
Combustor Pressure	1-3 bar
Air Inlet Temperature	300-423 K
Pressure Drop	3% - 5%
Air Flow Rate at 3% dP/P*	28-60 g/s
Fuel Flow Rates**	15-65 g/min
Global Equivalence Ratio	0.08-0.35

\*With flow split of ~80% main, 20% dilution

\*\*Fuel flow rates at each condition bounded by LBO and max combustor temperature

**High-Speed Multiphase Liquid Spray Imaging (Advanced Photon Source, Argonne National Laboratory)**

One of the unique capabilities afforded by the M1 is the ability to easily transport the combustor and supporting infrastructure to external facilities to perform specialized diagnostic measurements for characterization. One type of unique diagnostic capability that will be applied to the M1 combustor is high-speed phase contrast imaging using the Advanced Photon Source (APS) at ANL, one of the most powerful synchrotron light sources in the world for x-ray generation. The high brightness and spectral breadth of this source allows for a wide range of advanced diagnostics to be performed, most of which are difficult to perform on smaller, laboratory-scale sources with limited photon flux. The 7-BM beamline is utilized for imaging of the M1 at the APS and can support several time-resolved x-ray diagnostics. Specifically, phase contrast imaging is used to image the liquid spray breakup from the pressure-swirl atomizer inside the combustor. An overview of this approach is shown in Figure 3.

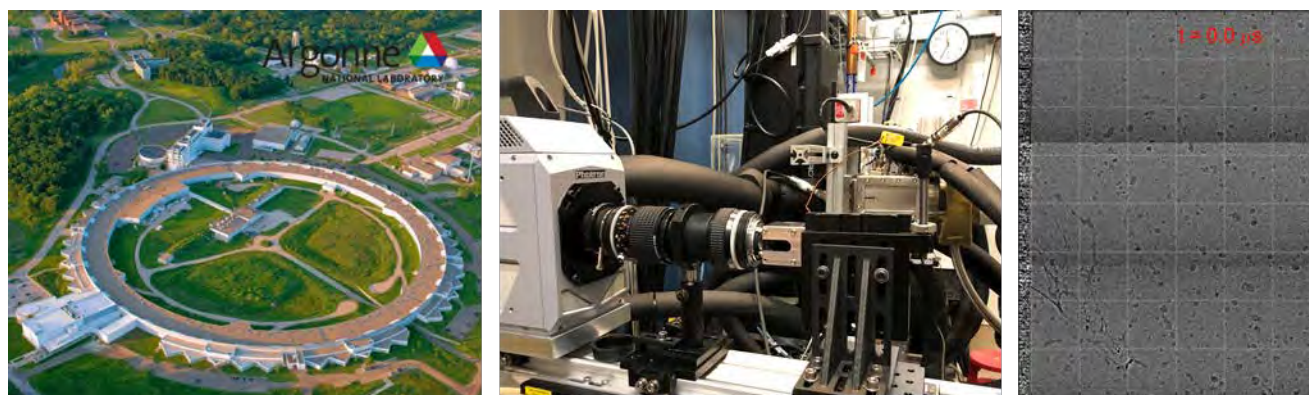


**Figure 3.** The Advanced Photon Source (APS) at Argonne National Laboratory (left); the ARC-M1 combustor installed at the 7-BM beamline at the APS (center); phase contrast image of fuel spray in the combusting ARC-M1 (right).

This technique utilizes the unfocused, raw emission from the bending magnet x-ray source (white beam) with beam power of approximately 600 mW/mm<sup>2</sup>, as measured at the scintillator crystal, which is used to convert the x-rays into visible light. This imaging technique relies on differences in the indices of refraction between the fuel and the surrounding heated air. While the primary interaction between the x-ray beam and the fuel is absorption, gradients in the indices of refraction, which primarily occur at the boundaries between the two fluids, causing phase shifts in the x-ray beam, resulting in a Fresnel diffraction pattern. Diffraction at the boundaries between liquid fuel and air results in enhanced contrast in the collected images. Using this technique, the fuel spray passing through the beam can be tracked in high-speed (90,517 Hz) images as it undergoes breakup. The imaging itself is conducted using a Photron SA-Z, which images a YAG:Ce scintillator crystal using

a reversed Nikkor 50mm f/1.2 lens and a forward Nikkor 105mm f/1.4 lens. The field of view is approximately 5.95 mm x 2.60 mm, with a resolution of 9.30  $\mu\text{m}/\text{pixel}$ . To allow the x-ray beam to pass into the combustor, the quartz windows typically used for other diagnostic techniques are replaced with Kapton windows. These windows are 0.127 mm thick with overall dimensions of 21.0 x 3.18 mm. Kapton is chosen for these windows because of its high x-ray transmissivity, ensuring the x-ray is minimally attenuated before or after passing through the fuel spray. This type of phase contrast imaging is only possible on the M1 combustor due to its unique ability for it and its entire control system to be easily transported to ANL to allow these experiments to be conducted. The information that is gained through this diagnostic technique is extremely unique and allows characterization of these liquid sprays in a combustor environment with unprecedented accuracy. This data will be the foundation of initial conditions that will be supplied to high-fidelity numerical simulations.

### High-Speed Diagnostic Techniques

In addition to the x-ray measurements at APS, high-speed laser and optical diagnostic techniques allow investigation into high-speed transient combustion phenomena that are critical for characterization of combustion performance but elusive to fully capture. These high-speed techniques have undergone tremendous development in the past decade, with new equipment allowing application at higher framerates than ever possible previously (routinely in the 10s of kHz and up to 1 MHz). The application of these techniques, including high-speed chemiluminescence, high-speed planar laser-induced fluorescence (PLIF), high-speed particle image velocimetry (PIV), and PDPA to the ARC-M1 combustor environment allow an extremely detailed understanding of the combustion environment and combustor boundary conditions. The design of the M1 has been specifically tailored to application of these diagnostic techniques with its large windows and multi-sided optical access. Figure 4 shows a sample image of high speed OH\* chemiluminescence at reference conditions, which will be retaken using PLIF at UIUC.

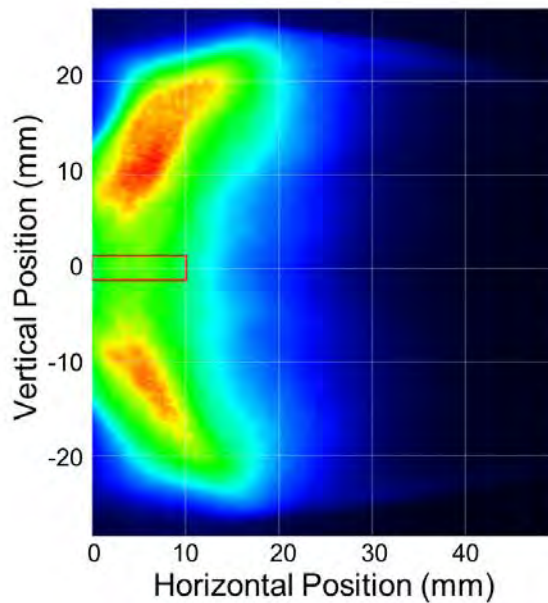


**Figure 4.** Average OH\* chemiluminescence image in the M1 combustor operating at reference conditions.

In addition to the combustion dynamics, we will systematically characterize the relevant flow fields which will be of critical importance for numerical simulation validation. Figure 5 shows initial PIV data that has been collected on the ARC M1. This serves as an example of the advanced diagnostic techniques which will be applied to the combustors as part of this project. Future efforts will focus on simultaneous application of PIV and other diagnostics including PLIF at high frame rates (>10 kHz). Using these diagnostics, we plan to investigate the specific flow velocities and combustion radicals present within an operating gas turbine combustor environment; this information allows study of the behavior leading to both combustor ignition and LBO in extreme environments. By gaining a deeper understanding of the flow behaviors leading to these events, future engine technologies can be optimized to reduce the likelihood of unexpected flame-out events and improve the reliability of relighting an engine in extreme high-altitude conditions. Additionally, the suitability of new alternative fuels with these engines can also be ascertained. These boundary conditions also allow for well-characterized high-fidelity

numerical simulations to be performed on this combustion environment, which can investigate combustion phenomena in ways that cannot be studied in experiments alone.

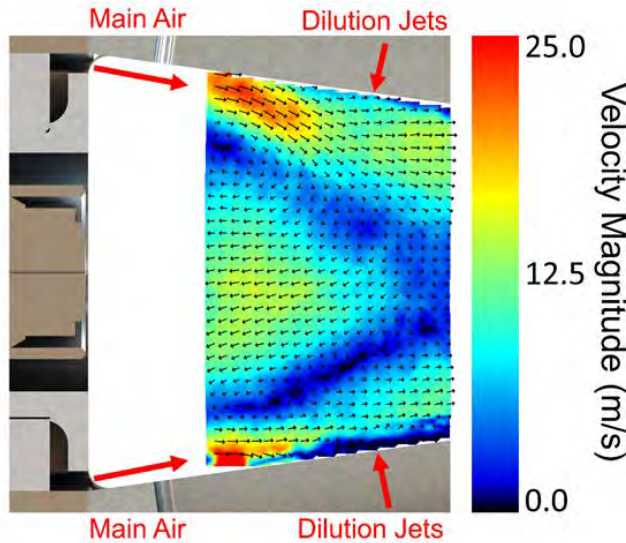


Figure 5. Average velocity from PIV in the M1 combustor operating at reference conditions.

The measurements proposed here ensure that M1 does not just become another combustor where fuels tests are reported. We will ensure that the M1 is the most extensively characterized combustor available so that the community can embrace its performance based on a firm scientific foundation and adapt further tests according to their needs.

**Milestones**

- 3 months: M1 combustor and control system setup and testing at UIUC.
- 6 months: Selection and testing of standardized testing conditions (basic LBO tests).
- 9 months: High altitude relight experiments at ARL.
- 12 months: APS x-ray measurements (depending on ANL reopening) and preliminary diagnostics measurements at UIUC.

**Major Accomplishments**

We are in the fifth month of the project. We have successfully operated the combustor and selected the test conditions. We have also been able to conduct some of the preliminary LBO measurements which will be shown in Task 2. At the outset of the project, we reassembled and received blessing of the original OEM, federal, and university team who participated in the M1 (we will keep them informed in the project).

**Publications**

N/A

**Outreach Efforts**

All test data will be made accessible through <https://altjetfuels.illinois.edu/>

**Awards**

None

**Student Involvement**

This project will be primarily conducted by two graduate students: Eric Wood (Ph.D.) and Jeongan Choi (Ph.D.).

### Plans for Next Period

We are at the very beginning of this project and the next task is to set up the diagnostics equipment at UIUC as well as conducting the high-altitude measurements at ARL and the x-ray imaging measurements at ANL.

## Task 2 – Measurements for Comparison with the Referee Combustor (NJFCP)

University of Illinois at Urbana-Champaign

### Objective

The objective here is the carry out baseline LBO and ignition measurements that were carried out in the referee combustor for comparison. This is to test how this smaller standard combustor compares to the referee rig at similar test conditions. We will also carry out high altitude measurements to ensure that the test results compare well with the trends we have observed in the referee combustor.

### Research Approach

Throughout the NJFCP, the referee combustor and several other combustors were carefully characterized in a variety of relevant operating regimes, including blowout and ignition. These studies were conducted at a variety of standard operating conditions which are relevant to gas turbine operational regimes that are likely to expose differences between fuels of varying properties. While these experiments in the referee combustor have provided valuable data about fuel effects near LBO, operating the referee rig comes with some disadvantages. The scale of the referee combustor brings large air and fuel flow rate requirements, which can make setup and operation expensive, especially when working with new alternatively derived fuels, which may be difficult to manufacture. As such, it would be beneficial if similar results could be obtained from a smaller combustor with reduced fuel and air requirements. By contrast, the ARC-M1 combustor uses significantly less air and fuel, reducing overall instrumentation expense and complexity, as well as reducing the volume of fuel needed to conduct tests over a range of conditions. This opens up the possibility that the M1 combustor could be used to evaluate performance of new fuels with much less fuel being used to conduct testing, reducing the supply requirements for a potential new fuel supplier. In order for this to happen, we need to ensure that the trends we see in a smaller combustor can convey the physics we saw in the referee combustor.

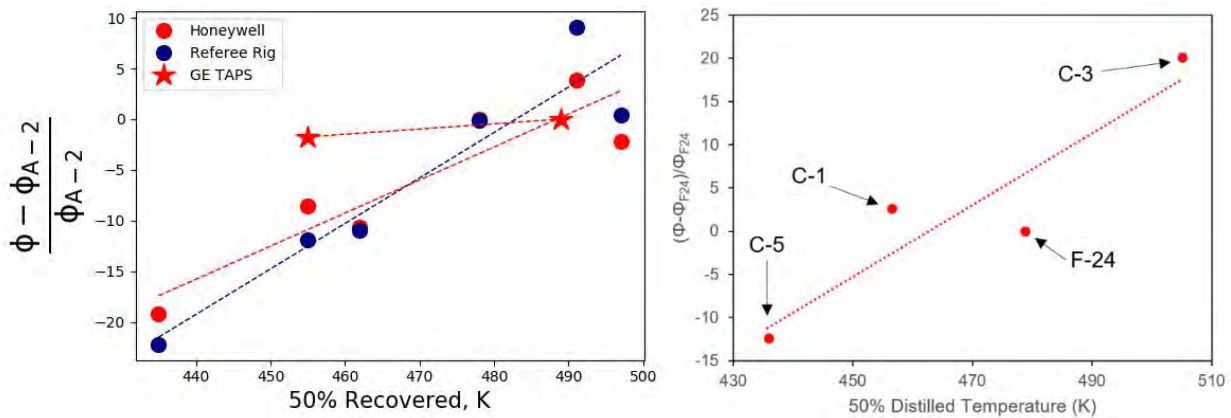


**Figure 6.** LBO data from several NJFCP rigs (left) and averaged data from the M1 combustor (right). Data from the M1 combustor was normalized using the F-24 data, as A-2 was not tested.

Testing of the ARC-M1 combustor will be conducted at near-LBO conditions to evaluate combustor performance and to facilitate comparisons to the referee combustor data that has been published as part of the NJFCP. These comparisons can give insight into how performance in the smaller combustion environment of the ARC-M1 compares to the larger referee rig. These comparisons will involve testing of the M1 combustor at identical conditions and evaluating how the performance across different fuels and different combustor operating conditions compares between the M1 and the referee rig data. Figure 6 shows some initial comparison data between the M1 and the referee rig. More in-depth comparisons will be

performed in the future to allow scientific performance evaluation of the effects of fuel properties and how these effects vary between the M1 combustor and the referee combustor.

### **Milestone(s)**

6 months: M1 combustor setup and shakedown and selection of test conditions.

9 months: Preliminary comparison measurements in the ARL high altitude chamber.

12 months: Comparison measurements of LBO for select NJFCP fuels in the M1 combustor for comparison with the referee combustor data.

### **Major Accomplishments**

Currently, we have only preliminary measurements shown in Figure 6. We had planned and executed a high altitude relight campaign in August 2020 but due to an unexpected fire at ARL's Aberdeen Proving Grounds, we had to cancel the campaign during the first week. We are set to go back to carry out the measurements in the first two weeks of November.

### **Publications**

N/A

### **Outreach Efforts**

All test data will be made accessible through <https://altjetfuels.illinois.edu/>

### **Awards**

None

### **Student Involvement**

This project will be primarily conducted by two graduate students: Eric Wood (Ph.D.) and Jeongan Choi (Ph.D.).

### **Plans for Next Period**

The very next task for execution is the high altitude relight campaign where two students will be traveling to the SmEARF high altitude facility at ARL with the M1 combustor. We anticipate that this campaign will take about three weeks followed by the analysis. After that, we will carry out the LBO measurements at UIUC along with a campaign at ARL's APS to investigate droplet behavior in near-LBO and ignition scenarios. Currently the APS is shut down for external researchers due to COVID-19, though we anticipate that this campaign will take place in the April-to-May 2021 timeframe.



# Project 66 Evaluation of High Thermal Stability Fuels

University of Dayton and University of Dayton Research Institute

## Project Lead Investigator

Joshua Heyne  
Associate Professor  
Mechanical Engineering  
University of Dayton  
300 College Park  
Dayton, OH 45458  
937 229-5319  
Jheyne1@udayton.edu

## University Participants

### University of Dayton

- P.I.s:
  1. Joshua Heyne, Associate Professor
  2. Randall Boehm, Research Engineer
- FAA Award Number: 13-C-AJFE-UD, Amendments 27 and 30
- Period of Performance: June 5, 2020 to August 10, 2021
- Tasks:
  1. Identify / create model of jet engine including all components necessary to accomplish evaluation of the impact of fuel properties.
  2. Build and apply heat transfer model of fuel system.
  3. Identify engine cooling trades that could be leveraged to optimize engine / aircraft system efficiency.
  4. Estimate gains in fuel efficiency.

## Project Funding Level

13-C-AJFE-UD-027 \$184,997  
13-C-AJFE-UD-030 \$100,000

Cost share is provided by the University of Dayton and DLR Germany.

## Investigation Team

- Joshua Heyne (University of Dayton) is the project lead investigator, responsible for building the team and coordinating team activities, driving toward completion of major milestones.
- Randall Boehm (University of Dayton) is a research engineer with 20 years of relevant industry experience and is responsible for leading the technical effort on this project.
- Logan Scholla (University of Dayton) is a graduate student research assistant who is currently responsible for properties databases with additional responsibilities to be added as per capability.
- Giacomo Flora (University of Dayton Research Institute) is a research engineer who is serving in an advisory capacity on this project.
- Lily Behnke (University of Dayton) is an undergraduate student research assistant who is collecting information related to fuel thermal stability.



## Project Overview

It has long been understood that increasing the reliance on jet fuel as a primary coolant for both the engine and the aircraft has significant performance and efficiency benefits relative to the use of air as a coolant [1]<sup>1</sup>, but fuel degradation and coking at high temperatures restricts how much heat can be put into the fuel. In some military applications, the performance benefits are large enough to justify the creation of specialty fuels such as JP7 and JPTS, which can tolerate much higher temperatures relative to petroleum-derived Jet A or Jet A1 (JP8) [2].<sup>2</sup> In land-based applications of gas turbines, weight is of little consequence, so the operations of waste heat recovery (WHR) for plant efficiency or the cooling of combustor inlet temperature for emissions reduction can be accomplished in a wide variety of ways, all of which are impractical for flight because of their impact on the mass of the power plant. Nonetheless, these applications provide some common examples of how controlling the air temperature along its flow path through the engine can have a large impact on performance, durability and energy efficiency [3]. The flurry of works relating to fuel deoxygenation [4], and other ways to decrease the coking propensity or its impacts [5] are largely motivated at the sponsorship level by these benefits.

More recently, sustainable alternative fuels (SAF) have received a lot of attention because they are, or can be, part of high-priority geopolitical goals to diversify energy supply chains and reduce greenhouse gas emissions. While the focus of most of these efforts have been around streamlining the evaluation and approval processes to use synthetic fuels at some blend ratio with petroleum-derived jet fuel to create a so-called drop-in fuel that can be used within existing infrastructure without objection from any of the stakeholders [6], there have also been discussions around characteristics of the synthetic blend component (such as low aromatics, high specific energy, and high thermal stability) that make them attractive to consider as potential specialty fuels (such as JPTS) or high performance fuels. Heyne, et al. recently published work highlighting the efficiency gain that can be expected to result from use of fuels with high specific energy, which all traces back to lower aircraft weight at take-off, meaning less mass to move and hold against the force of gravity [7].

The weight of the fuel uplifted to an aircraft, as necessary to complete its mission, is certainly an important component to the integrated engine and aircraft energy demand and efficiency. There is also expected to be an impact on the energy efficiency of the engine related to other properties of the fuel, including:

1. **Hydrogen/carbon (H/C) ratio.** Through its impact on combustor exhaust gas composition, this ratio has a small impact on the ratio of heat capacities ( $\gamma$ ) and combustor exit temperature, even when the total enthalpy created at the combustor is unchanged.
2. **Viscosity.** Viscosity impacts the heat transfer coefficients that ultimately determine how much waste heat is recovered by the fuel (coolant) and delivered back into the engine via the combustor
3. **Energy density.** Energy density, measured in joules per liter (J/L), impacts volumetric flow rates, which also impact heat transfer coefficients.
4. **Specific heat.** The specific heat also has some effect on heat transfer coefficients, but perhaps more importantly has a direct impact on the temperature rise in the fuel per unit of heat energy absorbed, which in turn may impact the coking rate.
5. **Coking rate.** Also known as fuel thermal stability, the coking rate drives several high-level design decisions relating to the thermal management of an engine.

## Task 1 – Identify/Create Model of Jet Engine Including All Components Necessary to Accomplish Evaluation of the Impact of Fuel Properties

University of Dayton

### Objectives

There are three primary objectives of this work. Phase 1 is to assess the potential impact of fully synthetic SAF to specific fuel consumption (SFC) of a jet engine with no associated change in engine design or logic. Phase 2 is to assess the impact of leveraging the high thermal stability of SAF candidates by increasing WHR up to a limit driven by the requirement that fuel vapor pressure must remain below the normal working fuel pressure at all operating conditions. To achieve the increased WHR, for this phase of the assessment only straight-forward, evolutionary design changes will be considered. In Phase 3, the coupled influence of increased WHR with optimized cooling flow schedules [8] will be identified and discussed.

### Research Approach

At some high level, one might argue that the maximum additional WHR is determined by the proposed shift in the maximum fuel temperature requirement; for instance,  $(160-127) \cdot C_p$ , where 160 C is what we are proposing for high thermal stability fuels, 127 C is the requirement corresponding to petroleum derived Jet A, and  $C_p$  is the heat capacity of the proposed fuel. While this is true at some level, it provides only part of the story. For this study, a fuel system thermal model (FSTM) was created to simulate the heat pickup of fuel in real engines. This model makes it possible to quantify the influence of fuel property variation on temperature rise and WHR within existing architectures. It also enables evaluations of conceptual level design changes that are intended to drive more heat into the fuel. A high-level engine performance model (EPM) was also created to enable evaluation and comparison of different conceptual designs that drive the same amount of total heat into the fuel (approximately  $33 \cdot C_p$  more than baseline), but taking that heat from difference sources. The EPM also enables evaluation of H/C impact on combustor exit temperature and turbine work extraction, which is usually neglected in performance models because it is thought to be a small impact, and the H/C of fuel onboard an aircraft is not generally known. The final piece to the overall impact on system efficiency is the weight, including the difference (decrease) in fuel weight necessary to complete the same representative mission, as well as the difference (increase) in weight created by the conceptual-level design changes that are considered.

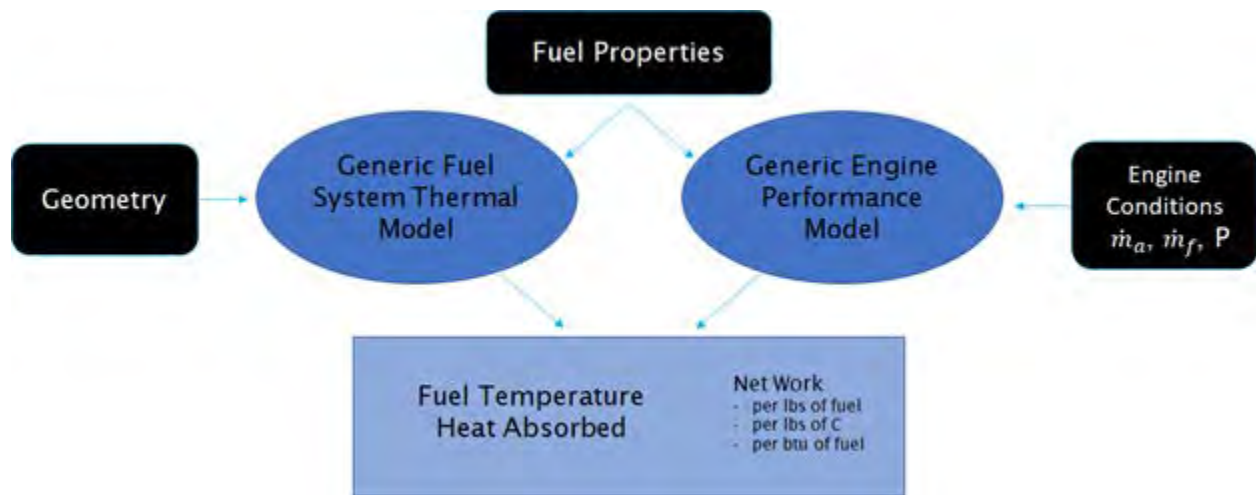


Figure 1. Fuels effects and conceptual design evaluation flow chart.

A distribution of properties, for potential SAF, is created by virtually blending individual molecules together by random association of mole fractions, whose values are also randomly determined, to each of forty-nine specific molecules with known physical and chemical properties [9]. Each fuel property of the mixtures is derived from the mixture definition and constituent properties according to ideal mixture blending rules which have been documented elsewhere [7]. This trial guess at a SAF candidate is then passed through a filter to determine whether it is expected to pass ASTM D1655 and ASTM D7566 fuel specifications. If it passes this filter, it is included within the distribution that is input to the FSTM and EPM as part of a Monte Carlo simulation. The motivation behind this approach was to maintain a physical link between different properties, as the full set of properties is derived from each fuel and the property variation is driven by fuel composition variation rather than arbitrary simulation. All liquid fuel properties include first-order temperature dependence, and none include pressure dependence.

For bookkeeping convenience, the total enthalpy supplied to the engine per unit time,  $(W_f \cdot LHV)$ , is to be conserved for all simulations. The net work per unit time  $(P_{net})$  from the engine (expansion plus compression) will vary in these simulations depending on fuel and conceptual design, which is counter to real applications where thrust \* air speed  $(\sim P_{net})$  would be conserved, and the fuel flow  $(W_f)$  would be changed to meet that demand.

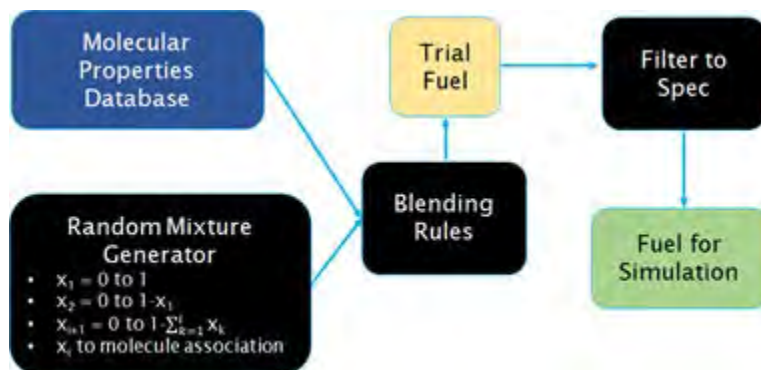


Figure 2. Monte Carlo fuel creation flow chart.

The Monte Carlo simulations will result in population distributions plotted against heat delivered to the combustor (H), covering the output from the FSTM, and to cover output from the EPM, the populations will be plotted against  $P_{net}$ . The predicted impact on fuel burn is determined by iteratively running the EPM until  $P_{net}$  of the trial fuel and design concept matches  $P_{net}$  of the reference fuel and design concept. The predicted savings depends on several assumptions that are part of the EPM. The impact of these assumptions on the target output of the study (fuel savings) will be discussed and evaluated for select cases by replacing the high-level EPM used for the Monte Carlo simulations, with a higher-fidelity engine performance model, built and simulated within the NPSS architecture distributed by NASA [10].

#### Progress toward assessment of SAF impacts on SFC

To date, significant milestones include: (1) the creation of the database of fully synthetic SAF candidates, (2) development and verification of the FSTM and EPM, and (3) completion of a case study which includes 2000 potential fuels.

The predictions suggest that viscosity has the largest impact on WHR at low power while volumetric flow rate (represented by energy density) has the largest impact on WHR at high power, as shown in Figure 3. A likely cause for the shift in the importance of viscosity is that flow throughout the fuel system transitions between laminar and turbulent when operating at low power conditions while it is fully turbulent at high power conditions. The net power is influenced most strongly by WHR when operating at low power and by H/C ratio (combustion products,  $C_p$ , and  $\gamma$ ) when operating at high power, as shown in Figure 4. A likely cause for the shift in the importance of WHR is that its variation is a larger fraction of  $P_{net}$  at low power conditions compared to high power conditions, while a likely cause for the shift in the importance of H/C ratio is that the fuel to air ratio is twice as high at high-power conditions relative to low-power conditions.

The impact to fuel energy consumption varies sharply with cycle conditions (low versus high), as well as engine design concept and component efficiencies. For the Phase 1 cases we have completed, given the set of assumptions we have made, the impact to fuel energy consumption ranges from -0.3% to +0.2% at high power. Application of this set of assumptions to Phase 2 (elimination of the air cooled oil cooler (ACOC) with concurrently a larger fuel cooled oil cooler (FCOC) installed) and Phase 3 (introduction of a FCOC to extract heat from the turbine cooling air and reduce its flow) efforts leads to a prediction of 10-15% savings at high power. Since this number is simply too high to believe, we are currently in the process of auditing our in-house EPM to understand why this prediction is so large, and concurrently we are working toward building the NPSS engine performance model.

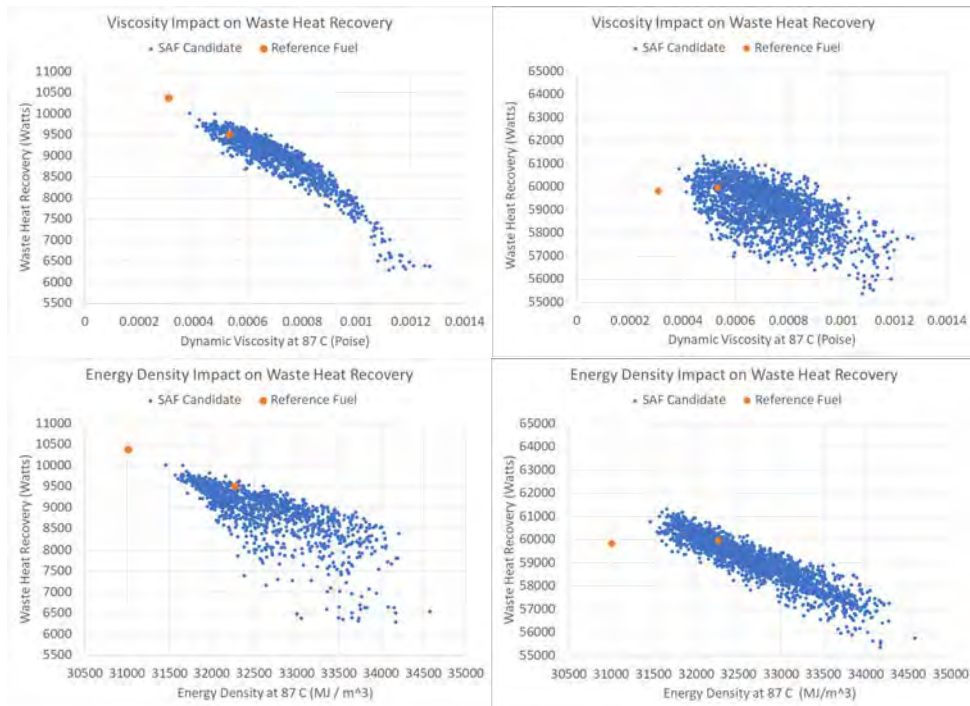


Figure 1. Main effects on waste heat recovery at low (left) and high (right) power.

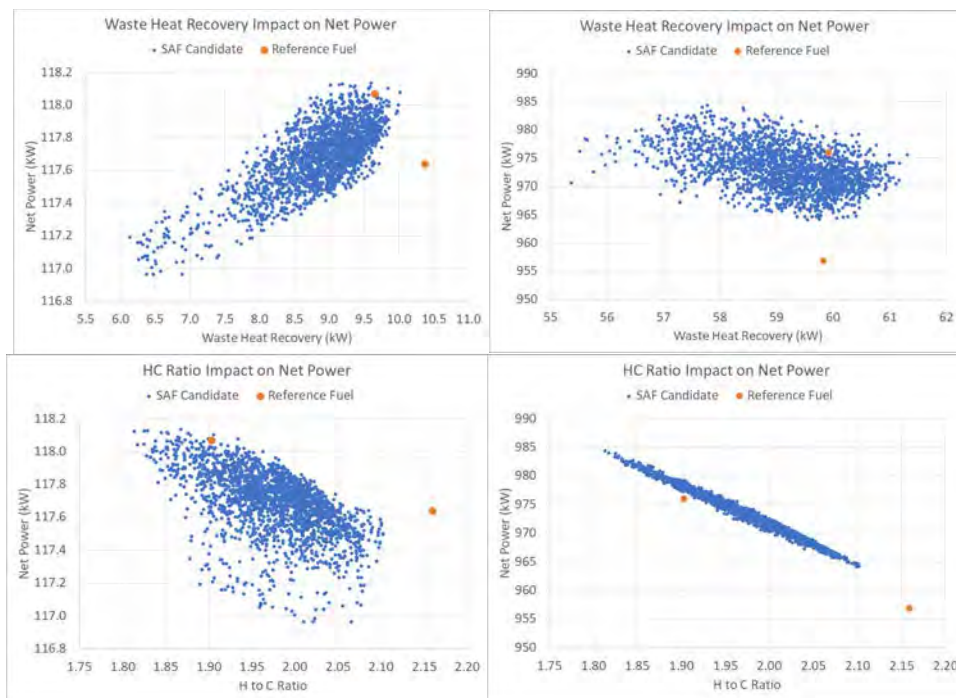


Figure 2. Main effects on net power from engine at low (left) and high (right) power.



## Milestones

- 1) The conceptual design of the model jet engine to serve as tool for evaluating the impact of fuel property variation on jet engine fuel efficiency was completed- 08/31/2020.
- 2) The preliminary construction of this model, including integration with Monte Carlo methods and verification of heat transfer coefficient correlations was completed- 10/29/2020.
- 3) Potential cooling trades leveraging active clearance control have been identified. A model to estimate W36/W3 as a function of heat extracted from the turbine cooling air, by the proposed FCOC has been built and will serve as a baseline for subsequent trades involving active clearance control.
- 4) The creation of the database of 2,000 fully synthetic SAF candidates and a variety of reference fuels was completed- 11/17/2020.
- 5) The simulations necessary to support Phase 1 of the project were completed- 11/25/2020.

## Major Accomplishments

Construction and verification of the FSTM and EPM and their integration with Monte Carlo methods was a major accomplishment, which was necessary to complete almost all of the remainder of this project.

## Publications

None

## Outreach Efforts

None

## Awards

None

## Student Involvement

- Logan Scholla (University of Dayton) is a graduate student research assistant who is currently responsible for properties databases with additional responsibilities to be added as per capability.
- Lily Behnke (University of Dayton) is an undergraduate student research assistant who is collecting information related to fuel thermal stability.

## Plans for Next Period

- Complete heat audit of the EPM and report its findings.
- Complete rollup of weight change estimates associated with the design changes considered for Phase 2 and the weight of fuel and document these estimates.
- Develop NPSS performance model of engine and collaborate with experts who are familiar with engine mission cycles and high-fidelity performance models in order to gain confidence in the assumptions used in this program.
- Write draft manuscript of first peer-reviewed article to result from this work.
- The framework for assessing the impact of cooling trades will be laid out and some examples will be described. For example, what if the ACOC is eliminated versus what if the turbine cooling air flow is reduced, as enabled by fuel cooling of some fraction of that bleed flow.
- Expand database of molecules used to create the SAF candidates and revise the filters based on what we have learned so far to create a second set of candidates that are more likely to result in significant fuel savings.
- Add to the database of reference fuels to provide additional fidelity to the comparisons drawn.

## References

1. Bruening, G. B. & Chang, W. S. Cooled cooling air systems for Turbine thermal management. *Proc. ASME Turbo Expo* 3, (1999).
2. Edwards, T. Advancements in gas turbine fuels from 1943 to 2005. *J. Eng. Gas Turbines Power* 129, 13–20 (2007).
3. Wilfert, G. *et al.* New Environmental Friendly Aero Engine Core Concepts. ISABE-2007-1120. *18th Int. Symp. Air Breath. Engines* 1–11 (2007).
4. Zabarnick, S., West, Z. J., Arts, A., Griesenbrock, M. & Wrzesinski, P. Studies of the impact of fuel deoxygenation on the formation of autoxidative deposits. *Proc. 16th Int. Conf. Stab. Handl. Use Liq. Fuels* (2019) doi:10.1021/acs.energyfuels.0c02603.



5. Stowell, R. & Sun, R. (12) United States Patent. 2, (2004).
6. Colket, M. *et al.* Overview of the National Jet Fuels Combustion Program. *AIAA J.* 55, 1087-1104 (2017).
7. Kosir, S. T. *et al.* Improvement in jet aircraft operation with the use of high-performance drop-in fuels. *AIAA Scitech 2019 Forum* (2019) doi:10.2514/6.2019-0993.
8. Paul J. Deveau, E. P. B., Greenberg, M. R. E. & Paolillo, Vernon, all of C. Gasturbine Engine Active Clearance Control. (1985).
9. Lemmon, E.W., Bell, I.H., Huber, M.L., McLinden, M. O. NIST Standard Reference Database 23: Reference Fluid Thermodynamic and Transport Properties-REFPROP. (2018).
10. Lytle, J. *et al.* Numerical Propulsion System Simulation (NPSS) 1999 Industry Review. *NASA Tech. Memo.* 1-96 (2000).



# Project 067 Impact of Fuel Heating on Combustion and Emissions

## Purdue University

### Project Lead Investigator

Robert P. Lucht  
Ralph and Bettye Bailey Distinguished Professor of Combustion  
School of Mechanical Engineering  
Purdue University  
West Lafayette, IN 47907-2088  
765-714-6020 (Cell)  
Lucht@purdue.edu

## University Participants

### Purdue University

- P.I.s: Dr. Robert P. Lucht
- FAA Award Number: 13-C-AJFE-PU-038
- Period of Performance: June 5, 2020 to June 4, 2021
- Task:
  1. Investigation of the effect of fuel heating on combustion and emissions for aviation gas turbines.

## Project Funding Level

Project 67 is funded by the FAA at the level of \$250,000 for the project period June 5, 2020 to June 4, 2021. The required cost sharing 1:1 match of \$250,000 is provided by Purdue University.

## Investigation Team

The principal investigator for the project is Prof. Robert P. Lucht and the co-principal investigator is Prof. Carson D. Slabaugh. Prof. Lucht is the major advisor for PhD graduate students Colin McDonald and Daniel Shin, and Prof. Slabaugh is the major advisor for PhD graduate students John Philo and Tristan Shahin. The graduate students are responsible for the design of system components such as the fuel heating system and will be responsible for executing test operations. Research Engineer Dr. Rohan Gejji is also working on the project and is helping the graduate students with their design projects and will be supervising the test operations.

## Project Overview

The goal of this project is to determine the effects of heating jet fuel prior to injection in an aviation gas turbine combustor. In an aircraft engine, heat which would conventionally be wasted can be directed into the fuel to increase its sensible enthalpy prior to injection. Thermochemistry dictates that this increase in sensible enthalpy leads to lower fuel consumption for a given combustor exit temperature. However, the effects of elevated fuel temperature on combustion performance characteristics (such as the fuel spray pattern, spatial distribution of reaction zones, pollutant emissions, and combustion dynamics) are not yet well-understood. We will perform experiments with heated fuels using a piloted, partially premixed fuel injector that is located in an optically accessible combustor. This will allow us to apply advanced laser diagnostic techniques to compare the behavior of the combustor at different fuel temperatures over a wide range of operating conditions.

The platform for the planned experiments is the Combustion Rig for Advanced Diagnostics, which is referred to as COMRAD. The test rig, shown in Figure 1, is designed to operate at steady-state conditions with thermal powers up to 8 MW, inlet air pressures up to 600 psi, and inlet air temperatures up to 1400 °F. To facilitate operation at these conditions, the test article



is made out of aviation-grade alloys and thoroughly water-cooled, and the inner windows are film-cooled with heated nitrogen. Prior to this project, extensive testing with ambient temperature fuels has been performed in this rig with a focus on 5 and 10 kHz particle image velocimetry (PIV) measurements in the downstream boundary condition window section and 50 and 100 kHz PIV measurements in the flame zone.

## Task 1 – Investigate the Effects of Fuel Heating on Combustion and Emissions for Aviation Gas Turbines

Purdue University

### **Objective**

The goal of this project is to determine the effects of fuel heating on the performance of aviation gas turbines. Heating the fuel can potentially lead to higher efficiency but may also lead to changes in the fuel distribution pattern and in the location of reaction zones in the combustor. These changes may also impact pollutant emissions and combustion dynamics during engine operation. We will perform experiments using heated fuels and measure the fuel distributions, reaction zone distributions, pollutant emissions, and combustion dynamics at a range of fuel temperatures from near room temperature to above the supercritical temperatures for hydrocarbon fuels.

### **Research Approach**

We will perform experiments with heated fuels using a piloted, partially premixed fuel injector that is located in an optically accessible combustor. This will allow us to apply advanced laser diagnostic techniques to compare the behavior of the combustor at different fuel temperatures over a wide range of operating conditions. These advanced diagnostic techniques include fuel planar laser-induced fluorescence (PLIF) imaging to monitor fuel distribution patterns, hydroxyl (OH) radical PLIF imaging to monitor reaction zones, and PIV to measure the flow fields. We will also measure emissions using probe sampling and pressure transducers to measure combustion dynamics.

### **Milestones**

The major milestones accomplished in the first three months of the project are:

1. The design of the fuel heater was completed and nearly all of the components have been ordered.
2. Operating conditions for our initial tests have been developed. These operating conditions were defined with the significant input from researchers at GE Aviation.
3. Major improvements to the COMRAD test rig and associated infrastructure were accomplished, including significant upgrades to the control system and the nitrogen supply for film cooling system.

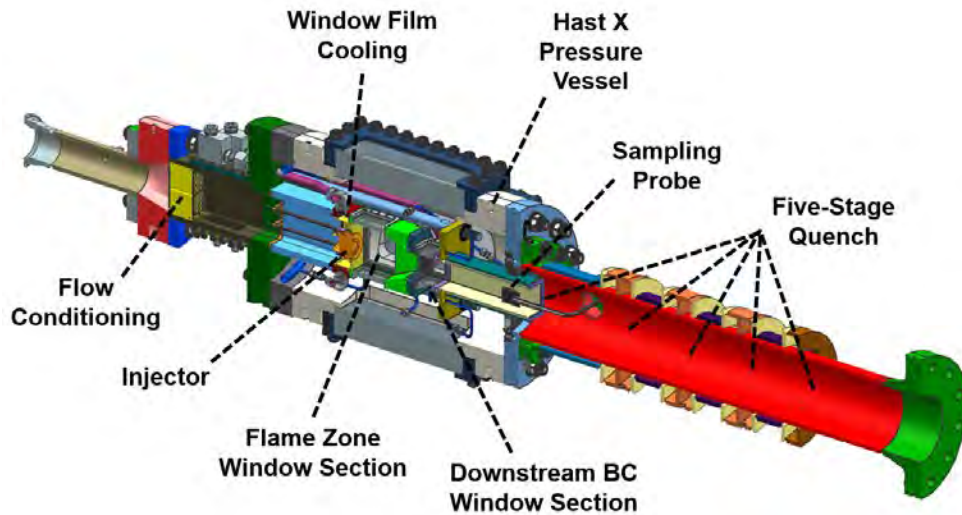


Figure 1. Schematic diagram of the Combustion Rig for Advanced Diagnostics (COMRAD).

### Major Accomplishments

The focus of the activities for this project to date have been the design of the fuel heating system and improvements to the test stand and facilities. The fuel heater design ensures that the goals of the project will be successfully met by developing the capability to provide heated fuels to the experiment at conditions of interest to both GE Aviation and the broader research community. The critical design review (CDR) for the fuel heater was completed on August 11. The facility improvements that have been completed will help to streamline test operations so we can more efficiently and reliably perform the experimental measurements for this project.

#### A. Fuel Heater Design

We began the fuel heater design by consulting with GE Aviation to determine target design conditions. These conditions are similar to those that have been previously tested in COMRAD. We plan to perform equivalence ratio sweeps from 0.50 to lean blow-out at the listed inlet air pressures and temperature. This will be repeated at multiple fuel temperatures, with a baseline of 200 °F and a more detailed study around 600-650 °F.

Table 1. Heated fuel operating condition limits.

Test Condition	$P_3$ (psia)	$T_3$ (°F)	Overall $\phi$	Total Fuel Flow Rate (pph)	Pilot/Total (%)
Cond001	150	900	0.37	117	30
Cond002	300			234	
Cond003	400			313	
Cond004	150		0.50	159	
Cond005	300			317	
Cond006	400			423	

We decided to design the fuel heater to supply fuel for the highest expected fuel flow rate condition at up to 800 °F, because at this point the fuel will be supercritical at injection. The maximum required power is 18.0 kW for the pilot fuel and 42.0 kW for the main fuel. Assuming a maximum heater efficiency of 80%, the heater has been sized for 27 kW of power for the pilot fuel circuits and 54 kW of power for the main fuel circuit.

The fuel heater configuration is based on prior experience testing heated fuels at our laboratory. The fuel flows through stainless steel tubes, which are sandwiched between a pair of copper blocks. Inserted into the copper blocks are 5/8-inch-diameter, 480-V cartridge heaters, which distribute the heat evenly over the entire length of tubing. There are three independent heater circuits, two for the pilot and one for the main, which consist of zones of five cartridges that are controlled remotely with PID controllers. Sheets of ceramic fiber insulation isolate the individual pairs of heater blocks.

**B. Nitrogen Heating System Improvements**

Our facility uses two separate natural gas-fired heaters for this project: one for heated air for the core flow and one for heated nitrogen for the window film cooling. In 2018, COMRAD was moved to a new test cell in ZL8, a building which recently opened adjacent to the building where the old test cell was located (ZL3). This required the piping downstream of the nitrogen heater to be reworked, because it is routed through the old test cells in ZL3. These changes have also required us to reroute tubing from our 6,000-psi nitrogen tank to the inlet of the heater, where the pressure is regulated to our target condition. Additionally, a control switching system was designed to switch control of the heater and the nitrogen system between the individual data systems in the ZL3 and ZL8 buildings. This is a significant upgrade to the capabilities of our facility, and it involved routing and landing many cables as well as wiring the control switching system. Presently, we are putting the finishing touches on this system and on the tubing to connect to the nitrogen system. We expect everything to be functional in mid-October.

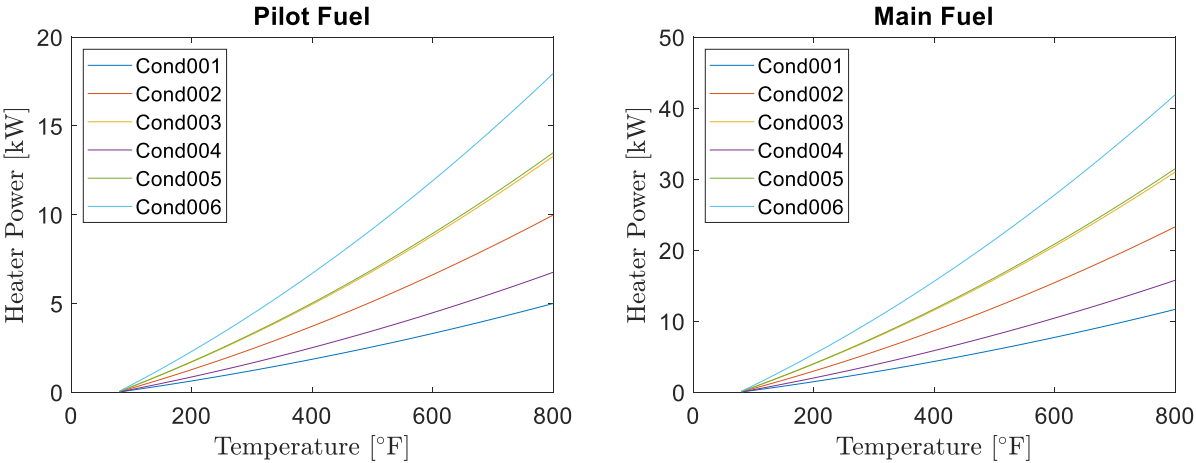


**Figure 2.** Required heater power for pilot and main fuel circuits.

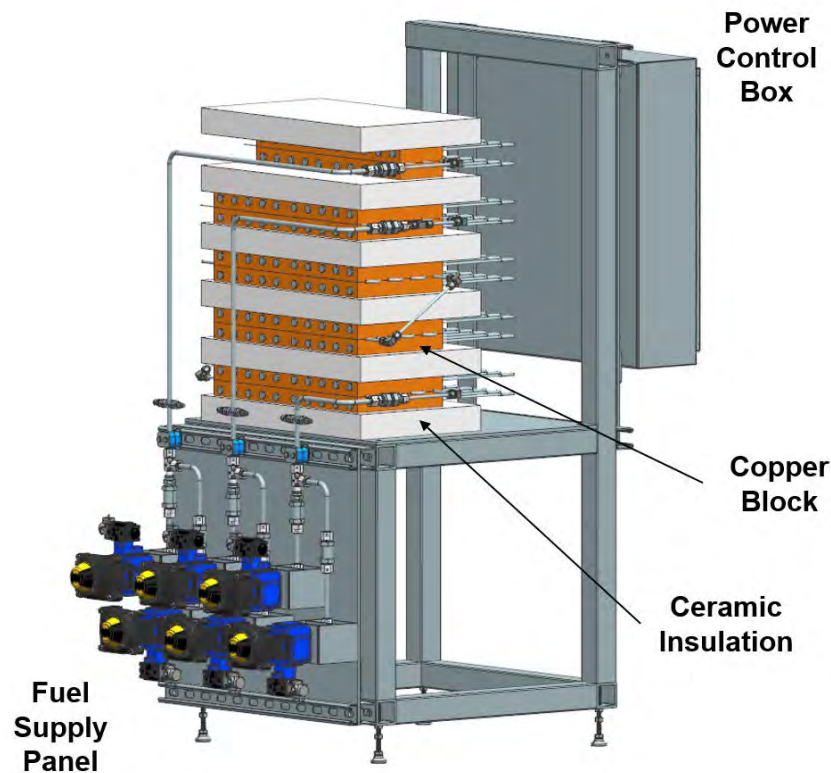


Figure 3. Schematic diagram of fuel heater design.

### Publications

We have not generated any publications thus far for Project 67.

### Outreach Efforts

We have not performed any outreach efforts thus far for Project 67.

### Awards

None

### Student Involvement

There are four PhD graduate students working on the project. The project provides outstanding research experiences for the graduate students including design of system components for and operation of a sophisticated aviation gas turbine combustion test rig, as well as application of advanced laser diagnostic methods for measurements in this test rig. As noted above, the graduate students have been responsible for the design of system components such as the fuel heating system and for the installation of components for the nitrogen window film cooling system. The students will be responsible for executing test operations.

### Plans for Next Period

Multiple tasks are ongoing in preparation to resume testing the experiment as currently configured as well as to begin testing with heated fuel. The primary item that needs to be completed before preliminary measurements can begin is the integration of the emissions sampling system. Completion of the fuel heater fabrication will follow, allowing testing with heated fuels to commence.



### A. Emissions Sampling System

For the planned test campaign, provisions have been made to install an emissions sampling probe designed by GE Aviation just downstream of the primary reaction zone. This probe will route a sample of exhaust gases to a Fourier-transform infrared spectrometer (FTIR) located near the test cell. The sample will be kept at 191 °C by electric heat tape to meet the inlet temperature required by the FTIR spectrometer. Installation of the heat tape, tubing, and valves needed for this system is in progress and is expected to be completed in early October.

### B. Fuel Heater Fabrication

The fabrication of the fuel heater and associated systems is currently underway. All of the major orders have been placed, and many components have been received. The fuel heater stand, shown in Figure 4, has been welded and is waiting to be powder coated. The cartridge heaters should be arriving within a week or two, at which point the machining of the copper blocks will begin. This makes it possible to verify the cartridge heater dimensions and ensure a good fit in the copper blocks. The disconnect switch and associated electrical components will arrive by the end of the month. An electrician has been contracted to perform the installation and wiring of the 480 V, three-phase power to the fuel heater after the required electrical components are delivered. Additionally, all of the required fluid components, except for the high temperature valves needed downstream of the heater, should arrive by the end of October.



Figure 4. Fuel heater stand fabrication.

### C. Summary and Timeline

After several months of work, we are very close to conducting our first measurements for this project. These first test operations will take place in mid-November 2020. Once the emissions system and the nitrogen heating system are ready for use, we are planning to run the experiment for 2-3 test days to obtain some data with ambient-temperature fuels. Data from these test days will complement past experiments with this hardware and allow us to try out the new facility systems before the fuel heater fabrication is completed. Planned milestones for the rest of the project period are listed in Table 2.



**Table 2: Project timeline**

Task	Planned Completion Date
<b>Initial testing with ambient-temperature fuel</b>	November 15, 2020
<b>Heated fuels test readiness review</b>	November 23, 2020
<b>Parametric survey testing with heated fuel:</b> Vary fuel temperature, pressure, and equivalence ratio with emissions measurements and chemiluminescence imaging	December 21, 2020
<b>Initial test operations with large-scale flow and flame diagnostics:</b> 10 kHz particle image velocimetry (PIV) and OH planar laser-induced fluorescence (PLIF) with chemiluminescence measurements	January 31, 2021
<b>Development of detailed operational test plan</b>	January 31, 2021
<b>Continued test operations with large scale flow and flame diagnostics:</b> Fuel PLIF, Mie scattering, and 100 kHz simultaneous OH PLIF/PIV measurements	June 4, 2021

# Project 068 Combustor Wall Cooling with Dirt Mitigation

## The Pennsylvania State University

### Project Lead Investigator

Karen A. Thole  
 Distinguished Professor  
 Department of Mechanical Engineering  
 The Pennsylvania State University  
 136 Reber Building  
 University Park, PA 16802-4400  
 Phone: (814) 865-2519  
 E-mail: kat18@psu.edu

### University Participants

#### The Pennsylvania State University

- P.I.s: Dr. Karen Thole, Dr. Stephen Lynch
- FAA Award Number: 13-C-AJFE-PSU-057
- Period of Performance: June 5, 2020 to June 4, 2021
- Tasks:
  - (1) Manufacture and test combustor liner cooling concepts with small coupons.
  - (2) Testing of optimal cooling concepts at engine-relevant conditions.
  - (3) Testing of scaled models of optimal cooling concepts for detailed boundary conditions.

### Project Funding Level

FAA funding to date \$150,000. Matching funds were provided by of \$150,000 Pratt & Whitney.

### Investigation Team

Name	Affiliation	Role	Tasks Responsible For
Distinguished Professor Karen A. Thole	The Pennsylvania State University	PI	Management, reporting, oversight of all technical tasks
Associate Professor Stephen Lynch	The Pennsylvania State University	Co-PI	Management, reporting, oversight of Tasks 1-3
Scott Fishbone	The Pennsylvania State University	Project Manager	Task 1 and 3
Brandon Fallon	The Pennsylvania State University	Graduate Student	Tasks 1-3

### Project Overview

A critical issue related to the operation of a gas turbine in today’s world is the ingestion of dirt and other fine particles that lead to blockages of cooling holes and passages required for effectively cooling the walls of the combustion chamber. Because the need to fly in dirty environments is on the rise, the criticality of operations in dirty environments is increasing. Modern gas turbine engines typically employ a double-walled combustor liner with impingement and effusion cooling plates whereby impingement cooling enhances the backside internal cooling and effusion cooling creates a protective film of coolant along the external liner walls. Dirt accumulation on the internal and external surfaces severely diminishes the heat transfer capability of these cooling designs. This study would initially investigate practical designs for reduced dirt accumulation at representative temperature conditions, and then explore how the designs are insensitive through detailed flow and heat transfer measurements on a scaled geometry.



## Task 1 – Manufacture and Test Combustor Liner Cooling Concepts with Small Coupons

The Pennsylvania State University

### Objective

The goal of this research is to produce an effective cooling design for combustor walls that is insensitive to dirt accumulation at existing or lower coolant flowrates. Various parameters such as dirt deposition, flow behavior, and heat transfer effectiveness will be investigated and quantified to compare the efficiency of candidate designs. Improved understanding of the reasoning behind dirt sensitivity and deposition behavior is also being sought.

### Research Approach

#### Background

The focus of the project is on the impacts of ingestion of dirt and other fine particulate matter in gas turbine engines. These particles are known to block cooling holes and passages needed to effectively cool combustion chamber walls. Gas turbine engines often utilize double-walled combustor liners comprised of impingement and effusion cooling plates, shown in Figure 1. The impingement plate enhances backside internal cooling and the effusion plate creates a protective film of coolant along the external liner walls. As particulate matter accumulates on these plates, the heat transfer performance severely diminishes, ultimately leading to component failure.

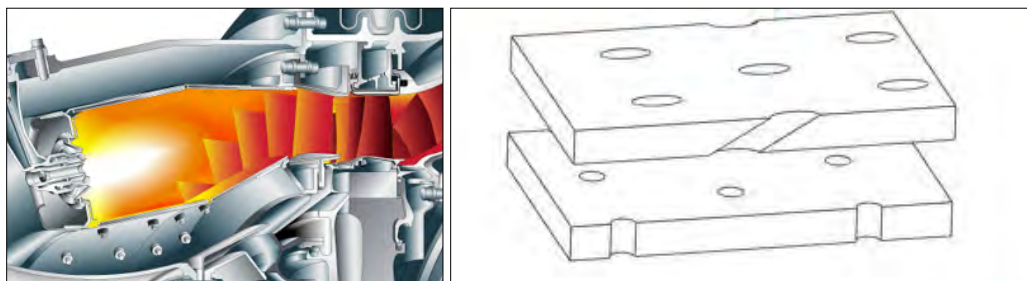
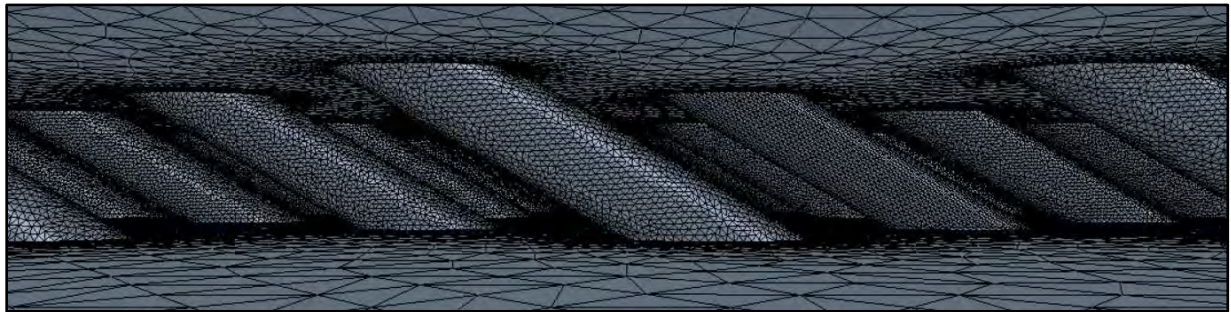


Figure 1. Schematic of double-walled combustor liner geometry.

#### Computational Simulations of Dirt Trajectories

Using a computational fluid dynamics (CFD) code called Star CCM+, pre-test prediction methods were utilized to study flow patterns and particle deposition behavior within the double-walled combustor liner. Simulations were performed on previously tested coupons to benchmark flow and deposition behavior. Development of said simulations required contriving a mesh to accurately define the coupon geometry while maintaining grid independence and determining the boundary conditions and physics models required to model previous experimental conditions. To achieve the mesh shown in Figure 2, an iterative approach was used. The parameters investigated were the cell count, base size, and cell shape. Of the shapes, it was found that the polyhedral mesh was approximately 0.4% more accurate than trimmer cells when compared to experimentally determined Reynolds numbers through the impingement jets. However, the computational time and storage space was dramatically increased. The polyhedral mesh utilized a base cell size of  $1.5e-4$  m, whereas the trimmer successfully reached a base size of  $8.0e-5$  m, pushing the cell count from 7.9 million to 11.9 million. Because the trimmer-based mesh was less computationally expensive, required less storage space, and had less than a 0.5% difference with the polyhedral mesh, the trimmer mesh was selected for the CFD predictions.



**Figure 2.** Final mesh of effusion holes selected for CFD predictions.

Once the geometry had a viable mesh, boundary conditions were needed to perform simulations. In previous experiments, the upstream and downstream pressure was controlled and held at a constant back flow margin (BFM). To model flow through the coupon, the simulation was set up such that the coupon was placed inside a wind tunnel matching the coupon dimensions. A stagnation inlet boundary condition was applied ten hole diameters upstream the coupon, and a pressure outlet boundary condition was applied ten hole diameters downstream the coupon.

### Dirt Simulation Test Facility

The dirt test facility incorporates both slug feed and continuous feed mechanisms to account for the various ways dirt may be ingested by a system. For the slug feed method, shown in Figure 3, dirt is introduced to the test facility in intervals. The dirt is sequentially placed inside a separate chamber attached to the main flow and pressurized slightly above the mainstream pressure. When opened, the slug is injected into the freestream.



**Figure 3.** Slug feed test facility.

In continuous feed tests, dirt is introduced through a constant stream. Shown in Figure 4, the continuous feed is accomplished by running air through a capillary tube directed at a plate containing a line of dirt. A stepper motor is attached to the capillary tube, allowing it to traverse the length of the plate, effectively blowing the dirt into the mainstream.

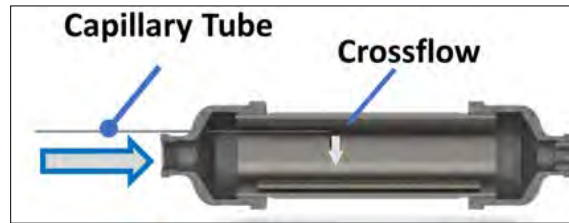


Figure 4. Continuous feed test facility.

A plenum is attached just below the slug feed entrance. To disperse the injected dirt, a splash plate is placed approximately a half-inch in front of the plenum entrance. The coupons, shown in Figure 5, consist of an effusion plate, spacer plate, and impingement plate stacked together. The impingement plate is placed first at the plenum's outlet, followed by the spacer, effusion plate, and bolts.

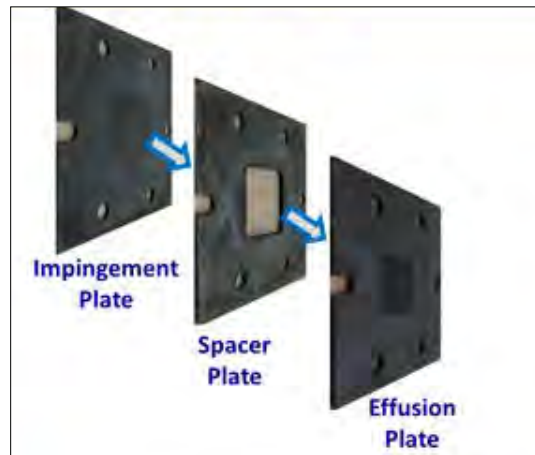


Figure 5. Experimental coupon geometry.

In the past, a horizontally orientated test facility was utilized to study dirt deposition behavior on test coupons, however, it was found that a high percentage of dirt stuck to the inner walls of the piping, causing less dirt to successfully reach the coupon. A vertical test facility will be used instead to facilitate improved dirt ingestion into the system. In a vertical setup, gravity acts parallel to the flow direction, influencing dirt to move toward the coupon rather than the pipe walls. The vertical test facility is shown below in Figure 6.



**Figure 6.** Vertical dirt test facility.

Currently, experiments are being performed using a cylindrical double-walled heat exchanger plenum. The new coupons will be substantially larger and require a new plenum to be built. The new plenum will incorporate a rectangular geometry, shown in Figure 7, to alleviate issues with dirt accumulation in areas outside the test region. This plenum will be made from clear acrylic, allowing researchers to more easily locate dirt post-test and creating an opportunity to use particle image velocimetry (PIV) laser measurements to more accurately track dirt behavior near the test coupons.

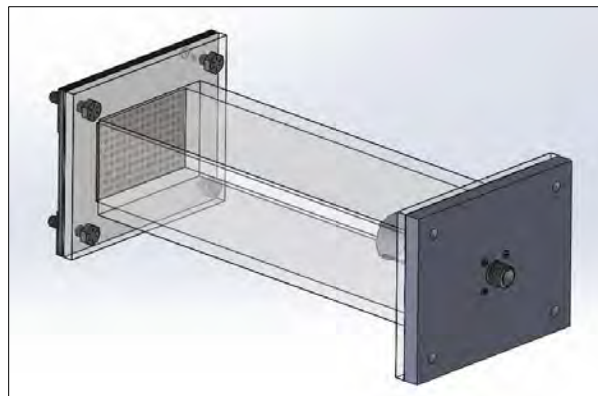


**Figure 7.** Rectangular acrylic plenum.

The dirt particles being used in these studies have an assumed mean diameter of 1.2  $\mu\text{m}$ . To effectively track the dirt, a filtered box meant to entangle dirt will be used. The dirt filter box is pressed against and bolted down to the outlet of the test coupons. Rectangular outlets with 0.5  $\mu\text{m}$  filter fabric placed over them allow the air to flow out of the box while providing a means of trapping the dirt. The large opening allows for easy access to bolts and can be sealed using a lid bolted against gasket material. Lastly, a pressure tap located to the side of the outlet is used to monitor downstream pressure.



### Data Collection and Analysis

Pressure measurements are recorded both upstream and downstream from the coupon and mainstream flow temperature is recorded using a k-type thermocouple offset 0.25 in from the coupon inlet. Alicat mass flow controllers are used to regulate and track the flow rate. Using a LabView code, the percent back flow margin (BFM) and pressure ratio (PR) can be controlled for the duration of the test. Each test is run at a specific BFM, which is calculated using Equation 1.

$$BFM = \left[ \frac{P_{up} + P_{down}}{P_{down}} - 1 \right] * 100 \quad (1)$$

Using the flow parameter (FP), each coupon's performance at various BFM's and dirt loadings can be evaluated. As dirt is ingested by the coupon, the FP reduces. This can be calculated using Equation 2.

$$FP = \frac{4\dot{m}\sqrt{T_{oc}R}}{\pi P_{up}ND^2} \quad (2)$$

In addition to FP, the capture efficiency, determined using Equation 3, will provide an additional means of quantifying the effectiveness of each coupon design. This is determined by subtracting the mass of the dirtied effusion plate by the mass of the clean effusion plate and dividing that quantity by the mass of dirt that successfully made its way to the effusion plate inlet. Any dirt that was found in the piping upstream from the effusion plate was removed from this calculation.

$$\eta_c = \frac{M_{eff} - M_{cl}}{D_{int}} * 100 \quad (3)$$

Upon the completion of each test, the test facility is dismantled and dirt is scraped out of the piping and measured. The goal is to locate at least 90% of the dirt to increase the reliability of the capture efficiency measurements. Once the dirt has been located, images of the dirt deposition patterns are taken using a laboratory microscope and can be used for qualitative analysis. Following this, the dirty effusion plate is scanned using a NextEngine 3D Scanner. Using an in-house MATLAB code, the thickness of the dirt across the plate can be evaluated by comparing the difference in depth between the clean and dirty plate, shown in Figure 8. From this information, the laterally averaged peak heights can be calculated.

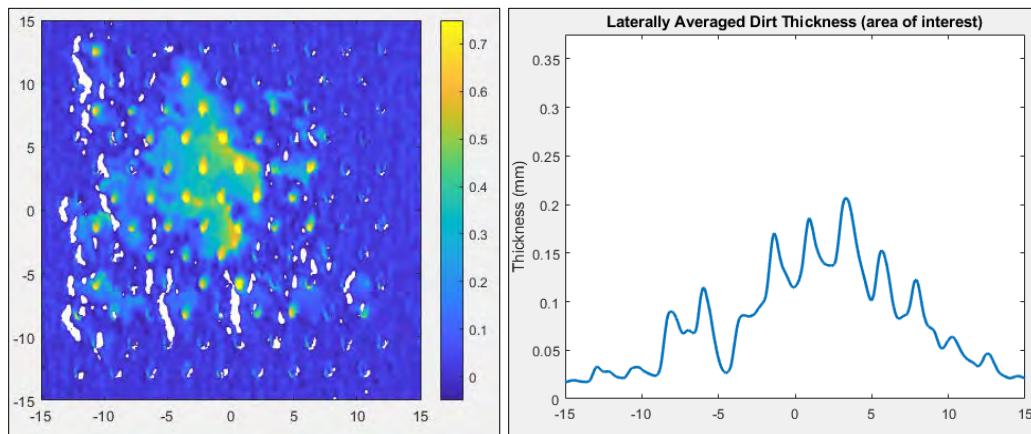


**Figure 8.** Post-test contour plot of dirt deposition locations and laterally averaged dirt thickness.



### Milestones

Milestone	Due Date	Estimated Date of Completion	Actual Completion Date	Status
Work plan	7/5/20	7/5/20	7/5/20	Complete
COE Meeting 1	10/1/20	10/1/20	10/29/2020	Complete
COE Meeting 2	4/1/21	4/1/21		
Annual Report	6/5/21	6/5/21		
Project Closeout	6/5/21	6/5/21		

### Major Accomplishments

The start of this research was focused on using the CFD code Star CCM+ to predict the flow field and particle deposition behavior through the double-walled liner geometry. In previous experimental studies, the Reynolds number through the impingement jets was measured and was used to benchmark the CFD predictions. The predictions for the Reynolds number achieved a nominal percent error of 15%. Figure 9 shows the velocity contours of the jets impinging on the effusion plate inlet face. These predictions show regions of low velocity in discrete locations which can be used to forecast where dirt may deposit. Figure 10 shows the predicted flow field in the space region between the impingement and effusion plates as well as the flow through the effusion holes. Velocity contours show a swirling effect that may be attributed to deposition behavior. Incident mass flux and particle studies were also performed using Lagrangian multiphase (LMP) physics models, but it was determined that the physics of the dirt particles themselves needed to be more thoroughly evaluated before proceeding further. Ultimately, it was determined that CFD predictions may provide a method for predicting flow and deposition behavior through these channels, but more work is required to refine these predictions.

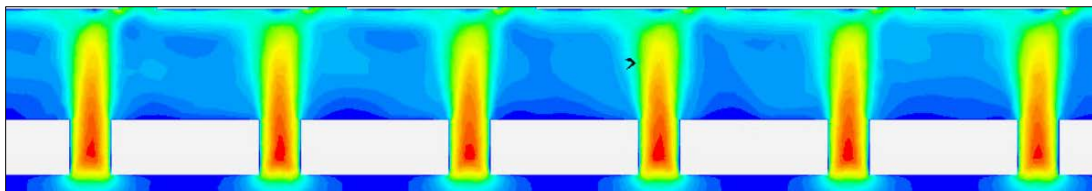


Figure 9. Velocity contours of flow through impingement jets and space region between plates.

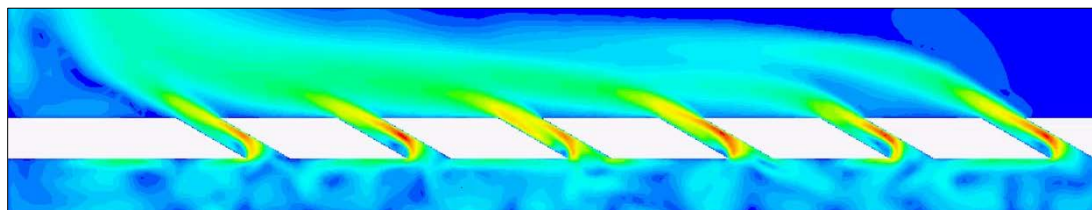
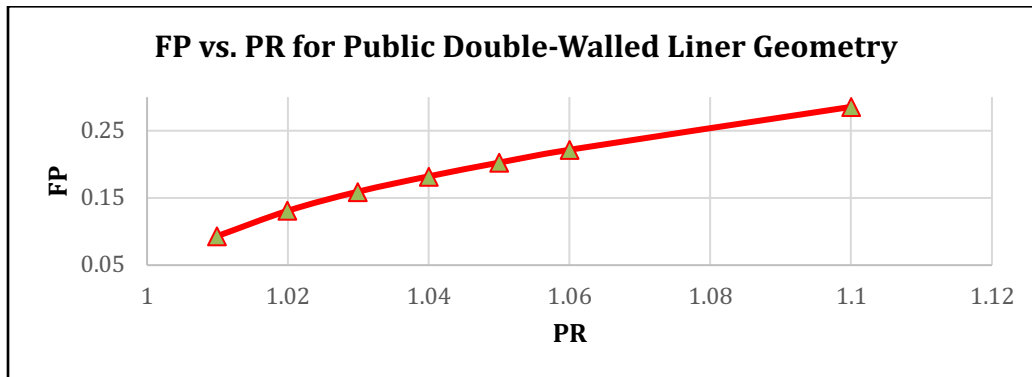


Figure 10. Velocity contours of flow through effusion holes.

The next major accomplishment was successfully transitioning the horizontally orientated test facility to a vertical test facility, shown in Figure 6. In addition, a new LabView code was developed to perform these tests and will be utilized for current and future experiments. Tests are actively being performed on this facility to validate the methods used in previous work [1]. A curve displaying the FP vs. PR for the public geometry, shown in Figure 11, was successfully created to evaluate the reduction in FP as dirt enters the system. Subsequent testing proved that FP comparisons are an effective means for comparing performance of various coupon designs. This is expected to be used as one of the primary modes to evaluate coupon performance going forward.



**Figure 11.** Flow parameter (FP) vs. pressure ratio (PR) curve for public geometry on vertically orientated test facility.

Microscopy is also being used to qualitatively inspect dirt deposition behavior on the effusion plates. Currently, the results of the vertical test facility are being compared to the horizontal facility to evaluate differences that occur due to the modified orientation. Figure 12 displays the results of three tests, one performed on the horizontal test facility and two performed on the vertical test facility. The horizontal test used 420 mg of dirt at a BFM of 1.33%, while the vertical tests used 105 mg and 420 mg at the same BFM. These studies showed that the vertical test with 105 mg of dirt more strongly resembled the horizontal test with 420 mg of dirt than the vertical test with 420 mg of dirt. It is believed that more dirt successfully reaches the coupon in the vertical facility because gravity now acts parallel to the flow rather than perpendicular. In these tests, less dirt was found in the piping upstream the coupon, indicating that the vertical test facility is more effective at supplying dirt to the coupons than the horizontal test facility for the slug feed tests. Because of this, the vertical facility will continue to be used in future tests. Efforts are also being dedicated towards producing reliable scans of dirt deposition to determine location and thickness of dirt deposited on the test coupons. This will provide an additional method of comparing the effectiveness of the various cooling designs.

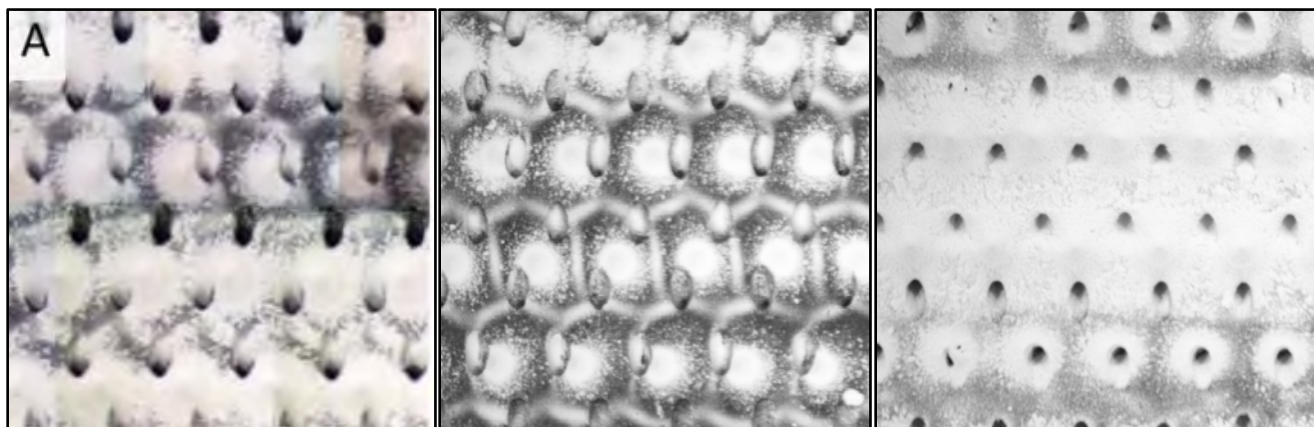


**Figure 12.** Dirt deposition behavior on effusion plate inlet face with horizontal and vertical test facilities at a BFM of 1.33%. Reading left to right: 420 mg of dirt in the horizontal facility (left), 105 mg of dirt in the vertical facility (middle), 420 mg of dirt in the vertical facility (right).

**Publications**

No publications to report yet.

**Outreach Efforts**

Bi-weekly presentations are given to Pratt & Whitney through this joint collaboration.

**Awards**

None

**Student Involvement**

The graduate student Brandon Fallon has taken on the role of performing CFD predictions, assembling and redesigning the test facility, and performing tests and analysis on the old and new liner geometry. This student will be the primary experimentalist going forward.

**Plans for Next Period**

Pratt & Whitney is actively working on getting new test coupons designed and fabricated. It is expected that the START Lab will receive these coupons in early 2021. Upon receiving the test coupons, the graduate student will begin by establishing a baseline FP vs. PR curve for each test coupon, which can be used to evaluate the reduction in FP as dirt is deposited on each coupon. Following this, each coupon will be tested at varying BFM's with various quantities of dirt, the exact amounts still to be determined. In the past, BFM's of 1.33% to 4.32% were tested with dirt loads ranging from 105 mg to 1260 mg. Currently, tests are being performed under ambient temperature conditions, and it is uncertain if this will be increased in the future. There have been discussions of incorporating particle image velocimetry (PIV) instrumentation to track and monitor dirt behavior in the freestream and near the surface of the effusion plate, however, it is not yet clear if this will be used in the future.

**Nomenclature**

$\dot{m}$	mass flow rate through test facility
$P_{up}$	upstream test facility pressure
$P_{down}$	downstream test facility pressure
$T_{oc}$	supply coolant temperature
$N$	number of impingement holes
$D$	cooling hole diameter
$\eta_c$	capture efficiency

**References**

[1] Cory, Trevor M., Thole, Karen A., Kirsch, Kathryn L., Lundgreen, Ryan, Prenter, Robin, and Kramer, Stephen. "Impact of Dust Feed on Capture Efficiency and Deposition Patterns in a Double-Walled Liner," GT2019-90981.



## Project 069 Transitioning a Research nvPM Mass Calibration Procedure to Operations

Missouri University of Science and Technology and Aerodyne Research Inc.

### Project Lead Investigator

Philip D. Whitefield  
Chancellor's Professor of Chemistry  
Missouri University of Science and Technology  
400 W 11<sup>th</sup> Street, Rolla, MO 65409  
573-341-4420  
pwhite@mst.edu

### University Participants

#### Missouri University of Science and Technology

- PI: Philip D. Whitefield, Chancellor's Professor of Chemistry
- FAA Award Number: 13-C-AJFE-MST Amendments: 014
- Period of Performance: June 5, 2020 to June 4, 2021
- Task:
  - Investigate the validity of the centrifugal particle mass analyzer (CPMA) mass calibration research approach for non-volatile particulate matter (nvPM) certification measurement systems. The assessment will extend across all nvPM mass ranges encountered during certification tests. The primary goal will be the successful transitioning of the research methodology to operations

### Project Funding Level

The total amount of funding from FAA is \$846,707. The matching funding of \$846,707 is from the Swiss Federal Laboratories for Materials Science and Technology (EMPA).

### Investigation Team

- Professor Philip Whitefield, Missouri University of Science and Technology
- Steven Achterberg, research technician, Missouri University of Science and Technology
- Max Trueblood, research technician, Missouri University of Science and Technology
- Dr. Richard Miake-Lye, subcontractor, Aerodyne Research Inc.
- Dr. Robert Howard, sub-contractor, Arnold Engineering Development Center (AEDC), USAF

### Project Overview

This project is designed to investigate the validity of the CPMA mass calibration research approach. The assessment will extend across all nvPM mass ranges encountered during certification tests. The primary goal will be the successful transitioning of the research methodology to operations. The project will begin with a laboratory assessment leading to a dedicated small engine as the test source at the USAF Arnold Engineering Development Complex.

The challenge mass devices for calibration (micro-soot sensor (MSS), laser-induced incandescence (LII), and cavity attenuated phase shift (CAPS)) will be provided by the North American Reference nvPM Measurement System and ancillary equipment along with the CPMA and other needed instruments such as a DMS500, and an aerosol mass spectrometer (AMS) and CAPS.

# Task 1 – Investigate the Validity of the Centrifugal Particle Mass Analyzer (CPMA) Mass Calibration Research Approach for nvPM Certification Measurement Systems

Missouri University of Science and Technology

### Objective

Acquire the components of a CPMA-based mass calibration system similar to that described in SAE E31 discussion paper DP-32 (presented by Dr. G. Smallwood) from the annual committee meeting June 17-21, 2019, Saclay, France. Assemble system and evaluate its performance.

### Research Approach

#### Subtask 1

Acquire the components of a CPMA-based mass calibration system similar to that described in SAE E31 discussion paper DP-32 (presented by Dr. G. Smallwood) from the annual committee meeting June 17-21, 2019, Saclay, France.

#### Subtask 2

Assemble and test the CPMA-based mass calibration system performance, at Missouri University of Science and Technology’s laboratories using a miniature combustion aerosol standard (mini-CAST) as the nvPM generation source (Figure 1).

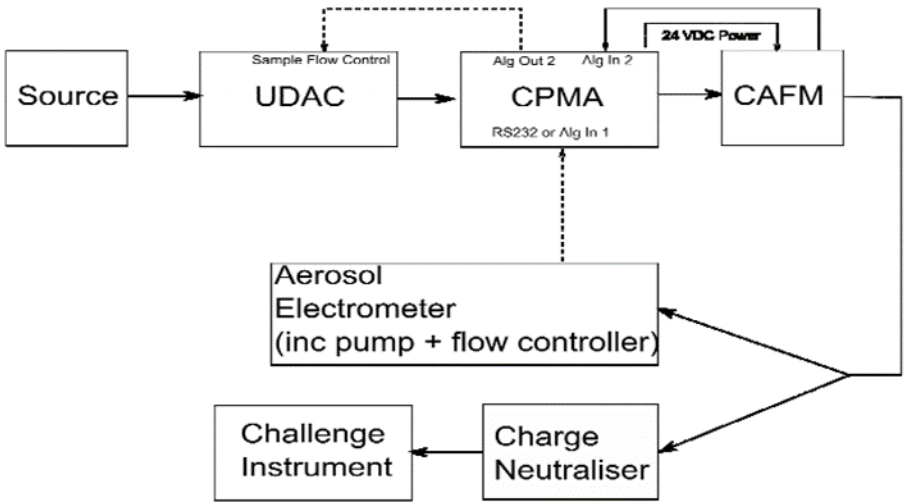


Figure 1. Schematic diagram of the CPMA-based mass calibration system.

#### Subtask 3

Investigate the validity of the CPMA mass calibration research approach across all nvPM mass ranges encountered during certification tests to successfully transition the methodology to operations.

#### Subtask 3a

Deploy (transport and install) the North American Reference System (NARS), including the CPMA-based mass calibration system and ancillary diagnostic suite, including the Air Force AVL nvPM measurement system, to engine testing facilities at Arnold Air Force Base, TN. Specifically, these engine testing facilities will include the J85 turbojet and a gas-turbine-based “start cart” as nvPM sources.



### **Subtask 3b**

Undertake performance evaluations of the CPMA-based mass calibration system, surveying across all mass ranges using the start cart as the nvPM source and compare these results with concomitant mass calibration data acquired using the SAE E-31 OCEC-based mass calibration methodology.

### **Subtask 3c**

Undertake performance demonstration by performing a mock-certification test on the J85 engine where the calibration will include the standard elemental carbon/organic carbon (EC/OC) analysis, as well as the CPMA-based calibration system described in document DP-32.

### **Subtask 3d**

De-couple the diagnostic suites from the Arnold AFB engine facilities and transport them back to Missouri and Massachusetts.

### **Subtask 4**

Analyze and interpret the data gathered in Tasks 2 and 3.

### **Subtask 5**

Prepare and deliver a final report.

## **Milestones**

- Components have been purchased and delivered.
- A straw man test protocol has been proposed and is under evaluation.
- An advisory team has been assembled to help with the evaluation of the various stages of this project. The team includes advisors from the Environmental Protection Agency (EPA) and the National Research Council (NRC) Canada. It meets virtually on a bi-weekly basis.

## **Major Accomplishments**

Having acquired the components, work on Tasks 2 and 3 is being pursued. Figure 2 is a schematic diagram of the source evaluation system exploring the dynamic range in nvPM mass concentration that can be employed in the laboratory-based studies in Task 2

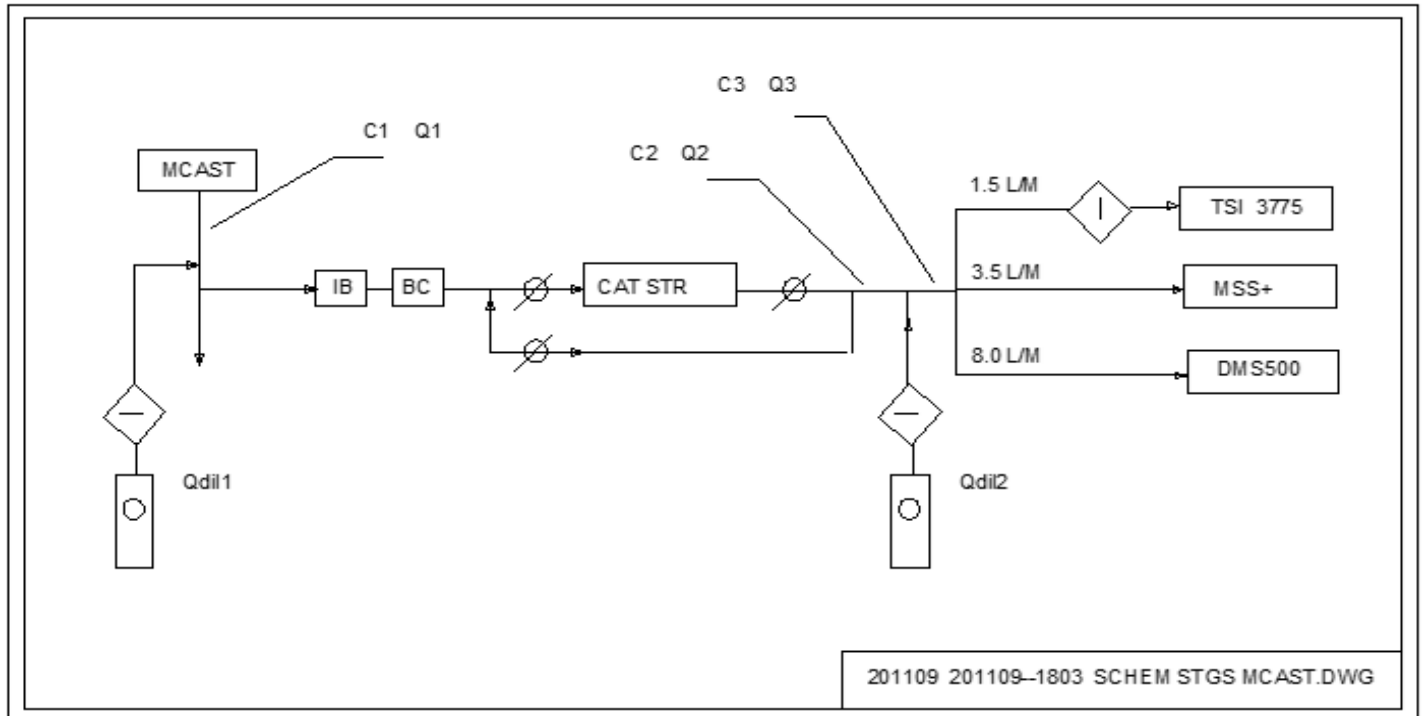


Figure 2. Schematic diagram of source evaluation studies in Task 2.

**Publications**

None

**Outreach Efforts**

Project 069 plan and progress was delivered as a recorded presentation at the virtual ASCENT advisory board meeting in April 2020.

**Awards**

None

**Student Involvement**

There are no graduate students currently assigned to this project. The restrictions imposed by the COVID-19 pandemic have prohibited the participation of undergraduate students.

**Plans for Next Period**

Continue to pursue the statement of work from Subtask 2 to Subtask 5 as described above.



# Project 070 Reduction of nvPM Emissions from Aero-Engine Fuel Injectors

## Georgia Institute of Technology

### Project Lead Investigator

Wenting Sun  
Associate Professor  
School of Aerospace Engineering  
Georgia Institute of Technology  
Phone: (404) 894-0524  
Fax: (404) 894-6596  
Email: wenting.sun@aerospace.gatech.edu

### University Participants

#### Georgia Institute of Technology

- P.I.: Dr. Wenting Sun
- FAA Award Number: 13-C-AJFE-GIT-080
- Period of Performance: August 11, 2020 to August 10, 2021
- Tasks:
  1. Measurements of non-volatile particulate matter (nvPM) formation and oxidation processes
  2. nvPM model development and validation
  3. Experimental facility development and operation

### Project Funding Level

The total amount of funding from FAA is \$500,000. The matching funding includes \$400,000 from Georgia Institute of Technology and \$100,000 from Honeywell.

### Investigation Team

Lead PI, Wenting Sun from the Georgia Institute of Technology will oversee the entire project and coordinate among different co-PIs. He will work with one graduate student and one research engineer to lead Task 3.

Co-PIs, Adam Steinberg, Ellen Yi Chen, Timothy Lieuwen, and Jechiel Jagoda from the Georgia Institute of Technology, will work with two graduate students to lead Task 1.

Co-PI, Rudy Dudebout from Honeywell, will lead Task 2.

### Project Overview

Reducing nvPM from gas turbine engines is essential for improving air quality and reducing the environmental impact of aviation. However, predicting and controlling nvPM remains a challenge due to the complicated physical and chemical processes at play. The proposed research will characterize the formation/oxidation of nvPM and optimize the design of an aeronautical gas turbine fuel injector to reduce nvPM at flight-relevant conditions. The goals of this project include:

- (1) conduct optical diagnostics to measure nvPM volume fraction and primary particle size; polycyclic aromatic hydrocarbon (PAH) and hydroxyl (OH) radical distributions; and the flow field for a set of fuel injectors.
- (2) develop empirical correlations describing nvPM formation/oxidation using data obtained in experiments.
- (3) validate computational fluid dynamics (CFD) simulations to facilitate fuel injector design optimization.

## Task 1 – Measurements of nvPM Formation and Oxidation Processes

Georgia Institute of Technology

### Objectives

In this task, laser-induced incandescence (LII) measurements will be conducted to quantify soot volume fraction and primary particle size; OH planar laser-induced fluorescence (PLIF) will be conducted to understand the soot oxidation process; PAH PLIF will be conducted to elucidate the formation pathway of soot; and particle image velocimetry (PIV) will be conducted to understand the fuel/air mixing process owing to the characteristics of fuel injectors.

### Research Approach

We will conduct LII to quantify soot volume fraction and primary particle size, PIV to measure flow fields, PAH PLIF and OH PLIF to understand the interaction between nvPM and important gas-phase species, and droplet Mie scattering to characterize the fuel spray. We will also conduct sampling measurements in the combustor exhaust to analyze the exhaust composition (via gas chromatography) and nvPM composition/morphology (via x-ray photoelectron spectroscopy (XPS) and scanning electron microscopy (SEM)), providing further understanding of nvPM kinetics. All measurements will be performed in a model aeronautical gas turbine combustor operated with a liquid jet fuel at engine-relevant operating conditions. All subtasks under Task 1 will proceed in parallel, as the ultimate aim is to measure multiple parameters simultaneously.

Since this is a new project, detailed results will be reported in the next report.

#### **Subtask 1.1 – LII Measurement**

LII utilizes short laser pulses to heat small particles to vaporization temperatures. The light emission, or incandescence, of the nvPM is then measured in order to deduce the relative volume fraction and primary particle size. Two-dimensional implementations of LII are performed by shaping the laser beam into a uniform sheet and capturing the incandescence at various wavelengths on sensitive time-gated cameras. The prompt emission immediately after the arrival of the laser pulse describes the volume fraction or spatial concentration of nvPM particles. By applying sufficient laser intensity to uniformly sublime the nvPM and by calibrating these measurements against emissions from known flames, it is then possible to determine absolute volume fractions.

For nvPM particle sizing, time-resolved LII (TiRe-LII) techniques can be used to obtain the incandescence decay over time. This approach utilizes the fact that small particles cool down faster than large ones after laser heating due to their larger surface-to-volume ratio. By solving energy and mass balances, the primary particle size can be evaluated. In order to measure the decays, which are on the order of several hundred nanoseconds in atmospheric pressure flames, ultra-high-speed cameras are necessary. Recently, we were able to demonstrate a single-camera single-laser-shot technique for making these measurements by capturing the decay time constants at 10 million-frames-per-second with a 50 ns gate. At these imaging rates, the flame motion appears stationary, enabling accurate pixel-by-pixel decay time measurements. The data from each pixel are then fit to a model to determine the instantaneous, primary nvPM particle sizes for the entire scene. The statistics for these images can then be compared to show regions of the flame where nvPM growth and nvPM oxidation typically occur.

For the high pressures associated with flight-relevant conditions, however, the incandescence time constants decrease to the order of ~50 ns. This is faster than the imaging rate of many single-chip ultra-high-speed cameras. In order to overcome this challenge and accurately measure the shorter time constants in these environments, a multi-camera variant of the TiRe-LII technique described above can be used. In this variant, two or more cameras sharing the same field-of-view can be gated to open a few tens of ns apart. The calibrated relative intensities of these images can then be used to estimate time constants and nvPM particle sizes. Hence, this method enables the determination of nvPM growth regions and oxidation regions, even in high-pressure environments.

The various LII measurements described in this subtask will be conducted using the fundamental 1064 nm output of a solid-state neodymium-doped yttrium aluminum garnet (Nd:YAG) laser operating at 5-10 kHz in order to avoid exciting the OH and PAH fluorescence. The laser beam will be formed into a sheet that is then passed through the combustor. The incandescence is then measured with time-gated cameras using the appropriate filters (near 640 nm) to avoid C<sub>2</sub> Swan band emissions. Calibrations using well-characterized laminar flames will be conducted to produce quantitative measurements for nvPM volume fraction and particle size in the gas turbine combustor at the conditions of interest.

### Subtask 1.2 – OH PLIF Measurement

Oxidation through reaction with OH is expected to be a critical pathway through which nvPM is destroyed in the flame. Understanding the relative trajectories of nvPM and OH through the combustor is therefore critical to predicting the final nvPM output.

Hydroxyl radicals, OH, form during high-temperature hydrocarbon oxidation, reaching super-equilibrium concentrations near the location of maximum heat release rate before relaxing to equilibrium in the products. Significant concentrations of OH occur in hot product gases at temperatures above  $\sim 1500$  K. Fortunately, owing to its strongly absorbing energy transitions at wavelengths that are relatively accessible to high-energy pulsed lasers, OH can be readily measured using PLIF. The main challenges with performing OH PLIF in the combustor of interest here are laser power absorption and signal trapping through the high-density gas at 10 bar.

We will perform OH PLIF measurements simultaneously with the 2D LII measurements to understand the interaction between nvPM and OH. Measurements will be made at a 5-10 kHz repetition rate using the frequency-doubled output of a dye laser (Rhodamine 6G), pumped by a frequency doubled solid-state laser (Nd:YAG). Over 7 W of ultraviolet (UV) laser light can be produced by our laser system, which is sufficient to acquire signal across the combustor domain. The laser beam will be formed into a sheet, made coincident with the LII laser sheet, and transmitted through the combustor. The OH PLIF signal will be filtered through an appropriate bandpass filter (around 307 nm) and recorded using a high-speed intensified camera. Appropriate corrections will be made for laser power absorption, intensity variations, and detector response. The resultant data will provide time-resolved 2D images of the OH distribution, which will be correlated to the nvPM dynamics to better understand the oxidation process and how specific trajectories influence the nvPM that is ultimately output from the combustor.

### Subtask 1.3 – PAH PLIF Measurement

PAHs occur naturally in jet fuel and also can be formed from small aliphatics during combustion. Since PAHs play a key role in nvPM growth, understanding their position relative to regions containing nvPM can help elucidate rate controlling processes.

PAH molecules have high absorption cross-sections across a wide range of wavelengths in the UV spectral range. It therefore is possible to perform PAH PLIF with a similar laser wavelength to that used for the OH PLIF, but slightly de-tuned from the narrow-band OH absorption line to avoid interference. Hence, PAH PLIF measurements will be acquired using the same experimental configuration as employed for the OH PLIF, but with a wavelength shift on the order of 0.1 nm. Measurements will be obtained simultaneously with the LII to elucidate the relative positions of nvPM and PAH during formation. While simultaneous OH and PAH PLIF will not be obtained, these species are related to different aspects of the nvPM dynamics and do not directly interact. Because the PAH PLIF laser beam is obtained by adjusting the wavelength of the OH PLIF beam, the different measurements can be obtained in close succession, thus maintaining identical operating conditions.

### Subtask 1.4 – PIV Measurement

Measuring the fluid velocity field is critical for understanding the influence of turbulence and mixing on nvPM dynamics. PIV measures the velocity field in a plane by tracking the motion of micron-scale particles that are seeded into the flow. Stereoscopic PIV (S-PIV) allows measurement of all three velocity components in the plane by simultaneously viewing the particle motion from two different viewing angles. While PIV (and S-PIV) has been successfully applied to study a wide range of flows, including in flames, its application in high-pressure fuel-rich combustion has been relatively limited. This is due to the high-intensity background luminescence from the flame, beam steering through index of refraction gradients, and fouling of the optical windows due to seed particle deposition. Despite these challenges, we recently demonstrated S-PIV in a 10-bar rich-burn gas turbine combustor similar to the one being studied in this work.

Here, S-PIV measurements will be made simultaneously with the LII and PLIF measurements. To enable these measurements, the flow will be seeded with micron scale  $ZrO_2$  tracer particles. The high melting point of  $ZrO_2$  mitigates window contamination relative to other commonly used solid tracers. Laser pulse pairs from a solid-state second-harmonic Nd:YAG laser will be formed into a sheet and transmitted through the combustor along the same path as those for the other measurement techniques. The particle-scattered light will be filtered through appropriate bandpass filters and collected by two high-speed cameras arranged in an angular stereoscopic viewing configuration. Image pre-processing routines—well established in our group—will be performed to reduce the effects of background flame luminosity and cross-signal interference, thus providing sharp particle images for subsequent vector processing. The resultant particle image pairs will

be converted to three-component velocity vectors using a multi-pass image cross-correlation algorithm implemented in LaVision DaVis, a commercial software package.

#### **Subtask 1.5 – Fuel Droplet Mie Scattering Measurement**

One important factor that controls nvPM formation is the mixing between the fuel from the injector spray and the air in the combustor. The fuel injector spray can be characterized by measuring the size and spatial distribution of liquid fuel droplets. Using Mie scattering imaging techniques, the spatial distribution of micro-sized fuel droplets can be determined via measurements of the elastic light scattering. However, quantification of the spray properties from Mie scattering is challenging, predominantly due to multiply scattered photons, interference from PIV seed particles, and the relationship between scattering intensity and droplet size. Here, the objective is to obtain qualitative information on the fuel spray trajectory, including spray angle, penetration, and the relative locations of the liquid fuel, flame, and nvPM.

To study fuel droplet distribution of different injectors at pressure in a non-reacting environment, the liquid fuel droplet distribution will be measured via Mie scattering at 5-10 kHz repetition rate. The second harmonic of an Nd:YAG laser will be formed into a sheet and transmitted through the spray inside the experimental facility. The scattered light will be imaged at an angle perpendicular to the laser propagation using a high-speed camera. This signal will then be separated from the PIV seed particle scattering using adaptive threshold-based segmentation techniques.

#### **Subtask 1.6 – Extractive Sampling Measurement**

In this task, exhaust gas samples will be extracted and analyzed via gas chromatography (gas phase), XPS (solid phase) and SEM (solid phase). The gas chromatography (Inficon Fusion  $\mu$ GC) analysis will reveal comprehensive information on large hydrocarbons formed during the combustion of Jet-A, such as detailed structure of PAHs, ethylene, and other intermediate species relevant to soot formation.

The XPS and SEM analyses will provide data on nvPM composition and morphology to help understand the detailed formation mechanism of nvPM. There are two possible mechanisms for nvPM formation that can be detected during the combustor test. The first is due to the liquid fuel impinging on the wall accompanied by chemical reactions at the wall. The other results from flame products such as soot or coked droplets. These two types of solid particles can be differentiated using chemical and morphology analysis. Solid particles formed due to wall wetting features lower carbon but significantly higher oxygen content (e.g., 70-80% carbon and 20% oxygen) and small amounts of hydrogen and nitrogen. This is due to incomplete oxidation of fuel at low temperatures. Solid particles formed from flame products feature high carbon and low oxygen content (e.g., 98% carbon and 2% oxygen). In terms of morphology, solid particles formed due to wall wetting exhibits amorphous structures while solid particles formed from flame products feature spherical particles with diameters that are typically 4-5 microns. For these experiments, a water-cooled sampling probe will be used to collect samples of exhaust gas from the pressure vessel.

## **Task 2 – nvPM Model Development and Validation**

Honeywell

This task involves the comparison of the experimental measurements obtained in Task 1 with detailed numerical simulations for the purpose of model development and validation. A numerical framework to model the gas turbine combustor system will be established based on Honeywell's previous experience. In this numerical framework, a commercial solver will be used to obtain CFD solutions with a large eddy simulation (LES) turbulence model using a dynamic Smagorinsky model. The combined heat release/turbulence model consists of non-premixed diffusion flamelets generated using a detailed Jet-A kinetic model that describes the formation of aromatic species up to pyrene. The simulation includes radiation with the discrete ordinate method due to  $H_2O$ ,  $CO_2$ , and nvPM (weighted-sum-of-gray-gases model (WSGGM)). The liquid fuel spray is modelled with Lagrangian tracking of droplets with stochastic secondary breakup, calibrated to experimental data. The domain is discretized using polyhedral cells and consists of the entire geometry from the inlet of the rig to the exhaust of the combustor. The simulation is initially converged with a Reynolds-averaged Navier-Stokes (RANS) solution, then run with five flow-throughs to initialize the solution and then a further five flow-throughs to obtain statistical averages. The numerical simulation will be compared with experimental results from optical measurements (LII, OH/PAH PLIF, S-PIV, and Mie scattering) at different flow conditions employing different fuel injectors. The numerical model will then be validated and optimized for further fuel injector design towards the minimization of nvPM emission.

Task 2 will be conducted in year two of this project after obtaining the proposed experimental results in Task 1.



## Task 3 – Experimental Facility Development and Operation

Georgia Institute of Technology

In this task, we will design and fabricate a high-pressure vessel and the model gas turbine combustor for the proposed measurement. The preliminary design of the high-pressure vessel is presented in Figure 1, featuring three large optical windows.

The combustor to be built will be comprised of a single fuel injector. This reflects a single injector of an annular Rich Burn, Quick Quench, Lean Burn (RQL) combustor architecture. The test rig will have provisions for routing air to cool the combustor walls and will provide air to the quench holes, the injector, and the swirler. The sidewalls will also incorporate optical access with suitable features to discourage accumulation of nvPM or S-PIV tracer particles. Non-optical components of the liner will be multi-holed angle cooled (i.e. effusion cooled) at an appropriate cooling flux with no additional thermal barrier coating. Honeywell will design the dome/bulkhead and fuel injector with replaceable screw-on injector swirlers. In addition, Honeywell will fabricate the fuel injector and screw-on injector swirlers. A combination of proprietary and public domain swirler configurations will be designed, fabricated, and tested. This will yield both data that are publishable and proprietary data that can directly translate to design improvements. The estimated design conditions are combustor inlet temperatures between 600 F to 800 F, combustor inlet pressures between 6 atm to 10 atm, pressure drop of approximately 3%, primary zone equivalence ratio of 1.2 to 1.8, and combustor exhaust temperatures of 2000 F to 3000 F.

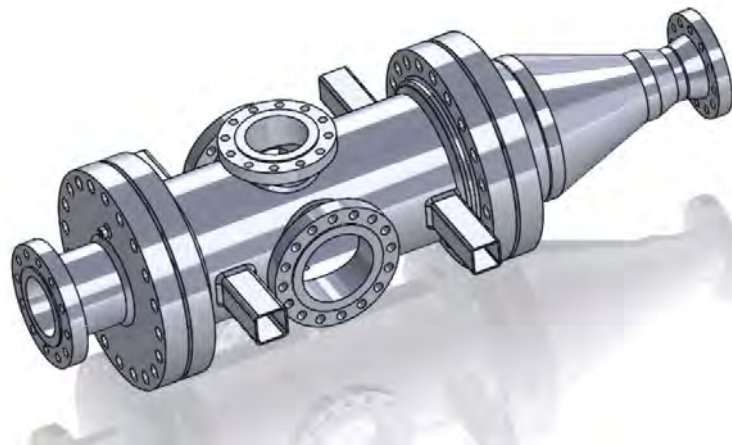


Figure 1. Rendering of high-pressure vessel.

### Milestones

Project 70 is a new project, so no milestones have been achieved yet.

### Major Accomplishments

Project 70 is a new project, so no accomplishments are reported.

### Publications

None

### Outreach Efforts

None

### Awards

None



**Student Involvement**

Project 70 is a new project. Students are being hired for this project.

**Plans for Next Period**

In the following year, Task 1 and Task 3 will be executed.



# Project 071 Predictive Simulation of nvPM Emissions in Aircraft Combustors

## Georgia Institute of Technology

### Project Lead Investigator

Suresh Menon  
Hightower Professor  
School of Aerospace Engineering  
Georgia Institute of Technology  
Phone: (404) 894-9126  
Email: suresh.menon@aerospace.gatech.edu

### University Participants

#### Georgia Institute of Technology

- PI: Suresh Menon
- FAA Award Number: 13-C-AJFE-GIT-067
- Period of Performance: Oct 1, 2019 – Sep 30, 2020
- Task(s):
  1. Implement high-fidelity method of moments with interpolative closure (MOMIC) model within large-eddy simulation (LES) to account for all physical processes such as nucleation, surface growth & oxidation, coagulation, and aggregation in soot formation.
  2. Evaluate soot/PAH (polycyclic aromatic hydrocarbon) chemistry model developed by Raytheon Technologies Research Center (RTRC) and soot model updates from University of Michigan (UM) and RTRC.

#### University of Michigan

- P. I.: Angela Violi
- FAA Award Number: 13-C-AJFE-GIT-067
- Period of Performance: One Year
- Task(s)
  1. Use Molecular Dynamics to assess parameters for nucleation process using RTRC's kinetics
  2. Collaborate with RTRC and GT to update MOMIC

### Project Funding Level

FAA funding is currently for one-year effort of \$500,000/year (Georgia Tech (GT): \$150,000, Raytheon Technology Research Center (RTRC): \$250,000 and University of Michigan (UM): \$100,000). Cost share of \$500,000 is also committed by participants.

The project started in late July 20 in GT and early September 2020 in RTRC and UM.

### Investigation Team

- Dr. Suresh Menon, Professor, Georgia Institute of Technology, Principal Investigator
- Dr. Miad Yazdani, United Technologies Research Center, Co-Principal Investigator
- Dr. Steve Zeppieri, United Technologies Research Center, Co-Principal Investigator
- Prof. Angela Violi, Professor, University of Michigan, Co-Principal Investigator
- Dr. Meredith (Med) Colket, Consultant, United Technologies Research Center, Co-Investigator

## Project Overview

This project will establish a new multi-scale approach to predict soot formation in aircraft combustors. A hierarchy of first principle simulation methods will be used to account for the multi-scale physics of the formation and transport of non-volatile particulate matter (nvPM, also called "soot" in the literature), and then use these methods to model the physics in large-eddy simulations (LES). This project will target and isolate the layers of empiricisms that currently exist, for example in particle inception models, in the role of precursors species in nucleation, particle shape assumptions and their impact on surface growth, the sensitivity of predictions to particle size distribution, and the ad hoc coagulation/coalescence mechanisms. All the relevant modeling tools already exist, but a systematic coupling of these tools in multi-scale, multi-physics strategy has yet to be accomplished by anyone. Hence, this study will establish a new predictive capability by integrating these capabilities.

We report here on the progress over a portion of this year because the project started officially in late July 2020 at GT and in September 2020 at the other team members' institutions. At GT, we are extending the Method of Moments with Interpolative Closure (MOMIC) approach based on first six moments of soot particle size distribution function and have completed some canonical OD, 1D and 3D tests. The six moment method is considered more accurate compared to the three moment method used earlier and is the most optimal method given the current state of knowledge. The MOMIC model accounts for all soot formation processes such as nucleation, coagulation, surface growth, and aggregation and is coupled with an in-house compressible reacting flow solver, which uses a computational code called LESLIE. The details about the LES-MOMIC approach and corresponding validation cases, along with results, are discussed in this report.

The present MOMIC method uses a simplified four-step Lindstedt soot model (Leung and Lindstedt, 1991) as well as 19-step ethylene-air reduced chemistry (Lu and Law, 2005) which does not account for details about the established aromatic soot precursors (Blanquart et. al., 2009). Therefore, RTRC and University of Michigan (UM) are working on developing improved soot kinetic models as well as a skeletal mechanism that accounts for details about the breakdown of fuel species to soot precursors such as polycyclic aromatic hydrocabons (PAHs). The identification of this detailed chemistry and the reduction to key species are briefly touched upon at the end of this report.

## Task 1 – LES-MOMIC of Sooting Flames

Georgia Institute of Technology

### Objective

The objective of this task is to establish the predictive capability of MOMIC within the LES code by simulating canonical sooting test cases.

### Research Approach

LES studies of turbulent sooting problems are very difficult due to the multi-scale nature of soot inception, coagulation, and surface growth that have to be modeled in a highly turbulent and reactive environment, typically in a complex combustor configuration. Most past studies have focused on global models that approximate the small-scale physics; as such, there are many models to account for the underlying physics. On the other hand, simulations will require some approximations because the computational resources will never meet the simulation requirements. In the current effort, we balance contributing to the prediction on soot formation physics with a need to obtain high-fidelity and reliable predictions using advanced models. To achieve this goal, we leverage our past LES capability and upgrade the models using the results from molecular dynamics (MD) and kinetic Monte Carlo (KMC) studies. MD studies will be conducted by the UM team in collaboration with the RTRC group that will work on KMC and PAH kinetics tools. These groups outputs will be used to adjust MOMIC at GT.

The current task involves key subtasks that were accomplished in the most recent quarter:

- 1) Assessment and improvement of the MOMIC method for first six moments of soot particle size distribution function (PSDF). Some optimizations are being performed to improve the performance and accuracy of the code. One-dimensional testcases were performed to verify predictions of the present solver with established results in the literature.
- 2) Augmentation of the MOMIC library with source terms accounting for agglomeration process.



- 3) Integration of simplified MOMIC approach within LES framework. Specifically, the objective is to carry the first six moments of the PSDF in the solver and establish a functional architecture for integration of the full-fledged MOMIC model within LESLIE.
- 4) Testing is performed to assess implementation of the LES-MOMIC model using a premixed flame-turbulence interaction study. The simulations are performed with a  $C_2H_4$ /air setup and reduced chemistry that includes the Leung and Lindstedt mechanism for soot formation and growth.

The MOMIC approach involves solving the moment equations in two limiting conditions. In the coalescent limit where the soot particles are assumed to conserve the spherical shape after collision, the equation for the  $r$ -th moment  $M_r$  is solved either in the subgrid or in the resolved space along with the LES equations. A general form is  $dM_r/dt = R_r + C_r + S_r + FM_r$ ,  $r = 0, 1, 2, 3, \dots$ , where  $M$  is the moment of the PSDF, and  $R$ ,  $C$ ,  $S$ , and  $F$  are respectively nucleation, coagulation (in the coalescent limit), surface growth, and subgrid turbulent mixing contributions to the  $r$ -th moment equation. When soot particles exceed a certain size limit ( $\sim 27.5$  nm), the particles start to aggregate into chain-like structures of fractal dimension  $D$  ( $\sim 1.8$ ). Then the above equations are replaced by another set of moment equations of similar form but with different source terms representing the aggregation rate, the coagulation rate, and the surface growth rate in the non-coalescent limit. The zeroth moment  $M_0$  represents the soot number density  $N_5$  defined by the number of soot particles per unit volume of the mixture. The first moment  $M_1$  represents the average total mass of soot particles  $m_5$  per unit volume. Thus, the soot mass fraction is  $Y_5 = M_1/\rho$ , where  $\rho$  is the mixture density. The average particle diameter is  $d_p = (6.0M_2/\pi\rho_{\text{soot}}M_1)^{1/3}$  (El-Asrag and Menon, 2009, Srinivasan and Menon, 2015).

The model accounts for the different soot formation processes such as nucleation, oxidation, surface growth, coagulation, and aggregation. Soot or nvPM transport by diffusion and thermophoretic forces are included to allow for complete description of the soot physical behavior in a turbulent reactive environment. The energy equation is supplied with an optically thin radiation model to account for the radiation effect by the soot particles. The choice of using the first six moments within the MOMIC approach implies that we solve for the whole moments and interpolate the fractional moments (Frenklach, 2002). Thus, this model is computationally efficient because only six additional equations are solved in the coalescent and nine equations in the non-coalescent limits, and the source terms can be computed using efficient parallel processing approach.

The following 0D, 1D, and 3D tests are performed to assess the implementation of the MOMIC model within the code. Results of each case study are provided in a side-by-side figures below the case study descriptions.

#### Case Study 1: Verification of Coagulation Source Terms

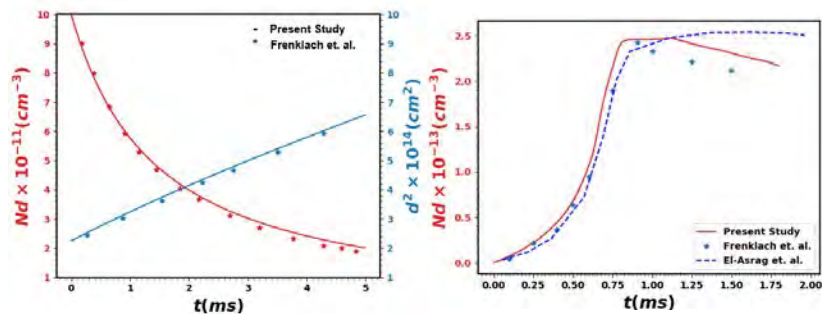
The free molecular coagulation model has been validated against one of the tests given by Frenklach and Harris, 1987. Consider a population of soot particles in a closed batch reactor where initially the particles have the same size (i.e., mono-dispersed), and the number density of the particles is  $10^{12}$   $\text{cm}^{-3}$ . The pressure and temperature of the reactor are kept constant at 1 atm and 1500 K, respectively. The bulk species comprising the soot particles are assumed as carbon atoms ( $m_0 = 3.18 \times 10^{-21}$  g) and the bulk density of the particle core  $\rho_s$  is  $1.8$   $\text{g/cm}^3$ . The time profiles of particle number density predicted with the present improved MOMIC library are compared in Figure 1(a) against results predicted by Frenklach and Harris using sectional methods. As can be witnessed from these results, the present study gives good comparison with the results by Frenklach and Harris, 1987 validating the implementation of coagulation source terms.

#### Case Study 2: Verification of MOMIC with simultaneous nucleation, surface growth, and coagulation

This example, shown in Figure 1(b), is based on results from shock tube data at 1800 K and presented as a verification test in Frenklach and Harris, 1987. Here, it assumed that for this verification study that soot particles with  $m = 4.784 \times 10^{-22}$  g and  $\rho = 1.86$   $\text{g/cm}^3$  are formed. We use the parameters/constants and assumptions from Frenklach and Harris (1987), which used a more complex sectional method to validate the model. The time dependent profile of particle inception (nucleation) rate is provided in the literature and therefore can be used for comparison with our more cost-effective MOMIC method. The source terms for the moment equations are calculated based on this nucleation time rate profile. The particles add carbon (C) by surface growth with rate constant  $k_s = 1 \times 10^{-4}$   $\text{g/cm}^2\text{s}$ . The particles are assumed to undergo coagulation in free molecular regime. The time profiles of number density evolution of soot particles obtained in the present 6-MOMIC study is compared to the earlier 3-moment (and more approximate) MOMIC method of El-Asrag et. al. (2007). Figure 1(b) shows this comparison. It is clear that the present 6-MOMIC is much more accurate than the 3-MOMIC when compared to the sectional method. A detailed comparison with new data (if available) will be addressed during this effort.

**Case Study 3: Verification of agglomeration coupled MOMIC approach for rich laminar premixed ethylene/air flame**  
 Ethylene/air laminar premixed flames, shown in Figure 2, are presented here for the purpose of verification of the MOMIC approach equipped with nucleation, coagulation, surface growth, and aggregation source terms embedded inside the LESLIE code. The test case considered here (Figure 2) is based on experimental configurations of Xu and Faeth, 2001 for laminar premixed sooting flames. The operating pressure considered is 101325 Pa. with the initial temperature of 400 K. The rich laminar 1D  $C_2H_4$ /air flame at an equivalence ratio ( $\Phi = 2.93$ ) is considered for the 1D simulations in the domain of 0.05 m in length. The domain is discretized using 500 cells. The inflow is treated as subsonic constant velocity inflow while the outflow is modelled with characteristic subsonic outflow boundary conditions. The solution is initialized with non-sooting flame profiles. The ethylene-air 19 species 15 step reduced mechanism is used to account for chemical pathways modelling the breakdown of fuel to the soot precursor assumed here as acetylene ( $C_2H_2$ ). The evolution of soot using the MOMIC model is compared against the experimental soot volume fraction as shown in Figure 2 and good agreements are observed.

**Case Study 4: Assessment of LES-MOMIC approach for rich turbulent premixed ethylene/air flame**  
 This proposed test intends to use the LES-MOMIC model with the finite rate chemistry for the premixed flame turbulence interaction problem (El-Asrag et. al., 2007). The schematic for the configuration is shown in Figure 3. The critical C/O ratio for ethylene-air premixed flames is 0.6. Therefore, for the current case, C/O ratio is fixed at 0.67 and the turbulence level will be varied so that the flame is in the thin reaction zone (TRZ) regime. The initial flame front is obtained from the laminar premixed flame solution and is specified at the center of the domain with the left side denoting the reactants and the right side denoting the products. The extent of the computational domain is 15 mm x 15 mm x 15 mm in the streamwise x, transverse y, and spanwise z directions. The flow field is initialized using von Karman-Pao energy spectrum. Characteristic inflow-outflow conditions are specified in the streamwise direction while periodic in the other two directions. The LES grid resolution chosen for the simulations is 64 x 64 x 64 number of LES cells with the assumption of quasi-laminar chemistry, meaning that no closure for subgrid turbulence-chemistry interactions is considered. Studies are still underway and will be reported soon.



(a) Case 1: Free molecular coagulation      (b) Case 2: nucleation, coagulation & surface growth

**Figure 1.** Verification of MOMIC Solver using 0D Testcases

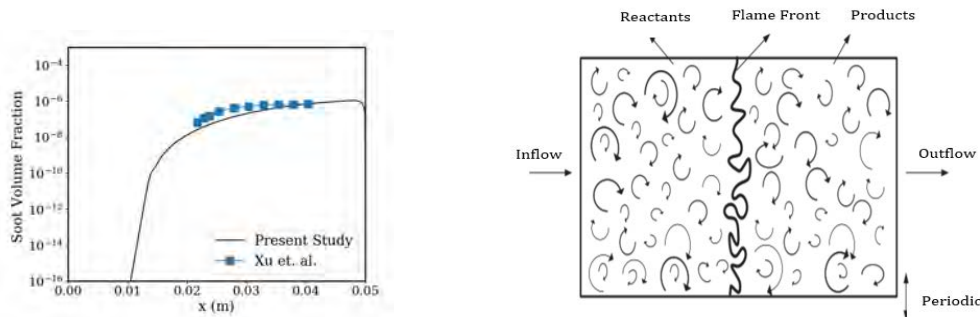


**Figure 3:** Case 3: Sooting Laminar Premixed Flames

**Figure 4:** Case 4: 3D turbulent premixed flame

In Case 4, rich premixed mixture enters the domain at a speed to approximately balance the forward propagation of the premixed flame and keep it statistically stationary in the middle of the domain, the combustion products leave the domain at the outflow. Inflow also contains turbulent fluctuations that wrinkle the premixed flame and soot formation occurs in the vicinity of this flame.

## Task 2 – Kinetic Activities at RTRC

### Objective

The goal of the effort is to identify one or two detailed ethylene/PAH kinetic mechanisms that handle both fuel decomposition and soot (PAH) growth reactions sufficiently so that the down-selected mechanism(s) can then serve as a basis for the reduced kinetic model ultimately to be used in the computational fluid dynamics (CFD)-based application.

### Research Approach

The research approach involves the assessment of published ethylene/PAH mechanisms, initiated in the current reporting period. In all, seven mechanisms were assembled for analysis:

- Abbel-Bockhorn-Frenklach (99 species/533 reactions)
- Wang-Frenklach (101 species/544 reactions)
- NJFCP Foundational Chemistry submodel with SERDP PAH reactions (166 species/504 reactions)
- NJFCP Foundational Chemistry submodel with KAUST PAH reactions (168 species/818 reactions)
- Full ARAMCO-KAUST C4 mechanism (581 species/3037 reactions)
- CREK Natural Gas mechanism (114 species/1999 reactions)
- UCONN (Lu) Skeletal C<sub>2</sub>H<sub>4</sub> mechanism (33 species/206 reactions)

(The Lu skeletal mechanism serves as a proxy for the reduced 19 species ethylene mechanism currently used at GT, because both mechanisms derive from the same fully detailed mechanism.)

These models have been benchmarked against published ethylene data sets for comparative analysis against both experimental data and relative performance against the various models. Current experimental data has been comprised primarily of shock tube data (Hidaka et al., 1999; Miller and Churchill, 1962; Skinner and Sokoloski, 1960) but comparison to well-stirred reactor, i.e., perfectly stirred reactors (PSR) (Dagaut et al., 1988; Westbrook et al., 1988) datasets have also been completed. The focus of the above analysis has been to assess the computational characteristic times of fuel decomposition and major product yields versus the experimental data. At present, one mechanism that is showing slightly better agreement to the various experiments is the CREK natural gas model, but analysis/comparisons utilizing all the above mechanisms continue.

### Milestones

Milestone	Planned Due Date
Establish the framework for MOMIC for LES	12/31/20
Extend the model to agglomeration effects	09/30/20
Simulate the test case(s) using the new MOMIC model	02/27/21
Identification of detailed ethylene-air mechanism	01/30/21
MD and KMC studies of nucleation	03/31/21

### Major Accomplishments

- Full inclusion of MOMIC with nucleation, surface growth, coagulation, and aggregation has been accomplished.
- Extensive validation studies with improved MOMIC.
- Basic LES-MOMIC framework is established and tested for a premixed flame turbulence interaction problem.
- Promising detailed kinetic mechanisms for fuel decomposition have been identified.



### **Publications:**

N/A

### **Outreach Efforts**

None

### **Awards**

None

### **Student Involvement**

Shubham Karpe is a PhD student at Georgia Institute of Technology.

Qi Wang is a PhD student at the University of Michigan

### **Plans for Next Period**

#### **MOMIC for CFD Applications (GT, RTRC, UM)**

The next steps in this activity will focus on developing postprocessing tools to quantify major features such as rates of different soot formation processes like nucleation, coagulation, and aggregation and how the soot is transported. These results will establish a baseline comparison testbed. The current MOMIC approach focuses on simplified soot model with reduced fuel chemistry. Therefore, improvements can be achieved in these two areas where the involvement of UM and RTRC is critical. Some of the important improvements planned for future work revolve along the following objectives:

- 1) Involvement of PAH species for soot precursor with inputs from RTRC.
- 2) Improvements in the nucleation and surface growth reactions and their rates using inputs from UM and RTRC.

#### **Kinetic Assessment of Ethylene/PAH Chemistry (RTRC)**

The next steps in this activity will now focus on more fuel-rich experiments, with the purpose of characterizing and assessing the reduced model generation of aromatic compounds (e.g., benzene, styrene, etc.) in order to understand their ability to ultimately characterize PAH production in relevant devices (e.g., aeroengine combustors). Once these fuel-rich comparisons are completed, a mechanism down selection will then be completed

#### **MD and KMC Simulations (UM and RTRC)**

The nucleation and surface growth models contain rate parameters that are being revisited with first principal studies using MD to establish the rate constants utilizing the kinetic models developed in RTRC. Then this model will be used in the KMC studies at RTRC to establish growth rate parameters in the inputs for the LES-MOMIC studies at GT.

### **References**

- Blanquart, G., Pepiot-Desjardins P. and Pitsch H. (2009) *Combustion and Flame* 156.3: 588-607.
- Dagaut, P., Cathonnet, M., Gaillard, J. (1988) *Combustion and Flame*, 71:295-312
- El-Asrag, H. and Menon, S. (2009) *Combustion and Flame*, 156: 385-395.
- El-Asrag, H., Lu, T., Law, C. K. and Menon, S. (2007) *Combustion and Flame*, 150: 108-126.
- Frenklach, M. (2002) *Chemical Engineering Science*. 57: 2229-2291.
- Frenklach, M., and Harris S. (1987) *Journal of colloid and interface science* 118.1: 252-261.
- Hidaka, Y., Nishimori, T., Sato, K., Henmi, Y., Okuda, R. and Inami, K. (1999) *Combustion and Flame*, 117:755-776.
- Leung, K. and Lindstedt, R. (1991) *Combustion and Flame*. 87: 289-305.
- Lu, T, and Law C. K. *Proceedings of the Combustion Institute* 30.1 (2005): 1333-1341.
- Miller, I.F., and Churchill, S. W. (1962) *AIChE Journal*, 8(2):201-204
- Srinivasan, S. and Menon, S. (2015) Soot modeling using the linear eddy model, CCL-TR-2015-03-10.
- Skinner, G. B., and Sokoloski, E. M. (1960), *Journal of Physical Chemistry*, 64(8):1028-1031
- Xu, F., and Faeth G. *Combustion and flame* 125.1-2 (2001): 804-819.
- Westbrook, C. K., Thornton, M. M., Pitz, W. J. and Malte, P.C. (1988) *Twenty-Second Symposium (International) on Combustion, The Combustion Institute*, 863-871.



# Project 072 Aircraft Noise Exposure and Market Outcomes in the U.S.

## Massachusetts Institute of Technology

### Project Lead Investigators

PI: R. John Hansman  
T. Wilson Professor of Aeronautics & Astronautics  
Department of Aeronautics & Astronautics  
Massachusetts Institute of Technology  
77 Massachusetts Avenue, 33-303  
Cambridge, MA 02139  
(617) 253-2271  
rjhans@mit.edu

Co-PI: Christopher R. Knittel  
George P. Shultz Professor of Applied Economics  
Sloan School of Management  
Massachusetts Institute of Technology  
77 Massachusetts Avenue, E62-527  
Cambridge, MA 02139  
(617) 324-0015  
knittel@mit.edu

Co-PI: Steven R. H. Barrett  
Professor of Aeronautics and Astronautics  
Department of Aeronautics and Astronautics  
Massachusetts Institute of Technology  
77 Massachusetts Avenue, 33-316  
Cambridge, MA 02139  
(617) 253-2727  
sbarrett@mit.edu

Co-PI: Jing Li  
Assistant Professor of Applied Economics  
Sloan School of Management  
Massachusetts Institute of Technology  
77 Massachusetts Avenue, E62  
Cambridge, MA 02139  
(617) 252-1131  
lijing@mit.edu

Co-PI: Florian Allroggen  
Research Scientist  
Department of Aeronautics and Astronautics  
Massachusetts Institute of Technology  
77 Massachusetts Avenue, 33-115A  
Cambridge, MA 02139  
(617) 715-4472  
fallrogg@mit.edu



## University Participants

### Massachusetts Institute of Technology

- P.I.s: Prof. R. John Hansman; co-PIs: Prof. Christopher R. Knittel, Prof. Steven Barrett, Prof. Jing Li, Dr. Florian Allroggen
- FAA Award Number: 13-C-AJFE-MIT, Amendment No. 075
- Period of Performance: August 11, 2020 to August 10, 2021
- Tasks:
  1. Literature review
  2. Empirical identification strategy and scope of dataset (*not reported; task planned to start in the next reporting period*)
  3. Calculation of noise impact metrics
  4. Cleaning and aggregation of housing transaction dataset (*not reported; task planned to start in the next reporting period*)
  5. Descriptive analysis of dataset (*not reported; task planned to start later*)
  6. Empirical analysis (*not reported; task planned to start later*)

## Project Funding Level

\$380,000 FAA funding and \$380,000 matching funds. Sources of match are approximately \$112,000 from MIT, plus third party in-kind contributions of \$268,000 from NuFuels LLC.

## Investigation Team

- Prof. R. John Hansman, PI, MIT (Tasks 1, 2, 3, 5, and 6)
- Prof. Christopher R. Knittel, co-PI, MIT (Tasks 1, 2, 4, 5, and 6)
- Prof. Steven R. H. Barrett, co-PI, MIT (Tasks 1, 5, and 6)
- Prof. Jing Li, co-PI, MIT (Tasks 1, 2, 4, 5, and 6)
- Dr. Florian Allroggen, co-PI, MIT (all tasks)
- Madeleine Jansson, Graduate Student, MIT (Tasks 1, 3, and 5)

## Project Overview

While enplanements at U.S. airports have increased by almost 50% over the past two decades, the number of Americans exposed to significant levels of aircraft noise has decreased substantially. However, there is still considerable concern within some airport communities about aircraft noise. This project leverages revealed-preference approaches to infer the “implicit price” of aircraft noise exposure from market outcomes in U.S. airport communities. More specifically, the research team is quantifying the capitalized disutility associated with aircraft noise exposure through analyzing the empirical relationship between aircraft noise exposure and transaction values for residential properties in communities surrounding U.S. airports. State-of-the-art empirical methods will be applied, which will leverage quasi-experimental settings of noise exposure changes. The project will empirically analyze the house price impacts of potential changes in noise exposure associated with the quasi-experimental settings. The results will provide insights into the average impacts of noise exposure on residential property values while also assessing dynamic adjustment processes and potential heterogeneities in revealed preferences, targeting factors such as time, location, or noise exposure patterns.

## Task 1 – Literature Review

Massachusetts Institute of Technology

### Objectives

The project team will review and summarize the existing body of literature in two topic areas:

- Empirical analyses of the impacts of noise exposure on residential property values.
- Noise exposure metrics.

### Research Approach

The research team will systematically review and summarize the existing literature. This entails:



1. Presenting a detailed overview of existing economic studies on the impacts of noise exposure on residential property values. This overview includes a review of both results and methods. In particular, the team will summarize results by comparing standardized metrics (e.g., noise depreciation index (NDI)). This enables analysis of trends that might be published in the existing body of work.
2. Comparing different noise metrics and their application. This will include, but is not limited to, metrics such as the day-night average sound level (DNL), equivalent sound level (LEQ), maximum sound levels (Lmax), and metrics which consider frequency and amplitude of noise events.

### **Milestone**

The research team started work in September 2020.

### **Major Accomplishments**

The research team prepared a high-level literature summary, which informed the presentation for the ASCENT Fall meeting (see below).

### **Outreach Efforts**

The team prepared a pre-recorded presentation for the ASCENT Fall Meeting (September 29-30, 2020). The presentation included a project overview and a high-level summary of the existing literature.

### **Plans for Next Period**

The team will continue to work towards completing this task.

## **Task 3 – Calculation of Noise Metrics**

Massachusetts Institute of Technology

### **Objective**

The goal of this task is to calculate aircraft noise exposure in communities surrounding selected U.S. airports. These analyses will be used to derive noise exposure changes associated with quasi-experimental changes in flight trajectories (e.g. due to new runways, new procedures). The team may develop models to compute exposure metrics that currently are not routinely calculated in the Aviation Environmental Design Tool (AEDT).

### **Research Approach**

The MIT team leverages existing DNL-based noise exposure maps shared by the FAA as a starting point of the analysis. If required, the AEDT is used to model noise exposure based on historical flight track data. If required, these flight tracks will be provided by the FAA for airports with Airport Surface Detection Equipment, Model X (ASDE-X) and different years between 2010 and 2019 (and future years as the study progresses).

The research team will also work with the FAA to examine older noise exposure data from 2000 to 2009. The goal is to explore how insights can be gained for this time period.

### **Milestone**

The research team started work in September 2020.

### **Major Accomplishments**

The team analyzed existing noise exposure maps provided by the FAA. Together with the FAA, the project team identified additional needs for noise analyses and coordinated next steps to obtain the required noise data.

### **Student involvement**

MIT graduate student Madeleine Jansson is conducting the research under this task.

### **Plans for Next Period**

The team will continue this task.



# Project 073 Fuel Composition Impact on Combustor Durability

## University of Dayton Research Institute

### Project Lead Investigator

Steven Zabarnick, Ph.D.  
Division Head, Fuels and Combustion Division  
University of Dayton Research Institute  
300 College Park  
Dayton, OH 45469-0043  
937-229-3961  
Steven.Zabarnick@udri.udayton.edu

### University Participants

#### University of Dayton Research Institute

- PI: Steven Zabarnick, Ph.D.
- FAA Award Number: 13-C-AJFE-UD, Amendment 029
- Period of Performance: August 11, 2020 to August 10, 2021
- Task:
  1. Radiation measurements of various fuel types will be performed in the referee combustor to evaluate the function of fuel composition on combustor liner lifetime.

### Project Funding Level

Initial Project Funding from FAA- \$299,148  
Cost share will come from Fuel Producers and Engine/Airframe OEMs. Cost share will be in fuel provided for testing and in fuel performance data provided for the evaluation.

### Investigation Team

Project Director/Principal Investigator: Steven Zabarnick  
Co-Investigator: Scott Stouffer  
Research Engineer: Tyler Hendershott  
Technician: Harry Grieselhuber  
Graduate Student: TBD  
Undergraduate Student: TBD

### Project Overview

In this study, the effect of fuel chemical composition on radiative heat transfer and the resulting combustor liner lifetime will be evaluated. Alternative fuels contain ratios of hydrocarbon types that may be quite different from familiar petroleum-based fuels. For petroleum-based fuels, it is known that higher aromatics levels contribute to greater radiative heat transfer and reduced combustor liner lifetime. As a result, aromatics are limited to 25 vol% in the ASTM D1655 jet fuel specification. Some candidate alternative fuels contain synthetically produced aromatics and cycloparaffins which need to be evaluated for their radiative heat transfer characteristics. The measurements taken in this project will provide insight into the effect of fuel type on the liner lifetime. Several fuel types will be investigated including an SAK (Synthetic Aromatic Kerosene), a baseline Jet A fuel, and a fuel that is high in cycloparaffins (e.g., the Shell IH<sup>2</sup> fuel). Diagnostic methods to be used in the investigation include the measurement of wall and gas temperatures, infrared (IR) cameras, and radiometers.

## Task 1 – Measurement of Radiative Heat Transfer in the Referee Rig

University of Dayton Research Institute

### Objective

The objective of this program is to provide insight into the effect of fuel type on engine combustor liner lifetime. The study will assure that candidate drop-in fuels will perform satisfactorily in jet engines and not increase engine maintenance nor decrease flight safety. The study may also show where fuel composition changes may reduce radiative heat transfer and therefore increase combustor liner lifetime.

### Research Approach

It is well known that fuel chemical composition strongly affects soot formation, smoke production, and radiative heat flux in gas turbine combustors (1). Studies of petroleum-based fuels with varying aromatics species levels have shown that these properties increase with overall aromatics species content. Other parameters such as hydrogen content, hydrogen: carbon (H/C) ratio, and smoke point have also been correlated with liner temperatures, but the effect of individual aromatics species types has not been well studied (2). Candidate alternative fuels may meet aromatics species overall limits but contain individual species or mixtures of species that are very different from those in petroleum-derived fuels. Radiation heat transfer to combustor liners is a major issue in the durability and operational envelope of gas turbine engines. Radiation can cause high heat fluxes resulting in localized heating, hot spots, and high thermal gradients along and across the liner. Increases in liner temperature can decrease the liner durability (3). The intense heating can cause problems with low cycle fatigue, cracking, and buckling of the liner, and in the extreme case can lead to localized melting of the liner. The walls of the combustor can be convectively cooled by effusion or film cooling, however the film cooling typically imposes a cycle performance penalty, along with elevated levels of CO and unburnt hydrocarbons, particularly at low power settings. Because of the concerns about fuel effects on radiation, the radiant heat flux is considered a Figure of Merit (FOM) by aircraft engine OEMs when evaluating alternative fuels for aircraft use (4).

The radiation from a gas turbine flame has two main components:

1. "Non-luminous" radiation from product gases such as CO<sub>2</sub>, H<sub>2</sub>O, and CO.
2. Luminous radiation from particulates (principally soot) (5).

The non-luminous radiation is in the infrared and has a spectral distribution, whereas the luminous radiation is broadband with a fraction of the radiation appearing in the visible wavelengths. Typically, as the pressure is increased, the luminous radiation from the soot particles becomes the dominant source of heat flux to the liner walls. While the convective component of the wall heat transfer is dependent on the fluid dynamics and gas temperature distribution near the walls, the peak radiant fluxes are related to the combinations of high temperature gas and particulates.

The emissivity of the combustion gases is typically related in an expression such as:

$$\epsilon_g = 1 - \exp[-aPL(qI)^{0.5}T_g^{-1.5}]$$

Where  $P$  = gas pressure, kPa

$l$  = a characteristic length factor, which is a function of combustor geometry

$T_g$  = gas temperature, K

$q$  = the fuel-to-air ratio

$L$  = the luminosity factor

The luminosity factor is set to one for gaseous emissivity. For sooting flames, associated with liquid aviation fuels, the luminosity is greater than one and can be correlated with the fuel composition. There are several relations for the luminosity versus fuel type in the literature (6-8). In general, the relations show a drop in the luminosity factor with increases in H/C ratio and decreases in the aromatic content of the fuel. Other correlations in the literature also address the relationship of correlation to smoke point and naphthalene content. While there has been use of IR as a diagnostic tool in basic flame experiments (9), there has been very little work reported in the literature using multiple radiometer and/or planar measurements of IR emissions in practical combustors. The Referee Rig Combustor is an ideal rig for assessing radiation heat transfer because the walls are heavily cooled, a condition that tends to suppress the convective component and thus the background radiant heating from opposing walls, so that the wall heat transfer is primarily from the flame radiation. Furthermore, the provision has been made for radiometer access to the combustor walls in the referee rig.

The team for the proposed effort has developed and used the Referee Rig Combustor to conduct experimental combustion research. Highlights of previous contributions to the evaluation of alternative fuels include:

1. Experimental measurements of lean blowout (LBO) for fuels at a condition of interest to the OEMs and the National Jet Fuels Combustion Program (NJFCP), which have resulted in an unexpected finding of a high correlation between the derived cetane number (DCN) and the LBO limit.
2. Experimental measurements of boundary conditions for the combustor including air flow splits to support numerical combustion modeling efforts.
3. Development of cold air and cold fuel capabilities for the facility to enable atmospheric cold start ignition experiments to be conducted over a range of conditions.
4. A further extension of the facility capability to enable altitude relight experiments to be conducted with a range of fuels at simulated altitudes of 25,000 ft.

The work with the Referee Rig Combustor has resulted in publications that detail cold start ignition (10), ignition at elevated temperatures (11), LBO characteristics (11-15), particulate and gaseous emissions (12), flow through the liner effusion passages (13), acoustic response (11-17), spray characteristics (16), and altitude relight (19).

**Milestones**

List of the anticipated major milestones and planned due dates.

Milestone	Planned Due Date
Test plan provided	1 Dec 2020
Testing performed over range of fuels	1 Aug 2021
Final report	31 Aug 2021

**Major Accomplishments**

The project has only just begun so there are no accomplishments yet.

**Publications**

The project has only just begun so there are no accomplishments yet.

**Outreach Efforts**

The project has only just begun so there are no outreach efforts yet.

**Awards**

None

**Student Involvement**

None

**Plans for Next Period**

The bulk of the project will be planned, conducted, analyzed, and reported in the next project period.

**References**

- (1) Lefebvre, A.H. Fuel Effects on Gas Turbine Combustion, AFWAL-TR-83-2004, 1983.
- (2) Rosfjord, T.J. Aviation-Fuel Property Effects on Combustion, NASA Contractor Report 168334, 1984.
- (3) Chin, J.S., and Lefebvre, A.H., "Influence of Fuel Composition on Flame Radiation in Gas Turbine Combustors," Journal of Propulsion and Power, Vol. 6, No. 4, pp. 497-503.
- (4) Boehm et al., "Development of Combustion Rules and Tools for the Characterization of Alternative Fuels, Phase 2A", AFRL-RQ-WP-TR-2013-0223, October 2013.
- (5) Gleason, G.C., and Bahr, D.W., "Fuel property effects on Life Characteristics of Aircraft Turbine Engine Combustors", ASME Paper 80-GT-55, 1980.
- (6) Lefebvre, A.H., "Gas Turbine Combustion (2nd edition)", Taylor and Francis, 1999.
- (7) Naegeli, D.W. and Moses, C.A., "Effects of Fuel Properties on Soot Formation in Gas Turbine Engines", ASME paper 80-GT-62, 1980.



- (8) Clark, J.A. "Fuel Property Effects on Radiation Intensities in a Gas Turbine Combustor", AIAA J. Vol. 20. No. 2, pp274-281, 1982.
- (9) Rankin, B.A., Blunck, D.L., Katta, V.R., Stouffer, S.D., Gore, J.P., Experimental and Computational Infrared Imaging of Bluff Body Laminar Diffusion Flames," Combustion and Flame, Vol. 159, pp2841-2843, 2012.
- (10) Hendershott, T.H., Stouffer, S.D., Monfort, J.R., Diemer, J., Busby, K.; Corporan, E., Wrzesinski, P.J., Caswell, A.W., "Ignition of Conventional and Alternative Fuel at Low Temperatures in a Single-Cup Swirl-Stabilized Combustor," 2018 AIAA Aerospace Sciences Meeting, AIAA 2018-1422
- (11) Stouffer, S.D., Hendershott, T.H., Monfort, J.R., Diemer, J. Edwin Corporan, E., Wrzesinski, P.J., Caswell, A., "Blowout and Ignition Characteristics of Conventional and Surrogate Fuels Measured in a Swirl Stabilized Combustor", AIAA Paper AIAA-2017-1954, AIAA SciTech Conference Jan 9-13, 2017.
- (12) Corporan, E., Edwards, J., Stouffer, S.D., DeWitt, M., West, Z., "Impacts of Fuel Properties On Combustor Performance, Operability and Emissions Characteristics, AIAA Paper AIAA-2017-0380, AIAA SciTech Conference Jan 9-13, 2017.
- (13) Alejandro M. Briones, A.M., Stouffer, S.D., Vogiatzis, K., Rein, K., Rankin, B.A., "Effects of Discrete Dome and Liner Cooling Momentum on Combustor Flow Fields", AIAA-2017-0781, AIAA SciTech Conference Jan 9-13, 2017.
- (14) Esclapez, L., Ma, P. C., Mayhew, E., Xu, R., Stouffer, S.D., Lee, T., Wang, H., and M. Ihme, M. "Fuel Effects on Lean Blow-out in a Realistic Gas Turbine Combustor" Accepted for publication in Combustion and Flame 2017.
- (15) Colborn, J.G., Heyne, J., Hendershott, T.H., Stouffer, S. D., Peiffer, E., and Corporan, E., "Fuel and operating condition effects on Lean Blowout in a Swirl-Stabilized Single Cup Combustor", AIAA 2020-1882, Presented at AIAA Scitech, January 9th 2020.
- (16) Mayhew, E., Mitsingas, C., McGann, B., Lee, T., Hendershott, T., Stouffer, S., Wrzesinski, P., and Caswell, A., "Spray Characteristics and Flame Structure of Jet A and Alternative Jet Fuels," AIAA Paper AIAA-2017-0148, AIAA SciTech Conference Jan 9-13, 2017.
- (17) Monfort, J.R., Stouffer, S.D., Hendershott, T.H., Wrzesinski, P.J., Foley, W.S., Rein, K., "Evaluating Combustion Instability in a Swirl-Stabilized Combustor Using Simultaneous Pressure, Temperature, and Chemiluminescence Measurements at High Repetition Rates," AIAA Paper AIAA 2017-1101, AIAA SciTech Conference Jan 9-13, 2017.
- (18) Erdmann, T.J., Burrus, D.L., Briones, A.M., Stouffer, S.D., Rankin, B.A., Caswell, A.W., "Experimental and Computational Characteristics of Flow Rates in a Multiple-Passage Gas Turbine Combustor Swirler," GT2017-65252, Proceedings of the ASME Turbo Expo 2017: Turbine Technical Conference & Exposition, June 26-30, Charlotte, NC.
- (19) Stouffer, S. D., Hendershott, T.H., Monfort, J., Colborn, J.G., Corporan, E., Paul Wrzesinski, P., Caswell, A. "Fuel Effects on Altitude Relight Performance of a Swirl Cup Combustor", AIAA 2020-1882 Presented at AIAA Scitech, January 9th 2020.



# Project 074 Low Emissions Pre-Mixed Combustion Technology for Supersonic Civil Transport

## Georgia Institute of Technology

### Project Lead Investigator

Adam Steinberg  
Associate Professor  
School of Aerospace Engineering  
Georgia Institute of Technology  
Phone: (404) 897-1130  
E-mail: adam.steinberg@gatech.edu

### University Participants

#### Georgia Institute of Technology

- P.I.: Dr. Adam Steinberg, Associate Professor, Daniel Guggenheim School of Aerospace Engineering
- FAA Award Number: 13-C-AJFE-GIT-079
- Period of Performance: August 11, 2020 to August 10, 2021
- Tasks:
  1. Overall program coordination
  2. Task 1: Experimental measurement of flame structure, combustion dynamics, and emissions

### Project Funding Level

FAA: \$1,000,000  
Georgia Institute of Technology: \$500,192  
GE Research: \$499,808

### Investigation Team

Dr. Adam Steinberg (PI), Georgia Tech  
Dr. Ellen Yi Chen Mazumdar (Co-PI), Georgia Tech  
Dr. Joseph Oefelein (Co-PI), Georgia Tech  
Dr. Jerry Seitzman (Co-PI), Georgia Tech  
Dr. Michael Benjamin (Co-PI), GE Aviation  
Dr. Krishna Venkatesan (Co-PI), GE Research  
Dr. Oleksander Bibik (Research Scientist), Georgia Tech  
Sriram Kalathoor (GRA), Georgia Tech  
Mitchell Passarelli (GRA), Georgia Tech  
Samuel Wonfor (GRA), Georgia Tech  
Andrew Zheng (GRA), Georgia Tech  
TBD (Research Engineer), GE  
TBD (Research Engineer), GE  
TBD (Research Engineer), GE

See Figure 1 for detailed task responsibilities.



	Project management											
	L	L	CL	L	L							
	Task 1: Experimental Measurements			ST1.1: Rig and Diagnostic Development			ST1.2: Experimental Campaigns			ST1.3: Data Processing and Analysis		
	Task 2: Large Eddy Simulations											
	ST2.1: Industrial-Scale LES			ST2.2: Research-Scale LES			ST2.3: LES Best Practices					
	Task 3: Thermoacoustic Modeling											
	ST3.1: Acoustic Response Modeling									ST3.2: Prediction, Assessment, Validation		
Adam Steinberg (PI)	L	L	CL	L	L						P	P
Ellen Mazumdar (Co-PI)		P	P	P	P							
Joseph Oefelein (Co-PI)						L	CL	L	L			
Jerry Seitzman (Co-PI)		P	P	P	P							
Oleksander Bibik (RE)		P	P	P	P							
Sriram Kalathoor (GRA)						P	P	P	P			
Mitchell Passarelli (GRA)		P	P	P	P						P	P
Samuel Wonfor (GRA)		P	P	P	P							
Andrew Zheng (GRA)		P	P	P	P							
Michael Benjamin (Co-PI)		P	P	P	P	P	P	P	P			
Krishna Venkatesan (Co-PI)	CL	CL	L	CL	P						CL	CL
TBD (RE)		P	P	P	P							
TBD (RE)						CL	L	CL	CL			
TBD (RE)											L	L

Figure 1. Responsibilities and roles of the research team.

## Project Overview

This project was initiated in Q3 of 2020; the report below summarizes initial activities.

Supersonic civilian transportation is an important growth area. However, combustor conditions experienced in supersonic engines are in a pressure-temperature range not encountered by existing subsonic engines. New combustor technologies are needed to optimize emissions of nitrogen oxides (NO<sub>x</sub>), carbon monoxide (CO), unburnt hydrocarbon (UHC), and non-volatile particulate matter (nvPM) across the flight mission, while achieving the necessary durability and stability. Fuel-lean premixed combustion is viewed as a key enabling technology. However, the ability of current design methodologies to predict the operability and emissions of these combustors at the relevant conditions is unproven. Hence, there is a critical need to generate high-quality experimental data at relevant conditions, coupled with the development/validation of computational fluid dynamics (CFD) simulations and reduced order thermoacoustic models. This project will fill this need through a combination of experiments, large eddy simulations (LES), and thermoacoustic modeling, all applied in a novel lean premixed combustor that is specifically designed for supersonic civilian transport. Figure 2 shows the elements of this research project.

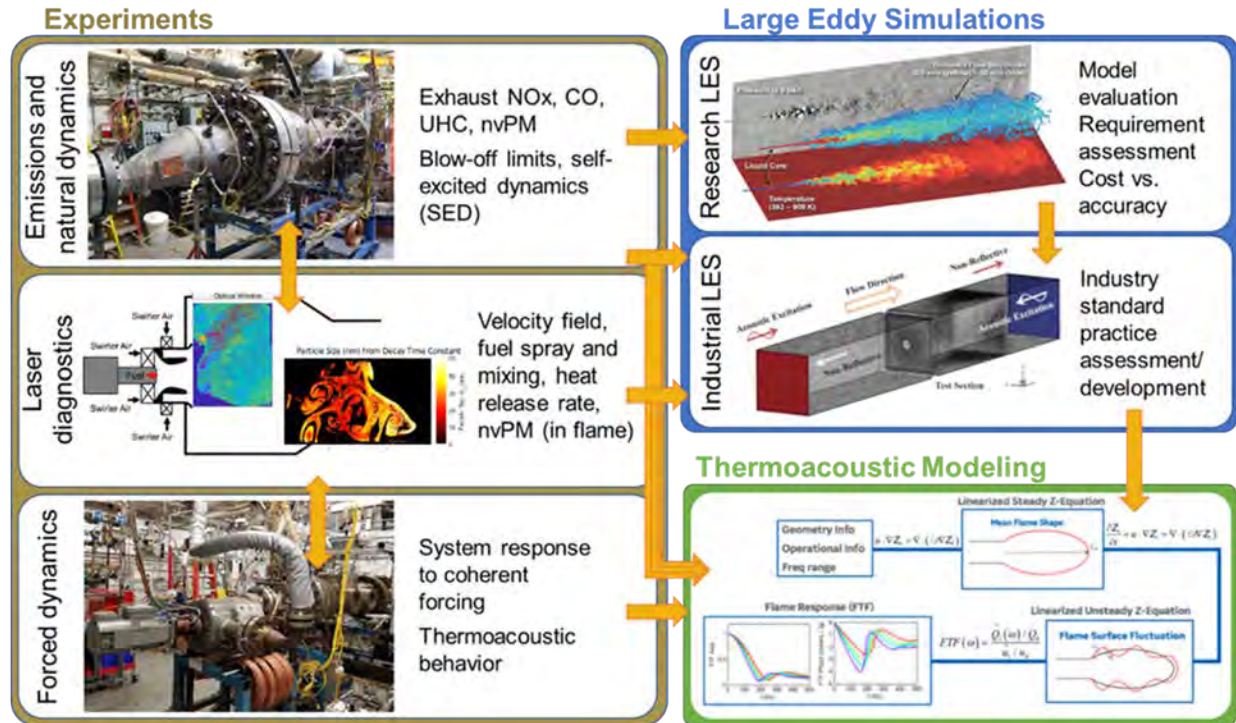


Figure 2. Elements of the research program.

## Task 1 – Experimental Measurements of Flame Structure, Combustion Dynamics, and Emissions

Georgia Institute of Technology

### Objective(s)

This task represents the experimental effort that will measure the flame structure, dynamics, and emissions in a novel micro-mixer combustor concept, designed specifically for low-emission operation at typical conditions encountered by supersonic engines. Experiments will be performed across pressures ranging from 80-150 psig (5.5-10 bar) and 600-1000 °F (590-810 K). Optical measurements of in-combustor processes and probe-based exhaust emissions measurements will be made, providing critical data for understanding these combustors and developing/validating the models in Tasks 2 and 3. Optical measurements to be deployed include stereoscopic particle image velocimetry (S-PIV), fuel droplet Mie scattering, OH\* chemiluminescence (FL), phase Doppler particle analysis PDPA, 2D time resolved laser induced incandescence (TiRe-LII), fuel planar laser induced fluorescence (PLIF), and filtered Rayleigh scattering (FRS).

### Research Approach

#### Rig and Diagnostic Development

Activities thus far have focused on designing and testing the laser diagnostics systems for transport and use in test cells at GE Research. To this end, we have deployed a new high-pressure laminar flame combustor that is capable of replicating the thermodynamic conditions of interest, but in a laboratory-scale facility that can be easily operated for diagnostic development. It is capable of operating with both gaseous and pre-vaporized liquid fuels. A schematic of the system is shown in Figure 3, along with the piping and instrumentation diagram (P&ID) for gaseous fuel operation.

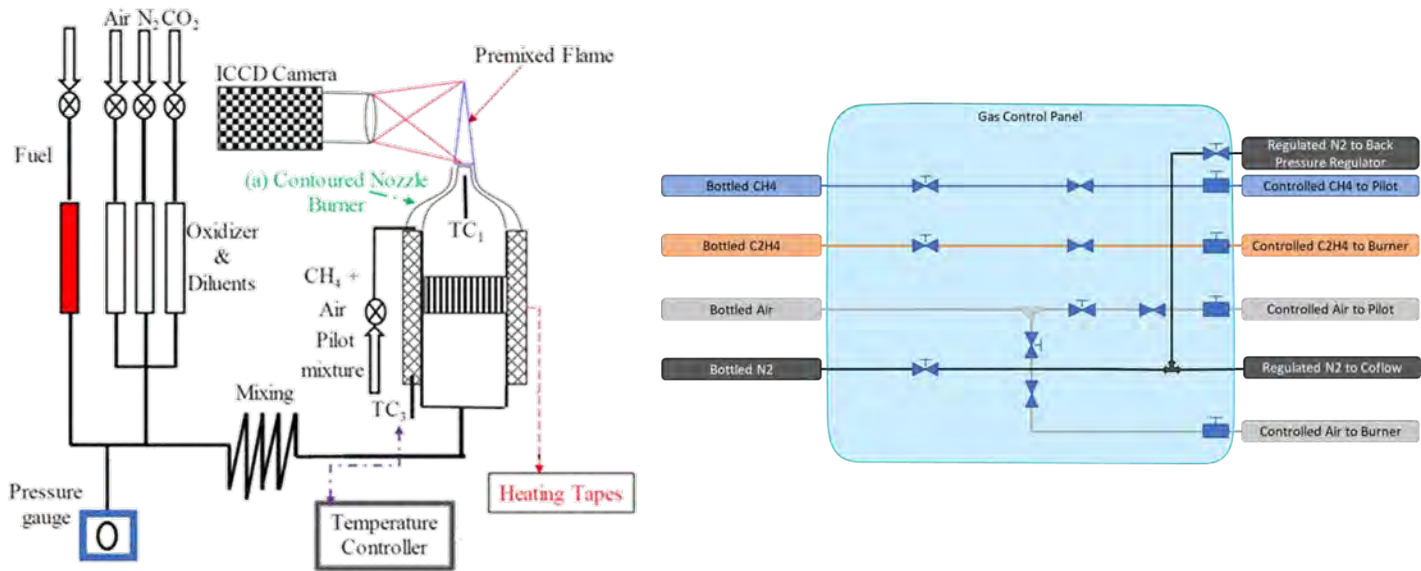


**Figure 3.** Layout and piping and instrumentation diagram (P&ID) for high-pressure calibration burner.

In addition to the rig design, we also are developing the theory, models, and algorithms required to apply the various laser diagnostics in the conditions of interest. Regarding FRS, we have designed and set up a unique experiment to measure Rayleigh-Brillouin scattering (RBS) spectra of combustion-relevant species at elevated temperatures and pressures. RBS spectral profiles are required to invert the fuel/air ratio from FRS data, which measure the convolution of the spectrum with a molecular iodine absorption filter. However, theoretical models only are validated for relatively simple species (i.e., diatomic gases) at or around atmospheric pressure [1]. Increasing the pressure causes a transition from a gas kinetic regime to a hydrodynamic regime, requiring more complicated model validation [2-4]. Unfortunately, the spectral features of interest are extremely narrow (e.g.,  $\mathcal{O}(10\text{ MHz})$  or  $\mathcal{O}(10\text{ fm})$ ) and cannot be measured using standard equipment.

Our experiment uses a novel virtually imaged phase array (VIPA) to disperse the RBS spectrum, providing unprecedented resolution and the ability to measure a complete spectrum in a single image. The layout of the experiment is shown in Figure 4 and a typical preliminary result using an unoptimized VIPA is shown in Figure 5. The latter demonstrates the RBS spectrum measured for nitrogen at 34 atm and 298 K. Clearly visible is a “triple Lorentzian” profile, generated by the combination of Doppler-shifted Rayleigh scattering and acoustic Brillouin scattering. We currently are in the process of measuring spectra for the relevant species at the temperatures and pressures to be studied in this work, which is essential for Year 2 measurement activities.

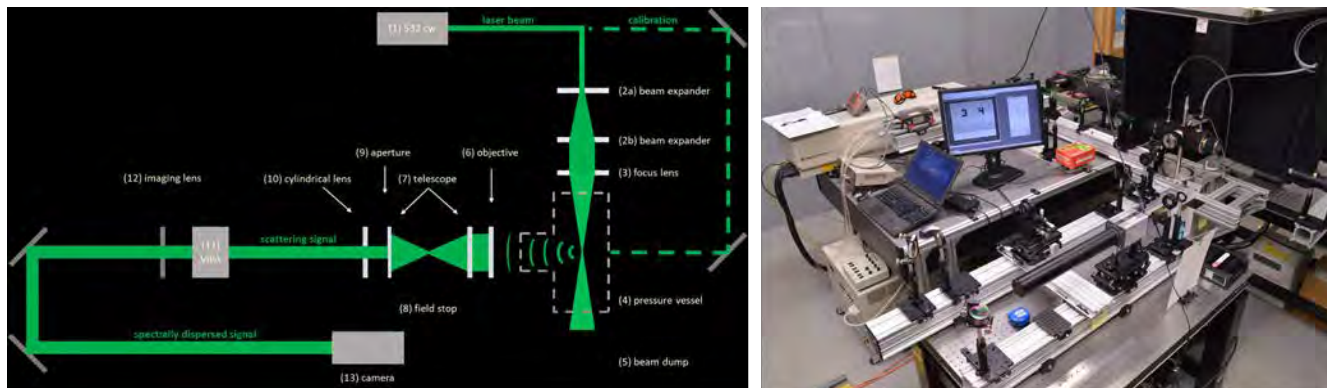


**Figure 4.** Layout of RBS spectrum measurement experiment.

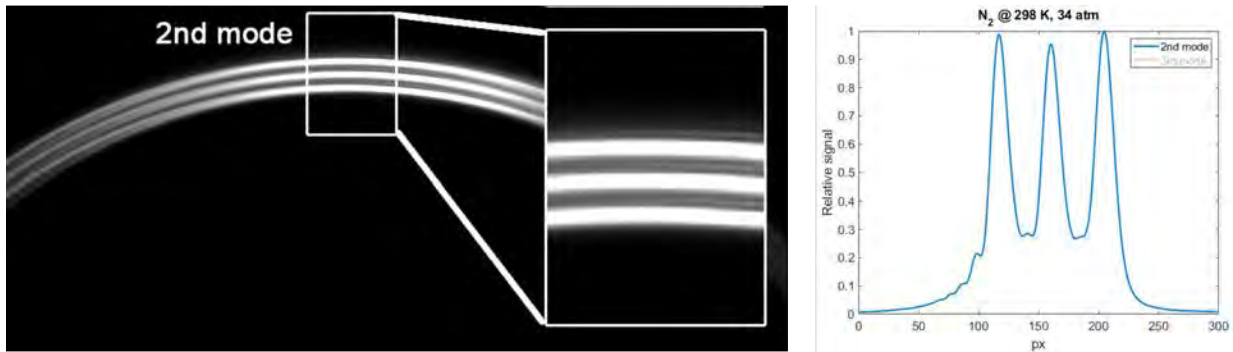


**Figure 5.** Measured RBS scattering spectra. Left: Raw signal dispersed by VPA. Right: Integrated spectrum.

We have also started developing a time-resolved laser-induced incandescence (TiRe-LII) model, which uses the incandescence decay profiles to determine soot properties like particle size. By combining this model with ultra-high-speed camera data at 10 MHz, it is possible to estimate planar or volumetric soot particle sizes in turbulent flames. The baseline model is based on work by Liu et al. [5] and includes laser absorption, conduction, and radiation elements. Additional heat transfer mechanisms, including sublimation, are currently being validated and integrated into the model in Figure 6. For lower laser fluences, the dominant heat transfer mechanism is conduction, which includes temperature dependent thermal conductivity and specific heat. We have also incorporated an iterative solver for determining the heat transfer contributions from the free molecular and continuum conduction regimes.

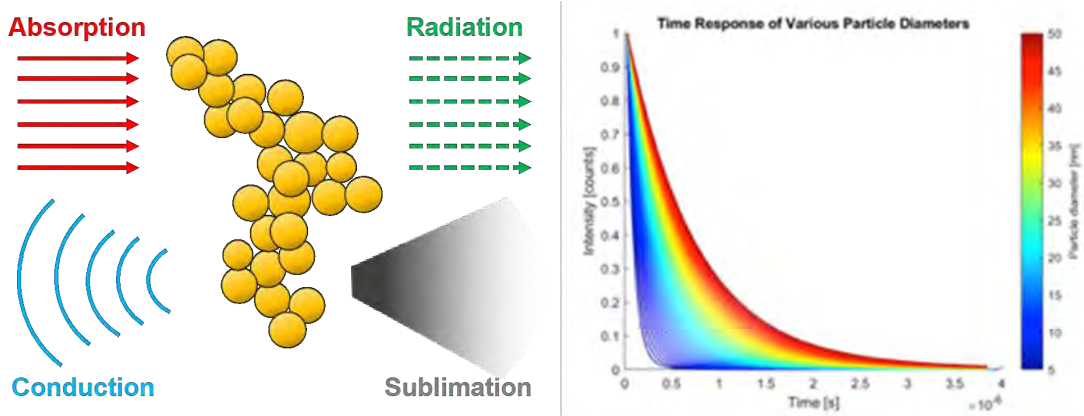


**Figure 6.** TiRe-LII concept. Left: Main physical process contributing to the LII signal. Right: Typical incandescence decay curves for different particle sizes.

To use this TiRe-LII model, several different fitting strategies can be adopted. One potential strategy is to use Bayesian inference to determine the most likely parameter values for a given decay profile. A second complementary approach is to obtain validation measurements of flame properties, such as temperature and soot agglomeration, to reduce the number of parameters that require fitting. For this preliminary TiRe-LII model, a simple fitting procedure was devised based on validation data from the literature. First, the temperature response of the model is calculated for different particle sizes. These temperature profiles are then converted to intensity profiles to create a “decay time-constant” to “soot particle size” library, as shown in Figure 6. Additional complexity can be added to this fitting procedure in the future that varies multiple parameters, such as aggregate size, local bath gas temperature, and particle size. For initial validation, ultra-high-speed camera data from two different flames from our previous work [6] were utilized. The first flame used a laminar ethylene flame burner, while the second flame utilized a turbulent non-premixed ethylene jet flame. A 1064 nm pulsed laser beam was then formed into a thin laser sheet to heat up the soot particles in the flame. Data were measured through a 640 nm (with 75 nm full width at half maximum) filter. The data were then captured at 10 MHz (50 ns exposure) on a non-intensified

ultra-high-speed camera (Shimadzu HPV-X2). Utilizing published values for soot aggregate size ( $N = 60$ ) and bath gas temperature (1850 K), we were able to fit our model library data to the incandescence decay at each pixel. This produced the soot particle sizes estimates shown in Figure 7. These preliminary estimates match well with literature values, which measure a soot particle size of  $\sim 32$  nm at the flame edge with a height of  $\sim 40$  mm above the burner.

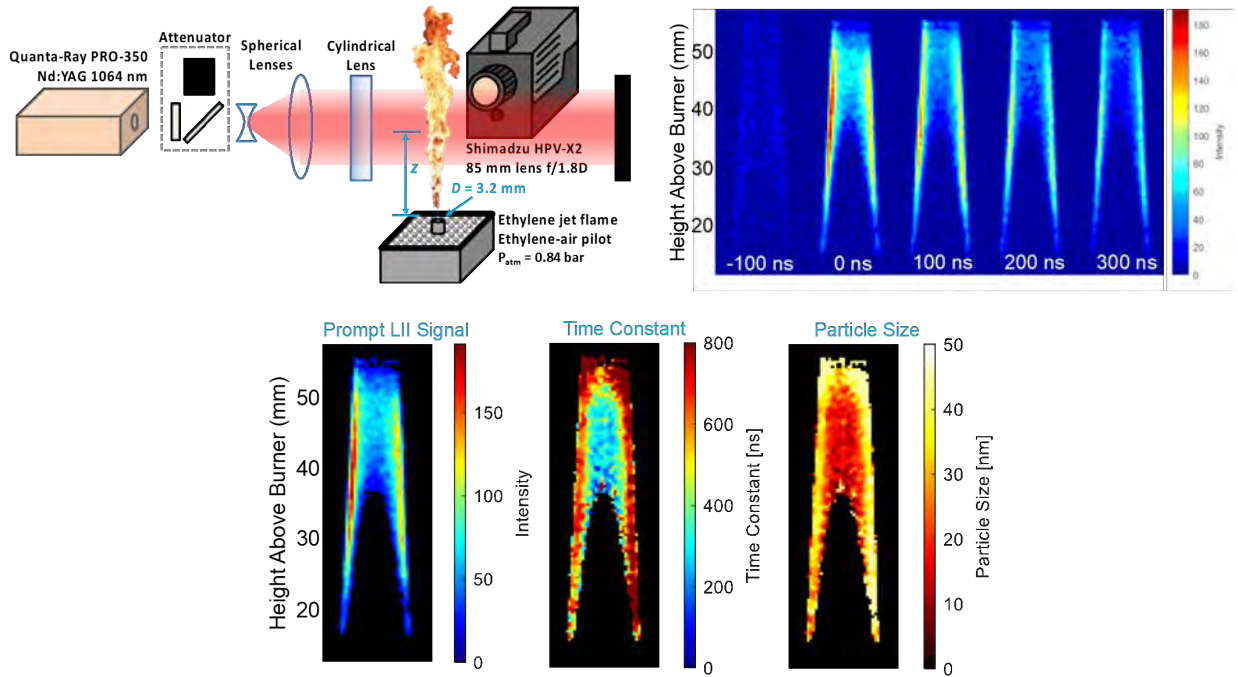


**Figure 7.** 2D TiRe-LII layout and typical results. Top left: Schematic of layout in jet flame experiment. Top right: Temporal decay measurements. Bottom: Data analysis and deduced particle sizes.

Similarly, soot particle size can be estimated in the atmospheric pressure turbulent jet flame. It is important to note that turbulent jet flames have temporally varying and spatially varying properties. However, if an average bath gas temperature of 1628 K is used [7], the TiRe-LII model produces the preliminary soot particle size estimates illustrated in Figure 8. The experimental data [6] looks at two different regions in the flame, one in the lower soot growth region and one in the higher soot oxidation region. By comparing estimates of the soot particle size, we can see that the particles are smaller on average in the growth region than in the oxidation region, which aligns with expectations. In the future, more work is needed to validate the bath gas temperature, soot agglomerate sizes, and other properties within the flame. Additional measurement complexities are also anticipated when working in high pressure combustors. We are currently working on fitting strategies and temperature measurement strategies, like two-color TiRe-LII, to improve our model estimates and reduce uncertainties.

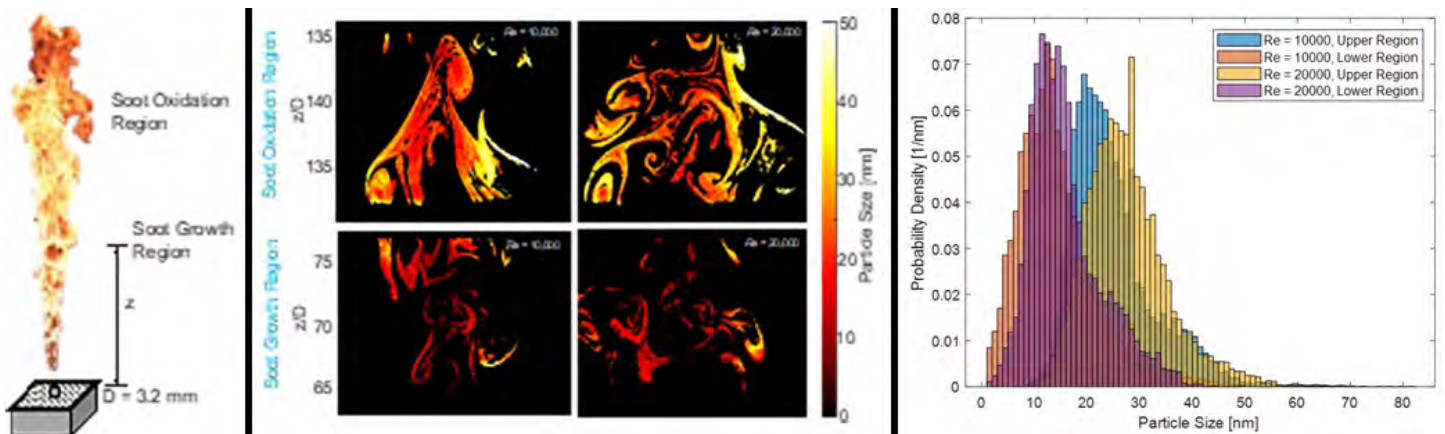


Figure 8. 2D TiRe-LII results in a turbulent jet flame. Left: Flame schematic. Middle: Typical instantaneous soot particle size snapshots at different Reynolds numbers and heights. Right: Particle size statistics.

### Milestones

N/A. Q1 has not been completed at the time of this report.

### Major Accomplishments

N/A. Q1 has not been completed at the time of this report.

### Publications

N/A. Q1 has not been completed at the time of this report.

### Outreach Efforts

N/A. Q1 has not been completed at the time of this report.

### Awards

N/A. Q1 has not been completed at the time of this report.

### Student Involvement

Samuel Wonfor (PhD Student), Georgia Tech: Design and fabrication of diagnostics test bed.

Andrew Zheng (PhD Candidate), Georgia Tech: Development of algorithms for TiRe-LII processing.

Sundar Ram Manikandan (MS Student), Georgia Tech: Assist in the design and fabrication of diagnostic test bed.

Rachel Thomas (BS Student), Georgia Tech: Assist in the development of post-processing algorithms to analyze thermoacoustic instabilities.

### Plans for Next Period

Over the next project period, we will complete the following activities:

- Test rig design, fabrication, and commissioning of combustor for studies without acoustic forcing.
- Measurement system design and testing; diagnostic post-processing algorithm development and validation.
- Experimental campaign measuring emissions and combustor behavior without acoustic forcing.
- Data analysis from experimental campaign.
- Initial design of combustor for studies with acoustic forcing.

### References

- [1] G. Tenti, Kinetic theory of molecular gases and application to light scattering experiments, Ph.D. thesis, University of Toronto, Toronto, 1974.
- [2] R. D. Mountain, "Spectral distribution of scattered light in a simple fluid," *Review of Modern Physics*, Vol. 38, No. 1, pp. 205-214, 1966.



- [3] N. A. Clark, "Inelastic light scattering from density fluctuations in dilute gases. The kinetic-hydrodynamic transition in a monatomic gas," *Physical Review A*, Vol. 12, No. 1, pp. 232-244, 1975.
- [4] V. Ghaem-Maghami, and A. D. May, "Rayleigh-Brillouin spectrum of compressed He, Ne, and Ar. I. Scaling," *Physical Review A*, Vol. 22, No. 2, pp. 692-697, 1980.
- [5] F. Liu, G. J. Smallwood, and D. R. Snelling, "Effects of primary particle diameter and aggregate size distribution on the temperature of soot particles heated by pulsed lasers," *Journal of Quantitative Spectroscopy and Radiative Transfer*, vol. 93, pp. 301-312, 2005.
- [6] Y. Chen, E. Cenker, D. R. Richardson, S. P. Kearney, B. R. Halls, S. A. Skeen, C. R. Shaddix, and D. R. Guildenbecher, "Single-camera, Single-shot, Time-resolved Laser-induced Incandescence Decay Imaging," *Optics Letters*, Vol. 43 (21), pp.5363-5366, 2018.
- [7] C. R. Shaddix, J. Zhang, R. W. Schefer, J. Doom, J. C. Oefelein, S. Kook, L. M. Pickett, and H. Wang, "Understanding and predicting soot generation in turbulent non-premixed jet flames," Technical Report SAND2010-7178 (Sandia National Laboratories, 2010).

## Task 2 – Large Eddy Simulations of Combustor Operation and Emissions

Georgia Institute of Technology

### Objectives

Simulation of advanced propulsion and power systems requires treatment of multiscale physics, in turn requiring trade-offs between cost and accuracy. Achieving the optimal balance is complicated due to the nonlinear nature of turbulent reacting flows, which involve multiphase mixtures, highly nonlinear chemical kinetics, multiscale velocity and mixing processes, turbulence-chemistry interactions, compressibility effects (density changes induced by changes in pressure), and variable inertia effects (density changes induced by changes in composition or heat addition). Coupling between processes occurs over a wide range of time and length scales, many being smaller than can be resolved in a numerically feasible manner. Further complications arise when liquid or solid phases are present due to the introduction of dynamically evolving interface boundaries and the resultant complex exchange processes.

The overarching objective of this task is to provide quantitative insights into the accuracy of select calculations and to assess critical trade-offs between cost and accuracy. One set of calculations is performed using preferred engineering LES solvers with the goal of minimizing cost for a targeted accuracy, as required by industry. A companion set of high-resolution LES calculations are performed using a research solver, the RAPTOR code at Georgia Tech (see Figure 9) [1,2], to provide detailed information beyond that available from the experiments alone. Complementary information from the first-principles LES and experimentally measured data provide a unique opportunity to understand the central physics of turbulent combustion processes in realistic parameter spaces and for making clear assessments of how a given combination of affordable engineering-based models perform. After achieving an adequate level of validation, results from the high-resolution LES calculations will provide fundamental information that cannot be measured directly and that is relevant to the development of lower-order engineering models. Thus, a strong link between theory, experiments, and relevant applications is established. The ultimate objectives of this task are to a) assess the model fidelity/attributes required to accurately simulate the operability and emissions; and b) assess the trade-offs between accuracy and cost.

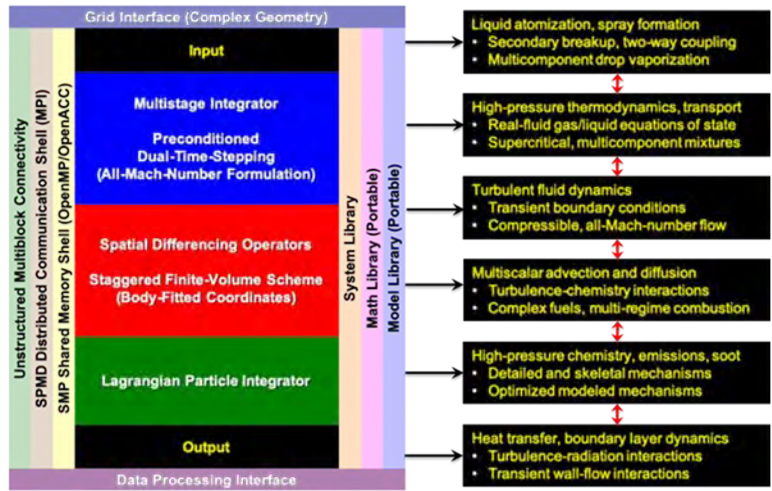


Figure 9. RAPTOR code structure highlighting the hierarchy of sub-models to be targeted for analysis.

## Research Approach

To establish a baseline starting point for Task 2, we are currently performing a set of verification studies that demonstrate the current capabilities of leading sub-models typically used for treatment of partially premixed flames in gas turbines. This includes the new high-pressure laminar flame combustor shown in Figure 3 at Georgia Tech. Calculations are being performed using the RAPTOR code framework, which is designed to provide solutions using “first principles” models in combination with the high-quality numerical methods required to provide maximum quality in the LES solutions. Simultaneously, we have begun training the GRA who will perform on the simulations (Kalathoor) in collaboration with Dr. Oefelein on the use of RAPTOR and the related models. The major goal is to stage the simulations toward fully coupled treatment of the targeted micro-mixer combustor, which will operate across pressures from 80-150 psig (5.5-10 bar) and temperatures of 600-1000 °F (590-810 K).

## Milestones

N/A. Q1 has not been completed at the time of this report.

## Major Accomplishments

N/A. Q1 has not been completed at the time of this report.

## Publications

N/A. Q1 has not been completed at the time of this report.

## Outreach Efforts

N/A. Q1 has not been completed at the time of this report.

## Awards

N/A. Q1 has not been completed at the time of this report.

## Student Involvement

Sriram Kalathoor (GRA, PhD Candidate), Georgia Tech: Baseline calculations with RAPTOR code.

## Plans for Next Period

Over the next project period, we will complete the following activities:

- LES of spray inflow conditions.
- Baseline RAPTOR LES of lean premixed combustor experiments.

## References

- [1] J. C. Oefelein, "Large eddy simulation of turbulent combustion processes in propulsion and power systems," *Progress in Aerospace Sciences*, vol. 41, no. 1, pp. 2-37, 2006.
- [2] J. C. Oefelein and R. Sankaran, "Large eddy simulation of reacting flow physics," in *Exascale Scientific Applications: Programming Approaches for Scalability, Performance, and Portability*, T. Straatsma, K. Antypas and T. Williams, Eds., Boca Raton, Taylor & Francis, pp. 231-256, 2018.

## Task 3 – Thermoacoustic Modeling

Georgia Institute of Technology

### Objective

Lean premixed combustors are susceptible to thermoacoustic instabilities, which increase emissions, decrease efficiency, reduce combustor life, and produce high-amplitude tonal noise. These instabilities occur in "islands" of the operating space that should be avoided during operation. Due to the wide range of potential operating conditions, it is not tractable to perform LES or experiments across all relevant conditions to assess instabilities; reduced order modeling tools (i.e., thermoacoustic solvers) must be used. However, these tools have not been validated for the conditions and configurations of relevance for lean premixed supersonic engine combustors. This task will develop, assess, and validate thermoacoustic solvers in this situation.

### Research Approach

A description of the acoustic response to heat release perturbations is required to close the feedback loop and predict the dynamics of the complete system. This will be obtained by constructing an acoustics model of the experimental test combustor section, forcing with a heat release perturbation at the flame location, and measuring the response of the acoustic pressure and velocity at locations of interest. The acoustic model will be a 3D model solved using the finite element method to capture 3D geometric features, mean flow fields, and appropriate boundary conditions which are applied at the inlets, outlets, and locations where acoustics losses occur due to pressure drops.

A unique time-domain approach will be employed to simulate the feedback loop between acoustics and flame responses. An important advantage to this approach is the direct inclusion of the effect of turbulent heat release on the dynamics of the system. Another advantage is the ability to rapidly calculate frequencies and amplitudes (as opposed to growth rates) for both stable and unstable operating conditions in a manner consistent with the physics of the real system. The output from this modeling process yields a time history of fluctuating velocity, pressure and heat release, which subsequently yields instability frequencies and amplitudes. The predicted frequencies and amplitudes will be validated against the experimental measurements. The validated analytical model can consequently be employed in the performance prediction of lean premixed combustion systems at conditions relevant to supersonic cruise flight operations.

To date, we have begun developing post-processing techniques to analyze experimental data at thermoacoustically unstable conditions. These techniques are being tested using data from previous collaborative experiments between Georgia Tech and GE, which focused on combustors for more conventional subsonic engines. Nevertheless, the currently available data are expected to share similar general features to those being collected during this program.

In particular, we have focused on techniques to analyze the non-linear cross-frequency thermoacoustic coupling mechanisms that become important at the high energy densities found in practical gas turbines. Such non-linear interactions allow coupling and "synchronization" between phenomena at different frequencies and in bands around integer frequency ratios that generally are not considered in thermoacoustic analysis [1]. However, our previous results have shown that they can drive the dominant dynamics at many conditions that exhibit intermittent bursts of combustion oscillations [2-3]. Understanding these interactions, therefore, is key to understanding the thermoacoustic behavior of the combustor and the thermoacoustic modeling efforts in Task 3.

To analyze these phenomena, we are employing a combination of spectral proper orthogonal decomposition (SPOD) [4] and synchronization analysis [5-6]. Coupling between oscillators with natural frequencies  $f_1^0$  and  $f_2^0$  that are related by  $f_1^0/f_2^0 \approx m/n$  (for integer values of  $m$  and  $n$ ) can be characterized through the generalized frequency detuning  $\Delta f^0 = mf_2^0 - nf_1^0$ . Since  $f_1^0$  and  $f_2^0$  are the natural frequencies of the independent oscillators,  $\Delta f^0$  does change due to coupling between the oscillators.



The parameter space over which synchronization occurs for harmonic ratio  $m:n$  is roughly V-shaped, as illustrated schematically in Figure 10, with the V-shaped synchronization region being largest for harmonic ratios. This figure demonstrates that coupling occurs for any nonzero coupling strength ( $B_D$  and  $B_R$ ), that coupling does not imply synchronization, and that synchronization is increasingly tolerant to  $\Delta f^0$  with increasing coupling strengths.

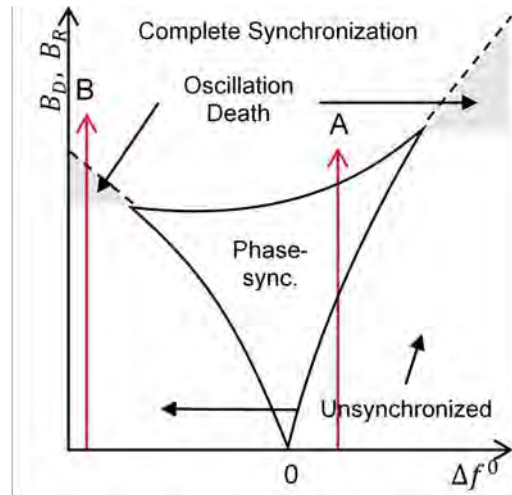


**Figure 10.** Example of synchronization characteristics as a function of frequency detuning and coupling strength.

Using this underlying theory, we are developing methods to unravel the complex couplings that occur in real gas turbines. An example is shown in Figure 11, which contains the short-time power spectra (spectrograms) of the pressure and velocity (measured using SPIV), as well as the SPOD spectra of the spray and heat release rate [3]. In the latter, the size and color of the dots represents the spectral coherence between SPOD mode pairs, and the energy represents the intensity of the velocity fluctuations in the mode pair.

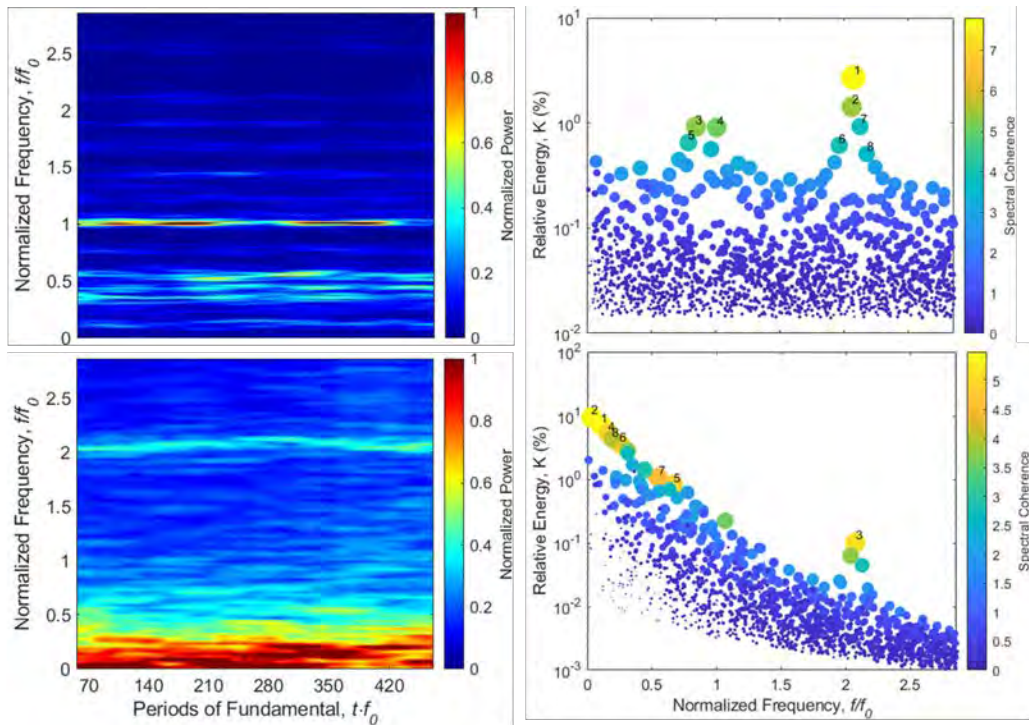


**Figure 11.** Example of thermoacoustic signatures in a pressurized gas turbine combustor. Left: Spectrograms of pressure (top) and velocity (bottom). Right: SPOD spectra of spray (top) and OH\* CL (bottom).

We find that the pressure field oscillates at frequency  $f_0$ , whereas the other phenomena (velocity, fuel, heat release) oscillate at a frequency around  $2f_0$ . This frequency is associated with a natural hydrodynamic instability in the system (not shown), which naturally occurs around  $2.1f_0$  in the non-reacting flow at the same operating conditions. The spectrograms demonstrate time-varying super-harmonic frequency detuning, correlated with time-varying oscillation amplitudes. Understanding these multi-physics interactions are critical for coupling the heat-release rate and acoustic oscillations in the thermoacoustic solver.

**Milestones**

N/A. Q1 has not been completed at the time of this report.

**Major Accomplishments**

N/A. Q1 has not been completed at the time of this report.

**Publications**

N/A. Q1 has not been completed at the time of this report.

**Outreach Efforts**

N/A. Q1 has not been completed at the time of this report.

**Awards**

N/A. Q1 has not been completed at the time of this report.

**Student Involvement**

Mitchell Passarelli (GRA, PhD Candidate), Georgia Tech: Development of post-processing algorithms to analyze thermoacoustic instabilities in gas turbine combustors.



### **Plans for Next Period**

Over the next project period, we will complete the following activity:

- Acoustic response to heat release dynamics modeling.

### **References**

- [1] N. Noiray, D. Durox, T. Schuller, and S. Candel, "A Unified Framework for Nonlinear Combustion Instability Analysis based on the Flame Describing Function", *Journal of Fluid Mechanics*, vol. 615, pp. 139-167, 2008.
- [2] M.L. Passarelli, J.D.M. Cirtwill, T. Wabel, A. M. Steinberg, and A.J. Wickersham, "Synchronization During Multi-Mode Thermoacoustic Oscillations in a Liquid-Fueled Gas Turbine Combustor at Elevated Pressure", *ASME Turbo Expo 2019*, Phoenix, 2019.
- [3] M.L. Passarelli, T. Wabel, A. Cross, K. Venkatesan, A. M. Steinberg, "Cross-frequency coupling during thermoacoustic oscillations in a pressurized aeronautical gas turbine model combustor", *Proceedings of the Combustion Institute*, In Press, 2020.
- [4] M. Sieber, C. O. Paschereit, and K. Oberleithner, "Spectral Proper Orthogonal Decomposition", *Journal of Fluid Mechanics*, vol. 792, pp. 798-828, 2016.
- [5] Balanov, N. Janson, D. Postnov, and O. Sosnovtseva, "Synchronization: From Simple to Complex", Springer Berlin, Heidelberg, 2009.
- [6] D. Volk, I. Dubinin, A. Myasnikova, B. Gutkin, and V. K. Nikulin, "Generalized Cross-Frequency Decomposition: A Method for the Extraction of Neuronal Components Coupled at Different Frequencies", *Frontiers in Neuroinformatics*, Vol. 12, no. 72, 2018.
- [7] K.T. Kim, "Nonlinear Interactions Between the Fundamental and Higher Harmonics of Self-Excited Combustion Instabilities", *Combustion Science and Technology*, vol. 189, no. 7, pp 1091-1106, 2018.



# Project 075 Improved Engine Fan Broadband Noise Prediction Capabilities

## Boston University & Raytheon Technologies Research Center

### Project Lead Investigator

Sheryl Grace  
Associate Professor  
Mechanical Engineering  
Boston University  
110 Cummington Mall, Boston, MA 02215  
Phone: 617-353-7364  
Email: sgrace@bu.edu

### University Participants

#### Boston University (BU)

- P.I.: Sheryl Grace – Associate Professor, Mechanical Engineering
- FAA Award Number: 13-C-AJFE-BU Amendment 022
- Period of Performance: 09/01/2020 – 8/31/2021
- Task(s):
  1. Fan wake surrogate model creation
  2. Improved low-order model

### Project Funding Level

First year's funding:

FAA: \$300,000 with \$115,000 allocated to BU and \$185,000 to Raytheon Technologies Research Center (RTRC).

Matching funds total \$300,000 with \$115,000 provided by BU (data sets, graduate student stipend, MS in Statistical Practice (MSSP) faculty/student time) and \$185,000 provided by RTRC (personnel time).

### Investigation Team

Sheryl Grace, BU: PD/PI. Tasks 1 and 2.

Jeff Mendoza, RTRC: Co PD/PI. Tasks 1 and 2.

Craig Aaron Reimann, RTRC: Staff Scientist. Tasks 1 and 2.

Julian Winkler, RTRC: Staff Scientist. Tasks 1 and 2.

### Project Overview

The noise signature of contemporary turbofan engines is dominated by fan noise, both tonal and broadband. Accepted methods for predicting the tone noise have existed for many years, and engine designers have developed methods for controlling or treating this tonal noise. Broadband noise, however, remains an outstanding problem. In order to enable design decisions that will achieve the goal of further reductions in engine noise, accurate prediction methods for broadband noise will accordingly be required. Interaction noise from the fan stage is a dominant broadband mechanism in a modern high bypass engine and is created by the interaction of the turbulence in the fan wakes with the fan exit guide vanes (FEGVs). This project will leverage prior development of low-order models for the prediction of fan broadband interaction noise. Gaps in the low-order approach will be addressed based on knowledge gained from computation and experimentation. In particular, a method for determining the inflow into the stator via a machine learning (ML) algorithm will be developed. The low-order method will also be validated against full-scale rig data and appropriate development undertaken based on the findings.

## Task 1– Fan Wake Surrogate Model Creation

Boston University and RTRC

### Objective

The goal is to build a surrogate model using ML that would work with performance level unsteady Reynolds-averaged Navier-Stokes (URANS) to specify the turbulent length scales and turbulence spectrum at locations along the helical fan wake path.

### Research Approach

#### **Subtask 1.1: Development of autoencoder**

When attempting to learn something about a flow field, there are often many inputs but relatively few outputs. This means that there is usually correlation among the input variables, which can be captured in a low-dimensional manifold using an autoencoder (AE). Many ML algorithms start by training an AE that provides dimension reduction of the input parameter space. In short, an AE takes input data and determines a low-dimensional representation of that data via an encoder. Students in the BU Masters in Statistics Program will assist the BU and RTRC researchers with the development of the autoencoder.

#### **Subtask 1.2: Development of decoder**

Once the AE is trained to find a good low-dimensional representation, it must be combined with a decoder to obtain the desired output. The second half, or decoder, of the ML algorithm must also be trained to provide the desired output.

#### **Subtask 1.3: Identification and creation of training data**

**Subtask 1.3.a: Existing training data:** BU and RTRC will work to collect relevant existing fan wake data sets.

**Subtask 1.3.b: Creation of additional training data:** RTRC will take the lead on producing new data sets.

#### **Subtask 1.4: Application of surrogate model to relevant fan geometries**

Cases that are used to produce training data can also be utilized during the validation stage, though further datasets will need to be identified for full validation. During later years of the project, the surrogate model, in particular, will be assessed against data obtained experimentally for modified fan rig trailing edge wake flows.

### Milestone

The initial milestone is to identify and access geometries and operating conditions that are relevant to study. The curation of data sets has begun. Both BU and RTRC are accumulating existing data sets and making plans to create new data sets.

### Major Accomplishments

- BU set up the internal portion of the grant and has begun to set up the subcontract to RTRC.
- BU MSSP is putting forward the AE development as a project to their students. A student group should be identified by December.
- RTRC has begun discussions with Pratt & Whitney to obtain access to past data sets.
- Source Diagnostic Test (SDT) fan geometry and flow path information is being obtained by BU and shared with RTRC so further computational runs can commence.
- File transfer methods have been set up between RTRC and BU so that data can be easily shared.

### Publications

None

### Outreach Efforts

None

### Awards

None

### **Student Involvement**

One undergraduate student has just begun to work with rotor wake data sets at BU. A new graduate student is currently being recruited to work on the project.

### **Plans for Next Period**

The milestones that have been set out for the first year of this project are:

- Identify and access geometries and operating conditions relevant to study.
- Prepare initial ML training datasets.
- Develop ML autoencoder. Begin feature extraction.
- Continued preparation of ML training datasets, initial training of ML decoder.
- First validation test of surrogate model.

## **Task 2 – Improvement of Low-order Model**

Boston University and RTRC

### **Objective**

The existing low-order methods are regularly applied to the SDT cases and as such have been well-validated against this test, which represents one scaled fan and multiple FEGVs. The low-order method must now be validated against full-scale test data. The low-order method might also require reformulation to account for other real-flow effects.

### **Research Approach**

BU will lead this task and will be provided geometry and comparison data by RTRC.

#### **Subtask 2.1: Ability to predict full-scale results**

The low-order method will be applied to a full-scale geometry with available validation data. Due to the difference in frequency range of interest for the full-scale case as compared to the scaled fans, it is surmised that the low-order method will require grid adjustments and integral extent adjustments. Such improvements to the low-order method will be completed as part of this task.

### **Milestones**

None

### **Major Accomplishments**

None

### **Publications**

None

### **Outreach Efforts**

None

### **Awards**

None

### **Student Involvement**

None

### **Plans for Next Period**

The milestones that have been set out for the first year of this project include validating the low-order model on a new geometry and testing rig scale versus full-scale applicability.



# Project 076 Improved Open Rotor Noise Prediction Capabilities

## Georgia Institute of Technology

### Project Lead Investigator

Principal Investigator:

Professor Dimitri N. Mavris

Director, Aerospace Systems Design Laboratory

School of Aerospace Engineering

Georgia Institute of Technology

Phone: (404) 894-1557

Fax: (404) 894-6596

Email: [dimitri.mavris@ae.gatech.edu](mailto:dimitri.mavris@ae.gatech.edu)

Co-Principal Investigator:

Dr. Jimmy Tai

Division Chief, Propulsion & Energy

Aerospace Systems Design Laboratory

School of Aerospace Engineering

Georgia Institute of Technology

Phone: (404) 894-0197

Fax: (404) 894-6596

Email: [jimmy.tai@ae.gatech.edu](mailto:jimmy.tai@ae.gatech.edu)

### University Participants

#### Georgia Institute of Technology

- P.I.s: Dr. Dimitri N. Mavris, Dr. Jimmy Tai
- FAA Award Number: 13-C-AJFE-GIT-078
- Period of Performance: August 11, 2020 to August 10, 2021
- Task(s):
  - Task 1: Literature Review
  - Task 2: Parametric CAD Model Creation
  - Task 3: CAA Case Setup and Validation

### Project Funding Level

The project funding is \$300,000 per year from the FAA. Cost share match amount is \$300,000 per year. The sources of match are cash and in-kind cost-share from an industry partner, General Electric (GE).

### Investigation Team

Dr. Dimitri Mavris, Professor, Georgia Tech (Project Management)

Dr. Jimmy Tai, Senior Research Engineer, Georgia Tech (Project Management)

Mr. Srujal Patel, Research Engineer II, Georgia Tech (Project Management, CAD, Computational Aeroacoustics)

Dr. Miguel Walter, Research Engineer II, Georgia Tech (Computational Aeroacoustics, Stochastic Methods)

Christopher Roper, Graduate Student, Georgia Tech (Computer Aided Design, Computational Fluid Dynamics)

Brenton Willier, Graduate Student, Georgia Tech (Computational Fluid Dynamics, Aeroacoustics)

Marcos Dos Santos, Graduate Student, Georgia Tech (Computational Fluid Dynamics, Rotor Performance)

Mariam Emara, Graduate Student, Georgia Tech (Tool-chain integration, Stochastic Methods)

Maxime Varoqui, Graduate Student, Georgia Tech (Aeroacoustics, Stochastic Methods)



## Project Overview

The Contra-Rotating Open Rotor (CROR) system has promising environmental benefits due to its ultra-high bypass ratio and high propulsive efficiency. The reduced fuel burn and emissions of the CROR compared to an equivalent thrust turbofan make it a viable economic and environmentally friendly propulsion alternative to traditional ducted systems. However, in the absence of a noise-conditioning duct, aerodynamic interactions within the CROR system, as well as between the system and surrounding installation components like the engine pylon, may result in noise penalties. If such a system configuration is not optimized, the added effect of flow asymmetry to the aerodynamic interactions could potentially result in severe noise penalties, making the CROR system infeasible for use in the aircraft industry. The proposed work will perform a sensitivity study on the design parameters of a CROR-eylon configuration. This study will leverage knowledge from past efforts with this type of configuration in order to narrow down the space of design parameters. High-fidelity computational aeroacoustics analyses will be carried out in order to analyze the effect of each of the chosen parameters on noise. This research is intended to provide both the FAA and industry with key insights necessary for the design optimization of the CROR system in the future.

## Task 1 – Literature Review

Georgia Institute of Technology

### Objective

The Georgia Tech research team will conduct a literature survey to summarize the state of the art in reducing open rotor source noise and will document the current best practices and processes used by various industry entities and researchers.

### Research Approach

The ongoing literature review is geared towards investigating the following questions:

- Q1. What are current experimental and computational approaches that researchers use to predict the noise of open rotor configuration?
- Q2. What parameters have been studied for noise sensitivity and what are the study findings?
- Q3. Are there any active flow control related technologies currently being implemented for open rotor noise reduction? If yes, what are the findings of such studies?
- Q4. What is the computational cost of performing a high-fidelity computational aeroacoustics study?
- Q5. What are the key performance and noise characteristics of the baseline geometry provided by GE?
- Q6. Which low-fidelity noise assessment tools are available to perform the preliminary level noise analysis to narrow the design space to select parameters for high-fidelity studies?

The current literature review is focused on Q1, Q2 and Q3. In particular, for Q2, the literature review effort is divided into three groups of parameters:

- i) Open rotor blade design parameters
- ii) Pylon effects related design parameters
- iii) Airframe integration related design parameters

### Milestone

We are currently compiling all the findings and are periodically sharing those with FAA during our bi-weekly telecons.

### Major Accomplishments

None

### Publications

None

### Outreach Efforts

None

### Awards

None

### **Student Involvement**

For this task, all five students are grouped into three design parameter categories as described above and are compiling and sharing their findings during the bi-weekly telecons.

### **Plans for Next Period**

We will continue investigating the answers for all questions in the next quarter. In particular, once the geometry is finalized by FAA, we should be able to answer Q5.

## **Task 2 – Parametric CAD Model Creation**

Georgia Institute of Technology

### **Objective**

The Georgia Tech research team will develop a fully parametric CAD model of the open rotor and pylon configuration so that it can be used for a computational aeroacoustics sensitivity study in the future.

### **Research Approach**

In this task, a fully parametric model of the baseline geometry of the CROR and pylon configuration will be generated. A CAD tool will be used for the model creation. During this step, emphasis will be placed on ensuring that the resulting geometry is an accurate representation of the physical design and is also suitable for CFD mesh generation. A scripting language such as Python may be used to automate the model update based on a design point. This is typically a time-consuming step because the mapping must be robust enough such that design variable instances do not lead to a geometry with undesirable imperfections, such as wrinkles or open surfaces, which might render them unsuited for CFD analysis.

While we are waiting on the final decision by FAA for the baseline geometry, we have already begun getting familiar with the CAD model creation process. Two software tools are under evaluation for the implementation work: CATIA V5 and Engineering Sketch Pad (ESP). CATIA V5 provides an industrial standard GUI-based platform to generate high-quality CAD geometries. As a second option, ESP, an open-source script-based and MDAO-friendly CAD tool is being evaluated as well; ESP has a more platform-independent framework, which is especially useful for cluster use. Some test geometries are being produced to identify the strengths and shortcomings of both CAD tools.

Also, in parallel, Python scripts are being generated to automate the CAD data extraction process so that once the baseline geometry is finalized, we can extract the section information from the existing STEP/IGES files.

### **Milestones**

This is currently work-in-progress and updates will be shared with FAA as milestones are reached in the following year.

### **Major Accomplishments**

None

### **Publications**

None

### **Outreach Efforts**

None

### **Awards**

None

### **Student Involvement**

For this task, two students are assigned: Chris Roper (CAD) and Brenton Willier (Python-based data extraction).

### **Plans for Next Period**

We will continue evaluating the CAD software and performing robust testing and shall have the scripts ready for the implementation work whenever we receive the baseline geometry from FAA/GE.

## **Task 3 – Computational Aeroacoustics (CAA) Case Setup and Validation**

Georgia Institute of Technology

### **Objective**

The Georgia Tech research team will set up a computational aeroacoustics case with the baseline parametric CAD model developed in the previous task and then will perform a validation study.

### **Research Approach**

This task covers all steps involved in setting up the aerodynamics as well as the aeroacoustics simulations. These steps include automatic mesh generation, selection of appropriate boundary conditions, study of mesh resolutions as well as finding solver parameters for the unsteady CFD simulations. Moreover, this task will also compare the numerical simulation results with available experimental data for validation. The main aim of this task is to provide evidence that the numerical simulation setup is robust and provides consistently accurate solutions. Such assurance is necessary before proceeding further with the sensitivity study runs in the future.

### **Milestones**

None

### **Major Accomplishments**

None

### **Publications**

None

### **Outreach Efforts**

None

### **Awards**

None

### **Student Involvement**

None

### **Plans for Next Period**

This task will be performed in last six months of the performance period. We anticipate completion of this task on time before the end of the performance period.



# Project 077 Measurements to Support Noise Certification for UAS/UAM Vehicles and Identify Noise Reduction Opportunities

## The Pennsylvania State University

### Project Lead Investigator

Eric Greenwood  
Assistant Professor of Aerospace Engineering  
Department of Aerospace Engineering  
The Pennsylvania State University  
229 Hammond Building  
University Park, PA  
Phone: (814) 863-9712  
Email: eric.greenwood@psu.edu

### University Participants

#### The Pennsylvania State University

- PI: Eric Greenwood, Assistant Professor of Aerospace Engineering
- FAA Award Number: 13-C-AJFE-PSU-067
- Period of Performance: August 11, 2020 to August 10, 2021
- Tasks:
  1. Review of Regulations, Standards, Literature, and Ongoing Research
  2. Computational Modeling of UAS and UAM Configurations
  3. Development of a Source Separation Process for Distributed Propulsion Vehicles
  4. Design and Development of a Reconfigurable Multirotor UAS Vehicle
  5. Microphone Type and Installation Investigation
  6. Baseline UAS Noise Measurement
  7. UAM Component Noise Measurement
  8. UAM Full-vehicle Noise Measurement

### Project Funding Level

\$500,000 awarded by FAA. \$500,000 in-kind matching from Beta Technologies for labor and flight test support.

### Investigation Team

- Eric Greenwood, PI, The Pennsylvania State University; acoustic measurement and analysis lead.
- Kenneth S. Brentner, Co-PI, The Pennsylvania State University; acoustic prediction lead.
- Eric N. Johnson, Co-PI, The Pennsylvania State University; UAS design and operations lead.
- Joel Rachaprolu, Graduate Research Assistant, The Pennsylvania State University; primarily responsible for developing noise source separation techniques for distributed propulsion vehicles.
- N. Blaise Konzel, Graduate Research Assistant, The Pennsylvania State University; primarily responsible for developing acoustic and atmospheric instrumentation for UAS and UAM flight testing.
- Keon Wong Hur, Graduate Research Assistant, The Pennsylvania State University; primarily responsible for developing UAS predictions to inform the development of experimental methods.



## Project Overview

The Pennsylvania State University will support the FAA in determining noise measurement and analysis methods that will allow the external noise radiation of a variety of Unmanned Aircraft System (UAS) and Urban Air Mobility (UAM) vehicles to be accurately characterized. Noise measurements will be collected for a wide range of UAS and UAM configurations across different operating modes, flight speeds, and altitudes. A reconfigurable multirotor UAS will be developed and tested in order to assess the effects of rotor number, blade design, and position on the radiated noise and the measurement and analysis process. The data analysis process developed through this project will allow the contributions of the individual rotor or propeller noise sources to be separated and modeled independently, allowing the variability in noise generation to be correlated to the variability in the vehicle flight state.

Measurement techniques for conventional propeller-driven aircraft and rotorcraft are well established. These techniques typically assume that the acoustic state of the vehicle does not change over the duration of a steady state pass over a microphone or microphone array. UAS and UAM platforms violate this steadiness assumption that has long been employed in the measurement and modeling of conventional aircraft noise. The rotor or propeller states, such as revolutions per minute (RPM) or blade pitch angle, will vary continuously and independently as the vehicle control system responds to atmospheric perturbations. Many of these vehicles employ distributed propulsion systems, where the rotors or propellers are not locked in phase. When multiple rotors or propellers operate at similar blade passing frequencies, coherent addition of the tonal noise will result in lobes of acoustic radiation that are tightly focused in certain directions. As the phase relationships between the rotors change over time, the directionality of these lobes will vary. Consequently, the noise cannot be modeled as a single stationary source, and no two flight passes will result in the same noise radiation pattern on the ground. Moreover, because there are numerous possible combinations of control inputs that result in the same flight condition, there is no longer a unique mapping of the flight condition of the vehicle as a whole to a corresponding acoustic state. This project aims to develop noise measurement techniques and data analysis methods that can reduce this variability, thereby allowing repeatable characterization of UAS and UAM noise for both noise certification standard and noise reduction purposes.

(Note: This project was awarded in August 2020, so this report only represents the first three months of effort.)

## Task 1 – Review of Regulations, Standards, Literature, and Ongoing Research

The Pennsylvania State University

### Objective

In this task, a comprehensive review will be conducted of past and ongoing activities closely related to this project to develop noise measurement methods to inform noise certification and noise reduction of UAS and UAM. This will include a review of existing noise certification standards for aircraft and rotorcraft, as well as existing industrial standards and published research regarding the measurement of aircraft noise. The applicability of these approaches to UAS and UAM noise measurement will be assessed, and the major limitations identified.

### Research Approach

The review task has been broadly divided into several categories. These include research on multirotor vehicle noise prediction, UAS noise measurements, acoustic instrumentation and installation effects, noise source separation techniques, aircraft noise characterization methods, and aircraft noise certification. Within each area, a broad search of the published literature will be conducted with the aim of identifying key research results, trends, and knowledge gaps. Research publications, regulations, standards, and advisory guidance relevant to the measurement, characterization, and noise certification of other aircraft types will also be reviewed and assessed to inform the development of measurement and characterization approaches suitable to UAS and UAM vehicles. The team will also identify ongoing research in noise measurement for UAS being conducted by FAA through the Integration Pilot Program, the NASA Ames, Glenn, and Langley Research Centers, the US Army Research Lab, other government agencies, and academic institutions. This research will be evaluated for lessons learned, to identify opportunities to engage with other ongoing research, and to develop the approach taken in the following tasks of this research project. The results of this review will be reported to FAA and may also be used to inform ongoing efforts to develop standards for UAS or UAM noise measurement, e.g., through the NASA UAM Noise Working Group.



## **Milestones**

This task will a) review the relevant literature related to the research conducted in this project and b) summarize these findings in reports or other publications.

## **Major Accomplishments**

Over 150 different publications, reports, and standards documents have been reviewed by the investigation team. An internal Penn State electronic repository has been established to organize the review activity allowing the team to share, organize, and summarize research materials as they are identified. Although the review is continuing, key results and knowledge gaps have been identified in each of the research areas:

### **Multicopter Vehicle Noise Prediction**

A growing number of research papers have been published on the topic of noise prediction for UAS and UAM vehicles. Of the papers on UAS noise prediction, the majority of the literature has focused noise predictions of isolated single rotors and has not addressed the potential for aerodynamic and/or acoustic interactions between the rotors of a multicopter vehicle. Recently, high fidelity computational fluid dynamics approaches have been applied to analyze the aeroacoustics of complete multicopter UAM configurations, indicating that aerodynamic interactions between the rotors, as well as the airframe, can cause high levels of unsteady loading noise which is highly dependent on the trim state of the vehicle [1]. In addition to the aerodynamic interactions, acoustic interactions between the rotor can cause the radiated noise to be strongly directional, as the coherent rotor tones add constructively in some directions and destructively in others [2]. Computational costs limit high fidelity predictions to purely periodic cases, where all rotors operate at precisely the same RPM and maintain a fixed phase relationship throughout the simulation. In reality, fixed-pitch multicopter UAS and UAM will need to continuously vary RPM in order to stabilize and control the flight of the vehicle, such that the phase relationships and resulting acoustic radiation will change throughout flight. Pascioni and Rizzi [3] employed a simplified propeller noise model to assess the effect of these phase relationships on the noise radiated to the ground for the multicopter GL-10 UAS aircraft. Figure 1, shown below, plots the instantaneous sound pressure level contours on the ground for the simulated GL-10 in the same cruise flight condition for three different randomized phase relationships. It is evident that these phase relationships have a dramatic impact on the directivity of the tonal noise component of multicopter vehicles.

While considerable research activity has been conducted in recent years to understand and predict the acoustic impacts of helicopters in maneuvering flight due to the significant increase in noise levels often observed when helicopters maneuver [4], no similar studies have been conducted for multicopter UAS or UAM aircraft. The noise generation of these aircraft is likely to be strongly influenced by maneuvering flight due to the high sensitivity of rotor noise generation to changes in RPM versus changes in blade pitch for the same change in thrust [2]. Unsteady flight effects have been shown to significantly affect the predicted noise—and its agreement with experiment—for conventional helicopters using the noise prediction system previously developed at Penn State under ASCENT Project 38 [5] and are likely to be at least as important for UAS and UAM vehicles. Measured acoustic data for complete multicopter UAS and UAM vehicles are not widely available, and to date most predictions for this class of vehicles have not been validated.

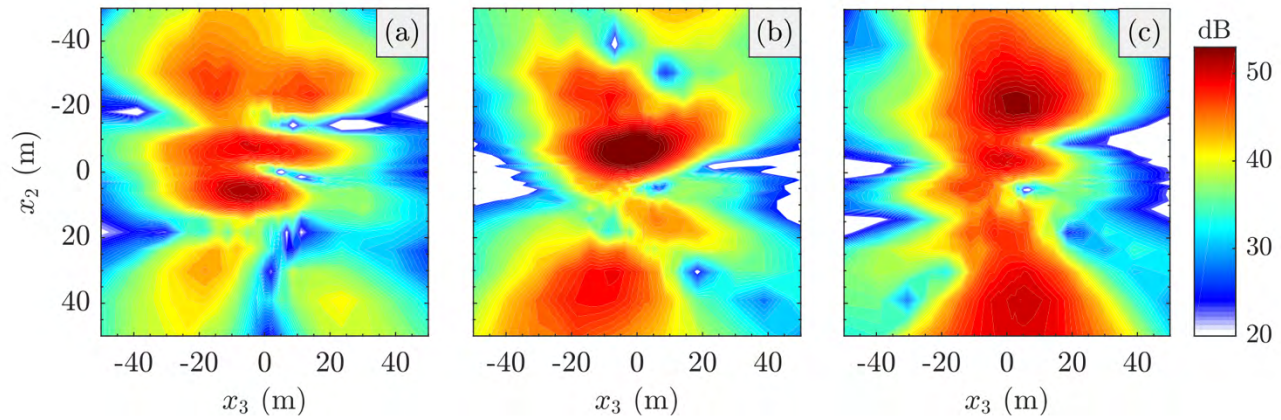


**Figure 1.** Predicted variation in ground noise levels for the 10-propeller GL-10 UAS with randomized phase relationships between the propellers. From Pascioni and Rizzi [3].

### UAS Noise Measurements

UAS noise measurements have been reported in numerous papers, though often for purposes such as the development and validation of Counter-UAS identification and localization algorithms rather than for the characterization and quantification of UAS noise and noise impacts. With a few exceptions [6], published UAS noise measurements have been limited to vehicles below 55 pounds gross weight, permitting these operations to be conducted under the FAA Part 107 “small UAS rule” without a waiver. Most studies looking at multirotor vertical lift UAS have focused on hovering flight conditions. A high degree of temporal unsteadiness is reported by many researchers, due to the fluctuation in rotor RPM required to stabilize multirotor vehicles, for example as shown in Figure 2 from Cabell, McSwain, and Grosveld [7].

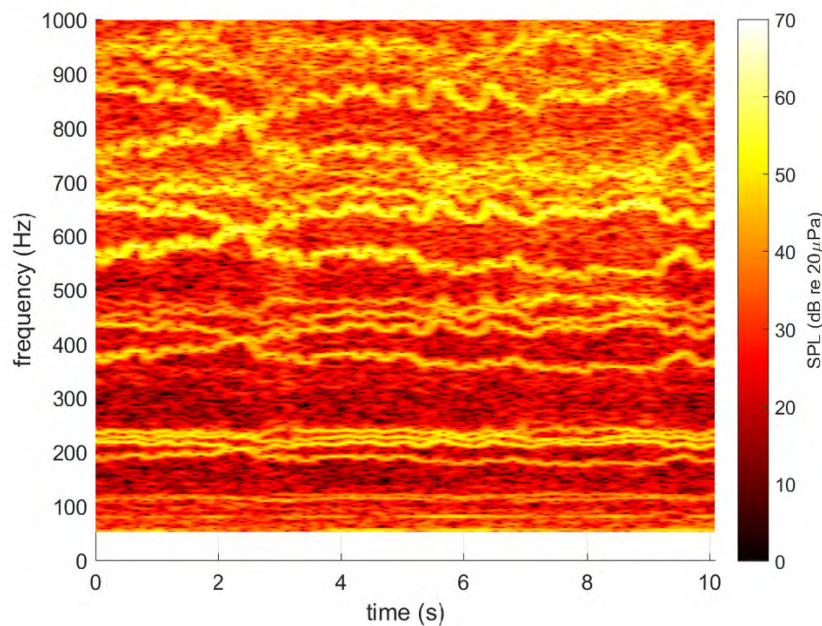


**Figure 2.** Spectrogram of noise from the DJI Phantom II quadcopter in hover from Cabell, McSwain, and Grosveld [7].



Some researchers report minimal variation in noise levels between hover and forward flight conditions [8], though other researchers report significant changes to the noise spectrum between hover and forward flight [9]. The potential for variations in noise levels and spectral content is supported by noise measurements for a complete SUI Endurance quadcopter tested by Pettingill and Zawodny in the NASA Langley Low Speed Aeroacoustic Wind Tunnel [10]. They reported a significant increase in broadband noise under certain forward flight conditions due to aerodynamic interactions between the rotors. Noise measurements conducted during the FAA Integration Pilot Program [11] found larger variations in the maximum noise level with speed for fixed wing UAS than vertical lift. In addition to hover and forward flight, the Integration Pilot Program also measured a wider range of operating conditions, including vertical climbs and approach trajectories than other reported studies, although detailed time series data were not reported. Repeated runs conducted on the same day demonstrated a variability in integrated noise metrics on the order of 2 dB, which is comparable to integrated noise measurement variability previously reported for helicopters [12]. However, one study by Alexander found large variations in multicopter noise measurements made on subsequent days [13], indicating some sensitivity to environmental conditions. UAS noise measurements reported to date have employed single or small arrays of closely spaced microphones; as a consequence, no significant directivity data have been reported for these vehicles.

### Acoustic Instrumentation and Installation Effects

Existing noise measurement standards and published research on microphone installations for aircraft noise measurements were reviewed. Elevated microphones, such as those used for noise certification of most aircraft categories, are known to be a poor representation of free-field noise due to interference between noise propagating along the direct ray between the vehicle and the microphone and that reflected from the ground. Flush mounting of the microphones on a rigid ground plane theoretically doubles the measured pressure at all frequencies, allowing for simple correction to the free-field, however edge diffraction effects from a finite sized ground plane do influence the response at higher frequencies.

Numerous techniques have been developed to minimize these edge diffraction effects by preventing them from adding coherently at the microphone, including offsetting the position of the microphone from the center of a circular ground board or more complex “daisy petal” geometries [14]. The literature in this area is limited, and few studies make comparisons between equivalent installations; however, it is clear that the size of the ground board has a dominant influence on the frequencies where edge diffraction effects are significant, with larger ground boards maintaining a flat frequency response across a wider range regardless of shape. As flush mounted microphones are difficult to package for outdoor noise measurements, alternative methods have been investigated, including lying a microphone on its side or inverting the microphone over the ground plane [15]. While the microphone-on-its-side method has been shown to significantly influence the frequency response of the installed microphone, the inverted microphone method is a close approximation to flush mounting over a frequency range determined by the spacing between the ground board and the microphone diaphragm [16]. The 7 mm spacing recommended by SAE ARP 4055 and incorporated by FAR Part 36 Appendix G appears to offer a relatively flat frequency response over the audible frequency range, as compared to the GRAS 67AX flush mounted microphone by Anderson et al. in Figure 3.

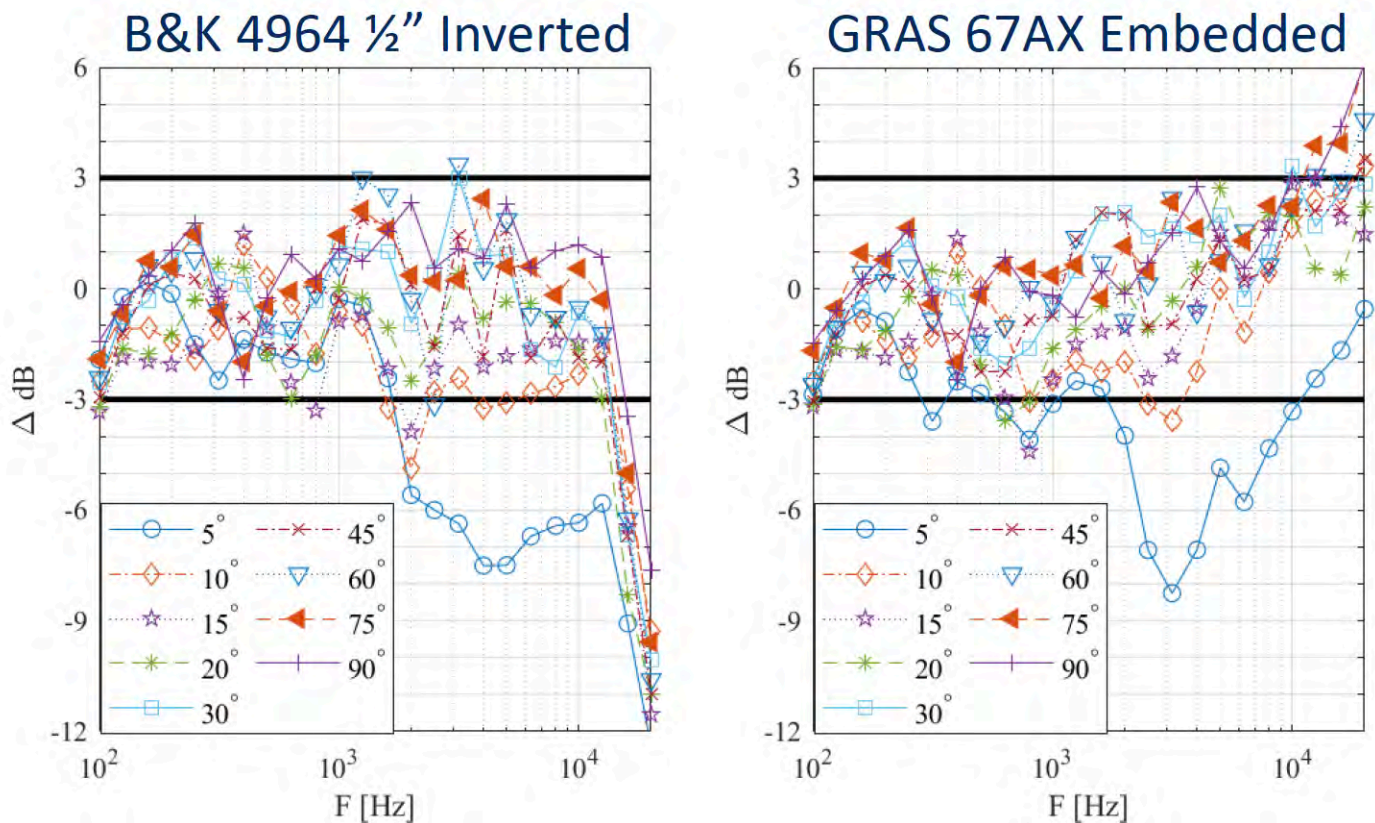


**Figure 3.** Comparison of measured level versus frequency at a variety of incidence angles between an inverted microphone and a true flush mounted microphone from Anderson et al. [16].

### Noise Source Separation

A review of techniques for harmonic noise separation methods was conducted in order to inform the approach to rotor noise separation being developed as a component of this project. Harmonic averaging techniques have long been applied to reduce the variability and suppress background noise in model helicopter rotor noise measurements conducted in anechoic wind tunnels. More recently, these techniques have been combined with time domain de-Dopplerization to separate noise radiated by the main rotor from that of the tail rotor [17]. This technique works most effectively when the radiated noise is nearly periodic, as pulse-to-pulse amplitude fluctuations will be averaged out by the method. The technique also relies on the fact that helicopter main and tail rotors operate at non-integral multiples of each other and would not be effective for rotors operating a similar RPM. Another technique using a time-varying Fourier decomposition of the signal has been shown to be more effective than harmonic averaging at extracting the energy from fluctuating tonal signals [18]; however, the method is numerically ill-conditioned when the rotor RPM are close to each other. An alternate method of source separation is the Vold-Kalman order tracking filter method [19]. This method employs a Kalman filtering technique to extract the harmonic components of the signal which track a phasor associated with the measured RPM of the rotating machinery from which the noise originates. A second generation “multi-shaft” Vold Kalman filtering approach has been very successfully applied to separate harmonic components of noise generated by a model counter-rotating open rotor [20] in a wind tunnel, even when the RPM of the two rotors were very close to one another, but continuously varying.

### Aircraft Noise Characterization

Numerous published techniques for aircraft noise characterization were reviewed. Most methods developed for rotorcraft map the measured noise emitted during steady flight to a spherical grid (or equivalent representation) traveling with the rotorcraft, with the aim of capturing the frequency and magnitude of noise as a function of directivity. Consequently, for a steady flight condition, a large linear array of microphones must be employed to capture the noise at various sideline angles

throughout the flyover [21]. These measurements are then “de-propagated” to normalize the levels to a single equivalent radiation distance and assigned to a radiation angle corresponding to the time of emission. When time-varying noise measurements are to be conducted, both lateral and longitudinal angles must be measured simultaneously, therefore requiring a planar acoustic array [22]. Noise measurements are typically collected across a wide range of operating conditions; for helicopters, both airspeed and sink rate are varied in steady flight, and quasistatic theory can then be employed to relate these parameters to the aerodynamic operating state of the main rotor and the corresponding noise radiation in maneuvering flight [23]. For vehicles with additional degrees of freedom, such as tilt rotors, additional flight states must be measured to fully characterize noise radiation characteristics over the entire operating envelope [24].

### **Aircraft Noise Certification**

Existing aircraft noise certification standards were reviewed, with a focus on Part 36 Appendices H and J (helicopters), K (tiltrotors), and G (light propeller aircraft) as these were most applicable to primarily propeller- or rotor-driven UAS and UAM. Additionally, the corresponding advisory guidance given in FAA Advisory Circular AC-36-4D and the ICAO AN/929 Environmental Technical Manual was reviewed. The standards and advisory guidance specify in detail characteristics such as the allowable terrain types and clearance from obstructions for noise measurement, acoustic instrumentation requirements, calibrations, and allowable corrections, meteorological measurements and limitations, flight conditions, time space position information (TSPI) requirements, and allowable deviations, and the required level of demonstrated repeatability.

Many of these specifications are likely applicable to UAS and UAM noise measurements without modification. However, some areas may need additional consideration. For example, small UAS noise levels are likely to be much lower than significantly larger crewed aircraft and as such, flight may need to be conducted at lower altitudes above ground to ensure adequate signal-to-noise at the microphones. This has significant implications for TSPI accuracy requirements, since errors in the vehicle position will have a greater influence on measured noise levels at shorter ranges; however, small UAS may be unable to carry precise tracking equipment without changing weight or drag in a way that influences acoustic emissions. Additionally, existing standards clearly define the flight condition of the vehicle throughout the data collection period. Where vehicles are over-actuated, the worst-case noise condition is usually sought; for example, when the pilot can directly control the RPM of the helicopter rotor, the highest normal RPM is to be maintained as that is generally the loudest operating condition. These conditions may not be so easy to define for UAS and UAM, which are likely to have many additional degrees of freedom, no obvious “worst case” acoustic configuration, and semi or fully autonomous operation. Representative operating conditions may vary considerably by vehicle configuration and planned mission. Atmospheric conditions may also strongly influence noise radiation characteristics for these vehicles in ways which are yet unknown; for example, while a procedure for tip Mach number corrections has been developed for helicopter noise certification to compensate for variations in speed or temperature, no such corrections have been developed for multirotor vehicles. Other factors, such as atmospheric turbulence intensity, may affect how the flight control system adjusts the rotor RPM to stabilize the vehicle, with corresponding impact on the measured noise levels.

### **Publications**

None

### **Outreach Efforts**

None

### **Awards**

None

### **Student Involvement**

All three graduate students have been actively involved in the research process. Keon Wong Hur has primarily focused on reviewing the literature on multirotor aircraft noise prediction. Joel Rachaprolu has been primarily responsible for the review of source separation techniques, and N. Blaise Konzel on acoustic measurement instrumentation and installations. All three students have reviewed material on UAS noise measurements. Regular meetings are held to discuss research findings and guide future research activities in addition to online collaboration through the internal Penn State repository established for this review.



## Plans for Next Period

Literature review activities will continue throughout the project. Additionally, the team will work to summarize the findings of the review into a publishable report or article of general interest to the aircraft noise research community. The team will also work to identify related ongoing research which may not have been published yet to identify opportunities for coordination and collaboration.

## References

- [1] Jia, Z., and Lee, S. Acoustic Analysis of a Quadrotor EVTOL Design via High-Fidelity Simulations. Presented at the 25th AIAA/CEAS Aeroacoustics Conference, Delft, The Netherlands, 2019.
- [2] Smith, B., Gandhi, D. F., and Niemiec, D. R. A Comparison of Multicopter Noise Characteristics with Increasing Number of Rotors. Presented at the Vertical Flight Society Forum 76, Virginia Beach, VA, 2020.
- [3] Pascioni, K., and Rizzi, S. A. Tonal Noise Prediction of a Distributed Propulsion Unmanned Aerial Vehicle. Presented at the 2018 AIAA/CEAS Aeroacoustics Conference, Atlanta, Georgia, 2018.
- [4] Greenwood, E., Schmitz, F. H., and Sickenberger, R. D. "A Semiempirical Noise Modeling Method for Helicopter Maneuvering Flight Operations." *Journal of the American Helicopter Society*, Vol. 60, No. 2, 2015, pp. 1-13. <https://doi.org/10.4050/JAHS.60.022007>.
- [5] Botre, M. C., Brentner, K. S., Horn, J., and Wachspress, D. A. Developing a Comprehensive Noise Prediction System for Generating Noise Abatement Procedures. Presented at the 25th AIAA/CEAS Aeroacoustics Conference, Delft, The Netherlands, 2019.
- [6] Senzig, D. A., Marsan, M., Downs, R. S., Hastings, A. L., Cutler, C. J., and Samiljan, R. W. *UAS Noise Certification and Measurements Status Report: Tigershark UAS Measurements, Tracking System Development and Certification Metrics Status*. Publication DOT-VNTSC-FAA-18-01. US Department of Transportation, 2017, p. 68.
- [7] Cabell, R., Grosveld, F., and McSwain, R. "Measured Noise from Small Unmanned Aerial Vehicles." *INTER-NOISE and NOISE-CON Congress and Conference Proceedings*, Vol. 252, No. 2, 2016, pp. 345-354.
- [8] Alexander, W. N., and Whelchel, J. "Flyover Noise of Multi-Rotor SUAS." *INTER-NOISE and NOISE-CON Congress and Conference Proceedings*, Vol. 259, No. 7, 2019, pp. 2548-2558.
- [9] Christian, A. W., and Cabell, R. Initial Investigation into the Psychoacoustic Properties of Small Unmanned Aerial System Noise. Presented at the 23rd AIAA/CEAS Aeroacoustics Conference, Denver, Colorado, 2017.
- [10] Pettingill, N. A., and Zawodny, N. S. Identification and Prediction of Broadband Noise for a Small Quadcopter. Presented at the Vertical Flight Society 75th Annual Forum, Philadelphia, PA, 2019.
- [11] Read, D. R., Senzig, D. A., Cutler, C., Elmore, E., and He, H. *Noise Measurement Report: Unconventional Aircraft - Choctaw Nation of Oklahoma; July 2019*. Publication DOT-VNTSC-FAA-20-03. Department of Transportation, 2020, p. 156.
- [12] Newman, J. S., and Locke, M. *Helicopter Noise Measurement Repeatability Program Final Report*. Publication FAA-EE-87-2. Department of Transportation, 1987.
- [13] Alexander, W. N., Whelchel, J., Intaratep, N., and Trani, A. Predicting Community Noise of SUAS. Presented at the 25th AIAA/CEAS Aeroacoustics Conference, Delft, The Netherlands, 2019.
- [14] Shivashankara, B. N., and Stubbs, G. W. "Ground Plane Microphone for Measurement of Aircraft Flyover Noise." *Journal of Aircraft*, Vol. 24, No. 11, 1987, pp. 751-758. <https://doi.org/10.2514/3.45517>.
- [15] Willshire Jr, W. L., and Nystrom, P. A. *Investigation of Effects of Microphone Position and Orientation on Near-Ground Noise Measurements*. Publication TP-2004. NASA, 1982.
- [16] Anderson, M., Stephenson, J. H., Zawodny, N. S., and Gee, K. L. "Characterization of the Effects of the Ground Boards on Acoustic Signals." *Journal of the Acoustical Society of America*, Vol. 146, 2019, p. 2761.
- [17] Greenwood, E., and Schmitz, F. H. "Separation of Main and Tail Rotor Noise from Ground-Based Acoustic Measurements." *Journal of Aircraft*, Vol. 51, No. 2, 2014, pp. 464-472. <https://doi.org/10.2514/1.C032046>.
- [18] Olsman, W. F. J. "Method for the Extraction of Helicopter Main and Tail Rotor Noise." *Journal of Aircraft*, Vol. 55, No. 2, 2017, pp. 805-816. <https://doi.org/10.2514/1.C034525>.
- [19] Leuridan, J., Kopp, G. E., Moshrefi, N., and Vold, H. "High Resolution Order Tracking Using Kalman Tracking Filters - Theory and Applications." *SAE Transactions*, Vol. 104, 1995, pp. 2390-2396.
- [20] Stephens, D. B., and Vold, H. "Order Tracking Signal Processing for Open Rotor Acoustics." *Journal of Sound and Vibration*, Vol. 333, No. 16, 2014, pp. 3818-3830. <https://doi.org/10.1016/j.jsv.2014.04.005>.
- [21] Conner, D., and Page, J. "A Tool for Low Noise Procedures Design and Community Noise Impact Assessment: The Rotorcraft Noise Model (RNM)." *Heli Japan*, 2002, pp. 11-13.
- [22] Guntzer, F., Spiegel, P., and Lummer, M. Genetic Optimizations of EC-135 Noise Avatement Flight Procedures Using and Aeroacoustic Database. Presented at the European Rotorcraft Forum 35, Hamburg, Germany, 2009.



- [23] Greenwood, E., and Rau, R. "A Maneuvering Flight Noise Model for Helicopter Mission Planning." *Journal of the American Helicopter Society*, Vol. 65, No. 2, 2020, pp. 1-10. <https://doi.org/10.4050/JAHS.65.022007>.
- [24] Conner, D., Marcolini, M., Edwards, B., and Brieger, J. "XV-15 Tiltrotor Low Noise Terminal Area Operations." *American Helicopter Society Forum* 53, May 1997.

## Task 2 – Computational Modeling of UAS and UAM Configurations

The Pennsylvania State University

### Objectives

The goal of this task is to develop several computational models of UAS and UAM aircraft with varied configurations in order to provide a simulated environment in which various noise measurement configurations and data processing methods can be rapidly investigated ahead of acoustic flight testing. The flight conditions and appropriate arrangement of microphones required to characterize the directivity of the vehicle will be evaluated. Additionally, data will be generated to validate efficacy of the rotor source separation process also being developed under this project.

### Research Approach

This task will leverage the UAM noise prediction system being developed by Penn State under ASCENT Project 49, with an emphasis on using the combined system of PSU-WOPOP and DEPSim to model the acoustic "beating" phenomena caused by the time varying RPM of multirotor UAS and UAM systems. The computational models will be used to identify requirements for microphone measurement arrays designed to capture variations in noise due to variations in flight condition and source directivity. A capability to generate synthetic background noise will be added to the prediction system to more realistically simulate a flight experiment. Finally, acoustic simulations will also provide details that are not available in the flight test measurements (e.g., noise predictions of isolated noise sources: thickness, loading, broadband, etc.; simple models to explore hypotheses of the impact caused by various aerodynamic and acoustic interactions, etc.) to help diagnose and analyze the noise from complicated UAS and UAM vehicles.

### Milestones

The milestones for this task consist of a) developing UAS and UAM models representative of vehicles for which noise measurements will be collected during this project, b) to conduct simulated experiments, and c) to identify best practices for UAS and UAM noise measurements by reviewing the simulated data.

### Major Accomplishments

A new module has been developed for PSU-WOPWOP which enables arbitrary Finite Impulse Response (FIR) filters to be applied to measured or predicted signals. This new capability is intended to be used to shape random "white" noise in the time domain to match typical ambient background noise levels expected during outdoor acoustic measurements. This will allow the effect of varying signal-to-noise on the noise measurement and data processing schemes to be evaluated in the simulation.

### Publications

None

### Outreach Efforts

None

### Awards

None

### Student Involvement

MS Student Keon Wong Hur is becoming familiar with using, and extending, the PSU-WOPWOP/DEPSim noise prediction system being developed under Project 49. He developed and implemented the initial FIR filtering module described in the previous section.



### **Plans for Next Period**

The next steps are to develop a representative UAS noise model for the noise prediction system and then to begin evaluating potential experimental approaches using the prediction tool.

## **Task 3 – Development of a Source Separation Process for Distributed Propulsion Vehicles**

The Pennsylvania State University

### **Objective**

The objective of this task is to develop a process for separating the noise generated by rotors or propellers at non-constant, but potentially similar, RPM from flyover measurements of UAS and UAM vehicles.

### **Research Approach**

The source separation process developed in this task will consist of two steps. The first step in this process will be a time domain de-Dopplerization method, allowing the ground-based measurements to be transformed to measurements analogous to stationary wind tunnel or inflight noise measurements. The second step of this method will be to develop an order-tracking filter approach that can separate out the contributions of each individual rotor or propeller from the transformed acoustic signal by relating the signals to the observed changes in rotor RPM at the time of emission. This process will be applied to predictions made by the computational models developed in the previous task. The accuracy and limitations of the source separation process will be assessed by comparing the output of the process to the predicted noise of the individual components.

### **Milestones**

The milestones for this task consist of a) developing a source separation process for stationary acoustic measurements, b) implementing a de-Dopplerization approach to convert non-stationary measurements to a stationary frame and c) applying the process to simulated and measured data to evaluate the effectiveness of the separation.

### **Major Accomplishments**

A single-shaft Vold-Kalman order tracking filter process has been developed. The process was applied to synthetically generated signals and was able to achieve an accurate separation. Acoustic data for one counter-rotating coaxial rotor from the Dragonfly UAS under development at Penn State was recently collected in the Penn State Flow-through Anechoic Chamber, as shown in Figure 4. Both rotors were equipped with tachometers and were rotated at the same nominal RPM, however small variations in speed naturally occurred, shown in Figure 5, since there was no mechanical coupling between the rotors. Figure 6 compares a spectrogram of the total noise measurement with both rotors operating to a spectrogram of the separated noise for just the front rotor. The order tracking filter appears to accurately separate the lower harmonics of the rotor noise from the total noise signal, but without further tuning was not able to extract the signal for the higher harmonics.



Figure 4. Counter-rotating coaxial rotor propeller noise measurement in the Penn State Flow-Through Anechoic Chamber.

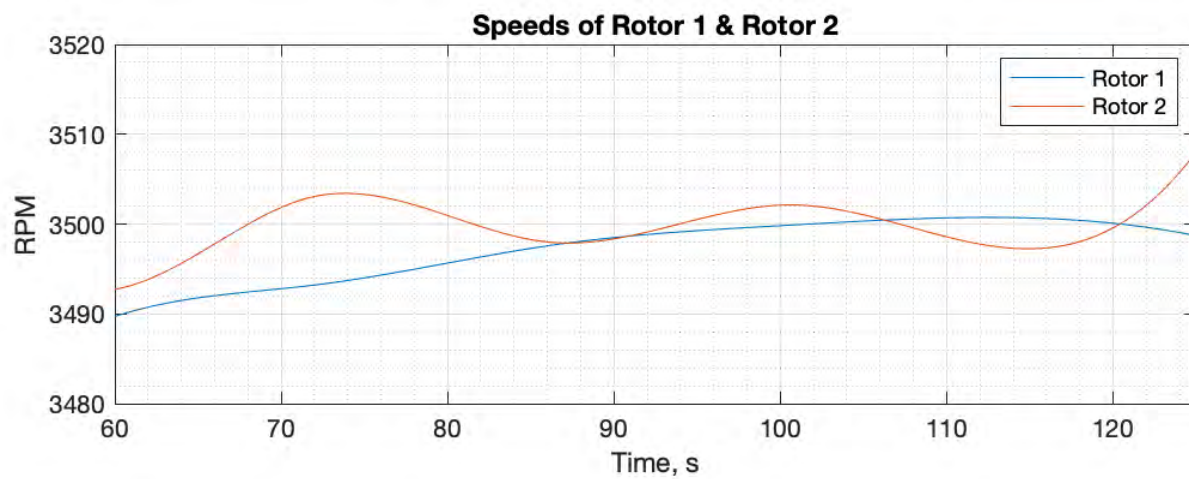


Figure 5. Rotor speed variations over time.

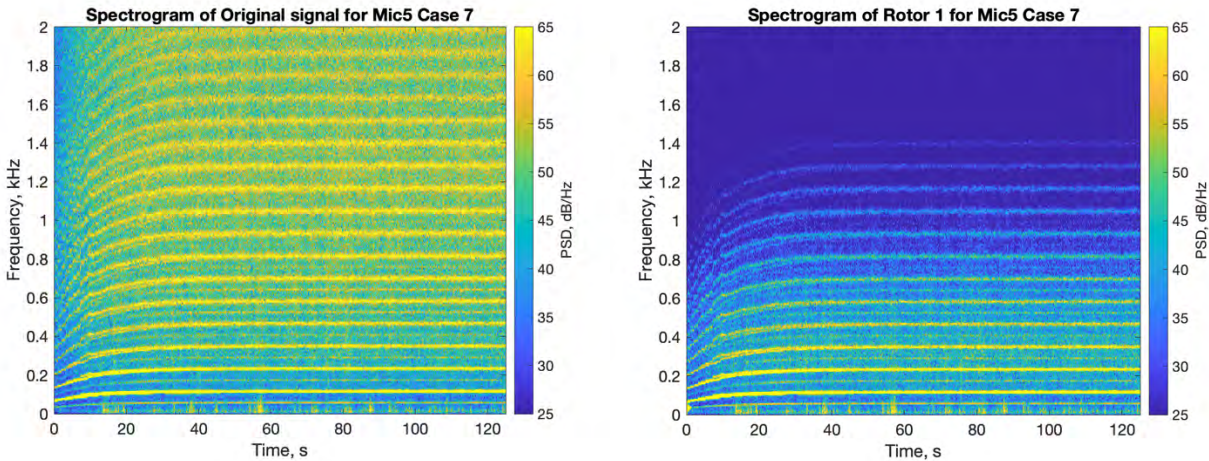


Figure 6. (Left) spectrogram of the total signal. (Right) spectrogram for single rotor.

### Publications

None

### Outreach Efforts

None

### Awards

None

### Student Involvement

MS Student Joel Rachaprolu developed the initial single-shaft Vold-Kalman filter implementation and has applied it to the test data set. He has begun implementing a second-generation multi-shaft filter in consultation with Håvard Vold.

### Plans for Next Period

The next step is to complete the implementation of a second-generation multi-shaft Vold-Kalman filter. Following that, a time-domain de-Dopplerization method will be implemented. Both processes will be applied to helicopter noise data collected during the joint NASA/FAA Helicopter Noise Abatement Flight Test in order to validate the method on well-separated rotor noise measurements during free flight. In conjunction with the previous task, the method will then be applied to simulated noise data in order to explore any limitations in the process. Finally, the method will be applied to UAS and UAM noise data collected in the following tasks.

## Task 4 – Design and Development of a Reconfigurable Multirotor UAS Vehicle

The Pennsylvania State University

### Objective

The objective of this task is to design and develop a multirotor UAS vehicle which can be easily reconfigured to explore the acoustic effects of different UAS vehicle configurations and their influence on the noise measurement and data processing approaches developed in this project.

### Research Approach

A UAS vehicle will be designed with adjustable rotor support arms, allowing the relative positions of the rotors to be easily reconfigured. The rotor shafts will be designed to allow rotors with different designs, e.g., different blade spacings, to be

mounted to the vehicle. The rotor shafts will be instrumented with encoders allowing for precise determination of the rotor RPM and shaft phase angle at a high sampling rate. The vehicle will also be instrumented with real-time kinematic differential GPS and an inertial measurement unit to provide a time-accurate position and state estimate which can then be correlated to the acoustic measurements.

Due to the reconfigurable nature of the vehicle, special consideration will be given to developing a control system capable of achieving stabilized flight across the range of possible configurations. Ground and flight testing of the vehicle will be conducted to ensure the vehicle systems and instrumentation are functioning nominally and to expand the vehicle operating envelope to cover the flight conditions for which noise measurements are to be made.

### **Milestones**

The milestones for this task consist of a) identifying acoustically significant configuration changes to be made on the vehicle, b) initial design of the vehicle and selection of sensors, c) control system design, and d) ground and flight testing.

### **Major Accomplishments**

None

### **Publications**

None

### **Outreach Efforts**

None

### **Awards**

None

### **Student Involvement**

This task has yet to begin and it has yet to be assigned to a suitable student.

### **Plans for Next Period**

This task will begin as soon as a suitable student completes onboarding.

## **Task 5 – Microphone Type and Installation Investigation**

The Pennsylvania State University

### **Objective**

The objective of this task is to assess several different microphone types and installation methods to determine their impact on the characterization of UAS and UAM vehicle noise.

### **Research Approach**

Several different microphone installations are routinely used for aircraft noise measurements, including the 4 feet elevated microphones prescribed by FAR 36 Appendix H, inverted microphones mounted over a ground board per SAE ARP 4055, and microphones flush-mounted in a ground board, such as the GRAS 67AX currently in use by the NASA Mobile Acoustics Facility. These installations present tradeoffs in terms of precision, effective frequency response, cost, test set up time, and operational use. Additionally, IEC 61672-1 specifies several classes of measurement microphones. Typically, Class 1 microphones are used for noise certification and research testing of aircraft; however, the cost of these microphones may be prohibitive for typical measurements of inexpensive small UAS, especially if a larger channel count is required to capture the directivity and variability of multirotor UAS noise. Testing and evaluation of different microphone types and installations will be conducted both in Penn State's anechoic chamber and throughout the outdoor acoustic measurements of UAS. The effect of the choice of installation on typical aircraft noise metrics, such as SEL or EPNL, will be assessed, as well as the effects on the source separation and characterization process. The ultimate aim will be to identify an accurate but cost-effective measurement approach for FAA and the UAS and UAM industries.



## **Milestones**

The milestones for this task consist of a) constructing several different types of microphone measurement installations, b) characterizing their acoustical properties, and c) evaluating the impact on UAS and UAM noise measurements.

## **Major Accomplishments**

An initial set of 12 ground plane microphone installations developed in accordance with SAE ARP 4055 has been developed and deployed for initial acoustic data collection. The installation consists of a plasma cut 16GA steel plate with rounded edges. Three mounting holes were drilled to support an inverted microphone tripod offset from the center of the circular plate. The tripod legs are made of 1/8 inch steel which are brazed to a 1/2 inch inner diameter shaft collar, securing the measurement microphone preamplifier with a set screw. The gap height is set in the field with a feeler gauge.

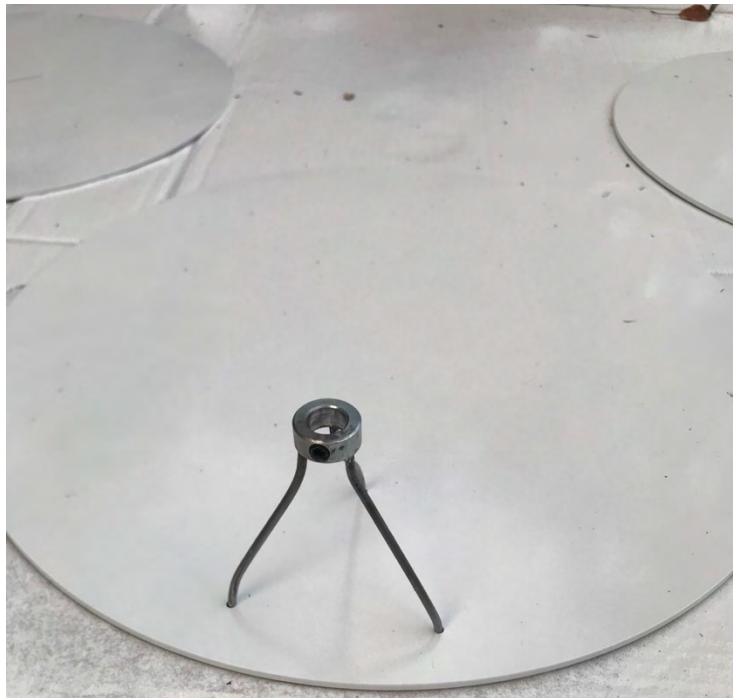


**Figure 7.** Ground plane microphone installation per SAE ARP 4055.

In field testing, several areas for improvement were identified. Although SAE ARP 4055 suggests that windscreens are not needed for inverted microphones, field testing with 14 knot winds at 10 m above ground level showed high wind noise levels for those microphone installations placed on smooth surfaces, such as asphalt. Lower noise levels were measured for nearby installations placed in mowed grass, but still significantly increased measured background noise levels relative to calm conditions. The current tripod mounting mechanism does not reliably return to the same gap height when removed from the ground board, which complicates set up, especially if the microphones need to be relocated frequently. The steel tripod legs were also difficult to manufacture consistently, so there was considerable variation between inverted microphone tripod geometries.

A new aluminum tripod leg design has been developed, along with a more repeatable manufacturing process. The new tripod legs have neodymium magnet feet, which allows a more consistent placement on the ground board with a repeatable gap height. Figure 8 shows a photograph of the new leg design.



Figure 8. Magnetic tripod leg design.

### **Publications**

None

### **Outreach Efforts**

None

### **Awards**

None

### **Student Involvement**

M.S. Student N. Blaise Konzel has developed the initial set of ground plane microphone hardware and is refining the design. He is also becoming familiar with the acoustic data acquisition equipment and calibration process.

### **Plans for Next Period**

Next steps are to develop several microphone windscreen concepts for inverted ground board microphones and test them in the Penn State Flow-through Anechoic Chamber. Experiments will be conducted to identify the appropriate microphone gap height and ground board configuration for small UAS noise measurements, and the data will be analyzed to assess the effect on noise certification metrics, such as sound exposure level (SEL) or effective perceived noise level (EPNL).



## Task 6 – Baseline UAS Noise Measurement

The Pennsylvania State University

### Objective

The objective of this task to conduct an acoustic flight test campaign to collect noise measurements for a variety of UAS vehicles under a variety of operating conditions and configurations.

### Research Approach

Acoustic measurements of flying UAS will occur at the nearby Mid-State Regional Airport. Noise measurements will be made for a variety of UAS in Penn State's fleet, including several configurations of the reconfigurable multirotor UAS platform developed in Task 4. Typically, Penn State's outdoor UAS research vehicles have inertial state measurements, barometers, magnetometers, and either WAAS or RTK augmented GPS, which are fused to provide 100 Hz vehicle position and state estimates. Several aircraft also include air data sensors, allowing airspeed, angle of attack, and sideslip to be estimated. The US Army Research Laboratory Vehicle Technology Directorate has also offered to make UAS available to Penn State for acoustic testing. Other opportunities for collaboration with US Government and industry UAS operators will be pursued in order to expand the variety of vehicles characterized. Each vehicle will be flown through a range of operating conditions, including hover, forward flight at several speeds, and any transition modes of the vehicle. Testing will be conducted at several altitudes, from near ground level to 400 feet above ground level in order to evaluate the ability to scale UAS noise measurements made at one flight altitude relative to another, given the relatively low noise levels of small UAS. Acoustic measurements will be made with Penn State's networked, battery-powered and field-deployable acoustic data acquisition system capable of sampling at up to 125 kHz at 24-bit resolution with subsample accurate GPS time synchronization across all nodes. The hardware will be configured to support at least 24 channels and can be expanded as required. The microphone array will be distributed so as to capture both spatial and temporal variations in the radiated noise. Weather instrumentation will be deployed, including ground level and 10 meter measurements of wind speed, direction, temperature, pressure, and humidity. High frequency ultrasonic 3D wind velocity measurements will also be made in order to relate the level of atmospheric turbulence to the fluctuations in the vehicle flight state and radiated noise.

### Milestone

The milestone for this task consists of collecting a baseline acoustic, performance, and meteorological data set of UAS noise measurements.

### Major Accomplishments

None

### Publications

None

### Outreach Efforts

None

### Awards

None

### Student Involvement

None

### Plans for Next Period

This task will commence following the development of an initial acoustic measurement configuration per Task 5.



## Task 7 – UAM Component Noise Measurement

The Pennsylvania State University

### Objective

Penn State will team with Beta Technologies to conduct an initial acoustic characterization of a single isolated rotor on BETA's UAM rotor test stand.

### Research Approach

Measurements will be conducted at Beta's test site in South Burlington, VT. The rotor test stand is mounted to a vehicle and can be operated in stationary or forward flight modes. These data will be used to establish a baseline set of noise data for a single rotor which will then be compared with data extracted from flyover measurement of the entire vehicle using the noise source separation processing developed in a previous task. Repeated measurements will be conducted to cover a range of rotor designs and operating conditions as Beta's development program advances.

### Milestone

The milestone for this task consists of collecting baseline noise measurements for isolated UAM rotors.

### Major Accomplishments

An initial data collection was conducted for one of Beta's ALIA-250 lifting rotor designs on the rotor test stand in a stationary configuration, as shown in Figure 9. RPM were varied from 1400 to 600 RPM; a spectrogram of the noise data during the sweep are shown in Figure 10. At low rotor speeds, most of the tonal content is concentrated in the first harmonic of the blade-passing frequency, however, broadband noise is prominent. As rotor RPM increases, the noise becomes more impulsive and higher harmonics of the blade-passing frequency become dominant. Further analysis will be conducted to determine directivity and tonal noise pulse shape in order to relate these characteristics to the physical mechanisms of noise generation.

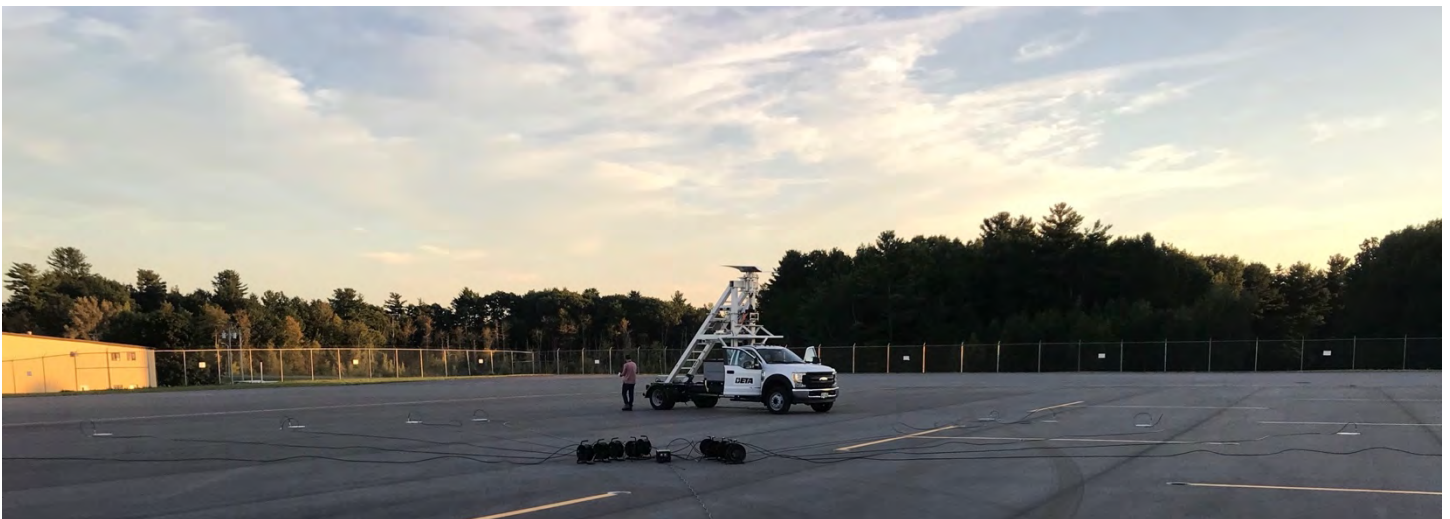


Figure 9. PSU noise measurement of Beta lifting rotor.

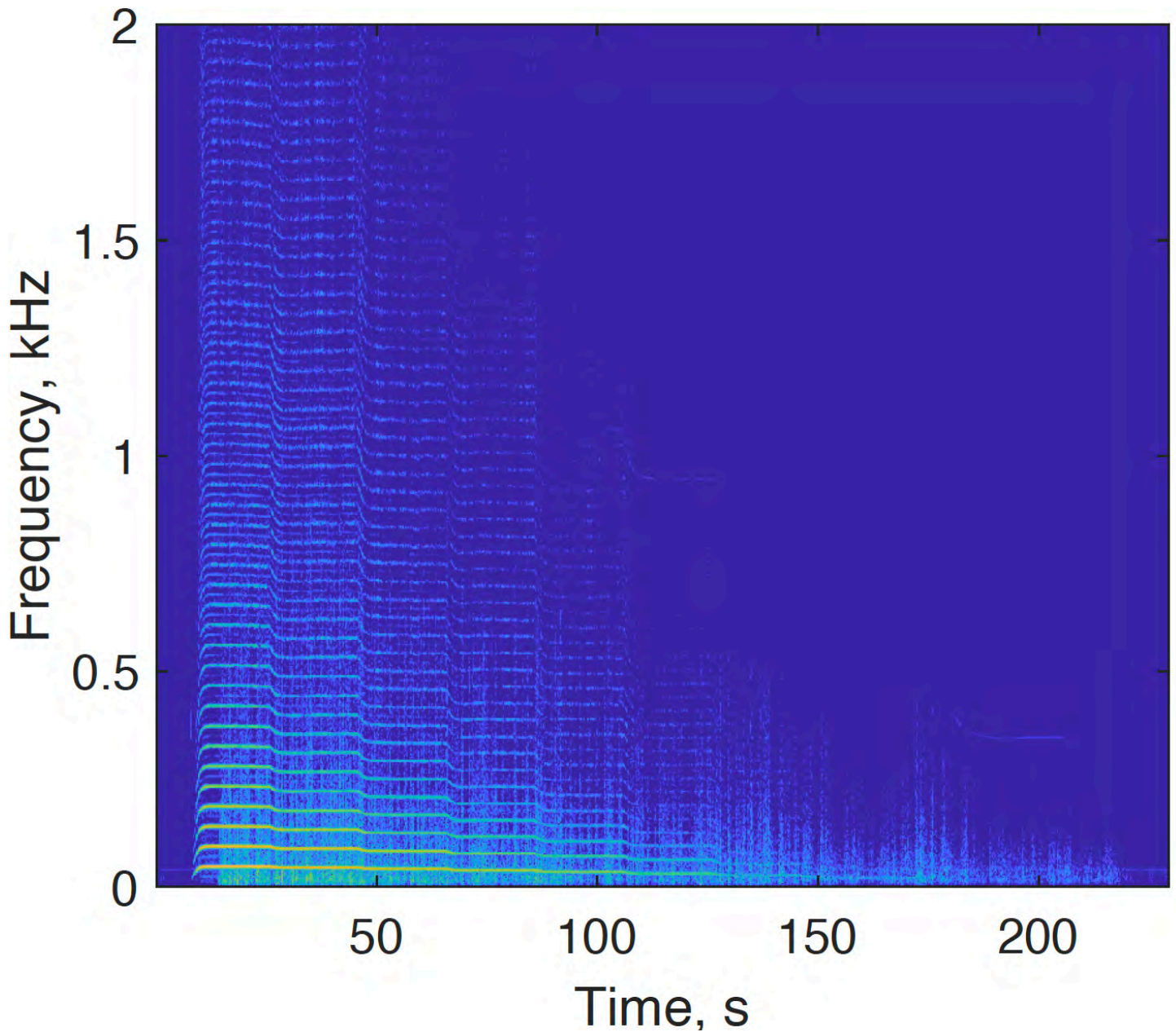


Figure 10. Spectrogram during RPM sweep from 1400 RPM to 600 RPM.

**Publications**

None

**Outreach Efforts**

None

**Awards**

None



### **Student Involvement**

N. Blaise Konzel and Joel Rachaprolu have begun analyzing the measured data in preparation for future noise measurements.

### **Plans for Next Period**

Follow on noise measurements will be conducted in conjunction with Beta Technologies as the company's rotor system develops.

## **Task 8 – UAM Full-Vehicle Noise Measurement**

The Pennsylvania State University

### **Objective**

The objective of this is to conduct an initial acoustic characterization of Beta Technologies' multirotor UAM vehicle in free flight.

### **Research Approach**

Measurements will be made at BETA's test site in Plattsburgh, NY. The vehicle's flight state and position will be recorded and correlated to the acoustic and weather measurements. Initial measurements will focus on characterizing the vehicle during cruising flight conditions. Measurements for transition and hover flight conditions will be conducted as the vehicle's flight envelope is expanded with the same ground-based sensors deployed in the UAS noise measurement task. However, the array configuration will be tailored to the larger size and higher speeds of Beta's UAM vehicle. The collected data will be analyzed and opportunities for noise reduction through design changes will be identified.

### **Milestone**

The milestone for this task consists of collecting a baseline acoustic, performance, and meteorological data set of UAM noise measurements across several operating modes.

### **Major Accomplishments**

Penn State collected initial noise measurements for a low-level flyover of the Beta ALIA-250 UAM vehicle in a fixed wing flight mode at Beta's test site in Plattsburgh, NY. The vehicle was configured with temporary wheeled landing gear for envelope expansion, as shown in Figure 11. The acoustic array was set up toward one side of the runway, with the other side left clear for the chase truck to pass during flyovers. The aircraft took off approximately 700 feet ahead of the array and landed approximately 300 feet after the array. Due to the restricted envelope of the vehicle, flyover altitudes were limited to between 15 feet and 40 feet wheels above ground. After several passes with the array on the port side of the vehicle, the array was redeployed on the starboard side. The acoustic and position tracking data are currently being analyzed.



**Figure 11.** Flyover noise measurement of the Beta ALIA-250 at Plattsburgh, NY.

### **Publications**

None

### **Outreach Efforts**

None

### **Awards**

None

### **Student Involvement**

M.S. Students N. Blaise Konzel and Joel Rachaprolu have begun analyzing the measured data in preparation for future noise measurements.

### **Plans for Next Period**

Follow on noise measurements will be conducted in conjunction with Beta Technologies for additional cruise, hover, and transition conditions as the operating envelope of the vehicle expands. The results of Tasks 1, 2, and 5 will influence the design and execution of future UAM flight tests.



## Publications Index

### Project 001

Eighteen graduate students and three undergraduate students involved.

#### Publications

- Choi, Y., D. Lambert, K. L. Jensen, C. D. Clark, B. C. English, and M. Thomas, 2020. Rank-Ordered Analysis of Consumer Preferences for the Attributes of a Value-Added Biofuel Co-Product. *Sustainability*, 12, 2363. doi:10.3390/su12062363.
- Gill, MacKenzie, K. L. Jensen, D. M. Lambert, S. Upendram, B. C. English, N. Labbé, S. Jackson, and R. J. Menard, 2020. Consumer Preferences for Eco-Friendly Attributes in Disposable Dinnerware. *Resources, Conservation and Recycling*, 161, 104965.
- Yu, T. E., B. C. English, J. Zhong, J. A. Larson, J. S. Fu, L. H. Lambert, and B. S. Wilson, 2021. High-resolution Multi-objective Optimization of Sustainable Supply Chains for a Large Scale Lignocellulosic Biofuel Industry, *Pursuing Sustainability: OR/MS Applications in Sustainable Design, Manufacturing, Logistics, & Resources*, C. Chen, V. Jayaraman, and Y. Chen, ed., Springer International Series in Operations Research and Management Science
- Sharma, B.P, T. E. Yu, B. C. English, C. Boyer, and J. A. Larson. 2020. Impact of Government Subsidies on a Cellulosic Biofuel Sector with Diverse Risk Preferences toward Feedstock Uncertainty, *Energy Policy*, 146, 111737. doi:10.1016/j.enpol.2020.111737
- Thomas, M., K.L. Jensen, M. Velandia, C. Clark, B. English, D. Lambert, and F.Walker. 2020. Outdoor Home Gardener Preferences for Environmental Attributes in Gardening Supplies and Use of Ecofriendly Gardening Practices. *HortTech*. 30(5):552-563.
- Thomas, M., K. L. Jensen, C. D. Clark, D. M. Lambert, B. C. English, and F. R. Walker. Consumer Preferences for Potting Mix with Biochar. *Journal of Cleaner Production*, In Review
- Gill, Mackenzie (August 2020). Consumer Preferences for Environmentally Friendly Disposable Dinnerware Alternatives, University of Tennessee M.S. Thesis.
- Patwary, A. Latif (May 2020). Efficiency Studies of the U.S. Transportation Sector, University of Tennessee M.S. Thesis.
- Robertson, A. (May 2020). Biomass Potential in Sustainable Aviation Fuel Development: Switchgrass Production Optimization and Carinata Oilseed Enterprise Viability Analysis, University of Tennessee M.S. Thesis
- Stevens J. and Taheripour F. (2020) A stochastic techno-economic analysis of aviation biofuel production from pennycress seed oil. Selected paper *presented at the 2020 Agricultural & Applied Economics Association Annual Meeting, Virtual Meeting August 10.*
- Taheripour, F., & Tyner, W. E. (2020). US biofuel production and policy: implications for land use changes in Malaysia and Indonesia. *Biotechnology for Biofuels*, 13, 11. doi:10.1186/s13068-020-1650-1
- Zhao X. Taheripour F., Malina R. Tyner W. (2020) Aviation biofuels: A viable and sustainable option to curb aviation emissions. Selected paper *presented at the 2020 Agricultural & Applied Economics Association Annual Meeting, Virtual Meeting August 10.*
- Taheripour F. Zhao X., Horridge M. Farrokhi F. Tyner W (2020) Land Use in Computable General Equilibrium Models. *Journal of Global Economic Analyses*, 5(2):63-109. doi:10.21642/JGEA.050202AF
- Fu, F., Summers, S., Morgan, T.J., Turn, S.Q., & Kusch, W. Fuel properties of *Milletia pinnata* seeds and pods grown in Hawaii. *Industrial Crops and Products*. In review.
- Fu, J., Summers, S., Turn, S.Q., & Kusch, W. Upgraded pongamia pod via torrefaction for the production of bioenergy. *Fuel*. In review.
- Bach, Q.V., Fu, J., & Turn, S.Q. Fuel Characterization of Construction and Demolition Wastes as Feedstock for Thermochemical Gasification, draft manuscript to be submitted to *Waste Management*.
- Brandt, K.L., Wooley, R.J., Geleynse, S.C., Gao, J., Zhu, J., Cavalieri, R.P., Wolcott, M.P. (2020). Impact of co-product selection on techno-economic analyses of alternative jet fuel produced with forest harvest residuals. *BioFPR*, 14(4):764-775.
- Geleynse, S., Jiang, Z., Brandt, K., Garcia-Perez, M., Wolcott, M., Zhang, X. (2020). Pulp Mill Integration with Alcohol-to-Jet Conversion Technology. *Fuel Processing Technology* 201:106338.
- Tanzil, A.H., X. Zhang, M. Wolcott and M. Garcia-Perez, Strategic Assessment of Sustainable Aviation Fuel Production Technologies: Yield Improvement and Cost Reduction Opportunities (*Submitted to Biomass and Bioenergy, 2020*)



- Tanzil, A.H., Zhang, X., Wolcott, M., Garcia-Perez, M. Evaluation of Biorefinery Alternatives for the Production of Sustainable Aviation Fuels in a Dry Grind Corn Ethanol Mill (*Submitted to Biomass and Bioenergy*)
- Tanzil, A.H., Zhang, X., Wolcott, M., Garcia-Perez, M. Evaluation of Biorefinery Alternatives for the Production of Sustainable Aviation Fuels in a Sugarcane Mill (*Internal review*)
- Tanzil, A.H., Zhang, X., Wolcott, M., Garcia-Perez, M. Evaluation of Biorefinery Alternatives for the Production of Sustainable Aviation Fuels in a Petroleum Refinery (*Internal review*)
- Mueller, D., Hoard, S., Roemer, K., Rijkhoff, S., Sanders, C. (2020). Quantifying the Community Capitals Framework: Strategic Application of the Community Assets and Attributes Model. Community Development. DOI: 10.1080/15575330.2020.1801785

## Reports

- Chan, S., Ogoshi, R. & Turn, S. Feedstocks for sustainable jet fuel production: An assessment of land suitability in Hawaii. Draft report. 82 pp.
- Potential Northwest Regional Feedstock and Production of Sustainable Aviation Fuel: 2019 Report from the Port of Seattle and Washington State University. Prepared February 2020.  
[https://www.portseattle.org/sites/default/files/2020-08/PofSeattleWSU2019updated\\_appendix.pdf](https://www.portseattle.org/sites/default/files/2020-08/PofSeattleWSU2019updated_appendix.pdf)
- CAEP/12-FTG04-IP08. Potential LCAF Technologies and Practices. June 2020.
- CAEP/12-FTG/02-WP/06. Summary of the work of CLCA-TG since FTG/01. September 2019.
- CAEP/12-FTG/03-IP/07. Summary of the work of CLCA-TG on co-processing since FTG/02. February 2020.
- CAEP/12-FTG/03-WP/04. Summary of the work of CLCA-TG since FTG/02. February 2020.
- CAEP/12-FTG/04-IP/07. Summary of progress since FTG/03 on calculating LCA values for fuels produced through co-processing of biogenic feedstock with petroleum feedstock. June 2020.
- CAEP/12-FTG/04-WP/05. Summary of the progress of the Core LCA Subgroup since FTG/03. June 2020.
- CAEP/12-FTG/05-WP/02. Summary of the progress of the Core LCA Subgroup since FTG/04. July 2020.
- CAEP/12-FTG/02-WP/09: Potential Methodology for the Fuel Production Evaluation Task
- CAEP/12-FTG/03-WP/10: Summary of the progress on inventory of techno-economic analyses on sustainable aviation fuel
- CAEP12/FTG04/WP03: Update on fuel production assessment and TEA
- CAEP12/FTG04/IP05 TPP Short Term Projections Database
- CAEP/12-FTG/03-WP/07 – “Progress on Modelling of ILUC values for CORSIA LCA”, Abu Dhabi, United Arab Emirates, February 2020.
- CAEP/12-FTG/03-WP/08 – “Progress of ILUC Subgroup on Low LUC Risk Practices”, Abu Dhabi, United Arab Emirates, February 2020.
- CAEP/12-FTG/03-WP/11 – “Guidance document for calculation and submission of LCA data for new pathways”, Abu Dhabi, United Arab Emirates, February 2020.
- CAEP/12-FTG/03-IP/04 – “Possible methodologies to derive regional ILUC values based on current modelling”, Abu Dhabi, United Arab Emirates, February 2020.
- CAEP/12-FTG/03-IP/05 – “Land Use Change Emission Accounting in GLOBIOM and GTAP-BIO”, Abu Dhabi, United Arab Emirates, February 2020.
- CAEP/12-FTG/03-IP/08 – “Method proposed for DLUC values”, Abu Dhabi, United Arab Emirates, February 2020.
- CAEP/12-FTG/04-WP/07 – “Guidance on Direct Land Use change calculation for Sustainability Criterion 2.2”, Virtual, June 2020.
- CAEP/12-FTG/04-WP/08 – “Expanding Regional ILUC Values Coverage Based On Model Simulations”, Virtual, June 2020.
- CAEP/12-FTG/04-IP/09 – “Progress on ILUC values for additional SAF pathways”, Virtual, June 2020.
- CAEP/12-FTG/04-IP/10 – “Low LUC risk practices: scoping for case studies analysis”, Virtual, June 2020.
- CAEP/12-FTG/05-WP/05 – “Updated ILUC values for carinata oil HEFA”, Virtual, July 2020.
- CAEP/12-FTG/05-WP/06 – “Updated ILUC values for ETJ perennial grass pathways”, Virtual, July 2020.
- CAEP/12-FTG/05-WP/07 – “DLUC safeguard for unused land approach in LMP”, Virtual, July 2020.
- CAEP/12-FTG/05-WP/08 – “Revised guidance on Direct Land Use Change calculation”, Virtual, July 2020.
- CAEP/12-FTG/05-IP/05 – “Overview of ILUC modelling assumptions applied across pathways”, Virtual, July 2020.
- Malina, R., Wolcott, M., Brandt, K. Update on TEA tool development. CAEP/12 Fuels Task Group, TPP subgroup. 20 May 2020.



## Presentations

- Stevens J. and Taheripour F. (2020) A stochastic techno-economic analysis of aviation biofuel production from pennycress seed oil. Selected paper *presented at the 2020 Agricultural & Applied Economics Association Annual Meeting, Virtual Meeting August 10.*
- Zhao X. Taheripour F., Malina R. Tyner W. (2020) Aviation biofuels: A viable and sustainable option to curb aviation emissions. Selected paper *presented at the 2020 Agricultural & Applied Economics Association Annual Meeting, Virtual Meeting August 10.*
- Taheripour attended the CRC meeting and made a presentation on regional land use change values. The meeting was in Argonne National Laboratory, Lemont, IL, October 15-17, 2019.
- Sharon Chan, Richard Ogoshi, Scott Turn. 2020. Feedstocks for Sustainable Jet Fuel Production: An Assessment of Land Suitability in Hawaii. Poster presented at the European Biomass Conference and Exhibition held virtually July 6-9, 2020. Received the **Best Visual Presentation Award.**
- Jinxia Fu, Sabrina Summers, Scott Q. Turn. 2020. Upgraded *Milletia Pinnata* Pod via Torrefaction for the Production of Bioenergy in Hawaii. Oral presentation at the *2020 Thermal & Catalytic Sciences Virtual Symposium.*
- Quang-Vu Bach, JinxiaFu and Scott Q. Turn. 2020. Construction and Demolition Waste as an Alternative Energy Source: Fuel Characterization and Ash Fusion Properties” Poster presented at the *2020 Thermal & Catalytic Sciences Virtual Symposium.*
- Quang-Vu Bach, Jinxia Fu, Lloyd S. Paredes and Scott Q. Turn. 2019. Investigation of Thermochemical Conversion of Construction and Demolition Waste using Chemical Equilibrium. Presented at the October 2019 *Thermochemical Biomass 2019* conference, in Chicago, Illinois.
- Turn, Information from this task was included in the talk, “Regional Supply Chain Analysis for Alternative Jet Fuel Production in the Tropics,” was presented at the Hawaii Aviation and Climate Action Summit, December 3, 2019, at the Hawaii State Capitol.
- Wolcott, M., Holladay, J. Supply chains for sustainable aviation fuels: Why, What, Who? CleanTech Alliance Breakfast. 11 December 2019. Seattle, WA.
- Wolcott, M., Brandt, K., Camenzind, D. Potential Northwest Regional Feedstock and Production of Sustainable Aviation Fuel. Energy and Sustainability Committee – WSU Briefing. 12 February 2020. Seattle, WA.
- Wolcott, M.P., K. Brandt, and D. Camenzind. Potential Northwest Regional Feedstock and Production of Sustainable Aviation Fuel: Port of Seattle. Washington State Aviation Biofuels Work Group. Virtual Meeting held on June 3, 2020.
- Wolcott, M. Potential Northwest Regional Feedstock and Production of Sustainable Aviation Fuel: Port of Seattle. Washington Clean Fuel Forum: 2021 Industry and Policy Forecast. 22 October 2020.

## Project 002

Three undergraduate students involved.

## Publications

- Prem Lobo, Lukas Durdina, Benjamin T. Brem, Andrew P. Crayford, Mark P. Johnson, Greg J. Smallwood, Frithjof Siegerist, Paul I. Williams, Elizabeth A. Black, Andrea Llamedo, Kevin A. Thomson, Max B. Trueblood, Zhenhong Yu, Donald E. Hagen, Philip D. Whitefield, Richard C. Miake-Lye, Theo Rindlisbacher. 2020. Comparison of standardized sampling and measurement reference systems for aircraft engine non-volatile particulate matter emissions. *Journal of Aerosol Science*, 145:105557. <https://doi.org/10.1016/j.jaerosci.2020.105557>
- John S. Kinsey, Robert Giannelli, Robert Howard, Brandon Hoffman, Richard Frazee, Michael Aldridge, Cullen Leggett, Katherine Stevens, David Kittelson, William Silvis, Jeffrey Stevens, Prem Lobo, Steven Achterberg, Jacob Swanson, Kevin Thompson, Timothy McArthur, Donald Hagen, Max Trueblood, Lindsay Wolff, David Liscinsky, Russell Arey, Kate Cerully, Richard Miake-Lye, Timothy Onash, Andrew Freedman, William Bachalo, Gregory Payne, Mikal Durllicki. 2020. Assessment of a regulatory measurement system for the determination of the non-volatile particulate matter emissions from commercial aircraft engines. *Journal of Aerosol Science*, 105734. In press, corrected proof. <https://doi.org/10.1016/j.jaerosci.2020.105734>



## Presentations

Presentations on the data analysis and interpretation to date have been made at:

- ASCENT virtual advisory board meetings held in April and September 2020
- AEC Roadmap virtual Meeting held in May 2020

## Project 003

Three graduate students involved.

## Presentations

- Peters JL, Hart J, Whitsel E, Laden F, Nguyen D, Kim C, Levy JI. Long-term aircraft noise exposure and the risk of hypertension in national US studies. UC Davis Aviation Noise and Emissions Symposium, San Diego, CA, March 2, 2020.

## Project 009

Three graduate students involved.

## Project 010

Eleven graduate students involved.

## Publications

- Jain, S., Ogunsina, K. E., Chao, H., Crossley, W. A., and DeLaurentis, D. A., Predicting Routes for, Number of Operations of, and Fleet-level Impacts of Future Commercial Supersonic Aircraft on Routes Touching the United States, 2020. <https://doi.org/10.2514/6.2020-2878>, URL <https://arc.aiaa.org/doi/abs/10.2514/6.2020-2878>.
- Mohammed Hassan, Holger Pfaender and Dimitri Mavris, "Design Tools for Conceptual Analysis of Future Commercial Supersonic Aircraft", AIAA Aviation 2020 Forum, AIAA 2020-2620, June 2020

## Submitted conference proceedings

- Jain, S., Mane, M., Crossley, W. A., & DeLaurentis, D. A. Investigating How Commercial Supersonic Aircraft Operations Might Impact Subsonic Operations and Total CO<sub>2</sub> Emissions. Abstract submitted to AIAA Aviation Forum for presentation in June 2021
- Mane M., Jain, S., Crossley, W. A. Estimating Market Size for Supersonic Passenger Transport Aircraft. Abstract submitted to AIAA Aviation Forum for presentation in June 2021

## Project 017

## Publications

- Smith, M., Rocha, S., Witte, M., & Basner, M. (2020). On the feasibility of measuring physiologic and self-reported sleep disturbance by aircraft noise on a national scale: A pilot study around Atlanta airport. *Science of the Total Environment*, 718: 137368

## Project 018

One graduate student and two undergraduate students involved.



## Project 019

### Publications

- Chowdhury G. Moniruzzaman, Jared Bowden, Saravanan Arunachalam. 2020. Aircraft landing and takeoff emission impacts on surface O<sub>3</sub> and PM<sub>2.5</sub> through aerosol direct feedback effects estimated by the coupled WRF-CMAQ model. Atmospheric Environment. 243:117859. <https://doi.org/10.1016/j.atmosenv.2020.117859>

## Project 020

One graduate student involved.

### Presentations

- Grobler, C. (presenter), Wolfe, P.J., Dasadhikari, K., Dedoussi, I.C., Allroggen, F., Speth, R.L., Eastham, S.D., Agarwal, A., Staples, M.D., Sabnis, J. and Barrett, S.R.H. Marginal climate and air quality costs of aviation emissions. Aerospace Europe conference in Bordeaux in February 2020.

## Project 021

One graduate student involved.

### Presentations

- Grobler, C. (presenter), Wolfe, P.J., Dasadhikari, K., Dedoussi, I.C., Allroggen, F., Speth, R.L., Eastham, S.D., Agarwal, A., Staples, M.D., Sabnis, J. and Barrett, S.R.H. Marginal climate and air quality costs of aviation emissions. Aerospace Europe conference in Bordeaux in February 2020.

## Project 022

One graduate student involved.

### Publications

- Zhang, J., Wuebbles, D. J., Kinnison, D. E., & Baughcum, S. L. Potential Impacts of Supersonic Aircraft Emissions on Ozone and Resulting Forcing on Climate. Volumes 1 and 2. Both papers are submitted to the Journal of Geophysical Research, September 2020.

## Project 023

Five graduate students involved.

## Project 025

Four graduate students involved.

### Publications

- N. Pinkowski, S. Cassady, D.F. Davidson, R.K. Hanson, "Spectroscopic inference of alkane, alkene, and aromatic formation during high-temperature JP8, JP5, and Jet-A pyrolysis," Fuel 269 117420 (2020). <https://doi.org/10.1016/j.fuel.2020.117420>
- Y. Wang, W. Wei, R.K. Hanson, "A new strategy of characterizing hydrocarbon fuels using FTIR spectra and generalized linear model with grouped-Lasso regularization," Fuel, accepted 9/30/2020.



## Project 027

Five graduate students involved.

### Publications

- N. Schorn, Z. Hoter, D. Blunck, "Turbulent Combustion Behavior of a Surrogate Jet Fuel," in preparation for submission to Fuels.
- Schorn, N., Bonebrake, J., Hoter, Z., Fillo, A., & Blunck, D. Pressure effects on the turbulent consumption speed of large hydrocarbon fuels. *AIAA Journal*, under review

## Project 029(A)

Three graduate students involved.

### Publications

- V. R. Hasti, R. P. Lucht, and J. P. Gore, "Large Eddy Simulation of Hydrogen Piloted CH<sub>4</sub>/Air Premixed Combustion with CO<sub>2</sub> Dilution," *Journal of the Energy Institute* **93**, 1099-1109 (2020). DOI: [10.1016/j.joei.2019.10.004](https://doi.org/10.1016/j.joei.2019.10.004)
- D. Shin, A. J. Bokhart, N. S. Rodrigues, P. E. Sojka, J. P. Gore, and R. P. Lucht, "Nonreacting Spray Characteristics for Alternative Aviation Fuels at Near-Lean Blowout Conditions," *AIAA Journal of Propulsion and Power* **36**, 323-334 (2020). DOI: 10.2514/1.B37712

## Project 031(A)

### Publications

#### Written reports

Evaluation of Integrated Hydropyrolysis and Hydroconversion (IH<sup>2</sup>®) Cycloparaffinic Kerosene (CPK-0), D4054 Phase 1 Research Report, May 2020.

## Project 033

One graduate student involved.

- Database made accessible through <https://altjetfuels.illinois.edu/>

## Project 034

Three graduate students involved.

### Publications

#### Peer-reviewed Journal Publications

- Colborn JG, Heyne JS, Stouffer SD, Hendershott TH, Corporan E. Chemical and physical effects on lean blowout in a swirl-stabilized single-cup combustor. *Proc Combust Inst* 2020. doi:10.1016/j.proci.2020.06.119.

### Presentations

#### Invited Talks:

- Heyne, J. (2020). Prescreening of sustainable aviation fuels. ACS Fall 2020 National Meeting & Exposition, San Francisco, CA.



### **Conference Presentations**

- Yang Z, Heyne J, Ave P, States U. A GCxGC Tier Alpha and Combustor Figure-of-Merit Approach on Sustainable Aviation Fuels Prescreening 2018:1–6. Eastern States Section of the Combustion Institute. University of South Carolina.

## **Project 036**

Three graduate students involved

### **Publications**

- Gao, Z., Behere, A., Li, Y., Lim, D., Kirby, M., & Mavris, D.M. Quantitative assessment of the new departure profiles with improved weight and thrust modeling. Journal of Aircraft, approved for publication.

## **Project 37**

No graduate students currently involved, Anticipated in 2021.

## **Project 038**

One graduate student involved.

## **Project 039**

Two graduate students involved.

### **Presentations**

- Cost-benefit analysis of naphthalene removal. Aviation Emissions Characterization (AEC) Roadmap annual meeting, May 2020.

## **Project 040**

Three graduate students and one undergraduate student involved.

## **Project 041**

One graduate student involved.

### **Presentations**

- V. Sparrow and K. Riegel, “2020 literature review of secondary sonic boom,” Written paper in Proc. 2020 e-Forum Acusticum (European Acoustics Association, Dec. 2020). This paper will be open-access, available online in 2021.

## **Project 043**

Six graduate students involved.



## Project 044

Four graduate students involved.

### Publications

- Thomas, J. & Hansman, R.J. (2020). Evaluation of the impact of transport jet aircraft approach and departure speed on community noise. MIT ICAT Report.
- Thomas, J. & Hansman, R.J. (2020). Modeling and assessment of delayed deceleration approaches for community noise reduction. AIAA AVIATION 2020 FORUM. <https://doi.org/10.2514/6.2020-2874>

### Presentations

- Thomas, J. & Hansman, R.J. (2020). Modeling and assessment of delayed deceleration approaches for community noise reduction. AIAA AVIATION 2020 FORUM. June 2020.

## Project 045

Six graduate students involved.

### Publications

- Ameya Behere, Loren Isakson, Tejas G. Puranik, Yongchang Li, Michelle Kirby, and Dimitri Mavris. Aircraft Landing and Takeoff Operations Clustering for Efficient Environmental Impact Assessment, AIAA AVIATION 2020 FORUM. June 2020, <https://doi.org/10.2514/6.2020-2583>

### Presentations

- Ameya Behere, Loren Isakson, Tejas G. Puranik, Yongchang Li, Michelle Kirby, and Dimitri Mavris. Aircraft Landing and Takeoff Operations Clustering for Efficient Environmental Impact Assessment, AIAA AVIATION 2020 FORUM. June 2020.

## Project 046

One graduate student and one undergraduate student involved.

## Project 047

Two graduate students involved.

### Presentations

- Laurens Voet, "Investigation of the effects of VNRS on LTO emissions of engines for supersonic transport aircraft," CAEP/12-WG3/5-ESTG meeting on November 3, 2020.

## Project 048

One graduate student involved.

### Publications

- Working Paper for CAEP/12-WG3-ECTG/5.



## Project 049

Two graduate students involved.

### Presentations

- B. Mukherjee, Z. F. T. Gan, J.-P. Theron, M. Botre, K. S. Brentner, E. Greenwood, and J. F. Horn, "A New Distributed Electric Propulsion Aircraft Simulation Tool for Coupled Flight Dynamics, Free Wake, and Acoustic Predictions," Vertical Flight Society 77th Annual Forum & Technology Display, May 11-13, 2021, *abstract submitted and under review*.
- Z. F. T. Gan, K. S. Brentner, and E. Greenwood, "Time Variation of Rotor Broadband Noise," Vertical Flight Society 8th Annual Electric VTOL Symposium, Jan. 26-28, 2021, *accepted for presentation*.

## Project 050

Six graduate students involved.

## Project 051

Two graduate students involved.

## Project 052

One graduate student involved.

## Project 053

Four graduate students and two undergraduate students involved.

## Project 054

Nine graduate students involved.

### Publications

- Behere, A., Bhanpato, J., Puranik, T.G., Li, Y., Kirby, M., Mavris D.N., "Data-driven Approach to Environmental Impact Assessment of Real-World Operations", in AIAA SciTech Forum 2021.

## Project 055

Three graduate students involved.

### Presentations

- Accepted submission to the 2021 AIAA SciTech virtual conference for the Flame Response Modeling task.
- Extended abstract submitted to AIAA Aviation 2021 Conference for work in the Turbine Interaction Modeling task.



## **Project 056**

One graduate student involved.

## **Project 057**

One graduate student involved.

## **Project 058**

Two graduate students involved.

## **Project 059**

Fourteen graduate students involved.

## **Project 060**

Three graduate students and three undergraduate students involved.

## **Project 061**

Three graduate students involved.

## **Project 062**

Four graduate students involved.

## **Project 063**

Two graduate students involved.

## **Project 064**

Two graduate students involved.

## **Project 065**

Four graduate students and one undergraduate student involved.

## **Publications**

- Yang, Z., Kosir, S., Stachler, R., Heyne, J., Shafer, L., and Anderson, C., "A GCxGC Tier Alpha Combustor Operability Prescreening Method for Sustainable Aviation Fuel," pp. 1-18. Fuel. (In review)



## **Presentations**

- ACS Fall 2020 National Meeting & Exposition, San Francisco, CA

## **Project 066**

One graduate student and one undergraduate student involved.

## **Project 067**

Four graduate students involved.

## **Project 068**

One graduate student involved.

## **Project 069**

There are no graduate students currently assigned to this project.

## **Project 070**

Graduate students: TBD

## **Project 071**

Two graduate students involved.

## **Project 072**

One graduate student involved.

## **Project 073**

Graduate student and undergraduate student: TBD

## **Project 074**

Five graduate students and one undergraduate student involved.

## **Project 075**

One undergraduate student involved.



## **Project 076**

Five graduate students involved.

## **Project 077**

Three graduate students involved.

## Project Funding Allocations by Federal Fiscal Year

### Breakout by Project

Project		Funding Based on award date							Total
		2014	2015	2016	2017	2018	2019	2020	
001	Alternative Jet Fuel Supply Chain Analysis	\$1,599,943	\$1,425,000	\$1,498,749	\$1,855,461	\$1,102,865	\$1,034,039	\$2,689,454	\$11,205,511
002	Ambient Conditions Corrections for Non-Volatile PM Emissions Measurements	\$2,800,000	\$750,000	-\$147,766	\$725,500	-	\$1,217,221	-	\$5,344,955
003	Cardiovascular Disease and Aircraft Noise Exposure	\$200,000	\$200,000	\$200,000	\$340,000	-	\$1,729,286	-	\$2,669,286
004	Estimate of Noise Level Reduction	\$150,000	-	-	-	-\$8,845	-	-	\$141,155
005	Noise Emission and Propagation Modeling	\$212,000	\$200,000	-	-	-	-	-	\$412,000
006	Rotorcraft Noise Abatement Operating Conditions Modeling	\$250,326	-	-	-	-	-	-	\$250,326
007	Civil, Supersonic Over Flight, Sonic Boom (Noise) Standards Development	\$100,000	\$200,000	-	-	-	-	-	\$300,000

Project		Funding Based on award date							Total
		2014	2015	2016	2017	2018	2019	2020	
008	Noise Outreach	\$ 30,000	\$ 50,000	\$ 75,000	\$ 25,000	-	\$ 30,000	-	\$210,000
009	Geospatially Driven Noise Estimation Module	-	-	-	-	-	-	\$250,000	\$250,000
010	Aircraft Technology Modeling and Assessment	\$549,979	\$550,000	\$310,000	\$669,567	\$764,185	-	\$2,747,116	\$5,590,847
011	Rapid Fleet-wide Environmental Assessment Capability	\$600,000	\$270,000	\$299,999	-	-	-	-	\$1,169,999
012	Aircraft Design and Performance Assessment Tool Enhancement	\$ 90,000	-	-	-	-	-	-	\$90,000
013	Micro-Physical Modeling & Analysis of ACCESS 2 Aviation Exhaust Observations	\$200,000	-	-	-	-	-	-	\$200,000
014	Analysis to Support the Development of an Aircraft CO2 Standard	\$520,000	-	-	-	-	-	-	\$520,000
017	Pilot Study on Aircraft Noise and Sleep Disturbance	\$154,000	\$343,498	\$266,001	\$134,924	-	-	-	\$898,423

Project		Funding Based on award date							Total
		2014	2015	2016	2017	2018	2019	2020	
018	Health Impacts Quantification for Aviation Air Quality Tools	\$150,000	\$150,000	\$200,000	\$270,000	-	-	\$1,299,991	\$2,069,991
019	Development of Aviation Air Quality Tools for Airport-Specific Impact Assessment: Air Quality Modeling	\$320,614	\$369,996	-	\$625,378	-	\$300,000	\$569,000	\$2,184,988
020	Development of NAS wide and Global Rapid Aviation Air Quality	\$150,000	\$200,000	\$250,000	\$250,000	-	-	-	\$850,000
021	Improving Climate Policy Analysis Tools	\$150,000	\$150,000	\$150,000	\$150,000	-	-	-	\$600,000
022	Evaluation of FAA Climate Tools	\$150,000	\$30,000	\$75,000	\$100,000	-	-	\$200,000	\$555,000
023	Analytical Approach for Quantifying Noise from Advanced Operational Procedures	-	\$286,711	\$250,000	\$250,000	-	\$250,000	\$500,000	\$1,536,711
024	Emissions Data Analysis for CLEEN, ACCESS, and Other Recent Tests	\$244,975	-	\$75,000	-	-	-	-	\$319,975

Project		Funding Based on award date							Total
		2014	2015	2016	2017	2018	2019	2020	
025	National Jet Fuels Combustion Program – Area #1: Chemical Kinetics Combustion Experiments	-	\$615,000	\$210,000	\$200,000	\$ 2,556	\$110,000	\$300,000	\$1,437,556
026	National Jet Fuels Combustion Program – Area #2: Chemical Kinetics Model Development and Evaluation	-	\$200,000	-	-	-\$ 2,556	-	-	\$197,444
027	National Jet Fuels Combustion Program – Area #3: Advanced Combustion Tests	-	\$1,010,000	\$580,000	\$265,000	-	\$ 30,000	-	\$1,885,000
028	National Jet Fuels Combustion Program – Area #4: Combustion Model Development and Evaluation	-	\$470,000	\$ 55,000	-	-	-	-	\$525,000
029	National Jet Fuels Combustion Program – Area #5: Atomization Tests and Models	-	\$640,000	\$360,000	\$150,000	-	\$120,000	-	\$1,270,000
030	National Jet Fuels Combustion Program – Area #6: Referee Swirl-Stabilized Combustor Evaluation/Support	-	\$349,949	-	-	-	-	-	\$349,949

Project		Funding Based on award date							
		2014	2015	2016	2017	2018	2019	2020	Total
031	Alternative Jet Fuels Test and Evaluation	-	\$489,619	\$744,891	\$999,512	\$183,019	-	\$2,976,134	\$5,393,175
032	Worldwide LCA of GHG Emissions from Petroleum Jet Fuel	-	\$150,000	-	-	-	-	-	\$150,000
033	Alternative Fuels Test Database Library	-	\$199,624	\$119,794	\$165,000	-	\$163,584	\$330,000	\$978,002
034	National Jet Fuels Combustion Program - Area #7: Overall Program Integration and Analysis	-	\$234,999	\$635,365	\$192,997	\$374,978	-	\$582,983	\$2,021,322
035	Airline Flight Data Examination to Improve flight Performance Modeling	-	\$150,001	-	-	-	-	-	\$150,001
036	Parametric Uncertainty Assessment for AEDT2b	-	\$65,000	\$175,000	\$380,000	-	\$300,000	-	\$920,000
037	CLEEN II Technology Modeling and Assessment	-	\$200,000	\$150,000	\$170,000	-	\$170,000	\$490,000	\$1,180,000
038	Rotorcraft Noise Abatement Procedures Development	-	\$150,000	\$150,000	\$150,000	\$150,000	-	\$300,000	\$900,000

Project		Funding Based on award date							
		2014	2015	2016	2017	2018	2019	2020	Total
039	Naphthalene Removal Assessment	-	-	\$200,000	\$290,000	-	\$350,000	-	\$840,000
040	Quantifying Uncertainties in Predicting Aircraft Noise in Real-world Situations	-	-	\$218,426	\$200,000	-	\$255,000	-	\$673,426
041	Identification of Noise Acceptance Onset for Noise Certification Standards of Supersonic Airplane	-	-	\$160,000	\$221,000	-	\$390,000	-	\$771,000
042	Acoustical Model of Mach Cut-off	-	-	\$255,000	\$150,000	\$170,000	-	-\$120	\$574,880
043	Noise Power Distance Re-Evaluation	-	-	\$150,000	\$75,000	-	\$220,000	\$400,000	\$845,000
044	Aircraft Noise Abatement Procedure Modeling and Validation	-	-	-	-	\$350,000	-	\$370,000	\$720,000
045	Takeoff/Climb Analysis to Support AEDT APM Development	-	-	\$250,000	\$75,000	\$8,845	\$175,000	-	\$508,845
046	Surface Analysis to Support AEDT APM Development	-	-	\$75,000	\$75,000	\$75,000	-	\$400,000	\$625,000

Project		Funding Based on award date							
		2014	2015	2016	2017	2018	2019	2020	Total
047	Clean Sheet Supersonic Engine Design and Performance	-	-	-	-	-	\$250,000	\$800,000	\$1,050,000
048	Analysis to Support the Development of an Engine nvPM Emissions Standards	-	-	\$150,000	\$200,000	-	\$200,000	\$200,000	\$750,000
049	Urban Air Mobility Noise Reduction Modeling	-	-	-	-	-	-	\$560,000	\$560,000
050	Over-Wing Engine Placement Evaluation	-	-	-	-	-	-	\$590,000	\$590,000
051	Combustion Concepts for Next-Generation Aircraft Engines	-	-	-	-	-	-	\$600,000	\$600,000
052	Comparative Assessment of Electrification Strategies for Aviation	-	-	-	-	-	-	\$600,000	\$600,000
053	Validation of Low Exposure Noise Modeling by Open Source Data Management and Visualization Systems Integrated with AEDT	-	-	-	-	-	-	\$569,903	\$569,903
054	AEDT Evaluation and Development Support	-	-	-	-	-	-	\$1,400,000	\$1,400,000

Project		Funding Based on award date							
		2014	2015	2016	2017	2018	2019	2020	Total
055	Noise Generation and Propagation from Advanced Combustors	-	-	-	-	-	-	\$2,999,984	\$2,999,984
056	Turbine Cooling through Additive Manufacturing	-	-	-	-	-	-	\$800,000	\$800,000
057	Support for Supersonic Aircraft En-route Noise Efforts in ICAO CAEP	-	-	-	-	-	-	\$420,000	\$420,000
058	Improving Policy Analysis Tools to Evaluate Higher-Altitude Aircraft Operations	-	-	-	-	-	-	\$500,000	\$500,000
059	Modeling and Measurements of Supersonic Civil Transport Jet Noise	-	-	-	-	-	-	\$749,956	\$749,956
060	Analytical Methods for Expanding the AEDT Aircraft Fleet Database	-	-	-	-	-	-	\$150,000	\$150,000
061	Noise Certification Streamlining	-	-	-	-	-	-	\$250,000	\$250,000
062	Noise Model Validation for AEDT	-	-	-	-	-	-	\$350,000	\$350,000

Project		Funding Based on award date							
		2014	2015	2016	2017	2018	2019	2020	Total
063	Parametric Noise Modeling for Boundary Layer Ingesting Propulsors	-	-	-	-	-	-	\$300,000	\$300,000
064	Alternative Design Configurations to Meet Future Demand	-	-	-	-	-	-	\$250,000	\$250,000
065	Fuel Testing Approaches for Rapid Jet Fuel Prescreening	-	-	-	-	-	-	\$559,998	\$559,998
066	Evaluation of High Thermal Stability Fuels	-	-	-	-	-	-	\$284,997	\$284,997
067	Impact of Fuel Heating on Combustion and Emissions	-	-	-	-	-	-	\$250,000	\$250,000
068	Combustor Wall Cooling with Dirt Mitigation	-	-	-	-	-	-	\$150,000	\$150,000
069	Transitioning a Research nvPM Mass Calibration Procedure to Operations	-	-	-	-	-	-	\$846,707	\$846,707
070	Reduction of nvPM Emissions from Aero-engine Fuel Injectors	-	-	-	-	-	-	\$500,000	\$500,000

Project		Funding Based on award date							Total
		2014	2015	2016	2017	2018	2019	2020	
071	Predictive Simulation of nvPM Emissions in Aircraft Combustors	-	-	-	-	-	-	\$500,000	\$500,000
072	Aircraft Noise Exposure and Market Outcomes in the United States	-	-	-	-	-	-	\$380,000	\$380,000
073	Fuel Composition Impact on Combustor Durability	-	-	-	-	-	-	\$299,148	\$299,148
074	Low Emissions Pre-Mixed Combustion Technology for Supersonic Civil Transport	-	-	-	-	-	-	\$1,000,000	\$1,000,000
075	Improved Engine Fan Broadband Noise Prediction Capabilities	-	-	-	-	-	-	\$300,000	\$300,000
076	Improved Open Rotor Noise Prediction Capabilities	-	-	-	-	-	-	\$300,000	\$300,000
077	Measurements to Support Noise Certification for UAS/UAM Vehicles and Identify Noise Reduction	-	-	-	-	-	-	\$500,000	\$500,000

## Breakout by University\*

University	Funding Based on award year								
	2013	2014	2015	2016	2017	2018	2019	2020	Total
Boston University	\$5,000	\$350,000	\$350,000	\$400,000	\$610,000	-	\$1,729,286	\$1,599,962.66	\$5,044,249
Georgia Institute of Technology	\$5,000	\$1,310,000	\$1,975,001	\$1,434,999	\$1,468,500	\$650,000	\$895,000	\$12,264,984	\$20,003,484
Massachusetts Institute of Technology	\$10,000	\$1,153,927	\$1,169,073	\$1,855,000	\$1,690,000	\$1,000,000	\$1,050,000	\$5,250,000	\$13,178,000
Missouri University of Science and Technology	\$5,000	\$2,800,000	\$750,000	-\$147,766	\$725,500	-	\$1,217,221	\$846,707	\$6,196,662
Oregon State University	\$5,000	-	\$160,000	\$80,000	\$59,000	-	-	-	\$304,000
Pennsylvania State University	\$5,000	\$862,301	\$766,711	\$958,426	\$890,424	\$320,000	\$797,623	\$2,845,000	\$6,794,485
Purdue University	\$5,000	\$389,979	\$1,030,000	\$763,750	\$747,067	\$114,185	\$605,000	\$1,220,116	\$4,875,097
Stanford University	\$5,000	\$380,000	\$1,155,000	\$345,000	\$200,000	-	\$110,000	\$1,069,903	\$3,264,903
University of Dayton	\$5,000	-	\$906,196	\$1,349,087	\$1,192,509	\$574,944	-	\$4,553,260	\$8,580,996
University of Hawaii	\$10,000	-	\$75,000	\$100,000	\$125,000	-	\$200,000	\$200,000	\$710,000

	<b>Funding Based on award year</b>								
<b>University</b>	<b>2013</b>	<b>2014</b>	<b>2015</b>	<b>2016</b>	<b>2017</b>	<b>2018</b>	<b>2019</b>	<b>2020</b>	<b>Total</b>
University of Illinois	\$5,000	\$349,943	\$553,000	\$375,000	\$265,000	-	\$130,000	\$879,956	\$2,557,899
University of North Carolina	\$5,000	\$320,614	\$369,996	-	\$625,378	-	\$300,000	\$569,000	\$2,189,988
University of Pennsylvania	\$5,000	\$154,000	\$343,498	\$266,001	\$134,924	-	-	-	\$903,423
University of Tennessee	\$5,000	\$200,000	\$100,000	\$100,000	\$225,000	-	\$260,000	\$500,000	\$1,390,000
University of Washington	\$5,000	\$60,000	\$29,997	\$15,000	-	-	-	-\$120.15	\$109,877
Washington State University	\$20,000	\$974,228	\$864,968	\$725,961	\$796,039	\$510,918	\$390,911	\$1,385,373	\$5,668,398

## Breakout by State\*

State	Funding Based on award year								
	2013	2014	2015	2016	2017	2018	2019	2020	Total
California	\$5,000	\$380,000	\$1,155,000	\$345,000	\$200,000	-	\$110,000	\$1,069,903	\$3,264,903
Georgia	\$5,000	\$1,310,000	\$1,975,001	\$1,434,999	\$1,468,500	\$650,000	\$895,000	12,264,984	\$20,003,484
Hawaii	\$10,000	-	\$75,000	\$100,000	\$125,000	-	\$200,000	\$200,000	\$710,000
Illinois	\$5,000	\$349,943	\$553,000	\$375,000	\$265,000	-	\$130,000	\$879,956	\$2,557,899
Indiana	\$5,000	\$389,979	\$1,030,000	\$763,750	\$747,067	\$114,185	\$605,000	\$1,220,116	\$4,875,097
Massachusetts	\$15,000	\$1,503,927	\$1,529,073	\$2,255,000	\$2,300,000	\$1,000,000	\$2,779,286	\$6,849,963	\$18,222,249
Missouri	\$5,000	\$2,800,000	\$750,000	-\$147,766	\$725,500	-	\$1,217,221	\$846,707	\$6,196,662
North Carolina	\$5,000	\$320,614	\$369,996	-	\$625,378	-	\$300,000	\$569,000	\$2,189,988
Ohio	\$5,000	-	\$906,196	\$1,349,087	\$1,192,509	\$574,944	-	\$4,553,260	\$8,580,996
Oregon	\$5,000	-	\$160,000	\$80,000	\$59,000	-	-	-	\$304,000
Pennsylvania	\$10,000	\$1,016,301	\$1,110,209	\$1,224,427	\$1,025,348	\$320,000	\$797,623	\$2,845,000	\$8,348,908
Tennessee	\$5,000	\$200,000	\$100,000	\$100,000	\$225,000	-	\$260,000	\$500,000	\$1,390,000
Washington	\$25,000	\$1,034,228	\$894,965	\$740,961	\$796,039	\$510,918	\$390,911	\$1385,253	\$5,778,275

\*Totals include administrative funds not associated with specific NFOs